

DTIC FILE COPY

MRS

ARs 27489.1-CHCF

MATERIALS
RESEARCH
SOCIETY

(2)

AD-A217 490

1-9-8-9

FALL MEETING

November 27 —
December 2, 1989
Boston Marriott Hotel/
The Westin Hotel
Copley Place
Boston, Massachusetts

DTIC
ELECTE
JAN 25 1990
S D

DISTRIBUTION STATEMENT A

Approved for public release
Distribution Unlimited

■ 1989 MRS OFFICERS ■

R.P.H. Chang
President

R.R. Chianelli
First Vice
President

J.B. Roberto
Second Vice
President

J.M. Phillips
Secretary

S.M. Kelso
Treasurer

J.E.E. Baglin
Past President

■ 1989 MRS COUNCILLORS ■

B.R. Appleton
David K. Biegelsen
Walter L. Brown
G. Slade Cargill
Charles B. Duke

Rodney C. Ewing
Robert A. Huggins
Herbert H. Johnson
Elton N. Kaufmann
S. Thomas Picraux

Gordon E. Pike
John M. Poate
Della M. Roy
Kathleen C. Taylor
C.W. White

THE MATERIALS RESEARCH SOCIETY

The Materials Research Society (MRS) is an organization of technical professionals from a wide variety of scientific and engineering disciplines. Its primary purpose is to hold symposia on topics of materials research which, because of their multidisciplinary nature, do not have adequate forums within the more traditional societies. Through these symposia, MRS attempts to promote interactions between chemists, physicists, metallurgists, engineers, etc., who are studying different aspects of a particular materials topic. Membership in the Materials Research Society is open to anyone who has an interest in materials development, processing, or characterization.

MEMBERSHIP BENEFITS INCLUDE:

1. Automatic mailing of the call of papers booklet and the preliminary program for both the Fall and Spring meetings.
2. A subscription to Journal of Materials Research, an archival interdisciplinary journal which is the official journal of the Materials Research Society.
3. The MRS BULLETIN, a monthly news publication which contains summaries of the Society symposia, news of Society members, announcements of meetings, and other activities sponsored or co-sponsored by MRS, and news about developments in research and industry.
4. A listing in and a copy of the MRS Membership Director, which is published yearly.
5. Opportunity to purchase MRS symposium proceedings, monographs, and videotapes at special member prices that are 15-25% off list price. This numbered series has become a standard reference in many areas of materials science. Over 126 volumes have been published in this well respected series.
6. Opportunity to purchase technical books from other scientific publishers at substantial savings.
7. Reduced subscription rates for journals published by the American Institute of Physics through the MRS affiliation with AIP.
8. Special personal subscription rates for Materials Letters, a letters journal published by North-Holland.

The membership fee is \$65 for the 1990 calendar year. Student membership is \$20 per year, but does not include a subscription to Journal of Materials Research. Student members of MRS may subscribe to JMR for \$15 in addition to their \$20 dues.

A free descriptive brochure on the Society is available. Contact:

Materials Research Society
9800 McKnight Road
Pittsburgh, Pennsylvania 15237 USA
(412) 367-3003
FAX (412) 367-4373

On-site meeting operations are handled by The Complete Conference, Sacramento, CA, Marilyn Hauck, President.

UNCLASSIFIED

MASTER COPY

FOR REPRODUCTION PURPOSES

SECURITY CLASSIFICATION OF THIS PAGE

REPORT DOCUMENTATION PAGE

1a. REPORT SECURITY CLASSIFICATION Unclassified		1b. RESTRICTIVE MARKINGS	
2a. SECURITY CLASSIFICATION AUTHORITY		3. DISTRIBUTION / AVAILABILITY OF REPORT Approved for public release; distribution unlimited.	
2b. DECLASSIFICATION / DOWNGRADING SCHEDULE			
4. PERFORMING ORGANIZATION REPORT NUMBER(S)		5. MONITORING ORGANIZATION REPORT NUMBER(S) ARO 27489.1-CH-CF	
6a. NAME OF PERFORMING ORGANIZATION Materials Research Society	6b. OFFICE SYMBOL (If applicable)	7a. NAME OF MONITORING ORGANIZATION U. S. Army Research Office	
6c. ADDRESS (City, State, and ZIP Code) Pittsburgh, PA 15237-6005		7b. ADDRESS (City, State, and ZIP Code) P. O. Box 12211 Research Triangle Park, NC 27709-2211	
8a. NAME OF FUNDING / SPONSORING ORGANIZATION U. S. Army Research Office	8b. OFFICE SYMBOL (If applicable)	9. PROCUREMENT INSTRUMENT IDENTIFICATION NUMBER DAAL03-89-G-0121	
8c. ADDRESS (City, State, and ZIP Code) P. O. Box 12211 Research Triangle Park, NC 27709-2211		10. SOURCE OF FUNDING NUMBERS	
		PROGRAM ELEMENT NO	PROJECT NO
11. TITLE (Include Security Classification) Materials Research Society Symposium on the Electrical, Optical and Magnetic Properties of Organic Solid State Materials			
12. PERSONAL AUTHOR(S) Long Y. Chiang (principal investigator)			
13a. TYPE OF REPORT Final	13b. TIME COVERED FROM 10/1/89 TO 9/30/90	14. DATE OF REPORT (Year, Month, Day) December 1989	15. PAGE COUNT 771
16. SUPPLEMENTARY NOTATION The view, opinions and/or findings contained in this report are those of the author(s) and should not be construed as an official Department of the Army position, policy, or decision, unless so designated by other documentation.			
17. COSATI CODES		18. SUBJECT TERMS (Continue on reverse if necessary and identify by block number)	
FIELD	GROUP	SUB-GROUP	
		Materials Areas, Electronic Materials, Polymers, Nuclear Waste, Cements	
19. ABSTRACT (Continue on reverse if necessary and identify by block number) The meeting's main focus was the technical symposia. Following the traditions of interdisciplinary programming, the symposia covered a very diverse materials area, ranging from electronic materials and polymers to nuclear waste and specialty cements. Oral presentations and posters kept the attendees informed of the latest breakthroughs, allowing maximum interaction among the researchers.			
20. DISTRIBUTION / AVAILABILITY OF ABSTRACT <input type="checkbox"/> UNCLASSIFIED UNLIMITED <input type="checkbox"/> SAME AS RPT. <input type="checkbox"/> DTIC USERS		21. ABSTRACT SECURITY CLASSIFICATION Unclassified	
22a. NAME OF RESPONSIBLE INDIVIDUAL		22b. TELEPHONE (Include Area Code)	22c. OFFICE SYMBOL

90 01 23 185

MRS

**MATERIALS
RESEARCH
SOCIETY**

1-9-8-9

FALL MEETING

November 27 —

December 2, 1989

Boston Marriott Hotel/

The Westin Hotel

Copley Place

Boston, Massachusetts

FINAL

PROGRAM

AND

ABSTRACTS

■ WELCOME TO THE MATERIALS RESEARCH SOCIETY'S 1989 FALL MEETING ■

Welcome to Boston for the 1989 Fall Meeting! The program is diverse — covering the familiar MRS Fall Meeting topics as well as several new symposium topics not previously covered in MRS meetings. We will also be experimenting with live video broadcasts of two Symposia between the Marriott and Westin Hotels. This meeting is comprised of 24 symposia with over 2,400 accepted papers, making it the largest MRS meeting to date!

On Monday evening we are delighted to welcome Robert N. Noyce, who will present the Plenary address. Noyce is a pioneer in the electronics industry; he is president and chief executive officer of SEMATECH as well as vice-chairman of Intel Corporation. The Von Hippel Award will be presented to honor both the Von Hippel winner and the Fall 1989 Graduate Student Award winners. Several evening poster sessions will be held in the Westin Hotel during the meeting; complimentary snacks and beverages will be served.

In addition to the oral and poster sessions, many other activities are scheduled to interest you. The Equipment Exhibit will be held Tuesday through Thursday in the Marriott Hotel. Symposium X will feature a series of authoritative reviews covering relevant topics for the non-specialist during the noon hours on Tuesday through Thursday. To complement the technical program, 22 MRS short courses are scheduled throughout the week.

Finally, we want to take this opportunity to thank the symposium organizers for assembling an excellent and stimulating program. The staff at MRS Headquarters and The Complete Conference have worked diligently to streamline this program into a coherent form. The MRS officers, Program Committee, Publicity Committee, Short Course Manager, and others have given invaluable help and advice. On behalf of the above, we welcome you to Boston and wish you a stimulating, productive, and enjoyable week.

Gary L. McVay
Pacific Northwest Laboratory

James C. Mikkelsen, Jr.
Xerox Palo Alto Research Center

Robert J. Nemanich
North Carolina State University

PRICE-\$20.00
SOLD BY: MATERIALS RESEARCH SOCIETY
9800 McKnight Rd.
Pittsburgh, PA. 15237

Accession For	
NTIS CRA&I	<input checked="" type="checkbox"/>
DTIC TAB	<input type="checkbox"/>
Unannounced	<input type="checkbox"/>
Justification	
By 20.00	
Distribution	
Availability Codes	
Dist	Availability for
A-1 21	



■CONTENTS■

About the Materials Research Society . . . inside front	Future Meetings769
Activities Locator inside back	Job Placement Centerx
Area Map770	MRS Proceedings Volumes762
Author/Speaker Index741	MRS Short Coursesxi
Corporate Affiliatesxii	Officers/Councillorsinside front
Equipment Exhibitx	Plenary Sessionviii
1989 Fall Meeting Chairsiv	Von Hippel Awardix
Fall Meeting Activitiesvii	1990 Spring Meeting767

SYMPOSIA

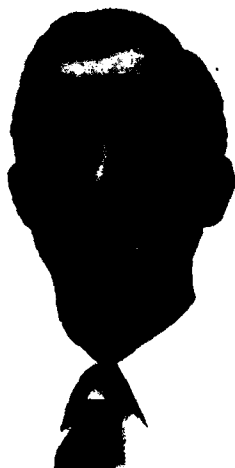
A. Beam-Solid Interactions, Physical Phenomena;	1
B. In-Situ Patterning, Selective Area Deposition and Etching;	55
C. Atomic Scale Structure of Interfaces;	83
D. Layered Structures, Heteroepitaxy, Superlattices, Strain and Metastability;	113
E. Properties of II-VI Semiconductors, Bulk Crystals, Epitaxial Films, Quantum Well Structures, and Dilute Magnetic Systems;	161
F. Diamond, Boron Nitride, Silicon Carbide and Related Wide Bandgap Semiconductors;	191
G. Impurities, Defects and Diffusion in Semiconductors, Bulk and Layered Structures;	225
H. Materials Issues in Microcrystalline Semiconductors;	285
I. Characterization of Plasma-Enhanced CVD Processes;	307
J. Neutron Scattering for Materials Science;	321
K. Advanced Electronic Packaging Materials; CVD;	347
L. Chemical Vapor Deposition of Refractory Metals and Ceramics;	365
M. High-Temperature Superconductors; Fundamental Properties and Novel Materials Processing;	385
N. Tailored Interfaces in Composite Materials;	489
O. Polymer Based Molecular Composites;	513
P. Optical Fiber Materials and Processing;	537
Q. Electrical, Optical, and Magnetic Properties of Organic Solid State Materials;	553
R. Materials Synthesis Utilizing Biological Processes;	593
S. Multi-Functional Materials;	611
T. Fractal Aspects of Materials;	625
U. Scientific Basis for Nuclear Waste Management; XIII;	653
V. Macromolecular Liquids;	685
W. Fly Ash and Coal Conversion By-Products Characterization, Utilization and Disposal VI;	713
X. Frontiers of Materials Research;	725
Y. Specialty Cements with Advanced Properties;	731

MRS would like to remind you that to attend MRS Symposia, you must be wearing your 1989 Fall Meeting Registration badge. If you have not registered, please do so. Registration is located on the fourth floor of the Boston Marriott. MRS appreciates your cooperation in not smoking or taking flash photographs in Symposium or Short Course rooms.

■ 1989 FALL MEETING CHAIRS ■



Gary L. McVay
Materials Sciences Department
Pacific Northwest Laboratory
P.O. Box 999
Richland, WA 99352
(509) 375-3762
FAX (509) 375-2059



James C. Mikkelsen, Jr.
Electronics & Imaging Laboratory
Xerox Palo Alto Research Center
3333 Coyote Hill Road
Palo Alto, CA 94304
(415) 494-4917
FAX (415) 494-4502



Robert J. Nemanich
Department of Physics
North Carolina State University
Box 8202
Raleigh, NC 27695-8202
(919) 737-3225
FAX (919) 737-7331

■ A MESSAGE FROM THE PRESIDENT ■

Over the last 12 months more than 100 people, including volunteer organizers and MRS staff members, have been preparing what we believe will be one of the most exciting Boston meetings to date. Over 2,400 abstracts are in the program, and we are projecting a record attendance of over 4,000 people.

The meeting's main focus is the technical symposia organized by Chairs Gary L. McVay of Pacific Northwest Laboratories, Robert J. Nemanich of North Carolina State University, and James C. Mikkelsen Jr. of Xerox. Following the traditions of interdisciplinary programming, the symposia will cover a very diverse materials area, ranging from electronic materials and polymers to nuclear waste and specialty cements. Oral presentations and posters will keep the attendees informed of the latest breakthroughs, allowing maximum interaction among the researchers.

The Society has invited Robert N. Noyce, a pioneer in the electronics industry and chief executive officer of SEMATECH, to present the Plenary Address on Monday evening, November 27. The 1989 Von Hippel Award will be presented to John Goodenough on Wednesday evening, November 29; the Graduate Student Award winners will be recognized, and the ceremonies will be followed by a wine and cheese reception.

Don't miss the special display of MRS Proceedings at both hotels for browsing and ordering; check the Short Course Program developed to complement the technical meeting, and be sure to visit the Equipment Exhibit and Job Placement Center. Many hours of work have been devoted to planning a meeting you won't want to miss. I look forward to meeting you.



R.P.H. Chang
1989 MRS President

■GRADUATE STUDENT AWARDS■

Outstanding performance by graduate students who are presenting significant and timely research and who are participating in the MRS 1989 Fall Meeting as an attendee and author or co-author of a symposium paper will receive their awards during the Von Hippel ceremony Wednesday evening.

■GRADUATE STUDENT MIXER■

All graduate students and members of MRS student chapters are invited to attend a reception on Tuesday, November 28, 5:00 - 6:30 p.m., in the Regis Room, Marriott Hotel. Refreshments will be served. Student chapters are a vital part of MRS providing discussion between students and faculty and promoting student interest in materials science. Don't miss this opportunity to meet with others involved in MRS student activities.

■SYMPOSIUM X■

MRS is pleased to announce that Symposium X will be broadcast live via satellite to selected university and industrial laboratories by PBS on Monday, November 27, 1989. To accommodate MRS meeting attendees interested in attending this popular noon-time symposium, it is held between noon and 1:30 p.m. daily in the Staffordshire Room at the Westin Hotel. Box lunches will be available at the symposium door for your convenience. Be sure to check the Meeting Guide available at the meeting for final scheduling details.

■SYMPOSIUM BROADCASTS■

Symposium M: High Temperature Superconductors, may be viewed simultaneously in the Marriott Hotel and the Westin Hotel; and Symposium F: Diamond, Boron Nitride, Silicon Carbide and Related Wide Bandgap Semiconductors, may be viewed simultaneously in the Marriott Hotel and the Westin Hotel. Check the Activities Locator in the Meeting Guide for daily locations at each hotel.

■ 1989 MRS FALL MEETING ACTIVITIES ■

Activity	Location	Time
Information Desk/Message Center	Fourth Floor Lobby, Marriott Hotel Third Floor Lobby, Westin Hotel	Sunday, 4:00 p.m.-9:00 p.m. Monday, 7:00 a.m.-7:00 p.m.
Meeting Registration	Fourth Floor Lobby, Marriott Hotel	Tuesday, 7:30 a.m.-5:00 p.m. Wednesday, 7:30 a.m.-5:00 p.m.
MRS Publication Sales	Fourth Floor Lobby, Marriott Hotel Third Floor Lobby, Westin Hotel (Monday - Friday)	Thursday, 7:30 a.m.-5:00 p.m. Friday, 7:30 a.m.-12:00 noon
Short Course Registration	Fourth Floor Lobby, Marriott Hotel	Sunday, 11:30 a.m.-1:30 p.m. and 4:00 p.m.-9:00 p.m. Monday, 7:00 a.m.-7:00 p.m. Tuesday, 7:30 a.m.-5:00 p.m. Wednesday, 7:30 p.m.-5:00 p.m. Thursday, 7:30 a.m.-5:00 p.m. Friday, 7:30 a.m.-9:00 a.m.
Short Course Program (Check with Information Desk for location of individual courses.)		Daily, 8:30 a.m.-4:30 p.m. Courses M-05 and C-09 will meet on Sunday November 26, 1:00 p.m.-6:00 p.m., and on Monday, November 27, 8:00 a.m.-4:30 p.m.
Manuscript Center	Cape Cod Room, Marriott Hotel St. George A, Westin Hotel	Open Monday-Friday 7:30 a.m. - 5:30 p.m.
Slide Preview Area	Near Information Desk Fourth Floor Lobby, Marriott Hotel Third Floor Lobby, Westin Hotel	Open Monday-Friday 7:30 a.m. - 5:00 p.m.
Symposium X Live National Satellite Broadcast	Staffordshire Room Westin Hotel	Monday, November 27 12:05 - 1:25 p.m. (Box lunches available for purchase at the door)
Symposium Broadcast: Wide Bandgap Semiconductors High Temperature Superconductors	Suffolk Room Marriott Hotel Essex North West America Lobby Westin Hotel	Tuesday-Friday noon Monday-Tuesday Wednesday-Friday
Equipment Exhibit <small>Deli-style lunch available daily in Equipment Exhibit, Noon-1:30 p.m.</small>	University Hall, Third Floor Marriott Hotel	Tuesday, 12:00 noon - 7:00 p.m. Reception, 5:00 p.m. - 7:00 p.m. Wednesday, 9:30 a.m. - 5:00 p.m. Thursday, 9:30 a.m. - 2:00 p.m.
Poster Sessions	America Ballroom, Fourth Floor Westin Hotel	Tuesday, 7:00 p.m. - 10:00 p.m. Wednesday, 8:00 p.m. - 10:00 p.m. Thursday, 7:00 p.m. - 10:00 p.m.
Plenary Session, Robert N. Noyce	Salon E, Marriott Hotel	Monday, 6:00 p.m.
Graduate Student Mixer	Regis Room, Marriott Hotel	Tuesday, 5:00 p.m. - 6:30 p.m.
Von Hippel Award Presentation and Lecture Graduate Student Awards	Salon E, Marriott Hotel	Wednesday, 6:00 p.m. Reception Following
Job Placement Center <small>Fee, \$5.00 for employment candidates, \$80.00 for employers</small>	Harvard Room, Third Floor Marriott Hotel	Tuesday-Thursday, 9:00 a.m. - 5:00 p.m.

■ PLENARY SESSION ■

Monday, November 27, 1989
6:00 - 7:00 p.m.
Boston Marriott Copley Place
Salon E



Robert N. Noyce
Chief Executive Officer, SEMATECH

Robert N. Noyce, a pioneer in the electronics industry, is President and CEO of SEMATECH and vice chairman of Intel Corporation.

Noyce graduated from Grinnell College with a BS degree in physics and mathematics and earned his Ph.D. in physical electronics at the Massachusetts Institute of Technology. Following graduation, Noyce engaged in research at Philco Corporation and Shockley Semiconductor Laboratory. He co-founded Fairchild Semiconductor Corporation in 1957 and with Jack Kilby of Texas Instruments invented the integrated circuit.

In 1968, Noyce co-founded Intel with long-time associate Gordon E. Moore with the objective of making large-scale integration a practical reality. Today, the company is the nation's third-largest semiconductor producer.

Noyce was a founding member and the first president of the Semiconductor Industry Association. He also was a member of the President's Committee on Industrial Competitiveness and the Defense Science Board.

Noyce is a member of the National Academy of Science, the National Academy of Engineering, the American Academy of Arts and Science, and holds 16 patents for semiconductor devices, methods and structures. He and Jack Kilby have jointly received the Ballantine Medal of the Franklin Institute and the Cledo Brunetti Award of the IEEE for inventing the integrated circuit. He and Gordon Moore have received the AFIPS Harry Goode Award for leadership in computer science. Noyce also has been awarded the National Medal of Technology, National Medal of Science, the I.E.E. Faraday Medal, and the IEEE Medal of Honor.

■ 1989 VON HIPPEL AWARD LECTURE ■

Wednesday, November 29, 1989

6:00 p.m.

Salon E

Marriott Hotel



John B. Goodenough
Virginia H. Cockrell
Centennial Chair of Engineering
University of Texas at Austin

The Materials Research Society proudly presents its 1989 Von Hippel Award to Professor John B. Goodenough. The Award honors his distinguished contributions to the field of solid state sciences, where his insights, ideas, knowledge and research have consistently drawn together the basic concepts of physics and chemistry in the conquest of wide-ranging fundamental topics. Through the years, his work can be said to have built the principal conceptual foundations of the science of solid state chemistry.

Professor Goodenough has made pioneering contributions in many experimental fields, including such diverse topics as development of ferrite-core random access memories, high pressure studies of perovskites, and the analysis of lithium ion conductivity in spinels. He has addressed the electronic structure of complex materials, with concepts fundamental to chemical bonding. In the days before band structure calculations were routine, Professor Goodenough succeeded in constructing, qualitatively, the band structures of most important semiconductors, oxides and metallic compounds. His 1963 book on "Magnetism and the Chemical Bond" remains a classic reference in the field. A similar intuitive approach underlies Professor Goodenough's classic analysis of superexchange mechanisms and of metal-insulator transitions. His work on Mott localization in oxides is of fundamental significance. Professor Goodenough's work on the electronic structure of transition metal compounds

has covered magnetic-exchange interactions, localized treatment of outer electrons, martensitic phase transformation mechanisms, and structure of ferroelectrics and bronzes. He has studied the electronic structure of metals based on the interactions of Fermi surfaces with Brillouin-zone surfaces in reciprocal space. He has recently investigated the electron pairing mechanism in high-T_c superconductor structures.

Professor Goodenough has also made key contributions in the field of materials for alternate energy technologies. These include solid electrolytes, solid-solution storage-cell electrodes, photoelectrolysis of water with sunlight, wavelength-selective coatings for solar collectors, zeolites for air conditioning with solar energy, catalytic electrodes and heterogeneous catalysis.

Professor Goodenough graduated from Yale University with a B.A. in Mathematics in 1943 and obtained his Ph.D. in Physics at the University of Chicago in 1952. His research in electronic materials (chemistry) continued at the Lincoln Laboratory until his move in 1976 to the University of Oxford as Professor and Head of the Inorganic Chemistry Laboratory. In 1986 he accepted the Virginia H. Cockrell Centennial Chair of Engineering at The University of Texas at Austin.

The Von Hippel Award of the Materials Research Society honors Professor Goodenough's accomplishments for their depth and diversity, exemplifying the possibilities of interdisciplinary materials research.

■JOB PLACEMENT CENTER■

The MRS Job Placement Center is organized and operated by the American Institute of Physics. The Center is conveniently located on the third floor of the Boston Marriott Copley Place and will be open from 9:00 a.m. - 5:00 p.m., Tuesday through Thursday. Individuals using the interviewing facilities to seek employment must register by completing an employment candidate form obtainable from MRS Information, Sunday afternoon and Monday.

■EQUIPMENT EXHIBIT■

Boston Marriott
Tuesday-Thursday, November 28-30, 1989

As part of the 1989 Fall Meeting, a major equipment exhibit will be held to display analytical and processing equipment closely paralleling the nature of the technical symposia. The exhibit will be on the third floor of the Boston Marriott Hotel, convenient to symposium meeting rooms. The technical program has been arranged to allow meeting participants ample opportunity to visit the exhibit.

Show Hours

Tuesday	12:00 noon - 7:00 p.m.
Reception	5:00 p.m. - 7:00 p.m.
Wednesday	9:00 a.m. - 5:00 p.m.
Thursday	9:00 a.m. - 2:00 p.m.

EXHIBITORS

Academic Press
Advanced Materials Engineering Research
AIXTRON GmbH
Alcatel Vacuum Products, Inc.
American Chemical Society
American Institute of Physics
Amplifier Research
Anatech Ltd.
APD Cryogenics, Inc.
Aries/QEI
ASTeX/Applied Science & Technology
ATM, Inc.
Balzers
Beam Alloy Corporation
Blake Industries, Inc.
Edmund Buehler Co. GmbH
Cahn Instruments, Inc.
Cameca Instruments, Inc.
Ceramaseal
Chapman and Hall
Commonwealth Scientific Corporation
CVC Products, Inc.
Denton Vacuum, Inc.
Duniway Stockroom Corporation
E.A. Fischione Instrument Manufacturing
Edwards High Vacuum International
EG&G Princeton Applied Research
Elsevier Science Publishing Company, Inc.
Charles Evans & Associates
FEI Company
Gatan, Inc.
Goodfellow Metals Cambridge Ltd.
Granville-Phillips Co.
High Vacuum Apparatus Manufacturing, Inc.
Hitachi Scientific Instruments
HPS Division
Huntington Laboratories

Image Micro Systems, Inc.
Implant Sciences Corporation
INEL, Inc.
Innovative Technology, Inc.
Instruments SA, Inc.
International Scientific Instruments, Inc.
Ion Tech, Inc.
Janis Research Company
JCPDS-ICDD
JEOL U.S.A., Inc.
Kaiser Systems, Inc.
Keithley Instruments
Kevex Instruments
Kimball Physics, Inc.
Kratos Analytical
Lake Shore Cryotronics, Inc.
Lambda Physik
Leighton Electronics, Inc.
Kurt J. Lesker Company
Leybold Inficon
Leybold Vacuum Products
Materials By Metron
McAllister Technical Services
MDC Vacuum Products Corporation
Microscience, Inc.
MKS Instruments
MMR Technologies, Inc.
National Electrostatics Corporation
Neslab Instruments
Netzsch Incorporated
NGS Associates, Inc.
Nicolet
North Eastern Analytical Corporation
Omicron Associates
Oxford Instruments
Oxford University Press
Peabody Scientific
Pergamon Press
Perkin-Elmer Corporation
Phillips Electronic Instruments
Physicon Corporation

Plasma Technology
Plenum Publishing Corporation
Princeton Gamma-Tech
Princeton Instruments, Inc.
Process Products Corporation
Quantachrome Corporation
Quantum Design, Inc.
RHK Technology, Inc.
Rigaku/USA
RMC-Cryosystems
Rudolph Instruments
Rudolph Research
Scientific Instruments
Scintag, Inc.
Siemens Analytical X-Ray
South Bay Technology, Inc.
Spectra Instruments
Spectra-Tech, Inc.
Spire Corporation
Springer-Verlag NY, Inc.
Structure Probe/SPI Supplies
SULA Technologies
Superconductive Components, Inc.
Sycon Instruments, Inc.
Tencor Instruments
Thermionics Laboratory
Ultra High Vacuum Instruments, Inc.
Vacuum Barrier Corporation
Varian/Vacuum Products
VAT, Inc.
VCR Group
VG Instruments
Virginia Semiconductor, Inc.
Voltaix, Inc.
Walf Associates
Waterloo Scientific
Wavemat, Inc.
John Wiley & Sons
Carl Zeiss, Inc.

■ MRS SHORT COURSE PROGRAM ■

1989 MRS FALL MEETING NOVEMBER 27 - DECEMBER 2 BOSTON MARRIOTT COPLEY PLACE

Title	At-Meeting Tuition	Title	At-Meeting Tuition
ADVANCED MATERIALS		C-20 Optical Characterization of III-V Semiconductor Epitaxial Layers	
M-04 Optoelectronic Materials, Processes, and Devices		Instructor: Gary W. Wicks	
Instructor: Mool C. Gupta		Friday, December 1	\$370
Friday-Saturday, December 1 - 2	\$535		
M-05 Fabrication, Characterization, and Applications of High-Temperature Superconducting Materials		PREPARATION AND FABRICATION OF MATERIALS	
Instructors: David A. Rudman and Robert E. Schwall		P-05 Plasma Enhanced CVD of Thin Films for Microelectronics	
Sunday-Monday, November 26 - 27	\$535	Instructor: Rafael Reif	
		Monday, November 27	\$370
M-06 Growth and Characterization of Diamond and Diamond-Like Films		P-06 Ion Implantation, Diffusion, Defects, and RTP	
Instructors: Daniel L. Flamm, Thomas R. Anthony, and Jeffrey T. Glass		Instructors: Nathan W. Cheung, Dennis M. Maher, and Steven C. Shatas	
Monday, November 27	\$425	Friday-Saturday, December 1 - 2	\$535
CHARACTERIZATION OF MATERIALS		P-12 Photon-Controlled Processing for Microelectronics	
C-01 Modern Materials Analysis Techniques		Instructor: Richard M. Osgood, Jr.	
Instructors: James A. Borders, Kenneth H. Eckelmeyer, and Suzanne H. Weissman		Friday, December 1	\$370
Monday-Wednesday, November 27 - 29	\$800	P-14 Film Formation, Adhesion, Surface Preparation, and Characterization of Thin Film Structures	
C-03 Surface and Thin Film Analysis		Instructor: Donald M. Mattox	
Instructors: Leonard C. Feldman and James W. Mayer		Friday-Saturday, December 1 - 2	\$560
Friday-Saturday, December 1 - 2	\$605	P-15 Ohmic Contacts to Compound Semiconductors	
C-06 Deep Level Transient Spectroscopy		Instructor: Peter A. Barnes	
Instructor: Charles E. Barnes		Friday, December 1	\$370
Monday, November 27	\$370	P-16 Epitaxial Growth of Compound Semiconductors	
C-08 Ceramic and Metal Matrix Composites		Instructors: L. Ralph Dawson, P. Dan Dapkus, and Gary W. Wicks	
Instructors: Jack Mecholsky and Maurice F. Amateau		Tuesday-Thursday, November 28 - 30	\$800
Friday-Saturday, December 1 - 2	\$535	F-01 Film and Coating Deposition Techniques	
C-09 Fractals: Concepts and Applications in Materials Science and Engineering		Instructor: Donald M. Mattox	
Instructors: James E. Martin and Alan J. Hurd		Tuesday-Wednesday, November 28 - 29	\$560
Sunday-Monday, November 26 - 27	\$535	F-02 Plasma Etching for Microelectronic Fabrication	
C-14 Scanning Tunneling Microscopy		Instructor: G. Kenneth Herb	
Instructor: Robert J. Hamers		Thursday, November 30	\$370
Monday, November 27	\$370	F-04 Microelectronic Packaging: Materials, Processing, and Reliability	
C-16 Scanning Electron Microscopy and X-Ray Microanalysis		Instructors: Shankara K. Prasad and Rama K. Shukla	
Instructors: David C. Joy and Dale E. Newbury		Thursday-Saturday, November 30 - December 2	\$800
Monday, November 27	\$390	F-08 Chemical Engineering Aspects of Silicon Integrated Circuit Fabrication	
C-19 Practical Transmission & Analytical Electron Microscopy - Theory, Practice and Specimen Preparation		Instructors: Isaac Trachtenberg and Dean P. Neikirk	
Instructors: Alton D. Romig, Jr., David B. Williams, and Ron M. Anderson		Monday-Wednesday, November 27 - 29	\$770
Tuesday-Thursday, November 28 - 30	\$800		

Advanced Control Systems Corporation
 Advanced Energy Industries, Inc.
 Aerospace Corporation
 AET addax, Inc.
 AG Associates
 Air Products & Chemicals, Inc.
 Aixtron, Inc.
 Alcatel NV
 Allied Signal, Inc.
 American Cyanamid Company
 American Fly Ash Company
 Amoco Chemical Corporation
 Amoco Oil Company
 Anatech Ltd.
 Anderson Physics Laboratories
 APD Cryogenics Inc.
 Applied Electron Corporation
 Applied Materials
 Applied Science and Technology, Inc.
 (ASTEX)
 Arco Solar, Inc.
 AT&T Bell Laboratories
 BASF Corporation
 Battelle Pacific Northwest Laboratories
 Bell Communications Research, Inc.
 Blake Industries, Inc.
 BP America, Inc.
 Brimrose Corporation of America
 Brush Wellman Engineered Materials
 Cabot Corporation
 Cameca Instruments, Inc.
 Chronar Corporation
 Commonwealth Scientific Corporation
 Conversion Technology
 Corning Glass Works
 Crystacomm, Inc.
 Crystallume
 CVC Products, Inc.
 Denton Vacuum Inc.
 Dow Chemical Company
 Dow Corning Corporation
 E.I. duPont de Nemours & Company
 Eaton Corporation
 EG&G Idaho, Inc.
 EG&G Princeton Applied Research
 Elatec, Inc.
 Electric Power Research Institute (EPRI)
 ElectroScan Corporation
 Emcore Corporation
 Engelhard Corporation
 EPI Systems Division (Chorus Corp.)
 Charles Evans & Associates
 Extrel Corporation
 Exxon Research & Engineering Co.
 E.A. Fischione Instruments Manu.
 Ford Motor Company
 Foster Miller, Inc.
 Fuji Electric Company, Ltd.
 Fuji Xerox Ltd.
 Fujitsu Ltd.
 Gas Research Institute
 Gatan, Inc.
 General Motors Corporation
 Genus Incorporated/Ionex
 Gerling Laboratories
 Getty Conservation Institute
 Glasstech Solar, Inc.

CORPORATE -AFFILIATES-

Goodfellow Corporation
 Granmont, Inc.
 Granville-Phillips Company
 GTE Laboratories, Inc.
 Heraeus Amersil
 High Voltage Engineering Europa B.V.
 Hitachi, Ltd.
 Hoechst Celanese
 Hoya Optics, Inc.
 HTR Sciences
 Hughes Aircraft Company
 Huntington Mechanical Laboratories
 IBM Corporation
 IBM Japan, Ltd.
 Imperial Chemical Industries
 Indium Corporation
 Innovative Technology, Inc.
 Instruments S.A., Inc.
 Intel Corporation
 International Centre for Diffraction Data
 (JCPDS)
 International Scientific Instruments, Inc.
 Ion Tech, Inc.
 Ionic Atlanta, Inc.
 Iowa Fly Ash
 James River Corporation
 Janis Research Company, Inc.
 JEOL (U.S.A.), Inc.
 Johnson & Johnson Orthopaedics
 Kanegafuchi Chemical Industry Co., Ltd.
 Kluwer Academic Publishers
 Kogaku Giken Company, Ltd.
 Kopin Corporation
 Kratos Analytical, Inc.
 Lake Shore Cryotronics, Inc.
 Lam Research Corporation
 Lambda Physik, Inc.
 Kurt J. Lesker Company
 Leybold Inficon, Inc.
 Leybold Vacuum Products, Inc.
 Los Alamos National Laboratory
 Magnesium Elektron, Inc.
 Martin Marietta Energy Systems, Inc.
 Materials Research Corporation
 Matheson Gas Products
 MDC Vacuum Products Corporation
 MEMC Electronic Materials Inc.
 Microelectronics & Computer Technology
 Corporation
 Microscience, Inc.
 Mitsui Petrochemical Industries, Ltd.
 MKS Instruments, Inc.
 Mobil Research & Development Corporation
 Molycorp Inc/Unocal Subsidiary
 Nano Instruments, Inc.
 National Electrostatics Corporation

Newport Corporation
 Nicolet
 Nimic, Inc.
 Nippon Denso Co., Ltd.
 Nippon Mining Company, Ltd.
 Nissei Sangyo America, Ltd.
 North Eastern Analytical Corporation
 Oak Ridge National Laboratory
 Ontario Research Foundation
 Ortech International
 Perkin-Elmer
 Pfizer, Inc.
 Philips Electronic Instruments Company
 PQ Corporation
 Process Products Corporation
 The Proctor & Gamble Company
 Questek, Inc.
 Raychem Corporation
 Raytheon Company
 Rhone-Poulenc, Inc.
 Rockwell International Science Center
 Sandia National Laboratories
 Sanyo Electric Co., Ltd.
 Schlumberger-Doll Research
 Schott Fiber Optics, Inc.
 Scienta Instruments AB
 Seiko Epson Corporation
 Siemens
 Solar Energy Research Institute
 Solarex Corporation
 Solecon Laboratories, Inc.
 South Bay Technology, Inc.
 Spire Corporation
 Springer-Verlag New York, Inc.
 Strem Chemicals, Inc.
 Sumitomo Electric U.S.A., Inc.
 Sumitomo Metal Mining Co., Ltd.
 Superconductive Components, Inc.
 Superconductivity Publications, Inc.
 Surface Science Instruments
 Tamarack Scientific Co., Inc.
 Tennessee Eastman Company
 Texas Instruments, Inc.
 3M Company
 Toei Industry Co., Ltd.
 Tonen Corporation
 Toray Industries (America), Inc.
 Toshiba Corporation
 Tosoh Corporation
 Tracor Northern, Inc.
 Ultra High Vacuum Instruments Ltd.
 Union Carbide Chemical & Plastics Co.
 United Technologies Research Center
 Universal Energy Systems, Inc.
 USG Corporation
 Vacuum Barrier Corporation
 Varian Extron
 Varian/Thin Film Tech Division
 VG Instruments, Inc.
 Voltaix, Inc.
 W.R. Grace & Company
 Wacker Siltronic Corporation
 Wavemat, Inc.
 Westinghouse Electric Corporation
 Xerox Corporation
 Carl Zeiss, Inc.

**SYMPOSIUM A:
BEAM-SOLID INTERACTIONS:
PHYSICAL PHENOMENA**

A

November 27 - December 1, 1989

Chairs

Peter Børgesen
Department of Materials
Science & Engineering
Cornell University
Ithaca, NY 14853
(607) 255-9168

Ray A. Zuhr
Building 3137
Oak Ridge National Laboratory
P.O. Box 2008
Oak Ridge, TN 37831
(615) 576-6722

James A. Knapp
Division 1111
Sandia National Laboratories
P.O. Box 5800
Albuquerque, NM 87185
(505) 844-2305

Symposium Support

Corning Cornell Ceramics Initiative

IBM Corporation

National Electrostatics Corporation

Oak Ridge National Laboratory

**Proceedings published as Volume 157
of the Materials Research Society
Symposium proceedings series.**

SESSION A1: ION ASSISTED DEPOSITION

Chairs: R. A. Zuhr and D. B. Poker
Monday Morning, November 27
Salon E (M)

8:30 ***A1.1**

LOW ENERGY ION BEAM SURFACE MODIFICATION, DEPOSITION, AND SYNTHESIS, J.J. Cuomo, IBM T.J. Watson Research Center, Research Division, Yorktown Heights, NY.

9:00 ***A1.2**

ION BEAM-ASSISTED MBE, E. Chason, J.Y. Tsao, K.M. Horn, D.K. Brice and S.T. Picraux, Sandia National Laboratories, Ion-Solid Interactions Department, Albuquerque, NM.

9:30 **A1.3**

LOW ENERGY ION BOMBARDMENT AND ISLAND COARSENING IN THIN FILMS, Chih H. Yang and Harry A. Atwater, California Institute of Technology, Applied Physics Department, Pasadena, CA.

9:45 **A1.4**

ION BEAM ASSISTED ZIRCONIUM NITRIDE FILMS, L.C. Oppenheim, The Johns Hopkins University, Materials Science and Engineering, Baltimore, MD; and K.R. Padmanabhan, Wayne State University, Department of Physics and Astronomy, Detroit, MI.

10:00 BREAK

10:30 ***A1.5**

IMPORTANCE OF SURFACE PREPARATION IN DIRECT ION BEAM DEPOSITION (IBD), Kiyoshi Miyake, Hitachi Ltd., Hitachi Research Laboratory, Ibaraki, Japan.

11:00 **A1.6**

PREPARATION AND CHARACTERIZATION OF ION BEAM ASSISTED ALUMINUM OXIDE FILMS, J.K. Hirvonen, T. Tetreault, G. Parker, B.W. Murray, Spire Corporation, Bedford, MA; and P. Revesz, Cornell University, Ithaca, NY.

11:15 **A1.7**

SILICON OXIDE FILM FORMATION BY THE SIMULTANEOUS USE OF A MICROWAVE ION SOURCE AND AN ICB SYSTEM, Gikan H. Takaoka, Hiroshi Tsuji and Junzo Ishikawa, Kyoto University, Kyoto, Japan.

11:30 **A1.8**

METASTABLE CrO₂ FILM FORMATION BY REACTIVE ION BEAM SYNTHESIS AND RAPID THERMAL ANNEALING, K.V. Ramanathan, C. Richard Guarnieri, J.J. Cuomo, D.A. Smith, and S. Shivashankar, IBM T.J. Watson Research Center, Research Division, Yorktown Heights, NY.

*Invited Paper

11:45 **A1.9**

ADHESION STUDIES OF Au FILMS ON GaAs USING ION-ASSISTED DEPOSITION TECHNIQUES, T.T. Bardin and J.G. Pronko, Lockheed Research and Development Division, Palo Alto, CA; A.J. Kellock and J.E.E. Baglin, IBM Almaden Research Center, San Jose, CA.

SESSION A2: ION INDUCED GROWTH/BURIED LAYERS

Chair: J. C. Barbour
Monday Afternoon, November 27
Salon E (M)

1:30 **A2.1**

IRRADIATION-INDUCED GRAIN GROWTH: THE ROLE OF DISLOCATIONS, Charles W. Allen and Lynn E. Rehn, Argonne National Laboratory, Materials Science Division, Argonne, IL.

1:45 **A2.2**

ION-BEAM-INDUCED EPITAXIAL CRYSTALLIZATION OF Ge_xSi_{1-x}/Si HETEROSTRUCTURES, R.G. Elliman, M.C. Ridgway, J.S. Williams, Royal Melbourne Institute of Technology, Microelectronics and Materials Technology Centre, Melbourne, Australia; and J.C. Bean, AT&T Bell Laboratories, Murray Hill, NJ.

2:00 **A2.3**

DEPENDENCE OF INTERFACE VELOCITY ON NOBLE METAL SEGREGATION DURING ION BEAM ENHANCED EPITAXY, J.S. Custer, Michael O. Thompson, Cornell University, College of Engineering, Department of Materials Science and Engineering, Ithaca, NY; J.M. Poate and D.C. Jacobson, AT&T Bell Laboratories, Murray Hill, NJ.

2:15 **A2.4**

ION BEAM INDUCED CRYSTALLIZATION IN PREAMORPHIZED BP(100), Naoto Kobayashi, Hisao Kobayashi, Hisao Tanoue, Nobuyuki Hayashi, Electrotechnical Laboratory, Ibaraki, Japan; and Yukinobu Kumashiro, Yokohama National University, Yokohama, Japan.

2:30 **A2.5**

AMORPHOUS TO POLYCRYSTAL TRANSITION ASSISTED BY ION BEAM IRRADIATION IN SILICON, C. Spinella, S. Lombardo and S.U. Campisano, Dip. di Fisica dell'Università, Catania, Italy.

2:45 **A2.6**

FORMATION OF BURIED ELEMENTAL LAYERS USING ION IMPLANTATION, D.W. Brown, Z.A. Munir, University of California, Davis, Division of Materials Science and Engineering, Mechanical Engineering Department, Davis, CA; R.G. Musket, Lawrence Livermore National Laboratory, Chemistry and Materials Department, Livermore, CA.

3:00 BREAK

3:30 A2.7
ION-BEAM-INDUCED EPITAXIAL CRYSTALLIZATION OF METAL SILICIDES, M.C. Ridgway, R.G. Elliman and J.S. Williams, Royal Melbourne Institute of Technology, Microelectronics and Materials Technology Centre, Melbourne, Australia.

3:45 A2.8
ION-BEAM SYNTHESIS OF BURIED YTTRIUM SILICIDE, T.L. Alford, Cornell University, Material Science and Engineering Department, Ithaca, NY; and J.C. Barbour, Sandia National Laboratories, Albuquerque, NM.

4:00 A2.9
ELECTRICAL TRANSPORT IN Si/CoSi₂/Si HETERO-STRUCTURES GROWN BY MESOTAXY, Alice E. White, M.L. Green, K. T. Short, D. Brasen AT&T Bell Laboratories, Murray Hill, NJ; and K. Maex, IMEC, Leuven, Belgium.

4:15 A2.10
ION BEAM ANNEALING OF Si CO-IMPLANTED WITH Ga AND As, S.P. Withrow, O.W. Holland and S.J. Pennycook, Oak Ridge National Laboratory, Solid State Division, Oak Ridge, TN; and J. Pankove, Solar Energy Research Institute, Golden, CO.

4:30 A2.11
EVOLUTION OF DIFFUSION AND SPUTTER LIMITED IMPLANTED IMPURITY DEPTH PROFILES DURING ION BEAM SYNTHESIS, P.L.F. Hemment, A.K. Robinson, U. Bussmann, K.J. Reeson, University of Surrey, Department of Electronic and Electrical Engineering, Guildford, Surrey, United Kingdom; R. Chater and J.A. Kilner, Imperial College, Department of Materials, London, United Kingdom.

4:45 A2.12
FORMATION OF BURIED AND SURFACE CoSi₂ LAYERS BY ION IMPLANTATION, M.F. Wu, A. Vantomme, G. Langouche, University of Leuven, Institut voor Kern-en Stralingsfysika, Leuven, Belgium; J. Vanhellemont, IMEC, Leuven, Belgium; J. Vanacken, H. Vloeberghs, and Y. Bruynseraede, University of Leuven, VSM, Belgium.

SESSION A3: ION BEAM MIXING

Chairs: P. Børgesen and D. A. Lilienfeld
Tuesday Morning, November 28
Salon E (M)

8:30 *A3.1
ION-BEAM MIXING AND PHASE FORMATION, L-U. Aaen Andersen, J. Bøttiger, K. Dyrbye, and J. Janting, University of Aarhus, Institute of Physics, Aarhus, Denmark.

9:00 *A3.2
THERMODYNAMIC ASPECTS OF ION MIXING IN METALLIC SYSTEMS, W.L. Johnson, California Institute of Technology, Keck Laboratory, Pasadena, CA.

9:30 A3.3
CRITICAL TEMPERATURES FOR RADIATION ENHANCED DIFFUSION AND EQUILIBRIUM PHASE FORMATION DURING ION BEAM MIXING, A.M. Vredenberg, R. de Reus, A.C. Voorrips, H.C. Tisink and F.W. Saris, FOM-Institute for Atomic and Molecular Physics, Amsterdam, The Netherlands.

9:45 A3.4
DIRECT OBSERVATION OF INTERMIXING IN GaAs/AlAs MULTILAYERS AFTER VERY LOW-DOSE ION-IMPLANTATION, M. Bode, A. Ourmazd, and J. Rentschler, AT&T Bell Laboratories, Holmdel, NJ; M. Hong, L.C. Feldman, and J.P. Mannaerts, AT&T Bell Laboratories, Murray Hill, NJ.

10:00 BREAK

10:30 A3.5
A STUDY OF THE DOMINANT MOVING SPECIES IN ION BEAM MIXING I: EFFECTS OF SAMPLE GEOMETRY AND ATOMIC MASS, G.W. Auner, Y.-T. Cheng, General Motors Research Laboratories, Warren, MI, and Wayne State University, Department of Physics and Astronomy, Detroit, MI; M.H. Alkisi and K.R. Padmanabhan, Wayne State University, Department of Physics and Astronomy, Detroit, MI.

10:45 A3.6
RELATIONSHIPS BETWEEN COHESIVE ENERGY, DEBYE TEMPERATURE, AND THE ONSET OF TEMPERATURE-DEPENDENT ION MIXING, Y.-T. Cheng, General Motors Research Laboratories, Physical Chemistry Department, Warren, MI.

11:00 A3.7
EFFECT OF CARBON ON ION BEAM MIXING OF FE-TI BILAYERS, J.-P. Hirvonen and M. Nastasi, Los Alamos National Laboratory, Materials Science and Technology Division, Los Alamos, NM.

11:15 A3.8
THE EFFECT OF SURFACE COATING ON ION BEAM DESORPTION OF HYDROGEN FROM TITANIUM, Richard E. Wistrom, Peter Børgesen and Herbert H. Johnson, Cornell University, Materials Science and Engineering, Ithaca, NY.

11:30 A3.9
ION-BEAM MIXING AND TRIBOLOGY OF Fe/B MULTILAYERS, Ren Yuan Hu, L.E. Rehn, G.R. Fenske and P.M. Baldo, Argonne National Laboratory, Materials Science Division, Argonne, IL.

11:45 **A3.10**
ION BEAM MIXING OF Sb SCHOTTKY CONTACTS ON n-Si, J.B. Malherbe, L.J. Bredell, K.P. Weimer, G. Myburg and E. Friedland, University of Pretoria, Department of Physics, Pretoria, South Africa.

SESSION A4: MODELLING/FUNDAMENTAL STUDIES

Chairs: M. O. Thompson and J. A. Knapp
Tuesday Afternoon, November 28
Salon E (M)

1:30 ***A4.1**
ION-SOLID INTERACTIONS AS VIEWED BY MOLECULAR DYNAMICS, Barbara J. Garrison, The Pennsylvania State University, Department of Chemistry, University Park, PA.

2:00 **A4.2**
COMPUTER SIMULATION OF IMPURITY SEGREGATION AT A RAPIDLY MOVING SOLID-LIQUID INTERFACE, Stephen J. Cook and Paulette Clancy, Chemical Engineering Department, Cornell University, Ithaca, NY.

2:15 **A4.3**
MOLECULAR DYNAMICS SIMULATIONS OF LOW-ENERGY ION/SURFACE INTERACTIONS DURING VAPOR PHASE CRYSTAL GROWTH: 10 eV Si INCIDENT ON Si(001) 2x1, M. Kitabatake, P. Fons, and J.E. Greene, University of Illinois, CSL, Urbana, IL.

2:30 **A4.4**
MOLECULAR DYNAMICS STUDY OF THE AMORPHIZATION OF CuTi, Michael J. Sabochick, U.S. Air Force Institute of Technology, Department of Engineering Physics, Wright Patterson AFB, OH; Nghi Q. Lam, Argonne National Laboratory, Materials Science Division, Argonne, IL.

2:45 **A4.5**
MOLECULAR DYNAMICS SIMULATIONS OF THE DISORDER FORMED IN SILICON BY HIGH-ENERGY ELECTRONS, A.M. Mazzone, CNR-Istituto LAMEL, Bologna, Italy.

3:00 BREAK

3:30 **A4.6**
SUPERHEATING AND SUPERCOOLING OF LEAD INCLUSIONS IN ALUMINIUM, E. Johnson, University of Copenhagen, Physics Laboratory, Copenhagen, Denmark; L. Gråbaek, J. Bohr, RISØ National Laboratory, Roskilde, Denmark; A. Johansen, L. Sarholt-Kristensen and H.H. Andersen, University of Copenhagen, Physics Laboratory, Copenhagen, Denmark.

3:45 **A4.7**
THERMAL ANNEALING OF SOLID Kr PRECIPITATES IN Ni, R.C. Birtcher, J. Rest, and D.S. Bergstrom, Argonne National Laboratory, Argonne, IL.

SESSION A5: NOVEL ANALYSIS TECHNIQUES/ UNIQUE STRUCTURES

Chairs: J. A. Knapp and M. O. Thompson
Tuesday Afternoon, November 28
Salon E (M)

4:00 **A5.1**
FABRICATION OF CRYSTALLINE-AMORPHOUS SUPERLATTICES BY DIFFERENTIAL ION-BEAM DAMAGE, J.M. Poate, D.J. Eaglesham, D.C. Jacobson, M. Cerullo, L.N. Pfeiffer and K.W. West, AT&T Bell Laboratories, Murray Hill, NJ.

4:15 **A5.2**
INTERNAL BLACKBODY EMISSION INTERFEROMETRY FOR MEASUREMENT OF CRYSTALLIZATION KINETICS AND OPTICAL PROPERTIES OF THIN FILMS, J.A. Roth and G.L. Olson, Hughes Research Laboratories, Malibu, CA.

4:30 **A5.3**
TRANSITION RADIATION FOR SURFACE ANALYSIS, John M. Macaulay and Julius J. Muray, SRI International, Physical Electronics Department, Menlo Park, CA.

4:45 **A5.4**
STM INVESTIGATIONS OF GRAPHITE SURFACES PREPARED BY 5 keV Ar⁺ ION BOMBARDMENT, Elliott A. Eklund, University of California, Department of Physics and Solid State Science Center, Los Angeles, CA; Eric J. Snyder and R. Stanley Williams, University of California, Department of Chemistry, Los Angeles, CA.

SESSION A6: POSTER SESSION I

Chairs: Peter Børgesen, James A. Knapp and Ray A. Zuhr

Tuesday Evening, November 28

7:00 p.m. - 10:00 p.m.

America Ballroom (W)

A6.1 GRAIN GROWTH AND PHASE FORMATION IN ION IRRADIATED/ANNEALED THIN NI-AL ALLOY FILMS, Dale E. Alexander and Gary S. Was, Department of Nuclear Engineering, University of Michigan, Ann Arbor, MI; and Lynn Rehn, Argonne National Laboratory, Materials Division, Argonne, IL.

A6.2 CESSATION AT HIGH TEMPERATURE OF RADIATION INDUCED DIFFUSION: THE ROLE OF DEFECT COMPLEX FORMATION, T.D. Andreadis and Mervine Rosen, Naval Research Laboratory, Washington, DC.

A6.3 VOID DENSITY REDUCTION DURING ION ASSISTED DEPOSITION, T.D. Andreadis, R.H. Bassel, Mervine Rosen, and J.A. Sprague, Naval Research Laboratory, Washington, DC.

A6.4 STUDIES ON ION SCATTERING AND SPUTTERING PROCESSES RELEVANT TO ION BEAM SPUTTER-DEPOSITION OF MULTICOMPONENT THIN FILMS, O. Auciello, North Carolina State University, Department of Materials Science, Raleigh, NC; and Microelectronics Center North Carolina, Research Triangle Park, NC; M.S. Ameen, North Carolina State University, Department of Materials Science, Raleigh, NC; A. R. Krauss, Argonne National Laboratory, Chemistry Division, Argonne, IL; and A.I. Kingon, North Carolina State University, Department of Materials Science, Raleigh, NC.

A6.5 INTERACTIONS OF LOW-ENERGY METAL IONS WITH SURFACES, P. Bai, Ch. Steinbruchel and T.-M. Lu, Rensselaer Polytechnic Institute, Center for Integrated Electronics, Troy, NY.

A6.6 ELECTRON BEAM INDUCED HOLE-DRILLING AND LITHOGRAPHY ON A NANOMETRE SCALE IN Al, MgO AND α -AlF₃ IN A STEM, Tim J. Bullough, Colin J. Humphreys and Robert W. Devenish, University of Liverpool, Department of Materials Science and Engineering, Liverpool, United Kingdom.

A6.7 THERMAL ANNEALING INVESTIGATION OF THE OPTICAL PROPERTIES OF B_{1-x}N_x FILMS FABRICATED BY ION BEAM ASSISTED DEPOSITION, C.A. Carosella, E.P. Donovan, and G.K. Hubler, Naval Research Laboratory, Washington, DC.

A6.8 MECHANISM OF ION-INDUCED SOLID-PHASE EPITAXIAL GROWTH, T.K. Chaki, State University of New York, Department of Mechanical & Aerospace Engineering, Buffalo, NY.

A6.9 STUDY OF THE ANODIC OXIDATION ON TI AND TA6V BY ION-IMPLANTED XE IONS MARKERS AND O¹⁸ TRACING TECHNIQUES, Heming Chen, Mingjiang Dai, Xinde Bai, Wangpei Li, Tsinghua University, Department of Material Science and Engineering, Beijing, China.

A6.10 CRYSTALLINE POLYMER THIN FILM DEPOSITION BY IONIZED CLUSTER BEAM, S.J. Cho, Kyungseong University, Department of Physics, Busan, Korea; H.S. Choe, Kyungsang University, Department of Physics, Jinju, Korea; H.K. Jang, S.S. Kim, C.N. Whang, Yonsei University, Department of Physics, Seoul, Korea; and D.S. Choi, Kangwon University, Dept. of Physics, Chuncheon, Korea.

A6.11 STRUCTURAL AND ELECTRICAL STUDIES OF EPITAXIAL PbTe FILMS GROWN BY ION-ASSISTED RF MAGNETRON SPUTTERING, J.G. Cook, S.R. Das, National Research Council of Canada, Laboratory for Microstructural Sciences, Ottawa, Canada; and M. Phipps, University of Ottawa, Department of Physics, Ottawa, Canada.

A6.12 OXIDATION BEHAVIOUR OF TITANIUM SURFACES COATED WITH BORON COMPOUNDS, M. Elena, L.A. Guzman, L. Moro, A. Tomasi, Institute for Scientific and Technological Research, Povo, Italy; S. Gialanella and P. Scardi, University of Trento, Department of Materials Science Engineering, Mesiano, Italy.

A6.13 ION-BOMBARDMENT EFFECTS ON FILM ADHESION, R.A. Erck, G.R. Fenske and A. Erdemir, Argonne National Laboratory, Materials and Components Technology Division, Argonne, IL.

A6.14 CARRIER LIFETIME DISTRIBUTIONS AND RECOMBINATION KINETICS IN SILICON ON INSULATOR (SIMOX) SUBSTRATES, M.A. Lourenço, K.P. Homewood, and P.L.F. Hemment, University of Surrey, Department of Electronic and Electrical Engineering, Guildford, Surrey, United Kingdom.

A6.15 SPONTANEOUS VITRIFICATION OF ION MIXED METASTABLE PHASES IN IRON-BASED ALLOY SYSTEMS, L.J. Huang, and H-D.Li, Tsinghua University, Department of Materials Science and Engineering, Beijing, China; and B.X. Liu, Tsinghua University, Department of Materials Science and Engineering, and Center of Condensed Matter and Radiation Physics, CCAST (World Lab.), Beijing, China.

A6.16 FOCUSED 0.5 MeV ION BEAM LINE WITH LOW ABERRATION QUADRUPOLE MAGNETS, Kiyotaka Ishibashi, Ken-ichi Inoue, Yutaka Kawata, Norio Suzuki, Kobe Steel, Ltd., Electronics Research Laboratory, Kobe, Japan; Mikio Takai and Susumu Namba, Osaka University, Faculty of Engineering Science and Research Center for Extreme Materials, Osaka, Japan.

A6.17 THE STRUCTURE AND PROPERTIES OF Ni FILMS GROWN BY ION BEAM ASSISTED DEPOSITION, R.A. Kant, G.P. Chambers and B.D. Sartwell, Naval Research Laboratory, Surface Modification Branch, Washington, DC.

A6.18 Ar⁺ INDUCED INTERFACIAL MIXING IN Pd/Cu SYSTEM, H.K. Kim, Korea Standards Research Institute, Taejon, Korea; J.H. Song, S.S. Kim, C.N. Whang, Yonsei University, Department of Physics, Seoul, Korea; J.J. Woo, Chonnam University, Department of Physics, Kwangju, Korea; and R.J. Smith, Montana State University, Department of Physics, Bozeman, MT.

A6.19 IN-SITU ION BEAM MEASUREMENTS OF DEUTERIUM LOADING IN THIN FOIL ELECTROCHEMICAL CELLS, J.A. Knapp, T.R. Guillinger, M.J. Kelly, D. Walsh, and B.L. Doyle, Sandia National Laboratories, Albuquerque, NM.

A6.20 ON THE STABILITY OF METASTABLE AND AMORPHOUS PVD-COMPOUND FILMS, Otto Knotek, Frank Jungblut, and Arman Barimani, Technical University Aachen, Aachen, West Germany.

A6.21 ANALYSIS OF ELEMENTS IN FINGERNAILS BY RUTHERFORD BACKSCATTERING SPECTROSCOPY, P. Madakson, IBM T.J. Watson Research Center, Yorktown, Heights, NY.

A6.22 SECONDARY IONIZATION DURING ION BOMBARDMENT OF Rh(111), Geoffrey P. Malafsky, Naval Research Lab, Washington, DC; and Nicholas Winograd, Pennsylvania State University, Department of Chemistry, University Park, PA.

A6.23 ION BEAM MIXING OF MULTILAYERED CoB THIN FILMS, G. Choe and R.M. Walser, The Univ. of Texas at Austin, Center for Materials Science & Engineering, Dept. of Electrical & Computer Engineering, Austin, TX.

A6.24 CHARGE STATES OF HEAVY IONS IN A UNIFORM ELECTRON GAS, A.M. Mazzone, CNR-Istituto LAMEL, Bologna, Italy.

A6.25 STUDY OF THE EVOLUTION OF THE BURIED SiO₂ LAYER FORMED BY MULTIPLE LOW DOSE OXYGEN IMPLANTATION INTO SILICON, F. Namavar and E. Cortesi, Spire Corporation, Bedford, MA.

A6.26 MICROSTRUCTURAL STUDIES OF MYLAR (PET) USING CRYOFRACTURING SYSTEM AND SEM, A.K. Nigam, Ramji Pathak, R.N. Chakraborty and U.K. Chaturvedi, Banaras Hindu University, VDG Lab., Department of Physics, Varanasi, India.

A6.27 FORMATION OF METASTABLE SILICIDE PHASE UNDER THERMAL ANNEALING AND BEAM IRRADIATION OF Ni/Si THIN FILM BILAYERS, Muhammad Z. Numan and Lim poh Leng, Indiana University of Pennsylvania, Physics Department, Indiana, PA.

A6.28 MICROSTRUCTURAL CHARACTERIZATION OF TEXTURE IN TUNGSTEN FILMS MADE BY ION-ASSISTED EVAPORATION, K. Rajan, Rensselaer Polytechnic Institute, Troy, NY; R.A. Roy, R. Petkie, and K.V. Ramanathan, IBM T.J. Watson Research Center, Research Division, Yorktown Heights, NY.

A6.29 DEPOSITION OF THIN METALLIC FILMS BY HIGH POWER ION BEAM TARGET EVAPORATION, A. N. Zakutaev, I.F. Isakov, G.E. Remnev, Nuclear Physics Institute, Tomsk, USSR.

A6.30 COMPUTER SIMULATION OF ION BEAM ENHANCED DEPOSITION OF TITANIUM NITRIDE FILMS, Wang Xi, Zhou Jiankun, Chen Youshan, Liu Xianghuai, and Zou Shichang, Shanghai Institute of Metallurgy, Ion Beam Laboratory, Shanghai, China.

A6.31 AES AND IR SPECTROSCOPIC STUDIES OF SOI STRUCTURES FORMED BY ION IMPLANTATION, Yu Yuehui, Lin Chenglu, and Zou Shichang, Shanghai Institute of Metallurgy, Ion Beam Laboratory, Shanghai, China; and P.L.F. Hemment, University of Surrey, Department of Electronic and Electrical Engineering, Guildford, Surrey, United Kingdom.

A6.32 FORMATION OF BURIED OXYNITRIDE LAYER INTO SILICA GLASS USING ION BEAM, Keiji Oyoshi, Takashi Tagami and Shuhei Tanaka, Nippon Sheet Glass Co., Ltd., Tsukuba Research Laboratory, Ibaraki, Japan.

A6.33 EVALUATION OF COMPOSITIONAL CHANGE IN MASKLESSLY DEPOSITED LINES BY MICRO-RBS ANALYSIS, A. Kinomura, Y.F. Lu, M. Takai, S. Namba, Osaka University, Faculty of Engineering Science and Research Center for Extreme Materials, Osaka, Japan; M. Satou and A. Chayahara, Government Industrial Research Institute Osaka, Osaka, Japan.

A6.34 DEPENDENCE OF COMPOSITION AND STRUCTURE OF ION-ASSISTED BORON NITRIDE THIN FILMS ON PROCESS PARAMETERS, T.G. Tetreault, J.K. Hirvonen, and G.R. Parker, Spire Corporation, Bedford, MA; P. Kullen, T. McDevitt, Mellon Institute, Pittsburgh, PA; and J.P. Hirvonen, Los Alamos National Laboratory, Los Alamos, NM.

A6.35 COBALT SILICIDE FORMATION ON Si SUBSTRATE HEAVILY DOPED WITH ARSENIC IONS, V.V. Tokarev, BSSR Academy of Sciences, Institute of Solid State and Semiconductor Physics, Minsk, USSR.

A6.36 TITANIUM SILICIDE FORMATION ON MONO- AND POLYCRYSTALLINE Si ENHANCED BY ARGON IMPLANTATION, V.V. Tokarev, A.I. Demchenko, U.Ch. Dulinets, BSSR Academy of Sciences, Institute of Solid State and Semiconductor Physics, Minsk, USSR.

A6.37 ION BEAM MIXING OF LANTHANUM OXIDES AND COPPER MULTILAYERS, J.P. Mathevet and A. Traverse, Centre de Spectrométrie Nucléaire et de Spectrométrie de Masse, Orsay, France.

A6.38 ION BEAM MIXING OF METALLIC MULTILAYERS, Agnès Traverse, Centre de Spectrométrie Nucléaire et de Spectrométrie de Masse, Orsay, France.

A6.39 EFFECT OF IMPLANTATION CONDITIONS ON THE MICROSTRUCTURE OF HIGH-DOSE OXYGEN IMPLANTED SILICON-ON-INSULATOR MATERIAL, S. Visitserngtrakul, Arizona State University, Department of Chemical, Bio and Materials Engineering, Tempe, AZ; B.F. Cordts, Ibis Technology Corporation, Danvers, MA; and S. Krause, Arizona State University, Department of Chemical, Bio and Materials Engineering, Tempe, AZ.

A6.40 THE CORROSION RESISTIVITY OF CERMET COATINGS MADE BY ION BEAM TREATMENT, Tian Wei, and Cai Weiping, Wuhan Iron and Steel University, Metallic Materials Department, Wuhan, China.

A6.41 INVESTIGATION OF OXIDE/METAL MULTILAYERS FOR SOFT X-RAY OPTICS FABRICATED BY ION BEAM SPUTTERING, I. Kataoka, K. Ito, T. Yonemitsu, K. Etoh, N. Hoshi, and I. Yamada, Japan Aviation Electronics Industry, Ltd., Research and Development Department, Tokyo, Japan.

A6.42 MOLECULAR DYNAMICS SIMULATIONS OF IONIZED CLUSTER BEAM DEPOSITION, Hongming Hsieh, R.S. Averback, Department of Materials Science and Engineering, University of Illinois, Urbana, IL; and R. Benedek, Argonne National Laboratory, Argonne, IL.

SESSION A7: BEAM MODIFICATION OF CERAMICS AND SUPERCONDUCTORS

Chairs: S. P. Withrow and C. J. McHargue
Thursday Morning, November 30
Salon E (M)

8:30 ***A7.1**
ION BEAM MODIFICATION OF HIGH T_c SUPERCONDUCTORS, O. Meyer, J. Geerk, G. Linker, B. Strehlau, X.X. Xi, Kernforschungszentrum Karlsruhe, Institut für Nukleare Festkörperphysik, Karlsruhe, West Germany.

9:00 ***A7.2**
STRUCTURE OF AMORPHOUS Al_2O_3 PRODUCED BY ION IMPLANTATION, C.J. McHargue, P.S. Sklad, P. Angelini, C.W. White and J.C. McCallum, Oak Ridge National Laboratory, Metals and Ceramics Division, Oak Ridge, TN.

9:30 **A7.3**
INFLUENCE OF ION BEAM MIXING ON THE GROWTH OF HIGH TEMPERATURE OXIDE SUPERCONDUCTING THIN FILM, N. Bordes, A.D. Rollet, M. Cohen, M. Nastasi, Los Alamos National Laboratory, Department MEE 11, Los Alamos, NM.

9:45 **A7.4**
INTERACTION BETWEEN IMPLANTED IONS AND INTRINSIC DEFECTS IN SILICA, R.H. Magruder, Belmont College, Nashville, TN; R.A. Weeks, Vanderbilt University, Nashville, TN; and R. Zuhr, Oak Ridge Laboratory, Oak Ridge, TN.

10:00 BREAK

10:30 **A7.5**
REFRACTIVE INDEX PROFILES OF HIGH DOSE Ti IMPLANTED OPTICAL WAVEGUIDES IN $LiNbO_3$, T. Bremer, Universität, FB. Physik, Osnabrück; and Ch. Buchal, R. Irmscher, KFA, Jülich, Institut für Schicht-und Ionentechnik, Jülich, West Germany.

10:45 **A7.6**
OPTICAL WAVEGUIDE FABRICATION BY STOICHIOMETRIC IMPLANTATION OF Ti AND O INTO $LiNbO_3$, D.B. Poker, Oak Ridge National Laboratory, Solid State Division, Oak Ridge, TN; and W. Xia, University of California-San Diego, Department of Electrical and Computer Engineering, La Jolla, CA.

11:00 **A7.7**
MODIFICATION OF THE WEAR PROPERTIES OF DIAMOND USING ION BEAM IRRADIATION, Gregory C. Anderson and Steven Prawer, Royal Melbourne Institute of Technology, Microelectronics and Materials Technology Centre, Melbourne, Australia.

11:15 **A7.8**
THE EFFECT OF ION INDUCED DAMAGE ON THE MECHANICAL PROPERTIES OF ZIRCONIA, E.L. Fleischer, T.L. Alford, P. Børgesen, P. Revesz, J.W. Mayer, Cornell University, Materials Science and Engineering, Ithaca, NY; and W. Hertl, Corning Inc., Corning, NY.

11:30 **A7.9**
THE FORMATION OF A SOLID LUBRICANT BORON NITRIDE IN B_4C BY ION IMPLANTATION AND LASER ANNEALING, Robert R. Reeber, Ning Yu, University of North Carolina, Department of Physics and Astronomy, Chapel Hill, NC; Weikan Chu, University of Houston, Texas Center for Superconductivity and Department of Physics, Houston, TX; and Robert P. Kusy, University of North Carolina, Dental Research Center, Chapel Hill, NC.

11:45 **A7.10**
CRYSTALLIZATION OF INTRINSIC AMORPHOUS LAYERS PRODUCED BY STOICHIOMETRIC IMPLANTATION OF Al AND O IONS IN a-AXIS ORIENTED Al_2O_3 SINGLE CRYSTALS, W. Zhou, D.X. Cao, and D.K. Sood, Royal Melbourne Institute of Technology, Microelectronics and Materials Technology Centre, Melbourne, Australia.

SESSION A8: BEAM MODIFICATION OF SEMICONDUCTORS

Chairs: E. Chason and M. J. Aziz
Thursday Afternoon, November 30
Salon E (M)

1:30 **A8.1**
AMORPHOUS TO CRYSTALLINE PHASE TRANSFORMATIONS IN HIGH DOSE ION IMPLANTED SILICON, R.P. Thornton, R.G. Elliman, Y.H. Li, A.P. Pogany, Royal Melbourne Institute of Technology, Microelectronics and Materials Technology Centre, Melbourne, Australia; E. Nygren, Ohio State University, Materials Science and Engineering, Columbus, OH; and J.S. Williams, Royal Melbourne Institute of Technology, Microelectronics and Materials Technology Centre, and Australian National University, Electronic Materials Engineering Department, Melbourne, Australia.

1:45 **A8.2**
STRESS AND PLASTIC FLOW IN SILICON DURING AMORPHIZATION BY ION-BOMBARDMENT, C.A. Volkert, AT&T Bell Laboratories, Murray Hill, NJ.

2:00 **A8.3**
STRUCTURAL CHARACTERIZATION OF DAMAGE IN Si(100) PRODUCED BY MeV Si⁺-ION IMPLANTATION AND ANEALING, M.K. El-Ghor, O.W. Holland, C.W. White, and S.J. Pennycook, Oak Ridge National Laboratory, Oak Ridge, TN.

2:15 **A8.4**
GETTERING OF CU AT BURIED DAMAGE LAYERS MADE BY SI SELF IMPLANTATION, J.R. Liefing, R.J. Schreutelkamp, W.X. Lu and F.W. Saris, FOM Institute for Atomic and Molecular Physics, Amsterdam, The Netherlands.

2:30 **A8.5**
ANNEALING TEMPERATURE DEPENDENCE OF THE ELECTRICAL ACTIVITY OF HIGH-DOSE Sb ION IMPLANTS IN (100) SILICON, S.N. Kumar, G. Chaussemy, A. Laugier, I.N.S.A. Lyon, Laboratoire de Physique de la Matière, Villeurbanne, France; M. Charbonnier, and M. Romand, CNRS, Laboratoire de Chimie Appliquée, Villeurbanne, France; and B. Canut, Université Claude Bernard, Laboratoire de Physique des Matériaux, Villeurbanne, France.

2:45 **A8.6**
ANNEALING BEHAVIOUR OF BURIED AMORPHOUS LAYERS FORMED BY MEV ¹¹⁵IN⁺ IMPLANTATION IN SI(100), R.J. Schreutelkamp, J.R. Liefing, FOM-Institute for Atomic and Molecular Physics, Amsterdam, The Netherlands; W.X. Lu, FOM-Institute for Atomic and Molecular Physics, Amsterdam, The Netherlands and Beijing Normal University, Beijing, China; and Z.L. Wang, B.X. Zhang, Beijing Normal University, Beijing, China.

3:00 BREAK

3:30 **A8.7**
KINETICS AND MICROSTRUCTURE OF TRANSIENTLY ANNEALED IMPLANTED POLYCRYSTALLINE SILICON LAYERS, J.M.C. England, P.J. Timans, R.A. McMahon, H. Ahmed, Cambridge University, Microelectronics Research Laboratory, Cambridge, United Kingdom; C. Hill, P.D. Augustus and D.R. Boys, Plessey Research, Allen Clerk Research Centre, Caswell, Towcester, United Kingdom.

3:45 **A8.8**
COMPARISON OF THE EFFECTS OF N-TYPE AND P-TYPE HYDROGENIC IMPURITY CONCENTRATIONS ON THE SOLID PHASE EPITAXIAL GROWTH OF AMORPHOUS SILICON, Young-Jin Jeon, University of Texas, Center for Materials Science and Engineering, Austin, TX; Won-Woo Park, M.F. Becker, and R.M. Walser, University of Texas, Department of Electrical and Computer Engineering, Austin, TX.

4:00 **A8.9**
COMPARISON OF MeV AND keV ION DAMAGE IN GaAs, S.T. Johnson, Royal Melbourne Institute of Technology, Microelectronics and Materials Technology Centre, Melbourne, Australia; J.S. Williams, Royal Melbourne Institute of Technology, Microelectronics and Materials Technology Centre, and Australian National University, Electronic Materials Engineering Department, Melbourne, Australia; and R.G. Elliman, Royal Melbourne Institute of Technology, Microelectronics and Materials Technology Centre, Melbourne, Australia.

4:15 **A8.10**
IN SITU CRYSTALLIZATION STUDY OF Kr ION AMORPHIZED Ge BY THERMAL ANNEALING WITH TEM, Lu-Min Wang, Robert C. Birtcher, and Lynn E. Rehn, Argonne National Laboratory, Materials Science Division, Argonne, IL.

4:30 **A8.11**
ION IMPLANT ACTIVATION AND REDISTRIBUTION IN Al_xGa_{1-x}As, S.J. Pearton, W.S. Hobson, A.E. Von Neida, AT&T Bell Laboratories, Murray Hill, NJ; N.M. Haegel, University of California, Department of Materials Science, Los Angeles, CA; K.S. Jones, University of Florida, Department of Materials Science, Gainesville, FL; N. Morris and B.J. Sealy, University of Surrey, United Kingdom.

4:45 **A8.12**
DOPANT SITE LOCATION IN DUAL-IMPLANTED GaP USING DEPTH OSCILLATIONS OF {111} PLANAR CHANNELING TECHNIQUE, N.R. Parikh, C.T. Kao, D.R. Lee, J. Muse, M.L. Swanson, Univ. of North Carolina, Department of Physics and Astronomy, Chapel Hill, NC; and T.E. Haynes, Oak Ridge National Lab., Oak Ridge, TN.

SESSION A9: POSTER SESSION II

Chairs: Peter Børgesen, James A. Knapp
and Ray A. Zuhr

Thursday Evening, November 30

7:00 p.m. - 10:00 p.m.

America Ballroom (W)

A9.1 IN-SITU STUDY OF RADIATION DAMAGE IN V₂O₅ INDUCED BY LOW ENERGY ELECTRONS, Hanjie Fan, Rebecca Ai and Laurence D. Marks, Northwestern University, Department of Materials Science and Engineering, Evanston, IL.

A9.2 AS AND B ION IMPLANTATION THROUGH Mo AND INTO Mo-SILICIDE LAYERS FOR SHALLOW JUNCTION FORMATION, R. Angelucci, M. Merli, S. Solmi, A. Armigliato, R. Fabbri, E. Gabilli and A. Poggi, CNR - Istituto LAMEL, Bologna, Italy.

A9.3 CHARACTERIZATION OF N AND B IMPLANTED FUSED SILICA, G.W. Arnold and R.K. Brow, Sandia National Laboratories, Albuquerque, NM.

A9.4 EXCIMER LASER INDUCED CRYSTALLIZATION OF AMORPHOUS SILICON NEAR THRESHOLD, R.Z. Bachrach, K. Winer, J.B. Boyce, F. Ponce, S.E. Ready, R.I. Johnson and G.B. Anderson, Xerox Palo Alto Research Center, Palo Alto, CA.

A9.5 ELECTRON BEAM INDUCED RADIATION DAMAGE IN SUPERCONDUCTORS, S. Basu, T. Roy, T.E. Mitchell and M. Nastasi, Los Alamos National Laboratory, Los Alamos, NM.

A9.6 DUAL IMPLANTATION OF Ti AND C INTO SINTERED α -SiC AND HOT PRESSED Si_3N_4 , R.S. Bhattacharya, A.K. Rai, and D. Patrizio, University Energy Systems, Inc., Dayton, OH.

A9.7 X-RAY AND RAMAN TOPOGRAPHIC STUDIES OF Si-ION IMPLANTED, PULSED-LASER-ANNEALED GaAs, R.C. Bowman Jr., P. Adams, J.T. Knudsen, Aerospace Corporation, Los Angeles, CA; H.D. Yao, University of Nebraska, Center for Microelectronic and Optical Materials Research, Lincoln, NE; and A.D. Compaan, University of Toledo, Physics and Astronomy Department, Toledo, OH.

A9.8 SURFACE REACTIONS OF NiO AND CoO IN THE ELECTRON MICROSCOPE ENVIRONMENT, Mary I. Buckett and L.D. Marks, Northwestern University, Department of Materials Science and Engineering, Evanston, IL.

A9.9 SUBNANOSECOND TIME-RESOLVED ELECTRON DIFFRACTION FROM THIN CRYSTALLINE GOLD FILMS, Hsiu-Cheng Chen, University of Rochester, Laboratory for Laser Energetics and Department of Physics and Astronomy, Rochester, NY; Gerard Mourou, University of Michigan, Department of Electrical Engineering and Computer Science, Ann Arbor, MI; and Robert Knox, University of Rochester, Department of Physics and Astronomy, Rochester, NY.

A9.10 IRRADIATION INDUCED METASTABLE PHASE FORMATION IN AMORPHOUS THIN FILMS DEPOSITED BY MAGNETRON COSPUTTERING, Qing-Ming Chen, Huazhong University of Science and Technology, Wuhan, China; Yu-Dian Fan and Heng-De Li, Tsinghua University, Beijing, China.

A9.11 CONDENSATION OF ULTRAFINE SILICA FROM A LASER-INDUCED PLUME, Gan-Moog Chow, Naval Research Laboratory, Composites and Ceramics Branch, Washington, DC; and Peter R. Strutt, University of Connecticut, Institute of Materials Science, Storrs, CT.

A9.12 LASER VAPORIZATION AND DEPOSITION OF LEAD ZIRCONATE TITANATE, Peter K. Schenck, Lawrence P. Cook, National Institute of Standards and Technology, Gaithersburg, MD; Jiarong Zhao, Chinese Academy of Science, Beijing, China; John W. Hastie, Edward N. Farabaugh, Chwan-Kang Chiang, Mark D. Vaudin, National Institute of Standards and Technology, Gaithersburg, MD; and Philip S. Brody, Harry Diamond Laboratories, Adelphi, MD.

A9.13 PHOSPHORUS IMPLANTATION OF 304L STAINLESS STEEL, E.C. Cooney, D.I. Potter, The University of Connecticut, School of Engineering, Institute of Materials Science, Metallurgy Department, Storrs, CT; N.L. Lee and G.B. Fisher, General Motors Research Laboratories, Physical Chemistry Department, Warren, MI.

A9.14 DENSITY OF AMORPHIZED SILICON AND ITS CORRELATION WITH STRUCTURE, J.S. Custer, Michael O. Thompson, Cornell University, College of Engineering, Department of Materials Science and Engineering, Ithaca, NY; J.M. Poate, D.C. Jacobson, AT&T Bell Laboratories, Murray Hill, NJ; S. Roorda, W.C. Sinke, FOM Institute for Atomic and Molecular Physics, Amsterdam, The Netherlands; and F. Spaepen, Harvard University, Cambridge, MA.

A9.15 NOBLE GAS ION IMPLANTATIONS IN LASER TREATED MATERIALS, J.Th.M. De Hosson, Materials Science Centre, Department of Applied Physics, Groningen, The Netherlands.

A9.16 FEMTOSECOND LASER MELTING OF GRAPHITE, D.H. Reitze, X. Wang, H. Ahn and M.C. Downer, University of Texas at Austin, Physics Department, Austin, TX.

A9.17 FORMATION OF DEFECT-FREE SHALLOW JUNCTIONS BY LOW-TEMPERATURE RAPID THERMAL ANNEALING, M.K. El-Ghor, S.J. Pennycook, and R.A. Zuhr, Oak Ridge National Laboratory, Oak Ridge, TN.

A9.18 A COMPARISON OF LOW AND HIGH DOSE GALLIUM ION IMPLANTED POLYCRYSTALLINE SILICON, H.B. Harrison, Griffith University, Microelectronics Department, Brisbane, Australia; A.P. Pogany, D.X. Cao, MMTL, RMIT, Melbourne, Australia; and Y. Komen, Technion, Israel.

A9.19 DIFFUSION OF CARBON IN TEMPERED MARTENSITIC STEEL DURING LASER MELTING, J.-P. Hirvonen, T.R. Jervis and T.G. Zocco, Los Alamos National Laboratory, Materials Science and Technology Division, Los Alamos, NM.

A9.20 RAPID THERMAL ANNEALING OF Si⁺ AND P⁺ DUALY IMPLANTED InP, Shen Honglie, Yang Genqing, Zhou Zuyao, and Zou Shichang, Shanghai Institute of Metallurgy, Ion Beam Laboratory, Shanghai, China.

A9.21 MODELING OF LOCALIZED MELTING OF THIN Si FILMS IN ZONE-MELTING RECRYSTALLIZATION, J.S. Im, Massachusetts Institute of Technology, Department of Materials Science and Engineering, Cambridge, MA, and Massachusetts Institute of Technology, Lincoln Laboratory, Lexington, MA; J.D. Lipman, I.N. Miaoulis, Tufts University, Mechanical Engineering Department, Medford, MA; C.K. Chen, Massachusetts Institute of Technology, Lincoln Laboratory, Lexington, MA; and C.V. Thompson, Massachusetts Institute of Technology, Department of Materials Science and Engineering, Cambridge, MA.

A9.22 EFFECTS OF NITROGEN ION IMPLANTATION IN 304 STAINLESS STEEL AT HIGH TEMPERATURES, Sadhna Shrivastava, Ram D. Tarey, M.C. Bhatnagar, Amitabh Jain and K.L. Chopra, Indian Institute of Technology, New Delhi, India.

A9.23 ANALYTICAL STUDY OF EFFECT OF ARSENIC CONCENTRATION ON SOLID PHASE EPITAXIAL GROWTH OF AMORPHOUS SILICON, Young-Jin Jeon, University of Texas, Center for Materials Science and Engineering, Austin, TX; M.F. Becker and R.M. Walser, University of Texas, Department of Electrical and Computer Engineering, Austin, TX.

A9.24 ION CHANNELING MEASUREMENTS OF STRAIN IN GERMANIUM IMPLANTED AND ANNEALED SILICON, E.A. Johnson and F. Namavar, Spire Corporation, Bedford, MA; and R.J. Culbertson, U.S. Army Materials Technology Laboratory, Watertown, MA.

A9.25 LOW ENERGY Si AND Sn IMPLANTATION OF GaAs, K.S. Jones, W.S. Rubart, L. Seiberling, University of Florida, Gainesville, FL; and D.K. Sadana, IBM T.J. Watson Research Center, Yorktown Heights, NY.

A9.26 HIGHLY STABLE W/p-In_{0.53}Ga_{0.47}As OHMIC CONTACTS FORMED BY RAPID THERMAL PROCESSING, A. Katz, R.F. Karlicek Jr., J.D. Wynn, B.E. Weir, D. Maher, P.M. Thomas, M. Soler, W.C. Dautremont-Smith, and L.C. Kimerling, AT&T Bell Laboratories, Murray Hill, NJ.

A9.27 MOSSBAUER STUDY OF THE DEFECT STRUCTURES AROUND Te IMPLANTED IN Al_x-Ga_{1-x}As, H. Bemelmans and G. Langouche, University of Leuven, Instituut voor Kern-en Stralingsfysica, Leuven, Belgium; and G. Borghs, IMEC, Leuven, Belgium.

A9.28 ION BEAM METHOD TO STUDY FRACTAL AGGREGATION OF MAGNETIC PARTICLES IN THIN FILMS, J.R. Ding, L.J. Huang, Tsinghua University, Department of Materials Science and Engineering, Beijing, China; and B.X. Liu, Tsinghua University, Department of Materials Science and Engineering, and Center of Condensed Matter and Radiation Physics, CCAST (World Lab.), Beijing, China.

A9.29 MODIFICATION OF NITRIDE CERAMIC STRUCTURE AND RESISTIVITY BY ION BEAMS, V.V. Lopatin and A.V. Kabyshev, High Voltage Institute, Tomsk, USSR.

A9.30 REDUCTION IN SECONDARY DEFECT FORMATION IN MEV ION IMPLANTED Si(100), W.X. Lu, R.J. Schreutelkamp, J.R. Liefing, and F.W. Saris, FOM-Institute for Atomic and Molecular Physics, Amsterdam, The Netherlands.

A9.31 AMORPHOUS METALLIC NiTi ALLOYS FORMED BY PLASMA ION MIXING, Xiaoci Zheng, R. Arthur Dodd, University of Wisconsin, Materials Science Department, Madison, WI; John R. Conrad and Frank Worzala, University of Wisconsin, NEEP and Materials Science Department, Madison, WI.

A9.32 LASER PULSE TRIGGERING OF THE EXPLOSIVE CRYSTALLIZATION IN AMORPHOUS Si AND Ge THIN FILMS, W. Marine and J. Marfaing, UA CNRS, Faculté des Sciences de Luminy, Département de Physique, Marseille, France.

A9.33 HREM OF ELECTRON BEAM INDUCED AMORPHIZATION AND PHASE TRANSFORMATION IN MoO₃ CRYSTAL, Shri R. Singh, Carnegie Mellon University, MEMS Department, Pittsburgh, PA; and Laurence D. Marks, Northwestern University, Center for Radiation Damage Studies, Department of Materials Science and Engineering, Evanston, IL.

A9.34 THE EFFECTS OF ANNEALING ON THE STRUCTURE AND DISTRIBUTION OF CHARGE STATES OF IRON IMPLANTED INTO α -Al₂O₃ AT 77K, C.J. McHargue, P.S. Sklad, J.C. McCallum and C.W. White, Oak Ridge National Laboratory, Metals and Ceramics Division, Oak Ridge, TN; A. Perez and G. Marest, University Claude Bernard, Villeurbanne, France.

A9.35 QUALITATIVE MODEL FOR SURFACE RIPPLING OF ZONE MELTING RECRYSTALLIZED SILICON-ON-INSULATOR LAYERS, Paul W. Mertens and Herman E. Maes, IMEC, Leuven, Belgium.

A9.36 PARAMETRIC STUDY OF THE ZONE-MELTING-RECRYSTALLIZATION PROCESS OF SOI STRUCTURES, Joseph Lipman, Ioannis N. Miaoulis, Tufts University, Mechanical Engineering Department, Medford, MA; and Jim S. Im, Massachusetts Institute of Technology, Materials Science and Engineering Department, Cambridge, MA.

A9.37 THE EFFECT OF CHROMIUM IMPLANTATION ON THE FRACTURE STRENGTH OF Al_2O_3 , M.E. O'Hern, C.J. McHargue, C.W. White, Oak Ridge National Laboratory, Oak Ridge, TN; and G.C. Farlow, Wright State University, Dayton, OH.

A9.38 ION-IMPLANTATION INDUCED AMORPHIZATION OF CERAMIC OXIDES, D.F. Pedraza, Oak Ridge National Laboratory, Metals and Ceramics Division, Oak Ridge, TN.

A9.39 METASTABLE STATES AND INCREASE IN CORROSION-MECHANICAL RESISTANCE IN STEELS IRRADIATED BY HIGH POWER ION BEAMS, A.D. Pogrebniak, V.P. Kushnarenko, N.N. Shabanov, Nuclear Physics Institute, Tomsk, USSR; A.K. Maksimov, Yu.M. Iesikov, V.M. Yugai, Tengizneftegas, Kulsary Department, Kaz, USSR.

A9.40 ION BEAM INDUCED CONDUCTIVITY CHANGES IN GLASSY CARBON, Douglas McCulloch and Steven Praver, Royal Melbourne Institute of Technology, Microelectronics and Materials Technology Centre, Melbourne, Australia.

A9.41 SYNTHESIS OF MoS_2 PHASE IN THE NEAR SURFACE REGION OF Al_2O_3 AND ZrO_2 BY ION IMPLANTATION, A.K. Rai, R.S. Bhattacharya, and D. Patrizio, Universal Energy Systems, Inc., Dayton, OH.

A9.42 EFFECT OF γ -RADIATION ON PHYSICO-CHEMICAL PROPERTIES OF LANTHANUM COBALTATE ($LaCoO_3$), B. Srinivas, V.R.S. Rao, and J.C. Kuriacose, Indian Institute of Technology, Department of Chemistry, Madras, India.

A9.43 STRUCTURAL AND THERMODYNAMIC PROPERTIES OF AMORPHIZED Si FORMED BY MeV Si BEAMS, S. Roorda, W.C. Sinke, FOM Institute for Atomic and Molecular Physics, Amsterdam, The Netherlands; J.M. Poate, D.C. Jacobson, S. Dierker, B.S. Dennis, AT&T Bell Laboratories, Murray Hill, NJ; P. Fuoss, AT&T Bell Laboratories, Holmdel, NJ; and F. Spaepen, Harvard University, Cambridge, MA.

A9.44 THE ROLE OF ION BEAMS IN CHANGING THE STATE OF RELAXATION OF AMORPHIZED Si, S. Roorda, W.C. Sinke, FOM Institute for Atomic and Molecular Physics, Amsterdam, The Netherlands; J.M. Poate, S. Dierker, B.S. Dennis, D.C. Jacobson, AT&T Bell Laboratories, Murray Hill, NJ; and F. Spaepen, Harvard University, Cambridge, MA.

A9.45 CONCENTRATION DEPENDENCE OF STRUCTURE AND CONTACT ELECTRONIC DENSITY IN IRON IMPLANTED SILICON, Francisco H. Sánchez and Marcela B. Fernández van Raap, Universidad Nacional de La Plata, Departamento de Física, La Plata, Argentina.

A9.46 CHANGE IN MAGNETIC CHARACTERISTIC OF 301 STAINLESS STEEL IRRADIATED WITH LASER AND ION BEAMS, H. Sanda, M. Takai and S. Namba, Osaka University, Faculty of Engineering Science and Research Center for Extreme Materials, Electrical Engineering Department, Osaka, Japan.

A9.47 TRANSIENT DIFFUSION IN BORON ION IMPLANTED SI(100), R.J. Schreutelkamp, FOM-Institute for Atomic and Molecular Physics, Amsterdam, The Netherlands; R.E. Kaim, J.F.M. Westendorp, Varian/Extrion Division, Beverly, MA; K.T.F. Janssen, J.J.M. Ottenheim, Philips Research Laboratories, Eindhoven, The Netherlands; and F.W. Saris, FOM-Institute for Atomic and Molecular Physics, Amsterdam, The Netherlands.

A9.48 RBS STUDIES OF DAMAGE BEHAVIOR IN SILICON INDUCED BY P_2^+ IMPLANTATION, Yang Gengqing, Lin Chenglu, Fang Ziwei, Zhou Zuyao, and Zou Shichang, Shanghai Institute of Metallurgy, Ion Beam Laboratory, Shanghai, China.

A9.49 INVESTIGATION ON MECHANISMS FOR ION BEAM INDUCED DEGRADATION OF POLYIMIDE, X.L. Xu, Zhou Zuyao, Chen Lizhi, Zou Shichang, Shanghai Institute of Metallurgy, Ion Beam Laboratory, Shanghai, China.

A9.50 EVALUATION OF SURFACE EFFECT ON DISLOCATION LOOP NUCLEATION, Naoto Shigenaka, Tsuneyuki Hashimoto, and Motomasa Fuse, Hitachi Ltd., Energy Research Laboratory, Ibaraki, Japan.

A9.51 STRUCTURAL ANALYSIS OF METASTABLE PHASES IN INTERMETALLIC ALLOYS PRODUCED BY ELECTRON IRRADIATION AND NON-EQUILIBRIUM PROCESSING, W. Sinkler and D.E. Luzzi, University of Pennsylvania, Department of Materials Science, Philadelphia, PA.

A9.52 SPATIAL DAMAGE DISTRIBUTION IN ELECTRON-BEAM PROCESSED GAAS-ALGAAS HETEROSTRUCTURES, EXPERIMENT AND THEORY, Doran D. Smith, U.S. Army, Electronics Technology and Devices Laboratory, Department SLCT-ED, Ft. Monmouth, NJ; Tobin Fink, New Jersey Institute of Technology, Physics Department, Newark, NJ; and W.D. Braddock, U.S. Army, Electronics Technology and Devices Laboratory, Department SLCT-ED, Ft. Monmouth, NJ and Cornell University, Ithaca, NY.

A9.53 ION IMPLANTATION INDUCED EFFECTS AT POLYSILICON GATE FEATURE EDGES, M.G. Stinson, Microelectronics Center of North Carolina, Research Triangle Park, NC, and North Carolina State University, Department of Electrical and Computer Engineering, Raleigh, NC; P.L. Smith, Microelectronics Center of North Carolina, Research Triangle Park, NC; and C.M. Osburn, Microelectronics Center of North Carolina, Research Triangle Park, NC, and North Carolina State University, Department of Electrical and Computer Engineering, Raleigh, NC.

A9.54 FAST TRANSIENT ANNEALING OF NEUTRON TRANSMUTATION DOPED InP, F.P. Korshunov, E.A. Kudriavtseva, N.A. Sobolev, T.A. Prokhorenko, and N.G. Kolin, Institute of Solid State and Semiconductor Physics, Minsk, USSR.

A9.55 EFFECTS OF LASER SURFACE MELTING ON STRUCTURE CHARACTER AND EROSION RESISTANCE OF PLASMA-SPRAYED CERAMIC COATINGS, Jia-Shu Sun, Tianjin Institute of Technology, Tianjin, China.

A9.56 MICROSTRUCTURAL ANALYSIS OF 1 MEV NITROGEN IMPLANTED FE AND TI SURFACES, A.M. Vredenberg and F.W. Saris, FOM-Institute for Atomic and Molecular Physics, Amsterdam, The Netherlands; N.M. v.d. Pers, Th.H. de Keijser, P.F. Colijn and E.J. Mittemeijer, Delft University of Technology, Laboratory of Metallurgy, Delft, The Netherlands.

A9.57 CHARACTERISTICS OF METAL-p⁺-GaAs SCHOTTKY BARRIER JUNCTION FORMED BY FOCUSED-ION-BEAM IMPLANTATION, Nobuo Watanabe, Takeo Tsukamoto and Masahiko Okunuki, Canon, Research Center, Kanagawa, Japan.

A9.58 STUDY OF Hf DIFFUSION IN α -Zr USING RUTHERFORD BACKSCATTERING SPECTROMETRY, M. Behar, P.L. Grande, F.C. Zawislak, Instituto de Física, UFRGS Porto Alegre, Brasil; F. Dymant and E. Savino Comisión Nacional de Energía Atómica, Buenos Aires, Argentina.

A9.59 COOPERATIVE BEHAVIOR IN AN ELECTRON STIMULATED Tl-Ba-Ca-Cu-O SUPERCONDUCTOR, J.P. Zhang and L.D. Marks, Northwestern University, Center for Surface Radiation Damage Studies, Department of Materials Science and Engineering, Evanston, IL.

A9.60 THE INTERACTION OF INERT GAS IONS WITH ADSORBATE-COVERED CRYOGENIC SURFACES, Patricia M. George, John M. Lindquist, Daryl L. Mossman, Gencorp Aerojet Electrosystems Co., Azusa, CA.

SESSION A10: FAST TRANSIENT PROCESSING

Chairs: P. S. Peercy and J. A. Knapp
Friday Morning, December 1
Salon E (M)

8:30 ***A10.1**
TRANSIENT CONDUCTANCE MEASUREMENTS, M.O. Thompson, Cornell University, Department of Materials Science and Engineering, Ithaca, NY.

9:00 **A10.2**
FREEZING IN SILICON AT LARGE UNDERCOOLING, A. Polman, P.A. Stolk and W.C. Sinke, FOM-Institute AMOLF, Amsterdam, The Netherlands.

9:15 **A10.3**
TRANSIENT CONDUCTANCE MEASUREMENTS OF SOLIDIFICATION VELOCITIES OF ELEMENTAL METALS, Harry A. Atwater, California Institute of Technology, Pasadena, CA; J.A. West, Patrick M. Smith, M.J. Aziz, Harvard University, Division of Applied Sciences, Cambridge, MA; J.Y. Tsao and P.S. Peercy, Sandia National Laboratories, Albuquerque, NM; and Michael O. Thompson, Cornell University, Department of Materials Science and Engineering, Ithaca, NY.

9:30 **A10.4**
OBSERVATION OF PULSED LASER-INDUCED MELTING OF SOLID SURFACES BY OPTICAL SPIN ORIENTATION, A. Vaterlaus, M. Lutz, D. Guarisco, M. Aeschlimann, M. Stampanoni, and F. Meier, ETH Hönggerberg, Laboratorium für Festkörperphysik, Zurich, Switzerland.

9:45 **A10.5**
SUB-MELTING LASER INDUCED GRAIN GROWTH, S.A. Ajuria, C.V. Thompson, Massachusetts Institute of Technology, Department of Materials Science and Engineering, Cambridge, MA.

10:00 BREAK

10:30 **A10.6**
PULSED LASER MELTING OF INTERMEDIATE Cu-Zn PHASES, D.M. Follstaedt and P.S. Peercy, Sandia National Laboratories, Albuquerque, NM; and J.H. Perepezko, University of Wisconsin, Department of Metallurgical and Mineral Engineering, Madison, WI.

10:45 **A10.7**
LASER MIXING OF TITANIUM ON SILICON CARBIDE, T.R. Jervis, J-P. Hirvonen, M. Nastasi and M.R. Cohen, Los Alamos National Laboratory, Materials Science and Technology Department, Los Alamos, NM.

11:00 **A10.8**
TEMPERATURE MEASUREMENT BY INFRARED TRANSMISSION FOR RAPID THERMAL PROCESSING APPLICATIONS, J.C. Sturm, P.V. Schwartz, and P.M. Garone, Princeton University, Dept. of Electrical Engineering, Princeton, NJ.

11:15 A10.9
METASTABLE GE-SN ALLOY LAYERS PREPARED BY PULSED LASER MELTING, I.T.H. Chang, B. Cantor, University of Oxford, Department of Metallurgy and Science of Materials, Oxford, United Kingdom; and A.G. Cullis, Royal Signals and Radar Establishment, Worcs, United Kingdom.

11:30 A10.10
CHARACTERIZATION OF PULSED LASER BEAM MIXED AuTeGaAs OHMIC CONTACTS, K. Wuyts, R.E. Silverans, K.U. Leuven, Physics Department, Leuven, Belgium; M. Van Hove, and M. Van Rossum, Interuniversity Microelectronics Center, Leuven, Belgium.

11:45 A10.11
MELTING OF ION IMPLANTED AND RELAXED AMORPHOUS SILICON, M.G. Grimaldi, P. Baeri, Dipartimento di Fisica, Catania, Italy; and G. Baratta, Istituto di Astronomia, Catania, Italy.

SESSION A11: BEAM MODIFICATION OF METALS

Chair: D. M. Follstaedt
Friday Afternoon, December 1
Salon E (M)

1:30 *A11.1
MARTENSITIC TRANSFORMATIONS IN ION IMPLANTED STAINLESS STEELS, E. Johnson, University of Copenhagen, Physics Laboratory, Copenhagen, Denmark.

2:00 A11.2
HARDNESS-DAMAGE CORRELATIONS IN Ta IMPLANTED SINGLE CRYSTAL Ni_3Al , Gary S. Was, University of Michigan, Departments of Nuclear Engineering and Materials Science and Engineering, Ann Arbor, MI; and S. Mantl, KFA Jülich, Institut für Schicht-und Ionentechnik, Jülich, West Germany.

2:15 A11.3
IRRADIATION-INDUCED AMORPHIZATION AND SHEAR ELASTIC INSTABILITY IN INTERMETALLIC COMPOUNDS, J. Koike, Los Alamos National Laboratory, Center for Materials Science, Los Alamos, NM; P.R. Okamoto, L.E. Rehn, R. Bhadra, M.H. Grimsditch, Argonne National Laboratory, Materials Science Division, Argonne, IL; and M. Meshii, Northwestern University, Department of Materials Science and Engineering, Evanston, IL.

2:30 A11.4
THE EFFECT OF MICROSTRUCTURE ON THE MORPHOLOGY AND KINETICS OF AMORPHIZATION INDUCED BY ION IRRADIATION, D.F. Pedraza and P.J. Maziasz, Oak Ridge National Laboratory, Metals and Ceramics Division, Oak Ridge, TN.

2:45 A11.5
EXTENDED SOLID SOLUTION FORMATION IN THE Ti-Co-Ni SYSTEM, David A. Lilienfeld and P. Børgesen, Cornell University, Ithaca, NY.

3:00 A11.6
CHARACTERIZATION OF HIGH-DOSE CARBON-ION-IMPLANTED AND ANNEALED Nb, J.S. Huang, Lawrence Livermore National Laboratory, Livermore, CA.

3:15 A11.7
STRENGTHENING OF ALUMINUM BY OXYGEN IMPLANTATION: EXPERIMENTAL RESULTS AND MECHANICAL MODELING, Roy J. Bourcier, Samuel M. Myers and David M. Follstaedt, Sandia National Laboratories, Albuquerque, NM; and Douglas H. Polonis, University of Washington, Material Science and Engineering Department, Seattle, WA.

3:30 A11.8
ION BEAM INDUCED PERCOLATION CLUSTERING IN Al-Fe-Cu ALLOY FILMS, C.H. Shang, Tsinghua University, Department of Materials Science and Engineering, Beijing, China; and B.X. Liu, Tsinghua University, Department of Materials Science and Engineering, and Center of Condensed Matter and Radiation Physics, CCAST (World Lab.), Beijing, China.

3:45 A11.9
UNUSUAL MICROSTRUCTURES OF A METASTABLE CRYSTALLINE $Pt_{50}Ti_{50}$ ALLOY UNDER ION BOMBARDMENT, Y.L. Chen, Y.-T. Cheng, J.V. Mantese, and A.B. Catalan, General Motors Research Laboratory, Warren, MI.

A1.1

LOW ENERGY ION BEAM SURFACE MODIFICATION, DEPOSITION, AND SYNTHESIS J. J. Cuomo, IBM Research Division, T. J. Watson Research Center, P.O. Box 218, Yorktown Heights NY 10598.

Energetic particle bombardment of surfaces will change the properties of that surface according to the particle and its energy. This paper is a review of low energy particle bombardment of surfaces during film growth. Property modifications, deposition and compound synthesis are presented. Energetic particle bombardment (100-1000 eV) during deposition alters film properties such as stress, density, electrical resistivity, chemical purity, hydrogen distribution, structure and composition. Physical properties as well as the hydrogen content of Nb, Cr, W, and Cu are controlled by ion bombardment during deposition. Energetic particle bombardment of a growing ZrO_2 film reduces its porosity and increase its index of refraction. Changes in microstructure and orientation are found in Nb, AlN and Group IV B nitride films. Synthesis of stable and metastable phases for high T_c superconductors, copper oxides, CrO_2 , AlN, and Group IV B mono and higher nitrides are also possible with energetic ion bombardment. Results on amorphous diamond-like carbon films deposited by ion beam deposition will also be presented.

A1.2

ION BEAM-ASSISTED MBE.* E. Chason, J.Y. Tsao, K.M. Horn, D.K. Brice and S.T. Picraux, Sandia National Laboratories, Albuquerque, NM 87185

Simultaneous growth and ion bombardment is shown to enhance the smoothening of surfaces during MBE growth under certain conditions. For example, a 500 eV Ar ion beam roughened surface at 500 C is smoothened after less than two monolayers of subsequent growth and bombardment. This beam-enhanced smoothening phenomenon is discussed in terms of a competitive balance between creation and annihilation of different types of surface defects; low energy ion beams create primarily vacancy-like defects while growth beams create adatom defects. The evolution of the surface is mediated by the interaction of these defects with each other and existing ledges and clusters.

Real-time measurements of the kinetics of surface roughening and smoothening made by RHEED (reflection high energy electron diffraction) are discussed in terms of this picture. During ion bombardment, surfaces are observed to reach a temperature dependent steady state roughness. A similar temperature dependence is observed for growth roughening. Yet, surprisingly, simultaneous ion bombardment and growth has been observed to lead to a smoothening of the surface. The energy and mass dependence of the beam assisted MBE results are compared with calculations of surface and bulk displacement thresholds.

*This work performed at Sandia National Laboratories supported by the U.S. Department of Energy under contract #DE-AC04076DP00789.

A1.3

LOW ENERGY ION BOMBARDMENT AND ISLAND COARSENING IN THIN FILMS, Chih H. Yang and Harry A. Atwater, California Institute of Technology, Pasadena, CA, 91125.

Low energy ion bombardment during thin film deposition has been shown to significantly modify the microstructure of deposited polycrystalline thin films. However, little of a fundamental nature is known about the interaction of a low energy ion beam with a discontinuous film at the early stages of growth, and the resulting effect on microstructure. We have modeled the effects of low energy ion bombardment on post-nucleation coarsening of islands in discontinuous films, using a procedure similar to the classical analysis of coarsening of Lifschitz, Slyozov and Wagner (LSW). Solution of a continuity equation, subject to the constraint of mass conservation, coupled with interface-limited and diffusion-limited rate laws for island coarsening allow vari-

ous types of ion-surface interactions and island size distributions to be modeled.

It has speculated that several different phenomena may occur as a result of low energy ion bombardment during film growth, including enhanced adatom diffusion, sputtering, dissociation of small islands and generation of new nucleation sites. Our analysis suggests that each of these phenomena leads to a unique kinetic path for coarsening and very different film microstructures. Hence it may be possible, through a study of island coarsening kinetics to assess the relative importance of adatom diffusion, sputtering, island dissociation, etc. in determining film microstructure resulting from ion assisted deposition.

A1.4

ION BEAM ASSISTED ZIRCONIUM NITRIDE FILMS.

I.C. Oppenheim, Materials Science and Engineering, The Johns Hopkins University, Baltimore, MD 21218; K.R. Padmanabhan, Department of Physics and Astronomy, Wayne State University, Detroit, MI 48202.

RF sputter deposition of 500nm thick zirconium films was carried on simultaneously with implantation of singly ionized molecular nitrogen. Samples were prepared at room temperature (23°C) with a nitrogen to zirconium arrival ratio varying from 2.7×10^{-2} to 4.4×10^{-1} and with the ion energy varying from 100 to 300 keV.

Stoichiometry of the films and ion concentration profiles were determined by Rutherford Backscattering Spectrometry. Results from a theoretical model for the ion concentration profiles will be compared to profiles derived from experiments. Grazing Angle X-Ray Diffraction was used to correlate nitride phase formation to processing parameters.

Knoop microhardness of films deposited on 304 stainless steel substrates were determined. The relative microhardness of the samples are studied as a function of parameters such as film stoichiometry and ion implantation energy.

A1.5

IMPORTANCE OF SURFACE PREPARATION IN DIRECT ION BEAM DEPOSITION (IBD) Kiyoshi Miyake, Hitachi Research Laboratory, Kuji-cho 4026, Hitachi, Ibaraki 319-12 JAPAN.

Firstly epitaxial growth of Si and Ge films using mass-separated low energy direct IBD method is discussed. Our IBD system provides an isotopically pure $^{74}Ge^+$ or $^{28}Si^+$ ion beam with 100-200 eV and 100-300 uA in 10^{-6} Pa vacuum pressure. Si epitaxial growth is possible at 740°C on Si(100) substrates using 200 eV $^{28}Si^+$ ion beam without special surface cleaning. The crystalline properties of the deposited films will be discussed from the view point of surface preparation and impurity inclusion problem.

Secondary a new attempt for Si surface cleaning method is presented which utilize low energy (0.5-1.0 keV) hydrogen ion irradiation to remove Si surface native oxide. In-situ AES analysis of SiO_2/Si layer under H_2^+ ion bombardment indicates that chemical sputtering of SiO_2 by ion implanted H ions at 450-500°C plays a great role to remove surface SiO_2 oxide.

Through these two discussions the importance of surface preparation in direct ion beam deposition will be stressed.

A1.6

PREPARATION AND CHARACTERIZATION OF ION BEAM ASSISTED ALUMINUM OXIDE FILMS. J. K. Hirvonen, T. Tetreault, G. Parker and B. W. Murray, Spire Corporation, Bedford, MA; P. Revesz, Cornell University, Ithaca, NY.

Dense, adherent, physically robust and high optical grade aluminum oxide coatings are required for protective coatings on optical reflecting surfaces. Electron beam evaporation of Al₂O₃ (or Al) has been used in conjunction with low energy (200-600 eV) oxygen ion bombardment from a Kaufman type ion source to produce such coatings for a range of evaporant to ion flux ratios on silicon and carbon substrates. The film's densities and stoichiometries have been measured using surface profilometry and RBS measurements and ellipsometry has been used to measure refractive indices. Mechanical characterization includes microhardness tests and adhesion tests. Initial results indicate that highly dense and adherent films with high refractive indices can be obtained using ion assisted deposition.

A1.7

SILICON OXIDE FILM FORMATION BY THE SIMULTANEOUS USE OF A MICROWAVE ION SOURCE AND AN ICB SYSTEM. Gikan H. Takaoka, Hiroshi Tsuji, and Junzo Ishikawa, Kyoto University, Sakyo, Kyoto 606, Japan

Silicon oxide (SiO₂) films, which are amorphous and insulating materials with a large band gap, have wide applications for functional coatings in semiconductor devices. We have prepared SiO₂ films at a substrate temperature of 100°C by the simultaneous use of a microwave ion source and an ICB system. The microwave ion source system is used to produce low energy (100-500 eV) oxygen ion beams in a high vacuum of about 10⁻⁵ Torr. In the ICB system, SiO₂-clusters are formed, and the ionized and neutral clusters are transferred to a substrate to make a contribution to the film formation.

By using oxygen ions, the transparent SiO₂ films could be obtained, and they showed a refractive index of 1.46. The chemical etching rate was low and similar to that of thermally grown films used in Si device processes. The bonding between Si and O atoms in these films could be enhanced by using both ionized clusters and oxygen ions, and the stoichiometric SiO₂ films were obtained. Also, the films showed an electric resistivity higher than 10¹⁴ Ω-cm, and a breakdown voltage was larger than 2 x 10⁶ V/cm. Furthermore, the surface state density calculated from the C-V characteristic for the film was found to be 6 x 10¹¹ cm⁻² eV⁻¹.

These results show that the simultaneous use of a microwave ion source and an ICB system has a high potential for preparing chemically stable SiO₂ films and that the films prepared can be applied to insulating and passivation coatings.

A1.8

METASTABLE CrO₂ FILM FORMATION BY REACTIVE ION BEAM SYNTHESIS AND RAPID THERMAL ANNEALING. K. V. Ramanathan, C. Richard Guarnieri, J. J. Cuomo, D. A. Smith, and S. Shivashankar, IBM Research Division, T. J. Watson Research Center, P.O. Box 218, Yorktown Heights NY 10598.

Metastable CrO₂ films are made by reactive ion beam synthesis followed by rapid thermal annealing. Both steps are required to obtain polycrystalline CrO₂ films. Amorphous films with some CrO₂ nuclei are grown by bombarding Cr deposited by thermal evaporation with low energy (< 500 eV) O₂ ions on substrates in the temperature range of 20-70°C. As deposited, these films are generally a mixture containing different phases of chromium oxide (CrO, Cr₂O₃, CrO₂, and Cr₂O₃). Substrate temperature, ion energy, and the arrival rates of O₂ to Cr influence the composition and structure of the as-deposited film. Rapid thermal annealing is necessary to separate and grow metastable structures like CrO₂ from the as depos-

ited oxide mixture. Soak temperatures of 400°C with rapid heating to 500°C are used in the rapid thermal annealing. However, films deposited at substrate temperatures greater than 70°C convert to Cr₂O₃ following annealing. Furnace annealing of as-deposited films also results in the equilibrium Cr₂O₃ phase.

A1.9

ADHESION STUDIES OF Au FILMS ON GaAs USING ION-ASSISTED DEPOSITION TECHNIQUES. T. T. Bardin, and J. G. Pronko Lockheed Research and Development Division, O/91-10, B203, 3251 Hanover St., Palo Alto, CA 94304-1191. A. J. Kellock and J. E. E. Baglin, IBM Almaden Research Center, K34/802, 650 Harry Road, San Jose, CA 95120-6099.

Previous work^{1,2} on the adhesion of Au metallization to GaAs indicated that bonding of the metallization is extremely sensitive to surface contamination. A series of experiments have been performed in an effort to understand the correlation between surface contamination, evaporation conditions, interface grain size, and film adhesion. These experiments include a study of the influence of *in situ* pre-sputtering of the semi-conductor surface with low-energy Ar ions prior to thermal deposition of Au films as well as ion-assisted thermal deposition of Au. Deposition conditions were varied in order to study the effects of substrate temperature, Ar ion bombarding energy and the relative flux of Ar ions to incident Au atoms. Adhesion was investigated using a peel test. In addition the interface of films processed under these various conditions was examined by XPS, RBS, and TEM methods. Film stress and interface grain size were studied by x-ray diffraction and x-ray rocking curve measurements. The results of these experiments will be discussed.

¹T. T. Bardin, J. G. Pronko, L. Senbetu, Mat. Res. Soc. Symp. Proc. 119 (1988) 147.

²T. T. Bardin, J. G. Pronko, and D. A. Kozak, Appl. Phys. Lett. 54 (1989) 173.

A2.1

IRRADIATION-INDUCED GRAIN GROWTH: THE ROLE OF DISLOCATIONS.* Charles W. Allen and Lynn E. Rehn, Materials Science Division, Argonne National Laboratory, Argonne, IL 60439.

Thermally activated grain growth generally occurs by a grain boundary migration mechanism and at temperatures typically in excess of a third to half the absolute melting point of the particular material. In contrast, irradiation-induced grain growth is nearly athermal. *In situ* observations during heavy ion irradiation of evaporated Au thin films in Argonne's HVEM-Tandem User Facility at temperatures as low as 10 K have clearly demonstrated that the irradiation-induced growth occurs both by grain boundary migration and by grain coalescence. Previous theories of irradiation-induced grain growth have assumed that growth occurs by the boundary migration mechanism alone and that only point defects created at a grain boundary contribute to the growth process. These *in situ* studies show that boundary migration is not the only operative mechanism, and direct observation of defect cluster dynamics strongly suggests that the basic assumptions of previous theories of irradiation-induced grain growth are at least not universal. A simple model, involving glide of dislocations resulting from the condensation of point defects, even far removed from a boundary, shows that glide of dislocations through a boundary produces local boundary migration while glide to a boundary with incorporation of the dislocations into the boundary structure changes the local specific grain boundary energy which can promote grain coalescence. In either event, the result is essentially the same as it would have been from the flux of the initial vacancies or self-interstitials through or to the boundary by bulk diffusion. It is suggested that the role of dislocations may be especially important in the case of irradiation-induced grain growth in gold in which growth rates are several times faster than in other pure metals such as Cu, Ag, Ni and Al and the visible dislocation activity during irradiation is extraordinary.

*Work supported by the U.S. Department of Energy, Basic Energy Sciences-Materials Sciences under Contract #W-31-109-ENG-38.

A2.2

ION-BEAM-INDUCED EPITAXIAL CRYSTALLIZATION OF $\text{Ge}_3\text{Si}_5/\text{Si}$ HETEROSTRUCTURES. R.G. Elliman, M.C. Ridgway, J.S. Williams, Microelectronics and Materials Technology Centre, Royal Melbourne Institute of Technology, GPO Box 2476V, Melbourne, Victoria 3001, Australia; and J.C. Bean, AT and T Bell Laboratories, Murray Hill, New Jersey 07974, USA

Ge_3Si_5 layers of approximately 100 nm thickness, grown epitaxially on (100) Si substrates by molecular beam epitaxy, were amorphized to either half their total thickness (thin) or completely amorphized to a depth beyond the GeSi/Si interface (thick) by Si implantation at -196°C . Ion-beam annealing of the amorphous GeSi alloys was then investigated for a variety of irradiation conditions. Samples were examined by high depth resolution Rutherford backscattering and channeling and by transmission electron microscopy. Such analysis revealed that ion-beam annealing caused epitaxial crystallization of both the thin and thick amorphous layers. The crystalline perfection of the regrown material and details of the commensurate/incommensurate transformation are reported for alloy compositions in the range $x = 0.1$ to $x = 0.8$.

A2.3

DEPENDENCE OF INTERFACE VELOCITY ON NOBLE METAL SEGREGATION DURING ION BEAM ENHANCED EPITAXY. J. S. Custer and Michael O. Thompson, Cornell University, Ithaca, NY; J. M. Poate and D. C. Jacobson, AT&T Bell Laboratories, Murray Hill, NJ.

Ion beam enhanced epitaxy (IBEE) of amorphous Si (a-Si) on crystal Si (c-Si) is a novel, low temperature crystal growth process, offering potential insights into long standing problems in basic crystal growth. Recent work has focussed on measuring the segregation and trapping of fast-diffusing noble metals (Cu, Ag, and Au) during MeV Ar induced IBEE, and comparing the results with classical segregation theory.

In this work we use MeV Si beams to induce IBEE of both intrinsic and doped a-Si layers while continuously monitoring the a-Si/c-Si interface position with the time resolved reflectivity technique. For Au doped layers, we observe a transient velocity enhancement of up to a factor of 2 during the build up of the Au segregation spike. The observed velocity changes for Au doped a-Si during IBEE are much less than the velocity enhancements observed for thermal anneals. The difference between the velocities for various impurities will be discussed.

Accurate velocity profiles are also required to sensitively compare impurity movement during IBEE with classical segregation theory. The apparent segregation coefficients and the effects of the interface velocity on the segregation will be presented.

A2.4

ION BEAM INDUCED CRYSTALLIZATION IN PREAMORPHIZED BP(100). Naoto Kobayashi, Hisao Kobayashi, Hisao Tanoue and Nobuyuki Hayashi, Electrotechnical Laboratory, Tsukuba, Ibaraki, Japan; Yukinobu Kumashiro, Yokohama National University, Yokohama, Kanagawa, Japan

Ion beam induced epitaxial crystallization (IBIEC) in pre-amorphized BP(100) have been investigated by means of RBS channeling method. BP is an attractive material which is a refractory wide bandgap semiconductor with melting point above 3000°C and bandgap of 2.1 eV.

BP(100) samples prepared by thermal CVD on Si(100) were preamorphized in the surface region with 70 keV Ar and 100 keV As ions. Re-crystallization was induced by subsequent ion bombardments with 400 keV Ar and 400 keV Kr at temperature range between 200°C and 400°C . The current densities of Ar and Kr ions were selected to give the same energy deposition rate in the elastic collision process ($4\mu\text{A}/\text{cm}^2$ for Ar^+ and $1\mu\text{A}/\text{cm}^2$ for Kr^+). Epitaxial crystallization was observed at temperatures much below those required for the thermal solid phase epitaxy (SPE) process (above 800°C). The critical temperature for crystallization at these current den-

sities was 230°C . The activation energy observed by both ion species bombardments was 0.17 ± 0.08 eV. The regrowth rate in the sample preamorphized with As ions was found to be 1.6 times as large as in the sample preamorphized with Ar ions. The regrowth rate as a function of the deposited energy density into nuclear collision at a given temperature was roughly one-quarter of that in the preamorphized Si(111) which was observed in comparison under the same experimental condition. On the same scale, Ar bombardments were found to be 2.7 times more effective in the regrowth rate than Kr ion bombardments.

A2.5

AMORPHOUS TO POLYCRYSTAL TRANSITION ASSISTED BY ION BEAM IRRADIATION IN SILICON. C. Spinella, S. Lombardo and S.U. Campisano, Dip. di Fisica dell'Università, corso Italia 57, I95129 Catania (ITALY).

The amorphous to polycrystal transition in chemical vapor deposited silicon films under Kr ion beam irradiation has been studied in the $320 - 450^\circ\text{C}$ temperature range. The grain size distribution is very narrow and the grain shape is cylindrical. Moreover the average grain diameter increases linearly with the ion dose. The growth rate is thermally activated with an activation energy of 0.28 eV, equal to that for the ion beam induced epitaxial layer by layer crystallization of amorphous silicon. The structure of the crystal grains has been studied in details and twins around (111) axis have been observed. This could explain why the absolute value of the grain growth rate is equal to that for ion beam assisted epitaxial crystallization on (111) substrate orientation. Data about the grain nucleation rate under ion beam irradiation are also reported and compared with those obtained for pure thermal processes. The results are explained in terms of a variation of the free energy difference between the amorphous and the crystal phase caused by the ion beam.

A2.6

FORMATION OF BURIED ELEMENTAL LAYERS USING ION IMPLANTATION. D.W. Brown* and Z.A. Munir, Div. of Materials Science and Engineering, Univ. of Calif. Davis, Davis, CA 95616, and R.G. Musket, Lawrence Livermore National Laboratory, P.O. Box 808, Livermore, CA 94550

We have shown that ion implantation can be used to form an essentially pure buried layer of an implanted element in a target material. Rutherford backscattering, cross-sectional transmission electron microscopy, scanning electron microscopy, and Auger electron spectroscopy revealed that a distinct aluminum layer was formed in single crystal beryllium during post-implant annealing (500°C , 1 hr) of samples implanted with 200 keV Al^+ . The Al-Be system is a representative of binary systems in which the elements have low mutual solubility and do not form intermediate phases. In such systems, precipitation of the implanted element can occur during implantation and/or post-implant annealing, creating the possibility of layer formation by processes that result in precipitate coalescence. For the Al-Be system, coalescence of the implanted aluminum into a layer during annealing was found to depend critically on dose for 50°C implants. Implantation at higher temperatures showed that layer formation was also dependent on the aluminum-precipitate/beryllium-matrix microstructure prior to annealing.

Considerations for the formation of buried elemental layers in other systems are discussed.

Work performed under the auspices of the U.S. Department of Energy by Lawrence Livermore National Laboratory under contract #W-7405-Eng-48.

*Current address: Lawrence Livermore National Laboratory, P.O. Box 808, Livermore, CA 94550.

A2.7

ION-BEAM-INDUCED EPITAXIAL CRYSTALLIZATION OF METAL SILICIDES. M.C. Ridgway, R.G. Elliman, and J.S. Williams, Microelectronics and Materials Technology Centre, Royal Melbourne Institute of Technology, GPO Box 2476V, Melbourne, Victoria 3001, Australia.

Ion-beam-induced epitaxial crystallization of disordered metal silicides has been investigated. Epitaxial NiSi_2 and CoSi_2 layers on (111) Si substrates were implanted with low energy Si ions to form a disordered surface layer containing both amorphous and heavily damaged crystalline material. Epitaxial recrystallization during subsequent high energy ion irradiation proceeded in a layer-by-layer manner from the original disordered/crystalline interface. For a disordered NiSi_2 layer at 450°C, 300 keV Si ion irradiation resulted in an ion-beam-induced growth rate of $14 \pm 6 \text{ nm}/10^{15} \text{ Si}/\text{cm}^2$. Dislocation densities of the ion-beam annealed layers were greater than those of the original epitaxial layers. Samples were analyzed with Rutherford backscattering spectrometry combined with channeling and transmission electron microscopy. Ion beam and thermal annealing are compared.

A2.8

ION-BEAM SYNTHESIS OF BURIED YTTRIUM SILICIDE. T. L. Alford, Material Science and Engineering Department, Cornell University, Ithaca, NY 14853; and J.C. Barbour, Sandia National Laboratories, Albuquerque, NM 87185

Metal silicides find useful applications in VLSI electronics as a result of their low resistivity and good stability at high temperatures. Several silicides form epitaxial layers on Si yielding nearly defect-free structures. We have investigated the formation of a buried $\text{YSi}_{1.7}$ layer in Si. The $\text{YSi}_{1.7}$ structure has a hexagonal lattice which can form epitaxially on Si(111) with $\approx 0.0\%$ mismatch. The epitaxial relationship between $\text{YSi}_{1.7}$ and Si is given by: $\text{YSi}_{1.7}(0001) // \text{Si}(111)$ and $\text{YSi}_{1.7}[10\bar{1}0] // \text{Si}[11\bar{2}]$. The buried silicide was formed by implanting 330 keV Y^+ ions into Si(111) substrates held at 450°C followed by a vacuum anneal at 1000°C. Samples were studied over the fluence range of $0.5 - 4 \times 10^{17} \text{ Y}/\text{cm}^2$. Concentration profiles were determined using RBS, and the crystalline quality was analyzed with ion channeling. A continuous buried layer (188 nm thick) was formed for a fluence of $4 \times 10^{17} \text{ Y}/\text{cm}^2$. The Si overlayer in this sample is 24 nm thick. RBS results from the samples with a fluence of $2 \times 10^{17} \text{ Y}/\text{cm}^2$ suggest that these samples are composed of a uniform buried $\text{YSi}_{1.7}$ layer with YSi_x precipitates above and below this layer. Ion channeling in the $\text{Si}\langle 111 \rangle$ direction showed that the uniform layers and the precipitates are aligned with the substrate, as depicted by a χ_{min} value of 7% in the Y signal. The perpendicular and parallel strains, ϵ^{\perp} and ϵ^{\parallel} , associated with the formation of $\text{YSi}_{1.7}$ were evaluated from x-ray rocking curves using a double crystal diffractometer. The following x-ray reflections were measured: $\text{YSi}_{1.7}(0004) // \text{Si}(333)$, and $\text{YSi}_{1.7}(10\bar{1}3)$ and $\text{Si}(331)$. The residual strains in the buried $\text{YSi}_{1.7}$ layer are: $\epsilon^{\perp} = 0\%$ and $\epsilon^{\parallel} = -1.0\%$.

This work was funded by the U.S. DOE under contract no. DE-AC04-76DP00789.

A2.9

ELECTRICAL TRANSPORT IN $\text{Si}/\text{CoSi}_2/\text{Si}$ HETEROSTRUCTURES GROWN BY MESOTAXY. Alice E. White, M. L. Green, K. T. Short, D. Brasen, and K. Maex*, AT&T Bell Laboratories, 600 Mountain Ave., Murray Hill, NJ 07974.

We have used mesotaxy, a technique which involves high dose implantation followed by high temperature annealing¹, to create thin ($< 500 \text{ \AA}$) layers of oriented single-crystal CoSi_2 buried beneath the surface of (100) silicon wafers. Several thousand angstroms of epitaxial silicon are then deposited using an RTCVD process. This results in a $\text{Si}/\text{CoSi}_2/\text{Si}$ heterostructure which is difficult to grow by UHV deposition and reaction. Rutherford backscattering and channeling measurements in conjunction with TEM observation indicate that the Si overlayer has threading dislocations at a density of $\sim 10^8/\text{cm}^2$. In addition, some SiC precipitates appear at the original Si surface. Nonetheless, Schottky barrier height measurements show that the lower CoSi_2/Si interface is of acceptable quality and efforts are underway to improve the upper CoSi_2/Si interface in order to make vertical transport measurements.

¹ Alice E. White, K. T. Short, R. C. Dynes, J. P. Garino, and J. M. Gibson, Appl. Phys. Lett. 50, 95 (1987).

*permanent address: IMEC, Leuven, Belgium

A2.10

ION BEAM ANNEALING OF Si CO-IMPLANTED WITH Ga AND As.* S. P. Withrow, O. W. Holland, and S. J. Pennycook, Solid State Division, Oak Ridge National Laboratory, Oak Ridge, TN 37831; and J. Pankove, Solar Energy Research Institute, Golden, CO 80401.

Beam-induced annealing resulting from high-energy, Si^+ -ion irradiation of amorphous Si layers heavily doped with electrically compensating impurities is discussed. Amorphous layers were formed by co-implantation of overlapping distributions of Ga and As in a fluence range which spanned well beyond the limits of solubility for these dopants in Si, especially for Ga. At substrate temperatures up to 400°C, recrystallization of the amorphous layer is shown to occur by solid-phase, epitaxial growth onto the single crystal substrate. The quality of the epitaxy and the extent of alloying and dopant redistribution during recrystallization are compared. These results have been characterized in co-implanted samples to ones which had been implanted only with a single gallium or arsenic impurity. Significant differences between the various types of implanted samples are detailed. Lack of impurity precipitation and segregation in the co-implanted samples, even at concentrations exceeding 5 at. %, are attributed to compensation effects most likely through clustering of the dissimilar dopants, both in the amorphous phase and in the recrystallized regions. Rutherford backscattering/ion channeling and transmission electron microscopy were used to characterize the samples. Electrical characterization was also done on selected samples.

*Research sponsored by the Division of Materials Sciences, U.S. Department of Energy under contract DE-AC05-84OR21400 with Martin Marietta Energy Systems, Inc.

A2.11

EVOLUTION OF DIFFUSION AND SPUTTER LIMITED IMPLANTED IMPURITY DEPTH PROFILES DURING ION BEAM SYNTHESIS. P L F Hemment, A K Robinson, U Bussmann, K J Reeson, Department of Electronic and Electrical Engineering, University of Surrey, Guildford, Surrey, GU2 5XH, UK; R Chater and J A Kilner, Department of Materials, Imperial College, London, UK.

The formation of compounds (eg SiO_2 , CoSi_2) by the implantation of high doses ($\geq 10^{18} \text{ cm}^{-2}$) of reactive ions is recognised as an important enabling technology for future generations of high performance microelectronic devices (eg CMOS/SIMOX). In order to develop predictive models describing the formation of these materials it is necessary to quantify the effects of sputtering, volume changes due to compound formation, radiation enhanced diffusion and segregation.

In this paper a systematic study of the effects of sputtering is reported. The evolution of profiles, where either sputtering or diffusion are the dominant mechanisms, have been studied by implanting reactive and chemically inert ion species into low sputter rate (bulk silicon) and high sputter rate (SiO_2 on Si) substrates. Depth profiles of $^{16}\text{O}^+$, $^{18}\text{O}^+$, N^+ , C^+ and Ar^+ ions implanted into (100) silicon to doses in the range 10^{17} to 10^{18} cm^{-2} at temperatures of up to 550°C have been determined by SIMS and RBS. The sensitivity of the implanted depth profiles to the values of physical parameters has been investigated using a computer model and the assumptions which must be made to achieve a good agreement with experimental profiles will be discussed.

A2.12

FORMATION OF BURIED AND SURFACE CoSi_2 LAYERS BY ION IMPLANTATION. M.F. Wu, A. Vantomme, G. Langouche, IKS, University of Leuven, Belgium; K. Maex, J. Vanhellemont, IMEC, Leuven, Belgium; J. Vanacken, H. Vloeberghs and Y. Bruynseraede, VSM, University of Leuven, Belgium.

The formation is studied of buried CoSi_2 layers and surface CoSi_2 layers formed by high dose ion implantation in an energy range of 30 to 160 keV, combined with conventional furnace annealing or with rapid thermal processing. The crystalline quality, the phase of the buried and surface silicide layers, the abruptness of the interfaces and the electrical transport properties are studied by RBS, channeling, cross-sectional TEM, Mössbauer spectroscopy and resistivity measurements. The stability of the buried and surface CoSi_2 layers at temperatures between 1000°C and 1200°C is also studied and compared with the results for MBE grown samples.

Low energy (30 keV) implantations with a dose of $5 \times 10^{16} \text{ atoms/cm}^2$ gave rise to continuous buried CoSi_2 layers as thin as 20 nm with good crystalline quality. High dose implantations, on the other hand, gave rise to surface CoSi_2 layers with crystalline quality and electrical properties comparable to those of MBE grown samples or buried CoSi_2 layers. It was found that buried CoSi_2 layers had better thermal stability than surface CoSi_2 layers with similar thickness. The disintegration was found to start by void formation at both CoSi_2/Si edges.

A3.1

ION-BEAM MIXING AND PHASE FORMATION.

L-U. Aaen Andersen, J. Böttiger, K. Dyrbye, and J. Janting, Institute of Physics, University of Aarhus DK-8000 Aarhus C, Denmark

The phase formation during ion-beam mixing of binary transition-metal alloys have been studied by use of 500-keV Ar^+ and Xe^+ and 200-keV Ne^+ in the temperature range 30-723 K. Especially the composition ranges, where only amorphous phases occur, i.e., the glass-forming ranges, have been investigated. Based on semiempirical data on free energies, metastable phase diagrams have been constructed and glass-forming ranges esti-

mated for the case of negative heat of mixing. Taking into account the quite large uncertainties of the applied thermodynamic data, reasonable agreement is observed between estimated and experimental glass-forming ranges.

In the case of positive heat of mixing, the initial thin-film structure is near thermodynamic equilibrium. However, for small values of the heat of mixing, it is still possible to form amorphous structures. In the absence of chemical driving forces, this formation cannot be explained in a similar way as in the case of negative heat of mixing.

As the nucleation of crystalline phases may differ with and without irradiation, irradiation of amorphous structures at elevated temperatures may create new metastable phases. Preliminary measurements of crystallization of metallic-glass films during irradiation are reported.

A3.2

THERMODYNAMIC ASPECTS OF ION MIXING IN METALLIC SYSTEMS. W.L. Johnson, 138-78 Keck Laboratory, California Institute of Technology, Pasadena, CA 91125 USA

Recent studies have clearly demonstrated that phenomena such as ion mixing in solids are in many cases dominated by events occurring in the late stages of collisional cascades, the so-called "quasithermal" or "thermal spike" stage.[1,2] In the case of all but the very low Z metals, it has been shown that ion mixing events take place predominantly in this regime. As a consequence, it has been found that thermochemical parameters must be incorporated into a description of compositional profiles and phase equilibria in ion irradiated materials. Studies of ion mixing in metal bilayers have led to the development of a phenomenological model of ion mixing which incorporates these thermochemical effects. The model has been tested in a wide variety of binary metal systems and found to give an excellent account of mixing in all but very low Z metals. The limits of validity of the model and its extension to nonmetallic systems will be discussed.

1. W.L. Johnson, in "Materials Modification by High-Fluence Ion Beams", eds. R. Kelly and M. Fernanda da Silva, NATO ASI series, (Kluwer Academic Publishers, Dordrecht, Boston, London, 1987), p. 405.

2. Y.T. Cheng, W.L. Johnson and M-A. Nicolet, Phys. Rev. Lett. **58**, 2083 (1987).

A3.3

CRITICAL TEMPERATURES FOR RADIATION ENHANCED DIFFUSION AND EQUILIBRIUM PHASE FORMATION DURING ION BEAM MIXING. A.M. Vredenberg, R. de Reus, A.C. Voorrips, H.C. Tisink and F.W. Saris, FOM-Institute for Atomic and Molecular Physics, Kruislaan 407, 1098 SJ Amsterdam, The Netherlands.

It is well known that in ion mixing two different temperature regimes are observed. Up to a critical temperature, T_c , ion mixing is almost temperature independent and may be characterized by a thermal spike model. For many systems ion mixing in this temperature regime leads to metastable alloy phases. Above T_c ion mixing becomes radiation enhanced and may be characterized by a thermally activated diffusion process. Although atomic mobility is enhanced, however, equilibrium phases do not necessarily form at these elevated temperatures.

In this paper we have compared T_c with the formation enthalpy of a hole of the size of the smaller constituent. A clear correlation was found, which implies, that at T_c the smaller atom becomes (thermally) mobile, leading to higher mixing rates, but not necessarily to equilibrium phases. For equilibrium phases to form, mobility of both constituents is required. Therefore, T_x , the temperature above which equilibrium phases will result from ion mixing, should be correlated with the formation enthalpy of a hole of the size of the larger atom. Thus, for every system a temperature window $T_c - T_x$ can be calculated from the hole formation enthalpies of

the constituents, in which ion induced mixing is enhanced, but metastable phases may still form.

Experimental support for the correlation between T_x and the larger-hole formation enthalpy was found by determining the crystallization temperatures, T_x , of amorphous Ta-Pd, Ni-Zr, Fe-Zr and Au-Zr mixtures under Xe or Ar bombardment.

A3.4

DIRECT OBSERVATION OF INTERMIXING IN GaAs/AlAs MULTILAYERS AFTER VERY LOW-DOSE ION-IMPLANTATION. *M. Bode, A. Ourmazd and J. Rentschler, AT&T Bell Labs, Holmdel, NJ 07733, M. Hong, L.C. Feldman and J.P. Mannaerts, AT&T Bell Labs, Murray Hill, NJ 07974.*

We combine chemical lattice imaging and digital vector pattern recognition to study, quantitatively, kinetic intermixing in GaAs/AlAs multilayers. We thus obtain, with atomic plane resolution and near-atomic sensitivity, composition profiles across each interface of the multilayer stack before and after ion-implantation. Our results show significant intermixing even when only one 320 keV Ga⁺ ion is implanted at 77 K into each 2000 Å² area of the interface. This corresponds to an incident ion dose of $5 \times 10^{12}/\text{cm}^2$.

The intermixing is not uniform along the interface. At each interface, we observe more intensely intermixed regions, whose widths correspond to those created by the damage track of a single implanted ion, as expected from Monte-Carlo simulations. It thus appears that we can directly image intermixing due to single energetic ions implanted into the multilayered GaAs/AlAs structure.

A3.5

A STUDY OF THE DOMINANT MOVING SPECIES IN ION BEAM MIXING I: EFFECTS OF SAMPLE GEOMETRY AND ATOMIC MASS. *G. W. Auner,* Y.-T. Cheng,** M. E. Alkisi,** and K. R. Padmanabhan***

* General Motors Research Laboratories, Warren, Michigan 48090.

** Department of Physics and Astronomy, Wayne State University, Detroit, Michigan 48202.

The factors determining the dominant moving species in ion mixing, such as the sample geometry, atomic mass, and thermodynamic parameters, have not been clarified. In order to identify the effect of sample geometry and atomic mass on the dominant moving species during ion beam mixing, bilayer samples with zero heats of mixing and similar cohesive energies were investigated using imbedded markers and Rutherford backscattering spectrometry. Samples with Hf on top of Zr and Zr on top of Hf irradiated with 150 keV Kr ions showed a small preferential inward movement of the top layer species with respect to the large amount of total mixing, regardless of species mass. This indicates that the dominant moving species in ion beam mixing is the result of a non-isotropic atomic transport determined by sample geometry instead of atomic mass.

A3.6

RELATIONSHIPS BETWEEN COHESIVE ENERGY, DEBYE TEMPERATURE, AND THE ONSET OF TEMPERATURE-DEPENDENT ION MIXING. *Y.-T. Cheng, General Motors Research Laboratories, Warren, Michigan 48090-9055.*

The mechanisms of ion mixing have been the subject of numerous studies. It is now generally accepted that collision cascade

and thermal spike effects dominate "low" temperature ion mixing, where ion mixing is basically temperature-independent. On the other hand, radiation-enhanced diffusion dominates "high" temperature ion mixing, where an Arrhenius-type temperature dependence is usually seen. A narrow temperature range defines a critical temperature T_c which separates these two regions. Two recently proposed relationships for the critical temperature T_c for the onset of radiation-enhanced diffusion in ion mixing are examined. The linear relationship between T_c and the cohesive energy E_{coh} is shown to be in agreement with experiment, while the relationship between T_c and the Debye temperature Θ_D is not. An unusual behavior of decreasing ion mixing rate with increasing temperature is also discussed.

A3.7

EFFECT OF CARBON ON ION BEAM MIXING OF FE-TI BILAYERS. *J.-P. Hirvonen and M. Nastasi, Materials Science and Technology Division, Los Alamos National Laboratory, Los Alamos, NM 87545*

Previous studies have shown that the mixing rate of evaporated carbon with iron and titanium is minimal in the temperature independent regime. In addition, in the nickel-silicon system, a thin evaporated carbon layer completely prevented mixing. Both of these results are at least in qualitative agreement with the thermodynamical model of ion beam mixing. However, the microscopic mechanism of this retarding of mixing is not understood.

In this work a bilayer Fe-Ti structure was implanted with a trace amount of ¹³C. The implantation energies were selected in such a way that the mean range of carbon ions was located either in the iron or in the titanium layer. The effect of this implanted carbon on mixing with 300 keV Ar⁺ ions was studied in the temperature range from 0 to 300 C using Rutherford backscattering spectroscopy at an energy of 5 MeV. The measurements revealed that mixing was not affected by carbon implanted into the titanium layer. However, carbon in the iron layer remarkably retarded mixing at all temperatures investigated. Changes in carbon concentration profiles were probed utilizing the resonance of the nuclear reaction ¹³C(p,γ)¹⁴N at a proton energy of 1.748 MeV. The results will be discussed in terms of the mobility of carbon as well as the defect-carbon interaction in the metals involved.

A3.8

THE EFFECT OF SURFACE COATING ON ION BEAM DESORPTION OF HYDROGEN FROM TITANIUM. *Richard E. Wistrom, Peter Børgesen, and Herbert H. Johnson, Materials Science and Engineering, Cornell University, Ithaca, NY 14853.*

Previous investigations reported that the mixing rate of Fe/Ti was reduced by a factor of 7 if the sample was charged with hydrogen. The mixing rate of similar samples of Ni/Ti was only reduced by a factor of 2. Hydrogen was lost from the samples during mixing. The hydrogen loss rate was significantly greater from Ni/Ti than from Fe/Ti.

Experiments were performed to determine whether the difference in mixing rates causes the difference in hydrogen loss rates or vice versa. Ti samples were coated with either Fe or Ni, hydrogen charged, and

irradiated with ions typically used for mixing. Hydrogen loss was measured as a function of irradiation fluence. Results provide an important clue as to how hydrogen reduces mixing rates.

A3.9

ION-BEAM MIXING AND TRIBOLOGY OF Fe/B MULTILAYERS.* RenYuan Hu, L. E. Rehn, G. R. Fenske and P. M. Baldo, Argonne National Laboratory, Argonne, IL 60439

Interdiffusion of Fe and B was studied during 1.5 MeV Kr ion bombardment. The square of the interdiffusion distance during mixing at 573 K was found to depend linearly on the irradiation dose. Arrhenius behavior with an apparent activation enthalpy of 0.7 eV was observed between 475 and 770 K. Electron microscopy of ion-beam mixed multilayer specimens revealed many crystalline iron-boride compounds, e.g. Fe₂B and Fe₃B, and an amorphous phase. Substantially improved adhesion and reduced friction were observed for ion-beam mixed Fe/B multilayers on M50 steel substrates.

*Work supported by the U.S. Department of Energy, Basic Energy Sciences-Materials Sciences and ECUT/Tribology Program under Contract #W-31-109-ENG-38.

A3.10

ION BEAM MIXING OF Sb SCHOTTKY CONTACTS ON n-Si. J.B. Malherbe, L.J. Bredell, K.P. Weimer, G. Myburg and E. Friedland, Department of Physics, University of Pretoria, Pretoria, 0002, South Africa.

Thin (100 nm) antimony Schottky contacts on n-Si have been bombarded with 100 and 120 keV Si⁺ ions, with doses ranging from 5×10^{13} to 1×10^{16} Si⁺ cm⁻². The extent of ion beam mixing has been determined by AES depth profiling and RBS. α -particle channeling has been employed to study the radiation damage caused by the bombarding ions in the silicon substrate. The ion bombardment had a pronounced effect on the electrical characteristics of the Schottky contacts. Changes in the ideality factor, Schottky barrier height and series resistance of the contacts are correlated to the AES, RBS and channeling results.

A4.1

ION-SOLID INTERACTIONS AS VIEWED BY MOLECULAR DYNAMICS. Barbara J. Garrison, Department of Chemistry, The Pennsylvania State University, University Park, PA 16802.

A microscopic picture of the ion-solid interactions as determined by molecular dynamics simulations will be presented. We plan to discuss examples from simulations on silicon^{1,2} and on rhodium³. In the case of Si we have investigated the process as a function of the primary particle energy. For 5-10 eV Si atom bombardment we find that the dimers on the Si{100}(2x1) face can be directly opened with the bombarding particle inserting into the dimer in the epitaxial position. As the energy increases to 15-20 eV, implantation begins to occur. For keV Ar bombardment we have found that the openness of the crystal controls many aspects of the ejection process including the depth of origin and the energy distributions of the ejected species. For both ejected Si and Rh atoms, the original crystal structure plays a dominant role in influencing their angular distributions. A combined theoretical-experimental approach has allowed us to determine the site and coverage of oxygen on Rh{111}.

1. B. J. Garrison, M. T. Miller and D. W. Brenner, Chem. Phys. Lett. **146** 553 (1988)

2. R. Smith, D. E. Harrison, Jr. and B. J. Garrison, Phys. Rev. B **40**, (July 1989).
3. C. T. Reimann, M. El-Maazawi, K. Walz, B. J. Garrison, N. Winograd and D. M. Deaven, J. Chem. Phys. **90** 2027 (1989).

A4.2

COMPUTER SIMULATION OF IMPURITY SEGREGATION AT A RAPIDLY MOVING SOLID-LIQUID INTERFACE. Stephen J. Cook and Paulette Clancy, Chemical Engineering Department, Cornell University, Ithaca, NY 14853.

A recently developed Non-Equilibrium Molecular Dynamics simulation method¹ has been used to study the thermodynamic and kinetic properties for alloyed materials undergoing rapid melting and subsequent resolidification, as occurs for example in laser annealing. Results will be presented for Lennard-Jones and Stillinger-Weber models of "alloys", A_xB_{1-x}, as paradigms of metal alloys and semiconductor alloys respectively. The two models exhibit strikingly different interface morphologies and hence form an interesting comparison. The effect of size differences between the solute B and substrate A atoms are studied for both the Lennard-Jones and Stillinger-Weber materials, as size is believed to play an important role in the enhanced partitioning of solute atoms at a rapidly moving interface, i.e. "solute trapping". Properties studied include calculations of the non-equilibrium segregation coefficient, k', and the interface position, velocity and temperature as a function of time. A computer graphics analysis highlights the nature of the interface morphology, the presence of defects and the occurrence of surface disorder.

1. D.K. Chokappa, S.J. Cook and P. Clancy, Phys. Rev. B., **42**, May 15 issue (1989).

A4.3

MOLECULAR DYNAMICS SIMULATIONS OF LOW-ENERGY ION/SURFACE INTERACTIONS DURING VAPOR PHASE CRYSTAL GROWTH: 10 eV Si INCIDENT ON Si(001)2x1. M. Kikabatake, P. Fons and J. E. Greene, CSL, University of Illinois, 1101 W. Springfield, Urbana, IL 61801.

Low-energy ion-irradiation is commonly used for modifying film microstructure and microchemistry during film growth by a variety of techniques including sputter deposition, plasma-assisted CVD, and MBE. We have used molecular dynamics simulations to investigate atomic-level phenomena associated with low-energy ion/surface interactions. In this paper, we present results for 10 eV Si ions incident on reconstructed Si(001)2x1 surfaces. Calculation of the positions and velocities of all atoms in the computational cell (up to 1000 atoms) were carried out using the many-body Tersoff potential for time steps of 1 femtosecond out to 0.8 picoseconds at which time all violent effects (collision cascade) subsided. Using the Tersoff potential, the (2x1) surface reconstruction was found to be stable with an energy gain of -0.61 eV per surface atom compared to the unreconstructed (1x1) surface. The sound velocity calculated by kinetic energy transfer in the z-direction was 80 Å/ps in good agreement with experimental data. 10 eV Si irradiation was sufficient to open surface dimers and result in an average maximum penetration depth, for normally incident ions, of 0.88 Å (72% of the distance from the surface to the 2nd layer). The number of defects produced per incident ion at 0 K was ~0.8. The nature of these defects (primarily split interstitials, hexagonal interstitials, and broken dimers) and their annealing characteristics as a function of temperature were investigated. No vacancies were observed, consistent with a Si atom displacement energy of 13-17 eV. Finally, ion-irradiation-induced epitaxial growth was observed when the incident ion interacted strongly with surface dimers.

A4.4

MOLECULAR DYNAMICS STUDY OF THE AMORPHIZATION OF CuTi. Michael J. Sabochick, Dept. of Engineering Physics, Air Force Institute of Technology, Wright Patterson AFB, OH 45433; Nghi Q. Lam, Materials Science Division, Argonne National Laboratory, Argonne, IL 60439.

It is well known that many alloys can be amorphized with electron and/or ion irradiation. Experiments on a variety of alloys have resulted in some generalizations about the phenomenon. For example, amorphization takes place at temperatures that are too low for long-range diffusion to occur; the onset of amorphization coincides with a volume expansion of a few percent; and alloys which do become amorphous obey certain laws regarding composition, structure, and the relationship between the components in the periodic table. Nevertheless, the fundamental cause of amorphization, whether it is due to chemical disordering or the introduction of lattice defects, is still not understood.

The purpose of the present work was to investigate this question by simulating the amorphization of a gamma-phase CuTi compound on the computer. An interatomic potential for this phase was developed using the embedded-atom method, and the heat of solution, density, and structure of the phase were reproduced within less than one percent. Two different approaches to amorphization were tried: one in which Cu and Ti atoms were randomly exchanged, and another in which Frenkel pairs were introduced at random. As atoms were exchanged with the first approach, many of the sharp peaks in the radial distribution function (RDF) were reduced, and some disappeared. Nevertheless, the RDF retained many peaks, suggesting that the alloy was chemically disordered but not amorphized. With sufficient numbers of lattice defects introduced with the second approach, the system experienced a volume expansion of about 2.3%, and an increase in potential energy of about 0.07 eV per atom. At about 0.2 dpa, the RDF lost almost all structure beyond the first nearest neighbor, indicating that the alloy had become amorphous, in agreement with experiment. Based on these results, the relative significance of chemical disordering versus the introduction of lattice defects in causing amorphization in alloys will be discussed.

A4.5

MOLECULAR DYNAMICS SIMULATIONS OF THE DISORDER FORMED IN SILICON BY HIGH-ENERGY ELECTRONS. A.M. Mazzone C.N.R.-Istituto LAMEL, Via de' Castagnoli 1 - 40126 Bologna, Italy.

Electron-phonon coupling is a point of major interest in many relaxation processes such, for instance, are the ones following high-energy implants or the passage of fission fragments.

In this work we present a molecular-dynamics simulation of the disorder generated in a silicon lattice by the passage of electrons with an energy well above the Fermi sea. The electrons are injected into the lattice at a given time and the lattice evolution is followed for times corresponding to typical phonon frequencies. The energy losses of the incoming electrons are accounted for by using a dielectric formulation. The interaction between these electrons and lattice atoms and the coupling between the lattice atoms are described by suitable interatomic potentials.

The work analyzes the influence on the lattice disordering of the various physical parameters of the process.

A4.6

SUPERHEATING AND SUPERCOOLING OF LEAD INCLUSIONS IN ALUMINIUM. E. Johnson¹, L. Gråbæk², J. Bohr², A. Johansen¹, L. Sarholt-Kristensen¹ and H.H. Andersen¹. ¹Physics Laboratory, University of Copenhagen, Denmark, ²RISØ National Laboratory, 4000 Roskilde, Denmark.

Ion implantation at room temperature of lead into aluminium leads to spontaneous phase separation and formation of lead precipitates growing epitaxially with the matrix. Unlike the highly pressurised solid noble gas inclusions, the pressure in the lead precipitates is indistinguishable from ambient.

Small implantation-induced lead precipitates embedded in an aluminium matrix were studied by X-ray diffraction. The (111) Bragg

peak originating from the lead crystals was followed during 4 temperature cycles, from room temperature to 678 K. The melting temperature for bulk lead is 601 K. In the first heating cycle we found a superheating of the lead precipitates of 47 K before melting occurred. During subsequent cooling a supercooling of 24 K below the solidification point of bulk lead was observed. In the subsequent heating cycles this hysteresis at the melting transition was reproducible. The full width of the hysteresis loop slowly decreased to 51 K while the mean size of the inclusions gradually increased from 14.3 nm to 23.0 nm. The phenomena of superheating and supercooling are thus most pronounced for the small crystallites. The persistence of the hysteresis loop over successive heating cycles demonstrate that its physical existence is genuine, and it is believed that it originates from the lack of free surfaces of the lead inclusions.

A4.7

THERMAL ANNEALING OF SOLID Kr PRECIPITATES IN Ni. R. C. Birtcher, J. Rest and D. S. Bergstrom, Argonne National Laboratory, Argonne, IL 60439

After implantation into Ni at room temperature, Kr condenses within small cavities as an fcc solid aligned with the Ni lattice. Evolution of these precipitates during subsequent thermal annealing to temperatures above 500°C has been followed with transmission electron microscopy. The results will be contrasted with precipitates produced by implantation at 500°C.

When Kr is implanted into Ni at 500°C, the precipitate size distribution is bimodal. The small precipitates are solid Kr and the large ones are faceted and nonsolid. Modelling with rate theory suggest that during the implantation solid Kr precipitates are immobile while nonsolid precipitates migrate by surface diffusion.

Room temperature implantation results in small solid Kr precipitates. Annealing to temperatures below 400°C after room temperature implantation produces a small upward shift in the monomodal size distribution and a decrease in the average, solid Kr density within the precipitates. Annealing above 500°C leads to precipitate coalescence that eliminates all small precipitates and results in large faceted cavities. The behavior of Kr atoms and precipitates during precipitation and annealing will be discussed on the basis of results from rate theory modelling.

*Work supported by U.S. DOE, Basic Energy Sciences-Materials Sciences under Contract #W-31-109-ENG-38.

A5.1

FABRICATION OF CRYSTALLINE-AMORPHOUS SUPERLATTICES BY DIFFERENTIAL ION-BEAM DAMAGE. J. M. Poate, D. J. Eaglesham, D. C. Jacobson, M. Cerullo, L. N. Pfeiffer, and K. W. West, AT&T Bell Laboratories, Murray Hill, NJ.

A study is presented of the build-up of ion-beam damage in multilayers and superlattices of elemental and compound semiconductors. MBE-grown superlattices of GeSi-Si and GaAs-AlAs are implanted with MeV ions and the build-up of damage is studied using a combination of RBS and channeling and TEM. The appearance of defects and amorphous regions in these layers is studied as a function of dose, implantation temperature, implanted species and layer compositions. It is shown that, where there is a significant difference in the damage rates for two materials, damage can be located almost entirely within the faster-damaging layer (i.e. damage occurs in GaAs and GeSi, respectively). In the case of GeSi-Si superlattices, damage is distributed evenly across a single layer, with no visible proximity effects at the interfaces. In GaAs-AlAs superlattices, on the other hand, damage is initiated at the center of the GaAs layers, and regions near the heterointerfaces require doses up to an order of magnitude higher to produce equivalent damage.

The distinction between these two systems is discussed in terms of the processes and migrating species involved in the build-up of damage. Finally, we show that for both GeSi-Si and GaAs-AlAs it is possible to create an amorphous-crystalline superlattice before the onset of significant damage in the slower-damaging layer.

A5.2

INTERNAL BLACKBODY EMISSION INTERFEROMETRY FOR MEASUREMENT OF CRYSTALLIZATION KINETICS AND OPTICAL PROPERTIES OF THIN FILMS. I.A. Roth and G.L. Olson, Hughes Research Laboratories, Malibu, CA.

The spectral emissivity of a semi-transparent thin film on a heated substrate varies with film thickness due to optical interference within the layer. This leads to oscillations in the emitted blackbody radiation intensity when the film thickness changes with time. Analysis of the time dependent change in emission intensity can be used to accurately determine the solid phase crystallization rate of an amorphous thin film or to obtain the growth rate of a film during vacuum deposition. In addition, since the blackbody emission spans a wide spectral range, the wavelength dependence of the emission can be used to obtain the absorption coefficient and index of refraction of an amorphous layer as a function of wavelength and temperature. In this paper we show how internal blackbody interferometry has been used to measure the crystallization kinetics and infrared optical properties of ion-implanted amorphous silicon and amorphous germanium thin films on crystalline substrates. A comparison of the blackbody emission interferometry data with time-resolved reflectivity measurements at 0.6328 μm and 1.15 μm shows that the blackbody emission results can be understood in terms of a straightforward optical model.

A5.3

TRANSITION RADIATION FOR SURFACE ANALYSIS. John M. Macaulay and Julius J. Muray, SRI International, 333 Ravenswood Ave., Menlo Park, CA 94025

The electron beam - material interaction gives rise to secondary electrons, backscattered electrons, cathodoluminescence, etc., all of which are used for analytical purposes. The interaction also produces transition radiation — dipole radiation produced by the movement of an energetic charged particle across an interface between two dielectrics (see, for example, M. L. Ter-Mikaelian 1972[†] for a full discussion). This paper reports on our investigation of the use of transition radiation, at optical wavelengths, for surface analysis.

We have used electron beams with energies up to 100 keV to produce transition radiation from metals, doped and undoped semiconductors, and insulators. The radiation is passed through a polarizer and a spectrometer — allowing a suitable spectral range to be determined for collecting transition radiation, in which luminescence, etc. is not observed. The low light levels, typical of transition radiation produced under these conditions, require the use of a single photon counting photomultiplier tube. The spectra are stored on a computer disk.

Theoretical transition radiation spectra are calculated, using published dielectric data, and are compared with the experimental spectra.

Experimental data from nanometer - thick surface layers and ion beam modified surfaces are presented and discussed. The depth and lateral resolutions of the technique are considered.

[†] M. L. Ter-Mikaelian 'High-Energy Electromagnetic Processes in Condensed Media' 1972 (Wiley - Interscience : New York)

A5.4

STM INVESTIGATIONS OF GRAPHITE SURFACES PREPARED BY 5 keV Ar⁺ ION BOMBARDMENT. Elliott A. Eklund, UCLA Dept. of Physics and Solid State Science Center, Los Angeles, CA; Eric J. Snyder and R. Stanley Williams, UCLA Dept. of Chemistry, Los Angeles, CA.

The processes of ion beam sputter deposition and sputter etching are used quite extensively in thin film growth and surface analysis. Despite increasing interest in this area,

the basic physics of these processes is still rather poorly understood.

In this study, the STM has been used to investigate surfaces of graphite prepared by 5 keV Ar⁺ ion bombardment. Several different surfaces have been prepared with sputtering rates from 2.4×10^{13} ions/cm²-sec. to 8.9×10^{14} ions/cm²-sec. while keeping the total dose of ions constant. STM images were taken in the constant height mode both before and after the sputter etching. The images of the ion bombarded graphite samples show a definite dependence of surface roughness on the rate of ion beam etching.

In addition, several images of different scale, ranging from $25\text{\AA} \times 25\text{\AA}$ to $500\text{\AA} \times 500\text{\AA}$, were taken for each sputtering rate used. This series of images shows that the surfaces produced have a self-similar or fractal nature. It is believed that results obtained with sputter etching, while important in themselves, also provide direct insight into the topography of surfaces that can be produced by ion beam sputter deposition. It is now clear that the sputtering rate plays a crucial role for both processes.

A6.1

GRAIN GROWTH AND PHASE FORMATION IN ION IRRADIATED/ANNEALED THIN NI-AL ALLOY FILMS. Dale E. Alexander and Gary S. Was, University of Michigan, Ann Arbor, MI, 48109; and Lynn Rehn, Argonne National Laboratory, Argonne, IL, 60439.

Ion irradiation and anneal studies have been performed on Ni, Ni-20 at.%Al multilayers and Ni-20 at.%Al co-evaporated thin films. Ni⁺, Kr⁺ and Xe⁺ ions were used to irradiate the films and homogenize the multilayers at room temperature. Irradiation of the alloy films resulted in the formation of a metastable, supersaturated solid solution of gamma phase and an HCP phase. Ion induced grain growth was observed and followed a power law dependence with dose. The presence of Al enhanced grain growth in alloy films. A factor of 2 greater grain growth was observed in Ni-Al multilayers compared with co-evaporated films irradiated to the same dose with the same ion species. Post irradiation annealing of the ion beam mixed samples at 450°C for 1 hour resulted in the formation of a dual phase gamma-gamma prime structure in which distinct, approximately equal size grains of both phases were identified. In order to understand the mechanism of the dual phase formation from a supposed compositionally homogenous film, a careful STEM characterization of the microstructure was undertaken following irradiation, both during and after annealing. CBED and ultra-fine probe EDS analyses were used to analyze the structure and composition of individual grains within the microstructure.

* This work supported under NSF grant DMR-8603174 and under DOE contract W-31-109-ENG-38.

A6.2

CESSATION AT HIGH TEMPERATURE OF RADIATION INDUCED DIFFUSION: THE ROLE OF DEFECT COMPLEX FORMATION. T.D. Andreadis and Mervine Rosen, Naval Research Laboratory, Washington DC, 20375-5000.

Recent work involving the ion bombardment of multi-layer NiAg indicates that radiation induced diffusion of Ag ceases when the temperature is increased from room temperature to 100° C. It has been speculated that this behavior is brought about by the dissociation at this temperature of a defect complex containing Ag which is responsible for the migration of Ag. Binding, formation, and migration energies of defects and complexes are calculated using Embedded Atom Potentials in Molecular Statics calculations. We investigate the diffusion of such defect complexes as a function of temperature.

A6.3

VOID DENSITY REDUCTION DURING ION ASSISTED DEPOSITION.
T.D. Andreadis, R.H. Bassel, Mervine Rosen, and J.A. Sprague, Naval Research Laboratory, Washington, DC, 20375-5000.

Computer simulations were used to examine the reduction of voids by thermal diffusion and athermal collision cascade mechanisms taking place during the Ion Beam Assisted Deposition (IBAD) of Ge films. Reduction of void density is of interest since it is accompanied by strengthened attachment of the deposited film to the substrate below. Void reduction may be accomplished by the trapping of collision cascade atoms in the void.

Simulations were made using the collision cascade code MARLOWE with realistic void size distributions to examine the reduction of void sizes solely due to the collision cascade and athermal vacancy-interstitial annihilations. The diffusion of residual interstitials and vacancies have been investigated.

A6.4

STUDIES ON ION SCATTERING AND SPUTTERING PROCESSES RELEVANT TO ION BEAM SPUTTER-DEPOSITION OF MULTICOMPONENT THIN FILMS: Q. Augello,^{1,2} M.S. Ameen,¹ A. R. Krauss,³ and A. I. Kingon.¹

(1) North Carolina State University, Department of Materials Science, Raleigh, NC 27665-7907. (2) Microelectronics Center North Carolina, RTP, NC 27709-2889. (3) Argonne National Laboratory, Chemistry Division, Argonne, IL 60439.

Several groups are now using high current (20-100 ma)/ low energy (1000-2000 eV) ion beams to deposit high T_c superconducting films by ion beam-induced sputtering of either bulk superconductor (i. e., $YBa_2Cu_3O_{7-\delta}$) or elemental (Y, Ba, Cu, etc.) targets. This technique is also being used for deposition of ferroelectric and optoelectronic ($KNbO_3$ for example) thin films. We are using a novel computer-controlled ion beam/rotatable target holder sputter-deposition technique, which involves sequential irradiation of elemental materials or their oxides. However, little information is available on basic ion scattering and sputtering processes occurring during deposition and their influence on film characteristics at these beam energies and ion fluxes. As part of our extensive research program on thin films related to materials mentioned above, we have performed computer modelling and made experimental measurements on sputtering and ion scattering using Ar^+ , Kr^+ , and Xe^+ ion beams on Y, Ba, Cu, KO_2 , Nb_2O_5 targets. The beam energy was varied from 1000-2000 eV and the angle of incidence was either 45° or 0° with respect to the target normal.

The data shows that, for 45° ion incidence on the target, significant gas incorporation and resputtering of the deposited film due to ion scattering occurs at the specular position, and substantially decreases towards the surface normal. The result is dependent on the mass of the incident ion and target atom, with Ar on Ba showing the most pronounced effects. The ion scattering effects were seen to diminish at normal incidence for all ion/target combinations. The sputtering yield is larger for polar angles in the range of specular reflection up to and including the surface normal for 45° bombardment.

The results above, coupled with measurements of the spatial distributions of sputtered species, have been used to determine the optimum deposition geometry and beam characteristics for ion beam sputter-deposition of high T_c superconducting and optoelectronic films.

A6.5

INTERACTIONS OF LOW-ENERGY METAL IONS WITH SURFACES.
P. Bai, Ch. Steinbruechel, and T.-M. Lu, Center for Integrated Electronics, Rensselaer Polytechnic Institute, Troy, NY 12180.

Recently, a growing number of techniques have employed self-ions, i.e., the ions derived from the deposition materials themselves, to concurrently bombard the surface during thin film growth in order to modify the film properties such as adhesion, impurity content, orientation, and epitaxy. The ion/atom ratio used in these techniques ranges from less than one percent to one hundred percent with the ion energy varying between a few eV and several keV. In this paper, we calculate the energy dependence of the self sputtering yield for metals based on a modified Sigmund linear cascade model. The results are compared to the existing experimental data and the results obtained from a Monte Carlo computer calculation (TRIM) on the self sputtering of carbon and copper. When the self sputtering yield is bigger than one, for a given ion energy there exists a critical ion/atom ratio above which there is no net deposition. The critical ion/atom ratio is plotted as a function of the ion energy for different materials. The

sputtering yield for surface impurities such as oxygen, carbon, and hydrogen by the incident metal ions is also studied. For a fixed density of impurities (oxygen and hydrocarbon) sitting on the surface, the minimum ion/atom ratio required to remove them is plotted as a function of the ion energy. Impurity removal at the growing surface during deposition is crucial in controlling the orientation and epitaxy of the films.

A6.6

ELECTRON BEAM INDUCED HOLE-DRILLING AND LITHOGRAPHY ON A NANOMETRE SCALE IN Al, MgO AND a- AlF_3 IN A STEM. Tim J. Bullough, Colin J. Humphreys and Robert W. Devenish, Department of Materials Science and Engineering, University of Liverpool, Liverpool L69 3BX, England.

A wide variety of materials including metals, alloys, semiconductors and ionic inorganic thin films which are inert under the electron beam in a conventional transmission electron microscope have been found to become damaged and/or "drill" under the high current density focused electron probe in a dedicated scanning transmission electron microscope operating at 100 kV. Typically, holes 1-5 nm in diameter can be formed in crystals many tens of nanometres in thickness. Controlled movement of the electron beam can produce features analogous to conventional lithographic structures but on a nanometre scale. Results of hole drilling experiments on Al, MgO and a- AlF_3 will be presented and possible mechanisms discussed.

In Al, holes ~5 nm in diameter initially form at the electron entrance surface, growing towards the electron exit surface with a row of dislocation loops distributed along the electron beam path. In contrast, faceted square cross-section holes in MgO grow in from the electron exit surface. Surfaces of MgO crystals can be atomically reconstructed and smoothed by scanning of the electron beam.

Holes form in a few milliseconds under the electron beam in many ionic inorganic evaporated thin films such as a- AlF_3 . By careful analysis of X-ray spectra acquired during hole drilling, coupled with computer control of the electron beam, it has been possible to obtain an insight into the mechanisms responsible for hole formation in such materials.

A6.7

THERMAL ANNEALING INVESTIGATION OF THE OPTICAL PROPERTIES OF $B_{1-x}N_x$ FILMS FABRICATED BY ION BEAM ASSISTED DEPOSITION. C. A. Carosella, E. P. Donovan and G. K. Hubler, Naval Research Laboratory, Washington, DC 20375-5000

The annealing behavior of the optical properties of boron nitride films ($B_{1-x}N_x$) is described for films fabricated by ion beam assisted deposition. The data are needed for the precise fabrication of coatings for optical components, such as antireflecting coatings.

Amorphous samples of boron nitride are deposited on silicon substrates. Spectra are taken from 400 to 25000 nm. and fits to the interference patterns are used to find index of refraction vs wavelength as a function of film nitrogen content. Changes in shapes of absorption bands at 7300 and 13300 nm, corresponding to BN vibrations, are monitored to indicate the onset of crystallization. Nitrogen atom fraction was varied from 0.2 to 0.5 by variation of the incident relative fluxes of nitrogen ion beam current to evaporant boron flux. The films were annealed in argon at 500 C, 700 C, 900 C and 1100 C and the measurements repeated. The systematic shifts in index of refraction with annealing temperature are described.

A6.8

MECHANISM OF ION-INDUCED SOLID-PHASE EPITAXIAL GROWTH. T.K. Chaki, Department of Mechanical and Aerospace Engineering, State University of New York, Buffalo, N.Y. 14260

A model is proposed to explain ion-induced solid phase epitaxial growth (SPEG). The crystallization is by the adjustment of atomic positions in the vicinity of the crystalline/amorphous interface due to self diffusion in amorphous solid. The driving energy of SPEG is the difference in free energies between the amorphous and crystalline solids. Irradiation increases the self diffusivity of the amorphous solid by generating point defects in the amorphous solid and thus enhances the crystallization. An expression for the velocity of epitaxial growth is derived. The model explains numerous experimental facts and at the limit of no irradiation, also gives a correct model of thermal solid phase epitaxial growth.

A6.9

STUDY OF THE ANODIC OXIDATION ON Ti AND TA6V BY ION-IMPLANTED Xe IONS MARKERS AND O⁺ TRACING TECHNIQUES. Author Heming Chen, Mingjiang Dai, Xinde Bai, Wangpei Li, Department of Material Science and Engineering, Tsinghua University, Beijing, China.

One Ion-Implanted Xe ions marker and two Ion-Implanted Xe ions markers as well as O⁺ tracing techniques are used to study the mechanism of anodic oxidation on Ti and TA6V. It is shown that in 5%wt ammonium citrate, the mechanism of anodic oxidation on Ti is very different from that on TA6V. For Ti, new oxide is mainly formed by the migration of Ti cations to the solution / oxide interface and the regions in which new oxide formed are at the solution / oxide interface and in old oxide near the interface. While for TA6V, new oxide is mainly formed by the migration of oxygen anions to the oxide / metal interface and the regions are at this interface and in old oxide near the interface. The transport numbers for Ti in solution of 1%wt KOH are calculated to reveal that temperature has an influence on it. At 3°C, its average is 0.32, while at 30°C, its average is 0.28. The current efficiency is above 99.8%. The result of AES spectrum shows that V and Al in oxide on TA6V present uniform distribution.

A6.10

CRYSTALLINE POLYMER THIN FILM DEPOSITION BY IONIZED CLUSTER BEAM. S. J. Cho, Department of Physics, Kyungseong University, Busan 608-020, Korea; H. S. Choe, Department of Physics, Kyungsang University, Jinju 660-300, Korea; H. K. Jang, S. S. Kim, C. N. Whang, Department of Physics, Yonsei University, Seoul 120-749, Korea; and D. S. Choi, Department of Physics, Kangwon University, Chuncheon 200-701, Korea.

Polyethylene (PE) and polyimide thin film are deposited by ionized cluster beam deposition (ICBD) technique. Polymerization and crystallization of PE and polyimide were investigated using TEM, FTIR and XRD, and the electronic structure of these polymer films were investigated using XPS. Films deposited at optimum ion acceleration voltage showed strong preferential crystal orientation. In the case of PE, orthorhombic structure was obtained at ion

acceleration voltage of 200V and the lattice parameter of PE film deposited by ICBD was close to that of the single crystal PE. Oxydianiline and pyromellitic dianhydride were co-deposited to fabricate polyimide film. Crystalline polyimide film was obtained at ion acceleration voltage of 700V.

A6.11

STRUCTURAL AND ELECTRICAL STUDIES OF EPITAXIAL PbTe FILMS GROWN BY ION-ASSISTED RF MAGNETRON SPUTTERING. J.G. Cook and S.R. Das, Laboratory for Microstructural Sciences, National Research Council of Canada, Ottawa, Canada K1A 0R6, and M. Phipps, Department of Physics, University of Ottawa, Ottawa, Canada K1N 6N5.

The growth of PbTe on (111) BaF₂ by means of rf magnetron sputtering has been studied. Low growth temperatures and high growth rates favour (100) growth, while high temperatures and low growth rates result in (111) growth. The application of a small negative substrate bias strongly encourages (111) growth, particularly at the lowest temperatures. With a -10V substrate bias, epitaxial (111) growth occurs at temperatures as low as 180°C. If no bias voltage is applied at such low temperatures, the growth is strongly (100) except at very low growth rates, for which it is of mixed orientation.

Hall effect studies are made on films grown at temperatures between 180°C and 400°C onto (111) BaF₂ which has been chemipolished to remove the cleavage ledges which are known to favour (100) growth. Below 180°C and without intentional doping the films are p-type, while above 300°C the films are n-type. The effect of a bias voltage on the surface morphology is examined. We also study the effect of a bias voltage applied only during the initial stages of film growth.

A6.12

OXIDATION BEHAVIOUR OF TITANIUM SURFACES COATED WITH BORON COMPOUNDS. M. Elena, L.A. Guzman, L. Moro, and A. Tomasi, Institute for Scientific and Technological Research - IRST, 38050 POVO (TN), Italy; and S. Gialanella, P. Scardi, Department of Materials Science Engineering, University of Trento, 38050 Mesiano (TN), Italy

Titanium is one of the most interesting materials for a wide range of high technology applications (e.g. in the aerospace sector, where its low density is an important characteristic). However, one of the main problems is its extremely high oxidation rate, which can limit its use especially in high temperature environments.

In the literature relatively few papers deal with this subject, and this can be understood in view of the recent widespread use of titanium in industrial applications, and to the difficulty of the task. In this paper we describe our attempts to protect titanium against oxidation using various surface treatments. In particular we have coated the metal with various compounds ranging from a Ti-B multilayer to BN, passing through TiB₂. Some films, obtained by RF sputtering, have also been ion bombarded in order to achieve a better uniformity and an increased adhesion to the substrate. In addition we have also used the Ion Beam Assisted Deposition technique (IBAD) to produce BN.

Our work shows the difficulty of obtaining an effective and complete solution to the problem of protecting titanium from oxidation, although some treatments have given promising results towards this goal.

A6.13

ION-BOMBARDMENT EFFECTS ON FILM ADHESION.* R.A. Erck, G. R. Fenske, and A. Erdemir, Materials and Components Technology Division, Argonne National Laboratory, Argonne, IL 60439

Ion-assisted processes, e.g., ion-assisted deposition (IAD), are becoming more common for the production of thin films. In IAD, a film is deposited by evaporation or sputtering while undergoing bombardment with inert or reactive energetic ions.

Good film adhesion is critical in many applications, particularly for lubricious metal films on ceramic substrates used at elevated temperatures. Many thin-film deposition techniques (e.g., evaporation) produce films with poor adhesion. Thus, energetic-beam deposition techniques such as IAD are being investigated because of their potential for improving the adhesion of the films to the substrate. Film adhesion in IAD can be improved by energetic-ion bombardment of the substrate prior to and during the start of deposition. However, the conditions (ion energy, flux, species) that produce the best adhesion at the start of deposition are not well understood.

In this work, a pull-type adhesion tester was used to measure the adhesion of various IAD films to Al_2O_3 and Si_3N_4 substrates. The effects of varying the current density and energy (100-1500 eV) of the ions (reactive and inert) are reported.

*Work supported by the U.S. Department of Energy, Energy Conversion and Utilization Technologies Division, under Contract W-31-109-Eng-38.

A6.14

CARRIER LIFETIME DISTRIBUTIONS AND RECOMBINATION KINETICS IN SILICON ON INSULATOR (SIMOX) SUBSTRATES. M A Lourenço, K P Homewood and P L F Hemment, Department of Electronic and Electrical Engineering, University of Surrey, Guildford, Surrey, GU2 5XH, UK.

Silicon on insulator (SOI) materials offer many advantages as substrates for small geometry MOS and bipolar circuits. During recent years SOI substrates formed by high dose oxygen implantation (SIMOX technology) have been shown to support high performance, fully depleted CMOS transistors and, recently, bipolar circuits also have been successfully fabricated.

During the preparation of the SIMOX substrates, involving ion implantation ($> 10^{14}$ O⁻ cm⁻²) and extended high temperature annealing ($\sim 1350^\circ\text{C}$), many defects are unintentionally introduced, which can act as trapping and recombination centres. In this paper the carrier lifetime distributions and recombination kinetics determined by Photoconductive Frequency Resolved Spectroscopy (PCFRS) are reported. Comparative measurements give lifetimes of 5 μs , 6 μs and 200 μs in bulk silicon, annealed bulk silicon and device quality SIMOX, respectively. In the annealed silicon and SIMOX the kinetics are observed to be second order whilst as expected being first order in unannealed bulk silicon.

Measurements on SIMOX material made as a function of temperature in the range 350 K to 90 K reveal a strong dependence of the lifetime distribution on temperature, confirming the dominance of carrier trapping. Trap parameters have been obtained from Arrhenius plots of the lifetime distribution and details of these will be presented.

A6.15

SPONTANEOUS VITRIFICATION OF ION MIXED METASTABLE PHASES IN IRON-BASED ALLOY SYSTEMS L.J.Huang, B.X.Liu(a) and H-D.Li, Department of Materials Science and Engineering, Tsinghua University, Beijing, 100084, CHINA; (a) also at Center of Conden-

sed Mater and Radiation Physics, CCAST(World Lab) Beijing, China.

Spontaneous vitrification was observed in some iron-based alloy films prepared by xenon ion mixing and hereafter annealed at low temperature.

It was found that the spontaneous vitrification could only be accessed when the system had a large elastic energy in addition to a pre-formed metastable phase by ion mixing. Firstly, the multilayered films were irradiated by xenon ions to certain dose and a uniform mixing was achieved. The films consisting of metastable phases were then subject to in situ annealing in transmission electron microscope to the temperature at which the metastable phases were stabilized. These films were kept at room temperature for months and re-examined again and a uniform spontaneous metastable crystalline to amorphous phase transformation was observed.

This paper presents the detailed process of metastable phase formation and transformation and the thermal stability of the observed vitrified phases. The kinetics of these phase transformations is also discussed.

A6.16

FOCUSED 0.5 MeV ION BEAM LINE WITH LOW ABERRATION QUADRUPOLE MAGNETS. Kiyotaka Ishibashi, Ken-ichi Inoue, Yutaka Kawata, Norio Suzuki, Electronics Research Laboratory, Kobe Steel, Ltd., Kobe 673-02, Japan; Mikio Takai and Susumu Namba, Faculty of Engineering Science and Research Center for Extreme Materials, Osaka University, Toyonaka, Osaka 560, Japan.

The techniques of Rutherford backscattering spectroscopy (RBS) and particle-induced X-ray emission spectroscopy (PIXE) using MeV ion microprobes are expected to play a very important role in the recent advancement of microelectronic materials and processes.

A microbeam line with 0.5 MeV helium ions has been developed and installed at the Research Center for Extreme Materials, Osaka Univ. The beam line consists of cylindrical objective slits, a magnetic quadrupole doublet with hyperbolic shaped pole pieces and a 5-axis goniometer newly designed for microchanneling measurements. A minimum beam spot size of $0.7\mu\text{m} \times 0.9\mu\text{m}$ was achieved by evaluating the spatial resolution of the secondary electron image, and a spot size of $1\mu\text{m}$ diameter with current of nearly 100pA has been steadily available. As an example of microbeam analysis, secondary electron and RBS mapping images of a $1\mu\text{m}$ gold pattern on a silicon substrate were demonstrated.

In this meeting, an optimum design of a quadrupole magnet using a 3-dimensional numerical magnetic analysis and comparison of spatial resolution between the two mapping images will be discussed.

A6.17

THE STRUCTURE AND PROPERTIES OF Ni FILMS GROWN BY ION BEAM ASSISTED DEPOSITION. R.A.Kani, G.P. Chambers, and B.D. Sartwell, Naval Research Laboratory, Code 4675, Washington DC 20375

The influence of ion bombardment on the properties of Ni thin films grown using ion beam assisted deposition has been studied for films grown under ion bombardment with high energy Ni ions (25 to 160 keV) and under Ar bombardment at

low energies (0.1 to 1.5 keV). Ni was selected for this study because it is a relatively unreactive metal. Ni and Ar ion bombardment were used in order to investigate ballistic effects with minimal influence due to compositional effects. Film microstructure was examined using transmission electron microscopy and electron diffraction. Substrates for the electron microscopy samples were single crystal sodium chloride with 7 nm of Ni deposited at 280 C. The observed microstructural characteristics include small grain size with strongly oriented crystal structure, microtwinning and a high density of defects. These features are discussed in terms of measured electrical conductivities and mass densities as a function of the ion to atom arrival ratio, ion energy, and substrate temperature. Samples prepared for electrical resistivity and density measurements were deposited on optically smooth single crystalline sapphire substrates at room temperature. Film densities were determined using step height measurements together with microbalance mass measurements; electrical conductivities were determined using the four-point-probe method. For the case of bombardment with low energy Ar ions, the mass density was observed to be strongly sensitive both to ion energy and to ion to metal atom ratio.

A6.18

Ar⁺ INDUCED INTERFACIAL MIXING IN Pd/Cu SYSTEM. H. K. Kim, Korea Standards Research Institute, Taejeon 302-340, Korea; J. H. Song, S. O. Kim, C. N. Whang, Department of Physics, Yonsei University, Seoul 120-749, Korea; J. J. Woo, Department of Physics, Chonnam University, Kwangju 500-757, Korea; and R. J. Smith, Department of Physics, Montana State University, Bozeman MT59717.

Evaporated Pd/Cu bilayer thin films are irradiated at room temperature using 80 keV Ar⁺ with doses in the range of 1×10^{15} to 1×10^{16} cm⁻². The Ar⁺ induced interfacial mixing behaviors are investigated using RBS technique, and phase formation by Ar⁺ bombardment is investigated using RBS and TEM techniques. RBS analysis shows that intermixing has occurred across the Pd/Cu interface, and the mixing variance increases with increasing dose of Ar⁺. This result agrees well with a model based on radiation enhanced diffusion mechanism. The phase of Cu₃Pd is found to be formed by Ar⁺ bombardment. This phase formation is discussed in terms of enhanced atomic mobility and thermodynamical driving force by introducing the concept of an effective heat of formation.

A6.19

IN-SITU ION BEAM MEASUREMENTS OF DEUTERIUM LOADING IN THIN FOIL ELECTROCHEMICAL CELLS. J.A. Knapp, T.R. Guillinger, M.J. Kelly, D. Walsh and B.L. Doyle, Sandia National Laboratories, Albuquerque, NM.

A key element of recent assertions of "cold fusion" has been the claim of electrochemical deuterium loading into Pd electrodes to levels exceeding 1.0 D:Pd. We have used external beam nuclear reaction analysis, in combination with electrochemical cells with a Pd foil electrode at one wall of the cell, to directly monitor the loading and unloading of D in the Pd foil as the cell is operated. Using a ³He ion beam in air, the deuterium in the outer 2 μm of the exposed Pd foil is measured using the D(³He,p) nuclear reaction. Typically, a 25 μm foil was observed to load to 0.6:1 (D:Pd) within a few minutes and reach 0.8-0.9 within several more minutes. No conditions were found which resulted in loadings higher than 0.9. Combined with reference electrode monitoring, this in-situ measurement of deuterium content for an operating Pd electrode provides a direct correlation between electrode loading and chemical

potential.

*This work was performed at Sandia National Laboratories supported by the U.S. Dept. of Energy, contract number DE-AC04-76DP00789.

A6.20

ON THE STABILITY OF METASTABLE AND AMORPHOUS PVD-COMPOUND FILMS. Otto Knotek; Frank Jungblut; Arman Barimani, Technical University Aachen, F.R.G.

Binary and quasibinary eutectic systems with small solubilities can create metastable phases as coatings using PVD-technology. They have sufficient thermal stability for tools, and for both wear- and corrosion-protection. Another special effect of those systems is the amorphous deposition from the gaseous phase. In this case, the thermal stability is increased due to the incorporation of small amounts of impurities. A specific transformation from the amorphous to the crystalline state can be achieved. Examples are given within the systems (Ti,Al)N, (Cr,Al)N and Al₂O₃. An example for the decomposition in coatings is to be given by the (Ti,Zr)N-system.

A6.21

Analysis of Elements in Fingernails by Rutherford Backscattering Spectroscopy P. Madakson IBM Research Division, Thomas J. Watson Research Center, Yorktown Heights, NY 10598.

The fingernails of several people were studied to determine the elements and their variations in composition and, with source and time. The common elements were found to be H, C, N, O, Ca and Fe. The first four elements have about the same composition for each of the fingernails studied and they do not vary significantly with time or source. In contrast, the compositions of Ca and Fe vary from person to person and with time, probably in line with changes in their amount in the body. Other elements found on some people are Bi, Si, Zn, Nb, Pb and Nd. Some of these are probably from external contamination of the fingernails and others from food or water intake.

A6.22

SECONDARY IONIZATION DURING ION BOMBARDMENT OF Rh(111), Geoffrey P. Malafsky(1) and Nicholas Winograd, Department of Chemistry, 152 Davey Laboratory, The Pennsylvania State University, University Park, PA 16802

Secondary ion mass spectrometry (SIMS) is a powerful technique for analyzing the atomic concentrations of thin films. However, SIMS is hampered by large differences in the ionization probabilities of different species. We report on the fundamental nature of the secondary ionization process during ion bombardment of a Rh(111) target. We describe the first direct comparison of measured energy and angle resolved secondary ion and neutral particle distributions from a single crystal sample. From this comparison, we identify a collisionally induced secondary ionization mechanism. This mechanism occurs during the collision cascade through certain high yield collision sequences which significantly disrupt the electronic structure of the lattice. These collision sequences produce anomalies in the energy and angular distributions of the ejected Rh⁺ ions which are not present in the Rh neutral particle distributions. The anomalous yields agree with a molecular dynamics simulation of the ion bombardment process.

(1) Present address: ONT Postdoctoral Fellow, Naval Research Lab, Code 6816, Wash, DC 20375

A6.23

ION BEAM MIXING OF MULTILAYERED Co-B THIN FILMS

G. Choe, Center for Materials Science and Engineering; R.M. Walser, Dept of Electrical and Computer Engineering. The University of Texas at Austin, Austin TX. 78712.

Magnetically soft, amorphous Co-B films, exhibiting a two-phase structure, have attracted attention because their specific morphological changes are associated with important changes in their soft magnetic properties¹. In this paper we report on investigation of the structural and magnetic properties of ion beam mixed Co-B films. Multilayered Co-B films were systematically prepared with various bilayer periods ($BP = T_{Co} + T_B$, $T_{Co}/T_B = 4$) and ratios of bilayer thickness (composition). These films were subsequently ion beam mixed with 150 keV 10^{16} Ar ions/cm². Microstructure and compositional modulation of the ion beam mixed films were investigated with TEM/TED, Auger depth profiling, and x-ray diffraction.

Although ion beam mixed films exhibited amorphous structures, the morphologies differed as a function of BP in the as-deposited state, possibly indicating a difference in atomic ordering due to different degrees of microscopic mixing. The ion beam mixed film with large BP (170Å) showed a microstructure composed of small spherical particles (60-150Å), whereas the ion beam mixed film with small BP (28Å) showed a two-phase separated, maze type microstructure. This morphological difference appeared to influence magnetic properties such as anisotropy and coercivity. Magnetization measurements of ion beam mixed films revealed that the atomic concentration at which ferromagnetism disappears extends to higher boron composition (≈ 55 at% B) than those of the reported melt-spun alloy (40 at% B)². These magnetic properties will be discussed in relationship to the morphological inhomogeneities.

1. D.Y. Kim and R.M. Walser, J. Appl. Phys., 64, 5676 (1988)

2. N.S. Kazama, T. Masumoto and M. Miura, J. Magn. Magn. Mat., 15, 1331 (1980)

A6.24

CHARGE STATES OF HEAVY IONS IN A UNIFORM ELECTRON GAS. A.M. Mazzone C.N.R-Istituto LAMEL, Via de' Castagnoli 1 - 40126 Bologna, Italy.

In this work a new formalism is presented for the evaluation of the effective charge of heavy ions with energy of few MeV.

Similarly to the theory of Guinea, Flores and Echenique the effect of the electron gas on the bound states of the ion is determined (i) by using a dielectric response in which free electrons are described by orthogonalized plane waves instead of plane waves and (ii) by including exchange and correlation effects between the orthogonalized plane waves and the bound states. The interaction between the electrons in the bound states is determined by using a variational procedure.

The stopping values corresponding to the this effective charge are used in a Monte Carlo simulation to calculate the ion range in silicon and gallium arsenide.

A6.25

STUDY OF THE EVOLUTION OF THE BURIED SiO₂ LAYER FORMED BY MULTIPLE LOW DOSE OXYGEN IMPLANTATION INTO SILICON*. F. Namavar and E. Cortesi, Spire Corporation, Patriots Park, Bedford, MA.

We have shown in our previous work [1] that it is possible to form high quality, low defect separation by implantation of oxygen (SIMOX) material with a three step oxygen implantation process (total dose of 1.1×10^{18} O⁺/cm²). In order to optimize this process, we have carried out an extensive study of the effect of parameters such as dose step, dose rate, implant angle, and annealing time and temperature, on the formation and quality of

the buried oxide layer and the quality of the silicon top layer.

We will present results of this work as obtained by RBS/channeling and TEM. Very high quality, low defect SIMOX material has been produced with a two step process (7×10^{17} O⁺/cm²). We will also discuss the formation and evolution of the buried SiO₂ layer at very low doses ($1-4 \times 10^{17}$ O⁺/cm²).

1. F. Namavar, E. Cortesi, and P. Sioshansi, Mat. Res. Soc. Symp. Proc. 128, 623 (1989).

* This work was supported in part by DOD/RADC at Hanscom AFB under contract No. F19628-86-C-0069.

A6.26

MICROSTRUCTURAL STUDIES OF MYLAR (PET) USING CRYOFRACTURING SYSTEM AND SEM. A.K. Nigam, Ramji Pathak, R.N. Chakraborty and U.K. Chaturvedi, VDG Lab., Deptt of Physics, B.H.U., Varanasi-221005, INDIA

To study the microstructure of the semicrystalline Polyethylene Terephthalate (PET) samples using versatile SEM technique a special cryofracturing system has been designed and fabricated. Using this system the thin 250 KeV H⁺ implanted polymer sheets can be broken at liquid N₂ temperature without disturbing their microstructural details as the sample becomes brittle at this temperature and can be fractured easily. Implantation causes blistering which may be exfoliated and flaked on further implantation. The SEM studies of these cryofractured samples have revealed evidences for the Brick Mortar structure of PET.

A6.27

FORMATION OF METASTABLE SILICIDE PHASE UNDER THERMAL ANNEALING AND BEAM IRRADIATION OF NI/SI THIN FILM BILAYERS. Muhammad Z. Numan and Lim poh Leng, Physics Dept., Indiana University of Pennsylvania, Indiana, PA 15705

Evaporated Ni Films on amorphous Si layers, prepared both by electron beam deposition on and ion implantation of <100> Si, were subjected to vacuum annealing and ion beam irradiation. The resulting planar silicide layer was characterized using Rutherford backscattering and cross-sectional transmission electron microscopy. The initial stage of nucleation and growth of the crystalline and amorphous silicide phases has been studied to understand the role of impurities and processing variables. A phenomenological model is proposed to explain the data.

A6.28

MICROSTRUCTURAL CHARACTERIZATION OF TEXTURE IN FUNGSTEIN FILMS MADE BY ION-ASSISTED EVAPORATION K. Rajan, Rensselaer Polytechnic Institute, Troy, NY, R. A. Roy, R. Petkie, and K. V. Ramanathan IBM Research Division, T. J. Watson Research Center, P.O. Box 218, Yorktown Heights NY 10598.

In previous work ion-assisted deposition of Nb, Cr, and W has been used to systematically control film stress by variation of deposition parameters such as ion flux, substrate temperature, and ion energy. Recently we established a general correlation between film fiber texture and stress in W films evaporated with concurrent ion bombardment. The films were deposited over a range of substrate temperatures and subjected to varying degrees of ion bombardment during growth.

In this paper the results of transmission electron microscopy studies of these films are presented. The effects of features such as grain boundary structure on texture are presented. The possible role of dislocations and dislocation-grain boundary interactions on the texture-stress relationship is also explored. Results will be discussed with respect to the dynamics of film growth during ion-assisted deposition.

A6.29

DEPOSITION OF THIN METALLIC FILMS BY HIGH POWER ION BEAM TARGET EVAPORATION. A.N.Zakutaev, I.F.Isakov, G.E.Remnev, Nuclear Physics Institute, 634050 Tomsk, P.O.Box 25, USSR.

The report deals with the results on production of thin films produced by high power ion beam target evaporation. The beam has the following parameters: 300 keV ion energy, 50 ns pulse duration, 100 to 200 A/cm² current density on the target. The beam consists of protons and carbon ions. In comparison with traditional vacuum evaporation techniques, the characteristic feature of employing those beams is high precipitation rate, exceeding 1 cm/s which guarantees production of dense and strong films. The transversal cross-section of the beam incident on the target was 20 cm², the substrate was positioned at a shallow angle to the target plane, at 2 and more cm distance. The films of plumbum, iron, cadmium, zinc and another materials were produced both by one pulse and by several pulses (to 100). In target evaporation, a droplet fraction was observed. The films showed a crystal structure with about 10² to 10³ Å crystallite dimensions. A correlation of metal non-annealed films with their growing rates was observed. The film profile followed the relief of the substrate surface in all the cases.

A6.30

COMPUTER SIMULATION OF ION BEAM ENHANCED DEPOSITION OF TITANIUM NITRIDE FILMS. WANG X1, ZHOU Jiankun, CHEN Youshan, LIU Xianghuai and ZOU Shichang, Ion Beam Laboratory, Shanghai Institute of Metallurgy, Academia Sinica, Shanghai 200050, China

A Monte-Carlo computer simulation has been performed to describe at atomic level the growth of titanium nitride films by ion beam enhanced deposition (IBED). The simulation is based on the assumption of a random target, fixed free path of moving particles and binary collisions. An alternate process of deposition of titanium atoms and implantation of nitrogen ions is applied to replace the actual continuous and synchronous process of IBED. According to the actual conditions, the adsorption of nitrogen, which has leaked out from the ion source, on the fresh titanium film surface has been considered. In addition, the change of the composition and density profiles during film growth has been taken into account. It is demonstrated that the width of the interface region between substrate and film increases with the increasing of the atomic arrival ratio R of the implanted nitrogen ions to deposited titanium atoms. When the titanium deposition rate is low, the nitrogen concentration of the films is not too sensitive to R, indicating that a considerable contribution to the nitrogen concentration is derived from the nitrogen gas leaked from the ion source. The obtained composition profiles are in agreement with the experimental measurements.

A6.31

AES AND IR SPECTROSCOPIC STUDIES OF SOI STRUCTURES FORMED BY ION IMPLANTATION. Yu Yuehui, Lin Chenglu and Zou Shichang, Ion Beam Laboratory, Shanghai Institute of Metallurgy, Academia Sinica, Shanghai 200050, China; and P.L.F. Hemment, Department of Electronic & Electrical Engineering, University of Surrey, Guildford, Surrey GU 5HX, U.K.

The chemical composition and structure of silicon on insulator (SOI) formed by O⁺ (200KeV, 1.8×10¹⁸cm⁻²) or N⁺ (190KeV, 1.8×10¹⁸/cm²) implantation into silicon have been investigated by AES, IR absorption and reflection spectroscopic measurements. For SOI structures produced by O⁺ implantation and annealing at 1300°C for 5 hours, the characteristic Auger spectrum for the interface between the top silicon layer and the buried oxide layer identified a chemical state of silicon whose major transition at 85eV is different from that of bulk silicon or silicon in SiO₂. This chemical state was also observed in the buried oxide layer and the ratio of the amplitude of the Si peak at 85eV to the Si peak at 76eV remains unchanged in the buried oxide layer, and the component ratio of SiO₂ phase in the buried oxide layer was determined to be 0.8. For SOI structures produced by N⁺ implantation and annealing at 1200°C for 2 hours, a nitrogen-rich layer was observed in the buried nitride layer. For both SOI structures, a strong asymmetry of the two main interfaces was observed. By IR absorption analysis, the activation energy of transformation of buried oxide layer into thermally oxidized SiO₂ was determined to be 0.13eV.

A6.32

FORMATION OF BURIED OXYNITRIDE LAYER INTO SILICA GLASS USING ION BEAM. Keiji Oyoshi, Takashi Tagami and Shuhei Tanaka, Tsukuba Research Laboratory, Nippon Sheet Glass Co., Ltd., 5-4 Tokodai, Tsukuba City, Ibaraki, 300-26 Japan

The depth profile of additionally implanted nitrogen was not a Gaussian-like distribution but a trapezoidal one at the dose of N⁺ ion, more than about 3×10¹⁶ ions/cm² (acceleration voltage, 150kV). The maximum concentration of nitrogen saturated at the ion dose. The concentration of implanted nitrogen drastically decreased after the annealing at 600°C.

In the case of silicon ion implantation before or after nitrogen ion implantation, the nitrogen depth profile was a Gaussian-like one, and the distribution of nitrogen did not change after the annealing at 900°C. The maximum nitrogen concentration was obtained in the case of nitrogen implantation after silicon implantation.

Moreover, bubbles appeared underneath the implanted surface at the condition of silicon to nitrogen ion dose ratio 0.75, total dose 4×10¹⁷ ions/cm², and acceleration voltages of silicon and nitrogen 100 and 50kV. The bubble formation was suppressed by the nitrogen ion implantation of two depths deeper and shallower than the peak of silicon concentration.

A6.33

EVALUATION OF COMPOSITIONAL CHANGE IN MASKLESSLY DEPOSITED LINES BY MICRO-RBS ANALYSIS. A. Kinomura, Y. F. Lu, M. Takai and S. Namba, Osaka University, Faculty of Engineering Science and Research Center for Extreme Materials, Toyonaka, Osaka 560, Japan; M. Satou and A. Chayahara, Government Industrial Research Institute Osaka, Ikeda, Osaka 563, Japan.

Oxygen contents in masklessly deposited tin oxide and silicon oxide lines were investigated by micro-RBS analysis using 1.5 MeV helium ion and proton microprobes. Since the micro-RBS analysis is free from the charge-up effect which is a serious problem in case of an Auger electron spectrometry, the micro-RBS is suitable for insulating materials. A spot size of the microprobe was $3 \mu\text{m} \times 3 \mu\text{m}$ with a beam current of 100 pA.

The tin lines were masklessly deposited on GaAs by an Ar^+ laser irradiation in an SnCl_4 atmosphere. Much oxygen content introduced from residual gas were found in the deposited lines. While Sn and SnO_2 are electrically conductive, SnO is an insulator. It is important to control the oxygen contents to obtain conductive lines.

The tin line deposited with a laser power of 350 mW was analyzed by the 1.5 MeV helium ion microprobe. Variation of the micro-RBS spectra due to the compositional change was observed when the microprobe was scanned across the deposited line. Stoichiometric SnO_2 was found at the center of the deposited line.

A6.34

DEPENDENCE OF COMPOSITION AND STRUCTURE OF ION-ASSISTED BORON NITRIDE THIN FILMS ON PROCESS PARAMETERS.* J.C. Tetreault, J.K. Hirvonen, and G.R. Parker, Spire Corporation, Bedford, MA; P. Kullen and T. McDevitt, Mellon Institute, Pittsburgh, PA; J.P. Hirvonen, Los Alamos National Laboratory, Los Alamos, NM.

Thin films of $\text{E}_x\text{N}_{(1-x)}$ have been deposited on a variety of substrates by the method of ion beam assisted deposition (IBAD). The process involves electron-beam evaporation of boron with simultaneous bombardment by a low-energy ($< 2\text{keV}$) non-mass analyzed nitrogen ion beam from a Kaufman-type ion source. The effect of process parameters, such as ion energy, ion/evaporant flux ratio, and substrate temperature, on the resulting film's stoichiometry and crystal structure is presented. X-ray diffraction, transmission electron microscopy, and Raman spectroscopy are used to investigate film microstructure while stoichiometric determination is provided by nuclear reaction resonance analysis. Other film characteristics which are reported include microhardness, friction and wear behavior, and optical properties.

* - This work sponsored in part by Department of Energy SBIR contract DE-AC02-87ER80449.

A6.35

COBALT SILICIDE FORMATION ON Si SUBSTRATE HEAVILY DOPED WITH ARSENIC IONS. V.V. Tokarev, Institute of Solid State and Semiconductor Physics, the BSSR Academy of Sciences, P. Brovka str. 17, Minsk, USSR, 220726.

Silicide films are gaining greater significance in the production of miniature devices. However silicide synthesis on heavily doped Si films is a matter of some definite difficulty which often can not be solved by traditional methods. The paper presented considers the processes

going on in heavily doped Si during its interaction with a metal film.

RBS, AES, x-ray diffraction and electrophysical measurements of film resistance and thickness were used to study the reaction of Co silicide formation with Si, heavily doped by As implantation (dose range $3 \cdot 10^{15} - 3 \cdot 10^{16} \text{ cm}^{-2}$). The reaction was enhanced by extra implantations of argon, oxygen and carbon in the dose range of $10^{14} - 10^{16} \text{ cm}^{-2}$ with energies ensuring $R_p = 0.5 d_{\text{Me}}, 1d_{\text{Me}}$ and $1.5 d_{\text{Me}}$, and also by rapid heating and annealing in diffusion furnace.

It is shown that every dopant used enhance the process of silicide formation on heavily doped Si, and the destabilisation of covalent bonds in Si is the main contribution rather than intermixing of metal-silicon layers.

A6.36

TITANIUM SILICIDE FORMATION ON MONO- AND POLY-CRYSTALLINE Si ENHANCED BY ARGON IMPLANTATION. V.V. Tokarev, A.I. Demchenko, U.Ch. Dulinets, Institute of Solid State and Semiconductor Physics, the BSSR Academy of Sciences, P. Brovka str. 17, Minsk, USSR, 220726.

Titanium silicide synthesis is a complex process, it is given much prominence in the production of IC. This paper gives the analysis of Ti silicide synthesis on mono- and polycrystalline Si, enhanced by argon implantation.

Electrophysical and analytical measurements made it possible to determine silicide film resistance and thickness, silicide phase, grain size, the structure and distribution of elements on silicide synthesis during solid phase reaction of mono- and polycrystalline silicon with 60 nm silicide film, implanted with argon ions to a dose range of $10^{14} - 10^{17} \text{ cm}^{-2}$ (energy range 30-200 keV) and heat treated in a diffusion furnace at 650°C and 850°C .

The investigations showed accelerated due to the implantation growth of silicide layers. This is caused by two processes: by intermixing metal atoms with Si atoms and by uniform dopant distribution in the mixed volume. There is presented a model of silicide synthesis, which also accounts for additive inclusion of Me-Si in the system.

A6.37

ION BEAM MIXING OF LANTHANUM OXIDES AND COPPER MULTILAYERS. J.P. Mathevet and A. Traverse, Centre de Spectrométrie Nucléaire et de Spectrométrie de Masse, Bât 108, 91405 Campus Orsay, France

The role of the energy deposition process (electronic versus nuclear), of the nature of created defects on ion beam mixing mechanisms of metallic and oxide layers are not yet well understood.

As lanthanum, copper and oxygen are components of high transition temperature superconductors, we have chosen to study their behavior under ion beam mixing. The effects of the initial oxygen content, the irradiation temperature and the density of deposited energy on the final composition and structure of the mixed layers are analysed. The possibility for preparing high T_c superconductors by this technique is discussed.

A6.38

ION BEAM MIXING OF METALLIC MULTILAYERS. Agnès Traverse, Centre de Spectrométrie Nucléaire et de Spectrométrie de Masse, Bât. 108, 91406 Campus Orsay, France

Experimental diffusion coefficients have been measured on metallic layered samples submitted to ion irradiation at low temperature, in different density of deposited energy regimes. The irradiated layers are chosen with enthalpy of mixing passing from positive to negative values: Ni/Pt, Ni/Pd, Ni/Au and Ni/Ag. A model for linear effects is presented through an analysis of the experimental results in terms of ballistic and chemical mechanisms.

A6.39

EFFECT OF IMPLANTATION CONDITIONS ON THE MICROSTRUCTURE OF HIGH-DOSE OXYGEN IMPLANTED SILICON-ON-INSULATOR MATERIAL. S. Visitsamrakul¹, B.F. Cordis², and S. Krause¹, ¹Department of Chemical, Bio and Materials Engineering, Arizona State University, Tempe, AZ.; ²Ibis Technology Corporation, Danvers, MA.

High-dose oxygen implantation in silicon, SIMOX (separation by implantation of oxygen), is a promising technique for producing silicon-on-insulator material. Most studies have examined SIMOX prepared with a traditional (lower current, lower temperature) implanter, which has beam current densities from 15-150 $\mu\text{A}/\text{cm}^2$. Recently, a high-current implanter with a density of 1 mA/cm^2 has been developed for commercial SIMOX fabrication. This machine shortens the implantation time and produces structural features not routinely observed in samples from traditional implanters. We have investigated SIMOX implanted at high-current densities and are reporting the effects of implantation dose, temperature, and beam current density on the structure using conventional and high resolution electron microscopy.

Most samples were implanted to a dose of $1.8 \times 10^{18} \text{ cm}^{-2}$, at 600°C, at 200 keV, and with the beam current density of 1 mA/cm^2 . The general structure of traditional and high current samples is the same with a 0.3 μm top Si layer, a 0.4 μm buried oxide layer, and damage zone below the buried oxide layer. However the top Si layer of the higher current samples has trails of bubbles at the surface with no defects, and large 0.1 μm multiply faulted defects extending outward from the buried oxide interface. In the top Si layer of traditional lower-current samples, there are short, 20 nm, defects throughout the layer and no bubbles are present. Annealing higher-current samples at 1300°C for 6 hours results in SIMOX with defect density of only 10^5 cm^{-2} which is four orders less than the traditional samples. This is attributed to the absence of defects at the surface in the newer samples. This effect will be discussed further.

When dose was varied from 0.3 to $1.8 \times 10^{18} \text{ cm}^{-2}$ in high current implanted samples, the structure of the top Si layer remained similar with bubbles and long multiple defects present for all doses. When beam current density was varied from 1 mA/cm^2 to 10 mA/cm^2 no significant structural changes occurred. When temperature was varied from 550 to 700°C, a large increase in final defect density occurred for samples implanted at 550°C. The effects of these implantation conditions on defect evolution will be discussed further.

A6.40

THE CORROSION RESISTIVITY OF CERMET COATINGS MADE BY ION BEAM TREATMENT. Tian Wei. Author, and Cai Weiping. Wuhan Iron and Steel University, Wuhan, China.

A cermet coating was obtained on a silicon-deposited pure iron surface by means of a single treatment integrating ion implantation and ion beam mixing. As compared with either simple ion implantation or simple ion beam mixing, the integrated treatment provides the cermet coating with an electrochemical performance far better than the simple treatments. Data as observed in the author's experimentation show that the integrated or, the 'dual treatment' exhibits the highest corrosion resistivity in aqueous solutions. In neutral aqueous solution, the specimen which has acquired its resistivity from the 'dual treatment' exhibits both a lower passivating current density I_c and a lower passivity-holding current density I_m than that of pure iron by more than two orders of magnitude; and the former shows a corrosive current density lower than that of simple ion beam mixed specimen by 8/9 with I_m and I_c lower by two orders of magnitude. Repeated voltametric graph shows its I_c to remain lower than that of pure iron after 13 sweeps, its I_m being 1/4 of

that of pure iron. All that has been mentioned above demonstrated that the 'dual treatment' imparts corrosion resistivity to the specimen which is far superior to those treated by other 'simple' treatments.

A6.41

INVESTIGATION OF OXIDE/METAL MULTILAYERS FOR SOFT X-RAY OPTICS FABRICATED BY ION BEAM SPUTTERING. I. Kataoka, K. Ito, T. Yamamitsu, K. Etoh, N. Hoshi, I. Yamada, Japan Aviation Electronics Industry, Ltd. 1-1, Musashino 3-chome, Akishima-shi, Tokyo, 196 Japan

Recently a number of studies of soft X-ray have been made. We are also investigating multilayers for these types of optics and have shown that high reflectivity can be obtained by using oxides or hydrides for space layers in the wavelength region from 2.33 nm to 4.4 nm because of these small absorption coefficients.

However, practically fabricated multilayers don't show such high reflectivities expected by calculation because of the roughness of interfaces and surfaces of multilayer.

Then, in this paper, we pay attention mainly to the problem of morphology of SiO_2/Ni and $\text{B}_2\text{O}_3/\text{Ni}$ multilayers fabricated by dual ion beam sputtering.

In the depositing process, oxygen ions and argon ions were supplied during the deposition of oxides and Ni respectively as a parameter of fabrication. We discuss the relation between conditions to deposit multilayers and their properties which are evaluated by using a radial distribution analysis system of RHEED pattern, an STM and X-ray diffractometer. Furthermore the reflectivity of multilayers was evaluated by X-ray reflectivity meter.

A6.42

MOLECULAR DYNAMICS SIMULATIONS OF IONIZED CLUSTER BEAM DEPOSITION. Horngming Hsieh and R. S. Averback, Department of Materials Science and Engineering, University of Illinois, Urbana, IL 61801; and R. Benedek, Argonne National Laboratory, Argonne, IL 60439.

Although ionized cluster beam deposition appears to be a promising method for thin film deposition, the physical processes of an energetic cluster containing tens to hundreds of atoms impinging on a surface are not understood. We have found that molecular dynamics simulation is a powerful technique for attacking such highly non-homogeneous many-body problems. In this investigation we have simulated the impingement of a cluster containing 100 atoms on a $\langle 100 \rangle$ surface of a fcc crystal using Lennard Jones potential and copper potential from the embedded atom method. The clusters with varying energies and with both the same and different lattice parameters than the substrate are studied. The simulations provide microscopic information about spreading of the cluster over the surface, epitaxial relationships, defect production, and atomic mixing between the cluster and the substrate.

Work supported by the U.S. Department of Energy, Basic Energy Sciences.

A7.1

ION BEAM MODIFICATION OF HIGH T_c SUPERCONDUCTORS. O. Meyer, J. Geerk, G. Linker, B. Strehlau, X.X. Xi, Kernforschungszentrum Karlsruhe, INFP, P.O. Box 3640, D-7500 Karlsruhe, FRG

Ion irradiation and implantation experiments of high temperature superconductors (HTSC) thin films resulted in many interesting effects. Among those are:

(i) the superlinear increase of the resistivity, ρ , with ion fluence, ϕ , leading to a metal to insulator transformation,

(ii) the large recovery below room temperature of the radiation induced increase of ρ (about 60%) as well as the recovery of the decrease of the transition temperature, T_c , and (iii) the large structural changes such as the increase of the c-axis lattice parameter with ϕ , the radiation induced orthorhombic to tetragonal phase transition, and the amorphization.

The T_c -depression rate and the change of the critical current depend on the initial state of the sample characterized by ρ , T_c , the residual resistivity ratio (ρ_{RT}/ρ_{100K}) and the grain boundary density. In order to separate the influence of percolation effects from intrinsic effects of the superconductor, high quality single crystalline films have been used in irradiation experiments. Displaced oxygen atoms play an important role for the observed property changes.

The ion induced metal to insulator transition is applied for ion beam patterning to fabricate narrow bridges and SQUID's. Low dose irradiation was used to improve the sensitivity of the SQUID's. The effectivity of defects as flux pinning centers to enhance the critical current in magnetic field is discussed.

A7.2

STRUCTURE OF AMORPHOUS Al_2O_3 , PRODUCED BY ION IMPLANTATION*. C. J. McHargue, P. S. Sklad, P. Angelini, C. W. White, and J. C. McCallum, Oak Ridge National Laboratory, P.O. Box 2008, Oak Ridge, TN 37831-6118.

The amorphous state can be produced in $\alpha-Al_2O_3$ (sapphire) by ion beam induced displacements at 77 K or by displacements combined with chemical effects at room temperature. Progress toward understanding the amorphization process has been made from studies of short-range order, electronic charge on implanted species, and the critical concentration for amorphization at 300 K.

Analysis of the fine structure of EELS spectra shows the $Al-O$ first nearest-neighbor distances to be different for amorphous Al_2O_3 , produced by implantation of iron and that produced by implantation of aluminum plus oxygen in the stoichiometric ratio at 77 K. Conversion electron Mössbauer spectroscopy has yielded information on the distribution of implanted iron and tin among various charge states (valences) and the symmetry of their surroundings. Analytical electron microscopy indicates the amorphous state to be produced at a critical concentration of zirconium implanted at 300 K.

*Research sponsored by the Division of Materials Sciences, U.S. Department of Energy, under contract DE-AC05-84OR21400 with the Martin Marietta Energy Systems, Inc.

A7.3

INFLUENCE OF ION BEAM MIXING ON THE GROWTH OF HIGH TEMPERATURE OXIDE SUPERCONDUCTING THIN FILM. N. Borges, A. D. Rollet, M. Cohen, M. Nastasi, Los Alamos National Laboratory, Los Alamos, NM 87545.

The superconducting properties of high temperature superconductor thin films are dependent on the quality of the substrate used to grow these films. In order to minimize the lattice matching between the superconducting film and the substrate, we have used a $YBa_2Cu_3O_7$ thin film deposited on (100) $SrTiO_3$ as a template. The first film was prepared by co-evaporation of Y, BaF_2 , and Cu on (100) $SrTiO_3$, followed by an anneal in "wet" oxygen at 850 C. This film showed a sharp transition at about 90K. A thicker layer of about 3000 Å was then deposited on top of this first 2000 Å film, using the same procedure. After the post anneal at 850 C, the transition took place at 77K and no epitaxy of the second film was observed. Ion

beam mixing at 400 C, using 400 keV O ions was done at the interface of the two films (the second one being not annealed). After the 850 C post anneal, the film displayed an improved T_c at 90K. Moreover, epitaxy was shown to take place from the interface $SrTiO_3$ -123 film towards the surface and was dependent on the dose. These results will be discussed from the data obtained from high energy backscattering spectroscopy combined with channeling experiments, x-ray diffraction and scanning electron microscopy observations.

A7.4

INTERACTION BETWEEN IMPLANTED IONS AND INTRINSIC DEFECTS IN SILICA. R. H. Magruder, Belmont College, Nashville, TN; R. A. Weeks, Vanderbilt University, Nashville, TN; R. Zuhr, Oak Ridge Laboratory, Oak Ridge, TN.

High purity silica (Spectrosil) samples were implanted with Ti, Cr, Mn, Fe and Cu at doses ranging from 1×10^{15} ions/cm² to 5×10^{15} ions/cm² at 160 KeV and approximately $2.6 \mu A/cm^2$. Backscattering measurements determined the concentration of implanted ions as a function of dose and depth. The optical absorption extinction coefficient per ion was measured from 1.8 to 6.0 eV. In all implanted samples there was an increase in absorption over unimplanted samples at energies ≥ 4.6 eV. By visual inspection a peak in the absorption was observed at ~ 5 eV for all samples and in the spectra of Mn samples at 5.8 eV. The increase in extinction coefficient per ion over an unimplanted sample was ion specific with the absorption of Cu implanted samples showing the least change and the largest increase in Cr implanted samples. We attribute the absorption at 5.0 eV to an E' center (B_2 center). The source of absorption at energies > 5.0 eV is due to several sources, one of which is E' absorption at 5.8 eV. At ~ 6 eV the first derivative, dEC/dE , where EC is the extinction coefficient and E is the photon energy, shows that the slope is positive in the absorptivities of all samples with the exception of those implanted with Mn and Cu. This positive slope indicates absorption due to bands with peaks at energies > 6.0 eV. As the absorption throughout the spectral range measured is ion specific, we attribute the different optical properties to differences in the interaction of the implanted ion with intrinsic defect centers such as E' and E' centers and to interactions with defects with energies greater than 6 eV.

This research was supported in part by NSF Contract #DMR-8513731 and in part by the Division of Materials Sciences, US DOE under contract #DE-AC05-84OR-21400 with Martin Marietta Energy Systems, Inc.

A7.5

REFRACTIVE INDEX PROFILES OF HIGH DOSE Ti IMPLANTED OPTICAL WAVEGUIDES IN $LiNbO_3$. T. Bremer, FB. Physik, Universität, D-4500 Osnabrück; and Ch. Buchal, R. Irmischer, Inst. Schicht- und Ionentechnik, KFA, D-5170 Jülich, W. Germany

Single crystalline y-cut substrates of $LiNbO_3$ have been implanted with ^{48}Ti ions at 200 keV and doses up to 4×10^{17} cm⁻². The implants have been performed at wafer temperatures of 77 K, 300 K and 620 K. Immediate subsequent processing at 1273 K in wet oxygen ambient led to good epitaxial regrowth at all doses, if sufficient time was allowed. Channeling and mode spectroscopy have been applied to monitor the regrowth process. Refractive index profiles have been calculated with an inverse WKB algorithm from measured dark line spectra. The maximum observed extraordinary refractive index change after regrowth is $\Delta n_e = 0.04$, indicating a solubility limit of 3.3×10^{21} Ti cm⁻³, corresponding to 18 % of Nb^{5+} replaced by Ti^{4+} . Even at the highest dose, some influence of dynamical annealing during implantation at 620 K is observed, leading to reduced post-implantation processing times.

A7.6

OPTICAL WAVEGUIDE FABRICATION BY STOICHIOMETRIC IMPLANTATION OF Ti AND O INTO LiNbO_3 . D. B. Poker, Solid State Division, Oak Ridge National Laboratory,* Oak Ridge, TN 37831-6057; and W. Xia, Department of Electrical and Computer Engineering, University of California, San Diego, La Jolla, CA 92093-0407.

X-cut substrates of LiNbO_3 have been implanted at 500°C with Ti and O to doses of 2.5 and 7.5×10^{17} ions/cm², respectively. The high substrate temperature during implantation ensures dynamic recrystallization, preserving the crystallinity of the LiNbO_3 . The stability of the stoichiometric implants is enhanced sufficiently that annealing at 1000°C proceeds with no surface degradation of the substrate. Annealing under identical conditions without the O implant usually results in phase separation of a Ti or Li oxide at the surface, even when annealing is performed immediately following implantation. Samples implanted with Ti and O to preserve the stoichiometric metal:oxygen ratio of the substrate can be stored at room temperature for several months without phase separation. Planar optical waveguides have been produced by stoichiometric implantation followed by annealing in water-saturated oxygen for one hour at temperatures of 900 and 1000°C. The sample annealed at 900°C supported a single lossy mode, while the 1000°C sample supported two propagating modes and one lossy mode at 0.6 μm .

* Operated by Martin Marietta Energy Systems, Inc. under contract DE-AC05-84OR21400 for the U.S. Department of Energy.

A7.7

MODIFICATION OF THE WEAR PROPERTIES OF DIAMOND USING ION BEAM IRRADIATION. Gregory C. Anderson and Steven Praver, Dept. of Applied Physics/Microelectronics and Materials Technology Centre, Royal Melbourne Institute of Technology, G.P.O. Box 2476V, Melbourne. Victoria 3001, AUSTRALIA.

Recent reports have suggested that ion implantation of diamond may significantly enhance its wear resistance. In an attempt to reproduce and extend these results natural diamond held at high temperature (800°C) has been subjected to implantation with various ion species. Scratch and indentation tests showed that the surface of diamond can indeed be toughened by ion beam irradiation.

Changes in the surface wear characteristics of the diamond have been determined using a 'Gatan' dimple grinder. Interferometric analysis of the dimples in the diamond has enabled the determination of the volume of diamond removed during grinding. Since it is possible to produce very shallow dimples, this method is much more sensitive to the ion beam modified surface than indentation or scratch testing.

Microstructural analytical techniques (RBS, RHEED and Raman Spectroscopy) have shown that even after high dose implantation the diamond is still single crystalline and has not undergone polycrystallisation, graphitisation or amorphisation due to the ion irradiation.

A7.8

THE EFFECT OF ION INDUCED DAMAGE ON THE MECHANICAL PROPERTIES OF ZIRCONIA. E. L. Fleischer, T. L. Alford, P. Børgesen, P. Revesz, J. W. Mayer, Materials Science and Engineering, Cornell University, Ithaca, NY; W. Herl, Corning Inc., Corning, NY.

Microhardness measurements were carried out on ion implanted single

crystal Y_2O_3 stabilized cubic ZrO_2 . Ions were implanted up to fluences of 3×10^{17} ions/cm². Comparison of the Knoop microhardness values of ZrO_2 implanted with various species over a range of fluences showed that the principle variable causing hardness changes for inert ion implantation is damage energy and not the ion fluence nor the ion species. For shallow inert ion implants, the hardness versus damage energy gives a unified plot. Hardnesses rise with increasing deposited damage energy to a value 15% higher than that of unimplanted zirconia. With additional damage the hardness drops to a value 15% lower than that of the unimplanted zirconia. Deep implants showed similar behavior but with the hardness increasing 50% over that of the unimplanted samples.

Friction and wear measurements of the shallow implants in a pin-on-disk assembly showed very different behavior for high dose versus unimplanted ZrO_2 . The unimplanted samples showed debris with an associated rise in friction. The implanted system showed much less debris and a constant value of friction even after 10,000 cycles.

A7.9

THE FORMATION OF A SOLID LUBRICANT BORON NITRIDE IN B_4C BY ION IMPLANTATION AND LASER ANNEALING. Robert R. Reeber, Ning Yu, Dept. of Physics & Astronomy, U. of North Carolina, Chapel Hill, NC 27599-3255; Wei-Kan Chu, Texas Center for Superconductivity and Dept. of Physics, U. of Houston, Houston, TX 77204-5506; and Robert P. Kusy, Dental Research Center, U. of North Carolina, Chapel Hill, NC 27599-7455.

A boron nitride (lubricant) thin layer (about 750 Å) has been formed at the surface of a B_4C substrate by implanting nitrogen ions at 100 keV with a total dose of 4×10^{17} N/cm² followed by XeCl laser annealing. The composition and the profile of the carbon, boron and implanted nitrogen, in the sample at various stages of our experiments were determined by Rutherford Backscattering (RBS). During XeCl laser annealing the deeply implanted nitrogen atoms diffused back to the surface and piled up there with about 50% of them lost from the surface. XPS measurements, combined with Ar sputtering, showed that a large amount of boron nitride (more than 70% of the remaining nitrogen) formed near the surface region after laser annealing.

A7.10

CRYSTALLIZATION OF INTRINSIC AMORPHOUS LAYERS PRODUCED BY STOICHIOMETRIC IMPLANTATION OF Al AND O IONS IN a-AXIS ORIENTED Al_2O_3 SINGLE CRYSTALS. W. Zhou, D.X. Cao and D.K. Sood, Microelectronics and Materials Technology Centre, Royal Melbourne Institute of Technology, 124 La Trobe Street, Melbourne, Victoria, 3000, Australia.

Damage free a-axis oriented single crystals of $\alpha\text{-Al}_2\text{O}_3$ were implanted at liquid nitrogen temperature with a stoichiometric implant (two parts Al to three parts oxygen with ion energies adjusted to give the same projected range), to produce an intrinsic amorphous phase (free of any impurities) of Al_2O_3 . Implant conditions, identical to those employed by White et al [1], were used: Al ions at 90 keV to a dose of 4×10^{16} Al ions/cm², and O ions at 55 keV to a dose of 6×10^{16} O ions/cm² to produce an amorphous layer approximately 130nm thick. Isothermal annealing was conducted at temperatures of 600, 700, 800 and 900°C for up to 24 hours in flowing high purity dry argon gas. Rutherford backscattering and channeling (RBS-C) and reflection high energy electron diffraction (RHEED) have been employed to investigate the crystallization behaviour.

The amorphous phase transforms directly to $\alpha\text{-Al}_2\text{O}_3$ at a well defined planar interface which moves towards the free surface. The interface velocity shows an Arrhenius behaviour with anneal temperature. An activation energy of about 0.7 eV has been determined. These results are remarkably different from those reported previously [1] for c-axis oriented Al_2O_3 substrates. Substrate orientation will be shown to play a dominant role in deciding the mode of crystallization as well as the kinetics of transformation.

[1] C.W. White et al, Mat. Res. Soc. Symp. Proc. 60, 337 (1986).

A8.1

AMORPHOUS TO CRYSTALLINE PHASE TRANSFORMATIONS
IN HIGH DOSE ION IMPLANTED SILICONR.P. Thornton¹, R.G. Elliman¹, Y.H. Li¹, A.P. Pogany¹,
E. Nygren² and J.S. Williams^{1,3}

1. Microelectronics and Materials Technology Centre, RMIT, Melbourne, 3000, Australia
2. Materials Science and Engineering, Ohio State University, Columbus, Ohio, 43210, USA
3. Electronic Materials Engineering, RSPHS, ANU, Canberra, 2600, Australia

The annealing of ion implanted amorphous silicon can result in varied and complex crystallization behaviour when the concentration of the implanted species exceeds the equilibrium solid solubility limit in the crystalline silicon phase. In this paper, we present and compare the crystallization behaviour for a number of implanted low melting point group III, IV and V impurities in silicon. A melt-mediated transformation from amorphous to fine grain polycrystalline silicon is observed in preference to epitaxial crystallization when the impurity concentration is high and the annealing temperature exceeds that of the elemental melting point of the implanted species. At lower concentrations, competition between retarded epitaxial growth and polycrystalline formation takes place. For high dose Sb, a solid phase amorphous to polycrystalline transformation occurs. The activation kinetics of all of these processes have been measured and data indicates that impurity diffusivity and solubility in amorphous silicon strongly determine the nature and kinetics of both epitaxy and nucleation and growth of polycrystalline silicon during annealing of high dose implanted silicon.

A8.2

STRESS AND PLASTIC FLOW IN SILICON DURING
AMORPHIZATION BY ION-BOMBARDMENT. C. A. Volkert,
AT&T Bell Laboratories, Murray Hill, NJ.

The stress in silicon wafers during ion-bombardment was determined by wafer curvature measurements using an in-situ laser-scanning technique. Measurements were made as a function of ion species (noble gases and Si), energy (1-3 MeV), fluence, flux, and sample temperature (100-400K). In a typical experiment, compressive stress was built-up in the bombarded region as a function of fluence, until a maximum was reached at approximately the dose required for the formation of a continuous buried amorphous layer. The magnitude of this maximum compressive stress (20-100 MPa) depended strongly on the flux. During further amorphization by continued bombardment, the stress decreased and eventually stabilized. If ion bombardment was interrupted during amorphization, a stress increase was observed over a period of several minutes; the magnitude of this change increased with the amount of damage in the silicon.

These changes in stress are interpreted in terms of ion beam induced defect creation and motion. The initial build-up of compressive stress is due to expansion of the bombarded region by the creation of defects and amorphous material. The subsequent relaxation is attributed to plastic flow under the ion beam. The stress increase that occurs when ion-bombardment is interrupted, may be due to redistribution of defects.

A8.3

STRUCTURAL CHARACTERIZATION OF DAMAGE IN
Si(100) PRODUCED BY MeV Si⁺-ION IMPLANTATION AND
ANNEALING.* M. K. El-Ghor, O. W. Holland, C. W. White, and
S. J. Pennycook, Oak Ridge National Laboratory, Oak Ridge, TN 37831.

Differences in the damage produced by implantation of MeV Si⁺ ions in silicon single crystals at room temperature and liquid nitrogen temperature are discussed. Damage morphology is characterized structurally both in the as-implanted condition and after post-implantation furnace annealing. During room temperature irradiation, a buried amorphous layer is formed near the end-of-range of the ions at moderate doses. The growth of this

layer is shown to occur by a layer-by-layer mechanism with relatively sharp interfacial transition regions. A wide region ahead of the buried amorphous region extending to the surface is observed to be free of any extended defects. Recrystallization of the damaged region during thermal annealing occurs by solid-phase epitaxial growth at both interfaces. Results of irradiation at liquid nitrogen temperature, on the other hand, show that nucleation and growth of the amorphous damage occurs over a wide region and is not confined to the interfacial region. This results in a very diffuse upper interface composed of a mixture of amorphous and crystalline phases. Substantial reordering is observed in this mixed-phase region at temperatures well below those required for annealing of continuous amorphous layers. Cross-sectional transmission electron microscopy, as well as Rutherford backscattering spectroscopy were used in this study. Damage nucleation/growth mechanisms at the two temperatures responsible for the different damage morphologies are discussed. The detailed microstructure of the damage is presented, and is related to its annealing behavior.

*Research sponsored by the Division of Materials Sciences, U.S. Department of Energy under contract DE-AC05-84OR21400 with Martin Marietta Energy Systems, Inc.

A8.4

GETTERING OF CU AT BURIED DAMAGE LAYERS MADE BY
SI SELF IMPLANTATION J.R. Liefting, R.J. Schreutelkamp, W.X.
Lu and F.W. Saris, FOM Institute for Atomic and Molecular Physics,
Kruislaan 407, 1098 SJ Amsterdam, The Netherlands

Channeled implants have been performed with 100keV ²⁸Si⁺ into p-type Si(100) to obtain a buried amorphous layer with a thickness of 1400 Å underneath a crystalline toplayer of 600 Å. Full recrystallization of this buried amorphous layer leads to a sharp buried interface at the depth where the two moving amorphous/crystalline interfaces meet. We have studied the gettering of Cu ions before and after recrystallization of the buried amorphous layer as a function of temperature and time.

The Cu was implanted at an energy of 15 keV at a dose ranging from 5E13 to 1E15 /cm² to obtain a high concentration of Cu in the near surface region. After the Cu implant annealings were performed at 490, 600 and 900°C for 10 min. to 18 hrs. Cu profiles before and after annealing were studied with Rutherford Backscattering Spectrometry and channeling analysis.

It is shown that, in case the Cu is implanted after recrystallization of the buried amorphous layer, the Cu will getter at the sharp buried interface. In case the Cu is implanted before recrystallization, the Cu will diffuse from the surface towards the substrate regions and is trapped inside the recrystallization buried amorphous layer. Full recrystallization leads to a broader buried interface with a higher amount of gettering of Cu ions.

A8.5

ANNEALING TEMPERATURE DEPENDENCE OF THE ELECTRICAL ACTIVITY
OF HIGH-DOSE Sb ION IMPLANTS IN (100) SILICON. S.N. KUMAR,
G. CHAUSSEMY, A. LAUGIER, Laboratoire de Physique de la
Matière, CNRS-358, I.N.S.A. Lyon, 69621 Villeurbanne; and
M. CHARBONNIER, M. ROMAND, Laboratoire de Chimie Appliquée,
CNRS-417 and B. CANUT, Laboratoire de Physique des Matériaux,
Université Claude Bernard, 69622 Villeurbanne, France.

The systematic of electrical activation by rapid thermal annealing (RTA) of the 40-120 keV Sb⁺ implants in (100) B-doped silicon is reported. A series of Sb⁺ implants (from 2x10¹⁴ to 1.2x10¹⁶ / cm²) were rapidly annealed for 10 s over a range of temperature, from 500 to 1100 °C, to study the implant behavior as a function of anneal temperature. The RBS and channeling data showed that, irrespective of the ion dose, the maximum fraction of Sb that can be substitutionally incorporated was achieved for RTA at 700 °C. The compositional depth profiles were obtained from XPS and SIMS analysis, and additional information about the chemical bonding between the Si, Sb and O atoms in the surface region was extracted from the angle-resolved X-ray

photoelectron spectroscopy (ARXPS) data.

Significant differences in the surface region composition between the Sb implants and the previously reported As implants¹ are observed. The Sb 3d_{5/2} line shape was well defined and line widths considerably smaller for the 700°C anneal when compared with those for the higher temperature anneals. The RBS, SIMS and ARXPS compositional data will be compared with the electrical characteristics of the MOS structures built on these samples.

- (1) S.N. Kumar, G. Chaussemy, B. Canut and A. Laugier, Appl. Phys. Lett. **53**, 2167 (1988); Appl. Surf. Sc. **36** 545 (1989); S.N. Kumar, G. Chaussemy, P. Roura and A. Laugier, MRS Proc. **136** (1989).

A8.6

ANNEALING BEHAVIOUR OF BURIED AMORPHOUS LAYERS FORMED BY MEV ¹¹⁵IN⁺ IMPLANTATION IN SI(100); R.J. Schreutelkamp¹, J.R. Liefing¹, W.X. Lu^{1,2}, B.X. Zhang², Z.L. Wang² and F.W. Saris¹; ¹FOM Institute for Atomic and Molecular Physics, Kruislaan 407, 1098 SJ Amsterdam, The Netherlands; ²Beijing Normal University, Beijing 100875, P.R. China

We have studied the annealing behaviour of buried amorphous layers formed by MeV ion implantation. In high (MeV) energy ion implantation a buried amorphous layer may be formed in silicon for a dose as low as 10¹⁴/cm². In general, a complex dislocation network is created when the buried amorphous layer is annealed. Such a defect layer seems to have a remarkably high thermal stability. The formation of a highly defected region close to the dopant profile may severely limit the formation of high quality heavily doped n⁺ or p⁺ layers in silicon.

In this paper we investigate the role of the dopant species on the formation of secondary defects during annealing of a buried amorphous layer in silicon. The buried amorphous layers were formed by 1.0 MeV ¹¹⁵In⁺ implantations in Si(100) with a dose of 10¹⁴/cm². By applying both TEM and RBS analysis the formation of secondary defects and precipitation of dopant atoms has been accurately determined as function of annealing temperature and time. A comparison is made with the annealing behaviour of buried amorphous layers formed by other dopants, like phosphorus, to account for the dependence on dopant species.

A8.7

KINETICS AND MICROSTRUCTURE OF TRANSIENTLY ANNEALED IMPLANTED POLYCRYSTALLINE SILICON LAYERS. J.M.C. England, P.J. Timans, R.A. McMahon and H. Ahmed, Cambridge University Microelectronics Research Laboratory, Science Park, Cambridge CB4 4FW, UK; C. Hill, P.D. Augustus and D.R. Boys, Plessey Research, Caswell, Northants NN12 8EQ, UK.

Microstructural changes occurring during the early stages of rapid thermal annealing of arsenic-implanted polysilicon bipolar emitters crucially affect the final dopant distribution¹ and hence device performance. The first stage of annealing is solid phase epitaxial regrowth (SPE) of the amorphised layer. In-situ studies using time resolved reflectivity, combined with XTEM of partly annealed structures, have been used to determine the effects of initial grain size (100Å-), amorphising species (Si or As), and temperature (600-850°C). Electron beam heating with high ramp rates (1600°C/s) was used to regrow specimens at constant temperature for times between 0.2 and 2000s.

The initial regrowth rate in polysilicon layers which had been pre-annealed at 1250°C to give complete epitaxial realignment to the (100) silicon substrate was $5 \times 10^{16} \exp(-2.71 \pm 0.05 \text{ eV}/kT)$ A/s. This is within 10% of the rate measured on similarly implanted (100) substrates, showing that impurities in the polysilicon

were not significant. The rate fell as the initial grain size was decreased, being ~20 times slower for 100Å grains at 620°C. All the polysilicon specimens showed much slower regrowth in the final stages. XTEM revealed that regrowth is non-planar, and that the lower rates are related to SPE from non-(100) oriented regions, either grains or twins. Quantitative data will be presented for both silicon and arsenic implants.

- (1) A.G.O'Neill, C.Hill, J.King, C.Please, J. Appl. Phys. **64**(1) 167 (1988)

A8.8

COMPARISON OF THE EFFECTS OF N-TYPE AND P-TYPE HYDROGENIC IMPURITY CONCENTRATIONS ON THE SOLID PHASE EPITAXIAL GROWTH OF AMORPHOUS SILICON. Young-Jin Jeon, Center for Materials Science and Engineering; Won-Woo Park, Dept. of Electrical and Computer Engineering; M. F. Becker, Dept. of Electrical and Computer Engineering; and R. M. Walser, Dept. of Electrical and Computer Engineering, The University of Texas, Austin, TX. 78712.

The solid phase epitaxial growth (SPEG) rates of self-ion amorphized layers in silicon wafers with <100> substrate orientation were measured previously by *in situ*, high precision, isothermal cw laser interferometry for temperatures from 450°C to 590°C, and concentrations in the range $5 \times 10^{18} \text{ cm}^{-3} < N < 3\text{--}4 \times 10^{20} \text{ cm}^{-3}$ for boron, phosphorous, and arsenic impurities.

At low impurity concentrations ($N < 4 \times 10^{19} \text{ cm}^{-3}$), the SPEG rate increased linearly with impurity concentration and satisfied the equation; $V/V_i = 1 + N/N_i$ where $N = \text{B, P, or As concentrations}$, $V_i(T)$ is the intrinsic growth rate and $N_i(T)$ is a temperature dependent quantity obtained from an activation plot of the intersections of the regrowth data with the concentration axis. To within experimental error, the activation energies and pre-exponential terms of the N_i 's for the three impurities were found to be identical. This clearly supports the view that impurity enhanced SPEG is a purely electronic effect. Surprisingly, this result also indicates that one-electron and one-hole effects on SPEG are not distinguishable for low values of N .

The SPEG rate varied quadratically with higher concentrations of ($4 \times 10^{19} \text{ cm}^{-3} < N < \sim 5 \times 10^{20} \text{ cm}^{-3}$) of the three impurities. The curvatures of the (V/V_i) vs (N/N_i) curves were also nearly the same, but that obtained for the acceptor (B) had the opposite sign of that obtained for the donors (P, As).

We interpret the result to indicate that processes associated with localized hole (electron) pairing, respectively accelerate (decelerate) the SPEG rate.

A8.9

COMPARISON OF MeV AND keV ION DAMAGE IN GaAs

S.T. Johnson¹, J.S. Williams^{1,2} and R.G. Elliman¹

1. Microelectronics and Materials Technology Centre, RMIT, Melbourne, 3000, Australia
2. Electronic Materials Engineering, RSPhysS, ANU, Canberra, 2601, Australia

The resultant damage to GaAs from an bombardment depends on the competition between defect production and dynamic (defect) annealing. Implantation parameters which have the dominant influence on damage production are ion mass, energy and dose. These give the deposited energy density about ion tracks and the integrated energy deposition. Additional parameters which influence dynamic annealing processes are ion dose rate and substrate temperature during implantation. In this paper, the nature and extent of MeV and keV ion damage in GaAs are compared as a function of ion mass, dose rate and temperature, using time resolved reflectivity, ion channeling and transmission electron microscopy techniques. In particular, the threshold conditions for amorphous phase production are measured and compared with various models.

A8.10

IN SITU CRYSTALLIZATION STUDY OF Kr ION AMORPHIZED Ge BY THERMAL ANNEALING WITH TEM* Lu-Min Wang, Robert C. Bircher and Lynn E. Rehn, Materials Science Division, Argonne National Laboratory, Argonne, IL 60439

The structural and morphological changes of Ge under 1.5 MeV Kr⁺ ion

irradiation at room temperature have been studied by in situ TEM. Amorphization in Ge was detectable after a Kr^+ dose of 8.5×10^{12} ions/cm², and was achieved after 1.2×10^{14} ions/cm². A high density of small void-like cavities, observed in the amorphous phase after 7×10^{14} ions/cm², grew into large holes transforming the irradiated Ge into a sponge-like porous material at a dose of 8.5×10^{15} ions/cm².

In this study, thermal annealing of 1.5 MeV Kr^+ ion amorphized Ge was carried out with TEM. Effects of ion dose and the morphology of the amorphous phase on crystallization have been studied. The variation of the temperature at which crystallization is complete, T_{Cr} , has been found to have three Kr^+ dose regimes. In the partially amorphized Ge, T_{Cr} increased with ion dose from 225°C to 400°C at 1.2×10^{14} ions/cm², where amorphization was complete. Between 1.2×10^{14} ions/cm² and 1×10^{15} ions/cm², T_{Cr} was constant within experimental uncertainty. In the third dose regime where large cavities have formed, T_{Cr} increased with ion dose. The sponge-like structure did not crystallize until the temperature reached 600°C. During annealing, the small cavities (3-10 nm in diameter) in the samples irradiated to $0.7-3 \times 10^{15}$ ions/cm² were expelled by the crystal growth front, and they coalesced into a few large holes. However, the sponge-like structure of the samples irradiated to higher doses ($\geq 8.5 \times 10^{15}$ ions/cm²) remained nearly unchanged after crystallization. The kinetics of crystallization in the three different dose regimes will be discussed.

*Work supported by the U.S. Department of Energy, BES-Materials Sciences, under Contract W-31-109-Eng-38.

A8.11

ION IMPLANT ACTIVATION AND REDISTRIBUTION IN $Al_xGa_{1-x}As$. S. J. Pearton, W. S. Hobson and A. E. Von Neida, AT&T Bell Laboratories, Murray Hill, NJ; N. M. Haegel, UCLA, Los Angeles, CA; K. S. Jones, University of Florida, Gainesville, FL; N. Morris and B. J. Sealy, University of Surrey, UK.

The electrical activation characteristics of implanted Be, Mg, Si and S in $Al_xGa_{1-x}As$ ($x = 0-1$) were investigated as a function of ion dose for rapid annealing in the range 600-950°C. The apparent activation energy for electrical activity of these species increases with increasing AlAs mole fraction. For Be this activation energy is 0.35 eV for GaAs and 0.49 eV for $Al_{0.54}Ga_{0.46}As$. Self-compensation is the predominant limiting mechanism for Si activation, as determined by the relative PL intensities of the Si_{Ga} -to- Si_{As} related transitions. No significant redistribution of implanted Si is observed for any AlAs mole fraction for RTA up to 900°C (5 sec) whereas S shows motion into the $AlGaAs$ and no tendency to outdiffuse. By contrast, both Be and Mg display loss of the dopant to the surface and little redistribution toward the bulk. Minimal damage is observed by TEM in as-implanted $AlGaAs$ for Be or Si doses below the amorphization threshold.

A8.12

DOPANT SITE LOCATION IN DUAL-IMPLANTED GaP USING DEPTH OSCILLATIONS OF {111} PLANAR CHANNELING TECHNIQUE. N. R. Parikh, C. T. Kao, D. R. Lee, J. Muse, M. L. Swanson, Dept. of Physics and Astronomy, University of North Carolina, Chapel Hill, NC 27599-3255, and T. E. Haynes, Oak Ridge National Laboratory, Oak Ridge, TN 37831-6048.¹

Previous studies have indicated that dual implantation can efficiently introduce group IV dopants onto selected sublattice sites and enhance electrical activation in III-V compound semiconductors. We have studied this phenomenon using Rutherford backscattering spectrometry to determine the lattice location of as-implanted Sn atoms in GaP. We used single crystals of GaP(100) which had been dual-implanted with $^{119}Sn^+$ following pre-implantation of either $^{69}Ga^+$ or $^{31}P^+$ at 400°C. Energies were selected for equivalent projected ranges, and all species were implanted with doses of 1×10^{15} ions/cm². The asymmetry in the angular dependence of the backscattering yield depth oscillations near the {111} planar channel was used to determine the sublattice site for the

implanted Sn. Preliminary results have suggested that the as-implanted Sn is predominantly on substitutional Ga sites after pre-implantation of either Ga or P.

¹ Research sponsored by the Division of Materials Sciences, U.S. Department of Energy under contract DE-AC05-84OR21400 with Martin Marietta Energy Systems, Inc.

A9.1

IN-SITU STUDY OF RADIATION DAMAGE IN V_2O_5 INDUCED BY LOW ENERGY ELECTRONS, Hanjie Fan, Rebecca Ai, and Laurence D. Marks, Department of Materials Science and Engineering, Northwestern University, Evanston, IL 60208

Radiation damage induced by low energy, low flux electrons has been studied by UHV-HREM. It is observed that irradiation by a 100eV electron beam at a flux of 10 μA for about 15min. induced changes only in the surface layer with a thickness that correlates to the electron mean free path. The surface damage follows the reduction route of, crystalline V_2O_5 \rightarrow amorphous, coupled with an ordered structure of oxygen vacancies. It is found that under irradiation of a 3keV electron beam at a flux of 50 μA for about 30min., the V_2O_5 surface transformed into a crystalline V_2O_5 phase. These observations suggest that desorption of oxygen from the surface and diffusion of oxygen to the surface from the bulk are two competing processes. Under low energy, low flux electron irradiation, oxygens desorb from the surface with a substantial faster rate than oxygens diffuse to the surface from the bulk, resulting a highly defect-containing surface which collapses into an amorphous phase. However, these two processes take place at a compatible rate under higher energy, higher flux electron irradiation, allowing formations of critical V_2O_5 nuclei which will grow upon further irradiation.

A9.2

As AND B ION IMPLANTATION THROUGH Mo AND INTO Mo-SILICIDE LAYERS FOR SHALLOW JUNCTION FORMATION. R. Angelucci, M. Merli, S. Solmi, A. Armigliato, R. Fabbri, E. Gabilli, and A. Poggi, CNR - Istituto LAMEL, Via Castagnoli 1, 40126 Bologna, Italy

Dopant ion implantation through refractory metal (ITM) films and implantation in silicide layers have been investigated as a viable approach to shallow junctions formation for VLSI applications.

As and B have been implanted through 40 nm e-gun evaporated Mo and into 100 nm thick $MoSi_2$ layer, obtained by RTA at 700°C, 60 s in nitrogen, to fabricate n⁺/p and p⁺/n circular diodes and test pattern for contact resistivity measurements. Post implantation annealing at 1000°C, 10 s and 1100°C, 2 s complete the fabrication process.

Measurements performed on diodes show a sensitivity of the junction characteristics to the fabrication process. In particular, the lowest values of leakage current, of the order of 1 nA/cm² at -1 V, are obtained for the implantation into silicide. Dopant distribution, measured by SIMS, and carrier concentration profiles, determined by incremental sheet resistance and Hall effect measurements, show a junction depth and a sheet resistivity of 130 nm and 26 Ω/\square for As and 170 nm and 30 Ω/\square for B after RTA at 1000°C, 10 s. No significant differences can be observed from the above mentioned carrier and dopant profiles for the two different junction formation procedures. The worst reverse current values for the ITM technology could be related to a different generation and evolution of the implantation damage. Electron microscopy observations and

Double crystal X-ray analysis are in progress to correlate residual damage and leakage current. The electrical activity of the deep levels, possibly introduced by the fabrication process, is being measured by Deep Level Transient Spectroscopy.

A9.3

CHARACTERIZATION OF N AND B IMPLANTED FUSED SILICA. C.W. Arnold and R.K. Brow, Sandia National Laboratories, Albuquerque, NM.

The formation of waveguides in glass by ion implantation is an attractive means for processing optical information in devices made by hybrid optoelectronic planar technology. Implanted species which are incorporated into the glass structure, such as B and N, result in greater index changes than are possible for ions producing changes through damage (compaction) alone. We have applied ion-beam analysis and XPS to the compositional and chemical characterization of 50 keV 1×10^{17} B and N/cm² implants into fused silica and have found clear evidence (XPS) for the formation of B₂O₃ and Si-oxyntiride. The N implanted samples exhibit two XPS peaks with ~50% of the N having a higher binding energy--which may be characteristic of unreacted N--than that for the SiO_xN_y peak. An implant of 1×10^{17} 95 keV Si/cm² or 1×10^{17} 120 keV Ar/cm² eliminates the unreacted N peak and results in a single Si-oxyntiride distribution which has a much greater N intensity than that for the combined original 2-peak distribution. Changes in the Si2p spectra are consistent with the formation of an oxyntiride layer. This result suggests that N precipitates formed at high ion fluences may be easily and efficiently incorporated into the modified glass structure and has important technological implications for the use of ion-implantation for optoelectronic purposes.

This work performed at Sandia National Laboratories supported by the U.S. Department of Energy under contract number DE-AC04-76DP00789.

A9.4

Excimer Laser Induced Crystallization of Amorphous Silicon Near Threshold. R.Z. Bachrach, K. Winer, J.B. Boyce, F. Ponce, S. E. Ready, R. I. Johnson, and G.B. Anderson, Xerox Palo Alto Research Center, 3333 Coyote Hill Road, Palo Alto Ca., 94304.

Experiments have revealed the near-threshold crystallization behavior of excimer laser irradiated thin amorphous silicon films deposited by plasma CVD (a-Si:H) and by LPCVD (a-Si). The intense, pulsed UV produced by the laser is highly absorbed by the thin amorphous material. TEM results indicate that crystallites nucleate in the surface region and X-ray analysis shows that the crystallites are randomly oriented. Following laser irradiation crystallites are produced whose structure and electrical characteristics vary according to starting material and laser scan parameters. Experiments relating crystallite grain size to other properties and characterizing the crystallized films using x-ray diffraction, Raman scattering, TEM, transport and other measurements will be described. Investigation of grain growth in crystallized a-Si:H and a-Si has shown the basic crystallization process exhibits a sharp threshold and increases as the square root of the laser energy density above threshold. Poor control of the laser beam can mask the threshold phenomena. Various dependences on material parameters such as doping and implanted Si concentration were also determined. Hydrogen is released from the film at a lower laser energy density than the onset of crystallization. Associated with the onset of crystallization is a sharp conductivity activation threshold phenomenon. TEM studies have identified that the threshold behavior of the crystallization process results in spatially abrupt interfaces between crystalline and amorphous material. Transient conductivity and absorption experiments investigating the kinetics of crystallization will also be presented.

A9.5

ELECTRON BEAM INDUCED RADIATION DAMAGE IN SUPERCONDUCTORS. S. Basu, T. Roy, T. E. Mitchell and M. Nastasi; Los Alamos National Laboratory, Los Alamos, NM 87545.

High temperature superconductors can be subjected to high energy radiation in certain potential applications. It has been demonstrated that electron beam radiation of superconducting samples in a transmission electron microscope can displace oxygen atoms in the lattice. This causes disordering of vacancies in the oxygen sublattice, leading to the orthorhombic to tetragonal transformation. This disordering can be monitored by changes in the b/a ratio. In some cases, prolonged radiation in the electron microscope has been known to cause oxygen loss and subsequent reordering of the Cu-O planes. In this study, the interaction of an electron beam with YBa₂Cu₃O₇ has been investigated as a function of electron energy, beam current, irradiation time and sample temperature.

A9.6

DUAL IMPLANTATION OF Ti AND C INTO SINTERED α-SiC AND HOT PRESSED Si₃N₄.* R. S. Bhattacharya, A. K. Rai, and D. Patrizio, Universal Energy Systems, Inc., 4401 Dayton-Xenia Road, Dayton, OH.

Ion implantation can be used to modify the near surface properties such as friction, wear, surface hardness and toughness of structural ceramics. Sintered α-SiC and hot pressed Si₃N₄ are known to amorphize under ion implantation resulting in softening of the surface layer. Thus, for improving surface hardness, toughness, friction and wear properties of these ceramics, dual implantations of appropriate elements are necessary to form hard second phases upon annealing induced recrystallization of the amorphous layer and chemical interaction of the implanted species. Dual implantations of Ti⁺ and C⁺ at energies of 175 keV and 50 keV respectively and at a dose of 1×10^{17} cm⁻² for each species have been performed into both SiC and Si₃N₄ substrates. The implanted samples were annealed at 1200°C for 2 hours in high vacuum (~1x10⁻⁶ torr) by placing them in Ta box. Rutherford backscattering analysis showed that no oxidation occurred during annealing and Ti diffused outward toward the surface in both SiC and Si₃N₄. Cross section TEM analysis revealed the formation of TiC precipitates in both SiC and Si₃N₄. A comparison of these results with that of single Ti implantation will be presented.

* This work was supported by the DOE, ECUT under Contract DE-AC05-84OR21400 with Martin Marietta Energy Systems, Inc.

A9.7

X-RAY AND RAMAN TOPOGRAPHIC STUDIES OF Si-ION IMPLANTED, PULSED-LASER-ANNEALED GaAs. R.C. Bowman, Jr, P. Adams, J.T. Knudsen, Aerospace Corp., Los Angeles, CA, H.D. Yao* and A.D. Compain, University of Toledo, Toledo, OH.

The lattice reconstruction of pulsed laser annealed, Si-ion implanted GaAs has been studied by both x-ray double crystal topography and Raman topography. The x-ray rocking curves show, for an implant dose of 2×10^{14} /cm², a maximum implantation-induced lattice dilation of 0.38%. At the center of the laser annealed spot for a pulse energy typically of 0.6 J/cm², the lattice strain is almost completely removed. However, concentric bands of reduced strain or a tilted lattice are observed surrounding the central annealed area. These characteristic bands are observed in regions where the pulsed laser energy density is in the range of 0.1-0.2 J/cm². The Raman topographs were obtained by raster scanning the sample with the spectrometer fixed at either the TO phonon frequency, LO frequency, or the amorphous band.

Correlation of the Raman results with the x-ray topographs show that the concentric bands correspond to the region in which some melting has occurred but epitaxial regrowth has not occurred since the melt front has not penetrated to the undamaged substrate. Further results obtained on higher dose Si implants up to $5 \times 10^{15}/\text{cm}^2$ will also be discussed.

* Present address: Center for Microelectronic and Optical Materials Research, University of Nebraska, Lincoln, NE.

A9.8

SURFACE REACTIONS OF NiO AND CoO IN THE ELECTRON MICROSCOPE ENVIRONMENT. Mary I. Buckett and L. D. Marks, Department of Materials Science and Engineering, Northwestern University, Evanston, IL 60208.

NiO and CoO surfaces react to form their respective Ni_3O_4 and Co_3O_4 spinel phases during irradiation in the electron microscope at a vacuum level of 10^{-7} Torr, but not at 10^{-10} Torr. Spinel formation occurring on (001), (110), and (111) profile surfaces of NiO and CoO have been examined in detail by through-focal series comparison of HREM experimental images with multislice image calculations. NiO surfaces tend to form (111) facets when exposed to the electron beam. Spinel formation is observed to nucleate preferentially at faceted (111) surfaces and at surface defects. Propagation into the bulk follows diffusion-controlled behavior. Once formed, Ni_3O_4 (001) and (110) surfaces appear to be stable in the electron beam. In contrast, the Ni_3O_4 (111) surface is seen to undergo dynamic reaction which reverts the surface 1 to 2 monolayers back to NiO. Ni_3O_4 spinel formation is reversible; the original NiO structure reappears with the beam removed. In CoO, faceting is not observed during electron irradiation. The spinel phase nucleates uniformly on all exposed (001), (110), and (111) surfaces. Unlike the case for NiO, Co_3O_4 spinel formation from CoO is irreversible.

In both cases, the surface-initiated formation of spinel phase appears to be a direct result of interaction between the sample surface and adsorbed species from the microscope environment. It is also strongly dependent on the incident electron flux, but not energy, which suggests an electron-stimulated reaction mechanism.

A9.9

SUBNANOSECOND TIME-RESOLVED ELECTRON DIFFRACTION FROM THIN CRYSTALLINE GOLD FILMS. Hsiu-Cheng Chen,* Gerard Mourou,† and Robert Knox,* Laboratory for Laser Energetics, University of Rochester, 250 East River Road, Rochester, New York 14623-1299

A 100-ps and 25.5-keV electron pulse was used to probe a 25-nm thick gold single crystal irradiated by a synchronized infrared optical pulse. The time-resolved changes in electron diffraction intensity following laser heating were interpreted in terms of temperature changes on a subnanosecond scale. An observed oscillatory behavior is believed to arise from the relaxation of a crystal lattice distortion in the surface region associated with surface plasmon generation. The relaxation of the surface layers of atoms appears to give rise to an oscillation in time of the scattered electron intensity. A preliminary theoretical interpretation is given using a modified Debye-Waller method.

*Also at: Department of Physics and Astronomy, University of Rochester, Rochester, New York 14627-0011.

†Present address: Department of Electrical Engineering and Computer

Science(E ECS), University of Michigan, Room 1116A, 1301 Beal Avenue, Ann Arbor, Michigan 48109-2122.

Acknowledgement: This work was supported by the Sponsors of the Laser Fusion Feasibility Project at the Laboratory for Laser Energetics. This work was also supported by the U.S. Air Force under contract F49620-87-C-0016.

A9.10

IRRADIATION INDUCED METASTABLE PHASE FORMATION IN AMORPHOUS THIN FILMS DEPOSITED BY MAGNETRON COSPUTTERING. Qing-Ming Chen, Huazhong University of Science and Technology, Wuhan, China; Yu-Dian Fan and Heng-De Li, Tsinghua University, Beijing, China.

Irradiation induced metastable phases in the amorphous thin Al-Fe, Al-Ni and Al-Co films have been studied in detail. The amorphous thin films were deposited by magnetron cosputtering onto the substrates which were kept at the liquid-nitrogen temperature. The composition of the samples in a total length of 200 mm spans the whole range of each binary phase diagram. The compositions and structures of the as-deposited thin films were determined by Rutherford backscattering analysis and by transmission electron microscopy. Then the amorphization range of each system was confirmed.

The amorphous samples of these three systems were irradiated with 300 keV Xenon ions to some four doses with the ion flux being less than $1 \mu\text{A}/\text{cm}^2$. After irradiation, all the samples were examined by transmission electron microscopy to detect the ion induced structures. The electron diffraction patterns of some irradiated samples revealed that crystalline structural phase transition took place in the samples and some non-equilibrium phases have been formed.

Finally, some phenomena in the structural phase transition have been discussed.

A9.11

CONDENSATION OF ULTRAFINE SILICA FROM A LASER-INDUCED PLUME. Gan-Moog Chow* and Peter R. Strutt, U-136 Institute of Materials Science, the University of Connecticut, Storrs, CT 06269.

A study of rapid condensation of silica from a plume produced by the interaction of a continuous-wave carbon dioxide laser beam with a ceramic target is presented. This process occurred in a reactive mixture gas environment (98.5% hydrogen, 1.5% methane). A heated tungsten filament was also placed in the proximity of the laser beam - material interaction zone. Silica deposited on a Ni alloy substrate exhibited different metastable morphologies, namely, nanometer-size amorphous fibers or linear-chain shape aggregates. There appeared to be a correlation between the morphology of the deposits and the position of the heated tungsten filament. When the tungsten filament was absent, silica was deposited in the form of clusters. In this case, depending on the beam-ceramic target interaction times, there was a shift in the Si-O stretching vibration characteristics. Sintering of these deposits was also observed at a hotter region on the substrate surface. It is proposed that chemical vapor transport reactions involving the heated tungsten filament affected the final morphology of the condensed silica. Mechanisms controlling the agglomeration of condensed silica are also discussed. Characterization techniques involved FTIR, X-ray diffraction, Auger and microprobe analysis, EDX and WDX analysis, SEM and TEM.

* Currently at Composites and Ceramics Branch, Code 6371, Naval Research Laboratory, Washington, D.C. 20375.

LASER VAPORIZATION AND DEPOSITION OF LEAD ZIRCONATE TITANATE. Peter K. Schenck, Lawrence P. Cook, Jiarong Zhao¹, John W. Hastie, Edward N. Farabaugh, Chwan-Kang Chiang and Mark D. Vaudin, National Institute of Standards and Technology, Gaithersburg, MD; and Philip S. Brody, Harry Diamond Laboratories, Adelphi, MD.

Laser induced vaporization of ceramic and refractory materials shows promise as a technique for the deposition of thin films of these materials. Critical to the utility of this technique is an understanding of the laser material interaction, plume formation and dynamics, material transport and how variations in the vaporization conditions effect the deposited film. Lead zirconate titanate (PZT, Zr/Ti~50/50) targets were irradiated using a q-switched Nd:YAG laser (10ns, 100mJ at 1.064 μ m). The deposition chamber was maintained at a pressure of 100 mTorr oxygen. Material from the plume was collected on single-crystal MgO substrates, suspended 1.0 - 2.0 cm above the target. The as-deposited films are being characterized by SEM/EDX, TEM, ESCA, x-ray diffraction and electrical measurements prior to and after annealing.

Temporally and spatially resolved spectra of the light emitted by the laser-generated plume were obtained with an optical multichannel analyzer (OMA) to yield information on the plume generation and chemistry of the deposition process. These spectra indicate that under these conditions a plasma is created above the target surface which persists for ~100 ns after the laser pulse.

¹ Guest Scientist, Chinese Academy of Science, Beijing, Peoples Republic of China.

PHOSPHORUS IMPLANTATION OF 304L STAINLESS STEEL. E. C. Cooney and D. I. Potter, Metallurgy Department, School of Engineering, Institute of Materials Science, The University of Connecticut, Storrs, CT, USA 06269-3136; N. L. Lee and G. B. Fisher, Physical Chemistry Department, General Motors Research Laboratories, Warren, MI, USA 48090-9055.

Electropolished 304L stainless steel specimens were implanted near room temperature with 175 keV phosphorus ions to fluences from 0.24×10^{17} P⁺/cm² to 4.0×10^{17} P⁺/cm². Microstructural characterization of the samples with an analytical electron microscope revealed an FCC to BCC transformation at fluences near 1.0×10^{17} P⁺/cm², followed by amorphous phase formation at 3.5×10^{17} P⁺/cm². Precipitation of a hexagonal phase, indexed as Fe₃P, from the amorphous matrix occurred at fluences of 3.75×10^{17} P⁺/cm². Anodic polarization measurements performed on specimens implanted to 3.5×10^{17} P⁺/cm² to generate amorphous phase showed no significant decrease in the critical anodic current density as compared to unimplanted 304L stainless steel. However, pitting corrosion was not seen on implanted specimens, whereas unimplanted specimens showed extensive pitting attack.

DENSITY OF AMORPHIZED SILICON AND ITS CORRELATION WITH STRUCTURE. J. S. Custer and Michael O. Thompson, Cornell University, Ithaca, NY; J. M. Poate and D. C. Jacobson, AT&T Bell Laboratories, Murray Hill, NJ; S. Roorda and W. C. Sinke, FOM Institute for Atomic and Molecular Physics, Amsterdam, The Netherlands; and F. Spaepen, Harvard University, Cambridge, MA.

The intrinsic density of amorphous Si (a-Si) is an important physical parameter. There is, however, a considerable spread in the density measurements with values ranging from 2-11% less dense than that of crystalline Si (c-Si). Moreover, there are computer simulations which indicate that a-Si should be denser than c-Si. To measure the intrinsic density it is essential that the a-Si layers be impurity and void free. We have achieved this using high energy Si implantation in Si.

Thick amorphous Si layers are created by multiple energy MeV Si self-

implantation using contact masks, resulting in sharp lateral amorphous-crystal boundaries. For thick Si substrates, the lateral dimensions are constrained and the majority of the density difference between the two phases is manifested as a surface step that can be measured using a surface profiler. These measurements indicate that as-implanted a-Si is 2% less dense than c-Si. Thermal anneals which lead to relaxation of the a-Si, but no measurable regrowth, result in a 10% decrease of the surface step heights. Once this initial decrease is over, the step heights scale linearly with a-Si thickness as the layer is regrown by solid phase epitaxy. Comparisons of these density changes with models, and the effects of post-relaxation ion irradiation will also be discussed.

NOBLE GAS ION IMPLANTATIONS IN LASER TREATED MATERIALS J. Th. M. De Hosson, Dept. of Applied Physics, Materials Science Centre, Nijenborgh 18, 9747 AG Groningen, The Netherlands.

Despite the advantages of laser processing for the production of wear resistant materials, laser surface melting results in tensile stresses because the melted layer shrinks during resolidification. These tensile stresses may lead to severe cracking of the material and to deleterious effects on the wear behaviour. Our basic idea presented in this paper is to convert the high tensile stresses in the laser melted surface into a compressive state after implantation.

When pressurized bubbles of implanted ions are nucleated in the surface layer, one can imagine that the corresponding compressive stress field may annihilate the tensile stress field of the laser melted materials. Furthermore, the surface layer might also be strengthened during wear, due to the interaction between moving dislocations and the bubbles. Results are presented of He and Ne implantations into laser treated materials.

FEMTOSECOND LASER MELTING OF GRAPHITE. D. H. Reitze, X. Wang, H. Ahn, and M. C. Downer, Physics Department, University of Texas at Austin, Austin, TX.

We report on the results of time-resolved reflectivity measurements on highly oriented pyrolytic graphite (HOPG) using 90 fs., 620 nm. pulses. In contrast to earlier picosecond melting experiments¹, we observe a large increase in reflectivity when the excitation pulse exceeds the critical fluence for melting ($F_m = 0.13$ J/cm²), suggestive of a liquid metallic phase², followed by a dramatic decrease in reflectivity caused by material ablation on the sample surface.

Differential reflectivity measurements on HOPG were performed over a wide range of excitation fluences. At excitation levels below F_m , the reflectivity decreases slightly initially and rapidly recovers in < 1 ps. When the critical fluence is reached, however, the initial reflectivity change is large and positive. For pump fluences slightly above F_m , the initial positive reflectivity phase persists for ~10 ps., crosses below the background value, and decreases to a small fraction of the background value at ~40 ps. As the pump fluence is increased, the crossing point occurs at earlier times, caused by the rapid ablation of surface material which obscures the surface.

Additional time-resolved experiments using a probe wavelength of 310 nm. as well as 620 nm probes with s and p polarizations were performed in order to elucidate the natures of the molten surface and the ablation cloud. Results of these measurements will be presented.

1. A. M. Malvezzi, N. Bloembergen, and C. Y. Huang, Phys. Rev. Lett. **57**, 146, (1986).

2. J. Heremans, C. H. Olk, G. L. Easley, J. Steinbeck, and G. Dresselhaus, Phys. Rev. Lett. **60**, 452, (1988).

A9.17

FORMATION OF DEFECT-FREE SHALLOW JUNCTIONS BY LOW-TEMPERATURE RAPID THERMAL ANNEALING.* M. K. El-Ghor, S. J. Pennycook, and R. A. Zuhr, Oak Ridge National Laboratory, Oak Ridge, TN 37831.

Low and high doses of As⁺ (3×10^{14} – 1×10^{16} cm⁻²) were implanted in Si single crystals in the energy range of 2 to 17.5 keV at room temperature. Defect-free shallow junctions with good electrical activation have been achieved at temperatures as low as 700°C by rapid thermal annealing. Cross-sectional transmission electron microscopy combined with in situ annealing has been used to distinguish the two possible mechanisms responsible for defect removal, bulk diffusion of point defects leading to defect annihilation, and glide of extended defects to the surface through the action of image forces. This latter mechanism is shown to become a more efficient means for defect removal as the junction becomes more shallow.

*Research sponsored by the Division of Materials Sciences, U.S. Department of Energy under contract DE-AC05-84OR21400 with Martin Marietta Energy Systems, Inc.

A9.18

A COMPARISON OF LOW AND HIGH DOSE GALLIUM ION IMPLANTED POLYCRYSTALLINE SILICON. H.B. Harrison, Microelectronics, Griffith University, Australia 4111, A.P. Pogany, D.X. CAO MMTL, RMIT, Melbourne, Australia 3000, and Y. Komen, Technion, Israel.

Gallium (Ga) implanted polycrystalline silicon is the subject of this investigation. Ga ions of 100keV and doses 3×10^{14} /cm² and 6×10^{15} /cm² (low and high dose respectively) have been studied with regard to their annealing properties. Previous reports by this group have concentrated on the higher dose regime, namely that of a liqued phase melt regime that determined the final morphology, and other physical and electrical properties.

Whilst the lower dose results in a similar damage layer albeit to a different depth, the annealing cycle tends to follow a more conventional solid phase epitaxial growth. However there are other interesting differences between the two doses regimes and it is the intent of this paper to highlight these differences and suggest speculative reasons for these physical and electrical differences.

A9.19

DIFFUSION OF CARBON IN TEMPERED MARTENSITIC STEEL DURING LASER MELTING. J.P. Hirvonen, T. R. Jervis, and T. G. Zocco, Materials Science and Technology Division, Los Alamos National Laboratory, Los Alamos, NM 87545

Migration of carbon is one of the most important factors determining the final microstructure of the laser melted surface of carbon steel. The formation and dissolution of carbides restricts the amount of carbon capable of diffusing during the melt duration (~ 100 nsec). This affects coarsening, composition, and microstructure of the modified surface layer.

Tempered martensitic steel with nominal composition: 1.05 wt. % C, 0.2 wt. % Si, and 0.3 wt. % Mn was implanted with ¹³C and subsequently laser melted with an excimer laser operating at 248 nm. The surface was exposed to five and ten pulses at an energy density of 1.2 J/cm² per pulse. The concentration profiles were measured utilizing the resonance of the nuclear reaction ¹³C(p,γ)¹⁴N at a proton energy of 1.948 MeV. From the measured concentration profiles the diffusion length per pulse as well as the fraction of carbon bonded to undissolved carbides were calculated. These results will be compared to similar studies in laser melted carbon implanted iron. Results of microstructural characterization of the surfaces using transmission electron microscopy will also be presented.

A9.20

RAPID THERMAL ANNEALING OF Si⁺ and P⁺ DUALY IMPLANTED InP. Shen Honglie, Yang Genqing, Zhou Zuyao and Zou Shichang, Ion Beam Laboratory, Shanghai Institute of Metallurgy, Academia Sinica, Shanghai, China 200050

150KeV Si⁺ ions and 160KeV P⁺ ions were implanted at 200°C with doses ranging from 1×10^{13} to 1×10^{15} /cm² to study the effect of dual implantations on the electrical properties of Fe doped InP. Samples were deposited with Si₃N₄ films of 1000Å by PECVD and annealed in a halogen tungsten lamp RTA system under flowing N₂ at different temperatures from 700 to 900°C for 5s. The samples were characterized by Hall measurements using the Van der Pauw method. To obtain carrier concentration profiles, differential Hall measurements were performed using 1:1 mixture of H₃PO₄:H₂O₂. It has been found that Si and P dual implantations in InP can results in an enhanced activation, particularly evident at high doses of implantation. The maximum dopant activation and average electron mobility for Si and P dual implants at doses of 1×10^{15} /cm² are 70% and 750cm²/vs, which corresponds to a peak carrier concentration of 5×10^{19} /cm³ while that for Si single implant at the same dose are 29% and 870cm²/vs, which corresponds to a peak carrier concentration of 1.2×10^{19} /cm³. It can be seen from the carrier concentration profiles that Si dopant is effectively prevented from interdiffusion with the help of rapid thermal annealing and P implantation.

A9.21

MODELING OF LOCALIZED MELTING OF THIN Si FILMS IN ZONE-MELTING RECRYSTALLIZATION. J.S. Im,^{a,c} J.D. Lipman,^b I.N. Misoulis,^b C.K. Chen,^c and C.V. Thompson.^a

^aDepartment of Materials Science and Engineering, Massachusetts Institute of Technology, Cambridge, MA 02139.

^bMechanical Engineering Department, Tufts University, Medford, MA 02155.

^cLincoln Laboratory, Massachusetts Institute of Technology, Lexington, MA 02173-0073.

Using the finite difference enthalpy method, we have developed a quantitative model that accounts for the localized melting behavior of thin Si films. The model incorporates radiative and conductive heat flow components and takes account of the phase changes that occur during zone-melting recrystallization. Emphasis is placed on the effects resulting from the differences in reflectivity and emissivity between solid and liquid Si. Quantitative information is provided concerning the temperature profile of the Si film and the configuration of the solid-liquid phase boundaries. The model shows the existence of two distinct types of melting behavior: reflectivity-change-dominated and emissivity-change-dominated. Partial melting and nonplanar solid-liquid interfaces are characteristic of reflectivity-change-dominated behavior, while "explosive" melting and hysteresis are characteristic of emissivity-change-dominated behavior.

The Lincoln Laboratory portion of this work was sponsored by the Rome Air Development Center.

A9.22

EFFECTS OF NITROGEN ION IMPLANTATION IN 304 STAINLESS STEEL AT HIGH TEMPERATURES. Sadhna Shrivastava, Ram D. Tarey, M.C. Bhatnagar, Amitabh Jain and K.L. Chopra, Indian Institute of Technology, Hauz Khas, New Delhi-110016, India.

Nitrogen ion implantation is an attractive technique for surface strengthening of metals and alloys. In order to achieve high throughputs, high dose rates are necessary and cooling of the target is often impractical. We present a study of the influence of target temperature on the stru-

cture and properties of nitrogen ion implanted 304 stainless steel. With a beam power of 0.1 W/cm^2 the target temperature is restricted to 150°C . At a dose of $3.5 \times 10^{17} \text{ N}_2/\text{cm}^2$, Glancing Angle X-ray Diffraction revealed the formation of ϵ -iron nitride and no nitrogen in solution. The microhardness measured at 10g increases by 15% . With a beam power of 1.1 W/cm^2 the target temperature is 550°C . At the same dose as before, the amount of ϵ -iron nitride produced is smaller but there is a few atomic percent nitrogen in solid solution. There is in addition the formation of chromium nitride. The increase in microhardness is 40% in this case. This enhanced hardening appears to be due to interstitial solid solution strengthening by nitrogen. The specimens contained a bcc phase which lends itself to such hardening. In general, Auger depth profiling revealed thermal redistribution effects and some loss of nitrogen through out-diffusion.

A specimen deformed by compression formed an enhanced oxide layer during ion implantation at a high beam power. There is no loss of nitrogen in this case. The oxide layer appears to have a capping action against out-diffusion.

A9.23

ANALYTICAL STUDY OF EFFECT OF ARSENIC CONCENTRATION ON SOLID PHASE EPITAXIAL GROWTH OF AMORPHOUS SILICON. Young-Jin Jeon, Center for Materials Science and Engineering; M. F. Becker, Dept. of Electrical and Computer Engineering; and R. M. Walser, Dept. of Electrical and Computer Engineering, The University of Texas, Austin, TX. 78712.

In this work we measured the functional dependence of the solid phase epitaxial growth (SPEG) of amorphous silicon on the concentration of implanted arsenic (n-type) impurity, N_{As} . The SPEG rates of self-ion amorphized layers in silicon wafers with $\langle 100 \rangle$ substrate orientation were measured by *in situ*, high precision, isothermal cw laser interferometry for temperatures from 470°C to 580°C , and concentrations in the range $5 \times 10^{17} \text{ cm}^{-3} < N_{\text{As}} < 3.8 \times 10^{20} \text{ cm}^{-3}$.

Changes in the SPEG velocity were not detected for $N_{\text{As}} < 6 \times 10^{18} \text{ cm}^{-3}$, but the growth rate increased linearly with arsenic concentrations in the range $6 \times 10^{18} \text{ cm}^{-3} < N_{\text{As}} < 2 \times 10^{19} \text{ cm}^{-3}$. In the linear region the SPEG data satisfied the equation; $V/V_i = 1 + N/N_i$, where $N_i(T)$ was fit to an Arrhenius form obtained from the temperature dependent intersections of the regrowth data with the concentration axis. In previous work we showed that the enhancement of the SPEG velocity by B and P could be described by an equation of the same form. For As, the activation energy and pre-exponential terms of N_i were 0.23 eV and $9.8 \times 10^{20} \text{ cm}^{-3}$; both values are only slightly smaller than those obtained for B and P implanted samples.

The activation energy for SPEG decreased for $N_{\text{As}} < 1 \times 10^{20} \text{ cm}^{-3}$ and increased for higher concentrations to $N_{\text{As}} = 3.8 \times 10^{20} \text{ cm}^{-3}$. The pre-exponential term for SPEG exhibited a similar variation with N_{As} . The SPEG rate varied nonlinearly with high arsenic concentrations ($N_{\text{As}} > 2 \times 10^{19} \text{ cm}^{-3}$) and a reduction in the rate of increase of the SPEG rate with N_{As} was observed. A similar effect was previously observed for P; another donor impurity. The quadratic fit of the data in the nonlinear range for both P and As suggests that processes involving localized electron pairing may have a deleterious effect on Si SPEG.

A9.24

ION CHANNELING MEASUREMENTS OF STRAIN IN GERMANIUM IMPLANTED AND ANNEALED SILICON. E.A. Johnson, and F. Namavar, Spire Corporation, Patriots Park, Bedford, MA; R.J. Culbertson, U.S. Army Materials Technology Laboratory, Watertown, MA.

We have used ion beam channeling (2 MeV He^+) to examine the surface of $\langle 100 \rangle$ silicon after low dose (10^{14} - $10^{15} \text{ atoms/cm}^2$) germanium implantation and annealing. After a moderate annealing regimen (850°C , $\leq 1 \text{ hr}$), backscattered particle channeling dips indicate that germanium atoms substitute into the silicon lattice. Aligned backscattering spectra show good channeling in the shallow, germanium implanted region with minimum yields comparable to pure, unimplanted silicon. At greater depths, beyond the projected

range of the germanium, aligned spectra exhibit ledges corresponding to somewhat higher dechanneling yields. We explore the orientation dependence of these ledges and propose a pseudomorphic lattice regrowth model to explain these observations.

A9.25

LOW ENERGY Si AND Sn IMPLANTATION OF GaAs. K.S. Jones, W.S. Rubart and L. Seiberling, University of Florida, Gainesville, Florida and D.K. Sadana, IBM T.J. Watson Research Center, Yorktown Heights, New York

Low energy Si^+ and Sn^+ implantation into GaAs has been studied extensively by cross-sectional and plan-view TEM. Comparisons of equivalent damage density distributions for the two species, formed by adjusting the implantation energy and dose over a three order of magnitude range, indicate ion beam induced epitaxial crystallization (IBIEC) greatly restricts the "window" for amorphous layer formation during room temperature implantation. For a 20 KeV Si^+ implant in GaAs only doses between $5 \times 10^{14} \text{ cm}^{-2}$ and $2 \times 10^{15} \text{ cm}^{-2}$ resulted in observation of an amorphous layer after implantation. A correlation between the existence of an amorphous layer and the subsequent extended defects observed upon annealing will be presented. When complete IBIEC induced regrowth of the amorphous layer occurred during the implantation, then extended defects formed upon rapid thermal annealing in an inert ambient. However, suppression of arsenic loss during rapid thermal annealing via use of either an arsine ambient or Si_3N_4 capping, suppresses or destabilizes extended defects. This elimination mechanism may be related to increasing the much more mobile Ga vacancy concentration which can dissolve the extrinsic, implant related dislocation loops. Finally RBS channeling results indicate suppression of arsenic loss during rapid thermal annealing results in a higher fraction of the implanted tin being substitutional which corresponds well with increased gallium vacancy formation. This was confirmed by observations of Sn precipitate concentrations in cross-sectional TEM. Hall effect results will also be presented on the activation of the implanted dopant.

A9.26

HIGHLY STABLE W/p-In_{0.53}Ga_{0.47}As OHMIC CONTACTS FORMED BY RAPID THERMAL PROCESSING. A. Katz, R.F. Kerlicek Jr., J.D. Wynn, B.E. Weir, D. Maher, P.M. Thomas, M. Soler, W.C. Dautremont-Smith and L.C. Kimmerling, AT&T Bell Laboratories, 600 Mountain Avenue, Murray Hill, NJ 07974.

Tungsten contacts to Zn doped $\text{In}_{0.53}\text{Ga}_{0.47}\text{As}$ have been formed by rapid thermal processing. Contacts to layers with Zn doping concentration of $5 \times 10^{18} \text{ cm}^{-3}$ were rectifying as sputter deposited as well as after heat treatments at temperatures lower than 450°C . Higher processing temperatures caused a linear decrease of the contact resistivity values from $0.6 \text{ } \Omega/\square$ as deposited to $0.15 \text{ } \Omega/\square$ after heating at 550°C . Rapid thermal processing at these higher temperatures stimulated the Schottky to ohmic contact conversion with minimum contact resistance value of $8.5 \times 10^{-5} \text{ } \Omega/\square$ and sheet resistance value of $150 \text{ } \Omega/\square$ as a result of heating at 600°C for 30 sec . By increasing the p-InGaAs doping level to $1 \times 10^{19} \text{ cm}^{-3}$ the specific contact resistance of this contact was dropped to the minimum of $7.5 \times 10^{-6} \text{ } \Omega/\square$ as a result of heating at 500°C for 30 sec . The W/p-In_{0.53}Ga_{0.47}As contact showed excellent thermal stability over the temperature range of 300 to 750°C , with an abrupt and almost unreacted metal-semiconductor interface. Heating at temperatures of 800°C or higher caused the degradation of the contact. This was reflected by a distinct increase in the heterostructure sheet resistance as a result of the intensive interfacial reaction which took place at the contact, accompanied by out diffusion of both In and As.

A9.27

MÖSSBAUER STUDY OF THE DEFECT STRUCTURES AROUND Te IMPLANTED IN $\text{Al}_x\text{Ga}_{1-x}\text{As}$. H. Bemelmans and G. Langouche, IKS, University of Leuven, Belgium; G. Borghs, IMEC, Leuven, Belgium.

^{125}Te atoms were implanted in $\text{Al}_x\text{Ga}_{1-x}\text{As}$ ($0 \leq x \leq 1$) with a dose of $2 \times 10^{15} \text{ atoms/cm}^2$. After rapid thermal annealing to 900°C , a variation in the Mössbauer spectra as a function of x is observed. For $0.2 \leq x \leq 0.7$, a component with a large electric field gradient is

dominant in the spectra, while for the other values of x an unsplit resonance dominates. The same component with the large electric field gradient was observed before [1] in the Mössbauer spectra of Te-implanted GaAs for concentrations exceeding 10^{19} atoms/cm³.

As the presence of this component is correlated with the presence of the DX-center, the hyperfine interaction parameters of the observed Mössbauer spectrum component will be discussed with respect to some of the existing models for the DX-center.

[1] G. Langouche, D. Schroyen, H. Bemelmans, M. Van Rossum, W. Deraedt and M. de Potter, *Mat. Res. Soc. Symp. Proc.* 104 (1988) 527.

A9.28

ION BEAM METHOD TO STUDY FRACTAL AGGREGATION OF MAGNETIC PARTICLES IN THIN FILMS J.R.Ding, L.J. Huang and B.X.Liu(a), Department of Materials Science and Engineering, Tsinghua University, Beijing 100084, CHINA; (a) also at Center of Condensed Matter and Radiation Physics, CCAST(World Lab.), Beijing.

Fractal aggregates of magnetic particles(Co and Fe) were observed in vapor-deposited Ag-Co and Fe-Cu alloy films, after the films had been irradiated at room temperature by 200 keV xenon ions to various doses. The fractal dimensions were determined with box-counting method to be 1.47 ± 0.02 and 1.42 ± 0.02 for Co and Fe, respectively. It was found that the fractals were formed through a cluster-cluster diffusion aggregation(CDLA) process. However, the dimensions observed were smaller considerably than the value of 1.72 expected by the CDLA model, because of the magnetic interaction among the aggregating particles. This is in agreement with the previous reported results.

The multiscaling properties of the observed fractals were also studied and showed some differences from those reported earlier.

A9.29

MODIFICATION OF NITRIDE CERAMIC STRUCTURE AND RESISTIVITY BY ION BEAMS. V.V.Lopatin, and A.V.Kabyshhev, High Voltage Institute, Tomsk, USSR

The ion implantation (The parameters of plasma-arc accelerator = 100 keV, 1-20 mA/cm², pulse duration = 250 μ s, frequency = 5-50 Hz) modifies structure and properties of a high dispersive nitride ceramics α -BN, AlN and Si₃N₄. In comparison with the heavy ions (Fe, Cu, Mo, W) the attack by light ions (Li, B, C, Al) modifies more significantly the structure and resistivity ρ_s inducing more thermostable coat.

The structure modification consists, generally, of grinding the crystallites up to formation of an amorphous film with the thickness that equals approximately the ion range (~ 30 nm). The ρ_s of coat increases at the depth of 300 to 500 nm.

As compared to the starting materials with $\rho_s = 10^{13} - 10^{14} \Omega$ growing dose from 10^{14} cm⁻² to 10^{17} cm⁻² results in the decreasing surface's ρ_s to $10^9 \Omega$. If C⁺-implantation occurs in the regime of ion mixing, for $D > 10^{15}$ cm⁻² new phases are synthesized as the flat crystals.

Post-implantation annealing increases the conductivity too, and allows to form the coat with the controllable $\rho_s = 10^3 - 10^9 \Omega$ and low temperature coefficient of resistivity (up to $10^{-4} K^{-1}$

within the temperature range to 1500 K). In this case the mechanism of conductivity changes due to the forming localized states within a wide band gap.

A9.30

REDUCTION IN SECONDARY DEFECT FORMATION IN MEV ION IMPLANTED Si(100)

W.X. Lu, R.J. Schreutelkamp, J.R. Liefsting and F.W. Saris, FOM Institute for Atomic and Molecular Physics, Kruislaan 407, 1098 SJ Amsterdam, The Netherlands

MeV ion implantation in Si above a dose of 10^{14} /cm² leads to secondary defect formation in a buried layer, which is rather stable. Annealing behaviour of Si(100) implanted with 1.0 and 2.0 MeV As⁺, B⁺ and Si⁺ ions at a dose above 10^{14} /cm² has been investigated by means of cross-sectional TEM. After annealing at 900°C for 15' elongated dislocation loops were found along [110] direction. A remarkable decrease in secondary defects has been observed if in addition a low energy silicon implantation was performed prior to annealing to form a sink for defects created during MeV implantation. The reduction of the secondary defect formation shows a strong dependence on the amount of disorder in the near surface region due to the low energy implant.

A9.31

AMORPHOUS METALLIC ALLOYS FORMED BY PLASMA ION MIXING. Xiaoci Zheng, R. Arthur Dodd, John R. Conrad, and Frank Worzala, University of Wisconsin, Madison, WI.

When plasma ions interact with layered Ni-based metallic films, the structures resulting from the ion-surface reactions vary with the ion dose and ion mass. For light ions, smaller grains are formed after plasma ion mixing, but no amorphous structure is observed. For heavy ions, an amorphous phase is obtained as long as the dose is larger than a critical value. The film structures are checked by TEM and electron diffraction.

The stability of the amorphous phase has been investigated by annealing the samples at various temperatures, and recrystallization is observed when the annealing temperature is above T_r . The grain sizes of recrystallized films are dependent on the annealing time.

A9.32

LASER PULSE TRIGGERING OF THE EXPLOSIVE CRYSTALLIZATION IN AMORPHOUS Si AND Ge THIN FILMS. W. Marine and J. Marfaing, UA CNRS 783, Faculté des Sciences de Luminy - Département de Physique - Case 901 - 13288 Marseille Cedex 9, France.

The first stage of triggering of the well known explosive crystallization is accelerated nucleation rate which generates large heat flow necessary to induce the intermediate melting. If in the ion implanted amorphous samples high nucleation rate can be explained by interfacial (amorphous-liquid-crystalline states) mechanisms, this nucleation is a purely thermal effect. Observed nucleation instabilities reported in this paper give an experimental evidence of the laser pulse length dependence of the nucleation rate.

The self-standing amorphous Ge and Si films has been crystallized in situ in transmission electronic microscope by

pulsed YAG laser ($\lambda = 0.53 \mu\text{m}$, pulse duration $\tau = 14 \text{ ns}$ and 30 ps (FWHM)). Parallely, crystallization has been obtained by rapid electron beam irradiation in order to compare the different nucleation modes. Under nanosecond laser and μs electron beam irradiation, a quasi-uniform repartition on the nucleation centres has been observed. The morphologies of the picosecond pulse crystallization is unambiguously defined by i) the existence of an amorphous-like zone in the central spot (at the crystallization threshold) or of a concentric ring with same amorphous-like structure under higher excitation near melted zone ; ii) the significative decrease of the dendritic area at the periphery of the crystallized zone, and subsequently the increase of the differently polycrystallized areas. The common particularity of the ps and ns irradiation is the well defined crystallization threshold for dendritic growth which is the result of competition between polycrystalline light induced nucleation and thermal explosive growth. The observations are discussed in the context of the heterogeneous nucleation theory.

A9.33

HREM OF ELECTRON BEAM INDUCED AMORPHIZATION AND PHASE TRANSFORMATION IN MoO_3 CRYSTAL. Shri R. Singh and Laurence D. Marks, Center for Radiation Damage Studies, Department of Materials Science & Engineering, Northwestern University, Evanston, IL.

The desorption induced by electronic transition (DIET) from MoO_3 crystal surfaces was studied by a UHV high resolution electron microscope. It was found that during the initial stages of desorption of oxygen from the surface generates number of dislocations in the structure and with further loss of oxygen the MoO_3 structure collapses to an amorphous like phase. The transformation to amorphous phase which is a metastable alternative polymorphic structure and does not require interdiffusion of species is a direct manifestation of rapid desorption of oxygen. The orientation dependence of transformation rate was investigated in terms structural model. The necessary condition for amorphization is (1) large disparity in the atomic diffusion rates of participating species and (2) an absence of polymorphic crystalline alternative as a final state. As irradiation dose increases, the diffusional process lead to the nucleation and growth of Mo microcrystallites of increasing size embedded in amorphous connective tissue. The Mo has well defined orientation relationship with MoO_3 , which is maintained throughout the transformation. The whole process is a continuous transformation consists of DIET from the surface leading to amorphization and subsequent diffusional process leading to nucleation and growth of Mo.

A9.34

THE EFFECTS OF ANNEALING ON THE STRUCTURE AND DISTRIBUTION OF CHARGE STATES OF IRON IMPLANTED INTO $\alpha\text{-Al}_2\text{O}_3$ AT 77 K .
C. J. McHargue, P. S. Sklad, J. C. McCallum, and C. W. White, Oak Ridge National Laboratory, P.O. Box 2008, Oak Ridge, TN 37831-6118; and A. Perez and G. Marest, University Claude Bernard, Lyon 1, Villeurbanne Cedex, France.

Implantation of iron into $\alpha\text{-Al}_2\text{O}_3$ at 77 K produces an amorphous state for fluences greater than $3 \times 10^{16} \text{ Fe/cm}^2$. Conversion electron Mössbauer spectroscopy (CEMS) was used to determine the distribution of the implanted iron among various charge (valence) states in as-implanted and annealed (in oxygen) samples. TEM and RBS were used to follow changes in the microstructure.

Iron in the as-implanted (amorphous) specimens was distributed among two Fe^{2+} , two Fe^{3+} , and the Fe^0 (metallic

clusters) states. The CEMS spectra for a sample containing $7 \times 10^{16} \text{ Fe/cm}^2$ shows all the iron to be converted to Fe^{2+} after annealing for 1 h at 700°C and above.

The TEM results show the structure to be mostly $\gamma\text{-Al}_2\text{O}_3$ after the 900°C anneal and all $\alpha\text{-Al}_2\text{O}_3$ after the 1100°C anneal.

*Research sponsored in part by the Division of Materials Sciences, U.S. Department of Energy, under contract DE-AC05-84OR21400 with the Martin Marietta Energy Systems, Inc.

A9.35

QUALITATIVE MODEL FOR SURFACE RIPPLING OF ZONE MELTING RECRYSTALLIZED SILICON-ON-INSULATOR LAYERS
Paul W. Mertens, Herman E. Maes, IMEC, Kapeldreef 75, B-3030 Heverlee, Belgium.

In the low power regime of ZMR the recrystallized layers show a regularly rippled surface. These surface undulations have considerably retarded the use of ZMR films for very-thin-film ($0.1 \mu\text{m}$) SOI processes. A better understanding of the underlying mechanism may help in reducing the magnitude of the phenomenon. In the present work, a possible qualitative model based on the interface energy equilibrium at the "triple" line defined as the intersection line between the solidification interface and the cap layer interface is presented.

In the regime under study the solidification interface is believed to consist of rounded segments with deep cusps in between which is typical for a cellular growth. The valleys of the surface ripples are believed to coincide with the locations of these cusps. Consider now the interface energy equilibrium along the triple line in a plane which is normal to this line. The liquid surface has a meniscus shape which is characterized by the typical "meniscus angle" at the triple line. This is easy to imagine for the forward tip of the curved segments. It merely means that the liquid surface has a positive slope as one looks into the scan direction. When considering points more closely to the center of a cusp, one can see that the liquid meniscus trapped between two neighbouring branches of the cusp becomes smaller and smaller. In order to maintain the continuity of the slope of the liquid surface, eventually the complete surface force equilibrium diagram (including the solid silicon - cap interface) will tend to rotate downward. This implies also that the surface of the laterally growing cells will be pushed downward leading to a dimple in the final film.

A9.36

PARAMETRIC STUDY OF THE ZONE-MELTING-RECRYSTALLIZATION PROCESS OF SOI STRUCTURES.
Joseph Lipman, Ioannis N. Miaoulis*, Mechanical Engineering Department, Tufts University, Medford, MA 02155; and Jim S. Im, Materials Science and Engineering Department, M.I.T., Cambridge, MA 02139

A numerical simulation of the Zone-Melting-Recrystallization (ZMR) thermal processing technique was developed. The finite difference algorithms used enabled the investigators to obtain temperature distributions in thin Silicon On Insulator structures. Effects not usually treated by the existing analytical and numerical solutions such as convective and radiative losses from the surface of the film, phase change, temperature dependent thermal properties, and significant optical property variations during phase change were included in the simulation. Different heat strip geometries and temperatures were simulated, and the results obtained matched experimental observations. The parametric study focused on four different areas: i) the relationship between the temperature of the heating source and the velocity; ii) the effects of the non-linearities induced by the treatment of the

thermal properties as temperature dependent; iii) the effects of the natural convection heat transfer from the structure to the inert gases typically used as atmospheres during processing, and iv) the heat conduction effects induced by the multilayer nature of the SOI structure to the temperature distribution. Results of this study are presented in graphical form and can be used by investigators to optimize ZMR processing. This research was supported by NSF grant MSM-8817949

*author to whom correspondence should be addressed

A9.37

THE EFFECT OF CHROMIUM IMPLANTATION ON THE FRACTURE STRENGTH OF Al_2O_3 .^{*} M. E. O'Hern, C. J. McHargue, C. W. White, Oak Ridge National Laboratory, P.O. Box 2008, Oak Ridge, TN 37831-6117, and G. C. Farlow, Wright State University, Dayton, OH 45435.

The fracture strength of two orthogonally oriented single crystals of sapphire implanted with 1×10^{17} Cr/cm² (180 keV) was determined by four-point bend testing. The fracture strength is increased by the chromium implantation. The effects of crystal orientation are addressed for both the implanted and unimplanted states.

The mechanisms responsible for the increase in transverse rupture strength are discussed and correlated with other measured mechanical properties.

^{*}Research sponsored by the Division of Materials Sciences, U.S. Department of Energy, under contract DE-AC05-84OR21400 with the Martin Marietta Energy Systems, Inc.

A9.38

ION-IMPLANTATION INDUCED AMORPHIZATION OF CERAMIC OXIDES.^{*} D.E. Pedraza, Metals and Ceramics Division, Oak Ridge National Laboratory, Oak Ridge, TN 37831-6376

A theoretical study of the mechanisms of ion-implantation induced amorphization of ceramic oxides is conducted based on the hypothesis that the production of highly localized and strongly anisotropic distortions causes lattice destabilization and the consequent transition to the amorphous state. α -alumina is taken as a model system to develop a detailed mathematical approach capable of predicting the kinetics of amorphization. It is known from experiment that many metallic and noble gas elements implanted at liquid nitrogen temperature to concentrations less than 3% induce amorphization. The effect of implantation is first studied at these low temperatures.

Two aspects of the implantation process are considered. One is the site location and the other is displacement damage caused by the bombarding species. The oxygen sublattice is taken as the reference lattice. Irradiation is assumed to produce only vacancies and interstitials, of both oxygen and aluminum, and also to displace already implanted impurities from the sites they are located. It is assumed that aluminum can be displaced into any of the available interstitial positions, but may not occupy oxygen sublattice sites. The implanted species is also assumed to be able to occupy only interstitial sites. Oxygen can be displaced into any interstitial site depending on the level of disorder of the aluminum sublattice. As a consequence, randomization of the aluminum sub-lattice is first produced. The atomic mechanism leading to localized distortions is assumed to be the accumulation of implanted impurities into tetrahedral interstices. It is postulated that once this accumulation reaches a critical value in a small region, amorphization of this region follows. The calculations yield a fast amorphization rate once the local impurity concentration reaches a certain level.

^{*}Research sponsored by the Division of Materials Sciences, U.S. Department of Energy, under Contract DE-AC05-84OR21400 with Martin Marietta Energy Systems, Inc.

A9.39

METASTABLE STATES AND INCREASE IN CORROSION - MECHANICAL RESISTANCE IN STEELS IRRADIATED BY HIGH POWER ION BEAMS. A.D. Pogrebnjak, V.P. Kushnarenko, N.N. Shabanov, Nuclear Physics Institute, 634050 Tomsk, P.O. Box 25, USSR; A.K. Maksimov, Yu.M. Iesikov, V.M. Yugai, Tengizmetgas, Kulsary department, Kaz.ASSR.

One of the promising ways to improve operation properties of structural materials is to irradiate alloy surfaces by high power ion beams (HPIB). Today the method to evaluate material resistance to corrosion cracking under low rate deformation of samples (10^{-5} to 10^{-4} s⁻¹) is being extensively developed. This method allows urgent information about corrosion cracking abilities of investigated materials or efficiency of protection methods when traditional methods cannot yield valuable information or need longer time of exposure. Effect of HPIB exposure on hydrogen cracking resistance of 45 steel has been investigated. Changes in physico-chemical surface properties were investigated using SIMS, microhardness measurements (Micromet), TEM and REM. Irradiation chamber of the modified TONUS accelerator was evacuated to 10 Torr, the beam parameters were: $E = 0.2$ to 0.5 MeV, $j = 20$ to 250 A/cm current density, $t = 60$ to 80 ns pulse duration. Corrosion cracking tests were performed in a hydrogen sulphide medium NACE, $pH = 3$, $T = 294K$, with 2×10^{-4} s⁻¹ deformation rate. Results of those tests evidenced increased corrosion resistance of investigated steel 45 after HPIB exposure, $j \geq 120$ A/cm (number of pulses exceeded 5). Amorphization of a surface layer ≤ 1 was observed in modified samples.

A9.40

ION BEAM INDUCED CONDUCTIVITY CHANGES IN GLASSY CARBON. Dougal McCulloch and Steven Prawer, Dept of Applied Physics/Microelectronics and Materials Technology Centre, Royal Melbourne Institute of Technology, G.P.O. Box 2476V, Melbourne, Victoria 3001, AUSTRALIA.

Glassy Carbon is produced by the controlled thermal degradation of specific polymer-type materials. Microstructurally it consists of a tangle of graphite-like ribbons or microfibrils. It is moderately hard, chemically inert, impermeable and biocompatible. Recent studies have shown that ion beam irradiation of Glassy Carbon significantly enhances its wear resistance making it a much more attractive material for bioengineering applications.

As part of an attempt to understand the mechanisms by which this enhancement occurs, the electronic structure of implanted GC has been investigated by surface resistivity measurements. Unirradiated GC has a resistivity of 4.5×10^{-3} ohm-cm. Ion beam irradiation of Glassy Carbon leads to an increase in the resistivity of the implanted layer of up to seven orders of magnitude.

This ion beam induced increase in the resistivity is concomitant with an increase in microstructural disorder as monitored by Raman Spectroscopy. Both the Raman and resistivity measurements suggest that the material undergoes an ion-beam induced transformation at damage levels of about 0.5 displacements per atom. At higher doses evidence exists for an ion beam induced annealing effect.

A9.41

SYNTHESIS OF MoS_2 PHASE IN THE NEAR SURFACE REGION OF Al_2O_3 AND ZrO_2 BY ION IMPLANTATION.* A. K. Rai, R. S. Bhattacharya and D. Patrizio, Universal Energy Systems, Inc., 4401 Dayton-Xenia Road, Dayton, OH.

Ion implantation has been widely used as a powerful technique to dope semiconductor surfaces. Also, new materials have been synthesized through the reaction of the implanted species with the substrate. Not much work has been done in utilizing ion implantation technique to synthesize new compound phases from implant constituent elements. This process can provide controlled incorporation of desired compounds in the near surface region of various materials. Surface sensitive properties of a particular material can thus be improved by choosing the proper compound.

The aim of this research work was to explore ion implantation technique to produce MoS_2 , a solid lubricant, in the near surface region of Al_2O_3 and ZrO_2 substrates. Dual implantations of Mo^+ and S^+ ions were performed in Al_2O_3 and ZrO_2 . The energies of the implants were adjusted to obtain overlapping profiles of Mo^+ and S^+ ions. Rutherford backscattering spectroscopy and Auger electron spectroscopy were used to determine the profiles of Mo^+ and S^+ before and after annealing. Formation of MoS_2 after post implant annealing was confirmed by transmission electron microscopy. Preliminary results of friction and wear measurements on the implanted and annealed substrates will be discussed.

* This work was supported by the DOE, ECUT Contract No. DE-AC02-88CE90026.

A9.42

EFFECT OF γ -RADIATION ON PHYSICO-CHEMICAL PROPERTIES OF LANTHANUM COBALTATE (LaCoO_3). B. Srinivas, V.R.S. Rao and J.C. Kuriacose, Department of Chemistry, Indian Institute of Technology, Madras-600 036, INDIA.

The decomposition of H_2O_2 on γ -irradiated LaCoO_3 has been studied. Pre-irradiation of LaCoO_3 in moist atmosphere leads to the formation of chemisorbed (surface excess) oxygen, transition metal reduction and enhanced catalytic activity. The enhancement in the catalytic activity is directly proportional to the amount of reduced metal.

The electrical conductivity of the sample pellets is found to decrease with increase in γ -dose. This is attributed to the trapping of charge carriers (electrons) by chemisorbed oxygen formed during γ -radiation. X-band ESR spectrum of γ -irradiated LaCoO_3 gives two signals $g_1 = 2.047$ and $g_2 = 2.006$ which are assigned to the superoxide ion (O_2^-). X-ray photoelectron spectroscopy was employed to investigate the possible surface modifications occurring during γ -irradiation. No significant change in the surface is noticed in LaCoO_3 irradiated in vacuum and dry oxygen. However, samples irradiated in air and moist oxygen show the following changes. The $0\ 1s$ region gives two peaks at 532.3 eV and 529.8 eV which are assigned to chemisorbed oxygen (O_2^-) and lattice oxygen (O^{2-}) respectively. The first peak steadily decrease when the sample is subjected to Ar^+ ion sputtering. The binding energy of $\text{Co}\ 2p_{3/2}$ shows a shift of 0.5 eV towards lower value. There is also a broadening of the peak which indicates reduction of Co^{3+} to Co^{2+} probably by hydrated electrons produced during γ -irradiation in moist atmosphere. Ar^+ ion sputtering increases the intensity of the $\text{Co}\ 2p$ signal implying cobalt metal ion segregation to the surface during γ -irradiation.

A9.43

STRUCTURAL AND THERMODYNAMIC PROPERTIES OF AMORPHIZED Si FORMED BY MeV Si BEAMS. S. Roorda and W. C. Sinke, FOM Institute for Atomic and Molecular Physics, Amsterdam, The Netherlands; J. M. Poate, D. C. Jacobson, S. Dierker, B. S. Dennis, AT&T Bell Laboratories, Murray Hill, NJ; P. Fuoss, AT&T Bell Laboratories, Holmdel, NJ; and F. Spaepen, Harvard University, Cambridge, MA.

Apart from its technological applications, amorphous (a) Si is of fundamental interest because it is the prototype of a covalently bonded disordered solid. Implantation with MeV Si ion beams can be used to form a-Si layers which are impurity and void free. In contrast, deposited a-Si layers will generally exhibit internal surfaces and will contain impurities from either the deposition process or in-diffusion. The implanted a-Si layers make it possible to study fundamental properties of a-Si, and especially variations in these properties as a result of annealing at moderate temperatures.

The a-Si layers were formed by ^{28}Si bombardments at energies as high as 8 MeV with the substrates held at 77K. Differential Scanning Calorimetry is used to determine the energy stored in the amorphous network, and to investigate the time evolution of structural relaxation. Raman spectroscopy is employed to characterize vibrational properties of a-Si in its different states of relaxation. The observed changes are consistent with, but do not unambiguously prove, a decrease in average bond angle distortion upon annealing. Finally, X-ray diffraction shows that differences in atomic structure are mainly due to reordering on a distance scale of more than one bond length.

A9.44

THE ROLE OF ION BEAMS IN CHANGING THE STATE OF RELAXATION OF AMORPHIZED Si. S. Roorda and W. C. Sinke, FOM Institute for Atomic and Molecular Physics, Amsterdam, The Netherlands; J. M. Poate, S. Dierker, B. S. Dennis, D. C. Jacobson, AT&T Bell Laboratories, Murray Hill, NJ; and F. Spaepen, Harvard University, Cambridge, MA.

A fundamental difference between amorphous Si prepared by Si implantation (amorphized Si) and crystalline Si lies in the fact that the ordered crystal is well defined, whereas the disordered amorphous state allows for a range of different structures. Consequently, many properties of a-Si are variable and depend on thermal history. The transition from a state with high internal energy to a low energy state is known as structural relaxation and is accompanied by a heat release of several kJ/mole.

Structural relaxation is generally interpreted as a decrease in average bond angle distortion in the amorphous network, but the role of defects such as floating and dangling bonds, interstitials and vacancies is unclear.

In this paper we show that relaxed, amorphized Si can be brought back to its high internal energy 'unrelaxed' state by irradiation with a variety of MeV ions such as He, C, Si and Ge. This phenomenon occurs at substantially lower fluences than are necessary for amorphization of c-Si and has been found to be due to nuclear rather than electronic energy losses. We will discuss, in the context of these results, the relationship between bond angle distortion and defects in a-Si.

A9.45

CONCENTRATION DEPENDENCE OF STRUCTURE AND CONTACT ELECTRONIC DENSITY IN IRON IMPLANTED SILICON. Francisco H. Sánchez, and Marcela B. Fernández van Raap, Departamento de Física, Facultad de Ciencias Exactas, Universidad Nacional de La Plata, La Plata, Argentina.

^{57}Fe Mössbauer data obtained from the $\text{Si}_{1-x}\text{Fe}_x$ system produced by iron implantation into silicon, have been analyzed

as a function of x in the range $0.001 < x < 0.40$. X-ray diffraction results suggest a high disordered, probably amorphous, system. It was found that both the Mössbauer isomer shift and the quadrupole splitting follow a logarithmic function of x with a change of slope in the vicinity of $x=0.20$, which was associated with a structural transformation. From the isomer shift data follows that the electronic charge density at the iron nuclear site increases linearly with $\ln(x)$ for x up to 0.20, and then decreases in the range $0.20 < x < 0.40$.

These results are discussed in terms of the type of atomic order, Si(Fe) band structure and electronic interactions, and the character, attractive or repulsive, of the Si-Fe and Fe-Fe interactions in the system.

A9.46

CHANGE IN MAGNETIC CHARACTERISTIC OF 301 STAINLESS STEEL IRRADIATED WITH LASER AND ION BEAMS. H. Sanda^{*}, M. Takai, and S. Namba, Faculty of Engineering Science and Research Center for Extreme materials, Osaka University, Toyonaka, Osaka, Japan.

301 stainless steel has two stable phases in room temperature, i.e., an austenitic phase which is a f.c.c. structure and nonmagnetic, and a martensitic phase which is a mixture of b.c.c. and b.c.t. structures and ferromagnetic. Cold-rolled 301 stainless steel foils, consisting of two mixed phases, were irradiated with laser or ion beams to investigate the magnetic modification accompanied with the phase transformations. The intensity of the magnetic signals related with the magnetic susceptibility of the samples decreased by irradiation with a focused Ar-ion laser beam from a laser power of 350mW to 550mW with a beam spot size of 13.2 μm (at 1/e intensity), indicating that the martensitic phase was transformed into the austenitic phase by laser annealing and quenching. On the other hand, the intensity of the magnetic signal of the sample increased by implantation at 3 MeV with Si^{4+} ions, indicating that the austenitic phase was transformed into the martensitic phase at the surface layer by ion induced stress. These results indicate that the beam induced phase-change in 301 stainless steel can be applied to read-only magnetic recording.

*On leave from Glory Ltd., Himeji, Hyogo, Japan

A9.47

TRANSIENT DIFFUSION IN BORON ION IMPLANTED SI(100): R.J. Schreutelkamp¹, R.E. Kaim², J.F.M. Westendorp², K.T.F. Janssen³, J.J.M. Ottenheim³ and F.W. Saris¹; 1-FOM Institute for Atomic and Molecular Physics, Kruislaan 407, 1098 SJ Amsterdam, The Netherlands; 2-Varian/Extrion division, 123 Brimbal Avenue, Beverly, MA 01915, USA; 3-Philips Research Laboratories, p.o. box 80.000, 5600 JA Eindhoven, The Netherlands

We have studied the transient diffusion behaviour of boron in silicon. The boron ions were implanted in Si(100) at energies of 5 and 10 keV and at a low dose of $1 \times 10^{13}/\text{cm}^2$. The implantations were done under both random and channelled condition. The channelled implantations were done along [100] direction. After RTA at a temperature ranging from 900°C to 1100°C we observe strong differences in

transient diffusion between the random and channelled implants. In this paper we discuss our results on basis of the different models for the transient diffusion mechanism. Our results support a model in which interstitial boron atoms are the cause of the transient diffusion.

A9.48

RBS STUDIES OF DAMAGE BEHAVIOR IN SILICON INDUCED BY P_2^+ IMPLANTATION. Yang Genqing, Lin Chenglu, Fang Ziwei, Zhou Zuyao and Zou Shichang, Ion Beam Lab., Shanghai Institute of Metallurgy, Academia Sinica, Shanghai 200050, China

The damage behavior of $\langle 100 \rangle$ -Si implanted with P_2^+ and P^+ at equivalent energies were investigated by 2MeV He^+ backscattering and channeling analysis. Different incident energies (25-180KeV) and intermediate doses (10^{13} - 10^{14}) were used for the implantation with sample holder being kept at a temperature ranging from 77K to 483K. In each monoatomic-diatomic comparison, the ion dose and the dose rate of P_2^+ were equal to half of those of P^+ ions in order to keep the total atomic number of the implants and the energy deposition rate unchanged. It has been shown that the damage created by P_2^+ implants is always greater than that of P^+ implants when the dosage is below the damage threshold fluence at which layered amorphization takes place, and furthermore, this damage enhancement phenomenon is strongly related with implantation temperature. It has been shown also that the annealing processes of the samples implanted with P_2^+ and P^+ at doses near damage threshold fluence behave differently. We attribute essentially the damage enhancement of diatomic ion implantation to the effects of simultaneous cascades overlap and the multiple collision between molecular fragments and target atoms.

A9.49

INVESTIGATION ON MECHANISMS FOR ION BEAM INDUCED DEGRADATION OF POLYIMIDE. X.L. Xu, Zhou Zuyao, Chen Lizhi, Zou Shichang, Ion Beam Lab., Shanghai Institute of Metallurgy, Academia Sinica Shanghai 200050, China

Three types of ions with different atomic masses (B, Ar, and As) were chosen to irradiate polyimide films in similar conditions in order to check the mechanisms of the formation of ion beam induced damage in polyimide. A four-point probe technique was used to measure sheet resistivities of implanted films. An ion mass effect on conductivity of ion irradiated polyimide film was discovered. The ion mass effect on ion beam induced change of conductivity and on the energy loss process of the ions in polyimide suggest that the electronic energy loss of incident ions is an important factor for the raise of conductivity of implanted polyimide, and the contributions of recoil ionization are restricted by the grave damages as a result of nuclear energy loss process of ions in targets. Our hypothesis are supported by the automatic spreading resistance measurement of B^+ implanted polyimide film coated on silicon substrate. The results of this work have been compared with the hypothesis of degradation through direct knock on of atoms in polyimide, proposed by D. Fink et al [Nucl. Instr. and Meth. B32 (1988) 125].

EVALUATION OF SURFACE EFFECT ON DISLOCATION LOOP NUCLEATION Naoto Shigenaka, Tsuneyuki Hashimoto and Motomasa Fuse, Energy Research Laboratory, Hitachi Ltd., 1168 Moriyama, Hitachi, Ibaraki, 316 Japan

Dislocation loop nucleation was investigated in type 304 stainless steel under ion irradiation. The 3mm ϕ disk specimens (0.1mm thick) were annealed at 1200°C for 10 hours, and irradiated with 300 keV He⁺ ions in the following ways.

Case I : The specimen was electro-polished for TEM observation prior to ion irradiation (thin foil irradiation case).

Case II : The specimen was irradiated, and then electro-polished from the unirradiated rear surface before TEM observation (thick foil irradiation case).

Ion irradiations were performed in the damage-rate range between 10⁻⁶ and 10⁻⁴ dpa/s, and temperature range between 300 and 450°C.

Dislocation loop density was measured and the following results were obtained.

Case I : The dislocation loop density was proportional to damage rate, and the apparent activation energy of dislocation loop nucleation was determined to be 0.8eV from the Arrhenius plot.

Case II : The density was proportional to the 0.66 power of the damage rate, and the apparent activation energy was 0.5eV.

These experimental observations were consistent with the predictions of a rate theory-based model in which a disinterstitial was assumed to be the nucleus of a dislocation loop and point defect flow toward the surface was included.

A9.51

STRUCTURAL ANALYSIS OF METASTABLE PHASES IN INTERMETALLIC ALLOYS PRODUCED BY ELECTRON IRRADIATION AND NON-EQUILIBRIUM PROCESSING. W. Sinkler and D.E. Luzzi. Dept. of Materials Science, University of Pennsylvania, Philadelphia, PA 19104-6272.

Electron imaging and diffraction are used to characterize and contrast the structures and microstructures of metastable intermetallic phases formed during electron irradiation and after quenching. Intermediate structures are formed during the early stages of electron irradiation induced amorphization in Cu-Ti intermetallic alloys which display a marked structural anisotropy. A similar observation has been made in quenched-Cr-Ti where the diffuse scattering from the quenched-in phase bears a striking resemblance to the diffuse scattering seen prior to amorphization in the Cu-Ti alloys (all of these phases are bcc-based structures). It has been reported in the literature that this quenched-in metastable Cr-Ti phase undergoes a spontaneous structural relaxation into the amorphous state during sub-eutectoid temperature anneals [1]. The interesting question as to the structural relationship between the pre-amorphized Cu-Ti phase and the quenched-in Cr-Ti phase is addressed. The dependences of these structures on the processing parameters (dose, quenching conditions, temperature) are characterized using electron diffraction and conventional and high-resolution imaging.

1. A. Blatter, M. von Allmen and N. Baltzer, J. Appl. Phys. 62 (1987) 276-280.

A9.52

SPATIAL DAMAGE DISTRIBUTION IN ELECTRON-BEAM PROCESSED GAAS-ALGAAS HETEROSTRUCTURES, EXPERIMENT AND THEORY. Doran D. Smith, Tobin Fink^{a)}, W. D. Braddock^{b)}, U S Army Electronics Technology and Devices Laboratory, Fort Monmouth, NJ 07703-5000, a) Permanent Address: New Jersey Institute of Technology, Newark, New Jersey 07102, b) On leave from Cornell University.

The effect of electron beam irradiation on the transport properties of HEMT structures has been studied. The data is found to agree with a model containing no free parameters which predicts the spatial extent and type of damage. As grown HEMT material was fabricated into Hall bars. The material was then characterized by measurement of 2D EG number density and drift mobility. The material was then irradiated at constant dose with electron energies between 2.5 and 20 keV. Damage was assessed by changes in the number density and mobility. The number density was unchanged at all energies. No change in mobility occurred for 2.5, 15, and 20 keV, however, a decrease in the mobility occurred for energies from 5.0 to 12.5 keV. Experimental data agrees with our theoretical model of the electrons energy loss as a function of its path length. Primary energy loss mechanism for higher energy electrons, $E > 1$ keV, is ionization of the stopping medium, while for low energy electrons single-particle and collective excitations become important. Low energy results are explained by the shallow penetration depth of the electrons. Lack of damage at high energies is explained by low energy deposition rates in the neighborhood of the 2D EG, and the increasing remoteness, with respect to the 2D EG, of the high damage areas. The damage is explained in terms of the creation of single Frenkel pairs, and thus is analyzed in terms of a single-vacancy and/or interstitial atom. After RTA at 450°C for 30 seconds, the damage effects were reduced or eliminated.

A9.53

ION IMPLANTATION INDUCED EFFECTS AT POLYSILICON GATE FEATURE EDGES. M. G. Stinson^{1,2}, P. L. Smith¹, and C. M. Osburn^{1,2}. ¹ Microelectronics Center of North Carolina (MCNC), P.O. Box 12889, Research Triangle Park, North Carolina 27709; ² Dept. of Electrical and Computer Engineering, North Carolina State University, Raleigh, North Carolina 27695-7911.

Recently, an enhanced leakage associated with ion implantation at polysilicon gate edges has been reported (1). In this study, TEM and SIMS characterization have been done to supplement electrical measurements in order to better understand the degradation. SIMS, XTEM, and TRIM analyses of arsenic implants through 7 nm gate oxides show considerable ion mixing. A roughening of the underlying silicon substrate leads to asperities which are believed to play an important role in enhancing leakage (2). XTEM analysis of a polysilicon gate edge also reveals the effects of volume expansion associated with the incorporation of both dopant and knock-on oxygen.

1. M. Stinson, and C. Osburn, submitted for publication.

2. D.J. DiMaria, and D.W. Dong, J. Appl. Phys., Vol. 51, No. 5, (1980).

A9.54

FAST TRANSIENT ANNEALING OF NEUTRON TRANSMUTATION DOPED INP. F.P. Korshunov, E.A. Kudriavtseva, N.A. Sobolev, T.A. Prokhorenko, N.G. Kolin. Institute of Solid State and Semiconductor Physics, 220726 Minsk, ul. P. Brovki, 17, USSR

Indium atoms have a very large capture cross section for thermal neutrons. This leads to the necessity of performing neutron transmutation doping (NTD) of A₃B₅ semiconductors with A₃=In in the shape of wafers and not of ingots. The most convenient procedure of radiation defect (RD) removing in the bulk of single wafers is the fast transient annealing (FTA). In the paper we

present investigations of defect annealing and impurity activation in NTD InP in the course of FTA by means of tungsten halogen lamps. InP crystals with NTD level of $7.8 \times 10^{17} \text{ cm}^{-3}$ have been used. Photoluminescence (PL) and Hall effect measurements have been performed at 4.2 K and in the range 77...300 K, respectively.

At FTA temperatures $T \geq 600^\circ \text{C}$ PL emerges and carrier concentration n starts to grow monotonically. The PL spectrum consists essentially of two broad bands - an exciton band with the intensity $I(\text{ex})$ and donor-acceptor recombination band $I(\text{da})$. The ratio $R = I(\text{da})/I(\text{ex})$ and n increase simultaneously and saturate at $T \geq 750^\circ \text{C}$. The absolute value of $I(\text{ex})$ rises up to $T \approx 800^\circ \text{C}$ and then starts to drop. The electron mobility μ increases with T in the range 600...750°C rapidly and at $T > 750^\circ \text{C}$ only slowly. The values of R , $I(\text{ex})$, n , μ and of compensation ratio obtained under optimum FTA conditions are the same as in the case of standard furnace annealing under equilibrium phosphorus vapour pressure.

The processes of defect annealing and electrical activation of the main transmuted impurity Sn are discussed.

A9.55

EFFECTS OF LASER SURFACE MELTING ON STRUCTURE CHARACTER AND EROSION RESISTANCE OF PLASMA-SPRAYED CERAMIC COATINGS. Jia-Shu Sun, Tianjin Institute of Technology, Hong Qi Nan Road, Nan Kai District, Tianjin 300191, Peoples Republic of China.

Alumina and zirconia powders were plasma sprayed onto sand-blasted steel substrates using a commercial EOKW arc plasma-sprayed unit. A 2KW CO₂ continuous wave laser was used to treat some of plasma-sprayed specimens. The micro-morphology, microstructure and crystalline characters of laser melted and unprocessed plasma-sprayed ceramic coatings were examined with electron microscope and X-ray diffractometer. The solid particles erosion tests were carried out in a rotating blade-wheel type erosion equipment. Quartz sand of 150 to 200µm in diameter was used as the erodent. The particles impact velocities from 30 to 70m/s were used. Results of this study have shown that laser surface melting has produced microstructure changes and significant improvement in solid particle erosion resistance of plasma-sprayed ceramic coatings. Erosion mechanisms of ceramic coatings were investigated.

In plasma spray process, the coating is built up particle by particle; each particle is frozen before the next particle arrives. This results in a layered structure and porosity of the plasma sprayed coatings, therefore, the erosion mechanisms are mainly micro-lamella spalling. Laser melting resulted in coalescence and porosity reduction of plasma-sprayed ceramic coatings, therefore, increasing hardness and erosion resistance of the ceramic coatings.

A9.56

MICROSTRUCTURAL ANALYSIS OF 1 MEV NITROGEN IMPLANTED FE AND TI SURFACES. A.M. Vredenberg and F.W. Saris, FOM-Institute for Atomic and Molecular Physics, Kruislaan 407, 1098 SJ Amsterdam, The Netherlands; N.M. v.d. Pers, Th.H. de Keijser, P.F. Collijn and E.J. Mittemeijer, Laboratory of Metallurgy, Delft University of Technology, Rotterdamseweg 137, 2628 AL Delft, The Netherlands

Nitrogen implantation is a well known technique to modify tribological properties of metal surfaces. Up to now for this purpose mostly medium energy, typically 100 keV, nitrogen beams are used. In this paper we will focus on the application of 1 MeV nitrogen beams, which modify much thicker surface regions than 100 keV beams.

It is shown that the hardness increment due to 1 MeV implantation is much larger than that due to 100 keV implantation. This may be attributed to the formation of nitrides (as observed with XRD), which are distributed over a much larger depth (typically 1 µm) than in the case of

100 keV implantation (typically 100 - 200 nm). At doses exceeding a certain threshold dose blisters were observed on the sample surface. It was found that blistering starts as soon as the nitrogen peak concentration reaches that in the nitrogen-richest nitride, i.e. 33 at.% N for Fe (Fe₃N) and 50 at.% N for Ti (TiN).

Furthermore, nitride precipitation was studied as a function of temperature during implantation. RBS was used to follow the evolution of the nitride concentration profile as a function of dose and XRD was applied to monitor the different nitride phases formed. XRD was also used to measure the residual stress before and after implantation, by using the $\sin^2\psi$ method. Although large volume changes deep beneath the sample surface, associated with high dose ($> 5 \times 10^{17}/\text{cm}^2$) MeV implantation, could in general induce large stress fields, only small changes in stress were observed, both for Fe and Ti. For all different implantation conditions an upper limit of average stress change in a surface layer of about 2 µm was found to be 10 MPa.

A9.57

CHARACTERISTICS OF METAL-p⁺-GaAs SCHOTTKY BARRIER JUNCTION FORMED BY FOCUSED-ION-BEAM IMPLANTATION Nobuo Watanabe, Takeo Tsukamoto and Masahiko Okunuki, Canon Research Center, 5-1, Morinosato-Wakamiya, Atsugi-shi, Kanagawa, Japan

We have investigated to form a metal-p⁺-GaAs Schottky barrier junction for our new cold cathode (GaAs avalanche type)¹⁾, which has a small p⁺-region fabricated by focused-ion-beam (FIB) implantation. The sample is Be ($1 \times 10^{16} \text{ atoms/cm}^3$) doped epitaxial layer grown by MBE on 7'off-sliced (100)GaAs wafer. The conditions of accelerating voltage, ion beam diameter and current density are 40kV(Be⁺), 0.2µm and 0.4A/cm², respectively. After the implantation, the sample is encapsulated with SiO₂ and annealed at 850°C for 1-min. Thin Aluminum film is evaporated to form the Schottky barrier junction. The Schottky barrier heights decrease gradually from 0.62 to 0.56V and the ideal factors increase from 1.09 to 1.19, following the doses from 8×10^{12} to $2 \times 10^{14} \text{ ions/cm}^2$. These phenomena are reasonable variations for the Schottky barrier junction in the high doped region. It is confirmed that the Schottky barrier junction can be formed on the surface under the FIB implantation with the high current density.

¹⁾Second International Conference on Vacuum Microelectronics, July 1989, Bath, England.

A9.58

STUDY OF Hf DIFFUSION IN α-Zr USING RUTHERFORD BACKSCATTERING SPECTROMETRY. F.Dyment¹, M.Behar², P.L.Grande², E.Savino¹, and F.C.Zawislak¹. 1) Comisión Nacional de Energía Atómica, Buenos Aires, 2) Instituto de Física, UFRGS, 91500 Porto Alegre, Brasil.

The diffusion of impurities in Zr and Zr alloys is of importance in nuclear technology. Earlier works have shown anomalous diffusion behaviours in α-Zr as well as in the α-phases of the other group IV A elements, Ti and Hf. A recent study of self diffusion in α-Zr single crystal¹ showed an Arrhenius plot curved downwards with decreasing temperature, corresponding to an increase of the activation energy (E_{act}) from 1.2 eV at about 1100 K to 3.5 eV at 800 K. More recently the diffusion coefficients of ⁵⁹Fe impurity in α-Zr single crystal were measured in the same range of temperatures. Again a similarly curved Arrhenius plot was obtained, but the

diffusion coefficients of Fe are 10^8 times larger than the self-diffusion ones.

The present contribution reports on measurements of the diffusion coefficients of Hf in α -Zr single crystal via the RBS technique. Films of 200 Å have been deposited on Zr and annealed at a pressure of 10^{-7} Torr. Our preliminary results also display a curved Arrhenius plot, the E_d increasing from about 0.5 eV at 1100 K to 2.5 eV at 800 K. In addition our data show that at 1100 K the diffusion coefficients of Hf are a factor 10^2 smaller than the self diffusion, but at 800 K both are equal.

1. J. Horvath et al., J. Nucl. Mat. 126 (1984) 206.
2. H. Nakajima et al., Phys. Mag. 58B (1988) 319.

A9.59

COOPERATIVE BEHAVIOR IN AN ELECTRON STIMULATED Tl-Ba-Ca-Cu-O SUPERCONDUCTOR. J. P. Zhang and L. D. Marks, Center for Surface Radiation Damage Studies, Department of Materials Science & Engineering, Northwestern University, Evanston IL 60208.

In this work we present an instantaneous phase transformation observed in $Tl_{0.5}Ba_{0.5}Ca_{0.5}Cu_{0.5}O_{1.5}$, which is produced by electron beam irradiation at 300 kv when the beam flux reaches 100 ± 15 A/cm². The remained products had been identified as $CaCuO$, and BaO by means of high resolution electron microscopy. The volume change and exhaustion of thallium from the transition area occurs in less than 1/30th of a second indicating a cooperative behavior in the electron stimulated (Tl-O) blocks. These results have been analyzed by treating the ground and excited states in an ionic crystal as the two states required in a Ising problem, then using the Bragg-Williams approximation to give a statistical estimation of the possibility of a phase transition. This theoretical model predicts the existence of a flux threshold, which is in qualitative agreement with the experimental results.

A9.60

THE INTERACTION OF INERT GAS IONS WITH ADSORBATE-COVERED CRYOGENIC SURFACES. Patricia M. George, John M. Lindquist, Daryl L. Mossman, Gencorp Aerojet ElectroSystems Co., P.O. Box 296, Azusa, Ca. 91702

We have studied the interaction of inert gas ion beams with adsorbate-covered, cryogenic optical surfaces. Parameters necessary to optimize removal of different adsorbates from Beryllium and gold-coated substrates will be presented. Mechanisms for the ion-adsorbate interaction and removal process will also be discussed. The experiments cover a range of ion beam voltages, currents etc. for neon, argon and helium with mirror temperatures ranging from room temperature to 25K \pm 5K. Adsorbate species include water, ammonia, hexane and variable mixtures of these gases. All ion beam experiments were performed in an ultra-high vacuum system, with a base pressure of 1×10^{-10} torr. During the ion bombardment the pressure rose to 1×10^{-7} torr. Adsorption and removal were monitored by X-Ray Photoelectron Spectroscopy. Ion-adsorbate reactions were also studied as a function of angle of incidence of the beam.

On reactive surfaces, such as Beryllium, argon ion beams were found to induce chemical reactions as low as 160K. As expected, at the lower temperatures argon gas condenses on the mirror surfaces. However, if these argon ions were provided with sufficient kinetic energy, e.g. 5keV the adsorbed gas could be removed. Neon and helium did not

stick and the data show that neon promises to be the best choice for removal of adsorbed species at the lower surface temperatures. The results also indicate that thermal mechanisms may be important in the removal process when surface temperatures reach 25K.

A10.1 ABSTRACT NOT AVAILABLE

A10.2

FREEZING IN SILICON AT LARGE UNDERCOOLING
A. Polman, P.A. Stolk and W.C. Sinke, FOM-Institute AMOLF, P.O. Box 41883, 1009 DB Amsterdam, The Netherlands

We have studied the motion of a Si liquid-solid interface under conditions of extreme undercooling. From measurements of the interface response function, which relates the freezing velocity to the temperature, it was possible to discriminate between kinetic models describing freezing in crystalline silicon (c-Si).

High-energy ion implantation was used to produce amorphous Si layers buried in a c-Si matrix. These structures were irradiated with a pulsed ruby laser. Transient reflectivity and conductivity measurements as well as channeling and cross-section TEM show that the buried layers can be crystallized via "epitaxial explosive crystallization". Crystallization velocity data were obtained using transient interference techniques and interface temperatures were derived from computer simulation.

The data show that the crystallization rate is remarkably constant at ~ 16 m/s over the entire temperature range from 150 to 225 K below the equilibrium melting point of c-Si. These data are compared with transition state theory (TST), diffusion limited freezing (Wilson-Frenkel) theory and a recent theory which takes into account the large density difference between solid and liquid Si (P.M. Richards, Phys. Rev. B38, 2727 (1988)).

Best agreement between theory and experiment is found using the latter model, which suggests that local transient density fluctuations at the freezing interface influence solidification on an atomic scale. A Wilson-Frenkel type formulation or a TST with an activation energy for the transition state of 0.6 eV are alternatives which however do not fit the data as well. An important implication of all three models is that the interface-limited freezing velocity in c-Si can never exceed ~ 16 -18 m/s.

A10.3

TRANSIENT CONDUCTANCE MEASUREMENTS OF SOLIDIFICATION VELOCITIES OF ELEMENTAL METALS.
Harry A. Atwater*, J.A. West, Patrick M. Smith, M.J. Aziz, Division of Applied Sciences, Harvard University, Cambridge MA; J.Y. Tsao and P.S. Peercy, Sandia National Laboratories, Albuquerque NM; and Michael O. Thompson, Department of Materials Science and Engineering, Cornell University, Ithaca NY.

We have performed nanosecond-resolution measurements of the lateral electrical resistivity of metal thin films on insulating substrates. Although the change of resistivity on melting of metals is much smaller than in Si, it is large enough to be detected by the transient conductance technique.

Comparison of transient conductance measurements with optical reflectivity measurements and heat-flow calculations permits the determination of the position and velocity of a planar crystal/melt interface during pulsed laser melting of metals such as Al, Ni, and Fe. This diagnostic should be useful in a number of techniques of solidification processing of pure metals and alloys.
*present address: MS 128-95, California Institute of Technology, Pasadena CA.

A10.4

OBSERVATION OF PULSED LASER-INDUCED MELTING OF SOLID SURFACES BY OPTICAL SPIN ORIENTATION.
A. Vaterlaus, M. Lutz, D. Guarisco, M. Aeschlimann, M. Stampanoni, and F. Meier, Laboratorium für Festkörperphysik, ETH Hönggerberg, 8093 Zürich, Switzerland.

Critical laser pulse energies for melting solid surfaces are accurately determined using the method of optical spin orientation. In this experiment electrons are optically excited to a spin-polarized final state. The polarization is given by the symmetry of the lattice. Upon melting, the structural disorder reduces the spin polarization to zero. By measuring the spin polarization of optically oriented photoelectrons information on the structural order of a thin surface sheet (10 - 20 Å) is obtained.

Melting of the sample surfaces was achieved using laser pulses of 20 ns and 70 ps duration. For Sn the polarization vs. pulse energy shows a step-function like behavior for both pulse durations with the discontinuity at the melting temperature. From the similarity of the two curves it is concluded that the structural disorder is established on a time-scale short even with respect to 20 ps. Positive ion emission starts at pulse energies close to but slightly below those where the drop of the polarization occurs.

An analogous experiment on p-doped Ge shows a qualitatively different dependence of the polarization vs. energy for the 30 ps and 20 ns pulses. Whereas for the 30 ps pulses the polarization is still at its low-intensity value at the onset of positive ion emission, the polarization of the electrons excited with 20 ns pulses vanishes for energies an order of magnitude lower than necessary for melting. Structure-unrelated electronic processes of ns-relaxation time are responsible for this phenomenon.

A10.5

SUB-MELTING LASER INDUCED GRAIN GROWTH. S.A. Ajuria, C.V. Thompson, Department of Materials Science and Engineering, Massachusetts Institute of Technology, Cambridge, MA.

The control of the microstructure of polycrystalline semiconducting thin films on insulator is of importance in establishing their electrical properties for several device applications. In this study, grain growth is thermally induced without melting by a CW Ar-ion laser ($\lambda=0.514\mu\text{m}$) in 1000Å CVD deposited polysilicon films encapsulated by Si_3N_4 . With irradiation times on the order of minutes, it is shown that it is possible to create and determine a steady-state temperature below melting, within the regime of grain growth.

A thermal model is developed to account for grain sizes seen at different laser powers. A direct relation is found between incident beam power and the steady-state temperature achieved within the film. The fit to experimental data is excellent.

The ability to reproducibly create a desired temperature in a small region can be used to tailor the microstructure of individual devices containing polycrystalline layers.

A10.6

PULSED LASER MELTING OF INTERMEDIATE Cu-Zn PHASES.
D. M. Follstaedt and P. S. Peercy, Sandia National Laboratories, Albuquerque, NM; and J. H. Perepezko, University of Wisconsin, Madison, WI.

We report quantitative studies of rapid melting and solidification in the Cu-Zn alloy system. In contrast to

most metals, the reflectance of Cu-Zn alloys increases upon melting. This novel behavior decreases the energy absorption upon melting, leading to well controlled molten layer thicknesses over a wide range of laser power without laser-induced damage. This feature, combined with the several distinct phases (stable and metastable) in Cu-Zn, offers a unique opportunity to study competition between resolidification of the initial phase and nucleation of metastable phases.

Melting and solidification were studied for γ -brass alloys (61 to 66.5 wt.% Zn) and β -brass (45.5 wt.% Zn) irradiated with 30 ns pulses at 694 nm. Melting was observed above ~ 1.0 and 3.0 J/cm^2 , respectively, for the two phases. The absorbed energy was measured calorimetrically and the increased reflectance of the liquid was used to measure the melt duration. The large difference between solid and liquid reflectances, e.g., from 0.83 to 0.89 for γ -brass with 66.5 wt.% Zn, yielded a well-defined melt onset and termination in the transient reflectance signature. These measurements, combined with the known thermodynamic parameters, permit quantitative characterization of the surface melting. In addition, microstructural (TEM) analysis of the phases which solidify will be presented.

This work supported by the U.S. Department of Energy under contract number DE-AC04-76DP00789 and by a Faculty Research Travel Appointment from Associated Western Universities.

A10.7

LASER MIXING OF TITANIUM ON SILICON CARBIDE. T. R. Jervis, J-P. Hirvonen, M. Nastasi, and M. R. Cohen, Materials Science and Technology Division, Los Alamos National Laboratory, Los Alamos, NM 87544

We have used excimer laser surface processing to melt and mix single Ti layers into the surface of polycrystalline SiC substrates. The mixing of Ti into the surface is very rapid and efficient. Examination of Rutherford backscattering (RBS) data shows the formation of a preferred composition at the Ti-substrate interface which propagates from the interface with further mixing. Reconstruction of the RBS spectrum indicates that a uniform layer of composition $\text{Ti}_{45}\text{C}_{37}\text{Si}_{18}$ is formed on the surface with full mixing. X-ray diffraction demonstrates the formation of crystalline phases of Ti silicides and possibly carbides. Profiling of C in both mixed and uncoated samples by 5 MeV He⁺ scattering demonstrates that laser processing of the SiC does not cause major changes in the stoichiometry of the substrate material.

A10.8

TEMPERATURE MEASUREMENT BY INFRARED TRANSMISSION FOR RAPID THERMAL PROCESSING APPLICATIONS -
J.C. Sturm, P.V. Schwartz, and P.M. Garone, Dept. of Electrical Engineering, Princeton University, Princeton, N.J. 08544

We here report a new non-invasive optical technique for the measurement of absolute temperature of silicon wafers in a rapid thermal processing environment. Absolute measurement of temperature has always been a difficult problem in rapid thermal processing systems. The traditional method, pyrometry, can give different results depending on what emissivity is used, and extreme care must be taken to avoid measuring radiation from the lamps. Pyrometry becomes even more difficult at low temperatures (600 - 700°C) since longer wavelengths are required. The problems are compounded when a quartz-walled chamber is used to contain a reactive gas species, as in epitaxial growth applications, because quartz is fairly opaque to wavelengths beyond 3 μm .

It is well known that as temperature increases the bandgap of silicon decreases and that its infrared transmission decreases. Because of the indirect gap, the absorption changes fairly gradually with photon energy at a fixed temperature. We have used these principles to measure silicon wafer temperature in a RTP system

with quartz walls by monitoring optical transmission at 1.5 μm . Modulating the light at high frequency makes the system immune to interference from the heating lamps. We now use this method for routine temperature monitoring from 400 to 800°C, with resolution on the order of one degree centigrade. Other temperature ranges are accessible with different wavelengths. Data for low temperature (<800°C) growth rates of epitaxial silicon and silicon-germanium using this system will be presented. This work has been supported by NSF and ONR.

A10.9

METASTABLE GE-SN ALLOY LAYERS PREPARED BY PULSED LASER MELTING. I.T.H. Chang, B. Cantor, Department of Metallurgy and Science of Materials, University of Oxford, Parks Road, Oxford OX1 3PH, UK; and A.G. Cullis, Royal Signals and Radar Establishment, St. Andrews Road, Malvern, Worc. WR14 3PS, UK.

Ge has a diamond cubic crystal structure while Sn exists in both the diamond cubic (α) and body centred tetragonal (β) allotropic forms. The solid solubilities between Ge and Sn are very small according to the equilibrium phase diagram. This paper describes an investigation of the manufacture of metastable crystalline microstructures in Ge-Sn alloys, using a variety of novel processing techniques. The main technique which has been studied is pulsed laser melting and this has been compared with other techniques, including melt-spinning and thermal co-evaporation. Cross-sectional and planview transmission electron microscopy have been used to characterise the microstructures of the different Ge-Sn alloy samples, with alloy compositions determined by energy-dispersive x-ray microanalysis. The variety of different metastable Ge-Sn alloy microstructures are discussed in details as a function of manufacturing technique and processing conditions.

A10.10

CHARACTERIZATION OF PULSED LASER BEAM MIXED AuTeGaAs OHMIC CONTACTS. K. Wuyts, R.E. Silverans, Phys.Dept. K.U.Leuven, Leuven; and M. Van Hove, M. Van Rossum, Interuniversity Microelectronics Center, Leuven, Belgium.

The formation of AuTe ohmic contacts on GaAs by pulsed laser beam mixing has been studied. Metallization of the GaAs was done by successive deposition of 500 Å Te and 1200 Å Au films on (100) oriented GaAs by resistive heating evaporation. Laser beam mixing of the layered structures was performed by focussed, visible as well as UV pulsed Nd:Yag-laserlight using single and multiple pulses with power densities (P_d) ranging from 40 MW/cm² to 800 MW/cm² per pulse. For comparison, short-time furnace alloyed ($t=15\text{s}$) contacts were prepared in a graphite strip heater at alloy-temperatures $300^\circ\text{C} \leq T_a \leq 550^\circ\text{C}$.

The transformation from Schottky to ohmic type contacts as a function of P_d , number of pulses or alloy-temperature was monitored by I-V measurements; the development of the interdiffusion of the contact constituents was observed by RBS-analysis using a 3 MeV He⁺⁺ beam. The onset of ohmicity, resp. for 5 pulses of $P_d \approx 40\text{ MW/cm}^2$ and for $T_a \approx 500^\circ\text{C}$, was governed by a similar interdiffusion behaviour; the laser beam mixed contacts however showed a strikingly narrower intermixed layer. The minimum values of the contact resistivities for the laser beam mixed AuTe contacts were equivalent to the furnace annealed AuTe contacts (as well as to identically processed AuGe contacts); however the morphological quality of the laser contacts was far superior.

A microscopic Mössbauer spectroscopy characterization revealed the formation of Au-doped Ga₂Te₃ structures; the doping level distribution was critically dependent upon the P_d - or T_a -values at conditions around the onset of ohmicity. These observations were

confirmed by XRD-measurements. The results of both macroscopic and microscopic analysis are combined to discuss the nature of the ohmic contacts in terms of possible conduction through a formed graded-heterostructure.

A10.11

MELTING OF ION IMPLANTED AND RELAXED AMORPHOUS SILICON M.G. Grimaldi and P. Baeri, Dipartimento di Fisica, Corso Italia 57, 195129 Catania, Italy; G. Baratta, Istituto di Astronomia, viale A. Doria, 195100 Catania, Italy

The melting temperature of ion implanted and relaxed amorphous silicon has been determined. Structural relaxation was induced by thermal treatment at low temperature (300, 400 and 500 °C) and was evaluated from the Raman linewidth of the transverse optic phonon in amorphous silicon. Pulsed laser irradiation ($\lambda=347\text{nm}$, $\tau=20\text{ns}$) has been used to induce surface melting in the amorphous layers and time resolved reflectivity to detect the melting onset. The threshold energy density for surface melting in the as-implanted amorphous is 10% lower than that of the relaxed one. Since this threshold depends on thermal conductivity we have precisely determined this parameter and a unique value of 0.013 W/(cm K) was found for both as-implanted and relaxed amorphous silicon. A comparison of the experimental results with heat flow calculations directly yields a melting temperature of 1450 ± 25 and 1600 ± 25 K for the as-implanted and relaxed amorphous silicon respectively. The difference in the melting temperature is consistent with the reduction in the internal energy of the relaxed amorphous as estimated from Raman spectrometry.

A11.1

MARTENSITIC TRANSFORMATIONS IN ION IMPLANTED STAINLESS STEELS. E. Johnson, Physics Laboratory, University of Copenhagen, Denmark.

Using ion implantation it is possible to induce martensitic transformations in austenitic stainless steels, where the implanted layer will undergo an fcc (γ) \Rightarrow bcc (α) transformation. The paper will review the various contributions to the driving force for the transformation. Stress provides the dominant contribution, while implantation-induced alloying only plays a significant role, when the composition obtained in the implanted layer directly favours formation of martensite. Implantations with noble gases — including helium — therefore provide very high transformation efficiency. The transformations resemble conventional martensitic transformations in stainless steels. Low nickel steels such as AISI 304 and 316 transform easily during implantation, while no transformation is observed in high nickel steels such as AISI 310.

The martensite content of the implanted layer and its extension in depth has been studied with several depth sensitive techniques: Cross-sectional TEM, energy selective CEMS and RBS/channeling analysis of single crystals. Formation of martensite starts at the surface and extends to larger depth with increasing ion fluence. The extent of the transformed layer coincides with the tails of the implant distributions, and the γ/α interface is rather sharp.

A11.2

HARDNESS-DAMAGE CORRELATIONS IN Ta IMPLANTED SINGLE CRYSTAL Ni₃Al. Gary S. Was, Departments of Nuclear Engineering and Materials Science and Engineering, University of Michigan, Ann Arbor, MI;

and S. Mantl, Institut für Schicht-und Ionentechnik, KFA Jülich, D-5170 Jülich, FRG.

Implantation of Ta into single crystal Ni₃Al was conducted to determine whether this would be an effective means of producing surface hardening in monolithic alloys. Ta was implanted at 400 keV to doses of 0.7, 3.6 and 25.2 x 10¹⁵ i/cm² along the <100> axis of a <100> crystal of Ni₃Al at room temperature. Composition vs depth profiles were made using RBS and lattice damage was analyzed using ion channeling. Surface hardness was measured using the ultra-low load indentation (nanoindentation) technique. Results show that the implanted surface is softer than the unimplanted surface (by 5-10%), and the hardness profile is extremely uniform over the depth of implantation (<90 nm). The minimum yield increases from 3% to about 30% and the half angle decreases from 0.74° to 0.66°. However, neither the surface hardness nor either of the channeling parameters show any dependence on dose even though the highest dose is a factor of 35 times the lowest. Following annealing at 1000°C for 1 hr, the surface hardness increases slightly over the as-implanted samples, the minimum yield recovers to 3-5% and the half-angle remains essentially the same. Softening is attributed to disordering of the structure which is partially compensated by the introduction of defects and the impurity.

A11.3

IRRADIATION-INDUCED AMORPHIZATION AND SHEAR ELASTIC INSTABILITY IN INTERMETALLIC COMPOUNDS. J. Koike*, P. R. Okamoto, L. E. Rehn, R. Bhadra, M. H. Grimsditch, Materials Science Division, Argonne National Laboratory, Argonne, IL 60439; and M. Meshii, Department of Materials Science and Engineering, Northwestern University, Evanston, IL 60208.

Previously some of us had reported a dramatic (~ 50 %) decrease in shear modulus prior to amorphization in Kr irradiated Zr₃Al, and proposed that amorphization is triggered when the crystalline lattice becomes unstable against shear stress. In the present work, the relation between amorphization and shear instability has been further investigated in additional compounds (FeTi, CuTi, NiAl) during room temperature irradiation with 1.7-MeV Kr. A shear modulus was measured using Brillouin scattering; structural information was obtained in situ in a high voltage electron microscope interfaced to a tandem accelerator. During irradiation of FeTi and CuTi, chemical disordering and a large (~ 40 %) decrease of shear modulus were observed, and amorphous phase developed subsequently. In contrast, NiAl remained chemically ordered, and exhibited only ~ 10 % decrease in shear modulus. Hence, these results provide further support for a shear instability mechanism for irradiation-induced amorphization.

* Present address: Center for Materials Science, Los Alamos National Laboratory, Los Alamos, NM 87545.

The work supported by DOE W-31-109-ENG-38 and DMR-8411178.

A11.4

THE EFFECT OF MICROSTRUCTURE ON THE MORPHOLOGY AND KINETICS OF AMORPHIZATION INDUCED BY ION IRRADIATION. D.E. Pedraza and P.J. Maziasz, Metals and Ceramics Division, Oak Ridge National Laboratory, Oak Ridge, TN 37831-6376

NiTi was irradiated with Ni ions in order to study the rate of amorphization as a function of temperature and to determine the temperature cutoff for this transition. A series of irradiation to various doses were conducted at different temperatures, from ambient up to

350°C. The irradiated specimens were observed by transmission electron microscopy. As expected, the kinetics slow as the temperature is increased. The fraction of material that becomes amorphous after irradiation at 250°C to a dose of 0.7 dpa is estimated to be 5 to 10%. Specimens irradiated at higher temperatures remain crystalline, even after doses as high as 4dpa.

Prior to irradiation, the specimens were given a thermal treatment which produced a high volume fraction of martensite. However, martensite entirely reverts to B2 within less than 20 minutes upon annealing at 80°C. Thus, during irradiation at temperatures of 80°C and above, all the specimens were entirely austenitic. Irrespective of the irradiation temperature, we found a very non-uniform distribution of amorphous regions that exhibited a morphology closely resembling the shape of prior (or, at room temperature, present) martensitic plates. These observations are discussed in terms of the effect of structural defects on the kinetics of amorphization.

* Research sponsored by the Division of Materials Sciences, U.S. Department of Energy, under Contract DE-AC05-84OR21400 with Martin Marietta Energy Systems, Inc.

A11.5

EXTENDED SOLID SOLUTION FORMATION IN THE TI-CO-NI SYSTEM. David A. Lilienfeld and P. Bergesen, Cornell University, Ithaca, N.Y.

A reasonable criterion for an alloy to form an amorphous phase during ion mixing is the presence of a complex phase at that composition. One such system is the Ti-Co-Ni system in which there exists a complex phase at the composition Ti₂(Co,Ni). Since this phase has a 96 atom unit cell, it is highly probable that room temperature ion mixing should produce an amorphous phase. Multilayer samples were fabricated. Surprisingly the diffraction patterns of the as-deposited samples consist of broad lines with an FCC structure. Room temperature ion mixing does not amorphize these samples but produces material with sharper diffraction lines than the as-deposited samples.

Ion irradiations carried out at liquid nitrogen temperature produced samples which contained a mixture of amorphous and crystalline structures but could not completely amorphize the samples. Elevated temperature ion mixing was performed. For substrate temperature below 300°C, the FCC phase remained. A 400°C irradiation produced the stable Ti₂(Co,Ni) structure. Composition and substrate temperature dependence of the FCC phase will be discussed in terms of a model which assumes that the FCC phase is a metastable extension of the high temperature Ti phase.

A11.6

CHARACTERIZATION OF HIGH-DOSE CARBON-ION-IMPLANTED AND ANNEALED Nb.* J.S. Huang, Lawrence Livermore National Laboratory, Livermore, CA

Polycrystalline niobium was implanted with 200-keV C⁺ ions to a total fluence of 7x10¹⁷ per cm² (maximum C content ~45 at.%). Auger electron spectroscopy analysis showed variation in C distribution of 5-45 % within a depth of ~3800 Å. Glancing-angle X-ray diffraction and transmission electron microscopy (TEM) analyses were conducted to characterize the phases and microstructures formed. Results indicated that a subsurface fcc NbC layer was formed, but neither the hcp or the orthorhombic Nb₂C phase reported in the equilibrium phase diagram was formed. The NbC phase has a minimum composition of about 36 at.% of C, which is outside the stoichiometry of the NbC phase reported in the equilibrium Nb-C phase diagram. The preference for formation of the NbC was discussed in terms of change of chemical free energy and strain energy associated with phase transformation.

The crystallographic relation between the subsurface NbC layer and the Nb matrix was also analyzed with TEM diffraction analysis. Analysis

results suggested that the transformation from the C-supersaturated bcc Nb lattice to the fcc NbC lattice was a Bain deformation that is typically observed in a diffusionless martensitic transformation.

Implanted samples were also annealed at temperatures of 973–1273 K. It was found that the NbC subsurface layer transformed into Nb₂C particles that had an hcp crystal structure; the crystallographic relation between the Nb matrix and the Nb₂C particles corresponded to that observed in the conventionally processed materials.

* Work performed under the auspices of the U.S. Department of Energy by the Lawrence Livermore National Laboratory under Contract W-7405-Eng-48.

A11.7

STRENGTHENING OF ALUMINUM BY OXYGEN IMPLANTATION: EXPERIMENTAL RESULTS AND MECHANICAL MODELING.

Roy J. Bourcier, Samuel M. Myers, and David M. Follstaedt, Sandia National Laboratories, Albuquerque, NM; and Douglas H. Polonis, University of Washington, Seattle, WA.

The influence of oxygen implantation on the mechanical properties of aluminum has been evaluated using ultra-low load microhardness indentation testing. A new approach has been employed to quantify the strength of the implanted layer in which the hardness data is combined with large-strain finite-element modeling of the resulting deformation. TEM techniques have been employed to characterize the microstructures after implantation and subsequent annealing. The implantation was performed at energies ranging from 25 to 200 keV to produce a flat oxygen concentration profile to a depth of ~ 500 nm; oxygen concentrations ranging from 5 to 20 at.% were investigated. Microhardness measurements were conducted on as-implanted Al and on specimens subsequently vacuum annealed at 723 and 823 K to produce dense distributions of Al₂O₃ precipitates 2-5 nm in diameter. The analysis shows that the flow stress of the implanted layer in the annealed specimens increases with oxygen content, reaching a value of ~ 1200 MPa for the 20 at.% composition, i.e. more than twice the strength level of conventional high strength Al alloys. The as-implanted, unannealed material exhibits even greater strength levels due to the high supersaturation and defective structure resulting from excess oxygen in solution. The strengths of the annealed material calculated from indentation measurements are in general agreement with values predicted on the basis of applying existing models for coherency and dispersion hardening to the observed microstructures.

This work was performed at Sandia National Laboratories and supported by the United States Department of Energy under Contract No. DE-AC04-76-DP00789

A11.8

ION BEAM INDUCED PERCOLATION CLUSTERING IN
Al-Fe-Cu ALLOY FILMS, C.H.Shang and B.X.Liu(a)
Department of Materials Science and Engineering,
Tsinghua University, Beijing 100084, CHINA; (a)
also at Center of Condensed Matter and Radiation
Physics, CCAST (World Lab.), Beijing.

Percolation clustering was observed in an Al-Fe-Cu alloy film, that had been irradiated by 180 keV xenon ions to a dose of 6×10^{15} Xe/cm² at LN₂ temperature, but not otherwise. At this critical dosage, the diffraction patterns of the percolation clustering showed strong diffuse bands, indicating that amorphous structure dominated the examined film. The bright field image of the percolation clustering was digitized with an M750 (VAX) image processor. The fractal dimension of the infinite cluster was calculated to be $D=1.88 \pm 0.06$, and the percolation threshold was $P_c=0.60 \pm 0.03$. These values are all in good agreement with the theoretical predictions. The percolation structures were thought to be formed during a crystalline-to-amorphous phase transition.

This paper presents the detailed experimental results and the possible mechanism responsible for the formation of fractal structures in the ion irradiated alloy films.

A11.9

UNUSUAL MICROSTRUCTURES OF A METASTABLE CRYSTALLINE Pt₅₀Ti₅₀ ALLOY UNDER ION BOMBARDMENT.
Y. L. Chen, Y.-T. Cheng, J. V. Mantese, and A. B. Catalan, General Motors Research Laboratories, Warren, Michigan 48090-9055.

A metastable nanocrystalline Pt₅₀Ti₅₀ alloy of an average grain size 2 nm was obtained by e-beam evaporation from two sources of Pt and Ti onto a single-crystal NaCl substrate at room temperature. This thin film Pt₅₀Ti₅₀ alloy was then bombarded by 400 keV Kr⁺⁺ to doses 5×10^{15} and 10^{16} Kr/cm² at room temperature. Transmission electron microscopy shows that, instead of ion beam induced amorphization or ion beam induced grain growth, the nanocrystalline Pt₅₀Ti₅₀ underwent unusual microstructural changes under ion bombardment: while maintaining the same crystal structure and an average grain size of 2 nm, the Pt₅₀Ti₅₀ thin film appeared to expand along the directions perpendicular to the ion beam direction, causing large ripples of sub-micron to micron size to develop. The origin of this unusual microstructural evolution under ion bombardment is being investigated.

SYMPOSIUM B:
IN-SITU PATTERNING:
SELECTIVE AREA DEPOSITION AND ETCHING

B

November 29-December 1, 1989

Chairs

Anthony F. Bernhardt
University of California
Lawrence Livermore National Laboratory
P.O. Box 5503 M/S L-271
Livermore, CA 94550
(415) 423-7801

Robert Rosenberg
IBM T.J. Watson Research Center
P. O. Box 218
Yorktown Heights, NY 10598
(914) 945-1888

Jerry G. Black
Massachusetts Institute of Technology
Lincoln Laboratory and
Nielsen-Kellerman Company
108 Trapelo Road
Lincoln, MA 01773
(617) 259-8329

Symposium Support

Air Force Office of Scientific Research

Amoco Technology Company

IBM Corporation

Lambda-Physik, Inc.

Newport Corporation

**Proceedings published as Volume 158
of the Materials Research Society
Symposium proceedings series.**

SESSION B1

Chairs: Anthony F. Bernhardt
Wednesday Morning, November 29
Salon E (M)

8:30 *B1.1

NOVEL PHOTOIMAGING SCHEMES AT POLYMER SURFACES, Gary Taylor, AT&T Bell Laboratories, Murray Hill, NJ.

9:00 *B1.2

X-RAY LITHOGRAPHY FOR THE 1990's...REAL OR NOT?, A. Wilson, IBM Research Division, T.J. Watson Research Center, Yorktown Heights, NY.

9:30 *B1.3

PULSED UV LASER PROCESSING FOR ULTRAHIGH-SPEED DEVICE TECHNOLOGY, T.W. Sigmon, Stanford University, Stanford Electronics Laboratory, Stanford, CA; Kurt H. Weiner, Lawrence Livermore National Laboratory, Physics Department, Livermore, CA; Paul G. Carey, Siemens, AG., Corporate Research and Technology, Munich, West Germany.

10:00 BREAK

10:30 B1.4

TIME-RESOLVED REFLECTANCE MEASUREMENTS OF THE MELTING OF METAL DEPOSITS DURING CONTINUOUS-WAVE LASER-INDUCED CHEMICAL VAPOR DEPOSITION, Paul B. Comita, IBM Almaden Research Center, Polymer Science and Technology Department, San Jose, CA; Peter E. Price Jr., University of Minnesota, Dept. of Chemical Engineering and Materials Science, Minneapolis, MN; and Toivo T. Kodas, University of New Mexico, Department of Chemical and Nuclear Engineering, Albuquerque, NM.

10:45 B1.5

IN SITU MEASUREMENT OF PULSED LASER INDUCED CARRIER GENERATION IN DOPED SILICON FILMS, T. Sameshima, M. Hara and S. Usui, Sony Research Center, Yokohama, Japan.

11:00 B1.6

SURFACE CHEMISTRY OF DIMETHYLALUMINUM HYDRIDE AND TRIMETHYLALUMINUM ON ALUMINUM, Daniel R. Strongin and Paul B. Comita, IBM Almaden Research Center, San Jose, CA.

*Invited Paper

Short Course P-12, "Photon-Controlled Processing for Microelectronics," and F-02, "Plasma Etching for Microelectronic Fabrication," may be of interest to symposium attendees. Details regarding course dates and instructors are provided in the short course section of this program.

11:15 B1.7

THE INTERACTION OF LASER-GENERATED METHYL RADICALS WITH Cd, Te, AND CdTe FILMS, J.J. Zinck, G.L. Olson, P.D. Brewer and J.E. Jensen, Hughes Research Laboratories, Malibu, CA.

11:30 B1.8

MECHANISM OF CHROMIUM DEPOSITION BY UV LASER LIGHT, Rainer Nowak and Peter Hess, University of Heidelberg, Institute of Physical Chemistry, Heidelberg, West Germany.

11:45 B1.9

SELECTIVE SURFACE MODIFICATION OF FLUOROCARBON RESIN USING EXCIMER LASER, Masayuki Okoshi and Masataka Murahara, Tokai University, Faculty of Engineering, Hiratsuka, Kanagawa, Japan; and Kouichi Toyoda, Riken, The Institute of Physical and Chemical Research, Wako, Saitama, Japan.

SESSION B2:

Chair: Jerry G. Black
Wednesday Afternoon, November 29
Salon E (M)

1:30 *B2.1

LASER SELECTED AREA PROCESSING FOR MICRO-ELECTRONICS APPLICATIONS, Shunji Kishida and Yukio Morishige, NEC Corporation, Optoelectronics Research Laboratories, Kawasaki, Japan.

2:00 B2.2

VISIBLE-WAVELENGTH LASER PHOTODEPOSITION OF COBALT INTERCONNECTS, M. Rothschild, J.H.C. Sedlacek, D.C. Shaver, and D.J. Ehrlich, Lincoln Laboratory, Submicrometer Technology Department, Lexington, MA; S.N. Bittenson, D. Edwards Jr. and N.P. Economou, Micrion Corporation, Peabody, MA.

2:15 B2.3

LASER-INDUCED CHEMICAL VAPOUR DEPOSITION OF INORGANICS/ORGANOMETALLICS FOR MICROELECTRONICS APPLICATIONS, J.G. Black, H.B. Harrison, P.C. Junk, A.E.W. Knight, R.I. McKay, C.L. Raston, Griffith University, Div. of Science and Technology, Brisbane, Australia.

2:30 B2.4

HIGH DEPOSITION RATE DIRECT WRITING OF AL ON Si, H.W. Lee and S.D. Allen, University of Iowa, Center for Laser Science and Engineering, Iowa City, IA.

2:45 B2.5

LASER CHEMICAL VAPOR DEPOSITION OF W ON Si AND SiO₂/Si, Jian-Yang Lin, Chung Cheng Institute of Technology, Department of Electrical Engineering, Taiwan, China; S.D. Allen, University of Iowa, Center for Laser Science and Engineering, Iowa City, IA.

3:00 BREAK

3:30 ***B2.6**
SELECTIVE AREA DEPOSITION BY ELECTRON BEAM ASSISTED DECOMPOSITION IN ADSORBED MOLECULAR LAYERS, F. Bozso, IBM T.J. Watson Research Center, Yorktown Heights, NY.

4:00 **B2.7**
SELECTIVE EPITAXY OF (Al,Ga)As AND (Al,Ga)As BASED STRUCTURES, T.F. Kuech, M. Goorsky and R. Potemski, IBM T.J. Watson Research Center, Yorktown Heights, NY.

4:15 **B2.8**
PATTERNING OF GaAs/AlGaAs WAFERS BY FOCUSED ELECTRON-BEAM INDUCED CHLORINE ETCHING AND SUBSEQUENT MBE GROWTH, M. Taneva, Y. Sugimoto, H. Hidaka, K. Akita, Optoelectronics Technology Research Laboratory, Tsukuba, Japan.

4:30 **B2.9**
EXCIMER LASER-INDUCED DEPOSITION OF GaN, A. Kobayashi, T. Asai, S. Kawai and P.J. Chong, Osaka University, The Institute of Scientific and Industrial Research, Osaka, Japan.

4:45 **B2.10**
HOLOGRAPHIC PATTERN ETCHING OF SILICON-CARBIDE BY EXCIMER LASERS, Masataka Murahara, Masaru Yonekawa, and Kouichi Shirakawa, Tokai University, Faculty of Engineering, Hiratsuka, Kanagawa, Japan.

SESSION B3

Chair: Susan D. Allen
Thursday Morning, November 30
Salon A/B (M)

8:30 ***B3.1**
LASER-BASED AREA-SELECTIVE PROCESSING FOR HIGH-DENSITY INTERCONNECTS, Y.S. Liu and H.S. Cole, G.E. Corporate Research and Development Center, Schenectady, NY.

9:00 **B3.2**
LASER DIRECT WRITING OF OPTICAL INTERCONNECTS IN POLYIMIDES AND SiO₂:TiO₂ COATINGS, D.W. Hewak and H. Jerominek, National Optics Institute, Sainte-Foy, Canada.

9:15 **B3.3**
SELECTIVE AREA DEPOSITION OF CONDUCTING PALLADIUM FILMS ON POLYIMIDE RESINS, Yoon-Gi Kim, S. Bialy, R. Miller, J.T. Spencer and P.A. Dowben, Syracuse University, Center for Molecular Electronics, Departments of Physics and Chemistry, Syracuse, NY.

9:30 **B3.4**
UV EXCIMER LASER INDUCED DEPOSITION OF PALLADIUM FROM SPIN-ON PALLADIUM-ACETATE FILMS, Hilmar Esrom and Georg Wahl, Asea-Brown-Boveri ABB-CRH, Eppelheimer Strasse, Heidelberg, West Germany; and Michael Stuke, Max-Planck-Institut für biophysikalische Chemie, Göttingen, West Germany.

9:45 **B3.5**
SELECTIVE CHEMICAL VAPOR DEPOSITION OF TUNGSTEN ON LASER-WRITTEN PRENUCLEATION PALLADIUM PATTERNS, Oliver Gottsleben and Michael Stuke, Max-Planck-Institut für biophysikalische Chemie, Göttingen, West Germany.

10:00 BREAK

10:30 **B3.6**
ANOMALOUSLY DEEP STRUCTURES PRODUCED BY III-V MATERIALS BY COMBINED FOCUSED ION BEAM IMPLANTATION AND DRY ETCHING, Lloyd R. Harriott, Henry Temkin and Yuh-Lin Wang, AT&T Bell Laboratories, Murray Hill, NJ.

10:45 **B3.7**
ULTRAHIGH VACUUM COMPATIBLE HALOGEN ETCHING PROCESS FOR SEMICONDUCTOR SURFACES, Andrew Freedman and Charter D. Stinespring, Center for Chemical and Environmental Physics, Aerodyne Research, Inc., Billerica, MA.

11:00 **B3.8**
CONTROL OF ETCHING RATE IN LASER-CHEMICAL REACTION OF Mn-Zn FERRITE BY MeV ION IMPLANTATION, Y.F. Lu, Mikio Takai, and S. Namba, Osaka University, Faculty of Engineering Science and Research Center for Extreme Materials, Osaka, Japan.

11:15 **B3.9**
PRECURSORS TO PHOTO-ABLATION OF SODIUM TRISILICATE GLASS DUE TO UV EXCIMER IRRADIATION, P.A. Eschbach, L.T. Dickinson S.C. Langford, Washington State University, Physics Department, Pullman, WA; and L.R. Pederson, Battelle-Pacific Northwest Laboratory, Richland, WA.

11:30 **B3.10**
X-RAY PHOTOEMISSION INVESTIGATION OF EXCIMER LASER-INDUCED ETCHING OF InP, R. Matz and J. Meiler, Research Laboratories of Siemens AG, Department 2FE F1 FKE 32, München, West Germany; and D. Haarer, Universität Bayreuth, Department Experimentalphysik IV, Bayreuth, West Germany.

11:45 **B3.11**
SELECTIVE ETCHING AND PHOTO-BLEACHING IN THIN AMORPHOUS Ge-Sb-S FILMS, Evdokia B. Savova and Boyill I. Pashmakoff, Institute of Solid State Physics, Sofia, Bulgaria.

12:00 **B3.12**
ULTRAFAST IMAGING OF ULTRAVIOLET LASER ABLATION AND ETCHING OF POLYMETHYL METHACRYLATE, Bodil Braren, R. Srinivasan, Kelly G. Casey, and Mildred Yeh, IBM T.J. Watson Research Center, Yorktown Heights, NY.

SESSION B4

Chair: Thomas F. Kuech
Thursday Afternoon, November 30
Salon A/B (M)

1:30 ***B4.1**
SELECTIVE SILICON EPITAXY FOR ADVANCED DRAM STRUCTURES, G. Bronner, IBM T.J. Watson Research Center, Yorktown Heights, NY.

2:00 **B4.2**
SURFACE REACTION MECHANISMS IN SELECTED AREA EPITAXY OF II-VI's, S.J.C. Irvine, H. Hill, J.E. Hails, S.J. Barnett and J.B. Mullin, Royal Signals and Radar Establishment, Worcestershire, United Kingdom.

2:15 **B4.3**
NOVEL STACKED CMOS PROCESS BY LOCAL OVERGROWTH, René P. Zingg, B. Höfflinger, Institute for Microelectronics, CMOS Technology, Stuttgart, West Germany; and G.W. Neudeck, Purdue University, Electrical Engineering Department, West Lafayette, IN.

2:30 **B4.4**
LASER ASSISTED MOLECULAR BEAM EPITAXY (LAMBE) GaAs ON SILICON PHOTODETECTORS, A. Christou, N.A. Papanicolaou, and G.W. Anderson, Naval Research Laboratory, Surface Physics Branch, Washington, DC.

2:45 **B4.5**
LASER SELECTIVE AREA EPITAXY FOR THE INTEGRATION OPTOELECTRONIC STRUCTURES, H. Liu, J.C. Roberts, J. Ramdani, and S.M. Bedair, North Carolina State University, Electrical and Computer Engineering Department, Raleigh, NC.

3:00 **B4.6**
LASER INDUCED SURFACE CHEMICAL EPITAXY, Charter D. Stinespring and Andrew Freedman, Center for Chemical and Environmental Physics, Aerodyne Research, Inc., Billerica, MA.

3:15 **B4.7**
LASER PROCESSED SILICIDES FOR GAAS HEMTS, W.T. Anderson, A. Christou, Naval Research Laboratory, Surface Physics Branch, Washington, DC; C. Michelakis, G. Kiriakidis, Research Center of Crete, Heraklion, Greece.

3:30 BREAK

4:00 **B4.8**
MASKLESS FORMATION OF TUNGSTEN FILM BY ION BEAM INDUCED DEPOSITION TECHNIQUE, Zheng Xu, Kenji Gamo and Susumu Namba, Osaka University, Faculty of Engineering Science, Osaka, Japan.

4:15 **B4.9**
NANOLOTHOGRAPHY BY STM ON $\text{Rb}_{0.3}\text{MoO}_3$, A CONDUCTING OXIDE, G. Rudd, D. Novak, S. Wang, S.H. Garofalini and E. Garfunkel, Rutgers University, Laboratory for Surface Modification and Center for Ceramics Research, Departments of Chemistry and Physics, Piscataway, NJ.

4:30 **B4.10**
COMBINING ELECTRON AND ION BEAM TECHNIQUES FOR THE PRODUCTION OF BURIED SINGLE-CRYSTAL METALLIC WIRES, S.D. Berger, Julita E. Woroniecka, H.A. Huggins, Alice E. White, K.T. Short, and D. Loretto, AT&T Bell Laboratories, Murray Hill, NJ.

4:45 **B4.11**
THE ROLE OF ADSORPTION AND VAPOR PRESSURE IN FOCUSED ION BEAM INDUCED DEPOSITION OF CARBON FILMS, S.J. Kirch, IBM General Technology Division, East Fishkill, Hopewell Junction, NY; and D.E. Seeger, IBM T.J. Watson Research Ctr., Yorktown Heights, NY.

5:00 **B4.12**
LASER ABLATION AND PLASMA HYBRID TECHNIQUE FOR DEPOSITING MULTILAYERED STRUCTURES, J. Krishnaswamy, S. Sharan, and J. Narayan, North Carolina State University, Raleigh, NC; and O.W. Holland, Oak Ridge National Laboratory, Solid State Div., Oak Ridge, TN.

SESSION B5: POSTER SESSION

Chair: Christopher Moylan
Thursday Evening, November 30
7:00 p.m. - 10 p.m.
America Ballroom (W)

B5.1 A NEW MODEL OF POLYMER PHOTOABLATION KINETICS, Sylvain Lazare, and Vincent Granier, Université de Bordeaux I, Laboratoire de Photophysique et Photochimie Moléculaire, Talence, France.

B5.2 A PROCESS MODEL FOR REACTIVE ION ETCHING AND STUDY OF THE EFFECTS OF MAGNETRON ENHANCEMENT, M. Meyvappan, Scientific Research Associates, Inc., Glastonbury, CT.

B5.3 SILICON FILM AS A NEW ETCHING MASK FOR InP DEVICES, X.S. Wu, Shanghai Institute of Metallurgy, Academia Sinica, Shanghai, China; Shuojin Wang, Zhejiang University, Hangzhou, China; Zhangde Lu, Shanghai Institute of Metallurgy, Academia Sinica, Shanghai, China; and Jun Chen, Fudan University, Institute of Materials Science, Shanghai, China.

B5.4 ETCHING OF GAAS ON AlGaAs IN RIE-MODE, G. Kaufel, E. Olander, Fraunhofer-Institut für Angewandte Festkörperphysik, Freiburg, West Germany.

B5.5 COPPER VAPOR LASER USED IN ETCHING AND DEPOSITION, Belgacem Haba, Brian W. Hussey, Arunava Gupta and Robert J. Baseman, IBM T.J. Watson Research Center, Yorktown Heights, NY.

B5.6 DOWNSTREAM ETCHING OF GaAs AND InP USING MOLECULAR CHLORINE AND CHLORINE RADICALS David G. Lishan and Evelyn L. Hu, University of California, Santa Barbara, Electrical and Computer Engineering Department, Santa Barbara, CA.

B5.7 COMBINING SPONTANEOUS MOLECULAR ASSEMBLY WITH MICROFABRICATION TO PATTERN SURFACES: COORDINATION CHEMISTRY OF FUNCTIONALIZED ISONITRILES TO Pt SURFACES, J.J. Hickman, C. Zou, D. Ofer and M.S. Wrighton, Massachusetts Institute of Technology, Department of Chemistry, Cambridge, MA; P. Laibinis, C. Bain and G.M. Whitesides, Harvard University, Department of Chemistry, Cambridge, MA.

B5.8 HOLLOW COLD CATHODE ION SOURCE FOR REACTIVE ION-BEAM ETCHING, A.I. Stognij and V.V. Tokarev, BSSR Academy of Sciences, Institute of Solid State and Semiconductor Physics, Minsk, USSR.

B5.9 LASER INDUCED FORWARD TRANSFER FOR THE DEPOSITION OF PATTERNED HIGH Tc SUPERCONDUCTOR THIN FILMS, E. Fogarassy, C. Fuchs, and S. De Unamuno, CRN, Laboratoire PHASE, Strasbourg, France; and J. Perriere, Université de Paris VII (G.P.S. de l'ENS), Paris, France.

B5.10 DIRECT EVIDENCE FOR THE CREATION OF MICROPORES IN UV-IRRADIATED POLY (METHYL METHACRYLATE), J.A. Moore and J.-O. Choi, Rensselaer Polytechnic Institute, Polymer Science and Engineering Program, Troy, NY.

B5.11 REACTIVE ION ETCHING OF In-BASED III-V SEMICONDUCTORS-COMPARISON OF Cl AND C₂H₆ CHEMISTRIES, S.J. Pearton, U.K. Chakrabarti, F.A. Baiocchi, and W.S. Hobson, AT&T Bell Laboratories, Murray Hill, NJ.

B5.12 ELEVATED TEMPERATURE REACTIVE ION ETCHING OF GaAs AND AlGaAs IN C₂H₆/H₂, S.J. Pearton, W.S. Hobson, AT&T Bell Laboratories, Murray Hill, NJ; and K.S. Jones, University of Florida, Gainesville, FL.

B5.13 CHARACTERIZATION OF SIDEWALL RESIDUE FILM AND ATOMIC STRUCTURE OF THE TRENCH FORMED BY BCl₃/Cl₂ REACTIVE ION ETCHING, Sun Jin Yun and Young-Jin Jeon, Electronics and Telecommunications Research Institute, Semiconductor Technology Division, Daejeon, Korea; Jeong Y. Lee, Korea Institute of Technology, Daejeon, Korea.

B5.14 SUBSTRATE HEATING EFFECTS IN EXCIMER LASER PLANARIZATION OF ALUMINUM, Robert J. Baseman and Joseph C. Andreshak, IBM T.J. Watson Research Center, Research Division, Yorktown Heights, NY.

B5.15 WHOLE COMPOSITION RANGE DEPOSITION OF THIN FILMS BY MAGNETRON COSPUTTERING AND ITS APPLICATIONS, Qing-Ming Chen, Huazhong University of Science and Technology, Wuhan, China; Yu-Dian Fan and Heng-De Li, Tsinghua University, Beijing, China.

B5.16 THE ETCHING OF Si(100) WITH A MOLECULAR BEAM OF F₂, K.B. Laughlin, M. McGonigal, D.J. Gladstone, M.T. Schulberg and S.T. Ceyer, Massachusetts Institute of Technology, Department of Chemistry, Cambridge, MA.

B5.17 SELECTIVE CHEMICAL VAPOR DEPOSITION OF TUNGSTEN FILMS ON TITANIUM ION-IRRADIATED SILICON DIOXIDE, H. Okuhira, S. Nishimatsu and K. Ninomiya, Hitachi, Ltd., Central Research Laboratory, Tokyo, Japan.

B5.18 STATISTICAL INTERPRETATION OF IR AND UV PHOTOABLATION, Ruediger Braun and Peter Hess, University of Heidelberg, Institute of Physical Chemistry, Heidelberg, West Germany.

B5.19 THE EFFECTS OF SOURCE GAS, TEMPERATURE AND PRESSURE ON THE SURFACE PLANARITY AND MICROSTRUCTURE OF SILICON SEG AND ELO, M.C. Arst, K.N. Ritz, J.T. Chen, S. Redkar, Philips Research Laboratories, Signetics Company, Sunnyvale, CA; J.O. Borland and J. Hann, Applied Materials, Inc., Epi Application Laboratory, Santa Clara, CA.

B5.20 IN-SITU CHARACTERIZATION OF CHEMICAL VAPOR DEPOSITION, R. Scarmozzino, T. Cacouris, and R.M. Osgood Jr., Columbia University, New York, NY.

B5.21 EDGE ENHANCED INTERLAYER DIFFUSION IN Al/Hf/Al VLSI METALLIZATION, X.S. Guo and W.A. Lanford, State University of New York at Albany, Albany, NY; and K.P. Rodbell, IBM-East Fishkill, Hopewell Junction, NY.

B5.22 LASER WRITING OF HIGH PURITY GOLD LINES, M. Jubber, J.I.B. Wilson, J.L. Davidson, P.A. Fernie, P. John, Heriot-Watt University, Riccarton, Edinburgh, Scotland.

B5.23 PHOTOSTIMULATED DEFECT-IMPURITY REACTIONS DURING ION BOMBARDMENT OF SI, Alex B. Danilin, Yuri N. Erokhin, Viktor N. Mordkovich, Institute of Microelectronics Technology and Superpure Materials, USSR Academy of Sciences, Moscow, USSR.

SESSION B6

Chair: Mordechai Rothchild
Friday Morning, December 1
Salon A/B (M)

8:30 ***B6.1**
GENERATION OF BLIND VIA-HOLES FOR A HIGH DENSITY MULTI-CHIP-MODULE USING EXCIMER LASERS, Friedrich G. Bachmann, Siemens AG, Corporate Production and Logistics Department, Munich, West Germany.

9:00 **B6.2**
UV LASER-INDUCED ETCHING OF FIRST-ROW TRANSITION METALS, G.W. Tyndall, IBM Almaden Research Center, San Jose, CA.

9:15 **B6.3**
PHOTOCHEMICAL AREA-SELECTIVE ETCHING OF Si AND SiO₂ USING SYNCHROTRON RADIATION, Junichi Takahashi, Yuichi Utsumi and Tsuneo Urisu, NTT, LSI Laboratories, Kanagawa, Japan.

9:30 **B6.4**
EXCIMER LASER-ASSISTED ETCHING OF SILICON USING CHLOROPENTAFLUOROETHANE, S.D. Russel, and D.A. Sexton, Naval Ocean Systems Center, Solid State Electronics Division, San Diego, CA.

9:45 **B6.5**
LOCALIZED LASER-ASSISTED ETCHING OF COPPER FILMS BY CHLORINE USING RAMAN SPECTROSCOPY FOR IN-SITU FILM ANALYSIS, Hua Tang and Irving P. Herman, Columbia University, Department of Applied Physics and the Microelectronics Sciences Laboratories, New York, NY.

10:00 BREAK

10:15 **B6.6**
SELECTIVE TUNGSTEN CVD ON A-SI:H BY PULSED UV LASER MODIFICATION OF THE NATIVE OXIDE, Arthur T. Howe, K.V. Reddy, Darrell L. Wuensch and Jeff T. Niccum, Amoco Technology Company, Technology Division, Naperville, IL; and Gerry W. Zajac, Amoco Corporation, Analytical Division, Naperville, IL

10:30 **B6.7**
WAVELENGTH-DEPENDENT AREA SELECTIVITY IN PHOTOCHEMICAL VAPOR DEPOSITION OF ALUMINUM FILMS, Mitsugu Hanabusa and Masahi Ikeda, Toyohashi University of Technology, Toyohashi, Japan.

10:45 **B6.8**
KrF EXCIMER LASER INDUCED DEPOSITION OF TITANIUM FROM TiCl₄, R. Izquierdo, M. Meunier and C. Lavoie, Ecole Polytechnique de Montreal, Groupe des Couches Minces et Département de Génie Physique, Montréal, Canada.

11:00 **B6.9**
SELECTIVE RAPID THERMAL CVD OF GERMANIUM, D.T. Grider, M.C. Ozturk, J.J. Wortman, North Carolina State University, Department of Electrical and Computer Engineering, Raleigh, NC; Y. Zhong, Liaoning University, Physics Department, Liaoning, China; D. Batchelor, and P. Russell, North Carolina State University, Department of Materials Science and Engineering, Raleigh, NC.

11:15 **B6.10**
LASER-INDUCED LOCAL DECOMPOSITION OF ADSORBED TUNGSTEN FLUORINE MOLECULES FOR METAL DEPOSITION ON SILICON, G. Auvert, D. Tonneau, and Y. Pauleau, C.N.E.T., Meylan, France.

11:30 **B6.11**
EXCIMER LASER INDUCED DEPOSITION OF TUNGSTEN FROM W(CO)₆ AND WF₆, B. Rager and F. Bachmann, Siemens AG, Corp. Production and Logistics Department, Munich, West Germany.

11:45 **B6.12**
DIRECT WRITING OF COPPER LINES USING ND:YAG LASER AND COPPER FORMATE PRECURSORS, Heinrich G. Müller and Siegfried Schuler, TU Berlin, Forschungsschwerpunkt Mikroperipherik, Berlin, West Germany.

SESSION B7

Chair: Robert Rosenberg
Friday Afternoon, December 1
Salon A/B (M)

1:30 ***B7.1**
LASER-INDUCED FORMATION AND SURFACE PROCESSING OF HIGH-TEMPERATURE SUPERCONDUCTORS, D.W. Bauerle, Angewandte Physik, Johannes-Kepler-Universität, Linz, Austria.

2:00 **B7.2**
LASER PATTERNING AND ELECTRICAL PROPERTIES OF SUBMICROMETERS LINES OF Y-Ba-Cu-O, J.P. Zheng, Q.Y. Ying, H.S. Kim, D.T. Shaw and H.S. Kwok, State University of New York at Buffalo, Institute on Superconductivity, Buffalo, NY.

2:15 **B7.3**
PULSED EXCIMER LASER ABLATION FOR THE DEPOSITION OF YBaCuO AND BiSrCaCuO COMPOUNDS: MATERIALS DISTRIBUTION AND STOICHIOMETRY, C. Fuchs and E. Fogarassy, CRN, Laboratoire PHASE, Strasbourg, France.

2:30 **B7.4**
(ABSTRACT WITHDRAWN)

2:45 BREAK

3:00 **B7.5**
TUNABLE UV LASER DECOMPOSITION OF GAS PHASE AND SURFACE ADSORBED ORGANOMETALLICS, Thomas Beuermann, Yanping Zhang, and Michael Stuke, Max-Planck-Institut für biophysikalische Chemie, Göttingen, West Germany.

3:15 **B7.6**
LOW TEMPERATURE INTERLEVEL SiO₂-LAYERS BY PHOTOINDUCED PROCESSING, H. Sigmund, A. Klumpp and G. Springholz, Fraunhofer-Institute for Solid State Technology, Munchen, West Germany.

3:30 **B7.7**
PHOSPHORUS DOPING INTO SILICON USING ArF EXCIMER LASER, A. Slaoui, E. Foulon, E. Fogarassy, and P. Siffert, Laboratoire PHASE, C.N.R.S., Strasbourg, France.

3:45 **B7.8**
ROLES OF GAS PHASE AND SURFACE PHOTOLYSIS IN LCVD FROM Fe(CO)₅, Xu Xin, Institute for Atomic Energy Research, Beijing, China and Massachusetts Institute of Technology, Department of Chemistry, Cambridge, MA; and J.I. Steinfeld, Massachusetts Institute of Technology, Department of Chemistry, Cambridge, MA.

4:00 **B7.9**
ROOM TEMPERATURE PHOTO-OXIDATION OF HYDROGENATED SILICON-CARBON ALLOYS, P. John, I.M. Odeh, A. Qayyum and J.I.B. Wilson, Heriot-Watt University, Riccarton, Edinburgh, Scotland.

4:15 **B7.10**
MECHANISM OF SELECTIVE AREA GROWTH OF ALUMINUM BY ORGANOMETALLIC CHEMICAL VAPOR DEPOSITION, Krishnan Raghavachari, G.S. Higashi, and M.L. Steigerwald, AT&T Bell Laboratories, Murray Hill, NJ.

4:30 **B7.11**
METAL DEPOSITION WITH INCOHERENT EXCIMER RADIATION, Hilmar Esrom, Asea-Brown-Boveri AG, Corporate Research Heidelberg, Heidelberg, West Germany; and Ulrich Kogelschatz, Asea-Brown-Boveri AG, Corporate Research Baden, Baden, Switzerland.

B1.1 ABSTRACT NOT AVAILABLE

B1.2

X-RAY LITHOGRAPHY FOR THE 1990's...REAL OR NOT?

Alan D. Wilson, IBM Research Division, T. J. Watson Research Center, P. O. Box 218, Yorktown Heights, New York 10598.

X-Ray Lithography has been a technology that was slated to be used at the limits of Optical Lithography and this was to be at the one micron or so minimum feature size which the industry reached in about 1986. X-rays are not used today so what happened and will they ever be used to make VLSI chips? To answer the first question is very easy...optical lithography did not reach its limit. To answer the second question is more difficult and that will be the goal of this paper, and, it will be shown that waiting for optical lithography to reach its limit may be the wrong thing to do. In addition to the usual resolution enhancements, x-ray lithography offers potential advantages in (1) yield, (2) process simplicity (and thus cost), and (3) chip size.

WHAT IS X-RAY LITHOGRAPHY?

X-ray lithography is a proximity printing process using $\sim 10 \text{ \AA}$ x-rays. Resolutions of 0.1 micron have been demonstrated in a number of laboratories around the world and a large, relative to optical lithography, depth of focus has been observed as well as 100% process latitude. This process latitude is an excellent attribute and has a significant role in the apparent insensitivity of x-rays to defects and excellent linewidth control achieved with x-rays. X-ray lithography does not employ any optical elements between mask and wafer which could limit the field size as in optical lithography. Chip or field size is limited by mask defect density or overlay. Intrinsic exposing rates, determined by the ratio of x-ray power to resist sensitivity, is on the order of $10 \text{ cm}^2/\text{sec}$. - a very suitable rate of exposure for manufacturing.

B1.3

PULSED UV-LASER PROCESSING FOR ULTRA-HIGH-SPEED DEVICE TECHNOLOGY. Thomas W. Sigmon, Stanford University, Stanford, CA; Kurt H. Weiner, LLNL, Livermore, CA.; and Paul G. Carey, Siemens, Munich, FRG.

Progress in high-speed device technology is occurring by both scaling of conventional devices, such as MOSFET and bipolar, and the development of new device structures which take advantage of multi-layer heterostructures. With scaling in the lateral dimensions producing devices with dimensions approaching $0.1 \mu\text{m}$, vertical scaling has become a topic of concern. This talk will focus on results obtained using pulsed uv-laser doping and selective epitaxy which addresses several of the problems faced in both the vertical scaling of junctions for silicon MOS and bipolar structures and in the fabrication of selective heterostructure layers. Following a brief historical overview and description of the process, successful applications in the fabrication of submicron MOSFETs and narrow base bipolar transistors in silicon will be presented. Results, both structural and electrical, on the fabrication of heterostructures layers in the $\text{Ge}_x\text{Si}_{1-x}$ and $\text{In}_x\text{Ga}_{1-x}\text{As}$ material systems will be presented.

B1.4

TIME-RESOLVED REFLECTANCE MEASUREMENTS OF THE MELTING OF METAL DEPOSITS DURING CONTINUOUS-WAVE LASER-INDUCED CHEMICAL VAPOR DEPOSITION

Paul B. Comita, IBM Almaden Research Center, 650 Harry Road, San Jose, CA 95120; Peter E. Price, Jr., Department of Chemical Engineering and Materials Science, University of Minnesota, Minneapolis, MN 55455; and Toivo T. Kodas, Department of Chemical and Nuclear Engineering, University of New Mexico, Albuquerque, NM.

We have observed the explosive melting of metallic gold during laser-induced chemical vapor deposition (LCVD) of gold on alumina surfaces, and have examined the time evolution of the phase change with reflectance measurements. The phase change has been observed when the continuous

wave laser light is modulated between approximately 0.5 Hz and 1 Mhz, and occurs with a substantial increase in emitted light at normal incidence to the laser-irradiated surface. This has been shown to be due to a change in the reflected laser light normal to the surface of the metal deposit. During the time the surface of a deposit is liquid or molten, the surface conforms to the substrate and the incident light is reflected primarily normal to the surface. When the surface of the deposit is a polycrystalline solid, the incident beam is scattered and reflected light normal to the surface is reduced. The increase in reflected laser light due to melting has been examined during the stationary growth of a gold deposit during single pulses of laser light. The reflected light at normal incidence to the surface has been determined as a function of laser fluence, wavelength in a two color experiment, length of duty cycle, and frequency of modulation. The laser light was modulated with a high power electro-optic modulator with a 20 Mhz bandwidth. The influence of this technique on the microstructure of gold deposited by LCVD has been examined in detail by scanning electron microscopy.

B1.5

In situ measurement of pulsed laser induced carrier generation in doped silicon films. T. Sameshima, M. Hara and S. Usui, Sony Research Center, Yokohama, Japan.

Very fast carrier generation during laser doping was established by transient conductance measurements. A non-doped SOS film with Al electrodes with a gap on the surface was coated with a thin boron film by decomposition of B_2H_6 gas using glow discharge. The conductance change of the silicon film between the Al electrodes was measured when the silicon surface was melted by irradiation with a pulsed XeCl excimer laser (30 ns FWHM) at an energy density of 1.0 J/cm^2 . The conductance associated with molten silicon first increased, then decreased. In the resolidification process, residual conductance caused by heavy boron doping was measured. Conductance was $0.05 \text{ S}/\square$ at the termination of melt, which was determined by the termination of high optical reflectivity associated with surface molten state using time resolve optical reflectivity measurements to be 400 ns after irradiation had ceased. This result indicates that the boron atoms diffused in the molten silicon from the surface were activated immediately after the molten silicon resolidified. Transient conductance measurements also showed that after the solidification, the conductance increased monotonously with time to reach $0.11 \text{ S}/\square$ at room temperature. The increase of conductance with time can be interpreted as the increase in the mobility of carriers as the silicon film cooled through heat diffusion to the underlying substrate.

B1.6

SURFACE CHEMISTRY OF DIMETHYLALUMINUM HYDRIDE AND TRIMETHYLALUMINUM ON ALUMINUM Daniel R. Strongin and Paul B. Comita, IBM Almaden Research Center, 650 Harry Road, San Jose, CA 95120.

The adsorption and reaction pathways of both dimethylaluminum hydride (DMAH) and trimethylaluminum (TMA) have been investigated on a polycrystalline aluminum surface with temperature programmed desorption, Auger electron spectroscopy, and secondary ion mass spectrometry. DMAH is adsorbed on the aluminum surface at 90 K in its monomeric, dimeric, and trimeric forms. TMA adsorbs primarily in the dimeric form and it desorbs from the aluminum surface at about 190 K. Secondary ion mass spectrometry and Auger electron spectroscopy show that carbonaceous deposits are left on the aluminum surface after TMA desorption. The temperature programmed desorption of DMAH from the aluminum surface results in the desorption of DMAH dimer

and trimer between 195 and 255 K. TMA is found to desorb as a reaction product at 230 K when DMAH reacts on the aluminum surface. This reaction channel to form TMA, from DMAH might provide a low temperature pathway for the production of aluminum metal.

B1.7

THE INTERACTION OF LASER-GENERATED METHYL RADICALS WITH Cd, Te, and CdTe FILMS. J.J. Zinck, G.L. Olson, P.D. Brewer, and J.E. Jensen, Hughes Research Laboratories, Malibu, CA.

Methyl radicals have been shown to be important species for gas phase (dry) etching of metal and semiconductor thin films. In this paper the interaction of excimer laser-generated methyl radicals with Cd, Te, and CdTe films is examined via studies of the adsorption of methyl radicals and desorption of reaction products from these surfaces in ultrahigh vacuum. Methyl radicals were produced by ArF excimer laser (193 nm) photodissociation of acetone molecules in a collisionless (molecular flow) environment. A surface-parallel irradiation geometry was used to dissociate the molecules in the gas phase without simultaneously inducing a transient temperature increase at the surface. Thermal desorption mass spectrometry and Auger electron spectroscopy were used to probe the surface chemistry of the undissociated parent molecule and the photodissociation products. Enhancement of the yield of desorbed metal alkyl reaction products was observed when the excimer laser was used to dissociate the parent molecule; the enhancement factor depended upon the substrate type, laser fluence and gas flux. The surface desorption results for Cd, Te, and CdTe will be presented, a mechanism which describes the interaction between the laser-generated radicals and the surface will be described, and the implications of these results for dry etching of metal and semiconductor thin films will be discussed.

B1.8

MECHANISM OF CHROMIUM DEPOSITION BY UV LASER LIGHT. Rainer Nowak and Peter Hess, Institute of Physical Chemistry, University of Heidelberg, Im Neuenheimer Feld 253, D-6900 Heidelberg, F.R.G.

The deposition of pure chromium films at low temperatures by LICVD is not only a challenge from a scientific point of view, but also of great interest for potential applications. Therefore, the deposition process was studied as a function of the important parameters such as UV laser fluence and repetition rate, gas flow, pressure, temperature etc. Nucleation and growth of the film were monitored in situ by measuring the transmission of a HeNe laser beam.

Impurity incorporation into the deposited film was determined by XPS analysis for different chromium complexes as precursors and buffer gases such as CO, rare gases and hydrogen. These experiments yielded detailed information on the variation of film composition, but also on the deposition rate and mechanism.

For higher buffer gas pressures the deposition process is diffusion limited. Chromium atoms and unsaturated complexes produced in the gas phase by UV laser photolysis seem to play a more important role for nucleation than for the growth process. There is a strong influence of surface chemistry on the chemical composition of the deposited films and indications for a catalytic activity of the surface.

B1.9

SELECTIVE SURFACE MODIFICATION OF FLUOROCARBON RESIN USING EXCIMER LASER.

M.OKOSHI, A graduate student of Faculty Eng. Tokai Univ.; M.Murahara, Faculty of Eng. Tokai Univ., 1117 Kitakaname, Hiratsuka, Kanagawa, 259-12, JAPAN; K.TOYODA, Riken, The Institute of Physical and Chemical Research, 2-1 Hirosawa, Wako, Saitama 351-01, JAPAN.

Fluorocarbon resin is very stable material chemically. Namely, it has chemical resistance and heat resistance. However, this material has no adhesion, and no affinity for oil or water.

So, we wish to report on the selective area modification of the fluorocarbon resin using ArF excimer laser beam and gaseous trimethyl boron ($B(CH_3)_3$). Then, ArF laser is irradiated on these resin surface, it is possible to cut the strong C-F bond. Even if this bond was cut, it would recombine immediately for high electronegativity of fluorine. Then, two kinds of decomposition of $B(CH_3)_3$ and $(C-F)_2$ were tried simultaneously by ArF laser irradiation. So F atoms were pulled out by B atoms. And all free positions F atoms were substituted by methyl-radicals. By this photochemical reaction, the surface of this resin was turned to oleophilic materials selectively.

In this experiment, the most effective experimental conditions are next; the fluence of ArF laser beam was 25 mJ/cm^2 , pulse repetition was 50 pps and irradiation time was 60 sec. And contact angle with oil was 0-10 degrees.

B2.1

LASER SELECTED AREA PROCESSING FOR MICROELECTRONICS APPLICATIONS. Shunji Kishida and Yukio Morishige, Opto-Electronics Research Laboratories, NEC Corporation, Kawasaki, Japan

Micron-scale thin film direct-patterning technology has a variety of applications in microelectronics. Excellent refractory metal patterning technologies of both projection printing and direct writing have been developed utilizing short pulse laser CVD. Promising practical results have been obtained for photomark clear defect repairing, LSI interconnection repairing, LSI failure analysis, and TFT fabrication.

For mask repairing, projection printing of high quality micron-scale Cr film has been achieved using high repetition rate (~kHz) laser pulse irradiation. In LSI interconnection application, pulsed-laser-CVD directly written W line allows large current flow ($\sim 10^4 \text{ mA}$), has sufficiently low contact resistance ($\leq 0.5 \Omega$) with Al interconnections, and reveals high reliability of passing aging test. These superior electrical characteristics make this technology applicable to a wide variety of microelectronics devices, including MOS, bipolar and analog LSIs.

B2.2

VISIBLE-WAVELENGTH LASER PHOTODEPOSITION OF COBALT INTERCONNECTS*, M. Rothschild, J. H. C. Sedlacek, D. C. Shaver, and D. J. Ehrlich, Lincoln Laboratory, Massachusetts Institute of Technology, Lexington, MA, and

S. N. Bittenson, D. Edwards, Jr., and
N. P. Economou, Micrion Corporation, Peabody, MA

The deposition of cobalt films from $\text{Co}_2(\text{CO})_8$ vapor has been developed. The new process is notable in that it is initiated photolytically with low-power visible argon-ion-laser radiation. Cobalt films 0.1- to 2- μm thick with resistivities of 30-50 $\mu\Omega\text{-cm}$ are deposited on glass, silicon or polyimide substrates. Scanning speeds for 0.5- μm -thick films are ~100 $\mu\text{m/s}$. We will discuss the current picture of the deposition mechanism, as determined with mass and infrared spectroscopies, and summarize studies of the electrical and material properties of the deposited films. We will also describe the recent application of the process to repair of flat panel displays.

* The Lincoln Laboratory portion of this work was sponsored by the Defense Advanced Research Projects Agency and the Department of the Air Force, in part under a specific program supported by the Air Force Office of Scientific Research.

B2.3

LASER-INDUCED CHEMICAL VAPOUR DEPOSITION OF INORGANICS/ORGANOMETALLICS FOR MICROELECTRONICS APPLICATIONS. J.G. Black, H.B. Harrison, P.C. Junk, A.E.W. Knight, R.I. McKay, C.L. Raston, Division of Science and Technology, Griffith University, Nathan 4111, Brisbane, Australia.

Inorganic/organometallic molecules have been targeted for laser-assisted metal deposition onto silicon surfaces using the following criteria: Favourable handling characteristics, ease of purification, sufficient vapour pressure for deposition of practical quantities of metal, and specific wavelength absorption characteristics to facilitate the laser-induced dissociation process. The inorganic/organometallic precursors are ideally required to undergo facile ligand-metal bond rupture so that contamination of the deposited metal by other reaction products (eg metal carbides) is minimized. Generated volatile material devoid of metal atoms is expected to be easily disposed without hindering the primary laser-induced deposition process.

In addition to deposition studies, photochemical mechanisms are being investigated using laser photofragmentation excitation spectroscopy, in consort with time of flight mass spectrometry. These studies are being undertaken in an attempt to design a more controlled experimental environment using photochemically driven fragmentation rather than the more commonly used thermolytic process.

Preliminary studies have succeeded in depositing thin lines of highly conductive material, with apparently little contamination. Precursors for the deposition of a range of materials suitable for microelectronics applications including aluminium, platinum and antimony are being developed.

B2.4 ABSTRACT NOT AVAILABLE

B2.5

LASER CHEMICAL VAPOR DEPOSITION OF W ON Si AND SiO_2/Si . Jian-Yang Lin, Dept. of Electrical Engineering, Chung Cheng Institute of Technology, Ta-Shi, Taiwan, R.O.C.; Susan D. Allen, The U. of Iowa, Iowa City, IA 52242-1294, U.S.A.

Deposition of W on bare Si and native- SiO_2/Si substrates has been investigated in an laser chemical vapor deposition (LCVD) system using a highly focused visible 514.5 nm cw Ar laser as the heat source. Temperature distributions on the Si substrate induced by the laser beam were calculated using a modified Lax formulation to study the deposition kinetics. W deposits on bare Si surface via the Si and/or H_2 reduction of WF_6 were self-limited in the thickness to 200 - 600 Å in both cases. Auger electron spectroscopic analysis showed that there was a trace amount of Si on the as-deposited W surface. Si-H bonds could be poisoning the further growth of W. W deposits on native- SiO_2/Si were only obtainable via the H_2 reduction of WF_6 in our laser direct-write system. Our experimental kinetic study indicated that HF desorption from the surface is the rate-controlling step for W deposition via the H_2 reduction of WF_6 . The as-deposited W lines were 2 - 10 μm wide, 0.2 - 6 μm thick with resistivities of 11 - 56 $\mu\Omega\text{-cm}$, depending upon the gas composition, the laser power level, and the laser scan speed. The growth rates of W lines achieved were as high as 2.2 mm/s. The nucleation and growth of W deposits have been observed with a high speed real-time optical monitoring and gating system as a function of the growth conditions.

B2.6

SELECTIVE AREA DEPOSITION BY ELECTRON BEAM ASSISTED DECOMPOSITION IN ADSORBED MOLECULAR LAYERS. F. Bozso, IBM Research Division, T. J. Watson Research Center, P.O. Box 218, Yorktown Heights, N.Y. 10598

Selected area deposition of thin films and material structures is possible with precise control over the material composition by using low energy electron beams to induce reactions in adsorbed molecular layers. Upon electron impact the adsorbed/coadsorbed molecules decompose into reactive species resulting in growth of a surface film. The composition of the film reflects that of the adsorbed molecular layer, which at cryogenic temperatures can very sensitively be controlled by the partial pressure of the reactant gases. We present detailed studies of the adsorption, co-adsorption and thermal and electron-beam induced dissociation of disilane, ammonia, nitric oxide, oxygen and decaborane on Si(100) and Si(111)-7x7 surfaces using X-ray and UV photoemission spectroscopy, thermal desorption spectroscopy and electron induced desorption. At room temperature the above gases adsorb mainly dissociatively whereas below 120K a layer of molecularly adsorbed species can be formed in equilibrium with the gas phase. We show that by proper choice of temperature, gas phase composition and electron beam, amorphous silicon, silicon nitride, silicon oxynitride and high concentration boron doped silicon films can be grown with a thickness control of nearly monolayer resolution.

B2.7

SELECTIVE EPITAXY OF (AL,Ga)AS AND (AL,Ga)AS BASED STRUCTURES, I.F.Kuech, M.Goorsky, and R.Potemski, IBM T.J.Watson Research Center, P.O.Box 218, Yorktown Heights, NY, 10598.

Selective Epitaxy is difficult to achieve in the conventional MOVPE based growth of GaAs and (Al,Ga)As. Both the high overall supersaturation of the growth ambient and the lack of a suitable back or etching reaction leads to the conformal deposition of the growing material under most growth conditions. We have recently demonstrated the selective area deposition of GaAs using diethyl gallium chloride (DEGACL). This precursor leads to the highly selective growth of GaAs with respect to a dielectric masking material. The use of diethyl aluminum chloride (DEALCL) does not however lead to the selective epitaxy of AlAs. The selective growth of the alloy, (Al,Ga)As, can be achieved under suitable growth conditions using both DEGACL and DEALCL. The HCl by-product from the decomposition of the DEGACL is thought to serve as an etchant, removing AlAs from the surrounding dielectric field regions. The alloy composition of the deposited material is a function of the growth conditions. The measured alloy composition will be compared to that predicted from the thermodynamic considerations. We have used this selective epitaxy technique to produce quantum well structures within localized regions of a substrate surface.

B2.8

PATTERNING OF GaAs/AlGaAs WAFERS BY FOCUSED ELECTRON-BEAM INDUCED CHLORINE ETCHING AND SUBSEQUENT MBE GROWTH. M.Taneya, Y.Sugimoto, H.Hidaka, K.Akita, Optoelectronics Technology Research Laboratory, Tsukuba, JAPAN

Focused electron-beam (FEB)-induced Cl_2 etching of $\text{Al}_x\text{Ga}_{1-x}\text{As}$ ($0 < x < 0.7$) was done for the purpose of in-situ patterning and subsequent crystal growth using a ultra-high vacuum multi-chamber system.

An FEB-induced Cl_2 etching of GaAs with an adsorbate layer at the surface was reported earlier.¹⁾ Achieving low-dimensional systems, such as quantum wires and boxes, requires the etching of layered structures consisting of AlGaAs and GaAs. When GaAs/AlGaAs wafers were exposed to a 10 keV-FEB and Cl_2 molecules, etching of AlGaAs was observed only in the FEB-scanned area. The etch rate of $\text{Al}_x\text{Ga}_{1-x}\text{As}$ ($0 < x < 0.7$) was about 30 nm/min, which is almost the same as that of GaAs. This indicates that patterning of GaAs/AlGaAs heterostructures is possible using FEB-induced Cl_2 etching.

The compatibility of the FEB-induced Cl_2 etching with subsequent MBE regrowth was tested by growing an AlGaAs layer on a GaAs layer previously patterned by FEB-induced Cl_2 etching. The surface of the regrown AlGaAs layer showed excellent morphology, which demonstrates that a surface suitable for the subsequent MBE growth can be obtained by FEB-induced Cl_2 etching.

1) M.Taneya et al. Jpn.J.Appl.Phys. 28,L429(1989).

B2.9

EXCIMER LASER-INDUCED DEPOSITION OF GaN. A. Kobayashi, T.Asai, S.Kawai and P.J.Chong, The Institute of Scientific and Industrial Research, Osaka University, Ibaraki, Osaka 567, Japan.

GaN films were prepared by laser-induced chemical vapour deposition (LICVD) technique from $\text{Ga}(\text{CH}_3)_3$ and NH_3 . Pulsed ArF excimer laser was used to induce gas phase reactions and the films were grown on the sapphire (0001) substrates at temperatures from 600 °C to 1000 °C. At high temperatures, GaN grew as islands and was polycrystalline. At low temperatures, GaN was deposited as a dense film and was a mixture of polycrystals and preferred oriented crystals. The films grown at around 800 °C were epitaxial with the (0001)-oriented layers. The surface morphology of these films was examined by a scanning electron microscope and a fine structure with the uniform grain size of about 0.6 μm was seen.

GaN films by the thermal CVD were also prepared under the same growth conditions and compared with the LICVD films. The results showed that crystallinity of the LICVD-grown GaN films was superior to that of the thermally grown ones. Moreover, the growth rate of the films was about 2.7 times faster (at 800 °C) under the laser gas-phase excitation.

Under the present conditions, the growth rate of the films was highly influenced by the deposition temperature. This indicates the growth rate is mainly determined by the surface reaction.

B2.10

HOLOGRAPHIC PATTERN ETCHING OF SILICON-CARBIDE BY EXCIMER LASERS

M.Murahara, Faculty of Eng., Tokai Univ., 1117 Kitakaname, Hiratsuka, Kanagawa 259-12, JAPAN., M.Yonekawa and K.Shirakawa, Graduate student of Faculty Eng., Tokai Univ., Kanagawa, JAPAN.

Silicon-carbide has high refractivity in the range of soft X-ray. But chemical etching of SiC is difficult. So we have been proposing to etch the SiC using two different wavelength excimer lasers and gaseous ClF_3 .

In this paper, we wish to report on fabrication of diffraction grating on SiC mirror by laser holographic method. The reflectance of this crystalline SiC mirror which was polished with a 1 Å accuracy was 30% in 249 nm (KrF) and in 193 nm (ArF) as high as 50%. On the other hand, the threshold fluence energy for etching was 800 mJ/cm² in 249 nm and in 193 nm as high as 7 J/cm². In these result, KrF laser is more effective than ArF laser. Then we applied three laser beams having different two wavelength to crystalline SiC in an atmosphere of ClF_3 gas. The XeF laser beam was used to photodissociate ClF_3 gas in the proximity of substrate. The divided two polarized KrF laser beams were interfered on the substrate, and it was used to locally excite the substrate.

Then, laser beams were irradiated; Fluence of KrF laser beam was 1 J/cm², XeF was 50 mJ/cm². And incidental angle of KrF laser beams were 20° and the grating gaps were 7170 Å, etching depth 1000 Å, and etching rate were 5 Å/pulse.

B3.1

LASER BASED AREA SELECTIVE PROCESSING FOR HIGH DENSITY INTERCONNECTS Y.S.LIU and H.S.Cole, GE Research and Development Center, Schenectady, N.Y.12345

The growing interest in laser processing in recent years has come from the increasing demand for an adaptive processing technology that offers capabilities of quick prototyping, rapid design and fabrication of relatively low volume application specific IC's, and the need for yield enhancement and circuit restructuring in fabrication of increasingly complex electronic devices and circuitry.

This paper reviews use of lasers for area selective processing for high density interconnect applications and discusses, specifically, several laser based techniques developed for patterned metallization using either direct or indirect two-step processes. Materials and processing requirements such as process speed, resolution, sensitivity and interface properties are addressed. Topics also include use of two-step laser catalyzed surface modifications for improving processing speed, metal/polymer interfaces, and high-speed UV laser via-drilling for multi-level interconnects.

* This work has been partially supported by ONR/SDIO under the contract number N00014-85-C-0890.

B3.2

LASER DIRECT WRITING OF OPTICAL INTERCONNECTS IN POLYIMIDES AND $\text{SiO}_2/\text{TiO}_2$ COATINGS. D.W. Hewak, and H. Jerominek, National Optics Institute, 369 rue Franquet, P.O. Box 9970, Sainte-Foy, Quebec, Canada G1V 4C5.

Laser direct-writing is an emerging technique for the fabrication of customized interconnect networks for VLSI circuits.

Fabrication of optical channel waveguides in commercially available polyimides and $\text{SiO}_2/\text{TiO}_2$ coatings by Ar^+ laser direct-writing is reported. Channels were fabricated on thermally oxidized Si wafers. Based on the transmission spectra of the materials used, the mechanism of writing was identified as thermal in origin and due to VIS light absorption. Post-writing development removed the untreated material leaving the desired channels.

Channel waveguides were fabricated with laser power up to 500 mW at 458 nm and scanning speeds up to 250 microns per sec. Adhesion of the channels to the substrate and complete removal of the untreated material were the major difficulties overcome in the fabrication procedure. Prism and butt-coupling techniques were used to study light propagation in the fabricated structures. The propagation loss measurements revealed that attenuation in channels was of the same order as in slab waveguides made of the same material, i.e. 1 - 5 dB/cm at 633 nm.

B3.3

SELECTIVE AREA DEPOSITION OF CONDUCTING PALLADIUM FILMS ON POLYIMIDE RESINS. Yoon-Gi Kim, S. Bialy, R. Miller, J.T. Spencer, and P.A. Dowben, Center for Molecular Electronics, Departments of Physics and Chemistry, Syracuse University, Syracuse, N.Y. 13244.

We have demonstrated that conducting palladium films can be selectively deposited on Kapton and Ultem 1000 (polyetherimide). The selective area deposition of palladium is undertaken from the UV photolysis ($\lambda = 337$ nm) of allylcyclopentadienyl palladium. The photolytic deposition process does not melt or damage the polyimide substrates and the conductivity of the resulting thicker

films ($\geq 500 \text{ \AA}$) is comparable to that of pure palladium ($\rho \approx 2\rho_{\text{Pd}}$).

From other studies [1,2] we know the process is not photopyrolytic and the films are largely free of oxygen and carbon contamination. The adhesion of the palladium films is very good and has been demonstrated to be suitable for applications as an interconnect or thin film resistor.

Deposition of palladium from $\text{Pd}(\text{C}_3\text{H}_5)(\text{C}_5\text{H}_5)$ is an alternative to deposition from palladium acetate which has also been proposed as an organometallic source compound for palladium deposition on polyimides [3].

[1] G.T. Stauff, P.A. Dowben, K.-H. Emrich, S. Barfuss, W. Hirschwald and N.M. Boag, J. Phys. Chem., 93, 749 (1989).

[2] K.-H. Emrich, G.T. Stauff, W. Hirschwald, S. Barfuss, P.A. Dowben, R.R. Birge, and N.M. Boag, Mat. Res. Soc. Symp. Proc., 131, 401 (1989).

[3] Y.S. Liu and H. Cole, Mat. Res. Soc. Symp. Proc., in Press.

B3.4 ABSTRACT NOT AVAILABLE

B3.5

SELECTIVE CHEMICAL VAPOR DEPOSITION OF TUNGSTEN ON LASER-WRITTEN PRENUCLEATION PALLADIUM PATTERNS

Oliver Gottsleben and Michael Stuke, Max-Planck-Institut für biophysikalische Chemie, P.O. 2841, D-3400 Göttingen, F.R. Germany

Laser-written palladium patterns on Al_2O_3 ceramic substrates are selectively amplified by tungsten using conventional chemical vapor deposition CVD with tungstenhexafluoride WF_6 and hydrogen H_2 . The palladium structures are formed by 248 nm UV excimer laser irradiation of spin-coated 1000 \AA palladium acetate films in air leading to a Pd-prenucleated substrate surface. Non-exposed palladium acetate film is removed by a solvent and the substrate transferred to a small vacuum chamber equipped with a heatable substrate holder and a WF_6/H_2 gas handling system. The dependence of the tungsten growth on the substrate temperature and the pressure of WF_6 and H_2 will be given. The selective growth of tungsten is self-limiting at a height of about 1000 \AA depending on experimental conditions. The height of the grown tungsten line increases with temperature and H_2 pressure and seems to be catalysed by the binding of hydrogen to palladium. Electron microscope pictures of generated palladium and tungsten patterns will be shown.

B3.6

ANOMALOUSLY DEEP STRUCTURES PRODUCED IN III-V MATERIALS BY COMBINED FOCUSED ION BEAM IMPLANTATION AND DRY ETCHING. Lloyd R. Harrison, Henryk Temkin, and Yuh-Lin Wang, AT&T Bell Laboratories, Murray Hill, New Jersey.

We have developed a direct patterning process for InP based materials which uses ion implantation followed by dry etching to produce surface topography. The substrate is first implanted with a 20 keV Ga^+ beam focused to 0.2 micron diameter. The surface pattern then developed in the substrate by etching with a low energy (25 - 100 eV) flood Ar^+ ion beam in a Cl_2 (5×10^{-4} Torr) atmosphere. This process has been integrated in a common vacuum chamber with a gas source molecular beam epitaxy (GSMBE) system. *In-situ* patterning and high quality overgrowth has been demonstrated for low Ar^+ ion energies during etching.

Step heights as large as 6000 \AA have been produced with this technique. The effect of the 20 keV Ga^+ ion beam clearly extends far

beyond its calculated projected range of 150 Å. The etched depth of the features increases rapidly for Ga^+ ion doses from 10^{13} to 10^{14} ions/cm². At doses above 2×10^{14} , the depth continues to increase but at a much slower rate. The etched depth of the features does not depend strongly on Ga^+ ion beam dose rate or angle of incidence (channeling). The step heights depend most strongly on the substrate temperature and Ar^+ ion energy during etching. Our observations seem to support a model of the etching process which includes point defect diffusion to explain the anomalously deep effect of the Ga^+ ion beam. We interpret the saturation of the etched depth at doses above 2×10^{14} as indicative of the formation of an amorphous layer in the substrate.

We will present data illustrating the step height dependence on ion implantation dose, dose rate, energy, and species as well as etching ion energy, substrate temperature and Cl_2 flow rate for several substrate materials.

B3.7

ULTRAHIGH VACUUM COMPATIBLE HALOGEN ETCHING PROCESS FOR SEMICONDUCTOR SURFACES. Andrew Freedman and Charter D. Stinespring, Center for Chemical and Environmental Physics, Aerodyne Research, Inc., Billerica, MA 01821

We will report on the development of an ultrahigh vacuum-compatible etching process using a combination of separate beams of halogen atoms/molecules and rare gas ions. The halogen atom source is based on a microwave discharge design (J. Vac. Sci. Technol. **A4**, 1946 (1986)) and can generate an effusive beam of fluorine or chlorine atoms admixed in argon or helium carrier gas. Typical fluxes of $1-5 \times 10^{14} \text{ cm}^{-2} \text{ s}^{-1}$ at a substrate-source aperture distance of 7 cm are obtained. We will describe results of quartz crystal microbalance measurements of chlorine atom/molecule-argon ion etching of aluminum and gallium arsenide. We will also report on x-ray photoelectron spectroscopy experiments aimed at understanding the basic microchemistry of chlorine interactions with both substrates.

This work is supported by the National Science Foundation under the Small Business Innovation Research Program.

B3.8

CONTROL OF ETCHING RATE IN LASER-CHEMICAL REACTION OF Mn-Zn FERRITE BY MeV ION IMPLANTATION. Y. F. Lu, M. Takai, and S. Namba, Faculty of Engineering Science and Research Center for Extreme Materials, Osaka University, Toyonaka, Osaka 560, Japan.

Single crystal ferrite is an important magnetic material which is used for magnetic head devices. Laser induced etching of Mn-Zn ferrite in H_3PO_4 aqueous solution by Ar^+ laser irradiation was found to result in the etching rate up to 340 $\mu\text{m/s}$ whereas the width of the etched groove is an order of 100 μm . The change in the etching rate due to the ion irradiation is considered to be an hopeful method to obtain ultra-fine structures of ferrite materials by combining laser etching techniques with FIB (focused ion beam) techniques.

The ferrite sample surface was implanted at 3 MeV with an O^+ dose of $1 \times 10^{17} \text{ cm}^{-2}$. The projected range of the ions was estimated to be 1.8 μm by a TRIM calculation and RBS measurements. Ferrite samples immersed in 85% H_3PO_4 solution was etched by scanning the focused laser beam with a diameter of 13.2 μm (at 1/e intensity) and a laser power ranging from 10 mW to 70 mW.

The laser induced etching is suppressed by the ion implantation. The etching rate in ion irradiated area decreased to less than 50 % of that in an unimplanted area. The etching rate is mainly suppressed at the surface layer thinner than the projected range, and the suppression decreased and vanished when the laser power was increased. Since the reflectivity of the sample

surface to the laser beam did not change after the ion irradiation, the etching rate suppression was considered mainly due to the crystallographic change in a surface layer.

B3.9

PRECURSORS TO PHOTO-ABLATION OF SODIUM TRISILICATE GLASS DUE TO UV EXCIMER IRRADIATION.* P. A. Eschbach, J. T. Dickinson, S. C. Langford, Physics Department, Washington State University, Pullman, WA 99164, and L. R. Pederson, Pacific Northwest Laboratory, Richland, WA 99352.

In previous work we examined the changes in the surface topography of sodium trisilicate glass ($\text{Na}_2\text{O} \cdot 3\text{SiO}_2$) with exposure to pulsed 248 nm (5eV/photon) excimer laser light at fluences of 2.6-5 J/cm², as well as the character of the products emitted from the glass surface (e.g., $+$ /- ions, electrons, ground state and excited neutral atoms and molecules). At these fluences, ablation readily occurs, accompanied by both photothermal and photochemical processes. In the current study, we examine the precursors of this high fluence behavior at fluences < 2.6 J/cm². The major products observed are photoelectrons and Na^+ . The Na^+ time-of-flight (TOF) position and shape is essentially constant over this fluence range (0.05-2.6 J/cm²) during the initial irradiation of both polished and fracture surfaces. This response is consistent with a photochemical (electronic) emission mechanism. As irradiation proceeds, the ion intensity gradually drops to very low levels, attributed to the depletion of Na in the surface region. At higher fluences (> 2.6 J/cm²) and additional bombardment, the Na^+ emission eventually regains and surpasses its initial intensity. The restored ion emission is accompanied by a visible plume due to Na D-line emission, the appearance of neutral Na Rydbergs, and the onset of surface etching. The number of laser pulses required to pass through the transition phase depends strongly on laser fluence. The role of photo-induced emission of electrons and Na^+ in the eventual onset of ablation will be discussed. Correlations of these studies with XPS and IR spectroscopy of the sodium trisilicate substrates will also be presented.

*Work supported by the National Science Foundation under Grant DMR 8601281, the Office of Naval Research under Contract N00014-87-K-0514, the Washington Technology Center, and NORCUS.

B3.10

X-RAY PHOTOEMISSION INVESTIGATION OF EXCIMER LASER-INDUCED ETCHING OF InP. R. Matz, J. Meiler, Research Laboratories of Siemens AG, Otto-Hahn-Ring 6, D-8000 München 83, F.R.G.; and D. Haarer, Universität Bayreuth, Lehrstuhl f. Experimentalphysik IV, Postf. 101251, D-8580 Bayreuth, F.R.G.

X-ray photoemission spectroscopy was used to reveal the reaction steps during laser-induced etching of (100)-InP in HBr and HCl gas atmosphere (0.1-1 mbar) by exposure to ArF excimer laser light of 193nm wavelength. Under direct exposure of the semiconductor surface, as employed for pattern transfer etching, pronounced etching occurs only above a laser threshold fluence which coincides with the energy density for transient surface melting. P depletion and formation of metallic In within the top surface layers are identified as first steps towards this efficient etching. The amount of In formed at various fluences is well correlated with the dependence of etch rate on laser fluence. In a second step, the halogen atoms generated by the laser pulse in the gas diffuse to the reaction sites on the surface to form InBr_3 or InCl_3 , respectively. The thickness of the reacted layer per laser pulse is on the monolayer scale. The layer is desorbed by either a sufficient background substrate temperature above 130°C or by the next laser pulse. When etching with a contact resist mask, exposure of the gas alone but not the surface is advantageous for resist protection. The halogen atoms then react with a stoichiometric InP surface. Also in this case, no reaction products with P are found which is probably due to the high vapour pressure of its halogenides. With the substrate at room temperature, however, an In halogenide layer grows under diffusion control up to a saturation thickness of about 20 monolayers. Growth of this layer can be avoided or its removal can be caused again by raising the substrate temperature above 130°C, where the halogenide vapour pressure exceeds the etch gas pressure. The temperature is well compatible with most photoresist processes.

In agreement with experiments, the results suggest that above the desorption temperature of the halogenides, the spatial resolution of the whole process is largely determined by lateral gas phase diffusion of the halogen atoms. Below this temperature, however, the In halogenide can be used to passivate unexposed surface areas so that the spatial resolution is improved.

B3.11

SELECTIVE ETCHING AND PHOTO-BLEACHING IN THIN AMORPHOUS Ge-Sb-S FILMS. Evdokia B. Savova and Boyvill I. Pashmakoff, Institute of Solid State Physics, 1784 Sofia, 72 Lenin Blvd., Bulgaria

A mechanism is proposed for the selective etching effects in thin amorphous Ge-Sb-S films based on the combined action of photostructural changes and alkaline solvent with a surface active substance. Evidence is given in support of the assertion that the same photostructural changes (namely, the breaking of Ge-Sb bonds under the action of UV light) are responsible for the irreversible photo-bleaching of these layers.

Five different compositions in the system Ge-Sb-S have been studied under different preparation conditions (thermal evaporation and laser-beam sputtering). Photostructural changes were induced by UV light and Nd-glass laser treatment. Infrared and Raman spectra of the layers are presented in support of the proposed model.

B3.12

ULTRAFast IMAGING OF ULTRAVIOLET LASER ABLATION AND ETCHING OF POLYMETHYL METHACRYLATE. Bodil Braren, R. Srinivasan, Kelly G. Casey, and Mildred Yeh, IBM, T. J. Watson Research Center Yorktown Heights, NY 10598

Ablation and etching of the surface of polymethyl methacrylate (=PMMA) by pulses of 248 nm laser radiation ~20 ns full width at half maximum (FWHM) have been probed by pulses of visible laser radiation (596 nm; <500 ps FWHM). The results were recorded photographically in real time with a set time delay between the 248 nm ablation pulse and the 596 nm probe pulse.

Modification of the surface structure of the polymer at a fluence ~ 3 J/cm² is first visible at 12 ns and appears to be complete in ~ 60 ns. The first manifestation of the ablation does not occur until the UV pulse is over and consists of a nearly transparent shock-wave that has an initial velocity of 6 x 10⁴ cm/sec. Solid material from the ablated zone begins to leave the surface at ~ 150 - 200 ns and reaches a maximum in intensity at 6 μs, continuing for ~ 20 μs. The average velocity of the solid material, which is probably a low molecular weight polymer of PMMA, is 1.5 x 10⁴ cm/sec.

The conclusion to be drawn from the present work is that the signal measured by photoacoustic detectors does not coincide with the bulk of the material leaving the surface.

B4.1

SELECTIVE SILICON EPITAXY FOR ADVANCED DRAM STRUCTURES. Gary Bronner, IBM Research Division, Yorktown Heights, N.Y.

In silicon microelectronics, memory cells and chips are used to develop the most advanced technology. In the future these chips will require truly three dimensional structures to achieve the needed density. This talk describes the use of selective silicon epitaxy to build three dimensional DRAM cells.

Selective silicon epitaxy is grown at reduced pressure and temperature (40 Torr and 900°C) in a SiCl₄ + H₂ ambient. SiCl₄ reacts with a silicon substrate to grow epitaxial silicon with HCl as a by-product. The HCl inhibits deposition of silicon on insulators leading to selective growth. Lateral growth of silicon epitaxy is achieved when the insulators are flush with the silicon

surface. The lateral growth rate and material quality of this overgrowth are strongly affected by the orientation of the silicon/insulator edge. Best material quality is achieved when (100) planes are allowed to grow laterally. Results are presented showing that silicon can be grown laterally with no defects. Defect etching, TEM, and electrical measurements are used to characterize the material.

The overgrown silicon material has been applied to the fabrication of a three dimensional DRAM cell. The cell consists of a trench capacitor which is overgrown with silicon selective epitaxy. A transistor and isolation are then built above the trench capacitor resulting in a cell that occupies the same area as the transistor alone. Fully functional memory cells have been built. The results show that selective silicon epitaxy is a realistic candidate for building three dimensional silicon devices.

B4.2

SURFACE REACTION MECHANISMS IN SELECTED AREA EPITAXY OF II-VI's. S. J. C. Irving, H. Hill, J. E. Hails, S. J. Barnett and J. B. Mullin, Royal Signals and Radar Establishment, Malvern, Worcestershire UK

Ultraviolet radiation can be used to enhance the growth rate of II-VI compounds such as CdTe and HgTe at temperatures below the precursor pyrolysis thresholds. The enhancement of growth rate is primarily a vapour absorption-decomposition reaction but the measured growth rates are approximately one tenth of those expected for diffusion limited growth. In the case of CdTe, the projection of a pattern by UV radiation onto a substrate can cause considerable enhancement in growth rate, leaving a well defined topographic pattern. This process relies on absorption of UV radiation, (a) in the vapour for photo-dissociation, and (b) on the substrate to overcome surface kinetics. Recent results will be presented for CdTe photo-epitaxy on (a) the effect of reduction in total irradiance in the vapour due to masking, (b) the effect of UV intensity on the surface and (c) surface absorption of visible radiation.

The extension of surface reaction mechanisms to other II-VI's will be discussed. Where the compound is weakly bonded, as is the case for Hg compounds, the surface kinetic suppression of growth rate is more severe. The potential for selected area epitaxy of HgTe should be more promising, but effects such as charge transfer assisted desorption of hydrocarbons may be more difficult to modulate optically due to the much higher intrinsic carrier concentration in this semimetallic compound. The potential for selected area epitaxial growth of II-VI's for in-situ processing of new opto-electronic device structures will be considered in the light of recent results.

B4.3

Novel Stacked CMOS Process by Local Overgrowth. René P. Zingg, B. Höfflinger, Institute for Microelectronics, D-7000 Stuttgart 80, FRG; and G. W. Neudeck, Purdue University, W. Lafayette, IN 47907, USA.

A new CMOS process has been developed to produce complementary devices on top of each other. The second silicon layer is grown by chemical vapor deposition (CVD) silicon epitaxy, where the growth is seeded with windows in a oxide film on a preprocessed wafer. The epitaxy progresses both vertically and laterally from the seed window, forming a crystalline film on this oxide. This growth is only seeded where devices will be built, to enable contact holes to devices realized in the substrate. A process with self-aligned source/drain and stacked gates, as well as one with a joint-gate between both channel types in the two device layers were realized. We observed no deterioration of bulk device characteristics associated with the fabrication steps necessary for the second active layer. The silicon-on-insulator (SOI) devices in the top layer exhibited mobilities comparable to transistors built in bulk material. Contrary to zone-melt recrystallization (ZMR) material, device parameters were very reproducible across the wafer and from lot to lot due to the defect-free crystalline material. SOI films with impurity levels of 8.8·10¹⁵/cm³ were produced by local silicon epitaxial overgrowth with trichlorosilane as source gas for selective epitaxy at 833-900°C. Trichlorosilane allows selective epitaxy without the addition of HCl gas, therefore lowering the impurity level of

the silicon considerably. The lateral epitaxy, which was restricted to device sites, was thinned to 0.7 μm thickness by chemo-mechanical polishing.

Surface channel mobilities of NMOS devices built in the bulk material were 700 cm^2/Vs and 165 cm^2/Vs for p-channel transistors in the SOI film, both for devices with top and submerged gates. Subthreshold slope was about 100 mV/dec for either channel type, threshold voltages were 0.5 V and -1.5 V, respectively, and leakage currents were well below 1 pA for 100 μm channel width devices in either layer.

B4.4

LASER ASSISTED MOLECULAR BEAM EPITAXY (LAMBE) GAAS ON SILICON PHOTODETECTORS, A. Christou, N.A. Papanicolaou, and G.W. Anderson, Naval Research Laboratory, Washington, DC, 20375, and A. Georgakilas, P. Panayiotas, Foundation for Research and Technology-HELLAS (F.O.R.T.H.) III-V Microelectronics Group, Crete, Greece

The monolithic integration of GaAs photonic devices and silicon electronic devices and circuits offers the potential of combining the superior speed and optoelectronic capabilities of GaAs based circuits with the sophistication of silicon VLSI technology. The first step toward the realization of this goal is the development of high performance optoelectronic devices such as photodetectors and lasers on GaAs material grown epitaxially on silicon substrates.

In this study various photodetector structures have been fabricated on LAMBE GaAs epitaxially grown on high resistivity silicon substrates. In realizing GaAs epitaxial layers grown on silicon by molecular beam epitaxy, it was necessary to initially optimize a GaAs nucleation layer deposited at 300°C followed by a strain accommodation layer grown at 620°C. An excimer laser at 248 nm and 120 mJ/cm² was used to assist in the growth of the nucleation and accommodation layers. A 300 Å GaAs nucleation layer was initially grown followed by a five period AlAs/GaAs multi-quantum well region, each 100 Å thick, for a total thickness of 1000 Å; finally a 2 μm undoped active layer followed by a 2000 Å thick n layer and a 500 Å thick n⁺ contact layer completed the structure.

The types of photodetectors investigated included linear photoconductors and three types of interdigitated finger devices: Metal-semiconductor-metal (MSM); Schottky diodes having one set of Schottky metal fingers and one set of ohmic fingers (S-O detectors); and photodetectors consisting of two sets of ohmic fingers (O-O detectors). The evaluation of the photodetectors was made using 840 nm wavelength pulsed light with a pulse width of 5 ns and rise (t_r) and fall (t_f) times of 200 ps. The t_r and t_f of both the linear and interdigitated devices fabricated in the undoped GaAs layer were in the 1-2 ns and 3-6 ns ranges, respectively. These results were comparable to those obtained for photoconductors fabricated on GaAs MBE layers grown on GaAs or made directly on semi-insulating substrate material using similar measurement techniques. The responsivity and quantum efficiency values of the photoconductors were in the ranges 0.6-0.9 A/W and 0.9-1.4, respectively.

B4.5

LASER SELECTIVE AREA EPITAXY FOR THE INTEGRATION OF OPTOELECTRONIC STRUCTURES. H. Liu, J.C. Roberts, J. Ramdani and S.M. Bedair, Electrical and Computer Engineering Department, N.C. State University, Raleigh, North Carolina

We report for the first time the selective epitaxy of device quality films using laser enhanced chemical vapor deposition. Selective and independent deposition of quantum wells, planar doped and p-i-n structures will be reported.

Sources used are TMG, AsH₃, PH₃, DMZn and SeH₂ for the growth of GaAs and GaAsP doped with Zn or Se. When the GaAs substrate is kept at a temperature less than 400°C, epitaxial growth takes place only on the area exposed to the Ar⁺ laser beam. Spot sizes in the range of 250 - 1000 μm were achieved and films were characterized by photoluminescence, Hall and C-V techniques.

GaAsP-GaAs-GaAsP single quantum wells with different well widths, thus emitting at different wavelengths, were selectively deposited on a GaAs substrate. Also, planar doped structures consisting of a planar sheet of Se atoms embedded between two undoped GaAs films were selectively deposited. Planar doping was achieved by simultaneous exposure to AsH₃ and SeH₂ during the LCVD process and a sheet carrier concentration in the 10¹²-10¹³/cm² range was obtained. Doping characteristics, especially for p-type dopants, were

found to be different from those obtained by MOCVD. This is attributed to different growth temperatures and the added photochemical enhancement inherent in the LCVD technique. We will report the processes involved in dopant incorporation.

Work is supported by SDIO and NSF

B4.6

LASER INDUCED SURFACE CHEMICAL EPITAXY. Charter D. Stinespring and Andrew Freedman, Center for Chemical and Environmental Physics, Aerodyne Research, Inc., Billerica, MA 01821

This paper describes ongoing experimental studies (Chem. Phys. Lett. **143**, 584 (1988); Appl. Phys. Lett. **52**, 1959 (1988)) of the thermal and UV photon-induced reactions of dimethyl cadmium (DMCd) and dimethyl tellurium (DMTe) on GaAs surfaces. The objectives of these studies are to provide an understanding of the underlying chemical mechanisms and to explore novel approaches to CdTe heteroepitaxy. The work focuses on CdTe heteroepitaxy because of the importance of this material in electro-optical systems. DMCd and DMTe were selected for investigation as precursor species because of their inherent scientific interest. The gas phase photochemistry of DMCd and DMTe has been extensively investigated; these molecules are known to undergo single rather than multi photon dissociation to produce ground state metal atoms. The basic questions we attempt to answer in this study are: i) How do DMCd and DMTe interact with the surface of a substrate or growing thin film? and ii) Is this interaction such that single photon (as opposed to multiphoton) processes can be used to produce metal adspecies and, ultimately, epitaxial CdTe thin films? Analysis of photodecomposition efficiency and product species distributions show widely different results for single and multiple adlayers. These results provide key insights into the underlying mechanisms of the photon-adspecies-substrate interaction.

This work is supported by the Air Force Office of Scientific Research.

B4.7

LASER PROCESSED SILICIDES FOR GAAS HEMTS, W.T. Anderson, A. Christou, Naval Research Laboratory, Washington, D.C.; and C. Michelakis, G. Kiriakidis, Research Center of Crete, Heraklion, Crete, Greece.

Laser annealed refractory metal gates have been developed for GaAs and high electron mobility transistors (HEMT) fabricated on MBE layers grown on laser desorbed substrates. Amorphous(a-) refractory metal silicide films were sputter deposited by a method in which the RF power to separate refractory metal and silicon targets were set at predetermined deposition rates and the substrates were rotated with respect to the sputter targets receiving a 0.2 to 0.5 nm film on each pass. This method has the following advantages over sputter deposition from a single target: (1) overall average composition can be better controlled by varying the power, and thus film thickness on each pass, to the separate targets, (2) amorphous films, which are desirable as diffusion barriers, are always obtained because a-Si is deposited on each pass of the Si target, and (3) because the substrate spends only a small time near the sputter target as it rotates, the surface temperature remains lower than if a single sputter target were used and photoresist can be employed to lift 1.0 μm long gates.

The a- silicide gates were laser annealed to reduce the gate resistance using a 308 nm excimer laser. Laser annealing has the advantage over rapid thermal anneal or oven anneal in that it is not necessary to heat the entire wafer and individual structures can be selectively annealed. Annealing is accomplished by adjusting the energy density to penetrate only part way into the film, ideally resulting in a phase change to polycrystalline material of lower resistivity, leaving the bottom part of the film as a well behaved amorphous diffusion barrier. In the case of films < 40 nm, the heat pulse reaches the a-

silicide/GaAs interface and Ohmic contact is formed by interdiffusion, as revealed by Rutherford Backscattering. HEMTs fabricated by these methods exhibited reduced light sensitivity compared to conventionally fabricated HEMTs.

B4.8

MASKLESS FORMATION OF TUNGSTEN FILM BY ION BEAM INDUCED DEPOSITION TECHNIQUE. Zheng Xu, Kenji Gamo and Susumu Namba, Faculty of Engineering Science, Osaka University, Toyonaka, Osaka 560, Japan.

The tungsten deposition using WF_6 is one of the promising ways for Schottky gate metallization in MESFET and heterostructure FET devices. Ion beam assisted deposition of tungsten using finely focused ion beams is particularly interesting because it provides a maskless metallization technique with submicrometer resolution.

In this study, tungsten film was deposited on n-type GaAs substrate by irradiating Ar^+ , H_2^+ beams in the WF_6 ambient. The low energy (500–2000 eV) was used to reduce the damage in the substrate. The damage in the substrate and annealing properties were examined by Schottky barrier characteristics, DLTS and C-V method, and the quality of deposited film was measured by XPS, RHEED and four probe point method.

W film with purity better than 90 % and resistivity of about 10^{-5} ohm.cm was obtained. Schottky barrier was formed by IBID for a 500 eV H_2^+ beam irradiation without any annealing, while almost ohmic contact was formed for 2 keV beam irradiation. In case of Ar^+ beam irradiation, almost ohmic contact was formed for both 500 eV and 2 keV beam, due to the heavier damage in the substrate. After annealing at 350°C for 10 min, most of the damage was annealed out for both 500 eV and 2 keV H_2^+ and Ar^+ irradiation, and all the contacts show Schottky characteristics. The n-factor ranges from 1.01 (500 eV Ar^+) to 1.61 (2 keV H_2^+). The barrier height was 0.67–0.88 eV for H_2^+ irradiation.

B4.9

NANOLITHOGRAPHY BY STM ON $Rb_{0.3}MoO_3$, A CONDUCTING OXIDE. G. Rudd, D. Novak, S. Wang, S.H. Garofalini and E. Garfunkel, Departments of Chemistry and Physics, Laboratory for Surface Modification, and Center for Ceramics Research, Rutgers University, Piscataway, NJ 08855.

We present results demonstrating the use of a scanning tunneling microscope (STM) to image and modify the surface of a conducting oxide ($Rb_{0.3}MoO_3$). We show that individual octahedral MoO_6 units of the oxide can be imaged. Under certain conditions controlled defects can be etched (written) on the surface which are stable in air. Features such as lines, holes, and squares as small as 1 nm deep and 7 nm across are observed. We also consider possible STM based mechanisms of writing on oxides such as abrasive etching, heating, and hot electron processes. Potential applications in nanolithography for memory storage and electronic devices which display various quantum size behavior are discussed.

B4.10

COMBINING ELECTRON AND ION BEAM TECHNIQUES FOR THE PRODUCTION OF BURIED SINGLE-CRYSTAL METALLIC WIRES. S. D. Berger, Julita E. Woroniecka, H.A. Huggins, Alice E. White, K.T. Short and D. Loretto. AT&T Bell Laboratories, Murray Hill, NJ.

We have fabricated single-crystal metallic wires of $CoSi_2$ buried beneath the surface of a Si wafer with widths down to ~100 nm. The wires are formed by a

novel technique which uses a combination of electron-beam lithography, reactive-ion etching and Co ion implantation.

Two different approaches have been taken. In one case the Co is selectively implanted by use of a mask. Structures produced in this way exhibit near perfect silicide/silicon interfaces which have not been subjected to any etching! In the second case the wires are defined by patterning a continuous silicide sheet. Here the structural quality of the edges of the wires is degraded by the reactive-ion etching.

A comparison of the transport properties of these wires both as a function of a size and also of method of construction will be discussed.

B4.11

THE ROLE OF ADSORPTION AND VAPOR PRESSURE IN FOCUSED ION BEAM INDUCED DEPOSITION OF CARBON FILMS. S. J. Kirch, IBM General Technology Division, T. J. Watson Research Center, Route 52, Hopewell Junction, NY 12533, and D. E. Savage, IBM Research Division, T. J. Watson Research Lab, Yorktown Heights, NY 10598.

Focused ion beam induced deposition of carbon films has become technologically important for the repair of lithographic masks. When an ion impinges on a substrate in the vicinity of an adsorbed molecule such as vinylbenzene (styrene), net deposition of carbon may occur. Recent studies [1] have stressed the importance of the pendant double bond of the vinyl substituent for deposition. This paper examines the differences in deposition characteristics of organic molecules which are similar to styrene, a material commonly used for this purpose, over a range of temperatures and pressures. The effect of vapor pressure was studied by examination of the series styrene, o-Cl styrene, and o-Br-styrene. The vapor pressure of these materials varies by more than an order of magnitude, while leaving the double bond of the vinyl substituent intact. The importance of the double bond was studied by comparison of the deposition characteristics of ethylbenzene and o-Br-ethylbenzene to the X-vinyl materials listed above. In contrast to recent studies [1], deposition is possible with all five materials. For each material, deposition yield is found to scale with the variation in vapor pressure over the temperature range studied (0–25°C). This behavior shows that physical adsorption rather than the presence or absence of the double bond plays the key role in determining deposition properties as shown in recent work involving ion beam induced deposition of gold [2].

[1] M.J. Vastle and L.R. Harriott, Proc. of the 33rd Int. Symp. on Electron Ion, and Photon Beams, Monterey, CA, May 1989 (to be published in IVS-3 B Nov/Dec 1989).

[2] A.D. Dubner and A. Wagner, J. Appl. Phys. 65 (9), pp. 3636.

B4.12

LASER ABLATION AND PLASMA HYBRID TECHNIQUE FOR DEPOSITING MULTILAYERED STRUCTURES. J. Krishnaswamy, S. Sharan and J. Narayan, Dept. of Materials Science and Engineering, North Carolina State University, Raleigh, NC 27695-7916; and O. W. Holland, Solid State Division, Oak Ridge National Laboratory, Oak Ridge, TN 37831-6118.

We have recently reported¹ a laser ablation and plasma hybrid technique of depositing hydrogen-free diamondlike, hard carbon films on room temperature substrates. The new technique enhances the non-equilibrium processes during laser ablation and further helps in depositing films with improved properties. In this paper we report on the deposition of a multilayered tungsten/carbon film. A 20 nsec (FWHM), 308 nm XeCl laser beam is sequentially focussed on closely placed tungsten and carbon targets to deposit a ~500 Å thick film with W/C multilayers. The

ablation circuit was configured in the laser ablation and plasma hybrid mode to form the film, since the laser energy alone was not sufficient to ablate tungsten. The films were characterized by RBS and transmission electron microscopy techniques.

1. J. Krishnaswamy, A. Rengan, J. Narayan, K. Vedam and C. J. McHargue, *Appl. Phys. Lett.*, **54**, 2455 (1989).

B5.1

A NEW MODEL OF POLYMER PHOTOABLATION KINETICS. Sylvain Lazare and Vincent Granier, Laboratoire de Photophysique et Photochimie Moléculaire, UA CNRS 348, Université de Bordeaux I, 351 Cours de la Libération, F-33405 Talence, France.

The amount of polymer ablated per pulse of the excimer laser radiation (193, 248 and 351 nm), was precisely measured over a large range of fluence, with the quartz crystal microbalance technique. These etch curves are analyzed with our new model of the Moving Interface, which provides β , screening coefficient and k , ablation rate constant (true ablation rate). This model allows for the first time the evaluation of the attenuation of the laser beam, due to the absorption of the radiation by the ablation products. Each couple of polymer and wavelength is characterized by a unique couple of β and k . Both β and k increase by shortening the wavelength. The influence of some polymer structural parameters is evidenced. At very high fluence, the appearance of a new etching mechanism (probably plasma) is revealed by the sudden acceleration of etch rate.

The model predicts that for high β polymers, products should strongly depend on fluence and wavelength. This is supported by the study of ablation products deposition. Spatial distribution, rate and yield vary with the mean size of the ablation products, since only large molecular fragments can deposit.

B5.2

A PROCESS MODEL FOR REACTIVE ION ETCHING AND STUDY OF THE EFFECTS OF MAGNETRON ENHANCEMENT, M. Mevyan, Scientific Research Associates, Inc., P. O. Box 1058, Glastonbury, CT 06033.

Reactive ion etching (RIE) has essentially replaced wet chemical etching as a preferable method for accomplishing fine-line lithography and selective etching. It has been shown [1] that use of a magnetic field (MIE) confines the electrons closer to the cathode, thus increasing ionization efficiently and offering low pressure, low bias etching. In both RIE and MIE, it is not well understood how various system parameters such as gas flow, pressure, bias voltage, magnetic field strength and magnets arrangement affect the etch rate, uniformity and selectivity.

We present a process model for the reactive ion etching and simulation results with and without the aid of magnetic enhancement. The model involves solution to the fluid flow and reactive species equations using a highly efficient finite difference algorithm. Results for the etching of GaAs using boron trichloride (BCl_3) plasma are presented. Proper dissociation kinetics and surface reactions leading to etching have been incorporated. For a 3" wafer, the computed etch rates are nearly uniform with slightly higher rates at the edges. This variation is a function of system pressure and flow rate, and the physics behind the observations are explained in the presentation. The computed rates are found to agree well

with previously published experimental results. A factor of four enhancement in etch rate is shown with the aid of a magnetic field.

1. D. C. Hison et al, *Semiconductor International*, Vol. 103, p.10, 1983.

B5.3

SILICON FILM AS A NEW ETCHING MASK FOR InP DEVICES, X.S. Wu, Shuojin Wang* and Zhongde Lu, Shanghai Institute of Metallurgy, Academia Sinica, Shanghai, China; and Jun Chen, Institute of Materials Science, Fudan University, Shanghai, China.

Silicon film as an etching mask or a diffusion mask for GaAs devices was reported previously. For similar reasons silicon also has been expected to be a good etching mask for InP based materials and devices.

On this letter, considerably different etching behaviors between silicon and InP were shown in several chemicals. On (100) InP substrates, silicon films were deposited by a rf (13.56 MHz) magnetron sputtering system at room temperature with a target of unintentionally doped silicon. For comparison, a SiO_2 mask was also deposited on InP substrate by CVD system at low temperature. The films were analyzed with SIMS, showing that the films were relatively pure silicon up to the interface or SiO_2 , respectively.

InP with Si mask or SiO_2 mask were etched in several conventional chemicals. The etched facets were observed by SEM. Their undersirable etched undercut were compared. It is shown that undercut of InP with Si Stripe mask is smaller than that with SiO_2 mask. In most of above chemicals, the undercut of Si/InP almost can't be observed as shown in the Figures of the paper. However, the biggest undercut of SiO_2 /InP is 0.83 in the solution of HCl and H_3PO_4 (1:1). The relatively stress of interface of Si/InP and SiO_2 /InP were measured. The relation between stress and etched undercut was discussed.

* Permanent address: Zhejiang University, Hangzhou, China

B5.4

ETCHING OF GAAS ON ALGAAS IN RIE-MODE G. Kaufel, E. Olander, Fraunhofer-Institut für Angewandte Festkörperphysik, Eckerstraße 4, D-7800 Freiburg, W. Germany.

This paper reports on the selective reactive ion etching (RIE) of GaAs on AlGaAs for recessed-gate GaAs MESFET technology.

MESFET or HEMT structures were grown, using MBE or MOCVD, including thin (3 nm) AlGaAs etch stop layers to precisely control the depth of the etched recess and hence the threshold voltage of the devices. The structure of interest for etching consists of an 80 nm GaAs layer ($n=3 \times 10^{18}/\text{cm}^3$), which is the contact layer of the recessed gate devices, and a 3 nm AlGaAs etch stop layer ($n=3 \times 10^{17}/\text{cm}^3$).

The structure below the etch stop layer is dependent on the particular device to be fabricated, but is irrelevant to the etching process.

We used a Leybold MPE 3003 Plasma Etcher which contains two etch modules and one deposition module. The etch gas used was CF_3Cl , for GaAs and Ar for AlGaAs. Etching was done at pressures between 30 mTorr and 100 mTorr and a self bias between 47 V and 250 V. The Etch Profile of the transistor gate recess varied with the pressure; the largest undercut is obtained at a pressure of 100 mTorr. We found that it was necessary to use self bias voltages below 150 Volts to stop the etching at the AlGaAs layer. Beyond a certain voltage there is a significant increase

in the etch rate of AlGaAs. Up to a power range between 0.20-0.30 W/cm², no radiation damage to a quantum well structure was observed using photoluminescence.

B5.5

COPPER VAPOR LASER USED IN ETCHING AND DEPOSITION. Belgacem Haba, Brian W. Hussey, Arunava Gupta, and Robert J. Baseman, IBM Thomas J. Watson Research Center Box 218, Yorktown Heights, New York 10598.

We have carried out experiments for etching manganese-zinc ferrite in aqueous KOH solutions using a copper vapor laser. The high repetition rate (5-10 KHz), the high peak power (~250 KW), and the short pulse length (10-15 ns) result in rapid etching of grooves with high aspect ratios. The depth of the grooves increased with laser power and slower scan speeds while, the width was limited to the laser beam focus. The etching process is believed to be purely thermal in nature and limited only by the removal of the molten material out of the grooves.

The copper vapor laser was also used as a source for projection deposition of various metals on quartz substrate by pure pyrolytic process. This system achieved patterns with fine feature sizes, good resolution, and metallic properties of the deposits. In this technique, both the spun-on organometallic films as well as LCVD were tried.

B5.6

DOWNSTREAM ETCHING OF GaAs AND InP USING MOLECULAR CHLORINE AND CHLORINE RADICALS. David G. Lishan and Evelyn L. Hu, ECE Dept., University of California, Santa Barbara, CA 93106.

We report a systematic study of downstream etching of GaAs and InP in a well controlled, load-locked environment. Base pressures of $\sim 5 \times 10^{-7}$ Torr are achievable. Molecular chlorine, hydrogen chloride and chlorine radicals are independently used to etch these materials and comparisons are made between their highly temperature dependent etch rates. A novel microwave source (McCarroll cavity) is used to generate the chlorine radicals in a region remote from the sample and thus eliminates physical sputtering mechanisms of etching. The technique of remote plasmas to generate reactive species has broad application to in situ deposition and etching and in this instance it will be compared to conventional reactive ion etching (RIE) of these materials.

In the GaAs system, the remote plasma enhances the etch rate by a factor of nearly three in the temperature range from room temperature to 250°C. However, InP data suggest that at temperatures below 140°C, chlorine radicals show no etch rate enhancement over molecular chlorine and perhaps even inhibit the etching rate. At temperatures above 140°C the etch rates using chlorine radicals is again slightly faster than with molecular chlorine. Under both of these etching conditions the temperature dependence is weak above this temperature. In contrast, RIE results indicate a rapid increase in the etch rate past 150°C. Changes in surface morphology and etch anisotropy as a function of temperature will be discussed.

B5.7

COMBINING SPONTANEOUS MOLECULAR ASSEMBLY WITH MICROFABRICATION TO PATTERN SURFACES: COORDINATION CHEMISTRY OF FUNCTIONALIZED ISONITRILES TO Pt SURFACES. J.J. Hickman, C. Zou, D. Ofer, and M.S. Wrighton, Department of Chemistry, Massachusetts Institute of

Technology, Cambridge, MA 02139; P. Laibinis, C. Bain, and G.M. Whitesides, Harvard University, Cambridge, MA 02138.

Pt electrodes can be functionalized by spontaneous binding of p-(ferrocenyl)phenyl-isonitrile, **I**, or m-chloro-p-(ferrocenyl)-phenylisonitrile, **II**, by reaction of pretreated Pt with ~1 mM **I** or **II** in CH₃CN at 298 K. FTIR is consistent with attachment of **I** or **II** via a -NC-Pt linkage. XPS, AES, and electrochemical characterizations are consistent with attachment of one monolayer of redox active material with a potential of ~+0.6 V vs. Ag due to the ferrocenyl moiety. XPS and AES show selective binding (>100:1) of **I** or **II** to Pt compared to the Si₃N₄ substrate of Pt microelectrode arrays. An AES line scan shows the isonitrile to only be on the eight Pt microelectrodes each ~2 μm x ~90 μm long x 0.1 μm thick and separated from each other by 1.4 μm. The data show that spontaneous self-assembly and microfabrication can be used to pattern surfaces with redox active molecular reagents.

B5.8

HOLLOW COLD CATHODE ION SOURCE FOR REACTIVE ION-BEAM ETCHING. Stognij A.I., Tokarev V.V., Institute of Solid State and Semiconductor Physics, the BSSR Academy of Sciences, P. Brovka str. 17, Minsk, USSR, 220726.

The paper reports the results of etching the polyimide film, sputtered onto the SiO₂/Si substrate with oxygen ion beam. The profile obtained has abrupt slopes. The paper studies the influence of ion beam energy and argon gas addition on the formation of the profile "valley" part.

Ion beam parameters were as follows: beam current density was up to 1.2 mA/cm², beam diameter was 12 cm, beam radial irregularity did not exceed 5%, energy range was 2-5 keV. Ion beam was extracted from a wide aperture source of reactive gas ions with a hollow cold cathode. The distinctive feature of the ion source is the use of double cascade self-maintained discharge at low pressure as an ion emitter. This ensures high beam operating parameters together with the simple construction of a diode type. Multipole magnet system having constant polarity is located along the hollow cathode periphery just near emission boundary and is employed to form constant density plasma emission boundary. The ion source ensures well collimated oxygen ion beam with O₂/O > 3 ratio, its contamination level is less than 2%. The source can continuously function for more than 100 hours.

B5.9

LASER INDUCED FORWARD TRANSFER FOR THE DEPOSITION OF PATTERNED HIGH T_c SUPERCONDUCTOR THIN FILMS. E. Fogarassy, C. Fuchs, S. De Unamuno CRN (IN2P3) Laboratoire PHASE (UPR n°292 du CNRS), BP 20, 67037 Strasbourg Cedex, France, and J. Perrière Université de Paris VII (G.P.S. de l'ENS) 2 place Jussieu 75251 Paris Cedex 05.

The laser induced forward transfer (LIFT) technique has been successfully applied, very recently (1), for depositing the new high T_c YBaCuO and BiSrCaCuO superconductor compounds. These materials are initially deposited in thin layer on an optically transparent support by laser evaporation or another more conventional technique. By irradiating under vacuum the film with a strongly absorbed single laser pulse, through the transparent support, we are able to remove the film

from the support to be transferred onto a selected target substrate, hold in contact with the original film. Using this new technique, we have successfully transferred with a one single ArF (193 nm) excimer laser pulse ($\geq 150 \text{ mJ/cm}^2$) YBaCuO and BiSrCaCuO precoated thin film ($\leq 0.5 \mu\text{m}$) from the transparent support onto various substrates. Transfer mechanism has been examined, in details, by using the one dimensional thermal diffusion equation to simulate the heating, melting and vaporization of these compounds, and possible consequences on their stoichiometry were analyzed.

Experiments were also performed in order to demonstrate the possibilities given by the LIFT technique for patterning the high Tc superconductor films either by passing the laser beam through a mask (mask patterning) or by focusing the beam with a lens system (direct patterning).

(1) E. Fogarassy, C. Fuchs, F. Kerherve, G. Hauchecorne and J. Perriere. *J. Mater. Res.* Vol. 4, n°5 Sep/Oct 1989.

B5.10

DIRECT EVIDENCE FOR THE CREATION OF MICROPORES IN UV-IRRADIATED POLY-(METHYL METHACRYLATE). J. A. Moore and J.-O. Choi, Rensselaer Polytechnic Institute, Polymer Science and Engineering Program, Troy, New York 12180-3590.

One rationale offered for the enhanced solubility of poly(methyl methacrylate) which has been exposed to ultraviolet radiation (Hg-Xe lamp) is that, in addition to a decrease in molecular weight caused by chain scission, volatile byproducts of the decomposition reaction create voids or micropores in the film which facilitate transport of solvent into the body of the film and thereby enhance dissolution.

Using azobenzene as a probe with an intense ultraviolet absorption we have accumulated direct evidence that a larger volume is available after irradiation. Azobenzene exists as the extended trans isomer under normal conditions, but upon irradiation at 335 nm it is isomerized to the compact cis isomer by rotation about the weakened N=N bond in the excited state. Clearly this isomerization process will be affected by the amount of space (free volume, microporosity) available on the molecular level as long as it is small compared to the molecular dimensions of the probe.

Films of PMMA including azobenzene were prepared by casting polymer solutions containing the probe or by exposing pre-irradiated films to the vapor of azobenzene. Under similar conditions, films which had been irradiated imbibed more azobenzene than annealed, unirradiated films or irradiated films which had been annealed above T_g . These materials were irradiated at 335 nm and the amount of trans azobenzene which had been formed was monitored spectrophotometrically. The largest amount of photoisomerization was observed for the pre-irradiated samples which had been penetrated by azobenzene from the vapor, indicating that the created free volume allowed the isomerization to proceed more easily.

B5.11

REACTIVE ION ETCHING OF In-BASED III-V SEMI-CONDUCTORS-COMPARISON OF Cl and C_2H_6 CHEMISTRIES. S. J. Pearton, U. K. Chakrabarti, F. A. Baiocchi and W. S. Hobson, AT&T Bell Laboratories, Murray Hill, NJ.

RIE of InP, InGaAs, InAlAs, InAs and InSb in CCl_2F_2 , SiCl_4 , Cl_2 , and $\text{C}_2\text{H}_6/\text{H}_2$ has been compared in terms of the relative etch rates, stoichiometry of the etch surface, and residual ion-induced disorder. The $\text{C}_2\text{H}_6/\text{H}_2$ mixture at the appropriate ratio (1:10) leads to smooth, controlled ($100\text{-}300 \text{ \AA} \cdot \text{min}^{-1}$) etching of these materials, while the Cl_2 -based mixtures lead to faster removal ($600\text{-}1000 \text{ \AA} \cdot \text{min}^{-1}$), but with generally rougher surface morphologies. Exposure to the $\text{C}_2\text{H}_6/\text{H}_2$ discharge leads to preferential removal of the group V elements to depths of $\leq 200 \text{ \AA}$ necessitating the removal of this non-stoichiometric layer in order to obtain acceptable Schottky diode behaviour. This is not necessary for Cl_2 -based etching, although the RIE samples show excess surface leakage current. Under low pressure discharge

conditions ion bombardment by hydrogen ions in the $\text{C}_2\text{H}_6/\text{H}_2$ plasma leads to reductions in carrier density in the first $\sim 1000 \text{ \AA}$ of the near-surface region of InP. This damage can be annealed out around 500°C , and appears to consist of point defects unobservable by TEM. The main advantage to the use of $\text{C}_2\text{H}_6/\text{H}_2$ is its better etching characteristics for InGaAs in comparison to the Cl_2 -based chemistries.

B5.12

ELEVATED TEMPERATURE REACTIVE ION ETCHING OF GaAs AND AlGaAs IN $\text{C}_2\text{H}_6/\text{H}_2$. S. J. Pearton, W. S. Hobson, AT&T Bell Laboratories, Murray Hill, NJ; K. S. Jones, University of Florida, Gainesville, FL

The etch rate, surface morphology and atomic composition, depth of hydrogen passivation and near-surface disorder in GaAs and $\text{Al}_x\text{Ga}_{1-x}\text{As}$ ($x = 0.09 - 1$) have been examined as a function of the sample temperature ($50\text{-}350^\circ\text{C}$) during reactive ion etching in $\text{C}_2\text{H}_6/\text{H}_2$. The etch rates are constant with time, show little temperature dependence and decrease with increasing Al content in the AlGaAs. The etched surfaces have smooth morphologies for C_2H_6 concentrations less than $\sim 40\%$ of the total gas volume. The As-to-Ga ratio in the near-surface region of GaAs remains unchanged over the temperature range investigated, and the depth of hydrogen passivation of shallow dopants is thermally activated ($D_H = 3.1 \times 10^{-5} \exp(-0.79 \text{ eV/kT})$ for GaAs and $1.8 \times 10^{-5} \exp(-0.85 \text{ eV/kT})$ for $\text{Al}_{0.28}\text{Ga}_{0.72}\text{As}$). A layer of sub-surface dislocations approximately 40 \AA deep were observed in GaAs by TEM for the highest power density discharges ($1.3 \text{ W} \cdot \text{cm}^{-2}$).

B5.13

CHARACTERIZATION OF SIDEWALL RESIDUE FILM AND ATOMIC STRUCTURE OF THE TRENCH FORMED BY BCl_3/Cl REACTIVE ION ETCHING. Sun Jin Yun and Young-Jin Jeon, Electronics and Telecommunications Research Institute, Daedog Danji P.O. Box 8, Daejeon City, Korea; and Jeong Y. Lee, Korea Institute of Technology, Daejeon City, Korea.

The silicon surface contamination and damage induced by trench etching in BCl_3/Cl reactive ion etching (RIE) process were characterized by means of x-ray photoelectron spectroscopy (XPS), secondary ion mass spectrometry (SIMS), and high resolution transmission electron microscopy (HRTEM).

The residue films at trench sidewall are $70 - 100$ angstroms thick and are composed of B and Cl. The residue at the upper region of trench sidewall is thicker than that of the lower region. The penetration of energetic ion species was investigated by SIMS depth profiling. Atomic configuration of a trench structure formed by BCl_3/Cl RIE was also observed by HRTEM. The surface roughness in sidewall caused by trench etching is severe more than 10 atomic layers and the near-surface region is heavily damaged.

B5.14

SUBSTRATE HEATING EFFECTS IN EXCIMER LASER PLANARIZATION OF ALUMINUM Robert J. Baseman and Joseph C. Andreshak IBM Research Division, IBM T.J. Watson Research Center, P.O. Box 218, Yorktown Heights, NY 10598

Substantial differences in excimer laser planarization processes are observed with substrate heating. Cavities, associated with filling of high aspect ratio vias at low substrate temperature, can be eliminated by substrate heating. Damage associated with pulse overlap regions can be temperature sensitive, and is reduced as substrate

temperatures are increased. While required fluences for planarization and sample damage both decrease as the sample temperature increases, the relative insensitivity of the damage threshold generally results in larger process windows at higher temperatures. We also report model calculations of the effect of substrate heating on sample temperature distributions and the durations of the laser driven melts.

B5.15

WHOLE COMPOSITION RANGE DEPOSITION OF THIN FILMS BY MAGNETRON COSPUTTERING AND ITS APPLICATIONS. Qing-Ming Chen, Huazhong University of Science and Technology, Wuhan, China; Yu-Dian Fan, and Heng-De Li, Tsinghua University, Beijing, China.

Magnetron cosputtering, i.e., simultaneous sputtering of two or more element targets, was employed to deposit alloy thin films of 17 binary systems such as Co-Mo and Cu-Mo. The films which allow the composition to cover the complete composition range of the phase diagram can be obtained at one time. The films were characterized with the help of transmission electron microscopy with hot stage, electron diffraction, and Rutherford backscattering spectrometry. Many amorphous phases and metastable phases were observed.

With the liquid-nitrogen cooling of substrates, magnetron cosputtering creates the nonequilibrium conditions of thin film growth. The nonequilibrium situation may result in an enhancement of the solid solubility, dramatic changes in the defect density, the formation of metastable crystal structures or amorphous phases, and changes in microstructure. All of these are the subjects of vital concern to the metallurgists. Magnetron cosputtering is a useful method for studying the subjects described above.

As an illustration, the present paper gives the nonequilibrium phase diagrams of the Fe-Bi and Cu-Mo systems which exhibit immiscibility in the equilibrium phase diagrams, and also gives the phase transition behaviours of the as-deposited metastable phases when annealed at the hot stage.

B5.16

THE ETCHING OF Si(100) WITH A MOLECULAR BEAM OF F₂. E.B. Laughlin, M. McConigal, D.J. Gladstone, M.T. Schulberg, and S.T. Leyer, Department of Chemistry, Massachusetts Institute of Technology, Cambridge, MA 02139.

The dissociative chemisorption of F₂ on Si(100) has been studied in order to investigate the potential of neutral molecular beams as a dry etching technique. The probability for dissociative chemisorption of F₂ on Si(100) at 250 K is about one for fluorine coverages less than 0.5 monolayer and is independent of F₂ kinetic energy. The sole desorption product observed under these conditions in a thermal desorption spectrum is SiF₂ at 800 K. Above 1 monolayer coverage, the dissociative chemisorption probability for SiF₂ formation drops to about 2×10^{-2} . However, further reaction of F₂ with a fluorinated silicon surface can be achieved by raising the kinetic energy of the incident F₂ to above 5-7 kcal/mole. At these higher F coverages, SiF₄ thermal desorption is also observed. The SiF₄ yield scales with normal incident kinetic energy of the incident F₂. These results suggest that etching of Si(100) by molecular F₂ can be enhanced by increasing the kinetic energy of the F₂ beam.

B5.17

SELECTIVE CHEMICAL VAPOR DEPOSITION OF TUNGSTEN FILMS ON TITANIUM ION IRRADIATED SILICON DIOXIDE. H. Okuhira, S. Nishimatsu, and K. Ninomiya, Central Research Laboratory, Hitachi, Ltd., Kokubunji, Tokyo 185, Japan.

We demonstrate the selective deposition of adherent tungsten (W) films on titanium (Ti) ion-irradiated silicon dioxide (SiO₂) using consecutive processes of ArF excimer laser chemical vapor deposition (CVD) and low-pressure (LP) CVD.

Ti ion irradiation is performed through a stencil metal mask in a CVD reaction chamber. Typical energy and ion doses are 600 eV and $1.1 \times 10^{14} \text{ cm}^{-2}$, respectively. Laser CVD with WF₆ and H₂ is then performed for 40 seconds at 400 K. After laser CVD, an ion irradiation pattern is clear but a metallic film is not observed. After subsequent LPCVD at 600 K, a 500 μm-wide and 20 nm-thick metallic pattern appears preferentially on the ion-irradiated SiO₂. Good adhesion of the deposited film is confirmed by a tape test.

Without the laser CVD step, the ion-irradiation pattern disappears during LPCVD and no W film deposition occurs. Therefore, laser CVD is essential. However, longer laser CVD times cause selectivity loss during LPCVD, and the deposition of weakly adherent film on the entire SiO₂ surface.

This study was performed through Special Coordination Funds of the Science and Technology Agency of the Japanese Government.

B5.18

STATISTICAL INTERPRETATION OF IR AND UV PHOTOABLATION. Ruediger Braun and Peter Hess, Institute of Physical Chemistry, University of Heidelberg, Im Neuenheimer Feld 253, D-6900 Heidelberg, F.R.G.

A photoablation model based on statistical concepts is presented. This model takes into account the optical, thermophysical and thermodynamic properties of the condensed film and uses statistics to calculate the number of ablated species and their kinetic energy.

Photoablation from condensed van der Waals films of benzene was studied employing a pulsed CO₂ laser in the IR and a pulsed KrF laser in the UV spectral region. The statistical model gives a reasonable description of the nonlinear fluence dependence of the ablation yield, which varies by more than five orders of magnitude in the fluence range studied. For this system, where no chemistry is involved, the fluence dependence of the kinetic energy of ablated species is investigated experimentally and compared with the theoretical model.

Polymer ablation was studied for polyimide films and foils with CO₂ laser and KrF laser pulses. The striking similarities in the etching behavior for IR and UV photoablation are discussed in the frame work of statistical concepts. The most interesting feature of these polymer ablation experiments is not the threshold behavior, but a similar slope in the etch rate versus fluence plot for IR and UV photoablation.

B5.19

THE EFFECTS OF SOURCE GAS, TEMPERATURE AND PRESSURE ON THE SURFACE PLANARITY AND MICROSTRUCTURE OF SILICON SEG AND ELO. M.C. Arsl, K.N. Ritz, J.T. Chen and S. Redkar, Philips Research Laboratories - Signetics Comp., Sunnyvale, CA.; and J.O. Borland and J. Hann, Applied Materials, Inc. - Santa Clara, CA.

The microstructure and surface planarity of selective silicon epitaxial growth (SEG) and epitaxial lateral overgrowth (ELO) have been analyzed via SEM and TEM. The samples in this study simulate size, structure and densities of transistor active areas in IC's. The epitaxial layers were processed in a low pressure CVD epi reactor (10-25 torr) using SiH_2Cl_2 (DCS) as a source gas and deposition temperatures from 860°C and 950°C. Results from this study show that epi/ SiO_2 interface faceting is strongly effected by the wafer loading (ratio of active silicon to non-active or field oxide regions) and by epi growth parameters. Faceting is less pronounced in samples with wafer loading values greater than 50 %. Processing parameters like reducing reactor pressure and HCl injection are also effective to minimize faceting. The addition of HCl during the epi growth cycle, which reduces the growth rate, also results in lower defect densities at the interfaces and the epi layer and creates ELO surfaces much smoother than that achieved by growth without HCl.

Applying these epitaxial techniques in IC processing requires to adjust growth parameters to the device lay-out "loading" in order to obtain after-epi wafer surfaces suitable for lithography. This effort of fine tuning of the epi processing parameters was complicated by planarizing SEG and ELO surfaces by standard silicon wafer polishing techniques. This step not only compensates for residual loading effects, but also eliminates layer thickness non-uniformities while providing the SEG and ELO layer with virgin wafer surface quality. Electrical performance of n-channel MOS transistors, built on as grown and surface polished SEG samples, were measured and compared to data from a standard MOS process with LOCOS isolation.

B5.20

IN-SITU CHARACTERIZATION OF CHEMICAL VAPOR DEPOSITION. R. Scarmozzino, T. Cacouris, R.M. Osgood Jr., Columbia University, New York, N.Y. 10027.

In-situ measurement of resistance has been used for the real-time monitoring of metallorganic chemical vapor deposition (CVD) growth characteristics. In particular, a novel technique for measuring CVD activation energies is presented. The micron scale geometry of the experiment makes it relevant to work in localized laser CVD. In this experiment, a thin conducting line is first deposited between test pads via laser photolysis of a metallorganic gas. By applying a voltage to the pads, a current is induced in the line which resistively heats it, causing pyrolysis and subsequent growth. By monitoring the current as a function of time, one simultaneously obtains information on the CVD growth rate and the power dissipation, which allows a measurement of the activation energy. The technique has been used to measure the CVD activation energy of the dimethylaluminum hydride (DMAIH).

B5.21

EDGE ENHANCED INTERLAYER DIFFUSION IN Al/Hf/Al VLSI METALLIZATION. X.S. Guo and W.A. Lanford, State U. of N.Y. at Albany, NY 12222, K.P. Rodbell, IBM-East Fishkill, Hopewell Junction, NY 12533

Al/Hf/Al multilayer were patterned and reactive ion etched into parallel stripes having stripe widths from 0.5 μm to 200 μm . Due to the ion bombardment and reactions between reactive ions and Al/Hf/Al stripes on the sidewalls of the stripe, there will be defects and damages near the edges of the stripe. These defects and damages will enhance the interlayer diffusion

between Al and Hf layers. A 2 MeV He beam was focused to 2 μm in diameter and scanned a few thousand \AA across the edge of a stripe, the RBS from the edge was compared with that from the center of a stripe. Stripes with different stripe width were also compared using RBS. It was found that the interlayer diffusion near the edge was enhanced, and the temperature where the edge interlayer diffusion started was 25 degree C below that at the center.

B5.22

LASER WRITING OF HIGH PURITY GOLD LINES. M Jubber, J I B Wilson, J L Davidson, P A Fernie, P John, Heriot-Watt University, Riccarton, Edinburgh EH14 4AS

Gold tracks have been deposited on thermally oxidised silicon wafers by pyrolytic decomposition of gaseous methyl (triethylphosphine)gold I, using focussed 514nm radiation from an argon ion laser. The precursor, $\text{AuMe}(\text{Et}_3\text{P})$, is a white crystalline solid with a relatively high vapour pressure and is one of a series of compounds being evaluated for laser deposition. Tracks were deposited at a speed of $35 \mu\text{ms}^{-1}$ with a spot size of $\approx 12 \mu\text{m}$. SIMS, EDAX and laser ionisation microprobe analysis (LIMA) were used to analyse the chemical composition of the tracks; the purity of better than 98% is consistent with the low value of room temperature resistivity ($4.2 \mu\Omega\text{cm}$, compared with bulk gold $\approx 2 \mu\Omega\text{cm}$). Stylus profilometry and SEM analysis showed the lines to have an almost rectangular cross-section suggesting that deposition is more rapid on the gold surface than on the SiO_2 substrate.

B5.23

PHOTOSTIMULATED DEFECT-IMPURITY REACTIONS DURING ION BOMBARDMENT OF SI. Alex B. Danilin, Yuri N. Erokhin, Viktor N. Mordkovich, Institute of Microelectronics Technology and Superpure Materials USSR Academy of Sciences, 142432, Chernogolovka, Moscow regn. USSR.

The influence of photoexcitation on the defect-impurity reactions during ion bombardment ($90 \pm 150 \text{ keV O}^+$, P^+ ions to a dose of $3 \times 10^{14} - 2 \times 10^{16} \text{ cm}^{-2}$) of Si was studied. Photoexcitation was performed by irradiation the sample with the light with the wavelength shorter than one corresponding to the Si energy bandgap.

It was shown that photoexcitation makes the strong influence on the formation of stable radiation defects (RDs) and their complexes with impurities and causes:
a) considerable reduction of the RDs accumulation in ion implanted layer; b) the increase of the dose of amorphization; c) non-monotonous change with the sample temperature in the region 500-700 K of the concentration of soluted oxygen during ion implantation; d) the change of velocity of oxygen atoms coagulation on precipitates; e) stimulates diffusion of oxygen atoms in Si.

The model, based on recombination-stimulated annealing of vacancy type point defects during ion implantation, explaining the decrease of RD accumulation during the early stages of ion implantation and increase of that on late ones is proposed.

On the correlation of profile of the deformation peak and spatial distribution of implanted species the influence of elastic force field on the kinetic of defect formation is discussed.

B6.1

GENERATION OF BLIND VIA-HOLES FOR A HIGH DENSITY MULT-CHIP-MODULE USING EXCIMER LASERS. Friedrich G. Bachmann, Siemens AG, Corp. Production and Logistics Dept., Munich, Fed. Rep. Germany

In recent years the on-chip delay has gone down

much more rapidly than the signal delay in packaged circuits. As a consequence of this the packaging delay times have had to be reduced drastically, which means that a greater packaging density has had to be implemented.

A novel planar packaging technique, used in the new SIEMENS main frame computer 7500 H 90 has led to considerable progress in solving this problem. An essential part of this system is a multi-chip-module which can hold up to 144 bare chips. The carrier of these IC's is a 16-layer high density multilayer printed circuit board, which is fabricated in a sequential process.

Interlayer contacts are formed by 80 μm wide blind via-holes, which are generated by excimer-laser ablation of the dielectric. The process described in this paper shows that it is possible to produce blind via-holes with an aspect ratio of about one in an extremely reliable and reproducible way.

This process is already being successfully run on a production line. It is to our best knowledge the first time excimer-lasers have been used on a large-scale in an industrial environment.

B6.2

UV LASER-INDUCED ETCHING OF FIRST-ROW TRANSITION METALS

George W. Tyndall IBM Almaden Research Center, 650 Harry Road, San Jose, CA 95120.

A quartz crystal microbalance (QCM) has been used to study the KrF^* (248 nm) laser-induced etching of Ti, Cr, Fe, Ni and Cu by bromine. The experiment consists of focusing the pulsed output of an excimer laser at normal incidence onto the surface of a quartz crystal coated with the transition metal. Absolute etch rates are determined from the change in the resonant frequency of the QCM over time. Each of the metals studied can be etched by bromine at laser fluences significantly below those required for ablation of the pure metal. The dependence of the etch rate on bromine pressure and laser fluence was measured to elucidate the etching mechanisms. The details of these etching mechanisms will be discussed.

B6.3

PHOTOCHEMICAL AREA-SELECTIVE ETCHING OF Si AND SiO_2 USING SYNCHROTRON RADIATION.

Jun-ichi Takahashi, Yuichi Utsumi, and Tsuneo Urisu, NTT LSI Laboratories, Kanagawa, Japan.

Material selectivity and the surface reaction scheme in the etching reaction are important factors for controllable area-selective processing. We have already reported [1,2] that photochemical etching using synchrotron radiation (SR) presents unique material selectivity, and that the surface reaction can be expressed as "photo-stimulated reactive desorption." This report discusses in some detail the mechanism involved in SR-stimulated area-selective etching of Si and SiO_2 using SF_6 gas.

Photon energy dependence of SiO_2 (thermal oxide) etching was studied to examine what kind of surface photo-excitation was dominant. Excitation wavelength range was selected by changing SR beam incident angles to Pt plane mirrors in the beam line. Experimental results indicate that the most important factor is core electron excitation of surface SiO_2 molecules. The influence of dopant in Si etching was also studied using B-doped, P-doped, and undoped poly-Si films. The etching rate decreased with increasing dopant concentration, independent of conduction type. This characteristic is quite different from the case for excimer laser or plasma etching. According to our reaction model this result can be

explained as active species quenching by majority carriers.

(1) T. Urisu et al. J. Vac. Sci. & Technol. B5 (1987) 1436. (2) J. Takahashi et al. Extended Abstracts 1988 Int. Conf. Solid State Devices & Mat. p.73.

B6.4

EXCIMER LASER-ASSISTED ETCHING OF SILICON USING CHLOROPENTAFLUOROETHANE. S. D. Russell, and D. A. Sexton, Solid State Electronics Division, Naval Ocean Systems Center, San Diego, CA.

Laser-assisted photothermal chemical reactions have been observed with silicon in a chloropentafluoroethane ambient using a KrF^* laser at 248 nm. Etching occurs only if the incident fluence exceeds the melt threshold ($\sim 0.75 \text{ J/cm}^2$), and is monitored by the change in silicon reflectance at 633 nm. Above the ablation threshold ($\sim 2.2 \text{ J/cm}^2$) increased surface roughness is observed. Etch rates $\sim 7 \text{ \AA/pulse}$ have been measured using both stylus profilometer and SEM cross-sectional techniques. The etch rate dependence on incident fluence, ambient pressure, doping concentration, crystal orientation and substrate temperature will be presented. This process allows single step patterning of silicon devices in a non-corrosive environment.

B6.5

LOCALIZED LASER-ASSISTED ETCHING OF COPPER FILMS BY CHLORINE USING RAMAN SPECTROSCOPY FOR *in situ* FILM ANALYSIS. Hua Tang and Irving P. Herman, Department of Applied Physics and the Microelectronics Sciences Laboratories, Columbia University, New York, NY.

Etching of copper films on glass was studied by localized laser substrate heating (4880 \AA) in the presence of chlorine gas. The spontaneous reaction of Cu with chlorine at room temperature forms a film [1], which was identified to be CuCl by Raman spectroscopy at 77 K. If the chlorine is then evacuated, laser heating can remove this CuCl film locally, down to the remaining copper film. If instead chlorine is present during laser heating, a bump is formed. In producing this feature, the CuCl layer and some of the underlying Cu film are converted to CuCl_2 , as identified by *in situ* Raman analysis at room temperature. After removal of the chlorine, etched CuCl/Cu regions are formed with micron-dimension patterns after subsequent *in situ* laser heating of these features or *ex situ* rinsing in solvents.

This work was supported by the Office of Naval Research and IBM.

[1] W. Sesselmann and T. J. Chuang, Surf. Sci. 176, 32 (1986).

B6.6

SELECTIVE TUNGSTEN CVD ON A-Si:H BY PULSED UV LASER MODIFICATION OF THE NATIVE OXIDE. Arthur T. Howe, K. V. Reddy, Darrell L. Wuensch and Jeff T. Niccum, Technology Division, Amoco Technology Company, PO Box 400, Naperville IL 60566; and Gerry W. Zajac, Analytical Division, Amoco Corporation, PO Box 400, Naperville IL 60566.

Laser patterning processes which use comparatively low laser intensities are of interest for applications requiring masks, or involving thermally sensitive devices. We have studied such a process involving the indirect control of tungsten chemical vapor deposition on a-Si:H by laser modification of the native oxide. The process has potential for use in the fabrication of active matrix flat panel displays.

Excimer laser pulses, of wavelengths 193, 248 and 308 nm, and fluences of approximately 100 mJ/cm^2 , were shown to cause slight growth of the native oxide on a-Si:H, and XPS studies of the effect will be described. The oxide growth was sufficient

to inhibit the reaction of WF_6 with the underlying silicon, thereby inhibiting tungsten growth on the regions exposed to the laser. Conditions under which patternability was achieved will be discussed.

B6.7

WAVELENGTH-DEPENDENT AREA SELECTIVITY IN PHOTO-CHEMICAL VAPOR DEPOSITION OF ALUMINUM FILMS.

Mitsugu Hanabusa and Masashi Ikeda, Toyohashi University of Technology, Tenpaku, Toyohashi 440, Japan.

We observed a wavelength-dependent thickness profile in photodeposition of aluminum thin films via photolysis of dimethylaluminum hydride by a deuterium lamp. Under illumination of the full spectrum including the VUV around 160 nm the deposit was formed preferentially in illuminated regions, while such area selectivity has been lost and uniform thickness was observed even outside the illuminated regions when the VUV was eliminated by a proper filter and the UV above about 180 nm was used.

The observed change in area selectivity reflects a shift in the relative importance of surface and gas phase reactions with wavelengths. With the VUV, nuclei can be formed via surface photolysis of adsorbates on silicon substrates, while with the UV only such nucleation is initiated only by arrival of photofragments produced in gas phase and diffused onto substrate surfaces. Once the nuclei are formed, the film growth continues with or without the VUV.

The observed effect offers an interesting possibility in controlling area selectivity in various applications. Also area selectivity is controlled by changing vapor pressures and substrate temperatures, as well. In combination of all these we can take a full advantage of photo-induced processes to control area selectivity.

B6.8

KrF EXCIMER LASER INDUCED DEPOSITION OF TITANIUM FROM $TiCl_4$. R. Izquierdo, M. Meunier and C. Lavoie, Groupe des Couches Minces et Département de Génie Physique, Ecole Polytechnique, Montréal, Canada H3C 3A7.

We have investigated the deposition of titanium from $TiCl_4$ induced by KrF excimer laser ($\lambda=248$ nm). Substrates used are: 1) glass; 2) crystalline silicon for possible formation of titanium silicides contacts; 3) $LiNbO_3$ for the formation of $Ti:LiNbO_3$ waveguides (1). When the laser with fluences of 1 mJ/pulse is focused, lines of 5 to 10 μm with and 1000 Å thick can be written at a speed of 5 μm /seconde on crystalline silicon and glass. However, the low damage threshold for $LiNbO_3$ requires to lower the input energy to < 0.01 mJ/pulse, thus reducing the film thickness to approximately 30 Ångströms at the same deposition speed.

In order to understand the basic mechanism of this deposition process, we have performed a preliminary study of the film by XPS and SEM. When the $LiNbO_3$ surface is exposed to 10 Torr of $TiCl_4$ and then evacuated, XPS shows that the adsorbed layer has $[Ti]/[Cl]=3$ and this ratio is not greatly affected when exposed to the unfocused laser in an evacuated cell. This suggests the importance of the gas phase chemistry. Moreover, at pressures higher than 5 Torr of $TiCl_4$, gas phase absorption leads to powder formation of 1 μm diameter deposited on the surface; XPS analysis shows that their composition is $[Ti]/[Cl]=10$. Possible deposition models based on this information will be presented.

(1) J.Y. Tsao et al. Appl. Phys. Lett. 42, 559 (1983).

B6.9

SELECTIVE RAPID THERMAL CVD OF GERMANIUM. D.T. Grider, M.C. Ozturk, J.J. Wortman, Y. Zhong*, North Carolina State University, Department of Electrical and Computer Engineering, Raleigh, NC 27695-7911, D. Batchelor, P. Russell, Department of Materials Science and Engineering, Raleigh, NC 27695-7907.

Selective depositions of germanium thin films have been investigated in a cold-wall rapid thermal processor using 3.0 - 8.0% GeH_4 diluted in a hydrogen carrier gas at pressures between 1.0 to 7.0 Torr and at temperatures up to 575°C. Deposition rates exceeding 3500 Å/min were obtained, making germanium compatible with the throughput requirements placed on single wafer manufacturing. Germanium growth progresses by the formation of germanium islands, which then grow both vertically and laterally, resulting in a rough surface. This roughness is deposition temperature dependent with smoother films being deposited at lower temperatures. Methods of improving the roughness of these films have been investigated.

Current silicided contacts to ultra shallow source/drain junctions are limited by the ability to controllably deposit thin metal layers to minimize silicon consumption. Selectively deposited germanium films can be used in current MOSFET technologies as a buffer layer between refractory metals and the underlying source/drain regions. With this goal, selective tungsten deposition on selective germanium has also been investigated.

* On leave from Liaoning University, Physics Department, China

B6.10

LASER-INDUCED LOCAL DECOMPOSITION OF ADSORBED TUNGSTEN FLUORINE MOLECULES FOR METAL DEPOSITION ON SILICON.

G. Auvert, D. Tonneau, Y. Pauleau, C.N.E.T. BP98,38243, Meylan, France.

Decomposition of tungsten hexafluoride on silicon substrates under cw argon laser irradiation in the visible domain has been extensively studied in presence of various buffer or reactive gases. Decomposition rate is found to be limited either by a mass transport phenomena or by a thermally activated process. It has been found that no photolytic decomposition process can be invoked as the limiting step in the decomposition rate.

Depending on the partial pressure of added hydrogen, irradiation proceeds either in a local etching of the silicon surface even through the native oxide or in a local deposition of tungsten lines with good electrical properties. In the high pressure domain, deposition kinetics are consistent with mechanisms invoked in conventional chemical vapor deposition reactors. A different mechanism which appears in a lower pressure domain will be tentatively interpreted in correlation with the laser-induced temperature.

B6.11

EXCIMER LASER INDUCED DEPOSITION OF TUNGSTEN FROM $W(CO)_6$ AND WF_6 . B. RAGER und F. Bachmann Siemens AG, Corp. Production and Logistics Dept. Otto-Hahn-Ring 6, 8000 Munich 83, FRG.

The ArF laser induced deposition of tungsten on Si-surfaces (with native oxide) from $W(CO)_6$ and WF_6 was investigated under various experimental deposition conditions. The dependence of the deposition rate on laserenergy fluence was studied. With an in-situ reflectivity measure-

ment the growth of the metallic layer could be monitored during the deposition process. We find that the initial stage of layer growth as well as the relative reflectivity as a function of deposition time critically depends on the laser fluence.

Model calculations have been performed to compare the measured reflectivity curves with the calculated curves.

The deposited tungsten layers have been analyzed by X-Ray-Photoelectron Spectroscopy and Auger-Electron Spectroscopy. The optical constants have been determined by ellipsometry. Resistivity values of about ten times of the bulk value have been measured by a four point probe.

In addition, experiments of direct pattern transfer deposition have also been carried out. The spatial resolution capability of the deposition process will be illustrated and discussed.

B6.12

DIRECT WRITING OF COPPER LINES USING ND:YAG LASER AND COPPER FORMATE PRECURSORS. Heinrich G. Müller and Siegfried Schuler, TU Berlin, Forschungsschwerpunkt Mikroperipherik, Berlin, FRG.

Laser direct writing techniques have been used for depositing copper lines from water soluble precursor films of copper formate. The deposition area is scanned with a cw Nd:YAG laser spot. By this method writing speeds of up to 50 mm/s and very good adhesion on alumina substrates could be reached.

The thin copper lines deposited using the above technique serve as seeds for further chemical copper deposition. The process offers great potential for thin film hybrid interconnects.

The details of the technique are discussed, including the formation of the precursor films, effects of the substrate surface, influence of the precursor film thickness on seed formation, and giving an analysis of the copper films obtained.

B7.1

LASER-INDUCED FORMATION AND SURFACE PROCESSING OF HIGH-TEMPERATURE SUPERCONDUCTORS. Dieter W. Bäuerle, Angewandte Physik, Johannes-Kepler-Universität, A-4040 Linz, Austria

Recent results on the *in-situ* deposition of thin extended films of Y-Ba-Cu-O and Bi-Sr-Ca-Cu-O using laser sputtering technique are presented. Surface patterning of these materials by laser-induced reduction, metallization, oxidation and ablation has been performed with both ceramic samples and thin films.

B7.2

LASER PATTERNING AND ELECTRICAL PROPERTIES OF SUBMICROMETER LINES OF Y-Ba-Cu-O. J.P. Zheng, Q.Y. Ying, H.S. Kim, D.T. Shaw and H.S. Kwok, Institute on Superconductivity, State University of New York at Buffalo, Bonner Hall, Buffalo, NY 14260

0.6 μm -wide lines of high T_c Y-Ba-Cu-O have been fabricated by direct laser writing on mirror-like thin films which were grown by laser

deposition without post annealing. The apparatus used in this study consisted of a single mode Q-switched Nd:YAG laser. The laser beam was focused to a diameter of 1 μm by a optical micro-objective lens. The film was translated by two computer-controlled stepper motors. The laser fluence was adjusted to slightly above the ablation threshold of 2 J/cm². The maximum scanning rate of the system was 0.5 mm/sec and was limited by the laser repetition rate of 1 kHz.

To characterize the patterning system, as well as the superconducting film, superconducting microstrips in the range of 0.6-85 μm wide were produced with a length of 100 μm . After patterning, the $T_c(R=0)$ decrease by less than 4 K from 81 K of original film for the 85-1.6 μm lines. However, for the 0.6 μm line, $T_c(R=0)$ decrease to 69 K. It is believed to be due to the finite grain size of the Y-Ba-Cu-O film. All the patterned lines showed J_c of $4 \times 10^6 \text{ A/cm}^2$ at 20 K. This value compares favorably with results using other patterning techniques. These patterned lines have been successfully applied to the study of optical detectors using Y-Ba-Cu-O films.

B7.3

PULSED EXCIMER LASER ABLATION FOR THE DEPOSITION OF YBaCuO AND BiSrCaCuO COMPOUNDS: MATERIALS DISTRIBUTION AND STOICHIOMETRY. C. Fuchs and E. Fogarassy, CRN (IN2P3), Laboratoire PHASE (UPR n°292 du CNRS), B.P. 20, 67037 Strasbourg Cedex, France

Pulsed laser ablation from solid targets appears to be a very convenient means to deposit thin films of a wide variety of materials including recently the new high T_c superconductor compounds (1).

The nature and the relative concentrations of atomic species and macroscopic size particles leaving the irradiated target surface and their spatial distribution, which are at the origin of the properties and quality of the deposit, depend on the various parameters involved in the laser-solid interaction.

We investigate, in this study the laser ablation processes for YBaCuO and BiSrCaCuO thin film deposition, using a pulsed ArF (193nm) excimer laser. The deposition parameters, especially those which are relevant to the geometrical configuration of the experimental set-up and laser irradiation conditions are examined in details. At low energy density ($< 0.5 \text{ J/cm}^2$), the evaporation process appears to be close to thermal equilibrium and characterized by a broad angular distribution ($\sim \cos \theta$) of the vaporized target material. At high energy density, a ionized plasma of elemental species is generated in front of the target surface and the ablated materials are ejected in a distribution which is strongly peaked ($\sim \cos^n \theta$, $n \gg 1$) in the direction normal to the target surface. The angular variation of the stoichiometry in the thin films are also measured and correlated both on the thermal emission law and plasma expansion dynamics. Finally the origin of the macroscopic spherical particles ($\sim 1 \mu\text{m}$ diameter) which are ejected with the atomic species from the irradiated target are discussed on the basis of our experimental results.

(1) See for example D. Bäuerle, Appl. Phys. A 48, 527, (1989).

B7.4

LASER PATTERNING OF HIGH T_c SUPERCONDUCTING THIN FILMS. G.G. Bentini, M. Bianconi, L. Corraa, S. Nicoletti(?), S. Naldini(?), CNR-Istituto LAMEL, Via Castagnoli, 1, I-40126 Bologna, Italy; (?) AUR.EL S.p.A, Via Casadei, 7, I-47015 Modigliana, Italy

High T_c superconducting thin films were prepared by laser ablation of bulk material on MgO and SrTiO₃ substrates. After the laser deposition the films were annealed in O₂ atmosphere to get a sharp resistivity vs. temperature transition and an high current density.

In order to obtain narrow lines of

superconducting material, the films were mounted onto an X-Y computer controlled stepping stage and irradiated with a pulsed laser beam focalized on the sample surface. The irradiations were performed under vacuum, inert or reactive atmosphere.

The patterning efficiency was measured as a function of the irradiation conditions (i.e. the number of pulses per frame, the laser fluence and the ambient atmosphere).

The electrical behaviour of the patterned film was studied as a function of line width for different film thicknesses and morphologies.

B7.5

TUNABLE UV LASER DECOMPOSITION OF GAS PHASE AND SURFACE ADSORBED ORGANOMETALLICS

Thomas Beuermann, Yanping Zhang, Michael Stuke
Max-Planck-Institut für biophysikalische Chemie, P.O. 2841,
D-3400 Göttingen, F.R. Germany

The metal alkyls trimethylaluminum (TMA), trimethylgallium (TMG) and trimethylindium (TMI) are decomposed by tunable UV laser light in the range 200 - 320 nm with collision-free product detection by laser mass spectroscopy using short and ultrashort laser pulses. In the gas phase, these compounds decompose via a one-photon process in the wavelength region studied. Using ultrashort laser pulses of 1 ps duration, unstable photoproducts like $\text{Al}(\text{CH}_3)_2$, $\text{Ga}(\text{CH}_3)_2$ and $\text{In}(\text{CH}_3)_2$ are detected with good signal to noise ratio, whereas they are not seen with ns laser sources. The photolysis laser wavelength dependence of the yields of atomic and molecular photofragments will be given. As a surprising result metal atoms Al, Ga and In are formed already at lower photon energies than the metal-monomethyl radicals AlCH_3 , GaCH_3 and InCH_3 . A mechanism, explaining the photolysis of trimethyl compounds of group III elements, is presented. Results on the tunable UV laser photoproduct distribution from surface adsorbed organometallics indicate, that some photoproducts are formed at lower threshold photon energy compared to the gas phase. A comparison between decomposition pathways of gas phase and surface adsorbed organometallics will be attempted.

B7.6

LOW TEMPERATURE INTERLEVEL SiO_2 -LAYERS BY PHOTOINDUCED PROCESSING. H. Sigmund, A. Klumpp and G. Springholz, Fraunhofer-Institute for Solid State Technology, Paul-Gerhardt-Allee 42, 8000 München 60

Deposition of SiO_2 from tetraethoxysilane (TEOS) by LPCVD and recently also by PECVD has become very conveniently as interlevel dielectric because of better step coverage properties of the films than corresponding films deposited from silane. Yet for low temperature planarizing ($< 400^\circ\text{C}$) SiO_2 layers multistep processing schemes such as deposit-etch-deposit by alternating plasma and thermal CVD ($\text{TEOS} + \text{O}_3$) are necessary to obtain the desired planarized profiles. Process flows are then more complex and throughput is reduced.

We studied photoinduced polymerization reactions of TEOS in order to deposit poly-siloxane layers with suitable viscosity properties and layer thicknesses. Dependent on the topological properties of the IC surface the viscosity and the film thickness can be controlled by the deposition parameters, so that different planarizing properties (step angle, step coverage)

may be adjusted. In a second processing step the poly-siloxane layers are then transformed in a combined thermal/photolytical or thermal/plasma treatment to SiO_2 . Typical examples for the planarizing properties of these techniques as IC interlayer dielectrics are presented. The physical and electrical properties (stress, etch rate, breakdown voltage) of these dielectric layers are given. These results are obtained with an experimental multichamber equipment.

B7.7

PHOSPHORUS DOPING INTO SILICON USING ArF EXCIMER LASER. A. Slaoui, F. Foulon, E. Fogarassy and P. Siffert, Laboratoire PHASE (UPR du CNRS n°292), CRN, 23 rue du Loess, 67037 Strasbourg Cedex, France.

Chemical doping of single - crystal Si in a PF_5 atmosphere is performed by irradiation with an ArF laser at 193 nm. We have investigated the dependence of doping parameters - laser fluence, number of pulses and PF_5 gas pressure - on the sheet resistance and the impurity concentration profiles. Two kinds of doping, the doping in PF_5 ambients and the doping using only the adsorbed layer, have been performed. From these results, it is found that phosphorus atoms are produced by pyrolysis of physisorbed layers of PF_5 formed on the silicon surface. As for the incorporation mechanism, it is shown that the process is mainly diffusion limiting. Electrical characteristics of n+p junctions formed by this technique seem to be strongly limited by the presence of point defects induced by laser irradiation.

B7.8

RÔLES OF GAS PHASE AND SURFACE PHOTOLYSIS IN LCD FROM $\text{Fe}(\text{CO})_5^*$. Xu Xin** and J.L. Steinfeld, Department of Chemistry, Massachusetts Institute of Technology, Cambridge, Massachusetts 02139.

Laser-driven deposition of metallic thin films from gas-phase precursors involves a complex interplay of gas-phase photodissociation and photolytic and thermal processes in the deposited films. We have been investigating these processes for deposition from iron carbonyl with argon fluoride and krypton fluoride excimer lasers, using profiling XPS and profiling auger electron spectroscopy to determine the chemical nature of the resulting films. The deposition is initiated by one- and two-photon sequential dissociation of $\text{Fe}(\text{CO})_5$, with both iron atoms and unsaturated $\text{Fe}(\text{CO})_x$ fragments depositing from the gas phase. Both thermal and photolytic processes take place in the growing iron film, with some of the carbon and oxygen driven off in molecular form and some being dissociated to form carbide and oxide moieties in the film. Some simple mathematical models have been developed to represent the dependence of growth rate and C/O content of the film on such parameters as laser fluence, laser wavelength, and substrate properties.

*Supported by National Science Foundation, Air Force Office of Scientific Research, and Digital Equipment Corporation.

**on leave from Institute for Atomic Energy Research, Beijing, People's Republic of China

B7.9

ROOM TEMPERATURE PHOTO-OXIDATION OF HYDROGENATED SILICON-CARBON ALLOYS. P. John, I. M. Odeh, A. Qayyum and J. I. B. Wilson, Heriot-Watt University, Riccarton, Edinburgh EH14 4AS

Hydrogenated amorphous silicon-carbon alloys, a-Si:C:H, have been deposited as thin films on crystalline silicon substrates from a capacitively coupled rf discharge in

silane-propane mixtures. Variations in the silicon-carbon ratios in the films were achieved by altering the SiH_4 to C_3H_8 flow rates at a substrate temperature, $T_s = 250 - 260^\circ\text{C}$, and total pressure, $P_t = 100$ mtorr. The stoichiometry of the allows was established by XPS and the hydrogen content by attenuated total reflectance infrared spectroscopy.

For values of the carbon content, $x_c \sim 0.3$, the films oxidize in air on illumination with the collimated output of a Xe-arc lamp at an irradiance of $\sim 30\text{mWcm}^{-2}$. Photo-oxidation also occurred with the frequency doubled (257nm) Ar^+ laser. In neither experiment did the measured or calculated surface temperature exceed 50°C .

The photostructural changes were investigated by ATR infrared spectroscopy. Inductive effects on the degenerate Si-H stretching modes were observed due to contiguously bound oxygen to SiH_3 groupings. In contrast, the structured band envelope of the C-H stretching mode remains unchanged during oxidation. The local bonding environment was also elucidated by measurement of the C(1s), Si(2s) and Si(2p) binding energies.

Contact photolithography demonstrated a spatial resolution of at least $5\mu\text{m}$ for the photo-oxidation process.

B7.10

MECHANISM OF SELECTIVE AREA GROWTH OF ALUMINUM BY ORGANOMETALLIC CHEMICAL VAPOR DEPOSITION
Krishnan Raghavachari, G. S. Higashi, and M. L. Steigerwald, AT&T Bell Laboratories, Murray Hill, NJ 07974

The pyrolysis of triisobutylaluminum occurs much more readily on the surface of Al than on the surface of an oxide. This propensity allows Al to be grown selectively on a wafer and may simplify certain metallization steps in integrated circuit manufacture. For example, the filling of high-aspect ratio via holes for applications in multilevel metallization might be performed using such an Al deposition technique.

In this study, ab-initio quantum chemical techniques have been used to elucidate why Al deposition is more facile on an Al surface than on an oxide surface. Such a deposition is governed principally by the activation barrier involved in a beta-hydrogen elimination reaction of the organometallic precursor (e.g., triisobutylaluminum). We have now calculated the transition states which determine this activation barrier for Al atoms in different chemical environments. Efficient gradient techniques have been used to determine the geometries of the transition states and the barriers have then been obtained by accurate calculations including the effects of electron correlation. Such molecular cluster calculations show that the transition state barrier for the beta-hydride elimination reaction increases substantially when comparing an Al atom bonded to other Al atoms vs. O atoms, explaining the observed surface selectivity. Detailed analysis of our results reveals that the relative beta-hydride elimination barriers in different environments are determined principally by the energetics of promoting an electron to the empty π^* -orbital on the Al.

B7.11

METAL DEPOSITION WITH INCOHERENT EXCIMER RADIATION. Hilmar Esrom and Ulrich Kogelschatz*, Asea-Brown-Boveri AG, Corporate Research Heidelberg, FRG Germany, *Corporate Research Baden, CH Switzerland

Recently we have shown /1/ that the incoherent UV radiation of a silent discharge excimer source is well suited for the photolytic decomposition of palladium acetate films. The discharge emits the second continuum of the Xe_2^* excimer peaking at 172 nm. Using the new excimer source in a reactor flooded with nitrogen structured and large area palladium deposits are obtained. The palladium layers were reinforced by electroless copper plating. Palladium deposition rates are measured as a function of the electrical input power of the silent discharge. It will also be shown that higher deposition rates can be obtained in the evacuated reactor. Also higher substrate temperatures have a considerable influence on the deposition rates. The quality of these films is compared to films obtained with excimer laser irradiation. With incoherent UV radiation extremely smooth films on various substrates were obtained while laser deposited films are discontinuous.

/1/ H. Esrom, G. Wahl and U. Kogelschatz, Euro-Conf. on CVD, Perpignan, June 1989, in print

SYMPOSIUM C: ATOMIC SCALE STRUCTURE OF INTERFACES

C

November 27 - 29, 1989

Chairs

R.D. Bringans
Xerox Palo Alto Research Center
3333 Coyote Hill Road
Palo Alto, CA 94304
(415) 494-4156

J.M. Gibson
Room 1C-325
AT&T Bell Laboratories
600 Mountain Avenue
Murray Hill, NJ 07974
(201) 582-5952

R.M. Feenstra
IBM T.J.Watson Research Center
P. O. Box 218
Yorktown Heights, NY 10598
(914) 945-2492

Symposium Support

Office of Naval Research

**Proceedings published as Volume 159
of the Materials Research Society
Symposium proceedings series.**

SESSION C1: INTERFACES AND HETEROEPITAXY

Chair: J. M. Gibson
Monday Morning, November 27
Salon A/B (M)

8:30 *C1.1
ONSET OF GaAs HOMOEPITAXY AND HETEROEPITAXY,
D.K. Biegelsen, Xerox Palo Alto Research
Center, Palo Alto, CA.

9:00 *C1.2
HIGH RESOLUTION ION SCATTERING STUDIES OF
THIN EPITAXIAL FILMS, Rued M. Tromp, IBM
Research Division, T.J. Watson Research
Center, Yorktown Heights, NY.

9:30 C1.3
ATOMIC STRUCTURE OF CaSi_2/Si INTERFACES,
Chris G. Van de Walle, Philips Laboratories,
Briarcliff Manor, NY.

9:45 C1.4
THE STRUCTURE AND CHEMISTRY OF THE Ge/SAP-
PHIRE INTERFACE, Geoffrey P. Malafsky and
David J. Godbey, Naval Research Laboratory,
Electronics Division, Washington, DC.

10:00 BREAK

SESSION C2: INITIAL STAGES
OF HETEROEPITAXY

Chair: R. Feenstra
Monday Morning, November 27
Salon A/B (M)

10:30 *C2.1
ENERGETICS AND ELECTRONIC STRUCTURE OF GaAs
ON Si, J.E. Northrup, Xerox Palo Alto
Research Center, Palo Alto, CA.

11:00 C2.2
STRUCTURAL ENERGIES OF ANTIPHASE DOMAIN
WALLS IN GaAs, David Vanderbilt and L. Brey,
Harvard University, Department of Physics,
Cambridge, MA.

11:15 C2.3
VERY THIN 2D GaAs FILMS ON Si DURING THE
EARLY STAGES OF GROWTH BY MBE, D.B. Fenner,
Xerox Palo Alto Research Center, Palo Alto,
CA, and Santa Clara University, Physics
Department, Santa Clara, CA; David K.
Biegelsen and B.S. Krusor, Xerox Palo Alto
Research Center, Palo Alto, CA.

*Invited Paper

Short Courses C-01, "Modern Materials
Analysis Techniques," C-14, "Scanning
Tunneling Microscopy," C-19, "Practical
Transmission & Analytical Electron Micros-
copy-Theory," and F-08, "Ceramic and Metal
Matrix Composites," may be of interest to
symposium attendees. Details regarding
course dates and instructors are provided in
the short course section of this program.

11:30 C2.4
 μm -SCALE LATERAL GROWTH OF Ga-MONOLAYERS
OBSERVED IN-SITU BY ELECTRON MICROSCOPY, J.
Osaka and N. Inoue, NTT, LSI Laboratories,
Atsugi City, Japan.

11:45 C2.5
THE INITIAL STAGES OF GROWTH OF InSb ON
GaAs(100) BY MBE - A HIGHLY LATTICE MIS-
MATCHED HETEROINTERFACE, C.J. Kiely, Univer-
sity of Liverpool, Department of Materials
Science and Engineering, Liverpool, United
Kingdom; A. Rockett, University of Illinois
at Urbana-Champaign, Material Sciences
Department, Urbana, IL; J-I. Chyi and H.
Morkoc, University of Illinois at Urbana-
Champaign, Coordinated Science Laboratory,
Urbana, IL.

SESSION C3: SURFACE STUDIES UNDER
GROWTH CONDITIONS

Chair: R. Tromp
Monday Afternoon, November 27
Salon A/B (M)

1:30 *C3.1
LOW ENERGY ELECTRON MICROSCOPY OF ATOMIC
SCALE STRUCTURES OF SURFACES, E. Bauer, M.
Altman, M. Mundschauf and W. Swiech, Tech-
nische Universität Clausthal, Physikalisches
Institut, Göttingen-Clausthal, West Germany.

2:00 C3.2
THE INITIAL STAGES OF GROWTH OF SI ON
SI(111) BY SPA-LEED, M. Horn von Hoegen,
IBM T.J. Watson Research Center, Yorktown
Heights, NY; M. Henzler, Universität Han-
nover, Institut fuer Festkoerperphysik,
Hannover, Germany.

2:15 C3.3
AUTOEPITAXY ON Au(111) STUDIED BY SCANNING
TUNNELING MICROSCOPY, M.M. Dovek, C.A. Lang,
J. Nogami and C.F. Quate, Stanford Univer-
sity, Department of Applied Physics, Stan-
ford, CA.

2:30 C3.4
STM OF GOLD ON GRAPHITE, P.A. Thomas, IBM
Corporation, East Fishkill, NY; W.H. Lee
and R.I. Masel, University of Illinois,
School of Chemical Sciences, Chemical En-
gineering Department, Urbana, IL.

2:45 C3.5
PHOTOEMISSION CHARACTERIZATION OF THIN FILM
NUCLEATION ON INERT SUBSTRATES, G. Haugstad,
A. Raisanen, C. Caprile, X. Yu, G. Ceccone
and A. Franciosi, University of Minnesota,
Department of Chemical Engineering and
Materials Science, Minneapolis, MN.

3:00 BREAK

SESSION C4: HETEROINTERFACE STRUCTURE

Chair: R. Bringans
Monday Afternoon, November 27
Salon A/B (M)

3:30 *C4.1

MEASUREMENT OF THE RELATIVE POSITION OF ADJACENT CRYSTALS, AND THE MODELLING OF INTERFACIAL STRUCTURE, R.C. Pond, University of Liverpool, Department of Materials Science and Engineering, Liverpool, United Kingdom.

4:00 C4.2

INTERFACE STRAIN AND THE VALENCE BAND OFFSET AT THE LATTICE MATCHED $\text{In}_{0.53}\text{Ga}_{0.47}\text{As}/\text{InP}$ INTERFACE, Mark S. Hybertsen, AT&T Bell Laboratories, Murray Hill, NJ.

4:15 C4.3

STRUCTURAL STUDIES OF EPITAXIAL METAL SEMICONDUCTOR INTERFACES USING TRANSMISSION ELECTRON SCATTERING, D. Loretto, J.M. Gibson and N. Chand, AT&T Bell Laboratories, Murray Hill, NJ; and S.M. Yalisove, University of Michigan, Department of Materials Science and Engineering, Ann Arbor, MI.

4:30 C4.4

HIGH-RESOLUTION IMAGING OF THE INTERFACES BETWEEN GaAs AND CoGa AND ErAs, Jane G. Zhu and Stuart McKernan, Cornell University, Department of Materials Science and Engineering, Ithaca, NY; Chris J. Palmstrøm, Bellcore, Red Bank, NJ; and C. Barry Carter, Cornell University, Department of Materials Science and Engineering, Ithaca, NY.

4:45 C4.5

PLAN-VIEW CBED STUDIES OF $\text{NiO-ZrO}_2(\text{CaO})$ INTERFACES, Vinayak P. Dravid, Michael R. Notis and Charles E. Lyman, Lehigh University, Department of Materials Science and Engineering, Bethlehem, PA; A. Revcolevschi, Université de Paris-Sud, Lab. de Chimie des Solides, Orsay, France.

SESSION C5: ENCAPSULATED SURFACES

Chair: J. M. Gibson
Tuesday Morning, November 28
Salon A/B (M)

8:30 *C5.1

INTERFACIAL SUPERSTRUCTURES STUDIED BY GRAZING INCIDENCE X-RAY DIFFRACTION, Koichi Akimoto, Jun'ichiro Mizuki, Ichiro Hirose and Junji Matsui, NEC Corporation, Fundamental Research Laboratories, Ibaraki, Japan.

9:00 C5.2

DIRECT OBSERVATION OF A 7×7 SUPERSTRUCTURE BURIED AT THE AMORPHOUS-Si/Si (111) INTERFACE, Akira Sakai, Toru Tatsumi and Koichi Ishida, NEC Corporation, Fundamental Research Laboratories, Ibaragi, Japan.

9:15 C5.3

TOPOGRAPHY OF Si(111): CLEAN SURFACE PREPARATION AND SILICON MOLECULAR BEAM EPITAXY, R.T. Tung, D.J. Eaglesham and F. Schrey, AT&T Bell Laboratories, Murray Hill, NJ.

9:30 C5.4

STRUCTURE AND COMPOSITION OF LIQUID/SOLID INTERFACES BY ION CHANNELING, M.M. Karmarkar, Ray Twisten and K.R. Padmanabhan, Wayne State University, Department of Physics and Astronomy, Detroit, MI.

9:45 C5.5

ELECTRONIC AND ATOMIC PROPERTIES OF THE a-C:H/Ge INTERFACE, M. Wittmer, IBM, T.J. Watson Research Center, Yorktown Heights, NY; D. Ugolini and P. Oelhafen, University of Basel, Institute of Physics, Basel, Switzerland.

10:00 BREAK

SESSION C6: SCANNING TUNNELING MICROSCOPY

Chair: R. Feenstra
Tuesday Morning, November 28
Salon A/B (M)

10:30 *C6.1

SEMICONDUCTOR INTERFACE ELECTRONIC STRUCTURE INVESTIGATION BY BALLISTIC-ELECTRON-EMISSION MICROSCOPY, L.D. Bell, M.H. Hecht, F.J. Grunthaner and William J. Kaiser, California Institute of Technology, Jet Propulsion Laboratory, Pasadena, CA.

11:00 *C6.2

T.E.M. IMAGING OF AN OPERATING S.T.M. STRAIN EFFECTS OF S.T.M., J.C.H. Spence, Arizona State University, Department of Physics, Tempe, AZ.

11:30 C6.3

SLIDING PLANES MODEL FOR STM IMAGING, John D. Todd and John B. Pethica, University of Oxford, Department of Metallurgy and Science of Materials, Oxford, United Kingdom.

11:45 C6.4

THE FORMATION OF $\text{Si}(111)1 \times 1\text{-Cl}$, John J. Boland and J.S. Villarrubia, IBM, T.J. Watson Research Center, Yorktown Heights, NY.

SESSION C7: PROBES OF CHEMISORBED LAYERS

Chair: W. Kaiser
Tuesday Afternoon, November 28
Salon A/B (M)

1:30 *C7.1

ATOMICALLY-RESOLVED SURFACE PHOTOVOLTAGE MEASUREMENTS BY OPTICALLY-EXCITED SCANNING TUNNELING MICROSCOPY, R.J. Hamers and K.M. Markert, IBM, T.J. Watson Research Center, Yorktown Heights, NY.

2:00 C7.2
PHOTOREFLECTANCE STUDIES OF ADSORPTION-INDUCED CHANGES IN SURFACE STATES ON GaAs(100), S. Sheu, K. Schultz and E.G. Seebauer, University of Illinois, Urbana, IL, Dept. of Chemical Engineering, Urbana, IL.

2:15 C7.3
THE FIRST MONOLAYERS OF Sb ON III-V-SEMICONDUCTORS STUDIED BY LIGHT SCATTERING, Michael Hünermann and Jean Geurts, RWTH Aachen, Aachen, West Germany; Wolfgang Richter, Institut für Festkörperphysik, Berlin, West Germany.

2:30 C7.4
STRUCTURAL AND ELECTRONIC CHARACTERIZATION OF METAL-ON-METAL INTERFACES, G. Vidali, P. Dowben and C.W. Hutchings, Syracuse University, Physics Department, Syracuse, NY.

2:45 C7.5
KINETICS OF BISMUTH OVERLAYER FORMATION ON GaAs(110) STUDIED USING LOW ENERGY ELECTRON DIFFRACTION AND TIME DEPENDENT MONTE CARLO SIMULATION, S.L. Chang, T. Guo, W.K. Ford, A. Bowler and E.S. Hood, Montana State University, Advanced Materials Center, Department of Physics and the Department of Chemistry, Bozeman, MT.

3:00 C7.6
IDEALLY HYDROGEN TERMINATED Si(111) SURFACES PREPARED USING HF ACID SOLUTIONS: PRODUCTION OF PERFECT CRYSTAL TERRACES?, G.S. Higashi, Y.J. Chabal, G.W. Trucks and Krishnan Raghavachari, AT&T Bell Laboratories, Murray Hill, NJ.

3:15 BREAK

SESSION C8: MOLECULAR DYNAMICS

Chair: J. Northrup
Tuesday Afternoon, November 28
Salon A/B (M)

3:30 *C8.1
MOLECULAR DYNAMICS STUDIES OF INTERFACE FORMATION DURING THIN FILM GROWTH, George H. Gilmer and Marcia H. Grabow, AT&T Bell Laboratories, Murray Hill, NJ; Aloysius F. Bakker, Delft Technical University, Applied Physics Department, Delft, The Netherlands.

4:00 C8.2
A MOLECULAR DYNAMICS STUDY OF WATER-Pt INTERFACE, K. Foster, K. Raghavan and M. Berkowitz, University of North Carolina, Department of Chemistry, Chapel Hill, NC.

4:15 C8.3
NON-EQUILIBRIUM MOLECULAR DYNAMICS SIMULATION OF THE RAPID SOLIDIFICATION OF METALS, Cliff F. Richardson and Paulette Clancy, School of Chemical Engineering, Cornell University, Ithaca, NY.

4:30 C8.4
PROPAGATION AND STABILITY OF MONATOMIC STEPS ON THE Si(001) SURFACE DURING MOLECULAR-BEAM EPITAXY, S. Clarke, M.R. Wilby and D.D. Vvedensky, Imperial College, The Blackett Laboratory and Semiconductor Materials IRC, London, United Kingdom.

4:45 C8.5
A NEW DEFECT ON THE RECONSTRUCTED Si(100) SURFACE; AN AB INITIO MOLECULAR-DYNAMICS STUDY, Sigeo Ihara and Shi Lun Ho, Hitachi Ltd., Central Research Laboratory, Tokyo, Japan; Tsuyoshi Uda and Masahiko Hirao, Hitachi Ltd, Advanced Research Laboratory, Tokyo, Japan.

SESSION C9: POSTER SESSION ATOMIC SCALE STRUCTURE OF INTERFACES

Chair: R. Bringans
Tuesday Evening, November 28
7:00 p.m. - 10:00 p.m.
America Ballroom (W)

C9.1 ELECTRONIC AND ATOMIC STRUCTURES OF SILICIDE/Si CONTACT SYSTEMS STUDIED BY SXS, H. Watabe, Matsuhita Electric Industrial Co., Ltd., Osaka, Japan; M. Iwami, M. Hirai and M. Kusaka, Okayama University, Faculty of Science, Research Laboratory for Surface Science, Okayama, Japan; H. Nakamura, Osaka Electro-Communication University, Osaka, Japan.

C9.2 COMPACT AND HIGH-RESOLUTION ION BACKSCATTERING ANALYSIS SYSTEM, CHIRIBAS, Y. Kido, I. Konomi, A. Kawano and J. Kawamoto, Toyota Central R&D Laboratories, Inc., Aichi-ken, Japan.

C9.3 TEMPERATURE DEPENDENT CURRENT-VOLTAGE CHARACTERISTICS IN THIN SiO₂ FILMS, Jin Zhao, New Jersey Institute of Technology, Microelectronics Center, Electrical Engineering Department, Newark, NJ; N.M. Ravindra, New Jersey Institute of Technology, Microelectronics Center, Physics Department, Newark, NJ.

C9.4 SPECTROSCOPIC ELLIPSOMETRY AS A NON-DESTRUCTIVE TECHNIQUE FOR CHARACTERIZATION OF ATOMIC-SCALE INTERFACES IN MULTI-LAYER STACKS, J.L. Stehle, J.H. Lecat, J.P. Piel, SOPRA, Bois-Colombes, France; L.C. Hammond, ARIES/QEI, Concord, MA.

C9.5 ADSORPTION AND TRIBOCHEMICAL REACTIONS, W.M. Mullins, Purdue University, School of Materials Engineering, West Lafayette, IN; T.E. Fischer, Stevens Institute of Technology, Department of Materials Science and Engineering, Hoboken, NJ.

C9.6 DIRECT REAL SPACE IDENTIFICATION OF THE PRODUCTS OF A SURFACE CHEMICAL REACTION USING SCANNING TUNNELING MICROSCOPY, John J. Boland and J.S. Villarrubia, IBM, T.J. Watson Research Center, Yorktown Heights, NY.

C9.7 DISCRIMINATION OF ATOMS ON THE SURFACE OF A TWO DIMENSIONAL SOLID SOLUTION WITH SCANNING TUNNELING MICROSCOPY, B.A. Parkinson, E. I. duPont de Nemours & Co., Inc., Central Research and Development Department, Wilmington, DE.

C9.8 A RAMAN SCATTERING STUDY OF INTER-FACE ROUGHNESS IN SMALL PERIOD GaAs/AlAs SUPERLATTICES, Daniel Gammon, B.V. Shanabrook and W. Tseng, Naval Research Laboratory, Washington DC.

C9.9 BISMUTH/InSb(110) INTERFACE STUDIED USING LOW-ENERGY ELECTRON DIFFRACTION, T. Guo and W.K. Ford, Montana State University, Advanced Materials Center and the Department of Physics, Bozeman, MT.

C9.10 UNDERSTANDING THE INFLUENCE OF INTERFACE PROPERTIES AND DEPOSITION PARAMETERS ON THE SELECTIVE GROWTH OF (100) AND (110) CoGa FILMS ON (100)GaAs, Young K. Kim, Delroy A. Baugh and R. Stanley Williams, University of California, Department of Chemistry and Biochemistry, Los Angeles, CA.

C9.11 OBSERVATION OF HETEROEPITAXIALLY GROWN ORGANIC ULTRATHIN LAYERS ON INORGANIC SUBSTATES BY IN-SITU RHEED AND UHV STM, Masahiko Hara, Hiroyuki Sasabe, Akira Yamada and Anthony F. Garito, The Institute of Physical and Chemical Research, Riken Institute, Frontier Research Program, Saitama, Japan.

C9.12 A NOVEL COMPUTATIONAL METHOD FOR EPITAXIAL ENERGY ON AN INCOMMENSURATE AND/OR COMMENSURATE INTERFACE, Sun M. Paik and Ivan K. Schuller, University of California, San Diego, Physical Department, La Jolla, CA.

C9.13 FULL POTENTIAL, LMTO CALCULATION OF TiC FRACTURE, D.L. Price and B.R. Cooper, West Virginia University, Department of Physics, Morgantown, WV.

C9.14 COMPARISON OF SURFACE ATOMIC GEOMETRIES OF TETRAHEDRALLY COORDINATED COMPOUND SEMICONDUCTORS WITH THOSE OF RUTILE STRUCTURE OXIDES, Charles B. Duke and Michael R. Thompson, Pacific Northwest Laboratory, Richland, WA.

C9.15 A CYCLIC-CLUSTER MINDO/3 COMPUTATION OF THE RELAXED EQUILIBRIUM STRUCTURE AND VIBRATIONS OF THE HYDROGENATED SILICON (111) SURFACE, Peter Deak, Physical Institute of the Technical University of Budapest Hungary, Budapest, Hungary; Lawrence C. Snyder, State University of New York at Albany, Chemistry Department, Albany, NY; Carlos O. Rodrigues, State University of New York at Albany, Physics Department, Albany, NY.

C9.16 STRUCTURAL AND ELECTRONIC PROPERTIES OF SEMICONDUCTOR-METAL AND SEMICONDUCTOR-INSULATOR INTERFACES AT MONOLAYER COVERAGE, Stefano Ossicini, C. Arcangeli and O. Bisi, Università di Modena, Dipartimento di Fisica, Modena, Italy.

C9.17 CALCULATIONS FOR MERCURY ADSORPTION ON COPPER, M. Karimi, Utica College, Physics Department, Utica, NY; G. Vidali, Syracuse University, Physics Department, Syracuse, NY.

C9.18 DOUBLE CRYSTAL X-RAY DIFFRACTION MEASUREMENT OF A TRICLINICALLY DISTORTED AND TILTED $\text{Al}_x\text{Ga}_{1-x}\text{As}$ UNIT CELL PRODUCED BY GROWTH ON OFFCUT GaAs SUBSTRATES, A. Leiberich and J. Levkoff, AT&T Bell Laboratories, Engineering Research Center, Princeton, NJ.

C9.19 A MECHANISM FOR SOLUTE SEGREGATION TO GRAIN BOUNDARIES, Chu Youyi and Zhang Sanhong, The Nonferrous Metals Society of China, Beijing, China.

C9.20 PHASE DIAGRAMS AND PHASE TRANSFORMATIONS FOR GRAIN BOUNDARIES IN HEXAGONAL CLOSE PACKED METALS, Kisoo Shin and A.H. King, State University of New York at Stony Brook, Department of Materials Science and Engineering, Stony Brook, NY.

C9.21 STRUCTURE OF PURE TILT AND TWIST BOUNDARIES GENERALIZATION AND COMMENTS ON THE STRUCTURAL UNIT MODEL, M. Khantha and V. Vitek, University of Pennsylvania, Department of Materials Science and Engineering, Philadelphia, PA.

C9.22 HIGH-RESOLUTION ELECTRON MICROSCOPY OF OLIVINE-MAGNETITE INTERFACES, Stuart McKernan and C. Barry Carter, Cornell University, Department of Materials Science and Engineering, Ithaca, NY; Daniel Ricoult, Corning-Europe, Avon, France; A.G. Cullis, Royal Signals and Radar Establishment, Worcs, United Kingdom.

C9.23 ATOMIC SCALE STRUCTURE OF TWIN BOUNDARY IN Y-Ba-Cu-O SUPERCONDUCTOR, Y. Zhu, M. Suenaga and Youwen Xu, Brookhaven National Laboratory, Upton, NY; M. Kawasaki, Jeol USA, Inc., Peabody, MA.

C9.24 STRUCTURAL STUDIES OF A TYPICAL LAYERED SEMICONDUCTOR (S_4In_2Zn) USING HIGH RESOLUTION ELECTRON MICROSCOPY AND CONVERGENT BEAM ELECTRON DIFFRACTION, Dwight R. Acosta, Universidad Nacional Autónoma de México, Instituto de Física, México, México; Mauro Briceño, Universidad de Los Andes, Facultad de Ciencias, Mérida, Venezuela.

C9.25 EFFECT OF B, C, P AND S ON INTERGRANULAR COHESION IN IRON, Genrich L. Krasko, U.S. Army Materials Tech. Lab, Metals Research Branch, Watertown, MA; G.B. Olson, Northwestern University, Department of Materials Science and Engineering, Evanston, IL.

C9.26 MODELING OF NANOPHASE CONNECTIVITY IN SUBSTANCE-VOID COMPOSITE BY OBLIQUE DEPOSITION, Tomoyoshi Motohiro, S. Noda, A. Isogai and O. Kamigaito, Toyota Central Research and Development Laboratories, Inc., Research Division IV, Materials Science Lab, Aichi-ken, Japan.

C9.27 DEFECT EVOLUTION IN Al/Cu AND Al/Ni BILAYERS DURING ANNEALING, Bent Nielsen, S.M. Heald, K.G. Lynn, E. Barrera and J. Jayanetti, Brookhaven National Laboratory, Upton, NY; W. Triftshäuser, Universität der Bundeswehr, Neubiberg, West Germany.

C9.28 NANOLAYER REACTIONS IN ALUMINUM-METAL INTERFACES, E.V. Barrera, M.W. Ruckman and S.M. Heald, Brookhaven National Laboratory, Upton, NY.

C9.29 INTERFACIAL STRUCTURE OF Er_2O_3 PRECIPITATES IN TITANIUM AND Ti-37Al, Daniel S. Schwartz and Shankar M.L. Sastry, McDonnell Douglas Research Laboratories, St. Louis, MO; P. Fraundorf, University of Missouri-St. Louis, Physics Department, St. Louis, MO.

C9.30 HIGH-RESOLUTION ELECTRON MICROSCOPY OF INTERFACES IN AlN-BRAZE METAL ALLOY SYSTEMS, A.H. Carim, University of New Mexico, Center for Micro-Engineered Ceramics and Department of Chemical and Nuclear Engineering, Albuquerque, NM.

C9.31 ATOMIC STRUCTURE OF CRYSTALLINE BORON NITRIDE INTERFACES WITH CERAMIC SUBSTRATES, L.F. Allard, Oak Ridge National Laboratory, High Temperature Materials Laboratory, Oak Ridge, TN; A.K. Datye and R.T. Paine, University of New Mexico, Center for Micro-Engineered Ceramics, Albuquerque, NM.

C9.32 SIMULATION AND QUANTIFICATION OF HIGH RESOLUTION Z-CONTRAST IMAGING OF SEMICONDUCTOR INTERFACES, David E. Jesson, S.J. Pennycook and M.F. Chisholm, Oak Ridge National Laboratory, Solid State Division, Oak Ridge, TN.

C9.33 SIMULATED IMAGE MAPS FOR USE IN EXPERIMENTAL HIGH-RESOLUTION MICROSCOPY, M.A. O'Keefe and U. Dahmen, University of California at Berkeley, Lawrence Berkeley Laboratory, National Center for Electron Microscopy, Berkeley, CA.

C9.34 LAYER CONTRAST IN InAs/GaAs SUPERLATTICES STUDIED BY TEM, C.J. Kiely, University of Liverpool, Department of Materials Science and Engineering, Liverpool, United Kingdom; K.C. Hsieh, University of Illinois at Urbana-Champaign, Department of Electrical Engineering, Urbana, IL; A. Rockett, University of Illinois at Urbana-Champaign, Department of Materials Science, Urbana, IL.

C9.35 ATOMIC STRUCTURE OF DISLOCATIONS AND INTERFACES IN SEMICONDUCTOR HETEROSTRUCTURES, J. Narayan, North Carolina State University, Department of Materials Science and Engineering, Raleigh, NC.

C9.36 PLATINUM SILICIDES FORMED BY RAPID THERMAL PROCESSING FOR SCHOTTKY BARRIERS, D.I. Zarovski, V.E. Borisenko, Minsk Radioengineering Institute, Minsk, USSR.

C9.37 XPS ANALYSIS OF THE CHEMISTRY OF THE SAPPHIRE SURFACE AS A FUNCTION OF HIGH TEMPERATURE VACUUM ANNEALING, Eliezer David Richmond, Naval Research Laboratory, Washington, DC.

C9.38 INFLUENCE OF PLASTICITY IN ADHESIVE BOND STRENGTH MEASUREMENTS USING SHOCK WAVES, Gerald L. Nutt and William Lai, Lawrence Livermore National Laboratory, Livermore, CA; and Kenneth E. Froschner, Martin, Froschner and Associates, Livermore, CA.

C9.39 ORIGIN OF ATOMIC RESOLUTION IN SCANNING TUNNELING MICROSCOPY, C. Julian Chen, IBM T.J. Watson Research Center, Yorktown Heights, NY.

C9.40 X-RAY REFLECTIVITY STUDIES OF THE Si(001)/ SiO_x INTERFACE, T.A. Rabedeau, I.M. Tidswell, P.S. Pershan, Harvard University, Department of Physics and Division of Applied Sciences, Cambridge, MA; J. Bevk, B.S. Freer, AT&T Bell Laboratories, Murray Hill, NJ; and A. Ourmazd, AT&T Bell Laboratories, Holmdel, NJ.

SESSION C10: SILICIDE INTERFACE
REACTIONS AND STRUCTURE

Chair: R. Pond
Wednesday Morning, November 29
Salon A/B (M)

8:30 *C10.1
INTERFACE STRUCTURES AND THEIR DEFECTS IN
CoSi₂/Si: DISLOCATIONS, DISCLINATIONS AND A
THIN-FILM PHASE TRANSFORMATION, David J.
Eaglesham, R.T. Tung, S.M. Yalisove, R.L.
Headrick and I.K. Robinson, AT&T Bell Labora-
tories, Murray Hill, NJ.

9:00 C10.2
ATOMIC STRUCTURES AT CoSi₂/Si(111) AND
CoSi/Si(111) INTERFACES, A. Catana and P.E.
Schmid, Swiss Federal Institute of Tech-
nology, Department of Applied Physics, Lau-
sanne, Switzerland; P. Stadelmann, Swiss
Federal Institute of Technology, Department
of Electron Microscopy, Lausanne, Switzer-
land.

9:15 C10.3
MICROSTRUCTURAL ASPECTS OF AMORPHOUS NICKEL
SILICIDE FORMATION IN EVAPORATED Ni-Si
MULTILAYERS, Karen Holloway, IBM, T.J.
Watson Research Ctr., Yorktown Heights, NY.

9:30 C10.4
NUMERICAL AUGER LINESHAPE ANALYSIS OF PHASE
FORMATION IN NI/SI(111), J.R. Butler, X.
Tong and P.A. Bennett, Arizona State Univer-
sity, Department of Physics, Tempe, AZ.

9:45 C10.5
X-RAY ABSORPTION STUDIES OF TITANIUM SILI-
CIDE FORMATION AT THE INTERFACE OF Ti DEPOS-
ITED ON Si, David Aldrich, Q. Islam, H.
Jeon, R. Nemanich and D.E. Sayers, North
Carolina State University, Department of
Physics, Raleigh, NC.

10:00 C10.6
SILICIDE FORMATION AND THERMAL STABILITY OF
Ni/Si/GaAs INTERFACES, Y. Yamamoto, K.
Ishibashi, Hosei University, Research Center
of Ion Beam Technology, Tokyo, Japan; S.
Suzuki, Advanced Materials Laboratory, Inc.,
Saitama, Japan; T.E. Shim, Samsung
Electronics, R&D Center, Semiconductor
Business, Seoul, Korea; and Waseda Univer-
sity, Tokyo, Japan.

10:15 BREAK

SESSION C11: ROUGHNESS AND INTERDIFFUSION

Chair: R. Hull
Wednesday Morning, November 29
Salon A/B (M)

10:30 C11.1
FRACTIONAL ATOMIC PLANES IN GaAs/Al As
SUPERLATTICES AND THEIR RELATIONSHIP TO
INTERFACIAL ROUGHNESS, Ivan K. Schuller,
University of California, San Diego, Physics
Department, La Jolla, CA; M. Grimsditch,
Argonne National Laboratory, Material Sci-
ence Division, Argonne, IL; F. Chambers and
G. Devane, Amoco Technology Company, Amoco
Research Center, Naperville, IL; H.
Vanderstraeten, D. Neerincx, J.-P. Locquet
and Y. Bruynseraede, Katholieke Universiteit
Leuven, Physics Department, Leuven, Belgium.

10:45 C11.2
STUDY OF INTERFACIAL SHARPNESS AND GROWTH IN
(AlAs)_m/(GaAs)_n SUPERLATTICES, W. Tseng, S.
Prokes, M. Fatemi, B.V. Shanabrook, B.
Wilkins and H. Dietrich, Naval Research
Laboratory, Washington, DC.

11:00 C11.3
A WEAK BEAM IMAGING TECHNIQUE FOR THE CHAR-
ACTERIZATION OF INTERFACIAL ROUGHNESS IN
(InGa)As/GaAs STRAINED LAYER STRUCTURES,
J.Y. Yao, T.G. Andersson and G.L. Dunlop,
Chalmers University of Technology, Depart-
ment of Physics, Göteborg, Sweden.

11:15 C11.4
THE OBSERVATION OF SURFACE ROUGHENING ON
ALUMINUM USING OPTICAL SECOND-HARMONIC
GENERATION, S. Janz, K. Pedersen and H. van
Driel, University of Toronto, Physics De-
partment, Toronto, Canada; R. Timsit, Alcan
Research and Development Centre, Kingston,
Canada.

11:30 C11.5
INTERFACIAL STABILITY AND INTERDIFFUSION IN
SEMICONDUCTOR SYSTEMS, Y. Kim and A.
Ourmazd, AT&T Bell Laboratories, Holmdel,
NJ.

11:45 C11.6
ATOMIC STRUCTURE AND CHEMISTRY OF INTERFACES
DETERMINED BY Z-CONTRAST STEM, M.F.
Chisholm, S.J. Pennycook and D.E. Jesson,
Oak Ridge National Laboratory, Solid State
Division, Oak Ridge, TN.

SESSION C12: OXIDE INTERFACES

Chair: R. Feenstra
Wednesday Afternoon, November 29
Salon A/B (M)

1:30 C12.1

THE USE OF FRESNEL CONTRAST TO STUDY THE INITIAL STAGES OF THE IN-SITU OXIDATION OF SILICON, F.M. Ross and W.M. Stobbs, Cambridge University, Department of Materials Science and Metallurgy, Cambridge, United Kingdom; J. Gibson, AT&T Bell Laboratories, Murray Hill, NJ.

1:45 C12.2

THE INITIAL STAGES OF FORMATION FOR THE Si/SiO₂ INTERFACE ON Si(111) 7X7, J.M. Gibson, AT&T Bell Laboratories, Murray Hill, NJ.

2:00 C12.3

ELECTRON SPIN RESONANCE STUDIES OF SILICON DIOXIDE FILMS ON SILICON IN INTEGRATED CIRCUITS USING SPIN DEPENDENT RECOMBINATION, Mark A. Jupina and Patrick M. Lenahan, Pennsylvania State University, University Park, PA.

2:15 C12.4

AN NMR STUDY OF HYDROGEN AT THE Si/SiO₂ INTERFACE OF THERMALLY GROWN OXIDES, David H. Levy and Karen K. Gleason, Massachusetts Institute of Technology, Department of Chemical Engineering, Cambridge, MA.

2:30 C12.5

ELECTRONIC STRUCTURE OF EPITAXIAL SiO₂/Si(100) INTERFACES, T. Motooka, University of Tsukuba, Institute of Applied Physics, Ibaraki, Japan.

2:45 C12.6

THE STRUCTURE OF INTERFACES IN OXIDE HETEROJUNCTIONS FORMED BY CVD, L.A. Tietz, S.R. Summerfelt and C.B. Carter, Cornell University, Department of Materials Science and Engineering, Ithaca, NY.

3:00 BREAK

SESSION C13: GRAIN BOUNDARIES AND NANOPHASE MATERIALS

Chair: C. B. Carter
Wednesday Afternoon, November 29
Salon A/B (M)

3:30 C13.1

THE STRUCTURE OF GRAIN BOUNDARIES IN ALUMINUM, M.J. Mills, Sandia National Laboratories, Materials Department, Livermore, CA; G.J. Thomas, Sandia National Laboratories, Theoretical Division, Livermore, CA; F. Cosandey, Rutgers University, Department of Mechanical and Material Science, Piscataway, NJ.

3:45 C13.2

ON THE ATOMIC STRUCTURE OF GRAIN BOUNDARIES IN SMALL METALLIC AND BIMETALLIC PARTICLES, Miguel Avalos, Roberto Hernández, Pablo Schabes, Armando Vázquez and Miguel José Yacamán, UNAM, Instituto de Física, Mexico, Mexico.

4:00 C13.3

STRUCTURE AND PROPERTIES OF THE (110) INVERSION DOMAIN BOUNDARY IN β -SiC, W.R.L. Lambrecht and B. Segall, Case Western Reserve University, Department of Physics, Cleveland, OH.

4:15 C13.4

MECHANICAL RESPONSE OF MATERIALS WITH INTERFACES, I. Alber, J.L. Bassani and J. Qu, University of Pennsylvania, Department of Mechanical Engineering and Applied Mechanics, Philadelphia, PA; V. Vitek and G.-J. Wang, University of Pennsylvania, Department of Materials Science and Engineering, Philadelphia, PA.

4:30 C13.5

ATOMISTIC SIMULATION STUDIES OF INTERFACES IN NANOPHASE COPPER AND SILICON, James A. Lupo and Michael J. Sabochick, Air Force Institute of Technology, Department of Engineering Physics, Wright Patterson AFB, OH.

4:45 C13.6

THE APPLICATION OF GLANCING ANGLE EXAFS TO STUDY THE STRUCTURE OF PLATINUM-NICKEL MULTILAYERS, G.M. Lamble and S.M. Heald, Brookhaven National Laboratory, Material Science Department, Upton, NY; B.M. Clemens, University of Stanford, Material Science and Engineering Department, Stanford, CA.

5:00 C13.7

THE ELECTRONIC STRUCTURE OF $\Sigma 5$ GRAIN BOUNDARIES IN CU, Erik C. Sowa and A. Gonis, Lawrence Livermore National Laboratory, Livermore, CA; X-G. Zhang, Northwestern University, Chicago, IL; and S.M. Foiles, Sandia National Laboratories Livermore, Livermore, CA.

C1.1

ONSET OF GaAs HOMOEPITAXY AND HETEROEPITAXY.**D. K. Biegelsen**

Xerox Palo Alto Research Ctr, Palo Alto, CA, 94304

Scanning tunneling microscopy results are presented for thin GaAs films grown by *in situ* molecular beam epitaxy on GaAs(100) and Si(100) substrates. Atomic arrangements are directly observed for the various surface reconstructions occurring as a function of surface stoichiometry. The homoepitaxial results are compared and contrasted with related images of As and GaAs deposited on on-axis and vicinal Si. In the earliest stages of heteroepitaxial growth a two dimensional film grows which is topographically uniform but chemically disordered. At coverages above approximately six monolayers a transition occurs to a three dimensional regime. We will try to delineate equilibrium and kinetic origins of the observed phenomena.

C1.2

HIGH RESOLUTION ION SCATTERING STUDIES OF THIN EPITAXIAL FILMS. **Ruud M. Tromp**, IBM Research Division, T.J. Watson Research Center Yorktown Heights, NY.

Medium Energy Ion Scattering (MEIS), in combination with channeling and blocking is eminently suited for the study of thin epitaxial films, with a depth resolution of 3-5 Å. In this talk I will present results obtained on the Si(111)-CaF₂ interface, grown *in situ* and analyzed with MEIS and photoemission techniques. We have determined the structure of this interface uniquely, and confirmed that the interface structure for much thicker is the same, using high resolution electron microscopy. Secondly, I will discuss the role of a surface active species ('surfactant') on the epitaxial growth process. In particular, I will address the dramatic changes in growth mode in the Si(001)/Ge/Si system, resulting from the presence of a segregating As monolayer during growth. Stranski-Krastanov and Volmer-Weber growth modes are changed to layer-by-layer growth under the influence of the As monolayer. These phenomena are interpreted using total energies calculated using self-consistent pseudopotential calculations in the local density approximation.

* Work performed in collaboration with M. Copel, M. Reuter, E. Kaziras and F.K. LeGoues.

C1.3

ATOMIC STRUCTURE OF CaSi₂/Si INTERFACES.**Chris G. Van de Walle**, Philips Laboratories, Briarcliff Manor, NY 10510.

When grown epitaxially on Si(111), metallic CaSi₂ assumes the trigonal-rhombohedral phase ($a=3.855$ Å, $c=30.6$ Å),¹ which is closely lattice-matched to Si (3.855 Å $\times \sqrt{2} = 5.45$ Å). The absence of *d* electrons makes CaSi₂ qualitatively different from the traditional transition-metal silicides. The atomic structure of the CaSi₂/Si interface is studied here with state-of-the-art theoretical techniques, based on pseudopotential-density-functional theory in a superlattice geometry. Various models for the interfacial structure are examined, in which the Ca atoms at the interface exhibit 5-, 6-, 7-, or 8-fold coordination. The configuration in which Ca has 7-fold coordination (as in bulk CaSi₂) has the lowest energy; the Si double layer at the interface can be considered to be a continuation of the CaSi₂ structure, but with a Si-Si distance very close to its value in bulk Si. This structure is consistent with results obtained from cross-sectional electron micrographs.¹ However, the structure in which interfacial Ca is 8-fold

coordinated is only ~0.1 eV higher in energy. The present results will be compared with the known structures of other silicides on Si. Values for Schottky barrier heights, calculated within the local-density approximation, will also be reported.

C1.4

THE STRUCTURE AND CHEMISTRY OF THE Ge/SAPPHIRE INTERFACE, **Geoffrey P. Malafsky**, ONT Postdoctoral Fellow; and **David J. Godbey**, Naval Research Laboratory, Code 6816, Wash, DC 20375

The molecular beam epitaxial (MBE) growth of silicon on sapphire (SOS) provides growth control on an atomic scale. This permits the study of the initial stages of heteroepitaxy. The growth of a crystalline epilayer is associated with a three dimensional growth mechanism and a large density of interfacial defects. Recently, it was shown that MBE grown germanium on sapphire (GOS) can produce a crystalline epilayer via an islanding growth mechanism. We examine the interfacial reactions of the new GOS system. We present an *in-situ* analysis of the chemical and structural bonding in the first few monolayers of the Ge epilayer. The interfacial chemistry is determined by X-ray photoelectron spectroscopy (XPS) and Auger electron spectroscopy (AES). The growth mechanism is revealed by the rate of attenuation of the sapphire peak signals.

C2.1

Energetics and Electronic Structure of GaAs on Si.**John E. Northrup**, Xerox Palo Alto Research Ctr, Palo Alto, CA, 94304

Total energy calculations have been performed using the density functional pseudopotential method for various possible two-dimensional phases of GaAs on Si(111) and Si(100). The two-dimensional phases which have been examined so far have positive formation energies with respect to bulk GaAs reservoirs (large GaAs islands) plus the As-terminated Si(111) or Si(100) surfaces. On the basis of these results one can estimate a critical number of GaAs pairs required to form stable GaAs islands on the As-terminated Si surface. The influence of the interface electrostatic dipole on the energetics and electronic structure of the overlayers has been examined.

C2.2

STRUCTURAL ENERGIES OF ANTIPHASE DOMAIN WALLS IN GaAs. **David Vanderbilt** and L. Brey, Department of Physics, Harvard University, Cambridge, MA 02138.

Local-density total-energy calculations of the structural properties of antiphase domain walls (ADW's) are carried out for GaAs, a prototypical III-V semiconductor. The ADW's, which are boundaries at which the assignment of species to sublattice becomes reversed, are problematic especially for growth of GaAs films on Si or Ge (100) substrates. We study a variety of superlattice structures containing ADW's oriented in the (100), (110), and (111) directions. The dependence of the ADW energy upon orientation, stoichiometry, and atomic structure is elucidated. Simple Ising-like models for the energetics of these interfaces are discussed and tested.

VERY THIN 2D GaAs FILMS on Si DURING the EARLY STAGES of GROWTH by MBE.

D.B.Fenner,*⁺ D.K. Biegelsen,* and B.S. Krusor;*

^{*}Xerox Palo Alto Research Center, Palo Alto, CA 94034.

⁺Physics Dept., Santa Clara University, Santa Clara, CA 95053.

GaAs samples deposited on Si by molecular beam epitaxy with a graded thickness of 0–3 nm initially show the presence of a metastable 2D layer containing Ga and As. In the thicker regions of the wedge samples, islands (3D topography) form in the presence of the 2D sea, i.e., Stranski–Krastanov growth. Compositional profiles of these wedges were made with *in situ* Auger electron spectroscopy (AES) which has allowed the identification of at least four regimes of growth; i) As termination of Si, ii) 2D–growth of a bilayer terrace, iii) followed by a second bilayer terrace, and finally iv) the nucleation of island growth. Lattice images from cross-sectional transmission electron microscopy are consistent with the AES profiles. Substrate temperature during deposition of the films has a strong effect on film topography, as does the beam–flux ratio on film stoichiometry.

DBF received support from the NSF (DMR–8822353).

C2.4

μm-SCALE LATERAL GROWTH OF Ga-MONOLAYERS OBSERVED IN-SITU BY ELECTRON MICROSCOPY J.Osaka, N.Inoue, NTT LSI Laboratories, Atsugi City, Japan

Terrace sizes on GaAs and AlGaAs surfaces have been limited to less than a few thousand and less than a few hundred Angstroms, respectively, by the small surface migration length of Ga and Al on surfaces covered with As. In this paper we show that the lateral growth of Ga(+Al) monolayer can be extended as far as several microns by using Ga(+Al) droplets.

Growth was performed in an MBE-SREM (Scanning Reflection Electron Microscope) system[1]. Surface atomic structures are observed in-situ at a resolution of about 1000 Å. When Ga is supplied for 2 layers on a surface covered with As, droplets are observed[2], spaced about 10 μm apart and sized about 1 μm at 600 °C. When As is supplied next, background areas are suddenly covered with As. However, it is found that bright areas appear around the droplets. These are Ga monolayers growing over the As. The gallium monolayers extend continuously until they finally cover the entire surface. It is shown that the size of the droplets, the spacing, and the monolayer extension in the case of AlGaAs are as large as those in GaAs. The very long diffusion length for the μm order is attributable to the fast diffusion of Ga and Al atoms on a Ga(+Al) overlayer on an As layer.

By taking advantage of this phenomenon, it is expected that terraces as large as several microns will be realized.

[1] K.Yamada, N.Inoue, J.Osaka, and K.Wada, Appl.Phys.Lett. 55 August 14 (1989)

[2] J.Osaka, N.Inoue, Y.Mada, K.Yamada, and K.Wada, ICCG-9 abstract No.FV-2, Sendai (1989)

C2.5

THE INITIAL STAGES OF GROWTH OF InSb ON GaAs(100) BY MBE - A HIGHLY LATTICE MISMATCHED HETEROINTERFACE.

C.J.Kiely, Department of Materials Science and Engineering, University of Liverpool; A.Rockett, J-I.Chyi and H.Morkoc, Coordinated Science Laboratory, University of Illinois at Urbana-Champaign.

Good quality epitaxial InSb can be grown on GaAs(100) by MBE despite the 14.6% lattice mismatch. We have previously reported TEM and electrical characterisation studies from thick InSb layers, in which we found quite high dislocation densities ($\sim 10^7 \text{ cm}^{-2}$) which limit electron mobilities [1]. In this present study, the initial stages of epitaxy have been investigated by plan view and cross-sectional microscopy of very thin InSb layers. The results have led us to deduce several key features related to defect formation in highly mismatched epitaxial overlayers.

InSb nucleates as three dimensional islands of well defined shape and grows pseudomorphically until a critical lateral dimension of $\sim 30 \text{ Å}$ is reached. After this, misfit is mainly accommodated by nucleating energetically favoured $a/2[011]$ edge-type dislocations at the periphery of the islands at regular intervals as strain periodically accumulates in the islands. Some 60° defects are noted at the interface however and are associated with dislocations and loops which thread through the epilayer. Evidence will be presented correlating the existence of these threading defects with (1) "misfit dislocation array mismatch" at coalescing islands, (2) interfacial steps, (3) residual strains in the islands at coalescence and (4) the thermal expansion coefficient mismatch between epilayer and substrate. Finally interface roughening effects which are seen to occur in this system during growth will be discussed.

[1] C.J.Kiely, J-I.Chyi, A.Rockett and H.Morkoc, Phil.Mag.A., (1989), in press.

C3.1

LOW ENERGY ELECTRON MICROSCOPY OF ATOMIC SCALE STRUCTURES OF SURFACES. E. Bauer, M. Altman, M. Mundschauf and W. Swiech, Physikalisches Institut, Technische Universität Clausthal, Clausthal-Zellerfeld and SFB 126, Göttingen-Clausthal, FRG.

Although low energy electron microscopy (LEEM) has presently only a lateral resolution of about 15 nm it can image atomic scale structures such as monoatomic steps or glide lines provided that their spacing is larger than 15 nm. The contrast is caused by the phase difference between the waves reflected from the terraces adjoining the step. Also interfaces are accessible to LEEM provided that they are parallel to the surface and not too far away from it. Their contrast is due to the quantum size effect.

The talk will be concerned mainly with the atomic step structure of Si(100), Si(111), Mo(110) and Pb(110) surfaces, its dependence on pre-treatment, its interaction with bulk defects and its significance for nucleation processes in surface phase transitions, segregation and film growth. Particular attention will be given to the modification of the atomic step structures by impurity-induced inhomogeneous sublimation and by interaction with strongly adsorbed atoms such as Au and Cu on Si(111) and Cu on Mo(110).

The interfacial structure will be discussed for the case of CoSi₂ on Si(111). A video tape will illustrate step-related processes.

THE INITIAL STAGES OF GROWTH OF SI ON SI(111) BY SPA-LEED. M. Horn von Hoegen, T. J. Watson Research Center, Yorktown Hgts, NY; M. Henzler, Institut fuer Festkoerperphysik, Universitaet Hannover, Germany.

LEED is used to investigate the initial stages of the growth of silicon on silicon (111) between 556K and 900K. The partial coverages θ_n of the growing film are derived out of the intensity oscillation of the 00- and 7x7-spot during evaporation.

We observe a preferred growth in the second layer long before the first layer is completed. Surface defects caused by superstructure disorder on the grown islands act as nucleation center for the diffusing adatoms. So at 633K the grown islands show no ordered superstructure, although the film is epitaxial. The 7x7-spots display all features of the diffraction of a substrate with a non scattering overlayer for coverages below 2 monolayers.

The grown films show below 650K an unordered superstructure, in an intermediate temperature range a mixture of 5x5- and 7x7-domains and finally above 870K the perfect 7x7- superstructure. The average size of islands increases from 30 up to 40000 atoms.

C3.3

AUTOEPITAXY ON AU(111) STUDIED BY SCANNING TUNNELING MICROSCOPY. M. M. Dovek, C. A. Lang, J. Nogami, and C. F. Quate, Department of Applied Physics, Stanford University, Stanford, California 94305

Using a scanning tunneling microscope in ultra-high vacuum, we have studied several stages of autoepitaxy on Au(111) from submonolayer up to twenty monolayer coverage at room temperature. The substrate, Au(111) epitaxially grown on mica, exhibits several hundred Å wide atomically flat terraces separated by monoatomic steps.

At submonolayer coverages, the gold nucleates into single layer clusters as small as 25 Å aligned preferentially in rows perpendicular to the <110> terrace edges. These clusters coalesce as the metal coverage increases. Higher layers start forming before the lower ones are completely filled. The number of incomplete layers increases with deposition rate and total thickness of the film. Room temperature diffusion smoothens the terrace structure over a period of several hours. The acceleration of this process by a moderate anneal is also observed.

Preliminary results on epitaxy of In and Ag on Au(111) will also be reported.

C3.4

STM OF GOLD ON GRAPHITE by P. A. Thomas, W. H. Lee, R. I. Masel, University of Illinois, Urbana II, 61801

Scanning Tunneling Microscopy was used to examine how evaporated gold films change when they are annealed at 600 C on graphite substrates. The evaporated films started out relatively smooth. However, after 1 hr of annealing, a series of dendrites were clearly visible on the surface of the films. With additional annealing, the dendrites got larger, until the film broke into particles. Particles then grew by a sintering process. After a long anneal, the surfaces of the larger particles became smooth again. However, the surfaces of the particles smaller than 50 Å remained rough. We believe that the difference in morphology of large and small particles may have some profound implications for shape selective catalysis.

C3.5

PHOTOEMISSION CHARACTERIZATION OF THIN FILM NUCLEATION ON INERT SUBSTRATES. G. Haugstad, A. Raisanen, C. Caprile, X. Yu, G. Ceccone and A. Franciosi, Dept. of Chemical Engineering and Materials Science, University of Minnesota, Minneapolis, MN 55455.

We have performed synchrotron radiation photoemission studies of the early stages of K, Mn, and Sm thin film growth on solid xenon substrates. In the coverage range explored (2×10^{13} - 1×10^{16} atoms/cm²), film growth is well approximated by a model in which the nucleation site density remains constant, and hemi-ellipsoidal clusters increase in size until coalescence is achieved. Site density and average cluster size were determined by comparing the experimental coverage-dependence of the metal and Xe core photoemission intensities with the predictions of the numerical model. The coverage-dependence of the effective core-level binding energies provide additional quantitative information on cluster size. We present a valence band photoemission analysis of the metal electronic structure as a function of cluster size and morphology in the 10^3 - 10^4 atom cluster size range. Furthermore, a deconvolution of the "screened" and "unscreened" contributions to the Xe core emission allowed us to probe directly the magnitude and the spatial extent of the metal-induced screening of the Xe core hole as a function of cluster size.

C4.1

MEASUREMENT OF THE RELATIVE POSITION OF ADJACENT CRYSTALS, AND THE MODELLING OF INTERFACIAL STRUCTURE. R.C. Pond, Department of Materials Science and Engineering, University of Liverpool, P.O. Box 147, Liverpool L69 3BX, England, U.K.

The relative position of adjacent crystals can be measured with high precision using transmission electron microscopy. The technique can be used in the case of grain boundaries where the relative orientation of the two crystals corresponds to a coincidence site lattice. Under these circumstances, sets of crystal planes which have the same spacing and orientation in the two crystals can be oriented simultaneously for two beam or systematic diffraction. The extinction distances for Bloch waves excited in the two crystals will be identical, but interference will occur if their phases are different. When the relative position of the two crystals is defined by a displacement p of one crystal with respect to the other, the phase difference will be equal to $2\pi g \cdot p$ for the reflection g . Providing the interface is inclined to the specimen surface, so called α -fringes will be observed in the image. By comparing simulated images with experimental observations, and using at least three independent reflections, the vector p can be determined. In favourable specimens, values of $g \cdot p$ as small as 0.02 can be detected. However, the technique is subject to possible ambiguities and imprecisions, particularly when high index reflections are used.

Determination of p enables interfacial structures to be modelled, and the technique has been used successfully to investigate the interfacial structure of grain boundaries in Al, Si and Ge for example. In addition, information concerning the structure of interfacial dislocations, and the excess free volume at interfaces has been obtained by these means.

C4.2

INTERFACE STRAIN AND THE VALENCE BAND OFFSET AT THE LATTICE MATCHED In_{0.53}Ga_{0.47}As/InP INTERFACE. Mark S. Hybertsen, AT&T Bell Laboratories, Murray Hill, NJ, 07974.

High resolution X-ray diffraction experiments on carefully grown In_{0.53}Ga_{0.47}As/InP heterostructures have shown an intrinsic

interface strain [1]. The growth sequence yields atomically abrupt interfaces with two types of interface layer: *PM* (where $M = \text{In}_{0.53}\text{Ga}_{0.47}$) and *AsIn*. In the present work, the interface energy as a function of strain for a 3×3 superlattice has been calculated using the local density functional approach (LDA). The alloy is treated within the virtual crystal approximation. In these preliminary studies, a simple one parameter structural model is examined: the *PM* distance is contracted by ϵ while the *InAs* distance is expanded by ϵ , preserving the *c*-axis lattice constant. The calculated strain which minimizes the total energy is similar to the strain found in the experiment. Furthermore, the calculated valence band offset (within the LDA) is found to be a sensitive function of the interface strain, varying by 150 meV for $0.0 \leq \epsilon \leq 0.08$. More detailed structural studies are underway and the interesting case where both interfaces have the same composition, e.g. *InAs* and *AsIn*, will be discussed.

[1] J.M. Vandenberg *et al.*, Appl. Phys. Lett. 53, 1920 (1988).

C4.3

STRUCTURAL STUDIES OF EPITAXIAL METAL SEMICONDUCTOR INTERFACES USING TRANSMISSION ELECTRON SCATTERING. D. Loretto, J. M. Gibson and N. Chand, AT&T Bell Labs., 600 Mountain Ave., Murray Hill, NJ 07974 and S. M. Yalisove, Dept. of Materials Science and Engineering, University of Michigan, 2300 Hayward Street, Ann Arbor MI 48109.

Epitaxial semiconductor/metal interfaces are usually studied in the transmission electron microscope (TEM) in two specimen geometries: planview and cross-section. In planview samples the electron beam impinges perpendicular to the plane of the interface, which allows for quantitative diffraction and conventional diffraction/imaging. In cross-section samples the electron beam is at grazing incidence and high resolution TEM images can be recorded. The advantages and limitations of each technique will be discussed using examples drawn from our continuing study of $\text{CoSi}_2/\text{Si}(001)$ $2 \times 1/1 \times 2^{(1)}$ and from work on $\text{Al/GaAs}(001)$. In particular we will discuss the relative sensitivity of HRTEM and planview transmission electron diffraction to atomic displacements at an epitaxial interface.

D. Loretto, J. M. Gibson and S. M. Yalisove, to appear in Phys. Rev. Lett. July 1989.

C4.4

HIGH-RESOLUTION IMAGING OF THE INTERFACES BETWEEN GaAs AND CoGa AND ErAs. Jane G. Zhu, Stuart McKernan, Chris J. Palmstrom* and C. Barry Carter, Department of Materials Science and Engineering, Cornell University, Ithaca, NY 14853; *Bellcore, Red Bank, NJ 07701.

Metallic compounds, including NiAl, NiGa, CoGa and CoAl, have numerous potential uses such as the incorporation of metal layers into semiconductor structures and the improvement of metal contacts for semiconductor devices. These compounds have the CsCl (i.e., simple cubic) structure. The arsenides of the trivalent rare earths, which are being studied for the same reasons, occur normally with the NaCl (f.c.c.) structure. The lattice constants, or for the materials with the CsCl structure, a sub-lattice constant, of these compounds are very close to the lattice constant of GaAs. For the purpose of investigating the structure and crystal quality of epilayers of these materials, CoGa and ErAs have been grown on GaAs (100) substrates by molecular-beam epitaxy. The misfit dislocations at these interfaces have been characterized and will be discussed in a companion paper. High-resolution transmission electron microscopy (HRTEM) has been used to study the atomic configuration and the abruptness of both the CoGa/GaAs and ErAs/GaAs interfaces.

The HRTEM images have been recorded using a JEOL 4000EX which has a point-to-point resolution of ~ 0.17 nm. The interface images have been simulated for a range of specimen and image conditions using the TEMPAS multislice program. The images of the materials on either side of the interface have also been simulated and compared to the experimentally obtained images. The position of the interface can be

located unambiguously in both the real and simulated images. The ErAs/GaAs interface appears to be very smooth, while the CoGa/GaAs interface does not appear to be as flat on an atomic scale. Interfaces have also been analyzed, in both simulated and experimental case, where steps were present on the original surface.

C4.5

PLAN-VIEW CBED STUDIES OF $\text{NiO-ZrO}_2(\text{CaO})$ INTERFACES. Vinayak P. Dravid, Michael R. Notis, Charles E. Lyman, Dept. of Materials Science & Engineering, Lehigh University, Bethlehem, PA 18015, USA, A. Revcolevschi, Lab. de Chimie des Solides, Universite de Paris-Sud, Orsay, FRANCE.

Lamellar interphase interfaces in the directionally solidified eutectic (DSE) $\text{NiO-ZrO}_2(\text{CaO})$ have been investigated using conventional TEM, convergent beam electron diffraction (CBED) and high resolution TEM. This DSE grows along $[1\bar{1}0] \text{ NiO} // [001] \text{ ZrO}_2$, with $[11\bar{2}] \text{ NiO} // [010] \text{ ZrO}_2$ and $[111] \text{ NiO} // [100] \text{ ZrO}_2$ // Interface normal. $(11\bar{1}) \text{ NiO} // (100) \text{ ZrO}_2$ has been identified as a low energy configuration with translation periodicity within the planar interface. The symmetry and relaxation mechanisms associated with this interface, in particular the three components of rigid body translation (RBT) have been investigated. CTEM and HRTEM indicated the dense nature of the core of the interface with minimum lattice expansion normal to the interface. Plan-view CBED has been used to identify in-plane RBT which generally lowers the holosymmetric bicrystal point group symmetry. The detailed methodology of plan-view CBED technique, its advantages and limitations will be compared with other experimental techniques.

C5.1

INTERFACIAL SUPERSTRUCTURES STUDIED BY GRAZING INCIDENCE X-RAY DIFFRACTION. Koichi Akimoto, Jun'ichiro Mizuki, Ichiro Hirose and Junji Matsui, NEC Corporation, 34, Miyukigaoka, Tsukuba city, Ibaraki 305, Japan

Surface superstructures (reconstructed structures) have been observed by many authors. However, it is not easy to confirm that a superstructure does exist at an interface between two solid layers. The present paper reports a direct observation, by a grazing incidence X-ray diffraction technique with use of a synchrotron radiation, of superstructures at the interface between two solid layers: amorphous silicon ($a\text{-Si}$)/ $\text{Si}(111)-7 \times 7$, $a\text{-Si}/\text{Ge}$, $a\text{-SiO}_2(111)-5 \times 5$, $a\text{-Si}/\text{B}(\sqrt{3} \times \sqrt{3})/\text{Si}(111)$, epitaxial $\text{Si}(111)/\text{B}(\sqrt{3} \times \sqrt{3})/\text{Si}(111)$, $\text{SiO}_2/\text{Si}(100)-2 \times 1$. In the case of $\text{B}(\sqrt{3} \times \sqrt{3})$, for instance, boron atoms are suggested to occupy substitutional sites, thus forming the $\sqrt{3} \times \sqrt{3}$ structure. Interfacial superstructures between Al (also Sb or Yb) and GaAs(100) have also been found. For the Yb/GaAs(100) contact system, different interfacial superstructures have been found with different Yb thickness giving rise to different Schottky-barrier heights. Such superstructures may be relevant for understanding Schottky-barrier formation. In addition, the interfaces of MOCVD-grown AlN/GaAs(100) have been found to have 1×4 or 1×6 superstructures.

C5.2

DIRECT OBSERVATION OF A 7x7 SUPERSTRUCTURE BURIED AT THE AMORPHOUS-Si/Si(111) INTERFACE. Akira Sakai, Toru Tsumi and Koichi Ishida, Fundamental Research Laboratories, NEC Corporation, Miyukigaoka, Tsukuba, 305 Japan.

Direct imaging of a 7x7 superstructure buried at the amorphous-Si/Si(111) interface has been demonstrated by cross-sectional high resolution transmission electron microscopy (HRTEM). The electron diffraction pattern of the interface region showed diffuse streaks of fractional order which suggested the existence of the superstructure at the interface. The <110> cross-sectional HRTEM image of the buried 7x7 superstructure in one domain showed saw-tooth like contrast which had a periodicity of 23 Å. This periodicity is 7 times the 1/3(422) periodicity which is 3.3 Å along the interface. The optical diffraction pattern of the image confirmed that the diffuse streaks of fractional order contributed to the image formation of the buried 7x7 superstructure. The origin of the image contrast will also be discussed.

C5.3

TOPOGRAPHY OF Si(111): CLEAN SURFACE PREPARATION AND SILICON MOLECULAR BEAM EPITAXY. R. T. Tung, D. J. Eaglesham and F. Schrey, AT&T Bell Labs., Murray Hill, N.J.

Recently it was shown that high quality single crystal NiSi_2 and CoSi_2 may be grown at room temperature on Si(111) by deposition of a few monolayers of metal, followed by co-deposition of silicide. Because of the absence of long range diffusion, imperfections on the original Si surface, such as steps, are preserved at the interface between silicide and silicon. These defects may be imaged by TEM to display the topography of the original surface. Large areas ($>100 \mu\text{m}^2$) of the surface may be examined at one time. The sense (up or down) of the steps may also be determined. In this paper, a comparison is made between Si(111) surfaces prepared by various techniques, including Shiraki oxidation, Si beam cleaning, etc. It is shown that the distribution of steps varies significantly depending on wafer misorientation, impurity particles, etc. Multiple steps and step bands are observed on surfaces with larger misorientation angles ($\sim 2-6^\circ$). The initial stages of Si MBE is studied in detail. Nucleation of Si islands on flat terraces is shown to depend on the terrace width as well as the character of prevalent steps. Preliminary result regarding the role played by 7x7 domain boundaries and impurities is also presented. With a high growth rate of $\sim 1 \text{ Å/sec}$, step-flow type growth is found for $> 700^\circ\text{C}$ and two dimensional nucleation and growth of Si islands on the terraces is found at $< 600^\circ\text{C}$. A discussion of the growth mode as a function of temperature, deposition rate, and step density is given.

C5.4

STRUCTURE AND COMPOSITION OF LIQUID / SOLID INTERFACES BY ION CHANNELING. M.M. Karmarkar, Ray Twetten and K.R. Padmanabhan, Department of Physics and Astronomy, Wayne State University, Detroit, MI 48202.

The liquid / solid interface is an active region in which the interaction between the liquid and the solid can lead to variations in the composition across the interface and possible atomic rearrangement in the underlying substrate. In this paper the application of ion channeling

technique to study interfacial structure and composition in situ at the liquid / solid interface is discussed.

Energetic He ions backscattered from a thin Si window cell¹ arrangement are used to characterize the liquid / solid interface after in situ anisotropic etching of the oxide layer. Analysis of the aligned and random backscattered energy spectrum of the ions after their interaction with the liquid at the interface indicates the growth of thin epitaxial metal films on Si from solutions. Experimentally measured χ min values of Si and metal atoms indicate that the metal atoms are deposited along the same direction (as the substrate atoms) up to several nm from a sharp interface. The lattice damage of the substrate during film growth from the solution appears significantly lower compared to that due to etching. Examples of this study for the deposition of epitaxial metal films of Cu, Ni, Pd and Au on Si from solutions of the metal halides are presented.

1. K.R. Padmanabhan, P.J. Drallos, R. B. Alexander and J. C. Buchholz, Appl. Phys. Lett., **48**, 578 (1986).

C5.5

ELECTRONIC AND ATOMIC PROPERTIES OF THE a-C:H/Ge INTERFACE. M. Wittmer, IBM T. J. Watson Research Center, Yorktown Heights, N.Y. 10598; D. Ugolini and P. Oelhafen, Institute of Physics, University of Basel, CH-4056 Basel, Switzerland.

The performance of Ge infrared optical components can be drastically improved by the use of a protective and antireflection coating made of a hydrogenated amorphous carbon (a-C:H) film. A primary concern in all applications a-C:H films is adhesion. The adhesion quality of thin coatings on a material depend to a large degree on the electronic and atomic properties of the interface. Since adhesion is promoted by chemical bonding and atomic intermixing in the interfacial layer, the absence of a stable germanium carbide compound surmises a poor adhesion of a-C:H films on Ge. We have investigated the properties of the interface with photoelectron spectroscopy, high resolution transmission electron microscopy and ion channeling technique and found the formation of a metastable phase and the existence of atomic intermixing in the interfacial layer. The reactive nature of the a-C:H/Ge interface is consistent with the good adhesion of our a-C:H films on Ge surfaces. The metastable phase is amorphous and the interfacial roughness amounts to less than 20 Å. The effect of substrate cleaning and deposition parameters on the interface properties will also be discussed.

C6.1

SEMICONDUCTOR INTERFACE ELECTRONIC STRUCTURE INVESTIGATION BY BALLISTIC-ELECTRON-EMISSION MICROSCOPY. L. D. Bell, M. H. Hecht, F. J. Grunthaner, and William J. Kaiser, Jet Propulsion Laboratory, California Institute of Technology, Pasadena, California.

Ballistic-Electron-Emission Microscopy (BEEM) is a three-terminal Scanning Tunneling Microscopy technique which enables imaging of buried interfaces with nanometer spatial resolution. Local BEEM spectroscopy of ballistic electron transport through interfaces allows direct, spatially-resolved measurements of critical interface properties including Schottky barrier height, semiconductor heterostructure band offset, and interface band structure.

Recent BEEM investigations of semiconductor heterostructure electronic properties will be discussed. Au/AlAs/GaAs heterostructures have been prepared by molecular-beam epitaxy (MBE) and in-situ processing techniques. BEEM transport spectroscopy results for these thin, MBE-grown heterostructure tunnel barriers will be described. BEEM reveals a dramatic dependence of the barrier transport spectra on layer thickness

for monolayer thickness variation. Finally, results employing new BEEM capabilities enabled by low-temperature operation will be presented.

*Research supported by ONR and SDIO/IST.

C6.2

T.E.M. IMAGING OF AN OPERATING S.T.M. STRAIN EFFECTS OF S.T.M. J.C.H. Spence, Arizona State University, Tempe, Arizona 85287-1504

An STM has been constructed which operates inside a TEM, during reflection electron microscope (REM) imaging (1,2). REM and STM images of the same region have been obtained. These show that, at a vacuum of about 10^{-7} Torr, reversible elastic strain sometimes accompanies tunneling. A Pt tip was used on InP. Video recordings have also been made during tunneling, and RHEED patterns are obtainable from the region imaged. We find that the strain decreases with increasing tunneling bias (larger gap). The possibility that these observations result from tunneling through an insulating adsorbate layer will be discussed. The implications of these strains for spectroscopy and work function measurements will be outlined.

1. M. Kuwabara, W. Lo and J.C.H. Spence. J.Vac. Sci. Tech. (1989) in press.
2. J.C.H. Spence. Ultramicros. 25, p. 165 (1988).

C6.3

SLIDING PLANES MODEL FOR STM IMAGING. John D. Todd and John B. Pethica, Department of Metallurgy and Science of Materials, University of Oxford, UK.

Scanning Tunneling Microscope Images of layered materials in a non-uhv environment exhibit various anomalous phenomena, including enhanced corrugation heights, periodicity over large areas and a marked absence of point defects. The recent images of Au(111) and Al(111) also show some of these properties. We have modified a precision indentation device to allow STM rastering of a tip across a surface, while simultaneously monitoring mechanical contact. Images we have obtained from this apparatus on a HOPG sample exhibit atomic scale resolution with contact areas much larger than a single atom.

Contrast in the image results from periodic conductance fluctuations as the layers of the sample undergo shear in the region of the tip. We provide a quantitative model for this process, which explains a variety of curious, and otherwise unrelated phenomena occurring during STM imaging of these materials.

C6.4

THE FORMATION OF Si(111)1x1-Cl, John J. Boland and J.S. Villarrubia, IBM Research Division, Thomas J. Watson Research Center, Yorktown Heights, NY 10598

Using scanning tunneling microscopy, we have studied the structural modifications induced by Cl upon reaction with Si(111)7x7. At low coverages reacted and unreacted sites are distinguishable in both current-voltage curves and topographs. At saturation coverage annealing produces extensive mass transport in which most of the adatom layer is stripped away and accumulated in pyramidal Si structures, permitting the complete underlying Si rest atom layer

to be imaged. Much of this layer initially exists as nearly adatom free Cl stabilized 7x7 domains, but further annealing converts it slowly to the more favorable bulk-like 1x1 structure. Structures intermediate between the 7x7 and 1x1 are observed.

C7.1

ATOMICALLY-RESOLVED SURFACE PHOTOVOLTAGE MEASUREMENTS BY OPTICALLY-EXCITED SCANNING TUNNELING MICROSCOPY. R.J. Hamers and K.M. Markert, IBM T.J. Watson Research Center, Yorktown Heights, N.Y.

Tunneling microscopy and tunneling spectroscopy have conventionally been applied to study the equilibrium properties of surfaces. However, many of the most important electronic properties at surfaces and interfaces are dynamic phenomena such as trapping and recombination. When a surface or interface is illuminated with visible light, the created electron-hole pairs will separate due to local band-bending, resulting in a photovoltage at the surface. The spatial dependence of the surface photovoltage (SPV) and its dependence on the illumination intensity can provide unique information about both the static and dynamic electronic properties of surfaces and interfaces.

We have used scanning tunneling microscopy, spectroscopy, and potentiometry to study the atomically-resolved surface photovoltage on both clean and chemically-modified silicon surfaces. At low illumination intensities, the SPV signals show a logarithmic dependence on the incident power. At higher intensities the SPV effect saturates as the bands are flattened, thereby allowing us to determine the absolute surface band-bending with atomic spatial resolution. Finally, at the highest intensities, partial inversion of the surface is sometimes observed. Large differences are observed in the photovoltage response at defects and other surface irregularities. These differences can be directly related to spatial variations in the local surface recombination rate and the local band-bending. Detailed measurements allow us to distinguish between these two possibilities.

C7.2

PHOTOREFLECTANCE STUDIES OF ADSORPTION-INDUCED CHANGES IN SURFACE STATES ON GaAs(100), S. Sheu, K. Schultz, and E. G. Seebauer, Department of Chemical Engineering, University of Illinois, Urbana, IL 61801.

Photoreflectance (PR) is a contactless optical technique that has traditionally been used for studies of the bulk electronic properties of semiconductors. Recent efforts in this laboratory have focused on using PR for adsorption measurements. In PR, the change in surface reflectance induced by a low-intensity laser is measured as a function of the wavelength of a tunable light source. At sufficiently high carrier concentrations (near 10^{16} cm⁻³) spectral features, known as Franz-Keldysh oscillations, appear due to quantum effects. In particular, the period and decay of the oscillations varies in response to adsorption of Ga and As, on GaAs(100) that can be interpreted quantitatively in terms of small changes in Fermi level pinning and changes in recombination rates mediated by surface states. The effects of surface recombination on the oscillations has been evaluated independently through studies of ion bombardment. Heavy bombardment with 1 keV Ar⁺ ions decreases surface carrier lifetime by about 20%. On semi-insulating samples, an optical interference effect in PR may be exploited to obtain estimates of how quickly charge in slow surface states equilibrates with the bulk. Adsorption-induced changes in this phenomenon due to Ga and As, are investigated as well.

C7.3

THE FIRST MONOLAYERS OF Sb ON III-V-SEMICONDUCTORS STUDIED BY LIGHT SCATTERING. Michael Hunermann, Jean Geurts, I. Phys. Inst. RWTH Aachen, FR Germany and Wolfgang Richter, Inst. Festkörperphysik, TU Berlin, FR Germany

Sb has been deposited under UHV conditions on cleaved (110) faces of GaAs, InP and GaP. Inelastic (Raman) and elastic light scattering was used to monitor the structural and morphological properties of the Sb overlayers. A sharp peak is observed in the Raman spectra at frequencies of 163 cm^{-1} (GaAs), 167 cm^{-1} (GaP) and 185 cm^{-1} (InP) already at submonolayer coverage. Its intensity turns out to be strongly polarisation dependent. From the attenuation of this peak with increasing Sb coverage, the dependence on deposition temperature, the variation with substrate and the correlation with growth morphology (deduced from elastic light scattering) this peak must be due to vibrations of Sb atoms at the III-V/Sb interface. The sharpness of this peak suggests an ordered arrangement of Sb atoms at the III-V interfaces as has been reported for Sb on GaAs in the literature. The appearance of such peaks on InP and GaP covered with Sb also suggests an ordered growth of the first Sb monolayer for these systems. However, the structural arrangement of this first Sb layer seems to be not the same for the three semiconductors studied. For larger coverages up to approximately 15 monolayers amorphous Sb is observed for all three systems in the Raman spectra, which crystallizes from thereon to rhombohedral Sb, as has been reported previously.

C7.4

STRUCTURAL AND ELECTRONIC CHARACTERIZATION OF METAL-ON-METAL INTERFACES*

G. Vidali, P. Dowben, and C.W. Hutchings, Syracuse University, Physics Dept., Syracuse, N.Y. 13244-1130.

We used Atomic Beam Scattering (ABS) and ARUPS to study the adsorption of Hg on Cu(100) at submonolayer coverages. ABS has been used to obtain structural information as well as to determine isosteric heats of adsorption at various coverages. Over a wide range of temperatures (from room temperature to 150K) we find that Hg forms a $c(2 \times 2)$ and a high density $c(4 \times 4)$ phase on Cu(100). The isosteric heat changes by 0.6 eV from a low disordered to a $c(4 \times 4)$ high density phase. The energetics and structural determinations are related to changes in the electronic structures determined by angle resolved photoemission.

* Sponsored by NSF Grant #DMR-8802512, DMR-8820729

C7.5

Kinetics of Bismuth Overlayer Formation on GaAs(110) Studied Using Low Energy Electron Diffraction and Time Dependent Monte Carlo Simulation, S. L. Chang, T. Guo, W. K. Ford, A. Bowler, and E. S. Hood, Advanced Materials Center, Department of Physics, and the Department of Chemistry, Montana State University, Bozeman, Montana 59717

Low energy electron diffraction spot profile analysis has been used to investigate the kinetics of overlayer growth for bismuth on GaAs(110). Electron diffraction from films deposited at low temperature was analyzed over the temperature range -100 C to 200 C. Adatom coverages of 0.4, 0.7, 1.0 and 1.5 monolayers have been studied. The experimental results indicate that sixth order spots begin to form at

coverages as low as 0.7 monolayers, with an ordering temperature of approximately -30 C. The sixth order diffraction arises due to the formation of 24 Å adatom chains along the $(1\bar{1}0)$ direction, the short direction in the gallium arsenide surface unit cell. Adatom induced substrate reconstruction, which is indicated by a loss of the (10) diffraction beam intensity, and spot profile narrowing upon annealing have been observed. Preliminary analysis of the spot profile data suggests that the dominant ordering mechanism is provided by an attractive, interchain interaction directed perpendicular to the chain axis. Advanced theoretical analysis using time dependent Monte Carlo simulations is currently underway to examine and to quantify the kinetics of overlayer formation and the development of ordered structure.

C7.6

IDEALLY HYDROGEN TERMINATED Si(111) SURFACES PREPARED USING HF ACID SOLUTIONS: PRODUCTION OF PERFECT CRYSTAL TERRACES? G. S. Higashi, Y. J. Chabal, G. W. Trucks and Krishnan Raghavachari, AT&T Bell Laboratories, Murray Hill, NJ 07974

Infrared absorption spectroscopy has been used to characterize the silicon hydrogen stretching vibrations due to H-termination of Si surfaces produced by HF acid etching. Normal HF acid etching (aqueous HF solutions of varying concentrations) results in surfaces which are atomically rough, exhibiting vibrational modes characteristic of mono-, di-, and tri-hydride Si termination. In contrast, pH modified HF solutions (pH = 9-10) produce ideally terminated Si(111) surfaces with silicon monohydride (Si-H) oriented normal to the surface. The surface is found to be homogeneous with low defect density ($< 0.5\%$) and extraordinarily narrow SiH vibrational linewidth (0.95 cm^{-1}). These surfaces are very stable; rinsing in H_2O , HCl , or NH_4OH for brief periods has little effect on the vibrations observed.

The implication of this finding is that the surfaces are extremely flat and have a high degree of crystalline perfection. The high degree of chemical and topological control of this interface suggest that this surface preparation technique may be useful for metal-oxide-semiconductor device applications.

C8.1

MOLECULAR DYNAMICS STUDIES OF INTERFACE FORMATION DURING THIN FILM GROWTH. George H. Gilmer and Marcia H. Grabow, AT&T Bell Laboratories, Murray Hill, NJ 07974, and Aloysius F. Bakker, Applied Physics Department, Delft Technical University, 2600 G A Delft, The Netherlands.

We have simulated the deposition of semiconductor thin films onto a variety of different substrates. Molecular dynamics techniques give information on the atomic-scale structures at all stages during the growth of the films, and some of these sequences will be illustrated in a videotape of the model. Simulations of large atomic systems over extended periods of time were made possible by the use of a special-purpose computer ATOMS which we constructed. The shared-memory architecture of ATOMS permits efficient use of parallel processing with a limited number of processor boards. We now have two machines operating, each of which runs our molecular dynamics code faster than the in-house supercomputer. These simulations reveal some of the atomistic mechanisms of crystal growth, impurity incorporation, defect generation and strain relaxation. Special emphasis is given to the effects of misfit between substrate and film, the strength of the bonds between the film atoms and the substrate, and dislocations and monatomic steps at the substrate surface. The stability of uniform films against islanding is also considered, and the influence of the deposition conditions on surface uniformity is examined.

C8.2

A MOLECULAR DYNAMICS STUDY OF WATER-Pt INTERFACE.

K. Foster, K. Raghavan and M. Berkowitz, Department of Chemistry, University of North Carolina, Chapel Hill, NC.

An analytical form of the interaction potential for studies of rigid surface-rigid water interface is prescribed. Using this potential the structure and dynamics of water lamina between the Pt(100) surfaces is investigated. The surface strongly influences the properties of two layers of water. The adjacent to the metal surface water layer has a crystal-like structure in two-dimensions parallel to the surface. Most of the molecules in this layer remain at the energetically favorable on-top sites over the duration of the simulation. The second layer is not crystal-like, although the remnants of the order imposed by the surface are clearly seen. Some of the molecules in the second layer are located above the water molecules of the first adsorption layer. Beyond the second layer water displays bulk-like character.

C8.3

NON-EQUILIBRIUM MOLECULAR DYNAMICS SIMULATION OF THE RAPID SOLIDIFICATION OF METALS. Cliff F. Richardson and Paulette Clancy, School of Chemical Engineering, Cornell University, Ithaca, NY 14853.

A recently developed non-equilibrium Molecular Dynamics computer simulation method¹ is used to study the rapid melting and resolidification of metals including copper, gold and aluminum. The interatomic forces between metal atoms are modeled with the density functional theory-derived Embedded Atom Method (EAM)². Two methods are used to parameterize the embedding function and pair potentials for the EAM: one is due to Foiles³ for liquid transition metals, the other was developed by Oh and Johnson⁴ for fcc and hcp metals. The results from the two models are compared to establish the importance of the hardness of the potential function. They are also compared to results for the simpler Lennard-Jones (LJ) model for the interatomic forces to determine the effect of the many-body forces which are present in EAM, but absent in LJ. A detailed description of the solid/liquid interface morphology will be made together with the calculation of the interface temperature and velocity to establish the rapid interface kinetics and their effect on the post-processed product. Comparison will be made with recent experimental results due to MacDonald et al⁵ for the picosecond laser melting of copper and gold.

1. D.K. Chokappa, S.J. Cook and P. Clancy, Phys. Rev. B., **40**, May 15 (1989).
2. M.S. Daw and M.I. Baskes, Phys. Rev. B., **29**, 6443 (1984).
3. S.M. Foiles, Phys. Rev. B., **32**, 3409 (1985).
4. D.J. Oh and R.A. Johnson, J. Mater. Res., **3**, 471 (1988).
5. C. MacDonald, A.M. Malvezzi and F. Spaepen, J. Appl. Phys., **65**, 129 (1989).

C8.4

PROPAGATION AND STABILITY OF MONATOMIC STEPS ON THE Si(001) SURFACE DURING MOLECULAR-BEAM EPITAXY. S. Clarke, M.R. Wilby, D.D. Vvedensky, The Blackett Laboratory and Semiconductor Materials IRC, Imperial College, London SW7 2BZ, United Kingdom.

The 2x1 dimer reconstruction of the Si(001) surface leads to the creation of two types of monatomic steps, those with dimers orientated normal to the step-edge (S_{\perp}) and parallel (S_{\parallel}). We present a Monte Carlo simulation of molecular beam epitaxy on vicinal Si(001) surfaces comprising an ordered array of monatomic steps. Comparison of simulated 2x1 domain coverage with half-order features in RHEED allows us to follow the propagation of steps at the surface. We observe preferential growth at S_{\parallel} steps for high fluxes, however for low fluxes this situation is reversed and growth is localized at S_{\perp} steps. Detailed reproduction of the surface

morphology, as observed by STM, enables a kinetic model of this phenomena to be proposed. Our study highlights the sensitivity of the solid-vacuum interface to the imposition of non-equilibrium constraints by the incident Si flux. We extend this analysis to bi-vicinal surfaces, in which the surface has been misorientated in two perpendicular directions.

C8.5

A NEW DEFECT ON THE RECONSTRUCTED Si(100) SURFACE; An AB INITIO MOLECULAR-DYNAMICS STUDY. Sigeo Ihara and Shi Lun Ho, Central Research Laboratory, Hitachi Ltd., Kokubunji, Tokyo, Japan; Tsuyoshi Uda and Masahiko Hirao, Advanced Research Laboratory, Hitachi Ltd., Kokubunji, Tokyo, Japan;

The modified method of Car and Parrinello [1] has been used to perform molecular-dynamics of Si(100) surface. In our method, the first order equation of motion is used for the electronic wave functions in contrast to the second order one in the original dynamical simulated annealing.

With this method the 2X1 reconstructed Si(100) surface is studied. We found a new type of defect on the surface; atoms which form the dimer are recessed from the surface, and are located at the interstitial sites. This recessed or interstitial dimer and the adjacent on-surface dimer are both symmetric. The energy difference per dimer between the recessed and the usual on-surface asymmetric dimer is less than 0.1 eV. Finite temperature simulations indicate that these interstitial dimers are stable.

The relationship of these new dimers to the missing dimers observed by STM [2] and the vacancy model proposed by Pandey[3] is discussed.

- [1] R. Car and M. Parrinello, Phys. Rev. Lett. **55**, 2471 (1985)
- [2] R. J. Hamers, R.J. Tromp, and J.E. Demuth, Phys. Rev. **B34**, 5343 (1985)
- [3] K.C. Pandey, in Proc. of the 17th Inter. Conf. on the Physics of Semiconductors, ed. by D.J. Chadi and W.H. Harrison (Springer-Verlag, New York 1985), p.55

C9.1

ELECTRONIC AND ATOMIC STRUCTURES OF SILICIDE/Si CONTACT SYSTEMS STUDIED BY SXS. H.Watabe, Matsu-shita Electric Industrial Co., Ltd., Osaka 540, Japan. M.Iwami, M.Hirai, M.Kusaka, Research Laboratory for Surface Science, Faculty of Science, Okayama University, Okayama 700 Japan and H.Nakamura, Osaka Electro-Communication University, Neyagawa, Osaka 572, Japan.

It has been clarified by some of the authors and others that Si-L_{2,3} valence band soft x-ray emission spectra (SXS) show a clear difference between several Si-compounds and a Si crystal[1]. An interesting point of our new application of SXS method to a hetero-interface system is that it is able to clarify either electronic or atomic structure of solid surfaces and interfaces non-destructively[1].

Several silicides/Si contact systems are studied by the SXS, XPS(x-ray photoelectron spectroscopy) and several other methods. Si-L_{2,3} SXS spectra of several silicides are composed of mainly three parts including a peak at photon energy of 100 eV, i.e., near E_F. Since the soft x-ray emission is induced by an electron transition from a valence band to a Si(2p) core hole, the SXS spectra are expected to reflect the valence band DOS(density of state) with an s- and d-symmetry due to a selection rule. Also, a d-like DOS of transition metals is expected to be near E_F. This indicates the d-like DOS near E_F is not due to a

nonbonding d-state but due to a bond formation between a transition metal and a Si atom. Interface structures will be discussed on this base.
[1] M.Iwami, et al., Surf. Sci. 199 (1988) 467.

C9.2

COMPACT AND HIGH-RESOLUTION ION BACKSCATTERING ANALYSIS SYSTEM, CHIRIBAS

Y.Kido, I.Konomi, A.Kawano, and J.Kawamoto
Toyota Central R & D Laboratories, Inc.,
Nagakute-cho, Aichi-gun, Aichi-ken, 480-11, Japan

The design and performance of CHIRIBAS (Compact and High-Resolution Ion Backscattering Analysis System) are presented. The system consists of a 50 kV duoplasmatron and energy analyzers connected to a personal computer. The 5-50 keV H^0 , He^0 , and He^+ beams are backscattered to 180° and their energies are analyzed by a time-of-flight technique or with an electrostatic deflector combined with a position sensitive micro-channel plate. The probing depth and depth resolution are estimated to be up to 50 and 0.5 nm, respectively. The computer-simulated spectrum analysis allows rapid and accurate determination of surface and interface structures such as lattice disorder and morphology. CHIRIBAS also allows the measurement of excited state populations using Stark ionization for the 5-10 keV H^0 neutralized at the exit surface. This technique provides the possibility to determine the energy and spatial distributions of the valence electrons extending outward from the top surface. The present study includes the discussion on the physical basis of ion-solid interactions and the preliminary data on surface structures obtained by CHIRIBAS.

C9.3

TEMPERATURE DEPENDENT CURRENT-VOLTAGE CHARACTERISTICS IN THIN SiO_2 FILMS, Jin Zhao and N.M. Ravindra. Microelectronics Center, New Jersey Institute of Technology, Newark, New Jersey 07102.

An analysis of the Fowler-Nordheim theory and its application to temperature dependent current-voltage characteristics, of very thin films of SiO_2 on silicon, is presented. The final results are believed to provide the most complete examination of Fowler-Nordheim-emission theory and predict the breakdown electric field in very thin (2.5-20 nm) SiO_2 films. The role of the roughness at the Si- SiO_2 interface, in determining the Fowler-Nordheim current in these structures is also discussed.

C9.4

SPECTROSCOPIC ELLIPSOMETRY AS A NON-DESTRUCTIVE TECHNIQUE FOR CHARACTERIZATION OF ATOMIC-SCALE INTERFACES IN MULTI-LAYER STACKS. J L Stehle, J H Lacat, J P Piel, SOPRA, 26/68 rue Pierre Joigneaux, 92270 Bois-Colombes, FRANCE. L C Hammond, ARIES/QEI, Concord MA 01742, USA.

Analysis of oxide interfaces with semiconductor substrates, such as crystalline silicon, gallium arsenide or indium phosphide is critical in processing and electrical performance. For various layer growth processes, interfaces can be characterized by spectroscopic ellipsometry (SE).

The wide spectral range (1.3 to 5.3 eV) of SE allows an optical penetration depth of 10nm to a few microns. It also allows coverage of the critical range of crystallinity peaks of silicon, germanium, gallium arsenide and indium phosphide.

A multilayer stack can be characterized in terms of its layer thicknesses and mixture compositions. As SE is a non-destructive technique, the physical

parameters thickness and composition must be calculated through a mathematical model. Linear regression analysis is used to minimize the differences between the measured spectrum and the calculated model. The error parameter term, is used as an indication of the quality of the fit. If necessary, an interlayer can be introduced into the model to enhance the fit. Its thickness can be measured with a sensitivity better than 2 Angstroms. Examples will be given.

C9.5

ADSORPTION AND TRIBOCHEMICAL REACTIONS. W. M. Mullins, Purdue University, West Lafayette, IN; and T. E. Fischer, Stevens Institute of Technology, Hoboken, NJ.

A model for chemisorption based on the Lewis theory is proposed and developed. The model reproduces the observed relationship between aqueous solubility and band gap for covalent oxides. A relationship is shown between the calculated free-energy of the surface reactions and the observed effect of water on the wear of these materials. This relationship is explained in terms of surface reaction rate and equilibrium. Similar calculations for the adsorption of $-COOH$ and $-CH_2-$ functional groups are presented. The results are compared to water adsorption calculations and related to experimental wear test results for model fluids on covalent oxides. The effect of water on lubricant adsorption is discussed.

C9.6

DIRECT REAL SPACE IDENTIFICATION OF THE PRODUCTS OF A SURFACE CHEMICAL REACTION USING SCANNING TUNNELING MICROSCOPY. John J. Boland and J.S. Villarrubia, IBM Research Division, Thomas J. Watson Research Center, Yorktown Heights, NY 10598

In this talk we show that it is possible to distinguish between the various products from the reaction of Cl with the adatom layer of the $Si(111)-7\times7$ surface. Initially the Cl reacts with the adatom dangling bond state but at higher coverages it inserts itself in the Si-Si bonds between the adatom and rest atoms layers. As a result there are three possible products reflecting adatoms which have reacted with one, two or three Cl atoms. These products, which correspond to three different Si adatom oxidation states, are characterized by different registries with respect to the underlying rest atom layer and appear in STM images as adatoms of different sizes. The origin of these differences is discussed.

C9.7

DISCRIMINATION OF ATOMS ON THE SURFACE OF A TWO DIMENSIONAL SOLID SOLUTION WITH SCANNING TUNNELING MICROSCOPY. B. A. Parkinson, E. I. DuPont de Nemours & Co., Central Research and Development Department, P. O. Box 80328, Wilmington, DE 19880-0328

Atomic resolution STM images of WS_2 , WSe_2 and the solid solution $WSeS$ were obtained in air. The statistical distribution of the peak tunneling currents at each atom location was much larger for the solid solution than for the pure phases. A clearly separated bimodal distribution was not observed for $WSeS$ and so surface occupancies could not be unambiguously assigned. A model relating the magnitude of the tunneling current of a given atom to its identity and nearest neighbor environment was then developed. Computer simulated images using this model were compared with the real images. Using the model sulfur and selenium positions for the imaged surface could then be deduced for >90% of the surface atoms. The occupancy appeared to be random as was expected for a solid solution. Speculative applications for the ability to discriminate surface atoms are discussed.

A Raman Scattering Study of Interface Roughness in Small Period GaAs/AlAs Superlattices

D. Gammon, B. V. Shanabrook and W. Tseng
Naval Research Lab, Washington DC 20375

Raman scattering (RS) has been used extensively to study the vibrational modes of $(\text{GaAs})_n(\text{AlAs})_m$ superlattices. Specifically, the energies of the confined optical phonons provide information about the interfacial roughness and the energies and intensities of the folded acoustic phonons provide information about the period and interfacial roughness of the superlattice. Because the energies of these modes are sensitive to the structural parameters of the superlattice, RS has considerable potential as a characterization technique. This is especially true for very small periods where luminescence and absorption spectra are difficult to interpret, and for small or thin structures where x-ray diffraction is less useful.

In this paper we review the properties of superlattice phonons which are useful for the characterization of superlattices, and we present the results of a study of interfacial sharpness in a series of samples grown by novel MBE techniques. A comparison of the advantages and disadvantages of RS relative to those of x-ray diffraction will be given.

* A detailed discussion of the x-ray results will also be given at the conference.

C9.9

Bismuth/InSb(110) Interface Studied Using Low-Energy Electron Diffraction - T. Guo and W. K. Ford, Advanced Materials Center and the Department of Physics, Montana State University, Bozeman, Montana 59717

Metals are not generally known to form ordered overlayers on the (110) surface of III-V semiconductors, largely because of the stability introduced by the charge redistribution that drives the reconstruction of the clean surface. Two semimetals, antimony and bismuth, are known counter examples. We report on a new interface system Bi/InSb(110), studied using quantitative low energy electron diffraction. LEED diffraction intensity analysis has been performed on cleaved samples with various coverages of bismuth overlayer deposited at room temperature. Our measured LEED intensity profiles show that, unlike the GaAs(110) case, there is no long-range order in the bismuth overlayers for as-deposited samples on InSb(110). However, following annealing, bismuth forms ordered overlayers with a (1x3) phase for one monolayer of bismuth and a (1x2) phase for two monolayers of bismuth. Furthermore, for either as-deposited or annealed samples, there is evidence that the InSb(110) clean surface reconstruction is not removed by the bismuth overlayers. Detailed experimental procedures and results, as well as a possible growth mechanism will be presented and discussed and compared to the bismuth on GaAs(110) system.

C9.10

UNDERSTANDING THE INFLUENCE OF INTERFACE PROPERTIES AND DEPOSITION PARAMETERS ON THE SELECTIVE GROWTH OF (100) AND (110) CoGa FILMS ON (100)GaAs. Young K. Kim, Delroy A. Baugh, and R. Stanley Williams, Department of Chemistry and Biochemistry, University of California, Los Angeles, CA 90024.

The codeposition of elemental Co and Ga by molecular beam epitaxy is used to selectively prepare (100) and (110) oriented CoGa films on

(100) GaAs surfaces. The propensity towards a particular orientation, (100) or (110) CoGa, is investigated as a function of the relative Co and Ga incident flux (i.e. the film stoichiometry), total deposition rate, and the surface temperature. The effects of predepositing one to several monolayers of Co or Ga on the clean GaAs surface prior to film growth is also studied in detail. The primary diagnostic techniques utilized in these experiments are Auger electron spectroscopy (AES), transmission electron microscopy (TEM), two theta x-ray diffractometry (XRD) and x-ray photoelectron spectroscopy (XPS). In addition, a quadrupole mass spectrometer (QMS) and a quartz crystal monitor (QCM) are used for precise on-line calibration of the relative and total beam flux.

Preliminary results indicate a strong dependence of the observed orientation specificity on the film stoichiometry and on interface reactions which appear to be controlled by the surface temperature. The lattice parameter of CoGa (cubic CsCl structure) varies over a rather wide range with the relative concentration of Co/Ga and is therefore expected to affect the dynamics leading to production of preferred orientations. TEM results have shown that in some circumstances interface reactions can also play an important role in this process. All aspects of the interface chemistry and physics and how they affect the orientation specificity will be discussed.

C9.11

OBSERVATION OF HETEROEPITAXIALLY GROWN ORGANIC ULTRATHIN LAYERS ON INORGANIC SUBSTRATES BY IN SITU RHEED AND UHV STM. Masahiko HARA, Hiroyuki SASABE, Akira YAMADA and Anthony F. GARITO, Frontier Research Program, The Institute of Physical and Chemical Research (RIKEN Institute), Wako, Saitama 351-01, JAPAN.

Heteroepitaxial growth of organic ultrathin layers on inorganic substrates was carried out in a newly developed organic molecular beam epitaxy (OMBE) system under a base pressure of ca. 2×10^{-10} torr. The positional and orientational order of the organic layers was determined during actual layer growth by in situ reflection high-energy electron diffraction (RHEED) from less than a monolayer. The two-dimensional diffraction pattern is stored in a microcomputer through a CCD camera for intensity analysis. The OMBE system has also a portable vacuum chamber so that the OMBE films can be transferred directly into a separate ultrahigh vacuum scanning tunneling microscope (UHV STM) system.

The RHEED pattern revealed that molecularly flat metallophthalocyanine (MPc) ultrathin layers have been grown heteroepitaxially on a cleaved surface of a transition metal dichalcogenide (MX_2) substrate. The MPc layer has its own lattice constant, which is completely different from that of MX_2 even at the initial deposition stage. This indicates that very large lattice mismatched structures can be obtained by this OMBE technique. Further in situ RHEED and UHV STM measurements are now in progress and an extended discussion will be reported in the symposium.

C9.12

A NOVEL COMPUTATIONAL METHOD FOR EPITAXIAL ENERGY ON AN INCOMMENSURATE AND/OR COMMENSURATE INTERFACE. Sun M. Paik and Ivan K. Schuller, Physics Department, B-019, University of California, San Diego, La Jolla, CA. 92093

A new "mapping technique" is introduced which allows the study of epitaxy on systems which are commensurate, axial commensurate or incommensurate. This method applied to the fcc (111)/bcc (110) system predicts a new epitaxial orientation, in good agreement with a recent experiment, as well as the well-known KS and NW orientations. An epitaxial orientational shift as a function of island size and system temperature is also predicted. These results are in good agreement with numerical model calculations. The study

of atomic force microscopy (and scanning tunnelling microscopy) using this technique and molecular dynamics simulation will also be discussed.

Work supported by the National Science Foundation
Grant # DMR 87-01921.

C9.13

FULL POTENTIAL, LMTO CALCULATION OF TiC FRACTURE D.L. Price and B.R. Cooper, Dept. of Physics, West Virginia University, Morgantown, WV 26506*

Fracture properties of structural materials such as the transition-metal carbides, and factors controlling such fracture, are of great interest. In the rocksalt carbides, the cleavage plane is the (001) plane, a result which is at first appearance surprising since (001) cleavage separates the largest number of covalent bonds per unit area. Here we report on an electronic structure calculation of the cleavage behavior of stoichiometric titanium-carbide along a (001) plane. This is accomplished by use of a repeated slab supercell calculation, in which the separation between slabs is varied to allow simulation of the cleavage process. At the the largest separations we then have a repeated slab calculation of the Ti-C/vacuum surface. As the surface separation is varied, we examine both the cleavage energy and cleavage forces and relate these properties to the behavior of the Ti d - C p covalent bonds at the surface.

The methodology is based on performing full-potential linear combination of muffin-tin orbitals calculations of total energy for TiC in a superlattice arrangement. Our LMTO implementation includes a true interstitial region. Besides incorporating a full potential, we provide for increased variational freedom in the basis set compared to standard LMTO practice, giving the ability to deal accurately with both bulk and surface atomic arrangements and the transition between these.

*Supported by AFOSR Grant AFOSR-87-0251.

C9.14

COMPARISON OF SURFACE ATOMIC GEOMETRIES OF TETRAHEDRALLY COORDINATED COMPOUND SEMICONDUCTORS WITH THOSE OF RUTILE STRUCTURE OXIDES, Charles B. Duke, and Michael R. Thompson, Pacific Northwest Laboratory, Richland, WA.

The cleavage surfaces of tetrahedrally-coordinated compound semiconductors are known to undergo extensive relaxations. These occur because of the possibility bond-length-conserving top-layer rotations associated with the existence of only three bonds for each surface atom in the truncated bulk structure. In rutile structure oxides (e.g., SnO_2 , GeO_2 , PbO_2 , TiO_2), however, the (110) and (100) the cleavage surfaces do not admit such bond-length-conserving relaxations. A series of tight-binding total-energy models which described quantitatively surface relaxations on tetrahedrally-coordinated ZnO has been extended to encompass rutile structure oxides. Calculations indicate that the (110) and (100) surfaces are not predicted to relax. Detailed analysis reveals that the absence of bond-length-conserving relaxations which yield more stable distorted local coordination is the reason for this behavior. This finding suggests fundamentally greater surface stability for rutile oxides relative to, e.g. wurtzite structure ZnO.

(1) C.B. Duke and Y.R. Wang, J. Vac. Sci. Technol. B 6, 1440 (1988).

* Operated by Battelle Memorial Institute for the US Department of Energy under Contract DE-AC06-76RL0-1830.

C9.15

A CYCLIC-CLUSTER MINDO/3 COMPUTATION OF THE RELAXED EQUILIBRIUM STRUCTURE AND VIBRATIONS OF THE HYDROGENATED SILICON (111) SURFACE. Peter Deák, Physical Institute of the Technical University of Budapest, Hungary1521; Lawrence C. Snyder, Chemistry Department, and Carlos O. Rodrigues, Physics Department, State University of New York at Albany, 1400 Washington Avenue, Albany NY 12222.

We have employed a slab shaped cyclic-cluster containing 54 silicon atoms (surface unit cell is 3×3 , width is 6 layers) covered by hydrogen atoms on both sides. We used the Modified Intermediate Neglect of Differential Overlap (MINDO/3) method to compute the relaxed equilibrium structure. The resulting surface electronic structure and vibrational modes are discussed.

C9.16

STRUCTURAL AND ELECTRONIC PROPERTIES OF SEMICONDUCTOR- METAL AND SEMICONDUCTOR-INSULATOR INTERFACES AT MONOLAYER COVERAGE. Stefano Ossicini, C.Arcangeli and O.Bisi, Dipartimento di Fisica, Università di Modena, 41100 Modena, Italy.

A theoretical study of the processes involved in the formation of epitaxial interfaces between Si and metals/insulators has been performed by the LMTO-ASA method, in a version suited to deal with solid-vacuum interfaces [1]. The investigated systems include the interface formed by 1 monolayer of Na or Ca on Si(111) and the adsorption of F on the Ca-Si(111) interface. The F-Ca-Si(111) system is formed at the initial stages of the CaF_2 -Si(111) interface formation.

The dispersion and the features of the metal induced interface states at different adsorption geometries have been studied and the effect of F interaction has been calculated. Our results provide an explanation for the existing experimental data of Na-Si(111), Ca-Si(111) and CaF_2 -Si(111) interfaces. The comparison with the calculation of the corresponding bulk compounds points out the features due to the interface.

[1] S.Ossicini and O.Bisi, Surf. Sci. 211/212, 572, 1989

C9.17

CALCULATIONS FOR MERCURY ADSORPTION ON COPPER.* M. Karimi, Utica College, Physics Dept., Utica, N.Y. and G. Vidali, Syracuse University, Physics Department, Syracuse, N.Y.

We have calculated the interaction between an Hg atom and a Cu(100) surface. We also calculated the interaction potential for He on a Hg-plated Cu surface. Using recent Helium beam scattering data (1), we are able to obtain structural and dynamical information on a Hg layer on Cu(100). Preliminary computer simulations will also be presented.

1) G. Vidali, C.W. Hutchings, C. Moses, in preparation.
* Sponsored by NSF Grant #8802512 and Sloan Foundation (G.V.)

DOUBLE CRYSTAL X-RAY DIFFRACTION MEASUREMENT OF A TRICLINICALLY DISTORTED AND TILTED $\text{Al}_x\text{Ga}_{1-x}\text{As}$ UNIT CELL PRODUCED BY GROWTH ON OFFCUT GaAs SUBSTRATES. A. Leiberich and J. Levkoff, AT&T Bell Laboratories, Engineering Research Center, Princeton, NJ.

Important corrections are required for double crystal X-ray diffraction characterization of epitaxial $\text{Al}_x\text{Ga}_{1-x}\text{As}$ layers grown on offcut GaAs substrates. These corrections can have technological impact for thin film fabrication where precise and reproducible process control is required. Double crystal X-ray diffraction measurements of epitaxial $\text{Al}_x\text{Ga}_{1-x}\text{As}$ grown on offcut (100) GaAs substrates are interpreted in terms of a triclinic distortion of the film unit cell with concurrent unit cell tilt. The results indicate that cell distortions and tilt angles oppose each other, but remain approximately colinear with the direction of the offcut angle alignment. Application of conventional formalism to this unit cell geometry can result in significant errors for the measurement of the film's stoichiometry and can lead to wrong assumptions about the epitaxial film's commensurability. A formalism is presented providing the correct crystallographic parameters and film stoichiometry. The results of this analysis provide a fundamental description of the epitaxial film/substrate crystal geometry valid for cubic semiconductor heteroepitaxy on offcut substrates.

A MECHANISM FOR SOLUTE SEGREGATION TO GRAIN BOUNDARIES CHU Youyi and ZHANG Sanhong, The Nonferrous Metals Society of China, 9 Xizhang Hutong, Xizhimennei Dajie, Beijing 100814, China

Boron is one of typical surface active solutes. Recently it has been found that there exist equilibrium and non-equilibrium segregations of boron at austenite grain boundaries after quenching from a high temperature, which would give strong effect on the structures of the grain boundaries and properties of the materials.

Based on the consideration of local equilibrium among vacancies, solute atoms and vacancy-solute atom complexes, a mechanism for solute segregation to grain boundaries has been suggested for a alloy system with binding energy of the complex $E_b \gg kT$. By using Fick's Second Law and Mass Conservation Law, a set of dynamic equations for grain boundary segregation has been derived, which can generally describe the dynamic process both including equilibrium and nonequilibrium segregation, if the equilibrium segregation is involved in the boundary condition.

Putting reasonable parameters for boron in δ -Fe and solving the equations by computer, the boron segregation at austenite grain boundaries has been calculated as functions of isothermal holding time, cooling rate and quenching temperature, which agree well with the corresponding experimental results.

PHASE DIAGRAMS AND PHASE TRANSFORMATIONS FOR GRAIN BOUNDARIES IN HEXAGONAL CLOSE PACKED METALS. Kisoo Shin and A.H. King, Department of Materials Science & Engineering, State University of New York at Stony Brook, Stony Brook, NY 11794-2275.

In HCP materials, three dimensional CSLs are only possible for rational values of $(c/a)^2$, except for rotations about the $[0001]$ axis. For real materials, which have irrational axial ratios, the concept of the constrained CSL (CCSL) is introduced in order to describe the structures of large angle grain boundaries. In earlier work, we have shown that dislocation spacing in high angle grain boundaries should change continuously as a function of misorientation and temperature (since the latter affects c/a). Because CCSLs occur in dense clusters in misorientation space, the energy change associated with varying dislocation densities can drive phase transformations which convert the structure from one CCSL (or Σ -value) to another.

In this paper, we calculate the elastic energies of dislocation arrays in

large angle grain boundaries in zinc, using a Read-Shockley approach. For a fixed grain boundary plane, energy surfaces are constructed as a function of temperature and misorientation. All possible dislocation structures within a CCSL cluster are compared with each other, eventually leading to a phase diagram for the grain boundary, in misorientation-temperature space. We demonstrate that for certain cases this approach should be entirely sufficient, because the grain boundary "core energy" is invariant so the only effect is that of the elastic energy of the dislocation array.

We present experimental evidence for an allotropic phase transformation of a grain boundary at reduced temperature, corresponding to our theoretical predictions.

Acknowledgement: This work is supported by the National Science Foundation under grant number DMR-8901994.

STRUCTURE OF PURE TILT AND TWIST BOUNDARIES - GENERALIZATION AND COMMENTS ON THE STRUCTURAL UNIT MODEL. M.Khantha and V.Vitek, Department of Materials Science and Engineering, University of Pennsylvania, Philadelphia, PA 19104-6272.

A systematic study of the structure of pure tilt boundaries with tilt axis $[112]$ is carried out in a fcc, bcc and simple cubic crystal structure. A simple way of obtaining the delimiting angles in a structural unit model (SUM) is presented and the results are compared with those of computer simulation.

A systematic study of the structure of twist boundaries is also carried out for a fcc crystal structure. The clusters of polyhedra that characterize a certain period vector are similar in both pure tilt and twist boundaries. This observation helps to identify the structure of filler units that are necessary in addition to delimiting boundary units in twist boundaries. A possible way of extending the SUM to other crystal structures is outlined.

HIGH-RESOLUTION ELECTRON MICROSCOPY OF OLIVINE-MAGNETITE INTERFACES. Stuart McKernan, C. Barry Carter, Daniel Ricoult*, and A. G. Cullis**, Department of Materials Science and Engineering, Cornell University, Ithaca, NY 14853. *Corning-Europe, 7bis Avenue de Valvins, AVON, F77210, France, **RSRE St. Andrews Rd. Worcs. WR14 3PS

The oxidation of iron-rich olivine to produce magnetite is a model system for the study of phase transitions involving mass transport. The two structures (olivine and spinel) can be grown in orientations such that the planar spacing for certain planes is nearly the same in both phases. The oxygen sublattice of the two systems is continuous across the phase boundary, although some slight displacement of the atoms occurs in the transformation from one phase to the other. The cation sublattice of both structures contains many structural vacancies which facilitates the movement of cations to the transformation front. The transformation from olivine to magnetite proceeds by the transport of Fe ions to the magnetite particles, and the removal of Mg and Si ions away from the magnetite. A knowledge of the interface structure and the structure of defects, such as steps or ledges, on these interfaces is essential in determining the mechanisms for the phase transformation in this model system.

HRTEM images have been obtained using a JEOL 4000EX from samples of internally oxidized iron-bearing olivine. Needle shaped magnetite precipitates are observed when the electron beam is oriented parallel to the olivine $[010]$ direction. The interface is found to be extremely sharp and atomically flat. Steps on the interface are frequently observed. Simulated images of the interface have been calculated for several models using the TEMPOAS program. These results will be presented, and the comparison between the experimental and calculated images will be discussed.

C9.23

ATOMIC SCALE STRUCTURE OF TWIN BOUNDARY IN Y-Ba-Cu-O SUPERCONDUCTOR. Y. Zhu, M. Suenaga, Youwen Xu, and M. Kawasaki* Department of Applied Science, Brookhaven National Laboratory, Upton, NY 11973
*Jeol USA, Inc. Peabody, MA 01960

Direct structural images of twin boundary have been obtained in $\text{YBa}_2\text{Cu}_3\text{O}_{7-\delta}$, $\text{YBa}_2(\text{Cu}_{0.98}\text{Zn}_{0.02})_3\text{O}_{7-\delta}$ and $\text{YBa}_2(\text{Cu}_{0.98}\text{Al}_{0.02})_3\text{O}_{7-\delta}$ ($\delta \approx 0$) superconducting ceramics by high-resolution transmission electron microscopy. It was found that the transition of the lattice planes of a twin domain across a twin boundary involves a shifting of the respective planes as well as a rotation across the boundary. The transition takes place within approximately 10 to 30 Å, which is considered as the twin boundary layer thickness and is in good agreement with our previous value of the twin boundary thickness estimated from measuring the length of the streak in the selected area diffraction patterns.¹ The difference of the twin boundary layer in pure "123" and Zn and Al doped "123" will be reported. A structure model of the twin boundary will also be proposed.

This research was performed under the auspices of the U.S. Department of Energy, Division of Materials Science, Office of Basic Energy Sciences under Contract No. DE-AC02-76CH00016.

1) Y. Zhu, M. Suenaga, Y. Xu, R.L. Sabatini, and A.R. Moodenbaugh, Appl. Phys. Lett. 54, 374 (1989).

C9.24

STRUCTURAL STUDIES OF A TYPICAL LAYERED SEMICONDUCTOR ($\text{S}_4\text{In}_2\text{Zn}$) USING HIGH RESOLUTION ELECTRON MICROSCOPY AND CONVERGENT BEAM ELECTRON DIFFRACTION. Dwight R. Acosta, Instituto de Física, Universidad Nacional Autónoma de México, A. P. 20-364, 01000 México, D. F., México. Mauro Bri- ceño, Universidad de Los Andes, Facultad de Ciencias, Mérida, Venezuela.

$\text{S}_4\text{In}_2\text{Zn}$ is a semiconductor material with a layered structure similar to a mica obtained after chemical transport reactions for crystal growing. Its laminar configuration makes the $\text{S}_4\text{In}_2\text{Zn}$ an ideal material for electron microscopy studies: wide planar zones and very thin as required for convergent beam electron diffraction and high resolution electron microscopy. $\text{S}_4\text{In}_2\text{Zn}$ crystallizes with a hexagonal structure ($a = 3.8\text{Å}$, $c = 37.0\text{Å}$) but some times presents rhombohedral structure and transform to a cubic one as temperature is increased (around 400°C). We report in this work electron microscopy measurements: thickness of layers, crystalline potential and full symmetry using convergent electron beam diffraction methods.

High resolution electron microscopy observations also were carried out from very thin layers and a wide variety of structural features were identified and characterized. Also defects like twins and dislocations were detected and quantified in order to correlate with some physical properties of $\text{S}_4\text{In}_2\text{Zn}$.

Optical diffractometry and image calculations were carried out together with high resolutions imaging in order to complete or corroborate information obtained from microscope observations.

C9.25

EFFECT OF B, C, P AND S ON INTERGRANULAR COHESION IN IRON. Genrich L. Krasko, Metals Research Branch, U.S. Army Materials Technology Laboratory, Watertown MA 02172 and G. B. Olson, Department of Materials Science and Engineering, Northwestern University, Evanston, IL 60208

LMTO-ASA spin-polarized calculations were performed on a simplified model of a (111) incoherent twin Σ3 grain boundary (GB) in SCC iron. The GB was modelled by a hexagonal 8-atom supercell, containing an

impurity atom (B, C, P or S) in the center of a capped trigonal prism of Fe atoms at the GB core. Contrary to earlier molecular cluster calculations, a strong charge transfer in the direction of Fe was discovered. The Wigner-Seitz spheres of B, C, P and S lose respectively 0.47, 0.25, 1.60 and 1.47 electrons. The s-electrons of the impurity atoms form filled bands separated from the valence bands (for B the gap is very small), while the p-electrons strongly hybridize with s-, p- and d- electrons of the nearest Fe atoms. As a result of this charge redistribution, strong ionic components are formed in Fe-P and Fe-S bonds. For B and C these are much weaker, the main bonding being covalent and metallic. The number of electrons occupying antibonding states increases steadily on moving from B to S. The magnetic moments of the Fe atoms nearest to the impurity are decreased. For B, C, P and S they are respectively 2.07, 1.88, 1.12 and $1.09 \mu_B/\text{atom}$, while the magnetic moment of a bulk Fe atom in

the BCC lattice is $2.24 \mu_B/\text{atom}$. This behavior is being compared with that of the corresponding (111) free surfaces in order to deduce the electronic basis of the influence of these impurities on the work of grain boundary separation.

C9.26

MODELING OF NANOPHASE CONNECTIVITY IN SUBSTANCE -VOID COMPOSITE BY OBLIQUE DEPOSITION. Tomoyoshi Motohiro, S. Noda, A. Isogai and O. Kamigaito, Toyota Central Res. & Develop. Labs., Inc. Nagakute-cho, Aichi-gun, Aichi-ken, 480-11, Japan.

Obliquely vapor deposited thin film is characterized by its unique inclined columnar structure. Recently one of the authors developed thin film optical quarter-wave plate by oblique deposition [1]. SEM observation revealed the inclined columns of ~10 nm in diameter and ~3 microns in length. Its birefringence indicates those columns are less closely spaced in the plane of vapor incidence (PVI) than normal to PVI, composing alternatively stacked substance layer (columns laterally connected with each other)-void layer (residual space) nanophase composite with 2-2 connectivity [2]. The growth mechanism of the inclined columnar structure has been successfully explained by the self-shadowing effect in 2D-space computer simulation in PVI [3]. However, the connectivity development perpendicular to PVI is not self-evident. In the present work, we performed simple 3D-space simulation of oblique deposition and observed substantial feature of the connectivity development and related features on this nanophase structure.

1. T. Motohiro and Y. Taga, to be appeared in Applied Optics-July 1, (1989).
2. R.E. Newnham, D.P. Skinner and L.E. Cross, Mat. Res. Bull., 13, 525 (1978). Pergamon Press, USA.
3. D. Henderson, M.H. Brodsky and P. Chaudhari, Appl. Phys. Lett. 25, 643 (1974).

C9.27

DEFECT EVOLUTION IN Al/Cu and Al/Ni BILAYERS DURING ANNEALING. Bent Nielsen, S. M. Heald, W. Triftshäuser*, K. G. Lynn, E. Barrera, and J. Jayanetti, Materials Science Division, Brookhaven National Laboratory, Upton, NY 11973.

*Universität der Bundeswehr, Neubiberg, FRG.

Thin bilayers of Al/Cu and Al/Ni were grown by evaporation on SiO_2 at ~300 K. A variable energy positron beam was utilized to probe the defect structure in the as grown layers and subsequently after heat treatment leading to significant interfacial reaction. The results strongly indicate that after the heat treatment microvoids are

formed in the Cu in the Al/Cu system and in the Al in the Al/Ni system.

This work was supported by the U.S. Department of Energy, Division of Materials Sciences, under Contract No. DE-AC02-76CH00016.

C9.28

NANOLAYER REACTIONS IN ALUMINUM-METAL INTERFACES. E. V. Barrera, M. W. Ruckman, and S. M. Heald, Brookhaven National Laboratory, Upton, NY 11973.

Surface Extended X-ray Absorption Fine Structure (SEXAFS) measurements on the nanometer level were made for Al/M interfaces where M was Cu, Cr or Ni. The samples were studied immediately after deposition and measurements were taken while varying thickness and after heat treatments. Significant differences in interface reactions were observed depending on deposition direction (Cu on Al or Al on Cu) and the amount of mixing was also related to whether M was Cu, Cr or Ni. The heat treatments further identified which interfaces were the more reactive. The SEXAFS measurements revealed that there were no detectable C or O present, suggesting that the interface structures were Al-M reactions and not associated with impurity effects. The results obtained from the as-deposited interfaces correlated well with data obtained from buried interfaces of like element combinations.

This work was supported by the U.S. Department of Energy, Division of Materials Sciences, under Contract Nos. DE-AS05-80ER10742 and DE-AC02-76CH00016.

C9.29

INTERFACIAL STRUCTURE OF Er_2O_3 PRECIPITATES IN TITANIUM AND Ti-37Al.* Daniel S. Schwartz, McDonnell Douglas Research Laboratories, St. Louis, MO; Shankar M. L. Sastry, McDonnell Douglas Research Laboratories, St. Louis, MO; and P. Fraundorf, University of Missouri-St. Louis, St. Louis, MO.

High-resolution transmission electron microscopy was used to study the structure of interfaces between Er_2O_3 precipitates and titanium alloy matrices at different stages in the growth of the precipitates. Rapid-solidification processing was used to create a metastable solid solution of 2 wt. % Er in both pure titanium and titanium 37 wt. % aluminum. Subsequent annealing causes the Er to scavenge O from the surrounding matrix and form a fine, mechanically beneficial dispersion of spherical Er_2O_3 precipitates, evenly distributed throughout the matrix. In the early stages of growth, the precipitates are found to be semi-coherent with the matrix in both alloys examined. Growth of the precipitates was controlled through the use of in situ heating, and the evolution of interfacial structure was traced as a function of precipitate size in the titanium and Ti-37Al matrices. Finally, the precipitate-matrix interfacial structure in pure titanium was compared to that in Ti-37Al.

*This work was supported by the Air Force Office of Scientific Research under Contract No. F49620-86-C-0108.

C9.30

HIGH-RESOLUTION ELECTRON MICROSCOPY OF INTERFACES IN AlN-BRAZE METAL ALLOY SYSTEMS. A. H. Carim, Center for Micro-Engineered Ceramics & Department of Chemical and Nuclear Engineering, University of New Mexico, Albuquerque, NM 87131.

An understanding of bonding between ceramics and metals requires knowledge of the interfacial structures that are present. In the work described here, the microstructural aspects of active brazing of AlN with a Ag-Cu-Ti alloy have been investigated. A series of reaction product

layers are formed. TiN is produced in contact with the polycrystalline, bulk AlN. High-resolution transmission electron microscopy and microdiffraction demonstrate that some of the TiN grains at the interface display specific orientation relationships with respect to the adjoining AlN crystallites. As has sometimes been observed in studies of epitaxy in other systems, these relationships are not necessarily those that provide the minimum geometrical mismatch between one or more sets of lattice planes. Farther from the substrate, an η -type nitride phase with composition $(\text{Ti,Cu,Al})_6\text{N}$ occurs as a reaction product. High-resolution images confirm the absence of amorphous or crystalline intervening phases at the TiN- η interface and at η grain boundaries.

C9.31

ATOMIC STRUCTURE OF CRYSTALLINE BORON NITRIDE INTERFACES WITH CERAMIC SUBSTRATES.* L. E. Allard, High Temperature Materials Laboratory, Oak Ridge National Laboratory, Oak Ridge, TN 37831; A. K. Datye and R. T. Paine, Center for Micro-Engineered Ceramics, University of New Mexico, Albuquerque, NM 87131.

Recent work has shown that BN prepared from polymeric precursors yields a pre-ceramic phase that melts below 1200°C. The BN polymeric melt can be applied to ceramic substrates to form thin, adherent, crystalline coatings. The structures of the BN ceramic coatings and BN/oxide substrate interfaces (such as BN/ Al_2O_3 , BN/MgO and BN/ TiO_2) have been investigated using submicron particles of simple geometry as model substrates. Using these model systems, all interface orientations that are thermodynamically stable can be studied using a single sample by high resolution TEM. Preliminary results indicate that the BN crystallizes in a hexagonal modification, with the BN basal plane always parallel to the oxide surface. Comparison of experimental images with calculated images permits determination of atomic structure at these ceramic-ceramic interfaces.

*Research sponsored in part by the U.S. DOE, Assist. Sec. for Conservation and Renewable Energy, Office of Transportation Systems, as part of the High Temperature Materials Laboratory User Program, under contract DE-AC05-84OR21400 with Martin Marietta Energy Systems, and by the Center for Micro-Engineered Ceramics, University of New Mexico

C9.32

SIMULATION AND QUANTIFICATION OF HIGH RESOLUTION Z-CONTRAST IMAGING OF SEMICONDUCTOR INTERFACES. David E. Jesson, S. J. Pennycook, and M. F. Chisholm, Oak Ridge National Laboratory, Oak Ridge, TN 37831.

Z-contrast STEM is a new technique for high-resolution electron microscopy giving images characterized by strong chemical sensitivity, high localization, and an incoherent character. There are no contrast reversals with defocus or sample thickness and no Fresnel fringe effects at interfaces, so that rigid shifts are independent of thickness and defocus. These characteristics arise from allowing only highly localized electron scattering to contribute to the image, so only the electron intensity close to the atom strings is important. It becomes very clear how these incoherent characteristics arise using a Bloch wave description since the dominant contribution to the image comes from the thickness integrated 1s state intensity. As a consequence, Z-contrast images may be predicted intuitively and simulated to high accuracy on a small computer. These calculations also demonstrate the strong localization of the image. Each atomic column is imaged practically independent of its neighbors, allowing "column by column" compositional mapping of interfaces. The implications of higher accelerating voltages for

improved resolution and localization are discussed.

*Research sponsored by the Division of Materials Sciences, U.S. Department of Energy under contract DE-AC05-84OR21400 with Martin Marietta Energy Systems, Inc.

C9.33

SIMULATED IMAGE MAPS FOR USE IN EXPERIMENTAL HIGH-RESOLUTION MICROSCOPY. M.A. O'Keefe and U. Dahmen, National Center for Electron Microscopy, Lawrence Berkeley Laboratory, University of California, Berkeley, CA 94720.

The variation of high resolution image contrast as a function of thickness and defocus for a given material can be plotted in a composite simulated image. Such simulations are useful as guiding maps during experimental high resolution microscopy. The use of these maps makes it possible to locate optimum imaging conditions even at foil thicknesses beyond the thin phase object limit. For perfect periodic crystals the contrast conditions repeat with thickness and defocus. The Fourier image distance $2d^2/\lambda$ for a crystal with period d is small enough to limit the size of a useful map to an array of about ten 100\AA defocus steps by ten 20\AA thickness steps (depending on extinction distance). However, due to their large period, defects such as grain boundaries have a much larger Fourier image distance. The image characteristics of a through-focus through-thickness map are thus particularly useful in optimizing defect contrast during operation of the microscope. Typical features of these maps and examples of recent applications at the NCEM will be discussed. This work was supported by the Director, Office of Energy Research, Office of Basic Energy Sciences of the U.S. Department of Energy under contract #DE-AC03-76SF00098.

C9.34

LAYER CONTRAST IN InAs / GaAs SUPERLATTICES STUDIED BY TEM

C.J. Kiehl, Department of Materials Science and Engineering, University of Liverpool; K.C. Hsieh, Department of Electrical Engineering, University of Illinois at Urbana-Champaign; A. Rockett, Department of Materials Science, University of Illinois at Urbana-Champaign.

Transmission Electron Microscopy studies have been carried out on a series of InAs / GaAs strained layer superlattices and effects such as anomalous layer contrast and asymmetries in interfacial sharpnesses have been observed. The technique of using (200) structure factor contrast for imaging layers in this system has been considered in detail since the layers exhibit contrast opposite to that predicted by kinematical theory. Using a theoretical Bloch wave approach we have systematically assessed the relative contributions to the layer contrast of factors such as (1) structure amplitudes, (2) absorption coefficients and Debye-Waller factors, (3) tetragonal distortion, (4) strain relief by misfit dislocations, (5) slight layer misorientations and (6) thin specimen surface relaxation effects. These results will be discussed fully and comparisons will be drawn from observations and calculations on the closely lattice matched AlAs / GaAs superlattice system.

The thermal stability and interfacial abruptness of InAs / GaAs SLS's grown by MOCVD as a function of growth temperature have been studied. Abrupt, symmetric interfaces are obtained at low growth temperatures (625°C) whereas more diffuse, asymmetric composition profiles are observed for those grown at high temperatures (800°C). This asymmetry occurs during growth and is not a result of bulk interdiffusion at elevated temperatures, as evidenced by analysis of samples grown at low temperatures and annealed at higher temperatures.

C9.35 ABSTRACT NOT AVAILABLE

C9.36

PLATINUM SILICIDES FORMED BY RAPID THERMAL PROCESSING FOR SCHOTTKY BARRIERS. D.I. Zarovski, V.E. Borisenko, Minsk Radioengineering Institute, P. Brovka 8, 220800 Minsk, USSR.

Platinum silicides were formed by rapid thermal processing of 35-45 nm platinum films deposited onto monocrystalline (111) phosphorus doped (2×10^{14} at/cm³) silicon substrates. Incoherent lights were used to process the samples for 5 - 30 s at induced temperatures ranging from 300 to 1050°C Schottky barriers with the active area of $500 \mu\text{m}^2$ were formed.

Phase composition and structure silicide layers were studied by RBS and TEM. I-V characteristics of Schottky barriers were measured. Silicide phases appear after processing at $400 - 450^\circ\text{C}$. The silicide layer growth follows parabolic kinetics characterized by the growth rate $v = 0.021 \exp(-1.0/kT)$ cm²/s at $400 - 600^\circ\text{C}$ when both Pt₃Si and PtSi were detected and $v = 0.014 \exp(1.1/kT)$ cm²/s at higher temperatures when only PtSi was formed.

The activation energy of recrystallization was estimated to be 0.75 eV. The mechanism of the recrystallization was predominantly coalescenced.

The Schottky barriers were characterized by the height of 0.65 - 0.66 eV and ideality factor of 1.04 - 2.6.

C9.37

XPS ANALYSIS OF THE CHEMISTRY OF THE SAPPHIRE SURFACE AS A FUNCTION OF HIGH TEMPERATURE VACUUM ANNEALING. Eliezer David Richmond, Naval Research Laboratory, Code 6816, Washington D.C. 20375-5000.

This represents the first XPS chemical analysis of the effects of in-situ high temperature vacuum annealing of (1102) sapphire substrates. Previously, the effects of high temperature vacuum annealing of a sapphire substrate in-situ of a VGB0 Si MEE system on the Si growth kinetics has been investigated¹, and the resultant material characterized for its crystalline quality, microstructural defects, and electrical properties². Three inch substrates were chemically cleaned and then inserted into the system load lock. The wafers were then annealed in a high temperature heating stage at 1450°C and 1300°C and analyzed with an ESCALAB Mk II using both Mg and Al excitation sources. Before chemical cleaning the surface of the wafer is contaminated with C. After the chemical clean the C peak disappears. This is in contrast to chemical cleaning of Si where a residual C contamination continues to exist. After the cleaning, a small residual F peak exists on the sapphire wafer. This F contamination disappears upon heating. For the 1450° annealed sample a loss of several percent of oxygen is found. This is accompanied by a slight increase in the Al(2p,2s) and O(1s) binding energies, which is consistent with a relaxation of the surface. Preliminary LEED results will be presented to investigate an accompanying reconstruction of the surface.

1. J.G. Pellegrino, E.D. Richmond, and M. Twigg, Materials Research Society Proc., vol. 116, p.395, 1988;

Eliezer D. Richmond, this conference, Session D.

2. E.D. Richmond, S. Quadri, A. Rudson, M. Twigg, N. Green, III International Si MEE Symposium, 30 May - 2 June 1989, Strasbourg France.

INFLUENCE OF PLASTICITY IN ADHESIVE BOND STRENGTH MEASUREMENTS USING SHOCK WAVES. Gerald L. Nutt and William Lai, Lawrence Livermore National Laboratory, P. O. Box 808, Livermore, CA 94550; and Kenneth E. Froschner, Martin, Froschner, and Associates, P. O. Box 17, Livermore, CA 94550.

We have developed a method of measuring the bond strength of metal/ceramic interfaces using a novel technique that employs shock waves to exfoliate metal films from ceramic substrates. The shock is generated by a magnetically accelerated projectile incident on a buffer material, which is used to adjust the amplitude and shape of the incident compressive wave. The buffer is coupled to the ceramic substrate. The compressive shock is phase shifted after reflection from the metal surface and becomes a triangular tensile pulse. When the tensile pulse passes through the metal/ceramic interface, and if the amplitude is sufficient, the metal film will spontaneously exfoliate from the substrate. Experimentally, measurements are taken of the free surface velocity of the spalled film using laser interferometry. The bond strength of the interface can be calculated based on the measured free surface velocity.

In this work, it was assumed that during the transit of the shock and rarefaction waves the material on either side of the interface did not reach the plastic state. We have attempted to verify this using transmission electron microscopy to measure the dislocation density near the interface before and after the spall process. We also report results of bond strength measurements on Ni/sapphire interfaces.

C9.39

ORIGIN OF ATOMIC RESOLUTION IN SCANNING TUNNELING MICROSCOPY C. Julian Chen, IBM Research Division, T.J. Watson Research Center, P.O. Box 218, Yorktown Heights, NY 10598.

Scanning tunneling microscopy (STM) has demonstrated *true* atomic resolution, i. e., 2-4 Å lateral resolution, on a number of solid surfaces. The observed resolution is far beyond the expectation of some well-known theoretical models of STM, for example, the s-wave theory of STM, i. e., based on consideration of local density of states (LDOS) of the sample, and the single-atom imaging model. In this paper, it is shown that true atomic resolution in STM originates from localized p_z or d_{z^2} states on the apex atom of the tip. Associated with these tip states, the tunneling matrix elements become proportional to the *derivatives* of sample wavefunction, i. e., $\partial\psi/\partial z$ and $\partial^2\psi/\partial z^2$ etc., rather than its amplitude. This results in much greater corrugation amplitudes than those of LDOS. The new theory is able to explain a large number of experimental results and provides insight into the origin, meaning and tip requirements of atomic-resolution STM.

C10.1

INTERFACE STRUCTURES AND THEIR DEFECTS IN CoSi_2/Si : DISLOCATIONS, DISCLINATIONS AND A THIN-FILM PHASE TRANSFORMATION.

D. J. Eaglesham, R.T. Tung, S.M. Yalisove, R.L. Headrick, and I.K. Robinson, AT&T Bell Laboratories, 600 Mountain Avenue, Murray Hill, NJ 07974.

The interface structures and interfacial defects in CoSi_2/Si heteroepitaxy have been the subject of intensive study for over a decade now, but the system continues to provide us with surprises. Here we will present the results of a study of the novel $\text{CoSi}_2/\text{Si}(110)$ interface, and revisit the much-studied

$\text{CoSi}_2/\text{Si}(111)$.

Although a large number of different silicide-silicon interfaces have been studied in the past, $\text{CoSi}_2/\text{Si}(110)$ differs crystallographically from all previously studied systems. Whereas for (111)B interfaces a twinning $1/6\langle 211 \rangle$ dislocation is needed to produce a step in the interface, and (100) interfaces require a $1/4\langle 111 \rangle$ dislocation at a step on the Si surface, the $1/4\langle 111 \rangle$ vector lies within a (110) interface, so that steps on the (110) surface are related by $1/2\langle 110 \rangle$, but there are two inequivalent interfaces on a given surface. The consequences of this symmetry for the (110) defect structure are described. For $\text{CoSi}_2/\text{Si}(111)$ B we describe a phase transformation into a low-symmetry structure for both the epilayer and the interface. The temperature at which low-symmetry films transform into the cubic silicide varies between $\approx 400^\circ\text{C}$ and $\approx 150\text{K}$, depending on the film composition and thickness. The low-temperature form does not correspond to any bulk phase of silicide and appears to be driven by the strain and interfacial free energy present in the thin film.

C10.2

ATOMIC STRUCTURES AT $\text{CoSi}_2/\text{Si}(111)$ AND $\text{CoSi}/\text{Si}(111)$ INTERFACES. A. Catana, P.E. Schmid and *P. Stadelmann, Institute of Applied Physics, *Institute of Electron Microscopy, Swiss Federal Institute of Technology, 1015 Lausanne, Switzerland.

$\text{CoSi}_2/\text{Si}(111)$ interfaces have been prepared by annealing of a UHV evaporated, Co layer at 400, 500, and 900°C for a few seconds. At low temperatures (400°C), the silicidation yields CoSi which is found to grow epitaxially on silicon. $\text{CoSi}_2/\text{Si}(111)$ and the more complex $\text{CoSi}/\text{Si}(111)$ interfaces are therefore well suited for the study of fundamental questions related to the interface composition and bonding configuration. At the same time, they offer the opportunity of studying atomic scale changes at interfaces in relation to the $\text{CoSi}-\text{CoSi}_2$ phase transformation.

Results are presented of a detailed high resolution study of both interfaces. Thin samples were prepared by conventional thinning techniques, as well as by cleavage of wedges. The second technique offers some advantages over the classic one such as the absence of ion-induced artefacts and a straightforward determination of sample thickness. Investigations were performed along both [110] and [112] silicon axes. The image contrast at the interface was analyzed using image simulations. Various bonding models are discussed and compared to experimental images. As a result, we show the occurrence of the sevenfold coordination of Co atoms at both A and B type interfaces. This is the first evidence of this interface geometry for CoSi_2 , others reports being in favor of Co-Si bonds and a 5-fold or 8-fold Co coordination.

C10.3

MICROSTRUCTURAL ASPECTS OF AMORPHOUS NICKEL SILICIDE FORMATION IN EVAPORATED Ni-Si MULTILAYERS. Karen Holloway, IBM Thomas J. Watson Research Center, Yorktown Heights, NY 10598

The formation of very thin (1-2 nm) amorphous intermixed layers at metal-silicon interfaces, and their growth at annealing temperatures below those at which crystalline silicides nucleate have attracted attention in recent years. This process constitutes the earliest stage of metal-silicon reaction in some systems, so its study is vital to the understanding of the formation of metal silicides for application in integrated circuits. Furthermore, as the growth of crystalline metal silicides has been extensively investigated, a knowledge of these systems can be applied to understand the process of diffusion by which these disordered layers expand. For example, the crystalline Ti silicides grow through the transport of silicon. The location of voids which appear during amorphization in Ti-Si multilayers suggest that this probably also proceeds via Si mobility. As Ni diffuses during the growth of nickel silicides, a study of the Ni-Si system complements those already performed on Ti-Si. To this end, the growth of thin interfacial amorphous nickel silicide layers in evaporated Ni-Si multilayer films of

various bilayer thicknesses has been investigated using cross-section transmission electron microscopy. This work focusses on the microstructure which evolves on rapid thermal annealing at temperatures low enough to suppress complete crystallization of the amorphous silicide (150-250°C). Crystalline Ni₂Si nucleates early in the reaction, forming a planar layer between the elemental nickel and the growing amorphous alloy. The formation of Kirkendall voids does not occur until the Ni is consumed by the crystalline silicide. These observations will be compared with the quite different microstructure which evolves during amorphization in Ti-Si multilayers.

C10.4

NUMERICAL AUGER LINESHAPE ANALYSIS OF PHASE FORMATION IN Ni/Si(111). J. R. Butler, X. Tong and P. A. Bennett, Department of Physics, Arizona State University, Tempe, Arizona 85287.

We show that numerical Auger lineshape analysis can quantitatively separate coexisting phases occurring in the thermal (contact) reaction of 0 - 30 Å nickel overlayers on Si(111). Measured Si LVV spectra are fit as linear combinations of measured "fingerprint" spectra for Ni₂Si, NiSi and NiSi₂ obtained by scraping bulk alloys in situ. We find that nickel reacts at room temperature to form Ni₂Si for all coverages from 0 to ~ 12 Å, at which point this reaction saturates, and pure nickel forms. We also find a cap of silicon on the A-type NiSi₂ structure, but not on the B-type when these are annealed at 500 C. Finally, NiSi forms at 300 C and coverages above 15 Å, but not at lower coverages. We present the data as a coverage vs. temperature kinetic phase diagram that provides a comprehensive view of phase formation in this ultrathin film system, and bridges a gap between monolayer and conventional (1000Å) thin film studies. By extrapolating from 1000Å film results, we can quantify a switch from bulk to surface diffusion and observe a variety of free energy and strain contributions to the nucleation rate for NiSi₂ formation.

C10.5

X-RAY ABSORPTION STUDIES OF TITANIUM SILICIDE FORMATION AT THE INTERFACE OF Ti DEPOSITED ON Si.* David Aldrich, Q. Islam, H. Jeon, R. Nemanich, and D.E. Sayers, North Carolina State University, Raleigh, NC 27595-8202

X-ray absorption measurements have been performed on the Ti K-edge for a series of titanium silicide samples. The samples were fabricated by depositing Ti on silicon wafers and subsequently annealing them up to temperatures from 100 to 900°C in UHV and Nitrogen. Measurements were done in the fluorescence and total electron yield modes at the X-11A beam line at the National Synchrotron Light Source. Using the different data collection techniques it is possible to examine the structure of the sample in different regions. Both EXAFS and near edge spectra (XANES) were acquired and analyzed. Comparisons with standard compounds have been made with the near edge data. The EXAFS data were analyzed using reference compounds. The XANES data showed a high sensitivity to changes in the film structure. Ti metallic bonding and Ti-Si bonds can be distinguished and their evolution traced as a function of annealing. The absorption spectra of samples annealed under N₂ are significantly different, indicating the possible presence of nitrides. Results are related to Raman and other measurements of the reaction process.

* Supported by the Division of Materials Science of the Department of Energy under contract DE-AS05-80ER10742

C10.6

SILICIDE FORMATION AND THERMAL STABILITY OF Ni/Si/GaAs INTERFACES.

Y. Yamamoto, K. Ishibashi, Res. Cntr. of Ion Beam Tech., Hosei Univ., Tokyo, Japan; S. Suzuki, Adv. Mat. Lab., Sohka, Japan; T. E. Shim¹, Waseda Univ., Tokyo, Japan.

Silicon and/or Ni were vacuum evaporated onto (100) GaAs. Interdiffusion and silicide formation processes in the system upon annealing were investigated using AES and X-ray diffractometry.

Thicknesses of Ni and Si were varied to examine how the interface reaction related to the relative amount of Ni to Si; (1) Si(1000 Å)/GaAs, (2) Ni(700 Å)/GaAs, (3) Ni(700 Å)/Si(1000 Å)/GaAs, (4) Si(1000 Å)/Ni(2000 Å)/GaAs, and (5) Ni(2000 Å)/Si(1000 Å)/GaAs.

AES measurement revealed that a Si/GaAs interface of sample (1) was stable after annealing at 850 C for 30 min. When the relative amount of Ni to Si is unity as sample (3), stable NiSi was formed and no reaction to GaAs was observed after annealing at 500 C for 2 hour.

When Ni was directly attached to GaAs, appreciable interdiffusion of GaAs and Ni was observed (samples (2), (4)), but in sample (4) Ga and As did not diffuse into the Ni₂Si surface layer at 500 C.

In the case that Ni was the outermost layer of which amount was in excess of Si as sample (5), the system was quite unstable at the same temperature; no clear silicide phase, no distinct interface, oxidation of the surface Ni layer.

¹Present address: Samsung Electronics, Seoul, Korea

C11.1

FRACTIONAL ATOMIC PLANES IN GaAs/AlAs SUPERLATTICES AND THEIR RELATIONSHIP TO INTERFACIAL ROUGHNESS. Ivan K. Schuller, Physics Department B-019, University of California, San Diego, La Jolla, CA.; M. Grimsditch, Material Science Division, Argonne National Labs., Argonne, IL.; F. Chambers, G. Devane, Amoco Research Center, Naperville, IL.; H. Vanderschueren, D. Neerincx, J.-P. Locquet and Y. Bruynseraede, Physics Department, Katholieke Universiteit Leuven, B-3030 Leuven, Belgium

We have grown high quality GaAs/AlAs superlattices with non-integral number of atomic planes in each layer of a superlattice. Diffraction studies of these superlattices show unusual structure, characteristic of the non-integral character of the superlattice, which may even be incommensurate. The results are in good agreement with structure factor calculations and show that this type of roughness cannot be determined by local measurements which only probe the structure of a single interface.

Work supported by the U.S. Department of Energy, Grant # DE FG03-87ER-45332 (at UCSD), Contract # W-31-109-ENG-38 (at ANL), the Belgian Inter-University Attraction Poles (IUAP) and Concerted Action (GOA) programmes. International travel was provided by NATO.

C11.2

STUDY OF INTERFACIAL SHARPNESS AND GROWTH IN (AlAs)_n / (GaAs)_n SUPERLATTICES W. Tseng, S. Prokes, M. Fatemi, B.V. Shanabrook, B. Wilkins and H. Dietrich, Naval Research Laboratory, Washington DC, 20375

A detailed investigation of x-ray diffraction has been made on (AlAs)_n / (GaAs)_n superlattices grown by three MBE techniques; normal growth, interrupted growth and atomic-layer-epitaxy (ALE). Theoretical simulations of the x-ray

diffraction scans have also been made to interpret the experimental data, in particular, the interfacial sharpness. Results indicate a roughness of three monolayers at the interface for normal growth conditions. The ALE growth gives improved interfacial sharpness, due to more precise control of shutter at slower growth rates and reduction of substrate temperatures during growth.

C11.3

A WEAK BEAM IMAGING TECHNIQUE FOR THE CHARACTERISATION OF INTERFACIAL ROUGHNESS IN (InGa)As/GaAs STRAINED LAYER STRUCTURES Yao I. Y. Andersson T. G. and Dunlop G. L. Department of Physics, Chalmers University of Technology, S-412 96 Göteborg, SWEDEN

A weak beam imaging technique in transmission electron microscopy (TEM) has been developed for the characterisation of interfacial roughness in lattice strained (InGa)As/GaAs multiple layered structures. In this technique, the heterointerfaces of (100) type strained layers are imaged in an inclined projection with a g_{311} diffracted reflection at off-Bragg conditions. It was found that the contrast that arose from variations in strained layer thickness was significantly increased in this imaging mode. Rough interfaces that resulted from growth in either a two or a three dimensional growth mode via island formation were observed. The interfacial roughness in terms of variations in strained layer thicknesses on a monolayer scale was imaged. The resolution of contrast in the plane of the interface was better than 10 nm. Such contrast improvement was attributed mainly to the enhancement of the contribution of diffracted electrons from the strained layers to the image. A theoretical calculation based upon kinematic theory was made in order to gain a better understanding of the contrast in this weak beam imaging mode. In principle, this imaging technique can be applied to other strained layer heterostructures.

C11.4

THE OBSERVATION OF SURFACE ROUGHENING ON ALUMINUM USING OPTICAL SECOND-HARMONIC GENERATION.* S. Janz, K. Pedersen, H. van Driel, University of Toronto, Toronto, Ontario; and R. Timsit, Alcan Research and Development Centre, Kingston, Ontario, Canada.

We report the use of optical second-harmonic generation (SHG) as an in situ probe of thermally induced changes in surface morphology. An incident beam from a synchronously pumped dye laser operating at a wavelength of 580 nm with a 3 picosecond pulse width was used to generate second-harmonic light at atomically clean Al (100), (110), and (111) surfaces. The SH light was collected using conventional photon counting techniques. As the temperature of the samples was ramped from room temperature to 620° C, the SH intensity increased dramatically at specific temperatures dependent on the crystal face. The SH intensity jumps occurred at 450° C for the (111) face, at 560° C for the (110) face and at 580° C for the (100) face. After the samples were quenched to room temperature, the SH signal decayed back to its initial value with a time constant of approximately 15 minutes. We interpret the rise in SH intensity as being caused by surface roughening due to a proliferation of steps as the temperature is increased beyond the roughening temperature characteristic of the crystal face. The decay of the surface roughness after quenching proceeds via a relatively slow self-diffusion process. The effect of surface morphology on optical SHG and its potential applications will be discussed.

* This work supported by the Natural Science and Engineering Research Council, the Ontario Laser and Lightwave Research Centre, and Alcan.

C11.5

INTERFACIAL STABILITY AND INTERDIFFUSION EXAMINED AT THE ATOMIC LEVEL. Y. Kim, A. Ourmazd, and J.A. Rentschler, AT&T Bell Labs, Holmdel, NJ 07733, and R. J. Malik, AT&T Bell Labs, Murray Hill, NJ 07974.

Modern crystal growth produces interfaces across which only the composition changes precipitously. Such systems are far from equilibrium and can relax by the introduction of extended defects, or by chemical interdiffusion. Here we investigate the chemical relaxation of interfaces, caused by interdiffusion between lattice-matched semiconductors.

Using chemical lattice imaging in combination with vector pattern recognition, we obtain quantitative profiles of the chemical change across single interfaces with atomic plane resolution. We thus study interdiffusion across single GaAs/AlGaAs interfaces as a function of temperature, depth of interface beneath the surface, and doping. Since our technique is sensitive to interdiffusion coefficients as small as 10^{-20} cm²/s, we can study atomic level changes at a single interface at the low temperatures used for many device processing steps (~700 C). Our results show interdiffusion, and hence the layer stability depend not only on temperature and doping, but also on the distance of the interface from the surface. The implications of these results for the stability of multilayered structures are discussed.

C11.6

ATOMIC STRUCTURE AND CHEMISTRY OF INTERFACES DETERMINED BY Z-CONTRAST STEM. M. F. Chisholm, S. J. Pennycook, and D. E. Jesson, Oak Ridge National Laboratory, Oak Ridge, TN 37831

The technique of Z-contrast STEM provides a fundamentally new and powerful approach to determining the atomic scale structure and chemistry of interfaces. In this paper we have applied the technique to a number of technologically important interfaces, including the direct imaging of interdiffusion in ultrathin (Si_mGe_n)_p superlattices, and the direct imaging of an interface reconstruction at a silicide/silicon interface. Since no contrast is seen within an amorphous layer, the technique is also a powerful way of studying amorphous/crystalline interfaces. Examples will be shown of Ge/SiO₂ interfaces produced by ion implantation and oxidation, Si/SiO₂ interfaces produced by oxidation, and the solid phase epitaxial growth front in ion-implanted, thermally annealed Si.

*Research sponsored by the Division of Materials Sciences, U.S. Department of Energy under contract DE-AC05-84OR21400 with Martin Marietta Energy Systems, Inc

C12.1

THE USE OF FRESNEL CONTRAST TO STUDY THE INITIAL STAGES OF THE *in situ* OXIDATION OF SILICON. E. M. Ross and W. M. Stobbs, Department of Materials Science and Metallurgy, Pembroke Street, Cambridge CB2 3QZ, UK; and J. M. Gibson, AT&T Bell Laboratories, 600 Mountain Ave., Murray Hill, NJ 07974.

The interface between silicon and its oxide has been studied extensively at different stages of growth using a variety of powerful analytical techniques. It has become clear that in order to understand the kinetics of thin oxide growth and the structure of the Si/SiO₂ interface, compositional information is required at atomic resolution to complement the interesting structural results already provided by high resolution electron microscopy. Unfortunately data is difficult to obtain at adequate resolution with techniques requiring a focussed probe because of the problems of beam broadening and damage to the oxide. However past analysis of oxides viewed edge-on in a conventional electron microscope has been accomplished by a different approach: utilising the sensitivity of the Fresnel contrast seen along a Si/SiO₂ interface to the composition change occurring at the interface. Information is extracted by matching the experimental fringes in low resolution defocused images to simulations from a simple computer model. This method has been used to determine the sharpness of

the Si/SiO₂ interface and to demonstrate changes in the relationship between the compositional and structural changes which both occur at the interface. The resolution achieved was sufficient to suggest a change in the oxidation kinetics between the ultra-thin (<3nm) and thin (3-30nm) growth regimes.

The weakness of this past work has been the uncertain nature of the initial silicon surface and damage associated with foil thinning. In the present study, rather than analysing formed oxides we describe observations of the growth *in situ* of oxide on a clean silicon surface in a microscope modified for ultra high vacuum. By analysing the Fresnel contrast along the edge of faceted regions of the specimen, compositional changes at the silicon surface can be observed while controlled amounts of oxide are grown. This growth under low oxygen pressures provides an interesting contrast to higher pressure thermal oxidation. We will discuss the implications of this work for theories of the growth of the first few monolayers of oxide.

C12.2

THE INITIAL STAGES OF FORMATION FOR THE Si/SiO₂ INTERFACE ON Si(111) 7x7. J. M. Gibson, AT&T Bell Laboratories, Murray Hill, NJ 07974

Using a UHV Transmission Electron Microscope we have studied the initial stages of Si oxidation by high-energy transmission electron diffraction and imaging. The atomic structure of the Si(111) 7x7 surface is monitored as it is converted to a 1x1 buried interface, using quantitative analysis of high-energy transmission diffraction data. Structural analysis involved Patterson functions, Fourier difference maps and least squares refinement from the electron data. We observe structural changes in the surface during O₂ exposure which go beyond simple random destruction of the adatoms or dimers, and have implication on the oxidation mechanism and interface structure.

C12.3

ELECTRON SPIN RESONANCE STUDIES OF SILICON DIOXIDE FILMS ON SILICON IN INTEGRATED CIRCUITS USING SPIN DEPENDENT RECOMBINATION. Mark A. Lupina and Patrick M. Lenahan, Pennsylvania State University, University Park, PA.

Although standard electron spin resonance (ESR) detection techniques have been quite successful in exploring the atomic scale structure of imperfections at or very near the Si/SiO₂ interface, these studies have been limited to extremely large surface areas (several cm²) with fairly large defect densities. The technique of spin dependent recombination (SDR) allows ESR observation of point defects in a single metal-oxide-semiconductor field-effect transistor (MOSFET) with surface areas of only 10⁻⁴ cm² and quite low interface state densities of ~10¹¹/cm². The two dominant paramagnetic defects found in the Si/SiO₂ system are the P_b center and the E' center. The P_b center is a trivalent silicon bonded to three other silicons at the Si/SiO₂ interface; the E' center is a trivalent silicon bonded to three oxygens in the oxide. With SDR's enhanced sensitivity, devices with different processing details are explored. Results show significant processing induced differences in the P_b and E' SDR spectra.

C12.4

AN NMR STUDY OF HYDROGEN AT THE Si/SiO₂ INTERFACE OF THERMALLY GROWN OXIDES. David H. Levy and Karen K. Gleason, Department of Chemical Engineering, MIT, Cambridge, MA.

Nuclear magnetic resonance (NMR) spectroscopy is used to study the incorporation of hydrogen at the silicon-silicon dioxide interface of thermal-

ly grown wet and dry oxides of silicon. A possible correlation between bonding structure (SiH vs. SiOH) and film stress is explored.

Hydrogen spatial distributions in the interfacial region are also examined by NMR. Since hydrogen is expected to cluster near defects as it does in the amorphous silicon hydride system, this may provide insight on the atomic scale structure of the Si/SiO₂ interface. An understanding of this interface is critical in explaining the growth kinetics of thin, low temperature oxides. Differences in the interfaces of wet and dry oxides are highlighted.

C12.5

ELECTRONIC STRUCTURE OF EPITAXIAL SiO₂/Si(100) INTERFACES. T. Motooka, Institute of Applied Physics, University of Tsukuba, Tsukuba, Ibaraki 305, Japan

The local densities of states (LDOS) of epitaxial SiO₂ layers on Si(100) surfaces have been calculated using the recursion method combined with the Harrison's universal tight-binding model. Clusters comprising ~10⁴ atoms were generated to describe possible crystalline SiO₂ layers on Si(100) substrates. In an epitaxial (√2x√2)R45° structure of β-cristobalite, only half of the surface Si atoms are connected to oxygen in SiO₂. The calculated LDOS associated with the remaining surface Si atoms showed that localized states due to the dangling bonds (P_s centers) appeared in the middle of the Si gap. These gap states were eliminated by terminating the dangling bonds with hydrogen consistent with the results of photoelectron spectroscopy measurements for H₂ annealed SiO₂/Si(100) interfaces. On the other hand, all the surface Si atoms are connected to the O atoms in a strained tridymite structure with an epitaxial relationship (001)[001]tridymite || (100)[110]Si. The interface states appeared near the Si conduction band edge and were primarily composed of the interface O 2p and surface Si 3s and 3p orbitals.

C12.6

THE STRUCTURE OF INTERFACES IN OXIDE HETEROJUNCTIONS FORMED BY CVD. L.A. Tietz, S.R. Summerfelt, and C.B. Carter, Department of Materials Science and Engineering, Cornell University, Ithaca, NY 14853.

The development of a network of misfit dislocations is an essential process in the formation of many types of phase boundaries during epitaxial growth. The introduction of misfit dislocations has been shown to affect not only the elastic energy of the interface but also the orientation relationship between the two phases. In this study, α-Fe₂O₃/α-Al₂O₃ heterojunctions are used as model interfaces for the study of misfit dislocation structures in oxides. α-Fe₂O₃ (hematite) and α-Al₂O₃ (sapphire) have the same crystal structure (S.G. = R3c; c/a = 2.73) but with a 5.5% lattice misfit.

A new, non-destructive method of preparing oxide heterojunctions for examination in the transmission electron microscope has been used to prepare the interfaces for this work. The technique involves deposition of thin oxide islands directly onto a TEM foil using CVD; in this case, hematite was deposited on (0001)-oriented sapphire. The hematite grew epitaxially with nearly exact alignment of the crystal axes. Island sizes

were predominantly in the range of 50 - 300 nm in diameter by <10 nm thick. In addition, all of the islands were attached to surface steps on the substrate. Weak-beam imaging has been used to characterize the dislocation structure parallel to both the (0001) terraces and the step faces. The influence of the dislocation structure on island orientation and morphology will be discussed.

C13.1

THE STRUCTURE OF GRAIN BOUNDARIES IN ALUMINUM*

M. J. Mills and G. J. Thomas, Sandia National Laboratories, Livermore, CA 94551-0969; and F. Cosandey, Rutgers University, Piscataway, NJ 08854.

A systematic study of the structure of tilt grain boundaries in aluminum has been initiated. High resolution transmission electron microscopy is being used to examine the interface structure of several bicrystals with <110> tilt axes. Specifically, the structure of a $\Sigma 9$ [1 $\bar{1}$ 0] 38.2° symmetric tilt boundary has been determined. The grain boundary plane, which appears wavy at lower magnification, is actually composed of atomically flat microfacets. Several different structures have been identified within individual microfacets: two distinct, symmetric structures with {221} boundary planes and an asymmetric structure in which the interface lies on a {111} of one of the crystals. These observations are being compared with calculated structures using the Embedded Atom Method. The quantitative comparison between the observed and predicted grain boundary structures is accomplished using multislice image simulations based on the calculated structures. The results of these comparisons and the evaluation of the relative energies of the microfacets will be discussed.

*This work is supported by the U. S. Department of Energy, BES-Materials Sciences, under contract number DE-AC04-76DP00789.

C13.2

ON THE ATOMIC STRUCTURE OF GRAIN BOUNDARIES IN SMALL METALLIC AND BIMETALLIC PARTICLES.

Miguel Avalos, Roberto Hernández, Pablo Schabes, Armando Vázquez and Miguel José Vacamán, Instituto de Física, Apdo. Postal 20364, UNAM.

The structure of small metallic and bimetallic particles of Pd, Ir, Rh, Ru, Pt and its alloys are studied using HREM. In particular the internal boundaries that are present in different structures are considered for a number of metals. In the case of bimetallic particles it is found that long period structures are produced in some regions of the particle. Different mechanisms for the formation of twin boundaries in these structures are discussed.

C13.3

STRUCTURE AND PROPERTIES OF THE (110) INVERSION DOMAIN BOUNDARY IN β -SiC. **W. R. L. Lambrecht** and B. Segall, Department of Physics, Case Western Reserve University, Cleveland, OH 44106.

The interface between two domains of β -SiC with inverted C and Si positions is called an Inversion Domain Boundary. It is one of the most frequently occurring planar defects in cubic SiC heteroepitaxially grown on a Si(001) substrate as a result of monoatomic steps. Results of density functional electronic structure and total energy calculations using the linear muffin-tin orbital method are presented for the (110) interface. The latter is a symmetry plane of the structure. This circumstance allows us to obtain the energy of formation of the

interface by subtracting the total energies of superlattices containing two equivalent interfaces and the corresponding perfect crystal. A simple model involving C-C and Si-Si bondlength relaxation by neighboring Si-C bond rotations is proposed. The calculations show that this lowers the total energy of formation of the defect from ~ 6 eV for the ideal structure to ~ 3 eV/interface unit cell area. Alternative structures are currently investigated by means of a valence force field approach. The interface is characterized by several occupied interface localized states in the bandgaps (both the semiconducting bandgap and the gap between the lower s-like and higher p-like valence bands). These are present even after relaxation of the structure. Layer projected densities of states and supercell band-structures will be presented. These states as well as the charge accumulation near the interface which leads to a potential barrier should have significant effects on the electronic transport. The high interface total energy also implies a weak bonding at this interface.

C13.4

MECHANICAL RESPONSE OF MATERIALS WITH INTERFACES

I. Alber, J. L. Bassani, and J. Qu, Department of Mechanical Engineering and Applied Mechanics, University of Pennsylvania; **V. Vittek and G.-J. Wang** Department of Materials Science and Engineering, University of Pennsylvania, Philadelphia, PA 19104.

Interfaces are regions of distinct atomic structure and, possibly, composition. They possess, therefore, properties which are different from those in the bulk. In continuum mechanics studies, the influence of an interface can be accounted for through displacement discontinuities, the magnitude of which depends both on tractions along the interface and the interfacial properties. The latter are controlled by the atomic structure of the interface and a relationship between the atomic scale properties and macroscopic mechanical response can thus be established.

In this paper we consider interfaces between misoriented crystals, i.e. grain boundaries. Their atomic structure is calculated using established methods of molecular statics with interatomic forces described by many-body potentials. The atomic level stresses and elastic constants are then calculated and on their basis the interfacial residual stresses and elastic moduli evaluated. These quantities are the interfacial properties needed when considering the mechanical response, and they are an input into the formulation of the boundary conditions for the corresponding continuum calculations.

Using the results of these studies effective elastic properties of bicrystals are deduced. The results are then generalized to properties of bimetals and composite materials.

This research was supported by the NSF Grant. no. 88-06966 and the MRL Program Grant DMR85-19059.

C13.5

ATOMISTIC SIMULATION STUDIES OF INTERFACES IN NANOPHASE COPPER AND SILICON. **James A. Lupo** and **Michael J. Sabochick,** Dept. of Engineering Physics, Air Force Institute of Technology, Wright Patterson AFB, OH 45433.

Nanophase copper and silicon were investigated using atomistic simulation. Nanophase materials have very small grains, and thus a significant fraction of the atoms are surrounded by an interface instead of a crystalline environment. The simulations employed an embedded-atom method potential for copper, and a modified Stillinger-Weber potential appropriate for crystalline and amorphous silicon. Computer "samples" of nanophase material were formed by compressing together three grains of several hundred atoms each, using Fletcher-Powell minimization and external pressures of 0.5, 1.5, and 4.5 GPa. All copper systems compressed to nearly the density of the perfect crystal, even with 8000-atom (50.0Å) grains. Silicon systems containing 105-atom (7.8Å) grains compressed to relative densities of 66%, 86% and 97% at the above pressures, as compared to the perfect crystal. Systems with 305-atom (11.3Å) grains compressed to relative densities of 70%, 72% and 75%. Large voids were observed in each case. Plots of atomic positions showed that crystalline order was maintained within the grains up to the interfaces. In other

words, no highly disordered interfaces were observed.

Bulk moduli and thermal expansion coefficients were calculated using molecular dynamics. Nanophase samples with relative densities near unity had bulk moduli close to that of the perfect lattice. Samples with relative densities less than unity showed correspondingly lower bulk moduli. For example, a silicon sample at 86% relative density had a bulk modulus 30% lower than the perfect lattice bulk modulus. In general, the bulk moduli seemed to be more affected by voids than by interfaces, even though all atoms are within a second-nearest neighbor distance of an interface in the 105-atom grain system. The thermal expansion coefficients of the nanophase silicon samples were generally larger than the perfect lattice expansion coefficient, by as much as a factor of two in some cases. Above 600K, the silicon samples showed evidence of annealing, and started to densify. The implications of these results and other calculations regarding the structure of interfaces and their effects on bulk properties will be discussed.

C13.6

THE APPLICATION OF GLANCING ANGLE EXAFS TO STUDY THE STRUCTURE OF PLATINUM-NICKEL MULTILAYERS. G. M. Lamble, North Carolina State University, Raleigh, NC 27695-8202, S. M. Heald, Brookhaven National Laboratory, Upton, NY 11973, and B. M. Clemens, University of Stanford, Stanford, CA 94305-2205

Recent reports have correlated the mechanical properties of multilayers with a structural expansion of the constituents. The nature of this expansion is under dispute, with conflicting theories by Clemens and Easley [1], who attribute the expansion to an interface effect, and Huberman and Grimsditch [2], who regard the expansion as a bulk effect. We apply the technique of glancing angle EXAFS to obtain detailed structural information, to appraise the ability of this technique to shed light on this controversy. We perform glancing angle EXAFS on platinum-nickel multilayers of varying bilayer thickness. Measurements are made by fluorescence detection of EXAFS beyond both the Pt L_{III} and the Ni K edges. Considerable interlayer mixing is evident, along with the retention of the bulk metallic character within the layers.

This work was supported by the U.S. Department of Energy, Division of Materials Sciences, under Contract Nos. DE-AS05-80ER10742 and DE-AC02-76CH00016.

- [1] Bruce M. Clemens and Gary L. Easley, Phys. Rev. Lett. 61, 2356 (1988).
- [2] M. L. Huberman and M. Grimsditch, Phys. Rev. Lett. 62, 1403 (1989).

C13.7

THE ELECTRONIC STRUCTURE OF $\Sigma 5$ GRAIN BOUNDARIES IN CU. Erik C. Sowa and A. Gonis, Lawrence Livermore National Laboratory, Livermore, CA; * X.-G. Zhang, Northwestern U., Chicago, IL; and S. M. Foiles, Sandia National Laboratories Livermore, Livermore, CA.†

We present first-principles calculations of the densities-of-states (DOS's) of unrelaxed and relaxed twist and tilt grain boundaries (GB's) in Cu. The relaxed configurations were obtained through the use of the Embedded Atom Method (EAM)¹, while the DOS's were calculated using the real-space multiple scattering theory (RS-MST) approach recently introduced² in the literature. The DOS's of GB's are compared against those of bulk materials as well as against one another. Although the RS-MST calculations are still not self-consistent, these comparisons allow us to verify certain expected trends in the DOS's, and to verify the usefulness and reliability of our method.

* Supported by US DOE under contract W-7405-ENG-48.

† Supported by Director, Office of Energy Research, Office of Basic Energy Sciences, Materials Science Division of the US DOE.

1. S. M. Foiles, submitted to Acta Met.

2. X.-G. Zhang and A. Gonis, Phys. Rev. Lett. 62, 1161-1164

SYMPOSIUM D:
LAYERED STRUCTURES - HETEROEPITAXY,
SUPERLATTICES, STRAIN AND METASTABILITY

D

November 27 - December 1, 1989

Chairs

Leo J. Schowalter
Physics Department and Center
of Integrated Electronics
Rensselaer Polytechnic Institute
Troy, NY 12180
(518) 276-6435

Brian W. Dodson
Division 1143
Sandia National Laboratories
P.O. Box 5800
Albuquerque, NM 87185
(505) 844-5459

Fred H. Pollak
Physics Department
Brooklyn College of SUNY
Brooklyn, NY 11210
(718) 780-5356

Jack E. Cunningham
Room 4B-513
AT&T Bell Laboratories
Crawfords Corner Road
Holmdel, NJ 07733
(201) 949-8236

Symposium Support

Aixtron, Inc.

ASTeX, Inc.

Blake Industries, Inc.

EPI Systems Division - Chorus Corporation

Emcore, Inc.

Instruments SA (Riber)

MDC Vacuum Products Corporation

VG Semicon, Ltd.

Varian, Inc.

Proceedings published as Volume 160
of the Materials Research Society
Symposium proceedings series.

SESSION D1: HETEROEPITAXY:

METAL/SEMICONDUCTORS

Chairs: T. L. Cheeks and R. W. Fathauer
Monday Morning, November 27
Salon C/D (M)

8:30 *D1.1

STABILITY OF METAL LAYERS EMBEDDED IN SEMICONDUCTORS, J.P. Harbison, T. Sands, C.J. Palmström, N. Tabatabaie, H.L. Gilchrist, L.T. Florez, T.L. Cheeks, R.E. Nahory, W.K. Chan, and V.G. Keramidas, Bellcore, Red Bank, NJ.

9:00 D1.2

ELECTRICAL AND OPTICAL CHARACTERIZATION OF MBE GROWN BURIED METAL (Al,Ga)As/NiAl/(Al,Ga)As DOUBLE SCHOTTKY DIODES, T.L. Cheeks, T. Sands, R. Nahory, J. Harbison, N. Tabatabaie, H. Gilchrist, and B. Wilkens, Bellcore, Red Bank, NJ.

9:15 D1.3

GROWTH AND CHARACTERIZATION OF GaAs/RARE-EARTH MONOARSENIDE/GaAs HETEROSTRUCTURES, C.J. Palmström, S. Mounier, T.G. Finstad, N. Tabatabaie, S.J. Allen, Jr., T. Sands, T.L. Cheeks, P.F. Miceli, Bellcore, Red Bank, NJ; J.G. Zhu, and C.B. Carter, Cornell University, Department of Materials Science and Engineering, Ithaca, NY.

9:30 D1.4

EPITAXIAL GROWTH OF MATCHED METALLIC $\text{ErP}_{0.6}\text{As}_{0.4}$ LAYERS ON GaAs AND $\text{ErP}_{0.5}\text{Sb}_{0.5}$ ON InP IN A MBE SYSTEM, A. Guivarc'h, A. Le Corre, J. Caulet, B. Guenais, M. Minier, G. Ropars, Centre National d'Etudes des Télécommunications, Lannion, France.

9:45 BREAK

10:15 D1.5

ANISOTROPIC STRAIN IN THIN EPITAXIAL $\text{CoSi}_2(110)$ FILMS GROWN ON $\text{Si}(110)$, S.M. Yalisove, University of Michigan, Department of Materials Science and Engineering, Ann Arbor, MI; D.J. Eaglesham, and R.T. Tung, AT&T Bell Laboratories, Murray Hill, NJ.

*Invited Paper

Short Course M-04, "Optoelectronic Materials, Processes, and Devices," C-20, "Optical Characterization of III-V Semiconductor Epitaxial Layers," and P-16, "Epitaxial Growth of Compound Semiconductors," may be of interest to symposium attendees. Details regarding course dates and instructors are provided in the short course section of this program.

10:30 D1.6

GROWTH OF EPITAXIAL CoSi_2 AND NiSi_2 ON (111), (100), AND (110) Si AT ROOM TEMPERATURE, R.T. Tung, and F. Schrey, AT&T Bell Laboratories, Murray Hill, NJ.

10:45 D1.7

FORMATION OF ULTRATHIN NICKEL AND COBALT SILICIDES ON $\text{Si}(111) \sqrt{3} \times \sqrt{3}$ -B AT ROOM TEMPERATURE, L. Luo, State University of New York at Albany, Department of Physics, Albany, NY; G.A. Smith, State University of New York at Albany, Department of Physics, Albany, NY and GE Corporate Research and Development Center, Schenectady, NY; Shin Hashimoto and W.M. Gibson, State University of New York at Albany, Department of Physics, Albany, NY.

11:00 D1.8

FORMATION OF HIGH QUALITY $\text{Si}/\text{CoSi}_2/\text{Si}$ DOUBLE HETERO-STRUCTURES BY SELF-ALIGNED AND TWO STEP MOLECULAR BEAM EPITAXY, M. Miyao, T. Ohshima, N. Nakamura and K. Nakagawa, Hitachi Ltd., Central Research Laboratory, Tokyo, Japan.

11:15 D1.9

GROWTH AND CHARACTERIZATION OF EPITAXIAL CoSi_2 ON $\text{Si}(100)$, Jorge R. Jimenez, L. Hsiung, K.V. Ramanathan, K. Rajan, L.J. Schowalter, Rensselaer Polytechnic Institute, Center for Integrated Electronics, Troy, NY; Shin Hashimoto, State University of New York, Physics Department, Albany, NY; R.D. Thompson, B.A. Ek, and S.S. Iyer, IBM T.J. Watson Research Center, Yorktown Heights, NY.

11:30 D1.10

EVOLUTION OF STRESS DURING HETEROEPITAXIAL GROWTH OF NiSi_2 ON (001) AND (111) SILICON SUBSTRATES, H.L. Ho, C.L. Bauer, S. Mahajan, Carnegie Mellon University, Department of Metallurgical Engineering and Materials Science, Pittsburgh, PA; A.G. Milnes, Carnegie Mellon University, Department of Electrical and Computer Engineering, Pittsburgh, PA.

11:45 D1.11

COLUMNAR EPITAXY OF CoSi_2 ON $\text{Si}(111)$, (100), and (110), R.W. Fathauer, California Institute of Technology, Jet Propulsion Laboratory, Pasadena, CA; C.W. Nieh, California Institute of Technology, Materials Science Department, Pasadena, CA; Q.F. Xiao and Shin Hashimoto, State University of New York at Albany, Physics Department, Albany, NY.

SESSION D2: HETEROEPITAXY: METALS,

SEMICONDUCTORS, AND INSULATORS

Chairs: R. T. Tung and R. F. C. Farrow
Monday Afternoon, November 27
Salon C/D (M)

1:30 D2.1

HIGH RESOLUTION X-RAY SCATTERING STUDIES OF STRAIN IN EPITAXIAL THIN FILMS OF YTTRIUM SILICIDE GROWN ON SILICON(111), L.J. Martinez-Miranda, University of Pennsylvania, Laboratory for Research on the Structure of Matter, Department of Electrical Engineering, Philadelphia, PA; M.P. Siegal, University of Pennsylvania, Laboratory for Research on the Structure of Matter, Department of Materials Science and Engineering, Philadelphia, PA; P.A. Heiney, University of Pennsylvania, Laboratory for Research on the Structure of Matter, Department of Physics, Philadelphia, PA; J.J. Santiago-Avilés, University of Pennsylvania, Laboratory for Research on the Structure of Matter, Department of Electrical Engineering, Philadelphia, PA; and W.R. Graham, University of Pennsylvania, Laboratory for Research on the Structure of Matter, Department of Materials Science and Engineering, Philadelphia, PA.

1:45 D2.2

SURFACE MORPHOLOGY OF TiSi_2 FORMED FROM UHV DEPOSITED Ti ON Si, Hyeon-taeg Jeon, North Carolina State University, Department of Materials Science and Engineering, Raleigh, NC; R.J. Nemanich, J.W. Honeycutt and G.A. Rozgonyi, North Carolina State University, Department of Physics and Department of Materials Science and Engineering, Raleigh, NC.

2:00 D2.3

EPITAXIAL GROWTH OF TbSi_2 ON Si(111), F.H. Kaatz, Laboratory for Research on the Structure of Matter and the University of Pennsylvania, Department of Materials Science, Philadelphia, PA; J. Van der Spiegel, Laboratory for Research on the Structure of Matter and the University of Pennsylvania, Department of Electrical Engineering, Philadelphia, PA; and W.R. Graham, Laboratory for Research on the Structure of Matter and the University of Pennsylvania, Department of Materials Science, Philadelphia, PA.

2:15 D2.4

GROWTH KINETICS OF Si ON SAPPHIRE BY MBE AS A FUNCTION OF SUBSTRATE IN-SITU HIGH TEMPERATURE SUBSTRATE ANNEAL, Eliezer David Richmond, Naval Research Laboratory, Washington, DC; Joseph G. Pellegrino, National Institute of Standards and Technology, Gaithersburg, MD; and Mark E. Twigg, GEO-Centers Inc., Fort Washington, MD.

2:30 D2.5

A HREM STUDY OF EPITAXIAL FLUORIDE / RARE EARTH / FLUORIDE / GaAs INTERFACES, C.J. Chien, Stanford University, Department of Materials Science and Engineering, Stanford, CA; R.F.C. Farrow, IBM Almaden Research Center, San Jose, CA; and J.C. Bravman, Stanford University, Department of Materials Science and Engineering, Stanford, CA.

2:45 D2.6

INFLUENCE OF OFF-ORIENTED SUBSTRATES ON HETEROEPITAXIAL GROWTH OF $(\text{Ca}, \text{Sr})\text{F}_2$ LAYERS ON Si(100), Tetsuro Minemura and Junko Asano, Hitachi, Ltd., Hitachi Research Laboratory, Ibaraki, Japan; Kazuo Tsutsui and Seijiro Furukawa, Tokyo Institute of Technology, Department of Applied Electronics, Yokohama, Japan.

3:00 BREAK

3:30 D2.7

STRAIN IN EPITAXIAL GaAs ON $\text{CaF}_2/\text{Si}(111)$, L.J. Schowalter, J.E. Ayers and S.K. Ghandhi, Rensselaer Polytechnic Institute, Center for Integrated Electronics, Troy, NY; Shin Hashimoto, W.M. Gibson, State University of New York at Albany, Physics Department, Albany, NY; F.K. LeGoues, IBM T.J. Watson Research Center, Yorktown Heights, NY; and P.A. Claxton, University of Sheffield, Dept. of Electronic and Electrical Engineering, Sheffield, United Kingdom.

3:45 D2.8

EPITAXIAL GROWTH OF (100) GaAs ON SOS USING A SPECIFICALLY DESIGNED MOCVD SYSTEM, T. Nishimura, K. Kadoiwa, K. Mitsui and T. Murotani, Mitsubishi Electric Corp., Optoelectronic and Microwave Devices R&D Lab., Hyogo, Japan.

4:00 D2.9

EFFECT OF STOICHIOMETRY ON THE ACTIVATION OF IMPLANTED Si IN MBE-GROWN GaAs ON Si, T.S. Kim and Y.C. Kao, Texas Instruments, Inc., Central Research Laboratories, Dallas, TX.

4:15 D2.10

SELECTIVE AREA GROWTH OF GaAs ON Si BY ELECTRON-CYCLOTRON-RESONANCE PLASMA-EXCITED MOLECULAR-BEAM-EPITAXY (ECR-MBE), Tomohiro Shibata, Naoto Kondo, Yasushi Nanishi and Masatomo Fujimoto, NTT Opto-electronics Laboratories, Kanagawa, Japan.

4:30 D2.11

ELECTRICAL PROPERTIES OF MESA DIODES ON EPITAXIAL GaAs/Si, K.L. Jiao, A.J. Soltyka, W.A. Anderson, State University of New York at Buffalo, Center for Electronic and Electro-optic Materials, Department of Electrical and Computer Engineering, Amherst, NY; and S.M. Vernon, Spire Corporation, Bedford, MA.

4:45 D2.12

HIGH QUALITY GaAs ON SOI BY MOCVD, N.H. Karam, V.E. Haven, S.M. Vernon, Spire Corporation, Bedford, MA; N.A. El-Masry, North Carolina State University, Raleigh, NC; and N. Haegel, University of California, Los Angeles, CA.

SESSION D3: FUTURE DEVELOPMENTS IN EPITAXIAL TECHNIQUES AND EQUIPMENT

Chairs: L.J. Schowalter and J.E. Cunningham
Monday Evening, November 27
8:00 p.m. - 10:00 p.m.
Salon C/D (M)

SESSION D4: GENERAL TOPICS IN STRAINED-LAYER EPITAXY

Chairs: C. P. Flynn and L. B. Freund
Tuesday Morning, November 28
Salon C/D (M)

8:30 *D4.1

FUNDAMENTAL ISSUES IN HETEROEPITAXY: A DOE COUNCIL OF MATERIALS SCIENCE PANEL REPORT, Paul S. Peercy, Sandia National Laboratories, Albuquerque, NM.

9:00 D4.2

THE ROLE OF AN INTERFACE MISFIT DISLOCATION IN BLOCKING THE GLIDE OF A THREADING DISLOCATION IN A STRAINED EPITAXIAL LAYER, L.B. Freund, J.C. Ramirez and A. Bower, Brown University, Division of Engineering, Providence, RI.

9:15 D4.3

SURFACE STRESS EFFECTS ON EPITAXY, K. Sieradzki and R.C. Cammarata, The Johns Hopkins University, Department of Materials Science and Engineering, Baltimore, MD.

9:30 D4.4

MICRODIFFRACTION FROM CLEAVED Si-Si_{1-x}Ge_x MULTILAYERS, W.T. Pike, Cambridge University, Department of Physics, Cavendish Laboratory, Cambridge, United Kingdom.

9:45 D4.5

ELECTRON CHANNELING ANALYSIS OF ELASTIC STRAINS IN InGaAs THIN FILMS, R. Keller, W. Zielinski, W.W. Gerberich, and J. Kozubowski, University of Minnesota, Department of Chemical Engineering and Materials Science, Minneapolis, MN.

10:00 BREAK

10:30 *D4.6

GROWTH AND RELAXATION OF STRAINED HETERO-STRUCTURES, J.Y. Tsao, Sandia National Laboratories, Albuquerque, NM.

11:00 D4.7

ALTERNATE ROUTES TOWARD MISMATCH ACCOMODATION IN STRAINED-LAYER STRUCTURES, Brian W. Dodson, Sandia National Laboratories, Albuquerque, NM.

11:15 D4.8

A STUDY OF DISLOCATION BENDING PROCESSES AT STRAINED LAYER INTERFACES, S.A. Hussien, N.A. El-Masry, J.C.L. Tarn, J.-R. Gong, and S.M. Bedair, North Carolina State University, Electrical and Computer Engineering Department, Raleigh, NC.

11:30 D4.9

DISLOCATION DENSITY REDUCTION IN GaAs EPI-LAYERS ON SILICON USING STRAINED LAYER SUPERLATTICES, S. Sharan, M. Sangneria, K. Jagannadham, and J. Narayan, North Carolina State University, Department of Materials Science and Engineering, Raleigh, NC.

11:45 D4.10

THE KINETICS OF STRAIN RELAXATION IN In-GaAs/GaAs STRAINED MULTILAYERS, David C. Paine and Morgan Kurk, Brown University, Engineering Department, Providence, RI; Robert N. Sacks, Timothy C. Eschrich and William J. Tanski, United Technologies Research Center, Electronic Material Department, East Hartford, CT.

SESSION D5: SiGe EPITAXY

Chairs: D. J. Eaglesham and S. M. Prokes
Tuesday Afternoon, November 28
Salon C/D (M)

1:30 *D5.1

PROPERTIES AND DEVICE APPLICATIONS OF Si_{1-x}Ge_x ALLOYS, Subramanian S. Iyer, IBM T.J. Watson Research Center, Research Division, Yorktown Heights, NY.

2:00 D5.2

THE GROWTH MECHANISM OF EPITAXIAL SiGe HETEROSTRUCTURES PRODUCED BY WET OXIDATION OF AMORPHOUS SiGe THIN FILMS, S.M. Prokes, U.S. Naval Research Laboratory, Washington, DC; and A.K. Rai, Universal Energy Systems, Inc., Dayton, OH.

2:15 D5.3

SOLID PHASE EPITAXIAL REGROWTH OF Ge_xSi_{1-x} ON [100] Si, Q.Z. Hong, A.J. Yu, J.W. Mayer, Cornell University, Department of Materials Science and Engineering, Ithaca, NY; J.M. Poate, J.C. Bean, and D.J. Eaglesham, AT&T Bell Laboratories, Murray Hill, NJ.

2:30 D5.4

SOLID PHASE EPITAXIAL REGROWTH OF SiGe STRAINED LAYERS AMORPHIZED BY ION IMPLANTATION, B.J. Robinson, B.T. Chilton, and D.A. Thompson, McMaster University, Centre for Electrophotonic Materials and Devices, Hamilton, Canada.

2:45 D5.5

REDUCTION OF DEFECT DENSITY IN HETEROEPITAXIAL $\text{Ge}_x\text{Si}_{1-x}$ GROWN ON PATTERNED Si SUBSTRATES, E.A. Fitzgerald, P.E. Freeland, Y.-H. Xie, AT&T Bell Laboratories, Murray Hill, NJ.

3:00 BREAK

3:30 *D5.6

EXPERIMENTAL STUDIES OF KINETIC EFFECTS IN STRAINED LAYER EPITAXY, R. Hull, and J.C. Bean, AT&T Bell Laboratories, Murray Hill, NJ.

4:00 D5.7

THE 2D-3D TRANSITION IN THE MBE GROWTH OF Ge/Si, D.J. Eaglesham, and M. Cerullo, AT&T Bell Laboratories, Murray Hill, NJ.

4:15 D5.8

MORPHOLOGY OF GE FILMS GROWN LAYER BY LAYER ON Si(001), F.K. LeGoues, M. Copel and R.M. Tromp, IBM T.J. Watson Research Center, Yorktown Heights, NY.

4:30 D5.9

MISFIT DISLOCATION NUCLEATION AND MULTIPLICATION AT $\text{Ge}_x\text{Si}_{1-x}$ /Si INTERFACES, D.D. Perovic, G.C. Weatherly, University of Toronto, Department of Metallurgy and Materials Science, Toronto, Canada; and D.C. Houghton, National Research Council, Division of Physics, Ottawa, Canada.

4:45 D5.10

DISLOCATION BEHAVIOUR IN $\text{Ge}_x\text{Si}_{1-x}$ EPILAYERS ON (001)Si; E.P. Kvam, The University of Liverpool, Department of Materials Science and Engineering, Liverpool, United Kingdom; and Lawrence Berkeley Laboratory, Berkeley, CA; D.M. Maher, The University of Liverpool, Department of Materials Science and Engineering, Liverpool, United Kingdom; and AT&T Bell Laboratories, Murray Hill, NJ; and C.J. Humphreys, The University of Liverpool, Department of Materials Science and Engineering, Liverpool, United Kingdom.

SESSION D6: METALLIC SUPERLATTICES

Chairs: R. C. Cammarata and A. F. Jankowski
Wednesday Morning, November 29
Salon C/D (M)

8:30 *D6.1

METASTABILITY IN SINGLE CRYSTAL EPILAYERS AND SUPERLATTICES GROWN BY MBE, R. Du and C.P. Flynn, University of Illinois at Urbana-Champaign, Materials Research Laboratory and Department of Physics, Urbana, IL.

9:00 D6.2

MICROSTRUCTURE OF FCC/BCC METAL MULTILAYERS, Nigel M. Jennett, D.J. Dingley, Bristol University, Department of Physics, Bristol, United Kingdom; and Y. Ando, Nagoya University, Department of Applied Physics, Nagoya, Japan.

9:15 D6.3

AN INVESTIGATION OF THE DISLOCATION STRUCTURE OF THE NI/AG PHASE BOUNDARY, Thomas A. Bamford, Wilkes College, School of Engineering and Applied Science, Wilkes-Barre, PA.

9:30 D6.4

EPITAXIAL GROWTH OF Cu-Ni SINGLE CRYSTAL ALLOYS AND SUPERLATTICES BY MOLECULAR BEAM EPITAXY, R.P. Burns, Research Triangle Institute, Research Triangle Park, NC, and North Carolina State University, Department of Physics, Raleigh, NC; Y.H. Lee, North Carolina State University, Department of Materials Science and Engineering, Raleigh, NC; N.R. Parikh, University of North Carolina, Department of Physics and Astronomy, Chapel Hill, NC; and J.B. Posthill, M.J. Mantini, and R.J. Markunas, Research Triangle Institute, Research Triangle Park, NC.

9:45 D6.5

STRUCTURAL AND ELECTRONIC PROPERTIES OF Pb/Cu MULTILAYERS, Dominique Neerincx, Kristiaan Temst, Hans Vanderstraeten, and Yvan Bruynseraede, Katholieke Universiteit Leuven, Laboratorium voor Vaste Stof-Fysika en Magnetisme, Leuven, Belgium; and Ivan K. Schuller, University of California-San Diego, Physics Department, La Jolla, CA.

10:00 BREAK

10:30 D6.6

SURFACE STRESS EFFECTS ON THE ELASTIC MODULI OF SUPERLATTICE THIN FILMS, R.C. Cammarata, K. Sieradzki, The Johns Hopkins University, Department of Materials Science and Engineering, Baltimore, MD; and F. Streitz, The Johns Hopkins University, Department of Physics and Astronomy, Baltimore, MD.

10:45 D6.7

ANALYSIS OF Au/Ni MULTILAYERS BY X-RAY DIFFRACTION, J. Chaudhuri, S. Shah, V. Gondhalekar, Wichita State University, The Institute for Aviation Research, Mechanical Engineering Department, Wichita, KS; and A.F. Jankowski, University of California, Lawrence Livermore National Laboratory, Livermore, CA.

11:00 D6.8
ELASTIC PROPERTIES OF FCC-FCC METALLIC MULTILAYERS, John R. Dutcher, Sukmock Lee, Jeha Kim, Craig D. England, George I. Stegeman and Charles M. Falco, University of Arizona, Optical Sciences Center and Department of Physics, Tucson, AZ.

11:15 D6.9
EPITAXIAL Fe/Ag AND Mn/Ag SUPERLATTICES, S. Nahm, and L. Salamanca-Young, University of Maryland, Department of Chemical and Nuclear Engineering, College Park, MD; and B.T. Jonker, J.J. Krebs, and G.A. Prinz, Naval Research Laboratory, Washington, DC.

11:30 D6.10
GROWTH AND CHARACTERIZATION OF (Mn/Ag) (001) SUPERLATTICES, B.T. Jonker, Y.U. Idzerda, J.J. Krebs, and G.A. Prinz, Naval Research Laboratory, Washington, DC.

11:45 D6.11
FORMATION AND STRUCTURE OF Mo THIN LAYERS ON Ni(001) AND Mo-Ni SUPERLATTICES, Y.H. Lee, North Carolina State University, Department of Materials Science and Engineering, Raleigh, NC; R.P. Burns, Research Triangle Institute, Research Triangle Park, NC, and North Carolina State University, Department of Materials Science and Engineering, Raleigh, NC; J.B. Posthill, M.J. Mantini, R.J. Markunas, Research Triangle Institute, Research Triangle Park, NC; and K.J. Bachmann, North Carolina State University, Department of Materials Science and Engineering, Raleigh, NC.

SESSION D7: III-V (A)

Chairs: C. Tu and W. Wang
Wednesday Afternoon, November 29
Salon C/D (M)

1:30 *D7.1
MATERIALS AND DEVICE PROPERTIES OF LATTICE-MATCHED AND PSEUDOMORPHIC InP BASED HETEROSTRUCTURES, Umesh K. Mishra, North Carolina State University, Department of Electrical and Computer Engineering, Raleigh, NC; and April S. Brown, Cornell University, Ithaca, NY.

2:00 D7.2
MATERIALS AND DEVICE CHARACTERISTICS OF PSEUDOMORPHIC AlGaAs-InGaAs-GaAs AND AllnAs-InGaAs-InP HIGH ELECTRON MOBILITY TRANSISTORS, J.M. Ballingall, Pin Ho, G.J. Tessmer, P.A. Martin, T. H. Yu, P.C. Chao, P.M. Smith and K.G.H. Duh, General Electric Company, Electronics Laboratory, Syracuse, NY.

2:30 D7.3
X-RAY DIFFRACTION STUDY OF InAlAs-InGaAs ON InP HIGH ELECTRON MOBILITY TRANSISTOR STRUCTURE PREPARED BY MOLECULAR-BEAM EPITAXY, H.Y. Liu, Y.C. Kao and T.S. Kim, Texas Instruments, Inc., Central Research Laboratories, Dallas, TX.

2:45 D7.4
STRUCTURAL AND ELECTRONIC PROPERTIES OF GaAs/InGaAs/GaAs HETEROSTRUCTURES, J.M. Bonar, R. Hull, R.J. Malik, and R.W. Ryan, AT&T Bell Laboratories, Murray Hill, NJ; and J.F. Walker, Laboratorio TASC, Trieste, Italy.

3:00 BREAK

3:30 D7.5
FIELD EFFECT TRANSISTOR STRUCTURE BASED ON STRAIN INDUCED POLARIZATION CHARGES, D.L. Smith, Los Alamos National Laboratory, Los Alamos, NM; R.T. Collins, T.F. Kuech, IBM T.J. Watson Research Center, Yorktown Heights, NY; C. Mailhot, Xerox Webster Research Center, Webster, NY.

3:45 D7.6
THE EFFECT OF INDIUM DEPLETION ON THE COMPOSITION OF OMVPE GROWN GaAs, P.D. Agnello, IBM T.J. Watson Research Center, Yorktown Heights, NY; P.B. Chinoy and S.K. Ghandhi, Rensselaer Polytechnic Institute, Troy, NY.

4:00 D7.7
HETEROJUNCTION STUDY OF $\text{Ga}_{0.9}\text{In}_{0.1}\text{As}(p^+)/\text{GaAs}(n)$ DIODES: CORRELATION OF ELECTRICAL AND STRUCTURAL CHARACTERISTICS, Y.W. Choi, C.R. Wie, State University of New York at Buffalo, Department of Electrical and Computer Engineering and Center for Electronic and Electrooptic Materials, Amherst, NY; K.R. Evans and C.E. Stutz, Wright-Peterson Air Force Base, OH.

4:15 D7.8
SURFACE CROSS-HATCHED MORPHOLOGY ON STRAINED III-V SEMICONDUCTOR HETEROSTRUCTURES, K.H. Chang, D. Srolovitz, R. Gibala, University of Michigan, Department of Materials Science and Engineering, Ann Arbor, MI; P.K. Bhat-tacharya, University of Michigan, Department of Electrical Engineering and Computer Science, Ann Arbor, MI; and J.F. Mansfield, University of Michigan, Electron Microbeam Analysis Laboratory, Ann Arbor, MI.

4:30 D7.9
THERMAL STABILITY OF STRAINED InGaAs/GaAs SINGLE QUANTUM WELLS, B. Elman, Emil S. Koteles, P. Melman, C.A. Armiento and C. Jagannath, GTE Laboratories, Inc., Waltham, MA.

4:45 **D7.10**

APPLICATION OF GaAs-AlGaAs SUPERLATTICE STRUCTURE FOR FABRICATING HIGH BREAKDOWN VOLTAGE POWER MISFET, W.C. Liu, W.S. Lour, R.L. Wang and W.C. Hsu, National Cheng Kung University, Department of Electrical Engineering, Tainan, Taiwan, China.

SESSION D8: III-V (B)

Chairs: A. C. Gossard and C. Fonstead
Thursday Morning, November 30
Salon C/D (M)

8:30 ***D8.1**

RESONANT TUNNELING TRANSISTORS AND QUANTUM EFFECT DEVICES, Federico Capasso, AT&T Bell Laboratories, Murray Hill, NJ.

9:00 ***D8.2**

DIFFRACTION STUDIES OF THE GROWTH OF STRAINED EPITAXIAL FILMS, G.J. Whaley and P.I. Cohen, University of Minnesota, Department of Electrical Engineering, Minneapolis, MN.

9:30 **D8.3**

EFFECTS OF SUBSTRATE MISORIENTATION AND THE GROWTH MECHANISM OF Si DOPED GaAs GROWN ON (111) A SUBSTRATE BY MBE, Y. Okano, H. Seto, M. Shigeta, S. Nishine, I. Fujimoto, ATR Optical and Radio Communications Research Laboratories, Kyoto, Japan; and T. Suzuki, Science and Technical Research Laboratories of NHK, Tokyo, Japan.

9:45 **D8.4**

ORDERED TERNARY ALLOYS BY ATOMIC LAYER EPITAXY, B.T. McDermott, K.G. Reid, A. Dip, N.A. El-Masry, S.M. Bedair, North Carolina State University, Electrical and Computer Engineering Department, Raleigh, NC; W. Duncan, Texas Instruments, Dallas, TX; X. Yin and F.H. Pollak, Brooklyn College of CUNY, Department of Physics, Brooklyn, NY.

10:00 BREAK

10:30 **D8.5**

InAs AND InGaAs GROWTH BY CHLORIDE ATOMIC LAYER EPITAXY, H. Shinawaki, NEC Corp., Microelectronics Research Laboratories, Kawasaki, Japan; Y. Kato and A. Usui, NEC Corporation, Fundamental Research Laboratories, Ibaraki, Japan.

10:45 **D8.6**

ELECTRICAL AND MATERIAL CHARACTERIZATION OF THE STABILITY OF ALGAAS AND INGAAS PLANAR DOPED STRUCTURES, Larry P. Sadwick, University of Utah, Department of Electrical Engineering, Salt Lake City, UT; and Dwight C. Streit, TRW Electronic Systems Group, Redondo Beach, CA.

11:00 **D8.7**

KINETICS OF QUANTUM WIRE GROWTH ON VICINAL SURFACES, K.J. Hugill, S. Clarke, D.D. Vvedensky, and B.A. Joyce, Imperial College, The Blackett Laboratory and Semiconductor Materials IRC, London, United Kingdom.

11:15 **D8.8**

LIQUID PHASE ELECTROEPITAXIAL (LPEE) GROWTH OF GaSb AND InGaAsSb, Shanthi N. Iyer, Ali Abul-Fadl, North Carolina A&T State University, Department of Electrical Engineering, Greensboro, NC; Albert T. Macrander, AT&T Bell Laboratories, Murray Hill, NJ; Jonathan H. Lewis and W. J. Collis, North Carolina A&T State University, Department of Electrical Engineering, Greensboro, NC.

11:30 **D8.9**

ENERGETICS AND RELAXATIONS OF ADATOM, DOPANT AND VACANCY RELATED COMPLEXES ON NORMAL AND STRAINED GaAs (001) SURFACE, S.B. Ogale, University of Southern California, Departments of Materials Science and Physics, Los Angeles, CA; and University of Poona, Department of Physics, Pune, India; A. Madhukar, University of Southern California, Departments of Materials Science and Physics, Los Angeles, CA; and R. Vishwanathan, University of Poona, Department of Physics, Pune, India.

11:45 **D8.10**

PULSED LASER ATOM PROBE ANALYSIS OF III-V COMPOUND SEMICONDUCTOR EPILAYERS, Ross A.D. Mackenzie, J. Alex Liddle, Chris R.M. Grovenor and Alfred Cerezo, Oxford University, Department of Metallurgy and Science of Materials, Oxford, United Kingdom.

SESSION D8: (CONT.) III-V (B)

Chairs: A. C. Gossard and C. Fonstead
Thursday Afternoon, November 30
Salon C/D (M)

1:30 **D8.11**

THE INTERACTION OF TRIMETHYLGALLIUM WITH CLEAN AND ADSORBATE COVERED SI(100) SUBSTRATES, T.R. Gow, R. Lin, L.A. Cadwell, F. Lee, R.I. Masel, University of Illinois, Urbana, IL.

1:45 **D8.12**

THERMAL DISORDERING OF MODULATION-DOPED AlAs/GaAs SUPERLATTICE, Kunihiro Hara, Hiroshi Ito, Shinya Ohmi and Takamasa Suzuki, Nippondenso Company, Ltd., Aichi-Ken, Japan.

**SESSION D9: SMALL ANGLE X-RAY
CHARACTERIZATION AND AMORPHOUS LAYERS**

Chairs: P. Persans and J. Kakalios
Thursday Afternoon, November 30
Salon C/D (M)

2:00 *D9.1

STRUCTURAL STABILITY OF AMORPHOUS SEMICONDUCTOR SUPERLATTICES, Peter D. Persans, Rensselaer Polytechnic Institute, Physics Department, Troy, NY; A.F. Ruppert, B. Abeles, Exxon Research and Engineering Company, Annandale, NJ; Y.-J. Wu and V. Pantojas, Rensselaer Polytechnic Institute, Physics Department, Troy, NY.

2:30 D9.2

A SYSTEMATIC METHOD FOR EXTRACTING STRUCTURAL PARAMETERS FROM LOW ANGLE X-RAY REFLECTIVITY MEASUREMENTS ON MULTILAYERS, L.M. Goldman, Harvard University, Division of Applied Sciences, Cambridge, MA; H.A. Atwater, California Institute of Technology, Thomas J. Watson Laboratory of Applied Physics, Pasadena, CA; and F. Spaepen, Harvard University, Division of Applied Sciences, Cambridge, MA.

2:45 D9.3

DETERMINATION OF 3-DIMENSIONAL DEFECT STRUCTURES IN GALLIUM ARSENIDE EPILAYERS ON SILICON USING WHITE BEAM SYNCHROTRON RADIATION TOPOGRAPHY IN BOTH TRANSMISSION GEOMETRY AND GRAZING BRAGG-LAUE GEOMETRY, M. Dudley, J. Wu, G.-D. Yao, State University of New York, Stony Brook, Department of Materials Science and Engineering, Stony Brook, NY; H.-Y. Liu and Y.C. Kao, Texas Instruments, Materials Science Laboratory, Dallas, TX.

3:00 D9.4

CHARACTERIZATION OF METAL/SEMICONDUCTOR MULTILAYERS BY RAMAN SPECTROSCOPY AND X-RAY DIFFRACTION, David D. Allred and Qi Wang, Brigham Young University, Department of Physics and Astronomy, Provo, UT.

3:15 BREAK

3:45 D9.5

(ABSTRACT WITHDRAWN)

4:00 D9.6

STRUCTURAL STABILITY OF HEAT TREATED W/B₄C MULTILAYERS, A.F. Jankowski, Lawrence Livermore National Laboratory, Chemistry and Materials Science Department, Livermore, CA.

4:15 D9.7

MULTILAYERED METALLIC THIN FILMS PREPARED BY DUAL-BATH ELECTRODEPOSITION, C.A. Ross, L.M. Goldman and F. Spaepen, Harvard University, Division of Applied Sciences, Cambridge, MA.

4:30 *D9.8

METASTABLE ELECTRONIC EFFECTS IN AMORPHOUS SUPERLATTICES, J. Kakalios, University of Minnesota, School of Physics and Astronomy, Physics Department, Minneapolis, MN.

SESSION D10: POSTER SESSION

Chairs: F. Pollak and B. W. Dodson
Thursday Evening, November 30
7:00 p.m. - 10:00 p.m.
America Ballroom (W)

D10.1 SILICIDE FORMATION AND THERMAL STABILITY OF Ni/Si/GaAs INTERFACES, Y. Yamamoto, K. Ishibashi, Hosei University, Research Center of Ion Beam Technology, Tokyo, Japan; S. Suzuki, Advanced Materials Laboratory, Inc., Saitama, Japan; T.E. Shim, Samsung Electronics, R&D Center, Semiconductor Business, Seoul, Korea; and Waseda University, Tokyo, Japan.

D10.2 EPITAXIAL GROWTH OF METALLIC LAYERS BY SOLID PHASE INTERDIFFUSION: STUDY OF THE Ni/GaAs AND Ni/AlAs SYSTEMS, R. Guérin, and S. Deputier, Campus de Beaulieu, Laboratoire de Chimie Minérale B, Rennes, France; J. Caulet, M. Minier, A. Poudoulec, Y. Ballini, V. Durel, G. Dupas, A. Guivarc'h, Centre National d'Etudes des Télécommunications, LAB/OCM/MPA, Lannion, France.

D10.3 LATTICE DISTORTION OF SINGLE-CRYSTAL CoSi₂ COLUMNS EMBEDDED IN SINGLE-CRYSTAL SILICON, Shin Hashimoto, Q.F. Xiao, W.M. Gibson, State University of New York at Albany, Physics Department, Albany, NY; C.W. Nieh, California Institute of Technology, Materials Science Department, Pasadena, CA; and R.W. Fathauer, California Institute of Technology, Jet Propulsion Laboratory, Pasadena, CA.

D10.4 STABILITY OF THE ELECTRICAL PROPERTIES OF PT-GA INTERMETALLICS ON ANNEALING CONDITIONS, Larry P. Sadwick, University of Utah, Department of Electrical Engineering, Salt Lake City, UT; and Young K. Kim, Delroy Baugh, and R. Stanley Williams, UCLA, Department of Chemistry and Biochemistry, Los Angeles, CA.

D10.5 CHARACTERIZATION OF ErAs/GaAs AND GaAs/ErAs/GaAs STRUCTURES, Jane G. Zhu, Cornell University, Department of Materials Science and Engineering, Ithaca, NY; Chris J. Palmstrøm, Suzanne Mounier, Bellcore, Red Bank, NJ; and C. Barry Carter, Cornell University, Department of Materials Science and Engineering, Ithaca, NY.

D10.6 SILICON CONSUMPTION DURING SELF-ALIGNED TITANIUM SILICIDE FORMATION ON SHALLOW JUNCTION, P.L. Smith, Microelectronics Center of North Carolina, Research Triangle Park, NC; and C.M. Osburn, North Carolina State University, Department of Electrical and Computer Engineering, Raleigh, NC, and Microelectronics Center of North Carolina, Research Triangle Park, NC.

D10.7 PREFERENTIAL GROWTH OF CoSi_2 IN Co/Si SOLID STATE INTERACTION, Liu Ping, Hong Feng, Li Bingzong, Fudan University, Department of Electronic Engineering, Shanghai, China; and Shen Xiaoliang, Fudan University, Center of Analyses and Measurements, Shanghai, China.

D10.8 EPITAXIAL GROWTH OF IrSi_3 ON Si(111), T.L. Lin, California Institute of Technology, Jet Propulsion Laboratory, Pasadena, CA; C.W. Nieh, California Institute of Technology, Keck Laboratory of Engineering, Pasadena, CA; Shin Hashimoto and Q.F. Xiao, State University of New York at Albany, Physics Department and Institute for Particle-Solid Interaction, Albany, NY.

D10.9 BORON $\sqrt{3} \times \sqrt{3}$ INTERFACE STRUCTURE ON Si(111): TWO-DIMENSIONAL ORDERED DOPING LAYER, R.L. Headrick, L.C. Feldman, I.K. Robinson, E. Vlieg, A.F.J. Levi, H.S. Luftman and J. Kovalchick, AT&T Bell Laboratories, Murray Hill, NJ.

D10.10 EPITAXIAL GROWTH OF (001) Cr ON (001) LiF, J. Mattson, Northwestern University, Department of Physics, Evanston, IL and MSD Argonne National Laboratory, Argonne, IL; B. Brodsky, MSD Argonne National Laboratory, Argonne, IL; and J.B. Ketterson, Northwestern University, Department of Physics, Evanston, IL.

D10.11 THE GERMANIUM GROWTH MECHANISM ON (1102) SAPPHIRE DEPOSITED BY MOLECULAR BEAM EPITAXY, David J. Godbey, Mark E. Twigg, Geoff P. Malafsky, and Syed B. Qadri, Naval Research Laboratory, Washington, DC.

D10.12 RAPID HETEROEPITAXIAL GROWTH OF Ge FILMS BY PULSED SUPERSONIC FREE JET CHEMICAL BEAM EPITAXY, Djula Eres, D.H. Lowndes, J.Z. Tischler, T.E. Haynes and M.F. Chisholm, Oak Ridge National Laboratory, Solid State Division, Oak Ridge, TN.

D10.13 SOLID PHASE EPITAXIAL GROWTH OF II-A FLUORIDES ON INP BY IN-SITU RAPID ISOTHERMAL PROCESSING, R. Singh, F. Radpour, A. Kumar, R.P.S. Thakur, University of Oklahoma, Department of Electrical Engineering and Computer Science, Norman, OK; J. Narayan, and A.R. Srivatsa, North Carolina State University, Department of Materials Science, Raleigh, NC; A.J. Nelson and H.S. Ullal, Solar Energy Research Institute, Golden, CO.

D10.14 STRAIN-CONTROLLED HIGH MOBILITY IN MODULATION DOPED $\text{Si}_{0.5}\text{Ge}_{0.5}/\text{Ge}/\text{Si}_{1-x}\text{Ge}_x$ HETERO-STRUCTURES, M. Miyao, E. Murakami, H. Etoh and K. Nakagawa, Hitachi Ltd., Central Research Laboratory, Tokyo, Japan.

D10.15 STRUCTURAL CHARACTERIZATIONS OF SYMMETRICALLY STRAINED Ge_mSi_n SUPERLATTICES, R.C. Bowman Jr., and P.M. Adams, The Aerospace Corporation, Los Angeles, CA; C.C. Ahn, California Institute of Technology, Keck Laboratory, Pasadena, CA; S.J. Chang, V. Arbet and K.L. Wang, University of California, Electrical Engineering Department, Los Angeles, CA.

D10.16 PLASTIC FLOW IN Si/Ge QUANTUM WELL STRUCTURES, Mark E. Twigg, GEO-Centers, Inc., Fort Washington, MD; and D.J. Godbey, Naval Research Laboratory, Washington, DC.

D10.17 THERMAL STABILITY OF $\text{Si}/\text{Si}_{0.85}\text{Ge}_{0.15}/\text{Si}$ MODULATION DOPED DOUBLE HETERO-STRUCTURES, P.J. Wang, B.S. Meyerson, P.M. Fahey, F. LeGoues, C.J. Scilla and J.M. Cotte, IBM T.J. Watson Research Center, Yorktown Heights, NY.

D10.18 EPITAXY OF Si_mGe_n ATOMIC LAYER SUPERLATTICES, J.-M. Baribeau, D.J. Lockwood, M.W.C. Dharma-wardana, D.C. Houghton and N.L. Rowell, National Research Council Canada, Division of Physics, Ottawa, Canada.

D10.19 MAGNETIC AFTEREFFECT IN COMPOSITIONALLY-MODULATED Ni/Cu MULTILAYERS PREPARED BY ELECTRODEPOSITION AND BY SPUTTERING, L.H. Bennett, L.J. Swartzendruber, National Institute of Standards and Technology, Gaithersburg, MD; and W. Abdul-Razzaq, West Virginia University, Morgantown, WV.

D10.20 THE KINETICS OF $\text{Si}_{1-x}\text{Ge}_x/\text{Si}$ RELAXATION USING LARGE AREA DISLOCATION IMAGING TECHNIQUES, D.C. Houghton, P. Timbrell and J.-M. Baribeau, National Research Council of Canada, Ottawa, Canada.

D10.21 STRUCTURAL PROPERTIES AND THERMAL EVOLUTION OF Fe/Ti MULTILAYERS, B. Rodmacq, J. Hillairet, J. Laugier, and A. Chamberod, CEN-Grenoble, DRF/SPH/MP, Grenoble, France.

D10.22 Ge TRANSPORT AND EPITAXY IN THE AMORPHOUS-Ge/Pd₂Si/[111] Si SYSTEM, Q.Z. Hong, J.G. Zhu, and J.W. Mayer, Cornell University, Department of Materials Science and Engineering, Ithaca, NY.

D10.23 MODEL FOR EPITAXIAL GROWTH OF CO ON CU(100), D.D. Vvedensky, and S. Clarke, Imperial College, The Blackett Laboratory and Semiconductor Materials IRC, London, United Kingdom.

D10.24 MAGNETIC PROPERTIES OF TbFeCo/Al MULTILAYER THIN FILMS, B.D. Yan, J.A. Barnard, M.H. Kim, and G.W. Warren, The University of Alabama, Department of Metallurgical and Materials Engineering, Tuscaloosa, AL.

D10.25 DEPENDENCE OF Mo/Si MULTILAYER MORPHOLOGY ON DEPOSITION ANGLE, Yuanda Cheng, Mary Beth Stearns and David J. Smith, Arizona State University, Department of Physics, Tempe, AZ.

D10.26 EFFECT OF SUBSTRATE MISORIENTATION ON HETEROEPITAXY WITH LARGE LATTICE MISMATCH: Ag/Si(111), D.C. McKenna, K.-H. Park, G.-C. Wang, Rensselaer Polytechnic Institute, Physics Department, Troy, NY; and G.A. Smith, State University of New York, Albany, Department of Physics, Albany, NY.

D10.27 X-RAY DIFFRACTION STUDIES OF PSEUDOMORPHIC α -Ge_xSn_(1-x) ON InSb(001), W. Lowe, E. Fitzgerald, P. Freeland, M. Asom and R. MacHarrie Jr., AT&T Bell Laboratories, Murray Hill, NJ.

D10.28 THERMODYNAMIC PHASE STABILITY ON GaAs OF INTERMETALLIC THIN FILMS OF CoGa WITH A LARGE RANGE OF COMPOSITIONS, Young K. Kim, Delroy Baugh and R. Stanley Williams, UCLA, Department of Chemistry and Biochemistry and Solid State Science Center, Los Angeles, CA.

D10.29 X-RAY TOPOGRAPHIC ANALYSIS OF STRAIN FIELDS DUE TO MICRON-SIZED GRATINGS ON Si(100) AND Al₂O₃ (1120) SURFACES, A. Peter Jardine, Michael Dudley, Gong-Da Yao and Lalita A. Balasubramanian, State University of New York, Stony Brook, Department of Materials Science and Engineering, Stony Brook, NY.

D10.30 FORMATION OF BURIED AND SURFACE CoSi₂ LAYERS BY ION IMPLANTATION, M.F. Wu, Peking University, Technical Physics Department, Beijing, China; A. Vantomme, G. Langouche, IKS University of Leuven, Leuven, Belgium; K. Maex, J. Vanhellemont, IMEC, Leuven, Belgium; J. Vanacken, H. Vloeberghs and Y. Bruynseraede, VSM, University of Leuven, Physics Department, Leuven, Belgium.

D10.31 ANISOTROPIC TRANSPORT IN In-GaAs/GaAs HETEROSTRUCTURES GROWN BY MOVPE, Qing Sun, D. Morris, C. Lacelle, and A.P. Roth, LMS, NRC, Ottawa, Canada.

D10.32 STRAINED InGaAs/GaAs QUANTUM WELLS WITH A 1.3 μ m BANDEDGE AT ROOM TEMPERATURE, P. Melman, B. Elman, C. Jagannath, Emil S. Koteles, A. Silletti, GTE Laboratories, Inc., Waltham, MA.

D10.33 A STABLE n-CHANNEL InP METAL-IN-SULATOR FIELD EFFECT TRANSISTOR WITH AN AMORPHOUS Si:H GATE, E. Roditi, Foundation for Research and Technology-Hellas, Heraklio, Greece; A.A. Iliadis, University of Maryland, Electrical Engineering Department, College Park, MD; and A. Christou, Naval Research Laboratory, Washington, DC.

D10.34 LATTICE MISMATCH EFFECTS IN GaAsP/GaAs AND GaAs/GaAsP/GaAs HETEROSTRUCTURES, Y.W. Choi, C.R. Wie, State University of New York at Buffalo, Department of Electrical and Computer Engineering and Center for Electronic and Electrooptic Materials, Amherst, NY; and S.M. Vernon, Spire Corporation, Bedford, MA.

D10.35 A TEM AND RHEED INVESTIGATION OF THE INITIAL STAGES OF InSb GROWTH ON GaAs(001) BY MOLECULAR BEAM EPITAXY (MBE), X. Zhang, A.E. Staton-Bevan, D.W. Pashley, Imperial College of Science, Technology and Medicine, Department of Materials, London, United Kingdom; S.D. Parker, R.L. Williams and R. Droopad, Imperial College of Science, Technology and Medicine, Department of Physics, London, United Kingdom.

D10.36 HETEROEPITAXIAL GROWTH OF InP ON GaAs WITH INTERFACE LAYER GROWN BY FLOW-RATED MODULATION EPITAXY, W.K. Chen, J.F. Chen, J.C. Chen, H.M. Kim, L. Anthony, C.R. Wie, and P.L. Liu, State University of New York at Buffalo, Department of Electrical and Computer Engineering, Amherst, NY.

D10.37 STRAIN AND LATTICE-MISMATCH IN (001) AND (111) GaInAs/GaAs STRAINED LAYER SUPERLATTICES, H.M. Kim and C.R. Wie, State University of New York at Buffalo, Department of Electrical and Computer Engineering, Amherst, NY; and C.G. Fonstad, Massachusetts Institute of Technology, Cambridge, MA.

D10.38 RAPID GROWTH OF THICK, IC QUALITY, GaAs LAYERS FROM A FLOWING SOLUTION, E.E. Crisman, J.T. Daly, H.J. Gerritsen, C. Roberts, and D. Schaafsma, Brown University Department of Physics, Providence, RI.

D10.39 METAL-ORGANIC CHEMICAL VAPOR DEPOSITION OF InP BY PULSING PRECURSORS, W.K. Chen, J.C. Chen, L. Anthony, and P.L. Liu, State University of New York at Buffalo, Department of Electrical and Computer Engineering, Amherst, NY.

D10.40 METALORGANIC MAGNETRON SPUTTER DEPOSITION (MOMS) OF $\text{In}_x\text{Ga}_{1-x}\text{Sb}$ ON (100)GaAs, R. Rousina, J.P. Noad, and J.B. Webb, National Research Council of Canada, Laboratory for Microstructural Sciences, Department of Physics, Ottawa, Canada.

D10.41 CRITICAL THICKNESS OF GaAs/InGaAs AND AlGaAs/GaAsP QUANTUM WELLS GROWN BY ORGANOMETALLIC CHEMICAL VAPOR DEPOSITION, Dan Bertolet, Jung-Kuei Hsu, and Kei May Lau, University of Massachusetts, Department of E.C.E., Amherst, MA; and Emil S. Koteles, GTE Laboratories Inc., Waltham, MA.

D10.42 OPTICAL SPECTROSCOPY OF 2D ELECTRONS CONFINED AT A GaAs/AlGaAs HETEROINTERFACE IN A TRANSVERSE ELECTRIC FIELD, Q.X. Zhao, P. Bergman, B. Monemar, Linköping University, Department of Physics and Measurement Technology, Linköping, Sweden; P.O. Holtz, Linköping University, Department of Physics and Measurement Technology, Linköping, Sweden and University of California at Santa Barbara, Department of Electrical and Computer Engineering, Santa Barbara, CA; C. Hallin, Linköping University, Department of Physics and Measurement Technology, Linköping, Sweden; M. Sundaram, J.L. Merz and A.C. Gossard, University of California, Santa Barbara, Department of Electrical and Computer Engineering, Santa Barbara, CA.

D10.43 HOT-CARRIER EFFECTS ON OPTICAL PROPERTIES OF GaAs/ $\text{Al}_x\text{Ga}_{1-x}\text{As}$ QUANTUM WELLS, W.M. Chen, B. Monemar, P.O. Holtz, Linköping University, Department of Physics and Measurement Technology, Linköping, Sweden; M. Sundaram, J.L. Merz and A.C. Gossard, University of California, Santa Barbara, Department of Electrical and Computer Engineering, Santa Barbara, CA.

D10.44 APPLICATION OF AN ULTRAHIGH RESOLUTION SPECTROMETER TO THE ANALYSIS OF PHONONS AND PHOTONS IN SOLIDS, J.L. Stehle, and P. Evrard, SOPRA, Bois-Colombes, France; and L.C. Hammond, and J.N. Willis, ARIES/QEI, Concord, MA.

D10.45 EFFECT OF ANNEALING ON STRAINED InGaAs/GaAs QUANTUM WELLS, Emil S. Koteles, B. Elman, P. Melman and C.A. Armiento, GTE Laboratories, Inc., Waltham, MA.

D10.46 CHARACTERIZATION OF MODULATION DOPED PSEUDOMORPHIC AlGaAs/InGaAs/GaAs HEMT STRUCTURES BY ELECTRON BEAM ELECTROREFLECTANCE AND PHOTOLUMINESCENCE, M.H. Herman, and I.D. Ward, Charles Evans and Associates, Redwood City, CA; R. Kopf, and S.J. Pearton, AT&T Bell Laboratories, Murray Hill, NJ; and E.D. Jones, Sandia National Laboratories, Albuquerque, NM.

D10.47 A NEW OXYGEN PLASMA SOURCE FOR "IN-SITU" GROWTH OF YBaCuO MOLECULAR BEAM EPITAXY LAYERS, M. Touzeau, D. Pagnon, Lab. de Phys des Plasmas, Parix XI, Orsay, France; P. Luzeau, A. Barski, ISA Riber, Rueil-Malmaison, France; A. Schuhl, R. Cabanel, S. Koch, J.P. Hirtz and G. Creuset, Thomson CSF, Orsay, France.

D10.48 GROWTH AND CHARACTERIZATION OF $\alpha\text{-Ge}_x\text{Sn}_{1-x}$ HETEROEPITAXIAL ALLOYS ON (001) InSb, E.A. Fitzgerald, P.E. Freeland, M.T. Asom, W. Lowe, R. MacHarrie Jr., A.R. Kortan, F.A. Thiel, L. Cooper, G.A. Thomas, K.A. Jackson, B.E. Weir and L.C. Kimerling, AT&T Bell Laboratories, Murray Hill, NJ.

D10.49 ELECTRODEPOSITED CERAMIC SUPERLATTICES, Jay A. Switzer, Michael J. Shane and Richard J. Phillips, University of Pittsburgh, Department of Materials Science and Engineering, Pittsburgh, PA.

D10.50 THERMAL STRAIN AND PHOTOLUMINESCENCE STUDY OF ALMOST LATTICE-MATCHED $\text{In}_y\text{Ga}_{1-y}\text{As}_{1-y}\text{P}_y$ EPITAXIAL FILMS GROWN ON InP SUBSTRATE, G. Bai, M-A. Nicolet, T. Vreeland Jr., California Institute of Technology, Pasadena, CA; S.-J. Kim, R.G. Sobers, J.W. Lee, M. Brelvi, P.M. Thomas and D.P. Wilt, AT&T Bell Laboratories, Murray Hill, NJ.

SESSION D11: OPTICAL CHARACTERIZATION OF STRAINED LAYERS, QUANTUM WELLS AND SUPERLATTICES

Chairs: D. J. Glembocki and E. Koteles
Friday Morning, December 1
Salon C/D (M)

8:30 ***D11.1**
STRAIN AND STRUCTURALLY INDUCED OPTICAL TRANSITIONS IN EPITAXIAL SEMICONDUCTORS, Thomas P. Pearsall, AT&T Bell Laboratories, Murray Hill, NJ.

9:00 **D11.2**
STRAIN-INDUCED PHOTOLUMINESCENCE IN Si/Ge SUPERLATTICES, G.F.A. van de Walle, E.A. Montie, D.J. Gravesteijn, and A.A. van Gorkum, Philips Research Laboratories, Eindhoven, The Netherlands.

9:15 D11.3
PHOTOLUMINESCENCE EXCITATION SPECTROSCOPY OF STRAINED InGaAs/GaAs QUANTUM WELLS, Emil S. Koteles, B. Owens, B. Elman, P. Melman, GTE Laboratories, Inc., Waltham, MA; D. Bertolet and Kei May Lau, University of Massachusetts, Compound Semiconductor Laboratory, Department of Electrical and Computer Engineering, Amherst, MA.

9:30 D11.4
CHARACTERIZATION OF INGAAS/GAAS STRAINED SL BY X-RAY DOUBLE CYRSTAL DIFFRACTION AND MODULATE PHOTOREFLECTION SPECTRA, L.S. Xiu, University of Science and Technology of China, Center for Fundamental Physics, Hefei, China; Y.T. Wang, Institute of Semiconductors, Chinese Academy of Science, Beijing, China; Z.Q. Wu, University of Science and Technology of China, Center for Fundamental Physics, Hefei, China; W.H. Zhuang, Institute of Semiconductors, Chinese Academy of Science, Beijing, China.

9:45 D11.5
OPTICAL CHARACTERIZATION OF GaAsP STRAINED LAYERS GROWN ON (111)-ORIENTED GaP, Mats-Erik Pistol, Maria Gerling, Anders Gustafsson, Gert Paulsson, Lars Samuelson, and Heinz Titze, University of Lund, Department of Solid State Physics, Lund, Sweden.

10:00 BREAK

10:30 D11.6
HIGH PRESSURE OPTICAL STUDIES OF GaSb-AlSb MULTIPLE QUANTUM WELLS, Benjamin Rockwell, H.R. Chandrasekhar, Meera Chandrasekhar, University of Missouri, Columbia, Department of Physics, Columbia, MO; Fred H. Pollak, H. Shen, Brooklyn College of CUNY, Physics Department, Brooklyn, NY; L.L. Chang, W.I. Wang and L. Esaki, IBM T.J. Watson Research Center, Yorktown Heights, NY.

10:45 D11.7
CHARACTERIZATION OF UNDOPED PSEUDOMORPHIC InGaAs/GaAs QUANTUM WELLS BY ELECTRON BEAM ELECTROREFLECTANCE (EBER) AND PHOTOLUMINESCENCE (PL), M.H. Herman, and I.D. Ward, Charles Evans and Associates, Redwood City, CA; and A. Dodabalapur, and B.G. Streetman, The University of Texas, Austin, TX.

11:00 D11.8
RAMAN CHARACTERIZATION OF InSb/GaAs GROWN BY METALORGANIC MAGNETRON SPUTTERING, Z.C. Feng and S. Perkowitz, Emory University, Physics Department, Atlanta, GA; T.S. Rao and J.B. Webb, National Research Council, Laboratory for Microstructural Science, Ottawa, Canada.

11:15 D11.9
ELECTRIC FIELD EFFECTS ON THE OPTICAL PROPERTIES OF InGaAs/GaAs STRAINED QUANTUM WELLS AND SUPERLATTICES, K. Gibb, C. Lacelle, and A.P. Roth, LMS, NRC, Ottawa, Canada; B. Soucail, N. Dupuis, and P. Voisin, GPS, ENS, Paris, France; and B.Y. Hua, and E. Fortin, University of Ottawa, Ottawa, Canada.

11:30 D11.10
RAMAN STUDY OF MOMBE AND PLASMA-MOVPE GROWN III-V LAYERS ON Si(100), J. Geurts, J. Finders, RWTH Aachen, I. Phys. Institut, Aachen, West Germany; H. Munder, M. Kamp, M. Oehlers, H. Lüth, KFA Jülich, ISI, Jülich, West Germany; J. Musolf, J. Leiber, A. Brauers, M. Weyers, P. Balk, RWTH Aachen, Inst. of Semiconductor Electronics, Inst. HL-Technik, Aachen, West Germany.

11:45 D11.11
MBE GROWN GaAs ON Si(100) STUDIED BY INFRARED SPECTROSCOPY, Thomas Eickhoff, I. Physics Institut, RWTH Aachen, Aachen, West Germany; Dietrich R.T. Zahn, and Wolfgang Richter, TU Berlin, Institut Festkörperphysik, Berlin, West Germany; David A. Woolf, David I. Westwood, and Robin H. Williams, University of Wales College of Cardiff, Physics Department, Cardiff, United Kingdom.

SESSION D12: OPTICAL CHARACTERIZATION OF EPITAXIAL LAYERS

Chairs: M. Chandrasekhar and F. Pollak
Friday Afternoon, December 1
Salon C/D (M)

1:30 D12.1
RAMAN SCATTERING FROM AN INTERFACIAL THIN LAYER OF GaAs HETEROEPITAXIALLY GROWN ON SILICON SUBSTRATE, Yoshiro Akagi, Mariko Ishino, Yoshiharu Nakajima, Sharp Corporation, Corporate R&D Group, Nara, Japan.

1:45 D12.2
STRESS EVALUATION METHOD USING RAMAN SPECTROSCOPY, Yohko Mashimoto, IBM Japan, Ltd., Shiga, Japan.

2:00 D12.3
ELECTRICAL AND OPTICAL CHARACTERIZATION OF InSb GROWN ON GaAs BY MBE, Phillip E. Thompson, James Waterman, D. Kurt Gaskill, Robert Stahlbush, and John Davis, Naval Research Laboratory, Washington, DC.

2:15 D12.4
INDEX OF REFRACTION ANISOTROPY IN MISMATCHED InGaAs/InP HETEROSTRUCTURES MEASURED BY ELLIPSOMETRY, Brian R. Bennett, Massachusetts Institute of Technology, Department of Materials Science and Engineering, Cambridge, MA; and Jesús A. del Alamo, Massachusetts Institute of Technology, Department of Electrical Engineering and Computer Science, Cambridge, MA.

2:30 BREAK

2:45 *D12.5
MODULATION SPECTROSCOPY OF LAYERED STRUCTURES, Orest J. Glembocki, Naval Research Laboratory, Washington, DC.

3:15 D12.6
CHARACTERIZATION OF AN ASYMMETRIC TRIANGULAR MULTIPLE QUANTUM WELL, BY VARIABLE ANGLE SPECTROSCOPIC ELLIPSOMETRY, Craig M. Herzinger, Paul G. Snyder and John A. Woollam, University of Nebraska, Department of Electrical Engineering, Lincoln, NE.

3:30 D12.7
PHOTOREFLECTANCE OF A GaAs/InGaP(ORDERED) SINGLE QUANTUM WELL GROWN BY ATOMIC LAYER EPITAXY, X. Yin, and F.H. Pollak, Brooklyn College of CUNY, Department of Physics, Brooklyn, NY; and B.T. McDermott, K.G. Reid, and S.M. Bedair, North Carolina State University, Raleigh, NC.

3:45 D12.8
MAGNETO-OPTICAL STUDIES OF 2-D ELECTRONS IN GaAsAlGaAs SINGLE HETEROJUNCTIONS, K-S. Lee, C.H. Perry, Northeastern University, Physics Department, Boston, MA; and J.M. Worlock, Bellcore, Red Bank, NJ.

4:00 D12.9
MAGNETO-OPTICAL STUDIES OF GaAs-AlGaAs MODULATION DOPED QUANTUM WELLS UNDER HYDROSTATIC PRESSURE, W. Zhou, C.H. Perry, Northeastern University, Boston, MA; and J.M. Worlock, Bellcore, Red Bank, NJ.

4:15 D12.10
SPATIALLY INDIRECT OPTICAL TRANSITIONS IN SEMICONDUCTOR QUANTUM WIRES, Joseph S. Weiner, G. Danan, A. Pinczuk, J. Valladares, L.N. Pfeiffer, K. West, AT&T Bell Laboratories, Murray Hill, NJ.

SESSION D12: OPTICAL CHARACTERIZATION OF EPITAXIAL LAYERS

Chairs: M. Chandrasekhar and F. Pollak
Friday Afternoon, December 1
Salon C/D (M)

1:30 D12.1
RAMAN SCATTERING FROM AN INTERFACIAL THIN LAYER OF GaAs HETEROEPITAXIALLY GROWN ON SILICON SUBSTRATE, Yoshiro Akagi, Mariko Ishino, Yoshiharu Nakajima, Sharp Corporation, Corporate R&D Group, Nara, Japan.

1:45 D12.2
STRESS EVALUATION METHOD USING RAMAN SPECTROSCOPY, Yohko Mashimoto, IBM Japan, Ltd., Shiga, Japan.

2:00 D12.3
ELECTRICAL AND OPTICAL CHARACTERIZATION OF InSb GROWN ON GaAs BY MBE, Phillip E. Thompson, James Waterman, D. Kurt Gaskill, Robert Stahlbush, and John Davis, Naval Research Laboratory, Washington, DC.

2:15 D12.4
INDEX OF REFRACTION ANISOTROPY IN MISMATCHED InGaAs/InP HETEROSTRUCTURES MEASURED BY ELLIPSOMETRY, Brian R. Bennett, Massachusetts Institute of Technology, Department of Materials Science and Engineering, Cambridge, MA; and Jesús A. del Alamo, Massachusetts Institute of Technology, Department of Electrical Engineering and Computer Science, Cambridge, MA.

2:30 BREAK

2:45 *D12.5
MODULATION SPECTROSCOPY OF LAYERED STRUCTURES, Orest J. Glembocki, Naval Research Laboratory, Washington, DC.

3:15 D12.6
CHARACTERIZATION OF AN ASYMMETRIC TRIANGULAR MULTIPLE QUANTUM WELL, BY VARIABLE ANGLE SPECTROSCOPIC ELLIPSOMETRY, Craig M. Herzinger, Paul G. Snyder and John A. Woollam, University of Nebraska, Department of Electrical Engineering, Lincoln, NE.

3:30 D12.7
PHOTOREFLECTANCE OF A GaAs/InGaP(ORDERED) SINGLE QUANTUM WELL GROWN BY ATOMIC LAYER EPITAXY, X. Yin, and F.H. Pollak, Brooklyn College of CUNY, Department of Physics, Brooklyn, NY; and B.T. McDermott, K.G. Reid, and S.M. Bedair, North Carolina State University, Raleigh, NC.

3:45 D12.8
MAGNETO-OPTICAL STUDIES OF 2-D ELECTRONS IN GaAsAlGaAs SINGLE HETEROJUNCTIONS, K-S. Lee, C.H. Perry, Northeastern University, Physics Department, Boston, MA; and J.M. Worlock, Bellcore, Red Bank, NJ.

4:00 D12.9

MAGNETO-OPTICAL STUDIES OF GaAs-AlGaAs MODULATION DOPED QUANTUM WELLS UNDER HYDROSTATIC PRESSURE, W. Zhou, C.H. Perry, Northeastern University, Boston, MA; and J.M. Worlock, Bellcore, Red Bank, NJ.

4:15 D12.10

SPATIALLY INDIRECT OPTICAL TRANSITIONS IN SEMICONDUCTOR QUANTUM WIRES, Joseph S. Weiner, G. Danan, A. Pinczuk, J. Valladares, L.N. Pfeiffer, K. West, AT&T Bell Laboratories, Murray Hill, NJ.

STABILITY OF METAL LAYERS EMBEDDED IN SEMICONDUCTORS. J.P. Harbison, T. Sands, C.J. Palmström, N. Tabatabaie, H.L. Gilchrist, L.T. Florez, T.L. Cheeks, R.E. Nahory, W.K. Chan, and V.G. Keramidas, Bellcore, 331 Newman Springs Rd., Red Bank, NJ 07701-7040.

One of the exciting challenges in the field of heteroepitaxy is the growth of two dissimilar materials in a single monocrystalline heterostructure. Perhaps the most interesting combination involves the growth of buried metal layers embedded in semiconductors, since such structures have the potential of opening up new classes of electronic and optoelectronic devices. We have concentrated on the III-V (Al,Ga,In)As semiconductor system which allows a wide range of possibilities both in heterostructure bandgap engineering and in variation of the lattice parameter. For the buried metallic layer we have concentrated for the most part on the intermetallic NiAl which has a cubic CsCl crystal structure with a unit cell only slightly larger (2.1%) than half that of GaAs and AlAs, and lattice-matched to In_{0.5}Ga_{0.5}As. Questions of stability of these thin metal layers, in particular during the elevated overgrowth temperatures of 400-600°C during which the metal is in intimate contact with the surrounding III-V, fall into two categories. First are questions of thermodynamic stability of the metal with respect to the adjacent semiconductor, and this concern is addressed by the proper initial choice of the metal. The second are questions of morphological stability: Will the thin film remain smooth and continuous or tend to agglomerate? The answers to these questions are more subtle, and depend on the exact sequences chosen for the overgrowth procedure. With a proper sequence, we are able to achieve buried NiAl layers electrically continuous as thin as 1 nm, opening up new measurement possibilities for metal films in the extreme quantum regime.

ELECTRICAL AND OPTICAL CHARACTERIZATION OF MBE GROWN BURIED METAL (Al,Ga)As/NiAl/(Al,Ga)As DOUBLE SCHOTTKY DIODES. T.L. Cheeks, T. Sands, R. Nahory, J. Harbison, N. Tabatabaie, H. Gilchrist, B. Wilkens, Bellcore, Red Bank, N.J.

The successful growth by MBE of buried metal heterostructures, such as (Al,Ga)As/NiAl/(Al,Ga)As, demonstrated that thin epitaxial and thermally stable metallic layers could be incorporated within GaAs. These new material structures have potential for metal base transistors and novel electronic and photonic devices. We have demonstrated that these materials behave as double Schottky barrier diodes from the current-voltage (I-V), capacitance-voltage (C-V) and internal photoemission (IPE) characteristics of a buried 200 Å NiAl layer. Using a selective etch process, three electrodes were defined in order to investigate the top and bottom diode characteristics of NiAl/AlAs/GaAs. An effective barrier height of about 1.1 eV was measured for both the top and bottom diodes with internal photoemission. This value was consistent with the I-V measurements ($n=1.1$ and $\phi_b = 0.982$) of the bottom diode and represented an enhancement in the barrier height due to the AlAs cladding layer. However, the effective barrier height of the top diode, measured by I-V, was lower than the bottom diode. This effect was investigated using RBS channeling, photoluminescence and TEM. The data suggested that the barrier height lowering could be attributed to planar defects which form at the NiAl/AlAs/GaAs interface due to the 2% lattice mismatch and the difference in symmetry. Further insight into the effect of defects on the transport properties at the interfaces and suggestions for improvements will be discussed.

GROWTH AND CHARACTERIZATION OF GaAs/RARE-EARTH MONOARSENIDE/GaAs HETEROSTRUCTURES. C.J. Palmström, S. Mounier, T.G. Finstad, N. Tabatabaie, S.J. Allen, Jr., T. Sands, T.L. Cheeks and P.F. Miceli, Bellcore, 331 Newman Springs Road, Red Bank, New Jersey 07701 and J.G. Zhu and C.B. Carter, Department of Materials Science and Engineering, Cornell University, Ithaca, NY 14853

The rare-earth monoarsenides (REAs) have high heats of formation and melting points. Furthermore, all but one have NaCl structures with a lattice parameter similar to that of GaAs, making them ideal candidates for buried epitaxial metallic layers in III-V semiconductors. For example, ErAs and LuAs have a lattice mismatch to GaAs of ~1.6% and ~0.4%, respectively. The effect of strain on the REAs growth itself can be ascertained by comparing growth of ErAs with LuAs on GaAs and on the subsequent GaAs overgrowth by characterizing the overgrown layers. A MBE growth chamber with a multiple crucible electron beam evaporation source was used to grow the GaAs/REAs/GaAs structures. The structural properties of the epitaxial layers were studied by RHEED during growth, in-situ Auger and LEED, and ex-situ by RBS, X-ray diffraction and TEM. RHEED oscillations during REAs growth are consistent with single layer by layer growth. RBS with channeling has shown that both LuAs and ErAs films grown on GaAs are good single crystals with minimum yields as low as ~7%. Cross sectional TEM studies show the interfaces to be atomically abrupt. ErAs and LuAs are found to be semi-metallic with room temperature resistivity ~70 and ~90 μΩ.cm, respectively. Electrical continuity has been found in buried REAs films as thin as 3 monolayers. This talk will emphasize the growth and characterization of GaAs/REAs/GaAs epitaxial structures.

EPITAXIAL GROWTH OF MATCHED METALLIC ErP_{0.6}As_{0.4} LAYERS ON GaAs AND ErP_{0.5}Sb_{0.5} ON InP IN A MBE SYSTEM. Quivarc'h A., Le Corre A., Caulet J., Guenais B., Minier M., Ropars G., Centre National d'Etudes des Télécommunications, BP 40, 22301 Lannion Cedex, France.

Abstract :

Very recent papers have reported the growth of YbAs and ErAs single-crystal films on (001) GaAs and the metallic behavior of these rare-earth monoarsenides. We show that several (rare-earth)-(V element) compounds can be used for this purpose. We carried out the epitaxial growths at 500°C of ErAs ($\rho = 60 \mu\Omega\text{cm}$), ErP ($\rho = 150 \mu\Omega\text{cm}$) and ErSb ($\rho = 60 \mu\Omega\text{cm}$) on GaAs or InP in a MBE system equipped with solid and gas sources.

Successful growth of ErP_{0.6}As_{0.4} films ($\rho = 80 \mu\Omega\text{cm}$) on GaAs with a reproducible lattice mismatch less than $5 \cdot 10^{-4}$ have been demonstrated. The ErP_{0.6}As_{0.4}/n-GaAs diode yield excellent I-V characteristics with a barrier height of 0.88 eV. In opposition to the ErAs layers, the ErP_{0.6}As_{0.4} films are stable in the atmosphere; thus, they are excellent candidates for epitaxial metal-semiconductor structures. The overgrowth of GaAs is found to be difficult in the case of a (001) GaAs substrate (island growth) but rather good for (111) GaAs.

In the case of InP substrates, equivalent structures were obtained by using a ErP_{0.5}Sb_{0.5} ternary compound.

We present the results of the various characterizations performed by using a set of complementary methods (RBS, TEM, x-ray diffraction, R_{\square} , I-V...).

D1.5

ANISOTROPIC STRAIN IN THIN EPITAXIAL CoSi_2 (110) FILMS GROWN ON Si(110). S.M. Yalisove, Department of Materials Science and Engineering, University of Michigan, 2300 Hayward St., Ann Arbor, MI 48109-2136, D.J. Eaglesham, and R.T. Tung, AT&T Bell Laboratories, 600 Mountain Ave., Murray Hill, NJ 07974-2070

Growth of single domain epitaxial CoSi_2 films on Si(110) has been recently demonstrated. These films contain two distinct sets of interfacial defects which are generated to relieve misfit strain at two different critical thicknesses and in orthogonal directions, the $\langle 011 \rangle$ and $\langle 100 \rangle$. Films which are 30 to 80 Å thick contain only one of these sets of misfit relieving defects. Consequently, the misfit strain is relieved in only one direction in the film. Rutherford backscattering (RBS) rocking curves were collected about channeling directions in two orthogonal planes to measure the orthorhombic distortion caused by this defect structure for two thicknesses of these films. Films were studied at a variety of different thicknesses to compare the RBS results with transmission electron microscopy (TEM) images of the same samples. Results will be presented which show that the 80 Å films are fully relieved in the $\langle 110 \rangle$ direction and almost fully strained in the $\langle 100 \rangle$ direction. These measurements will be shown to be entirely consistent with TEM results.

D1.6

GROWTH OF EPITAXIAL CoSi_2 AND NiSi_2 ON (111), (100), and (110) Si AT ROOM TEMPERATURE. R. T. Tung and F. Schrey, AT&T Bell Laboratories, Murray Hill, N.J. 07974

The formation of NiSi_2 and CoSi_2 from evaporated metal films on single crystal Si requires an anneal at high temperatures (750°C for NiSi_2 and 550°C for CoSi_2). A high temperature is required because the nucleation and diffusion processes need large thermal activation. In this paper, we show that the "reaction" of these silicides proceeds quite adequately at room temperature. It is known that deposition of a few monolayers (ML) of Co on Si(111) leads to the formation of epitaxial CoSi_2 at room temperature. Here, following the metal deposition, co-deposition of stoichiometric CoSi_2 at room temperature leads to the growth of thick layers (>200 Å) of single crystal epitaxial silicide. High quality NiSi_2 may also be grown at room temperature on Si(111) by the deposition of ML Ni and subsequent NiSi_2 co-deposition. This observation is suggestive of NiSi_2 formation at room temperature upon ML Ni deposition, a subject which is presently controversial. On Si(100) and (110), nucleation of the disilicide phase does not occur at room temperature. However, using annealed thin layers (< 20 Å) of CoSi_2 and NiSi_2 as templates, it is shown that homoepitaxial growth of these two silicides take place at room temperature along both (100) and (110) directions. Very high crystalline quality is found for these room temperature NiSi_2 and CoSi_2 layers. Ion channeling χ_{min} 's of 2-3% are common. TEM analyses show (111) films have the type B orientation and the interface dislocations to correspond faithfully to steps on original surface. Thick (100) and (110) layers grown at room temperature are single crystals whose defect structures conform to the original thin templates. A discussion of the silicide reaction is also given.

D1.7

FORMATION OF ULTRATHIN NICKEL AND COBALT SILICIDES ON Si(111) $\sqrt{3} \times \sqrt{3}$ -B AT ROOM TEMPERATURE. L. Luo, G. A. Smith*, Shin Hashimoto and W. M. Gibson, Department of Physics, SUNY at Albany, Albany, NY

The MeV ion channeling technique is sensitive to the small displacement perpendicular to the direction of incident ion beam and, therefore, is an excellent and straightforward probe of structure quality of thin films and buried interface. This was used, combined with Monte Carlo computer simulations, to study the crystalline quality, the phase of the surface and the buried ultrathin metal (Ni and Co) silicide layers which form upon room

temperature deposition on Si(111) $\sqrt{3} \times \sqrt{3}$ -B reconstructed surfaces. The results indicate that in some cases the metal atoms initially deposited on Si diffuse to reaction sites in the fourth layer where the metal silicides growth begins. Further deposition of the metal leads to the growth of metal silicides which is thought to be a diffusion barrier that stops the supply of Si atom from bulk onto the surface at 300°K and soon terminates the formation of metal silicides. Subsequent deposition of the metal atoms (>4ML) forms a pure metal film on top of the thin disordered silicides.

* Also at GE Corporate Research and Development Center, Schenectady, NY

D1.8

FORMATION OF HIGH QUALITY Si/CoSi₂/Si DOUBLE HETERO-STRUCTURES BY SELF-ALIGNED AND TWO STEP MOLECULAR BEAM EPITAXY. M. NIYAO, T. OHSHIMA, N. NAKAMURA and K. NAKAGAWA, Cent. Res. Labo., Hitachi Ltd., Kokubunji, Tokyo, Japan

The formation and application of high quality Si/CoSi₂/Si double hetero-structures are comprehensively studied. In these experiments, grooved patterns, with different dimensions of line & space (submicron - a few μm), were formed on Si (111) substrates and then CoSi₂ was grown by molecular beam epitaxy (MBE) under a stoichiometric beam condition (Co/Si=1/2). At growth temperatures higher than 400°C, the CoSi₂ films deposited on the side walls ($\langle 211 \rangle$ orientation) of the grooves agglomerated to reduce the interface energy between the CoSi₂ and Si. However, on the flat (111) Si surfaces, pin hole free CoSi₂ films were obtained up to 500°C. In this way, fine patterning of CoSi₂ electrodes becomes possible under self-aligned MBE growth by choosing a growth temperature in the range 400°C - 500°C. In the further experiment, 2-step MBE growth was used to obtain high quality Si overlayers on the CoSi₂/Si substrates. Here, very thin Si layers were grown at low temperatures (300 - 400°C) to stabilize the surface atoms of CoSi₂ and then, on top, thick Si layers have grown at high temperatures (500 - 600°C). RHEED and SEM observations showed that the Si/CoSi₂/Si structure has good crystallinity and morphology. In addition cross-sectional TEM observation revealed that both the upper and lower interfaces between the CoSi₂ and Si are atomically abrupt and smooth. Finally, permeable base transistors (PBT) were fabricated utilizing this newly developed MBE process. A high performance from the PBT's ($G_m = 42 \text{ mS/mm}$) was obtained, which agreed well with the computer simulations. This work was performed under the management of the R&D Associ. for Future Elec. Dev. as a part of the R&D of Basic Tech. for Future Indus. supported by New Ener. and Indus. Tech. Devel. Organ.

D1.9

GROWTH AND CHARACTERIZATION OF EPITAXIAL CoSi₂ ON Si(100). Jorge R. Jimenez, L. Hsiung, K.V. Ramanathan, K. Rajan, L.J. Schowalter, Center for Integrated Electronics, Rensselaer Polytechnic Institute, Troy, NY 12180; Shin Hashimoto, Physics Department, State University of New York, Albany, NY 12222; R.D. Thompson, B.A. Ek, and S.S. Iyer, IBM T.J. Watson Research Center, Yorktown Heights, NY 10598.

Epitaxial CoSi₂ on silicon is a system of considerable interest, because of possible novel device applications such as 3-D interconnects and the metal-base transistor. While much work has been done on CoSi₂/Si(111), relatively little has been done on CoSi₂/Si(100), which is considerably more difficult to grow, but may be the technologically more important system. We have grown films of CoSi₂ on Si(100) by MBE and studied them using LEED, RBS, TEM, SEM and resistivity measurements. The use of a template method, where a thin (10-15 Å) CoSi₂ film is codeposited at room temperature before annealing and further codeposition, improves film quality in terms of ion channeling and resistivity, compared to those grown by straight Co deposition.

The number and size of grains of other orientations are also substantially reduced, but are not completely removed. Schottky barrier heights of ≈ 0.7 eV have been determined from I-V and C-V measurements, although the heights obtained from C-V measurements are higher by as much as 0.1 eV. We have also observed unusually large tetragonal strain ($\epsilon_T = 2.6\%$) in films ≈ 120 Å thick. The dislocation densities observed along the interface by TEM on these same films is of the order of $10^6/\text{m}$. Assuming all these are misfit dislocations uniformly distributed with Burger's vector $\frac{1}{2}[011]$ at the interface gives a strain of $\epsilon_{\parallel} \approx 1\%$. It has been found through detailed examination of TEM diffraction patterns that metastable cobalt silicide stoichiometries may exist suggesting metastabilities which have not been reported for epitaxial CoSi_2 growth on $\text{Si}(111)$.

D1.10

EVOLUTION OF STRESS DURING HETEROEPITAXIAL GROWTH OF NiSi_2 ON (001) AND (111) SILICON SUBSTRATES. H.L. Ho, C.L. Bauer, S. Mahajan, Department of Metallurgical Engineering and Materials Science, and A.G. Milnes, Department of Electrical and Computer Engineering, Carnegie Mellon University, Pittsburgh, PA. 15213.

Thin film stress accompanying the heteroepitaxial nucleation and growth of NiSi_2 resulting from the interaction of polycrystalline nickel films with (001) and (111) silicon substrates has been measured through the use of a levered optical beam technique in the temperature range of 770 - 910°C. Results indicate that stress decreases during growth of NiSi_2 on (001) and (111) oriented silicon substrates whereupon stress remains constant after complete formation of NiSi_2 . However, stress reduction is considerably larger during the formation of NiSi_2 on (111) silicon ($\geq 300 - 400$ MPa), whereas a comparatively small stress reduction (≤ 100 MPa) is observed for NiSi_2 on (001) silicon. Furthermore, increasing temperature increases the magnitude of stress reduction of NiSi_2 on (111) silicon while virtually no effect is found for NiSi_2 on (001) silicon. TEM studies reveal that for NiSi_2 on (111) silicon, $a/6\langle 112 \rangle$ Shockley partial dislocations are associated with steps at the $\text{NiSi}_2/(111)$ silicon interface. It is argued that the larger decrease in stress of NiSi_2 grown on (111) silicon is the result of interfacial glide of Shockley partial (winning) dislocations along the (111) composition plane with concomitant migration of steps. In contrast, the smaller decrease in stress during the formation of NiSi_2 on (001) silicon is attributed to the presence of non-gleing interfacial dislocations of the type $a/4\langle 111 \rangle$.

The authors gratefully acknowledge the financial support of the IBM Center for Thin Film Sciences at Carnegie Mellon University.

D1.11

COLUMNAR EPITAXY OF CoSi_2 ON $\text{Si}(111)$, (100), and (110).*

R. W. Falbauer, Jet Propulsion Laboratory, California Institute of Technology, Pasadena, CA; C. W. Nieh, California Institute of Technology, Pasadena, CA; and Q. F. Xiao and Shin Hashimoto, State University of New York at Albany, Albany, NY.

Codeposition of cobalt and silicon with Si:Co ratios ranging from 12 to 60 on silicon substrates held at 640-800°C in ultra-high vacuum is found to result in epitaxial columns of cobalt disilicide surrounded by epitaxial silicon. On $\text{Si}(111)$, planar transmission electron microscopy (TEM) analysis reveals no extended defects in either the silicide or silicon matrix for growth at 700-800°C. However, growth at 640°C results in a high density of planar twins in the silicon. Rutherford backscattering analysis reveals channeling minimum yields for the Co signal as low as 4% and yields for the Si signal as low as 2% for (111)-oriented samples. Independent control of column diameter and spacing is possible through selection of Si:Co ratio and growth temperature. Average column diameters ranging from 25 to 130 nm with spacings of 80 to 230 nm have been demonstrated.

The shapes of the silicide grains vary considerably for (111), (100), and (110) silicon. Both twinned (type B) and untwinned (type A) silicide grains have been observed on all three orientations. Most of the grains on $\text{Si}(111)$ are type B, but roughly equal numbers of type A and type B grains are observed on $\text{Si}(100)$ and (110). On $\text{Si}(100)$, type-B grains assume the shape of platelets with four variants, due to twinning about the four (111) planes inclined to the surface (100) plane. Type A grains on $\text{Si}(100)$ exhibit serrated edges due to faceting on (111) planes, as revealed by high-resolution TEM.

*Work supported by SDIO and NASA.

D2.1

HIGH RESOLUTION X-RAY SCATTERING STUDIES OF STRAIN IN EPITAXIAL THIN FILMS OF YTTRIUM SILICIDE GROWN ON SILICON(111). L. J. Martinez-Miranda*, M. P. Siegal**, P. A. Heiney***, J. J. Santiago-Avilés* and W. R. Graham**, Laboratory for Research on the Structure of Matter, *Department of Electrical Engineering, **Department of Materials Science and Engineering, ***Department of Physics, University of Pennsylvania, Philadelphia, PA 19104.

We have used high resolution grazing incidence x-ray scattering (GIXS) to study the in-plane structure of epitaxial YSi_2 -x films grown on $\text{Si}(111)$, with thicknesses ranging from 85 Å to 510 Å. These films were prepared from a 34 Å template layer of YSi_2 -x annealed at 700°C, onto which additional Y was deposited at about 300°C, a temperature high enough to induce silicide formation. All films were annealed at 850°C to achieve epitaxy, with chi-minimum of 3-4% as measured from backscattering spectrometry.

YSi_2 -x crystallizes in the AlB_2 structure, which is hexagonal, with bulk lattice parameters $a = 3.842$ Å / $c = 4.414$ Å respectively. This should result in an almost perfect lattice match to $\text{Si}(111)$. Our results indicate that the films are strained, and that film strain increases as a function of thickness, with lattice parameters varying from $a = 3.846$ Å / $c = 4.142$ Å for the 85 Å film to $a = 3.877$ Å / $c = 4.121$ Å for the 510 Å film. We correlate these results with an increase in pinhole areal coverage as a function of thickness. In addition, our measurements show no evidence for the existence of ordered silicon vacancies in the films.

Work supported by an IBM Program of Support for the Materials and Processing Sciences Grant; NSF-MRL Grant No. DMR-85-19059; and University of Puerto Rico ARO Grant No. P-22681-MS.

D2.2

SURFACE MORPHOLOGY OF TiSi_2 FORMED FROM UHV DEPOSITED Ti ON Si. Hyeonjae Jeon, R. J. Nemanich, J.W. Honeycutt and G. A. Rozgonyi, North Carolina State University, Department of Physics and Department of Materials Science and Engineering, Raleigh, NC 27695-8202

Of the silicides often considered for IC applications, TiSi_2 films formed by reaction of Ti on Si exhibit lower resistivity and higher temperature stability. An aspect important for the application is that significant surface roughening has been observed after annealing to form the silicides. In this study the island formation mechanisms and the morphology of TiSi_2 on Si are examined and related to the nucleation and growth properties of the TiSi_2 film. Ti is deposited on clean, reconstructed Si substrates (ie. 2×1 on $\text{Si}(100)$ and 7×7 on $\text{Si}(111)$) at room temperature and also at high substrate temperature (500°C-800°C). The TiSi_2 formation process is monitored with in-situ LEED, AES and ex-situ Raman and the surface morphology is examined with ex-situ SEM and TEM. Ti thicknesses between 50 Å and 400 Å were examined. The TiSi_2 formation process involves Si diffusion at temperatures <400°C, formation of a meta-stable TiSi_2 phase at $\sim 500^\circ\text{C}$, and transformation to the stable TiSi_2 phase at $\sim 700^\circ\text{C}$. At $\sim 700^\circ\text{C}$, in situ LEED measurements show diffraction corresponding to the reconstructed substrate. This indicated the formation of islands with clean substrate regions between the islands. The high temperature required for nucleation of the stable phase is interpreted as an indication of high surface energy. The microscopy results show smooth surfaces for TiSi_2 formation at annealing temperature $\sim 500^\circ\text{C}$, and TiSi_2 island formation at annealing temperatures between 600°C and 900°C depending on the film thickness. The island formation process is described in terms of a wetting model, and the surface energies for nucleation and island formation are related.

*This work was supported in part by the National Science Foundation through grant DMR 8717816 and CDR 8721505.

D2.3

EPITAXIAL GROWTH OF TbSi_2 ON $\text{Si}(111)$. F. H. Kaatz, J. Van der Spiegel, and W. R. Graham, Laboratory for Research on the Structure of Matter and the University of Pennsylvania, Philadelphia, PA 19104.

We provide the first description of the epitaxial growth of TbSi_2 on $\text{Si}(111)$. TbSi_2 crystallizes in the hexagonal AlB_2 structure with a 0.05 mismatch to the $\text{Si}(111)$ bulk lattice. In this study, terbium is evaporated onto Shiraki cleaned silicon wafers and annealed in UHV to form TbSi_2 films of 200 Å in thickness with the pressure maintained below 5×10^{-10} torr during all procedures. Low energy electron diffraction (LEED) shows single crystal growth with a sharp $\sqrt{3} \times \sqrt{3}$ pattern after an 850°C anneal. Auger electron spectroscopy (AES) indicates intermixing at room temperature with growth following a nucleation type mechanism. We describe growth procedures leading to a Rutherford backscattering minimum channeling yield of 7-8 %. X-ray and transmission electron diffraction (TEM) analyses show the formation of single-crystalline TbSi_2 with an orientation of $\text{TbSi}_2(0001) \parallel \text{Si}(111)$ and $\text{TbSi}_2(10\bar{1}0) \parallel \text{Si}(1\bar{1}2)$. TEM also reveals pinhole formation with an average size of less than 0.5 μm , with no evidence of an ordered vacancy network in these films. We also present the first electrical measurements on TbSi_2 .

This work is supported in part by the NSF-MRL under grant # DMR 8819885.

D2.4

GROWTH KINETICS OF Si ON SAPPHIRE BY MBE AS A FUNCTION OF SUBSTRATE IN-SITU HIGH TEMPERATURE SUBSTRATE ANNEAL. Eliezer David Richmond, Naval Research Laboratory, Code 6816, Washington D.C. 20375-5000, Joseph G. Pellegrino, NIST, Gaithersburg, MD 20889, Mark E. Twigg, GEO-Centers Inc., Fort Washington MD. 20744.

The effects of high temperature vacuum annealing of a sapphire substrate in-situ of a VG80 Si MBE system on the growth kinetics has been preliminarily investigated¹ and the resultant material characterized for its crystalline quality, microstructural defects, and electrical properties². Here we present a more detailed investigation of the growth kinetics of MBE Si on (1102) sapphire. The substrates are annealed in a vacuum of 10^{-7} to 10^{-8} mbar for 30 minutes at 1100°C, 1300°C, and 1450°C. Si films are grown with a thickness ranging from 3 nm to 40 nm. The films are found to grow by a Volmer Weber process. For a given substrate annealing temperature, the island size increases and the island density decreases with increasing film thickness. As the annealing temperature of the substrate decreases the island size distribution has several properties: 1) The center of the distribution shifts to smaller diameters; 2) The peak height of the distribution increases; and 3) the standard deviation of the distribution decreases.

1. J.G. Pellegrino, E.D. Richmond, and M. Twigg, Materials Research Society Proc., vol. 116, p.395, 1988.
2. E.D. Richmond, S. Quadri, A. Knudson, M. Twigg, N. Green, III International Si MBE Symposium, 30 May - 2 June 1989, Strasbourg France.

D2.5

A HREM STUDY OF EPITAXIAL FLUORIDE / RARE EARTH / FLUORIDE / GaAs INTERFACES. C.J. Chien, R.E.C. Farrow*, J.C. Bravman Department of Materials Science and Engineering, Stanford University, Stanford, CA 94305. *IBM Research Center, 650 Harry Road, San Jose, California 95120-6009.

Ultrathin epitaxial rare earth films buried in a host matrix of rare earth fluorides exhibit magnetic properties significantly different from bulk crystals. In this paper we report a HREM study of such structures which

complements grazing incidence X-ray diffraction and in situ RHEED studies of films grown by molecular beam epitaxy.

We find that in $\text{NdF}_3/\text{Y}/\text{NdF}_3$ structures grown on GaAs (111) substrates that the GaAs- NdF_3 interface is atomically rough with a random distribution of steps and microfacets arising from the initial heat-cleaning stage of sample preparation in UHV. The NdF_3 does not replicate this rough interface and by 70 Å thick the NdF_3 surface roughness is on the order of a single monolayer. Epitaxy of the rare earth film on the fluoride is sometimes accompanied by interfacial replacement reactions evident from large local variations in lattice parameter within the metal film near the interface.

A detailed picture of the defect structure of these novel structures is developed from this study and the magnetic implications of the defect structure is discussed.

D2.6

INFLUENCE OF OFF-ORIENTED SUBSTRATES ON HETERO-EPITAXIAL GROWTH OF $(\text{Ca}, \text{Sr})\text{F}_2$ LAYERS ON $\text{Si}(100)$. Tetsuroh Minemura and Junko Asano, Hitachi Research Laboratory, Hitachi, Ltd., Hitachi-shi, Japan; Kazuo Tautsui and Seiji Kurokawa, Tokyo Institute of Technology, Yokohama-shi, Japan.

Heteroepitaxial growth of $(\text{Ca}, \text{Sr})\text{F}_2$ layers on $\text{Si}(100)$ has been investigated for applying it to GaAs/fluoride/Si structures. $\text{Si}(100)$ substrates off-oriented toward $\langle 011 \rangle$ have a considerable effect on reducing crystal defects in the epitaxial GaAs layers on them. In this paper, we will report that the influence of off-oriented substrates on the epitaxy of $(\text{Ca}, \text{Sr})\text{F}_2/\text{Si}(100)$ is quite different from that for GaAs/Si.

$(\text{Ca}_x, \text{Sr}_{1-x})\text{F}_2$ layers were grown on exact and off-oriented $\text{Si}(100)$ substrates by molecular beam epitaxy (MBE). Rutherford backscattering spectroscopy was employed for evaluating the crystallinity of the layers.

The minimum channeling yields (χ_{min}) for CaF_2 layers grown on the exact and off-oriented $\text{Si}(100)$ substrates are small, 0.1-0.15, which shows no influence of off-oriented substrates on their crystallinities. On increasing the mixing composition of Sr, the χ_{min} 's for $(\text{Ca}_x, \text{Sr}_{1-x})\text{F}_2$ layers grown on the off-oriented $\text{Si}(100)$ substrates get large, about 0.9, although those grown on the exact $\text{Si}(100)$ are kept small. This influence of off-oriented substrates for $(\text{Ca}_x, \text{Sr}_{1-x})\text{F}_2/\text{Si}(100)$ is quite the reverse of GaAs/Si.

D2.7

STRAIN IN EPITAXIAL GaAs ON $\text{CaF}_2/\text{Si}(111)$. L.J. Schowalter, J.E. Ayers, and S.K. Ghandhi. Ctr. for Integrated Electronics, Rensselaer Polytechnic Institute, Troy, NY 12180; Shin Hashimoto and W.M. Gibson, Physics Department, State University of New York at Albany; F.K. LeGoues, IBM T.J. Watson Research Ctr.; and P.A. Claxton, Dept. of Electronic & Electrical Eng., U. Sheffield.

While direct heteroepitaxy of GaAs on Si already has demonstrated suitable properties for many applications, the high density of threading dislocations ($\approx 10^7 \text{ cm}^{-2}$) and high stress ($\approx 10^9 \text{ dynes/cm}^2$) will make it difficult to fabricate minority carrier devices (such as lasers and solar cells) with reasonable yield and lifetimes. To overcome this problem, we have attempted to use epitaxial CaF_2 as an epitaxial buffer layer between the GaAs and Si substrate. Layers of (111) GaAs of approximately 1 μm were grown on CaF_2 layers which were 140 and 380 nm thick. The best nucleation conditions for the GaAs on $\text{CaF}_2/\text{Si}(111)$ we have observed were at a substrate temperature of 600 °C which resulted in high quality GaAs films which exhibited channeling minimum yields of 4% and x-ray rocking curve FWHM in the range of 500 arc seconds. The density of threading dislocations in the 1 μm thick GaAs layers was observed by TEM to be $10^7/\text{cm}^2$. No

strain was measured in both sets of GaAs samples within the accuracy ($\pm 1.2 \times 10^{-4}$) of double-crystal x-ray diffraction measurements. Ion channeling, however, revealed a large tetragonal strain of 3.5×10^{-3} in the thinner (160 nm) CaF_2 buffer layers. No strain was observed in either the CaF_2 layer or the GaAs layer for samples grown on the thicker CaF_2 buffer layer. We have modeled our results in terms of the strain relief mechanisms for GaAs and CaF_2 which are in good agreement with the observed results.

D2.8

EPITAXIAL GROWTH OF (100) GaAs ON SOS USING A SPECIFICALLY DESIGNED MOCVD SYSTEM. T. Nishimura, K. Kadoiwa, K. Mitsui and T. Murotani, Optoelectronic & Microwave devices R & D Lab., Mitsubishi Electric Corp. Mizuhara, Itami, 664, Japan.

There have been two main problems in applying the GaAs-on-Si technique to monolithic microwave integrated circuits (MMIC's) and digital IC's. One is the poor resistivity of Si substrate and the other is the wafer warpage and the cracks of the GaAs layer due to the difference of thermal expansion coefficients between Si and GaAs. Sapphire is a good candidate for the substrate, since it is an insulator and has a thermal expansion coefficient close to that of GaAs. In earlier studies (111) GaAs has been grown on sapphire. In this study we have grown (100) GaAs on Si-on-sapphire (SOS), where various techniques for GaAs on Si can be easily applied.

In order to get a high quality GaAs layer on SOS with good reproducibility, we introduced the new MOCVD system specifically designed for GaAs on Si technique. This is a full load locked and automated MOCVD system with two reactors (one is for Si cleaning, the other is for the growth).

In spite of thick GaAs layer over than $15\mu\text{m}$, no crack of the GaAs layer and bending of $1/2$ as much as that on the Si substrate are observed. PL characteristics show much smaller residual stress. The X-ray FWHM is reduced by the annealing from 140 arcsec to 65 arcsec at $10\mu\text{m}$ of the GaAs thickness, which is surprisingly narrow data in highly mismatched systems. The dislocations are effectively reduced to $3 \times 10^6 \text{ cm}^{-2}$ by the annealing and strained layer superlattice.

D2.9

EFFECT OF STOICHIOMETRY ON THE ACTIVATION OF IMPLANTED Si IN MBE-GROWN GaAs ON Si. T.S. Kim and Y.C. Kao, Central Research Laboratories, P.O. Box 655936, MS 147, Texas Instruments Inc., Dallas, TX 75265

In this work, activation of Si implanted into GaAs-on-Si layers grown by molecular beam epitaxy (MBE) is studied. It is found that the Si activation is lower in GaAs on Si than in bulk GaAs and varies widely. To examine if the low activation of implanted Si is due to the amphoteric behavior of Si and not due to the defects unique to GaAs on Si, activation of non-amphoteric dopants such as Be and S is also studied. Be occupies Ga sublattice and is an acceptor, while S occupies As sublattice and is a donor. The activation of implanted Be in GaAs on Si is as good as in bulk GaAs, while S shows much higher activation in GaAs on Si than in bulk GaAs. These results suggest that no donor- or acceptor-like defects exist in high concentration in GaAs on Si and that the amphoteric behavior of Si is the major compensation mechanism in MBE-grown GaAs on Si. The increased Si-acceptor concentration and S activation in GaAs on Si are apparently due to the high density of As vacancies.

To determine if the high concentration of As vacancies is due to the threading dislocations or due to the growth conditions for GaAs on Si, we examine the activation of Si implanted into GaAs on GaAs MBE-layers grown under the conditions similar to those for GaAs on Si. It is found that the Si activation varies substantially depending on the $V(\text{As})/III(\text{Ga})$ flux ratio during the MBE growth and layers grown with the V/III flux ratio used for GaAs on Si shows substantially lower Si activation than bulk GaAs. These results indicate

that the high density of As vacancies in GaAs on Si is a result of the growth conditions which require low V/III flux ratio for good surface morphology. The effect of the threading dislocations does not appear to be significant compared to that of As vacancies and no clear correlation is found between the density of threading dislocations and implanted Si activation.

D2.10

SELECTIVE AREA GROWTH OF GaAs ON Si BY ELECTRON-CYCLOTRON-RESONANCE PLASMA-EXCITED MOLECULAR-BEAM-EPITAXY (ECR-MBE) Tomohiro Shibata, Naoto Kondo, Yasushi Nanishi, and Masatomo Fujimoto; NTT Opto-electronics Laboratories, Atsugi-shi, Kanagawa, 243-01 Japan

The GaAs-on-Si heterostructure is one of the most promising systems for monolithic integration of electronic and optical devices. For practical applications, a selective area growth technique is considered to be essential. In addition, this technique is widely known to reduce dislocations, cracks, and warpage induced by thermal stress. Low-temperature Si surface cleaning has also been the focus of much interest as a key technique for avoiding degradation of Si devices during heat treatment at around 900°C ; such heat treatment is thought to be inevitable to obtain a clean surface prior to GaAs growth.

In this study, selective area growth of GaAs on Si was successfully performed by ECR-MBE at 630°C , the highest temperature throughout the growth process. This study builds on the authors' previous work using ECR-MBE: low-temperature GaAs growth including surface cleaning, and selective area GaAs homoepitaxial growth. GaAs was selectively grown on Si masked with 100-nm-thick SiN film. The SiN mask was patterned with $1\text{-}\mu\text{m}$ lines and spaces. The substrate was cleaned at 630°C by hydrogen ECR plasma exposure prior to growth, which yields a clean hetero-interface with no detectable pile-up of either carbon or oxygen. The growth temperature was kept constant without employing a two-step growth method. A cross-sectional SEM image revealed that the GaAs layer was selectively grown only on the unmasked areas, while no GaAs was deposited on the masked areas. No anomalous growth at the mask edge was observed in contrast to conventional MOCVD. The mechanisms of low-temperature plasma cleaning and selective area growth will be discussed in terms of the surface reactions and kinetics.

D2.11

ELECTRICAL PROPERTIES OF MESA DIODES ON EPITAXIAL GaAs/Si. K.L. Jiao, A.J. Solyka and W.A. Anderson, Center for Electronic and Electro-optic Materials, Department of Electrical and Computer Engineering, State University of New York at Buffalo, Bonner Hall, Buffalo, NY 14260; and S.M. Vernon, SPIRE Corp., Patriots Park, Bedford, MA 01730

Deep level transient spectroscopy (DLTS) and current-voltage-temperature (I-V-T) studies were performed on MOCVD-grown GaAs multilayer diodes on GaAs or Si substrates to study the influence of heteroepitaxy on electrical properties. A deep level ($E_c - 0.65 \text{ eV}$) was found for both GaAs/GaAs and GaAs/Si structures and is hence related to inherent defects of the GaAs epitaxial layer. For GaAs/Si, a continuous distribution of trap levels was also observed which could be attributed to misfit dislocations. I-V-T data revealed the saturation current density of GaAs/Si diodes to be four orders in amplitude higher and less temperature dependent than for GaAs/GaAs ones. The diode ideality factor (n) increased linearly with $1/T$ for GaAs/Si diodes but was relatively temperature independent for GaAs/GaAs diodes. The slopes of the I-V data were invariant with temperature for GaAs/Si diodes indicating tunneling to be the predominant mechanism. For GaAs/GaAs diodes at high forward bias, SRH recombination due to deep levels was observed. Arrhenius plots indicated an activation energy (E_A) of 0.60 eV . At low forward bias voltages, the slopes of the I-V data showed less temperature dependence, multiple mechanisms, and activation energies of 0.27 eV and 0.36 eV . A model using intraband multistep tunneling is utilized in explaining the data.

D2.12

HIGH QUALITY GaAs ON SOI BY MOCVD. N.H. Karam, V.E. Haven, S.M. Vernon, Spire Corporation, Patriots Park, Bedford, MA 01730; N.A. El-Masry, North Carolina State University, Raleigh, NC 27615; and M. Baegel, University of California, Los Angeles, CA 90024.

Epitaxial GaAs films have been successfully deposited on 3-inch diameter silicon wafers with a buried oxide by MOCVD. This is important due to the potential for three-dimensional integration of optical and electronic devices in addition to combining two technologies for radiation hardness. The silicon on insulator wafers were prepared using the Separation by Implantation of Oxygen process. Direct (100) silicon and 2 degrees off (100) towards (110) wafers were implanted with oxygen. The implanted wafers were then annealed at 1300°C for 6 hours in a nitrogen ambient to form a continuous buried oxide typically 4000 Å thick and a regrown Si over layer approximately 1400 Å.

The MOCVD deposition of GaAs on SOI took place in a SPI-MO CVDTM 450 reactor operated at atmospheric pressure using the standard two-step deposition technique for GaAs on Si. The surface morphology of the deposited films was found comparable to state of the art GaAs on Si films grown in the same reactor. Transmission Electron Microscopy (TEM) showed that the deposited films are of single domain and are of excellent quality. We have employed defect reduction techniques such as thermal cycle growth and strained layers to improve the quality of the deposited films. Two orders of magnitude reduction in defect density and a factor of 50X increase in the photoluminescence intensity have been observed. We will report on our progress in producing high quality GaAs on SOI and the comparison with GaAs on Si.

D4.1

FUNDAMENTAL ISSUES IN HETEROEPITAXY: A DOE COUNCIL OF MATERIALS SCIENCE PANEL REPORT. Paul S. Peercy, Sandia National Laboratories, Albuquerque, NM, (Panel Chairman)

A Panel comprised of members from academia, government labs and industry was convened by the Department of Energy Council on Materials Science January, 1989, to assess the current understanding of epitaxy and, based on this understanding, to recommend potentially fruitful research directions in this area.

Panel members were: E. G. Bauer (Tech. Universitat Clausthal), B. W. Dodson (Sandia National Laboratories), D. J. Ehrlich (MIT Lincoln Laboratory), L. C. Feldman (AT&T Bell Laboratories), C. P. Flynn (U. Illinois), M. W. Geis (MIT Lincoln Laboratory), J. P. Harbison (Bellcore), R. D. Kelley (DOE- Basic Energy Sciences), R. Matyi (U. Wisconsin), P. M. Petroff (U. California-SB), J. M. Phillips (AT&T Bell Laboratories), P. S. Peercy - Chairman (Sandia National Laboratories), G. B. Stringfellow (U. Utah) and A. Zangwill (Georgia Inst. Technology).

The Panel considered heteroepitaxy between metals, insulators and semiconductors and the new types of artificially structured materials which can now be grown by advanced epitaxy techniques. The principal findings of the Panel, with emphasis on future directions identified by the Panel, will be summarized in this presentation.

D4.2

THE ROLE OF AN INTERFACE MISFIT DISLOCATION IN BLOCKING THE GLIDE OF A THREADING DISLOCATION IN A STRAINED EPITAXIAL LAYER. L. B. Freund, J. C. Ramirez and A. Bower, Division of Engineering, Brown University, Providence, RI.

A general definition of the driving force for glide of a threading dislocation in a strained epitaxial layer is adopted to consider the interaction of dislocations on intersecting glide planes. This definition of driving force includes the possibility of glide through a region of spatially nonuniform stress, which is the situation in such an interaction. The analysis is based on the theory of elastic dislocations.

For the case of materials with cubic symmetry and an interface with normal direction [001], a straight 60 degree misfit dislocation is assumed to exist at the interface. This dislocation is supposed to have been formed by glide on a {111} plane. A threading dislocation on an intersecting {111} plane, which also leaves behind a 60 degree interface misfit dislocation, approaches the stationary dislocation. The traction induced on the glide plane of the threading dislocation by the stationary dislocation is determined for all combinations of Burgers vectors for the interacting dislocations, and the influence of this traction on glide is assessed. The results indicate that the effect is significant in blocking the glide of the threading dislocation for large mismatch strain and for layer thickness near the critical thickness.

For the case of an embedded strained layer, a kinetic law for thermally activated glide is invoked to study the change in shape of the threading dislocation during interaction with a stationary misfit dislocation. Results are obtained by imposing the kinetic law pointwise along the line of the threading dislocation, where the influence of the induced traction calculated in the foregoing interaction analysis is included in the driving force. The process is simulated numerically, and the results support the conclusion that the interaction can significantly retard the progress of a threading dislocation.

D4.3

SURFACE STRESS EFFECTS ON EPITAXY. K. Sieradzki and R. C. Cammarata, Department of Materials Science and Engineering, The Johns Hopkins University, Baltimore Maryland 21218, USA

We present an analysis of the thickness dependence on misfit required for the maintenance of epitaxy for the simple overlayer-substrate system. The analysis is similar to conventional equilibrium elastic theories except that we include an extra term into the overall energy balance which arises from surface stress effects. As an approximation we assume linear elastic behavior of the film. Physically, the effect of the surface stress is to introduce a thickness dependent lattice parameter for the free standing overlayer, i.e., for an overlayer disconnected from the substrate. Consequently, a completely incoherent interface is not defined as an overlayer which is relaxed to its bulk equilibrium lattice parameter, but rather an overlayer relaxed to a thickness dependent lattice parameter which is set by the magnitude of the surface and interfacial stress for interfaces in the system. Our results indicate that surface stress effects can have a significant effect on critical thickness. For example using typical values of the relevant parameters for metals, a 0.004 positive misfit ($a_{\text{substrate}} > a_{\text{film}}$) results in a critical thickness of ≈ 4.5 nm when surface stress effects are included, compared to a value of 12 nm when surface stress effects are ignored. For a 0.004 negative misfit the critical thickness is predicted to be ≈ 18 nm. Incorporation of non-linear elastic effects into the surface stress term would alter these predictions, and these studies are presently underway.

D4.4

MICRODIFFRACTION FROM CLEAVED $\text{Si-Si}_{1-x}\text{Ge}_x$ MULTILAYERS. W. T. Pike, Cavendish Laboratory, Madingley Road, Cambridge

Using the nanometer probe available in the dedicated scanning transmission electron microscope local structural information can be obtained from individual layers in [100] grown $\text{Si-Si}_{1-x}\text{Ge}_x$ multilayer structures. Furthermore the small probe size enables cleaved specimens with their very large wedge angles to be analyzed in cross-section. Diffraction patterns are shown from multilayers of varying composition

and periodicity. Analysis of the patterns concentrates on the higher order Laue zone (holz) reflections in the high angle excess ring rather than the holz deficit lines in the zero order beam more usually recorded, as it has proved difficult to obtain consistently clear deficit patterns. The behaviour of the excess holz reflections indicates the transition from a strained layer superlattice to a dislocated structure as the thickness of the layers increases for a given composition. These results are discussed with respect to possible strain relaxation mechanisms in these samples.

D4.5

ELECTRON CHANNELING ANALYSIS OF ELASTIC STRAINS IN InGaAs THIN FILMS. B. Keller, W. Zielinski, W.W. Gerberich, and J. Kozubowski, University of Minnesota, Minneapolis, MN.

Elastically-strained layers in thin film systems have received a great deal of attention recently. Of particular interest are the opto-electronic processes in these strained systems and their potential failure due to defect mechanisms. Proper characterization of the elastic and plastic strain fields arising from lattice-mismatched epitaxy is therefore essential to a better understanding of these items.

In_xGa_{1-x}As (x=0.05) thin films were grown by MBE on (100) GaAs substrates. The associated 1.3% lattice mismatch resulted in the development of an elastic strain field in the system. Electron channeling patterns (ECP) were then obtained from these samples in an SEM at different accelerating voltages. This allowed ECP's to be obtained from various information depths within the samples. Crystallographic data was therefore collected from both sides of the InGaAs/GaAs interface after the entire system was produced. An image analysis system was used to measure interplanar spacings and hence elastic strains from the patterns.

Lateral strains parallel to the interface varied with distance from the interface. The strain fields also varied with film thickness. Implications on misfit dislocation formation and the relevance of the ECP technique for elastic strain characterization will be discussed.

D4.6

GROWTH AND RELAXATION OF STRAINED HETEROSTRUCTURES. J.Y. Tsao, Sandia National Laboratories, Albuquerque, NM 87185.

How growth conditions correlate with the structural perfection of strained epitaxial films is an interesting and fundamental materials science question. The original equilibrium theories of van der Merwe, Matthews, and coworkers predicted that, below a critical thickness, lattice mismatch would be accommodated entirely by film strain. Above this thickness, film strain would be partly relieved by misfit dislocations.

In many semiconductor systems of interest, however, these theories are too simple. Often, structures which should exhibit strain relief do not, and other structures which should not, do. The issue is not merely an academic one: current state-of-the-art heterostructure devices require epitaxial layers as highly strained as possible. In this talk, recent work will be reviewed which has helped resolve this question, and which has led to a unified view of the stability and metastability of strained epitaxial films.

This work was performed at Sandia National Laboratories and was supported by the U.S. Department of Energy under Contract DE-AC04-76DP00789.

D4.7

ALTERNATE ROUTES TOWARD MISMATCH ACCOMODATION IN STRAINED-LAYER STRUCTURES. Brian W. Dodson, Sandia National Labs, Albuquerque, NM 87185

A great deal of work on the problem of stability and relaxation of strained-layer structures has recently been carried out. This has led to a basic understanding of mismatch accommodation via biaxial strain and the mechanisms and associated kinetics of structural relaxation via plastic flow. Accommodation of lattice mismatch, however, need not be accomplished solely by biaxial strain and/or glissile misfit dislocations. Other possible approaches include interdiffusion, formation of ordered alloys, spinodal decomposition, lattice tilt, and various forms of pseudomorphic growth. In this paper, the roles of lattice tilt, 3-d growth mode, and glissile generation of edge dislocations will be discussed, based on continuum and atomistic models of the energetics of the competing structures.

This work was performed at Sandia National Laboratories and was supported by the U.S. Department of Energy under Contract DE-AC04-76DP00789.

D4.8

A STUDY OF DISLOCATION BENDING PROCESSES AT STRAINED LAYER INTERFACES. S.A. Hussien, N.A. El-Masry, J.C.L. Tarn, J.-R. Gong and S.M. Bedair, Electrical and Computer Engineering Department, N.C. State University, Raleigh, North Carolina

An energy model was developed to evaluate the minimum critical layer thickness in strained layer structures that is required to block threading dislocations. The model calculates the change in the system energy that results from the presence of a bent dislocation segment at the strained interface. Calculations show that a threading dislocation has to overcome an energy barrier before gliding along the interface, indicating that the bending process is thermally activated. Also, bending of the dislocations becomes more favorable by increasing the value of the strain and/or thickness of the strained film.

The predictions of this model were experimentally verified by investigating the interaction of dislocations with strained layer superlattices in GaAs grown on Si. Three sets of GaAsP/InGaAs strained superlattice buffer layer structures were epitaxially stacked, with layers having the lowest strain closest to the GaAs/Si interface. The values of the strain used in this study were 0.0075, 0.0108 and 0.0135. Such structures were studied by TEM, both as grown and after cycle annealing. We found that the length of the bent dislocation segment increases with the value of strain, and annealing greatly enhances the process of dislocation bending.

We will report on how the above findings can impact in the quality of GaAs grown on Si substrates.

D4.9

DISLOCATION DENSITY REDUCTION IN GaAs EPILAYERS ON SILICON USING STRAINED LAYER SUPERLATTICES. S. Sharan, M. Sanganeria, K. Jagannadham and J. Narayan, Dept. of Materials Science and Engineering, North Carolina State University, Raleigh, NC 27695-7916

We have investigated the role of strained layer superlattices (InGaAs/GaAs) in reducing the threading dislocation density in GaAs epilayers grown on silicon substrates by Organometallic Chemical Vapor Deposition. Various combinations of superlattice layers have been used to study the effect of superlattice period,

thickness and composition on the reduction of dislocation density. The interaction of threading dislocations with the strained layer superlattices has been studied using cross-section and plan view transmission electron microscopy. The use of the strained layer superlattices is found to lower the threading dislocation density in the epilayers. The period and the thickness of the superlattice layers have been tailored such that misfit dislocations are formed by the bending of threading dislocations and not by nucleation of misfit dislocations. We have developed a model for analyzing the bending of threading dislocations at the strained superlattice interfaces. This model is based on the energy balance between the coherent energy of the superlattice and the energy required to bend threading dislocations at the superlattice interface.

D4.10

THE KINETICS OF STRAIN RELAXATION IN InGaAs/GaAs STRAINED MULTILAYERS David C. Paine and Morgan Kurk, Brown University, Providence, Rhode Island, and Robert N. Sacks, Timothy C. Eschrich, and William J. Tanski, United Technologies Research Center, East Hartford, Connecticut.

In this paper we report on our studies of strain relaxation in highly strained $\text{In}_x\text{Ga}_{1-x}\text{As}/\text{GaAs}$ ($0.1 < x < 0.3$) multilayers grown by MBE on GaAs at 420°C . We have characterized defect densities and strain relaxation using, principally, TEM and double crystal X-ray techniques. The thickness of the films that were studied (20 periods repeating with $\approx 10\text{ nm InGaAs}/10\text{ nm GaAs}$) far exceeds the critical thickness predicted by strain energy calculations. Nevertheless, the as-grown misfit dislocation density that was measured is well below this level due to limited defect nucleation and growth kinetics at the deposition temperature. We have studied the rate at which strained films relax as a function of post-growth annealing time and temperature.

A global activation energy was determined for dislocation nucleation and growth in our system by determining the degree of relaxation (dislocation density) as a function of time and temperature. To do this we performed proximity anneals at temperatures between 500 and 1100°C in a RTA and measured, by plan view TEM, the resulting dislocation density. In addition, long time anneals (from 1 to 48 hrs) at the growth temperature (420°C) were used to accurately determine the rate of defect nucleation and growth that is expected during multilayer deposition in the MBE.

In addition, defect interaction and multiplication mechanisms have been documented. For example, cross-sectional TEM micrographs have been obtained that strongly suggest a mechanism for the formation of "v"-shaped defects in the GaAs buffer layer. We have shown that the strain field around certain groups of dislocations in the multilayers can locally force a misfit (with a perpendicular line direction and parallel Burgers vector) lying in the substrate/multilayer interface into the substrate.

D5.1

PROPERTIES AND DEVICE APPLICATIONS OF $\text{Si}_{1-x}\text{Ge}_x$ ALLOYS. Subramanian S. Iyer, IBM Research Division, T.J. Watson Research Center, PO Box 218 Yorktown Heights, NY 10598.

Using low temperature epitaxial growth techniques, pseudomorphic $\text{Si}_{1-x}\text{Ge}_x$ alloys may be grown either on Si substrates or on suitably modified relaxed buffer layers of differing composition and lattice constant. It is thus possible to synthesize heterostructures with a wide variety of bandgaps and relative band alignments. Such structures have several device applications, such as heterojunction bipolar transistors and resonant tunnelling diodes. In this paper we review the properties of $\text{Si}_{1-x}\text{Ge}_x$ heterostructures in the context of device processing. These include considerations for the growth of abrupt heterostructures, and the stability of the heterostructures to thermal processing and oxidation. Heterojunction bipolar transistors with $\text{Si}_{1-x}\text{Ge}_x$ bases and resonant tunnelling devices have been fabricated. We review the design criteria and present some principal results. It will be shown that the use of $\text{Si}_{1-x}\text{Ge}_x$ alloys can provide significant leverage in Si technology.

D5.2

THE GROWTH MECHANISM OF EPITAXIAL SiGe HETEROSTRUCTURES PRODUCED BY WET OXIDATION OF AMORPHOUS SiGe THIN FILMS. S.M. Prokes, U.S. Naval Research Laboratory, Washington, D.C. 20375; and A.K. Rai, Universal Energy Systems, Inc., Dayton, OH 45432.

Epitaxial SiGe/Si structures have been formed by annealing from amorphous SiGe films deposited on a $\text{Si}(100)$ substrate at a pressure of 1×10^{-7} Torr. Under vacuum or nitrogen ambient annealing, the resultant films were polycrystalline, but when subjected to wet oxidation at 900°C , they were found to be epitaxial. The results which will be discussed indicate that the presence of an initial native oxide precludes solid phase epitaxy (SPE) under standard annealing conditions, but epitaxy can be achieved under oxidation conditions. The effect of initial Ge concentration on the oxidation rate, oxide trapping of Ge, and the epitaxial growth rate will also be covered. The analysis techniques applied include reflection electron diffraction (RED), ellipsometry, cross-sectional and plan-view TEM, and Rutherford Backscattering.

D5.3

SOLID PHASE EPITAXIAL REGROWTH OF $\text{Ge}_{1-x}\text{Si}_x$ ON $[100]$ Si Q.Z. Hong, A.J. Yu, J.W. Mayer, Department of Materials Science and Engineering, Cornell University, Ithaca, New York 14853; J.M. Poate, J.C. Bean, D.J. Eaglesham, AT&T Bell Labs, Murray Hill, New Jersey 07974

Solid phase epitaxial regrowth of $\text{Ge}_{1-x}\text{Si}_x$ ($4\% < x < 60\%$) on Si has been investigated. The MBE grown $\text{Ge}_{1-x}\text{Si}_x$ was first amorphized by 300-500 keV Si ion beams before being annealed in a vacuum furnace in the temperature range of 475 to 575°C . For samples with low Ge content ($x < 8\%$), the epitaxial regrowth proceeded in a layer by layer fashion, with the regrowth rate linearly proportional to the annealing time. The minimum yield recovered to 4% when the entire film was recrystallized. However samples with more Ge concentrations exhibited a non-planar-recrystallization behavior, as indicated by both Rutherford backscattering spectrometry and transmission electron microscopy. Furthermore the minimum yield of the Ge rich samples after regrowth was several times larger than that in the as-deposited state.

D5.4

SOLID PHASE EPITAXIAL REGROWTH OF SiGe STRAINED LAYERS AMORPHIZED BY ION IMPLANTATION. B. J. Robinson, B.T. CHILTON & D.A. Thompson, Centre for Electrophotonic Materials and Devices, McMaster University, Hamilton, Ont., Canada L8S 4M1.

Capped strained layers of $\text{Si}_{1-x}\text{Ge}_x$ on (100) Si grown by molecular beam epitaxy and initially coherent have been amorphized by ion implantation at 40K with 120 keV As^+ . Subsequently, the structures have been regrown by solid phase epitaxy at 600°C for 300s. Rutherford backscattering/channeling and transmission electron microscopy have been used to characterize the structure of the layer before and after implantation, and after regrowth. The measurements yield the range of concentration and strained layer thickness over which solid phase epitaxy can be used to recover the initial coherency strain. Results are compared with theoretical models of equilibrium and metastable strain states.

D5.5

REDUCTION OF DEFECT DENSITY IN HETEROEPITAXIAL $\text{Ge}_x\text{Si}_{1-x}$ GROWN ON PATTERNED Si SUBSTRATES. E.A. Fitzgerald, P.E. Freeland, Y.-H. Xie, AT&T Bell Laboratories, Murray Hill, NJ 07974.

We have grown MBE $\text{Ge}_x\text{Si}_{1-x}$ semiconductor alloys on mesas fabricated on (001) Si substrates. Single layer films with $x < 0.5$ were deposited on mesas 25-200 microns in lateral dimensions, as well as large area control specimens. Threading dislocation densities were measured with chemical etching and transmission electron microscopy (TEM), and misfit dislocations were revealed using chemical etching and plan-view TEM.

For low strain levels, we see a reduction in misfit and threading dislocation densities as compared with the unpatterned, large area growth. Wet-etching shows a large decrease in threading dislocation density, and we observe mesas in TEM which are dislocation-free. The effect of heterogeneous nucleation sources of misfit dislocations are limited to the mesa which contains the source; i.e. the yield of low defect density area increases due to the confinement of the dislocation source.

For high strain levels, the average misfit dislocation length becomes much less than our 25 micron mesa, resulting in less effective defect reduction. We will discuss our latest results concerning defect reduction for layers with higher misfit stress.

By examining relaxation of heteroepitaxial films with a range of strain levels on mesas, a clear correlation is made between the amount of relaxation in a strained film and the available sources for misfit dislocation nucleation.

D5.6

EXPERIMENTAL STUDIES OF KINETIC EFFECTS IN STRAINED LAYER EPITAXY R.Hull and J.C. Bean, AT&T Bell Laboratories, 600 Mountain Avenue, Murray Hill, NJ 07974.

The relaxation kinetics of strained layer epitaxy in the $\text{Ge}_x\text{Si}_{1-x}/\text{Si}$ system is studied by transmission electron microscopy (TEM) of structures which are annealed both in-situ and ex-situ from the microscope. In-situ annealing in the TEM allows direct dynamic observation of the introduction, propagation and interaction of misfit dislocations. Annealing in the original molecular beam epitaxy growth chamber serves as a control for the in-situ annealing experiments, and also allows us to investigate the effects of the presence/absence of an amorphous surface native oxide on dislocation nucleation and propagation.

The in-situ experiments enable us to quantify and to decouple dislocation nucleation, propagation and interaction processes. The relative importance of these processes depends crucially upon layer thicknesses and compositions and upon the structure geometry. At low lattice mismatch strains ($x < \sim 0.25$ in $\text{Ge}_x\text{Si}_{1-x}$), relaxation is nucleation-limited as the density of pre-existing defect sources in the material is insufficient to allow effective relaxation. At higher strains extra sources, such as half-loop nucleation at the growth surface, are generated. Dislocation velocities vary widely from $\text{\AA} \cdot \text{sec}^{-1}$ to $\mu\text{m} \cdot \text{sec}^{-1}$ at the growth temperature of 550°C , depending upon the structure geometry. Single $\text{Ge}_x\text{Si}_{1-x}$ layers grown upon a free Si surface are very thermally unstable: annealing to temperatures \geq the initial growth temperature immediately initiates motion of pre-existing dislocations. Comparable $\text{Ge}_x\text{Si}_{1-x}$ layers buried beneath a Si cap of the order of thousands of \AA thick, however, exhibit far greater thermal stability, with dislocation velocities three orders of magnitude lower than in the single interface structure. Finally, we find that dislocation interactions can be the crucial limiting process in determining the strain relaxation rate in very thin epilayers, inter-dislocation forces defining an effective "critical thickness" below which defects may pin each others motion.

D5.7

THE 2D-3D TRANSITION IN THE MBE GROWTH OF Ge/Si D.J. Eaglesham and M. Cerullo, AT&T Bell Laboratories, 600 Mountain Avenue, Murray Hill, NJ 07974, USA

The growth of Ge and high Ge content alloys on Si is a subject of increasing technological interest, particularly at high Ge

levels where the band offsets are large. The maximum Ge content attainable during growth of such films is normally imposed by the transition from 2D layer-by-layer growth to 3D island growth. Previous RHEED and RBS studies of very thin Ge layers have suggested that islands forming at this unwetting transition are already relaxed by misfit dislocations.

Here we present a study of the nucleation and growth of Ge (and high-Ge alloys) on Si (and SiGe) by MBE. A combination of in-situ RHEED and Auger with ex-situ TEM is used to study the kinetics of the transformation as a function of temperature, and surface cleanliness. It is shown that islands are dislocation-free when formed, and grow without the introduction of misfit dislocations up to island thicknesses far in excess of the critical thickness (up to $\sim 10 h_c$). This phenomenon is explained in terms of strain relaxation by island deformation. The implications of these observations for the growth of high-Ge alloys are discussed.

D5.8

MORPHOLOGY OF GE FILMS GROWN LAYER BY LAYER ON $\text{Si}(001)$ F.K. LeGoues, M. Copel and R.M. Tromp IBM Research Division, Thomas J. Watson Research Center, Yorktown Heights, NY 10598.

The preferred mode of growth for germanium on $\text{Si}(001)$ is layer by layer for three monolayers, followed by islanding. The resulting morphology consists of a completely relieved Ge layer, where the relief is accomplished by a network of dislocations. In the present work, we have studied the morphology of 15 monolayers thick Ge films that have been forced to grow layer by layer by saturating the Si surface with As prior to Ge growth. In this case, no dislocations are observed. Instead, the strain is relieved by a novel, never before observed defect, consisting of two $\Sigma 9$ boundaries and a twin plane. These defects are formed catastrophically and only involve local rearrangement of atoms. We explain this unusual morphology by the absence of nucleation sites for dislocations during layer by layer growth. This also means that islanding, or rather, the edges of island must be a necessary condition for dislocation formation during MBE.

D5.9

MISFIT DISLOCATION NUCLEATION AND MULTIPLICATION AT $\text{Ge}_x\text{Si}_{1-x}/\text{Si}$ INTERFACES. D.D. Perovic, G.C. Weatherly, Dept. of Metallurgy and Materials Science, University of Toronto, Toronto Canada M5S 1A4; and D.C. Houghton, Division of Physics, National Research Council, Ottawa Canada K1A 0R6.

In the study of elastic strain relaxation in semiconductor heterostructures, a number of misfit dislocation generation mechanisms have been suggested to account for the high interfacial dislocation density observed in these almost defect-free crystals. Several $\text{Ge}_x\text{Si}_{1-x}/\text{Si}$ heterostructures, both in the as-grown and annealed condition have been studied using transmission electron microscopy. The results indicate that some of the popular theories of dislocation generation are less important or not applicable based on both theoretical and experimental considerations. Specifically, it will be shown that (i) heterogeneous sources in these so-called "perfect" crystals play a dominant role in the operative nucleation mechanisms, (ii) the Hagen-Strunk dislocation nucleation mechanism is inoperative under most conditions in this system and (iii) the strain relaxation behaviour during growth may be different from that observed in metastable structures annealed after growth.

D5.10

DISLOCATION BEHAVIOUR IN $\text{Ge}_x\text{Si}_{1-x}$ EPILAYERS ON $(001)\text{Si}$: E.P. Kvan[†], D.M. Maher[‡], and C.J. Humphreys^{*}, ^{*}Department of Materials Science and Engineering, The University, Liverpool L69 3BX, [†]Lawrence Berkeley Laboratory, 1 Cyclotron Road, Berkeley, CA 94720, [‡]AT&T Bell Laboratories, 600 Mountain Ave., Murray Hill, NJ 07974

We have observed that the nature of misfit dislocations introduced near the critical thickness in $\text{Ge}_x\text{Si}_{1-x}$ alloys on $(001)\text{Si}$ changes markedly in the region $0.4 \leq x \leq 0.5$. At or below the lower end of this compositional range, the observed microstructure is comprised almost entirely of 60° type dislocations, while at the high end, the dislocation

structure is almost entirely Lomer edge type. As a consequence of this change, the dislocation density at the top of the epilayer varies by a factor of 1000. Similarly, several other observables (e.g. dislocation length and spacing) also change appreciably.

Part of the reason for the morphological variation seems to be a change in the source for dislocation introduction, in conjunction with a change in glide behaviour of dislocations as a function of film thickness. Evidence will be presented that indicates strain, as well as thickness, has a critical value for some dislocation introduction mechanisms, and that these together determine the resulting microstructure.

Furthermore, it appears unlikely that the edge-type Lomer dislocations which appear at about $x = 0.5$ are either introduced directly by climb, or grown in, as in the three-dimensional island growth and coalescence which occurs when x approaches unity. Instead, a two-step mechanism involving glissile dislocations is proposed and discussed.

D6.1

METASTABILITY IN SINGLE CRYSTAL EPILAYERS AND SUPERLATTICES GROWN BY MBE. R. Du and C.P. Flynn
Materials Research Laboratory and Department of Physics,
University of Illinois at Urbana-Champaign, 104 S. Goodwin,
Urbana, IL 61801

We have discovered that the (1102) planes of hexagonal metals can be grown tilted on the 211 planes of bcc metals. The epilayer grows as a coherent, unstrained single crystal. In effect it forms a low angle asymmetrical tilt boundary with the substrate. A regular arrangement of dislocations evidently glides to the interface driven by the long range epitaxial strain, thereby relieving the elastic strain energy. Tilt angles up to 7° can be designed, and the angle predicted from the requirement of interfacial coherence with zero long range strain. In the tilt angle range $0-7^\circ$ the observed tilt angles agree with the predictions to 0.1° . Interfacial processes with this elegance, precision and simplicity do not appear to have been observed before. The selection of one of two equivalent tilts involves a symmetry breaking that depends on the miscut of the sapphire substrates employed here for bcc growth. Possible applications of superlattices prepared in this way for x-ray and neutron optics are discussed.

This research was supported in part by the Department of Energy, Division of Materials Science contract DE-AC02-76ER01198.

D6.2

MICROSTRUCTURE OF FCC/BCC METAL MULTILAYERS. Nigel M. Jennett and D.J. Dingley, Dept. Physics, Bristol University, England. Y. Ando, Dept. Applied Physics, Nagoya University, Japan.

Metal multilayers of Fe/Cu, V/Cu and Fe/Ni have been grown in either HV or UHV evaporators for the investigation of magnetic properties. A buffer layer of 800-1500 Å Cu was used between mica substrate and multilayer. Systematic experiments were performed to investigate microstructure as a function of vacuum quality and substrate temperature.

Cu/Fe foils grown between 100°C and 500°C at $2-4 \times 10^{-7}$ mbar exhibited a complex structure in which the Cu grew in (111) epitaxy and the Fe divided between the Kurdjumov-Sachs and Nishiyama-Wassermann orientation relationships and with a lath-like microstructure reminiscent of martensitic needles in ferritic steels. These laths grew laterally with increasing foil thickness, approximately maintaining a constant aspect ratio and perturbed the foil surface such that the surface morphology, as observed by SEM, corresponded closely to the lath distribution. In general, perfection of microstructure was much improved by growing in UHV conditions. Lower contamination rates allowed a slower evaporation, a higher surface mobility and thus a reduction in the substrate temperature necessary to achieve epitaxy. With increasing temperature, foils were polycrystalline and of uniform thickness ($<100^\circ\text{C}$); rough with columnar grains of

increasing size ($150^\circ\text{C} < 300^\circ\text{C}$); flat with simultaneously good epitaxy (approx. 300°C); perfect epitaxy but discontinuous as material migrated over the surface into single crystal islands ($>345^\circ\text{C}$). The window of conditions for complete coverage by flat single crystal is narrow and shifts with changes in surface nucleation density. Subsequent layers follow the buffer layer morphology closely therefore flat, almost perfect-crystal buffer layers were grown and then recrystallised, without roughening, by an in situ anneal.

D6.3

AN INVESTIGATION OF THE DISLOCATION STRUCTURE OF THE NI/AG PHASE BOUNDARY. Thomas A. Bamford, Wilkes College, Wilkes-Barre, PA.

The Ni/Ag interphase boundary structure in the parallel cube-on-cube orientation was studied for the boundary planes (001) and (011). Coarsely spaced dislocations were found in all annealed interfaces; the origin of these was apparently differential thermal expansion of the bicrystal film. A detailed search for intrinsic periodic structure consistent with the O-lattice construction was made using X-ray diffraction, electron diffraction and transmission electron microscopy. No evidence for this could be found; such a relaxation, if present, is very weak. It is unlikely that such a small relaxation could account for the relative energy minimum associated with the parallel cube-on-cube orientation found by previous investigators.

D6.4

EPITAXIAL GROWTH OF Cu-Ni SINGLE CRYSTAL ALLOYS AND SUPERLATTICES BY MOLECULAR BEAM EPITAXY.

R.P. Burns, Research Triangle Institute, Research Triangle Park, NC and Department of Physics, North Carolina State University, Raleigh; Y.H. Lee, Department of Materials Science and Engineering, North Carolina State University, Raleigh; N.R. Parikh, Department of Physics and Astronomy, University of North Carolina, Chapel Hill; J.B. Posthill, M.J. Mantini, R.J. Markunas, Research Triangle Institute, Research Triangle Park, NC

Epitaxial growth in the Cu-Ni system is presently being explored as a means of fabricating a lattice matched, defect free substrate for either the direct deposition of diamond, or for deposition of a suitable interlayer to promote diamond nucleation. Epitaxial metal films have been grown by molecular beam epitaxy which are of higher quality than commercially-available single crystal substrates. Since the lattice constants of Cu ($a_0 = 0.3615$ nm) and Ni ($a_0 = 0.3524$ nm) straddle that of diamond ($a_0 = 0.3567$ nm), lattice-matched epitaxial alloys can be fabricated for a wide range of diamond growth parameters. Cu-Ni epitaxial alloys of varying composition have been grown at the $150-300^\circ\text{C}$ range to investigate the possible occurrence of spinodal decomposition, which has been reported in the literature. Spinodal decomposition has not been detected with transmission electron microscopy. Strained layer superlattices have also been grown in order to potentially deflect dislocations originating at the substrate/epilayer interface. Multilayers and superlattices of varying composition and thicknesses will be discussed. *In vacuo* cleaning techniques and subsequent characterization by AES, XPS, and LEED of the bulk substrates have been developed and will be described. Determination of the structural quality of the grown films has been made by XRD, SEM, TEM, RBS/channeling, and LEED. AES and XPS demonstrate that epitaxial metal films can be grown free of impurities (particularly carbon) that are normally found in bulk substrates.

D6.5

STRUCTURAL AND ELECTRONIC PROPERTIES OF Pb/Cu MULTILAYERS. Dominique Neerincx, Kristiaan Temst, Hans Vanderstraeten, Yvan Bruynseraede, Laboratorium voor Vaste Stof-Fysika en Magnetisme, Katholieke Universiteit Leuven, B-3030 Leuven, Belgium; and Ivan K. Schuller, Physics Department - B019, University of California-San Diego, La Jolla, California 92093, USA.

We have prepared Pb/Cu multilayered structures on liquid nitrogen cooled substrates (for layer thicknesses below 200 \AA) and on

room temperature substrates. The high angle X-ray diffraction spectrum indicates the presence of interfacial disorder of a continuous kind (crystalline/amorphous like). In the low angle spectrum pronounced minima occur at positions given by $q=2\pi/\Lambda$, where Λ is the bilayer thickness. This is in contradiction with Pb/Ge (crystalline/amorphous) multilayers, where minima are observed at positions $q=2\pi/D$ with D the Pb thickness. This behavior is explained by taking into account the optical properties of the individual layers. The electronic elastic mean free path in the individual layers, obtained from resistivity measurements, is limited by the layer thickness for the thinnest samples, while a saturation occurs for the thicker layers. This saturation is probably due to the poorer structural quality of the thicker samples.

This work is supported by the Belgian Concerted Action (G.O.A.), Inter-University Attraction Poles (I.U.A.P.) and I.I.K.W. programs. (at K.U. Leuven) and the U.S. Department of Energy grant # DE-FG03-87ER45 (at U.C.S.D.). International travel was provided by NATO. D.N. is a Research Assistant of the Belgian N.F.W.O. and K.T. and H.V. are Research Fellows of the Belgian I.I.K.W.

D6.6

SURFACE STRESS EFFECTS ON THE ELASTIC MODULI OF SUPERLATTICE THIN FILMS. R.C. Cammarata, K. Sieradzki, and F. Streitz, The Johns Hopkins University, Baltimore, MD 21218.

A model is presented which predicts a significant sample-size effect on the elastic moduli of superlattice thin films possessing small layer repeat lengths. Due to the presence of incoherent interfacial stresses, biaxial in-plane elastic strains are created which are approximately inversely proportional to the layer repeat length Λ . When Λ is of the order of 1 nm, these strains can be of the order of 1%, inducing nonlinear elastic behavior. This model is able to explain in a semi-quantitative way the supermodulus effect in certain metallic superlattices.

D6.7

ANALYSIS OF Au/Ni MULTILAYERS BY X-RAY DIFFRACTION. J. Chaudhuri, S. Shah, V. Gondhalekar, Mech. Eng. Dept. and The Inst. for Aviation Research, The Wichita State Univ., Wichita, KS 67208; and A. F. Jankowski, Lawrence Livermore National Laboratory, Livermore, CA 94550.

Profiles of strain within individual layers in Au/Ni multilayer system were obtained by iterative fitting of the experimental diffraction pattern with a kinematic model. The depth profile of strain in the modulation direction was obtained for these metallic multilayers with repeat periodicities ranging from 1.19 nm to 4.26 nm. An attempt was made to correlate the "supermodulus effect" present in the Au/Ni system with the strain distributions obtained from this kinematic model. A significant volume fraction of interfaces is present in these nanometric scaled periodic structures.

D6.8

ELASTIC PROPERTIES OF FCC-FCC METALLIC MULTILAYERS[†]. John R. Dutcher, Sukmock Lee, Jeha Kim, Craig D. England, George I. Stegeman and Charles M. Falco, Optical Sciences Center and Department of Physics, University of Arizona, Tucson, AZ 85721.

The surface acoustic phonon modes of sputter-deposited Ag-Pd and Cu-Co multilayers were studied using Brillouin light scattering. Both of these metal combinations are fcc-fcc. Enhancements of the biaxial modulus (the "supermodulus effect") have been reported for Ag-Pd¹ and other fcc-fcc multilayers near a multilayer modulation

wavelength value of $\Lambda = 25\text{\AA}$. We have measured the dispersion of the phonon mode velocities for Ag-Pd and Cu-Co multilayers as a function of Λ for samples with Λ in the range 10\AA to 100\AA . The Λ -dependence of the effective elastic constants of the multilayer samples, which was obtained by comparing the data with calculated dispersion curves for the phonon modes, will be discussed.

[†]work supported by Office of Naval Research grant N00014-88-K-0298

¹G.E. Henein and J.E. Hilliard, J. Appl. Phys. 54, 728 (1983).

D6.9

EPITAXIAL Fe/Ag AND Mn/Ag SUPERLATTICES. S. Nahm, and L. Salamanca-Young, University of Maryland, College Park, MD 20742; and B. T. Jonker, J. J. Krebs, and G. A. Prinz, Naval Research Laboratory, Washington, DC 20375-5000.

We studied the epitaxial growth and structural properties of Fe/Ag and Mn/Ag superlattices grown on (001) GaAs substrates using Transmission Electron Microscopy. A buffer layer of either Ag or ZnSe was grown on the (001) GaAs substrate before the growth of the superlattice to obtain good quality films.[1],[2] Both Fe/Ag and Mn/Ag superlattices with Ag buffer layer show very sharp interfaces. In the Fe/Ag superlattice the in-plane $\langle 100 \rangle$ direction of Fe is parallel to the $\langle 110 \rangle$ direction of Ag. In this configuration the Fe layer maintains its bulk bcc structure. On the contrary, in the Mn/Ag superlattice our results show that the growth of the Mn layer is pseudomorphic with the Mn layer being fct rather than bct. Both fct and bct structures had been suggested to be possible structures for this layer.[2] The structure of the Mn layers in the superlattice is studied as a function of Mn layer thickness. Our TEM results show that both kinds of superlattices have similar densities of dislocations of $\approx 10^9\text{cm}^{-2}$. Some of the dislocations originate within the superlattice film and others in the Ag buffer layer. The dislocations are edge dislocations with Burgers vectors along $\langle 110 \rangle$ directions. The densities of dislocations for the Fe/Ag superlattices grown on a ZnSe buffer layer were $\approx 10^9\text{cm}^{-2}$. We will present detailed studies of the interfaces in the superlattices as well as the interface between the Fe seed layer and the GaAs substrate.

The work by S. N. and L-S-Y was supported by the National Science Foundation No. DMR-87-10817.

[1] J.J. Krebs, B.T. Jonker, and G.A. Prinz, J. Appl. Phys, 63, 3467, (1988).

[2] B. T. Jonker, J.J. Krebs, and G.A. Prinz, Phys. Rev. B39, 1399,(1989).

D6.10

GROWTH AND CHARACTERIZATION OF (Mn/Ag) (001) SUPERLATTICES,* B.T. Jonker, Y.U. Idzerda, J.J. Krebs and G.A. Prinz, Naval Research Laboratory, Washington, D.C. 20375-5000.

In an attempt to stabilize the bcc phase of Mn, predicted to be ferromagnetic,^{1,2} we have grown single crystal Mn films and coherent (Mn/Ag) superlattices on Ag(001) by MBE.³ In a simple constant volume approximation based on the Wigner-Seitz radius of α -Mn, one would expect a bcc lattice constant of 2.89\AA , while recent total energy calculations predict an equilibrium lattice constant of 2.79\AA .² Thus the 2.89\AA square surface net of the Ag(001) plane is expected to provide a good template with which to stabilize the bcc structure.

The Ag(001) substrate films were grown on 5 monolayer (ML) Fe(001) seed layers grown on ZnSe(001) epilayers, which were grown in turn on bulk GaAs(001) substrates. The superlattices had 20 to 100 periods, with periods consisting of 1, 2, 3, 5 and 14 ML's of Mn and 10 - 15 ML's of Ag. The structure of the samples was determined from a combination of RHEED, x-ray diffraction, and conversion electron extended x-ray absorption fine structure measurements. X-ray θ -2 θ scans show prominent and well-resolved multiple satellite structure around the high angle Ag Bragg peaks, as well as low angle diffraction peaks produced by the superlattice period. We find that although the Mn(001) films are pseudomorphic with the substrate and exhibit the desired 2.89\AA square

surface net, they are tetragonally distorted along the surface normal, with an out-of-plane lattice parameter which decreases with increasing film thickness up to 5 ML. Films thinner than 3 ML (corresponding to one complete unit cell) are nearly fcc, while by 5 ML they exhibit a body-centered tetragonal structure which does not change with additional thickness. Beyond approximately 14 ML, the films cannot maintain the single crystal phase. These results are compared with corresponding x-ray photoelectron diffraction data. We detect no significant ferromagnetic contribution at temperatures down to 5 K.

1. G. Fuster *et al.*, Phys. Rev. B 38, 423 (1988).

2. V.L. Moruzzi and P.M. Marcus, Phys. Rev. B 38, 1613 (1988).

3. B.T. Jonker, J.J. Krebs and G.A. Prinz, Phys. Rev. B 39, 1399 (1989).

* This work was supported by the Office of Naval Research.

D6.11

FORMATION AND STRUCTURE OF Mo THIN LAYERS ON Ni(001) AND Mo-Ni SUPERLATTICES. Y.H. Lee, Department of Materials Science and Engineering, North Carolina State University, Raleigh, NC; R.P. Burns, Research Triangle Institute, Research Triangle Park, NC and Department of Physics, North Carolina State University, Raleigh; J.B. Posthill, M.J. Mantini and R.J. Markunas, Research Triangle Institute, Research Triangle Park, NC; K.J. Bachmann, Department of Materials Science and Engineering, North Carolina State University, Raleigh, NC.

For heteroepitaxial diamond growth, Mo along with certain other transition metals are considered to be possible substrates because of their reactivity with carbon. However, Mo is not lattice-matched to diamond. The formation of a metastable, pseudomorphic overlayer of Mo (normally bcc, $a_0=0.314\text{nm}$) on diamond-lattice-matching single crystal surfaces like Ni (fcc, $a_0=0.352\text{nm}$) and metallic multilayers represents a possibility for combining enhanced chemical reactivity with lattice matching. Ultrathin ($<2\text{nm}$) overlayers of Mo have been grown by molecular beam epitaxy on single crystal Ni(001) substrates. A systematic study by in situ LEED, XPS and AES on overlayers of varying thicknesses was used to determine the nucleation and growth processes of these thin films. Thicker layers of Mo ($>50\text{nm}$) and superlattices of Mo-Ni system were also grown on Ni(001). Assessment of the Mo/Ni(001) system and the Mo/Ni/Mo/Ni(001) superlattices was made utilizing LEED, SEM, TEM and XRD. Composition was determined via in situ XPS and AES.

D7.1

MATERIALS AND DEVICE PROPERTIES OF LATTICE-MATCHED AND PSEUDOMORPHIC InP BASED HETEROSTRUCTURES

Umesh K. Mishra and April S. Brown
N.C.State University, Raleigh N.C.
Cornell University, Ithaca, N.Y.

GaInAs based HEMTs and HBTs are superior for high frequency applications than GaAs based devices because of the better electronic transport properties in GaInAs. The electron mobility is $13,000\text{ cm}^2/\text{V}\cdot\text{s}$ and the conduction band discontinuity between $\text{Al}_{0.48}\text{In}_{0.52}\text{As}$ and $\text{Ga}_{0.47}\text{In}_{0.53}\text{As}$ is 0.51eV , all higher than the GaAs based system. Furthermore, the low bandgap of GaInAs (0.74eV) reduces the emitter-base turn-on voltage of the HBT, substantially reducing the power dissipation. The large conduction band discontinuity coupled with the high doping possible in $\text{Al}_{0.48}\text{In}_{0.52}\text{As}$ ($\text{Nd} > 1 \times 10^{19}\text{ cm}^{-2}$) provides for large two dimensional electron gas (2DEG) concentrations in modulation doped structures. 2DEG channels formed at single heterostructures have exhibited sheet resistances as low as 130 ohm/sq. compared to 700 ohm/sq. obtained from AlGaAs/GaAs structures. By growing pseudomorphic (In rich) $\text{Ga}_{0.47}\text{In}_{0.53}\text{As}$ on $\text{Al}_{0.48}\text{In}_{0.52}\text{As}$ enhancements in conduction band discontinuity, electron mobility, 2DEG density and electron confinement are realized. These materials properties have been utilized to produce discrete HEMTs with $f_T > 200\text{GHz}$, ring oscillators with room temperature gate delay of 6pS and frequency dividers operating at 26.7GHz . Discrete HBTs have demonstrated a f_T of

49GHz and a f_{max} of 62GHz whereas static frequency dividers have operated at 15GHz . Optimization of MBE growth conditions of GaInAs and AlInAs on (100) InP and vicinal substrates and their impact on device performance will be discussed.

D7.2

MATERIALS AND DEVICE CHARACTERISTICS OF PSEUDOMORPHIC AlGaAs-InGaAs-GaAs and AlInAs-InGaAs-InP HIGH ELECTRON MOBILITY TRANSISTORS. J.M. Ballingall, Pin Ho, G.J. Tessler, P.A. Martin, T.H. Yu, P.C. Chao, P.M. Smith, and K.G.H. Duh, General Electric Electronics Laboratory, Syracuse, NY 13221 (INVITED).

High electron mobility transistors (HEMTs) with single quantum well active layers composed of pseudomorphic InGaAs grown on GaAs and InP are establishing new standards of performance for microwave and millimeter wave applications. This is due to recent progress in the molecular beam epitaxial growth of strained InGaAs heterostructures coupled with developments in short gate length (sub- $0.2\mu\text{m}$) device fabrication technology. This paper reviews this progress and the current state-of-the-art for materials and devices.

The critical thickness for strained layer structures is now generally recognized to be a function of epitaxial growth conditions, with growth temperature being the key parameter. Apparently controlling misfit dislocation kinetics. This has enabled the growth of InGaAs quantum wells with higher InAs mole fractions (and hence strains) than previously attainable, resulting in metastable strained layer HEMTs, i.e., with strains exceeding the currently accepted limits for stability against misfit dislocation formation. While dislocations can now be controlled to a greater extent than previously, there is mounting evidence that strain strongly influences growth kinetics and hence layer quality, independent of dislocation formation.

Increasing the InAs mole fraction of the quantum well provides substantial enhancement of the active layer electron confinement potential and the effective electron velocity, more than offsetting any deleterious effects of strain on transistor performance. While strain is generally considered a risk factor for the reliability of electronic devices, it is notable that the reliability of HEMTs with active layer strains exceeding 2% appears to be comparable to conventional GaAs field effect transistors. This research is partially supported by the Air Force Office of Scientific Research (AFSC) Contract F49620-88-C-0054.

D7.3

X-RAY DIFFRACTION STUDY OF InAlAs-InGaAs ON InP HIGH ELECTRON MOBILITY TRANSISTOR STRUCTURE PREPARED BY MOLECULAR-BEAM EPITAXY. H. Y. LIU, Y. C. Kao and T. S. Kim. Central Research Laboratories, P.O. Box 655936, MS 147, Texas Instruments Inc., Dallas, TX 75265

High-Electron Mobility Transistors (HEMTs) can be prepared by growing alternating epitaxial layers of InAlAs-InGaAs-InAlAs on InP substrates. Lattice matched HEMTs are obtained by growing layers of $\text{In}_{1-x}\text{Al}_x\text{As}$ and $\text{In}_y\text{Ga}_{1-y}\text{As}$ with $x \approx 0.523$ and $y \approx 0.532$. Varying the values of x and y by controlling the individual flux during molecular-beam epitaxial (MBE) growth, one can obtain pseudomorphic HEMTs. Pseudomorphic HEMTs may have superior electronic transport properties and larger conduction band discontinuity compared to an unstrained one. The precise control of the composition is thus important to the properties of HEMTs. This control is however very difficult and the values of x and y may vary from run to run.

In this paper we will study the effect on the electrical properties of HEMTs due to the structure variation of x and y values as well as the thickness of the InGaAs layer. We will demonstrate that all this structure information: including composition and thickness of both the buffer and top InAlAs layers and the active channel InGaAs layer, can be obtained by double crystal x-ray diffraction. They can be revealed from the analysis of the fine features of the double-crystal rocking curves (DCRCs). These structure parameters are obtained by comparing the experimental DCRC with the one from computer simulation according to semi-kinematical approximation. During the simulation one or more of these structure parameters are adjusted until the best fitted DCRC is obtained. Hall measurements will be used to correlate with x-ray diffraction results. The limitation of DCRC in measuring small variations in channel layer thickness and small changes in composition for both InAlAs and InGaAs layers will also be discussed.

STRUCTURAL AND ELECTRONIC PROPERTIES OF GaAs/InGaAs/GaAs HETEROSTRUCTURES. J.M. Bonar, R. Hull, R.J. Malik, and R.W. Ryan, AT&T Bell Labs, Murray Hill NJ; and J.F. Walker, Laboratorio TASC, Trieste, Italy.

We have examined a series of samples consisting of 200Å $\text{In}_x\text{Ga}_{1-x}\text{As}$ layered in a hetero-junction bipolar transistor (HBT) structure ($\text{In}_x\text{Ga}_{1-x}\text{As}$ on GaAs, followed by GaAs, AlGaAs and a GaAs cap) in order to correlate structural, electronic, and device properties with In concentration. In this study, x was varied from 0 to 0.5, which spans the range from pseudomorphic growth to layers well above the critical thickness.

Dislocation densities were measured by Transmission Electron Microscopy (TEM). The average distance between dislocations was found to be greater than the TEM detection limit for $x < 0.30$. For $x = 0.30$, the distance between dislocations was on the order of 1-5 microns, with the dislocations observed being of the expected $1/2\langle 110 \rangle$ type. For a layer thickness of 200Å, 30% In exceeds the equilibrium definition of critical thickness. The dislocation density observed also exceeds the expected density if the only dislocation sources are threading defects from the substrate. One possible extra source we have observed is misfit dislocations which are associated with stacking faults. For $x \geq 0.40$, the distance between dislocations was much less, on the order of thousands of angstroms or less, the dislocation structure was more disordered, and the samples showed evidence of 3-dimensional growth. Several of the samples were annealed in the microscope in order to gain insight into how dislocations form and move in this system.

Hall measurements were made on structures with p-type doped In layers. The hole mobility initially increased with addition of In, peaking at $x = 0.10$, with a corresponding drop in sheet resistance. N-p-n HBT structures were also made, these devices showed substantial improvement in gain with the addition of some In, rising from $\beta = 149$ at $x = 0$ to $\beta = 190$ at $x = 0.1$, then monotonically dropping with In concentration to $\beta = 1$ at $x = 0.5$. The fact that the electrical characteristics and device performance degraded before the dislocation density was high enough to be measured by TEM demonstrates that for mismatched systems with low defect levels, electrical and device performance are far more sensitive measures of dislocation formation.

D7.5

FIELD EFFECT TRANSISTOR STRUCTURE BASED ON STRAIN INDUCED POLARIZATION CHARGES D.L. Smith, Los Alamos National Laboratory, Los Alamos, NM, 87545, R.T. Collins, T.F. Kuech, I.B.M. T.J. Watson Research Center, Yorktown Heights, NY, 10598 C. Mailhot, Xerox Webster Research Center, Webster, NY, 14580.

Strained layers have been utilized in many device structures. The tunability of the bandgap with layer strain has been the focus of most of these device related studies. However, when growth of the strained layer structure occurs along a polar direction of the crystal internal electric fields arising from the piezo-electric effect can be internally generated by the induced polarization charges. We suggest a new field effect transistor structure based on strain induced polarization charges. The structures utilize the pseudo-morphic growth of a barrier layer on a substrate oriented in a polar direction (i.e. $\langle 111 \rangle$, $\langle 211 \rangle$, ...). Polarization charges are generated in large bandgap material, used as a gate insulator. A 2D electron gas, whose density can be modulated by an external bias, forms at the hetero-interface to screen the polarization charges. Zero bias densities of several times $10^{11}\text{e}/\text{cm}^2$ and turn-off threshold voltages of 0.5V can be achieved in the $\text{Ga}_{1-x}\text{In}_x\text{As}-\text{AlIn}_{1-x}\text{As}$ model system. Both normally-on and normally-off structures are possible.

D7.6

THE EFFECT OF INDIUM DEPLETION ON THE COMPOSITION OF OMVPE GROWN GaAs. P.D. Agnello, T.J. Watson Research Center, IBM, Yorktown Heights, NY; P.B. Chinoy and S.K. Ghandhi, Rensselaer Polytechnic Institute, Troy, New York 12180.

We present an experimental and theoretical study of the nature of Indium depletion in the OMVPE growth of GaInAs from triethylindium (TEI), trimethylgallium (TMI) and arsine (AsH_3). A mathematical model, including the effects of homogeneous and het-

erogeneous decomposition of the In species, was developed for this purpose. Several different mechanisms are postulated, based on experimental data obtained from a mass spectrometric study. The activation energies for the decomposition reactions were obtained by fitting the theoretical composition of GaInAs with the experimental values for growth at 700°C. These models were then compared with experimental results over a wide range of growth parameters such as susceptor temperature, susceptor slope, reactor pressure and reactant partial pressure. Excellent correlation was obtained for a model based on the homogeneous decomposition of a TEI- AsH_3 adduct to a stable product via an irreversible bimolecular reaction, with an activation energy of 11.9 kcal/gmol.

This study resulted in the development of a model which describes the nature of the chemical processes that lead to indium depletion. The rate expression for this depletion can be used to predict the growth rate and composition of GaInAs for a wide range of reactor parameters.

D7.7

HETEROJUNCTION STUDY OF $\text{Ga}_{0.9}\text{In}_{0.1}\text{As}(p^+)/\text{GaAs}(n)$ DIODES: CORRELATION OF ELECTRICAL AND STRUCTURAL CHARACTERISTICS. Y.W. Choi and C.R. Wie, State University of New York at Buffalo, Department of Electrical and Computer Engineering and Center for Electronic and Electrooptic Materials, Amherst, New York 14260; K.R. Evans and C.E. Stutz, Wright-Peterson Air Force Base, Ohio

The effects of in-plane lattice mismatch in electrical characteristics have been studied for MBE grown $\text{Ga}_{0.9}\text{In}_{0.1}\text{As}(p^+)/\text{GaAs}(n)/\text{GaAs}(n^+)$ samples. Different in-plane mismatch was introduced by a variation of epilayer thickness ($h = 0.1, 0.25, 0.5$ and $1\text{ }\mu\text{m}$). Double crystal X-ray rocking curve (XRC), Optical Beam Induced Current (OBIC), and Nomarski Micrograph were used for structural characterization. The depth-dependent OBIC images show that the photo-induced carriers are not sensitive to the surface cross-hatched patterns. The lifetime of photo-induced carriers are strongly affected only in regions near the mismatched hetero-interface due to the misfit dislocations. Capacitance-Voltage measurements at different frequencies show a higher frequency dispersion for a greater lattice mismatch. From the frequency dependence of the C-V curve, we obtain the interface state density as a function of the in-plane mismatch. Interface state density was estimated using the effective parallel capacitance and conductance components and a bulk series resistance. We also report the temperature dependent Current-Voltage characteristics.

D7.8

SURFACE CROSS-HATCHED MORPHOLOGY ON STRAINED III-V SEMICONDUCTOR HETEROSTRUCTURES. K.H. Chang, D. Srolovitz, R. Gibala, Department of Materials Science and Engineering, P. K. Bhattacharya, Department of Electrical Engineering and Computer Science, and J. F. Mansfield, Electron Microbeam Analysis Laboratory, The University of Michigan, Ann Arbor, MI 48109-2136.

An important phenomenon of the growth of strained heteroepitaxial III-V compound semiconductors is "surface perturbation". The surface morphology of the strained epitaxial layer is generally mirror-like when observed by regular optical microscopy, but a surface cross-hatched pattern is revealed when Nomarski interference is applied. This quasi-periodic perpendicular surface pattern propagates along $[110]$ and $[1\bar{1}0]$ directions with the (001) growth orientation. This unique surface morphology can greatly affect device fabrication processing. In this paper, heteroepitaxial strained $\text{In}_x\text{Ga}_{1-x}\text{As}$ layers, with x varying from 0 to 0.5, were grown on (001) GaAs substrates by molecular beam epitaxy (MBE). We present results of the correlation between the surface morphology and the interfacial line defects produced in the strained

growth by Nomarski interference optical microscopy and transmission electron microscopy (TEM) studies. Three aspects of surface cross-hatched patterns have been studied: the dependency of the growth temperature, the misfit percentage and the strained layer thickness. The surface pattern is clearly seen on samples grown at high temperature (520°C) and those with small lattice-mismatched ($\epsilon < 2\%$) systems. A poorly defined cross-hatched morphology was found on layers grown at relatively low temperature (400°C). As the lattice mismatch of the strained layer becomes larger than 2%, a roughly textured surface morphology is commonly observed in place of actual cross hatching. Few threading dislocations are observed in the strained layer when the cross-hatched surface morphology exists. It is also noted that the surface cross-hatched pattern develops after the majority of the interfacial misfit dislocations are generated. The result suggests that the surface cross-hatch pattern is directly related to the generation of interfacial misfit dislocations.

D7.9

THERMAL STABILITY OF STRAINED InGaAs/GaAs SINGLE QUANTUM WELLS B. Elman, Emil S. Koteles, P. Melman, C.A. Armiento, and C. Jagannath, GTE Laboratories Inc., Waltham, MA

The stability of strained layer structures with respect to high temperature anneals is of particular importance because of its implications in device fabrication. In this work we present interesting results on the structural stability of InGaAs/GaAs strained single quantum wells (SQW) with a variety of indium compositions and well widths close to critical thickness values. The samples were grown by molecular beam epitaxy and were subjected to furnace annealing or ion implantation with ^{75}As at 35 keV followed by rapid thermal annealing. Photoluminescence (PL) measurements were used to monitor excitonic transitions. As a result of heat treatment, changes in low temperature PL spectra were observed and used to evaluate the stability of strained SQWs. We report on both strain relief and strain recovery. Strain relief was observed in wide SQWs. Narrow PL peaks from these as-grown quantum wells were split into a broad peak at lower energy and a narrow peak at higher energy which is consistent with partial relaxation toward the equilibrium condition as a result of heat treatment. Strain recovery was observed in higher indium composition narrow quantum wells which were grown partially relaxed (with a low dislocation density). In this case, significant narrowing in PL linewidths was observed indicating that thermal annealing of dislocations was taking place. We emphasize that although strained layers provide enhanced flexibility in band-structure engineering, these structures can be significantly modified (even degraded) during commonly used processing procedures.

D7.10

APPLICATION OF GaAs-AlGaAs SUPERLATTICE STRUCTURE FOR FABRICATING HIGH BREAKDOWN VOLTAGE POWER MISFET. W.C. Liu, W.S. Lour, R.L. Wang, and W.C. Hsu, Department of Electrical Engineering, National Cheng Kung University, Tainan, Taiwan, Republic of China.

A new power MISFET with undoped GaAs-AlGaAs superlattice gate "insulator" and buffer structure has been fabricated successfully. The superlattice gate "insulator" exhibits a much higher gate breakdown voltage ($> 35\text{V}$) with very low prebreakdown leakage current and a lower gate capacitance (C_{gs}). Due to the existence of gate "insulator", a higher carrier concentration can be used in the active channel which improves the output drain current drivability and transconductance. If the gate length is reduced to 1 μm , a higher transconductance up to 330 mS/mm can be obtained. An output power density of 0.7 W/mm has been achieved by the nonoptimized structure and dimension.

The insertion of superlattice buffer structure, between active channel and buffer layer, offers an

excellent carrier confinement and provides an interface degraded region smaller than 40 Å. In addition, the superlattice buffer structure can getter greatly deep level impurities and defects from substrate or buffer layer.

In summary, the GaAs-AlGaAs superlattice structure is suitable for fabricating high power, high frequency and low noise MISFET.

D8.1

Resonant Tunneling Transistors and Quantum Effect Devices

Federico Capasso

AT&T Bell Laboratories
Murray Hill, NJ 07971

Recent advances in quantum electron devices are presented.¹ This new class of structures has potential for circuits with greatly reduced complexity and multiple valued logic. Resonant tunneling bipolar transistors, microwave multistate transistors, and their circuit applications, and superlattice base transistors* will be discussed.

1. F. Capasso et al., IEEE Trans. Electron. Dev., Special Issue on Heterostructure Transistors, 1980. In Press.

D8.2

DIFFRACTION STUDIES OF THE GROWTH OF STRAINED EPITAXIAL FILMS.* G.J. Whaley and P.I. Cohen, Department of Electrical Engineering, University of Minnesota, Minneapolis, MN 55455

Reflection high-energy electron diffraction (RHEED) is sensitive to the changes in lattice constant, growth mode, surface morphology, and surface structure that occur during the growth of lattice-mismatched epitaxial films. During the growth of InGaAs on GaAs(100) by molecular beam epitaxy the diffracted intensity of the specular beam is observed to oscillate in time corresponding to layer-by-layer growth. The intensity decreases more sharply than the homoepitaxial case, perhaps due to a change in the surface Debye-Waller factor. The beams broaden, depending upon the scattering angle, indicating an increase in the surface step density. The background intensity increases due to an increased density of point defects. The separation of the diffracted beams, to within the limits of the technique, are unchanged up until a strain determined thickness. At this thickness, which depends upon temperature, the growth mode and the lattice constant change. Past the critical thickness (113) faceted islands are observed. By growing at lower temperatures these changes can be inhibited. Measurements are compared to the relaxation theory of Tsao and Dodson [1]. Using RHEED changes in lattice constant as small as 0.0003 nm can be resolved. We measure an activation energy for the dislocation glide velocity of 3.5 eV. An important issue is whether the strain drives segregation to grade the film.

1. J.Y. Tsao, B.W. Dodson, S.T. Picraux, D.M. Cornelson, Phys. Rev. Lett., **52**, 2455 (1987).

* Partially supported by NSF grant DMR-8615207 and the Minnesota Center for Interfacial Engineering (NSF)

EFFECTS OF SUBSTRATE MISORIENTATION AND THE GROWTH MECHANISM OF Si DOPED GaAs GROWN ON (111)A SUBSTRATE BY MBE. Y. Okano, H. Seto, M. Shigetani, S. Nishine, I. Fujimoto, ATR Optical and Radio Communications Research Laboratories, Sanpeidani, Inuidani, Seika-cho, Soraku-gun, Kyoto 619-02, Japan; and T. Suzuki, Science and Technical Research Laboratories of NHK, Kinuta, Setagaya-ku, Tokyo 157, Japan

Si has been widely used as an n-type dopant in GaAs grown by MBE on a GaAs (100) substrate. The incorporation site of this dopant, however, is greatly affected by the substrate orientation. It has been reported that Si acts as an acceptor in the growth on (111)A, (211)A and (311)A substrates. The results were explained in terms of the ratio of (111)A-like bonding sites to (100)-like bonding sites. In the growth on slightly (1-5°) misoriented (111)A substrates, however, it was found that the incorporation behavior of this amphoteric dopant changed largely as compared with the growth on exactly (111)A oriented substrate.

In the growth on exactly (111)A oriented substrate at low flux ratio (As_4/Ga), substantially all the Si atoms act as acceptors. With increase of the degree of misorientation, and with increase of the flux ratio, the number of donor-site Si atoms increased. Further, surface morphology has been improved by increasing the degree of misorientation.

We suppose that the dissociation rate of As_4 molecule plays an important role in the site selection of Si atoms. Since the valence electron density in a Ga single dangling bond site on an ideally flat (111)A surface is considered to be very small, dissociation of As_4 on this surface must be fairly slow. Introduction of surface steps with (100)-like bonding geometry may promote the dissociation of As_4 at the steps and cause lateral growth from the steps. Details will be discussed.

ORDERED TERNARY ALLOYS BY ATOMIC LAYER EPITAXY. B.T. McDermott, K.G. Reid, A. Dip and S.M. Bedair, Electrical and Computer Engineering Department, N.C. State University, Raleigh, North Carolina. W. Duncan, Texas Instruments, Dallas, Texas. X. Yin and F.H. Pollak, Brooklyn College of Cuny, Brooklyn, NY.

ALE of ternary alloys proceeds by the deposition of one atomic layer in a self-limiting manner per growth cycle and thus offers the ultimate technique in studying ordered structures. The low temperature growth of In-As-Ga-As and Ga-P-In-P by ALE will be reported. We found that both the structural and bandgap properties of these ALE ordered alloys to be different from that reported by MOCVD and MBE techniques.

Ga-P-In-P ordered alloy, for example, has been grown by ALE on GaAs at 500°C using organometallic and hydride sources. This has been achieved by sequential exposure of GaAs substrate to TMG, PH_3 , TEIn and PH_3 . TEM showed that the structure is deposited in an ordered fashion. X-ray diffraction also showed the lattice constant of the deposited films corresponds to $In_{0.5}Ga_{0.5}P$. These results were found to be independent of the mole fractions of the precursors in the gas phase. The bandgap of the ALE ordered alloy measured by the modulated photoreflectance at room temperature and photoluminescence (liquid He) techniques are 1.78 eV and 1.85 eV respectively. These values are considered to be the lowest reported bandgap for this ordered alloy. These results can be due to the ability of ALE to produce structures with a high degree of ordering. We will report on the properties of these ALE ordered structures grown both on 100 and (111) GaAs oriented substrates.

This work is supported by ONR/SDIO.

INAs AND InGaAs GROWTH BY CHLORIDE ATOMIC LAYER EPITAXY. H. Shimawaki, Microelectronics Res. Labs. NEC Corp., Kawasaki, Japan. Y. Kato and A. Usui, Fundamental Res. Labs. NEC Corp., Tsukuba, Japan.

InAs chloride atomic layer epitaxy (ALE) was carried out in detail, which resulted in the first successful preparation of $(GaAs)_n(InAs)_m$ for $n=1$ and 2 on (111)B InP substrates. Crystal growth techniques with strictly controlled thickness and crystal composition are required for high performance heterojunction device realization. ALE is suitable to this purpose, because the monolayer (ML) growth process is repeated, based on a self-limiting mechanism.

InAs was grown by 400 ALE cycles on (100), (111)A and (111)B InAs substrates at an InCl and AsH_3 pressure of 7.5×10^{-4} atm and 1.4×10^{-3} atm, respectively, with an alternate supply of InCl and AsH_3 . Growth rates for the (111)B substrates showed a constant value of 0.9 monolayer/cycle at temperatures below 375 °C. Growth rates for the (100) and (111)A substrates, on the other hand, decreased steadily with an increase in the growth temperature. At 375 °C, the growth rates for the (111)B substrates were independent of InCl pressure, suggesting that InAs ALE has a self-limiting growth factor on (111)B substrates.

$(GaAs)_1(InAs)_1$ and $(GaAs)_2(InAs)_2$ layered structures were prepared on (111)B InP substrates at 375 °C. GaCl and InCl were fed in alternately, not simultaneously, at 1.2×10^{-4} atm and 1.2×10^{-3} atm, respectively. There were 300 ALE cycles for $(GaAs)_1(InAs)_1$ and 150 cycles for $(GaAs)_2(InAs)_2$. In each case, Ga compositions (x) and growth rates (v), calculated by the X-ray diffraction peaks of the grown layers, agreed well with expected values. $x=0.49$ and $v=2.0$ ML/cycle were obtained for $(GaAs)_1(InAs)_1$, and $x=0.49$ and $v=4.2$ ML/cycle were obtained for $(GaAs)_2(InAs)_2$. These results indicate that chloride ALE is highly controllable in $(GaAs)_n(InAs)_m$ preparation, which allows achieving heterojunction devices with excellent carrier transport characteristics.

ELECTRICAL AND MATERIAL CHARACTERIZATION OF THE STABILITY OF ALGaAs AND InGaAs PLANAR DOPED STRUCTURES. Larry P. Sadwick, Department of Electrical Engineering, University of Utah, Salt Lake City, Utah 84112; and Dwight C. Streit, TRW Electronic Systems Group, One Space Park, Redondo Beach, California 90278.

Recently Schubert et. al. [1] have used planar (δ) doping as a tool to study the diffusion of atomic Si in GaAs by capacitance-voltage (C-V) measurements on room temperature and annealed samples. In this work we extend and augment this technique to both AlGaAs and InGaAs planar doped structures grown by molecular beam epitaxy (MBE). In addition to the C-V measurements, X-ray, Photoluminescence, SIMS and Hall measurements have been employed to investigate and determine both the stability and diffusion of Si in ternary GaAs compound semiconductors. The demonstrated improvement in planar doped HEMT devices provided the initial motivation for this study. The techniques and the methodology used in this paper also permit direct measurements of the epitaxial crystal quality relationships to both the planar doping parameters and the MBE growth conditions. The combination of techniques described above provides an excellent method to determine the optimum growth conditions and parameters so as to achieve both the abrupt doping transitions and good crystal quality required to maintain application-dependent device quality transport properties. A matrix of both single and multiple (periodically spaced) planar doped structures have been grown. The crystal quality degradation and induced strain of highly doped planar structures will also be discussed. The results presented for both lattice matched and pseudomorphic structures should be of significant use for HEMT and superlattice design considerations.

1. E.F. Schubert, T.H. Chiu, J.E. Cunningham, B. Tell, and J.B. Stark, Jour. of Elec. Mat., Vol. 17, No. 6, 1988.

KINETICS OF QUANTUM WIRE GROWTH ON VICINAL SURFACES

K.J. Hugill, S. Clarke, D.D. Vvedensky, B.A. Joyce, The Blackett Laboratory and Semiconductor Materials IRC, Imperial College, London SW7 2BZ, United Kingdom.

The growth of quantum wires by molecular-beam epitaxy on vicinal surfaces is studied with a Monte Carlo simulation of growth. Wire quality is characterized in terms of two quantities, one which simply measures the percentage of atoms in the correct positions for an ideal quantum wire, and one that characterizes the connectivity of the wire. The conclusions drawn from our study are the same regardless of how quantum wire quality is characterized. Beginning with a simplified situation in which two species are distinguished only by a label, and not by different mobilities, we find that wire quality is maximized at a single temperature, which is beam-flux-dependent. At low temperatures, growth by the formation and coalescence of islands inhibits wire quality, while at high temperatures the enhanced fluctuations in the step edge profile lead to correlated lateral shifts in the wires on adjacent terraces, which also degrades wire quality. Interspersing the growth with periods of recovery lowers the temperature for wire quality, but also lowers the maximum wire quality. Modelling the situation with two species with different mobilities, which would be applicable for the case of GaAs/AlAs quantum wires, reveals that the temperature at which wire quality is maximized can be estimated accurately from the quality of the wires in the separated systems.

D8.8

LIQUID PHASE ELECTROEPITAXIAL (LPEE) GROWTH OF GaSb and InGaAsSb. Shanthi N. Iyer, Ali Abul-Fadl, *Albert T. Macrander, Jonathan H. Lewis and W. J. Collis, Department of Electrical Engineering, North Carolina A&T State University, Greensboro, NC 27411, *600 Mountain Avenue, AT&T Bell Laboratories, Murray Hill, NJ 07974

Experimental results of the InGaAsSb phase diagram near 580°C will be reported. GaSb and InGaAsSb alloys of composition close to GaSb corner of the phase diagram, have been grown lattice matched to (100) GaSb successfully by LPEE technique. Growth rates were found to increase with current density, typical value being $\sim 1 \mu\text{m}/\text{min}$ at a current density of $10 \text{ A}/\text{cm}^2$. The layers have been assessed using both double crystal x-ray diffraction and high resolution x-ray diffraction. Finally, results on the low temperature photoluminescence spectra of these samples will also be presented.

Financial support for this work was provided by Air Force Office of Scientific Research, Washington, D.C. (Contract No. 49620-89-C-0004) which is gratefully acknowledged.

D8.9

ENERGETICS AND RELAXATIONS OF ADATOM, DOPANT AND VACANCY RELATED COMPLEXES ON NORMAL AND STRAINED GaAs (001) SURFACE. S.B. Ogale*, A. Madhukar* and R. Vishwanathan*, * Departments of Materials Science and Physics, University of Southern California, Los Angeles, CA 90089; + Department of Physics, University of Poona, Pune, India.

Surface complexes involving Ga and Si adatoms, Si dopant, Ga and As antisite replacements and vacancies at the GaAs (001) surface are examined for their energetics and associated structural relaxations by employing semiempirical two and three body potential energy functions¹. The energy minimization is achieved via simulated annealing Monte Carlo procedure². An $8 \times 8 \times 8$ GaAs matrix is used as the substrate with periodic boundary conditions in the lateral plane. The adatom, dopant or vacancy is added to the system after allowing the top two surface layers to

reconstruct into a $c(2 \times 2)$ pattern. The suitably chosen neighborhood of the modified spot is then allowed to relax to a minimum energy configuration. The complexes are studied for both the unstrained as well as strained surfaces. The results of these studies will be presented and their consequences for the understanding of Molecular Beam Epitaxial growth will be discussed.

1. D.K. Choi, S.M. Koch, T. Takai, T. Halicioğlu and W.A. Tiller, J. Vac. Sci. Technol. B6 (4), 1140 (1988).
2. S. Kirkpatrick, C.D. Gelatt, Jr., M.P. Vecchi, Science, 220, 671 (1983).

D8.10

PULSED LASER ATOM PROBE ANALYSIS OF III-V COMPOUND SEMICONDUCTOR EPILAYERS. Ross A.D. Mackenzie, J. Alex Liddle, Chris R.M. Grovenor and Alfred Cerezo, Department of Metallurgy and Science of Materials, Oxford University, Parks Road, Oxford OX3 1PH

The growth of III-V epilayer materials on indium phosphide substrates often requires the epilayer to be grown in a miscibility gap. The presence of this miscibility gap has led to the suggestion that the material may spinodally decompose or undergo phase separation either during growth or during subsequent processing. Electron microscopy techniques have shown the presence of contrast fluctuations on scales of a few tens of nanometers and a few nanometers. The larger scale variations are amenable to compositional analysis using high resolution scanning transmission electron microscopy techniques, but the finer scale variations are not. The pulsed laser atom probe has both the spatial resolution and chemical resolution to permit the fine scale contrast in these materials to be examined.

Epilayers of a variety of materials have been examined, and results will be presented which show the scale of the fluctuations and also give an indication of the extent to which these materials deviate from their nominal (lattice matched) compositions. The correlation between the atom probe microanalysis data and the fine scale contrast in electron microscopy will also be shown.

D8.11

THE INTERACTION OF TRIMETHYLGALLIUM WITH CLEAN AND ADSORBATE COVERED Si(100) SUBSTRATES

by: T. R. Gow, R. Lin, L. A. Cadwell, F. Lee, R. I. Masel, University of Illinois, Urbana IL, 61801

Pulsed beam methods are used to examine the initial stages of GaAs growth on silicon substrates by MOMBE. A pulsed beam of trimethylgallium (TMGa) was directed onto a heated Si(100) substrate which was partially covered by various adsorbates, and the resultant reaction products were examined by mass spectroscopy. X-ray photoemission spectroscopy (XPS) was also used to examine the growing film. It is found that at TMGa exposures of 1×10^{13} molecules/cm² or less, the decomposition process on a hot Si(100) substrate is very similar to the decomposition process reported previously [1,2] when TMGa is adsorbed onto a cold Si(100) substrate, then the substrate is heated. However, at higher exposures the chemistry changes. It is possible to transiently populate a weakly bound state which we assign to TMGa adsorption in the second monolayer. If the sample is below 450 K, the TMGa in the second monolayer desorbs. However, at temperatures between 500 and 700 K the TMGa in the second monolayer reacts to form a CH₃ group ($x=3,4$) and a dimethylgallium radical. The dimethylgallium and CH₃ groups desorb. However, some of the CH₃ groups remain bound to the substrate leading to extra carbon incorporation. At higher temperatures, the TMGa in the second monolayer pyrolyses to dimethylgallium and methyl radicals, some of which desorb, and some of which get incorporated into the surface. There also is evidence for formation of traces of monomethylgallium. These results indicate that

flux of TMGa could have an important influence on carbon incorporation in MOMBE.

- 1) F. Lee, T. R. Gow, R. Lin, A. L. Backman, D. Lubben, and R. I. Masel *Proc. MRS.*, 131, 339-344 (1989).
- 2) F. Lee, A. Backman, R. Lin, T. R. Gow, R.I. Masel *Surface Sci.*, to appear

D8.12

THERMAL DISORDERING OF MODULATION-DOPED AlAs/GaAs SUPERLATTICE. Kunihiro Hara, Hiroshi Ito, Shinya Ohmi and Takamasa Suzuki, NIPPONDENSO CO., LTD., Kariya, Aichi, Japan

The effect of modulation-doping on thermal stability of interface structure in a heterojunction, especially in multi quantum well superlattices has not been clear yet. The purpose of this paper is to clarify the effect of Si doping on interdiffusion in the modulation-doped multi quantum well (MQW) superlattices by photoluminescence (PL) spectra.

AlAs barrier layers (100 Å) and GaAs well layers (60 Å) were grown on a GaAs substrate by MBE. The AlAs layer was doped with Si at a concentration of $1 \times 10^{18} \text{ cm}^{-3}$ with and without undoped AlAs spacer layer (20 Å) on both sides. An undoped MQW sample was also prepared for comparison. Annealing was carried out at various temperatures between 730°C and 850°C.

The PL peak corresponding to interband transition defined by 60 Å well layer disappeared completely after annealed at 850°C for 5 min. in the modulation-doped sample without spacer layer, while PL peak shift was observed in other samples after annealed at 850°C for 1 to 20 min. The diffusion coefficient was estimated at 1.5×10^{-17} , 9.0×10^{-18} and $1.5 \times 10^{-18} \text{ cm}^2/\text{sec}$. in the modulation-doped sample without spacer, with spacer and in the undoped sample, respectively.

D9.1

STRUCTURAL STABILITY OF AMORPHOUS SEMICONDUCTOR SUPERLATTICES. Peter D. Persans*, A. F. Ruppert*, B. Abeles*, Y.-J. Wu* and V. Pantofaru*. *Physics Department, Rensselaer Polytechnic Institute, Troy, NY; *Exxon Research and Engineering Co., Annandale NJ.

We report the results of recent Raman scattering and x-ray diffraction experiments on the structure and thermal stability of amorphous semiconductor/insulator periodic multilayer structures based on a-Si:H, a-Ge:H and a-SiO₂:H. By varying the superlattice repeat distance for bi-layer structures from 2 nm to 50 nm it is possible to extract information on the range of relaxation and interdiffusion and on the influence of interfaces and composition gradients on relaxation.

Thermal restructuring is found to occur in at least three stages. First, a low activation energy local relaxation step is observed in which atoms move by a few angstroms to lower energy sites. This is observed in changes in the average density and compositional mixing of atoms near interfaces. Second, long range (>2 nm) diffusion of network atoms is observed which may in some cases wash out compositional variations. Third, crystallization of one or both sub-layer materials may occur. The crystallization and interdiffusion processes can occur in parallel and relative activation energies can be determined by measuring the temperature and repeat distance dependence of mixed crystal versus pure crystal fractions of the annealed superlattices.

D9.2

A SYSTEMATIC METHOD FOR EXTRACTING STRUCTURAL PARAMETERS FROM LOW ANGLE X-RAY REFLECTIVITY MEASUREMENTS ON MULTILAYERS. L.M. Goldman, H. A. Atwater* and F. Spaepen, Division of Applied Sciences, Harvard University, Cambridge, MA 02138

X-ray diffraction is one of the main methods of determining the structure of multilayers. Low angle reflectivity measurements are particularly useful for multilayers containing polycrystalline or amorphous constituents, and for obtaining specific structural data, such as surface roughness or diffuseness. Although many analyses of low angle reflectivity have been published, the agreement between model and data is not perfect. We will present a method, based on both kinematic and dynamic scattering calculations that produces the best agreement so far, and use it to extract specific structural parameters such as the roughness or diffuseness of the external surface, the thickness of the constituent layers, the average electron density, the difference in electron density between the constituent layers, and the roughness or diffuseness of the internal interfaces. Results will be given for a sputtered Al/Al₂O₃ multilayer. Application to other systems as well as the utility of this procedure to the study of non-linear diffusion will be discussed.

* Present address: Thomas J. Watson Laboratory of Applied Physics, California Institute of Technology, Pasadena, CA 91125

D9.3

DETERMINATION OF 3-DIMENSIONAL DEFECT STRUCTURES IN GALLIUM ARSENIDE EPILAYERS ON SILICON USING WHITE BEAM SYNCHROTRON RADIATION TOPOGRAPHY IN BOTH TRANSMISSION GEOMETRY AND GRAZING BRAGG-LAUE GEOMETRY. M. Dudley, J. Wu and G.-D. Yao, Dept. of Materials Science and Engineering, SUNY at Stony Brook, Stony Brook NY; H.-Y. Liu and Y.C. Kao, Materials Science Laboratory, Texas Instruments, Dallas, TX.

White beam synchrotron topography in both transmission and grazing Bragg-Laue geometries has been used to reveal the 3-dimensional defect structure in MBE grown GaAs epilayers on Si. In the grazing Bragg-Laue case, manipulation of geometry enabled depth profiling of defect structures in both epilayer and substrate. Defects observed include substrate threading dislocations, interfacial dislocations and epilayer planar defects. Dislocation line direction and Burgers vector analysis was performed. Clear continuity between substrate threading dislocations and interfacial dislocations was established. Overall defect structures were then correlated with processing conditions.

This technique affords a rapid and non-destructive way of quantitatively characterizing processing induced damage in such systems.

Research Funded in part by the NSF under contract # DMR 8506948, and performed on beamline X-19C at the NSLS which is funded by DOE under contract # DE-FG02-84ER45098.

D9.4

CHARACTERIZATION OF METAL SEMICONDUCTOR MULTILAYERS BY RAMAN SPECTROSCOPY AND X-RAY DIFFRACTION. David D. Allred and Qi Wang, Department of Physics and Astronomy, Brigham Young University, Provo, UT.

We have used Raman spectroscopy and x-ray diffraction in the characterization of W/C multilayers used in soft x-ray optics. The main Raman band is from a-C and consists of a broad peak at about 1580 cm^{-1} (G-line) and a shoulder at about 1380 cm^{-1} (D-line). It was found that the D-line to G-line intensity ratio of W/C multi-

layers with thin tungsten layer (about 20 Å) was higher than that of single carbon layers deposited on thick tungsten layer (about 400 Å). This indicates that the carbon in multilayer samples may be more disordered. The x-ray diffraction study of samples showed that in the former case the tungsten is a-W and in the latter case it is crystalline. This means that the interfacial effect may cause the difference in the structure of carbon layers.

D9.5 ABSTRACT WITHDRAWN

D9.6

STRUCTURAL STABILITY OF HEAT TREATED W/B₄C MULTILAYERS. A.F. Jankowski, Lawrence Livermore National Laboratory, Livermore, California.

An application of multilayer structures takes form in x-ray microscopy as artificial Bragg diffractors. The performance of such optical systems depends on the stability of the multilayer structure.

One of the most widely used multilayer combinations for highly reflective, x-ray mirrors is W/C. The layers within the vapor deposited multilayers are typically amorphous. Studies have shown, however, an amorphous to crystalline transition in the W layers with increasing thickness. Heat treatments of the W/C multilayers have been shown to produce similar effects, crystallinity in the W layers and the presence of W-C intermetallics, as well as change the repeat periodicity of the superlattice.

An alternative to the W-C multilayer combination is W-B₄C. The measured reflectivity of x rays (>705eV) from W/B₄C multilayers have been measured to equal or exceed W/C, for mirrors with identical dimensions. The relative stability of W/B₄C may additionally be enhanced, following a kinetic argument requiring the decomposition of B₄C before the formation of WC. In this study, multilayers of W/C and W/B₄C will be vacuum heat treated, then structurally examined. A comparison of pre- and post- heat treatments will be accomplished using depth profiling and cross-section microscopy.

This work was performed under the auspices of the U.S. Department of Energy by Lawrence Livermore National Laboratory under Contract No. W-7405-Eng-48.

D9.7

MULTILAYERED METALLIC THIN FILMS PREPARED BY DUAL-BATH ELECTRODEPOSITION C.A. Ross, L. M. Goldman and F. Spaepen, Division of Applied Sciences, Harvard University, Cambridge, MA 02138

Electrodeposition is a fast and relatively inexpensive method for making artificial metal multilayered films. We present a dual bath electrodeposition technique capable of producing crystalline Ni/amorphous NiP_x multilayers with repeat lengths of 20 Å and above, of sufficient quality to give several low-angle x-ray reflections. In this method, a multilayer is made on a disc-shaped substrate which rotates over two nozzles. A different electrolyte (plating bath) circulates through each nozzle. Deposition occurs only on those parts of the substrate exposed to the electrolytes, directly above the nozzles, so a multilayer is formed as the substrate rotates. The compositional and structural modulations of the films are analysed using x-ray diffraction and microscopy, and the effects of deposition parameters, such as the current density, are examined. The P content of the NiP_x layers varies between 10 at.% and 25 at.% as the current density varies between 400 Am⁻² and 3000 Am⁻², allowing compositionally modulated, fully amorphous NiP_x/NiP_y films to be deposited. The dual bath technique can, in principle, be used to make multilayers from any pair of materials which can be electrodeposited, and its utility in the production of other multilayer systems will be assessed.

D9.8

METASTABLE ELECTRONIC EFFECTS IN AMORPHOUS SUPERLATTICES. J. Kakalios, School of Physics and Astronomy, University of Minnesota, Minneapolis, MN 55455.

There has recently been considerable interest in the electrical and optical properties of amorphous semiconductor superlattices. This talk will review some novel electronic

effects observed in amorphous multilayers which challenge our understanding of these materials. Quantum size effects have been found in heterostructures consisting of alternating layers of a small band gap amorphous semiconductor and a wide band gap amorphous insulator; the amorphous analogs of GaAs/GaAlAs crystalline superlattices. The absorption spectrum shifts to higher energies as the thickness of the amorphous semiconductor layer is reduced below 50 Å, which has been interpreted as a quantum size effect. However, transport data indicates that the electronic phase coherence length is much less than the semiconductor layer spacing, which directly conflicts with the quantum well interpretation. Various efforts to resolve this contradiction will be reviewed. Doping modulated amorphous multilayer structures, consisting of alternating layers of n-type and p-type doped amorphous silicon, display an enhanced dark conductivity after illumination termed persistent photoconductivity (PPC). After a brief (a few seconds) exposure to white light, the dark conductivity parallel to the layers increases by several orders of magnitude. This PPC takes several days to decay at room temperature but is reversed upon annealing above 400°K. PPC has been extensively studied in crystalline semiconductor structures, and the models proposed to account for PPC involve either charge separation by internal electric fields or charge trapping in a defect which undergoes a large lattice relaxation (the DX center). Studies of PPC in amorphous doping superlattices support the latter model, and enable a microscopic determination of the process responsible for PPC.

D10.1

SILICIDE FORMATION AND THERMAL STABILITY OF Ni/Si/GaAs INTERFACES.

Y. Yamamoto, K. Ishibashi, Res. Cntr. of Ion Beam Tech., Hosei Univ., Tokyo, Japan; S. Suzuki, Adv. Mat. Lab., Sohka, Japan; T. E. Shim¹, Waseda Univ., Tokyo, Japan.

Silicon and/or Ni were vacuum evaporated onto (100) GaAs. Interdiffusion and silicide formation processes in the system upon annealing were investigated using AES and X-ray diffractometry.

Thicknesses of Ni and Si were varied to examine how the interface reaction related to the relative amount of Ni to Si; (1) Si(1000 Å)/GaAs, (2) Ni(700 Å)/GaAs, (3) Ni(700 Å)/Si(1000 Å)/GaAs, (4) Si(1000 Å)/Ni(2000 Å)/GaAs, and (5) Ni(2000 Å)/Si(1000 Å)/GaAs.

AES measurement revealed that a Si/GaAs interface of sample (1) was stable after annealing at 850 C for 30 min. When the relative amount of Ni to Si is unity as sample (3), stable NiSi was formed and no reaction to GaAs was observed after annealing at 500 C for 2 hour.

When Ni was directly attached to GaAs, appreciable interdiffusion of GaAs and Ni was observed (samples (2), (4)), but in sample (4) Ga and As did not diffuse into the Ni₂Si surface layer at 500 C.

In the case that Ni was the outermost layer of which amount was in excess of Si as sample (5), the system was quite unstable at the same temperature; no clear silicide phase, no distinct interface, oxidation of the surface Ni layer.

¹Present address: Samsung Electronics, Seoul, Korea

D10.2

EPITAXIAL GROWTH OF METALLIC LAYERS BY SOLID PHASE INTERDIFFUSION: STUDY OF THE Ni/GaAs AND Ni/AlAs SYSTEMS Guérin R. and Deputier S., Laboratoire de Chimie Minérale B - Campus de Beaulieu - 35042 Rennes Cedex, France - Caulet J., Minier M., Poudoulec A., Ballini Y., Durel V., Dupas G., Guivarc'h A., Centre National d'Etudes des Télécommunications, LAB/OCM/NPA, BP 40, 22301 Lannion Cedex, France

An ideal M/SC III V contact should be made by stable and

epitaxial metallic films. In principle, such a contact may be obtained by the solid state interdiffusion of a metal film with a III V SC substrate. By using a set of complementary methods (RBS, TEM, X-ray diffraction...) we explored the possibilities offered by the two systems Ni/GaAs and Ni/AlAs annealed up to 600°C. Our starting point was the experimental determination of the Ni-Ga-As ternary phase diagram. Five ternary phases which are structurally derived from the hexagonal NiAs type were evidenced. This diagram provides the absolutely required basis for understanding the sequence of phase formation in the Ni/GaAs system. The Ni-Al-As diagram was studied for the same purpose. The main steps of the interaction appear to be different in the two systems. During the Ni/GaAs one, three successive steps as a function of the annealing temperature are observed: first a mixture of a Ga-rich ternary phase (phase C) + NiAs, then phase C + NiAs + NiGa and at last the two binaries NiAs + NiGa where the reaction stops. In the case of the Ni/AlAs reactions, the three steps successively correspond to a mixture of NiAl + a As-rich ternary phase (phase B) then NiAl + phase B + NiAs and finally NiAl + NiAs. NiAs and NiAl are the key compounds in Ni/GaAs and Ni/AlAs reactions respectively and all the reaction compounds are either highly textured (pseudocubic NiAs and ternaries) or epitaxial (cubic binaries NiGa and NiAl).

D10.3

LATTICE DISTORTION OF SINGLE-CRYSTAL CoSi_2 COLUMNS EMBEDDED IN SINGLE-CRYSTAL SILICON.*

Shin Hashimoto, Q.F. Xiao, and W.M. Gibson, State University of New York at Albany, Albany, NY; C.W. Nieh, California Institute of Technology, Pasadena, CA; and R.W. Fathauer, Jet Propulsion Laboratory, California Institute of Technology, Pasadena, CA.

Codeposition of Si and Co on a heated Si(111) substrate with a Si:Co ratio greater than 3 results in epitaxial columns of cobalt disilicide (with a channeling minimum yield of approximately 4%) embedded in high quality epitaxial Si (with a channeling minimum yield of approximately 3%). The average diameter and density of the silicide columns can be controlled by deposition parameters such as the Co:Si flux ratio and the deposition temperature.

The average lattice distortion (or strain) in the silicide columns is measured by ion channeling. Due primarily to constraints of the surrounding Si lattice, the unit cell of the cobalt disilicide lattice in the columns is elongated perpendicular to the substrate when the average aspect ratio (height:diameter) of the columns is greater than approximately 1.4. This is in contrast to the case of the cobalt disilicide lattice in ordinary two-dimensional films where the unit cell is elongated parallel to the substrate due to the smaller lattice constant of cobalt disilicide compared to Si and to constraints at the planar interface. This indicates a different type of mismatch accommodation, unlike the usual accommodation in two-dimensional epitaxial films grown on planar substrates.

* Work partially supported by SDIO and NASA.

D10.4

STABILITY OF THE ELECTRICAL PROPERTIES OF Pt-Ga INTERMETALLICS ON ANNEALING CONDITIONS. Larry P. Sadwick, Department of Electrical Engineering, University of Utah, Salt Lake City, Utah 84112; Young K. Kim, Delroy Baugh and R. Stanley Williams, UCLA Department of Chemistry and Biochemistry 2080 Young Hall, Los Angeles, CA 90024

Ambient dependent annealing studies of the electrical properties of thin films of single phase platinum-gallium (Pt-Ga) intermetallics (PtGa_2 , PtGa, and Pt_2Ga) on GaAs are investigated. The thin Pt-Ga films have been grown on GaAs by molecular beam epitaxy by co-evaporation of the elements. The motivation behind this study is to determine the thermodynamic stability of the single phase Pt-Ga intermetallic family members as potential candidates for high temperature stable contacts to GaAs. Our previous work [1] has established that Pt_2Ga on GaAs is not stable on GaAs when annealed in nitrogen gas while both PtGa_2 and PtGa

appear to be stable to approximately 450 C and 600 C, respectively. As expected from the Pt-Ga-As ternary phase diagram, no PtAs_2 phases were observed for either PtGa_2 or PtGa. The work presented in this talk will focus on both the electrical properties and the chemical and phase transformations which occur upon temperature annealing under different ambients of the thin (1000 to 2000 Angstrom) films on GaAs. The primary material and surface science characterization tools employed in this study are two theta x-ray diffraction (XRD), x-ray photoemission spectroscopy (XPS), and Auger electron spectroscopy (AES). The barrier height and the ideality factor of these films, among other electrical data are monitored after each anneal cycle.

1. L.P. Sadwick, Y.K. Kim, D.K. Shuh, K.L. Wang, and R.S. Williams, 1989 Electronic Material Conference, Boston, Mass.

D10.5

CHARACTERIZATION OF ErAs/GaAs and GaAs/ErAs/GaAs STRUCTURES. Jane G. Zhu, Chris J. Palmstrom*, Suzanne Mounier* and C. Barry Carter, Department of Materials Science and Engineering, Cornell University, Ithaca, NY 14853; *Bellcore, Red Bank, NJ 07701.

Rare-earth metal arsenides have recently been grown epitaxially on GaAs. Such materials provide the potential of incorporating rare-earth mono-arsenides into semiconductor heterostructures. These structures may also provide means for improving metal contacts to compound semiconductor devices. ErAs has NaCl structure, which, like GaAs, is face-centered cubic but with a different two-atom basis. The lattice constant of ErAs is only 1.6% larger than that of GaAs.

Smooth epitaxial layers of ErAs have been grown with different thicknesses on GaAs (100) substrates by molecular-beam epitaxy. The misfit dislocations at the ErAs/GaAs interface have been characterized by weak-beam dark-field imaging for plane-view samples and by high-resolution transmission electron microscopy for cross-section samples. The misfit dislocations lie primarily along the common $\langle 001 \rangle$ directions when the ErAs layer is thin. However, as the thickness of the ErAs increases, the dislocations become more irregular and some of the dislocations then lie on $\langle 011 \rangle$ orientations. A model of the formation of these misfit dislocations will be presented.

GaAs/ErAs/GaAs with different thicknesses of the ErAs well have also been characterized. At present, when GaAs is overgrown on the ErAs layer, it tends to be heavily twinned. The top GaAs layer is also faceted which presumably is the result of the island growth. The GaAs grown on ErAs has a tendency to be epitaxially aligned with the ErAs, i.e., GaAs(100)//ErAs(100). However, areas of GaAs(111)//ErAs(100) or GaAs(122)//ErAs(100) have been observed. The origin of the defects will be discussed.

D10.6

SILICON CONSUMPTION DURING SELF-ALIGNED TITANIUM SILICIDE FORMATION ON SHALLOW JUNCTION. P.L. Smith¹, C.M. Osburn^{1,2}, ¹Microelectronics Center of North Carolina (MCNC), P.O. Box 12889, Research Triangle Park, North Carolina 27709, ²Department of Electrical and Computer Engineering, North Carolina State University, Raleigh, North Carolina 27695-7911.

Silicon consumption during the self-aligned-silicide process using titanium reaction with silicon has been studied. The self-aligned silicide (SALICIDE) process was developed to overcome the conductivity and contact resistance limitations associated with very shallow junctions. Typical one micrometer CMOS technology employing junctions deeper than 0.25 μm with sheet resistances below 100 ohm might only derive modest benefit from this process. Half-micrometer technology however, with junction depths below 0.2 μm and sheet resistances of a few hundred ohms/sq is an ideal candidate for this process. A fundamental limitation of the Salicide process is the silicon required to selectively react with metal to form the silicide. As junction scale to smaller dimensions, the silicon consumption must also be scaled so that the silicide does not penetrate the junction. This study was initiated to better quantify the silicon consumption occurring during titanium silicide formation, to examine techniques to reduce the silicon consumption during silicidation, and to define the maximum permissible silicide thickness on ultra shallow ($<100\text{nm}$) junction as might be needed for quarter-micrometer and smaller devices. Results indicate that: (1) Silicon consumption in

boron and arsenic shallow junction regions is larger, by 70%, than can be explained simply on the basis of silicide formation. (2) The annealing gas atmosphere has an important influence on the amount of excess silicon consumption. (3) Lateral loss of silicon and loss from the TiON etching must be considered.

D10.7

PREFERENTIAL GROWTH OF CoSi_2 IN Co/Si SOLID STATE INTERACTION. Liu Ping, Hong Feng, Li Bingzong, and Shen Xiaoliang, Fudan University, Shanghai, P.R.China

In recent years, CoSi_2 has been studied intensively because of its possible application in microelectronics. In this work the CoSi_2 thin film growth by Co/Si solid state interaction was investigated. Four-point probe, AES, XRD and other techniques were used to characterize the electrical and crystalline properties of the films formed on (111) and (100) Si substrates. A strong preferential CoSi_2 (111) orientation grain growth was observed on (111) Si substrate. The formed CoSi_2 film is highly conductive with a resistivity of about 15 $\mu\text{m}\cdot\text{cm}$. The behaviors of oxygen and other impurities during Co/Si interaction has also been studied and the snow-plow effect of some impurities was observed.

D10.8

EPITAXIAL GROWTH OF IrSi_3 ON Si (111). T.L. Lin, Jet Propulsion Laboratory, California Institute of Technology, Pasadena, CA ; C. W. Nieh, Keck Laboratory of Engineering, California Institute of Technology, Pasadena, CA ; Shin Hashimoto, and Q. F. Xiao, Physics Department and Institute for Particle-Solid Interaction, State University of New York at Albany, Albany, NY.

IrSi_3 has a hexagonal crystal structure and the lattice mismatch between the IrSi_3 (0001) plane and the Si (111) plane is about -1.8% at room temperature along all three $\langle 1\bar{1}0 \rangle$ Si directions. Localized epitaxial growth of IrSi_3 on (111) and (100) Si has been previously reported by Chu *et al.* with epitaxial regions consisting of three dominant modes and 40 μm in size after annealing iridium thin films on Si at 1000 $^\circ\text{C}$ [1].

We are studying the epitaxial growth of single-phase IrSi_3 layers on Si(111) by two growth techniques : reaction deposition epitaxy and molecular beam epitaxy. The samples were characterized *in-situ* by reflection high energy electron diffraction, and *ex-situ* by scanning electron microscopy, Rutherford backscattering spectroscopy (RBS), and transmission electron microscopy (TEM).

Epitaxial growth of IrSi_3 films on Si(111) were achieved at growth temperatures ranging from 630 to 800 $^\circ\text{C}$. Good surface morphology was observed for IrSi_3 layers grown at temperatures below 680 $^\circ\text{C}$. TEM analysis reveals that the IrSi_3 layers grow epitaxially on Si(111) with three epitaxial modes and a minimum channeling yield of 52% was observed for the samples grown at 630 $^\circ\text{C}$ by RBS.

**This work was sponsored by NASA and SDIO as part of JPL's Center for Space Microelectronics Technology.

1. J. J. Chu and L. J. Chen, J. Appl. Phys., 63 (4), 1163 (1988)

D10.9

BORON $\sqrt{3}\times\sqrt{3}$ INTERFACE STRUCTURE ON Si(111): TWO-DIMENSIONAL ORDERED DOPING LAYER. R.L. Headrick, L.C. Feldman, I.K. Robinson, E. Vlieg, A.F.J. Levi, H.S. Luftman and J. Kovalchick, AT&T Bell Laboratories, Murray Hill, N.J. 07974.

The $\sqrt{3}\times\sqrt{3}$ reconstruction of boron on Si(111) remains ordered during room temperature deposition of Si, and forms an ordered Si(111) $\text{B}\sqrt{3}\times\sqrt{3}$ /a-Si interface with 1/3 monolayer boron at the interface. In-situ synchrotron x-ray diffraction measurements during growth of the Si(111)B/a-Si interface were used to determine the interface structure. The Si(111)B $\sqrt{3}$ surface is transformed to the Si(111)B/a-Si ordered interface via the removal of Si adatoms from the surface which then become part of the amorphous Si layer. The data is consistent with an abrupt crystalline/amorphous interface. This leaves a two-dimensional $\sqrt{3}\times\sqrt{3}$ boron array in normal fourfold coordinated substitutional sites at the interface. Since substitutional boron is a p-type dopant in crystalline silicon, the reconstruction layer is expected to be electrically active. Hall effect measurements at 4 $^\circ\text{K}$ show a high p-type carrier density ($>10^{14}/\text{cm}^2$) at the Si(111) $\text{B}\sqrt{3}\times\sqrt{3}$ /a-Si interface.

D10.10

EPITAXIAL GROWTH OF [001] Cr ON [001] LiF. J. Mattson[†]; M. B. Brodsky^{**}; J. B. Ketterson[†].

The temperature and growth-rate dependence of e-beam deposited Cr on LiF [001] substrates has been studied with *in situ* RHEED, X-ray diffraction, and magneto-transport measurements. RHEED measurements indicate that in the temperature range 500 $^\circ\text{C}$ $>$ T $>$ 400 $^\circ\text{C}$ and with evaporation rates $<$ 1 $\text{\AA}/\text{s}$, epitaxial growth occurs. These same measurements also indicate that there is a thickness region where layer-by-layer growth is observable along the [110] direction before being observed along the [010] direction, at 60 \AA and 100 \AA respectively. There is evidence in these films for surface reconstruction, and work is presently being done to establish the nature of this surface reconstruction. Resistivity measurements have shown that as the degree of epitaxy is improved and the thickness increases, the residual resistance ratio, $\rho(300\text{K})/\rho(4.2\text{K})$ also increases from 5 (at 500 \AA) to more than 50 (at 2000 \AA).

[†] Dept. Physics, Northwestern University, Evanston, IL

^{**} MSD Argonne National Laboratory, Argonne, IL

* This work supported by the U.S. Department of Energy under contract No. W-31-109-ENG-38

D10.11

THE GERMANIUM GROWTH MECHANISM ON (1102) SAPPHIRE DEPOSITED BY MOLECULAR BEAM EPITAXY. David J. Godbey, Mark E. Twigg, Geoff P. Malafsky, and Syed B. Qadri, Naval Research Laboratory, Code 6816, Washington, D.C. 20375

Single crystal germanium films have been successfully grown on the (1102) sapphire face using molecular beam epitaxy. The growth mechanism is 3 dimensional at high temperatures, but approaches 2 dimensional growth at lower temperatures. Islands were formed on a film grown at 800 C and 5 nm thick that had a mean diameter of 22+4 nm, while islands on a film 40 nm thick had a mean diameter of 110+70 nm. Scanning electron microscopy shows that the films grown at 800 C have a rough surface. Growth at temperatures of 400 C

produced smooth surfaces, but resulted in polycrystalline films. By using solid phase epitaxy techniques, we have succeeded in growing singly oriented films with good surface properties at 350 C. The use of germanium on sapphire as a substrate for MBE grown gallium arsenide has been explored, and will also be addressed.

D10.12

RAPID HETEROEPITAXIAL GROWTH OF Ge FILMS BY PULSED SUPERSONIC FREE JET CHEMICAL BEAM EPITAXY. Diula Eres, D. H. Lowndes, J. Z. Tischler, T. E. Haynes, and M. F. Chisholm, Oak Ridge National Laboratory, P. O. Box 2008, Solid State Division, Oak Ridge, TN.

Epitaxial Ge thin film growth rates (0.25 $\mu\text{m/s}$) that are significantly higher than attainable by conventional vapor phase epitaxial growth methods were achieved by utilizing a pulsed supersonic free jet expansion. The Ge-bearing source molecules (Ge_2H_6) were seeded in a helium carrier gas (5% Ge_2H_6). A pulsed free jet expansion of this gas mixture was directed toward the surface of a heated GaAs (100) substrate where Ge film growth took place by surface induced thermal decomposition of the impinging Ge_2H_6 molecules. The growth mechanism is believed to be governed by molecular scattering events involving thermal decomposition products and undecomposed Ge_2H_6 molecules, rather than by solid-gas equilibrium thermodynamics. The microstructural properties of the films were investigated by double crystal x-ray diffractometry, cross-section transmission electron microscopy and Rutherford backscattering spectrometry.

*Research sponsored by the Division of Materials Sciences, U.S. Department of Energy under contract DE-AC05-84OR21400 with Martin Marietta Energy Systems, Inc.

D10.13

SOLID PHASE EPITAXIAL GROWTH OF II-A FLUORIDES ON InP BY IN-SITU RAPID ISOTHERMAL PROCESSING. R. SINGH, F. Radpour, A. Kumar, R.P.S. Thakur, University of Oklahoma, Norman, OK; J. Narayan, A.R. Srivatsa, North Carolina State University, Raleigh, NC; A.J. Nelson and H.S. Ullal, Solar Energy Research Institute, Golden, CO.

Availability of epitaxial dielectrics on crystalline conductors, superconductors and semiconductors in any desired sequence (e.g. dielectric on semiconductor etc. and vice-versa) can result into new and improved microelectronic, optoelectronic, superconducting electronic devices and circuits as well as integration of diverse technologies on the same substrate. Out of the various potential epitaxial dielectrics, group II-A fluorides (CaF_2 , BaF_2 , SrF_2 , and their mixtures) have shown promising results. Reduced thermal budget (product of processing time and temperature) processing techniques are essential for the next generation of devices and circuits. A number of undesirable phenomenon can be minimized if the dielectric is deposited at room temperature followed by solid phase epitaxial growth. We have used in-situ rapid isothermal processing for in-situ cleaning the substrate, and anneal the room temperature deposited II-A fluoride films on (100) and (111) InP. In this paper for the first time we report the solid phase epitaxial growth of II-A

fluorides on InP. The X-ray diffraction, SEM, TEM, XPS and high frequency capacitance-voltage results are presented.

This work is supported by SDIO/IST and managed by the ARO.

D10.14

STRAIN-CONTROLLED HIGH MOBILITY IN MODULATION DOPED $\text{Si}_{1-x}\text{Ge}_x$ / Ge / $\text{Si}_{1-x}\text{Ge}_x$ HETERO-STRUCTURES. M. MIYAO, E. MURAKAMI, H. ITOH, and K. NAKAGAWA, Cent. Res. Lab. Hitachi Ltd., Kokubunji, Tokyo 185, Japan

Comprehensive studies of $\text{Si}_{1-x}\text{Ge}_x$ / Ge / $\text{Si}_{1-x}\text{Ge}_x$ hetero-structures are described. In these experiments, $\text{Si}_{1-x}\text{Ge}_x$ buffer layers (200nm) were grown on (100) Ge substrates by molecular beam epitaxy (520°C) and then Ge films (20nm) and modulation doped (Ga) - $\text{Si}_{1-x}\text{Ge}_x$ (30nm) films were grown (400°C) commensurately. Strains generated by the hetero-structure were monitored using Raman spectroscopy. In addition, two dimensional hole mobilities at the $\text{Si}_{1-x}\text{Ge}_x$ / Ge interface were evaluated by Hall measurements.

In the Raman spectra, peaks from 4 different lattice vibrations, i.e. Si-Si, Si-Ge, Ge-Ge and strained Ge-Ge, were observed. The frequency difference between the strained Ge-Ge peak from the MBE grown Ge films and the strain free Ge-Ge peak from Ge substrates was found to be proportional to the x-values in the buffer $\text{Si}_{1-x}\text{Ge}_x$ layers.

The relation between the strains (ϵ) and x-values was obtained as $\epsilon(\%) = 3.8(x-1)$. In this way, accurate control of strain in the Ge films becomes possible by changing the x-value in the buffer layer.

Two dimensional hole mobilities measured at 77K increased with strain in the low strain region (0.35% - 0.95%). This suggests that the band gap and/or band structure of the $\text{Si}_{1-x}\text{Ge}_x$ / Ge hetero-interface is strongly influenced by the stress field. However, in the high strain region (0.95% - 1.52%), hole mobility decreased due to the formation of dislocations. The maximum hole mobility (77K) obtained was $2400\text{cm}^2/\text{V.s}$ at the strain value of 0.95%. This mobility is 4 times higher than that reported for the modulation doped p-Si / $\text{Si}_{1-x}\text{Ge}_x$ / Si hetero-structure[1].

[1] R. People et al. Appl. Phys. Lett. 45, 1232, (1984)

D10.15

STRUCTURAL CHARACTERIZATIONS OF SYMMETRICALLY STRAINED Ge_mSi_n SUPERLATTICES. R. C. BOWMAN JR. and P.M. Adams, The Aerospace Corporation, Los Angeles, CA; C.C. Ahn, California Institute of Technology, Pasadena, CA; S.J. Chang, V. Arbet, and K.L. Wang, University of California, Los Angeles, CA.

Ge_mSi_n strained layer superlattices have been prepared by MBE. These Ge_mSi_n heteroepitaxial superlattices were grown on relaxed $\text{Ge}_y\text{Si}_{1-y}$ buffer layers in order to symmetrize the strain distribution and thus obtain pseudomorphic growth of nominal 300nm thick superlattices. Samples with different superlattice periodicities and different individual layer thickness ratios were prepared. Cross-sectional transmission electron microscopy, x-ray diffraction, and Raman scattering spectroscopy have been used to characterize these samples.

This paper describes the geometrical properties (i.e., layer thickness, uniformity, homogeneity, and interface abruptness) and crystalline perfection of the superlattice layers as deduced from these measurements. The compositions and defect structures of the $\text{Ge}_y\text{Si}_{1-y}$ buffer layers were found to have significant influence on the quality of the superlattices. In particular, more disorder was

apparent for superlattice structures grown on $\text{Ge}_{0.5}\text{Si}_{0.5}$ buffers than those grown on buffer layers with significantly higher or lower Ge contents. The effects of thermal anneals on the stability and relaxation behavior will also be reported.

D10.16

PLASTIC FLOW IN Si/Ge QUANTUM WELL STRUCTURES. Mark E. Twigg, GEO-Centers, Inc., Fort Washington, Md 20744; and D. J. Godbey Naval Research Laboratory, Washington, D. C. 20375.

Understanding plastic flow in semiconductor quantum well structures is an important step in developing a successful model for the mechanical stability of more complicated modulated device structures. As the first step in conducting such a fundamental study, we have used molecular beam epitaxy in growing a simple quantum well structure on a (001) silicon substrate that consists of a 100nm Si buffer, a 60nm $\text{Si}_{0.7}\text{Ge}_{0.3}$ quantum well, and 500nm of epitaxial Si. We grew this structure at a deposition rate of 0.2nm/sec and a growth temperature of 500°C. In order to study subsequent plastic flow, the as-grown material was subjected to four different annealing treatments: 800°C for 30 minutes, 850°C for 30 minutes, 900°C for 30 minutes, and 1200°C for 30 seconds. From measurements of the dislocation density using plan-view transmission electron microscopy, we found the strain relief in the as-grown film to be 4×10^{-3} . For all four annealing treatments we found that the strain relief increased to a value of 2×10^{-4} . Because all dislocations observed in these films occurred as paired misfit dislocation dipoles, plastic flow in this system must be due to the propagation of double kinks. It is our conjecture that such low observed values for strain relief, in annealed quantum well structures, can be explained in terms of a new mechanical stability criterion for double kink extension.

D10.17

THERMAL STABILITY OF $\text{Si}/\text{Si}_{0.8}\text{Ge}_{0.15}/\text{Si}$ MODULATION DOPED DOUBLE HETEROSTRUCTURES. P.J. Wang, B.S. Meyerson, P.M. Fahey, F. LeGoues, C.J. Scilla, and J.M. Cotte, IBM T.J. Watson Research Center, P.O. Box 218, Yorktown Heights, NY 10598

Si/SiGe heterostructures have potential applications for many advanced devices. Since Si and SiGe are lattice-mismatched, heterostructures based on these alloy systems are metastable. Several growth techniques, such as molecular beam epitaxy (MBE) and ultra high vacuum/ chemical vapor deposition (UHV/CVD), have been demonstrated to enable the growth of coherently strained Si/SiGe at low temperatures. The low growth temperature provides insufficient energy for atoms to overcome a kinetic barrier and inhibits the structural relaxation process. However, these strained heterostructures are inclined to relax if they are subjected to temperatures well above the growth temperature.

The thermal stability of $\text{Si}/\text{Si}_{0.8}\text{Ge}_{0.15}/\text{Si}$ p-type modulation doped double heterostructures grown by the UHV/CVD technique has been examined by Hall measurement, transmission electron microscopy, and secondary ion mass spectroscopy. As-grown heterostructures showed two-dimensional hole gas (2DHG) conduction at abrupt Si/SiGe and SiGe/Si interfaces. An anneal at 800 °C for 1 hr. promoted the migration of boron acceptors to the heterointerfaces. This degraded the electrical properties of heterostructures but they still retained 2DHG conduction. Rapid redistribution of boron and the disappearance of 2DHG conduction was observed after a 900 °C, 0.5 hr. anneal. No misfit dislocations were observed for all the annealed heterostructures demonstrating the defect-free crystal quality of these as-grown strained heteroepitaxial layers. The problems associated with interdiffusion of Ge is examined and will be discussed.

D10.18

EPITAXY OF Si_mGe_n ATOMIC LAYER SUPERLATTICES. L.-M. Baribeau, D.J. Lockwood, M.W.C. Dharma-wardana, D.C. Houghton and N.L. Rowell, Division of Physics, National Research Council Canada, Ottawa, K1A 0R6, CANADA.

In recent years there has been much interest in the synthesis of semiconductor superlattices for use in device applications. Strained-layer superlattices are of particular interest because strain adds an extra degree of freedom to bandgap engineering. $\text{Si}/\text{Si}_{1-x}\text{Ge}_x$ strained heteroepitaxy has been studied extensively and novel devices based on that materials system have been proposed. Recently, it has also been predicted that due to zone folding effects, very short period $(\text{Si}_m\text{Ge}_n)_p$ atomic layer superlattices (ALS), made of p periods of alternating m and n monolayers of Si and Ge, may have optical properties not observed in the host materials. In particular it is expected that for certain values of m and n and specific strain conditions, quasi-direct band gap could be obtained in these ALS. In this paper we report the molecular beam epitaxy growth of various $(\text{Si}_m\text{Ge}_n)_p$ ALS and their characterization by Raman scattering spectroscopy, double crystal X-ray diffraction, transmission electron microscopy and photoluminescence. The ALS were prepared on (100) Si, (100) Ge and on $\text{Si}_{1-x}\text{Ge}_x$ buffers to study the substrate dependence of their structural and optical properties. Annealing treatments were also performed to study interdiffusion and strain relaxation. Planar growth was observed on Ge substrates but the microstructures showed some waviness on Si substrates and a high defect density on alloy buffers. Phonon peaks due to folding of acoustic modes were seen by Raman scattering spectroscopy in the frequency range 60-200 cm^{-1} . The observed Raman spectra from the ALS were interpreted on the basis of an analysis of theoretical spectra of these systems. This analysis provided an estimation of the interfacial blurring in the ALS. The PL investigation revealed no strong luminescent features that could be related to a direct band gap transition.

D10.19

MAGNETIC AFTEREFFECT IN COMPOSITIONALLY-MODULATED Ni/Cu MULTILAYERS PREPARED BY ELECTRODEPOSITION AND BY SPUTTERING. L.H. Bennett, L. J. Swartzenduber, NIST, Gaithersburg, MD 20899 and W. Abdul-Razzaq, West Virginia University, Morgantown, WV 26506

There has been a large body of studies of the magnetic properties of Ni/Cu superlattices produced from the vapor phase by sputtering or other deposition. A much smaller body of data is available on these compositionally-modulated alloys produced by electrodeposition. Therefore, when it was discovered¹ that there was a relaxation of the magnetic moment upon field changes in the electrodeposited Ni/Cu, the question arose as to whether or not the effect might be unique to the deposition process. For example, could it be that the electrodeposition process caused hydrogen to be imbedded in the multilayers, and that this hydrogen was somehow related to the magnetic aftereffect observed in electrodeposited Ni/Cu? We now have discovered the same magnetic relaxation in sputtered Ni/Cu. Thus the effect, which is of some importance to the application of magnetic multilayers to magnetic recording, does not appear to be an artifact of the preparation process.

L. V. Atzmony, L.J. Swartzenduber, L.H. Bennett, M.P. Dariel, D.S. Lashmore, M. Rubinstein, and P. Lubitz, J. Mag. Magn. Matls. 69, 237 (1987).

D10.20

THE KINETICS OF $\text{Si}_{1-x}\text{Ge}_x/\text{Si}$ RELAXATION USING LARGE AREA DISLOCATION IMAGING TECHNIQUES. D.C. Houghton, P. Timbrell and J.-M. Baribeau, National Research Council of Canada, Ottawa, Ontario K1A 0R6, Canada.

Annealing experiments in the 600-900°C temperature range on MBE grown SiGe/Si heterostructures have revealed an abrupt transition from stable to relaxed microstructure. Transitions occurring at unique strain-thickness values for uncapped SiGe epilayers, buried strained layers and

superlattices provide the thermodynamic equilibrium critical thicknesses for these geometries. Single misfit dislocations at densities $\leq 1 \text{ cm}^{-2}$ have been observed using Nomarski interference microscopy of defect etched surfaces and charge collection microscopy (EBIC) in the SEM. In addition, X-ray topography and both plan view and cross sectional TEM have been used to characterize the dislocation structures. The kinetics of misfit accommodation by dislocation glide can be characterized by a relaxation temperature which for 30 minute furnace anneals and excess stresses below $\sim 10^{-2} \text{ G}$ is $600^\circ\text{C} \pm 25^\circ\text{C}$. A comparison of the sensitivities obtained by each technique is made. The extent of relaxation (misfit dislocation density) for various anneal cycles and values of excess stress is discussed together with the implications for processing of devices such as the SiGe heterojunction bipolar transistor (HBT).

D10.21

STRUCTURAL PROPERTIES AND THERMAL EVOLUTION OF Fe/Ti MULTILAYERS. Rodnacq B., Hillairet J., Laugier J. and Chamberod A., CEN-Grenoble, DRF, SPH, 85 X, 38041 Grenoble Cédex, France.

Fe/Ti metallic multilayers deposited by sputtering technique at the $\text{Fe}_{33}\text{Ti}_{67}$ average composition have been studied by X-ray diffraction, Mössbauer spectroscopy and electrical resistivity as a function of the period. For $\Lambda \leq 4 \text{ nm}$, an amorphous-like structure is observed, although the modulation of composition still exists along the growth direction. For larger Λ , crystalline Ti appears, first with a bcc structure ($\Lambda = 4 \text{ nm}$), then with the stable hcp structure ($\Lambda = 6 \text{ nm}$) the c-axis lying along the multilayer growth direction. At a period of 8 nm, the iron-rich layer in turn crystallizes to a bcc phase inducing a texture change of the Ti layer, the c-axis lying now preferentially in the plane. Anomalies in both the lattice parameters and crystallite size occur from this period up to about 12 nm. For larger periods, one tends towards layers of practically pure hcp Ti and bcc Fe respectively.

The thermal behaviour depends strongly on the period, too. For $\Lambda < 8 \text{ nm}$, an interdiffusion of iron and titanium from 500 K leads to a metastable bcc solid solution $\text{Fe}_{33}\text{Ti}_{67}$. Above 700 K, the equilibrium phases $\alpha\text{-Ti}$ and FeTi appear. On the contrary, for $\Lambda > 8 \text{ nm}$, it seems that titanium preferentially diffuses into Fe at short distance. As a result, the equilibrium phases are formed directly although composition modulation along the growth direction is still observed. Above 700 K, the increase of the grain size parallels the disappearance of the composition modulation.

D10.22

Ge TRANSPORT AND EPITAXY IN THE AMORPHOUS-Ge/Pd₂Si/[111] Si SYSTEM. Q.Z.Hong, J.G.Zhu and J.W.Mayer, Department of Materials Science and Engineering, Cornell University, Ithaca, New York 14853

Solid phase epitaxy (SPE) of Ge-Si alloy on [111] Si substrates was achieved in the amorphous-Ge/Pd₂Si/[111] Si system. Channeled Rutherford backscattering Spectrometry and high resolution cross section transmission electron microscopy were used to investigate the reaction process. The SPE started with the migration of Ge atoms into the epitaxial Pd₂Si layer at 600 °C. Then single crystalline Ge islands were formed on the Si substrate. Finally the Ge islands coalesced to form a uniform epitaxial $\text{Ge}_{70}\text{Si}_{30}$ layer on the [111] Si substrate. In the meantime, the Pd₂Si exchanged positions with the Ge layer, leading to a final configuration of Pd₂Si/epi- $\text{Ge}_{70}\text{Si}_{30}$ /[111] Si. The minimum yield of the epitaxial layer was 0.42, measured in the presence of the top polycrystalline Pd₂Si.

D10.23

MODEL FOR EPITAXIAL GROWTH OF CO ON CU(100). D.D. Vvedensky and S. Clarke, The Blackett Laboratory and Semiconductor Materials IRC, Imperial College, London SW7 2BZ, United Kingdom

The kinetics of growth of Co on Cu(100) are investigated with a kinetic solid-on-solid model. By an appropriate choice of mobility parameters that reflects the adatom-substrate interaction and the relative surface free energies of the two materials, the surface step density is found to reproduce qualitatively all of the important features of recent *in-situ* He-atom scattering experiments. Our study suggests that growth is initiated by regions where second and possibly third layers of Co are formed while other regions of the Cu substrate are uncovered. Once the substrate has been covered, growth proceeds in a conventional layer-by-layer manner. This interpretation is in agreement with the conclusions of Steigerwald and Egelhoff from their studies of growth of Fe on Cu(100). By identifying the pertinent physical mechanism governing the early stage of growth, we are able to provide an estimate of the diffusion barrier of Co on Co overlayers that agrees well with an Arrhenius analysis of the experimental data.

D10.24

MAGNETIC PROPERTIES OF TbFeCo/Al MULTILAYER THIN FILMS. B.D. Yan, J.A. Barnard, M.H. Kim, and G.W. Warren, Department of Metallurgical and Materials Engineering, The University of Alabama, Tuscaloosa, AL 35487-0202.

A series of periodic multilayer TbFeCo/Al thin films have been prepared by DC magnetron sputtering using sequential deposition techniques. The nominal area composition of the alloy target was $\text{Tb}_{20}\text{FeCo}_{80}$. The configuration of the films is of the form $(x\text{A}/y\text{B})_n$, where x and y are the thicknesses of the A and B layers respectively, and n is the number of bilayer units used in constructing the film. The individual layers are from 2-10nm thick; the total thickness of the TbFeCo alloy is kept constant at 80nm for all samples regardless of the thickness of the individual layers. The magnetic properties of the films (eg., saturation magnetization, magnetic anisotropy, and coercivity) have been measured as a function of TbFeCo and Al layer thicknesses by vibrating sample and torque magnetometry. The quality of the multilayers (periodicity of the superlattice and sharpness of the interfaces) has been ascertained by X-ray diffraction and cross-sectional TEM. An 80nm thick homogeneous thin film of the TbFeCo alloy was also grown under identical sputtering conditions as a reference and was found to have in-plane easy magnetization. Very pronounced interfacial and/or reduced dimension effects have been found in the multilayer systems. These include evidence for a "dead layer" in the interface regions (2-3nm thick) and reversal of the direction of easy magnetization from in-plane (in the homogeneous thin film samples) to strongly perpendicular in the multilayer configuration. The details of the hysteretic behavior of multilayer samples depend sensitively on the individual layer thicknesses. These results demonstrate the potential for growing new materials with precisely tailored properties using multilayer thin films.

D10.25

DEPENDENCE OF Mo/Si MULTILAYER MORPHOLOGY ON DEPOSITION ANGLE. Yuanda Cheng, Mary Beth Stearns and David J. Smith, Dept. of Physics, Arizona State Univ., Tempe, AZ 85287

Mo/Si multilayer films (ML) are one of the highest reflectivity systems being used for soft X-ray optical elements. Studies show that the ML produced by sputtering have slightly wider Si on Mo interfaces and narrower Mo on Si interfaces than those produced by e-beam evaporation. In order to investigate whether this is due to the wider spread of incident angles in sputtering, a series of Mo/Si ML have been fabricated in a UHV e-beam evaporation system at different deposition angles. The substrate temperature

(T_s) was varied between 300K and 550K and the deposition angle (α) was varied from 0° (normal incidence) to 60° by tilting the substrate. The films were studied by cross-sectional high resolution electron microscopy.

For $T_s=300K$, the interfaces became smoother and the Mo crystallites became more spherical in shape as α was varied from 0° to 60°. Some "columnar" structure was seen in some samples. For $T_s=550K$, which is the optimum temperature for 0°, the Mo on Si interfaces broadened as α increased. Beyond 30° the Mo layers were amorphous and the Mo and Si were highly diffused. Higher α thus produces behavior similar to that due to higher T_s . Some of the differences between ML produced by sputtering and by vapor deposition can now be explained.

D10.26

EFFECT OF SUBSTRATE MISORIENTATION ON HETEROEPI TAXY WITH LARGE LATTICE MISMATCH: Ag/Si(111). D.C. McKenna, K.-H. Park, G.-C. Wang, Physics Department, Rensselaer Polytechnic Institute, Troy, NY, and G.A. Smith, Department of Physics, State University of New York, Albany, NY

Epitaxial films of Ag were grown by Molecular Beam Epitaxy on small angle misoriented Si(111) substrates. The surface normal was tilted 0 to 6° away from the Si(111) axis toward the $[1\bar{1}2]$ direction. Despite the large lattice mismatch (~25%), good quality Ag films, 600 to 1200 Å thick, were grown on the misoriented Si(111) substrates. From X-ray pole figure analysis, the epitaxial relationship is found to be Ag(111)//Si(111):Ag $[01\bar{1}]$ //Si $[01\bar{1}]$ with smaller amounts of a twinning structure - Ag(111)//Si(111):Ag $[0\bar{1}1]$ //Si $[01\bar{1}]$. Interestingly, the angle between the Si(111) axis of the substrate and the Ag(111) axis of the film (the misalignment angle) is not zero. In contrast to the perfect alignment of Ag(111) on a flat Si(111) substrate,¹ the Ag(111) axis is tilted away from the Si(111) axis toward the surface normal. Axial MeV He ion channeling shows the misalignment angle (up to 6°) increases linearly with substrate misorientation angle (~1/10 substrate misorientation angle). Possible structural models consistent with the observations will be discussed.

¹K.-H. Park, D.C. McKenna, H.S. Jin, G.-C. Wang, K. Rajan, G. Smith, L. Luo and W.M. Gibson, Mat. Res. Soc. Symp. Proc. 138, 545 (1989).

D10.27

X-RAY DIFFRACTION STUDIES OF PSEUDOMORPHIC α -Ge_xSn_(1-x) ON InSb(001) W. Lowe, E. Fitzgerald, P. Freeland, M. Asom and R. MacHarrie, Jr., AT&T Bell Laboratories, Murray Hill, NJ 07974

Using MBE, thick layers of α -Ge_xSn_(1-x) ($x \leq .13$) have been grown on InSb(001) substrates. The layers have been characterized by x-ray diffraction with respect to their perpendicular lattice constant a_{\perp} . For samples with compositions of $x = .04$ and $.08$ a notable tetragonal distortion is observed. The origin of the distortion is the in-plane strain-epitaxy of the α -Ge_xSn_(1-x) to the lattice constant of the InSb. The x-ray data shows that as much as 8% Ge can be incorporated into the α -Sn before the β phase becomes significant. Above 8% the diffraction peaks become broad indicating degradation of the diffracted domains. It is believed that the present growth temperature limits Ge content to 8%. However, in samples grown to contain more than 8% Ge only 8% Ge is incorporated in the α -Sn. The excess Ge is possibly expelled from the sample. Data will also be presented on α -Sn/Sn_xGe_{1-x} superlattices.

D10.28

THERMODYNAMIC PHASE STABILITY ON GaAs OF INTERMETALLIC THIN FILMS OF CoGa WITH A LARGE RANGE OF COMPOSITIONS. Young K. Kim, Delroy Baugh and R. Stanley Williams, Department of Chemistry and Biochemistry and Solid State Science Center, UCLA, Los Angeles, CA.

Crystalline thin films of CoGa with different compositions have been grown on GaAs (100) by co-deposition of Co and Ga. The phase transformations upon annealing were studied using two theta X-ray diffraction (XRD), Auger electron spectroscopy (AES), X-ray photoemission spectroscopy (XPS) and Transmission electron microscopy (TEM). One of the most interesting features of the CoGa phase is the large composition range over which an ordered structure is stable. For the 1:1 stoichiometric compounds Co and Ga atoms form interpenetrating primitive cubic lattices, but for deviations from 1:1 stoichiometry there must be structural defects in the lattices.

This presentation will focus on the chemical and phase transformations which occur upon annealing of the CoGa thin films on GaAs. The stability of these thin films as a function of the varying stoichiometries will be discussed by considering the thermodynamic properties and defect-related chemical reactions at the interface between CoGa and GaAs.

D10.29

X-RAY TOPOGRAPHIC ANALYSIS OF STRAIN FIELDS DUE TO MICRON-SIZED GRATINGS ON Si(100) AND Al₂O₃ (1120) SURFACES. A. Peter Jardine, Michael Dudley, Gong-Da Yao and Lalita A. Balasubramanian, Dept. of Materials Science, SUNY Stony Brook, Stony Brook NY 11794.

In a previous synchrotron X-ray topographic examination of Si(100) samples, in which 0.3µm deep concentric circular gratings were etched into the surface by plasma CVD, it was shown that the diffraction contrast was consistent with a radial strain field. Recently, we have also observed diffraction contrast from identical circular gratings sputtered into single-crystal sapphire, and from linear gratings etched into Si(100) using plasma CVD. Analysis of white beam transmission and reflection topographs enabled characterization of the three dimensional distribution of the strain field associated with the presence of the gratings. Mass transport processes can be studied through the analysis of the decay of sinusoidally shaped grating surfaces and so the presence of strain fields and their characterization is of interest. Similarly, the presence of strain fields may be a significant factor in epitaxial crystal growth. The origin and nature of these strain fields will be discussed.

Experiments performed on the X-ray topography beamline (X-19C) at the NSLS is supported by D.O.E.(DE-FG02-84ER45098). Support from NSF (M.D, G-D.Y, DMR 8506948) is gratefully acknowledged.

D10.30

FORMATION OF BURIED AND SURFACE CoSi₂ LAYERS BY ION IMPLANTATION. M.F. Wu, A. Vantomme, G. Langouche, IKS, University of Leuven, Belgium; K. Maex, J. Vanhellemont, IMEC, Leuven, Belgium; J. Vanacken, H. Vloeberghs and Y. Bruynseraede, VSM, University of Leuven, Belgium.

The formation is studied of buried CoSi₂ layers and surface CoSi₂

layers formed by high dose ion implantation in an energy range of 30 to 160 keV, combined with conventional furnace annealing or with rapid thermal processing. The crystalline quality, the phase of the buried and surface silicide layers, the abruptness of the interfaces and the electrical transport properties are studied by RBS, channeling, cross-sectional TEM, Mössbauer spectroscopy and resistivity measurements. The stability of the buried and surface CoSi_2 layers at temperatures between 1000°C and 1200°C is also studied and compared with the results for MBE grown samples.

Low energy (30 keV) implantations with a dose of 5×10^{16} atoms/cm² gave rise to continuous buried CoSi_2 layers as thin as 20 nm with good crystalline quality. High dose implantations, on the other hand, gave rise to surface CoSi_2 layers with crystalline quality and electrical properties comparable to those of MBE grown samples or buried CoSi_2 layers. It was found that buried CoSi_2 layers had better thermal stability than surface CoSi_2 layers with similar thickness. The disintegration was found to start by void formation at both CoSi_2/Si edges.

D10.31

ANISOTROPIC TRANSPORT IN InGaAs/GaAs HETERO-STRUCTURES GROWN BY MOVPE. Qing Sun, D. Morris, C. Lacelle, and A. P. Roth, LMS, NRC, Ottawa, Canada

Anisotropic electron transport has been observed in $\text{In}_{x-1}\text{Ga}_x\text{As}$ /GaAs heterostructures grown by MOVPE on (100) and intentionally misoriented GaAs substrates. The low field electron mobilities in two perpendicular directions are found to be higher in the [110] direction than in the [1 $\bar{1}$ 0] direction, while the degree of anisotropy decreases with increasing carrier concentration. The ratio of $\mu_{[110]}/\mu_{[1\bar{1}0]}$ derived from Hall measurements at both 300K and 77K can be related to the degree of substrate misorientation as well as epilayer composition, which varies in the range of $0 < x < 0.24$.

Drastic differences are also observed in the photoluminescence spectra of layers grown on substrates with different orientations. These anisotropic properties are directly related to the anisotropy of [110] and [1 $\bar{1}$ 0] dislocations due to lattice mismatch between the substrates and the layers.

D10.32

STRAINED InGaAs/GaAs QUANTUM WELLS WITH A 1.3 μm BANDEDGE AT ROOM TEMPERATURE P. Melman, B. Elman, C. Jagannath, Emil S. Koteles, A. Silletti, GTE Laboratories Inc., 40 Sylvan Rd., Waltham, MA. 02254

The fabrication of long wavelength optoelectronic devices on GaAs substrates is an attractive method for the monolithic integration of optical and electronic devices on a single chip for applications in telecommunications. Strained InGaAs quantum wells (QW) grown on GaAs substrates can be used for engineering the bandgap required for 1.3 μm transitions at room temperature. We have grown and characterized QW structures with this bandgap using a technique of spatial strain separation to avoid the stringent restriction of critical thickness which limits the achievable bandgap energy in this material system.

The samples were grown by MBE on GaAs substrates with a InGaAs buffer layer designed to relieve part of the strain generated by the large lattice constant mismatch. The indium concentration in this layer was about 25% and the dislocations were terminated by a 2/2 nm InGaAs/GaAs superlattice. The InGaAs QW, grown on this buffer layer, was 6 nm wide with an indium composition of 45%. The QW, which was analysed using low temperature PL and room temperature transmission spectroscopy, had a bandedge around 1.3 μm at room temperature. The PL spectra show broadening attributed to incomplete termination of misfit dislocations by the

superlattice layer. A strain symmetrized superlattice should improve the quality of the QW. This is the longest wavelength reached with InGaAs/GaAs QWs and this structure promises to be suitable for the fabrication of long wavelength optoelectronics on GaAs substrates.

D10.33

"A STABLE n-CHANNEL InP METAL-INSULATOR FIELD EFFECT TRANSISTOR WITH AN AMORPHOUS Si:H GATE. E. Koditi, Foundation For Research and Technology-Illias, Iliraklio Grece, Greece. A. A. Iliadis, Electrical Engineering Department, University of Maryland, College Park, MD 20742 and A. Christou, Naval Research Laboratory, Washington, DC 20375

Indium Phosphide and its ternary and quaternary lattice matched systems have wide potential applications in optoelectronic, high speed digital and microwave technologies. Conventional n-channel MESFET's have not been fully developed due to a low Schottky barrier ($\Phi_b < 0.5$ eV) resulting in an excessively high reverse bias leakage current. In order to correct the leakage problem, insulated gate systems have been developed based on deposited insulators⁽¹⁾ or epitaxially grown wide band gap semiconductors. The deposited insulators continue to exhibit a high interface state density and drift in the gate. The epitaxially grown semiconductors are usually lattice mismatched to InP which results in strain induced interface states and thermal instabilities. Amorphous semiconductors have distinct advantages over the epitaxially grown semiconductors because of lower deposition temperatures, easier passivation and lower stress induced interface states.

In this work, we report for the first time the fabrication and dc characteristics of a highly stable n-channel InP FET using a hydrogenated amorphous silicon gate (a-Si:H).

The devices were made on Si implanted ($N_D \cdot N_A = 5 \times 10^{16} \text{ cm}^{-3}$) semi-insulating (100) InP substrates after nitride encapsulation and annealing. The a-Si:H was deposited by dc Magnetron sputtering in H_2 ambient at 200°C, followed by the deposition of the Pt/Au gate metals. The 1 μm gates were defined by standard photolithography and lift-off techniques. The I-V characteristics of the devices showed channel pinch-off at $V_{GS} = -7\text{V}$ and a maximum transconductance (g_m) between 30 and 38 mS/mm. The transfer characteristics showed a flat g_m region for V_{GS} between -2 and -4V. The I_{DS} drift of the FET's was tested at $V_{GS} = 0$ and -3 V. No observable change in I_{DS} was measured in the first 300 hours. After the first 300 hours of testing a 3% increase was indicated for $V_{GS} = -3\text{V}$. The high stability of this gate system is attributed to the low temperature of deposition and the particular passivation of the InP surface followed here, as shown by Auger and Low-Energy Electron Probe analysis.

The combination of the stable characteristics and the good pinch-off voltages make this device the best reported to date with a-Si:H gates⁽²⁾.

1. K. Oigawa, S. Uekusa, Y. Sugiyama and M. Tacano, Jap. J. Appl. Phys., 26, 1719 (1989).
2. S. Loualiche, C. Vaudry, L. Henry and A. LeCorre, Electronics Lett., 22, 896 (1986)

D10.34

LATTICE MISMATCH EFFECTS IN GaAsP/GaAs AND GaAs/GaAsP/GaAs HETEROSTRUCTURES. Y.W. Choi and C.R. Wie, State University of New York at Buffalo, Dept. of Electrical and Computer Engineering and Center for Electronic and Electrooptic Materials, Amherst, New York 14260; S.M. Vernon, Spire Corporation, Bedford, MA 01730

Structural and electrical characteristics of the $\text{GaAs}_{1-x}\text{P}_x/\text{GaAs}$ and $\text{GaAs/GaAs}_{1-x}\text{P}_x/\text{GaAs}$ ($x=0.02, 0.05, 0.07, 0.17$ and 0.31) heteroepitaxial systems have been investigated using X-ray rocking curve technique, Optical Beam Induced Current (OBIC) technique, and I-V-T and C-V measurements. The rocking curve Full Width Half Maximum of the $\text{GaAs}_{1-x}\text{P}_x$ epilayer increased sharply at $x=0.17$ due to a decreased layer thickness and increased in-plane mismatch. As the lattice mismatch increased, crosshatch pattern density in the OBIC image and Nomarski Micrograph increases and the ideality factor for Au-GaAsP/GaAs and $\text{Au-GaAs/GaAsP/GaAs}$ Schottky diodes increases. The minority carrier diffusion length, measured by the light beam traveling method, decreased with increasing in-plane mismatch. Fermi-level pinning by misfit dislocation was observed for the higher phosphorus composition GaAsP/GaAs samples. $\text{Au-GaAs/GaAsP/GaAs}$ Schottky diodes show an excess current at a low temperature and high field range which is believed to be due to defect related tunneling.

D10.35

A TEM AND RHEED INVESTIGATION OF THE INITIAL STAGES OF InSb GROWTH ON GaAs(001) BY MOLECULAR BEAM EPITAXY (MBE). X. Zhang,* A.E. Staton-Bevan,* D.W. Pashley,* S.D. Parker,* R.L. Williams,† and R. Droopad,†, Imperial College of Science, Technology and Medicine, London, SW7 2BZ, U.K. (*Department of Materials, †Department of Physics).

The narrow-gap semiconductor, InSb, shows potential for monolithic, integrated, optoelectronic device applications. The present study focuses attention on the very early stages of MBE growth of InSb on GaAs(001), using the complementary techniques of in-situ RHEED and plan-view and cross-sectional TEM. These techniques provide clear evidence for island growth, rather than monolayer or Stranski-Krastanov growth. A study of the island morphology and defect structure has been made as a function of the amount of InSb deposited. Results to be presented will include clear evidence for {113} and {111} facets, details of linear and planar defects in the InSb and evidence for the presence of an additional epitaxial sphalerite phase.

D10.36

HETEROEPITAXIAL GROWTH OF InP ON GaAs WITH INTERFACE LAYER GROWN BY FLOW-RATED MODULATION EPITAXY. W. K. Chen, J. F. Chen, J. C. Chen, H. M. Kim, L. Anthony, C. R. Wie, and P. L. Liu, Department of Electrical and Computer Engineering, SUNY at Buffalo, Amherst, NY.

Heteroepitaxy adds a new dimension to material growth and device applications. We can use the unique features of several semiconductors and combine them to realize new devices, such as OEIC's. For heteroepitaxy in MOCVD, the two-step growth technique is widely used. A thin interface layer is first grown at low temperatures prior to a high temperature growth. The interface layer affects the quality of the film.

In our experiments, InP epilayers were grown on GaAs substrates by using the two-step technique in an MOCVD system. However, the interface layer was grown by the flow-rated modulation epitaxy technique. The crystallinity of the film increases initially with the thickness of the interface layer. High quality films were obtained with an interface layer thicker than 500 Å. Different from the conventional MOCVD, the quality of the film does not deteriorate when the thickness of interface layer is further increased. The FWHM's of the x-ray rocking curve (Fe K α_1 line) and 10 K PL spectrum for a 6.2- μ m-thick InP/GaAs are 144 arcsec and 1.28 meV, respectively. They are quite compatible to that of InP homoepitaxy. A Schottky diode made on the heteroepitaxial film shows an ideality factor of 1.42, a barrier height of 0.5 eV, and a leakage current of 2.92×10^{-3} A/cm² at a reverse bias of 0.5 V.

D10.37

STRAIN AND LATTICE-MISMATCH IN (001) AND (111) GaInAs/GaAs STRAINED LAYER SUPERLATTICES. H. M. Kim and C. R. Wie, State University of New York at Buffalo, Dept. of Electrical and Computer Engineering, Bonner Hall, Amherst, New York, 14260; C. G. Fonstad, Massachusetts Institute of Technology, Cambridge, Massachusetts, 02139

GaInAs/GaAs strained layer superlattices (SLSs) grown by molecular-beam epitaxy on (001) and (111) GaAs substrates are characterized using double crystal X-ray rocking curve (XRC), for the first time on (111)-oriented GaInAs/GaAs SLSs. The rocking curve broadening of the (111)-oriented GaInAs/GaAs SLS is much greater than that of the (001) SLS, indicating that the layer quality is better for the SLS grown on a (001) substrate than for those grown on a (111) substrate. This seems

to be mainly due to the degree of lattice relaxation in each SLS. The computer simulation based on the dynamical X-ray diffraction theory indicates a nearly pseudomorphic tetragonal distortion for the (001)-oriented SLS and a partially-relaxed rhombohedral distortion for the (111)-orientation. The plain and graded buffer layers are partially relaxed for (111)-oriented SLSs. We show the influence of random fluctuations of layer thicknesses in the higher order SLS peaks in the rocking curves of the (001)-oriented sample. The in-plane elastic strains obtained from XRC are in good agreement with data obtained from Raman spectroscopy.

D10.38

RAPID GROWTH OF THICK, IC QUALITY, GaAs LAYERS FROM A FLOWING SOLUTION, E. E. Crisman, J. T. Daly, H. J. Gerritsen, C. Roberts and D. Schaafsma, Department of Physics, Brown University, Providence, RI 02912

A novel liquid phase epitaxy (LPE) technique has been demonstrated which is capable of rapid growth of layers of GaAs many microns thick. By using a flowing, gallium rich solution of Ga and As, rather than the traditional stationary 'melt' for liquid phase epitaxy, the width of the solute depleted layer at the liquid/solid interface is both reduced and held constant during the LPE growth process. This permits the initially high growth rate ($\sim 8 \mu\text{m}/\text{min}$) to be sustained for the entire term of the growth cycle. In comparison, static solution growth LPE rates are of the order of $10 \mu\text{m}/\text{hr}$ when layers of several micron thickness are required. Since no arsenic overpressure is needed at the growth temperature ($700^\circ\text{C} - 800^\circ\text{C}$), excess arsenic is not observed in the resulting thick film layers. Such films have been demonstrated to be of a crystallographic and electronic quality comparable to good MOCVD and MBE layers, and therefore, are directly suitable for use in IC device fabrication. Because the initial capital outlays as well as safety considerations are much less than required for MOCVD and/or MBE systems, the additional high throughput capability of this LPE technology might make it economically competitive with current processes.

A brief description will be given of the mathematical model on which the growth chamber design is based, along with comparisons between predicted and measured growth rates. Diagrams of the growth chamber will also be presented. Photoluminescence (PL) spectra of doped and undoped layers will be compared with PL responses of high quality commercial grade GaAs epitaxial layers (MOCVD and MBE). Mobility values and other data, relative to electronic performance and crystallographic perfection will also be discussed.

D10.39

METAL-ORGANIC CHEMICAL VAPOR DEPOSITION OF InP BY PULSING PRECURSORS. W. K. Chen, J. C. Chen, L. Anthony, and P. L. Liu, Department of Electrical and Computer Engineering, SUNY at Buffalo, Amherst, NY.

By pulsing precursors alternately into an MOCVD system, we have grown InP. Since precursors are separately introduced, prereaction is effectively suppressed. The growth temperature is substantially lowered in comparison with the conventional MOCVD. It is mass-transported limited above 410°C , which is 140°C lower than that of conventional MOCVD. The process is kinetic-controlled with an activation energy of 19 Kcal/mol at low temperatures. Apparently, the surface catalytic effect greatly enhances the decomposition of reactants, particularly, PH_3 .

At 340°C , the growth rate in each switching cycle saturated at exactly one monolayer. At such a low temperature, the TMI is partially pyrolyzed. It suggests that the methylindium radicals rather than the In atoms play the crucial role in the self-limiting process of InP atomic layer epitaxy.

D10.40

METALORGANIC MAGNETRON SPUTTER DEPOSITION (MOMS) OF $\text{In}_{0.1}\text{Ga}_{0.9}\text{Sb}$ ON (100)GaAs. R. Rousina, J.P. Noad* and J.B. Webb, Laboratory for Microstructural Sciences, Div. of Physics, National Research Council Canada, 100 Sussex Dr., Ottawa. K1A 0R6.

This work reports for the first time, the epitaxial growth of $\text{In}_{0.1}\text{Ga}_{0.9}\text{Sb}$ on (100)GaAs by Metalorganic Magnetron Sputtering. Epilayers with thicknesses of 1-3 μm were deposited by magnetron sputtering a solid antimony target in a reactive atmosphere of trimethylindium (TMI), trimethylgallium (TMG) and an argon carrier gas. High quality "mirror-like" films could be deposited on GaAs over the entire compositional range despite the large lattice mismatch between film and substrate (14.6% for InSb and 7.8% for GaSb). All films were deposited under antimony stabilised conditions. Growth temperatures of 400 - 500°C and TMG/(TMI + TMG) flux ratios of 0 - 1 were investigated to determine the growth conditions for optimal surface morphology and crystallinity of the InGaSb layers. The composition of these layers was found to be directly related to the TMG/(TMG + TMI) flux ratio at constant growth temperature. Growth rates of 1 $\mu\text{m/hr}$ for the GaSb and 2.8 $\mu\text{m/hr}$ for the InSb were observed. The crystal quality was evaluated using x-ray diffraction and electron channeling and the composition by EDX and SIMS. The results of these studies are will be discussed in detail.

+Advanced Devices and Reliability Directorate, Communications Research Centre, Ottawa, Canada K2H 8S2.

D10.41

CRITICAL THICKNESS OF GaAs/InGaAs AND AlGaAs/GaAsP QUANTUM WELLS GROWN BY ORGANOMETALLIC CHEMICAL VAPOR DEPOSITION Dan Bertolet, Jung-Kuei Hsu, and Kei May Lau, University of Massachusetts, Department of E.C.E., Amherst, MA 01003; and Emil S. Koteles, GTE Laboratories Inc., Waltham, MA 02254

We present a study of strained GaAs/ $\text{In}_{0.11}\text{Ga}_{0.89}\text{As}$ and $\text{Al}_{0.35}\text{Ga}_{0.65}\text{As}/\text{GaAs}_{0.82}\text{P}_{0.18}$ single quantum wells (QW) with thicknesses exceeding the critical thickness (h_c) for misfit dislocation formation predicted by the force-balance model. The $\text{In}_{0.11}\text{Ga}_{0.89}\text{As}$ QW layers are subjected to biaxial compression, as opposed to the $\text{GaAs}_{0.82}\text{P}_{0.18}$ QW layers, which are under biaxial tension. Samples were grown by atmospheric pressure OMVCD on (100) $2^\circ \rightarrow (110)$ oriented GaAs substrates, and characterized by photoluminescence (PL), photoluminescence excitation (PLE) and optical microscopy. For both material systems, as the strained QW layer thickness (L_z) increased beyond h_c , the typical crosshatch surface morphology was observed, indicating the presence of misfit dislocations. However, the QW PL peak positions did not shift in energy, as would be expected if the material was relaxed to some extent. In the $\text{GaAs}_{0.82}\text{P}_{0.18}$ QW's, the strain-dependent energy separation between light- and heavy-holes was measured by PLE, and did not decrease for samples over the critical thickness, again implying no loss of strain. The PL intensity from a GaAs/ $\text{In}_{0.11}\text{Ga}_{0.89}\text{As}$ QW with $L_z \approx 2 \times h_c$ was reduced by more than two orders of magnitude, presumably caused by dislocations acting as non-radiative recombination centers. The PL intensity from a $\text{Al}_{0.35}\text{Ga}_{0.65}\text{As}/\text{GaAs}_{0.82}\text{P}_{0.18}$ sample with $L_z \approx 2 \times h_c$ however, was not reduced. To test the stability of the samples, they were annealed at 850°C in an AsH_3 ambient for ten minutes. None of the PL spectra changed significantly, indicating that these strained QW structures are temperature stable up to 850°C.

D10.42

OPTICAL SPECTROSCOPY OF 2D ELECTRONS CONFINED AT A GaAs/AlGaAs HETEROINTERFACE IN A TRANSVERSE ELECTRIC FIELD. Q.X. Zhao^{a)}, P. Bergman^{a)}, B. Monemar^{a)}, P.-O. Holtz^{a,b)}, C. Hallin^{a)}, M. Sundaram^{b)}, J.L. Merz^{b)} and A.C. Gossard^{b)}, ^{a)}Dept. of Physics and Measurement Technology,

Linköping University, S-581 83 Linköping, SWEDEN. ^{b)}Dept. of Electrical and Computer Engineering, University of California, Santa Barbara, California 93106, USA.

Radiative recombination and decay time measurements of the two dimensional electron gas in a GaAs-AlGaAs heterojunction (the so called H-band) has been studied under transverse electric field perturbation in specially optimized structures prepared by molecular beam epitaxy. The heterointerface was created between 50 nm undoped GaAs and 8 nm of undoped $\text{Al}_{0.35}\text{Ga}_{0.65}\text{As}$ followed by 70 nm Si-doped $\text{Al}_{0.35}\text{Ga}_{0.65}\text{As}$. Both positive and negative gate voltages have been applied to the GaAs-AlGaAs interface, and shifts of the H-band energy position depending on the gate voltage are induced by the corresponding changes in the heterointerface 2D potential. For different gate voltages the excitation power dependence of the H-band energy position is quite similar, since only the lowest 2D subband is occupied in these samples. It is demonstrated that a transverse electric field allows a simple way to modify the 2D heterointerface potential, so that detailed spectroscopy can be done on the recombination of carriers localised in such a potential. Another interesting phenomenon is that the gate voltage can increase the luminescence of the active 50nm-GaAs layer. This indicates that the electric field makes the "3D" recombination more dominant by changing the potential. To obtain information about the dynamical behaviour of the interface recombination we have performed both timeresolved spectral measurements and time decay measurements with and without an applied electric field. The decay time has been measured at different energy positions in the broad H-band luminescence, and is found to have a non-exponential decay with values of decay time varying from a few ns at high energies, to hundreds of ns in the lower energy region.

D10.43

HOT-CARRIER EFFECTS ON OPTICAL PROPERTIES OF GaAs/ $\text{Al}_x\text{Ga}_{1-x}\text{As}$ QUANTUM WELLS. W.M. Chen, B. Monemar, P.O. Holtz, Department of Physics and Measurement Technology, Linköping University, S-581 83 Linköping, SWEDEN; and M. Sundaram, J.L. Merz and A.C. Gossard, Department of Electrical and Computer Engineering, University of California, Santa Barbara, California 93106, USA.

In this paper we report a study of hot-electron effects on optical properties of GaAs/ $\text{Al}_x\text{Ga}_{1-x}\text{As}$ quantum wells, by photoluminescence (PL) in presence of an external magnetic field and a microwave (MW) field. Both single quantum wells (SQWs) and multiple quantum wells (MQWs), grown by molecular beam epitaxy (MBE) with modulated doping, were studied in this work. A profound enhancement of the free exciton (FE) emission from both SQWs and MQWs is observed with MW irradiation. This is attributed to effects of hot-electrons, which are cyclotron resonance accelerated in the MW electric field, as evident from the characteristic dependence on a static magnetic field. The mechanism responsible for the giant enhancement in PL emission intensity of the QWs in the presence of hot-carriers is studied in detail, and is discussed in terms of the following two main contributions. First of all, impact ionization of excitons (FEs or excitons bound at shallow impurities (BEs)) and/or of shallow impurities in the $\text{Al}_x\text{Ga}_{1-x}\text{As}$ energy barriers is readily realizable with the experimental conditions, as can be directly seen by a strong quenching of luminescence from the barrier. This process blocks, at least partly, the shunt pass of the photoexcited free carriers in the barrier so that they are mainly accommodated in the GaAs energy well. Secondly, an increase of free electron temperature T_e in the barriers may result in an increase in the diffusion into the well, and consequently enhances the number of the excitons in the well. The direct role of the external perturbations (magnetic field and MW) on the exciton formation and recombination in the well (via modifying the electronic energy and wavefunction of the excitons) is also studied, via resonant optical excitation of the excitons.

D10.44

APPLICATION OF AN ULTRAHIGH RESOLUTION SPECTROMETER TO THE ANALYSIS OF PHONONS AND PHOTONS IN SOLIDS. J. L. Stehle, P. Evrard, SOPRA, 26/68 rue Pierre Joigneaux, 92270 Bois-Colombes, FRANCE. L. C. Hammond, J. N. Willis, ARIES/QEI, 5A1 Damonmill Square, Concord MA 01742, USA.

A new, powerful double spectrometer, in double pass (DMDP), has been designed for the analysis of transparent vitreous materials. Intensity and position of longitudinal and transverse Brillouin modes can be analyzed, with a resolution of 0.03

cm^{-1} . Throughput and stray-light rejection exceed those of a Fabry-Perot with an equivalent resolution.

In a single scan, it is possible to analyze low frequency Raman and Brillouin lines, on the Stokes and anti-Stokes sides, from 0.1 to 2000 cm^{-1} . With a slit width of 1mm, sample alignment and incident power density are no longer critical. An intensity of 10^4 photons/second is easily achieved with a resolution of 1 cm^{-1} . The spectral range of 0.2 to 1.5 microns covers the interesting resonance zones for semiconductors, superconductors and superlattices.

The monochromator can also be used in photoluminescence and time-resolved fluorescence. By using a CCD detector, imaging of samples can be achieved for one vibrational band. Some Brillouin and low frequency Raman applications will be discussed and spectra of germanium, silicon and superlattices will be presented.

D10.45

EFFECT OF ANNEALING ON STRAINED InGaAs/GaAs QUANTUM WELLS Emil S. Koteles, B. Elman, P. Melman, and C.A. Armiento, GTE Laboratories Inc., Waltham, MA 02254

The ability to modify the optical properties of epitaxial semiconductor heterostructures in a spatially selective manner has many potential device applications. We have investigated the effects of shallow ion implantation and rapid thermal annealing (RTA) on strained InGaAs/GaAs quantum wells (QW) as a means of achieving this goal.

The samples consisted of MBE grown single quantum wells and ion beam irradiation was performed using ^{75}As ions with energies low enough (35 keV) that the disordered regions were well separated spatially from the QWs. RTA was performed at 750° to 850° C for 15 seconds. Low temperature photoluminescence (PL) and PL excitation spectroscopies were used to monitor excitonic energies. After RTA, exciton energies shifted significantly to higher values only in the implanted regions. The magnitudes of the shifts were dependent on QW widths, indium compositions in the wells, and implantation fluences. They were interpreted as resulting from the modification of the shapes of the as-grown QWs from square (abrupt interfaces) to rounded (gradual interfaces) due to enhanced In diffusion out of the well layers in irradiated areas as a consequence of the diffusion of vacancies generated near the surface by the implantation. This technique promises simultaneous patterning, interdiffusion and modification of optical and electronic properties of quantum well materials, annealing of implantation induced defects and activation of dopants when electrically active ions are used for implantation.

D10.46

CHARACTERIZATION OF MODULATION DOPED PSEUDOMORPHIC AlGaAs/InGaAs/GaAs HEMT STRUCTURES BY ELECTRON BEAM ELECTROREFLECTANCE AND PHOTOLUMINESCENCE. M. H. HAKMAN, I. D. Ward, Charles Evans & Associates, Redwood City, CA; R. Kopf, S. J. Pearton, AT&T Bell Laboratories, Murray Hill, NJ; and E. D. Jones, Sandia National Laboratories, Albuquerque, NM.

We have investigated the optical transitions present in MBE-grown modulation doped pseudomorphic $\text{Al}_{1-x}\text{Ga}_x\text{As}/\text{In}_{1-y}\text{Ga}_y\text{As}/\text{GaAs}$ HEMT structures of 120Å InGaAs thickness, y values 0.10 to 0.20, and x values 0.20 to 0.30. From both 300K EBER and 4K PL measurements we observe transitions from the InGaAs strained quantum well layer. The intensity and lineshape of the InGaAs transition in both optical spectra is affected by

processing temperatures, and provides an indication of the quality of the HEMT.

In addition to strong, sharp features arising from the GaAs substrate and the superlattice buffer, the EBER data shows important characteristics of the AlGaAs layer which are unavailable from the PL. The latter include the presence of Franz-Keldysh oscillations, from which the crystal quality, composition, and electric field strength within the AlGaAs can be assessed. Specifically, when the growth temperatures are excessive, the disappearance of the Franz-Keldysh oscillations is associated with outdiffusion of In from the strained layer, and consequent deterioration of active device performance.

D10.47

A NEW OXYGEN PLASMA SOURCE FOR "IN-SITU" GROWTH OF YBaCuO MOLECULAR BEAM EPITAXY LAYERS. M. TOUZEAU*, D. PAGNON*, P. LUZEAU*, A. BARSKI*, A. SCHUHL*, R. CABANEL*, S. KOCH*, J.P. HIRTZ* and G. CREUSET*

* Lab. de Phys des Plasmas, Paris XI, 91405 Orsay Cédex France
* ISA RIBER, 133-137 Bd National 92503 Rueil Malmaison France
* Thomson CSF, Domaine de Corbeville 91404 Orsay Cédex France

We present an oxygen introduction cell used for in-situ growth of epitaxial thin films of High Tc superconductors in a MBE system. Since such a machine is not compatible with high pressure, active oxygen is needed in order to obtain good oxydation of the cations. Atomic oxygen is produced using a DC plasma source located in the growth chamber. A quartz tube with a U-form contains oxygen gas at a pressure between 30 and 300 Pascal. The electrodes made in platinum are distant of 12 cm. We typically used a DC current in the plasma of the order of 25 mA.

The design of this cell is specially conceived for the safety of the MBE system. In the plasma, the atomic oxygen concentration, deduced from optical absorption measurements, lies between 5 and 10% depending on the experimental conditions.

The outcoming oxygen rate is between 5×10^{17} and 5×10^{18} molecules per 10^{16} second which gives, on the sample a flux higher to 10^{16} at / sec. cm^2 in the best experimental conditions.

We have produced superconducting films of DyBaCuO directly in the growth chamber using this cell.

D10.48

GROWTH AND CHARACTERIZATION OF $\alpha\text{-Ge}_x\text{Sn}_{1-x}$ HETEROEPITAXIAL ALLOYS ON (001) InSb. E.A. Fitzgerald, P.E. Freeland, M.T. Asom, W. Lowe, R. MacHarrie, Jr., A.R. Kortan, F.A. Thiel, L. Cooper, G.A. Thomas, K.A. Jackson, B.E. Weir, and L.C. Kimerling, AT&T Bell Laboratories, Murray Hill, NJ 07974.

We have grown MBE $\alpha\text{-Ge}_x\text{Sn}_{1-x}$ ($0 < x < 0.16$) alloys on (001) InSb despite the nearly complete immiscibility of Ge and Sn. $\alpha\text{-Ge}_x\text{Sn}_{1-x}$ alloys were stabilized due to a relatively close lattice match with the InSb.

We observe three stages of growth with reflection high energy electron diffraction (RHEED). The growth commences two-dimensionally, and a gradual shift to three-dimensional growth with thickness is observed. Upon continued growth, twinning occurs and finally phase separation. Generally, for alloys with $0 < x < 0.14$, the twinning stage occurs between 1200Å and 2000Å. For $0.13 < x < 0.16$, only 100Å is grown before the twinning phase is reached.

Double and triple crystal x-ray results show that totally strained (up to $x=0.84\%$), $\alpha\text{-Ge}_x\text{Sn}_{1-x}$ is stabilized with $x \leq 0.08$. A mixture of $\beta\text{-Sn}$ and $\alpha\text{-Ge}_x\text{Sn}_{1-x}$ is observed for $x > 0.08$, in contrast to the RHEED results, which show single-crystalline growth.

Hall effect and reflectivity measurements indicate that the carrier concentration increases with x , with a maximum of approximately 10^{22} cm^{-3} at $x=0.08$. The carrier mobility ($T=85\text{K}$) decreases to $< 1000 \text{ cm}^2/\text{V-sec}$ in this composition

range. These transport results suggest an increasing overlap of the conduction and valence bands and semimetallic behavior.

In-situ and ex-situ stability measurements were also performed. 1200Å thick films with $0.04 \leq x \leq 0.13$ were stable to 120-130°C. A thermodynamic model is derived which follows the experimental trends of stability as a function of film thickness, temperature, and Ge concentration.

D10.49 ABSTRACT WITHDRAWN

plays a subsidiary role to symmetry in determining the optical properties. First principles theoretical studies of these new materials have provided an important base of understanding of how properties of the constituent bulk semiconductors can be used to predict the electronic structure of these superlattices.

D11.2

STRAIN-INDUCED PHOTOLUMINESCENCE IN Si/Ge SUPERLATTICES.

G.F.A. van de Walle, E.A. Montie, D.J. Gravesteijn and A.A. van Gorkum, Philips Research Laboratories Eindhoven, The Netherlands

The luminescence of short period Si/Ge superlattices has been studied as a function of superlattice period, composition and strain. The superlattices were grown by MBE on a SiGe buffer layer, with constant or graded Ge fraction, deposited on 4" and 6" substrates. During part of the deposition process the substrate rotation was stopped, causing a systematic variation in superlattice period (30%) and in relative mismatch between superlattice and buffer ($0 < \delta a/a < 0.013$).

Rutherford backscattering spectrometry (RBS) was used to analyse the composition and crystallinity of the samples. The superlattice period and the strain in both superlattice and buffer layer was obtained from X-ray diffractometry (XRD). Transmission electron microscopy (TEM) was used to assess the morphology of the layers, while Raman scattering was used to characterize the interface sharpness. Photoluminescence (PL) bands are observed around 0.8 eV for several samples of differing composition. The signal is only present in those samples in which the superlattice has an average perpendicular lattice constant different from that in the buffer. As there are no indications of resulting misfit dislocations from TEM, the luminescence is concluded to be strain-induced. Furthermore, the signal disappears when the superlattice is removed from the buffer layer by etching, indicating that the luminescence originates from the superlattice.

D11.3

PHOTOLUMINESCENCE EXCITATION SPECTROSCOPY OF STRAINED InGaAs/GaAs QUANTUM WELLS Emil S. Koteles, D. Owens, B. Elman, and P. Melman, GTE Laboratories Inc., Waltham, MA 02254 and D. Bernolet and Kei May Lau, The University of Massachusetts, Amherst, MA 01003

There has been much interest lately in compound semiconductor quantum wells (QW) subjected to biaxial strain due to lattice mismatch between the barrier and well layers. The addition of strain in the well layers of such pseudomorphic (lattice matched but strained) QWs modifies confined energy levels and is a useful additional parameter in the design of devices. The characterization of such structures is complicated by the addition of strain which affects conduction, light-, and heavy-hole valence bands differently. This also leads to questions concerning the band offsets in these heterostructures. Calculations indicate that the heavy-hole exciton (commonly measured using photoluminescence (PL) spectroscopy) is much less sensitive to such concerns than the light-hole transition. Therefore, we have measured the PL excitation spectra of a series of $\text{In}_{0.1}\text{Ga}_{0.9}\text{As}/\text{GaAs}$ QWs, grown by MOCVD and MBE, with nominal widths ranging from 1.1 to 36 nm. We have observed peak and bandedge-like structure at energies much above the heavy-hole exciton energy which we attribute to the ground state of the light-hole exciton. As expected the energy of the light-hole exciton is very sensitive to the band offset and the difference between the light-hole and heavy-hole exciton energies for wide wells is an accurate and independent measure of the strain in the well layer.

D11.1

STRAIN AND STRUCTURALLY INDUCED OPTICAL TRANSITIONS IN EPITAXIAL SEMICONDUCTORS. Thomas P. Pearsall, ATT Bell Laboratories, Murray Hill, New Jersey, 07974

Strained-layer epitaxy can be used to introduce internal levels of compressive or tensile strain on the order of several percent. This is large enough to shift some conduction and valence band energy levels in commonly used semiconductors by as much as 500meV. By changing the symmetry of the crystal, the strain also causes mixing of these energy levels, which in turn changes the optical transition matrix element. The importance of this effect depends both on the magnitude of the strain and the relative orientation of the strain field relative to the crystalline axes of the material.

Yield strength of most semiconductors limits the symmetry changes to distortions of a few percent. However, grown-in transformations of the symmetry by creating artificial crystal structures can be used to redefine the allowed set of electronic wavefunctions producing dramatic changes in the electronic energy spectrum. This is Wavefunction Engineering, examples of which have now been demonstrated in III-V and group IV materials. In such artificially structured materials, strain

D11.4

CHARACTERIZATION OF INGAAS/GAAS STRAINED SL BY X-RAY DOUBLE CRYSTAL DIFFRACTION AND MODULATE PHOTOREFLECTION SPECTRA. L. S. Xu; Y. T. Wang; Z. Q. Wu; W. H. Zhuang; * University of Science and Technology of China, P. R. China; ** Institute of Semiconductors, Chinese Academy of Science, P. R. China.

With the kinematical theory model we did computer simulation of the X-ray double crystal diffraction of InGaAs/GaAs MQW. From the diffraction angle of the satellites one got period of MQW ($L_z + L_s$) and from the relative intensity I_n/I_{n+1} one got L_z/L_s . The obtained results L_z and L_s are consistent with the experimental value from photoreflection and photoluminescence spectra.

D11.5

OPTICAL CHARACTERIZATION OF GaAsP STRAINED LAYERS GROWN ON (111)-ORIENTED GaP. Mats-Erik Pistol, Maria Gerling, Anders Gustafsson, Gert Paulsson, Lars Samuelson, and Heinz Titze, University of Lund, Department of Solid State Physics, P. O. Box 118, S-221 00 Lund, SWEDEN.

Strained layers of III-V semiconductors grown on (111)-oriented substrates are of considerable interest due to the piezoelectric field expected to be present. The strain situation is different from similar structures grown on (100)-oriented substrates and no splitting of the X conduction band is expected for the (111) case. The critical thickness of (111)-grown samples is expected to be different from samples grown on (100) substrates. We have grown thin strained layers of indirect bandgap GaAsP on (111)-oriented GaP with different compositions and thicknesses. These structures have been characterized by photoluminescence, electroluminescence and wavelength-resolved cathodoluminescence, all at low temperature, as well as secondary ion mass spectroscopy. The photoluminescence emission involving transitions from the X conduction band to the valence band is strong and often persisting to room temperature. The strain shift of the X conduction band as a function of composition has been followed. Electroluminescence shows transitions involving resonant quantised states in the quantum well formed from the Γ band. The energy of the states in the resonant Γ band well can, hence, also be traced as a function of composition and strain of the layers. These shifts of the different band edges are compared with calculations. Cathodoluminescence studies, detecting the emission from the layer, reveal the onset of dislocation formation at the critical thickness and is shown to be a sensitive method to measure very low densities of dislocations where the separation of the dislocation lines is greater than 20 μm . A comparison of dislocation generation is made of GaAsP layers grown on (111)-, and (100)-oriented substrates.

D11.6

HIGH PRESSURE OPTICAL STUDIES OF GaSb-AlSb MULTIPLE QUANTUM WELLS. Benjamin Rockwell, H.R. Chandrasekhar and Meera Chandrasekhar, Department of Physics, University of Missouri - Columbia, Columbia, MO 65211; Fred H. Pollak and H. Shen, Physics Department, Brooklyn College of CUNY, Brooklyn, N.Y. 11210; L.L. Chang, W.I. Wang and L. Esaki, IBM Thomas J. Watson Research Center, Yorktown Heights, N.Y. 10598-0218

Photoreflectance (PR) and Photoluminescence (PL) studies of GaSb-AlSb multiple quantum well structures under hydrostatic pressure at cryogenic temperatures are presented. Due to the lattice mismatch between the GaSb and AlSb layers, the light (LH) and heavy (HH) hole valence bands split leading to a light hole derived ground state for the multiple Quantum Well (MQW) structure. A large number of excitonic transitions from the conduction sub-bands (CB) to the LH and HH sub-bands are observed in

PR. In contrast, the transition from the ground sub-band from the CB to the LH dominates the PL. The PL intensity drops dramatically as the direct Γ CB crosses the L CB at $\sim 10\text{kBars}$ but the PR intensity does not. However a large drop in intensity of PR is observed as the X CB crosses each sub-band energy. The pressure coefficients (α) get progressively smaller for the higher sub-band transitions. Several competing effects such as pressure induced changes in the electron effective mass, the excitonic Rydberg, the lattice parameters and interface effects lead to the variation of α .

H.R.C. was supported by a grant from the U.S. Department of Energy under grant no. DE-AC02-84ER45048 and M.C. was supported by the U.S. Army under contract no. DAAL03-86-K-0083.

D11.7

CHARACTERIZATION OF UNDOPED PSEUDOMORPHIC InGaAs/GaAs QUANTUM WELLS BY ELECTRON BEAM ELECTROREFLECTANCE (EBER) AND PHOTOLUMINESCENCE (PL). M. H. Haxman, I. D. Ward, Charles Evans & Associates, Redwood City, CA; and A. Dodabalapur, B. G. Streetman, The University of Texas, Austin, TX.

We have investigated the interband optical transitions within undoped pseudomorphic InGaAs/GaAs quantum wells of a range of thickness from 50Å to 150Å, and y values 0.1 to 0.2. From PL, we identify the lowest interband transitions. Electron beam electroreflectance (EBER) modulation spectroscopy is utilized to detect the lowest and the higher energy interband transitions within the quantum wells. We compare the measured interband energies to those calculated theoretically.

D11.8

RAMAN CHARACTERIZATION OF InSb/GaAs GROWN BY METALORGANIC MAGNETRON SPUTTERING. Z. C. Feng and S. Perkowitz, Physics Department, Emory University, Atlanta, GA 30322; T. S. Rao and J. B. Webb, Laboratory for Microstructural Science, National Research Council, Ottawa K1A 0R6, Canada.

Despite the large (14%) lattice mismatch between InSb and GaAs, high quality films of InSb, with various thicknesses of 0.17 - 2.67 microns, have been deposited on (100) GaAs substrates using metalorganic magnetron sputtering (MOMS). The MOMS-grown layers have been studied by Raman and resonance Raman scattering at 50 - 300K, performed in the near-backscattering geometry with an Ar^+ ion laser. The Raman spectra for the InSb/GaAs layers show a narrow (about 4 cm^{-1}) LO line and obey the expected selection rules, indicating the films to be of high crystalline quality with (100) orientation. An initial increase in the compressive stress appears to be related to a combination of 3-dimension island growth kinetics and the thermal expansion differences of the InSb and GaAs. A relaxation of this stress is observed in thicker films.

D11.9

ELECTRIC FIELD EFFECTS ON THE OPTICAL PROPERTIES OF InGaAs/GaAs STRAINED QUANTUM WELLS AND SUPERLATTICES. K. Gibb, C. Lacelle and A.P. Roth, LMS, NRC, Ottawa, Canada; B. Soucail, N. Dupuis and P. Voisin, GPS, ENS, Paris, France; B.Y. Hua* and E. Fortin, University of Ottawa, Ottawa, Canada.

Strained multiple quantum wells (SMQW) and superlattices (SLS) of InGaAs/GaAs have been studied using Photoluminescence Excitation (PLE) and Photocurrent (PC) spectroscopy. Applying a longitudinal electric field in SMQW structures (ie with wide barriers (> 20 nm)), produces a red shift of the exciton due to the quantum

confined Stark effect. In contrast, in SLS structures (ie with narrow barriers ($< 10\text{nm}$)), the electric field decouples the wells and a blue shift of the absorption edge is expected.

We have studied several samples with various well and barrier width at zero field using PLE and as a function of applied bias in a Schottky diode configuration using PC. Optical transitions involving both confined and unconfined states are observed and in SLS structures the first electron miniband width can be directly measured. Transitions between confined electrons and heavy holes (type I) behave as expected under applied electric field, whereas the situation is more complex for transitions involving unconfined heavy holes or light holes (type II).

* Present Address : Beijing Polytechnic University, Beijing, China.

D11.10

RAMAN STUDY OF MOMBE AND MOVPE GROWN III-V LAYERS ON Si(100). J.Geurts, J.Finders I.Phys. Inst. RWTH Aachen (F.R.G.) H.Münder, M.Kamp, M.Oehlers, H.Lüth, ISI, KFA Jülich (F.R.G.) J.Musolf, J.Leiber, A.Brauers, M.Weyers P.Balk, Inst. Semicond. Electronics, RWTH Aachen, (F.R.G.)

We characterized MOMBE and MOVPE GaAs layers on Si(100), grown by a two step method (buffer and epi-layer). In MOVPE the buffer growth was plasma stimulated. As group III source either TMC or TEG was used. Further, we investigated plasma-MOVPE InP layers on top of GaAs layers on Si.

The crystalline quality was determined by Raman scattering from the III-V phonons, using the intensity of the symmetry forbidden TO phonon and the width of the allowed LO phonon as a measure for non-ideality. Our results are consistent with double crystal x-ray diffraction (DCXD) linewidths. Besides, we observe characteristic spectra from disturbed regions like buffer layers, which give no DCXD peaks. Thereby, we can visualize the transition from buffer to epi-layer. The depth resolution is obtained by varying the light penetration depth, using different laser lines. For appropriate epilayer thickness, the TO/LO ratio increases by a factor 2 when the penetration depth is changed from $0.07\text{ }\mu\text{m}$ to $0.31\text{ }\mu\text{m}$, reflecting the worse buffer quality.

InP layers were studied with lateral resolution by Raman-microprobe. They show well defined LO peaks, which however have a distinct spectral splitting and local inhomogeneities.

D11.11

MBE GROWN GaAs ON Si(100) STUDIED BY INFRARED SPECTROSCOPY, Thomas Eickhoff, I.Phys. Inst. RWTH Aachen, FR Germany, Dietrich R.T. Zahn and Wolfgang Richter, Inst. Festkörperphysik, TU Berlin, FR Germany, David A.Woolf, David I.Westwood and Robin H. Williams, Physics Dept. U of Wales college of Cardiff, UK

GaAs layers were deposited onto Si (100) substrates using molecular beam epitaxy. The growth parameters varied were: (i) substrate misorientation, (ii) substrate preparation by using different etching procedures, and (iii) buffer layer growth conditions (deposition rates from 0.1 to $1.0\text{ }\mu\text{m/h}$ and growth temperature from 550 to 650 K). Infrared reflectivity spectra were taken in the range from 50 to 500 cm^{-1} on the $0.1\text{ }\mu\text{m}$ thick buffer layers as well as on the active layers which were grown on top of the

buffer at 850 K , with a rate of $0.1\text{ }\mu\text{m/h}$ up to thicknesses of $4\text{ }\mu\text{m}$.

The infrared active phonon of GaAs can be observed already on the thin buffer layers. A harmonic oscillator and Drude fitting procedure is used to determine layer thickness, carrier concentration and damping constant. The latter correlates well with the layer quality as determined from spectroscopic ellipsometry data and Raman scattering spectra.

D12.1

RAMAN SCATTERING FROM AN INTERFACIAL THIN LAYER OF GaAs HETEROEPITAXIALLY GROWN ON SILICON SUBSTRATE. Yoshiro Akagi, Mariko Ishino, Yoshiharu Nakajima, Sharp Corporation, Corporate R&D Group, Tenri, Nara, 632 JAPAN

Heteroepitaxial GaAs grown on silicon substrate attracting recent interest, however, suffers several difficulties: (1) high dislocation density ($\sim 10^6\text{ cm}^{-2}$) due to large lattice mismatch (4%) between GaAs and Si, (2) residual stress in GaAs originating from the difference in thermal expansion coefficients between them, (3) antiphase domain (APD). Considerable efforts have been made to suppress these problem and several techniques have been found to be successful. In addition, we investigated interfacial thin layer of GaAs (100nm - 300nm) by using Raman scattering and photoluminescence (PL) to characterize an interface. Specimen of nondoped GaAs ($2\text{ }\mu\text{m}$) was directly grown on Si(100) with 2° off towards $\langle 011 \rangle$ by two-step MOCVD. Layer of GaAs was chemically etched by $\text{NH}_4\text{OH-H}_2\text{O}_2$ until an interface become observable.

In GaAs layer less than 300nm , broad scattering centered around 700 cm^{-1} and TO-like phonon were observed as well as LO phonon spectrum which is only allowed in our scattering geometry. Above 300nm in thickness of GaAs layer, both of these spectra slightly shifted and disappeared, approaching to a spectrum observed for a bulk material. PL spectra of these interfacial GaAs layer shifted towards higher energy which shows an elevation of quasi-Fermi level. These experimental results can be explained by n-carrier generation of 10^{18} cm^{-3} only within interfacial GaAs layer less than 300nm because of auto-doping of Si atoms from substrate during growth near 700°C .

D12.2

STRESS EVALUATION METHOD USING RAMAN SPECTROSCOPY. Yokko Mashimoto IBM Japan, Ltd. (Yasu Site), Yasu, Shiga, Japan.

Recently local stress measurement/evaluation method is considered to be very important to evaluate electrical property of semiconductor. Raman spectroscopic method has been established for evaluation of the local stresses with $1\text{ }\mu\text{m}$ in diameter. The measurement problems caused by equipment itself was solved by the followings.

- Ar Plasma line was utilized to calibrate wave number.
- Data was fitted with Gaussian and Lorentz distribution to determine the peak top accurately.

This method with introduction of a certain assumption can be applied to the stress measurement not only for Silicon single

crystal like trench structure, but also for laminated thin layers like silicon oxide or silicon nitride on silicon.

In this paper, measurement and data processing methods are described and also application results to the thin layer of semiconductor and packaging plastic material are reported.

D12.3

ELECTRICAL AND OPTICAL CHARACTERIZATION OF InSb GROWN ON GaAs BY MBE. Phillip E. Thompson, James Waterman, D. Kurt Gaskill, Robert Stahlbush, and John Davis. Code 6823, Naval Research Laboratory, Washington, DC 20375-5000

InSb has been grown on semi-insulating GaAs substrates by molecular beam epitaxy. By growing an InSb buffer layer at 300°C prior to the main InSb layer growth at 420°C, the effect of the 14% lattice mismatch between GaAs and InSb was minimized. A typical 5 μm InSb film had a room temperature carrier concentration and electron Hall mobility of $2 \times 10^{16}/\text{cm}^3$ and $6 \times 10^4 \text{ cm}^2/\text{Vs}$, respectively. At 77°K these values became $2 \times 10^{15}/\text{cm}^3$ and $1.1 \times 10^5 \text{ cm}^2/\text{Vs}$. For a 10 μm film the 77°K mobility was $1.5 \times 10^5 \text{ cm}^2/\text{Vs}$. Temperature dependent Hall measurements revealed a peak in the mobility at 85°K and 70°K for the 5 and 10 μm samples, respectively. Optical characterization by room temperature IR transmission spectroscopy showed a broad absorption edge, with an absorption coefficient of $1.4 \times 10^3/\text{cm}$ at a wavelength of 6 μm . Epilayer thickness was determined from observed interference fringes and corresponded to the calculated epitaxial layer thickness. Capacitance-voltage measurements using MIS capacitors and Schottky diodes produced 77°K carrier concentrations in agreement with the Hall measurements. Carrier lifetimes were determined by photoconductive response and capacitance transient measurements. Lifetimes of 20 ns and 50 ns were determined for the 5 and 10 μm films, respectively. For comparison, the carrier lifetime in bulk n-type InSb was found to be 200 ns.

D12.4

INDEX OF REFRACTION ANISOTROPY IN MISMATCHED InGaAs/InP HETEROSTRUCTURES MEASURED BY ELLIPSOMETRY. Brian R. Bennett and Jesús A. del Alamo, Mass. Inst. of Tech., Cambridge, MA.

We have applied ellipsometry to characterize $\text{In}_x\text{Ga}_{1-x}\text{As}$ grown by molecular beam epitaxy on (001) InP. The epitaxial layer thickness varied from 0.3 to 1.1 μm and x ranged from 0.46 to 0.61. The index of refraction, n , of the epilayers was measured by ellipsometry at 0.633 μm as a function of ϕ , the azimuth angle. We found that for mismatched samples ($1 \pm 1.2 \times 10^{-4}$) n is a strong function of ϕ , reaching a maximum when the incident beam is parallel to the [110] direction and a minimum for orthogonal directions. Variations of n with ϕ are often as large as 0.1, far exceeding changes typically produced by electric fields or free carriers.

Our results can be explained by piezo-optical (photoelastic) effects. The lattice-constant mismatch between the substrate and epitaxial layer results in a strained epitaxial layer. The epitaxial layers are thicker than the critical layer thickness, suggesting the presence of misfit dislocations. These dislocations partially relieve strain and are known to form more readily in the [110] direction than in the orthogonal [110] direction, resulting in anisotropic strain and refractive index. The existence of misfit dislocations in the samples exhibiting optical anisotropy is confirmed by measurements of large double-crystal x-ray FWHM values and lattice constant mismatch parallel to the interface.

D12.5

MODULATION SPECTROSCOPY OF LAYERED STRUCTURES. Orest J. Glembocki, Naval Research Laboratory, Code 6833, Washington DC 20375.

Layered semiconductor structures have been of fundamental and applied interest for over a decade. The ability to grow high quality layers that exhibit novel electronic and optical properties has been made possible by the development of growth techniques such as molecular beam epitaxy and chemical vapor deposition. This success is possible because of the close interaction between the growth effort and the materials characterization.

Photoreflectance and electoreflectance are two optical modulation techniques, which have proven to be useful in the study of layered structures. Modulation techniques exploit a periodic variation in some property of the sample to obtain derivative-like optical spectra, which have enhanced sensitivity to weak transitions, which may otherwise be difficult to observe. Because the reflectivity is commonly measured, modulation techniques can be used over a wide spectral range, normally not accessible to luminescence or absorption. Furthermore, modulation spectra contain information in the spectral position of a given line and in its line shape. These facts have been important in the study of quantum wells and superlattices. Spectrally, modulation techniques have allowed for room temperature determinations of the well and barrier parameters, including well widths, barrier heights and barrier thicknesses. The form of the line shapes in modulation spectroscopy contains information about the effects of the applied modulation. The phase of the line shape and its dependence on the frequency of modulation have been used to study the effects of the applied perturbation. In particular effects of light on NIPI structures, electric fields in coupled wells and light effects on impurities have been studied.

Finally, it will be shown that a comparison of several techniques, such as PR and piezomodulation can provide even more detailed information about the sample of interest.

D12.6

CHARACTERIZATION OF AN ASYMMETRIC TRIANGULAR MULTIPLE QUANTUM WELL, BY VARIABLE ANGLE SPECTROSCOPIC ELLIPSOMETRY.* Craig M. Herzinger, Paul G. Snyder, and John A. Woolam, University of Nebraska, Lincoln, NE 68588-0511.

Variable angle spectroscopic ellipsometry (VASE) was used to characterize a 20 period $\text{GaAs-AlGa}_{1-x}\text{As}$ multiple quantum well (MQW) structure, grown by molecular beam epitaxy. The barriers were nominally 200 \AA $\text{Al}_{0.25}\text{Ga}_{0.75}\text{As}$, and the well regions were grown to approximate a linearly graded composition, from $x=0$ to $x=0.25$, with total well width 200 \AA . A strong HH1-CB1 excitonic transition was observed at 1.53 eV, with the weaker LH1-CB1 transition near 1.54 eV. These are consistent with a multiband effective mass theory calculation. A small, narrow feature was also observed at the AlGaAs bandgap energy (E_g), which we ascribe to a weak Franz-Keldysh effect in the barriers.

VASE data were analyzed using a model which explicitly included the full MQW structure, with graded wells. Bulk optical constants were used. This model could fit the data quantitatively over the photon energy range above E_g , and qualitatively below E_g . In a second model, the entire MQW was treated as a single layer, and its optical constants obtained in the exciton region. A third model was used to solve for the optical constants within the wells. The relative merits of these models will be discussed.

1. G.D. Sanders and K.K. Bajaj, J. Vac. Sci. Technol. B2, 1295 (1987).

* Work supported by NASA Lewis Grant NAG-3-154.

D12.7

PHOTOREFLECTANCE OF A GaAs/InGaP(ORDERED) SINGLE QUANTUM WELL GROWN BY ATOMIC LAYER EPITAXY. X. Yin and E.H. Pollak, Brooklyn College of CUNY, Brooklyn, NY 11210; B.T. McDermott, K.G. Reid and S.M. Bedair, North Carolina State University, Raleigh, NC 27695

The photoreflectance (PR) spectrum of a GaAs/InGaP (ordered) single quantum well has been measured at 300K. We have observed three quantum transitions from the GaAs well in addition to a peak from the InGaP barrier layer. Good agreement between the experimental data and a theoretical calculation is obtained for a conduction band offset parameter $Q_C < 0.1$. The parameter $Q_C = \Delta E_C / (\Delta E_C + \Delta E_V)$, where ΔE_C and ΔE_V are the conduction and valence band discontinuities, respectively.

The total structure was built by ALE on (100) GaAs substrates in a layer by layer fashion at 500°C using TEI, PH₃ and TMG sources. The growth proceeded by the deposition of a monolayer of In then P then Ga and then P. The cycle was repeated for 100 times. This was followed by eleven ALE cycles of GaAs and then a second 100 cycles of the In-P-Ga-P ordered alloy.

From a detailed lineshape fit to the experimental spectrum we have obtained transition energies of 1.468 ± 0.01 eV, 1.585 ± 0.01 eV, 1.615 ± 0.02 eV and 1.797 ± 0.01 eV. The latter feature corresponds to the fundamental gap of the InGaP barrier while the former three structures are identified as 11H, 11L and 12H quantum transitions. The notation mnH(L) denotes transitions between the mth conduction and nth valence subbands of heavy(H)- or light(L)- hole character. Good agreement between experiment and a calculation based on the envelope function model is achieved for $Q_C \sim 0.05$ and a well width of 35 Å. This value of Q_C is considerably smaller than those obtained from measurements of GaAs/InGaP(random) heterojunctions.

D12.8

MAGNETO-OPTICAL STUDIES OF 2-D ELECTRONS IN GaAs-AlGaAs SINGLE HETEROJUNCTIONS.

K.-S. Lee[†], C.H. Perry[†], Northeastern University, Boston, MA 02115, and J.M. Worlock[†], Bellcore, Red Bank, NJ 07701

We report low temperature magneto-photoluminescence investigations of the exciton spectra of high mobility n-doped (AlGa)As-GaAs single heterojunctions up to 23 Tesla. At zero field, the PL spectrum is dominated by the bulk exciton transitions, but the radiative transitions between the two dimensional electron gas (2DEG) and the photoexcited holes are not discernable. In the presence of magnetic fields, applied perpendicular to the interface, Landau transitions (LT) appear at the fields which are dependent on the sample parameters¹. With low incident laser power, intensity oscillations are observed as the LT lines cross the bulk exciton lines; this behaviour may be associated with some type of resonant tunneling of the 2DEG from the quantum well region to bulk GaAs. The possibility of screening by the long range random potential fluctuation² is excluded because the period of oscillation is not related to the filling factor of the 2DEG. The cyclic effect of the magnetic field on the PL efficiency or on the efficiency of non-radiative recombination processes remains unexplained and is under further investigation.

¹ I. Kukushkin, V. Timofeev, K. Klitzing, and K. Ploog, *Advances in Solid State Physics* 28, 21 (1988).

² T. Ando, *J. Phys. Soc. Jap.* 37, 1044 (1974).

[†] Guest Scientists at the Francis Bitter National Magnet Laboratory, MIT; supported by NSF under grant # DMR - 8604706.

D12.9

MAGNETO-OPTICAL STUDIES OF GaAs-AlGaAs MODULATION DOPED QUANTUM WELLS UNDER HYDROSTATIC PRESSURE

W. Zhou[†], C.H. Perry[†], Northeastern University, Boston, MA 02115, and J.M. Worlock[†], Bellcore, Red Bank, NJ 07701

We report magneto-photoluminescence studies of n-type modulation doped GaAs-AlGaAs multiple quantum well (MQW) heterostructures under hydrostatic pressure from 0-30 kbars. A pressure-induced metal-insulator transition is observed^{1,2}; this transition is monitored by investigation of the dramatic changes that take place in the different spectral features (energy and line-width) as a function of magnetic field. These changes can be correlated with the tuning of the carrier concentration with pressure. Analysis of the free Landau PL recombination indicates a transformation to magneto-excitonic-like behaviour at about 10 kbars at low temperatures in a MQW with an electron density of $n_e = 5 \times 10^{11} \text{ cm}^{-2}$ and $x=0.21$.

1 J.M. Mercy et al. *Surface Science* 142, 298 (1984).

2 C.H. Perry, B.A. Weinstein, S.K. Hark and C. Mailhot, 18th Int. Conf. on the Physics of Semiconductors (ed O. Engstrom, World Scientific, Singapore, 1987), p.687

[†] Guest Scientists at the Francis Bitter National Magnet Laboratory, MIT; supported by NSF under grant # DMR - 8604706.

D12.10

SPATIALLY INDIRECT OPTICAL TRANSITIONS IN SEMICONDUCTOR QUANTUM WIRES. Joseph S. Weiner, G. Danan, A. Pinczuk, J. Valladares, L. N. Pfeiffer, K. West, AT&T Bell Laboratories, Murray Hill, NJ.

In optical experiments with laterally patterned modulation-doped GaAs/AlGaAs quantum wells we observe spatially separate confinement of electrons and holes in one-dimensional quantum wires.

The sample was fabricated from a high mobility modulation doped GaAs/AlGaAs single quantum well heterostructure. 1000 Å lines with 2000 Å period were patterned using electron-beam lithography, followed by ion-milling to selectively deplete the electron gas in the unmasked regions. The resulting lateral modulation of the charge density induces a periodic lateral potential which confines the electron gas to one dimension.

The photoluminescence (PL) from the quantum wires exhibits an onset at the bandgap, followed by a cutoff at the Fermi level characteristic of the electron gas. Unlike the two-dimensional electron gas, the intensity of the PL from the quantum wires increases above the bandgap, reaching a maximum just below the Fermi level. This behavior is due to spatially indirect transitions between electrons and holes that are separately confined in a type II lateral multiple quantum wire superlattice. Resonant inelastic light scattering spectra exhibit new peaks due to intersubband excitations of the one-dimensional electron gas. From the optical measurements we obtain the Fermi energy as well as the subband spacings and determine the one-dimensional electron density.

SYMPOSIUM E:
PROPERTIES OF II-VI
SEMICONDUCTORS: BULK CRYSTALS, EPITAXIAL
FILMS, QUANTUM WELL STRUCTURES, AND
DILUTE MAGNETIC SYSTEMS

E

November 27 - December 1, 1989

Chairs

Jan F. Schetzina
Department of Physics - Cox Hall
North Carolina State University
Raleigh, NC 27695-8202
(919) 737-3314

Herb F. Schaake
Texas Instruments
MS 147
P.O. Box 655936
Dallas, TX 75265
(214) 995-5842

Fil J. Bartoli, Jr.
Naval Research Laboratory
4555 Overlook Avenue, Code 6551
Washington, DC 20375
(202) 767-3276

Symposium Support

Air Force Office of Scientific Research

Army Research Office

DARPA

Office of Naval Research

Texas Instruments

Proceedings published as Volume 161
of the Materials Research Society
Symposium proceedings series.

**SESSION E1: BULK CRYSTAL GROWTH
AND PROPERTIES**

Chair: J. F. Schetzina
Monday Morning, November 27
Salon H/I (M)

8:30 *E1.1

GROWTH OF LARGE-DIAMETER CdZnTe AND CdTeSe BOULES FOR $Hg_{1-x}Cd_xTe$ EPITAXY: STATUS AND PROSPECTS, S. Sen, S.M. Johnson, J.A. Kiele, W.H. Konkel and J.E. Stannard, Santa Barbara Research Center, Advanced Development Lab, Goleta, CA.

9:15 *E1.2

BULK CRYSTAL GROWTH OF LATTICE-MATCHED CDZnTE FOR HGZnTE EPITAXY, S. McDevitt, J. Sepich and D. John, II-VI Incorporated, Materials R&D Department, Saxonburg, PA; A. Sher and A. Raizman, Soreq Nuclear Research Center, Solid State Physics Department, Yavne, Israel.

9:45 E1.3

ON THE RELATIONSHIP BETWEEN DISLOCATION DENSITY AND X-RAY FULL WIDTH HALF MAXIMUM IN HORIZONTAL BRIDGMAN GROWN CdTe AND CdZnTe, H.F. Schaaake and H.-Y. Liu, Texas Instruments Inc., Central Research Laboratories, Dallas, TX.

10:00 BREAK

10:30 E1.4

PHOTOLUMINESCENCE DETECTION OF NATIVE DEFECTS IN THE SURFACE REGION OF BULK CdTe, P.M. Amirtharaj and N.K. Dhar, U.S. Army Center for Night Vision and Electro-Optics, Fort Belvoir, VA.

10:45 E1.5

PHOTOLUMINESCENCE STUDIES IN $Zn_xCd_{1-x}Te$ SINGLE CRYSTALS, J. González-Hernández, Brigham Young University, Physics and Astronomy, and Center for X-ray Imaging, Provo, UT and Centro de Investigación y Estudios Avanzados del IPN, México, México; David D. Allred, Brigham Young University, Physics and Astronomy, and Center for X-ray Imaging, Provo, UT; Elías López-Cruz, Universidad Autónoma de Puebla, Depto. de Física, Instituto de Ciencias, Puebla, México; and Worth P. Allred, Galtech Semiconductor Materials Corporation, Mt. Pleasant, UT.

11:00 E1.6

NONDESTRUCTIVE COMPOSITIONAL AND DEFECT CHARACTERIZATION OF ZnCdTe ALLOYS USING PHOTOLUMINESCENCE SPECTROSCOPY, W.M. Duncan, R.J. Koestner, J.H. Tregilgas, H.-Y. Liu and M.-C. Chen, Texas Instruments, Inc., Central Research Laboratories, Dallas, TX.

*Invited Paper

11:15 E1.7

GETTERING EXPERIMENTS ON CdTe, M.H. Jin, K. James and J.L. Merz, University of California, Santa Barbara, Electrical and Computer Engineering Department, Santa Barbara, CA; C. Jones, Santa Barbara Research Center, Goleta, CA.

11:30 E1.8

PHOTOPLASTIC BEHAVIOR OF TYPE II-VI SEMICONDUCTORS, T.J. Garosshen, C.S. Kim and J.M. Galligan, University of Connecticut, Department of Metallurgy and Institute of Materials Science, Storrs, CT.

11:45 E1.9

PREPARATION AND CHARACTERIZATION OF $(ZnTe)_x(CdSe)_{1-x}$ SINGLE CRYSTALS, V.K. Madhusmitha Rani, R.P. Vijaya Lakshmi, D. Raja Reddy and B.K. Reddy, S.V. University College, Department of Physics, Tirupata, India.

**SESSION E2: OPTICAL AND
ELECTRICAL PROPERTIES**

Chair: M. Tamargo
Monday Afternoon, November 27
Salon H/I (M)

1:30 *E2.1

RECENT ADVANCES IN STRAINED WIDE-GAP II-VI SEMICONDUCTOR SUPERLATTICES, A.V. Nurmikko, Brown University, Providence, RI; R.L. Gunshor, M. Kobayashi, Purdue University, Lafayette, IN; and L.A. Kolodziejewski, Massachusetts Institute of Technology, Cambridge, MA.

2:15 E2.2

DEEP LEVEL LUMINESCENCE MEASURING OF MBE CdTe GROWTH QUALITY AND PROCESSING, J.L. Shaw and L.J. Brillson, Xerox Webster Research Center, Electronic Marketing Lab, Webster, NY; S. Sivananthan and J.P. Faurie, University of Illinois at Chicago, Physics Department, Chicago, IL.

2:30 E2.3

STRUCTURAL AND VIBRATIONAL PROPERTIES OF ZnTe EPITAXIAL LAYERS GROWN BY MBE, J. Petruzzello, D. Olego, Philips Laboratories, North American Philips Corporation, Briarcliff Manor, NY; X. Chu and J.P. Faurie, University of Illinois at Chicago, Physics Department, Chicago, IL.

2:45 E2.4

HIGH RESOLUTION AND ANALYTICAL ELECTRON MICROSCOPY OF MULTILAYER HETEROEPITAXIAL SEMICONDUCTORS, H.-J. Kleebe, University of California, Santa Barbara, Materials Department, Engineering III, Santa Barbara, CA; W.J. Hamilton, W.L. Ahlgren and S.M. Johnson, Santa Barbara Research Center, Goleta, CA; and M. Rühle, University of California, Santa Barbara, Materials Department, Engineering III, Santa Barbara, CA.

3:00 BREAK

3:30 *E2.5

SOLUBILITY OF IMPURITIES AND DEFECT IMPURITY INTERACTION IN II-VI SEMICONDUCTORS, Yves Marfaing, CNRS, Laboratoire de Physique des Solides de Bellevue, Meudon, France.

4:15 E2.6

MOCVD GROWTH OF $\text{Cd}_{1-y}\text{Zn}_y\text{Te}$ EPITAXIAL LAYERS USING A VERTICAL FLOW/HIGH-SPEED HORIZONTAL ROTATING DISK REACTOR, W.L. Ahlgren, S.M. Johnson, W.J. Hamilton, A. Szilagyi, Santa Barbara Research Center, Goleta, CA; G.S. Tompa and P.D. Reinert, EMCORE Corporation, Somerset, NJ; C.K. Ziegler and W.J. Lick, University of California, Santa Barbara, Department of Mechanical and Environmental Engineering, Santa Barbara, CA.

4:30 E2.7

THICKNESS MEASUREMENT OF THIN FILMS BY X-RAY ABSORPTION, J. Chaudhuri and S. Shah, The Wichita State University, Mechanical Engineering Department, Wichita, KS.

4:45 E2.8

TILT GROWTH OF CdTe EPILAYERS ON SAPPHIRE SUBSTRATES BY MOCVD, Kenji Maruyama, Hiroji Ebe, Yoshito Nishijima and Koji Shinohara, Fujitsu Laboratories Ltd., Atsugi, Japan.

SESSION E3: DOPING OF II-VI MATERIALS

Chair: H. Schaake

Tuesday Morning, November 28

Salon H/I (M)

8:30 *E3.1

NOVEL APPROACHES TO DOPING OF II-VI COMPOUNDS GROWN BY MBE, Maria C. Tamargo, Bellcore, Red Bank, NJ.

9:15 *E3.2

MOCVD GROWTH AND DOPING OF ZnSe AND RELATED II-VI MATERIALS, H. Kukimoto, Tokyo Institute of Technology, Imaging Science and Engineering Laboratory, Yokohama, Japan.

10:00 BREAK

10:30 *E3.3

GROWTH AND DOPING OF ZINC SELENIDE BY MOLECULAR BEAM EPITAXY, J.M. DePuydt, H. Cheng, M.A. Haase and J.E. Potts, 3M Company, Basic Technologies Laboratory, St. Paul, MN.

11:00 E3.4

DEPOSITION OF ZINC SELENIDE BY ATOMIC LAYER EPITAXY FOR MULTILAYER X-RAY OPTICS, J. Kevin Shurtleff, David Allred, Raymond Perkins and James Thorne, Brigham Young University, Departments of Chemistry and Physics, Provo, UT.

11:15 E3.5

OPTIMIZED MIS CHARACTERISTICS OF AS-GROWN EPITAXIAL ZnSe/EPITAXIAL GaAs HETEROSTRUCTURES, J. Qiu, Q.-D. Qian, M. Kobayashi, R.L. Gunshor, D.R. Menke, D. Li and N. Otsuka, Purdue University, West Lafayette, IN.

11:30 E3.6

PSEUDOMORPHIC ZnTe/AlSb/GaSb: GROWTH AND CHARACTERIZATION, D.L. Mathine, J. Han, M. Kobayashi, R.L. Gunshor, D.R. Menke and M. Vaziri, Purdue University, Electrical Engineering Department, West Lafayette, IN; J. Gonsalves and N. Otsuka, Purdue University, Materials Engineering Department, West Lafayette, IN; Q. Fu, M. Hagerott and A.V. Nurmikko, Brown University, Division of Engineering, Providence, RI.

11:45 E3.7

TRANSMISSION ELECTRON MICROSCOPY OF II-VI/III-V SEMICONDUCTOR INTERFACES, D. Li, N. Otsuka, M. Kobayashi, R.L. Gunshor and L.A. Kolodziejski, Purdue University, Department of Materials Engineering and Science, West Lafayette, IN.

SESSION E4: THIN FILMS AND HETEROSTRUCTURES I

Chair: R. L. Gunshor

Tuesday Afternoon, November 28

Salon H/I (M)

1:30 *E4.1

RECENT ADVANCES IN WIDE-BAND GAP II-VI'S FOR VISIBLE LIGHT EMITTERS, T.C. McGill.

2:15 E4.2

SURFACE MORPHOLOGY AND PHOTOLUMINESCENCE SPECTRA OF ZnSe AFTER EXCIMER LASER ANNEALING, G.-J. Yi and G.F. Neumark, Columbia University, Metallurgy and Materials Science Department, New York, NY; Z. Lu, Columbia University, Electrical Engineering Department, New York, NY; P.R. Newbury, Philips Laboratories, Materials Physics Department, Briarcliff Manor, NY; C.F. Yu, Columbia University, Electrical Engineering Department, New York, NY; B.J. Fitzpatrick, M. Shone and A. Sicignano, Philips Laboratories, Materials Physics Department, Briarcliff Manor, NY.

2:30 E4.3

PLASMA-ASSISTED EPITAXIAL GROWTH OF ZnSe FILMS IN HYDROGEN PLASMA, Satoshi Yamauchi and Takashi Hariu, Tohoku University, Department of Electronic Engineering, Sendai, Japan.

2:45 **E4.4**
EFFECT OF Se PRECURSORS AND PROCESSING CONDITIONS ON OPTOELECTRONIC PROPERTIES OF ZnSe GROWN BY MOVPE, Konstantinos P. Giapis, AT&T Bell Laboratories, Murray Hill, NJ; and Klavs F. Jensen, Massachusetts Institute of Technology, Department of Chemical Engineering, Cambridge, MA.

3:00 **E4.4A**
GROWTH OF $\text{ZnS}_x\text{Se}_{1-x}$ BY MBE USING AN ELECTRO-CHEMICAL SULPHUR SOURCE, J. Wallace, K. Prior, B. Cavenett, J. Hunter, S. Adams and M. Haines, Heriot-Watt University, Department of Physics, Edinburgh, United Kingdom.

3:15 BREAK

3:30 ***E4.5**
ALE/MBE GROWTH AND CHARACTERIZATION OF ZN-CHALCOGENIDE SUPERLATTICE STRUCTURES, T. Yao, M. Fujimoto, H. Izumiya, H. Tanino and Y. Okada, Electrochemical Laboratory, Ibaraki, Japan.

4:15 **E4.6**
SELECTIVE-AREA DEPOSITION OF METALS, PASSIVANTS, INSULATORS, AND EPITAXIAL FILMS OF II-VI COMPOUND SEMICONDUCTORS, D.L. Dreifus, North Carolina State University, Department of Electrical and Computer Engineering, Raleigh, NC; Y. Lansari, J.W. Han, J.W. Cook Jr. and J.F. Schetzina, North Carolina State University, Physics Department, Raleigh, NC.

4:30 **E4.7**
SPATIAL LIGHT MODULATOR USING A CdS THIN FILM PHOTOCAPACITOR, Joseph Reichman, Grumman Corporation, Corporate Research Center, Bethpage, NY.

4:45 **E4.8**
PHOTOLUMINESCENCE PROPERTIES OF GRADED COMPOSITION $\text{Mg}_x\text{Zn}_{1-x}\text{Se}$ CRYSTALS, H.J. Lozykowski, Ohio University, Electrical and Computer Engineering Department, Athens, OH; X.D. Tiang, University of Heilongjian, Harbin, China; and J.L. Merz, University of California, Santa Barbara, Santa Barbara, CA.

**SESSION E5: THIN FILMS
AND HETEROSTRUCTURES II**

Chair: T. C. McGill
Wednesday Morning, November 29
Salon H/I (M)

8:30 ***E5.1**
ATOMIC LAYER EPITAXY OF WIDE BANDGAP II-VI COMPOUND SEMICONDUCTOR SUPERLATTICES, M. Konagai, Y. Takemura, R. Kimura, N. Teraguchi and K. Takahashi, Tokyo Institute of Technology, Department of Electrical and Electronic Engineering, Tokyo, Japan.

9:15 **E5.2**
GROWTH OF LATTICE-MATCHED ZnSe-ZnS STRAINED-LAYER SUPERLATTICES ONTO GaAs AS AN ALTERNATIVE TO ZnS_{1-x}Se_x ALLOYS, H. Oniyama, S. Yamaga and A. Yoshikawa, Chiba University, Department of Electric and Electronics Engineering, Chiba, Japan.

9:30 **E5.3**
STRUCTURAL AND ELECTRICAL CHARACTERIZATION OF CdSe THIN FILMS, Miltiadis K. Hatalis, Fuyu Lin, Lehigh University, Sherman Fairchild Laboratory, Department of Electrical Engineering, Bethlehem, PA; and Michael R. Westcott, Litton Systems Canada Ltd., Display Systems Engineering, Rexdale, Canada.

9:45 **E5.4**
U.S. POLYCRYSTALLINE THIN FILM SOLAR CELL PROGRAM, Harin S. Ullal, Kenneth Zweibel and Richard L. Mitchell, Solar Energy Research Institute, Golden, CO.

10:00 **E5.5**
A STRUCTURAL STUDY OF EPITAXIAL LAYERS OF CdSe AND CdS GROWN ON GaAs, A.G. Cullis, P.J. Parbrook, P.W. Smith, B. Cockayne, P.J. Wright and G.M. Williams, Royal Signals and Radar Establishment, Worcs, United Kingdom.

10:15 BREAK

10:30 ***E5.6**
EXCITONIC PROPERTIES IN ZnSe-ZnS STRAINED-LAYER SUPERLATTICES AND A FIBONACCI SEQUENCE, Tsunemasa Taguchi and Yoichi Yamada, Osaka University, Faculty of Engineering, Department of Electrical Engineering, Osaka, Japan.

11:15 **E5.7**
OPTICAL PROPERTIES OF CdZnS-ZnS STRAINED LAYER SUPERLATTICES, Yasuyuki Endoh and Tsunemasa Taguchi, Osaka University, Faculty of Engineering, Department of Electrical Engineering, Osaka, Japan.

11:30 **E5.8**
PRECISE MEASUREMENTS OF MINORITY CARRIER LIFETIMES IN II-VI FILMS AND SUPERLATTICES, W.O. Doggett, Michael W. Thelander and J.F. Schetzina, North Carolina State University, Physics Department, Raleigh, NC.

11:45 **E5.9**
NONLINEARITY OF BOUND EXCITON STIMULATED EMISSION INDUCED BY NONEQUILIBRIUM ACOUSTIC PHONONS, N.N. Zinov'ev, D.I. Kovalev and I.D. Yaroshetskii, Academy of Sciences of the USSR, A.F. Ioffe Physico-Technical Institute, Leningrad, USSR.

SESSION E6: NOVEL GROWTH
AND CHARACTERIZATIONS

Chair: F. Bartoli Jr.
Wednesday Afternoon, November 29
Salon H/I (M)

1:30 *E6.1
PHOTOASSISTED MBE OF II-VI SEMICONDUCTOR FILMS AND SUPERLATTICES, N.C. Giles, R. L. Harper, J.W. Han and J.F. Schetzina, North Carolina State University, Physics Department, Raleigh, NC.

2:15 E6.2
GROWTH AND INITIAL CHARACTERIZATION OF NOVEL HGTE-BASED II-VI MATERIALS, F.G. Moore, Naval Research Laboratory, Washington, DC; J.C. Abele, Lewis and Clark College, Portland, OR; and P.E. Kremer, Crystal Specialties Intl., Colorado Springs, CO.

2:30 E6.3
USE OF ATOM PROBE TECHNIQUES IN THE STUDY OF II-VI SEMICONDUCTORS, Ross A.D. Mackenzie, Chris R.M. Grovenor and J. Alex Liddle, Oxford University, Department of Metallurgy and Science of Materials, Oxford, United Kingdom.

3:00 BREAK

3:15 *E6.4
MBE GROWTH OF HgCdTe FOR INFRARED DETECTOR APPLICATIONS, J.M. Arias, S.H. Shin, J.G. Pasko, M. Zandian, and R.E. DeWames, Rockwell International Science Center, Thousand Oaks, CA.

4:00 E6.5
ELECTRICAL PROPERTIES OF MBE-GROWN HgCdTe, S. Hwang, Jeong W. Han, J.W. Cook Jr. and J.F. Schetzina, North Carolina State University, Department of Physics, Raleigh, NC.

4:15 E6.6
FIRST AND SECOND ORDER RAMAN STUDIES OF COMPOSITION AND STRUCTURAL ORDERING IN $Hg_{1-x}Cd_xTe$, A. Compaan, University of Toledo, Physics and Astronomy Department, Toledo, OH; Robert C. Bowman Jr., The Aerospace Corporation, Chemistry and Physics Lab, Los Angeles, CA.

4:30 E6.7
TEMPERATURE-DEPENDENT INFRARED ABSORPTION OF HG-BASED II-VI SEMICONDUCTOR SUPERLATTICES, Z. Yang, Y. Lansari, J.W. Han and J.F. Schetzina, North Carolina State University, Physics Department, Raleigh, NC.

4:45 E6.8
PROPERTIES OF MODULATION DOPED HgCdTe, Jeong W. Han, S. Hwang, Y. Lansari, J.W. Cook Jr. and J.F. Schetzina, North Carolina State University, Physics Department, Raleigh, NC.

SESSION E7: HgCdTe: SURFACES,
PASSIVANTS, AND PROCESSING

Chair: S. Hwang
Thursday Morning, November 30
Salon H/I (M)

8:30 *E7.1
SHOCKLEY-READ RECOMBINATION IN P-TYPE HgCdTe, Y. Nemirovsky and R. Fastow, Technion-Israel Institute of Technology, Department of Electrical Engineering, Haifa, Israel.

9:15 E7.2
THE EFFECT OF SURFACE LAYERS IN EPITAXIAL n-TYPE HgCdTe, K.K. Parat, N.R. Taskar, I.B. Bhat and S.K. Ghandhi, Rensselaer Polytechnic Institute, Troy, NY.

9:30 E7.3
SURFACE ELECTRONS IN INVERTED LAYERS OF P-HGCDTE, S.E. Schacham and E. Finkman, Technion-Israel Institute of Technology, Department of Electrical Engineering, Haifa, Israel.

9:45 E7.4
ELECTRICAL CHARACTERIZATION OF P-TYPE $Cd_xHg_{1-x}Te$ GROWN BY MOVPE (IMP), A. Royle, J.S. Gough, S.J.C. Irvine and J.B. Mullin, Royal Signals and Radar Establishment, Worcestershire, United Kingdom.

10:00 E7.4A
MBE GROWTH: SURFACE ROUGHNESS THEORY, A. Sher, Srinivasan Krishnamurthy, Martha A. Berding, SRI International, Menlo Park, CA; A.-B. Chen, Auburn University, Auburn, AL; and Archibald Fripp, National Aeronautics and Space Administration, Langley Research Center, Hampton, VA.

10:30 E7.5
LANGMUIR-BLODGETT FILM PASSIVATION ON CATHODICALLY CLEANED MCT AND PC-TYPE DEVICES, Kengo Shimano, Tetsuya Suzuki, Taizo Hoshino and Masao Sakashita, Nippon Steel Corporation, R&D Labs.-I, Kawasaki, Japan.

10:45 E7.6
ENHANCED METALLIZATION STABILITY ON MERCURY-CADMIUM-TELLURIDE, A. Raisanen, G. Haugstad, X. Yu and A. Franciosi, University of Minnesota, Department of Chemical Engineering and Materials Science, Minneapolis, MN; D.J. Peterman, McDonnell Douglas Research Labs, St. Louis, MO.

11:00 E7.7
GROWTH OF HIGH QUALITY LWIR FILMS BY LIQUID PHASE EPITAXY, Dipankar Chandra, Texas Instruments, Dallas, TX.

11:15 **E7.8**
CHARACTERIZATION OF (Hg,Cd) Te FOR INFRARED FOCAL PLANE ARRAY APPLICATIONS, A.J. Syllaios, V.C. Lopes and W.H. Wright, Texas Instruments, Inc., Dallas, TX.

11:30 **E7.9**
EFFECTS ON DEFECTS ON METAL-INSULATOR-SEMI-CONDUCTOR PROPERTIES OF HgCdTe FILMS GROWN BY LIQUID PHASE EPITAXY, Dipankar Chandra and Michael W. Goodwin, Texas Instruments, Inc., Dallas, TX.

11:45 **E7.10**
LOW-TEMPERATURE PROCESSING TECHNOLOGY FOR II-VI SEMICONDUCTORS, D.L. Dreifus and R.M. Kolbas, North Carolina State University, Department of Electrical and Computer Engineering, Raleigh, NC; B.P. Sneed and J.F. Schetzina, North Carolina State University, Department of Physics, Raleigh, NC.

SESSION E8: HgCdTe: EITAXIAL GROWTH

Chair: J. Arias

Thursday Afternoon, November 30
Salon H/I (M)

1:30 ***E8.1**
RECENT PROGRESS IN THE OMVPE GROWTH OF HgCdTe, S.K. Ghandhi, Rensselaer Polytechnic Institute, Troy, NY.

2:15 **E8.2**
VAPOUR PRESSURE MEASUREMENTS ON ORGANOTELLURIUM PRECURSORS FOR MOVPE, J.E. Hails, S.J.C. Irvine and J.B. Mullin, Royal Signals and Radar Establishment, Worchestershire, United Kingdom.

2:30 **E8.3**
INFLUENCE OF SUBSTRATE QUALITY IN THE METAL ORGANIC CHEMICAL VAPOUR DEPOSITION OF HgCdTe, M.J. Bevan and N.J. Doyle, Westinghouse Science and Technology Center, Pittsburgh, PA.

2:45 **E8.4**
TEM CHARACTERIZATION OF DEFECTS IN HgCdTe GROWN ON (001) CdTe AND (111)B CdZnTe SUBSTRATES BY MOCVD, Anthony Hobbs, O. Ueda, K. Maruyama, S. Murakami and K. Shinohara, Fujitsu Laboratories Ltd., Atsugi, Japan.

3:00 BREAK

3:30 **E8.5**
STRUCTURAL AND ELECTRICAL PROPERTIES OF HETEROEPITAXIAL HgCdTe/CdZnTe/GaAs/Si, S.M. Johnson, W.L. Ahlgren, M.H. Kalisher, W.J. Hamilton Jr. and J.B. James, Santa Barbara Research Center, Goleta, CA.

3:45 **E8.6**
PROPERTIES OF HgTe-ZnTe STRAINED LAYER SUPERLATTICES GROWN BY MOVPE, J.T. Mullins, P.A. Clifton, P.D. Brown, K. Durose and A.W. Brinkman, University of Durham, Applied Physics Group, S.E.A.S., Durham, United Kingdom.

4:00 **E8.7**
MBE GROWTH AND CHARACTERIZATION OF SMALL BAND GAP HgTe-HgCdTe SUPERLATTICES, Y. Lansari, Z. Yang, S. Hwang, J.W. Cook Jr. and J.F. Schetzina, North Carolina State University, Physics Department, Raleigh, NC.

4:15 **E8.8**
PHASE DIAGRAM LATTICE PARAMETER AND OPTICAL OPTICAL ENERGY GAP VALUES FOR THE $Hg_{2x}(CuIn)_yMn_{2z}Te_2$ ($x+y+z=1$) ALLOYS, Pedro Grima Gallardo, Universidad de Los Andes, Centro de Estudios en Semiconductores, Fac. Ciencias. Dpto. Física., Laboratorio de Cristales, Mérida, Venezuela.

4:30 **E8.9**
ON THE FIELD EMISSION FROM HgTe-CdTe SUPERLATTICES WITH GRADED STRUCTURES UNDER MAGNETIC QUANTIZATION, Kamakhya P. Ghatak, University of Jadavpur, Department of Electronics Engineering, Calcutta, India; Sambhu N. Biswas, Bengal Engineering College, Department of Electronics and Telecommunication Engineering, West Bengal, India.

4:45 **E8.10**
INVESTIGATION OF LIQUID ENCAPSULANT FOR CdTe AND $Cd_xHg_{1-x}Te$ MELT, Wang Caihao and Wu Wenhai, Shanghai University of Science and Technology, Department of Materials Science, Shanghai, China.

5:00 **E8.11**
MBE GROWTH AND CHARACTERIZATION OF HIGH QUALITY EPITAXIAL $Hg_{1-x}Cd_xTe$ THIN FILMS, M.B. Lee, J. De Carlo, D. Di Marzio and M. Kesselman, Grumman Corporate Research Center, Bethpage, NY.

SESSION E9: Hg-BASED SUPERLATTICES: DMS MATERIALS

Chair: Y. Lansari

Friday Morning, December 1
Salon H/I (M)

8:30 ***E9.1**
FREE-CARRIER INDUCED OPTICAL NONLINEARITIES IN NARROW BANDGAP SEMICONDUCTORS, S.Y. Auyang, Massachusetts Institute of Technology, Cambridge, MA; and P.A. Wolff, NEC Research Institute, Princeton, NJ.

9:00 **E9.2**

NARROW-GAP NONLINEAR OPTICAL MATERIALS, E.R. Youngdale, C.A. Hoffman, J.R. Meyer, F.J. Bartoli, Naval Research Laboratory, Washington, DC; J.W. Han, J.W. Cook Jr., and J.F. Schetzina, North Carolina State University, Raleigh, NC; and A. Martinez, Naval Surface Weapons Center, Silver Spring, MD.

9:15 ***E9.3**

TRANSPORT PROPERTIES OF Hg-BASED SUPERLATTICES, C.A. Hoffman, J.R. Meyer and F.J. Bartoli, Naval Research Laboratory, Washington, DC.

9:45 **E9.4**

HgTe-CdTe MULTIPLE QUANTUM WELLS, C.A. Hoffman, D.J. Arnold, J.R. Meyer, F.J. Bartoli, Naval Research Laboratory, Washington, DC; Y. Lansari, J.W. Cook, Jr., and J.F. Schetzina, North Carolina State University, Raleigh, NC.

10:00 **E9.5**

ELECTRIC FIELD EFFECTS IN Hg-BASED AND NON-Hg-BASED II-VI SEMICONDUCTOR QUANTUM WELLS, Z. Yang, J.F. Schetzina, North Carolina State University, Physics Department, Raleigh, NC.

10:15 BREAK

10:30 ***E9.6**

NEW DEVELOPMENTS IN II-VI-BASED DILUTED MAGNETIC SEMICONDUCTORS, J.K. Furdyna and N. Samarth, University of Notre Dame, Physics Department, Notre Dame, IL.

11:00 **E9.7**

MAGNETIC PROPERTIES OF NOVEL III-V DILUTED MAGNETIC SEMICONDUCTORS, S. von Molnar, H. Munekata, H. Ohno and L.L. Chang, IBM T.J. Watson Research Center, Yorktown Heights, NY.

11:15 **E9.8**

TEM STUDY OF DEFECTS IN CdTe/CdMnTe SUPERLATTICES ON (100) InSb, S. Diamond and J.W. Steeds, University of Bristol, Physics Department, Bristol, United Kingdom.

11:30 **E9.9**

IN AND Ga AUTODOPING OF CdMnTe EPILAYERS GROWN ON InSb AND GaAs SUBSTRATES, J.J. Dubowski, J.M. Wrobel, S. Rolfe, National Research Council of Canada, Division of Physics, Laboratory for Microstructural Sciences, Ottawa, Canada; J.A. Jackman, CANMET, Metals Technology Laboratories, Ottawa, Canada; and J.H. Mazur, University of Southern California, Materials Science and Engineering Department, Los Angeles, CA.

11:45 **E9.10**

PHOTOLUMINESCENCE STUDIES OF DILUTED MAGNETIC SEMICONDUCTORS UNDER HYDROSTATIC PRESSURE: $\text{Cd}_{1-x}\text{Mn}_x\text{Te}$, M. Prakash, M. Chandrasekhar and H.R. Chandrasekhar, University of Missouri, Columbia, MO; I. Miotkowski and A.K. Ramdas, Purdue University, West Lafayette, IN.

SESSION E10: DMS MATERIALS

Chair: S. von Molnar

Friday Afternoon, December 1

Salon H/I (M)

1:30 **E10.1**

OBSERVATION OF Mn^{2+} TRIPLET CLUSTERS AND NON-NEAREST NEIGHBOR EXCHANGE EFFECT IN $(\text{Cd}, \text{Mn})\text{Te}$, Xiaomei Wang, D. Heiman, S. Foner and P. Becla, Massachusetts Institute of Technology, Francis Bitter National Magnet Laboratory, Cambridge, MA.

1:45 **E10.2**

THE EFFECT OF DZYALOSHINSKI-MORIYA INTERACTION ON THE MAGNETIZATION OF DILUTE MAGNETIC SEMICONDUCTORS, C.R. McIntyre, Massachusetts Institute of Technology, Physics Department, Cambridge, MA; P.A. Wolff, NEC Research Institute, Princeton, NJ; and Y. Shapira, Tufts University, Physics Department, Medford, MA.

2:00 **E10.3**

IN-SITU STUDIES OF SEMIMAGNETIC HETEROJUNCTION PARAMETERS, Xiaohua Yu, A. Raisanen, G. Haugstad, N. Troullier and A. Franciosi, University of Minnesota, Department of Chemical Engineering and Materials Science, Minneapolis, MN.

2:15 **E10.4**

NOVEL PROPERTIES OF MAGNETIC SEMICONDUCTORS GROWN BY MONOLAYER DEPOSITION USING LASER-TARGET ABLATION, X.-L. Zheng, C.A. Huber and D. Heiman, Massachusetts Institute of Technology, Francis Bitter National Magnet Laboratory, Cambridge, MA.

2:30 **E10.5**

PHOTOLUMINESCENCE OF ZnSe FILMS AND ZnSe/ZnMnSe STRAINED LAYER SUPERLATTICES UNDER HYDROSTATIC PRESSURE, Judah A. Tuchman, Zhifeng Sui, Irving P. Herman, Columbia University, Department of Applied Physics, New York, NY; R.L. Gunshor, Purdue University, School of Electrical Engineering, West Lafayette, IN; L.A. Kolodziejski, Massachusetts Institute of Technology, Department of Electrical Engineering, Cambridge, MA.

2:45 **E10.6**

MAGNETO-OPTICAL STUDIES OF ZnFeSe/ZnSe/ZnFeSe QUANTUM WELL STRUCTURES, X. Liu and A. Petrou, SUNY at Buffalo, Department of Physics and Astronomy, Buffalo, NY; B.T. Jonker, G.A. Prinz and J.J. Krebs, Naval Research Laboratory, Washington, DC; and J. Warnock, IBM T.J. Watson Research Center, Yorktown Heights, NY.

3:00 BREAK

3:30 **E10.7**

TRANSITION METAL DONOR LEVELS IN II-VI SEMICONDUCTORS, D. Heiman, M. Dahl, J. Perkins, X. Wang, X.-L. Zheng, P. Becla, Massachusetts Institute of Technology, Francis Bitter National Magnet Laboratory, Cambridge, MA; K. Smith, J. Marsella, K. Dwight, A. Wold, Brown University, Chemistry Department, Providence, RI; and A. Mycielski, Academy of Science, Institute of Physics, Warsaw, Poland.

3:45 **E10.8**

MAGNETIC STUDY OF Fe-BASED II-VI DILUTED MAGNETIC SEMICONDUCTORS, H.J.M. Swagten, Eindhoven University of Technology, Department of Physics, Eindhoven, The Netherlands; A. Twardowski, Warsaw University, Institute of Experimental Physics, Warsaw, Poland; C.E.P. Gerrits and W.J.M. de Jonge, Eindhoven University of Technology, Department of Physics, Eindhoven, The Netherlands.

4:00 **E10.9**

ENERGY LEVEL SPECTRA OF TRANSITION METAL IONS IN DILUTED MAGNETIC SEMICONDUCTORS, Murielle Villeret, S. Rodriguez, Purdue University, Department of Physics, West Lafayette, IN; and E. Kartheuser, Université de Liège, Liège, Belgium.

4:15 **E10.10**

RAMAN SPECTROSCOPY OF A NOVEL DILUTED MAGNETIC SEMICONDUCTOR: CUBIC $\text{Cd}_{1-x}\text{Mn}_x\text{Se}$, R.G. Alonso, E.-K. Suh, Purdue University, Department of Physics, West Lafayette, IN; H. Pascher, University of Bayreuth, Bayreuth, West Germany; E. Oh, A.K. Ramdas, Purdue University, Department of Physics, West Lafayette, IN; N. Samarth, H. Luo and J.K. Furdyna, University of Notre Dame, Notre Dame, IN.

4:30 **E10.11**

THE INFLUENCE OF Fe DONORS IN HgSe ON FREE-CARRIER SCATTERING MECHANISM, Qian Dingrong, Zhang Jiamin, Zhou Qun, Liu Kun, Shanghai Institute of Technical Physics, Academia Sinica, Lab for Infrared Physics, Shanghai, China; W. Szuszkiewicz, Warsaw University, Institute of Experimental Physics, Warsaw, Poland; and A. Mycielski, Science Academia of Poland, Institute of Physics, Warsaw, Poland.

4:45 **E10.12**

FREE EXCITON MAGNETOSPECTROSCOPY OF CdFeSe DILUTED MAGNETIC SEMICONDUCTOR, A. Twardowski, K. Pakula, Warsaw University, Institute of Experimental Physics, Warsaw, Poland; M. Arciszewska and A. Mycielski, Polish Academy of Sciences, Institute of Physics, Warsaw, Poland.

E1.1

GROWTH OF LARGE-DIAMETER CdZnTe AND CdTeSe BOULES FOR Hg_{1-x}Cd_xTe EPITAXY: STATUS AND PROSPECTS. S. Sen, S.M. Johnson, J.A. Kiele, W.H. Konkel and J.E. Stannard, Santa Barbara Research Center, 75 Coromar Dr., B2/8, Goleta, CA 93117

Single crystals of CdTe or dilute alloys of Cd_{1-y}Zn_yTe ($y \leq 0.04$) and CdTe_{1-z}Se_z ($z \leq 0.04$) with low defect density and large single-crystal area ($>30 \text{ cm}^2$) are required as substrates for high-quality epitaxial Hg_{1-x}Cd_xTe thin films in the infrared (IR) detector industry. Bridgman or gradient freeze has been the most common current technique used for growing these materials. This paper reviews the current status and the evolution at SBRC of one variation of the Bridgman technique, viz., vertical modified Bridgman (VMB), for producing large-area substrates with excellent uniformity and reproducibility. CdTe, Cd_{1-y}Zn_yTe ($y \leq 0.04$) and CdTe_{1-z}Se_z ($z \leq 0.04$) boules of 5-7.5 cm diameter have been grown unseeded in the present version of the VMB growth system. In general, under optimum growth conditions, the boules have the smallest grain structure (several grains) at the tip end with enhancement of grain selection as the cylindrical body of the boule is approached, resulting in one predominant and large grain occupying 70-80 percent of the entire boule volume; {111}-oriented Cd_{1-y}Zn_yTe and CdTe_{1-z}Se_z substrates with single-crystal areas as large as 50-60 cm² have been obtained from these boules. Crystal quality characterized by x-ray rocking curve, IR transmission (2.5-20 μm), low-temperature photoluminescence, and Hall-effect measurements as a function of temperature, showed a strong correlation with the starting material quality (especially that of elemental Te and Se). Analyses of the thermal history during growth reveals that the presence of the ampoule (with charge) increases the temperature inside the furnace by 10 to 15 degrees. The temperature gradient at the tip was measured to be 8-10° C/cm and it dropped to 4-5° C/cm beyond 2.5 cm from the tip -- where rapid enhancement of grain selection takes place in most boules. This agrees with the prediction from the numerical thermal model that was developed for the growth process with radiative and conductive heat transfer included and using a temperature profile similar to that existing in the actual growth furnace. Conditions for maximizing the fraction solidifying with a slightly convex interface, hence maximizing the single crystal yield, will be presented.

E1.2

BULK CRYSTAL GROWTH OF LATTICE-MATCHED CDZNTe FOR HgZnTe EPITAXY. S. McDevitt, J. Sepich, D. John, II-VI Incorporated, Saxonburg, PA; and A. Sher, A. Raizman, Solid State Physics Department, Soreq Nuclear Research Center, Yavne, Israel.

Lattice-matched Cd_{1-x}Zn_xTe substrates have been shown to improve morphology of HgCdTe and HgZnTe epilayers. Currently, Cd_{0.96}Zn_{0.04}Te, chosen for its lattice match to Hg_{0.8}Cd_{0.2}Te, is widely available as a substrate material and has been statistically proven to have lower dislocation densities and x-ray rocking curves as compared to CdTe.

Hg_{1-x}Zn_xTe epilayers, $0.16 \leq x \leq 0.19$, can be lattice matched to Cd_{1-x}Zn_xTe substrates, $0.20 \leq x \leq 0.24$. Bulk crystal growth of Cd_{0.8}Zn_{0.2}Te is more difficult than Cd_{0.96}Zn_{0.04}Te because of its increased tendency to crack during cooldown. In addition, the segregation coefficient of Zn in CdTe limits the lattice matched portion to approximately 45% of the total ingot.

Cd_{0.8}Zn_{0.2}Te has been successfully grown, characterized and fabricated into substrates specially chosen for their lattice match to Hg_{1-x}Zn_xTe, $0.16 \leq x \leq 0.19$. The relatively large number of substrates with the same composition and same quality have provided the opportunity to test processes of epitaxial growth and annealing of HgZnTe. Hg annealed epilayers grown on (111)B Cd_{1-x}Zn_xTe, $0.24 \leq x \leq 0.20$, have shown p-type conductivity with carrier concentration, carrier mobility and minority carrier lifetime comparable with the best results quoted for HgCdTe epilayers.

E1.3

ON THE RELATIONSHIP BETWEEN DISLOCATION DENSITY AND X-RAY FULL WIDTH HALF MAXIMUM IN HORIZONTAL BRIDGMAN GROWN CdTe and CdZnTe. H.F. Schaake and H.-Y. Liu, Texas Instruments Inc., Dallas, Texas 75265

The full width half maximum (FWHM) of the x-ray double crystal rocking curve is a frequently used measure of crystal quality. We have measured the relationship between the dislocation density as determined by defect etching using the Nakagawa etch and the FWHM measured at the same spot on horizontal Bridgman grown CdTe and CdZnTe. We find that there is no simple relationship between the two measurements. For example, one sample with a FWHM of 10 arc-seconds had a dislocation density $6 \times 10^5 \text{ cm}^{-2}$ while another with the same FWHM had less than 10^5 cm^{-2} . However, a large number of data points were scattered about the straight line, $\rho_d = 3 \times 10^5 \text{ FWHM}$.

The lack of a simple relationship results from a failure to consider the Burgers vectors of the dislocations. The observed distribution of dislocations can be considered to be the sum of a group of dislocations whose average Burgers vector is zero (i.e., randomly distributed) and one in which all of the Burgers vectors are the same. The first distribution will give rise to a broadening proportional to the square root of the dislocation density while the second will give rise to a broadening proportional to the density. Comparison with theoretical models shows that the second type of distribution generally, but not always, dominates in the samples we have measured.

The two distributions can be separated by making measurements of the FWHM as a function of the x-ray beam width. We will report on these measurements.

E1.4

PHOTOLUMINESCENCE DETECTION OF NATIVE DEFECTS IN THE SURFACE REGION OF BULK CdTe. P.M. Amirtharaj and N.K. Dhar, U.S. Army Center for Night Vision and Electro-Optics, Fort Belvoir, VA.

High resolution, low temperature photoluminescence (8-40K) measurements were performed on a series of bulk CdTe samples that were doped with In to a density of $1 \times 10^{15} \text{ cm}^{-3}$; the initial reference surface was obtained by cleaving the crystal in an inert atmosphere of N₂ or Ar and subsequent changes resulting from chemical etches (Br/MeOH, KOH/MeOH, Na₂S₂O₄/NaOH/H₂O, K₂Cr₂O₇/HNO₃/H₂O) and aging extending over several weeks were investigated. The major difference between the as-cleaved and the other sample spectra is the presence of a distinct peak at 1.5896 eV. Previous investigations involving annealing procedures have assigned this feature to originate in Cd vacancies. On this basis, it is strongly suspected that etching and aging lead to a loss of Cd from the surface region. The preferential loss of Cd in the near surface region ($\leq 50\text{\AA}$) due to Br/MeOH is a well known phenomena. However, the current investigation suggests that the effect may extend much deeper and is not particular to Br/MeOH treatment. Implications of this result in the formation of electrical contacts, device properties and the long term stability of CdTe will be discussed.

E1.5

PHOTOLUMINESCENCE STUDIES IN Zn_xCd_{1-x}Te SINGLE CRYSTALS. J. González-Hernández, David D. Allred, Physics and Astronomy, and Center for X-ray Imaging, Brigham Young University, Provo, UT, 84602; Elías López-Cruz, Depto. de Física, Instituto de Ciencias, Universidad Autónoma de Puebla, Puebla, México and

Worth P. Allred*, Galtech Semiconductor Materials Corp., Mt. Pleasant, UT, 84647.

The crystalline quality of $Zn_xCd_{1-x}Te$ single crystals grown by a modified Bridgman technique with x in the range of $0 \leq x \leq 0.10$ was analyzed using photoluminescence (PL), electrical and optical transmission measurements. A typical PL spectrum shows two groups of emission line: the narrow lines peaking at higher energies attributed to exciton recombination and the broader bands at lower energies which have been previously ascribed to band-to-acceptor radiative transitions. Emission below the band-to-acceptor transitions, generally associated with structural defects in CdTe, were not observed in our materials. The analysis of the emission intensity as a function of both the excitation intensity and the sample temperature was used to identify the origin of the various lines in the spectra. In the exciton emission region, one sees sharp lines due to free and bound exciton transitions. Furthermore, emission involving excited states of the free exciton are observed in our $Zn_xCd_{1-x}Te$ with x up to 0.05. To our knowledge, this is the first time that those transitions are observed in this ternary compound, regardless of the preparation method. The latter is a good indication of the high crystalline perfection of these materials. Similar to the PL, optical transmission and electrical measurements also indicate a high crystalline quality of the $Zn_xCd_{1-x}Te$. Effects of implantation doping will also be discussed.

†Also Centro de Investigación y Estudios Avanzados del IPN, 07900 México, D.F.

E1.6

NONDESTRUCTIVE COMPOSITIONAL AND DEFECT CHARACTERIZATION OF $ZnCdTe$ ALLOYS USING PHOTOLUMINESCENCE SPECTROSCOPY. W.M. Duncan, R.J. Koestner, J.H. Tregilgas, H.-Y. Liu and M.-C. Chen. Central Research Laboratories, Texas Instruments, Inc., Dallas, TX 75265

Alloys of $ZnCdTe$ are important substrate materials for growth of epitaxial thin films of $HgCdTe$ for infrared detector applications. In order to attain close lattice match between $ZnCdTe$ and nominally 10 μm $HgCdTe$, alloys containing a few percent of Zn are needed. In this work, photoluminescence (PL) spectroscopy has been developed as a nondestructive contactless method for precise determination (± 0.002 in X) of $ZnTe$ mole fraction.

Although photoluminescence has been used widely for qualitative evaluation of II-VI binary and ternary materials, the methodology developed in this work allows quantitative composition measurements to be performed at room temperature. Because of the high spatial resolution obtainable with the method, microscopic as well as macroscopic inhomogeneities can be readily examined. For example, microscopic PL behavior with micron scale spatial resolution has been studied for material with and without Te precipitation. Also, determination of an effective Zn segregation coefficient for crystals grown by the horizontal Bridgman method has been possible.

In order to determine the accuracy of these measurements, we have correlated photoluminescence results to precision lattice constant X-ray measurements and to theoretical bandgap versus composition behavior. In addition room temperature results have been correlated to high resolution helium temperature PL measurements and to transport measurements. From these latter comparisons, it is found that room temperature PL lineshapes and intensities provide in addition qualitative insight into impurity and defect properties of these substrates. A correlation is also found between Te precipitate density and the 1.09 eV defect band intensity at helium temperature.

E1.7

GETTERING EXPERIMENTS ON CdTe M.H. Jin, K. James, and J.L. Merz, Electrical & Computer Engineering Department, University Of California, Santa Barbara, CA 93106

We report the first observation of ion-implantation damage gettering of impurities in CdTe to provide better substrates for epitaxial growth or for other applications. In this report we describe the results of photoluminescence (PL) experiments that were performed on samples of

Bridgman-grown CdTe to study the annealing behavior and gettering effects of the material. Cathodoluminescence (CL) experiments were also performed, and the results were consistent with those obtained by PL.

CdTe is an extremely useful material for optical devices which require a direct bandgap in the near infrared. Bulk CdTe is of interest as a substrate for the epitaxial growth of $HgCdTe$ and for formation of superlattices in combination with other II-VI compounds. However, in order to properly control the liquid-phase epitaxial (LPE) growth of $HgCdTe$ on CdTe, a knowledge of the annealing behavior of the CdTe substrate is essential. It is also necessary to identify and eliminate unwanted impurities if the CdTe is to become technologically important for this purpose.

From PL and CL experiments the annealing behavior of bulk CdTe material was studied. It was found that impurity gettering can occur at the temperature at which liquid phase epitaxy takes place (500°C). It was also found that the optimum anneal time is four hours at this temperature. This gettering of impurities should provide improved substrates for epitaxial growth.

E1.8

PHOTOPLASTIC BEHAVIOR OF TYPE II-VI SEMICONDUCTORS. T.J. Garosshen, C.S. Kim and J.M. Galligan, Department of Metallurgy and Institute of Materials Science, University of Connecticut, Storrs, CT 06269-3136.

An interesting phenomenon related to charged dislocations in type II-VI semiconductors is the increase in flow stress which occurs when a crystal, which is plastically deforming, is irradiated with light. This effect is quite large; for example, CdS exhibits as much as a 100% increase in flow stress when irradiated with white light with an intensity of 0.02 watts/cm².

The results of experiments on the effects of temperature, slip systems, and defect concentration on the extent of the photoplastic effect and related kinetic behavior, will be presented for CdS. Measurements of the current associated with dislocation motion will also be presented, along with a discussion of the pertinent mechanism(s).

In addition, methods of exploiting photoplastic behavior to improve device performance will be presented.

E1.9

PREPARATION AND CHARACTERISATION OF $(ZnTe)_x(CdSe)_{1-x}$ SINGLE CRYSTALS. V.K.MADHUSMITHA RANI, R.P. VIJAYA LAKSHMI, D.RAJA REDDY AND B.K.REDDY. DEPARTMENT OF PHYSICS, S.V.UNIVERSITY COLLEGE, TIRUPATI -517 502 INDIA.

The title material is one of the least studied among II - VI alloy systems. Due to auto compensation, so far it has not been possible to prepare $ZnTe$ in n-type and $CdSe$ in p-type. More over $ZnTe$ crystallizes in Zinc blend where as $CdSe$ crystallizes in wurtzite structure. Because of the varied nature of the end compounds, an attempt has been made to prepare single crystals of $(ZnTe)_x(CdSe)_{1-x}$ system in the entire range of 'x'. The alloy material in entire range of composition in the single crystal form was grown by a modified Piper-Polich method. The grown crystals of this alloy system have been subjected to chemical analysis. DTA and DTG studies carried out on these alloys did not shows any phase transitions. However, two Exothermic peaks associated with increase in mass were noticed. This has been attributed to oxidation effects of Se/Te or Cd/Zn. XRD data though showed some regularity near the end compositions

there is still some ambiguity for the middle compositions. Energy gap obtained from reflection spectra and also photocurrent spectral response showed bowing. However, there is a marked different feature at one the end regions. The growth and the results of all the above mentioned investigations are presented and discussed in this paper.

E2.1

RECENT ADVANCES IN STRAINED WIDE-GAP II-VI SEMICONDUCTOR SUPERLATTICES. A.V. Nurmikko, Brown University, Providence RI, R.L. Gunshor and M. Kobayashi, Purdue University, Lafayette IN, L.A. Kolodziejski, M.I.T., Cambridge, MA.

We review recent work in wide-gap II-VI heterostructures with focus on ZnSe/ZnTe, ZnTe/MnTe, and CdTe/MnTe superlattices and quantum wells. The ZnSe/ZnTe system has been studied in the limit of ultrathin layers of one or two monolayers of ZnTe imbedded into ZnSe films or quantum wells; the electronic properties of such structures reflect the 'isoelectronic delta-doping' by nearly 2-dimensional arrays of Te strong exciton self-trapping and high radiative efficiencies. A good microscopic understanding of such centers has been obtained through steady-state and transient spectroscopies.

ZnTe/MnTe and CdTe/MnTe heterostructures have been prepared as single quantum wells (SQW) with relatively thin (<40Å) MnTe barrier layers. While bulk MnTe crystallizes in the hexagonal layered (NiAs) form, its pseudomorphic growth in the zincblende form has been realized in these structures. As one consequence, the optical gap of MnTe increases from approximately 1.3 eV to 3.2 eV. The SQW's exhibit strong electronic confinement; CdTe/MnTe, for example, shows optical emission up to about 2.0 eV while bulk CdTe bandgap is at 1.6 eV. Photoluminescence and resonant Raman techniques have been used to elucidate the electronic and optical phonon states. Strong exciton-phonon coupling is in evidence. Magneto-optical methods have yielded partial insight to the question of interface coherence and magnetic ordering in these highly strained heterostructures.

Research supported by DARPA, ONR, and NSF

E2.2

DEEP LEVEL LUMINESCENCE MEASUREMENTS OF MBE CdTe GROWTH QUALITY AND PROCESSING. J. L. Shaw and L. J. Brillson, Xerox Webster Research Center, Webster, NY 14580; and S. Sivanathan and J. P. Faurie, University of Illinois at Chicago, Chicago, IL 60680

We have used luminescence spectroscopies to characterize the deep levels within MBE-grown CdTe epilayers as a function of growth and subsequent processing conditions. Clear differences in deep level emission energies and intensities are evident as a function of growth orientation, temperature, and Te background pressure. We have also investigated the effect of Br-methanol etching and subsequent thermal desorption of excess Te on the deep level emission. Photoluminescence (PL) spectra of etched CdTe surfaces measured at 80 K in ultrahigh vacuum (UHV) after thermal desorption are sensitive to crystal surface stoichiometry. Auger electron spectra (AES) show that Br-methanol etching in a N₂ atmosphere produce surfaces free of C and O but rich in Te. PL spectra after Te desorption at 250 °C exhibit a sharp, intense band edge peak characteristic of clean surfaces with minimal band bending/surface states. Unlike UHV-cleaved surfaces of commercial bulk-grown CdTe, the cleaned (100) MBE surfaces show very little emission below the band edge (1.55 eV), indicating the relatively high quality of the MBE-grown epilayer. Exposure of the films to a 1 kV electron beam virtually eliminates the near band edge emission and introduces new mid-gap spectral features. Further heating undamaged MBE films produces changes in near band edge emission lines due to stoichiometry changes

below AES detectability and significant mid-gap emission above 450 °C. Thus deep level luminescence techniques are sensitive indicators of MBE growth quality and potentially powerful tools for optimizing growth and processing.

E2.3

STRUCTURAL AND VIBRATIONAL PROPERTIES OF ZnTe EPITAXIAL LAYERS GROWN BY MBE. J. Petruzzello, D. Olego, Philips Laboratories, North American Philips Corp., Briarcliff Manor, NY; X. Chu and J. P. Faurie, University of Illinois at Chicago.

We have investigated the structural and vibrational properties of ZnTe thin films, grown by molecular beam epitaxy, with transmission electron microscopy and Raman spectroscopy. The ZnTe films were grown from a compound source on (100) GaAs substrates and have thicknesses in excess of 2 μm. These layers were studied as a function of growth temperature, T_s, ranging from 250 to 350 °C.

The structural properties of the GaAs - ZnTe interface and bulk of the films are similar throughout the range of growth temperatures. Misfit dislocations are found at the interface and threading dislocations are found throughout the bulk of the ZnTe. The ZnTe films displayed a pronounced difference, however, in the structural properties of the near surface region as a function of growth temperature. The films grown at T_s ≥ 300 °C show precipitates, with dimensions of about 500 Å in width, embedded in the ZnTe lattice and associated with the threading dislocations. The precipitates are crystalline Te as determined by energy dispersive x-ray analysis and electron diffraction. In high resolution micrographs of the ZnTe - Te precipitate interfaces some degree of coherency exists. The chemical nature of the precipitates is confirmed by the appearance of strong Te modes in the Raman spectra. The Te modes are shifted to higher frequencies due to tensile strain as a result of the lattice mismatch with ZnTe. In addition to the Te precipitates there was a very thin film ≈ 50 Å over the entire surface of the ZnTe. This layer was found to be epitaxial and have a smaller lattice parameter than the ZnTe by high resolution microscopy. The chemical nature of this film is under investigation. The precipitates and thin film formation are avoided when the films are grown with substrate temperatures ≤ 275 °C. In light of this temperature dependence we conclude that the Te diffuses through the film and precipitates near the top surface at higher growth temperatures. This process appears to be facilitated by threading dislocations present in the bulk of the film.

E2.4

HIGH RESOLUTION AND ANALYTICAL ELECTRON MICROSCOPY OF MULTILAYER HETEROEPITAXIAL SEMICONDUCTORS. H.-J. Klesche*, W.J. Hamilton**, W.L. Ahlgren**, S.M. Johnson**, M. Rühle*; *UCSB, Materials Dept., Eng. III, Santa Barbara, CA; and **=Santa Barbara Research Center, Goleta, CA.

Development of thin-film epitaxial layers on silicon substrates is being actively pursued as an alternative to bulk substrates for potential improvements in size, strength, monolithic signal processing, and cost of infrared detectors. This study has investigated the structural and chemical properties of films of CdTe / CdZnTe grown on GaAs/Si wafers by metal organic chemical vapor deposition (MOCVD) followed by the growth of HgCdTe by liquid-phase epitaxy (LPE). Key to the success in achieving high quality transmission electron microscope (TEM) images of these multilayer structures was the development of a specimen preparation method that provides a great deal of rigidity and strength during mechanical and ion thinning.

Using TEM with ancillary analytical methods, parallel electron energy-loss spectroscopy (PEELS) and energy-dispersive x-ray spectroscopy (EDS), a number of observations have been made. Low magnification images show broad area relationships of the layers and structural defects. High resolution imaging of cross sections of the multilayers shows a

number of phenomena: most of the heteroepitaxial misfit is relieved by misfit dislocations at the interfaces; many stacking faults and threading dislocations propagating across the films appear to be related to interface structural anomalies; there is some evidence of contamination at interfaces, but interface defects mainly appear to be extremely minute pits or hillocks. EDS and PEELS investigations of interface regions have demonstrated a redistribution of material close to interfaces.

E2.5

SOLUBILITY OF IMPURITIES AND DEFECT IMPURITY INTERACTION IN II-VI SEMICONDUCTORS. Yves Marfaing, Laboratoire de Physique des Solides de Bellevue, CNRS, Meudon, France.

Impurity doping in II-VI semiconductors is characterized by two aspects: limited solubility of electrically active impurities, strong interaction of impurities with native defects. Examples are found in the whole range of materials from narrow band gap alloys (CdHgTe) to wide band gap compounds (ZnTe, ZnSe): net donor or acceptor concentration is at most equal to a few 10^{18} cm^{-3} while, in extreme cases, self compensation of impurities prevents conversion of conductivity type.

First the specific properties of the II-VI semiconductors at the origin of the observed effects will be discussed: energies of formation and migration of defects, position of the associated electronic levels, energy of mixing with foreign elements.

Then in the light of that analysis the particular aspects presented by the methods of growth at low temperature (MBE, MOCVD) will be considered.

Finally the problem of impurity incorporation under non-equilibrium conditions will be addressed. One process is ion implantation followed by rapid thermal annealing. Another interesting phenomenon is related to the change in the charge state of defects caused by excess charge carriers. This could possibly lead to photo-induced doping.

E2.6

MOCVD GROWTH OF $\text{Cd}_{1-y}\text{Zn}_y\text{Te}$ EPITAXIAL LAYERS USING A VERTICAL FLOW/HIGH-SPEED HORIZONTAL ROTATING DISK REACTOR. W. L. Ahlgren, S. M. Johnson, W. J. Hamilton, and A. Szilagyi, Santa Barbara Research Center, Goleta, CA 93117; G. S. Tompa and P. D. Reinert, EMCORE Corp., Somerset, NJ 08873; C. K. Ziegler and W. J. Lick, University of California, Santa Barbara, CA 93106.

$\text{Cd}_{1-y}\text{Zn}_y\text{Te}$ grown epitaxially on GaAs or GaAs/Si is a substrate material for $1\mu\text{m}$ - Cd_xTe thin film growth. For this application, the crystal lattice perfection and alloy compositional uniformity are of primary importance. Superior compositional uniformity should be achieved in a vertical flow/high-speed horizontal rotating disk reactor, for which the substrate surfaces are uniformly accessible (heat and mass transfer rates are uniform over the radius of the disk). Using such a reactor, a parametric study of $\text{Cd}_{1-y}\text{Zn}_y\text{Te}$ deposition on GaAs and GaAs/Si substrates has been carried out. The parameters varied were reactant concentrations and substrate temperature. In addition, a variety of substrate orientations and pre-growth cleaning procedures were used. Layer characteristics to be presented include alloy composition and uniformity, Ga and As content, crystal lattice perfection, and surface morphology. Alloy composition and uniformity are determined by mapping the bandgap and lattice constant using photoluminescence and x-ray techniques. Profiles of Ga, As, and other impurities in the CdZnTe layers are derived from SIMS measurements. Crystal lattice perfection is established using x-ray and electron beam techniques, including TEM (high-resolution cross-sectional lattice imaging) and SEM (cathodoluminescence and electron beam channeling). Surface morphology is assessed on the basis of micrographs and haze measurements derived from a light-scattering technique. These layer attributes will be correlated with growth parameters using response surface methodology. The growth experiments were carried out following a Central Composite design. Growth rate and composition uniformity will be compared against a computer model that combines convective-diffusive transport of reactants (including buoyancy effects) with the assumption of thermodynamic equilibrium at the growth interface.

E2.7

THICKNESS MEASUREMENT OF THIN FILMS BY X-RAY ABSORPTION. J. Chaudhuri and S. Shah, Mech. Engr. Dept., The Wichita State University, Wichita KS 67208.

An X-ray diffraction method is described for determining thicknesses of thin films grown on single crystal substrates. The equations, based on the kinematical theory of X-ray diffraction and a mosaic crystal model, were developed. The thickness of the thin film was computed from the absorption of the integrated diffracted X-ray intensity from the single crystal substrate due to double traverse through the film. Since the diffracted intensity from the film is not required, the film does not have to be single crystal in nature. Thus, thicknesses of less ordered, polycrystalline or even amorphous films can be measured with high precision by this technique.

E2.8

TILT GROWTH OF CdTe EPILAYERS ON SAPPHIRE SUBSTRATES BY MOCVD. Kenji Maruyama, Hiroji Ebe, Yoshito Nishijima, and Koji Shinohara, Fujitsu Laboratories Ltd., Atsugi, Japan.

We have evaluated the characteristics of CdTe epitaxial layers grown on sapphire substrates by MOCVD. Tilt growth of the CdTe epilayers with respect to vicinal surface sapphire substrates were observed. We used sapphire substrates with offset angles of $1-3^\circ$. We measured the angular differences between epilayers and substrates with double crystal X-ray diffraction. The direction of tilt of CdTe epilayers correspond to the offset directions in sapphire substrates. A representative tilt angle in a CdTe epilayer shows 2.78° , which is larger than the offset angle of 1.75° in the sapphire substrate. In addition, the tilt of the epilayers is proportional to the offset of the substrates and is inversely proportional to the thickness of epilayers. A $5 \mu\text{m}$ -thick epilayer has no tilt.

Cross-sectional Transmission Electron Microscopy observation showed lamella-twinning regions in CdTe epilayers near the CdTe/sapphire interface. The FWHMs in (331) diffraction are lower than those in (333) diffraction in $1 \mu\text{m}$ -thick epilayers. Thus, the interface regions are distorted in the thin epilayers. The 3.8% lattice mismatch in CdTe/sapphire heteroepitaxy is accommodated by the tilt of the epilayers.

E3.1

NOVEL APPROACHES TO DOPING OF II-VI COMPOUNDS GROWN BY MBE. Maria C. Tamargo, BELLCORE, 331 Newman Springs Road, Red Bank, New Jersey.

Doping of II-VI compounds has been an obstacle for the realization of semiconductor devices made from these materials. The occurrence of self compensation usually limits the levels of doping that can be achieved and restricts the doping to only one type. ZnSe, for example, can be made n-type but it has been virtually impossible to be doped p-type. Thus, recently, novel methods to affect the dopant incorporation have been developed which have led to specific successes in some material systems as well as to new insight into the general problem. Two of these methods, which involve molecular beam epitaxy (MBE), are the light assisted doping method developed by Bicknell, et al, and the planar doping method developed by deMiguel, et al. In the first, by irradiating the sample with light during MBE growth, the incorporation process for both the n-type and the p-type dopants in CdTe was modified to obtain higher carrier concentrations and reduced deep level emission in photoluminescence. Well behaved p-n junctions in CdTe have been

made by this method. In the second, by incorporating the Ga dopant in spatially separated sheets deposited on a particular ZnSe surface termination, higher doping levels and reduced deep level emission were also obtained for n-type ZnSe. These two recent breakthroughs are now in the early stages of understanding. Models are being developed which point to exciting new directions in which to approach the issue of doping and self compensation in II-VI compounds. We will review these results and extract some ideas about the general processes involved. We will use these concepts to discuss recent results we have obtained in the doping of ZnSe with As to produce acceptors in ZnSe.

E3.2

MOCVD GROWTH AND DOPING OF ZnSe AND RELATED II-VI MATERIALS. H. Kukimoto, Imaging Science and Engineering Laboratory, Tokyo Institute of Technology, 4259 Nagatsuda, Midori-ku, Yokohama 227, Japan

Recent progress in metalorganic chemical vapor deposition (MOCVD) of wide bandgap II-VI materials, especially of ZnSe, ZnS and their alloys, is reviewed with emphasis on the general principles for obtaining uniform and high quality epitaxial layers and the current major issue of conductivity control.

The surface morphology and crystalline quality can be improved by a suitable choice of source materials and by lattice-matching the epitaxial layer to the substrate. Photo-assisted growth is effective for a remarkable reduction of the growth temperature.

By using appropriate sources, high conductivity n-type epitaxial layers of ZnSe and ZnS doped with impurities from group III and VII of the periodic table have been successfully grown by low temperature MOCVD.

We have also grown p-type ZnSe layers with carrier concentration ranging from low 10^{16} to high 10^{17} cm⁻³ using LiN₃ as the dopant. Extensive studies are now focussed on the better p-type control. High purity source materials, appropriate p-type dopants and low temperature growth are important keys.

E3.3

GROWTH AND DOPING OF ZINC SELENIDE BY MOLECULAR BEAM EPITAXY. J.M. DePuydt, H. Cheng, M.A. Haase, and J.E. Potts, 3M Company, St. Paul, MN.

Zinc selenide (ZnSe) has long been recognized as a potentially useful compound for the fabrication of short wavelength (460 nm), solid-state, light-emitting devices. Even though it has been identified as a technologically important material and a great deal of research has been devoted to it, development of practical devices from ZnSe has not ensued. The major obstacles which hindered progress with ZnSe were difficulties in producing large, high quality crystals and in controlling the doping of this wide bandgap semiconductor.

Recently, with the advent of thermal nonequilibrium growth techniques like molecular beam epitaxy (MBE) and metalorganic chemical vapor deposition (MOCVD), great progress has been made in overcoming some of the problems traditionally encountered in the growth and doping of ZnSe. Breakthroughs have been made in several areas including the deposition of high quality undoped films, with intentional n-type doping and, most significantly, with p-type doping. In our presentation we will review some of the recent progress made by various workers in the MBE growth and doping of ZnSe epitaxial films.

In addition to describing contributions made elsewhere, we will discuss some recent results obtained in our labs on the MBE growth of ZnSe. We will describe our production of low resistivity p-ZnSe films by Li doping and will discuss the junction characteristics and electroluminescence obtained from ZnSe pn junctions. Finally, we will describe some problems which we feel are limiting the performance of our ZnSe light emitting diodes and the approaches which may be used to overcome these problems.

E3.4

DEPOSITION OF ZINC SELENIDE BY ATOMIC LAYER EPITAXY FOR MULTILAYER X-RAY OPTICS. J. Kevin Shurtleff, David Allred, Raymond Perkins, and James Thorne, Brigham Young University Departments of Chemistry and Physics, Provo, UT 84602.

Atomic layer epitaxy is a chemical vapor deposition technique which deposits a single layer of atoms during each process cycle. The thickness of a film deposited by atomic layer epitaxy depends on the number of process cycles and is independent of other process parameters. The precise thickness control possible with atomic layer epitaxy makes it an excellent technique for producing multilayer x-ray optics.

The theory of atomic layer epitaxy suggests that a single layer of atoms is strongly bound to the substrate by chemisorption during each process cycle. Atoms which are weakly bound by physisorption are removed during the purge step between cycles. A better understanding of atomic layer epitaxy requires examination of the chemisorption and physisorption of atoms.

We have designed and built an atomic layer epitaxy system which will allow us to observe the chemisorption and physisorption of atoms during deposition. With this system we have deposited ZnSe layer pairs from diethyl zinc and hydrogen selenide.

E3.5

Optimized MIS characteristics of as-grown epitaxial ZnSe/epitaxial GaAs heterostructures J. Qiu, Q.-D. Qian, M. Kobayashi, R. L. Gunshor, D. R. Menke, D. Li, and N. Otsuka, Purdue University, West Lafayette, Indiana, 47907 USA

Pseudomorphic ZnSe layers have been grown on GaAs epilayers and nearly ideal C-V profiles have been observed from the epilayer/epilayer MIS structure. In our previous work, a post-growth annealing procedure was required to achieve the desired C-V characteristics. In this report, the nearly ideal C-V characteristics were obtained from as-grown samples without the necessity of a post-growth annealing. In a series of experiments, the surface stoichiometry of the GaAs epilayers was systematically modified prior to the nucleation of ZnSe. The various GaAs surfaces were characterized by RHEED reconstruction patterns. TEM was used to observe differences in the microstructure of the interfaces corresponding to the various nucleation conditions. Starting with a (2x4) surface, the electrical characteristics improved as the GaAs surface became increasingly Ga rich. Such as-grown MIS structures exhibited an integrated interface state density of less than 4×10^{11} cm⁻² which is comparable to the interface state densities reported for the (Al,Ga)As/GaAs interface. No hysteresis and very little frequency dispersion was observed in the C-V curves.

The research was supported by DARPA/ONR URI contract N00014-86-K0760, and AFSOR grant AFOSR-85-0185.

E3.6

PSEUDOMORPHIC ZnTe/AlSb/GaSb: GROWTH AND CHARACTERIZATION D. L. Mathine, J. Han, M. Kobayashi, R. L. Gunshor, D. R. Menke, and M. Vaziri (Elect. Eng., Purdue Univ.), J. Gonsalves, and N. Otsuka, (Materials Eng., Purdue Univ., West Lafayette, IN 47907),

Q. Fu, M. Hagerott, and A. V. Nurmikko (Division of Eng., Brown Univ., Providence, RI 02912).

A wide band-gap light emitter has many potential optoelectronic device applications. Computer simulations indicate that the p-ZnTe/n-AlSb interface appears favorable for the injection of electrons into ZnTe. As a means of achieving this objective, ZnTe epitaxial layers have been grown on GaSb substrates, GaSb epitaxial layers, and on pseudomorphic AlSb/GaSb epitaxial heterostructures. ZnTe nucleated on GaSb substrates shows a three-dimensional behavior while ZnTe nucleated on epitaxial layers of either GaSb or AlSb has a two-dimensional characteristic. The two-dimensional nucleation is confirmed by RHEED intensity oscillations. The microstructural quality of these epitaxial layers has been examined using TEM and x-ray rocking curves. Free exciton related features have been observed in the photoluminescence of both thick (strain relaxed) and pseudomorphic ZnTe epilayers. Doping and transport experiments involving ZnTe, AlSb, and GaSb grown on Si-GaAs substrates will be discussed. Hall data shows p-type carrier concentrations as low as $8.5 \times 10^{14} \text{ cm}^{-3}$ for undoped ZnTe epitaxial layers.

This research was supported by DARPA/ONR URI contract N00014-86-K0760, AFOSR-85-0185 grant, (NSF)-MRG grant DMR-8520868, and NSF equipment grant ECS-8606241.

E3.7

TRANSMISSION ELECTRON MICROSCOPY OF II-VI/III-V SEMICONDUCTOR INTERFACES. D. Li, N. Otsuka, M. Kobayashi, R. L. Gunshor, L. A. Kolodziejski, Purdue University, W. Lafayette, IN 47907.

At present, great efforts are directed to the development of new electronic and optical devices utilizing II-VI/III-V semiconductor heterojunctions. The most important step for achieving this goal is the preparation of high quality interfaces having low interface state densities. In the present study, atomic structures of ZnSe/GaAs and CdTe/InSb interfaces have been analyzed in order to investigate the structural mechanism of accommodation of valence mismatch at these interfaces. Samples of pseudomorphic II-VI epilayers grown on III-V epilayers by MBE were observed by cross-sectional TEM. HREM images show coherent lattice structures of the interfaces, but dark bands with thicknesses of a few monolayers appear along the interfaces in these images. Interfaces appear as bright lines in dark field images of 200 type reflections, while dark field images of 400 type reflections show dark contrasts at the interfaces. These observations are explained by the existence of very thin interfacial layers of In_2V_3 compounds (Ga_2Se_3 , In_2Te_3) whose cation sublattices have structural vacancies resulting from the valence mismatch of constituent elements. Based on the result, effects of growth and annealing conditions of the interface atomic structures are discussed.

E4.1 ABSTRACT NOT AVAILABLE

E4.2

SURFACE MORPHOLOGY AND PHOTOLUMINESCENCE SPECTRA OF ZnSe AFTER EXCIMER LASER ANNEALING. G.-J. Yi, G.F. Neumark, Z. Lu, P.R. Newbury, and C.F. Yu, Columbia University, New York, NY; B.J. Fitzpatrick, M. Shone, A. Sicignano, Philips Laboratories, Briarcliff Manor, NY.

It is generally known that good bipolar conductivity has not been obtained in any wide-band-gap semiconductor due to problems such as self-compensation and solubility. Thus non-equilibrium impurity incorporation is required. It is well known that lasers, and particularly excimer lasers, provide a convenient approach toward achieving this. We have therefore tested such lasers on ZnSe. One concern regarding compound semiconductors is disproportionation, particularly for materials such as ZnSe which,

at atmospheric pressure, sublime prior to melting. From the observation of the surface morphology, specifically the twinning structure, we have determined that melting and re-crystallization can be obtained. Specifically, we can obtain this at atmospheric pressure, without use of an encapsulating layer. Another important question is whether laser annealing can lead to the desired non-equilibrium impurity incorporation. To check this, we have investigated Na doped ZnSe, since it has been predicted that for amphoteric impurities, such as Na, high temperatures would favor the substitutional (acceptor) location vs. the interstitial (donor) one. The evidence from donor-acceptor pair (DAP) spectra shows that there does not appear to be appreciable site transfer of this type at the lower laser power levels, even where regrowth is obtained. However, the higher power levels do give indications of such transfer.

1. G.F. Neumark, J. Appl. Phys. 51, 3383 (1980).

E4.3

PLASMA-ASSISTED EPITAXIAL GROWTH OF ZnSe FILMS IN HYDROGEN PLASMA
Satoshi Yamauchi, and Takashi Hariu, Department of Electronic Engineering, Tohoku University, Sendai 980, Japan

The advantages of plasma-assisted epitaxy (PAE) are low temperature epitaxial growth and efficient doping among others. The epitaxial growth of ZnSe on GaAs substrates was realized above 200°C in hydrogen plasma. Although the grown layers are characterized with strong exciton emissions in photoluminescence at 4.2K, it was found the quality of ZnSe films is sensitive to plasma conditions, particularly to hydrogen gas flow rate. The dominant exciton emission changes from donor-bound exciton emission (I_X , I_2) to free exciton emission (I_X) as hydrogen gas flow rate is increased. Hydrogen plasmas mixed with about 2% HCl and N₂ respectively resulted in highly conductive ($610 \Omega^{-1} \text{cm}^{-1}$) n-type layers and nitrogen-acceptor (acceptor level ~100meV) doped layers. The electrical conductivity of n-type films can be well controlled by the content of HCl in H₂. Nitrogen-acceptor doping can be achieved only in the H₂+N₂ mixed plasma, but not in non-excited H₂+N₂ mixed gas flow. The photoluminescent properties of nitrogen-acceptor doped films depends not only upon the content of N₂ in H₂ but also upon the Se/Zn supply ratio and rf power applied to excite the plasma. Optical emission spectroscopy employed for plasma diagnosis detected SeN which is produced by the reaction between N₂⁺ and Se or SeH, and which can be responsible for effective nitrogen doping.

E4.4

EFFECT OF Se PRECURSORS AND PROCESSING CONDITIONS ON OPTOELECTRONIC PROPERTIES OF ZnSe GROWN BY MOVPE. Konstantinos P. Giapis, AT&T Bell Laboratories, 600 Mountain Ave., Murray Hill, NJ 07974, and Klaus E. Jensen, Department of Chemical Engineering, Massachusetts Institute of Technology, Cambridge, MA 02139.

The growth of ZnSe on (100) GaAs substrates by low pressure organometallic vapor phase epitaxy (MOVPE) was investigated in a vertical downflow reactor. Dimethylzinc (DMZn) was used as the Zn source while four selenium sources were employed: diethylselenide (DESe), methylallyl selenide (MASE), diallylselenide (DASE), and hydrogen selenide (H₂Se). H₂Se produced material with excellent electrical properties and photoluminescence (PL) characteristics. Diethylselenide always produced highly resistive films but the PL spectra indicated low impurity incorporation. The use of methylallylselenide resulted in heavily carbon contaminated ZnSe films.

A lower growth temperature was needed with DASE and improved PL characteristics were obtained in comparison to results from MASE.

Growth with H_2Se produced material with very weak deep level emission in both the 300 K and the 9 K photoluminescence spectra. With increasing growth temperature, the dominant donor-bound excitonic emission (I_x) was seen to decrease in intensity and the free exciton became the dominant emission. Selectively-excited photoluminescence revealed chlorine to be the main donor impurity associated with the I_x . The optoelectronic properties deteriorated at higher growth temperatures ($>350^\circ C$). This coincided with a dramatic increase in the intensity of the Y_0 peak, attributed to complex dislocation tangles and other structural defects.

The effect of nitrogen impurities in ZnSe were investigated by NH_3 doping. Besides incorporating nitrogen into the films, the addition of NH_3 had the advantage of eliminating hillock formation. The nitrogen incorporation produced a shallow acceptor-bound exciton which dominated the near-band-edge PL emission spectra.

E4.4A

GROWTH OF ZnS_xSe_{1-x} BY MBE USING AN ELECTROCHEMICAL SULPHUR SOURCE. J. Wallace, K. Prior, B. Cavenett, J. Hunter, S. Adams and M. Haines, Department of Physics, Heriot-Watt University, Edinburgh, U.K.

In this paper we describe the use of an electrochemical sulphur cell to grow ZnS_xSe_{1-x} alloys on GaAs substrates. The cell uses the ionic transport of Ag ions in Ag_2S to produce a sulphur flux which depends on the applied voltage and the advantages and disadvantages of this type of solid state source will be discussed. In particular, results will be given showing the use of the cell to produce lattice matched material with $x \approx 0.055$ which has been characterized by photoluminescence, Raman and X-ray measurements. We also demonstrate the versatility of the cell for fabricating $ZnS_xSe_{1-x}/ZnS_ySe_{1-y}$ multilayers as well as more complex profiles.

E4.5

ALE/MBE GROWTH AND CHARACTERIZATION OF ZN-CHALCOGENIDE SUPERLATTICE STRUCTURES (INVITED). T. Yao, M. Fujimoto, H. Izumiya, H. Tanino, and Y. Okada, Electrotechnical Laboratory, Tsukuba, Ibaraki 305, Japan.

This paper will report the ALE/MBE growth of Zn-chalcogenide superlattice structures including $ZnSe/ZnTe$ and $ZnS/ZnSe$ systems. Structural and optical characterization of the superlattices using RHEED "in situ" observation, X-ray diffraction, Raman scattering, and photoluminescence techniques will be reported.

E4.6

SELECTIVE-AREA DEPOSITION OF METALS, PASSIVANTS, INSULATORS, AND EPITAXIAL FILMS OF II-VI COMPOUND SEMICONDUCTORS.*

D.L. Dreifus, Department of Electrical and Computer Engineering; Y. Lansari, J.W. Han, J.W. Cook, Jr. and J.F. Schetzina, Department of Physics, North Carolina State University, Raleigh, NC 27695-8202

II-VI semiconductor surface passivants, insulators and epitaxial layers have been deposited onto selective substrate areas by employing new masking and lift-off techniques. The II-VI layers were grown by either conventional or photoassisted molecular beam epitaxy (MBE). Low resistance, unannealed ohmic contacts to wide-bandgap p-type CdTe have also been realized through the use of selectively-placed thin films of the semi-metal HgTe followed by thermal evaporation of indium. CdTe, considered a prime candidate for the surface passivation of HgCdTe due to its close lattice-match, has been selectively-deposited as 5 μm thick rings with outer diameters in the range between 20 μm and 100 μm in outer diameter on (100) oriented CdTe substrates.

Room temperature layers of insulating ZnS, deposited onto the active gate region between the source and drain, have been used to successfully fabricate MIS field-effect transistors from HgCdTe. Thicker layers

of insulating ZnS have been employed as an inter-level metal dielectric for advanced multilevel metallization device processing.

Epitaxial layers of HgCdTe have also been grown onto selective areas of (100) CdTe substrates at $125^\circ C$. The 125 μm square mesa structures are typical dimensions for infrared detector elements, which can now be formed without chemical etching. In addition, 10 μm stripes composed of HgTe-CdTe superlattices have also been selectively grown by photo-assisted MBE using the new selective-area deposition techniques developed at NCSU.

*Work supported by NSF grant DMR-88-13525 and DARPA contract DAAL03-86-K-0146.

E4.7

SPATIAL LIGHT MODULATOR USING A CdS THIN FILM PHOTOCAPACITOR. Joseph Reichman, Corporate Research Center, Grumman Corporation, Bethpage, N.Y.

We have developed an optically addressed Spatial Light Modulator (SLM) that uses a thin film of CdS as the photosensor and a liquid crystal as the electro-optic material. The device spatially and temporally modulates a read light beam in accordance with a write light beam. Switching of an applied AC voltage to the liquid crystal layer takes place when the CdS is illuminated with photons of energies greater than its bandgap. The required high dark impedance is achieved by the creation of a depletion region in the CdS thin film by surface acceptor states. This is in contrast to previously reported work on optically addressed SLM's where the high impedance depletion region is created by a Schottky barrier or p-n junction structure. The complex impedance as a function of frequency and illumination was determined. Analysis of the results indicate that the reduction in impedance with illumination is due to shrinkage of the depletion width with the resultant change in capacitance. This is attributed to capture of photogenerated holes by deep acceptor states and forward biasing due to the generated photovoltage.

The SLM displays photoelectrochemical cell characteristics. A photovoltage, dark rectification, and a photocurrent proportional to the illumination intensity was obtained. Photoluminescence and transient photocurrent measurements were found consistent with an acceptor surface state model for the CdS thin film.

E4.8

PHOTOLUMINESCENCE PROPERTIES OF GRADED COMPOSITION $Mg_xZn_{1-x}Se$ CRYSTALS. H. J. Lozykowski, Ohio University; X. D. Tang, University of Heilongjiang, Harbin, PRC; J. L. Merz, University of California, S. Barbara.

The photoluminescence properties of $Mg_xZn_{1-x}Se$ solid solution grown on ZnSe substrate by a closed solid-state diffusion technique have been investigated. The depth profiles of the diffusion region (were determined with an electron probe microanalyzer) shows well distinguish surface layer and thick graded layer. The PL spectra of $Mg_xZn_{1-x}Se$ side of the sample excited with a wide range of excitation energy shift the edge emission band toward longer wavelengths with decreasing excitation energy. The experimental observation are discussed on the basis of the funnel shape band-gap of the graded $Mg_xZn_{1-x}Se$ crystal. The edge emission spectrum was found to shift toward the shorter wavelength with electric field applied parallel to the compositional gradient of $Mg_xZn_{1-x}Se-ZnSe$ heterostructure. It is concluded that hole transport in the grade-band-gap regions cause by the effective electric field is responsible for the spectral shifts.

E5.1

ATOMIC LAYER EPITAXY OF WIDE BANDGAP II-VI COMPOUND SEMICONDUCTOR SUPERLATTICES. M.Konagai, Y.Takemura, R.Kimura, N.Teraguchi and K.Takahashi; Tokyo Institute of Technology, Meguro-ku, Tokyo, JAPAN

ZnSe, ZnTe thin films and ZnSe-ZnTe strained layer superlattices(SLS) have been successfully grown by atomic layer epitaxy(ALE) using molecular beam epitaxy. The ideal ALE growth, i.e., one monolayer per cycle by opening and closing the shutters of the constituent elements, was obtained for ZnSe and ZnTe over a range of substrate temperatures 250-350°C and 240-280°C, respectively. The surface morphology of ALE-ZnSe grown under optimized conditions was very specular without any structures. However, for ZnTe, it was found that precise control of the Te beam intensity is essential to eliminate hillocks. $(\text{ZnSe})_m(\text{ZnTe})_n$ ($m, n=1-4$) SLSs were grown by ALE. The PL intensity of the SLS grown by ALE is more than ten times greater than that of the SLS grown by the conventional MBE method. In this paper, optical properties of these SLSs will be reported in detail.

ZnS and ZnSe were also prepared by ALE using metalorganic molecular beam epitaxy(MOMBE). Diethylzinc(DEZn), diethylsulfur(DES) and diethylselenium(DESe) were used as source gases for Zn, S and Se. The pyrolysis of DEZn, DES and DESe was carried out. The ALE growth of ZnSe was achieved at substrate temperatures between 250-300°C which are about 150°C lower than those in conventional MOMBE. Under optimum growth conditions, the surface of ZnSe were very specular without any structure. The preparation of ZnS-ZnSe SLSs by MOMBE-ALE will be also reported.

E5.2

GROWTH OF LATTICE-MATCHED ZnSe-ZnS STRAINED-LAYER SUPERLATTICES ONTO GaAs AS AN ALTERNATIVE TO ZnSSe ALLOYS: H.Oniyama, S.Yamaga and A.Yoshikawa
Faculty of Eng., Chiba University

This paper describes the results on the first attempt to fabricate misfit-dislocation-free epi-layers of a wide bandgap II-VI semiconductor on GaAs by utilizing the ZnSe-ZnS strained-layer superlattice (SLS) structure.

ZnSe layers are usually grown on GaAs substrates, since "substrate-grade" ZnSe bulk crystals can not be obtained. Lattice-mismatch between ZnSe and GaAs causes misfit-dislocations which deteriorate the quality and electrical properties of the ZnSe layers. In order to control the properties, especially to obtain low-resistive p-type layers, a precise lattice-matching between the epi-layers and GaAs is required. We propose here a new idea that ZnSe-ZnS SLSs can be an alternative to the lattice-matched ZnSSe alloys.

SLSs consisting of 200Å-ZnSe and 10Å-ZnS layer in one period, which were theoretically estimated to be lattice-matched to GaAs, were grown on GaAs by metalorganic molecular beam epitaxy. In the SLSs, the ZnSe well-layers are much thicker than the ZnS barrier-layers, resulting in little carrier confinement effects. Hence, from the viewpoint of bandgap energy, the SLSs are rather regarded as "ZnSe epi-layers" grown coherently on GaAs. It has been found from the photoluminescence spectra and electron beam induced current image observation that the SLSs can be grown on GaAs without the generation of misfit-dislocations. This shows that the ZnSe-ZnS SLSs can be a promising alternative to the lattice-matched ZnSSe ternary alloys on GaAs.

E5.3

STRUCTURAL AND ELECTRICAL CHARACTERIZATION OF CdSe THIN FILMS. Miltiadis K. Hatalis, Fuyun Lin, Lehigh University, Bethlehem, PA; and Michael R. Westcott, Litton Systems Canada, Rexdale, Ontario, Canada.

We have studied the structural and electrical characteristics of 25 nm thick undoped and indium-doped CdSe films deposited on glass substrates. Transmission Electron Microscopy has revealed that the as-deposited films are microcrystalline with a grain size ~10 nm. Distinctively different grain growth has been observed in the doped and undoped films after thermal annealing. Grain growth in the undoped CdSe was found to stop when the average grain size became equal to the film thickness.

Enhanced grain growth has been observed in the indium doped CdSe. In contrast to undoped films, grain growth in doped CdSe is not limited by the film thickness but depends primarily upon annealing time and temperature. An average grain size larger than the film thickness has been achieved. Furthermore, an abnormal grain growth resulting in grains with sizes much larger (>20X) than the film thickness has been observed. The density of these grains, their crystal structure and TEM observations of in-situ annealed films will be discussed. The possibility of obtaining large area single crystal CdSe will also be discussed.

The channel resistance of the indium doped CdSe for various electrode spacings was characterized. After annealing the resistance decreased for short (<25 µm) electrode separation whereas it increased for larger ones. Possible explanations of our results will be presented.

E5.4

U.S. POLYCRYSTALLINE THIN FILM SOLAR CELL PROGRAM. Harin S. Ullal, Kenneth Zweibel and Richard L. Mitchell, Solar Energy Research Institute, 1617 Cole Boulevard, Golden, CO 80401

Substantial technical progress has been made in polycrystalline thin film solar cells in the past year. Two materials that have been investigated extensively for solar cell applications are copper indium diselenide (CIS) and cadmium telluride (CdTe).

In the area of CIS, dramatic improvements have occurred in both high efficiency and long-term reliability. For laboratory devices, 14.1% efficiency has been reported for CIS solar cells. For solar power modules, a world record aperture area efficiency of 8.5% and a module output of 33.8 watts has been verified at SERI for modules of 1 ft x 4 ft. Outdoor reliability testing of CIS modules exposed to natural sunlight for several months have also demonstrated no degradation.

Rapid advances have also been made by II-VI based solar cells and related alloys. In the case of CdTe solar power modules, aperture area efficiency of 7.3% have been achieved for about 1 ft x 1 ft module; and for small devices total area efficiency of 12.3% has been verified by SERI.

Work supported by the U.S. Department of Energy under contract # DE-AC02-83CH10093.

E5.5

A STRUCTURAL STUDY OF EPITAXIAL LAYERS OF CdSe AND CdS GROWN ON GaAs. A.G. Cullis, P.J. Parbrook, P.W. Smith, B. Cockayne, P.J. Wright and G.M. Williams, Royal Signals and Radar Establishment, St Andrews Road, Malvern, Worcs WR14 3PS, UK

Both CdSe and CdS are wide band-gap semiconductors and epitaxial layers of these compounds have potential applications for the fabrication of photovoltaic devices. The preparation of superlattices would also give the possibility of production of light-emitting devices and optical switches. Accordingly, growth of layers of these materials has been undertaken by MOCVD using substrates of single crystal GaAs. In the present paper we report transmission electron microscopy studies of the layers produced in this way. Careful investigations have been carried out of the morphology and structure of the layers at various stages in their growth. Initial nucleation is followed by the development of characteristic layer microstructures, including dislocations at the heterointerfaces which relieve lattice misfit stresses between the different materials. We shall give a comprehensive description of the defect structures which form. The nature of superlattices based upon alternating layers of the two II-VI compounds will also be described.

E5.6

EXCITONIC PROPERTIES IN ZnSe-ZnS STRAINED-LAYER SUPERLATTICES AND A FIBONACCI SEQUENCE. Tsunemasa TAGUCHI and Yoichi YAMADA, Department of Electrical Engineering, Faculty of Engineering, Osaka University, Suita, Osaka 565, JAPAN.

Type I band structure ZnSe-ZnS strained-layer superlattice (SLS) is the most fundamental example for understanding "excitons" in wide band-gap II-VI SLSs whose binding energy is larger than 70 meV. A fluctuation of the heterointerface between the ZnSe well and the ZnS barrier layers can be completely controlled within one monolayer. We review optical properties of 2D excitons on the basis of our recent results [1] of low temperature exciton luminescence, absorption and excitation spectra. The present SLSs were fabricated by low-pressure MOCVD technique using all gaseous sources onto (100) GaAs or ZnS substrates. We demonstrate a new kind of heterostructure, a Fibonacci superlattice, which consists of alternating layers of ZnSe and ZnS for the first time [2]. The talk is concentrated on the following subjects:

- (1) Determination of the interface and the critical thickness by ion-channelling and transmission electron microscope
- (2) Band offset and strains revealed by exciton absorption as a function of ZnSe well thickness
- (3) Excitonic behaviour under high excitation and Stark effect
- (4) Temperature dependence of excitons; exciton binding energy and linewidth
- (5) Optical properties of Fibonacci superlattices

[1] Y.Yamada and T.Taguchi, Proc. Int. Conf. on II-VI Compounds, 1989, Berlin.

[2] Y.Yamada and T.Taguchi, Phys. Rev. to be published.

E5.7

OPTICAL PROPERTIES OF CdZnS-ZnS STRAINED-LAYER SUPERLATTICES. Yasuyuki ENDOH and Tsunemasa TAGUCHI, Faculty of Engineering, Osaka University, Suita, Osaka 565, JAPAN.

I would like to present the results of the growth and optical properties of $\text{Cd}_x\text{Zn}_{1-x}\text{S}$ -ZnS strained-layer superlattices (SLSs) by low-pressure metalorganic chemical vapour deposition (MOCVD). Both electrons and holes are confined in the CdZnS well layers, namely, a type I structure, and the bandgap of $\text{Cd}_x\text{Zn}_{1-x}\text{S}$ at R.T. changes from about 3.6 eV (at $x=0$) to about 2.4 eV (at $x=1$). Consequently, high-efficiency blue and ultraviolet emissions due to the quantum confinement effect can be expected by varying the mole-fraction x . Recently, we have succeeded in the growth of

$\text{Cd}_x\text{Zn}_{1-x}\text{S}$ -ZnS SLS in the range $0.1 < x < 0.5$ for the first time. Especially at $x=0.3$, high-quality SLS was obtained.

In the PL spectra of $\text{Cd}_{0.3}\text{Zn}_{0.7}\text{S}$ -ZnS SLS at 4.2 K, sharp-emission peak above the bandgap of the well layer appeared and no deep-level was observed compared to that of $\text{Cd}_{0.3}\text{Zn}_{0.7}\text{S}$ thin film. Dependence of the well-layer thickness was also observed and this proves that the type I SLS structure is certainly realized. This fact was also confirmed by the higher-order satellite peaks of the X-ray diffraction spectrum. While, from the temperature dependence of the PL peak intensity, a large activation energy which is about 70 meV for the thermal quenching of exciton, was obtained. This large binding energy shows the possibility of the application to the exciton devices, such as quantum-laser and fast response optical switch. The effect of the external electric field is also demonstrated to get more information of the SLS.

E5.8

PRECISE MEASUREMENTS OF MINORITY CARRIER LIFETIMES IN II-VI FILMS AND SUPERLATTICES.* W.O. Doggett, Michael W. Thelander and J.F. Schetzina, North Carolina State University, Raleigh, North Carolina.

HgCdTe and CdTe have long been known as excellent materials for use in infrared detectors, solar cells and various thermal-imagery devices. One of the key parameters in determining the effectiveness of these devices is the lifetime of the minority carriers in the material. This paper will describe a system for accurately measuring the carrier lifetimes by the transient photoconductivity decay method over a temperature range of 77-300K by using a cavity dumped argon ion laser and digital recording equipment. Lifetimes in HgCdTe and CdTe films and HgTe-CdTe superlattices grown at North Carolina State University by the photo-assisted MBE method will be reported which range from tens of nanoseconds for some of the Hg-based multilayers to several microseconds for the CdTe thin films.

Several high-frequency problems had to be resolved in order to obtain an accurate determination of short carrier lifetimes. Various pulse reflections and other problems can easily occur in bringing a signal from low temperature out of a dewar's cold chamber. Solutions to these problems will be presented which include precise impedance matching and use of a fast sampling oscilloscope. The accuracy of this method is demonstrated by our ability to determine the shape of a 10 ns laser pulse (as measured by a rapid-risetime silicon detector) by using a standard HgCdTe sample with a 300 ns lifetime and a deconvolution method to extract the laser pulse from the signal. This method also allows us to record photo-resistive changes during the laser pulse itself and to determine carrier life-times on the order of the laser pulse width or less.

*Work is supported by NSF grant DMR-88-13525 and DARPA contract DAAL03-87-K-0153.

E5.9

NONLINEARITY OF BOUND EXCITON STIMULATED EMISSION INDUCED BY NONEQUILIBRIUM ACOUSTIC PHONONS. N.N. Zingray, D.I. Kovalev, I.D. Yaroshetskii, A.F. Ioffe Physico-Technical Institute, Academy of Sciences of the USSR, 19421 Leningrad, USSR

Among the generation processes of acoustic phonons in condensed matter, laser-like emission of phonons could become the most interesting. So it is great interest to learn whether such a process takes place at two-quantum (phonon+photon) optical decay. The possible way to investigate these phenomena is to study the luminescence under injection of "probe" nonequilibrium acoustic phonons into the sample. The kinetic of bound exciton luminescence and spectral changes induced by the "probe" phonons were studied at wide range of exciton densities at $T=1.3\text{K}$ in order to identify the nature of radiative transition. The spectrum of the "probe" was controlled independently. The spectral

broadening of the phonon-assisted luminescence band induced by the "probe" phonons was found to grow nonlinearly up to and more than the Debye energy with increasing optical pumping of the sample. To summarize, the luminescence mechanism of the M-band in CdS has been identified as nonlinear radiative recombination of bound excitons with the emission of acoustic phonons. The obtained data indicate that acoustic phonons with occupation numbers $n_{ph} \gg 1$ are generated in this recombination process.

E6.1

PHOTOASSISTED MBE OF II-VI SEMICONDUCTOR FILMS AND SUPERLATTICES. * N. C. Giles **, R.L. Harper, J.W. Han and J.F. Schetzina, North Carolina State University, Raleigh, NC.

A survey will be presented of recent growth of II-VI semiconductors using photoassisted molecular beam epitaxy (MBE), a growth technique in which the substrate is illuminated during the entire film deposition. The materials that will be discussed include undoped and As-doped CdTe, As-doped HgCdTe, and In-doped HgCdTe. A variety of structures including heterojunctions and modulation-doped superlattices have been grown.

The use of photoassisted MBE has allowed a substantial reduction in substrate growth temperatures. Undoped CdTe epilayers exhibiting bright excitonic photoluminescence (PL) peaks at low temperature (5 K) have been grown at 125 °C. Highly conducting p-type CdTe:As epilayers with room temperature hole concentrations as high as $6.2 \times 10^{18} \text{ cm}^{-3}$ have been grown at 180 °C.

Both p-type and n-type Hg-based modulation-doped superlattices have been prepared, using As and In for p-type and n-type dopants, respectively. Low temperature infrared PL measurements have been performed on a series of Hg-based epilayers and quantum well structures. Selected samples were cleaved and mounted for optically-pumped stimulated emission experiments, using the 1.06 μm output from a cw Nd:YAG laser. Stimulated emission has been successfully observed at 2.8 μm .

*Work supported by NSF grant DMR-8813525 and DARPA contract DAAL03-86-K-0146.

**Present address: West Virginia University, Morgantown, WV.

E6.2

GROWTH AND INITIAL CHARACTERIZATION OF NOVEL HGTE-BASED II-VI MATERIALS. F.G. Moore*, Naval Research Laboratory, Washington, D.C.; J.C. Abele, Lewis and Clark College, Portland, OR.; and R.E. Kremer, Crystal Specialties, Colorado Springs, CO.

$\text{Hg}_{1-x}\text{A}_x\text{Te}$ materials where $\text{A} = (\text{Mg}, \text{Ba}, \text{Sr}, \text{Ca})$ have been synthesized by the vertical Bridgman technique. Hydrostatic density measurements showing segregation are presented for all materials and a distribution coefficient of ~ 1.005 is obtained for HgMgTe. For Hg_{1-x}Te a relationship between bandgap E_g and composition x , is developed based on FTIR measurements of cut-on wavelengths. The variation of energy gap with composition is found to be comparable to that of HgMnTe and twice as rapid as that of HgCdTe. Variation of lattice parameter a_0 with composition is also discussed. Carrier concentration and mobility data from room temperature and 77K Hall measurements are presented both for as-grown materials, and for samples annealed in a saturated overpressure of Mercury.

*National Research Council Postdoctoral Associate

E6.3

USE OF ATOM PROBE TECHNIQUES IN THE STUDY OF II-VI SEMICONDUCTORS. Ross A D Mackenzie, Chris R M Grovener and J Alex Liddle, Department of Metallurgy and Science of Materials, Oxford University, Parks Road, Oxford OX3 1PH

The Atom Probe Field Ion Microscope (APFIM) permits the microchemistry of materials to be determined with both high spatial and chemical resolution. Pulsed laser atom probe has been used in the investigation of elemental and III-V compound semiconductors, where it has been possible to study interfacial roughness in quantum well structures, and small scale compositional fluctuational variations in epilayer materials.

These techniques are now being applied to bulk and epilayer binary and ternary II-VI alloys. Using results obtained from the study of binary alloys the conditions needed for the controlled evaporation process can be determined. A controlled evaporation is required if accurate compositional information is to be obtained. The technique can then be applied to the observation of composition fluctuations in both bulk and epilayer materials. Preliminary results from this investigation will be presented, and the potential of these techniques for the analysis of II-VI materials shown.

E6.4

MBE GROWTH OF HgCdTe FOR INFRARED DETECTOR APPLICATIONS. J.M. Arias, S.H. Shin, J.G. Pasko, M. Zandian and R.E. DeWames, Rockwell International Science Center, Thousand Oaks, CA 91360.

Device quality MBE HgCdTe must be demonstrated as the first step toward the fabrication of the next generation of large-area, high-performance IR focal plane arrays. We have carried out HgCdTe MBE growth studies which have lead us to device quality HgCdTe epilayers. Long- (8-14 μm) and middle (3-5 μm) wavelength IR photovoltaic diodes fabricated in these epilayers have performance (R_0A product values, quantum efficiency, etc.) comparable to those obtained using material grown by the more mature liquid phase epitaxy technique (LPE). These results represent a significant step toward the demonstration of MBE as a viable growth technique for the fabrication of large IR focal plane arrays.

Undoped MBE $\text{Hg}_{1-x}\text{Cd}_x\text{Te}$ ($0.20 < x < 0.30$) epilayers were grown on the (211)B orientation of CdZnTe and GaAs substrates. Epilayers up to 25 μm thick have been grown at a rate of 4-6 $\mu\text{m/h}$, at 195 °C. Alloy compositional uniformity is good; for $x=0.24$, the standard deviation of x was found to be 0.0017 for a $3.5 \times 1.5 \text{ cm}^2$ wafer. The epitaxial surface morphology was smooth and free from macroscopic defects which occur on other more common orientations. HgCdTe structural properties were measured by double crystal x-ray rocking curve and dislocation etching (EPD). FWHM and EPD values as low as 34 arc-sec and $1 \times 10^5 \text{ cm}^{-2}$ were obtained for the epilayers grown on lattice-matched CdZnTe, while those grown on GaAs substrates yielded values of 60 arc-sec and $6 \times 10^6 \text{ cm}^{-2}$, respectively. Homojunctions (p^+-n and n^+-p) were formed by arsenic diffusion and ion-implantation. We show that diodes fabricated on GaAs substrates have R_0A values that approach theoretical values when they are operating in the diffusion regime. This result is significant to imaging applications where the ability to grow acceptable devices on GaAs provides new possibilities in hybrid and monolithic technologies. Diodes fabricated on HgCdTe grown on CdZnTe substrates exhibited good diode performance even at lower operating temperatures ($T \leq 77\text{K}$). In this talk we will describe our most recent MBE growth studies, discuss their implications and present current material quality and diode characteristics.

E6.5

ELECTRICAL PROPERTIES OF MBE-GROWN HgCdTe S. Hwang, Jeong W. Han, J.W. Cook, Jr., and J.F. Schetzina, Department of Physics, North Carolina State University, Raleigh, NC 27695-8202

A detailed analysis of Hall effect data obtained at temperatures between 20K and 300K has been made for HgCdTe thin films prepared by molecular beam epitaxy. Based on a theoretical calculation for intrinsic concentrations that takes into account the non-parabolicity of the conduction band, the electron concentrations are shown to follow nicely the model for semiconductors in their extrinsic and intrinsic temperature range. The scattering mechanisms in these materials are studied through the analysis of electron mobility. Polar mode, deformation-potential acoustic, piezoelectric, and impurity scattering are included. The calculation is done by solving the Boltzmann equation with an iteration method that incorporates the two-mode nature of the optical phonons and the non-parabolicity of the conduction band. The results indicate that,

even at 77K, the scattering is dominated by polar optical phonon scattering.

Work is supported by NSF grant DMR-88-13525 and DARPA contract DAALO3-87-K-0153

E6.6

FIRST AND SECOND ORDER RAMAN STUDIES OF COMPOSITION AND STRUCTURAL ORDERING IN $\text{Hg}_{1-x}\text{Cd}_x\text{Te}$. A. Compaan, U. Toledo, Toledo, OH; R. C. Bowman, Jr., Aerospace Corp., Los Angeles, CA.

Alloy fluctuations, defect densities, and clustering are sensitive to crystal growth conditions. The resonance behavior of first and second order LO and TO Raman scattering has been shown to be quite sensitive to these properties in $\text{Hg}_{1-x}\text{Cd}_x\text{Te}$ (MCT). We have studied MCT for x -values between 0.20 and 0.32 and for photon energies from 2.35 to 2.7 eV and for samples prepared by a wide range of techniques—LPE, MOCVD, MBE, bulk growth, and pulsed laser annealing. In addition to the HgTe-like TO and LO modes and the CdTe-like LO mode, we have studied the resonance behavior of the mode at 133 cm^{-1} , which has been identified as originating from the preferential clustering of 3 Hg and 1 Cd about the Te.¹ We find that the intensity of this peak for various bulk and epitaxially grown samples is unusually large only near the E_1 resonance.² Pulsed laser annealing with a Nd:YAG-pumped dye laser strongly suppresses this mode in all samples suggesting that extremely rapid epitaxial regrowth may inhibit the 3:1 cluster formation. Second order Raman scattering also shows a strong resonance at the E_1 gap but this intensity is suppressed by the pulsed laser anneal.

¹ P. M. Amirtharaj, et al, *J. Vac. Sci. Technol.*, A3, 226 (1985.)

² A. Compaan, R. C. Bowman, Jr., & D. E. Cooper in Proc. Conf. Narrow Gap Semicond. & Related Materials, (Gathersburg, 12-15 June 1985.)

E6.7

TEMPERATURE-DEPENDENT INFRARED ABSORPTION OF HG-BASED II-VI SEMICONDUCTOR SUPERLATTICES* Z. Yang, Y. Lansari, J. W. Han and J. F. Schetzina, Physics Department, North Carolina State University, Raleigh, NC. 27695-8202

Optical absorption spectra for a series of $\text{HgTe}/\text{Cd}_{0.85}\text{Hg}_{0.15}\text{Te}$ superlattices (SL's) have been measured in the spectral region from 1 to $12\text{ }\mu\text{m}$, and at temperatures ranging from room temperature (RT) down to 77 K. First, the optical constants of each substrate at RT were obtained by measuring its transmission and reflection, along with its transmission spectra at T below RT. The SL's were then grown on these substrates and the absorption coefficient and refraction index of the SL's at RT were obtained by measuring the transmission and reflection spectra and using the exact formulae for the transmission and reflection of a two-layer system. The transmission spectra of the SL-substrate samples were then measured at temperatures $T = 77\text{--}300\text{ K}$. The transmission spectra of the corresponding substrates were used to correct the spectra of the samples and the absorption spectra of the SL's were thus obtained.

The absorption coefficient of the SL's show clear step-like features which are typical in SL's due to the transitions of electrons from different subbands. The transitions from the first heavy hole subband (hh1) and the first light hole subband (lh1) to the first conduction subband (c1) are clearly evident in the spectra. The observed transitions at RT agree well with the theoretically-predicted selection rules and transition energies. A value of 350 meV for the valence band offset between HgTe and CdTe is used. When the temperature decreases, the overall intensity of the absorption increases. This is due to the fact that fewer thermally excited electrons are in the conduction subbands and fewer holes are in the valence subbands. Below 240 K, two new exciton-like absorption lines appear near the energy of the $\text{hh1} \rightarrow \text{c1}$ transition. These features were observed in all three SL's studied to date. Because of the presence of the two lines it is difficult to determine with high accuracy how the energy of the $\text{hh1} \rightarrow \text{c1}$ transition changes with temperature. However, our results to date are consistent with a large (350 meV) and relatively temperature-independent

valence band offset for the HgTe/CdTe SL's. Additional samples are presently being studied to further clarify this point.

* This work was supported by NSF grant DMR-88-13525 and DARPA contract DAALO3-87-K-0153

E6.8

PROPERTIES OF MODULATION DOPED HgCdTe . Jeong W. Han, S. Hwang, Y. Lansari, J.W. Cook, Jr., and J.F. Schetzina, Department of Physics, North Carolina State University, Raleigh, N.C. 27695-8202

We have employed photoassisted molecular beam epitaxy to prepare both p-type and n-type modulation doped HgCdTe . All samples are superlattices of twenty double layers consisting of $\text{Hg}_{0.15}\text{Cd}_{0.85}\text{Te}/\text{Hg}_{1-x}\text{Cd}_x\text{Te}$ ($x=0.16\text{--}0.25$). As and In were used as p-type and n-type dopants, respectively. Dopant oven temperatures were changed systematically to obtain a range of carrier concentrations and mobilities.

Double crystal x-ray rocking curves exhibit very sharp main peaks (20-30 arcsec) with up to seven orders of satellites. Also, vertical cross-section TEM studies indicate that the superlattices are of very high structure quality with sharp interfaces. No evidence of Hg-interdiffusion was found in the TEM studies. The high structural quality is due to the low growth temperature ($T_s=150^\circ\text{C}$) associated with the photoassisted molecular beam epitaxy technique and very stable source fluxes. Hall effect measurements at low temperatures ($20^\circ\text{K}\text{--}100^\circ\text{K}$) yielded carrier concentrations independent of temperature for both n-type and p-type samples. The absence of carrier freeze-out indicates that modulation doping in HgCdTe was successfully achieved. Hole mobilities ranged from $200\text{ cm}^2/\text{Vs}$ to $400\text{ cm}^2/\text{Vs}$. Electron mobilities as large as $1.3 \times 10^5\text{ cm}^2/\text{Vs}$ were measured. These mobilities are comparable to carrier mobilities in bulk HgCdTe with the same carrier concentrations.

We will also report results of a systematic study of mobilities in modulation doped HgCdTe single heterostructures, in which we have changed the undoped spacer thickness, dopant oven temperatures, and Cd compositions in the channel. Mobilities dependent upon spacer thickness and sheet carrier densities at $\sim 30^\circ\text{K}$ will be reported.

*Work is supported by NSF grant DMR-88-13525 and DARPA contract DAALO3-87-K-0153

E7.1

SHOCKLEY-READ RECOMBINATION IN P-TYPE HgCdTe , Y. Nemi-rovsky and R. Fastow, Microelectronics Research Center, Technion - I.I.T, Haifa 32000, Israel.

The excess carrier lifetime in semiconductors and the related processes of generation and recombination determine directly device performance. In particular, it is very important to determine the excess carrier lifetime and the mechanism which limits the lifetime in p-type $\text{Hg}_{1-x}\text{Cd}_x\text{Te}$ with $x=0.225$, since currently modern focal plane arrays for detection of radiation in the $8\text{--}12\text{ }\mu\text{m}$ spectral region are based on this material.

Experimental studies of excess carrier lifetime in p-type HgCdTe indicate that Shockley-Read (S-R) recombination is the dominant mechanism at low temperature. Several experiments have been undertaken to measure the excess carrier lifetime in p-type HgCdTe . However, the results appear contradictory and the reported excess carrier lifetimes span 3 orders of magnitude, from $\sim \text{ns}$ to $\sim \mu\text{sec}$ at 77 K.

It appears that the major cause of controversy in the reported lifetime results, stem from lack of a unified approach to the definition of S-R lifetimes. Different time-constants measured in various studies and in versatile and diverse experiments, are referred by the common name "lifetime", and this has been a major cause for controversy and misunderstanding.

The purpose of this paper is to define the various "lifetimes" which are pertinent to the S-R model, and to pre-

sent various measurements on doped as well as undoped material. The time-constant measured in each experiment is theoretically defined and related to the physical parameters of the material. In particular, trapping effects will be considered.

E7.2

THE EFFECT OF SURFACE LAYERS IN EPITAXIAL n-TYPE HgCdTe, K.K. Parat, N.R. Taskar, I.B. Bhat and S.K. Ghandhi, Rensselaer Polytechnic Institute, Troy, New York 12180.

The presence of a low mobility n-type surface layer on n-HgCdTe is generally not apparent in the Hall Constant (R_H) vs. temperature curve for this material, or in the μ vs. temperature data. However, the influence of this layer is clearly seen by a study of the dependence of R_H as a function of the B field.

This talk will outline the use of this diagnostic method for evaluating epitaxial HgCdTe layers grown by organometallic vapor phase epitaxy, which have been previously converted to n-type by annealing in a Hg overpressure. The B field dependence of R_H was analyzed to extract the bulk and surface carrier concentrations, and also their respective mobilities. The effect of anodic sulfide passivation on the B field dependence of the Hall Constant will also be outlined. In these layers, the measured electron concentration and mobility values approach that of bulk HgCdTe. Additionally, details of the passivation technique will be presented in this talk.

E7.3

SURFACE ELECTRONS IN INVERTED LAYERS OF P-HGCDTE. S.E. Schacham and E. Finkman, Technion, Haifa, Israel.

A small concentration of surface electrons can cause strong anomalous behavior and even make p-type samples appear like n-type. Studying the nature of interface electrons we found that their properties depend on surface potential (electron concentration) in the inversion layer. Anodic sulfide passivation may give flatband conditions with hardly noticeable inversion layer. Samples with acceptor concentration as low as $8 \cdot 10^{14} \text{cm}^{-3}$ are characterized by completely normal behavior of the Hall coefficient. Annealing these samples in 70-120°C for several hours resulted in increasing number of n-skin electrons. Surface passivated using anodic oxide gave strongly inverted surfaces, with n-type behavior at all temperatures under the highest magnetic field used ($\sim 1\text{T}$). Analysis of magnetic field dependence of transport parameters show that properties of bulk material remained unchanged for the various surface treatments, indicating that the only change is induced near the interface, increasing the surface charge density and the depth of the band bending at the interface. The density of surface electrons was below $5 \cdot 10^{11} \text{cm}^{-2}$ for the anodic sulfide, and up to $5 \cdot 10^{12} \text{cm}^{-2}$ for the oxide interface. When surface concentration is small, the electron mobilities were lower than those obtained in same composition bulk n-type material, as can be anticipated (e.g. $\mu = 1 \cdot 5 \cdot 10^4 \text{cm}^2/\text{v.s}$ at 77K). However, increasing band bending and skin electrons in the induced well near the surface, resulted in very high mobility skin electrons (e.g. $1.5 \cdot 10^5 \text{cm}^2/\text{v.s}$ at 77K, and $3 \cdot 10^5$ at 13K, for composition $x=0.22$), as in the best n-type material. It is concluded that this is the result of lowering the dimensionality of the electrons while gradually increasing their confinement near the interface. Presently we intend to verify the 2D character of these electrons by performing transport studies at high magnetic fields, and Shubnikov-de Haas experiments.

E7.4

ELECTRICAL CHARACTERISATION OF P-TYPE $\text{Cd}_x\text{Hg}_{1-x}\text{Te}$ GROWN BY MOVPE (IMP). A. Royle, J S Gough, S J C Irvine and J B Mullin. Royal Signals and Radar Establishment, Malvern, Worcestershire UK

Detailed electrical characterisation and analysis of results on a series of epitaxial layers grown by MOVPE (IMP) on CdTe substrates has

been carried out. The growth programme was aimed at achieving low carrier concentration p-type material with a low x alloy composition, in some cases x was as low as $x = 0.19$. The design of high operating temperature (HOT) IR detectors requires material with this specification.

Temperature dependent Hall measurements over the 4.2 to 300K range were carried out on a series of layers. At low temperatures, surface and interface effects can dominate the complex Hall coefficient as this technique measures both p-type bulk properties and surface inversion layers in parallel. In an attempt to suppress these effects a series of layers have been grown with thin epitaxial caps and buffers.

The best Hall data, viz R_H positive at very low temperatures has been obtained on layers with $x \sim 0.22$ and using the cap and buffer structure. The acceptor concentration was typically $5 \times 10^{14} \text{cm}^{-3}$. These results will be compared with layer of lower x and uncapped structures. Theoretical fits to the best p-type data have been attempted; values of the extrinsic hole concentration and acceptor ionization potential have been obtained. A value of the intrinsic carrier concentration (n_i) is a required parameter for the fitting equations and the best fits suggest that there is either a discrepancy in the determination of alloy composition or the published values of n_i (x, T).

E7.4A

MBE GROWTH: SURFACE ROUGHNESS THEORY*

**A. Sher, Srinivasan Krishnamurthy and Martha A. Berding
SRI International, Menlo Park, California 94025**

**A.-B. Chen, Auburn University, Auburn, Alabama 36849
Archibald Fripp
National Aeronautics and Space Administration
Langley Research Center
Hampton, Virginia 23665**

In this paper, we consider the surface entropy to be related to the arrangement of atom pairs rather than the more traditionally used total number of configurations. This important correction is applied to the simplest theory of nucleation of solids and their growth rate. The purpose of this paper is to demonstrate, within the context of a simple and physically transparent model, the arguments needed to improve the surface entropy calculations and a range of resulting effects. The major changes introduced are a reduction of the rough to smooth critical transition temperature, smooth limit islands with fewer point defects, direct demonstration of layer by layer growth, and a relation between the effect of energy assisted MBE and entropy equilibration.

*This work has been supported in part by the National Aeronautics and Space Administration under Contract NAS1-18226 and ONR Contract N00014-88-C0096.

E7.5

LANGMUIR-BLODGETT FILM PASSIVATION ON CATHODICALLY CLEANED MCT AND PC-TYPE DEVICES. Kengo Shimano, Tetsuya Suzuki, Taizo Hoshino and Masao Sakashita; R&D Labs. -I, Nippon Steel Corp., 1618 Ida, Nakahara-ku, Kawasaki 211, Japan

Surface passivation of semiconductors $Hg_{1-x}Cd_xTe$ (MCT) is of importance for their utilization as IR detectors. This work reports MCT surface passivation technique combined with cathodic surface cleaning and Langmuir-Blodgett film formation. Characteristics of PC-type devices are also discussed.

N-type MCT ($x=0.20$) substrates were chemically etched with methanol solution containing 0.5% of bromine after mechanical polishing. The surface oxides on MCT were reduced electrochemically in a pH 5.0 acetic acid - acetate buffer solution at a voltage (vs. Ag/AgCl) between -0.85 and -1.00 V. By using XPS, it is confirmed that the cathodically reduced surface is oxide free. Indium electrodes were formed on MCT substrate where the active area was 1 mm^2 . 10,12-heptacosadienic acid (a diacetylene compound) was used as the amphiphilic compound for LB film formation. This type of diacetylene was polymerized by irradiation with UV light. Such a polymerization increases mechanical strength of the LB film. Fig. 1 shows the characteristic of a PC-type device passivated by the LB film of 41 layers as a relative response to a thermopile. These MCT devices exhibit sufficient sensitivity to detect IR radiation in the atmospheric window.

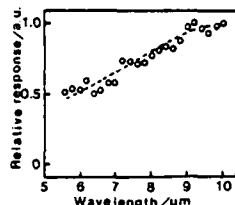


Fig. 1 Spectroscopic characteristics of LB/MCT sensor.

E7.6

ENHANCED METALLIZATION STABILITY ON MERCURY-CADMIUM-TELLURIDE. A. Raisanen, G. Haugstad, X. Yu, and A. Franciosi, Dept. of Chem. Engineering and Materials Science, U. of Minnesota, Minneapolis, MN 55455; and D.J. Peterman, McDonnell Douglas Research Labs, St. Louis, MO 63166.

$Hg_{1-x}Cd_xTe$ (MCT) semiconductor alloys are widely used for high-performance infrared detectors. Deposition of metals such as Al, In, and Cr onto MCT surfaces yields atomic interdiffusion and a preferential metal-Te reaction causing Hg-depletion of the surface layer, with a severe effect on junction properties. Semi-empirical calculations of binary thermodynamic reaction enthalpies using Miedema's model suggest that thin rare earth metal interlayers may act as diffusion barriers at metal/MCT junctions due to the large rare earth-Te and rare earth-Hg reaction enthalpies. Our synchrotron radiation photoemission studies of metal/MCT contacts involving Al, In, Cr, and Ag metallizations with and without thin (1-15 Å) Yb interlayers indicate that Yb acts as an effective diffusion barrier on the MCT surface, preventing metal-Te reaction, Hg-depletion of the semiconductor near-surface layer, and, in general, atomic interdiffusion across the junction.

E7.7

GROWTH OF HIGH QUALITY LWIR FILMS BY LIQUID PHASE EPITAXY. Dipankar Chandra, Texas Instruments Inc., Dallas, Tx.

Growth of long wavelength infra-red mercury cadmium telluride films by liquid phase epitaxy has usually yielded films of inferior electrical properties as evidenced

by Hall mobilities lower than theoretical values by factors of 5 or more at 77 K. In addition the Hall behavior over the entire temperature range did not follow classical behavior. A systematic series of investigations was conducted to improve the electrical performance of these films by four methods: i) growth of $HgZnTe$ films, where the cadmium was replaced by zinc, ii) growth at temperatures $>550^\circ\text{C}$, iii) growth at a slow rate on a $CdZnTe$ substrate following 'cleaning' in the melt of the substrate surface and iv) doping the film by controlled levels of indium or gallium.

The first method did not lead to any improvements in the Hall behavior. In addition, the films grown displayed varying dislocation densities. The second method led to a small but definite increase in the yield of non-anomalous or classical films (5%). The third method yielded films with classical or non-anomalous Hall behavior about 20% of the time. The last method consistently led to films with classical Hall behavior. This was accomplished with indium doping levels at $1.5 \times 10^{14}/\text{cm}^3$. Preliminary data indicate that it will be possible to go to still lower doping levels while maintaining classical Hall behavior. Similar data were observed for gallium doping. The segregation coefficients controlling the doping levels and their concentration dependence were also precisely determined during these investigations. The improvement in the electrical properties of these epilayers can be attributed to the reduction or elimination of type inhomogeneities known to degrade Hall mobilities in films grown by liquid phase epitaxy.

E7.8

CHARACTERIZATION OF $(Hg,Cd)Te$ FOR INFRARED FOCAL PLANE ARRAY APPLICATIONS. A. J. Syllaios, V. C. Lopes, W. H. Wright, Texas Instruments Inc., Dallas, Texas 75265

Material characterization has an important role in the use of $(Hg,Cd)Te$ for Infrared Detector Focal Plane Array applications. It addresses both the evaluation of material preparation processes and the selection of material suitable for the construction of detector arrays. A comprehensive characterization effort includes the use of simple prototype detector devices and the use of a series of non-invasive characterization techniques.

One prototype detector, the Metal Insulator Semi-conductor (MIS) device, is used to establish correlations between material parameters and focal plane array performance. Such MIS device characteristics as dark current, breakdown voltage and photoresponse are correlated to optical and electrical material properties, as well as to the density of crystal defects. Spatially resolved MIS device, FTIR transmission, minority carrier lifetime and surface recombination velocity measurements will be reviewed. Recent results will be presented for n-type bulk $(Hg,Cd)Te$ with a Cd concentration of $x=0.22$ and a 77 K cutoff wavelength of 10 μm , grown by the Solid State Recrystallization process or by the Travelling Heater Method.

E7.9

EFFECTS OF DEFECTS ON METAL-INSULATOR-SEMICONDUCTOR PROPERTIES OF $HgCdTe$ FILMS GROWN BY LIQUID PHASE EPITAXY. Dipankar Chandra and Michael W. Goodwin, Texas Instruments Inc., Dallas, Texas.

A comprehensive study of all materials parameters influencing metal-insulator-semiconductor (MIS) properties of n-type $HgCdTe$ films grown by liquid phase epitaxy from tellurium rich melts was conducted. When the epitaxy process was optimized to grow films free of inclusions and terracing, the first indications of the MIS properties to be expected could be obtained from the temperature dependence of the Hall electron mobility.

Films displaying an anomalous dependence of the Hall mobility on temperature yielded non-classical low frequency MIS properties with little or no measurable 'dark' storage times ($< 2 \times 10^{-6}$ second). The MIS performance of these films appeared relatively independent of other materials parameters; remaining, for example, virtually unaffected by the film dislocation density changing between $5 \times 10^4/\text{cm}^2$ and $2 \times 10^6/\text{cm}^2$.

Films displaying a classical dependence of the Hall mobility on temperature yielded drastically improved classical high frequency MIS properties. For these films, the

MIS performance appeared almost exclusively dependent on dislocation density levels as long as the donor density remained lower than $1 \times 10^{15}/\text{cm}^3$. The dark storage time of classical films increased continuously with decreasing dislocation density levels, rising to 100 μs for a dislocation density level of $1 \times 10^5/\text{cm}^2$ for materials with a 77 K IR cutoff wavelength of 10.5 μm . A simple monotonic relationship could be established between the MIS performance parameters and the dislocation density over the entire measurement span: from $5 \times 10^4/\text{cm}^2$ to $2.5 \times 10^6/\text{cm}^2$.

E7.10

LOW-TEMPERATURE PROCESSING TECHNOLOGY FOR II-VI SEMICONDUCTORS.*

D.L. Dreifus and R.M. Kolbas, Department of Electrical and Computer Engineering; B.P. Sneed and J.F. Schetzina, Department of Physics, North Carolina State University Raleigh, NC 27695-8202

A new low-temperature (<60°C) processing technology that avoids potentially damaging processing steps such as ion-implantation and elevated-temperature-annealing has been developed at NCSU. The technology includes: 1) photolithographic transfer of patterns with geometries as small as 2 μm , 2) calibrated etchants with etching rates as low as 40 Å/s and compatible with photolithography, 3) a metallization lift-off process using a photoresist profiler, 4) an interlevel metal dielectric for advanced structures requiring multilevel metallizations, and 5) an insulator technology for metal-insulator-semiconductor (MIS) structures.

A number of devices have been fabricated from II-VI epitaxial layers grown by photoassisted molecular beam epitaxy and processed using the technology described above. This has resulted in several first demonstrations of II-VI semiconductor devices such as CdTe metal-semiconductor field-effect transistors (MESFETs), CdTe p-n junctions, CdMnTe MESFETs, and HgCdTe metal-insulator-semiconductor field-effect transistors (MISFETs). Optimization of the processing steps has resulted in device yields in excess of 75% on recent device structures, including HgCdTe MISFET devices from which digital logic circuits have been successfully fabricated and tested.

*Work supported by NSF grant DMR-88-13525 and DARPA contract DAAL03-86-K-0146.

E8.1

RECENT PROGRESS IN THE MOVPE GROWTH OF HgCdTe (Invited), S.K. Ghandhi, Rensselaer Polytechnic Institute, Troy, New York 12180.

This talk will present recent progress in the direct alloy growth of HgCdTe, by organometallic vapor phase epitaxy. Issues of compositional uniformity have essentially been solved, and the focus of efforts is now on annealing of as-grown material, and on extrinsic doping. The annealing of epitaxial layers has proved to be considerably more difficult than for bulk material. Problems with the full annealing of as-grown p-type HgCdTe layers to n-type will be outlined, and techniques described for overcoming them. Extrinsic n- and p-type doping of HgCdTe will also be described, using arsine gas as the dopant species for p-type, and trimethylindium for n-type HgCdTe. Properties of extrinsic layers will be described, both for as-grown layers and also for layers which have been subjected to heat treatment.

Finally, progress in the growth of HgCdTe at reduced temperatures will be presented. Crystal properties as well as electrical characteristics will be presented for HgTe and HgCdTe layers, grown in the 240-320°C range. The advantages of growth at reduced temperatures will be outlined, as well as its associated problems.

E8.2

VAPOUR PRESSURE MEASUREMENTS ON ORGANOTELLURIUM PRECURSORS FOR MOVPE J.E. Hails, S. J. C. Irvine and J. B. Mullin, Royal Signals and Radar Establishment, St Andrews Road, Malvern, Worcs, UK

A well accepted objective for improved material quality in the MOVPE growth of the infra-red detector material (Hg,Cd)Te is

deposition at lower temperatures. This will lead to reduction and control of the equilibrium mercury vacancy concentration allowing greater control of the electrical properties. Lowering the growth temperature would also reduce the interdiffusion between substrates and epitaxial layers thus enabling more complex structures to be grown. There are two ways in which the growth temperature can be lowered:

- use of less stable precursors for thermal growth
- photolytic growth.

Both of these routes will require the use of alternative precursors.

Before an organometallic compound can be used as a precursor, certain basic properties need to be known and one of the most important of these for MOVPE growth is vapour pressure. An MOVPE system for precursor assessment which has facilities for the measurement of vapour pressure will be described. The technique used can also give information on the photo and thermal stabilities of the organotellurium compounds. Results on the assessment of some new organotellurium compounds will be reported.

E8.3

INFLUENCE OF SUBSTRATE QUALITY IN THE METAL ORGANIC CHEMICAL VAPOUR DEPOSITION OF HgCdTe, M.J. Bevan and N.J. Doyle, Westinghouse STC, Pittsburgh, PA.

The quality and uniformity of HgCdTe IR detectors are thought to be limited by structural defects. MOCVD technology has advanced to the state that HgCdTe is limited by the crystal quality and uniformity of the substrate material. Foreign substrates such as GaAs is used but the large mismatch is only partly accommodated, resulting in films with double crystal rocking curve widths greater than 1 arcmin. Using lattice-matched substrates, CdZnTe and CdTeSe (nominally 4.5% Zn or Se), (100) 2° oriented epilayers have comparable rocking curve widths (ca. 25 arcsec), but have pyramidal facets (>10 μm). The hillocks are avoided by using the (111)B orientation, but HgCdTe has a rotational twinned structure. Specular films have been grown free of twinning by MOCVD on (211)B substrates, combining the attributes of both (111) and (100)-oriented HgCdTe.

Characterisation of substrate material continues to reveal a range of undesirable properties, potentially detrimental to epitaxial growth, both structurally and chemically. Using x-ray techniques, the range of defects observed in commercially-available material include, for example, precipitates and inclusions, microcracks and microtwins, sub-grain structure and non-uniformity in double crystal rocking curves. Unintentional impurity doping of the substrate material give rise to low resistivity (<100 ohm cm) and these impurities can ultimately dope the subsequent HgCdTe epilayer. Electrical evaluation of as-grown and Hg-annealed films has suggested the presence of dopants arising from the substrate.

E8.4

TEM CHARACTERIZATION OF DEFECTS IN HgCdTe GROWN ON (001) CdTe AND (111)B CdZnTe SUBSTRATES BY MOCVD, Anthony Hobbs, O.Ueda, K.Maruyama, S.Murakami and K.Shinohara; Fujitsu Laboratories Ltd., Japan.

Transmission Electron Microscopy (TEM) has been used to characterize epilayers of $\text{Hg}_{1-x}\text{Cd}_x\text{Te}$ ($x=0.16$) grown on both (001) CdTe and (111)B $\text{Cd}_{0.97}\text{Zn}_{0.03}\text{Te}$ substrates by MOCVD. Growth on (001) CdTe is found to give rise to epilayers which contain a large number of grain boundaries in the surface region with associated boundary dislocations. Many dense dislocation bands have also been identified at these boundaries. The grains themselves are often oblong in shape with the long axis in just one <110> direction. In addition, a high density of dislocation loops are associated with the boundary dislocation network.

By contrast, growth on (111)B $\text{Cd}_{0.97}\text{Zn}_{0.03}\text{Te}$ substrates results in double-position twinning at

the surface. The surface morphology consists of roughly circular hillocks with a twinned relationship to the surrounding material. Several types of twin-boundaries are evident; these are often accompanied by dislocation networks. Grain boundaries and dislocation loops of the type seen in the (001) epilayers are not generally present although localized regions containing large numbers of dislocation segments and loops are found.

The formation mechanism for the defect structure in both (001) and (111) epilayers will be discussed.

E8.5

STRUCTURAL AND ELECTRICAL PROPERTIES OF HETEROEPITAXIAL HgCdTe/CdZnTe/GaAs/Si. S.M. Johnson, W.L. Ahlgren, M. H. Kalisher, W. J. Hamilton, Jr., and J. B. James, Santa Barbara Research Center, 75 Coromar Dr., B2/8, Goleta, CA 93117

The growth of HgCdTe on Si-based substrates is now being strongly pursued to provide an alternative to bulk CdZnTe substrates for improvements in size, strength, monolithic signal processing, and cost of infrared detector arrays. We are using a hybrid growth approach by which epitaxial CdZnTe is grown on GaAs/Si wafers by metal-organic chemical vapor deposition (MOCVD) followed by the growth of HgCdTe by the more mature liquid-phase epitaxy (LPE) technology. The structural properties of these layers were characterized using high-resolution x-ray rocking-curve analysis. The commercial GaAs/Si wafers used as starting substrates were oriented (100) 3° toward [111] with typical rocking-curve full-width at half-maximum (FWHM) of 150-200 arc-sec. High-resolution x-ray measurements show that the GaAs layer is tilted 0.24° further toward [111] with respect to the Si and that the (100) CdZnTe layer is tilted by 4.1° back towards [111] with respect to the GaAs, apparently to reduce the interfacial energy associated with the large lattice mismatch. Perpendicular and parallel strain measurements show that there is some tetragonal distortion (elastic strain) of the GaAs layer; however, the 14.6 % lattice mismatch between CdZnTe and GaAs is almost entirely relieved by plastic deformation (misfit dislocations). X-ray FWHM values of as low as 85 arc-sec have been obtained for the heteroepitaxial CdZnTe layers. We have also found that the FWHM of the HgCdTe layer is typically lower than that of the CdZnTe layer, which is due to both an annealing effect during the LPE growth and an improvement in material quality with increased thickness. LPE-grown In-doped, n-type, Hg_{0.7}Cd_{0.3}Te layers with 77K mobilities of 4×10^4 cm²/V-sec and carrier concentrations of 4×10^{15} cm⁻³ were obtained on the heteroepitaxial substrates; these properties are nearly identical to those of layers grown simultaneously on bulk CdZnTe substrates. The variations in the HgCdTe electrical properties with the structural quality of the heteroepitaxial substrates will be discussed.

E8.6

PROPERTIES OF HgTe-ZnTe STRAINED LAYER SUPERLATTICES GROWN BY MOVPE J.T. Mullins, P.A. Clifton, P.D. Brown, K. Durose and A.W. Brinkman, Applied Physics Group, S.E.A.S. University of Durham, South Road, Durham DH1 3LE, U.K.

The HgTe-ZnTe strained layer superlattice system is a possible alternative to mercury cadmium telluride (MCT) as a long wavelength infra-red material and is of interest in its own right as an example of a highly strained type III superlattice. The interdiffusion coefficient between HgTe and ZnTe is sufficiently low to allow growth at typical MOVPE temperatures. By producing a superlattice of the two binary compounds rather than a ternary alloy, it is possible to tailor the effective energy gap of the material independently of the composition by appropriate choice of well and barrier thicknesses. For a given cutoff wavelength the resulting material is more structurally stable than MCT as less mercury is required and the destabilising effect of Cd on the weak Hg-Te bond is eliminated.

In this work the properties of HgTe-ZnTe superlattices grown by Metal Organic Vapour Phase Epitaxy at temperatures down to 325°C are reported. Their structure was characterised by cross-sectional transmission electron microscopy and X-ray diffraction. Infra-red transmission measurements were made to determine the optical absorption coefficient as a function of wavelength and show maximum absorption coefficients comparable to those of MCT. Their electrical properties and the effect on the electronic structure of the anisotropy dictated by the superlattice periodicity were assessed by high field magneto-transport measurements.

E8.7

MBE GROWTH AND CHARACTERIZATION OF SMALL BAND GAP HgTe-HgCdTe SUPERLATTICES.* Y. Lansari, Z. Yang, S. Hwang, J.W. Cook, Jr., and J.F. Schetzina, North Carolina State University, Raleigh, NC 27695-8202.

A series of undoped and In-doped HgTe-Hg_{0.15}Cd_{0.85}Te superlattices (SLs) of varying well and barrier thicknesses has been grown by molecular beam epitaxy (MBE) and photo-assisted MBE.

Double-crystal x-ray rocking curve measurements were performed on all the SLs and full widths at half maxima of the main diffraction peaks as low as 28 arcs were measured, indicative of very high structural quality. X-ray satellite peaks were observed for all of the SLs studied, which allowed accurate determination of the SL double-layer thickness.

For different SLs, the HgTe layer thickness ranged from 67 Å-160 Å, while the Hg_{0.15}Cd_{0.85}Te layer thickness ranged from 35 Å to 102 Å, leading to small band gaps, as calculated using the k-p model. In this band gap regime, unique electrical properties including highly anisotropic effective masses and very high mobilities are expected to occur. All of the SLs were n-type with carrier concentrations ranging from 10^{16} - 10^{17} cm⁻³ (30-295 K). Mobilities as large as 1×10^5 cm²/Vs (30-60 K) were measured using standard van der Pauw techniques.

Transmission and reflection data (300 K) were used to obtain absorption coefficient versus photon energy curves which clearly show large step-like features due to the 2D electronic transitions between the superlattice valence and conduction subbands. New features associated with the near-zero gap nature of the SLs were also observed and will be discussed.

*Work supported by NSF grant DMR-88-13525 and DARPA contract DAAL03-87-K-0153.

E8.8

PHASE DIAGRAM, LATTICE PARAMETER, AND OPTICAL OPTICAL ENERGY GAP VALUES FOR THE Hg_{2x}(CuIn)_yMn_{2z}Te₂ (x+y+z=1) ALLOYS. Pedro Grima Gallardo, Fac. Ciencias, Dpto. Física, Laboratorio de Cristales, Centro de Estudios en Semiconductores, Universidad de Los Andes, Mérida, Venezuela.

Polycrystalline samples of the diluted semimagnetic semiconductor alloys Hg_{2x}(CuIn)_yMn_{2z}Te₂ are prepared by the melt and anneal technique. Measurements of differential thermal analysis (DTA), Guinier x-ray photographs and optical absorption are carried out in order to obtain the lattice parameters, optical energy gaps (E_g) and phase transition temperature values.

The results shown four single-phase fields, namely ordered zincblende (β), ordered chalcopyrite (α'), disordered zincblende (β) and disordered chalcopyrite (α) in the composition range of interest. For higher z values the field is two phases. It is shown that while the manganese ordering has little effect on the lattice parameters, it has appreciable effect on the values of E_g . This is demonstrated by the different aiming points at z=1 for the E_g vs z lines in the different fields.

Sections of the general T(x,y,z) phase diagram are presented in order to visualize the different fields.

E8.9

On the field emission from HgTe-CdTe superlattices with graded structures under magnetic quantization. Kamakhyia P. Chatak, Department of electronics Engineering, University of Jaiyapur, Calcutta-700032, India; and Sambhu N. Biswas, Department of Electronics and Telecommunication Engineering,

Bengal Engineering College, Shibpur, Howrah-711103, West Bengal, INDIA.

HgTe/CdTe superlattices (SL's) have received a great deal of attention since 1979 when they were first suggested as a promising new materials for long-wave length infrared detectors and other opto-electronic applications. These features arise from the unique zero-band gap material HgTe and direct band-gap semiconductor CdTe whose energy band structure could be described by three band Kane model. All the works have been reported with the assumption that the interfaces between the layers are sharply defined with zero thickness, so as to be devoid any interface effects. Thus an intermediate potential region exists for the carriers which influences all the transport properties.

It is well-known that at field strength of the order of 10^9 V/m, the potential barrier at the surfaces of metal, alloys and semiconductor heterostructures usually become thin and result in field emission of the electrons due to tunnel effect. In the present paper, we studied the magnetic field emission from HgTe/CdTe SL and compared the same with the bulk specimens of constituting materials. The field emitted current density increases with electron concentration and field strength in an oscillatory manner. The field emission in HgTe/CdTe SL is greater than that of the constituting materials and the theoretical results are in agreement with the experimental observations as reported elsewhere.

E8.10

INVESTIGATION OF LIQUID ENCAPSULANT FOR CdTe AND $\text{Cd}_{1-x}\text{Hg}_x\text{Te}$ MELT. Wang Caihao and Wu Wenhui, Department of Materials Science, Shanghai University of Science and Technology, Jiading, Shanghai 200180, China.

The LEC technique has not been able to be used successfully for the crystal growth of II-VI compounds due to the lack of suitable encapsulant having the following characteristics at the crystal pulling temperature: lower melting point than the crystal grown, smaller specific gravity than the II-VI compound melt, high boiling point, low vapor pressure, transparent, wetting the SiO_2 container and the II-VI melt, but not reacting with them nor insoluble with the II-VI melt. The encapsulant generally used for the III-V compounds, B_2O_3 , has not all these characteristics.

According to the above requirements, among the IA- and IIA-halides only the chlorides can be considered. Thermodynamic calculation shows that IA and IIA elements can not be replaced from their chlorides by Hg or Cd, and that IA- or IIA-chlorides does not react with SiO_2 . A lot of mixtures, each composed of two chlorides, were tested. The eutectic composition of these mixtures were selected to lower the melting point. Experimental results show that from them three mixtures of chlorides can satisfy the demands of the encapsulant for CdTe and $\text{Cd}_{1-x}\text{Hg}_x\text{Te}$ melt.

E8.11

MBE GROWTH AND CHARACTERIZATION OF HIGH QUALITY EPITAXIAL $\text{Hg}_{1-x}\text{Cd}_x\text{Te}$ THIN FILMS. M.B. Lee, J. De Carlo, D. Di Marzio, and M. Kesselman, Grumman Corporate Research Center, M/S A02-026, Bethpage, N.Y. 11714

Reproducible and highly uniform epilayers of $\text{Hg}_{1-x}\text{Cd}_x\text{Te}$ up to 11 μm thick have been grown on (100) CdTe substrates using molecular beam epitaxy. These

epilayers were characterized in detail using a wide variety of structural, optical, and electronic techniques. Compositions as low as $x=0.153$ have been achieved with sharp IR absorption cutoffs and good uniformity over a 1cm x 1cm square area. Double crystal x-ray rocking curve measurements indicate that the epilayers are of good crystallinity. Hall mobility of as-grown epilayers is $\sim 10^6 \text{ cm}^2/\text{Vsec}$ while the carrier concentration is $\sim 10^{15} \text{ cm}^{-3}$ at 10 K. In addition, EDAX scanning electron microscopy data, as well as preliminary results of temperature dependent EXAFS measurements will be presented. Corresponding characterization of these epilayers after post growth Hg vapor annealing will also be discussed.

E9.1

FREE-CARRIER INDUCED OPTICAL NONLINEARITIES IN NARROW BANDGAP SEMICONDUCTORS. S. Y. Auyang and P. A. Wolff*, Massachusetts Institute of Technology, Cambridge, MA 02139

We have studied a variety of fast, free-carrier induced third order optical nonlinearities in semiconductors by four-wave mixing experiments using CO_2 lasers. Among the materials studied, HgTe and HgCdTe compounds yielded the largest nonlinearities, partly because of their small energy bandgaps and effective masses. Third order nonlinear optical susceptibilities in excess of 2×10^{-3} esu have been observed in HgCdTe epitaxial layers. Free carrier nonlinear processes are fast, with relaxation times in the picosecond range. They are capable of inducing huge perturbations in the dielectric function because they do not saturate at high laser intensities, as the slower processes do. The large nonlinearities we observe are nonresonant and operate at room temperature. They do not require exact matching of the material parameter to the light frequency, although optimizing the energy band structures in superlattices can further enhance the optical nonlinearity. These nonlinear processes have potential application in optical data processing.

* Present address: NEC Research Institute, Princeton, NJ.

E9.2

NARROW-GAP NONLINEAR OPTICAL MATERIALS. E. R. Youngdale, C. A. Hoffman, J. R. Meyer, and F. J. Bartoli, Naval Research Laboratory, Washington, D. C.; J. W. Han, J. W. Cook, Jr., and J. F. Schetzina, North Carolina State University, Raleigh, NC; A. Martinez, Naval Surface Weapons Center, Silver Spring, MD.

We discuss an experimental study of optical nonlinearities in HgTe-CdTe superlattices grown by MBE and $\text{Pb}_{1-x}\text{Sn}_x\text{Se}$ grown by hot-wall epitaxy. These systems are attractive candidates for nonlinear optical applications, since the electron effective masses are very light in the region near zero energy gap. Third-order nonlinear susceptibilities ($\chi^{(3)}$) have been determined by the non-degenerate four-wave mixing technique, using a pair of grating-tuned, Q-switched CO_2 lasers. Measurement of the dependence of $\chi^{(3)}$ on frequency difference $\Delta\omega$ has yielded relaxation times (τ) for the dominant nonlinear mechanisms. In the superlattices τ is found to decrease with increasing energy gap, reaching a value of ≈ 1 ps in the wider gap samples. Open-gap superlattices show a stronger dependence on laser power and temperature than do zero-gap superlattices, in agreement with a theoretical calculation based on the optical heating of carriers. $\chi^{(3)}$ up to 4×10^{-5} esu is observed. A large $\chi^{(3)}$ is also obtained in $\text{Pb}_{0.8}\text{Sn}_{0.2}\text{Se}$ ($\approx 2 \times 10^{-5}$ esu). The nonlinear prop-

erties were studied in a Fabry-Perot configuration, and enhancement of the four-wave signal will be discussed. The optical nonlinearities in both HgTe-CdTe superlattices and $\text{Pb}_{1-x}\text{Sn}_x\text{Se}$ films show no saturation at power densities up to 400 kW/cm^2 .

E9.3

TRANSPORT PROPERTIES OF Hg-BASED SUPERLATTICES. C. A. Hoffman, J. R. Meyer, and F. J. Bartoli, Naval Research Laboratory, Washington, D. C.

The present understanding of band edge and free carrier properties in Hg-based superlattices such as HgTe-CdTe is reviewed. We emphasize the large number of striking experimental results that have been demonstrated in this material system, such as extremely high hole mobility, equal electron and hole mobilities, mass broadening of holes and a double transition of the superlattice from semiconducting to semimetallic and back to semiconducting with increasing HgTe well width. These results are related to distinctive aspects of the superlattice band structures obtained theoretically. One finds that nearly all of the main experimental results are qualitatively consistent with band structures calculated assuming a large valence band offset, but are difficult to explain if the offset is small. The band structure for Hg-based superlattices thus appears to be fairly well understood, and the theoretical results imply a number of unique properties which are not attainable in other materials. Potentially, these may be exploited in new types of devices.

E9.4

HgTe-CdTe MULTIPLE QUANTUM WELLS. C. A. Hoffman, D. J. Arnold, J. R. Meyer, and F. J. Bartoli, Naval Research Laboratory, Washington, D. C.; Y. Lansari, J. W. Cook, Jr., and J. F. Schetzina, North Carolina State University, Raleigh, NC.

A series of high-quality HgTe-CdTe multiple quantum wells have been grown by MBE onto lattice-matched $[100] \text{Cd}_{1-x}\text{Zn}_x\text{Te}$ substrates. While most previous studies of the HgTe-CdTe system have involved superlattices with relatively thin ($\leq 60 \text{ \AA}$) CdTe barriers, the $\approx 100 \text{ \AA}$ barriers of the present samples prevent significant tunneling between neighboring wells. Since the energy bands then have no dispersion in the growth direction, the "mass-broadening" phenomenon which has a large effect on the transport and magneto-optical properties of HgTe-CdTe superlattices, is eliminated. Detailed magneto-transport measurements as a function of magnetic field and temperature have been treated by a mixed conduction analysis. Accurate energy gaps have been obtained from the temperature dependence of the intrinsic carrier density. Although samples with well thicknesses $d_w = 68$ and 160 \AA are found to have gaps near zero, an energy gap of 16 meV has been determined for a structure with intermediate d_w (128 \AA). This represents the first experimental confirmation of a second semiconducting region which had been predicted theoretically. We also find that for the range of well thicknesses studied, the temperature at which the electron mobility has its peak is more sensitive to the band structure than to the particular scattering mechanisms. Due to the negative temperature coefficient of the effective mass, μ_n in thick-well samples increases with T well into the region where phonon scattering dominates the momentum relaxation.

E9.5

ELECTRIC FIELD EFFECTS IN Hg-BASED AND NON-Hg-BASED II-VI SEMICONDUCTOR QUANTUM WELLS*. Z. Yang, J. F. Schetzina, Physics Department, North Carolina State University, Raleigh, NC. 27695-8202

We report here a theoretical study on the effects of an external electric field applied across an asymmetric quantum well (QW) structure composed of II-VI semiconductors. An asymmetric QW structure is made of two thin well layers with different thicknesses

separated by a thin barrier layer and sandwiched between two barrier layers. Each layer thickness is $\sim 30 - 100 \text{ \AA}$. Several QW's made of different II-VI semiconductors were studied to explore their applications in electrooptics at wavelengths ranging from 0.5 to 10 \mu m .

A typical structure studied is a Hg-based multi-QW with two well layers of $\text{Cd}_{0.18}\text{Hg}_{0.82}\text{Te}$ (75 \AA) and $\text{Cd}_{0.18}\text{Hg}_{0.82}\text{Te}$ (100 \AA), separated by a $\text{Cd}_{0.85}\text{Hg}_{0.15}\text{Te}$ (30 \AA) barrier layer and sandwiched between two $\text{Cd}_{0.85}\text{Hg}_{0.15}\text{Te}$ layers. At zero electric field, the band gap of the QW structure is 120 meV at $T = 300 \text{ K}$ which corresponds to a 10 \mu m absorption edge. The band gap changes by more than 25 meV when the field strength is increased to 100 KV/cm . Whether the band gap increases or decreases depends on the direction of the applied field. Similar QW's with higher x -value can cover the wavelength region up to 1 \mu m . CdMnTe can be used as a barrier material for even shorter wavelengths. In the green and blue spectral region, ZnTe/ZnSe QW's can be used. Large band gap shifts exist in all the asymmetric QW's studied.

Potential applications of these QW's include high speed optical modulators for fiber optic telecommunication, nonlinear optical devices, and even logic units with lasers, detectors and modulators all fabricated on a single substrate.

* This work was supported by NSF through grant DMR-88-13525 and DARPA contract DAAL03-87-K-0153

E9.6

NEW DEVELOPMENTS IN II-VI-BASED DILUTED MAGNETIC SEMICONDUCTORS. J. K. Furdyna and N. Samarth, Physics Department, University of Notre Dame, Notre Dame, IN 46556.

The most commonly studied diluted magnetic semiconductor (DMS) alloys belong to the $\text{A}^{II}_{1-x}\text{Mn}_x\text{B}^{VI}$ family of materials. These systems have been investigated for several years, and have been extensively reviewed. In this paper, we describe recent developments in both bulk and epitaxial growth of II-VI-based DMS alloys, focusing on two nascent areas of research: a) crystal phases such as cubic (zinc-blende) $\text{Cd}_{1-x}\text{Mn}_x\text{Se}$ which were previously inaccessible by conventional bulk growth techniques but which can be stabilized by molecular beam epitaxy and b) DMS alloys such as $\text{Cd}_{1-x}\text{Fe}_x\text{Se}$ and $\text{Zn}_{1-x}\text{Co}_x\text{Se}$ that contain the magnetic ions Fe^{2+} and Co^{2+} instead of Mn^{2+} . We will describe the growth of these systems, and their characterization by x-ray diffraction, transmission electron microscopy, reflectivity, magnetization, Raman scattering and neutron scattering.

E9.7

MAGNETIC PROPERTIES OF NOVEL III-V DILUTED MAGNETIC SEMICONDUCTORS. S. von Molnár, H. Munekata, H. Ohno and L. L. Chang, IBM Research Division, T. J. Watson Research Center, Yorktown Heights, NY 10598, USA.

The temperature and magnetic field dependence of the semiconductors InAs and GaAs containing up to 10% Mn are reported. All samples were $\sim 2\text{-}\mu\text{m}$ thin films prepared by molecular beam epitaxy (MBE) at growth temperatures varying between $150\text{-}400^\circ\text{C}$ (1). Major results may be summarized as follows: 1) The magnetization of the materials are extremely sensitive to small ($\sim 50^\circ\text{C}$) changes in growth temperature; 2) Higher growth temperatures lead to two distinguishable contributions to the magnetization. The major component is ferromagnetic with $T_c \approx 300\text{K}$, similar to MnAs, while the remainder obeys a Curie-Weiss law; 3) Lower growth temperature leads to alloy formation as evidenced by typical Curie-Weiss behavior with $\Theta_p \approx 22 \pm 5 \text{ K}$ and Curie constant $C \approx 0.01 \pm 0.0015 \text{ K}^{-1}$ for a sample containing 9% Mn. These properties will be compared to the more conventional diluted II-VI systems.

(1) H. Munekata et. al., submitted to 10th MBE Workshop, Raleigh, N.C., September 1989.

E9.8

TEM STUDY OF DEFECTS IN CdTe/CdMnTe SUPERLATTICES ON (100) InSb . S. Diamond & J.W. Steeds, Physics Department, University of Bristol, Bristol S8 1TL, UK

$\text{CdTe/Cd}_{1-x}\text{Mn}_x\text{Te}$ superlattices with $x \sim 0.2$ and well/barrier thicknesses ranging from 20Å to 300Å were examined via plan and cross-sectional TEM in analytical instruments capable of EDX and CL. Misfit, inclined and threading dislocations were observed with a net density of around 10^9 cm^{-2} .

It was observed that the sense of the {111} plane involved, in terms of the CdTe crystal polarity, affected the behaviour of these dislocations. These dislocations running on {111} B-type Te terminated planes tended to dissociate into $\frac{1}{6}\langle 112 \rangle$ type Shockley partials with the generation of a stacking fault, whereas those on {111} A-type terminated planes did not. No correlation was seen between quantum well thickness and defect density and the good quality of interface sharpness and quantum well thicknesses were not affected by dislocations.

In this system the lattice mismatch of $\sim 4.10^{-3}$ between $\text{Cd}_{0.8}\text{Mn}_{0.2}\text{Te}$ and CdTe is more important than that of $2.5 \cdot 10^{-4}$ between CdTe and InSb . Consequently, of the misfit dislocations observed, most were seen at the interface between the CdTe and CdMnTe buffer layers, and within the superlattice rather than at the substrate and CdTe interface. This suggests that half loop dislocations glide in from the surface rather than from sources within the crystal.

E9.9

IN AND Ga AUTODOPING OF CdMnTe EPILAYERS GROWN ON InSb AND GaAs SUBSTRATES. J.J. Dubowski, J.M. Wrobel, S. Rolfe, Laboratory for Microstructural Sciences, NRCC, Ottawa, Canada, J.A. Jackman, Metals Technology Laboratories, CANMET, Ottawa, Canada; and J.H. Mazur, University of Southern California, Materials Science and Engineering Department, Los Angeles, CA.

Epitaxial layers of $\text{Cd}_{1-x}\text{Mn}_x\text{Te}$ ($0 \leq x < 0.60$) were grown on (111) GaAs and (001) InSb substrates by pulsed laser evaporation and epitaxy (PLEE). Autodoping of the layers with In and Ga, and the quality of the interface were both investigated with secondary ion mass spectroscopy (SIMS), low-temperature photoluminescence (PL) and high resolution transmission electron microscopy (HRTEM). The layers were grown at a rate of $\sim 1 \mu\text{m/h}$ on substrates held at temperatures ranging from 200 to 300 °C. The study were carried out on as-grown layers and samples annealed at 400 - 700 °C.

A significant concentration of Ga and In was found in the layers grown on both GaAs and InSb substrates. This confirms earlier observations concerning CdTe grown on GaAs and InSb . Ion imaging studies revealed that Ga and In most often accumulate near the film surface at localized spots of up to about $5 \mu\text{m} \times 5 \mu\text{m}$ in size. Sometimes channels of accumulated Ga and In impurities extended from the surface to the layer-substrate interface. Annealing of the samples does not seem to affect the size of precipitated 'hot spots' of Ga and In, however, it causes the average concentration of Ga and In in the layers to increase above 10^{16} cm^{-3} .

Photoluminescence spectra show that in some cases annealing replaces the sharp excitonic lines with a broad band at a lower energy. Most likely this band results from the formation of Ga and In related complexes.

E9.10

PHOTOLUMINESCENCE STUDIES OF DILUTED MAGNETIC SEMICONDUCTORS UNDER HYDROSTATIC PRESSURE: $\text{Cd}_{1-x}\text{Mn}_x\text{Te}$. M. Prakash, M. Chandrasekhar, and H.R.

Chandrasekhar, University of Missouri, Columbia, MO ; I. Miotkowski and A.K. Ramdas, Purdue University, W. Lafayette, IN.

We report photoluminescence studies of the diluted magnetic semiconductor alloy $\text{Cd}_{1-x}\text{Mn}_x\text{Te}$ for $x = 0.05, 0.15$ and 0.20 , under hydrostatic pressure in a diamond anvil cell at 5 to 100K. The alloys were p-doped so as to allow a study of the acceptor bound magnetic polaron (ABMP). We can clearly observe the A^0X and the $e-A^0$ transitions. The separation between these transitions has a Coulombic part (which is temperature independent) and a magnetic part (which decreases with increasing temperature)¹. The magnetic part is due to the binding energy of the ABMP.

We find that the separation between the exciton and $e-A^0$ decreases as a function of pressure (from 47 to 40 meV for $x = 0.05$). This is clearly not a lattice constant effect, since a decreasing separation between Mn^{2+} ions would increase the binding energy. We expect mechanisms such as changes in the dielectric constant, exchange integrals and wavefunction overlap to play competing roles. The pressure coefficients of both the exciton and the $e-A^0$ transition have a predominantly linear term, and small sublinear bowing.

¹ M. Bugajski, P. Becla, P.A. Wolff, D. Heiman and L. R. Ram-Mohan, Phys. Rev. B 38, 10512 (1988).

The work at the University of Missouri was supported by the U.S. Army Research Office under grant number DAAL03-86-K0083 and the U.S.DOE under grant number DE-AC02-84ER45048; the work at Purdue University was supported by the National Science Foundation grant number DMR-85-20866.

E10.1

OBSERVATION OF Mn^{2+} TRIPLET CLUSTERS AND NON-NEAREST NEIGHBOR EXCHANGE EFFECT IN $(\text{Cd}, \text{Mn})\text{Te}$. Xiaomei Wang, D. Heiman, S. Foner, and P. Becla, MIT Francis Bitter National Magnet Laboratory, Cambridge, MA 02139

Diluted magnetic semiconductors are excellent hosts for the study of the quantum structures of spin clusters. Here we provide quantitative evidence of magnetic ion triplet clusters and of the saturation of magnetic ion pairs. Magnetization measurements using a Faraday rotation technique on $\text{Cd}_{1-x}\text{Mn}_x\text{Te}$ up to 60 T at liquid helium temperature are reported. The magnetic fields were furnished by the pulsed-field facility at the MIT Francis Bitter National Magnet Laboratory.

For $x = 0.1$, the measured magnetization $M(B)$ versus field B is composed of three different linear regimes. The increase of slope at ~ 30 T corresponds to the onset of open triplet clusters, and the decrease of the slope at ~ 52 T is attributed to the saturation of pairs. The experimental data is compared to calculated contributions from different types of clusters in a nearest-neighbor cluster model. Overall good agreement is obtained.

Further-neighbor interactions are included by introducing an average exchange bias field Δ . This bias field is more pronounced in the present experiment, with higher x and higher B than previous pair-step experiments. By quantitative analysis of the data for pairs, we find a linear relation between Δ and M , independent of x (for $x \leq 0.1$). This relation allows us to determine the coupling constant of next-nearest-neighbor interactions, $J_2/k_B = -1.1$ K, within a mean-field model.

This work was supported by NSF under Grant No. DMR-8807419, and DARPA-N00014-86-0760.

E10.2

THE EFFECT OF DZIALOSHINSKI-MORIYA INTERACTION ON THE MAGNETIZATION OF DILUTE MAGNETIC SEMICONDUCTORS. C. R. McIntyre*, M.I.T.; P. A. Wolff, M.I.T., Cambridge, MA; Y. Shapira, Tufts University, Medford, MA.

A theoretical investigation of the effect of Dzyaloshinski-Moriya (DM) interaction on Mn^{2+} spin pairs will be presented. The DM interaction is an anisotropic superexchange mechanism responsible

for weak ferromagnetism in antiferromagnetic insulators.¹ Recently, theoretical and experimental investigations on dilute magnetic semiconductors (DMS) have focused on DM interactions.^{2,3} This interaction can couple states of different total spin, thereby affecting the magnetization of DMS. We investigate the coupling of the ground state $S=0$ to the $S=1$ level for Mn^{2+} pairs in the presence of a magnetic field. Calculations have shown the field- and superexchange-dependent energies and eigenstates of spin pairs. The differential magnetization has been calculated and will be compared with results from pulsed magnetic field experiments. Implications for spin-lattice relaxation via the DM interaction will be mentioned.

*IBM Graduate Fellow

1. T. Moriya, in *Magnetism*, ed. G.T. Rado and H. Suhl, (Academic Press, New York, 1963), vol. 1.
2. B. E. Larson, Ph.D. thesis, Harvard Univ., 1988.
3. Y. Shapira et al., to be published in *Solid State Communications*.

E10.3

IN-SITU STUDIES OF SEMIMAGNETIC HETEROJUNCTION PARAMETERS. Xiaohua Yu, A. Raisanen, G. Haugstad, N. Troullier, and A. Franciosi, Dept. of Chemical Engineering and Materials Science, University of Minnesota, Minneapolis, MN 55455.

We have conducted a systematic study of $Ge-Cd_{1-x}Mn_xTe$ heterostructures prepared *in-situ* by deposition of polycrystalline Ge onto atomically clean $Cd_{1-x}Mn_xTe(110)$ surfaces. We examined by means of high resolution synchrotron radiation photoemission the valence band offset ΔE_v as a function of the substrate composition x ($x=0, 0.35$, and 0.60) and bandgap E_g ($E_g=1.47, 1.93$, and 2.13 eV), and probed atomic interdiffusion across the interface by monitoring the coverage-dependence of the characteristic overlayer and substrate core emission. We find $\Delta E_v=0.54\pm0.15$ eV in all cases, no dependence of ΔE_v on substrate E_g within experimental uncertainty, no evidence of Te-Ge interdiffusion, and limited Cd outdiffusion in the Ge overlayer. These findings indicate that within the range of validity of the transitivity rule, $Cd_{1-x}Mn_xTe-Cd_{1-y}Mn_yTe$ heterojunctions may actually follow the much maligned common-anion rule.

E10.4

NOVEL PROPERTIES OF MAGNETIC SEMICONDUCTORS GROWN BY MONOLAYER DEPOSITION USING LASER-TARGET ABLATION. X.-L. Zheng, C.A. Huber, and D. Heiman, MIT Francis Bitter National Magnet Lab., Cambridge, MA 02139

Ordered crystal structures such as $Cd,MnTe$, have several advantages. Short-range ordering of magnetic ions in Cu_2GeMnS_4 has been shown to give magnetic enhancements (10X), which may lead to similar enhancements in $(Cd,Mn)Te$ of magneto-optical properties like Faraday rotation and magnetically-tunable lasers. Although being more difficult to achieve, long-range ordering of the cations in alloys like $(Zn,Mn)Se$ or $(In,Ga)As$ should reduce alloy-related carrier scattering and level broadening. This is important for effects that require resonant energy levels. One method of generating such ordering is by sequential layering of different atomic monolayers using epitaxial crystal growth. Layer-by-layer growth using laser-ablated targets has some advantages over other epitaxial techniques like MBE. A multiple-target UHV growth apparatus at MIT exploits these

aspects for epitaxial growth of semiconductors alloyed with transition metals and doped with impurities. Doping of II-VI semiconductors relies on targets of Zn_3P_2 or Zn_3As_2 for p-doping, and GaSe or InSe for n-doping. We report results for these systems grown by laser ablation techniques.

Work supported by NSF DMR-8807419 and DARPA N00014-86-0760.

E10.5

PHOTOLUMINESCENCE OF ZnSe FILMS AND ZnSe/ZnMnSe STRAINED LAYER SUPERLATTICES UNDER HYDROSTATIC PRESSURE. Judah A. Tuchman, Zhifeng Sui, Irving P. Herman, Department of Applied Physics, Columbia University, New York, NY; R. L. Gunshor, School of Electrical Engineering, Purdue University, West Lafayette, IN; L. A. Kolodziejski, Department of Electrical Engineering, Massachusetts Institute of Technology, Cambridge, MA.

Strained and unstrained ZnSe films and ZnSe/ZnMnSe strained layer superlattices grown on GaAs by molecular beam epitaxy have been studied by photoluminescence (PL) as a function of hydrostatic pressure. Measurements were made at 9 K up to pressures of ~40 kbar using a diamond anvil cell. The energy of each of the excitonic features of unstrained ZnSe films was found to increase by ~6.4 meV/kbar, while those in ZnSe/ $Zn_{0.67}Mn_{0.33}Se$ SSL's appeared to increase slower with pressure, ~6.0 meV/kbar. Moreover, the broad and asymmetric PL spectrum of this SSL at ambient pressure was found to become narrower and more symmetric with increasing pressure.

This work was supported at Columbia by the Joint Services Electronics Program Contract DAAL03-88-C-0009 and at Purdue by the Office of Naval Research Contract N00014-82-K0563.

E10.6

MAGNETO-OPTICAL STUDIES OF ZnFeSe/ZnSe/ZnFeSe QUANTUM WELL STRUCTURES. X. Liu and A. Petrou, SUNY at Buffalo, NY; B.T. Jonker, G.A. Prinz and J.J. Krebs, NRL, Washington, D.C.; and J. Warnock, IBM, Yorktown Heights, NY.

Magneto-reflectance studies were carried out on three ZnFeSe/ZnSe/ZnFeSe quantum well structures with $L(ZnFeSe)=100\text{\AA}$ and $L(ZnSe)=100, 150$ and 200\AA grown by MBE. The Fe molar concentration was 0.1. The spin splittings of the heavy hole excitons were studied at $T=4.2$ K in magnetic fields up to 8T. The heavy hole excitons in the Faraday geometry split into two components. A lower energy one with polarization $\delta_{+}(-3/2 \rightarrow -1/2)$ and a higher component with polarization $\delta_{-}(3/2 \rightarrow 1/2)$. The two components show a marked asymmetric behavior as function of magnetic field B. The δ_{+} component shows a strong magnetic red shift, and becomes weaker with increasing field. The δ_{-} component, on the other hand, initially shows a magnetic blue shift up to $B=2$ T and then saturates. This behavior can be quantitatively understood as follows: The magnetic field induced splitting of the heavy holes inside the ZnFeSe layers overwhelms the zero-field band offset at a relatively modest applied field. The $-3/2$ holes become localized in the ZnFeSe layers while the $+3/2$ holes remain in the ZnSe layer. In the conduction band, however, the two spin components of the electrons remain localized in the ZnSe layer. This results in type-I behavior for the δ_{-} and type-II for the δ_{+} components of the heavy hole excitons. The asymmetry associated with the spin segregation of the heavy holes provides an accurate measure of the valence band offset in this system.

E10.7

TRANSITION METAL DONOR LEVELS IN II-VI SEMICONDUCTORS. D. Heiman, M. Dahl, J. Perkins, X. Wang, X.-L. Zheng, and P. Becla, MIT Francis Bitter National Magnet Lab., Cambridge, MA 02139; K. Smith, J. Marsella, K. Dwight, and A. Wold, Chemistry Department,

Brown University, Providence, RI 02912; A. Mycielski, Institute of Physics, Academy of Science, Warsaw

Transition metal impurities (Sc, V, Ti, Fe) provide dense donor levels in II-VI semiconductors. We examine two configurations — donor levels that lie above the conduction band (e.g. HgSe:Fe and CdTe:Sc) and midgap donor levels (e.g. CdSe:Fe and ZnSe:V). In HgSe:Fe the mixed-valence $\text{Fe}^{2+}/\text{Fe}^{3+}$ system allows for Coulomb repulsion between Fe^{3+} ionized donors which induces spatial charge ordering. We report results of studies of 2D heterostructures such as CdSe:Fe/HgSe in which the screening donor electrons are removed from the Fe^{3+} in the CdSe barrier layer and fall into the 2D quantum well in the HgSe layer. This type of 2D structure shows charge-ordered mobility enhancements at temperatures higher than those observed in 3D materials. In other systems, in which the transition metal has a mid-bandgap donor level, an important process is the optical transition [$\text{Fe}^{3+} \rightarrow$ conduction band] and the transition [valence band $\rightarrow \text{Fe}^{3+}$]. Examples of optical pumping on these systems will be presented.

Supported by DMR-8601345, DMR-8813164, NSF DMR-8807419 and DARPA N00014-86-0760.

E10.8

MAGNETIC STUDY OF Fe-BASED II-VI DILUTED MAGNETIC SEMICONDUCTORS. H.J.M. Swagten, Department of Physics, Eindhoven University of Technology, The Netherlands, A. Twardowski, Institute of Experimental Physics, Warsaw University, Poland, C.E.P. Gerrits and W.J.M. de Jonge, Department of Physics, Eindhoven University of Technology, The Netherlands.

The Fe-based Diluted Magnetic Semiconductors (DMS) represent a novel class of materials. In contrast to Mn, the additional electron of the $3d^6$ -configuration of the Fe^{2+} occupies e-orbitals located above the valence bands. The position of the energy levels of the magnetic ions with respect to the band structure is generally assumed to be intimately related to the character and strength of the d-d interaction. On the other hand, Wei and Zunger have suggested a negligible hybridization of these states with the band structure and consequently, the energy gap of Fe-DMS should not influence the magnetic properties drastically.

Magnetically, various compounds of the II-VI group Fe-DMS have been studied in a detailed way, such as $\text{Zn}(\text{Fe})\text{Se}$, $\text{Zn}(\text{Fe})\text{S}$, $\text{Cd}(\text{Fe})\text{Se}$ and $\text{Hg}(\text{Fe})\text{Se}$. In all these systems it seems that for low Fe concentrations the magnetic properties are dominated by the crystal-field induced singlet ground state of the Fe^{2+} -ion. It should also be emphasized that no effect of the energy gap is clearly visible in the data, which is consistent with the above-mentioned small hybridization of the e-orbitals. The thermodynamic properties can, in principle, be described by the crystal-field model including an AF interaction between the spins, which is roughly a factor two larger than it was for Mn.

For higher concentrations evidence for the AF interaction between Fe ions is visible, for instance in the decrease of the excess specific heat per Fe-ion with the Fe-concentration, but also in the strong reduction of the magnetization. For $\text{Zn}(\text{Fe})\text{Se}$ in high magnetic fields, the crystal-field model predicts steps in the magnetization, at $B \approx 35$ T, which is not reflected by the data. In this respect, the role of the orientation of the sample will be discussed.

E10.9

ENERGY LEVEL SPECTRA OF TRANSITION METAL IONS IN DILUTED MAGNETIC SEMICONDUCTORS. Murielle Villeret, S. Rodriguez, Purdue University, West Lafayette, IN; and E. Kartheuser, Université de Liège, Liège, Belgium.

We present a study of the low lying energy levels of Fe^{2+} , Co^{2+} , Ni^{2+} and Cu^{2+} in diluted magnetic semiconductors such as $\text{Cd}_{1-x}\text{Co}_x\text{Te}$ and $\text{Cd}_{1-x}\text{Co}_x\text{Se}$ and their counterparts. In the first of these compounds the magnetic ion sits on a site of symmetry T_d while in the second the symmetry is trigonal (C_{3v}). We develop a formulation that permits a continuous variation from T_d to C_{3v} symmetry. Comparison with experimental data in $\text{Cd}_{1-x}\text{Co}_x\text{Se}$ shows that the C_{3v} distortion amounts to about 10% of the crystal potential at the Co^{2+} site. Our study of the energy spectra of Fe^{2+} in T_d and C_{3v} crystal potentials reveals

that, even in the cubic field, the levels exhibit an anisotropy which manifests itself in an anisotropy of the magnetization, M , in the regime in which M is not a linear function of the magnetic field B . The study includes all the levels in the lowest terms of the $(3d)^6$ ($n=6,7,8,9$) configurations. The calculations are carried out to second order in the spin-orbit interaction and in B for the lowest orbital states and to first order in B for the excited states. The g-factors of all the levels are obtained including their anisotropy for the Co^{2+} and Cu^{2+} Γ_8 states.

This work supported by the National Science Foundation (Grant No. DMR 86-16787) and by the North Atlantic Treaty Organization (Research Grant No. 0759/87).

E10.10

RAMAN SPECTROSCOPY OF A NOVEL DILUTED MAGNETIC SEMICONDUCTOR: CUBIC $\text{Cd}_{1-x}\text{Mn}_x\text{Se}$. R.G. Alonso, E.-K. Suh, H. Pascher*, E. Oh and A.K. Ramdas, Purdue University, West Lafayette, IN; and N. Samarth, H. Luo and J.K. Furdyna, University of Notre Dame, Notre Dame, IN.

In contrast to the bulk diluted magnetic semiconductor (DMS) $\text{Cd}_{1-x}\text{Mn}_x\text{Se}$ which occurs with the wurtzite structure, its epilayers grown on (001) GaAs substrate by Molecular Beam Epitaxy exhibit the cubic zinc blende structure [Samarth *et al.* Appl. Phys. Lett. 54, 2680 (1989)]. Raman spectroscopy and photoluminescence studies on this novel DMS show (1) a "two mode" behavior of the zone center optical phonons, (2) large Raman shifts associated with the spin-flip of donor-bound electrons and (3) huge Zeeman shifts of an excitonic component. The large magnetic field dependence in (2) and (3) and saturation at high fields and low temperatures show that the large sp-d exchange interaction characteristic of DMS's is also manifested strikingly in the zinc blende phase of $\text{Cd}_{1-x}\text{Mn}_x\text{Se}$. The paper will also present results on superlattices consisting of $\text{Cd}_{0.9}\text{Zn}_{0.1}\text{Se}/\text{Cd}_{0.9}\text{Mn}_{0.1}\text{Se}$ and $\text{Cd}_{0.9}\text{Mn}_{0.1}\text{Se}/\text{ZnSe}$ where the constituent layers have the zinc blende structure.

* Permanent address: University of Bayreuth, Federal Republic of Germany.

Research supported by DARPA-URI (ONR Contract No. N00014-86-K-0760); NSF Grant Nos. DMR-86-16787 and DMR-85-20866.

E10.11

THE INFLUENCE OF Fe DONORS IN HgSe ON FREE-CARRIER SCATTERING MECHANISM. Qian Dingrong, Zhang Jiamin, Zhou Qun, Liu Kun, Lab for Infrared Physics, Shanghai Institute of Technical Physics, Academia Sinica, China; W. Szuszkiewicz, Institute of Experimental Physics, Warsaw University, Warsaw, Poland; A. Mycielski, Institute of Physics, Science Academia of Poland, Warsaw, Poland.

It was previously reported that Dingle temperature in HgSe sample with iron concentration higher than about $5 \times 10^{18} \text{ cm}^{-3}$ strongly decreases at low temperature while the electron mobility apparently increases. This has been accounted for by a model of "charge-superlattice" formed by the ionized resonant Fe donors in the lattice of crystal. The space ordering of ionized Fe donors, in return, excludes the low-momentum-transfer scattering processes, and hence should substantially affect free-carrier absorption in view of the fact that the exchange of momentum with lattice is crucial

for a band electron to be excited by a photon to higher state in energy band.

A comprehensive infrared study on HgSe:Fe samples with Fe concentration ranging from $1.5 \times 10^{18} \text{ cm}^{-3}$ to $7 \times 10^{19} \text{ cm}^{-3}$ has been performed, for the first time, in the temperature range $1.8\text{K} < T < 300\text{K}$ for transmission spectra, and at room temperature for reflectivity spectra, respectively. It has been found that the scattering mechanism in samples with Fe density less than $5 \times 10^{18} \text{ cm}^{-3}$ is ionized-impurity scattering at all measured temperatures, while it is no longer ionized-impurity scattering at low temperatures for samples with Fe density higher than $5 \times 10^{18} \text{ cm}^{-3}$. This is a new evidence of the "charge-superlattice" model.

It has also been found that Drude theory describes the measured free-carrier absorption and reflectivity in HgSe:Fe very well and the predominant scattering mechanism at room temperature is ionized-impurity scattering for all samples. However, for samples with Fe density less than $5 \times 10^{18} \text{ cm}^{-3}$, the damping parameters are wavelength-dependent, while for samples with Fe density higher than $5 \times 10^{18} \text{ cm}^{-3}$, the damping parameters are wavelength-independent which means that the carriers in samples encounter scattering differently. In other words, the momentum relaxation time changes from energy-dependent to energy-independent while the Fermi level is approaching Fe level.

In conclusion, Fe ions play a remarkable role in the scattering processes in HgSe.

E10.12

FREE EXCITON MAGNETOSPECTROSCOPY OF CdFeSe DILUTED MAGNETIC SEMICONDUCTOR. A. Twardowski, K. Pakula, Institute of Exp. Physics, Warsaw University, Warsaw, Poland, M. Arciszewska, A. Mycielski, Institute of Physics, Polish Academy of Sciences, Warsaw, Poland

A novel class of Fe-based Diluted Magnetic Semiconductors (DMS) attracted recently a considerable interest. The Fe^{2+} substitutional ions in these compounds possess both spin and orbital momenta ($S=2$, $L=2$), which leads to substantially different, in respect to Mn-based DMS, magnetic behaviour of these materials. The optical properties, specially those concerning the s-d exchange interaction between the Fe ions and the band electrons, are relatively unexplored yet. In particular the s-d exchange involving valence band electrons (which is related to d-d exchange between the Fe ions) has been studied only for cubic ZnFeSe so far. In this paper we report the free exciton magnetospectroscopy results for hexagonal $\text{Cd}_{1-x}\text{Fe}_x\text{Se}$ ($x < 0.08$) obtained at $T=1.9\text{K}$ and magnetic fields up to 5T, for both magnetic field parallel and perpendicular to the crystal c axis. Strong exciton splitting in a magnetic field is observed, generally in accordance with the situation encountered for ZnFeSe. The exciton splittings reveal strong anisotropy depending on magnetic field orientation, as expected for hexagonal crystals. Combining the spectroscopic data with the magnetization measured on the very same samples we determine the s-d exchange interaction parameters for CdFeSe. We also discuss the chemical trends of the s-d and d-d parameters within the Fe-based DMS class.

SYMPOSIUM F:
DIAMOND, BORON NITRIDE, SILICON CARBIDE
AND RELATED WIDE BANDGAP SEMICONDUCTORS



November 28 - December 1, 1989

Chairs

Jeffrey T. Glass
Department of Materials
Science & Engineering
North Carolina State University
Raleigh, NC 27695-7907
(919) 737-7216

Naoji Fujimori
Sumitomo Electric Industries
1-1, 1-Chome Koyakita
Itami, Hyogo, Japan 661
(0727) 71-0621

Russell Messier
Materials Research Laboratory of
The Pennsylvania State University
University Park, PA
(814) 865-3704

Symposium Support

Kobe Steel, Ltd.

Sumitomo Electric Industries, Ltd.

**Proceedings published as Volume 162
of the Materials Research Society
Symposium proceedings series.**

SESSION F1: DIAMOND FOR ELECTRONICS:
GROWTH AND CHARACTERIZATION
Tuesday Morning, November 28
America South (W)

SYMPOSIUM F presentations
may be viewed simultaneously
in the Suffolk Room,
Marriott Hotel.

8:30 *F1.1
THE ELECTRONIC AND OPTICAL PROPERTIES OF
DIAMOND; DO THEY FAVOUR DEVICE APPLICATIONS?
A.T. Collins, King's College London, Wheat-
stone Physics Laboratory, London, United
Kingdom.

9:00 *F1.2
ATOMIC HYDROGEN IN CVD DIAMOND GROWTH,
Thomas R. Anthony, General Electric Cor-
porate Research and Development Center,
Schenectady, NY.

9:30 F1.3
THERMODYNAMICS AND THE CVD OF DIAMOND,
Walter A. Yarbrough, Pennsylvania State
University, Materials Research Laboratory,
University Park, PA.

9:45 F1.4
STUDIES OF DIAMOND GROWTH PROCESSES FROM
CHEMICAL VAPOR DEPOSITION, C. Judith Chu,
Benjamin J. Bai, Robert H. Hauge, Mark P.
D'Evelyn, and John L. Margrave, Rice Univer-
sity, Department of Chemistry, Houston, TX.

10:00 BREAK

10:30 F1.5
SCANNING TUNNELING MICROSCOPY INVESTIGATION
OF DIAMOND FILMS ON HIGHLY ORIENTATED PYROL-
YTIC GRAPHITE SUBSTRATES, A. Peter Jardine,
Fen-Chu Tseng and F.F.Y. Wang, State Univer-
sity of New York, Stony Brook, Department of
Materials Science, Stony Brook, NY.

10:45 F1.6
ADSORPTION OF HYDROCARBON RADICALS ON THE
HYDROGENATED DIAMOND SURFACE, Mark R.
Pederson, Kobiari A. Jackson and Warren E.
Pickett, Naval Research Laboratory, Complex
Systems Theory Branch, Washington, DC.

*Invited Paper

Short Course M-06, "Growth and Characteriza-
tion of Diamond and Diamond-Like Films," may
be of interest to symposium attendees.
Details regarding course dates and instruc-
tors are provided in the short course sec-
tion of this program.

11:00 F1.7
MICROWAVE CVD OF DIAMOND USING METHANOL-RARE
GAS MIXTURES, M. Buck, T.J. Chuang and H.
Seki, IBM Almaden Research Center, San
Jose, CA.

11:15 F1.8
EFFECTS OF O₂ ADDITION ON DIAMOND GROWTH: IN
SITU SPECIES MEASUREMENTS AND MODELING,
Stephen J. Harris, General Motors Research
Labs, Physical Chemistry Department, Warren,
MI.

11:30 F1.9
MORPHOLOGY OF DIAMOND FILMS GROWN BY DC
PLASMA JET CVD, Kazuaki Kurihara, Ken-ichi
Sasaki, Montonobu Kawarada and Nagaaki
Koshino, Fujitsu Laboratories, Functional
Material Laboratory, Atsugi, Japan.

11:45 F1.10
OXYGEN EFFECT IN DIAMOND DEPOSITION AT LOW
TEMPERATURES, Y. Liou, A. Inspektor, R.
Weimer, D. Knight, and R. Messier, The
Pennsylvania State University, Materials
Research Laboratory, University Park, PA.

SESSION F2: DIAMOND GROWTH
AND CHARACTERIZATION
Tuesday Afternoon, November 28
America South (W)

SYMPOSIUM F presentations
may be viewed simultaneously
in the Suffolk Room,
Marriott Hotel.

1:30 F2.1
ELECTRON CONTROLLED CHEMICAL VAPOR DEPOSI-
TION OF DIAMOND THIN FILMS ON VARIOUS SUB-
STRATES, Yong-Hee Lee, Klaus J. Bachmann,
and Jeffrey T. Glass, North Carolina State
University, Department of Materials Science
and Engineering, Raleigh, NC.

1:45 F2.2
KrF* LASER-INDUCED CHEMICAL VAPOR DEPOSITION
OF DIAMOND, George W. Tyndall and Nigel P.
Hacker, IBM Almaden Research Center, San
Jose, CA.

2:00 F2.3
INVESTIGATIONS OF EXCIMER LASER EFFECTS ON
CVD DIAMOND GROWTH, P.E. Pehrsson, H.H.
Nelson, F.G. Celii, Naval Research Labora-
tory, Washington, DC.

2:15 F2.4
AN NMR STUDY OF DIAMOND THIN FILMS, Karen M.
McNamara and Karen K. Gleason, Massachusetts
Institute of Technology, Department of
Chemical Engineering, Cambridge, MA.

2:30 BREAK

2:45 **F2.5**

DIAMOND POLYTYPISM: DIFFRACTION, VIBRATION-AL BEHAVIOR, AND OPTICAL PROPERTIES, A.W. Phelps, Diamond Materials, Inc., State College, PA; K.E. Spear, W. Howard, D. Huang, and W.B. White, The Pennsylvania State University, University Park, PA.

3:00 **F2.6**

DOMAIN SIZE DETERMINATION IN DIAMOND THIN FILMS, Y.M. LeGrice, R.J. Nemanich, North Carolina State University, Department of Physics, Raleigh, NC.

3:15 **F2.7**

CHARACTERIZATION OF THIN FILM AND SINGLE-CRYSTAL CVD DIAMOND BY ABSORPTION AND LUMINESCENCE SPECTROSCOPY, A.T. Collins, King's College London, Wheatstone Physics Laboratory, London, United Kingdom; M. Kamo and Y. Sato, NIRIM, Ibaraki, Japan.

3:30 **F2.8**

EFFECT OF DOPING WITH NITROGEN AND BORON ON CATHODOLUMINESCENCE WITH CVD-DIAMOND, Yoshihiro Yokota, Hiroshi Kawarada, Yusuke Mori, and Akio Hiraki, Osaka University, Department of Electrical Engineering, Faculty of Engineering, Suita, Osaka, Japan.

3:45 **BREAK**

4:00 **F2.9**

PHOTOLUMINESCENCE SPECTROSCOPY OF DIAMOND FILMS, J.A. Freitas, Jr., Sachs/Freeman Associates, Landover, MD; J.E. Butler, S.G. Bishop, Naval Research Laboratory, Washington, DC; W.A. Carrington, University of South Florida, Tampa, FL; and U. Strom, Naval Research Laboratory, Washington, DC.

4:15 **F2.10**

CW FOUR-WAVE MIXING IN SYNTHETIC DIAMOND, D.A. Redman and S.C. Rand, University of Michigan, Department of EECS, Ann Arbor, MI.

4:30 **F2.11**

MODELLING OF A Ag/DIAMOND/n-GaAs PHOTODIODE WITH GRATING COUPLING OF THE INCIDENT LIGHT TO SURFACE PLASMA WAVES, D. Barman, M. Rahman, A.S. Karakashian, A. Altshuler and S. Broude, University of Lowell, Department of Physics and Applied Physics, Lowell, MA.

4:45 **F2.12**

OPTICAL CHARACTERIZATION OF NICKEL IN DIAMOND, M.H. Nazaré, A.J. Neves, Universidade de Aveiro, Departamento e Centro de Física, Aveiro, Portugal; and Gordon Davies, King's College London, Department of Physics, London, United Kingdom.

SESSION F3: POSTER SESSION

Tuesday Evening, November 28

7:00 p.m.- 10:00 p.m.

America Ballroom (W)

F3.1 A STUDY OF THE ELECTRONIC STRUCTURE NEAR INDIVIDUAL DISLOCATIONS IN DIAMOND BY ENERGY LOSS SPECTROSCOPY, J. Bruley, and P.E. Batson, IBM T.J. Watson Research Center, Yorktown Heights, NY.

F3.2 CHARACTERIZATION OF HEAVY METAL CONTAMINATION IN DIAMOND FILMS USING SIMS AND TOTAL REFLECTION X-RAY FLUORESCENCE (TXRF), R.S. Hockett, Charles Evans and Associates, Redwood City, CA; and James Knowles, Crystallume, Inc., Menlo Park, CA.

F3.3 MODELLING OF DIAMOND HETEROSTRUCTURES FOR ELECTRO-OPTICAL APPLICATIONS, A. Altshuler, S. Broude, C. Hantzis, A.S. Karakashian, University of Lowell, Physics Department, Lowell, MA.

F3.4 INFRARED AND RAMAN CHARACTERIZATION OF THE HYDROGEN ENVIRONMENTS IN DIAMOND AND DIAMOND-LIKE FILMS. Y.M. LeGrice, E.C. Buehler, R.J. Nemanich, North Carolina State University, Department of Physics, Raleigh, NC; J.T. Glass, North Carolina State University, Department of Materials Science and Engineering, Raleigh, NC; K. Kobashi, Kobe Steel, Ltd., Electronics Technology Center, Kobe, Japan; F. Jansen and M.A. Machonkin, Xerox Corporation, Webster, NY.

F3.5 ELECTRONIC STRUCTURE AND ENERGY PARAMETERS OF DIAMOND NUCLEI - A FIRST PRINCIPLES CLUSTER APPROACH, A. Altshuler, M. Wilner, C.C. Ai and Y.C. Yang, University of Lowell, Physics Department, Lowell, MA.

F3.6 EFFECT OF DIFFERENT H₂-CH₄ GAS COMPOSITIONS ON THE MORPHOLOGY AND GROWTH RATE OF DIAMOND GROWN BY HOT FILAMENT CVD, Edward N. Farabaugh and Albert Feldman, National Institute of Standards and Technology, Optical Materials Group, Gaithersburg, MD.

F3.7 DEPOSITION OF DIAMOND FILMS BY A SCANNING OXYGEN-ACETYLENE FLAME, Yonhua Tzeng, Calvin Cutshaw and Richard Phillips, Auburn University, Electrical Engineering Department, Auburn, Alabama.

F3.8 ENHANCEMENT OF DIAMOND SP³ BONDING IN RF SPUTTERED CARBON FILMS WITH NITROGEN GAS ADDED, C.J. Torng, T. Yeh, J.M. Sivertsen, University of Minnesota, Department of Chemical Engineering and Materials Science, Minneapolis, MN; and J.H. Judy, University of Minnesota, Department of Electrical Engineering, Minneapolis, MN.

F3.9 IMPORTANCE OF FILAMENT REACTIVITY FOR CVD DIAMOND GROWTH, M. Sommer and F.W. Smith, City College of New York, Department of Physics, New York, NY.

F3.10 HIGH-RATE DEPOSITION OF DIAMOND BY DC ARC DISCHARGE IN HYDROGEN-METHAN MIXTURE GAS, Xiang-Liu Jiang, Beijing Institute of Science and Technology, Beijing, China; Fang-Qing Zhang, Ying-Hu Yang, Jing-Qi Le and Bing Yang, Lanzhou University, Department of Physics, Lanzhou, China.

F3.11 INTRA- AND INTERGRANULAR FRACTURE OF DIAMOND THIN FILMS, H.A. Hoff, A.A. Morrish, J.E. Butler, B.B. Rath, Naval Research Laboratory, Washington, DC; W.A. Carrington, University of Florida, Tampa, FL.

F3.12 APPLICATION OF A THERMOBALANCE FOR STUDYING DEPOSITION KINETICS OF DIAMOND FILMS, Jerry Czarnecki and David Thumim, Cahn Instruments, Cerritos, CA.

F3.13 FAR INFRARED LASER MEASUREMENTS OF DIAMOND FILMS, Lawrence P. Bourget, Richard S. Post, Applied Science and Technology, Inc., Woburn, MA; Robert Giles, Andrew Gatesman and Greg Phillips, Lowell University, Department of Physics, Lowell, MA.

F3.14 CHARACTERIZATION OF HOLLOW-CATHODE DC DISCHARGE GROWTH OF DIAMOND, H.N. Chu, A.R. Lefkow, R. Redwing, L.W. Anderson, M.G. Lagally and J.E. Lawler, University of Wisconsin, Department of Physics, Madison, WI.

F3.15 FREE-STANDING CVD DIAMOND SHAPES AND COATINGS, Donald E. Patterson, Robert H. Hauge and John L. Margrave, Rice University and the Houston Area Research Center, The Woodlands, TX.

F3.16 (ABSTRACT WITHDRAWN)

F3.17 LASER ASSISTED TECHNIQUES FOR DIAMOND AND DIAMONDLIKE THIN FILMS, J. Krishnaswamy, A. Rengan, G. Matera, M. Longo, A. Srivatsa and J. Narayan, North Carolina State University, Department of Materials Science and Engineering, Raleigh, NC; and R. Nemanich, North Carolina State University, Department of Physics, Raleigh, NC.

F3.18 LASER-FLASH METHOD FOR INVESTIGATING THE THERMAL CONDUCTIVITIES OF DIAMOND THIN FILMS SYNTHESIZED BY EA-CVD, Yang Peichun, Pu Xin, Xuan Zhenwu, Qi Lichang, Research Institute of Synthetic Crystals, Beijing, China; and Hou Li, Pennsylvania State University, Materials Research Laboratory and Department of Engineering Science and Mechanics, University Park, PA.

F3.19 STUDY FOR GROWING DIAMOND FILMS (DF) ON SURFACES OF VARIOUS MATERIALS, Pu Xin, Yang Peichun, Xuan Zhenwu, Qi Lichang, Research Institute of Synthetic Crystals, Beijing, China; and Hou Li, Pennsylvania State University, Materials Research Laboratory and Department of Engineering Science and Mechanics, University Park, PA.

SESSION F4: DIAMOND FOR ELECTRONICS

Wednesday Morning, November 29
America South (W)

SYMPOSIUM F presentations
may be viewed simultaneously
in the Suffolk Room,
Marriott Hotel.

8:30 ***F4.1**
HOMOEPITAXIAL DIAMOND FILMS, M.W. Geis, Lincoln Laboratory, Massachusetts Institute of Technology, Lexington, MA.

9:00 **F4.2**
ELECTRICAL PROPERTIES OF HOMOEPITAXIAL DIAMOND FILMS, G.Sh. Gildenblat, S.A. Grot, C.W. Hatfield, C.R. Wronski, A.R. Badzian, T. Badzian, and R. Messier, The Pennsylvania State University, University Park, PA.

9:15 **F4.3**
IN-SITU CHARACTERIZATION OF THIN POLYCRYSTALLINE DIAMOND FILM QUALITY BY THERMAL WAVE AND RAMAN TECHNIQUES, R.W. Pryor, P.K. Kuo, L. Wei, R.L. Thomas, and P.L. Talley, Wayne State University, Institute for Manufacturing Research and Department of Physics, Detroit, MI.

9:30 **F4.4**
REGROWTH OF RADIATION DAMAGED LAYERS IN DIAMOND PRODUCED BY ION IMPLANTATION AT LIQUID NITROGEN TEMPERATURE, G.S. Sandhu, B. Liu, M.L. Swanson, University of North Carolina, Department of Physics and Astronomy, Chapel Hill, NC; and W.K. Chu, University of Texas, Texas Center for Superconductivity, Houston, TX.

9:45 **F4.5**
D.C. AND A.C. CONDUCTIVITY OF DIAMOND FILMS, G.A. Sokolina, A.A. Botev, L.L. Bouilov, S.V. Bantsekov, O.I. Lazareva, and I.G. Teremetskaya, Institute of Physical Chemistry of the Academy of Sciences of the USSR Moscow, USSR.

10:00 BREAK

10:30 **F4.6**
SELECTIVE NUCLEATION BASED EPITAXY OF CVD DIAMOND AND ITS APPLICABILITY TO SEMICONDUCTING DEVICE, H. Kawarada, J.S. Ma, Osaka University, Faculty of Engineering, Suita, Osaka, Japan; T. Yonehara, Canon Inc. Tamura, Hiratsuka, Kanagawa, Japan; Y. Yokota, Y. Mori, J. Wei, and A. Hiraki, Osaka University, Faculty of Engineering, Suita, Osaka, Japan.

10:45 **F4.7**
ELECTRICAL PROPERTIES OF THIN FILM AND BULK DIAMOND TREATED IN HYDROGEN PLASMA, Sacharia Albin and Linwood Watkins, Old Dominion University, Department of Electrical and Computer Engineering, Norfolk, VA.

11:00 **F4.8**
DEEP LEVEL TRANSIENT SPECTROSCOPY STUDY OF THIN FILM DIAMOND, K. Srikanth and S. Ashok, Pennsylvania State University, Department of Engineering Science and Mechanics and Center for Electronic Materials and Processing, University Park, PA; A. Badzian, T. Badzian and R. Messier, Pennsylvania State University, Materials Research Laboratory, University Park, PA.

11:15 **F4.9**
N-TYPE DOPING AND DIFFUSION OF IMPURITIES IN DIAMOND, S. Kajihara, A. Antonelli and J. Bernholc, North Carolina State University, Department of Physics, Raleigh, NC.

11:30 **F4.10**
DEPOSITION AND CHARACTERIZATION OF UNDOPED AND NITROGEN-DOPED DIAMOND THIN FILMS, Joseph B. Milstein, University of Lowell, Department of Electrical Engineering, Lowell, MA; Lian Li, Ye-Yung Teng and Anatoly M. Altshuler, University of Lowell, Department of Physics and Applied Physics, Lowell, MA.

11:45 **F4.11**
DOPING OF DIAMOND BY CO-IMPLANTATION OF DOPANT ATOMS WITH CARBON, G.S. Sandhu, M.L. Swanson, University of North Carolina, Department of Physics and Astronomy, Chapel Hill, NC; and W.K. Chu, University of Houston, Texas Center for Superconductivity, Houston, TX.

SESSION F5: ELECTRICAL PROPERTIES AND DEVICES IN DIAMOND AND DIAMOND-LIKE MATERIALS

Wednesday Afternoon, November 29
America South (W)

SYMPOSIUM F presentations
may be viewed simultaneously
in the Suffolk Room,
Marriott Hotel.

1:30 ***F5.1**
ELECTRONIC PROPERTIES OF DIAMOND/NICKEL AND DIAMOND/BORON NITRIDE INTERFACES, Warren E. Pickett and Steven C. Erwin, Naval Research Laboratory, Washington, DC.

2:00 **F5.2**
PSEUDOMORPHIC DIAMOND, PREDICTIONS OF STRUCTURE AND PROPERTIES, A.M. Altshuler and A.S. Karakashian, University of Lowell, Physics Department, Lowell, MA.

2:15 **F5.3**
CYCLIC-CLUSTER MINDO/3 COMPUTATIONS OF THE LATTICE CONSTANT AND BAND STRUCTURE OF BORON NITRIDE, DIAMOND, SILICON CARBIDE AND RELATED WIDE GAP SEMICONDUCTORS, Lawrence C. Snyder, State University of New York at Albany, Albany, NY; Arthur H. Edwards, University of North Carolina at Charlotte, Department of Electrical Engineering, Charlotte, NC; and Peter Deák, Physical Institute of the Technical University of Budapest, Hungary.

2:30 **F5.4**
ELECTRICAL CHARACTERIZATION OF METAL CONTACTS ON DIAMOND THIN FILMS, D. Narducci, J.J. Cuomo, C. Richard Guarnieri, and S.J. Whitehair, IBM T.J. Watson Research Center, Research Division, Yorktown Heights, NY.

2:45 **F5.5**
CONTACT RESISTIVITY OF B DOPED CVD GROWN DIAMOND FILMS, K. Nishimura, North Carolina State University, Materials Science and Engineering, Raleigh, NC, and Kobe Steel Ltd., Japan; K. Das and J.T. Glass, North Carolina State University, Materials Science and Engineering, Raleigh, NC.

3:00 **F5.6**
METALLIZATION OF SEMICONDUCTING DIAMOND: Mo, Mo/Au, Mo/Ni/Au, K.L. Moazed, North Carolina State University, Raleigh, NC; J.R. Zeidler and M.J. Taylor, Naval Ocean Systems Center, San Diego, CA.

3:15 **F5.7**
PROPERTIES OF CVD DIAMOND-METAL INTERFACE, Yusuke Mori, Hiroshi Kawarada, Yoshihiro Yokota, and Akio Hiraki, Osaka University, Department of Electrical Engineering, Faculty of Engineering, Suita, Osaka, Japan.

3:30 BREAK

4:00 *F5.8
EPITAXIAL GROWTH OF DIAMOND AND DIAMOND DEVICES, Naoji Fujimori, Sumitomo Electric Ind. Ltd., Itami Research Laboratory, Itami, Hyogo, Japan.

4:30 F5.9
BLUE LIKE DIAMOND LIGHT EMITTING DEVICES TO BE MASS-PRODUCED, Masaya Kadono, Shigenori Hayashi, Kenji Itoh, Takashi Inushima and Shumpei Yamazaki, Semiconductor Energy Laboratory Co., Ltd., Kanagawa, Japan.

4:45 F5.10
ELECTRICAL BEHAVIOR OF DIFFUSED IMPURITIES IN DIAMOND SINGLE-CRYSTALS, D. Narducci, J.J. Cuomo, IBM T.J. Watson Research Center, Yorktown Heights, NY.

5:00 F5.11
A DIAMOND SILICON HETEROJUNCTION DIODE, C.L. Ellison, Norton Company, Salt Lake City, UT; R.M. Cohen, University of Utah, Materials Science Department, Salt Lake City, UT; and J.T. Hoggins, Norton Company, Salt Lake City, UT.

5:15 F5.12
SCHOTTKY DIODES FABRICATED IN THIN CARBON FILMS CONTAINING POLYCRYSTALLINE DIAMOND GRAINS, G.A.J. Amaratunga, W.I. Milne, K.K. Chan, K.J. Clay, A. Putnis and M.E. Welland, Engineering Department, Cambridge, United Kingdom.

SESSION F5: (CONT.) ELECTRICAL PROPERTIES AND DEVICES IN DIAMOND AND DIAMOND-LIKE MATERIALS
Thursday Morning, November 30
America South (W)

SYMPOSIUM F presentations
may be viewed simultaneously
in the Suffolk Room,
Marriott Hotel.

8:30 F5.13
THE IMPACT OF β -SiC, DIAMOND AND c-BN ON POWER ELECTRONICS, Richard Koba and William Russell, Diamond Materials, Inc., State College, PA.

8:45 *F5.14
SIMPLE GRAPHITIC NETWORK MODELS OF "DIAMOND-LIKE" CARBON, M.A. Tamor and C.H. Wu, Research Staff, Ford Motor Company, Dearborn, MI.

9:15 F5.15
DOPING EFFECT IN HYDROGENATED AMORPHOUS CARBON THIN FILMS BY ION IMPLANTATION, S.P. Wong, The Chinese University of Hong Kong, Department of Electronics, Hong Kong, China; and Peng Shaoqi, Zhongshan University, Department of Physics, Guangzhou, China.

9:30 F5.16
OPTICAL BAND GAP OF DIAMOND-LIKE CARBON FILMS AS A FUNCTION OF RF SUBSTRATE BIAS, Paul Pastel and Walter Varhue, University of Vermont, Department of Electrical Engineering, Burlington, VT.

9:45 F5.17
STUDY OF AMORPHOUS CARBON THIN FILMS ON METALS, INSULATORS AND SEMICONDUCTORS, A. Martin, X.-M. Wu, G.-R. Yang, A. Tu, P. Persans and T.-M. Lu, Rensselaer Polytechnic Institute, Center for Integrated Electronics and Physics Department, Troy, NY.

10:00 BREAK

SESSION F6: SILICON-CARBIDE: GROWTH, CHARACTERIZATION ELECTRICAL PROPERTIES, AND DEVICES

Thursday Morning, November 30
America South (W)

SYMPOSIUM F presentations
may be viewed simultaneously
in the Suffolk Room,
Marriott Hotel.

10:30 *F6.1
STEP-CONTROLLED EPITAXIAL GROWTH OF SiC, Hiroyuki Matsunami, Tetsuzo Ueda, and Hironori Nishino, Kyoto University, Kyoto, Japan.

11:00 *F6.2
EPITAXIAL GROWTH AND DOPING OF AND DEVICE DEVELOPMENT IN MONOCRYSTALLINE BETA-SiC SEMICONDUCTOR THIN FILMS, Robert F. Davis, North Carolina State University, Department of Materials Science and Engineering, Raleigh, NC.

11:30 F6.3
INNOVATIVE LOW-TEMPERATURE MOCVD (LTMOCVD) AND PLASMA-ENHANCED LTMOCVD ROUTES TO THE FABRICATION OF DEVICE QUALITY ELECTRONIC MATERIALS, Alain E. Kaloveros, Paul J. Toscano, Richard Single and Victor Tulchinsky, State University of New York at Albany, Physics and Chemistry Departments, Albany, NY; and Marianne Holma, University of Illinois at Urbana-Champaign, Physics Department, Urbana, IL.

11:45 F6.4
GROWTH OF 6H-SiC ON CVD-GROWN 3C-SiC SUBSTRATES, Woo Sik Yoo and Hiroyuki Matsunami, Kyoto University, Department of Electrical Engineering, Kyoto, Japan.

SESSION F6: (CONT.) SILICON-CARBIDE:
GROWTH CHARACTERIZATION ELECTRICAL
PROPERTIES, AND DEVICES

Thursday Afternoon, November 30
America South (W)

SYMPOSIUM F presentations
may be viewed simultaneously
in the Suffolk Room,
Marriott Hotel.

1:30 *F6.5
SOME OBSERVATIONS ON THE ELECTRICAL CHARACTER OF THE HETEROEPITAXIALLY GROWN CUBIC SiC, B. Molnar and G. Kelner, Naval Research Laboratory, Washington, DC.

1:45 F6.6
NATIVE DEFECTS, DIFFUSION, SELF-COMPENSATION, AND BORON DOPING IN CUBIC SILICON CARBIDE, C. Wang, J. Bernholc, North Carolina State University, Department of Physics, Raleigh, NC; and R.F. Davis, North Carolina State University, Department of Materials Science, Raleigh, NC.

2:00 F6.7
DEEP-LEVEL DOMINATED ELECTRICAL CHARACTERISTICS OF Au CONTACTS ON β -SiC, K. Das, H.S. Kong, J.B. Petit, J.W. Baumgarner and R.F. Davis, North Carolina State University, Department of Materials Science and Engineering, Raleigh, NC; L.G. Matus, National Aeronautics and Space Administration, Lewis Research Center, Cleveland, OH.

2:15 F6.8
A NEW DEEP ACCEPTOR IN EPITAXIAL CUBIC SiC, J.A. Freitas, Jr., Sachs/Freeman Associates, Inc., Landover, MD; S.G. Bishop, Naval Research Laboratory, Washington, DC.

2:30 F6.9
ELECTRONIC STRUCTURE OF HIGH BANDGAP SEMICONDUCTOR INTERFACES: SiC/AlN, SiC/BP, C/BN, W.R.L. Lambrecht and B. Segall, Case Western Reserve University, Department of Physics, Cleveland, OH.

2:45 F6.10
SILICON CARBIDE/((In₂O₃)_x(SnO₂)_{1-x}) DEVICES FOR THE DETECTION OF ULTRAVIOLET RADIATION, James V. Masi, Western New England College, Springfield, MA.

3:00 BREAK

3:15 F6.11
OHMIC CONTACTS ON β -SiC, M. Iqbal Chaudhry, Clarkson University, Department of Electrical and Computer Engineering, Postdam, NY; W.B. Berry and M.V. Zeller, University of Notre Dame, School of Engineering, Notre Dame, IN.

3:30 F6.12
HIGH AND MEDIUM ENERGY ION SCATTERING STUDY OF Mo/3C-SiC CONTACT, S. Hara and I. Ohdomari, Waseda University, Shinjuku-ku, Tokyo, Japan; W. Slijkerman, J.F. van der Veen, FOM Institute, Amsterdam, The Netherlands; S. Misawa, E. Sakuma and S. Yoshida, Electrotechnical Laboratory, Tukuba-shi, Ibaraki, Japan.

3:45 F6.13
DOPED AMORPHOUS SiC, MIXED CARBIDE AND OXYCARBIDE THIN FILMS BY A LIQUID ROUTE, C-J Chu, E. Liimatta and J.D. Mackenzie, University of CA, Department of Material Science and Engineering, Los Angeles, CA.

4:00 F6.14
LIQUID PHASE HOMOEPITAXIAL GROWTH OF 4H-SiC CRYSTALS AND FABRICATION TECHNIQUES OF BLUISH-PURPLE LIGHT EMITTING DIODES, Y. Ueda, T. Nakata, K. Koga, Y. Matsushita, Y. Fujikawa, T. Uetani, T. Yamaguchi, and T. Niina, Sanyo Electric Co., Ltd., Semiconductor Research Center, Hirakata, Osaka, Japan.

4:15 BREAK

SESSION F7: OTHER WIDE BAND-GAP
SEMICONDUCTORS I
Thursday Afternoon, November 30
America South (W)

SYMPOSIUM F presentations
may be viewed simultaneously
in the Suffolk Room,
Marriott Hotel.

4:30 *F7.1
GALLIUM NITRIDE, A WIDE BAND-GAP SEMICONDUCTOR, Jacques I. Pankove, University of Colorado, Boulder, CO.

5:00 F7.2
GROWTH OF CUBIC GaN BY REACTIVE-ION MOLECULAR BEAM EPITAXY, R.C. Powell, G.A. Tomasch, Y.W. Kim, J.A. Thornton, and J.E. Greene, University of Illinois, Coordinated Science Laboratory, Urbana, IL.

5:15 F7.3

HETEROEPITAXIAL GROWTH AND CHARACTERIZATION OF GaN ON SAPPHIRE SUBSTRATES, T.P. Humphreys, C.A. Sukow and R.J. Nemanich, North Carolina State University, Department of Physics, Raleigh, NC; J.B. Posthill, R.A. Rudder, S.V. Hattangady and R.J. Markunas, Research Triangle Institute, Research Triangle Park, NC.

SESSION F8: POSTER SESSION

Thursday Evening, November 30

7:00 p.m. - 10:00 p.m.

America Ballroom (W)

F8.1 LOW TEMPERATURE SELECTIVE GROWTH OF β -SiC USING $\text{SiH}_2\text{Cl}_2/\text{C}_3\text{H}_8/\text{HCl}/\text{H}_2$ GAS SYSTEM, Y. Ohshita, Fundamental Research Laboratory, NEC Corporation, Kawasaki, Japan.

F8.2 ANNEALING AND CRYSTALLIZATION PROCESSES IN A HYDROGENATED AMORPHOUS SILICON-CARBON ALLOY FILM, D.K. Basa, Utkal University, Department of Physics, Bhubaneswar, India; F. W. Smith, The City College of New York, Dept. of Physics, New York, NY.

F8.3 A COMPARISON OF THE MICROSTRUCTURE OF SiC GROWN ON (001) Si, (111) Si, AND 6H-SiC SUBSTRATES BY CVD, J. Yang, P. Pirouz, Case Western Reserve University, Department of Materials Science and Engineering, Cleveland, OH; and J.A. Powell, NASA Lewis Research Center, Cleveland, OH.

F8.4 THE FORMATION OF HELICAL DISLOCATIONS IN SILICON SUBSTRATES DURING THE EPITAXIAL DEPOSITION OF BETA SILICON CARBIDE, M. Aindow, T.T. Cheng, and P. Pirouz, Case Western Reserve University, Department of Materials Science and Engineering, Cleveland, OH.

F8.5 COMPOSITION AND STRUCTURE OF HIGHLY ORIENTED β -SiC FILMS GROWN ON Si SUBSTRATES BY REACTIVE MAGNETRON SPUTTERING, O.U. Wahab, Linköping University, Department of Physics, Linköping, Sweden; Y. Yamamoto, Linköping University, Department of Physics, Linköping, Sweden, and Nippon Sheet Glass Co., Ltd., Tsukuba, Japan; T.I. Selinder, M. Willander, and J.-E. Sundgren, Linköping University, Department of Physics, Linköping, Sweden.

F8.6 GROWTH OF EPITAXIAL SiC LAYERS ONTO ON- AND OFF-AXIS 6H-SiC SUBSTRATES BY ION BEAM DEPOSITION, K.L. More, S.P. Withrow, T.E. Haynes, and R.A. Zuhr, Oak Ridge National Laboratory, Oak Ridge, TN.

F8.7 SEM OBSERVATION OF GROWTH AND DEFECT FORMATION ON HETEROEPITAXIALLY GROWN SiC ON(100) SILICON, B. Molnar and L.M. Shirey, Naval Research Laboratory, Washington, DC.

F8.8 THE EFFECTS OF POWER DENSITY ON THE PROPERTIES OF DIAMONDLIKE FILMS, Shuguang Chen, Shuhan Lin and Yangming Guo, Zhongshan University, Department of Physics, Guangzhou, China; Kaiming Zhang, Guangdong Engineering College, Chemical Engineering Department, Guangzhou, China.

F8.9 SUBSTRATE AND TEMPERATURE DEPENDENT MORPHOLOGY OF rf-SPUTTERED INDIUM NITRIDE FILMS, T.J. Kistenmacher, D. Dayan, R. Fainchtein, W. A. Bryden and T.O. Poehler, The Johns Hopkins University, Applied Physics Laboratory, Laurel, MD.

F8.10 TRANSMISSION ELECTRON MICROSCOPY OF InN THIN FILMS, J.S. Morgan, T.J. Kistenmacher, W.A. Bryden and T.O. Poehler, The Johns Hopkins University, Applied Physics Laboratory, Laurel, MD.

F8.11 VIBRATIONAL SPECTROSCOPY OF BORON NITRIDE AT HIGH TEMPERATURES AND PRESSURES, Gregory J. Exarhos, Battelle-Pacific Northwest Laboratory, Richland, WA; and Nancy J. Hess, University of Washington, Mineral Physics Group, Department of Geology, Seattle, WA.

F8.12 MOCVD OF WIDE BANDGAP III-V SEMICONDUCTORS BY USING NOVEL PRECURSORS, Kwok-Lun Ho, Klavs F. Jensen, Massachusetts Institute of Technology, Department of Chemical Engineering, Cambridge, MA; Wayne L. Gladfelter, David Boyd, and John Evans, University of Minnesota, Department of Chemistry, Minneapolis, MN.

F8.13 THEORETICAL INVESTIGATION OF GRAPHITIC BeO, Renata M. Wentzcovitch, University of Chicago, The James Franck Institute and Department of Physics, Chicago, IL; Alessandra Continenza and Arthur J. Freeman, Northwestern University, Department of Physics and Astronomy, Evanston, IL.

SESSION F9: OTHER WIDE BAND-GAP SEMICONDUCTORS II

Friday Morning, December 1

America South (W)

SYMPOSIUM F presentations
may be viewed simultaneously
in the Suffolk Room,
Marriott Hotel.

9:00 *F9.1
CUBIC BORON NITRIDE PN DIODE MADE AT HIGH PRESSURE, Osamu Mishima, National Institute for Research in Inorganic Materials, Tsukuba, Japan.

9:30 F9.2

A NEW OPTOELECTRONICS SEMICONDUCTOR CUBIC BN: PROPERTIES OF N.I.R.I.M. MADE CRYSTALS AND POTENTIALITIES, Koh Era and Osamu Mishima, National Institute for Research in Inorganic Materials, Tsukuba, Ibaraki, Japan.

9:45 F9.3

CONDUCTIVITY OF FILMS OF BORON NITRIDE, G.A. Sokolina, O.I. Lazareva, and S.V. Bantsekov, Institute of Physical Chemistry of the Academy of Sciences of the USSR, Moscow, USSR; and D. Pott, Technische Hochschule, Strasse der Nationen, DDR.

10:00 F9.4

POLYCRYSTALLINE α -BN: STRUCTURE, CONDUCTION, AND THE BAND GAP ENERGETIC STATES, V.V. Lopatin, High Voltage Institute, Tomsk, USSR.

10:15 F9.5

GROWTH AND PHYSICAL PROPERTIES OF rf-MAGNETRON SPUTTERED InN SEMICONDUCTING FILMS, W.A. Bryden, J.S. Morgan, T.J. Kistenmacher, D. Dayan, R. Fainchtein and T.O. Poehler, The Johns Hopkins University, Applied Physics Laboratory, Laurel, MD.

10:30 BREAK

11:00 *F9.6

BORON PHOSPHIDE AS A REFRACTORY SEMICONDUCTOR, Y. Kumashiro, Yokohama National University, Yokohama, Japan; M. Hirabayashi, Electrotechnical Laboratory, Ibaraki, Japan; S. Takagi, Daido Steel Co. Ltd., Nagoya, Japan.

11:15 F9.7

THERMAL AND ION BEAM INDUCED REACTIONS IN Ni ON BP, Naoto Kobayashi, Electrotechnical Laboratory, Ibaraki, Japan; Yukinobu Kumashiro, Yokohama National University, Yokohama, Japan; Peter Revesz, Jian Li and James W. Mayer, Cornell University, Ithaca, NY.

11:30 F9.8

BORON PHOSPHIDE ON SILICON FOR RADIATION DETECTORS, J.C. Lund, K.S. Shah, F. Olschner, Radiation Monitoring Devices, Inc., Research Department, Watertown, MA; and F. Ahmed, Devcom Inc., Framingham, MA.

11:45 F9.9

ZnGeP_2 : A WIDE BANDGAP CHALCOPYRITE STRUCTURE SEMICONDUCTOR FOR NONLINEAR OPTICAL APPLICATIONS, G.C. Xing and K.J. Bachmann, North Carolina State University, Department of Materials Science and Engineering, Raleigh, NC; and J.B. Posthill, Research Triangle Institute, Research Triangle Park, NC.

F1.1

THE ELECTRONIC AND OPTICAL PROPERTIES OF DIAMOND; DO THEY FAVOUR DEVICE APPLICATIONS? A T Collins, Wheatstone Physics Laboratory, King's College London, Strand WC2R 2LS, UK.

Diamond is a wide-bandgap material; natural semiconducting diamond has a high room-temperature hole mobility ($2000 \text{ cm}^2 \text{V}^{-1} \text{s}^{-1}$) and exhibits blue cathodoluminescence. The resistivity of p-type natural diamond is fairly high at room-temperature, but drops by two orders of magnitude at 300°C and is still quite low at 1000°C . By doping with boron, semiconducting single-crystal diamond can be produced by high-pressure synthesis and semiconducting epitaxial films grown by chemical vapour deposition. At first sight diamond would therefore seem to be an ideal material for high-temperature devices and blue light emitting diodes.

The reality is less promising. A recent analysis of mobility measurements for natural p-type diamond will be presented. This shows that the room-temperature value is dramatically reduced by quite low concentrations of ionised impurities. This explains why values measured for synthetic and CVD material are substantially less than $2000 \text{ cm}^2 \text{V}^{-1} \text{s}^{-1}$. The analysis also emphasises the rapid reduction in mobility with increasing temperature, even for a high quality natural diamond (e.g. $\sim 100 \text{ cm}^2 \text{V}^{-1} \text{s}^{-1}$ at 550°C). The blue luminescence is also rapidly quenched by increasing temperatures.

Nitrogen behaves as a donor in diamond, but the centres are very "deep" and it has not proved possible to grow diamonds by any technique (using N or other dopants) which have appreciable n-type conductivity. Rectifying junctions can therefore only be fabricated using Schottky barriers.

Although several diamond devices have been demonstrated in the laboratory the electronic and optical properties of diamond do not favour their commercial development.

F1.2

ATOMIC HYDROGEN IN CVD DIAMOND GROWTH

Thomas R. Anthony
General Electric Corporate Research & Development Center
River Road, Schenectady, New York, 12309, USA
(518) 387-6160

Abstract

Diamond can be grown metastably at subatmospheric pressures and moderate temperatures from hydrocarbon gases in the presence of atomic hydrogen. Atomic hydrogen serves many roles in CVD diamond growth, namely: 1.) stabilization of the diamond surface, 2.) reduction of the size of the critical nucleus, 3.) "dissolution" of carbon in the gas, 4.) production of carbon solubility minimum, 5.) generation of condensable carbon radicals in the gas, 6.) abstraction of hydrogen from hydrocarbons attached to surface, 7.) production of vacant surface sites, 8.) etching of graphite.

Atomic hydrogen can carry out these functions because of favorable relationships between energies for carbon-carbon, carbon-hydrogen and hydrogen-hydrogen bonds. An examination of bond energies of other carbon-X systems indicates that potential atomic hydrogen substitutes exist for some functions of atomic hydrogen in CVD diamond growth but that no substitute fills all the roles that hydrogen does. There are many ways to generate atomic hydrogen and each way provides a new but related CVD diamond method.

F1.3

THERMODYNAMICS AND THE CVD OF DIAMOND. Walter A. Yarbrough, Materials Research Laboratory, The Pennsylvania State University, University Park, PA 16802

Bulk diamond is unstable relative to bulk graphite except at high pressure and temperature. In spite of this well crystallized diamond has been grown using numerous CVD methods, most of which have in common the production of atomic hydrogen and hydrocarbon radicals in regimes where solid carbon is expected to be a stable product. Two fundamentally different points of view have emerged in the effort to explain why well crystallized diamond, and not graphite or vitreous carbon, is observed in these experiments. The first argues that a metastable stationary equilibrium is established in which graphite is "etched" by atomic hydrogen at a rate higher than diamond and hence diamond is kinetically stable with respect to graphite. With the assumption that diamond formation is controlled by relative kinetics the deposition mechanism becomes critically important and much debate has centered on the mechanism and species involved. If this is correct then the vapor phase growth of relatively defect free, single crystal diamond becomes problematic. The entropy production required by irreversible thermodynamics for any finite growth rate is normally minimized for the growth of well crystallized, defect free materials by ensuring that local thermodynamic equilibrium is attained or that departures from equilibrium are small. However this approach applies only if the desired phase is thermodynamically stable and the growth of other phases can be ignored. A second postulate is reformulated and defended in this paper. This is that at the growth interface, and under the conditions found successful for its growth, hydrogenated diamond surfaces are thermodynamically stable with respect to graphite. If this result is correct then a global understanding of the parameters important to the growth of diamond can be obtained without detailed kinetic analyses. A semi-empirical method was used to estimate enthalpies of formation for the three hydrogenated low index surfaces of diamond and graphite with the result that the diamond surfaces have lower enthalpies of formation. Assuming that bulk diamond is kinetically stable it is shown that at least qualitatively many of the experimental observations made in this laboratory and elsewhere are more consistent with this view than with the idea that the formation of diamond instead of graphite is kinetically controlled. With this result it can be argued that relatively defect free, single crystal diamond films by CVD are possible in spite of the bulk instability of diamond relative to graphite. In addition this suggests general principles which might be applied to the growth of other metastable phases - notably cubic boron nitride.

F1.4

STUDIES OF DIAMOND GROWTH PROCESSES FROM CHEMICAL VAPOR DEPOSITION. C. Judith Chu, Benjamin J. Bai, Robert H. Hauge, Mark P. D'Evelyn, and John L. Margrave, Rice University, Department of Chemistry, P. O. Box 1892, Houston, Texas 77251.

Synthesis of diamond thin films has been studied using hot-filament-assisted chemical vapor deposition with a variety of hydrocarbon precursors. Carbon-13-labeled diamond films were synthesized using mixtures of $^{13}\text{CH}_4$ and $^{12}\text{CH}_4$ in H_2 . The Raman peak at 1332 cm^{-1} for ^{12}C -diamond was found to shift by 50 cm^{-1} to 1282 cm^{-1} for pure ^{13}C -diamond, and the diamond peak shifts linearly within these limits with the ^{13}C mole fraction. This linear correlation has been used to study the incorporation efficiencies of various growth precursors by means of isotopic labeling, i.e., the incorporation efficiency of C-13-methane is compared to C-12-precursors such as acetylene, ethane, ethylene, acetone, carbon monoxide, and other hydrocarbons by investigating the C-13 mole fraction of the resulting diamond thin film.

Investigations of the gaseous species generated during the hot-filament-assisted CVD of diamond from mixtures of C-13-labeled methane and C-12-labeled acetylene indicate that the C-13 mole fraction in the resulting diamond thin film correlates with the C-13 mole fraction of the methane in the gas phase and not that of the acetylene. It appears that under the hot-filament-assisted CVD conditions, methyl radicals derived from methane are primarily responsible for diamond growth.

SCANNING TUNNELING MICROSCOPY INVESTIGATION OF DIAMOND FILMS ON HIGHLY ORIENTATED PYROLYTIC GRAPHITE SUBSTRATES. A. Peter Jardine, Fen-Chu Tseng and F.F.Y. Wang, Dept. of Materials Science, SUNY Stony Brook, Stony Brook, NY 11794.

The (0001) graphite surface has been extensively studied by Scanning Tunneling Microscopy (STM) making it a natural candidate for high resolution surface studies on the initial formation of Diamond films and surface phase identification. In particular, STM studies can yield atomic information on the relative abundances of diamond, diamond-like carbon, amorphous or graphitic regions of a surface. Diamond films were deposited onto heated, highly oriented pyrolytic graphite surfaces using a microwave assisted CVD. A selection of films were grown where processing variables such as the presence of Si, H₂ and CH₄ gas concentrations and microwave power inputs were varied. STM images of samples with short deposition times were taken. Correlations of film phases to processing variables are discussed.

F1.6

ADSORPTION OF HYDROCARBON RADICALS ON THE HYDROGENATED DIAMOND SURFACE.* Mark R. Pederson, Koblar A. Jackson*, and Warren E. Pickett, Complex Systems Theory Branch, Naval Research Laboratory, Washington D. C. 20375-50000.

Recently, it has been established that growth of diamond via chemical vapor deposition may be enhanced in the presence of a hydrogen gas or plasma. In order to gain insight into this phenomenon, we have studied a variety of hydrocarbon adsorption processes on a hydrogenated diamond crystallite surface. The Local Spin Density approximation has been employed with a localized basis set to calculate adsorption potentials and equilibrium separations for several hydrocarbon radicals. While the adsorption height of a single methane radical onto a single dangling bond is found to be in excellent agreement with the bulk-diamond bond length, the back-bonded hydrogens of adjacent adsorbed methane radicals repel one another which suggests diamond growth via methyl radicals only may be unfavorable. In contrast, adjacent acetylinic adsorbates do not repel each other but lead to the introduction of double carbon bonds and misplaced carbon atoms above the active layer. We present adsorption potentials, equilibrium bondlengths and vibrational spectra for H, C, CH₃ and C₂H radicals and discuss interactions between neighboring adsorbates.

*Supported in part by SDIO/IST contract N00014-89-WX-2C023.

*NRL-NRC Research Associate.

F1.7

MICROWAVE CVD OF DIAMOND USING METHANOL-RARE GAS MIXTURES. M. Buck, L.L. Chuang and H. Seki, IBM Research Division, Almaden Research Center, San Jose, CA.

The deposition of diamond from a reactive vapor phase has been dominated by the use of gas mixtures containing very small amounts of carbon containing molecules in a sea of hydrogen molecules. In most cases the carbon containing gas is a simple hydrocarbon such as methane, but more recently there have been reports using nitrogen and oxygen containing simple organics such as amines and alcohols¹. The graphite removing role of atomic hydrogen has generally been recognized as playing a key role in the successful deposition of diamond, and the few models proposed for the deposition process are

all based on this central theme. However the possible role of other atoms and molecules in the deposition process is less clear. There is need for more experimental data to further our understanding in this regard. Here we give a preliminary report on our investigation of deposition from methanol - rare gas mixtures using a small microwave reactor. An important result is that diamond of high purity, based on the sharpness of the 1332cm⁻¹ line and the background level of the Raman spectra, could be deposited without any additional hydrogen. We have also compared this result with those by other gas mixtures, in which the atomic ratio of carbon, hydrogen and oxygen are equivalent to methanol, in order to assess the significance of the parentage of these atoms in the diamond formation.

1) Y. Hirose and Y. Terasawa, J.J.A.P. Letter 25, (1986) L519.

F1.8

EFFECTS OF O₂ ADDITION ON DIAMOND GROWTH: IN SITU SPECIES MEASUREMENTS AND MODELING. Stephen J. Harris, General Motors Research Labs, Warren, MI 48090.

Recent studies have shown that addition of oxygen to diamond growth environments can have significant effects on the growth. These studies have attributed the effects of O₂ to removal of non-diamond carbon from the surface, formation of a more reactive surface, formation of additional radicals in the gas phase, and destruction of gas phase pyrocarbon-forming species. The purpose of this work is to determine how oxygen addition affects the gas phase chemical environment at the substrate surface in a filament-assisted diamond growth system in order to understand better the interesting effects of O₂ on the kinetics of growth and quality of the diamond film.

A small hole in a substrate on the tip of a quartz microprobe allows gas molecules present at the substrate surface to enter the probe, and those molecules are subsequently detected by a mass spectrometer. This *in situ* technique allows detection of stable hydrocarbons and permits us to test our chemical kinetics modeling which we use to estimate concentrations of radical species.

Our measurements show that the concentrations of small hydrocarbons (methane, ethylene, acetylene) decrease monotonically as O₂ is added, while CO concentrations increase. Agreement between experiment and model for these species is very good and encourages us that the model's predictions for species which were not measured are reasonably accurate. Calculated H and CH₃ radical concentrations rise monotonically with increasing O₂, although the percentage rise is greater for H. This rise in radical concentration depends on the CH₄/H₂ ratio. Comparison between species measurements and growth kinetics shows a complex behavior.

F1.9

MORPHOLOGY OF DIAMOND FILMS GROWN BY DC PLASMA JET CVD. Kazuaki Kurihara, Ken-ichi Sasaki, Motonobu Kawarada, and Nagaaki Koshino, FUJITSU LABORATORIES LTD. Atsugi, JAPAN.

There have been some interesting attempts to use thermal plasma for diamond synthesis. The biggest advantage of these methods is the high growth rate. No reports of the effects of important deposition parameters, such as methane concentration and substrate temperature, have been published, however.

Our research focused on the effects of methane concentration, substrate temperature, and the cooling rate of plasma on the morphology of diamond films synthesized by dc plasma jet CVD.

To change the cooling rate of the plasma, we changed the distance between the plasma torch and substrate. We looked at the surfaces and cross sections with SEM. Optical emission was also used to analyze the plasma jet and the diamond growth mechanism.

With increased methane concentration, the diamond films grew faster, but over a certain concentration, growth rate stopped increasing. At lower methane concentrations, (111) planes tend to be obtained and, at higher concentrations, (100) planes. The lower cooling rate decreased the growth rate and formed (100) planes. The transparency of the synthesized diamond films is better at lower methane concentrations and lower pressures.

F1.10

OXYGEN EFFECT IN DIAMOND DEPOSITION AT LOW TEMPERATURES. Y. Liou, A. Inspektor, R. Weimer, D. Knight and R. Messier, Materials Research Laboratory, The Pennsylvania State University, University Park, PA 16802

Diamond thin films were deposited on different substrates at low temperatures (<400°C) by microwave plasma enhanced chemical vapor deposition system. The deposited films were either amorphous carbon films or diamond films depending on the different gas mixtures being used. The concentration of the oxygen in the gas mixtures is critical for diamond growth. The etching rate of the non-diamond carbonic compounds in the coating was higher with more oxygen addition in the gas mixtures. Different ratios of the methane to oxygen concentration on different substrates at different temperatures have been studied. Raman spectroscopy, X-ray diffraction and scanning electron microscopy have been used to characterize the deposited films.

F2.1

ELECTRON CONTROLLED CHEMICAL VAPOR DEPOSITION OF DIAMOND THIN FILMS ON VARIOUS SUBSTRATES. Yong-Huee Lee, Klaus J. Bachmann and Jeffrey T. Glass, North Carolina State University, Department of Materials Science and Engineering, Raleigh, N.C. 27695-7907

Electrons can affect the hot filament assisted growth of diamond films in several ways, including acceleration of gas species dissociation, creating damage at the growth surface, etc. Thus, electron controlled chemical vapor deposition (ECCVD) has been utilized to deposit diamond on scratched (001) Si substrates. Current-voltage characteristics of the ECCVD system indicated a DC plasma was generated under certain conditions. Diamond film quality was correlated with biasing conditions. Highly faceted diamond growth exhibiting only a sharp Raman line at 1332 cm^{-1} was obtained under certain conditions. However, biasing which created a DC plasma resulted in spherulitic growth incorporating graphitic carbon into the diamond film. Extensive chemical, structural and optical characteristics of the films will be described. Diamond film deposition on various single crystal substrates of interest for heteroepitaxial growth has also been attempted. Not only lattice matching but also bond energy considerations have been utilized in choosing these substrates. The film quality and the characteristics of the interfacial carbide formation will be discussed. Finally, homoepitaxial diamond films have also been deposited on natural type IIa diamond substrates. Characteristics of the grown films are described for diamond substrates of different orientations.

F2.2

KrF* LASER-INDUCED CHEMICAL VAPOR DEPOSITION OF DIAMOND
George W. Tyndall and Nigel P. Hacker IBM Almaden Research Center, 650 Harry Road, San Jose, CA 95120.

A KrF* laser-based process for the deposition of diamond is reported. The experiment consists of focusing the pulsed excimer laser beam at normal incidence onto the surface of a room temperature silicon substrate in the presence of an organic precursor. The presence of diamond in the deposited films were verified using Raman Spectroscopy and Auger Electron Spectroscopy.

F2.3

INVESTIGATIONS OF EXCIMER LASER EFFECTS ON CVD DIAMOND GROWTH. P. E. Pehrsson, H. H. Nelson, F. G. Celii,* Naval Research Laboratory, Washington, D.C. 20375; *NRC/NRL Post-Doctoral Fellow

One of the principal problems associated with the nucleation and growth of CVD diamond films is the necessity of growing on a substrate heated to about 800 C. The use of excimer laser radiation as an alternative energy source allowing lower growth temperatures has been reported,¹ although another claim was subsequently retracted.

We used a variety of laser conditions to modify the surface and gas phase chemistry in a diamond growth apparatus, including those reported to have enhanced growth. The laser wavelength, precursor gas (and hence the gas-phase absorption), laser intensity and orientation with respect to the substrate, flow rate, and gas inlet orientation with respect to the filament were varied. The samples were analyzed using Optical and Scanning Electron Microscopy, the Scanning Auger Microprobe, and Micro-Raman Scattering.

In all cases, the laser had either no effect or actually suppressed diamond growth in comparison to the adjacent unirradiated regions. Interestingly, the crystals that did grow in the irradiated regions were similar in size and morphology to those from the unirradiated areas, suggesting possible mechanisms by which the laser suppressed diamond nucleation. Variations in the types of carbon observed across the samples are discussed. These results are interesting not only because they conflict with previous encouraging claims, but also because they may provide clues to the diamond nucleation process.

1. Y. Goto, T. Yagi and H. Nagai, Mater. Res. Soc. Symp. Proc. (1988) in press.

F2.4

AN NMR STUDY OF DIAMOND THIN FILMS. Karen M. McNamara and Karen K. Gleason, Department of Chemical Engineering, MIT, Cambridge, MA.

Nuclear magnetic resonance (NMR) spectroscopy is used to study the incorporation of ^{13}C and ^1H into diamond thin films grown in a hot filament reactor. Quantitative values for the ratio of sp^3/sp^2 carbon and hydrogen content will be obtained. NMR linewidths will indicate the degree of disorder in the system, as well. The carbon-13 source is acetone, isotopically labeled at either the carbonyl or methyl carbons. Thus, carbon-13 contents will indicate the relative role of CH_3 and CO derived precursors in diamond deposition, shedding light on the mechanisms of diamond growth. Understanding of these mechanisms is essential in exploiting the potential of diamond as a semiconductor.

F2.5

DIAMOND POLYTYPISM: DIFFRACTION, VIBRATIONAL BEHAVIOR, AND OPTICAL PROPERTIES* A. W. Phelps, Diamond Materials, Inc., 2820 East College Avenue, State College, PA. 16801; K. E. Spear, W. Howard, D. Huang, and W. B. White, The Pennsylvania State University, University Park, PA. 16802.

Polytypism is a well-known phenomenon in SiC. It is important to semiconductor applications of SiC because the bandgap and electron/hole mobilities are a strong function of polytype.

Polytypism has recently been identified in monocrystalline diamond particles formed by homogeneous nucleation. Structural models have been used to determine the likely response of hexagonal and rhombohedral diamond polytypes during x-ray or electron diffraction, Raman and infrared spectroscopy, and optical measurements. Many physical properties of diamond are affected by the degree of hexagonal character and space group symmetry of these polytypes. Diffraction patterns for two diamond polytypes, 15R and 21R, have been calculated and indicate that lines not allowed in hexagonal polytypes become allowed and will appear in diffraction of these rhombohedral polytypes.

The vibrational behavior of diamond polytypes should be closely tied to the degree of hexagonal character in a particular polytype. Some polytypes will have so called 'weak modes' present in their Raman spectra as the result of a 'zone folding' mechanism like that seen in the Raman spectra of SiC polytypes. The refractive indices and birefringence are expected to be controlled by the degree of hexagonal character of the specific polytype.

The variation in properties with diamond polytypism may provide a number of useful methods for the identification of these materials as well as provide new fundamental information about the materials themselves and polytypic materials in general.

* This research was co-sponsored by: (i) the Ben Franklin Partnership Program of Pennsylvania, (ii) the Office of Naval Research (with funding from SDIO/IST) under contract #N00014-86-K-0443, and (iii) Diamond Materials, Inc.

F2.6

DOMAIN SIZE DETERMINATION IN DIAMOND THIN FILMS. Y.M. LeGrice, R.J. Nemanich, Dept. of Physics, North Carolina State University, Raleigh, NC 27695.

Diamond films deposited by CVD methods usually have some sp^2 bonded carbon incorporated in them. Raman scattering measurements are able to display both the diamond and sp^2 bonded regions in these samples. Previous studies have shown that in order to determine the ratio of the sp^2 to sp^3 bonded regions, the domain sizes must be known. In this study the linewidth of the diamond peak at 1332 cm^{-1} is used to determine diamond domain sizes, while the intensity of the disorder induced scattering is related to the size of the sp^2 bonded regions. We have carried out detailed calculations of the effect based on the phonon dispersion curves of diamond and breakdown of wavevector selection rules in Raman scattering. The results enable us to determine domain sizes of the diamond regions in the films. The linewidths of samples prepared by various methods were calculated, and the dimensions of the diamond regions were obtained. From these results, it was determined that there is an inverse relationship in the domain sizes of the diamond and sp^2 domain sizes. When the diamond regions are large, sp^2 regions are small, and vice-versa. The changes in the domain sizes with growth conditions are correlated to the growth process.

F2.7

CHARACTERISATION OF THIN FILM AND SINGLE-CRYSTAL CVD DIAMOND BY ABSORPTION AND LUMINESCENCE SPECTROSCOPY. A T Collins, Wheatstone Physics Laboratory, King's College London, Strand, London WC2R 2LS, UK; M Kamo and Y Sato, NIRM, 1-1 Namiki, Tsukuba, Ibaraki 305, Japan.

Polycrystalline films and single crystals of diamond produced by the decomposition of methane-hydrogen mixtures in a microwave plasma, with CH_4 concentrations between 0.3 and 3.0%, have been examined using optical absorption and cathodoluminescence (CL) spectroscopy from 900 to 200 nm (1.4 to 5.6 eV).

In absorption all samples show a continuously increasing absorption from low energies to high energies, right up to the fundamental absorption edge at 5.5 eV. The strength of this absorption (which may be associated with carbon double bonds) increases as the concentration of CH_4 in the gas mixture is increased.

Blue CL from the films and the crystals is associated with donor-acceptor pair recombination. The single-crystals also exhibit strong "edge emission" which is characteristic of

defect-free material, but this luminescence is not detected from any of the films. As the CH_4 concentration in the starting gas is increased, CL characteristic of nitrogen-, interstitial- and vacancy-related optical centres is observed from the diamond films. A CL line at 1.681 eV, which is also observed in absorption in some films, has been attributed previously to a defect involving silicon.

We have also studied defects produced by radiation damage (using 2 MeV electrons) and thermal annealing. The absorption and CL spectra of the crystals show all the systems characteristic of irradiated type IIa natural diamond with extremely low impurity concentrations.

F2.8

EFFECT OF DOPING WITH NITROGEN AND BORON ON CATHODOLUMINESCENCE OF CVD-DIAMOND. Yoshihiro Yokota, Hiroshi Kawarada, Yusuke Mori and Akio Hiraki, Dept. of Electrical Eng., Faculty of Eng., Osaka Univ., Suita, Osaka 565, Japan.

Nitrogen (N) and boron (B) are the electrically and optically active impurities in diamond. We have investigated cathodoluminescence (CL) of the diamonds doped with them formed with microwave plasma chemical vapor deposition (CVD).

In the undoped specimens, the CL spectra have only one peak at 2.8-2.9 eV classified as "band-A". These are the same spectra as natural typeIIa diamonds where dislocations correspond to the emission areas. The specimens doped with B show the intense CL spectra with a peak at about 2.4 eV in addition to the 2.9 eV-band. In the CL spectra of N-doped specimens, three peaks appear at about 2.9, 2.1 and 1.7 eV. The 2.9 eV-peak is the same as undoped specimens. The 2.1 eV-peak is attributed to N-related center. The 1.7 eV-peak is attributed to the isolated neutral vacancy (V) called "GR1" center. In the specimens doped with N and B at the same time, there exist three peaks at about 2.4 eV, 2.1 and 1.7 eV, which have been recognized above.

Other N-related strong emission centers such as H3 (2.46 eV) and N-V (1.94 eV) have not been observed. These results show that, although neutral V are present, N-V complexes are not formed during CVD process. The fabrication of these centers has been also tried to introduce enough V using high energy electron irradiation.

F2.9

PHOTOLUMINESCENCE SPECTROSCOPY OF DIAMOND FILMS. J.A. Freitas, Jr.*, J.E. Butler, L.M. Hanssen, S.G. Bishop, and U. Strom, Naval Research Laboratory, Washington, DC 20375-5000. * Sachs/Freeman Associates, Landover, MD 20785-5396.

Photoluminescence (PL) spectroscopy has been used to characterize polycrystalline diamond films prepared by filament-assisted vapor deposition (FACVD) and by a combustion technique (CT) in an oxyacetylene flame. The 20-30 μm thick films generally consisted of microcrystallites with grain sizes ranging from 10-200 μm . The temperature range of interest was 6K-300K.

The PL spectra of the FACVD films are dominated by a defect band with a strong zero-phonon line at 1.67 eV and phonon replica at lower energies. This band (GR1), identified with a neutral vacancy, is observed in crystals prepared by other techniques, after electron irradiation.

The CT films exhibit two PL lines near 1.95 eV and 2.16 eV, respectively. The 1.95 eV band has been tentatively identified as a nitrogen-vacancy

pair. This band has been observed in natural diamond which has been irradiated and subsequently annealed at elevated temperatures. We have observed a strong dependence of the PL spectra radially across a given CT film and associate this with details of the flame chemistry.

F2.10

CW FOUR-WAVE MIXING IN SYNTHETIC DIAMOND. D. A. Redman and S. C. Rand, University of Michigan, Department of EECS, 1301 Beal Avenue, Ann Arbor, MI 48109-2122.

We report efficient CW optical phase conjugation and resonantly enhanced four-wave mixing spectroscopy of the N-V color center in synthetic diamond.

An ultra-narrow resonance is observed in the room temperature nearly degenerate four-wave mixing spectrum upon excitation within the vibronic band at 590 nm, furnishing the triplet manifold decay rate.

F2.11

"MODELLING OF A Ag/DIAMOND/n-GaAs PHOTODIODE WITH GRATING COUPLING OF THE INCIDENT LIGHT TO SURFACE PLASMA WAVES" D. Barman, M. Rahman, A.S. Karakashian, A. Altshuler and S. Broude, University of Lowell, Department of Physics and Applied Physics, Lowell, MA 01854

A theoretical model has been developed to design a metal/insulator/semiconductor narrow band photodiode with grating coupling of the incident light to surface plasma waves (SPW). The insulating layer consists of a thin polycrystalline diamond film which is deposited on an n-GaAs substrate with a grating having optimal parameters etched into it. A silver barrier contact on the diamond film also serves as the active medium for the SPW. This type of device is an angle of incidence, wavelength and polarization sensitive photodetector. It has an enhanced quantum efficiency compared to a flat surface detector. This design is also compared to similar Ag/Insulator/n-GaAs detectors for insulators other than diamond.

F2.12

OPTICAL CHARACTERISATION OF NICKEL IN DIAMOND MH Nasaré, AJ Neves Departamento e Centro de Física (INIC), Universidade de Aveiro, 3800 Aveiro, Portugal and Gordon Davies, Department of Physics, King's College London, Strand, London WC2R 2LS, UK

We show that when diamonds are synthesised using a solvent-catalyst which contains nickel, individual atoms of Ni may be grown into the diamonds. The presence of the nickel atoms may be identified and their concentrations estimated in a non-destructive manner using optical spectroscopy.

The characterising optical signal is absorption or photoluminescence with sharp (zero-phonon) lines in the near-infrared at 1.401 and 1.404 eV. Using synthetic diamonds which have unusually low internal strains, we show that the lines contain fine structure which is produced by the five natural isotopes of Ni, unambiguously establishing that the lines are produced by nickel. There is evidence for only one Ni atom in the optical center producing the 1.4 eV lines.

Stresses of up to 1 GPa applied along the $\langle 001 \rangle$, $\langle 111 \rangle$ and $\langle 110 \rangle$ axes of the diamond show that the Ni atom is in a trigonal environment: if the Ni atom substitutes for a carbon atom it is displaced out of the lattice site (qualitatively like the single nitrogen atom in diamond). The effects of the stresses establish that the ground state of the optical transition is an orbital doublet, split by a spin-orbit coupling of 3 meV to produce the two lines at 1.401 and 1.404 eV. The excited state is an orbital singlet. Magnetic fields up to 6 Tesla produce clear splittings of the lines, and confirm the trigonal environment.

Using the measured radiative decay time of the 1.4 eV luminescence, we show that the absorption coefficient μ (in cm^{-1}) integrated over both lines (photon energy E in meV) is related to their concentration C (cm^{-3}) by

$$C = 5 \times 10^{19} \int dE \mu(E).$$

F3.1

A STUDY OF THE ELECTRONIC STRUCTURE NEAR INDIVIDUAL DISLOCATIONS IN DIAMOND BY ENERGY LOSS SPECTROSCOPY. J. Bruley, and P.E. Batson. IBM Research Division, Thomas J. Watson Research Center, Yorktown Heights, NY 10598.

Spatially resolved electron energy loss spectra recorded from very small volumes of diamond containing individual dislocations show extra intensity within the band-gap just below the 1s to bulk conduction band threshold energy, when compared to spectra recorded from neighboring defect free regions. This is interpreted as direct evidence for the presence of vacant defect states associated with the dislocation structure. The contribution of the π^* states from the surface layers to this region of the spectra is completely removed by calculating the difference between the spectra recorded on and off the defect. A comparison is drawn between the measured near edge structure and calculations of local density of states reported in the literature.

F3.2

CHARACTERIZATION OF HEAVY METAL CONTAMINATION IN DIAMOND FILMS USING SIMS AND TOTAL REFLECTION X-RAY FLUORESCENCE (TXRF). R. S. Hockett, Charles Evans & Associates, Redwood City, CA; and James Knowles, Crystallume, Inc., Menlo Park, CA.

Processes for diamond film growth on silicon substrates may introduce heavy metal contamination at the interfaces or in the film itself. These metals may or may not be detrimental for the application of the diamond film, but the measurement of the metals is required before such an assessment can be adequately made. This paper will address the usefulness of Secondary Ion Mass Spectrometry (SIMS) and of a new technique called Total Reflection X-Ray Fluorescence (TXRF) for the characterization of heavy metal contamination in diamond films prepared by different processes, including microwave and dc sputter deposition, where contamination was intentionally introduced. Characterization of these films by more commonly used techniques will also be reported.

F3.3

MODELLING OF DIAMOND HETEROSTRUCTURES FOR ELECTRO-OPTICAL APPLICATIONS. A. Altshuler, S. Broude, C. Hantzis, A.S. Karakashian, Physics Dept., University of Lowell, Lowell, MA 01854

A theoretical model has been developed for a diamond/semiconductor heterojunction based on a molecular dynamics and pseudo-potential approach. Characteristics of the structure are estimated and the performance in electro-optical applications such as wave-guides, detectors, LEDs and quantum-well devices is predicated.

F3.4

INFRARED AND RAMAN CHARACTERIZATION OF THE HYDROGEN ENVIRONMENTS IN DIAMOND AND DIAMOND-LIKE FILMS. Y.M. LeGrice, E.C. Buehler, R.J. Nemanich, Dept. of Physics, North Carolina State University, Raleigh, NC 27695; J.T. Glass, Dept of Materials Science and Engineering, North Carolina State University; K. Kobashi, Electronics Technology Center, Kobe Steel, Ltd., Kobe, Japan, 651; F. Jansen and M.A. Machonkin, Xerox Corp., Webster, NY 14580.

It is well known that H plays an important role in the growth of diamond and diamond-like thin films by activated CVD processes. We have investigated films prepared under varying conditions with IR and Raman spectroscopy. The growth temperatures were varied in one series, while the concentration of CH_4/H_2 was varied in another. In the IR, two bands at approximately 2880 and 2970 cm^{-1} were observed, due to the stretching mode of the C-H and C-H₂ bonds. From this it was determined that the C-H and C-H₂ environments were present, and that the carbon was sp^3 bonded. The intensity of this absorption band was then correlated to the Raman scattering spectrum. It was found in the Raman measurements that there was a natural progression from diamond-like films to diamond films. This progression was observed as H incorporation was decreased, so that films containing the largest amount of H were more diamond-like than those with little H. No sharp transition of the H incorporation vs the growth parameters was observed. Aspects of the growth process are discussed based on these results.

*Supported in part by SDIO/IST through the ONR under contract N00014-86-K-0666.

F3.5

ELECTRONIC STRUCTURE AND ENERGY PARAMETERS OF DIAMOND NUCLEI: A FIRST PRINCIPLES CLUSTER APPROACH. A. Altshuler, M. Wilner, C.C. Ai and Y.C. Yang, Physics Department, University of Lowell, Lowell, MA.

We present results of Multiple-Scattering X-alpha Self-Consistent Field (MS-Xa-SCF) calculations of electronic states and total energies of small clusters of carbon atoms arranged in diamond-lattice positions. Relaxation of bond lengths gives the equilibrium structure of the diamond clusters, considered as nucleation centers. Comparison of total energies of clusters of increasing size enables us to estimate the surface energy of these nucleation centers, which are to be used as parameters in a thermodynamic theory of diamond nucleation and growth.

We present results of similar calculations on these same clusters modified to simulate their embedding in bulk diamond. We obtain in this way a small-cluster model of bulk diamond, and identify molecular orbital precursors of conduction and valence bands.

F3.6

EFFECT OF DIFFERENT CH_4/H_2 GAS COMPOSITIONS ON THE MORPHOLOGY AND GROWTH RATE OF DIAMOND GROWN BY HOT FILAMENT CVD. Edward N. Farabaugh and Albert Feldman, National Institute of Standards and Technology, Gaithersburg, MD

Diamond film growth has been carried out on single crystal Si and polycrystalline mullite substrates by hot filament chemical vapor deposition. Both substrates offer a good thermal expansion match to diamond. Gas mixture ratios of CH_4/H_2 ranged from 0.1-1.0%. The remaining deposition parameters were: substrate temperature, 750°C; filament temperature, 1800°C; gas pressure, 40 torr; gas flow rate, 52 sccm except for the 0.1% CH_4/H_2 ratio deposition in which the flow rate was 120 sccm. Film thicknesses were determined from cross sectional SEM micrographs. The average growth rates on the mullite increased with increasing CH_4 gas fraction, ranging from 0.05 $\mu\text{m/hr}$ to 0.21 $\mu\text{m/hr}$. Growth rates on the Si substrates were slightly lower for identical growth conditions. Surface SEM micrographs revealed that the roughness of the films decreased with increasing CH_4 gas fraction during deposition. X-ray diffraction patterns showed that crystalline grain size in the films decreased with increasing CH_4 gas fraction. No preferred crystallographic orientation was seen in the diffraction patterns. Isolated particles were also grown on Si substrates under the same deposition conditions as the film growth. As the CH_4 gas fraction increased, the

particle growth displayed increasing rates of secondary particle nucleation resulting in a less well faceted morphology.

F3.7

DEPOSITION OF DIAMOND FILMS BY A SCANNING OXYGEN-ACETYLENE FLAME. Yonhua Tzeng, Calvin Cutshaw, and Richard Phillips, Electrical Engineering Department, Auburn University, Alabama 36849.

Diamond films of high quality have been deposited on various substrates, e.g. silicon, by an oxygen acetylene flame operating at one atmosphere pressure in air as well as oxygen rich or oxygen deficient ambient. High quality diamond films are composed of well defined octahedral or cuboctahedral diamond crystallites that are optically transparent in the visible light range and are characterized by a Raman peak similar to that for natural diamond. The physical properties as well as surface morphology of diamond films are strongly dependent on the experimental parameters such as substrate temperature, flame composition, gas flow speed, distance between the inner cone of the flame and the substrate, the tilted angle of the flame with respect to the substrate and the ambient gas composition which can be varied by flowing gases towards the substrate through the flame that is tilted at an angle wrt to substrate.

By varying the flame composition with time and scanning the flame across the substrate, diamond films can be deposited in several minutes on silicon substrates. We will discuss the microstructures of diamond crystallites and the physical and electrical properties of diamond films based on data obtained from Raman spectroscopy, I-V, SEM, surface profilometry and optical emission spectroscopy. The advantages and disadvantages of the flame CVD technique will be presented.

F3.8

ENHANCEMENT OF DIAMOND sp^3 BONDING IN RF SPUTTERED CARBON FILMS WITH NITROGEN GAS ADDED : C. J. TORNG, T. YEH and J. M. SIVERTSEN, DEPT. OF CHEM. ENG. AND MAT. SCI., U. OF MINNESOTA, J. H. JUDY, DEPT. OF ELEC. ENG., U. OF MINNSOTA, MINNEAPOLIS, MN 55455

Thin carbon films were prepared by RF diode sputtering of a graphite target in a mixed nitrogen/argon plasma. A series of carbon thin films were deposited as a function of nitrogen partial pressure. The substrates were Corning #2 cover glass. We observed a systematic variation of the properties of the carbon thin films with increasing nitrogen partial pressure. Auger electron spectroscopy (AES), X-ray photoelectron spectroscopy (XPS), TEM diffraction study showed that nitrogen stabilizes the sp^3 diamond bonding in some instances more than in a-C:H films.

From AES studies, it was shown that as the nitrogen partial pressure increases to 1 mtorr or above, in a total sputtering pressure of 10 mtorr, the carbon Auger spectrum (in fine structure) is identical to the diamond Auger spectrum. XPS studies also show that the diamond phase (which has a binding energy of 287.28 eV) is present, and its amount increased as the nitrogen partial pressure increased. Further characterization of these carbon thin films by TEM diffraction, optical ellipsometry and dielectric constant measurements also will be discussed in this paper.

REFERENCES :

1. T. Mori and Y. Namba, J. Appl. Phys. 55, 3276 (1984).

F3.9

IMPORTANCE OF FILAMENT REACTIVITY FOR CVD DIAMOND GROWTH. M.Sommer and F.W.Smith, Department of Physics, City College of New York, Convent Ave. & 138th St., New York, NY 10031.

We report on an investigation of the behavior of a W filament heated in mixtures of CH_4 and H_2 (1200 to 2500K, 9 and 25 Torr, $\text{CH}_4/\text{H}_2 = 1\%$ and 3%). After the filament has been thermally converted to W_2C (14×10^{-2}), evidence for the existence of a layer of graphitic carbon on the filament surface has been obtained from emissivity measurements. The removal of the C deposit at a high enough temperature (2250-2280K) has been observed from emissivity and also from resistance, power consumption and reactivity studies. The reactivity of the filament surface (i.e. its efficiency in dissociating H_2 and CH_4) increases dramatically when regions of the surface become C-free. The transition temperature from deposition to etching (i.e. from a C-covered to a C-free filament surface) and its dependence on the CH_4/H_2 ratio are in good agreement with our thermodynamic model¹. Since atomic hydrogen plays a vital role in CVD diamond growth, our results show the importance of operating the filament using conditions where the surface is clean and hence most reactive. We will indicate how measurements of filament resistance and power consumption can be used in a simple manner to monitor the C coverage, and hence reactivity, of the filament surface.

I. M. Sommer, K. Mui & F. W. Smith, Solid State Communications, 69 (7) 775-8 (1989)

F3.10

HIGH-RATE DEPOSITION OF DIAMOND BY DC ARC DISCHARGE IN HYDROGEN-METHAN MIXTURE GAS Xiang-Liu JIANG, Beijing Institute of Science and Technology, Beijing, China; Fang-Qing ZHANG, Ying-Hu YANG, Jing-Qi LE, and Bing YANG, Lanzhou University, Department of Physics, Lanzhou, China.

The preparation of diamond films with applicable structure, properties, uniformity and repeatability is undoubtedly required for the fabrication of electronic devices using the diamond films as the structural layers.

In this study, the polycrystalline diamond films with high growth-rate have been synthesized by dc arc discharge plasma CVD in a mixture gas of $\text{CH}_4(1\%)$ and $\text{H}_2(99\%)$. The diamond films are deposited on water-cooled silicon and molybdenum substrates at gaseous pressure of 200 Torr. The typical arc discharge is performed at 200V and 4A, while the hydrogen flow rate is about 3000-3500 sccm. The crystallinity of diamond films prepared are characterized well by X-ray diffraction (XRD), Raman spectroscopy, and scanning electron microscopy (SEM). It is verified by XRD and Raman measurements that the synthesized diamond films are identified as natural cubic diamond structure and contain substantially no graphite or amorphous carbon. SEM photographs show that the crystal grain size reaches 50-60 μm and the average growth rate of diamond films, deposited during 4 hours, is about 40-60 $\mu\text{m/h}$. However, it is observed that the crystal grain size and the film thickness are not proportional to the deposition time.

The characterization results of structure and physical properties for the prepared diamond films are reported, and the possible applications for electronic device fabrication are discussed.

F3.11

INTRA- AND INTERGRANULAR FRACTURE OF DIAMOND THIN FILMS. H.A. Hoff, A.A. Morrish, J.E. Butler, and B.B. Rath, Naval Research Laboratory, Washington, DC; and W.A. Carrington, University of Florida, Tampa, FL.

Diamond thin films have been synthesized at low pressures by chemical vapor deposition (CVD) and, recently, at ambient atmosphere with an oxygen-acetylene welding torch, both on Si as a substrate. By the application of appropriate thermal or mechanical stresses to the substrate, the diamond films can be delaminated. The delaminated films even when only a few microns thick can be handled easily without fracturing.

Scanning electron microscopy (SEM) examination of fractured CVD diamond films shows the presence of both intra- and inter-granular fracture attesting to the inherent strength of the films. Using transmission electron microscopy (TEM), twinning and stacking faults are seen within the crystallites of the films. By combining SEM and TEM examination, the relative degree of intragranular fracture found in films synthesized by both CVD and oxygen-acetylene torch has been investigated. Possible mechanisms for the intragranular fracture and the relative strength of such films will be discussed.

F3.12

APPLICATION OF A THERMOBALANCE FOR STUDYING DEPOSITION KINETICS OF DIAMOND FILMS. Jerry Czarnecki, David Thumim; Cahn Instruments, 16207 Carmenita, Cerritos, CA 90701

In spite of the tremendous progress in the field of deposition of diamond films, full control of the processes involved is still to be developed. The ultimate goal: monocrystalline growth of diamond on non-diamond substrates requires better insight into the elementary processes. Due to the limitations in the presently available instrumentation, too little is known about kinetics of diamond deposition.

Thermobalances present large potential for studying kinetics of diamond growth, as they provide continuous monitoring of the process, as well as temperature- and environment control, especially in Hot Filament-, and Laser-Enhanced CVD. A Cahn thermobalance type TG-171 has been applied to study HFE CVD deposition of diamond and diamond-like films from CH_4 . Changes in the deposition rates during each individual process may indicate three stages of the deposition kinetics: 1- generation of nuclei (slow, linear); 2- growth on nuclei (exponential); 3- growth on the surface of diamond film, completely covering the substrate (fast, linear). An attempt to determine the concentration of graphite in the deposited layer, based on differences in oxidation rates of diamond and graphite has been proposed, as supplementary to X-ray diffraction method.

F3.13

FAR INFRARED LASER MEASUREMENTS OF DIAMOND FILMS. Lawrence P. Bourget and Dr. Richard S. Post, Applied Science and Technology, Inc., 35 Cabot Road, Woburn, MA 01801; and Dr. Robert Giles, Andrew Gatesman, and Greg Phillips, Department of Physics, Lowell University, Lowell, MA 01854.

This paper will discuss polycrystalline diamond deposited onto silicon using a high pressure microwave plasma source. These films were characterized using ellipsometric measurement techniques with far infrared (300 GHz - 3000 GHz) laser sources, as well as FTIR.

The deposited films were found to be only weakly absorbing in this band.

The film characteristics and their dielectric properties will be presented.

F3.14

CHARACTERIZATION OF HOLLOW-CATHODE DC DISCHARGE GROWTH OF DIAMOND - H.N. Chu, A.R. Lefkow, R. Redwing, L.W. Anderson, M.G. Lagally, J.E. Lawler, Department of Physics, University of Wisconsin, Madison WI 53706

Diamond films have been grown by a variety of methods. Of these, especially interesting is the work reported on the use of hollow-cathode discharges. We have grown diamond on Si (100) using a Ta spiral hollow cathode and 0.5% CH₄ in H₂ at 30 Torr and 80 sccm, with 150V potential and a 1 cm substrate-cathode spacing. The substrate temperature is 900 C and the growth rate is about 0.5 um/hr. The existence of diamond was verified with both Raman scattering and scanning electron microscopy. We have also used a solid Cu electrode with an abnormal glow discharge. In order to attempt to understand the plasma chemistry, we have made emission measurements of the different glow regions. We observe a glow near the cathode, a dark space, and a second glow near the anode. We shall describe emission measurements as a function of anode-cathode spacing and attempt to relate them to the growth rate of the diamond film.

Research Supported by NSF Grant No. CDR-8721545 in support of the Engineering Research Center - Plasma Aided Manufacturing.

F3.15

FREE-STANDING CVD DIAMOND SHAPES AND COATINGS. Donald E. Patterson, Robert H. Hauge, and John L. Margrave. Rice University and the Houston Area Research Center, 4802 Research Forest Dr., The Woodlands, TX 77381.

Free-standing CVD diamond film cylinders have been prepared via the hot filament technique. The cylinders have been characterized by both Raman spectroscopy and X-ray diffraction. The cylinders have been prepared to have either a rough interior and a smooth exterior or vice versa. The rough side is used to form physical bonds to a second surface. Methods of transferring and bonding diamond cylinders to another cylinder will be discussed. Other free-standing diamond forms, bonding techniques, and potential coatings applications will also be discussed.

F3.16 ABSTRACT WITHDRAWN

F31.7

LASER ASSISTED TECHNIQUES FOR DIAMOND AND DIAMOND-LIKE THIN FILMS J. Krishnaswamy, A. Rengan, G. Matera, M. Longo, A. Srivatsa and J. Narayan, Dept. of Materials Science and Engineering and R. Nemanich, Dept. of Physics, North Carolina State University, Raleigh, N. C. 27695-7916.

We describe preliminary results of diamond and diamond-like thin films produced by laser assisted, hot filament CVD and laser ablation & plasma hybrid techniques. The hot filament CVD films are deposited from hydrocarbon precursors on a continuously excimer illuminated silicon substrate and the diamond-like films are deposited using a laser ablation and plasma hybrid technique wherein graphite targets are ablated in hydrogen and hydrogen free ambients. Microhardness and optical band gap measurements of the laser deposited films show an inverse correlation as a function of substrate temperature. Microstructure and property correlations of the films as characterized by TEM, FTIR, SIMS, and Raman techniques

are discussed. We compare hydrogen incorporation in diamond films prepared by CVD, amorphous hydrogen free and hydrogenated films by laser ablation and plasma hybrid technique(1) and hydrogenated amorphous DLC films by soft vacuum, CW electron beam cracking of methane and acetylene (2). The nature of diamond epitaxy on various substrates will be addressed.

References:

1. J. Krishnaswamy, A. Rengan, J. Narayan, K. Vedam and C. McHargue. Appl. Phys. Lett., 54,2445 (1989).
2. J. Krishnaswamy, L. Andriunas, H. Zarnani, C. Collins and M. Caolo, 1988 Spring Meeting of MRS, Nevada

F3.18

Laser-Flash Method for Investigating the Thermal Conductivities of Diamond Thin Films Synthesized by EA-CVD. Yang Peichun Pu Xin Xuan Zhenwu Qi Lichang and Hou Li Research Institute of Synthetic Crystals P.O. Box 733, Beijing 100018 P.R. China.

Natural IIA diamond crystal exhibits extremely high thermal conductivity, which ($\lambda = 21 \text{ W/CM K}$) is five times higher than that of copper at room temperature. So, it is very important to make relative precise measurement of thermal conductivities of the diamond thin films for its use as semiconductor materials, especially as heat sinks used in electronic devices. In this report, the thermal conductivities of diamond thin films (diamond thin films was etched from Si substrate by mixed solution of HNO₃ and HF 3:1 in Volume) which synthesized by EA-CVD under different deposition conditions were investigated by Laser-Flash method. The influences of deposition conditions, such as, the concentration of hydrocarbon gases, substrate temperatures and crystallography structures of the films on their thermal conductivities were analysed. The results provide some effective information for the application of diamond thin films in electronic devices.

F3.19

Study for Growing Diamond Films (DF) on Surfaces of Various Materials. Pu Xin Yang Peichun Xuan Zhenwu Qi Lichang and Hou Li Research Institute of Synthetic Crystals, P.O. Box 733, Beijing 100018, P.R. China.

In this paper, deposition of DF on surface of some materials as substrates by electron-assisted CVD technique is reported. The materials used as substrates were Si, Mo, Cu, Diamond Ceramics and quartz glass, etc. In the experiment, H₂, CH₄, and C₂H₅OH were used as gas sources. The tungsten filament heated up to 2000°C was adopted for thermal decomposition device, and a direct voltage between filament and holder below the substrate was applied. The filament is negative and holder positive. The elementary parameters of experiments are as following: total flow of gases 50-200 cc/min; the content of hydrocarbon in gases 0.5-2.0%; the temperature of substrates 600-900°C; The voltage between filament and holder 50-150 V. The 1333 cm⁻¹ peak in Raman spectrum of samples obtained at precious conditions show that they are polycrystalline diamond films. The crystallography morphology was observed with SEM. Results of the experiments showed that differences of the forming nucleation and depositing processes by changing operative parameters were quite obvious. Especially, they were different between each other for various substrates, although the operative conditions were similar. The present research is

important in increasing speed of growth and improving quality of growing DF and is quite valuable in application.

F4.1

HOMOEPITAXIAL DIAMOND FILMS, M. W. Geis, Lincoln Laboratory, Massachusetts Institute of Technology, Lexington, Massachusetts 02173

Homoepitaxial growth techniques are being developed to obtain device quality films. The hot filament technique was used to produce epitaxial films on (100)-, (110)-, and (111)-oriented, type-IIa diamond substrates. Hydrogen, containing 3% acetone, was used to grow the films and $B(OCH_3)_3$ was added to the gas mixture when boron-doped films were desired. The filament temperature was 2200 °C, as determined by an optical pyrometer, and the substrates were placed on a 850 °C carbon substrate holder, 0.4 cm below the filament. The system was operated at a pressure of 0.2 bar and the residence time of the gases in the chamber was 10 minutes. Films as thick as 20 μm have been obtained without cracking or polycrystalline growth. For undoped films, growth rates of 1.3, 4.1, and 1.8 $\mu m h^{-1}$ were obtained on (100)-, (110)-, and (111)-oriented substrates, respectively. The growth on the (100)-oriented substrates was smooth while films on (110)-, and (111)-oriented substrates were rough. With the addition of $B(OCH_3)_3$, growth rates of 6.6, 14, <0.7 $\mu m h^{-1}$ were obtained on (100), (110), and (111) substrates, respectively. Films on (100)- and (110)-oriented substrates were smooth while those on (111) substrates were very rough. The undoped films were insulating and the doped films had resistivities on the order of $3 \times 10^{-3} \Omega cm$ with boron concentrations in excess of $10^{20} cm^{-3}$. The films were epitaxial as determined by x-ray and reflection-electron diffraction. Twinning occurred only in the boron-doped films grown on (111) substrates. Dislocation densities less than $10^8 cm^{-2}$ were obtained with the undoped films on (100)-oriented substrates, as determined by transmission electron microscopy. Initial results of secondary ion mass spectrometry indicate that the films contain only carbon and boron. This presentation will discuss the epitaxial growth, and requirements for semiconductor quality material.

*This work was sponsored by SDIO/OST through the Office of Naval Research.

F4.2

ELECTRICAL PROPERTIES OF HOMOEPITAXIAL DIAMOND FILMS.

G. Sh. Gildenblat, S. A. Grot, C. W. Hatfield, C. R. Wronski, A. R. Badzian, T. Badzian, and R. Messier, The Penn State University, University Park, PA 16802.

We describe the results of electrical characterization of homoepitaxial diamond films. This includes measurements of film resistivity, I-V and C-V-F characteristics of Schottky diodes with a homoepitaxial diamond base, ohmic contact characterization using a modified Shockley ladder structure and the effect of surface treatments on film properties.

Single crystal and polycrystalline homoepitaxial diamond films were grown using a microwave plasma assisted chemical vapor deposition process. Single crystal diamond (100)-oriented substrates were obtained by cutting natural industrial type diamond. Both doped and undoped diamond films were investigated. The doping was achieved by placing boron powder on the substrate holder inside the deposition chamber. The diamond nature of the films was confirmed using Raman spectroscopy, x-ray diffraction and other methods.

Evaporation of gold, aluminum, and titanium through shadow masks was used to form test structures for the electrical characterization of the films. Schottky diodes with excellent rectifying characteristics were obtained using a single crystal homoepitaxial base. As in the case of Schottky diodes with a polycrystalline diamond base, diode characteristics are controlled by deep acceptors.

Additional treatment of the homoepitaxial film surface can induce the transition from rectifying to ohmic behavior of the metal/CVD diamond contacts.

F4.3

IN-SITU CHARACTERIZATION OF THIN POLY-CRYSTALLINE DIAMOND FILM QUALITY BY THERMAL WAVE AND RAMAN TECHNIQUES.

R.W. Pryor, P.K. Kuo, L. Wei, R.L. Thomas and P.L. Talley, Institute for Manufacturing Research and Department of Physics, Wayne State University, Detroit, MI 48202, USA

In this paper, the thermal wave technique and microfocus Raman spectroscopy are applied to the measurement of the relative quality of thin diamond films deposited on silicon and other substrate materials. The thermal wave technique uses a modulated heating laser beam, normal to the diamond film surface, to initiate a thermal wave which propagates into the film and the substrate. The resulting modulated surface temperature profile launches a thermal wave in the overlying gas(es). The accompanying modulated gas density is then interrogated by a second (probe) laser beam. The probe beam is deflected by the corresponding periodic changes in the gradient of the refractive index of the gas. The probe beam deflection versus offset position information is fitted, using a theoretical solution of the three-dimensional thermal diffusion equation for the gas / film / substrate system. The physically important parameter for this application of the method is the value obtained for the diffusivity of the measured diamond film. Thermal conductivities derived from our diffusivity measurements using this method compare well to previous measurements on similarly prepared films by other methods. Currently measured values for the thermal conductivity of high-quality polycrystalline diamond films are of the order of 9 W/cm.K.

A multiscan, microfocus Raman spectroscopy technique is also applied to the same films to determine the diamond to "graphite" ratio for a relative film quality assessment. Measured values of thermal conductivity for lower diamond content films range between the 9 W/cm.K value and the thermal conductivity of graphite. Measurements have also been made on bulk diamond using the thermal wave technique.

This work was supported by the Institute for Manufacturing Research, Wayne State University and by the Army Research Office under Contract No. DAAL03-88-K-0089

F4.4

REGROWTH OF RADIATION DAMAGED LAYERS IN DIAMOND PRODUCED BY ION IMPLANTATION AT LIQUID NITROGEN TEMPERATURE. G.S. Sandhu, B. Liu, M.L. Swanson Department of Physics and Astronomy, University of North Carolina, Chapel Hill, NC; and W.K. Chu, Texas Center for Superconductivity, University of Houston, TX. 77204-5506, USA

The recrystallization of radiation damaged layers in natural diamond created by ion implantation is an interesting problem due the inherent instability of the diamond phase at normal temperatures and pressures. Recent successes with the CVD deposition of diamond films and doping of natural diamond by ion implantation have brought diamond microelectronics closer to practical realization. Unfortunately, diffusion of interstitials and vacancies as well as identification of various defects in diamond are not very well understood problems. We have used RBS/Channeling and optical absorption to study the regrowth of disordered layers in diamond produced by implantation at 77K with carbon, or carbon plus boron ions. Post implantation annealing has shown a large annealing step at 500 °C which could arise due to interstitial/vacancy diffusion. The effect of furnace annealing versus RTA will be discussed in terms of interstitial and vacancy diffusion in diamond. Optical measurements on the boron plus carbon ion implanted samples after RTA have shown large new absorption bands around 1060 cm^{-1} which could be due to the formation of boron related defects in diamond.

F4.5

D.C. AND A.C. CONDUCTIVITY OF DIAMOND FILMS. G.A. Sokolina, A.A. Botev, L.L. Bouilov, S.V. Bantsekov, O.I. Lazareva, I.G. Teremetskaya. Institute of Physical Chemistry of the Academy of Sciences of the USSR, Leninsky Prospekt, 31, Moscow 117915, USSR.

Owing to the finding in the field of diamond synthesis from an activated gaseous phase, diamond polycrystalline films (DPF) can be obtained on heterogeneous substrates on areas measured in cm^2 . We studied the influence of temperature T on static G_{dc} and dynamic G_{ac} electrical conductivity of diamond films in the system: tungsten substrate-diamond film-aquadag electrode. DPF were obtained by the method of chemical crystallization from an electrically activated gaseous phase. Tungsten substrates with an area of 0.5 cm^2 were used. The temperature of the substrates (T_c) was varied from 800°C to 1200°C .

The structure of the films was studied by the methods of fractography and X-ray diffractometry. The visible dimensions of the crystallites and the dimensions of the regions of coherent scattering (RCS) were determined. $G_{dc}(T)$ and $G_{ac}(T)$ of DPF were measured in the temperature range $T = (300-900)\text{K}$ for diamond films obtained for different T_c . In the studied temperature range $(300-900)\text{K}$ there are two temperature regions, in each of these regions G_{ac} is described by the exponent with its own activation energy value E . According to obtained data the law of the change of $G_{ac}(f)$ can be written as $G_{ac} = f \cdot T^E$, where the power index decreases with increasing T . Experimental results of temperature variation of conductivity are considered on basis of grain-boundary model.

F4.6

SELECTIVE NUCLEATION BASED EPITAXY OF CVD DIAMOND AND ITS APPLICABILITY TO SEMICONDUCTING DEVICE

H. Kawarada, J.S. Ma, *T. Yonehara, Y. Yokota, Y. Mori, J. Wei and A. Hiraki, Faculty of Engineering, Osaka University, Suita, Osaka 565, Japan., *Canon Inc. Tamura, Hiratsuka, Kanagawa 254, Japan.

A substrate paved with large single crystal grains ($>10 \mu\text{m}$) with equal size in a periodic array has a lot of properties equivalent to single crystal. This kind of structure has been firstly fabricated in Si using selective nucleation based epitaxy (SENTAXY) and the device performance is equivalent to that of single crystal.

We have fabricated a periodic array of nearly single crystal diamond particles of $10 \mu\text{m}$ using plasma CVD on the Si substrate with finely patterned dots (less than $2 \mu\text{m}$). The edges or corners of dots are subjected to change to suitable nucleation sites during the pretreatment with abrasive powders. The nucleation sites retain only at these parts during the oblique irradiation of Ar. Single nuclei can be formed at small dots and nearly single crystal particles grow until they come in contact with one another. The superiority of the edge or corner nucleation is that the well-controlled selective growth occurs in one dimension or on desired points.

One of the advantages of SENTAXY in CVD diamond has been obtained in the luminescent properties. The cathodoluminescence intensity has been increased by at least several times in the arrayed particles formed with SENTAXY compared with the polycrystalline films with random nucleation sites deposited at the same condition. Since the grain boundaries are supposed to be act as nonradiative recombination center due to conductive layer, the much lower density of the boundaries in the former sample is crucial for the efficient luminescence of the CVD diamond. For the same reason, the better junction properties of semiconductor are expected.

F4.7

ELECTRICAL PROPERTIES OF THIN FILM AND BULK DIAMOND TREATED IN HYDROGEN PLASMA. Sacharia Albin and Linwood Watkins. Department of Electrical and Computer Engineering, Old Dominion University, Norfolk, VA 23529.

Current-voltage characteristics of type Ia synthetic diamond, type IIb natural diamond and free-standing diamond films are measured. The diamond films are polycrystalline, deposited on sacrificial silicon substrates using a microwave chemical vapor deposition process. These samples are subjected to hydrogen plasma treatment under varying conditions. A 20 minute exposure to a hydrogen plasma induced by 50W rf power is sufficient to increase the conductivity of all the samples by five orders of magnitude. Furnace annealing in a nitrogen ambient show that hydrogen is retained by all the samples up to 400°C . Apart from these two common features among the samples, their I-V characteristics show considerable difference. The forward and reverse characteristics of the polycrystalline film are identical and the increase in conductivity may be due to the passivation of grain boundaries; a similar effect has been observed in the case of polycrystalline silicon. The bulk diamond samples show asymmetrical I-V characteristics. The forward current for type Ia diamond is an order of magnitude higher than the reverse current whereas it is about five orders of magnitude higher in the case of type IIb diamond. The significance of these results, along with the effect of hydrogen plasma conditions is discussed. Results of control experiments to understand the role of atomic hydrogen in diamond will be presented.

F4.8

DEEP LEVEL TRANSIENT SPECTROSCOPY STUDY OF THIN FILM DIAMOND. K. Srikanth and S. Ashok, Department of Engineering Science & Mechanics and Center for Electronic Materials & Processing, A. Badzian, T. Badzian and R. Messier, Materials Research Laboratory, the Pennsylvania State University, University Park, PA 16802

Metal contacts on polycrystalline, semiconducting diamond thin films have been shown to exhibit rectification, and such Schottky contacts are useful in realizing metal-semiconductor field effect transistors (MESFET) for high-temperature electronics. We have carried out a deep level transient spectroscopy (DLTS) study of poly-diamond synthesized by a plasma enhanced chemical vapor deposition process.

Au and Al Schottky contacts were used on the undoped (p-type) poly-diamond, and the DLTS spectra were measured at various reverse bias voltages in the temperature range $100 - 450 \text{ K}$. From the DLTS measurements at 1 V reverse bias, a very prominent peak is seen corresponding to a majority carrier trap 316 meV above the valence band minimum. The trap concentration determined at 400/s rate window is $8 \times 10^{13} \text{ cm}^{-3}$. This trap concentration decreases to $3 \times 10^{13} \text{ cm}^{-3}$ with 3 - 10 V reverse bias. Along with the drop in trap concentration with increasing depth, the activation energy also decreases from 311 meV at 3 V to 286 meV at 10 V.

From low-temperature capacitance-voltage (C-V) measurements, a strong dependence of the slope of $1/C^2$ versus voltage plots is seen as a function of temperature. This is consistent with the deep energy level of p-type dopant in diamond.

F4.9

N-TYPE DOPING AND DIFFUSION OF IMPURITIES IN DIAMOND. S. Kajihara, A. Antonelli, and J. Bernholc, NC State University, Raleigh, NC 27695-8202.

For many electronic applications of diamond technology it is necessary to dope diamond n-type. However, n-type doping of diamond is very difficult and the only confirmed shallow n-type dopant is Li, which is believed to occupy an

interstitial position and to diffuse rapidly at elevated temperatures. In our search for a suitable donor for high temperature applications, we have investigated theoretically a number of potential n-type dopants, such as P, Li, and Na, as well as common contaminants, such as N. The CarParinello method was used to calculate the equilibrium atomic positions of the impurities and of the surrounding carbon atoms in a 64-atom supercell.

For substitutional impurities, our previous work on self-diffusion in diamond has shown that interstitial-mediated diffusion pathways are much less favorable than the ones involving a vacancy. However, even the vacancy pathway results in a rather high activation energy for diffusion. Larger substitutional impurities, such as P, introduce substantial strain fields into diamond, resulting in a positive incorporation energy. These results suggest that larger dopants should be introduced into the material by ion implantation or other non-equilibrium methods.

F4.10

DEPOSITION AND CHARACTERIZATION OF UNDOPED AND NITROGEN-DOPED DIAMOND THIN FILMS.* Joseph B. Milstein, Lian Li, Ye-Yung Teng, and Anatoly M. Altshuler, University of Lowell, Lowell, MA

We have investigated the deposition of diamond, with no intentional doping and with nitrogen doping, in a low pressure radio-frequency plasma assisted CVD deposition system operating at 440 KHz. Substrates of aluminum oxide and *in-situ* deposited silicon nitride on silicon wafers have been employed. The depositions have been carried out with substrate temperatures in the range of 700 to 1200 °C.

Characterization of the films has been performed by a variety of techniques including x-ray diffraction, ellipsometry, electrical measurements, and optical absorption.

*Supported in part by Sanders Associates, Nashua, NH.

F4.11

DOPING OF DIAMOND BY CO-IMPLANTATION OF DOPANT ATOMS WITH CARBON. G.S. Sandhu, M.L. Swanson Department of Physics and Astronomy, University of North Carolina, Chapel Hill, NC; and W.K. Chu, Texas Center for Superconductivity, University of Houston, TX. 77204-5506, USA

We have investigated the challenging problem of doping diamond by co-implanting boron, nitrogen and phosphorus with carbon into natural insulating type IIa diamonds. All the implantations were done at liquid nitrogen temperature and some of the samples were then rapidly heated to 1100 °C. Unlike the previous attempts to dope diamond by room temperature and high temperature ion implantations, this method is expected to yield a higher doping efficiency for the implanted atoms. We have characterized the implanted diamonds with optical absorption, photo-conductivity, cathode-luminescence and electrical measurements. Boron doped samples showed new large optical absorption bands in the

infrared around 1060 cm⁻¹ and 2960 cm⁻¹ and electrical resistivities less than 200 ohm-cm, indicating a high substitutional fraction of boron atoms. Results of various measurements performed on nitrogen and phosphorus doped samples will also be discussed.

F5.1

ELECTRONIC PROPERTIES OF DIAMOND/NICKEL AND DIAMOND/BORON NITRIDE INTERFACES. Warren E. Pickett and Steven C. Erwin, Code 4692, Naval Research Laboratory, Washington, DC 20375-5000.

The preparation and many applications of epitaxial diamond (Di) films requires an understanding of the bonding and electronic characteristics of the interface between diamond and other solids. We have recently applied two *ab initio* methods to study two such interfaces: the Di/Ni (001) interface as a canonical Di/metal system, and earlier the Di/BN (110) interface as a system involving two wide bandgaps. The near lattice match, favorable surface properties, and recent experimental studies suggested the Di/Ni system. Using a superlattice geometry with 4 layers of Di and 3 layers of Ni, it was found that more Di layers were necessary to allow some C atoms to approximate the bulk in Di. Results for the bonding, interface states, and an estimate of the Schottky barrier height from a 6-Di/5-Ni layer superlattice will be presented and analyzed. The characteristics of the interface will be contrasted with previous results on the Di/BN interface. A general result suggested by these calculations is that the satisfaction of Di dangling bonds by the Ni atoms may play little role in the bonding. The narrow (5 eV) d bands are confined to the Di gap region, whereas the Di s-p bands span a 20 eV region lying below the d bands and thus bond only indirectly. Establishing the principles which determine bonding of C atoms to foreign surfaces is a priority in this study.

Supported by the SDIO/IST program through The Office of Naval Research.

F5.2

PEUDOMORPHIC DIAMOND, PREDICTIONS OF STRUCTURE AND PROPERTIES. A.M. Altshuler, A.S. Karakashian, Physics Department, University of Lowell, MA.

Electronic and Atomic structure of strained layers of Diamond have been calculated by means of an "ab initio" pseudopotential approach. Some thermodynamic, electronic and optical characteristics are estimated. Promising applications of pseudomorphic diamond' electronic and electrooptical structures will be discussed.

F5.3

CYCLIC-CLUSTER MINDO/3 COMPUTATIONS OF THE LATTICE CONSTANT AND BAND STRUCTURE OF BORON NITRIDE, DIAMOND, SILICON CARBIDE AND RELATED WIDE GAP SEMICONDUCTORS. Lawrence C. Snyder, Chemistry Department, State University of New York at Albany, 1400 Washington Avenue, Albany NY 12222; Arthur H. Edwards, Department of Electrical Engineering, University of North Carolina at Charlotte, Charlotte N.C. 28223; and Peter Deák, Physical Institute of the Technical University of Budapest, Hungary 1521.

We have employed a 32 atom cyclic-cluster and the Modified Intermediate Neglect of Differential Overlap (MINDO/3) method to compute the lattice constant and

band structure for boron nitride, diamond, silicon carbide and other III-V wide gap semiconductors. Other properties of these crystals have also been calculated. The computational scheme we choose allows inexpensive study of defects in these materials. The results presented here justify it from the viewpoint of representing the host.

F5.4

ELECTRICAL CHARACTERIZATION OF METAL CONTACTS ON DIAMOND THIN FILMS. D. Narducci, J. J. Cuomo, C. Richard Guarnieri, S. J. Whitehair, IBM Research Division, T. J. Watson Research Center, P.O. Box 218, Yorktown Heights NY 10598.

Polycrystalline boron-doped diamond thin films were prepared by microwave-enhanced plasma-assisted chemical vapor deposition. Ti, V, Ta, Nb, Al, Mo and W contacts were prepared by physical vapor deposition and their behavior was studied as a function of the annealing temperature, atmosphere and duration. For Ti contacts, short heat treatments (less than 60 minutes) at 500°C under argon atmosphere were found to make ohmic contacts for applied voltages up to 50 V. Longer annealing times, more reactive atmospheres, and higher temperatures degraded the contact characteristics. In order to obtain a more complete picture of the interface structure, the capacity-voltage characteristics and the impedance spectra of the systems were measured between 10 K and 1000 K. The interface contribution to the overall dielectric behavior of the system shows much shallower depletion widths in Ti-diamond (ohmic) contacts than with the non-linear Nb and Ta contacts. The higher values of the contact resistance and the shallower depletion width with Ti can be explained in terms of formation of a thin carbide-like region at the metal-semiconductor interface. The space-charge region width as well as the distribution of localized states in the band gap were also determined. The effect of the microstructure on the electrical properties of the systems is discussed in comparison with the behavior of metal contacts on single-crystal diamonds.

F5.5

CONTACT RESISTIVITY OF B DOPED CVD GROWN DIAMOND FILMS. K. Nishimura⁺, K. Das and J. T. Glass, Materials Science and Engineering, North Carolina State University, Raleigh, NC, 27695-7907, ⁺ visiting from Kobe Steel Ltd. in Japan

The contact resistivity (R_c) of various metal electrodes on B doped CVD grown diamond films were measured. The B doped diamond films were grown by microwave plasma CVD using 0.5 % CH_4 in H_2 and varying concentrations of Diborane (B_2H_6) in the gas phase. The substrate temperature was approximately 800 C and the growth time was 7 hours. All of the films were polycrystalline with clear mixtures of (111) and (100) facets on the surface.

The metals investigated included Pt, $TaSi_2$, Ni and Al. They were deposited by RF sputtering in order to achieve good adhesion between the contact and the film. Transmission Line Mode (TLM) patterns to measure R_c were fabricated on the diamond films by conventional photolithography. The dimensions of the electrodes were $300 \mu m \times 120 \mu m$ and distances between electrodes were 50 μm , 30 μm , 20 μm , 10 μm , and 5 μm . Film thickness of these electrodes were about 2,000 Å. In the case of as-deposited Pt contacts, R_c was $8.6 \times 10^{-4} \Omega cm^2$ for a B/C ratio of 400 ppm and $2.5 \times 10^{-2} \Omega cm^2$ for a B/C ratio of 40 ppm. R_c increased monotonically when the B/C ratios decreased. This suggests that tunneling effect is a dominant transport mechanism at the Pt/B doped diamond film interface for these doping concentrations. Other metal contacts were deposited on the films synthesized with a gas phase B/C ratio of 200 ppm. The orders of R_c were $Pt < TaSi_2 < Ni < Al$ for as-deposited contacts at room temperature. Annealing effects for these contacts will also be presented.

Acknowledgements: The authors wish to thank A. Nakae, K. Kobashi, K. Miyata, K. Kumagai of Kobe Steel, Ltd. and R. F. Davis of NCSU. Financial Support of Kobe Steel, Ltd. is also gratefully acknowledged.

F5.6

METALLIZATION OF SEMICONDUCTING DIAMOND: Mo, Mo/Au, Mo/Ni/Au. K.L. Moazed, North Carolina State University, Raleigh, NC 27695-7916; J.R. Zeidler,

Code 7601; and M.J. Taylor, Code 561, Naval Ocean Systems Center, San Diego, CA 92152-5000.

Ohmic contacts to semiconducting diamond have been fabricated using photolithographic techniques that parallel conventional manufacturing practice.

Thin metallic films of molybdenum, molybdenum/gold, and molybdenum/nickel/gold were evaporated onto the diamond surface in an ion-pumped ultrahigh vacuum system. The samples were annealed in a tube furnace in an atmosphere of flowing purified hydrogen gas. The current-voltage response of the samples were measured as a function of annealing temperature and of isothermal annealing time.

Ohmic response is obtained after high temperature annealing and the resistance of the contacts is decreased by approximately ten orders of magnitude relative to the unannealed condition. The measured resistance is comparable to the sheet resistance of the semiconducting natural diamond.

Examination of the diamond/molybdenum interface provides strong evidence that molybdenum has reacted with diamond to produce a metal carbide phase.

Partial funding of this research by SDIO/IST managed by M. Yoder, ONR Scientific Officer, is gratefully acknowledged.

F5.7

Properties of CVD Diamond-Metal Interface Yusuke Mori, Hiroshi Kawarada, Yoshihiro Yokota and Akio Hiraki. Department of Electrical Eng., Faculty of Eng. Osaka University, Suita, Osaka 565, Japan.

Diamond is considered to be a central material in the field of Schottky barrier theory, because of its unique character—wide bandgap but zero ionicity. In this experiment, p-type semiconducting epitaxial and polycrystalline diamond films have been synthesized using microwave plasma chemical vapour deposition. CO/H_2 and CH_4/H_2 mixtures were used as reaction gas and B_2H_6/H_2 mixture as dopant gas. Much better rectifying property due to Schottky barrier has been obtained in the films formed with $CO(5\%)/H_2$, compared with $CH_4(0.5\%)/H_2$. From the point of Raman scattering, the crystal qualities of both films are in the same level. The difference in the electric structure of local areas such as grain boundary or surface is crucial for the barrier formation. In the case of polycrystalline, the choice of metal which exhibits higher barrier height in single crystal diamond is also important to obtain good rectifying property.

Moreover, electroluminescence (EL) between blue and green has been observed at both forward (25v) and reverse (15v) biased metal/diamond interface, when Pt or Au is used as point-contact. EL spectra depends on the amounts of boron doping and they have similar spectra compared with those of cathodoluminescence.

F5.8

EPITAXIAL GROWTH OF DIAMOND AND DIAMOND DEVICES. Naoki Fujimori, Itami Research Laboratory, Sumitomo Electric Ind. Ltd., 1-1, 1-chome Koyakita, Itami, Hyogo 664, JAPAN.

To make diamond devices, it is important to get a good epitaxial layer, because properties of the devices will be determined by the properties of the active layer. Microwave plasma assisted CVD seems to be

suitable method for growing epitaxial layers. The substrate plane strongly affects the surface roughness and the crystallinity of the epitaxial layers. (100) plane was found to be better than (110) or (111) plane. The properties of diamond epitaxial layer are also affected by the deposition conditions. Shiomi et al. reported the effect of CH_4 concentration in the reactant gas. 6% was found to be the best methen concentration. Doping of element atoms is easily carried out during epitaxial growth. B makes diamond p type semiconductor with resistivity which varies from 10^{-2} to $10^5 \Omega\text{cm}$. The authors found that P makes a diamond layer n type but the resistivity of the film was higher than $10^5 \Omega\text{cm}$. The properties of the diamond epitaxial layer will be summarized. Some devices were tried to make using the diamond epitaxial layer. Nishibayashi et al. developed a emission device, successfully, using shottky junction. This device emitted light which peaked at 530nm. Recent developments of other devices will be reported.

F5.9

BLUE LIKE DIAMOND LIGHT EMITTING DEVICES TO BE MASS-PRODUCED. Masaya Kadono, Shigenori Hayashi, Kenji Itoh, Takashi Inushima and Shumpei Yamazaki, Semiconductor Energy Laboratory Co., Ltd., 398 Hase Atsugi-shi, Kanagawa, 243 Japan.

Recently, blue light emitting devices (LED) of diamond have been developed. We have been studying diamond thin films as LED, formed by the magnet-active microwave plasma CVD method.

The advantages brought by our proposal are to deposit diamond thin films on large area. Actually, we succeeded in deposition of them on Si wafers of 4 inches in diameter. And the disparity of the film in thickness and quality is limited within 10%. The diamond was analyzed by SEM, X-ray diffraction, and Raman spectroscopy. If 0.8mm square chips are made by using the developed diamond, it is possible to produce about 10,000 LED in one wafer.

Blue like light has been observed by means of both cathode-luminescence (CL) and electro-luminescence (EL). It is expected that LED of diamond is produced as mass production scale. The details of our experiment will be reported in the lecture.

F5.10

ELECTRICAL BEHAVIOR OF DIFFUSED IMPURITIES IN DIAMOND SINGLE-CRYSTALS D. Narducci, J. J. Cuomo IBM Research Division, T. J. Watson Research Center, P.O. Box 218, Yorktown Heights NY 10598

The dependence of the electrical properties on the evolving doping profile during diffusion processes was studied, as well as the role of the vacancies in determining the electrical properties of diamonds. To this aim, P, B and Ge were deposited on diamond single-crystal by physical vapor deposition. The elements were then thermally diffused into diamond at 800°C under helium atmosphere. The deposited layer was finally removed and subsequent annealing cycles were carried out. The diffusion profiles were tracked by Nuclear Analysis Techniques. For comparison, the same elements were implanted in diamonds at 70 K and at room temperature. Electrical contacts of different metals were deposited on diamond and the current-voltage and the capacity-voltage characteristics were measured as a function of

temperature between 10 K and 1000 K. A comparative analyses of the electrical behavior of implanted and diffused samples was carried out, which elucidated the electronic activity of point defects in diamond.

F5.11

A DIAMOND SILICON HETEROJUNCTION DIODE. C.L. Ellison, Norton Company, 2532 South 3270 West, S.L.C., Ut. 84119; and R.M. Cohen, University of Utah, Materials Science Dept., S.L.C., Ut. 84112. J.T. Hoggins, Norton Company, 2352 South 3270 West, S.L.C., Ut. 84119.

Thin diamond films were grown on low resistivity p-type silicon wafers by microwave plasma assisted chemical vapor deposition (MPACVD). Using gold contacts, diode behavior was observed and forward bias current densities in excess of 5 amps/cm² were obtained. Reverse bias current densities were as low as 5 mamps/cm². Photocurrent was measured when photon energies larger than the silicon band gap, 1.12eV, were used to illuminate the surface. Photocurrent continued to be measured even when the illumination spot was moved several centimeters away from the metal-diamond contact. The photovoltage was positive on the silicon. No photocurrent was observed when illuminating the area around one contact of a diamond film grown on AlN. We conclude the diamond-silicon heterojunction forms a diode.

F5.12

Schottky diodes fabricated in thin Carbon films containing polycrystalline Diamond grains

G.A.J. Amarasinga, W.I. Milne, K.K. Chan, K.J. Clay A. Putnis and M.E. Welland

Dept. of Engineering, Trumpington St., Cambridge CB2 1PZ, U.K.

Formation of Schottky diodes on 30nm - 50nm thick C films deposited from a capacitively coupled CH_4/Ar rf plasma is reported. Transmission electron microscopy and Auger electron spectroscopy show the smooth opaque films to be comprised of crystalline diamond grains ranging from 10nm - 200nm diameter. The films were deposited on n-type and p-type Si substrates. Schottky junctions are formed by evaporating 1mm diameter Al dots using a shadow mask.

The thin films are found to be n-type (Phosphorous) or p-type (Boron) doped form the underlying Si substrate, as previously reported by Gildenblat et al¹. Film resistivity in the order of 10^{-2} - $10^5 \Omega\text{cm}$ is observed at room temperature. Using the 1-5 Ωcm resistive n-type and p-type Si substrates as ohmic contacts, the I-V characteristics of the sandwich cell are measured. These characteristics show n-type and p-type diode behaviour for the Al/C film/Si structures. The highest reverse breakdown voltages observed for the n-type and p-type diodes are 65V and 150V respectively. A current density of 75mA/cm² is obtained at a forward bias voltage of 5V for the n-type diodes and 20V for the p-type diodes.

1. G.Sh.Gildenblat et al. App.Phys.Letts., 53(7), 1988.

F5.13

THE IMPACT OF β -SiC, DIAMOND AND c-BN ON POWER ELECTRONICS. Richard Koba and William Russell, Diamond Materials, Inc., 2820 East College Ave., State College, PA, 16801; *35 Cherry Hill Dr., Danvers, MA, 01923.

β -SiC, diamond and c-BN are the three ultimate semiconductors. All three materials share many properties in common. Diamond and SiC both exhibit polytypism. c-BN can be synthesized with rocksalt structure, and 2H BN is synthesized by shock methods. However, for most high-performance semiconductor applications, the 3C polytypes of diamond, BN and SiC are preferred. Useful semiconductor devices can be made from these three materials because they can be doped. Nitrogen and aluminum atoms are donors and acceptors for β -SiC, respectively. Boron is the most shallow acceptor for diamond and beryllium and silicon atoms have been used as acceptors and donors in c-BN.

This talk will review Diamond Materials' efforts on the synthesis of each of these materials. Although only the monocrystalline forms of each material will be useful for high performance devices, these materials will also be of great importance as polycrystalline sheets. Because of their high thermal conductivity and low electrical conductivity, diamond and c-BN sheets will play a critical role in the packaging of β -SiC, diamond and c-BN semiconductor devices.

A conventional Si power FET is compared theoretically to an equivalent diamond FET. Assuming that the diamond die temperature can operate 200°C hotter than the Si die, and that the operating voltage of the diamond is 10 times greater than that of the Si, then the calculations indicate that a diamond FET can dissipate ~ 25 times more thermal power than the Si FET. This increased thermal dissipation results in the diamond FET delivering 35 times more power-to-load than the Si FET.

F5.14

SIMPLE GRAPHITIC NETWORK MODELS OF "DIAMONDLIKE" CARBON. M. A. Tamor and C. H. Wu, Research Staff, Ford Motor Company, Dearborn, MI 48121-2053.

The atomic structure of "diamondlike" carbon (DLC) is not well understood. It is well established that the visible and near infrared optical properties of DLC are determined by small graphite-like aromatic clusters linked in a transparent matrix. For hydrogenated DLC (a-C:H), spectroscopic studies show that the aromatic clusters are linked by aliphatic structures. In hydrogen-free DLC (a-C) some spectroscopic methods indicate a high degree of "amorphous diamond" sp^3 coordination, while local probes indicate little or no fourfold carbon coordination. We describe a very simple structural model based on a graphitic network in which π -electrons are strongly localized by non-aromatic defects. Guided by experiment only in the choice of defect, this "defected graphite" model reproduces many important properties of DLC and reconciles several conflicting observations.

F5.15

DOPING EFFECT IN HYDROGENATED AMORPHOUS CARBON THIN FILMS BY ION IMPLANTATION. S.P. Wong, Dept. of Electronics, The Chinese University of Hong Kong, Hong Kong; and Peng Shaoqi, Dept. of Physics, Zhongshan University, Guangzhou, China.

Hydrogenated amorphous carbon (a-C:H) thin films have been prepared by rf glow discharge decomposition of $C_6H_5CH_3$ gas at 13.6 MHz. Multi-energy boron or phosphorus implantation into these films have been performed to achieve a relatively flat impurity profile and the doping effect as a function of implanted concentration has been studied. It is found that there are critical values of the implanted boron and phosphorus concentration below which there are no significant changes observed in the electrical conductivity and the conductivity activation energy. Once the impurity concentration exceeds the critical values, the conductivity activation energy decreases drastically and the room temperature conductivity increases abruptly by two to three orders of magnitude. The doping

mechanism leading to these behaviours will be discussed. Comparison between results obtained by B^+ and BF_2^+ implantation will also be presented.

F5.16

OPTICAL BAND GAP OF DIAMOND-LIKE CARBON FILMS AS A FUNCTION OF RF SUBSTRATE BIAS. Paul Pasetl and Walter Varhue, Dept. of Electrical Engineering, Univ. of Vermont, Burlington, VT.

The optical band gap of diamond-like carbon films are significantly less than the band gap of diamond. Ion energy is believed to have significant influence on the optical bandgap of plasma deposited DLC films. This investigation systematically measures the effect that energetic ion bombardment during growth has on the optical band gap of DLC films.

The material is prepared by Electron Cyclotron Resonance Plasma Enhanced Chemical Vapor Deposition at low pressure, (1 to 300 mTorr) and low temperature, (below 150 °C). ERCPECVD allows one to decouple the production of reactive species from the energetic ion bombardment of the substrate. Reactive species production is controlled by reactor pressure and input microwave power. The ion energy incident on the substrate is controlled by the divergence of the magnetic field and by the degree of bias applied to the substrate. Because the DLC films are insulating the biasing must be performed with an RF power supply.

Transmission measurements with a spectrophotometer are used to determine optical bandgap.

F5.17

STUDY OF AMORPHOUS CARBON THIN FILMS ON METALS, INSULATORS AND SEMICONDUCTORS A. Martin*, X.-M. Wu, G.-R. Yang, A. Tu, P. Persans, and T.-M. Lu, Center for Integrated Electronics and Physics Department, Rensselaer Polytechnic Institute, Troy, NY 12180.

Because of their many desirable properties, such as hardness, chemical inertness, and optical transparency, amorphous carbon (α -carbon) films have important applications to the areas of protective coatings, surface passivation, and X-ray lithography masks. We have employed a simple DC glow discharge technique to deposit α -carbon on a variety of metal, insulating and semiconducting substrates using a methane and argon plasma. At appropriate deposition conditions, the films adhere very well to practically all substrate materials including: Si, Al, Cu, Ta, SiO_2 , polyimide, and paralyne. The bias potential applied to the substrates ranged from several hundred volts to over one kilovolt. These films normally contain both broad sp^2 and sp^3 peaks in their Raman spectra. Peculiar types of films containing only a broad sp^2 peak in the Raman spectra have also been observed. I-V measurements of α -carbon deposited on silicon substrates exhibit a Frenkel-Poole electron transport phenomenon. Possible mechanisms that lead to the observed field-enhanced thermal excitation of trapped electrons into the conduction band will be discussed.

* also IBM Advanced Semiconducting Technology Center

F6.1

STEP-CONTROLLED EPITAXIAL GROWTH OF SiC. Hirovuki Matsunami, Tetsuzo Ueda and Hironori Nishino, Kyoto University, Yoshidahonmachi, Sakyo, Kyoto, Japan.

Single crystals of 6H-SiC can be grown on step-controlled 6H-SiC(0001) substrates at 1300-1500°C by chemical vapor deposition (CVD) using a $\text{SiH}_4\text{-C}_3\text{H}_8\text{-H}_2$ system. This temperature is lower by 300-400°C compared with well-known typical growth temperature of 6H-SiC by CVD. The density of surface steps was controlled by the introduction of off-orientation into (0001) substrates. 6H-SiC is grown laterally from the steps inheriting the stacking order of the substrates. On uncontrolled (0001) substrates, 3C-SiC with twin structures are grown, probably through nucleation on terraces. Polytypes of the grown layers are changed by the surface-step density. Surface morphology varied with the direction of off-orientation of the step-controlled substrates, which indicates the merge of different polytypes during the growth. The growth mechanism will be discussed.

The crystal quality of epitaxial layers was examined using X-ray, RHEED and photoluminescence measurements. P-n junctions of 6H-SiC fabricated by doping impurities during epitaxial growth have extremely good rectification. Pn junction diodes show blue-light emission. Details of crystal quality and diode characteristics are also described.

F6.2

Epitaxial Growth and Doping of and Device Development in Monocrystalline Beta-SiC Semiconductor Thin Films, Robert F. Davis, Department of Materials Science and Engineering, North Carolina State University, Raleigh, NC 27695-7907

High purity monocrystalline β -SiC films have been chemically vapor deposited on Si (100) and α -SiC (0001) at 1660K-1823K and 0.1 MPa using SiH_4 and C_2H_4 carried in H_2 . Films grown on the on-axis Si (100) contained substantial concentrations of dislocations, stacking faults and antiphase boundaries; those deposited on α -SiC (0001) contained primarily double positioning boundaries. These boundaries were eliminated by using off-axis orientations of the respective substrates. Films produced on Si (100) have also been doped during growth and via ion implantation with B or Al (p-type) or P or N (n-type) at liquid nitrogen, room and elevated temperatures. Results from the former procedure showed the ionized dopant/total dopant concentration ratios for N, P, B and Al to be 0.1, 0.2, 0.002 and 0.01, respectively. The solubility limits of N, P and B at 1660K were determined to be $\sim 2 \times 10^{20}$, 1×10^{18} and $8 \times 10^{18} \text{ cm}^{-3}$, respectively; that of Al exceeds $2 \times 10^{19} \text{ cm}^{-3}$. High temperature ion implantation coupled with dynamic and post annealing resulted in a markedly reduced defect and precipitate concentrations relative to that observed in similar research at the lower temperatures. Dry etching in CF_4 and NF_3 by reactive ion etching (RIE) and in SF_6 by plasma etching have also been conducted. Device-compatible surface impurity chemistry and morphology were only obtained using RIE and NF_3 combined with a C cathode. Schottky diode, p-n junctions, MESFET and MOSFET devices have been fabricated. The p-n junctions have the characteristics of insulators containing injected carriers. The current-voltage characteristics of the MESFETs measured from 298 to 623K indicated reasonable performance throughout this range. The maximum transconductance was 1.6 mS/mm; the value of this parameter decreased with temperature. Similar data were obtained on both enhancement mode and depletion mode MOSFETs; the latter operated continuously as high as 923K - the highest temperature ever reported for a semiconductor field effect device. Transconductances as high as 11.90 mS/mm were achieved.

F6.3

INNOVATIVE LOW-TEMPERATURE MOCVD (LTMOVCVD) AND PLASMA-ENHANCED LTMOVCVD ROUTES TO THE FABRICATION OF DEVICE QUALITY ELECTRONIC MATERIALS. Alain E. Kaloyeros, Paul J. Toscano, Richard Single, and Victor Tulchinsky, Physics and Chemistry Departments, State University of New York at Albany, Albany, NY, and Marianne Holma, Physics Department, University of Illinois at Urbana-Champaign, Urbana, IL.

We have developed new methodology to produce device-quality doped and undoped semiconductor materials at temperatures as low as 100-150°C, well below those of conventional "high temperature" CVD and MOCVD techniques, by low-

temperature metal-organic chemical vapor deposition (LTMOVCVD) and plasma-enhanced LTMOVCVD from designed organometallic compounds. LTMOVCVD not only displays the attractive features associated with the high temperature MOCVD process, but also possesses many unique advantages. These include its ability to produce compound semiconductor and superconductor materials with variable composition, e.g. silicon carbide $\text{Si}_x\text{C}_{1-x}$ and gallium arsenide $\text{Ga}_x\text{As}_{1-x}$, on thermally fragile or chemically sensitive substrates. In addition, the precursors employed are safe, non-toxic, non-hazardous and easy to handle; single source precursors containing all the elemental constituents desired in the target material can be employed in most cases to fabricate compound electronic materials. For example, preliminary work by the present researchers showed that epitaxial growth of GaAs can be achieved from organometallic precursors of the type $(\text{C}_6\text{F}_5)(\text{CH}_3)_2\text{GaAs}(\text{C}_2\text{H}_5)_3$, where Ga and As are already directly bonded by coordination strength in the ratio 1/1 in the precursor. This approach eliminates the inherent limitations of conventional MOCVD where separate precursors are used for each of the individual components of the desired compound.

In this paper, we present microstructural and microchemical analyses results for high quality silicon carbide films produced by LTMOVCVD from the single organometallic precursor tetraethynylsilane, $\text{Si}(\text{C}_2\text{H})_4$, in the temperature range 300-450°C. Controlled variations in the deposition parameters (temperature, pressure, flow, plasma...) yielded a series of films with variable composition (C/Si ratio) and structure (amorphous or crystalline).

F6.4

GROWTH OF 6H-SiC ON CVD-GROWN 3C-SiC SUBSTRATES. Woo Sik Yoo and Hiroyuki MATSUNAMI, Department of Electrical Engineering, Kyoto University, Yoshidahonmachi, Sakyo, Kyoto 606 Japan.

Polytype control and crystal growth on 3C-SiC substrates have been investigated in a sublimation method. Polytypes of grown crystals were controlled 3C- and 6H-modifications for the first time and its reproducibility was confirmed with many growth runs.

Single crystalline 3C-SiC(100) films ($\sim 10 \mu\text{m}$ thick) grown on Si(100) were used as substrates after removing Si in a $\text{HF}+\text{HNO}_3$ mixture. Crystal growth was carried out with various parameters of temperature (1800~2400°C), pressure (50~760 Torr) and time (0.5~6h).

Polytypes of grown crystals on 3C-SiC(100) were examined by photoluminescence (PL) measurements, Raman scattering, X-ray diffraction and RHEED analyses. Crystallinity and electrical properties were also investigated by using various characterization techniques. Polytypes of grown crystals change from cubic 3C-modification to hexagonal 6H-modification with temperature increase: polytype can be controlled by selecting growth parameters. 6H-SiC(0114) planes can be grown on 3C-SiC(100). Starting from the growth of 3C-SiC on Si substrate, we have succeeded in polytype-controlled growth of 6H-SiC ingots up to 20mm in diameter and 10mm in length for 6 hours.

Characterization results of 6H-SiC crystals grown on 3C-SiC will be described. The growth mechanism of 6H-SiC on 3C-SiC will be also discussed based on experimental study on thermal stability of 3C-SiC.

F6.5

SOME OBSERVATIONS ON THE ELECTRICAL CHARACTER OF THE HETEROEPITAXIALLY GROWN CUBIC SiC. B. Molnar, G. Kelner, Naval Research Laboratory, Washington, DC 20375-5000

This paper re-examines the electrical characterization of thin layers of cubic SiC, grown at 1380°C on (100) Si substrates. All undoped SiC films are invariable n-type. The thermal ionization energy, E_d , of the dominant donors, as deduced from Hall measurements, is significantly different from that inferred from photoluminescence measurements. The residual donors have been assigned to either nitrogen or structural defects. The temperature dependent electron concentrations as derived from the Hall measurements clearly indicate a minimum, which suggest a transition to impurity band conduction. In this case the temperature dependence of the directly measurable resistivity could be used to derive an activation energy e_1 . This energy e_1 and the thermal ionization energy E_d should be in agreement only

in samples where the donor concentration is sufficiently low. In our most homogeneous samples activation energy was in the range of 0.032-0.025 eV. The decrease in activation energy has been associated with an increase in nitrogen concentration using both ESR and SIMS measurements. The nitrogen concentrations in these epitaxially grown SiC layers are in the so called intermediate range, where the activation energy is strongly dependent on the concentration. In such samples the e_1 activation energy represents the transition from the top of a quasi-continuum impurity band to the conduction band and not from the ground state to the conduction band which is inferred from PL measurement as 0.053 eV. The concentration of the nitrogen in the samples is believed to be the most likely reason for the conflicting values reported for the dominant donor ionization energy by Hall and the PL measurements.

F6.6

NATIVE DEFECTS, DIFFUSION, SELF-COMPENSATION, AND BORON DOPING IN CUBIC SILICON CARBIDE. C. Wang, J. Bernholc, and R. F. Davis, NC State University, Raleigh, NC 27695-8202.

We report the results of a comprehensive theoretical investigation of the effects of stoichiometry and boron doping on the properties of cubic SiC. Since SiC is a two-component material, the nature of the dominant native defects strongly depends on the stoichiometry of the material. In addition, the formation energy of charged defects also depends on the position of the Fermi level.

Supercell calculations using first-principles pseudopotentials show that the lowest energy defect in Si-rich n-type and intrinsic SiC is the electrically inactive Si antisite, while the doubly-positively charged carbon vacancy is the lowest energy defect in p-type SiC. The electrons released by the vacancies compensate acceptor dopants and lead to strong self-compensation effects when doping occurs during growth of the crystal. In C-rich SiC, the dominant defect for all Fermi level positions is the electrically inactive C antisite.

Si atoms in pure SiC are found to diffuse via a mechanism involving a C vacancy and a Si antisite, while C atoms diffuse with help of a C vacancy. These results are in good agreement with experimental data. We have also calculated the activation barriers for several diffusion mechanisms in boron doped material, and will discuss the origin of the experimentally observed enhancement of diffusion in boron doped SiC.

F6.7

DEEP-LEVEL DOMINATED ELECTRICAL CHARACTERISTICS OF Au CONTACTS ON β -SiC. K. Das, H. S. Kong, J. B. Petit, J. W. Baumgarner, and R. F. Davis, Department of Materials Science and Engineering, North Carolina State University, Raleigh, NC 27695-7907, and L. G. Matus, National Aeronautics and Space Administration, Lewis Research Center, Cleveland, Ohio 44135

Device quality heteroepitaxial films of β -SiC on Si substrates are being routinely grown in a number of laboratories. These films have various defects that could affect the characteristics of fabricated devices. In order to assess the effect of these defects on the electronic quality of the films, a study of the current-voltage characteristics of Au contacts formed on films grown heteroepitaxially on both nominally (100) oriented and off-axis (100) silicon substrates has been conducted. These contact diodes are rectifying and particularly in off-axis silicon substrates very low reverse leakage currents are observed. The diode ideality factor is between 1.3 and 2.0 in all cases except in nominal (100) silicon substrates where it is greater than two. Logarithmic plots of the I-V characteristics in the forward direction indicate space charge limited current conduction through the active volume of the diodes. These plots also indicate the presence of allowed states in the band-gap. The β -SiC films grown on nominally (100) oriented substrates show the presence of two deep levels located approximately between 0.26 eV and 0.38 eV below the conduction band edge. In some films on nominal (100) substrates, the I-V characteristics are also influenced by some additional traps which are exponentially distributed in energy with a maximum occurring at the

conduction band edge. In contrast the films deposited on off-axis substrates have only one deep level located approximately below 0.49 eV for the 2° off (100) substrates and at 0.57 eV for the 4° off (100) substrates. Previous microstructural analysis revealed that the nature and density of defects in the β -SiC heteroepitaxial films on both nominal and off-axis (100) silicon are similar except that the films on nominal (100) substrates have a high density of antiphase domain boundaries. Therefore, the presence of the shallower deep-level states observed in the β -SiC films grown on nominal (100) substrates is speculated to be due to the electrical activity of antiphase domain boundaries.

F6.8

A NEW DEEP ACCEPTOR IN EPITAXIAL CUBIC SiC*
J.A. Freitas, Jr., Sachs/Freeman Associates, Inc., Landover, MD 20785, and S.G. Bishop, Naval Research Laboratory, Washington, DC 20375-5000

We have investigated the temperature and excitation intensity dependence of photoluminescence (PL) spectra in several undoped and lightly Al-doped thin films of cubic SiC grown by chemical vapor deposition on Si substrates. The low power PL spectra in all samples studied exhibit a deep donor-acceptor pair PL band which involves a previously undetected deep acceptor ($E_A = 470$ meV). This deep acceptor is found in every film we have studied, doped and undoped, independent of growth reactor. Its pervasive character indicates that it is probably associated with a nonstoichiometric defect rather than a background impurity and suggests the possibility that it is at least partially responsible for the high compensation observed in undoped n-type films of cubic SiC.

* Partially supported by the Office of Naval Research

F6.9

ELECTRONIC STRUCTURE OF HIGH BANDGAP SEMICONDUCTOR INTERFACES: SiC/AlN, SiC/BP, C/BN.
W. R. L. Lambrecht and B. Segall, Department of Physics, Case Western Reserve University, Cleveland, OH 44106.

Electronic structure and total energy calculations are presented for SiC/AlN, SiC/BP and C/BN heterojunctions. Cubic crystal structures are assumed. The (110) interface is chosen because it is the simplest interface characterized by III-IV and IV-V bond compensation which is expected to be energetically favorable but requires chemical restructuring for other low-index interfaces. The interfaces are modeled with superlattices of 1 to 9 layers of each material. The linear muffin-tin orbital band-structure method is used in the local density functional framework. The energy of formation of the superlattices is studied as a function of thickness and the energy of formation per interface in the limit of isolated interfaces is combined with estimates of the surface cleavage energies to discuss the adhesion. The interface energies per interface unit cell are found to be 0.45, 0.50 and 0.94 eV for SiC/AlN, SiC/BP and C/BN, assuming the most favorable interface configuration. The latter is found to be Si-N, Al-C for SiC/AlN and Si-B, C-P for SiC/BP and is discussed in terms of electrostatic and band-structure effects. The alternative bonding configurations are found to be several eV higher in energy. The band-offsets are calculated using the recently developed self-consistent dipole theory. The bandgaps used are calculated including approximate self-energy corrections. The band-alignments are found to be of type II (same sign for valence and conduction band offset) for C/BN and SiC/BP and of type I (large bandgap enclosing small one) for SiC/AlN. Implications for device applications will be discussed. Layer projected densities of states and superlattice band structures will be presented.

F6.10

SILICON CARBIDE/((In₂O₃)_x(SnO₂)_{1-x}) DEVICES FOR THE DETECTION OF ULTRAVIOLET RADIATION. James V. Masi, Western New England College, Springfield, MA. 01119

Heterojunctions of both n- and p-type silicon carbide with oxide mixtures of indium and tin have been formed on single crystal substrates of both alpha and beta phase silicon carbide, both seed and plasma deposited. Both n+/n and n+/p structures were formed by vapor phase deposition and attendant annealing of the structures for varying times at 400°C in air. Metallurgical preparation and affixing of ohmic contacts of both silicides and Au/Ta was accomplished by physical vapor deposition. Electrical device characteristics were measured along with their respective spectral response characteristics both normal to and edge-on with the junction plane. Device characteristics are somewhat typical of expected heterojunctions between these materials, with the exception of the spectral response, which has a distinct bimodal response in both the visible and ultraviolet regions of the spectrum. Results of the electrical and optical properties as well as a discussion of proposed modeling variations are given. Prospects for other types of devices based on this system are also discussed.

F6.11

OHMIC CONTACTS ON β -SiC. M. Iqbal Chaudhry, Department of Electrical and Computer Engineering, Clarkson University, Potsdam, NY 13676; W. B. Berry, and M. V. Zeller, School of Engineering, University of Notre Dame, Notre Dame, IN 46556.

We report on ohmic contacts on β -SiC. The contacts were formed using Ni, NiCr, W, Ti, WSi_2 and $TiSi_2$. Contact resistance measurement and Auger Electron Spectroscopy (AES) were used to study the annealing effect on the contact materials.

Auger analysis of Ni-SiC system indicates that during the heat treatment, Ni reacts with Si to form silicide. Similar results are found for NiCr-SiC system.

Minimum contact resistance of tungsten and titanium on SiC is 6.1×10^{-3} ohm/cm² and 7.6×10^{-3} ohm/cm², respectively. High temperature annealing deteriorates both contacts although for titanium contacts the resistance increases less dramatically as compared to the tungsten contact. The silicides of tungsten and titanium yield lower resistance than metallic W and Ti contacts. The contact resistance for WSi_2 and $TiSi_2$ after heat treatment decreases to 3.0×10^{-4} ohm/cm² and 1.1×10^{-4} ohm/cm² respectively.

F6.12

HIGH AND MEDIUM ENERGY ION SCATTERING STUDY OF MO/3C-SiC CONTACT. S. Hara and I. Ohdomari, Waseda Univ., Ohkubo, Shinjuku-ku, Tokyo 169, Japan; W. Slijkerman and J.F. van der Veen, FOM Institute, 1098 SJ Amsterdam, The Netherlands; S. Misawa, E. Sakuma, and S. Yoshida, Electrotechnical Laboratory, Umezono, Tukuba-shi, Ibaraki 305, Japan.

Refractory-metal/3C-SiC contacts are good candidates for electrodes of high temperature devices. We present here a result of study on Mo/SiC interfaces for thick and thin Mo layer cases by high and medium energy ion scattering spectroscopies, Auger electron spectroscopy, X-ray diffraction, and low energy electron diffraction. We show that the behavior of carbon is quite different from that of silicon in terms of diffusion.

In the case of thick Mo layer (200nm), a carbide/silicide/SiC multilayer is formed by heat treatment at 1200°C for 1 hour after the Mo deposition. Carbon accumulates gradually into the surface region of a Mo overlayer by annealing at 900°C, finally forming a carbide/silicide/SiC layer similar to the structure of the annealing at 1200°C.

In the case of thin Mo (7×10^{18} atoms/cm²), the composition of SiC surfaces makes influences on the behavior of carbon and silicon diffusion. Carbon diffusion toward a Mo overlayer is observed after the Mo deposition onto carbon-rich surfaces while no silicon diffusion occurs. For a silicon-rich surface, 1ML intermixing between the Mo overlayer and the silicon topmost layer of the substrate takes place, acting as diffusion barrier in annealing stages.

In conclusion, carbon diffuses much faster than silicon in the Mo overlayer, thereby accumulating near the surface region.

F6.13

DOPED AMORPHOUS SiC, MIXED CARBIDE AND OXYCARBIDE THIN FILMS BY A LIQUID ROUTE. C-J Chu, E. Liimatta and J.D. Mackenzie, Department of Material Science and Engineering, University of California, Los Angeles, CA 90024

Advanced ceramics like carbides and nitrides can be obtained by the pyrolysis of metal-organic polymers. An intermediate amorphous phase is obtained after the removal of the organic components and before crystallization. By this polymer process, amorphous SiC thin films have been deposited on different substrates using metal-organic solutions. Amorphous mixed carbides and oxycarbides films have also been prepared by the addition of a variety of alkoxides, such as Ti, Al and Zr to the SiC polymer precursor.

Dopants such as B and P have been introduced into the structure of the SiC polymer precursor by a solution method. N-type and P-type thin films have been prepared. The electrical and optical properties of these films have been studied and compared with the amorphous SiC film by vapor route. P-N junction diodes that contain these new materials have been fabricated and the current-voltage (I-V) characteristics have been studied.

F6.14

LIQUID PHASE HOMOEPITAXIAL GROWTH OF 4H-SiC CRYSTALS AND FABRICATION TECHNIQUES OF BLuish-PURPLE LIGHT EMITTING DIODES. Y. Ueda, T. Nakata, K. Koga, Y. Matsushita, Y. Fujikawa, T. Uetani, T. Yamaguchi, and T. Niina, Semiconductor Research Center, Sanyo Electric Co., Ltd. 1-18-13 Hashiridani, Hirakata, Osaka 573 Japan

4H-SiC single crystals have been successfully fabricated on the seeds of 6H-type crystals by the vacuum sublimation method at a temperature of 2400°C and under a pressure of 7-60mbar in an argon atmosphere. Liquid phase epitaxy was attempted by using a dipping method with the 4H-SiC crystals. As we reported previously at ICACSC'88, the off-angle substrate is crucial and/or key technology for the accomplishment of this attempt. The conditions of the crystals growth on the 4H-SiC substrate at 5° off-angle were the same as those of the 6H-type crystals growth. The temperature for melting Si was 1700°C in both cases. Undoped grown crystals showed n-type conduction. We observed the surface morphology and the etch pits of the crystals. The structure of the grown crystals were found to be the 4H-type through the measurements of Hall mobility, photoluminescence and Raman scattering.

P-n junctions were epitaxially obtained on 4H-SiC substrates. Aluminum and nitrogen were doped as acceptors and donors, respectively. But aluminum was also added to n-type layers to make D-A pairs. I-V and C-V characteristics were measured after the LED chips were molded to lamps by clear resin. The diffusion potential was found to be 2.7eV, which was larger than that of a 6H-SiC

blue LED by 0.2eV. The LED fabricated in this study emitted bluish-purple light with a brightness of 1mcd at the forward current of 20mA. Other characteristics were as follows: 420nm peak wavelengths, 90% color purity, and light output was 1.7μW.

F7.1

GALLIUM NITRIDE, A WIDE BAND-GAP SEMICONDUCTOR.
Jacques I. Pankove, University of Colorado, Boulder, CO 80309-0425
and SERI, Golden, CO 80401

This talk will present a historical perspective on the technology, understanding and device applications of GaN. GaN has a direct energy gap of 3.4 eV. The direct gap allows efficient optical transitions both in absorption and luminescence. Laser emission in the UV has been obtained as well as electroluminescence over the visible spectrum. In particular, efficient blue-emitting LEDs have been made. This material is suitable for a variety of other applications such as electron-ballistic devices, electro-optic modulators and acousto-electric devices. Negative electron affinity has been demonstrated with a cesiated surface.

GaN has been grown on sapphire by various deposition methods, yielding large-area single crystals with the wurtzite structure. More recently, the cubic form of GaN has been grown on a nearly lattice-matching single crystal of β-SiC.

F7.2

GROWTH OF CUBIC GaN BY REACTIVE-ION MOLECULAR BEAM EPITAXY. R.C. Powell, G.A. Tomasch, Y.W. Kim, J.A. Thornton* and J.E. Greene Coordinated Science Laboratory, University of Illinois, Urbana, IL.
*Deceased.

Zinc-blende structure epitaxial GaN films have been grown by reactive-ion molecular-beam epitaxy in which Ga is supplied by evaporation from an effusion cell while the nitrogen is provided by an ultra-high vacuum hot-cathode ion source. Mass and energy analysis of the ion beam shows it to be approximately 85% N₂⁺ and 15% N⁺ with an energy spread of ~ 5eV. Films grown on MgO(100)1x1 substrates at temperatures T_s between 650 and 800°C, nitrogen ion acceleration voltages of 35 V, and growth rates between 0.2 and 0.6 μm h⁻¹ were single crystals. The films exhibited the zinc-blende structure with a lattice constant of 0.446 nm. Cross-sectional transmission electron microscopy examination of ~ 0.7-μm-thick epitaxial layers show smooth abrupt interfaces with the primary defects being (111) microtwins. Room-temperature resistivities could be varied between 2.7x10² and 1.1x10⁴ Ω-cm by increasing the incident N/Ga ratio from 1.0 to 2.8 at T_s = 700°C. Photoconductivity decay experiments show the presence of deep traps.

F7.3

HETEROEPITAXIAL GROWTH AND CHARACTERIZATION OF GaN ON SAPPHIRE SUBSTRATES.

T.P. Humphreys, C.A. Sukow, and R.J. Nemanich, Department of Physics, North Carolina State University, Raleigh, NC 27695-8202, J.B. Posthill, R.A. Rudder, S.V. Hattangady, and R.J. Markunas,

Research Triangle Institute, Research Triangle Park, NC 27709

Epitaxial GaN films have been grown by plasma-enhanced chemical vapor deposition (PECVD) at the Research Triangle Institute. The growth procedure utilizes an inert gas discharge (He) combined with the down stream introduction of a trimethylgallium (TMGa) and nitrogen mixture. Growth temperatures were varied in the 500-650°C range. Both cubic [111] and wurtzite [0001] GaN epitaxial films have been achieved on basal plane sapphire substrates. Differences in the substrate growth temperature and variations of the flow rates of the reactant gases can account for the different observed phases. Phase identification, crystallographic orientation relationships and microstructure characterization have been accomplished with transmission electron microscopy. Microtwins, stacking faults, and double-position boundaries are observed in cubic GaN, whereas threading dislocations are the predominant defects found in wurtzitic GaN epitaxial films. The optical properties of the grown films were investigated using Raman spectroscopy. The first reported Raman results from cubic GaN will be presented along with spectra from wurtzitic GaN. The observation of the respective Raman-active phonon modes can also be used for phase identification. Further characterization of the grown films was accomplished with x-ray diffraction, scanning electron microscopy, Hall measurements, and surface analytical techniques.

F8.1

LOW TEMPERATURE SELECTIVE GROWTH OF β-SiC USING SiH₂Cl₂/C₃H₈/HCl/H₂ GAS SYSTEM. Y. Ohshita, Fundamental Res. Lab., NEC Corp., Miyazaki 4-1-1, Miyamae-ku, Kawasaki 213, Japan

β-SiC is grown on a Si(100) substrate by chemical vapor deposition method under reduced pressure using SiH₂Cl₂/C₃H₈/H₂/HCl gas system. A cold type vertical CVD reactor by radiant heating method is used for the present work. The addition of HCl to SiH₂Cl₂/C₃H₈/H₂ gas system makes it possible to obtain a stoichiometric β-SiC film at low growth temperature of 900°C. The ratio of silicon to carbon is examined by Auger electron spectroscopy. The deposited film without HCl gas contains much excess silicon. On the other hand, the silicon to carbon ratio is remarkably improved as increasing the HCl flow rate. Excess silicon, nucleated without carbonization at low growth temperature, seems to be etched away from the film surface by HCl gas. The film is found to be highly (100)-oriented polycrystalline β-SiC on a Si(100) substrate by electron diffraction pattern.

Moreover, β-SiC selective growth on a Si(100) surface, with no nucleation on a SiO₂ surface, is achieved. Without HCl gas, SiC is deposited on a silicon surface and the whole SiO₂ area. According to the increase of the HCl gas flow rate, the density of SiC nucleation on a SiO₂ surface is much decreased. Perfect selective β-SiC film with a mirror surface is obtained in more than 1.5% HCl concentration.

F8.2

ANNEALING AND CRYSTALLIZATION PROCESSES IN AN HYDROGENATED AMORPHOUS SILICON-CARBON ALLOY FILM*

D.K. Basa, Department of Physics, Utkal University, Bhubaneswar 751004, India and F.W. Smith, Department of Physics, The City College of CUNY, New York, NY 10031, U.S.A.

An hydrogenated amorphous silicon-carbon alloy film ($a\text{-Si}_{1-x}\text{C}_x\text{H}$, with $x = 0.29$) was prepared by glow discharge decomposition of a silane and ethylene gas mixture. A careful and detailed investigation of the infrared absorption was undertaken in the range 400 to 4000 cm^{-1} for both the as-deposited ($T = 250^\circ\text{C}$) and annealed (up to 1200°C) film. In addition to the changes in the local bonding brought about by annealing, the study demonstrates clearly that there is a change from amorphous to microcrystalline at $T_a = 800^\circ\text{C}$ and then to crystalline phase at $T_a = 1200^\circ\text{C}$.

*This research was carried out at the City College of New York and was supported by the U.S. Department of Energy under Grant No. DE-FG02-84ER45168.

F8.3

A COMPARISON OF THE MICROSTRUCTURE OF SiC GROWN ON (001) Si, (111) Si, AND 6H-SiC SUBSTRATES BY CVD. J. Yang, P. Pirouz, Department of Materials Science and Engineering, Case Western Reserve University, Cleveland, OH 44106; and J. A. Powell, NASA Lewis Research Center, Cleveland, OH 44135.

3C-SiC has been grown on (001) Si, (111) Si and (0001) 6H-SiC substrates by CVD. The microstructure of the films has been investigated by Nomarski differential interference contrast microscopy, SEM and TEM. On the (001) Si substrate, the 3C-SiC film is single crystalline with a parallel epitaxial relationship with respect to the substrate. The film grown on (111) Si substrate is predominantly in parallel epitaxy, however, small misoriented grains are also present. In the case of growth on the 6H-SiC substrate, the close-packed planes and directions of the film are parallel to those of the substrate. A wide variety of line defects and planar faults occur in the 3C-SiC epilayers. Stacking faults are common to all the epilayers. Inversion domain boundaries (IDBs) and IDB dislocations occur in films grown on on-axis (001) Si but, as expected, are absent in those grown on (111) Si, 6H-SiC, and off-axis (001) Si. Double positioning boundaries occur in films grown on (111) Si and 6H-SiC substrates. These faults have been investigated by TEM, and misfit dislocations at the epilayer/substrate interface are characterized by HREM. In addition, 6H-SiC has been grown epitaxially on off-axis 6H-SiC substrates. The defect density is extremely low in the latter films. The mode of growth (two- or three-dimensional) of these films is discussed and the formation of various defects are related to the growth mode.

F8.4

THE FORMATION OF HELICAL DISLOCATIONS IN SILICON SUBSTRATES DURING THE EPITAXIAL DEPOSITION OF BETA SILICON CARBIDE M. Aindow, T.T. Cheng and P. Pirouz, Department of Materials Science and Engineering, Case Western Reserve University, Cleveland, OH 44106, USA.

Conventionally, electron microscopy studies on epitaxial deposits of semiconducting materials concentrate on defects within the deposit as these features can alter the electrical characteristics of devices fabricated in such materials. However, in some systems examination of microstructural changes in the substrate can provide useful information about deposition mechanisms. One such example is the formation of pits during the initial stages of deposition of beta SiC on Si.

An electron microscopy study will be presented of the dislocation content of silicon substrates used for the deposition of beta SiC. It is shown that dislocations lying parallel to the interface in the silicon wind up into helical configurations during the initial stages of growth in which only a carbon source gas is used. These observations are rationalised in terms of the climb of screw components by a flux of silicon vacancies to

pinned segments of pre-existing dislocations. Evidence for such a process is presented in terms of a dependence of the helix radius and pitch upon the deposition temperature. Mechanisms for the introduction and pinning of dislocations and the subsequent formation of helices will be discussed.

F8.5

COMPOSITION AND STRUCTURE OF HIGHLY ORIENTED β -SiC FILMS GROWN ON Si SUBSTRATES BY REACTIVE MAGNETRON SPUTTERING. O.U. Wahab, Y. Yamamoto*, T.I. Selinder, M. Willander and J.-E. Sundgren, Dept. of Physics, Linköping University, S-581 83 Linköping, Sweden.

SiC films grown on Si substrates by reactive magnetron sputtering have been investigated. The studied films were grown in mixed Ar/CH₄ discharges on both (100) and (111) oriented Si substrates kept at temperatures T_s ranging from 700 to 1250°C . The results show that the carbon content in the films, as determined by Auger electron spectroscopy, increased rapidly as the CH₄ pressure, P_{CH_4} , was increased and that films with a close to stoichiometric composition could be grown in a narrow range of P_{CH_4} . As T_s was increased the required CH₄ pressure necessary to obtain stoichiometric SiC films was found to decrease. Also the plasma conditions affected this pressure and a more intense plasma resulted in lower P_{CH_4} -values. This demonstrates that the CH₄ decomposition necessary for carbon incorporation into the growing film both occurs through pyrolysis and through decomposition in the plasma. X-ray diffraction and transmission electron microscopy studies showed that single phase β -SiC films could be grown on both type of substrates. Only the (100) oriented substrates resulted in highly oriented β -SiC films. These films exhibited, however, small randomly located regions of non-oriented β -SiC. These latter regions were found to be associated with thermal etch pits in the substrates originating from the substrate cleaning procedure. Also T_s was critical for growth of β -SiC films and values higher than approximately 1100°C was necessary to obtain single phase highly oriented films. For lower T_s multi-phase films with several different SiC polymorphs were observed and for $T_s < 800^\circ\text{C}$ the films were amorphous. The film surface morphologies as viewed by scanning electron microscopy showed smooth films in the amorphous region, rough surface morphologies in the multi-phase region and relatively smooth surfaces for the single phase β -SiC films. * Permanent address; Nippon Sheet Glass Co., Ltd., 5-4 Tokodai, Tsukuba-city, Ibaraki-pref. 300-26, Japan.

F8.6

GROWTH OF EPITAXIAL SiC LAYERS ONTO ON- AND OFF-AXIS 6H-SiC SUBSTRATES BY ION BEAM DEPOSITION. K.L. More, S.P. Withrow, T.E. Haynes, and R.A. Zuhr, Oak Ridge National Laboratory, P.O. Box 2008, Oak Ridge, TN 37831-6064

Thin films of β -SiC have been grown epitaxially onto on-axis 6H-SiC substrates using ion beam deposition (IBD). The IBD technique involves the direct deposition of alternating layers of $^{13}\text{C}^+$ and $^{30}\text{Si}^+$. The carbon and silicon ions were obtained from an ion implanter by decelerating mass-analyzed ion beams to 40 eV. The SiC substrate was held at $\sim 700^\circ\text{C}$. Thin films of α -SiC (predominantly 4H) were obtained following deposition onto off-axis ($\sim 2^\circ$) 6H-SiC under the same processing conditions. High resolution electron microscopy and Rutherford backscattering techniques were used to determine the structure and crystalline perfection of the resulting layers.

Research sponsored by the Division of Materials Sciences, U.S. Department of Energy and the Assistant Secretary for Conservation and Renewable Energy, Office of Transportation Systems, as part of the High Temperature Materials Laboratory Program under Contract DE-AC05-84OR21400 with Martin Marietta Energy Systems, Inc.

F8.7

SEM OBSERVATION OF GROWTH AND DEFECT FORMATION ON
HETEROEPI TAXIALLY GROWN SiC ON (100) SILICON. B. Malnar and
L.M. Shirey, Naval Research Laboratory, Washington, D.C. 20375

The starting surfaces of the heteroepitaxially grown cubic SiC films on (100) Si by a two step CVD, using a $C_3H_8-SiH_4/H_2$ reaction gas system at about 1370°C were studied. A highly conductive layer on the SiC at the Si/SiC interface was observed using differential Hall measurements. To determine the origin of this conduction, scanning electron microscopy (SEM) was used to show the morphology of both the (100) Si and the SiC surfaces at the Si/SiC interface. A novel method was developed to make the SiC surfaces at the Si/SiC interface observable by direct SEM examination. The SiC surfaces appeared smooth under the optical microscope, but SEM revealed growth features. The typical SiC's grown at different laboratories vary somewhat in appearance, indicating some differences in the "carbonization process". The observed growth features are related to the characteristic rectangular shallow pits present on the (100) Si substrate surfaces. The SEM image of the SiC surface is the reverse of that of the Si. All or a portion of each growth feature protrudes from the smooth grown SiC surface, indicating that these growth features extend into the underlying pits in the Si substrate. Most of the pits on the (100) Si surface are pyramidal in shape, bounded by {111} planes, with a linear dimension between 1000-6000 Å. The growth features either fill or border similar rectangles with crystallographic patches of material but after certain growth only smaller, unresolvable patches with different densities could be observed. On a vicinal (100) Si surface that is a few degrees toward {110}, the pits are similarly shaped. The equal presence of two antiphase domains on (100) Si became dominated by single domains on such an off axis grown SiC. These features have consequences for the initial nucleation of SiC and the development of associated growth defects.

F8.8

THE EFFECTS OF POWER DENSITY ON THE PROPERTIES
OF DIAMONDLIKE FILMS*, Shuguang Chen, Shuhan Lin
and Yangming Guo, Department of Physics,
Zhongshan University, Guangzhou, China; Kaiming
Zhang, Chemical engineering Department,
Guangdong Engineering College, Guangzhou, China.

The diamond-like carbon films were prepared by
radio frequency plasma CVD. The feedstock was
mixture of butane and hydrogen, and the
substrates were kept at room temperature during
the deposition.

The dependence of deposition rate, conductivity,
and activity energy on power density has been
studied. The results showed that the deposition
rate increased, the conductivity decreased first
and then increased, and the activity energy
decreased rapidly with the increase of power
density in our study range.

The dependence of optical properties on the
power density has been studied using a
spectroscopic ellipsometer. We found the
refractive index decreased slightly, but the
absorption coefficient increased rapidly with
photo energy. The results have been discussed.

* This work was partly supported by NSFC and by
Guangdong NSF.

F8.9

SUBSTRATE AND TEMPERATURE DEPENDENT MORPHOLOGY OF
rf-SPUTTERED INDIUM NITRIDE FILMS. T. J. Kistenmacher,
D. Dayan, R. Fainchtein, W. A. Bryden, and T. O. Poehler,
Applied Physics Laboratory, The Johns Hopkins University,
Laurel, MD 20707-6099

The morphology of rf-sputtered films of the wide bandgap
semiconductor InN on a variety of substrates over a range of
substrate temperatures (50-600 °C) have been studied by X-
ray scattering and scanning tunneling microscope (STM). For
films deposited on fused quartz and the {111} face of
silicon, there is a transition from an off-normal inclina-

tion to a fully textured (0002) film with increasing sub-
strate temperature. In contrast, films deposited on the
(0001) face of sapphire are mixtures of textured and hetero-
epitaxial domains. The volume and quality of epitaxial
grains are maximized in the substrate temperature range
300-400 °C and the rotation of the reciprocal lattice of InN
by 30° to that of the sapphire substrate was determined by
X-ray precession photography. Finally, STM has proven to be
a particularly powerful method for determining the substrate
and temperature dependence of the grain size, surface rough-
ness on the angstrom scale, and inter-grain architecture of
the textured and hetero-epitaxial domains of these rf-
sputtered films.

Supported in part by the U. S. Dept. of Navy under contract
N00039-89-C-5301.

F8.10

TRANSMISSION ELECTRON MICROSCOPY OF InN THIN FILMS. J. S.
Morgan, T. J. Kistenmacher, W. A. Bryden, and T. O. Poehler,
Applied Physics Laboratory, The Johns Hopkins University,
Laurel, MD 20707-6099.

This paper describes growth morphology and structure of rf-
magnetron sputtered thin films of InN, studied by plan-view
transmission electron microscopy. Films deposited on TEM
grids, (0001) sapphire, {111} silicon and amorphous quartz
were prepared for TEM by mechanical abrasion of the substr-
ate followed by sputter etching.

At low deposition temperatures (< 400 °C), films consisted
of small basal-oriented, columnar grains. Above 400 °C to
500 °C, depending on substrate type, growth consisted of
larger, faceted, basal-oriented, globular grains. Selected
area diffraction on individual grains yielded diffraction
patterns from several reciprocal lattice zones. Dark field
micrographs revealed high dislocation densities within
grains. TEM observations of growth morphology and defect
structure were correlated with compositional analysis (i.e.,
oxygen impurity concentration) and transport properties.

Supported in part by the U. S. Dept. of the Navy under con-
tract N00039-89-C-5301.

F8.11

VIBRATIONAL SPECTROSCOPY OF BORON NITRIDE AT HIGH
TEMPERATURES AND PRESSURES. Gregory J. Exarhos, Pacific
Northwest Laboratory, P. O. Box 999, MS K2-44, Richland, WA
99352; and Nancy J. Hess, Mineral Physics Group, Department
of Geology, University of Washington, Seattle, WA 98195.

A relatively high refractive index and enhanced thermal
stability make boron nitride an attractive coating material
for optical film applications. Raman scattering
measurements have been used to distinguish between
crystalline and amorphous phases in boron nitride coatings
and bulk materials. The response of boron nitride to
applied stress (temperature, pressure) is evaluated from
measured changes in the vibrational spectrum.

Raman scattering from the hexagonal phase of boron nitride
coatings on graphite substrates has been measured to 2500 K
using a pulsed-excitation gated-detection technique. The E_2
mode frequency decreases monotonically by nearly 100 cm^{-1} ,
while the linewidth increases by a factor of three. The
phase stability of boron nitride at high temperatures is
confirmed by these measurements, which are in agreement with
a simple phonon decay model for the excitation.

Raman spectra of boron nitride as a function of applied
pressure to 100 kbar were acquired from samples mounted in a
diamond anvil cell. Stability of the hexagonal phase under
hydrostatic conditions was confirmed. Current work involves
Raman measurements of samples subjected to uniaxial stress
where transformation to an amorphous phase has been
predicted. The pressure-induced frequency shift of the
observed E_2 mode can be used to determine strain and strain
heterogeneity in deposited films.

MOCVD OF WIDE BANDGAP III-V SEMICONDUCTORS BY USING NOVEL PRECURSORS. Kwok-Lun Ho, Klavs F. Jensen, Department of Chemical Engineering, Massachusetts Institute of Technology, Cambridge, MA 02139, Wayne L. Gladfelter, David Boyd, and John Evans Department of Chemistry, University of Minnesota, Minneapolis, MN 55455.

Wide bandgap III-V compound semiconductors, specifically the ternary compound $\text{Al}_x\text{Ga}_{1-x}\text{N}$ are potential materials for optoelectronic devices operating in the blue to ultraviolet range. Conventional growth techniques require high temperatures which are suspected of introducing nitrogen vacancies in the materials. As an alternative, we present organometallic chemical vapor deposition (MOCVD) growth of AlN and GaN based on novel precursors designed to decompose at relatively low temperatures. Furthermore, instead of introducing separate sources for nitrogen (e.g. NH_3) and the group III metal (e.g. $\text{Al}(\text{CH}_3)_3$), these new source compounds already contain the metal-nitrogen bond. A large number of suitable sources have been evaluated and of these we focus on diethylaluminumazide (Et_2AlN_3) which gives pure AlN films.

The growth rate mechanism for formation of AlN has been investigated. The ethyl groups leave predominantly by β -elimination and the azide group evolves nitrogen leaving hydrogenated AlN behind. Reasonable growth rates ($> 0.1 \mu\text{m/hour}$) are observed at temperatures starting at 450°C . The growth process appears to be limited by chemical kinetics with an apparent activation energy of 30 kcal/mole except at high temperatures ($> 600^\circ\text{C}$) where mass transfer influences the growth process. At the low temperatures the films are amorphous and contain hydrogen as determined by FTIR. The hydrogen content decreases and the crystallinity of the film increases with temperature. Films grown on (0001) sapphire substrates at temperatures above 850°C show good crystalline properties. The optical properties of the as-grown material are discussed in terms of deposition conditions.

F8.13

THEORETICAL INVESTIGATION OF GRAPHITIC BeO . Renata M. Wentzcovitch,* The James Franck Institute and Department of Physics, The University of Chicago, Chicago, IL 60637; Alessandra Continenza and Arthur J. Freeman, Department of Physics and Astronomy, Northwestern University, Evanston, IL 60208.**

The question of whether BeO , a wide gap semiconductor (7.8 - 10.7 eV), could exist or not in the layered graphitic phase, like the other members of the family of first row solids C and BN, is still an open point. In this work we investigate this possibility through a first principles, all-electron, total energy LDA study of the electronic structure of the compounds in this series in the layered and in the dense wurtzite-like phases. We obtain the minimum energy path between these phases in BeO and compare with those of C and BN. The chemical trends responsible for relative metastability along the series are revealed after a detailed analysis of the differences of the energy components of the compounds in the two phases. We also offer a process for the synthesis of BeO which is based on recent progresses in the synthesis of new graphitic materials by Chemical Vapor Deposition.

* Present address: Brookhaven National Laboratory, Physics Department 510A, Upton, NY 11973.

** Work supported by NSF through NWUMRC grant # DMR88-21571.

F9.1

CUBIC BORON NITRIDE PN DIODE MADE AT HIGH PRESSURE Osamu Mishima, National Institute for Research in Inorganic Materials, 1-1 Namiki, Tsukuba, 305 Japan

The fabrication of a c-BN pn junction diode with the temperature difference solvent method at about 50 kbar and 1700°C will be reviewed. The obtained diode was functional as a high-temperature (650°C)

rectifier and as an UV LED, which proved that the c-BN can be a good potential candidate as an electronic and optoelectronic material.

Purity and perfection of the c-BN crystals were not optimum and productivity of the high-quality c-BN crystals at a high pressure was limited due to the present experimental difficulties. Some of the works that are being made on the refinement of the diode production will be reported.

Surface morphology and crystallographic polarity of the c-BN crystals will be also discussed.

F9.2

A NEW OPTOELECTRONICS SEMICONDUCTOR CUBIC BN: PROPERTIES OF N.I.R.I.M. MADE CRYSTALS AND POTENTIALITIES. Koh Era and Osamu Mishima, National Institute for Research in Inorganic Materials, Namiki 1-1, Tsukuba, Ibaraki 305, Japan.

Optoelectronic properties have been studied on undoped, Be-doped(p), Si-doped(n), and their junction crystals made by a method of ultra-high pressure synthesis. Main emission bands of our forward-biased pn junctions peak at 315 or 255 nm (calibrated), depending on crystals. The 315 nm band appears often. Tails of the emission bands extend towards infrared. A small peak is observed at around 475 nm in 315 nm crystals. Emission power efficiency is estimated to be ppm or less. Under reverse-bias or cathode ray excitation, a weak emission appears in longer wavelength region. Attempts have not been succeeded in obtaining photoluminescence. Relatively high efficiency of injection excitation for the UV bands seems exceptional among various excitation conditions. Excited state processes which bring about these characteristics must be governed strongly by substantial amounts of crystal imperfections coming from the present preparation conditions. Such excited state processes are discussed.

Though the observed blue emission and potential of blue-emitting LED of cBN have attracted much attention, we believe that significance of this material lies in its ultraviolet, particularly in 200 nm range, injection emission nature. Cubic BN can be recognized as almost only material with which both p- and n-type semiconductors are certainly made, having very wide bandgap (estimated to be 7 eV). Whereas, as the blue-emitting LED material, cBN seems to have little advantage on the whole in comparison with SiC. Discussions are made on potentialities as a material for novel optoelectronics devices and on problems to realize them.

F9.3

CONDUCTIVITY OF FILMS OF BORON NITRIDE. G.A. Sokolov, O.I. Lazareva, S.V. Bantsekov, Institute of Physical Chemistry of the Academy of Sciences of the USSR, Moscow 117915, Leninsky Prospekt, 31 and D. Pott, Technische Hochschule 9010 Karl-Marx-Stadt, Strasse der Nationen 62, DDR.

Films of amorphous boron nitride were obtained by the method of ion-assisted deposition. A few of μm thick films with high adhesion were deposited on tungsten carbide.

The transverse current has been measured in the system WO substrate-BN film-electrode of aquadag or Ag. The temperature dependence of the static $G_{sc}(T)$ and dynamic $G_{ac}(T)$ conductivity was measured at low electric field intensity in the linear region of the current-voltage characteristic. Temperature variation of d.c. conductivity $G_{sc}(T)$ was obtained over the whole range $300 < T < 900 \text{ K}$, while $G_{ac}(T) \sim 150 < T < 900 \text{ K}$ at frequencies $f = 10^2 - 10^4 \text{ Hz}$. Experimental data on $G_{sc}(T)$ and $G_{ac}(T)$ were analyzed on the basis of model suggested by Davis and Mott for the density of states in forbidden gap of non-crystalline materials.

We concluded, that there are three different mechanisms of transport by charge carriers: a) $T < 250$ K: conductivity due to carriers hopping between localized states near the Fermi energy; b) over the whole range $250 < T < 700$ K: conductivity due to carriers excited into the localized states at the band edges; c) at $T > 700$ K conductivity due to transport by carriers into non-localized states.

F9.4

POLYCRYSTALLINE δ -BN: STRUCTURE, CONDUCTION, AND THE BAND GAP ENERGETIC STATES. V.V. Lopatin. High Voltage Institute, Tomsk, USSR.

Pyrolytic boron nitride (PBN) prepared by a vapour-phase deposition possesses the unique thermal physical, and dielectric properties which are determined not only by electronic structure but also by anisotropic structure; viz. the crystallite sizes, boundary conditions, and texture.

The paper presents the results of measurements of the dielectric PBN properties in the range to 2000 K. The peculiarities of the electronic structure and texture are analyzed as the cause of the conductivity anisotropy σ . The expressions allowing to define a conduction of anisotropic polycrystals by the measured texture function and σ of single crystals are given.

The modulation thermoactivation spectroscopy was used to determine the energetic and kinetic parameters of the centres of trapping and recombination of the charge carriers, which are placed in a band gap and take part in charge transport. It was found that the holes play a main part in the charge transport in the temperature range to 650 K.

F9.5

GROWTH AND PHYSICAL PROPERTIES OF rf-MAGNETRON SPUTTERED INN SEMICONDUCTING FILMS. W. A. Bryden, J. S. Morgan, T. J. Kistnermacher, D. Dayan, R. Fainchtein, and T. O. Poehler, Applied Physics Laboratory, The Johns Hopkins University, Laurel, MD 20707-6099.

InN films have been grown using reactive rf-magnetron sputtering and characterized by the measurement of their optical, electrical, structural and compositional properties. Films have been prepared on fused quartz, silicon (111) and sapphire (0001). Optical absorption and reflectance have been performed on the samples. Electrical properties (resistivity and Hall effect) have been measured from 1.4K to 500K. Structural characterization has been carried out using X-ray scattering, SEM, TEM and STM. Deposition at 50 °C results in films with a columnar growth morphology, a high carrier density and low mobility. As the temperature of deposition is increased an abrupt change in the growth is evident near 400 °C that is manifested in a change in the structural properties and the electrical transport. At higher temperatures, the film properties steadily improve until at 550 °C the films grown on (0001) oriented sapphire show grains that are epitaxial, with a tenfold decrease in carrier density and an increase of mobility by a factor of four. While the variation in deposition temperature improves the physical properties of the material the carrier density remains high and the mobility relatively low. Auger analysis of the films shows a highly oxygenated surface layer which extends significantly into the bulk of the films. The oxygen impurity severely degrades the semiconducting properties of the material and modifications are underway that will lead to InN films that are of much higher quality.

Supported in part by the U. S. Dept. of Navy under contract N00039-89-C-5301.

F9.6

BORON PHOSPHIDE AS A REFRACTORY SEMICONDUCTOR. Y. Kumashiro, Yokohama National University, Yokohama, Kanagawa; M. Hirabayashi, Electro-technical Laboratory, Tsukuba, Ibaraki; S. Takagi, Daido Steel Co. Ltd., Nagoya, Aichi.

The present paper, first, reviews our results on refractory semiconductor of boron phosphide single crystalline wafers. The crystal growth by CVD process, characterization by Bond method, electrical properties by van der Pauw method, thermoelectrical properties, thermal properties by a unique ring-flash light method and Schottky diode characteristics are mentioned. The following results are concluded.

1. The results of the precise measurements of lattice constant would explain the conduction type and isotope substitution effect in BP.
2. Some electronic transport properties such as donor and acceptor levels and lattice scattering process before and after thermal neutron experiments are clarified. Thermal conductivity shows a pronounced temperature dependence due to phonon scattering.
3. Mobility of $30 \text{ cm}^2/\text{s}\cdot\text{V}$ at 850°C and high thermoelectric power of $\sim 500 \mu\text{V/K}$ indicate the promising materials for devices operated at high temperatures, while high thermal conductivity of $4.0 \text{ W/cm}\cdot\text{K}$ for heat-sink for semiconductor devices.
4. Schottky diodes of n-BP-Sb and -Au shows excellent characteristics and barrier height of n-BP is independent of material and two-thirds of energy bandgap.

In addition to review talk, recent results on thermoelectric properties of sintered BP specimen are mentioned. The highest thermoelectric power of 2 mV/K and high thermoelectric figure of merit reflect promising materials for thermoelectric device.

F9.7

THERMAL AND ION BEAM INDUCED REACTIONS IN Ni ON BP.

Naoto Kobayashi, Electrotechnical Laboratory, Tsukuba, Ibaraki, Japan; Yukinobu Kumashiro, Yokohama National University, Yokohama, Kanagawa, Japan; Peter Revesz, Jian Li and James W. Mayer, Cornell University, Ithaca, NY, USA

In order to study the basic reaction mechanism of metals with refractory wide bandgap semiconductor BP (bandgap with 2.1 eV and melting point above 3000°C) which is of interest from the view of the device application, solid phase reactions of Ni thin films with epitaxially grown BP(100) were investigated both in thermal treatment and ion beam induced process with RBS, AES, XRD and XPS.

In thermal processing, reactions of Ni thin films with BP started between 350°C and 400°C . Ni is found to be the moving species at these temperatures. The formation of the fully reacted crystalline phase with the mixture of NiB and Ni₃P was observed at 450°C . Depth profile measurements with RBS, AES and XPS have revealed uniform mixture of the two phases in depth. At elevated temperatures above 600°C , mixture of phases with less Ni content was found to be formed.

Ion beam induced reactions with 800 keV Xe bombardments were observed at temperatures between 77K and 200°C at the fluence with $5 \times 10^{16} \text{ ions/cm}^2$. Below room temperature the reaction was found to be inhomogeneous and showed an amorphous phase with the same composition as the first thermal phase. The reaction induced at 200°C showed crystalline phase with the same composition and the same XRD pattern as those reacted thermally at 450°C . The reacted layer thickness as a function of the ion beam fluence at 200°C increased linearly with the fluence, which can suggest interface reaction mechanism in this system.

F9.8

BORON PHOSPHIDE ON SILICON FOR RADIATION DETECTORS. J.C. Lund, K.S. Shah, F. Olschner, Radiation Monitoring Devices, Inc., Watertown, MA 02172; and F. Ahmed, Devcom Inc., Framingham, MA 01701

We report on radiation detectors fabricated from boron phosphide (BP) layers. These devices were fabricated by growing 1 to 10 micron thick layers of BP by chemical vapor deposition (CVD) on (100) oriented n-type silicon substrates. Ohmic contacts were applied to the Si (Au-Sb) and Schottky barrier contacts (also Au-Sb) were applied to the BP layer. After extensive electrical and physical characterization, the resulting devices were tested as radiation detectors and were found to be capable of detecting individual 5.5 MeV alpha particles. With some improvements we hope to fabricate neutron detectors from these devices, making use of the very high cross-section of boron for thermal neutrons.

F9.9

ZnGeP₂: A WIDE BANDGAP CHALCOPYRITE STRUCTURE SEMICONDUCTOR FOR NONLINEAR OPTICAL APPLICATIONS. G.C. Xing and K.J. Bachmann, Department of Materials Science and Engineering, North Carolina State University, Raleigh, NC27695; and J.B. Posthill, Research Triangle Institute, Research Triangle Park, NC27709.

ZnGeP₂ is a chalcopyrite structure semiconductor with a bandgap of 1.99eV at room temperature. Since ZnGeP₂ has the second largest birefringence of the known II-IV-V₂ chalcopyrite structure semiconductors, it is of interest in the context of nonlinear optical applications. Efforts have been made in improving the quality of ZnGeP₂ single crystals. In this paper we report the growth and characterization of ZnGeP₂ epitaxial layers by open tube MOCVD and ZnGeP₂ single crystals by high-pressure vapor transport. The electrical and optical properties have been investigated by Hall measurements, absorption spectroscopy, photoconductivity and photoluminescence spectroscopy, and compared with those of the crystals grown from melt. Both the melt-grown crystals and epitaxial layers show extended band tailing in the transparency range of ZnGeP₂. In contrast, the high-pressure vapor transported single crystals exhibits substantially lower sub-bandgap absorption. X-ray diffraction and transmission electron microscopy have been used for the structural characterization of these crystals. The results show that both the epitaxial films and the high-pressure vapor transported crystals crystallized in the chalcopyrite structure.

SYMPOSIUM G:
IMPURITIES, DEFECTS AND DIFFUSION
IN SEMICONDUCTORS: BULK AND
LAYERED STRUCTURES

G

November 27 - December 1, 1989

Chairs

J. Bernholc
Department of Physics
North Carolina State University
Raleigh, NC 27695-8202
(919) 737-3126

D. J. Woford
IBM T.J. Watson Research Center
P. O. Box 218
Yorktown Heights, NY 10598
(914) 945-2553

E. E. Haller
Department of Materials Science
and Lawrence Berkeley Laboratory
University of California at Berkeley
Berkeley, CA 94720
(415) 486-5294

Symposium Support

Air Force Office of Scientific Research

IBM Corporation

Office of Naval Research

Proceedings published as Volume 163
of the Materials Research Society
Symposium proceedings series.

IMPURITIES, DEFECTS AND DIFFUSION
IN SEMICONDUCTORS: BULK AND
LAYERED STRUCTURES

November 27 - December 1, 1989

SESSION G1: ELECTRONIC STRUCTURE -
DEEP LEVELS I

Chair: D. J. Wolford
Monday Morning, November 27
Salon F (M)

8:30 *G1.1
HIGH RESOLUTION SPECTROSCOPY OF POINT
DEFECTS IN SEMICONDUCTORS, H.G. Grimmeiss,
M. Kleverman and J. Olajos, University of
Lund, Department of Solid State Physics,
Lund, Sweden.

9:00 G1.2
INFRARED ABSORPTION STUDY OF ZINC-DOPED
SILICON, E. Merk, J. Heyman and E.E.
Haller, University of California at
Berkeley, Center for Advanced Materials,
Materials and Chemical Sciences Division,
Lawrence Berkeley Laboratory, Berkeley, CA.

9:15 G1.3
INFRARED STUDIES OF THE DOUBLE ACCEPTOR ZINC
IN SILICON, A. Dörnen, R. Kienle, and K.
Thonke, Universität Stuttgart, Physikal-
isches Institut, Stuttgart, West Germany; P.
Stolz and G. Pensl, University of Erlangen,
Institut für Angewandte Physik, Erlangen,
West Germany; D. Grünebaum and N.D.
Stolwijk, University of Münster, Institut
für Metallforschung, Münster, West Germany.

9:30 G1.4
PRESSURE DEPENDENCE OF A DEEP EXCITONIC
LEVEL IN SILICON, G.A. Northrop and D.J.
Wolford, IBM T.J. Watson Research Center,
Yorktown Heights, NY.

9:45 G1.5
NEW ODMR OBSERVATIONS IN Zn-DOPED LEC InP
AND Cr- AND Te- DOPED GaAs, J.M. Trombetta
and T.A. Kennedy, Naval Research Laboratory,
Washington, DC.

10:00 BREAK

*Invited Paper

Short Courses C-06, "Deep Level Transient
Spectroscopy," and P-06, "Ion Implantation,
Diffusion, Defects, and RTP," may be of
interest to symposium attendees. Details
regarding course dates and instructors are
provided in the short course section of this
program.

SESSION G2: ELECTRONIC STRUCTURE -
DEEP LEVELS II

Chair: J. M. Langer
Monday Morning, November 27
Salon F (M)

10:15 *G2.1
COMPLEX DEFECTS IN SEMICONDUCTORS, B.
Monemar, Linköping University, Department of
Physics and Measurement Technology, Linköp-
ing, Sweden.

10:45 G2.2
THE ELECTRONIC STRUCTURE OF INTERSTITIAL
IRON IN SILICON, M. Kleverman, A-L
Thilderkvist, G. Grossmann, J. Olajos and
H.G. Grimmeiss, University of Lund, Depart-
ment of Solid State Physics, Lund, Sweden.

11:00 G2.3
D-BAND LUMINESCENCE IDENTIFIED WITH TRANSI-
TION METAL DECORATED, AS DISTINCT FROM
UNDECORATED DISLOCATIONS, V. Higgs and E.C.
Lightowers, King's College London, Physics
Department, London, United Kingdom.

11:15 G2.4
PHOTOLUMINESCENCE EXCITATION SPECTROSCOPY OF
MOCVD-GROWN GaAs:V, Y.J. Kao, N.M. Haegel,
University of California, Los Angeles,
Department of Materials Science and En-
gineering, Los Angeles, CA; and W.S. Hobson,
AT&T Bell Laboratories, Murray Hill, NJ.

11:30 G2.5
RADIATIVE AND NON-RADIATIVE RECOMBINATIONS
AT ER CENTERS IN GaAlAs, Taha Benyattou,
Ejelloul Seghier, and Gérard Guillot, INSA
de Lyon, LPM Department, Villeurbanne,
France; Pierre Galtier and Marie-Noëlle
Charasse, Thomson CSF/LCR, Orsay, France.

11:45 G2.6
CHARACTERIZATION OF DEEP-LEVEL DEFECTS IN
SEMI-INSULATING GaAs AND InP BY PHOTOINDUCED
TRANSIENT SPECTROSCOPY (PITS), Paweł
Kaminski, Institute of Electronic Materials
Technology, Physical Investigations Depart-
ment, Warszawa, Poland.

SESSION G3: ELECTRONIC STRUCTURE -
SHALLOW IMPURITIES

Chair: M. L. W. Thewalt
Monday Afternoon, November 27
Salon F (M)

1:30 *G3.1
ENHANCEMENT OF MINORITY CARRIER LIFETIMES IN
 $n^+/n/n^+$ GaAs HOMO-STRUCTURES, Leigh M. Smith
and D.J. Wolford, IBM T.J. Watson Research
Center, Yorktown Heights, NY; R.
Venkatasubramanian and S.K. Ghandhi, Rensse-
laer Polytechnic Institute, Troy, NY.

2:00 G3.2
EVIDENCE FOR STRONG TRAPPING BY IONIZED DONORS OF FREE EXCITONS IN EXCITED STATES, S. Zemon and G. Lambert, GTE Laboratories, Waltham, MA.

2:15 G3.3
FORMATION OF THREE RED-SHIFT EMISSIONS IN HEAVILY GERMANIUM-DOPED P-TYPE GAAS GROWN BY MBE, Y. Makita, A. Yamada, H. Shibata, N. Ohnishi, A.C. Beye and K.M. Mayer, Electrotechnical Laboratory, Photopress Section, Ibaraki, Japan.

2:30 G3.4
ELECTRICAL PROPERTIES OF HEAVILY Be-DOPED GaAs GROWN BY MOLECULAR BEAM EPITAXY, H. Shibata, Y. Makita, A. Yamada, N. Ohnishi, M. Mori, Y. Nakayama, A.C. Beye, and K.M. Mayer, Electrotechnical Laboratory, Ibaraki, Japan.

2:45 G3.5
PHOTOLUMINESCENCE STUDY OF GaAs DIFFUSED WITH Li, H.P. Gislason and E.Ö. Sveinbjörnsson, University of Iceland, Science Institute, Reykjavik, Iceland; B. Monemar and M. Ahlström, Linköping University, IFM, Linköping, Sweden.

3:00 G3.6
LASER-THERMAL IMPURITY PUMPING OF SHALLOW DONORS IN ULTRAPURE GERMANIUM, T. Theiler and F. Keilmann, Max-Planck-Institut für Festkörperforschung, Stuttgart, West Germany.

3:15 BREAK

SESSION G4: ELECTRONIC STRUCTURE - NATIVE DEFECTS AND TRANSITION METALS IN III - V's

Chair: S. G. Bishop
Monday Afternoon, November 27
Salon F (M)

3:30 G4.1
VACANCY-TYPE DEFECTS IN PLASTICALLY DEFORMED GaAs, P. Mascher, S. Dannefaer and D. Kerr, University of Winnipeg, Department of Physics, Winnipeg, Canada.

3:45 G4.2
ODMR STUDIES ON BULK GALLIUM PHOSPHIDE, Keith L. Brower, Sandia National Laboratories, Albuquerque, NM.

4:00 G4.3
THE ROLE OF OXYGEN IN p-TYPE InP, J. Michel, J. Jeong, K.M. Lee and L.C. Kimerling, AT&T Bell Laboratories, Murray Hill, NJ.

4:15 G4.4
MID-INFRARED SPECTRAL PHOTO RESPONSE OF SEMI-INSULATING GaAs, G.J. Brown, and W.C. Mitchel, U.S. Air Force, Wright Research and Development Center, Materials Laboratory (WRDC/MLPO), Wright-Patterson AFB, OH.

4:30 G4.5
ASSOCIATION OF THE 0.8eV EMISSION BAND TO THE EL₆ CENTER IN GAAS, S. Alaya, M.A. Zaïdi, G. Marrakchi, H. Maaref, Faculté des Sciences, Physique Department, Monastir, Tunisia; H.J. Von Bardeleben and J.C. Bourgoin, Université Paris VII, Groupe Physique des Solides (ENS), Paris, France.

4:45 G4.6
THE ELECTRONIC STRUCTURE OF THE "0.15eV" Cu ACCEPTOR LEVEL IN GaAs, E. Janžén, M. Linnarsson and B. Monemar, Linköping University, Department of Physics and Measurement Technology, Linköping, Sweden; M. Kleverman, University of Lund, Department of Solid State Physics, Lund, Sweden.

SESSION G5: ELECTRONIC STRUCTURE - COMPLEX DEFECTS IN Si

Chair: M. Stavola
Tuesday Morning, November 28
Salon F (M)

8:00 *G5.1
PHOTOLUMINESCENCE CHARACTERIZATION OF IMPURITIES AND DEFECTS IN SEMICONDUCTORS, M.L.W. Thewalt, Simon Fraser University, Department of Physics, Burnaby, Canada.

8:30 G5.2
GENERATION AND DISSOCIATION OF IRON-BORON PAIRS IN SILICON, M. Suezawa and K. Sumino, Tohoku University, Institute for Materials Research, Sendai, Japan.

8:45 G5.3
THEORETICAL INVESTIGATIONS OF THE METASTABILITY OF IRON-GROUP III ACCEPTOR PAIRS IN SILICON, J.R. Leite and L.V.C. Assali, Universidade de São Paulo, Instituto de Física, São Paulo, Brazil.

9:00 G5.4
PHOTOCONDUCTIVITY STUDY OF CrB AND Cr_i IN SILICON, A. Schlette, R. Kienle, A. Dörnen, and K. Thonke, Universität Stuttgart, Physikalisches Institut, Stuttgart, West Germany.

9:15 *G5.5
FORMATION OF In-Cu PAIRS IN SILICON DURING CHEMO-MECHANICAL POLISHING, Th. Wichert, R. Keller, M. Deicher, W. Pfeiffer, H. Skudlik and D. Steiner, Universität Konstanz, Fakultät für Physik, Konstanz, West Germany.

9:45 BREAK

SESSION G6: HYDROGEN IN Si. I

Chair: M. Stavola
Tuesday Morning, November 28
Salon F (M)

10:15 *G6.1
FERMI RESONANCE EFFECTS ON THE VIBRATION MODES OF HYDROGEN-PASSIVATED BORON IN SILICON, G.D. Watkins, W.B. Fowler, G.G. DeLeo, M. Stavola and D.M. Kozuch, Lehigh University; S.J. Pearton, J. Lopata, AT&T Bell Laboratories, Murray Hill, NJ.

10:45 G6.2
OPTICALLY DETECTED MAGNETIC RESONANCE OF A HYDROGEN-RELATED COMPLEX DEFECT IN SILICON, W.M. Chen, O.O. Awadelkarim, B. Monemar, Linköping University, Department of Physics and Measurement Technology, Linköping, Sweden; J.L. Lindström, Swedish Defence Research Establishment, Linköping, Sweden; and G.S. Oehrlein, IBM T.J. Watson Research Center, Yorktown Heights, NY.

11:00 *G6.3
HYDROGEN BEHAVIOUR IN SILICON, Guido L. Chiarotti, F. Buda, R. Car and M. Parrinello, International School for Advanced Studies, Condensed Matter Department, Trieste, Italy.

11:30 G6.4
HYDROGEN DIFFUSION IN B-DOPED SILICON, C.P. Herrero, C.S.I.C., Instituto de Ciencia de Materiales, Madrid, Spain; M. Stutzmann and A. Breitschwerdt, Max-Planck-Institut für Festkörperforschung, Stuttgart, West Germany.

11:45 G6.5
MODELING OF THE DIFFUSION OF HYDROGEN IN SILICON, D. Mathiot, CNET-CNS, Meylan, France; and D. Ballutaud, P. de Mierry and M. Aucouturier, CNRS, Laboratoire Physiques des Solides, Meudon, France.

SESSION G7: HYDROGEN IN Si. II

Chair: E. E. Haller
Tuesday Afternoon, November 28
Salon F (M)

1:30 *G7.1
THE STRUCTURES OF ISOLATED HYDROGEN CENTERS IN SEMICONDUCTORS INFERRED FROM MUONIUM, T.L. Estle, Rice University, Physics Department, Houston, TX; R.F. Kiefl, TRIUMF and University of British Columbia, Vancouver, Canada; J.W. Schneider, Universität Zürich, Zürich, Switzerland; and C. Schwab, CRN, Strasbourg, France.

2:00 G7.2
ELECTRONIC STRUCTURE AND HYPERFINE PARAMETERS FOR HYDROGEN AND MUONIUM IN SILICON, Chris G. Van de Walle, Philips Laboratories, Briarcliff Manor, NY.

2:15 G7.3
HYDROGEN IN CRYSTALLINE SILICON UNDER COMPRESSION AND TENSION, C.S. Nichols and D.R. Clarke, IBM T.J. Watson Research Center, Yorktown Heights, NY.

2:30 G7.4
ANALYSIS OF REAL-TIME HYDROGENATION DATA FROM P AND N-TYPE SILICON, Carleton H. Seager and Robert A. Anderson, Sandia National Laboratories, Albuquerque, NM.

2:45 G7.5
HYDROGEN SEGREGATION AT AL/SI INTERFACE STUDIED BY NUCLEAR RESONANT REACTION, Joyce C. Liu, A.D. Marwick and F.K. LeGoues, IBM T.J. Watson Research Center, Yorktown Heights, NY.

3:00 G7.6
DISSOCIATION KINETICS OF SHALLOW ACCEPTOR-HYDROGEN PAIRS IN SILICON, T. Zundel and J. Weber, Max-Planck-Institut für Festkörperforschung, Stuttgart, West Germany.

3:15 BREAK

SESSION G8: HYDROGEN IN III-V SEMICONDUCTORS

Chair: E. E. Haller
Tuesday Afternoon, November 28
Salon F (M)

3:45 *G8.1
HYDROGEN COMPLEXES IN III-V SEMICONDUCTORS, Bernard Pajot, Université Paris, Groupe de Physique des Solides de l'ENS, Paris, France.

4:15 G8.2
Sn-H COMPLEXES IN GaAs, D.M. Kozuch, Lehigh University, Sherman Fairchild Laboratory, Physics Department, Bethlehem, PA; M. Stavola, S.J. Pearton, C.R. Abernathy and J. Lopata, AT&T Bell Laboratories, Murray Hill, NJ.

4:30 G8.3
REASSESSMENT OF ACCEPTOR PASSIVATION MECHANISM IN p-TYPE HYDROGENATED GaAs, I. Szafranek and G.E. Stillman, University of Illinois at Urbana-Champaign, Department of Materials Science and Engineering, Center for Compound Semiconductor Microelectronics, Materials Research Laboratory and Coordinated Science Laboratory, Urbana, IL.

4:45 G8.4
HYDROGEN PASSIVATION OF INTERFACIAL DEFECTS IN MOCVD GROWN GaAs/InP, V. Swaminathan, U.K. Chakrabarti, W.S. Hobson, R. Caruso, J. Lopata and S.J. Pearton, AT&T Bell Laboratories, Murray Hill, NJ.

5:00 G8.5
PASSIVATION OF Zn ACCEPTORS IN InGaAs DURING
RIE WITH CHF_3/H_2 AND CH_4/H_2 , Martin Möhrle,
Heinrich-Hertz-Institut, Berlin, West Ger-
many.

SESSION G9: COMPOUND SEMICONDUCTORS
POSTER SESSION

Chairs: D. J. Wolford and E. E. Haller
Tuesday Evening, November 28, 1989
7:00 p.m. - 10:00 p.m.
America Ballroom (W)

G9.1 OPTICAL ABSORPTION OF DEEP DEFECTS
IN NEUTRON IRRADIATED SEMI-INSULATING GaAs,
M.O. Manasreh, U.S. Air Force, WRDC/MLPO,
Wright-Patterson AFB, OH; and P.J. Pearah,
Spectrum Technology Inc., Holliston, MA.

G9.2 RECOVERY FROM THE METASTABLE EL2
DEFECT IN GaAs UNDER MONOCHROMATIC LIGHT
ILLUMINATION, M.O. Manasreh and D.W.
Fischer, U.S. Air Force, WRDC/MLPO, Wright-
Patterson AFB, OH.

G9.3 EL-2 DEFECT FORMATION AND CARBON
INCORPORATION IN GaAs GROWN BY ORGANO-
METALLIC VAPOR PHASE EPITAXY, R.
Venkatasubramanian, Research Triangle Park,
NC; J.M. Borrego and S.K. Ghandhi, Rens-
selaer Polytechnic Institute, Troy, NY.

G9.4 DX-CENTER IN Se-DOPED $\text{Al}_x\text{Ga}_{1-x}\text{As}$,
Thomas Hanak, University of Denver, Depart-
ment of Physics, Denver, CO; Assem Bakry,
Richard K. Ahrenkiel, Solar Energy Research
Institute, Golden, CO; and Michael L.
Timmons, Research Triangle Institute,
Research Triangle Park, NC.

G9.5 A MODEL OF Si DIFFUSION IN GaAs
BASED ON THE FERMI-LEVEL EFFECT, Shaofeng
Yu, Ulrich M. Gösele and Teh Y. Tan, Duke
University, Department of Mechanical En-
gineering and Materials Science, Durham, NC.

G9.6 BURIED AMORPHOUS LAYERS IN GALLIUM
ARSENIDE, Dipankar Sengupta, Mark C.
Ridgway, John M. Zemanski and Steven T.
Johnson, Royal Melbourne Institute of Tech-
nology, Microelectronics and Materials
Technology Centre, Melbourne, Australia.

G9.7 NEW GERMANIUM-RELATED DONOR IN
NEUTRON-IRRADIATED GALLIUM PHOSPHIDE, J.
Barczynska and E. Goldys, Warsaw University,
Institute of Experimental Physics, Warsaw,
Poland.

G9.8 DIFFUSION OF Ga VACANCIES AND Si IN
GaAs, K.B. Kahen, D.J. Lawrence, D.L.
Peterson and G. Rajeswaran, Eastman Kodak
Company, Corporate Research Laboratories,
Rochester, NY.

G9.9 MECHANISM FOR THE DIFFUSION OF Zn
IN GaAs, K.B. Kahen, Eastman Kodak Company,
Corporate Research Laboratories, Rochester,
NY.

G9.10 DEFECTS IN THE NEAR-SURFACE REGION
OF $2.5 \text{ MeV}^{16}\text{O}^+$ IMPLANTED n-GaAs, C.C. Tin
and P.A. Barnes, Auburn University, Depart-
ment of Physics, Auburn, AL; T.T. Bardin and
J.G. Pronko, Lockheed Research and Develop-
ment Division, D91-10, B203, Palo Alto, CA.

G9.11 DEEP LEVEL LUMINESCENCE IN InP:
PHONON FEATURE ANALYSIS, S. Banerjee, A.K.
Srivastava and B.M. Arora, Tata Institute of
Fundamental Research, Bombay, India.

G9.12 OPTICAL ABSORPTION AND PHOTOLUMI-
NESCENT FROM LOCALIZED STATES IN HEAVILY
DOPED InGaAsP:Ge, R. Rajalakshmi and B.M.
Arora, Tata Institute of Fundamental
Research, Bombay, India.

G9.13 VOID FORMATION AND THE CORRELATION
WITH THE REDUCTION OF CARRIER CONCENTRATION
IN Si-IMPLANTED GaAs, Kei-Yu Ko, Samuel
Chen, S.-Tong Lee, Longru Zheng, Eastman
Kodak Company, Corporate Research Labora-
tories, Rochester, NY; and T.Y. Tan, Duke
University, Department of Mechanical En-
gineering and Materials Science, Durham, NC
and Microelectronics Center of North Caro-
lina, Research Triangle Park, NC.

G9.14 DISORDER INDUCED BAND TAILING
EFFECTS ON DEEP LEVELS IN SEMICONDUCTORS,
A.A. Teate and N.C. Halder, University of
South Florida, Department of Physics, Tampa,
FL.

G9.15 SURFACE AND INTERFACE DAMAGE CHARA-
CTERIZATION OF REACTIVE ION ETCHED MBE
REGROWN GaAs, M.W. Cole, M. Dutta, U.S. Army
Electronics Technology and Devices Labora-
tory, Department of Elect. Materials Branch,
Ft. Monmouth, NJ; J. Rossabi, Institution
Quest Tech, Inc. Eatontown, NJ; Doran D.
Smith, U.S. Army Electronics Technology and
Devices Laboratory, Department of Elect.
Materials Branch, Ft. Monmouth, NJ; J.L.
Lehman, Institution JEOL USA Inc., Depart-
ment Applications, Peabody, MA.

G9.16 DIFFUSION OF ION-IMPLANTED TIN IN
GALLIUM ARSENIDE, E.L. Allen, Stanford
University, Department of Materials Science
and Engineering, Stanford, CA; M.D. Deal and
J.D. Plummer, Stanford University, In-
tegrated Circuits Laboratory, Stanford, CA.

- G9.17** Pd/Au:Be OHMIC CONTACTS TO p-TYPE GaAs, K.M. Schmitz, K. Jiao, R. Sharma and W.A. Anderson, State University of New York at Buffalo, Center for Electronic and Electro-optic Materials, Department of Electrical and Computer Engineering, Buffalo, NY; G. Rajeswaran and L.R. Zheng, Eastman Kodak Company, Corporate Research Laboratories, Rochester, NY; M.W. Cole, U.S. Army Electronics Technology and Devices Laboratory, Fort Monmouth, NJ.
- G9.18** VOID FORMATION, ELECTRICAL ACTIVATION AND LAYER INTERMIXING IN Si-IMPLANTED GaAs/AlGaAs SUPERLATTICES, S.-Tong Lee, Samuel Chen, Kei-Yu Ko, Mary L. Ott, G. Braunstein, Eastman Kodak Company, Corporate Research Laboratories, Rochester, NY; and T.Y. Tan, Duke University, Department of Mechanical Engineering and Materials Sciences, Durham, NC and Microelectronics Center of North Carolina, Research Triangle Park, NC.
- G9.19** REDUCTION OF DX CENTER CONCENTRATION IN Sn-DOPED AlGaAs GROWN BY LPE AND ITS MEANING, In Duk Hwang and Sin Chong Park, Electronics and Telecommunications Research Institute, Basic Research Department, Dajeon, Korea.
- G9.20** HOT-CARRIER EFFECTS ON OPTICAL PROPERTIES OF GaAs/Al_xGa_{1-x}As QUANTUM WELLS, W.M. Chen, B. Monemar and P.O. Holtz, Linköping University, Department of Physics and Measurement Technology, Linköping, Sweden; M. Sundaram, J.L. Merz and A.C. Gossard, University of California, Santa Barbara, Department of Electrical and Computer Engineering, Santa Barbara, CA.
- G9.21** THE NATURE OF NATIVE DEFECTS IN LEC GROWN SEMI-INSULATING GaAs BY THERMALLY STIMULATED CURRENT SPECTROSCOPY, Zhaoqiang Fang, Lei Shen, T.E. Schlesinger and A.G. Milnes, Carnegie Mellon University, Department of Electrical and Computer Engineering, Pittsburgh, PA.
- G9.22** PRESSURE EFFECTS ON DEEP LEVELS IN SEMICONDUCTORS, Ken-ichi Takarabe, Shigeru Minomura, Okayama University of Science, Department of Physics, Okayama, Japan; Masahiko Kusaka, Okayama University, Department of Physics, Okayama, Japan; Koichiro Matsuda, Horiba Ltd., 1st R&D Department, Kyoto, Japan.
- G9.23** IMPROVED HOLE DIFFUSION LENGTHS IN BULK n-TYPE GaAs FOR HIGH EFFICIENCY SOLAR CELLS, D. Wong, T.E. Schlesinger and A.G. Milnes, Carnegie Mellon University, Department of Electrical and Computer Engineering, Pittsburgh, PA.
- G9.24** THE STUDY OF CONTAMINATION OF CARBON, BORON, AND OXYGEN IN LEC-GAAS, Yoshiko Itoh, The Institute of Physical and Chemical Research, Saitama, Japan; Yoshinori Kadota, Sumitomo Metal Mining Company, Ltd., Hokkai-doh, Japan; Hiroto Fukushima, Japan Analysis Center, Chiba, Japan; and Mikio Takai, Osaka University, Engineering Department, Osaka, Japan.
- G9.25** THE ROLE OF CHARGED POINT DEFECTS ON THE DIFFUSION BEHAVIOR OF SILICON IN GaAs, Jeff J. Murray, David A. Stevenson, Stanford University, Department of Materials Science and Engineering, Stanford, CA; and Michael D. Deal, Stanford University, Center for Integrated Systems, Department of Electrical Engineering, Stanford, CA.
- G9.26** MAGNETICALLY STABILIZED KYROPOULOS GROWTH OF InP, Steven Bachowski, Brian S. Ahern, Robert M. Hilton, Joseph A. Adamski, Rome Air Development Center, Hanscom AFB, MA.
- G9.27** TEMPERATURE DEPENDENCE OF SCATTERED LIGHT INTENSITY BY PRECIPITATES ALONG DISLOCATIONS IN AN In DOPED LEC GaAs CRYSTAL, Kazufumi Sakai and Tomoya Ogawa, Gakushuin University, Department of Physics, Tokyo, Japan.
- G9.28** X-ALPHA CALCULATIONS OF Sn DOPING IN GaAs, D.M. Union and M. Wilner, University of Lowell, Physics Department, Lowell, MA.
- G9.29** BERYLLIUM DOPING IN MBE GROWN GaAs AND AlGaAs, Joseph Pellegrino, National Institute of Standards and Technology, Gaithersburg, MD; James Griffin and Micheal Spencer, Howard University, MSRCE, Washington, DC.
- G9.30** ANOMALOUS LUMINESCENCE PROPERTIES OF GaAs GROWN BY MOLECULAR BEAM EPITAXY, I. Szafranek, University of Illinois at Urbana-Champaign, Department of Materials Science and Engineering, Coordinated Science Laboratory, Urbana, IL; M.A. Plano, M.J. McCollum, S.L. Jackson, K.-Y. Cheng, and G.E. Stillman, University of Illinois at Urbana-Champaign, Department of Electrical and Computer Engineering, Urbana, IL.
- G9.31** POOLE-FRENKEL EFFECT ON THE DX CENTERS IN III-V TERNARY ALLOYS, H. Altelaarrea, J. Bosch, A. Pérez, J. Samitier, and J.R. Morante, Universitat de Barcelona, Departament de Física Aplicada i Electrònica, Barcelona, Spain.

- G9.32** DEEP-LEVEL DOMINATED CURRENT-VOLTAGE CHARACTERISTICS OF NOVEL AND IMPORTANT SEMICONDUCTOR HETEROSTRUCTURES, K. Das, North Carolina State University, Department of Materials Science and Engineering, Raleigh, NC.
- G9.33** MOBILITY-LIFETIME PRODUCT OF PHOTO-EXCITED ELECTRONS IN GaAs: THE ROLE OF EL2, George C. Valley, University Paris XI, Institut d'Optique, Paris, France, and Hughes Research Laboratories, Malibu, CA; H.J. Von Bardeleben, Centre National de la Recherche Scientifique, Groupe de Physique des Solides de l'Ecole Normale Supérieure, Paris, France.
- G9.34** OPTICAL CHARGE TRANSFER PROCESSES IN SEMI-INSULATING GaAs, E. Christoffel, T. Benchiguer, A. Goltzené, and C. Schwab, Université Louis Pasteur, CRN, Groupe Recherches Physiques et Matériaux, Strasbourg, France; K. Chino and K. Satoh, Sumitomo Metal Mining Company, Ltd., Tokyo, Japan; P. Bunod and E. Molva, IRDI-CEA, CENG Department, Division d'Electronique de Technologie et d'Instrumentation, Grenoble, France.
- G9.35** COMPARATIVE OPTICAL STUDIES OF Cu, Mn, AND C IMPURITIES IN BULK LEC GROWN GaAs BY ELECTRON BEAM ELECTROREFLECTANCE (EBER) AND PHOTOLUMINESCENCE (PL), M.H. Herman and I.D. Ward, Charles Evans and Associates, Redwood City, CA; and P.J. Pearah, Spectrum Technology, Holliston, MA.
- G9.36** CORRELATION OF FREE CARRIER CONCENTRATION MEASUREMENTS IN GaAs BY NON-CONTACT OPTICAL ELECTRON BEAM ELECTROREFLECTANCE (EBER) AND PHOTOREFLECTANCE (PR) TO ELECTRICAL HALL EFFECT, D.K. Gaskill, N. Bottka, and R.S. Sillmon, Naval Research Laboratory, Washington, DC; M.H. Herman and I.D. Ward, Charles Evans and Associates, Redwood City, CA; and C.L. Reynolds, AT&T Bell Laboratories, Reading, PA.
- G9.37** Ge RELATED DEEP LEVEL LUMINESCENCE IN InGaAs LATTICE MATCHED TO InP, S.S. Chandvankar, A.K. Srivastava, B.M. Arora, and D.K. Sharma, Tata Institute of Fundamental Research, Bombay, India.
- G9.38** CARBON DOPING IN InGaAs GROWN BY MBE, Hiroshi Ito and Tadao Ishibashi, NTT, LSI Laboratories, Kanagawa, Japan.
- G9.39** SURFACE STRUCTURE OF SULFUR COATED GaAs, Yoshihisa Fujisaki and Shigeo Goto, Hitachi Ltd., Central Research Laboratory, Tokyo, Japan.
- G9.40** ELECTRICAL AND PHOTOLUMINESCENCE PROPERTIES OF Mg^{+} AND C^{+} IMPLANTED ACCEPTORS IN InP, A.C. Beve, A. Yamada, A. Shimizu, H. Shibata, H. Tanoue, K.M. Mayer, H. Sugiyama, K. Kamijoh, T. Oda, O. Arriga and Y. Makita, Electrotechnical Laboratory, Ibaraki, Japan.
- G9.41** QUALITATIVE PHYSICS OF DEEP LEVELS IN HETEROSTRUCTURES, Harold P. Hjalmarson, I.J. Fritz, J.F. Klem and T.M. Brennan, Sandia National Laboratories, Albuquerque, NM.
- G9.42** Ge TRANSPORT AND EPITAXY IN THE AMORPHOUS-Ge/Pd₂Si/(111) Si SYSTEM, Q.Z. Hong, J.G. Zhu and J.W. Mayer, Cornell University, Department of Materials Science and Engineering, Ithaca, NY.
- G9.43** ELECTRICAL AND MATERIAL CHARACTERIZATION OF THE STABILITY OF ALGaAs AND INGaAs PLANAR DOPED STRUCTURES, Larry P. Sadwick, University of Utah, Department of Electrical Engineering, Salt Lake City, UT; and Dwight C. Streit, TRW Electronic Systems Group, Redondo Beach, CA.
- G9.44** NON-LINEAR DIFFUSION IN HgCdTe/CdTe MULTILAYERS, Y. Kim, A. Ourmazd, R.D. Feldman and J.A. Rentschler, AT&T Bell Laboratories, Holmdel, NJ.
- G9.45** CHARACTERIZATION OF RAMAN SCATTERING SPECTRA IN AlGaP TERNARY ALLOYS, Devki N. Talwar, and T.D. Fang, Indiana University of Pennsylvania, Department of Physics, Indiana, PA; and M. Vandevyver, CEA-CEN de Saclay, Gif-sur-Yvette, France.
- G9.46** ELECTRONIC STRUCTURE OF Li-IMPURITIES IN ZnSe, Tamio Oguchi, Taizo Sasaki, National Research Institute for Metals, Tokyo, Japan; and Hiroshi Katayama-Yoshida, Tohoku University, Department of Physics, Sendai, Japan.
- G9.47** THE DEEP 0.11 eV MANGANESE ACCEPTOR LEVEL IN GaAs, M. Kleverman, University of Lund, Department of Solid State Physics, Lund, Sweden; E. Janzen, M. Linnarsson and B. Monemar, Linköping University, Department of Physics and Measurement Technology, Linköping, Sweden.
- G9.48** IDENTIFICATION OF SURFACE-RELATED ELECTRON TRAPS IN UNDOPED GaAs BY DEEP LEVEL TRANSIENT SPECTROSCOPY, K.C. Shin and I.S. Park, Goldstar Cable Research Laboratory, Semiconductor Department, Kyungki, Korea.

G9.49 PHOTOLUMINESCENCE STUDIES OF IMPURITIES AND DEFECTS IN MERCURIC IODIDE, X.J. Bao, T.E. Schlesinger, Carnegie Mellon University, Department of Electrical and Computer Engineering, Pittsburgh, PA; R.B. James, Sandia National Laboratories, Livermore, CA; A.Y. Cheng and C. Ortale, EG&G Energy Measurements, Goleta, CA.

G9.50 TRANSIENT CURRENT AND TRANSIENT CAPACITANCE MEASUREMENTS OF DEFECTS IN AlGaAs MODFETS, R. Magno and R. Shelby, Naval Research Laboratory, Washington, DC.

G9.51 ELECTRONIC AND OPTICAL PROPERTIES OF DEEP DONORS IN HYDROGENATED $\text{Al}_x\text{Ga}_{1-x}\text{As}$ DOPED WITH SILICON, R. Moustefaoui, R. Legros, J. Chevallier, LPSB, CNRS, Meudon, France; C.W. Tu and R.F. Kopt, AT&T Bell Laboratories, Murray Hill, NJ.

G9.52 LUMINESCENCE DUE TO Mn DOPPED GaP, Teresa Monteiro and Estela Pereira, Universidade de Aveiro, Departamento de Física, Aveiro, Portugal.

G9.53 ZEEMAN STUDY OF THE 1.040 eV PHOTOLUMINESCENCE BAND IN CU DOPED SILICON, K.G. McGuigan, M.O. Henry, School of Physical Sciences, National Institute for Higher Education, Dublin, Ireland; M.H. Nazaré, Universidade de Aveiro, Departamento de Física, Aveiro, Portugal; and E.C. Lightowers, King's College, Department of Physics, London, United Kingdom.

SESSION G10: DIFFUSION IN Si

Chair: J. Bernholc

Wednesday Morning, November 29

Salon F (M)

8:00 ***G10.1**
ATOMIC DIFFUSION AND DEFECT REACTIONS IN SILICON, Sokrates T. Pantelides, IBM T.J. Watson Research Center, Yorktown Heights, NY.

8:30 **G10.2**
PRESSURE AND STRAIN EFFECTS ON DIFFUSION, A. Antonelli and J. Bernholc, North Carolina State University, Department of Physics, Raleigh, NC.

8:45 **G10.3**
LOW-TEMPERATURE DIFFUSION OF DOPANTS IN SILICON, P. Fahey and M. Wittmer, IBM T.J. Watson Research Ctr., Yorktown Heights, NY.

9:00 **G10.4**
DETERMINATION OF THE FRACTIONAL INTERSTITIALCY COMPONENT OF DIFFUSION FOR ARSENIC, M. Heinrich, M. Budil, H.W. Pötzl, TU-Wien, Wien, Austria.

9:15 **G10.5**
MEASUREMENTS OF ENHANCED AND RETARDED DIFFUSION OF BURIED LAYERS IN SILICON MEMBRANE STRUCTURES DURING OXIDATION, Scott T. Dunham, Anuradha M. Agarwal, and Nanseng Jeng, Boston University, Electrical, Computer and Systems Engineering, Boston, MA.

9:30 **G10.6**
MIGRATIONS OF INTERSTITIAL ATOMS IN SEMICONDUCTORS, T. Wada, A. Takeda and M. Ichimura, Nagoya Institute of Technology, Department of Electrical and Computer Engineering, Nagoya, Japan; M. Takeda, Government Industrial Research Institute, Nagoya, Japan.

9:45 BREAK

SESSION G11: DIFFUSION IN Si

Chair: J. Bernholc

Wednesday Morning, November 29

Salon F (M)

10:15 **G11.1**
MEASUREMENTS OF ENHANCED OXYGEN DIFFUSION IN SILICON DURING THERMAL DONOR FORMATION: NEW EVIDENCE FOR POSSIBLE MECHANISMS, A.R. Brown, R. Murray, R.C. Newman and J.H. Tucker, Imperial College of Science, The Blackett Laboratory, Interdisciplinary Research Centre Semiconductor Materials, London, United Kingdom.

10:30 **G11.2**
A STEADY-STATE MODEL FOR COUPLED DEFECT-IMPURITY DIFFUSION IN SILICON, F.F. Morehead and R.F. Lever, IBM East Fishkill Facility, Hopewell Junction, NY.

10:45 **G11.3**
HIGH AND LOW TEMPERATURE MEASUREMENTS OF THE CHROMIUM DIFFUSIVITY IN SILICON, J. Zhu and D. Barbier, Institut National des Sciences Appliquées de Lyon, Laboratoire de Physique de la Matière, Villeurbanne, France.

11:00 **G11.4**
THE FORMATION OF SILICON-RICH SILICIDES, Maria Ronay, IBM T.J. Watson Research Center, Yorktown Heights, NY.

11:15 **G11.5**
PRECIPITATION OF COPPER AND COBALT AT GRAIN BOUNDARIES IN SILICON, U. Jendrich, H.J. Möller, Case Western Reserve University, Department of Materials Science and Engineering, Cleveland, OH; and T. Tütken, University of Göttingen, IV. Physical Institute, Göttingen, West Germany.

11:30 G11.6

ANNEALING OF ION IMPLANTED TIN IN SILICON: A RBS/CHANNELING, MOSSBAUER SPECTROSCOPY AND TEM INVESTIGATION OF SOLUBILITY AND RESIDUAL DEFECTS, P. Kringhøj, A. Nylandsted Larsen, and J.W. Petersen, University of Aarhus, Institute of Physics, Aarhus C, Denmark.

11:45 G11.7

EXTREME SUPERSATURATION OF OXYGEN IN LOW-TEMPERATURE EPITAXIAL SILICON AND SILICON-GERMANIUM ALLOYS, P.V. Schwartz, J.C. Sturm, and P.M. Garone, Princeton University, Department of Electrical Engineering, Princeton, NJ; S.A. Schwarz, Bellcore, Red Bank, NJ.

SESSION G12: DIFFUSION IN COMPOUNDS

Chair: L. C. Kimerling

Wednesday Afternoon, November 29
Salon F (M)

1:30 *G12.1

DIFFUSION IN INHOMOGENEOUS SYSTEMS, STUDIED AT NEAR-ATOMIC RESOLUTION, A. Ourmazd, J. Cunningham, Y. Kim and M. Bode, AT&T Bell Laboratories, Holmdel, NJ.

2:00 G12.2

GROWTH OF GaAs ON Ge SUBSTRATES BY ATOMIC LAYER EPITAXY, J. Ramdani, B.T. McDermott, N. El-Masry, and S.M. Bedair, North Carolina State University, Electrical and Computer Engineering Department, Raleigh, NC.

2:15 G12.3

EXTREMELY RAPID SN DIFFUSION IN GAAS AND (AL,Ga)AS, T.F. Kuech, M. Goorsky, F. Cardone, G. Scilla and R. Potemski, IBM T.J. Watson Research Center, Yorktown Heights, NY.

2:30 G12.4

DIFFUSION OF ION IMPLANTED MAGNESIUM AND BERYLLIUM IN GALLIUM ARSENIDE, Heyward G. Robinson, Michael D. Deal and David A. Stevenson, Stanford University, Department of Materials Science and Engineering, Stanford, CA.

2:45 G12.5

DEFECT FORMATION DURING Zn DIFFUSION INTO GaAs, M. Luysberg, W. Jäger, and K. Urban, KFA Jülich, Institut für Festkörperforschung, West Germany; M. Perret, N. Stolwijk, and H. Mehrer, Universität Münster, Institut für Metallforschung, Münster, W. Germany.

3:00 G12.6

ROOM-TEMPERATURE DIFFUSION OF Mn IN CdTe AND THE FORMATION OF $Cd_{1-x}Mn_xTe$, A. Wall, A. Raisanen, G. Haugstad and A. Franciosi, University of Minnesota, Department of Chemical Engineering and Material Science, Minneapolis, MN.

3:15 BREAK

SESSION G13: ORDERING IN ALLOYS

Chair: K. E. Newman

Wednesday Afternoon, November 29
Salon F (M)

3:45 *G13.1

ORDERING IN III/V ALLOYS, G.B. Stringfellow, University of Utah, College of Engineering, Salt Lake City, Utah.

4:15 G13.2

COMPARISON OF ORDERED AND MODULATED STRUCTURES IN InGaP ALLOY SEMICONDUCTORS GROWN BY MOCVD, CHLORIDE-VPE AND LPE METHODS, Q. Ueda, M. Hoshino, M. Takechi, and M. Ozeki, Fujitsu Laboratories Ltd., Atsugi, Japan; T. Kato and T. Matsumoto, Yamanashi University, Engineering Department, Kofu, Japan.

4:30 G13.3

ATOMIC ORDERING AND ALLOY CLUSTERING IN MBE-GROWN $InAs_ySb_{1-y}$ EPILAYERS, T.Y. Seong, A.G. Norman, G.R. Booker, University of Oxford, Department of Metallurgy and Science of Materials, Oxford, United Kingdom; R. Droopad, R.L. Williams, S.D. Parker, P.D. Wang and R.A. Stradling, Imperial College of Science, Technology and Medicine, Department of Physics, London, United Kingdom.

SESSION G14: SUPERLATTICES -
ELECTRONIC STRUCTURE

Chair: K. K. Bajaj

Thursday Morning, November 30
Salon F (M)

8:00 *G14.1

LIGHT- AND HEAVY-HOLE BOUND EXCITON TRANSITIONS AND FREE TO BOUND TRANSITIONS IN $Ga_xAl_{1-x}As/GaAs$ QUANTUM WELLS, Donald C. Reynolds, Wright Research and Development Center, Electronic Technology Laboratory, Wright-Patterson AFB, OH; and Krishan K. Bajaj, Arizona State University, Tempe, AZ.

8:30 G14.2

DECAY MEASUREMENTS ON FREE AND BOUND EXCITON RECOMBINATION IN DOPED GaAs/AlGaAs QUANTUM WELLS, P. Bergman, P.O. Holtz, B. Monemar, Linköping University, Department of Physics and Measurement Technology, Linköping, Sweden; M. Sundaram, J.L. Merz and A.C. Gossard, University of California at Santa Barbara, Department of Electrical and Computer Engineering, Santa Barbara, CA.

8:45 G14.3

EFFECTS OF CONFINEMENT ON THE OPTICAL PROPERTIES OF A SHALLOW ACCEPTOR AND ITS BOUND EXCITON IN GaAs/AlGaAs QUANTUM WELLS, P.O. Holtz, Linköping University, Department of Physics and Measurement Technology, Linköping, Sweden and University of California, Santa Barbara, Department of Electrical and Computer Engineering, Santa Barbara, CA; M. Sundaram, J.L. Merz and A. C. Gossard, University of California, Santa Barbara, Department of Electrical and Computer Engineering, Santa Barbara, CA.

9:00 G14.4

OPTICAL SPECTROSCOPY OF 2D ELECTRONS CONFINED AT A GaAs/AlGaAs HETEROINTERFACE IN A TRANSVERSE ELECTRIC FIELD, Q.X. Zhao, P. Bergman, B. Monemar, Linköping University, Physics and Measurement Technology, Linköping, Sweden; P.-O. Holtz, Linköping University, Physics & Measurement Technology, Linköping, Sweden and University of California, Santa Barbara, Electrical & Computer Engineering, Santa Barbara, CA; C. Hallin, Linköping University, Physics & Measurement Technology, Linköping, Sweden; M. Sundaram, J.L. Merz and A.C. Gossard, University of California, Santa Barbara, Electrical & Computer Engineering, Santa Barbara, CA.

9:15 G14.5

DEFECT INDUCED LUMINESCENCE FROM MBE PREPARED Si/Si_{1-x}Ge_x SUPERLATTICES, G.A. Northrop, S.S. Iyer, and D.J. Wolford, IBM T.J. Watson Research Center, Yorktown Heights, NY.

9:30 *G14.6

SHALLOW-DEEP TRANSITIONS AND DEEP LEVELS IN SUPERLATTICES, John D. Dow, S.Y. Ren, J. Shen, R.-D. Hong, D.A. Drabold, O.F. Sankey, M.-H. Tsai, S. Klemm and P.A. Fedders, University of Notre Dame, Department of Physics, Notre Dame, IN.

10:00 BREAK

SESSION G15: DX CENTERS I

Chair: H. P. Hjalmarson
Thursday Morning, November 30
Salon F (M)

10:30 *G15.1

THE DX CENTER: EVIDENCE FOR CHARGE CAPTURE VIA AN EXCITED INTERMEDIATE STATE, T. N. Theis and Patricia M. Mooney, IBM T.J. Watson Research Ctr., Yorktown Heights, NY.

11:00 G15.2

EFFECT OF LOCAL ATOMIC CONFIGURATION ON DX ENERGY LEVEL, T. Baba and M. Mizuta, NEC Corporation, Fundamental Research Laboratories, Ibaraki, Japan; T. Fujisawa, J. Yoshino and H. Kukimoto, Tokyo Institute of Technology, Yokohama, Japan.

11:15 G15.3

ELECTRIC FIELD ENHANCEMENT OF THE EMISSION RATE OF DX CENTERS, Mimoun Zazoui, Song L. Feng, Jacques C. Bourgoin, and Hans J. Von Bardeleben, Université Paris VII, Centre National de la Recherche Scientifique, Groupe de Physique des Solides de l'Ecole Normale Supérieure, Paris, France.

11:30 G15.4

OPTICALLY DETECTED MAGNETIC RESONANCE OF GROUP IV AND GROUP VI DONORS IN Al_xGa_{1-x}As/GaAs (x≥0.35) HETEROSTRUCTURES, E. Glaser, T.A. Kennedy and B. Molnar, Naval Research Laboratory, Washington, DC.

11:45 G15.5

OPTICAL PROPERTIES OF EXTREMELY HEAVILY DOPED n-GaAs, Huade Yao, University of Nebraska, Center for Microelectronic and Optical Materials Research, Lincoln, NE; and Alvin Compaan, University of Toledo, Department of Physics and Astronomy, Toledo, OH.

SESSION G16: DX CENTERS II

Chair: P. M. Mooney
Thursday Afternoon, November 30
Salon F (M)

1:30 *G16.1

THEORY OF EL2 AND DX CENTERS, D.J. Chadi, Xerox, Palo Alto Research Center, Palo Alto, CA.

2:00 G16.2

IS DX(Te) CENTER IN Al_xGa_{1-x}As A NEGATIVE-U DEFECT? L. Dobaczewski, J.E. Dmochowski, P. Kaczor, J. Wróbel and J.M. Langer, Polish Academy of Sciences, Institute of Physics, Warsaw, Poland.

2:15 G16.3

PHOTOIONIZATION AND PHOTOCAPTURE TESTS OF DX-CENTER MODELS, Harold P. Hjalmarson, S.R. Kurtz and T.M. Brennan, Sandia National Laboratories, Albuquerque, NM.

2:30 G16.4

MOSSBAUER STUDY OF THE DEFECT STRUCTURES AROUND Te IMPLANTED IN Al_xGa_{1-x}As, H. Bemelmans and G. Langouche, IKS, University of Leuven, Leuven, Belgium; and G. Borghs, IMEC, Leuven, Belgium.

2:45 G16.5

THE METASTABILITY OF THE EL2 DEFECT IN GaAs 3-5 ALLOYS, Hans J. Von Bardeleben and Jacques C. Bourgoin, Université Paris VII, Centre National de la Recherche Scientifique, Groupe de Physique des Solides de l'Ecole Normale Supérieure, Paris, France.

3:00 BREAK

SESSION G17: EL2 DEFECTS

Chair: D. J. Chadi

Thursday Afternoon, November 30

Salon F (M)

3:30 *G17.1

PROGRESS IN UNDERSTANDING THE OPTICAL PROPERTIES OF EL2, G.A. Baraff, AT&T Bell Laboratories, Murray Hill, NJ.

4:00 G17.2

DIRECT OPTICAL DETERMINATION OF THE CROSS-SECTION FOR LIGHT INDUCED METASTABLE TRANSITION OF THE EL2 DEFECT, W. Kuszko, M. Jezewski, J.M. Baranowski; Warsaw University, Institute of Experimental Physics, Warsaw, Poland.

4:15 G17.3

THE DOUBLE DONOR ISSUE OF THE EL2 DEFECT IN GaAs, M.O. Manasreh and Gail J. Brown, U.S. Air Force, WRDC/MLPO, Wright-Patterson AFB, OH.

4:30 G17.4

ABSOLUTE PRESSURE DEPENDENCE OF THE SECOND IONIZATION LEVEL OF EL2 IN GaAs, D.E. Bliss, W. Walukiewicz, D.D. Nolte and E.E. Haller, University of California, Berkeley, Department of Materials Science and Mineral Engineering, and the Center for Advanced Materials, Lawrence Berkeley Laboratory, Berkeley, CA.

4:45 *G17.5

THE SYMMETRY OF THE EL2 DEFECT IN GaAs, P. Trautman and J.M. Baranowski, Warsaw University, Institute of Experimental Physics, Warsaw, Poland.

SESSION G18: GROUP IV SEMICONDUCTORS
AND HYDROGEN - POSTER SESSION

Chair: J. Bernholc

Thursday Evening, November 30

7:00 p.m. - 10:00 p.m.

America Ballroom (W)

G18.1 AN ANOMALOUS VACANCY DIFFUSION IN SILICON DURING THE ANTIMONY DRIVE-IN DIFFUSION, W. Wijaranakula and J.H. Matlock, SEH America, Inc., Materials Characterization Laboratory, Vancouver, WA.

G18.2 A COMPARISON OF THE DIFFUSIVITY OF AS AND GE IN SI AT HIGH DONOR CONCENTRATIONS, K. Kylliesbech Larsen, P. Gaiduk, and A. Nylandsted Larsen, University of Aarhus, Institute of Physics, Aarhus C, Denmark.

G18.3 ANOMALOUS TRANSIENT TAIL DIFFUSION OF BORON IN SILICON: CONCENTRATION DEPENDENCE VERSUS SPATIAL DEPENDENCE, N.E.B. Cowern, Nederlandse Philips Bedrijven, Corp. OSA CAD Centre, CFT Automation Eindhoven, The Netherlands; H.F.F. Jos, Philips Components, Nijmegen, The Netherlands; and K.T.F. Janssen, Philips Research Laboratories, Eindhoven, The Netherlands.

G18.4 RAPID THERMAL PROCESS-INDUCED DEFECTS: GETTERING OF THE INTERNAL AND EXTERNAL CONTAMINANTS, B. Hartiti, W. Eichhammer, J.C. Muller, and P. Siffert, CNRS, Laboratoire PHASE, Strasbourg, France.

G18.5 OXYGEN AND IRON REDISTRIBUTION UPON THERMAL TREATMENT IN IRON IMPLANTED SILICON, B. Pivac, A. Borghesi, Università di Pavia, Dipartimento di Fisica, Pavia, Italy; L. Ottolini, CNR, Centro di Studio per la Cristallografia Strutturale del CNR, Pavia, Italy; M. Geddo, A. Piaggi and A. Stella, Università di Pavia, Dipartimento di Fisica, Pavia, Italy.

G18.6 ION BEAM ETCHING OF SILICON: IMPLANTATION AND DIFFUSION OF NOBLE GAS ATOMS, AND GETTERING OF COPPER, William D. Sawyer and Jörg Weber, Max-Planck-Institut für Festkörperforschung, Stuttgart, West Germany.

G18.7 BEHAVIOR OF POINT DEFECTS IN FZ AND CZ Si CRYSTALS, Takao Abe, Shin-Etsu Handotai, R&D Center, Isobe, Japan.

G18.8 AN IMPROVED MODEL FOR COMPUTER SIMULATION OF OXYGEN PRECIPITATION PHENOMENA, M. Schrems, P. Pongratz, H.W. Pötzl, TU-Vienna, Vienna, Austria; E. Guerrero, D. Huber, Wacker, Chemitronic/AT, Burghausen, West Germany.

G18.9 FAILURE OF THE "KICK-OUT" MODEL FOR THE DIFFUSION OF Au INTO Si WHEN TESTED BY MONTE CARLO SIMULATION, Uwe Schmid, Max-Planck-Institut für Festkörperforschung, Stuttgart, West Germany; and James A. Van Vechten, Oregon State University, Department of Electrical and Computer Engineering, Corvallis, OR.

G18.10 DIFFUSION OF POINT DEFECTS IN A STRESSED SIMPLE CUBIC LATTICE, Dimitris Maroudas and Robert A. Brown, Massachusetts Institute of Technology, Department of Chemical Engineering, Cambridge, MA.

G18.11 COMPUTER CALCULATION OF DIFFUSIVITY, EFFECTIVE ACTIVATION ENERGY AND OF ACTIVATION ENERGY DIMINUTION FROM MEASURED PROFILE OF IMPURITY DISTRIBUTIONS IN SILICON, D.K. An, Microelectronics Company, Budapest, Hungary.

G18.12 DEFECTS IN DOPED SILICON EPILAYERS STUDIED WITH VARIABLE-ENERGY POSITRONS AND MeV IONS, P.J. Simpson, P.J. Schultz, R.W. Hunt, I.V. Mitchell, University of Western Ontario, Ontario, Canada; T.E. Jackman, and G.C. Aers. National Research Council of Canada, Ontario, Canada.

G18.13 ANGLE RESOLVED XPS ANALYSIS OF SURFACE DEFECTS IN HIGH-DOSE Sb^+ IMPLANTED MONOCRYSTALLINE SILICON, S.N. Kumar, G. Chaussemy, A. Laugier, I.N.S.A. Lyon, Laboratoire de Physique de la Matière, Villeurbanne, France; M. Charbonnier, CNRS, Université Lyon I, Département de Chimie Appliquée et Génie Chimique, Villeurbanne, France; B. Canut, Université Claude Bernard - Lyon I, Département de Physique des Matériaux, Villeurbanne, France.

G18.14 MODIFIED OPTICALLY DETECTED MAGNETIC RESONANCE TECHNIQUE FOR STUDIES OF DEFECTS IN Si AND GaAs, W.M. Chen and B. Monemar, Linköping University, Department of Physics and Measurement Technology, Linköping, Sweden.

G18.15 OPTICAL PROPERTIES OF NOVEL VIBRONIC BANDS IN ELECTRON-IRRADIATED TIN DOPED SILICON, J.H. Svensson, B. Monemar, Linköping University, Department of Physics and Measurement Technology, Linköping, Sweden; B.G. Svensson, The Royal Institute of Technology, Department of Solid State Electronics, Kista, Sweden.

G18.16 A NEW METASTABLE DEFECT IN SILICON, AN OPTICAL STUDY AND AN INVESTIGATION OF THE MECHANISM CAUSING THE CONFIGURATIONAL CHANGE, J.H. Svensson and B. Monemar, Linköping University, Department of Physics and Measurement Technology, Linköping, Sweden.

G18.17 NOVEL LUMINESCENCE BAND IN SILICON IMPLANTED WITH PHOSPHORUS AND BORON, A.K. Srivastava, D.K. Sharma, and K.L. Narasimhan, Tata Institute of Fundamental Research, Bombay, India; D. Sarkar and V. Premchandran, Indian Telephone Industries, Bangalore, India.

G18.18 UNIAXIAL STRESS AND ZEEMAN MEASUREMENTS ON THE 0.943eV LUMINESCENCE BAND IN SILICON, M.C. do Carmo, Universidade de Aveiro, Departamento de Física, Aveiro, Portugal; K.G. McGuigan, M.O. Henry, Dublin City University, School of Physical Sciences, Dublin, Ireland; G. Davies and E.C. Lightowers, Kings College, Department of Physics, London, United Kingdom.

G18.19 STRAIN INDUCED INTRINSIC QUANTUM WELLS AS THE ORIGIN OF BROAD BAND PHOTOLUMINESCENCE IN SILICON CONTAINING EXTENDED DEFECTS, Helge Weman and Bo Monemar, Linköping University, Department of Physics and Measurement Technology, Linköping, Sweden.

G18.20 A HVEM STUDY OF THE ELECTRON IRRADIATED DEFECTS IN NITROGEN DOPED FZ-Si, Gao Yuzun, General Research Institute for Non-Ferrous Metals, Beijing, China; and T. Takeyama, Hokkaido University, HVEM Lab, Sapporo, Japan.

G18.21 IDENTIFICATION OF RADIATION-INDUCED DEFECTS IN Si:Al, Ya.I. Latushko, V.V. Petrov, Lenin Byelorussian State University, Laboratory Spectroscopy of Semiconductors, Minsk, USSR.

G18.22 DEFECT-FORMATION DEPENDENCE ON GROUP V-DOPANT ATOMS IN ELECTRON-IRRADIATED SILICON, O.O. Awadelkarim, A. Henry, B. Monemar, Linköping University, Department of Physics and Measurement Technology, Linköping, Sweden; and J.L. Lindström, Swedish Defence Research Establishment, Linköping, Sweden.

G18.23 ELECTRONIC STRUCTURE OF VACANCY-PHOSPHORUS IMPURITY COMPLEXES IN SILICON, Hongqi Xu, University of Lund, Department of Theoretical Physics, Lund, Sweden; and U. Lindefelt, ABB Corporate Research, Västerås, Sweden.

G18.24 A SIMPLE MODEL FOR DEFECT STRUCTURES IN SILICON, G.J. Ackland and V. Vitek, University of Pennsylvania, Department of Materials Science and Engineering, Philadelphia, PA.

G18.25 NEW DLTS PEAKS ASSOCIATED WITH NEW DONORS AND ROD-LIKE DEFECTS IN CZOCHRALSKI SILICON, Yoichi Kamiura, Fumio Hashimoto and Minoru Yoneta, Okayama University, Faculty of Engineering, Okayama, Japan.

G18.26 MULTICONFIGURATIONAL CARBON-GROUP V PAIR DEFECTS IN SILICON, E. Güre and B.W. Benson, Lehigh University, Physics Department, Bethlehem, PA.

G18.27 THE ROLE OF FOUR-MEMBER RING DEFECT STRUCTURES CONTAINING CARBON, NITROGEN, AND OXYGEN IN CRYSTALLINE SILICON, Lawrence C. Snyder, Rongzhi Wu, and Peter Deak, State University of New York at Albany, Chemistry Department, Albany, NY; and James W. Corbett, State University of New York at Albany, Albany, NY.

G18.28 MOLECULAR DYNAMICS STUDIES OF DISLOCATION CORES IN SI, M.S. Duesbery, D.J. Michel, Naval Research Laboratory, Washington, DC; and B. Joos, Ottawa-Carleton Institute for Physics, Ottawa, Canada.

G18.29 HYDROGEN INDUCED DEFECTS AT SILICON EPITAXIAL SURFACES AND BURIED MISFIT DISLOCATIONS, Tian-Qun Zhou, Zbigniew J. Radzinski, Zhigang Xiao, George A. Rozgonyi, North Carolina State University, Department of Materials Science and Engineering, Raleigh, NC.

G18.30 TEM INVESTIGATION OF SECONDARY DISLOCATIONS IN GRAIN BOUNDARIES IN GERMANIUM, M. Griess, M. Seibt, University of Göttingen, IV. Physikalisches Institut, Göttingen, West Germany; H.J. Möller, Case Western Reserve University, Department of Materials Science and Engineering, Cleveland, OH.

G18.31 AC PHOTOVOLTAIC INSPECTION OF P-N JUNCTIONS HAVING HIGH LEAKAGE CURRENT, N. Honma, H. Shimizu, C. Munakata, Hitachi, Ltd., Central Research Laboratory, Tokyo, Japan; and M. Ogasawara, Hitachi, Ltd., Device Development Center, Tokyo, Japan.

G18.32 RIBBON-LIKE DEFECTS IN HIGH-DOSE OXYGEN IMPLANTED SILICON-ON-INSULATOR MATERIAL, S. Visitserngtraku, AZ State University, Department of Chemical, Bio and Materials Engineering, Tempe, AZ; J. Barry, University of Queensland, Electron Microscope Centre, Brisbane, Australia and AZ State University, Ctr. for Solid State Science, Tempe, AZ; S. Krause, AZ State University, Department of Chemical, Bio and Materials Engineering, Tempe, AZ.

G18.33 THE ENHANCEMENT OF THE INTERDIFFUSION IN Si/Ge AMORPHOUS MULTILAYERS BY ADDITIONS OF Au AND B, B. Park and F. Spaepen, Harvard University, Division of Applied Sciences, Cambridge, MA; J.M. Poate and D.C. Jacobson, AT&T Bell Laboratories, Murray Hill, NJ.

G18.34 STRUCTURAL TRANSITIONS IN TITANIUM/AMORPHOUS-SILICON MULTILAYER THIN FILMS, L.A. Clevenger, E. Ma and C.V. Thompson, MA Institute of Technology, Department of Materials Science and Engineering, Cambridge, MA; R.R. deAvillez, Pontificia Universidade Catolica, Departamento de Ciencia dos Materiais e Metalurgia, Rio de Janeiro, Brazil; and K.N. Tu, IBM T.J. Watson Research Ctr., Yorktown Heights, NY.

G18.35 INTERFACIAL REACTION BETWEEN Ni/Ge BILAYER AND SILICON (100) SUBSTRATE, Jian Li, Q.Z. Hong, and J.W. Mayer, Cornell University, Department of Materials Science and Engineering, Ithaca, NY.

G18.36 POSITRON ANNIHILATION IN DIAMONDS, U. Karfunkel, M.C. Stemmet, S.H. Connell, J.P.F. Sellschop, University of the Witwatersrand, Schonland Research Centre, Johannesburg, South Africa; and M. Moussavi-Madani, University of Bophuthatswana, Department of Physics, Bophuthatswana, South Africa.

G18.37 STRUCTURAL AND ELECTRONIC PROPERTIES OF SUBSTITUTIONAL DEFECTS IN DIAMOND, Koblar A. Jackson, Mark R. Pederson, Naval Research Laboratory, Complex Systems Theory Branch, Washington, DC; and Joseph G. Harrison, University of Alabama-Birmingham, Birmingham, AL.

G18.38 SURFACE AND BULK PROPERTIES WHICH INFLUENCE ION-BEAM HYDROGENATION OF SILICON, Robert A. Anderson and Carleton H. Seager, Sandia National Laboratories, Albuquerque, NM.

G18.39 ELECTRONIC AND VIBRATIONAL PROPERTIES OF GROUP V DONOR-HYDROGEN COMPLEXES IN CRYSTALLINE SILICON, L.V.C. Assali, E.C.F. da Silva, and J.R. Leite, Universidade de São Paulo, Instituto de Física, São Paulo, Brazil.

G18.40 EXTREME SUPERSATURATION OF OXYGEN IN LOW-TEMPERATURE EPITAXIAL SILICON AND SILICON-GERMANIUM ALLOYS, P.V. Schwartz, J.C. Sturm and P.M. Garone, Princeton University, Department of Electrical Engineering, Princeton, NJ; S.A. Schwarz, Bellcore, Red Bank, NJ.

G18.41 SURFACE PROTECTION DURING PLASMA HYDROGENATION FOR ACCEPTOR PASSIVATION IN InP, J. Lopata, W.C. Dautremont-Smith, S.J. Pearton, J.W. Lee, N.T. Ha, and H.S. Luftman, AT&T Bell Laboratories, Murray Hill, NJ.

G18.42 INTERDIFFUSION MEASUREMENTS IN Si-Ge/Si STRAINED LAYER SUPERLATTICES, S.M. Prokes, M. Fatemi, U.S. Naval Research Laboratory, Washington, DC; and K. Wang, University of California, Los Angeles, Department of Electrical Engineering, Los Angeles, CA.

G18.43 ELECTRONIC STRUCTURE OF AN ISO-ELECTRONIC CENTER IN SULPHUR-DOPED SILICON STUDIED BY OPTICAL DETECTION OF MAGNETIC RESONANCE, W.M. Chen, A. Henry, B. Monemar, Linköping University, Department of Physics and Measurement Technology, Linköping, Sweden; and M.L.W. Thewalt, Simon Fraser University, Department of Physics, Burnaby, Canada.

G18.44 AN ELECTRON PARAMAGNETIC RESONANCE INVESTIGATION OF IRON-INDIUM PAIRS IN SILICON, W. Gehlhoff, Academy of Sciences of GDR., Centre for Scientific Instruments, Berlin, East Germany; P. Emanuelsson, P. Omling and H.G. Grimmeiss, University of Lund, Department of Solid State Physics, Lund, Sweden.

G18.45 THE VERY EARLY STAGES OF INITIAL OXIDATION OF SILICON (111) IN ATOMIC OXYGEN, Bhola N. De, Jane E. Peterkin, Jane Hruska, Yong Zhao, N.J. Ianno, and John A. Woollam, University of Nebraska, Center for Microelectronics and Optical Materials Research and Department of Electrical Engineering, Lincoln, NE.

G18.46 HYDROGEN PASSIVATION STUDIES IN DISLOCATED CZ AND FZ SILICON, C. Dubé, J.P. Kalejs, and S. Rajendran, Mobil Solar Energy Corporation, Billerica, MA.

G18.47 ENHANCEMENT OF OXYGEN PRECIPITATION IN QUENCHED CZOCHRALSKI SILICON CRYSTALS, A. Hara, T. Fukuda, I. Harai, and A. Ohsawa, Fujitsu Laboratories Ltd., Kawasaki, Japan.

G18.48 DIVACANCY TRANSFORMATIONS IN ELECTRO-IRRADIATED SILICON, J.H. Robison and A.E. Jaworowski, Wright State University, Physics Department, Dayton, OH.

G18.49 DETERMINATION OF 3-DIMENSIONAL DEFECT STRUCTURES IN GALLIUM ARSENIDE EPI-LAYERS ON SILICON USING WHITE BEAM SYNCHROTRON RADIATION TOPOGRAPHY IN BOTH TRANSMISSION GEOMETRY AND GRAZING BRAGG LAUE GEOMETRY, M. Dudley, J. Wu and G.-D. Yao, State University of New York at Stony Brook, Department of Materials Science and Engineering, Stony Brook, NY; H.-Y. Liu and Y.C. Kao, Texas Instruments, Materials Science Laboratory, Dallas, TX.

G18.50 DIFFUSION OF Au IN AMORPHOUS Si MEASURED BY THE COMPOSITION MODULATION TECHNIQUE, E. Nygren, Ohio State University, Department of Materials of Science and Engineering, Columbus, OH; B. Park and F. Spaepen, Harvard University, Division of Applied Sciences, Cambridge, MA.

G18.51 HYDROGEN DIFFUSION AND COMPLEX FORMATION IN SILICON, J.T. Borenstein, Mobil Solar Energy Corporation, Billerica, MA; D. Tulchinski and J.W. Corbett, State University of New York at Albany, Physics Department, Albany, NY.

SESSION G19: DOPING IN III-V's

Chair: R. C. Newman
Friday Morning, December 1
Salon F (M)

8:30 ***G19.1**
ELECTRON SCATTERING BY NATIVE DEFECTS IN UNIFORMLY- AND MODULATION-DOPED SEMICONDUCTOR STRUCTURES, W. Walukiewicz, Lawrence Berkeley Laboratory, Center for Advanced Materials, Materials and Chemical Sciences Division, Berkeley, CA.

9:00 **G19.2**
ACCEPTOR DELTA-DOPING IN GaAs, W.S. Hobson, S.J. Pearton, and C.R. Abernathy, AT&T Bell Laboratories, Murray Hill, NJ; and G. Cabaniss, Solecon Laboratories, San Jose, CA.

9:15 **G19.3**
PRECIPITATION PHENOMENA ASSOCIATED WITH ULTRA-HIGH Be DOPING OF $\text{Ga}_{0.47}\text{In}_{0.53}\text{As}$ BY MBE, C.M. Cotell, M.B. Panish, R. A. Hamm, L.C. Hopkins and J.M. Gibson, AT&T Bell Laboratories, Murray Hill, NJ.

9:30 **G19.4**
CHARACTERISTICS OF DOPING AND DIFFUSION OF HEAVILY DOPED N AND P TYPE InP AND InGaAs EPITAXIAL LAYERS GROWN BY METALORGANIC CHEMICAL VAPOR DEPOSITION, C.J. Pinzone, N.D. Gerrard, R.D. Dupuis, N.T. Ha and H.S. Luftman, AT&T Bell Laboratories, Materials Science Research Department, Murray Hill, NJ.

9:45 **G19.5**
EFFECTS OF Si INCORPORATION AND ELECTRICAL ACTIVATION ON INTERSUBBAND OPTICAL ABSORPTION IN GaAs/AlGaAs MULTIPLE QUANTUM WELLS, J.D. Ralston, H. Ennen, M. Maier, M. Ramsteiner, B. Dischler, and P. Koidl, Fraunhofer-Institut für Angewandte Festkörperphysik, Freiburg, West Germany.

10:00 BREAK

SESSION G20: SUPERLATTICES - DIFFUSION

Chair: J. A. Van Vechten
Friday Morning, December 1
Salon F (M)

10:30 ***G20.1**
IMPURITY-INDUCED LAYER DISORDERING: CURRENT UNDERSTANDING AND AREAS FOR FUTURE INVESTIGATION, L.J. Guido and N. Holonyak, Jr., University of Illinois, Department of Electrical Engineering, Urbana, IL.

11:00 **G20.2**

BEHAVIOR OF DOPANT-RELATED DEFECTS IN AlGaAs SUPERLATTICES, N.D. Theodore, Cornell University, Department of Materials Science and Engineering, Ithaca, NY; P. Mei, Columbia University, Department of Electrical Engineering, New York, NY; C.B. Carter, Cornell University Department of Materials Science and Engineering, Ithaca, NY; C. Palmstrom, S.A. Schwarz, J.P. Harbison, L.T. Florez, Bell Communications Research Inc., Redbank, NJ.

11:15 **G20.3**

INTERDIFFUSION BEHAVIOR OF SYMMETRICALLY STRAINED $\text{Ge}_{\text{m}}\text{Si}_{\text{m}}$ SUPERLATTICES, P.M. Adams, R.C. Bowman Jr., The Aerospace Corporation, Los Angeles, CA; S.J. Chang, V. Arbet and K.L. Wang, University of California, Los Angeles, Department of Electrical Engineering, Los Angeles, CA.

11:30 ***G20.4**

DIFFUSION MECHANISMS IN GaAs AND GaAs-BASED LAYERED STRUCTURES, U. Gösele, Duke University, School of Engineering, Durham, NC; and T.Y. Tan, Duke University, School of Engineering, Durham, NC, and Microelectronics Center of North Carolina, Research Triangle Park, NC.

G1.1

HIGH RESOLUTION SPECTROSCOPY OF POINT DEFECTS IN SEMICONDUCTORS. H. G. Grimmeiss, M. Kleverman and J. Olajos, Department of Solid State Physics, University of Lund, Box 118, S-221 00 LUND, Sweden.

For a better understanding of the behavior of defects and impurities in semiconductors a variety of measuring techniques have been developed for characterizing and identifying their electronic properties. In general, a comprehensive characterization and identification of shallow and deep centers is only possible if several different measurement techniques are applied.

In this paper we illustrate and discuss briefly recent developments in high resolution spectroscopy of point defects with particular emphasis on photothermal ionization spectroscopy (PTIS). PTIS and absorption possess many common features, but nevertheless have interesting differences. Both techniques give very detailed information on the energy structures of defects. For purposes of chemical identification and correlation we also present results which have been obtained from other experimental methods such as EPR, photo-EPR and junction space charge techniques. All centers discussed in this paper show a manifold of sharp lines in PTIS and absorption which allow a detailed analysis not only of the energy structure, but also of the symmetry and charge state. Both interstitial and substitutional as well as pairs of defects have been studied. Impurities from different groups of the Periodic Table and in particular of different transition metals in silicon are used as examples in order to illustrate the importance of combining different measurement techniques for a comprehensive identification and characterization of point defects.

G1.2

INFRARED ABSORPTION STUDY OF ZINC-DOPED SILICON. E. Merk, J. Heyman, and E.E. Haller, Center for Advanced Materials, Materials and Chemical Sciences Division, Lawrence Berkeley Laboratory, and University of California, Berkeley, CA 94720

We report high resolution infrared absorption spectra associated with the deep Zinc acceptor in silicon. The optical transitions between ground and excited "p-like" states of the neutral helium-like double acceptor Zn^0 center have been observed for the first time. The absorption cross section for the hole transition is found to be very small, of the order of 10^{-17} cm^2 . Energy spacings of the $P_{3/2}$ Rydberg series are very similar to the spacings of the group-III acceptors, suggesting, that, in spite of the large ground state binding energy, effective-mass approximation still applies to the excited states. This represents one more case where the strong central cell potential does not disturb the neutral helium-like excited states. Similar observations have been made for the less deep neutral double acceptor Be, and for the chalcogen donors S, Se, and Te.

The optical ionization energy of $Zn^{0/-}$ has been determined to be 2575 cm^{-1} (0.319 eV).

In addition two other sets of absorption lines related to zinc have been observed at 2130 cm^{-1} and 2750 cm^{-1} and their origin will be discussed.

* supported by National Swiss Foundation for the Research.

G1.3

INFRARED STUDIES OF THE DOUBLE ACCEPTOR ZINK IN SILICON. A. Dörnen, R. Kienle, K. Thonke (4. Phys. Inst. Univ. Stuttgart, D-7000 Stuttgart, FRG), P. Stolz, G. Pensl (Inst. für Angewandte Physik, Univ. Erlangen, D-8520 Erlangen, FRG), D. Grünebaum, N.D.

Stolwijk (Inst. für Metallforschung, Univ. Münster, D-4400 Münster, FRG)

The neutral charge state of the double acceptor zink in silicon is investigated by infrared absorption and photoconductivity measurements. In both types of experiments the photoionization of the Zn^0 center is observed. The spectral line shape and the numerical value of the optical cross section agrees with the previously reported photo capacitance data.

In infrared absorption and photoconductivity measurements bound-to-bound transitions of the Zn^0 center are observed. The excited states are described by effective mass theory, as in the case of hydrogen-like shallow single acceptors. The observation of Fano resonances of the O^+ phonon (64.3 meV) underlines the effective-mass-like character of the wave functions. The ionization energy of the Zn^0 acceptor state is found to be $319.1 \pm 0.2 \text{ meV}$.

Similar to the double acceptor zink in germanium a splitting of ground state due to the hole-hole-interaction is observed.

G1.4

PRESSURE DEPENDENCE OF A DEEP EXCITONIC LEVEL IN SILICON.* G.A. Northrop and D.J. Wolford, IBM Thomas J. Watson Research Center, Yorktown Heights, NY 10598.

Certain optically active defects in silicon provide a unique opportunity to observe, in detail, the effect of hydrostatic pressure on a deep level. These defects are weakly coupled to the lattice and produce strong luminescence signals, with intense no-phonon transitions precisely marking the excitonic level. Here we present a photoluminescence (5 - 100K) study of one such defect - the I_1 radiation-damage center - under high hydrostatic pressures (1-50 kbar). Surprisingly, the luminescence intensity of I_1 drops by 3 orders of magnitude over that range, becoming undetectable well-before level crossing with continuum states, while the free exciton remains largely unchanged. We find an initial pressure coefficient of $\sim 0.47 \text{ meV/kbar}$, a result deviating considerably from the -1.66 meV/kbar we derive from the free exciton for the indirect X bandgap, and thus indicating the presence of multi-band contributions characteristic of deep levels. Above $\sim 20 \text{ kbar}$ the I_1 slope decreases to $\sim 0.25 \text{ meV/kbar}$, which is suggestive of a crossing between radiative and nonradiative levels of the defect. However, the PL temperature dependence and phonon-sideband structure show no change with pressure that would be consistent with such a crossing. Likewise, no decrease in thermal binding energy with increasing pressure is observed. Luminescence lifetime, for which preliminary results will be presented, is the most sensitive test of any change in the internal efficiencies of recombination at this defect. Other mechanisms for the drop in I_1 intensity, such as reduced capture efficiency, will also be discussed.

*Supported in part by the U.S. Office of Naval Research under contract N00014-85-C-0868.

G1.5

NEW ODMR OBSERVATIONS IN Zn-DOPED LEC InP AND Cr- AND Te-DOPED GaAs. J. M. Trombetta* and T. A. Kennedy, Naval Research Laboratory, Washington, DC, 20375.

While deep recombination centers in InP and GaAs have been studied extensively with Optically Detected Magnetic Resonance (ODMR), the participation of shallow centers has received limited attention. In this work, we report an ODMR feature on the donor-acceptor pair (DAP) emission at 1.37 eV in Zn-doped LEC-grown InP, having a g-value of 1.21 ± 0.01 , near the predicted conduction electron value ($g=1.20$). Previously observed as a sharp line¹, it is accompanied in our measurements by an underlying broader peak which varies in intensity and width with microwave modulation frequency and optical excitation intensity. This broader feature is interpreted as the unresolved electron-hole exchange-split resonances of electrons bound to residual shallow donors, having a range of separations from the acceptors. A new photoluminescence-increasing detection of this resonance observed at

higher modulation frequencies (e.g. 40 kHz) is tentatively assigned to the spin dependence of the DAP emission itself while a decreasing signal observed only at lower frequencies demonstrates the existence of an additional competing recombination process. An observation of a new broad resonance in a Te- and Cr- doped LEC GaAs sample near the predicted conduction electron g-value of 0.4 will also be discussed.

This work sponsored in part by the Office of Naval Research
* NRC-NRL Resident Research Associate

1. L. H. Robins, P. C. Taylor, and T. A. Kennedy, Phys. Rev. B **38**, 13227 (1988)

G2.1

COMPLEX DEFECTS IN SEMICONDUCTORS.

B. Monemar, Dept. of Physics and Measurement Technology, Linköping University, S-581 83 Linköping, SWEDEN.

Recent advances in the understanding of electronic structure of complex defects in semiconductors are reviewed, in connection with new optical data for such defects both in III-V compounds and silicon. In GaP neutral complexes related to As_G antisites and Ga_i interstitials have been investigated, and general trends for their properties may be observed. Dynamical processes relevant for carrier capture and recombination via such defects have also been investigated. In silicon detailed information on complex defects may be obtained from bound exciton spectroscopy on the neutral charge state. An interesting example involving neutral chalcogen pairs, exhibiting both metastability and final state excitation effects, will be discussed.

G2.2

THE ELECTRONIC STRUCTURE OF INTERSTITIAL IRON IN SILICON

M. Kleverman, A-L Thilderkvist, G. Grossmann, J. Olajos, and H. G. Grimmeiss, Department of Solid State Physics, University of Lund, Box 118, S-221 00 LUND, Sweden.

A donor-like line spectrum in Fe-doped silicon has been studied by high-resolution Zeeman spectroscopy. Previous work unambiguously identified the center as the interstitial iron impurity and suggested that the spectrum is due to the transitions $Fe_i^0 + h\nu \rightarrow Fe_i^+ + e^-$, where the excited electron enters shallow effective-mass-like donor states. In the optical excitation, different final core states (Fe_i^+) are reached giving rise to several superimposed shallow-donor spectra.

The Zeeman splitting patterns show this interpretation to be basically correct. The $2p_{\pm}$ lines show a splitting similar to that for shallow donors, e.g. quadratic shifts and the characteristic avoided crossing with the $3p_0$ line due to the non-linear terms in the Zeeman Hamiltonian.

This simple donor model is the basis for an analysis of the spectrum where all lines are observed to split into more components than given by the effective-mass approximation. This is especially notable for the $2p_0$ line for which three non-thermalizing components are clearly observed. This additional splitting, attributed to the internal degrees of freedom of the Fe_i^+ core, provides new detailed insight into the level structure of the defect.

G2.3

D-BAND LUMINESCENCE IDENTIFIED WITH TRANSITION METAL DECORATED, AS DISTINCT FROM UNDECORATED DISLOCATIONS. **V. Higgs**, and E.C. Lightowers, Physics Dept., King's College London, Strand, London, WC2R 2LS, U.K.

Luminescence features associated with dislocations in Si, the D-bands, have been investigated in several laboratories during the past 13 years

[1], and there has been considerable speculation concerning the relationship between the spectral features observed and specific dislocation types and the nature of the electronic transitions involved. In a recent investigation of Si grown by molecular beam epitaxy [2] it was noted that the D-band luminescence features were absent in the as-grown material, in spite of dislocation densities in the range 10^4 - 10^5 cm⁻², but that they could be introduced by deliberate contamination with Cu, Fe and Ni. It was concluded that the D-bands must be associated with decorated, as distinct from undecorated, dislocations.

In this paper we show that high purity FZ Si, free of transition metal contamination, carefully cleaned and then plastically deformed in a clean metal-free environment to produce dislocation densities in the range 10^4 - 10^8 cm⁻², does not show D-band luminescence, only a broadening of the free and donor and acceptor bound-exciton features. Very sharp D-band features can be created by subsequent deliberate contamination with Cu, Fe or Ni. The relative intensities of the luminescence feature vary with the dislocation density, but are virtually identical for the different metals except for a very small shift in energy. Work is in progress aimed at creating specific types of dislocations to investigate the possibility of developing a qualitative, or even quantitative, photoluminescence assessment technique for dislocations in both Si and Ge. The state of progress will be reported.

[1] R. Sauer, J. Weber, J. Stolz, E.R. Weber, K.H. Kusters and H. Alexander, Appl. Phys. A **36** 1 (1985)

[2] V. Higgs, E.C. Lightowers, G. Davies, F. Schaffler and E. Kasper, Semicond. Sci. Technol. In the press.

G2.4

PHOTOLUMINESCENCE EXCITATION SPECTROSCOPY OF MOCVD-GROWN GaAs:V. **Y.J. Kao**, and **N.M. Haegel**, Dept. of Materials Science and Engineering, University of California - Los Angeles, Los Angeles, CA; and **W.S. Hobson**, AT&T Bell Laboratories, Murray Hill, NJ.

Vanadium is a substitutional impurity in GaAs which is known to have a strong intracenter luminescence transition centered at 1.8 μ m. In this study, photoluminescence (PL) and photoluminescence excitation (PLE) spectroscopies have been used to study the characteristic V emissions of MOCVD-grown GaAs:V. Some of the samples were additionally doped with Si and/or Be in order to systematically vary the Fermi levels in the epitaxial layer and change the charge state of the vanadium.

An analysis of the PLE spectrum with below-band-edge excitation showed that the dominant V emission band of semi-insulating and p-type samples arises from crystal-field transitions of $V^{3+}(3d^3)$ ions. With above-band-edge excitation, an oscillatory behavior in the PLE spectrum of most samples was observed, similar to phenomena which have been reported in PLE studies of EL2. The intensity of these oscillatory bands gradually diminished as the concentration of vanadium in the sample was increased.

G2.5

RADIATIVE AND NON RADIATIVE RECOMBINATIONS AT ER CENTERS IN GaAlAs. **Taha Benyattou, Djelloul Seghier, Gérard Guillot**, INSA de Lyon, LPM, 69621 Villeurbanne Cédex (France); and **Pierre Galtier, Marie-Noëlle Charasse**, Thomson CSF/LCR, 91404 Orsay Cédex (France).

Photoluminescence (PL) of MBE Er doped $Ga_{0.55}Al_{0.45}As$ has been studied under continuous and pulsed laser excitation. We report PL spectra attributed to transitions from the two first excited states $^4I_{11/2}$ and $^4I_{13/2}$ to the ground state $^4I_{15/2}$. The PL intensity of these transitions shows a square root dependence on the excitation power. The lifetime of these two levels have been measured as a function of temperature and are found to be respectively 0.5ms and 1ms at 10K

which is comparable to decay times observed in insulators.

We have performed two beam-experiments in order to study and to find the origin of the non radiative processes. A pump beam is used to create a constant population of Er ($4f_{13/2}$) and a probe beam is used to create electron-hole pairs. We found a decrease of PL intensity induced by the probe beam so we conclude to the existence of losses associated with free carriers (ie. Auger effect).

From pulsed experiments using pulsed pump beam, we have shown that the Auger effect occurs during the PL excitation. In view of recent results indicating that rare earths (RE) create an attractive potential for the electrons, we propose the following model for the Er PL excitation process: excitons bound to Er are created and decay non radiatively by energy transfer to the rare earth (which is the cause of the Er observed PL) or to free carriers by Auger effect (which is the cause of the observed losses). This model explains the square root dependence and can be a good approach for all other RE doped III-V materials since most of them present a sublinear PL dependence law.

G2.6

CHARACTERIZATION OF DEEP-LEVEL DEFECTS IN SEMI-INSULATING GaAs AND InP BY PHOTOINDUCED TRANSIENT SPECTROSCOPY (PITS). Paweł Kamiński, Institute of Electronic Materials Technology, ul. Konstruktor-ska 6, 02-673 Warszawa, Poland

Semi-insulating (SI) GaAs and InP are substrate materials for manufacturing high speed electronic devices. Properties of these compounds, however, are controlled by deep-level impurities and native defects. This paper is aimed at showing the potentialities of Photoinduced Transient Spectroscopy (PITS) for investigation of residual deep-level defects in SI materials. We use the double-gated box-car integrator to process the photocurrent transient similarly as in DLTS technique.

The PITS spectra for Cr-doped and undoped LEC SI GaAs are compared. In the former, apart from chromium acceptor level (0.88 eV) a number of other traps are observed including that corresponding to iron contamination (0.52 eV) and to native defects - EL2 (0.74 eV) and EL6 (0.31 eV). The defect structure of the latter is also very complex and together with EL2 and EL6 several other traps occur. The effect of the Fermi-level position and charge carrier lifetime on PITS spectrum is discussed.

The PITS spectrum for Fe-doped LEC SI InP is shown. The traps with thermal emission activation energies of 0.71 eV and 0.64 eV correspond, respectively, to hole and electron emission from deep acceptor level associated with Fe in (0/-) charge state. The 0.35 eV and 0.23 eV traps are presumably attributed to some Fe-related complexes.

G3.1

ENHANCEMENT OF MINORITY CARRIER LIFETIMES IN n⁺/n/n⁺ GaAs HOMO-STRUCTURES. LEIGH M. SMITH† and D.J. WOLFORD†, IBM T. J. Watson Research Center, Yorktown Heights, NY; R. VENKATASUBRAMANIAN† and S.K. GHANDHI† Rensselaer Polytechnic Institute, Troy, NY.

We show that the radiative efficiency and lifetimes of photoexcited carriers in epitaxial GaAs can be enhanced by 3 to 4 orders-of-magnitude by the preparation of n⁺ "spike-doped" layers at surfaces and substrate interfaces. Samples were MOVCD-prepared with n-region thicknesses of 3-10 μm , and Si- or S-doped to n⁺ concentrations of $5 \times 10^{18} \text{ cm}^{-3}$. Time-resolved luminescence in such structures, under both surface and bulk (near-band-edge) excitation conditions, reveal near-edge-excitonic or band-to-band-dominated recombination spectra, with carrier lifetimes ranging from 1.5 nsec at 1.5 K to greater than 1 μsec at room temperature. This is in contrast to the subnanosecond lifetimes typical in conventionally grown bulk GaAs, but is comparable to the best reported for high-purity LPE grown GaAs/

Al_xGa_{1-x}As double heterostructures. The spatial distributions of photoexcited carriers in these structures are observed to expand by over an order of magnitude during their 1 μsec room temperature lifetime. The expansion is diffusive, with a measured diffusion constant of 14 cm^2/s at 300 K. This corresponds to a room temperature mobility of 525 cm^2/Vsec , comparable to previously measured hole mobilities in bulk p-type GaAs of similar purity. These results are clear evidence that the narrow, heavily doped layers effectively shield minority carriers from the interfaces, thereby reducing interface recombination.

This work was supported in part by the Office of Naval Research under contract N00014-85-C-0868;† The Solar Energy Research Institute, Golden, CO under contract XL-5-05018-2;‡ and Agreement 970-ERER-ER-87 with the New York State Energy Research and Development Authority.‡

G3.2

EVIDENCE FOR STRONG TRAPPING BY IONIZED DONORS OF FREE EXCITONS IN EXCITED STATES. S. Zemon and G. Lambert, GTE Laboratories, 40 Sylvan Road, Waltham, MA

A striking enhancement has been observed in the intensity of donor-related, photoluminescence transitions in undoped (10^{14} - 10^{15} cm^{-3}), epitaxial GaAs for excitation energies (E_e) in the vicinity of the band-gap energy (E_g). Enhancement data will also be presented for a variety of other samples, including GaAs heterostructures, substrates, and GaAs/Si as well as AlGaAs. In some cases dramatic intensity increases of over two orders of magnitude have been found, with donor-related transitions dominating acceptor-related ones in the excitonic region of even low-compensation, p-type material. The strong effects observed have been correlated to the presence of ionized donors (D^+). The enhancement was most readily observed for (D^+, h) and/or (D^+, X). Photoluminescence excitation (PLE) spectra at 4.2 K showed that the effect has a maximum consistent with excitation of the n=3 state of the free exciton ($X_{n=3}$) and decreases monotonically as E_e increases to values as much as 12 meV above E_g . A strong effect was also observed when pumping the $X_{n=2}$ transition, but only a weak one when pumping $X_{n=1}$. The two main PLE features at $X_{n=2,3}$ are interpreted in terms of an enhancement of donor transitions due to trapping of $X_{n=2,3}$ by D^+ . Subsequently, this complex can transform into ($D^+, X_{n=1}$) as well as (D^+, h). The trapping of $X_{n=2,3}$ by D^+ is apparently much more effective than that of $X_{n=1}$. Since the long range attraction between D^+ and X_n is due to interaction with the induced dipole, then the interaction should be stronger as the exciton radius (and therefore n) increases. Temperature, polarization, and magnetic field data will be discussed.

G3.3

FORMATION OF THREE RED-SHIFT EMISSIONS IN HEAVILY GERMANIUM-DOPED P-TYPE GAAS GROWN BY MBE. Y. MAKITA, A. YAMADA, H. SHIBATA, N. OHNISHI, A. C. BEYE, and K. M. MAYER, Electrotechnical Laboratory, 1-1-4 Umezono, Tsukuba-shi, 305, Japan.

Molecular beam epitaxy (MBE) of p-type GaAs doped with Ge was made, in which Ga to As₄ flux ratio, γ , Ge concentration, [Ge] and growth temperature were used as parameters. Photoluminescence (PL) spectra at 2K for slightly doped GaAs revealed that for $\gamma=1$ the emission of excitons bound to neutral Ge acceptors (A^0, X) was dominant. With increasing γ , (A^0, X) was steeply suppressed and the exciton emission at ionized Ge donors (D^+, X) was gradually enhanced and for $\gamma=11$, (D^+, X) became most dominant. In van der Pauw measurements, samples having [Ge] around $1 \times 10^{17} \text{ cm}^{-3}$ presented the p- to n- type conversion at $\gamma=1.7$, which was also specified in PL spectra as the quenching of a characteristic emission, [g-g] and the formation of an emission reflecting the increased number of donors, (B-B). [g-g] is formed just below (A^0, X) and exhibits a strong energy shift towards lower energy sides with increasing [Ge], which presumes that [g-g] is due to the pairs between excited-state acceptors. [g-g] has been proved to be easily quenched by small amount of donors being effective even by a factor of 30 smaller than that of acceptors. The formation of predominant [g-g] for $\gamma=1$ assures that extremely low-compensated p-type samples were grown by using an amphoteric impurity, which was established upto [Ge] = $1 \times 10^{18} \text{ cm}^{-3}$. In these samples four emission series exhibited significant energy shifts with increasing [Ge]. From [Ge] $\sim 1 \times 10^{16} \text{ cm}^{-3}$, the above [g-g] appears as a dominant emission and

at $[Ge] \sim 1 \times 10^{17} \text{ cm}^{-3}$, another red shift emission, $[g-g]_2$ begins to be formed on the higher energy side of $[g-g]_1$. It is interesting to note that both $[g-g]_1$ and $[g-g]_2$ seem to be totally quenched by the further increase of $[Ge]$. The emission due to band to Ge acceptor, (e, Ge) does not change its central energy till $[Ge] = 5 \times 10^{16} \text{ cm}^{-3}$ and for larger $[Ge]$ it turns into a new broad emission, $[g-g]_3$ displaying a steep red energy shift. The last emission, $[g-g]_4$ indicates a steady blue energy shift with growing $[Ge]$ larger than $1 \times 10^{16} \text{ cm}^{-3}$, which was theoretically explained in terms of the pairs between ground-state acceptors.

G3.4

ELECTRICAL PROPERTIES OF HEAVILY Be-DOPED GaAs GROWN BY MOLECULAR BEAM EPITAXY. H. Shibata, Y. Makita, A. Yamada, N. Ohnishi, M. Mori, Y. Nakayama, A. C. Beye and K. M. Mayer. Electro-technical Lab. 1-1-4 Umezono, Tsukuba-shi, 305, JAPAN

Electrical properties of heavily Be-doped GaAs grown by molecular beam epitaxy (MBE) were investigated in a wide range of carrier concentration $[A]$ from 1×10^{14} up to $1 \times 10^{20} \text{ cm}^{-3}$ at the sample temperature between 10K and room temperature (RT). The hole mobility at RT exhibits a maximum value of $308 \text{ cm}^2/\text{Vs}$ at $[A] = 7.2 \times 10^{15} \text{ cm}^{-3}$. The dependence of RT hole concentration on Be effusion cell temperature was nearly coincident with that of Be vapor pressure, which suggests that the doping of Be is governed by the Be arrival rate over the entire $[A]$ range studied. Raman scattering measurements were also carried out to examine the properties of distorted lattice due to the heavy doping.

Photoluminescence measurements were made at 2K in which several new peaks were discovered in the near-band-edge emission region. The emission band named by $[g-g]$ was observed for $[A]$ between 4.8×10^{16} and $7.0 \times 10^{17} \text{ cm}^{-3}$ which exhibited weak red shift with increasing $[A]$. This red shift was ascribed to the formation of the pairs between excited-states acceptors. The emission bands denoted by $[g-g]_1$ and $[g-g]_2$ were obtained for $[A]$ larger than $1.8 \times 10^{18} \text{ cm}^{-3}$ and presented strong blue and red shifts, respectively. The red shift of $[g-g]_2$ was recently explained in terms of the pair between ground-states acceptors. The emission band denoted by $[g-g]_3$ began to appear for $[A]$ larger than $2.6 \times 10^{19} \text{ cm}^{-3}$ but indicated no energy shift. Precise informations on the energy shift and the spectral evolution of these plural emissions as the function of $[A]$ enable one to estimate the carrier concentration by a non-destructive and contactless method with high spatial resolution.

G3.5

PHOTOLUMINESCENCE STUDY OF GaAs DIFFUSED WITH Li. H.P. Gislason and E.Ö. Sveinbjörnsson, U. of Iceland, Reykjavik, Iceland, B. Monemar and M. Ahlström, Linköping U., Linköping, Sweden.

We present a detailed study of the photoluminescence (PL) properties of a wide range of GaAs material diffused with the group-I element Li. Li is known to compensate both n- and p-type GaAs, and our starting material includes different n-type and p-type GaAs as well as semi-insulating material. Little work has been reported on the properties of Li in GaAs recently despite extensive studies in the seventies. Optical properties have mainly been studied by local-mode IR spectroscopy [1]. The only photoluminescence study so far on Li diffusion in GaAs [2] was done in Cu-doped samples with emphasis on Cu rather than Li. In the present study the Li doping of GaAs is investigated through its effect on existing PL bands in the as-grown material and the appearance of new such bands.

A dramatic example of spectral changes in GaAs upon Li doping is the gradual disappearance of the 1.36 eV PL band which is usually present through inadvertent Cu contamination of the samples. New PL bands resulting from the Li doping of n-type horizontal Bridgman material include a strong band at 1.34 eV and shallower bands at 1.45 and 1.48 eV. The doping procedure suggests that these bands are Li related, and since they appear only in n-type material the responsible centres are concluded to have acceptor character. The dependence of the PL intensity and energy positions of these bands on excitation intensity suggests that the deepest one represents transitions to a localized acceptor level, which we attribute to a deep Li_{Ga} acceptor. The shallower bands are assigned to pair transitions involving shallower Li-related centres. An analysis of the dependence of the PL intensity on temperature in the range between 4 K

and room temperature supports this model. The correlation between the different starting material and PL properties will be used to characterize the corresponding levels. The microscopic identity of the centres will be discussed in relation to earlier work on Li in GaAs.

1. M.E. Levy and W.G. Spitzer, J. Phys. Chem. Solids 6, 3223 (1973)
2. H.P. Gislason *et al.*, J. Appl. Phys. 58, 240 (1985)

G3.6

LASER-THERMAL IMPURITY PUMPING OF SHALLOW DONORS IN ULTRAPURE GERMANIUM. T. Theiler and F. Keilmann, Max-Planck-Institut für Festkörperforschung Stuttgart, FRG; E. E. Haller, Lawrence Berkley Labs, CA

Extremely narrow far-infrared lines $1/\lambda$ of OH-donors in ultrapure Germanium are used to probe the fundamental dynamic processes of impurities. For measurement we use PTIS modified by using frequency-fixed lasers and Zeeman-tuning of the impurity transition. We observe, for the first time, a change of the (lifetime dominated) resonance lineshape in the intensity region near 10^{-4} W/cm^2 . This effect can be quantitatively understood in a rate equation model, which shows that at the critical intensity the ground state becomes depleted and the dependence of the recombination on the degree of ionization becomes important. Therefore the effect depends also on compensation.

A quite distinct mechanism starts to broaden the line at much higher intensities near 10^{-1} W/cm^2 . This is identified as the equalization of ground and excited state population and thus, the results yield information on the thermal ionization of the excited state. This latter ionization step can also be accomplished in a further experiment by using a second far infrared laser to yield a "photo-photo-ionization-spectrum".

Reference

- 1/* H. Navarro, E. E. Haller, F. Keilmann; Phys. Rev. B37, p. 10822 1988

G4.1

VACANCY-TYPE DEFECTS IN PLASTICALLY DEFORMED GaAs. P. Mascher, S. Dannefaer and D. Kerr, Department of Physics, University of Winnipeg, Winnipeg, MB R3B 2E9, Canada

Semi-insulating GaAs has been investigated by positron lifetime spectroscopy in various states of plastic deformation. In the as-deformed samples large vacancy clusters could be detected as one of the defect components emerging for strains above the upper yield point. As expected from theory, the positron response from these traps shows a strong dependence on the measuring temperature between 30 and 350 K which allows an estimate of the void size of about 50 Å.

A significant decrease of the (retained) concentration of these defects with increasing deformation temperature ($450^\circ\text{C} \leq T_D \leq 600^\circ\text{C}$) suggests an annealing stage in this temperature range. Presently, both isochronal and isothermal annealing studies are in progress to obtain information on the migrating species and the kinetics of the process.

G4.2

ODMR STUDIES ON BULK GALLIUM PHOSPHIDE. Keith L. Brower, Sandia National Laboratories, Albuquerque, NM.

We have observed new optically detected magnetic resonances (ODMR) in n-type, sulfur doped 0.08 ohm-cm bulk gallium phosphide. The ODMR spectrum was observed at 1.3 K using 20.4 GHz, 50 mW, 280 Hz square-wave modulated microwaves with 50 mW of either 514.5, 488.0, 457.9, or 363.8 nm light illumination from an Ar ion laser. Within our 1.8 - 0.8 micron detection range, the ODMR luminescence is strongest near 800 nm using a Ge detector and 514.5 nm light illumination. No ODMR signals could be detected under

subbandgap illumination with 50 mw of light from a dye laser between approximately 800 and 900 nm.

The ODMR spectrum appears to be indicative of two distinct centers. One spectrum is characterized by an isotropic resonance having a g value of approximately 2.0125 and a linewidth of approximately 200 G; this resonance tends to be skewed to lower magnetic fields. The other, weaker spectrum appears to be an isotropic 2-line hyperfine spectrum at $g = 1.98$. The hyperfine lines are separated by approximately 485 G and have a linewidth of approximately 250 G. The isotropic nature of the spectra and the lack of forbidden transitions suggest spin 1/2 centers. The hyperfine spectrum might arise from a P-related defect in GaP.

This work performed at Sandia National Laboratories supported by the U.S. Department of Energy under contract number DE-AC04-76DP00789.

G4.3

THE ROLE OF OXYGEN IN p-TYPE InP. J. Michel, J. Jeong, K. M. Lee and L. C. Kimerling, AT&T Bell Laboratories, Murray Hill, NJ 07974.

We have studied the influence of oxygen on the electrical and optical properties of Be- and As-doped InP. The initial p-type InP [Be,As] shows a strong deep photoluminescence (PL) band at 1.5 μ m. This PL-band was related to the P_{1b} antisite defect by optically-detected magnetic resonance (ODMR) measurements. As the oxygen concentration increases, the 1.5 μ m PL-band disappears and a new PL-band at 1 μ m appears. Hall effect and resistivity measurements show that an increase in oxygen concentration results in a conversion from p-type to n-type material. We attribute the disappearance of the 1.5 μ m PL-band to a shift of the Fermi-level and the introduction of the 1 μ m band to an oxygen-related center.

G4.4

MID-INFRARED SPECTRAL PHOTO RESPONSE OF SEMI-INSULATING GaAs. G.J. Brown, and W.C. Mitchel, Materials Laboratory (WRDC/MLPO), Wright Research and Development Center, Wright-Patterson AFB, OH. 45433-6533

We have developed a characterization technique using mid-infrared, fourier transform photoconductivity (PC) that is capable of identifying deep energy levels in gallium arsenide. Our technique requires less sample processing than deep level transient spectroscopy (DLTS) and can be used on semi-insulating (SI) gallium arsenide. Using this technique we have observed evidence of several below mid-gap energy levels in undoped SI gallium arsenide. Spectral PC measurements were made on SI GaAs before and after illuminating the cooled samples with high intensity white light at 8K. The PC spectrum typically showed a broad photoresponse from 2 to 20 microns that was attributed to multiple energy levels in the material. The observed energy levels were 0.55 eV, 0.44 eV, 0.24 eV and a range from 0.15 to 0.06 eV. However, the shallow photoresponse from the carbon acceptor was not observed after illumination. The most striking spectral feature was a sharp ionization edge at about 0.44 eV in all of the samples studied. This energy level agrees well with the 0.43 eV level that has been observed by temperature dependent Hall effect measurements. The 0.43 eV Hall effect level is an intrinsic defect level and is postulated to be the 0.35 eV EL6 level observed by DLTS. The 0.44 eV level was also observed in our PC spectrum of a n-type Bridgman grown sample that had shown the 0.43 Hall effect level. The presence of additional deep levels in concentrations comparable to those of EL2 and carbon indicates that the simple model for compensation in SI GaAs which invokes only EL2 and shallow impurities needs revision.

G4.5

ASSOCIATION OF THE 0.8eV EMISSION BAND TO THE EL₆ CENTER IN GAAS. S. Alaya, M.A.Zaïdi, G.Marrakchi, H.Maaref, Faculté des Sciences Monastir (TUNISIA), H.J.Von Bardeleben and

J.C.Bourgoin. Groupe Physique des Solides de l'ENS. Tour 23. 2 Place Jussieu 75 251 PARIS (FRANCE).

The role of native defects as electrically active centers has long been known in GaAs. The EL₆ center which is commonly found in LEC and H.B grown GaAs is the most ubiquitous center other than the well known EL₂ center.

Two experimental techniques are used in this study in order to well establish the optical and electrical properties of this center.

The correlation of our photoluminescence and DLTS results of various S.I and n-type GaAs samples either grown by LEC or HB technique and the analysis of the thermal annealing effects on these samples led us to unambiguously relate the 0.8eV PL band to the EL₆ center. We have found that the appearance of the 0.8eV PL band is related to the Fermi-level position. We propose a configuration coordinate model which explains both all the characteristic electrical properties of the EL₆ center and the established properties of the 0.8eV PL band. A radiative recombination mechanism of this deep PL band is also proposed.

G4.6

THE ELECTRONIC STRUCTURE OF THE "0.15 eV" Cu ACCEPTOR LEVEL IN GaAs. E. Janzén, M. Linnarsson, B. Monemar, Linköping University, Linköping, Sweden and M. Kleverman, Lund University, Lund, Sweden.

Cu-diffused GaAs-samples have been investigated using different kinds of FTIR techniques and photoluminescence. Line spectra observed in absorption can be interpreted as transitions from the ground state to the excited effective mass like $2P_{3/2}$, $2P_{5/2}(\Gamma_8)$, and $2P_{5/2}(\Gamma_7)$ states of a neutral substitutional Cu_{Ga} acceptor. One LO-phonon higher in energy - interfering with the continuum - the Fano replicas of these transitions are visible. The binding energy of 157.8 meV has been obtained by adding the effective mass value of the $2P_{5/2}(\Gamma_8)$ state to the energy position of the corresponding absorption line.

All transitions to the excited states have replicas 0.84 meV higher in energy. The replicas are of electronic nature, as can be seen from uniaxial stress measurement.

Photoconductivity spectra showing oscillating photoconductivity will also be presented. The distance between two neighbouring dips is 36.4 meV, which is similar to the energy of an LO-phonon. The extrapolated "binding energy" obtained from the oscillations is 164.2 meV. The discrepancy between the binding energies will be discussed in terms of a <100> Jahn-Teller distortion.

Uniaxial stress and Zeeman measurements of the FTIR line spectra will be presented. These results allow us to give a detailed description of the electronic structure of the Cu-center.

G5.1

PHOTOLUMINESCENCE CHARACTERIZATION OF IMPURITIES AND DEFECTS IN SEMICONDUCTORS. M.L.W. Thewalt, Department of Physics, Simon Fraser University, Burnaby, B.C., Canada V5A 1S6.

Photoluminescence spectroscopy has become a well developed and widely applied tool for the study and characterization of defects and impurities in semiconductors. The field remains very dynamic, with advances being made both in the techniques themselves as well as in the breadth and complexity of the centres to which they can be applied.

One recent trend in photoluminescence spectroscopy has been the use of Fourier transform interferometric techniques, which previously had been developed primarily for mid- and far-infrared absorption spectroscopy. Interferometric photoluminescence spectroscopy can be advantageous not only for longer wavelength studies and for broad spectral scans, but

also in situations where very high spectral resolution and accuracy are required.

These topics will be illustrated with reference to a number of new photoluminescence studies. In Ge we will demonstrate the utility of photoluminescence for donor and acceptor characterization in high and ultra high purity material, as well as the first observation of a triple acceptor bound exciton. In Si, results for several new complex defect systems including the O-related thermal donors will be discussed. Finally we will illustrate the application of interferometry to high resolution photoluminescence and magnetophotoluminescence in high purity epitaxial GaAs.

G5.2

GENERATION AND DISSOCIATION OF IRON-BORON PAIRS IN SILICON. M. Suezawa and K. Sumino, Institute for Materials Research, Tohoku University, Sendai 980, Japan

This paper reports the kinetics of generation and dissociation processes of Fe-B pairs in Si studied by means of electron spin resonance (ESR). A specimen of B-doped float-zone-grown Si sealed into an evacuated quartz capsule together with a piece of Fe was quenched into ice-water from 1300°C. Changes in the concentrations of Fe-B pairs, electrically neutral Fe (Fe^0) and singly ionized Fe (Fe^+) due to various heat-treatments of the quenched specimen were determined from ESR measurements with an X-band spectrometer at 10 K. In contrast to a result previously published by Weber, the ESR absorption due to Fe-B pairs is not detected in an as-quenched specimen and only absorptions due to Fe^0 and Fe^+ are observed. This seems to mean that the high temperature state in which Fe atoms and B atoms are individually distributed within the crystal is effectively frozen in the crystal due to our quenching procedure. Isochronal annealing of the quenched specimen reveals that Fe-B pairs are generated at a temperature as low as 40°C. The concentration of Fe-B pairs increases with an increase in annealing temperature and achieves the maximum at about 100°C. Annealing at higher temperatures leads to a reduction in the concentration of Fe-B pairs. On the other hand, the concentrations of Fe^0 and Fe^+ are observed to show the behavior reverse to that of Fe-B pairs: Namely, they decrease due to annealing at temperatures lower than 100°C and increase at higher temperatures. However, they decrease again due to annealing at temperatures higher than 150°C. The latter may be attributed to clustering or precipitation of Fe in such a temperature range. Isothermal annealing of the quenched specimen reveals that the generation process of Fe-B pairs obeys the first order reaction kinetics. Mean separation of B atoms estimated from the time constant of Fe-B pair generation is found to be comparable to that determined from the concentration of B atoms in the specimen. This again supports the idea that Fe and B atoms are randomly distributed in the as-quenched specimen. The activation energy of Fe migration is determined to be 0.65 eV from this work. This magnitude is consistent to that determined by diffusion experiments.

G5.3

THEORETICAL INVESTIGATIONS OF THE METASTABILITY OF IRON-GROUP III ACCEPTOR PAIRS IN SILICON. J.R. Leite and L.V.C. Assali, Instituto de Física da Universidade de São Paulo, CP 20516, 01498 São Paulo, SP, Brazil.

The metastability of the Fe-Al, Fe-Ga and Fe-In pairs in silicon has been observed from DLTS and EPR experiments. It has been found that these pairs are stable in both, the $\langle 111 \rangle$ or $\langle 100 \rangle$ axial symmetry configurations, indicating that they may consist of a substitutional acceptor with the Fe impurity occupying the nearest or next-nearest neighbor interstitial site, respectively.

Recently we have reported the first rigorous electronic-state calculations for the Fe-B pair, one of the most investigated complexes in silicon. Preliminary attempts to correlate the electronic structure of this pair in both, the $\langle 111 \rangle$ and $\langle 100 \rangle$ axial symmetries have also been made. The aim of the present paper is to report on the results of our systematic studies of the electronic struc-

ture of the Fe-B, Fe-Al and Fe-Ga pairs in silicon. Rigorous SCF calculations have been carried out for the pairs in C_{3v} and C_{2v} symmetries in order to investigate the bistability of these systems. For each pair, results are presented for the one-electron energy gap levels and resonances, donor and acceptor transitions, Fermi hyperfine contact fields at the iron and the acceptor nuclei, total spins, Mott-Hubbard potentials and total energies.

G5.4

PHOTOCONDUCTIVITY STUDY OF Cr_2B AND Cr_1 IN SILICON

A. Schlette, R. Kienle, A. Dörnen, and K. Thonke
4. Physikalisches Institut, Universität Stuttgart,
Pfaffenwaldring 57, 7000 Stuttgart-80 (FRG)

Chromium is known to form complexes with different acceptors in silicon. By DLTS and Hall measurements a level at $E_v + 0.28\text{eV}$ (0/+ transition) is found for the chromium-boron complex. In photoluminescence (PL), a spectrum with zero phonon transition at 844 meV shows up.

We find in our photothermal ionisation spectroscopy (PTIS) experiments a resonance at the same energy as PL observes, exhibiting the identical 5-fold finestructure. Approx. 9 meV higher in energy a weak negative peak due to a forbidden transition is found. The ionisation threshold is observed as a step in the PTIS signal at ~ 874 meV. Fano resonances due to 'f' and 'g' phonons for all these features indicate clearly, that this spectrum belongs to effective-mass-like states of a donor. So chromium acts as a deep donor with a level at $E_v + 295\text{meV}$ and excited EMT-like states. Uniaxial stress measurements confirm the conduction band-like behaviour of the excited state and reveal the additional $\langle 111 \rangle$ -axis of the defect core.

In n-type samples, two thresholds at energies of 200 meV and 430 meV occur, the latter being followed by a sequence of modulations due to LO phonons. These energies were previously ascribed to Cr_1 and Cr_2 , respectively.

G5.5

FORMATION OF In-Cu PAIRS IN SILICON DURING CHEMO-MECHANICAL POLISHING. Th. Wichert, R. Keller, M. Deicher, W. Pfeiffer, H. Skudlik, and D. Steiner, Fakultät für Physik, Universität Konstanz, D-7750 Konstanz, FRG.

Following 200 eV Cu^+ implantation of Si, doped with radioactive ^{111}In atoms, the formation of In-Cu pairs is observed using the perturbed $\gamma\gamma$ angular correlation technique (PAC). The pairs exhibit axial symmetry about the $\langle 111 \rangle$ lattice direction and have a dissociation energy of 0.69 eV, assuming an attempt frequency of 10^{12} Hz . Using the three measured Cu specific interaction frequencies of $\nu_Q = 237, 334$, and 408 MHz ($T_M = 78\text{ K}$) it is shown that these pairs are identical with the In-X pairs observed after chemo-mechanical polishing of Si wafers (M. Deicher et al., Institute of Physics Conference Series, Vol. 95 (1989) 155). This identification implies that at 273 K Cu atoms in Si possess a much higher diffusivity, being about 4 orders of magnitude higher, than expected from extrapolating diffusion data measured at 1000 K. Possible explanations of this phenomenon will be discussed and comparisons with other experiments indicating the presence of Cu in Si will be made.

G6.1

FERMI RESONANCE EFFECTS ON THE VIBRATION MODES OF HYDROGEN-PASSIVATED BORON IN SILICON*. G. D. Watkins, W. B. Fowler, G. G. DeLeo, M. Stavola, and D. M. Kozuch, Dept. of Physics, Lehigh University, Bethlehem, Pa. 18015; S. J. Pearton and J. Lopata, AT&T Bell Laboratories, Murray Hill, N. J. 07974

^{10}B - ^{11}B isotope shifts have been reported recently for the ^1H and ^2H vibrational frequencies of the H-B complex in silicon¹. The $^{10}\text{B}^2\text{H}$ - $^{11}\text{B}^2\text{H}$ shift was found to be anomalously large. We show that this effect finds a natural explanation in a phenomenon called "Fermi resonance"², arising from a weak anharmonic coupling between the second harmonic of the transverse B vibration and the longitudinal H vibration. We first present a simple classical explanation of the effect in terms of a "parametric oscillator", or a child pumping himself on a swing. We then outline a simple quantum mechanical treatment that provides a satisfactory quantitative explanation of the results. Our calculations also predict infrared absorption at the boron second harmonic frequencies. These are observed for both ^{10}B and ^{11}B with intensities and polarization as predicted, providing direct confirmation of the interpretation. The Pankove Si-H-B model³, therefore, remains intact. Our results, in fact, provide further confirmation of its validity in the sense that we have confirmed for the first time that the boron vibrations are perpendicular to the Si-H-B bond.

*Research at Lehigh University supported by Office of Naval Research Contract N00014-84K-0025.

1. B. Pajot, A. Chari, M. Aucouturier, M. Astier and A. Chantre, Sol. St. Comm. 67, 855 (1988).
2. E. Fermi, Z. Phys. 71, 250 (1931).
3. J. I. Pankove, D. E. Carlson, J. E. Berkeyheiser, and R. O. Wance, Phys. Rev. Lett. 51, 2224 (1983).

G6.2

OPTICALLY DETECTED MAGNETIC RESONANCE OF A HYDROGEN-RELATED COMPLEX DEFECT IN SILICON. W.M. Chen, O.O. Awadelkarim, B. Monemar, Department of Physics and Measurement Technology, Linköping University, S-581 83 Linköping, SWEDEN; J.L. Lindström, Swedish Defence Research Establishment, P.O. Box 1165, S-581 11 Linköping, SWEDEN; and G.S. Oehrlein, IBM Research Division, T.J. Watson Research Center, Yorktown Heights, N.Y. 10598 USA

Hydrogen in semiconductors has recently received great attention, not only because of its fascinating physical properties, but also due to its technological importance, e.g. in passivating a variety of defects in semiconductors. Despite numerous studies a microscopic identification of H-induced defects by magnetic resonance techniques is still absent. This is a key problem for a better understanding of the properties of hydrogen. In this paper, we present the first optically detected magnetic resonance (ODMR) studies of a hydrogen-related defect in semiconductors. The defect is present in hydrogenated boron-doped silicon single crystals, after room-temperature electron-irradiation. A spin-triplet ($S=1$) is shown to be the electronic state responsible for the observed ODMR spectrum. A detailed angular dependence study of the ODMR spectrum reveals a C_{2v} defect symmetry. The defect is argued to be a di-hydrogen-vacancy complex (VH_2), in which the hydrogen atoms passivate two dangling bonds of the lattice vacancy. The presence of H in the defect complex is evidenced by the resolved hyperfine structure of the ^1H atom with nuclear spin $I=1/2$ (99.985% naturally abundant). The energy levels of this complex in the forbidden gap and their important role as strong non-radiative recombination channels are also discussed.

G6.3

HYDROGEN BEHAVIOUR IN SILICON. Guido L. Chiarotti, F. Buda, R. Car and M. Parrinello, Int'l School for Advanced Studies, Trieste, Italy

The role of Hydrogen in Silicon has been the subject of extensive experimental and theoretical investigations. Both in crystalline (c-Si) and in amorphous (a-Si) phases the behaviour of H has technological relevance. In fact in c-Si H is capable of passivating defect related states. In a-Si instead H plays a crucial role in the doping process. We discuss both the cases of c-Si:H and a-Si:H, that we have investigated by means of ab-initio Molecular Dynamics simulation. Within this computational scheme the interatomic potential is obtained from accurate local density functional calculations, and dynamical finite temperature effects are completely taken into account.

For c-Si we restrict to the study of H^+ in the high temperature regime. The results can be summarized as follows: (i) The diffusion proceeds via a jump-like mechanism. (ii) The diffusion path is substantially different from that inferred from zero temperature total energy calculations, demonstrating the importance of dynamical effects. (iii) The computed diffusion coefficient and its temperature dependence are in good agreement with the high temperature available experimental data, and confirm the high mobility of H in c-Si. We also suggest that scattering experiments may distinguish between different diffusion mechanisms.

By rapid quench from the melt we have obtained an a-Si:H sample. We will discuss some structural and electronic properties of this system.

G6.4

HYDROGEN DIFFUSION IN B-DOPED SILICON. C. P. Herrero*, M. Stutzmann, and A. Breitschwerdt, Max-Planck-Institut für Festkörperforschung, D-7000 Stuttgart 80, FRG.

We have measured the IR reflectance of hydrogen passivated boron-doped silicon for different B-concentrations and passivation conditions (temperature and exposure time). From the observed features in the IR spectra, we can obtain hydrogen depth profiles in passivated samples, and effective diffusion coefficients can be deduced. We find that the diffusion of hydrogen in B-doped c-Si can be described by the same parameter as in undoped Si ($D = D_0 \exp(-E_M/kT)$) with $D_0 = 2.4 \times 10^{-7} \text{ cm}^2\text{s}^{-1}$, $E_M = 0.43 \text{ eV}$, provided that trapping of H at substitutional acceptor sites is correctly taken into account. From the trap-limited diffusion analysis, a binding energy for B-H pairs of 0.6 eV is found, in agreement with theoretical calculations.

In the course of these investigations we have also observed that surface oxide layers can hinder completely the diffusion of H into the silicon bulk. An analysis of this hindered diffusion in samples under different biases will be presented.

* Present address: Instituto de Ciencia de Materiales, CSIC, Serrano 115 dpdo, 28006 Madrid, Spain

G6.5

MODELING OF THE DIFFUSION OF HYDROGEN IN SILICON. D. Mathiot, CNET - CNS, BP: 98, 38243 Meylan Cedex (France), and D. Ballutaud, P. de Mierry and M. Aucouturier, Labo. Physiques des Solides, CNRS, 1 Place A. Briand, 92195 Meudon Principal (France).

A model is proposed to describe the behaviour of H in Si at moderate temperatures. It is assumed that H has both a donor and an acceptor level in the band gap, and thus it can exist in the three charge states H^0 , H^+ and H^- . The bulk diffusion of hydrogen is slowed down by the formation of H_2 molecules, as well as by interactions with the dopant atoms. In the surface region the high surface concentration measured by SIMS is

attributed to the trapping of H atoms on plasma induced extended defects.

Good simulations are obtained in both n- and p-type Si, for various doping levels. In lightly doped samples a comprehensive description of the behaviour of H⁰ is obtained with parameters consistent with the high temperature data. In order to obtain the most reliable values for the parameters governing the behaviour of H⁺ and H⁻ we will report simulations of experimental results (SIMS diffusion profiles) covering a wide range of substrate doping levels.

G7.1

THE STRUCTURES OF ISOLATED HYDROGEN CENTERS IN SEMICONDUCTORS INFERRED FROM MUONIUM. T. L. Estle, Rice Univ., Houston, TX; R. F. Kieff, TRIUMF, Vancouver, B. C., Canada; J. W. Schneider, Univ. of Zurich, Zurich, Switzerland; and C. Schwab, CRN, Strasbourg, France.

The study of isolated hydrogen in semiconductors is difficult because of the tendency for hydrogen to form complexes. The detailed structural information usually obtained from EPR and ENDOR has been absent with the single exception of hydrogen in silicon¹. An alternative to direct studies of hydrogen exists in the form of muon spectroscopic studies of muonium in semiconductors². In such experiments the muon is essentially an isotope of hydrogen with $\frac{1}{9}$ th the mass of the proton. Twenty isolated muonium centers have been observed in tetrahedrally-coordinated crystals ranging from Si and other group-IV crystals to the copper halides (11 crystals total). Muon level-crossing resonance (μ LCR) has provided detailed structural models for neutral interstitial muonium at a bond center in silicon³ (the analog of the hydrogen center seen by EPR¹) and very near a bond center in GaP and GaAs⁴.

This paper will review these measurements and discuss the structures and their metastabilities. Comparison will be made to the EPR work on Si¹ and to theoretical studies of Si and initial ones on Ge and GaAs. In addition recent μ LCR results on the metastable and stable muonium centers in the copper halides will be presented.

¹ Yu. V. Gorenkinskiy and N. N. Nevynnyi, Sov. Tech. Phys. Lett. 13, 45 (1987).

² R. F. Kieff and T. L. Estle, in *Hydrogen in Semiconductors*, ed. by J. I. Pankove and N. M. Johnson, Academic Press, to be published.

³ R. F. Kieff, et al., Phys. Rev. Lett. 60, 224 (1988).

⁴ R. F. Kieff, et al., Phys. Rev. Lett. 58, 1780 (1987).

G7.2

ELECTRONIC STRUCTURE AND HYPERFINE PARAMETERS FOR HYDROGEN AND MUONIUM IN SILICON.

Chris G. Van de Walle, Philips Laboratories, Briarcliff Manor, NY 10510.

We show that parameter-free spin-density-functional calculations can yield accurate results for hyperfine parameters of defects in semiconductors. First-principles calculations¹ have recently produced a conclusive picture of the structural properties of hydrogen (or its pseudo-isotope, muonium) as an impurity in crystalline Si. The calculated structures were compared with those obtained from an analysis of muon-spin-rotation experiments,² a technique (analogous to electron spin resonance) which probes the interaction between electronic wavefunctions and nuclear spins. An even more direct link between theory and experiment can be established if hyperfine parameters for various defect structures can also be calculated from first principles. Pseudopotential-spin-density-functional supercell calculations are used here to obtain values for isotropic (contact interaction) and anisotropic (dipole-dipole) components of the hyperfine interaction. Both types of paramagnetic centers, corresponding to the tetrahedral interstitial site ("normal muonium") and the bond-center position ("anomalous muonium") yield results which are in good agree-

ment with those obtained from muon-spin-rotation. The agreement found in this case instills confidence in the general use of spin-density-functional calculations for predicting hyperfine parameters of defects.

¹C. G. Van de Walle, P. J. H. Denteneer, Y. Bar-Yam, and S. T. Pantelides, Phys. Rev. B. 39, 10791 (1989).

²R. F. Kieff, M. Celio, T. L. Estle, S. R. Kreitzman, G. M. Luke, T. M. Riseman, and E. J. Ansaldo, Phys. Rev. Lett. 60, 224 (1988).

G7.3

HYDROGEN IN CRYSTALLINE SILICON UNDER COMPRESSION AND TENSION C. S. Nichols and D. R. Clarke IBM Research Division, T. J. Watson Research Center, Yorktown Heights, NY 10598, USA

The behavior of hydrogen in crystalline silicon (c-Si) has been investigated as a function of pressure using first-principles total-energy methods. The calculations combine density-functional theory with norm-conserving pseudopotentials and large supercells to explore the stable site for hydrogen as a function of the hydrogen charge state, the Fermi level, and the lattice constant.

It is found that, for moderate pressures, the hydrogen minimum energy position undergoes a transition from the tetrahedral interstitial site to the bond-center site. For the positive and neutral charge states, this transition occurs under compression, whereas for the negative charge state, it occurs under hydrostatic tension.

These results are used to make predictions about hydrogen solubility in c-Si and to investigate hydrogen behavior in the stress fields of dislocations, grain boundaries, and crack tips. Specifically, application of hydrostatic pressure to p-type Si should have little effect on the hydrogen solubility (up to $\approx 5\%$ strain), whereas hydrogen in n-type Si becomes less soluble with application of pressure. Furthermore, we predict that hydrogen in n-type Si should form a Cottrell atmosphere around an isolated dislocation core, but that no such effect should be present in p-type Si. These findings may be generalized to the case of a grain boundary, which can be viewed as an array of dislocation cores, to conjecture that grain boundaries in n-type material may be more readily passivated than those in p-type material. Finally, we predict that hydrogen preferentially moves to the bond-center position in p-type Si affecting the energy of cleavage and thereby altering the fracture resistance. No such effect is expected in n-type Si.

This work was supported in part by ONR Contract No. N00014-88-C-0176.

G7.4

ANALYSIS OF REAL-TIME HYDROGENATION DATA FROM P AND N-TYPE SILICON.* Carleton H. Seager and Robert A. Anderson, Sandia National Laboratories, Albuquerque, NM.

The results of analyzing the charge density data obtained on p and n-type silicon Schottky-barrier structures during H implantation will be discussed. In p-type samples, the depletion field induced drift of positive H species is consistent with a high ($\approx 10^{-10}$ cm²/sec) value of the hydrogen diffusivity at 300K. Capture of these positive species by ionized acceptors proceeds with the large capture radius (50-70 Å) expected for a coulomb assisted process. At low electric fields, evidence for diffusion of neutral H is also seen. Furthermore, we observe that a substantial fraction of hydrogenated boron acceptors (10-20%) convert to a negative charge state in the presence of mobile hydrogen.

In n-type diodes, H passivation of phosphorus donors proceeds largely by diffusion of neutral species; in contrast to p-type diodes, high depletion fields noticeably retard passivation, indicating that occasional conversion of neutral hydrogens to protons is occurring. The density of positive species is enhanced near the metal/silicon interface, apparently due to electron tunneling. This causes negative voltage shifts of Mott-Schottky capacitance plots and enough narrowing of the diode depletion region to

substantially lower the diode resistance. These latter effects have also been observed on diodes not H implanted but merely fabricated on wet-etched silicon surfaces. These effects disappear after short, low-temperature anneals which out-diffuse the hydrogen.

*This work was performed at Sandia National Laboratories, supported by the U. S. Department of Energy under Contract No. DE-AC04-76DP00789.

G7.5

HYDROGEN SEGREGATION AT AL/SI INTERFACE STUDIED BY NUCLEAR RESONANT REACTION.

Joyce C. Liu, A. D. Marwick, and F. K. LeGoues, IBM Thomas J. Watson Research Center, Yorktown Heights, New York 10598

Hydrogen segregation at the interface between an epitaxial Al film and a Si(111) wafer is studied by using $^1\text{H}(^{15}\text{N}, \alpha\gamma)^{12}\text{C}$ nuclear resonant reaction analysis. The hydrogen atoms are introduced by either low energy (500 eV) implantation or cathodic charging in H_2SO_4 . Hydrogen depth profiles show that hydrogen atoms diffuse through the 150 nm thick Al layer during the hydrogenation and are trapped at the Al/Si interface. The amount of hydrogen in the vicinity of the interface is in the order of $10^{14}/\text{cm}^2$ after a sample is implanted with $7 \times 10^{17} \text{ H}/\text{cm}^2$. A reduction in H concentration at the interface is observed after thermal annealing and the binding energy of the hydrogen atom to the interface is then determined from kinetic data. Ion channeling and high resolution transmission electron microscopy are also used to characterize the microstructures of the epitaxial Al film and the Al/Si interface.

G7.6

DISSOCIATION KINETICS OF SHALLOW ACCEPTOR-HYDROGEN PAIRS IN SILICON.

Zundel T. and Weber J., Max-Planck-Institut für Festkörperforschung, Heisenbergstr.1, D-7000 Stuttgart 80, Federal Republic of Germany

We determine the thermal dissociation kinetics of the shallow electrically neutral acceptor-hydrogen complexes (AH) in silicon doped with A=B, Al, Ga, or In. Annealing of hydrogenated p-type crystalline silicon with a reverse bias applied to a Schottky diode leads to a reactivation of the acceptor within the space charge region. The hydrogen-acceptor complex can thermally dissociate, and the released positively charged hydrogen drifts out of the space charge region under the electric field. Due to the drift effect the concentration of H is negligible in the high-field region, and the reaction $\text{AH} \rightleftharpoons \text{A} + \text{H}$ only proceeds to the right. Therefore the dissociation of the AH complex follows first-order kinetics throughout the entire annealing time. The first-order kinetics permits us to precisely determine the dissociation frequency ν_A of the AH pairs. The temperature-dependent values of ν_A satisfy the relation $\nu_A = \nu_{0A} \exp(-E_A/kT)$, with $\nu_{0B} = 2.8 \cdot 10^{14} \text{ s}^{-1}$, $\nu_{0Al} = 3.1 \cdot 10^{13} \text{ s}^{-1}$, $\nu_{0Ga} = 6.9 \cdot 10^{13} \text{ s}^{-1}$, and $\nu_{0In} = 8.4 \cdot 10^{13} \text{ s}^{-1}$. The dissociation energies E_A depend only weakly on the acceptors: $E_B = (1.28 \pm 0.03) \text{ eV}$, $E_{Al} = (1.44 \pm 0.02) \text{ eV}$, $E_{Ga} = (1.40 \pm 0.03) \text{ eV}$, and $E_{In} = (1.42 \pm 0.05) \text{ eV}$. In addition, similar measurements on acceptor-deuterium complexes will be presented.

G8.1

HYDROGEN COMPLEXES IN III-V SEMICONDUCTORS.

Bernard Pajot, Groupe de Physique des Solides de l'ENS, Tour 23, Université Paris 7, 2 place Jussieu, 75251 Paris Cedex 05, France.

Hydrogen can bind to atoms from intrinsic or extrinsic centers

in III-V compounds. This generally neutralizes the electrical activity of such centers and the understanding of this neutralization goes through the knowledge of the microscopic structure of the H-related complexes. Vibrational spectroscopy of the H bonds, alone or coupled with uniaxial stressing of the samples, is well suited to this purpose as its results are reasonably independent from the electrical activity of the complexes.

Results are presented on the occurrence,

structure, stability and atomic reorientation of the H-related complexes associated with dopant atoms or with lattice defects and they are correlated with those from other techniques and also compared with theoretical estimates.

G8.2

Sn-H COMPLEXES IN GaAs. D. M. Kozuch, Sherman Fairchild Laboratory, Lehigh University, Bethlehem, PA; M. Stavola, S. J. Pearton, C. R. Abernathy, and J. Lopata, AT&T Bell Laboratories, Murray Hill, NJ.

Infrared absorption bands due to the H vibrations of Sn-H complexes in GaAs have been found near 1328 and 749 cm^{-1} for Sn-doped epilayers exposed to an H_2 plasma. These bands are assigned to H stretching and wagging, respectively, for the Sn-H complex. The bands shift to lower frequency upon substitution of D for H confirming that they are H vibrations. The Sn-H complexes anneal out near 200°C which corresponds to a dissociation energy of 1.5 eV .

It is interesting to compare the properties of donor-H complexes in Si with those in GaAs. The donor-H complexes in Si have nearly identical vibrational frequencies (~ 1560 and 810 cm^{-1} for P, As, and Sb donors). In GaAs, there is a pronounced dependence of the frequencies upon the identity of the donor [the Si-H complex in GaAs has vibrations at 1717 and 897 cm^{-1} , Pajot et al., Phys. Rev. B37, 4188 (1988), which are very different from those of Sn-H given above]. From a comparison to the vibrations of other dopant-H complexes whose structures are known, the vibrational characteristics suggest that the H occupies an antibonding site in all of the donor-H complexes. However, it is known only for GaAs:Si-H that the H is at the antibonding site adjacent to the donor and not at a more distant antibonding site. The implications of the donor-dependence of the vibrational frequencies for the structures of the donor-H complexes in the two hosts will be discussed.

G8.3

REASSESSMENT OF ACCEPTOR PASSIVATION MECHANISM IN p-TYPE HYDROGENATED GaAs. L. Szafrank and G.E. Stillman, Center for Compound Semiconductor Microelectronics, Materials Research Laboratory and Coordinated Science Laboratory, University of Illinois at Urbana - Champaign, Urbana, IL 61801.

The relative thermodynamic stability of passivating complexes of hydrogen with various shallow acceptors in p-type GaAs has been investigated. High-resolution, liquid-He temperature photoluminescence studies of hydrogenation and of the recently reported light-induced reactivation¹ reveal, that group III_B substitutional acceptors Be, Mg and Zn are neutralized less effectively and are more susceptible to the athermal reactivation effect than group IV_A impurities - C, Si and Ge. Moreover, significant differences in the rate and extent of the reactivation have been observed between Mg and Be, as well as between Si and C. The presently accepted microscopic models of acceptor passivation in p-type GaAs, that imply bond rearrangements and changes in a local lattice coordination in order to satisfy the covalent nature of hydrogen bonding in

the defect site, cannot fully account for these new experimental results.

We propose a modified chemical structure of the passivating hydrogen-acceptor complex in p-type GaAs. In this model the electrical neutralization is simply a result of Coulomb attraction-assisted close pairing between compensated hydrogen donors and acceptor impurities. According to Hopfield's analysis², in such associated ionized donor-acceptor pairs the compensation would become passivation for pair separation shorter than the effective Bohr radius of an acceptor. The model allows for a semiquantitative prediction of the relative affinity to hydrogenation and the stability of the resulting neutralizing complexes, based on the electronegativity of acceptor species, in general agreement with our measurements. Kinetic and thermodynamic aspects of acceptor passivation and reactivation, consistent with the proposed binding configuration of hydrogen-acceptor complexes, will be discussed.

This work was supported by the Joint Services Electronics Program, under contract N00015-84-C-0149, the National Science Foundation, under grants DMR 86-12860 and CDR 85-22666 and by SDIO/IST contract DAAL 03-87-K-0013.

1. I. Szafrank, S.S. Bose and G.E. Stillman, submitted to Appl. Phys. Lett.
2. J.J. Hopfield, in "Physics of Semiconductors" (Proc. 7th Int. Conf.), p. 725 (Dunod, Paris and Academic Press, New York, 1964).

G8.4

HYDROGEN PASSIVATION OF INTERFACIAL DEFECTS IN MOCVD GROWN GaAs/InP. V. Swaminathan, U. K. Chakrabarti, W. S. Hobson, R. Caruso, J. Lopata, and S. J. Pearton, AT&T Bell Laboratories, Murray Hill, NJ 07974

The results of a low temperature (5K) photoluminescence study of hydrogenation of GaAs on InP grown by metal organic chemical vapor deposition are presented. An emission band at ~ 1.42 eV originating from the GaAs/InP interfacial region shows a 30 fold increase in intensity relative to the GaAs band edge emission after exposure to hydrogen plasma for 30 min at 250 °C. This improvement in intensity is attributed to hydrogen passivation of defects at the heterointerface caused by the large ($\approx 4\%$) lattice mismatch between GaAs and InP. The passivation effect recovers on annealing the hydrogenated sample at 350 °C. Excitation dependence of the 1.42 eV band suggests that the interfacial region consists of a compositionally graded layer. Further, this band shifts to higher energy on annealing the sample in the temperature range 150–450 °C with the hydrogenated sample exhibiting a larger shift than the untreated sample. The possible reasons for these annealing induced peak shifts are discussed in terms of the modifications of the interfacial region.

G8.5

PASSIVATION OF Zn ACCEPTORS IN InGaAs DURING RIE WITH CHF_3/H_2 AND CH_4/H_2 . Martin Möhrle, Heinrich-Hertz-Institut, Berlin, FRG

Reactive ion etching (RIE) of dielectric layers and of InP related compounds with gas mixtures of CHF_3/H_2 and CH_4/H_2 , respectively, are well established techniques for fine-line pattern transfer. However, we found that the use of such hydrogen-containing plasmas leads to a strong decrease of the electrically active acceptor concentration at the surface of highly Zn-doped InGaAs.

LPE-grown $\text{In}_{0.53}\text{Ga}_{0.47}\text{As}$ layers, epitaxially doped with Zn to a level of $p = 1 \cdot 10^{19} \text{ cm}^{-3}$, as well as samples with hole concentrations above 10^{20} cm^{-3} , achieved by additional Zn diffusion from the vapour phase, were exposed to CHF_3/H_2 and CH_4/H_2 plasmas, respectively, for 3...9 min in a parallel-plate RIE system operating at 13.56 MHz. Electrochemical C-V profiling revealed a reduction of the carrier concentration by about two orders of magnitude at the surface. The depleted regions extended to a depth of 30...80 nm into the layer. Moreover Ti/Pt/Au contacts applied to p-InGaAs after RIE etching using the above gas mixtures exhibited strongly non-ohmic characteristics, whereas on as-diffused samples a linear behaviour with low resistivities of typically $< 10^{-6} \Omega \text{ cm}^2$ is obtained. No such effects were observed after RIE with CF_4 or CF_4/O_2 , which indicates that hydrogen plays a crucial rôle for the

observed passivation of Zn acceptors.

A moderate temperature treatment (330 °C, 20 min) resulted in a complete reactivation of the passivated acceptors, as inferred from profile measurements. Furthermore the linearity of contact characteristics was re-established by this annealing procedure.

G9.1

OPTICAL ABSORPTION OF DEEP DEFECTS IN NEUTRON IRRADIATED SEMI-INSULATING GaAs. M. O. Manasreh, Materials Laboratory (WRDC/MLPO), Wright Research and Development Center, Wright-Patterson Air Force Base, Ohio 45433-6533, and P. J. Pearah, Spectrum Technology Incorporated, 6 October Hill Drive, Holliston, MA 01746.

Two defects were observed in thermal neutron irradiated semi-insulating LEC GaAs materials by using the infrared absorption technique. The first defect was observed before thermal annealing and it has a broad peak at ~ 0.83 eV. The second defect was observed after annealing the sample at 250 °C for 15 min. The latter defect is an EL2-like defect, but is thermally unstable at 400 °C with a concentration of about an order of magnitude larger than [EL2] observed in as grown LEC materials. Both defects were found to photoquench with white light or 1.1 eV monochromatic light at 9 K and thermally recovered at 150 K. The concentration of the EL2-like defect is reduced from $8.5 \times 10^{16} \text{ cm}^{-3}$ after annealing the sample at 300 °C for 15 min to $2 \times 10^{16} \text{ cm}^{-3}$ after annealing at 400 °C for 15 min. This defect becomes unquenchable after the latter annealing conditions. An explanation for this behavior is offered.

G9.2

RECOVERY OF THE METASTABLE EL2 DEFECT IN GaAs UNDER MONOCHROMATIC LIGHT ILLUMINATION. M. O. Manasreh and D. W. Fischer, Materials Laboratory (WRDC/MLPO), Wright Research and Development Center, Wright-Patterson Air Force Base, Ohio 45433-6533.

The infrared absorption technique is used to study the recovery of the EL2 metastable state in semi-insulating GaAs under monochromatic light illumination. The induced optical recovery is monitored after low intensity ($\leq 2 \text{ mW/cm}^2$) irradiation in the energy range of $0.7 \leq h\nu \leq 1.5$ eV. The data exhibit a complex structure consisting of a broad band around 0.9 eV and a set of multiple sharp peaks between 1.44 and 1.5 eV. This recovery is strongly dependent on the sample, temperature and illumination time. The present results suggest that a) the existing data and theoretical predictions for the As_{Ga} antisite structure are not compatible with the optical recovery data, b) EL2 is affected dramatically by other defects (traps) present in the sample and c) the peaks observed in the optical recovery data are coincident with the arsenic vacancy energy levels and therefore the present results support the proposed complex models involving an arsenic vacancy.

G9.3

EL-2 DEFECT FORMATION AND CARBON INCORPORATION IN GaAs GROWN BY ORGANOMETALLIC VAPOR PHASE EPITAXY. R. Venkatesubramanian, Research Triangle Park, NC; J.M. Borrego and S.K. Ghandhi, Rensselaer Polytechnic Institute, Troy, NY 12157.

A study of impurities and defects in epitaxial GaAs grown by organometallic vapor phase epitaxy (OMVPE), which provides information about the nature of organometallic growth process, is presented.

EL-2 is a commonly observed deep-level and carbon is an important residual acceptor impurity in OMVPE grown n-GaAs. A concurrent

monitoring of the concentration of these two defects, as a function of growth conditions such as arsine partial pressure, TMGa partial pressure and growth temperature, has been used to understand the thermochemistry of arsine in the OMVPE GaAs process. The concentration of EL-2 in unintentionally doped n-GaAs, as measured by Deep Level Transient Spectroscopy, has been evaluated in samples grown under conditions where intrinsic carrier levels exist. An anti-site (As_{Ga}) defect formation mechanism during OMVPE growth, at various growth temperatures, is developed based on these results.

The relative variation of carbon levels was monitored by photoluminescence measurements taken at 4K, under the same set of growth conditions. Based on this study and the EL-2 study, it is concluded that the increase in carbon levels with growth temperature is due to gas-phase loss of the H radical from As-H growth species.

G9.4

DX-CENTER IN Se-DOPED $Al_xGa_{1-x}As$. Thomas Hanak*, University of Denver, Department of Physics, University Park, Denver, CO 80210; Assem Bakry and Richard K. Ahrenkiel, Solar Energy Research Institute, 1617 Cole Blvd., Golden, CO 80401; and Michael L. Timmons, Research Triangle Institute, Research Triangle Park, NC, 27709-2194. *Work performed at the Solar Energy Research Institute.

We report the measurement of the activation energy for the DX-center in Se-doped $Al_xGa_{1-x}As$ grown by metal-organic chemical vapor deposition (MOCVD) for different alloy compositions. The peaks obtained from conventional DLTS are often asymmetric with shoulders on one or both sides. These shoulders often arise from two or more traps which are active in the same temperature range.

The capacitive transients are recorded digitally and analyzed directly by applying a nonlinear double exponential fitting routine to the data. This fitting produces two Arrhenius plots and yields the densities of the defect states. From the Arrhenius plots, the capture cross sections at infinite temperature and the activation energies are calculated. These results are then used to simulate the DLTS spectra. Excellent agreement between real and simulated spectra is shown.

G9.5

A MODEL OF Si DIFFUSION IN GaAs BASED ON THE FERMI-LEVEL EFFECT. Shaofeng Yu, Ulrich M. Gösele, and Teh Y. Tan. Department of Mechanical Engineering and Materials Science, Duke University, Durham, NC 27706

We propose a quantitative model for Si diffusion in GaAs. In this model we incorporate the experimental result that Si is an amphoteric impurity which constitutes a shallow donor when occupying the Ga site, Si_{Ga} , and a shallow acceptor when occupying the As site, Si_{As} . At high concentrations Si_{Ga}^+ and Si_{As}^- coexist. The amphoteric behavior of Si may be viewed as an effect of the Fermi-level. We assume that Si_{Ga}^+ and Si_{As}^- diffuse respectively on the Ga and As sublattices. That is, the diffusion of Si_{Ga}^+ and Si_{As}^- is governed by the variously charged Ga_{Ga} vacancies and As_{As} vacancies (or self-interstitials) respectively. The experimentally observed Si diffusivity is concentration dependent which results from the Si amphoteric nature as well as from another effect of the Fermi-level, which is its influence on the concentrations of the charged point defect species. Satisfactory quantitative descriptions of available experimental results are obtained. An analysis of the data on Si diffusion into a Sn-doped GaAs substrate has led us to believe that the previously proposed Si-pair diffusion model may no longer be favored.

G9.6

BURIED AMORPHOUS LAYERS IN GALLIUM ARSENIDE. Dipankar Sengupta, Mark C. Ridgway, John M. Zemanski and Steven T. Johnson, Microelectronics and Materials Technology Centre, Royal Melbourne Institute of Technology, Melbourne, Victoria, 3000, Australia.

It has been possible to produce buried amorphous layers in semi-insulating Gallium Arsenide (GaAs) by implanting 150keV Oxygen (O^+) ions to a dose of $7 \times 10^{15}/cm^2$ at room temperature. The layers are usually of $\sim 3500\text{\AA}$ thickness and the interface with crystalline material lies at a depth of $\sim 2000\text{\AA}$ from the surface. Implantations carried out at lower sample temperatures resulted in a continuous amorphous layer formation starting at the surface. When implantation was done at higher sample temperatures no amorphous layer was formed due to self-annealing.

The regrowth characteristics of the amorphous layer into crystalline material are now being studied using time resolved reflectivity and Rutherford backscattering spectroscopy combined with channeling. The regrowth of amorphous material in contact with the bulk undamaged GaAs (deep amorphous/crystalline interface) shows a temperature dependence with the activation energy of 1.3eV which is in reasonable agreement with earlier works [1]. The regrowth rate shows an interesting depth dependence to be presented in the paper. The regrowth behaviour of amorphous material in contact with the heavily damaged surface layer (shallow amorphous/crystalline interface) is now under detailed investigation.

The results of these experiments will help clarify whether the damage present in the crystalline layer has any effect on the kinetics of the regrowth process.

[1]C. Licoppe, Y.I. Nissim and C. Meriadec, J. Appl. Phys. **58**, 3094 (1985) and references therein.

G9.7

NEW GERMANIUM-RELATED DONOR IN NEUTRON-IRRADIATED GALLIUM PHOSPHIDE. J. Barczynska and E. Goldys, Institute of Experimental Physics, Warsaw University, 00-681 Warsaw, Hoza 69, Poland.

Neutron transmutation doping is a standard method to obtain n-type silicon. The similar procedure of thermal neutron irradiation and subsequent annealing has been applied to GaP. Ga and P atoms transmute to Ge and S which are both substitutional donors in GaP. The concentration of Ge in our samples was $1.1 \cdot 10^{18}/cm^3$, the additional S concentration was $7 \cdot 10^{16}/cm^3$. The side effect of the irradiation is the creation of different structural defects leading to the lowering of the Fermi level into the midgap. The induced defects disappear almost completely after annealing for 1h at 800°C. The annealing in itself does not lead to defect creation. We have measured the absorption coefficient and photoconductivity for photon energies between 0.25 eV and 2.2 eV, the dependence of resistivity vs. temperature and the sign of thermoelectric power for such irradiated and annealed samples. The dominant feature in the absorption spectra resembles the photoionisation of a moderately deep (0.45 eV) center. The similar structure can be also observed in photoconductivity. The sign of thermoelectric power indicates that the samples are n-type. The resistivity is thermally activated with the activation energy 0.43 eV. These results can be interpreted as due to the donor level at 0.43 eV under the c. b. which is photoionised by light with energy greater than about 0.5 eV. Large concentration of this center suggest that it is germanium-related.

G9.8

DIFFUSION OF Ga VACANCIES AND Si IN GaAs. K.B. Kahan, D.J. Lawrence, D.L. Peterson, and G. Rajeswaran, Corporate Research Laboratories, Eastman Kodak Company, Rochester, New York, 14650.

All impurity diffusion processes involve the motion of intrinsic point defects, such as vacancies. The specific example of Si diffusion in GaAs will be examined. Using the Si-pair diffusion formalism of Greiner and Gibbons, a new Si diffusion model is developed based on the dominant diffusion species being Si_{Ga}-V_{Ga} pairs, where V_{Ga} is the Ga vacancy. In the model, the unknown parameters are the pair diffusion coefficient (D_p) and the equilibrium constant, which are fitted to the experimental data. D_p is derived to be equal to one-half the Ga vacancy diffusivity. Next, an experiment to determine the V_{Ga} diffusivity, D_v , is described, and it is shown that the fitted D_p values approximately equal 0.5 D_v . The derivation of D_v is based on the observation that capping a GaAs quantum well sample with SiO₂ enhances the thermal intermixing of the wells. This enhancement is assumed to result from the introduction of additional V_{Ga} into the sample. The intermixing was monitored by measuring the photoluminescence shifts of the first electron-heavy hole peaks following annealing of the samples from 800 to 1025°C. The measured shifts were compared with the theoretical predictions. A relation for D_v of the form $0.962 \exp(-2.72 \text{ eV/KT}) \text{ cm}^2/\text{s}$ was obtained. Using this result, the equilibrium V_{Ga} concentration (C_v) was computed via an ensemble Monte Carlo simulation. The derived expression for C_v was $1.25 \times 10^{31} \exp(-3.28 \text{ eV/KT}) \text{ cm}^{-3}$.

G9.9

MECHANISM FOR THE DIFFUSION OF Zn IN GaAs. K.B. Kahan, Corporate Research Laboratories, Eastman Kodak Company, Rochester, New York, 14650-2011.

The diffusion profile of Zn in GaAs is kinked for most processing conditions. A model is presented to explain this phenomenon. The basis for the model is that Zn diffuses by an interstitial-substitutional mechanism. The Frank-Turnbull mechanism is invoked to govern the interchange between interstitial Zn (Zn_i) and substitutional Zn (Zn_s), via the Ga vacancies (V_{Ga}). These vacancies are proposed to be either neutral or singly-ionized, depending on the position of the Fermi-level. The temperature dependence of the ionization level is given by the Van Vechten-Thurmond model of the entropy of defects. In addition, two physical phenomena are proposed. Interstitial Zn is generated not only at the sample surface but also by the thermal dissociation of Zn_s into Zn_i and V_{Ga}. The second phenomenon is the formation of a neutral Coulomb pair between the donor, Zn_i⁺, and the acceptor, Zn_s⁻. This pairing is favored energetically since it reduces the number of isolated point charges. The pairing leads to the diffusivity of Zn_i being a decreasing function of the concentration of Zn_s since Zn_s is relatively immobile. The results of the model are compared with the kinked Zn profiles of Tiwari et al. (1). A fit is made to the data at one temperature. The results of the model are shown to be in good agreement with the profiles at other temperatures using only one adjustable parameter, the diffusivity of Zn_i in undoped GaAs.

1. S. Tiwari, J. Hintzman, and A. Callegari, Appl. Phys. Lett. 51, 2118 (1987).

G9.10

DEFECTS IN THE NEAR-SURFACE REGION OF 2.5 MeV ¹⁶O⁺ IMPLANTED n-GaAs. C.C. Tin and P.A. Barnes, Dept. of Physics, Auburn University, AL 36849; T.T. Bardin and J.G. Pronko, Lockheed Research &

Development Div., D91-10, B203, 3251 Hanover St., Palo Alto, CA 94304.

MeV ion implantation in GaAs is known to cause amorphization of the region at the end of the ion range. The near-surface region, however, is still crystalline albeit heavily compensated. We have carried out deep level transient spectroscopy (DLTS) studies of the defect levels in the near-surface region of n-GaAs samples implanted with different doses of 2.5 MeV ¹⁶O⁺ ions.

A comparison between the defect structures in the original and the implanted samples shows that implantation produced a broad range of defect levels ranging from 0.58 to 0.3 eV from the conduction band edge. This broad range of defects has an unusually large capture cross-section. The intensities of the DLTS peaks increase with the dose of ¹⁶O⁺ ions. The presence of EL2, which was present in the original samples, was not observed in the implanted samples.

Results from measurements made on samples that have been implanted at 200 °C and on implanted samples subjected to rapid thermal annealing will also be discussed.

G9.11

DEEP LEVEL LUMINESCENCE IN InP: PHONON FEATURE ANALYSIS S. Banerjee, A.K. Srivastava and B.M. Arora, T.I.F.R., Homi Bhabha Road, Bombay, India.

There are several recent reports on deep level luminescence in InP. The deep level luminescence in InP is characterised by broad overlapping bands which have been assigned to native defects and impurities like Fe, Mn, etc. Presence of several bands in random proportions in different samples has caused problem in obtaining their parameters uniquely. Strong phonon features for Fe and Mn in InP have been identified; however, the reported results do not agree due to lack of detailed lineshape analysis. The lineshape analysis of the band C related to a native defect is far from satisfactory. Hence, there is a need to obtain accurate parameters which can describe the experimental spectra due to these impurities or defects, uniquely.

We have measured photoluminescence of deep levels due to Fe, Mn and band C in InP at 10K. For the first time, lineshape analysis using configuration coordinate model has resulted in consistent parameters (see Table) describing each defect uniquely. Strong TO phonon coupling in all three defects was observed in all samples. The spectral features obtained for several samples can be consistently described by a composite of one or more of these defects present in different proportions.

Band	Zero Phonon Energy (eV)	Phonon Energy (eV)	Huang-Rhys Coeff
Fe	1.142	0.039	2
Mn	1.185	0.039	1.4
Band C	1.113	0.039	1.5

G9.12

OPTICAL ABSORPTION AND PHOTOLUMINESCENCE FROM LOCALIZED STATES IN HEAVILY DOPED InGaAsP:Ge. R. Rajalakshmi, and B.M. Arora, T.I.F.R., Bombay, India.

The absorption spectra (80K-300K) of heavily doped In_{0.72}Ga_{0.28}As_{0.40}P_{0.60}:Ge shows a prominent Urbach tail and the photoluminescence (14K-200K) shows a broad-band emission below the band gap energy. The experimental results are compared with the calculated spectra involving transitions between the conduction band states and the disorder induced tail

states above the valence band edge.

Photoluminescence calculation shows that the observed band is a superposition of several Stokes-shifted phonon replicas with the Huang-Rhys factor=3. The zero phonon line shape is obtained by assuming an exponential density of states at valence-band edge, a constant transition matrix element, and a non-equilibrium distribution function for holes which takes into account the capture and emission kinetics of the tail states.

The absorption spectra are calculated considering band-to-band transitions as well as tail-to-band transitions accompanied by phonon interaction. A peculiarity of these materials is that to obtain good quality fitting of the calculated spectra to the measured results, a reduced value of the electron Fermi level is necessary as compared to the value obtained from the Hall-electron concentration.

G9.13

VOID FORMATION AND THE CORRELATION WITH THE REDUCTION OF CARRIER CONCENTRATION IN SI-IMPLANTED GaAs. Kei-Yu Ko, Samuel Chen, S.-Tong Lee, Longru Zheng, Corporate Research Laboratories, Eastman Kodak Company, Rochester, New York 14650, and T.Y. Tan, Department of Mechanical Engineering and Materials Science, Duke University, Durham, NC 27706, and Microelectronics Center of North Carolina, Research Triangle Park, NC 27709.

Small, near-spherical voids were recently observed in the near-surface region of ion-implanted and annealed GaAs. We report the measurements of dopant and carrier concentration profiles of GaAs implanted with 220 keV Si at doses varying from 3×10^{13} cm⁻² to 1×10^{15} cm⁻² and annealed at 850°C for one hour. In high-dose implanted samples voids were found in the near-surface region by transmission electron microscopy. In the same region secondary ion mass spectroscopy measurement revealed an inhibition of dopant diffusion while C-V profiling measurement showed a severe reduction of carrier concentration. The correlation between the presence of voids and the suppression of carrier concentration is discussed.

G9.14

DISORDER INDUCED BAND TAILING EFFECTS ON DEEP LEVELS IN SEMICONDUCTORS. A. A. Teate and N.C. Halder, Department of Physics, Univ. South FL, Tampa, FL 33620.

We have investigated the effects of disorder induced band tailing on deep levels in compound semiconductor alloys, such as Al_xGa_{1-x}As and In_xGa_{1-x}As. In particular, we have eliminated the assumption of Gaussian broadening of the defect density of states proposed earlier by others on the basis of the central limit theorem. Since in GaAs, GaAs-alloys, and many disordered systems exponential absorption edges have been observed, we expect the density of states (DOS) should asymptotically exhibit this behavior, which may be represented by the convolution of the sharp level DOS and the disordered broadening function extending well into the energy gap. The expressions derived for the transient capacitance in the presence of the

disorder induced band tailing are quite different from the results published previously by Das et al. We applied this theory to investigate the deep level transient spectra (DLTS) and isothermal capacitance transient spectra (ICTS) in Al_xGa_{1-x}As and In_xGa_{1-x}As. Our results indicate that standard experimental measurements with DLTS and ICTS, in general, can overestimate the activation energy, capture cross-section, etc even in the case of weak disorder. Finally, a comparison between the simulated and measured DLTS and ICTS show some new results.

G9.15

SURFACE AND INTERFACE DAMAGE CHARACTERIZATION OF REACTIVE ION ETCHED MBE REGROWN GaAs. M.W. Cole, M. Dutta, J. Rossabi*, Doran, D. Smith and J.L. Lehman*, US Army ETDL, Ft. Monmouth, N.J. 07703, Quest Tech, Inc., Eatontown, N.J. 07724, + JEOL, USA Inc., Peabody, Mass 01960.

In this study damage resulting from reactive ion etching (RIE) and wet etching of MBE grown GaAs and the defects generated in subsequent regrowth has been evaluated by several techniques. The four MBE grown GaAs samples analyzed were cleaved from the same wafer, three of which were reactively etched with HCl at 300W and 150W, Cl₂ at 150W while the fourth was wet etched in a solution of H₂O:H₃PO₄:H₂O₂ as a comparison. All were then regrown together to keep the growth conditions the same. Photoluminescence (PL) spectra were taken at different temperatures and a fit was obtained to the temperature dependence of the PL intensities. The LO phonon intensities measured by room temperature Raman spectroscopy showed a strong correlation to the relative PL intensities, where the HCl sample was found to be inferior to the others. TEM microstructural evaluation showed both HCl RIE samples to have significant interface roughness, with the sample etched at 300W showing the most structural damage in the regrowth region. Defects were dominated by microtwins on {111} planes with average width of 85nm (300W) and 50nm (150W). High densities of dislocation tangles were evident in the 150W HCl sample. Defect densities for the Cl₂ and wet etched samples were three times lower than that of the HCl etched samples. Lattice damage in the Cl₂ and the wet etched samples consisted primarily of dislocations emanating from the interface region and a few narrow 18nm microtwins. The extent of disorder in the regrowth region was largest for the HCl sample (233nm) versus narrower defect band for the Cl₂ and wet etch samples of 142nm and 166nm respectively.

G9.16

DIFFUSION OF ION-IMPLANTED TIN IN GALLIUM ARSENIDE. E.L. Allen, Department of Materials Science and Engineering, Stanford University; M.D. Deal and J.D. Plummer, Integrated Circuits Laboratory, Stanford University, Stanford, CA 94305.

Group IV atoms are used as n-type dopants in GaAs, but their diffusion behavior is not well understood. The diffusion mechanism of all Group IV n-type dopants appears to be the same, and by studying tin, which has a high diffusivity, the relative effect of implant damage on diffusion can be extracted.

The diffusion of ion implanted tin in gallium arsenide was investigated as a function of temperature, dose, background doping, and encapsulant properties. The chemical depth profiles were determined with SIMS and the carrier profiles were determined by Polaron CV Profiling. The data was fit using a numerical process simulator, SUPREM 3.5. Tin diffusivity was found to depend on the square of the electron concentration via the Fermi level effect. Implant damage plays a significant role in limiting diffusion in the near-surface

implanted region, while enhancing diffusion on the bulk side of the implant.

In this paper the results of the tin diffusion experiments are presented and discussed. The behavior of tin is compared to that of ion-implanted germanium and silicon.

G9.17

Pd/Au:Be OHMIC CONTACTS TO p-TYPE GaAs. K.M. Schmitz, K. Jiao, R. Sharma and W.A. Anderson, Center for Electronic and Electro-optic Materials, Department of Electrical and Computer Engineering, State University of New York at Buffalo, Buffalo, NY 14260; G. Rajeswaran and L.R. Zheng, Corporate Research Laboratory, Eastman Kodak Company, Rochester, NY 14650; M.W. Cole, U.S. Army Electronics Technology and Devices Laboratory, Fort Monmouth, NJ 07703.

Stable, low resistance ohmic contacts to p-type GaAs were studied for use in semiconductor laser applications. Comparison was made between Cr/Au, Pd/Au, Au:Be and Pd/Au:Be metallizations. Regions of P^+ were formed in N-type GaAs by ion implantation of Zn followed by rapid anneal at 900°C for 5s compared to a spin-on source which was rapid diffused at 950°C for 6s. Surface doping of 2×10^{19} - 2×10^{20} /cm³ and junction depths of 0.2-0.4 μ m were determined by SIMS, groove and stain, and electrochemical profile. Metallizations were accomplished by thermal evaporation with a base pressure of 2.4×10^{-6} Torr. Sintering of the metallizations was done by furnace or RTA at 350°C. This sintering temperature was selected after RBS studies predicted an absence of significant interdiffusion. Pd/Au:Be gave the best result of $1 \mu\Omega\text{-cm}^2$ based upon transmission line, cross-bridge Kelvin and van der Pauw studies. A layer of BeO was revealed on the surface of Au:Be contacts by Auger studies. Cross-section TEM studies on Pd/Au:Be revealed a uniform layer of alloyed Ga-As-Au with an absence of spiking. Pd/Au and Au:Be metallizations were inferior to the Pd/Au:Be due to spiking and other imperfections. Stability is related to interdiffusion and alloying phenomena.

G9.18

VOID FORMATION, ELECTRICAL ACTIVATION AND LAYER INTERMIXING IN SI-IMPLANTED GaAs/AlGaAs SUPERLATTICES. S.-Tong Lee, Samuel Chen, Kei-Yu Ko, Mary L. Ott, G. Braunstein, Corporate Research Laboratories, Eastman Kodak Company, Rochester, NY 14650, and T. Y. Tan, Department of Mechanical Engineering and Materials Sciences, Duke University, Durham, NC 27706 and Microelectronics Center of North Carolina, Research Triangle Park, NC 27709

We have found small, near-spherical voids in the near-surface region of ion-implanted and annealed GaAs/AlGaAs superlattices and GaAs. Voids were generally observed in annealed samples implanted with 220 keV Si to a dose $\geq 3 \times 10^{14}/\text{cm}^2$. We have suggested that, because of its internal surfaces, the voids can act as sinks for vacancies, trap impurities and suppress dopant activation. C-V profiling results showed that electrical activation of Si implants by thermal annealing was severely suppressed in the near-surface region of superlattices where voids and mixing inhibition were found. The reduction in carrier concentration, attributable to the presence of voids, is used to explain the anomalous phenomenon of the inhibition of enhanced layer intermixing in the near-surface region of superlattices.

G9.19

Reduction of DX center concentration in Sn - doped AlGaAs grown by LPE and its meaning. In Duk Hwang, and Sin Chong Park, Basic Research Department, ETRI, P.O.Box 8, Daedog Danji, Dajeon, Chungnam, Korea

DX centers in Sn-doped $\text{Al}_x\text{Ga}_{1-x}\text{As}$ grown on the GaAs substrates of different orientations are studied for the first time by Capacitance-Voltage method and Deep Level Transient Spectroscopy. In AlGaAs:Sn grown on (100) substrates, two types of traps, trap A and trap B, are observed to have strong dependence on Al mole fraction x . The concentration of trap B showing its DLTS peak at $\sim 160\text{K}$ is much higher than that of trap A for $x > 0.3$.

Unexpectedly, the concentration of both trap A and trap B in the (111) Ga and (111) As face samples with $x > 0.3$ are observed to be one order of magnitude lower than those in the (100) face samples with the same Al composition, even though the DLTS activation energies of three groups of samples are observed to be the same.

Believing this result is caused by the difference in the atomic arrangement around a Sn atom, a new model for the DX center is proposed. In this model, a Sn atom acts as a DX center when the second nearest neighbor Al and Ga atoms have an anisotropic ordering.

G9.20

HOT-CARRIER EFFECTS ON OPTICAL PROPERTIES OF GaAs/Al_xGa_{1-x}As QUANTUM WELLS. W.M. Chen, B. Monemar, P.O. Holtz, Department of Physics and Measurement Technology, Linköping University, S-581 83 Linköping, SWEDEN; and M. Sundaram, J.L. Merz and A.C. Gossard, Department of Electrical and Computer Engineering, University of California, Santa Barbara, California 93106, USA.

In this paper we report a study of hot-electron effects on optical properties of GaAs/Al_xGa_{1-x}As quantum wells, by photoluminescence (PL) in presence of an external magnetic field and a microwave (MW) field. Both single quantum wells (SQWs) and multiple quantum wells (MQWs), grown by molecular beam epitaxy (MBE) with modulated doping, were studied in this work. A profound enhancement of the free exciton (FE) emission from both SQWs and MQWs is observed with MW irradiation. This is attributed to effects of hot-electrons, which are cyclotron resonance accelerated in the MW electric field, as evident from the characteristic dependence on a static magnetic field. The mechanism responsible for the giant enhancement in PL emission intensity of the QWs in the presence of hot-carriers is studied in detail, and is discussed in terms of the following two main contributions. First of all, impact ionization of excitons (FE:s or excitons bound at shallow impurities (BE:s)) and/or of shallow impurities in the Al_xGa_{1-x}As energy barriers is readily realizable with the experimental conditions, as can be directly seen by a strong quenching of luminescence from the barrier. This process blocks, at least partly, the shunt pass of the photoexcited free carriers in the barrier so that they are mainly accommodated in the GaAs energy well. Secondly, an increase of free electron temperature T_e in the barriers may result in an increase in the diffusion into the well, and consequently enhances the number of the excitons in the well. The direct role of the external perturbations (magnetic field and MW) on the exciton formation and recombination in the well (via modifying the electronic energy and wavefunction of the excitons) is also studied, via resonant optical excitation of the excitons.

THE NATURE OF NATIVE DEFECTS IN LEC GROWN SEMI-INSULATING GaAs BY THERMALLY STIMULATED CURRENT SPECTROSCOPY. Zhaoliang Fang, Lei Shen, T.E. Schlesinger and A.G. Milnes, Department of Electrical and Computer Engineering, Carnegie Mellon University, Pittsburgh, PA 15213.

In-doped semi-insulating GaAs has a low dislocation density but this does not necessarily correlate with a low trap density. This has been studied by thermally stimulated current spectroscopy (TSC) with intrinsic (1.96 eV) and extrinsic (1.15 eV) light for both In doped and undoped LEC materials grown under various non-stoichiometric conditions. Significant differences are seen in the bulk trap spectra associated with Ga-rich and As-rich material and with isoelectronic In doping. Proximity wafer-annealing at 950° C has been shown to improve minority carrier lifetime in n-type GaAs and we show that in semi-insulating GaAs this causes changes in trap structure. From such thermal studies and the effects of non-stoichiometric growth, the probable nature of the traps commonly seen is inferred. Traps T2 (0.49eV), T3 (0.33-0.44eV), T5 (0.26eV), and T6 (0.21eV) are tentatively identified as As^{++} , a V_{As} -related complex, V_{Ga} and Ga_{As}^{--} respectively.

G9.22

PRESSURE EFFECTS ON DEEP LEVELS IN SEMICONDUCTORS Ken-ichi TAKARABE and Shigeru MINOMURA, Department of Physics, Okayama University of Science, Okayama 700; Masahiko Kusaka, Okayama University, Okayama 700; Koichiro MATSUDA, Horiba Ltd., Kyoto 601

Pressure has been a powerful tool better to understand semiconducting properties. We here report that the pressure effect on the deep D center found in In-doped ZnSe, and the DX center in $Al_xGa_{1-x}As:Si$. Isothermal pressure derivative of emission rates The carrier concentrations of epitaxial layers of ZnSe grown on (001)GaAs substrates by low-pressure vapor-phase epitaxy were systematically controlled from 10^{16} to 10^{18} cm⁻³ tuning the In cell temperatures. Upon the incorporation of In, the deep electron trap ($E_T=0.7$ eV), D center, is induced. It was found that the loading of pressures up to 1.5GPa decrease the emission rate from 10^3 to 10^0 sec⁻¹ by a factor of 10^{-3} . The observed large reduction of emission rate upon pressures is interpreted as indicating that the emission of electron from the D center accompanies with the large change in activation volume. By general thermodynamical relations, the activation volume is evaluated to $16A^3$, and equivalent to the change of 8% in the bond-length of ZnSe. Multiplicity of DX center of Si-doped $Al_xGa_{1-x}As$ The recent DLTS studies show two closely-spaced DX centers in Si-doped $Al_xGa_{1-x}As$. It was previously found that the pressure induce the metastable DX center in Si-doped GaAs, however the multiplicity of metastable DX center is not resolved. We will present the experimental results on the multiplicity using the isothermal transient capacitance spectroscopy under pressure.

IMPROVED HOLE DIFFUSION LENGTHS IN BULK n-TYPE GaAs FOR HIGH EFFICIENCY SOLAR CELLS. D. Wong, T.E. Schlesinger, and A.G. Milnes, Carnegie Mellon University, Pittsburgh, PA 15213.

We report on a simple method of wafer annealing which is effective in raising minority carrier diffusion lengths in n-type bulk GaAs to above the value necessary for efficient solar cell performance. This treatment also decreases the concentration of many deep level defects observed by deep level transient spectroscopy in bulk GaAs (both electron and hole traps) and may prove useful in preprocessing of GaAs for applications other than photovoltaics. Wafers of n-type LEC and HB GaAs were given proximity anneals in sealed quartz ampoules at 950°C for periods of 1 to 64 hours. 16 hour anneals were found to be optimum at this temperature and brought about an increase in hole diffusion lengths of up to a factor of 3 from starting values of L_p of between 0.6 μ m and 1.1 μ m to as high as 3.0 μ m as determined by electron beam induced current measurements. Both Te and Si doped specimens annealed under identical conditions were found to show this improvement even for wafers obtained from boules which had been given an ingot anneal by the manufacturer. A minority carrier trap which we have labeled HCX ($E_T+0.29$ eV) appears to be the lifetime-limiting defect in this material. We have also measured the photoresponse of improved material using an electrochemical (transparent) diode and with p+n diffused junction solar cells. A significant improvement in the photoresponse, especially for the long wavelength portion of the spectrum has been observed.

G9.24

THE STUDY OF CONTAMINATION OF CARBON, BORON, AND OXYGEN IN LEC-GAAS. Yoshiko Iton, The Institute of Physical and Chemical Research, Wako, Saitama, Yosunori Kadota, Sumitomo Metal Mining Co., Ltd., Kunitomi, Hokkaido, Hiroto Fukushima, Japan Analysis Center, Sanno, Chiba, and Mikio Takai, Osaka University, Toyonaka Osaka.

It is important to control and suppress residual impurities such as carbon, boron and oxygen in a LEC-GaAs crystal. To date, however, the contamination behavior of such impurities has not been clarified, since direct measurements of such impurities were not possible. In this study, the concentrations of carbon, boron and oxygen in samples pulled by the various experimental conditions were measured by a newly developed CPAA (charged particle activation analysis) method. The reactions used were $^{12}C(d,n)^{13}N$, $^{10}B(d,\alpha)^8Li$ and $^{16}O(^3He,p)^{17}F$ for carbon, boron, and oxygen, respectively.

Carbon in LEC GaAs was found to be introduced as CO from the ambient atmosphere; the oxygen concentration in the crystals was related to the concentration of water in 3_2O_3 and decreased with the duration of melting. An equilibrium distribution coefficient of oxygen in GaAs crystals at solidification ratio of 0.5 was found by our direct measurements to be 0.08, the value of which was smaller by a factor of 3.5 than that reported before.

G9.25

THE ROLE OF CHARGED POINT DEFECTS ON THE DIFFUSION BEHAVIOR OF SILICON IN GaAs. Jeff J. Murray, David A. Stevenson, Department of Materials Science and Engineering, Stanford University, Stanford CA and Michael D. Deal, Center for Integrated Systems, Stanford University, Stanford, CA.

Since silicon is a commonly used dopant in the fabrication of GaAs M⁺FET and JFET devices, its diffusion behavior is of great technological importance. It has been known for some time that the diffusion behavior of implanted silicon is markedly different from that observed from controlled solid source

experiments. In order to understand this difference a close look at the defect chemistry of the GaAs is required.

In the current study we have used several types of dopants to modify the point defect chemistry of the GaAs prior to implantation and subsequent annealing. We have noted enhanced silicon diffusion for different n-type GaAs substrates and retarded silicon diffusion for p-type substrates.

In addition, we have used MOCVD and MBE grown structures with stepped silicon doping behavior. These structures allow us to study silicon diffusion behavior in well controlled silicon concentration gradients at specific silicon doping levels. As a result we can predict the diffusivity of silicon as a function of background doping or more explicitly as a function of the Fermi level position in the crystal.

G9.26

MAGNETICALLY STABILIZED KYROPOULOS GROWTH OF InP. Steven Bachowski, Brian S. Ahern, Robert M. Hilton, Joseph A. Adamski, Rome Air Development Center, Hanscom AFB MA 01731

A new crystal growth furnace with axial magnetic fields of 4.3 kGauss has been applied to the growth of 50 and 70mm diameter InP crystals by the Liquid Encapsulated Kyropoulos (MLEK) technique. This method has resulted wafers with low and uniform dislocation densities. Results will be presented showing how strong axial fields have reduced the buoyancy driven convection and how the dislocation density has been reduced as a result of the the lowering of the thermal gradients with the LEK method.

G9.27

TEMPERATURE DEPENDENCE OF SCATTERED LIGHT INTENSITY BY PRECIPITATES ALONG DISLOCATIONS IN AN In DOPED LEC GaAs CRYSTAL. Kazufumi Sakai and Tomoya Ogawa, Department of Physics, Gakushuin University, Mejiro, Tokyo 171, Japan

IR light scattering technique was used and developed to observe the dislocations as well as micro-precipitates such as swirls and growth striations in the semiconductors. Clear images of dislocations inside GaAs crystals by the technique are going to use detection of the micro-defects. However, the scattering mechanism of the light are dependent upon types of defects and frequency of incident deams, while it should include many informations about the scatterers. One of the models was proposed by Ogawa[1] to explain the mechanism of the light scattering process, which obeyd the resonance scattering formula related between the scattered intensity and adsorption coefficient of light with a function of temperature of the specimen.

In this paper, intensity scattered from the precipitates along dislocations in an In-doped LEC GaAs crystal were precisely measured as a function of the temprature with three different frequencies of IR lasers. The peaks at 90, 123, 210, and 255K for $1.32\mu\text{m}$ radiation are with a similarity obtained by other two laser beams operated at $1.15\mu\text{m}$ and $1.06\mu\text{m}$, where the corresponding peaks slightly shift to low temperature side. The resonance frequency and damping coefficient were evaluated by using the resonance scattering model, since they show the abrupt change at about 150K. These temperature dependence can be numerically explained by Ogawa's model.

1) T. Ogawa: Jpn. J. Appl. Phys., 25, 1986, L916

G9.28

X-ALPHA CALCULATIONS OF Sn DOPING IN GaAs. D.M. Union and M. Willner, Physics Department, University of Lowell, Lowell, MA.

We report on Multiple-Scattering X-alpha Self-Consistent-Field calculations of Sn doping, including formation energies, in 17- and 29- atom cluster models of GaAs, both as a substitutional and an interstitial defect. Results for lattice substitution share many qualitative similarities with those reported in the literature for other substitutional amphoteric defects. Comparisons are made between various ways of simulating the embedding of the clusters in bulk GaAs.

G9.29

BERYLLIUM DOPING IN MBE GROWN GaAs AND AlGaAs. Joseph Pellegrino, NIST, Gaithersburg, Md.; James Griffin and Micheal Spencer, Howard Univ. MSRCE, Washington D.C.

Beryllium is an effective p dopant in GaAs and AlGaAs and plays an important role in the device characterizations of hetero bipolar transistors. This work examines the room temperature and liquid nitrogen hole mobility for two series of beryllium doped samples; GaAs and AlGaAs. Both series were grown by MBE with active layer thicknesses ranging between 0.5 - 1.5 μm . Within each series the doping ranged between $3.0 \times 10^{15} \text{cm}^{-3}$ to levels greater than $1.0 \times 10^{19} \text{cm}^{-3}$. Mobility and carrier concentrations were obtained through Hall measurements and an additional measure of the concentration profile was obtained using polaron measurements. Ohmic contacts for the Hall measurements were obtained using a Zn-In alloy. The mobility measurement results suggest the onset of carrier compensation and possible type conversion at higher doping levels. One possible explanation for this result is that at elevated doping concentrations some beryllium is incorporated as interstitial donors or defect complexes. The results for both the GaAs and AlGaAs series will be presented and discussed.

G9.30

ANOMALOUS LUMINESCENCE PROPERTIES OF GaAs GROWN BY MOLECULAR BEAM EPITAXY. L. Szafrank, M.A. Plano, M.J. McCollum, S.L. Jackson, K.Y. Cheng and G.E. Stillman, Center for Compound Semiconductor Microelectronics, Materials Research Laboratory and Coordinated Science Laboratory, University of Illinois at Urbana - Champaign, Urbana, IL 61801.

GaAs layers grown by MBE possess unique photoluminescence (PL) features associated with unidentified shallow defects. The best known are the series of lines in the 1.504-1.511 eV range, induced by defect-bound excitons (Künzel-Ploog peaks¹) and broad bands in the 1.466-1.482 eV region, originating, presumably, in related "defect-complexes".² Recently, we have reported that the "g" peak at the high energy limit of the Künzel-Ploog series is due to recombination of excitons bound to the shallowest known acceptor-like defect in GaAs, labeled "A".³ The activation energy of this defect is ~24.8 meV, about 1.7 meV less than that of C_{As}.

Additional low temperature PL studies have revealed that incorporation of this very common center results in dramatic changes in the optical properties of p-type MBE GaAs, most of which have been frequently observed in the past, but never related to the presence of the "A" defect. We have found that with increasing concentration of the "A" defect: 1) the relative intensity of the free exciton band goes through a maximum, where it dominates the near band-edge PL spectrum, and its lineshape transforms into a single, narrow peak; 2) a new, sharp line emerges at 1.513g eV; 3) neutral and ionized donor-bound exciton transitions dissappear almost completely, regardless of the actual donor concentration and compensation ratio, determined independently by Hall-effect measurements. This anomalous behaviour has led to many reports, concerning characterization of MBE GaAs and the nature of free exciton recombination, which in view of our results were based on misinterpretation of PL

data. A simple model will be proposed to explain the observed quenching of the donor-related exciton transitions. The possibility of suppression of the "A" defect incorporation by appropriate choice of growth parameters will be demonstrated.

This work was supported by the Joint Services Electronics Program, under contract N00015-84-C-0149, the National Science Foundation, under grants DMR 86-12860 and CDR 85-22666 and by DIO/IST contract DAAL 03-87-K-0013.

1. H. Künzel and K. Ploog, *Appl. Phys. Lett.* **37**, 416 (1980).
2. F. Briones and D.M. Collins, *J. Electron. Mater.* **11**, 847 (1982).
3. I. Szafranek, M.A. Plano, M.J. McCollum, S.L. Jackson, K.Y. Cheng and G.E. Stillman, 1989 *Electron. Mater. Conf.*, Boston, MA (to be published).

G9.31

POOLE-FRENKEL EFFECT ON THE DX CENTERS IN III-V TERNARY ALLOYS. H. Altelaarrea, J. Bosch, A. Pérez, J. Samitier and J.R. Morante. Departament de Física Aplicada i Electrònica. Universitat de Barcelona. Diagonal 645-647. Barcelona 08028. SPAIN.

By means of the isothermal transients, ITS, and their differences, DITS, the electrical parameters determination associated to the DX center are reviewed. The dependence of the DX centers thermal emission rates on the electric field is reported to follow a Poole-Frenkel model applied to a level attached to L minima. The time constant distribution originated by this feature has been found to be the most significative in order to explain the non-exponential emission transient and, on the other hand, the thermal activation energy shows a value which is in agreement with the Hall data.

Likewise, the thermal cross section does not show dependence on the temperature in the interval measured, while the thermal activation of the capture time constant is determined by the free carriers activation from the absolute minimum up to L minima. These two aspects fit the capture kinetic whose parameters are found to indicate rather a small relaxation unless high energy phonons are involved in the multiphonon mechanism.

Both data, emission and capture, allow to discuss a revision of the previous results deduced from the DLTS spectra whose behaviour is explained and, at the same time, point out a more simple model for the DX centers that those suggested assuming broadening, cross section distribution or fine structure.

G9.32

DEEP-LEVEL DOMINATED CURRENT-VOLTAGE CHARACTERISTICS OF NOVEL AND IMPORTANT SEMICONDUCTOR HETEROSTRUCTURES. K. Das, Department of Materials Science and Engineering, North Carolina State University, Raleigh, NC 27695-7907

Various novel semiconductor heterostructures are currently being developed for: (1) applications in extreme radiation environments, (2) high speed applications, (3) optoelectronic applications, and (4) monolithic integration of Si-based electronics with GaAs-based optoelectronics. With silicon-on-insulator and GaAs-on-silicon-on-insulator composite structures, integration of radiation-hard, latch-up-free, submicron CMOS technology with optoelectronic devices could become a viable technology. Silicon substrates with buried implanted oxide layers and silicon-on-sapphire with GaAs heteroepitaxial films are potentially important materials systems for the above applications. In order to characterize these materials electrically, a study of current-voltage characteristics of metal-semiconductor contacts formed on these various semiconductor films has been carried out. The dominant transport mechanism in all these films appears to be deep-level-dominated, space-charge-limited-current conduction. The deep-level parameters, which were determined using a straight-forward analysis, appear to be sensitive to the type of crystallographic defects initially present in a film and the defects introduced or removed by subsequent annealing and processing. In some cases, the determined discrete levels using the present approach are in excellent agreement with reported DLTS data. In particular, the analysis of the I-V characteristics obtained from heteroepitaxial MBE

GaAs grown on commercially-available silicon-on-sapphire indicates the presence of one discrete deep-level state located 0.28eV below the conduction band edge, which is within 0.01eV of the E1 center unique to MBE GaAs-on-silicon. Certain types of crystallographic defects appear to contribute greatly to states distributed in energy within the band gap. These electrically active defects are expected to influence the characteristics of devices fabricated in these novel materials.

G9.33

MOBILITY-LIFETIME PRODUCT OF PHOTOEXCITED ELECTRONS IN GaAs: THE ROLE OF EL2. George C. Valley*, Hughes Research Laboratories, Malibu, CA 90265, USA; H. J. von Bardeleben, Groupe de Physique des Solides de l'Ecole Normale Supérieure, Centre National de la Recherche Scientifique², Tour 23, 2 place Jussieu, 75251 Paris Cedex 05, France.

The mobility lifetime products for photo-electrons in semi-insulating GaAs, which fit successfully the results of photo-refractive studies undertaken in the presence of large AC electric fields or with a DC electric field and moving fringes are three orders of magnitude smaller than those inferred from transport measurements or from the photorefractive effect with no applied electrical field.

Consideration of enhanced recombination via EL2 effective-mass states linked to the L-conduction band minimum allows us to fit the dependence of photorefractive beam coupling gain coefficient on grating period for both AC fields and moving gratings. This cascade-capture process, which is three orders of magnitude faster than recombination by multiphonon emission from the Γ band to EL2, leads to greatly reduced mobility-lifetime products for field strengths greater than 1 kV/cm. Our results establish the dominant influence of the EL2 defect properties on the recombination process of photocarriers. The detailed understanding of defect recombination processes is essential for modelling and optimizing the photorefractive effect in semi-insulating GaAs.

* Visiting Professor at the Université Paris XI, Institut d'Optique during part of this work.

² associé à l'Université Paris VII.

G9.34

OPTICAL CHARGE TRANSFER PROCESSES IN SEMI-INSULATING GaAs. E. Christoffel, T. Benchiguer, A. Goltzené and C. Schwab, Groupe "Recherches Physiques et Matériaux", C.R.N., Université Louis Pasteur, 23, rue du Loess, 67037 Strasbourg Cedex France; K. Chino and K. Satoh, Electronics Materials Laboratory, Sumitomo Metal Mining Co., Ltd. 1-6-1 Suehiro-cho, Ohme-shi, Tokyo 198, Japan; P. Bunod and E. Molva, Division d'Electronique de Technologie et d'Instrumentation, IRDI-CEA, CENG, 38041 Grenoble Cedex, France.

The optical charge transfer processes is studied by means of the Electron Paramagnetic Resonance (EPR) technique on purposely prepared samples chiefly containing photoquenchable grown-in As_{Ga}^{+} and electron-induced ST1 paramagnetic centers. This mechanism is described quantitatively by a model taking into account the well-known similarity between the optical behaviors of the mid-gap donor EL2 and the photoquenchable antisites. It leads to a determination of the total content of the latter independent of initial paramagnetic fraction. ST1 becomes paramagnetic by capture of a hole, thus we infer it to be paramagnetic in its neutral acceptor state, ST1⁰.

This approach is then used for analysing the compensation mechanism between donor and acceptor states in post-growth annealed materials. Under illumination, an intricate interplay between several assumed intrinsic defects like As_{Ga} , ST1, SF, FR1, FR2 and FR2' and extrinsic ones like Fe^{3+} is revealed. Here the peculiarities of the model appear

as an efficient tool for separating the various signals and for identifying the electrical nature of the corresponding defects. Balancing released and trapped carriers in terms of defect concentrations may further help identification of spectra of insufficient EPR signature.

G9.35

COMPARATIVE OPTICAL STUDIES OF Cu, Mn, AND C IMPURITIES IN BULK LEC GROWN GAAS BY ELECTRON BEAM ELECTROREFLECTANCE (EBER) AND PHOTOLUMINESCENCE (PL). M. H. Herman, I. D. Ward, Charles Evans & Associates, Redwood City, CA; and P. J. Pearah, Spectrum Technology, Holliston, MA.

We have used both 300K and 100K Electron Beam Electroreflectance (EBER) and 4K photoluminescence (PL) to measure optical transitions. A series of LEC grown GaAs were studied which have been contaminated primarily by the individual elements Cu, Mn, and C at levels above $10^{15}/\text{cm}^3$. In an uncontaminated control sample, we find evidence for strong excitonic effects in the EBER lineshape, even at 300K. For the contaminated samples, we find evidence for characteristic optical impurity transitions below the E_g band gap of the GaAs in both spectroscopies. However, in general the estimated impurity binding energies by EBER are not equivalent to established PL or DLTS values.

The correlated appearance of impurity peaks below the split-off $E_g + \Delta_g$ band may allow their assignment to either donors or acceptors in modulated reflectance studies [1]. None of the present cases showed corresponding transitions below $E_g + \Delta_g$, suggesting that the impurity features below E_g possibly arise from acceptor transitions. Alternatively, the reduction of light penetration into the GaAs above the E_g band gap, reducing the sample interaction volume, may also explain this null observation.

[1] M. Cardona, K. L. Shaklee & F. H. Pollak, Phys. Rev. 154(3) 696, 1967.

G9.36

CORRELATION OF FREE CARRIER CONCENTRATION MEASUREMENTS IN GaAs BY NON-CONTACT OPTICAL ELECTRON BEAM ELECTROREFLECTANCE (EBER) AND PHOTOREFLECTANCE (PR) TO ELECTRICAL HALL EFFECT. D. K. Gaskill, N. Bottka, R. S. Sillmon, Naval Research Lab, Washington, DC; M. H. Herman, I. D. Ward, Charles Evans & Associates, Redwood City, CA; and C. L. Reynolds, AT&T Bell Laboratories, Reading, PA.

We have used the non-contact modulation spectroscopies electron beam electroreflectance (EBER) and photoreflectance (PR) to measure optical transitions at the E_g band gap in a series of N-type Si-doped GaAs. The free carrier concentrations within these samples were measured by Hall effect to cover a range between 10^{15}cm^{-3} and $2 \times 10^{17}\text{cm}^{-3}$. We find consistent agreement between the electrical Hall measurements and the optical estimates of the carrier concentration by both independent modulation spectroscopies.

The method of optical carrier concentration measurement is based upon the field-dependent Franz-Keldysh oscillations which exist above the E_g band gap. From the depletion region model, the surface electric field F_s , arising from the difference between the pinned surface Fermi level and that of the bulk, decreases linearly from the surface. Using the heavy-hole and electron reduced mass, the electric field is calculated from EBER and PR spectra by established methods. The optically estimated electric field is found to lie between the calculated F_s and an estimated mean field $F_s/\sqrt{3}$. We present an empirical relationship between the EBER, PR and Hall measurements, from which very accurate estimations of carrier concentration can be made optically.

G9.37

Ge RELATED DEEP LEVEL LUMINESCENCE IN InGaAs LATTICE MATCHED TO InP. S.S. Chandvankar, A.K. Srivastava, B.M. Arora and D.K. Sharma, Tata Institute of Fundamental Research, Homi Bhabha Road, Bombay 400005, India.

There is considerable interest in the study of deep levels in III-V compound alloys. We have studied the deep level luminescence associated with the amphoteric dopant Ge in InGaAs grown lattice matched to InP.

The InGaAs layers are grown by liquid phase epitaxy on InP substrates. Ge is added to the melt prior to growth. InGaAs layers grown with different amounts of Ge are studied by Hall measurement and photoluminescence. Results of Hall measurements show that Ge doping produces net p-type conduction. The samples show a wide range of carrier concentration starting with $n = 8 \times 10^{16}\text{cm}^{-3}$ for the undoped sample to $p = 5 \times 10^{17}\text{cm}^{-3}$ for the sample with the highest Ge doping. The layers are, however, highly compensated.

The PL measurements are made at 10K. The Ge doped samples show a broad deep level luminescence band covering the energy range 0.55 - 0.75 eV. The peak of luminescence shifts to lower energy with increasing p-type doping due to Ge. The PL spectra also show strong dependence on the excitation power. The peak of luminescence shifts to higher energy with increasing excitation power. The spectra show the existence of several deep levels. Preliminary analysis of the data resulted in the luminescence peaks at 0.73, 0.70, 0.68 and 0.66 eV. We think that Ge doping gives rise to complex formation which depending upon the atomic configuration of its neighbours creates several deep levels. Similar effects have been seen in ZnSse mixed crystals.

G9.38

CARBON DOPING IN InGaAs GROWN BY MBE. Hiroshi Ito and Tadao Ishibashi, NTT LSI Laboratories, 3-1 Morinosato Wakamiya, Atsugi-shi, Kanagawa, 243-01 JAPAN

Carbon doping in $\text{In}_{1-x}\text{Ga}_x\text{As}$ was investigated using solid source MBE for the first time. A graphite filament was used as a carbon source. Indium mole fraction x from 0 (GaAs) to 1 (InAs) were tested. Epi-layers were grown directly on semi-insulating GaAs substrates. Growth temperature was varied between 400°C and 650°C depending on mole fraction x . Resultant V/III ratio was about 5. Free carrier concentrations and mobilities were measured by the van der Pauw method.

Under a constant doping concentration ($6 \times 10^{18}\text{cm}^{-3}$), free carrier concentration decreases as x increases from 0 to 0.54. In this region, conduction type is p. Hole mobility also decreases with increasing x . When x is higher than 0.68, conduction type is n. Electron concentration and electron mobility increase with increasing x . These results indicate that conduction type inversion, which occurs when x is about 0.6, is due to a self-compensation. Occupation probability of III or V site by C atoms is thought to change gradually depending on the binding energy difference among C-Ga, C-As and C-In.

G9.39

SURFACE STRUCTURE OF SULFUR COATED GAAS. Yoshihisa FUJISAKI, Shigeo GOTO, Central Research Lab., Hitachi Ltd., Kokubunji, Tokyo, JAPAN

Recently, sulfur passivation of GaAs crystal has got a great attention since it improves the quality of GaAs surfaces. It is thought to be

attributed to the termination of dangling bonds of the surface atoms by sulfur. However, the detailed surface structure has not been clarified enough. Actually, two models have been proposed on the termination of free bonds. In this study, the surface structure of sulfur coated GaAs was investigated using photoluminescence (PL), X-ray photoelectron spectroscopy (XPS), and RHEED. The specimen used were (100), (111)A, and (111)B GaAs wafers. The sulfur passivation was performed in $(\text{NH}_4)_2\text{S}_x$ at 50°C for 10 minutes. The enhancement of PL intensity was remarkable for the sulfur treated (111)A wafer, but it's not so obvious for (111)B wafers. Due to RHEED observation, the sulfur treated (111)A surface has 1x1 non-reconstructed structure, whose clean surface is 2x2. This non-reconstructed structure implies the termination of Ga dangling bonds on the A surfaces, which decreases the surface state density of a crystal and enhances the PL intensity. To the contrary, both patterns corresponding to sulfur treated and untreated (111)B surfaces were halo. This is due to the thick oxide upon the (111)B surface.

In the XPS study, the smaller amount of sulfide and oxide were found on the sulfur treated (111)A surface compared with those on the sulfur treated (111)B, which coincides with the RHEED data.

G9.40

ELECTRICAL AND PHOTOLUMINESCENCE PROPERTIES OF Mg^+ and C^+ IMPLANTED ACCEPTORS IN InP . A.C. Beve, A. Yamada, A. Shimizu, H. Shibata, H. Tanoue, K.M. Mayer, H. Sugiyama, K. Kamijoh, T. Oda, O. Arriga and Y. Makita, Electrotechnical Laboratory, 1-1-4 Umezono, Tsukuba-shi, Ibaraki-ken, 305 Japan.

Ion-implantation is carried out in nominally undoped bulk InP substrates with single energy of 100 keV for Mg^+ whereas flat profile C^+ implantation is obtained using several energies up to 400 keV. The net carrier concentration profile at 300K is measured by C-V method. The photoluminescence (PL) is collected from the etched area where the carrier concentration is comparable to that of the unimplanted wafer ($4.9 \times 10^{15} \text{ cm}^{-3}$). The ground and excited states binding energies of Mg and C acceptors are accurately determined by low-temperature selective excitation of PL using an Ar^+ pumped dye laser. In addition, a sharp emission line peaking at 1.3968 eV is found to be dominant in the annealed samples. Its energy position and spectral shape (with a low energy shoulder) are similar to those of isoelectronic Bi bound exciton line well characterized in intentionally Bi-doped InP . Its intensity is found to decrease with increasing C^+ dose from $5.9 \times 10^{11} \text{ cm}^{-3}$ to $5.9 \times 10^{13} \text{ cm}^{-3}$ confirming that C is not involved. This emission band is not detected in the unannealed virgin wafer. Finally, its detection in annealed and unimplanted bulk InP clearly indicates an annealing induced-activation process of displaced Bi impurity off to regular substitutional site. These results strengthen the key role of optical spectroscopy, particularly resonant excitation of PL as a characterization method of such neutral point defects which are not detectable through electrical measurements.

G9.41

QUALITATIVE PHYSICS OF DEEP LEVELS IN HETEROSTRUCTURES* Harold P. Hjalmarson, I. J. Fritz, J. F. Klem, and T. M. Brennan, Sandia National Laboratories, Albuquerque, NM 87185.

The qualitative physics of deep levels in heterostructures will be described. Using a tight-binding method, energies for both deep and resonant levels have been calculated for substitutional impurities in GaAs/AlAs superlattices. Generalizing these results, it is found that an impurity in

a semiconductor layer has nearly the same average binding energy as it would in the bulk semiconductor equivalent of that layer. Also, an impurity forms a resonance state attached to each quantum well subband. Quantum size effects displace the actual bandedges from their corresponding virtual bandedges and thus can convert a resonance level into a deep level. Furthermore, binding energies have oscillatory deviations from the average binding energy described above. These deviations can be correlated with the nodal positions of the quantum well states, and thus the binding energy of a deep level depends on the position of the impurity within the quantum well.

Interface roughness can act as a deep level by binding or localizing an electronic state. The effect of interface roughness on low field mobility, high field drift velocity, and photoluminescence of quantum wells will be analyzed. In particular, the role of interface roughness in controlling the saturated drift velocity of light holes in InGaAs/GaAs quantum wells will be described.

*Supported by US DOE under Contract DE-AC-04-76DP00789.

G9.42

Ge TRANSPORT AND EPITAXY IN THE AMORPHOUS- $\text{Ge/Pd}_{30}\text{Si}_{70}/[111] \text{ Si}$ SYSTEM Q.Z. Hong, J.G. Zhu and J.W. Mayer, Department of Materials Science and Engineering, Cornell University, Ithaca, New York 14853

Solid phase epitaxy (SPE) of Ge-Si alloy on $[111] \text{ Si}$ substrates was achieved in the amorphous- $\text{Ge/Pd}_{30}\text{Si}_{70}/[111] \text{ Si}$ system. Channelled Rutherford backscattering spectrometry and high resolution cross section transmission electron microscopy were used to investigate the reaction process. The SPE started with the migration of Ge atoms into the epitaxial $\text{Pd}_{30}\text{Si}_{70}$ layer at 600 °C. Then single crystalline Ge islands were formed on the Si substrate. Finally the Ge islands coalesced to form a uniform epitaxial $\text{Ge}_{0.5}\text{Si}_{0.5}$ layer on the $[111] \text{ Si}$ substrate. In the meantime, the $\text{Pd}_{30}\text{Si}_{70}$ exchanged positions with the Ge layer, leading to a final configuration of $\text{Pd}_{30}\text{Si}_{70}/\text{epi-Ge}_{0.5}\text{Si}_{0.5}/[111] \text{ Si}$. The minimum yield of the epitaxial layer was 0.42, measured in the presence of the top polycrystalline $\text{Pd}_{30}\text{Si}_{70}$.

G9.43 ABSTRACT NOT AVAILABLE

G9.44

NON-LINEAR DIFFUSION IN HgCdTe/CdTe MULTILAYERS. Y. Kim, A. Ourmazd, R.D. Feldman, and J.A. Rentschler, AT&T Bell Labs, Holmdel, NJ 07733.

We apply the combination of chemical lattice imaging and vector pattern recognition to the HgCdTe/CdTe system, to determine as a function of annealing temperature, the composition of individual atomic planes across each interface of a multi-quantum well stack. The resultant composition profiles, which directly reveal the chemical change across each interface at near-atomic resolution and sensitivity, are analysed in terms of linear and non-linear diffusion theory, to deduce the interdiffusion coefficient and its activation energy.

Our results show interdiffusion to be a sensitive function of the interface depth beneath the surface. Analysis in terms of linear diffusion theory yields a depth-dependent activation energy. This depth dependence implies a dramatic change of up to $10^5 \times$ in the stability of a quantum well as its depth beneath the surface is varied.

A rigorous analysis in terms of non-linear diffusion theory yields depth-independent enthalpies and entropies for diffusion, and a depth-dependent pre-exponential factor. This indicates the depth-dependence of the interdiffusion to arise from an inhomogeneous, depth-dependent distribution of the point defects involved in the diffusion process. With certain assumptions, our results essentially allow the investigation of the native defect concentration atomic plane by atomic plane. Such unique measurements provide a valuable link with theory, and are vital for a detailed understanding of diffusion at the atomic level.

G9.45

CHARACTERIZATION OF RAMAN SCATTERING SPECTRA IN AlGaP TERNARY ALLOYS. Devki N. Talwar, T. D. Fang, Department of Physics, Indiana University of Pennsylvania, Indiana PA; and M. Vandevyver, CEA- CEN de Saclay, B.P. # 2, 91191, France.

Recently, remarkable success has been achieved in the growth processes of ternary alloys and good quality of AlGaP samples are prepared by the organometallic vapor phase epitaxy (OMVPE) technique. The knowledge of their basic physical properties (viz., lattice dynamics, band structure, elastic stiffness constants etc.) is, however, still meager. Although, inelastic neutron scattering data of phonon dispersions do not exist for Al-pnictides some information for their optical phonon mode behavior has, however, been obtained through infrared (IR) and Raman scattering (RS) methods. The knowledge of impurity induced first-order Raman scattering (IFOR) in the low frequency region is not known at this time but is very much needed for material characterization of device structures.

Based on the Green's function formalism, a theory of IFOR in mixed crystals is developed and applied to $Al_xGa_{1-x}P$. The required host lattice Greens functions are obtained in terms of a realistic lattice dynamical model and the self energy functions, needed in the explicit expressions for the scattering intensities in each Raman active representations are evaluated to first order in x . The calculated results in the low composition region x are compared and discussed with the existing Raman data.

G9.46

ELECTRONIC STRUCTURE OF Li-IMPURITIES IN ZnSe. Tamio Oguchi and Taizo Sasaki, National Research Institute for Metals, Tokyo 153; and Hiroshi Katayama-Yoshida, Department of Physics, Tohoku University, Sendai 980, Japan.

Properties of lithium impurity in zinc selenide is recognized as a crucial problem in fabricating a p-type material for the blue color light-emitting-diode. Only little is known on the electronic structure and the stability of the lithium impurity in ZnSe.

Electronic structure of lithium impurities in ZnSe has been studied by using the density-functional molecular-dynamics method proposed by Car and Parrinello, with a supercell model and a norm-conserving pseudopotential method.

Total energies and electronic properties are calculated for substitutional and interstitial impurity configurations as well as for vacancy systems, by taking lattice relaxation into account. The stable site and the migration path for a lithium atom are discussed in detail. Analysis on the numerical convergency and the validity of the model employed is also presented.

G9.47

THE DEEP 0.11 eV MANGANESE ACCEPTOR LEVEL IN GaAs. M. Kleverman, Lund University, Lund, Sweden and E. Janzén, M. Linnarsson, B. Monemar, Linköping University, Linköping, Sweden.

We have used FTIR absorption and FTIR photoconductivity together with photoluminescence to investigate GaAs doped with manganese. In absorption we find four distinct peaks just below the ionization limit. We interpret the peaks as due transitions from the ground state to the excited effective mass like $2P_{3/2}$, $2P_{5/2}(\Gamma_8)$, $2P_{5/2}(\Gamma_7)$ and $3P_{5/2}(\Gamma_8)$ states of the substitutional Mn_{Ga} acceptor. By adding the effective mass value of the $2P_{5/2}(\Gamma_8)$ state to the energy position of the corresponding absorption

peak we arrive at a ground state binding energy of 112.4 meV.

At the energy distance of an LO-phonon from the excited states we find their Fano replicas. In photoconductivity even higher order replicas are visible. In absorption the replica of the $2P_{3/2}$ state is weak and can only be seen as a small dip whereas the replicas of the other excited states are quite strong. In the photoconductivity measurements the replica of the $2P_{3/2}$ transition is the strongest. Besides the LO-phonon replicas of the excited state transitions another set of replicas is visible in the photoconductivity measurements. Since the distance between the two sets is 3 meV it might be TO-phonon replicas. At lower energies there are structures we tentatively ascribe to Fano replicas of the $2S_{3/2}$ state. The binding energy of the $2S_{3/2}$ state would then be 25.2 meV, which is considerably deeper than the effective mass value of 7.7 meV.

The oscillating photoconductivity above the ionization limit is rather weak. The period is 36.3 meV, which is close to the energy of the LO-phonon. The extrapolated limit is 110.2 meV, which is 2.2 meV below the ionization limit.

The results of uniaxial stress and Zeeman measurements of the absorption lines allow us to present a detailed description of the electronic structure of the Mn_{Ga} acceptor in GaAs.

G9.48

IDENTIFICATION OF SURFACE-RELATED ELECTRON TRAPS IN UNDOPED GAAS BY DEEP LEVEL TRANSIENT SPECTROSCOPY. K.C.Shin and I.S.Park, Goldstar Cable Research Laboratory, Anyang, Kyungki, Korea

Electron traps present in the melt-grown, undoped n-type GaAs have been studied by deep level transient spectroscopy(DLTS). Of these electron traps with energies ranging from 0.14 to 0.81 eV from the conduction band, some are believed to be related to the surface damage.

To see clearly which electron traps are related to surface damage, we prepared grain boundary Schottky barrier sample in the measurement of DLTS, thereby removing the possible effects of surface damage which can be introduced in the formation of Schottky barrier of ordinary sample with Au contact. The DLTS signal measured with increasing depletion depth of grain boundary Schottky barrier sample was compared to that of ordinary Au contact Schottky barrier sample and surface damage related electron traps were distinguished from bulk related ones.

G9.49

PHOTOLUMINESCENCE STUDIES OF IMPURITIES AND DEFECTS IN MERCURIC IODIDE. X.J. Bao, T.E. Schlesinger, Carnegie Mellon University, Pittsburgh PA 15213, R.B. James, Sandia National Laboratories, Livermore CA 94551, A.Y. Cheng C. Ortale, EG&G Energy Measurements, Goleta CA 93116.

Mercuric Iodide (HgI_2) has gained increasing attention because of its use as a material for the fabrication of room temperature X-ray and gamma ray detectors. The fabrication of high quality detectors is often limited, however, not only by intrinsic defects in the material but also by defects introduced during processing. We report on the observation of several new lines in the near-band-edge low temperature photoluminescence

spectrum of mercuric iodide. Further we have studied the effects of vacuum exposure, bulk heating, and chemical etching on the PL spectrum of this material. We find that the near surface region has a different defect structure than the bulk which we attribute to iodine deficiency. Bulk heating for times ranging from 10 minutes to several hours modifies the defect structure while vacuum exposure does not, though the latter does cause material loss from the surface of a sample. The effects of metal contact on mercuric iodide have also been studied. Metals investigated include Pd, Cu, Sn, In, and Al. All these metals cause reproducible characteristic changes in the luminescence spectrum or introduce new emission bands into the spectrum. These changes may be due to the introduction of the metal by diffusion into the mercuric iodide, reaction between the mercuric iodide and the metal, or possibly strain at the metal semiconductor interface. These studies provide guidance in choosing contact material and proper processing conditions for the fabrication of high quality nuclear detectors.

G9.50

TRANSIENT CURRENT AND TRANSIENT CAPACITANCE MEASUREMENTS OF DEFECTS IN AlGaAs MODFETS. R. Magno and R. Shelby, Naval Research Laboratory, Washington, DC, 20375.

The defects present in AlGaAs MODFET devices subjected to accelerated lifetime tests have been studied by transient current and when possible by transient capacitance techniques. By measuring transient source-drain currents following the application of a voltage pulse to the gate, it is possible to perform a Deep Level Transient Spectroscopy (DLTS) experiment on MODFET devices which are too small for the conventional capacitance DLTS. As a first step, unstressed control devices large enough for both DLTS methods were examined in order to understand the similarities and differences between the two techniques. Both the capacitance and current spectra contain the AlGaAs DX defect. By comparison, the current DLTS spectra for stressed devices contain the DX defect and an additional feature which is not found in the capacitance DLTS experiments. This additional feature is anomalous in that the transient has a sign which is opposite to that expected for a majority carrier trap. An analysis of the properties of the new defect suggest that it is located in the channel between the gate and either the source or the drain.

G9.51

ELECTRONIC AND OPTICAL PROPERTIES OF DEEP DONORS IN HYDROGENATED Al_{0.37}Ga_{0.63}As DOPED WITH SILICON; R. Mostefaoui, R. Legros, J. Chevallier, LPBH, CNRS, 1 place A. Briand, 92195 Meudon Cedex, FRANCE; and C.W. Tu, R.V. Kopf, ATT Bell Laboratories, Murray Hill, New Jersey, 07874, USA.

Si doped Al_{0.37}Ga_{0.63}As epilayers (x=0.37) have been exposed to a R.F. hydrogen plasma. It is known that such a treatment generates a neutralisation of the D-X centers by the in-diffused hydrogen atoms [1,2]. In this work, we report the electronic and optical properties of the dominant deep donors remaining after hydrogenation.

The binding energy of these donors is similar to that of the D-X centers measured on a reference sample. However, the photoconductivity, at a given temperature, is much less persistent in the hydrogenated sample: the electron recapture time is 4 to 5 orders of magnitude lower in the hydrogenated sample if compared to the reference

sample. This means that the barrier height for electron capture by the deep donors is lower compared to that of the D-X centers. Moreover, the photon energy dependence of the deep donor optical ionization cross-section is shifted by 0.2 eV towards higher with respect to the D-X center cross-section variation. Thus, the physical properties of the deep donors remaining after hydrogenation are different from that of the D-X centers. Modifications of the D-X center properties brought by hydrogen atoms located in the vicinity might be at the origin of these effects.
[1] J.C. Nabity et al.: A.P.L., 50, 921 (1987)
[2] R. Mostefaoui et al.: J.A.P., 64, 207 (1988)

G9.52

LUMINESCENCE DUE TO Mn DOPPED GaP. Teresa Monteiro; and Estela Pereira, Departamento de Física, Universidade de Aveiro, 3800 Aveiro, Portugal.

Manganese usually gives rise to strong emission bands in the near infrared in most host crystals. In the III-V materials manganese is known to originate a deep centre due to Mn²⁺ only in GaP. The only study on this emission is due to A.T. Vink and G.G.P. van Gorkom (J. Luminescence, 5, 399 (1972)), in spite of the interest that a detailed study of the band may provide to a better understanding of the location and nature of levels found in Mn doped GaP.

In this work we present a detailed study of the characteristics of the Mn²⁺ luminescence band in samples with different concentrations of Mn and of donors. The temperature dependence of the luminescence band and its lifetime is discussed. The mechanism of thermal quenching of the luminescence is also discussed.

In an attempt to correlate the luminescence data with former EPR results the magnetic field splitting of the emission lines of Mn²⁺ and the ESR signals of the same samples in the dark and upon band gap excitation is discussed.

G9.53

ZEEMAN STUDY OF THE 1.040 eV PHOTOLUMINESCENCE BAND IN CU DOPED SILICON. K.G. McGuigan, M.O. Henry, School of Physical Sciences, National Institute for Higher Education, Collins Avenue, Dublin 9, Ireland; M.H. Nazaré, Departamento de Física, Universidade de Aveiro, 3800 Aveiro, Portugal; and E.C. Lightowler, Department of Physics, King's College, Strand, London, WC2R 2LS, England.

The major features in the photoluminescence spectrum of silicon doped with copper are the 1.014 eV and the .943 eV bands. The former is thought to occur at copper pairs. The second is the dominant feature in lightly doped samples. A third band with sharp transitions at 1.040 and 1.034 eV is also seen in copper doped samples that have been heated at 1000 C for very short times (one minute) or annealed for 10 minutes at 700 C.

We report on the temperature dependence of this luminescence band and on the effects of an applied magnetic field.

The two transitions at 1.040 and 1.034 eV are found to occur from two excited states into a common ground state and the observed thermal activation energy agree reasonably well with the measured spectroscopic separation.

Zeeman measurements are reported on the 1.040 and 1.034 eV lines showing that the lower energy line involves a spin triplet excited state and the higher energy line a spin singlet excited state.

G10.1

ATOMIC DIFFUSION AND DEFECT REACTIONS IN SILICON Sokrates T. Pantelides, IBM Research Division, Thomas J. Watson Research Center, P. O. Box 218, Yorktown Heights, NY 10598

In recent years, it has been possible to carry out first-principles calculations of many key properties that relate to defect reactions and atomic diffusion, e.g. self-diffusion and the diffusion of various impurities (dopants, hydrogen, fluorine, oxygen, chalcogens, transition metals). A number of long-standing controversies have been resolved, several puzzles have been elucidated and a number of predictions have been made. Representative results will be described to convey a sense of the state of the art. Current directions and new results will also be discussed.

Acknowledgement: This work was supported in part by the Office of Naval Research under contract No. N00014-84-C-0396. It is a pleasure to acknowledge the following collaborators in various aspects of this work: Y. Bar-Yam, J. Bernholc, P. Bloechl, R. Car, P. J. H. Denteneer, J. D. Joannopoulos, P. J. Kelly, F. R. McFeely, M. Needels, C. S. Nichols, A. Oshiyama, and C. G. Van de Walle.

G10.2

PRESSURE AND STRAIN EFFECTS ON DIFFUSION. A. Antonelli and J. Bernholc, NC State University, Raleigh, NC 27695-8202.

When pressure is applied to a crystal, the formation enthalpy of a vacancy increases by the term pV_{at} , where V_{at} is the atomic volume, because the formation of a vacancy results in a transfer of an atom to the surface. Similarly, the formation enthalpy of an interstitial decreases by pV_{at} , while this term is absent in the activation enthalpy for the concerted exchange. Our first-principles calculations for Si show that the pV_{at} dominates the pressure induced changes, i.e. the activation energy for self-diffusion increases for the vacancy mechanism, decreases for the interstitial mechanism and remains approximately constant for the concerted exchange. Since the pressure dependence of each mechanism is different, the present results suggest that a set of experiments carried out at different pressures can unravel their relative contributions to self-diffusion. In addition, we find that the pressure derivative of the formation energy of the vacancy is negative, implying an *inwards* relaxation of the nearest neighbors of the vacancy.

Pseudomorphic growth on non-Si substrates often results in substantial changes in the lattice constants parallel and perpendicular to the substrate and induces large non-hydrostatic strains. We have carried out calculations for Si strained to correspond to growth on a Ge_xSi_{1-x} substrate and find that the formation energy of the interstitial goes substantially down when the mole-fraction of Ge is increased, while the formation energy of the vacancy remains approximately constant. In general, the results predict a sizable enhancement in the self-diffusion coefficient for Si grown pseudomorphically on any substrate with larger lattice spacing in the growth plane.

G10.3

LOW-TEMPERATURE DIFFUSION OF DOPANTS IN SILICON P. Fahey and M. Wittmer, IBM T. J. Watson Research Center, Yorktown Heights, N.Y. 10598.

It has been recently reported that diffusion of substitutional dopant atoms in silicon occurs during the formation of transition-metal silicides at temperatures below 300°C. Though it has been postulated

that the mechanism for the low-temperature diffusion is related to defect-enhanced diffusion, evidence for this mechanism is still lacking. We have created buried marker layers by molecular beam epitaxy to test the postulated model. The silicon samples contain a delta-shaped distribution of dopant atoms that is used to probe the diffusion enhancement. Our results show that the enhancement is unquestionably due to point defects generated by the silicide formation. We observed the effect for different dopant atoms and found an asymmetrical broadening of the diffusion profile, where diffusion is mainly directed towards the surface. This is the first experimental evidence for a 'wind effect' which has been discussed theoretically in the literature. We present the results of simulating the asymmetrical broadening by solving continuity equations for the diffusion of point defects and dopant atoms including their strong coupling.

G10.4

DETERMINATION OF THE FRACTIONAL INTERSTITIALCY COMPONENT OF DIFFUSION FOR ARSENIC M. Heinrich, M. Budil, H.W. Pötzl, TU-Wien, Gußhausstrasse 27-29, A-1040 Wien, Austria

In analyzing the experiments of Fahey et al. (1985)¹ it is shown, that the discrepancies in determination of the fractional interstitialcy component of diffusion of arsenic f_I^{As} arise due to the assumption $\frac{C_I^{As}}{C_I^{Si}} = \frac{C_{AsI}}{C_{SiI}}$ in the equation $\frac{D_{As}}{D_{Si}} = (1 - f_I^{As}) \frac{C_{AsV}}{C_{SiV}} + f_I^{As} \frac{C_{AsI}}{C_{SiI}}$ made by the authors to analyze their experiments. This assumption has been made in almost all previous works analyzing diffusion under nonequilibrium conditions. In simulating the experimental data by means of the pair diffusion model of Budil et al. (1989)², which accounts for the concentration of the dopants, the point defects and the dopant-defect pairs we find the abovementioned assumption not justified. A consistent treatment shows that the supersaturation of dopant-point defect pairs during nonequilibrium conditions and the supersaturation of point defects do not show the same behavior, as the number of dopant atoms is limited and therefore sets a natural limit for the dopant-point defect pair supersaturation. A unique value for f_I^{As} is presented which makes it possible to explain the diffusion enhancement under surface nitridation as well as surface oxynitridation in one model.

[1] P. Fahey, G. Barbuscia, M. Moslehi, R.W. Dutton. Appl. Phys. Lett. 46(8), 15 April 1985, p. 734

[2] M. Budil, H. Pötzl, G. Stingeder, M. Grasserbauer, K. Goser. Materials Science Forum Vols. 38-41 (1989) pp. 719-724

G10.5

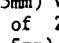
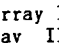
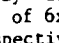
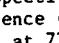
MEASUREMENTS OF ENHANCED AND RETARDED DIFFUSION OF BURIED LAYERS IN SILICON MEMBRANE STRUCTURES DURING OXIDATION. Scott T. Dunham, Anuradha M. Agarwal and Nanseng Jeng, Electrical, Computer and Systems Engineering Department, Boston University, Boston, MA.

Calculations of the diffusion coefficient of silicon self interstitials vary over several orders of magnitude at temperatures of interest for integrated circuit fabrication. Previously, these differences have been explained by invoking a bulk trapping phenomenon. An alternative explanation is suggested by the observation that lower values of interstitial diffusivity are calculated from experiments in which interstitial concentration is monitored near non-oxidizing SiO_2 interfaces and higher values are calculated when monitored in the bulk; thereby possibly indicating that the interactions of interstitials with the SiO_2 film may be more complicated than a constant interface regrowth velocity. In this work, in order to distinguish between bulk and interface interactions, we measure the enhanced and retarded diffusion, respectively, of phosphorus and antimony buried layers while interstitials are injected at a wafer surface via thermal oxidation. The starting substrates were

float-zone silicon and Czochralski silicon with or without pre-treatment to precipitate excess oxygen. The samples were prepared by implantation of P or Sb followed by the growth of an epitaxial layer. They were then etched anisotropically from the backside to yield membrane structures. Local oxidation is performed on either the front or back side of each wafer and buried layer diffusion is monitored, yielding information about interstitial diffusion in silicon and how it depends on bulk properties.

G10.6

MIGRATIONS OF INTERSTITIAL ATOMS IN SEMICONDUCTORS. T. Wada, A. Takeda, M. Ichimura, Nagoya Institute of Technology, Showa, Nagoya, 466, Japan; and M. Takeda, Government Industrial Research Institute, Nagoya, 462, Japan.

Zn and Ge atoms were introduced into the unirradiated regions of GaAs at 50°C and Si wafers at 140°C, respectively by using the electron-beam doping method. The surfaces of GaAs substrates (undoped (100), LEC) with an area of 13x20mm² (t=0.6mm) and Si wafers (area 17x30mm², t=0.25mm) were covered partially (like ) by the overlayers of Zn sheet (5x5mm², t=0.5mm) and Ge wafer (10x10mm², t=0.5mm), respectively. The only surfaces of the Zn and Ge sheets were irradiated locally with the fluences of 5x10¹⁸ (in water bath) and 1x10¹⁸ electrons/cm² (in vacuum) at 7MeV, respectively. Even at a distance of 0.10mm from the irradiated overlayers in the GaAs and Si substrates, Zn and Ge atoms respectively, whose interstitials may migrate the unirradiated regions, were detected by SIMS measurements. On the other hand, the surfaces of only GaAs wafers (6x12mm²) without Zn sheet (array I, ) and Zn (5x5mm², t=0.5mm)/GaAs (13x20mm²) (array II, ) and Zn (6x6mm², t=0.5mm)/Zn/GaAs (6x12mm²) (array III, ) were irradiated partially at 50°C by the area of 6x6mm² for arrays I and III, and 5x5mm² for array II, respectively. In the case of arrays I and II, the photoluminescence (PL) for the GaAs substrates disappeared in every region at 77K before annealing. However, it should be emphasized for array III that PL large peaks attributed to Ga antisite defects (Ga_{As}) at 1.445eV were observed even at a distance of ~5mm from the irradiated regions before annealing. The concentration of Ga_{As} created by the reaction of the kick-out mechanism in array III, Zn_iZn_s+Ga_{As}, is much higher than that produced in arrays I and II, where subscripts of i and s mean interstitial and substitutional states. Then, Ga_i diffuses into the unirradiated regions and Ga_{As} defects may be introduced by a reaction, Ga_iZn_sGa_{As}+As_i.

G11.1

MEASUREMENTS OF ENHANCED OXYGEN DIFFUSION IN SILICON DURING THERMAL DONOR FORMATION: NEW EVIDENCE FOR POSSIBLE MECHANISMS. A.R. Brown, R. Murray, R.C. Newman and J.H. Tucker, Interdisciplinary Research Centre Semiconductor Materials, Imperial College, The Blackett Laboratory, Prince Consort Road, London, SW7 2BZ, U.K.

Recently it has been shown that heat treatment of Czochralski silicon in a hydrogen plasma enhances the rates of thermal donor formation and the loss of oxygen from solution by factors of 5, 30 and 300 at 450, 400 and 350°C respectively. The inference is that TD-formation is controlled by long range diffusion of interstitial oxygen atoms, since ENDOR studies show oxygen to be present in the defects. We have, therefore, re-appraised and extended measurements of the rate of loss of oxygen in furnace annealed samples at low temperatures down to 315°C. The new data indicate an activation energy close to 1.8eV, the value found for TD-formation. There is also an indication that a previously proposed model of oxygen dimer formation is incorrect.

Ancillary experiments involving 2MeV electron irradiation and H⁺ plasma treatments of samples provide no evidence that the enhanced diffusion results from the presence of either self interstitials or vacancies. It is possible that hydrogen impurities may be responsible for the observed effects, although it is not

implied that hydrogen is a constituent of TD-centres. The enhancement cannot be due to an intrinsic property of the oxygen as it is necessary to account for the results of the relaxation of stress-induced dichroism which show normal diffusion jump rates in some samples.

G11.2

A STEADY-STATE MODEL FOR COUPLED DEFECT-IMPURITY DIFFUSION IN SILICON. F. F. Morehead and R. F. Lever, IBM East Fishkill Facility, Hopewell Junction, NY.

We extend and generalize our earlier model which was proposed to explain tails in the diffusion profiles of high concentration boron and phosphorus in silicon. Our quasi-steady-state approach is generalized to include both vacancies (V) and self-interstitials (I) at equivalent levels. I-V recombination is regarded as near local equilibrium, occurring through reactions of the defects with defect-impurity pairs. This approach leads directly to important details such as the well-known plateau, kink and tail in high concentration phosphorus diffusions in silicon and to the less well recognized tails in boron as well, with no additional ad hoc assumptions. Our extended model, in its simplest form, allows a more complete and less restrictive treatment than the usual combination of "kick-out" and Frank-Turnbull models of gold in diffusion in silicon. An important advantage is the direct inclusion of these defect-impurity interactions and the resulting gradients in the defect concentrations, which gradients are ignored even in the latest versions of popular process simulation programs, such as SUPREM IV. Our model provides insights that are unique to this approach and yields details of the diffusion process which would be otherwise accessible only to a full-blown model tracking all of the diffusing species, defects and defect-impurity pairs. Such a model would consume about a million times more computer processing time than our more transparent steady-state approach.

G11.3

HIGH AND LOW TEMPERATURE MEASUREMENTS OF THE CHROMIUM DIFFUSIVITY IN SILICON. J. Zhu, D. Barbier, Laboratoire de Physique de la Matière, Bât. 502, Institut National des Sciences Appliquées de Lyon, 20 Avenue Albert Einstein, F69621 Villeurbanne Cedex, France.

The diffusivity of most of the 3d metals in Silicon have been already assessed in the high temperature range with however a very poor accuracy, making the extrapolation toward low temperature hazardous. Moreover, low temperature measurements achieved only in the case of Fe, disagreed by several order of magnitude with the diffusivity law derived from the fit of high temperature data.

In this work, the diffusivity of Chromium in Silicon has been studied in the 20-1050 °C range. Chromium films were sputtered onto one face of Boron-doped Silicon samples which were subsequently annealed and quenched in a Rapid Thermal Processor. The diffusion coefficients between 850 and 1050 °C were obtained by erfc fitting of the Chromium-Boron pair profiles, measured by means of Deep Level Transient Spectroscopy a few days after diffusion. Low temperature diffusivities were derived from the rate constant of the diffusion-limited Chromium-Boron pairing reaction, monitored by Deep Level Transient Spectroscopy in Chromium-contaminated specimens at fixed temperatures of the 20-100 °C interval.

Whereas our high temperature diffusivity values were in close agreement with the early determinations of Bendik and Würker, we measured low temperature diffusivities at least one order of magnitude higher than those extrapolated from the high temperature diffusivity law. Due to a more expanded 1/T interval in the low temperature range, the Arrhenius fit of the data points from 20 to 1050 °C is likely to be more reliable than the previous high temperature determinations. Thus, our results suggest that the energy barrier for the jump of Chromium atoms between two adjacent interstitial sites should be rather 0.85 eV than 1.0 eV so far assumed.

G11.4

THE FORMATION OF SILICON-RICH SILICIDES. Maria Ronay, IBM T.J. Watson Research Center, Yorktown Heights, NY.

While it is known that the formation of transition-metal (TM) disilicides between silicon single crystals and thin polycrystalline TM overlayers takes place by silicon diffusion at a temperature as low as 450°C for CrSi_2 , and as high as 750 °C for HfSi_2 , such formation temperatures are hard to reconcile with the large activation energy for silicon self-diffusion (4.1 to 5.1 eV). I find that the formation temperature of disilicides correlates with the size of the TM atom, suggesting that TM diffusion may be the rate limiting step. Transition metals diffuse interstitially in silicon with an activation energy as low as 0.43 eV for the small copper ion and as high as 1.5 eV for the large titanium atom.

In order to investigate this suggestion we choose rhenium as an example for a relatively slow diffusing TM. We studied the formation of ReSi_2 alone, and we studied it by adding fast-diffusing copper to the system. Using thin film layered structures, inert gas annealing and Auger electron spectroscopy combined with sputter profiling and x-ray analysis, we found that for Re-Si diffusion couples the formation temperature of ReSi_2 is 900°C, the highest reported for a disilicide. In the case of Cu-Re-Si or Re-Cu-Si diffusion 'couples' the formation temperature of ReSi_2 is reduced to 400-500°C. While in both cases ReSi_2 forms by silicon diffusion, in the presence of copper this is preceded by copper diffusing into silicon. Structural relations indicate that the formation of Cu_3Si precipitate injects silicon self-interstitials into the silicon lattice, a fast diffusing species, which then forms the ReSi_2 at much lower temperature than without copper. Theoretical results of Joannopoulos *et al.*, Pantelides *et al.* and Baraff *et al.* predict very low barriers to the migration of silicon self-interstitials. The results reported here suggest that the diffusion of TM atoms (ions) into silicon precedes and promotes the diffusion of silicon into the TM films by forming silicon interstitials or by otherwise weakening the silicon bonds.

G11.5

PRECIPITATION OF COPPER AND COBALT AT GRAIN BOUNDARIES IN SILICON. U. Jendrich, H.J. Möller. Department of Materials Science and Engineering, Case Western Reserve University, Cleveland, OH 44106; and T. Tüken, IV. Physics Institute, University of Göttingen, 3400 Göttingen, FRG.

Many of the electronic properties of polycrystalline semiconductors are related to grain boundary phenomena. Recent experimental results indicate that segregating shallow and deep level impurities like phosphorous or transition metal impurities are more important for their electrical properties than has been previously assumed, however, little is known about the segregation behavior of many of these impurities. This study will present experimental results on the interaction of copper and cobalt with grain boundaries in silicon.

Czochralski grown bicrystals containing a single coincidence grain boundary and large grained polycrystalline silicon were used for the gettering experiments. The metals were diffused in the crystal from a surface source at temperatures between 850° and 1050° C until a homogeneous distribution of the impurities in the bulk was achieved. In the case of cobalt a radioactive isotope ^{57}Co was used and the distribution of the element in the bulk analysed by a tracer technique combined with Mössbauer spectroscopy, which allowed a quantitative analysis even at very low impurity levels. Depending on the temperature and cooling rate the metallic impurities accumulate inhomogeneously at the grain boundary forming metal silicide precipitates. TEM investigations were carried out to analyse the distribution, morphology, size and the crystallographic structure of the precipitates.

The results show that structural features in the grain boundary like dislocations and steps facilitate the nucleation and lead to the inhomogeneous distribution, and that the gettering depends strongly on the thermal history of the specimens. The results obtained so far are discussed from the perspective of the electrical transport properties of grain boundaries.

G11.6

Annealing of ion implanted tin in silicon: A RBS/channeling, Mössbauer spectroscopy and TEM investigation of solubility and residual defects.

P. Kringhøj, A. Nylandsted Larsen, and J. W. Petersen, Institute of Physics, University of Aarhus, DK-8000 Aarhus C, Denmark

This work reports results from an investigation over a wide concentration range of the Si-Sn system produced by ion implantation of Sn into $\langle 100 \rangle$ silicon.

A homogeneous profile to a depth of 2000 Å of ^{119}Sn was obtained by a triple implantation technique. Samples with concentrations in the range $3.0 \cdot 10^{20} \text{ cm}^{-3}$ to $1.7 \cdot 10^{21} \text{ cm}^{-3}$ were RTA or furnace annealed. The samples were investigated with the following technique: RBS/channeling, Mössbauer spectroscopy and TEM.

By following the formation and subsequent dissolution of $\beta\text{-Sn}$ precipitates as a function of annealing time and temperature, the solubility of Sn in Si was determined in the temperature range 1000 to 1200°C.

For temperatures at or above 1000°C and for Sn concentrations below $6 \cdot 10^{20} \text{ cm}^{-3}$ perfect regrowth of the implanted layer and removal of residual defects was achieved for annealing times larger than ~10s. This leads us to propose Sn as an ideal preamorphization candidate.

G11.7

EXTREME SUPERSATURATION OF OXYGEN IN LOW-TEMPERATURE EPITAXIAL SILICON AND SILICON-GERMANIUM ALLOYS - P.V. Schwartz, J.C. Sturm, P.M. Garone, Dept. of Electrical Engineering, Princeton University, Princeton, N.J. 08544; and S.A. Schwarz, Bellcore, Red Bank, N.J. 07701

The solid solubility of oxygen in silicon has a well accepted maximum of approximately $2 \times 10^{18} \text{ cm}^{-3}$. Using a combination of rapid thermal processing and chemical vapor deposition known as Limited Reaction Processing, we have grown epitaxial silicon and silicon-germanium strained layer alloys with oxygen concentrations up to 10^{21} cm^{-3} (over 1% of the atomic composition). The concentrations were measured by SIMS calibrated against implant standards.

Although the exact nature of the oxygen is not known, it is thought that the oxygen does not exist in precipitate form, even though conventional theories would predict a large number of precipitates given the extreme supersaturation and thermal history of the samples. No precipitates have yet been seen by TEM. IR transmission shows a large peak shifted from that of normal interstitial oxygen in silicon, and suggests that hydrogen may be playing an important role. This is consistent with the fact that the source of the oxygen is thought to be water vapor adsorbed on the quartz walls of the growth chamber.

Despite these large oxygen concentrations, layers may be grown without stacking faults or dislocations. Electron channeling patterns are indistinguishable from those of bulk wafers. Further, high quality electrical devices such as heterojunction bipolar transistors have been made in these films. This work has been supported by ONR and NSF.

G12.1

DIFFUSION IN INHOMOGENEOUS SYSTEMS, STUDIED AT NEAR-ATOMIC RESOLUTION. A. Ourmazd, J. Cunningham, Y. Kim, and M. Bode, AT&T Bell Labs, Holmdel, NJ 07733.

Modern materials and devices are highly inhomogeneous systems. It is thus necessary to investigate diffusion at extremely high spatial

resolution, and hence sensitivity. We have developed a technique based on chemical lattice imaging, that can quantitatively measure diffusivities as small as $10^{-20} \text{ cm}^2/\text{s}$, sampling regions $\sim 10^{-19} \text{ cm}^3$ in volume. This method essentially maps the composition of materials with atomic sensitivity, and reveals the atomistic details of the diffusion process.

The application of our approach to intermixing in the GaAs/AlGaAs and the HgCdTe/CdTe systems shows the interdiffusion coefficient to be a sensitive function of the interface distance from the surface. Similarly, we are able to observe the kinetic intermixing induced in multilayered systems, when a single energetic ion enters each 2000 \AA^2 of the interface. Finally, we can image δ -doped layers in GaAs, directly determining their width, the in-plane distribution of the dopants, and their outdiffusion during different growth procedures, or subsequent anneals.

In this paper we describe how such measurements can shed light on the details of diffusion and intermixing in semiconductor multilayers, systems that are highly inhomogeneous and far from equilibrium.

G12.2

GROWTH OF GaAs ON Ge SUBSTRATES BY ATOMIC LAYER EPITAXY*. J. Ramdani, B.T. McDermott, N. El-Masry and S.M. Bedair, Electrical and Computer Engineering Department, N.C. State University, Raleigh, North Carolina

The GaAs/Ge system suffers from problems such as epilayer crystalline quality and interdiffusion of Ge, Ga and As. Atomic Layer Epitaxy (ALE) can offer improved GaAs/Ge interfaces because of its two dimensional growth nature and its ability for low temperature deposition.

GaAs was grown on Ge at 300°C and 400°C using TEG and TMG respectively. This low deposition temperature has resulted in the near elimination of the outdiffusion of Ge into the GaAs epilayers. SIMs data indicated a drop in the Ge concentration by five orders of magnitude in the GaAs film over a thickness of 150 \AA away from the Ge interface. This represents a substantial improvement over other GaAs films grown by ALE at 450°C or by MOCVD at 550°C . TEM data also showed that ALE-grown GaAs/Ge interfaces are almost free from stacking faults and antiphase domains. The I-V characteristics of GaAs/Ge junctions were thyristor-like, diffused or abrupt junctions, depending on the ALE growth temperatures.

We will report on the use of the ALE self-limiting adsorption process of TMG to control the indiffusion of Ga into an n-type Ge substrate at the monolayer levels. This was followed by low temperature ALE growth of GaAs which resulted in an improved $\text{nn}^+ \text{ GaAs-p}^+ \text{ n Ge}$ heterojunction.

*Supported by ONR/SDIO Contract N00014-88-K-0527

G12.3

EXTREMELY RAPID SN DIFFUSION IN GAAS AND (Al,Ga)AS I.F. Kuech, M. Goorsky, F. Cardone, G. Scilla, and R. Potemski, IBM T.J. Watson Research Center, P.O. Box 218, Yorktown Heights, NY, 10598.

Tin is a n-type dopant in GaAs and (Al,Ga)As. It has been recently studied in the growth of (Al,Ga)As in conjunction with its characteristics as a DX center. We have studied the diffusion of Sn in both GaAs and (Al,Ga)As grown by metal-organic vapor epitaxy (MOVPE). Unlike other group IV dopants in GaAs, Sn is an extremely fast diffuser at both low temperatures and low Sn concentrations. It diffuses much more rapidly than Zn or Mg in similar structures under like annealing

conditions. We have measured the diffusion of Sn in both GaAs and (Al,Ga)As as a function of alloy composition, annealing temperature, and Sn concentration. This matrix of samples and annealing conditions allows for the study of influence of the bandgap on the diffusion characteristics. The Sn diffusion coefficient is found to be highly concentration dependent as well as dependent on the alloy composition. The Sn diffusion coefficient in (Al,Ga)As is also sensitive to the electrical characteristics (i.e. Fermi level) of the matrix into which it is diffusing. A higher diffusion coefficient was found for diffusion into n-type $\text{Al}_{0.4}\text{Ga}_{0.6}\text{As}$ than nominally undoped or p-type material. Both the modeling of the diffusion profiles and a discussion of the results in terms of the current models of fast diffusion in GaAs will be given.

G12.4

DIFFUSION OF ION IMPLANTED MAGNESIUM AND BERYLLIUM IN GALLIUM ARSENIDE. Heyward G. Robinson, Michael D. Deal, and David A. Stevenson, Stanford University, Stanford CA.

Magnesium and beryllium are finding increasing use as p-type dopants in gallium arsenide. The annealing behavior of samples implanted with these dopants has been studied extensively by several researchers but the basic mechanisms governing their redistribution have not been fully understood. In this paper we report on some recent progress in this area.

Magnesium implants show three diffusion regions: 1) rapid uphill diffusion in the peak of the implant; 2) rapid concentration-independent diffusion in the tail; and 3) slow concentration-dependent diffusion in between. Beryllium, in contrast, shows only concentration dependent diffusion. Uphill diffusion can be induced in beryllium implants by co-implanting with a heavier element such as argon. Paradoxically, this retards the concentration dependent diffusion. This behavior can be explained with the Substitutional-Interstitial-Diffusion (SID) mechanism and an understanding of the defect chemistry after implantation. In the region of uphill diffusion, the dopants are seen to getter from areas of excess interstitials to areas of excess vacancies. A critical concentration of damage is required to initiate uphill diffusion which explains why it is observed in magnesium implants and only in beryllium implants when argon is co-implanted. The implant damage reduces the concentration dependent diffusion by shifting dopant atoms from interstitial to substitutional sites.

G12.5

DEFECT FORMATION DURING Zn DIFFUSION INTO GaAs. M. Luysberg, W. Jäger, K. Urban, Institut für Festkörperforschung, KFA Jülich; M. Perret, N. Stolwijk, and H. Mehrer, Institut für Metallforschung, Universität Münster, F.R. Germany.

The microstructural evolution during Zn diffusion into semi-insulating GaAs single crystals at 1170 K was characterized for various diffusion times $t < 1740 \text{ min}$ by analytical electron microscopy. The results were compared with Zn concentration profiles obtained by spreading resistance measurements (SRM) on the same samples.

Crystal lattice defects were observed only in the depth region between the surface and the diffusion front which could be identified unambiguously by SRM. The diffusion front was found to be characterized by the presence of prismatic interstitial-type dislocation loops and of cavities partly filled with Ga. Behind the diffusion front

a dislocation network was observed. The dislocations were decorated and surrounded by Ga-enriched precipitates. Closer to the surface the dislocation density decreased and faceted voids and vacancy-type dislocation loops were observed. Just below the surface SRM yielded a Zn concentration plateau and electron microscopy showed a high density of Zn-rich precipitates.

A model is presented which accounts for these observations. It is based on fast interstitial Zn diffusion and the kick-out mechanism for interstitial-substitutional exchange. A possible contribution of the Frank-Turnbull mechanism well behind the diffusion front is discussed.

G12.6

Room - Temperature Diffusion of Mn in CdTe and the Formation of $Cd_{1-x}Mn_xTe$. A. Wall, A. Raisanen, G. Haugstad, and A. Franciosi, Department of Chemical Engineering and Materials Science, University of Minnesota, Minneapolis, MN 55455.

Deposition of Mn at room temperature onto atomically clean CdTe (110) surfaces yields atomic interdiffusion for metal coverages $\theta \leq 3 \text{ \AA}$ with Mn atoms occupying cation sites within the surface and near-surface layers of the semiconductor, and the displaced Cd atoms migrating away from the surface. Synchrotron radiation photoemission studies of the surface region as a function of the photoelectron escape depth, and parallel studies of bulk ternary alloys cleaved in-situ, indicate room-temperature diffusion lengths for Mn larger than 18 Å, and the formation of relatively homogeneous ternary semimagnetic semiconductor surface alloys throughout the $0 < x < 0.95$ composition range. The highest Mn concentration observed far exceed those obtainable with bulk crystal growth methods, indicating that the surface free energy plays an important role in determining the stability of the ternary surface layer. The resulting simplified atomic-layer-epitaxy method holds promise for the synthesis of a wide variety of semimagnetic semiconductor superlattices.

G13.1

ORDERING IN III/V ALLOYS. G.B. Stringfellow, College of Engineering, University of Utah, Salt Lake City, Utah 84112

Simple calculations using the delta-lattice-parameter (DLP) model indicate that the enthalpy of mixing is invariably larger than or equal to zero for III/V alloys, and increases with increasing difference in lattice constant for the constituent binary compounds. In terms of the regular solution model this suggests the occurrence of miscibility gaps. Solid phase immiscibility has indeed been observed in a number of systems. Nevertheless, such alloys can be grown by OMVPE, including the highly metastable alloys GaPSb and InPSb. Initially surprising was the occurrence of ordered structures in these same alloys. The regular solution model apparently specifically excludes immiscibility and ordering in the same system. However, when the positive enthalpy of mixing is due to strain energy effects, as in III/V alloys, Hume-Rothery recognized very early that such phenomena should be anticipated. This was later confirmed by detailed first principles calculations. In fact, the tendency for ordering is anticipated to increase as the difference in tetrahedral radii of the elements sharing a common sublattice increases. Thus, it is somewhat surprising that ordering was first observed in the AlGaAs system where Al and Ga have nearly equal sizes. Ordered structures have now been observed in several III/V alloy systems including the ternary systems GaAsSb and GaInP and the quaternaries GaInAsP, GaInAsSb, and AlGaInP. In this paper, ordering in other alloy systems such as InPSb,

InAsSb, and GaAsP will be described. Surprisingly, no strong correlation between atomic size difference and the degree of ordering has been observed. Another unexpected observation is that the preferred ordered structure for the ternaries GaInP, InPSb, InAsSb, and GaAsP involves ordering along the {111} directions. Both first principles total energy and simple strain energy calculations indicate that such ordered structures are only slightly more stable than the disordered solid solution. Other ordered structures, including $L1_0$, where ordering occurs along the {100} directions, are considerably more stable. Both phenomena must be explained in terms of the surface kinetic processes occurring during epitaxial growth. Such an explanation is supported by the importance of kinetic parameters such as growth rate, temperature, and substrate orientation in determining both the degree of order and the specific ordered structures observed.

G13.2

COMPARISON OF ORDERED AND MODULATED STRUCTURES IN InGaP ALLOY SEMICONDUCTORS GROWN BY MOCVD, CHLORIDE-VPE AND LPE METHODS. O. Ueda, M. Hoshino, M. Takechi, and M. Ozeki, Fujitsu Laboratories Ltd., 10-1 Morinosato-Wakamiya, Atsugi 243-01, Japan; and T. Kato and T. Matsumoto, Yamanashi University, 4-3-11 Takeda, Kofu 400, Japan.

Ordered and modulated structures in InGaP alloy semiconductors grown on (001)GaAs substrates by metalorganic chemical vapor deposition (MOCVD), chloride-vapor phase epitaxy (VPE) and liquid phase epitaxy (LPE) have been systematically studied by transmission electron diffraction (TED) and high resolution transmission electron microscopy.

In MOCVD-InGaP crystals ($T_g = 630^\circ\text{C}$), strong ordering (CuPt-type) has been observed, which is associated with an abnormality in the photoluminescence (PL) peak energy as previously reported. For Chloride-VPE-InGaP crystals, CuPt-type ordered structures have also been observed. However, the degree of ordering is weaker in the latter case and crystals grown at $576-740^\circ\text{C}$ exhibit normal PL peak energies. On the other hand, in LPE-InGaP crystals, no superstructure spots are found in the (110) TED patterns, and the crystals exhibit normal PL peak energies. Modulated structures do not depend on the growth method since they are observed in all crystals. From these results, one can conclude that the ordered structures are not generated under thermal equilibrium conditions but rather by the diffusion and reconstruction of deposited atoms on the growth surface.

G13.3

ATOMIC ORDERING AND ALLOY CLUSTERING IN MBE-GROWN $InAs_ySb_{1-y}$ EPILAYERS. T.Y. Seong, A.G. Norman, G.R. Booker, Dept. of Metallurgy and Science of Materials, University of Oxford, U.K.; R. Droopad, R.L. Williams, S.D. Parker, P.D. Wang and R.A. Stradling, Dept. of Physics, Imperial College of Science, Technology and Medicine, University of London, U.K.

We report the first observation by transmission electron diffraction (TED) of CuPt-type atomic ordering in MBE-grown $InAs_ySb_{1-y}$ epitaxial layers. The layers corresponded to the composition range $y = 0.2$ to 0.8 . TED patterns obtained from all the epitaxial layers contained strong $1/2(111)$ superstructure spots. This is consistent with ordering on (111) planes of the group V sublattice with alternating As-rich and Sb-rich (111) planes. Ordering occurred on only two of the four possible (111) planes. The intensity of the superstructure spots exhibited a maximum for $y \approx 0.5$. This could be due to an increase in either the volume fraction of the ordered phase or the degree of ordering. A fine scale ($\approx 15\text{nm}$) strain contrast was observed by

transmission electron microscopy in all the epitaxial layers. This contrast is attributed to alloy clustering possibly occurring as a result of spinodal decomposition. The 77K carrier mobility decreased smoothly from $5 \times 10^4 \text{ cm}^2 \text{Vs}^{-1}$ for $x = 0$, to $1 \times 10^3 \text{ cm}^2 \text{Vs}^{-1}$ for $x = 0.5$, and then increased to $5 \times 10^4 \text{ cm}^2 \text{Vs}^{-1}$ for $x = 1$. Mechanisms for the coexistence of the atomic ordering and alloy clustering in the epitaxial layers, and also possible correlations between the structural and electrical properties, are discussed.

G14.1

LIGHT- AND HEAVY-HOLE BOUND EXCITON TRANSITIONS AND FREE TO BOUND TRANSITIONS IN $\text{Ga}_{1-x}\text{Al}_x\text{As/GaAs}$ QUANTUM WELLS. Donald C. Reynolds, Wright Research and Development Center, Electronic Technology Laboratory, Wright-Patterson AFB OH, and Krishan K. Bajaj, Arizona State University, Tempe AZ.

Excitons bound to neutral donors in $\text{Al}_{1-x}\text{Ga}_x\text{As/GaAs}$ quantum wells were observed by high resolution resonant excitation photoluminescence, and temperature dependent photoluminescence measurements. Changes in the binding energy of excitons are observed when the donors are located in the center of the well, at the edge of the well, or in the center of the barrier. The variations in these binding energies are reported as a function of well size from 75-350Å. The binding energies increased as the well size was reduced to about 100Å, with further reductions in well size they decreased.

Light-hole free excitons bound to neutral donors were observed in $\text{Al}_{1-x}\text{Ga}_x\text{As/GaAs}$ quantum wells. The transitions were observed, using selective excitation photoluminescence spectroscopy, in the energy region between the light-hole and heavy-hole free exciton transitions where no other intrinsic transitions exist. The neutral donor-bound heavy-hole free-exciton transitions were also observed when the light-hole bound exciton transitions were observed. Quantum well structures which showed no evidence of a heavy-hole donor bound exciton also showed no evidence of a light-hole donor bound exciton.

Free to bound transitions, free hole to bound electron, have also been observed in the $\text{Al}_{1-x}\text{Ga}_x\text{As/GaAs}$ quantum wells. The diamagnetic shift of these transitions was used to identify them from excitonic transitions.

G14.2

DECAY MEASUREMENTS ON FREE AND BOUND EXCITON RECOMBINATION IN DOPED GaAs/AlGaAs QUANTUM WELLS. P. Bergman, P.O. Holtz, B. Monemar, Dept. of Physics and Measurement Technology, Linköping University, S-58183 Linköping, SWEDEN; M. Sundaram, J.L. Merz and A.C. Gossard. Dept. of Electrical and Computer Engineering, University of California at Santa Barbara, Santa Barbara, CA 93106, USA.

We have studied the decay kinetics of the free exciton (FE) and the acceptor bound exciton (BE) in a $\text{GaAs/Al}_{0.3}\text{Ga}_{0.7}\text{As}$ quantum well (QW). The QWs were grown by molecular beam epitaxy (MBE) in a Varian Gen II system and doped in the central 20% of the QW with a Be-concentration of 10^{17} cm^{-3} . The measurements were performed on different samples with a QW width ranging from 50 Å up to 150 Å.

At low temperatures the decay time of the BE was found to be in the range of 350-550 ps with a weak tendency of increased decay time with an increased QW width. The FE decay at low temperatures is close to our measuring resolution (250 ps). At higher temperatures the FE decay increases due to the change in the energy distribution of the FEs. Our measurements show that the measured decay time of the BE also increases correspondingly, and at temperatures above 20 K the decay time of the BE and the FE are identical in all samples.

The temperature dependence of the decay times is explained by a model assuming thermalization between the FE and the BE. This results in a thermal equilibrium between these states at elevated temperatures,

which in turn gives rise to the similar decay time observed. CW photoluminescence measurement comparing the relative intensity of the FE and BE recombination at different temperatures support the suggested model.

G14.3

EFFECTS OF CONFINEMENT ON THE OPTICAL PROPERTIES OF A SHALLOW ACCEPTOR AND ITS BOUND EXCITON IN GaAs/AlGaAs QUANTUM WELLS. P.O. Holtz^{a,b}, M. Sundaram^b, J.L. Merz^b, and A.C. Gossard^b. a) Department of Physics and Measurement Technology, Linköping University, S-58183 Linköping, Sweden, b) Department of Electrical and Computer Engineering and Materials Department, University of California, Santa Barbara, CA 93106

The binding energy of an impurity confined in a quantum well (QW) is strongly dependent on the thickness of the QW. The effect of the confinement on the impurity binding energy has been calculated in several theoretical papers, but these predictions have been experimentally verified only in a few cases, mainly for donors.

We report in this study the observation of transitions from the ground state to excited states of the Be-acceptor confined in narrow GaAs/AlGaAs QWs via two independent spectroscopic techniques: Two hole transitions (THTs) of the acceptor bound exciton (BE) measured by selective photoluminescence and resonant Raman scattering (RRS) observed at dye-laser excitation resonant with or close to the BE. The same transitions are observed at almost identical transition energies with these two techniques. The effect of confinement on the acceptor transitions has been investigated by varying the thickness of the QWs in the range 50 - 138 Å for samples doped in the central 20% of the QWs. The provided experimental results are also compared with the theoretical predictions.

The dependence of the binding energy of the exciton bound to the investigated Be-acceptor on the transition energies as determined from the above described THT and RRS measurements has also been investigated. An almost linear relationship between these quantities was derived, which implies that a correspondence to Haynes' rule in bulk material could be applied also to these QW systems, but in this case for the same acceptor at different binding energies due to the effect of confinement.

G14.4

OPTICAL SPECTROSCOPY OF 2D ELECTRONS CONFINED AT A GaAs/AlGaAs HETEROINTERFACE IN A TRANSVERSE ELECTRIC FIELD. Q.X. Zhao^a, P. Bergman^a, B. Monemar^a, P.-O. Holtz^{a,b}, C. Hallin^a, M. Sundaram^b, J.L. Merz^b and A.C. Gossard^b. a) Dept. of Physics and Measurement Technology, Linköping University, S-581 83 Linköping, SWEDEN. b) Dept. of Electrical and Computer Engineering, University of California, Santa Barbara, California 93106, USA.

Radiative recombination and decay time measurements of the two dimensional electron gas in a GaAs-AlGaAs heterojunction (the so called H-band) has been studied under transverse electric field perturbation in specially optimized structures prepared by molecular beam epitaxy. The heterostructure was created between 50 nm undoped GaAs and 8 nm of undoped $\text{Al}_{0.35}\text{Ga}_{0.65}\text{As}$ followed by 70 nm Si-doped $\text{Al}_{0.35}\text{Ga}_{0.65}\text{As}$. Both positive and negative gate voltages have been applied to the GaAs-AlGaAs interface, and shifts of the H-band energy position depending on the gate voltage are induced by the corresponding changes in the heterostructure 2D potential. For different gate voltages the excitation power dependence of the H-band energy position is quite similar, since only the lowest 2D subband is occupied in these samples. It is demonstrated that a transverse electric field allows a simple way to modify the 2D heterostructure potential, so that detailed spectroscopy can be done on the recombination of carriers localised in such a potential. Another interesting phenomenon is that the gate voltage can increase the luminescence of the active 50nm-GaAs layer. This indicates that the electric field makes the "3D" recombination more dominant by changing the potential. To obtain information about the dynamical behaviour of the interface recombination we have performed both time-resolved spectral measurements and time decay measurements with and without an applied electric field. The decay

time has been measured at different energy positions in the broad H-band luminescence, and is found to have a non-exponential decay with values of decay time varying from a few ns at high energies, to hundreds of ns in the lower energy region.

G14.5

DEFECT INDUCED LUMINESCENCE FROM MBE PREPARED $\text{Si/Si}_{1-x}\text{Ge}_x$ SUPERLATTICES.* G.A. Northrop, S.S. Iyer, and D.J. Wolford, IBM Thomas J. Watson Research Center, Yorktown Heights, NY 10598.

We report the first definitive observation of photoluminescence (10 K) from Si/SiGe superlattice heterostructures. Samples consisting of thin alternating layers of $\text{Si/Si}_{1-x}\text{Ge}_x$ were prepared by molecular beam epitaxy on (001) Si. Radiation damage, in the form of implantation with $3 \times 10^{12}/\text{cm}^2$ Si^+ , at 50 keV, followed by annealing at 200°C , was used to produce centers responsible for the sharp I_1 and G excitonic lines, often observed in similarly damaged silicon. Superlattices with periods as short as 200 Å exhibit significant recombination at both centers. We find the G-line is not measurably shifted or spectrally broadened, thus suggesting that such recombination may be localized to the unstrained, pure silicon layers. In contrast, the shallower I_1 center displays two components -- a sharp line similar to that of G, centered on a broadened, but distinct, luminescence background. This we interpret as recombination at centers localized to both the silicon and the alloy layers, respectively, thus proving deep-level recombination occurs from within the heterostructures. Use of these defects as potential probes of very narrow-period and symmetrically strained superlattices will be discussed, as will possibility of quantum-size effects in these structures.

*Supported in part by the U.S. Office of Naval Research under contract N00014-85-C-0868.

G14.6

SHALLOW-DEEP TRANSITIONS AND DEEP LEVELS IN SUPERLATTICES. John D. Dow, S. Y. Ren, J. Shen, R.-D. Hong, D. A. Drabold, O. F. Sankey, M.-H. Tsai, S. Klemm, and P. A. Fedders, U. of Notre Dame*, Notre Dame, IN.

Substitutional impurities in semiconductors that are s- and p-bonded generally produce four deep levels with energies in the vicinity of the fundamental band gap (one s-like and three p-like). If none of these levels lies within the gap and the impurity comes from a different Column of the Periodic Table from the atom it replaces, then the impurity is termed a "shallow impurity"; otherwise it is a "deep trap" or an "isoelectronic center". Artificially layered materials such as superlattices offer an opportunity to change the character of an impurity from "shallow" to "deep" by driving one of its deep levels from within the host bands into the gap. This can be done by engineering the thicknesses of the artificial layers. The superlattice band edges are relatively more sensitive to the layer thicknesses than the energies of the deep levels, allowing one to move a band edge through a deep level, changing the character of the impurity. For example, Si on a Ga site in a GaAs quantum well of a GaAs/AlAs superlattice will have its s-like deep level above the conduction band edge of the superlattice for thick quantum wells, but in the superlattice's band gap for thin wells, being "shallow" in the former case but "deep" in the latter. This impurity makes the quantum well n-type for thick wells but semi-insulating for thin ones. (Similar behavior, as a function of alloy composition, is observed for Si in $\text{Al}_x\text{Ga}_{1-x}\text{As}$ alloys and N in $\text{GaAs}_{1-x}\text{P}_x$.) We speculate that similar shallow-deep transitions can be employed to circumvent the resistance of some II-VI semiconductors to p-type doping and to explain the low doping efficiency of amorphous Si.

G15.1

THE DX CENTER: EVIDENCE FOR CHARGE CAPTURE VIA AN EXCITED INTERMEDIATE STATE. Thomas N. Theis and Patricia M. Mooney, IBM Research, T.J. Watson Research Center, P.O. Box 218, Yorktown Heights, NY.

We review diverse experimental observations which suggest that charge capture to the deep donor level (DX center) in GaAs and $\text{AlGa}_{1-x}\text{As}$ occurs via an intermediate excited state. The observations include: 1. The alloy and pressure dependence of the activation energies for capture and emission. 2. The non-exponential broadening of the capture transients, corresponding to an exponential dependence of the capture rate on the quasi-Fermi level. 3. The electric field and lattice temperature dependence of the hot electron capture rates. All of these observations support the large lattice relaxation picture, but multiphonon capture must occur from an excited state which lies well above the lowest conduction band edge, and which approximately tracks the DX level.

What suppresses multiphonon capture from the Γ valley? Many authors have suggested that capture occurs via conduction states of the higher lying L-valley, but recent experiments indicate DX involves no unusual weighting of L-like basis states. A natural mechanism for suppressing such transitions is that capture to DX involves more than one electron. Simultaneous capture of two electrons from the Γ valley is improbable, and the dominant capture process involves occupation of a localized resonant state, which can relax to the DX state upon capture of a second electron. Such a picture is completely consistent with a "negative U" model for the DX center, as proposed by Chadi and Chang. Furthermore, the inferred configuration coordinate diagram is precisely analogous to that calculated for the arsenic antisite by Dabrowski and Scheffler. This supports the idea that the neutral arsenic antisite (EL2) and negatively charged substitutional donor (DX) are similar defects.

G15.2

EFFECT OF LOCAL ATOMIC CONFIGURATION ON DX ENERGY LEVEL. T. Baba and M. Mizuta, NEC Corporation, Tsukuba, Japan; and T. Fujisawa, J. Yoshino and H. Kukimoto, Tokyo Institute of Technology, Yokohama, Japan.

In this paper we have successfully determined energy levels of Si-DX centers with specific local environments, specifically the Si-DX center surrounded only by the Ga 2nd nearest neighbors (nn) is located 295 meV above the Γ conduction band edge of GaAs. The energy level moves downward when coordinated by an Al and Ga mixed-environment by as much as 120 meV. We will further report similar experiments for the case of a Te donor and will compare this with Si. The main concern of this paper is the different behaviors of the two donors due to the different substitutional sites between Si (group III site) and Te (group V site).

Using a sample consisting of a monolayer of AlAs and 14 monolayers of GaAs with Si or Te as a dopant, DLTS measurements were conducted under various hydrostatic pressures. The energy level for the Te-DX center surrounded only by Ga was found to be higher than the energy of the Si-DX center in GaAs. Downward movement of the Te-DX center when associated with Al as the 1st nn was also observed. On the other hand, different from the Si-DX center, a very large shift of the activation energy for electron emission with pressure was found for the Te-DX center surrounded by the mixed-environment. This will be discussed in relation to the lattice relaxation of the relevant DX centers.

G15.3

ELECTRIC FIELD ENHANCEMENT OF THE EMISSION RATE OF DX CENTERS. Mimoun Zazoui, Song L. Feng, Jacques C. Bourgoin and Hans J. von Bardeleben, Groupe de Physique des Solides de l'Ecole Normale Supérieure, Centre National de la Recherche Scientifique^a, Tour 23, 2 place Jussieu, 75251 Paris Cedex 05, France.

We have investigated the electric field enhancement of the electron emission rate of DX centers in MBE and LPE Si and Te doped GaAlAs layers for different alloy compositions. In Te doped layers, in a specific alloy composition range, this enhancement is found to obey to the Poole Frenkel effects. The reason this effect is operative for special alloy compositions and natures of the impurity will be explained. The consequences of the fact that DX center emission is sensitive to the Poole Frenkel effect will be developed. It will be deduced that the DX center can only be a single donor state, as is the shallow effective-mass state associated with the lowest conduction band. It will therefore be concluded that the DX level is the effective-mass state associated with the L band which is deepened by intervalley mixing.

^a associé à l'Université Paris VII.

G15.4

OPTICALLY DETECTED MAGNETIC RESONANCE OF GROUP IV AND GROUP VI DONORS IN $\text{Al}_{1-x}\text{Ga}_x\text{As}/\text{GaAs}$ ($x \geq 0.35$) HETEROSTRUCTURES. E. GLASER, T.A. Kennedy, and B. Molnar, Naval Research Laboratory, Washington, D.C., 20375-5000.

The influence of different chemical species on the nature of shallow donor states in $\text{Al}_{1-x}\text{Ga}_x\text{As}/\text{GaAs}$ heterostructures has been investigated by optically detected magnetic resonance (ODMR). ODMR experiments were performed on as-grown and implanted Si- and S-doped epitaxial layers (1-5 μm) of AlAs and $\text{Al}_{1-x}\text{Ga}_x\text{As}$ ($x \geq 0.35$) grown on (001) GaAs substrates. The results are compared with the predicted behavior of shallow donor states associated with group IV and group VI impurities in III-V semiconductors.

Angular rotation studies of the Si donor ODMR reveal the heteroepitaxial strain of the $\text{Al}_{1-x}\text{Ga}_x\text{As}/\text{GaAs}$ structures and demonstrate explicitly the X-minimum symmetry of the shallow donor state.¹ This donor can be described by an independent valley model for $x \geq 0.75$ since the valley-orbit interaction is negligible.

The donor g-value anisotropy is much reduced for the S-doped samples as compared to the Si-doped samples with similar aluminum mole fraction. For example, $\Delta g = 0.008$ as the magnetic field is rotated from $[1\bar{1}0]$ to $[001]$ for $\text{Al}_{0.4}\text{Ga}_{0.6}\text{As:S}$ as compared to $\Delta g = 0.019$ for $\text{Al}_{0.4}\text{Ga}_{0.6}\text{As:Si}$. In addition, the linewidths of the resonances are significantly larger for the S-doped samples. These data suggest that the valley-orbit splitting of the ground singlet (A_1) state and the excited doublet (E_2) state for the S donor in $\text{Al}_{1-x}\text{Ga}_x\text{As}$ is 10-15 meV, similar to values reported for group VI donors in GaP.

1. E. Glaser *et al.*, Phys. Rev. B (Aug. 15, 1989)

The work was supported in part by ONR

G15.5

OPTICAL PROPERTIES OF EXTREMELY HEAVILY DOPED n-GaAs. Huade Yao* and Alvin Compaan, University of Toledo, Toledo, OH.

It is generally accepted that the DX center lies ~160 meV below the L-band edge in GaAs. Therefore carrier concentrations of n-GaAs can not exceed $\sim 2 \times 10^{19}/\text{cm}^3$ provided there is little distortion of the conduction band at high dopant densities. However, pulsed-laser annealing on ion-implanted GaAs can produce carrier concentrations beyond this limit. Recently, we obtained extremely heavily

doped n-GaAs by pulsed-dye-laser annealing ($\lambda = 728 \text{ nm}$) on Si-implanted GaAs. Electron concentrations exceed $3 \times 10^{19}/\text{cm}^3$. Raman studies indicate that the highest frequency of the Raman plasmon mode (L^+) is at $\sim 1700 \text{ cm}^{-1}$, much higher than any previous reports. Our photoluminescence (PL) studies show that in very heavily doped n-GaAs, the electron-hole recombination is dominated by non-momentum-conservation transitions. The PL spectra indicate a bandgap narrowing, due to heavy n-type doping, which is approximately proportional to the square root of the electron concentration. For a carrier concentration of $3.2 \times 10^{19}/\text{cm}^3$, the bandgap shrinkage exceeds ~180 meV. The PL data show that the Fermi level exceeds 420 meV at the highest carrier concentration. This is indirect evidence of a conduction band "stretch" between the Γ and L-valley of GaAs. If the Γ -band edge shifts much more than the L-band edge during the course of bandgap narrowing, the energy difference between the DX center and Γ -band edge increases significantly. Then carrier concentrations exceeding $\sim 2 \times 10^{19}/\text{cm}^3$ are possible without the Fermi energy exceeding the DX center energy.

* Present address: Center for Microelectronic and Optical Materials Research, University of Nebraska, Lincoln, NE.

G16.1

THEORY OF EL2 AND DX CENTERS. D. J. Chadi, Xerox Palo Alto Research Center, Palo Alto, CA.

The doping of GaAs with Group IV or VI elements generally leads to shallow donor levels with binding energies of $\approx 7 \text{ meV}$. These shallow levels are associated with substitutional site impurity atoms. A very interesting shallow-deep transition is experimentally observed to occur at pressures exceeding 24 kbars. In the absence of pressure, the same type of transition is observed to occur when a fraction larger than 22% of the Ga atoms are replaced by Al, i.e., the donor binding-energy increases with Al concentration reaching a peak value of about 160 meV. The microscopic nature of atomic distortions responsible for the formation of these deep DX centers in Si and S doped GaAs and AlGaAs alloys were examined via *ab initio* self-consistent total-energy calculations. Defect formation is found to be accompanied by a large bond rupturing lattice distortion involving the donor and one of its nearest neighbors. The proposed atomic structure for DX is shown to provide a satisfactory explanation for nearly all of its experimentally observed properties. The similarities and common physical origins of DX and As-antisite derived EL2 defect centers are emphasized. Our most recent calculations show that a similar type of lattice distortion also occurs in p-doped ZnSe where it leads to acceptor self-compensation.

G16.2

IS DX(Te) CENTER IN $\text{Al}_x\text{Ga}_{1-x}\text{As}$ A NEGATIVE-U DEFECT? L. Dobaczewski, J. E. Dmochowski, P. Kaczor, J. Wróbel, and J. M. Langer, Institute of Physics, Polish Academy of Sciences, Warsaw, POLAND.

DX centers in AlGaAs attract significant attention caused by their atypical behavior for defect states as well as their technological importance. Among many open problems concerning their nature one has attracted particular attention recently. It is a possibility of a negative-U character of this defect. It is our aim to provide analysis of several experiments aimed to resolve this puzzle as well as to discuss implication of the negative-U for recombination processes.

Careful analysis of the Hall concentration (particularly lack of a double slope in the high temperature region for all known data indicating an omnipresent high compensation being quite natural for a negative-U system) gives support to this model. A seemingly indicative mobility changes are

consistent with this model but do not provide a clear cut argument.

Most significant piece of evidence for the negative-U is given by the absence of the Poole-Frenkel effect in the ground state (localized) of DX center in contrast to a standard P-F effect occurring at the metastable hydrogenic X-like D^0 state.

The supposition that the DX center in the ground state binds two electrons is also consistent with a strong dependence of a capture rate on a high magnetic field. There is also quite significant evidence that a photoionization of DX center is a two-step process (with an intermediate state being a neutral D^0 state).

G16.3

PHOTOIONIZATION AND PHOTOCAPTURE TESTS OF DX-CENTER MODELS. Harold P. Hjalmarson, S. R. Kurtz, and T. M. Brennan, Sandia National Laboratories, Albuquerque, New Mexico 87185.

The DX-center photoionization cross-section has a large threshold energy (approximately 1 eV) which is much larger than its thermal binding energy (approximately 0.1 eV). This data can be explained by a large-lattice relaxation model in which strong coupling to the lattice drives a resonance state into the bandgap. In the trapped bipolaron model, the large lattice relaxation occurs only, if a second electron is captured by the neutral DX-center.

These models can be distinguished by detailed measurements of the photoionization or photocapacitance cross-section. We show that further analysis of the original LLK model shows that it predicts a phenomenon which we term photocapture. In this phenomenon, absorption of light induces transitions between conduction band-edge states and unrelaxed DX-center states lying within the conduction band. The net result in the ideal model is that absorption of light can fill the DX-center. The modified photoionization cross-section for the LLK model will be shown to disagree with photocapture data. Furthermore, the photoionization cross-section for the trapped bipolaron model will also be described; it disagrees with photoionization data.

1. D. V. Lang, R. A. Logan, M. Jaros, Phys. Rev. B **19**, 1015 (1979).
2. D. J. Chadi and K. J. Chang, Phys. Rev. Lett. **61**, 873 (1988).

*This work was supported by the U. S. Department of Energy under contract number DE-AC-04-76DP00789.

G16.4

MÖSSBAUER STUDY OF THE DEFECT STRUCTURES AROUND Te IMPLANTED IN $Al_xGa_{1-x}As$. H. Bemelmans and G. Langouche, IKS, University of Leuven, Belgium; G. Borghs, IMEC, Leuven, Belgium.

^{129m}Te atoms were implanted in $Al_xGa_{1-x}As$ ($0 \leq x \leq 1$) with a dose of 2×10^{13} atoms/cm². After rapid thermal annealing to 900°C, a variation in the Mössbauer spectra as a function of x is observed. For $0.2 \leq x \leq 0.7$, a component with a large electric field gradient is dominant in the spectra, while for the other values of x an unsplit resonance dominates. The same component with the large electric field gradient was observed before [1] in the Mössbauer spectra of Te-implanted GaAs for concentrations exceeding 10^{19} atoms/cm³.

As the presence of this component is correlated with the presence of the DX-center, the hyperfine interaction parameters of the observed Mössbauer spectrum component will be discussed with respect to some of the existing models for the DX-center.

[1] G. Langouche, D. Schroyen, H. Bemelmans, M. Van Rossum, W. Deraedt and M. de Potter, Mat. Res. Soc. Symp. Proc. **104** (1988) 527

G16.5

THE METASTABILITY OF THE EL2 DEFECT IN GaAs AND 3-5 ALLOYS. Hans J. von Bardeleben and Jacques C. Bourgoin, Groupe de Physique des Solides de l'Ecole Normale Supérieure, Centre National de la Recherche Scientifique², Tour 23, 2 place Jussieu, 75251 Paris Cedex 05, France

The microscopic structure of the EL2 defect and its relation to the metastability has turned out to be one of the key problems in the study of this defect. The two currently discussed models, the isolated arsenic antisite As_{Ga} and the pair model $As_{Ga}-As_i$, predict different metastable configurations: the gallium vacancy-arsenic interstitial pair and the split interstitial As_i-As_i respectively.

We present in this paper an analysis of the alloy and pressure dependence of the EL2 properties in the stable and metastable configuration. We show that these variations, which have not been included in the previous modelling of EL2, can be quantitatively interpreted if the EL2 metastable state is attributed to the $Al(1s)$ effective-mass state associated with the L conduction band minimum. The apparent contradiction on the point symmetry of EL2, deduced from optical absorption and ODENDOR measurements, find a simple explanation within this model. The origin of this metastability implies it to be a property concerning not only the double donor EL2 but the much wider class of donor defects in 3-5 compounds.

² associé à l'Université Paris VII.

G17.1

PROGRESS IN UNDERSTANDING THE OPTICAL PROPERTIES OF EL2. G. A. Baraff, AT&T Bell Laboratories, Murray Hill, N.J., 07974

Many experimental techniques have been used to probe EL2 in an attempt to determine its exact microscopic identity, the exact position of nearby atoms for both its normal and metastable configurations, and the exact mechanism by which it transforms between the two. Part of the reason for our difficulty in reaching full understanding of this defect may be that our knowledge of basic defect processes has been built on experience with systems for which standard simplifying approximations have been valid. For that reason, we may have been unprepared to cope with a defect for which these simplifications do not work.

In this talk, we shall review experimental features of the optical absorption of EL2 in the normal state. We shall exhibit some of the seeming internal inconsistencies that appear in interpreting them. We shall then show how some of these inconsistencies trace back to the breakdown of familiar ideas which we have carried over from the study of similar, but better behaved, systems. Finally, we shall present an account of recent progress towards refining our understanding of the EL2 optical absorption spectrum and its response to hydrostatic and uniaxial stress.

G17.2

DIRECT OPTICAL DETERMINATION OF THE CROSS-SECTION FOR LIGHT INDUCED METASTABLE TRANSITION OF THE EL2 DEFECT. W. Kuszko, M. Jezewski, J. M. Baranowski, Institute of Experimental Physics, Warsaw University, Warsaw, Poland.

The characteristic absorption spectrum of the EL2 defect in GaAs quenches proportionally when the defect undergoes a transition to a metastable state during illumination of a crystal at low temperature. This feature was used to measure a spectral dependence of an absolute value of a cross-section σ^* for the light induced metastable transition. The

spectrum of σ^* exactly renders the shape of the band of the EL2 intracenter absorption with its fine structure. This is a strong evidence that both the fine structure and the broad band of the intracenter absorption are due to the same transition within the defect. It is also ruling out the possibility that the excited state of this transition is a strongly delocalized level.

It is concluded that the EL2 defect reaches its metastable configuration relaxing from the excited state of the intracenter transition which is in agreement with the recent theoretical results by Chadi et al. and Dabrowski et al. A comparison of the value of σ^* with the value of the cross-section of the intracenter absorption shows that the effectiveness of this channel of relaxation is in the order of a few percent.

G17.3

THE DOUBLE DONOR ISSUE OF THE EL2 DEFECT IN GaAs. M. O. Manasreh and Gail L. Brown, Materials Laboratory (WRDC/MLPO), Wright Research and Development Center, Wright-Patterson Air Force Base, Ohio 45433-6533.

Photo-induced changes in the infrared (IR) absorption spectrum of the EL2 defect in undoped and lightly alloyed unannealed GaAs materials grown by the liquid-encapsulated Czochralski technique were observed under a monochromatic light irradiation. These changes were attributed to the change of the charge states of EL2. The spectrum which is believed to be due to the charged EL2 exhibits a complex structure with two peaks at 1.07 and 1.32 eV and a shoulder at 0.94 eV. The $EL2^+ \rightarrow EL2^0$ and $EL2^+ \rightarrow EL2^0$ were obtained by illuminating the sample with $0.7 \leq h\nu \leq 0.95$ eV and $1.3 \leq h\nu \leq 1.5$ eV, respectively. The transformation $EL2^+ \leftrightarrow EL2^0$ can be achieved in less than 10 sec and can be repeatedly switched back and forth between the two states. Fourier-transform photoconductivity (FTPC) measurements were performed on a large number of samples both semi-insulating and n-type. Two broad peaks were observed in the FTPC spectra with thresholds at ~ 0.78 and ~ 0.95 eV. The photoquenching and thermal recovery properties of these two peaks are identical to those of EL2. Both IR and FTPC results suggest strongly that EL2 is a double donor.

G17.4

ABSOLUTE PRESSURE DEPENDENCE OF THE SECOND IONIZATION LEVEL OF EL2 IN GaAs. D.E. Bliss, W. Walukiewicz, D.D. Nolte, and E.E. Haller, Dept. of Materials Science and Mineral Engineering, University of California at Berkeley and the Center for Advanced Materials, LBL.

We report the results of DLTS experiments under uniaxial stress on the second ionization level of EL2 in p-type GaAs. We measured the shift in the hole emission rate as a function of stress applied in the [100] and [110] directions. By modeling the valence band with two independently displacing bands and appropriately derived thermal effective masses, we obtain a small absolute hydrostatic pressure derivative for the defect, 36 ± 15 meV GPa⁻¹. The shear contribution is negligible. This result is very different from the measured absolute pressure derivative of 90 ± 15

meV GPa⁻¹ for the first ionization level. We propose that it indicates that the strong lattice coupling of EL2 occurs in the neutral charge state.

*Supported by US DOE
contract DE-AC03-76SF00098.

G17.5

THE SYMMETRY OF THE EL2 DEFECT IN GaAs. P. Trautman and J.M. Baranowski, Institute of Experimental Physics, Warsaw University, Warszawa, Poland

Linear dichroism has been measured in the broad absorption band of the EL2 defect in GaAs under uniaxial stress. In addition, the splittings of the EL2 zero-phonon line (ZPL) at 8378cm^{-1} under uniaxial stress applied along [100], [111], and [110] directions have been measured. Splitting of the ZPL under [100] stress is over one order of magnitude smaller than under [111] stress, on the other hand, the linear dichroism in the broad absorption band is roughly equal for these two directions of stress. This is an evidence for the quenching of the coupling to tetragonal strains due to interaction with trigonal modes of the lattice (the Ham effect). Therefore, it is established, that the excited T_2 state of EL2 is an localized state subject to dynamical Jahn-Tell' coupling to trigonal modes of the lattice. The possibility that the excited T_2 state has hydrogenic nature associated with the L minima is ruled out by the present results. The observed splittings of the ZPL together with polarization selection rules clearly indicate the tetrahedral T_d symmetry of the EL2 defect ruling out any other point group in particular trigonal C_{3v} . In view of the presented experimental results, their interpretation, and recent theoretical investigations, the isolated arsenic antisite As_{Ga} most successfully accounts for the properties of the neutral charge state of the EL2 defect.

G18.1

AN ANOMALOUS VACANCY DIFFUSION IN SILICON DURING THE ANTIMONY DRIVE-IN DIFFUSION: W. Wijaranakula and J.H. Matlock, Materials Characterization Laboratory, SEH America, Inc., 4111 NE 112th Ave., Vancouver, WA 98662, USA.

In the junction-isolated bipolar integrated circuit device fabrication, a low-resistivity buried layer diffusion is the first processing step prior to epitaxial layer growth. In the region underneath the antimony buried layer, enhanced oxygen thermal donor generation and retardation of the oxygen precipitation were observed. The effect of oxygen outdiffusion could explain one of the phenomena, but not both simultaneously, because they seemingly contradict to each other. If it is assumed that the electronic defects responsible for the donor activity are related to silicon interstitials, an enhanced thermal donor generation could occur as a result of vacancy undersaturation. This assertion appears to be the most plausible one because it is consistent with an observed retardation of the oxygen precipitation.

From the above observations, it is hypothesized that the depletion of intrinsic vacancies in the region underneath the buried layer occurs during an antimony drive-in diffusion. In this region, the diffusion of ionized vacancies could be enhanced by the build-in electric field originating from the antimony buried layer. In the buried layer, a Sb^+V^- complex formation is also hypothe-

sized. Assuming the proposed mechanism is to prevail, the intrinsic vacancy concentration could play a significant role in the generation of the oxygen thermal donors in silicon.

G18.2

A COMPARISON OF THE DIFFUSIVITY OF AS AND GE IN SI AT HIGH DONOR CONCENTRATIONS. K. Kylliesbech Larsen, P. Gaiduk, and A. Nylandsted Larsen, Institute of Physics, University of Aarhus, DK-8000 Aarhus C, Denmark

The aim of this paper is to compare the diffusivity of As and Ge in Si at high donor concentration: $\sim 10 < n/n_i < \sim 60$, where n and n_i are respectively the actual and intrinsic carrier concentration at the diffusion temperature. Such a comparison is interesting for many reasons, suffice it to mention here that these two impurities have almost the same mass and tetrahedral covalent radius (both bigger than the one for Si) but that Ge is electrically neutral as a substitutional impurity in Si whereas As is positively charged, hence Coulomb-interaction related differences in the diffusivities can be, in principle, studied.

We have previously demonstrated that for $\sim 20 < n/n_i < \sim 60$ the diffusivities of Sn, As, and Sb in Si at 1050°C depend on $(n/n_i)^2$, where S is significantly higher than 2, the value which should be expected for diffusion via doubly charged negative vacancies. In the present paper we include data for Ge and will perform a detailed comparison between the measured diffusivities of Ge and As in Si as well as a comparison with theoretical estimates.

G18.3

ANOMALOUS TRANSIENT TAIL DIFFUSION OF BORON IN SILICON: CONCENTRATION DEPENDENCE VERSUS SPATIAL DEPENDENCE. N.E.B. Cowern, Philips CFT Automation, Eindhoven, The Netherlands; H.F.F. Jos, Philips Components, Nijmegen, The Netherlands; and K.T.F. Janssen, Philips Research Laboratories, Eindhoven, The Netherlands.

Boron transient diffusion exhibits an anomalous 'tail' diffusion, in which the low-concentration part of the B profile diffuses much faster than the 'peak' region. Currently available models of this effect either assume that it arises from inhomogeneity in the silicon crystal due to damage [1,2], or that it is due to spatial variation in B substitutionality after ion implantation [3].

Recent observations suggest that at damage levels below the amorphisation threshold, the response of B doping atoms to implantation damage depends mainly on the B concentration. Specifically, implantation of a low dose of Si ions into the near-surface region of a substitutional B profile appears to cause B transient diffusion which is inversely dependent on B concentration [4]. This behavior is not consistent with any of the models so far proposed for the anomalous B peak-tail diffusion [1-3].

To clarify this issue we report further, more critical measurements on the concentration dependence of anomalous B transient diffusion, using a range of shallow Si implant doses into deep substitutional B profiles. We also report on the evolution of the electrical activation as a function of B concentration and time, using SIMS and spreading-resistance techniques. We discuss the physical basis for alternative models of the observed behavior, and present numerical simulations based on one such model.

1. R.B. Fair, J.J. Wortman and J. Liu, J. Electrochem. Soc. **131**, 2387 (1984).
2. A.E. Michel, Nucl. Instrum. Meth. **B37/38**, 379 (1989).
3. W.K. Hofker, H.W. Werner, D.P. Oosthoek and H.A.M. de Grefte, Appl. Phys. **2**, 265 (1973).
4. N.E.B. Cowern, H.F.F. Jos and K.T.F. Janssen, Proc. E-MRS Meeting, Symposium B, Strasbourg, May 30-June 2 1989.

G18.4

RAPID THERMAL PROCESS-INDUCED DEFECTS: GETTERING OF THE INTERNAL AND EXTERNAL CONTAMINANTS. B. Hartiti, W. Eichhammer, J.C. Muller and P. Siffert, CRN (IN2P3) Laboratoire PHASE (UPR n° 292 du CNRS) BP 20, 67037 Strasbourg Cedex, France.

In recent years, rapid thermal processes (RTP) have been widely studied with the aim to replace conventional thermal processes. As RTP inherently include quenching steps at the end of the thermal cycle, the determination of the origin of RTP-related defects in silicon is of great importance for many device applications. RTP-induced defects were in general analyzed by means of Deep Level Transient Spectroscopy (DLTS) in the near surface region. A number of energy levels were detected, varying from one author to the other, which were believed to be either intrinsic or impurity-related defects without excluding a possible contribution of surface contaminants.

Here, we will demonstrate that the RTP-induced defects are related to residual impurities present in the as-grown material, and, hence are dependent on the origin of the silicon wafer. For one particular material an activation of a specific residual metallic impurity was observed in the temperature range $800 - 1000^\circ\text{C}$. A complete picture of what is occurring in RTP was obtained by a systematic serial sectioning in steps of about $25\mu\text{m}$ over the whole sample thickness. In particular, we were able to separate three different effects: the activation of residual bulk defects, the inhomogeneous redistribution of these defects by a gettering effect of the surface, and the occurrence of surface contamination during the sample preparation.

The annealing of the activated bulk defects as well as the possible passivation of these defects by means of low-energy hydrogen ion implantation are discussed.

G18.5

OXYGEN AND IRON REDISTRIBUTION UPON THERMAL TREATMENT IN IRON IMPLANTED SILICON. B. Pivac*, A. Borghesi*, L. Ottoloni**, M. Geddo*, A. Piaggi* and A. Stella*, *Dipartimento di Fisica-Universita' di Pavia Via A. Bassi 6, I-27100 Pavia, ITALY; **Centro di Studio per la Cristallografia Strutturale del C. N. R., I-27100 Pavia, ITALY

As an iron is a fast diffuser in silicon, the prevention of silicon contamination with iron during technological processes is very difficult. In order to study the iron-oxygen interaction in silicon, different doses of 100 keV iron ions have been implanted into CZ silicon substrates, and subsequently annealed. The redistribution of iron and oxygen upon thermal treatment in nitrogen atmosphere was monitored with SIMS and FTIR measurements. A significant gettering of iron as well as of oxygen into the layer close to the implanted surface has been found only for doses exceeding the critical fluences, therefore indicating that the structural disorder and associated lattice strain field are the main driving force for gettering mechanism. It has been found, however, that for doses above the critical fluences not all iron ions have been trapped into the damaged region, but a significant part of them have diffused into the bulk of material, unaffected with gettering oxygen.

G18.6

ION BEAM ETCHING OF SILICON: IMPLANTATION AND DIFFUSION OF NOBLE GAS ATOMS, AND GETTERING OF COPPER William D. Sawyer and Jörg Weber Max-Planck-Institut für Festkörperforschung Heisenbergstr. 1, 7000 Stuttgart 80, Federal Rep. of Germany

Using photoluminescence (PL), Rutherford backscattering (RBS) and transmission electron microscope imaging (TEM), we investigate defects which are introduced into silicon by ion beam etching. The RBS results show that during the ion beam etch a highly damaged surface layer is formed which contains a large concentration of Ar atoms. The Ar atoms then diffuse out of the surface and into the crystalline bulk by some form of radiation enhanced diffusion. Annealing of the etched samples at 350°C results in the formation of noble gas defects known from previous PL studies of ion implanted silicon. When the samples are annealed at 650°C new defects are formed. Although little is

known about the structure of these defects, we show that the new Ar defect getters a small copper contamination very effectively. Further annealing of the Ar etched samples at 1050°C causes the formation of Ar bubbles with an average diameter of about 5 nm.

G18.7

BEHAVIOR OF POINT DEFECTS IN FZ AND CZ Si CRYSTALS

Takao Abe,

Shin-Etsu Handotai, Annaka, Gunma 379-01, JAPAN.

FZ Si crystals containing both swirls (A-defect) and D-defect, which are 3mm thick wafers cut vertically to the growth direction, are annealed in wet O₂ and N₂ ambient, and then are observed by x-ray topograph following Cu decoration using 1mm thick specimens cut parallel to the growth direction. A-defect formation is enhanced and D-defect region is reduced when FZ wafers are annealed in wet O₂ at 1000°C, whereas shrunken A-defect and enhanced D-defect are observed by the annealing in N₂ at 1000°C. It is clearly demonstrated from the above results that A-defects are formed by excess Si interstitials and D-defects by excess vacancies.

By reheating of CZ grown crystal ingots in the same grown-furnace, the ring-like OSF region is generated with steep thermal gradient in the growth direction, whereas the anomalously oxygen-precipitated (AOP) region is produced with the rapid cooling from near melting temperature in the same manner of detaching from the melt.

A-defect formation is attributed to steep thermal gradient of the periphery of ingot, whereas D-defect to mild thermal gradient at the center of ingot. It is concluded that A-defect and ring-like OSF region are composed of excess Si interstitials and D-defect and AOP region is related to excess vacancies. Only an essential factor for point defect formation is the thermal gradient in the growing crystals.

G18.8

AN IMPROVED MODEL FOR COMPUTER SIMULATION OF OXYGEN PRECIPITATION PHENOMENA

M. Schrems, P. Pongratz, H.W. Pötzl, TU-Vienna, Austria;
E. Guerrero, D. Huber, Wacker Chemitronic, Burghausen, FRG.

Oxygen Precipitation is of considerable importance for VLSI processing ("Gettering", "Denuded Zone Formation"). A model which has been presented at the EMRS 1989 in Strasbourg has been further improved. The model differs from most of the other precipitation models currently used in literature, since it describes growth and decay of an ensemble of oxygen precipitates statistically by a Fokker-Planck equation. The coefficients of the Fokker-Planck equation contain the Gibbs energies of precipitates, which are modelled as the sum of volume-, interfacial- and stress energy terms. Energy contributions of point defects are also considered. Model parameters are determined from single step annealing experiments. Then experimentally observed phenomena in multi step annealing like the "oxygen precipitation retardation/recovery phenomenon" [1] and the "nucleation incubation phenomenon" [2] are studied. Our model can quantitatively account for experimentally determined interstitial oxygen data and precipitate densities. Furthermore a selection of a complete numerical analysis of experimental data (comprising size distribution of precipitates, precipitated oxygen, precipitate densities, average precipitate radius and critical precipitate radius all as a function of time) will be given and discussed.

- [1] T.Y. Tan and C.Y. Kung, J. Appl. Phys., Vol. 59 (1986) pp. 3974
- [2] N. Inoue et al., J. Cryst. Growth, Vol. 84 (1987) pp. 21

G18.9

FAILURE OF THE "KICK-OUT" MODEL FOR THE DIFFUSION OF Au INTO Si WHEN TESTED BY MONTE CARLO SIMULATION.

Uwe Schmid, and James A. Van Vechten, Oregon State University, Corvallis, OR 97331-3202, U.S.A.

We have developed VIDSIM, a Monte Carlo simulation program for the creation, interaction, migration and reaction of point defects in Si and GaAs type lattices. This 'C'-program can do large simulations on PCs at almost no cost by running continuously in the background with multitasking software. It is available at the cost of the media to anyone wishing to test the relationship between any particular complete set of atom level assumptions and their microscopic consequences.

We have applied VIDSIM to the controversial case of Au diffusion into Si [1,2]. At this writing, we have finished the formation of $1.4 \cdot 10^4$ Au substitutionals (Aus) at 1368 K in a sample of $6.4 \cdot 10^8$ sites through approx. $8 \cdot 10^8$ discrete events via the "kick-out" hypothesis with parameters as suggested by U. Gösele. A real sample would have melted to the Au-Si eutectic before this. The result is dramatically at odds with the properties claimed by the proponents of that model re: 1) the profile of Au interstitials, which decays exponentially and never becomes flat; 2) the variation with time of the Au concentration in the center of the sample, which is linear at all times and never becomes \sqrt{t} ; 3) the effect of Aus on the outdiffusion of Si interstitials, which is only quantitative and not qualitative; 4) the Au profile itself, which we find to be much more exponential and less U-shaped than claimed.

Our VIDSIM simulation of the "Frank-Turnbull" model [1] goes much slower and showed an initial behavior which was at odds with both experiment and the claims of its proponents. As the simulation continues, it is showing sign of turning toward experiment and claim. In contrast to the kick-out, it also produces a U-profile from a one-sided diffusion.

- [1] F. A. Huntley and A. F. W. Willoughby, J. Electrochem. Soc. 120, 414 (1973)
- [2] A. Seeger, Phys. Stat. Sol. (a), A 61, 521 (1980)

* Present address: Max-Planck-Institut für Festkörperforschung, Stuttgart, F.R.G.

G18.10

DIFFUSION OF POINT DEFECTS IN A STRESSED SIMPLE CUBIC LATTICE.

Dimitris Maroudas and Robert A. Brown, Department of Chemical Engineering, Massachusetts Institute of Technology, Cambridge, MA 02139.

Systematic theoretical and computational procedures are presented for the analysis of point defect diffusion in the presence of an applied potential that is superimposed onto the perfect lattice potential. The procedure starts with the formulation of a conservation equation for the number density of point defects. The method of moments is used to derive expressions for the diffusivity tensor D as a function of equilibrium ensemble averages of the displacement vector of the defect. The components of D are computed by a dynamic Monte Carlo simulation with the proper introduction of the time variable.

Results are demonstrated for a simple cubic structure characterized by a spatially periodic lattice potential in the absence of imperfections. For a constant applied potential the diffusivity tensor is isotropic. For a linear potential it is anisotropic, but homogeneous and the sizes of its components relative to the isotropic value vary significantly depending on the magnitude and the direction of the potential gradient. Continuum modelling, jump rate theory and the solution of the homogeneous problem are combined to form a constitutive model for the dependence of D on the potential gradient. This model can be used for the solution of problems, such as the diffusion of substitutional impurities in semiconductor crystals and the calculation of the concentration field of point defects in the vicinity of dislocations.

G18.11

COMPUTER CALCULATION OF DIFFUSIVITY, EFFECTIVE ACTIVATION ENERGY AND OF ACTIVATION ENERGY DIMINUTION FROM MEASURED PROFILE OF IMPURITY DISTRIBUTIONS IN SILICON. D.K.An, Microelectronics Company P.O.Box. 21, H-1325 Budapest Hungary

The exact dopant profile carries all the information about diffusion process, but in order to get that information it is necessary to have a consistent model to analyzing the measured profiles. The aim of this work is to analyze the measured profiles of impurities in the anomalous diffusion processes on computer. The work starts with the discussion about Boltzmann-Mantano method for the anomalous diffusion process including the kink-tail profile case. Using this method the diffusivities of the dopants were calculated, then the effective activation energies and the decrease of the activation energies of three dopants (Boron Phosphorus, Arsenic) have been calculated on the base of a diffusion model given by the author. The pre-diffusion factors were estimated and finally expressions for the diffusivities of the impurities are given. Some results can be seen on Fig.1,2,3,4.

G18.12

DEFECTS IN DOPED SILICON EPILAYERS STUDIED WITH VARIABLE-ENERGY POSITRONS AND MeV IONS. P.J.Simpson, P.J.Schultz, R.W.Hunt and I.V.Mitchell, University of Western Ontario, T.E.Jackman and G.C.Aers, National Research Council of Canada.

Properties of semiconductors grown by molecular beam epitaxy (MBE) are strongly affected by defects, and few non-destructive techniques exist to study these. The relatively new variable-energy positron beam technique provides such a probe of near surface defects and impurities, even at low concentrations ($\approx 10^{-6}$ atomic concentration). Rutherford backscattering of light ions and nuclear reaction analysis provide complementary information regarding the depth profile of dopants and impurities.

Silicon epilayers grown by MBE at the National Research Council were studied at UWO using both positron annihilation and ion beam techniques. Measurements were made following a high temperature anneal in order to examine dopant migration and defect recovery.

G18.13

ANGLE RESOLVED XPS ANALYSIS OF SURFACE DEFECTS IN HIGH-DOSE Sb^{+} IMPLANTED MONOCRYSTALLINE SILICON. S.N.KUMAR, G. CHAUSSEMY, A. LAUGIER, Laboratoire de Physique de la Matière, CNRS URA 358, INSA LYON, 69621 Villeurbanne Cedex; M. CHARBONNIER, Département de Chimie Appliquée et Génie Chimique, CNRS URA 417, B. CANUT, Département de Physique des Matériaux, Université Claude Bernard - LYON I, 69622 Villeurbanne Cedex, France.

Defects in shallow surface regions, whose depths are comparable to the mean free path of photoelectrons, can be precisely examined by angle-resolved X-ray photoelectron spectroscopy (ARXPS) wherein, by sensing the photoelectrons at

low take-off angles, the signal arising from the deeper layers is effectively quenched. We report the ARXPS analysis of the implantation induced damage resulting from high-dose Sb ion implants in (100) p-Si. Surface regions of silicon implanted with 2×10^{14} , 1.2×10^{15} , 5.4×10^{15} and 1.4×10^{16} Sb^{+}/cm^2 and subsequently rapidly annealed at $1100^{\circ}C$ for 10s were studied by analyzing the Si 2p, O 1s and Sb 3d_{5/2} photoelectron spectra at various take-off angles. In particular, the Si 2p peaks revealed two lines corresponding to the elemental and oxidized states in all the samples. The binding energy shift between these two lines was ~ 1 eV less for the 2×10^{14} Sb^{+}/cm^2 sample than for others and the Si/SiO_x ratio decreased systematically with increasing ion dose. The O concentration increased by nearly one order of magnitude between the 1.2×10^{15} and 1.4×10^{16} Sb^{+}/cm^2 implanted samples. The results of RBS, SIMS and ARXPS are interpreted in terms of the formation of a highly disordered surface region for doses higher than a critical value of $\sim 10^{15}$ Sb^{+}/cm^2 . These data will also be compared with the electrical characteristics of the N⁺/P diodes and MOSFET structures constructed on the activated implanted samples.

G18.14

MODIFIED OPTICALLY DETECTED MAGNETIC RESONANCE TECHNIQUE FOR STUDIES OF DEFECTS IN Si AND GaAs. W.M. Chen and B. Monemar, Department of Physics and Measurement Technology, Linköping University, S-581 83 Linköping, SWEDEN.

Optically detected magnetic resonance (ODMR) has been proven to be a powerful technique for studies of electronic structure and microscopic identification of defects in many semiconductors. Its application to the technologically important materials Si and GaAs as well as their related heterostructures has been very limited so far, however. This is mainly because the ODMR spectrum is commonly dominated by a strong background signal, which obscures any possible detection of defect-related ODMR signals. In this paper we shall discuss the physical mechanisms responsible for the background signal, based on hot-carrier effects in a microwave field. A modified technique, a multiply pulsed ODMR system, which has been proven to be very successful in overcoming the difficulties of ODMR in Si and GaAs, has been developed in this work. A number of defects in these materials have been discovered and investigated by this new technique. These defects could not be studied by conventional ODMR technique. A few examples of such studies will be demonstrated. A universal application of this technique to other high dielectric loss materials is also emphasized. This work therefore provides a breakthrough in ODMR studies of defects in semiconductors.

G18.15

OPTICAL PROPERTIES OF NOVEL VIBRONIC BANDS IN ELECTRON-IRRADIATED TIN DOPED SILICON. J.H. Svensson, B. Monemar, Department of Physics and Measurement Technology, Linköping University, S-581 83 Linköping, SWEDEN and B.G. Svensson, Department of Solid State Electronics, The Royal Institute of Technology, P.O. Box 1298, S-164 28 Kista, SWEDEN.

New vibronic bands have been investigated in 2 MeV electron irradiated Czochralski grown silicon doped with tin. Two no-phonon lines are observed at 341,6 meV and 509,8 meV, each with strong coupling to phonons. At low temperatures (T=6 K) the phonon sideband spectrum is completely dominated by a single vibrational mode with a quantum energy of 8.6 and 8.7 meV for the two no-phonon lines respectively. Coupling to four and six phonon quanta are observed for the no-phonon lines. At higher temperatures coupling to thermally excited single vibrational modes in the ground state is observed for both no-phonon lines.

The temperature dependence of the absorption has been studied between 6 and 190 K. The intensity relation between the two absorption structures is also found to be dependent on the optical excitation of the sample. When the sample is cooled in darkness the no-phonon peak at lowest energy has a minimum in intensity. After optical excitation the intensity increases at the expense of the intensity of the no-phonon peak at higher energies. These peaks have also been observed in photoluminescence. The defect causing the transitions is suggested to be a complex defect involving tin as, at least, one of the constituents.

G18.16

A NEW METASTABLE DEFECT IN SILICON, AN OPTICAL STUDY AND AN INVESTIGATION OF THE MECHANISM CAUSING THE CONFIGURATIONAL CHANGE. J. H. Svensson and B. Monemar, Department of Physics and Measurement Technology, Linköping University, S-581 83 Linköping, SWEDEN.

Recently a new no-phonon peak was discovered in electron irradiated silicon (1). Optical studies of this peak displayed metastable properties of the defect causing the electronic transition. In this work we present detailed information about the transition and the processes governing the observed change of the configuration of the defect only observed at temperatures below 70 K and during optical above band gap excitation. Experimental results explaining the change in configuration as caused by free excitonic recombination at the defect is presented.

A detailed temperature dependence of the no-phonon peak and the absorption structure related to it from 4.2 to 70 K, where thermal quenching of the structure starts to occur, is also presented. Experimental results from uniaxial stress studies of the transition from the metastable state will be discussed.

(1) J. H. Svensson and B. Monemar (Accepted Phys. Rev. B, Rapid Communications)

G18.17

NOVEL LUMINESCENCE BAND IN SILICON IMPLANTED WITH PHOSPHORUS AND BORON. A.K. Srivastava, D.K. Sharma and K.L. Narasimhan, Tata Institute of Fundamental Research, Homi Bhabha Road, Bombay 400005, D. Sarkar and V. Premchandran, Indian Telephone Industries, Doorvani Nagar, Bangalore 560016, India.

There is considerable interest in the study of processing related defects in silicon. We report the results of photoluminescence measurements on ion implanted silicon. The samples are implanted with P (energy 180 keV; dose 10^{15} atoms/cm²) and B (energy 80 keV; dose 10^{15} atoms/cm²) and annealed at 900°C for 30 min. followed by slow cooling. Some samples implanted with only P or B were also studied.

The photoluminescence measurements were made at 10K using He Ne laser as the excitation source. A liq. N₂ cooled Ge detector was used to measure the signal.

The double implanted sample shows a very strong luminescence line at 1.017 eV with phonon replicas at 0.998, 0.978 and 0.965 eV. The luminescence intensity of the no phonon (NP) 1.017 eV line is nearly one order of magnitude larger than the TO phonon line in the unimplanted sample. The temperature dependence of the NP line shows excitonic behaviour. The intensity is nearly constant up to a temperature of 25K

and then falls rapidly with an activation energy of 56 meV in the 50-100K range.

The samples implanted only with either P or B do not show the novel luminescence. We think that there is a complex involving both the P and B which is giving rise to the new luminescence band.

G18.18

UNIAXIAL STRESS AND ZEEMAN MEASUREMENTS ON THE 0.943eV LUMINESCENCE BAND IN SILICON. M.C. do Carmo, Departamento de Fisica, Universidade de Aveiro, 3800 Aveiro, Portugal; K.G. McGuigan and M.O. Henry, School of Physical Sciences, Dublin City University, Dublin 9, Ireland; G. Davies and E.C. Lightowers, Department of Physics, Kings College, Strand, London WC2R 2LS, UK.

Copper is a common contaminant in silicon crystals and several copper-related luminescence bands have been reported [1,2]. In this paper we present new data on the 943meV band which dominates the luminescence of samples lightly doped with copper and rapidly quenched from 1100°C. Uniaxial stress measurements on two of the zero-phonon lines in the spectrum show that the luminescence transitions occur from T to A states at a tetrahedral centre. Zeeman measurements reveal some novel features which will be analysed and compared with corresponding data for other transition metal related luminescence bands. The physical mechanisms for the stability of these defects in silicon will be inferred.

1. J. Weber, H. Bauch and R. Sauer, Phys. Rev. B **25**, 7688 (1982)
2. K.G. McGuigan, M.O. Henry, E.C. Lightowers, A.G. Steele and M.L.W. Thewalt
Solid State Comm. **68**, 7 (1988)

G18.19

STRAIN INDUCED INTRINSIC QUANTUM WELLS AS THE ORIGIN OF BROAD BAND PHOTOLUMINESCENCE IN SILICON CONTAINING EXTENDED DEFECTS. Helge Weman and Bo Monemar, Department of Physics and Measurement Technology, Linköping University, S-581 83 Linköping, SWEDEN.

In this work we present a new recombination mechanism that can occur in semiconductors containing extended defects.

The model is based on experimental data both from hydrogen plasma treated silicon, containing extended defects like platelets and gas bubbles, and from oxygen precipitated silicon. The photoluminescence (PL) spectra of these samples contain broad bands, typically around 0.9 eV, with a halfwidth (FWHM) of as much as 100 meV.

The origin of these broad PL bands we attribute to electron-hole recombination in the heavily damaged region surrounding the extended defects, where the electrons and holes can be localized in strain induced potential wells.

The experimental data from the plasma treated silicon [1], are supported by a theoretical calculation based on the compressive strain induced bending of the conduction and valence bands around (111) and (100) platelets, resulting in a local bandgap reduction of as much as 0.3 eV. The model is also consistent with the observed temperature and excitation intensity dependence of the broad PL bands.

This recombination mechanism is believed to occur also in other semiconductors since it is not related to the electrical potentials of the defects, but is of an "intrinsic" nature.

[1] H. Weman, J. L. Lindström, and G. S. Oehrlein, Proc. E-MRS 1989 Spring Meeting, Symp. B, Strasbourg, May/June 1989.

A HVEM STUDY OF THE ELECTRON IRRADIATED DEFECTS IN NITROGEN DOPED FZ-Si. Gao Yuzun, General Research Institute for Non-Ferrous Metals, Beijing, China; and T. Takeyama, HVEM Lab, Hokkaido University, Sapporo, Japan.

The nitrogen doped FZ-Si single crystal has excellent strength properties against thermo-mechanical deformation (1). Under certain conditions, nitrogen and vacancies in Si can form deep energy level defects (2). In the present work, a high voltage transmission electron microscope (JEM-1000) has been used to investigate the electron irradiated defects in p-type FZ-Si and nitrogen doped FZ-Si. The concentration of nitrogen in the latter was $1E+15$ at./cm³. The specimens were irradiated in the condition of 1000 kV and the dose of 0.1 dpa/min in HVEM.

The obtained results were as follows:

1. The electron irradiated defects were bar-like defects along $\langle 110 \rangle$ directions, dislocation loops and stacking faults on $\{113\}$ planes in the two kinds of Si.
2. When the irradiated conditions were the same, the irradiated defects were easier to be produced in the FZ-Si than in nitrogen doped FZ-Si in the temperature range 573-773 K.
3. The migration energy of vacancies in the temperature range 573-773 K was 0.34 and 0.58 eV for FZ-Si and nitrogen doped FZ-Si respectively. It seems to indicate that there was some interaction between vacancies and nitrogen atoms in the nitrogen doped FZ-Si. The results have clearly proved that the nitrogen doped FZ-Si has excellent property against electron irradiation.

Reference

- (1) K. Sumino, et al., J. Appl. Phys. 54(1983), 5016
- (2) M. Tajima, et al., Jpn. Appl. Phys. 20(1981), L423

G18.21

IDENTIFICATION OF RADIATION-INDUCED DEFECTS IN Si:Al. Ya. I. Latushko, V. V. Petrov. Lenin Byelorussian State University, Minsk, 220080, USSR

Radiation defects (RD) in Si:Al have been studied by means of IRA and PL techniques. It is found that the main Al-containing RD in electron irradiated Si is an interstitial Al atom (Al_i). The Al_i-Al_i pair formation takes place during annealing at a temperature of 225 °C. This has led to the shift of the helium-like IRA spectrum to a higher energy region and to the disappearance of PL lines. The value of activation energy of Al_i-Al_i pair formation is 0.95 eV which corresponds to the migration of Al_i along hexagonal interstitials.

Besides this RD and the defect with energy level $E_v+0.21$ eV a number of new ones with the IRA lines in the range of 0.1-1.0 eV and the PL lines in the range of 0.5-1.2 eV was observed in neutron-irradiated Si. Taking into account the annealing data and the results obtained from piezospectroscopic studies the classification of this RD has been established. The obtained results confirmed that transitions at Al_i correspond to the T_d symmetry center. Piezospectroscopic investigations of neutron-irradiated Si have shown that uniaxial stress leads to the removal of both electron and orientational degeneration of defect energy levels. The RD under study are found to have symmetry of at least four types: tetrahedral; monoclinic; rhombic 1; triclinic. The values of piezospectroscopic tensor components lie in the interval from 0.1 to 50 meV/GPa.

G18.22

DEFECT-FORMATION DEPENDENCE ON GROUP V-DOPANT ATOMS IN ELECTRON-IRRADIATED SILICON. O. O. Awadelkarim, A. Henry, B. Monemar, Department of Physics and Measurements Technology, Linköping University, S-581 83 Linköping, SWEDEN and J. L. Lindström, Swedish Defence Research Establishment, P.O. Box 1165, S-581 11 Linköping, SWEDEN.

The defect states introduced in P-, As- and Sb-doped silicon upon room-temperature electron-irradiation are studied by deep-level transient spectroscopy (DLTS). Evidence is provided for involvement of the P-atom and the vacancy in the defect complex giving rise to the prominent electron trap commonly observed at $E_c-0.4$ eV (E_c being the edge of the conduction band). It could not be concluded, however, whether the complex comprises only a phosphorus-vacancy pair, as in the E-centre. This electron trap together with another at $E_c-0.30$ eV, apparently phosphorus related, exhibit configurationally metastable behaviour. The configurational metastability, a phenomenon observed here only in P-doped material, is argued to have arisen from the presence of a P atom in the defect complexes. Other electron traps observed at $E_c-0.27$ eV and $E_c-0.34$ eV in As-doped material and $E_c-0.51$ eV in Sb-doped material are discussed in terms of complexes involving As or Sb. Data on the stability of the observed traps, their carrier capture cross sections, production and annealing properties are presented.

G18.23

ELECTRONIC STRUCTURE OF VACANCY-PHOSPHORUS IMPURITY COMPLEXES IN SILICON. Hongqi Xu, Department of Theoretical Physics, University of Lund, Sweden; and U. Lindefelt, ABB Corporate Research, Västerås, Sweden.

The vacancy-P impurity related complex in silicon has recently been investigated experimentally. /1/ We present a systematic theoretical investigation of the four vacancy-P, $n=1, 2, 3, 4$, complexes in silicon using a self-consistent semi-empirical tight-binding method. The calculations are based on Lanczos algorithm and a continued-fraction Green's function method, which is very well suited for studying complex defects.

The energy levels in the band gap for the five cases vacancy and vacancy-P, $n=1, 2, 3, 4$, show a remarkable regularity. For $n=1$ (point-symmetry group C_{3v}) and $n=2$ (C_{2v}) an e^- and b_2^- level, respectively, are found at practically the same energy as the t_2^- vacancy gap level (T_d). Furthermore, for $n=2, 3$ (C_{3v}) and 4 (T_d) we find a b_1^- , e^- and t_2^- level, respectively, all at practically the same position just above the top of the valence band. For the intermediate cases $n=1, 2$ and 3 there is also an a_1 gap level with increasing energy.

We shed light on this regularity by related it to the localization of the wave functions on the Si and P atoms surrounding the vacancy. We also discuss the effect of lattice distortion and compare our results with experimental works.

/1/ O. O. Awadelkarim and B. Monemar, Phys. Rev. B 38, 10116 (1988).

G18.24

A SIMPLE MODEL FOR DEFECT STRUCTURES IN SILICON. G. J. Ackland and V. Vitek, Department of Materials Science and Engineering, University of Pennsylvania, Philadelphia, PA

We have shown that the results of theoretical, *ab initio* structural stability and point defect calculations can easily be reproduced without any angular dependent terms, using a

simple, parameterised short-ranged, pairwise potential in which the bonding is restricted to four bonds. These two-body terms have a clear physical interpretation in covalently bonded materials and the present model provides an extremely clear picture of the cohesion.

The model predicts reconstructions of the (001) and (111) surfaces which are consistent with experimental observation. Surprisingly, the model (which is biased towards fourfold coordination) sometimes prefers reconstructions to threefold coordinated surfaces over fourfold coordination. For point defect calculations we find that the lowest energy structure is often of rather low symmetry, and not the high symmetry structures which are usually examined based on intuition from the metallic case. We also show that small clusters tend to have a close-packed form rather than being akin to pieces of the diamond structure.

While we do not expect quantitative accuracy for formation energies, the reliability of the model in predicting ground state structures, combined with its extreme simplicity, make it a valuable guide to intuition for examining possible starting configurations in more accurate total energy calculations.

G18.25

NEW DLTS PEAKS ASSOCIATED WITH NEW DONORS AND ROD-LIKE DEFECTS IN CZOCHRALSKI SILICON.

Yoichi Kamiura, Fumio Hashimoto and Minoru Yoneta, Faculty of Engineering, Okayama University, Okayama 700, JAPAN.

We have studied the effects of preannealing at temperatures 450-520°C on the new donor (ND) formation at 650°C by a combination of electrical measurements, deep-level transient spectroscopy (DLTS), preferential etching and transmission electron microscopy (TEM). Prolonged annealing at 450°C produced a new kind of thermal donors (NTDs) with simultaneous annihilation of so-called thermal donors (TDs) that have extensively been studied by many investigators. TDs and NTDs exhibited qualitatively the same kinetic behavior, but NTDs had smaller generation rates and higher thermal stability. In such long-preannealed samples, the ND formation was greatly enhanced, and two new DLTS peaks arising from shallow donor levels always appeared in closely correlation with the enhanced ND formation. They were also correlated with the formation of <110> elongated rod-like defects (RLDs) and associated dislocation dipoles, both of which were observed by TEM and also were revealed as triangular etch pits by the Wright etching. For not preannealed samples, we have never observed such DLTS peaks, RLDs and etch pits even after extended annealing at 650°C. Instead, we observed only weak continuous DLTS spectra often reported previously and silicon oxide precipitates revealed as black spots by TEM. We tentatively attribute these new DLTS peaks to small oxygen precipitates nucleated at NTDs, and continuous DLTS spectra to those formed by homogeneous nucleation.

G18.26

MULTICONFIGURATIONAL CARBON-GROUP V PAIR DEFECTS IN SILICON. E. Güler and B. W. Benson, Lehigh University, Bethlehem PA 18015.

Three different multiconfigurational defects were observed in carbon rich, electron irradiated silicon, doped with the three group V elements, phosphorus^{1,2,3}, antimony⁴ and arsenic⁵. They appear in DLTS and TSCAP spectra after the anneal of interstitial carbon at 350K. We identify them as interstitial carbon - substitutional group V pairs. Each of these defects has a stable configuration with an energy level near 0.4 eV below conduction band and converts to other configurations upon injection of minority carriers at

certain temperatures. Although the overall properties of these defects are similar, energy levels corresponding to the metastable configurations and barriers for the conversions among them are different for pairs with each group V atom. In the case of C_i - Sb_s and C_i - As_s, two of the configurations form a bistable pair with close similarity to the properties of C_i - C_s pair⁶, suggesting a similar molecular bond switching mechanism. The shifts in the electrical level positions for the pair formation and conversion suggest Coulomb interactions between the constituents at different lattice separations as proposed for Fe - acceptor pairs⁷.

1. Song et.al. Appl. Phys. Lett. 51, 1155 (1987).
2. Asom et.al. Appl. Phys. Lett. 51, 256 (1987).
3. Güler et.al. B. Am. Phys. Soc. 34, 834 (1989).
4. Benson et.al. Materials Science Forum 38-41, 391 (1989).
5. Güler et.al. B. Am. Phys. Soc. 34, 834 (1989).
6. Song et.al. Phys. Rev. Lett. 60, 460 (1988).
7. Chantre et.al. Phys. Rev. B 31, 7979 (1985).

Work supported by the U.S. Office of Naval Research Contract No. N00014-84K-0025

G18.27

THE ROLE OF FOUR-MEMBER RING DEFECT STRUCTURES CONTAINING CARBON, NITROGEN, AND OXYGEN IN CRYSTALLINE SILICON. Lawrence C. Snyder, Rongzhi Wu, and Peter Deak, Chemistry Department, and James W. Corbett, Physics Department, State University of New York at Albany, 1400 Washington Avenue, Albany NY 12222.

In molecular cluster calculations employing the MINDO/3 method to describe carbon, nitrogen, and oxygen containing defects in crystalline silicon, we have found defects containing two of these first row atoms in a four-member ring to be stable. The O-Si-O-Si(-O) four-member ring is proposed to be a rapidly diffusing species. The C-Si-O-Si(-O) four-member ring is shown to be a probable structure for the Si-G15 defect. The N-Si-N-Si(-N) four-member ring is shown to exhibit an infrared spectrum very close to that observed for nitrogen "dimer" in silicon.

G18.28

MOLECULAR DYNAMICS STUDIES OF DISLOCATION CORES IN SI. M.S. Duesbery, D.J. Michel, Naval Research Laboratory, Washington D.C. 20375; and B. Joos, Ottawa-Carleton Institute for Physics, Ottawa, Ontario, Canada K1N 9B4.

The structure and mobility of dislocation cores in a Stillinger-Weber¹ Si model are examined at an atomistic level using molecular dynamics. Straight and double-kinked 30° and 90° partial dislocation glide dipoles are modelled in a strain-free environment: reconstruction and anti-phase defects are found to be present for 30° partial dislocations. The effects of applied shear strains and of temperatures up to the melting point are considered also.

1. F.H. Stillinger and T.A. Weber, Phys. Rev. B31, 5262 (1985).

G18.29

HYDROGEN INDUCED DEFECTS AT SILICON EPITAXIAL SURFACES AND BURIED MISFIT DISLOCATIONS. Tian-Qun Zhou, Zbigniew J. Radzinski, Zhigang Xiao, George A. Rozgonyi, Dept. of Materials Science and Engineering, North Carolina State University, Raleigh, NC 27695-7916

A novel silicon epitaxial structure containing spatially confined arrays of misfit dislocations has been

fabricated in order to investigate the interaction between hydrogen and individual extended defects. The effect of hydrogenation using different plasma implantation doses was studied using secondary ion mass spectroscopy (SIMS), transmission electron microscope (TEM) and scanning electron microscope in electron beam induced current mode (EBIC/SEM). SIMS was used to determine the hydrogen profile, TEM to reveal hydrogen induced defects and surface radiation damage due to the high dose hydrogen plasma process, while EBIC/SEM provided imaging of the electrical activities of individual defects. For the sample treated with a high dose plasma, SIMS indicates that hydrogen is concentrated in the near surface region to a depth of 2500 Å, where TEM micrographs show that the sample is heavily damaged. An unusual EBIC/SEM contrast effect was obtained due to the existence of a surface inversion layer following high dose hydrogenation. The buried misfit dislocations are decorated with hydrogen-induced defect or hydrogen stabilized defects.

G18.30

TEM INVESTIGATION OF SECONDARY DISLOCATIONS IN GRAIN BOUNDARIES IN GERMANIUM. M. Griess, M. Seibt, IV. Physikalisches Institut, University of Göttingen, 3400 Göttingen, FRG; H.J. Möller, Department of Materials Science and Engineering, Case Western Reserve University, Cleveland, OH 44106.

Transition metal and other impurities can be gettered by grain boundaries in semiconductors and alter their electrical properties. Recent studies of the segregation process indicate that the distribution of precipitated impurities is rather inhomogeneous and facilitated by dislocations and other structural features in the grain boundaries.

The objective of the present investigation is the characterization of grain boundary dislocations to get more insight in the structural features of arbitrary grain boundaries and their gettering properties. For this purpose near-coincidence [011] - tilt grain boundaries in germanium have been grown by the two seed Czochralski technique at misorientation angles of about 40°. A number of dissociated grain boundaries were observed with angular deviations to the coincidence orientations $\Sigma 3$, $\Sigma 9$, $\Sigma 19$, and $\Sigma 27$ below about 30. The secondary dislocations in some of the grain boundaries were studied by conventional and high resolution TEM. The combination of both methods allowed to determine the Burger's vectors of some of the dislocations and to relate them to corresponding DSC lattice vectors. The main results are that non-primitive Burger's vectors are observed and that they do not always belong to the DSC lattice of the nearest coincidence orientation. Furthermore the result is discussed in comparison with earlier observations of a $\Sigma 27$ grain boundary, which indicate that the dislocation type and structure changes with the misorientation angle.

G18.31

AC PHOTOVOLTAIC INSPECTION OF P-N JUNCTIONS HAVING HIGH LEAKAGE CURRENT. N. Honma, Shimizu, C. Munakata, Central Research Laboratory, Hitachi Ltd., Kokubunji, Tokyo 185 and M. Ogasawara, Device Development Center, Hitachi Ltd., Oume, Tokyo 198

Junction leakage is one of the most severe yield-limiting mechanisms in the fabrication of VLSI circuits. A technique for imaging the distribution of ac photovoltages induced by irradiation with a chopped photon beam (PB) in a Si wafer has been applied to the nondestructive inspection of junction leakage. A cathode ray tube (CRT) or a He-Ne laser is utilized to generate photovoltages in junctions. Ac photovoltages are measured capacitively through a 25 µm air gap between the wafer surface and the transparent electrode. Junctions are formed on a p-type Si wafer with a resistivity of 0.1 Ωm. Arsenic ions are implanted to form n-type surface layers. The junctions are surrounded by a 500 nm-

thick field oxide layer, under which boron ions are heavily implanted to make a channel stopper.

When a junction leakage current is large, the induced photovoltage should decrease because of reduction in the junction impedance. However, it is found that photovoltages become high when leaky junctions are irradiated by the chopped PB. The photovoltages for the leaky junctions are higher than those for normal junctions not only in the junction areas but also in the field oxide regions around the junctions. This indicates that dense positively charged traps exist at the interface between the boron-doped Si substrate and the field oxide layer around the leaky junction, and that the traps cause the increase in both the junction leakage current and the photovoltage.

G18.32

RIBBON-LIKE DEFECTS IN HIGH-DOSE OXYGEN IMPLANTED SILICON-ON-INSULATOR MATERIAL. S. Visitserngrakul¹, J. Barry^{2,*}, and S. Krause¹, ¹Dept. Chemical, Bio and Material Engineering, Arizona State University, Tempe, AZ; ²Center for Solid State Science, Arizona State University, Tempe, AZ.

High-dose oxygen implantation in silicon, SIMOX (separation by implantation of oxygen), is a leading technique for producing silicon-on-insulator material. The implantation generates defects not only in the top Si layer, but also in the Si substrate beneath the buried oxide layer. A prominent defect found in the substrate is of a ribbon-like configuration. Although commonly observed, it has not yet been investigated in detail. We report here high resolution electron microscopy observations that lead to a structural identification of these ribbon-like defects.

The Si (100) wafers were implanted by a recently developed high-current (40 mA) implanter, at 575°C, at 180 keV to the dose of $2 \times 10^{18} \text{ cm}^{-2}$. They were examined from cross-section samples using a Philips 400T at 120 keV and a JEOL 200CX at 200 keV for high resolution images. Numerous ribbon-like defects were observed in the Si substrate, of a density of 10^{11} cm^{-2} and a length varying in between 10 to 40 nm.

The ribbon-like defects in bulk Si were assigned to layers of interstitial atoms incorporated in between {113} or {115} habit planes. In a thin precipitate layer, the interstitials are disordered. However, for a sufficient thickness the interstitials may order into a crystalline configuration previously assumed to be hexagonal. Our observations in SIMOX show that two crystalline phases are present in the defect. The interstitials may either preserve the cubic diamond structure, or they may induce local phase transformation into hexagonal silicon. The observations presented, supported by an image simulation, actually identify the presence of both crystalline structures from differences in contrast as well as periodicity of the images. In cubic regions, the {111} lattice fringes of the defect appear uniformly. The transformation occurs through the twin operation across {115} planes which intersect {111} planes at 75°. Even if the cubic structure is slightly tilted, the cross {111} lattice fringes will appear evenly in one direction. In distinct contrast, in the hexagonal structure a slight tilt by as little as 0.7° from the exact <011> axis will strongly excite the kinematically forbidden spot of (001)_h. The basal plane now produces double-periodicity images along the c-axis of the hexagonal phase. The atomic structure model of the interface in both regions will also be discussed.

* Present address: University of Queensland, Electron Microscope Centre, St. Lucia, Brisbane, Queensland 4067, Australia.

G18.33

THE ENHANCEMENT OF THE INTERDIFFUSION IN Si/Ge AMORPHOUS MULTILAYERS BY ADDITIONS OF Au AND B. R. Park, F. Spaepen, Division of Applied Sciences, Harvard University, Cambridge, MA 02138; J.M. Poate, D.C. Jacobson, AT&T Bell Laboratories, 600 Mountain Avenue, Murray Hill, NJ 07974.

Amorphous Si/amorphous Ge artificial multilayers were prepared by ion beam sputtering. Boron or gold impurities were introduced into the Si-Ge multilayers by ion implantation or during the sputter deposition. Diffusion coefficients were determined by measuring the decrease in the intensity of the first order X-ray diffraction peak resulting from the composition modulation.

It was found that the interdiffusion of Si and Ge in their amorphous phase can be enhanced by doping with Au or B. The enhancement factor in these experiments is independent of the degree of structural relaxation of the amorphous phase, as observed by the decrease of the diffusivity with time, which can be explained by trapping of electrons or holes,

introduced by the dopants, by pre-existing neutral dangling bonds (structural defects).

Work at Harvard has been supported by the National Science Foundation through the Materials Research Laboratory, under contract number DMR-86-14003.

G18.34

STRUCTURAL TRANSITIONS IN TITANIUM/AMORPHOUS-SILICON MULTILAYER THIN FILMS
L.A. Clevenger¹, E. Ma and C.V. Thompson, Department of Materials Science and Engineering, Massachusetts Institute of Technology, Cambridge, MA 02139, R.R. deAvillez, Departamento de Ciencia dos Materiais e Metalurgia, Pontificia Universidade Catolica, 22452-Rio de Janeiro, RJ-Brazil and K.N. Tu, I.B.M T.J. Watson Research Center, Yorktown Heights NY, 10598

The formation and growth of both amorphous-titanium-silicide and crystalline C49-TiSi₂ in titanium/amorphous-silicon multilayer thin films and structural transitions that occur in these phases upon heating was investigated using a combination of differential scanning calorimetry, thin film X-ray diffraction, Auger depth profiling, and cross-sectional transmission and scanning transmission electron microscopy. The multilayer films had atomic concentration ratios of either 1 Ti atom to 2 Si atoms, 1 Ti atom to 1 Si or 2 Ti atoms to 1 Si atom and modulation periods ranging from 10 to 100 nm. In the as-deposited condition, a thin amorphous-titanium-silicide layer was found to exist between the titanium and silicon layers. Heating the multilayer film caused the amorphous-silicide to grow by an exothermic reaction at low temperatures and to undergo an endothermic structural relaxation at high temperatures which was related to a densification and/or compositional homogenization in the amorphous phase. Heating to temperatures over approximately 800 K caused C49-TiSi₂ to form at the amorphous-titanium-silicide/amorphous-silicon interface with an activation energy of 3.1±0.1 eV. The temperatures for the completion of the growth of the amorphous-titanium-silicide, endothermic structural relaxation in the amorphous-titanium-silicide and for the formation of C49-TiSi₂ were found to decrease with decreasing modulation period. This was interpreted to be due to the shorter diffusion distances in smaller modulation period films.

¹ Present address: I.B.M. T.J. Watson Research Center, Yorktown Heights, NY 10598

G18.35

INTERFACIAL REACTION BETWEEN Ni/Ge BILAYER AND SILICON (100) SUBSTRATE. JIAN LI, Q.Z. Hong AND J.W. MAYER, Department of Materials Science and Engineering, Cornell University, Ithaca, NY 14853, USA.

The sequential formation and dissociation of intermetallic compounds in the Ni/Ge/Si(100) system have been studied by using Rutherford backscattering spectroscopy, Auger depth profiling, and X-ray diffraction. Layer structures of NiGe/NiSi/Si(100) were formed after thermal annealing at 350°C. Upon annealing from 350°C to 425°C, the NiGe phase dissociated, providing more free Ni atoms for the further growth of NiSi phase at the nickel germanide/Si(100) interface. The NiSi phase grows with a (time)^{1/2} dependence and with an activation energy of 2.1 eV. The dissociation of NiGe led to an extensive redistribution of Ge and Ni with a configuration of Ge_{0.4}Ni_{1.1}Si_{1.7}/NiSi/Si(100) and this layer structure remained stable until 580°. After annealing at temperatures between 680°C and 720°C, homogenization of Ge in the film occurred. Further phase identification is in progress to clarify whether high temperature annealing can induce a ternary phase or a mixture of NiSi and Si-Ge solid solutions in this system.

G18.36

POSITRON ANNIHILATION IN DIAMONDS.

U. Karfunkel, M.C. Stemmet, S.H. Connell, J.P.F. Sellschop, University of the Witwatersrand, P O Wits 2050, Johannesburg, South Africa; and M. Moussavi-Madani, Department of Physics, University of Bophuthatswana, Mafikeng, Bophuthatswana.

Positron annihilation using Doppler broadening was applied to natural and artificial diamonds. The line-shape parameter F was determined as function of the annealing temperature between room temperature and 700°C. While certain of the measured overall characteristics of F vs. temperature such as the prevacancy region and the fast rising at about 500 to 600°C are qualitatively similar for the various types of diamond, other properties depend in a very specific way on the type of diamond probed. Thus in natural type IIa diamond (which is known to be relatively pure) the method shows with extreme sensitivity some details depending on the diffusion of interstitials in the diamond and their interaction with vacancies, and at some higher temperature the migration of vacancies and the rapid formation of vacancy based centres by solid state reactions. On the other hand, some of these finer details are missing in the artificial diamond, while other novel structural characteristics are found, which are interpreted as being due to the submicroscopic metal inclusions that are present in the artificial diamond. It is suggested to utilise these type of novel phenomena for the probing of similar composite systems.

G18.37

STRUCTURAL AND ELECTRONIC PROPERTIES OF SUBSTITUTIONAL DEFECTS IN DIAMOND.* Koblar A. Jackson* and Mark R. Pederson, Complex Systems Theory Branch, Naval Research Laboratory, Washington D.C. 20375-5000, and Joseph G. Harrison, University of Alabama-Birmingham, Birmingham, Alabama 35294.

We have performed first-principles quantum mechanical calculations to determine the structural and electronic properties of the nitrogen and phosphorous substitutional impurities in diamond. The calculations are performed within a local basis framework, using the Local Density Approximation (LDA). We study impurity properties by performing parallel calculations on hydrogen terminated finite clusters of carbon atoms, replacing the central carbon atom with an impurity atom in the defect clusters. We find defect-related deep levels in the host gap in both the nitrogen and phosphorous impurity systems, at 0.82 and 1.16eV below the conduction band, respectively. From total energy studies on C₅H₁₂-based clusters, we find the on-site diamond lattice position to be stable for both the nitrogen and phosphorous impurities in the ground state; evidence from these calculations suggests, however, that low-lying excited states have a stable off-center position. We will discuss the question of lattice relaxation in these systems, and the effect relaxation has on impurity properties, and address the cluster-size dependence of our results.

*Supported in part by SDIO/IST contract N00014-89-WX-2C023.

*NRC-NRL Research Associate

G18.38

SURFACE AND BULK PROPERTIES WHICH INFLUENCE ION-BEAM HYDROGENATION OF SILICON.* Robert A. Anderson and Carleton H. Seager, Sandia National Laboratories, Albuquerque, NM.

We are studying hydrogen motion and bonding in silicon by means of rapid 1 Mhz capacitance-voltage profiling of Schottky barriers. Our results display the time evolution of dopant passivation when low-energy H ions are implanted directly into the silicon through the front-electrode metallization. These data are compared with numerical transport simulations in order to determine the charge state, diffusivity, and trapping parameters appropriate to

the hydrogenation process in p and n-type material. The analysis is complicated by the dual importance of boundary conditions which establish the surface hydrogen concentration and bulk processes which deplete the hydrogen as it moves through the lattice. We assume that the metal-silicon interface is a perfect sink for hydrogen which diffuses back to the surface from the H-implantation depth. Accordingly, a nearly time independent concentration is established within a second at the implantation range, which supplies hydrogen to the bulk. Our data indicate that some of the mobile hydrogen is in a positively charged state. The application of a bias voltage therefore influences not only the transport of hydrogen within the lattice, but also the fraction of implanted hydrogen which escapes to the surface. Furthermore, the data suggest that other trapping events, in addition to reactions with unpassivated shallow donor or acceptor levels, must be considered in the analysis.

*This work was performed at Sandia National Laboratories, supported by the U. S. Department of Energy under Contract No. DE-AC04-76DP00789.

G18.39

ELECTRONIC AND VIBRATIONAL PROPERTIES OF GROUP V DONOR-HYDROGEN COMPLEXES IN CRYSTALLINE SILICON. L.V.C. Assali, E.C.F. da Silva, and J.R. Leite, Instituto de Física da Universidade de São Paulo, CP 20516, 01498 São Paulo, SP, Brazil.

The fact that H can passivate the electrical activity of p-type and n-type Si has attracted a great deal of attention in the last years. Contrary to the passivation of group III acceptors, which has been studied extensively, the passivation of group V donors is not very well investigated. It seems to be currently accepted that the passivation effects are consequence of pair formations where the H atom is attached to one of the donor's Si nearest neighbors in an antibonding position along the $\langle 111 \rangle$ axis. Although this microscopic structure has been confirmed for the P-H complex in Si by the application of an ab initio pseudopotential method, the calculated H-stretch vibrational frequency, 400cm^{-1} , is in clear contrast with the measured value, 1555.2cm^{-1} .

In this work the electronic structure and the vibrational properties of the group V donor-H pair complexes in Si are investigated. The calculations discussed here for the pair electronic states were carried out within the framework of the multiple-scattering X α molecular cluster model. The Green's-function technique and a valence-force field Hamiltonian have been adopted to obtain the vibrational energies of the pairs.

G18.40 ABSTRACT NOT AVAILABLE

G18.41

SURFACE PROTECTION DURING PLASMA HYDROGENATION FOR ACCEPTOR PASSIVATION IN InP. J. Lopata, W. C. Dautremon-Smith, S. J. Pearton, J. W. Lee, N. T. Ha, and H. S. Luftman, AT&T Bell Laboratories, Murray Hill, NJ 07974.

Various dielectric and metallic films were examined as H-permeable surface protection layers on InP substrates during H_2 or D_2 plasma exposure for passivation of acceptors in the InP. Plasma deposited SiN_x , SiO_2 , and a-Si films ranging in thickness from 85 to 225 Å were used to protect p-InP during D_2 plasma exposure at 250°C. Optimum protective layer thicknesses were determined by a trade-off between the effectiveness of the layer to prevent P loss from the wafer surface and the ability to diffuse atomic H or D at a rate greater than or equal to that in the underlying InP. SIMS and capacitance-voltage depth profiling were used to determine the extent of D in-diffusion and acceptor passivation respectively. Sputter deposited W and e-beam evaporated Ti films ~100 Å thick were also evaluated as surface protection layers for InP.

The W coated sample yielded similar results to those with dielectric films in that acceptors in p-InP were passivated to a similar depth for the same plasma exposure. The 100 Å Ti film, however, did not allow the D to diffuse into the InP substrate. It is surmised that the Ti film trapped the D, thus preventing diffusion into the substrate.

G18.42

INTERDIFFUSION MEASUREMENTS IN SiGe/Si STRAINED LAYER SUPERLATTICES. S.M. Prokes, M. Fatemi, U.S. Naval Research Laboratory, Washington D.C., 20375; and K. Wang, University of California, Los Angeles, CA 90024.

Interdiffusion measurements in $\text{Si}_{1-x}\text{Ge}_x/\text{Si}$ strained-layer systems have been obtained from X-ray diffraction measurements. Mixing of the superlattices has been monitored using X-ray powder diffractometry, double crystal X-ray diffraction, and XTEM, when applicable. In the powder diffractometer method, both "small-angle" and "high-angle" superlattice peaks were monitored allowing comparisons of thermal mixing in the near-surface layers versus mixing of the complete superlattice. Measurements have been made at annealing temperatures as low as 550°C, and noticeable differences in the X-ray spectra have been seen. Results indicate that these changes do not stem from dislocation formation or propagation, and they must be considered when interpreting diffusion data.

G18.43

ELECTRONIC STRUCTURE OF AN ISOELECTRONIC CENTER IN SULPHUR-DOPED SILICON STUDIED BY OPTICAL DETECTION OF MAGNETIC RESONANCE. W.M. Chen, A. Henry, B. Monemar, Department of Physics and Measurement Technology, Linköping University, S-581 83 Linköping, Sweden; and M.L.W. Thewalt, Department of Physics, Simon Fraser University, Burnaby, B.C., Canada V5A 1S6.

We report an investigation on the electronic structure of an isoelectronic center in S-doped Si, by optical detection of magnetic resonance (ODMR). A spin-triplet ($S=1$) has been identified to be the lowest electronic excited state of the defect, giving rise to deep photoluminescence (PL) emissions (S_A at 968.24 meV and S_B at 811.96 meV) [1] when it decays to the diamagnetic ($S=0$) crystal ground state. This is in full agreement with recent Zeeman measurements [2]. A small zero-field splitting of the spin-triplet as well as a weak anisotropy of the magnetic interaction of the defect (not possible to resolve in Zeeman data) has been revealed, which leads directly to the determination of the symmetry for the defect. A S-related complex model is suggested as the identity of the defect. A critical test of two possible metastable configurations of the constituents of a single defect is undertaken. This work provides the first case where ODMR of an electronic state can be observed directly from its radiative transitions in Si.

[1] M.L.W. Thewalt, M. Nissen, D.J.S. Beckett and S. Charbonneau, in Proc. the 3rd Int. Conf. on Shallow Impurities in Semiconductors, Ed. by B. Monemar (Inst. of Phys. Conf. Series Vol. 95, Bristol, 1989) p. 505.

[2] M. Singh, E.C. Lightowers and G. Davies, Proc. E-MRS 1989 Spring Meeting, May 30-June 2, Strasbourg, France.

G18.44

AN ELECTRON PARAMAGNETIC RESONANCE INVESTIGATION OF IRON-INDIUM PAIRS IN SILICON. W. Gehlhoff, Academy of Sciences of the GDR, Centre for Scientific Instruments, Rudower Chaussee 6, Berlin 1199, GDR; and P. Emanuelsson, P. Omling and H. G. Grimmeiss, Department of Solid State Physics, University of Lund, Box 118, S-221 00 Lund, Sweden.

Silicon crystals co-doped with iron and indium were investigated by Electron Paramagnetic Resonance (EPR). Three different EPR signals originating from iron-indium pairs, two with orthorhombic symmetry and one with trigonal symmetry, were found. The chemical identity of the EPR-centres were determined from the hyperfine splitting caused by ^{113}In , ^{115}In and, in isotope doped samples, by ^{57}Fe . The trigonal⁽¹⁾ and one of the orthorhombic⁽²⁾ signals are reported before. This "old" orthorhombic signal shows to be, in contrary to what was originally concluded⁽²⁾, an excited state and the new orthorhombic signal is found to be the corresponding ground state. The three spectra will be analyzed in detail and the effective g-values will be explained using crystal field theory. Finally, the zero-field splitting between the two orthorhombic states will be estimated from the temperature dependence of the two signals.

- 1) P. Omling, P. Emanuelsson, W. Gehlhoff and H. G. Grimmeiss, Solid State Communications **70**, (1989).
- 2) G. W. Ludwig and H. H. Woodbury, Solid State Physics **13**, 223 (1962).

G18.45

THE VERY EARLY STAGES OF INITIAL OXIDATION OF SILICON (111) IN ATOMIC OXYGEN*, B. Ola N. De, Jane E. Peterkin, Jane Hruska, Yong Zhao, N.J. Ianno and John A. Woollam, Center for Microelectronics and Optical Materials Research, and The Department of Electrical Engineering, U. of Nebraska, Lincoln, NE 68588-0511

According to the recently proposed model of Muraly and Murarka (1986), the very early stages of initial oxidation of silicon involves the diffusion of oxygen through a very thin barrier of silicon oxide into a volume of silicon near the oxide-silicon interface when the oxidation is relatively faster than at the later stages (when the oxidation is confined only at the interface and hence much slower). Using monolayer sensitive Variable Angle Spectroscopic Ellipsometry (VASE), we have examined the validity of this model for early oxidation by "ashing" Si(111) in atomic oxygen in a pure oxygen plasma asher. The data shows that the initial oxide growth on Si can be divided into two linear regions and at later stages it becomes parabolic as a function of time. These results are in agreement with the predictions of the theory. *Research supported by NASA Grant NAG-3-95.

G18.46

HYDROGEN PASSIVATION STUDIES IN DISLOCATED Cz AND Fz SILICON. C. Dubé, J.P. Kalejs and S. Rajendran Mobil Solar Energy Corporation, 4 Suburban Park Drive, Billerica, MA 01821

Hydrogen passivation using a Kaufmann ion source has been carried out on Cz and Fz silicon dislocated by four point bending in the temperature range from 800-1000 C. The lifetime improvement after passivation is examined as a function of dislocation density up to about $1 \times 10^7/\text{cm}^2$ using the EBIC technique applied to the sample cross

section. Minority carrier diffusion lengths in this material are degraded to 10-20 microns both as a result of the thermal treatment accompanying the stress application and by the dislocations. Differences in the degradation are not observed as a function of the oxygen content of the silicon. Hydrogen passivation for 2 minutes at 400 C produces an increase in the diffusion length of 5-10 microns that is small compared to that observed in silicon grown by the Edge-defined Film-fed Growth (EFG) technique (1) with comparable levels of dislocations and pre-passivation diffusion lengths. However, the penetration depth of the passivation front through the wafer thickness is not observed to be dependent on the dislocation density and the passivation appears to extend through the entire wafer thickness of 400 microns in all cases. This is very different from the case of the EFG material, for which the penetration depth in highly dislocated regions is of the order of 100-150 microns under comparable passivation temperatures and times. A model for hydrogen diffusion and trapping is applied to the study of the differences observed between these materials, and the model results are used to argue that these differences are not produced by hydrogen transport effects in the bulk.

1C. Dubé & J. Hanoka, Appl. Phys. Lett. **45**, 1135 (1984).

G18.47

ENHANCEMENT OF OXYGEN PRECIPITATION IN QUENCHED CZOCHRALSKI SILICON CRYSTALS. A. Hara, T. Fukuda, I. Hirai and A. Ohsawa, Fujitsu Laboratories Ltd., Kamikodanaka, Nakahara -ku, Kawasaki 211, Japan.

We found that oxygen precipitation of CZ-Si crystals can be enhanced by rapid cooling from solution annealing temperature ($>1200^\circ\text{C}$). Quenching ($1700^\circ\text{C}/\text{min}$) from 1290°C increases oxygen precipitation at $700^\circ\text{C}/360\text{h}$ to about 5 times that of slow cooling ($8^\circ\text{C}/\text{min}$). The enhancement effects of quenched-silicon disappeared by solution annealing and followed slow cooling. We found that oxygen precipitation of the quenched sample is not influenced by preannealing at temperatures below 900°C , and decrease at temperatures above 900°C . Preannealing is carried out before precipitation annealing at $700^\circ\text{C}/20\text{h} + 1000^\circ\text{C}/10\text{h}$.

Quenching from high temperatures introduces defects, which increase oxygen precipitation and disappear by solution annealing and followed slow cooling. We estimate that the defects could be aggregation of intrinsic point defects because the aggregation may enhance oxygen precipitation and is stable to above 900°C . The defects are not vacancies, self-interstitials or simple complexes such as A-centers and divacancies, because they are not stable to 900°C . The defects are neither impurities such as metal impurities and carbon nor small oxygen precipitate so called embryos, because fewer impurities and embryos are introduced by quenching than by slow cooling.

The oxygen precipitation was able to be controlled according to initial oxygen concentration by introducing the quenching process before precipitation annealing. Thus we can overcome the problem of thermal history in the intrinsic gettering.

G18.48

DIVACANCY TRANSFORMATIONS IN ELECTRON-IRRADIATED SILICON. J.H. Robison* and A.E. Jaworowski, Physics Department, Wright State University, Dayton, OH; *Present address: Anser, Division SDTD, 1215 Jefferson Davis Highway, Arlington, VA.

Real-time electric field drift measurements, capacitance-voltage profiling and deep-level transient spectroscopy have been used to observe interactions of hydrogen with divacancy in 2-MeV electron-irradiated silicon samples. We found that in the presence of mobile hydrogen the divacancy existed in two distinct states,

H₁ and H₂, which occurred near the temperature where previously the divacancy was observed. The correlation between the "free" hydrogen concentration and the H₁ and H₂ levels has been examined in the reverse bias annealed samples. The production of H₁ level is favored at depth which have a higher concentration of hydrogen. The sum of the two concentrations remaining constant throughout the sample, supports the assumption that the H₁ and H₂ are different states of the same defect, namely the divacancy.

G18.49

DETERMINATION OF 3-DIMENSIONAL DEFECT STRUCTURES IN GALLIUM ARSENIDE EPILAYERS ON SILICON USING WHITE BEAM SYNCHROTRON RADIATION TOPOGRAPHY IN BOTH TRANSMISSION GEOMETRY AND GRAZING BRAGG LAUE GEOMETRY. M. Dudley, J. Wu and G.-D. Yao, Dept. of Materials Science and Engineering, SUNY at Stony Brook, Stony Brook NY; H.-Y. Liu and Y.C. Kuo, Materials Science Laboratory, Texas Instruments, Dallas, TX.

White beam synchrotron topography in both transmission and grazing Bragg-Laue geometries has been used to reveal the 3-dimensional defect structure in MBE-grown GaAs epilayers on Si. In the grazing Bragg-Laue case, manipulation of geometry enabled depth profiling of defect structures in both epilayer and substrate. Defects observed include substrate threading dislocations, interfacial dislocations and epilayer planar defects. Dislocation line direction and Burgers vector analysis was performed. Clear continuity between substrate threading dislocations and interfacial dislocations was established. Overall defect structures were then correlated with processing conditions.

This technique affords a rapid and non-destructive way of quantitatively characterizing processing induced damage in such systems.

Research funded in part by the NSF under contract # DMR 8506948, and performed on beamline X-19C at the NSLS which is funded by DOE under contract # DE-FC02-84SF45098.

G18.50

DIFFUSION OF Au IN AMORPHOUS Si MEASURED BY THE COMPOSITION MODULATION TECHNIQUE. E. Nygren^{a)}, B. Park and F. Spaepen, Division of Applied Sciences, Harvard University, Cambridge, MA 02138

Compositionally modulated amorphous Si/amorphous Si(0.7 at. % Au) multilayers with a repeat length of 46Å have been fabricated by ion beam sputtering system. The change, with annealing time, in the intensity of the first X-ray diffraction peak resulting from the composition modulation is used to determine the diffusion coefficients of Au in amorphous Si. Diffusion lengths scale on the order of an interatomic distance can be measured. The diffusivities over the temperature range 200 to 260°C have an Arrhenius-type temperature dependence with an activation enthalpy of 1.2 eV. The diffusivities are in agreement with the extrapolation of high temperature data taken by RBS in ion-implanted amorphous Si, and are smaller than those in the crystalline Si.

a) Present Address: Department of Materials of Science and Engineering, The Ohio State University, Columbus OH 43210

G18.51

HYDROGEN DIFFUSION AND COMPLEX FORMATION IN SILICON. J.T. Borenstein, Mobil Solar Energy Corporation, 4 Suburban Park Drive, Billerica, MA 01821; D. Tulchinski and J.V. Corbett, Physics Department, SUNY at Albany, Albany, NY 12222.

The kinetics of hydrogen diffusion and complex formation in crystalline silicon are investigated using a model previously developed to explain the influence of dopant type and concentration on observed deuterium profiles in silicon. The predictions of the model are shown to be in close agreement with recent SIMS profiles of deuterated FZ-Si crystals. The in-diffusion process is dominated by trapping at impurity sites and by the formation of immobile hydrogen molecules. Charge state effects are shown to control the kinetics of hydrogen-acceptor and hydrogen-donor deactivated complexes.

Previous studies have treated the surface concentration of hydrogen and the capture radii of hydrogen at complexes as free kinetic parameters. We present an analytic relationship between the diffusion coefficient D of neutral hydrogen and both the hydrogen surface concentration and the capture radius for molecule formation. The consequences of fixing D at the known high-temperature value for the diffusion coefficient in the model are determined. The existence of this analytic relation reduces the number of free parameters in the kinetic model and leads to an improved understanding of hydrogen reactions in silicon.

G19.1

ELECTRON SCATTERING BY NATIVE DEFECTS IN UNIFORMLY- AND MODULATION-DOPED SEMICONDUCTOR STRUCTURES. W. Walukiewicz, Center for Advanced Materials, Materials and Chemical Sciences Division, Lawrence Berkeley Laboratory, 1 Cyclotron Rd., Berkeley, CA 94720

The effect of charged native defects on electron mobility of a 3-D electron gas in uniformly doped (UD) thin layers and a 2-D electron gas in modulation doped heterostructures (MDH) is calculated. The concentrations of native defects are found using the recently proposed model of amphoteric native defects.¹ According to the model, the single most important parameter controlling the defect formation is the location of the Fermi level measured with respect to an internal energy reference, Fermi level stabilization energy (E_{FS}). We find that in the case of UD n-type GaAs, the electron concentration saturates at high doping levels. The saturation results from increased formation of compensating native acceptors. These acceptors act as efficient electron scattering centers leading to an abrupt decrease of electron mobility for doping levels exceeding 10¹⁹ cm⁻³. Based on the same model of defect formation, we can also explain differences between electron mobility in "normal" and "inverted" MDHs. In inverted MDH, the undoped GaAs quantum well is grown in the presence of free electrons which facilitate the formation of native defects. Scattering by those defects reduces the 2-D electron mobility. In normal MDH, the undoped GaAs layer is grown prior to n-type doped AlGaAs, therefore no electrons are present in the quantum well during the growth. As a consequence, the concentration of native defects is much lower and electron mobilities much higher than in the inverted MDH.

Work supported by US DOE under Contract No. DE-AC03-76SF00098.

[1] W. Walukiewicz, Appl. Phys. Lett. 54, 2099 (1989).

G19.2

ACCEPTOR DELTA-DOPING IN GaAs. W. S. Hobson, S. J. Pearton and C. R. Abernathy, AT&T Bell Laboratories, 600 Mountain Ave, Murray Hill, NJ. G. Cabaniss, Solecon Laboratories, San Jose, CA.

We have investigated the formation and diffusion of delta-doped layers in GaAs employing the acceptors Zn, Cd, and C. MOCVD was used for the growth of the Zn and Cd δ-doped layers while MOMBE was utilized to achieve C δ-doping. The narrowest atomic profiles for Zn had full width at half maxima of 60Å for peak Zn concentrations of $\leq 3 \times 10^{18}$ cm⁻³, as measured by SIMS. An effective diffusion coefficient of $\leq 7 \times 10^{17}$ cm²/s is estimated for a growth temperature of 625°C, based on multiple Zn δ-doped

layers. For carbon, a doping spike of $7 \times 10^{19} \text{ cm}^{-3}$ with a full width at half maximum of 50 Å, as measured by electrochemical capacitance voltage profiling, was achieved and represents the highest doping level yet reported for planar doping. Diffusion of the carbon was negligible under RTA for 5 s at 900°C. By contrast, it was difficult to achieve doping levels $\geq 5 \times 10^{17} \text{ cm}^{-3}$ for Cd due to its high vapor pressure.

G19.3

PRECIPITATION PHENOMENA ASSOCIATED WITH ULTRA-HIGH Be DOPING OF $\text{Ga}_{0.47}\text{In}_{0.53}\text{As}$ BY MBE. C. M. Cotell, M. B. Panish, R. A. Hamm, L. C. Hopkins, and J. M. Gibson, AT&T Bell Laboratories, Murray Hill, NJ 07974.

Ultra-high Be doping ($\geq 1 \times 10^{20} \text{ cm}^{-3}$) of $\text{Ga}_{0.47}\text{In}_{0.53}\text{As}$ has a number of potentially desirable applications including use in high speed heterostructure bipolar transistors. In this paper, we report the results of a study of Be doping of $\text{Ga}_{0.47}\text{In}_{0.53}\text{As}$ as a function of temperature between 365 and 500°C. The $\text{Ga}_{0.47}\text{In}_{0.53}\text{As}$ samples used in this study were grown by gas source molecular beam epitaxy (GSMBE) using decomposed AsH_3 and PH_3 for generation of As_2 and P_2 beams and elemental effusion cells for the Ga, In and Be sources. The samples were characterized by TEM and SIMS and their electrical properties were determined by Hall measurements. It was found that for each growth temperature there exists a maximum hole concentration. Increasing the Be flux above that which produced the maximum hole concentration resulted in precipitation and the nucleation of dislocations at the precipitates. The occurrence of precipitation may be related to the rate of surface diffusion of Be and, therefore, may depend upon temperature. The nucleation of dislocations at precipitate sites is apparently dependent upon precipitate size.

G19.4

CHARACTERISTICS OF DOPING AND DIFFUSION OF HEAVILY DOPED N AND P TYPE InP AND InGaAs EPITAXIAL LAYERS GROWN BY METALORGANIC CHEMICAL VAPOR DEPOSITION. C.J. Pinzone, N.D. Gerrard, R.D. Dupuis, N.T. Ha and H.S. Lufman, AT&T Bell Laboratories, Murray Hill, NJ

Electronic and photonic device applications of the InP/InGaAs semiconductor materials system requiring the growth of epitaxial material doped to or near the saturation limit of the impurity in the host material present an extreme challenge for the crystal grower. To produce device heterostructures with abrupt dopant profiles, preserve the junction during subsequent growth, and retain a high degree of crystalline perfection it is necessary to understand the limits of dopant incorporation, the behavior of the impurity in the material, and the influence of adjacent layers on the dopant distribution.

N and p type doping above 10^{19} has been achieved in InP and InGaAs grown by MOCVD. Growth conditions and electrical characterization results for doping near the electrical saturation limit will be presented.

homo and heterojunctions of InP and InGaAs doped at various levels were prepared by MOCVD. Secondary Ion Mass Spectroscopy (SIMS) was used to determine the degree of dopant diffusion in these structures and the role of the doping level of adjacent layers in enhancing or retarding this diffusion. These results, and techniques for control of impurity distributions will be presented.

G19.5

EFFECTS OF Si INCORPORATION AND ELECTRICAL ACTIVATION ON INTERSUBBAND OPTICAL ABSORPTION IN GaAs/AlGaAs MULTIPLE QUANTUM WELLS. J.D. Ralston, H. Ennen, M. Maier, M. Ramsteiner, B. Düscher, and P. Koidl, Fraunhofer-Institut für Angewandte Festkörpersphysik, Eckerstraße 4, 7800 Freiburg, West Germany.

In the past five years, several groups have successfully demonstrated efficient infra-red detection at $3-12 \mu\text{m}$ based on intersubband absorption in GaAs/AlGaAs quantum wells. Typical structures contain GaAs QW's doped with Si to a level on the order of 10^{18} cm^{-3} . Utilizing SIMS profiling, Hall measurements, electronic Raman scattering, and infra-red absorption, we will present a detailed study of the effects of Si dopant behaviour on intersubband absorption in GaAs/AlGaAs MQW's. The peak wavelength and integrated intensity of the infra-red absorption are found to be strongly dependent upon the incorporation and electrical activation of Si in doped GaAs QW's, which in turn are greatly influenced by the epitaxial growth conditions.

Six samples of identical design were grown on undoped GaAs substrates by MBE. Each sample contained a 10 period MQW region, consisting of 140 Å undoped $\text{Al}_{0.3}\text{Ga}_{0.7}\text{As}$ barrier layers and 70 Å GaAs QW's doped in the center 50 Å with Si at a concentration of $2 \times 10^{18} \text{ cm}^{-3}$. The MQW region was grown at a different substrate temperature for each sample, varying between 520 and 680°C. SIMS profiling clearly reveals that, with

increasing substrate temperature, the Si doping profile broadens extensively and shifts towards the sample surface. This behaviour is attributed to Si segregation on the growing surface, and leads to substantial unintended doping of the AlGaAs barrier layers. This implies that the actual free carrier population may be due to a combination of intentional doping in the QW and unintentional modulation doping from the barriers. The SIMS results also indicate that, although extensive Si segregation appears to occur through the QW interfaces during MBE growth, no resolvable Al-Ga interdiffusion between the well and barrier layers occurs.

The wavelength at which the maximum intersubband absorption occurs is determined by a coupling of the bare intersubband transition and the two-dimensional free carrier plasma in the QW. The resulting depolarization shift of the infra-red absorption peak, as a function of substrate temperature, has been determined by electronic Raman scattering, providing data on the variations in free carrier concentration for the same nominal Si doping. Free carrier concentrations were also measured directly via Hall measurements. The results indicate clearly that at both very low and very high substrate temperatures the 2-dimensional electron concentration is markedly reduced in the QW's. This behaviour is tentatively attributed, at low growth temperatures, to electron capture by deep defects in the AlGaAs barrier layers. At high growth temperatures, loss of free electrons is attributed to degraded activation of, or incomplete electron transfer from Si atoms incorporated in the AlGaAs barriers. In the present study, a substrate temperature of 620°C yielded both the highest free carrier concentration and the largest integrated infrared absorption intensity. This work highlights the importance of thoroughly characterized epitaxial growth in optimizing the performance of intersubband infrared detectors.

G20.1

IMPURITY-INDUCED LAYER DISORDERING: CURRENT UNDERSTANDING AND AREAS FOR FUTURE INVESTIGATION. L. J. Guido and N. Holonyak, Jr., University of Illinois, Urbana, IL

The study of impurity-induced layer disordering (IILD) has led to the successful application of heterolayer interdiffusion to the fabrication of optoelectronic devices. Ordinarily, this type of layer interdiffusion is undesirable in the active region of quantum well heterostructure (QWH) devices but can be masked (prevented) and be "turned-on" where desired. The acceptance of IILD as a device fabrication technology has occurred because: (1) it provides a means for selective bandgap, refractive index, and conductivity-type "engineering" parallel to the crystal growth plane, (2) it employs simple integrated circuit-style processing, and (3) it has been achieved in many III-V semiconducting compounds using a variety of agents (e.g., shallow impurities, native defects). The purpose of this work is threefold. First is to identify important contributions to the current phenomenological understanding of IILD. For example, the determination of the temperature and impurity concentration dependence of the Al-Ga interdiffusion coefficient, the identification of the crystal surface-ambient interaction and the Fermi-level effect, and the comparison of thermal annealing-induced and impurity-diffusion-induced layer disordering. Second is to review the strengths and weaknesses of existing IILD models in consideration of the above mentioned experimental data. Third is to present performance data for $\text{Al}_{1-x}\text{Ga}_x\text{As-GaAs}$ QWH devices that have been fabricated using these "IILD concepts". The device results are encouraging, but suggest that higher levels of sophistication will require a more complete understanding and further development of IILD.

G20.2

BEHAVIOR OF DOPANT-RELATED DEFECTS IN AlGaAs SUPERLATTICES. N.D. Theodore, P. Mei*, C.B. Carter, C. Palmstrom**, S.A. Schwarz**, J.P. Harbison**, L.T. Florez**, Department of Materials Science and Engineering, Bard Hall, Cornell University, Ithaca, NY 14853; *Department of Electrical Engineering, Mudd Building, Columbia University, NY 10027; **Bell Communications Research Inc., 331 Newman Springs Rd., Redbank, NJ 07751.

The presence of silicon dopant atoms is known to increase the diffusion of Al in the AlGaAs/GaAs superlattice system. This phenomenon has been used in the past to induce dopant-enhanced mixing of AlGaAs/GaAs superlattices. A previous study characterized the mixing behavior of AlGaAs superlattices at high Si-doping levels.¹ Defects such as dislocation loops and Si-rich precipitates were found to form in the highly doped superlattices upon annealing. The presence of the defects was found to be related to changes in mixing behavior. In the present study, transmission electron microscopy has been used to characterize the defects. Superlattices with varying silicon doping levels have been annealed at different temperatures for varying time-periods, to observe the temperature-time behavior of the dislocation-loops. The superlattice

geometry has been varied to confirm or deny the tentative observation of a preponderance of defects in GaAs as opposed to AlAs in the superlattice. These results will be presented. The vacancy/interstitial nature of the loops will also be discussed.

1. N.D. Theodore, C.B. Carter, P. Mei, S.A. Schwarz, T. Venkatesan, J.P. Harbison, Proc. Mat. Res. Soc. Symp. 1988 (in press).

G20.3

INTERDIFFUSION BEHAVIOR OF SYMMETRICALLY STRAINED Ge_mSi_m SUPERLATTICES. P.M. Adams and R.C. Bowman, Jr., The Aerospace Corporation, Los Angeles, CA; S.J. Chang, V. Arbet, and K.L. Wang, University of California, Los Angeles, CA.

X-ray diffraction and Raman scattering have been used to study interface mixing between the Ge and Si layers in symmetrically strained Ge_mSi_m superlattices during thermal anneals. The superlattices had been grown by MBE procedures on relaxed $\text{Si}_{0.5}\text{Ge}_{0.5}$ alloy buffer layers. In order to extract the bulk interdiffusion coefficients from the intensity changes of the x-ray satellites, samples with nominal periodicities between 1.4nm and 5.6nm have been prepared. Initial analyses of the temperature dependences of these satellites yielded an activation energy of 3.0eV for the interdiffusion coefficient. This value is essentially equivalent to that previously obtained¹ for a Ge/Si superlattice grown on a $\text{Ge}_{0.4}\text{Si}_{0.6}$ alloy buffer. From comparisons with diffusion parameters for crystalline Si and Ge it is concluded that intermixing in these Ge/Si superlattices are dominated by the diffusion of Si atoms into the Ge layers via a vacancy mechanism. Intermixing also produced significant changes in the Raman spectra. Namely, the intensity of the zone-fold acoustic peaks decreased while the optical mode associated with the Ge-Si vibration systematically increased during the annealing. In addition, shifts in the optic mode energies that can be attributed to alloy formation at the interfaces were also observed.

1. S.J. Chang, et al., Appl. Phys. Lett. 54, 1235 (1989)

G20.4

DIFFUSION MECHANISMS IN GaAs AND GaAs-BASED LAYERED STRUCTURES. U. Gösele and T. Y. Tan†, School of Engineering, Duke University, Durham, NC; ‡also at the Microelectronics Center of North Carolina, Research Triangle Park, NC.

It has taken more than twenty years to demonstrate that both vacancies and self-interstitials are important for understanding the mechanisms of self- and impurity diffusion in the elemental semiconductor silicon. Similarly, for a long time diffusion processes in GaAs and other III-V compounds have almost exclusively been discussed in terms of mechanisms involving vacancies. Only in the last couple of years the phenomenon of impurity-diffusion-induced disordering of GaAs-based superlattices have allowed to study self-diffusion processes much more closely than previously possible and to arrive at detailed conclusions concerning Ga self-diffusion and a number of impurity diffusion mechanisms. Under intrinsic and n-type doping conditions Ga self-diffusion is dominated by a mechanism involving triply negatively charged gallium vacancies, whereas under heavy p-type doping Ga self-interstitials govern Ga self-diffusion.

Concerning impurity diffusion mechanisms we will shortly discuss silicon diffusion in GaAs and then concentrate on Zn and Be diffusion both of which appear to be governed by the 'kick-out' mechanism. We will specifically deal with the different diffusion behavior in the presence or absence of an outside source and with the influence of zinc in-diffusion on the diffusion behavior of Be or Zn incorporated in a buried layer.

SYMPOSIUM H:
MATERIALS ISSUES IN
MICROCRYSTALLINE SEMICONDUCTORS

H

November 29 - December 1, 1989

Chairs

Philippe M. Fauchet
Department of Electrical Engineering
Princeton University
Princeton, NJ 08544
(609) 258-4416

Chuang Chuang Tsai
Xerox Palo Alto Research Center
3333 Coyote Hill Road
Palo Alto, CA 94304
(415) 494-4515

Kazunobu Tanaka
Electrotechnical Laboratory
1-1-4, Umezono, Tsukuba-Shi
Ibaraki, 305, Japan
0298-54-5243

Symposium Support

Sanyo Electric Company, Limited

Solar Energy Research Institute

Tonen Corporation

Xerox Corporation

**Proceedings published as Volume 164
of the Materials Research Society
Symposium proceedings series.**

SESSION H1: MICROCRYSTALLINE SILICON:

GROWTH

Chair: C. C. Tsai
Wednesday Morning, November 29
Salon J/K (M)

8:15 INTRODUCTORY REMARKS

8:30 *H1.1

ROLE OF SURFACE AND GROWTH-ZONE REACTIONS IN THE FORMATION PROCESS OF $\mu\text{c-Si:H}$, Akihisa Matsuda, Electrotechnical Laboratory, Materials Science Division, Ibaraki, Japan; and Toshio Goto, Nagoya University, Electronics Department, Nagoya, Japan.

9:00 H1.2

OPTO-ELECTRONIC PROPERTIES OF $\mu\text{c-Si}$ GROWN FROM SiF_4 and H_2 BY PECVD, Y. Okada, I.H. Campbell, P.M. Fauchet, and S. Wagner, Princeton University, Department of Electrical Engineering, Princeton, NJ.

9:15 H1.3

SUBSTRATE TEMPERATURE DEPENDENCE OF THE RAMAN SPECTRA FOR MICROCRYSTALLINE SILICON FILMS PRODUCED BY REACTIVE MAGNETRON SPUTTERING, C.Wang, G.N. Parsons, E.C. Buehler, G. Lucovsky and R.J. Nemanich, North Carolina State University, Department of Physics and Material Science and Engineering, Raleigh, NC.

9:30 H1.4

PREPARATION AND CHARACTERIZATION OF HIGHLY CONDUCTIVE (100 S/cm) PHOSPHORUS DOPED $\mu\text{c-Si:H}$ FILMS DEPOSITED USING THE VHF-GD TECHNIQUE, K. Prasad, F. Finger, H. Curtins, A. Shah, Institut of Microtechnology, Neuchatel, Switzerland; and J. Bauman, University of Konstanz, Physics Institut, Konstanz, West Germany.

9:45 H1.5

COMPOSITION DETERMINATION OF MICROCRYSTALLINE TWO-PHASE SILICON RICH OXIDES, D. Bouldin, C.H. Lam, IBM, Essex Junction, VT; K.-T. Chang and K. Rose, Rensselaer Polytechnic Institute, Center for Integrated Electronics, Troy, NY.

10:00 BREAK

10:30 *H1.6

CHEMISTRY AND SOLID STATE PHYSICS OF MICROCRYSTALLINE SILICON, Stan Veprek, Technical University Munich, Institute for Chemistry of Information Recording, Munich, West Germany.

*Invited Paper

11:00 H1.7

ELECTRONIC AND STRUCTURAL PROPERTIES OF $\mu\text{c-Si:H}$ FILMS PREPARED BY RF GLOW DISCHARGE WITH HYDROGEN DILUTION, S. Aljishi, Shu Jin, M. Stutzmann and L. Ley; Max-Planck-Institut für Festkörperforschung, Stuttgart, West Germany.

11:15 H1.8

THE FORMATION OF SILICON CLUSTERS IN P.E.C.V.D. Si:O:H:F ALLOYS, A.G. Dias and J. Figueiredo, Centro de Fisica Molecular das Universidades de Lisboa, Instituto Nacional de Investigacao Cientifica, Complexo I (I.S.T.) Lisboa, Portugal.

11:30 H1.9

PREPARATION OF CRYSTALLINE Si THIN FILMS BY SPONTANEOUS CHEMICAL DEPOSITION, Tohru Komiya, Akira Kamo, Hiroshi Kujirai, Tokyo Institute of Technology, Imaging Science and Engineering Laboratory, Yokohama, Japan; Isamu Shimizu, Tokyo Institute of Technology, Imaging Science and Engineering Laboratory and Graduate School at Nagatsuta, Yokohama, Japan; and Jun-ichi Hanna, Tokyo Institute of Technology, Imaging Science and Engineering Laboratory, Yokohama, Japan.

11:45 H1.10

MICROCRYSTALLINE SILICON FILMS PRODUCED BY RF MAGNETRON SPUTTERING AND THE EFFECT OF DIFFERENT AMBIENTS ON THEIR CONDUCTIVITY, Ratnabali Banerjee, A.K. Bandyopadhyay, S.N. Sharma, A.K. Batabyal, and A.K. Barua, Indian Association for the Cultivation of Science, Energy Research Unit, Calcutta, India.

SESSION H2: SEMICONDUCTOR COMPOUNDS:

NANOCRYSTALS

Chair: P.M. Fauchet
Wednesday Afternoon, November 29
Salon J/K (M)

1:30 *H2.1

LINEAR AND NONLINEAR OPTICAL PROPERTIES OF QUANTUM SEMICONDUCTOR CRYSTALLITES, Louis Brus, AT&T Bell Laboratories, Murray Hill, NJ.

2:00 H2.2

ELECTRODEPOSITION OF 3-DIMENSIONAL SIZE QUANTIZED CdS AND CdSe FILMS, G. Hodes and T. Engelhard, The Weizmann Institute of Science, Department of Materials Research, Rehovot, Israel.

2:15 H2.3

STRUCTURAL AND ELECTRICAL CHARACTERIZATION OF CdSe THIN FILMS, Miltiadis K. Hatalis, and Fuyun Lin, Lehigh University, Department of Electrical Engineering, Bethlehem, PA; and Michael R. Westcott, Litton Systems Canada Limited, Rexdale, Canada.

2:30 H2.4

A STUDY OF THE PRESSURE-INDUCED PHASE TRANSITION IN BULK AND NANOCRYSTALLINE CdS, Xue-Shu Zhao, John Schroeder, P.D. Persans, and Enlian Lu, Rensselaer Polytechnic Institute, Physics Department, Troy, NY.

2:45 H2.5

TIME-RESOLVED SPECTRA OF EDGE EMISSION OF CdSe MESOSCOPIC CLUSTERS IN GeO₂ GLASS MATRIX, Takao Inokuma, Akinori Tanaka, Toshihiro Arai, University of Tsukuba, Institute of Applied Physics, Ibaraki, Japan; and Mitsuru Ishikawa, Hamamatsu Photonics K.K., Tsukuba Research Laboratory, Ibaraki, Japan.

3:00 BREAK

3:30 *H2.6

OPTICAL PROPERTIES OF II-VI SEMICONDUCTOR-DOPED GLASS, P.D. Persans, An Tu, T. Driscoll, M. Lewis, and R. Redwing, Rensselaer Polytechnic Institute, Physics Department and Center for Integrated Electronics, Troy, NY.

4:00 H2.7

FABRICATION AND CHARACTERIZATION STUDIES OF SEMICONDUCTOR-IMPREGNATED POROUS VYCOR GLASS, C.A. Huber, Massachusetts Institute of Technology, Francis Bitter National Magnet Laboratory, Cambridge, MA and University of Puerto Rico, Department of Physics, Rio Piedras, Puerto Rico; T.E. Huber, Harvard University, Department of Physics, Cambridge, MA and University of Puerto Rico, Department of Physics, Rio Piedras, Puerto Rico; A.P. Salzberg and J.A. Perez, University of Puerto Rico, Department of Physics, Rio Piedras, Puerto Rico.

4:15 H2.8

SYNTHESIS, STRUCTURAL AND OPTICAL CHARACTERIZATION OF SMALL PARTICLE III-V SEMICONDUCTOR CLUSTERS INCLUDED IN POROUS HOSTS, James E. MacDougall, Hellmut Eckert, William T.A. Harrison, Galen D. Stucky, University of California, Santa Barbara, Department of Chemistry, Santa Barbara, CA; Norman Herron, Ying Wang, E.I. duPont de Nemours and Co., Inc., Central Research and Development Department, Wilmington, DE; Karin Moller and Thomas Bein, University of New Mexico, Department of Chemistry, Albuquerque, NM.

4:30 H2.9

THE PREPARATION OF COLLOIDAL III-V SEMICONDUCTORS IN AQUEOUS SOLUTION, Toby J. Cumberbatch and Michael D. Spencer, Cambridge University, Engineering Department, Cambridge, United Kingdom; and Andrew Putnis, Cambridge University, Department of Earth Sciences, Cambridge, United Kingdom.

SESSION H3: MICROCRYSTALLINE

SILICON: PROPERTIES

Chair: K. Tanaka

Thursday Morning, November 30

Salon J/K (M)

8:30 *H3.1

THE GROWTH AND STABILITY OF MICROCRYSTALLINE SILICON, S. Wagner and S. Wolff, Princeton University, Department of Electrical Engineering, Princeton, NJ.

9:00 H3.2

MICROCRYSTAL SILICON FILMS PREPARED BY REMOTE PLASMA CVD, Sung Chul Kim, Jung Tae Hwang, Seung Kyu Lee, Chang Young Jung, Sung Moo Soe, Sung Ok Koh, Kwan Soo Chung, and Jin Jang, Kyung Hee University, Department of Physics and Electronics, Seoul, Korea.

9:15 H3.3

FRACTAL-LIKE STRUCTURES PRESENT IN HYDROGEN-ATED AMORPHOUS AND MICROCRYSTALLINE SILICON, R.C. van Oort, J.C. van den Heuvel and M.J. Geerts, Delft University of Technology, Faculty of Electrical Engineering, Delft, The Netherlands.

9:30 H3.4

ROLE OF HYDROGEN IN THE PROCESS OF EXCIMER-LASER-INDUCED CRYSTALLIZATION OF a-Si:H, K. Winer, R. Bachrach, R. Johnson, S. Ready, G. Anderson and J. Boyce, Xerox Palo Alto Research Center, Palo Alto, CA.

9:45 H3.5

HYDROGEN PASSIVATION OF UNDOPED AND DOPED μ c-Si, M. Stutzmann, C.P. Herrero, M. Ingels and A. Breitschwerdt, Max-Planck-Institut für Festkörperforschung, Stuttgart, West Germany.

10:00 BREAK

10:30 *H3.6

CONTROL OF CHEMICAL REACTIONS FOR GROWTH OF c-Si AT LOW SUBSTRATE TEMPERATURE, I. Shimizu, J. Hanna, and H. Shirai, Tokyo Institute of Technology, Yokohama, Japan.

11:00 H3.7

EFFECTS OF HYDROGEN ATOMS ON PASSIVATION AND GROWTH OF MICROCRYSTALLINE Si, Toshimichi Ito, Tatsuro Yasumatsu and Akio Hiraki, Osaka University, Department of Electrical Engineering, Osaka, Japan; and Hirokuni Watabe, Matsushita Electric Industrial Company, Limited, Osaka, Japan.

11:15 H3.8

A DISCUSSION OF ELECTRONIC OPTICAL ABSORPTION SPECTRA OF NANOCRYSTALLINE THIN FILMS, E. Bustarret, Max-Planck-Institut für Festkörperforschung, Stuttgart, West Germany; and M.A. Hachicha, CNRS-LEPES, Grenoble, France.

11:30 H3.9

GROWTH OF MICROCRYSTALLINE SILICON IN ULTRA-THIN LAYERS, Youn-Jung Wu, P.D. Persans, Rensselaer Polytechnic Institute, Physics Department, Troy, NY; B. Abeles, Exxon Research and Engineering Company, Annandale, NJ; and Shu-Lin Wang, University of Chicago, James Franck Institute, Physics Department, Chicago, IL.

11:45 H3.10

PHOTOMODULATION STUDY OF NANOCRYSTALLINE HYDROGENATED SILICON, L. Chen, J. Tauc, Brown University, Providence, RI; and Z. Vardeny, University of Utah, Salt Lake City, UT.

SESSION H4: OPTICAL PROPERTIES

Chair: P. Persans

Thursday Afternoon, November 30

Salon J/K (M)

1:30 *H4.1

PROPERTIES OF BINARY Si:H MATERIALS PREPARED BY HYDROGEN PLASMA SPUTTERING, Shoji Furukawa and Tatsuro Miyasato, Kyushu Institute of Technology, Fukuoka-ken, Japan.

2:00 H4.2

CRITICAL REVIEW OF RAMAN SPECTROSCOPY AS A DIAGNOSTIC TOOL FOR SEMICONDUCTOR NANOCRYSTALS, P.M. Fauchet, Princeton University, Department of Electrical Engineering, Princeton, NJ.

2:15 H4.3

RAMAN SCATTERING FROM MICROCRYSTALLINE FILMS: CONSIDERATIONS OF COMPOSITE STRUCTURES WITH DIFFERENT OPTICAL ABSORPTION PROPERTIES, R.J. Nemanich, Y.M. LeGrice, R.E. Shroder, North Carolina State University, Department of Physics and Department of Materials Science and Engineering, Raleigh, NC; and J.B. Boyce, Xerox Palo Alto Research Center, Palo Alto, CA.

2:30 H4.4

PHONON STATES IN SiC SMALL PARTICLES, Y. Sasaki, C. Horie, Ishinomaki Senshu University, Basic Science Department, Ishinomaki, Japan; and Y. Nishina, Tohoku University, IMR Department, Sendai, Japan.

2:45 H4.5

MODELLING INTERBAND OPTICAL SPECTRA OF MICROCRYSTALLINE WIDE BAND GAP SEMICONDUCTORS (V₂O₅, AlN, BN) USING THE COHERENT POTENTIAL APPROXIMATION, Carolyn Rubin Aita, University of Wisconsin-Milwaukee, Materials Department and the Laboratory for Surface Studies, Milwaukee, WI.

3:00 H4.6

NONLINEAR OPTICAL PROPERTIES OF STRUCTURED NANOPARTICLE COMPOSITES, Meyer H. Birnboim, Wei Ping Ma, and Guang Mei, Rensselaer Polytechnic Institute, Department of Mechanical Engineering, Troy, NY.

SESSION H5: SILICON ALLOYS

Chair: I. Shimizu

Thursday Afternoon, November 30

Salon J/K (M)

3:45 *H5.1

OPTOELECTRONIC AND PHOTOVOLTAIC APPLICATIONS OF MICROCRYSTALLINE SiC, Y. Hamakawa, G. Hirata, Y. Matsumoto, M.K. Han and H. Okamoto, Osaka University, Faculty of Engineering Science, Osaka, Japan.

4:15 H5.2

THE EFFECT OF HYDROGEN ON THE STRUCTURE OF AMORPHOUS AND MICROCRYSTALLINE SiC PREPARED BY THE POLYMER ROUTE, C-J. Chu, Florence Bobonneau and J.D. Mackenzie, University of California, Department of Material Science and Engineering, Los Angeles, CA.

4:30 H5.3

CHARACTERIZATION OF AMORPHOUS CARBON THIN FILMS, N.-H. Cho, K.M. Krishnan, D.K. Veirs, M.D. Rubin, Lawrence Berkeley Laboratory, Mechanical Engineering Department, Berkeley, CA; B. Bushan, IBM Research Division, San Jose, CA; and D.B. Bogy, University of California at Berkeley, Department of Mechanical Engineering, Berkeley, CA.

4:45 H5.4

THE EFFECT OF HYDROGEN ON THE STRUCTURE AND ELECTRO-OPTICAL PROPERTIES OF SILICON-GERMANIUM ALLOYS, I.H. Campbell, P.M. Fauchet, Princeton University, Department of Electrical Engineering, Princeton, NJ; C.M. Fortmann, and D.E. Albright, University of Delaware, Department of Electrical Engineering, Newark, DE.

SESSION H6: POSTER SESSION

MICROCRYSTALLINE SEMICONDUCTORS

Chairs: P.M. Fauchet, K. Tanaka
and C.C. Tsai

Thursday Evening, November 30

7:00-10:00 p.m.

America Ballroom (W)

H6.1 OPTICAL PROPERTIES OF MICROCRYSTALLINE SILICON, Martin Ingels, Martin Stutzmann and Stefan Zollner, Max-Planck-Institut für Festkörperforschung, Stuttgart, West Germany.

H6.2 ROOM TEMPERATURE EXCITONIC ABSORPTION IN SMALL CdS CRYSTALLITES, D.K. Rai and Binod Kumar, University of Dayton Research Institute, Dayton, OH.

H6.3 PARTICLE-SIZE DISTRIBUTION OF CdSe QUANTUM DOTS DETERMINED BY PHOTOLUMINESCENCE SPECTROSCOPY, E.N. Prabhakar, Massachusetts Institute of Technology, Francis Bittner National Magnet Laboratory, Cambridge, MA and California Institute of Technology, Department of Physics, Pasadena, CA; C.A. Huber, Massachusetts Institute of Technology, Francis Bitter National Magnet Laboratory, Cambridge, MA and University of Puerto Rico, Rio Piedras, Puerto Rico; and D. Heiman, Massachusetts Institute of Technology, Francis Bitter National Magnet Laboratory, Cambridge, MA.

H6.4 THERMALLY GROWN OXIDE LAYERS ON a-GaAs FILMS FOR MASKING AND PATTERN GENERATION IN VLSI, S.V. Avadhani and B.S.V. Gopalam, Indian Institute of Technology, Physics Department, Madras, India.

H6.5 STUDIES OF FORMATION AND STRUCTURE OF $\text{GeS}_2\text{-GaS}_{1.5}\text{-CdS}$ SEMICONDUCTING GLASSES, Suzanne Barnier, Micheline Guittard, Faculté des Sciences Pharmaceutiques et Biologiques de Paris, Laboratoire de Chimie Minérale, Paris, France; and Christian Julien, Université Pierre et Marie Curie, Laboratoire de Physique des Solides, Paris, France.

H6.6 OPTICAL AND MICROSTRUCTURAL CHARACTERIZATION OF THIN FILM CuInSe_2 FOR PHOTO-VOLTAIC APPLICATIONS, John R. Tuttle, David S. Albin, and Rommel Noufi, Solar Energy Research Institute, Solid State Research, Golden, CO.

H6.7 THERMAL ANNEALING OF AMORPHOUS CoMnNiO FILMS ON OXIDIZED Si SUBSTRATE, Tan Hui, Tao Mingde, Qin Dong, Han Ying, Xinjiang Institute of Physics, Academia Sinica, Xinjiang, China; Lin Chenglu and Zou Shichang, Shanghai Institute of Metallurgy, Ion Beam Laboratory, Shanghai, China.

H6.8 THE GRAPHITIZATION OF A-C:H FILMS DURING THERMAL ANNEALING, Shuhan Lin, Shuguang Chen and Dang Mo, Zhongshan University, Department of Physics, Guangzhou, China.

H6.9 PREPARATION AND CHARACTERIZATION OF COLLOIDAL MoS_2 MICROCRYSTALS, Enlian Lu, P.D. Persans, Rensselaer Polytechnic Institute, Physics Department, Troy, NY; A. Ruppert and R. Chianelli, Exxon Research and Engineering Company, Annandale, NJ.

H6.10 TRANSPORT PROPERTIES OF B-, p-DOPED, AND UNDOPED 50kHz PECVD MICROCRYSTALLINE SILICON, M.A. Hachicha, CNRS-LEPES, Grenoble, France; and E. Bustarret, Max-Planck-Institut für Festkörperforschung, Stuttgart, West Germany.

H6.11 SUPPRESSION OF ACCEPTOR DEACTIVATION IN SILICON BY ION IMPLANTATION DAMAGE, K. Srikanth and S. Ashok, Pennsylvania State University, Department of Engineering Science and Mechanics and Center for Electronic Materials and Processing, University Park, PA.

H6.12 ENHANCED NONLINEAR OPTICAL RESPONSE OF COATED NANOPARTICLES, N. Kalyaniwalla, J.W. Haus, M.H. Birnboim, W.P. Ma, Rensselaer Polytechnic Institute, Physics Department, Troy, NY; and R. Inguva, University of Wyoming, Laramie, WY.

H6.13 THE EFFECT OF MICROCRYSTALLINITY ON INTERBAND OPTICAL TRANSITIONS IN SPUTTER DEPOSITED ZIRCONIA, C.-K. Kwok, C.R. Aita, University of Wisconsin-Milwaukee, Materials Department and Laboratory for Surface Studies, Milwaukee, WI; and E. Kolawa, California Institute of Technology, Pasadena, CA.

H6.14 PREPARATION AND CHARACTERIZATION OF MICROCRYSTALLINE SiC:H FILMS, S.V. Rajarshi, F. Mohammad, R.O. Dusane, V.G. Bhide, University of Poona, School of Energy Studies, Pune, India; S.V. Ghaisas, P. Kulkarni and A.S. Nigavekar, University of Poona, Department of Physics, Pune, India.

H6.15 RAMAN STUDIES OF MICROSTRUCTURAL CHANGES IN AMORPHOUS SILICON-BORON ALLOYS DUE TO ANNEALING, G. Yang, P. Bai, Rensselaer Polytechnic Institute, Center for Integrated Electronics and Physics Department, Troy, NY; B.Y. Tong, S.K. Wong, J. Du, University of Western Ontario, Center for Chemical Physics, London, Canada; and I. Hill, University of Western Ontario, Surface Science Laboratory, London, Canada.

SESSION H7: DEVICES AND APPLICATIONS

Chair: S. Wagner

Friday Morning, December 1

Salon J/K (M)

8:30 ***H7.1**

PREPARATION OF HIGH-QUALITY POLY-Si AND $\mu\text{-Si}$ AND $\mu\text{-Si}$ FILMS BY THE SPC METHOD, T. Matsuyama, M. Nishikuni, M. Kameda, S. Okamoto, M. Tanaka, S. Tsuda, M. Ohnishi, S. Nakano and Y. Kuwano, Sanyo Electric Company, Ltd., Functional Materials Research Center, Osaka, Japan.

9:00 **H7.2**

CHARACTERISTICS OF HYDROGENATED MYCROCRYSTALLINE Si FOR Si HBTs, H. Fujioka, M. Itoh, and K. Takasaki, Fujitsu Limited, Advanced Technology Development Division, Kanagawa, Japan.

9:15 H7.3
DOPANT SEGREGATION AT POLYCRYSTALLINE SILICON GRAIN BOUNDARIES IN DEVICE FABRICATION PROCESSES, M. Itoh, I. Aikawa, N. Hirashita and T. Ajioka, Oki Electric Industry Company, Ltd., VLSI R&D Laboratory, Tokyo, Japan.

11:45 H7.11
DEVELOPMENT OF THE VERY THIN MICROCRYSTALLINE N-LAYER AND ITS APPLICATION TO THE STACKED SOLAR CELL, F. Nakabeppu, T. Ishimura, K. Kumagai and K. Fukui, CRDL TONEN Corporation, Saitama, Japan.

9:30 H7.4
CORRELATIONS BETWEEN OPTICAL, ELECTRICAL, AND STRUCTURAL PROPERTIES OF IN-SITU PHOSPHORUS-DOPED HYDROGENATED MICROCRYSTALLINE SILICON - EFFECTS OF RAPID THERMAL ANNEALING ON MATERIAL PROPERTIES, D.E. Kotecki, S.J. Jeng, IBM, Semiconductor Development Laboratory, Hopewell Junction, NY; J. Kanicki, IBM T.J. Watson Research Center, Yorktown Heights, NY; C.C. Parks, V. Phan, W. Rausch, K. Seshan and J. Tien, IBM, Semiconductor Development Laboratory, Hopewell Junction, NY.

9:45 H7.5
SILICON RE-CRYSTALLIZATION CONTROL FOR VLSI/ULSI'S WITH SOI-LIKE STRUCTURES, Jun'ichi Matsunaga, Shigeru Kanbayashi and Shinji Onga, Toshiba Corporation, ULSI Research Center, Kawasaki, Japan.

10:00 BREAK

10:30 H7.6
SELECTIVE DEPOSITION OF N-DOPED μ C-Si:H:F BY RF PLASMA CVD ON Si AND SiO_x SUBSTRATES, K. Baert, P. Deschepper, J. Nijs and R. Mertens, I.M.E.C., Department MAP/SMG, Heverlee, Belgium.

10:45 H7.7
SELECTIVE GROWTH OF Si CRYSTALS OVER AMORPHOUS SUBSTRATES SEEDED BY SOLID-STATE AGGLOMERATION OF PATTERNED Si, K. Yamagata and T. Yonehara, Canon Inc., R/D Headquarters, Kanagawa, Japan.

11:00 H7.8
THE CRYSTAL-AXIS-ROTATION OF LASER-RECRYSTALLIZED SILICON ON INSULATOR, K. Sugahara, T. Ipposhi, Y. Inoue, T. Nishimura, and Y. Akasaka, Mitsubishi Electric Company, LSI R&D Laboratory, Itami, Japan.

11:15 H7.9
NEW MODEL FOR POLY-SILICON THIN FILM TRANSISTORS FOR USE WITH SPICE, M. Izzard, W.I. Milne, and P. Migliorato, Cambridge University, Engineering Department, Cambridge, United Kingdom.

11:30 H7.10
ELECTRICAL PROPERTIES OF SIPOS FILMS DEPOSITED ON CRYSTALLINE SILICON, Tien-Min Chuang, Kenneth Rose, and Ronald J. Gutmann, Rensselaer Polytechnic Institute, Center for Integrated Electronics, Troy, NY.

H1.1

ROLE OF SURFACE AND GROWTH-ZONE REACTIONS IN THE FORMATION PROCESS OF $\mu\text{-Si:H}$. Akihisa Matsuda, Electrotechnical Laboratory, Tsukuba, Japan; and Toshio Goto, Nagoya University, Nagoya, Japan.

Diode-laser-absorption technique was used in the SiH_4/H_2 plasmas under various ratios of SiH_4/H_2 to detect SiH_3 and SiH_2 radicals. SiH_3 of 10^{12} - $10^{11}/\text{cm}^3$ was detected in all SiH_4/H_2 conditions, while SiH_2 was not observed within the detection limit of this method ($6 \times 10^9/\text{cm}^3$) in all conditions, indicating that SiH_3 is the responsible radical for the film growth even in the $\mu\text{-Si:H}$ growth condition.

The surface-loss (β), the recombination (γ) and the sticking (s) probabilities of incident SiH_3 radicals were estimated by means of the step-coverage experiments on a c-Si wafer, which were performed under a wide range of substrate temperatures. It was found that β does not show a temperature dependence for the a-Si:H deposition conditions, while it does decrease slightly with an increase in the temperature for the $\mu\text{-Si:H}$ conditions. On the other hand, s shows a strong temperature dependence in the temperature range between 350°C and 460°C for a-Si:H, and it shows small temperature dependence for $\mu\text{-Si:H}$.

These results are interpreted in terms of a difference in the growing surface between $\mu\text{-Si:H}$ and a-Si:H depositions in a unified manner.

H1.2

OPTO-ELECTRONIC PROPERTIES OF $\mu\text{-Si}$ GROWN FROM SiF_4 AND H_2 BY PECVD. Y. Okada, I. H. Campbell, P. M. Fauchet and S. Wagner, Department of Electrical Engineering, Princeton University, Princeton, NJ 08544

Microcrystalline silicon ($\mu\text{-Si}$) has been drawing attention as a candidate for the p-layer of amorphous silicon (a-Si) solar cells [1] and the emitter of silicon heterojunction transistors [2].

To understand the relation between opto-electronic properties and microstructure, we have grown $\mu\text{-Si}$ films from SiF_4 with H_2 -dilution using plasma-enhanced chemical vapor deposition (PECVD). The substrate temperature and SiF_4/H_2 flow ratio were varied from 200 to 350 °C and from 0.09 to 0.5, respectively. The crystallinity and crystallite size were evaluated by Raman spectroscopy. The electrical conductivities lie in the range from 10^{-11} to $10^{-2} \text{ S}\cdot\text{cm}^{-1}$ (a-Si to $\mu\text{-Si}$). The highest conductivity of $\mu\text{-Si}$ is much higher than that of polycrystalline silicon (poly-Si) grown by conventional CVD ($\sim 10^{-6} \text{ S}\cdot\text{cm}^{-1}$) and is not explained by the traditional conduction model for poly-Si [3].

H1.3

SUBSTRATE TEMPERATURE DEPENDENCE OF THE RAMAN SPECTRA FOR MICROCRYSTALLINE SILICON FILMS PRODUCED BY REACTIVE MAGNETRON SPUTTERING. C. Wang, G.N. Parsons, E.C. Buehler, G. Lucovsky and R.J. Nemanich, Department of Physics, and Material Science and Engineering, North Carolina State University, Raleigh N.C. 27695-8202

Microcrystalline silicon is typically deposited at low temperatures by glow discharge, using a hydrogen to silane ratio greater than 10. We have used reactive magnetron sputtering, with a substrate temperature (T_s) between 240°C and 650°C, and a hydrogen pressure of 0.4 mTorr to deposit amorphous and microcrystalline silicon films. Raman spectroscopy was used to investigate the vibrational spectrum, and hence, the amorphous or crystalline

nature of the films. The hydrogen content was determined using ir. At $T_s=240^\circ\text{C}$, the films are "electronic-grade" hydrogenated amorphous silicon with 12 at.% H, and no crystalline features in the Raman spectrum. At $T_s=450^\circ\text{C}$, the Raman spectrum shows only amorphous features, and hydrogen is not detected by ir. At $T_s=550^\circ\text{C}$, the films have a dramatically different Raman spectrum, indicating an abrupt change in the film structure. These films are microcrystalline, with a large silicon TO peak at 518 cm^{-1} (full width at half max. $\approx 10 \text{ cm}^{-1}$), and a shoulder at 495 cm^{-1} . At $T_s=650^\circ\text{C}$, the TO peak at 518 cm^{-1} becomes more narrow (full width at half max. $\approx 6.5 \text{ cm}^{-1}$), and features due to 2-phonon scattering in crystalline silicon become distinct. We will discuss the effect of hydrogen partial pressure, on the deposition temperature at which the abrupt change in microstructure occurs in reactive magnetron sputtered silicon films.

H1.4

PREPARATION AND CHARACTERISATION OF HIGHLY CONDUCTIVE (100 S/cm) PHOSPHORUS DOPED $\mu\text{-Si:H}$ FILMS DEPOSITED USING THE VHF-GD TECHNIQUE. K. Prasad, F. Finger, H. Curtins, A. Shah, Institut of Microtechnology, Rue Breguet 2, 2000 Neuchâtel, Switzerland; and J. Bauman, Physics Inst., Univ. of Konstanz, 7750 - Konstanz, W. Germany.

The Very High Frequency Glow Discharge (VHF-GD : 70 MHz) technique has been used to deposit phosphorus doped $\mu\text{-Si:H}$ films. Conductivities as high as 100 S/cm have been obtained using low RF power (25 mW/cm^2 or 15 mW/cm^3) for film thicknesses of 0.5 and $1.5 \mu\text{m}$ at a deposition temperature of 300°C and phosphine to silane doping ratio of 1.5%. For these samples an average grain size of 150 Å is deduced from X-ray diffraction measurements. The conductivities are considerably higher (factor 5 to 10) than those obtained by the standard GD at 13.56 MHz , which require much higher RF-power densities (factor 10 higher). Our results are comparable to those obtained using an ECR plasma [1], and to the best conductivities reported for in-situ P doped polysilicon deposited by pyrolysis at 600°C and annealed at 700°C [2]. The possibility of producing this material at such low temperatures (300°C) opens new prospects for its applications in microelectronics.

H1.5

COMPOSITION DETERMINATION OF MICROCRYSTALLINE TWO-PHASE SILICON RICH OXIDES. D. Bouldin and C.H. Lam, IBM, 1000 River Road, Essex Junction, VT 05452; and K.-T. Chang and K. Rose, Center for Integrated Electronics, Rensselaer Polytechnic Institute, Troy, NY 12181.

HRTEM measurements of silicon rich oxides (SRO) show silicon microcrystals in an oxide matrix¹. Simple, reliable characterization of the composition of this two phase material has been a problem. Ellipsometric measurement of the refractive index is a convenient method for characterizing SRO films. Film composition can be related to the refractive index by Bruggeman's effective medium approximation. In this paper we demonstrate correlation of film compositions obtained by this technique with those obtained by Auger electron spectroscopy (AES) and Rutherford back scattering (RBS). We further demonstrate regimes of LPCVD growth where simple correlation of film composition with $[\text{N}_2\text{O}]/[\text{SiH}_4]$ gas ratios are and are not reliable.

H1.6

CHEMISTRY AND SOLID STATE PHYSICS OF MICROCRYSTALLINE SILICON. Stan Vepřek, Institute for Chemistry of Information Recording, Technical University Munich, Lichtenbergstrasse 4, D-8046 Garching-Munich, F.R.G.

Firstly, I shall discuss the various preparation methods or the deposition of micro- (nano-) crystalline silicon with emphasis on their merits and demerits regarding the control of material's quality and possibility of scaling up to large area applications.

The talk will concentrate on the fundamental understanding of the parameters controlling the structural, chemical and related physical properties of the deposited $\mu\text{-Si}$. The formation of a pure microcrystalline phase requires the deposition to occur close to the partial chemical equilibrium at the position of the substrate. The experimental possibilities of establishing such conditions will be outlined. The

pure microcrystalline material free of amorphous tissue can be deposited via chemical transport in hydrogen plasma. The reaction mechanism and the rate determining steps of the deposition will be explained on the basis of experimental facts and outlined theoretically.

The chemical and physical properties of $\mu\text{-Si}$ are directly related to the structural properties of the material and, in particular, to the nature of the grain boundaries. Therefore, the control of the structure of the grain boundaries and the lattice dilatation will be outlined first. It will be shown that the bond length dilatation within the grain boundaries is the origin of many physical properties, such as electric conductivity, optical absorption, elastic and Raman scattering of light. It is also the origin of the incorporation of oxygen into the material during its long term exposure to air. This problem can be easily avoided by the application of a negative bias during the deposition. The resultant compressive stress in the films strongly influences their physical properties.

H1.7

ELECTRONIC AND STRUCTURAL PROPERTIES OF $\mu\text{-Si:H}$ FILMS PREPARED BY RF GLOW DISCHARGE WITH HYDROGEN DILUTION. S. Aljishi, Shu Jin, M. Stutzmann, and L. Ley: Max-Planck-Institut für Festkörperforschung, Heisenbergstr. 1, D-7000 Stuttgart 80, F.R.G.

Total photoelectron yield spectroscopy, photothermal deflection spectroscopy and the constant photocurrent technique are utilized to evaluate the electronic density of bandgap states (DOS) in $\mu\text{-Si:H}$ films prepared by RF glow discharge in SiH_4 diluted with H_2 . The spectra provide a measure of the defect density in the amorphous matrix and the degree of microcrystallinity and show strong correlation with structural properties of the films (microcrystal size, volume fraction) as measured by Raman and X-ray diffraction spectroscopies. Raman measurements are also used to identify the hydrogen bonding configurations in the material. Three series of films are grown to study the effects of the H_2 dilution ratio, substrate temperature, and RF power density on the structure and the DOS. Comparisons are made to un-hydrogenated microcrystalline films prepared by high temperature anneals of a-Si:H.

H1.8

THE FORMATION OF SILICON CLUSTERS IN P.E.C.V.D. SiO:H:F ALLOYS. A.G. Dias and J. Figueiredo; Centro de Física Molecular das Universidades de Lisboa, Instituto Nacional de Investigação Científica, Complexo I (I.S.T.) Av. Rovisco Pais 1000 Lisboa PORTUGAL.

In this paper we report on the results of a study of a new SiO:H:F alloy produced by Plasma Enhanced Chemical Vapour Deposition in $\text{SiH}_4/\text{F}_2/\text{Ar}$ gas mixtures. The oxidation of these films, associated with residual oxygen and oxygenated compounds from the fluorine container (Matheson gas with 98% of purity) and to the etching of the Pyrex wall of the deposition chamber, is enhanced by the presence of the fluorinated species in the active discharge zone.

The optoelectronic and structural properties of these alloys are coherently interpreted taking into account respectively the results from dark conductivity and optical absorption measurements and from X-ray diffraction, infrared and Raman spectroscopy studies. These results have shown that films produced with a F_2/SiH_4 gas ratio (r) lower or equal than 0.4 are amorphous semiconducting SiO:H:F alloys, whereas films deposited with $r \geq 0.5$ exhibit a multiphase structure consisting of silicon clusters embedded in an

amorphous insulating fluorine doped silicon oxide tissue. The formation of silicon clusters within the amorphous SiO:H:F matrix, resulting from a segregation process of the oxygen and fluorine atoms, is also discussed.

H1.9

PREPARATION OF CRYSTALLINE Si THIN FILMS BY SPONTANEOUS CHEMICAL DEPOSITION
TOHRU KOMIYA, AKIRA KAMO, HIROSHI KUJIRAI, ISAMU SHIMIZU*, AND JUN-ICHI HANNA
Tokyo Institute of Technology
Imaging Science and Engineering Laboratory and
Graduate School at Nagatsuta*
Nagatsuta, Midori-ku, Yokohama, 227 Japan

We have established a new preparation technique for the preparation of Si thin films based on a gas phase reaction of SiH_4 with F_2 at the reduced pressure. This technique provides us a variety of the films from "amorphous" to "single crystalline" in epitaxial manner.

Microcrystalline films could be deposited on the glass substrate at the rate of 12 Å/sec under the condition of SiH_4 (100%, 30 sccm), F_2 (10%-He, 30 sccm), $T_s = 340^\circ\text{C}$, and $P_{\text{res}} = 550 \text{ mtorr}$. The transition temperature from "amorphous" to "microcrystalline" shifted down as a gas flow ratio, SiH_4/F_2 was decreased or the pressure was decreased. Even at the temperature of 505°C on the substrate, the films could be prepared at the rate of 30 Å/sec when the flow ratio of 2 was selected.

The epitaxial growth of the Si films was observed at the same condition for preparing the microcrystalline films on the glass substrate when the Si wafers treated by the RCA cleaning method and then dipped into HF solution were applied as the substrate.

The experimental results suggested that fluorine played a very important contribution into the relaxation of the Si-networks on the growing surface, leading to the crystallization.

H1.10

MICROCRYSTALLINE SILICON FILMS PRODUCED BY RF MAGNETRON SPUTTERING AND THE EFFECT OF DIFFERENT AMBIENTS ON THEIR CONDUCTIVITY. Ratnabali Banerjee, A.K. Bandyopadhyay, S.N. Sharma, A.K. Batabyal and A.K. Barua; Energy Research Unit, Indian Association for the Cultivation of Science, Calcutta-700 032, India.

Hydrogenated microcrystalline silicon films were prepared in an rf magnetron sputtering system using a single crystal silicon wafer (4" diameter) target. The sputtering gas was a mixture of argon and hydrogen. Highly conducting films ($\sim 10^{-3} \Omega^{-1} \text{cm}^{-1}$) with low bonded hydrogen content (~ 5 at %) were obtained at fairly low rf power density of 1.2 W/cm^2 for high hydrogen partial pressures. The target voltage increased with increasing hydrogen partial pressure when the rf power was kept constant. The effect of variation of gas composition with constant power density and constant target voltage was compared.

For films with lower conductivity values ($\sim 10^{-5} \Omega^{-1} \text{cm}^{-1}$), an increase was observed in the conductivity (more than two orders in magnitude) when left in ordinary atmosphere. The effect was stalled in vacuum and got

accelerated in a simulated humid ambient. In contrast to that observed for hydrogenated amorphous silicon films, the effect was not reversed on annealing in vacuum at 150°C/200°C. The films with initial conductivity of $10^{-9} \Omega^{-1} \text{cm}^{-1}$ did not exhibit this temporal change in conductivity.

H2.1

LINEAR AND NONLINEAR OPTICAL PROPERTIES OF QUANTUM SEMICONDUCTOR CRYSTALLITES. Louis Brus, AT&T Bell Laboratories, Murray Hill, N.J.

Powders of purified II-VI semiconductor crystallites, with a narrow size distribution and the surface chemically bonded to chosen organic species (ie, "capped"), can be prepared using inverse micelle and organometallic reactions. The crystallites show a three dimensional quantum size effect, with a partially discrete electronic absorption spectrum and an apparent band gap that increases with decreasing diameter. The crystallites are structurally characterized by NMR, TEM, x-ray, and Raman methods. Transient photophysical hole-burning optical measurements reveal the homogeneous absorption spectra of individual crystallites. Picosecond and shorter transient absorption experiments probe the nonlinear response to intense resonant and nonresonant optical pulses, and the fast excited state relaxation phenomena.

H2.2

ELECTRODEPOSITION OF 3 DIMENSIONAL SIZE QUANTIZED CdS AND CdSe FILMS. G. Hodes and T. Engelhard, Department of Materials Research, The Weizmann Institute of Science, Rehovot 76100, Israel

Electrodeposition of CdS and CdSe from non aqueous electrolytes containing a Cd salt and elemental S or Se gives transparent, adherent films made up of aggregates of ca. 5 nm crystallites. These films exhibit a blue shift in their optical absorption spectra of ca. 0.2 eV due to 3 dimensional size quantization in the individual crystallites. This blue shift occurs for films deposited from electrolytes containing a strongly adsorbing anion (e.g. Cl^-) but much less so, or not at all, for those with a weakly adsorbing anion (e.g. ClO_4^-). We discuss a mechanism for the growth of these microcrystalline films based on the anion adsorption properties.

While these layers have a high electrical resistance due, at least in part, to the poor electrical contact between individual crystallites (which is the cause for the size quantization), photovoltaic activity is obtained in a liquid-junction (photoelectrochemical) configuration. This behavior can be understood in terms of the intimate contact between electrolyte and individual crystallites in the microporous semiconductor film. A change from n-type to apparent p-type behavior often occurs after etching the films in dilute HCl. This is treated by considering the films as made up of isolated colloidal crystallites with little, or no, band bending in the film.

Optical properties of the films, including variation of the blue shift with preparation conditions and correlation of absorption and photoluminescence spectra will also be treated.

H2.3

STRUCTURAL AND ELECTRICAL CHARACTERIZATION OF CdSe THIN FILMS. Miltiadis K. Hatalis, Fuyu Lin, Lehigh University, Bethlehem, PA; and Michael R. Westcott, Litton

Systems Canada, Rexdale, Ontario, Canada.

We have studied the structural and electrical characteristics of 25 nm thick undoped and indium-doped CdSe films deposited on glass substrates. Transmission Electron Microscopy has revealed that the as-deposited films are microcrystalline with a grain size ~10 nm. Distinctively different grain growth has been observed in the doped and undoped films after thermal annealing. Grain growth in the undoped CdSe was found to stop when the average grain size became equal to the film thickness.

Enhanced grain growth has been observed in the indium doped CdSe. In contrast to undoped films, grain growth in doped CdSe is not limited by the film thickness but depends primarily upon annealing time and temperature. An average grain size larger than the film thickness has been achieved. Furthermore, an abnormal grain growth resulting in grains with sizes much larger (>20X) than the film thickness has been observed. The density of these grains, their crystal structure and TEM observations of in-situ annealed films will be discussed. The possibility of obtaining large area single crystal CdSe will also be discussed.

The channel resistance of the indium doped CdSe for various electrode spacings was characterized. After annealing the resistance decreased for short (<25 μm) electrode separation whereas it increased for larger ones. Possible explanations of our results will be presented.

H2.4

A STUDY OF THE PRESSURE-INDUCED PHASE TRANSITION IN BULK AND NANOCRYSTALLINE CdS. Xue-Shu Zhao, John Schroeder, P.D. Persans and Enlian Lu, Physics Department, Rensselaer Polytechnic Institute, Troy, NY.

We have used resonant Raman scattering induced by pressure tuning to study the pressure-induced phase transition in bulk and 6 nm diameter colloidal microcrystalline CdS. We observe that bulk CdS undergoes a well-defined first order phase transition at 27 kbar and that the intensity of the zone-center LO phonon Raman scattering increases when the level of the intermediate state (bound exciton I_2) is close to the photon energy. Above 27 kbar the Raman scattering and photoluminescence completely disappear. The phase transition in colloidal CdS is quite different from the bulk. There is no sharp transition; it appears to occur over a wide pressure range up to and above 50 kbar. We attribute the different pressure behavior in colloidal CdS to the effect of surface reconstruction and surface distortion energy in microcrystals. Both bulk and colloidal CdS reverse to the original wurtzite phase after the pressure is released.

H2.5

RESOLVED SPECTRA OF EDGE EMISSION OF CdSe MESOSCOPIC CLUSTERS IN GeO_2 GLASS MATRIX. Takao Inokuma, Akinori Tanaka, Toshihiro Arai, Inst. of Appl. Phys., Univ. of Tsukuba, Tsukuba, Ibaraki 305, Japan; and Mitsuru Ishikawa, Tsukuba Research Lab., Hamamatsu Photonics K.K., Tsukuba Ibaraki, 305, Japan

Time-resolved photoluminescence spectra of CdSe microcrystals in GeO_2 glass matrix were measured at liq. N₂ temperature. The size of microcrystals was controlled by varying the annealing temperature and the duration time. The average sizes of contained crystals in samples were in the range between 3-16 nm in diameter. For the excitation of photoluminescence, 514.5 nm line of a mode locked Ar⁺ laser which has about 50 ps pulse width and 82 MHz repetition rate was used. The steady-state photoluminescence spectrum shows two peaks. Both peaks shift to higher energy side with decreasing the crystal size. The luminescence in higher energy side may correspond to the edge emission in a bulk crystal. The decay profile of this emission involves a fast decay

component which has similar shape to the exciting light and two slow components. The shapes of spectra at various times after excitation do not change. This fact shows that both fast and slow decay components are originated by the transition between the same energy levels. The decay times of the slow components, τ_1 and τ_2 , increased with decreasing of the crystal size. In the sample containing crystal which has smaller diameter than the effective Bohr diameter of the exciton in a bulk, d_0 , one of the slow component disappeared. The time-integrated intensity ratio I_1/I_2 increases with increasing crystal size. This variation occurs intensively in the samples which contain smaller size crystal than d_0 . These variation will be discussed with the quantum confinement effect for exciton.

H2.6

OPTICAL PROPERTIES OF II-VI SEMICONDUCTOR-DOPED GLASS. P. D. Persans, An Tu, T. Driscoll, M. Lewis, and R. Redwing, Physics Department and Center for Integrated Electronics, Rensselaer Polytechnic Institute, Troy, NY 12180

We discuss the effects of size and electron-phonon interactions on the electronic properties of isolated nanometer-sized $\text{CdS}_x\text{Se}_{1-x}$ semiconductor particles embedded in glass. Optical absorption and cw photoluminescence experiments have been performed on a series of samples of glass containing $\text{CdS}_x\text{Se}_{1-x}$ microcrystals in the temperature range of 77K-450K. Photomodulated transmission measurements have also been carried out. For pump and probe photon energies within 200 meV above the band-edge we observe photoinduced bleaching which we attribute to a band-filling mechanism. The data show that there is a blue-shift of the band-edge due to the quantum size effect, but the photoluminescence peak and photoinduced transmission peak widths are much broader than theory predicts for bulk samples. The Urbach tail width in optical absorption shows the same type of behavior. It has been found that both homogeneous and inhomogeneous mechanisms contribute to broadening of the optical spectra. We attempt to separate these two mechanisms by studying the temperature dependence of the Urbach tail, cw photoluminescence and photoinduced absorption. These measurements have been carried out on materials which have been structurally characterized by a number of techniques including x-ray diffraction, small-angle x-ray scattering, electron microscopy and Raman scattering.

H2.7

FABRICATION AND CHARACTERIZATION STUDIES OF SEMICONDUCTOR-IMPREGNATED POROUS GLASS. *

C. A. Huber[#], T. E. Huber⁺, A. P. Saltsberg and J. A. Perez, Department of Physics, University of Puerto Rico, Rio Piedras, PR 00931.

Novel semiconductor-silica composites have been fabricated from porous Vycor glass of 50 Å characteristic pore diameter. The Vycor glass is impregnated by pressure forcing the non-wetting semiconductor melt into the interconnected pores. Dense semiconductor mesh-like microstructures can be fabricated by this technique. Characterization measurements on selenium-, tellurium- and preliminary results on gallium antimonide-impregnated Vycor show the composites to be suitable for both optical and electrical transport studies, particularly those with specific interest in quantum confinement of carriers in this type of materials.

H2.8

SYNTHESIS, STRUCTURAL AND OPTICAL CHARACTERIZATION OF SMALL PARTICLE III-V SEMICONDUCTOR CLUSTERS ENCLOSED IN POROUS HOSTS.

James E. MacDougall, Hellmuth Exert, William T. A. Harrison, Galer D. Stucky, Department of Chemistry, University of California, Santa Barbara, CA; Norman Heaton, Ying Wang, Central Research and Development Department, E. I. duPont de Nemours and Co., Wilmington, DE; Karin Moller, and Thomas Bein, Department of Chemistry, University of New Mexico, Albuquerque, NM.

Standard MOCVD type reactions have been carried out within the pores of both crystalline and amorphous hosts to form small particle III-V and II-VI semiconductors. These "Size Quantized" semiconductors have been studied by solid state magic angle spinning (MAS) NMR, UV-Vis and IR spectroscopy, as well as X-ray diffraction attempting to correlate structure property relationships. Details of the synthetic methods as well as the results of both spectroscopic and diffraction techniques will be discussed.

H2.9

THE PREPARATION OF COLLOIDAL III-V SEMICONDUCTORS IN AQUEOUS SOLUTION. Toby J. Cumberbatch and Michael D. Spencer, Engineering Department, Cambridge University, Cambridge, England; and Andrew Putnis, Department of Earth Sciences, Cambridge University, Cambridge, England.

Colloidal suspensions of indium arsenide (InAs) and gallium arsenide (GaAs) have been prepared by passing arsine (AsH_3) through dilute aqueous solutions of the metal nitrates. The possibility of producing ternary materials such as GaInAs is also being investigated. Small aqua-ligand exchange rates ($\log_{10}k_{\text{ex}}$: $\text{Ga}^{3+} \approx 3.3$; $\text{In}^{3+} \approx 4.3$) coupled with a low concentration of arsenide anions make the rate of precipitation very slow. As expected, no reaction was observed in an aqueous aluminium solution for which $\log_{10}k_{\text{ex}}$: $\text{Al}^{3+} = -0.8$. To increase the nucleation rate, mixed solvent systems have been investigated as a means of increasing the ligand exchange rate, as have alternative sources for the arsenide ions.

Examination of the precipitates by transmission electron Microscopy shows that the microcrystalline particles are uniform, with an average diameter of 15nm, and of single phase. The electron diffraction patterns were indexed to InAs and GaAs and in agreement with the corresponding X-ray diffraction powder patterns.

Optical absorption data from an electrophoretically deposited layer of GaAs confirm that the material is a semiconductor with a band gap of $\approx 1.45\text{eV}$. Low temperature photoluminescence is being used for a more detailed analysis of both materials.

H2.1

THE GROWTH AND STABILITY OF MICROCRYSTALLINE SILICON. S. Wagner and S. Wolf, Princeton University, Princeton, NJ.

Two questions must be answered to understand the structure of $\mu\text{-c-Si}$: How does it form? and why is it stable? We study the first question by observing the transition from epitaxial growth on crystalline Si to disordered growth as the c-Si substrate is covered with hydrogen. The key result is that hydrogen coverage disrupts crystalline and promotes microcrystalline growth.

To understand the stability of $\mu\text{-c-Si}$ we focus on the equilibrium between $\mu\text{-c-Si}$ and an a-Si:H matrix. Typical material contains three phases, i.e., $\mu\text{-c-Si}$, a-Si:H and H_2 . We investigate the conditions of co-existence of these three phases in function of the size of the microcrystals and of the hydrogen bonding in the a-Si:H. The most stable configuration appears to be one where hydrogen-free microcrystals are embedded in an a-Si:H matrix that is saturated with H.

This work is supported by the Electric Power Research Institute.

H3.2

MICROCRYSTAL SILICON FILMS PREPARED BY REMOTE PLASMA CVD
Sung Chul Kim, Jung Tae Hwang, Seung Kyu Lee, Chang Young Jung, Sung Moo Soe, Sung Ok Koh, Kwan Soo Chung, Jin Jang
Dept. of Physics & Dept. of Electronics, Kyung Hee University
Dongdaemoon-ku, Seoul 130-701, Korea

Hydrogen dilution in a glow-discharge silane plasma is known to prepare microcrystal silicon film at low substrate temperatures (200 - 300°C). We studied the application of the remote plasma enhanced chemical vapor deposition (remote PECVD) to the growth of intrinsic and doped microcrystal silicon films. Lucovsky's group has developed a remote PECVD technique, in which plasma generating region is connected upstream of a remote deposition chamber. Silane and hydrogen mixture are introduced into the downstream reactor and helium passes through the plasma generating region.

In the present study the influences of deposition temperature, hydrogen dilution ratio (H_2/SiH_4), discharging power, and total pressure on the structural, optical and electrical properties of the Si thin films prepared by a remote PECVD. The results are compared with the behavior in the glow discharged microcrystal films. The growth of microcrystal Si is enhanced by increasing the hydrogen dilution ratio, rf power, and by decreasing the total pressure. It was found that microcrystal Si films were grown over the deposition temperature range 200 - 300 °C when the hydrogen dilution ratio was higher than 30. The deposited microcrystal Si films show a sharp Raman peak near 520 cm^{-1} and only 2090 cm^{-1} Si-H modes in the infrared optical absorption and high room temperature conductivity of $>1S/cm$. The roles of hydrogen and helium on the growth of microcrystal Si will be discussed.

H3.3

FRACTAL-LIKE STRUCTURES PRESENT IN HYDROGENATED AMORPHOUS AND MICROCRYSTALLINE SILICON.
R.C. van Oort, J.C. van den Heuvel, M.J. Geerts,
Delft University of Technology, Faculty of
Electrical Engineering, Mekelweg 4, Delft,
the Netherlands.

The film surface of a-Si:H and μ c-Si:H films etched in a hydrogen rf plasma were examined by using scanning electron microscopy. Hydrogenated amorphous silicon (a-Si:H) generally is regarded as a material consisting of two phases. One phase of a high electrical quality and a low structural disorder, and a second phase of poor quality, containing a lot of hydrogen and many microvoids. This phase is of a low structural order. A hydrogen plasma is able to etch a-Si:H at a rate of 1 Å/s. The etch rate of microcrystalline silicon (μ c-Si:H) is 0.2 Å/s. The μ c-Si:H is a mixture of crystals imbedded in an a-Si:H matrix. This difference can only be explained by the fact that the crystals, a material of a high structural order, are practically not etched. Due to the fact that a-Si:H is a mixture of material with different degrees of structural order a coarsened a-Si:H film surface is revealed by SEM after etching a-Si:H films in a hydrogen plasma. The structures visible are fractal-like. The same is found for μ c-Si:H films. The amount of fractals and the size can be changed by adjusting the deposition conditions, influencing the microstructure of the layers. The fractals in μ c-Si:H form a closed network. This is an indication that the fractal-like structures are crystalline.

H3.4

ROLE OF HYDROGEN IN THE PROCESS OF EXCIMER-LASER-INDUCED CRYSTALLIZATION OF a-Si:H. K. Winer, R. Bachrach, R. Johnson, S. Ready, G. Anderson, and J. Boyce, Xerox Palo Alto Research Center, Palo Alto, CA.

Hydrogen evolution spectra and hydrogen concentration depth profiles are correlated with carrier transport and average grain size measurements in order to investigate the role of hydrogen in dopant activation and grain growth upon crystallization by pulsed-excimer-laser-induced surface heating of hydrogenated amorphous silicon (a-Si:H) thin films grown by plasma-enhanced chemical vapor deposition.

Hydrogen depletion from a-Si:H occurs only above a well-defined laser energy density threshold, increases slowly with increasing laser energy and shot densities, and is enhanced by the presence of dopants which is to be expected from the Fermi-level-dependent hydrogen diffusion coefficients observed in bulk a-Si:H. While the average grain size increases monotonically with increasing laser energy density and is nearly independent of dopant concentration, the room temperature dc dark conductivity exhibits a sharp transition marking the onset of crystallization and dopant activation at laser energy densities which decrease logarithmically with increasing dopant concentration.

A comparison between the role of hydrogen in the process of excimer-laser-induced crystallization of a-Si:H and the growth of microcrystalline silicon by hydrogen dilution will be made, and a model of hydrogen incorporation in silicon based on a simplified Si-H phase diagram and chemical equilibrium principles will be discussed.

H3.5

HYDROGEN PASSIVATION OF UNDOPED AND DOPED μ c-Si.
M. Stutzmann, C.P. Herrero, M. Ingels, and A. Breitschwerdt, Max-Planck-Institut für Festkörperforschung, D-7000 Stuttgart 80, FRG.

We have investigated the effects of hydrogen plasma treatment on the electronic and structural properties of doped (n- and p-type) as well as undoped microcrystalline silicon. Samples were prepared by recrystallization of a-Si:H films at 800°C. For the characterization of the samples before and after passivation we have used IR reflectance, spectroscopic ellipsometry, photothermal deflection spectroscopy, and Raman scattering. Results on subgap absorption (defect and free carrier), free carrier plasma reflection, and on the local vibrational modes of dopant atoms and hydrogen will be presented and discussed in terms of corresponding results in monocrystalline silicon.

H3.6

CONTROL OF CHEMICAL REACTIONS FOR GROWTH OF c-Si AT LOW SUBSTRATE TEMPERATURES. T. Shimizu, J. Hamada, and H. Shirai, Tokyo Institute of Technology, Yokohama, Japan

Chemical reactions and their control have been investigated on the growth of crystalline Si thin film at substrate temperature as low as 300 °C, for the purpose of developing preparation technique of Si thin film for the electronic devices requiring large area, i.e., display devices, sensors or solar cells.

The precursors given in the form of SiH_nF_{4-n} ($n=1,2,3$) were made by decomposing a gaseous mixture of SiF_4 and H_2 by plasma or mixing F_2 with SiH_4 . By supplying atomic hydrogen or F-related agents, c-Si thin film was grown at a growth rate of more than 20 Å/s with these precursors on the substrate at such a low temperature. Si-epitaxy was performed on a c-Si(100) substrate at 300 °C with the aid of the topological restriction on the substrate surface. Some local equilibrium is considered to be preserved between sticking and chemical etching for these precursors to promote the two dimensional

crystal growth. Highly ordered structure was observed in the epi-Si films by the measurements with RHEED, X-ray diffraction and Raman scattering. Hall mobility of more than 150 cm²/Vs was also obtained in the epi-Si film. Chemical affinity of the surface was also assessed as an important factor for the epitaxial growth since it was difficult to make the epi-Si from the precursors, SiH₄ and F₂, on either CaF₂ or Sapphire with the lattice constant similar to that of c-Si. We will discuss the concept of "chemical annealing and sintering" in respect to the structural relaxation for making crystalline Si-network at low temperature..

H3.7

EFFECTS OF HYDROGEN ATOMS ON PASSIVATION AND GROWTH OF MICROCRYSTALLINE SI. Toshiyuki ITO, Tatsuro YASUMATSU and Akio HIRAKI. Osaka University, Suita, Osaka, Japan, and Hirokuni WATABE, Matsushita Electric Industrial Co. Ltd., Osaka, Osaka, Japan.

Because effects of bonded H atoms on Si surfaces are important to understand passivation effects as well as growth mechanism of microcrystalline Si, we have investigated H-covered micro-surfaces of crystalline Si by means of infrared spectroscopy, diffraction technique and thermal analysis as well as a cluster calculation of molecular orbitals. The system treated here includes anodized porous crystalline Si which has huge surface area (~200 - 800 m²/cm³) almost completely covered with H atoms, and is compared with microcrystalline Si:H. Actually, infrared spectra measured show almost the same features for the porous Si and the microcrystalline Si:H.

Calculation results indicate the following: (1) Si bonding to a surrounding Si atom is weaker with increase in number of H atoms bonded to the Si atom concerned; (2) Such weak Si-Si bondings are also easily broken by attack of O atoms; (3) Furthermore, the oxidation of the H-covered Si at Si backbonds of SiH₃ (n=1-3) is energetically advantageous, compared with that at the Si-H bonds. Experimental results on the initial oxidation process of the porous Si, which are clearly shown mainly by means of infrared analysis of Si-H stretching vibration band located at 2000 - 2300 cm⁻¹, have been consistent with the calculation results above. Results on analysis of isothermal desorption of H can also be explained consistently. Charge redistributions calculated are addressed in relation to origins of peak shifts of infrared spectra observed. Furthermore, the cluster calculation predicts possible stable H sites at Si surfaces, or Si-H bondings. From those results, possible effects of H on the growth mechanism of the microcrystalline Si:H are also discussed.

H3.8

A DISCUSSION OF ELECTRONIC OPTICAL ABSORPTION SPECTRA OF NANOCRYSTALLINE THIN FILMS.

E. Bustarret, Max-Planck-Institut für Festkörperforschung, D-7000 Stuttgart 80, FRG, M.A. Hachicha, LEPES-CNRS, BP 166X, F-38042 Grenoble, France.

Both fully crystallized^(*) microcrystalline layers with an average grain size L ranging between 10 and 100 nm and mixed-phase hydrogenated nanocrystalline silicon (doped and undoped) films have been studied at room temperature by Photothermal Deflection Spectroscopy, Transmission Spectroscopy and Spectroscopic Ellipsometry. The resulting spectra are compared with similar data obtained on monocrystalline and hydrogenated amorphous silicon.

We discuss the various extrapolation procedures used for the definition of an optical gap in such widely differing system. We then focus on near- and below-the-gap absorption, and particularly on the respective roles of free carriers, grain boundary disorder and hydrogen.

H3.9

GROWTH OF MICROCRYSTALLINE SILICON IN ULTRATHIN LAYERS. Yeun-Jung Wu*, P. D. Persans*, B. Abeles*, Shu-Lin Wang*. *Physics Dept., Rensselaer Polytechnic Institute, Troy NY; **Exxon Research and Engineering Co., Annandale NJ; *Physics Dept., University of Chicago, Chicago IL.

Microcrystalline silicon particles of different sizes have been made by thermal annealing of amorphous silicon/silicon dioxide multi-

layer structures at temperatures up to 1000°C. The Si layer thickness was varied from around 4 nm to 10 nm. Crystallization temperature measurements confirm our previous result that thinner layers are more stable against crystallization. Studies of optical phonon Raman scattering peak shift and broadening through different annealing stages have been related to phonon coherence length. Comparable peak shift and broadening of different samples at different annealing temperatures and progressive shift and broadening within one sample reveal the growth dynamics of microcrystal grain boundaries. Optical transmission and photothermal deflection spectroscopy studies have also been performed to extract the volume fraction of microcrystal Si. We model the whole system as amorphous/microcrystal composite and discuss the nature of grain boundaries and thin film stability.

H3.10

PHOTOMODULATION STUDY OF NANOCRYSTALLINE HYDROGENATED SILICON. L. Chen and J. Tauc, Brown University, Providence, RI; Z. Vardeny, University of Utah, Salt Lake City, UT.

Steady state and transient photomodulation (PM) spectra were measured in nanocrystalline Si:H (nc-Si:H) films in the spectral range from 0.25 to 1.25 eV, temperature range from 80 to 300 K and time domain from 10⁻⁷ to 10⁻² sec. The crystalline grain size of the samples varied from 70 to 830 Å. In the spectra one can see the features of two phases: amorphous and crystalline. A PM band at high energy (0.8 to 1.0 eV) was observed which is similar to that in a-Si:H and is ascribed to the amorphous phase. Photoinduced absorption $\Delta\alpha \propto \omega^{\beta}$ was seen at low energy (0.25 to 0.5 eV) and is interpreted as due to free carriers in the crystalline phase. Their decays above 150 K can be described by a stretched exponential $\Delta\alpha \propto \exp[-(t/\tau)^{\gamma}]$ which extends into much longer times than the exponential decays due to the recombination in crystalline Si. A model for trapping and recombination processes associated with the presence of the two phases is proposed and compared with the experimental results. The results of this study are shown to be compatible with a two phase model. They also explain why the steady state PM response is much larger in nc-Si:H than in c-Si.

H4.1

PROPERTIES OF BINARY Si:H MATERIALS PREPARED BY HYDROGEN PLASMA SPUTTERING. Shoji Furukawa and Tatsuro Miyasato, Kyushu Institute of Technology, 680-4, Kawazu, Iizuka-shi, Fukuoka-ken 820, Japan.

We have prepared the binary Si:H materials by means of a reactive sputtering technique in hydrogen gas onto a low temperature (about 100 K) substrate. The obtained materials were observed by optical absorption, Raman scattering, and X-ray diffraction. The former measurement showed that the materials have a wide optical gap of up to 2.4 eV, and contain a large amount of hydrogen atoms. These features are quite similar to those of the polysilane alloys prepared by disilane-plasma CVD (1). However, the latter two measurements showed that the silicon atoms in the materials are crystallized, and form small crystalline particles surrounded by hydrogen atoms. From the infrared absorption data, the hydrogen atoms are bonded in the form of SiH₃ or SiH₂, and the absorption relevant to polysilane chains is hardly observed. Moreover, the infrared absorption wavenumbers corresponding to bending modes shift to higher wavenumber side compared with those of the polysilane alloys. These data clearly show the difference between the polysilane alloys and the present Si:H, and support the microscopic model stated above. The formation of microcrystalline Si:H by the hydrogen plasma sputtering with a moderate growth

rate may be possible because of a chemical process.

H4.2

CRITICAL REVIEW OF RAMAN SPECTROSCOPY AS A DIAGNOSTIC TOOL FOR SEMICONDUCTOR NANOCRYSTALS. P.M. Fauchet, Princeton U., Princeton NJ 08541.

Raman spectroscopy has been used extensively to investigate various properties of nanocrystalline semiconductors, such as size, shape, composition, orientation, and stress. Simple theories have been developed and applied successfully to the determination of grain size and shape [1]. There remain several unsettled issues, especially concerning the influence of grain boundaries and free surfaces on the Raman spectrum. It appears clear that the vibrational properties of the atoms on the outer shell of the grains reflect the nature of the bonding at the grain boundaries which in turn control the electronic properties of microcrystalline semiconductors. In this presentation, a critical review of Raman spectroscopy as a diagnostic tool for nanocrystalline objects is given.

H4.3

RAMAN SCATTERING FROM MICROCRYSTALLINE FILMS: CONSIDERATIONS OF COMPOSITE STRUCTURES WITH DIFFERENT OPTICAL ABSORPTION PROPERTIES. R.J. Nemanich, Y.M. LeGrice and R.E. Shroder, Dept. of Physics, and Dept. Materials Science and Engineering, North Carolina State University, Raleigh, NC 27695; and J.B. Boyce, Xerox Palo Alto Research Center, Palo Alto, CA 94304

Raman scattering measurements are often used to characterize the atomic bonding in semiconducting films. One aspect that is often ignored is the different optical absorption of the amorphous and crystalline components of the films. A model is described which addresses the properties of Raman scattering from composites of materials of different optical absorption. The analysis shows that the observed spectra is dependent on both the percentage of the components and in the domain size of the more highly absorbing materials. Experimental measurements were made on composite samples prepared from powders of diamond and graphite. This system is an extreme example of the problem, and excellent agreement is obtained between the model and the experimental results. The results are applied to the analysis of carbon films which exhibit diamond and disordered graphitic structures and microcrystalline silicon prepared by magnetron sputtering or excimer laser exposure of hydrogenated Si. The results were analyzed in terms of the model for Raman scattering from composite materials. The experimental results reflect the length scales of the domains and vibrational excitations.

H4.4

PHONON STATES IN SiC SMALL PARTICLES. Y. Sasaki and C. Horie, Ishinomaki Senshu University, Ishinomaki 986, Japan; and Y. Nishina, IMR, Tohoku University, Sendai 980, Japan.

Size dependence of optical phonon frequencies and phonon dampings of SiC small particles has been studied by analysing their Raman data taken at room temperature. The particle size ranges from 30 nm to 1 μ m. The decrease in the particle size yields the result that (1) the TO-phonon frequency decreases, (2) the damping increases, and (3) the splitting between the LO- and TO-phonon frequencies (LT splitting) decreases. The damping up to 800 K includes a temperature-independent term besides the temperature-dependent term which is present in the bulk crystal. These results, except (3), clearly show the evidence that the TO-phonon

(polariton) is scattered at the particle surface. The decrease in the LT splitting is attributed to absence of the macroscopic electric field which would be present due to surrounding atoms in the case of the bulk crystal. It is noted that the particle consists of a number of crystallites and that the Raman spectra are characterized by the particle size rather than the size of crystallites constituting the particle. This result suggests that the surface phonon-polariton mode at the interface between the crystallites plays a minor role in the Raman spectrum of particles consisting of a number of microcrystals.

H4.5

MODELLING INTERBAND OPTICAL SPECTRA OF MICROCRYSTALLINE WIDE BAND GAP SEMICONDUCTORS (V_2O_5 , AlN, BN) USING THE COHERENT POTENTIAL APPROXIMATION. Carolyn Rubin Aita, Materials Department and the Laboratory for Surface Studies, University of Wisconsin-Milwaukee, P.O. Box 784, Milwaukee, Wisconsin 53201.

This paper deals with the use of the coherent potential approximation for analysis of the ultraviolet-visible optical absorption spectra of several microcrystalline wide band gap semiconductors. The spectra of these materials, V_2O_5 , AlN, BN, have a long low energy exponential tail followed by a higher energy region in which the absorption coefficient varies slowly with incident photon energy. The Tauc model, which is based on a random phase approximation, fails to present an integrated picture of absorption in both regions. Using the coherent potential approximation (1), we determine three interrelated optical parameters for each material: the energy band gap of the perfect virtual crystal, the energy band gap of the disordered microcrystalline material, and the slope of the exponential increase of the absorption coefficient with increasing energy at the onset of the fundamental optical absorption edge. The types of disorder implied by this model are discussed.

H4.6

NONLINEAR OPTICAL PROPERTIES OF STRUCTURED NANOPARTICLE COMPOSITES. Meyer H. Birnboim, Wei Ping Ma and Guang Mei, Rensselaer Polytechnic Institute, Troy NY.

The effective nonlinear susceptibility $\chi^{(3)}$ for a composite of a dilute suspension of structured metal/semiconductor nanoparticles that utilizes the surface mediated plasmon resonance can be enhanced by orders of magnitude compared to the intrinsic $\chi^{(3)}$ for a film of the same semiconductor. Calculated enhancements as large as 10^4 have previously been reported for concentric sphere polymeric containing nanoparticles¹. Here we report calculations for various nanoparticle models consisting of concentric spheres with a semiconductor core and metallic shell, or a metallic core and semiconductor shell. Other geometries include the concentric ellipsoid and dumbbell models. The semiconductors are CdS and CdS_xSe_{1-x} and the metals are Al, Au and Ag. Enhancements are obtained in both $\chi^{(3)}$ and figure of merit with no degradation in the intrinsic speed of the nonlinearity.

The choice of geometrical parameters and of component materials permit tailoring of the wavelength dependence and bandwidth characteristics of the nonlinear response. However, fabrication of these structured nanoparticle suspensions remains the key challenge.

H5.1

OPTOELECTRONICS AND PHOTOVOLTAIC APPLICATIONS OF MICROCRYSTALLINE SiC. Y. Hamakawa, G. Hirata, Y. Matsumoto, M.K. Han and H. Okamoto, Faculty of Engineering Science, Osaka University, Toyonaka, Osaka, 560, Japan

A review is given on the recent progress of the physics and technology of microcrystalline silicon carbide (μ c-SiC) and their application to optoelectronic devices. First, historical background of glow discharge μ c-Si and their preparation technology transition up to ECR (Electron Cyclotron Resonance) CVD are briefly demonstrated together with their physical properties and solar cell applications as a highly conductive electrode. Second, a series of technical data on highly conductive P and N type μ c-SiC prepared by ECR plasma CVD has been presented together with their optical and electrical properties, and also valency electron controllability. Finally, recent achievements of optoelectronic devices applications are presented.

In the solar cell application field, 15.5% and 12% efficiency have been achieved with the structure of ITO/P type μ c-SiC/N type poly Si and P type μ c-SiC/I type a-Si/N type μ c-Si heterojunction cell respectively. A visible light injection type Electroluminescence Thin Film Diode might also be a promising optoelectronic device as an application of μ c-SiC. Possibility of other devices such as an imaging device will be also overviewed and discussed from the current R&D aspects.

H5.2

THE EFFECT OF HYDROGEN ON THE STRUCTURE OF AMORPHOUS AND MICROCRYSTALLINE SiC PREPARED BY THE POLYMER ROUTE. C.-J. Chu, Florence Bobonneau and C.M. Mackenzie, Department of Material Science and Engineering, University of California, Los Angeles, CA 90024

Amorphous SiC:H thin films have been deposited on different substrates using metal-organic solutions. Dopants, such as B, P have been introduced at the molecular level during the preceramic polymer synthesis. After different firing schedules, microcrystalline SiC with varying crystallite size can be produced.

Using electron spin resonance the major defect in these polymer synthesized ceramics is identified as C-dangling bonds. Additionally, the ESR results show that heat treatment in hydrogen can decrease the C-dangling bond content. Presumably the C-dangling bonds are eliminated through C-H bond formation. IR spectra confirm the increase in H concentration produced through heat treatment. Electrical and optical properties of the hydrogenated amorphous SiC have also been studied.

H5.3

CHARACTERIZATION OF AMORPHOUS CARBON THIN FILMS. N.-H. Cho, K.M. Krishnan, D.K. Veirs, M.D. Rubin, Lawrence Berkeley Laboratory, Berkeley, CA 94720; B. Bushan, IBM Research Division, San Jose, CA 95120; and D.B. Bogy, Dept. of Mechanical Engineering, Univ. of Cal. at Berkeley, CA 94720

Amorphous carbon films have recently received considerable attention due to their unusual and attractive properties, e.g. extreme hardness, high electrical resistivity, infrared transparency and chemical inertness. These macroscopic

properties have been explained by suggesting that the amorphous state of carbon contains graphitic microcrystals with extensive sp^3 cross-linking.

In this study, a systematic approach is being taken to investigate the microstructure, electronic bonding, and the physical and optical properties of amorphous carbon thin films. The films are grown on Si and NaCl substrates using ion-beam sputtering deposition techniques. The effects of hydrogen concentration, sputtering power density and substrate temperature on the film properties are being investigated. Each series of films are produced by varying one parameter and keeping all the other parameters fixed.

Films vary over a wide range as a function of the deposition conditions. In particular, the hydrogen content plays a critical role in the properties of these films. The microstructure and the electronic bonding of the films are characterized using electron energy loss spectroscopy, Raman spectroscopy, and optical spectroscopy. The relationship between the chemical structure and the properties are examined. Finally, the correlation between these different characterization techniques are evaluated in this paper.

H5.4

THE EFFECT OF HYDROGEN ON THE STRUCTURE AND ELECTRO-OPTICAL PROPERTIES OF SILICON-GERMANIUM ALLOYS. L.H. Campbell, P.M. Fauchet, Princeton U., Princeton NJ 08544; and C.M. Fortmann, D.E. Albright, U. Delaware, Newark DE 19716.

Photo-CVD is used to deposit microcrystalline (μ c) and amorphous SiGe:H films. Temperature, pressure and hydrogen dilution control the final hydrogen content, and thus the optical bandgap and electronic transport. We have identified the conditions that lead to the targetted H content and we have been able to relate the film composition and properties to the deposition chemistry thanks to the well defined gas phase chemistry. The bonding of H is studied by IR absorption, Raman scattering and H thermal evolution, and the H content is measured by SIMS and IR absorption.

In Si-Ge alloys, H is found to bond preferentially to Si while Si and Ge mix randomly resulting in a statistical distribution of clusters. At the highest H radical fluxes, the selective etching of "amorphous" surface atoms leads to microcrystallinity and reduced H concentration. The etch rate is studied as a function of the reaction conditions. In μ c alloys, H forms polyhydrides at the grain boundaries. The electrical transport (measured by the $\mu\tau$ product) of μ c alloys is inferior to that of amorphous alloys having the same Si-Ge composition. The effect on the electrical properties of annealing at moderate temperature to drive off the polyhydrides will be reported.

H6.1

OPTICAL PROPERTIES OF MICROCRYSTALLINE SILICON. Martin Ingels, Martin Stutzmann, and Stefan Zollner, Max-Planck-Institut für Festkörperforschung, D-7000 Stuttgart 80, FRG.

We have studied the optical properties of μ c-Si in the energy range between 0.4 and 6 eV by a combination of photothermal deflection spectroscopy, optical transmission measurements, and spectroscopic ellipsometry. In addition, structural features of our samples were probed with Raman spectroscopy. μ c-Si samples were obtained by recrystallization of thin a-Si:H films at various temperatures, in order to produce μ c-Si with different crystallite sizes.

The optical data indicate that the absorption coefficient in the sub-gap region ($h\nu < 1$ eV) is fairly independent of the crystallite size and even changes very little across the amorphous-to-microcrystalline transition. Larger changes occur in the energy region between the indirect gap and

the first direct gap of crystalline Si ($E_1 \approx 3.4$ eV). It is also found that the width of the E_1 peak in the spectra of the imaginary part, ϵ_2 , of the dielectric constant provides a good measure for the crystallite size as determined from Raman experiments.

H6.2

ROOM TEMPERATURE EXCITONIC ABSORPTION IN SMALL CdS CRYSTALLITES. D.K. Rai and Binod Kumar, University of Dayton Research Institute, Dayton, OH 45469

The absorption characteristics of commercial CdS-containing yellow glass which shows constant transmitted intensity (intensity limiting) over a range of incident CW laser intensity (at a few watts) have been studied at room temperature. Though the thick specimen ($t > 0.5$ mm) shows only a broad step-like feature near $\lambda > 460$ nm, a thin ($t \sim 0.09$ mm) shows two absorption features which can be interpreted as the first two quantum-confined exciton absorption features corresponding to a crystallite size of ~ 45 Å. The absorption spectrum of a sample ($t \sim 0.5$ mm) heated for 15 min. at 700°C shows two new absorption features at 440 nm and 380 nm, which correspond to a much smaller crystallite size of ~ 25 Å. This reduction in size is not inconsistent with estimates made from a well-known model for crystallite growth. Some consequences of these changes in the absorption features on the optical nonlinearities of the glass will be discussed.

H6.3

PARTICLE-SIZE DISTRIBUTION OF CdSe QUANTUM DOTS DETERMINED BY PHOTOLUMINESCENCE SPECTROSCOPY. E.N. Prabhakar, C.A. Huber, and D. Heiman, Francis Bitter National Magnet Laboratory, MIT, Cambridge, MA 02139

Particle size distribution effects on the energy levels of semiconductor quantum dots are investigated. By examining the low temperature photoluminescence spectra of microcrystals of the binary semiconductor CdSe embedded in a glass matrix, the distribution of energy levels due to three dimensional confinement is determined. Calculations of the electron-hole pair ground state energy provide a relation between confinement energy and particle diameter. This allows conversion of the photoluminescence lineshape directly into a distribution of particle radii and facilitates analysis of the observed properties of the material.

H6.4 ABSTRACT NOT AVAILABLE

H6.5

STUDIES OF FORMATION AND STRUCTURE OF $\text{GeS}_2\text{-GaS}_{1.5}\text{-CdS}$ SEMICONDUCTING GLASSES. Suzanne Barnier, Micheline Guittard, Laboratoire de Chimie Minérale, Faculté des Sciences Pharmaceutiques et Biologiques de Paris V, 4 av. de l'Observatoire, 75270 Paris Cedex 06, France, and Christian Julien, Laboratoire de Physique des Solides, Université Pierre et Marie Curie, 4 pl. Jussieu, 75252 Paris Cedex 05, France.

The glass formation domain of the $\text{GeS}_2\text{-GaS}_{1.5}$ semiconducting glasses doped with CdS has been studied over a wide range of composition. The ternary system has been synthesized by dissolving cadmium sulphide with up to 40% CdS. Differential thermal analysis is used to investigate the crystallization behaviour of these glasses. Structural studies have been done by means of infrared and Raman scattering spectroscopies. In these experiments, informations on the modifying role of cadmium sulphide addition in the binary matrix have been studied. The GeS_4 tetrahedral units remain upon CdS doping but at high concentration a new manifestation of the dopant is the appearance of S-S bonds.

H6.6

OPTICAL AND MICROSTRUCTURAL CHARACTERIZATION OF THIN FILM CuInSe_2 FOR PHOTOVOLTAIC APPLICATIONS. John R. Tuttle, David S. Albin, and Rommel Noufi, Solar Energy Research Institute, Golden, CO

Thin film CuInSe_2 based photovoltaic devices exhibit efficiencies exceeding 14%. The electro-optical and microstructural properties of the material are highly dependent on film stoichiometry and deposition parameters, and are dominated by the degree and manner of microcrystallinity, such as rough surfaces and secondary phases ($\text{Cu}_2\text{-}_6\text{Se}$) at free surfaces and grain boundaries. Electro-optical and structural characterization of thin film CuInSe_2 as a function of composition is accomplished, in part, by spectrophotometry, Hall effect, and X-Ray diffraction measurement techniques.

For very Cu-poor material (at.% Cu < 22) with high bulk ρ , the electro-optical behavior is characterized by a microstructure of small multi-phase grains of a mixed tetragonal/cubic nature, free of secondary precipitates. For intermediate bulk ρ 's and compositions ($22 < \text{at.\% Cu} < 25$), the microstructure appears as larger grains of a mixed tetragonal/cubic nature, with an increasing amount of $\text{Cu}_2\text{-}_6\text{Se}$ at grain boundaries. The $\text{Cu}_2\text{-}_6\text{Se}$ may, or may not, contribute to electrical conduction and/or the absorption of light. For Cu-rich compositions (at.% Cu > 25), the microcrystalline structure may take on a profoundly different character. The near stoichiometric single phase grain is now a component of a mixed phase aggregate that includes semi-metallic $\text{Cu}_2\text{-}_6\text{Se}$ sufficient to dominate the conductivity and optical behavior. The mixed phase aggregate is not optimal for photovoltaic applications.

In this report, a full discussion of, but not limited to, the above phenomena and their effects on photovoltaic device performance will be presented.

H6.7

THERMAL ANNEALING OF AMORPHOUS CoMnNiO FILMS ON OXIDIZED Si SUBSTRATE. Tan Hui, Tao Mingde, Qin Jiong, and Han Ying, Xinjiang Institute of Physics, Academia Sinica, Wulumuqi 830011, Xinjiang, China; and Lin Chenglu, and Zou Shichang, Ion Beam Laboratory, Shanghai Institute of Metallurgy, Academia Sinica, Shanghai 200050, China

Amorphous CoMnNiO films have been shown to be a suitable material for fabrication negative temperature coefficient thermistor. The CoMnNiO films were deposited on oxidized Si substrate by rf sputtering equipment. A sinter mixture of Co_2O_3 , MnO_2 , and NiO was used as the target. The sample were thermally annealed at $550\text{-}1100^\circ\text{C}$ for 4 hours and rapid thermally annealed at $1000\text{-}1200^\circ\text{C}$ for 30 seconds in O_2 or Ar atmosphere. Using x-ray diffraction, infrared absorption, Auger, Raman and resistance measurements, we have studied the compositions, structures and electrical properties of the CoMnNiO films. It is found that the atomic ratio of Co, Mn, Ni, and O is 7:6:2:10. The structure of the as-deposited films is amorphous state. A phase transition from amorphous to polycrystalline states is observed after thermal annealing at $800\text{-}1100^\circ\text{C}$ for 4 hours and rapid thermal annealing at $1000\text{-}1100^\circ\text{C}$ for 30 seconds. The analytical results show that the polycrystalline states are NiMn_2O_4 , CoMn_2O_4 and CoO . The conductivity of the films decreases after annealing at temperature below 600°C and higher than 800°C . However, after annealing at $600\text{-}800^\circ\text{C}$ the conductivity increases. Using the CoMnNiO films we have fabricated the thermistor, which exhibits a short responsive time and a good stability.

THE GRAPHITIZATION OF A-C:H FILMS DURING THERMAL ANNEALING. * Shuhan Lin, Shuguang Chen, and Dang Mo, Department of Physics, Zhongshan University, Guangzhou, China.

The diamond-like A-C:H films were obtained from the decomposition of acetylene or benzene. Annealing was carried out in Ar ambient. The optical properties (e.g. the optical gap E_{opt} , the extinction coefficient K , and the refraction index n) were measured by a spectroscopic ellipsometer. The electrical conductivity was provided by dc conduction measurement in planar or sandwich structure. The structure of the films was characterized by Raman spectroscopy, infrared absorption, and scattering electronic microscope.

We found that not only the optical properties, but also the electrical conductivity, the Raman spectra and the infrared spectra changed remarkably when the annealing temperature was over a critical value.

The results indicate that the incorporated hydrogen concentration is an important parameter in determining the structure and properties of the films. Once most of the hydrogen has been driven out, as indicated by infrared absorption of C-H bond, the graphitization takes place and the microcrystal graphite can be found in the annealed samples. It is the structure change which causes the properties change of the films.

PREPARATION AND CHARACTERIZATION OF COLLOIDAL MoS_2 MICROCRYSTALS. Enlian Lu*, P.D. Persans*, A. Ruppert* and R. Chianelli*, *Physics Department, Rensselaer Polytechnic Institute, Troy NY; *Exxon Research and Engineering Co., Annandale NJ.

Transition metal sulfides, such as MoS_2 , consist of two-dimensional chalcogen-metal-chalcogen layers which are weakly bonded to one another in the third dimension. Their optical, electronic and mechanical properties are therefore quite anisotropic. These materials are also of wide practical interest with applications including lubricant additives, battery electrodes and hydrotreating catalysts.

We have prepared MoS_2 microcrystalline colloids by a variety of techniques including direct chemical synthesis and chemically, thermally and ultrasonically-aided splitting of larger crystals. We have performed temperature-dependent optical absorption, photoluminescence and resonant Raman scattering on both suspended and dried colloidal dispersions in order to elucidate the effects of particle size, surfaces, and phase. Dielectric effective medium effects are particularly important because the particles are platelet-shaped and have large ϵ_2 in the wavelength region of interest. We have observed a small resonant enhancement of the vibrational Raman mode at 409 cm^{-1} as the excitation energy is tuned through the B exciton peak at room temperature whereas no resonant enhancement is observed for the 383 cm^{-1} mode. We will discuss Raman scattering results in terms of exciton-phonon coupling.

TRANSPORT PROPERTIES OF B-, P-DOPED, AND UNDOPED 50 kHz PECVD MICROCRYSTALLINE SILICON. M.A. Hachicha, E. Bustarret, LEPES-CNRS, BP 166X, F-38042 Grenoble, France.

Undoped silicon layers with a crystalline fraction around 95% are obtained at 350°C by 50 kHz triode PECVD in a H_2/SiH_4 mixture. Their average grain size is 20 nm, with H contents below 2 at% and spin densities in the 10^{16} cm^{-3} range. These 500 nm-thick films yield at room temperature (rt) a dc conductivity of $3 \times 10^{-2}\Omega^{-1}\text{cm}^{-1}$ and a Hall mobility of $8 \times 10^{-2}\text{ cm}^2\text{V}^{-1}\text{s}^{-1}$.

The study by SIMS, infrared absorption, grazing angle X-ray and Ra-

man scattering spectroscopies of the doped samples as a function of the B_2H_6/SiH_4 and PH_3/SiH_4 ratios shows how the crystalline fraction and the grain size drop with doping. The presence of phosphorus induces a transfer of the infrared Si-H stretching mode absorption from the 2100 to the 2000 cm^{-1} line while retaining the 111 texture of the undoped layer. This texture is gradually lost upon boron doping, while the hydrogen bonding is affected only at our maximum B_2H_6/SiH_4 ratio of 10^{-2} . In this particular case, the rt dc conductivity is $2\Omega^{-1}\text{cm}^{-1}$ and the Hall mobility $15\text{ cm}^2\text{V}^{-1}\text{s}^{-1}$ for a solid phase density of 10^{19} boron cm^{-3} . At the maximum P incorporation ($8 \times 10^{20}\text{ cm}^{-3}$), the rt dc conductivity reaches $30\Omega^{-1}\text{cm}^{-1}$ for a Hall mobility of $55\text{ cm}^2\text{V}^{-1}\text{s}^{-1}$.

SUPPRESSION OF ACCEPTOR DEACTIVATION IN SILICON BY ION IMPLANTATION DAMAGE. K. Srikanth and S. Ashok, Department of Engineering Science & Mechanics and Center for Electronic Materials & Processing, The Pennsylvania State University, University Park, PA 16802

The introduction of atomic hydrogen in Si by ion implantation or plasma processing results in a number of interesting phenomena, including donor generation, acceptor neutralization, and defect/grain boundary passivation. While studying atomic hydrogen passivation of Ar ion implant damage in Si, we have found evidence of suppression of acceptor deactivation by the previous Ar implanted surface layer.

(100) p-Si wafers of 1-10 ohm-cm resistivity were implanted at room temperature with 20 keV Ar ($10^{12} - 10^{15}\text{ cm}^{-2}$ dose), followed by H implantation at 0.4 keV from a Kaufmann source to a fluence on the order of 10^{18} cm^{-2} . The samples were evaluated by spreading resistance as well as the properties of subsequently fabricated Schottky contacts.

Spreading resistance measurements indicate deactivation of acceptor dopants on samples that were hydrogenated without Ar implants, as has been widely reported in the literature. The depth of the acceptor deactivation is about $6\mu\text{m}$, while the surface concentration of holes drops by a factor of 200. However, the deactivation is considerably reduced in samples that were pre-implanted with Ar, and is almost fully suppressed for an Ar dose of 10^{15} cm^{-2} .

The results tend to support the presence of Si microcrystallites in ion implanted (but unannealed) layers, as well as the passivation of their grain boundaries by atomic hydrogen along with the suppression of H migration further into Si by the microcrystallites. Additional results to be presented include the effect of hydrogen implants on polycrystalline Si deposited on crystalline Si, and dopant-implanted crystalline Si.

ENHANCED NONLINEAR OPTICAL RESPONSE OF COATED NANOPARTICLES. N. Kalyaniwalla, J.W. Haus, M.H. Birnboim and W.P. Ma, Rensselaer Polytechnic Institute, Troy, NY and R. Inguva, University of Wyoming, Laramie, WY

We study coated, nanometer-size, ellipsoidal particles that have a semiconductor or polymer core surrounded by a metal coating. We predict that composite materials containing these particles will have much larger enhancement of the nonlinear optical response than had previously been found by using semiconductor colloid suspensions or semiconductor - doped glasses. The enhancement is due to the surface plasmon resonance from the metal dielectric constant that increases the local field in the core material. The frequency of the resonance and the enhancement depend upon the particle shape and the coating thickness, as well as on the specific materials.

We demonstrate the enhancement by calculating the optical phase conjugate signal using an effective medium approximation. The effective Kerr coefficient can be much larger than for semiconductor - doped glass alone and the response time remains fast.

Also, we discuss a novel optical bistability for these new materials and show that the threshold intensity for optical bistability can be greatly reduced by using the coated particles. The switching intensity can be reduced below 100KW/cm^2 .

THE EFFECT OF MICROCRYSTALLINITY ON INTERBAND OPTICAL TRANSITIONS IN SPUTTER DEPOSITED ZIRCONIA. C.-K. Kwoh and C.R. Alta, Materials Department and Laboratory for Surface Studies, University of Wisconsin-Milwaukee, PO Box 784, Milwaukee, WI 53201¹. E. Kolawa, California Institute of Technology, 116-81, Pasadena, CA 91125.

The formation of a β phase in coexistence with an α phase in sputter deposited zirconia films is a consequence of microcrystallinity, resulting from the dominance of the surface free energy contribution to the Gibbs free energy when the crystallite surface area-to-volume ratio exceeds a critical value. This paper relates changes in the fundamental optical absorption band to these different structural forms. θ - 2θ x-ray diffraction was used to obtain crystallographic data, Rutherford backscattering spectrometry for chemical analysis, and UV-visible spectrophotometry for determining transmission and reflection, from which the optical absorption coefficient was calculated. The initial exponential rise of the absorption band and the energy² of two transitions across the band gap are discussed in terms of microcrystallite size of the α phase and a recently calculated band structure and density of states for the zirconia polymorphs³.

H6.14

PREPARATION AND CHARACTERISATION OF MICROCRYSTALLINE SiC:H FILMS. S.V. Rajarshi, F. Mohammad, R.O. Duseane, V.G. Bhide, School of Energy Studies, University of Poona, PUNE-411007, India and S.V. Ghaisas, P. Kulkarni and A.S. Nigavekar, Department of Physics, University of Poona, PUNE-411007, India.

Microcrystalline SiC:H and μ c-Si:H films are prepared by r.f. glow discharge method. The dependence of microcrystallinity on the relative flowrates of hydrogen, silane and methane as well as r.f. power are investigated. Characterization is done using low angle x-ray diffraction, Spectroscopic Ellipsometry (SE), conductivity and photoconductivity, x-ray photoelectron spectroscopy (XPS) and ultraviolet photoelectron spectroscopy (UPS). Role of unintentionally incorporated carbon and oxygen is also investigated.

The analysis of the data leads to the structural model of μ c-SiC:H which is similar to that of μ c-Si:H. Dependence of microcrystallinity on the growth parameters for μ c-Si:H and μ c-SiC:H is used to investigate role of carbon on the formation of micro-crystalline matrix. Effects of boron doping are studied and compared with the observed boron segregation in μ c-Si:H toward amorphous region.

H6.15

RAMAN STUDIES OF MICROSTRUCTURAL CHANGES IN AMORPHOUS SILICON-BORON ALLOYS DUE TO ANNEALING. G. Yang, P. Bai, Center for Integrated Electronics and Physics Department, Rensselaer Polytechnic Institute, Troy, NY 12180; B. Y. Tong, S. K. Wong, J. Du, Center for Chemical Physics, and I. Hill, Surface Science Laboratory, University of Western Ontario, London, Ontario, Canada.

Amorphous $\text{Si}_{1-x}\text{B}_x$ alloy films with boron composition x ranging from 0.01 to 0.5 were deposited on the Si substrates at a temperature of 480°C in a low pressure chemical vapor deposition (LPCVD) system. Those films were annealed in a nitrogen ambient for 30 minutes at various temperatures between 600°C and 900°C. Raman scattering experiments were carried out on both as-deposited and annealed films where the spectra of the Si-Si TO-like vibrational mode at around 480 cm^{-1} was specifically studied to obtain the information on the microstructure of the films.

The structural disorder of the as-deposited amorphous $\text{Si}_{1-x}\text{B}_x$ alloy films was observed to increase, as we reported in a previous paper, with an increase of the boron content. It was further concluded that the boron content x can be roughly divided into three regions, 1) $x \leq 3\%$, 2) $3\% \leq x \leq 30\%$, and 3) $x \geq 30\%$, in which the boron induced structural disorder behaves differently as a function of the boron

content. Microcrystalline and polycrystalline films can be obtained from annealing of those films. The required annealing temperature, however, was different, depending on the boron content in the films. Studies on films with the various boron contents showed that while, in general, the higher the boron content, the harder is to crystallize, the plot of the TO-like mode FWHM as a function of the boron content for a given annealing temperature suggested that there was a threshold boron content below which microcrystalline or polycrystalline films were obtained. This threshold boron content increased with an increase of the annealing temperature. For those high boron content films that remained amorphous after annealing, however, an enhancement of the local order was observed. A detailed analysis will be presented.

H7.1

Preparation of High-quality poly-Si and μ c-Si films by the SPC Method: T. Matsuyama, M. Nishikuni, M. Kameda, S. Okamoto, M. Tanaka, S. Tsuda, M. Onnishi, S. Nakano and Y. Kuwano

Functional Materials Research Center, Sanyo Electric Co., Ltd.
1-18-13 Hashiridani, Hirakata, Osaka 573, Japan

Abstract

In order to improve the conversion efficiency of silicon solar cells, it is necessary to develop materials with high-photosensitivity in the long wavelength region for an increase in I_{sc} . It is also important to develop window materials with high conductivity and wide bandgap for an increase in V_{oc} . Firstly, we describe Solid Phase Crystallization (SPC) method which enables us to grow a Si crystal at a low temperature down to 650°C. Using this method we have obtained thin-film polycrystalline silicon (poly-Si) with high-photosensitivity in the long wavelength region and Hall mobility of 70 $\text{cm}^2/\text{V}\cdot\text{sec}$, and confirmed the photovoltaic effect in the thin-film poly-Si structure for the first time. Secondly, we have succeeded in preparing a device-quality p-type microcrystalline silicon (μ c-Si) by the SPC method at 650°C for 7 hours from the conventional plasma-CVD p-type amorphous silicon (a-Si) without any post-doping process. This is also the first success in the world. Obtained properties of $\sigma_d = 1 \times 10^{-3} (\Omega\cdot\text{cm})^{-1}$ and a high optical transmittance in a 2.0~3.0eV range are more excellent as a window material compared to the conventional p-type μ c-Si:H. Detailed structural characterization using Raman spectroscopy and TEM will be given. Finally, advantages and limitations of SPC method as a new technique to prepare μ c-Si as well as poly-Si are discussed from the viewpoints of device applications.

H7.2

CHARACTERISTICS OF HYDROGENATED MICROCRYSTALLINE Si FOR Si HBTs. H. Fujioka, M. Itoh, K. Takasaki, Advanced Technology Development Division, Fujitsu Limited, 1015 Kamikodanaka, Nakanara-ku, Kawasaki, Kanagawa, Japan 211

C and F were doped into μ c-Si:H films to improve their thermal stability. The use of μ c-Si:H films as wide-gap emitters for Si HBTs is promising for future high speed LSIs. However, the poor thermal stability of the μ c-Si:H film is a serious problem for the practical use. To improve the thermal stability, it is desirable to add C or F to μ c-Si:H film. (1) In this paper we report on the effect of C or F doping on the properties of the μ c-Si:H film. The μ c-Si:H films were deposited using a conventional plasma CVD apparatus at a substrate temperature of 230 °C to 480 °C. The deposition gases were SiH_4 - SiF_4 - PH_3 - H_2 for F doped μ c-Si:H, SiH_4 - CH_4 - PH_3 - H_2 for C doped μ c-Si:H. The structural and electrical properties were investigated using XTEM, RHEED, X ray diffraction and sheet resistance measurement. μ c-Si:H/crystalline-Si heterodiodes and HBTs were fabricated to estimate the junction properties. Experimental results indicate that the addition of CH_4 to the reaction gases suppresses the crystallization and increases the resistivity of the

film. On the contrary, the addition of SiF_4 to the reaction gases has a small influence both on the crystallization and the resistivity of the $\mu\text{-Si:H}$ film.

H7.3

DOPANT SEGREGATION AT POLYCRYSTALLINE SILICON GRAIN BOUNDARIES IN DEVICE FABRICATION PROCESSES, M. ITOH, I. AIKAWA, N. HIRASHITA, AND T. AJIOKA, Oki Electric Industry Co., Ltd., VLSI R&D Laboratory, 550-1, Higashiasakawa, Hachioji, Tokyo 193, Japan

Dopant segregation at the grain boundaries of polycrystalline silicon (poly-Si) causes an unfavorable increase in resistivities of poly-Si. The dopant segregation at the grain boundaries in device fabrication processes has been studied with a new approach using spreading resistance (SR) measurements, SIMS and cross-sectional TEM (XTEM). Phosphorus was implanted with dose $1.5 \times 10^{16} \text{ cm}^{-2}$ at 40 keV into LPCVD poly-Si films with thickness of 1 μm on SiO_2 . Then the samples were annealed at 900°C – 1000°C in N_2 for 30 min. Although SR measurements exhibited that electrically active dopant concentration was constant in depth within the poly-Si films, the phosphorus concentration, measured by SIMS, increased gradually with increasing depth. XTEM observations reveal that the grain size decreases with increasing depth. The phosphorus depth concentration is found to be a linear relationship with a reciprocal grain size corresponding to the same depth. Since the reciprocal grain size is proportional to area of grain boundaries, the linear relationship indicates that the number of segregated phosphorus atoms per unit area is unique within poly-Si films. Both phosphorus concentration in the grains (N_G) and phosphorus concentration segregated at the grain boundaries (N_{GB}) can be evaluated from the relation. The segregation ratios of N_{GB}/N_G range from 4.33 to 1.06 between annealing temperatures of 900°C and 1000°C , and the heat of segregation of 1.7 eV is obtained. Our results indicate that carrier concentration in the poly-Si is very sensitive to annealing temperature in device fabrication processes.

H7.4

CORRELATIONS BETWEEN OPTICAL, ELECTRICAL, AND STRUCTURAL PROPERTIES OF IN-SITU PHOSPHORUS-DOPED HYDROGENATED MICROCRYSTALLINE SILICON – EFFECTS OF RAPID THERMAL ANNEALING ON MATERIAL PROPERTIES. D.E. Kotecki, S.J. Jeng, J. Kanicki, C.C. Parks, V. Phan, W. Rausch, K. Seshan and J. Tien, IBM, Semiconductor Development Laboratory, Hopewell Junction, NY, (*) IBM, T.J. Watson Research Center, Yorktown Heights, NY.

Films of in-situ phosphorus-doped hydrogenated microcrystalline silicon ($n\text{-}\mu\text{-Si:H}$) have been deposited by plasma enhanced chemical vapor deposition (PECVD) on Si(100) and fused quartz substrates from reactive gas mixtures consisting of $\text{PH}_3/\text{SiH}_4/\text{H}_2$. All films were grown at a constant RF power density of 0.1 W-cm^{-2} and a total pressure of 1.0 Torr, while the substrate temperature and (1% PH_3/SiH_4) / H_2 dilution were varied between 200°C and 400°C , and 1% and 10% respectively. Films with a thickness ranging from 250 Å to 1 μm were investigated. The $n\text{-}\mu\text{-Si:H}$ films were subjected to rapid thermal anneal (RTA) at temperatures from 600 – 1000°C for durations of 10–30 seconds.

The deposited films are characterized, both before and after RTA, in terms of their optical band-gap, electrical conductivity and Hall mobility. The interfacial structure, grain size and orientation are investigated by cross-sectional high resolution TEM, and the hydrogen and phosphorus profiles are measured by SIMS.

For pre-annealed films, lattice image TEM confirms the presence of a mixed phase material. For thick films ($> 0.4 \mu\text{m}$), microcracks and voids are observed either in the film or at the interface. No such defects are detected in thin ($< 500 \text{ Å}$) films. The optical band-gap of the pre-annealed films is $\approx 1.8 \text{ eV}$ and strong correlations are observed between the film microstructure and the electrical transport properties. The effects of RTA are shown to significantly alter film morphology and microstructure, increase electrical conductivity, and decrease the optical band-gap. For thin $n\text{-}\mu\text{-Si:H}$ films, RTA produced smooth recrystallized films with the crystal orientation aligned with the substrate. For thick

$n\text{-}\mu\text{-Si:H}$ films, RTA produced large voids within the recrystallized regions, which are believed due to trapped H_2 bubbles, resulting in rough surfaces.

H7.5

SILICON RE-CRYSTALLIZATION CONTROL FOR VLSI/ULSI'S WITH SOI-LIKE STRUCTURES. Jun'ichi Matsunaga, Shigeru Kanbayashi, and Shinji Onga, ULSI Research Center, TOSHIBA Corporation, Kawasaki-city, 210 JAPAN.

A silicon re-crystallization technology for a thin film transistor (TFT), an SOI-like-structure device, which is one of realistic solutions for realizing attractive system on silicon (SOS) with higher packing density, higher operation speed and more variety of functionality in a single chip, is described.

For gaining a higher performance TFT, a grain size control of silicon crystal on an insulator film is required. Then, a process of re-crystallization of amorphous silicon film which is deposited on an oxide film at a lower temperature with an LPCVD method is observed especially utilizing a TEM analysis. As a result, it is found that the behaviour of re-crystallization depends strongly on initial Si deposition conditions, for examples, deposition temperature, the state of deposition surface, namely, oxide film surface, and annealing conditions such as annealing temperature and annealing time. From their analytical results and corresponding electrical characteristics of TFT's, a mechanism of re-crystallization process during annealing procedure and an optimum condition for TFT's are discussed.

In addition, a possibility of an SOS device fascinating and challenging to a trend of conventional down-scaled Si devices will also be presented based on their electrical data.

H7.6

SELECTIVE DEPOSITION OF N-DOPED $\mu\text{-Si:H:F}$ BY RF PLASMA CVD ON Si AND SiO_2 SUBSTRATES. K. Baert, P. Deschepper, J. Nijts, R. Mertens, I.M.E.C. Kapeldreef 75, 3030 Leuven, Belgium.

It is well established that high quality $\mu\text{-Si:H:F}$ can be deposited by rf plasma CVD of fluorinated gas sources like SiF_4 and SiH_2F_2 , mixed with H_2 and/or SiH_4 . However, this growth process is usually not selective, which means layers are deposited on SiO_2 as well as on Si substrates. In this paper, selective growth from $\text{SiF}_4 + \text{SiH}_4$ gas source is reported.

In general, selective deposition can be obtained by balancing a etch process with a deposition process. It was found that in a pure SiF_4 plasma, Si as well as SiO_2 were etched and the etch rate could be controlled from 0 to 3 nm/min by controlling the SiF_4 flow, rf power and temp. When 0–6 sccm of 100 ppm PH_3 in SiH_4 was added, n-doped $\mu\text{-Si:H:F}$ with a conductivity up to 100 S/cm was deposited on c-Si or poly-Si substrates, whereas no deposition happened on thermal SiO_2 , CVD SiO_2 or on glass. The balance between selective and non-selective deposition could be tuned by changing the temp (which controls the etch rate) and the SiH_4 flow (which controls the deposition rate). It is thought that the selective growth happens because nuclei initially formed on the SiO_2 type substrate are less stable and can be etched away more easily, whereas nuclei on Si substrate are more strongly bonded to the substrate and can grow to up to the critical radius necessary for film formation.

This process was successfully applied for the self-aligned deposition of source and drain regions of poly-Si thin film transistors on insulating substrate. The method provides an alternative for the ion implantation technique, since it can be applied to large area substrates and does not require subsequent annealing.

H7.7

SELECTIVE GROWTH OF Si CRYSTALS OVER AMORPHOUS SUBSTRATES SEED BY SOLID-STATE AGGLOMERATION OF PATTERNED Si. K. Yamagata and T. Yonehara, R&D Headquarters, Canon Inc., 6770 Tamura Hiratsuka-city, Kanagawa-Pref., 254, Japan

The phenomenon of agglomeration is known such that continuous films are altered to discrete islands in the solid state, well below the melting point. The phenomenon is driven by surface-energy minimization followed by large mass-transport. It is found that annealing ambients strongly affect the temperatures at which the agglomeration starts, and that impurity in the initial films influences the mass-transport. Polycrystalline Si 100nm-thick films were readily agglomerated by annealing in H_2 ambient, but in contrast, the phenomenon hardly took place in N_2 ambient. Phosphorus impurity in the Si films enhanced the mass-transport. Thus, thicker films can be agglomerated by doping phosphorus in Si. Most significantly, the agglomerated Si semi-spherical islands were confirmed single domain crystals (i.e. no grain boundary in the islands) by transmission electron microscope.

We will demonstrate selective growth of a matrix of large Si crystal islands over amorphous substrates, seeded by the agglomerated single domain Si crystals. Fine polycrystalline Si films were deposited on SiO_2 by LPCVD and patterned into small portions, 1.2 μm in diameter, a hundred μm apart in lattice points. These were agglomerated to form single crystal seeds by annealing in H_2 ambient at 1000 $^{\circ}C$. Si was grown selectively on the each seeds and overgrowth proceeded up to 100 μm by CVD selective epitaxial growth technique, resulting in a matrix of uniformly sized islands. These highly faceted crystals were classified into three crystalline forms, single-crystals, primary twins and multiple twins. However, most were single crystals with a specific orientation of $\langle 110 \rangle$ normal to the substrate surface.

H7.8

THE CRYSTAL-AXIS-ROTATION OF LASER-RECRYSTALLIZED SILICON ON INSULATOR. K. Sugahara, T. Ipposhi, Y. Inoue, T. Nishimura, and Y. Akasaka LSI R&D Lab. Mitsubishi Electric Corp. 4-1 Mizuhara Itami 664 JAPAN

The laser-recrystallized SOI is an important material for fabricating 3-D ICs. We reported that laterally growth from $\langle 001 \rangle$ Si seed in the $\langle 100 \rangle$ direction on an insulating film provided the highest quality of single crystalline SOI film without any obvious defects. However, we found that the crystal axis of the recrystallized Si film gradually changed from $\langle 001 \rangle$ toward $\langle 011 \rangle$. This seemed to be a texture rotation around $\langle 010 \rangle$ axis, and the rotation always occurred in the same direction (anisotropy) whether the growth direction was varied by changing the direction of the laser beam scan. Slower growth speed and higher laser power contributed to make smaller the rotation angle. The temperature distributions numerically simulated from those conditions indicate that the temperature gradient between a top and bottom surface of the SOI film becomes large, as the crystallographic change becomes large. This implies that the crystallographic change is caused by the accumulation of small change in bond angles of each stacked Si atom due to different conditions of thermal expansion in the Si film.

While, in the case of the $\langle 100 \rangle / \langle 001 \rangle$ growth direction, the right position and the bond angles of the Si atom coming from the liquid Si is definitely determined by two atoms already arranged at a liquid-solid interface, and any mutual relation among Si atoms in a same plane is not required for a growth procedure. This assures the crystal growth at laser beam scanning as fast as several tens cm/sec. Therefore the anisotropy is considered to be due to the preferential crystal growth in $\langle 100 \rangle$ direction, and hence, it is also speculated that the initial stage of crystal growth in any crystallographic direction was controlled by crystal growth in $\langle 100 \rangle$ direction. This work was supported by NEDO under the management of FED.

H7.9

'NEW MODEL FOR POLY-SILICON THIN FILM TRANSISTORS FOR USE WITH SPICE' M. Izzard, W. I. Milne, P. Migliorato, Cambridge University Engineering Department, Cambridge England.

The electrical characteristics of the poly-Si thin film transistor (TFT) have been modelled using equations based on the 'volume average defect density' assumptions used by many theorists (eg. Migliorato and Meakin [1]) for the saturation and sub-threshold regime. The off-characteristics have been modelled in a semi-empirical manner to reflect the anomalous off-current. Transient effects are dealt with using charge-control in the body of the TFT. The model is simple to use and may be applied to a wide range of devices by altering model parameters.

In this paper the approximations used are compared to the full numerical integrations of the relationships. We will discuss the model, its implementation and use, and give some examples of circuits that have been simulated using SPICE and manufactured with poly-Si on glass.

H7.10

ELECTRICAL PROPERTIES OF SIPOS FILMS DEPOSITED ON CRYSTALLINE SILICON Tien-Min Chuang, Kenneth Rose and Ronald J. Gutmann, Center for Integrated Electronics, Rensselaer Polytechnic Institute, Troy, NY 12181

SIPOS is composed of silicon microcrystals in an oxide matrix. Undoped SIPOS is important as a passivant in high-voltage planar devices; doped SIPOS shows promise as an electron emitter for BiCMOS devices. Carrier transport and trapping are more complex and less understood in these two-phase materials than simple oxides. Both bulk and interface properties play a role. We present transport and trapping studies on undoped and phosphorus-doped SIPOS films deposited on n-type and p-type Si by LPCVD. Electrical properties have been characterized by C-V, ω , I-V, DLTS, spreading resistance, and photo-induced microwave reflection techniques.

Our C-V and DLTS data on undoped SIPOS indicate interface traps with a density of $5 \times 10^{12} \text{ cm}^{-2} \text{ eV}^{-1}$ and a response time between 1 and 10 μsec exist near midgap of the SIPOS. We find that the polarity of fixed charges in the SIPOS near the interface is tied to the type of the Si substrate. Unlike MOS structures, deep depletion occurs due to the nonlinear conduction of the SIPOS under high field stress.

n⁺-SIPOS/p-Si samples show diode I-V characteristics with ideality factor of 1.1 to 1.2 and reverse leakage current on the order of $100 \mu\text{A}/\text{cm}^2$ after annealing in the forming gas. We believe this reverse leakage is correlated with interface traps. Photo-induced microwave reflection transient-waveform shows an order of magnitude increase in photoconductivity recovery time with doped SIPOS films. This indicates either a lower surface recombination velocity or an increased trapping with the doped SIPOS films, with important implications for high frequency emitter structures.

DEVELOPMENT OF THE VERY THIN MICROCRYSTALLINE
N-LAYER AND ITS APPLICATION TO THE STACKED SOLAR CELL.

F. Nakabeppu, T. Ishimura, K. Kumagai and K. Fukui,
CRDL TONEN Corp., 3-1 Nishi-turugaoka 1-chome,
Ohi-mati, Iruma-gun, Saitama-ken, Japan, 354.

Amorphous-microcrystalline mixed-phase hydrogenated silicon ($\mu\text{c-Si:H}$), which was developed by Electrotechnical Lab. and us for the first time in the world, is now widely used as the ohmical connection layer of the stacked solar cell. Improvement of the efficiency of the stacked solar cell will be realized by reducing the light absorption loss of p-n layer which does not work as the active layer. But in general, as the microcrystalline film becomes thinner, its conductivity rapidly decreases. Consequently, J_{sc} increases but V_{oc} and FF decrease due to the lack of good ohmical connection. Therefore, establishing the preparation method of the high conductive very thin $\mu\text{c-Si:H}$ film is essential for the improvement of the efficiency of the stacked solar cell.

This work has been done according to the idea that microcrystalite size must be smaller than the film thickness to obtain the high conductive thin $\mu\text{c-Si:H}$ film. The relationship between the amount of H ions in the plasma and the microcrystalite size was reported by A. Matsuda. The experimental results, increasing the amount of H ions induces decreasing the size of μc , show the possibility of microcrystalite size control. Addition of Ar gas to the plasma was selected as the easy way to increase the amount of ions and its effect on the film structure was investigated. It was demonstrated that even 150A film showed good σ and the ring pattern in RHEED measurement which means that the film is μc . This newly developed n-layer was applied to fabricate the stacked solar cell and J_{sc} increased by 5-6% because of the reduction of light absorption loss keeping V_{oc} and FF constant.

SYMPOSIUM I: CHARACTERIZATION OF PLASMA-ENHANCED CVD PROCESSES

November 27-28, 1989

Chairs

Dale E. Ibbotson
Room 6F-317
AT&T Bell Laboratories
600 Mountain Avenue
Murray Hill, NJ 07974-2070
(201) 582-2838

Gerald Lucovsky
Department of Physics
North Carolina State University
Box 8202
Raleigh, NC 27695-8202
(919) 737-3301

Dennis W. Hess
Department of Chemical Engineering
University of California, Berkeley
116 Gilman Hall
Berkeley, CA 94720-9989
(415) 642-4862

Symposium Support

Office of Naval Research

**Proceedings published as Volume 165
of the Materials Research Society
Symposium proceedings series.**

SESSION 11: DIAGNOSTICS AND MODELLING

Chair: Dennis Hess
Monday Morning, November 27
Yarmouth/Vineyard (M)

8:30 *I1.1

PECVD RF DISCHARGE MODELS REVIEW, Alan Garscadden, Wright Research and Development Center, Wright-Patterson AFB, OH.

9:00 *I1.2

RF DISCHARGE MODELING, J.-P. Boeuf, Université P. Sabatier, Centre de Physique Atomique de Toulouse, Toulouse, France.

9:30 I1.3

THE EFFECT OF REACTOR PRESSURE ON THE GROWTH OF GLOW DISCHARGE a-SiN:H, Walter J. Varhue, University of Vermont, Department of Electrical Engineering, Burlington, VT; Kiril Pandelisev, Johnson Matthey Electronics, Trail, Canada.

9:45 I1.4

INFRARED LASER ABSORPTION STUDIES OF RADICAL CONCENTRATIONS IN CH₄ RADIO FREQUENCY PLASMAS, Joda C. Wormhoudt, Aerodyne Research, Inc., Center for Chemical and Environmental Physics, Billerica, MA.

10:00 BREAK

10:15 *I1.5

SILANE PLASMA CHEMISTRY ONE STEP AT A TIME: SILICON HYDRIDE RADICAL-MOLECULE KINETICS, Joseph M. Jasinski, IBM Research Division, Thomas J. Watson Research Center, Yorktown Heights, NY.

10:45 I1.6

LASER-INDUCED FLUORESCENCE OF SILICON AND SILICON MONOXIDE IN A GLOW DISCHARGE, Anthony J. Hynes, Georgia Tech Research Institute, Molecular Sciences Branch, Atlanta, GA.

11:00 I1.7

SPATIAL GENERATION PROFILES OF ACTIVE RADICALS IN PLASMA-ENHANCED CVD OF a-Si:H, D. Mataras, S. Cavadias, and D.E. Rapakoulias, Institute of Chemical Engineering and High Temperature Chemical Processes, Patras, Greece.

*Invited Paper

Short Course P-05, "Plasma Enhanced CVD of Thin Films for Microelectronics," may be of interest to symposium attendees. Details regarding course dates and instructors are provided in the short course section of this program.

11:15 *I1.8

ELECTRONIC AND CHEMICAL PROPERTIES OF SILICON CLUSTERS IN REACTIONS WITH SILANE, M.L. Mandich, W.D. Reents Jr. and K.D. Kolenbrander, AT&T Bell Laboratories, Murray Hill, NJ.

11:45 I1.9

IN-SITU SUBSTRATE TEMPERATURE MEASUREMENT DURING a-SiN PLASMA CVD FROM N₂ ROTATIONAL TEMPERATURE, Shin-ichiro Ishihara, Akira Otsuka and Seiichi Nagata, Matsushita Electric Industrial Company, Central Research Laboratories, Osaka, Japan.

SESSION 12: PECVD OF SILICON OXIDES AND NITRIDES

Chair: Alain Harrus
Monday Afternoon, November 27
Yarmouth/Vineyard (M)

1:30 *I2.1

SILICON TECHNOLOGY AND PECVD MATERIALS: ISSUES AND CHALLENGES, Alain S. Harrus, and Graham W. Hills, AT&T Bell Laboratories, Allentown, PA.

2:00 *I2.2

PLASMA DEPOSITION OF Si_xH_y: PROCESS CHEMISTRY VS. FILM PROPERTIES, Donald L. Smith, Xerox Palo Alto Research Center, Electronics and Imaging Lab, Palo Alto, CA.

2:30 I2.3

PLASMA DEPOSITED SILICON NITRIDE FILM CHEMISTRY, Justin N. Chiang and Dennis W. Hess, University of California, Berkeley, Chemical Engineering Department, Berkeley, CA.

2:45 I2.4

NITROGEN INCORPORATION REACTIONS IN HYDROGENATED AMORPHOUS SILICON, NITROGEN ALLOYS PRODUCED BY REMOTE PECVD, G.N. Parsons and G. Lucovsky, North Carolina State University, Department of Physics, Raleigh, NC.

3:00 BREAK

3:15 *I2.5

MICROWAVE AND ECR PLASMA DEPOSITION OF Si_xN_y FOR OPTOELECTRONICS, Steven Dzioba, Bell-Northern Research Ltd., Advanced Technology Lab, Ottawa, Ontario, Canada.

3:45 I2.6

CHARACTERIZATION OF Si₃N₄ FILMS DEPOSITED USING AN ELECTRON CYCLOTRON RESONANCE (ECR) PLASMA, J.P. Simko, Y.-Z. Hu, J.W. Andrews, E.A. Irene, and T.M. Mayer, University of North Carolina, Department of Chemistry, Chapel Hill, NC.

4:00 I2.7
CHARACTERIZATION OF THE PLASMA CHEMISTRY AND FILM COMPOSITION OF PECVD SILICON NITRIDE DEPOSITED FROM SILANE-NITROGEN AND SILANE-AMMONIA MIXTURES WITH ARGON ADDITIONS, W.E. Quinn, B.G. Bagley, B.J. Wilkens, Bellcore, Semiconductor Materials Research Department, Red Bank, NJ; and B.M. Gallois, Stevens Institute of Technology, Materials and Metallurgical Engineering Department, Hoboken, NJ.

4:15 I2.8
DIRECTIONAL DEPOSITION OF SILICON OXIDE BY A PLASMA ENHANCED TEOS PROCESS, Julian J. Hsieh, D.E. Ibbotson, D.L. Flamm and J.A. Mucha, AT&T Bell Laboratories, Murray Hill, NJ.

4:30 I2.9
RF POWER DEPENDENCE OF THE MATERIAL PROPERTIES OF PECVD SILICON DIOXIDE, J.D. Chapple-Sokol, IBM General Technology Division, Hopewell Junction, NY; E. Tierney and J. Batey, IBM T.J. Watson Research Center, Yorktown Heights, NY.

4:45 I2.10
EVIDENCE FOR STRONGLY ENHANCED DEFECT CREATION IN LOW-TEMPERATURE PECVD SiO₂ FILMS, R.A.B. Devine, Centre National d'Etudes des Telecommunications, Meylan, France; and R.L. Pfeiffer, U.S. Army ETDL, Fort Monmouth, NJ.

SESSION I3: SEMICONDUCTORS

Chair: Dale Ibbotson

Tuesday Morning, November 28
Yarmouth/Vineyard (M)

8:45 *I3.1
THE ROLE OF LOW-ENERGY ION/SURFACE INTERACTIONS DURING CRYSTAL GROWTH FROM THE VAPOR PHASE; EFFECTS ON MICROCHEMISTRY AND MICROSTRUCTURE, Joe E. Greene, University of Illinois, Department of Materials Science, the Coordinated Science Laboratory, and the Materials Research Laboratory, Urbana, IL.

9:15 *I3.2
ION BOMBARDMENT EFFECTS ON SURFACE COMPOSITION AND STRUCTURE IN PLASMA PROCESSING, Thomas M. Mayer, University of North Carolina, Department of Chemistry, Chapel Hill, NC.

9:45 I3.3
REMOTE PLASMA-ENHANCED CHEMICAL VAPOR DEPOSITION OF EPITAXIAL SILICON ON SILICON (100) AT 150°C, T. Hsu, B. Anthony, L. Breaux, S. Banerjee and A. Tasch, University of Texas, Microelectronics Research Center, Department of Electrical and Computer Engineering, Austin, TX.

10:00 BREAK

10:30 I3.4
REACTION KINETICS OF EPITAXIAL SILICON DEPOSITION AT 200-400°C USING REMOTE PLASMA ENHANCED CHEMICAL VAPOR DEPOSITION, B. Anthony, T. Hsu, L. Breaux, S. Banerjee and A. Tasch, University of Texas, Microelectronics Research Center, Department of Electrical and Computer Engineering, Austin, TX.

10:45 *I3.5
DEVELOPMENT OF REMOTE PLASMA ENHANCED CVD PROCESSES THROUGH THE USE OF IN-VACUO ELECTRON DIFFRACTION AND SURFACE ANALYTICAL TECHNIQUES, R.A. Rudder, G.G. Fountain, S.V. Hattangady, J.B. Posthill and R.J. Markunas, Research Triangle Institute, Research Triangle Park, NC.

11:15 I3.6
HIGH RATE DEPOSITION OF HYDROGENATED AMORPHOUS SILICON FILMS BY ECR PLASMA CVD, S. Ozaki, T. Akahori, T. Tani and S. Nakayama, Sumitomo Metal Industries Ltd., Hyogo, Japan.

11:30 I3.7
THE ELECTRICAL AND OPTICAL PROPERTIES OF AMORPHOUS SILICON ALLOYS BY PLASMA-ENHANCED CVD METHOD, M. Kapur, Guang H. Lin and J.O'M. Bockris, Texas A&M University, Department of Chemistry, College Station, TX.

11:45 I3.8
POLYHYDRIDE BONDING GROUPS IN PECVD AMORPHOUS Si THIN FILMS, B.N. Davidson, G.N. Parsons, C. Wang and G. Lucovsky, North Carolina State University, Department of Physics, Raleigh, NC.

SESSION I4: NOVEL MATERIALS/APPLICATIONS

Chair: Gerald Lucovsky

Tuesday Afternoon, November 28
Yarmouth/Vineyard (M)

1:30 *I4.1
DIAMOND FORMING DISCHARGES, Peter K. Bachmann, Philips Research Laboratories, Aachen, West Germany.

2:00 *I4.2
THE PLASMA DEPOSITION OF SEMICONDUCTOR MULTI-LAYER STRUCTURES, Masataka Hirose and Seiichi Miyazaki, Hiroshima University, Department of Electrical Engineering, Saijochi, Higashi-Hiroshima, Japan.

2:30 I4.3
FORMATION OF MULTILAYER HETEROSTRUCTURES BY CONTROL OF PATHWAYS IN REMOTE PECVD, D.V. Tsu, J.A. Theil, S.S. Kim and G. Lucovsky, North Carolina State University, Department of Physics and Materials Science and Engineering, Raleigh, NC.

2:45 I4.4
WIDE AREA DISC SHAPED PLASMA SOURCE FOR
ENERGY ASSISTED MOCVD OF GaAs, B. Pihlstrom,
T. Sheng, Z. Yu and G.J Collins, Colorado
State University, Department of Electrical
Engineering, Fort Collins, CO.

3:00 BREAK

3:30 I4.5
LOW TEMPERATURE CLEANING OF Ge AND GaAs
SURFACES USING HYDROGEN DISSOCIATED WITH A
REMOTE NOBLE-GAS DISCHARGE, S.V. Hattangady,
R.A. Rudder, M.J. Mantini, G.G. Fountain,
J.B. Posthill and R.J. Markunas, Research
Triangle Institute, Research Triangle Park,
NC.

3:45 I4.6
LOW-TEMPERATURE PECVD Si_3N_4 FILMS FOR GaAs
ENCAPSULATION AND PASSIVATION, R.L. Pfeffer,
R.A. Lux, K.A. Jones, US Army ETDL, Fort
Monmouth, NJ; R.A.B. Devine, Centre National
d'Etudes des Telecommunications, Meylan,
France.

4:00 I4.7
STRUCTURE AND MORPHOLOGY OF VITREOUS
CHALCOGENIDE THIN FILMS OBTAINED BY PLASMA-
ENHANCED CVD, Bernard Cros, Serge Peytavin,
Michel Ribes, Universite des Sciences et
Techniques du Languedoc, Laboratoire de
Physicochimie des Matériaux Solides,
Montpellier, France; Henri Camon, Alain
Mosset and Jean-Louis Balladore,
C.E.M.E.S.-L.O.E., Toulouse, France.

4:15 *I4.8
SYNTHESIS AND PHYSICAL PROPERTIES OF POLYMER
FILMS WITH METAL INCLUSIONS, Eric Kay, IBM
Almaden Research Center, Physical Science
Department, San Jose, CA.

4:45 I4.9
FTIR INVESTIGATIONS OF PLASMA MODIFIED
POLYMER SURFACES AND THEIR INTERFACES WITH
PLASMA DEPOSITED TUNGSTEN, Klavs F. Jensen,
Massachusetts Institute of Technology,
Department of Chemical Engineering, Cam-
bridge, MA; Jihperng Leu and Manoj Dalvie,
University of Minnesota, Department of
Chemical Engineering and Materials Science,
Minneapolis, MN.

11.1

PECVD RF DISCHARGE MODELS REVIEW. Alan Garscadden, Wright Research and Development Center, Wright-Patterson AFB, OHIO

Rapid progress has been made recently in the understanding of the essential features of RF discharges. The discharge has been studied by several distinct approaches ranging from circuit models, diffusion models, Monte-Carlo, and one-dimensional Boltzmann models. The coupling of experimental data from improved diagnostic methods has resulted in a convergence of the conclusions from these different theoretical approaches. A self-consistent treatment of the ionization and the electric field distribution by Boeuf and Belenger (1989) has clarified the importance of the various mechanisms coupling energy into the plasma. A two group model was used to describe the fast electrons released from the electrodes and the sheaths by ion bombardment and the slow electrons of the bulk plasma. The transport equations describing the two electron groups have been coupled with the continuity and momentum transfer equation and Poisson's equation. There resulted four distinct electron energy gain regimes: a time dependent plasma excitation; fast electron excitation from secondary emission; wave-riding on the sheath oscillation (collisional: Kushner) and a non-collisional electron) sheath interaction (Godyak). The relative contributions are sensitive functions of pressure, frequency and RF voltage. On the other hand if the discharge is strongly electronegative the plasma approximation is quite good. Similar progress on understanding of the homogeneous plasma chemistry also will be illustrated. There still remain the problems of coupling of the actual deposition or etching effects to the plasma conditions. While there are some examples of these effects, improvements in the last area depend on experimentalists providing kinetic data for well-defined conditions. Some consideration of modeling the practical problem of particle contamination is also made.

11.2

RF DISCHARGE MODELING. J.-P. Boeuf, Centre de Physique Atomique de Toulouse, (CNRS, URA 277), Université P. Sabatier, 118 Route de Narbonne, Toulouse, France.

Since the publication of the first self-consistent model of rf glow discharges by Graves and Jensen in 1986, a number of papers have been devoted to rf discharge models. These works have contributed to clarify a number of points concerning the electrical properties of these discharges: space and time variations of the electric field and charged particle densities, role of the sheath field and of the plasma bulk field in the power deposition. These results will be summarized in this lecture.

However, several questions are still open concerning the results obtained with the different existing models and the "future" of rf discharge modeling.

The first question is related to the physical basis of the fluid models. Considering the wide variety of physical assumptions which are used in different works, it might be difficult for the non specialist to have a global idea of the capability of the models, and of their accuracy and reliability.

The second concerns the validity domain of the fluid models, and the problem of the practical use of more refined models (Monte Carlo, particle in cell) when fluid models are no longer valid (e.g. low pressure).

The third question is related to the plasma chemistry and to what can be expected concerning the modeling of practical plasma processing conditions.

These questions will be discussed and illustrated with recent results.

11.3

THE EFFECT OF REACTOR PRESSURE ON THE GROWTH OF GLOW DISCHARGE a-SiN:H. Walter J. Varhue, Dept. of Electrical Eng., Univ. of Vermont, Burlington, VT; and Kiril Pandelisev, Johnson Matthey Electronics, P. O. Box 3000, Trail, B. C., Canada.

Thin films of a-SiN:H have been prepared by PECVD using a capacitively coupled RF glow discharge. The reactor pressure was varied from 30 to 300 mTorr. Electrical characterization of the films included a determination of the trapped electron density and electrical resistivity. Also measured was the SiN bond and total bonded H concentration by FTIR spectroscopy. The change in reactor pressure effects the character of the glow discharge by increasing the mean free path of both ions and electrons. This in turn effects the electron energy distribution which influences the production rate of reactive species and the energetic ion bombardment which influences several physical processes occurring at the growth surface. In this investigation the plasma potential and density have been determined for both Ar and SiH₄/NH₃ rf discharges as a function of pressure with an emissive Langmuir Probe.

Film resistivity and SiN bond concentration have been found to decrease monotonically with increasing reactor pressure. Total bonded H content in the film however increases with reactor pressure. Trapped electron density does not appear to be significantly effected by reactor pressure.

The plasma potential for the SiH₄/NH₃ discharge initially decreases with reactor pressure as also observed with the Ar, yet then is found to increase with further increase of reactor pressure. The plasma density increase for both Ar and the SiH₄/NH₃ discharge as reactor pressure is increased.

11.4

INFRARED LASER ABSORPTION STUDIES OF RADICAL CONCENTRATIONS IN CH₄ RADIO FREQUENCY PLASMAS. Joda G. Wormhoudt, Center for Chemical and Environmental Physics, Aerodyne Research, Inc., Billerica, MA 01821

Infrared tunable diode laser absorption studies of process plasmas are being carried out in a laboratory reactor which allows a long absorption path. In this paper we report studies of CH₄ radio frequency plasmas. For these studies, the reactor had an absorption path length of about 48 m. It has an active volume 1 m in length and 15 cm diameter, excited by 13.56 MHz RF with input power levels of 100 to 1000 W. The electrodes are shielded from the plasma by a teflon liner.

The molecular species whose concentrations have been measured include CH₃, and C₂H₂ as well as CH₄. Other CH₄ plasma species for which we plan spectral searches include CH₂, C₂H₄ and C₂H₆. Observations are made for ranges of reactor parameters, including RF power, dilution by Ar or H₂, total pressure, and O₂ addition. Estimation of the plasma temperature from rotational line absorption intensities will also be discussed.

Recently, several groups have undertaken detailed chemical kinetic modeling of CH₄ discharges. The model concentrations presented here should be of use in assessing the predictive capabilities of the models. We will discuss some preliminary comparisons between models and experiment.

11.5

SILANE PLASMA CHEMISTRY ONE STEP AT A TIME: SILICON HYDRIDE RADICAL-MOLECULE KINETICS Joseph M. Jasinski, IBM Research Division, Thomas J. Watson Research Center, P. O. Box 218, Yorktown Heights, NY 10598

In order to propose and quantitatively test models for the plasma induced growth of silicon containing thin films, it is desirable to understand which silicon radical species are generated in the gas and how quickly they are removed by gas phase radical-molecule

reactions, since these processes ultimately determine the flux of reactive species to the film growth surface. Electron impact dissociation of silane readily generates all possible mono-silicon radical species, SiH_x ($x = 1-3$). Over the past several years we have developed flash kinetic spectroscopy techniques to generate, directly detect and measure absolute reaction rate constants for these radicals. Results of these studies for the SiH , SiH_2 and SiH_3 radicals will be presented.

Silyldiyne, SiH , is generated in the excimer laser photolysis of disilane and phenylsilane and detected by laser induced fluorescence. Silylene, SiH_2 , is generated in the excimer laser photolysis of disilane, phenylsilane or iodosilane and is detected by cw laser resonance absorption. Silyl, SiH_3 , is generated by chlorine atom abstraction from silane or by excimer laser photolysis of bromosilane and is detected by infrared diode laser spectroscopy. Absolute reaction rate constants for the removal of these radicals by a variety of reaction partners have been measured at room temperature. The results provide a new understanding of the thermochemistry and reactivity of these radicals and a simple explanation for the silicon radical concentrations which have thus far been observed in silane deposition plasmas. They also lead to the possibility of two different film growth mechanisms, which will be discussed briefly.

11.6

Laser-Induced Fluorescence of Silicon and Silicon Monoxide in a Glow Discharge. Anthony J. Hynes, Molecular Sciences Branch, Georgia Tech Research Institute, Georgia Tech, Atlanta, Ga. 30332.

Laser-induced fluorescence (LIF) shows great potential as a sensitive, specific and potentially non-intrusive diagnostic in plasma enhanced chemical vapor deposition (PECVD). In this work, we report the observation of LIF from Si and SiO, two potentially important gas-phase intermediates in a variety of PECVD systems.

Si was detected in a low pressure glow discharge in an Ar/SiH_4 mixture. Fluorescence was excited using a frequency-doubled Nd-Yag pumped dye laser exciting the $4^3\text{P}_2 - 3^3\text{P}_2$ transitions at ≈ 252 nm and monitoring both spectrally resolved and total fluorescence.

SiO was detected in a low pressure discharge in an $\text{Ar/SiCl}_4/\text{O}_2$ mixture. Fluorescence was excited via the $A^1\pi - X^1\Sigma^+$ transition at ≈ 230 nm with dispersed fluorescence being monitored.

We have also studied Si atom production in the multi-photon dissociation of SiCl_4 , SiH_4 and $\text{Si}(\text{CH}_3)_4$ at 193 and 252 nm. The implications of this process for non-intrusive LIF diagnostics of Si atoms will be discussed.

11.7

SPATIAL GENERATION PROFILES OF ACTIVE RADICALS IN PLASMA-ENHANCED CVD OF a-Si:H. D. Mataras, S. Cavadias, D.E. Rapakoulis, Institute of Chemical Engineering and High Temperature Chemical Processes, Greece.

Laser Induced Fluorescence (LIF) and Optical Emission Spectroscopy (OES) have been applied in an rf silane discharge, for the simultaneous detection of spatially resolved, relative concentration profiles of both ground state and electronically excited SiH radicals. These measurements were carried out in low power low

depletion conditions, for pressures ranging from below 20 mTorr to approximately 0.5 Torr, in pure silane as well as in mixtures with He, Ar and H_2 . LIF spatial profiles present a maximum located at approximately 10 millimetres from the rf electrode. The position of this maximum is insensitive to variations of pressure, power, dilution, buffer gas and interelectrode gap. To the contrary the emission profile is sensitive to pressure. The observed differences in the behaviour of ground state SiH and electronically excited SiH are attributed to the anisotropy of the electron swarm, together with the different generation thresholds of the two radicals. Considering the fact that reactive dissipation dominates over diffusional transport for SiH_n ($n < 3$) radicals, under usual deposition conditions, spatial profiles represent the stationary silane fragment generation pattern. The dependence of these profiles on dilution and chamber geometry will be further discussed.

11.8

ELECTRONIC AND CHEMICAL PROPERTIES OF SILICON CLUSTERS IN REACTIONS WITH SILANE. M. L. Mandich, W. D. Reents, Jr., and K. D. Kolenbrander, AT&T Bell Laboratories, Murray Hill, NJ.

Formation of hydrogenated silicon dust in silane plasmas poses formidable quality control problems in the subminiaturization of silicon devices. Plasma diagnostic studies suggest that this dust begins as small subsilane ions which grow incrementally by reactions with silane. Such a growth process must involve small hydrogenated silicon clusters which are crucial in determining the growth rates and structures of larger particles.

Our studies focuses on the electronic and chemical properties of small bare and hydrogenated silicon cluster ions. Charged silicon clusters and subsilane cations are prepared and reacted with silane in the ion cell of a Fourier transform mass spectrometer. Sequential reactions to form larger hydrogenated silicon clusters observed at room temperature. All of the clustering sequences, however, encounter early kinetic bottlenecks which prevent further growth.

Ab initio electronic structure calculations are used together with phase space theoretical calculations to elucidate the potential surfaces for silicon cluster reactions with silane. Two unforeseen mechanisms are uncovered for activation of silane by silicon centers: one involves four center transition states, the other involves strong bridging silicon-hydrogen bonds. Larger hydrogenated silicon clusters exist as highly branched, cyclic, or compact species. Such structures are formed at the expense of the highly reactive silicon centers required for activation of the Si-H bonds of silane.

Our findings indicate that sequential clustering of small silicon clusters and subsilane cations with silane does not lead to formation of the deleterious hydrogenated dust observed in silane plasmas. Furthermore, the microscopic surfaces of these small silicon clusters offer a model for studying chemistry at highly reactive silicon centers.

11.9

"in situ" SUBSTRATE TEMPERATURE MEASUREMENT DURING a-SiN PLASMA CVD FROM N_2 ROTATIONAL TEMPERATURE. Shin-ichiro Ishihara, Akira Otsuka & Seiichi Nagata Matsushita Electric Industrial Co. Central Research Laboratories Moriguchi City, Osaka JAPAN

PECVD a-SiN film is characterized as good passivation film for IC, deposited at low temperatures. The a-SiN is also used for gate insulator of a-Si:H TFT which is applied to LCD-TV addressing. Film characteristics are largely depend on its deposition temperatures. We suggest "in situ" measuring method of a-SiN surface temperatures through neighboring gas temperatures during rf (13.56MHz) deposition.

Rotational temperature of $\text{N}_2(^1\text{N} - ^3\Pi_g)^{0-3}$ is known to be a transfer of N_2 gas temperature (T_g). Its lifetime is 40nsec, so N_2 emits light as soon

as the N_2 is excited to this state. There are no other ways to release the energy. The other gases temperatures should be the same because of many collisions in glow discharge ambient (≈ 100 Pa). The emission spectrum at 406nm were not affected by SiH_4 , NH_3 & H_2 mixing as a-SiN raw gases.

Major emission in the rf plasma was N_2 and H_2 . T_g near the substrates was increased with H_2 ratio of H_2+N_2 mixture. Higher $N_2/(H_2+N_2)$ ratio deposition decreased etching rate of the a-SiN by HF and NH_4F mixture, and increased in the film density, similar to the phenomena increasing in setting substrate temperatures which were also observed in T_g . In addition, T_g brought a lot of knowledge about thermal transfer in the specific PCVD chamber which can be used for the "in situ" monitoring of PCVD a-SiN deposition.

I2.1

SILICON TECHNOLOGY AND PECVD MATERIALS: ISSUES AND CHALLENGES Alain S. Harnus, and Graham W. Hills AT&T Bell Laboratories, 555 Union Boulevard, Allentown PA 18103

The trend toward increased complexity of silicon VLSI technology, driven by submicron design rules and multiple levels of interconnects, is giving Plasma Enhanced CVD processes a predominant role. Three major categories of materials are emerging as crucial to successful manufacturing: (a) Dielectrics for interlevel isolation and passivation, away from active structures, such as TEOS-based oxide (PETEOS), and silicon nitride; (b) Closer to the gate/transistor structure, Dielectrics for isolation, such as PETEOS and borate/phosphate-doped oxide (BPSG), or gate-quality oxides, such as downstream Silane-based oxide; (c) Conductors, such as Tungsten or Silicon. The drive to plasma enhanced deposition is irreversible.

In this paper we review some of the current issues and challenges with emphasis on interlevel dielectrics and passivation. No final answer will be given but hopefully discussion will be generated. A few topics that will be illustrated are outlined below.

- Film quality requirements, although extensive, are fairly well defined. What is the most efficient plasma generation to achieve them? Should the reactor design be specific or generic?
- Will the understanding of mechanisms (such as step coverage) dictate discharge characteristics? Is the required step coverage incompatible with film quality? Should we aim for maximum or minimum step coverage?
- The issue of contaminants (metals, mobile ions) is not clearly resolved. Will it slow down the frantic push to integrated processing? How will integrated processing affect device fabrication strategies?
- How does surface conditioning (both substrate and hardware) affect the process results? Will plasma induced damage to the device be a major concern? What is known?

I2.2

PLASMA DEPOSITION OF SiN_xH_y : PROCESS CHEMISTRY VS. FILM PROPERTIES. Donald L. Smith, Xerox Palo Alto Research Center, Palo Alto, CA 94304.

"Silicon nitride" films deposited by plasma-enhanced chemical vapor deposition have been studied for over two decades as diffusion barrier and insulating layers in integrated circuitry, yet the chemistry of the deposition process has been investigated only recently. We have analyzed the plasma composition using special mass spectrometric techniques and have correlated it with the deposition rate and properties of the films to identify the film-forming precursor species and their surface reactions. SiN_xH_y deposited from SiH_4 in excess NH_3 was found to involve the gas-phase precursor radical triaminosilane, $Si(NH_2)_3$, which adsorbs with a very low sticking probability and then chemically condenses towards Si_3N_4 on hot substrates with the evolution of ammonia. High-power, SiH_4 -lean plasma conditions that maximize reaction to triaminosilane result in near-unity utilization of SiH_4 and produce N-rich films that contain none of

the Si-H bonding that has been associated with electrical defects. When N_2 is used instead of NH_3 , no gas-phase Si-N compounds are formed, and deposition occurs instead by the reaction of SiH_n radicals with N atoms at the surface. In either process, insufficient power or too much SiH_4 make the reaction of Si with N incomplete, leading to Si-H bonding and lower N/Si ratio in the films. These compositional changes were found to significantly affect the rate of charge injection and trapping in electrical stressing tests on MIS structures. Material deposited from a SiH_4 -lean, high power NH_3 plasma has much lower a trapping rate for both electrons and holes than does SiN_xH_y deposited under conditions that give a "stoichiometric" N/Si ratio of 4/3, and it also contains much less grown-in positive charge.

I2.3

PLASMA DEPOSITED SILICON NITRIDE FILM CHEMISTRY. Justin N. Chiang, Dennis W. Hess, Chemical Engineering Dept., University of California, Berkeley, Berkeley, CA 94720.

The structure and composition of plasma deposited (PD) silicon nitride thin films, formed using NH_3/SiH_4 , N_2/SiH_4 , and $N_2/SiH_4/H_2$ discharges are compared. The effect of a DC grounded stainless steel screen placed directly over the substrate in the rf glow discharge is also discussed. Chemical structure and composition of these films were measured using X-ray Photoelectron Spectroscopy and Fourier Transform Infrared Spectroscopy. Significant changes are observed in film composition with both changes in gas composition and with utilization of the screen. When the screen is invoked, variations in film composition are more pronounced for PD silicon nitride films formed using N_2 . An increase in the N:Si ratio occurs for all films deposited using the screen. This is reflected in increased N-H and decreased Si-H bonding. Similar changes are also observed for films deposited from a $N_2/SiH_4/H_2$ discharge as compared to films formed using a N_2/SiH_4 discharge.

I2.4

NITROGEN INCORPORATION REACTIONS IN HYDROGENATED AMORPHOUS SILICON, NITROGEN ALLOYS PRODUCED BY REMOTE PECVD. G.N. Parsons and G. Lucovsky, Department of Physics, North Carolina State University, Raleigh N.C. 27695

Hydrogenated amorphous silicon (a-Si:H), and amorphous silicon nitrogen (a-Si,N:H) alloys for thin film device applications are typically produced by direct plasma-enhanced CVD, or glow discharge (GD). As an alternative deposition process, we have found that remote plasma-enhanced CVD offers significant advantages by providing increased control over gas phase and surface reactions. In the remote PECVD process, silane is not excited in the plasma-glow, but is indirectly excited by species extracted from a remote, noble gas plasma. By using SiH_4/N_2 (He or Ar) or SiH_4/NH_3 (He or Ar) mixtures introduced downstream from a He plasma, we have used the remote PECVD process to produce a-Si,N:H alloys containing up to 30 at.% nitrogen and 8 to 13 at.% hydrogen. We have investigated the bonding environments for Si, N, and H using ir, and determined the nitrogen and hydrogen concentrations, [N] and [H], respectively, using SIMS. We have related these results to the gas phase excitation of N_2 and NH_3 , and to nitrogen incorporation reactions at the growth surface. Using N_2 as the source gas, we find that with increasing [N]: 1) the Si-H stretching mode shifts continuously from 1990 cm^{-1} at [N]=0 at.% to 2100 cm^{-1} at [N]=30 at.%; 2) the absorbance of the Si-H bending mode begins to decrease at [N] = 5 at.%, and disappears for [N] > 25%; and 3) N-H features are never observed. The shift of the stretching mode and the decrease in the bending mode absorbance result from fluctuation and coupling, respectively, when N is "back-bonded" to an Si-H group. These results demonstrate that at the deposition surface, nitrogen bonds preferentially to silicon (and not to hydrogen), and that Si-N bond formation is statistical, i.e., Si-N bonds are distributed randomly in an a-Si:H host matrix. When a small amount of NH_3 is used as the feed gas instead of N_2 , the nitrogen incorporation rate is enhanced by a factor of about two, and the nitrogen bonding at low concentrations (up to 5 at.%) is different, in that nitrogen atoms appear to favor silicon sites which are spatially removed from hydrogen atoms.

12.5

MICROWAVE and ECR PLASMA DEPOSITION of SiN_x for OPTOELECTRONICS. Steven Dzioba, Bell-Northern Research, Ottawa, Ont., K1Y 4H7, Canada.

Motivated by incongruent loss of Group V elements at high temperature and susceptibility to plasma damage, downstream microwave and ECR plasma processes have been developed for dielectric deposition for optoelectronic devices.

High quality SiN_x and SiO_xN_y thin films have been deposited on MOCVD grown InP/InGaAs layers at 300°C and/or without intentional substrate heating. Pinhole-free, low hydrogen content ($<10^{21} \text{ cm}^{-3}$) SiN_x films can be prepared using both high pressure (1 Torr) downstream microwave plasmas and under low pressure (1 mTorr) ECR conditions. However, using ECR, with low energy (50 eV) ion bombardment, films show a decrease in wet etch rate by a factor of 10 indicating denser films. Stress for ECR deposited films is 2×10^9 dynes/cm² and compressive.

Further physical/chemical film characterization illustrates the role of ion bombardment versus activated metastable species in SiN_x film properties.

These techniques have been used to prepare Zn diffusion masks for p-i-n detectors, passivation layers and high quality optical coatings for diode lasers and other optoelectronic devices.

12.6

CHARACTERIZATION OF Si_3N_4 FILMS DEPOSITED USING AN ELECTRON CYCLOTRON RESONANCE (ECR) PLASMA. J. P. Simko, Y.-Z. Hu, J. W. Andrews, E. A. Irene, T. M. Mayer, Dept. of Chemistry, Univ. of North Carolina, Chapel Hill, NC 27599

Silicon nitride films were deposited on silicon substrates in a microwave ECR plasma at different temperatures and microwave power density. The chemical composition of the deposited films were measured using x-ray photoelectron spectroscopy (XPS) and attenuated total reflectance (ATR) infrared spectroscopy. In-situ spectroscopic ellipsometry was also used to monitor film composition as deposition proceeded. The films were deposited in the afterglow of an ammonia or nitrogen discharge with silane introduced above the sample surface. Deposition rates of two hundred angstroms per minute were obtained with little dependence on temperature, in the range 150 - 450°C. Films deposited at $<250^\circ$ showed severe cracking while films deposited at higher temperature did not. Correlation between XPS and ATR results show a high degree of Si-N bonding in the films with Si-O bonding primarily at the surface due to surface oxidation. ATR results indicate that the concentration of Si-H and N-H bonding concentrations in films were higher for low temperature deposited films and were still detectable at 450°. Ellipsometry is shown to be sensitive to composition changes in the film, such as H incorporation, during growth.

12.7

CHARACTERIZATION OF THE PLASMA CHEMISTRY AND FILM COMPOSITION OF PECVD SILICON NITRIDE DEPOSITED FROM SILANE-NITROGEN AND SILANE-AMMONIA MIXTURES WITH ARGON ADDITIONS. W. E. Quinn, B. G. Bagley, B. J. Wilkens, Bellcore, Red Bank, NJ; and B. M. Gallois, Stevens Institute of Technology, Hoboken, NJ.

Silicon nitride films deposited from silane-nitrogen and silane-ammonia mixtures by PECVD contain large amounts of

hydrogen. We have determined that adding argon to the gas mixture reduces the amount of hydrogen in the resulting films. Differences in film composition are obviously due to changes in the chemistry of the discharge which was characterized by line-of-sight mass spectrometry, optical emission spectroscopy and plasma double probe measurements. Substrate temperature was fixed at 325 °C, pressure was 500 mtorr, the RF power was 0.25 watts cm⁻², the silane to nitrogen ratio was varied from 0.003 to 0.02, the silane to ammonia ratio was varied from 0.01 to 0.5, and the argon additions were 10% of the total flow. Argon additions to the discharge increased the plasma density in both ammonia and nitrogen plasmas. Optical emission from N₂ and SiH species increased upon addition of 10% argon to the silane-nitrogen discharge, whereas the NH emission decreased upon 10% argon addition to the silane-ammonia discharge. Infrared transmission spectra of films deposited with and without argon show no change in peak position or intensity of Si-H and N-H absorption bands in the spectral range studied, despite a large (up to 20 atom%) reduction in hydrogen content, as determined by nuclear profiling, upon the addition of argon. These results suggest that a substantial fraction of the hydrogen in the films is not infrared active. We propose that the reduction in hydrogen content is due to bombardment of the growing films by argon ions, which sputter the adsorbed hydrogen molecules.

12.8

DIRECTIONAL DEPOSITION OF SILICON OXIDE BY A PLASMA ENHANCED TEOS PROCESS Julian J. Hsieh, D. E. Ibbotson, D. L. Flamm and J. A. Mucha AT&T Bell Laboratories, 600 Mountain Ave, Murray Hill, NJ 07974

Plasma enhanced deposition of silicon oxide using TEOS (tetraethoxysilane) has gained wide acceptance as a coating process for interlevel dielectric applications. Its advantages include low temperature processing and void-free filling for medium aspect ratio features (up to ~0.8). However, future devices will require higher density metal interconnection and it becomes more difficult to deposit void-free coatings over surfaces with severe topography. Even a perfectly conformal deposition process can produce coatings with voids and regions of high stress on features of high aspect ratios (>1). One potential solution to this problem is to engineer a directional deposition process followed by a planarization step.

This paper describes the deposition of silicon oxide from TEOS using helium/oxygen mixtures in a parallel plate rf plasma reactor. Under appropriate process conditions, highly directional deposition of low-stress, stoichiometric silicon oxide is achieved. The step coverage profiles and the chemical and physical properties of these SiO_2 films were studied to gain an understanding of the origin of preferential vertical deposition. The typical deposition conditions used in this study were 1 torr total pressure, 320°C substrate temperature, 1-9% TEOS, 0-80% O₂, high (14 MHz) or low (150 kHz) applied frequency and low power density (~0.1 W/cm²). Step coverage, chemical stability and film stress were found to be most dependent on discharge frequency and O₂ flow. This dependence will be explained by the various effects involved in the oxide deposition mechanism.

12.9

RF POWER DEPENDENCE OF THE MATERIAL PROPERTIES OF PECVD SILICON DIOXIDE. J.D. Chapple-Sokol, IBM General Technology Division, Hopewell Junction, NY; E. Tierney and J. Batey, IBM T.J. Watson Research Center, Yorktown Heights, NY.

In direct RF plasma enhanced chemical vapor deposition (PECVD), the RF power can couple both with gas-phase species and with the evolving film surface. By consequence, changing the power density in a PECVD system can have a large effect on both the nature of the film precursors and on the structure of the film itself. These effects can be observed in the chemical, electrical, and physical structure of the film.

We have examined the power dependence of the PECVD reaction of a dilute mixture of silane and nitrous oxide in helium to deposit silicon dioxide films. This reaction process has been used previously to deposit near thermal quality films with excellent electrical properties¹. A commercial single wafer reactor was used at power densities ranging from 0.2 to 5 Watts/cm².

A number of techniques were employed to examine the films, including chemical and structural evaluation by infrared spectroscopy, stress measurements, and etch rates. Electrical properties of the films were measured using I-V and C-V techniques.

The broad range of power densities used in this study permitted a substantial expansion of the range of process conditions under which high quality oxide films can be deposited. Electrically 'thermal-like' films were deposited under conditions that led to widely varying physical properties. The properties of these PECVD films will be compared with those of other deposited films and thermally grown SiO_2 .

I2.10

EVIDENCE FOR STRONGLY ENHANCED DEFECT CREATION IN LOW-TEMPERATURE PECVD SiO_2 FILMS. R. A. B. Devine* and R. L. Pfeiffer, US Army ETDL, Fort Monmouth, NJ.

Amorphous SiO_2 films have been deposited by plasma enhanced chemical vapor deposition ($\text{N}_2\text{O}:\text{SiH}_4$ flow ratio of 40:1) then ^{60}Co gamma irradiated. We observe paramagnetic defects similar to oxygen vacancy centers which are created at least 100 times more efficiently in as-deposited oxide than in the same oxide annealed for 1 hr at 950°C in Ar. Positive fixed oxide charge creation in samples irradiated in the unbiased mode has a fractional yield of 0.018 and a flatband voltage variation with dose of 8 mV/krad for an 1100 Å thick capacitor. The positive fixed oxide charge and paramagnetic defects do not appear to have the same (defect) origin.

I3.1

THE ROLE OF LOW-ENERGY ION/SURFACE INTERACTIONS DURING CRYSTAL GROWTH FROM THE VAPOR PHASE: EFFECTS ON MICROCHEMISTRY AND MICROSTRUCTURE. L. E. Greene, Department of Materials Science, the Coordinated Science Laboratory, and the Materials Research Laboratory, University of Illinois, 1101 W. Springfield Ave., Urbana, Illinois 61801.

Low-energy ($\leq 200\text{eV}$) ion irradiation during crystal growth from the vapor phase plays an important and sometimes dominant role in controlling the growth kinetics and physical properties of films deposited by glow discharge and ion beam sputter deposition, molecular beam epitaxy using accelerated dopants, and plasma-assisted chemical vapor deposition. Ion/surface interaction effects, including trapping, preferential sputtering, collisional mixing, and surface segregation are used to interpret and model experimental results concerning the effects of low-energy particle bombardment on nucleation kinetics, growth kinetics, enhanced diffusion at interfaces, elemental incorporation probabilities, and dopant depth distributions. Of particular interest are the results of recent experiments designed to: (1) determine elemental incorporation probabilities and depth profiles of accelerated dopants in MBE Si as a function of acceleration energy E_a and growth temperature T_g , (2) investigate nucleation and growth kinetics of In overlayers using primary-ion deposition as a function of E_a and T_g on clean $\text{Si}(100)2\times 1$ surfaces, (3) use molecular dynamics and Monte Carlo simulations to investigate microstructure evolution, and (4) investigate the role of low-energy ion irradiation in reducing dislocation densities in epitaxial $\text{TiN}(100)$ layers.

I3.2

ION BOMBARDMENT EFFECTS ON SURFACE COMPOSITION AND STRUCTURE IN PLASMA PROCESSING. Thomas M. Mayer, Department of Chemistry, University of North Carolina, Chapel Hill, NC 27599

Bombardment of the substrate by energetic ions occurs in all plasma processes in which the substrate is in contact with the plasma. The flux, energy and identity of these ions depends greatly on the type of plasma and operating conditions. Ion energies can range from about keV in low frequency, low pressure discharges, such as sputter etching, to a few eV in high frequency, magnetically confined discharges such as microwave ECR. It has been shown that structural damage to crystalline substrates can occur in the form of point defects, extended defects, and amorphous film formation to depths

roughly corresponding to the range of the ion in the solid. Compositional modifications are induced by ion implantation, ion mixing of interfaces, segregation, and preferential sputtering effects. The magnitude and depth of these effects are mitigated also by movement of the interface, as in an etching or deposition process. We will consider examples primarily from etching of Si surfaces using inert and reactive gases, contrasting high ion energy bombardment in reactive ion etching environment and low energy bombardment in microwave ECR environment. In-situ ellipsometric techniques for evaluation the extent of ion bombardment induced modifications will also be discussed.

I3.3

REMOTE PLASMA-ENHANCED CHEMICAL VAPOR DEPOSITION OF EPITAXIAL SILICON ON SILICON (100) AT 150°C . T. Hsu, B. Anthony, L. Breaux, S. Banerjee, and A. Tasch, University of Texas, Austin, TX

Low temperature silicon epitaxy is critical to future generation ultra-large scale integrated circuits and silicon-based heterostructures. In this study, remote plasma-enhanced chemical vapor deposition has been used to demonstrate silicon homoepitaxial films at temperatures as low as 150°C , the lowest temperature reported for silicon epitaxy. The process relies on a stringent ex-situ preparation and loading of samples as well as an in-situ remote hydrogen plasma clean of the surface prior to epitaxy. An ultra-high vacuum environment (10^{-10} Torr) is utilized to achieve and maintain atomically clean surfaces.

Substrates are prepared with degreasing followed by an RCA clean. Prior to loading, the samples undergo a dilute HF etch to remove the native oxide and to passivate the surface with hydrogen. The samples are then loaded in a nitrogen-purged glove box. The in-situ clean is performed at temperatures at or below 300°C with a total pressure of 45 mTorr for 30 minutes at low rf powers ($<15\text{ W}$). The growth proceeds by remotely exciting the source gas, silane, with energetic species extracted from the noble gas plasma, such as Ar metastable gas atoms and energetic electrons, as well as increasing adatom mobility on the surface via collisions with the energetic species. Typical parameters for the growth include a total pressure of 200 mTorr, total flow rate of 360 sccm and a silane flow of 0.3 sccm. Characterization of the films has been done in-situ using RHEED and AES and ex-situ using TEM and Nomarski interference contrast microscopy. The films grown at 150°C to date have a thickness of 250 Å - 350 Å and show excellent crystallinity by the above methods. Growth at temperatures below 150°C have yielded amorphous films. Excellent quality epitaxial films have been grown in the temperature range 150°C to 400°C .

I3.4

REACTION KINETICS OF EPITAXIAL SILICON DEPOSITION AT $200-400^\circ\text{C}$ USING REMOTE PLASMA ENHANCED CHEMICAL VAPOR DEPOSITION. B. Anthony, T. Hsu, L. Breaux, S. Banerjee, and A. Tasch, Microelectronics Research Center, Department of Electrical and Computer Engineering, The University of Texas, Austin, TX 78712.

In this paper we will discuss the reaction kinetics of Remote Plasma-enhanced Chemical Vapor Deposition (RPCVD). In RPCVD, an argon glow discharge is generated remotely from the substrate using radio frequency (r-f) excitation. Excited species such as argon metastables and energetic electrons are transported to the substrate through a pyrex tube. Silane is introduced through a gas dispersal ring immediately upstream from the substrate and is never exposed directly to the glow discharge. Thus the excitation of the silane is limited to interaction with the plasma-excited argon gas over a distance of 5-10 cm between the gas ring and the substrate. This interaction distance is variable giving additional control over gas phase reactions.

The growth rate has been found to be dependent on temperature, r-f power, and the silane flow rate. The effects of these variables have been studied over a range of $200-400^\circ\text{C}$, 5-30W r-f power, and 5-30 sccm of silane at constant pressure. The deposition rate has been found to increase sharply with increased r-f power which implies that energetic electrons are more important than argon metastables since metastable concentration is maximized at low r-f power. A plot of deposition rate vs. temperature

yields a very small activation energy ($E_a=0.25$ eV) which is much smaller than that of thermal CVD (2.2 eV) or plasma-enhanced CVD (0.61 eV) in the 600-700°C temperature range [1]. It is believed that this low E_a is associated with plasma-enhanced desorption of hydrogen from the silicon surface.

I3.5

DEVELOPMENT OF REMOTE PLASMA ENHANCED CVD PROCESSES THROUGH THE USE OF IN-VACUO ELECTRON DIFFRACTION AND SURFACE ANALYTICAL TECHNIQUES. R.A. Rudder, G.G. Fountain, S.V. Hartangady, J.B. Posthill, and R.J. Markunas, Research Triangle Institute, Research Triangle Park, NC 27709-2184

Remote plasma enhanced chemical vapor deposition is now being used in a wide variety of materials processing. The materials deposited can be amorphous such as SiO_2 , Si_3N_4 , silicon oxynitrides, or a-Si:H. Or, the materials deposited can be epitaxial such as Si, Ge, dilute SiC alloys (carbon < 5%), or GaN. The wide variety of materials deposited necessitates a variety of gaseous reagents and processing conditions be employed. Arriving at conditions suitable for the deposition of one particular material has been assisted through the use of *in situ* and *in vacuo* electron diffraction and surface analytical techniques. Unlike molecular beam techniques, real time analysis of the surfaces under processing is not possible due to the high pressures employed. Instead, one has to develop processes using sequential sampling where the CVD process is interrupted to allow evacuation and analysis of the surface structure and chemistry.

This paper discusses the development of remote plasma CVD processes using both *in situ* and *in vacuo* surface analysis techniques. Specifically, the development of low-temperature Si processing involving homoepitaxy: below 800°C and SiO_2 deposition will be discussed. Plan and cross-sectional transmission electron diffraction, reflection high energy electron diffraction, and electrical mobility data will be given supporting the quality of the low temperature epitaxy. High frequency and quasistatic capacitance-voltage measurements are used to evaluate the density of interface state traps at the SiO_2/Si interface. In both the homoepitaxy and the dielectric depositions, surface cleaning processes based on remote plasma activation of hydrogen has been critical. Without the cleaning, homoepitaxy is inhibited, and SiO_2/Si interfaces have exceedingly high densities of interface state traps. Interface trap densities as low as $2 \times 10^{12}/\text{cm}^2\text{-eV}$ are routinely obtained.

I3.6

HIGH RATE DEPOSITION OF HYDROGENATED AMORPHOUS SILICON FILMS BY ECR PLASMA CVD. S.Ozaki, T.Akahori, T.Tani and S.Nakayama, Sumitomo Metal Industries Ltd., Amagasaki, Hyogo, Japan

Hydrogenated amorphous silicon (a-Si:H) films have been prepared by an RF plasma CVD system. It was applied to many devices such as photoreceptors and photovoltaic cells. However, deposition rate of the RF plasma CVD is in order of 100Å/min to 1000Å/min.

Newly developed ECR plasma CVD system has high powered microwave generator and high exhaust property in order to obtain high deposition rate.

By using this system, deposition rate linearly increases with the increase in the introduced microwave power and high deposition rate of 1µm/min was achieved at microwave power of 2.5kW. Usually, in the case of the RF plasma CVD, it is well-known that photosensitivity is deteriorated when deposition rate extremely increases. In the case of the ECR plasma CVD, this phenomenon was not appeared. Photoconductivity (σ_p) increases with the increase in the microwave power. σ_p is strongly influenced by the concentration of Si-H₂ bonds which decrease with the increase in the microwave power. Darkconductivity (σ_d) is independent of the microwave power and keeps low value of 10^{-12}S/cm . Films prepared at deposition rate of 1µm/min has excellent photosensitivity of $\log(\sigma_p/\sigma_d) \geq 6$ (σ_p is measured under AM1 solar

simulator). The deposition yield of SiH_4 gas is more than that of conventional CVD and polymerization in a gas phase generated Si powder is not observed.

I3.7

THE ELECTRICAL AND OPTICAL PROPERTIES OF AMORPHOUS SILICON ALLOYS BY PLASMA-ENHANCED CVD METHOD. M. Kapur, Guang H. Lin, and J. O'M. Bockris, Department of Chemistry, Texas A&M University, College Station, TX 77843

High and low bandgap amorphous silicon thin film alloys (a:SiAl, a:SiSe, a:SiS, a:SiGa and a:SiAs) were prepared by plasma-enhanced chemical vapor deposition. It was found that Al, As, and Ga amorphous silicon alloys are low bandgap materials whereas a:SiS and a:SiSe are high bandgap semiconductor. The optical band gap of these alloys changes from 1.1 eV to 2.1 eV, depending on the alloying element and its concentration in the film. The dark to light conductivity ratio, the activation energy and the Urbach edge were measured for different alloys at various compositions. The structural properties and chemical composition were also analyzed by FTIR, XPS, SIMS and EPMA techniques. The results show that these amorphous silicon alloys are promising materials for multi-bandgap photovoltaic devices.

I3.8

POLYHYDRIDE BONDING GROUPS IN PECVD AMORPHOUS Si THIN FILMS. B.N.Davidson, G.N. Parsons, C. Wang and G. Lucovsky, Department of Physics, North Carolina State University, Raleigh, N.C. 27695-8202

In glow-discharge deposition (GD) of a-Si:H alloys, the concentration of electronically-active defects increases as the incorporation of bonded hydrogen in polymerized dihydride groups, $(\text{SiH}_2)_n$ increases. Since the fraction of dihydride groups increases strongly with decreasing substrate temperature (T_s), the incorporation of these bonding groups can only effectively be reduced by restricting T_s to about 230°C or higher. We have found that a-Si:H films produced by remote plasma-enhanced chemical-vapor deposition (remote PECVD) are qualitatively different than the GD films in the following ways: 1) the amount of bonded hydrogen for $T_s > 100^\circ\text{C}$ is less by about a factor of about two; and 2) the fraction of polyhydride bonding is also significantly less than the monohydride fraction for $T_s > 100^\circ\text{C}$. By extending our studies to sputtered films, we have shown that the fraction of polyhydride bonding groups scales with the total concentration of bonded hydrogen, $[\text{H}]$, rather than any particular deposition variable. We have developed a statistical model that provides a basis for translating any process-dependent representation of data for the polyhydride fraction into a universally-obeyed scaling relationship in which the independent variable is $[\text{H}]$. We have used two complementary approaches: 1) a monte carlo method based on a finite matrix of bonding sites and 2) an analytical formalism for an infinite matrix of bonding sites. The agreement between the analytical model and the experimental data supports our observation that the fraction of polyhydride bonding is not determined simply by T_s , but is a function of the particular reaction pathways in a deposition process chemistry. Our studies of the remote PECVD process are consistent with a reduced availability of hydrogen at the growth surface during film deposition. We propose that the initial step in the heterogeneous surface chemistry involves the fragmentation of an excited silane molecule, SiH_4^* into SiH_2 and molecular hydrogen, H_2 . In contrast in the GD process, there is a broader spectrum of deposition precursors, and in general more hydrogen is available at the growth surface, and hence in the deposited thin films.

I4.1

DIAMOND FORMING DISCHARGES. Peter K. Bachmann
Philips Research Laboratories, Aachen, West Germany.

The modern era of metastable diamond growth began when Russian scientists published papers on diamond deposition from the gas phase in 1976 and 1981 [1]. They suggested to produce the necessary quantities of atomic hydrogen required for diamond deposition by means of electrical discharges. Researchers in Japan subsequently utilized microwave plasmas for this purpose [2]. By now, numerous groups have confirmed that diamond is formed from hydrogen/hydrocarbon gas mixtures by means of discharges. Other carbon carriers along with oxygen/hydrogen mixtures were successfully introduced. Polycrystalline coatings were formed on substrates ranging from insulators to metals and from glasses to single crystals.

A wide variety of plasma deposition methods were applied for diamond deposition. Included are low pressure DC-, RF-, and microwave plasma CVD from non-isothermal plasmas, as well as the utilization of arc discharges, plasma jets and thermal RF plasmas. The different diamond forming discharges will be compared with respect to both their characteristics and their suitability for diamond growth. Special emphasis will be on microwave plasma CVD and DC plasma jet deposition. A brief summary of the properties, the characterization and practical applications of diamond thin films will also be included in this presentation.

I4.2

THE PLASMA DEPOSITION OF SEMICONDUCTOR MULTILAYER STRUCTURES. Masataka Hirose and Seiichi Miyazaki, Department of Electrical Engineering, Hiroshima University, Higashi-Hiroshima 724, Japan.

Very early stages of the plasma enhanced CVD of silicon based materials have been characterized on atomic scale by using the ultra thin multilayer structures. The thickness of the respective layer was in the range of 10 to 100 Å. The topological aspects of the deposited layers have been studied by the x-ray interference and diffraction. The chemical bonding features and the compositional abruptness in the heterojunction interfaces have been clarified by high resolution x-ray photoelectron spectroscopy. The results have revealed that the reactive species impinging from the plasma homogeneously cover the substrate surface and layer by layer growth takes place on atomic scale. The island growth, which is a known mechanism in metal thin film deposition, is very unlikely in the case of semiconductors and insulators. Also, inter-diffusion or compositional mixing of the constituent atoms in the interface is negligible and the interface is atomically abrupt. From these it becomes evident that the plasma enhanced CVD technique can offer an extremely uniform ultra thin film because of rather high mobility of reactive species on the growing surface.

I4.3

FORMATION OF MULTILAYER HETEROSTRUCTURES BY CONTROL OF PATHWAYS IN REMOTE PECVD. D.Y. Tsu, J.A. Thell, S.S. Kim, and G. Lucovsky, Departments of Physics, and Materials Science and Engineering North Carolina State University, Raleigh, NC 27695-8202

Studies of reaction pathways for the deposition of silicon suboxides (SiO_xH) by remote PECVD have shown that two simultaneous, and independent reactions control thin film deposition, one for the SiO_2 "alloy"

component (Si-O-Si bonds), and a second for the a-Si:H component (Si-Si, and Si-H bonds). In a Remote PECVD process for SiO_2 , an upstream rf plasma discharge of an O_2/He mixture results in the formation of metastable O_2 species; these interact with unexcited silane at the substrate surface, downstream from the plasma-glow, producing the film. We find that changing the O_2/He ratio, alters only the deposition rate and not the thin film bonding groups. In the a-Si:H process, the silane must be plasma-activated; i.e., thin film deposition can occur only when the He plasma after-glow extends downstream into the deposition region and interacts with the silane. By biasing a grid placed between the plasma source and the deposition region, the plasma after-glow can be electrically switched from either extending or not extending beyond the grid, thereby respectively opening or closing the a-Si:H deposition channel. Using gas mixtures for which $[\text{O}_2] \ll [\text{SiH}_4]$ provides an opportunity to electrically switch the film composition between SiO_xH and SiO_2 without changing any other deposition process parameter. To illustrate these aspects of the Remote PECVD process reactions, we have formed $\text{SiO}_2\text{-SiO}_x\text{H-SiO}_2$ heterostructures and performed CV measurements of their properties. The injection of charge into the SiO_x layer (200Å), and its trapping time in that layer are controlled by varying the thickness of the first SiO_2 layer, while maintaining a relatively thick second SiO_2 layer (200Å). For example a thickness of about 50Å allows tunneling into the suboxide layer and is sufficiently thick to maintain charge storage, where thicker layers (100Å) prevent tunnel injection, and thinner layers (25Å) allow substantial charge release out of the suboxide layer.

I4.4

WIDE AREA DISC SHAPED PLASMA SOURCE FOR ENERGY ASSISTED MOCVD OF GaAs, * B. Pihlstrom, T. Sheng, Z. Yu and G. J. Collins, Dept. Electrical Engineering, Colorado State University, Fort Collins, CO 80523

A wide area disc shaped plasma source of 20cm in diameter generated by a ring shaped cathode electron beam is used to decompose Trimethylgallium (TMGa) and Trimethylarsenic (TMAs). Volume photo-absorption of VUV photons and sensitized atom-molecule collisions with excited species and radicals can all assist dissociation of the organometallic feedstock reactants. In addition, the excited radical flux and VUV impingement on the film may also assist heterogeneous surface reactions and increase surface mobility of adsorbed species. Mass spectrometry studies using deuterium as a replacement for hydrogen as a trace gas allowed for the elicitation of decomposition pathways of TMGa and TMAs. Byproducts of hydrogen and helium plasmas were also studied as well as low temperature homoepitaxial GaAs film deposition.

I4.5

LOW TEMPERATURE CLEANING OF Ge AND GaAs SURFACES USING HYDROGEN DISSOCIATED WITH A REMOTE NOBLE-GAS DISCHARGE. S.V. Hattangady, R.A. Rudder, M.J. Mantini, G.G. Fountain, J.B. Posthill, and R.J. Markunas, Research Triangle Institute, Research Triangle Park, NC 27709-2194.

The native oxides of Ge and GaAs have long been known to preclude the formation of suitable MIS structures. Furthermore, these oxides are detrimental to low temperature homo- and hetero-epitaxy processes. The removal of these native oxides is therefore critical to epitaxy and MIS processing.

In situ cleaning of Ge and GaAs surfaces has been achieved at 300-375 °C using a novel technique employing hydrogen that is dissociated using a remote Ar discharge. Such a technique circumvents the problems of cross contamination introduced from a directly excited hydrogen discharge due to erosion of the quartz tube walls by the active hydrogen. Reconstructed surfaces characteristic of clean Ge and GaAs surfaces have been observed with Reflection High Energy Electron Diffraction (RHEED) following such a treatment. Auger and X-ray Photoelectron Spectroscopy

(XPS) analyses show that such a treatment removes both oxygen and carbon contamination from the surface. XPS window scans on the Ga-3d and the As-3d peaks show that the treatment is successful in removing oxygen bonded to both Ga and As on the GaAs surface.

I4.6

LOW-TEMPERATURE PECVD Si_3N_4 FILMS FOR GaAs ENCAPSULATION AND PASSIVATION. R. L. Pfeffer, R. A. Lux, K. A. Jones, and R. A. B. Devine*, US Army ETDL, Fort Monmouth, NJ.

We have begun a detailed study of the physical properties of Si_3N_4 films deposited at low temperatures using a PECVD process based on dilution of reactive gases with inert carrier gas¹ in order to investigate their feasibility for use as post-implant encapsulants and/or device passivation layers for GaAs. The films and substrates are analyzed by ion channeling, ellipsometry, IR spectrometry, ESR, RBS, and SEM to evaluate implantation-induced substrate and interface damage as well as the films' optical properties, surface morphology, stoichiometry, uniformity, stress, and electrical trapping characteristics. Following furnace or RTA annealing they are recharacterized, adding SIMS to evaluate As diffusion into the films. Both Schottky and ohmic contacts are then formed and used to measure Hall mobility, trap density and 1/f noise. Preliminary results of these studies are presented and compared with those obtained using other techniques such as wafer-to-wafer As entrapment, arsine overpressure, or conventional CVD.

I4.7

STRUCTURE AND MORPHOLOGY OF VITREOUS CHALCOGENIDE THIN FILMS OBTAINED BY PLASMA-ENHANCED CVD. Bernard CROS, Serge PEYTAVIN, Michel RIBES, Laboratoire de Physicochimie des Matériaux Solides, U.R.A. D0407, USTL, place Eugène-Bataillon, 34060 Montpellier Cedex 1, France; and Henri CAMON, Alain MOSSET, Jean-Louis BALLADORE, C.E.M.E.S.-L.O.E., 29, rue Jeanne-Marvig, 31055 Toulouse, France.

Germanium chalcogenide glasses present interesting properties as negative photoresists when they are silver sensitized. In this work, thin films were deposited on 4 inches diameter wafers in an industrial hot wall glow discharge equipment. Reactive gases are germane and hydrogen selenide. The layers are characterized by various techniques: EXAFS, LAXS, SEM, TEM. EXAFS and LAXS studies allow a comparison between the structures of thin films and those of homologous bulk glasses. Morphology studies by SEM and TEM on GeSe_3 and $\text{GeSe}_{5.5}$ compositions reveal an heterogeneous structure explained by a demixtion. The microlithographic influence of the properties of PECVD chalcogenide films on the microlithographic properties of chalcogenide films obtained by PECVD were compared with those of sputtering deposited glasses and discussed.

I4.8

SYNTHESIS & PHYSICAL PROPERTIES OF POLYMER FILMS WITH METAL INCLUSIONS. Eric Kay, IBM Almaden Research Center, San Jose, CA 95120

The ability to produce metal clusters uniformly dispersed throughout a polymeric matrix by reactive chemical etching/sputtering and simultaneous plasma polymerization in a r.f. capacitively coupled diode system will be described. The utility of optical emission spectroscopy to monitor both the polymerization precursors and metal atoms arriving at the film growing surface will be mentioned. Characterization of the metal containing plasma polymerized films was realized using X-ray photo

electron spectroscopy, X-ray fluorescence, Raman spectroscopy, electron microscopy and diffraction.

The size and volume fraction of the metal particles in the organic matrix can be controlled over a wide range and the resultant changes in optical, electrical and magnetic properties of the composite films can be examined. Dielectric breakdown, electrical percolation phenomena, resonant absorption and magnetic phase transitions as a function of metal particle size and volume fraction will be discussed. Hydrocarbon versus fluorocarbon matrices will be compared.

I4.9

FTIR INVESTIGATIONS OF PLASMA MODIFIED POLYMER SURFACES AND THEIR INTERFACES WITH PLASMA DEPOSITED TUNGSTEN Jihpeng Leu, Manoj Dalvie, Department of Chemical Engineering and Materials Science, University of Minnesota, Minneapolis, MN 55455, and Klavs E. Jensen, Department of Chemical Engineering, Massachusetts Institute of Technology, Cambridge, MA 02139.

Surface modification of polyimide in a downstream microwave $\text{CF}_4/\text{NF}_3/\text{O}_2/\text{Ar}$ plasma has been studied *in situ* by Fourier transform infrared (FTIR) reflection-absorption spectroscopy. Thin polymer films (100Å-2000Å) were prepared by spin coating gold covered silicon substrates. Etch rates and the chemical structure of the polymer surface were monitored as function of gas phase composition, plasma treatment conditions and time. NF_3/Ar and CF_4/Ar plasmas produced significant surface fluorination in terms of polyfluorinated alkyl and aryl compounds as well as acyl and benzoyl fluorides. The surface fluorination decreased with O_2 content in the etching gas. The effect of humidity on the plasma modified polymers was evaluated by comparing infrared spectra collected *in situ* and after air exposure.

Tungsten was deposited on the surface modified polymer surfaces in a radial flow parallel plate radio frequency (13.56 MHz) WF_6/H_2 discharge at 150 °C. WF_6/H_2 ratios less than 1/10 produced good tungsten films. The nucleation of the tungsten films has been investigated as a function of polyimide surface treatment and plasma conditions. The interface between the tungsten film and the polymer surface was characterized by *ex situ* reflectance-absorbance FTIR measurements through the back side of the Si/polymer/metal sandwich and comparison with physical vapor deposited tungsten. Fluorinated species were detected at the metal polymer interface. The surface/interface chemistry is related to the nucleation and adhesion of the tungsten to the polyimide.

SYMPOSIUM J: NEUTRON SCATTERING FOR MATERIALS SCIENCE

J

November 27-30, 1989

Chairs

Stephen M. Shapiro
Department of Physics (510B)
Brookhaven National Laboratory
Upton, NY 11973
(516) 282-3822

James D. Jorgensen
Materials Science Division
Argonne National Laboratory
700 S. Cass Avenue
Bldg. 223
Argonne, IL 60439
(312) 972-5513

Simon C. Moss
Physics Department
University of Houston
Houston, TX 77204-5504
(713) 749-2840

Symposium Support

Argonne National Laboratory

Army Research Office

Brookhaven National Laboratory

Los Alamos National Laboratory

National Institute for Standards and Technology

Oak Ridge National Laboratory

**Proceedings published as Volume 166
of the Materials Research Society
Symposium proceedings series.**

SESSION J1: INTRODUCTION TO NEUTRON
SCATTERING AND EXPERIMENTAL TECHNIQUES

Chair: S. M. Shapiro
Monday Morning, November 27
Salon J/K (M)

8:30 *J1.1

NEUTRONS: THE KINDER, GENTLER PROBE OF
CONDENSED MATTER, John D. Axe, Brookhaven
National Laboratory, Department of Physics,
Upton, NY.

9:00 *J1.2

NEUTRON SCATTERING INSTRUMENTATION, Roger
Pynn, Los Alamos National Laboratory,
LANSCÉ, Los Alamos, NM.

9:30 *J1.3

THE ADVANCED NEUTRON SOURCE, John B. Hayter,
Oak Ridge National Laboratory, Solid State
Division, Oak Ridge, TN.

10:00 BREAK

10:30 J1.4

THE APPLICATION OF NEUTRON TOPOGRAPHY TO THE
STUDY OF X-RAY SENSITIVE ORGANIC SINGLE
CRYSTALS - A POSSIBLE ALTERNATIVE TO X-RAY
TOPOGRAPHY, M. Dudley, State University of
New York at Stony Brook, Department of
Materials Science and Engineering, Stony
Brook, NY.

10:45 J1.5

MULTIPLE SMALL ANGLE NEUTRON SCATTERING
CHARACTERIZATION OF THE DENSIFICATION OF
ALUMINA, S. Krueger and G.G. Long, National
Institute of Standards and Technology,
Gaithersburg, MD; and R.A. Page, Southwest
Research Institute, San Antonio, TX.

11:00 J1.6

THERMAL DIFFUSE SCATTERING IN NEUTRON TIME-
OF-FLIGHT POWDER PATTERNS, Michael J. Radler
and Jerome B. Cohen, Northwestern Univer-
sity, The Technological Institute, Depart-
ment of Materials Science and Engineering, Evans-
ton, IL; and John Faber Jr., Argonne Nation-
al Laboratory, Materials Science Division,
Argonne, IL.

11:15 J1.7

REAL SPACE METHOD OF POWDER DIFFRACTION FOR
NON-PERIODIC AND NEARLY-PERIODIC MATERIALS,
T. Egami, B.H. Toby, W. Dmowski, University
of Pennsylvania, Department of Materials
Science and Engineering, Philadelphia, PA;
Chr. Janot, Institut-Laue-Langevin,
Grenoble, France; and J.D. Jorgensen, Ar-
gonne National Laboratory, Division of
Materials Science, Argonne, IL.

11:30 J1.8

NEUTRON RIETVELD ANALYSIS OF ANION AND
CATION DISORDER IN THE FAST-ION CONDUCTING
PYROCHLORE SYSTEM $Y_2(Zr_xTi_{1-x})_2O_7$, Sossina
M. Haile and B.J. Wuensch, Massachusetts
Institute of Technology, Department of
Materials Science and Engineering, Cam-
bridge, MA; and E. Prince, National In-
stitute of Standards and Technology, Reactor
Radiation Division, Gaithersburg, MD.

11:45 J1.9

SMALL ANGLE NEUTRON SCATTERING INVESTIGA-
TIONS OF NANOPHASE Ti, TiO_2 AND Pd, J.E.
Epperson, Argonne National Laboratory,
Materials Science Division, Argonne, IL;
J.W. White, Australian National University,
Research School of Chemistry, Canberra,
Australia and Argonne Fellow, Argonne Na-
tional Laboratory, Argonne, IL; R.W. Siegel,
J.A. Eastman, Argonne National Laboratory,
Materials Science Division, Argonne, IL;
Y.X. Liao, Sichuan University, Measure and
Testing Center, Chengdu, China and Argonne
National Laboratory, Materials Science
Division, Argonne, IL; and A. Narayanasamy,
University of Madras, Department of Nuclear
Physics, Madras, India and Argonne National
Laboratory, Materials Science Division,
Argonne, IL.

SESSION J2: SURFACES, FILMS AND INTERFACES

Chair: Gian Felcher
Monday Afternoon, November 27
Salon J/K (M)

1:30 *J2.1

SURFACES INVESTIGATION BY NEUTRON REFLEC-
TION, B. Farnoux, CEN SACLAY, Laboratoire
Leon Brillouin, Gif-sur-Yvette, France.

2:00 J2.2

VIBRATIONAL SPECTROSCOPY OF SURFACE SPECIES:
INELASTIC NEUTRON SCATTERING, J. Tomkinson,
Rutherford Appleton Laboratory, United
Kingdom; and G.J. Kearley, Institut Laue
Langevin, Grenoble, France.

2:15 J2.3

INTERDIFFUSION OF CADMIUM ARACHIDATE IN
LANGMUIR-BLODGETT FILMS, P. Stroeve, J.F.
Rabolt, IBM Almaden Research Center, San
Jose, CA; R.O. Hilleke, G.P. Felcher, Ar-
gonne National Laboratory, Material Science
Division, Argonne, IL; and S.H. Chen,
Massachusetts Institute of Technology,
Nuclear Engineering Department, Cambridge,
MA.

*Invited Paper

2:30 J2.4
NEUTRON REFLECTIVITY STUDY OF GD-Y INTER-FACE, J.F. Ankner and H. Zabel, University of Illinois at Urbana-Champaign, Urbana, IL; D.A. Neumann, C.F. Majkrzak, National Institute of Standards and Technology, Gaithersburg, MD; A. Matheny, J.A. Dura and C.P. Flynn, University of Illinois at Urbana-Champaign, Urbana, IL.

2:45 J2.5
NEUTRON DIFFRACTION STUDIES OF $\text{Cd}_{1-x}\text{Mn}_x\text{Se}$ EPILAYERS AND ZnSe/MnSe MULTILAYERS, T.M. Giebultowicz, University of Notre Dame, Physics Department, Notre Dame, IN and National Institute of Standards and Technology, Reactor Radiation Division, Gaithersburg, MD; P. Klosowski, University of Notre Dame, Physics Department, Notre Dame, IN; J.J. Rhyne, National Institute of Standards and Technology, Reactor Radiation Division, Gaithersburg, MD; N. Samarth, H. Luo and J.K. Furdyna, University of Notre Dame, Physics Department, Notre Dame, IN.

3:00 BREAK

3:30 J2.6
LOCAL ENVIRONMENTAL EFFECTS IN MAGNETIC ALLOYS AND MULTILAYERS: CALCULATIONS OF THE STATIC RESPONSE FUNCTIONS, D.D. Johnson, Sandia National Laboratories, Livermore, CA; J.B. Staunton, University of Warwick, Coventry, United Kingdom; B.L. Györffy, University of Bristol, Bristol, United Kingdom; F.J. Pinski, University of Cincinnati, Cincinnati, OH; and G.M. Stocks, Oak Ridge National Laboratory, Oak Ridge, TN.

3:45 J2.7
DETERMINATION OF HYDROGEN DENSITY PROFILES IN THIN FILMS AND MULTILAYERS BY NEUTRON REFLECTION, C.F. Majkrzak, S. Satija, D. Neumann, J. Rush, D. Lashmore, C. Johnson, National Institute of Standards and Technology, Reactor Radiation Division, Gaithersburg, MD; J. Bradshaw, Optoline, Andover, MA; L. Passell and R. DiNardo, Brookhaven National Laboratory, Upton, NY.

4:00 J2.8
MAGNETOELASTIC EFFECTS IN RARE-EARTH MULTILAYERS AND FILMS, R.W. Erwin, J.J. Rhyne, National Institute of Standards and Technology, Gaithersburg, MD; J. Borchers, R. Du, M.B. Salamon, and C.P. Flynn, University of Illinois at Urbana-Champaign, Urbana, IL.

4:15 J2.9
THE MORPHOLOGY OF SYMMETRIC DIBLOCK COPOLYMERS AS REVEALED BY NEUTRON REFLECTIVITY, S.K. Satija and C.F. Majkrzak, National Institute of Standards and Technology, Reactor Radiation Division, Gaithersburg, MD; S.H. Anastasiadis and T.P. Russell, IBM Almaden Research Center, San Jose, CA.

4:30 J2.10
A NEUTRON REFLECTIVITY STUDY OF THE ORDER-DISORDER TRANSITION IN THIN FILM DIBLOCK COPOLYMER FILMS, S.H. Anastasiadis, T.P. Russell, IBM Almaden Research Center, San Jose, CA; S.K. Satija and C.F. Majkrzak, National Institute of Standards and Technology, Gaithersburg, MD.

4:45 J2.11
THE STUDY OF SURFACES AND INTERFACES ON THE REFLECTOMETER CRISP AT THE ISIS PULSED NEUTRON SOURCE, J. Penfold, Rutherford Appleton Laboratory, Oxon, United Kingdom.

SESSION J3: PHASE TRANSFORMATIONS AND HIGH T_c

Chair: J. B. Cohen
Tuesday Morning, November 28
Salon J/K (M)

8:30 *J3.1
MARTENSITIC PHASE TRANSITIONS, PHONONS AND DIFFUSION PROPERTIES IN BCC METALS, W. Petry, Institut Laue-Langevin, Grenoble, France.

9:00 J3.2
STRESS DEPENDENCE OF THE SOFT PHONON BRANCH IN MARTENSITICALLY TRANSFORMING $\text{Ni}_{62.5}\text{-Al}_{37.5}$, S.M. Shapiro, Brookhaven National Laboratory, Department of Physics, Upton, NY.

9:15 J3.3
POLARIZATION RELAXATION OF THE FERROELECTRIC KD_2PO_4 USING NEUTRON SCATTERING, Ron Edge and Vicki Homer, University of South Carolina, Physics Department, Columbia, SC.

9:30 J3.4
PHASE DEVELOPMENT OF AN Al-Ti COMPOSITE DURING HEATING UP TO 1400°C , H.-G. Brokmeier, TU Clausthal, Department of Physical Metallurgy, and GKSS Research Center, Geesthacht, West Germany; M. Klatt, GKSS Research Center, Geesthacht, West Germany; and C. Ritter, Institute Laue Langevin, Grenoble, France.

9:45 BREAK

10:00 *J3.5
NEUTRON POWDER DIFFRACTION: A POWERFUL MATERIALS RESEARCH TECHNIQUE, W.I.F. David, Rutherford Appleton Laboratory, Oxon, United Kingdom.

10:30 J3.6

NEUTRON SCATTERING STUDY OF THE STRUCTURE OF $\text{Y}_2\text{BaCuO}_{7-\delta}$ AT 294 K AND 77 K, S.L. Town, B.A. Hunter, University of New South Wales, Advanced Electronic Materials Group, School of Physics, Kensington, Australia; R.L. Davis, Australian Institute of Nuclear Science and Engineering, Menai, Australia; and K.N.R. Taylor, University of New South Wales, Advanced Electronic Materials Group, School of Physics, Kensington, Australia.

10:45 J3.7

STRUCTURE OF $\text{ErBa}_2\text{Cu}_3\text{O}_x$ IN THE COMPOSITION RANGE $6.1 < x < 7.0$, E. Pörschke, P. Meuffels, Institut f. Festkörperforschung, Jülich, West Germany; and B. Rupp, Paul Scherrer Institut, Labor für Festkörperforschung, Villingen, Switzerland.

11:00 J3.8

NEUTRON POWDER DIFFRACTION STUDY OF THE STRUCTURES OF $\text{La}_{1.9}\text{Ca}_{1.1}\text{Cu}_2\text{O}_6$ AND $\text{La}_{1.9}\text{Sr}_{1.1}\text{Cu}_2\text{O}_6$, A. Santoro, F. Beech, National Institute of Standards and Technology, Reactor Radiation Division, Gaithersburg, MD; and R.J. Cava, AT&T Bell Laboratories, Murray Hill, NJ.

11:15 J3.9

NEUTRON DEPOLARIZATION BY FLUX LATTICES IN HI-Tc MATERIALS, S.J. Pickart, A.C. Nunes, M.L. Crow, University of Rhode Island, Physics Department, Kingston, RI; T.R. McGuire, S. Shinde and S.A. Shivashankar, IBM T.J. Watson Research Center, Yorktown Heights, NY.

11:30 J3.10

USE OF NEUTRON DIFFRACTION IN DETERMINING STRAINS IN HIGH-TEMPERATURE SUPERCONDUCTING COMPOSITES, D.S. Kupperman, J.P. Singh, Argonne National Laboratory, Materials and Components Technology Division, Argonne, IL; J. Faber Jr., and R.L. Hitterman, Argonne National Laboratory, Materials Science Division, Argonne, IL.

11:45 J3.11

HIGH RESOLUTION NEUTRON POWDER DIFFRACTION STUDIES OF THE FERROELASTIC PHASE TRANSITION IN LaNbO_4 , W.I.F. David, Rutherford Appleton Laboratory, Oxon, United Kingdom.

SESSION J4: ALLOYS I

Chair: G. Kostorz

Tuesday Afternoon, November 28

Salon J/K (M)

1:30 *J4.1

LATTICE DEFECTS STUDIED BY DIFFUSE NEUTRON SCATTERING, J. Peisl, Sektion Physik, LM Universität, München, West Germany.

2:00 J4.2

NEUTRON SCATTERING STUDY OF THE EQUILIBRIUM DEFECT STRUCTURE IN UNDERSTOICHIOMETRIC MnO , D. Schuster, Enka, Wuppertal, West Germany; R. Dieckmann, Cornell University, Ithaca, NY; W. Schilling, W. Schweika, IFF-KFA Jülich, Jülich, West Germany.

2:15 J4.3

SHORT-RANGE ORDER IN α -BRASS, Leszek Reinhard, University of Houston, Department of Physics, Houston, TX; Bernd Schönfeld, Gernot Kostorz, ETH Zürich, Angewandte Physik, Zürich, Switzerland; and Willi Bührer, LNS der ETH Zürich, Paul-Scherrer-Institut, Würenlingen, Switzerland.

2:30 J4.4

SHORT RANGE ORDER IN CU-ZN: A COMPARISON OF NEUTRON DIFFUSE SCATTERING DATA WITH FIRST PRINCIPLES RESULTS, M. Sluiter, Lawrence Berkeley Laboratory, Berkeley, CA and Lawrence Livermore National Laboratory, Condensed Matter Division, Livermore, CA; P.E.A. Turchi, Lawrence Livermore National Laboratory, Condensed Matter Division, Livermore, CA; D.M. Nicholson and G.M. Stocks, Oak Ridge National Laboratory, Metals and Ceramics Division, Oak Ridge, TN; D.D. Johnson, Sandia National Laboratories, Livermore, CA; and F.J. Pinski, University of Cincinnati, Department of Physics, Cincinnati, OH.

2:45 J4.5

ORDERING MECHANISM IN SUBSTITUTIONAL Ni-Cr ALLOY: EXPERIMENTS AND THEORY, P.E.A. Turchi, Lawrence Livermore National Laboratory, Condensed Matter Division, Livermore, CA; R.H. Howell, Lawrence Livermore National Laboratory, Physics Department, Livermore, CA; A.L. Wachs, M.J. Fluss, Lawrence Livermore National Laboratory, Condensed Matter Division, Livermore, CA; F.J. Pinski, University of Cincinnati, Department of Physics, Cincinnati, OH; D.M. Nicholson and G.M. Stocks, Oak Ridge National Laboratory, Metals and Ceramics Division, Oak Ridge, TN; and W. Schweika, Institut für Festkörperforschung der Kernforschungsanlage Jülich, Jülich, West Germany.

3:00 J4.6

PHONON DISPERSION IN THE ALLOY $\text{Cu}_{0.85}\text{Al}_{0.15}$, Henry Chou, S.M. Shapiro, Brookhaven National Laboratory, Department of Physics, Upton, NY; S.C. Moss, University of Houston, Physics Department, Houston, TX; and M.E. Mottoller, Oak Ridge National Laboratory, Solid State Division, Oak Ridge, TN.

3:15 BREAK

3:45 J4.7

COMPOSITION AND TEMPERATURE DEPENDENCE OF THE SHORT RANGE ORDER DIFFUSE SCATTERING IN $Al_c Ag_{1-c}$ ALLOYS, G.M. Stocks and D.M. Nicholson, Oak Ridge National Laboratory, Oak Ridge, TN; F.J. Pinski, University of Cincinnati, Cincinnati, OH; J.B. Staunton, University of Warwick, United Kingdom; D.D. Johnson, Sandia National Laboratory, Livermore, CA; and B.L. Gyorffy, University of Bristol, United Kingdom.

4:00 J4.8

PHASE DIAGRAMS AND DIFFUSE NEUTRON SCATTERING, R. Caudron, F. Solal, A. Pinel and M. Sarfaki, ONERA, Chatillon, France.

4:15 J4.9

DIFFUSE NEUTRON SCATTERING STUDY OF THE SHORT-RANGE ORDER IN Fe 20at% Al ALLOY, Werner E. Schweika, Institut für Festkörperforschung, KFA Jülich GmbH, Jülich, West Germany.

4:30 J4.10

LATTICE MISFIT AND DECOMPOSITION IN NI-AL-MO ALLOYS, Hector Calderon and Gernot Kostorz, ETH Zürich, Angewandte Physik, Zürich, Switzerland.

4:45 J4.11

INFLUENCE OF INTERSTITIAL OXYGEN ON THE LATTICE PARAMETERS OF SOLUTION-TREATED AND AGED Ti-8.6AL ALLOYS, George T. Gray III and A.C. Lawson, Los Alamos National Laboratory, Los Alamos, NM.

5:00 J4.12

IN-BEAM SMALL-ANGLE SCATTERING STUDIES OF PHASE SEPARATION IN NI-TI SINGLE CRYSTALS, Alberto Cerri, University of Vienna, Solid State Physics Department, Wien, Austria; Bernd Schöfeld and Gernot Kostorz, ETH Zürich, Angewandte Physik, Zürich, Switzerland; Albert F. Wright, Institut Laue-Langevin, Grenoble, France.

SESSION J5: ALLOYS II AND RESIDUAL STRESS

Chair: B. Wuensch

Wednesday Morning, November 29

Yarmouth/Vineyard (M)

8:30 *J5.1

COMPOSITION AND PROFILE DETERMINATION OF LIGHT ELEMENTS BY NEUTRON ABSORPTION REACTIONS, R. Gregory Downing, George P. Lamaze, John K. Langland and Brent L. Grazman, National Institute of Standards and Technology, Gaithersburg, MD.

9:00 J5.2

DISTRIBUTION OF BORON IN ION IMPLANTED $Hg_{1-x}Cd_xTe$, Robert C. Bowman Jr. and John F. Knudsen, The Aerospace Corporation, El Segundo, CA; and R. Gregory Downing, National Institute for Standards and Technology, Gaithersburg, MD.

9:15 J5.3

SANS MEASUREMENT OF HYDROGEN-DISLOCATION CORRELATION IN PALLADIUM, Brent J. Heuser, G.C. Summerfield, J.S. King, University of Michigan, Department of Nuclear Engineering, Ann Arbor, MI; and J.E. Epperson, Argonne National Laboratory, Material Science/IPNS Department, Argonne, IL.

9:30 J5.4

STUDY OF PREFERRED ORIENTATION IN GEOLOGICAL SAMPLES WITH PULSED NEUTRONS, Allen C. Larson, Phillip J. Vergamini, Manuel Lujan Jr., Los Alamos National Laboratory, Neutron Scattering Center (LANSCE), Los Alamos, NM; Rudy Wenk, University of California, Berkeley, Department of Geology and Geophysics, Berkeley, CA.

9:45 BREAK

10:00 *J5.5

RESIDUAL AND APPLIED STRESS ANALYSIS, Aaron D. Krawitz, University of Missouri, Department of Mechanical and Aerospace Engineering, Columbia, MO.

10:30 J5.6

RESIDUAL STRESS MEASUREMENTS BY MEANS OF NEUTRON DIFFRACTION, H.J. Prask and C.S. Choi, National Institute of Standards and Technology, Reactor Radiation Division, Gaithersburg, MD.

10:45 J5.7

RESIDUAL STRESS ANALYSIS BY NEUTRON TIME-OF-FLIGHT AT A REACTOR SOURCE, H.G. Priesmeyer, Institut für Reine und Angewandte Kernphysik, Universität Kiel, Geesthacht, West Germany; and J. Schröder, Institut für Werkstofforschung, Geesthacht, West Germany.

11:00 J5.8

EFFECT OF HEAT TREATMENT AND UNIAXIAL COMPRESSION ON THE RESIDUAL STRESSES IN U-0.8 wt. % Ti ALLOY MEASURED BY NEUTRON DIFFRACTION, A. Salinas-Rodriguez, T.M. Holden, J.H. Root, S.R. MacEwen, Chalk River Nuclear Laboratories, Ontario, Canada; and G.M. Ludtka, Martin-Marietta Energy Systems, Oak Ridge, TN.

11:15 J5.9

NEUTRON MEASUREMENT OF RESIDUAL STRESSES IN A USED RAILWAY RAIL, Peter J. Webster, Keng S. Low, Gordon Mills, University of Salford, Department of Civil Engineering, Salford, United Kingdom; and George A. Webster, Imperial College, Department of Mechanical Engineering, London, United Kingdom.

11:30 J5.10

NEUTRON DIFFRACTION ANALYSIS OF RESIDUAL STRESS IN CORROSION RESISTANT ALLOYS, Michael P. Anderson, Exxon Research and Engineering Company, Annandale, NJ; Maurice Watkins, Exxon Production Research Company, Houston, TX; and David Vakmin, Brookhaven National Laboratories, Upton, NY.

11:45 J5.11

NEUTRON DIFFRACTION MEASUREMENT OF STRESS FIELD DURING FATIGUE CYCLING OF A CRACKED TEST SPECIMEN, M.T. Hutchings, C.A. Hippsley, and V. Rainey, Harwell Laboratory, Materials Physics and Metallurgy Division, Didcot, United Kingdom.

SESSION J6: POLYMERS AND DISORDERED SYSTEMS

Chair: G. G. Long

Wednesday Afternoon, November 29

Yarmouth/Vineyard (M)

1:30 *J6.1

DYNAMICS OF STAR-BRANCHED POLYMERS IN SOLUTION, J.S. Huang and L.J. Fetters, Exxon Research and Engineering Company, Annandale, NJ; D. Richter and B. Farago, Institut Laue-Langevin, Grenoble, France; and B. Ewen, Max Planck Institut Fur Polymerforschung, Mainz, West Germany.

2:00 J6.2

MICROSTRUCTURE AND ISOTOPIC LABELING EFFECTS ON THE MISCIBILITY OF POLYBUTADIENE BLENDS STUDIED BY THE SMALL ANGLE NEUTRON SCATTERING TECHNIQUE, S. Sakurai, H. Hasegawa, T. Hashimoto, I.G. Hargis, S.L. Aggarwal and C.C. Han, National Institute of Standards and Technology, Polymers Division, Gaithersburg, MD.

2:15 J6.3

CHARACTERIZATION OF MOLECULAR NETWORK OF THERMOSETS USING NEUTRON SCATTERING, Wen-li Wu, National Institute of Standards and Technology, Polymers Division, Gaithersburg, MD.

2:30 J6.4

SHEAR INDUCED PHASE BEHAVIOR OF POLYMER BLENDS BY SMALL ANGLE NEUTRON SCATTERING, Alan I. Nakatani, Hongdoo Kim, and Charles C. Han, National Institute of Standards and Technology, Polymers Division, Gaithersburg, MD.

2:45 J6.5

THERMODYNAMIC INTERACTION PARAMETERS OF STEREOREGULAR PMMA, James M. O'Reilly, Eastman Kodak Company, Corporate Research Laboratories, Rochester, NY; Hsinjin Yang, Eastman Kodak Company, Commercial Systems Information Group, Rochester, NY; and David Teegarden, Eastman Kodak Company, Corporate Research Laboratories, Rochester, NY.

3:00 BREAK

3:15 *J6.6

STRUCTURE AND DYNAMICS OF GLASSES AND LIQUIDS, David L. Price, Argonne National Laboratory, Materials Science Division, Argonne, IL.

3:45 J6.7

CROSSOVER IN THE VIBRATIONAL DENSITY OF STATES OF SILICA AEROGELS STUDIED BY HIGH-RESOLUTION NEUTRON SPECTROSCOPY, H. Conrad, Argonne National Laboratory, Materials Science Division, Argonne, IL; R. Schatzler, Institut für Festkörperforschung der KFA Jülich, Jülich, West Germany; and J. Fricke and G. Reichenauer, Physikalisches Institut der Universität Würzburg, Am Hubland, Würzburg, West Germany.

4:00 J6.8

VIBRATIONAL EXCITATIONS OF WEAKLY CONNECTED SOLIDS, D.W. Schaefer, C.J. Brinker, and C.S. Ashley, Sandia National Laboratories, Albuquerque, NM; D. Richter and B. Farago, Institute Laue-Langevin, Grenoble, France.

4:15 J6.9

VIBRATIONAL SPECTRA FOR HYDROGENATED AMORPHOUS SEMICONDUCTORS, W.A. Kamitakahara, R. Biswas, A.M. Bouchard, Iowa State University, Ames Laboratory and Microelectronics Research Center, Ames, IA; F. Gompf and J.B. Suck, Kernforschungszentrum Karlsruhe, INFP, Karlsruhe, West Germany.

4:30 J6.10

INELASTIC NEUTRON SCATTERING STUDIES OF NONLINEAR OPTICAL MATERIALS: p-NITROANILINE ADSORBED IN ALPO-5, Jacqueline M. Nicol, University of Maryland, College Park, MD and National Institute of Standards and Technology, Reactor Radiation Division, Gaithersburg, MD.

4:45 J6.11

DIFFUSE NEUTRON SCATTERING FROM EXCESS OXYGEN IN $UO_{2.13}$, J.P. Goff and M.T. Hutchings, Harwell Laboratory, Materials Physics and Metallurgy Division, Didcot, United Kingdom; and W. Hayes, Clarendon Laboratory, Oxford, United Kingdom.

5:00 J6.12

COMPARISON OF NEUTRON ELASTIC AND INELASTIC SCATTERING FROM FUSED QUARTZ, CAB-O-SIL AND AEROGEL, John H. Root, William J.L. Buyers, Atomic Energy of Canada Ltd., Chalk River, Canada; John H. Page, University of Manitoba, Winnipeg, Canada; Dale W. Schaefer and C.J. Brinker, Sandia National Laboratories, Albuquerque, NM.

SESSION J7: POLYMERS AND DISORDERED MEDIA

Chair: T. P. Russell

Thursday Morning, November 30

Yarmouth/Vineyard (M)

8:30 J7.1

STUDY OF THERMAL EXPANSION OF GRAPHITE AND HNO₃-GIC BY NEUTRON DIFFRACTION, Haim Pinto, Mordechai Melamud, and Hagai Shaked, Negev Nuclear Research Centre, Beer-Sheva, Israel.

8:45 J7.2

CHARACTERIZATION OF SOL-CLAY COMPOSITES BY SMALL-ANGLE NEUTRON SCATTERING, Ahmad Moini and Thomas J. Pinnavaia, Michigan State University, Department of Chemistry and Center for Fundamental Materials Research, East Lansing, MI; and P. Thiyagarajan, Argonne National Laboratory, IPNS Division, Argonne, IL.

9:00 J7.3

NEUTRON SCATTERING STUDY OF LAYERED SILICATES PILLARED WITH MULTIMETHYLAMMONIUM IONS, D.A. Neumann, J.J. Rush, National Institute of Standards and Technology, Reactor Radiation Division, Gaithersburg, MD; J.M. Nicol, National Institute of Standards and Technology, Reactor Radiation Division, Gaithersburg, MD and University of Maryland, College Park, MD; Y.B. Fan, H. Kim, S.A. Solin, T.J. Pinnavaia, Michigan State University, Department of Physics, East Lansing, MI; N. Wada, Colorado School of Mines, Department of Physics, Golden, CO; and S.F. Trevino, National Institute of Standards and Technology, Gaithersburg, MD and ARDEC, Picatinny Arsenal, NJ.

9:15 J7.4

OBSERVATION OF MICELLAR FORMATION IN THE CAVITY OF POROUS SILICA GLASS, Kenneth Bradley, Argonne National Laboratory, Argonne, IL; Sow-Hsin Chen, Massachusetts Institute of Technology, Nuclear Engineering Department, Cambridge, MA; and Pappannan Thiyagarajan, Argonne National Laboratory, Argonne, IL.

9:30 J7.5

ANALYSIS OF SANS FROM CONTROLLED PORE GLASSES, N.F. Berk, C.J. Glinka, W. Haller and L.C. Sander, National Institute of Standards and Technology, Gaithersburg, MD.

9:45 J7.6

CHARACTERIZATION OF CHEMICALLY MODIFIED PORE SURFACES BY SMALL ANGLE NEUTRON SCATTERING, C.J. Glinka, L.C. Sander, N.F. Berk and W. Haller, National Institute of Standards and Technology, Reactor Radiation Division, Gaithersburg, MD.

10:00 BREAK

10:15 J7.7

PRECURSOR MORPHOLOGY AND MICROSTRUCTURE EVOLUTION IN POROUS SILICA BY SMALL ANGLE SCATTERING, G.G. Long, S. Krueger, D.R. Black, and J.P. Cline, National Institute of Standards and Technology, Gaithersburg, MD; R.A. Gerhardt, Rutgers University, Piscataway, NJ; and P.R. Jemian, Northwestern University, Evanston, IL.

10:30 J7.8

SMALL ANGLE NEUTRON SCATTERING STUDY OF CRITICAL BINARY FLUIDS IN POROUS GLASSES, S.B. Dierker and P. Wiltzius, AT&T Bell Laboratories, Murray Hill, NJ.

10:45 J7.9

SMALL ANGLE NEUTRON SCATTERING STUDY OF SOL-GEL GLASSES, P. Wiltzius and S.B. Dierker, AT&T Bell Laboratories, Murray Hill, NJ.

11:00 J7.10

USE OF NEUTRON DIFFRACTION AND RIETVELD ANALYSIS TO STUDY THE BEHAVIOR OF NEUTRON IRRADIATED URANIUM SILICIDES, R.C. Birtcher, M.H. Mueller, J.W. Richardson Jr., Argonne National Laboratory, Materials Science Division, Argonne, IL; and J. Faber Jr., Amoco Research Center, Naperville, IL.

11:15 J7.11

HELIUM DENSITIES IN BUBBLES PRODUCED IN IRRADIATED NICKEL MEASURED BY SMALL ANGLE NEUTRON SCATTERING, Q. Li, HMI Berlin GmbH, Metallische Werkstoffe, Berlin, West Germany; D. Schwahn, H. Schroeder, W. Kesternich, and H. Ullmaier, KFA Jülich GmbH, Institut für Festkörperforschung, Jülich, West Germany.

11:30 J7.12

SURFACE EVAPORATION IN A POLYMER MIXTURE OF LONG AND SHORT CHAINS, Russell J. Composto and Richard S. Stein, University of Massachusetts, Polymer Research Institute, Amherst, MA; G.P. Felcher, A. Mansour, and A. Karim, Argonne National Laboratory, Argonne, IL.

11:45 J7.13

TRANSESTERIFICATION KINETICS OF A MAIN CHAIN AROMATIC POLYESTER, W. A. MacDonald, ICI Advanced Materials, Materials Research Centre, Cleveland, United Kingdom; G. McLean, A.D.W. McLenaghan, and R.W. Richards, University of Strathclyde, Department of Pure and Applied Chemistry, Glasgow, United Kingdom.

12:00 J7.14

SANS STUDY OF CAPILLARY CONDENSATION IN PORUS MEDIA, M.Y. Lin, National Institute of Standards and Technology, Gaithersburg, MD, and Princeton University, Department of Physics, Princeton, NJ; S.K. Sinha, J.S. Huang, B. Abeles and J.M. Drake, Exxon Research and Engineering Company, Annandale, NJ.

J1.1

NEUTRONS: THE KINDER, GENTLER PROBE OF CONDENSED MATTER. John D. Axe, Brookhaven National Laboratory, Upton, NY.

Neutrons are a nearly ideal structural probe of bulk condensed matter. They are electrically neutral, penetrate deeply and interact weakly (but precisely) with the atomic nuclei. Light atoms and neighboring atoms in the Periodic Table can be readily distinguished. Because neutrons have a magnetic moment, the magnetic arrangement of electrons (and even of nuclei!) can also be probed. Being relatively massive, (unlike x-rays and electrons), neutrons with wave-lengths comparable to interatomic distances have meV rather than keV or eV energies, allowing inelastic scattering studies of phonons, spin waves and other thermal excitations. For areas as diverse as depth profiling and residual stress analysis to the structure of polymers and glasses, neutrons provide unique and indispensable information. This talk will try to provide an overview of the versatility and subtlety of modern thermal neutron scattering techniques, and their present and future role in condensed matter research.

J1.2

NEUTRON SCATTERING INSTRUMENTATION. Roger Pynn, LANSCE, Los Alamos National Laboratory, Los Alamos, NM87545.

Because neutron scattering is a signal-limited technique, specialized instrumentation has been developed to measure various features of the fluctuation spectra of materials. In spite of this diversity, most neutron scattering spectrometers are constructed from a small number of optical elements each of which serves to define either the energy or the trajectory of a neutron beam. A variety of the optical elements which are in use at reactor-based installations and pulsed spallation sources will be discussed in this talk. In addition, I will describe the way in which powder and single-crystal diffraction, small angle scattering, reflectometry and some types of inelastic scattering are carried out in practice at both types of source. I will also consider the limitations which current neutron scattering spectrometers place on our ability to obtain information from the technique. This part of the presentation should permit potential users to better assess whether neutron scattering can contribute to a solution of their research problems.

J1.3

THE ADVANCED NEUTRON SOURCE. John B. Hayter, Solid State Division, Oak Ridge National Laboratory, P.O. Box 2008, Oak Ridge, Tennessee 37831-6393.

The Advanced Neutron Source (ANS) is a new user experimental facility planned to be operational at Oak Ridge in the late 1990's. The centerpiece of the ANS will be a steady-state research reactor of unprecedented thermal neutron flux ($\phi_{th} = 9 \cdot 10^{19} \text{ m}^{-2} \cdot \text{s}^{-1}$) accompanied by extensive and comprehensive equipment and facilities for neutron-based research. The ANS provides the first opportunity in more than two decades to construct a neutron research facility in which the reactor, beamlines and instruments are designed as an optimal integrated package, taking advantage of the many new techniques which have been developed since the advent of the ILL high flux reactor in Grenoble ($\phi_{th} = 1.5 \cdot 10^{19} \text{ m}^{-2} \cdot \text{s}^{-1}$). State-of-the-art facilities will be provided for fundamental and nuclear physics studies, materials irradiation, radioisotope and transuranic element production, and materials analysis, but the primary role of the ANS will be to support neutron scattering for condensed-matter research.

Neutron spectra will be available in all energy ranges of interest to materials science. A hot source ($T > 2000 \text{ K}$) will be instrumented for studies of magnetic and other excitations up to about 100 meV energy transfer, as well as for diffraction, while thermal beams ($T = 320 \text{ K}$) will provide the

best available facilities for conventional neutron scattering studies at the atomic or small-molecule scale. The most extensive instrumentation will be for studies of materials on the nm to μm scale, for example, colloids, polymers, ceramics, alloys and composites. These instruments will be situated in a low-background guide hall, into which beams from two cold sources ($T = 20 \text{ K}$) will be carried by neutron guides. There will be routine provision of neutron polarization analysis, an extremely important technique which to date has suffered from marginal intensity at existing sources. Polarization analysis has obvious applications in all studies of magnetic materials, but it has equally powerful, though less well-known, applications in non-magnetic studies, for example of subtle structural correlation effects in polymers.

J1.4

THE APPLICATION OF NEUTRON TOPOGRAPHY TO THE STUDY OF X-RAY SENSITIVE ORGANIC SINGLE CRYSTALS - A POSSIBLE ALTERNATIVE TO X-RAY TOPOGRAPHY. M. Dudley, Dept. of Materials Science and Engineering, SUNY at Stony Brook, Stony Brook NY.

Neutron topography has been carried out on organic single crystals of varying X-ray sensitivity, in order to test the feasibility of the technique as an alternative to X-ray topography for the study of the influence of defects on the solid state reactivity of X-ray sensitive single crystals. Specimens studied include the diacetylene PTS, and Pyrene. A comparison of the strain sensitivity and spatial resolution of the neutron and X-ray based techniques is made. Preliminary results of dynamic neutron topographic studies of the UV induced polymerization in PTS are presented. These results are compared to those obtained from similar X-ray topographic studies.

Results indicate that the neutron technique is a useful ally technique to the analogous X-ray techniques in studies of the influence of defects on reactivity in specimens of moderate X-ray sensitivity. In cases of extreme sensitivity, the neutron technique is the only one available for studies of this nature.

Synchrotron topography performed in part on beamline X-19C at the NSLS which is funded by DOE under contract # DE-FG02-84ER45098. Neutron topography experiments were performed at ILL, Grenoble, and were funded by the SERC.

J1.5

MULTIPLE SMALL ANGLE NEUTRON SCATTERING CHARACTERIZATION OF THE DENSIFICATION OF ALUMINA. S. Krueger and G.G. Long, National Institute of Standards and Technology (formerly NBS), Gaithersburg, MD; and R.A. Page, Southwest Research Institute, San Antonio, TX.

Multiple small angle neutron scattering (MSANS) was used to characterize the pore evolution of $\alpha\text{-Al}_2\text{O}_3$ sintered to densities ranging from 57 to 99% of theoretical density (TD). When multiple scattering dominates the total scattering cross-section, effective radii for the pore size distributions are obtained by measuring the wavelength dependence of the shape of the scattering curves at low scattering vector. The size regime available to this technique lies between 0.08 and 10 μm , which is the relevant microstructure size range in ceramics, compared to the 1 to 100 nm range generally available with small angle neutron scattering methods.

Conventionally sintered Al_2O_3 samples were studied, and the results indicated an initial decrease in the effective pore radius from 0.19 μm at 57% TD to 0.17 μm at 79% TD. As the sample density further increases, the effective pore radius grows more rapidly to >0.5 μm at 99% TD. Standard Porod analysis on the high angle portion of the

scattering curves shows a gradual increase in the effective pore radius as the sample density increased from 57% to 79% TD, and then a more rapid increase upon further densification. Both results indicated a clear break between the intermediate and final stages of processing. The MSANS and Porod analyses are combined to model the total pore size distribution during each stage of thermal processing.

J1.6

THERMAL DIFFUSE SCATTERING IN NEUTRON TIME-OF-FLIGHT POWDER PATTERNS, Michael J. Radler and Jerome B. Cohen, Department of Materials Science & Engineering, The Technological Institute, Northwestern University, Evanston, IL 60208, and John Faber, Jr., Materials Science Division, Argonne National Laboratory, Argonne, IL 60439

Cation interstitial site occupations at elevated temperatures (1123 to 1673 K) in the nonstoichiometric transition metal monoxides, Co_{1-x}O , Mn_{1-x}O , and Fe_{1-x}O , have been studied with in-situ time of flight neutron powder diffraction. Inelastic scattering from lattice phonons contributes a sizeable fraction of the observed Bragg intensity at large scattering vector, Q . Ignoring this thermal diffuse scattering (TDS) leads to errors in the site occupations and temperature factors. The intensity from one phonon TDS has been calculated as a function of time-of-flight and used to correct the measured intensities. A brief review of the theory and calculation of the TDS spectra will be presented. Examples of calculated TDS spectra for these rocksalt structure oxides and the effect of the correction will be discussed.

J1.7

REAL SPACE METHOD OF POWDER DIFFRACTION FOR NON-PERIODIC AND NEARLY-PERIODIC MATERIALS, T. Egami, B. H. Toby, W. Dmowski, University of Pennsylvania, Philadelphia, PA; Chr. Janot, Institut-Langevin, Grenoble, FR; J. D. Jorgensen, Argonne National Laboratory, Argonne, IL

A large number of materials are either non-crystalline or are strongly deviated from perfect periodicity. If we apply a crystallographic method of structural analysis to these materials we have to make an awkward assumption of pseudo-periodicity, since these analyses rely heavily upon the assumption of periodicity. Instead, however, it is most useful to go through an intermediate step of obtaining the atomic pair distribution function (PDF) by the direct Fourier transformation of the normalized intensity. This method, the real space method, has been applied so far primarily on non-crystalline materials, but it was shown recently that they are equally effective in analyzing the structure of crystalline solids with internal randomness. We discuss our recent results of the PDF analysis of superconducting oxides carried out using a pulsed neutron source (IPNS) and a hot thermal neutron source (ILL). With the pulsed source the PDF was obtained from the total scattering intensity including both the elastic and inelastic scattering intensities, while with the hot thermal source only the elastic scattering intensity determined by a triple-axis spectrometer was used in calculating the PDF. It was found that high T_c oxides such as $\text{Th}_2\text{Ba}_2\text{CaCu}_2\text{O}_8$ have a significant displacive atomic short range order, which appear to change anomalously with temperature. The displacive ordering lowers the local symmetry, for instance from tetragonal to orthorhombic. The effect of such short range ordering on the superconductivity will be discussed.

J1.8

NEUTRON RIETVELD ANALYSIS OF ANION AND CATION DISORDER IN THE FAST-ION CONDUCTING PYROCHLORE SYSTEM $\text{Y}_2(\text{Zr}_{1-x}\text{Ti}_x)\text{O}_7$, Sossina M. Haile and B. J. Wuench, Department of Materials Science and Engineering, M.I.T., Cambridge, MA, and E. Prince, Reactor Radiation Division, National Institute of

Standards and Technology, Gaithersburg, MD.

The cubic pyrochlore structure type $\text{A}_2\text{B}_2\text{O}_7$, space group $\text{Fd}3\text{m}$, is a superstructure with lattice constant double that of a fluorite-like array of ions. Cations A and B order in positions 16c and 16d; oxygen ions are ordered in 48f and 8a, leaving an anion vacancy (relative to fluorite) at 8b. $\text{Y}_2\text{Ti}_2\text{O}_7$ is a fully-ordered pyrochlore, whereas $\text{Y}_2\text{Zr}_2\text{O}_7$ is fully disordered and statistically has the fluorite structure. Intermediate solid solutions have partial order. Moon and Tuller [*Solid State Ionics* 28-30 (1988) 470] found a progressive increase in ionic conductivity by two and one-half orders of magnitude ($1.6 \cdot 10^{-5}$ to $5.0 \cdot 10^{-3} \text{ ohm}^{-1}\text{cm}^{-1}$ at 1000°C) to accompany the disorder. Powder diffraction patterns obtained with 1.553\AA thermal neutrons have been subjected to Rietveld analysis to permit correlation of ionic conductivity and structure. Typical residuals are $R_{\text{Bragg}} = 2.17\%$, $R_{\text{WP}} = 9.96\%$ and $R_E = 7.36\%$. Most of the information on ordering is contained in the superstructure intensities. Identically zero in the disordered fluorite state, the magnitudes of the superstructure intensities are determined by the difference between the scattering length of the cation species which order in the A or B site and the average cation scattering length for a given composition. The scattering length of Ti is negative (-0.3438) relative to values 0.775 and 0.716 for Y and Zr, respectively. The average cation length is consequently small, and the difference between individual and average scattering lengths unusually large. The superstructure maxima are thus as much as three times more intense than the fluorite-type substructure intensities. Neutron scattering is therefore an especially sensitive measure of order in the present system.

J1.9

SMALL ANGLE NEUTRON SCATTERING INVESTIGATIONS OF NANOPHASE Ti, TiO_2 AND Pd, J. E. Epperson, J. W. White*, R. W. Siegel, J. A. Eastman, Y. X. Liao†, and A. Narayanasamy†, Materials Science Division, Argonne National Laboratory, Argonne, IL 60439

The microstructural characteristics of nanophase Ti, TiO_2 and Pd have been investigated by small angle neutron scattering (SANS) techniques. Nanophase particles of Ti and Pd were prepared by evaporation of the respective metal and by condensation in an inert gas atmosphere; for preparation of TiO_2 , oxidation of the nanophase Ti to TiO_2 was carried out in the fabrication apparatus. Particles were collected and compacted into thin disks appropriate for SANS samples. For the TiO_2 and Pd, SANS investigations were carried out after selected sintering anneals in air. For the nanophase Ti, the SANS investigations were carried out after incremental dosing with small, measured amounts of oxygen. The maximum entropy method was used to analyze the sintering data. The results for TiO_2 are interpreted in terms of a microstructural model consisting of nanometer sized grains separated by about 0.5 nm wide boundary regions, the boundary regions containing small voids or pores, and material that was at most some 60-70 percent of the bulk density. Because of the volume expansion upon reaction, oxidation of nanophase Ti resulted in gradual closing of the originally accessible pores. For practical purposes, oxidation at ambient temperature ceased until the protective oxide coating was breached.

J2.1

SURFACES INVESTIGATION BY NEUTRON REFLECTION, A. FARNoux, Laboratoire Léon Brillouin, CEN SACLAY, 91191 GIF-SUR-YVETTE Cedex (France)

Several phenomena analogous to those observed in classical optics, such as reflection, refraction and interferences, are also observed with slow neutrons. Information on surface organisation, described by a refractive index profile, can be extracted from reflection experiments. These information are similar to those obtained by X-rays reflection; however there are some instances where the new neutron method provides a distinct advantage. The refractive index is simply related to the scattering length density, a parameter which describes the neutron-matter interaction. Due to the magnetic interaction, magnetic materials have a neutron spin dependent refractive index, and a critical reflection of polarised neutrons is a particularly sensitive probe of surface magnetism. On the other hand, in contrast

to X-rays, neutron scattering length values vary randomly from element to element; isotopic substitution can then produce large contrast in the scattering length density. Of particular importance is the large difference between hydrogen and Deuterium. This is used with a distinct advantage to study many problems in surface chemistry, particularly in the polymer field.

J2.2

VIBRATIONAL SPECTROSCOPY OF SURFACE SPECIES: INELASTIC NEUTRON SCATTERING. J. Tomkinson, Rutherford Appleton Laboratory, UK; and G. J. Kearley, ILL, Grenoble, France.

Recent results on the vibrational spectroscopy of adsorbates on catalytically active surfaces shall be presented. These were obtained on the TFXA spectrometer ISIS, UK. This spectrometer covers the molecular vibrational frequency range, 20 to 4000 cm^{-1} , with the highest resolution presently available. The role of model compounds will be included. Calculated neutron spectra, using CLIMAX etc. (with overtones, combinations, and phonon wings) ensures consistent assignments. Spectroscopists now have access to the vibrations of molecules adsorbed on "commercial" catalysts.

J2.3

INTERDIFFUSION OF CADMIUM ARACHIDATE IN LANGMUIR-BLODGETT FILMS.

P. Stroeve, J.F. Rabolt IBM-ARC, R.O. Hilleke, G.P. Felcher, Argonne National Laboratory and S.H. Chen, MIT

The interdiffusion of Cadmium Arachidate (CdA) in Langmuir-Blodgett films has been studied by neutron reflection at the Intense Pulsed Neutron Source. One of the samples consisted of a few layers of perhydro H-CdA deposited on a silicon support, overlaid with a few layers of perdeutero D-CdA, for a total thickness of ~300 Angstroms. In a second sample the layers of perhydro- and perdeutero- CdA were separated by two monolayers of H-n-octadecene /co-maleic acid copolymer. When heated for 15 minutes at 70° C, well below the disorder temperature¹, approximately 25% of the D-CdA molecules were replaced by H-CdA molecules, although the overall Langmuir-Blodgett film structure is known to remain unchanged¹. The presence of copolymer layers limited the interdiffusion process to about 5%.

J2.4

NEUTRON REFLECTIVITY STUDY OF GD-Y INTERFACE J.F. Ankner and H. Zabel, University of Illinois at Urbana-Champaign, Urbana, IL; D.A. Neumann and C.F. Majkrzak, National Institute of Standards and Technology, Gaithersburg, MD; and A. Matheny, J.A. Dura, and C.P. Flynn, University of Illinois at Urbana-Champaign, Urbana, IL.

In recent years, there has been a great deal of interest in surface, interface, and thin film magnetism. Using neutron reflectometry and grazing-angle diffraction, one can determine the magnetic structure of surface and subsurface layers in these types of systems. We have studied, using spin-polarized neutron reflectometry, the interface between Y(0001) and Gd(0001) single-crystal films grown by molecular-beam epitaxy (MBE). Bulk gadolinium is a ferromagnet with $T_c = 293\text{K}$. Below T_c , we observe, as expected, that the Gd layer, except for the

region near the Y interface, exhibits a uniform magnetic moment. We will compare the depth-dependence of the magnetization at the Y interface with the chemical interdiffusion as determined by x-ray reflectometry. Weller, et al. have observed a surface magnetic moment above T_c on Gd(0001) films in vacuum.¹ We have searched for such a state at $T=295\text{K}$ and find, within experimental uncertainty, no net moment at the Gd-Y interface. This result is in agreement with results obtained for Gd-Y superlattices studied by polarized neutron diffraction and suggests that the Gd-Y interface is indeed different than the surface of Gd in vacuum. We will also discuss complementary grazing-angle neutron diffraction experiments.

J2.5

NEUTRON DIFFRACTION STUDIES OF $\text{Cd}_{1-x}\text{Mn}_x\text{Se}$ EPILAYERS AND ZnSe/MnSe MULTILAYERS. T.M. Giebultowicz, Univ. of Notre Dame, Notre Dame, IN, and National Instit. of Standards and Technology, Gaithersburg, MD; P. Klosowski, Univ. of Notre Dame; J.J. Rhyne, Natl. Inst. of Standards and Technology; N. Samarth, H. Luo, and J.K. Furdyna, Univ. of Notre Dame.

We report neutron diffraction studies of crystallographic and magnetic properties of MBE-grown $\text{Cd}_{1-x}\text{Mn}_x\text{Se}$ epilayers and ZnSe/MnSe superlattices. Unlike bulk $\text{Cd}_{1-x}\text{Mn}_x\text{Se}$ crystals which exist only in the wurtzite structure up to $x=0.50$, epilayers grown on (100) GaAs can be obtained in the zinc-blende type form with x as high as $x \leq 0.75$ (with thicknesses up to 1.5 μm). In ZnSe/MnSe multilayers, the MnSe and the ZnSe layers grow both in the zinc-blende structure, although bulk MnSe forms only NaCl-type crystals. We have investigated superlattices containing 100-200 ZnSe/MnSe bilayers with thicknesses 60-105 Å and MnSe layer thicknesses 22-49 Å. Nuclear diffraction patterns from the multilayers exhibit a number of satellite lines well resolved from the GaAs Bragg reflections, in good agreement with theoretical calculations. At low T we have observed additional diffraction maxima, clearly indicating an antiferromagnetic Type III spin structure in the MnSe layers. The positions of the magnetic peaks show that there is a significant tetragonal distortion these layers. In contrast, diffraction data from the $\text{Cd}_{1-x}\text{Mn}_x\text{Se}$ epilayers showed no such distortion, despite the rather large lattice mismatch (~5%) between the epilayer material and the GaAs substrate. Broadening of the nuclear reflections shows, however, that the mismatch produces a considerable strain in the epilayers. In samples with $x=0.70$ and 0.75 at low T we have observed Type III diffraction maxima with no excess width, indicating the existence of a long-range antiferromagnetism which has never been observed in any other material from the $\text{Al}_{1-x}\text{Mn}_x\text{B}$ class.

J2.6

LOCAL ENVIRONMENTAL EFFECTS IN MAGNETIC ALLOYS AND MULTILAYERS: CALCULATIONS OF THE STATIC RESPONSE FUNCTIONS. D.D. Johnson, Sandia National Laboratories, Livermore, CA; J. B. Staunton, University of Warwick, Coventry, U.K.; B. L. Györfy, University of Bristol, Bristol, U.K.; F. J. Pinski, University of Cincinnati, Cincinnati, OH; G. M. Stocks, Oak Ridge National Laboratory, Oak Ridge, TN.

We present results of first-principles calculations of 'local' response functions in magnetic alloys, such as the change in the local magnetic moments, or hyperfine fields, due to changes in the local chemical environment. These response functions, which may be directly compared to neutron-scattering experiments, are derived via a mean-field statistical mechanical description of compositional fluctuations in alloys. The thermal averages are performed via the Korringa-Kohn-Rostoker coherent potential approximation, which incorporates the electronic structure of the high-temperature, chemically disordered state. As a first application of the theory, we have investigated FeV alloys and multilayers and compared our results with experiments on multilayers and a set of first-principle 'supercell' calculations. All experimental trends for the magnitude of the moments and the effects of the interface and interfacial alloying are reproduced, and there is good quantitative agreement with the 'supercell' calculations. These results suggest the utility of these response functions for investigating the effects of changes in the chemical environment on the

alloy moments and for aiding experimental interpretation in other multilayer systems that are less experimentally amenable than FeV.

J2.7

DETERMINATION OF HYDROGEN DENSITY PROFILES IN THIN FILMS AND MULTILAYERS BY NEUTRON REFLECTION. C.F. Majkrzak, S. Satija, D. Neumann, J. Rush, D. Lashmore, C. Johnson, NIST, Gaithersburg, MD; J. Bradshaw, Optoline, Andover, MA; L. Passell, R. DiNardo, BNL, Upton, NY

The density of hydrogen in thin films or multilayers of metal hydrides can be inferred from an expansion of the host lattice as measured by conventional x-ray diffraction techniques. However, because hydrogen and deuterium have scattering lengths for neutrons that are comparable to those of most metal nuclei, unlike the corresponding case for x-ray atomic scattering amplitudes, the hydrogen density profile normal to the surface of a flat, thin film can be determined directly from neutron reflectivity measurements. The hydrogen density modulation in an artificial superlattice along the growth direction can also be determined in this manner. Furthermore, the thin films or multilayers need be neither crystalline nor metallic: for example, the H composition profile in a H-Si superlattice created by chemical vapor deposition can be obtained by neutron reflection.

Often hydrogen can be loaded into a film or multilayer in either a gas cell or electrolytically, in situ, thereby making possible real time measurements of hydrogen concentration profiles in active electrodes. The latter configuration can be realized in practice by using a single crystal substrate (e.g., silicon), which is nearly transparent to neutrons, as the incident medium. The sensitivity of this method will be discussed and the results of specific measurements on several materials, including a Ni-Ti multilayer electrolytically charged with H and D, will be reported.

J2.8

MAGNETOELASTIC EFFECTS IN RARE-EARTH MULTILAYERS AND FILMS. R.W. Erwin, J.J. Rhyne, National Institute of Standards and Technology, Gaithersburg, MD; J. Borchers, R. Du, M.B. Salamon and C.P. Flynn, University of Illinois at Urbana-Champaign, Urbana, IL.

Neutron scattering and SQUID magnetometry studies of [Dy|Y] and [Er|Y] multilayers and Dy and Er films have provided insight into the interplay of magnetoelastic and exchange interactions in rare-earths as the magnetic structures are strongly perturbed by elastic constraints. We are now able to show that the suppression of the ferromagnetic transitions and the temperature dependence of the turn angles can be calculated for the Dy materials by applying epitaxial conditions to the standard theories. Quantitative calculations are also in agreement with the observed critical fields in these materials. However, the energetics determining the magnetic structure in Er films and multilayers cannot be explained by magnetoelasticity alone, since anomalous critical fields have been reported by Borchers et al.¹ The turn angle in the Er multilayers is nearly temperature independent near the $2\pi/7$ lockin value, while in the thin films the turn angles move closer to the bulk values. There is also a 30%-50% reduction of the basal plane ordering temperatures compared to bulk Er.

J2.9

THE MORPHOLOGY OF SYMMETRIC DIBLOCK COPOLYMERS AS REVEALED BY NEUTRON REFLECTIVITY. S.K. Satija and C.F. Majkrzak, National Institute of Standards and Technology, Gaithersburg, MD 20899; S.H. Anastasiadis and T.P. Russell, IBM Research Division, Almaden Research Center, San Jose, Ca

We report neutron reflectivity (NR) studies on thin films of polystyrene/polymethylmethacrylate (PS/PMMA) diblock copolymers. Due to chemical differences of the constituent blocks and the different interactions of the blocks with the air and substrate interfaces, these thin films, once heated above the glass transition temperature, form a multilayer morphology. NR studies were made on a series of symmetric, diblock PS/PMMA copolymers where the molecular weight of the individual blocks was varied from 15,000 to 150,000. All specimens were heated to 170°C for at least 72 hours to achieve full orientation of the microdomains and reach equilibrium. It was found that the long period, characterizing the center-to-center distance of the PMMA lamellae, varied as $N^{0.65}$. It was also found that the interface between the PS and PMMA microdomains was 47 ± 4 Å independent of the molecular weight of the copolymers. In addition, the interface between PS and PMMA homopolymers was found to be 47 Å. In all cases, a hyperbolic tangent function closely described the variation in the composition across the interface. While the functional form of the interface and its invariance with molecular weight are consistent with theoretical predictions, the magnitude of the interface measured is nearly twice the theoretical value derived from the statistical segment lengths of and the interaction parameter between the PS and PMMA. This discrepancy points to a misunderstanding of current ideas on the interfacial behavior of copolymers.

J2.10

NEUTRON REFLECTIVITY STUDY OF THE ORDER-DISORDER TRANSITION IN THIN FILM DIBLOCK COPOLYMER FILMS. S.H. Anastasiadis and T.P. Russell, IBM Research Division, Almaden Research Center, San Jose, CA; S.K. Satija and C.F. Majkrzak, National Institute of Standards and Technology, Gaithersburg, MD.

Symmetric, diblock copolymers undergo a transition from an ordered, lamellar microdomain morphology to a phase mixed morphology at the microphase separation transition temperature (MST). The MST corresponds to the temperature at which $\chi N = 10.5$ where χ is the binary, Flory-Huggins interaction parameter and N is the number of segments in the copolymer. In the ordered state symmetric, diblock copolymers of polystyrene and polymethylmethacrylate (PS/PMMA) are known to produce a lamellar morphology oriented parallel to the substrate surface. In the disordered state the oscillations in the composition of PS and PMMA as a function of distance from the interface (air or substrate) are exponentially damped. In this study the order-disorder transition in thin films of PS/PMMA diblock copolymers was investigated by variation of temperature or molecular weight of the copolymer. Either will produce a change in χN . Neutron reflectivity profiles from films of these copolymers are well described by a scattering length density profile where the volume fraction of the PS or PMMA as a function of the distance, z , from air or substrate interface is given by $\bar{\phi} + \phi_E \exp(-z/\xi)$

$\cos^2(2\pi z/L)$ where L is the period of the oscillations, $\bar{\phi}$ is the average composition, ϕ_E is the excess surface concentration and ξ is the correlation length. Slight changes in L were found with increasing temperature and ξ was found to decrease markedly with increasing temperature. It was found, regardless of the molecular weight copolymer, that ξ^{-1} varied linearly with $((\chi N)_s - (\chi N))^{1/2}$ where $(\chi N)_s$ is the value of χN at the MST. Thus, at the MST, ξ is infinite and the ordered morphology propagates through the entire thickness of the specimen as observed. These results are in very good agreement with recent theoretical arguments.

J2.11

THE STUDY OF SURFACES AND INTERFACES ON THE REFLECTOMETER CRISP AT THE ISIS PULSED NEUTRON SOURCE. J Penfold
Rutherford Appleton Laboratory, Chilton, Didcot, Oxon, UK

The study of surfaces and interfaces using the specular reflection of neutrons on the reflectometer CRISP at the ISIS pulsed neutron source is described.

The instrumentation and recent developments in analysis techniques are described.

A wide ranging experimental programme is now well established. Examples from that programme will be presented, and will include surfactant adsorption at the air-liquid and liquid-solid interfaces, solid polymer films, and surface magnetism.

J3.1

MARTENSITIC PHASE TRANSITIONS, PHONONS AND DIFFUSION PROPERTIES IN BCC METALS. W. Petry, Institut Laue-Langevin, 156X, 38042 Grenoble Cedex, France.

Phonon spectroscopy on in situ grown bcc single crystals of the group 4 metals Ti, Zr, Hf show a band of low energy and strongly damped phonons. Geometrical considerations show how these damped lattice vibrations achieve the displacements necessary for the two martensitic phase transitions from bcc to ω (under pressure) and from bcc to hcp (upon lowering the temperature). Different to theoretical predictions, no elastic precursors of the new phase are observed.

Quasielastic incoherent neutron scattering indicates in a very direct way that diffusion in these metals takes place via jumps into nearest neighbor vacancies. These diffusion jumps are strongly enhanced by the soft phonons. Following an idea of Herzig and Köhler it is shown that this model of phonon enhanced diffusion explains the diffusion anomalies of all bcc metals.

J3.2

STRESS DEPENDENCE OF THE SOFT PHONON BRANCH IN MARTENSITICALLY TRANSFORMING $\text{Ni}_{62.5}\text{Al}_{37.5}$ S. M. Shapiro, Brookhaven National Laboratory*, Upton, NY 11973.

In the alloy $\text{Ni}_{62.5}\text{Al}_{37.5}$, which exhibits a Martensitic transformation near $T_M=80\text{K}$, the $[\zeta\zeta 0]$ transverse phonon branch with polarization along the $[110]$ shows a considerable amount of softening as T_M is approached. In particular, a minimum in the dispersion curve occurs near $\zeta=1/6$. Accompanying this softening is intense diffuse elastic scattering which peaks at the same wave vector. Recent inelastic neutron scattering experiments with applied uniaxial stress have shown that when the stress is applied along the $[001]$ direction, perpendicular to the soft direction, additional softening occurs. In addition the diffuse scattering also changes. Results of measurements along other branches and temperature dependence will also be presented.

J3.3

POLARIZATION RELAXATION OF THE FERROELECTRIC KD_2PO_4 USING NEUTRON SCATTERING. Ron Edge, Dept. of Physics, USC, Columbia, SC; and Vicki Homer, Dept. of Physics, USC, Columbia, SC.

Previously, the polarization switching of KD_2PO_4 was studied using ESR. This required the use of crystals doped with arsenic and then irradiated with x-rays, to create the necessary paramagnetic centers. For such crystals, back-relaxation was determined to be insignificant.

We have used the single crystal time-of-flight neutron scattering facility at Argonne to observe the polarization behavior of pure KD_2PO_4 , for crystals cooled below the Curie point. Initial studies of the splitting of appropriate Bragg peaks show clearly the four domain types, and their response to applied electric fields. As opposed to crystals prepared for ESR work, the pure crystals display strong back-relaxation, indicating that the kinetics of polarization reversal differs significantly for the pure crystals.

Complementary studies of changes in the low frequency dielectric constant as a function of polarization level explore further the difference in polarization behavior between pure and treated KH_2PO_4 and KD_2PO_4 .

J3.4

PHASE DEVELOPMENT OF AN AL-TI COMPOSITE DURING HEATING UP TO 1400°C . H.-G. Brokmeier, Department of Physical Metallurgy TU Clausthal and GKSS Research Center, Postfach 1160, D-2054 Geesthacht, FRG; M. Klatt, GKSS Research Center, Postfach 1160, D-2054 Geesthacht, FRG; and C. Ritter, Insitute Laue Langevin, 156X Centre de tri, 38042 Grenoble Cedex, France

In the system Al-Ti several intermetallic compounds have been observed, see par example Murray (1). The constitution of intermetallic compounds such as $\gamma\text{-TiAl}$ can be realised by two different procedures:

1) arc melting

2) powder metallurgy

In both cases the phase development to reach the phase equilibrium is quite different. But material properties, microstructure and texture will be influenced strongly.

The investigated Al-Ti composite was prepared by powder metallurgical methods and consists of 50 Vol.% Al and 50 Vol.% Ti respectively. By cold extrusion of pure Al and pure Ti no intermetallic compounds were formed. The investigations were carried out in a temperature range between 20°C - 1400°C . The phase determinations were performed at D1B, a powder diffractometer of the ILL in Grenoble, which was equipped with a high vacuum furnace and a linear position sensitive detector (LPSD) in horizontal geometry. Hence, every minute a diffraction pattern can be measured. In that way the kinetic of the phase transformation was obtained. Neutron diffraction was preferred in order to measure a bulk sample for minimizing grain growth effects and the influence of an expected Al loss at the sample surface.

This paper will discuss the path during the Ti-Al phase diagram from the outgoing two-phased Al-Ti composite to the two-phased material at 1400°C which consists of $\gamma\text{-TiAl}$ and $\alpha\text{-Ti(Al)}$.

J3.5

NEUTRON POWDER DIFFRACTION: A POWERFUL MATERIALS RESEARCH TECHNIQUE. W. I. F. David, ISIS Facility, Rutherford Appleton Laboratory, Chilton Didcot, Oxon, UK.

Neutron powder diffraction is a powerful technique that provides a detailed description of moderately complex crystal structures. This is nowhere more apparent than in the area of high temperature superconductors where neutron powder diffraction has provided precise structural and magnetic information, not only under ambient conditions but also at high and low temperatures and high pressures. Outside superconductor research, the variety of materials studied by neutron powder diffraction is equally impressive including zeolites, fast ionic conductors, permanent magnets and materials undergoing phase transitions. Recent advances that include high resolution studies and real-time crystallography will be presented. Future possibilities of neutron powder diffraction will be discussed.

J3.6

NEUTRON SCATTERING STUDY OF THE STRUCTURE OF $\text{Y}_2\text{BaCuO}_{7.8}$ AT 294 K AND 77 K. S.L. Town, B.A. Hunter, R.L. Davis* and K.N.R. Taylor, Advanced Electronic Materials Group, School of Physics, University of New South Wales, P.O. Box 1, Kensington, NSW, 2033, Australia, *Australian Institute of Nuclear Science and Engineering, Private Mail Bag 1, Menai, NSW, 2234, Australia.

Using the high resolution powder diffractometer (HRPD) attached to the HIFAR reactor at the Australian Nuclear Science and Technology Organisation, results have been obtained from $\text{Y}_2\text{BaCuO}_{7.8}$ at both room temperature and 77 K. We present here the data refined using the Rietveld method, illustrating the structure at both room temperature and 77 K to be Pnma, having lattice parameters at room temperature of $a=7.1222\text{\AA}$, $b=12.68\text{\AA}$ and $c=5.61\text{\AA}$.

J3.7

STRUCTURE OF $\text{ErBa}_x\text{Cu}_{1-x}\text{O}_7$ IN THE COMPOSITION RANGE 6.1×7.0 . E. Porschke, P. Meuffels, Institut für Festkörperforschung, KFA Jülich, D-5170 Jülich, F.R.G.; and B. Rupp, Paul Scherrer Institut, Labor für Festkörperforschung, CH-5234 Villigen PSI, Switzerland.

The structure of a series of homogeneous orthorhombic and tetragonal $\text{ErBa}_x\text{Cu}_{1-x}\text{O}_7$ powder samples (6.1×7.0) has been determined by elastic neutron scattering using the Rietveld method of profile refinement. All samples were prepared in the same apparatus by a careful absorption-desorption procedure.

By removing oxygen the cell parameter c expands, while the $\text{Cu}(2)\text{-Cu}(2)$ and the Ba-Ba distances shrink. Accordingly the most significant changes in atomic distances occur between the $\text{Cu}(2)\text{-O}(2,3)$ planes and the $\text{Cu}(1)\text{-O}(4)\text{-Cu}(1)$ chains. With decreasing oxygen content the distance increases and the oxygen $(0,0,z)$ apex atom $\text{O}(1)$ moves closer to the Cu-O-Cu chains going away from the Cu-O planes. The $\text{O}(1)\text{-plane}$ and $\text{O}(1)\text{-chains}$ distances are monotonous functions of the oxygen content, but the concentration dependence of these bonding lengths seems to be much stronger below $x < 6.5$. The change of the interatomic distances can be correlated to the suppression of superconductivity, which in the case of $\text{ErBa}_x\text{Cu}_{1-x}\text{O}_7$ occurs within the orthorhombic phase.

J3.8

NEUTRON POWDER DIFFRACTION STUDY OF THE STRUCTURES OF $\text{La}_{1.9}\text{Ca}_{0.1}\text{Cu}_2\text{O}_6$ AND $\text{La}_{1.9}\text{Sr}_{0.1}\text{Cu}_2\text{O}_6$. A. Santoro and F. Beech, NIST, Reactor Division, Gaithersburg, MD 20899 and R.J. Cava, AT&T, 600 Mountain Ave., Murray Hill, N.J. 07974

The title compounds are structurally isomorphous and their structure can be derived from that of La_2CuO_4 by substituting the layers of composition CuO_2 present in La_2CuO_4 with a block of three layers having composition and sequence $(\text{CuO}_2) - (\text{M/La}) - (\text{CuO}_2)$, where M is either Ca or Sr and M/La indicates that the site may be occupied by an M and/or a La atom. Although the general structural configuration of $\text{La}_{1.9}\text{M}_{0.1}\text{Cu}_2\text{O}_6$ is the same for $\text{M} = \text{Ca}$ or Sr , the distribution of the atoms is different in the two cases. More specifically, in $\text{La}_2\text{CaCu}_2\text{O}_6$ the perovskite-type layers form blocks with sequence $-(\text{CuO}_2) - (\text{Ca}) - (\text{CuO}_2) -$ and these blocks are separated from each other by rock-salt blocks of two layers $-(\text{LaO}) - (\text{LaO}) -$. In $\text{La}_2\text{SrCu}_2\text{O}_6$, on the other hand, the perovskite-type blocks have composition $-(\text{CuO}_2) - (\text{La}) - (\text{CuO}_2) -$ and they are separated by blocks

$-(\text{NO}) - (\text{NO}) -$ where $\text{N} \approx 70\% \text{La} + 30\% \text{Sr}$. The different distribution of atoms in the structure can be easily explained in terms of the ionic radii of the cations.

J3.9

NEUTRON DEPOLARIZATION BY FLUX LATTICES IN HI-T_c MATERIALS. S. J. Pickart, A. C. Nunes and M. L. Crow, University of Rhode Island*, Kingston, RI; and T. R. McGuire, S. Shinde and S.A. Shivashankar, IBM Thomas J. Watson Research Center, Yorktown Heights, NY.

Recently we reported¹ observation of neutron depolarization by a YBaCuO 123 composition below its T_c of 86K. We have further explored this effect as a function of applied field and temperature in 123 material, and observed it in Bi 2212 compositions ($T_c \approx 110\text{K}$) as well. We believe our results reflect flux line lattice behavior and may thus bear on the issue of critical current densities.

Samples, prepared and characterized at IBM, were of various flat-plate shapes of 1 mm thickness. Depolarization was observed only after cooling in a weak field and subsequently applying a larger field (1400 oe). In the 123 sample at 4K depolarization coincided with H_{c1} and showed hysteresis, indicating that flux penetration and pinning are involved. The effect disappeared at 55K, well below T_c , and we speculate that this results from short-scale field inhomogeneities associated with flux lattice melting².

Depolarization has also been observed in samples of Bi 2212 composition at 77K. Two samples with different critical currents were measured, with the degree of depolarization differing slightly. These measurements are currently being extended to 4K to explore more fully the indicated correlation between depolarization and critical current density.

J3.10

USE OF NEUTRON DIFFRACTION IN DETERMINING STRAINS IN HIGH-TEMPERATURE SUPERCONDUCTING COMPOSITES. D. S. Kupperman and J. P. Singh, Materials and Components Technology Division; and J. Faber Jr. and R. L. Hitterman, Materials Science Division, Argonne National Laboratory, Argonne, Illinois 60439

The Intense Pulsed Neutron Source and the General Purpose Powder Diffractometer at Argonne National Laboratory were used to show that neutron diffraction techniques can be applied to YBCO/Ag composites to measure bulk residual strains in the constituent parts. We have observed residual tensile strains in Ag as a function of crystallographic direction: three strains range from as high as 0.085% in 15% Ag samples to as low as about 0.02% in a 30% Ag sample. Compressive strains in the YBCO (111) crystallographic direction were approximated by correcting for the diffraction peak shift due to changes in stoichiometry with varying Ag content. The estimated compressive-strain values vary from 0.04% (15% Ag) to 0.09% (20% Ag) to 0.01% (30% Ag), with an uncertainty of about 0.03%. The decrease in strain in YBCO for the 30% Ag composite is consistent with the decrease in Ag strain and may be due to microcracking of the composite or to inhomogeneities in the distribution of YBCO and Ag . *Work supported by the U.S. Department of Energy, Office of Energy Storage and Distribution, Conservation and Renewable Energy, under Contract W-31-109-Eng-38. This work has benefited from the use of the Intense Pulsed Neutron Source at Argonne National Laboratory.

J3.11

HIGH RESOLUTION NEUTRON POWDER DIFFRACTION STUDIES OF THE FERROELASTIC PHASE TRANSITION IN LaNbO_4 . W I F David, Rutherford Appleton Laboratory, Chilton, Didcot, Oxon, UK

Many diffraction patterns obtained on very high resolution diffractometers ($\Delta d/d < 0.001$) reveal a rich variety of sample-dominated line broadening. Most existing analyses treat these effects as isotropic. However, in a substantial number of cases observed on the high resolution powder diffractometer (HRPD) at ISIS, the hkl-dependence of the peak broadening is complex and initially unknown. In this poster a modification of the traditional Rietveld method is presented that permits simultaneous analysis of the crystal structure and the hkl-dependent broadening in a model-independent manner. The principal difference is that all peak widths may be refined as independent variables. Structural parameters may thus be obtained that are unbiased by an imposed peak-broadening model, and the refined peak widths may be examined to determine the origin of the sample-dependent broadening

High-resolution neutron powder diffraction data were collected at a series of temperatures from a 1 cm sample of LaNbO_4 on HRPD at ISIS. The data collected at temperatures around the phase transition showed significant broadening, particularly of some hkl reflections. Use of the refinement method described above yielded significantly superior profile fitting. Analysis of the peak broadening indicated a broadening mechanism dominated by strain. Incorporating a second rank strain tensor description of peak broadening into our Rietveld code revealed that the strain broadening principal axes were collinear with the principal axes of the ferroelastic strain tensor. This unexpected result is discussed within the context of the mechanism of the ferroelastic phase transition.

J4.1

LATTICE DEFECTS STUDIED BY DIFFUSE NEUTRON SCATTERING. J. Peisl, Sektion Physik, LM Universität, München, FRG.

Deviations from the regular arrangement of atoms in solids give rise to a diffuse scattered intensity between the Bragg peaks. Lattice vibrations cause an inelastic contribution which can be experimentally separated in a purely elastic neutron scattering experiment. Crystal lattice defects lead to an elastic diffuse scattering. It contains information on point defects and small clusters. The defect structure, i.e. the lattice location, the displacements of the near neighbours, the strength and the symmetry of the long ranged displacement field can be determined. Also defect correlations occurring on formation of defect-pairs, trapping of defects or generally non-random defect concentration distributions can be deduced.

The strength and the limits of this type of investigations will be demonstrated by reporting on experimental results. Light interstitials in bcc metals (Nb, Ta) are located on octahedral sites (O, N) or tetrahedral sites (H, D). Their displacement fields show some peculiarities which will be discussed.

In metal hydrogen systems the lattice distortions induce an indirect elastic interaction between the dissolved hydrogen atoms which is responsible for a novel type of phase transitions. Macroscopic hydrogen density modes as predicted for the new phase have been observed by neutron radiography.

For highly mobile defects the displacement fields have a finite life time which depends on the jump frequency and on the lattice relaxation time. This effect has recently been observed as a quasielastic broadening of the energy width of the diffuse neutron scattering.

J4.2

NEUTRON SCATTERING STUDY OF THE EQUILIBRIUM DEFECT STRUCTURE IN UNDERSTOICHIOMETRIC MnO , D. Schuster, Enka, D-5600 Wuppertal, West Germany; R. Dieckmann, Cornell University, Ithaca, USA; W. Schilling, W. Schweika, IFF-KFA Jülich, D-5170 Jülich, West Germany,

Model calculation [A.M. Stoneham et al. in Physics of Disordered Materials, ed. D. Adler et al, Plenum Publ. Corp (1985) p. 243] predict 4:1-vacancy clusters to dominate - like in $\text{Fe}_{1-\Delta}\text{O}$ - the cation sublattice disorder of $\text{Mn}_{1-\Delta}\text{O}$ at high temperatures. To test this prediction diffuse neutron scattering experiments have been performed on single crystal $\text{Mn}_{1-\Delta}\text{O}$ held at 1400°C under controlled oxygen partial pressures. By changing the oxygen partial pressures deviations from stoichiometry Δ , i.e. cation vacancy concentrations could be fixed to 0.3%, 1.6% and 6.4%. Using time of flight techniques the elastic diffuse scattering could be separated from the inelastic contributions. The differences in the elastic diffuse intensities measured at different values of Δ yield differential scattering cross sections per vacancy for scattering vectors \vec{Q} ranging from 0.1 to 3.5 \AA^{-1} in the (100)- and (211)-lattice plane. Broad maxima of the disorder scattering are observed near $|\vec{Q}| = 1.6 \cdot 2\pi/a$ in the $\langle 100 \rangle$ - and near $|\vec{Q}| = 1.6 \cdot \sqrt{2} \cdot 2\pi/a$ in the $\langle 110 \rangle$ -direction. No increase of the scattering towards small \vec{Q} -values could be detected. The results can be interpreted as the scattering from randomly distributed Mn-vacancies which induce relative displacements of their nearest neighbour O and Mn-ions of +8% and -5% respectively. The presence of larger numbers of vacancy clusters can be excluded.

J4.3

SHORT-RANGE ORDER IN α -BRASS. Leszek Reinhard, ETH Zürich, now at Dept. of Physics, Univ. of Houston, Houston, TX; Bernd Schönfeld, Gernot Kosterz, Angewandte Physik, ETH Zürich, CH-8093 Zürich, and Willi Bührer, LNS der ETH Zürich, CH-5303 Würenlingen, Switzerland.

States of equilibrium in α -brass single crystals of different composition (Cu-31.1 at.% Zn and Cu-22.4 at.% Zn, using the isotope Cu-65 to enhance the scattering contrast) were investigated by elastic diffuse neutron scattering. The scattering contributions due to short-range order and linear atomic displacements were separated by a least-squares fitting procedure.

The short-range order intensity showed four maxima in the (001) plane around the 110 position. These maxima are due to the flat portions of the Fermi surface along the $\langle 110 \rangle$ directions. Fermi vectors deduced from their location are in good agreement with results of positron annihilation experiments. The intensity modulations are smaller for the sample with the lower Zn concentration.

Effective pair potentials were determined based on the approximation-free inverse Monte-Carlo method and the high temperature approximation of Clapp and Moss. A dominant nearest-neighbour interaction is found, and there are no signs of a distinct dependence on Zn concentration. Based on a Monte-Carlo simulation, a low-temperature phase Cu_3Zn with D_{023} structure is suggested.

J4.4

SHORT RANGE ORDER IN CU-ZN: A COMPARISON OF NEUTRON DIFFUSE SCATTERING DATA WITH FIRST PRINCIPLES RESULTS. M. Sluiter, Lawrence Berkeley Laboratory, Berkeley, CA 94720, and Lawrence Livermore National Laboratory, Livermore, CA 94550, P.E.A. Turchi, Lawrence Livermore National Laboratory, Livermore, CA 94550, D.M. Nicholson and G.M. Stocks, Oak Ridge National Laboratory, Oak Ridge, TN 37831-6114, D.D. Johnson, Sandia National Laboratory, Livermore, CA 94550, F.J. Pinski, University of Cincinnati, Cincinnati, OH 45221.

Recently, measurements of short range order (SRO) neutron diffuse scattering intensity have been performed on quenched Cu-Zn alloys with 22.4 to 31.1 at. % Zn and pair interactions were obtained by Inverse Monte Carlo simulation [1]. These results will be compared to SRO intensities and effective pair interactions obtained from first-principles electronic structure calculations. The theoretical interactions were obtained with the KKR-CPA-Generalized Perturbation Method (GPM). The theoretical SRO intensities were calculated with the Cluster Variation Method in the tetrahedron-octahedron approximation with first-principles pair interactions as input. More generally, phase stability in the Cu-Zn alloy system, using the energetic properties obtained with the KKR-CPA-GPM, will be discussed.

J4.5

ORDERING MECHANISM IN SUBSTITUTIONAL Ni-Cr ALLOY: EXPERIMENTS AND THEORY. P.E.A. Turchi, R.H. Howell, A.L. Wachs, M.J. Fluss, LLNL, Livermore, CA; F.J. Pinski, University of Cincinnati, OH; D.M. Nicholson and M.G. Stocks, ORNL, Oak Ridge, TN; W. Schweika, IFKJ, Jülich, FRG.

Recent measurements of short range order (SRO) - Diffuse neutron scattering intensity have been performed on quenched Ni-Cr alloys in the range 11 to 25 at. % in Cr [1]. Typical behavior of the pair interactions, as obtained from Inverse Monte-Carlo simulations, strongly indicates the existence of a well defined flat sheet of the Fermi surface, primarily normal to the $\{110\}$ direction. These results are compared with first principles KKR-CPA band structure calculations of the Bloch spectral function as well as effective pair interactions deduced from the Generalized Perturbation Method. Furthermore, two-dimensional angular correlation of positron annihilation radiation measurements allow us to investigate the fermiology of this alloy system and confirm the above results. Hence, we prove the major role played by specific features of the Fermi Surface in driving SRO in disordered alloys and establish a clear connection between neutron scattering, positron annihilation spectroscopy and theoretical investigations of ordering processes in substitutional alloys.

J4.6

PHONON DISPERSION IN THE ALLOY $\text{Cu}_{0.85}\text{Al}_{0.15}$. Henry Chou, S. M. Shapiro, Brookhaven National Laboratory, S. C. Moss, University of Houston, and M. E. Mostoller, Oak Ridge National Laboratory.

X-ray scattering¹ revealed diffuse satellites which were attributed² to screening singularities associated with parallel flat sections of the Fermi surface, in analogy with Kohn anomalies. We have confirmed the elastic nature of this scattering with neutrons and made detailed measurements of phonon dispersion curves on a large single crystal of $\text{Cu}_{0.85}\text{Al}_{0.15}$ at room temperature. Phonon frequencies were ascertained to better than ± 0.03 meV but no clear anomaly was observed near the expected wave vector $q=2k_F$. Near the zone boundaries the phonon energies were significantly lower than the corresponding phonons in pure Cu. This is attributed to mode repulsion from high frequency localized vibrational modes of the Al atom in the Cu host lattice³.

Inter-atomic force constants and vibrational density of states were obtained by performing a Born-von Karman analysis on the complete set of phonon dispersion curves. Implication of these results on the short range order in this alloy will be discussed.

J4.7

COMPOSITION AND TEMPERATURE DEPENDENCE OF THE SHORT RANGE ORDER DIFFUSE SCATTERING IN $\text{Al}_x\text{Ag}_{1-x}$ ALLOYS.* G. M. Stocks and D. M. Nicholson, Oak Ridge National Laboratory, Oak Ridge, TN; F. J. Pinski, University of Cincinnati, Cincinnati, OH; J. B. Staunton, University of Warwick, United Kingdom; D. D. Johnson, Sandia National Laboratory, Livermore, CA; and B. L. Gyorffy, University of Bristol, United Kingdom.

We show results of calculations for the temperature and composition dependence of the short range order (SRO) diffuse scattering in $\text{Al}_x\text{Ag}_{1-x}$ solid solutions. The calculations are based on the ab initio concentration functional theory of Gyorffy and Stocks. The complex temperature and concentration dependence of the diffuse scattering argues for experimental studies of the SRO at temperature in the Al-rich solid solution phase in order to confirm the suggestions that the origin of Guinier-Preston zone formation in these alloys lies in concentration rather than displacement fluctuations.

J4.8

PHASE DIAGRAMS AND DIFFUSE NEUTRON SCATTERING R. Caudron, F. Solal and A. Finel, ONERA, B.P.72, 92322 Chatillon (France)

The order properties of compounds or solid solutions are important ingredients of the phase diagrams. For alloys of normal and transition metals, they can be described in terms of interaction potentials between the atomic species present in the alloys. Within this framework, phase diagram should be deducible from these potentials. In our laboratory, calculation techniques, using tight binding, C.P.A. and G.P.M. approximations have been developed to deduce interaction potentials from the electronic structure of the alloys. These techniques are valid for transition metal alloys, being based on the tight binding method. Experimentally, our purpose is to obtain interaction potentials through the measurements of the short range order parameter, in order to check them against the calculated orders of magnitude and, ultimately, to build phase diagrams. As an example, we describe our diffuse neutron scattering measurements at high temperature on single crystals of Ni_3Cr , Pd_3V and Ni_3V . The latter alloys exhibit a first order transition from the disordered FCC solid solution to DO_{22} , a FCC based superstructure. For each sample at each temperature, we explored the (100) and the (110) planes of the reciprocal space, and we submitted the intensities measured to a linear least squares fitting procedure, using a model including short range order parameters $\alpha(R)$ and first order displacement parameters. For Ni_3V and Ni_3Cr , the diffuse maxima occur at the expected $(1\frac{1}{2}0)$ positions, as the ordered state is DO_{22} . For Pd_3V , they surprisingly occur at (100) positions: the mean field theory leads to a correct prediction for Ni_3V and Ni_3Cr , but not for Pd_3V : we present better thermodynamical models (C.V.M and Monte Carlo simulations), yielding potentials and transition temperatures

J4.9

DIFFUSE NEUTRON SCATTERING STUDY OF THE SHORT-RANGE ORDER IN Fe 20at% Al ALLOY. Werner E. Schweika, KFA Jülich GmbH, Institut für Festkörperforschung, 5170 Jülich, FRG

The short-range order in a Fe 20at% Al single crystal has been studied as a function of the temperature in the ferromagnetic and paramagnetic phases by diffuse neutron scattering. The experiments have been performed at the instrument for diffuse neutron scattering (DNS) at the cold

beam of the Jülich research reactor. The energy of the scattered neutrons has been analysed by the time-of-flight method.

Above the Curie temperature T_C a diffuse peak due to short-range order is found at the zone boundary points 100. A least squares analysis yields parameters for short-range order and lattice displacements. Effective pair-potentials are obtained by the inverse Monte Carlo method.

Below T_C the expected usual increase of the 100 peak is not found when the temperature is lowered. Instead the intensity at $\frac{111}{222}$ increases with an onset of long-range ordering below $T \approx 350^\circ\text{C}$. The observed new phase seems to be metastable, since after long annealing finally the intensity of the 100 peak grows as well and the DO_3 structure is formed. The influence of the ferromagnetic interaction on the chemical ordering is discussed.

J4.10

LATTICE MISFIT AND DECOMPOSITION IN NI-AL-MO ALLOYS
Hector Calderon and Gernot Kosterz, Angewandte Physik, ETH Zürich, CH-8093 Zürich, Switzerland.

The effect of lattice mismatch δ between the γ -matrix and γ' -precipitates on the decomposition process of Ni-Al-Mo alloys has been investigated by means of small-angle neutron scattering (SANS) and transmission electron microscopy (TEM). The role of the elastic strains induced by δ on the precipitate arrangement, morphology and coarsening kinetics is not yet clear. Recent theoretical work by Johnson and by Kawasaki has shown that a comparison between the predicted influence of interparticle interactions and experiment is already possible.

Single crystalline specimens with various compositions were used for the SANS experiments. The lattice mismatch δ was varied by Mo addition. It ranged from 1.2% (binary Ni-12.6 at.% Al) to 0%. All specimens were aged in-beam at 833 K or at 883 K.

The experimental SANS results obtained at the Institut Laue-Langevin, Grenoble, France, show that the shape, arrangement and coarsening rate of the γ' -particles are very sensitive to coherency strains. The scattering patterns for alloys with $\delta = 1.2$ and 0.6%, respectively, are anisotropic with sharp peaks along $\langle 100 \rangle$. This suggests that even very small γ' -particles are not spherical and arranged along specific directions. Alloys with $\delta \approx 0$ give rise to isotropic scattering patterns, which indicates a spherical particle shape and no orientational preference. Furthermore, the reduction of δ apparently slows down the coarsening rate by a factor of 23. High-resolution and dark-field TEM, results on precipitate shape and arrangement will also be presented.

J4.11

INFLUENCE OF INTERSTITIAL OXYGEN ON THE LATTICE PARAMETERS OF SOLUTION-TREATED AND AGED Ti-8.6Al ALLOYS.* George T. Gray III and A.C. Lawson, Los Alamos National Laboratory, Los Alamos, New Mexico 87545

Interstitial oxygen has long been known to have a pronounced influence on the structure and mechanical properties of titanium alloys, particularly those containing the ordered Ti_3Al (hereafter α_2) phase. Systematic studies on binary Ti-Al alloys have suggested that a major portion of this influence is related to the fact that oxygen stabilizes α_2 and is qualitatively linked to an increased tendency for inhomogeneous slip in alloys containing >6 wt% Al. Electron microscopy studies of α -alloys have further suggested that oxygen and/or aluminum ordering may be occurring.

To investigate possible aluminum and oxygen ordering in Ti-8.6Al, neutron diffraction experiments were conducted on Ti-8.6Al alloys containing three oxygen contents, 500 ppm, 1000 ppm, and 2000 ppm in the solution-treated condition and aged to precipitate α_2 . Neutron diffraction data were obtained on HIPD at LANSCE and the data refined using GSAS.

The lattice parameters "a" and "c" were observed to vary as a function of oxygen content and heat treatment condition. Consistent with literature data on pure Ti, the "a" lattice parameter of the solution-treated Ti-8.6Al material is seen to be relatively insensitive to oxygen while the "c" parameter increases with oxygen content. Following aging to precipitate the α_2 , the "c" lattice parameter is seen to still exhibit a positive dependence on oxygen content with aging and a slight "c" parameter increase compared to the solution-treated material. The "a" lattice parameter of the aged Ti-8.6Al alloys show decreased "a" values with increasing oxygen content. The LANSCE data will be discussed in light of parallel TEM results and literature data.

J4.12

IN-BEAM SMALL-ANGLE SCATTERING STUDIES OF PHASE SEPARATION IN NI-TI SINGLE CRYSTALS. Alberto Cerri, ETH Zürich, now at University of Vienna, Festkörperphysik, A-1090 Wien; Bernd Schönfeld and Gernot Kosterz, Angewandte Physik, ETH Zürich, CH-8093 Zürich, Switzerland; Albert F. Wright, Institut Laue-Langevin, F-38042 Grenoble, France.

Phase separation of quenched supersaturated Ni-(9.5-12.0) at.% Ti single crystals was followed by small-angle neutron scattering (SANS) during in-beam aging at 773, 813 and 853 K. Because Ni and Ti differ appreciably in scattering length, very sensitive measurements were possible. With the incident beam along $\langle 110 \rangle$, scattering maxima in $\langle 100 \rangle$ directions were observed from the earliest stages of decomposition.

While the results obtained at 773 K may be compatible with the general features of spinodal decomposition, the behavior at 813 and 853 K may be interpreted on the basis of the two-phase model with homogeneous precipitates in a depleted matrix. Here, the integrated SANS intensity reaches a constant level after several hours. Later stages should be controlled by Ostwald ripening. Though scaling may be shown to hold (with a certain choice of scaling variables), the ageing kinetics is considerably slower than expected. This may be related to a stabilizing effect of elastic coherency stresses due to the lattice mismatch of precipitates and matrix.

J5.1

COMPOSITION AND PROFILE DETERMINATION OF LIGHT ELEMENTS BY NEUTRON ABSORPTION REACTIONS. R. Gregory Downing, George P. Lamaze, John K. Langland and Brent L. Grazman, National Institute of Standards and Technology, Bldg. 235, Rm B108, Gaithersburg, MD 20899.

A second generation neutron depth profiling (NDP) facility has been constructed on a "cold" (i.e. low energy) neutron port as part of the Cold Neutron Research Facility (CNRF) at NIST. The increased neutron flux density and reaction rate enables the nondestructive determination of concentration versus depth profiles of ^3He , ^6Li , ^7Be , ^{10}B , ^{14}N , and ^{22}Na with analysis times and resolution comparable to those of RBS. At somewhat longer times for data acquisition, ^{35}Cl and ^{17}O can be profiled as well. By exploiting the intrinsic properties of cold neutrons, energy sensitive samples such as polymer films are nondestructively analyzed using NDP and the exact same sample volume successively studied with other analytical techniques.

The new NDP facility is designed to enable positioning of

individual samples in the target chamber while maintaining a high vacuum environment. Programmable temperature control of the sample holder during analysis allows the study of solid state diffusion in real time. The target chamber has several discrete charged particle detector systems including coincidence detection for analyzing self-supporting thin films and time-of-flight energy analysis for high resolution near-surface analysis. The simultaneous use of multiple detectors give an optimized depth resolution in the minimum amount of analysis time. Position sensitive detectors are being used to perform channelling measurements and eventually, multidimensional profile characterization of the sample. Other tools are being incorporated in the instrument for *in situ* cleaning and sputtering of the sample surface.

J5.2

DISTRIBUTION OF BORON IN ION IMPLANTED $Hg_{1-x}Cd_xTe$, Robert C. Bowman, Jr., and John F. Knudsen, The Aerospace Corporation, El Segundo, CA; and R. Gregory Downing, National Institute for Standards and Technology, Gaithersburg, MD.

Boron ion implantation is often used to fabricate n-p junctions in $Hg_{1-x}Cd_xTe$ for its use as infrared photovoltaic detectors. The distributions of the implanted species as well as accompanying lattice damage are important parameters with regards to subsequent performance of these devices. Multiple energy (50-400 keV) boron implants were made into bulk and epitaxial $Hg_{0.7}Cd_{0.3}Te$ as well as CdTe single crystals. A nondestructive neutron depth profiling (NDP) method has been used to measure the boron (^{10}B) concentration profiles before and after post-implant anneals. When the NDP results are compared with theoretical ion ranges obtained by the TRIM Monte Carlo computer simulations, the profiles correspond closely to the calculated boron distributions.

The behavior of boron implants through photochemically deposited SiO_2 passivation films on $Hg_{0.7}Cd_{0.3}Te$ has also been evaluated. The distributions of boron within each of the layers were monitored by combined profiling and etching experiments and were compared with the prediction from the TRIM simulations. The SiO_2 film acts primarily like a neutral region that shifts the boron profiles toward the surface. Some effects of this shift on the electrical parameters of $Hg_{0.7}Cd_{0.3}Te$ will be described.

J5.3

SANS MEASUREMENT OF HYDROGEN-DISLOCATION CORRELATION IN PALLADIUM. Brent J. Hansen, G. C. Summerfield, J. S. King, University of Michigan, Ann Arbor, MI; and J. E. Apperson, Argonne National Laboratory, Argonne, IL.

Small angle neutron scattering measurements have been made on deformed polycrystal palladium samples with and without deuterium (and hydrogen) dissolved in the solution phase (α) at room temperature. Deformation was produced in one set of samples by cold rolling to 65% CW, and in a second set by a hydriding-dehydriding cycle ($\alpha/\beta/\alpha$). Solubility enhancements above that for well annealed samples (Sievert's law) were found to be about 30% for CW samples and 40% for ($\alpha/\beta/\alpha$) samples. These are in reasonable agreement with results published by Lynch[1] and Flanagan[2] for gas atom concentrations near 5,000 ppm, and attributed by these authors as due solely to the presence of dislocations. Concentrations were held constant during SANS experiments in an equilibrium gas pressure cell. The difference in scattered intensity from the same deformed sample before and after gas loading was determined as a function of Q ($Q=2\pi/\lambda \sin \theta$). The difference scattering was strongest for the ($\alpha/\beta/\alpha$) samples and reveals a $1/Q$ behavior with a lowest angle component of stronger inverse Q dependence. The CW

samples show qualitatively the same pattern but the data taken thus far are hampered by poor statistics. The Q dependencies and their interpretation will be discussed.

J5.4

STUDY OF PREFERRED ORIENTATION IN GEOLOGICAL SAMPLES WITH PULSED NEUTRONS. Allen C. Larson and Phillip J. Vergamini, Manuel Lujan, Jr. Neutron Scattering Center (LANSCE), Los Alamos National Laboratory, Los Alamos, NM 87545; Rudy Wenk, Department of Geology and Geophysics, University of California, Berkeley, CA 94720.

The single crystal diffractometer, (SCD) at LANSCE provides an ideal capability for the study of preferred orientation in geological samples. The 2-d position sensitive detector with the large wavelength range available at the pulsed neutron source allows one to measure the complete distribution of intensities for several poles very quickly. Each histogram covers about $\frac{\pi^2}{16}$ Radians of reciprocal space and will contain information from all possible poles visible with the wavelength range used, usually about 0.5 to 5.0 Å. With this method complete, pole figures of many lattice planes can be constructed from only 12 to 20 sample orientations as compared to over 1000 per lattice plane using conventional diffractometers.

Pole figures from measurements of experimentally deformed standard samples of calcite and quartzite with a known history of deformation will provide information about deformation mechanisms and their temperature/strain history. This information can be applied to interpret preferred orientation in naturally deformed rocks.

J5.5

RESIDUAL AND APPLIED STRESS ANALYSIS. Aaron D. Krawitz, University of Missouri, Columbia, MO 65211

The use of neutrons for stress measurements began about ten years ago and has been increasingly employed. The lower absorption of neutrons by most engineering materials extends the sampling depth from microns to millimeters and enables the study of new types of problems. It is particularly suitable for triaxial macrostresses and stress gradients into the depth of engineering components, volumetric microstresses, and for systems containing heavy elements, such as tungsten and uranium.

One major application involves depth profiling of macrostress gradients through the thickness of parts by the use of small probe regions created via slits or apertures. Such gradients arise, for example, in welded or heat-treated components. Another is the characterization of differential thermal microstresses created upon fabrication of metal matrix composites reinforced with fibers, whiskers, or particles. In this case the whole sample is irradiated as in conventional powder diffraction. The technique has also been used to study the response of single or multiphase alloys to applied stress through the use of *in situ* tensile test devices.

After an introduction to triaxial stress measurement methodology, and the use of neutrons for this purpose, examples of macro- and microstress analysis in alloys and composites will be presented as well as applied stress work. Measurements at both steady state and pulsed sources will be included.

J5.6

RESIDUAL STRESS MEASUREMENTS BY MEANS OF NEUTRON DIFFRACTION
H.J. Prask, and C.S. Choi, Reactor Radiation Division,
National Institute of Standards and Technology,
Gaithersburg, MD 20899

Neutron diffraction is analogous to x-ray diffraction in methodology and analytical formalism; however, in the wavelength regime appropriate to diffraction, neutrons are typically about a thousand times more penetrating. The neutron diffraction technique is also nondestructive. Energy-dispersive neutron diffraction has been developed at the NIST reactor as a probe of sub- and near-surface residual stresses in technological samples. Application of the technique has been made to a variety of metallurgical specimens, and includes the determination of tri-axial stresses as a function of depth in a number of uranium-3/4wt%Ti samples with different thermo-mechanical histories, and in two types of 7075-T6 aluminum "ogives" of interest to the Army. Also determined was a bi-axial stress distribution vs. depth in an induction-hardened-steel test specimen (for the SAE). Details of the technique and applications will be presented.

J5.7

RESIDUAL STRESS ANALYSIS BY NEUTRON TIME-OF-FLIGHT AT A REACTOR SOURCE. H.G. Priesmeyer, Institut für Reine und Angewandte Kernphysik, Universität Kiel; J. Schröder, Institut für Werkstofforschung, OKSS-FORSCHUNGSZENTRUM, P.B. 11 60, D-2054 Geesthacht/FRG

A high-resolution neutron time-of-flight powder diffractometer has been installed at the FRG-1 research reactor (5 MW) in Geesthacht. The instrument is a Fourier correlation spectrometer, operating in the reverse time-of-flight (RTOF) mode. Correlation spectrometry is known to be very neutron-efficient in the low-energy-range, so that extensive stress profiling can be done on small or medium size neutron sources in acceptable measuring times. The neutron time-of-flight has important advantages for strain measurements:

- the "white" reactor neutron spectrum allows simultaneous investigation of many reflexions;
- the scattering volume is ideally defined in 90 ° geometry;
- fixed geometry eases setups for special environments;
- there is no high-order contamination;
- the resolution is almost constant over the whole energy range.

Details of the instrumental setup and first experimental results will be presented.

J5.8

EFFECT OF HEAT TREATMENT AND UNIAXIAL COMPRESSION ON THE RESIDUAL STRESSES IN U-0.8 wt.% Ti ALLOY MEASURED BY NEUTRON DIFFRACTION. A. Salinas-Rodriguez, J. H. Root, T.M. Holden, S.R. MacEwen, Chalk River Nuclear Laboratories, Ontario, Canada K0J 1J0; and G.M. Ludtka, Martin-Marietta Energy Systems, P.O. Box 2004, Oak Ridge, Tennessee, U.S.A.

The residual stress distribution in 17 mm thick-walled, γ -quenched U-0.8Ti alloy tubes was studied using neutron diffraction techniques. Additional measurements were made after the as-quenched tubes were stress levelled at room temperature (0.015 strain in compression), or aged at 658 K followed by immersion quenching, or after combined stress levelling and aging. The stresses were calculated with the isotropic bulk values of the elastic constants for U-0.8Ti alloys given strains measured from shifts in the (110), (111) and (112) Bragg peaks

Quenching from the γ field resulted in a biaxial stress state at every point across the wall of the tube. The

radial stress was negligible. The axial and circumferential stresses were equal, reaching 700 MPa in compression at the tube outer surface and 500 MPa in tension in the interior. After the tube was aged at 658 K for 4 hours and immersion quenched to room temperature the residual stresses were about 30% lower than those observed in the as-quenched condition. Stress levelling relieved all the residual stresses within experimental uncertainty.

J5.9

NEUTRON MEASUREMENT OF RESIDUAL STRESSES IN A USED RAILWAY RAIL. Peter J. Webster, Keng S. Low, Gordon Mills, Department of Civil Engineering, University of Salford, Salford M5 4WT, UK; and George A. Webster, Department of Mechanical Engineering, Imperial College, London SW7 2AZ, UK.

The high resolution neutron diffraction technique has been applied to determine non-destructively the residual stress distribution developed in the head of a railway rail after normal service.

Measurements were made, using the neutron strain scanner at the Institut Laue Langevin, Grenoble, on a transverse slice of rail 12mm thick taken from a section of straight track. The rail head was scanned in the three principal orientations in a series of parallel traverses sufficiently close to enable a two dimensional matrix of data to be accumulated and vertical, transverse and longitudinal residual stress contours to be drawn.

Substantial residual compressive and tensile stresses and steep stress gradients were observed related to the depth below the top surface, distance from the running line and shape of the rail head. The highest stresses and stress gradients were observed in transverse and vertical directions but significant stresses were also retained in the longitudinal (12mm thick) direction of the rail.

The results demonstrate the effectiveness and unique characteristics of the neutron technique to determine non-destructively and continuously the residual stresses inside engineering components.

J5.10

Neutron Diffraction Analysis of Residual Stress in Corrosion Resistant Alloys. Michael P. Anderson Exxon Research and Engineering Co., Annandale, NJ, Maurice Watkins, Exxon Production Research Co., Houston, TX, and David Vakmin, Brookhaven National Laboratories, Upton, NY

Reserves being produced by oil companies contain chemical species, such as hydrogen sulfide, that aggressively attack traditional materials. To deal effectively with these environments, a new materials technology utilizing corrosion-resistant alloys based upon nickel, iron, chromium, and molybdenum is being developed. Because these materials are strengthened by cold work, complex residual stress states occur. These stresses can influence performance by affecting susceptibility to environmental cracking. Therefore, a study was undertaken to accurately measure residual stress distributions as a function of processing where the principal variable examined was the method of tube production. A methodology based upon neutron scattering was used to measure the through-wall distribution of residual stresses. The results show that the residual stress patterns are a function of the deformation mode. Tubulars that are cold worked by pilgering have large compressive stresses on the inner diameter and large tensile stresses on the outer diameter. In contrast, tubulars that

are drawn have tensile stresses on the inner diameter and compressive stresses on the outer diameter.

J5.11

NEUTRON DIFFRACTION MEASUREMENT OF STRESS FIELD DURING FATIGUE CYCLING OF A CRACKED TEST SPECIMEN. M.T. Hutchings, C.A. Hipsley and V. Rainey, Materials Physics and Metallurgy Division, Harwell Laboratory, Didcot, OX11 0RA, UK.

Neutron diffraction provides a unique method of measuring the internal stress field within metallic components⁽¹⁾, and hence of testing values of stress hitherto only determined by theoretical calculation.

The triaxial stress tensor along the line of cracking at two stages of a fatigue cycle applied to a fatigue test specimen of ferritic steel has been determined. The experiments were performed with high volume resolution of $\sim 1\text{mm}^3$ on a sample of size $\sim 13 \times 31 \times 49\text{mm}^3$ using the D1A diffractometer at the Institut Laue Langevin, Grenoble. A wavelength of 1.91\AA was used and the strains calculated from a comparison of the (211) Bragg reflection angles with those from an annealed piece of steel of the same composition. With the assumption that the principal strains lie along the symmetry axes of the specimen, the strain field was first measured at the maximum applied stress intensity, the sample being held at maximum load by a bolt. The applied load was then relieved by removal of the bolt, and the strain field remeasured. The triaxial strain tensors, at intervals of 0.5-mm , were converted to stress tensors using standard theory and values of $E = 207\text{ GPa}$ and $\nu = 0.28$. These experimentally determined stress fields are compared with those expected from standard analysis.

J6.1

DYNAMICS OF STAR-BRANCHED POLYMERS IN SOLUTION. J. S. Huang and L. J. Fetters, Exxon Research and Engineering Company, Rt. 22E, Annandale, NJ 08801; D. Richter and B. Farago, Institut Laue-Langevin, 156X, 38042 Grenoble Cedex, France; and B. Ewen, Max Planck Institut Fur Polymerforschung, 6500 Mainz, FRG.

We have studied 12-arm star-branched polymers using elastic and quasi-elastic small angle neutron scattering. By selectively labeling a single arm as well as labeling of the center core of the star polymer, we accessed the static and dynamic properties of the constituents of the star. We have investigated the relaxation between the static structure of the star and its initial dynamic response as measured by neutron spin echo spectroscopy. In the frame work of the random phase approximation, the initial relation rates for the various partial structure factors have been obtained for a Gaussian star, including the effects of hydrodynamic interaction. The Q-dependence of the relaxation rates under various solvent contrast conditions can be quantitatively accounted for.

J6.2

MICROSTRUCTURE AND ISOTOPIC LABELING EFFECTS ON THE MISCIBILITY OF POLYBUTADIENE BLENDS STUDIED BY THE SMALL-ANGLE NEUTRON SCATTERING TECHNIQUE. S. Sakurai, H. Hasegawa, T. Hashimoto, I. G. Hargis, S. L. Aggarwal and C. C. Han, Polymers Division, National Institute of Standards and Technology, Gaithersburg, Md 20899.

Deuterated polybutadiene and protonated polybutadiene (PBD/PBH) blends with various microstructures have been studied by the small-angle neutron scattering experiments. Correlation length, ξ , zero-wavenumber structure factor, $S(q=0)$, and interaction parameter, χ_{blend} have been obtained. All PBD/PBH blends exhibit UCST behavior. With

the use of random copolymer theory, the interaction parameter, χ_{blend} , has been successfully separated into χ_1 , χ_2 and χ_3 which are interaction parameters between the same isotope labeled 1,2-unit and 1,4-unit, opposite isotope labeled 1,2-unit and 1,4-unit, and opposite isotope labeled 1,2-unit with 1,2-unit or 1,4-unit with 1,4-unit, respectively.

It can be concluded that; (1) The random copolymer theory of ten Brinke, Karasz and MacKnight works well for this case; (2) The intramolecular interaction between different microstructure pairs gives negative contribution to the total interaction parameter, χ_{blend} ; (3) The magnitude of the individual χ which is due to microstructure effect is much bigger than that due to the isotope-labeling effect.

J6.3

CHARACTERIZATION OF MOLECULAR NETWORK OF THERMOSETS USING NEUTRON SCATTERING. Yan-li Wu, Polymers Division, NIST, Gaithersburg, MD 20899.

Neutron scattering measurements were conducted to investigate the conformation of the molecular network in an epoxy and a cyanate ester resins. These resins were all cured through a homo-polymerization process and all the starting monomers were partially deuterated to provide the scattering contrast. No amine chain was introduced into the network.

It was observed that the crosslinking process resulted in a significant change in the scattering intensity over a Q range from 0.005 to 1.5 \AA^{-1} . These results were analyzed using a scheme based on Random Phase Approximation (RPA) to obtain the intra-network correlation function. The results indicated that crosslinking caused an increase in the end to end distance of the monomer. In addition, the crosslinking was also found to induce density fluctuation, its effect on the validity of RPA will be discussed.

J6.4

SHEAR INDUCED PHASE BEHAVIOR OF POLYMER BLENDS BY SMALL ANGLE NEUTRON SCATTERING. Alan I. Nakatani, Hongdoo Kim, and Charles C. Han, Polymers Division, National Institute of Standards and Technology, Gaithersburg, MD 20899.

The phase behavior of polymer blends and solutions can be changed dramatically by deformation using a variety of flow geometries. Unlike simple binary fluids which require extremely high shear rates to produce extremely small shifts in the phase boundary, polymer phase behavior may be influenced by as much as 10 degrees with the application of much lower shear rates. However, there is a large body of conflicting data concerning the nature of these shear effects in polymers.

Here we report on the effects of shear on the phase behavior of polymer blends by small angle neutron scattering (SANS). Experiments were conducted using a specially constructed, concentric cylinder apparatus for in situ studies of concentrated polymer solutions and melts. Two separate systems will be discussed: 1) a blend of polystyrene and polybutadiene. 2) a blend of polystyrene and poly(vinylmethylether). Both systems exhibit shifts in the phase behavior which indicate shear induced mixing in agreement with previous results obtained by other techniques. These results will be interpreted in context with existing theories of shear induced phase behavior.

J6.5

THERMODYNAMIC INTERACTION PARAMETERS OF STEREOREGULAR PMMA. James M. O'Reilly,* Hsinjin Yang,** and David Teegarden,* *Corporate Research Laboratories, **Commercial Systems Information Group, Eastman Kodak Company, Rochester, NY 14650

Stereoregular PMMA have been extensively studied by SANS and other techniques. In these studies we report the measurement of the Flory-Huggins interaction parameters by SANS using the RPA method. Blends of deuterated atactic PMMA and hydrogenous isotactic and syndiotactic PMMA and blends of deuterated isotactic PMMA with atactic PMMA were prepared, and scattering measurements were made on these blends. The interaction parameter for atactic and syndio χ s varies from -4.2×10^{-3} to -5.8×10^{-3} with increasing concentration of syndio. The interaction parameter for isotactic and syndio χ s ranges from -2.4×10^{-4} to -4.3×10^{-4} with increasing isotactic concentration. We observe the familiar concentration dependence of χ which is sometimes attributed to the differences in the lattice (molar) volume of the monomer units. In this case since the monomer units have the same molecular weight and the densities of the polymers differ by less than 5%, it is unlikely that the concentration dependence of χ is due to this cause. It is likely that the concentration dependence of χ is due to the different environments which occur as a function of concentration. χ is less than χ s, reflecting a stronger interaction between isotactic and syndio segments. The χ s can be analyzed using the copolymer interaction model and these interaction parameters will be compared with similar data in the literature.

J6.6

STRUCTURE AND DYNAMICS OF GLASSES AND LIQUIDS. David L. Price, Materials Science Division, Argonne National Laboratory, 9700 South Cass Avenue, Argonne, IL 60439.

Neutron diffraction provides information about the instantaneous structure of a disordered material. Information obtained in reciprocal space can be directly informative, e.g., as regards diffraction peaks at low angles which can reveal intermediate-range order in the system. Alternatively, the diffraction patterns can be Fourier transformed to give the real-space distribution functions which contain information about short-range order, i.e., near-neighbor bond distances and angles. Inelastic neutron scattering shows how these structures evolve with time. The energy dependence of this scattering gives the density of states of vibrational motions; in the case of liquids, the quasielastic scattering is related to diffusive motions. The wave vector-dependence of the scattering gives information about the structural entities associated with these different types of motion.

J6.7

CROSSOVER IN THE VIBRATIONAL DENSITY OF STATES OF SILICA AEROGELS STUDIED BY HIGH-RESOLUTION NEUTRON SPECTROSCOPY H. Conrad*, R. Schätzler, Institut für Festkörperforschung der Jülich, West Germany; and J. Fricke, G. Reichenauer, Physikalisches Institut der Universität Würzburg, Am Hubland, D-87600 Würzburg, West Germany.

A vibrational density of states analysis of neutrons inelastically scattered from silica aerogels has revealed a crossover from a Debye law to a different power law at crossover frequencies ν_{co} depending on sample density. Both these frequencies and the spectral exponents are determined for three base-catalysed aerogels. The resemblance of the observed behaviour to a phonon-fracton crossover is discussed. The effective sound velocities are determined from the ratio of total elastic to total inelastic scattering and are in good agreement with ultrasonic data.

J6.8

VIBRATIONAL EXCITATIONS OF WEAKLY CONNECTED SOLIDS. D. W. Schaefer, C. J. Brinker, and C. S. Ashley, Sandia National Laboratories, Albuquerque, NM 87185; and D. Richter and B. Farago, Institute Laue-Langevin, 38042 Grenoble Cedex, France.

Because of the rich chemistry of solution prepared silicate glasses, it is possible to prepare highly porous solid materials where the topology of the continuous phase is controlled by the precursor chemistry. Porosity can range from bubble-like pores to highly dispersed polymeric networks. In the case of the latter materials, these are ideal materials to search for the existence of fracton excitations. These excitations represent the flopping and breathing modes of the weakly connected network structure and are the solid state analogs of the Rouse-Zimm modes observed in polymers in solution.

We use spin-echo neutron scattering techniques to study these low energy excitations in a polymeric aerogel, the material which we believe would show the highest probability of network modes. We observed intense inelastic scattering in the μ ev range that is strongly dependent on temperature. These modes were analyzed in the incoherent approximations using the Carpentier-Pelizzari formulation for phonon-like scattering from amorphous systems.

Assuming fracton excitations, we find that the data is adequately characterized by assuming a fracton dimension of 1.5. The temperature dependence of the excitations follows the Debye-Waller factor as expected for phonon like excitations.

J6.9

VIBRATIONAL SPECTRA FOR HYDROGENATED AMORPHOUS SEMICONDUCTORS. W. A. Kamitakahara, R. Biswas, and A. M. Bouchard, Ames Laboratory and Microelectronics Research Center, Iowa State University, Ames, IA 50011; F. Gompf and J. B. Suck, Kernforschungszentrum Karlsruhe, INF, Postfach 3640, D-7500 Karlsruhe, Federal Republic of Germany.

Hydrogen vibration spectra have been measured by time-of-flight neutron spectroscopy for several amorphous semiconductors, including a-Ge:H and a-Si:H. The sputtered samples contain about 10 at. % H. The results of realistic computer simulations, which use structural models generated by molecular dynamics, will be presented for comparison with the a-Ge:H spectrum, as well as with previously obtained data on a-Si:H. The primary Si-H and Ge-H bond-bending features at 645 and 570 cm^{-1} have substantial widths that arise from the variable local environments of the H atoms. The a-Ge:H spectrum shows unexpected features at 350 and 430 cm^{-1} which are identified by the simulations as dihydride "rocking" modes, in which two H atoms bonded to the same Ge atom make in-phase transverse motions. In the case of a-Si:H, features at 650 and 950 cm^{-1} can be directly used to estimate the relative numbers of H atoms bonded to Si and C atoms.

The Division of Materials Sciences, U.S. Dept. of Energy (USDOE) provided support for work at the Ames Laboratory, which is operated by Iowa State University for the USDOE under contract W-7405-Eng-82. Work at the Microelectronics Research Center was supported by the Air Force Office of Scientific Research.

J6.10

INELASTIC NEUTRON SCATTERING STUDIES OF NONLINEAR OPTICAL MATERIALS: p-NITROANILINE ADSORBED IN ALPO-5. Jacqueline M. Nicol, University of Maryland/NIST, Gaithersburg, MD, Terrence J. Udovic and John J. Rush, NIST, Gaithersburg, MD, and Sherman D. Cox and Galen D. Stucky, University of California, Santa Barbara, CA.

The adsorption of para-nitroaniline (p-NA) into the channels of the molecular sieve ALPO-5 results in nonlinear optical properties of the system that are very different from those of either the individual guest molecules or the host molecular sieve. Inelastic neutron scattering has been used to characterize the vibrational spectroscopy (below 2000 cm^{-1}) of p-NA adsorbed in ALPO-5 at both 3% and 13% weight loadings, which represent the onset of and the maximum in the nonlinear optical coefficient, respectively. In

addition, the spectra of pure p-NA and ALPO-5 were obtained for comparison. Spectral differences in the region of 30 - 60 meV for the two p-NA loadings are interpreted in terms of a different alignment and ordering of the p-NA molecules inside the confines of the ALPO-5 channels.

J6.11

NEUTRON SCATTERING FROM EXCESS OXYGEN IN $UO_{2.13}$. J.M. Goff and M.J. Hutchings. Materials Physics and Metallurgy Division, Harwell Laboratory, Didcot, OX11 0RA, UK, and W. Hayes, Clarendon Laboratory, Parks Road, Oxford, OX1 3PU, UK.

A knowledge of the thermophysical properties of hyperstoichiometric $UO_{2.13}$ is important in reactor fuel studies. Of special interest is the oxygen mobility and thermal conductivity of oxidised fuel. As an initial stage of an investigation using neutron techniques, the disordered structure of the excess oxygen ions in a single crystal of $UO_{2.13}$ at temperatures in the range 1173K-1573K has been studied by coherent diffuse scattering. At ambient temperature the excess oxygen is largely in the form of UO_6 , but in the region above ~900K the oxygen diffuses more uniformly into the lattice. The scattering distribution in the (110) plane was measured using the θ -axis spectrometer at PLUTO.

Earlier diffraction results of Willis⁽¹⁾ have suggested that the excess oxygen ions formed defect clusters of the 2:2:2 type, with equal numbers of vacancies: interstitials: relaxed ions. A comparison of the present diffuse scattering data with calculated intensity distributions and with data from other pure⁽²⁾ and doped fluorite systems confirms that the defective ions form clusters with one or two interstitials, probably with a more extended relaxation field of the 8:1:8 or 8:3:8 type. The formation and temperature dependence of this clustering have been investigated, and show that when the sample is cooled the UO_6 phase reappears with considerable hysteresis.

J6.12

COMPARISON OF NEUTRON ELASTIC AND INELASTIC SCATTERING FROM FUSED QUARTZ, CAB-O-SIL AND AEROGEL. John H. Root and William J. L. Buyers, Atomic Energy of Canada Ltd., Chalk River, Ontario; John H. Page, University of Manitoba, Winnipeg, Manitoba; Dale W. Schaefer and C. J. Brinker, Sandia National Laboratories, Albuquerque, NM.

Neutron scattering experiments have been performed to study the structure and dynamics of three preparations of silica: a dense glass (fused quartz), a flame-hydrolyzed aggregate (Cab-O-Sil, grade M5) and a polymeric aerogel. The experiments were performed at temperatures 300 K, 77 K and 4.2 K on the three materials. Neutron inelastic scattering was measured at Q values 1.5, 2.5, 2.9 and 4.0 \AA^{-1} .

The elastic scattering indicates a systematic decrease in positional correlations on progressing from fused quartz through Cab-O-Sil to aerogel. The inelastic scattering was analyzed with the Buchenau model (1) to obtain the sample and temperature dependences of the density of states, $g(\nu)$.

At frequencies less than 1.5 THz $g(\nu)$ is proportional to a power of ν for all forms of silica and there is no significant temperature dependence of the exponent. From data measured at $Q \approx 2.5 \text{ \AA}^{-1}$ the exponents for fused quartz, Cab-O-Sil and aerogel are found to be 2.6 ± 0.1 , 2.03 ± 0.03 and 1.64 ± 0.09 respectively. These cross through the Debye value of 2 and are all higher than the value 1/3 conjectured for fractions. In the aerogel the exponent drops to 1.20 ± 0.03 at $Q = 1.5 \text{ \AA}^{-1}$ and $g(\nu)$ is observed to vary in detail for each Q value studied. We conclude that the Buchenau analysis is not appropriate for aerogel.

J7.1

STUDY OF THERMAL EXPANSION OF GRAPHITE AND HNO_3 -GIC BY NEUTRON DIFFRACTION: Haim Pinto, Mordechai Melamed, and Hagai Shaked, Nuclear Res Centre - Negev, Beer-Sheva, Israel.

The temperature dependence of the lattice parameter c of pristine graphite and of HNO_3 -Graphite Intercalation Compounds (GIC) stages 3 and 4 are studied in the range 10 to 300 K, using neutron diffraction. The thermal expansion of the HNO_3 layers is extracted from the "difference" between stage 3 and stage 4 data. Also the liquid-to-solid 2D phase transition of the layers is studied. Three samples were used: A sample of pristine graphite in the form of HOPG with $\sim 3.5^\circ$ mosaic spread, a sample of stage 3 and a sample of stage 4 HNO_3 -GIC which were prepared from the same batch of pristine graphite [1,2]. Neutron diffraction ($\lambda = 2.4 \text{ \AA}$) patterns were taken on the KANDI III neutron diffractometer at the IRR-2 reactor. The samples were cooled from 300 K to 10 K in steps of $\sim 1 \text{ K}$ and remained $\sim 1 \text{ hr}$ at each temperature step ensuring temperature stabilization ($\pm 0.2 \text{ K}$) and equilibration. The temperature dependence of the lattice parameter c was determined from the temperature dependence of the Bragg angles of (00 ℓ) reflections with $\ell = 4, 18, 33$ for graphite, stage 3, stage 4, respectively.

The lattice parameter versus temperature curves were fitted to fourth degree polynomials up to 250 K (where the melting phase transition occurs). The dependence of the thermal expansion coefficients on temperature was obtained by taking the logarithmic derivatives of these polynomials. It is found that the thermal expansion coefficient of the graphite layers in the GIC is similar to that for pristine graphite, whereas the coefficient of the HNO_3 layers is much larger.

J7.2

CHARACTERIZATION OF SOL-CLAY COMPOSITES BY SMALL-ANGLE NEUTRON SCATTERING. Ahmad Moali and Thomas J. Pinnavaia, Department of Chemistry and Center for Fundamental Materials Research, Michigan State University, East Lansing, MI 48824; and P. Thiyagarajan, IPNS Division, Argonne National Laboratory, Argonne, IL 60439.

A series of silica sol-clay composites were characterized by small-angle neutron scattering (SANS). These complex materials were formed by reacting uniform spherical silica sol particles ($< 100 \text{ \AA}$) with suspensions of the 2:1 layered silicate Na-montmorillonite ($< 2 \mu$). The resulting composites are 3-dimensional, highly porous networks of platelets and spheres. SANS studies on the pure silica sols and the sol-clay suspensions showed an increase in the degree of sol dispersion upon interaction with clay. The dispersion was also found to be highly dependent on the pH and the aging time of the suspensions. SANS studies on hydrolyzed sol-clay powder samples provided insights on the degree of clay stacking/aggregation, as well as on the size and shape of the silica particles. Several clays of different particle size and charge density were examined, and their effects on the formation of sol-clay composite products were studied.

J7.3

NEUTRON SCATTERING STUDY OF LAYERED SILICATES PILLARED WITH MULTIMETHYLAMMONIUM IONS. D.A. Neumann, and J.J. Rush, National Institute of Standards and Technology, Gaithersburg, MD 20899; J.M. Nicol, NIST and University of Maryland, College Park, MD 20742; Y.B. Fan, H. Kim, S.A. Solin, and T.J. Pinnavaia, Michigan State University, E. Lansing, MI 48824; N. Wada, Colorado School of Mines, Golden, CO 80401; and S.F. Trevino, NIST and ARDEC, Picatinny Arsenal, NJ 07806.

Montmorillonite and vermiculite are members of a naturally occurring class of expandable layered silicates widely known as clays in which the two-

dimensional oxyanions are separated by layers of intercalated cations. Permanent porosity can be induced in these minerals by exchanging large cations, such as tetramethylammonium, for the naturally occurring ions, e.g. Na. The resulting material is known as a "pillared clay" and the cations which prop the layers apart are referred to as "pillars". Here we present an incoherent, inelastic neutron scattering study of montmorillonite pillared with tetramethylammonium ions and vermiculite pillared with trimethylammonium ions. These spectra yield information on the pillar-host interaction and on the orientation of the pillars in these systems. In addition, we will present elastic scattering results which show that the ion-exchange in these systems is not complete, a fact which could have practical consequences for the further development of pillared clays as tailored catalysts and molecular sieves.

J7.4

OBSERVATION OF MICELLAR FORMATION IN THE CAVITY OF POROUS SILICA GLASS. Kenneth Bradley, Brown University, Providence, RI; Sow-Hsin Chen, MIT, Cambridge, MA; Pappannan Thiagarajan, Argonne National Laboratory, Argonne, IL.

Small angle neutron scattering has been used to characterize the microstructure of porous silica glass (Corning Glass, Vycor brand, no. 7930). Analysis of the empty Vycor data adopts the scattering formalism developed by Berk which uses Cahn's scheme for simulating the morphology of isotropic spinodal decomposition. Micellar formation in the glass pores is observed by contrast matching the silica with a H_2O/D_2O mixture. In the case of cationic surfactants, CTAB and DTAB, no micellar formation was observed and the surfactant molecule merely coats the interior surface of the pore. In the case of the anionic surfactant, SDS, evidence of micellar formation is obtained from observation of the intermicellar correlation peaks which arise from inter- and intra-cavity micelle correlations.

J7.5

ANALYSIS OF SANS FROM CONTROLLED PORE GLASSES. N. F. Berk, C. J. Glinka, W. Haller, and L. C. Sander, Natl. Institute of Standards and Technology, Gaithersburg, MD 20899.

Small angle neutron scattering measurements have been performed on several samples of silica controlled pore glasses with pore sizes ranging from roughly 70 to 300 Å. The scattering intensity is strongly peaked at small Q and shows approximate Porod law behavior at large Q . Contrast variation measurements have shown that the pore space in these samples is entirely interconnected and thus forms a bicontinuous microstructure. The scattering data have been analyzed using the leveled wave method based on an early scheme for representing two-phase microstructures resulting from spinodal decomposition. In this approach interfaces are modeled by the contours of a stochastic standing wave composed of plane wave components propagating in random directions with random phases and having wave numbers distributed according to a given probability density, $P(k)$. We have determined model $P(k)$ functions by fitting the SANS data with the leveled wave scattering function and then used these to construct leveled wave images of the corresponding porous structures. The average pore sizes obtained by measuring chord lengths in the computer models turn out to agree with the values determined for these glasses by mercury porosimetry.

J7.6

CHARACTERIZATION OF CHEMICALLY MODIFIED PORE SURFACES BY SMALL ANGLE NEUTRON SCATTERING. C. J. Glinka, L. C. Sander, N. F. Berk and W. Haller, Natl. Institute of Standards and Technology, Gaithersburg, MD 20899.

Small angle neutron scattering has been used to characterize the structure of linear hydrocarbon chains chemically grafted to the internal pore surfaces of microporous silica particles. The aim of this work has been to relate the structure of the bonded adsorbate layers in these particles to their performance in, for example, reverse phase liquid chromatography. By filling the remaining pore space in the particles with a solution that matches the scattering density of the silica framework, the scattering from the adsorbate layers is enhanced and provides a sensitive probe of the effective thickness, uniformity and degree of solvent penetration in the layers. Results will be presented for monomeric phases of alkyl chains ranging from C4 to C30 bonded to various types of porous silica.

J7.7

PRECURSOR MORPHOLOGY AND MICROSTRUCTURE EVOLUTION IN POROUS SILICA BY SMALL ANGLE SCATTERING. G. G. Long, S. Krueger, D. R. Black, and J. P. Cline, National Institute of Standards and Technology (formerly NBS), Gaithersburg, MD; R. A. Gerhardt, Rutgers Univ., Piscataway, NJ; and P. R. Jemian, Northwestern Univ., Evanston, IL.

Porous silica was studied by means of small angle scattering to determine the microstructure of the precursor bodies as a function of the chemistry of the starting materials, and, in a separate experiment, to follow the microstructure evolution as a function of thermal processing (sintering) during the intermediate and final stages. The morphology of the precursor bodies was followed as a function of the ratio of colloidal silica to potassium silicate in the Shoup processing. For 10% colloidal silica, a broad size distribution was found for the radii of the silica aggregates. However, a narrower size distribution was found for 30% colloidal silica. The results show that the largest measurable particle radius goes as the inverse of the fraction of colloidal silica.

The new technique of multiple small angle neutron scattering (MSANS) offers the possibility of investigating microstructure in the size regime between 0.08 and 10 μm , which is the relevant microstructure size range in ceramics. Such sizes were previously inaccessible without increasing the resolution of the currently available SANS instruments. This study indicated that densification during the intermediate stages of sintering of porous silica is accompanied by pore coarsening to radii $>0.22 \mu m$. In the late stages of sintering, there are no detectable pores with radii $>0.08 \mu m$, and radii of gyration on the order of 30 nm were measured using conventional SANS methods.

J7.8

SMALL ANGLE NEUTRON SCATTERING STUDY OF CRITICAL BINARY FLUIDS IN POROUS GLASSES. S. B. Dierker and P. Wiltzius, AT&T Bell Laboratories, Murray Hill, NJ.

We have previously found that for binary liquid mixtures of 2,6 lutidine and water imbibed into porous VYCOR glass, the phase behavior as well as the temperature dependence of composition fluctuations exhibit a wealth of novel features.¹ These can be understood as resulting from a combination of finite size and random field effects. Elastic light scattering measurements have provided important evidence for a transition from complete to partial wetting behavior.² However, SANS is better matched to studying the short length scale structure of the fluid mixture inside the porous medium.

We measured with SANS the static structure factor $S(q)$ as a function of temperature and composition. By choosing appropriate mixtures of regular and heavy water we adjusted the scattering length densities of the liquid and the glass to be equal on average. The thus determined $S(q)$ of the liquid changes from a Lorentzian in the one phase region to a Lorentzian squared at the random field transition, in agreement with predictions of the Random Field Ising Model. Measurements of the evolution of $S(q)$ and of the correlation length with temperature will be presented and discussed.

The work has benefitted from the use of facilities at the Los Alamos Neutron Scattering Center, a national user facility funded as such by the DOE/Office of Basic Energy Sciences.

1. S. B. Dierker and P. Wiltzius, Phys. Rev. Lett. **58**, 1865 (1987).
2. P. Wiltzius, S. B. Dierker, and B. S. Dennis, Phys. Rev. Lett. **62**, 804 (1989).

J7.9

SMALL ANGLE NEUTRON SCATTERING STUDY OF SOL-GEL GLASSES. P. Wiltzius and S. B. Dierker, AT&T Bell Laboratories, Murray Hill, NJ.

The basic steps in fabricating sol-gel glasses involve forming a solution of material that undergoes gelation and subsequent drying of the gel. These porous quartz structures have morphologies which are strongly dependent on preparation conditions and characterization on submicron length scales is of great importance. Electron microscopy on these insulating materials is plagued by charging effects and radiation damage. Small Angle X-Ray Scattering techniques are impaired by large absorption, which leaves Small Angle Neutron Scattering (SANS) as a valuable tool. We are going to present SANS data on a variety of sol-gel glasses covering two decades in q -space ($30 \text{ \AA} \leq \text{length scales} \leq 2000 \text{ \AA}$). The results indicate, e. g., that fast gelation produces a clumpy glass, where the building blocks of the network are 80 - 100 Å diameter SiO_2 aggregates. Slow gelation produces a smoother internal surface, which is random down to the smallest length scales probed. Our results do not support the concept that the internal surfaces are rough and have fractal geometry.

The work has benefitted from the use of facilities at the Los Alamos Neutron Scattering Center, a national user facility funded as such by the DOE/Office of Basic Energy Sciences.

J7.10

USE OF NEUTRON DIFFRACTION AND RIETVIED ANALYSIS TO STUDY THE BEHAVIOR OF NEUTRON IRRADIATED URANIUM SILICIDES.* R. C. Bircher, M. H. Mueller, J. W. Richardson, Jr., and J. Faber, Jr., Argonne National Laboratory, Argonne, IL 60439.

Uranium silicides have been considered as potential reactor fuels for high flux reactor based neutron sources. However, U_3Si was found to become amorphous under irradiation and to become mechanically unstable to rapid growth by plastic flow. The stability of U_3Si_2 is also uncertain. In this experiment, we are following in detail the behavior of U_3Si , U_3Si_2 and precipitates of U_3Si_2 in U_3Si irradiated with fast neutrons at room temperature. The specimens contain highly depleted Uranium. Damage is primarily produced by fast fission and spallation of the Uranium atoms, and will be identical to that produced in a reactor. Structural changes are monitored by power neutron diffraction at the Intense Pulsed Neutron Source at Argonne National Laboratory. The data is analyzed with standard Rietvied refinement techniques. Results from these neutron scattering measurements are being correlated with the results of *in situ* electron microscopy study of ion irradiations.

The irradiations are being performed in small steps ($< 3 \times 10^{-8}$ U burn up) in order to closely follow changes in the crystal structures. We have detected a broadening and shifting of Bragg peaks in both irradiated U_3Si and U_3Si_2 . The U_3Si was also found to contain precipitates of U_3Si_2 under tensile strain. This tensile strain is being relieved by the irradiation. Some of the U atom sites in U_3Si , but not U_3Si_2 , have very anisotropic Debye Waller factors which increase with irradiation. During the continuing irradiation,

we will look for chemical disordering and elastic softening that may serve as a precursor for phase changes and amorphization.

J7.11

HELIUM DENSITIES IN BUBBLES PRODUCED IN IRRADIATED NICKEL MEASURED BY SMALL ANGLE NEUTRON SCATTERING.

Q. Li¹, D. Schwahn, H. Schroeder, W. Kesternich, and H. Ullmaier

IFF - KFA Jülich GmbH, 5170 Jülich, FRG

¹HMI Berlin GmbH, 1000 Berlin 39, West-Berlin

The density of He in bubbles produced in irradiated Ni, their size and density have been determined with neutron small angle scattering. We have used nickel specimens implanted with He^3 and He^4 thus creating different scattering contrasts. The scattering measurements were performed before and after isochronal anneals between 400 °C and 900 °C. After the 400 °C treatment only displacement damage was visible. At higher annealing temperatures (between 450 °C and 650 °C) He bubbles were formed; however, there exists still a large number of other defects. Above 700 °C the defects disappear, and a growth of bubbles with a bimodal size distribution is dominating. The size of the larger and smaller bubbles is of the order of 100 Å, and 10 Å and smaller, respectively. TEM studies indicate that the large bubbles appear around grainboundaries and at the surface. The smaller ones appear in the bulk. The experimentally determined gas density in the large bubbles is consistent with the calculated equilibrium value.

J7.12

SURFACE EVAPORATION IN A POLYMER MIXTURE OF

LONG AND SHORT CHAINS. Russell J. Composto and Richard S. Stein, Polymer Research Institute, University of Massachusetts, Amherst, MA*; G. P. Felcher, A. Mansour and A. Karim, Argonne National Laboratory, Argonne, IL**

Neutron reflection measurements were taken on a thin (800 Å) layer of a polymer blend deposited on a silicon substrate. The blend consisted of a deuterated polystyrene of low molecular weight (720) and a protonated polystyrene of high molecular weight (910,000), where the volume fraction of d-PS was 0.20. Our objective was to observe surface enrichment¹ of the short chains upon annealing this mixture of extremely different molecular weights above the glass transition temperature. Instead, when annealed at 180 °C, the sample gradually lost the lighter(deuterated) component without any appreciable excess at the surface. This surprising result spurred a systematic program, where the surface evaporation for melts was tested as a function of the weight of the lighter component as well as the annealing temperature.

J7.13

TRANSESTERIFICATION KINETICS OF A MAIN CHAIN AROMATIC POLYESTER. W. A. MacDonald, ICI Advanced Materials, Wilton, UK; G. McLean; A.D.W. McLenaghan; and R.W. Richards, Dept. Pure and Applied Chemistry, University of Strathclyde, Glasgow G1 1XL, UK

Main chain liquid crystal polymers (MCLCP's) are of interest due to possibility of improved strength, compared to conventional polymers, due to their ability to form highly oriented extended chain structures. Much experimental work has been reported on the organisation of large scale structures in these materials. We are concerned here with a molecular aspect of MCLCP's which may be relevant to their use in polymers and blends.

At high temperatures main chain aromatic polyesters undergo transesterification wherein ester linkages break and reform. Recombination occurs randomly and leads to scrambling of the chemical sequence in the molecule. Using small angle neutron scattering (SANS), we have investigated the kinetics and energetics of this process. In brief, blends of deuterated and hydrogenous aromatic polyester were annealed for known times at selected temperatures. The SANS data for the quenched specimens was analysed following the suggestion of Benoit et al which provided rate constants and the average number of reactions per molecule for the transesterification process. The activation energy obtained is 71 kJmol⁻¹, polyethylene terephthalate has an activation energy of 152 kJmol⁻¹.

J7.14

SANS STUDY OF CAPILLARY CONDENSATION IN POROUS MEDIA. M.Y. LIN, *National Institute of Standards and Technology, React A106, Gaithersburg, MD 20889 and Department of Physics, Princeton University, Princeton, NJ 08544*, S.K. SINHA, J.S. HUANG, B. ABELES AND J.M. DRAKE, *Exxon Research and Engineering Co., Rt. 22 E, Annandale, NJ 08801*.

With small angle neutron scattering (SANS) we study the capillary condensation of fluids in porous media. We use Vycor glasses with a porosity of ~ 0.31. By choosing an appropriate mixture of Hexane and deuterated Hexane, the scattering length density of the mixture is adjusted to be equal to that of Vycor in average. The condensation is controlled by changing the vapor pressure of the mixture in Vycor. As the fluids condenses on the Vycor surface, we use SANS to determine the change in effective porosity, surface roughness and internal surface area as a function of vapor pressure p ($0 < p < p_0$ where p_0 is the saturated vapor pressure). In addition,

results from other independent measurements of the same system, e.g., isotherm measurements, will also be discussed and compared with the SANS data.

SYMPOSIUM K:
ADVANCED ELECTRONIC
PACKAGING MATERIALS

K

November 27-29, 1989

Chairs

Che-Yu Li
Department of Materials
Science & Engineering
Cornell University
Bard Hall
Ithaca, NY 14853
(607) 255-4349

C. Julian Chen
IBM T.J. Watson Research Center
P. O. Box 218
Yorktown Heights, NY 10598
(914) 945-2935

Julian P. Partridge
IBM T.J. Watson Research Center
P. O. Box 218
Yorktown Heights, NY 10598
(914) 945-3113

Andrew Barfknecht
Conductus, Inc.
969 W. Maude Avenue
Sunnyvale, CA 94086
(408) 732-3181 ext. 163

Symposium Support

National Science Foundation

**Proceedings published as Volume 167
of the Materials Research Society
Symposium proceedings series.**

SESSION K1: OVERVIEW

Chairs: Donald E. Barr and C. A. Neugebauer
Monday Morning, November 27
Provincetown/Orleans (M)

8:30 *K1.1

FUTURE PACKAGING DIRECTIONS IN THE 1990's AND THEIR MATERIALS CHALLENGES, Dean E. Eastman, IBM T.J. Watson Research Center, Logic, Memory AND Packaging, Yorktown Heights, NY.

9:15 *K1.2

MATERIAL DEVELOPMENT CHALLENGES IN HIGH-DENSITY PACKAGING OF ADVANCED VLSI MEMORY DEVICES, Steven D. Prough, Intel Corporation, Components Technology Development Group, Plastic Package Engineering, Chandler, AZ.

10:00 *K1.3

MATERIALS, MECHANICAL AND THERMAL CONSIDERATIONS OF HIGH DENSITY MULTI-CHIP ELECTRONIC PACKAGES, J.P. Krusius, Cornell University, School of Electrical Engineering, Ithaca, NY.

10:45 BREAK

11:00 *K1.4

POLYIMIDE-CERAMIC SUBSTRATE FOR SUPERCOMPUTER PACKAGING, K. Kimbara, A. Dohya, T. Watari, NEC Corporation, Computer Engineering Division, Tokyo, Japan.

11:30 *K1.5

GLASS-CERAMICS FOR MICROELECTRONIC PACKAGING, John F. MacDowell and George H. Beall, Corning Incorporated, Research Department, Corning, NY.

SESSION K2: OPTOELECTRONICS

Chairs: Carolyn A. Paddock and John J. Ritsko
Monday Afternoon, November 27
Provincetown/Orleans (M)

1:30 *K2.1

OPTICAL INTERCONNECT TECHNOLOGY FOR MULTI-PROCESSOR NETWORKS, John D. Crow, IBM T.J. Watson Research Center, Yorktown Heights, NY.

*Invited Paper

Short Courses P-15, "Ohmic Contacts to Compound Semiconductors," and F-04, "Micro-electronic Packaging: Materials, Processing, and Reliability," may be of interest to symposium attendees. Details regarding course dates and instructors are provided in the short course section of this program.

2:15 *K2.2

FEMTOSECOND TIME DOMAIN TECHNIQUES FOR CHARACTERIZATION OF LINEAR AND NONLINEAR OPTICAL PROPERTIES IN GaAs WAVEGUIDES, K.K. Anderson, M.J. LaGasse, H.A. Haus, and J.G. Fujimoto, Massachusetts Institute of Technology, Department of Electrical Engineering and Computer Science, and Research Laboratory of Electronics, Cambridge, MA.

2:45 *K2.3

OPTICAL WAVEGUIDES IN THE COMPUTER ENVIRONMENT, Modest M. Oprysko, IBM T.J. Watson Research Center, Yorktown Heights, NY.

3:15 BREAK

3:30 *K2.4

INTEGRATED OPTICAL DEVICES IN SEMICONDUCTOR MATERIALS, Thomas L. Koch, AT&T Bell Laboratories, Holmdel, NJ.

4:00 *K2.5

OPTICAL INTERCONNECT SWITCH, Paul R. Prucnal, Princeton University, Department of Electrical Engineering, Princeton, NJ.

4:30 *K2.6

GLASS SEALING OF OPTICAL FIBERS, Kathleen S. Abbott, E.I. duPont de Nemours & Co., Inc., Engineering Development Laboratory, Wilmington, DE.

SESSION K3: POLYMERS

Chair: Paul S. Ho
Tuesday Morning, November 28
Provincetown/Orleans (M)

8:30 *K3.1

PHOTOSENSITIVE POLYIMIDES, Hiroo Hiramoto, Toray Industries, Inc., Electronic and Imaging Materials Research Laboratories, Shiga, Japan.

9:00 *K3.2

STRUCTURE AND PROPERTIES OF LIQUID CRYSTAL POLYMERS, Samuel I. Stupp, University of Illinois at Urbana-Champaign, Department of Materials Science & Engineering Urbana, IL.

9:30 K3.3

NEW PHOTOSENSITIVE POLYIMIDE (SIM2000XL-RTS) FOR PACKAGING APPLICATIONS, H.S. Kwok, State University of New York at Buffalo, Institute on Superconductivity, Amherst, NY; S. Jeng, M. Xu, P.L. Liu, State University of New York at Buffalo, Department of Electrical and Computer Engineering, Amherst, NY; C.J. Lee, Occidental Chemical Corporation, Technology Center, Grand Island, NY.

9:45 K3.4

ENVIRONMENTALLY STABLE POLYMERS FOR ELECTRONIC PACKAGING FROM SOLUBLE INTERMEDIATES, C.K. Ober, T. Mates, and H. Martin, Cornell University, Department of Materials Science and Engineering, Ithaca, NY.

10:00 **K3.5**

THE PREPARATION AND PROPERTIES OF A NEW FAMILY OF AMORPHOUS FLUOROPOLYMERS: TEFLON AF, Paul R. Resnick, E. I. duPont de Nemours & Co., Inc., Polymer Products Department, Wilmington, DE.

10:15 BREAK

10:30 **K3.6**

INELASTIC DEFORMATION AND FRACTURE OF POLYMER COMPOSITES, D.M. Shinozaki, University of Western Ontario, Department of Materials Engineering, London, Canada.

11:00 **K3.7**

SOLVENT DIFFUSION IN SELECTED POLYIMIDE FILMS, W.P. Pawlowski, M.I. Jacobson, M.E. Teixeira and K.G. Sakorafos, IBM Corporation, Systems Technology Division, Endicott, NY.

11:15 **K3.8**

SOLVENT-INDUCED DAMAGE IN POLYIMIDE THIN FILMS, Mu-San Hu, University of California, Santa Barbara, Materials Department, Santa Barbara, CA.

11:30 **K3.9**

DELAMINATION OF METAL-POLYMER INTERFACES WITH SMALL GEOMETRIES, Shih-liang Chiu, Y.H. Jeng, Raul E. Acosta and Paul S. Ho, IBM T.J. Watson Research Center, Yorktown Heights, NY.

11:45 **K3.10**

ORGANIC DIE COAT MATERIALS FOR PLASTIC PACKAGES, R. Padmanabhan, Motorola, Final Manufacturing Research and Development, Physical Electronics and Packaging Laboratory, Phoenix, AZ.

SESSION K4: COMPOSITES

Chairs: Edward A. Giess and C. A. Steidell
Tuesday Afternoon, November 28
Provincetown/Orleans (M)

1:30 ***K4.1**

CERAMIC/POLYMER NANOCOMPOSITE PROPERTIES FOR MICROELECTRONIC PACKAGING, Robert E. Newnham, A. Das, T.T. Srinivasan, Pennsylvania State University, Materials Research Laboratory, University Park, PA.

2:00 ***K4.2**

CHARACTERIZATION OF DIELECTRICS OVER BROAD ELECTRICAL BANDWIDTHS, G. Arjavalingam, Y. Pastol, J.-M. Halbout and G.V. Kopcsay, IBM T.J. Watson Research Center, Yorktown Heights, NY.

2:30 **K4.3**

A NEW MULTILAYERED MATERIAL WITH LOW DIELECTRIC PERMITTIVITY BASED ON INTERCALATION PROPERTIES OF LAYERED COMPOUNDS, Vivek Mehrotra and Emmanuel P. Giannelis, Cornell University, Department of Materials Science and Engineering, Ithaca, NY.

2:45 **K4.4**

CERAMIC FIBER COMPOSITES FOR ELECTRONIC PACKAGING: THERMAL TRANSPORT PROPERTIES, Hongmei Zhang, and David G. Onn, University of Delaware, Applied Thermal Physics Laboratory, Department of Physics AND Astronomy, Newark, DE; and John Bolt, E.I. duPont de Nemours and Company, Experimental Station, Wilmington, DE.

3:00 **K4.5**

PREPARATION OF Al_2O_3 -COATED METAL SUBSTRATE FOR HIGH DENSITY ELECTRONIC ASSEMBLY, K. Nakada, M. Ono and S. Kosuge, NKK Corporation, Steel Research Center, Kawasaki, Japan.

3:15 **K4.6**

METAL MATRIX COMPOSITE MATERIALS FOR ELECTRONIC PACKAGING, M.N. Gungor, Westinghouse Science and Technology Center, Pittsburgh, PA; and J.D. Gardner, Westinghouse Electronics Systems Group, Baltimore, MD.

3:30 BREAK

3:45 ***K4.7**

ADHESION, REACTION AND STABILITY OF METAL/POLYMER INTERFACES, J. Kim, S.P. Kowalczyk, IBM T.J. Watson Research Center, Yorktown Heights, NY; Y.H. Kim, IBM T.J. Watson Research Center, Yorktown Heights, NY and KAIST, Chung-Ryang, Seoul, Korea; T.S. Oh and G.F. Walker, IBM T.J. Watson Research Center, Yorktown Heights, NY.

4:15 **K4.8**

X-RAY DIFFRACTION STUDIES OF THE DELAMINATION OF COPPER THIN FILMS FROM GLASS AND SILICA SUBSTRATES, Alan G. Fox, Naval Postgraduate School, Department of Mechanical Engineering, Monterey, CA; and Rowland M. Cannon, University of California, Lawrence Berkeley Laboratory, Center for Advanced Materials, Berkeley, CA.

4:30 **K4.9**

THE EFFECT OF N_2 ADDITION ON SPUTTERED TITANIUM BORIDE FILMS, N.C. Saha and R.K. Sharma, Motorola Inc., Phoenix, AZ.

4:45 K4.10

RBS ANALYSIS OF PHOSPHOR PACKAGES FOR LASER-HEAT TL DOSIMETRY, Stanley H. Stern, Jack L. Price, Naval Surface Warfare Center, White Oak Laboratory, Nuclear Branch, Silver Spring, MD; Donald G. Simons, Naval Surface Warfare Center, White Oak Laboratory, Nuclear Branch, Silver Spring, MD and Catholic University of America, Physics Department, Washington, DC; David J. Land and Veerendra K. Mathur, Naval Surface Warfare Center, White Oak Laboratory, Nuclear Branch, Silver Spring, MD.

SESSION K5: POSTER SESSION
ADVANCED PACKAGING MATERIALS

Chair: A. Barfknecht
Tuesday Evening, November 28
7:00 p.m. - 10:00 p.m.
America Ballroom (W)

K5.1 DIELECTRIC PROPERTIES OF SINTERED AlN, R.D. Harris, R.C. Enck and J.L. Fields, BP Research, Cleveland, OH.

K5.2 TIME-RESOLVED LUMINESCENCE OF OXYGEN-RELATED DEFECTS IN ALUMINUM NITRIDE, J.H. Harris and R.A. Youngman, BP Research, Cleveland, OH.

K5.3 A TECHNIQUE FOR BRAZING ALUMINUM NITRIDE SUBSTRATES, M. Grant Norton, Cornell University, Department of Materials Science and Engineering, Ithaca, NY; Jacek M. Kajda, Brian C.H. Steele, Imperial College of Science, Technology and Medicine, Department of Materials, London, United Kingdom.

K5.4 THE MICROSTRUCTURE AND MICROCHEMISTRY OF TUNGSTEN AND TUNGSTEN COMPOUND REACTIONS WITH ALUMINUM NITRIDE, A. Stair D. Westwood and Michael R. Notis, Lehigh University, Whitaker Lab #5, Department of Materials Science and Engineering, Bethlehem, PA.

K5.5 LOW TEMPERATURE SILVER-GLASS DIE ATTACH MATERIAL, Mark Blocker and My N. Nguyen, Johnson Matthey Electronics, San Diego, CA.

K5.6 FAST FIRING OF A LOW TEMPERATURE DIELECTRIC BASED ON LEAD MAGNESIUM TUNGSTEN ZIRCONATE TITANATE, S. Mansfield, A.M. Barus, S.M. Landin, and J.A.T. Taylor, Alfred University, New York State College of Ceramics, Department of Ceramic Engineering, Alfred, NY.

K5.7 DENDRITIC FORMATION AND GROWTH OF Si IN THE Cu_3Si MATRIX INDUCED BY ION IRRADIATION AND THERMAL ANNEALING, Jian Li, S. Russell, and J.W. Mayer, Cornell University, Department of Materials and Engineering, Ithaca, NY.

K5.8 OXIDATION OF PB-SN AND PB-SN-X ALLOYS: BULK VS. GRAIN BOUNDARY REGIONS, D.A. Sluzewski, Y.A. Chang, University of Wisconsin, Madison, Department of Materials Science and Engineering, Madison, WI; and V.C. Marcotte, IBM General Technology Division, East Fishkill Facility, Hopewell Junction, NY.

K5.9 NEW TYPE POLYIMIDE FOR MULTI CHIPS MODULE APPLICATION, Hidetaka Satou, and Daisuke Makino, Hitachi Chemical Company Ltd., Yamazaki Works; and Toru Kikuchi, and Takayuki Saito, Hitachi Chemical Company Ltd., Ibaraki Research Laboratory, Ibaraki, Japan.

K5.10 COMPLEXITIES OF COPPER THICK FILM PROCESSING FOR MULTI-LAYER MICROCIRCUITS, Ronald P. Anjard, CPT, Oceanside, CA.

K5.11 INFLUENCE OF FIRING GAS PRESSURE ON THE MICROSTRUCTURE AND THERMAL CONDUCTIVITY OF AlN CERAMICS, E. Udagawa, Fujitsu Laboratories Ltd., Inorganic Materials Laboratory, Kanagawa, Japan; H. Makiyama, N. Kamehara and K. Niwa, Fujitsu Laboratories Ltd., Atsugi, Japan.

K5.12 ION EXCHANGE REACTION IN A THIN FILM OF POLYIMIDE, Yoshiro Akagi, Mariko Ishino, Yasunari Okaoto, Hiroshi Taniguchi, Kohji Ooka and Yoshiharu Nakajima, Sharp Corporation, Corporate Research and Development Group, Nara, Japan.

SESSION K6: ALUMINUM NITRIDE

Chair: John C. Hurt
Wednesday Morning, November 29
Provincetown/Orleans (M)

8:45 *K6.1
ALUMINUM NITRIDE: A REVIEW OF THE KNOWLEDGE BASE FOR PHYSICAL PROPERTY DEVELOPMENT, G.R. Miller, The Carborundum Company, Phoenix, AZ.

9:15 K6.2
TEMPERATURE DEPENDENCE OF THE THERMAL CONDUCTIVITY OF ALUMINUM NITRIDE SUBSTRATES: MEASURING AND MODELLING EFFECTS OF MICROSTRUCTURE AND IMPURITIES, Ralph B. Dinwiddie and David G. Onn, University of Delaware, Applied Thermal Physics Laboratory, Department of Physics and Astronomy, Newark, DE.

9:30 K6.3
TEMPERATURE DEPENDENCE OF THERMAL CONDUCTIVITY OF ELECTRONIC CERAMICS BY AN IMPROVED FLASH DIFFUSIVITY TECHNIQUE, R.C. Enck and R.D. Harris, BP Research, Cleveland, OH.

9:45 **K6.4**
STRUCTURE AND PROPERTIES OF C-AXIS ORIENTED ALN FILMS REACTIVELY DEPOSITED BY DC PLANAR MAGNETRON SPUTTERING, T. Takahashi, Toyama University, Electrical Engineering Department, Toyama, Japan; Fumio Takeda, Toyama Technical College, Electrical Engineering Department, Toyama, Japan; Masahiko Naoe, Tokyo Institute of Technology, Physical Electronics Department, Tokyo, Japan.

10:00 **K6.5**
ON THE STRUCTURE OF PLANAR DEFECTS IN ALN, Stuart McKernan and C. Barry Carter, Cornell University, Department of Materials Science and Engineering, Ithaca, NY.

10:15 BREAK

10:45 **K6.6**
PLANAR AND CURVED DEFECTS IN ALUMINUM NITRIDE: THEIR MICROSTRUCTURE AND MICROCHEMISTRY, Alistair D. Westwood, and Michael R. Notis, Lehigh University, Department of Materials Science and Engineering, Whitaker Lab #5, Bethlehem, PA.

11:00 **K6.7**
INVERSION DOMAIN BOUNDARIES AND OXYGEN ACCOMMODATION IN ALUMINUM NITRIDE, R.A. Youngman, J.H. Harris, BP Research, Cleveland, OH; P.A. Labun and R.J. Graham, Arizona State University, Center for Solid State Science, Tempe, Az.

11:15 **K6.8**
THE LOAD DEPENDENCE OF Ti/Al₂O₃ AND Ti/AlN INTERFACIAL CRACK PROPAGATION, Tao Liu, Michael R. Notis and Y.T. Chou, Lehigh University, Whitaker Lab #5, Department of Materials Science and Engineering, Bethlehem, PA.

11:30 **K6.9**
THICK FILM METALLIZATION OF ALUMINUM NITRIDE, M. Grant Norton, Cornell University, Department of Materials Science and Engineering, Ithaca, NY; Brian C.H. Steele, Imperial College of Science, Technology and Medicine, Department of Materials, London, United Kingdom.

SESSION K7: METALLIZATION AND INTERCONNECTS

Chairs: Caroline A. Kovac
Wednesday Afternoon, November 29
Provincetown/Orleans (M)

1:30 ***K7.1**
ELECTROLESS METAL DEPOSITION - CHALLENGES & OPPORTUNITIES, Mahadevaier Krishnan, and R. Jagannathan, IBM T.J. Watson Research Center, Yorktown Heights, NY.

2:00 **K7.2**
ELECTROLESS PLATING OF COPPER INTERCONNECTIONS ON ION BEAM CATALYZED POLYIMIDE, T. Flottmann, Akzo Research Laboratories, Department ARLO-C/NM, Obernburg, West Germany; A. Tulke, Akzo Research Laboratories, Department ARLO-PA, Obernburg, West Germany; E. Esper, Akzo Research Laboratories, Department ARLO-C/NM, Obernburg, West Germany; W. Lohmann, Akzo Research Laboratories, Department ARLO-PA, Obernburg, West Germany.

2:15 **K7.3**
REAL-TIME INVESTIGATION OF SOLID AND LIQUID STATE REACTIONS IN AU-SN/CU SYSTEM, Seyong Oh, Igor Y. Khandros, IBM T.J. Watson Research Center, Yorktown Heights, NY; and Janet L. Poetzinger, IBM GTD, Hopewell Junction, NY.

2:30 **K7.4**
OXIDATION KINETICS OF (Pb,In) SINGLE-PHASE ALLOYS, M.-X. Zhang, Y.A. Chang, University of Wisconsin, Madison, Department of Materials Science and Engineering, Madison, WI; and V.C. Marcotte, IBM General Technology Division, East Fishkill Facility, Hopewell Junction, NY.

2:45 **K7.5**
PHASE STABILITY AND MECHANICAL BEHAVIOR OF TERNARY BISMUTH-LEAD-TIN SOLDERS, W.J. Whealon, D.S. Stone, Y.A. Chang, University of Wisconsin, Madison, Department of Materials Science and Engineering, Madison, WI.

3:00 BREAK

3:30 **K7.6**
CONTACT REACTIONS AT THIN FILM ALUMINUM-TRANSITION METAL INTERFACES, Bernd Schuhmacher and Uwe Köster, University of Dortmund, Department of Chemical Engineering, Dortmund, West Germany.

3:45 **K7.7**
RESIDUAL STRESSES IN FILAMENT-EVAPORATED ALUMINUM FILMS ON SINGLE CRYSTAL SILICON WAFERS, Hai Woong Park and Steven Danyluk, University of Illinois at Chicago, Department of Civil Engineering, Mechanics, and Metallurgy, Chicago, IL.

4:00 **K7.8**
ELECTROMIGRATION IN THIN FILMS OF Au ON GaAs, P.F. Tang, A.G. Milnes, Carnegie Mellon University, Department of Electrical and Computer Engineering, Pittsburgh, PA; C.L. Bauer, and S. Mahajan, Carnegie Mellon Univ., Department of Metallurgical Engineering and Materials Science, Pittsburgh, PA.

4:15 **K7.9**
INTERDIFFUSION OF Cu/Co, Co/Au AND Cu/Co/Au THIN FILMS, P. Madakson and J. Liu, IBM T.J. Watson Research Center, Yorktown Heights, NY.

K1.1

FUTURE PACKAGING DIRECTIONS IN THE 1990's AND THEIR MATERIALS CHALLENGES

Dean E. Eastman, Vice-President, Logic, Memory & Packaging, IBM, T.J. Watson Research Center, Yorktown Heights, NY 10598

As we enter the 1990's, Si IC technology continues to rapidly advance from VLSI towards ULSI, e.g., to the 64 Mb DRAM chip and beyond. With these Si advances in density, performance and cost reduction, packaging technology will also have to rapidly advance to meet packaged electronics systems requirements, ranging from supercomputers, mainframes, and workstations to consumer electronics. Metals, polymers and ceramics will be used in increasingly more dense and complex package structures to support ULSI interconnection, cooling, reliability and physical support functions. New and improved materials synthesis, characterization, and especially processing of these complex package structures of films and interfaces will be required. An overview of packaging materials and processing trends and challenges, both development and manufacturing, in the 1990's will be described.

K1.2

MATERIAL DEVELOPMENT CHALLENGES IN HIGH-DENSITY PACKAGING OF ADVANCED VLSI MEMORY DEVICES. Steven E. Frough, Intel Corp; Components Technology Development Group, Chandler, Arizona 85226

Design objectives for semiconductor memory systems using DRAM or SRAM technologies have traditionally been focussed on density, cost and reliability factors. Component packaging played a major role in determination of reliability and cost, while density was primarily driven by chip level integration. Future systems for hand held, laptop, and disk replacement applications based on new, nonvolatile technologies will put much more emphasis on package densification. Credit card sized modules with capacity up to 50 megabytes are in the concept stages based on announced plans of semiconductor manufacturers to develop ever denser, higher capacity chips.

Material challenges will derive from the need to significantly shrink component packages to minimum size needed to support chip-to-system interconnects. This will have to be achieved without sacrificing reliability, yet cost per bit will be expected to continue its downward trend. The initial response is already evident in development of small, ultra-thin plastic surface mount component (PSMC) packages which are only slightly larger than the IC chips (dies) embedded in them. Problems that are exacerbated by this miniaturization include: moisture absorption rate, fragility of terminal leads and sensitivity to thermal stress in SMT assembly and field service. Material and design improvements will be required to mitigate these effects and increase stress

Strategies which seem likely to be employed include tape automated bonding (TAB), die coating and support structures for outer lead terminals. This paper presents a rationale for each strategy and discusses synergies leading to an optimized packaging system.

K1.3

MATERIALS, MECHANICAL, AND THERMAL CONSIDERATIONS OF HIGH DENSITY MULTI-CHIP ELECTRONIC PACKAGES.* J.P. Krusius, Cornell University, School of Electrical Engineering, Ithaca, New York 14853.

Advanced electronic systems increasingly derive their performance gains from density on all packaging levels. This trend is particularly pronounced for first level packages and has lead to an enhanced research effort on multi-chip modules. Fundamental limits studies have shown that density improvements by orders of magnitude are possible [1]. Recent analyses of multi-chip packages using package system simulation [2], a

new systematic design methodology for electronic packaging, have concluded that comparable performance goals can be met with several competing solutions differing in their materials, mechanical, thermal and manufacturability characteristics. Complex design tradeoffs will thus determine future high density multi-chip modules. A set of such competing modules solutions will be found for high density CMOS and bipolar based IC technologies using package system simulation. Materials, mechanical, and thermal tradeoffs will then will be identified and discussed. Based on this, the competing multi-chip modules will be ranked and compared with current trends in existing multi-chip module technologies. Finally, materials research issues will be identified.

K1.4

POLYIMIDE-CERAMIC SUBSTRATE FOR SUPERCOMPUTER PACKAGING

K. Kimbara, A. Dohya, T. Watari, NEC Corporation
1-10, Nisshin-Cho, Fuchu City, Tokyo 183 JAPAN

This paper introduces the Polyimide-Ceramic substrate for the NEC SX Supercomputers. In case of high performance system such as supercomputers and top end machines in general purpose computers, sophisticated packaging technologies are essential to achieve fastest operations as well as to use highest-speed, highly integrated LSIs. Wiring substrate which mounts and interconnects LSIs is the key to back up LSI's higher logical-operations. The high speed interconnection wirings and high density LSI mounting are requested for the substrate. The Polyimide-Ceramic substrate had been developed to meet these demands and have many features of high density thin film wirings, high power supply, high thermal conductivity and huge number of I/Os, in addition to high speed wirings.

25 μ m wide, 75 μ m center-to-center spacings, up to four signal layers, 6ns/cm signal transmissions, 2.5W/cm² to 6.5W/cm² high power density, 2177 to 11500 I/Os on a 10cm to 22.5cm square substrate have been achieved by using this super substrate technology.

The packaging hierarchy, the first level packaging of TAB LSI, the second level of multi-chip packaging by using Polyimide-Ceramic substrate and liquid cooling module, and the third level of board assemblies are introduced.

K1.5

GLASS-CERAMICS FOR MICROELECTRONIC PACKAGING. John F. MacDowell and George H. Beall, Corning Incorporated, Corning, NY.

Glass-ceramics appear to constitute a new generation in microelectronic packaging materials. Some recently developed glass-derived ceramic materials with low dielectric constants and thermal expansivities matching silicon are described. These materials include cordierite solid solutions, boron phosphates, fluorimicas, and microfoams.

A distinction is made between glass-ceramics derived via internal nucleation and crystallization of bulk glass and those formed by sintering and surface devitrification of glass particulates.

Sintered mixtures of glass and crystalline particulates, although not glass-ceramics, are also described.

K2.1

OPTICAL INTERCONNECT TECHNOLOGY FOR MULTI-PROCESSOR NETWORKS John D. Crow, IBM, Watson Res. Ctr, P.O. Box 218, Yorktown Heights, NY

The interconnection of many processors in order to increase the computing power of the ensemble is of growing importance in the data processing industry. For higher speed networks, optical interconnects will be attractive if they can be implemented with Gigabit/sec speed, highly integrated components, packaged onto compact modules, compatible with DP equipment cards and assembly processes. The technology must also demonstrate high reliability and almost error free operation in the computing system environment. Adapting the current long-transmission distance optimized optical technology, consisting of discrete devices, custom assembled into hybrid packages, with sub-micron optical alignments, seems ill suited to the near-term realization of an optical interconnect technology which will be competitive with electrical wiring approaches.

At IBM we have developed an optimized optical technology for short distance, highly integrated, Gigabit/sec speed links. We have used a $1\ \mu\text{m}$ GaAs E/D MESFET with SBL and DCS logic families to fabricate Tx and Rx chips with most of the link adapter functions (i.e. serialization, clocking, line driving, and receiving) required to interface a data bus with a fiber optic network.

K2.2

FEMTOSECOND TIME DOMAIN TECHNIQUES FOR CHARACTERIZATION OF LINEAR AND NONLINEAR OPTICAL PROPERTIES IN GaAs WAVEGUIDES. K. K. Anderson, M. J. LaGasse, H. A. Haus, and J. G. Fujimoto, Massachusetts Institute of Technology, Dept. of Electrical Engineering and Computer Science, and Research Laboratory of Electronics, Cambridge, MA 02139.

Femtosecond time domain measurements can provide a powerful approach for characterizing both the nonlinear as well as linear optical properties of waveguide devices. Measurements of the nonresonant χ_3 or nonlinear index are of central importance for applications in all optical switching. We describe a new approach for directly measuring nonlinear index in waveguide devices using femtosecond pump probe time division interferometry. This technique achieves high sensitivity and reduces acoustic and thermal fluctuation artifacts in an interferometric measurement by using time division multiplexing and differential detection. Sensitivities of $\lambda/500$ are obtained without active stabilization. Combining this technique with a wavelength tunable femtosecond laser source permits measurements to be performed as a function of wavelength. We describe studies of the nonresonant nonlinear index in bulk GaAlAs waveguides as well as preliminary measurements in MQW waveguides. In addition to interferometry, pump probe measurements of induced absorption can provide information on the dynamics of carrier generation and state filling. Finally, time of flight or multiple echo studies of pulse propagation in the waveguide are a measurement of loss and dispersion. Systematic measurements of the wavelength dependence of nonlinear index n_2 , two-photon absorption β , as well as simple linear measurements of absorption α can provide a comprehensive characterization of the waveguide device.

K2.3

OPTICAL WAVEGUIDES IN THE COMPUTER ENVIRONMENT? Modest M. Oprysko, IBM Research Division, T.J. Watson Research Center, P.O. Box 218, Yorktown Heights, NY 10598.

It is anticipated that optics will play an increasing role in future high performance computer systems. However, the incompatibility of today's optoelectronic packaging technology with high performance microelectronic packaging is an impediment to the introduction of optics in the computer environment. Optical waveguides may provide a natural path for the integration of electrical and optical devices. These optical waveguides should be capable of providing high density optical interconnect, be thermally stable, compatible with standard electronic packaging processes, etc. Progress in optical waveguide work for computer applications from several laboratories will be presented.

K2.4 ABSTRACT NOT AVAILABLE

K2.5

OPTICAL INTERCONNECT SWITCH. Paul R. Prucnal, Dept. of Electrical Engineering, Princeton University, Princeton, NJ 08544.

The speed of VLSI circuits is experiencing a diminishing growth rate due to electrical I/O bottlenecks at the chip and board levels. It is well-known that this electrical pin-out problem can be remedied with fiber-optic interconnects, since the information capacity of a single optical fiber is several orders of magnitude greater than an electrical transmission line. However, the increase in channel capacity offered by optical fibers does not, by itself, solve the pin-out problem. It is important that the interconnections be reconfigurable, so that different functions can be performed without physically restructuring the interconnection. The reconfiguration of interconnects can be performed, for example, by using a photonic switch. Photonic switches have been shown to have a very large transmission bandwidth and faster reconfiguration time than their electronic counterparts, but photonic switches with high-interconnect capability have not yet been demonstrated. The integration of switch arrays with large dimension is limited by the minimum physical dimension of an individual optical switching element, as well as by its crosstalk and the waveguide propagation loss. These factors restrict the dimension of a monolithic $N \times N$ optical switch array to about $N=10$ input/output ports. In this talk, the experimental demonstration of a novel switching architecture for optical interconnects is reported. This switch multiplexes the signals from all input ports onto a common optical transmission channel. The multiplexed signals are then broadcast to all output ports. The switching function is achieved by demultiplexing the desired input port, making high-dimensionality switches feasible.

K2.6

GLASS SEALING OF OPTICAL FIBERS. Kathleen S. Abbott, E. I. du Pont de Nemours & Co. (Inc.), Engineering Development Laboratory 101 Beech Street, P.O. Box 80840 Wilmington, Delaware, 19880-0840

As a replacement for metallized fibers soldered into packages, a method was developed to glass-seal bare optical fibers into metal tubes. The glass seal protects the package hermetically from the environment and eliminates the use of epoxies and metallization techniques. Much work was done to test the influence of system variables on the functionality and long-term life of the seal. Results indicate a stable product from the standpoint of temperature, mechanical stability and optical signal integrity.

The design challenge lay in the choice of both the metal tube and

the solder glass. Correct material and processing selection resulted in a highly stable fiber subassembly versatile enough for use in many optoelectronic, electro-optic and like devices.

Packaging and optical alignment required that the seal maintain a high degree of hermeticity, pure optical integrity before and after sealing, ability to withstand temperature cycling, and geometric centering of the optical fiber within the glass seal. The product, which has been developed and tested by Du Pont in collaboration with British Telecom Research Labs, meets all these requirements and is being manufactured at BT&D.

K3.1

PHOTOSENSITIVE POLYIMIDES Hiroo Hiramoto, Toray Industries, Incorporated, Sonoyama, Otsu City, Shiga 520, Japan

Photosensitive polyimides are used as interdielectrics and protection coatings of electronic devices. They can easily give fine-patterned films with excellent characteristics of polyimides by photolithographic procedure.

Photosensitive polyimides are composed of polyimides or polyimide precursors with photosensitive groups and can be converted into polyimides by heat curing. Photosensitive groups such as double bonds, azides, o-naphthoquinonediazides or o-nitrobenzyl are incorporated to polymer chains through covalent bonds or acid-amine salts. Some polyimides have photosensitivity even without specially introduced photosensitive groups. Most of photosensitive polyimides are negative-working, but a few of them are positive-working.

Characteristics of photosensitive polyimides are fixed by two factors, the method of introducing photosensitive group and the structure of polyimide backbone chain. Photosensitivity, resolution, purity, easiness of imide conversion reaction depend mainly on the former factor. The film properties after curing are mainly determined by the latter and are also affected by the former when imide cyclization is imperfect.

Photosensitive polyimides are widely used as buffer coatings and interdielectrics of LSI, interdielectrics of LSI assembly packages for computers, and protection coatings of electronic devices such as linephotosensors.

K3.2

STRUCTURE AND PROPERTIES OF LIQUID CRYSTAL POLYMERS. Samuel I. Stupp, Department of Materials Science and Engineering, University of Illinois at Urbana-Champaign, Urbana, IL

Thermotropic liquid crystal polymers are a new class of polymeric substances which may find application as advanced electronic packaging materials. This possibility is based on the thermo-mechanical and dielectric properties of some of these new materials. Aromatic polyesters are one of the chemical families of thermotropic liquid crystal polymers and these are at the moment commercially available in the USA, Europe and Japan. These materials are particularly interesting because of their high thermal stabilities as solids and because they melt into fluids with relatively low viscosities given their nematic nature. Upon solidification the ordered fluids crystallize partially yielding materials of high strength and low coefficients of thermal expansion. One of the aromatic polyesters, the homopolymer of p-hydroxybenzoic acid, has one of the highest ambient temperature thermal conductivities known for polymeric materials. Also many of these new materials exhibit excellent chemical resistance and low dielectric constants. The lecture will discuss some of the fundamental links between the observed properties and the molecular constitution of these materials. Another topic to be covered is the impact of surfaces and external forces on the molecular orientation of thin layers.

K3.3

NEW PHOTOSENSITIVE POLYIMIDE (SIM2000XL-RTS) FOR PACKAGING APPLICATIONS. H.S. Kwok, S. Jeng, M. Xu and P.L. Liu, Department of Electrical and Computer Engineering, State University of New York at Buffalo, Amherst, N.Y.; C.J. Lee, Occidental Chemical Corporation, Technology Center, Grand Island, N.Y.

Polyimides are finding increased use as dielectric materials in multi-level metalization technology, which is the key to high-density packaging applications for microelectronics.

Newly developed photosensitive polyimidesiloxane (SIM2000XL-RTS) has been evaluated in terms of thermal stability, photosensitivity and lithography as well as electrical breakdown properties. The sensitivity to N₂ laser exposure has been measured under optimized process conditions. We also find that SIM2000XL-RTS can be processed up to 350°C without significant decomposition. Micron-scale contact images can be successfully patterned by both N₂ laser and conventional UV exposure. The electrical breakdown field strength of SIM2000XL-RTS is about 4 MV/cm by sandwich measurements.

K3.4

ENVIRONMENTALLY STABLE POLYMERS FOR ELECTRONIC PACKAGING FROM SOLUBLE INTERMEDIATES. C. K. Ober, T. Mates, and H. Martin, Materials Science & Engineering, Cornell University, Ithaca, NY 14853-1501

We are investigating new polymers based on poly(phenylene vinylene), PPV and poly(phenylene), PP. Like Kapton, the well known polyimide, these polymers can be spincoated from soluble intermediates and converted to their thermally stable forms by elimination of small groups during a heating cycle. As such, these polymers are insulating. Unlike Kapton, both poly(phenylene vinylene) and poly(phenylene) have the potential for metallic conductivity when properly doped.

During curing, the complete removal of the leaving groups is important in determining the final behavior of the cured polymer film. Elimination of the leaving groups was followed by means of Rutherford Backscattering analysis for various curing conditions and environments. We will describe the curing and film-forming properties of these polymers, and discuss both their dielectric characteristics and thermal stability as a function of the curing conditions.

K3.5

THE PREPARATION AND PROPERTIES OF A NEW FAMILY OF AMORPHOUS FLUOROPOLYMERS: TEFLON® AF. Paul R. Resnick, E. I. Du Pont de Nemours & Company, Inc., Polymer Products Department, P. O. Box 80353, Wilmington, DE. 19808-0353

Teflon® AF is a new family of amorphous fluoropolymers based on bis-2,2-trifluoromethyl-4,5-difluoro-1,3-dioxole which has unusual properties. In addition to the

superior electrical (e.g. dielectric constant = 1.934 @ 1 MHZ), chemical resistance and thermal properties associated with fluoropolymers the Teflon[®] AF family possesses glass transition temperatures as high as 300° resulting in improved physical characteristics. The polymers have extremely high optical clarity and have limited solubility in some commercially available perfluorinated ethers. Teflon[®] AF polymers may be either solution cast into clear micron thin films or melt processed into a variety of forms.

K3.6

INELASTIC DEFORMATION AND FRACTURE OF POLYMER COMPOSITES. D.M. Shinozaki Department of Materials Engineering, University of Western Ontario, London, Ontario, N6A5B8 CANADA

The study of the mechanical integrity of multi-phase systems such as polymer-metal, polymer-ceramic and polymer-polymer composites involves some aspects of both continuum mechanics and materials science. A review of some topics which relate these two general approaches will emphasize methods to measure useful parameters. Some important considerations which are often overlooked, and which should be evaluated are the pressure dependence of inelastic deformation, non-constant volume plastic flow, time and temperature dependent response and inhomogeneity of plasticity. The need for including these considerations will be discussed briefly.

K3.7

SOLVENT DIFFUSION IN SELECTED POLYIMIDE FILMS. W.P. Pawlowski, M.I. Jacobson, M.E. Teixeira, and K.G. Sakorafos, IBM Systems Technology Division, Endicott, NY 13760

The absorption of several solvents including methylene chloride (MC), methyl chloroform (MCF), γ -butyrolactone (BLO), dibromomethane (DBRO), 1,2-dichloroethane (DCE), and 1,2-dichloropropane (DCP) in Kapton H[™], Upilex S[™], and Upilex R[™] polyimide film was measured gravimetrically. A significant difference in the rate and amount of absorption of these chemicals by the various films was observed. The difference in chemical structure, method of imidization, and film formation play a major role in the absorption properties of the polyimide. The diffusion of MC and DBRO in Kapton H was shown to be Case II by both gravimetric and Rutherford backscattering spectrometry (RBS) analysis. In addition, RBS measurements of DBRO diffusion into the rough (drum) and smooth (air) side of Kapton H film showed that solvent penetrating from the rough side initially penetrates more rapidly. MC diffusion in Upilex R was found to be intermediate between Fickian and Case II using RBS. Although Upilex S showed no MC or DBRO weight gain gravimetrically, RBS analysis showed a small weight gain after extended exposure.

K3.8

SOLVENT-INDUCED DAMAGE IN POLYIMIDE THIN FILMS. Mu-San Hu, Materials Department, University of California, Santa Barbara, CA 93106.

Solvent (e.g.: xylene) induced damage bands formed in residually strained polyimide thin films on Al substrates have been studied. Microscopy studies showed that these damage bands resemble crazes. A mechanics approach is taken to understand this phenomenon.

The characteristics of the damage bands have been compared with the behavior of cracks in brittle thin films. The critical strain for damage formation has been identified. This strain tends to diminish with increase in exposure time. In contrast to the cracking of brittle films, the critical strain exhibits only weak dependence

on the film thickness over a wide range. Strain-enhanced diffusion of solvent into the films is considered to be responsible for the property degradation that leads to damage propagation.

K3.9

DELAMINATION OF METAL-POLYMER INTERFACES WITH SMALL GEOMETRIES. Shih-liang Chu, Y.H. Jeng, Raul E. Acosta and Paul S. Ho. IBM Thomas J. Watson Research Center, Yorktown Heights, NY 10598

Metal-polymer multilayered structures are increasingly used in electronic packaging. The mechanical integrity of such structures is an important concern, particularly regarding the effect due to dimensional reduction on the delamination behavior of the metal-polymer interface. This problem has been investigated using a stretch-deformation method on samples with fine metal lines patterned on polyimide substrates. The samples with patterns of equal-line-space of 4-16 μ m of Au/Cr laminate were photolithographically fabricated on the PMDA-ODA substrate. Preliminary results show that the mode of interfacial failure depend on the line width of the Au/Cr line and the orientation of the metal line with respect to the stretching direction. Only cracking is observed when the orientation of metal lines is parallel to the stretching direction. In the perpendicular direction, the failure behavior changes from a pure delamination mode to a mixed mode of cracking and delamination as the line width decreases from 16 μ m to 4 μ m. Results can be qualitatively accounted for using a simplified model based on two-dimensional stress analysis and the Poisson ratio mismatch between metal and polymer.

K3.10

ORGANIC DIE COAT MATERIALS FOR PLASTIC PACKAGES. R. Padmanabhan, Final Manufacturing Research & Development, Mail Drop B-136, Motorola, 5005 E. McDowell Rd., Phoenix, AZ 85008.

The role of organic materials in electronic packages is constantly being expanded. A fairly recent application is the use of these materials for encapsulating high lead count IC dice, like TAB chips that are bonded directly to the board in plastic packages. Since these packages are non-hermetic, some special constraints are placed in the selection of these die coat materials. Reliability issues that have to be addressed include compatibility with the underlying dielectric medium, chemical resistance, low moisture absorption, corrosion protection and resistance to thermal stresses. This paper discusses some of these concerns and reviews the suitability of different categories of die coat materials for this application. Examples are given from three classes of materials that were investigated in this study, viz., epoxy resins, polysiloxymides and silicones. Results of chemical resistance, thermal cycle, temperature-humidity-bias and other tests are discussed and some suggestions are made for future research in this area.

K4.1

CERAMIC/POLYMER NANOCOMPOSITE PROPERTIES FOR MICROELECTRONIC PACKAGING. Robert E. Newnham, Amitabh Das, Thallam T. Srinivasan, Materials Research Laboratory, The Pennsylvania State University, University Park, PA 16802

The thermal expansion and dielectric properties of various polymer/fumed silica composites have been studied. Both thin film and bulk samples were prepared and the fine silica was dispersed and mixed with the aid of solvents and ultrasonification respectively. TEM micrographs showed the evidence of the formation of a nanocomposite. The dielectric properties were low which is suitable for substrates, but they did not conform to any mixing rules, which are used for micro, or macro composites. The thermal expansion coefficients similarly did not follow any of the composite rules, predicted by effective medium theory and others. An anomalous behavior in the thermal expansion coefficient

was observed, well below the T_g of the polymer. An attempt is made in this study to explain the unique properties of nanocomposites, which cannot be predicted by conventional composite modeling of properties.

K4.2

CHARACTERIZATION OF DIELECTRICS OVER BROAD ELECTRICAL BANDWIDTHS G. Arijalingam, Y. Pastol, J.-M. Halbout, and G.V. Kopcsay, IBM Thomas J. Watson Research Center, Yorktown Heights, New York 10598.

There is considerable recent interest in the dielectric properties of materials measured over broad electrical bandwidths. This follows from advances made in the performance of electronic devices which now produce pulses with risetimes in the order of 5 picoseconds. It is essential to know the dielectric constants and loss properties of the materials used in fabricating these devices and their interconnection structures, up to frequencies of about 100 GHz. In this talk we will describe a novel technique for measuring these properties, from 10 GHz to about 125 GHz, in a single experiment.

The technique is based on transient electromagnetic pulses radiated and received by broadband antennas. The antenna structures are integrated with the high-speed optoelectronic devices used for both electrical pulse generation and for electrical sampling. The radiated electromagnetic pulses have frequency components between 0 and 150 GHz. When a sample is inserted in the microwave beam, the received time-domain signal undergoes attenuation and time delay caused by the absorption and the dispersion of the material respectively. From this, the loss coefficient and dielectric constant can be determined separately, over the wide available bandwidth, using Fourier analysis. Since the radiation is highly polarized, we can also characterize the orientation dependent dielectric properties of anisotropic materials.

We will describe the experimental set-up and the analysis used to make the broadband dielectric characterization, and present results, obtained for the first time at these frequencies, for several materials including polymers, ceramics, and uniaxial crystals.

K4.3

A NEW MULTILAYERED MATERIAL WITH LOW DIELECTRIC PERMITTIVITY BASED ON INTERCALATION PROPERTIES OF LAYERED COMPOUNDS. Vivek Mehrotra and Emmanuel P. Giannelis, Department of Materials Science and Engineering, Cornell University, Ithaca, NY 14853.

Microelectronic packaging in the next generation of very high speed ICs will require materials with very low dielectric constant and loss tangent. New materials based on a series mode in which layers of the two components are stacked alternately with the electric field normal to the layers have been proposed for reducing the dielectric permittivity. Intercalation compounds formed by the insertion of atomic or molecular layers of a guest species in the galleries of the host are excellent precursors for the realization of such superlattices with atomically sharp interfaces.

We have fabricated multilayered films with Angstrom range periodicity by intercalating discrete molecular layers of a polymer in the galleries of insulating layered silicates. The resulting structure exhibits good dimensional stability, good metal adhesion and a very low dielectric constant. The dielectric properties of the pristine layered host, guest species and the intercalated compound will be presented and discussed.

K4.4

CERAMIC FIBER COMPOSITES FOR ELECTRONIC PACKAGING: THERMAL TRANSPORT PROPERTIES. Hongmei Zhang, David G. Onn, ATPL, Department of Physics & Astronomy, University of Delaware, Newark, DE 19716 and John Bolt, Experimental Station, E.I. Du Pont de Nemours and Co., Wilmington, DE, 19898.

Composites which combine the high thermal conductivity of ceramic fibers with the low dielectric constant of polymers are attractive candidates for electronic packaging applications. We have measured the anisotropic thermal diffusivity between 20 K and 500 K of uniaxial, quasi-isotropic and random fiber composites containing various volume fractions of alumina and other fibers. The x-axis and y-axis diffusivities were obtained from a modified Angstrom's Bar while the z-axis diffusivity and specific heat were obtained from an Electronic Pulse technique. The anisotropic thermal conductivities were then obtained from the diffusivities, the density and the specific heat. The uniaxial x-axis conductivities were analyzed using the "parallel model" permitting extraction of the temperature dependence of the fiber conductivities. The y-axis, z-axis and random fiber conductivities were very dependent on the composite microstructure and required more complex composite transport models for analysis. For uniaxial composites the y-axis and z-axis conductivities did not agree for higher fiber loadings as the influence of the anisotropic pre-preg structure influenced the transport properties.

K4.5

PREPARATION OF Al_2O_3 -COATED METAL SUBSTRATE FOR HIGH DENSITY ELECTRONIC ASSEMBLY. K.Nakada, M.Ono and S.Kosuge, NKK Corporation, Kawasaki-ku, Kawasaki, 210, Japan.

The appearance of the higher density assembly together with recent advances in electronic devices has demanded the substrates with higher thermal conductivity. We have succeeded in preparing the new metal substrates insulated with Al_2O_3 thin film by a CO_2 laser evaporation process which was newly developed by authors and characterized by the high deposition rate of ceramics compared with the other conventional deposition processes.

The Al_2O_3 films deposited on Al substrates were examined in terms of chemical composition, microstructure, density, hardness, breakdown voltage, thermal conductivity and so on. The major results are as follows.

- (1) The composition of Al_2O_3 films was nearly stoichiometric relationship.
- (2) Al_2O_3 films were amorphous.
- (3) Al_2O_3 films with 3-15 μm thick were very dense (pore free) and very hard ($H_v = 2000 \text{ kgf/mm}^2$).
- (4) The breakdown voltage was over 100V per $1 \mu m$ thick, which was much higher than that of Al_2O_3 bulk.
- (5) The thermal conductivity was about five times as high as that of Al_2O_3 substrates.

These results lead to the conclusion that this new metal substrate could be very effective for high density electronic assembly.

K4.6

METAL MATRIX COMPOSITE MATERIALS FOR ELECTRONIC PACKAGING.
M. N. Gungor, Westinghouse Science and Technology Center,
Pittsburgh, PA and J. D. Gardner, Westinghouse Electronics
Systems Group, Baltimore, MD.

Due to increased demand for lightweight, high performance integrated circuits, the design of electronics and microwave packaging systems requires lightweight, thermally manageable, fabricable and cost effective materials. Engineered metal matrix composites reinforced with fibers, whiskers and particulates offer new opportunities for design engineers to meet these design criteria. The presence of a low coefficient of thermal expansion reinforcement phase and high thermal conductivity metal matrix allow the packaging to be thermally stable to semiconductor devices and provide heat transfer paths to surroundings. In addition, low density and high modulus of the composites provide weight savings for the package design which is particularly important for space and aerospace electronics systems applications. Because of low cost of fabrication, one particular composite material system of interest for applications is particulate reinforced metal matrix composites.

In this paper, the results of CTE behavior of ceramic particulate reinforced Al metal matrix composites are presented. The effects of reinforcement chemistry, volume fraction, and matrix chemistry are discussed.

K4.7

ADHESION, REACTION and STABILITY of METAL POLYMER INTERFACES J. Kim, S. P. Kowalczyk, Y. H. Kim*, J. S. Oh and G. E. Walker IBM T. J. W. Research Center, P.O. Box 218, Yorktown Heights, NY 10598. (* KAIST, Chung-Ryang P.O. Box 131, Seoul, Korea.

Polyimide has been of great interest to the microelectronic industry due to its unique properties such as high temperature stability, excellent low dielectric constant and easy processibility. When coupled with thin conducting metal films, there are basically two types of interfaces between metal and polyimide: first, the interface formed by the vapor deposition of metal films on cured polyimide (metal-on-polyimide interface) and, second, the interfaces created by spin coating of a polyimide precursor onto a metal film followed by curing to form the polyimide (polyimide-on-metal interface). The present work addresses the characteristics of these two types of polyimide interfaces with several metals in terms of: (1) their unique interfacial chemical reaction mechanisms, (2) correlation of the interfacial reactions with their adhesion strengths and (3) consequence of the interfacial reaction for stability of the interfaces and for reliability of microelectronic devices. This paper is to summarize the interface related issues in microelectronic industry mostly published elsewhere.

K4.8

X-RAY DIFFRACTION STUDIES OF THE DELAMINATION OF COPPER THIN FILMS FROM GLASS AND SILICA SUBSTRATES.
Alan G. Fox and Rowland M. Cannon, Center for Advanced Materials,
Lawrence Berkeley Laboratory, University of California, Berkeley
CA94720.

Double-cantilever-beam (DCB) samples for fracture toughness studies have been made from thin films of copper on glass or silica substrates so that during testing the fracture event passes exactly along the copper/glass (SiO_2) interface. The strength of these Cu/glass (SiO_2) interfaces is governed primarily by the amount and type of impurities present when the thin film is prepared and the environment in which the DCB test is performed. In the present work X-ray diffractograms were taken from regions of the thin Cu films which had 'seen' fracture events and compared with those (from the same sample) which had not, and the results correlated with the measured fracture toughnesses. The X-ray diffraction lines from the copper films which had not been subjected to a fracture event were shifted and broadened (relative to strain-free copper) due to the differences in thermal expansion coefficient between the Cu

film and the substrate. As expected, these residual stresses were found to be greater for the silica substrates than for glass. A transmission electron microscope (TEM) study of the films in cross-section confirmed that the defects associated with the line broadening were twin faults and dislocations. The effect of the passage of the fracture event along the Cu/ceramic interfaces was to significantly reduce the extent of line shift, but only to slightly reduce the extent of broadening. This result suggests that although the overall mean strain in the Cu is reduced by the passage of the fracture event along the copper thin-film/ceramic interface, the non-uniform strain is not much affected. This occurs because, as expected, dislocations are generated in the thin copper film as the crack extends along the interface. This was also confirmed by TEM studies. It was also found that the greater the strength of the interface, the greater was the reduction in mean strain due to the fracture event; this, of course, is consistent with the generation of greater numbers of dislocations in the copper films by the fracture events along interfaces of higher strength.

K4.9

THE EFFECT OF N_2 ADDITION ON SPUTTERED TITANIUM BORIDE FILMS. N. C. Saha and R. K. Sharma,
Motorola Inc., Phoenix, Arizona.

Thin films of titanium boride were deposited onto SiO_2 substrate by sputtering from a TiB_2 target in (0-100%) Ar/N_2 gas mixtures. The film properties such as composition, crystallinity and sheet resistance were significantly changed upon addition of N_2 in the sputter gas. These changes in composition and crystallinity were evaluated by x-ray photoelectron spectroscopy (XPS) and x-ray diffraction (XRD) techniques.

The film deposited in argon was stoichiometric TiB_2 and polycrystalline in nature. Addition of nitrogen led to decomposition of TiB_2 , formation of BN and TiN compounds, loss of crystallinity, and increase in the film sheet resistance. The changes in properties of these films as a function of deposition conditions are directly attributable to the film compositions.

K4.10

RBS ANALYSIS OF PHOSPHOR PACKAGES FOR LASER-HEAT THERMOLUMINESCENCE DOSIMETRY. Stanley H. Stern, Jack L. Price, Donald G. Simons*, David J. Land, and Veerendra K. Mathur, U.S. Naval Surface Warfare Center, White Oak Laboratory, Silver Spring, MD 20903-5000.

Components and packages of phosphors being developed by International Sensor Technology, Inc., for a laser-heat thermoluminescence radiation-dosimetry system have been analyzed with Rutherford Backscatter Spectrometry (RBS) and complementary measurements of Particle-Induced X-ray Emissions (PIXE). Samples consist of ~50-micron diameter powder grains of $\text{CaSO}_4:\text{Tm}$, of mixtures of $\text{CaSO}_4:\text{Tm}$ and $\text{LiF}:\text{Ti,Mg}$, or of $\text{MgB}_2\text{O}_7:\text{Tm}$ respectively embedded in a transparent silicone adhesive matrix (Dow-Corning 96-083). The matrix with phosphor is pressed and cured at 150°C and 400°C on a ~1000-Å thick Al heat sink evaporated on a substrate of Dupont KAPTON VN.

Our principal finding with regard to morphology indicates an inhomogeneous outer layer ~100 $\mu\text{g}/\text{cm}^2$ of silicone binder that covers the phosphor-matrix bulk. Such encapsulation might explain dosimeter robustness vis-à-vis possible humidity degradation. A second significant finding is the spectrometric suggestion of Be and B in the binder. If their presence is confirmed, these elements might be respectively related to observed large-background "zero" radiation-dose BeO thermoluminescence and to potential ^{10}B thermal-neutron absorption.

K5.1

DIELECTRIC PROPERTIES OF SINTERED AlN, R.D. Harris, R.C. Enck, and J.L. Fields, BP Research, Cleveland, OH 44128.

AlN has been proposed as a high thermal conductivity substrate material for the electronics packaging industry. In order to make use of AlN in this application, it is extremely important to have a thorough understanding of its electrical properties. We have initiated a study of the ac electrical properties (dielectric constant and dielectric loss) and the dc resistivity of sintered AlN. For this study, we have used samples purchased commercially as well as samples made by the Carborundum Company, a member of the BP Group. Measurements have been carried-out as a function of temperature and frequency. Using photolithographically defined sputtered gold electrodes in a guard ring geometry (yielding ϵ to better than $\pm 1\%$), we find variations in the room temperature dielectric constant for AlN substrates obtained from different sources. The source-to-source range is from 8.5 to 8.7. This variation has not been previously reported, with 8.8 being the generally reported value in the product literature. We find similar source-to-source variations in the room temperature dielectric loss. All of the samples show thermally activated behavior in the dc resistivity. The activation energy observed for most samples is similar; however, different pre-exponential factors are apparent. As a result, there are large variations in the measured room temperature resistivities for samples from different sources.

K5.2

Time-Resolved Luminescence of Oxygen-Related Defects in Aluminum Nitride L.H. Harris and R.A. Youngman, BP Research, Cleveland, OH.

The luminescence of aluminum nitride doped with approximately 1wt/o oxygen consists of an intense, very broad (1eV), spectral line in the near UV centered at 375 nm. Though there is little doubt that this transition is associated with oxygen incorporation in the AlN lattice, both the anomalous width of this feature and the specific complex from which it originates, have been a matter of debate over the past decade^{1,2}. In this paper we present time-resolved luminescence data, over millisecond time scales, which strongly suggests that the 375 nm peak is due to a donor to acceptor transition, as originally described by Thomas et al. for GaP³. The major evidence for this conclusion is the observation of significant shifts in the peak position as a function of delay time. This model is further shown to be consistent with a mechanism for oxygen accommodation in AlN where charge balance is achieved via the formation of aluminum vacancies in the lattice.

K5.3

A TECHNIQUE FOR BRAZING ALUMINUM NITRIDE SUBSTRATES, M. Grant Norton, Jacek M. Kajda, Brian C. H. Steele, Department of Materials, Imperial College of Science, Technology and Medicine, Prince Consort Road, London, SW72BP, England.

A technique for brazing aluminum nitride (AlN) using conventional (non-active) brazing alloys has been investigated. The process involves the *in-situ* decomposition of a metal hydride. This process alters the surface chemistry of the substrate and improves the wettability of the molten braze. The development of high strength bonding between braze and ceramic results. The ceramic-braze interface was studied using scanning electron microscopy (SEM). The nature of the interfacial reactions and the reaction products have been identified using x-ray diffraction (XRD). The progress of the reaction has been followed using differential thermal analysis (DTA).

The experimental results have been correlated with thermodynamic predictions of the reaction process. In addition to joining ceramic to ceramic, braze joints of AlN to copper and to a low expansion iron-nickel lead frame alloy were made.

K5.4

THE MICROSTRUCTURE AND MICROCHEMISTRY OF TUNGSTEN AND TUNGSTEN COMPOUND REACTIONS WITH ALUMINUM NITRIDE. Alistair D. Westwood & Michael R. Notis, Dept. of Materials Science & Engineering, Whitaker Lab #5, Lehigh University, Bethlehem, PA 18015

A clear understanding of the bonding mechanism in the

co-fired tungsten-aluminum nitride metallization system is not currently available. Using a variety of electron optical and analytical techniques, we have performed microstructural and microchemical studies on both cofired thick film tungsten/AlN interfaces, and on AlN substrates containing Y_2O_3 , $CaWO_4$, and WO_3 as sintering aids. Based on these results, a model is proposed to explain the reaction sequence and the nature of the bonding mechanism that produces adhesion at the tungsten-aluminum nitride metallization interface. The effect of the morphology and microchemistry at the interface region on thermal resistance at the interface will also be discussed.

K5.5

LOW TEMPERATURE SILVER-GLASS DIE ATTACH MATERIAL. Mark Blocker and My N. Nguyen, Johnson Matthey Electronics, San Diego, California.

A new silver-lead vanadate glass die attach material is discussed. Its sintering characteristics is examined by dilatometry and electron microscopy. Sintering is found to occur at lower temperature than conventional silver-glass system. This is caused by the reaction between silver and one of the glass component during the heat treatment. The sintering characteristics can be altered using appropriate additives leading to crack free die bonding without sacrificing adhesion.

The new glass combined with a more volatile organic system has produced a single pass die attach material which can be fired at temperature as low as 360 C. In addition, the sintering rate is controlled by additives to provide the stress relief for large area dice.

K5.6

FAST FIRING OF A LOW TEMPERATURE DIELECTRIC BASED ON LEAD MAGNESIUM TUNGSTEN ZIRCONATE TITANATE; S. Mansfield, A.M. Barus, S.M. Landin, J.A.T. Taylor, New York State College of Ceramics at Alfred University, Alfred, NY 14802

The possibility of fast firing a relaxor dielectric to mitigate the lead loss and reduce the cost of sintering has been investigated. A binder burnout prefire is required to prepare the tape cast laminates for fast firing. The dielectric formulation, $Pb(Mn_{0.33}Nb_{0.67})_{0.02}(Mg_{0.5}W_{0.5})_{0.48}Zr_{0.23}Ti_{0.27}O_3$, shows superior properties when fired conventionally, if processing procedures are carefully controlled, including using the columbite precursor method to avoid the creation of excess pyrochlore. The data from X-ray diffraction, scanning electron microscopy and impedance analysis at various temperatures and frequencies are presented for various fast firing profiles.

K5.7

DENDRITIC FORMATION AND GROWTH OF Si IN THE Cu₃Si MATRIX INDUCED BY ION IRRADIATION AND THERMAL ANNEALING. JIAN LI, S. RUSSELL AND J.W. MAYER, Department of Materials and Engineering, Cornell University, Ithaca, NY 14853, USA.

Cu₃Si bilayer samples with overall compositions Cu_{1-x}Si_x (0 < x < 1), determined by Rutherford backscattering spectrometer, have been irradiated at room temperature to a dose of 5x10¹⁵ Kr/cm². After irradiation, transmission electron microscopy (TEM) results showed that the Cu₃Si phase was formed between the Cu and amorphous Si film. Subsequent room temperature aging led to the formation of dendritic patterns in the Cu₃Si matrix. These dendritic patterns were identified as amorphous Si precipitates. Upon further annealing at 450°C, these dendritic patterns branch out at the tips. The TEM results showed that the new branches of Si dendritic patterns are crystalline and the original dendritic patterns remained amorphous. The kinetics of the dendritic growth and the recrystallization of amorphous Si in the Cu₃Si matrix have been studied.

K5.8

OXIDATION OF Pb-Sn AND Pb-Sn-X ALLOYS: BULK VS. GRAIN BOUNDARY REGIONS. D.A. Sluzewski, Y.A. Chang, Department of Materials Science and Engineering, University of Wisconsin-Madison, Madison, WI 53706, and V.C. Marcotte, IBM General Technology Division, East Fishkill Facility, Hopewell Junction, NY 12533.

Vacuum fatigued Pb-Sn alloys show marked increase in fatigue life when compared with air fatigued samples. Oxygen interactions at the grain boundaries appear to play a role in reduced lifetime. For these reasons, the oxidation behavior of Pb-Sn and Pb-Sn-X single phase alloys was characterized using a scanning Auger multiprobe (SAM) system. Using conventional Auger spectroscopy combined with argon ion sputtering, the compositions and thickness of the surface oxides for various times and temperatures were determined. Utilizing the small beam size (~0.1 micron) of the SAM, the regions at the grain boundaries were examined. By combining these techniques, the different oxidation behavior of the bulk and grain boundary regions will be illustrated.

K5.9

NEW TYPE POLYIMIDE FOR MULTI CHIPS MODULE APPLICATION. H. SATOU, D. MAKINO, T. KIKUCHI, AND T. SAITO, HITACHI CHEMICAL COMPANY LTD., IBARAKI JAPAN

In this paper we will describe a new type low dielectric constant polyimide for Multi Chips Module application. As well known, Fluorine containing polyimide indicates low dielectric constant, however one disadvantage is weak resistance to solvent compared to aromatic type polyimide.

New type polyimide shows 2.7 as dielectric constant and has the strong solvent resistance by using p-Terphenyl-tetracarboxylic Dianhydride as a new acid monomer.

K5.10

Complexities of Copper Thick Film Processing for Multi-layer Microcircuits. Dr. Ronald P. Anjard, Director/CPT. While thick film materials have been used in microcircuits for over 15 years, the use of copper has been a long desired alternative to the precious metal systems such as gold, platinum-gold, palladium-silver and others, on both functional and cost basis.

However, there have been numerous major technological considerations which have greatly impacted the replacement of these precious metal systems with copper. Complicating this, in recent years there has been the added technology of multi-level microcircuits using the thick film technology. In this case multiple layers are developed with intermediate barriers as well as special interconnections. These added operations have further complicated the effective utilization of thick film copper materials. At this point in time, very few multi-level thick film manufacturers use copper as an effective alternative. This paper will deal with technical and quality factors affecting and allowing the utilization of copper thick film systems in complex multi-level circuits as well as the mere traditional yet high volume single layer thick film circuit systems.

K5.11

INFLUENCE OF FIRING GAS PRESSURE ON THE MICROSTRUCTURE AND THERMAL CONDUCTIVITY OF AlN CERAMICS. E. Udagawa*, H. Makiyama, N. Kamehara, and K. Niwa, Fujitsu Laboratories Ltd., Morinosato-Wakamiya 10-1, Atsugi, Japan

The thermal conductivity of AlN is significantly affected by its purity. In particular, a small amount of oxygen decreases thermal conductivity. We used CaCO₃ as an additive to decrease oxygen impurity. Calcium alminate (Ca_xAl_yO_z) is formed by the reaction of Al₂O₃ and CaO during firing. We investigated the influence of gas pressure during firing on the microstructure and on the thermal conductivity of AlN ceramics. Thermal conductivity exceeded 260 W/m K was obtained, with a firing pressure of 700 kPa. This value is a 30% higher than that obtained at atmospheric pressure. And remaining oxygen take a minimum value at same pressure. We confirmed that the composition of the remaining impurity is C₃A(3CaO Al₂O₃).

K5.12

ION EXCHANGE REACTION IN A THIN FILM OF POLYIMIDE. Yoshiro Akagi, Mariko Ishino, Yasunari Okamoto, Hiroshi Taniguchi, Kohji Ooka, Yoshiharu Nakajima, Sharp Corporation, Corporate R&D Group, Tenri, Nara, 632 JAPAN

Polyimide resin is now widely used at various fields in electronic applications because of its stability against temperature. This material generally serves as a dielectric insulator between circuit electrodes. Usually, the dielectric layer has been exposed to a number of wet chemical processes including immersion in organic solvents and/or in aqueous solutions.

We examined a relationship between imidification of polyimide and adsorption of sodium ion in thin films of polyimide. Samples of aromatic polyimide with and without siloxane modification were prepared by spin-coating method on silicon wafers, followed by ring-condensation at high temperatures above and below 200°C. Then thin films of polyimide of about 100nm whose imidification were previously determined by ir absorption, were soaked in dilute aqueous solution of sodium hydroxides. Adsorbed quantity of sodium ion was determined by various methods, such as atomic-absorption method.

From above experiments, obvious correlation between degree of imide-ring-condensation and adsorbed quantity of sodium ion was found in both types of polyimide resin.

These correlation cannot be explained only by a simple adsorption or permeation, but should be interpreted by chemical ion-exchange-reaction between sodium ion and remaining carboxyl-group of uncondensed polyamic acid.

K6.1

ALUMINUM NITRIDE: A REVIEW OF THE KNOWLEDGE BASE FOR PHYSICAL PROPERTY DEVELOPMENT. G.R. Miller, The Carborundum Company, Phoenix, AZ.

Aluminum nitride has generated a great amount of interest in both the research and business communities because of its high thermal conductivity and relatively good electrical insulation properties. Its use in microelectronic packages requires a detailed understanding of the raw material - process - property relationships so as to fit within the complex constraints demanded in packages. This paper presents a status report of the public knowledge base for developing the requisite properties of aluminum nitride for advanced electronic packages. Emphasis is given the use of standard materials science, social state physics and physical chemistry tools in the development and understanding of microstructures, thermal conductivities, electrical characteristics, and mechanical properties of this material. Additionally of some of the surface characteristics of this material as relates to the aluminum nitride/metal interface are discussed.

K6.2

TEMPERATURE DEPENDENCE OF THE THERMAL CONDUCTIVITY OF ALUMINUM NITRIDE SUBSTRATES: MEASURING AND MODELLING EFFECTS OF MICROSTRUCTURE AND IMPURITIES Ralph B. Dinwiddie and David G. Onn, Applied Thermal Physics Laboratory Department of Physics & Astronomy, University of Delaware, Newark, DE 19716

For several years now aluminum nitride has been a prime candidate material for thermal management applications in advanced electronic packaging. The high thermal conductivity of pure single crystal AlN is not easily achieved in a sintered substrate

although some commercial products are now exceeding 50% of the single crystal value. The room temperature thermal conductivity is inhibited primarily by impurities but is also affected by grain size effects. In order to clearly separate these effects we have measured the in-plane thermal conductivity of a comprehensive set of experimental and commercially available AlN substrates between 20 K and 500 K (-250 C to 230 C) using a precision Guarded Longitudinal Bar method. Comparison with our own out-of-plane Laser Flash values indicates the substrates are thermally isotropic. The temperature dependent thermal conductivity data is analyzed using a non-linear least-squares fit to the Klemens-Callaway model the parameters of which include crystallite size and impurity concentration. The resulting crystallite size and impurity parameters are compared with values obtained from such material characterization techniques as SEM, XRD and PIXE.

K6.3

TEMPERATURE DEPENDENCE OF THERMAL CONDUCTIVITY OF ELECTRONIC CERAMICS BY AN IMPROVED FLASH DIFFUSIVITY TECHNIQUE, R.C. Enck and R.D. Harris, BP Research, Cleveland, OH 44128.

The thermal conductivity of ceramic materials used for IC substrates and packages has increased in importance as chip sizes have decreased and heat loads have risen. AlN (room temperature (RT) thermal conductivity (λ) greater than 200 W/m K) and BeO (λ (RT) ~ 260 W/m K) are the major candidates for applications demanding high conductivity. Conflicting reports of the temperature dependences of λ for these materials over the range of interest for packaging use (< 200°C) have been published, with some reports suggesting a crossover in λ . These reported differences may be due to the reported problems in measuring λ in AlN using the flash diffusivity method. For the present experiments, we have used a new long wavelength laser flash diffusivity system which has been shown to determine thermal diffusivity to better than $\pm 3\%$ for AlN with sample thicknesses ranging from 0.3 mm to 5 mm. No absorbing coatings are required and no correction factors are needed to fit the data to theory. We report λ from room temperature to 200°C for AlN from the Carborundum Company, a member of the BP Group, and a number of other commercial sources, and for BeO and SiC. Over this temperature range, the thermal conductivities of AlN and BeO both show linear dependences on inverse temperature. The slope of this dependence increases with RT thermal conductivity so that the ratio of BeO to AlN thermal conductivities is much smaller at 200°C than at room temperature. No crossover in the thermal conductivities is observed. Our results are supported by recent steady state heat flow measurements which agree with our thermal conductivity values in regions of overlap rather than with previous literature values.

K6.4

STRUCTURE AND PROPERTIES OF C-AXIS ORIENTED AlN FILMS REACTIVELY DEPOSITED BY DC PLANAR MAGNETRON SPUTTERING. T. Takahashi, Toyama Univ.; F. Takeda, Toyama Tech. College, Toyama, JAPAN; and M. Naoe, Tokyo Institute of Technology, Tokyo, JAPAN.

AlN films have passivation, insulating and high thermal conductive properties. It is very important to investigate effects of depositing conditions on the structure and the properties of AlN film from the viewpoint of packaging design and reliability. AlN films have been deposited by reactive DC planar magnetron sputtering at a low substrate temperature of 80°C. An Al disk and either N₂ or NH₃ were used as a target and an ambient gas, respectively. In films deposited in N₂, the c-axis of AlN crystallites whose sizes decreased from 450 to 300 Å with increasing N₂ pressure from 0.3 to 40 mTorr was perpendicular to the film plane. On the other hand, in NH₃, the c-axis of crystallites whose sizes increased from 150 to 200 Å with increasing NH₃ pressure from 0.3

to 40 mTorr was parallel to the film plane. The surface and the cross-sectional microstructures of AlN films deposited in N_2 were significantly different from that deposited in NH_3 . The surface of films deposited in NH_3 was smoother than that deposited in N_2 . The transmittance of films deposited in NH_3 was superior to that in N_2 in wave length of 275~450m μ . The resistivity of films deposited in N_2 and in NH_3 were 10^{14} ~ 10^{15} Ω ·cm. Dielectric constants of films deposited in N_2 and that in NH_3 were 9.7 and 9, respectively, in the frequency range of 20 kHz to 20 MHz. The structure and the properties of AlN films deposited by this method depended on a kind of ambient gas.

K6.5

ON THE STRUCTURE OF PLANAR DEFECTS IN ALN. Stuart McKernan and C.Barry Carter, Department of Materials Science and Engineering, Cornell University, Ithaca, NY 14853

Aluminum nitride is of great interest as a modern, electronic packaging material. The mechanical strength, high thermal conductivity and electrical resistivity of AlN and the relatively small thermal expansion coefficient make this material extremely well suited as a semiconductor substrate material. It has the hexagonal, wurtzite structure rather than the cubic structure more common in commercial semiconductors, and is also a polar material. In polycrystalline, sintered AlN material, several different planar defects have previously been identified. Anti-phase boundaries (which have the same configuration as basal twins) and stacking-faults have been identified in this material. More complex "dome-like defects" have also been reported. The association of oxygen impurities with these extended defects has been proposed.

The "dome-like defects" have been observed to lie on the (0001) plane and two {10 $\bar{1}$ 1} planes; these are all polar planes in this structure. The bonding across the planes that form these defects will be either all Al-Al bonds or all N-N bonds. Convergent beam electron diffraction experiments have been performed at the {1120} orientation on either side of the defect planes. By comparing the intensity distribution in the CBED patterns with calculated diffraction patterns the absolute orientation of the AlN may be determined. Models for the different possible configurations of these interfaces will be presented, and the possibility of oxygen inclusion at these defects, for example by forming an Al-O-Al layer at the interface, will be discussed.

K6.6

PLANAR AND CURVED DEFECTS IN ALUMINUM NITRIDE: THEIR MICROSTRUCTURE AND MICROCHEMISTRY. Alistair D. Westwood and Michael R. Notis, Department of Materials Science & Engineering, Whitaker Lab #5, Lehigh University, Bethlehem, PA 18015.

A microstructural and microchemical analysis of planar and curved defects in aluminum nitride will be discussed, highlighting the similarities and differences between these two types of defects. The crystallographic nature of these defects has been investigated using CTEM and CBED techniques, showing them both to be inversion boundaries. The rigid body translation at the interface has been studied in both defect types.

A microchemical analysis of the two defect types reveals segregation of oxygen to the planar defect, but no segregation effects were seen at the curved defect.

Analysis of unsintered aluminum nitride powder, and the structural and chemical studies reported here have led to a proposed model for the formation of these two types of defects. The effect of these defects on thermal conductivity will also be discussed.

K6.7

Inversion Domain Boundaries and Oxygen Accommodation in Aluminum Nitride R.A. Youngman and J.H. Harris, BP Research, Cleveland, OH; P.A. Labun and R.J. Graham, Arizona State University, Tempe, AZ.

Aluminum nitride is known to have a large affinity for oxygen as an impurity. At high levels (>4wt/o) the oxygen is incorporated in the form of planar stacking faults where "pure" 2H AlN is regularly interspersed with a layer of oxygen at the faults¹. At oxygen levels lower than ~4wt/o the structure is thought to consist of "pure" 2H AlN interspersed with a random distribution of such oxygen containing stacking faults². Liquid-phase sintering of aluminum nitride often produces a final microstructure containing a high density of inversion domain boundaries³(IDBs) and few (if any) stacking faults. These boundaries are significantly aplanar (indicating a low interface energy), and often have precipitates and other, faceted defects associated with them. We have investigated these defects both structurally and chemically by electron optical methods (TEM, STEM, HREM, CBED, EDS, and EELS). The structural nature of the boundaries, in the absence of oxygen, requires Al-Al and/or N-N bonds to occur with some frequency across the boundary. Such bonding is unlikely due to the excess energy required. Chemical analysis (EELS) reveals that oxygen is often associated with the boundaries and may mediate the bonding at the boundary. A model is proposed for the IDB which includes structural aspects combined with considerations of stoichiometry in an effort to understand the origin and energetics of this defect.

K6.8

THE LOAD DEPENDENCE OF Ti/Al₂O₃ AND Ti/AlN INTERFACIAL CRACK PROPAGATION. Tao Liu, Michael R. Notis, and Y. T. Chou, Department of Materials Science & Engineering, Lehigh University, Bethlehem, PA 18015.

The Ti/Al₂O₃ system is important in microelectronic applications where Ti is used for thin film metallization on polycrystalline Al₂O₃ (or single crystal sapphire) substrates. More recently interest has also been shown in the Ti/AlN system for applications requiring higher thermal conductivity. Both of these systems are chemically reactive with intermediate phases forming at the interface. In this report, a Nikon QM high temperature microhardness tester is used to measure the fracture toughness, at elevated temperatures, of the interface between a thin Ti film and the substrate. The temperature effects on adhesion are now being studied.

In addition, a nanoindenter is being employed to explore interfacial crack propagation between the Ti thin film and the substrate materials. Crack propagation at or near the interface is investigated as a function of indentation load, and the mechanisms that trigger this crack propagation are proposed.

K6.9

THICK FILM METALLIZATION OF ALUMINUM NITRIDE. M. Grant Norton, Brian C. H. Steele, Department of Materials, Imperial College of Science, Technology and Medicine, Prince Consort Road, London, SW72BP, England.

A widely used technique to metallize substrates for electronic packaging applications is thick film technology. The interaction between commercial thick film materials and aluminum nitride (AlN) has been undertaken and an in depth investigation of the glass/ceramic reactions which occur in frit bonded films. The experimental results have been correlated with thermodynamic predictions of the reaction processes. The standard glasses were found to react with the substrate causing blistering, foaming or dewetting. Following from these studies a model glass system was developed and reactions of this glass with AlN have been investigated using scanning electron microscopical techniques and hot stage microscopy. Thick film inks have been developed using this glass system which are compatible with AlN substrates.

K7.1

ELECTROLESS METAL DEPOSITION - CHALLENGES & OPPORTUNITIES R. Jagannathan and M. Krishnan, Electrochemical Processes Group, IBM T.J. Watson Research Center Yorktown Heights, N.Y. 10598

Applications of electroless deposition of metals in microelectronic industry have become increasingly attractive due to several important considerations such as process simplicity and cost effectiveness. Many applications in advanced packaging technologies demand more stringent requirements in terms of material compatibility, quality of metallurgy and process performance. This development has provided excellent opportunities for inventing new concepts and ideas in developing electroless processes that can meet the challenges. This presentation reviews the present state of the art in electroless deposition of metals pertaining to high performance packaging. An overview of the major challenges will also be discussed.

K7.2

ELECTROLESS PLATING OF COPPER INTERCONNECTIONS ON ION BEAM CATALYZED POLYIMIDE. T. Flottmann, A. Tulke, E. Esper, W. Lohmann, Akzo Research Laboratories, 8753 Obernburg, Fed. Rep. Germany

Additive plating of interconnections on printed wiring boards is gaining attention as fabrication technology. It can be combined with physical techniques, such as laser or ion beam irradiation, to obtain fine-line conductor patterns without employing conventional photoresist processes.

In this paper an ion beam resist method is presented. Decomposition of a palladium compound by ion irradiation has been used to catalyze electroless plating on polyimide. First palladium-acetylacetonate or -acetate is spin-coated on a polyimide substrate. The thin resist film is then irradiated through a mask with He or Ar ions at 100 KeV energy. After washing off the film parts which were not exposed to the ion beam, copper is deposited on the catalyzed polyimide substrate in an alkaline electroless plating bath. When using alkaline resistant polyimide, several microns thick copper lines can be plated. The chemical surface composition of the Pd-compounds after ion beam exposure has been investigated with ESCA. It has been found that metallic Pd can be formed with a high concentration. Pd-acetate is more effective to form catalytic sites than Pd-acetylacetonate.

K7.3

REAL-TIME INVESTIGATION OF SOLID AND LIQUID STATE REACTIONS IN AU-SN/CU SYSTEM. Seyong Oh, Igor Y. Khandros, IBM T.J. Watson Research Center, Yorktown Heights, NY; and Janet L. Poetzinger, IBM GTD, Hopewell Junction, NY.

Joining with eutectic Au-Sn alloy is of interest when solder hierarchy is involved. This study addresses kinetics of transformations in Au-Sn system, and liquid and solid state reactions with Cu.

For that purpose, a real-time X-ray analysis technique has been developed and employed for in-situ investigation of reactions in Au-Sn/Cu system as a function of temperature. The specimens were mounted on the automated goniometers for uncoupled scan and heated with hot helium gas. Count rate vs. time at 2θ corresponding to major diffraction peaks was used for monitoring phase transformation.

Typically, 1 μm eutectic Au-Sn films were deposited on 1.5 μm Cu layers on Si wafers. Phase changes of Au-Sn films on Cu from room temperature to above the eutectic point, then to room temperature have been investigated.

Au and AuSn, major phases in as-deposited condition, turned to Au₃Sn and AuSn as temperature increased, and formed Cu-Sn intermetallics above the eutectic temperature. Diffusion of Cu into Au-Sn layer during the heating increased melting point. Dissolution of Cu in liquid Au-Sn as well as solid state diffusion turned binary Au-Sn into ternary Au-Sn-Cu and created Cu-Sn intermetallics. The effect of heating rate on the melting temperature of the bilayer structure and the underlying reactions will be discussed.

K7.4

OXIDATION KINETICS OF (Pb,In) SINGLE-PHASE ALLOYS. M.-X. Zhang, Y. A. Chang, Department of Materials Science and Engineering, University of Wisconsin-Madison, Madison, WI 53706, and V. C. Marcotte, IBM General Technology Division, East Fishkill Facility, Hopewell Junction, NY 12533

The solid state oxidation kinetics of Pb-In single-phase alloys was studied with AES (Auger Electron Spectroscopy) depth profiling technique. The samples containing 3, 30 and 64 at% In were oxidized in air from room temperature up to 275°C. At room temperature, the oxidation for all the three compositions was found to obey the logarithmic law. With increasing the temperature, the kinetics change from logarithmic to parabolic behavior. The transition for Pb-3 at% In alloys occurs between 150°C to 175°C, while the transition for Pb-30 at% In and Pb-64 at% In alloys occurs below 100°C.

K7.5

PHASE STABILITY AND MECHANICAL BEHAVIOR OF TERNARY BISMUTH-LEAD-TIN SOLDERS. W. J. Whealon, D. S. Stone, Y. A. Chang, Department of Materials Science and Engineering, University of Wisconsin, Madison, WI 53706.

A phase stability study of the Pb-Sn-Bi ternary system and mechanical testing of the Pb-Sn-Bi eutectic alloy (52.5% Bi-32% Pb-15.5% Sn) were done. A ternary phase (X) was found to form at 103°C by means of a Class III type reaction. The ternary eutectic composition consists of Sn, Bi, and X (~54% Pb-42% Bi-4% Sn) in equilibrium in a temperature range from its formation temperature (96°C) to 78°C. At 78°C the X phase decomposes eutectoidally into Sn, Bi, and β with β being the peritectic phase seen in the Pb-Bi binary system. These transformations, and particularly the difference in composition of the equilibrium phases of the ternary eutectic at different temperatures, lead to marked changes in the mechanical properties of this electronic solder alloy on cooling. Upon solidification, and before cooling, the solder behaves in a brittle manner, showing no ductility, with a cleavage-type relationship between the fracture surface and dendrites formed during solidification. Holding the solder at above 78°C does not decrease the brittleness shown. After cooling to room temperature the solder behaves extremely ductily, possibly even superplastically. Upon reheating to above 78°C the solder shows a subtle loss in ductility although brittle fracture does not occur. It is concluded that the fragmentation of the dendritic solidification structure into fine (1-5 μm) equiaxed grains causes the dramatic changes in the mechanical behavior of this solder. This fragmentation is caused by the solid state decomposition of the X phase at 78°C into three phases of very different compositions. This causes precipitation of very fine equiaxed grains which prevent an easy crack path.

K7.6

CONTACT REACTIONS AT THIN FILM ALUMINUM-TRANSITION METAL INTERFACES: Bernd Schuhmacher & Uwe Köster, Department of Chemical Engineering, University of Dortmund, D-4600 Dortmund 50, F.R. Germany

Contact reactions at thin film Al/TM interfaces (TM = W, Cr, Co, Zr and Ta) have been studied by means of cross sectional transmission electron microscopy. In all cases the first phase formed at the interface was the most aluminum-rich compound as given in the corresponding phase diagram: In the case of Al/W, Al/Cr as well as Al/Co contacts rather smooth, planar growth of Al₁₂W, Al₇Cr and Al₉Co₂, respectively, has been observed; parabo-

lic growth rates indicate a diffusion controlled reaction. On the other hand, Al/Zr and Al/Ta contacts exhibit a rather irregular growth morphology of Al₃Zr and Al₃Ta, respectively.

In addition the precipitation behavior of rapidly solidified supersaturated solid solutions upon thermal annealing has been studied, in order to get a better insight on preferred orientation relationships between the aluminum matrix and the aluminides as well as on the influence of defects, e.g. grain boundaries.

Based on the observed morphologies and orientation relationships as well as on the kinetics of the reaction a model will be proposed for the different modes of interfacial reactions, i.e. planar or irregular growth.

K7.7

RESIDUAL STRESSES IN FILAMENT-EVAPORATED ALUMINUM FILMS ON SINGLE CRYSTAL SILICON WAFERS. Hai Woong Park and Steven Danyluk, University of Illinois at Chicago, Department of Civil Engineering, Mechanics, and Metallurgy, P.O. Box 4348, MC: 246, Chicago, Illinois 60680.

Residual and thermal stresses have a substantial influence on the damage, fracture and lifetime of electronic components. These stresses form during processing of individual components or during the operation of electronic devices. The detection and elimination of residual stresses is therefore critical to the reliability of electronic packaging materials. The present study was initiated to develop a non-destructive interferometric technique (Shadow Moire) to measure stresses at metal/ceramic and polymer/ceramic layered structures and chip-to-package interconnections.

The Shadow Moire technique has been applied to a measurement of in-plane residual stresses of thin aluminum films, vapor deposited on single crystal silicon wafers. Stresses were determined over large spatial areas and varying geometries in order to model the stress distributions and develop the technique so that the stresses in complicated geometries could be measured. For example, 780 nanometers thick vapor deposited aluminum films increase the residual stresses by 30%; these stresses vary with position on the wafer and may have significant effect on the long-term operation of devices.

K7.8

ELECTROMIGRATION IN THIN FILMS OF Au ON GaAs. P. F. Tang, A. G. Milnes, Dept. of Electrical and Computer Engineering, and C. L. Bauer, S. Mahajan, Dept. of Metallurgical Engineering and Materials Science, Carnegie Mellon Univ. Pittsburgh, PA 15213

Evolution of the fractional change of electrical resistance $\Delta R/R_0$ in thin films of Au on (001) GaAs has been investigated as a function of time t , temperature T , and current density j . Initially $\Delta R/R_0$ increases linearly with increasing t for constant T and j , and exponentially with increasing T for constant t and j . An analytical model based on formation of cylindrical hole/hillocks at grain boundary triple junctions due to atomic flux imbalance resulting from variations of grain boundary inclinations defining triple junctions, and variations of grain boundary diffusivities, is developed to quantitatively relate the $\Delta R/R_0$ to the corresponding microstructure. Using a Monte Carlo method, systems of a large number of conductor lines, each containing a certain number of triple junctions whose inclinations and orientations with respect to the current are randomly distributed, are simulated. The distribution of atomic flux divergence along each line determines $\Delta R/R_0$ and hole

distribution at a given time while the maximum hole size controls the lifetime of that particular line. The cumulative failure of all the conductor lines shows a log-normal like behavior and predicts the mean-time-to-failure and standard deviation. Generally, the model is in good agreement with experimental observations.

K7.9

Interdiffusion of Cu/Co, Co/Au and Cu/Co/Au Thin Films P. Madakson and J. Liu, IBM Research Division, Thomas J. Watson Research Center, Yorktown Heights, NY 10598.

Thin films of Cu/Co, Co/Au and Cu/Co/Au were deposited on oxidized silicon substrates by e-beam evaporation. They were annealed at temperatures ranging from 300 to 550°C in helium. Detailed analysis was carried out using four-point probe resistance measurements and Rutherford backscattering spectroscopy (RBS). No interdiffusion of Cu/Co or Cu/Co/Au was observed at $\leq 400^\circ\text{C}$ but severe intermixing of Co/Au occurred. This was found to be associated with the grain structure of the films. Larger grains result in low diffusion because they have fewer grain boundaries which are favored diffusion paths for the atoms.

SYMPOSIUM L:
CHEMICAL VAPOR DEPOSITION OF
REFRACTORY METALS AND CERAMICS



November 29 - December 1, 1989

Chairs

Theodore M. Besmann
Metals and Ceramics Division
Oak Ridge National Laboratory
MS 6063
P. O. Box 2008
Oak Ridge, TN 37831-6063
(615) 574-6852

Bernard M. Gallois
Department of Materials
& Metallurgical Engineering
Stevens Institute of Technology
Hoboken, NJ 07030
(201) 420-5263

Symposium Support

Directorate of Electronic and
Materials Sciences - Air Force Office
of Scientific Research
Army Research Office

**Proceedings published as Volume 168
of the Materials Research Society
Symposium proceedings series.**

SESSION L1: FUNDAMENTALS/MODELING

Chairs: B. Gallois and F. Rosenberger
Wednesday Morning, November 29
Essex Northwest (W)

8:00 *L1.1

INTERESTS AND LIMITS OF THE THERMODYNAMIC APPROACH FOR C.V.D. PROCESSES, C. Bernard, Laboratoire de Thermodynamique et Physico-Chimie Métallurgiques, Saint-Martin-d'Heres, France; and R. Madar, Laboratoire des Matériaux et du Génie Physique ENSPG, Saint-Martin-d'Heres, France.

8:30 *L1.2

PREDICTING THE CHEMISTRY IN CVD SYSTEMS, K.E. Spear, The Pennsylvania State University, Ceramic Science and Engineering, University Park, PA.

9:00 *L1.3

MODELS OF CHEMICAL REACTIONS AND TRANSPORT PROCESSES UNDERLYING CHEMICAL VAPOR DEPOSITION, Klavs F. Jensen, Massachusetts Institute of Technology, Department of Chemical Engineering, Cambridge, MA; Dimitrios I. Fotiadis, Erik O. Einset, and T.J. Mountziaris, University of Minnesota, Department of Chemical Engineering and Materials Science, Minneapolis, MN.

9:30 L1.4

GAS PHASE REACTIONS RELEVANT TO CHEMICAL VAPOR DEPOSITION: NUMERICAL MODELING, D. Burgess, Jr. and M.R. Zachariah, National Institute of Standards and Technology, Center for Chemical Technology, Gaithersburg, MD.

9:45 L1.5

A UNIFIED MODEL FOR CVD PROCESSES BASED ON BOND GRAPH METHODS, S.R. Kalidindi, Massachusetts Institute of Technology, Department of Mechanical Engineering, Cambridge, MA; and S.B. Desu, Virginia Polytechnic Institute and State University, Department of Materials Engineering, Blacksburg, VA.

10:00 L1.6

CALCULATION OF TRANSPORT-SHIFTED CVD-PHASE DIAGRAMS, Joshua Collins and Daniel E. Rosner, Yale University, Department of Chemical Engineering, New Haven, CT.

10:15 BREAK

10:30 L1.7

TRANSPORT PROPERTIES OF CVI PREFORMS AND COMPOSITES, T.L. Starr, G.B. Freeman and T.C. Elston, Georgia Tech Research Institute, Georgia Institute of Technology, Atlanta, GA.

*Invited Paper

10:45 L1.8

3-D MODELING OF FORCED FLOW, THERMAL GRADIENT CVI FOR CERAMIC COMPOSITE FABRICATION, T.L. Starr and A.W. Smith, Georgia Tech Research Institute, Georgia Institute of Technology, Atlanta, GA.

11:00 L1.9

CHEMICAL VAPOR INFILTRATION OF POROUS PREFORMS: EVOLUTION OF DENSIFICATION, Herman C.T. Cheng, E.I. duPont de Nemours & Co., Inc., Department ETL, Wilmington, DE; Brian Heble and Stanley Middleman, University of California, San Diego, Chemical Engineering Department, LaJolla, CA.

11:15 L1.10

ANALYTICAL SIMULATION OF AN IMPROVED CVI PROCESS FOR FORMING HIGHLY DENSIFIED CERAMIC COMPOSITES, Nyan-Hwa Tai and Tsu-Wei Chou, University of Delaware, Center for Composite Materials and Department of Mechanical Engineering, Newark, DE.

11:30 L1.11

A MODEL FOR CHEMICAL VAPOR INFILTRATION OF FIBROUS SUBSTRATES, Rajesh R. Melkote, University of Minnesota, Department of Chemical Engineering and Materials Science, Minneapolis, MN; and Klavs F. Jensen, Massachusetts Institute of Technology, Department of Chemical Engineering, Cambridge, MA.

11:45 L1.12

MODELLING TRANSPORT, REACTION, AND PORE STRUCTURE EVOLUTION DURING DENSIFICATION OF CELLULAR OR FIBROUS STRUCTURES, Stratis V. Sotirchos and Manolis Tomadakis, University of Rochester, Department of Chemical Engineering, Rochester, NY.

SESSION L2: DIAGNOSTICS

Chairs: E. A. Whittaker and L. C. Hammond
Wednesday Afternoon, November 29
Essex Northwest (W)

1:30 L2.1

SURFACE CHEMISTRY OF ALN PRECURSORS ON SILICA, M.E. Bartram, T.A. Michalske, and J.W. Rogers Jr., Sandia National Laboratories, Albuquerque, NM.

1:45 L2.2

SURFACE COMPOSITION BY RESONANT SUM FREQUENCY GENERATION DURING CHEMICAL VAPOR DEPOSITION, Karen L. Carleton and William J. Marinelli, Physical Sciences, Inc., Andover, MA.

2:00 L2.3

INTERACTION OF BORAZINE WITH A RE(0001) SURFACE, STUDIED BY LEED, TPD, AES, AND ELS, J.-W. He and D.W. Goodman, Texas A&M University, Department of Chemistry, College Station, TX.

2:15 L2.4
EARLY GROWTH IN THE CHEMICAL VAPOR DEPOSITION OF TiN, TiC AND SiC AND MONITORING BY LASER SCATTERING, Max Klein and Bernard Gallois, Stevens Institute of Technology, Department of Materials Science and Engineering, Hoboken, NJ.

2:30 L2.5
LIGHT SCATTERING MEASUREMENTS OF CVD SILICON CARBIDE, B.W. Sheldon and T.M. Besmann, Oak Ridge National Laboratory, Metals and Ceramics Division, Oak Ridge, TN.

2:45 L2.6
IN SITU GROWTH MONITORING OF TUNGSTEN BY REFLECTOMETRY, Albert Hasper, Jisk Holleman, Jan Middelhoek, University of Twente, Department EL, Enschede, The Netherlands.

3:00 BREAK

3:30 L2.7
A NEW APPLICATION OF SPECTROSCOPIC ELIPSOMETER: A FAST, NON-DESTRUCTIVE TECHNIQUE FOR SURFACE RECOGNITION AND CLASSIFICATION, J.L. Stehle, J.H. Lecat, J.P. Piel, SOPRA, Bois-Colombes, France; and L.C. Hammond, ARIES/QEI, Concord, MA.

3:45 L2.8
INITIAL STAGES IN THE GROWTH OF OXIDE THIN FILMS BY CVD, L.A. Tietz, S.R. Summerfelt, G.R. English, and C.B. Carter, Cornell University, Department of Materials Science and Engineering, Ithaca, NY.

4:00 L2.9
MECHANISTIC STUDIES OF THE CHEMICAL VAPOR DEPOSITION OF AlN FILMS USING ORGANOMETALLIC PRECURSORS: $[R_2AlNH_2]_3$, Carmela C. Amato, Leonard V. Interrante, and John B. Hudson, Rensselaer Polytechnic Institute, Departments of Chemistry and Materials Engineering, Troy, NY.

4:15 L2.10
MECHANISTIC ASPECTS OF THE DEPOSITION OF THIN ALUMINA FILMS DEPOSITED BY MOCVD, R.W.J. Morssinkhof, T. Fransen, M.M.D. Heusinkveld and P.J. Gellings, University of Twente, Enschede, The Netherlands.

4:30 L2.11
GAS PHASE CHARACTERIZATION IN LP CVD PROCESSES BY A PERFORMANT RAMAN EQUIPMENT, R. Gauffrès, P. Huguet, U.S.T.L., Montpellier, France; D. Boya and J. Lafforêt, Comurhex, Pierrelatte, France.

4:45 L2.12
GAS PHASE REACTIONS RELEVANT TO CHEMICAL VAPOR DEPOSITION: OPTICAL DIAGNOSTICS, D. Burgess Jr., National Institute of Standards and Technology, Center for Chemical Technology, Gaithersburg, MD.

5:00 L2.13
SMALL SCALE FABRICATION AND CHARACTERIZATION OF CERAMIC MATERIALS, Jerry Czarnecki, Edgardo Francisco, and David Thumim, Cahn Instruments, Carmenita, CA.

SESSION L3: PROCESS-MICROSTRUCTURE RELATIONSHIPS

Chairs: W. J. Lackey and N. A. Scoville
Thursday Morning, November 30
Essex Northwest (W)

9:00 *L3.1
CORRELATION AMONG PROCESS ROUTES, MICROSTRUCTURES AND PROPERTIES OF CHEMICALLY VAPOR DEPOSITED SILICON CARBIDE, Robert F. Davis, North Carolina State University, Department of Materials Science and Engineering, Raleigh, NC.

9:30 L3.2
MICROSTRUCTURAL CHARACTERIZATION OF MULTI-PHASE COATINGS PRODUCED BY CHEMICAL VAPOR DEPOSITION, K.L. More, R.A. Lowden, T.M. Besmann, and R.D. James, Oak Ridge National Laboratory, Metals and Ceramics Division, Oak Ridge, TN.

9:45 L3.3
CHEMICAL VAPOR DEPOSITION OF SILICON BORIDES, T. Goto, M. Mukaida, and T. Hirai, Tohoku University, Institute for Materials Research, Sendai, Japan.

10:00 BREAK

10:30 L3.4
CHARACTERIZATION OF SILICIDE FORMATION OF LPCVD-W BY MEANS OF RBS AND XRD, S-L. Zhang and R. Buchta, Swedish Institute of Microelectronics, Kista, Sweden; and M. Ostling, The Royal Institute of Technology-Electrum, Solid State Electronics, Kista, Sweden.

10:45 L3.5
MICROSTRUCTURE OF CVD - Al_2O_3 , J.N. Lindström, C. Chatfield, and M.E. Sjöstrand, AB Sandvik Coromant, Stockholm, Sweden.

11:00 L3.6
SELECTIVE CHEMICAL VAPOUR DEPOSITION OF TUNGSTEN USING SiH_4/WF_6 CHEMISTRY, C.A. van der Jeugd, G.J. Leusink, G.C.A.M. Janssen, S. Radelaar, Delft University of Technology, Centre for Submicron Technology, The Netherlands.

11:15 L3.7
STUDY OF $W_{20}O_{58}$ OXIDE PHASE OBSERVED IN CVD W FILMS, M. Lawrence A. Dass, Siva Sivaram, and Bryan Tracy, Intel Corporation, Santa Clara, CA.

11:30 L3.8
INVESTIGATION OF CVD β -SiC SURFACES PRODUCED VIA A "NOVEL" SURFACE REPLICATION PROCESS, Aliki K. Collins, Joseph T. Keeley, Michael A. Pickering and Raymond L. Taylor, Morton Thiokol, Inc./CVD, Woburn, MA.

11:45 L3.9
INFLUENCE OF IMPURITIES AND MICROSTRUCTURE ON THE RESISTIVITY OF LPCVD TITANIUM NITRIDE FILMS, M.J. Buiting and A.H. Reader, Philips Research Laboratories, Eindhoven, The Netherlands.

SESSION L4: MICROSTRUCTURE-MECHANICAL PROPERTY RELATIONSHIPS

Chairs: P. N. Dyer and F. S. Galasso
Thursday Afternoon, November 30
Essex Northwest (W)

1:30 *L4.1
DESIGN AND DEVELOPMENT OF CVD COATINGS, V.K. Sarin, Boston University, College of Engineering, Boston, MA.

2:00 L4.2
INDENTATION ADHESION OF DIAMOND FILMS ON THE VARIOUS SUBSTRATES, Tyan-Ywan Yen, Cheng-Tzu Kuo, National Chiao Tung University, Institute of Mechanical Engineering, HsinChu, Taiwan, China; and S.E. Hsu, Cheng Shan Institute of Science and Technology, Lungtan, Taiwan, China.

2:15 L4.3
TUNGSTEN CARBIDE EROSION RESISTANT COATING FOR AEROSPACE COMPONENTS, D. Garg and P.N. Dyer, Air Products and Chemicals, Inc., Allentown, PA.

2:30 L4.4
(ABSTRACT WITHDRAWN)

2:45 BREAK

3:15 L4.5
INTERNAL STRESSES IN AMORPHOUS SiO_2 FILMS DEPOSITED BY THE PYROLYSIS OF ORGANOMETALLIC PRECURSORS AT LOW PRESSURES, S.B. Desu, Virginia Polytechnic Institute and State University, Department of Materials Engineering, Blacksburg, VA.

3:30 L4.6
INFLUENCE OF SUBSTRATE AND PROCESS PARAMETERS ON THE PROPERTIES OF CVD-SiC, A. Parretta, V. Adoncchi, E. Cappelli, G. Giunta, and V. Vittori, Eniricerche S.p.A., Rome, Italy.

3:45 L4.7
EFFECTS OF DEPOSITION CONDITIONS ON THE MICROSTRUCTURE AND PROPERTIES OF CVD SiC, E. Minford, Robert E. Stevens, Vincent L. Magnotta, and Paul N. Dyer, Air Products and Chemicals, Inc., Allentown, PA; Thomas Watkins and David J. Green, Pennsylvania State University, University Park, PA.

4:00 L4.8
INTERACTION OF TITANIUM WITH SiC COATED BORON FIBERS, Lewis Hwan and Beng Jit Tan, University of Connecticut, Department of Chemistry, Storrs, CT; Francis S. Galasso, United Technologies Research Center, East Hartford, CT; and Steven L. Suib, University of Connecticut, Departments of Chemistry and Chemical Engineering, Storrs, CT.

4:15 L4.9
OXIDATION RESISTANT COATINGS PRODUCED BY CHEMICAL VAPOR DEPOSITION: IRIIDIUM AND ALUMINUM NITRIDE/ALUMINA COATINGS, P. Netter

4:30 L4.10
CHEMICAL VAPOUR DEPOSITION OF TITANIUM CARBIDE, K. Singh, A.K. Suri, D.K. Bose and C.K. Gupta, Bhabha Atomic Research Centre, Metallurgy Division, Bombay, India.

SESSION L5: NOVEL/LARGE-SCALE TECHNOLOGIES

Chairs: T. M. Besmann and D. Gaillard
Friday Morning, December 1
Essex Northwest (W)

8:00 *L5.1
APPLICATION OF AI CONTROL TO THE VLS SiC WHISKER PROCESS, P.D. Shalek and W.J. Parkinson, Los Alamos National Laboratory, Los Alamos, NM.

8:30 L5.2
MORPHOLOGICAL EVOLUTION OF TITANIUM CARBIDE WHISKERS, R. Mathur and Bernard Gallois, Stevens Institute of Technology, Department of Materials Science and Engineering, Hoboken, NJ.

8:45 L5.3
CHARACTERIZATION OF CERAMIC MATRIX COMPOSITES FABRICATED BY CHEMICAL VAPOR INFILTRATION, D.P. Stinton, D.M. Hembree, Jr., K.L. More, and T.M. Besmann, Oak Ridge National Laboratory, Department of Metals and Ceramics, Oak Ridge, TN.

9:00 L5.4
THE EMERGENCE OF PLASMA ENHANCED CHEMICAL VAPOR DEPOSITION (PECVD) AS A VIABLE INDUSTRIAL COATING PROCESS, George Engle, GEC, Inc., Phoenix, AZ; James W. Warren, Composite Innovations Corporation, Woodland Hills, CA.

9:15 L5.5
DEPOSITION AND CHARACTERIZATION OF SILICON NITRIDE SINGLE CRYSTAL FILMS, Joseph B. Milstein, Lian Li, Ye-Yung Teng and Anatoly M. Altshuler, University of Lowell, Lowell, MA.

9:30 L5.6
LASER CHEMICAL VAPOR DEPOSITION OF TIN FILMS, B. Chen, N. Biunno, R.K. Singh and J. Narayan, North Carolina State University, Department of Materials Science and Engineering, Raleigh, NC.

9:45 L5.7
LASER-INDUCED PHOTOCHEMICAL VAPOR DEPOSITION OF TUNGSTEN, A.J.P. van Maaren and W.C. Sinke, FOM-Institute for Atomic and Molecular Physics, Amsterdam, The Netherlands.

10:00 BREAK

10:30 L5.8
STRUCTURAL CONTROL OF MATERIALS SYNTHESIZED BY LASER EVAPORATION AND RAPID CONDENSATION, Tongsan D. Xiao and Peter R. Strutt, University of Connecticut, Institute of Materials Science, Storrs, CT.

10:45 L5.9
REACTIVE CHEMICAL VAPOR DEPOSITION AS A METHOD FOR COATING CARBON FIBER WITH CARBIDES, J. Bouix, C. Vincent, H. Vincent and R. Favre, Universite de Lyon I, Laboratoire de Physicochimie Minerale, Villeurbanne, France.

11:00 L5.10
THIN FILM OF YTTRIA STABILIZED ZIRCONIA BY MODIFIED CVD, F. Cellier.

11:15 L5.11
SOLUTION PRECURSOR - LOW PRESSURE CHEMICAL VAPOR DEPOSITION OF TITANIUM OXIDE FILMS, Jiong Ping Lu, Jengdaw Wang, and Rishi Raj, Cornell University, Department of Materials Science and Engineering, Ithaca, NY.

11:30 L5.12
AMORPHOUS INSULATING NBO FILMS BY REACTIVE EVAPORATION, B.X. Liu, Tsinghua University, Center of Condensed Matter and Radiation Physics, CCAST (World Lab.), Beijing and Department of Materials Science and Engineering, Beijing, China; J.R. Ding, X. Zhou and J.N. Bai, Tsinghua University, Department of Materials Science and Engineering, Beijing, China.

11:45 L5.13
A LOW TEMPERATURE CVD PROCESS FOR TIN COATING, A. Agüero, D. Little and P. Lowden, Liburdi Engineering Ltd., Hamilton, Canada.

SESSION L6: METAL-ORGANIC CHEMICAL VAPOR DEPOSITION

Chairs: K. Gonsalves and D.P. Stinton
Friday Afternoon, December 1
Essex Northwest (W)

1:30 *L6.1
LOW TEMPERATURE MOCVD OF TRANSITION METAL CARBIDES, BORIDES AND OXIDES, G.S. Girolami.

2:00 L6.2
METALORGANIC CHEMICAL VAPOR DEPOSITION OF SILICON BASED CERAMICS USING METHYLSILAZANE, Honghua Du, Bernard Gallois, and Kenneth Gonsalves, Stevens Institute of Technology, Hoboken, NJ.

2:15 L6.3
CHARACTERIZATION OF MOCVD GROWN EPITAXIAL CERAMIC OXIDE THIN FILMS, J.C. Parker, H.L.M. Chang, J.J. Xu, and D.J. Lam, Argonne National Laboratory, Materials Science Division, Argonne, IL.

2:30 L6.4
PREPARATION, STRUCTURE AND PROPERTIES OF VO_x AND TiO₂ THIN FILMS BY MOCVD, H.L.M. Chang, J.C. Parker, J.J. Xu, and D.J. Lam, Argonne National Laboratory, Materials Science Division, Argonne, IL.

2:45 BREAK

3:15 L6.5
STRUCTURE, COMPOSITION, AND PROPERTIES OF CVD ZrO₂ FILMS OBTAINED FROM ZIRCONIUM ACETYLACETONATES, S.B. Desu, and T. Shi, Virginia Polytechnic Institute and State University, Department of Materials Engineering, Blacksburg, VA.

3:30 L6.6
TITANIUM NITRIDE THIN FILMS: PROPERTIES AND APCVD SYNTHESIS USING ORGANOMETALLIC PRECURSORS, Renaud M. Fix, Roy G. Gordon, and David M. Hoffman, Harvard University, Department of Chemistry, Cambridge, MA.

3:45 L6.7
CHEMICAL VAPOR DEPOSITION OF NIOBIUM CARBIDE USING A NOVEL ORGANOMETALLIC PRECURSOR, P.D. Stupik and A.R. Barron, Harvard University, Department of Chemistry, Cambridge, MA.

4:00 L6.8
LOW TEMPERATURE ORGANOMETALLIC CHEMICAL VAPOR DEPOSITION (OMCVD) OF RHODIUM AND IRIIDIUM THIN FILMS, D.C. Smith, C.J. Burns, and A.P. Sattelberger, Los Alamos National Laboratory, Inorganic and Structural Chemistry Group, Los Alamos, NM; S.G. Pattillo, D.W. Carroll, and J.R. Laia, Los Alamos National Laboratory, Material Science and Technology Division, Los Alamos, NM.

4:15 L6.9

ORGANOMETALLIC CHEMICAL VAPOR DEPOSITION OF STRONTIUM TITANATE THIN FILMS, W.A. Feil, Northwestern University, Department of Materials Science and Engineering, Evanston, IL; L.M. Tonge, Northwestern University, Department of Chemistry and Materials Research Center, Evanston, IL; B.W. Wessels, Northwestern University, Department of Materials Science and Engineering, Evanston, IL; and T.J. Marks, Northwestern University, Department of Chemistry and Materials Research Center, Evanston, IL.

4:30 L6.10

HIGHLY RESOLVED GRADIENT PATTERNS IN GLASS BY MEANS OF CHEMICAL VAPOR DEPOSITION, Harry D. Gafney, Edgar Mendoza, Eugene Wolkow, Queens College of CUNY, Department of Chemistry, Flushing, NY; and Peter Wong, Queensborough Community College, Department of Chemistry, Bayside, NY.

4:45 L6.11

SMALL ANGLE X-RAY SCATTERING (SAXS) FROM METAL IMPREGNATED POROUS VYCOR GLASS, D. Sunil, Queens College, Department of Physics, Flushing, NY; J. Sokolov, Queens College, Department of Physics, Flushing, NY, and DAS, BNL, Upton, NY; M.H. Rafailovich, E. Mendoza, E. Wolkow, H.D. Gafney, Queens College, Department of Physics, Flushing, NY; G. Long, NIST; P. Jemian, Northwestern University; and A. Hansen, Brookhaven National Laboratory.

L1.1

Interests and limits of the thermodynamic approach for C.V.D. processes. C. Bernard and R. Madar*, Laboratoire de Thermodynamique et Physico-Chimie Métallurgiques ENSEEG, BP 75, 38402-Saint-Martin-d'Hères Cedex, France
* Laboratoire des Matériaux et du Génie Physique ENSPG, BP 46, 38402-Saint-Martin-d'Hères Cedex, France

The principles of the thermodynamic analysis which can be done ab initio in order to help the selection :
- the material to be deposited for a well defined application,
- the nature of reactants,
- the experimental parameters range of the experimental parameters,
will be developed and illustrated by some examples.

The main problems linked to the data selection will be emphasized : assessments, availability of coherent data, sensitiveness of the results to the data accuracy...

Finally, the validity of a thermodynamic approach performed at equilibrium in view to optimize a dynamic non equilibrium process will be discussed.

L1.2

PREDICTING THE CHEMISTRY IN CVD SYSTEMS.

Karl E. Spear, Ceramic Science and Engineering, The Pennsylvania State University, University Park, PA 16802

Tailoring the chemical and physical nature of CVD deposits for specific applications requires understanding and controlling the chemical processes occurring in a reactor. This implies an understanding of the combined equilibrium, kinetic, and transport processes. The processes occurring produce composition gradients in the reactor which can cause variations in the deposition chemistry. Examples will be given to illustrate predictions of limits on the chemical behavior of CVD systems by using partial equilibrium concepts. A comparison of these limits with experimental observations can be used to hypothesize deposition mechanisms. Derived physical and mathematical models of the mechanisms provide the critical tool for manipulating and controlling the chemical and physical nature of CVD deposits.

L1.3

MODELS OF CHEMICAL REACTIONS AND TRANSPORT PROCESSES UNDERLYING CHEMICAL VAPOR DEPOSITION.

Klavs F. Jensen, Department of Chemical Engineering, Massachusetts Institute of Technology, Cambridge, MA 02139. Dimitrios I. Fotiadis, Erik O. Einset, and T.J. Mountziaris, Department of Chemical Engineering and Materials Science, University of Minnesota, Minneapolis, MN 55455.

Detailed physicochemical models of chemical vapor deposition (CVD) processes are presented. Finite element computations based on two- and three-dimensional transport-reaction descriptions are used to elucidate flow effects in horizontal and vertical CVD reactors operating at atmospheric and low pressures. The development of buoyancy driven flows caused by large temperature gradients is described. These flows are superimposed on the main flow and the resulting complex mixed convection flows adversely affect film thickness and composition uniformity. The existence of transverse and longitudinal rolls in horizontal reactors is predicted in agreement with experimental observations. For vertical pedestal reactors the computations demonstrate that wall effects, susceptor heating and buoyancy driven recirculations lead to reduced and nonuniform growth rates as well as the development of three-dimensional non-axisymmetric flow fields. In addition to buoyancy driven flows due to thermal gradients, buoyancy driven flows caused by concentration gradients are also demonstrated. This effect will be important in systems with a heavy species in a light carrier gas.

The thermophoretic transport of tracer particles used for flow visualization or particle contaminants generated in the processes is also considered. The thermophoretic effect confounds smoke test visualizations, but it has the advantage of reducing particle contamination in the growing film. The combination of transport models with detailed chemical mechanisms is described and illustrated with examples primarily relevant to electronic

materials processing. The extension of the modelling approach to CVD systems for ceramics is discussed.

L1.4

GAS PHASE REACTIONS RELEVANT TO CHEMICAL VAPOR DEPOSITION: NUMERICAL MODELING. D. Burgess, Jr. and M.R. Zachariah. National Institute of Standards and Technology, Gaithersburg, MD 20899.

Numerical modeling of gas phase chemical kinetics was used to suggest appropriate experimental conditions and to interpret species concentrations measurements in the systems: $\text{SiH}_4 \rightarrow \text{Si}$ and $\text{SiH}_4 + \text{NH}_3 \rightarrow \text{Si}_3\text{N}_4$. The modeling used kinetic information largely compiled by Coltrin et al. The effects of temperature, pressure, and concentrations on kinetic pathways and reactive intermediates were investigated. A comparison was made between gas phase chemistry at low temperatures (700-1000K), at higher temperatures (1200-1800K), and due to laser-initiated photofragmentation. These processes are relevant, respectively, to silicon/silicon-nitride chemical vapor deposition (CVD), to flame-driven gas phase silicon-based particle nucleation, and to laser-induced processes for materials fabrication.

For silane decomposition at lower temperatures, the Si_2H_6 isomers were found to be important intermediates, while at higher temperatures Si_2H_2 and Si were active species. The presence of relatively small amounts of hydrogen (H_2) at lower temperatures has the effect of slowing net decomposition rates of products such as Si_3H_8 and reducing the transient concentrations of intermediates such as Si_2H_4 . At higher temperatures, much larger H_2 concentrations are necessary to reduce transient intermediates such as Si. For laser-initiated processes (e.g. $\text{SiH}_4 + h\nu \rightarrow \text{SiH}_2 + \text{H}_2$), it was found that increasing fragmentation leads to kinetic processes similar to those found at higher temperatures. The utility of employing this modeling approach to the silicon-nitride system is currently being investigated.

L1.5

A UNIFIED MODEL FOR CVD PROCESSES BASED ON BOND GRAPH METHODS. S.R.Kalidindi, Department of Mechanical Engineering, Massachusetts Institute of Technology, Cambridge, MA; and S.B.Desu, Department of Materials Engineering, Virginia Polytechnic Institute and State University, Blacksburg, VA.

The CVD processes are highly complicated involving several phenomena, but only few of them are required in describing a given CVD process. However, in most cases the relative dominance of these phenomena are not known apriori. Therefore the modeling of a specific CVD process (whose kinetics are not known) involves a laborious process of repeated guesses at the dominant phenomena supplemented by good numerical techniques. Most often for different guesses, different formulations of the numerical technique are required, which involves considerable effort.

A unified approach to model the general CVD process using the versatility and flexibility of bond graph method will be presented. Development of some of the important bond graph elements to represent convection, diffusion, migration, homogeneous reaction, and heterogeneous reaction will be shown. The use of the elements will be illustrated through a few simple examples ranging from diffusion only processes to convection-diffusion processes with gas phase and surface reactions. It will also be shown that a single bond graph program with changes in input can handle all these different cases with little time and effort.

CALCULATION OF TRANSPORT-SHIFTED CVD-PHASE DIAGRAMS. Joshua Collins and Daniel E. Rosner

High Temperature Reaction Engineering Laboratory
Department of Chemical Engineering, Yale University
New Haven, CT 06520-2159 Y.S., U.S.A.

A non-iterative method is presented for the construction of so-called "CVD-phase diagrams", including the systematic effects of segregation of chemical elements across the non-isothermal vapor diffusion boundary layer. Element segregation is shown to induce important shifts in the equilibrium deposit phases predicted from the actual local gas composition at the deposition surface, as opposed to the element ratios corresponding to the input ("feed") gas composition, as is commonly done. Both multicomponent Fick and Soret diffusion are assumed to act across a 'chemically frozen' mass transfer boundary layer, with local thermochemical equilibrium imposed only at the deposition surface (i.e. a 'cold-wall reactor with a 'hot' substrate). As a specific example, this model is applied to the deposition of titanium boride from $\text{TiCl}_4(\text{g})$ and $\text{BCl}_3(\text{g})$ in $\text{H}_2(\text{g})$ onto fibers for ceramic composite material applications. A flow-reactor geometry of particular interest is a long cylindrical vessel with a resistively heated coaxial fiber for the deposition substrate, however, the method presented here is general in that both the chemical system and CVD-reactor geometry can be changed to any other system of interest provided adequate thermochemical and thermophysical data are available, and the deposition rate is vapor transport controlled with estimable convective diffusion mass- and heat-transfer coefficients.

L1.7

TRANSPORT PROPERTIES OF CVI PREFORMS AND COMPOSITES, T. L. Starr, G. B. Freeman and T. C. Elston, Georgia Institute of Technology, Atlanta, GA 30332

Chemical vapor infiltration (CVI) is an effective and versatile technique for fabrication of ceramic matrix composites. The transport properties - gas permeability, thermal conductivity and effective diffusivity - of the preform, and partially densified composite control the uniformity of the infiltration process. These properties, in turn, are controlled by the material microstructure. We have developed a simple model, based on the physical microstructure, that predicts the anisotropic transport properties of cloth lay-up composites.

An anisotropic material is modeled as a layer structure consisting of two, or more, isotropic components. Composite transport coefficients perpendicular and parallel to the layers are given by "series" and "parallel" combining laws involving the isotropic coefficients of these component materials and their volume fractions. These component material properties are determined using microstructural information and fundamental material properties.

Model calculations are compared to experimental measurements for thermal conductivity and gas permeability. Predictions for effective diffusivity are presented. Application of this model into an finite element process model is outlined.

L1.8

3-D MODELING OF FORCED FLOW, THERMAL GRADIENT CVI FOR CERAMIC COMPOSITE FABRICATION, T. L. Starr and A. W. Smith, Georgia Institute of Technology, Atlanta, GA 30332

Forced flow, thermal gradient CVI (FCVI) has demonstrated excellent potential for fabrication of high strength, high toughness ceramic composites. Extension of this process to large and complex shapes is facilitated by use of a computer model to optimize process conditions and hardware for rapid, uniform infiltration.

A 3-D model has been developed using a "finite volume" formulation. A steady-state solution for heat conduction and Darcy's law permeation produces temperature and gas flow distributions within the fiber preform. These are used to generate matrix deposition rates within each volume

element. By "marching" through time, a complete simulation of the densification process is obtained.

The model is demonstrated for a FCVI system with cylindrical symmetry and compared to experimental results obtained at the Oak Ridge National Laboratory. The model successfully predicts the effects of variation in process conditions and in infiltration hardware configurations.

L1.9

CHEMICAL VAPOR INFILTRATION OF POROUS PREFORMS: EVOLUTION OF DENSIFICATION. Herman C.T. Cheng, E.I. du Pont de Nemours & Co., Wilmington, DE; and Brian Heble and Stanley Middleman, University of California, San Diego, La Jolla, CA.

Composite materials can be prepared starting with a porous textile preform upon which chemical vapor deposition occurs. Infiltration of the porosity by the precursor gases permits solid film growth within the preform. Resistance to diffusion within the porous structure limits the rate of densification, and has the potential to severely affect the uniformity of densification throughout the evolving solid structure.

Using a simple model of the geometry of a densifying structure we have developed a method of simulating the rate and spatial uniformity of densification of the evolving structure. Two example simulations are presented in answer to two questions we have raised:

- How can an *initially* nonuniform preform be selected that will evolve toward a uniformly densified structure?
- How does the *variance* of an initially nonuniform preform evolve in time?

L1.10

ANALYTICAL SIMULATION OF AN IMPROVED CVI PROCESS FOR FORMING HIGHLY DENSIFIED CERAMIC COMPOSITES. Nyan-Hwa Tai and Tsu-Wei Chou, Center for Composite Materials & Department of Mechanical Engineering, University of Delaware, Newark, DE, 19716

Among the various chemical routes for forming ceramic composites, the chemical vapor infiltration (CVI) technique is attractive because of its relatively low process temperature. The properties of the ceramic composites which are formed by the CVI process, are strongly influenced by the fabrication parameters. These parameters include the temperature boundary conditions, concentration of the vapor species, pressure adjustment during processing, fiber diameter, fiber content, and the spatial arrangement of fibers in the preform. In the present work, Darcy's law has been adopted to simulate the flow field in the fibrous preform; furthermore, the temperature and density distributions within the fibrous preform during processing are also investigated. A 3-D unit cell has been used for simulating the fiber arrangement in the preform. The advancement of the solidified front from high temperature region to low temperature region has been determined. Highly densified ceramic composites can be fabricated by the CVI process through the adjustment of temperature boundary conditions and concentrations of the vapor species. The flow field and solidified front growth after preform reorientation will also be reported.

L1.11

A MODEL FOR CHEMICAL VAPOR INFILTRATION OF FIBROUS SUBSTRATES. Rajesh R. Melkote, Department of Chemical Engineering and Materials Science, University of Minnesota, Minneapolis, MN 55455, and Klavs F. Jensen, Department of Chemical Engineering, Massachusetts Institute of Technology, Cambridge, MA 02139.

Chemical vapor infiltration (CVI) is growing in importance as a viable means of producing fiber-reinforced composites, but the process is far from completely understood. A model is presented here for the CVI of random short-fiber substrates which includes, for the first time, the calculation of internal void formation responsible for undesirable "residual porosity" in the final composite. The gas-phase precursor continuity equation is solved along with the equations for local fiber growth due to solids deposition over an isotropic fully penetrable cylinders (FPC) medium representing the actual preform. The transport and accessibility characteristics of the FPC model are evaluated by

Monte Carlo simulation, and the geometric properties are calculated using derived analytical expressions.

Results will be presented for internal deposition profiles as well as less-readily available quantities such as surface area as a function of process variables such as temperature, pressure, and initial porosity. The percolation threshold of the FPC structure is shown to imply an upper densification limit which is less than the theoretical maximum. The relationship between substrate density increase and open porosity during infiltration, which to date has been empirically fit, is predicted here from first principles. Under isothermal conditions, diffusion limitations result in gradients in matrix deposit density, with preferential deposition on the outer surface, especially at high temperatures. This necessitates periodic machining to open pathways to the interior. Imposition of an adverse thermal gradient across the slab will be shown to circumvent this primary disadvantage of the isothermal technique by allowing better control of intrasubstrate deposition rates.

L1.12

MODELLING TRANSPORT, REACTION, AND PORE STRUCTURE EVOLUTION DURING DENSIFICATION OF CELLULAR OR FIBROUS STRUCTURES, Stratis V. Soteriophos and Manolis Tomadakis, Department of Chemical Engineering, University of Rochester, Rochester, NY 14627

Mathematical models describing mass transport, heat transport, reaction, and pore structure evolution in porous media of initially fibrous or cellular structure are developed. The models are used to theoretically investigate the transient behavior of the densification process during preparation of refractory ceramics by chemical vapor infiltration of fibrous or cellular preforms. Monte Carlo simulation methods are employed to determine the variation of the local average structural properties of the porous structure (porosity, internal surface area, accessible porosity, accessible internal surface area, etc.) and of the effective diffusivity in the porous medium with the local extent of densification. Assemblages of spherical cavities overlapping with populations of cylindrical capillaries are used to model the structure of cellular preforms. The information obtained from the above computations is then used in a macroscopic reaction and diffusion model to predict densification and closed porosity profiles in the substrate. The results of our mathematical models are compared with experimental data reported in the literature for SiC/SiC composites manufactured by densifying preforms of silicon carbide fibers. On the basis of our simulation results, optimal reaction temperature, temperature gradient, and pressure histories are proposed for reducing the processing time needed for obtaining "uniformly" densified composites.

L2.1

SURFACE CHEMISTRY OF AlN PRECURSORS ON SILICA, M.E. Bartram, T.A. Michalske, and J.W. Rogers, Jr., Sandia National Laboratories, Albuquerque, NM 87185.

FTIR, TPD, and XPS have been used to study the nucleation and decomposition of AlN precursors on the surface of silica. NH_3 reacts selectively with the aluminum alkyl surface complex produced by trimethylaluminum (TMA) chemisorption to form a new product on the surface that is stable in high vacuum at 300 K. The vibrational spectrum of this species is similar to that of the TMA: NH_3 adduct known in the condensed phase and may be consistent with the formation of an analogous structure that is bonded to the surface via an Al-O-Si linkage. Formation of this surface adduct alters the chemistry of the aluminum alkyl component and leads to $-\text{NH}_2-$ cross-linking between the aluminum centers by 550 K. This surface chemistry will be compared to that of the analogous systems, NH_3 + triethylaluminum and triisobutylaluminum on silica.

L2.2

SURFACE COMPOSITION BY RESONANT SUM FREQUENCY GENERATION DURING CHEMICAL VAPOR DEPOSITION, Karen L. Carleton and William J. Marinelli, Physical Sciences Inc., Andover, MA 01810

Second harmonic generation (SHG) and sum frequency generation (SFG) are used to probe the initial stages of growth of metal films on silicon (100) surfaces. The metal is deposited by thermal decomposition of organometallic species such as trimethylaluminum. These nonlinear optical probes of the aluminum overlayer may be resonantly enhanced by tuning the probe laser in resonance with aluminum atomic transitions. This yields chemically specific detection of the surface composition. The SFG method will be correlated with Auger measurements of the deposited overlayer under UHV conditions. However, the technique is also applicable under actual CVD growth conditions.

L2.3

INTERACTION OF BORAZINE WITH A RE(0001) SURFACE, STUDIED BY LEED, TPD, AES AND ELS, J.-W. He and D. W. Goodman, Department of Chemistry, Texas A&M University, College Station, Texas 77843.

The interaction of borazine ($\text{N}_3\text{B}_3\text{H}_6$) with a Re(0001) surface has been studied by low energy electron diffraction (LEED), thermal desorption spectroscopy (TDS), Auger electron spectroscopy (AES) and electron energy loss spectroscopy (ELS). Two LEED patterns have been observed following borazine adsorption and annealing. One is the 2×2 structure, assigned to arise from atomic nitrogen. The other is the 3×21 pattern and is related to boron. The appearance of the two patterns indicates that borazine dissociates below 570K. With a high exposure ($>6\text{L}$) of borazine and a subsequent annealing, only the well formed 3×21 pattern is observed. Completion of this boron structure depends on both the surface boron coverage and the annealing temperature. Thermal desorption spectra show three states for borazine (α , β_1 and β_2) and three states for hydrogen (α , β_1 , β_2). The α state in the borazine desorption spectrum is due to desorption of multilayers of borazine. The β state hydrogen is shown to correspond primarily to decomposition of borazine. Two desorption states of nitrogen at $T > 1300\text{K}$ are also observed and correspond to the decomposition of borazine. AE data show that borazine decomposes to boron nitride when irradiated with a 2keV e^- -beam. Chemisorbed borazine, on the other hand, without e^- -beam irradiation, dissociates into atomic nitrogen and boron upon annealing to $T > 450\text{K}$. ELS results corroborate the LEED, TDS, and AES data that borazine adsorbs on Re(0001) non-dissociatively at 115K and dissociates into N and B upon annealing to $\sim 600\text{K}$.

L2.4

EARLY GROWTH IN THE CHEMICAL VAPOR DEPOSITION OF TiN, TiC AND SiC AND MONITORING BY LASER SCATTERING, Max Klein, and Bernard Gallois, Department of Materials Science and Engineering, Stevens Institute of Technology, Hoboken, NJ.

The early growth of TiN, TiC and SiC coatings by CVD on various substrates has been studied to gain an understanding of the development of growth morphologies. While continued growth of these coatings generally results in columnar grains, such morphologies do not necessarily originate at the substrate/coating interface. Rather, deposition begins on the substrate at a low rate, often as fine grains, and can continue to deposit for a short time before the onset of columnar grain growth, which continues at a higher rate.

A laser scattering technique has been developed as a tool for characterizing the early growths

through their surface roughness. This non-contact method is being used as an in-situ diagnostic by detecting changes in the growing deposit surface. For the earliest growths, a set of surface statistics, including rms roughness and lateral spacing of features, can be calculated.

L2.5

LIGHT SCATTERING MEASUREMENTS OF CVD SILICON CARBIDE.
H. W. Sheldon and T. M. Besmann, Metals and Ceramics Division, Oak Ridge National Laboratory, Oak Ridge, TN 37831.

Surface morphologies created by the chemical vapor deposition of silicon carbide were examined with light scattering. Silicon carbide was deposited from methyltrichlorosilane under various conditions, and for various lengths of time to create different surfaces. A HeNe laser source was used, and the scattered light was measured over a range of scattering angles. These measurements are compared to SEM observations and profilometer measurements of the same surfaces. In theory, the scattered light contains all of the information needed to provide a statistical description of a given surface, however, a complete vector theory for the scattering phenomena is too complex to provide any simple basis for experimental analysis. The application and limits of existing descriptions of scattering from a rough surface are discussed. The possible future use of light scattering for in-situ CVD measurements is also discussed.

L2.6

IN SITU GROWTH MONITORING OF TUNGSTEN BY REFLECTOMETRY
Albert Hasper, Jisk Holleman, Jan Middelhoek, University of Twente, Enschede, The Netherlands.

Reflectometry has already been proven to be a valuable tool for measuring deposition and etch rates of (semi)transparent layers e.g. SiO₂ on Si. It has also been demonstrated that etch rates of mono Si can be measured by using a grating as a mask.

In the Tungsten case which has a high extinction coefficient 3 applications of reflectometry will be presented:

1 End point detection of Tungsten growth via Si reduction.

The reflection versus time curve for a Si wafer with or without a native oxide shows strong differences due to the retarding by the native oxide of the reduction process.

2 In situ Tungsten surface roughness measurement for the H₂ and SiH₄ reduction case.

The surface roughness, σ is given by:

$$\sigma = \frac{0.12\lambda}{\cos\phi} \{10 \log(R_0/R)\}^{1/2}$$

Surface roughness from 5 to 100 nm can be measured in situ. The effect of renucleation can be studied

3. In situ selective growth rate measurement by using an SiO₂ grating as a mask.

When tungsten is grown selectively on a substrate masked by an SiO₂ grating the 0-order reflection versus time shows a sinusoidal wave given by:

$$R = 1/4 \left| \frac{r_1 + r_2 \exp(j2\beta)}{r_1 + r_1 r_2 \exp(j2\beta) + r_3 \exp(j2\gamma)} \right|^2$$

From this the growth rate can be calculated.

L2.7

A NEW APPLICATION OF SPECTROSCOPIC ELLIPSOmetry: A FAST, NON-DESTRUCTIVE TECHNIQUE FOR SURFACE RECOGNITION AND CLASSIFICATION. J L Stehle, J H Lecat,

J P Piel, SOPRA, 26/68 rue Pierre Joigneaux, 92270 Bois-Colombes, FRANCE. L C Hammond, ARIES/QEI, 5A1 Damonmill Square, Concord MA 01742, USA.

Spectroscopic ellipsometry (SE) has been used for accurate measurement of thickness and refractive indices, N and K, over the spectral range 1.3 to 5.3 eV. By drawing curves of N and K against wavelength, it is possible to recognize the nature of a surface as a unique 'fingerprint'.

Material surfaces will have a characteristic fingerprint in the complex plane of the refractive index. Families of materials such as metals, semiconductors, dielectrics, polymers, silicides, etc. have different characteristics.

The spectrum can be measured rapidly by an instrument such as the MOSS (Multilayer Optical Spectrometric Scanner) from SOPRA; in less than 1 second for a multichannel model.

Subsequent data analysis will allow the calculation of (1) N and K of a substrate, (2) N and thickness, T, (3) N and K of a layer where the thickness is known. Refractive index values for each energy step are plotted in the N and K plane and are compared with 'families' of curves of indices of other materials to determine its nature.

L2.8

INITIAL STAGES IN THE GROWTH OF OXIDE THIN FILMS BY CVD. L.A. Tiriz, S.R. Summerfelt, G.R. English, and C.B. Carter, Department of Materials Science and Engineering, Cornell University, Ithaca, NY 14853.

A technique has been developed for studying the early stages of the hetero-epitactic nucleation and growth of oxide thin films by transmission electron microscopy (TEM). Chemical vapor deposition (CVD) has been used to grow hematite (α -Fe₂O₃) on self-supporting, ion-thinned, sapphire TEM foils. Prior to deposition, the foils were given a special cleaning and annealing treatment to produce "clean", well-defined, stepped surfaces. Observations of α -Fe₂O₃ grown on four different orientations of sapphire -- (0001), {1102}, {1010}, and {1120} -- using bright-field imaging and selected-area diffraction (SAD) are discussed in this paper.

The α -Fe₂O₃ grew in an island-growth mode on all four substrate orientations. α -Fe₂O₃ and α -Al₂O₃ have the same corundum-type structure with a 5.5% lattice misfit. Analysis of moiré fringes and SAD patterns showed hetero-epitactic growth on each type of substrate, but different, distinctive, island morphologies. The island morphology on the two prismatic surfaces of sapphire indicated a strong preference for growth parallel to (0001) under our growth conditions. On (0001) substrates, all of the islands were associated with surface steps indicating preferential nucleation at these sites. Pronounced facetting of the islands parallel to low-index planes was observed. In contrast, α -Fe₂O₃ grown on the {1102} surface of alumina exhibited a more irregular morphology and distorted moiré fringe patterns.

L2.9

MECHANISTIC STUDIES OF THE CHEMICAL VAPOR DEPOSITION OF ALN FILMS USING ORGANOMETALLIC PRECURSORS: $[R_2AlNH_2]_3$, Carmela C. Amato, Leonard V. Interrante, and John B. Hudson, Departments of Chemistry and Materials Engineering, Rensselaer Polytechnic Institute, Troy, NY 12180-3590.

The gas phase and surface chemistries of a series of organometallic precursors to AlN, i.e. $[R_2AlNH_2]_3$, (where R is methyl, ethyl, iso-butyl, or tert-butyl), are currently under investigation. The volatile precursor, $[Me_2AlNH_2]_3$, deposits AlN films on silicon substrates at temperatures varying from 400°-800°C in a low pressure (ca. 80-100 mtorr) chemical vapor deposition system. The gaseous products are analyzed by GC-FTIR. The mechanistic and kinetics of this OMCVD process are studied using a molecular beam UHV system. Detection of the reaction products is performed by mass spectrometry.

L2.10

MECHANISTIC ASPECTS OF THE DEPOSITION OF THIN ALUMINA FILMS DEPOSITED BY MOCVD.

R.W.J. Morssinkhof, T. Fransen, M.M.D. Heusinkveld and P.J. Gellings. University of Twente, P.O. Box 217, 7500 AE Enschede, The Netherlands.

Thin alumina films were deposited on stainless steel by Metal Organic Chemical Vapor Deposition, using Aluminum-Tri-Isopropoxide as reactant. The aim of this research was to prepare the alumina films, and to optimize the process parameters for obtaining the best coatings with respect to the protective properties in oxygen and sulphur containing atmospheres. For this optimization, the reaction mechanism of the decomposition of ATI and deposition of Al_2O_3 have been studied by thermogravimetry, differential scanning calorimetry and mass spectrometry.

The experiments indicate that the optimum reaction conditions involve two steps: the decomposition of ATI to $Al(OH)_3$, followed by diffusion to and reaction at the substrate surface. Above 235 °C amorphous Al_2O_3 films are formed. The deposition experiments show that the reaction in the gas phase is an important factor. It determines the homogeneity of the deposition rate along the reactor, and the quality of the coating. Due to lack of a gas phase reaction below 300 °C, the order of the surface reaction could be determined and appeared to be 2. Also the activation energy was determined, and was found to be 15 kJ/mol. This low value is in contradiction with the observed homogeneous coating, indicative of reaction limited growth.

The conclusion is that the reaction mechanism may be explained by Langmuir type adsorption followed by the reaction of two adsorbed species at the surface.

L2.11

GAS PHASE CHARACTERIZATION IN LP CVD PROCESSES BY A PERFORMANT RAMAN EQUIPMENT. P. Gaufres and P. Huguet, U.S.T.L., 34060 MONTPELLIER CEDEX 1 (France). D. Boya and J. Lafforêt, Comurhex, BP 29, 26701 PIEPRELATTE CEDEX (France).

Spontaneous Raman scattering may be used as a technique for the characterization of gas phase in LP CVD processes, provide that the performances of the equipment are somewhat improved, in comparison with common designs. It thus appears as a lower cost and simpler technique than CARS.

A reactor, which reproduces the industrial conditions of W deposition from WF_6 and H_2 , is put into the cavity of an argon laser. The spectra are recorded with a multichannel spectrometer, equipped of an intensified detection. Spectra of satisfactory S/N ratio are obtained with pressures down to 1 mbar and temperatures up to 1000 K.

Temperature and composition may be measured as a function of the distance from the substrate. It has been found that, at a pressure of 40 mbar of pure hydrogen, the rotational temperature of the gas is higher, by about 100 K, than the temperature of the substrate, at a distance of about 3 mm. This phenomenon, very important in the interpretation of

CVD mechanism, will be discussed in terms of collisional effects and relaxation.

L2.12

GAS PHASE REACTIONS RELEVANT TO CHEMICAL VAPOR DEPOSITION: OPTICAL DIAGNOSTICS. D. Burgess, Jr., National Institute of Standards and Technology, Gaithersburg, MD 20899.

Optical emission and laser-induced fluorescence (LIF) have been used to study thermal- and laser-driven chemical processes in the gas phase pertaining to the systems: $SiH_4 \rightarrow Si$ and $SiH_4 + NH_3 \rightarrow Si_3N_4$. These processes are important to silicon/silicon-nitride chemical vapor deposition (CVD), to flame-driven gas phase silicon-based particle nucleation, and to laser-induced processes for materials fabrication.

UV laser (193 nm) photolysis was used to generate reactive SiH_3 and NH_3 species. Emission from NH (A-X) near 338 nm was by far the most intense. In addition, more complex emission from vibrational bands of the NH_2 ($\tilde{A}-\tilde{X}$) transition in the region 600-800 nm was observed. A number of bands ($v_2'=4-9$) in the progression $(0, v_2', 0) \rightarrow (0, 0, 0)$ were found with those transitions originating in $v_2'=4-6$ being much more intense. Narrow band emission with well defined heads (suggesting diatomic) from Si-containing species was recorded at 375/381, 387, and 418/430/437 nm. These were tentatively identified as hot bands ($v'=2,3$) of the SiH (A-X) system, although many Si_2 (H-X) transitions are also known in the 390-430 nm region. The kinetics of a number of important reactions: $NH_2 + SiH_4$, $SiH_2 + SiH_4$, and $SiH_2 + SiH_2$ are currently being investigated using a photolysis/LIF pump/probe experiment under low concentration/pressure conditions (0.01-1 torr). These experimental results are being used in conjunction with an ongoing chemical kinetics modeling program.

L2.13

SMALL SCALE FABRICATION AND CHARACTERIZATION OF CERAMIC MATERIALS. Jerry Czarnecki, Edgardo Francisco, David Thumm, Calm Instruments, 14207 Calmenita, Cerritos, CA 90701

Fabrication of ceramic and composite materials involves many variables, so optimization of the process requires many tests using very expensive equipment and significant amounts of costly precursors. Experiments with environment-controlled vacuum furnaces are lacking very important kind of information, that is in most cases there is no continuous monitoring of the kinetics of the deposition process.

A high-capacity, high-temperature thermobalance, equipped with a controller of gas and vapor composition and pressure has been applied for monitoring of a high-temperature metal-ceramic composite material. CVD process of subsequent deposition of tungsten, tungsten carbide (interlayer) and Al_2O_3 (coating) has been monitored gravimetrically.

In the second stage of the experiment the same thermobalance has been used for characterization of the oxidation rate of the product obtained, allowing fast prediction of the service life as function of the CVD process used to fabricate that part.

L3.1

CORRELATION AMONG PROCESS ROUTES, MICROSTRUCTURES AND PROPERTIES OF CHEMICALLY VAPOR DEPOSITED SILICON CARBIDE. Robert E. Davis, North Carolina State University, Box 7907, Raleigh, NC

Chemically vapor deposited silicon carbide is simultaneously a strong, oxidation resistant, diffusion limiting coating and composite matrix and a wide bandgap semiconductor for high-temperature, -power, -frequency and radiation hard applications. The former is produced, usually from trimethyldichlorosilane carried in H_2 . It normally possesses a highly faulted, columnar microstructure containing a random mixture of the cubic beta (3c) and hexagonal or rhombohedral alpha (of which 6H is dominant) polytypes. Deformation of this material at high temperatures (1848 - 2023K) and stresses (110 - 220 MN/m²) occurs by dislocation glide controlled by the Peierls stress. By contrast, high purity, low defect density, single crystal films of pure beta or 6H-SiC can be grown on monocrystalline Si(100) or SiC (0001) substrates. Doping, oxidation and device fabrication procedures have been developed which have resulted in power and light emitting diodes as well as field effect transistors. Various process routes will be discussed and accompanied by the results of various analytical and physical property results.

L3.2

MICROSTRUCTURAL CHARACTERIZATION OF MULTIPHASE COATINGS PRODUCED BY CHEMICAL VAPOR DEPOSITION. K.L. More, R.A. Lowden, T.A. Besmann, and R.D. James, Metals and Ceramics Division, P.O. Box 2008, Oak Ridge National Laboratory, Oak Ridge, TN 37831-6064.

Chemical vapor deposition (CVD) has been utilized to produce multiphase coatings of various compositions within a given system using several processing conditions. The coating systems to be discussed include Si-Mo-C, Si-Cr-C, and Si-Ti-C. Thermodynamic calculations have been made for a variety of experimental conditions within each system. Scanning electron microscopy, transmission and analytical electron microscopy, and x-ray diffraction techniques have been used to thoroughly characterize the microstructures and to determine compositions of the coatings as a function of CVD processing conditions.

L3.3

CHEMICAL VAPOR DEPOSITION OF SILICON BORIDES. T. GOTO, M. MUKAIDA AND T. HIRAI, INSTITUTE FOR MATERIALS RESEARCH, TOHOKU UNIVERSITY, JAPAN.

Silicon borides are a candidate for high-temperature thermoelectric materials because of their superior oxidation resistance and high Seebeck coefficients. Many kinds of silicon borides such SiB_4 , SiB_6 and SiB_{14} are known, however their intrinsic thermoelectric properties have not been well understood. In the present work, high-purity and high-density SiB_4 and SiB_6 thick plates were prepared by chemical vapor deposition, and their thermoelectric properties were measured.

The silicon borides (SiB_4 and SiB_6) were prepared using $SiCl_4$, B_2H_6 and H_2 on graphite substrates. The deposition temperature ranged from 1323 to 1773K, total gas pressure from 4 to 40kPa, and the B to Si molar ratio in the source gases from 0.2 to 2.8.

The CVD conditions to prepare the monolithic SiB_4 and SiB_6 were shown. The lattice parameters and densities were in agreement with literature values. The composition of the CVD- SiB_6 was stoichiometric, but that of the CVD- SiB_4 varied depending on CVD conditions. The Seebeck coefficient of the CVD- SiB_4 was nearly constant (about 100 μ V/deg), but that of the CVD-

SiB_6 increased with increasing temperature from 200 μ V/deg (at 400K) to 300 μ V/deg (at 900K). The measurements of Hall mobilities suggest that the conduction mechanism of the SiB_6 is hopping.

L3.4

CHARACTERIZATION OF SILICIDE FORMATION OF LPCVD-W BY MEANS OF RBS AND XRD. S.-L. Zhang and R. Buchta, Swedish Institute of Microelectronics, 164 21 Kista, Sweden; M. Östling, The Royal Institute of Technology-Electrum, Solid State Electronics, 164 28 Kista, Sweden.

The WSi_2 formation has been studied by means of RBS and XRD techniques. The silicide was formed by annealing 200 nm to 750 nm thick LPCVD-W films deposited on 1.5 - 4.0 Ω cm p-type <100>-Si substrates. Deposition temperatures were 300 - 350 °C. The thickness of the formed WSi_2 was observed to increase parabolically with the annealing time. This agrees with the behavior found in the literature for sputter deposited W films.

The crystal structures of the grown WSi_2 and the remaining W films were studied by XRD. The structure is strongly dependent on the thermal history of the samples. The as-deposited W films become more oriented to the <100> direction with increasing film thickness. When a 200 or 750 nm thick W film sample was annealed at temperatures from 700 to 800°C the remaining W films became more oriented to the <100> direction with decreasing W film thickness. The preferred orientation of the grown WSi_2 films was also found to vary with the silicidation conditions. This indicates that the simple method of comparing the W diffraction peaks of the remaining W film after heat treatment to a reference sample will unavoidably introduce large errors. Therefore, compensation of the orientation change of the W and WSi_2 films during heat treatment is required if XRD is employed to study the kinetics of the WSi_2 formation.

L3.5

MICROSTRUCTURE OF CVD - Al_2O_3 . J.A. Lindstrom, C. Charfield and M.F. Sjöstrand, AB SANDVIK COROMANT, Box 42056, S-126 12 STOCKHOLM, Sweden

Chemical Vapor Deposition of alumina on cemented carbide cutting tools has been industrial praxis for more than 10 years and the wear properties of Al_2O_3 as well as of TiC and TiN have been discussed extensively in the literature. However, little has been mentioned about the kinetics, stability and microstructure of the different alumina phases and how the formation of these phases depends on the deposition process. Alumina crystallizes in several different phases. The α -structure (Corundum) is the stable phase at typical deposition temperatures (950-1050°C). The metastable χ -phase is the second most commonly occurring alumina modification in CVD- Al_2O_3 . Other infrequently occurring types are θ , γ and δ .

Alumina is usually deposited on cemented carbide pre-coated with TiC. The conditions during the early nucleation stage determine whether the α - or the χ -phase or a mixture thereof is going to grow. Thermodynamic calculations show e.g. that the presence of small amounts of H_2O in H_2 has a drastic effect. At about 30 ppm H_2O can oxidize the TiC surface into Ti_2O_3 which favors the α -phase to grow. A second source of oxidation is CO_2 in the process gas. Most likely CO_2 adsorbs and decomposes on the TiC surface before the surface is covered with Al_2O_3 and protected. The latter oxidation is enhanced by the presence of Co, Cobalt, in small amounts originating from the cemented carbide substrate, is usually unevenly distributed over the TiC surface. This results in enhanced local oxidation and, consequently, α - Al_2O_3 is going to grow at certain locations in the form of "spots".

The α -phase exhibits a more coarse-grained structure and has a higher density than the χ -phase. χ -phase nucleates on a "pure" TiC surface with good lattice matching. An interesting observation is that χ -phase may transform into α -phase during the subsequent growth of the coating. However, the microstructure of this transformed α -phase differs from the α -phase that was nucleated directly on the TiC (Ti_2O_3) surface; it is fine-grained and shows almost the same morphology as the χ - Al_2O_3 .

L3.6

SELECTIVE CHEMICAL VAPOUR DEPOSITION OF TUNGSTEN USING SiH_4/WF_6 CHEMISTRY. C.A. van der Jeugd, G.J. Leusink, G.C.A.M. Janssen, S. Radelaar, Centre for Submicron Technology, Delft University of Technology, P.O. box 5046, 2600 GA Delft, The Netherlands.

Results obtained on selective CVD of tungsten using the SiH_4/WF_6 chemistry are presented. We investigated the deposited films by room temperature resistivity measurements, Electron Probe Micro Analysis (EPMA), Auger spectroscopy, Rutherford Back Scattering (RBS) and by measuring the resistivity of the layers between 10 K and 330 K. It was found that the room temperature resistivity depends strongly on the deposition temperature. At deposition temperatures below 475 °C the resistivity is higher than the resistivity obtained with the H_2 process. The room temperature resistivity increases from 10 $\mu\Omega\cdot\text{cm}$ at 475 °C to ~ 50 $\mu\Omega\cdot\text{cm}$ at 325 °C for a $\text{SiH}_4/\text{WF}_6=0.6$ ratio. This resistivity increase is, according to the EPMA analysis, due to the incorporation of Si (from 0.5 at% at 475 °C to 3 at% at 325 °C). The RBS data showed the layers to be compact with the Si incorporated throughout the whole layer with, according to the Auger analysis, an increase in Si concentration at the surface. Finally the low temperature resistivity measurements of the SiH_4 reduced W films showed an anomalous temperature dependence. The films deposited at deposition temperatures between 325 °C and 475 °C at a $\text{SiH}_4/\text{WF}_6=0.6$ ratio showed an unexpected increase in resistivity when the temperature decreases below ~ 250 K. The magnitude of this resistivity step increases with decreasing deposition temperature i.e. increasing Si content.

L3.7

STUDY OF W_2O_5 OXIDE PHASE OBSERVED IN CVD W FILMS. M. Lawrence A. Dass, Siva Sivaram and Bryan Tracy, 3065 Bowers Avenue, Intel Corporation, Santa Clara, CA 95051

Chemical vapor deposited tungsten (CVD W) films are extensively used in VLSI devices as metallizations due to their attractive properties such as excellent step coverage and low resistivity. Reduction of tungsten hexafluoride can be accomplished using either hydrogen or silane. Transmission electron microscopy has been used to characterize the microstructures of both hydrogen and silane reduced CVD W films. Electron diffraction results show the presence of extra rings in addition to fundamental rings which correspond to matrix W. The spacings of these rings correspond to W_2O_5 oxide phase. Dark field imaging of the extra ring shows that the oxide phase is present as particles. The oxide phase particles are uniformly distributed within the film. The average particle size of the oxide particle is about 75 Å, and is found to vary with thickness of W films. Oxygen profiles obtained from Secondary Ion Mass Spectrometry have shown the presence of oxygen which is consistent with the microstructural observations. Both microstructural and structural characteristics of the tungsten and the oxide phases and their correlation with the physical properties are presented.

L3.8

INVESTIGATION OF CVD β -SiC SURFACES PRODUCED VIA A "NOVEL" SURFACE REPLICATION PROCESS. Alik J. Collins, Joseph T. Keeley, Michael A. Pickering, and Raymond L. Taylor, Morton Thiokol, Inc./CVD, Woburn, MA. 01801

A novel replication process for Silicon Carbide surfaces was developed in our Research Center. A polished polycrystalline Chemical Vapor Deposited β -SiC surface was reproduced by a two step pretreatment process followed by CVD of SiC.

In this paper we describe the process and present characterization data of both the substrate and the replica surfaces. The characterization data include XRD, Auger, ESCA, Raman, and reflectivity spectra both in the infrared and the ultra violet region. Based on the characterization results we

developed a model to describe what happens in terms of reactions and microstructure during the replication process.

L4.1

DESIGN AND DEVELOPMENT OF CVD COATINGS. V.K. Sarin, College of Engineering, Boston University, Boston, MA.

The efficacy and economic benefits accompanying the application of CVD coatings, especially in tribological applications, is well established. In spite of their tremendous commercial success, a basic understanding of structure/property relationships, and adhesive characteristics, are still incomplete. This information limitation has been an impediment to systematic design of new and improved coatings. However, since these coatings (typically 5-10 μ) do not necessarily exhibit bulk material properties, measurement of both mechanical properties and adhesion in itself present a major technical challenge. This has resulted in a two-fold problem, mainly development of unique techniques to characterize both properties and performance, before any substantive structure/property correlations can be established. Coating design, structure/property relationships and characterization techniques will be reviewed and discussed.

L4.2

INDENTATION ADHESION OF DIAMOND FILMS ON THE VARIOUS SUBSTRATES. Tyan-Ywan Yen, Cheng-Tzu Kuo, National Chiao Tung University, Institute of Mechanical Engineering, HsinChu, Taiwan, R.O.C.; and S. E. Hsu, Cheng Shan Institute of Science and Technology, Lungtan, Taiwan 32526, R.O.C.

The microwave plasma-assisted chemical vapor deposition was used to deposit diamond films to investigate the mechanisms of indentation adhesion on the various substrates. Indentation was conducted by employing Rockwell brale indenter. The critical loads for crack initiation and propagation of the films under different deposition conditions were determined. SEM, AES, XRD and Raman spectrometer were used to characterize the surfaces before and after the substrate pretreatments and diamond deposition; and to correlate with the adhesion measurements.

The adhesion of diamond films to the substrates was found to be significantly depending upon the substrate material and its pretreatments, and the deposition conditions. The possible adhesion mechanisms would be discussed.

L4.3

TUNGSTEN CARBIDE EROSION RESISTANT COATING FOR AEROSPACE COMPONENTS. B. Gung and P. N. Sanyal, Sanyal Process and Chemicals, Inc., 7701 Hamilton Boulevard, Allentown, PA 18106

An increasing problem faced by the aerospace industry is the erosive wear of engine components. Various CVD deposited protection coatings have been used previously to combat this wear problem, but with limited success. This paper presents results obtained with a low temperature CVD deposited, erosion resistant, multilayer tungsten carbide coating system. The coating can be deposited at temperatures below 1000°C on various alloys used in the aerospace industry. The low temperature of deposition eliminates the problem of degradation of mechanical properties that occurs with normal high temperature CVD processes. High cycle fatigue strength and other mechanical property data are presented for coated stainless steel, as well as erosion resistant data for both mild and harsh erosive environments.

L4.4 ABSTRACT WITHDRAWN

L4.5

INTERNAL STRESSES IN AMORPHOUS SiO_2 FILMS DEPOSITED BY THE PYROLYSIS OF ORGANOMETALLIC PRECURSORS AT LOW PRESSURES. S.B. Iksu, Department of Materials Engineering, Virginia Polytechnic Institute and State University, Blacksburg, VA.

Amorphous SiO_2 films were deposited by the low pressure pyrolysis of organometallic precursors such as diacetoxydi-*t*-butoxy silane at temperatures of 400°C to 500°C. Films were deposited on both single crystal silicon and fused quartz substrates. Film stress at room temperature after cooling from deposition temperature, as well as stress as a function of anneal temperature were measured using the curvature method.

As deposited films were under significant tensile stress of the order of 400 MPa. The film stress at room temperature following deposition, increases as the deposition temperature decreases and deposition pressure increases. Dopants like B_2O_3 and P_2O_5 , at small concentrations, significantly decreased the intrinsic stress of as deposited films. Stress reduction was also achieved by post deposition annealing. The silica film stress is correlated to the structure of the film, more specifically to the Si-O-Si angle distribution.

Interrelations between film stress, deposition conditions, post deposition treatments, and film structure will be discussed.

L4.6

INFLUENCE OF SUBSTRATE AND PROCESS PARAMETERS ON THE PROPERTIES OF CVD-SiC. A. Parretta, V. Adoncccchi, E. Cappelli, G. Giunta and V. Vittori, Eniricerche S.p.A., via E. Ramarini 32, 00015 Monterotondo (Roma).

The microstructure and mechanical properties (adhesion, hardness) of beta-SiC coatings, prepared in a cold wall reactor starting from two different CVD processes, were studied by examining different substrates and deposition process conditions.

Hard (3500 HK), fine grained beta-SiC coatings, with a good oxidation resistance at 1273 K, were deposited onto graphite substrates at relatively high deposition temperatures (1473-1673 K) using SiCl_4 , C_3H_8 , H_2 gas mixtures.

The thermal decomposition of methyltrichlorosilane (MTS) in hydrogen and argon allowed the production of beta-SiC coatings onto a variety of substrate materials in the temperature range 1173-1373 K. The growth mechanisms of SiC deposited from MTS/ H_2 /Ar system onto graphite and polycrystalline alpha-SiC substrates were studied. At low (~ 40 kPa) and atmospheric pressures, the growth kinetics are surface limited. Also, a strong dependence of the microstructure and crystallographic orientation on the deposition parameters was observed.

Hard metals (WC/Co) were successfully coated with beta-SiC using the MTS/ H_2 /Ar system. Problems of chemical compatibility and thermal expansion mismatch between the substrates and the beta-SiC coating were minimized by the deposition of intermediate layers.

The adhesion of the coatings was evaluated using mechanical "scratch test" measurements.

L4.7

ROLE OF DEPOSITION CONDITIONS ON THE MICROSTRUCTURE AND PROPERTIES OF CVD-SiC. E. A. Minter, Robert F. Stevens, Vincent L. Magnotta, and Paul M. Dyer, Air Products and Chemicals, Inc., Allentown, PA. And Thomas Watkins and David J. Green, Pennsylvania State University, University Park, PA.

Ceramic coatings are finding application in a wide variety of uses. Key to the successful utilization of these coatings is an understanding of the interaction of thermomechanical properties of the coating and the substrate as well as the effects of processing conditions on the adhesion and on the residual stress state in both the coating and the substrate. A

lack of appreciation of these factors has led to coating spallation or cracking and resulting failure in service.

The results of recent experiments to determine the tensile and compressive strength and elastic modulus of SiC coatings applied on graphite substrates via chemical vapor deposition will be analyzed with respect to the effects of these properties on residual stresses.

L4.8

Interaction of Titanium with SiC Coated Boron Fibers

Lewis Hwan¹, Beng Jit Tan¹, Francis S. Galasso² and Steven L. Suib³, 1. Dept. of Chemistry, U-60, University of Connecticut, Storrs, CT 06269-3060. 2. United Technologies Research Center, East Hartford, CT 06108. 3. Dept. of Chem. Eng., U-60, University of Connecticut, Storrs, CT 06269-3060.

Silicon carbide (SiC) coated boron fibers have been imbedded in titanium by hot pressing and have been coated with titanium using a chemical vapor deposition. Room temperature tensile strength measurements have shown that silicon carbide coated boron (SiCABO) fibers coated with titanium are stable after thermal treatments at 1000°C for 24 hours. These coated fibers have been studied with X-ray powder diffraction, tensile strength measurements, thermal studies, X-ray photoelectron spectroscopy and scanning Auger microscopy. Depth profiles of the coated fibers have been used to study the interaction of titanium with the SiCABO fibers. Scanning Auger microscopy studies have shown that the SiCABO fibers have a carbon rich surface as compared to another more well known silicon carbide coated boron fiber (BORSIC). A comparison of these two types of fibers will be made and factors responsible for the significantly higher tensile strengths after heating in titanium with the SiCABO fibers will be discussed.

L4.9

OXIDATION RESISTANT COATINGS PRODUCED BY CHEMICAL VAPOR DEPOSITION: IRIIDIUM AND ALUMINIUM NITRIDE / ALUMINA COATINGS P. NETTER and Ph. CAMPROS, Vapometallurgy Division, COMURHEX, BP 29, 26701 PIERRELATTE Cedex (FRANCE)

Oxidation resistant coatings of iridium on graphite, carbon/carbon or molybdenum and of aluminium nitride/alumina on graphite and carbon/carbon have been produced by low pressure CVD from halide starting compounds (IrF_6 and AlCl_3). The resulting deposits are adherent, non porous and have proved impervious to oxygen in subsequent heating to 2000° C in air for more than 30 minutes (no evidence of deterioration).

These coatings materials are promising for effective protection against oxidation for rocket engines, gas turbines, thermal protection system tiles of space shuttle or against corrosion in the glass industry (iridium).

Schematics of the CVD processes are described as well as analysis and characterization techniques used in order to determine layers structures and compositions (optical microscopy, SEM, XPS and ESCA, SAM and SIMS). Results of oxidation tests performed by induction heating in air are also given

L4.10

CHEMICAL VAPOUR DEPOSITION OF TITANIUM CARBIDE, R. Singh, A.K. Suri, D.K. Bose and C.K. Gupta, Metallurgy Division, Bhabha Atomic Research Centre, Trombay, Bombay 400 085.

This paper deals with a process for chemical vapour deposition of titanium carbide using titanium tetraiodide as a titanium source.

In the process investigated titanium tetraiodide as synthesized in-situ by passing vapours of iodine over heated titanium and the iodide is transported to other interconnected reactor where it reacts with hydrogen and hydrocarbon bearing gas to form titanium carbide on heated stainless steel substrates. This process offers an advantage of carrying out reaction under lower temperature conditions as compared to the conventionally used titanium chloride as the titanium bearing source.

The paper reports on the influence of various parameters on the carbide deposition process and establishes the optimum conditions. The paper also incorporates characterisation studies carried out by various physico-mechanical tests.

L5.1

APPLICATION OF AI CONTROL TO THE VLS SiC WHISKER PROCESS. E. D. Shalek and W. J. Parkinson, Los Alamos National Laboratory, Los Alamos, NM 87545.

Silicon carbide whiskers have excellent mechanical and chemical properties giving them much potential, some already commercially proven, as a reinforcement for structural ceramic composite materials. Los Alamos has developed a batch process for producing very high quality SiC whiskers by the vapor-liquid-solid (VLS) method; however, the process has rather complex chemistry and has been difficult to make reproducible over the long term, reproducibility being an important consideration for process scale-up.

The process is difficult to model mathematically, so optimum conditions have been derived from relating the many process parameters to product results to establish a set of rules that will be used to run the process. These are incorporated in a two-phase expert system designed to guide inexperienced users. In Phase 1, an expert consultant program provides the user with information that enables him to set up the run. This information is incorporated into the rule base that makes up Phase 2- the control system. At present, the operator functions as the controller by responding to the decisions of the expert system; automation can be added later.

Although the external process conditions have always been monitored during a run, the recent installation of a gas chromatograph to sample the reactor gases has been the single most valuable contributor to process control and reproducibility. By comparing the inlet and outlet gas stream compositions, we can quantify the reactions taking place and directly relate the process conditions to SiO generation and subsequent nucleation and growth phenomena.

L5.2

MORPHOLOGICAL EVOLUTION OF TITANIUM CARBIDE WHISKERS. R. Mathur, and Bernard Gallois, Department of Materials Science and Engineering, Stevens Institute of Technology, Hoboken, NJ.

The early growth of titanium carbide whiskers from a mixture of $TiCl_4$ - CH_4 - H_2 was investigated, using fine nickel particles as the catalytic agent in a hot-wall CVD reactor. This study confirms that whisker growth is initiated by the VLS growth mechanism in the temperature range of 1273-1423 K, well below the Ti-Ni-C ternary eutectics as reported in the literature. The initial growth proceeds by diffusion of the constituent species through a Ni-Ti liquid droplet and is characterized by a rapid increase in length at near constant diameter. A gradual coarsening of features is observed at latter stages. The whiskers exhibit extensive branching and kinking and a $\langle 100 \rangle$ primary growth direction.

L5.3

CHARACTERIZATION OF CERAMIC MATRIX COMPOSITES FABRICATED BY CHEMICAL VAPOR INFILTRATION.* D. P. Stinton, D. M. Hembree, Jr., K. L. More, and T. M. Besmann, Oak Ridge National Laboratory, Oak Ridge, TN.

Composites consisting of silicon carbide (SiC) matrices reinforced with continuous Nicalon fibers are being developed for many high-temperature structural applications. An attractive process for fabricating these fiber-reinforced composites is chemical vapor infiltration (CVI), because it is one of only a few processes capable of incorporating continuous ceramic fibers in a ceramic matrix without damaging the relatively fragile reinforcing fibers. This investigation applied Raman spectroscopy, transmission electron microscopy, and optical microscopy to study the morphology of the SiC matrix in ceramic matrix composite materials.

L5.4

THE EMERGENCE OF PLASMA ENHANCED CHEMICAL VAPOR DEPOSITION (PECVD) AS A VIABLE INDUSTRIAL COATING PROCESS. George Engle, GEC, Inc., 2650 S. 47th Street, Suite 103, Phoenix, AZ 85034 and James W. Warren, Composite Innovations Corporation, 24300 Aetna Street, Woodland Hills, CA 91367.

The potential of Chemical Vapor Deposition, as a process for applying erosion and corrosion resistant ceramic and metal coatings to ferrous and non-ferrous alloys has long been recognized. Unfortunately, the high deposition temperatures (900°-1000°C) cause deleterious and generally nonreversible metallurgical changes in the coated parts. Corresponding shape stability and dimensional tolerances are also lost. For more than twelve years, Plasma Enhanced Chemical Vapor Deposition (PECVD) technology has evolved from the laboratory into production operations within the semiconductor industry.

This acceptance is primarily due to the low PECVD deposition temperatures (<450°C). The PECVD processes have recently demonstrated an adaptability to coating alloy components and carbon-ceramic fibers with a wide range of carbide, boride, nitride, oxide and metal coatings to render them corrosion and erosion resistant. Typical Knoop hardness control of silicon carbide coatings can be controlled from about 2300 to more than 7000 kgfmm⁻² at 10 μ m penetration of the indenter while fiber coating thickness and uniformity can be controlled from 300A \pm 5%. Selected coatings applications and performance are described.

L5.5

DEPOSITION AND CHARACTERIZATION OF SILICON NITRIDE SINGLE CRYSTAL FILMS. Joseph B. Milstein, Lian Li, Ye-Yung Teng, and Anatoly M. Altschuler, University of Lowell, Lowell, MA

We have investigated the deposition of single crystal silicon nitride in a low pressure radio-frequency plasma assisted CVD deposition system operating at 440 KHz in an atmosphere of nitrogen and hydrogen. Substrates consisting of single crystal silicon wafers have been employed. The depositions have been carried out with substrate temperatures in the range of 300 to 1200 °C. We find that the reaction of the silicon wafer with the nascent nitrogen produced in this system appears to be self-quenching at low substrate temperatures.

Characterization of the films has been performed by a variety of techniques including x-ray diffraction, ellipsometry, electrical measurements, and optical absorption.

L5.6

LASER CHEMICAL VAPOR DEPOSITION OF TIN FILMS
B.Chen, N. Biunno, R.K. Singh, and J.Narayan Dept. of Materials Science and Engineering, North Carolina State University, Raleigh, NC 27695-7916

We have investigated the growth of titanium nitride thin films using the laser-induced chemical vapor deposition technique. A CO₂ laser ($\lambda=10.6\mu\text{m}$) operating in both continuous wave and pulsed modes was employed to induce localized heating of the molybdenum and stainless steel substrates. The flow rates of TiCl₄ and NH₃ were controlled to optimize the deposition of TiN films. The substrate temperature during deposition was varied from 700°C and 1200°C by controlling the laser power density and the pulse duration. The effect of various processing parameters (gas flow rates, substrate temperature, flow geometry, etc) on the stoichiometry and microstructure of the TiN was analyzed by Auger Electron Spectroscopy, Transmission Electron Microscopy, Rutherford Backscattering Spectroscopy, & Scanning Electron Microscopy. The nature of the interface between the substrate and the film as a function of temperature will also be discussed. Simple thermal calculations correlating the deposition characterized with the laser power density will also be included in the presentation.

L5.7

LASER-INDUCED PHOTOCHEMICAL VAPOR DEPOSITION OF TUNGSTEN. A.J.P. van Maaren and W.C. Sinke, FOM-Institute for Atomic and Molecular Physics, kruislaan 407, 1098 SJ Amsterdam, The Netherlands.

Laser-induced photochemical vapor deposition can impart an important contribution to refractory metals CVD technology. It enables deposition at lower substrate temperatures and offers the possibility of projection patterning or direct writing.

We have employed an ArF excimer laser, aligned parallel to the substrate, to perform blanket deposition of tungsten on silicon using WF₆ and H₂ as reaction gases. The experiments were performed in a cold-wall reactor, with a base pressure of 10⁻⁸ mbar. In this reactor high quality W films have been deposited at substrate temperatures as low as 200 °C. We have performed depositions at different substrate temperatures and laser-pulse frequencies. Film thickness and morphology have been studied with RBS and cross-section SEM. Resistivities as low as 9.0 $\mu\Omega\text{cm}$ have been obtained. We will show that, after deposition over the native oxide, the roughness at the W-Si interface of laser deposited W films is clearly reduced in comparison with thermally deposited films.

In addition we have determined the contribution of the Si-reduction reaction to the total W deposition. In these experiments W was deposited on the mono-crystalline Si top-layer of a marker sample, and the buried marker in the substrate was used as a reference for RBS measurements.

L5.8

STRUCTURAL CONTROL OF MATERIALS SYNTHESIZED BY LASER EVAPORATION AND RAPID CONDENSATION

Tongsan D. Xiao & Peter R. Strutt, The University of Connecticut, Institute of Materials Science, Storrs, CT 06268.

As uniquely demonstrated by Chow and Strutt, rapid condensation of species from a high-power cw CO₂ laser plume may be exploited to synthesize novel new materials. Of specific interest was the synthesis of a nanoscale composite containing 25 to 100 nm. diameter silica fibers and a metal matrix. Recent studies now show that similar structures can be generated using a modified procedure, providing a greater degree of flexibility and control of process variables.

One feature of the modified technique is independent substrate heating. This replaces the use of a laser beam for combined (i) substrate heating, and (ii) ceramic target interaction to form a plume. Results will be presented showing how the morphology and growth rate of deposited layers depends on the (i) substrate temperature, (ii) chamber pressure, and (iii) geometrical configuration in the reaction zone. Attention is devoted to the cross-sectional uniformity of fibers, where, it is proposed, the effect of interfacial chemistry on surface tension influences fiber surface stability. A diversity of microstructural and analytical techniques have been used to characterize morphological structures. These include transmission electron microscopy, auger spectroscopy, XPS, and fourier transform infrared spectroscopy.

L5.9

REACTIVE CHEMICAL VAPOR DEPOSITION AS A METHOD FOR COATING CARBON FIBER WITH CARBIDES. J. BOUX, C. VINCENT, H. VINCENT, R. FAVRE, LABORATOIRE DE PHYSICOCHIMIE MINERALE (URA 116 DU CNRS), UNIVERSITE DE LYON 1, 43 Boulevard du 11 Novembre 1918, 69622 VILLEURBANNE CEDEX (FRANCE).

Carbon fibre is an ideal material for reinforcing inorganic matrix composites, specially for high temperatures. Its main drawback is its susceptibility to oxidation and to reaction with metals.

Our challenge was to perfect a method of producing a carbon fibre in which each elementary filament is covered and protected by a very thin and adherent layer of a refractory carbide such as SiC, B₄C, etc.

In this purpose, we use reactive chemical vapor deposition (RCVD) in which only the M element of the M_nC carbide is carried by the gas phase, carbon being supplied by the fibre itself. The growth rate is self regulated by the solid state diffusion.

This method has been developed in a continuous reactor with ex-PAN (6 K) or ex-PITCH (2 K) fibers.

L5.13

A LOW TEMPERATURE PVD PROCESS FOR TIN COATING

A. Agüero, D. Little, and P. Lowden,
Liburdi Engineering Limited, Hamilton, Ontario.

The mechanical behaviour of the coated fibers is very near that of the starting ones, but their oxidation rate at 600°C is 100 times lower.

L5.10 ABSTRACT NOT AVAILABLE

L5.11

SOLUTION PRECURSOR - LOW PRESSURE CHEMICAL VAPOR DEPOSITION OF TITANIUM OXIDE FILMS. Jiong Ping Lu, Jengdaw Wang and Rishi Raj, Dept. of Materials Sci. & Eng. Cornell Univ. Ithaca, NY 14853.

A novel technique for performing Low Pressure Chemical Vapor Deposition (LPCVD) has been set up. The apparatus consists of a vertical - cold wall reactor, which uses liquid solutions as precursors. Solution precursors are converted into vapor right before entering the reactor. Deposition takes place on substrates held at temperatures higher than the vaporization temperature. A LPCVD process using liquid solution precursors will be referred to as Solution Precursor - LPCVD. It has some advantages over conventional LPCVD, including easy control of film composition, less restriction on precursor compounds, simplicity of apparatus and improved safety.

Solution Precursor - LPCVD method has been applied for depositing titanium oxide films on Si(100) and glass substrates. The precursor used is titanium isopropoxide, $Ti[OCH(CH_3)_2]_4$, dissolved in toluene solvent. The base pressure of the reactor is 0.5 torr, and operating pressure is in the range of 2.0 - 3.0 torr. The precursor is vaporized at 150°C, and films deposited in the temperature range of 300 - 550°C. Rutherford Back-Scattering (RBS) analysis of the deposited films show that the stoichiometry is TiO_2 . A wide range of deposition rate has been achieved by changing the concentration of the precursor solution. X-ray Diffraction (XRD) experiments indicate that the structure is anatase. No other phase can be detected. In the temperature range of 300 - 350°C, randomly oriented polycrystalline films are obtained; while at higher temperatures (450 - 550°C), the films are textured. The preferential orientation exists on both Si(100) and glass substrates, eliminating the substrate orientation effect. The textured films have columnar structure, and show very different morphology as compared to randomly oriented films.

L5.12

AMORPHOUS INSULATING NbO FILMS BY REACTIVE EVAPORATION. B.X.Liu, Center of Condensed Matter and Radiation Physics, CCAST (World Lab.), Beijing and Department of Materials Science and Engineering, Tsinghua University, Beijing 100084, CHINA; J.R.Ding, X.Zhou and J.N.Bai, Department of Materials Science and Engineering, Tsinghua University, Beijing 100084, CHINA

Reactive Evaporation technique was employed to prepare directly the amorphous NbO films for the usage of insulating layers.

It was found that the sheet electrical resistance of the amorphous NbO films was much greater than that of the crystalline counterparts, indicating that the amorphous NbO films are more suitable for being used as an insulating layer in junction devices.

Both thermal and irradiation stabilities of the prepared amorphous NbO films were studied. The recrystallization temperature of the films was 1120 ± 50 K, and the films also crystallized upon heavy ion irradiation at room temperature.

This paper presents the detailed procedure of the film preparation and the properties of the amorphous NbO films.

A novel low temperature process for the chemical vapor deposition of titanium nitride films has been developed. Titanium sub-halides generated "in-situ" by chlorination of titanium pellets are subsequently reacted with a nitrogen source at reduced pressure and temperatures of 550 - 600°C. The coatings have excellent adhesion and no wear resistance.

A description of the process and the properties of coatings produced by it will be presented.

L6.1 ABSTRACT NOT AVAILABLE

L6.2

METALORGANIC CHEMICAL VAPOR DEPOSITION OF SILICON BASED CERAMICS USING METHYLSILAZANE. Honghua Du, Bernard Gallois, and Kenneth Gonsalves, Stevens Institute of Technology, Hoboken, NJ.

Silicon nitride and silicon carbonitride ceramic films have been deposited using a methylsilazane prepolymer, $[CH_3SiH_2NH]_n$, with NH_3 and H_2 as the carrier gases in a cold-wall, resistance-heated quartz reactor at 873-1073 K.

When NH_3 is used, silicon nitride is obtained. The Si-C and Si-H bonds in the prepolymer can be effectively cleaved and the associated C and H removed. The residual N-H bonds detected in the silicon nitride phase can be attributed to the high bond strength or excess NH_3 present in the reaction system.

When H_2 is used, silicon carbonitride is obtained. Cleavages of the C-H and N-H bonds in the prepolymer are effective on pyrolysis, and the associated H is removed as H_2 . Partial cleavages of the Si-NH and Si-CH₃ bonds in the prepolymer and removal of N and C species are also evidenced by the high Si atomic composition, compared with N and C, in the film deposited.

The silicon carbonitride film density increases with temperature, in contrast to a constant silicon nitride film density. It is believed that the rupture of the cyclic structure of the prepolymer is dominated by the nucleophilic effect in NH_3 , and by thermal dissociation in H_2 .

L6.3 ABSTRACT NOT AVAILABLE

L6.4 ABSTRACT NOT AVAILABLE

L6.5

STRUCTURE, COMPOSITION, AND PROPERTIES OF CVD ZrO_2 FILMS OBTAINED FROM ZIRCONIUM ACETYLACETONATES. S.B.Desu and T.Shi, Department of Materials Engineering, Virginia Polytechnic Institute and State University, Blacksburg, VA.

ZrO_2 films were deposited on silicon and quartz substrates at temperatures of 350°C to 550°C by the pyrolytic decomposition of zirconium acetylacetonates. Depositions were carried out at both atmospheric and low pressures. The optical properties, structure, microstructure and composition of films were characterized by ellipsometer, X-ray diffraction, scanning electron microscopy (SEM), and X-ray photoelectron microscopy (XPS), respectively.

The deposition rate was kinetically controlled at low temperatures and mass transfer controlled at high temperatures. Use of zirconium (IV) acetylacetonate resulted in cubic ZrO_2 with some carbon contamination whereas, monoclinic, pure ZrO_2 films were obtained with the precursor zirconium (IV) trifluoroacetylacetonate. The monoclinic ZrO_2 films are fine grained and showed preferential orientation. The measured values of dielectric constant, refractive index, and electrical resistivity of ZrO_2 films are 18, 2.2, and $5E13$ Ohm.cm, respectively.

The results are explained in the light of decomposition mechanisms of the organometallic precursors.

L6.6
TITANIUM NITRIDE THIN FILMS: PROPERTIES AND APCVD SYNTHESIS USING ORGANOMETALLIC PRECURSORS. Renaud M. Flx, Roy G. Gordon, David M. Hoffman, Department of Chemistry, Harvard University, Cambridge, MA 02138.

A unique combination of properties makes titanium nitride (TiN) thin films an attractive material for a wide range of applications. Current CVD processes, however, require temperatures too high for thermally sensitive substrates such as plastics, or aluminized silicon microcircuits. In this paper we present a new low-temperature atmospheric pressure CVD synthesis of TiN thin films, which uses organometallic compounds as precursors.

Film depositions were carried out at temperatures from about 100 to 300 °C on substrates such as silicon wafers, glass, vitreous carbon, and boron. Growth rates, film thicknesses and surface morphology (by SEM) will be reported. The characterization of the films by electron microprobe analysis, RBS, XPS and XRD will be discussed. The electrical and optical properties of the films will also be described.

L6.7
CHEMICAL VAPOR DEPOSITION OF NIOBIUM CARBIDE USING A NOVEL ORGANOMETALLIC PRECURSOR. P.D. Stupik and A.R. Barron*, Department of Chemistry, Harvard University, Cambridge, MA 02138.

A method for the preparation of niobium carbide films at less than 500°C has been developed. The use of volatile organo-niobium compounds as single component precursors, in an atmospheric pressure laminar flow CVD apparatus yielded adherent films of niobium carbide on single crystal silicon and glass substrates. XPS studies indicate that the films contain a carbide phase and a nearly stoichiometric ratio of niobium to carbon. The morphology of the films has been examined by SEM.

L6.8
LOW TEMPERATURE ORGANOMETALLIC CHEMICAL VAPOR DEPOSITION (OMCVD) OF RHODIUM AND IRIUM THIN FILMS. D.C. Smith, C. J. Burns, and A. P. Sattelberger, Inorganic and Structural Chemistry Group (INC-4), Los Alamos National Laboratory, Los Alamos, NM 87545; and S. G. Pattillo, D. W. Carroll, and J. R. Laia, the Material Science and Technology Division, Los Alamos National Laboratory, Los Alamos, NM 87545.

We will describe new low temperature (≤ 300 °C) routes to rhodium and iridium thin films from volatile organometallic precursors that have been developed at Los Alamos. The following topics will be discussed: (1) synthesis and characterization of the organometallic precursors, (2) the conditions of film growth and the types of substrates used, (3) experimental variables (e.g., pressure, substrate temperature, hydrogen concentration, etc.) and their effect on film quality and film deposition rates, and (4) experimental characterization of the metal films by X-ray diffraction, scanning electron microscopy, and Auger spectroscopy.

L6.9

ORGANOMETALLIC CHEMICAL VAPOR DEPOSITION OF STRONTIUM TITANATE THIN FILMS. W. A. Feil,^a L. M. Tonge,^b B. W. Wessels,^a and T. J. Marks,^b Northwestern University, Evanston, IL 60208

SrTiO₃ thin films were deposited by low pressure organometallic chemical vapor deposition on sapphire and silicon substrates using the volatile metalorganic precursors titanium isopropoxide and Sr (dipivaloylmethanate)₂. Oxygen and water vapor were used as reactant gases and argon was used as a carrier gas. Growth rates ranging from 0.3 - 5.0 $\mu\text{m/hr}$ were obtained at 600 - 850°C. Highly c-axis oriented SrTiO₃ was obtained on (0001) sapphire, while no preferred orientation could be observed for the films grown on silicon. Both the growth rate and growth temperature influenced the phases stabilized and the surface morphology of the as-deposited films grown on sapphire. SrTiO₃ films deposited on silicon substrates exhibited resistivities greater than 10^9 ohm-cm and dielectric constants up to 100.

L6.10
HIGHLY RESOLVED GRADIENT PATTERNS IN GLASS BY MEANS OF CHEMICAL VAPOR DEPOSITION. Harry D. Gafney, Edgar Mendoza, Eugene Wolkow, Department of Chemistry, Queens College of CUNY, Flushing, N.Y. 11367; and Peter Wong, Department of Chemistry, Queensborough Community College, Bayside, N.Y. 11364

Recent experiments have established that highly resolved patterns of refractive index gradients can be produced in glass by photolysis and subsequent heat treatment of vapor deposited organometallic reagents on porous Vycor glass (PVG) or dried porous silica gels. The comparative topographies of the porous adsorbents and consolidated glasses were observed by optical and scanning electron microscopy (SEM) and conclusions were drawn with respect to resolution of patterns as a function of chemical behavior of absorbate. The photochemical and thermal reactions, which lead to consolidated glass formation, as well as the synthesis of sol-gels will be described. Comparisons between glasses made by critical cooling of melts (ccm), such as vycor, and the sol-gel method (sgm) will be discussed with respect to their compositions and topographies.

L6.11
SMALL ANGLE X-RAY SCATTERING (SAXS) FROM METAL IMPREGNATED POROUS VYCOR GLASS.* D. Sunil, J. Sokolov*, M.H. Rafailovich, E. Mendoza, E. Wolkow, H.D. Gafney, Queens College, G. Long, NIST, P. Jemian, Northwestern University, A. Hansen, Brookhaven National Laboratory,

We have obtained highly resolved patterns by photolysis of iron and tin compounds vapor deposited onto porous Vycor glass, (PVG). In order to study the nature of the surface chemical process and its relationship to the morphology of the glass, the samples were studied by various complementary techniques. SAXS clearly shows that the Sn impregnated glass retains the morphology of the spinodally decomposed phase of the PVG even after consolidation at 1200°C. In contrast, the Fe impregnated sample has this structure only for $T \leq 650$ °C and is then collapsed to a uniform

glass at 1200°C. Rutherford backscattering in conjunction with X-Ray micrography show the Sn oxides to be uniformly distributed in a granular glass matrix, while the Fe oxides are incorporated into a smooth glass substrate, forming a uniform, 400 μ thick layer situated several hundred angstroms below the glass surface. We conclude that the Sn oxides are more strongly bound to the glass thereby modifying its surface and inhibiting the consolidation process. Similar studies on impregnated glass gels will be presented and compared with scanning electron micrographs of the samples.

**SYMPOSIUM M:
HIGH-TEMPERATURE SUPERCONDUCTORS:
FUNDAMENTAL PROPERTIES AND NOVEL
MATERIALS PROCESSING**

M

November 27 - December 1, 1989

Chairs

Jagdish Narayan
Department of Materials
Science & Engineering
North Carolina State University
Raleigh, NC 27695-7916
(919) 737-7874

Paul Chu
Texas Center for Superconductivity
University of Houston
Houston, TX 77204-5506
(713) 749-2842

Lynn Schneemeyer
AT&T Bell Laboratories 1A-363
600 Mountain Avenue
Murray Hill, NJ 07974
(201) 582-5318

David Christen
Solid State Division MS 6061
Oak Ridge National Laboratory
Oak Ridge, TN 37831-6061
(615) 574-6269

Symposium Support

Oak Ridge National Laboratory/Through the
High-Temperature Superconductor Pilot Center/
Department of Energy

**Proceedings published as Volume 169
of the Materials Research Society
Symposium proceedings series.**

SESSION M1: THEORY AND EXPERIMENT

Chairs: P. Chu and F. Fradin
Monday Morning, November 27
Salon G (M)

SYMPOSIUM M presentations
may be viewed
simultaneously in the
Essex North West Room,
Westin Hotel.

8:30 *M1.1

MYTH AND REALITY IN HIGH T_c , Philip W. Anderson, Princeton University, Department of Physics, Princeton, NJ.

9:00 *M1.2

SOME THEORIES OF HIGH TEMPERATURE SUPERCONDUCTIVITY, Marvin L. Cohen, University of California, Berkeley, and Materials and Chemical Sciences Division, Lawrence Berkeley Laboratory, Department of Physics, Berkeley, CA.

9:30 M1.3

RENORMALIZATION FROM DENSITY FUNCTIONAL THEORY TO STRONG COUPLING MODELS FOR THE ELECTRONIC STRUCTURE OF La_2CuO_4 , Mark S. Hybertsen and Michael Schluter, AT&T Bell Laboratories, Murray Hill, NJ; E.B. Stechel and D.R. Jennison, Sandia National Laboratories, Solid State Theory Division 1151, Albuquerque, NM.

9:45 BREAK

10:00 *M1.4

EXPERIMENTAL EVIDENCE FOR VORTEX-GLASS SUPERCONDUCTIVITY IN $YBaCuO$, R. Koch, IBM T.J. Watson Research Center, Yorktown Heights, NY.

10:30 M1.5

ELECTRONIC STRUCTURE OF $La_{2-x}Sr_xNiO_4$ SUPERCONDUCTING MATERIALS, Yuejin Guo and William A. Goddard III, California Institute of Technology, Arthur Amos Noyes Laboratory of Chemical Physics, Pasadena, CA.

10:45 M1.6

VORTEX PHASES AND DISSIPATION IN HIGH TEMPERATURE SUPERCONDUCTING OXIDES, N.C. Yeh, IBM T.J. Watson Research Center, Yorktown Heights, NY.

***Invited Paper**

Short Course M-05, "Fabrication, Characterization, and Applications of High-Temperature Superconducting Materials," may be of interest to symposium attendees. Details regarding course dates and instructors are provided in the short course section of this program.

11:00 M1.7

EVIDENCE OF KOSTERLITZ-THOULESS TRANSITION AND FLUCTUATIONS IN HIGH TEMPERATURE SUPERCONDUCTING THIN FILMS, Q.Y. Ying and H.S. Kwok, State University of New York at Buffalo, Institute on Superconductivity, Buffalo, NY.

11:15 M1.8

PHONON ANOMALY ACROSS T_c IN $Y(Er)Ba_2Cu_3O_{7-\delta}$, R.P. Sharma, L.E. Rehn, P.M. Baldo and J.Z. Liu, Argonne National Laboratory, Materials Science Division, Argonne, IL.

11:30 M1.9

REPRODUCIBLE TUNNELING DATA ON CHEMICALLY ETCHED SINGLE CRYSTALS OF $YBa_2Cu_3O_7$, J.M. Valles Jr., M. Gurvitch, A.M. Cucolo, R.C. Dynes, J.P. Garno, L.F. Schneemeyer, J.V. Waszczak, AT&T Bell Laboratories, Murray Hill, NJ.

11:45 M1.10

HIGH QUALITY SINGLE CRYSTALS OF $Y_1Ba_2Cu_3O_y$ WITH SUPERIOR MICROWAVE PROPERTIES, Dong Ho Wu, W. Kennedy and S. Sridhar, Northeastern University, Physics Department, Boston, MA.

SESSION M2: NOVEL MATERIALS

Chairs: L. Schneemeyer and J. Jorgenson
Monday Afternoon, November 27
Salon G (M)

SYMPOSIUM M presentations
may be viewed
simultaneously in the
Essex North West Room,
Westin Hotel.

1:30 *M2.1

CRYSTAL CHEMISTRY OF OXIDE SUPERCONDUCTORS, Arthur W. Sleight, Oregon State University, Department of Chemistry, Corvallis, OR.

2:00 M2.2

SUPERCONDUCTIVITY IN BISMUTH-LEAD-ANTIMONY BASED PEROVSKITES, R.J. Cava, B. Batlogg, J.J. Krajewski, W.F. Peck Jr., L.W. Rupp Jr., AT&T Bell Laboratories, Murray Hill, NJ.

2:30 M2.3

$PrBa_2Cu_3O_7$ AND $CmBa_2Cu_3O_7$: THE ABSENCE OF SUPERCONDUCTIVITY IN $YBa_2Cu_3O_7$ -RELATED COMPOUNDS, L. Soderholm, G.L. Goodman, Argonne National Laboratory, Chemistry Division, Argonne, IL; U. Welp, Argonne National Laboratory, Materials Sciences Division, Argonne, IL; and C.-K. Loong, Argonne National Laboratory, IPNS Division, Argonne, IL.

2:45 **M2.4**

THE EFFECTS OF OXYGEN AND STRONTIUM VACANCIES ON THE SUPERCONDUCTIVITY OF SINGLE CRYSTALS OF $\text{Bi}_2\text{Sr}_{2-x}\text{CuO}_{6-y}$, B.C. Sales, B.C. Chakoumakos and Edward Sonder, Oak Ridge National Laboratory, Solid State Division, Oak Ridge, TN.

3:00 **M2.5**

STRUCTURE PROPERTY RELATIONSHIPS IN THE ONE-LAYER BISMUTH STRONTIUM CUPRATE SUPERCONDUCTOR, Steven A. Sunshine, Robert Fleming, Lynn Schmeemeyer and Theo Siegrist, AT&T Bell Laboratories, Murray Hill, NJ.

3:15 BREAK

3:30 ***M2.6**

CERTAIN NOVEL ASPECTS OF THALLIUM AND BISMUTH CUPRATE SUPERCONDUCTORS, C.N.R. Rao, Indian Institute of Science, Solid State and Structural Chemistry Unit, Bangalore, India.

4:00 **M2.7**

INFLUENCE OF THE PARTIAL SUBSTITUTION OF SMALL RARE EARTHS FOR Ca IN THE SUPERCONDUCTIVE Bi-Sr-Ca-Cu-O COMPOUND, M.J. Casanove, P. Baules, E. Snoeck and C. Roucau, CNRS, CEMES-LOE, Toulouse, France; P. Millet, R. Enjalbert and J. Galy, LCC, Toulouse, France.

4:15 **M2.8**

SYNTHESIS AND CHARACTERIZATION OF $\text{Nd}_{1-x}\text{Ce}_x\text{CuO}_{4+x}$, T.A. Vanderah, Naval Weapons Center, Research Department, China Lake, CA; and M.S. Osofsky, Naval Research Laboratory, Washington, DC.

4:30 **M2.9**

SUPERCONDUCTIVITY IN $(\text{Nd,Ce,Ca})_2\text{CuO}_{4-z}$, T. Sakurai, T. Yamahita, S. Ikegawa and H. Imauchi, International Superconductivity Technology Center, Superconductivity Research Laboratory, Tokyo, Japan.

4:45 **M2.10**

SUPERCONDUCTING BEHAVIOR OF TETRAGONAL (T') $\text{Eu}_{2-x}\text{Ce}_x\text{CuO}_{4+\delta}$, V.J. Melim, Weimin Peng and C.W. Kimball, Northern Illinois University, Department of Physics, Dekalb, IL; and B. Dabrowski, Y. Zheng and D.G. Hinks, Argonne National Laboratory, Argonne, IL.

5:00 **M2.11**

CERAMIC MATERIALS WITH T' -CRYSTAL STRUCTURE IN THE $\text{Ln}_{2-x}\text{M}_x\text{CuO}_{4-y}$ ($\text{Ln}=\text{Pr,Nd}$; $\text{M}=\text{Ce, Pb, Sn}$) SYSTEM, R. Oviedo-Roa, L. Govea, and R. Escudero, Universidad Nacional Autonoma De Mexico, Instituto de Investigaciones en Materiales, Solid State Department, Mexico, D.F., Mexico.

SESSION M3: THIN FILM DEPOSITION:

LASER ABLATION TECHNIQUE

Chairs: J. Narayan and T. Venkatesan
Tuesday Morning, November 28
Salon G (M)

SYMPOSIUM M presentations
may be viewed
simultaneously in the
Essex North West Room,
Westin Hotel.

8:00 ***M3.1**

PULSED LASER TECHNIQUE FOR DEPOSITION OF SUPERCONDUCTING THIN FILMS: DEPOSITION PHYSICS AND IN-SITU PROCESSING, R.K. Singh and J. Narayan, North Carolina State University, Department of Materials Science and Engineering, Raleigh, NC.

8:30 **M3.2**

SYNTHESIS AND PROPERTIES OF $\text{Y}_{1-x}\text{Pr}_x\text{Ba}_2\text{Cu}_3\text{O}_{7-x}$ THIN FILMS, X.D. Wu, M.S. Hegde, A. Inam and X.X. Xi, Rutgers University, Physics Department, Piscataway, NJ; T. Venkatesan and C.C. Chang, Bellcore, Red Bank, NJ.

8:45 **M3.3**

IN SITU GROWTH OF HIGH QUALITY EPITAXIAL $\text{YBa}_2\text{Cu}_3\text{O}_{7-x}$ FILMS AT MODERATE SUBSTRATE TEMPERATURES AND OVER LARGE AREAS BY PULSED LASER ABLATION, Douglas H. Lowndes, J.W. McCamy, D.P. Norton, R. Feenstra, J.D. Budai and D.N. Mashburn, Oak Ridge National Laboratory, Solid State Division, Oak Ridge, TN.

9:00 **M3.4**

TAILORED HIGH- T_c SUPERCONDUCTING THIN FILMS MADE BY LAYER-BY-LAYER DEPOSITION WITH EXCIMER LASER, Tomoji Kawai, Masaki Kanai, Hitoshi Tabata and Shichio Kawai, Osaka University, The Institute of Scientific and Industrial Research, Osaka, Japan.

9:15 **M3.5**

IN SITU PREPARATION OF SUPERCONDUCTING Y-Ba-Cu-O THIN FILMS ON SILICON SINGLE CRYSTALS, H.-U. Habermeyer and G. Mertens, Max-Planck-Institut, Stuttgart, West Germany.

9:30 **M3.6**

MACROSCOPIC PERSISTENT CURRENTS IN LASER ABLATED $\text{YBa}_2\text{Cu}_3\text{O}_{7-x}$ FILMS, B. Stritzker, J. Fröhlingdorf, U. Krüger, Institut für Schicht- und Ionentechnik, KFA Jülich, West Germany; P. Leiderer, Universität Konstanz, Fakultät für Physik, Konstanz, West Germany; R. Feile, Universität Mainz, Institut für Physik, Mainz, West Germany; and W. Zander, Institut für Schicht- und Ionentechnik, KFA Jülich, West Germany

9:45 BREAK

10:00 ***M3.7**

STUDY OF IN-SITU LASER-DEPOSITION OF SUPERCONDUCTING THIN FILMS BY IN-SITU RESISTANCE MEASUREMENT, Q.Y. Ying, H.S. Kim, D.T. Shaw and H.S. Kwok, State University of New York at Buffalo, Institute on Superconductivity, Buffalo, NY.

10:30 **M3.8**

IN-SITU GROWN YBCO FILMS AND BUFFER LAYERS ON SILICON BY PULSED LASER DEPOSITION, G.A.N. Connell, J.B. Boyce, Xerox Palo Alto Research Center, Palo Alto, CA; F. Bridges, Xerox Palo Alto Research Center, Palo Alto, CA and University of California, Physics Department, Santa Cruz, CA; D.B. Fenner, Xerox Palo Alto Research Center, Palo Alto, California and Santa Clara University, Physics Department, Santa Clara, CA; and D.K. Fork, Xerox Palo Alto Research Center, Palo Alto, California and Stanford University, Department of Applied Physics, Stanford, CA.

10:45 **M3.9**

ArF LASER ABLATION OF $\text{YBa}_2\text{Cu}_3\text{O}_{7-x}$ AS STUDIED BY EMISSION SPECTROSCOPY, SEM AND EDAX, Alon Hoffman, Royal Melbourne Institute of Technology, Department of Applied Physics, Melbourne, Australia; and Rafael Manory, Royal Melbourne Institute of Technology, Department of Metallurgy Engineering, Melbourne, Australia.

11:00 **M3.10**

THE PROCESSING OF SUPERCONDUCTING THIN FILMS OF Pb-Bi-Sr-Ca-Cu-O USING LASER ABLATION TECHNIQUES, F. Beech, M. Brown, R. Jackman, I.W. Boyd, University College London, Department of Electronic and Electrical Engineering, London, United Kingdom; and F. Saba, Imperial College, Department of Materials, London, United Kingdom.

11:15 **M3.11**

ION TIME OF FLIGHT STUDY FROM LASER ABLATED $\text{Y}_1\text{Ba}_2\text{Cu}_3\text{O}_7$, R.A. Neifeld, A. Tauber, U.S. Army LABCOM, ETDL, Fort Monmouth; W.T. Hill III, B. Turner, University of Maryland, Institute of Physical Science and Technology, College Park, MD.

11:30 **M3.12**

CHARACTERIZATION OF THE TARGET-SUBSTRATE BIAS POTENTIAL DEPENDENCE OF PULSED LASED DEPOSITION OF $\text{YBa}_2\text{Cu}_3\text{O}_{7-g}$, D.B. Chrisey, K.S. Grabowski, Naval Research Laboratory, Surface Modification Branch, Washington, DC; M.S. Osofsky, Naval Research Laboratory, Materials Physics Branch, Washington, DC; J.A. Sprague and C.R. Gossett, Naval Research Laboratory, Surface Modification Branch, Washington, DC.

11:45 **M3.13**

PREPARATION AND PROPERTIES OF EPITAXIAL THIN FILMS OF SUPERCONDUCTING $\text{Nd}_{1-x}\text{Ce}_x\text{CuO}_{4-y}$, A. Gupta, G. Koren, C.C. Tsuei, A. Segümler and T.R. McGuire, IBM T.J. Watson Research Center, Yorktown Heights, NY.

SESSION M4: BULK MATERIALS

Chairs: D. Ginley and H. O'Bryan

Tuesday Afternoon, November 28

Salon G (M)

SYMPOSIUM M presentations
may be viewed
simultaneously in the
Essex North West Room,
Westin Hotel.

1:30 ***M4.1**

THE STUDY OF THE SYNTHESIS AND MEASUREMENT OF HIGH T_c BULK MATERIALS, P.H. Hor, University of Houston, Houston, TX.

2:00 **M4.2**

FABRICATION OF TEXTURED MICROSTRUCTURES IN $\text{YBa}_2\text{Cu}_3\text{O}_{6+x}$ BY LIQUID-PHASE SINTERING, Lijie Zhang, Martin P. Harmer and Helen M. Chan, Lehigh University, Department of Material Science, Bethlehem, PA.

2:15 **M4.3**

SYNTHESIS OF UNIDIRECTIONALLY SOLIDIFIED Y-Ba-Cu-O BULK SUPERCONDUCTORS WITH HIGH CRITICAL CURRENT DENSITY, E. Yanagisawa, S. Kondoh, J. Shimoyama, J. Kase, T. Matsubara and T. Morimoto, Asahi Glass Company, Ltd., Research Center, Yokohama, Japan.

2:30 **M4.4**

PROCESSING OF HIGH CURRENT DENSITY $\text{YBa}_2\text{Cu}_3\text{O}_x$ SUPERCONDUCTORS, V. Selvamanickam and K. Salama, University of Houston, Texas Center of Superconductivity, Department of Mechanical Engineering, Houston, TX.

2:45 **M4.5**

FABRICATION OF $\text{YBa}_2\text{Cu}_3\text{O}_{7-x}$ FILAMENTS BY EXTRUSION OF A $\text{Cu}_3\text{O}_3\text{Ba}_2\text{Y}(\text{meOEt})_7$ (meOEt IS 2-METHOXYETHANOL) PRECURSOR, M.W. Rupich, S.F. Cogan, B. Lagos and J.P. Hachey, EIC Laboratories, Inc., Norwood, MA.

3:00 BREAK

3:15 ***M4.6**

THE DEPENDENCE OF T_c FOR CERAMIC HIGH- T_c SUPERCONDUCTORS ON ELECTRONIC PARAMETERS, B.C. Giessen and R.S. Markiewicz, Northeastern University, Barnett Institute and Departments of Chemistry and Physics, Materials Science Division, Boston, MA.

3:45 **M4.7**

THE EFFECT OF THE DISTRIBUTION OF DOPANTS IN HIGH T_c BI-COMPOUND SUPERCONDUCTORS, Alexis S. Nash, Marquette University, ECBE Department, Milwaukee, WI; Kenneth C. Goretta, Argonne National Laboratory, Ceramics Section, Materials and Components Technology Division, Argonne, IL; Philip Nash, Illinois Institute of Technology, Metallurgical and Materials Engineering, Chicago, IL; Roger B. Peoppel and Donglu Shi, Argonne National Laboratory, Ceramics Section, Materials and Components Technology Division, Argonne, IL.

4:00 **M4.8**

A NOVEL SPRAY PYROLYSIS SYSTEM FOR THE DEPOSITION OF HIGH T_c SUPERCONDUCTORS, Toby J. Cumberbatch, Cambridge University, I.R.C. in Superconductivity, Cambridge, United Kingdom; Stephen Deane and Paul E. Barden, Cambridge University, Engineering Department, Cambridge, United Kingdom.

4:15 **M4.9**

HIGH TEMPERATURE SUSPENSION MELTING TREATMENT OF SUPERCONDUCTING POWDER (HTSM), Zhang Jiangou, Zhou Yiru, Wang Junsheng, Yan Junlian, Liu Ansheng, Zhang Baoren and Xu Yalan, General Research Institute for Non-Ferrous Metals, Beijing, China.

4:30 **M4.10**

REACTIONS AT CERAMIC SUPERCONDUCTOR/METAL INTERFACES, Min-Seok Oh and Michael R. Notis, Lehigh University, Department of Materials Science and Engineering, Bethlehem, PA.

4:45 **M4.11**

$YBa_2Cu_3O_7$ FILAMENT-SUPERPLASTIC ALLOY COMPOSITES, Emilio Orgaz and Miguel A. Ocampo, Condumex Research and Development Center, Department of Materials, México, D.F., México; David Rios-Jara and Tatsuo Akachi, IIM-UNAM, Department of Metals and Ceramic Materials, México City, México.

5:00 **M4.12**

SILVER IN Y-Ba-Cu-O: SUBSTITUTION, MICROSTRUCTURE, AND SUPERCONDUCTING PROPERTIES, B.R. Weinberger, L. Lynds, D.M. Potrepka, R. Cipolli, D.B. Snow, C.T. Burila, H.E. Eaton, United Technologies Research Center, East Hartford, CT; Z. Tan and J.I. Budnick, University of Connecticut, Department of Physics, Storrs, CT.

5:15 **M4.13**

MICROSTRUCTURAL ANALYSES AND MAGNETIC MEASUREMENTS OF $Ag/YBa_2Cu_3O_{7-x}$ COMPOSITES, V.S. Achuthuraman, Y.J. Zhang, M.L. Mecartney, University of Minnesota, Department of Chemical Engineering and Materials Science, Minneapolis, MN; and J. McArdle, Q. Chen, B. Koepke, Honeywell, Inc., Minneapolis, MN.

**SESSION M5: THIN FILM DEPOSITION:
OTHER TECHNIQUES**

Chairs: R. C. Dynes and D. K. Christen
Wednesday Morning, November 29
Salon G (M)

SYMPOSIUM M presentations
may be viewed simultaneously
in the America Ballroom Lobby
Westin Hotel.

8:00 ***M5.1**

IN-SITU GROWTH OF $Y_1Ba_2Cu_3O_{7-x}$ FILMS BY MOLECULAR BEAM EPITAXY WITH AN ACTIVATED OXYGEN SOURCE, J. Kwo, AT&T Bell Laboratories, Murray Hill, NJ.

8:30 **M5.2**

SUPERCONDUCTORS AND INSULATORS IN RUBIDIUM BARIUM BISMUTH OXIDE FILMS GROWN IN-SITU BY MOLECULAR BEAM EPITAXY, E.S. Hellman, E.H. Hartford, R.M. Fleming, AT&T Bell Laboratories, Murray Hill, NJ.

8:45 **M5.3**

AS-DEPOSITED SUPERCONDUCTING Y-Ba-Cu-O FILMS ON GaAs SUBSTRATE BY HIGH PRESSURE DC SPUTTERING PROCESS, R.J. Lin and P.T. Wu, Industrial Technology Research Institute, Materials Research Laboratories, Hsinchu, Taiwan, China.

9:00 **M5.4**

HIGH- T_c $YBa_2Cu_3O_7$ THIN FILMS PRODUCED BY MULTILAYER SPUTTER DEPOSITION, Mark S. DiIorio, Kai-Yueh Yang, Andrew N. Erickson, Biomagnetic Technologies Inc., San Diego, CA; Patricia Tsai, M. Brian Maple, University of California-San Diego, Department of Physics, LaJolla, CA.

9:15 **M5.5**

HIGH CRITICAL CURRENT DENSITY IN ULTRATHIN YBCO FILMS, X.X. Xi, Rutgers University, Physics Department, Piscataway, NJ; W. Schauer, Institut fuer Technische Physik, Karlsruhe, West Germany; J. Geerk, Kernforschungszentrum Karlsruhe, Institute fuer Nukleare Festkoeperphysik, Karlsruhe, West Germany; Q. Li, Rutgers University, Physics Department, Piscataway, NJ; G. Linker and O. Meyer, Kernforschungszentrum Karlsruhe, Institute fuer Nukleare Festkoeperphysik, Karlsruhe, West Germany.

9:30 **M5.6**
SYNTHESIS AND PROPERTIES OF $\text{YBa}_2\text{Cu}_3\text{O}_{7-x}$ THIN FILMS GROWN IN-SITU BY SINGLE TARGET MAGNETRON SPUTTERING, C.B. Eom, J. Sun, K. Yamamoto, T.H. Geballe, Stanford University, Center for Materials Research, Stanford, CA; and S.S. Laderman, Hewlett-Packard Company, Palo Alto, CA.

9:45 BREAK

10:00 ***M5.7**
IN-SITU PREPARATION OF THIN FILMS OF HIGH T_c MATERIALS, T. Geballe, Stanford University, Stanford, CA.

10:30 **M5.8**
ION BEAM CO-DEPOSITION OF $\text{YBa}_2\text{Cu}_3\text{O}_{6+x}$ FILMS, B.J. Kellett, J.H. James, A. Gauzzi, B. Dwir and D. Pavuna, Swiss Federal Institute of Technology, Institute of Micro and Optoelectronics, Lausanne, Switzerland.

10:45 **M5.9**
IN-SITU PREPARATION AND CHARACTERIZATION OF SUPERCONDUCTING THIN FILMS AND RELATED MATERIALS BY MOCVD FOR THE DEVELOPMENT OF THREE TERMINAL SWITCHING DEVICES, R. Singh, S. Sinha, N.J. Hsu, P. Chou, R.P.S. Thakur, A. Kumar, University of Oklahoma, Department of Electrical Engineering and Computer Science, Norman, OK; J. Narayan and R.K. Singh, North Carolina State University, Department of Materials Science, Raleigh, NC.

11:00 **M5.10**
LOW TEMPERATURE PREPARATION OF Y-Ba-Cu-O THIN FILMS BY OMCVD, Taiji Tsuruoka, Ryoudou Kawasaki, Hitoshi Abe and Susumu Shibata, Oki Electric Industry Company, Ltd., Research Laboratory, Tokyo, Japan.

11:15 **M5.11**
PREPARATION OF SUPERCONDUCTING Y-Ba-Cu-O THIN FILMS BY MOCVD, H. Ohnishi, Y. Kusakabe, M. Kobayashi and S. Hoshinouchi, Mitsubishi Electric Corporation, Manufacturing Development Laboratory, Hyogo, Japan; H. Harima and K. Tachibana, Kyoto Institute of Technology, Department of Electronics, Kyoto, Japan.

11:30 **M5.12**
INNOVATIVE LOW-TEMPERATURE METAL-ORGANIC CHEMICAL VAPOR DEPOSITION (LTMOCVD) ROUTES TO THE FABRICATION OF DEVICE QUALITY HIGH TEMPERATURE OXIDE SUPERCONDUCTORS, Alain E. Kaloyeros, Aiguo Feng, Jonathan Garhart, State University of New York at Albany, Physics Department, Albany, NY; Marianne Holma, University of Illinois at Urbana-Champaign, Physics Department, Urbana, IL; and Kenneth Brooks, University of Illinois at Urbana-Champaign, Chemistry Department, Urbana, IL.

11:45 **M5.13**
IN-SITU GROWTH OF $\text{YBa}_2\text{Cu}_3\text{O}_{7-x}$ FILMS BY METAL ORGANIC CHEMICAL VAPOR DEPOSITION USING VERTICAL, HIGH-SPEED ROTATING DISK REACTOR, D.W. Noh, B. Gallois, Stevens Institute of Technology, Department of Materials Science and Engineering, Hoboken, NJ; C. Chern, B. Kear, Rutgers University, Department of Materials Science, Piscataway, NJ; G.S. Tompa, P. Norris and P. Zawadzki, EMCORE, Somerset, NJ.

SESSION M6: CRYSTAL CHEMISTRY
Chairs: A. Sleight and T. Vanderah
Wednesday Afternoon, November 29
Salon G (M)

SYMPOSIUM M presentations
may be viewed simultaneously
in the America Ballroom Lobby
Westin Hotel.

1:30 ***M6.1**
STRUCTURAL ASPECTS OF THE PHASE SEPARATION IN $\text{La}_2\text{CuO}_{4.032}$, C. Chaillout, Grenoble, France.

2:00 **M6.2**
CRYSTAL CHEMISTRY AND SUB-SOLIDUS PHASE RELATIONS IN $(\text{La},\text{RE})_2\text{CuO}_4$ SYSTEMS, Joseph F. Bringley, Steven S. Trail, Michael W. McElfresh and Bruce A. Scott, IBM T.J. Watson Research Center, Yorktown Heights, NY.

2:15 **M6.3**
A THERMOCHEMICAL INVESTIGATION OF THE La-Sr-Cu-O SYSTEM, Joseph Bularzik, Alexandra Navrotsky, Princeton University, Geology and Geophysical Science, Princeton, NJ; and Bruce Scott, Joe Bringley and Steve Trail, IBM T.J. Watson Research Center, Yorktown Heights, NY.

2:30 **M6.4**
STRUCTURAL AND MAGNETIC PROPERTIES OF UNTWINNED $\text{YBa}_2\text{Cu}_3\text{O}_{6+x}$ SINGLE CRYSTALS, Debra L. Kaiser, Frank W. Gayle, Lydon J. Swartzendruber and Winnie Wong-Ng, National Institute of Standards and Technology, Ceramics Department, Gaithersburg, MD; Steven F. Watkins and Frank R. Fronczek, Louisiana State University, Department of Chemistry, Baton Rouge, LA.

2:45 **M6.5**
 $\text{Ba}_2\text{YCu}_3\text{O}_{7-\delta}$ CRYSTAL SURFACE LAYERS; ORTHORHOMBIC SPLITTING, DISLOCATIONS, AND CHEMICAL ETCHING, D.J. Werder, C.H. Chen, M. Gurvitch, B. Miller, L.F. Schneemeyer and J.V. Waszczak, AT&T Bell Laboratories, Murray Hill, NJ.

3:00 BREAK

3:15 ***M6.6**
STRUCTURAL PHASE DIAGRAM AND SUPERCONDUCTING BEHAVIOR IN THE $Ba_{1-x}K_xBiO_3$ SYSTEM, J.D. Jorgensen, Shiyou Pei, D.G. Hinks, B. Dabrowski, D.R. Richards, A.W. Mitchell and D.T. Marx, Argonne National Laboratory, Materials Science Division, Argonne, IL; S.K. Sinha, J.M. Newsam, D. Vaknin and A.J. Jacobson, Exxon Research and Engineering Company, Annandale, NJ.

3:45 **M6.7**
ELECTRON-PHONON COUPLING IN SUPERCONDUCTING $Ba_{1-x}K_xBiO_3$: A RAMAN-SCATTERING STUDY, K.F. McCarty, Sandia National Laboratories, Livermore, CA; H.B. Radousky, Lawrence Livermore National Laboratory, Livermore, CA; D.G. Hinks, Y. Zheng, A.W. Mitchell, Argonne National Laboratory, Argonne, IL; T.J. Folkerts and R.N. Shelton, University of California-Davis, Department of Physics, Davis, CA.

4:00 **M6.8**
MAGNETIZATION MEASUREMENTS OF 5 μm $Ba_{0.6}K_{0.4}BiO_3$ CRYSTALS: APPROACH TO INTRINSIC BEHAVIOR WITH DECREASING SIZE? G.S. Grader, A.F. Hebard and L.F. Schneemeyer, AT&T Bell Laboratories, Murray Hill, NJ.

4:15 **M6.9**
HIGH TEMPERATURE NEUTRON DIFFRACTION STUDY OF THE FORMATION REACTION OF BISMUTH SUPERCONDUCTORS, M.F. Garbauskas, R.H. Arendt, General Electric Company, Corporate Research and Development, Schenectady, NY; J.D. Jorgensen and R.L. Hitterman, Argonne National Laboratory, Argonne, IL.

4:30 **M6.10**
MODELS FOR OXYGEN ORDERING AND DIFFUSION IN $Ba_2YCu_3O_x$ AND $Ba_2YCu_{3-y}MyO_x$ ($M=Fe, Co, Al, Ga$), A. Santoro, National Institute of Standards and Technology, Reactor Radiation Division, Gaithersburg, MD.

4:45 **M6.11**
INFRA-RED INVESTIGATIONS ON THE LATTICE INSTABILITY OF SINGLE PHASE $(Bi, Pb)_2Sr_2Ca_2-Cu_3O_{10+x}$ SUPERCONDUCTING CERAMIC, He Aisheng, North University of Technology, Physics Department, Beijing, China; Zhang Jincang, Chang Fanggao, Henan Normal University, Physics Department, Xinxiang, China; Xiang Jiong and He Yusheng, Tsinghua University, Physics Department, Beijing, China.

SESSION M7: POSTER SESSION
Chairs: D. K. Finnemore, B. Batlogg, J. Budai, R. Singh and W. K. Chu
Wednesday Evening, November 29
8:00 p.m. - 10:00 p.m.
America Ballroom (W)

M7.1 ELECTRONIC STRUCTURE CALCULATIONS OF THE COPPER-OXYGEN PLANES IN $YBa_2Cu_3O_{6+y}$ FOR $0 < y < 1$, J.A. Cogordan, Universidad Nacional Autónoma de México, Instituto de Investigaciones en Materiales, México, México.

M7.2 ON THE NATURE OF HOLES IN $YBa_2-Cu_3O_{7-x}$, E.E. Alp, J.C. Campuzano, G. Jennings, J. Guo, L. Beaulaigue, S.M. Mini, Argonne National Laboratory, Materials Science Division, Argonne, IL; M. Faiz, Y. Zhou, University of Illinois at Chicago, Chicago, IL; and J.Z. Liu, Northwestern University, Evanston, IL.

M7.3 BAND DISPERSION AND THE FERMI SURFACE OF $YBa_2Cu_3O_{6.9}$, J.C. Campuzano, G. Jennings, M. Faiz, L. Beaulaigue, B.W. Veal, A.P. Paulikas, J.Z. Liu, H. Claus and K. Vandervoort, Argonne National Laboratory, Materials Science Division, Argonne, IL; A.J. Arko, R.S. List, R.J. Bartlett and S.W. Cheong, Los Alamos National Laboratory, Los Alamos, NM; C.G. Olson, A.B. Yang, R. Liu and C. Gu, Ames National Laboratory, Ames, IA.

M7.4 HIGH TEMPERATURE CERAMIC SUPERCONDUCTORS AND EXACT SOLUTIONS OF THE NON-LINEAR LANDAU-GINZBURG EQUATIONS, Jack A. Tuszynski, University of Alberta, Edmonton, Canada; and John M. Dixon, University of Warwick, Coventry, United Kingdom.

M7.5 HOLE CONCENTRATION AND SUBSTITUTIONAL DISORDER IN COMPENSATION DOPED $NdBa_2-Cu_3O_y$, T. Penney, M.W. Shafer and B.L. Olson, IBM T.J. Watson Research Center, Yorktown Heights, NY.

M7.6 ELECTRONIC STRUCTURES OF Ga- AND Zn-SUBSTITUTED $YBa_2Cu_3O_7$ SUPERCONDUCTORS, Yong-nian Xu and W.Y. Ching, University of Missouri-Kansas City, Department of Physics, Kansas City, MO; and K.W. Wong, University of Kansas, Department of Physics and Astronomy, Lawrence, Kansas.

M7.7 STUDIES OF THE ELECTRONIC STRUCTURE OF HTSC AND RELATED COMPOUNDS BY X-RAY PHOTOELECTRON SPECTROSCOPY, S. Myhra, A.E. Bocquet, J.F. Dobson and P.C. Healy, Griffith University, Division of Science and Technology, Queensland, Australia; P. Goodman and T.J. White, Melbourne University, School of Physics, Victoria, Australia; A.M. Stewart, Australian National University, Research School of Physics, ACT, Australia; J.G. Thompson, Australian National University, Research School of Chemistry, ACT Australia.

M7.8 THE EFFECT OF MAGNETIC FIELD ON THE CRITICAL CURRENT DENSITY OF BULK SUPERCONDUCTING WIRES, M.T. Lanagan, U. Balachandran, C.A. Youngdahl, J.T. Dusek, J.J. Picciolo and R.B. Poeppel, Argonne National Laboratory, Materials and Components Department, Argonne, IL.

M7.9 SANDWICH EXCITONS AS THE MECHANISM OF SUPERCONDUCTIVITY IN CUPRATES AND BIS-MUTHATES, Brent A. Richert, U.S. Air Force Academy, Department of Physics, Colorado Springs, CO; Ewald Schachinger, Technische Universität Graz, Institut für Theoretische Physik, Graz, Austria; and Roland E. Allen, Texas A&M University, Department of Physics, College Station, TX.

M7.10 AC SUSCEPTIBILITY STUDIES OF THE HIGH T_c SUPERCONDUCTORS: DISSIPATIVE EFFECTS IN THE $La_{2-x}Sr_xCuO_{4-y}$ AND $YBa_2Cu_3O_{7-y}$ SYSTEMS, Xinsheng Ling, Mark Filipkowski, Joseph I. Budnick, University of Connecticut, Department of Physics and Institute of Materials Science, Storrs, CT.

M7.11 TRANSPORT CRITICAL CURRENT OF SINTERED $YBa_2Cu_3O_x$ IN TIME-VARYING MAGNETIC FIELDS, P.D. Hambourger, J. DiCillo, M. Gibberman, J. Marino, L.P. Valek, Cleveland State University, Department of Physics, Cleveland, OH; and Michael A. Centanni, Ferro Corporation, Independence, OH.

M7.12 INFLUENCE OF METALLIC SILVER INFILTRATION ON THE MICROSTRUCTURE AND TRANSPORT PROPERTIES OF $YBaCuO$, L. Ryelandt, M. Cassart, A. Vandenbosch, F. Delannay and J-P. Issi, Université Catholique de Louvain, Unité de Physico-Chimie et de Physique des Matériaux, Louvain-la-Neuve, Belgium.

M7.13 COMPARISON OF FLUX DYNAMICS IN TWO SAMPLES OF $YBa_2Cu_3O_7$ WITH DIFFERENT PINNING, M. Turchinskaya, L.H. Bennett, L.J. Swartzendruber, A. Roitburd, C.K. Chiang, M. Hill, J.E. Blendell, National Institute of Standards and Technology, Gaithersburg, MD; and K. Sawano, Nippon Steel Corporation, Kawasaki, Japan.

M7.14 FLUX PINNING AND WEAK LINK STRUCTURE IN $Ca_2Cu_1O_3$ DOPED $LnBa_2Cu_3O_{7-y}$ ($Ln=La, Y$), Fumio Mizuno, Hiromu Masuda, Izumi Hirabayashi and Shoji Tanaka, Superconductivity Research Laboratory, Nagoya Division, Nagoya, Japan.

M7.15 EASILY ACTIVATED FLUX CREEP AND ANISOTROPIC FLUCTUATION IN $NdCeCuO$ THIN FILMS, S. Hatta, S. Hayashi, H. Adachi and K. Wasa, Matsushita Electric Industrial Company, Ltd., Central Research Laboratories, Osaka, Japan.

M7.16 MAGNETIZATION AND FLUX BEHAVIOUR OF $YBa_2Cu_3O_{7-y}$ SUPERCONDUCTING RINGS, Shoichi Yokoyama, Kenji Shimohata, Toshie Ushijima and Tadatoshi Yamada, Mitsubishi Electric Corporation, Central Research Laboratory, Hyogo, Japan.

M7.17 VORTEX STRUCTURE: LATTICE, GLASS, OR LIQUID? Robert J. Soulen Jr. and S.A. Wolf, Naval Research Laboratory, Superconducting Materials Section, Washington, DC.

M7.18 THE UPPER CRITICAL MAGNETIC FIELD OF SUPERCONDUCTING $YBa_2(Cu_{1-x}Ni_x)_3O_7$, Youwen Xu, A.R. Moodenbaugh and M. Suenaga, Brookhaven National Laboratory, Material Science Division, Upton, NY.

M7.19 FLUX LATTICE MELTING IN ANISOTROPIC HIGH T_c SUPERCONDUCTORS, R.S. Markiewicz, Northeastern University, Physics Department and Barnett Institute, Boston, MA.

M7.20 HIGH TEMPERATURE DEFECT CHEMISTRY OF UNDOPED AND Ce-DOPED Nd_2CuO_4 , D.J.L. Hong, A. Mehta and D.M. Smyth, Lehigh University, Whitaker Lab #5, Materials Research Center, Bethlehem, PA.

M7.21 TRANSPORT AND DIAMAGNETIC PROPERTIES OF 2:2:1:2 AND 2:2:2:3 (Bi,Pb)-Sr-Ca-Cu-O SUPERCONDUCTING MATERIALS, R. Ibáñez, M.J. Sanchis, F. Sapiña, D. Beltrán, A. Beltrán, UICBM, Universitat de Valencia, Dpt. Química Inorgánica, Valencia, Spain; C. Rillo, J. Bartolomé, F. Lera, R. Navarro, ICMA, CSIC-Universidad de Zaragoza, Zaragoza, Spain; G.F. de la Fuente, Fibertek, Inc., Materials Department, Herndon, VA.

M7.22 CRITICAL CURRENT DENSITIES IN $Bi_2Sr_2CaCu_2O_{8+d}$, Shunji Nomura, Yutaka Yamada, Tomohisa Yamashita, Eriko Yoneda, Hisashi Yoshino and Ken Ando, Toshiba Corporation, Research and Development Center, Kawasaki, Japan.

M7.23 CORRELATIONS BETWEEN THE Cu-O BONDING STATES AND THE SUPERCONDUCTIVITY, S.C. Han, Shanghai Institute of Metallurgy, Chinese Academy of Sciences, Shanghai, China and Xsirius Superconductivity, Inc., Scottsdale, AZ; D.Z. Liu, Shanghai Institute of Testing Technology, Shanghai, China; X. X.M. Xie, Z.L. Wu, Shanghai Institute of Metallurgy, Chinese Academy of Sciences, Shanghai, China; and G.C. Huth, Xsirius Superconductivity, Inc., Scottsdale, AZ.

M7.24 CRITICAL CURRENT AND PROCESSING TEMPERATURE IN ALIGNED SINTERED COMPACTS OF $\text{YBa}_2\text{Cu}_3\text{O}_{7-\delta}$ J.E. Tkaczyk, K.W. Lay, GE Corporate R&D Schenectady, NY.

M7.25 GROWING OF $\text{Nd}_{2-x}\text{Ce}_x\text{CuO}_y$ SINGLE-CRYSTALS BY A FLUX METHOD, S. Pinol and C. Miravittles, ICMB-CSIC, Barcelona, Spain; J. Fontcuberta, Universitat de Barcelona, Department Fisica Fonamental, Barcelona, Spain; and D. Paul, University of Warwick, Department of Physics, Coventry, United Kingdom.

M7.26 MAGNETIC AND PHONON SCATTERING IN $\text{Nd}_{2-x}\text{Ce}_x\text{CuO}_{4-\delta}$: NORMAL STATE AND SUPERCONDUCTING PROPERTIES, J.L. Peng, R.N. Shelton, University of California, Davis, Department of Physics, Davis, CA; and H.B. Radousky, Lawrence Livermore Laboratory, Livermore, CA.

M7.27 SEMICONDUCTOR-METAL-SUPERCONDUCTOR TRANSITIONS IN UNDOPED AND Ce-DOPED Nd_2CuO_4 , A. Mehta, D.J.L. Hong and D.M. Smyth, Lehigh University, Whitaker Lab #5, Materials Research Center, Bethlehem, PA.

M7.28 ANISOTROPIC THERMAL CONDUCTIVITY OF SUPERCONDUCTING LANTHANUM CUPRATE, D.T. Morelli, G.L. Doll and J.P. Heremans, General Motors Research Laboratories, Physics Department, Warren, MI; M.S. Dresselhaus, A. Cassanho, D.R. Gabbe and H.P. Jenssen, Massachusetts Institute of Technology, Center for Materials Science and Engineering, Cambridge, MA.

M7.29 INFRARED AND RAMAN SPECTROSCOPY OF PHONONS IN $(\text{Nd/Pr})_2\text{CuO}_4$ AND $(\text{Ca}_{0.86}\text{Sr}_{0.14})\text{-CuO}_2$, M.K. Crawford, E. I. duPont de Nemours and Co., Inc., Corporate Research and Development Department, Experimental Station, Wilmington, DE; Gerald Burns, IBM T.J. Watson Research Center, Yorktown Heights, NY; E.M. McCarron, E. I. duPont de Nemours and Co., Inc., CR&D Department, Experimental Station, Wilmington, DE; G.V. Chandrasekhar, IBM T.J. Watson Research Center, Yorktown Heights, NY; W.E. Farneth, E. I. duPont de Nemours and Co., Inc., CR&D Department, Experimental Station, Wilmington, DE; T.M. Shaw, IBM T.J. Watson Research Center, Yorktown Heights, NY.

M7.30 THE SEARCH FOR VERY HIGH TEMPERATURE SUPERCONDUCTIVITY IN THE TITANIUM BORIDE SYSTEM, Brian S. Ahern, Steven Bachowski, Rome Air Development Center, Electronic Materials Division, Hanscom AFB, MA.

M7.31 EFFECTS OF OXYGEN STOICHIOMETRY ON THE MAGNETIC ORDERING OF $\text{La}_2\text{Ni}_{1-y}\text{Cu}_y\text{O}_{4+x}$, J. Zhao and M.S. Seehra, West Virginia University, Physics Department, Morgantown, WV; A.F. Hepp and J.R. Gaier, NASA Lewis Research Center, Cleveland, OH; and R.M. Richman, Mount St. Mary's College, Science Department, Emmitsburg, MD.

M7.32 THE TRANSPORT PROPERTIES AND DEFECT CHEMISTRY OF $(\text{La}_{1-x}\text{Sr}_x)_2\text{CuO}_{4-\delta}$, Ming-Jinn Tsai, Elizabeth J. Opila and Harry L. Tuller, Massachusetts Institute of Technology, Department of Materials Science and Engineering, Cambridge, MA.

M7.33 SUPERLATTICE MODULATION IN Nd_2CuO_4 AND THE ELECTRON-DOPED SYSTEMS $\text{Nd}_{2-x}\text{Ce}_x\text{CuO}_4$ AND $\text{Nd}_2\text{CuO}_{4-x}\text{F}_x$, C.H. Chen, D.J. Werder, A.C.W.P. James, D.W. Murphy, S. Zahurak, R.M. Fleming, B. Batlogg and L.F. Schneemeyer, AT&T Bell Laboratories, Murray Hill, NJ.

M7.34 $\text{La}_{2-x}\text{Ba}_x\text{Sr}_{1-x}\text{Y}_x\text{Cu}_2\text{O}_6$ AND $\text{M}_2\text{SrCu}_2\text{O}_6$ ($\text{M}=\text{Pr}$ AND Nd); NEW LAYERED COPPER-OXIDES WITH THE $\text{La}_2\text{SrCu}_2\text{O}_6$ STRUCTURE, Eric A. Hayri, Brookhaven National Laboratory, Chemistry Department, Upton, NY.

M7.35 THE STRUCTURE OF THE 50K SUPERCONDUCTOR $(\text{Y}_{1-x}\text{Ca}_x)\text{Ba}_2\text{Cu}_3\text{O}_{6+\delta}$ ($\delta < 0.2$), John B. Parise, State University of New York at Stony Brook, Earth and Space Sciences, Stony Brook, NY; and Eugene M. McCarron III, E.I. duPont de Nemours and Co., Inc., Central Research and Development Department, Experimental Station, Wilmington, DE.

M7.36 $\text{Nd}_{1.85-x}\text{Bi}_x\text{Ce}_{0.15}\text{CuO}_{4-\delta}$: PREPARATION AND PROPERTIES, M. Greenblatt, J.G. Lee and K.V. Ramanujachary, Rutgers University, Chemistry Department, New Brunswick, NJ.

M7.37 STRUCTURAL ANALYSIS OF $\text{Nd}_{2-x}\text{Ce}_x\text{CuO}_4$ ($x=0.15$) SUPERCONDUCTORS, Delei Li, M.Y. Su and L.D. Marks, Northwestern University, Science and Technology Center for Superconductivity, Department of Materials Science, Evanston, IL; B. Krause, Northern Illinois University, Department of Physics, Dekalb, IL.

M7.38 SUPERCONDUCTING AND STRUCTURAL PROPERTIES OF $(\text{Ba}_{1-x}\text{K}_x)(\text{Bi}_{1-y}\text{My})\text{O}_3$ SYSTEM ($M=\text{Tl, Pb and Sb}$), B. Dabrowski, D.G. Hinks, S. Pei, J.D. Jorgensen, D.R. Richards, Y. Zheng, C.W. Kimball and A.W. Mitchell, Argonne National Laboratory, Materials Science Division, Argonne, IL.

M7.39 THERMODYNAMIC PROPERTIES OF OXYGEN IN $\text{YBa}_2\text{Cu}_3\text{O}_x$, P. Meuffels and R. Naeven, Institut für Festkörperforschung, Jülich, West Germany.

M7.40 LOW TEMPERATURE BEHAVIOR OF $\text{YBa}_2\text{Cu}_3\text{O}_{6+2x}$ PHASE DIAGRAM, Ryoichi Kikuchi, UCLA, Materials Science and Engineering, Los Angeles, CA; and Jae-Sung Choi, University of Washington, Washington Technology Center, Materials Science and Engineering, and Advanced Materials Technology Program, Seattle, WA.

M7.41 GROWTH, ANNEAL AND PROPERTIES OF SINGLE CRYSTAL $\text{YBa}_2\text{Cu}_3\text{O}_x$, Jingwen Zhang, Ping Wang, Academia Sinica, Institute of Chemistry, Beijing, China; and Zhongxian Zhao, Academia Sinica, Institute of Physics, Beijing, China.

M7.42 OXYGEN EVOLUTION FROM $\text{YBa}_2\text{Cu}_3\text{O}_{7-\delta}$ SUPERCONDUCTING POWDERS GENERATED BY AEROSOL ROUTES, Pratim Biswas and Derong Zhou, University of Cincinnati, Dept. of Civil and Environmental Engineering, Cincinnati, OH; Jeff Grothaus, Procter and Gamble, Cincinnati, OH; Punit Boolchand and Darl McDaniel, University of Cincinnati, Department of Electrical Engineering, Cincinnati, OH.

M7.43 INHOMOGENEOUS SINTERING IN $\text{YBa}_2\text{Cu}_3\text{O}_{6+x}$, Laura C. Stearns, Martin P. Harmer and Helen M. Chan, Lehigh University, Bethlehem, PA.

M7.44 HIGH T_c OXIDE SOLID STATE REACTION KINETICS VIA COMPLEX IMPEDANCE SPECTROSCOPY, E.A. Cooper, T.O. Mason, Northwestern University, Department of Materials Science and Engineering, Evanston, IL; U. Balachandran and M.L. Kullberg, Argonne National Laboratory, Argonne, IL.

M7.45 THE EFFECTS OF THE SOLUTION STRUCTURE ON THE MICROSTRUCTURE AND PROPERTIES OF SINTER FORGED SOL-GEL-DERIVED SUPERCONDUCTORS, D. Kenzer, M. Teepe, G. Moore, G. Kordas, University of Illinois at Champaign-Urbana, Department of Materials Science and Engineering, Urbana, IL; M.E. Biznek, U. Balachandran, M.L. Kullberg, R.B. Poeppel, Argonne National Laboratory, Dept. of Materials and Components Technology Division, Argonne, IL; Y.L. Jeng and D.L. Johnson, Northwestern University, Dept. of Materials Science and Engineering, Evanston, IL.

M7.46 ROUTES TO OXIDE FILMS FOR THE PROTECTION OF CUPRATE SUPERCONDUCTORS, Ronald H. Baney, Debora F. Bergstrom, Dow Corning Corporation, Electronics Research Department, Midland, MI; Leslie E. Carpenter, Donald R. Petersen, Dow Corning Corporation, Process Engineering Department, Midland, MI; Dennis F. Elwell, Andrew A. Shapiro and Paul F. Fleishner, Hughes Aircraft Company, Microelectronic Circuits Department, Newport Beach, CA.

M7.47 $\text{Ag-YBa}_2\text{Cu}_3\text{O}_7$ POWDER GENERATION BY AEROSOL DECOMPOSITION, Toivo T. Kodas, Altaf H. Carim, University of New Mexico, Center for Micro-Engineered Ceramics, Farris Engineering Center, Albuquerque, NM; and Kevin Ott, Los Alamos National Laboratory, Exploratory Research and Development Center for High Temperature Superconductors, Los Alamos, NM.

M7.48 CONTROL OF MICROSTRUCTURES AND GRAIN BOUNDARY PHASES IN THE $\text{MBa}_2\text{Cu}_3\text{O}_{7-\sigma}$ SYSTEMS, A.I. Kingon, C. Davis, M. Lawrence, T. Hare, C.C. Koch and D.G. Haase, North Carolina State University, Department of Materials Science and Engineering, Raleigh, NC.

M7.49 EFFECT OF PURITY OF RAW MATERIALS AND PROCESSING ON THE MICROSTRUCTURE AND PROPERTIES OF HIGH T_c $\text{YBa}_2\text{Cu}_3\text{O}_{7-\delta}$, Ph. Dumas and J.A.T. Taylor, New York State College of Ceramics at Alfred University, Ceramics Engineering, Alfred, NY.

M7.50 SYNTHESIS OF 1-2-3 POWDER BY SPRAY CALCINATION OF AEROSOLS OF PRECURSOR SOLUTIONS, R.L. Lakis and S.R. Butler, Lehigh University, Materials Research Center, Bethlehem, PA.

M7.51 PROCESSING AND FABRICATION OF $\text{YBa}_2\text{Cu}_4\text{O}_x$ AND $\text{YBa}_2\text{Cu}_4\text{O}_x/\text{YBa}_2\text{Cu}_3\text{O}_y$ COMPOSITES, U. Balachandran, M.E. Biznek, K.C. Goretta, D. Shi, R.B. Poeppel, Argonne National Laboratory, Materials and Components Department, Argonne, IL; and T.O. Mason, Northwestern University, Evanston, IL.

M7.52 CRYSTALLITE ORIENTATION IN YBaCu CERAMIC LAYERS SINTERED ON SILVER SUBSTRATES, Claus Schüler, Felix Greuter and Petra Kluge-Weiss, ABB Corporate Research, Baden, Switzerland.

M7.53 PHASE STABILITY OF $\text{LnBa}_2\text{Cu}_3\text{O}_y$ AND $\text{Ln}_2\text{BaCuO}_5$ ($\text{Ln} = \text{Dy, Er, Eu, Gd, Ho, Sm, Yb}$), Kiichi Yoshiara, Fusaoki Uchikawa, Kiyoshi Yoshizaki, Mitsubishi Electric Corporation, Materials and Electronic Devices Laboratory, Kanagawa, Japan; Kiyotaka Nakahigashi, University of Osaka Prefecture, Department of Materials Science, Osaka, Japan.

M7.54 STUDY OF CARBONATES USED IN THE PREPARATION OF SUPERCONDUCTORS, Phillip G. Wahlbeck, Dwight L. Myers and R. Ronald Richards, Wichita State University, Department of Chemistry and the Institute for Aviation Research, Wichita, KS.

M7.55 ONE-STEP SYNTHESIS AND DENSIFICATION OF BULK $\text{YBa}_2\text{Cu}_3\text{O}_{7-x}$ /Ni COMPOSITE SUPERCONDUCTORS, C. Gelin and B. Champagne, National Research Council Canada, Boucherville, Canada.

M7.56 IN-SITU PROCESSING AND REACTION OF CO_2 WITH $\text{YBa}_2\text{Cu}_3\text{O}_{7-x}$, C. Michael Greenlief, University of Missouri, Department of Chemistry, Columbia, MD; Joseph F. Bringley, Stephen M. Gates, Bruce A. Scott, Steven S. Trail and Christopher D'Emic, IBM T.J. Watson Research Center, Yorktown Heights, NY.

M7.57 A SYSTEMATIC STUDY OF THE EFFECTS OF METAL SUBSTITUTIONS FOR Cu IN $\text{YBa}_2(\text{Cu}_{1-x}\text{M}_x)_3\text{O}_{7-\delta}$, M=Al, Ga, Fe, Ni, Zn, Youwen Xu, A.R. Moodenbaugh, Y.L. Wang, M. Suenaga and R.L. Sabatini, Brookhaven National Laboratory, Materials Science Division, Upton, NY.

M7.58 PREPARATION OF Ca-SUBSTITUTED $\text{YBa}_2\text{Cu}_3\text{O}_8$, T. Miyatake, K. Yamaguchi, T. Takata, S. Gotoh, N. Koshizuka and S. Tanaka, Superconductivity Research Laboratory (SRL), ISTEK, Division I, Tokyo, Japan.

M7.59 ROLE OF SILVER IN $\text{YBa}_2\text{Cu}_3\text{Ag}_x\text{O}_{7-\delta}$ COMPOSITE SUPERCONDUCTORS, L. Ganapathi, Ashok Kumar and J. Narayan, North Carolina State University, Department of Materials Science and Engineering, Raleigh, NC.

M7.60 SOL-GEL PREPARATION, MICROWAVE SINTERING AND MICROWAVE PROPERTIES OF SUPERCONDUCTING POWDER, Fathi Selmi, H.S. Dewan, The Pennsylvania State University, Research Center for the Engineering of Electronic and Acoustic Materials, University Park, PA; S. Komarneni, The Pennsylvania State University, Materials Research Laboratory, University Park, PA; V.K. Varadan and V.V. Varadan, The Pennsylvania State University, Research Center for the Engineering of Electronic and Acoustic Materials, University Park, PA.

M7.61 PHASE RELATIONSHIPS IN THE Y-Ba-Cu-O IN WET CO_2 ENVIRONMENTS, J.J. Simmins, Eutech Engineering Technologies, Alfred, NY; G.S. Fischman and R.L. Snyder, New York State College of Ceramics at Alfred University, Alfred, NY.

M7.62 PREPARATION OF FIBROUS Bi(Pb)-Sr-Ca-Cu-O CRYSTALS CONTAINING THE HIGH- T_c PHASE, Ichiro Matsubara, Hideo Tanigawa, Toru Ogura, Hiroshi Yamashita, Makoto Kinoshita, Government Industrial Research Institute, Osaka, Glass-Ceramics Materials, Osaka, Japan; Tomoji Kawai, Osaka University, The Institute of Scientific and Industrial Research, Osaka, Japan.

M7.63 PRELIMINARY INVESTIGATION OF PROCESSING AND PHASE DIAGRAM CONSTRUCTION IN THE Y-Sr-Cu-O SYSTEM, T.D. Rolin, F.S. Cheng, J.R. Ashburn, H.Y. Cheng, E.E. Anderson, The University of Alabama in Huntsville, Chemistry Department, Huntsville, AL.

M7.64 OXIDATION AND REDUCTION KINETICS OF $\text{Bi}_2\text{SrCuO}_{6-y}$ CRYSTALS, Edward Sonder, B.C. Chakoumakos and B.C. Sales, Oak Ridge National Laboratory, Solid State Division, Oak Ridge, TN.

M7.65 HIGH-TEMPERATURE DEFORMATION OF $\text{YBa}_2\text{Cu}_3\text{O}_{7-\delta}$ WITH Ag ADDITIONS, J.L. Routbort, K.C. Goretti, J. Sulek and J.P. Singh, Argonne National Laboratory, Materials Science Division, Argonne, IL.

M7.66 BULK MODULUS OF THE YBACUO OXIDE SUPERCONDUCTOR OBTAINED FROM MAGNETIC MEASUREMENTS, Bokhimi, U.N.A.M., Instituto de Física, México City, México.

M7.67 ULTRASONIC STUDY OF THE LOW TEMPERATURE STRUCTURAL PHASE TRANSITION IN $\text{YBa}_2\text{Cu}_3\text{O}_{7-\delta}$ AND ITS DEPENDENCE ON OXYGEN CONCENTRATION, J. Toulouse and X.Q. Wang, Lehigh University, Physics Department, Bethlehem, PA; D.J.L. Hong, Lehigh University, Materials Research Center, Bethlehem, PA.

M7.68 MAGNETIC ANISOTROPY AND OXYGEN STOICHIOMETRY IN $\text{YBa}_2\text{Cu}_3\text{O}_{7-y}$, J.R. Ashburn, F.S. Cheng, T.D. Rolin, H.Y. Cheng, E.E. Anderson, The University of Alabama in Huntsville, Physics Department, Huntsville, AL.

M7.69 OXYGEN ORDERING IN $\text{YBa}_2\text{Cu}_3\text{O}_x$, D. de Fontaine, University of California, Berkeley and Lawrence Berkeley Laboratory, Department of Materials Science and Mineral Engineering, Berkeley, CA; M.E. Mann, University of California, Berkeley and Lawrence Berkeley Laboratory, Department of Physics, Berkeley, CA; and G. Ceder, University of California, Berkeley and Lawrence Berkeley Laboratory, Department of Materials Science and Mineral Engineering, Berkeley, CA.

M7.70 Fe DOPANT LARGELY REPLACES Cu(2) PLANAR SITES IN AEROSOL PRODUCED $\text{YBa}_2(\text{Cu}_{1-x}\text{Fe}_x)_3\text{O}_{7-\delta}$ SUBMICRON GRAINS AND DESTROYS SUPERCONDUCTIVITY, P. Boolchand, P. Biswas, D. Zhou, W. Huff, D. McDaniel and K. Eglaid, University of Cincinnati, Electrical Engineering Department, Cincinnati, OH.

M7.71 OXYGEN CONTENT VARIATION IN CATION-DEFICIENT AND CHEMICALLY-DOPED HIGH- T_c Y-Ba-Cu-O SUPERCONDUCTORS, Y.H. Kao, L.W. Song and Y.D. Yao, State University of New York at Buffalo, Department of Physics, Buffalo, NY; Z. Tao and K.W. Jones, Brookhaven National Laboratory, Upton, NY.

M7.72 LUMINESCENCE FROM DEFECTS AND IMPURITY CENTERS IN Y_2O_3 , M.S. Jahan, D.W. Cooke, B.L. Bennett, W.L. Hults, M.A. Maez, K.C. Ott and J.L. Smith, Los Alamos National Laboratory, Department MP-14, Los Alamos, NM.

M7.73 RELATION BETWEEN THE CHARACTERISTICS OF POWDER AND MICROSTRUCTURE; PROPERTIES OF CERAMICS FOR $\text{YBa}_2\text{Cu}_3\text{O}_x$ SUPERCONDUCTORS, Meiyu Zhao, Chengen Li, Xingyun Jin and Yeming Huang, Shanghai Institute of Ceramics, Electronic Ceramics Department, Shanghai, China.

M7.74 LOW-RESISTIVITY CONTACTS TO HIGH-TEMPERATURE SUPERCONDUCTORS, T.H. Tiefel, S. Jin, M.E. Davis, R.B. van Dover, R.C. Sherwood, H.M. O'Bryan, G.W. Kammlott and R.A. Fastnacht, AT&T Bell Laboratories, Murray Hill, NJ.

M7.75 OXYGEN ORDERING AND SAMPLE INHOMOGENEITY IN $\text{YBa}_2\text{Cu}_3\text{O}_{7-\delta}$, Y. Bruynseraede, J. Vanacken and B. Wuyts, K.U. Leuven, Department of Physics, Leuven, Belgium; I.K. Schuller, University of California-San Diego, Physics Department, La Jolla, CA.

M7.76 MAGNETIC FIELD CONTROLLED LEVITATION AND SUSPENSION OF A MAGNET ABOVE AND BELOW TYPE II SUPERCONDUCTORS, Takeshi Takamori, John J. Boland and Derek B. Dove, IBM T.J. Watson Research Center, Yorktown Heights, NY.

M7.77 INTERACTIONS BETWEEN SILVER AND $\text{YBa}_2\text{Cu}_3\text{O}_{7-\delta}$, A.H. Carim, University of New Mexico, Center for Micro-Engineered Ceramics and Department of Chemical and Nuclear Engineering, Albuquerque, NM; R.E. Loehman, Sandia National Laboratories, Albuquerque, NM; A.P. Tomsia and J.A. Pask, Pask Research and Engineering, Pinole, CA.

M7.78 TEMPERATURE DEPENDENT FAR INFRARED STUDIES OF MAGNETICALLY-ORIENTED $\text{YBa}_2\text{Cu}_3\text{O}_{7-\delta}$, F. Lu, C.H. Perry, K. Chen and R.S. Markiewicz, Northeastern University, Physics Department, Boston, MA.

M7.79 HIGH-TEMPERATURE INTERACTIONS BETWEEN OXIDE SUPERCONDUCTORS AND ELECTRICAL CONTACT MATERIALS, R.D. Ray II and E.E. Hellstrom, University of Wisconsin-Madison, Department of Materials Science and Engineering, Madison, WI.

M7.80 EFFECT OF SURFACE ROUGHNESS ON PENETRATION DEPTH IN THE Y AND Bi HIGH-TEMPERATURE SUPERCONDUCTORS, J.W. Purpura and T.R. Clem, Naval Coastal Systems Center, Materials Science Department, Panama City, FL.

M7.81 ANALYSIS OF LOW TEMPERATURE PHASE TRANSITION PRIOR TO SUPERCONDUCTIVE BEHAVIOR IN HIGH TEMPERATURE SUPERCONDUCTORS, M.A. Rodriguez and R.L. Snyder, New York State College of Ceramics at Alfred University, Alfred, NY.

M7.82 MAGNET REPLICA BY HIGH T_c SUPERCONDUCTORS, R. Weinstein, In-Gann Chen, J. Liu and D. Parks, University of Houston, Institute of Beam Particle Dynamics/Texas Center for Superconductivity, Houston, TX.

M7.83 DISTRIBUTION OF IRON OVER COPPER SITES IN $\text{GdBa}_2(\text{Cu}_{1-x}\text{Fe}_x)_3\text{O}_{7-\delta}$, H.J. Bornemann and G. Czjzek, Kernforschungszentrum Karlsruhe, Department INFP, Karlsruhe, West Germany; and R. Kmiec, Institute of Nuclear Physics, Krakow, Poland.

M7.84 MAGNETIC PHASE DIAGRAM OF $\text{YBa}_2(\text{Cu}_{1-x}\text{Fe}_x)_3\text{O}_y$ AND $\text{YBa}_2(\text{Cu}_{1-x}\text{Co}_x)_3\text{O}_y$, Masao Doyama, Masaaki Matsui, Hiroshi Matsuoka, Kazuhito Ishikawa and Eiji Hayashi, Nagoya University, Faculty of Engineering, Department of Materials Science, Nagoya, Japan.

M7.85 ATOMISTIC DEFECT MODELS OF $\text{YBa}_2\text{Cu}_3\text{O}_7$, Roger C. Baetzold, Eastman Kodak Company, Corporate Research, Rochester, NY.

M7.86 ELECTRON MICROSCOPIC STUDY OF OXYGEN-VACANCY ORDERING IN $\text{YBa}_2\text{Cu}_3\text{O}_{6+x}$ with $x > 0.3$, P. Peng, D.J.L. Hong, A. Mehta, H.M. Chan and D.M. Smyth, Lehigh University, Whitaker Lab #5, Materials Research Center, Bethlehem, PA.

M7.87 THERMOGRAVIMETRIC STUDY OF OXYGEN DIFFUSION IN SUPERCONDUCTING $\text{YBa}_2\text{Cu}_3\text{O}_{7-\delta}$ OXIDES, L.T. Shi and K.N. Tu, IBM T.J. Watson Research Center, Yorktown Heights, NY.

M7.88 OXYGEN DISTRIBUTION NEAR METAL M SUBSTITUTED SITES IN $\text{YBa}_2(\text{Cu}_{1-x}\text{M}_x)_3\text{O}_{7+\delta}$ AS DETERMINED BY X-RAY ABSORPTION MEASUREMENTS, C.Y. Yang, Brookhaven National Laboratory, Materials Science Department, Upton, NY and University of Michigan, Ann Arbor, MI; Y.L. Wang, S.M. Heald, Youwen Xu, A.R. Moodenbaugh, D.O. Welch and M. Suenaga, Brookhaven National Laboratory, Materials Science Division, Upton, NY.

M7.89 VARIATION IN T_c AND CARRIER CONCENTRATION CAUSED BY CHANGE OF OXYGEN CONTENT IN Tl-BASED SUPERCONDUCTORS, Y. Shimakawa, Y. Kubo, T. Manako and H. Igarashi, NEC Corporation, Fundamental Research Laboratories, Kawasaki, Japan.

M7.90 SUPERCONDUCTIVITY OF Bi-Sr-Ca-Cu-O DOPED WITH Ag IONS, Teruo Kato, Yukio Kazumata and Hiroshi Maeta, Japan Atomic Energy Research Institute, Department of Physics, Ibaraki, Japan.

M7.91 DOMAIN STRUCTURES AND PINNING IN OXIDE SUPERCONDUCTORS, Alexander Roitburd, National Institute of Standards and Technology, Metallurgy Division, Gaithersburg, MD.

M7.92 FIELD ORIENTED GRAINS OF RARE EARTH DOPED HIGH T_c SUPERCONDUCTORS, F. Chen, Northeastern University, Barnett Institute, Department of Chemistry, Boston, MA; R.S. Markiewicz, Northeastern University, Barnett Institute, Physics Department, Boston, MA; and B.C. Giessen, Northeastern University, Barnett Institute, Department of Chemistry, Boston, MA.

M7.93 EFFECT OF HIGH TEMPERATURE DEFORMATION ON GRAIN BOUNDARY DEFECTS IN $\text{YBa}_2\text{Cu}_3\text{O}_{7-x}$, Krishna Rajan, Rensselaer Polytechnic Institute, Materials Engineering Department, Troy, NY.

M7.94 MICROSTRUCTURAL EVOLUTION OF $\text{Ba}_2\text{YCu}_3\text{O}_7$ SUPERCONDUCTOR BY ELECTRON IRRADIATION IN A TRANSMISSION ELECTRON MICROSCOPE, Kensuke Shiraishi and Hiroshi Itoh, Japan Atomic Energy Research Institute, Takasaki Radiation Chemistry Research Establishment, Takasaki, Japan.

M7.95 A STUDY OF THE THERMODYNAMIC STABILITY OF $\text{Y}_1\text{Ba}_2\text{Cu}_4\text{O}_8$, K.P. Atwal, R. Gronsky, University of California, and National Center for Electron Microscopy, Materials and Chemical Sciences Division, Lawrence Berkeley Laboratory, Department of Materials Science and Mineral Engineering, Berkeley, CA; J. Nickel, A. Markelz, University of California, Physics Division, Lawrence Berkeley Laboratory, Berkeley, CA.

M7.96 THE COLOR OF POLARIZATION IN HIGH TEMPERATURE SUPERCONDUCTORS, M.S. Osofsky, H.A. Hoff, Naval Research Laboratory, Superconducting Materials Section, Washington, DC; and W.L. Lechter, Sachs/Freeman Associates, Inc., Landover, MD.

M7.97 X-RAY ABSORPTION STUDIES OF VANADIUM SUBSTITUTION IN $\text{YBa}_2\text{Cu}_3\text{O}_{7-\delta}$ SUPERCONDUCTORS, Zhengquan Tan and J.I. Budnick, University of Connecticut, Department of Physics and Institute of Materials Science, Storrs, CT; B.R. Weinberger and L. Lynds, United Technologies Research Center, East Hartford, CT.

M7.98 ON THE STABILITY AND TRANSPORT PROPERTIES OF $\text{Y}_1\text{Ba}_2\text{Cu}_3\text{O}_{7-x}$ PHASES COMBINED WITH REFRACTORY CERAMICS, P. Del Angel, J.M. Domínguez, O. Guzmán, A. Montoya, L. Vicente, Instituto Mexicano del Petróleo, ICA, México, México.

M7.99 THE ELECTROCHEMICAL RESPONSE OF $\text{YBa}_2\text{Cu}_3\text{O}_{7-x}$ IN AQUEOUS SOLUTIONS, T.S. Chin, National Tsing Hua University, Department of Materials Science and Engineering, Hsinchu, Taiwan, China; C.A. Lin, M.P. Hung, National Cheng Kung University, Department of Materials Engineering, Tainan, Taiwan, China.

M7.100 RAMAN AND FLUORESCENCE SPECTRA OBSERVED IN LASER MICROPROBE MEASUREMENTS OF COMPOUNDS IN THE Ln-Ba-Cu-O SYSTEM, Edgar S. Etz, National Institute of Standards and Technology, Center for Analytical Chemistry, National Measurement Laboratory, Gaithersburg, MD; Winnie Wong-Ng, National Institute of Standards and Technology, Ceramics Division, Institute for Materials Science and Engineering, Gaithersburg, MD; and Thomas D. Schroeder, Shippensburg University of Pennsylvania, Department of Chemistry, Shippensburg, PA.

M7.101 MICROANALYSIS OF CUPRATE SUPERCONDUCTORS USING THE COLOR OF POLARIZATION, H.A. Hoff, M.S. Osofsky, Naval Research Laboratory, Materials Science and Technology Division, Washington, DC; and W.L. Lechter, Sachs/Freeman Associates, Inc., Landover, MD.

M7.102 HARMONIC GENERATION IN THE ALTERNATING MAGNETIC RESPONSE OF HIGH- T_c SUPERCONDUCTORS, A. Shaulov, R. Bhargava and D. Dorman, North American Philips Corporation, Philips Laboratories, Materials Physics Department, Briarcliff Manor, NY.

M7.103 PARTIAL SUPERCONDUCTIVITY IN $\text{YBa}_2\text{Cu}_3\text{O}_7$ AT $90 < T < 300$ K, R. Munger and H.J.T. Smith, University of Waterloo, Department of Physics, Waterloo, Canada.

M7.104 THERMAL EXPANSION OF $\text{Pb}_2\text{Sr}_2\text{Y}_{1-x}\text{Ca}_x\text{Cu}_3\text{O}_{8+\delta}$, H.M. O'Bryan and P.K. Gallagher, AT&T Bell Laboratories, Department GD-307, Murray Hill, NJ.

M7.105 MECHANISM OF TWIN FORMATION AND NATURE OF TETRAGONAL TO ORTHORHOMBIC TRANSFORMATION IN $\text{YBa}_2\text{Cu}_3\text{O}_{7-x}$, Mehmet Sarikaya, Ryoichi Kikuchi and I.A. Aksay, University of Washington, Department of Materials Science and Engineering, and Washington Technology Center, Seattle, WA.

M7.106 MAGNETIC INTERACTIONS IN $\text{Y}_{1-x}\text{Pr}_x\text{Ba}_2\text{Cu}_3\text{O}_7$: UPPER CRITICAL FIELD AND HEAT CAPACITY STUDIES, H.B. Radousky, Lawrence Livermore National Laboratory, Livermore, CA; N.E. Phillips, R.A. Fisher, R. Caspary and A. Amato, University of California, Berkeley, Materials and Chemical Sciences Division, Lawrence Berkeley Laboratory, Berkeley, CA; J.L. Peng and R.N. Shelton, University of California, Davis, Department of Physics, Davis, CA.

M7.107 MAGNETIZATION AND LOW TEMPERATURE SPECIFIC HEAT OF ORTHORHOMBIC AND TETRAGONAL $\text{RBa}_2\text{Cu}_3\text{O}_x$ ($R=\text{Y}, \text{Ho}$), H.R. Khan, FEM, Gmuend, West Germany; and R. Kuentzler, CNRS, I.P.C.M.S., Strasbourg, France.

M7.108 IN-SITU TRANSMISSION ELECTRON MICROSCOPY AND COMPUTER SIMULATION STUDY OF THE KINETICS OF OXYGEN LOSS IN $\text{YBa}_2\text{Cu}_3\text{O}_2$, C.P. Burmester, University of California, Berkeley, and the National Center for Electron Microscopy, Department of Materials Science and Mineral Engineering, Berkeley, CA; L.T. Wille, Florida Atlantic University, Department of Physics, Boca Raton, FL; and R. Gronsky, University of California, Berkeley, and the National Center for Electron Microscopy, Department of Materials Science and Mineral Engineering, Berkeley, CA.

M7.109 ELASTICITY STUDIES ON LATTICE INSTABILITY OF HIGH T_c OXIDE SUPERCONDUCTORS, Ye-Ning Wang, Hui-Min Shen, Xiao-Hui Chen, Lin-Hai Sun and Zi-Ran Xu, Nanjing University, Institute of Solid State Physics, Nanjing, China.

M7.110 PROPERTIES AND MICROSTRUCTURE OF SUPERCONDUCTING OXIDES PREPARED BY OXIDATION OF LIQUID QUENCHED ALLOY PRECURSORS, J.S. Luo, D. Michel and J-P. Chevalier, CNRS CECM, Vitry, France.

M7.111 CRYSTAL CHEMISTRY AND PHASE EQUILIBRIA STUDIES OF THE Ba-R-Cu-O SYSTEMS, Winnie Wong-Ng, Robert S. Roth, Lawrence P. Cook, Boris Paretkin, Michael Hill and E.R. Fuller Jr., National Institute of Standards and Technology, Ceramics Division, Gaithersburg, MD.

M7.112 RAMAN STUDIES ON Y_{123} AS A FUNCTION OF ANNEALING, G. Burns, F.H. Dacol, C.A. Feild, A. Gupta, F. Holtzberg, G. Koren, R.B. Laibowitz and T.K. Worthington, IBM T.J. Watson Research Center, Yorktown Heights, NY.

M7.113 HIGH RESOLUTION TRANSMISSION ELECTRON MICROSCOPY STUDY OF DEFECT STRUCTURES IN MULTI-PHASE YBaCuO , M. Fendorf and R. Gronsky, University of California, and National Center for Electron Microscopy, Lawrence Berkeley Laboratory, Department of Materials Science and Mineral Engineering, Berkeley, CA.

M7.114 COMPLEX DEFECTS IN Y-Ba-Cu-O SINGLE CRYSTALS, Philippe Galez, CEA-Saclay, CPCM, Gif sur Yvette, France; P. Schweiss, CEA-Saclay, L.L.B. and K.F.N. Karlsruhe, Gif sur Yvette, France; J.-F. Marucco, Université Paris-Sud Laboratoire Composés non-stoéchiométriques, Orsay, France; and G. Collin, Université Paris-Sud, Laboratoire Physique Solides and C.P.C.M., Orsay, France.

M7.115 CRYSTAL CHEMICAL AND FUNCTIONAL REPRESENTATION OF HIGH- T_c SUPERCONDUCTORS AND RELATED PHASES, J. Sigalovsky, and B.C. Giessen, Northeastern University, Barnett Institute and Department of Chemistry, Materials Science Division, Boston, MA.

M7.116 ULTRASONIC STUDY OF ELASTIC ANISOTROPY AND LATTICE INSTABILITY OF SINGLE CRYSTAL $\text{Bi}_2\text{Sr}_2\text{CaCu}_2\text{O}_8$, Jin Wu, Ye-Ning Wang, Hui-Min Shen, Jin-Song Zhu, Nanjing University, Institute of Solid State Physics, Nanjing, China.

M7.117 IRRADIATION EFFECTS IN $\text{Tl}_2\text{Ca}_2\text{Ba}_2\text{Cu}_3\text{O}_{10}$ SUPERCONDUCTORS, J.C. Barbour, J.F. Kwak, E.L. Venturini, D.S. Ginley and P.S. Peercy, Sandia National Laboratories, Albuquerque, NM.

M7.118 MAGNETIC PENETRATION DEPTHS OF ALIGNED COMPOSITES OF THE HIGH TEMPERATURE SUPERCONDUCTOR $\text{Tl}_2\text{Ca}_2\text{Ba}_2\text{Cu}_3\text{O}_{10+\delta}$, J.R. Thompson, Oak Ridge National Laboratory, Oak Ridge, TN and University of Tennessee, Department of Physics, Knoxville, TN; D.K. Christen, Oak Ridge National Laboratory, Oak Ridge, TN; H.A. Deeds, Y.C. Kim, University of Tennessee, Department of Physics, Knoxville, TN; J. Brynestad, S.T. Sekula, H.R. Kerchner and J.D. Budai, Oak Ridge National Laboratory, Oak Ridge, TN.

M7.119 SUPERSTRUCTURE AND LONG PERIOD ANTIPHASE BOUNDARIES IN $\text{Bi}_2\text{Sr}_2\text{CaCu}_2\text{O}_{8+x}$, R. Herrera, P. Schabes-Retchkiman, J. Reyes-Gasga and M.J. Yacamán, UNAM, Instituto de Física, Mexico, Mexico.

M7.120 TRANSMISSION ELECTRON MICROSCOPY STUDY OF Fe-DOPED BiCaSrCuO. K. Fortunati, R. Gronsky, University of California, and National Center for Electron Microscopy, Lawrence Berkeley Laboratory, Department of Materials Science and Mineral Engineering, Berkeley, CA; R.L. Meng, C.W. Chu, University of Houston, Texas Center for Superconductivity, Houston, TX.

M7.121 HIGH RESOLUTION CALORIMETRY IN HIGH T_c SUPERCONDUCTORS, J-P. Ribeaucourt, Laboratoire de Physique des Solides, Orsay, France; X.-L. Shen, Tongji University, Physics Department, Shanghai, China; and P. Garoche, Laboratoire de Physique des Solides, Orsay, France.

M7.122 PROCESSING AND CHARACTERISATION OF SINGLE PHASE SUPERCONDUCTING THIN FILMS IN THE Bi-Sr-Ca-Cu-O SYSTEM FROM CHEMICAL PRECURSORS, T.E. Bloomer, S.J. Golden, F.F. Lange and K.J. Vaidya, University of California at Santa Barbara, Materials Department, Santa Barbara, CA; W.L. Olson, Superconductor Technologies, Inc., Santa Barbara, CA.

M7.123 MAGNETIC AND ^{119}Sn MOSSBAUER EFFECT STUDY OF Sn-DOPED $\text{Pb}_2\text{Sr}_2\text{Eu}_{0.5}\text{Ca}_{0.5}\text{Cu}_{3-x}\text{Sn}_x\text{O}_{8+z}$ ($x=0.1$) SUPERCONDUCTOR, P.P. Vaishnava, GMI Engineering and Management Institute, Physics Department, Flint, MI; C.D. Nelson and W.P. Pratt Jr., Michigan State University, Department of Physics and Astronomy, East Lansing, MI.

M7.124 PHYSICAL PROPERTIES OF $\text{Bi}_2\text{Sr}_2\text{CuO}_6$, THE SEMICONDUCTING PHASE, STRUCTURALLY DISTINCT FROM THE $N=1$ Bi-CUPRATE SUPERCONDUCTOR, Bryan C. Chakoumakos, Brian C. Sales and Edward Sonder, Oak Ridge National Laboratory, Solid State Division, Oak Ridge, TN.

M7.125 RF SURFACE RESISTANCE MEASUREMENTS IN THE Pb-Bi-Sr-Ca-Cu-O SYSTEM, M.T. Lanagan, Argonne National Laboratory, Materials and Components Department, Argonne, IL; C.T. Bohn, J.R. Delayen, M.C. Einloth, R.N. Vogt and U. Balachandran, Argonne National Laboratory, Engr. Physics Department, Argonne, IL.

M7.126 MAGNETIC PROPERTIES OF $\text{Pb}_2\text{Sr}_{2-x}\text{Eu}_x\text{Ca}_x\text{Cu}_3\text{O}_{8+z}$ SUPERCONDUCTORS, C.D. Nelson, W.P. Pratt Jr., Michigan State University, Department of Physics and Astronomy, East Lansing, MI; and P.P. Vaishnava, GMI Engineering and Management Institute, Flint, MI.

M7.127 INVESTIGATIONS ON SUPERCONDUCTIVITY IN Pb-Sr-R-Ca-Cu-O ($R=Y, \text{Gd}, \text{Dy}$) OXIDE SYSTEM, Ram Prasad and N.C. Soni, Bhabha Atomic Research Centre, Metallurgy Division, Bombay, India.

M7.128 HIGHLY TEXTURED SUPERCONDUCTING $\text{Bi}_2\text{Sr}_2\text{Ca}_1\text{Cu}_2\text{O}_y$ CRYSTALS PREPARED BY UNIDIRECTIONAL SOLIDIFICATION PROCESSING, T. Oyama, M. Nakagawa, T. Suga, K. Ishige, S. Nagaya, Superconductivity Research Laboratory (SRL), International Superconductivity Technology Center (ISTEC), Tokyo, Japan; M. Miyajima, I. Hirabayashi, Superconductivity Research Laboratory (SRL), International Superconductivity Technology Center (ISTEC), Nagoya Division, Nagoya, Japan; Y. Shiohara, and S. Tanaka, Superconductivity Research Laboratory (SRL), International Superconductivity Technology Center (ISTEC), Division IV, Tokyo, Japan.

M7.129 FLUX-ASSISTED PREPARATION OF POWDERED BISMUTH SUPERCONDUCTORS, R.H. Arendt, M.F. Garbaskas and L.L. Schilling, General Electric Company, Corporate Research and Development, Schenectady, NY.

M7.130 SYNTHESIS AND PROCESSING OF Bi-Sr-Ca-Cu-O POWDERS, S.M. Johnson, M.I. Gusman, L. Liu and R.H. Lamoreaux, SRI International, Department of Materials Research Laboratory, Menlo Park, CA; C.B. Eom, Stanford University, Stanford, CA.

M7.131 SYNTHESIS, MICROSTRUCTURE AND CRITICAL CURRENT DENSITY OF CRYSTALLIZED GLASSES IN Bi-Sr-Ca-Cu-O SYSTEM, Donglu Shi, M.S. Boley, J.G. Chen, Ming Xu, U. Welp and K. Vandervoort, Argonne National Laboratory, Materials Science Division, Argonne, IL.

M7.132 CRYSTAL GROWTH OF HIGH T_c SUPERCONDUCTORS IN THE SYSTEM Bi-Ca-Sr-Cu-O, P.D. Han and D.A. Payne, University of Illinois at Urbana-Champaign, Department of Materials Science and Engineering, Materials Research Laboratory, and Science and Technology Center for Superconductivity, Urbana, IL.

M7.133 EVOLUTION OF THE HIGH T_c PHASE IN RAPIDLY SOLIDIFIED Bi-Ca-Sr-Cu OXIDES, A. Asthana, P.D. Han, Z. Xu, L. Chang and D.A. Payne, University of Illinois at Urbana-Champaign, Department of Materials Science and Engineering, Materials Research Laboratory, and Science and Technology Center for Superconductivity, Urbana, IL.

M7.134 SPECIAL TREATMENT ON BiCaSrCuO SUPERCONDUCTORS, X.W. Wang, M. Scott, C. Moore, R. Snyder, Alfred University, Electrical Engineering, Alfred, NY.

M7.135 PREPARATION OF BiPbSrCaCuO SUPERCONDUCTORS BY LASER PEDESTAL GROWTH METHOD, K. Hayashi, H. Nonoyama, M. Ueyama, M. Nagata, H. Hitotsuyanagi, Sumitomo Electric Industries, LTD., Osaka Research Laboratories, Osaka, Japan.

M7.136 NEW METHOD FOR SYNTHESIZING Bi-Sr-Ca-Cu-O SUPERCONDUCTOR, M. Tanaka and K. Habu, SONY Corporation, Research Center, Tokyo, Japan.

M7.137 ELECTRICAL AND MICROSTRUCTURAL CHARACTERISTICS OF REGRADED Bi-Pb-Sr-Ca-Cu-O SUPERCONDUCTOR PREPARED BY RAPID THERMAL MELT PROCESSING, B.M. Moon, B. Lalevic, Y. Lu, Rutgers University, Department of Electrical Engineering, Piscataway, NJ; B.H. Kear, L.E. McCandlish, Rutgers University, Department of Materials Science, Piscataway, NJ; A. Safari and M. Meskoob, Rutgers University, Department of Ceramics, Piscataway, NJ.

M7.138 THE PREPARATION OF Bi-Pb-Sr-Ca-Cu-O SUPERCONDUCTING POWDER FOR THICK FILM PASTES, J. Hagberg, A. Uusimäki, J. Levoska and S. Leppavuori, University of Oulu, Microelectronics and Material Physics Laboratories, Oulu, Finland.

M7.139 PHASE CHEMISTRY, MICROSTRUCTURE AND PROPERTIES OF DIRECTIONALLY SOLIDIFIED SUPERCONDUCTING $\text{Bi}_2\text{Sr}_2\text{CaCu}_2\text{O}_8$, H.M. Chow, X.P. Jiang, M.J. Cima, J.S. Haggerty and M.C. Flemings, Massachusetts Institute of Technology, Department of Materials Science and Engineering, Cambridge, MA; H.D. Brody, University of Pittsburgh, Department of Materials Science and Engineering, Pittsburgh, PA.

M7.140 MELT PROCESSING OF SUPERCONDUCTORS IN THE Bi-Ca-Sr-Cu-O_x SYSTEM, J.P. Cronin, S. West, E. Roberts, S. Rosenfelder and D.R. Uhlmann, The University of Arizona, Arizona Materials Laboratories, Tucson, AZ; O.H. El-Bayoumi and R.J. Andrews, Solid State Sciences Directorate, Rome Air Development Center, Hanscom Air Force Base, MA.

M7.141 CATION DISORDERING IN Tl SUPERCONDUCTORS, B. Morosin, R.J. Baughman, D.S. Ginley, J.F. Kwak, J.E. Schirber, C.P. Tigges and E.L. Venturini, Sandia National Laboratories, Division 1153, Albuquerque, NM.

M7.142 CRYSTAL STRUCTURES AND SOLID SOLUTION BETWEEN Tl-Sr-Ca-Cu-O and Tl-Ba-Ca-Cu-O SUPERCONDUCTORS, A. Soeta, T. Suzuki, S. Takeuchi, T. Kamo, S. Matsuda, Hitachi Ltd., Hitachi Research Laboratory, Ibaraki, Japan.

M7.143 ORIENTATION PROCESS OF Bi-TYPE OXIDE SUPERCONDUCTOR AND ITS HIGH-FIELD TRANSPORT PROPERTIES, N. Enomoto, H. Kikuchi, K. Imai, H. Takami and N. Uno, Furukawa Electric Co., Ltd., Yokohama Research and Development Laboratories, Yokohama, Japan.

M7.144 EFFECT OF OXYGEN PARTIAL PRESSURE ON STABILITY OF HIGH-TC PHASE IN SINTERED Bi-Pb-Sr-Ca-Cu-O SUPERCONDUCTORS, H.K. Lee, K.W. Lee, D.H. Ha and J.C. Park, Korea Standards Research Institute, Taejeon, Korea.

M7.145 THE SUPERCONDUCTIVITY OF $\text{Bi}_{1.6}\text{Pb}_{0.4}\text{Sr}_2\text{Ca}_2(\text{Ca}_{1-x}\text{Ag}_x)_3\text{O}_y$ AND $\text{Bi}_{1.6}\text{Pb}_{0.4}\text{Sr}_2\text{Ca}_2\text{Cu}_3\text{O}_y$ + wt% Ag, Chongde Wei, Chin Lin, Qingrong Feng, Zunxiao Liu, Jian Lan, Yunxi Sun, Guozhong Li, Ke Wu, Lixin Xue, Zizhao Gan, Peking University, Department of Physics, Beijing, China.

M7.146 SYNTHESIS OF VARIOUS Bi-SYSTEMS FROM NITRATES BY USING A SPRAY-DRYING PROCESS, Jens Hyldtoft, Svend Dahl-Petersen, Torsten Freltoft, Liselotte Lorenzen and Per Vase, NKT A/S, Department of Research and Development, Broendby, Denmark.

M7.147 THE EFFECTS OF TRANSITION METAL SUBSTITUTIONS FOR COPPER IN THE Bi-Sr-Ca-Cu-O SUPERCONDUCTING SYSTEM, J.C. Bennett, F.W. Boswell, J.M. Corbett, S. Kohara, University of Waterloo, Waterloo, Canada; and F.S. Razavi, Brock University, St. Catharines, Canada.

M7.148 THE EFFECTS OF SEEDING ON THE FORMATION OF HIGH- T_c Bi-Pb-Sr-Ca-Cu-O COMPOUNDS, Cheol J. Kim and Mark R. DeGuire, Case Western Reserve University, Department of Materials Science and Engineering, Cleveland, OH; and Narottam P. Bansal, NASA Lewis Research Center, Ceramics Branch, Cleveland, OH.

M7.149 OPTIMIZING THE MACHINING PROPERTIES OF HIGH T_c BS₂CCO, R.J. Rayne, L.E. Toth, B.A. Bender, R.J. Soulen Jr., Naval Research Laboratory, Washington, DC.

M7.150 THE EFFECT OF THE DISTRIBUTION OF DOPANTS IN HIGH T_c BI-COMPOUND SUPERCONDUCTORS, Alexis S. Nash, Marquette University, ECBE Department, Milwaukee, WI; Kenneth C. Goretta, Argonne National Laboratory, Ceramics Section, Materials and Components Technology Division, Argonne, IL; Philip Nash, Illinois Institute of Technology, Metallurgical and Materials Engineering, Chicago, IL; Roger B. Poeppel and Donglu Shi, Argonne National Laboratory, Ceramics Section, Materials and Components Technology Division, Argonne, IL.

M7.151 HIGH RESOLUTION NEUTRON POWDER DIFFRACTION STUDY OF THE TUBULAR PHASE $\text{Bi}_4\text{Sr}_8\text{Cu}_6\text{O}_{19+x}$, M.T. Caldes, J.M. Navarro, A. Fuertes, X. Obradors, C. Miravittles, Institut de Ciència de Materials de Barcelona (CSIC), Barcelona, Spain; J. Rodriguez-Carvajal, Institut Max von Laueaul Langevin, Grenoble, France; M. Vallet, J. González-Calbet, Laboratorio de Magnetismo Aplicado (RENFE-UCM), Madrid, Spain.

M7.152 PREPARATION OF HIGH-PURITY $\text{Tl}_2\text{Ca}_n\text{-Ba}_2\text{Cu}_{n+1}\text{O}_{6+2n}$ ($n=1,2$) POWDERS FROM STOICHIOMETRIC REACTANT MIXTURES, Nae-Lih Wu, National Taiwan University, Department of Chemical Engineering, Taipei, Taiwan, China; Y.D. Yao, Academia Sinica, Department of Physics, Taipei, Taiwan, China; E. Ruckenstein, State University of New York at Buffalo, Department of Chemical Engineering, Amherst, NY.

M7.153 SOLID STATE FORMATION OF SUPERCONDUCTING PHASES IN THE Tl-Ca-Ba-Cu-O SYSTEM, T.W. Huang, M.P. Hung, Cheng Kung University, Department of Material Engineering, Tainan, Taiwan, China; T.S. Chin, National Tsing Hua University, Department of Materials Science and Engineering, Hsinchu, Taiwan, China; H.C. Ku, National Tsing Hua University, Department of Physics, Hsinchu, Taiwan, China; P.C. Yao, S.E. Hsu, Chun Shan Institute of Science and Technology, Material Research and Development Center, Lung-Tang, Taiwan, China.

M7.154 PHASE EQUILIBRIA IN THE SYSTEM Tl-Ca-Ba-Cu-O , Lawrence P. Cook, Chwan K. Chiang, Winnie Wong-Ng and Lawrence H. Bennett, National Institute of Standards and Technology, Ceramics Department, Gaithersburg, MD.

M7.155 Tl-Ba BASED HIGH TEMPERATURE SUPERCONDUCTORS: PREPARATIONS AND PROPERTIES, M. Greenblatt S. Li, L. McMills, M.H. Pan and K.V. Ramanujachary, Rutgers University, Chemistry Department, New Brunswick, NJ.

M7.156 HYPER- AND HYPOBARIC PROCESSING OF Tl-Ba-Ca-Cu-O SUPERCONDUCTORS, K.C. Goretta, Argonne National Laboratory, Materials and Components Department, Argonne, IL; J.L. Routbort, Donglu Shi, M.C. Hash and Ira Bloom, Argonne National Laboratory, Materials Science Department, Argonne, IL.

M7.157 VARIATION OF T_c IN $\text{Tl-RICH Tl-Ca-Ba-Cu-O}$ SINGLE CRYSTALS, E.L. Venturini, R.J. Baughman, B. Morosin, D.S. Ginley, J.F. Kwak, J.E. Schirber and C.P. Tigges, Sandia National Laboratories, Division 1153, Albuquerque, NM.

M7.158 PREPARATION OF $\text{Ba}_2\text{YCu}_3\text{O}_{6.9}$ THIN FILM SUPERCONDUCTORS USING SOLUBLE ARYLOXIDE PRECURSORS, Mary Rose Scozzafava, Massachusetts Institute of Technology, Ceramics Processing Research Laboratory, Cambridge, MA; Michael J. Cima, Wendell E. Rhine, Massachusetts Institute of Technology, Department of Material Science, Cambridge, MA.

M7.159 METAL-ORGANIC DECOMPOSITION AND MICROSTRUCTURE DEVELOPMENT IN $\text{Ba}_2\text{YCu}_3\text{O}_{7-x}$ FILMS FROM METAL TRIFLUORACETATE PRECURSORS, Paul C. McIntyre, Raymond C. Chiu, Michael J. Cima, Wendell E. Rhine, Massachusetts Institute of Technology, Ceramics Processing Research Laboratory, Cambridge, MA.

M7.160 PREPARATION OF Y-Ba-Cu-O FILMS BY A MODIFIED CHEMICAL VAPOR DEPOSITION METHOD, T.S. Chin, L.H. Perng, C.H. Lin, Tsing Hau University, Department of Materials Science and Engineering, Hsinchu, Taiwan, China; T.W. Huang, C.H. Hsu, M.P. Hung, Cheng Kung University, Department of Material Engineering, Tainan, Taiwan, China; and Z.H. Hung, Cheng Hung University, Department of Chemical Engineering, Tainan, Taiwan, China.

M7.161 EFFECT OF GLOW DISCHARGE CURRENT ON COMPOSITION Y-Ba-Cu-O FILMS BY HIGH PRESSURE DC SPUTTERING PROCESS, R.J. Lin and P.T. Wu, Industrial Technology Research Institute, Materials Research Laboratories, Hsinchu, Taiwan, China.

M7.162 PREPARATION AND PROPERTIES OF HIGH T_c YBCO POLY-CRYSTAL THIN FILMS BY IN-SITU METHOD, N. Harada, K. Satou, K. Yamamoto, Furukawa Electric Co., Ltd., Yokohama Research and Development Laboratories, Yokohama, Japan.

M7.163 ELECTROPHORETIC DEPOSITION OF HIGH-TEMPERATURE SUPERCONDUCTOR THICK FILMS, J.B. Mooney, A. Sher, M.L. Riggs, K.A. Sabo, A. Rosengreen, B. Kingsley and J.C. Terry, SRI International, Menlo Park, CA.

M7.164 THE FABRICATION OF $\text{YBa}_2\text{Cu}_3\text{O}_7$ THIN FILMS BY PHYSICAL VAPOR DEPOSITION, De Huai Chen, R.L. Sabatini and H. Wiesmann, Brookhaven National Laboratory, Materials Science Division, Upton, NY.

M7.165 ORIENTED MICROSTRUCTURE OF $\text{YBa}_2\text{-Cu}_3\text{O}_{7-x}$ THICK FILMS, F. Wellhofer, T.C. Shields, J.S. Abell, K.N.R. Taylor, University of Birmingham, School of Metallurgy and Materials, Birmingham, United Kingdom; and D. Holland, University of Warwick, School of Physics, Coventry, United Kingdom.

M7.166 THE SPUTTER DEPOSITION AND CHARACTERIZATION OF EPITAXIAL MAGNESIUM OXIDE THIN FILMS AND THEIR USE AS A SAPPHIRE/YBCO BUFFER LAYER, G.W. Morris, R.E. Somekh, Z.H. Barber and J.E. Evetts, Cavendish Laboratories, Interdisciplinary Research Centre in Superconductivity, and University of Cambridge, Department of Materials Science and Metallurgy, Cambridge, United Kingdom.

M7.167 $Y_1Ba_2Cu_3O_{7-x}$ FILMS FROM NITRATE SOLUTION USING RF PLASMA DEPOSITION, A. Shah, T. Haugan, S. Witanachchi, S. Patel and D.T. Shaw, State University of New York at Buffalo, Institute on Superconductivity, Buffalo, NY.

M7.168 IN SITU PREPARATION OF Y-Ba-Cu-O SUPERCONDUCTING THIN FILMS BY DC-MAGNETRON SPUTTERING, L.F. Chen, L. Zhou, S.J. Pang, Y.H. Kuo, L. Li, B.R. Zhao and Y.Z. Zhang, Academia Sinica, Beijing Laboratory of Vacuum Physics, General Research Institute of Non-ferrous metals, Beijing, China; Peking University, Department of Physics, Beijing, China; Academia Sinica, Institute of Physics, Beijing, China.

M7.169 MULTILAYER E-BEAM DEPOSITION AND ANNEALING OF $YBa_2Cu_3O_{7-\delta}$ THIN FILMS ON $LaGaO_3$ SUBSTRATES, Richard DeVito, Brian G. Pazol, John H. Chaffin, Litton/Itek Optical Systems, Lexington, MA; Roger F. Belt and Robert Uhrin, Litton/Airtron, Morris Plains, NJ.

M7.170 PREPARATION OF $YBa_2Cu_3O_x$ SUPERCONDUCTING THIN FILMS BY MEANS OF SINGLE TARGET RF-SPUTTERING, H. Weyten, University of Antwerp (UIA), Department of Chemistry Antwerp, Belgium; R. De Batist, P. Nagels, University of Antwerp (RUCA), Antwerp, Belgium; and J. Cornelis, SCK/CEN, Materials Development Department, Mol, Belgium.

M7.171 RAPID CHEMICAL VAPOR DEPOSITION OF $YBa_2Cu_3O_x$ COATINGS, W.J. Lackey, W.B. Carter, D.N. Hill, E.K. Barefield, J.A. Haniogofsky, M.J. Shapiro, T.S. Moss III, A.J. Green and D.F. O'Brien, Georgia Institute of Technology, Georgia Tech Research Institute, Atlanta, GA; R.A. Jake and K.R. Efferson, American Magnetics, Inc., Oak Ridge, TN.

M7.172 LOW TEMPERATURE GROWTH OF SUPERCONDUCTING $YBa_2Cu_3O_{7-x}$ THIN FILMS BY METALORGANIC CHEMICAL VAPOR DEPOSITION, Keiichi Kanehori, Nobuyuki Sugii and Katsuki Miyauchi, Hitachi, Ltd., Central Research Laboratory, Tokyo, Japan.

M7.173 PARTIAL REDUCTION-REOXIDATION PROCESSING OF Y-Ba-Cu-O SPUTTERED THIN FILMS, F.H. Garzon, J.G. Beery, D.K. Wilde and I.D. Raistrick, Los Alamos National Laboratory, NM.

M7.174 COMPOSITIONAL CONTROL OF Y-BA-CU-O FILMS EMPLOYING A SINGLE OXIDE TARGET, A.J. Drehman, J.A. Horrigan, M.W. Dumais, B.L. MacDonald, R.J. Andrews, Rome Air Development Center, Solid State Sciences Directorate, Hanscom AFB, MA; P.M. Tedrow, Massachusetts Institute of Technology Francis Bitter National Magnet Laboratory, Cambridge, MA; and M.N. Alexander, Rome Air Development Center, Solid State Sciences Directorate, Hanscom AFB, MA.

M7.175 SPRAY PYROLYSIS TECHNIQUE FOR THE DEPOSITION OF SUPER CONDUCTING FILMS, Marc Soller, Larry P. Moy, Michael R. Squillante, Radiation Monitoring Devices, Inc., Watertown, MA; and James Marzik, U.S. Army Materials Technology Laboratory, Watertown, MA.

M7.176 $YBa_2Cu_3O_{7-x}$ THIN FILMS PREPARED BY MULTILAYER DEPOSITION, Valentin Garcia-Vazquez and Charles M. Falco, University of Arizona, Optical Science Center and Arizona Research Laboratories, Department of Physics, Tucson, AZ.

M7.177 HIGHLY ORIENTED $YBa_2Cu_3O_{7-x}$ THIN FILMS PREPARED BY UNBALANCED DC MAGNETRON SPUTTERING FROM SINGLE STOICHIOMETRIC TARGET, N. Savvides, D.W. Hensley, C. Andrikidis, R. Driver and J.C. Macfarlane, CSIRO, Division of Applied Physics, Sydney, Australia; N.X. Tan and A.J. Bourdillon, University of New South Wales, Sydney, Australia.

M7.178 CRUCIBLELESS LIQUID PHASE GROWTH OF (00L) $YBaCuO$ FILMS ON POLYCRYSTALLINE SUBSTRATES, F.C. Chen, L.H. Perng, T.S. Chin, C.P. Perng, C.M. Wu, T.B. Wu, and C.H. Lin, National Tsing Hua University, Hsinchu, Department of Materials Science and Engineering, Hsinchu, Taiwan, China.

M7.179 HIGH T_c SUPERCONDUCTOR FILMS GROWN BY THE LPE TECHNIQUE, A.S. Yue and C.S. Yang, University of California, Department of Materials Science and Engineering, Los Angeles, CA.

M7.180 PREPARATION OF Y-Ba-Cu-O HIGH T_c SUPERCONDUCTING FILMS BY PLASMA-ENHANCED ORGANOMETALLIC CHEMICAL VAPOR DEPOSITION, J. Zhao, L.M. Tonge, H.O. Marcy, B.W. Wessels, T.J. Marks and C.R. Kannewurf, Northwestern University, Materials Research Center and Science and Technology Center for Superconductivity, Materials Science and Engineering, Evanston, IL.

M7.181 SUPERCONDUCTING $\text{YBa}_2\text{Cu}_3\text{O}_{7-y}$ THIN FILM ON METAL SUBSTRATE BY CHEMICAL VAPOR DEPOSITION PROCESS, T. Yamaguchi, S. Aoki, N. Sadakata, and O. Kohno, Fujikura Ltd., Tokyo Laboratory, Tokyo, Japan.

M7.182 SUPERCONDUCTING HIGH T_c THIN FILMS PREPARED BY LASER DEPOSITION: COMPARISON OF LASER SOURCES, L. Lynds, B.R. Weinberger, G.G. Peterson and D.M. Potrepka, United Technologies Research Center, East Hartford, CT.

M7.183 IN-SITU GROWTH OF $\text{YBa}_2\text{Cu}_3\text{O}_7$ BY LASER ABLATION, D.K. Fork, Xerox Palo Alto Research Center, Palo Alto, California and Stanford University, Department of Applied Physics, Stanford, CA; K. Char, Conductus, Inc., Sunnyvale, CA; J.B. Boyce, Xerox Palo Alto Research Center, Palo Alto, CA; F. Bridges, Xerox Palo Alto Research Center, Palo Alto, CA and University of California, Physics Department, Santa Cruz, CA; G.A.N. Connell, Xerox Palo Alto Research Center, Palo Alto, CA; and T.H. Geballe, Stanford University, Department of Applied Physics, Stanford, CA.

M7.184 VERSATILE LASER DEPOSITION CHAMBER FOR IN-SITU FABRICATION OF BUFFER LAYERS AND SUPERCONDUCTING THIN-FILMS, R.E. Russo, R.P. Reade and J.M. McMillan, Lawrence Berkeley Laboratory, Berkeley, CA; and B.L. Olsen, Lawrence Livermore National Laboratory, Livermore, CA.

M7.185 IN-SITU LASER DEPOSITION OF $\text{YBa}_2\text{Cu}_3\text{O}_{7-\delta}$ AND $\text{HoBa}_2\text{Cu}_3\text{O}_{7-\delta}$ HIGH- T_c SUPERCONDUCTING THIN FILMS ON Si (100) AND KTaO_3 (100), A.K. Singh, C. Lee, J. Narayan, North Carolina State University, Department of Materials Science and Engineering, Raleigh, NC; and L.A. Boatner, Oak Ridge National Laboratory, Ceramics and Interface Section, Oak Ridge, TN.

M7.186 LONG-LASER-PULSE METHOD OF PRODUCING Y-Ba-CuO SUPERCONDUCTING FILMS, R.E. Russo, M. Balooch and D.R. Olander, University of California and Lawrence Berkeley Laboratory, Berkeley, CA.

M7.187 IN-SITU DEPOSITION OF HIGH TEMPERATURE SUPERCONDUCTORS ON LaAlO_3 SUBSTRATES, P. Tiwari, A.K. Singh, C.B. Lee and J. Narayan, North Carolina State University, Department of Materials Science and Engineering, Raleigh, NC.

M7.188 PULSED LASER DEPOSITION OF HIGH- T_c SUPERCONDUCTING THIN FILMS, M. Grant Norton, Lisa A. Tietz and C. Barry Carter, Cornell University, Department of Materials Science and Engineering, Ithaca, NY; Stephen E. Russek and Robert A. Buhrman, Cornell University, School of Applied and Engineering Physics, Ithaca, NY.

M7.189 UNIFORMITY CONSIDERATIONS OF "IN-SITU" LASER-ABLATED $\text{Y}_1\text{Ba}_2\text{Cu}_3\text{O}_{7-x}$ FILMS OVER THREE INCH WAFERS, James A. Greer and Jerrold Van Hook, Raytheon Company, Research Division, Lexington, MA.

M7.190 IN-SITU PROCESSING OF TEXTURED AND EPITAXIAL SUPERCONDUCTING Ho-Ba-Cu-O THIN FILMS ON (100) MgO AND YS-ZrO_2 SUBSTRATES IN THE TEMPERATURE RANGE 500-650°C, R.K. Prasad, A.K. Singh and J. Narayan, North Carolina State University, Department of Materials Science and Engineering, Raleigh, NC.

M7.191 SOFT X-RAY STUDIES OF Y-Ba-Cu-O THIN FILMS PREPARED BY LASER ABLATION, A. Krol, State University of New York at Buffalo and Stony Brook, Department of Physics, Buffalo, NY; G. Smith, Brookhaven National Laboratory, Department of Instrumentation, Upton, NY; C.J. Sher, D.R. Storch, L.W. Song, Y.H. Kao, S. Witanachchi, Y.Z. Zhu, S. Patel and D.T. Shaw, State University of New York at Buffalo and Stony Brook, Department of Physics, Buffalo, NY.

M7.192 IN SITU GROWTH OF EPITAXIAL SUPERCONDUCTING $\text{YBa}_2\text{Cu}_3\text{O}_{7-x}$ FILMS ON INSULATING, SEMICONDUCTING AND FERROELECTRIC KTaO_3 BY PULSED LASER ABLATION, J.W. McCamy, David P. Norton, Douglas H. Lowndes, L.A. Boatner, R. Feenstra and J.D. Budai, Oak Ridge National Laboratory, Solid State Division, Oak Ridge, TN.

M7.193 CHARACTERIZATION OF GROUND STATE NEUTRAL AND ION TRANSPORT DURING LASER ABLATION OF 1:2:3 SUPERCONDUCTORS BY TRANSIENT OPTICAL ABSORPTION SPECTROSCOPY, D.B. Geohegan, D.N. Mashburn, Oak Ridge National Laboratory, Solid State Division, Oak Ridge, TN.

M7.194 LASER INTERFEROMETRIC MEASUREMENT OF SUBSTRATE TEMPERATURE DURING GROWTH OF HIGH T_c SUPERCONDUCTOR FILMS, K.L. Saenger, J. Gupta, J.P. Doyle, R.A. Roy and J.J. Cuomo, IBM T.J. Watson Research Center, Yorktown Heights, NY.

M7.195 HIGHLY ORIENTED SUPERCONDUCTING Bi-Sr-Ca-Cu OXIDE THIN FILMS BY THE SOLUTION SOL-GEL PROCESS, P. Ravindranathan, S. Komarneni, A.S. Bhalla and R. Roy, The Pennsylvania State University, Materials Research Laboratory, University Park, PA.

M7.196 THE USE OF BaF_2 BUFFER LAYERS FOR THE SPUTTER-DEPOSITION OF TlCaBaCuO THIN-FILM SUPERCONDUCTORS, K.M. Hubbard, P.N. Arendt, Los Alamos National Laboratory, Materials Science and Technology Division, Los Alamos, NM; E.J. Peterson, Los Alamos National Laboratory, Exploratory Research and Development Center, Los Alamos, NM; G.A. Reeves, N.E. Elliott, Los Alamos National Laboratory Materials Science and Technology Division, Los Alamos, NM; D.W. Cooke, Los Alamos National Laboratory, Meson-Physics Facility, Los Alamos, NM; D.R. Brown, Los Alamos National Laboratory, Mechanical and Electrical Engineering Division, Los Alamos, NM; and M. Nastasi, Los Alamos National Laboratory, Materials Science and Technology Division, Los Alamos, NM.

M7.197 AS-GROWN SUPERCONDUCTIVITY OF Bi-SYSTEM THIN FILMS PREPARED BY MAGNETRON SPUTTERING WITH Pb DOPED THREE TARGETS: $(\text{Bi}_{1.6}\text{Pb}_{0.4})_{1+a}(\text{SrCa})_2\text{Cu}_3\text{O}_x$, $(\text{Bi}_{1.6}\text{Pb}_{0.4})_{1-b}(\text{SrCa})_{2+c}\text{Cu}_3\text{O}_x$ AND $(\text{Bi}_{1.6}\text{Pb}_{0.4})_1(\text{Sr-Ca})_{2-c}\text{Cu}_3\text{O}_x$ ($a=0.5$, $b=1$, $c=1.5$) Ken'ichi Kuroda, Masami Tanioku, Kazuyoshi Kojima, and Koichi Hamanaka, Mitsubishi Electric Corporation, Central Research Laboratory, Hyogo, Japan.

M7.198 EVALUATING THE CHEMICAL COMPATIBILITY OF POTENTIAL SUBSTRATE MATERIALS FOR Bi-Sr-Ca-Cu-O FILMS, K.E. Williams, M.M. Matthiesen, D.A. Rudman, Massachusetts Institute of Technology, Department of Materials Science and Engineering, Cambridge, MA.

M7.199 IN-SITU GROWTH OF SUPERCONDUCTING Bi-Sr-Ca-Cu-O THIN FILMS BY ACTIVATED REACTIVE CO-EVAPORATION, K. Yoshikawa, T. Satoh, N. Sasaki and M. Nakano, Fujitsu Ltd., Kawasaki, Japan.

M7.200 HIGH- T_c SUPERCONDUCTING Bi-(Pb-)Sr-Ca-Cu-O FILMS DEPOSITED BY PULSED Nd:YAG LASER ABLATION, J. Levoska, J. Hagberg, P. Pusa, A. Uusimäki and S. Leppävuori, University of Oulu, Microelectronics Laboratory, Oulu, Finland.

M7.201 IN SITU REACTIVE SPUTTER DEPOSITION OF SUPERCONDUCTING Bi-Sr-Ca-Cu-O THIN FILMS ON SILICON SUBSTRATES, M. Migliuolo, D.W. Greve, T.E. Schlesinger, Carnegie Mellon University, Department of Electrical and Computer Engineering, Pittsburgh, PA; J.A. Brewer, R.M. Belan, Kurt J. Lesker Company, Clairton, PA.

M7.202 IN-SITU AND POST ANNEALED SUPERCONDUCTING THIN FILMS OF BiSrCaCuO BY PULSED LASER DEPOSITION, L. DiDomenico and X.D. Wu, Rutgers University, Physics Department, Piscataway, NJ; T. Venkatesan, Bellcore, Red Bank, NJ.

M7.203 THERMAL EXPANSION OF $\text{YBa}_2\text{Cu}_3\text{O}_7$, G.A. Ramadass, V. Ramachandran and R. Srinivasan, I.I.T., Department of Physics, Madras, India.

M7.204 THIN-FILM DEPOSITION AND TRANSPORT IN $2223 \text{ Bi-Sr-Ca-Cu-O}$, J.T. Kucera, D.G. Steel, J.M. Graybeal, Massachusetts Institute of Technology, Physics Department, Cambridge, MA; T.P. Orlando, Massachusetts Institute of Technology, EECS Department, Cambridge, MA; and D.A. Rudman, Massachusetts Institute of Technology, Materials Science Department, Cambridge, MA.

M7.205 CRITICAL CURRENT DENSITY MEASUREMENTS OF LASTER DEPOSITED SUPERCONDUCTING THIN FILMS, C.B. Lee, A.K. Singh, R.K. Singh and J. Narayan, North Carolina State University, Department of Materials Science and Engineering, Raleigh, NC.

M7.206 THE DETERMINATION OF OXYGEN STOICHIOMETRY OF HIGH TEMPERATURE SUPERCONDUCTING THIN FILMS BY NUCLEAR SCATTERING OF 3 MEV PROTONS ON OXYGEN, H.-S. Jin and T. Yan, Brooklyn College of The City University of New York, Department of Physics, Brooklyn, NY.

M7.207 RECRYSTALLIZATION OF NON VACUUM DERIVED $\text{Ba}_2\text{YCu}_3\text{O}_{7-\delta}$ FILMS, M.F. Ng, S.C. Peterson, M.J. Cima, Massachusetts Institute of Technology, Ceramics Processing Research Laboratory, Cambridge, MA.

M7.208 TWO NON-CONTACT TECHNIQUES FOR CHARACTERIZATION OF THIN FILMS OF YBCO, C.A. Weiss, W.L. McLean, X.D. Wu, Rutgers University, Physics Department, Piscataway, NJ; J. Barner and T. Venkatesan, Bellcore, Red Bank, NJ.

M7.209 STRUCTURAL AND SUPERCONDUCTING PROPERTIES OF YBCO THIN FILMS ON Zr(Y)O_2 SUBSTRATES, Q. Li, Rutgers University, Physics Department, Piscataway, NJ; G. Linker, J. Geerk, O. Meyer, Kernforschungs-zentrum Karlsruhe, Institute fuer Nukleare Festkoeperphysik, Karlsruhe, West Germany; and X.X. Xi, Rutgers University, Physics Department, Piscataway, NJ.

M7.210 ANNEALING BEHAVIOR OF $\text{Ba}_2\text{YCu}_{3+x}\text{O}_{7+y}$ THIN FILMS, T. Siegrist and E. Coleman, AT&T Bell Laboratories, Murray Hill, NJ.

M7.211 PROPERTIES OF THIN FILMS OF $\text{YBa}_2\text{-Cu}_3\text{O}_7$ PREPARED BY COEVAPORATION OF Y, Cu AND BaF_2 , I.D. Raistrick, D.N. Sinha, F.H. Garzon, J.G. Beery and D.K. Wilde, Los Alamos National Laboratory, Los Alamos, NM.

M7.212 EFFECT OF BUFFER LAYERS ON THE SUPERCONDUCTING PROPERTIES OF YBCuO FILMS ON METALLIC SUBSTRATES, S. Witanachchi, J. Chang, Y.Z. Zhu, S. Patel and D.T. Shaw, State University of New York at Buffalo, Institute on Superconductivity, Buffalo, NY.

M7.213 INTERFACES IN THIN FILM HIGH- T_c SUPERCONDUCTORS, Lisa A. Tietz, M. Grant Norton and C. Barry Carter, Cornell University, Department of Materials Science and Engineering, Ithaca, NY.

M7.214 OXYGEN RESONANCE STUDY IN YBaCuO HIGH- T_c FILMS, Hiroki Kuwano, Jian Li, Peter Revesz, James W. Mayer, Cornell University, Materials Science and Engineering, Ithaca, NY; Yasuhiro Nagai, Nippon Telegraph and Telephone Corporation, NTT Applied Electronics Laboratories, Tokyo, Japan.

M7.215 LINE BROADENING ANALYSES OF VARIOUSLY PREPARED YBaCuO SUPERCONDUCTING FILMS, M. Ece and R.W. Vook, Syracuse University, Physics Department, Syracuse, NY; John P. Allen, CVC Products, Inc., Rochester, NY.

M7.216 CATION INTERDIFFUSION AT YBCO/MgO INTERFACES, M. Lanham, J. Mayer, S.J. Golden, A.G. Evans, University of California, Materials Department, Santa Barbara, CA; and M. Rühle, Max-Planck Institute, Metallforschung Department, Stuttgart, West Germany.

M7.217 MICROSTRUCTURE OF Y-Ba-Cu-O THIN FILMS GROWN ON SINGLE CRYSTAL $SrTiO_3$, Siu-Wai Chan, D.M. Hwang and S.M. Sempere, Bellcore, Red Bank, NJ.

M7.218 XPS ANALYSIS OF Y-Ba-Cu-O AND Zr-O THIN FILMS AND INTERFACES WITH SILICON SUBSTRATES, D.B. Fenner, Xerox Palo Alto Research Center, Palo Alto, California and Santa Clara University, Physics Department, Santa Clara, CA; A.M. Viano, Santa Clara University, Physics Department, Santa Clara, California and Xerox Palo Alto Research Center, Palo Alto, CA; J.B. Boyce and G.A.N. Connell, Xerox Palo Alto Research Center, Palo Alto, CA.

M7.219 THE INFLUENCE OF THE SUBSTRATE SURFACE ON THE NUCLEATION AND GROWTH OF SUPERCONDUCTING THIN FILMS, S. Basu, N. Bordes, M. Cohen and M. Nastasi, Los Alamos National Laboratory, Los Alamos, NM.

M7.220 MICROSTRUCTURES OF Y123 FILMS ON $SrTiO_3$ AND $LaGaO_3$, T. Roy, T.E. Mitchell and I.D. Raistrick, Los Alamos National Laboratory, Los Alamos, NM.

M7.221 INVESTIGATION OF POTENTIAL DIFFUSION BARRIERS BETWEEN $YBa_2Cu_3O_{7-x}$ AND SILICON, A. Lubig, Ch. Buchal and B. Stritzker, Institut für Schicht- und Ionentechnik, Jülich, West Germany.

M7.222 EPITAXIAL AND SUPERCONDUCTING PROPERTIES OF $Y_1Ba_2Cu_3O_{7-x}$ FILMS ON FIVE PEROVSKITE SUBSTRATES, R. Feenstra, J.D. Budai, S.J. Pennycook, M.F. Chisholm, M.D. Galloway, D.K. Christen, D.P. Norton, J.W. McCamy, D.H. Lowndes and L.A. Boatner, Oak Ridge National Laboratory, Oak Ridge, TN.

M7.223 THE INTERFACE BETWEEN SILVER CONTACTS AND HIGH T_c SUPERCONDUCTORS, M.D. McConnell and W.G. Morris, General Electric Company, Research and Development, Schenectady, NY.

M7.224 STUDY OF EPITAXY OF $YBa_2Cu_3O_{7-x}$ BY THERMAL REGROWTH OF ION IMPLANTED AMORPHOUS LAYERS, J.A. Martinez, UNLP, Department de Física, Argentina; A. Inam and X.D. Wu, Rutgers University, Physics Department, Piscataway, NJ; B. Wilkens, N.G. Stoffel, D. Hart, D.M. Hwang, L. Nazar and T. Venkatesan, Bellcore, Red Bank, NJ.

M7.225 VERY LOW RESISTANCE ELECTRICAL CONTACTS TO Tl -BASED HIGH T_c FILMS, J.F. Kwak, R.P. Hellmer, T.R. Castillo, R. Padilla and D.S. Ginley, Sandia National Laboratories, Division 1152, Albuquerque, NM.

M7.226 MEASUREMENTS OF SURFACE RESISTANCE OF HTS THIN FILMS FROM 0.5 TO 40 GHz, J. Steinbeck, Hanscom Air Force Base, RADC/EEAC, Hanscom, MA; D.E. Oates and A.C. Anderson, Massachusetts Institute of Technology, Lincoln Laboratory, Lexington, MA.

M7.227 ELECTRIC-FIELD MODULATION OF A Bi-Sr-Ca-Cu-O FILM WITH A PLASMA POLYMERIZED FILM AS AN INSULATOR, Shin'ichi Morohashi, Hideo Suzuki, Kohtaroh Gotoh, Norio Fujimaki and Shinya Hasuo, Fujitsu Laboratories Limited, Atsugi, Japan.

M7.228 RESISTANCE TRANSITIONS OF ION-BEAM THINNED $YBa_2Cu_3O_7$ FILMS - AN APPROACH TO THE LIMITING THICKNESS OF ONE LATTICE CONSTANT, A.F. Hebard, R.H. Eick, T. Siegrist and E. Coleman, AT&T Bell Laboratories, Murray Hill, NJ.

M7.229 TRANSPORT MEASUREMENTS ON SUPERCONDUCTING $YBa_2Cu_3O_7$ LINES, STEP EDGE STRUCTURES, AND ION BEAM DAMAGED LINES, Brian Moeckly, Daniel K. Lathrop, Gregory F. Redinbo, Stephen E. Russek, R.A. Buhrman, Cornell University, Department of Applied and Engineering Physics, Ithaca, NY.

M7.230 CRITICAL CURRENT DENSITY OF NARROW SUPERCONDUCTING THIN FILMS FABRICATED BY LASER ABLATION TECHNIQUES, L.W. Song, Y.H. Kao, Q.Y. Ying, J.P. Zheng, H.S. Kwok, Y.Z. Shu and D.T. Shaw, State University of New York, Department of Physics, Buffalo, NY.

M7.231 MAGNETIC EFFECT ON LOW-RESISTIVITY METAL-HIGH T_C SUPERCONDUCTOR CONTACTS, Yonhua Tzeng, Mitch Belser, Auburn University, Department of Electrical Engineering, Auburn, AL.

M7.232 WET CHEMICAL ETCHING OF HIGH-TEMPERATURE SUPERCONDUCTING FILMS IN EDTA SOLUTION, F.K. Shokoohi, L.M. Schiavone, Bellcore, Quantum Structure Research Department, Red Bank, NJ; C.T. Rogers, Bellcore, Solid State Physics Research Department, Red Bank, NJ; A. Inam, X.D. Wu, Rutgers University, Physics Department, Piscataway, NJ; L. Nazar and T. Venkatesan, Bellcore, Red Bank, NJ.

M7.233 CHARACTERIZATION OF HIGH-TEMPERATURE SUPERCONDUCTING MATERIALS IN Y-Ba-Cu-O SYSTEMS, Hiroshi Kezuka, Tokyo Engineering University, Department of Electronics, Tokyo, Japan; and Tomomi Masaki, Nippon Electronics Engineering College, Tokyo, Japan.

M7.234 $YBa_2Cu_3O_{7-x}$ THIN-FILM dc SQUIDS WITH FOCUSED ION BEAM FABRICATED WEAK-LINKS, B. Dutta, Middlebury College, Physics Department, Middlebury, VT; C.T. Rogers, A. Scherer and T. Venkatesan, Bellcore, Red Bank, NJ; X.D. Wu, Rutgers University, Physics Department, Piscataway, NJ.

M7.235 FABRICATION AND PROPERTIES OF HETERO-EPITAXIAL MULTILAYER STRUCTURES OF METAL-OXIDE SUPERCONDUCTORS, H. Dorsett, A. Inam and X.D. Wu, Rutgers University, Physics Department, Piscataway, NJ; C.T. Rogers and T. Venkatesan, Bellcore, Red Bank, NJ.

M7.236 IONIZING RADIATION EFFECTS ON THIN FILM TEMPERATURE SUPERCONDUCTORS, Steven D. Mittleman, Barry A. Kirby, Alvin J. Drehman, Bruce L. MacDonald, Robert J. Andrews, Michael N. Alexander, Rome Air Development Center, Solid State Sciences Directorate, Hanscom AFB, MA.

M7.237 FABRICATION OF HIGH T_C SUPERCONDUCTING COMPOSITE STRUCTURES, D.T. Shaw, S. Patel, J. Chang, S. Witanachchi, Y.Z. Zhu, L. Song and Y.H. Kao, State University of New York at Buffalo, Institute on Superconductivity, Buffalo, NY.

M7.238 INFLUENCE OF METALLIC SILVER INFILTRATION ON THE MICROSTRUCTURE AND TRANSPORT PROPERTIES OF $YBaCuO$, L. Ryelandt, M. Cassart, A. Vandenbosch, F. Delannay and J-P. Issi, Université Catholique de Louvain, Unité de Physico-Chimie et de Physique des Matériaux, Louvain-la-Neuve, Belgium.

M7.239 HIGH T_C SUPERCONDUCTOR FIBERS FROM METALLO-ORGANIC PRECURSORS, K.C. Chen and K.S. Mazdiyasn, General Atomics, Department of Defense Materials, San Diego, CA.

M7.240 FORMATION OF SPUTTERED Y-BA-CU-O SUPERCONDUCTING THIN FILM ON METAL SUBSTRATE, H. Hayakawa, Y. Iijima, N. Sadakata and O. Kohno, Fujikura Ltd., Tokyo Laboratory, Tokyo, Japan.

M7.241 A MULTIFILAMENT SUPERCONDUCTING WIRE OF Y-Ba-Cu-o, L.R. Motowidlo, G.M. Ozeryansky, IGC, Advanced Superconductors, Inc., Waterbury, CT; R.D. Blaughter, D.W. Hazelton, J.A. Rice, Intermagnetics General Corporation, Guilderland, NY.

M7.242 110K SUPERCONDUCTING FIBERS OF $[Bi,Pb(Sb)]_2 Sr_2Ca_2Cu_3O_{10+x}$, Zhang Jincang, Henan Normal University, Physics Department, Xinxiang, China; He Aisheng, North University of Technology, Physics Department, Beijing, China; Hu Yujing, Xiang Jiong and He Yusheng, Tsinghua University, Beijing, China.

M7.243 COILS OF YBCO TEXTURED BY PARTIAL MELTING, Ningxia Tan, Antony J. Bourdillon, State University of New York at Stony Brook, Department of Materials Science and Engineering, Stony Brook, NY; and N. Savvides, CSIRO, Division of Applied Physics, Sydney, Australia.

M7.244 THERMAL ANNEALING STUDY OF HIGH- T_C $YBaCuO$ AND $BiSrCaCuO$ SUPERCONDUCTING WIRES, Y.D. Yao, Academia Sinica, Institute of Physics, Taipei, Taiwan, China; J.W. Chen, National Taiwan University, Department of Physics, Taipei, Taiwan, China; Y.Y. Chen, W.S. Pern, Academia Sinica, Institute of Physics, Taipei, Taiwan, China; I.N. Lin, P.C. Yao, S.J. Yang and S.E. Hsu, Chung Shan Institute of Science and Technology, Materials Research and Development Center, Lung-Tan, Taiwan, China.

M7.245 STUDIES ON MICROSTRUCTURE - PROPERTY RELATIONSHIP OF $YBa_2Cu_3O_{7-x}$ + Ag COMPOSITE WIRE, S. Samajdar and S.K. Samanta, The University of Michigan, Plasticity Laboratory, Department of Mechanical Engineering and Applied Mechanics, Ann Arbor, MI.

M7.246 MICROWAVE PROPERTIES OF HIGH QUALITY Y-Ba-Cu OXIDE THIN FILMS FROM 1-100 GHz, A. Inam and X.D. Wu, Rutgers University, Physics Department, Piscataway, NJ; L. Nazar and T. Venkatesan, Bellcore, Red Bank, NJ.

M7.247 MICROSTRUCTURE AND FLUX PINNING CHARACTERISTICS OF HIGH-T_c SUPERCONDUCTING TAPE PREPARED BY THE DIRECTIONAL MELT-GROWTH TECHNIQUE, M. Okada, R. Nishiwaki, T. Matsumoto, T. Kamo, K. Aihara and S. Matsuda, Hitachi Ltd., Hitachi Research Laboratory, Ibaraki, Japan; and M. Seido, Hitachi Cable Ltd., Metal Research Laboratory, Ibaraki, Japan.

M7.248 REPRODUCIBLE, LARGE-SCALE PRODUCTION OF THALLIUM-BASED HIGH TEMPERATURE SUPERCONDUCTORS, R.L. Gay, D. Stelman, J.C. Newcomb, J.M. Pechenik and L.F. Grantham, Rockwell International, Rocketdyne Division, Canoga Park, CA.

M7.249 FABRICATION OF Bi₂Sr₂Ca_nCu_{n+1}O_x THIN FILMS BY LASER ABLATION, J. Chang, S. Witanachchi, S. Patel and D.T. Shaw, State University of New York at Buffalo, Institute on Superconductivity, Buffalo, NY.

M7.250 FORMATION OF 2223 PHASE IN Bi(Pb)-Sr-Ca-Cu-O SYSTEM DURING ANNEALING PROCESS, Chen Liqun, Huang Zuwei, Huang Yuzhen, Bi Jianqing, Ni Rongming and Zhao Zhong-xian, Academia Sinica, Institute of Physics, Beijing, China.

M7.251 ROUTES TO HIGH T_c SUPERCONDUCTING Tl-Ba-Ca-Cu-O FILMS USING ORGANOMETALLIC CHEMICAL VAPOR DEPOSITION, Darrin S. Richeson, Lauren M. Tonge, Northwestern University, Department of Chemistry, Evanston, IL; Jing Zhao, Jiming Zhang, Northwestern University, Department of Materials Science and Engineering, Evanston, IL; Henry O. Marcy, Northwestern University, Department of Electrical Engineering and Computer Science, Evanston, IL; Tobin J. Marks, Northwestern University, Department of Chemistry, Evanston, IL; Bruce W. Wessels, Northwestern University, Materials Science and Engineering Department, Evanston, IL; and Carl R. Kannevurf, Northwestern University, Science and Technology Center for Superconductivity and the Materials Research Center, Department of Electrical Engineering and Computer Science, Evanston, IL.

M7.252 EFFECT OF PROCESSING PARAMETERS AND POSTPROCESSING THERMAL CYCLING ON THE SUPERCONDUCTING PROPERTIES OF Ag/YBa₂Cu₃O_{7-x} WIRES, Miguel A. Ocampo, Emilio Orgaz, Centro de Investigación y Desarrollo COMDUMEX, México, México; and Tatsuo Akachi, Instituto de Investigaciones en Materiales, UNAM, México, México.

M7.253 THE ROLE OF STRUCTURAL DEFECTS IN FLUX PINNING AND HIGH J_c IN THIN FILM Y-Ba-Cu-O SUPERCONDUCTORS, R. Ramesh, D. M. Hwang, A. Inam, P. England and T. Venkatesan, Bellcore, Red Bank, NJ.

M7.254 ELECTRON MICROSCOPY OF (Bi,Pb)-Sr-Ca-Cu-O WIRES WITH VARYING SINTER TIME, Y. Feng, R.E. Smallman, I.P. Jones, F. Wellhofer, University of Birmingham, Superconductivity Research Group and School of Metallurgy and Materials, Birmingham, United Kingdom; N. McN. Alford, and T.W. Button, ICI Advanced Materials, Cheshire, United Kingdom.

M7.255 FIELD AND TEMPERATURE-DEPENDENT SUSPENSION STUDIES OF HIGH TEMPERATURE SUPERCONDUCTORS, S.A. Solin, Michigan State University, East Lansing, MI and NEC Research Institute, Princeton, NJ; and Y. Huang, Michigan State University, East Lansing, MI.

M7.256 X-RAY DIFFRACTION STUDY OF THE CRYSTALLIZATION PROCESS OF HIGH T_c SUPERCONDUCTING Bi-GLASS CERAMICS, Winnie Wong-Ng, Chwan K. Chiang, Stephen W. Freiman and Lawrence P. Cook, National Institute of Standards and Technology, Gaithersburg, MD.

M7.257 ON THE IMPROVEMENT OF DyBa₂Cu₃O_{7-δ} PROPERTIES THROUGH BETTER SINTERING, J.M. Seuntjens and D.C. Larbalestier, University of Wisconsin, Applied Superconductivity Center and Department of Material Science and Engineering, Madison, WI.

M7.258 SOME OBSERVATIONS OF THE EFFECTS OF HIGH PRESSURES AND TEMPERATURES ON THE STABILITY OF Y Ba₂Cu₃O_{7-x}, R.K. Williams, K.B. Alexander, J. Brynstad, T.J. Henson, D.M. Kroeger, G.C. Marsh and J.O. Scarbrough, Oak Ridge National Laboratory, Oak Ridge, TN.

SESSION M8: DISSIPATION

Chairs: R. Koch and W. Skoepol
Thursday Morning, November 30
Salon G (M)

SYMPOSIUM M presentations
may be viewed simultaneously
in the America Ballroom Lobby
Westin Hotel.

8:00 *M8.1

CONSIDERATIONS LIMITING CRITICAL CURRENTS IN HIGH TEMPERATURE SUPERCONDUCTORS, M. Tinkham, Harvard University, Department of Physics, Cambridge, MA.

8:30 **M8.2**
FLUX MOTION AND DISSIPATION IN CUPRATE
SUPERCONDUCTORS, B. Batlogg, T.T.M. Palstra
and L.F. Schneemeyer, AT&T Bell Laborator-
ies, Murray Hill, NJ.

9:00 **M8.3**
HYSTERETIC DEPENDENCE OF CRITICAL CURRENT ON
APPLIED MAGNETIC FIELD AND MAGNETIC IRREVER-
SIBILITY LINE CROSSINGS IN POLYCRYSTALLINE
 $\text{YBa}_2\text{Cu}_3\text{O}_7$, Thomas R. Askew and Richard B.
Flippen, E. I. duPont de Nemours & Co.,
Inc., Central Research and Development
Department, Wilmington, DE.

9:15 **M8.4**
DISSIPATIVE EFFECTS OF VORTEX MOVEMENTS IN
 $\text{YBa}_2\text{Cu}_3\text{O}_7$ MEASURED BY MAGNETOTHERMAL EF-
FECTS, Izio Rosenman and Charles Simon,
Université Paris 7, Groupe de Physique des
Solides, Paris, France; Gaston Collin,
Université Paris - Sud, Laboratoire de
Physique des Solides, Orsay, France.

9:30 ***M8.5**
CRITICAL CURRENTS IN THIN FILMS AND SINGLE
CRYSTALS OF HIGH TEMPERATURE SUPERCONDUCT-
TORS, P.H. Kes, Leiden University, Kamer-
lingh Onnes Laboratory, Leiden, The Nether-
lands.

10:00 BREAK

10:15 ***M8.6**
ON THE RESISTIVE STATE OF HIGH TEMPERATURE
SUPERCONDUCTORS IN MAGNETIC FIELD, Yasuhiro
Iye, The University of Tokyo, The Institute
for Solid State Physics, Tokyo, Japan.

10:45 **M8.7**
ELECTRICAL TRANSPORT DISSIPATION EFFECTS IN
EPITAXIAL $\text{Y}_{1-x}\text{Ba}_x\text{Cu}_3\text{O}_{7-x}$ THIN FILMS, D.K.
Christen, C.E. Klabunde, Oak Ridge National
Laboratory, Oak Ridge, TN; J.R. Thompson,
Oak Ridge National Laboratory, Oak Ridge, TN
and University of Tennessee, Knoxville, TN;
H.R. Kerchner, S.T. Sekula, R. Feenstra and
J.D. Budai, Oak Ridge National Laboratory,
Oak Ridge, TN.

11:00 **M8.8**
LOW FIELD RESISTIVE BEHAVIOR OF $\text{Bi}_2\text{Sr}_2\text{CaCu}_2\text{-}$
 O_8 , R.B. Van Dover, L.F. Schneemeyer and
J.V. Waszczak, AT&T Bell Laboratories,
Murray Hill, NJ.

11:15 **M8.9**
MAGNETIC RELAXATION IN $\text{Bi}_2\text{Sr}_2\text{CaCu}_2\text{O}_{8+x}$
SINGLE CRYSTALS, E. Agostinelli, P. Filaci,
D. Fiorani, A.M. Testa, C.N.R., I.T.S.E.,
Rome, Italy; G. Balestrino, Università di
Salerno, Dip. di Fisica, Salerno, Italy; P.
Paroli, II Università di Roma, Dip.
d'Ingegneria Meccanica, Rome, Italy; J.
Tejada, Dep. de Fisica Fonamental, Bar-
celona, Spain.

SESSION M9: THIN FILM CHARACTERIZATION AND COMPOSITE MATERIALS

Chairs: K. N. Tu and A. Dasgupta
Thursday Afternoon, November 30
Salon G (M)

SYMPOSIUM M presentations
may be viewed simultaneously
in the America Ballroom Lobby
Westin Hotel.

1:30 ***M9.1**
ATOMIC SCALE CHARACTERIZATION OF DEFECTS AND
INTERFACES BY Z-CONTRAST STEM, S.J.
Pennycook, M.F. Chisholm, D.E. Jesson, R.
Feenstra, D. Mashburn, D.P. Norton, J.W.
McCamy and D.H. Lowndes, Oak Ridge National
Laboratory, Oak Ridge, TN.

2:00 **M9.2**
CHARACTERIZATION OF SUPERCONDUCTING
 $\text{YBaCu}(\text{F})\text{O}$ THIN FILMS WITH THREE DIFFERENT
ORIENTATIONS, X.K. Wang, D.X. Li, D.Q. Li,
Y.H. Shen, J.Q. Zheng, R.P.H. Chang and J.B.
Ketterson, Northwestern University, Mate-
rials Research Center and Science and Tech-
nology Center for Superconductivity, Evans-
ton, IL.

2:15 **M9.3**
DIRECT OBSERVATION BY TRANSMISSION ELECTRON
MICROSCOPY OF THE EARLY STAGES OF GROWTH OF
SUPERCONDUCTING THIN FILMS, M. Grant Norton,
Lisa A. Tietz, Scott R. Summerfelt and C.
Barry Carter, Cornell University, Department
of Materials Science and Engineering, Itha-
ca, NY.

2:30 **M9.4**
CHARACTERIZATION OF CROSS-SECTIONS OF
 TlBaCaCuO THIN FILMS ON MgO SUBSTRATES BY
ANALYTICAL AND HIGH RESOLUTION ELECTRON
MICROSCOPY, J. Mayer, M. Lanham, University
of California, Materials Department, Santa
Barbara, CA; T.W. James, Superconductor
Technologies, Inc., Santa Barbara, CA; A.G.
Evans, University of California, Materials
Department, Santa Barbara, CA; M. Rühle,
Max-Planck-Institut für Metallforschung,
Stuttgart, West Germany.

2:45 **M9.5**
GRAIN BOUNDARY MODELLING AND CORRELATIONS
WITH CRITICAL CURRENT DEFECTS IN HIGH-Tc
SUPERCONDUCTORS, K. Jagannadham and J.
Narayan, North Carolina State University,
Department of Materials Science and En-
gineering, Raleigh, NC.

3:00 LATE NEWS

3:30 BREAK

3:45 ***M9.6**
THE PREPARATION OF $\text{Bi}_2\text{Sr}_2\text{CaCu}_2\text{O}_8$ FIBERS BY THE FLOAT ZONE PROCESS, Linda Moulton, Joseph Brenner, Stanford University, Material Science Department, Stanford, CA; Perla Peszkin, Robert S. Feigelson, Stanford University, Center for Materials Research, Stanford, CA; and Dan Gazit, Nuclear Research Center Negev, Beer Sheva, Israel.

4:15 **M9.7**
110K Bi-Ca-Sr-Cu-O SUPERCONDUCTING FIBERS BY GLASS-TO-CERAMIC PROCESS, Haixing Zheng, Yi Hu, Yun-Seung Choi, Ren Xu, Patrick Lin and J.D. Mackenzie, University of California-Los Angeles, Department of Materials Science and Engineering, Los Angeles, CA.

4:30 **M9.8**
DEVELOPMENT OF A COMPOSITE TAPE CONDUCTOR OF Y-Ba-Cu-O, R.D. Blaugher, D.W. Hazelton, J.A. Rice, Intermagnetics General Corporation, HiT Superconducting Materials, Guilderland, NY.

4:45 **M9.9**
PREPARATION OF HIGH T_c OXIDE SUPERCONDUCTING TAPE BY RF MAGNETRON SPUTTERING, M. Fukutomi, Y. Tanaka, T. Asano, H. Maeda, National Research Institute for Metals, Tsukuba Laboratories, Ibaraki, Japan; H. Takahara, Mitsui Mining and Smelting Company Ltd., Central Research Laboratory, Saitama, Japan.

5:00 **M9.10**
PROCESSING AND PERFORMANCE OF METAL-CERAMIC FIBER REINFORCED HIGH TEMPERATURE SUPERCONDUCTOR, S. Salib, C. Vipulanandan, and T. Stone, University of Houston, Texas Center for Superconductivity, Houston, TX.

5:15 **M9.11**
PREPARATION OF HIGH T_c Bi-Pb-Sr-Ca-Cu-O SUPERCONDUCTING FIBER BY LASER HEATED PEDESTAL GROWTH METHOD, K. Tomomatsu, A. Kume and H. Tominaga, Fujikura Ltd., Tokyo Laboratory, Tokyo, Japan.

SESSION M10: THIN FILMS: Bi AND Tl COMPOUNDS

Chairs: D. Gubser and C. C. Koch
Friday Morning, December 1
Salon G (M)

SYMPOSIUM M presentations
may be viewed simultaneously
in the America Ballroom Lobby
Westin Hotel.

8:00 ***M10.1**
THIN FILM PROCESSING FOR HIGH- T_c SUPERCONDUCTORS OF Bi-SYSTEM, Kiyotaka Wasa, Matsushita Electric Co., Ltd., Central Research Laboratories, Osaka, Japan.

8:30 ***M10.2**
PROCESSING AND PROPERTIES OF Bi-Sr-Ca-Cu-Oxide SUPERCONDUCTING THIN FILMS, D.A. Rudman, Massachusetts Institute of Technology, Department of Materials Science and Engineering, Cambridge, MA; J.T. Kucera, Massachusetts Institute of Technology, Department of Physics, Cambridge, MA; M.M. Matthiesen, Massachusetts Institute of Technology, Department of Materials Science and Engineering, Cambridge, MA; D.G. Steel, Massachusetts Institute of Technology, Department of Physics, Cambridge, MA; L.M. Rubin, Massachusetts Institute of Technology, Department of Materials Science and Engineering, Cambridge, MA; D.W. Face, Massachusetts Institute of Technology, Center for Material Science and Engineering, Cambridge, MA; J.M. Graybeal, Massachusetts Institute of Technology, Department of Physics, Cambridge, MA; T.P. Orlando, Massachusetts Institute of Technology, Department of Electrical Engineering and Computer Science, Cambridge, MA.

9:00 **M10.3**
HIGH- T_c UNDOPED AND PB-DOPED BI-SR-CA-CU-O THIN FILMS PREPARED BY ORGANOMETALLIC CHEMICAL VAPOR DEPOSITION, J.M. Zhang, H.O. Marcy, L.M. Tonge, B.W. Wessels, T.J. Marks and C.R. Kannewurf, Northwestern University, Center for High Temperature Superconductivity and Materials Research Center, Materials Science and Engineering, Evanston, IL.

9:15 **M10.4**
PREPARATION OF Bi-Sr-Ca-Cu-O SUPERCONDUCTING THIN FILMS BY MOCVD, Shinji Gohda and Yasuhiro Maeda, Hoxan Corporation, Hoxan Research Laboratories, Sapporo, Japan.

9:30 **M10.5**
THE SYNTHESIS OF THE HIGH- T_c PHASE OF Bi-Pb-Ca-Sr-Cu-O THIN FILM BY SINGLE TARGET MAGNETRON SPUTTERING, R.L. Meng, Li Gao, P.H. Hor, Y.Y. Sun, Y.Q. Wang and C.W. Chu, University of Houston, Texas Center for Superconductivity, Houston, TX.

9:45 **M10.6**
MOLECULAR BEAM EPITAXY OF LAYERED Bi-Sr-Ca-Cu-O COMPOUNDS, D.G. Schlom, Stanford University, Department of Electrical Engineering, Stanford, CA; J.T. Sizemore, Stanford University, Department of Materials Science, Stanford, CA; A.F. Marshall, Stanford University, Center for Materials Research, Stanford, CA; Z.J. Chen, J.S. Harris Jr., Stanford University, Department of Electrical Engineering, Stanford, CA; J.C. Bravman, Stanford University, Department of Materials Science, Stanford, CA; M.R. Beasley, T.H. Geballe, Stanford University, Department of Applied Physics, Stanford, CA; J.N. Eckstein, I. Bozovic, K.E. von Dessenneck, Varian Research Center, Palo Alto, CA.

10:00 BREAK

10:15 ***M10.7**

APPLICATIONS OF RAPID THERMAL PROCESSING (RTP) TO HIGH TEMPERATURE SUPERCONDUCTORS, D.S. Ginley, J.F. Kwak, E.L. Venturini, R.J. Baughman and B. Morosin, Sandia National Laboratories, Organization 1144, Albuquerque, NM; J.W. Halloran and M.J. Neal, CPS Superconductor, Inc., Milford, MA.

10:45 **M10.8**

A NEW HYBRID PVD/OMCVD ROUTE TO HIGH- T_c SUPERCONDUCTING THIN FILMS OF Tl-Ba-Ca-Cu-O, D.S. Richeson, L.M. Tonge, Northwestern University, Department of Chemistry, Evanston, IL; X.K. Wang, Northwestern University, Materials Science and Engineering Department, Evanston, IL; H.O. Marcy, Northwestern University, Electrical Engineering and Computer Science Department, Evanston, IL; T.J. Marks, Northwestern University, Chemistry Department, Evanston, IL; R.P.H. Chang, Northwestern University, Materials Science and Engineering Department, Evanston, IL; J.B. Ketterson, Northwestern University, Department of Physics and Astronomy; and C.R. Kannewurf, Northwestern University, Science and Technology Center for Superconductivity and the Materials Research Center, Chemistry Department, Evanston, IL.

11:00 **M10.9**

THE EFFECT OF ANNEALING CONDITIONS ON MAGNETRON SPUTTERED SUPERCONDUCTING TL-BASED THIN FILMS, S.H. Liou, University of Nebraska-Lincoln, Department of Physics, Lincoln, NE.

11:15 **M10.10**

ATOMIC RESOLUTION ELECTRON MICROSCOPY OF BICUPRATES, R. Ramesh, B.G. Bagley and J.M. Tarascon, Bellcore, Red Bank, NJ; C.J.D. Hetherington, B. Simion and G. Thomas, National Center for Electron Microscopy, Materials and Chemical Sciences Division, Berkeley, CA.

11:30 **M10.11**

STUDY ON THE ELEMENTARY STEPS OF THE EPITAXIAL GROWTH OF Bi-Sr-Ca-Cu-O ON THE SURFACE OF Si AND MgO BY MEANS OF RHEED AND PHOTO-ELECTRON SPECTROSCOPIES, Takashi Hanada, Maki Kawai, Tokyo Institute of Technology, RLEM, Yokohama, Japan; Tsutomu Goda, and Shousuke Teratani, Tokyo Gakugei University, Tokyo, Japan.

11:45 **M10.12**

TEM STUDY OF CVD-GROWN Bi-Sr-Ca-Cu-O THIN FILMS ON (001) MgO SUBSTRATES, O. Ueda, T. Kimura, H. Yamawaki, M. Ihara and M. Ozeki, Fujitsu Laboratories Ltd., Atsugi, Japan.

SESSION M11: THIN FILMS: PROPERTIES AND DEVICES

Chairs: D. M. Kroeger and M. Suenaga
Friday Afternoon, December 1
Salon G (M)

SYMPOSIUM M presentations
may be viewed simultaneously
in the America Ballroom Lobby
Westin Hotel.

1:00 ***M11.1**

PROXIMITY-EFFECT AND TUNNELING IN $\text{YBa}_2\text{Cu}_3\text{O}_{7-x}$ /METAL LAYERED STRUCTURES, L.H. Greene, W.L. Feldmann, J.B. Barner, L.A. Farrow, P.F. Miceli, R. Ramesh, B.J. Wilkens, B.G. Bagley, Bellcore, Red Bank, NJ; M. Giroud, CRTBT-CNRS, Grenoble, France; and J.M. Rowell, Conductus, Sunnyvale, CA.

1:30 **M11.2**

MAGNETIC FLUX PINNING IN $\text{YBa}_2\text{Cu}_3\text{O}_x$ FILMS, H.R. Kerchner, R. Feenstra, Oak Ridge National Laboratory, Solid State Division, Oak Ridge, TN; J.O. Thomson, J.R. Thompson, Oak Ridge National Laboratory, Solid State Division, Oak Ridge, TN and University of Tennessee, Knoxville, TN; D.K. Christen, S.T. Sekula and L.A. Boatner, Oak Ridge National Laboratory, Solid State Division, Oak Ridge, TN.

1:45 **M11.3**

CRITICAL CURRENT DENSITY AND MICROSTRUCTURE OF $\text{YBa}_2\text{Cu}_3\text{O}_{7-x}$ THIN FILMS AS A FUNCTION OF FILM THICKNESS, A. Mogro-Campero, L.G. Turner, E.L. Hall and N. Lewis, GE Research and Development Center, Schenectady, NY.

2:00 **M11.4**

MICROSTRUCTURE AND PROPERTIES OF MIXED $\text{YBa}_2\text{Cu}_3\text{O}_{7-x}$ AND $\text{Y}_2\text{Ba}_4\text{Cu}_8\text{O}_{16}$ THIN FILMS, A.F. Marshall, A. Kapitulnik, Stanford University, Stanford, CA; K. Char, R.W. Barton, Conductus, Inc., Sunnyvale, CA; and S.S. Laderman, Hewlett-Packard Company, Palo Alto, CA.

2:15 **M11.5**

A STUDY OF GRAIN BOUNDARIES IN HIGH T_c SUPERCONDUCTING $\text{YBa}_2\text{Cu}_3\text{O}_{7-x}$ THIN FILMS USING HIGH RESOLUTION ANALYTICAL STEM, D.H. Shin, J. Silcox, S. Russek, D. Lathrop and R.A. Buhrman, Cornell University, Department of Applied Physics, Ithaca, NY.

2:30 ***M11.6**

EXPITAXIAL GROWTH OF HIGH T_c THIN FILMS AND SUPERLATTICES PROGRESS TOWARDS THE ARTIFICIAL CONSTRUCTION OF HIGH T_c SUPERCONDUCTORS, Jean-Marc Triscone, Michael G. Karkut, Olivier Brunner, Louis Antognazza and Øystein Fischer, Université de Genève, DPMC, Genève, Switzerland.

3:00 BREAK

3:15 *M11.7

FABRICATION AND EVALUATION OF DEVICE STRUCTURES ON THIN FILMS OF YBCO, P. Mankiewicz, Boston University, Boston, MA.

3:45 M11.8

TUNNELLING MEASUREMENTS ON THIN FILMS OF $\text{YBa}_2\text{Cu}_3\text{O}_{7-\delta}$, A.M. Cucolo, J.M. Valles, J.M. Phillips, M. Gurvitch, R.C. Dynes and J.P. Garno, AT&T Bell Laboratories, Murray Hill, NJ.

4:00 M11.9

USE OF Si-YBaCuO INTERMIXED SYSTEM FOR PATTERNING OF SUPERCONDUCTING THIN FILMS, Q.Y. Ma, E.S. Yang, G.V. Treyz, C. Shu and R.M. Osgood Jr., Columbia University, Microelectronics Sciences Laboratories and Center for Telecommunication Research, New York, NY; Chin-An Chang, IBM T.J. Watson Research Center, Yorktown Heights, NY.

4:15 M11.10

HIGH SPEED INFRARED DETECTORS USING Y-Ba-Cu-O THIN FILMS, J.P. Zheng, Q.Y. Ying and H.S. Kwok, State University of New York at Buffalo, Institute on Superconductivity, Buffalo, NY.

4:30 M11.11

JOSEPHSON WEAK-LINKS FABRICATED FROM HETERO-EPITAXIAL $\text{YBa}_2\text{Cu}_3\text{O}_{7-x}/\text{PrBa}_2\text{Cu}_3\text{O}_{7-x}/\text{YBa}_2\text{Cu}_3\text{O}_{7-x}$ MULTILAYERS, C.T. Rogers and T. Venkatesan, Bellcore, Red Bank, NJ; A. Inam, Rutgers University, Physics Department, Piscataway, NJ.

4:45 M11.12

HIGH T_c SUPERCONDUCTOR MULTILEVEL STRUCTURES FORMED WITH Ta_2O_3 SPACER LAYERS, Rabi S. Bhattacharya, Universal Energy Systems, Inc., Dayton, OH; Peter B. Kosel, University of Cincinnati, Department of Electrical Engineering, Cincinnati, OH; and T. Peterson, Wright Patterson Air Force Base, WRDC/MLPO, Dayton, OH.

M1.1

MYTH AND REALITY IN HIGH T_c . Philip W. Anderson, Dept. of Physics, Princeton University, Princeton, N.J. 08544

I will discuss constraints on theoretical models mandated by the experimental facts on high T_c . The resistivity anisotropy and the magnitude of the Drude conductivity reject the hypothesis that the normal state is a Fermi liquid; the heuristics of transition temperatures require a 3-dimensional, interlayer mechanism for T_c ; and many different types of data—photoemission, NMR, the high T_c itself—suggest that some very low energy, unconventional excitations are present. Some new theoretical speculations will also be discussed.

M1.2

SOME THEORIES OF HIGH TEMPERATURE SUPERCONDUCTIVITY. Marvin L. Cohen, Department of Physics, University of California and Materials and Chemical Sciences Division, Lawrence Berkeley Laboratory, Berkeley, CA.

A brief review of some historical aspects of theoretical research on superconductivity and of some features of BCS theory will be given followed by a discussion of pairing mechanisms.

For phonon induced pairing, there are limitations on the transition temperature T_c arising from possible lattice instabilities. For specific materials measured properties such as the isotope effect put limits on T_c and on the possible role of phonons as a pairing Boson. Some of these conditions change when anharmonicity, defects, or lower dimensionality are considered.

A proposal will be presented for observing $T_c \geq 200$ K in metallic hydrogen based on a phonon pairing mechanism.

A discussion of electronic pairing mechanisms such as plasmons, excitons and demons and magnetic or spin induced pairing will be given. The role of weak or strong coupling and other properties will be discussed in an effort to suggest possible experimental probes to find the dominant pairing mechanism.

Some general comments will be made about the oxide systems and the use of theory to calculate T_c 's for those materials.

Work supported by NSF Grant DMR88-18404 and DOE Contract No. DE-AC03-76SF00098.

M1.3

RENORMALIZATION FROM DENSITY FUNCTIONAL THEORY TO STRONG COUPLING MODELS FOR THE ELECTRONIC STRUCTURE OF La_2CuO_4 . Mark S. Hybertsen and Michael Schluter, AT&T Bell Laboratories, Murray Hill, NJ. 07974; E.B. Stechel and D.R. Jennison, Sandia National Laboratories, Albuquerque, NM, 87185.

Starting from a realistic quantum-chemical description of the Cu-O based superconductors, strong coupling models are derived. The Local Density Functional approach, which has been shown to accurately describe the cohesive properties of these materials e.g. La_2CuO_4 , is the starting point. These results are mapped onto a multiband Hubbard model providing a complete set of numerical parameters which represent the specific features of the Cu-O planes. The properties of the model are in good agreement with experiments probing high (1-10 eV) energies. A second step of mapping is carried out with exact diagonalization studies of finite clusters within the Hubbard model in order to study effective one-band models which describe the low energy (≤ 1 eV) properties. The insulating phase is well described by a Heisenberg model and the value derived for the exchange coupling is in excellent agreement with experiment. The spectra for added carriers are well described by effective one band models. Specific values for the parameters are obtained which have implications for possible descriptions of the superconducting state.

M1.4 ABSTRACT NOT AVAILABLE

M1.5

ELECTRONIC STRUCTURE OF $\text{La}_{2-x}\text{Sr}_x\text{Ni}_2\text{O}_4$ SUPERCONDUCTING MATERIALS. Yuejin Guo and William A. Goddard III, Arthur Amos Noyes Laboratory of Chemical Physics, California Institute of Technology, Pasadena, California 91125.

We have examined $\text{La}_{2-x}\text{Sr}_x\text{Ni}_2\text{O}_4$ systems to determine whether they might be high temperature superconductors. Using ab initio electronic methods (generalized valence bond and configuration interaction) for various clusters representing the $\text{La}_2\text{Ni}_2\text{O}_4$ and $\text{La}_{1.8}\text{Sr}_{0.2}\text{Ni}_2\text{O}_4$ nickel oxide superconducting materials, we find that (1) in the parent compound, $\text{La}_2\text{Ni}_2\text{O}_4$, the O(2p) levels are filled, leading to two unpaired spins on each Ni (Ni^{II} (d^8) oxidation state). The Ni spins are coupled antiferromagnetically to the spins of adjacent Ni^{II} sites.

(2) oxidation beyond the nickelous (Ni^{II}) state leads not to Ni^{III} d^7 but rather to oxidized oxygen atoms (denoted O^+) with a highly mobile $\text{O}2p\pi$ hole bridging two Ni^{II} sites, $\text{Ni}^{II} - \text{O}^+ - \text{Ni}^{II}$. (3) the $\text{O}2p\pi$ hole at these oxidized sites ($\text{Ni}^{II} - \text{O}^+ - \text{Ni}^{II}$) is ferromagnetically coupled to the adjacent Ni^{II} d electrons despite the fact that this is opposed by the direct dd exchange. This coupling induces an attractive interaction between conduction electrons that is responsible for the superconductivity.

Therefore, we find interactions comparable with the magnon pairing mechanism of superconductivity proposed by us for the Cu (214) and (123) materials. The calculations suggest that the Ni 214 system can have a higher T_c than the Cu 214 system.

M1.6 ABSTRACT NOT AVAILABLE

M1.7

EVIDENCE OF KOSTERLITZ-THOULESS TRANSITION AND FLUCTUATIONS IN HIGH TEMPERATURE SUPERCONDUCTING THIN FILMS. Q.Y. Ying and H.S. Kwok, Institute on Superconductivity, State University of New York at Buffalo, Bonner Hall, Buffalo, NY 14260

In the last decade, there has been considerable effort to investigate both theoretically and experimentally the Kosterlitz-Thouless properties in superconductors. There have also been studies of K-T transition on granular thin high T_c superconducting films. In here, we report some experimental evidence of K-T transition in Y-Ba-Cu-O thin superconducting films.

The films were deposited by laser evaporation method. The R-T relation was measured. In the vicinity of transition temperature T_c which was below the mean-field transition temperature T_{c0} , the resistance dropped exponentially with the inverse square root of the reduced temperature when the sample was cooled down. A stronger evidence was the power law dependence of the voltage-current relationship. It was found that the exponent decreased from near 10 far below T_c to 3 at T_c , and suddenly dropped to 1 above T_c . This corresponded to the unbinding of vortex-antivortex pairs to form a vortex plasma near T_c .

Broadening of the transition at high temperature was also observed. The R-T relation in this region showed fluctuations of superconducting carrier nucleation.

M1.8

PHONON ANOMALY ACROSS T_c IN $\text{Y}(\text{Er})\text{Ba}_2\text{Cu}_3\text{O}_{7-\delta}$. R. P. Sharma, L. E. Rehn, P. M. Baldo, and J. Z. Liu, Argonne National Laboratory, Argonne, IL 60439

Ion channeling in single crystals of $Y(Er)Ba_2Cu_3O_{7.8}$ provides a direct method to investigate atomic vibrations. Angular channeling scans with 1.5 MeV He across the [001] direction as a function of temperature (300 \rightarrow 40 K) revealed an abrupt decrease in Cu-O vibrational amplitudes of $\sim 30\%$ across the superconducting transition temperature ($T_c \sim 92$ K). When the oxygen content in the sample was reduced to O_6 , the specimen became nonsuperconducting, and the above anomalous change disappeared. In $ErBa_2Cu_3O_{7.8}$, the two major [001] rows of Cu-O and Er-Ba followed a different temperature dependence. A normal Debye-type behavior was found for the Er-Ba vibrational amplitudes (u_1), but a substantially stronger than normal temperature dependence was observed for the Cu-O rows, i.e. an $\sim 80\%$ decrease in u_1 between 300 \rightarrow 100 K. A channeling measurement with $CuK\alpha$ X-rays using 6.55 MeV He confirmed the anomalous vibrational behavior of Cu-atoms in the Cu-O rows in $YBa_2Cu_3O_{7.8}$. Similar angular scans using resonance elastic scattering from oxygen provided additional confirmation. The observed anomaly can be explained on the basis of strong correlated atomic motion in the [001] Cu-O rows in the superconducting state.

*Work supported by the U.S. Department of Energy, Basic Energy Sciences-Materials Sciences under Contract #W-31-109-ENG-38.

M1.9

REPRODUCIBLE TUNNELING DATA ON CHEMICALLY ETCHED SINGLE CRYSTALS OF $YBa_2Cu_3O_7$ J. M. Valles, Jr., M. Gurrvitch, A. M. Cucolo, R. C. Dynes, J. P. Garno, L. F. Schneemeyer, J. V. Waszczak AT&T Bell Laboratories, Murray Hill, NJ 07974

We have fabricated tunnel junctions between chemically etched single crystals of $YBa_2Cu_3O_7$ (YBCO) and evaporated metal counterelectrodes which exhibit reproducible characteristics. Above the bulk critical temperature YBCO, T_c , the conductance $G(V)$, has a linear dependence with voltage and has some asymmetry. Below T_c , additional structure associated with the superconductivity appears in $G(V)$. At $T \ll T_c$ there is a reproducible finite zero bias conductance which suggests that there are states at the Fermi energy in superconducting YBCO. Junctions with Pb, Sn, Bi, Sb, PbBi, and Au counterelectrodes all show qualitatively similar behavior.

M1.10

HIGH QUALITY SINGLE CRYSTALS OF $YBa_2Cu_3O_7$ WITH SUPERIOR MICROWAVE PROPERTIES* Dong Ho Wu, W. Kennedy and S.Sridhar, Physics Department, Northeastern University, Boston, MA 02115.

We have fabricated¹ high quality single crystals of $YBa_2Cu_3O_7$, which display extremely sharp microwave (10 GHz) transitions. A variety of electrodynamic measurements have been performed on these crystals: radio frequency penetration depth λ and its temperature and field dependence, lower critical field H_{c1} and microwave surface resistance R_s . The temperature dependence and anisotropy of these parameters was measured between 4.2K and T_c .

The best crystals possess low $\lambda_{ab}(0) = 1400$ Å and $R_s \ll 400$ $\mu\Omega$, and $H_{c1\perp}(0) = 250$ G. The temperature dependence of these quantities is also in good agreement² with BCS calculations. In contrast, in poor quality crystals, λ and R_s can be orders of magnitude higher, and H_{c1} much lower ($\sim 5-20$ G). In poor crystals and also polycrystals, the electrodynamic can be understood^{1,3} in terms of Josephson junctions of size $\sim 2-4 \mu m^2$.

* Supported by NSF-ECS-88-11254

1. Dong Ho Wu, W.Kennedy, C.Zahopoulos and S.Sridhar, Appl. Phys. Lett., (to appear, Aug. 1989)
2. S.Sridhar, Dong Ho Wu and W.Kennedy, (to be published).
3. Dong Ho Wu, C.A. Shiffman and S.Sridhar, Phys. Rev. B, **38**, 9311 (1988)

M2.1

CRYSTAL CHEMISTRY OF OXIDE SUPERCONDUCTORS.
Arthur W. Sleight, Oregon State University, Corvallis, OR.

Structure-property relationships for oxide superconductors and related materials will be discussed using the latest available data. In this regard, important deviations from ideal structure and composition will be considered. Both point defects and extended defects can strongly influence properties. The absence of thermodynamic stability for the high T_c superconductors will also be discussed. Those superconductors with the highest T_c seem to be examples of entropy stabilized phases which can only exist as defect ridden materials.

M2.2

SUPERCONDUCTIVITY IN BISMUTH-LEAD-ANTIMONY BASED PEROVSKITES. R. J. Cava, B. Batlogg, J. J. Krajewski, W. F. Peck, Jr., L. W. Rupp, Jr., AT&T Bell Laboratories, 600 Mountain Avenue, Murray Hill, New Jersey, 07974.

Superconducting $BaPb_{0.75}Bi_{0.25}O_3$, with a T_c of 12K is now widely viewed as the precursor to the recent explosive appearance of copper-oxide superconductors with record high T_c 's. The observation of superconductivity near 30K in $Ba_{0.8}K_{0.2}BiO_3$ has led to a debate on the pairing mechanism in this class of materials which is far from settled. We have recently reported the occurrence of superconductivity at 3.5K in $BaPb_{0.75}Sb_{0.25}O_3$. Comparison of these three materials is of considerable interest to us and we will present our most recent results.

The Sb-O bond might generally be considered to be more ionic than the Bi-O bond, but in the $Ba(Pb,Bi)O_3$ and $Ba(Pb,Sb)O_3$ perovskites the covalency of the bonds might be similar. The variation of lattice parameters in the $Ba(Pb,Sb)O_3$ solid solution obeys the same principle that is observed in $Ba(Pb,Bi)O_3$. In both cases the implied average Bi-O or Sb-O bond length is what would be expected on accommodation of these atoms into $BaPbO_3$ in a mixed valence state. We will present recent results aimed at clarification of the bonding - charge disproportionation issues in these materials.

M2.3

$PrBa_2Cu_3O_7$ AND $CmBa_2Cu_3O_7$: THE ABSENCE OF SUPERCONDUCTIVITY IN $YBa_2Cu_3O_7$ -RELATED COMPOUNDS. L. Soderholm, G.L. Goodman, U. Welp and C.-K. Loong. Argonne National Laboratory, Argonne, IL 60439.

$PrBa_2Cu_3O_7$ is the only member of the $Y123O_7$ -series which is orthorhombic, but not superconducting. The absence of superconductivity in the Pr-compound has been attributed to the ease with which Pr^{3+} can be oxidized. However, magnetic inelastic neutron scattering provides evidence that this anomalous behaviour is the result of strong interactions between the Pr f-electrons and electrons of the CuO planes. Curium has chemical properties similar to Pr, but a different f-electron radial distribution. Therefore we suspected that $Cm123O_7$ should form, and that it should be superconducting. Indeed, we have successfully synthesized $^{248}Cm123O_7$, but it does not superconduct. $X\alpha$ Discrete Variational cluster calculations reveal that the Pr 4f-wavefunctions strongly hybridize with those of

the CuO planes and that this type of hybridization is even stronger for Cm123O_7 . We conclude that in both Pr123O_7 and Cm123O_7 it is magnetic pair breaking that suppresses superconductivity.

This work is supported by DOE-BES under contract No. W-31-109-ENG-38.

M2.4

THE EFFECTS OF OXYGEN AND STRONTIUM VACANCIES ON THE SUPERCONDUCTIVITY OF SINGLE CRYSTALS OF $\text{Bi}_2\text{Sr}_{2-x}\text{CuO}_{6-y}$. B. C. Sales, B. C. Chakoumakos and Edward Soder, Solid State Division, Oak Ridge National Laboratory*, Oak Ridge TN 37831-6056.

Singles crystals of $\text{Bi}_2\text{Sr}_{2-x}\text{CuO}_{6-y}$ were grown from CuO-rich melts. The Sr content of the crystals was varied from $x=0.1$ to $x=0.5$ by adjusting the starting composition of the melt and the oxygen content was reversibly adjusted between $y=0$ and $y=0.5$ by an appropriate heat treatment of the crystals in a thermogravimetric system. With decreasing Sr content the superconducting transition temperature, T_c , of the crystals decreased rapidly from 9 K to below 4.2 K, and the resistivity in the *a-b* plane changed from metallic (linear in *T* from 30-300 K) to semiconducting. Reducing the oxygen content in the crystals had a similar effect on the resistivity. Only crystals with close to the maximum oxygen content ($y=0$) were superconducting, and removal of oxygen from previously superconducting crystals resulted in a rapid decrease of T_c , and the eventual loss of superconductivity. A bond-valence sum analysis suggests that oxygen is removed from the Bi_2O_2 layers. The relevance of the phenomenon of "weak localization" to the upturn in the resistance at low temperatures of oxygen or strontium deficient crystals will also be discussed.

M2.5

STRUCTURE PROPERTY RELATIONSHIPS IN THE ONE-LAYER BISMUTH STRONTIUM CUPRATE SUPERCONDUCTOR. Steven A. Sunshine, Robert Fleming, Lynn Schneemeyer, and Theo Siegrist, AT&T Bell Laboratories, Murray Hill, N. J. 07974

The one-layer strontium bismuth cuprates (the so-called 2201 phase) have been reported to exhibit a wide variety of properties and structures. This material is of particular interest because it allows for the study of low temperature normal state properties in a "high T_c " superconductor. We have carefully examined the structure property relationships in this system.

Studies have been conducted on both ceramic samples as well as single crystals. Ceramic samples have been prepared in 4, 20, and 100% O_2 . Single crystals have been synthesized by both flux growth (NaCl) and melt techniques. These materials vary from insulating to superconducting depending on both metal and oxygen stoichiometry. The single crystals have been structurally characterized and changes in the structure have been related to the diverse physical properties.

M2.6

CERTAIN NOVEL ASPECTS OF THALLIUM AND BISMUTH CUPRATE SUPERCONDUCTORS. C.N.R. Rao, Indian Institute of Science, Bangalore-560012, India.

Properties of the novel series of thallium cuprate superconductors of the general formula $\text{TlCa}_{1-x}\text{Ln}_x\text{Sr}_2\text{Cu}_2\text{O}_y$ (*Ln* = rare earth) will be discussed. Specially interesting is the change in the sign of the thermopower

shown by these cuprates with change in *x*. $\text{TlSr}_{n+1-x}\text{Ln}_x\text{Cu}_n\text{O}_y$ constitutes a new series of thallium cuprates without either Ca or Ba. The $n=1$ (1021) and $n=2$ (1122) members have been characterized. The 1021 member with *Ln* = La shows a change in the sign of the thermopower with change in *x*. The 1021 members have a T_c of ~40K and 1122 members have a T_c of ~80K. $\text{Bi}_{2-x}\text{Pb}_x\text{CaSr}_2\text{Cu}_2\text{O}_y$ and $\text{Bi}_{2-x}\text{Ca}_{1-y}\text{Ln}_y\text{Sr}_2\text{Cu}_2\text{O}_y$ show change in the sign of thermopower with change in *x* or *y*, the $x=y=0.0$ parent cuprates itself showing negative thermopower from 300K down to T_c . Dielectric and other properties of glassy and crystalline Bi cuprates will be examined.

M2.7

INFLUENCE OF THE PARTIAL SUBSTITUTION OF SMALL RARE EARTHS FOR Ca IN THE SUPERCONDUCTIVE Bi-Sr-Ca-Cu-O COMPOUND. M.J. Casanove, P. Baules, E. Snoeck, C. Roucau, CEMES-LOE, BP 4347, 31055 Toulouse Cedex, France ; P. Millet, R. Enjalbert, J. Galy, LCC, 205 Rte de Narbonne, 31077 Toulouse Cedex, France.

Superconductive 2:2:1:2 phases of the type $\text{Bi}_2\text{Sr}_2\text{Ca}_{1-y}\text{Ln}_y\text{Cu}_2\text{O}_{8+x}$, where *Ln* stands for Yb or Er, have been synthesized and characterized by X-ray diffraction. The small rare earth atoms prove to substitute preferentially in the Ca site. The samples including Yb atoms are single phased until a content $y = 0.5$ while complete substitution can be achieved with Er cations. The electrical properties of these compounds are affected by the rare earth content. Their structural characteristics and in particular the incommensurate modulation have been investigated by electron microscopy. The results are in favour of an atomic displacive one-dimensional modulation with both transverse and longitudinal components. It has been observed that the wave length of the modulation decreases with increasing *y* (until $y = 0.5$), in the case of a substitution by Yb atoms. Simultaneously, the critical temperature of these samples diminishes until $y = 0.5$, the compounds presenting a semi-conductor behaviour for higher Yb contents.

M2.8

SYNTHESIS AND CHARACTERIZATION OF $\text{Nd}_{1.85}\text{Ce}_{0.15}\text{CuO}_{4+x}$; T.A. Vanderah, Naval Weapons Center, China Lake, CA; M.S. Ososky, Naval Research Laboratory, Washington, D.C..

Nd_2CuO_4 and its Ce-doped, n-type superconducting derivative were synthesized by solid state reaction of Nd_2O_3 , CuO, and "active" CeO_2 . Samples were characterized by X-ray diffraction, thermogravimetry, and measurements of resistivity and magnetic susceptibility.

$\text{Nd}_{1.85}\text{Ce}_{0.15}\text{CuO}_{4+x}$, as prepared by high-temperature solid state reaction of the component oxides in air, is a 6 K superconductor, but careful annealing at lower temperatures under an inert gas containing a low partial pressure of oxygen raises the T_c to 24 K.

Our objective was to measure the average formal copper valence in the parent compound as well as its superconducting derivative. Since Ce^{4+} oxidizes iodide ion, oxygen content was measured by thermogravimetric analysis under hydrogen rather than iodometric-type titrimetry methods.

According to our results and those published by the discoverers of the Nd-Ce-Cu-O system, reduction of the average formal copper valence to +1.7 from +2.0 in the parent Nd_2CuO_4 is prerequisite for stabilization of the "phase-pure" 24 K superconductor. The synthetic difficulties encountered in this system seem to be particularly representative of the metastable nature of these unusual superconducting oxides.

M2.9

Superconductivity in $(\text{Nd,Ce,Ca})_2\text{CuO}_{4-z}$: T. Sakurai, T. Yamahita, S. Ikegawa and H. Yamauchi, Superconductivity Research Laboratory, International Superconductivity Technology Center, 10-13 Shinonome 1-Chome Koto-ku, Tokyo 135 JAPAN

The relationship between carrier density and superconductivity transition temperature (T_c) for the conventional p-type oxide superconductors such as $\text{La}_{1.85}\text{Sr}_{0.15}\text{CuO}_4$ has been well established. The same relationship for the newly discovered n-type superconductors, i.e. $\text{Nd}_{2-x}\text{Ce}_x\text{CuO}_{4-z}$ of the T' phase structure exhibits a peculiar feature, that is, a discontinuity in the T_c -vs-[carrier density] curve. It is not clearly known if such a feature is essential for n-type superconductors.

In this work, we controlled the carrier (electron) density in Nd_2CuO_4 by substituting Ca as well as Ce into the Nd-sites, and studied the T_c -[carrier density] relationship. The phase relations in the $(\text{Nd,Ce,Ca})_2\text{CuO}_{4-z}$ system were studied by obtaining the tie-lines using X-ray diffraction and electron probe microanalysis techniques, and the region where only T' phase is stable was established in the phase diagram. Specimens of the $\text{Nd}_{1.82-x}\text{Ce}_{0.18}\text{Ca}_x\text{CuO}_{4-z}$ system which is included in the T' single phase region were synthesized to control the excess carriers due to the Ca substitution. Hall coefficients and DC resistivity of specimens were measured to elucidate the relation between the carrier density and T_c .

M2.10

SUPERCONDUCTING BEHAVIOR OF TETRAGONAL (T') $\text{Eu}_{2-x}\text{Ce}_x\text{CuO}_{4\pm\delta}$ * V.J. McIlm, Weimin Peng and C.W. Kimball, Northern Illinois University, DeKalb, IL and B. Dabrowski, Y. Zheng and D. G. Hinks, Argonne National Laboratory, Argonne, IL

$\text{Eu}_{2-x}\text{Ce}_x\text{CuO}_4$ ($0 \leq x \leq 0.17$) has been synthesized with the tetragonal T' structure. These compounds are analogues of the n-type superconductor $\text{Nd}_{2-x}\text{Ce}_x\text{CuO}_4$ in which the Cu-O coordination is square planar rather than pyramidal or octahedral. AC susceptibility and resistance measurements show that $\text{Eu}_{2-x}\text{Ce}_x\text{CuO}_{4\pm\delta}$ becomes superconducting with $T_c \sim 13\text{K}$ for $x = 0.15$ and 0.17 , when prepared under reducing conditions. Subsequent low temperature O_2 annealing increases the superconducting fraction but does not change T_c . The ^{151}Eu Mossbauer shift indicates that Eu has a valence near $3+$ for all x . The change in both shift and quadrupole splitting are small as the Ce spans the nonsuperconducting to superconducting concentrations. The relationship of superconducting behavior to preparation conditions, electronic structure, volume change and magnetic behavior will be discussed.

*Work supported by the National Science Foundation (DMR87-19738; OSTC-STC-8809854) and the US Dept. of Energy, BES (#W-31-109-ENG-38)

M2.11

CERAMIC MATERIALS WITH T'-CRYSTAL STRUCTURE IN THE $\text{Ln}_{2-x}\text{M}_x\text{CuO}_{4-y}$ ($\text{Ln}=\text{Pr,Nd}$; $\text{M}=\text{Ce, Pb, Sn}$) SYSTEM. R. Oviedo-Roa, L. Govea and R. Escudero, Instituto de Investigaciones en Materiales, UNIVERSIDAD NACIONAL AUTONOMA DE MEXICO. Apdo. Postal 70-360, Mexico, D.F., 04510, Mexico.

We have prepared single phase T'-crystal structure in the system $\text{Ln}_{2-x}\text{M}_x\text{CuO}_{4-y}$ where $\text{Ln}=\text{Pr, Nd}$, and $\text{M}=\text{Ce, Pb}$ and Sn for the compositions $x=0, 0.10, 0.13, 0.15, 0.17, 0.3$ and 0.4 . We observed that all series of compounds are isostructural to the T'-phase of Nd_2CuO_4 . In some cases we found impurity phases in very small amounts. The most interesting of these compounds is the formation of the single phase with Pb and Sn ; although, they are not superconductors.

We also determined the oxygen content and the copper oxidation state in terms of the $[\text{Cu-O}]^{+p}$ charge by a double iodometric titration technique. The structure and lattice parameters of the compounds were studied by X-ray powder diffractometry and the superconducting properties by electrical resistance measurements.

A discussion about the role of Pb and Sn in the structure formation is given in terms of oxidation states of these atoms.

M3.1

PULSED LASER TECHNIQUE FOR DEPOSITION OF SUPERCONDUCTING THIN FILMS: DEPOSITION PHYSICS AND IN-SITU PROCESSING. R.K. Singh and J. Narayan, Department of Materials Science and Engineering, North Carolina State University, Raleigh, NC 27695-7916

We have theoretically and experimentally analyzed the laser induced evaporation process for the deposition of superconducting thin films from bulk targets. A theoretical model based on the generation and expansion of a high temperature and high pressure gas in vacuum is developed. This model correctly predicts most of the characteristic features of the films fabricated by the technique including (i) the dependence of ion velocity on the pulse energy density and (ii) spatial thickness and compositional variations in superconducting thin films as a function of energy density. The fabrication of in-situ single crystal superconducting thin films at low substrate temperatures by the laser evaporation technique will also be discussed. By applying a dc bias to an interposing ring, epitaxial films were produced at substrate temperatures as low as 500°C . The films deposited at 650°C exhibited critical current density values of $5.0 \times 10^6 \text{ A/cm}^2$ and $1.0 \times 10^6 \text{ A/cm}^2$ on (100) SrTiO_3 and (100) YSZ substrates, respectively. X-ray diffraction, transmission electron microscopy, electron channeling patterns and Rutherford backscattering/channeling showed excellent epitaxial quality of films on SrTiO_3 and YSZ substrates with best values of minimum ion channeling yield of 3.5% on (100) SrTiO_3 substrates. The deposition conditions and the microstructure will be correlated with the superconducting properties.

M3.2

SYNTHESIS AND PROPERTIES OF $Y_{1-x}Pr_xBa_2Cu_3O_{7-x}$ THIN FILMS. X. D. Wu, M. S. Hegde, A. Inam, and X. X. Xi, Physics Department, Rutgers University, Piscataway, NJ 08854; T. Venkatesan, and C. C. Chang, Bellcore, Red Bank, NJ 07707

The $Y_{1-x}Pr_xBa_2Cu_3O_{7-x}$ system offers the exciting possibility of being used as an epitaxial junction barrier between two superconducting $YBa_2Cu_3O_{7-x}$ layers since the system has virtually no change in its orthorhombic structure. $Y_{1-x}Pr_xBa_2Cu_3O_{7-x}$ thin films were prepared in-situ by a pulsed laser deposition technique. The films showed metallic behavior in resistivity vs temperature for $x \leq 0.4$. The superconducting transition temperature decreases progressively as the Pr concentration is increased, as has been found for bulk samples. Ion beam channeling (2 MeV He^+) studies indicate that the films grow epitaxially on (100) $SrTiO_3$ substrate, showing minimum yield of 4-5%. This is confirmed by x-ray diffraction data which show the films to be highly oriented with their c-axes perpendicular to the surface. Moreover, the study reveals a systematic decrease in the intensity ratio of (200) to (100) x-ray lines with increasing values of x, which is explained on the basis of an increase in the symmetry along the c-axis.

M3.3

IN SITU GROWTH OF HIGH QUALITY EPITAXIAL $YBa_2Cu_3O_{7-x}$ FILMS AT MODERATE SUBSTRATE TEMPERATURES AND OVER LARGE AREAS BY PULSED LASER ABLATION.* Douglas H. Lowndes, J. W. McCamy, D. P. Norton, R. Feenstra, J. D. Budai, and D. N. Mashburn, Solid State Division, Oak Ridge National Laboratory, Oak Ridge, TN 37831-6056.

Pulsed KrF (248 nm) excimer laser ablation of $YBa_2Cu_3O_{7-x}$ (Y-123) target pellets has been used for in situ growth of smooth, high-quality Y-123 epitaxial films with primarily c-axis-normal orientation and variable thickness on $SrTiO_3$, $KTaO_3$, MgO , $LaGaO_3$, and $LaAlO_3$ substrates, without high-temperature post-annealing. A rotating target pellet, line focusing, laser beam scanning over the target, and high laser energy densities (~ 3.5 J/cm²) can be combined to yield films of nearly uniform composition over areas ~ 8 cm²; scaleup to >20 cm² area is being studied. "Baseline" Y-123 films grown on both $SrTiO_3$ and $KTaO_3$ at $T_{heater} \sim 700$ °C (estimated $T_{substrate} \sim 625$ -650 °C), followed by O_2 post-annealing at lower temperatures, have T_c (midpoint) > 90 K, and ΔT_c (10%-90%) ~ 1.0 -1.5 K. Omission of the O_2 post-annealing step results in only a small (~ 2 -3 K) reduction of T_c , and in very smooth films with lateral features only on the ~ 150 nm length scale. Results of detailed microstructural and crystallographic film characterization by SEM, RBS and x-ray diffractometry will be presented, together with superconducting transport measurements.

*Research sponsored by the Division of Materials Sciences, U.S. Department of Energy under contract DE-AC05-84OR21400 with Martin Marietta Energy Systems, Inc.

M3.4

TAILORED HIGH- T_c SUPERCONDUCTING THIN FILMS MADE BY LAYER-BY-LAYER DEPOSITION WITH EXCIMER LASER. Tomoji Kawai, Masaki Kanai, Hitoshi Tabata and Shichio Kawai, The Institute of Scientific and Industrial Research, Osaka University, Mihogaoka, Ibaraki, Osaka 567 Japan.

In the copper containing high T_c oxide-superconductors, the number and the distance of $Cu-O_2$ layers and carrier concentration have relations with the value of the superconducting transition temperature. Thus, it is important to control these parameters independently in order to elucidate the superconducting mechanism and to exploit a new superconductor.

We have artificially formed five different Bi(Pb)-Sr-Ca-Cu-O films containing one to five $Cu-O_2$ layers between Bi_2O_2 layers by a successive deposition method at low temperatures (500°C) taking advantage of laser ablation method in the presence of N_2O . In these compounds, hole concentration has been independently changed by doping Pb at the Bi_2O_2 layer with controlling the numbers of the $Cu-O_2$ layer.

Using the layer-by-layer technique, the control of the composition in the atomic layer scale is also possible by the incorporation of atoms and ions to the crystal structure to form "tailored superconducting films". Site-selective substitution of Ba for Sr or Ca in layered $(Bi-Pb)_2Sr_2Ca_1Cu_2O_y$ has been performed to control the superconducting properties

M3.5

IN SITU PREPARATION OF SUPERCONDUCTING Y-Ba-Cu-O THIN FILMS ON SILICON SINGLE CRYSTALS. H.-U. Habermeier and G. Mertens, Max-Planck-Institut/FKF, D 7000 Stuttgart-80, FRG.

Superconducting Y-Ba-Cu-O thin films with critical temperatures exceeding 80 K are deposited on silicon single crystal substrates using the laser deposition technique. Deposition from a sintered $YBa_2Cu_3O_7$ target in oxygen ambient of 0.1-5 mbar at

temperatures in the range of 700°C to 820°C forms crystalline material in which the target composition of the metallic constituents is preserved and critical temperatures up to 86 K are achieved¹. X-ray analysis as well as Raman spectroscopy reveal that specimens prepared at optimum conditions are single phase c-axis oriented, no traces of a second phase occur. Investigations of the surface morphology show granular surface structures in contrast to films grown in a similar way on MgO or $SrTiO_3$ single crystals. The surface morphology, however, is strongly influenced by the deposition temperature of the films and an optimization procedure for the film deposition has to take into account this issue. The films prepared by this in situ technique are quite stable against conventional chemicals used in photolithographic patterning, however, a strong correlation between film quality before patterning and a degradation after patterning is observed. To prevent this an in situ technique for the protection of the superconducting film is developed.

1. H.-U. Habermeier and G. Mertens, Proceedings of the HTM²SC Conference, Stanford, 1989.

M3.6

MACROSCOPIC PERSISTENT CURRENTS IN LASER ABLATED $YBa_2Cu_3O_{7-x}$ FILMS.

J. Fröhlingdorf*, U. Krüger, P. Leiderer†, R. Feile††, W. Zander*, B. Stritzker*
* Institut für Schicht- und Ionentechnik, KFA Jülich, FRG
† Fakultät für Physik, Universität Konstanz, FRG
†† Institut für Physik, Universität Mainz, FRG

Thin films of $\text{YBa}_2\text{Cu}_3\text{O}_{7-x}$ have been produced in situ by laser ablation without further low temperature annealing. Films were found to be polycrystalline with the c-axis preferentially oriented normal to the substrate plane on single crystalline (001)- SrTiO_3 and (random)- ZrO_2 . Complete superconducting transitions above 92 K with transition widths of about 1 K have been observed even on YSZ substrates. Critical current densities, j_c (77 K), of more than $1.5 \times 10^6 \text{ A/cm}^2$ could be obtained on SrTiO_3 -substrates. This new technique enables deposition of films as thin as 10 nm with excellent superconducting properties; it requires short process times (< 5 min) and is a versatile method which is also applicable to other materials. The high quality of the thin films over large areas was demonstrated by the measurement of persistent superconducting current densities (77 K) in the order of 10^5 A/cm^2 in a 1 mm broad ring of 9 mm diameter. No dissipation of this persistent current could be observed during one hour.

M3.7

STUDY OF IN-SITU LASER-DEPOSITION OF SUPERCONDUCTING THIN FILMS BY IN-SITU RESISTANCE MEASUREMENT. Q.Y. Ying, H.S. Kim, D.T. Shaw and H.S. Kwok, Institute on Superconductivity, State University of New York at Buffalo, Bonner Hall, Buffalo, NY 14260

An in-situ resistance measurement was made during the deposition of superconducting films. Silver leads were thermally evaporated before the deposition of the HTS film. For normal deposition conditions, leading to in-situ as-deposited HTS films, i.e. 5 mTorr O_2 pressure and $\sim 600^\circ\text{C}$ substrate temperature, the resistivity dropped sharply at the beginning of deposition and reached a minimum. After that, it increased slowly as the deposition continued. The initial decrease was due to the formation of the first few layers of HTS material. The minimum value of the resistivity was comparable to the typical value of Y-Ba-Cu-O thin films exhibiting superconductivity. However, the slow increase of the resistance indicated that the oxygen inside the film was constantly diffusing out during deposition. Immediately after the deposition, oxygen was filled into the chamber up to 100 Torr. The resistivity dropped to a steady value in a few seconds. It was the result of oxygen in-diffusion leading to the final superconducting film.

Measurement was also done at low oxygen pressure during deposition. It was found that in this case the film showed a semiconducting behavior even with otherwise identical deposition conditions. The behavior of the in-situ resistance change was also different.

M3.8

IN-SITU GROWN YBCO FILMS AND BUFFER LAYERS ON SILICON BY PULSED LASER DEPOSITION* G. A. N. Connell¹, J. B. Boyce¹, F. Bridges^{1,2}, D. B. Fenner^{1,3}, and D. K. Fork^{1,4}. (1)Xerox Palo Alto Research Center, Palo Alto, CA 94304; (2)Physics Dept. Univ. of California, Santa Cruz, CA 95064; (3)Physics Dept., Santa Clara Univ., Santa Clara CA 95053; (4)Dept. of Appl. Phys., Stanford Univ., Stanford, CA 94305

Attempts to grow high quality films of the high temperature superconductors on bare silicon have been hindered by substrate-film interdiffusion and by thermal expansion mismatch. In an

effort to circumvent these problems, buffer layers have been introduced as part of the thin film growth process. The buffer layer and the superconducting layer are sequentially deposited using a multi-target pulsed laser deposition system. Transition temperatures of up to 88K and a large degree of c-axis orientation are observed despite the presence of a 140Å amorphous SiO_2 layer beneath the buffer layer. Growth conditions and properties of various buffer layers, including zirconia-based buffers, as measured by x-ray diffraction and TEM will be presented. In addition, the results of the characterization of the superconducting properties of the films will be discussed.

* Supported in part by the Air Force Office of Scientific Research under Contract F49620-89-C-0017.

M3.9

ArF LASER ABLATION OF $\text{YBa}_2\text{Cu}_3\text{O}_{7-x}$ AS STUDIED BY EMISSION SPECTROSCOPY, SEM AND EDAX. Alon Hoffman, and Rafael Manory, Dept. of Applied Physics, Royal Melbourne Institute of Technology, G.P.O BOX 2476V, Melbourne, Victoria, 3001, Australia.

The fluorescence emission spectra from the plasma plume induced by ArF Eximer laser irradiation of $\text{YBa}_2\text{Cu}_3\text{O}_{7-x}$, Y, YO, Cu, CuO and YCuO were studied. Based on a comparison between the spectra obtained for the different materials, the peaks in the spectrum obtained for $\text{YBa}_2\text{Cu}_3\text{O}_{7-x}$ were assigned. The only oxide species detected was YO. Spatially resolved measurements from the plasma plume emanating from the irradiated $\text{YBa}_2\text{Cu}_3\text{O}_{7-x}$ sample were performed. The emission spectra from the plasma plume were recorded as a function of distance from the ablated surface. The variation in the spectra with distance were tentatively interpreted in terms of the temperature profile, different relaxation times of excited states and chemical reactions occurring within the plume.

The influence of laser ablation on the morphology and composition of the irradiated $\text{YBa}_2\text{Cu}_3\text{O}_{7-x}$ material was studied by SEM and EDAX. It was found that the 1-2-3 composition ratio of the near surface region after ablation was maintained. Changes in the morphology were observed and four distinctive regions could be identified: (i) the inner track region in which the laser intensity is at its maximum inducing evaporation, (ii) the track rim region where melting occurs, (iii) the near track region, extending out to about 0.3 mm from the rim in which the temperature is below the melting point and grain growth is induced, and (iv) the unaffected region, in which the structure is that of the original sintered material.

M3.10

THE PROCESSING OF SUPERCONDUCTING THIN FILMS OF Pb-Bi-Sr-Ca-Cu-O USING LASER ABLATION TECHNIQUES. F. Rees, M. Brown, R. Jackman, I. W. Boyd. Department of Electronic and Electrical Engineering, University College London, Torrington Place, London WC1E 7JE, UK, and F. Saba, Department of Materials, Imperial College, London SW7, UK.

In this presentation we shall discuss the processing of the Bi-Sr-Ca-Cu-O superconductors into thin films using Laser ablation techniques. In particular we will discuss the attempts to optimize both the critical temperatures and critical currents of films of the lead doped BSCCO

material. We also intend to discuss some recent results we have obtained on the basic physical processes operating in the ablation process. In particular we wish to discuss the relationship between the shape profile of the plume of the ablated material and the surface damage on the target pellet caused by the laser. We also intend to highlight recent theoretical work which suggests an elegant method for extending the technique to the deposition of high quality films, of uniform thickness, over large areas.

M3.11 ABSTRACT NOT AVAILABLE

M3.12

CHARACTERIZATION OF THE TARGET-SUBSTRATE BIAS POTENTIAL DEPENDENCE OF PULSED LASER DEPOSITION OF $\text{YBa}_2\text{Cu}_3\text{O}_{7-\delta}$. D.B. Chrisey, K.S. Grabowski, M.S. Osofsky, J.A. Sprague, and C.R. Gossett, Naval Research Laboratory, Washington, DC 20375-5000

Pulsed laser deposition of high T_c materials offers many advantages not found in conventional deposition techniques such as stoichiometric deposition in a high oxygen background pressure. In addition, the nonthermal distribution in energy of neutral material and the presence of positive ions in the laser-produced plume can also be effective in lowering the substrate processing temperature. We have deposited $\text{YBa}_2\text{Cu}_3\text{O}_{7-\delta}$ thin films in situ onto (100) MgO and (100) SrTiO_3 substrates using PLD while varying the target-substrate bias potential, oxygen background pressure, and substrate temperature in an effort to fabricate high quality films at lower substrate temperatures. The transport and microstructural properties of the resulting films suggest that there is an optimum temperature for in situ deposition of $\text{YBa}_2\text{Cu}_3\text{O}_{7-\delta}$.

M3.13

PREPARATION AND PROPERTIES OF EPITAXIAL THIN FILMS OF SUPERCONDUCTING $\text{Nd}_{1-x}\text{Ce}_x\text{CuO}_y$. A. Gupta, G. Koren, C.C. Tsuei, A. Segmüller, and T. R. McGuire, IBM Thomas J. Watson Research Center Box 218, Yorktown Heights, New York 10598.

Thin films of the electron-doped superconductor, $\text{Nd}_{1-x}\text{Ce}_x\text{CuO}_y$, have been deposited on SrTiO_3 substrates using the laser ablation technique. The deposited films grow epitaxially with the c-axis normal to the substrate on (100) oriented SrTiO_3 , and with (103) orientation on (110) substrates. The transport and magnetic properties of the film are very sensitive to the concentration of oxygen vacancies. Films deposited and cooled in presence of 150 mTorr of oxygen exhibit localization behavior with no evidence of superconductivity down to 5 K. Superconductivity is observed on annealing the films in vacuum or under a reducing atmosphere. The best films, with composition of $\text{Nd}_{0.85}\text{Ce}_{0.15}\text{CuO}_y$, on (100) SrTiO_3 , show zero resistance at 20 K with a transition width of 1 K. The normal-state resistivity shows metallic behavior with approximately T^2 temperature dependence. Such a dependence suggest strong electron-electron interaction in this system. The critical current density in zero magnetic field has been measured to be $2 \times 10^5 \text{ A/cm}^2$ at 5.5 K.

M4.1 ABSTRACT NOT AVAILABLE

M4.2

FABRICATION OF TEXTURED MICROSTRUCTURES IN $\text{YBa}_2\text{Cu}_3\text{O}_{6+x}$ BY LIQUID-PHASE SINTERING. Lijie Zhang, Martin P. Harmer and Helen M. Chan, Lehigh University, Bethlehem, PA 18015.

It is well-recognized that conventionally prepared bulk $\text{YBa}_2\text{Cu}_3\text{O}_{6+x}$ samples exhibit values of critical current density (J_c) which are too low for practical applications. However, Jin et. al. have shown that melt-processing produces a high degree of grain alignment, with J_c on the order of $17,000 \text{ A/cm}^2$. In this study, textured microstructures have been developed using liquid phase sintering, where samples are sintered close to the peritectic temperature and then slowly cooled. This process produces "domains" of large plate-shaped aligned grains. The effects of variables such as sintering time, temperature, and cooling rate on the degree of texture have been studied. Also, a series of quenching experiments were conducted in order to determine how the microstructure develops during the course of the heat treatment. The relationship between the degree of texture and the electrical properties will be discussed, together with possible mechanisms for the texture development.

M4.3

SYNTHESIS OF UNIDIRECTIONALLY SOLIDIFIED Y-Ba-Cu-O BULK SUPERCONDUCTORS WITH HIGH CRITICAL CURRENT DENSITY. E. Yanagisawa, S. Kondoh, J. Shimoyama, J. Kase, T. Matsubara and T. Morimoto, Research Center, Asahi Glass Co. Ltd., Hazawa-cho, Kanagawa-ku, Yokohama 221, Japan.

Critical current density, J_c , of bulk high- T_c oxides is limited within low level which is too low to be applied for the practical use. To overcome the problem, we tried to synthesize bulk material with single crystal like textures by the unidirectional solidification of Y-Ba-Cu-O system. Starting mixtures of Y_2O_3 , BaCO_3 and CuO with nominal composition of $\text{Y}_{1-x}\text{Ba}_2-x\text{Cu}_3-2x\text{O}_y$ ($x < 0.4$) were sintered at $900-950^\circ\text{C}$ and melt solidified in certain temperature gradients by conventional floating zone method above 1000°C . Then, bulk materials of about $5 \times 5 \times 20 \text{ mm}^3$ without appreciable cracks or pores were obtained. These materials have single crystal like microtextures, where a number of small ($20 \mu\text{m}$) particles of Y_2BaCuO_5 homogeneously precipitate. The small pieces of about $1 \times 0.15 \times 2 \text{ mm}^3$ were cut from the ingots, and the J_c was measured by the conventional four terminal resistivity measurement. The value of J_c of our specimen is more than 4600 A/cm^2 under the applied field of 10 kOe at 77 K. The effects of the doping of lanthanid atoms doping on the J_c will also be discussed.

M4.4

PROCESSING OF HIGH CURENT DENSITY $\text{YBa}_2\text{Cu}_3\text{O}_x$ SUPERCONDUCTORS. V. Selvamanickam and K. Salama, Department of Mechanical Engineering, Texas Center of Superconductivity, University of Houston, Houston, Texas 77004.

A liquid phase processing method has been developed to fabricate oriented grained $\text{YBa}_2\text{Cu}_3\text{O}_x$ samples with high current density [1]. The current density in these samples, however, is found to be sensitive to microstructure which is controlled by processing parameters. Random grain growth, restriction of orientation to the surface and crystallographically mismatched domains of locally aligned grains can be avoided by a proper combination of these processing parameters. Cooling rate through the peritectic temperature is found to be a crucial factor in controlling the extent of grain orientation. Samples rapidly cooled and sintered at 930 C are found to exhibit no grain orientation due to the randomness in the recrystallization process. When the cooling rate is decreased considerably, a microstructure with grains as long as 1 to 1.5 cm oriented along the length of the sample over a width of 0.5 to 1 cm can be obtained. The grains are plate shaped and the fracture surface lies on the a-b plane. The decrease in the cooling rate apparently allows more time for recombination of the decomposed phases into the superconducting phase and also permits sufficient time for mass transport along the fast growth a-b plane yielding elongated grains. Quenching studies from different temperatures during the slow cooling process reveals that a significant undercooling is required for grain nucleation and this determines the temperature range for the cooling process. The samples prepared by the slow cooling process repeatedly exhibit very high current densities at 77 K. A significant anisotropy in the resistivity across the grains is observed, but transport and inductive measurements reveal a very high value of supercurrent density in excess of 10^4 A/cm^2 in this orientation. This suggests that the nature of grain boundaries of the material fabricated by this process is very different from those studied earlier.

I. K. Salama, V. Selvamanickam, L. Gao, and K. Sun, *Applied Physics Letters*, 54, 2352 (1989)

M4.5

FABRICATION OF $\text{YBa}_2\text{Cu}_3\text{O}_x$ FILAMENTS BY EXTRUSION OF A $\text{Cu}_2\text{O}_3\text{Ba}_2\text{Y}(\text{meOEt})$, (meOEt IS 2-METHOXYETHANOL) PRECURSOR. M. W. Rupich, S. F. Cogan, B. Lagos, and J. P. Hachey, EIC Laboratories, Inc., Norwood, MA 02062

Superconducting $\text{YBa}_2\text{Cu}_3\text{O}_x$ filaments were fabricated by the thermal pyrolysis and oxidation of precursor filaments formed by room temperature extrusion of a molecular $\text{Cu}_2\text{O}_3\text{Ba}_2\text{Y}(\text{meOEt})$, (meOEt is 2-methoxyethanol) complex. The molecular precursor, $\text{Cu}_2\text{O}_3\text{Ba}_2\text{Y}(\text{meOEt})$, was synthesized by the reaction of a soluble copper(II) oxide polymer, $(\text{CuO})_n$, with $\text{Ba}(\text{meOEt})_2$ and $\text{Y}(\text{meOEt})_3$ in a pyridine/2-methoxyethanol solvent mixture. The structure of the molecular $\text{Cu}_2\text{O}_3\text{Ba}_2\text{Y}(\text{meOEt})$ precursor is believed to consist of a two dimensional array of CuO_2 layers formed by the cross-linking of the linear Cu-O-Cu-O chains by $\text{Ba}(\text{meOEt})_2$ and $\text{Y}(\text{meOEt})_3$. The polymeric structure of the precursor promotes the orientation and alignment of the $\text{YBa}_2\text{Cu}_3\text{O}_x$ microstructure. Extrusion, pyrolysis and oxidation of the $\text{Cu}_2\text{O}_3\text{Ba}_2\text{Y}(\text{OR})$ precursor results in the formation of a $\text{YBa}_2\text{Cu}_3\text{O}_x$ grain structure consisting of platelets which are predominantly oriented along the filament axis. The degree of grain orientation in the filaments and the filament density depend on the pyrolysis conditions and filament diameter.

Superconducting $\text{YBa}_2\text{Cu}_3\text{O}_x$ filaments with diameters of 75 to 500 μm were fabricated and characterized. The filaments showed transition temperatures (onset) above 90 K and reached zero resistance at 89 K. Critical current densities of $\sim 300 \text{ A/cm}^2$ have been obtained at 77 K. The physical and chemical properties of the precursor filaments and the pyrolysis and oxidation conditions that yield oriented superconducting filaments will be presented. The major advantage of the process is the ability to influence the orientation of the $\text{YBa}_2\text{Cu}_3\text{O}_x$ grain structure of the filaments through the structure of the precursor.

I. M. W. Rupich et al., *Appl. Phys. Lett.* (submitted).

M4.6

THE DEPENDENCE OF T_c FOR CERAMIC HIGH- T_c SUPERCONDUCTORS ON ELECTRONIC PARAMETERS. B.C. Glessen and R.S. Markiewicz, Materials Science Division, Barnett Institute and Departments of Chemistry and Physics, Northeastern University, Boston, MA 02115

Even in the absence of a detailed microscopic theory, attempts to find a unifying description for T_c in high- T_c superconducting oxides have been quite successful. The relation of T_c to hole (or electron) concentration, especially the occurrence of a maximum value of T_c within a given compound and the correlation of T_c with both the percentage of "active" material (e.g., CuO_2^{2-} layers) and the hole concentration within the active material can be qualitatively understood in terms of concepts successfully used for intercalation compounds. Including explicitly the splitting effect of interlayer coupling, we have recently proposed a universal correlation of T_c with the hole concentration per active layer which generates a set of T_c curves that represent the experimental data well.

Based on this model, we examine or re-examine structural and electronic parameters characterizing the occurrence of high- T_c superconductivity, with special emphasis on its frequent and fundamental correlation with structural instabilities.

M4.7

THE EFFECT OF THE DISTRIBUTION OF DOPANTS IN HIGH T_c BI-COMPOUND SUPERCONDUCTORS. Alexis S. Nash, Marquette University, Milwaukee, WI, Kenneth C. Goretta, Argonne National Laboratory, Argonne, IL, Philip Mash, Illinois Institute of Technology, Chicago, IL, Roger B. Poeppel and Donglu Shi, Argonne National Laboratory, Argonne, IL.

A series of 4336 Bi-Sr-Ca-Cu oxide samples doped with either 1 to 10% metallic silver or 1 to 10% SnO_2 were prepared using a solid state reaction method. The distribution of cationic dopants, the microstructure and the crystal structure of the samples was studied using energy dispersive spectrometry, scanning electron and optical microscopy and x-ray diffractometry.

The dependence of microstructure and T_c on the type and the distribution of dopant and on firing schedules have been determined. The grain morphology was found to depend upon the type of dopant, varying from plates to irregular chunks. Addition of silver leads to a marked increase in preferred orientation with (001) planes perpendicular to the pressing direction in sintered pellets. This was confirmed by scanning electron microscopy.

The resistivity-temperature data show an enhanced T_c in Ag-doped samples under certain conditions. Energy dispersive spectrometry indicates that the dopants mostly segregate to the grain boundaries.

M4.8

A NOVEL SPRAY PYROLYSIS SYSTEM FOR THE DEPOSITION OF HIGH T_c SUPERCONDUCTORS. Toby J. Cumberbatch, I.R.C. in Superconductivity, Cambridge University, Cambridge, England; Stephen Deane and Paul E. Barden, Engineering Department, Cambridge University, Cambridge, England

A spray pyrolysis system has been developed in which the use of airless atomisation and optical heating permits the deposition of thin film superconductors at growth surface temperatures of up to 650°C. This is sufficient to drive a pyrolytic decomposition reaction to completion and obviates the need for a subsequent high temperature anneal to form the desired oxide. A fine aerosol is generated with a commercial centrifugal atomisation system and the cross section is controlled by an annular gas

shower of oxygen or nitrogen. The atomisation process is further assisted by an electrostatic field which charges the droplets so reducing coalescence within the aerocolloidal suspension. The substrates rest on a partially transparent sheet of ceramic and are heated from above and below by tungsten halogen lamps. For optically transparent substrates, the energy is coupled directly into the nascent film which provides a higher heat flux to the growth surface than is available from diffusion through the substrate. Local variations in the droplet flux density are alleviated by the substrate executing a trochoid in the horizontal plane whilst the position of the spray gun is fixed.

Dense YBCO films, comprising a mixture of ternary oxides, have been deposited directly on to glass substrates at 500°C. Results will be presented from the new system for a range of superconducting materials, deposited at higher temperatures, on to conventional substrates.

M4.9

HIGH TEMPERATURE SUSPENSION MELTING TREATMENT OF SUPERCONDUCTING POWDER (HTSM). Zhang Jiangou, Zhou Yiru, Wang Junsheng, Yan Junlian, Liu Ansheng, Zhang Baoren and Xu Yalan. 208A204 Lab. General Research Institute for Non-Ferrous Metals. Beijing 100088, China.

This work explored a high temperature suspension melting process to prepare YBCO superconducting powder, and the powder was analyzed and observed by TEM, SEM, X-ray diffraction technique and optical microscope. It is hard to obtain ideal superconductors with uniform and pure superconducting phase using the normal powder preparing processes. In this paper, we have investigated the effects of both non-uniform composition of the original powder and low portion of superconducting phase on J_c of bulk material. A new process -- HTSM has been discovered. HTSM process is such a way that the normal superconduct powder is suspended in a special high temperature furnace, melted and recrystallized instantaneously in a rich oxygen environment, and then quenched rapidly. The experiment indicated that HTSM process is the powder comes not into contact with any crucible in the whole process and hence avoids contamination. In the case of preparing YBCO superconducting powder by HTSM process, the powder can be purified, the uniformity of the bulk material can be improved, the portion of superconducting phase and the critical current density can be increased. The critical current density values of the bulk materials were increased about 2~3 times, and the J_c value of its tape came up to 7800A/cm².

M4.10

REACTIONS AT CERAMIC SUPERCONDUCTOR/METAL INTERFACES. Min-Seok Oh and Michael R. Notis, Lehigh University, Dept. Materials Science & Engineering, Whitaker Lab #5, Bethlehem, PA 18015

Joining technology for ceramic superconductors is currently a major problem. At least two problem areas have emerged: reactions which occur at ceramic/metal interfaces formed during composite wire fabrication, and preparation of contacts with low contact resistance for measurement of physical properties. Characterization techniques to examine the microstructure and microchemistry associated with ceramic superconductor/metal interfaces will be described. These include

quantitative analysis using Electron Probe Micro analysis (EPMA) and x-ray color mapping methods to visualize the spatial distribution of reaction products. The possible reactions which occur at ceramic superconductor/metal interfaces will be discussed and examples will be shown of interfaces between Ba-Y-Cu-O and Bi-Sr-Ca-Cu-O vs. a series of metals (Ag, Ni, Cu) now being considered for joining and cladding applications. In a composite configuration, Ag metal interlayers are found to promote interfacial reactions.

M4.11

YBa₂Cu₃O₇ FILAMENT-SUPERPLASTIC ALLOY COMPOSITES. Emilio Orgaz, Miguel A. Ocampo, Centro de Investigación y Desarrollo CONDUMEX, Blvd. Cervantes Saavedra 255, 11520 México D.F., México., David Rios-Jara, and Tatsuo Akachi. Instituto de Investigaciones en Materiales, UNAM, Apdo Postal 70-360, 04510, México D.F., México.

Composites formed by superconducting filaments clad with superplastic alloys were prepared. YBa₂Cu₃O₇ powder was obtained by standard solid state reaction and was used to extrude green filaments. After sintering and oxygenation, the filaments showed superconductivity at 90K (zero resistance).

A novel clad was tested using low melting point superplastic alloys. This cold process preserves the YBa₂Cu₃O₇ from deoxygenation. The composites showed superconductivity at T_c higher than 85K. The resistivity ratio between the YBa₂Cu₃O₇ ceramic material in the normal state and the metal clads ranges from 5 to 50. This provides the current by-pass when the superconductivity is locally lost. The metal-ceramic interface was characterized by electrical transport measurements and microstructural observations. Critical current density determinations are under way and will be presented.

M4.12

SILVER IN Y-Ba-Cu-O: SUBSTITUTION, MICROSTRUCTURE, AND SUPERCONDUCTING PROPERTIES. B. R. Weinberger, L. Lynds, D. M. Potrepka, R. Cipolli, D. B. Snow, C. T. Burila, H. E. Eaton, United Technologies Research Center, East Hartford CT 06108; Z. Tan, J. I. Budnick, Department of Physics, University of Connecticut, Storrs, CT 06268.

Ag/Y-Ba-Cu-O composites have been proposed for a variety of applications. Unlike virtually all other metals (gold being the other notable exception), when subject to high temperature synthesis processes, Ag/YBa₂Cu₃O_{7-x} composites display no degradation of superconducting T_c and some enhancement of J_c . The composite material consists of basically single phase YBa₂Cu₃O_{7-x} and Ag metal.

To be presented is experimental evidence that Ag actually exists in three distinct environments in such composites: in metallic clumps filling voids in the Y-Ba-Cu-O matrix, along Y-Ba-Cu-O grain boundaries, and minimally substituted in the lattice of YBa₂Cu₃O_{7-x}. To be detailed are studies of the microstructure of Ag/Y-Ba-Cu-O composites made by cold-pressing and hot isostatic pressure processing (HIP) including: X-ray diffractometry, EXAFS, light and transmission electron microscopy, electron microprobe studies. These structural properties will be correlated with magnetometry, resistivity and critical current measurements.

MICROSTRUCTURAL ANALYSES AND MAGNETIC MEASUREMENTS OF Ag/YBa₂Cu₃O_{7-x} COMPOSITES.

V.S.Achuthuraman, Y.J.Zhang, M.L.Mecartney, Dept. of Chem. Eng. & Mat. Sci., University of Minnesota, Minneapolis, MN 55455, and J.McArdle, Q.Chen, B.Koepeke, Honeywell Inc., Minneapolis, MN 55428.

The addition of silver or silver oxide to YBa₂Cu₃O_{7-x} powders before sintering has been observed to enhance densification and grain growth. This enhancement has been postulated to occur via a liquid phase sintering mechanism. We have undertaken studies on the wetting behavior of Ag on YBa₂Cu₃O_{7-x} at various temperatures and the effect of quench rate on the wetting behavior. In addition, the grain boundary structure of Ag/YBa₂Cu₃O_{7-x} composites and distribution of silver have been analyzed by SEM and TEM. Lastly, effects on magnetic susceptibility and flux creep due to modification of the microstructure of YBa₂Cu₃O_{7-x} by the addition of silver have been investigated.

M5.1

IN-SITU GROWTH OF Y₁Ba₂Cu₃O_{7-x} FILMS BY MOLECULAR BEAM EPITAXY WITH AN ACTIVATED OXYGEN SOURCE.

J. Kwo,* AT&T Bell Laboratories, Murray Hill, New Jersey 07974

High quality, superconducting Y₁Ba₂Cu₃O_{7-x} thin films have been successfully produced by molecular beam epitaxy on MgO(100) at a substrate temperature ~ 650°C. The in-situ growth was achieved by incorporating neutral oxygen radicals produced by a remote microwave-excited plasma in a flow-tube reactor. By enhancing the flow speed of the O₂ stream to minimize recombinations, we have demonstrated remarkable improvements in the superconducting properties. The main chamber pressure during growth is maintained at 5x10⁻⁶ torr, compatible with standard MBE operation. Films 500Å thick show reproducible sharp transitions (R=0) at 89K, and low resistivities of ρ(300K) = 202 μΩ-cm, ρ(100K) = 70 μΩ-cm. The epitaxial order of (001) orientation was characterized by x-ray diffraction and ion channeling. Furthermore, the qualities of interfacial sharpness and surface morphology are significantly improved over the ex-situ annealed films. In-situ reflection high energy electron diffraction indicated that a layer-by-layer type of growth has produced a highly ordered, atomically smooth film surface. The tunnel junction experiments were recently conducted. The results of single particle tunneling and quasiparticle tunneling will be reported.

* Work done in collaborating with M. Hong, T. A. Fulton, D. J. Trevor, R. M. Fleming, A. E. White, A. R. Kortan, R. C. Farrow, and K. T. Short.

M5.2

SUPERCONDUCTORS AND INSULATORS IN RUBIDIUM BARIUM BISMUTH OXIDE FILMS GROWN IN-SITU BY MOLECULAR BEAM EPITAXY. E. S. Hellman, E. H. Hartford, R. M. Fleming, AT&T Bell Laboratories, Murray Hill, NJ 07974.

Investigations of epitaxial growth in the rubidium barium bismuth oxide material system have shown it to be a powerful synthetic technique. The simple cubic perovskite (Rb,Ba)BiO₃ can be grown at temperatures below 350°C by molecular beam epitaxy using an RF plasma atomic oxygen source. Films with metallic normal state conductivity and superconducting onsets in resistivity as high as 27K are obtained without annealing. The epitaxy proceeds in the normal (1 0 0) orientation on (1 0 0) SrTiO₃, despite a 10% lattice mismatch. (1 1 0) epitaxy is obtained on (1 0 0) MgO substrates, despite the good lattice match for (1 0 0) growth. Bismuth rich films are generally not superconducting and contain a phase with a 9.5Å lattice spacing which appears to be related to the hexagonal solid solution phase known in the barium bismuth oxide system. Films with moderate bismuth deficiency are also superconducting, and show both (1 0 0) and (2 2 1) texture on SrTiO₃ in reflection high energy electron diffraction (RHEED) patterns and x-ray diffraction scans. Films with large bismuth deficiency are perovskite-like but are insulating and unstable in air. This picture of the "phase diagram" for epitaxy, along with an understanding of the influence of growth conditions, can be used to achieve control of the composition and properties of the films.

M5.3

AS-DEPOSITED SUPERCONDUCTING Y-Ba-Cu-O FILMS ON GaAs SUBSTRATE BY HIGH PRESSURE DC SPUTTERING PROCESS. R.J. Lin and P.T. Wu, Materials Research Laboratories, Industrial Technology Research Institute, Chungtung, Hsinchu, Taiwan, R.O.C.

The superconducting Y-Ba-Cu-O thin films on (100)GaAs substrate have been reproducibly prepared by high pressure DC sputtering process without further post-annealing treatment. The targets were Y-Ba-Cu-O compounds made by solid state reaction. The sputtering gases were Ar-50%O₂, and total gas pressure was 1-2 torr. The substrate temperature was lower than 450°C. By now, the superconductivity of the films is T_c(onset) = 95K and T_c(zero) = 40K. The thickness of the films is 1-2μm. The detailed process and results of X-ray diffraction, magnetization, SEM and TEM micrographs of the films will be discussed.

M5.4

HIGH-T_c YBa₂Cu₃O₇ THIN FILMS PRODUCED BY MULTILAYER SPUTTER DEPOSITION. Mark S. Dilorio, Kai-Yueh Yang, Andrew N. Erickson, Biomagnetic Technologies, Inc., San Diego, CA; Patricia K. Tsai, M. Brian Maple, University of California San Diego, La Jolla, CA.

We have fabricated thin films of YBa₂Cu₃O₇ using multilayer sequential sputtering from three metallic targets in a load-locked deposition system. The films that are sputter-deposited at room temperature in argon and post-annealed in flowing oxygen show zero resistance at 86 K on yttria-stabilized zirconia (YSZ) substrates. The technique is very reproducible and produces moderately smooth films whose stoichiometry is determined by electron microprobe to be close to 1:2:3 over relatively large (>2") substrate areas. Films sputter-deposited in mixed oxygen and argon at 450 °C and post-annealed in oxygen show a shiny smooth surface, improved film stability, and zero resistance at 84 K on YSZ substrates. The structure of these films was studied by x-ray diffraction, which shows a polycrystalline structure in most of the films, and a partial c-axis orientation in films annealed at higher temperatures. We have also patterned input coupling coils from films deposited on relatively large area (1" x 0.5") YSZ substrates for use in SQUID magnetometers.

M5.5

HIGH CRITICAL CURRENT DENSITY IN ULTRATHIN YBCO FILMS X.X. Xi, W. Schauer*, J. Geerk, Q. Li*, G. Linker and O. Meyer, Kernforschungszentrum Karlsruhe, Institute fuer Nukleare Festkoeperphysik, *Institut fuer Technische Physik, P.O.Box 3640, D-7500 Karlsruhe, FRG. *Physics Department, Rutgers University, Piscataway, NJ08854, U.S.A.

Ultrathin $\text{YBa}_2\text{Cu}_3\text{O}_{7-x}$ films were produced on (100) SrTiO_3 and (100) MgO substrates by hollow-cathode magnetron sputtering. Metallic temperature-dependence of the resistivity and full superconducting transition above 4.2 K were obtained in films as thin as about 3 nm (e.g. $T_{\text{CO}}=62\text{K}$ for a film of 3.5 nm) on (100) SrTiO_3 . Due to the bigger mismatch between YBCO films and (100) MgO substrates and the dislocation layers at the film substrate interface produced thereby, the full superconductivity can be obtained on MgO substrates only in films thicker than 6nm. The critical current density, J_{C} , of a 30nm thick film on (100) SrTiO_3 had a value of $2 \times 10^6 \text{ A/cm}^2$ at 77K and zero field which is comparable to that of the thicker films though the J_{C} degraded in thinner films. However, a relatively high J_{C} of $3.5 \times 10^5 \text{ A/cm}^2$ was still obtained in a 5nm film at 4.2K and zero field. The field-dependence of J_{C} for the 5nm film was measured and was found to be very much different from that of the thicker films. We speculate that it is partly due to the increasing importance of flux pinning when the film thickness is decreased.

M5.6

SYNTHESIS AND PROPERTIES OF $\text{YBa}_2\text{Cu}_3\text{O}_{7-x}$ THIN FILMS GROWN *IN-SITU* BY SINGLE TARGET MAGNETRON SPUTTERING. C.B. Eom, J. Sun, K. Yamamoto, and T.H. Geballe, Stanford University, Stanford, CA 94305; and S.S. Laderman, Hewlett-Packard Co., Palo Alto, CA 94304.

Using single target off-axis sputter deposition, high quality superconducting films of $\text{YBa}_2\text{Cu}_3\text{O}_{7-x}$ were made *in situ* on $\text{MgO}(100)$ substrates.⁽¹⁾ These films have properties which are distinctly different from those of bulk ceramics and of post-deposition annealed films. Their superconducting resistive transitions range from 75 to 86K and remain sharp regardless of the value of T_{C} . Normal state conductivities are as high as the best single crystals. Their critical current densities are higher than $6 \times 10^7 \text{ A/cm}^2$ at 4.2 K.

We have studied the thickness dependence of superconducting properties (T_{C} , J_{C}) from 30Å to 5000Å thickness. Although T_{C} starts degrading below 200Å, the transition temperature of a 30Å film was still 30 K. However, the J_{C} drops linearly below 1500 Å. The dependence of thickness upon nucleation, growth and surface coverage is under investigation.

We measured transport properties of these films in magnetic fields of up to 8 T. The resistive transition broadens with field perpendicular to ab plane, although much less than in post-annealed films on $\text{SrTiO}_3(100)$ substrates. We observed a broadening which shows sign of saturation under the condition of $H \parallel J$ in the ab plane. We studied flux creep and flow behavior of these films from I-V characteristics and resistivity measurements at various temperatures and magnetic fields.

(1) C.B. Eom and et al., Appl. Phys. Lett. to be published (Aug. 7, 1989)

M5.7 ABSTRACT NOT AVAILABLE

M5.8

Ion Beam Co-deposition of $\text{YBa}_2\text{Cu}_3\text{O}_{6+x}$ Films B.J. Kellett, J.H. James, A. Gauzzi, B. Dwir, and D. Pavuna, Institute of Micro and Optoelectronics, Swiss Federal Institute of Technology, Lausanne CH 1015, Switzerland.

Superconducting $\text{YBa}_2\text{Cu}_3\text{O}_{6+x}$ films have been deposited by a four ion beam deposition system. Three ion beams are used for sputtering while the fourth, directed at the substrate, is used for etching, oxygen assisted growth, and patterning. As deposited superconducting films have been grown on SrTiO_3 and Si with oxide buffer layers (buffer layers were ion-beam deposited). Both oxide and metallic targets, O_2 background gas, O_2 assist, and substrate temperature have been studied to determine effects on oxygen stoichiometry, critical current (J_{C}) and superconducting transition temperature (T_{C}). Auger electron spectroscopy (AES) X-ray diffraction (XRD) and SEM have been employed to refine processing conditions and determine optimum processing routes for Hybrid device structures for applications in optoelectronics.

M5.9

IN-SITU PREPARATION AND CHARACTERIZATION OF SUPERCONDUCTING THIN FILMS AND RELATED MATERIALS BY MOCVD FOR THE DEVELOPMENT OF THREE TERMINAL SWITCHING DEVICES. R. Singh, F. Radpour, S. Sinha, N.J. Hsu, P. Chou, R.P.S. Thakur, A. Kumar, University of Oklahoma, Norman, OK; J. Narayan and R.K. Singh, North Carolina State University, Raleigh, NC.

High throughput, low temperature deposition, sharp interfaces, and selective deposition with direct ion, electron and photon beam controlled techniques are some of the key driving forces for the development of superconducting thin films by MOCVD technique. Thus, MOCVD, in addition to well established roles in semiconductor and optoelectronics industry, can play a similar major role in the superconductivity industry. We have successfully used MOCVD for the deposition of Y-Ba-Cu-O superconducting thin films, BaF_2 as a buffer layer and as a dielectric material and Y_2O_3 (preferred as a gate dielectric material due to higher dielectric constant of about 16). As deposited Y-Ba-Cu-O films on BaF_2/YSZ substrates have zero resistance at 80K and exhibit texture of growth with either c or a axis perpendicular to the substrate. In this paper we will present preparation and characterization of Y-Ba-Cu-O and other related material deposited by MOCVD. Based on our experimental work, it appears that these materials have the potential of realizing hybrid semi-conductor/superconductor three terminal switching devices.

M5.10

LOW TEMPERATURE PREPARATION OF Y-Ba-Cu-O THIN FILMS BY OMCVD. Taiji Tsuruoka, Ryoudou Kawasaki, Hitoshi Abe, and Susumu Shibata, Research Laboratory, Oki Electric Industry Co., Ltd. Tokyo, Japan.

We have developed the low temperature preparation of YBaCuO thin films by organo-metallic chemical vapor deposition (OM-CVD) using N_2O gas. The films were fabricated at a low substrate temperature as 650°C. For the deposition of YBaCuO films, we used β -diketonate metal chelates of 2,2,6,6-tetramethyl-3,5-heptanedione-barium, -yttrium, -copper. Critical temperature of this film without after annealing was 80K. By x-ray diffraction (XRD), we observed that c-axis of the crystal is perpendicular to the surface of (100) SrTiO₃ substrate. Even though the films grown at 600°C, small XRD peaks of YBaCuO crystal can be observed.

By using O_2 gas, the lowest temperature to prepare YBaCuO thin films with high T_c on SrTiO₃ substrate without after annealing was 750°C. Meanwhile, it is well known that N_2O gas decomposes into N_2 and O (single atom) above 500°C. Here we observed that the reduction of growth temperature of YBaCuO films by using N_2O gas depended on presence of active oxygen atom, because other deposition conditions of both cases (using O_2 gas and using N_2O gas) were quite the same.

The experimental results show that the use of active oxygen makes it possible to crystallize YBaCuO thin films at a low temperature. This low temperature is compatible with semiconductor device processing and reduces film contamination due to substrate diffusion.

M5.11 ABSTRACT NOT AVAILABLE

M5.12

INNOVATIVE LOW-TEMPERATURE METAL-ORGANIC CHEMICAL VAPOR DEPOSITION (LTMO-CVD) ROUTES TO THE FABRICATION OF DEVICE QUALITY HIGH TEMPERATURE OXIDE SUPERCONDUCTORS. Alain E Kaloyeros, Aiguo Feng, and Jonathan Garhart, Physics Department, State University of New York at Albany, Albany, NY, and Marianne Holma and Kenneth Brooks, Physics and Chemistry Departments, University of Illinois at Urbana-Champaign, Urbana, IL.

We have developed methodology to produce high quality superconductor thin films on complex shapes and forms by low-temperature metal-organic chemical vapor deposition (LTMO-CVD) from designed organometallic compounds. Preliminary results will be presented from the successful growth of high-purity, high-quality Y-Ba-Cu-O films (T_c -89K, J_c -20,000A/cm²) by simultaneous LTMO-CVD of three metal β -diketonate precursors, namely, Cu(acac)₂, Y(acac)₃ and Ba(fod)₂, with and without oxygen atmosphere. The deposition was carried out at temperatures of 300-400°C and on a variety of substrates that included (100) MgO, SrTiO₃, and ZrO₂-stabilized silicon. Typical deposition rate and film thickness, for films produced at a working pressure of 10^{-6} - 10^{-5} torr, were, respectively, 2-3nm and 1-2 μ m. The thickness variation across a typical substrate was also investigated and found to be <5%/cm over the whole substrate. The electrical properties of the films were quite sensitive to the temperature and duration of the post-deposition high-temperature annealing step. The best transition temperature of ~89K, and the sharpest transition, were obtained for film annealed using a one-step slow anneal at 850°C in 100% oxygen atmosphere.

The quality of the LTMO-CVD-produced Y-Ba-Cu-O films was investigated by performing microstructural and microchemical analyses and elemental concentration profiling on films deposited on MgO substrates at 350°C and annealed according to the scheme described earlier. The films were characterized by Auger electron spectroscopy (AES), scanning electron microscopy (SEM), and energy-dispersive x-ray spectroscopy (EDXS). AES and EDXS in-depth and lateral (x-y) quantitative analyses were in excellent agreement. They showed that film composition was practically constant over the entire film and independent of lateral or depth position. AES quantitative analysis yielded a composition of Y_{1.0}Ba_{2.0}Cu_{3.18}O_x, while EDXS yielded a composition of Y_{1.0}Ba_{2.0}Cu_{3.15}O_x. SEM results showed that the film exhibits a typical pattern of oriented needles with an extremely smooth texture and a very small concentration of voids. These preliminary studies showed that the films had a constant composition over the whole substrate area and that LTMO-CVD-produced films might be excellent candidates for, for example, photolithography and patterning applications.

M5.13

IN-SITU GROWTH OF YBa₂Cu₃O_{7-x} FILMS BY METAL ORGANIC CHEMICAL VAPOR DEPOSITION USING VERTICAL, HIGH-SPEED ROTATING DISK REACTOR. D. W. Noh, B. Gallois, Stevens Institute of Technology, Hoboken, NJ; C. Chern, B. Kear, Rutgers University, Piscataway, NJ; G. S. Tompa, P. Norris, P. Zawadzki, EMCORE, Somerset, NJ.

Superconducting thin films of YBa₂Cu₃O_{7-x} were grown on MgO (100) and YSZ(100) substrates without post-annealing by metal organic chemical vapor deposition using vertical high-speed (1100 rpm) rotating disk reactor. The source materials were Y(tmhd)₃, Ba(tmhd)₂, and Cu(tmhd)₂, which were kept at 135 °C, 240 °C, and 120 °C respectively. The precursors were transported using nitrogen as the carrier gas and introduced separately into the stainless steel cylindrical chamber, which was maintained at 60 torr. The oxygen partial pressure was 30 Torr. The substrates were heated resistively at 800°C. After the growth the films were cooled down at a rate of 5 °C/min under 1 atmospheric pressure of pure oxygen.

The X-ray diffraction pattern of the films showed primarily orientation of c-axis perpendicular to the substrates with weak peaks of (h00) corresponding to a-axis orientation. Scanning Electron Microscopy of the films showed well-developed a-axis and c-axis plate structure which appeared as rectangular micron-sized features on the MgO surface. On the YSZ substrates a-axis and c-axis plate-like projection were also observed, with the dense plate-like c-axis orientation dominant. Four probe resistance measurement showed T_c at 91.8 K (ΔT_c =2.2 K) and 85 K (ΔT_c =7 K) on YSZ and MgO substrates respectively.

M6.1 ABSTRACT NOT AVAILABLE

M6.2

CRYSTAL CHEMISTRY AND SUB-SOLIDUS PHASE RELATIONS IN (La,RE)₂CuO₄ SYSTEMS. Joseph F. Bringley, Steven S. Trail, Michael W. McElfresh and Bruce A. Scott I.B.M. Research Division, T. J. Watson Research Center, Yorktown Heights, NY 10598.

There are three closely related (RE)₂CuO₄ (RE = rare earth) structure-types presently known which exhibit superconductivity at appropriate levels of electron or hole doping. Each contain isolated sheets of either 4-fold (T'), 5-fold (T*), or 6-fold (T) Cu-O coordination. In an effort to determine the factors which influence their stabilities, a range of doped and undoped (La,RE)₂CuO₄ (RE = Nd to Y) systems were investigated, with particular focus on the crystal chemistry of the La,Nd system.

For La_{2-x}Nd_xCuO₄, the structure remains that of La₂CuO₄ (T) and the degree of orthorhombicity increases with increasing x for 0.0 ≤ x ≤ 0.4. The structure transforms to that of Nd₂CuO₄ (T') for x ≥ 0.5. However, careful examination of the x-ray powder diffraction data for samples with La/Nd ratios ≈ 1.0 revealed yet a third phase whose structure corresponded to that of T*. Studies of the remaining (La,RE)₂CuO₄ systems under a variety of conditions including high oxygen pressure, resulted in the observation of several new T* phases in these systems as well, but single phase materials with this structure could not be obtained in most cases. Isolation of nearly pure T* LaDyCuO₄ suggests that RE cation-ordering may be playing a role in its stabilization.

An investigation of La_{1.45x}Nd_{0.55x}CuO₄ and Nd_{1.45x}La_{0.55x}CuO₄ systems revealed that the T and T' phases are stabilized electronically by doping. The T-structure is stabilized only by hole doping, whereas the T'-structure is stabilized only by electron doping. In addition, the solid solution limits of the doped-phases could be extended by employing high-pressure (40-70 kbar) during synthesis. It was found that the critical temperature for superconductivity (T_c) decreased gradually with increasing Nd content in La_{1.45x}Nd_{0.55x}CuO₄, but that

substitution of La for Nd in $\text{Nd}_{1.85-x}\text{La}_x\text{Ce}_{0.15}\text{CuO}_4$ did not significantly affect T_c . The importance of cation size ratio, electronic factors and oxygen fugacity for the crystal chemistry and superconductivity of these systems will be presented and discussed.

M6.3

A THERMOCHEMICAL INVESTIGATION OF THE La-Sr-Cu-O SYSTEM. Joseph Bularzik and Alexandra Navrotsky, Princeton University, Princeton, NJ; and Bruce Scott, Joe Bringley and Steve Trail, IBM Thomas J. Watson Research Center, Yorktown Heights, NY.

The perovskite related La_2CuO_4 oxides substituted with alkali earth metals were one of the first classes of high temperature superconductors discovered. As with many of the high temperature superconductors the crystal structure is well known and there are many studies on the electronic and magnetic properties. The thermodynamic properties are also very important to understand the ability and superconducting mechanism of these structures.

Solution calorimetry using a lead borate solvent has been performed on La_2CuO_4 and the related Sr substituted oxides. The variation of the heat of solution with the Sr content will be discussed. Calorimetric measurements on the oxide components (CuO , La_2O_3 , $\text{La}(\text{OH})_3$, SrCO_3) yield heats of formation.

The oxygen content in the superconducting phases can be varied, changing the properties, the T_c for example. An accurate analysis is necessary for meaningful thermodynamic data. X-ray analysis, iodometric titrations and TGA were used.

M6.4

STRUCTURAL AND MAGNETIC PROPERTIES OF UNTWINNED $\text{YBa}_2\text{Cu}_3\text{O}_{6+x}$ SINGLE CRYSTALS. Debra L. Kaiser, Frank W. Gayle, Lydon J. Swartzendruber and Winnie Wong-Ng, National Institute of Standards and Technology, Gaithersburg, MD 20899; and Steven F. Watkins and Frank R. Fronczek, Dept. of Chemistry, Louisiana State University, Baton Rouge, LA 70803.

We have developed a thermomechanical process for the complete removal of twins from $\text{YBa}_2\text{Cu}_3\text{O}_{6+x}$ single crystals. Single crystal x-ray diffraction studies on untwinned crystals with superconducting transitions at 54 and 91 K have revealed that oxygen atoms in the O(4) positions in the basal plane are offset from the crystallographic mirror plane in the a direction, leading to "zig-zag" Cu-O chains. Other structural features will be described in detail. Preliminary magnetic susceptibility measurements on untwinned crystals have shown that twin boundaries are not the principal flux pinning sites in this material. Anisotropy in the magnetic properties along the a , b and c crystallographic directions will be discussed.

M6.5

$\text{Ba}_2\text{YCu}_3\text{O}_{7-\delta}$ CRYSTAL SURFACE LAYERS; ORTHORHOMBIC SPLITTING, DISLOCATIONS, AND CHEMICAL ETCHING. D.J. Werder, C. H. Chen, M. Gurvitch, B. Miller, L. F. Schneemeyer and J. V. Waszczak, AT&T Bell Laboratories, 600 Mountain Avenue, Murray Hill, NJ 07974.

We find by transmission electron diffraction that the orthorhombic splitting of the upper surface layers ($< 1 \mu\text{m}$) of single crystal $\text{Ba}_2\text{YCu}_3\text{O}_{7-\delta}$ is reduced, differing by 10 to 30 percent from the bulk value. We also find by transmission electron microscopy that in general the surfaces are of inferior quality, and thus, not representative of the bulk. These results have important consequences for those experiments that probe only the upper surface layers. By etching with $\text{Br}/\text{ethanol}$ and $\text{HClO}_4/\text{NaClO}_4$ the poor quality surfaces are removed.

M6.6

STRUCTURAL PHASE DIAGRAM AND SUPERCONDUCTING BEHAVIOR IN THE $\text{Ba}_{1-x}\text{K}_x\text{BiO}_3$ SYSTEM. J. D. Jorgensen, Shiyu Pei, D. G. Hinks, B. Dabrowski, D. R. Richards, A. W. Mitchell, and D. T. Marx, Materials Science Division, Argonne National Lab., Argonne, IL 60439; and S. K. Sinha, J. M. Newsam, D. Vaknin, and A. J. Jacobson, Exxon Research and Engineering Co., Annandale, NJ 08801.

We have determined the structures of five phases in the $\text{Ba}_{1-x}\text{K}_x\text{BiO}_3$ system for $0 < x < 0.5$ and temperatures of 10 to 500 K. Superconductivity occurs only in a cubic perovskite phase for $x > 0.37$. T_c is 30 K at the phase boundary and decreases with increasing x until a solubility limit for K is reached near $x = 0.5$. For decreasing x , at room temperature, the cubic phase transforms first to an orthorhombic Ibmm phase and then to a monoclinic I2/m phase involving rotational and then breathing-mode distortions of the BiO_6 octahedra, respectively. The occurrence of semiconducting behavior in the Ibmm phase, where only rotational distortions are present, cannot be explained on the basis of conventional band theory and raises intriguing questions about the existence of local or fluctuating Bi charge disproportionation which could play an important role in the superconducting behavior.

M6.7

ELECTRON-PHONON COUPLING IN SUPERCONDUCTING $\text{Ba}_{1-x}\text{K}_x\text{BiO}_3$: A RAMAN-SCATTERING STUDY.* K. F. McCarty, Sandia Nat. Lab., Livermore, CA; H. B. Radousky, Lawrence Livermore Nat. Lab., Livermore, CA; D. G. Hinks, Y. Zheng, and A. W. Mitchell, Argonne Nat. Lab., Argonne, IL; T. J. Folkerts and R. N. Shelton, U.C.-Davis, Davis, CA.

The isotropic perovskite $\text{Ba}_{1-x}\text{K}_x\text{BiO}_3$ has been studied at temperatures down to 4 K by use of Raman spectroscopy. Polycrystalline samples were prepared by two different methods and characterized by x-ray diffraction and magnetization measurements. Selected samples were characterized by neutron diffraction. The superconducting phases ($0.375 \leq x \leq 0.5$) are cubic with T_c 's approaching 30 K. The Raman spectra of these phases are a combination of intense electronic scattering and disorder-induced phonon scattering. The noncubic $\text{Ba}_{1-x}\text{K}_x\text{BiO}_3$ phases ($0 \leq x < 0.375$) have an additional, intense Raman peak at 569 cm^{-1} arising from the breathing-mode vibration of the oxygen octahedra. All $\text{Ba}_{1-x}\text{K}_x\text{BiO}_3$ phases have a Raman band around 325 cm^{-1} associated with an optical phonon dominated by oxygen vibration.

As superconducting $\text{Ba}_{0.6}\text{K}_{0.4}\text{BiO}_3$ is cooled, the phonon band at 348 cm^{-1} (43 meV) develops the distinctive Fano lineshape. This lineshape occurs when scattering from an electronic continuum interferes with scattering from a discrete phonon. Observation of a Fano lineshape is persuasive evidence for strong coupling between the phonon and electronic states. Significantly, the same phonon was not observed to be strongly coupled to the electronic states for nonsuperconducting $\text{Ba}_{0.8}\text{K}_{0.2}\text{BiO}_3$ at temperatures down to 4 K. The strong coupling of the optical phonon at 348 cm^{-1} is suggestive of phonon involvement in the superconducting state. Interestingly, electron-phonon coupling has been reported in the literature at nearly the identical frequency (340 cm^{-1}) for the triple perovskite $\text{YBa}_2\text{Cu}_3\text{O}_7$ as observed here for the Bi-based perovskite.

*Supported by the USDOE, OBES, Div. of Mat. Sciences under contracts DEAC04-76DP00789 (SNL) and W-31-109-ENG-38 (ANL) and USDOE under contract W-7405-ENG-48 (LLNL and UC-Davis).

M6.8

MAGNETIZATION MEASUREMENTS OF $5\mu\text{m}$ $\text{Ba}_{0.6}\text{K}_{0.4}\text{BiO}_3$ CRYSTALS: APPROACH TO INTRINSIC BEHAVIOR WITH DECREASING SIZE? G. S. Grader, A. F. Hebard and L. F. Schneemeyer, AT&T Bell Labs, Murray Hill, NJ 07974.

Magnetization measurements on cubic $\text{Ba}_{0.6}\text{K}_{0.4}\text{BiO}_3$ crystals, approximately $5\mu\text{m}$ in size, have been obtained using a recently-developed electrodynamic force balance technique. In the presence of a fixed magnetic field gradient, a uniform magnetic field is ramped and the initial field, $H_{c1}(T)$, at which flux enters the levitated crystal is determined as a function of temperature. The onset of flux entry is marked by a pronounced deviation from a linear magnetization together with a noticeable reorientation of the crystal near $H = 0$, a reorientation caused by a field-induced torque on the remanent moment. The dependence of H_{c1} on temperature is linear over the temperature range $7\text{K} \leq T \leq 30\text{K}$ with a slope approximately a factor of three higher than published values. These higher values of H_{c1} imply either intrinsically cleaner material with a reduced Ginzburg-Landau parameter κ or higher surface critical fields. In addition, our failure to observe time-dependent flux creep (with a resolution of 100 ms after applying a field) is to be contrasted with published results on polycrystalline material where flux creep is detectable at significantly longer (hours) time scales. These results, a higher H_{c1} and extremely rapid flux entry, suggest that the intrinsic properties of high- T_c superconductors may be more accurately reflected in small crystals which are more likely to be of higher quality than larger crystals.

M6.9

HIGH TEMPERATURE NEUTRON DIFFRACTION STUDY OF THE FORMATION REACTION OF BISMUTH SUPERCONDUCTORS, M. F. Garbauskas and R. H. Arendt, General Electric Company, Corporate Research and Development, P. O. Box 8, Schenectady, NY 12301, J. D. Jorgensen and R. L. Hitterman, Argonne National Laboratory, 9200 S. Cass Ave., Argonne, IL 60439-4814.

A number of species have been identified in the (Bi,Pb)-Ca-Sr-Cu-O system which superconduct with transition temperatures ranging from ~ 10 to $\sim 110\text{K}$. The mechanism of the formation of these different compounds is not well understood. Further, it is not known if the species, both superconducting and non-superconducting, observed at room temperature are the same as those existent at the formation temperatures. The course of the chemical reaction of the 110K superconducting compound was followed using high temperature neutron diffraction. The identity and evolution of the phases formed during the reaction will be discussed.

This work has benefitted from the use of the Intense Pulsed Neutron Source at ANL which is funded by DOE, BES-Materials Science, Contract W-31-109-ENG-38.

M6.10 ABSTRACT NOT AVAILABLE

M6.11

INFRA-RED INVESTIGATIONS ON THE LATTICE INSTABILITY OF SINGLE PHASE (Bi,Pb) $_{1-x}\text{Sr}_x\text{Ca}_1\text{Cu}_1\text{O}_{10+x}$ SUPERCONDUCTING CERAMIC. He Aisheng, North University of Technology, Beijing, China; Zhang Jincang and Chang Fanggao, Henan Normal University, Xinxiang, China; Xiang Jiong and He Yusheng, Tsinghua University, Beijing, China

Temperature dependent infra-red absorption experiments were conducted on a single phase (Bi,Pb) $_{1-x}\text{Sr}_x\text{Ca}_1\text{Cu}_1\text{O}_{10+x}$ sample. Typical spectra showed that three absorption peaks

can be seen at 293K . The one at 610cm^{-1} (A1) is remarkable whereas the other two (A2= 1020cm^{-1} , A3= 1490cm^{-1}) are small but distinguishable. The peaks keep no change until 205K , where a new peak A2'= 900cm^{-1} appears. It is interesting to point out that as the temperature was stabilized at $203.5 \pm 0.5\text{K}$ for more than 30 minutes, the gradual growth of A2' peak, and the vanishing of A2 peak can be clearly seen, implying a quasi-isothermal process. This is in agreement with the results of time dependent ultrasonic measurements at $209.0 \pm 0.1\text{K}$ on the similar samples, in which the isothermal-like changes in both attenuation and velocity of both longitudinal and shear waves can last for more than 20 minutes. Specific heat anomalous hump and lattice constants anomalous increases appeared also near this temperature, indicating a possible phase transition taking place. It is also apparent that followed the sudden changes both A1, A2' showed rapid fluctuations until $150\text{--}140\text{K}$, which is consistent with those observed in ultrasonic and x-ray study. Dmowski et al proposed a model of short-range ordering due to displacements of Tl (or Bi in our case) and O atoms [Phys. Rev. Lett. 61(1989) 2608]. Such displacements of Bi and O atoms might take place at about 200K , leading to the structure phase transition and the tunneling motion of the atoms between their two equivalent positions could result in the observed unstable behavior between $200\text{--}150\text{K}$.

M7.1

ELECTRONIC STRUCTURE CALCULATIONS OF THE COPPER-OXYGEN PLANES IN $\text{YBa}_2\text{Cu}_3\text{O}_{6+y}$ FOR $0 < y < 1$. J. A. Cogordan, Instituto de Investigaciones en Materiales, Universidad Nacional Autónoma de México, Apdo. Postal 70-360, 04510 México D.F., México.

Molecular *ab initio* self-consistent field calculations, on clusters, simulating the copper-oxygen planes in the $\text{YBa}_2\text{Cu}_3\text{O}_{6+y}$ are reported. The changes in the electronic structure are studied as a function of the variation of the lattice parameters due to oxygen concentration, $0 < y < 1$.

Open and Closed shell calculations are performed, and it is found that the open shell states are energetically favored for $.4 < y < .9$.

M7.2

ON THE NATURE OF HOLES IN $\text{YBa}_2\text{Cu}_3\text{O}_{7-x}$

E.E. Alp, J.C. Campuzano, G. Jennings, J. Guo, L. Beaulaigue, S.M. Mini, Argonne National Laboratory, Argonne IL 60439; M. Faiz, Y. Zhou, University of Illinois at Chicago, P.O. Box 4348, Chicago, IL 60680; J.Z. Liu, Northwestern University, Evanston, IL 60201.

Angle-resolved oxygen K-edge x-ray absorption spectroscopy measurements were performed on single crystals of $\text{YBa}_2\text{Cu}_3\text{O}_{7-x}$. The crystals were cleaved in situ, under ultra-high vacuum, while the sample stage was cooled to 20K . Measurements were carried out both at low temperature and at room temperature. It was found that there are two distinct transitions between 526 and 531eV . The peaks in $\text{YBa}_2\text{Cu}_3\text{O}_{7-x}$ show strong orientation dependence, as well as an energy dispersion of 2eV . One of the peaks disappears after the sample is heated to room temperature. Comparison of the experimental results to a transition-state calculation of the absorption cross section shows good agreement with the data. It is found that there are holes of s-symmetry on all Cu-O bonds.

Work supported by U.S. DOE, BES-Materials Sciences Contract #W-31-109-ENG-38

M7.3

BAND DISPERSION AND THE FERMI SURFACE OF YBa₂Cu₃O_{6.9}

I.C. Campuzano, G. Jennings, M. Faiz, L. Beaulaigue, B.W. Veal, A.P. Paulikas, J.Z. Liu, H. Claus, K. Vandervoort, Argonne National Laboratory, Argonne, IL 60439; A.J. Arko, R.S. List, R.J. Bartlett, S.W. Cheong, Los Alamos National Laboratory, Los Alamos, NM 87545; C.G. Olson, A.B. Yang, R. Liu, C. Gu, Ames National Laboratory, Ames, IA 50011

VUV Photoemission spectroscopy measurements of YBa₂Cu₃O_{6.9} single crystals cleaved in situ while cooled to 20K in ultra-high vacuum were carried out. Under these conditions, oxygen loss is minimised, and the surface is representative of the bulk superconductor. The measurements reveal that YBa₂Cu₃O_{6.9} is a good metal, while YBa₂Cu₃O₆ is a highly correlated insulator. The bands show dispersions in YBa₂Cu₃O_{6.9} as large as 0.22 eV, in agreement with band structure calculations using the local density approximation. The bandwidth is also in good agreement at the centre of the Brillouin zone. By monitoring the dispersion of the bands as they cross the Fermi energy, the Fermi surface is mapped. The Fermi surface so obtained shows good agreement with the predictions of LDA band structure calculations, and also shows good agreement with the Fermi surface measured by positron annihilation experiments

Work supported by U.S. DOE, BES-Materials Sciences Contract #W-31-109-ENG-38

M7.4

HIGH TEMPERATURE CERAMIC SUPERCONDUCTORS AND EXACT SOLUTIONS OF THE NON-LINEAR LANDAU-GINZBURG EQUATIONS. Jack A. Tuszynski, University of Alberta, Edmonton, Canada; and John M. Dixon, University of Warwick, Coventry, U.K.

A direct link has been established between an effective microscopic BCS Hamiltonian and a Landau-Ginzburg (LG) order parameter description of both standard and high temperature superconductors. Using very recent mathematical discoveries, which have used the Symmetry Reduction Method to find exact solutions of highly non-linear partial differential equations, we have found a complete set of one-dimensional analytical solutions of the equation of state for the LG free energy density. This has been done both in the absence and presence of superconducting currents. For the two-dimensional case we have provided asymptotic and approximate expressions.

We distinguish two qualitatively distinct types of behaviour. When the effective mass of the Cooper pairs, $m^* > 0$, we find a mean field ground state, homogeneous in space, which corresponds to standard superconductor theory; when $m^* < 0$ the ground state is highly inhomogeneous and leads to a penetration field which is periodically damped and much larger in high T_c materials. In this latter case the dependence of the critical current may take a variety of forms as a function of reduced temperature and the coherence length is orders of magnitude shorter, as observed. We conjecture that to explain high temperature superconductivity one should assume $m^* < 0$ and close to $T = T_c$ ($m^* \rightarrow m_0(T_c)$), so that the normal-to-superconducting transition is driven by the temperature dependence of the effective mass. In this case the mean field coefficient A , in the vicinity of $T = T_c$, would then only be weakly temperature dependent.

M7.5

HOLE CONCENTRATION AND SUBSTITUTIONAL DISORDER IN COMPENSATION DOPED NdBa₂Cu₃O_y. T. Penney, M. W. Shafer, and B. L. Olson, IBM Research Division, T. J. Watson Research Center, Yorktown Heights, NY 10598 USA

The purpose of this work is to determine the effects of hole concentration and substitutional disorder on the transition temperature, T_c , in high temperature superconductors, by several compensation doping experiments. In order to obtain reliable hole concentrations we have measured the total holes by iodometric titration and the mobile holes by the Hall effect. The Hall constant for YBa₂Cu₃O_y is temperature dependent, so the hole concentration is undetermined, by Hall measurements alone. We have found that for various substitutions of the form Nd_(1-x)-Ca_xBa_{2-x}Cu_{3-z}Zn_zO_y with all Y replaced by Nd, the temperature dependence of the Hall constant is small at 100K so a unique Hall number is determined. We find that the Hall number correlates well with the number of mobile holes on the planes as calculated from the total chemical holes by the recipe of Tokura et al. From our work and the work of others, for a variety of materials with the YBa₂Cu₃O_y structure, there is a dome shaped master curve of T_c vs hole concentration, with a maximum at about 90K and 0.2 holes / plane Cu.

We have made several double doping experiments to test the validity and form of the master curve and to compare substitutions on and off the Cu-O planes. Substitution of Nd for Ba reduces the number of mobile holes and T_c . However when Ca compensates for some of the Nd, the number of mobile holes and T_c increase. In YBa₂Cu_{3-x}Zn_xO_y the number of holes increases and T_c decreases but one can not separate the effect of the hole concentration from that of the disorder due to Zn at least partially on the Cu-O planes. Our new compensation system is Nd_{1.1}Ba_{1.9}Cu_{3-z}Zn_zO_y which lies on the left side of the dome. With increasing Zn, holes and T_c initially increase following the master curve, but then between $z = 0.01$ and 0.05 falls 20K below the curve, unambiguously showing the effect of substitutional disorder.

M7.6

ELECTRONIC STRUCTURES OF Ga- AND Zn- SUBSTITUTED YBa₂Cu₃O₇ SUPERCONDUCTORS. Yong-nian Xu and W.Y. Ching, University of Missouri-Kansas City; Department of Physics, Kansas City, Mo 64110; K.W. Wong, University of Kansas, Lawrence, Ks 66045

The electronic band structures of YBa₂Cu₃O₇ superconductor in which one of the Cu atom was replaced by Ga or Zn have been studied by means of the first-principles orthogonalized LCAO method. Both cases of substitution involving the Cu on the chain site and the Cu on the plane site were investigated. Our results show significant modifications in the electronic structure due to the site-specific substitution. The Ga substitution reduces the density of states (DOS) at the Fermi level by more than a factor of 2. For the Zn substitutions, the reductions of DOS at the Fermi level are smaller. Ga substitution at the chain site results in the complete removal of the one dimensional chain band near and above the Fermi level. These and other results will be discussed together with current experimental observations on substituted YBa₂Cu₃O₇ samples.

* Supported by DOE Grant No. DE-FG02-84ER45170

M7.7

STUDIES OF THE ELECTRONIC STRUCTURE OF HTSC AND RELATED COMPOUNDS BY X-RAY PHOTOELECTRON SPECTROSCOPY. S. Myhra, A.E. Bocquet, J.F. Dobson and P.C. Healy, Griffith University, Queensland, Australia; P. Goodman and T.J. White, Melbourne University, Victoria, Australia; A.M. Stewart and J.G. Thompson, Australian National University, ACT, Australia.

A range of HTSC compounds have been studied by XPS (La_{2-x}(Sr,Ba)_xCuO₄, RE-1-2-3, Bi-2-2-0-1, Bi-2-2-1-2 and Tl-2-2-1-2). It is found that low binding energy contributions to the O 1s and alkaline earth (Ca,Sr,Ba) core photoelectron lines are features common to all these compounds. The observations are consistent with initial

state screening mechanisms. The additional charge on or near the alkaline earth sites should be very polarizable. This may either cause electron or hole pairing in other layers of the compound, or may enhance a tendency to pair by some other mechanism. The structurally related Aurivillius phases and the $\text{Ca}(\text{Ba}, \text{Sr})\text{TiO}_3$ perovskites which are insulators, do not exhibit these features. However, the compound $\text{La}_{1-x}\text{Sr}_x\text{CoO}_3$, which is "metallic" but not superconducting, also have low binding energy O 1s and Sr 3d components. Thus it may be that these XPS fingerprints are characteristic of the wider class of "metallic" oxides, and are necessary, but not sufficient, indicators of HTS.

These studies have recently been extended to the $\text{RE}_{2-x}\text{Ce}_x\text{CuO}_4$ compounds (RE=Pr, Sm and Nd). Results for semiconducting as well as e- and p-type HTSC preparations will be reported.

M7.8

THE EFFECT OF MAGNETIC FIELD ON THE CRITICAL CURRENT DENSITY OF BULK SUPERCONDUCTING WIRES. M. T. Lanagan, U. Balachandran, C. A. Youngdahl, J. T. Dusek, J. J. Picciolo, and R. B. Poeppel, Argonne National Laboratory, Argonne, IL.

Bulk $\text{YBa}_2\text{Cu}_3\text{O}_{7-x}$ (YBCO) wires were fabricated by a conventional extrusion technique and sintered above 900°C. Critical current density (J_c) was measured as a function of applied magnetic field at 77 K and was found to decrease significantly at fields below 100 G. Such degradation of J_c has been attributed to weak link behavior at the grain boundaries.

Two different diameter wires were processed identically, and the smaller-diameter wire had the higher J_c . It has been suggested that magnetic fields, which are generated by electrical current, limit the current-carrying capacity of the wire. Magnetic fields on the order of 10 G have been generated by currents in bulk wire, and fields of this magnitude have been observed to significantly decrease J_c .

A YBCO tube was fabricated and a copper wire was placed down the center of the tube. A concentric magnetic field was generated by a current in the wire and could interfere constructively or destructively with the magnetic field in the tube. J_c increased by 10% when the current in the YBCO tube was opposite to the current in the copper wire. The enhancement of J_c was attributed to the partial cancellation of the magnetic field in the YBCO tube.

Work supported by the U. S. Department of Energy, Office of Energy Storage and Distribution, Conservation and Renewable Energy, under Contract W-31-109-Eng-38.

M7.9

Sandwich Excitons as the Mechanism of Superconductivity in Cuprates and Bismuthates.* Brent A. Richert, Department of Physics, U.S. Air Force Academy, Colorado Springs, Colorado 80840; Ewald Schachinger, Institut für Theoretische Physik, Technische Universität Graz, Austria; and Roland E. Allen, Department of Physics, Texas A&M University, College Station, Texas 77843.

We consider an excitonic model in which the electron is localized in a d orbital on a metal site, and the hole is in a linear combination of p orbitals on the surrounding oxygen sites, with both electron and hole in an insulating LaO , BaO , etc. layer adjacent to a metallic CuO_2 or BiO_2 plane. Even for rather large effective dielectric constants, some of the excitons are found to be tightly bound and consequently to have sizable transition densities $\alpha(x)\beta(x)$. We calculate the attractive carrier-carrier interaction $V(q)$, and use it to estimate the superconducting T_c as a function of the parameters in the model. This excitonic mecha-

nism appears to provide a natural and consistent interpretation of high-temperature superconductivity in both the cuprates and bismuthates.

*Supported by Office of Naval Research (N00014-82-K-0447).

M7.10

AC SUSCEPTIBILITY STUDIES OF THE HIGH T_c SUPERCONDUCTORS: DISSIPATIVE EFFECTS IN THE $\text{La}_{2-x}\text{Sr}_x\text{CuO}_{4-y}$ AND $\text{YBa}_2\text{Cu}_3\text{O}_{7-y}$ SYSTEMS. Xinsheng Ling, Mark Filipkowski, Joseph I. Budnick, Department of Physics & Institute of Materials Science, Univ. of Connecticut, Storrs, CT.

We present ac susceptibility results of the $\text{La}_{2-x}\text{Sr}_x\text{CuO}_{4-y}$ (2-1-4): $x=0.07, 0.1$ and the $\text{YBa}_2\text{Cu}_3\text{O}_{7-y}$ (1-2-3) high- T_c superconductors. The data of the out-of-phase component χ'' of the susceptibility in zero field of sintered solids of the two systems show that the energy dissipation below T_c is very large in the 2-1-4 materials but very small in the 1-2-3 materials. We discuss the possible origins of this difference between the 2-1-4 and the 1-2-3 systems based on several models in high T_c superconductivity.

M7.11

TRANSPORT CRITICAL CURRENT OF SINTERED $\text{YBa}_2\text{Cu}_3\text{O}_x$ IN TIME-VARYING MAGNETIC FIELDS. P. D. Hambourger, J. DiCillo, M. Gibberman, J. Marino, L. P. Vitek, Cleveland State Univ., Cleveland, OH 44115;* and Michael A. Centanni, Ferro Corporation, Independence, OH 44131.

Susceptibility data by many authors¹ suggest that oscillating (10 Hz-10 kHz) magnetic fields are more effective in penetrating bulk YBCO than are static fields of the same magnitude. If so, transport critical current (J_c) might be more severely reduced by time-varying fields than by static fields. We have measured direct-current four-lead J_c in sintered samples at 77 K using steady and sinusoidally-time-dependent (5-100 Hz) magnetic fields of up to 40 G - sufficient to suppress J_c to ~20% of its zero-field value. The field was oriented either parallel or perpendicular to the current. In all cases, the magnetic field strength required for a given reduction of J_c was independent of frequency to within ~10%. Data taken at lower temperatures and with non-sinusoidal field waveforms will be presented.

*Supported in part by the Ohio Board of Regents Research Challenge Program and by NASA (Grants NCC-3-19 and NAG-3-873).

¹See, for example, R. B. Goldfarb et al, Extended Abstracts, Symposium S, 1987 Fall Meeting, Materials Research Society, p. 261.

M7.12

INFLUENCE OF METALLIC SILVER INFILTRATION ON THE MICROSTRUCTURE AND TRANSPORT PROPERTIES OF YBaCuO . L. Ryelandt, M. Cassart, A. Vandenbosch, F. Delannay and J-P. Issi, Unité de Physico-Chimie et de Physique des Matériaux, 1 Place Croix du Sud, B-1348 Louvain-la-Neuve, Belgium,

Wires of $\text{YBa}_2\text{Cu}_3\text{O}_{7-\delta}$ have been prepared by swaging using silver for the metal sheath. The influence of the heat-treatment conditions on the microstructure and transport properties (i.e. thermal conductivity, thermoelectric power and electrical

resistivity) has been investigated. The same measurements have been performed on bulk samples pressed and sintered between two silver sheets.

Due to the infiltration of silver into the superconductor, composite materials were obtained. The electrical resistivity was found to decrease by more than one order of magnitude. It was observed that the presence of silver inside the bulk of the superconducting ceramic affects the grain growth and the porosity, that it does not reduce the T_c and J_c values, and that it leads to a very small contact resistance between the oxide and the metal.

M7.13

COMPARISON OF FLUX DYNAMICS IN TWO SAMPLES OF $YBa_2Cu_3O_7$ WITH DIFFERENT PINNING. M. Turchinskaya, L.H. Bennett, L.J. Swartzendruber, A. Roitburd, C.K. Chiang, M. Hill, and J.E. Blendell, NIST, Gaithersburg, MD, 20899, and K. Sawano, Nippon Steel Corp., Kawasaki 211, Japan.

The flux dynamics in two samples of $YBa_2Cu_3O_7$, with very similar equilibrium superconducting properties, but with substantially different pinning structures, are compared. One sample was produced by a melt growth process¹ (MGP) and the other by a solid state reaction² (SSR). Measurements by ac susceptibility with an applied field of 0.5 Oe gave sharp transitions for both samples. The onset temperatures were 92 K with transition widths (10%-90%) less than 2 K. Both were fully diamagnetic for temperatures less than about 85 K. Hysteresis loops and magnetization vs. time data were obtained at various temperatures for a number of applied fields. Magnetization as a function of time showed the characteristic $\ln(t)$ behavior for both samples. At low temperatures ($T < 40$ K) $dM/d\ln(t)$ was nearly equal for both samples and was a linear function of T . Also for $T < 40$ K hysteresis loops for both samples were well described by the critical-state model. At 77 K, the SSR sample showed large deviations from this model, whereas the MGP sample retained significant pinning and was still describable by the critical-state model. The MGP sample exhibited attractive levitation at 77 K. There is also a large difference in transport critical current at this temperature.

1. M. Murakami, M. Morita, K. Doi and K. Miyamoto, Jpn. J. Appl. Phys., to be published.
2. J.S. Wallace, E.R. Fuller, Jr., A.S. Raynes, S.W. Freiman, J.E. Blendell, M. Balmer, and M. Hill, Proc. TMS Symposium on High Temperature Superconducting Oxides: Processing and Properties, Las Vegas, March, 1989.

M7.14

FLUX PINNING AND WEAK LINK STRUCTURE IN $Ca_2Cu_1O_3$ doped $LnBa_2Cu_3O_{7-y}$ ($Ln=La, Y$). Fumio Mizuno, Hiromu Masuda, Izumi Hirabayashi, and Shoji Tanaka, Superconductivity Research Laboratory, Nagoya Division, ISTE, 2-4-1, Mutsuno, Atsuta-ku, Nagoya 456, Japan.

The effect of Ca doping on the flux pinning and the weak link structure of the $LnBa_2Cu_3O_{7-y}$ ($Ln=La, Y$) system have been studied. The magnitude and the magnetic field dependence of the critical current density were improved by Ca doping. A small amount of impurity phases of Ca-related compounds such as $Ca_2Cu_1O_3$ may work as a desirable flux pinning center. Moreover, it was found that the current-temperature characteristics for Ca-doped samples showed the evidence of two kinds of superconductor phases which have different transition temperatures T_c and T_c' . The experimental result agreed well with the Ambegaokar-Baratoff theory for asymmetric Josephson junctions (S-I-S) in the temperature range of $T < T_c'$ and with proximity junction theory (S-N-S) in the range of $T_c' < T < T_c$.

M7.15

EASILY ACTIVATED FLUX CREEP AND ANISOTROPIC FLUCTUATION IN $NdCeCuO$ THIN FILMS S. Hatta, S. Hayashi, H. Adachi and K. Wasa Central Research Laboratories of Matsushita Electric Industrial Co., Ltd., Moriguchi, Osaka 570, JAPAN

We report magnetic properties of $NdCeCuO$ thin films with electron doped type. For the film of $Nd_{1.855}Ce_{0.145}Cu_{1.2}$, the sharp transition was observed at 22K. According to Bean model, J_c at 4.2K was estimated to be 10^4 A/cm². In configuration H // c, the logarithmic time dependence of diamagnetization was observed below 300 Oe. The activation energy could be estimated to be 0.01 eV, which was much lower than other superconducting films with hole doped type. When H was increased more than 400 Oe, the diamagnetization did not show any smooth time dependence, but it revealed largely fluctuating change. In the case of H \perp c, definite diamagnetization was obtained for the film thicker than the penetration depth. Different from the H//c configuration, both the relaxation and the fluctuation were poor. This anisotropic field effect was also observed in the temperature dependence of diamagnetization. At H=1kOe, the diamagnetization decayed within several K in H//c configuration, while it held out up to T_c in the case of H \perp c. Such a field effect seemed to be enhanced in the $NdCeCuO$ films, compared to other films. This suggests that the flux creep might be dominant in a weak field, however, that the fluctuation mechanism caused by H would be likely in the relatively high field.

M7.16

MAGNETIZATION AND FLUX BEHAVIOUR OF $YBa_2Cu_3O_{7-x}$ SUPERCONDUCTING RINGS. Shoichi Yokoyama, Kenji Shimohata, Toshie Ushijima and Tadatosh Yamada, Central Research Laboratory, Mitsubishi Electric Corporation, AMAGASAKI, HYOGO, 661 JAPAN

The magnetization and flux creep measurements at 77K were carried out for the ring and powder of $YBa_2Cu_3O_{7-x}$. Samples of $YBa_2Cu_3O_{7-x}$ rings (OD19xID13x7mm) were made by the sintering process. The magnetic fields of central region of the ring were measured by a Hall device. In order to measure the flux creep of the samples, we applied the external fields of 2kG to the samples, and decreased the fields to the lower fields between zero and 800G. Samples of plates (13x4mm) were made by cold-pressing the powder that was obtained by crushing the rings. The Hall device was set between the two plates. The magnetization and flux creep of the plates were measured by the same method for the ring. The critical current density (J_c) of about 200 A/cm² at zero external field for the rings was estimated by hysteresis of the magnetization. The flux creep equation is given by Anderson and Kim model as $M(t)/M(0) = 1 - kT/U_0 (\ln t)$ where k is Boltzmann's constant, T is temperature, U_0 is pinning potential, t is the time and $M(t)$ is magnetization. The flux creep data of rings and plates were almost agreed with this equation. The pinning potentials U_0 of 1.2eV for the ring and 0.9eV for the plate at zero external field were obtained from the flux creep data. The dependence of U_0 on external field for the ring was greater than that for the plate.

M7.17

VORTEX STRUCTURE: LATTICE, GLASS, OR LIQUID?

Robert J. Soulen, Jr., S.A. Wolf, Naval Research Laboratory, Washington, DC.

Recent measurements of the dissipation of vibrating reeds coated with cuprate superconductors in a magnetic field have been interpreted as providing evidence for the presence of new phases in type II superconductors: flux liquids or flux glasses. Further evidence has been cited on the basis of resistivity. We present data and a model which suggest that a more conventional interpretation in terms of the electro-dynamics of the vortices can adequately account for all the observations.

M7.18

THE UPPER CRITICAL MAGNETIC FIELD OF SUPERCONDUCTING $\text{YBa}_2(\text{Cu}_{1-x}\text{Ni}_x)_3\text{O}_7$, Youwen Xu, A.R. Moodenbaugh, and M. Suenaga, Material Science Division, Brookhaven National Laboratory, Upton, NY 11973*

The upper critical magnetic field H_{c2} of a series samples of $\text{YBa}_2(\text{Cu}_{1-x}\text{Ni}_x)_3\text{O}_7$ is measured. Other related parameters, such as the lower critical magnetic field H_{c1} , the Ginsberg-Landau parameter κ and the jump in the specific heat dc/T_c , are calculated. Preliminary results show that the temperature dependence of the magnetization $M(T)$ is linear from a few degrees below T_c to 10 to 12 K below T_c . The field dependence $dM/dH(T)$ near T_c is linear with a constant slope. With 2% of Cu replaced by Ni, the value of H_{c2} is the same as the non-substituted sample. While the value of κ increases result in a lower H_{c1} .

*Supported by the U.S. DOE office of Basic Energy Sciences, Division of Materials Science, under contract No. DE-AC02-76CH00016.

M7.19

FLUX LATTICE MELTING IN ANISOTROPIC HIGH T_c SUPERCONDUCTORS. R.S. Markiewicz, Physics Department and Barnett Institute, Northeastern University, Boston, MA 02115

The Lindeman criterion for flux lattice melting in a uniaxially-anisotropic superconductor is found to give good agreement with experiment, both as to the shape of the melting phase diagram and as to the weak anisotropy of the transition. Studies of the flux lattice dispersion relations reveal further interesting features: a 'second sound' mode and a magnetoroton-like dip in the helicon branch.

M7.20

HIGH TEMPERATURE DEFECT CHEMISTRY OF UNDOPED AND Ce-DOPED Nd_2CuO_4 . D. J. L. Hong, A. Mehta, and D. M. Smyth, Materials Research Center, Whitaker Lab #5, Lehigh University, Bethlehem, PA 18015.

It has been reported that $\text{Nd}_{1.85}\text{Ce}_{0.15}\text{CuO}_4$ is superconducting below 24 K if it is annealed in a reducing atmosphere ($P(\text{O}_2) < 10^{-4}$ atm) at 1000°C [1]. This study correlates the high temperature defect structure of undoped and Ce-doped Nd_2CuO_4 with its electrical properties.

Equilibrium electrical conductivities of undoped and doped samples were measured as a function of temperature ($500 < T < 900^\circ\text{C}$) and oxygen partial pressure ($10^{-3} < P(\text{O}_2) < 1$ atm). Over most of the measurement region undoped Nd_2CuO_4 shows an n-type, semiconducting behavior, but for highly reducing conditions, i.e., below 10^{-3} atm and 900°C , it exhibits metallic behavior. At low temperatures ($< 500^\circ\text{C}$) and high oxygen partial pressure (1 atm), the material becomes a p-type semiconductor. In the doped material ($\text{Nd}_{1.85}\text{Ce}_{0.15}\text{CuO}_4$), the carrier concentration is fixed by the donor concentration, and it exhibits metallic behavior.

[1] Y. Tokura, H. Takagi, and S. Uchida. *Nature*, **337**, 345-347 (1989).

(Supported by the Division of Materials Research, NSF, and the Lehigh University Consortium for Superconducting Ceramics.)

M7.21

TRANSPORT AND DIAMAGNETIC PROPERTIES OF 2:2:1:2 AND 2:2:2:3 (Bi,Pb)-Sr-Ca-Cu-O SUPERCONDUCTING MATERIALS. R. Ibáñez, M. J. Sanchis, F. Sapiña, D. Beltrán, A. Beltrán, UICBM, Dpt. Química Inorgánica, Universitat de Valencia, C/Dr. Moliner 50, 46100 Burjassot (Valencia), Spain; C. Rillo, J. Bartolomé, F. Lera, R. Navarro, ICMA, CSIC-Universidad de Zaragoza, 50009 Zaragoza, Spain; G. F. de la Fuente, Fibertek, Inc., 510-A Herndon Parkway, Herndon, VA, USA.

The nature of the high T_c superconductive materials makes it difficult to densify them in wire-like form while maximizing their critical current densities. We have recently shown that the Laser Floating Zone (LFZ) method allows the growth of oriented polycrystalline fibers of the bismuth cuprate superconductive phases. The influence of the precursor composition and its preparation technique, as well as the effect of the LFZ growth parameters and post-growth annealing on the characteristics of the resultant fibers have been studied.

Results from a complete study of the evolution of the transport properties and the diamagnetism of "2212" and "2223" bismuth cuprate materials along their preparation procedure (including powder, sintered pellets and fibers) will be presented. In addition, the effect of Pb(Bi) and Ln(Ca) substitutions will also be discussed. The anisotropy in the diamagnetic properties of the fibers has been carefully determined by a.c. magnetic susceptibility and magnetization measurements, and the results will be related to their composition and microstructure.

M7.22

CRITICAL CURRENT DENSITIES IN $\text{Bi}_2\text{Sr}_2\text{CaCu}_2\text{O}_{8+d}$. Shunji Nomura, Yutaka Yamada, Tomohisa Yamashita, Eiko Yoneda, Hisashi Yoshino and Ken Ando, Research and Development Center, Toshiba Corporation, Komukai-Toshiba cho, Kawasaki, Kanagawa, 210 JAPAN

$\text{Bi}_2\text{Sr}_2\text{CaCu}_2\text{O}_{8+d}$ single crystal has been grown by a self-flux method. Transport phenomena and the magnetization of the single crystal have been studied. We have measured the temperature dependence of resistivities, critical fields (H_{c1} and H_{c2}) and critical current densities at 77K by transport in a field up to 14 T as well as by M-H loops in a field up to 5 T.

Three different critical current densities were obtained depending on the relative orientation of the current, the magnetic field and the Cu-O planes. The magnetic field dependence for the critical current densities was stronger at 77K than that at 10K.

An anisotropy in the critical current densities within the c plane and along the c axis was found to be approximately 10 in the critical current density ratios in

quantitative agreement with the anisotropy in the normal-state resistivity.

The magnetic field dependences of the critical current densities within the c plane measured in the fields applied within the c plane and along the c axis, where Lorentz forces could be caused in both directions, were quite different and the dependencies could be explained by the difference in upper critical fields.

The angular dependence of the critical current densities along the c axis in fields applied within the c basal plane obviously appeared in the single crystals. The anisotropy in flux pinning force density is found to be $F_p b/F_p a=3$. The data provide strong evidence for flux pinning by the incommensurate modulated structure in this system.

M7.23

CORRELATIONS BETWEEN THE Cu-O BONDING STATES AND THE SUPERCONDUCTIVITY. S.C.Han^{1,3}, D.Z.Liu², X.M.Xie¹, Z.L.Wu¹, G.C.Huth³. 1) Shanghai Institute of Metallurgy, Chinese Academy of Sciences, Shanghai, China; 2) Shanghai Institute of Testing Technology, Shanghai, China; 3) Xsunus Superconductivity, Inc., 7590 E. Gray Road, Suite 103, Scottsdale, AZ 85260

X-ray photoelectron core-level spectra (XPS) has been measured for CuO , $\text{YBa}_2\text{Cu}_3\text{O}_x$, $\text{Bi}_2(\text{Sr,Ca})_2\text{Cu}_2\text{O}_x$ and $\text{Bi}_2\text{Sr}_2\text{Ca}_2\text{Cu}_2\text{O}_x$ in order to observe the correlation between the Cu-O bonding states and the superconductivity. Both the $\text{Cu } 2p_{3/2}$ and $\text{O } 1s$ lines are found to be composed of three Gaussian peaks, which are related to the $3d^{10}L$, $3d^9L$ and $3d^{10}$ initial states (L indicates a ligand hole in the O $2p$ band). In the insulator CuO , the $\text{Cu } 2p_{3/2}$ line shows an essential feature of the $3d^9$ and $3d^{10}L$ initial states. The $3d^9L$ feature is only observed in YBCO and BSCCO compounds. In $\text{Bi}_2\text{Sr}_2\text{Ca}_2\text{Cu}_2\text{O}_x$, the $3d^{10}$ signal diminishes, whereas the $3d^{10}L$ and $3d^9L$ states are dominant. These results confirm that a localized picture is necessary for CuO . The $3d^9$ and $3d^{10}L$ states in CuO can be treated as quasiparticles (neutral fermions with spin 1/2). The insulating behavior is determined by a gap of charge-transfer from the $3d^9$ to the $3d^{10}L$ states. Hole-doping produces the $3d^9L$ state which is a sort of bosonic quasiparticle carrying a unit of positive charge $1e$ and spin 0 or 1. Pairing of the $3d^9L$ bosons gives rise to the "p-type" superconductivity, and T_c seems to increase with the density of the $3d^9L$ state. The charge is both distributed on copper and oxygen sites. Overdoping reduces the $3d^9L$ density and thus T_c . Symmetrically, electron-doping produces the $3d^{10}$ bosons with charge e and spin 0 or 1. The $3d^{10}$ bosons are probably responsible for the "n-type" superconductivity. However, since in most of the copper oxides both the hole-like $3d^9L$ and the electron-like $3d^{10}$ states are present, the single-carrier model is not appropriate, and the possibility of the $3d^9L$ "hole" superconductivity in the "n-type" materials still can not be ruled out.

M7.24

CRITICAL CURRENT AND PROCESSING TEMPERATURE IN ALIGNED SINTERED COMPACTS OF $\text{YBa}_2\text{Cu}_3\text{O}_{7-\delta}$. J.E. Tkaczyk, K.W. Lay, GE Corporate Research and Development, Schenectady, NY.

Magnetically aligned as well as non-aligned $\text{YBa}_2\text{Cu}_3\text{O}_{7-\delta}$ ceramics were prepared through a powder processing method using a range of sintering and annealing temperatures. A rapid rise in density for samples sintered above 900 C signals the onset of liquid phase sintering. Accompanying the decrease in porosity is a drop in the room temperature resistivity and a increase in the critical current density. A oxygen anneal at 890C improved performance as compared to anneals at 500C possibly due to the high temperature decomposition of carbonates. The anisotropic properties of the Josephson coupling across grain boundaries as well as the anisotropy of the intragranular critical current accounts for the improved performance observed in the aligned materials. Through reduction of self-field effects, critical currents over 10^3 A/cm^2 at 77K are reproducibly obtained. The maximum J_c in a 1/4 tesla magnetic field was 16 and 200 A/cm^2 attained in the non-aligned and aligned materials respectively, for sintering temperatures of 950 and 980C. The reduction in J_c at higher sintering temperatures is attributed to increased microcracking of larger grains and to incongruent melting at the grain boundaries.

* Partial Support provided by the Defense Advanced Research Projects Agency contract # N00014-88-C-000681.

M7.25

GROWING OF $\text{Nd}_{2-x}\text{Ce}_x\text{CuO}$ SINGLE-CRYSTALS BY A FLUX METHOD. S. Pinol and C. Miravittles, ICMB-CSIC Avda Marti i Franques S/N Barcelona (08028) Spain. J. Fontcuberta, Dept Fisica Fonamental Univ de Barcelona, Diagonal 647 Barcelona (08028) Spain. D. Paul, Dept of Physics, Univ of Warwick Coventry CV47AL, U.K.

We have investigated single-crystals growth of $\text{Nd}_{2-x}\text{Ce}_x\text{CuO}$ by using a flux method. The phase diagram $\text{Nd}_2\text{O}_3\text{-CuO}$ has been determined for a number of compositions. In addition, the corresponding diagram for some $\text{Nd}_2\text{O}_3\text{-CeO}_2$ compositions will be also reported. Plate single crystals having dimensions up to $5 \times 5 \times 0.2 \text{ mm}^3$ have been prepared by cooling the alumina crucibles containing the melt mixtures, from 1250 °C to 800 °C at a rate of 5 °C/h.

Crystals has been characterized by EDAX, Magnetic Susceptibility and Resistance Measurements. The yield of x values in the starting compositions and the corresponding values in the crystals has been investigated in order to optimize starting compositions to improve superconducting properties. Superconducting single crystals have been found for flux compositions 70% CuO , (30-x)% Nd_2O_3 and z% of CeO_2 with $3.75 < z < 5$

M7.26

Magnetic and Phonon Scattering in $\text{Nd}_{2-x}\text{Ce}_x\text{CuO}_{4-\delta}$: Normal State and Superconducting Properties. J.L. PENG AND R.N. SHELTON, Department of Physics, University of California, Davis, CA 95616; H.B. RADOUSKY, Lawrence Livermore Laboratory, Livermore, CA 94578.

Samples of $\text{Nd}_{2-x}\text{Ce}_x\text{CuO}_{4-\delta}$ ($0 \leq x \leq 0.2$) were prepared by annealing both in air and under vacuum (10^{-5} torr). Powder x-ray diffraction patterns indicated that all samples consisted of a single phase Nd_2CuO_4 - type tetragonal structure with crystal symmetry $14/mmm$. Electrical resistivity measurements showed that all Ce doped $\text{Nd}_2\text{CuO}_{4-\delta}$ samples annealed in air and those annealed in vacuum with $x < 0.17$ demonstrate a Kondo effect resulting from the combination of magnetic and phonon scattering. Magnetic susceptibility and electrical resistivity measurements reflect the influence of crystal field effects below 55 K. The linear temperature dependent term of the resistivity typical of metallic behavior in the high- T_c oxides exists across the whole range of Ce concentration, with the exception of the host compound $\text{Nd}_2\text{CuO}_{4-\delta}$ which is an insulator. This indicates that a model of metal-insulator transition is not appropriate in describing the occurrence of superconductivity in $\text{Nd}_{2-x}\text{Ce}_x\text{CuO}_{4-\delta}$.

M7.27

SEMICONDUCTOR-METAL-SUPERCONDUCTOR TRANSITIONS IN UNDOPED AND Ce-DOPED Nd_2CuO_4 . A. Mehta, D. J. L. Hong, and D. M. Smyth, Materials Research Center, Whitaker Lab #5, Lehigh University, Bethlehem, PA 18015.

Nd_2CuO_4 behaves primarily as an oxygen-deficient, n-type material. It is observed that undoped Nd_2CuO_4 undergoes a semiconductor to metal transition at large carrier concentrations ($n > 7 \text{ mole}\%$). The large electron concentration required to transform the material to a metal can be created either by doping (Ce) or by sufficient reduction. Insufficient Ce doping ($< 7 \text{ mole}\%$) or reduction result in non-superconducting n-type semiconductors.

When the metallic samples are cooled at constant oxygen activity, the conductivity begins to decrease for temperatures below 500°C, apparently as a result of the trapping of charge carriers. For samples with increasing amounts of reduction, the trapping phenomenon becomes less significant.

The relationship between the metal-semiconductor transition and the "trapping" phenomenon to the superconducting transition in Nd_2CuO_4 will be discussed.

(Supported by the Division of Materials Research, NSF, and the Lehigh University Consortium for Superconducting Ceramics.)

M7.28

ANISOTROPIC THERMAL CONDUCTIVITY OF SUPERCONDUCTING LANTHANUM CUPRATE D. T. Morelli, G. L. Doll, and J. P. Heremans, Physics Department, General Motors Research Laboratories; M. S. Dresselhaus, A. Cassanho, D. R. Gabbe, and H. P. Jenssen, Center for Materials Science and Engineering, Massachusetts Institute of Technology,[†] Cambridge, MA 02139

We present the first measurements of the anisotropic thermal conductivity of a high- T_c superconducting material. The thermal conductivity of a Sr-doped, single crystal of lanthanum cuprate has been measured from room temperature to 4 K for the [100] and [001] tetragonal crystallographic directions. The sample has a nominal stoichiometry of $\text{La}_{1.0}\text{Sr}_{0.04}\text{CuO}_4$ and a superconducting onset temperature of 25 K, with zero resistance attained below 9 K. We observe that the thermal conductivity at room temperature for the [001] symmetry is a factor of three smaller than the [100] direction, and the anisotropy increases to over an order of magnitude in the liquid helium temperature range. This anisotropy is in contrast to the thermal conductivity of an undoped, semiconducting lanthanum cuprate (La_2CuO_4) crystal. We tentatively associate the anisotropy to a stronger phonon-phonon scattering in the [001] direction. In addition, we observe a small anomaly in the [100] conduction near T_c , whereas no corresponding effect is observed along the [001] direction.

[†] MIT work funded by the NSF under grant DMR87-FG05-85ER45151.

M7.29

INFRARED AND RAMAN SPECTROSCOPY OF PHONONS IN $(\text{Nd}/\text{Pr})_2\text{CuO}_4$ AND $(\text{Ca}_{0.86}\text{Sr}_{0.14})\text{CuO}_2$ M. K. Crawford*, Gerald Burns**, E. M. McCarron*, G. V. Chandrasekhar**, W. E. Farneth*, and T. M. Shaw**, *E. I. du Pont de Nemours & Co., Inc., P. O. Box 80356, Wilmington, DE 19880-0356; **IBM Research Division, T. J. Watson Research Center, Yorktown Heights, NY 10598-0218.

We report measurements of infrared (IR) and Raman active phonons in the (nominally) undoped electron superconductors Nd_2CuO_4 and Pr_2CuO_4 (T' structure), for ceramics and ab plane oriented crystals. Symmetry assignments are given based upon these results. Based upon ^{18}O substitution and comparison with other systems, phonon assignments are made. The effect of electron doping on the infrared and Raman active phonons will be described. Finally, a comparison to the $(\text{Ca}_{0.86}\text{Sr}_{0.14})\text{CuO}_2$ system, which has similar Cu-O planes is made. In the CaCuO_2 structure there are five IR active and no Raman active modes, in agreement with our experimental results. We assign the IR active phonons in $(\text{Ca}_{0.86}\text{Sr}_{0.14})\text{CuO}_2$ to specific structural elements. The similarities and differences seen in comparison with the T' materials will be related to details of the crystal structure.

M7.30

THE SEARCH FOR VERY HIGH TEMPERATURE SUPERCONDUCTIVITY IN THE TITANIUM BORIDE SYSTEM. Brian S. Ahern, Steven Bachowski, Rome Air Development Center, Hanscom AFB MA 01731

Early claims of anomalous conductivity within a high pressure phase of Tiboride compounds have never been verified. In this study a range of compounds within the Titanium Boride system have been evaluated for possible high temperature superconducting applications. TiB_2 and Ti_3B_4 samples were synthesized by a variety of techniques. TiB_2 was prepared in single crystal form via a high pressure float zone technique. The compounds were subjected to pressures as high as 350,000psi at room temperature in an attempt to discover a high pressure phase. Results will be presented on the electrical, magnetic and crystallographic characterizations of the crystals.

M7.31

EFFECTS OF OXYGEN STOICHIOMETRY ON THE MAGNETIC ORDERING OF $\text{La}_2\text{Ni}_{1-y}\text{Cu}_y\text{O}_{4+x}$ J. Zhao and M.S. Seehra, Physics Department, West Virginia Univ., Morgantown, WV 26506; A.F. Hepp and J.R. Gaier, NASA Lewis Research Center, Cleveland, OH 44135; and R.M. Richman¹, Mount St. Mary's College, Emmitsburg, MD 21727.

We present results of magnetic susceptibility and x-ray diffraction measurements of $\text{La}_2\text{Ni}_{1-y}\text{Cu}_y\text{O}_{4+x}$. Synthesis of title compounds was accomplished using standard solid state reaction methods with oxides and doping Cu for Ni, $y = 0.002$ to 0.05. After firing at 1200°C and regrinding three times, samples were quenched from 1000°C in either air or N_2 . We find the magnetic ordering to be very sensitive to the oxygen stoichiometry of the samples. Antiferromagnetic order is found below 10K in a liquid nitrogen-quenched sample and disappears when excess oxygen is introduced; the transition, however, is not affected by the presence of copper. Our data show that the magnetic properties and phase diagram of $\text{La}_2\text{NiO}_{4+x}$ are similar to the magnetic properties and phase diagram of $\text{La}_2\text{CuO}_{4+x}$, the parent compound of the 40K superconductors, as inferred from analogous literature data. We did not observe superconductivity² in any of our samples of $\text{La}_2\text{Ni}_{1-y}\text{Cu}_y\text{O}_{4+x}$.

1. Work performed at NASA Lewis Research Center as a Case-NASA Summer Faculty Fellow, 1988.
2. See: Z. Kakol, J. Spalek, and J.M. Honig, J. Solid State Chem 79, 1 (1989) for a report on the observation of diamagnetism in $\text{La}_{2-x}\text{Sr}_x\text{NiO}_4$.

M7.32

THE TRANSPORT PROPERTIES AND DEFECT CHEMISTRY OF $(\text{La}_{1-x}\text{Sr}_x)_2\text{CuO}_{4-\delta}$ Ming-Jinn Tsai, Elizabeth J. Opila and Harry L. Tuller, Department of Materials Science and Engineering, MIT, Cambridge, MA 02139

A study of the $(\text{La}_{1-x}\text{Sr}_x)_2\text{CuO}_{4-\delta}$ system has been carried out to determine the roles of dopants and oxygen stoichiometry on the transport properties and defect chemistry of this system. A series of ceramic samples were prepared using a solution method with x varying between 0 and 0.5 at 0.05 intervals. Electrical measurements included 4-probe dc resistance and thermoelectric power (TEP) measurements conducted under controlled oxygen partial pressures (10^{-4} - 1 atm) over a wide temperature range (25-1000 °C). The conductivity

was found to reach a maximum for $0.15 < x < 0.2$ which we interpret as reflecting a change from electronic to ionic compensation of Sr. High sensitivity TGA measurements are used to confirm the dopant compensation by oxygen vacancies at high x. A transition from metal to semiconductor occurs at reduced temperature for $x > 0.25$. The conductivity and TEP of La_2CuO_4 show a $1/6$ power dependence on PO_2 and an independence of temperature, implying that 1) the hole concentration is controlled by the redox reaction, 2) the hole mobility is insensitive to both PO_2 and temperature, and surprisingly, 3) the enthalpy of the redox reaction is nearly zero. We discuss the role of Sr in modifying the defect and transport characteristics of La_2CuO_4 .

M7.33

SUPERLATTICE MODULATION IN Nd_2CuO_4 AND THE ELECTRON-DOPED SYSTEMS $\text{Nd}_{2-x}\text{Ce}_x\text{CuO}_4$ AND $\text{Nd}_2\text{CuO}_{4-x}\text{F}_x$. C.H. Chen, D.J. Werder, A.C.W.P. James, D.W. Murphy, S. Zahurak, R.M. Fleming, B. Baolgg, and L.F. Schneemeyer, AT&T Bell Laboratories, 600 Mountain Ave., Murray Hill, NJ 07974

We have observed a periodic superlattice modulation in Nd_2CuO_4 and in the electron doped $\text{Nd}_{2-x}\text{Ce}_x\text{CuO}_4$ and $\text{Nd}_2\text{CuO}_{4-x}\text{F}_x$ systems by electron diffraction and microscopy. The superlattice appears identical in all the systems studied; it was found in both superconducting and nonsuperconducting samples, but most of the samples examined were not homogeneous with respect to the superlattice. The superlattice modulation is characterized by a wave vector $q = (1/4, 1/4, 0)$ parallel to the Cu-O plane; it exists in four possible variants with its c-axis parallel to the four equivalent [111] zone axes of the underlying tetragonal lattice. Samples quenched from high temperature invariably showed no superlattice or superconductivity; bulk superconductivity and regions of superlattice were observed on annealing in the range 250-750 °C. We believe that oxygen diffusion is responsible for this disproportionation into superlattice and nonsuperlattice regions.

M7.34

$\text{La}_{2-x}\text{Ba}_x\text{Sr}_{1-x}\text{Y}_x\text{Cu}_2\text{O}_6$ AND $\text{M}_2\text{SrCu}_2\text{O}_6$ (M=Pr and Nd); NEW LAYERED COPPER-OXIDES WITH THE $\text{La}_2\text{SrCu}_2\text{O}_6$ STRUCTURE. Eric A. Hayri, Chemistry Department, Brookhaven National Laboratory, Upton, N.Y. 11973.

$\text{La}_{2-x}\text{Ba}_x\text{Sr}_{1-x}\text{Y}_x\text{Cu}_2\text{O}_6$ ($0 \leq x \leq 0.5$) solid solutions, $\text{M}_2\text{SrCu}_2\text{O}_6$ (M=La, Pr, Nd) and other doped La-Ba-Sr-Y-Cu-O compounds of the $\text{La}_2\text{SrCu}_2\text{O}_6$ structure have been prepared and characterized by X-ray powder diffraction, electrical resistivity and magnetic susceptibility measurements. All samples are semiconductors. $\text{La}_2\text{SrCu}_2\text{O}_6$ has a room temperature resistivity of $\sim 10^{-2} \Omega\text{-cm}$ while the corresponding Pr and Nd compounds are $\sim 1 \Omega\text{-cm}$. Doped and oxygen annealed samples show little change in physical properties. Possible reasons for the absence of superconductivity in a structure closely related to many known high- T_c materials is discussed.

M7.35

The Structure of the 50K Superconductor $(\text{Y}_{1-x}\text{Ca}_x)\text{Ba}_2\text{Cu}_3\text{O}_{6.8}$ ($0 < x < 0.2$). John B. Parise, Earth and Space Sciences, State University of New York at Stony Brook, NY 11794 and Eugene M. McCarron III, Central Research and Development Department, E. I. Du Pont de Nemours & Company, Experimental Station, P. O. Box 80356, Wilmington, Delaware 19880-0356

Replacing Y(III) by Ca(II) in $(\text{Y}_{1-x}\text{Ca}_x)\text{Ba}_2\text{Cu}_3\text{O}_6$ induces superconductivity. A solid solution limit exists, as is evidenced by the lack of variation in unit cell parameters for values of $x > 0.3$. At low doping levels ($x < 0.2$ nominal), materials prepared by solid state techniques consist of a complex intergrowth of Ca-rich and Ca-poor 123-type phases, as well as pure $\text{YBa}_2\text{Cu}_3\text{O}_6$ and BaCuO_2 . At higher doping levels the Ca content of the samples becomes constant ($x \sim 0.30$). Structural refinements using data collected by X-ray and neutron powder diffractometry are consistent with Ca-doping causing oxidation only of Cu in the sheet leaving the copper in the so-called chain-site as Cu(I). Many of the structural changes occurring in this system upon oxidation, such as flattening of the CuO_2 -sheets and contraction of the in-plane Cu-O distance, also occur in the structurally related superconducting system, $\text{Pb}_2\text{Sr}_2(\text{Y}_{1-x}\text{Ca}_x)\text{Cu}_3\text{O}_8$. Consideration of structural changes in several systems leads to the conclusion that there exists an optimum level of oxidation for the CuO_2 -sheets which results in the highest values of T_c ; the optimum value is close to a formal oxidation state of +2.5 for Cu in the sheets.

M7.36

$\text{Nd}_{1.85-x}\text{Bi}_x\text{Ce}_{0.15}\text{CuO}_{4.5}$: PREPARATION AND PROPERTIES. M. Greenblatt, J.G. Lee and K.V. Ramanujachary, Chemistry Department, Rutgers University, New Brunswick, NJ 08893.

Effects of Bi addition on the transport properties of the electron doped $\text{Nd}_{1.85}\text{Ce}_{0.15}\text{CuO}_{4.5}$ are investigated. Polycrystalline samples were prepared by both conventional high temperature solid state synthesis and by the decomposition of nitrate solutions containing stoichiometric amounts of component ions. Both the normal state resistivity behavior and the bulk volume fraction of the superconducting phase are shown to improve with the amount of Bismuth in a narrow compositional range. Results of these investigations will be presented with a special emphasis on the electrical and magnetic properties.

M7.37

STRUCTURAL ANALYSIS OF $\text{Nd}_{2-x}\text{Ce}_x\text{CuO}_4$ ($x=0.15$) SUPERCONDUCTORS. Dejei Li, M.Y. Su and L. D. Marks, Science and Technology Center for Superconductivity, Department of Materials Science, Northwestern University, Evanston, IL 60208, and B. Krause, Dept. of Physics, Northern Illinois University, Dekalb, IL 60115

Experimental results on the structure of superconducting and non-superconducting $\text{Nd}_{2-x}\text{Ce}_x\text{CuO}_4$ using electron microscopy are reported. Three different structures have been observed by conventional and convergent beam electron diffraction; a 4mm phase similar to Nd_2CuO_4 ; a 2mm phase where the four-fold rotational symmetry element is lost; and one- and two-dimensional modulated structures where the modulation wavelength is four times the unit cell and takes place on either or both the a and b axes. Comparison of different samples indicates that the modulated structure is more common in samples with worse superconducting properties and contains approximately the same cerium content as the unmodulated material. This is interpreted as due to Ce²⁺ doping where there is a small displacement in the Ce positions (and presumably additional oxygen) leading to the modulated structure; numerical simulated high resolution images based upon this model show fair agreement with the experimental results. A more detailed analysis will be presented.

M7.38

SUPERCONDUCTING AND STRUCTURAL PROPERTIES OF $(\text{Ba}_{1-x}\text{K}_x)(\text{Bi}_{1-y}\text{M}_y)\text{O}_3$ SYSTEM ($\text{M}=\text{Tl}$, Pb and Sb)*. B. Dabrowski, D.G. Hinks, S. Pei, J.D. Jorgensen, D.R. Richards, Y. Zheng, C.W. Kimball and A.W. Mitchell, Materials Science Division, Argonne National Laboratory, Argonne, IL 60439, USA

Single phase samples of $(\text{Ba}_{1-x}\text{K}_x)(\text{Bi}_{1-y}\text{M}_y)\text{O}_3$ ($\text{M}=\text{Tl}^{+3}$, Pb^{+4} and Sb^{+5}) have been synthesized over wide compositional range using a two-step procedure. In the first step, K is incorporated into the O-deficient Bi-reduced material during a nitrogen firing at 700°C. Low-temperature oxygen annealing removes the oxygen vacancies and increases average Bi oxidation state. For $y=0$ and $x>0.35$, samples have a simple cubic structure and are bulk superconductors with T_c gradually decreasing from 30 to 22K as x increases to 0.50. For $y>0$ samples are superconducting only in a simple cubic structure with T_c gradually decreasing as y increases for fixed x . There is no apparent relation between Bi content or oxidation state to T_c . The highest T_c is found in the compositional range adjacent to the structural phase transition into the lower symmetry nonsuperconducting phase. These results support our earlier conjecture that optical phonons (polarons) are responsible for superconductivity in $\text{Ba}_{1-x}\text{K}_x\text{BiO}_3$ system.

*Supported by National Science Foundation-Office of Science and Technology Centers under contract #STC-8809854 (BD, SP) and DMR87-19738 (CWK) and U.S. Department of Energy, BES, under contract #W-31-109-ENG-38 (DGH, JDJ, YZ, AMM).

M7.39

THERMODYNAMIC PROPERTIES OF OXYGEN IN $\text{YBa}_2\text{Cu}_3\text{O}_x$. P. Meuffels and R. Naeven, Institut für Festkörperforschung, KFA Jülich, D-5170 Jülich, F.R.G.

The oxygen content x ($6.15 < x < 7$) in $\text{YBa}_2\text{Cu}_3\text{O}_x$ was measured as a function of oxygen pressure for temperatures between 400 and 750 °C. The orthorhombic-to-tetragonal (O-T) phase boundary was determined as a function of oxygen stoichiometry between 550 and 700 °C. From these results the concentration dependence of the chemical potential and the solution enthalpy and entropy of oxygen in $\text{YBa}_2\text{Cu}_3\text{O}_x$ were derived for both phases.

In both the orthorhombic and tetragonal phase the chemical potential increases monotonously with increasing x . The chemical potential is continuous at the O-T transition point, but the solution enthalpy and entropy undergo a steplike discontinuity. These results are quite coherent with an interpretation of the phase transformation as an order-disorder transition. Lattice gas models, as proposed in literature, explain some features of the experimental observations, if one assumes repulsive interactions between oxygen atoms on nearest-neighbouring sites. These models, however, provide only a semiquantitative description. It will be shown that deviations between experimental and theoretical data cannot be explained by merely adopting concentration dependent oxygen site energies. There seem to be entropic contributions to the chemical potential, perhaps due to the Cu-sublattice, which also have to be considered.

M7.40

LOW TEMPERATURE BEHAVIOR OF $\text{YBa}_2\text{Cu}_3\text{O}_{6+2x}$ PHASE DIAGRAM. Ryoichi Kikuchi* and Jae-Sung Choi, Department of Materials Science and Engineering, and Advanced Materials Technology Program, Washington Technology Center, University of Washington, Seattle, WA 98195

The phase diagram of the Cu-O plane of $\text{YBa}_2\text{Cu}_3\text{O}_{6+2x}$ is presented with the emphasis on the low temperature behavior. The model is the same as the one used by de Fontaine and coworkers; namely the O-O interaction (V_2) through Cu is attractive while the nearest-neighbor O-O bond (V_1) and the second-neighbor O-O bond (V_3) are repulsive. It is shown that the orthorhombic II phase (O_{II}) with the double periodicity is stable and is surrounded by orthorhombic I phase (O_I) both for the small and large O densities. The boundaries are at $x = 0.125$ and 0.375 in low temperatures. The constant μ (chemical potential) curves in the phase diagram for $\mu = V_2$ and $\mu = V_2 + 2V_3$ lie near the O_I - O_{II} boundaries in the O_I phase sides, and are particularly of importance. Numerical calculations are done using the cluster variation method with the same basic cluster combinations, a square and a cross, as was used by de Fontaine et al. Different from previous papers, however, a special program has been devised to avoid computer underflow even for very low temperatures, and thus we can calculate low temperature phase boundaries.

*After August 1989: Department of Materials Science and Engineering, UCLA, Los Angeles, CA 90024

M7.41

GROWTH, ANNEAL AND PROPERTIES OF SINGLE CRYSTAL $\text{YBa}_2\text{Cu}_3\text{O}_x$. Jingwen Zhang and Ping wang, Institute of Chemistry, Academia Sinica, Beijing, China; Zhongxian Zhao, Institute of Physics, Academia Sinica, Beijing, China

As the compound $\text{YBa}_2\text{Cu}_3\text{O}_x$ (YBCO) is the typical of high T_c superconductor. The single crystals with large size, good quality and two kinds of shapes in YBCO oxides have been prepared by flux method with the extra $\text{BaO}+\text{CuO}$ as solvent. The typical size was $5 \times 1.2 \times 0.7$ mm for the bar-shaped crystal and $2.5 \times 1.5 \times 0.01$ mm for the flake one. Both of them exhibit a transition from metal to superconductor at 85 K after annealing in an O flow, but before annealing the transition is at 59 K. An important factor is that the quenching rather than slowly cooling after the annealing.

To observe the behaviour of copper ions which are believed to play an important role in the mechanism of superconductors. The ESR measurements on the crystal samples as function of temperature have been done. They showed notable anisotropy. The 117, 139, 165, 195, 235 cm^{-1} peaks of Raman spectra have been observed and showed the strong electron-phonon coupling and charge transfer transition. The space image with atom level of resolution was observed by STM (Scanning Tunnel Microscope).

M7.42

OXYGEN EVOLUTION FROM $\text{YBa}_2\text{Cu}_3\text{O}_{7-\delta}$ SUPERCONDUCTING POWDERS GENERATED BY AEROSOL ROUTES. Pratim Biswas and Derong Zhou, Department of Civil & Environmental Engineering, University of Cincinnati; Jeff Grothaus, Procter & Gamble, Cincinnati; Punit Boolchand, Darl McDaniel, Univ. of Cincinnati; Cincinnati, Ohio 45221-0071.

A novel aerosol process¹ has been used to generate sub-micron sized powders of $\text{YBa}_2\text{Cu}_3\text{O}_{7-\delta}$. There is evidence of a correlation between the critical temperature, crystallographic structure, and oxygen content of these superconducting powders. Oxygen evolution rates of the aerosol generated superconducting powders have been measured using a thermogravimetric analyzer (TGA). The results are compared to those of a solid state sintered superconducting powder.

The temperature of a known amount (30-35 mg) of superconducting powder was increased in a reducing atmosphere (N_2) at a constant rate of $10^\circ\text{K}/\text{min}$ in a Mettler TGA. The amount of oxygen released and the rate of weight loss of the sample is measured as a function of temperature.

From an Arrhenius plot, the activation energy and preexponential factor are determined assuming first order oxygen evolution kinetics. These are used to calculate ΔH , ΔS , and ΔG for each peak. ΔH was of the order of 0.8 eV and ΔG about 3 eV. Assuming end products of Y_2O_3 , Cu and BaO, δ was calculated to be 0.05 for the aerosol samples. These results on aerosol produced samples will be compared to conventional solid state reacted samples to elucidate possible oxygen bonding configurations.

¹Biswas et al.; Superconducting Powders Generated by an Aerosol Process; in press, Materials Letters, 1989.

M7.43

INHOMOGENEOUS SINTERING IN $YBa_2Cu_3O_{6+x}$. Laura C. Stearns, Martin P. Harmer, and Helen M. Chan, Lehigh University, Bethlehem, PA.

One area of the much-studied $YBa_2Cu_3O_{6+x}$ superconductors which is not well understood is their sintering behavior and microstructural development. Since the microstructures of these materials tend to be rather non-ideal, this study focuses on the effects of heterogeneities on sintering. In particular, coarse inclusions have been deliberately introduced into the starting powders in order to examine their influence on sintering. The effects of variables such as volume fraction, size, and density of inclusions have been studied. Two different starting powders were investigated; one compositionally stoichiometric and the other rich in CuO so that a liquid would form during sintering. The role of this Cu-containing liquid in the sintering of these heterogeneous structures will be discussed.

M7.44

HIGH T_c OXIDE SOLID STATE REACTION KINETICS VIA COMPLEX IMPEDANCE SPECTROSCOPY. E. A. Cooper and T. Q. Mason, Northwestern University, Evanston, IL; U. Balachandran and M. L. Kullberg, Argonne National Laboratory, Argonne, IL; NSF Science and Technology Center for Superconductivity.

Complex impedance spectroscopy was used to follow the kinetics of solid state reaction of the Y-Ba-Cu oxide superconductor from oxide precursors. Carefully classified and sized large particles of CuO (25-150 μm) were imbedded in finely dispersed matrices of yttrium and barium oxides. These matrix materials were prepared by a variety of means, including solid state reaction of yttrium oxide and barium carbonate and sol-gel route, with and without vacuum calcination to remove carbonate. Cold-pressed pellets were prepared and placed between platinum electrodes in a complex impedance apparatus and were sintered in situ. The impedance unit consisted of an IBM PC-compatible controlled HP-4192A. Data were analyzed via EQUIVCRT, a commercially available software package.

A single arc impedance spectrum was obtained at short and intermediate times, from which a characteristic resistance could be obtained. The inverse, or conductance, scaled with the fraction of superconductor produced. Results were analyzed in terms of solid state reaction kinetic theory for activation energy and particle size effect.

M7.45

THE EFFECTS OF THE SOLUTION STRUCTURE ON THE MICROSTRUCTURE AND PROPERTIES OF SINTER FORGED SOL-GEL-DERIVED SUPERCONDUCTORS. D. Kanzer, M. Teepe, G. Moore and G. Kordas, University of Illinois, Urbana, IL 61805; M. E. Bismek, U. Balachandran, M. L. Kullberg, and R. B. Poeppel, Argonne National Laboratory, Argonne, IL 60439; and Y. L. Jeng and D. L. Johnson, Northwestern University, Evanston, IL 60208

Powders of Y-Ba-Cu-O system have been derived from sols with controlled morphology that have been prepared using Y-methoxyethoxide, Ba-methoxide, and Cu-ethoxide. The powders have been annealed at 300°C under high vacuum (<10⁻⁵ Torr). Following this treatment, the powders were sinter forged. The microstructure and properties of the resulting superconductors have been studied as a function of the sol-structure and sinter forging conditions. The results will be discussed in the context of the processing parameters and microstructure.

Work supported by the National Science Foundation, Office of Science and Technology Centers, under Contract #DMR-8809864 (DK, MT, GM, and GK, Science and Technology Center for Superconductivity - University of Illinois at Champaign-Urbana; MEB, Science and Technology Center for Superconductivity - Argonne National Laboratory; YLJ and DLJ, Science and Technology Center for Superconductivity - Northwestern University); the U. S. Dept. of Energy, Office of Energy Storage and Distribution, Conservation and Renewable Energy (UB and RBP), Laboratory Management Division (MLK), under Contract W-31-109-Eng-38; the Amoco Chemical Company (MLK); and partial support from the Division of Educational Programs, Argonne National Laboratory (MEB).

M7.46

ROUTES TO OXIDE FILMS FOR THE PROTECTION OF CUPRATE SUPERCONDUCTORS. Ronald H. Baney, Debora F. Bergstrom, Leslie E. Carpenter, and Donald R. Petersen, Dow Corning Corporation, Midland MI, Dennis F. Elwell, Andrew A. Shapiro, and Paul F. Fleishner, Hughes Aircraft Company, Newport Beach, CA.

The cuprate superconductors rapidly degrade in moisture and in the presence of organic compounds. We have a method of protection which consists of coatings and a coating process using sol/gel routes to the low temperature formation of oxide films. In contrast to traditional organic protective films, amorphous silica films formed from a variety of precursors gave excellent protection and caused little degradation of bulk and film superconductors.

The protective ability of the films were assessed by monitoring the degradation of $Y_1Ba_2Cu_3O_{7-d}$ in the presence of 85% relative humidity at 85 °C. Volume magnetic susceptibility, four-point probe resistivity, current density measurements and x-ray diffraction were performed. Without protection, degradation was almost complete within one hour of exposure. With protection, superconducting properties were maintained even after 48 hours of exposure.

M7.47

Ag- $YBa_2Cu_3O_7$ POWDER GENERATION BY AEROSOL DECOMPOSITION. Toivo T. Kodas and Altaf H. Carim, Center For Micro-Engineered Ceramics, University of New Mexico, Albuquerque, NM; Kevin Ott, Exploratory Research and Development Center For High Temperature Superconductors, Los Alamos National Laboratory, Los Alamos, NM.

The properties of metal-superconductor composites are of interest for a variety of reasons. Interfaces between superconductors and metals determine the integrity of electrical contacts and are of importance for composite materials which can provide improved mechanical properties relative to the pure

superconductor. In an effort to study these composite materials, we have produced $\text{Ag-YBa}_2\text{Cu}_3\text{O}_7$ powders by decomposing metal nitrate solution droplets in a gaseous flow system. The powders were characterized by x-ray diffraction and by analytical and high-resolution transmission electron microscopy. Particles consisting of nanocrystalline Ag and $\text{YBa}_2\text{Cu}_3\text{O}_7$ with grain sizes of 10 to 100 nm could be formed. For temperatures above the melting point of Ag, each polycrystalline $\text{YBa}_2\text{Cu}_3\text{O}_7$ particle had associated with it a single Ag crystallite. The effect of reactor operating parameters such as residence time and temperature on the formation of secondary phases and particle morphology will be discussed. The use of the particles for studies of metal-superconducting ceramic interfaces will also be discussed.

M7.48

CONTROL OF MICROSTRUCTURES AND GRAIN BOUNDARY PHASES IN THE $\text{MBa}_2\text{Cu}_3\text{O}_{7-\sigma}$ SYSTEMS. A.I. Kingon, C. Davis, M. Lawrence, T. Hare, C.C. Koch and D.G. Haase, Department of Materials Science and Engineering, North Carolina State University, Raleigh, NC 27695

In polycrystalline $\text{YBa}_2\text{Cu}_3\text{O}_{7-\sigma}$, critical currents continue to be limited by both random grain orientation, and grain boundary phase(s) which are present on a significant fraction of the boundaries. The origin of these grain boundary phases are investigated. In materials produced by the mixed oxide route, these are shown to correspond to local compositional variations, consistent with the high temperature phase equilibria. The grain boundary phases are characterized by their thermal signatures, as well as by TEM, XPS and scanning Auger microprobe. The phases have a significant and characteristic effect on the sintering process, and therefore upon the microstructural evolution. It is also shown that their presence reduces J_c significantly. The $\text{YBa}_2\text{Cu}_3\text{O}_{7-\sigma}$ materials prepared by the mixed oxide process are compared with those prepared by chemical precipitation. In the case of one "chemical" process route, the amount of grain boundary phases are significantly reduced, altering the sintering process. J_c values also increase significantly.

Reaction with CO_2 is shown to result in a Ba-Cu-C-O phase which melts at $\sim 965^\circ\text{C}$ in O_2 , and is extremely difficult to remove.

Results for $\text{YBa}_2\text{Cu}_3\text{O}_{7-\sigma}$ are compared with $\text{GdBa}_2\text{Cu}_3\text{O}_{7-\sigma}$, which has a significant range of cation solid solution. The latter is therefore more tolerant of the mixed oxide process route.

M7.49

EFFECT OF PURITY OF RAW MATERIALS AND PROCESSING ON THE MICROSTRUCTURE AND PROPERTIES OF HIGH TC $\text{YBa}_2\text{Cu}_3\text{O}_{7-\delta}$. Ph. DUMAS* and J. A. T. TAYLOR, N. Y. S College of Ceramics at Alfred university, ALFRED N. Y., 14 802.

Microstructure and properties of high TC $\text{YBa}_2\text{Cu}_3\text{O}_{7-\delta}$ ceramics were studied as a function of purity of raw materials and processing conditions. Technical and reagent grade raw materials were used to prepare the precursor superconducting powder, the characteristics of which were monitored by XRD, chemical analysis, thermal analysis and SEM.

Bulk specimens were then prepared with these two master batches by conventional solid state sintering. Superconducting properties were examined by T-resistivity studies and by magnetic susceptibility. Microstructure was characterized by SEM and phase identification by XRD and EDS.

The effects of impurities on microstructure and electrical properties will be discussed.

M7.50

SYNTHESIS OF 1-2-3 POWDER BY SPRAY CALCINATION OF AEROSOLS OF PRECURSOR SOLUTIONS. R. L. Lakis and S. R. Butler, Materials Research Center, Lehigh University, Bethlehem, PA 18015.

We have prepared submicron powders of orthorhombic Y-Ba-Cu oxide by generating a submicron droplet aerosol of precursor solutions. The aerosol droplets are carried in an oxygen stream into a high temperature furnace where they are directly converted to 1-2-3 powder. The powder is collected on a filter after a cooling section downstream from the furnace. Both nitrate and mixed anion solutions have been investigated. Process parameters investigated include: spraying rate, average droplet size, furnace temperature, furnace residence time (oxygen flow rate), and precursor solution composition and concentration. For a typical concentration and droplet size (~ 0.3 micron), we calculate a powder particle size of 100 nm. High resolution SEM results confirm this as an "average" particle size for 950°C furnace temperatures. Some larger agglomerates (~ 1 -2 microns) are seen. Their origin in the process will be discussed. Characterization of the powders by X-ray diffraction and several particle size measurement methods will be presented. Sintering behavior and final microstructures of bodies prepared from the powders will be discussed.

(Supported by the Lehigh University Consortium on Superconducting Ceramics.)

M7.51

PROCESSING AND FABRICATION OF $\text{YBa}_2\text{Cu}_4\text{O}_x$ AND $\text{YBa}_2\text{Cu}_4\text{O}_x/\text{YBa}_2\text{Cu}_3\text{O}_y$ COMPOSITES. U. Balachandran, M. E. Biznek, K. C. Goretta, D. Shi, R. B. Poeppel, Argonne National Laboratory, Argonne, IL; and T. O. Mason, Northwestern University, Evanston, IL.

Powders of $\text{YBa}_2\text{Cu}_4\text{O}_x$ ("124") were prepared via a solid state reaction from a mixture of Y_2O_3 , BaCO_3 , and CuO in the 1-2-4 stoichiometric amount. The calcined powders were characterized by thermal analyses and x-ray diffraction. Pellets sintered in oxygen at $\sim 950^\circ\text{C}$ exhibited a sharp superconducting transition at 87 K. $\text{YBa}_2\text{Cu}_4\text{O}_x/\text{YBa}_2\text{Cu}_3\text{O}_y$ composites were made with varying amounts of 124 and 123 powders and sintered over a range of temperatures and oxygen pressures. Upon sintering, these composites exhibited superconductivity \sim about 87 K with a sharp transition despite the multiphase structure. The experimental results are discussed in relation to the microstructures obtained.

Work supported by the U. S. Department of Energy, Office of Energy Storage and Distribution, Conservation and Renewable Energy (UB, KCG, RBP), Office of Basic Energy Sciences -- Materials Science (KCG, DS), under Contract W-31-109-Eng-38, and the National Science Foundation, Office of Science and Technology Centers, under Contract #STC-8809854 (MEB, Science and Technology Center for Superconductivity -- Argonne National Laboratory; TOM, Science and Technology Center for Superconductivity -- Northwestern University). MEB acknowledges partial support from the Division of Educational Programs, Argonne National Laboratory.

M7.52

CRYSTALLITE ORIENTATION IN YBaCu CERAMIC LAYERS SINTERED ON SILVER SUBSTRATES. Claus Schüller, Felix Greuter and Petra Kluge-Weiss, ABB Corporate Research, Baden, Switzerland

A stoichiometric precursor powder of YBaCu with 0.8 - 0.1 μm grain size was prepared by coprecipitation of oxalates in organic liquids, followed by calcination at 580°C. Stable suspensions of this powder were obtained in i-Propanol and used in a controlled dip coating process. Well packed powder layers formed on Ag foils. During reactive sintering of such layers, a small volume of a transient liquid phase develops close to 920°C, the BaCuO₂/CuO eutectic temperature. This phase induces oriented nucleation and growth of crystallites on the Ag surface before it is consumed by the progression reaction. At completion of the reactive sintering, a dense, single phase, polycrystalline ceramic layer has formed consisting of highly oriented crystallites with their a, b-axis parallel to the substrate surface.

YBaCu layers 5-10 μm thick on Ag strips 50 μm thick, 3 mm wide have $T_c = 90\text{ K}$ ($\Delta T \sim 2\text{ K}$) and $j_c > 1000\text{ A/cm}^2$ as measured with dc and magnetization.

Details of their microstructure and further data of their s.c. properties will be reported.

M7.53

PHASE STABILITY OF LNBA₂CU₃O₇ AND LN₂BACUO₅ (Ln = Dy, Er, Eu, Gd, Ho, Sm, Yb). Kiichi Yoshiara, Fusaoki Uchikawa, Kiyoshi Yoshizaki, Materials and Electronic Devices Laboratory, Mitsubishi Electric Corporation, Sagami-hara-city, Kanagawa, Japan; Kiyotaka Nakahigashi, Department of Materials Science, University of Osaka Prefecture, Sakai-city, Osaka, Japan

Phase stability of a series of LnBa₂Cu₃O₇ and Ln₂BaCuO₅ (Ln=Dy,Er,Eu,Gd,Ho,Sm,Yb) has been studied as a function of oxygen partial pressure and temperature by X-ray diffraction, thermal gravimetric and differential thermal analyses. In the above materials, a phase decomposition with decreases of a sample weight took place at high critical temperatures T_c (we define here T_{c1} as the decomposed temperature for LnBa₂Cu₃O₇, and T_{c2} for Ln₂BaCuO₅). In the case of Ln=Dy,Er,Ho and Yb, for example, the LnBa₂Cu₃O₇ decomposed into Ln₂BaCuO₅ and liquid phase containing BaCuO₂ and CuO at T_{c1} and the Ln₂BaCuO₅ decomposed into Ln₂O₃ and another liquid phase containing BaO, CuO and Cu₂O at T_{c2} , which was higher than T_{c1} . The critical temperature $T_{c1,2}(\text{K})$ was changed depending strongly on the oxygen partial pressure $P(\text{atm})$ and an effective ionic radius $R(0.1\text{nm unit})$ of Ln atom which was eightfold for LnBa₂Cu₃O₇, sevenfold for Ln₂BaCuO₅, coordinated by oxygen atoms. The observed values of $T_{c1,2}$ for all the systems, together with those of YBa₂Cu₃O₇ and Y₂BaCuO₅ reported previously, were well reproduced by following relation, respectively.
 $T_{c1} = -3325.7R^2 + 7870.8R - 3260.1 + 17.8\ln(P)$
 $T_{c2} = -17493R^2 + 34582R - 15489 + 20.8\ln(P)$
 The reliability index R_p was 0.5% for T_{c2} .

M7.54

STUDY OF CARBONATES USED IN THE PREPARATION OF SUPERCONDUCTORS. Phillip G. Wahlbeck, Dwight L. Myers, and R. Ronald Richards, Department of Chemistry and the Institute for Aviation Research, Wichita State University, Wichita, KS 67208.

Studies utilizing thermal analyses and Knudsen effusion cell mass spectrometry have been

performed on samples of YBa₂Cu₃O_{7-x} prepared using solid state reaction methods. The starting materials were the oxides CuO(s) and Y₂O₃(s) and either the usual BaCO₃ or Ba(NO₃)₂. The study was performed to examine the effects of the carbonate on residual materials in the samples after syntheses.

The course of the synthetic chemical reaction was studied by thermal analyses. Mass spectrometry was used to study residual materials in the samples; comparative data for carbon-oxygen species will be presented. In addition, scanning electron microscopy coupled with energy dispersive X-ray analysis (SEM-EDAX) was used to analyze the surfaces of the two materials. The significance in materials preparation will be discussed.

M7.55

ONE-STEP SYNTHESIS AND DENSIFICATION OF BULK YBa₂Cu₄O₈/Ni COMPOSITE SUPERCONDUCTORS. C. Ge-linas and B. Champagne, National Research Council Canada, Boucherville, Quebec, Canada, J4B 6Y4.

The fabrication of bulk YBa₂Cu₃O_x/metal composite superconductors is not a straightforward process because of the high oxygen-temperature dependence of the YBa₂Cu₃O_x phase. After fabrication of the composite at high temperature, it is almost impossible to diffuse oxygen through the metal envelope into the densified compound to restore the required oxygen content for superconductivity above 77K. To overcome this drawback, it is possible to synthesize YBa₂Cu₄O₈ under high oxygen pressure. This compound is a more stable oxygen stoichiometry phase and could remain superconductive after densification at high temperature.

In this work, hot isostatic pressing (HIPing) was used to synthesize and densify YBa₂Cu₄O₈/Ni composite superconductors in a single step. The choice of the starting materials was made in order to generate various oxygen pressures within Ni cans during HIPing. Two different types of precursors were used: oxide powders mixed in stoichiometric amounts (Y₂O₃, BaO₂, CuO and Cu₂O) and YBa₂Cu₃O_x with CuO and BaO₂.

Depending on the precursors and the HIPing parameters, various Y-Ba-Cu-O phases are formed: YBa₂Cu₄O₈, Y₂Ba₄Cu₇O_{15-x} and Y₂BaCuO₅. Microstructure and superconductive properties of these HIPed HTSC/Ni composites are presented.

M7.56

IN-SITU PROCESSING AND REACTION OF CO₂ WITH YBa₂Cu₃O_{7-x}. C. Michael Greenlief, Joseph F. Bringley, Stephen M. Gates, Bruce A. Scott, Steven S. Trail, and Christopher D'Emic, I.B.M. Research Division, T. J. Watson Research Center, Yorktown Heights, NY 10598.

The recent discovery of high temperature superconductivity near 90 K in the Y-Ba-Cu-O and related systems has generated tremendous amounts of new experimental and theoretical research on these materials. The properties of polycrystalline YBa₂Cu₃O_{7-x} can be strongly influenced by the absorption of ambient gases during processing and measurement. Studies of these ambient "impurity" effects in carbonate-prepared YBa₂Cu₃O_{7-x} under ultra-clean conditions has been studied in a two part ultra-high vacuum chamber in which ceramics and thin films can be exposed to various gases at temperatures up to 1200 K and pressures up to 1 atm. The chamber can then be evacuated to UHV for Temperature-Programmed-Desorption (TPD) and/or four-point resistivity measurements. The volatile impurity levels, and reactions with, YBa₂Cu₃O_{7-x} were studied in the chamber as different processing procedures were performed.

Heating of superconducting YBa₂Cu₃O_{7-x} to temperatures of up to 925 K show that CO₂ and H₂O are the major volatile impurities observed in TPD. Their level can be reduced greatly by repeated annealing of the samples in oxygen (100 Torr, 673 K). In-situ resistivity measurements show that as these impurity levels are decreased, the superconducting transition sharpens; however, no change in T_c is observed. TPD was also used to monitor the out-diffusion of O₂, which occurred with a activation energy of 1.8 eV. Both the fully oxidized (

YBa₂Cu₃O₇) and YBa₂Cu₃O_{6.5} form of the material were exposed to CO₂ at mild temperatures (325-725 K). TPD measurements show that the latter absorbs significantly more CO₂. Indirect evidence by TPD and by X-ray powder diffraction will be presented which suggests that CO₂ can insert into oxygen vacancies in the partially reduced material. Furthermore, the absorption of CO₂ impedes the kinetics of subsequent oxygen-uptake in this temperature range. CO₂ is found to be a reducing agent for Y-Ba-Cu-O system under relatively mild conditions. Preliminary experiments with YBa₂Cu₃O₆ indicate that CO₂ causes appreciable reduction to copper metal at temperatures as low as 716 K.

*Present Address: Department of Chemistry, University of Missouri, Columbia, MO 65211.

M7.57

A SYSTEMATIC STUDY OF THE EFFECTS OF METAL SUBSTITUTIONS FOR Cu IN YBa₂(Cu_{1-x}M_x)₃O_{7-δ}, M=Al, Ga, Fe, Ni, Zn. Youwen Xu, A. R. Moodenbaugh, Y. L. Wang, M. Suenaga, and R. L. Sabatini, Materials Science Division, Brookhaven National Lab., Upton, NY 11973.*

A series of Cu-substituted samples was prepared using well controlled and reproducible procedures^{1,2}. These preparation methods resulted in samples with typical grain sizes of >5μm. This relatively large grain size allowed microprobe studies of individual grains to determine composition of the 1:2:3 phase. Microprobe was also used to check for additional phases. Solubility limits of substitutions for Cu in these samples are estimated. Superconducting transition temperatures and lattice parameters are presented. It is suggested that some of the wide discrepancies among reported T_c's reported in the literature may, at least in part, be due to variation in oxygen content of samples prepared differently. In the case of Ga, a smooth variation of T_c and lattice parameters for x≤0.10, has been widely assumed to be good evidence for a significant solid solution. However our microprobe studies show no evidence for Ga content of the 1:2:3 phase down to the x=0.01 level. Preliminary studies also show no evidence for solid solution above x=0.01 when substituting Mn, Cr, Zr, and Ti for Cu in 1:2:3.

*Supported by the US DOE Office of Basic Energy Sciences, Division of Materials Science, under Contract DE-AC02-76CH00016.

¹Youwen Xu, et al., Phys. Rev. B38, 7084, 1988.

²Youwen Xu, et al., Phys. Rev. B39, 6667, 1989.

M7.58

PREPARATION OF Ca-SUBSTITUTED YBa₂Cu₄O₈. T. Miyatake, K. Yamaguchi, T. Takata, S. Gotoh N. Koshizuka and S. Tanaka, Superconductivity Research Laboratory (SRL), ISTE, 1-10-13, Shinonome, Koto-ku, Tokyo, 135, Japan

Synthesis of bulk superconducting YBa₂Cu₄O₈ ("1-2-4"), containing double Cu-O chains, has been so far done by following two methods; high oxygen pressure annealing method [1-2], and ambient oxygen reaction method with alkali carbonate [3]. In this report, we describe a preparation method combined with the two methods and properties of Ca-substituted "1-2-4" compound.

Samples with various compositions were prepared by the solid state reaction method starting with Y₂O₃, Ba(NO₃)₂, CuO and CaCO₃. High quality polycrystalline materials were obtained when HIP treatment in Ar+O₂ gas environment was performed after the ambient oxygen reaction. X-ray diffraction showed that each sample had the "1-2-4" structure, with no second phase. We also discuss about the superconducting properties of Ca-substituted "1-2-4" samples.

[1] J. Karpinski et al.; NATURE, 336 (1989) 660.

[2] R. M. Hazen et al.; Appl. Phys. Lett., 54 (1989) 1057.

[3] R. J. Cava et al.; NATURE, 338 (1989) 328.

M7.59

ROLE OF SILVER IN YBa₂Cu₃Ag_xO_{7-δ} COMPOSITE SUPERCONDUCTORS. L. Ganapathi, Ashok Kumar and J. Narayan, Department of Materials Science and Engineering North Carolina State University, Raleigh, N. C. 27695-7916

Superconducting properties and microstructures of the YBa₂Cu₃Ag_xO_{7-δ} composites have been studied as a function of silver content, 0 < x < 6, using a variety of techniques. The superconducting transition temperature, T_c, of these composites was found to be the same, ~ 90 K, for the above range of compositions. The composites with x > 3 are found to have resistivity behavior identical to silver metal above the superconducting transition temperature. The peritectic transformation temperature of the 123 material in the composite is lowered. Alloy formation between Ag and Cu is proposed to take place triggering the peritectic transformation at lower temperatures. The silver is observed in the form of precipitates at very low concentrations of silver, indicating that silver does not substitute for copper in YBa₂Cu₃O₇. Lattice parameters of the composites were found to be invariant throughout the above composition range. The addition of Ag₂O in the starting composition seems to stabilize the stoichiometric YBa₂Cu₃O₇ by way of decomposition to Ag and O, also, the better diffusion of oxygen through silver in comparison with that through the superconductor helps the regeneration of superconductivity in the composite superconductor.

M7.60

SOL-GEL PREPARATION, MICROWAVE SINTERING AND MICROWAVE PROPERTIES OF SUPERCONDUCTING POWDER. Fathi Selmi, H.S. Dewan, *S. Komarneni, V.K. Varadan and V.V. Varadan, Research Center for the Engineering of Electronic and Acoustic Materials, 149 Hammond Building, * Materials Research Laboratory, The Pennsylvania State University, University Park, PA 16802.

Ultra-pure superconducting, Y Ba₂ Cu₄ O_x, powder was synthesized using the sol-gel technique. Conventional and microwave sintering of both commercial and sol-gel prepared powders were investigated and the sintered samples were characterized and compared in terms of densification and particle size. The dielectric properties were also studied at microwave frequencies as a function of temperature and preparation conditions.

M7.61

PHASE RELATIONSHIPS IN THE Y-Ba-Cu-O IN WET CO₂ ENVIRONMENTS. J.J. SIMMINS, Eutech Engineering Technologies, Alfred, NY 14802. G.S. FISCHMAN, and R.L. SNYDER, N.Y.S. College of Ceramics at Alfred University, Alfred, NY 14802.

Reactions involving carbon dioxide with compounds in the Y-Ba-Cu-O system are currently under investigation. Several interesting phenomena have been discovered. For example, it has been found that the decomposition of Y₁Ba₂Cu₃O_{8+δ} in wet CO₂ proceeds by a step-wise process involving intermediate compounds. It has also been observed that decomposition does not take place readily, at high temperatures, without the presence of water vapor in the system. The decomposition of the 211 "green phase" proceeds in a single step.

Simultaneous thermal analysis (STA) was performed in both wet and dry CO₂ environments to determine the kinetics of reaction and activation energies for CO₂ decomposition. In the case of Y₁Ba₂Cu₃O_{6+y} profile fitting of the STA data was needed to determine the rates of the individual reactions. In-situ as well as post mortem X-ray diffraction was used to confirm these mechanisms.

Experimental results as well as techniques will be discussed.

M7.62

PREPARATION OF FIBROUS Bi(Pb)-Sr-Ca-Cu-O CRYSTALS CONTAINING THE HIGH-T_c PHASE. Ichiro Matsubara, Hideo Tanigawa, Toru Ogura, Hiroshi Yamashita, Makoto Kinoshita, Government Industrial Research Institute Osaka, Ikeda City, Osaka; and Tomoji Kawai, Osaka University, Ibaraki City, Osaka.

Fibrous crystals containing the high-T_c phase of Bi(Pb)-Sr-Ca-Cu-O superconductor have been prepared by heating a glassy melt-quenched plate in a stream of oxygen gas. Each fiber is composed of several platelike single crystals which are stacked in layer structure. The dimension of the fibers are 2-10 μm x 10-300 μm x 3-15 mm. The fibers shows a remarkable resistance drop at 105 K and T_c(end) at 70 K. The high-T_c phase is detected on a micro area X-ray diffractometer and the High-T_c crystals are stacked between the low-T_c platelike crystals. The fibers have a single crystal nature and can be bent to a radius of curvature (R) of 0.4 mm without a decrease in the T_c value. The highest J_c is 67000 A/cm² (63 K, zero magnetic field) in a nonbending state. It surpasses 35000 A/cm² even in a bending state of R > 1 mm and finally decreases down to 3200 A/cm² for R = 0.4 mm.

M7.63

PRELIMINARY INVESTIGATION OF PROCESSING AND PHASE DIAGRAM CONSTRUCTION IN THE Y-Sr-Cu-O SYSTEM. T. D. Rolin, F. S. Cheng, J. R. Ashburn, H. Y. Cheng, E. E. Anderson, The University of Alabama in Huntsville, Huntsville, AL 35899.

We have investigated the Y-Sr-Cu-O system which forms a K₂NiF₄ 40 K superconducting phase in addition to an 80 K phase of hypothesized stoichiometry Y_{1+x}Sr_{2-x}Cu₃O₇. Difficulties in processing single phase materials by standard solid state reaction of carbonates and oxides have compelled us to explore other methods. A two-step solid state processing technique as well as a coprecipitation method will be discussed including the relative advantages and disadvantages of each. We will also report results of preliminary TGA/DTA measurements of samples with several Y to Sr ratios. From data obtained we have mapped some of the ternary phase diagram, particularly encompassing the region expected to be favorable for nonstoichiometric crystal growth. This region of interest includes [pseudo]binary cuts along Y₁Sr₁Cu₄O₇-CuO and Y₁Sr₂Cu₃O₇-CuO.

M7.64

OXIDATION AND REDUCTION KINETICS OF Bi₂Sr₂CuO_{6+y} CRYSTALS. Edward Sonder, B.C. Chakoumakos, and B.C. Sales, Solid State Division, Oak Ridge National Laboratory, P.O. Box 2008, Oak Ridge, TN 37831-6056.

The oxygen content of Bi₂Sr₂CuO_{6+y} single crystals can be reversibly varied between y=0 and y=0.4 by suitable heat treatment in either oxygen or helium gas. Only crystals with close to the maximum oxygen content (y=0) are superconducting above 4.2 K. A thermogravimetric study was made of the oxidation and reduction kinetics of a group of small single crystals with typical dimensions of 5 x 5 x 0.05 mm. For these measurements the oxygen content of the crystals was repeatedly changed from y=0 to y=0.4. Oxidation rates were studied in flowing oxygen over the temperature range 450-800°C, and reduction rates were investigated in flowing helium gas over the temperature range 740-800°C. The activation energy for oxidation was 1 eV/atom, which was much smaller than the activation energy for reduction of 5 eV/atom. Attempts to remove more than 0.5 oxygens per formula unit resulted in decomposition of the Bi₂Sr₂CuO_{6+y} structure and the formation of orthorhombic Bi₂Sr₂O₅.

*Research sponsored by the Division of Materials Sciences, U.S. Department of Energy under contract DE-AC05-84OR21400 with Martin Marietta Energy Systems, Inc.

M7.65

HIGH-TEMPERATURE DEFORMATION OF YBa₂Cu₃O_{7-δ} WITH Ag ADDITIONS. J. L. Routhort, K. C. Goretta, J. Sulek, and J. P. Singh, Argonne National Laboratory, Argonne, IL 60439

Second phase silver additions have been observed to increase the density of YBa₂Cu₃O_{7-δ} (123) and result in enhanced room-temperature fracture toughness, strength and critical current density (J_c). Further increase in J_c can be achieved by the texture, which can be induced by plastic deformation. Therefore, the steady-state flow stress of 1-2-3 samples containing 10 and 20 vol. % Ag has been measured in direct compression in air at constant strain rates. The results are compared with those obtained from unalloyed 1-2-3 between 870°C and 930°C for strain rates of 5 x 10⁻⁶ to 4 x 10⁻⁵ s⁻¹.

*Work supported by the U.S. Department of Energy, Basic Energy Sciences-Materials Sciences under Contract #W-31-109-ENG-38.

M7.66

BULK MODULUS OF THE YBACUO OXIDE SUPERCONDUCTOR OBTAINED FROM MAGNETIC MEASUREMENTS. Bokhimi, Instituto de Fisica UNAM, a.p. 20-364, 01000 Mexico D.F., Mexico.

The Bulk modulus of any system is normally obtained from measurements of its thermodynamic or mechanical properties. In this work it is shown that starting from magnetic measurements of the YBACUO oxide superconductors, it is possible to obtain their Bulk modulus. The magnetic susceptibility at high temperatures of the Y₁Ba₂Cu₃O_{7-x} oxide superconductors is temperature independent for each oxygen deficiency x. This fact is explained if one assume that the charge carriers in this system have a free-electron like behavior. With this assumption the transition temperature to the superconducting state changes linear with the charge carriers density. It is known that when an external pressure is applied to superconducting samples of YBACUO, their transition temperatures to the superconducting state change linear with pressure. If it supposed that in this system the pressure produces only a change in the volume of the unit cell, but not in the number of its charge carriers, then for this system it is found a relation between the Bulk modulus and the magnetic susceptibility at high temperatures. The values that are obtained for the Bulk modulus of the Y₁Ba₂Cu₃O_{7-x} oxide superconductors by this method, using measurements of the magnetic susceptibility at room temperature for different oxygen deficiencies, are of the same order of magnitude to those reported in the literature, which were obtained from sound-velocity and hydrostatic pressure measurements.

M7.67

ULTRASONIC STUDY OF THE LOW TEMPERATURE STRUCTURAL PHASE TRANSITION IN $\text{YBa}_2\text{Cu}_3\text{O}_{7-x}$ AND ITS DEPENDENCE ON OXYGEN CONCENTRATION. J. Toulouse and X. Q. Wang, Physics Department, Bethlehem, Pennsylvania, 18015; and D. J. L. Hong, Materials Research Center, Lehigh University, Bethlehem, Pennsylvania, 18015.

Elastic and structural instabilities have been reported in $\text{YBa}_2\text{Cu}_3\text{O}_{7-x}$ between 210 and 270K. In order to better characterize these instabilities, we have carried out an ultrasonic study as a function of both oxygen concentration and annealing temperature. Measurements of the sound velocity and ultrasound attenuation have been performed with simultaneous resistance measurements. The attenuation measurements reveal two major peaks. The upper peak occurs above 200K. It is relatively narrow ($\sim 25^\circ\text{K}$) and its position, T_p , shifts downwards with decreasing oxygen concentration. An analysis of the results suggests that the upper peak is associated with an athermal (martensitic-type) transition starting at a temperature T_s , just above T_p . The onset of the transformation also appears to correspond to the beginning of a steep rise in the sound velocity. Finally, a linear relationship is obtained between the upper peak temperature, T_p , and the superconducting transition temperature, T_c , suggesting that the second phase formed is essential for the high T_c .

M7.68

MAGNETIC ANISOTROPY AND OXYGEN STOICHIOMETRY IN $\text{YBa}_2\text{Cu}_3\text{O}_{7-y}$. J. R. Ashburn, F. S. Cheng, T. D. Rolin, H. Y. Cheng, E. E. Anderson, The University of Alabama in Huntsville, Huntsville, AL 35899.

We have investigated the interrelationship between the anisotropy of the magnetic properties and the oxygen stoichiometry in single crystals of $\text{YBa}_2\text{Cu}_3\text{O}_{7-y}$ for y between zero and 0.6. The crystals were grown from a nonstoichiometric melt with the oxygen content adjusted by quenching from appropriate temperatures. Magnetization (in fields up to 5 T) and susceptibility (from 4.2 to 100 K) were measured with a SQUID magnetometer. Diamagnetic shielding remains near 100% for y less than 0.5 while Meissner signals in low fields decrease in a stepwise fashion paralleling the decrease in T_c . Preliminary observations indicate an exponentially increasing anisotropy in the lower critical field with increasing y . However, the lower critical fields and magnetic relaxation both parallel and perpendicular to the c -axis appear to vary non-monotonically with increasing y in a manner reminiscent of the behavior of the normal state conductivity and suggestive of a dependence on oxygen ordering.

M7.69

OXYGEN ORDERING IN $\text{YBa}_2\text{Cu}_3\text{O}_x$. D. de Fontaine*, M.E. Mann** and G. Ceder* *Department of Materials Science & Mineral Engineering, U.C. Berkeley and Lawrence Berkeley Lab, Berkeley, CA 94720; and **Dept. of Physics, U.C. Berkeley and Lawrence Berkeley Lab, Berkeley, CA 94720.

Oxygen ordering in the symmetry plane of $\text{YBa}_2\text{Cu}_3\text{O}_x$ has been studied by the Cluster Variation Method (CVM) and by Monte Carlo simulation in an anisotropic two-dimensional Ising model. The orthorhombic (Ortho I) to tetragonal transition is found to be second order at high temperature and another phase, Ortho II, becomes stable at stoichiometry $x=6.5$ at intermediate temperatures. States of partial order are also found at low temperatures as a direct consequence of the strong anisotropy of the second neighbor effective oxygen interactions.

Models based on symmetric Ising models are incapable of producing ordered states beyond Ortho I, stable or metastable, recent claims to the contrary notwithstanding. The present model reproduces the essential features of TEM micrographs and diffraction patterns of $\text{YBa}_2\text{Cu}_3\text{O}_x$ samples aged at low temperature.

M7.70

Fe DOPANT LARGELY REPLACES Cu(2) PLANAR SITES IN AEROSOL PRODUCED $\text{YBa}_2(\text{Cu}_{1-x}\text{Fe}_x)_3\text{O}_{7-x}$ SUBMICRON GRAINS AND DESTROYS SUPERCONDUCTIVITY. P. Boolchand, P. Biswas, D. Zhou, W. Huff, D. McDaniel, K. Eglaid, Univ. of Cincinnati, Cincinnati, OH 45221-0071.

Several groups¹ have examined Fe metal doping effects in the indicated cuprate superconductor produced by conventional solid state reaction of powders. In such samples, there is a general consensus that Fe dopant largely ($>85\%$) enters in CuO_2 chains with the remainder present in CuO_2 planes. At $x=0.015$, the transition temperature T_c remains nearly the same as that of the pristine $\text{YBa}_2\text{Cu}_3\text{O}_{7-x}$ material of $\sim 90\text{K}$.

We have now prepared submicron grains of indicated superconductor using nitrate and Fe-chloride precursors in an aerosol reactor. At an Fe dopant concentration of $x=0.015$, T_c is found to drop sharply to $<11\text{K}$, from a value of 65K for the pristine aerosol sample. ⁵⁷Fe dopant site distribution in the aerosol sample displays largely a unimodal distribution with the planar - B site ($\delta=0.02\text{ mm/s}$ and $\Delta=0.41\text{ mm/s}$) as the principal site. These results suggest that aerosol processing leads to Fe dopant largely present in CuO_2 planes. The loss of superconductivity in such samples would appear to be consistent with the idea of a magnetic ion inducing pair-breaking in the CuO_2 planes, as in a conventional Nb-based low-temperature superconductor.

¹P. Boolchand and D. McDaniel in Vol. 4 of "Studies of High Temperature Superconductors", Editor A. Narlikar (in press), 1989.

M7.71

OXYGEN CONTENT VARIATION IN CATION-DEFICIENT AND CHEMICALLY-DOPED HIGH- T_c Y-Ba-Cu-O SUPERCONDUCTORS. Y.H. Kao, L.W. Song, Y.D. Yao, State University of New York at Buffalo; and Z. Tao, K.W. Jones, Brookhaven National Laboratory, Upton, NY.

Oxygen content in a variety of high- T_c superconductors has been determined by using a charged particle activation method¹. Compounds studied in this experiment include Cu-deficient Y-Ba-Cu-O, Cu/Bi-deficient Bi-Sr-Ca-Cu-O and some systems doped with Cr, Ni, Nb, Ag, and Pb. Using the oxygen content variation in Cu- and Bi-deficient compounds as a basis, the net effects of chemical doping on the formal valence of cations in Y-Ba-Cu-O and Bi-Sr-Ca-Cu-O are compared for different types of impurity atoms. In the case of Bi-Sr-Ca-Cu-O compounds, Cu- and Bi- deficiencies give rise to different variations in the oxygen content. When each kind of deficiency is replaced by a given dopant (e.g. Ag or Pb), the net results are significantly different. This observation suggests that there exists a compatibility condition between each kind of cation-deficiency and a given dopant atom.

This research is supported by DOE and AFOSR.

1. Z. Tao, D.E. Alburger, K.W. Jones, Y.D. Yao, and Y.H. Kao, Appl. Phys. Lett. **53**, 1440 (1988).

M7.72

LUMINESCENCE FROM DEFECTS AND IMPURITY CENTERS IN Y_2O_3 . M. S. Jahan*, D. W. Cooke, B. L. Bennett, W. L. Hults, M. A. Maez, K. C. Ott, and J. L. Smith, Los Alamos National Laboratory, Los Alamos, NM 87545.

Unreacted Y_2O_3 is frequently found in sintered $YBa_2Cu_3O_x$ superconductors as an unwanted second phase. Removal of this insulating impurity, especially at the surface, is important for achieving low values of surface resistance. A convenient method for detecting the presence of insulating material at the surface is that of thermally stimulated luminescence (TSL). Following γ irradiation at RT and subsequent heating to 350°C, Y_2O_3 emits characteristic luminescence, which can be used to identify its presence in high-temperature superconductors. Additionally, the purity of the Y_2O_3 starting material can also be determined by the TSL technique. Our investigations show that defects and impurities exist even for 99.999% pure material.

The characteristic TSL glow curve of Y_2O_3 consists of a main peak at 115°C and a knee at 190°C. The corresponding spectral emission is comprised of broad bands at 490 and 630 nm, and a narrow band with well-resolved peaks at 543 and 550 nm. An additional band, associated with the 190°C peak only, is observed at 590 nm. These emission spectra have been previously associated with Tb^{3+} . Based upon x-ray fluorescence and chemical analyses of Y_2O_3 , we conclude that Tb^{3+} is not the main impurity. This conclusion is further supported by the fact that intentional doping of Y_2O_3 with Tb^{3+} does not alter the intensity of the characteristic emission spectra. A model based upon electron centers (F and F^+), an unknown impurity, and Tb^{3+} as a deep trap, can adequately explain our data.

* Permanent Address: Memphis State University, Memphis, TN 38152.

Research Supported by U.S.D.O.E. and USA/SDC.

M7.73

RELATION BETWEEN THE CHARACTERISTICS OF POWDER AND MICRO-STRUCTURE; PROPERTIES OF CERAMICS FOR $YBa_2Cu_3O_x$ SUPER-CONDUCTORS Meiyu Zhao, Chengen Li, Xingyun Jin, Yeming Huang Shanghai Institute of Ceramics, Shanghai 200050, P.R. CHINA

Four kinds of $YBa_2Cu_3O_x$ (YBCO) superconducting powders with different particle sizes, shapes and different amounts of twins have been prepared in this work. The density, grain sizes, XRD of phase composition, configuration of twins of the ceramics have been investigated. The relation between the characteristics of YBCO powders and the microstructure, current density of the bulk materials are also discussed. In contrast to the improved YBCO powder prepared by solid state method, the YBCO powders through the improved coprecipitation approach have less impurities, smaller particle size, and much more amounts of twins, as well as the sintered pellets show a higher density (the highest density around 97% of the theoretical density), an orthorhombic single phase, and moreover, the pellets have finer grain boundaries and well developed twins. As a result, these samples exhibit current densities (about 1500 A/cm²) higher than those prepared by solid state method. Using BaO , instead of $BaCO_3$ as the starting material, a more dense bulk YBCO ceramics with orthorhombic single phase and J_c (about 1,000 A/cm²) can have also been fabricated by solid state method.

M7.74

LOW-RESISTIVITY CONTACTS TO HIGH-TEMPERATURE SUPERCONDUCTORS. T. H. Tiefel, S. Jin, M. E. Davis, R. B. van Dover, R. C. Sherwood, H. M. O'Brien, G. W. Kammlott and R. A. Fastnacht, AT&T Bell Laboratories, Murray Hill, NJ, 07974.

An essential requirement in evaluation of the current carrying capability (J_c) as well as for actual high-current applications of the high T_c oxide superconductors is the preparation of robust, low-resistance

electrical contacts to the superconductor. In this paper convenient in-situ preparation methods for obtaining extremely-low-resistivity contacts to bulk high T_c superconductors (ρ_c in the range of 10^{-12} to 10^{-11} Ω -cm²) are described. Three different configurations of silver contact metal in Y-Ba-Cu-O have been employed, i.e., embedded Ag wire, embedded Ag particles, and selectively patterned Ag-clad on superconductor wire. In all three cases, the low-resistivity, metallic contacts are formed during the sintering or melt-processing of the superconductor, thus eliminating the need for separate steps of contact preparation such as vacuum deposition of contact metal and additional heat treatment. The distribution and morphology of the silver contacts will be discussed. The measured contact resistivities in the present work are the lowest reported for the high T_c superconductors, and these methods may serve as a useful basis for important contact technologies needed for bulk superconductor applications.

M7.75

OXYGEN ORDERING AND SAMPLE INHOMOGENEITY IN $YBa_2Cu_3O_{7-\delta}$. Y. Bruynseraede, J. Vanacken, B. Wuyts and I.K. Schuller*, Laboratorium voor Vaste Stof-Fysika en Magnetisme, Katholieke Universiteit Leuven, 3030 Leuven, Belgium; *Physics Department - B019, University of California - San Diego, La Jolla, California 92093, USA.

Gas evolution, x-ray diffraction and critical temperature measurements are reported on two sets of $YBa_2Cu_3O_{7-\delta}$ samples as a function of oxygen and metal ion composition. The oxygen deficient samples were prepared by annealing (at 400°C) in vacuum ($\approx 10^{-6}$ Torr) for varying lengths of time. Initially, a large change in "chain" occupancy accompanied by a decrease in T_c from 90 K to 60 K is observed. Longer annealing yields a decrease of the 60 K superconducting fraction, probably due to oxygen ordering effects since the oxygen content stays constant. In one set of $YBa_2Cu_3O_{7-\delta}$ samples, and probably due to inhomogeneities, we observed the coexistence of two superconducting phases in the temperature region 90 K - 60 K. Y-substitutions with different Pr concentration in $YBa_2Cu_3O_{7-\delta}$ were also investigated. The presence of Pr strongly affects T_c while the oxygen evolution behavior does not change at all.

This work is supported by the Belgian Inter University Institute for Nuclear Sciences (I.I.K.W.), the Inter University Attraction Poles (I.U.A.P.) and Concerted Action (G.O.A.) Programs (at K.U.L.) and the U.S. Office of Naval Research under contract number N00014-88K-0480 (at U.C.S.D.). International travel was provided by NATO. Two of us (J.V. and B.W.) would like to thank the Belgian I.W.O.N.L. and F.K.F.O. for financial support.

M7.76

MAGNETIC FIELD CONTROLLED LEVITATION AND SUSPENSION OF A MAGNET ABOVE AND BELOW TYPE II SUPERCONDUCTORS. Takeshi Takamori, John J. Boland and Derek B. Dove, IBM Research Division, Thomas J. Watson Research Center, Yorktown Heights, NY 10598

Levitation and suspension of a permanent magnet can be controlled by combination of a variable magnetic field and a type II superconductor ($YBa_2Cu_3O_x$). It has been observed that a continuous range of distances exists where stable levitation and suspension may be obtained, and that the orientation of magnetic moment of the levitated or suspended magnet is also adjustable over a range of angles. The incorporation of the magnetic element makes it possible to suspend much higher mass than reported previously. Observations are presented with a short movie.

M7.77

INTERACTIONS BETWEEN SILVER AND $YBa_2Cu_3O_{7-\delta}$

A. H. Carim, Center for Micro-Engineered Ceramics & Department of Chemical and Nuclear Engineering, University of New Mexico, Albuquerque, NM 87131; R. E. Loehman, Dept. 1840, Sandia National Laboratories, P.O. Box 5800, Albuquerque, NM 87185; A. P. Tomsia and J. A. Pask, Pask Research and Engineering, Pinole, CA.

Given the importance of the $Ag-YBa_2Cu_3O_{7-\delta}$ system for electrical contacts to the superconductor, metal-clad wires, and high-ductility composites, the reactions that occur between the two materials are of substantial interest. We have utilized a variety of techniques, including sessile-drop experiments, SEM/EDS, electron microprobe, and TEM to characterize the interaction of silver with $YBa_2Cu_3O_{7-\delta}$ (123). The contact angle of a liquid Ag droplet on the 123 surface decreases with increasing oxygen partial pressure and with time at high temperature. Silver rapidly penetrates the pores and grain boundaries in the sintered superconductor pellet at temperatures at or above 940°C. The mechanism for wetting by silver is the reaction of Ag with oxygen supplied by the ambient or from reduction of nearby 123 grains. This apparently leads to a decomposition of the superconductor into Y_2BaCuO_5 (211) and a liquid rich in Ba and Cu, which in turn solidifies as $BaCuO_2$ and other products. X-ray maps, microprobe line scans, and TEM confirm that grains surrounded by silver have been reduced to 211 and furthermore indicate the presence of $BaCuO_2$ particles nearby. Less decomposition of 123 is observed at higher oxygen partial pressures, since the ambient provides a greater supply of oxygen.

M7.78

TEMPERATURE DEPENDENT FAR INFRARED STUDIES OF MAGNETICALLY-ORIENTED $YBa_2Cu_3O_{7-\delta}$

F. Lu*, C.H. Perry*, K. Chen and R.S. Markiewicz
Physics Department, Northeastern University, Boston MA 02115

The polarized ($E \parallel \hat{c}$ and $E \perp \hat{c}$) optical response of magnetically-oriented ($> 95\% \hat{c}$ -axis) $YBa_2Cu_3O_{7-\delta}$ 93K superconductor are reported over a wide energy range from 2-3000 meV¹. Our far infrared reflectivity studies have been extended from 300- 10K. Strong anisotropic changes in the low frequency spectra are observed between the normal and the superconducting states; the most pronounced are associated with the $E \perp \hat{c}$ spectrum. The latter also displays well defined phonons in contrast to the high conductivity ab-plane. Various model parameters associated with the phonons, plasma frequencies and relaxation rates have been deduced from fits to the data.

¹ F. Lu, C.H. Perry, K. Chen, and R.S. Markiewicz, J.O.S.A. B6, 39G, (1989)

*Supported in part by NSF grant #DMR 8604706 and Northeastern University Research and Development Fund.

M7.79

HIGH-TEMPERATURE INTERACTIONS BETWEEN OXIDE SUPERCONDUCTORS AND ELECTRICAL CONTACT MATERIALS. R.D. Ray II and E.E. Hellstrom, Department of Materials Science and Engineering, University of Wisconsin-Madison, 1509 University Ave., Madison, WI 53706.

Electronic devices and high-field applications of high-temperature superconductors require contact between the superconductor and a metal conductor. Some processing steps require that this contact be heated to elevated temperatures. Whereas at room temperature, no reaction was observed between 123 and a sputtered overlayer of Au or Ag, we have shown that Au can extract Cu from 123 at 875°C, causing it to decompose. With Ag we observe Ba loss from 123 at 875°C. The decomposition products with Au and Ag are being studied with x-ray diffraction, microprobe analysis, and Auger and

Raman spectroscopy to identify the phases that form. We are also investigating the mechanism by which Cu diffuses through the Au. The various applications require different superconductor/metal contact configurations that see different environments. This can influence the superconductor/metal interaction. Specifically, our experiments have the superconductor completely surrounded by metal (metal clad wire), the metal completely surrounded by superconductor (metal powder additions to the superconductor), and a planar interface between the metal and superconductor (electrical contact for devices).

M7.80

EFFECT OF SURFACE ROUGHNESS ON PENETRATION DEPTH IN THE Y AND Bi HIGH-TEMPERATURE SUPERCONDUCTORS. J.W. Purpura and T. R. Clem, Naval Coastal Systems Center, Panama City, FL.

Bulk polycrystalline tubes of Y-Ba-Cu-O and Bi-Sr-Ca-Cu-O high-temperature superconductors were fabricated with varying degrees of inner wall surface roughness. The tubes are evaluated by means of SQUID magnetometry. Estimates of the intergranular penetration depth are given based on measurements of the temperature variation of the axial magnetic field trapped within the center bores of the tubes. Deviations from the Gorter-Casimir temperature dependence are discussed. The superconducting phases within the samples were identified by x-ray powder diffraction. Scanning electron microscopy was performed to measure surface roughness, grain size, and grain size uniformity. Four-point resistivity measurements were conducted to determine critical temperature. The effect of surface properties on magnetic hysteresis is also examined.

M7.81

ANALYSIS OF LOW TEMPERATURE PHASE TRANSITION PRIOR TO SUPERCONDUCTIVE BEHAVIOR IN HIGH TEMPERATURE SUPERCONDUCTORS. M.A. RODRIGUEZ and R. L. SNYDER, N.Y.S. College of Ceramics at Alfred University, Alfred, N.Y. 14802.

Recent reports have discussed the possibility of a low temperature phase transition in the high temperature superconductors just prior to the illustration of superconductive behavior.

This presentation will attempt to confirm this phenomena for the 123 compound in the Y-Ba-Cu-O system as well as investigate the possibility of this transition in other high T_c materials such as the Bismuth and Thallium compounds. Phases to be investigated in these systems include 2201, 2212, and 2223 compounds.

Synchrotron radiation shall be used for data collection. Experiments shall be run at the NSLS located Brookhaven National Labs.

M7.82

MAGNET REPLICA BY HIGH T_c SUPERCONDUCTORS R. Weinstein, In-Gann Chen, J. Liu, and D. Parks, Institute of Beam Particle Dynamics/Texas Center for Superconductivity, University of Houston, Houston, TX 77204

When a superconductor (SC) has imperfections, the field may be contained, or pinned. This "Incomplete Meissner Effect" allows the production of magnet replicas, which are bulk superconductor with persistent internal currents which reproduce the parent magnetic field. The field remains in place due to pinning and is an excellent copy of the parent field, independent of the shape of the SC. This phenomenon has been demonstrated on low T_c SCs with fields up to 2.25T. An extension of this study to high T_c SCs has been conducted. Magnetic fields trapped in both longitudinal and transverse directions are measured in hollow cylindrical samples and other configurations. Effect of Ag addition and grain size on the amount of field trapped have also been studied. Magnetic fields of over 100 gauss have been detected for samples with large grains and Ag addition. Giant flux creep effect associated with the high T_c SCs has been studied by the field vs. time measurements. Significantly slower flux creep rate is observed in samples with Ag addition and large grains. Calculations of the internal current indicate that magnetic field higher than 1 T can be achieved by materials produced by the partial melting process, in which transport J_c higher than

10^4 amp/cm² at 77 K and low field have been measured.⁽¹⁾ It is suggested that this method can be used to characterize the bulk transport current and homogeneity of SC samples. It is experimentally noted that magnetic field can be added by attaching more than one SC samples together. The application of this magnet replica technique can be very significant in many areas due to its low energy consumption, low weight, and good multipole reproduction. No direct electricity to the magnet is needed. Maintaining the LN temperature is the only energy consumption. Prominent applications include high efficiency motor/generator, MRI magnets, and particle beam steering devices.

(1) Salama et al, *Appl. Phys. Lett.*, June 1989.

M7.83

DISTRIBUTION OF IRON OVER COPPER SITES IN $GdBa_2(Cu_{1-x}Fe_x)_3O_{7-\delta}$. H.J. Bornemann and G. Czizek, Kernforschungszentrum Karlsruhe, INFP, P.O.B. 3640, D-7500 Karlsruhe, FRG; and R. Kmiec, Institute of Nuclear Physics, ul. Radzikowskiego 152, 31-342 Kraków, Poland.

Iron doped compounds $GdBa_2(Cu_{1-x}Fe_x)_3O_{7-\delta}$ with $0.03 \leq x \leq 0.25$ and $\delta < 0.1$ as well as with $\delta > 0.7$ have been investigated by Mössbauer spectroscopy with ¹⁵⁵Gd and with ⁵⁷Fe. For each iron concentration x , samples with different transition temperatures T_c (at constant oxygen content, $\delta < 0.1$) were prepared and investigated. Samples were reduced to an oxygen deficiency $\delta > 0.7$ either at 650°C under vacuum or at 950°C in an N₂ atmosphere, followed by a quench to room temperature.

A comparison of ⁵⁷Fe Mössbauer spectra for samples treated by these different procedures has yielded an unambiguous determination of the fraction of iron atoms occupying Cu(2) sites. This fraction extrapolates to ~4% for $x=0$. It increases monotonously with x to ~17% for $x=0.12$. In samples reduced at 950°C for 44 hours, the fraction of iron on Cu(2) sites is doubled, and this large Cu(2) site occupancy is maintained when the material is reoxidized at 450°C.

From the systematic variation of the parameters associated with the remaining quadrupole doublets with iron concentration x and with T_c (for constant x), tentative assignments of the doublets to specific oxygen coordinations of Fe on Cu(1) sites were derived.

For ¹⁵⁵Gd, both the quadrupole splitting and the isomer shift vary smoothly with iron concentration. No influence of an extra charge associated with iron on Cu(2) sites in the vicinity of Gd nuclei is discernible.

M7.84

MAGNETIC PHASE DIAGRAM OF $YBa_2(Cu_{1-x}Fe_x)_3O_y$ and $YBa_2(Cu_{1-x}Co_x)_3O_y$. Masao Doyama, Masaaki Matsui, Hiroshi Matsuoka, Kazuhito Ishikawa and Eiji Hayashi, Department of Materials Science, Faculty of Engineering, Nagoya University, Furocho, Chikusa-ku, Nagoya 464-01 JAPAN. $YBa_2(Cu_{1-x}Fe_x)_3O_y$ ($x=0-0.12$) and $YBa_2(Cu_{1-x}Co_x)_3O_y$ ($x=0-0.15$) are prepared by mixing the oxides of 4N-Y₂O₃, BaCO₃, CuO and other oxide for doping (Fe₂O₃ or CoO), calcined twice at 900°C for 16 hours and 500°C for 2 hours in air and by slowly cooling, pressed into a pellet, again sintered. Electrical resistivity, lattice parameters, magnetic susceptibility are measured as a function of temperature.

As the amount of doping was increased, diamagnetism was decreased. At a lower magnetic field, magnetization changed from negative to positive. Apparent H_{c2} becomes lower. The volume fraction of superconducting phase rapidly decreased. In all specimens, the paramagnetic susceptibility above T_c can be expressed as $\chi = C/(T-\theta) + \chi_0$ where χ_0 is independent of temperature.

Magnetic phase diagram was determined by the measurements of magnetic susceptibility and positive muon spin relaxation. At low temperatures, spin glass phase transition was found and both superconducting phase and spin glass phase are coexistent.

M7.85

ATOMISTIC DEFECT MODELS OF $YBa_2Cu_3O_{7-x}$. Roger C. Baetzold, Eastman Kodak Company, Rochester, NY 14650-02001.

Atomistic Defect Calculations have been presented for $YBa_2Cu_3O_{7-x}$ within the framework of the shell-model description of ionic bonding. The short-range potentials are utilized within the electron-gas calculation and then optimized to allow the best fit to crystal structure. This presentation will focus on phonon dispersion relations determined with the original and improved potential models. Comparison to Raman and infrared experimental vibration frequencies are made. In addition, the mechanisms of oxygen ion diffusion in the crystal are examined with interstitial and vacancy models. Within the crystal planes an oxygen ion vacancy mechanism having an activation barrier of 1 eV is computed. These and other computed properties will be compared to experiment.

1. R.C. Baetzold, *Phys. Rev. B* 38,11304 (1988).

M7.86

ELECTRON MICROSCOPIC STUDY OF OXYGEN-VACANCY ORDERING IN $YBa_2Cu_3O_{6+x}$ with $x > 0.3$. P. Peng, D. J. L. Hong, A. Mehta, H. M. Chan, and D. M. Smyth, Materials Research Center, Whitaker Lab #5, Lehigh University, PA 18015.

It is widely accepted that $YBa_2Cu_3O_{6+x}$ undergoes an orthorhombic to tetragonal transition on chemical reduction. Most X-ray diffraction results locate this transition at an oxygen content of $x \sim 0.6$. However, recent high temperature defect modeling of oxygen nonstoichiometry in $YBa_2Cu_3O_{6+x}$ indicates that the orthorhombic order persists to much lower oxygen contents; at least down to $x \sim 0.3$ for all temperatures above 300°C. One possible explanation for this discrepancy is that at lower oxygen contents the scale of the orthorhombic order in $YBa_2Cu_3O_{6+x}$ becomes very fine, and due to low spatial resolution of x-ray diffraction the short range orthorhombic structure is "averaged out" as tetragonal. Furthermore, theoretical calculations by Morris and Khachaturyan [1] predict that below 100°C, the orthorhombic phase decomposes spinodially into a two-phase mixture of orthorhombic and tetragonal structures.

A systematic study was undertaken on $YBa_2Cu_3O_{6+x}$, with oxygen contents varying from $x = 0.3$ to 0.9, using electron diffraction and convergent beam electron diffraction in the transmission electron microscope. Particular attention was paid to superstructures arising from the ordering of oxygen vacancies.

[1] A. G. Khachaturyan, S. V. Semenovskaya and J. W. Morris, Jr., *Phys. Rev.*, B37(4), p. 2243 (1988).

(Supported by the Division of Materials Research, NSF; and the Lehigh University Consortium for Superconducting Ceramics.)

M7.87

THERMOGRAVIMETRIC STUDY OF OXYGEN DIFFUSION IN SUPERCONDUCTING $YBa_2Cu_3O_{7-\delta}$ OXIDES. L.T. Shi and K.N. Tu, IBM T. J. Watson Research Center, Yorktown Heights, NY 10598

The oxides of oxygen-deficient $YBa_2Cu_3O_{7-\delta}$ with $\delta \approx 0.32$ in both powder and chunk form were annealed in ambient oxygen to investigate the behavior of oxygen in-diffusion. Thermogravimetric measurements were used to monitor in-situ weight gain during the annealing at constant heating rates between room temperature and 580°C. The temperature for achieving a definite oxygen

stoichiometry changes with the heating rates, which were varied from 0.1 to 15°C/min. By measuring the rate dependence, the activation energy of oxygen diffusion in the powder oxide was determined to be 1.25 ± 0.05 eV, in good agreement with the value obtained by the previous resistivity measurements. However, the activation energy obtained from the chunk oxide is higher, i.e. 1.52 ± 0.06 eV. A longer diffusion distance in the chunk oxide which requires diffusion across grains might be responsible for this discrepancy. In addition, the oxygen out-diffusion was studied by annealing the oxide in ambient helium at constant temperatures. The results will be reported.

M7.88

OXYGEN DISTRIBUTION NEAR METAL M SUBSTITUTED SITES IN $YBa_2(Cu_{1-x}M_x)_3O_{7+\delta}$ AS DETERMINED BY X-RAY ABSORPTION MEASUREMENTS. C. Y. Yang*, Y. L. Wang, S. M. Heald, Youwen Xu, A. R. Moodenbaugh, D. O. Welch, and M. Suenaga, Materials Science Division, Brookhaven National Lab., Upton, NY 11973.*

X-ray absorption measurements have been performed on $YBa_2(Cu_{1-x}M_x)_3O_{7+\delta}$, $M = Fe$ ($x \leq 0.15$), Co ($x \leq 0.28$), Ni ($x \leq 0.08$), and Zn ($x \leq 0.04$). Changes in oxygen distribution near the metal substituted sites were found to depend on the substituting element M . It is clear that the oxygen coordination near Fe^{1+} and Co (which substitute predominately in trivalent states), increases with M content x . However, no change in oxygen coordination near Ni or Zn sites is observed as a function of composition x . These atoms are primarily divalent. The relationships among M valence state, M concentration x , and oxygen distribution are examined. Several microscopic models of the local environment for each case are evaluated for consistency with the data.

* also University of Michigan, Ann Arbor, MI 48109.

* Supported by the US DOE Office of Basic Energy Sciences, Division of Materials Science, under Contract DE-AC02-76CH00016.

† C. Y. Yang, et al., Phys. Rev. B **39**, 6681 (1989).

M7.89

VARIATION IN T_c AND CARRIER CONCENTRATION CAUSED BY CHANGE OF OXYGEN CONTENT IN TI-BASED SUPERCONDUCTORS. Y. Shimakawa, Y. Kubo, T. Manako and H. Igarashi, NEC Corporation, 4-1-1 Miyazaki, Miyamae-ku, Kawasaki 213, Japan

Some TI-based superconductors have a notable feature that they show various T_c values with almost the same crystal structures. This variation in T_c and the correlations among T_c , carrier concentration and structure were studied. In particular, in $Tl_2Ba_2CuO_6$, a wide range of T_c values between zero and 85K was observed¹⁾. It was revealed that oxygen desorption and absorption caused the change of carrier concentration, and thus T_c value changed. Clear correlations among T_c , oxygen content and c-axis length were found. A fully oxygen-annealed sample shows metallic non-superconducting behavior. Decrease in oxygen content of about 0.1 per formula unit, which corresponds to decrease in $[Cu-O]^+$ hole concentration of 0.2, increases T_c up to about 80K, and elongates c-axis by about 0.4%.

In $Tl_2Ba_2CaCu_2O_8$, a similar behavior of T_c (85-110K) was observed. Variation in T_c appeared in other TI-based superconductors and comparison among them will also be reported.

1) Y. Shimakawa et al., Physica C **157**(1989)279.

M7.90

SUPERCONDUCTIVITY OF Bi-Sr-Ca-Cu-O DOPED WITH Ag IONS. Teruo KATO, Yukio KAZUMATA and Hiroshi MAETA, Japan Atomic Energy Research Institute, Tokai-mura, Naka-gun, Ibaraki-ken, 319-11, Japan.

In Bi-Sr-Ca-Cu-O (BSCCO) two superconducting phases with different T_c 's of 85 and 110 K are usually observed, but the concentration of the high T_c phase increases with the dope of Pb ions. This increase of the high T_c phase presumably has a certain relation with the valence of Bi ions. The valence states of these ions are assumed to be the mixture of Bi^{+3} and Bi^{+5} , and this mixed valence state will affect the valence of Cu ions. In this paper, we report the difference of superconductivity between the two samples prepared from two different powders of CuO and Cu_2O , and also the characteristic of superconductivity in BSCCO doped with Ag ions.

In $BiSrCaCu_xO_y$ ($x=2,3,4,5$) prepared from CuO , T_c decreases with an increase of Cu content, while the opposite phenomenon is observed in the samples prepared from Cu_2O , that is, T_c increases with an increase of Cu content. On the dope of Ag ions, $BiSrCaCu_2O_y + Ag_x$ ($x=0,1,1.5,2.0$), the maximum ratio of high T_c to low T_c phase in volume is obtained at Ag content between 1.5 and 2.0. From these experiments, the strong correlation between the high T_c phase and Cu^+ valence state is suggested.

M7.91

DOMAIN STRUCTURES AND PINNING IN OXIDE SUPERCONDUCTORS. Alexander Roitburd, NIST, Gaithersburg, MD, 20899.

The domain structure of oxide superconductors arises as a result of twinning associated with the tetragonal-orthorhombic transition inside a restricted volume (a grain in a polycrystal or a part of an initial single crystal). A thermodynamic theory of the size and arrangement of the domains has been developed. Two types of interfaces in domain structures are considered as obstacles to the movement of vortices: (1) coherent twin boundaries without microstresses and (2) noncoherent twin boundaries and boundaries between polydomain layers with microstresses. Magnetic and elastic vortex-interface interactions have been considered. The role of the interfaces in the pinning of the array of vortices is discussed with a comparison between the theoretical results and the available experimental data.

M7.92

FIELD ORIENTED GRAINS OF RARE EARTH DOPED HIGH T_c SUPERCONDUCTORS. E. Chen^(a,c), R.S. Markiewicz^(b,c), and B.C. Giessen^(a,c), Departments of Chemistry (a) and Physics (b) and Barnett Institute (c), Northeastern University, Boston, MA 02115

A strong magnetic field causes grains of $YBa_2Cu_3O_{7-\delta}$ (YBCO) or of the Bi or Tl families of high- T_c superconductors to orient¹, with the crystalline c-axis parallel to the field direction. Some rare earth (RE) substituted YBCO compounds are known to orient with c-axis perpendicular to the field, due to crystal field effects on the magnetic ion. From a detailed x-ray diffraction study, we find that different RE's lead to orientation along different directions in the a,b-plane. Moreover, the same RE can lead to orientation along different axes when substituted in YBCO vs. a Bi or Tl-based superconductor.

1. Farrell, et al., Phys. Rev. B **36**, 4025 (1987).

2. Livingston, et al., J. Appl. Phys. **64**, 5806 (1988).

M7.93

EFFECT OF HIGH TEMPERATURE DEFORMATION ON GRAIN BOUNDARY DEFECTS IN $\text{YBa}_2\text{Cu}_3\text{O}_{7-x}$. Krishna Rajan, Materials Engineering Department, Rensselaer Polytechnic Institute, Troy, NY 12180-3590.

The results of transmission electron microscopy studies on $\text{YBa}_2\text{Cu}_3\text{O}_{7-x}$ subjected to high temperature extrusion are presented. Particular emphasis is put on high temperature accommodation processes of lattice dislocations into sub-grain boundaries. It is suggested from the electron microscopy observations that stress induced climb mechanisms for dislocations are operative. Also presented is evidence of localized lattice distortions near twin boundaries due to isothermal high temperature deformation. Preliminary results on the structure of grain boundary facets and steps is described. The implications of these results for texture development in bulk ceramic superconductors is also discussed.

M7.94

MICROSTRUCTURAL EVOLUTION OF $\text{Ba}_2\text{YCu}_3\text{O}_7$ SUPERCONDUCTOR BY ELECTRON IRRADIATION IN A TRANSMISSION ELECTRON MICROSCOPE. Kensuke Shiraishi and Hiroshi Itoh, Takasaki Radiation Chemistry Research Establishment, Japan Atomic Energy Research Institute, Watanuki-machi, Takasaki, Gunma 370-12, JAPAN

The specimen for transmission electron microscopy was prepared from single phased $\text{Ba}_2\text{YCu}_3\text{O}_7$ sintered pellet by thinning with low-energy Ar-ion bombardment. The microstructural observation and electron irradiation were performed with JEM 2000FX-II operating at 200 kV. Electrons with about $5 \times 10^{22} \text{ m}^{-2} \text{ s}^{-1}$ in flux were irradiated to the specimen in the direction almost normal to a {113} plane with near (110) system reflections.

Small defect clusters of several nm in size observed with a (110) reflection were appreciably increased in the number density by the electron irradiation to about $1.5 \times 10^{22} \text{ m}^{-2}$. Upon further irradiation, the clusters gradually grew larger with a little increase in the number density. Twinning was promoted during electron irradiation up to 10^{22} m^{-2} and planar defects were appeared to form on the plane. Precipitation along the grain boundary was also induced by the electron irradiation in the microscope.

The microstructural evolution in the ion-milled specimen will be discussed in terms of superconducting properties modified by electron and ion irradiations, comparing with the microstructure observed in the specimens prepared without ion-bombardment.

M7.95

A STUDY OF THE THERMODYNAMIC STABILITY OF $\text{Y}_1\text{Ba}_2\text{Cu}_4\text{O}_8$ K.P. Atwal, R. Gronsky, J. Nickel*, A. Markelz* Department of Materials Science and Mineral Engineering, University of California, and National Center for Electron Microscopy, Materials and Chemical Sciences Division * Physics Division, Lawrence Berkeley Laboratory, 1 Cyclotron Road, Berkeley, CA 94720

The YBaCuO family of superconductors now contains at least three members and that number is likely to increase. The phases found to date are commonly referred to as 123, 124 and 247 because of their cation ratios. In this study the thermodynamic stability of the 124 phase, ($\text{Y}_1\text{Ba}_2\text{Cu}_4\text{O}_8$) is investigated, with respect to decomposition to the well known 123 structure.

Bulk samples with a 124 structure were made by annealing precursor 123 material in high pressure oxygen gas. The presence of high oxygen pressure led to the formation of extra Cu_2O layers in the 123 material, converting it to the 124 phase. The samples were subsequently heated under vacuum for several different times. The bulk samples were then characterized by x-ray diffraction and high resolution transmission electron microscopy. Computer simulation is used to verify the structure of phases observed in high resolution images.

Unlike the 123 phase, the 124 structure does not appear to show variable oxygen stoichiometry. From the presence of additional superconducting Cu_2O planes higher T_c and critical current may be expected, yet the opposite is actually observed. This result may be associated with the stability of the 124 phase and its by-products, and may be the limiting factor in practical applications.

This work was supported by the Director, Office of Energy Research, Office of Basic Energy Sciences, Materials Science Division, of the U.S. Department of Energy under Contract No. DE-AC03-76SF00098.

M7.96

THE COLOR OF POLARIZATION IN HIGH TEMPERATURE SUPERCONDUCTORS. M.S. Osofsky, H.A. Hoff, Naval Research Laboratory, Washington, DC; and W.L. Lechter, Sachs/Freeman Associates, Inc, Landover, MD

Earlier work has demonstrated that high- T_c cuprate superconductors exhibit similar reflectivity spectra in the visible when viewed through crossed polarizers (ie. they have similar colors of polarization). Here, we extend our initial studies, which were done using a quartz halogen light source, by presenting reflectivity spectra of superconducting and non-superconducting layered cuprates made using a brighter xenon source. Possible correlations of these spectra with the material's superconducting and normal state properties as well as their origins will then be discussed.

M7.97

X-RAY ABSORPTION STUDIES OF VANADIUM SUBSTITUTION IN $\text{YBa}_2\text{Cu}_3\text{O}_{7-\delta}$ SUPERCONDUCTORS(*) Zhengquan Tan and J. I. Budnick, Department of Physics and Institute of Materials Science, University of Connecticut, Storrs, CT; B. R. Weinberger and L. Lynds, United Technologies Research Center, East Hartford, CT.

$\text{YBa}_2\text{Cu}_3\text{O}_{7-\delta}$ materials with vanadium nominally substituting Cu, Y and Ba respectively have been synthesized. Bulk superconductivity with sharp transition at $T_c = 93 \text{ K}$ is maintained at low vanadium concentrations. V, Cu and Y K-edge x-ray absorption spectra have been measured on these materials to determine the local environment of vanadium and the effect of V-substitution on the atomic structures. Identical V XANES (x-ray absorption near-edge structure) spectra are observed independent of whether the vanadium nominally substitutes Cu, Y or Ba, suggesting that the V enters a unique local environment. The observed prominent 1s-3d pre-edge peak, stronger than that in V_2O_5 , shows that the V atom is very likely to have four oxygen nearest neighbors. However, the combined Cu and Y extended x-ray absorption fine structure results are incompatible with V exclusively substituting the four-oxygen-coordinated Cu(1) in the $\text{YBa}_2\text{Cu}_3\text{O}_7$ structure. Both the Cu and Y EXAFS spectra are affected significantly by the V-substitution and will be discussed in terms of the Cu and Y local environments.

(*) Work carried out at Beam Line X-11 at the National Synchrotron Light Source and supported by the U. S. Department of Energy under Contract No. DE-AS05-80-ER10742.

M7.98

ON THE STABILITY AND TRANSPORT PROPERTIES OF $Y_{1-x}Ba_xCuO_{7-x}$ PHASES COMBINED WITH REFRACTORY CERAMICS. P. Del Angel, J.M. Domínguez, O. Guzmán, A. Montoya, L. Vicente, Instituto Mexicano del Petróleo, ICA, Apdo. Postal 14-805, 07730 México, D. F. and C. Falcony, CINVESTAV, México D. F.

A systematic modification of the transport properties of $Y_{1-x}Ba_xCuO_{7-x}$ superconductor system was studied. Some partial resistivity losses occur, together with a decrease of the critical temperature (T_c) as $x \rightarrow 0$ when a pure orthorhombic $Y_{1-x}Ba_xCuO_{7-x}$ phase is combined with an increasing amount of refractory ceramics impurities (Al_2O_3 , SiC).

The solids were characterized by secondary electron imaging and EDS technics, X-ray diffraction and thermal analysis. From the results a percolation model emerges to explain the partial resistivity falls, while a cation substitution model is more probable for the systematic decrease of (T_c) as $x \rightarrow 0$. The partial resistivity losses observed at higher temperatures in other superconducting systems might in fact be the result of partial superconductive phases entrapped in non superconducting ceramic masses.

+ permanent address : Facultad de Química, UNAM, 04510 México, D. F.

M7.99

THE ELECTROCHEMICAL RESPONSE OF $YBa_2Cu_3O_{7-x}$ IN AQUEOUS SOLUTIONS T.S. Chin, Dept. Mat. Sci. Eng., Natn'l Tsing Hua Univ., Hsinchu, 30043, Taiwan; C.A. Lin, M.P. Hung, Dept. Mat. Eng., Natn'l Cheng Kung Univ., Tainan, 70100, Taiwan, R.O.C.

Electrochemical properties of Y-Ba-Cu-O superconductor which being intrinsically unstable in water were elucidated by using potentiodynamic scanning in different aqueous solutions with 0.1 M concentration.

The electrochemical stability of the $YBa_2Cu_3O_{7-x}$ compound was found to be superior in both salt solutions of NaCl and KCl, and alkaline solutions of NaOH and NH_4OH . Extremely low corrosion current of 2.86 $\mu A/sq.cm$ was observed in 0.1 M NaCl solution. The corrosion potential in the above solutions ranges from 36 - 92 mV. Polarization wasn't possible in these solutions. However the E_{corr} raised up to 360 - 960 mV in acid solutions including sulfuric, sulfuric, phosphoric and nitric acids depicting more passive behavior. Polarization was observed in sulfuric and phosphoric acids indicating their potential to be used as etching solution in lithography. The electrochemical behavior of the Y-Ba-Cu-O compound in the HCl solution is peculiar and informative. It showed three transitions in the polarization curve, corresponding to 272, 756, and 1013 mV, respectively. This is related to the transition in the valence of copper ions during dissolution, which is depressed in the acid solutions which are oxidizing in nature.

The Galvanic current decreases at an order of $Al > Cu > Ag$, when the $YBaCuO$ is coupled with each of them in 1 M phosphoric acid solution and 0.1 M HCl.

M7.100

RAMAN AND FLUORESCENCE SPECTRA OBSERVED IN LASER MICRO-PROBE MEASUREMENTS OF COMPOUNDS IN THE Ln-Ba-Cu-O SYSTEM. Edgar S. Etz and Winnie Wong-Ng, National Institute of Standards and Technology, Gaithersburg, MD, and Thomas D. Schroeder, Shippensburg University of Pennsylvania, Shippensburg, PA.

We are investigating by Raman microprobe measurements the superconducting and related phases in the $LnBa_2Cu_3O_{7-x}$ (for $x=0$ to 1) system where yttrium has been replaced by several of the lanthanide (Ln), or rare earth, elements. These studies are aimed at relating the observed optical spectra (Raman and fluorescence) to the compositional and structural aspects of these ceramics. We are examining the structure-specific rare earth ion fluorescence spectra of the various phases and compositions which we will illustrate for the erbium and europium analogs of the yttrium 1:2:3 system. Of interest is the substitutional chemistry of these isostructural systems, examining the changes in the spectra, and establishing the micro-analytical usefulness of these spectra, especially for the detection of impurity phases. In the case of the Er^{3+} -substituted materials, for example, the cw laser-excited (argon ion, at 488 or 514.5 nm) green and red fluorescence emissions, when observed, originate from the $^4S_{3/2}$ and $^4F_{9/2}$ emissive states, respectively.

M7.101

MICROANALYSIS OF CUPRATE SUPERCONDUCTORS USING THE COLOR OF POLARIZATION. H.A. Hoff, M.S. Osofsky, Naval Research Laboratory, Washington, DC; and W.L. Lechter, Sachs/Freeman Associates, Inc., Landover, MD.

A technique for the identification of individual anisotropic grains in a heterogeneous and opaque material involves the observation of grain color in reflected light through crossed polarizers (color of polarization). Such colors are generally characteristic of particular phases. Of the many members of the class of hole carrier cuprate superconductors examined so far, only one characteristic color of polarization has been observed. This same color has also been observed in a member of the electron carrier cuprate superconductors that we have examined.

We have studied the presence of color in many of these cuprates and found a strong correlation between color and the existence of superconductivity. The gradation in color from insulator to superconductor and the presence of identifying colors for secondary phases facilitates the selection of grains for microanalysis. The changes in composition corresponding to the changes in color and the variations in composition of recognizable cuprate superconductors found by quantitative Energy Dispersive X-ray Spectroscopy will be discussed.

M7.102

HARMONIC GENERATION IN THE ALTERNATING MAGNETIC RESPONSE OF HIGH- T_c SUPERCONDUCTORS. A. Shaulov, R. Bhargava, and D. Dorman, Philips Laboratories, North American Philips Corporation, Briarcliff Manor, NY.

We have developed a novel ac technique for characterizing the magnetic behavior of high- T_c superconductors. This technique is based on monitoring the spectrum of the magnetic response of these materials to small sinusoidal fields. A nonlinear magnetic behavior is indicated by the appearance of harmonic components in the spectrum. Measurements of these harmonics as a function of bias field, temperature and frequency provide valuable information about the processes of flux penetration, flux pinning and flux creep in these materials.

Measurements on sintered Y-Ba-Cu-O samples have shown that the application of a steady bias field, above a certain threshold, causes the generation of odd harmonic components in the alternating magnetic response of the material. These harmonics sharply disappear as the temperature is raised above a certain point, indicating a transition to a linear behavior. The transition temperature is strongly frequency dependent and shifts up as the frequency increases. The new transition exhibited by the harmonic components is interpreted as signifying a transition from a state of flux pinning to a state of dissipative flux motion without pinning. These measurements demonstrate a new method for accurate determination of the lower critical field and the "irreversibility" field below which irreversibility in the magnetization sets in as a result of flux pinning.

M7.103

Partial Superconductivity in $\text{YBa}_2\text{Cu}_3\text{O}_7$ at $90 < T < 300$ K.

R. Munger and H.J.T. Smith <GWP>², University of Waterloo, Waterloo, Ontario.

The presence of partial superconductivity in $\text{YBa}_2\text{Cu}_3\text{O}_7$ in the temperature range $90 < T < 300$ K has been investigated by various techniques. The current voltage characteristics of polycrystalline $\text{YBa}_2\text{Cu}_3\text{O}_7$ were studied at temperatures above the 90 K superconducting transition. It was found that the IV curves are non-linear and that the non-linearity is temperature dependent. For a constant current bias the voltage across the sample increases when microwaves are applied. The induced voltage is proportional to the bias current and the proportionality constant (ΔR) is temperature dependent. ΔR increases slowly between 300 K and 120 K and has a sharp increase as T approaches T_c . The simultaneous application of microwaves and a magnetic field also result in a non-zero value of ΔR . For small magnetic fields and at room temperature ΔR increases rapidly for $0 < H < 20$ G and oscillates with a period of 40 G for $15 < H < 135$ G. For larger magnetic fields ΔR also oscillates with a period of 1.5 to 2.0 KG for $0 < H < 7.0$ KG. Between 7 and 9 KG ΔR is constant. Measurements at all temperatures above 90 K show similar behaviour. These results will be discussed in terms of weakly linked islands of superconductivity in a normal matrix.

M7.104

THERMAL EXPANSION OF $\text{Pb}_2\text{Sr}_2\text{Y}_{1-x}\text{Ca}_x\text{Cu}_3\text{O}_{8+\delta}$. H. M. O'Bryan and P. K. Gallagher, AT&T Bell Laboratories, Murray Hill, NJ, 07974.

The thermal expansion of $\text{Pb}_2\text{Sr}_2\text{Y}_{1-x}\text{Ca}_x\text{Cu}_3\text{O}_{8+\delta}$ has been measured between 25 and 700°C for $x = 0, .2$ and $.4$. Measurements were made on ceramic samples with $\delta = 0$ during heating at 4°/min in N_2 and O_2 atmospheres. In N_2 the coefficient of thermal expansion is ~ 13 ppm/°C for all compositions. In O_2 the expansion varies greatly with temperature as the samples undergo both oxidation and reduction. The expansion mimics previously reported gravimetric data. Two maxima of $\sim 1.4\%$ are found near 550°C and 700°C. The lattice expansion on oxidation contrasts to the shrinkage observed when $\text{Ba}_2\text{YCu}_3\text{O}_{6.2}$ is oxidized.

M7.105

MECHANISM OF TWIN FORMATION AND NATURE OF TETRAGONAL TO ORTHORHOMBIC TRANSFORMATION IN $\text{YBa}_2\text{Cu}_3\text{O}_{7-x}$. Mehmet Sarikaya, Ryoichi Kikuchi, and I. A. Aksay, Dept. of Materials Science & Eng. FB-10, and Washington Technology Center, Univ. of Washington, Seattle, WA 98195.

Nucleation and growth of twins in the $\text{YBa}_2\text{Cu}_3\text{O}_{7-x}$ system have been theoretically studied on the basis of transmission electron microscopy observations. The shape of the tips of the twinned domains is predicted from two types of strain: one is associated with the twin boundary and the other with the lattice at the tip region. From the model, the tangent of the angle at the tip is calculated to be 1/9 the orthorhombic phase is analyzed with an energy minimization approach by which one can also predict the mechanism of growth of the twinned domains. The variations in microstructures and twins that are developed via different transformation routes (isothermal and athermal) are correlated with models and TEM observations. The similarities of transformation characteristics in this system are discussed with those of other systems in which the major part of the transformation involves a shear.

M7.106

MAGNETIC INTERACTIONS IN $\text{Y}_{1-x}\text{Pr}_x\text{Ba}_2\text{Cu}_3\text{O}_7$: UPPER CRITICAL FIELD AND HEAT CAPACITY STUDIES. H. B. Radousky, Lawrence Livermore National Laboratory, Livermore, CA 94550; N. E. Phillips, R. A. Fisher, R. Caspar and A. Amato, Materials and Chemical Sciences Division, Lawrence Berkeley Laboratory, UC-Berkeley, Berkeley, CA 94720; J. L. Peng and R. N. Shelton, Department of Physics, UC-Davis, Davis CA 95616

Substitution of Pr for Y in $\text{Y}_{1-x}\text{Pr}_x\text{Ba}_2\text{Cu}_3\text{O}_7$ depresses T_c with superconductivity disappearing for $x \geq 0.5$. Upper critical field measurements were obtained from magnetization data for a series of seven samples with $0 \leq x \leq 0.45$. The H_{c2} results show a linear behavior with temperature up to $x = 0.2$, but change dramatically in character for the $x \geq 0.3$ compositions. For $x = 0.3$ and greater the curves are no longer monotonically increasing and show the "bell" shaped behavior reminiscent of the magnetic superconductors RERh_4B_4 and REMo_6S_8 (RE = rare earth). This result is interpreted to mean that magnetic interactions are important in the $\text{Y}_{1-x}\text{Pr}_x\text{Ba}_2\text{Cu}_3\text{O}_7$ system. Heat capacity measurements have been performed on the $x = 0.3$ sample from 0.3 to 65K in fields up to 7T. Initial results indicate no discontinuity at $T_c = 42$ K. This result is unusual based on the observed Meissner fraction and values of the Sommerfeld gamma derived from the Pauli susceptibility. The low temperature heat capacity shows a large upturn below 2 K which is strongly enhanced by a 7T field. Further heat capacity work on more dilute Pr substituted samples is in progress and will be reported as available.

Work at Livermore and Davis performed under auspices of U.S. DOE at Lawrence Livermore National Laboratory under contract No. W-7405-ENG-48; work at Berkeley supported by U.S. DOE, Office of Basic Energy Science under contract No. DE-AC03-76SF00098.

M7.107

MAGNETIZATION AND LOW TEMPERATURE SPECIFIC HEAT OF ORTHORHOMBIC AND TETRAGONAL $\text{RBa}_2\text{Cu}_3\text{O}_x$ (R = Y, Ho). H.R. Khan*, FEM, Katharinenstrasse 17, 7070 Schwaebisch Gmuend, FRG and R. Kuentzler, I.P.C.M.S., LA 306 du CNRS, 3 rue de l, Universite, 67084 Strasbourg, France.

Orthorhombic and tetragonal compounds of compositions $\text{RBa}_2\text{Cu}_3\text{O}_x$ (R = Y and Ho) are prepared and characterized by X-ray diffraction, Optical and SE-microscopy and EDXA. The $T_c(\text{mid})$ of the orthorhombic phases is about 92 K (A.C. susceptibility). The magnetic moments of Cu and Ho

as well as Curie-Weiss temperatures are determined from the Curie-Weiss plots. The electronic specific heat coefficients of the orth. and tetr. YBCO are determined from the specific heat measurements (1.5 - 20 K) and the values are 0.95 and 1.70 mJ/gat¹K⁻² respectively. HoBCO compounds show Schottky specific heat anomalies in both orth. and tetr. phases due to the interaction of the magnetic moment of the Ho ion with the crystalline electric field (CEF). The specific heat and magnetic data in relation to superconductivity will be discussed.

*And Dept. of Physics & Astronomy, University of TN, Knoxville, Tennessee.

M7.108

IN-SITU TRANSMISSION ELECTRON MICROSCOPY AND COMPUTER SIMULATION STUDY OF THE KINETICS OF OXYGEN LOSS IN YBa₂Cu₃O₇. C. P. Burmesier¹, L. T. Wille², and R. Gronsky¹, ¹Department of Materials Science and Mineral Engineering, University of California, and the National Center for Electron Microscopy, Berkeley, CA; ²Department of Physics, Florida Atlantic University, Boca Raton, FL.

Oxygen ordering in the basal plane plays a vital role in determining the superconducting properties of the YBa₂Cu₃O₇ system. Upon cooling from the disordered, tetragonal phase, parallel O-Cu-O chains develop leading to the formation of the orthorhombic phase (OrthoI), a 90K superconductor, near z = 7. At lower oxygen content, a doubling of the orthorhombic unit cell leads to the formation of the orthorhombic OrthoII phase, a 60 K superconductor, near z = 6.5. Thus an understanding of thermodynamics of oxygen ordering is essential for the development and control of superconducting properties in this material.

High resolution transmission electron microscopy is used to study the kinetics of oxygen loss associated with the low temperature OrthoI to OrthoII transition. Oxygen loss in YBa₂Cu₃O₇ is induced by in-situ beam heating in the electron microscope. As the material transforms from YBa₂Cu₃O₇ to YBa₂Cu₃O_{6.5}, the evolution of transient and equilibrium structures is observed directly using real-time atomic resolution video imaging and microdiffraction analysis.

Results from an Ising model Monte Carlo simulation of oxygen ordering in this material are used to interpret observed structures and transient ordering. The simulation is also used to extrapolate experimentally observed behavior to values of temperature and oxygen concentration not explicitly examined in this study. Qualitative agreement between simulation and experiment is excellent.

This work is supported the Director, Office of Basic Energy Sciences, Materials Sciences Division of the U. S. Department of Energy under Contract Number DE-AC03-76SF00098. One of us, (L. T. W.) is supported by grant No. MDA 972-88-J-1006 from DARPA.

M7.109

ELASTICITY STUDIES ON LATTICE INSTABILITY OF HIGH T_c OXIDE SUPERCONDUCTORS. Ye-Ning WANG, Hui-Min SHEN, Xiao-Hui CHEN, Lin-Hai SUN, and Zi-Ran XU, Institute of Solid State Physics, Nanjing University, P.R.China.

There exist a few broad internal friction peaks (ultrasonic attenuation as well) at 120K, 230K in YBCO; at 95K, 130K, 250K in BSCCO and at 90K, 135K, 180~280K in TBCCO, which have been confirmed to be induced by phase-like transition (PLT) of first order. X-ray diffraction studies indicate that the PLT is characterized by abrupt change of lattice parameters instead of change of crystal symmetry. Tensile tests show elastic softening associated with PLT. However, elastic modulus curves measured at kHz and MHz frequency ranges reveal somewhat different behavior at PLT, although the overall trend of stiffening are the same for ceramic materials. This has been analyzed in terms of the different mechanism of damping due to PLT for the two frequency ranges as well as the different results for single crystal and polycrystalline materials.

There always occurs an internal friction peak associated with PLT at T_m about 10-30K above T_c for superconducting phase, whereas disappears in nonsuperconducting phase as shown in the table.

	TABLE	
	T _c	T _m
YBa ₂ Cu ₃ O _x	90K	120K
	60K	75K
Bi-Sr-Ca-Cu-O	107K	130K
	83K	95K
Tl-Ba-Ca-Cu-O	115K	135K
	?	90K

The coexistence of the PLT and superconducting transition exhibits that both have the common intrinsic factor such as the electronic state varied by oxygen doping.

M7.110

PROPERTIES AND MICROSTRUCTURE OF SUPERCONDUCTING OXIDES PREPARED BY OXIDATION OF LIQUID QUENCHED ALLOY PRECURSORS. J.S. LUO, D. MICHEL AND J-P. CHEVALIER, CNRS CECM, 15 Rue G. Urbain, 94407 VITRY (FRANCE)

We have produced various high T_c superconductors through oxidation of alloy precursors obtained by planar flow casting. It is found that this preparation method can improve homogeneity, modify the morphology, and can be readily carried out under controlled atmosphere. For EuBa₂Cu₃O₇, we have observed a substantial increase in critical current, which can be attributed to the uniform grain size and composition. In the case of multi-component systems such as Bi-Pb-Sr-Ca-Cu and Pb-Sr-Ca-Y-Cu, good chemical homogeneity can be ensured by passage through the liquid state. Finally, although the ductility of the precursor alloys significantly varies as a function of the system, the resulting oxides are all brittle.

M7.111

Crystal Chemistry and Phase Equilibria Studies of the Ba-R-Cu-O systems. Winnie Wong-Ng, Robert S. Roth, Lawrence P. Cook, Boris Paretzkin, Michael Hill and E.R. Fuller, Jr., Ceramics Division, National Institute of Standards and Technology, MD 20899.

Knowledge of the phase compatibility and melting relationships of compounds formed in the Ba-R-Cu-O systems, where R=lanthanides and yttrium, is essential for understanding material properties and controlling processing parameters for the high T_c superconductor phases Ba₂RCu₃O_{6+x}. The present paper reports the influence of the size of R on the phase formation, phase compatibilities and melting relationships in these systems. In addition, since the extent to which change in the Gibbs energy of R-substituted mixtures results in an altered primary phase field is of great practical interest, possible primary phase field of mixed-lanthanides superconductor phases such as Ba₂(Nd,Y,Eu)Cu₃O_{6+x} will also be presented. Experimental results of specimens equilibrated in air will be summarized.

M7.112

RAMAN STUDIES ON Y123 AS A FUNCTION OF ANNEALING. G. Burns, F. H. Dacol, C. A. Feild, A. Gupta, F. Holtzberg, G. Koren, R. B. Laibowitz and T. K. Worthington, IBM Research Division, T. J. Watson Research Center, Yorktown Heights, NY 10598, USA.

We have studied the behavior of $\text{YBa}_2\text{Cu}_3\text{O}_{7-\delta}$ (Y123) for fully oxygenated ($\delta \approx 0.0$) single crystals and films as a function of annealing temperature (T_A). The samples were annealing for 16 hours at T_A in flowing helium gas. For each T_A , we have measured the Raman spectra on the films, and on the large face and small edge of the crystals, this yields all five Raman active modes ($4A_{1g} + B_{1g}$). We also measured the corresponding superconducting transition temperatures (T_c).

The Raman results can be divided into three ranges for the crystals and films. (a) Results from material with the highest T_c (fully oxygenated), and (b) from the plateau region ($T_c \approx 60$ to 50 K). In these ranges, some of the phonon lines shift in frequency. (c) In the region where T_A is high enough, so that T_c goes to zero, there are large changes in intensity of most of the Raman lines; the low frequency Ba-Ba and high frequency $\text{O}_2 - \text{O}_2$ vibrations become very weak.

These results are consistent with a change of the crystal structure from orthorhombic (superconducting) to another orthorhombic (superconducting) structure and then to a tetragonal (semiconducting) structure. We will relate our findings to other results.

M7.113

HIGH RESOLUTION TRANSMISSION ELECTRON MICROSCOPY STUDY OF DEFECT STRUCTURES IN MULTI-PHASE YBaCuO. M. Fendof and R. Gronsky, Department of Materials Science and Mineral Engineering, University of California, and National Center for Electron Microscopy, Lawrence Berkeley Laboratory, Berkeley, CA. 94720

It is now known that superconducting YBaCuO exists in at least three well characterized phases with differing copper and oxygen content. Due to the cation ratios (Y:Ba:Cu) these compounds are commonly referred to as the "123", "124", and "247" phases. When YBaCuO crystals are grown in practice, an intergrowth of more than one structure frequently occurs in order to accommodate local deviations from these ideal stoichiometries.

High Resolution Transmission Electron Microscopy is used to study the crystallographic defects in YBaCuO which are induced when phases with differing lattice parameters exist in an intimate mixture. Computer simulation of high-resolution images is utilized in order to verify the phases present in various regions of actual TEM images.

The "123" and "124" phases are related by a $1/2[100]$ partial dislocation, and TEM images confirm that when the two phases grow together laterally, defects of this type are present in the specimen. When larger domains of these two phases meet, a low angle misorientation boundary is found. Such boundaries are formed in a manner which allows continuity of atomic planes between phases to be preserved as much as possible, with a corresponding minimization of the interfacial surface energy. An atomic model for this type of interface is developed, leading to implications for the structural nature of the transformation from the "124" phase to the "123" phase.

The defects observed in multi-phase YBaCuO are likely to have significant effects on the superconducting properties of the material. In particular, they are expected to contribute to limitations on critical current values.

This work is supported by the Director, Office of Basic Energy Sciences, Materials Sciences Division of the U.S. Department of Energy under Contract Number DE-AC03-76SF00098.

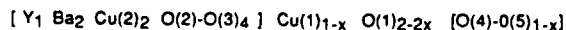
M7.114

COMPLEX DEFECTS IN Y-Ba-Cu-O SINGLE CRYSTALS. Philippe Galez, P. Schweiss, J.-F. Marucco and G. Collin, C.P.C.M., DPhG, C.E.A. Saclay, B1 563, 91191. Gif sur Yvette, France.

The crystal structure of twenty Y-Ba-Cu-O type single crystals are examined by neutron diffraction on four-circle diffractometer. These

crystals with volume from $\approx 10\text{mm}^3$ up to 500mm^3 are obtained by a flux method ($\text{BaCuO}_2\text{-CuO}$) and reannealed in flowing oxygen or nitrogen in a thermobalance in order to get the required oxygen composition.

For compositions $\text{YBa}_2\text{Cu}_3\text{O}_{6+x}$ with $x \geq 0.40$ the crystals are orthorhombic twinned. An exact solution is used for the refinement including incoherent superposition of domains, which leads to the structure of the individual orthorhombic sample. An outstanding result is the systematic occurrence of a complex defect associated to a copper deficiency (x) on the Cu(1) site: a $2(x)$ deficiency on the bridging oxygen and a deficiency (x) on the sum $\text{O}(4)+\text{O}(5)$ of the two oxygen sites around Cu(1), with a maximum occupancy of (x) on the "forbidden" O(5) site. The formula should then be written for a maximum oxygenation:



This copper deficiency is found in the range 3-6%, in agreement with X-ray results and is due to a copper fugacity on the weakly bound Cu(1) site. $\text{Cu}^{+3d^{10}}$ only surrounded by two oxygen at the high temperature used to prepare single crystals, even in an excess of CuO. It should be noted that we never observed any deficiency on the Y, Ba, Cu(2) and O(2)-(3) sites. This result is also valid for yttrium rare earth such as Dy, Ho, Er. This defect results in a lowering of T_c , a broadening of the superconducting transition and a reduced Meissner effect observed in "large" single crystals as compared to ideal ceramics or to "small" ($v < 1\text{mm}^3$) single crystals prepared at lower temperature. For lower oxygen content and down to $\text{O}_{6.4}$ only the chain oxygen site O(4) is stable but the vacancies on Cu(1) and bridging oxygen O(1) remain.

In addition we observe a change in the in-plane anisotropy, especially on the U_{11} term, of the chain oxygen with oxygen concentration and very small change in distance at low temperature.

M7.115

CRYSTAL CHEMICAL AND FUNCTIONAL REPRESENTATION OF HIGH- T_c SUPERCONDUCTORS AND RELATED PHASES. J. Sigalovsky and B.C. Giessen, Materials Science Division, Barnett Institute and Department of Chemistry, Northeastern University, Boston, MA 02115

The diversity of cuprates, bismates, thallates, and related ceramic superconductors and the strong effects of compositional variations such as cation substitution, oxygen content and intercalation suggest the need for an efficient characterization and cataloging system based on compositional, crystallographic and functional criteria. Compositional factors include element content, stoichiometry, or groups of elements occupying specific atomic positions. Crystallographic criteria include crystal system, unit cell size, space group, and structural subunits. Functional characterizations are based on the geometry of specific functional groups (metal-oxygen polyhedra or networks, counterions, intercalants) and atomic connectivity or unit dimensionality (isolated ions, chains, layers or three-dimensional networks).

Additional classification is based on electronic characteristics. Within any scheme, compounds are identified by a digital code for cross-referencing. A well designed system should also be useful for the description of "missing" phases that might form in constrained, metastable equilibrium.

M7.116

ULTRASONIC STUDY OF ELASTIC ANISOTROPY AND LATTICE INSTABILITY OF SINGLE CRYSTAL $\text{Bi}_2\text{Sr}_2\text{CaCu}_2\text{O}_8$. Jin WU, Ye-Ning WANG, Hui-Min SHEN, Jin-Song ZHU, Institute of Solid State Physics, Nanjing University, Nanjing, P.R.China.

Both the longitudinal and transverse sound velocities vs temperature along two perpendicular directions in the a-b plane of $\text{Bi}_2\text{Sr}_2\text{CaCu}_2\text{O}_8$ single crystal with $T_c=84.5\text{K}$ have been measured by pulse echo technique, using the PZT(longitudinal wave, 7.5MHz) and quartz(shear wave, 10MHz) transducers. X-rays diffraction experiments determined the directions which ultrasonic wave propagated along and showed that the specimen is a fairly good monocrystal.

The elastic constants C_{11} , C_{12} , C_{22} and C_{66} vs temperature have been calculated from the velocity data. The elastic softening minimum around 250K and elastic anisotropy are obviously observed in the a-b plane. The phase-like transition as we called near 250K is characterized by the jump of lattice parameters but with symmetry unchanged. It was also found that the sound velocity minimum results primarily from a shear instability, which is consistent with the appearance of internal friction peak and ferro-elastic stress-strain loop around 250K induced by the motion of interfaces of two phases with slight different lattice parameters, because the mobility of interfaces often originate from shear deformation.

M7.117

IRRADIATION EFFECTS IN $\text{Tl}_2\text{Ca}_2\text{Ba}_2\text{Cu}_3\text{O}_{10}$ SUPERCONDUCTORS. J. C. Barbour, J. F. Kwak, E. L. Venturini, D. S. Ginley, and P. S. Peercy, Sandia National Laboratories, Albuquerque, NM 87185.

The effects of ion irradiation on T_c , J_c , and flux pinning were studied in thin superconducting films of $\text{Tl}_2\text{Ca}_2\text{Ba}_2\text{Cu}_3\text{O}_{10}$. Our previous studies of O-irradiation were extended to other ions and energies to separate the effects of energy deposition into ionization and atomic displacements. We also looked for flux pinning from low fluence He irradiation. The range of the ions was chosen to be greater than the 0.2 to 0.7 μm thickness of the highly oriented polycrystalline films on SrTiO_3 substrates. Comparison of 760 keV O and 2 MeV He ion irradiations shows comparable decreases in T_c for comparable energy into atomic displacements, suggesting that ionization effects are negligible. The zero resistance state is suppressed at a damage level of 0.028 dpa for 760 keV O irradiation. The behavior of the ρ vs. T curve was found to depend sensitively on both the microstructure and quality of interconnections between grains. $T_c(\rho=0)$ and $T_c(\text{onset})$ decreased smoothly without structure in the $\rho(T)$ curves for 0.7 μm films which had high substrate coverage and broad grain interconnections. In contrast, $T_c(\text{onset})$ remained approximately constant while $T_c(\rho=0)$ decreased and extra structure appeared in the $\rho(T)$ curves for 0.2 μm films which had $\approx 75\%$ substrate coverage and narrow grain interconnections. Finally, no effect on the 44 meV pinning barrier in a 0.5 kG field was observed for fluences up to 1×10^{15} He/cm² (2 MeV He), which decreased T_c by $\approx 10\%$ and the magnetic shielding current by 15%. We speculate that grain boundary pinning is sufficient to mask effects of ion-induced defects on the pinning.

This work was funded by the U.S. DOE under contract no. DE-AC04-76DP00789.

M7.118

MAGNETIC PENETRATION DEPTHS OF ALIGNED COMPOSITES OF THE HIGH TEMPERATURE SUPERCONDUCTOR $\text{Tl}_2\text{Ca}_2\text{Ba}_2\text{Cu}_3\text{O}_{10+\delta}$. J. R. Thompson^{a,b}, D. K. Christen^a, H. A. Deeds^b, Y. C. Kim^b, J. Brynastad^a, S. T. Sekula^a, H. R. Karchner^a, and J. D. Budai^a, ^aOak Ridge National Laboratory, Oak Ridge TN 37831 and ^bDept. of Physics, University of Tennessee, Knoxville.

Polycrystalline sintered samples of the high temperature superconducting compound $\text{Tl}_2\text{Ca}_2\text{Ba}_2\text{Cu}_3\text{O}_{10+\delta}$ were synthesized

with relatively high phase purity, ground to a fine powder, and used to form an axially aligned composite by suspending it in liquid epoxy in the presence of an aligning magnetic field. X-ray diffraction with scattering along the alignment axis gave only (00L) reflections with rocking curve widths of 1° FWHM, indicating good c-axis alignment. The transition temperature T_c , defined by extrapolating the diamagnetic signal to zero, was 123.5 K.

The magnetization $M(H,T)$ was investigated in a SQUID magnetometer for fields $H < 50$ kOe and temperatures $T < 130$ K. Using the analysis of Kogan et al. [Phys. Rev. B 38, 11958 (1988)], we obtained values for the penetration depth $\lambda(T)$ as function of temperature. For $H \parallel$ c-axis with induced supercurrents in the ab plane, the corresponding penetration depth $\lambda_{ab}(T)$ was evaluated and compared with various theoretical results for the temperature dependence. BCS weak coupling results in the clean limit appeared to give a better description of the data than two fluid, dirty limit, or strong coupling calculations. An extrapolation to $T = 0$ K gave a value for $\lambda_{ab}(0) = 0.17 \mu\text{m}$. Analogous results for the penetration depth corresponding to vortex supercurrents along the c-axis will be discussed.

*Research sponsored by the Division of Materials Sciences, U. S. Department of Energy under contract DE-AC05-84OR21400 with Martin Marietta Energy Systems, Inc.

M7.119

SUPERSTRUCTURE AND LONG PERIOD ANTIPHASE BOUNDARIES IN $\text{Bi}_2\text{Sr}_2\text{CaCu}_2\text{O}_{8-x}$. R. Herrera, P. Schabes-Retchkiman, J. Reyes-Gasca, and M. J. Yacamán, Instituto de Física, U.N.A.M., Apdo. Postal 20-364, 01000, Mexico, D.F., Mexico

The occurrence of a superstructure in the electron diffraction patterns along the b-axis in the Bi based high- T_c superconductors has been reported by several groups. Although several models have been proposed, no agreement has been reached on the type of superstructure.

We have analyzed the structure of the $\text{Bi}_2\text{Sr}_2\text{CaCu}_2\text{O}_{8-x}$ from the long-period superstructure point of view. An incommensurate modulation along the b-axis has been found with mean size for the antiphase boundaries of $M=5/2$. It is concluded that the superstructure is consistent with a long-period structure based on planar defects such as antiphase boundaries. Calculated diffraction patterns and images using this model are in full agreement with the experimental results obtained by several groups. We conclude that the incommensurate structure along the b-axis observed in these materials can be explained in terms of a simple defect structure.

M7.120

TRANSMISSION ELECTRON MICROSCOPY STUDY OF Fe-DOPED BiCaSrCuO . K. Fortunati, R. Gronsky, R.L. Meng*, and C.W. Chu*, Department of Materials Science and Mineral Engineering, University of California, and National Center for Electron Microscopy, Lawrence Berkeley Laboratory, Berkeley, CA 94720; *Texas Center for Superconductivity, University of Houston, Houston, Texas 77204

Large-angle grain boundaries have been frequently observed in high-resolution transmission electron microscope images of iron-doped BiCaSrCuO (BCSCO) high-temperature superconductors. When the matrix is viewed along the [001] crystallographic orientation, a direct view of the c-plane stacking is observed in small, high aspect-ratio grains. These perpendicularly oriented grains have widths along the [001] direction on the order of hundreds of Angstroms. This type of microstructure has not been found in BCSCO doped (five atomic percent, with respect to copper) with other metals (Co, Ni, Zn and Ga), nor in undoped material. Therefore, its presence suggests that the introduction of iron must cause some change in the surface energy, and hence microstructure, of the material. This study attempts to explain this microstructure, and to correlate it to measured electronic properties.

The microstructure found in the Fe-doped materials may have significant effects on superconducting properties, due to weak conduction links and flux pinning at the grain boundaries. The superconducting transition temperature of the Fe-doped material is markedly lower than the undoped material. Although the increased grain boundary area of this microstructure may be responsible for some of the lowering of the transition temperature, its effect on the critical current and critical magnetic field of the superconductor is expected to be much more dramatic.

This work was supported by a University of Houston (TCSUH) subcontract under DARPA Grant No. MDA972-88-J-1002, and by U.S. Department of Energy Contract No. DE-AC03-76SF00098.

M7.121 ABSTRACT NOT AVAILABLE

M7.122

PROCESSING AND CHARACTERISATION OF SINGLE PHASE SUPERCONDUCTING THIN FILMS IN THE Bi-Sr-Ca-Cu-O SYSTEM FROM CHEMICAL PRECURSORS. T. E. Bloomer, S. J. Golden, F. F. Lange and K. J. Vaidya. UCSB, Materials Dept., Eng III, Santa Barbara, CA 93106 and W. L. Olson. Superconductor Technologies, Inc., 460 Ward Drive, Suite F, Santa Barbara, CA 93111.

Single phase, superconducting thin films in the Bi-Sr-Ca-Cu-O system have been fabricated by the spin-pyrolysis of ethyl hexanoate liquid precursors on single-crystal MgO. Thin films were characterized by a variety of techniques. In addition, a parallel study of bulk material was carried out using high temperature X-ray diffraction and differential thermal analysis. It was found that single-phase films (by X-ray diffraction and scanning electron microscopy), with a T_c ($R = 0$) of 86K, were obtained only with Sr-deficient, Bi-rich compositions (cf. '2212'). With these film compositions, a wide temperature range was found to exist over which single-phase, two-layer c-axis oriented films could be obtained; 745–840 C. Thin film data relating to the two-layer composition range and temperature range of formation are interpreted in terms of differential thermal analysis and high temperature X-ray diffraction data; possible phase relations pertinent to the formation of the two-layer phase are discussed.

Work supported by US DARPA under contract No. N00014 88 C 0713.

M7.123

MAGNETIC AND ^{119}Sn MOSSBAUER EFFECT STUDY OF $\text{Sn-DOPED Pb}_2\text{Sr}_{2-x}\text{Eu}_{0.5}\text{Ca}_{0.5}\text{Cu}_{3-x}\text{Sn}_x\text{O}_{8+z}$ ($x = 0.1$) SUPERCONDUCTOR. P. P. Vaishnava, GMI Engineering and Management Institute, Flint, MI 48504; and C. D. Nelson and W. P. Pratt, Jr., Dept. of Physics and Astronomy, Michigan State University, East Lansing, MI 48824.

X-ray diffraction, magnetic susceptibility and ^{119}Sn Mossbauer effect measurements have been performed for the titled superconductor. From the x-ray diffraction measurements, it was found that the sample is a single-phase material. To obtain information about the diamagnetic shielding and Meissner effects, susceptibility measurements were performed in a) the field-cooled and b) zero-field-cooled modes. The ^{119}Sn Mossbauer effect spectrum showed the presence of Sn in the $4+$ state. No evidence was found for the $2+$ state of Sn.

Work supported by the MSU Center for Fundamental Materials Research.

M7.124

PHYSICAL PROPERTIES OF $\text{Bi}_2\text{Sr}_2\text{CuO}_6$, THE SEMICONDUCTING PHASE, STRUCTURALLY DISTINCT FROM THE $N=1$ Bi-CUPRATE SUPERCONDUCTOR. Bryan C. Chakoumakos, Brian C. Sales, and Edward Sonder. Solid State Division, Oak Ridge National Laboratory*, P.O. Box 2008, Oak Ridge, TN 37831-6056.

The stable phase that forms near 2-2-1 in the Bi-Sr-Cu oxide system is now recognized as a semiconducting phase structurally distinct from the $n = 1$ Bi-cuprate superconductor, whose actual composition ($\text{Bi}_2\text{Sr}_{2-x}\text{CuO}_{6-y}$, $x = 0.1-0.25$, $y = 0-0.5$) is deficient in Sr. The 2-2-1 phase forms by a slow solid-state replacement of the superconducting phase for compositions near 2-2-1. It also has been grown from melt compositions (2-2-1 ranging to 2-2.25-1.5), but single-phase products are not obtained, implying incongruent melting. Alumina and zirconia crucibles promote the growth of the superconducting phase by reacting with the melt to remove Sr, whereas Au crucibles promote the growth of the 2-2-1 phase. Owing to its fine-grained, fibrous habit, structural characterization has been difficult. Of the unit cells proposed, that of Roth et al. provides the best fit to our x-ray powder data, $a = 24.654(2)$, $b = 5.4074(8)$, $c = 22.241(7)$ Å, $\beta = 106(1)^\circ$. Although, the superconducting $n = 1$ Bi-cuprate exhibits variable Sr and O contents, the 2-2-1 phase appears to be a single composition with no oxygen exchange observed by TGA. The 2-2-1 phase is semiconducting as determined by electrical resistivity measurements.

*Research sponsored by the Division of Materials Sciences, U.S. Department of Energy under contract DE-AC05-84OR21400 with Martin Marietta Energy Systems, Inc.

M7.125

RF SURFACE RESISTANCE MEASUREMENTS IN THE Pb-Bi-Sr-Ca-Cu-O SYSTEM. M. T. Lanagan, C. T. Bohn, J. R. Delany, M. C. Einloth, R. N. Vogt, and U. Balachandran, Argonne National Laboratory, Argonne, IL.

Superconducting $\text{Bi}_2\text{Sr}_2\text{CaCu}_2\text{O}_x$ (BSCCO) specimens were fabricated by melting and recrystallization. The melting operation required that BSCCO be placed on a compatible substrate, for which silver was found to be suitable. Silver substrates up to 6 in. in diameter were coated with BSCCO thick films and subsequently fired at 850 to 910°C. Samples were characterized by scanning electron microscopy, x-ray diffraction, and critical current density. The rf surface resistance was measured by replacing the bottom of a TE-mode resonant cavity with a BSCCO thick-film specimen. A sharp transition in rf surface resistance was observed at 80 K.

Pb-doped $\text{BiSrCaCu}_1.8\text{O}_x$ did not require melting and could be sintered without a substrate. Organics were added to the Pb-doped BSCCO powder, and a plastic mass was extruded into wire. Various heat treatments were carried out for sintering times of up to 14 days. The wire was then placed as the center conductor in a resonant coaxial cavity, and surface resistance at 1 GHz was measured as a function of temperature from 4 to 120 K. Rf surface resistance data revealed that the onset of superconductivity occurred at 105 K and that the transition was very broad. This is in contrast to undoped BSCCO specimens measured earlier. The rf surface resistance will be compared with copper, $\text{YBa}_2\text{Cu}_3\text{O}_{7-x}$, and other superconducting materials.

Work supported by the U. S. Department of Energy, Office of Energy Storage and Distribution, Conservation and Renewable Energy, under Contract W-31-109-Eng-38.

M7.126

MAGNETIC PROPERTIES OF $\text{Pb}_2\text{Sr}_2\text{Eu}_{1-x}\text{Ca}_x\text{Cu}_3\text{O}_{8+z}$ SUPERCONDUCTORS. C.D. Nelson and V.P. Pratt, Jr., Dept. of Physics and Astronomy, Michigan State University, East Lansing, MI 48824; and P.P. Vaishnava, GMI Engineering and Management Institute, Flint, MI 48504.

X-ray diffraction and magnetic measurements using a SQUID magnetometer have been performed on $\text{Pb}_2\text{Sr}_2\text{Eu}_{1-x}\text{Ca}_x\text{Cu}_3\text{O}_{8+z}$ ($0 < x < 0.9$) superconductors. For $x = 0, 0.1, 0.3, 0.5$, and 0.7 , we have single phase materials. However, a small percentage of an impurity phase is noticed in the $x = 0.7$ sample, and the $x = 0.9$ sample is clearly not a single phase material. The onset temperature for the superconducting transition becomes higher as the Ca concentration is increased. To obtain information about the diamagnetic shielding and Meissner effects, the susceptibility of all the samples was measured under two protocols: zero-field-cooling and field-cooling. The Meissner fraction was always less than 100%, but this fraction increased as the Ca concentration was made larger. From our susceptibility versus magnetic field measurements, we have obtained values for H_{c1} and H_{c2} .

Work supported by MSU Center for Fundamental Materials Research.

M7.127

INVESTIGATIONS ON SUPERCONDUCTIVITY IN Pb-Sr-R-Ca-Cu-O ($R=\text{Y, Gd, Dy}$) OXIDE SYSTEM, Ram Prasad and N.C. Soni, Metallurgy Division, Bhabha Atomic Research Centre, Trombay, Bombay 400 085.

The effect of sintering temperature, furnace atmosphere and composition on the superconducting transition temperature of several members of the series $\text{Pb}_2\text{Sr}_2\text{R}_{1-x}\text{Ca}_x\text{Cu}_3\text{O}_z$ ($0.0 < x < 0.7$, $R = \text{Y, Gd, Dy}$) has been investigated. The shape of the resistivity temperature curve and the zero resistance temperatures are found to be extremely sensitive to the synthesis parameters employed. Superconductivity is not observed in the samples treated in oxidizing atmosphere or heated at very high temperature. Samples sintered in flowing nitrogen atmosphere showed incomplete transitions starting at about 75 K and extending down to 15 K. We have developed a new and comparatively simple synthesis procedure involving treatment of the sample in vacuum to obtain nearly single phase materials showing metallic behaviour and superconductivity. The superconducting onset temperature is found to be about 75 K and the zero resistance temperature is 50 K. With this procedure, samples of the composition $\text{Pb}_2\text{Sr}_2\text{YCu}_3\text{O}_z$ also show superconductivity. The effect of replacement of calcium by other ions will also be discussed.

M7.128

HIGHLY TEXTURED SUPERCONDUCTING $\text{Bi}_2\text{Sr}_2\text{Ca}_1\text{Cu}_2\text{O}_y$ CRYSTALS PREPARED BY UNIDIRECTIONAL SOLIDIFICATION PROCESSING.

T.Oyama, M.Nakagawa, T.Suga, K.Ishige, S.Nagaya, M.Miyajima, I.Hirabayashi, Y.Shiohara, and S.Tanaka, Superconductivity Research Laboratory (SRL), International Superconductivity Technology Center (ISTEC), 1-10-13 Shinonome, Koto-ku, Tokyo 135, JAPAN.

Unidirectional solidification processes, for making high T_c superconductive oxides have been investigated. The potential importance of solidification processing route was revealed by the high critical current densities demonstrated by S. Jin *et al.* and M. Murakami *et al.* in textured $\text{YBa}_2\text{Cu}_3\text{O}_{7-x}$. In this report, we present effects of solidification processing parameters on texture, morphology, grain size, and structure of crystals grown unidirectionally. Processing parameters include growth rate (R), liquid/solid interface temperature gradient (G), rod diameter (d), and rod initial composition (C_0). The ratio G/R adjusts the texture, morphology, and structure of the crystals. The texture of the processed rods of $\text{Bi}_2\text{Sr}_2\text{Ca}_1\text{Cu}_2\text{O}_y$ was with the c-axis normal to the rod axis. The higher the G/R, the more highly the crystals grow unidirectionally. The crystal grains become larger and longer with decreasing the growth rate. Interrelation between textured structure and superconducting behavior will be presented.

Work supported in part by the Ministry of International Trade and Industry (MITI) through the New Energy and Industrial Technology Development Organization (NEDO)

M7.129

FLUX-ASSISTED PREPARATION OF POWDERED BISMUTH SUPERCONDUCTORS, R. H. Arendt, M. F. Garbaskas and L. L. Schilling, General Electric Company, Corporate Research and Development, P. O. Box 8, Schenectady, NY 12301.

Results are presented on efforts to prepare both the 80K and 110K transition temperature bismuth superconducting species in either phase pure or nearly phase pure, powdered form. Such material can be used to fabricate superconducting structures, such as metal sheathed wire and tapes. Two solvent systems were investigated. It was found that the 110K species could not be prepared with either flux system. In contrast, the 80K species could be prepared with either flux. In one case, the final product was the nearly phase pure, with highly reproducible superconducting characteristics. Data will be presented on the effects of variation of the reaction temperature and duration, solvent content, and of post-synthesis anneals of the product materials.

M7.130

SYNTHESIS AND PROCESSING OF Bi-Sr-Ca-Cu-O POWDERS.

S. M. Johnson, M. I. Gusman, L. Liu, R. H. Lamoreaux, SRI International, Menlo Park, CA; and C.B. Eom, Stanford University, Stanford, CA.

Powders in the Bi-Sr-Ca-Cu-O and related systems have been synthesized by freeze-drying. The properties of these powders are compared to those of powders in the Y-Ba-Cu-O system. Bi-based powders have a larger particle size ($>1\mu\text{m}$) than Y-Ba-Cu-O powders because calcining temperatures are close to the melting point. The effects of sintering temperature on critical transition temperature have been studied. Powders containing lead have also been prepared.

An overview of the powder synthesis method will be presented, followed by data on the effects of the processing conditions on the superconducting properties.

This research is supported by the Electric Power Research Institute.

M7.131

SYNTHESIS, MICROSTRUCTURE AND CRITICAL CURRENT DENSITY OF CRYSTALLIZED GLASSES IN Bi-Sr-Ca-Cu-O SYSTEM.* Donglu Shi, M. S. Boley, J. G. Chen, Ming Xu, U. Welp, and K. Vandervoort, Argonne National Laboratory, Argonne, Illinois 60439.

Materials in the Bi-Sr-Ca-Cu-O system with various nominal compositions have been completely melted and rapidly solidified by using splat quenching technique to produce highly dense and homogeneous glasses. Desired superconducting phases with single resistive and magnetization shielding transitions at 110 K and 85 K have been obtained through subsequent crystallization anneals. With highly controlled microstructures, the flux pinning strength is greatly increased resulting in a 30 times increase in intragrain critical current density from 10^5 A/cm² to 10^7 A/cm² at 5 T at 10 K. Two types of microstructural changes have been observed, which are likely to be responsible for the rapid increase of critical current density. Large amounts of finely dispersed precipitates have been found in the sample matrix, and the density of the precipitates greatly increases with the calcium and copper concentration in the starting material. Extra calcium and copper supersaturated in the sample matrix also causes severe lattice distortion and forms large quantity of surface defects. These atomic lattice defects are also believed to increase the flux pinning strength.

M7.132

CRYSTAL GROWTH OF HIGH T_c SUPERCONDUCTORS IN THE SYSTEM Bi-Ca-Sr-Cu-O. P.D. HAN and D.A. PAYNE, Department of Materials Science and Engineering, Materials Research Laboratory, and Science and Technology Center for Superconductivity, University of Illinois at Urbana-Champaign, Urbana, IL 61801.

Systematic investigation of crystal growth in the system Bi-Ca-Sr-Cu-O is reported. Centimeter size single crystals of $\text{Bi}_2\text{CaSr}_2\text{Cu}_2\text{O}_8$ (2122, $T_c=80\text{K}$) and $\text{Bi}_2\text{Sr}_2\text{CuO}_6$ (2021, $T_c=12\text{K}$) were grown from off-stoichiometric and stoichiometric melts. Data are reported for the fluxes used and developed. Millimeter size crystals of $\text{Bi}_2\text{Ca}_2\text{Sr}_2\text{Cu}_3\text{O}_{10}$ (2223, $T_c=110\text{K}$) were grown by crystallization of amorphous precursors in the solid state. The three types of superconducting crystals were characterized by OM, XRD, SEM, TEM, SQUID and resistivity measurement. Data are reported also for the influences of growth parameters and chemical additions (e.g., Pb, Sb, Ge, Sn) on superconducting characteristic and growth mechanisms.

M7.133

EVOLUTION OF THE HIGH T_c PHASE IN RAPIDLY SOLIDIFIED Bi-Ca-Sr-Cu OXIDES. A. Asthana, P.D. Han, Z. Xu, L. Chang and D.A. Payne, Department of Materials Science and Engineering, Materials Research Laboratory, and Science and Technology Center for Superconductivity, University of Illinois at Urbana-Champaign, IL 61801.

Materials in the Bi-Ca-Sr-Cu-O system were prepared by rapid solidification. Specific heat-treatment conditions for the crystallization of the various superconducting phases ($\text{Bi}_2\text{Sr}_2\text{CuO}_6$, $\text{Bi}_2\text{Ca}_1\text{Sr}_2\text{Cu}_2\text{O}_8$, $\text{Bi}_2\text{Ca}_2\text{Sr}_2\text{Cu}_3\text{O}_{10}$) were identified. The effect of heat-treatment conditions and chemical additives on the superconducting properties was studied.

Emphasis was placed on optimizing processing conditions for enhancing the content of the high T_c ($\text{Bi}_2\text{Ca}_2\text{Sr}_2\text{Cu}_3\text{O}_{10}$) phase. A number of starting compositions were used in order to maximize the fraction of the high T_c phase. Intergrowths of lower T_c phases, and precipitation of extraneous phases such

as CuO and $(\text{Ca,Sr})_2\text{CuO}_5$, complicated efforts to obtain the high T_c phase in pure form. The effect of dopants (such as Pb, Sb, Sn, Ge) on stabilization of the high T_c phase was also investigated. A coexisting liquid phase was observed during heat-treatment, and might play an important role in the formation of the high T_c phase. Results will be discussed with respect to data on superconducting properties as a function of microstructure evolution.

M7.134

SPECIAL TREATMENT ON BiCaSrCuO SUPERCONDUCTORS. X.W. Wang, M. Scott, C. Moore, R. Snyder, Alfred University, N.Y. 14802

After initial studies on BiCaSrCuO superconductors¹, we have obtained some new results under two special treatments. The first technique is the glass ceramic BiCaSrCuO with magnetic treatment. It is observed that the crystal orientation and grain sizes are different from that under no magnetic treatment. The phase formation condition will be discussed.

The second technique is the metal doping in BiCaSrCuO system. It is observed that under Al doping, the mechanical strength of Bi compound is increased². Furthermore, Pb doping has a stronger effect on the phase formation. The mechanical strength is also enhanced when Pb concentration is not too high. A detailed study of superconductivity, crystal structure and morphology will be presented.

¹ X.W. Wang, et al, "Studies of the BiCaSrCuO Materials", in "Superconductivity and its Applications", ed. H. Kwok et al (Elsevier, New York, 1988).

² X.W. Wang, et al, "Some Physical Properties of Ceramic Superconductors", in "8th Joint Symposium on Materials Science", June 1989, Rochester, N.Y.

M7.135

PREPARATION OF BiPbSrCaCuO SUPERCONDUCTORS BY LASER PEDESTAL GROWTH METHOD: K. Hayashi, H. Nonoyama, M. Ueyama, M. Nagata, H. Hitotsuyanagi Sumitomo Electric Industries, LTD. 1-3, Shimaya, Ichome, Konohanaku, Osaka 554 JAPAN

BiPbSrCaCuO crystals were prepared by laser pedestal growth method. Crystal structure and superconducting properties (T_c, J_c) were studied as a function of crystal growth and post annealing conditions.

Nominal composition of $\text{Bi}_{1.4}\text{Pb}_{0.6}\text{Sr}_2\text{Ca}_2\text{Cu}_3\text{O}_x$ was typically chosen for this study. The heat source was CO₂ laser which melt the top of the feed rod. The sample obtained by this method was about 2.5mm diameter and 90mm long. Pb and Bi were slightly evaporated from the melt, but the macroscopic composition shown by ICP analysis did not change during crystal growth. As-grown crystal consisted of SrCaCuO and 2212 phase which were aligned to longitudinal direction of the sample. After annealed in air, SrCaCuO and 2212 phases reacted each other and 2223 phase was grown between them. As the annealing time became longer, the volume fraction of 2223 phase became larger. Up to now, T_c of 106K and J_c of 1560A/cm^2 at 77.3K without magnetic field are obtained.

This study was carried out as a part of "R&D program for superconductive generation equipment and materials" under the Moonlight Project of Agency of Industrial Science and Technology, MITI and also being commissioned by the New Energy and Industrial Technology Development Organization (NEDO).

NEW METHOD FOR SYNTHESIZING Bi-Sr-Ca-Cu-O SUPERCONDUCTOR.
M. Tanaka, and K. Habu,
SONY Corporation Research Center, Tokyo, Japan.

It is well known that Bi-Sr-Ca-Cu-O (BSCCO) superconductor ceramics consist of $\text{Bi}_2\text{Sr}_2\text{Ca}_2\text{Cu}_3\text{O}_x$ (2223), $\text{Bi}_2\text{Sr}_2\text{Ca}_2\text{Cu}_2\text{O}_x$ (2212), and oxides of constituent elements. The single phase ceramics with high T_c of about 107 K were fabricated only in BSCCO with Pb. It is likely that this superconductor is the alloy with the composition of $(\text{Bi}, \text{Pb})_2(\text{Pb}, \text{Sr}, \text{Ca})_4\text{Cu}_3\text{O}_{10}$. The superconductor with Pb may have properties different from those of the pure BSCCO.

In this work the processes for preparing the oxide superconductor with high T_c are studied in the BSCCO ceramics without Pb. We have obtained the BSCCO ceramics with the ratio (2223)/(2212)=1.5 - 1.8 in the nominal composition of 2:2:2:3 or 2:2:3:4 for Bi:Sr:Ca:Cu after the sintering for about 30 hr. It is likely that the crystal growth of (2223) is not depending on the nominal composition but the sintering conditions. Our results predict that synthesizing (2223) ceramics without Pb is possible. The key conditions of our processes are as follows; 1) Sr-Ca-Cu-O precursor oxide and Bi_2O_3 are used for raw materials of the sintering process. 2) The partial pressure of O_2 are arranged 0.08-0.10 atm. in the sintering process. The superconducting critical temperature T_c determined by a.c. magnetic susceptibility measurement is 107 K for (2223) and 80 K for (2212). The anomalous decrease of magnetic susceptibilities is observed at the temperature below 50 K, and is very sensitive to the applied magnetic field. The origin of this phenomenon is under examination.

ELECTRICAL AND MICROSTRUCTURAL CHARACTERISTICS OF REGRADED Bi-Pb-Sr-Ca-Cu-O SUPERCONDUCTOR PREPARED BY RAPID THERMAL MELT PROCESSING
B. M. Moon, B. Lalevic, Y. Lu, *B.H. Kear, *L.E. McCandlish, **A. Safari, and **M. Meskoob. Department of Electrical Engineering, *Department of Materials Science, **Department of Ceramics. Rutgers University, P.O. Box 909, Piscataway, New Jersey 08855-0909

Properties of rapidly melted Bi-Pb-Sr-Ca-Cu-O ceramics have been studied. Sintered pellets were melted at 1200C, cooled rapidly, then annealed. As-melt crystal exhibits a semiconductor behavior and melt-annealed samples are superconducting at 105K ($T_c=0$). Rapid Thermal Melt Processing (RTMP) has the potential of overcoming many problems, such as porosity, poor current carrying capacity, and poor mechanical properties. This is due to the crystal growth at a controlled rate to an essentially uniform size distribution while embedded in a virtually pore-free matrix during RTMP and subsequent heat-treatment.

In this paper, The correlations between electrical and microstructural characteristics of RTMP-annealed samples will be discussed. Also, X-ray diffraction, SEM, magnetic susceptibility, DC resistance, and critical current density data will be presented.

THE PREPARATION OF Bi-Pb-Sr-Ca-Cu-O SUPERCONDUCTING POWDER FOR THICK FILM PASTES. J. Hagberg, A. Uusimäki, J. Levoska and S. Leppävuori, Microelectronics and Material Physics Laboratories, University of Oulu, Oulu, Finland

Fine grained and homogeneous (Bi-Pb)-Sr-Ca-Cu-O powders with nominal compositions near by $\text{Bi}_2\text{Pb}_{0.4}\text{Sr}_2\text{Ca}_2\text{Cu}_3\text{O}_y$ were made via the oxalate route. In this route, nitrates of bismuth, lead, strontium, calcium and copper and oxalic acid were used as the starting materials. The pH of the solutions made from starting materials was regulated with ammonium hydroxide around a value of 3. The oxalate precipitates were filtered, washed and dried. The powders were then annealed at below 700 °C to decompose them to oxide powders. The powders were investigated by TGA, TDA, XRD and TEM, and particle size and surface area measurements were carried out. The effect of the production parameters, such as washing conditions of the residue and the decomposition annealing temperature of the oxalate powder on the particle size of the powder, was studied.

The decomposed powders were found to have particle sizes from about 50 nm up to 750 nm, and the particles formed agglomerates with the largest dimension being up to 2 µm. These powders were mixtures of oxides or oxides and carbonates depending on the decomposition annealing temperature. The size of particle agglomerates was found to be controllable. The properties of thick film pastes made from oxalate based powders were found to be superior to the mixed oxide/carbonate based pastes.

PHASE CHEMISTRY, MICROSTRUCTURE AND PROPERTIES OF DIRECTIONALLY SOLIDIFIED SUPERCONDUCTING $\text{Bi}_2\text{Sr}_2\text{CaCu}_2\text{O}_8$. H.M. Chow, X.P. Jiang, M.J. Cima, J.S. Haggerty, and M.C. Flemings, Department of Materials Science and Engineering, Massachusetts Institute of Technology, Cambridge, MA 02139; H.D. Brody, University of Pittsburgh, Pittsburgh, PA 15261.

Ceramic rods of $\text{Bi}_2\text{Sr}_2\text{CaCu}_2\text{O}_8$ (2212) were directionally solidified by laser-heated float-zone crystallization. The microstructure of the resulting material can be controlled through variation of growth parameters such as growth rate and oxygen partial pressures. Highly textured samples composed of the 2212 phase are produced at growth rates less than 0.1 cm/h. At these low growth rates, the solidification front proceeds along the (200) axis of the 2212 grains. Faster growth rates are accompanied by the appearance of minor amounts of other phases in a matrix of highly-textured 2212 which accommodates the necessary change in stoichiometry. $\text{Bi}_2\text{Sr}_2\text{CaO}_6$ was the only other phase observed at 0.2cm/h. Four other phases were found at 0.7cm/h; $\text{Bi}_2\text{Sr}_2\text{CaO}_6$, $\text{Bi}_2\text{Sr}_{0.7}\text{CaO}_{4.7}$, $\text{Bi}_{4.5}\text{Sr}_{2.7}\text{Cu}_2\text{O}_x$, and $\text{Sr}_{1.4}\text{CaCu}_{3.9}\text{O}_x$. Several of these phases are previously unreported but do have analogs with binary oxides in this system. The secondary phases can be removed through annealing with associated impact on the microstructure. Very high growth rates (16cm/h) yield samples that contain only $\text{Bi}_5\text{Sr}_3\text{Ca}_{12.5}\text{O}_{12.5}$, $\text{Bi}_{4.3}\text{Sr}_3\text{Cu}_2\text{O}_x$, and $\text{Sr}_3\text{Ca}_2\text{Cu}_5\text{O}_x$ and no 2212.

MELT PROCESSING OF SUPERCONDUCTORS IN THE Bi-Ca-Sr-Cu-O_x SYSTEM. J.P. Cronin, S. West, E. Roberts, S. Rosenfelder and D.R. Uhlmann, The University of Arizona, Arizona Materials Laboratories, 4715 E. Ft. Lowell Road, Tucson, AZ; O.H. El-Bayoumi and R.J. Andrews, Solid State Sciences Directorate, Rome Air Development Center, Hanscom Air Force Base, MA

Glass formation in the Bi-Ca-Sr-Cu-O_x system has been explored as a function of composition. Also investigated were the effects of selected dopants on glass formability. Upon reheating the glasses, they were observed to crystallize readily. The morphology and composition of the crystalline phases were investigated as a function of overall chemistry, melting conditions and heat treatment. The chemistry and microstructures of the phases are compared with measurements of the critical current density and critical temperature for superconducting behavior.

M7.141

CATION DISORDERING IN TI SUPERCONDUCTORS*

B. Morosin, R. J. Baughman, D. S. Ginley, J. F. Kwak, J. E. Schirber, C. P. Tigges and E. L. Venturini, Sandia National Laboratories, Albuquerque, NM 87185

Detailed structure determinations on crystals grown from melts with different metal oxide ratios suggest cation solid solution (or disorder) occurs in Ti-Ca-Ba-Cu-O high-T_c superconductors. Such disorder together with varying oxygen vacancies alters the carrier concentration, producing a wide range of T_c's for individual crystals belonging to the identical structure-type or phase. These small stoichiometric differences are also reflected in the lattice parameters values reported by different laboratories for a particular phase. The effect of pressure on T_c has been determined using an R.F. technique. On the Ti₂CaBa₂Cu₂O₈ phase, a Ti-rich/Ca-poor crystal with a T_c of 95K had dT_c/dp = 0.33±0.04 K/kbar while a more stoichiometric material with T_c of 106K had a smaller value of 0.20±0.04K/kbar. Such large differences in the pressure derivative of T_c may result from such cation disordering. Vacuum and oxygen annealing studies on well-characterized crystals are being explored to better understand the relationship to superconducting properties.

M7.142

CRYSTAL STRUCTURES AND SOLID SOLUTION BETWEEN Ti-Sr-Ca-Cu-O AND Ti-Ba-Ca-Cu-O SUPERCONDUCTORS. A. Soeta, I. Suzuki, S. Takeuchi, I. Kamo, S. Matsuda, Hitachi Research Laboratory, Hitachi Ltd., Hitachi-shi, Ibaraki 319-12, Japan

We report the superconductivity and crystal structures in Ti-(Ba,Sr)-Ca-Cu-O(TBSCC) system. The samples were prepared by a conventional powder-mixed method. The atomic ratio of Ti:(Ba+Sr):Ca:Cu was 2:2:2:3, corresponding to Ti₂Ba₂Ca₂Cu₃O_x phase, and the Ba/Sr ratio was varied at 1/4, 2/3, 1/1, 3/2 and 4/1. Electrical resistance was measured by the standard four-probe method and susceptibility change by the standard AC method. In the case of TBSCC system, the single phase was obtained more easily compared with the Ti-Sr-Ca-Cu-O(TSCC) and Ti-Ba-Ca-Cu-O(TBCC) systems. As a result we achieved the high superconducting volume fraction, 95% above 100K. The T_c decreased gradually from both TBCC and TSCC sides as a function of the Ba/Sr ratio. The T_c value changed discontinuously at Ba/Sr=1.0, which was caused by the crystallographic transformation. By the X-ray diffraction and TEM analysis, the crystal structure was determined to be the 2223 phase consisting of three CuO₂ planes sandwiched by Ti-O bilayers in the Ba rich side, and the 1223 phase consisting of three CuO₂ planes sandwiched by Ti-O monolayer in the Sr rich side. The crystallographic transformation is responsible for the discontinuity of the T_c.

M7.143

ORIENTATION PROCESS OF Bi-TYPE OXIDE SUPERCONDUCTOR AND ITS HIGH-FIELD TRANSPORT PROPERTIES N. Enomoto, H. Kikuchi, K. Imai, H. Takami and N. Uno Yokohama R&D Labs. Furukawa Electric Co., Ltd., 2-4-3 Okano Nishiku, Yokohama 220 Japan.

We have been studying both improvement of alignment of crystal grain and reduction of weak-link in grain boundary in order to increase superconductivity of bulk. In this case it is effective to improve oriented crystal grain.

In case of Bi-type oxide, heat treatment including liquid phase was quite effective to obtain both low-T_c and high-T_c phase as single phase, without Pb-doping. By a modified powder in tube process using Ag, Bi-type calcined powder was processed into tape wire with 0.1-0.5 mm thick. The details of the reaction involved here were made clear by using TG/DTA, EPMA, XPS, XRD, etc. By XRD and SEM revealed were c-axis oriented texture perpendicular to wire axis and aligned grain structure, which was supposed to be formed through reactive sintering including liquid phase. J_c values were measured at 77 and 4.2 K upto 31 T. 5×10⁴ A/cm² was obtained over 20 T at 4.2 K, in which working mechanism for pinning will be presented.

This work was conducted as collaboration with Tokyo Electric Power Co. Ltd

M7.144

EFFECT OF OXYGEN PARTIAL PRESSURE ON STABILITY OF HIGH-T_c PHASE IN SINTERED Bi-Pb-Sr-Ca-Cu-O SUPERCONDUCTORS. H.K. Lee, K.W. Lee, D.H. Ha, and J.C. Park, Korea Standards Research Institute, P.O. Box 3, Taedok Science Town, Taejeon, 305-340, Korea

The effect of oxygen partial pressure on stability of high-T_c phase in Bi-Pb-Sr-Ca-Cu-O system has been investigated using x-ray diffraction, resistivity and a.c. susceptibility measurements. It was found that part of the high-T_c phase (> 100 K) in Bi-Pb-Sr-Ca-Cu-O system was transformed into low-T_c phase (~80 K) and insulating phase by heating in the temperature range 820 °C to 880 °C in O₂ of one atmosphere. This transformation resulted in sensitive dependence of zero resistance temperature in low magnetic field as well as the decrease of zero resistance temperature of the superconductor. The a.c. susceptibility measurements indicated that the transformation occurred mainly in the coupled phase between high-T_c grain phases. It is shown that the original high-T_c phase can be restored upon retreatment at 840 °C in low oxygen partial pressure of 0.1 atmosphere. The reversible superconducting phase transformation is discussed in conjunction with the formation mechanism of the high-T_c phase in Bi-Pb-Sr-Ca-Cu-O system.

M7.145

THE SUPERCONDUCTIVITY OF Bi_{1.6}Pb_{0.4}Sr₂Ca₂(Ca_{1-x}Ag_x)₃O_y AND Bi_{1.6}Pb_{0.4}Sr₂Ca₂Cu₃O_y + x wt% Ag. Chongde Wei, Chin Lin, Qingrong Feng, Zunxiao Liu, Jian Lan, Yunxi Sun, Guozhong Li, Ke Wu, Lixin Xue, Zizhao Gan, Department of Physics, Peking University, Beijing, China.

Both interstitially Ag-doped Bi_{1.6}Pb_{0.4}Sr₂Ca₂Cu₃O_y + x wt% Ag with x=0.5, 1.0, 5.0, 10.0, 15.0, and substitutionally doped Bi_{1.6}Pb_{0.4}Sr₂Ca₂(Cu_{1-x}Ag_x)₃O_y with x=0.025, 0.05, 0.10, 0.20, 0.40, systems were studied. For interstitially Ag-doping all samples have the structure of 2223

phase, for substitutionally doping the samples with $x=0.025$, 0.05 , and 0.10 have the structure of 2223 phase, while the samples with $x=0.2$ and 0.4 are mixture of 2223 phase and 212 phase. Semi-quantitative analysis shows that silver atoms distribute both in the grain boundaries and in the grains, the distribution is inhomogeneous.

Magnetic susceptibility measurements indicate that both the interstitial and substitutional Ag-doping yield much higher diamagnetic signal for ZFC in a field of 60 Oe at 5K. At 80K, $-4\pi M/H$ was also enhanced by Ag-doping for $H \leq 200$ Oe. Magnetic critical current J_c was calculated from magnetization curves at 1.5K. Substitutional Ag-doping increases J_c for $x \leq 0.2$. Possible explanation was discussed.

M7.146

SYNTHESIS OF VARIOUS Bi-SYSTEMS FROM NITRATES BY USING A SPRAY-DRYING PROCESS. Jens Hyldtoft, Svend Dahl-Petersen, Torsten Freltoft, Liselotte Lorenzen, and Per Vase, NKT A/S, Sognevej 13, DK-2605, Broendby, Denmark.

Solutions of the Bi, (Pb), Sr, Ca, and Cu nitrates were mixed, spray-dried, decomposed, and finally sintered in various atmospheres.

The two compositions (2212) and (2223) were produced with a 20% Pb substitution for Bi in the (2223) compound.

The materials were characterized by X-ray diffraction, AC susceptibility and transmission electron microscopy, including EDX analyses.

The spray-drying process has several advantages compared to traditional wet or dry milling processes.

Most importantly, the initial material composition can be controlled very accurately which is of specific importance for obtaining pure phases.

Secondly, a nearly perfect mixing is achieved in the solution making lower temperatures and shorter sintering times possible.

Finally, the process is much cleaner since contamination from carbonate sources can be totally avoided. This has great importance for obtaining high J_c values.

M7.147

The Effects of Transition Metal Substitutions for Copper in the Bi-Sr-Ca-Cu-O Superconducting System. J.C. Bennett, F.W. Boswell, J.M. Corbett, S. Kohara, University of Waterloo, Waterloo, Ontario; and F.S. Razavi, Brock University, St. Catharines, Ontario, Canada.

The effects of transition metal dopants on superconductivity in samples of nominal composition $Bi_2CaSr_{1-x}M_xO_{8.5}$ with $M = Co, Fe, Ni$ and Zn have been investigated for $0 \leq x \leq 1$. Co and Fe additions were found to progressively suppress the T_c of the doped material and result in semiconducting behaviour for $x \geq 0.2$. Magnetic susceptibility measurements confirm the depression in T_c and also indicate the proportion of superconducting material of 4.2 K decreases rapidly with dopant concentration, probably due to inhomogeneity effects. The measured Meissner effect for $x \leq 0.05$ is about 35% suggesting these compounds are bulk superconductors. For $x \geq 0.10$, the Meissner fraction is much smaller indicating the material is less homogeneous, consisting of semiconducting and superconducting regions. In the ranges of dopant concentration $0 \leq x \leq 0.07$ and near $x = 1.0$, x-ray powder diffraction reveals the doped samples remain

essentially single phase 2122 but are multiphase for all other dopant concentrations. Energy dispersive x-ray analysis in the TEM indicates Co and Fe substitute for Cu in near the nominal concentrations. For the Ni and Zn doped compounds, resistance measurements show only a slight depression in T_c for nominal dopant concentrations $0 \leq x \leq 0.5$. However, EDX analyses reveal Ni and Zn are only incorporated into the superconducting phase at about 10% or less of the nominal concentration for the preparation conditions used. Further microstructural characterization of the doped compounds by TEM will also be discussed.

M7.148

THE EFFECTS OF SEEDING ON THE FORMATION OF HIGH- T_c Bi-Pb-Sr-Ca-Cu-O COMPOUNDS, Cheol J. Kim and Mark R. De Guire, Case Western Reserve University, Cleveland, OH; and Narottam P. Bansal, NASA Lewis Research Center, Cleveland, OH.

The difficulty of obtaining Bi-Sr-Ca-Cu-O superconductors with large fractions of the "2223" phase (i.e., the phase with $T_c \approx 110$ K, a characteristic lattice spacing of 3.7 nm, and a reported stoichiometry of $Bi_2Sr_2Ca_2Cu_3O_{10+y}$) is well recognized. Very long annealing times within a narrow temperature range, careful composition and/or atmosphere control, and Pb doping have variously been reported as being necessary to obtain single-phase 2223 materials. This study was undertaken to determine whether the formation of this phase could be accelerated through heterogeneous nucleation by previously synthesized 2223 crystals. Nearly single-phase powder of Pb-doped 2223 with T_c of 109 K has been added to two types of materials with the 2223 composition: rapidly quenched glass, and sintered multiphase crystalline powder. These materials were then annealed at various temperatures and times. The resulting microstructures were characterized using XRD, SEM, EDS, and TEM. In particular, the boundary region between the seed crystals and the matrix was studied to identify the products and understand the mechanisms of the interfacial reactions. These findings could be useful for single crystal growth or for enhancing the production of 2223 materials.

Work supported by NASA Lewis Research Center.

M7.149

OPTIMIZING THE MACHINING PROPERTIES OF HIGH T_c BSCCO. R. J. Ruys, L. E. Toth, B. A. Bender, R. J. Soulen Jr., Naval Research Laboratory, Washington D.C.

BSCCO has excellent machinability characteristics and can be cut and shaped with conventional metal working machines and steel tools. Also, the machinability of BSCCO is comparable and perhaps better than the widely used Macor, a glass-ceramic produced by Corning, Inc. Because BSCCO is this machinable it may have applications other than in superconducting devices. The best method to prepare BSCCO for machining is to cast it and then heat treat it. This results in a dense material with a random network of platelets. It is this random network of platelets that accounts for the machinability. BSCCO prepared by sintering also yields a machinable material, but due to its lower density it is weaker than BSCCO prepared by casting followed by a heat treatment. Superconducting parts machined at NRL and being tested at other labs include a SQUID shield with a 1.27 cm bore and a closed end, and a microwave cavity; tolerances are held to ± 0.002 cm.

M7.150

THE EFFECT OF THE DISTRIBUTION OF DOPANTS IN HIGH T_c Bi-COMPOUND SUPERCONDUCTORS. Alexis S. Nash, Marquette University, Milwaukee, WI, Kenneth C. Goretti, Argonne National Laboratory, Argonne, IL, Philip Nash, Illinois Institute of Technology, Chicago, IL, Roger B. Poeppel and Donglu Shi, Argonne National Laboratory, Argonne, IL.

A series of 4336 Bi-Sr-Ca-Cu oxide samples doped with either 1 to 10% metallic silver or 1 to 10% SnO_2 were prepared using a solid state reaction method. The distribution of cationic dopants, the microstructure and the crystal structure of the samples was studied using energy dispersive

spectrometry, scanning electron and optical microscopy and x-ray diffractometry.

The dependence of microstructure and T_c on the type and the distribution of dopant and on firing schedules have been determined. The grain morphology was found to depend upon the type of dopant, varying from plates to irregular chunks. Addition of silver leads to a marked increase in preferred orientation with {001} planes perpendicular to the pressing direction in sintered pellets. This was confirmed by scanning electron microscopy.

The resistivity-temperature data show an enhanced T_c in Ag-doped samples under certain conditions. Energy dispersive spectrometry indicates that the dopants mostly segregate to the grain boundaries.

M7.151

HIGH RESOLUTION NEUTRON POWDER DIFFRACTION STUDY OF THE TUBULAR PHASE $\text{Bi}_2\text{Sr}_2\text{Ca}_2\text{Cu}_3\text{O}_{10-x}$. M.T. Caldés, J.M. Navarero, A. Fuertes, I. Obradors, C. Miravittles, Institut de Ciència de Materials de Barcelona (C.S.I.C.), C/Martí i Franqués s/n, 08028 Barcelona, Spain; J. Rodríguez-Carvajal, Institut Max von Laue-Paul Langevin, 156 X, 38042 Grenoble CEDEX, France; M. Vallet, J. González-Calbet, Laboratorio de Magnetismo Aplicado (RENFE-UCM), 28290 Las Matas, Madrid, Spain.

$\text{Bi}_2\text{Sr}_2\text{Ca}_2\text{Cu}_3\text{O}_{10-x}$ is a non-superconducting oxide closely related to the superconducting $\text{Bi}_2\text{Sr}_2\text{CuO}_8$. The crystal structures of both phases are based on the stacking of multiple perovskite and Bi-O layers, but in $\text{Bi}_2\text{Sr}_2\text{Ca}_2\text{Cu}_3\text{O}_{10-x}$ the presence of extra perovskite layers arranged perpendicularly to the CuO_2 planes breaks the two-dimensional character of the structure, common to all high T_c superconducting copper oxides. Recently we have reported the crystal structure determination of this compound by single crystal X-ray diffraction, and the study of the structural and physical properties by means of electron microscopy, electrical resistivity and magnetic susceptibility^{1,2}. Here we present the investigation of the exact location of the oxygen atoms in the structure by means of neutron diffraction experiments, and the comparison of these results with the superconducting phases in the Bi-Sr-Ca-Cu-O system. The high temperature behavior of this material by time-resolved neutron powder diffraction measurements will be also presented.

References: 1. A. Fuertes et al., *Physica C* 157 (1989), 525.
2. M.T. Caldés et al., *Physica C*, in the press.

M7.152

PREPARATION OF HIGH-PURITY $\text{Tl}_2\text{Ca}_n\text{Ba}_2\text{Cu}_{n+1}\text{O}_{6+2n}$ ($n=1,2$) POWDERS FROM STOICHIOMETRIC REACTANT MIXTURES. Nae-Lih Wu, NTU, Taiwan; Y. D. Yao, Academia Sinica, Taiwan; and E. Ruckenstein, SUNY at Buffalo, U.S.A.

Novel solid state reaction methods have been developed for preparing high-purity $\text{Tl}_2\text{CaBa}_2\text{Cu}_2\text{O}_8$ (the 2122) and $\text{Tl}_2\text{Ca}_2\text{Ba}_2\text{Cu}_3\text{O}_{10}$ (the 2223) powders from stoichiometric reactant mixtures. Single-phase 2122 powders with superconducting temperatures (both zero-resistivity and diamagnetic onset temperatures) above 110 K are prepared at 830 °C by the following reaction: $\text{CaBa}_2\text{CuO}_4 + \text{Tl}_2\text{O}_3 + \text{CuO} \rightarrow \text{Tl}_2\text{CaBa}_2\text{Cu}_2\text{O}_8$. On the other hand, single-phase 2223 powders with superconducting temperatures above 115 K are produced via the intercalation of CaO and CuO into the existing 2122 grains at 870 °C. Powder melting and Tl loss via vaporization, both of which are strongly associated with the conventional methods, are greatly suppressed in the new methods. For either the 2122 or 2223 compound, powders thus prepared typically show a complete Meissner effect of 20% of $(-1/4 \pi)$ at a field of 20 G.

M7.153

SOLID STATE FORMATION OF SUPERCONDUCTING PHASES IN THE Tl-Ca-Ba-Cu-O SYSTEM T.W. Huang, M.P. Hung, Dept. Mat. Eng., Cheng Kung Univ., Tainan, Taiwan; T.S. Chin, Dept. of Mat. Sci. Eng., H.C. Ku, Dept. of Phys., Tsing Hua Univ., Hsinchu, 30043, Taiwan; P.C. Yao, S.E. Hsu, Mat. R & D Center, Chung Shan Inst. of Sci. & Tech. Lung-Tang, 32526, Taiwan, ROC

Solid state formation of superconducting phases in the Tl-Ca-Ba-Cu-O system was studied with a closed oxygen flowing system both in synthesis and DTA/TG analyses. The phase analyses were done with XRD.

It was found that the high T_c 2223 and low T_c 2122 phases were formed at around 900 and 840 °C, respectively, at a heating rate of 10 °C/min. The activation energy of the formation reaction was calculated with the Kissinger's peak shift method. It was 50 and 35 kcal/mole for the 2223 and 2122, respectively. Since the activation energy is low as compared to that of superconducting Y-Ba-Cu-O³, short period of reaction time (within 30 minutes) is needed to form the superconducting Tl-Ca-Ba-Cu-O phases.

Different precursors were used to prepare the Tl-Ca-Ba-Cu-O superconducting phase. It was found that $\text{Ca}_3\text{BaCu}_3\text{O}_7$ is the best one.

M7.154

Phase Equilibria in the System Tl-Ca-Ba-Cu-O. Lawrence P. Cook, Chwan K. Chiang, Winnie Wong-Ng, and Lawrence H. Bennett, National Institute of Standards and Technology, Gaithersburg, MD 20899.

Phase equilibria related to the stability of the high T_c phases in the system Tl-Ca-Ba-Cu-O are being investigated by high temperature synthesis in an apparatus constructed primarily of MgO. The apparatus employs a buffering technique in which $P_{\text{Tl}_2\text{O}}$ is held constant by vaporization

equilibria in a separate reservoir and P_{O_2} is held at 1

atm. In principle, equilibrium can be bracketed with reversibility experiments in which the results of thallium loss and thallium gain are compared. *In situ* resistivity measurements are being used to monitor phase changes as thallium mass transport occurs. Phase assemblages are being characterized by x-ray powder diffraction, SEM/EDX analysis, and a.c. magnetic susceptibility measurements.

M7.155

Tl-BASED HIGH TEMPERATURE SUPERCONDUCTORS: PREPARATIONS AND PROPERTIES. M. Greenblatt, S. Li, L. McMills, M. H. Pan and K. V. Ramanujachary, Chemistry Department, Rutgers University, New Brunswick, NJ 08893.

Novel synthetic routes have been worked out for single phase Tl-based 2201, 2212, 2223, Bi and Pb stabilized 1212 compounds and their substitutional analogs both as bulk polycrystalline materials and thin film samples. Sharp resistive transitions, high zero resistance temperature and high superconducting bulk fractions are observed. Results of substitutional studies to enhance the superconducting properties will be presented.

M7.156

HYPER- AND HYPOBARIC PROCESSING OF Tl-Ba-Ca-Cu-O SUPERCONDUCTORS. K. C. Goretti, J. L. Routbort, Donglu Shi, M. C. Hash, and Ira Bloom, Argonne National Laboratory, Argonne, IL.

Phase-pure Tl-based superconductors have not been synthesized at atmospheric pressure. For example, compositions rich in Ca and Cu have generally been used to form the 120-K phase $Tl_2Ba_2Ca_2Cu_3O_x$. In this work, precursor powders of $Ba_2Cu_3O_5$, Ca_2CuO_3 , and " Ba_2CuO_3 " were synthesized by solid-state reaction and then mixed with Tl_2O_3 and CuO in a cation stoichiometry of Tl:Ba:Ca:Cu equal to 2:2:2:3. The powders were cold-pressed into pellets and sintered in oxygen atmospheres of 10^4 to 2×10^6 Pa at temperatures of 830 to 930°C. The resulting specimens were characterized by x-ray diffraction, scanning electron microscopy, and density measurement, and analyzed for the superconducting properties of Meissner fraction, transition temperature, and critical current density at 77 K.

Work supported by the U. S. Department of Energy, Office of Basic Energy Sciences -- Materials Science, and the Office of Energy Storage and Distribution, Conservation and Renewable Energy, under Contract W-31-109-Eng-38.

M7.157

VARIATION OF T_c IN TI-RICH TI-Ca-Ba-Cu-O SINGLE CRYSTALS. E. L. Venturini, R. J. Baughman, B. Morosin, D. S. Ginley, J. F. Kwak, J. E. Schirber, and C. P. Tigges, Sandia National Laboratories, Albuquerque, NM 87185.

Meissner effect data are compared for single crystals with different structure types and stoichiometry in the Ti-Ca-Ba-Cu-O system of high-temperature superconductors. There is a wide range of onset temperatures (T_c) and a multiple step temperature dependence of the Meissner signal for Ti-rich crystals with the same structure type such as $Tl_2CaBa_2Cu_2O_x$ (Ti-2122). Energy dispersive X-ray analysis (EDS) was used to establish the stoichiometry of both surfaces for each crystal plate, and X-ray precession photography determined the structure type. The relative Ba and Cu concentrations are constant within experimental error in crystals with a common structure type, as is the sum of the Ti and Ca. However, the Ti/Ca ratio shows considerable variation: substitution of Ti on the Ca sites is suggested by a Ti-rich EDS composition and is demonstrated by detailed structure determinations for several specimens using single crystal X-ray diffraction data.

The replacement of Ca^{+2} with Tl^{+3} is assumed to alter the carrier concentration since the oxygen content of the as-grown crystals is similar. This site substitution is reflected in the Meissner data. For example, crystals with the Ti-2122 structure type have been grown where 25-30% of the Ca is replaced by Tl. At least 80% of the volume in such crystals remains nonsuperconducting above 75 K, while the remainder has an onset of superconductivity near 95 K. In contrast, Ti-2122 crystals with much lower Ti substitution show single Meissner transitions with onsets between 105 and 110 K. Our current explanation is that there are gradients in the Ti substitution on the Ca site in Ti-rich crystals, leading to complex temperature dependence for the Meissner signal. Less substitution of Ti on Ca sites in bulk ceramics may explain the appreciably higher T_c 's compared to single crystals with the same structure type.

This work was performed at Sandia National Laboratories, supported by the U. S. Department of Energy, Office of Basic Energy Sciences, under Contract No. DE-AC04-76DP00789.

M7.158

PREPARATION OF $Ba_2YCu_3O_{7-x}$ THIN FILM SUPERCONDUCTORS USING SOLUBLE ARYLOXIDE PRECURSORS, Mary Rose Scozzafava, Michael J. Cima, Wendell E. Rhine, Ceramics Processing Research Laboratory, Massachusetts Institute of Technology, Cambridge, Massachusetts

Use of metal alkoxide precursor solutions for the preparation of high T_c superconducting materials is attractive because of the potential low carbon content in the prefired films. However, the insolubility of copper alkoxides have made application of this method difficult. We have improved the solubility of copper alkoxide and aryloxy complexes by using nitrogen-containing compounds as ligands. Solutions of copper, barium, and yttrium aryloxides (with copper concentrations of 0.7 mol/L) have been

used as precursors to $Ba_2YCu_3O_{7-x}$ superconductors. Preparation and characterization of spin-coated and dip-coated superconducting films which are derived from such precursor solutions are described.

M7.159

METAL-ORGANIC DECOMPOSITION AND MICROSTRUCTURE DEVELOPMENT IN $Ba_2YCu_3O_{7-x}$ FILMS FROM METAL TRIFLUOROACETATE PRECURSORS. Paul C. McIntyre, Raymond C. Chiu, Michael J. Cima, Wendell E. Rhine, Ceramics Processing Research Laboratory, Massachusetts Institute of Technology, Cambridge, MA.

Decomposition of metal-organic precursors to $Ba_2YCu_3O_{7-x}$ films is difficult because of the high reaction temperature required to decompose $BaCO_3$, which forms as an intermediate compound during conversion. The recently proposed use of metal trifluoroacetate (TFA) solutions offers an alternative path to barium-containing superconducting films. The TFA salts decompose to the metal fluorides forming BaF_2 , eliminating $BaCO_3$ from the system. Ultimate conversion to BYC, however, is shown not only to depend on hydrolysis of the BaF_2 at high temperatures, but also hydrolysis of copper trifluoroacetate at low temperatures to prevent the volatilization of $Cu(TFA)_2$. These processes result in unique microstructural behavior which can be characterized by electron microscopy and Auger spectroscopy. Effects due to substrate interactions have been eliminated by use of a chemically inert substrate material, $BaZrO_3$.

M7.160

PREPARATION OF Y-Ba-Cu-O FILMS BY A MODIFIED CHEMICAL VAPOR DEPOSITION METHOD T.S. Chin, L.H. Perng, C.H. Lin, Dept. Mat. Sci. Eng., Tsing Hua Univ., Hsinchu, Taiwan; T.W. Huang, C.H. Hsu, M.P. Hung, Dept. Mat. Eng. Cheng Kung Univ., Z.N. Hung, Dept. Chem. Eng. Cheng Kung Univ., Tainan, Taiwan, ROC

A modified chemical vapor deposition method was developed to prepare superconducting Y-Ba-Cu-O thin films. In this method, aqueous solution containing 0.03N nitrates of Y, Ba, Cu in a ratio of 1:2:3 (the 123 solution) or 1:3:2 (the 132 solution) diluted with equal part of ethanol was atomized into droplet of few microns and then carried into a high temperature reaction chamber where pyrolysis occurred and deposition onto substrates was possible at suitable reaction temperatures.

YSZ single crystal and 96% alumina substrate were used. The optimum reaction temperature is 350 °C for YSZ substrate, 320 - 370 °C for alumina substrate. The 132 solution yielded better film stoichiometry than the 123 solution. Heat treatment was found to be necessary. An annealing at 900 °C for 3 minutes was found enough to result in good quality superconducting 123 phase. Measured T_c was 70 °K onset, 50 °K for zero resistance from films grown on YSZ substrate. Detailed SEM microstructure, and the effect of processing parameters on film properties are discussed.

M7.161

EFFECT OF GLOW DISCHARGE CURRENT ON COMPOSITION OF Y-Ba-Cu-O FILMS BY HIGH PRESSURE DC SPUTTERING PROCESS. R.J. Lin and P.T. Wu, Materials Research Laboratories, Industrial Technology Research Institute, Chutung, Hsinchu, Taiwan, R.O.C.

The Y-Ba-Cu-O films were grown on (100)MgO substrates by high pressure DC planar diode sputtering process. The targets were Y-Ba-Cu-O compounds made by solid state reaction. The sputtering gases were Ar-50%O₂, and total pressure was 1.5 torr. For $Y_2Ba_2Cu_3O_{7-x}$ target, the atomic ratio Ba/Y in the films almost remains constant (Ba/Y = 1.7), and Cu content monotonically increases with increasing

discharge current(0.4-0.8A). The Cu content in the film approaches to that of target at low discharge current. Additionally, the Cu content in the films monotonically decreases with reducing the Cu content of target(Ba/Y = 2). The possible reason for getting Cu-rich films will be discussed.

M7.162

PREPARATION AND PROPERTIES OF HIGH T_c YBCO POLY-CRYSTAL THIN FILMS BY IN-SITU METHOD. N.Harada, K.Satou, K.Yamamoto, YOKOHAMA R&D LABORATORIES, FURUKAWA ELECTRIC Co.Ltd., 2-4-3, Okano, Nishi-ku, Yokohama, 220 Japan

In order to fabricate the high T_c superconductor films onto metal substrates, (a) in-situ process without post annealing is indispensable for suppress the diffusion of metallic elements from substrates to films. (b) While the films on the metal substrate is likely to be poly-crystalline, high J_c poly-crystal films should be a first milestone in course of the development of flexible conductors and so on.

We prepared high T_c YBCO films by co-evaporating method for in-situ process. MgO single crystal was used for the substrates and it was kept at 650-750 °C in the ozone pressure of 10^{-5} - 10^{-6} Torr during the film growth. After the evaporation, the substrate heater was turned off at about 2Torr ozone pressure in order to promote the oxidation of the film. Tests were done comparatively by using other oxygenating gases.

TEM and RHEED studies showed that the films were poly-crystalline and the direction of the a,b axes were not according to that of MgO substrate. Conventional DC transport measurements showed that the zero-resistance T_c was 85K and the critical current density J_c was up to 7×10^4 A/cm² at 77K. This suggests the possibility of fabricating the high J_c poly-crystal films on metal substrate. Details on analyses of will be provided.

This study was conducted on the collaboration basis with Tokyo Electric Power Co.Ltd.

M7.163

ELECTROPHORETIC DEPOSITION OF HIGH-TEMPERATURE SUPERCONDUCTOR THICK FILMS. J.B. Mooney, A. Sher, M.L. Riggs, K.A. Sabo, A. Rosengreen, B. Kingsley, and J.C. Terry, SRI International, 333 Ravenswood Ave., Menlo Park, CA 94025.

Thick films of high-temperature superconductors have been in the past prepared by spraying, spinning, settling, spreading, screen printing, and electrophoresis. Most of these processes make use of preprepared superconducting powders; consequently, advances in superconductivity are immediately adaptable to the process.

SRI has used electrophoretic deposition (as developed for liquid-toned office copiers) to form films that are denser than those created by other means; this is because our highly charged particles are driven onto the substrates by high fields ($< 5 \times 10^5$ V/cm). The substrates can be silver or nonmetallic (e.g., ZrO_2) with a thin silver layer to function as an electrode. We are also able to deposit on thin dielectric films on conductors, either by applying voltage to the conducting substrate or by charging the surface. The films can be patterned to micrometer dimensions and submicrometer tolerances through electrostatic latent images, patterned electrodes, or electron-beam exposure of the binder that functions as an electron resist. The binder that provides smear protection in office copying also aids in charge direction and lends green strength to the deposit for convenient post-deposition processing.

Experiments with $YBa_2Cu_{(7-x)}$ films and magnetic orientation studies are discussed.

M7.164

THE FABRICATION OF $YBa_2Cu_3O_7$ THIN FILMS BY PHYSICAL VAPOR DEPOSITION. De Hua Chen, R. L. Sabatini, and H. Wiesmann, Materials Science Division, Brookhaven National Laboratory, Upton, NY 11973.

A series of thin films of $YBa_2Cu_3O_7$ were fabricated by the technique of Physical Vapor Deposition (PVD). PVD is an attractive deposition technique which has not been described in the literature. A high vacuum stainless steel chamber, with three individual thermal sources was constructed. Tungsten metal boats were used for the evaporation of yttrium and barium and an aluminum oxide coated basket was used for the evaporation of copper. A quartz crystal rate monitor and high current silicon controlled rectifier (SCR) was associated with each source allowing the depositions to be automatically controlled in a negative feedback loop configuration. The barium and copper sources exhibited long operating lifetimes. The lifetime of the yttrium source was limited by the oxygen partial pressure in the evaporation chamber. During the depositions oxygen gas was admitted into the chamber at a pressure of $\sim 5 \times 10^{-5}$ Torr and evaporation rates of a few angstroms per second were typical. Films have been successfully deposited on both aluminum oxide and yttrium stabilized zirconia substrates. T_c onsets of ~ 80 K and ~ 90 K have been achieved on these substrates respectively. The morphology of these films has been characterized by SEM photomicrographs and X-ray diffraction. Data is also presented describing the quality of the superconducting transition.

This work was supported by the U.S. Department of Energy, Division of Materials Sciences, under Contract No. DE-AC02-76CH00016.

M7.165

ORIENTED MICROSTRUCTURE OF $YBa_2Cu_3O_{7-x}$ THICK FILMS. F. Wellhofer, T.C. Shields, J.S. Abell, K.N.R. Taylor, School of Metallurgy and Materials, University of Birmingham, U.K. and D. Holland, School of Physics, University of Warwick, U.K.

The fabrication of screen printed superconducting thick films of YBCO on zirconia substrates is described. Processing close to the peritectic transition has produced highly oriented microstructures induced by partial melting and subsequent nucleation and growth. These films exhibit enhanced superconducting properties with critical current densities in excess of 500 Acm^{-2} at 77 K. The influence of sinter temperature and time, oxygen partial pressure and cooling rates on the prevailing microstructure has been studied. The role of the interfacial reaction layer in determining the solidification behaviour is assessed.

M7.166

THE SPUTTER DEPOSITION AND CHARACTERISATION OF EPITAXIAL MAGNESIUM OXIDE THIN FILMS AND THEIR USE AS A SAPPHIRE/YBCO BUFFER LAYER. G.W. Morris, R.E. Somekh, Z.H. Barber and J.E. Evetts, Interdisciplinary Research Centre in Superconductivity, West Site, Madingley Road, Cambridge, England and Department of Materials Science and Metallurgy, New Museums Site, Pembroke Street, Cambridge, England.

Sapphire has dielectric properties that make it attractive as a substrate for superconducting electronic applications. It is difficult, however, to form high quality yttrium barium copper oxide (YBCO) on sapphire because of reaction with the substrate and because epitaxy is not readily achieved. We have deposited thin films of magnesium oxide, by UHV reactive d.c. magnetron sputtering, on M (10 $\bar{1}$ 0), R (10 $\bar{1}$ 2), C (0001), and A (11 $\bar{2}$ 0) -plane sapphire substrates, initial results on the development of a suitable epitaxial (110) on M-plane buffer layer being reported at [1]. The orientational relationships of sapphire and magnesia and the nature and microstructure of their interfaces are reported as a function of substrate type and temperature, of deposition rate and conditions and of post deposition treatment. The results of investigation of these films as a buffer between sapphire substrates and subsequently deposited thin films of YBCO are reported.

[1] "Optimisation of thin film $\text{YBa}_2\text{Cu}_3\text{O}_x$ deposition by d.c. sputtering onto sapphire substrates." E J Tomlinson *et al IEEE Trans. Magn.* 25 (1989) 2530 - 2533.

M7.167

$\text{Y}_1\text{Ba}_2\text{Cu}_3\text{O}_{7-x}$ FILMS FROM NITRATE SOLUTION USING RF PLASMA DEPOSITION. A. Shah, T. Haugan, S. Witanachchi, S. Patel and D. T. Shaw, Institute on Superconductivity, State University of New York at Buffalo, Bonner Hall, Buffalo, NY 14260

A nitrate solution of Y, Ba and Cu was atomized and introduced into an inductively coupled argon-oxygen plasma operated at 3 to 7 kw at 13.56 MHz under atmospheric pressure. As-deposited superconducting films were grown on (100) YSZ substrates heated to 650°C. Critical temperatures of 82K and critical current density of 4.5×10^3 amp/cm² at 40K have been achieved. X-ray diffraction show the films to be oriented c-axis perpendicular to the substrate surface. The effects of solution composition, aerosol concentration, rf power and substrate temperatures on the superconducting properties and microstructures will be discussed.

M7.168

IN SITU PREPARATION OF Y-Ba-Cu-O SUPERCONDUCTING THIN FILMS BY DC-MAGNETRON SPUTTERING

L.F.Chen, L.Zhou, S.J.Pang, Y.H.Kuo, L.Li, B.R.Zhao, and Y.Z.Zhang, Beijing Laboratory of Vacuum Physics, Academia Sinica; General Research Institute of Non-ferrous metals, Beijing, China; Department of Physics, Peking University, Beijing, China; Institute of Physics, Academia Sinica, Beijing, China.

Y-ba-cu-o thin films have been epitaxially grown by dc-magnetron sputtering. The epitaxial orientation were varied by controlling substrate temperature, oxygen partial pressure and The substrate orientation is not facing the cathode. Optimum preparation condition were a low discharge(120v), a high oxygen partial pressure in an oxygen argon mixture($\text{Ar}/\text{O}_2=2:1$) and substrate temperatures at 785°C. The compositional and structural properties were determined by X-fluorescence and X-ray diffraction. The films exhibit zero resistance at 90k. The supercurrent at 78k has reached $8.9 \times 10^5 \text{A}/\text{cm}^2$.

M7.169

MULTILAYER E-BEAM DEPOSITION AND ANNEALING OF $\text{YBa}_2\text{Cu}_3\text{O}_{7.8}$ THIN FILMS ON LaGaO_3 SUBSTRATES. Richard DeVito, Brian G. Pazol, John H. Chaffin, Litton/Itek Optical Systems, Lexington, MA; Roger F. Belt and Robert Uhrin, Litton/Airtron, Morris Plains, NJ.

Thin films of $\text{YBa}_2\text{Cu}_3\text{O}_{7.8}$ have been deposited on samples of LaGaO_3 substrates by multilayer E-beam evaporation. Alternating layers of Cu, Y_2O_3 , and BaF_2 were deposited on polished (100) substrates. An annealing study was performed to thoroughly blend the layers and minimize substrate interdiffusion. Films were prepared by annealing in wet oxygen at temperatures between 800 °C and 1000 °C.

Four point resistance versus temperature curves were obtained to determine the superconducting transition temperature and transition width. Critical current measurements and I-V curves were also made in addition to resistivity measurements to give better determination of sample quality.

Auger depth profiling was performed as a function of annealing cycle to determine the amount of blending of the layers and quantify any substrate diffusion. Since LaGaO_3 is a close lattice match to $\text{YBa}_2\text{Cu}_3\text{O}_{7.8}$, SEM and x-ray diffraction studies were used to reveal the crystallographic and epitaxial qualities.

M7.170

PREPARATION OF $\text{YBa}_2\text{Cu}_3\text{O}_x$ SUPERCONDUCTING THIN FILMS BY MEANS OF SINGLE TARGET RF-SPUTTERING. H. Weyten, University of Antwerp (UIA), Dep. of Chemistry, 2610 Wilrijk, Antwerp, Belgium; R. De Batist, P. Nagels, University of Antwerp (RUCA), 2020 Antwerp, Belgium; J. Cornelis, SCK/CEN, Materials Development Dep., 2400 Mol, Belgium.

High T_c superconducting thin films have been deposited on sapphire (single crystal Al_2O_3) by means of RF-sputtering from a single stoichiometric target of $\text{YBa}_2\text{Cu}_3\text{O}_x$ composition. The $\text{YBa}_2\text{Cu}_3\text{O}_x$ films were grown in an argon-oxygen atmosphere on a substrate which reached a temperature of $\pm 400^\circ\text{C}$ during deposition.

The study of stoichiometry and homogeneity of the as-deposited films, by means of electromicroprobe analysis (EMPA) was used to optimize the sputtering parameters of the system.

To achieve superconductivity, with an onset of ± 90 K, a high temperature, post-deposition thermal treatment in oxygen is necessary. Resistivity measurements show that the temperature at which zero resistivity is reached, is lower with respect to the bulk samples ($T_c(R=0)=89$ K) as a result of interaction with the substrate.

Following thermal treatment, the superconductive films were further analysed by SEM/EDX and EMPA in order to determine stoichiometry, homogeneity and texture. The results were used to optimize the conditions for thermal treatment of the films.

* Work supported in part by the Belgian Government (IUAP-Programme Antwerp)

M7.171

RAPID CHEMICAL VAPOR DEPOSITION OF $\text{YBa}_2\text{Cu}_3\text{O}_x$ COATINGS. W.J. Lackey, W.B. Carter, D.N. Hill, E.K. Barefield, J.A. Hanigofsky, M.J. Shapiro, T.S. Moss III, A.J. Green, and D.F. O'Brien, Georgia Institute of Technology, Atlanta, GA 30332; and R.A. Jake and K.R. Efferson, American Magnetics, Inc., Oak Ridge, TN 37831.

Chemical vapor deposition (CVD) is extensively used commercially for preparation of numerous electronic, optical, tribological, and chemically protective coatings. Compared to other coating processes CVD is often faster, yields higher quality, more adherent films, and can be used to coat multiple irregularly shaped substrates. About a dozen investigators have reported on the CVD of superconducting $\text{YBa}_2\text{Cu}_3\text{O}_x$. Some of these films have very high critical current densities ($\sim 10^5 \text{A}/\text{cm}^2$) even in strong magnetic fields. Typical reagents have been metal complexes of various β -diketonate ligands. These are solids at room temperature which slowly sublime when heated to $\sim 100\text{-}300^\circ\text{C}$; the vapor is then swept into the CVD system by a carrier gas. Without exception, however, the very low vapor pressure of the Y, Ba, and Cu precursor reagents has restricted deposition rates to low values, e.g., $1 \mu\text{m}/\text{h}$. Furthermore, the vapor pressures of the precursors are strongly dependent on temperature and are subject to change as a result of thermal-environmental induced degradation during sublimation. Hence, process control and repeatability are unusually poor.

A rapid, controllable process for CVD of superconducting $\text{YBa}_2\text{Cu}_3\text{O}_x$ has been developed. The new process relies on slowly feeding and pneumatically transporting powdered solid reagents directly into the CVD furnace; a vaporizer is not used. Deposition rates two orders of magnitude greater than those achievable by reagent sublimation have

been obtained using a powder feed mixture of Y, Ba, and Cu TMHD complexes (TMHD is tetramethylheptanedionate). Potentially, the process is applicable to thermally unstable, less volatile lower cost reagents such as the acetates.

This work was supported by Dr. Kay R. Adams of DARPA and Dr. Wallace A. Smith of ONR under Contract Number N00014-88-C-0615.

M7.172

LOW TEMPERATURE GROWTH OF SUPERCONDUCTING $\text{YBa}_2\text{Cu}_3\text{O}_{7-x}$ THIN FILMS BY METALORGANIC CHEMICAL VAPOR DEPOSITION. Keiichi Kanehori, Nobuyuki Sugii and Katsuki Miyauchi, Central Research Laboratory, Hitachi, Ltd., Tokyo, Japan.

Metalorganic chemical vapor deposition (MOCVD) is thought to be one of the most desirable methods to grow oxide superconductor thin films because it has high composition controllability, high reliability and high productivity. However, a concerted effort is required to decrease deposition temperature in order to apply MOCVD in microelectronics processes. This paper reports influence of deposition temperature on crystallographic and electrical properties of Y-Ba-Cu-O thin films.

Thin films were grown by a low pressure MOCVD apparatus in the temperature range from 550 °C to 800 °C. β -diketonate complexes of Y, Ba and Cu were employed as source materials.

Thin films grown in the temperature range from 550 °C to 800 °C had the orthorhombic $\text{YBa}_2\text{Cu}_3\text{O}_{7-x}$ structure. However, thin film grown at 550 °C showed semiconductive electrical properties. The superconducting transition was observed for the films grown above 600 °C. The onset temperature for these films agreed with around 90 K. On the other hand, the zero resistivity temperature depended on deposition conditions. The zero-resistivity temperatures for the films grown at 600 °C, 650 °C and 700 °C were 11 K, 71 K and 83 K, respectively.

M7.173

PARTIAL REDUCTION - REOXIDATION PROCESSING OF Y-Ba-Cu-O SPUTTERED THIN FILMS. F. H. Garzon, J. G. Beery, D. K. Wilde and I. D. Raistrick, Los Alamos National Laboratory, NM.

Thin films of Y-Ba-Cu-O were produced by rf sputtering of $\text{YBa}_2\text{Cu}_3\text{O}_{7-x}$ ceramic targets, using a variety of plasma compositions, pressures, rf power levels, and substrate temperatures. Post-annealing of these films in oxygen produced superconducting films with T_c values between 40-60 K, broad transition widths and semiconductor-like electrical behavior above T_c . Subsequent annealing at 850°C in an inert gas with a residual oxygen pressure of -10 ppm followed by an oxygen anneal produced high quality thin films: $T_c > 85$ K with narrow transition widths. The structure and morphology of these films during this reduction-oxidation processing were studied using X-ray diffraction and electron microscopy.

M7.174

COMPOSITIONAL CONTROL OF Y-BA-CU-O FILMS EMPLOYING A SINGLE OXIDE TARGET. A.J. Drehman, J.A. Horrigan, M.W. Dumais, B.L. MacDonald, R.J. Andrews, P.M. Tedrow* and M.N. Alexander Solid State Sciences Directorate Rome Air Development Center Hanscom AFB, MA 01731

Superconducting films were fabricated by R-F diode sputtering from a single Y-Ba-Cu oxide target that was both Ba and Cu rich. By controlling the sputter deposition parameters we were able to control the film composition as determined by EDX and X-ray diffraction. A particularly useful parameter is the bias of the substrate table. By applying a small negative bias, the film uniformity is improved and, more importantly, back-sputtering is reduced. By controlling bias, sputter gas pressure and oxygen content, target-substrate separation, target voltage and substrate temperature, we find that a single oxide target can be used to produce stoichiometric $\text{YBa}_2\text{Cu}_3\text{O}_x$ films under various processing conditions. Resulting microstructures, superconducting transitions and critical currents are presented.

*MIT Francis Bitter National Magnet Laboratory. AFSC University Resident Research Fellow at RADC

M7.175

SPRAY PYROLYSIS TECHNIQUE FOR THE DEPOSITION OF SUPER CONDUCTING FILMS. Marc Soller, Larry P. Moy and Michael R. Squillante, Radiation Monitoring Devices, Inc., Watertown, MA 02172, and James Marzik, U.S. Army Materials Technology Laboratory, Watertown, MA 02172.

Research has been performed on the use of chemical spray pyrolysis for depositing thin and thick films of superconducting YBCO. The effects of reagent concentration, deposition rate, substrate temperature and substrate type were investigated. Superconducting films from 0.5 to 10 microns thick were deposited on single crystal strontium titanate, polycrystalline alumina and Type 304 stainless steel. The films have been characterized for their physical and superconducting properties.

M7.176

$\text{YBa}_2\text{Cu}_3\text{O}_x$ THIN FILMS PREPARED BY MULTILAYER DEPOSITION.* Valentin Garcia-Vazquez and Charles M. Falco, Department of Physics, Optical Science Center and Arizona Research Laboratories, University of Arizona, Tucson, AZ 85721

We have used a combination of BaF₂ evaporation and DC triode sputtering of Y and Cu to produce high temperature superconducting thin films. Post-annealed films on single crystal SrTiO_3 (100) substrates exhibit a 92 K superconducting onset. Rutherford backscattering spectroscopy was used to analyze the stoichiometry of films deposited on carbon substrates. X-ray diffraction on post-annealed films shows preferential orientation of the c-axis. Annealing conditions to optimize the superconducting properties will be reported. We are also studying the annealing conditions for other substrates, such as sapphire, MgO and YSZ.

*Supported by the U. S. Department of Energy under contract No. DE-FG02-87ER45297. One of us (V. G.-V.) has benefited from a CONACYT-Mexico fellowship.

M7.177

HIGHLY ORIENTED $\text{YBa}_2\text{Cu}_3\text{O}_{7-x}$ THIN FILMS PREPARED BY UNBALANCED DC MAGNETRON SPUTTERING FROM SINGLE STOICHIOMETRIC TARGET. N. Savvides, D.V. Hensley, C. Andrikidis, R. Driver and J.C. Macfarlane, CSIRO Division of Applied Physics, Sydney 2070, Australia; N.X. Tan and A.J. Bourdillon, University of New South Wales, Sydney 2033, Australia.

Resputtering of material from the film surface during deposition has been a persistent problem in conventional dc and rf single-target sputtering systems. Energetic heavy particles (ions and neutrals), arising from the plasma or produced at the cathode, bombard the growing film causing preferential resputtering of Ba and Cu and consequently alter its composition. We have attacked this problem by altering the sputtering process of dc magnetrons.

Thin films of $\text{YBa}_2\text{Cu}_3\text{O}_{7-x}$ were reproducibly prepared with metal stoichiometry close to 1-2-3 by dc magnetron sputtering from a single stoichiometric target. To circumvent the resputtering effects, the magnetron used an unbalanced magnetic field configuration to direct the plasma away from the substrate. Energy dispersive spectroscopy was used to determine the composition of as-deposited and post-annealed films. Highly oriented films with the c-axis perpendicular to the film plane were obtained by depositing onto $\text{MgO}(100)$, $\text{YSZ}(100)$ and $\text{SrTiO}_3(100)$ substrates followed by post-annealing at 850-950 °C in flowing oxygen. The best films have $T_c=91-93$ K, sharp transition width $\Delta T_c(90\%-10\%)=0.5$ K, and metallic resistivity above the transition with resistivity ratio $\rho_{300}/\rho_{100}=2-3$. The critical current density J_c , measured on unpatterned films 2-5 mm wide and 12 mm long, was 1.5×10^5 A cm^{-2} at 77 K and 1.5×10^6 A cm^{-2} at 4.2 K.

M7.178

CRUCIBLELESS LIQUID PHASE GROWTH OF (00L) YBaCuO FILMS ON POLYCRYSTALLINE SUBSTRATES. K.C. Chen, L.H. Perng, T.S. Chin, C.P. Perng, C.M. Wu, T.B. Wu, and C.H. Lin, Dept. of Materials Sci. & Eng., National Tsing Hua Univ., Hsinchu, Taiwan, R.O.C.

Oxide superconductor thin films can be fabricated by liquid phase growth (LPG) using suitable fluxes. However, the extremely reactivity of the melt with crucible limit the availability. In this study, a crucibleless method of growing YBaCuO thin films by LPG is successfully developed.

Pellets of suitable weight composed of raw constituents were put onto a polycrystalline alumina substrate. After liquifying at 1100 °C for 10 min., they were cooled down at different rates to around 960 - 930 °C (depending on composition), the substrate holder was turned 90° over to let the melt flow. Thin and thick films were thus obtainable.

All the thin and thick films showed very strong (00L) orientation of the 123 superconducting phase on rough 96% alumina substrates, dense polished 99% alumina substrates, and MgO single crystals, if suitable buffer layer(s) was applied. $T_{c,0}$ of 60 °K was routinely obtainable from 96% alumina substrate coated with Au then 2115 underlayers. Higher T_c is available using MgO single crystal with thin Au underlayer. Detailed microstructure and processing parameters relating to orientation growth superconducting properties are discussed.

Part of binary phase diagram of the $\text{YBa}_2\text{Cu}_3\text{O}_7 - \text{BaCuO}_2$ system was constructed.

M7.179

HIGH T_c SUPERCONDUCTOR FILMS GROWN BY THE LPE TECHNIQUE. A.S. Yue and C.S. Yang, Department of Materials Science & Engineering, University of California, Los Angeles, CA 90024-1595.

High T_c $\text{YBa}_2\text{Cu}_3\text{O}_7$ and Bi-Ca-Sr-CuO Superconductor films have been grown by the liquid-phase-epitaxial (LPE) technique. The success in growing these films is based on detailed determinations of the peritectic portions of the pseudo-binary phase diagrams in the $\text{Y}_2\text{O}_3\text{-CuO-BaO}$ and $\text{Bi}_2\text{O}_3\text{-CuO-(SrCa)O}$ ternary systems. The LPE-grown films on sapphire and silicon substrates were prepared by cooling the off-peritectic melts from 1050°C to 950°C and from 890°C to 870°C at an average rate of 10°C per hour.

Representative X-ray diffraction patterns of the LPE-grown $\text{YBa}_2\text{Cu}_3\text{O}_7$ and Bi-Ca-Sr-CuO films on sapphire substrates show the existence of two split (013) and (103) peaks at $2\theta = 32.6^\circ$ and 32.8° , respectively. This indicates that these films have orthorhombic crystal structures of the $\text{YBa}_2\text{Cu}_3\text{O}_7$ and BCSCO phases in agreement with those reported previously. Plots of resistance against temperature for LPE-grown films without post-annealing show that the resistances decrease linearly from room temperature to 90°K and 110°K, respectively. Below these temperatures, they deviate from linearity with a downward curve to a zero-resistance value of 78°K for the $\text{YBa}_2\text{Cu}_3\text{O}_7$ film and 80°K for the BCSCO film. To substantiate these critical temperatures at $R=0$ data, we have performed the a.c. susceptibility versus temperature experiments on the LPE-grown films. It was found that their transition temperatures are also near 80°K in good agreement with the resistivity versus temperature data.

M7.180

PREPARATION OF Y-Ba-Cu-O HIGH T_c SUPERCONDUCTING FILMS BY PLASMA-ENHANCED ORGANOMETALLIC CHEMICAL VAPOR DEPOSITION. J. Zhao, L. M. Tonge, H. O. Marcy, B. W. Wessels, T. J. Marks and C. R. Kannewurf, Materials Research Center and Science and Technology Center for Superconductivity, Northwestern University, Evanston, IL 60208

A plasma-enhanced organometallic chemical vapor deposition process for the preparation of $\text{YBa}_2\text{Cu}_3\text{O}_7$ thin films using the volatile metal-organic precursors $\text{Y}(\text{dipivaloyl-methanate})_3$, $\text{Ba}(\text{dipivaloyl-methanate})_2$, and $\text{Cu}(\text{acetylacetonate})_2$ has been developed. At deposition temperatures as low as 650°C, as-deposited films show formation of the crystalline 1-2-3 phase along with other impurity phases, as indicated by the x-ray diffraction patterns. Auger electron spectroscopy indicates that the films have a very low carbon content. Superconducting films with c axes oriented perpendicular to the yttria-stabilized zirconia (YSZ) substrate surface were obtained after appropriate post-annealing.

M7.181

SUPERCONDUCTING $\text{YBa}_2\text{Cu}_3\text{O}_{7-y}$ THIN FILM ON METAL SUBSTRATE BY CHEMICAL VAPOR DEPOSITION PROCESS T. Yamaguchi, S. Aoki, N. Sadakata and O. Kohno, Tokyo Laboratory, Fujikura Ltd., Tokyo 135, Japan

Formation of Y-Ba-Cu-O thin film by chemical vapor deposition (CVD) process has been investigated. Application of the high- T_c superconducting materials for conductor requires uniform formation of the substance. The material has some intrinsic properties such as anisotropic current flow and weak links at grain boundaries which may result large reduction of the transport J_c , therefore it is necessary to eliminate these defects. Thin film fabricating methods are favorable because highly oriented and clean grain boundaries could be obtained. Among these methods, CVD

process is advantageous because the deposition rate is larger than the other thin film processes. In this study, superconducting $\text{YBa}_2\text{Cu}_3\text{O}_{7-y}$ thin films have been prepared by CVD process using beta-diketonate chelates of Y, Ba and Cu on both single-crystalline SrTiO_3 substrates and metal substrates. As-deposited film on SrTiO_3 showed poor superconducting properties with low T_c , though consequent annealing improved the zero-resistive T_c at 89K. The film on metal substrate with SrTiO_3 buffer layer also showed good superconductivity of zero resistance at 85K. These films had (110) orientation to the basal plane. The growth rate of the films was quite fast about 30 microns per hour or more.

M7.182

SUPERCONDUCTING HIGH T_c THIN FILMS PREPARED BY LASER DEPOSITION: COMPARISON OF LASER SOURCES.
L. Lynds, B. R. Weinberger, G. G. Peterson and D. M. Potrepka, United Technologies Research Center, E. Hartford, CT 06108.

Pulsed laser ablation of targets to produce high quality superconducting thin films is being performed in many laboratories. Properties of deposited superconducting materials depend critically on the nature of laser radiation used in the ablation process and on the intervening reaction conditions. We have observed significant differences in the ablation process between a free-running Nd:YAG laser (1064 nm) and an excimer (248 nm) laser equipped with unstable resonator optics. It was then possible to compare effects of pulse dynamics within the same range of fluence (1 - 100 J/cm²). Ablation occurs through threshold-dependent interactions with the targets and produces a non-equilibrium distribution of energy amongst ejected atoms and molecules appearing, primarily, in translation energy (1 - 15 eV). The angular distribution of product states suggests that the coupling of the optical radiation to the target may proceed through stimulated Brillouin scattering. Effects of optical parameters on the nature of thin film morphology/structure and superconductivity will be discussed.

M7.183

IN-SITU GROWTH OF $\text{YBa}_2\text{Cu}_3\text{O}_x$ BY LASER ABLATION*. D. K. Fork^{1,2}, K. Char³, J. B. Boycel¹, F. Bridges^{1,4}, G. A. N. Connell¹, and T. H. Geballe². (1) Xerox Palo Alto Research Center, Palo Alto, CA 94304; (2) Dept. of Appl. Phys, Stanford Univ., Stanford, CA 94305; (3) Conductus, Inc., Sunnyvale, CA 94086; (4) Physics Dept., Univ. of California, Santa Cruz, CA 95064.

$\text{YBa}_2\text{Cu}_3\text{O}_x$ has been grown *in-situ* on Al_2O_3 (1102) by laser ablation. The effects of oxygen pressure and substrate temperature on the growth of $\text{YBa}_2\text{Cu}_3\text{O}_x$ were studied. Substrate temperature and laser energy density play important roles in getting well-oriented $\text{YBa}_2\text{Cu}_3\text{O}_x$ thin films with the c-axis perpendicular to the substrate. Typical resistivity curves shows $\rho \sim 300 \mu\Omega\text{-cm}$ at 300K and $\rho \sim 120 \mu\Omega\text{-cm}$ at 100K. The superconducting transition width is less than 1K and T_c is a little depressed to 87K. Compositional and structural differences for *in-situ* $\text{YBa}_2\text{Cu}_3\text{O}_x$ thin films on other substrates such as MgO , YSZ , SrTiO_3 and LaAlO_3 will be also presented as well as studies of grain boundary defects and interface defects using x-ray

diffraction, TEM, and compositional analysis. The in-plane epitaxial relationships will be discussed in terms of both deposition parameters and the electrical transport properties, such as the resistivity and the critical current density.

* Supported in part by the Air Force Office of Scientific Research under Contract F49620-89-C-0017.

M7.184

VERSATILE LASER DEPOSITION CHAMBER FOR IN-SITU FABRICATION OF BUFFER LAYERS AND SUPERCONDUCTING THIN-FILMS.
B.E. Russo, R.P. Reade, and J.M. McMillan, Mail Stop 90-2024, Lawrence Berkeley Laboratory, Berkeley, CA 94720, and B.L. Olsen, Lawrence Livermore National Laboratory, L-350, Livermore, CA 94550.

Pulsed laser deposition is a demonstrated technique for the fabrication of thin-film high temperature superconductors. The films are normally deposited on single crystal substrates placed several centimeters from the bulk target material. We have developed a deposition chamber with the capability of rotating four bulk materials separately into the path of an excimer laser beam. The target holder allows in-situ laser deposition of several materials without exposing the chamber (and films) to the atmosphere between layers. Using this system, we have deposited buffer layers of several materials before depositing the superconducting films. In addition, protective cover layers have been deposited over the superconducting film without removing the film from the clean chamber environment. As-deposited superconducting thin-films have been deposited on laser-deposited metal layers. For example, YBCO films have been deposited on Ag buffer layers. The silver films were laser deposited on MgO immediately before the YBCO film. The deposition parameters for metal buffer layers have been optimized and are significantly different than those employed for the superconducting material. A description of the system and results for several metal buffer layers and multilayered film compositions will be described.

M7.185

IN-SITU LASER DEPOSITION OF $\text{YBa}_2\text{Cu}_3\text{O}_{7-\delta}$ AND $\text{HoBa}_2\text{Cu}_3\text{O}_{7-\delta}$ HIGH- T_c SUPERCONDUCTING THIN FILMS ON Si (100) AND KTaO_3 (100). A.K. Singh, C. Lee, J. Narayan, Department of Materials Science and Engineering, Raleigh, N.C. 27695-7916; L.A. Boatner, Ceramics and Interface Section, Oak Ridge National Laboratory, Oak Ridge, TN 37831.

We have developed a biased laser deposition method for the in-situ deposition of High- T_c superconducting $\text{YBa}_2\text{Cu}_3\text{O}_{7-\delta}$ and $\text{HoBa}_2\text{Cu}_3\text{O}_{7-\delta}$ thin films on Si (100) and KTaO_3 (100) substrates. The deposition was aimed towards the growth of textured film on Si and epitaxial film on KTaO_3 . The lattice parameter of the superconductor ($a \approx 3.85\text{\AA}$) and KTaO_3 ($a=3.99\text{\AA}$) are close to each other. A XeCl excimer laser ($\lambda=308\text{nm}$) was used with pulse duration of ~ 40 ns. The energy density of the laser impacting the target was adjusted to be 2.5 J/cm^2 . The deposition was done in a precleaned chamber with an oxygen atmosphere at 200 mT. The target and substrate were parallel and 4.85 cm apart. For lower temperature (500-550°C) depositions, an electrically biased (+300 V) metallic ring was used to accomplish deposition. The ring was placed at a distance of 0.6 cm from the target. The nature of epitaxial and textured growth was determined by X-ray diffractometry, transmission electron microscopy, and Rutherford Backscattering techniques. The films were textured with 'c' axis perpendicular to the plane of the film. The transition temperature T_c was determined by resistivity vs temperature measurements using conventional four-probe method. The T_c values ($R=0$) for superconducting films on KTaO_3 was ~ 84 K and 77 K for films deposited

on Si. The J_c values of the films were determined by patterning the film by covering the substrate with a suitable mask. The details regarding the above results will be discussed.

M7.186

LONG-LASER-PULSE METHOD OF PRODUCING Y-Ba-Cu-O SUPERCONDUCTING FILMS. R. E. Russo, M. Balooch and D. R. Olander, University of California and Lawrence Berkeley Laboratory, Berkeley, CA.

Deposition of superconducting thin films from $\text{YBa}_2\text{Cu}_3\text{O}_x$ target using a long-pulse (ms) Nd-glass laser with 50 J/pulse energy has been demonstrated. The deposition rate was approximately 100 nm/pulse. A film produced by four pulses on a SrTiO_3 substrate, held at 540 °C, and post-annealed at 850 °C for about two hours exhibited an onset transition at 78K and zero resistance at 61K. The angular distribution up to 40° with respect to normal was diffuse with and no significant variation in composition. Scanning electron microscopy showed no cracks but revealed spherical inclusions on the order of microns in the film. Scanning tunneling microscopy in air showed a terrace-ledge structure with about 12 Å height on the uniform portion of the film.

Evaporated species and their velocity distributions of the laser-target interaction were obtained by a quadrupole mass spectrometer utilizing time-of-flight technique. The time dependence of the target temperature was monitored by a fast optical pyrometer. Among the detectable molecules by the mass spectrometer were Cu, Ba, Y, BaCuO and YBaO_2 . Low-energy laser pulse generated neutrals only. At high energies neutrals and ions were emitted from the target.

M7.187

IN-SITU DEPOSITION OF HIGH TEMPERATURE SUPERCONDUCTORS ON LaAlO_3 SUBSTRATES.

P. Tiwari, A.K. Singh, C.B. Lee and J. Narayan, Department of Materials Science and Engineering, North Carolina State University, Raleigh, N.C. 27695-7916.

Excellent quality $\text{YBa}_2\text{Cu}_3\text{O}_{7.8}$ superconducting thin films have been fabricated in-situ on low dielectric constant Lanthanum Aluminate substrate (cubic, $a = 3.79 \text{ \AA}$, dielectric constant=16) using pulsed laser ablation ($\lambda=308\text{nm}$, $t = 45 \text{ ns}$, energy $> 2.5 \text{ J cm}^{-2}$). The films on LaAlO_3 were fabricated at different oxygen partial pressure (100 - 200 mTorr) and substrate temperatures (500-650°C). The epitaxial nature and crystallinity of the film were analyzed by X-ray diffraction, transmission electron microscopy, and Rutherford backscattering spectrometry. The transition temperature, T_c , was determined by resistivity vs temperature measurements using conventional four-probe method and the films exhibited excellent superconductivity with zero resistance at about 90K. The films were patterned by covering the substrate with a suitable mask for critical current density measurements. The details of microstructures and chemical compositions will be correlated with superconducting properties.

M7.188

PULSED LASER DEPOSITION OF HIGH- T_c SUPERCONDUCTING THIN FILMS. M. Grant Norton, Lisa A. Tietz, C. Barry Carter Department of Materials Science and Engineering, Stephen E. Russek and Robert A. Buhrman, School of Applied and Engineering Physics, Cornell University, Ithaca, NY 14853.

Smooth, high- T_c thin films of Y-Ba-Cu-O have been deposited by pulsed laser evaporation of stoichiometric bulk samples. The films were deposited onto (001)-oriented MgO and (001)-oriented SrTiO_3 in an oxygen ambient using a pulsed XeF excimer laser. Superconducting films could be deposited at substrate temperatures from 580-700°C. The films, which were between 200-300 nm thick, had critical temperatures above 80K. In addition to describing the experimental techniques, film characterization is reported. The surface morphology was examined using scanning electron microscopy (SEM). Film composition was determined using x-ray diffraction (XRD) and Rutherford backscattering

spectroscopy (RBS). The microstructures of the films including grain-boundary structures and film-substrate interfaces have been studied by examination of cross-sectional and plan view samples using transmission electron microscopy (TEM).

M7.189

UNIFORMITY CONSIDERATIONS OF "IN-SITU" LASER-ABLATED $\text{Y}_{1.2}\text{Ba}_{2.0}\text{Cu}_{3.0}\text{O}_x$ FILMS OVER THREE INCH WAFERS. James A. Greer and Jerrold Van Hook, Raytheon Research Division, Lexington, MA

This paper will discuss the uniformity of a variety of properties of "in-situ" laser-ablated $\text{Y}_{1.2}\text{Ba}_{2.0}\text{Cu}_{3.0}\text{O}_x$ thin films deposited on three inch wafers. A novel deposition chamber has been developed which incorporates a programmable mirror which allows us to raster a focused excimer laser beam (248 nm) over a radii of a rotating 3.5 inch stoichiometric target. The substrate is also rotated and sits 12.7 cm above the target. Thickness uniformity of $\pm 5\%$ over three inch wafers has been demonstrated. The composition uniformity is better than $\pm 1\%$ as determined by EDX, and the nominal metal ion composition is $\text{Y}_{1.2}\text{Ba}_{2.0}\text{Cu}_{3.0}$.

In order to grow films "in-situ" the system incorporates an RF atomic oxygen source capable of producing fluxes of over 10^{18} atoms/cm² at the substrate surface given the source efficiency and chamber pumping speed. Typical growth parameters are a laser pulse rate of 20 PPS yielding an average growth rate of 0.5 $\mu\text{m}/\text{hour}$. Growth temperatures are about 575 °C yielding films with a high degree of \hat{c} -axis orientation. The best films grown to date have been on 3 inch (1102) sapphire wafers. The uniformity in the room temperature resistivity of these films is $1.1 \pm 0.1 \text{ m}\Omega\text{-cm}$. The films are weakly metallic in behavior and the temperature of zero resistance varies from 65 K at the outer edge of the wafer to 45 K in the center. The effects of a variety of buffer layers such as MgO and ZrO_2 on the HTS film properties will also be discussed.

This work is the first demonstration that the laser-ablation process can be scaled up to substrate sizes compatible with semiconducting process technology. Thus, a number of HTS microwave devices such as strip line resonators or filters could be fabricated from a single substrate.

M7.190

"IN-SITU PROCESSING OF TEXTURED AND EPITAXIAL SUPERCONDUCTING Ho-Ba-Cu-O THIN FILMS ON (100) MgO and YS-ZrO_2 SUBSTRATES IN THE TEMPERATURE RANGE 500-650°C. R.K. Prasad, A.K. Singh, and J. Narayan, Department of Materials Science and Engineering, North Carolina State university, Raleigh, N.C. 27695-7916.

Thin films of $\text{HoBa}_2\text{Cu}_3\text{O}_{7.8}$ were deposited on (100) MgO and (100) YS-ZrO_2 substrates using laser ablation technique. High powered pulsed XeCl excimer laser ($\lambda=0.308\mu\text{m}$, $t=45$ nanoseconds and average energy density $= 2.5 \text{ J/cm}^2$) was used to ablate bulk superconducting targets onto an appropriate substrate placed parallel to the target at a distance of 4.85 cm. The films were deposited at 500-650 °C in an oxygen atmosphere of 0.2 Torr in the presence of a biased ring. The thickness of the superconducting films were varied from 500-6000 Å. The superconducting transition temperature T_c ($R=0$) was measured to be 84-86K for the various substrates. The critical current density (J_c) $\geq 10^6 \text{ J/cm}^2$ at 77K was measured in these films. X-ray diffraction pattern showed films on all three substrates to be highly textured. The nature of epitaxial growth was studied using Transmission Electron Microscopy (TEM) and Rutherford Backscattering Spectrometry (RBS) techniques. The results on microstructures and superconducting properties of these films and bulk will be discussed.

M7.191

SOFT X-RAY STUDIES OF Y-Ba-Cu-O THIN FILMS PREPARED BY LASER ABLATION. A. Krol, G. Smith*, C.J. Sher, D.R. Storch, L.W. Song, Y.H. Kao, S. Witanachchi, Y.Z. Zhu, S. Patel, and D.T. Shaw, State University of New York at Buffalo and Stony Brook, NY; and *Brookhaven National Laboratory, Upton, NY.

Soft x-ray fluorescence, total electron yield, and scattering were measured for the development of techniques specifically useful for atomic-scale characterization of oxide thin films. By using a new parallel plate avalanche counter to measure the fluorescence yield around the oxygen K edge, and by a comparison of results obtained with these different techniques, it is possible to probe directly the oxygen deficiency near the film surface. By taking x-ray data at different photon energies and as a function of grazing incidence angle, useful information on the superconducting film can be obtained, including oxygen depth profile, film thickness, surface roughness, optical constants, etc.

Thin films of Y-Ba-Cu-O were made on MgO and ZrO₂ substrates by laser ablation. The film structure is characterized by diffraction, electron microscopy, and EDAX. Superconducting properties are investigated by electrical and magnetic measurements. Soft x-ray experiments were carried out at the U-15 Beamline at the National Synchrotron Light Source. Possible correlations between x-ray results and superconducting properties will be discussed.

This research is supported by DOE and AFOSR.

M7.192

IN SITU GROWTH OF EPITAXIAL SUPERCONDUCTING YBa₂Cu₃O_{7-x} FILMS ON INSULATING, SEMICONDUCTING AND FERROELECTRIC KTaO₃ BY PULSED LASER ABLATION.* J.W. McCamy, David P. Norton, Douglas H. Lowndes, L. A. Boatner, R. Feenstra, and J. D. Budai, Solid State Division, Oak Ridge National Laboratory, Oak Ridge, TN 37831-6056.

KTaO₃ is an interesting substrate for potential applications of epitaxial thin film 123-materials because of relatively small mismatches of lattice parameters and thermal expansion coefficients and low chemical reactivity at elevated temperatures. More importantly, large single crystals of KTaO₃ are easily grown with optical quality, and can be doped to form an n-type semiconductor and/or a ferroelectric with variable ferroelectric T_c. Thus, optoelectronic devices that utilize a superconducting epitaxial film on top of a ferroelectric and/or semiconducting substrate seem possible. As an initial step in exploring such applications, we have carried out what are believed to be the first epitaxial growth experiments of Y-123 films on both insulating and doped (semiconducting) KTaO₃-family single crystals by pulsed laser ablation. Preliminary results show that primarily c-axis-normal epitaxial films can be grown with T_c(R=0) ~90 K and ΔT_c(10%-90%) ~1 K, and that these films are comparable to the best films grown on SrTiO₃ in terms of smoothness and surface morphology. Results of microstructural (SEM, RBS, x-ray) and superconducting transport property (T_c, J_c) measurements for several film-substrate combinations will be presented.

*Research sponsored by the Division of Materials Sciences, U.S. Department of Energy under contract DE-AC05-84OR21400 with Martin Marietta Energy Systems, Inc.

M7.193

CHARACTERIZATION OF GROUND STATE NEUTRAL AND ION TRANSPORT DURING LASER ABLATION OF 1:2:3 SUPERCONDUCTORS BY TRANSIENT OPTICAL ABSORPTION SPECTROSCOPY.* D.B. Geohegan and D. N. Mashburn, Solid State Division, Oak Ridge National Laboratory, Oak Ridge TN 37831-6056.

The transport of ground state Y, Ba, and Cu neutrals and Y⁺, and Ba⁺ ions following excimer laser ablation of Y₁Ba₂Cu₃O_{7-x} oxide superconductor pellets has been studied using optical absorption spectroscopy. Spatially resolved absorption measurements following the laser pulse (1mm, 20 ns resolution) indicate significant ground state number densities at times up to an order of magnitude longer than the fluorescence from excited states in the laser plume. The time-of-flight absorbance profiles result in velocity distributions which are broadened significantly toward lower velocities with a low velocity component (< 10⁵ cm s⁻¹) to the ablation process which is not observed using emission spectroscopy. Spectrally broadened emission and absorption lines are used to estimate electron, ion and neutral densities in different regions of the plume. A correlation of the absorption data with ion probe measurements will be presented. The observation of collisions, detection of YO, BaO, and CuO, and the effects of oxygen background pressure as measured by the absorption technique will also be discussed. The application of this technique as an in situ monitor of the kinetic energy of species during low temperature deposition of epitaxial 1:2:3 superconducting thin films will be described.

*Research sponsored by the Division of Materials Sciences, U.S. Department of Energy under contract DE-AC05-84OR21400 with Martin Marietta Energy Systems, Inc.

M7.194

LASER INTERFEROMETRIC MEASUREMENT OF SUBSTRATE TEMPERATURE DURING GROWTH OF HIGH T_c SUPERCONDUCTOR FILMS K. L. Saenger, J. Gupta, J. P. Doyle, R. A. Roy, and J.J. Cuomo, IBM Research Division, T. J. Watson Research Center, P.O. Box 218, Yorktown Heights NY 10598.

Substrate temperature during film growth is an important processing parameter for vapor deposited films of the high T_c superconductors. Required substrate temperatures reported for "superconducting-as-deposited" films are in the range of 400 - 700°C, with the lower temperatures corresponding to increasing oxygen availability. In this presentation we describe a novel, non-contact optical thermometry technique in which the temperature of a transparent substrate is determined from its laser interferometrically measured thermal expansion. The technique is easy to implement and extremely accurate. Temperatures measured with this technique are reported for MgO (100) and YSZ substrates and compared to those measured conventionally by optical pyrometry or thermocouples in close proximity to the sample. The effect of the deposited film on the actual and apparent substrate temperature will also be discussed.

M7.195

HIGHLY ORIENTED SUPERCONDUCTING Bi-Sr-Ca-Cu OXIDE THIN FILMS BY THE SOLUTION SOL-GEL PROCESS. P. Ravindranathan, S. Komarneni, A.S. Bhalla, and R. Roy, Materials Research Laboratory, The Pennsylvania State University, University Park PA 16802.

Reproducible synthesis of homogeneous superconducting Bi-Sr-Ca-Cu oxide films is essential to the development of high T_c superconductive devices. Highly oriented Bi₂Sr₂CaCu₂O_{8+x} films were prepared on MgO and SrTiO₃ substrates by the solution sol-gel (SSG) method. A multiple sol of the superconductor was prepared using bismuth nitrate, copper acetate, strontium and calcium metals. The sol was coated on the substrates by spin casting and calcined at different temperatures. Films calcined at 870 C for 10 minutes showed the formation of the superconducting phase with preferential orientation along C-axis. These films were characterized by X-ray powder diffraction, scanning electron microscopy and resistance measurements. The resistance measurement showed the onset temperature

was 90 K for a film coated on MgO substrate. The details of the superconducting film preparation by SSG processing will be discussed.

M7.196

THE USE OF BaF_2 BUFFER LAYERS FOR THE SPUTTER-DEPOSITION OF TiCaBaCuO THIN-FILM SUPERCONDUCTORS. K.M. Hubbard^a, P.N. Arendt^a, E.J. Peterson^b, G.A. Reeves^a, N.E. Elliott^a, D.W. Cooke^c, D.R. Brown^d, and M. Nastasi^a, Los Alamos National Laboratory, Los Alamos, NM.

Results have shown that Ti-based superconducting films with a thickness of less than one micron often have poor electrical properties because of film-substrate interdiffusion during the annealing process. In an effort to improve the properties of thin films, we have experimented with the use of BaF_2 buffer layers as a diffusion barrier. Thin films of TiCaBaCuO have been grown by dc magnetron sputtering onto YSZ, MgO, and Ag substrates, both with and without a spin-deposited BaF_2 buffer layer. Films were also deposited on SrTiO_3 for use as a reference. The composition of the films, and the degree of interdiffusion, were determined by high-energy elastic backscattering analysis. Electrical properties were determined by both four-point probe and eddy-current measurements. In addition, structural analysis was performed on selected samples by XRD and TEM. The results indicate that the use of BaF_2 buffer layers can significantly improve the electrical properties of TiCaBaCuO thin-film superconductors.

a:Materials Science and Technology Division
b:Exploratory Research and Development Center
c:Meson-Physics Facility
d:Mechanical and Electrical Engineering Division

M7.197

AS-GROWN SUPERCONDUCTIVITY OF Bi-SYSTEM THIN FILMS PREPARED BY MAGNETRON SPUTTERING WITH Pb DOPED THREE TARGETS: $(\text{Bi}_{1.6}\text{Pb}_{0.4})_{1+a}(\text{SrCa})_2\text{Cu}_3\text{O}_x$, $(\text{Bi}_{1.6}\text{Pb}_{0.4})_1(\text{SrCa})_{2+c}\text{Cu}_3\text{O}_x$ and $(\text{Bi}_{1.6}\text{Pb}_{0.4})_1(\text{SrCa})_2\text{Cu}_{3+c}\text{O}_x$ ($a=0.5$, $b=1$, $c=1.5$) Ken-ichi Kuroda, Masami Tanioku, Kazuyoshi-Kojima, and Koichi Hamanaka, Cent. Res. Lab., Mitsubishi Electric Corp., Tsukaguchi, Amagasaki, Hyogo, JAPAN

It was demonstrated that high quality oxide superconducting thin films of both $\text{BiSrCaCuO}^{1,2)}$ and $\text{YBaCuO}^{3)}$ were grown by the multi-target sputtering method with calcined targets.

In this paper, we report on the as-grown Bi-system thin films prepared with Pb doped three targets. These three targets were simultaneously discharged and the heated $\text{MgO}(100)$ substrate was rotated above these targets. The staying time on each target was adjusted to precisely control the chemical composition of the film. The thickness of the film was 100 nm. For the optimized sample, the surface of the film was as smooth as the surface of Ref.1. The c axis of the film was 3.74nm and highly oriented normal to the substrate. The zero resistivity was obtained at 72 K in a as-grown state. From the ICP analysis, none of Pb was detected in the film grown at 650°C.

REFERENCES

- 1) K.Kojima, K.Kuroda, M.Tanioku and K.Hamanaka, Jpn.J.Appl.Phys.28(1989)L643. 2) K.Kuroda, et al., to be published in Jpn.J.Appl.Phys. 3) K.Kuroda, et al., to be published in Jpn.J.Appl.Phys.

M7.198

EVALUATING THE CHEMICAL COMPATIBILITY OF POTENTIAL SUBSTRATE MATERIALS FOR Bi-Sr-Ca-Cu-O FILMS.*

K.E. Williams, M.M.Matthiesen, D.A. Rudman, Department of Materials Science and Engineering, MIT, Cambridge, MA 02139.

Most of the recently discovered high T_c oxide superconductors react with technologically important substrate materials used in thin film applications. In particular, the $\text{Bi}_2\text{Sr}_2\text{CaCu}_2\text{O}_8$ (BSCCO) superconductor is chemically incompatible with Al_2O_3 , Si and SiO_2 . In order for BSCCO to be commercially useful, compatible substrates must be identified. Because thin films studies are not suited for quickly surveying a large number of materials, this investigation uses powder processing methods. Candidate substrates that were investigated include metals such as Ag and Ta and insulators such as Y_2O_3 and ZrO_2 . Pressed pellets containing 50 vol. % of the substrate material and 50 vol. % of BSCCO powders were sintered at 850° C in air for up to four days. Chemical compatibility was then evaluated using SQUID magnetometer, x-ray diffraction, and SEM characterization techniques. The validity of this technique was verified by conducting experiments with Al_2O_3 , which is known to be incompatible with BSCCO, and MgO, which is known to be compatible. Other investigations using this method have shown that Ag is chemically compatible with BSCCO, while Ta is not. The results of investigations of Y_2O_3 and ZrO_2 , silicide compounds (which are compatible with Si), and gallate compounds (which exhibit low microwave losses) will also be reported.

*Research supported by the U.S. Army Strategic Defense Command through Babcock and Wilcox.

M7.199

IN-SITU GROWTH OF SUPERCONDUCTING Bi-Sr-Ca-Cu-O THIN FILMS BY ACTIVATED REACTIVE CO-EVAPORATION. K. Yoshikawa, T. Satoh, N. Sasaki and M. Nakano Fujitsu Ltd., 1015 Kamikodanaka Nakahara-ku, Kawasaki. 211. JAPAN

In-situ growth of superconducting Bi-Sr-Ca-Cu-O thin films have been successfully realized with good reproducibility. The obtained films had a $T_c(\text{onset})$ of 90K and a $T_c(\text{zero})$ of 45K.

The films were fabricated using activated co-evaporation technique. The film thickness was from 700 to 1000 Å. The machine has two electron-beam guns, two resistively heated boats and rf power supply. Bi_2O_3 and SrF_2 were evaporated from EB guns. Cu and Ca metal were evaporated from resistively heated boats. Oxygen gas was directly introduced onto substrate. A plasma was generated between the evaporation sources and the substrate by rf power supply to enhance oxidation. The F was not detected in the film from EDX analysis. SrF_2 was dissociated by the rf plasma. The substrate temperature during deposition was 680 °C, and growth rate was 0.2 Å/s. Re-evaporation of Bi from growing film was suppressed by using Bi_2O_3 as a source.

The film on (100)MgO substrate showed the orientation with the c-axis perpendicular to the film surface. This indicates that the film was epitaxially grown. The surface of the film was much smoother than that of the films fabricated with post-annealing.

M7.200

HIGH- T_c SUPERCONDUCTING Bi-(Pb)-Sr-Ca-Cu-O FILMS DEPOSITED BY PULSED Nd:YAG LASER ABLATION. J. Levoska, J. Hagberg, P. Pusa, A. Uusimäki and S. Leppävuori, *Microelectronics and Material Physics Laboratories, University of Oulu, SF-90570 Oulu, Finland*

High T_c superconducting Bi-(Pb)-Sr-Ca-Cu-O thin films were made on MgO using laser ablation deposition. A pulsed beam from the Nd:YAG laser at 1064 or 532 nm was scanned over a sintered, high T_c superconducting target. The target materials, $\text{BiSrCaCu}_2\text{O}_y$ and compositions near $\text{Bi}_{2-x}\text{Pb}_x\text{Sr}_2\text{Ca}_2\text{Cu}_{3.4}\text{O}_y$ ($x \leq 0.6$, $d \leq 0.6$) made by the mixed oxide route, had zero resistivity temperatures of 80 - 82 K and 101 - 105 K, respectively. Films were deposited on MgO (100) single crystal substrates at room temperature. The amorphous films were crystallized by annealing at 850-920 °C followed by slow cooling. The effects of laser parameters and annealing conditions were investigated. The films were studied by XRD, SEM, EPMA and resistivity measurements.

The chemical composition of the as-deposited films were found to correspond with those of the target materials. The best films containing no Pb were obtained by allowing the film to melt, followed by a long annealing below the solidus temperature. These films consisted mainly of the 2212 phase and had T_c (midpoint) at 81 K and zero resistivity at 77 K. The best Pb doped films were annealed near 850 °C and they consisted mainly of the 2223 phase. These films had T_c (midpoint) at 107 K and zero resistivity at 100 K. The superconducting phases in the annealed films were strongly oriented with their c-axes perpendicular to the substrate surface.

M7.201

IN SITU REACTIVE SPUTTER DEPOSITION OF SUPERCONDUCTING Bi-Sr-Ca-Cu-O THIN FILMS ON SILICON SUBSTRATES. M. Migliuolo, D.W. Greve, T.E. Schlesinger, Carnegie Mellon University, Pittsburgh PA 15213, J.A. Brewer, R.M. Belan, Kurt J. Lesker Company, 1515 Worthington Ave, Clairton PA 15025

Thin films of the Bi-Sr-Ca-Cu-O (BSCCO) superconductor have been fabricated on silicon substrates by in situ reactive magnetron sputtering. Superconducting films of thickness less than 1 μm were obtained by simultaneous sputtering from Bi, Sr/Ca, Sr/Cu and Ca/Cu targets. These targets are mounted in a cluster of four Torus® sources in a Kurt J. Lesker Supersystem III. The effects on composition of partial oxygen pressure, substrate temperature, and relative target power levels have been studied in detail in order to allow for the selective deposition of the two higher temperature phases of the BSCCO. Film composition was determined by energy dispersive x-ray fluorescence spectroscopy and film texture and morphology were investigated by x-ray, TEM, and SEM techniques. Superconductor-substrate interactions occurring at higher substrate temperatures were minimized by the use of magnesium oxide and yttria stabilized zirconium oxide buffer layers. The buffer layers were deposited in the same deposition system from a Torus® source, and crystallized in situ.

M7.202

IN-SITU AND POST ANNEALED SUPERCONDUCTING THIN FILMS OF BiSrCaCuO BY PULSED LASER DEPOSITION. L. DiDomenico, and X. D. Wu, Physics Department, Rutgers University, Piscataway, NJ 08854, T. Venkatesan, Bellcore, Red Bank, NJ 07701

Three different superconducting phases have been found in the Bi based oxide system. The intergrowth of high and low T_c phases makes the preparation of a pure high T_c phase difficult. So far, there are no reports about in-situ growth of good high T_c (110 K) films.

The pulsed laser deposition method was used to prepare Bi based thin films with high temperature processing. The composition of the targets (2212, 2223 and Pb doped 2223) can be reproduced in the films up to temperature after which the compound begins to decompose. It was found that the deposition temperature is very critical for the formation of Bi based superconducting thin films. The 2212 phase is easily formed unlike the 2223 phase. The onset of the superconductivity in 2223 phase is about 110 K while the transition width is very wide. We will present the superconducting properties obtained from the thin films prepared under different oxygen pressure and temperature. The detailed characterization (X-ray, RBS and SEM) results of the films will be also presented.

M7.203

THERMAL EXPANSION OF $\text{YBa}_2\text{Cu}_3\text{O}_7$. G.A. Ramadass, V. Ramachandran and R. Srinivasan Department of Physics, I.I.T., MADRAS 600 036, India.

The variation of linear thermal expansion coefficient α , of the single phase high temperature superconductor $\text{YBa}_2\text{Cu}_3\text{O}_7$ with temperature has been studied using the Pizeau's optical interference method in the temperature range 85 to 300 K. Effect of oxygen deficiency on thermal expansion has also been studied by quenching the superconducting materials from high temperatures (600 °C) and repeating the experiments. The linear thermal expansion coefficient was found to decrease with decrease in temperature. But there seems to be an anomaly in this behaviour at about 220 K which is reproducible. When the samples were rendered non-superconducting by quenching from high temperature this anomaly was found to be more pronounced. It is interesting to note that some anomalies were reported in the literature in the measurements of specific heat, lattice parameters, attenuation of sound and sound velocity at about 220 K on $\text{YBa}_2\text{Cu}_3\text{O}_7$.

M7.204

THIN-FILM DEPOSITION AND TRANSPORT IN 2223 Bi-Sr-Ca-Cu-O. J.T. Kucera, D.G. Steel, J.M. Graybeal, T.P. Orlando, and D.A. Rudman; MIT, Cambridge, MA.

We have reproducibly prepared thin films of Bi-Sr-Ca-Cu-O with $T_c \geq 105\text{K}$. Depositions were done at ambient temperature with a subsequent post-deposition anneal, and did not include lead substitution. X-ray diffraction data indicates a majority fraction of the 2223 phase. These films possess very large grains of the order of 20-30 μm in size. Post-deposition annealing conditions are a sensitive function of composition. Detailed transport measurements as a function of temperature and magnetic field have been obtained.

M7.205

CRITICAL CURRENT DENSITY MEASUREMENTS OF LASER DEPOSITED SUPERCONDUCTING THIN FILMS. C.B. Lee, A.K. Singh, R. K. Singh, and J. Narayan, Department of Materials Science and Engineering, North Carolina State University, Raleigh, N.C. 27695-7916.

Transport critical current density (J_{c1}) measurements were performed on epitaxial and textured $\text{RBA}_2\text{Cu}_3\text{O}_7$ ($R = \text{Y}$, and Ho) superconducting thin films deposited by pulsed laser evaporation technique ($\lambda = 308\text{nm}$, $\tau = 45\text{ns}$).

Epitaxial films by lattice matching (SrTiO_3 , LaAlO_3 , KTaO_3), and planar matching (YSZ), and textured thin films on lattice mismatched substrates (MgO , Si) were fabricated by this technique at low processing temperatures ranging between 500-650 °C. Various models used to explain the critical current density data as a function of temperature will be presented. The role of flux creep and SNS behavior in controlling the critical current densities was investigated. The effect of Ag-doping in $\text{YBa}_2\text{Cu}_3\text{O}_7$ on the critical current will also be presented as intergrain or intragrain phenomena.

Part of this research has been sponsored by the Office of Energy Systems Research, the Division of Energy Conversion and Utilization Technologies (ECUT) programs, under subcontract number 19X-4337 C, and the U.S. Department of Energy, Martin Marietta Energy Systems, Inc.

M7.206

THE DETERMINATION OF OXYGEN STOICHIOMETRY OF HIGH TEMPERATURE SUPERCONDUCTING THIN FILMS BY NUCLEAR SCATTERING OF 3 MEV PROTONS ON OXYGEN. H.-S. Jin and T. Yan, Department of Physics, Brooklyn College of The City University of New York, Brooklyn, NY 11210.

A simple method is presented to measure the oxygen stoichiometry of high temperature superconducting thin films. It is an undestructive and absolute method, and as simple as traditional RBS techniques. By using the nuclear scattering of 3 MeV protons on oxygen, the relative sensitivity to oxygen has been enhanced. By taking the oxide substrates as references, the uncertainty due to charge integration has been avoided and the accuracy has thus been improved. The accuracy of this method simply depends on the accuracies in the data on atomic stopping power, the chemical composition of the substrates and the background subtraction.

M7.207

RECRYSTALLIZATION OF NON VACUUM DERIVED $\text{Ba}_2\text{YCu}_3\text{O}_{7-x}$ FILMS. M. F. Ng, S. C. Peterson, M. J. Cima, Ceramics Processing Research Laboratory, Massachusetts Institute of Technology, Cambridge, MA.

Recrystallization occurring during high temperature treatment of superconducting films is associated with texture development. X-ray diffraction and microscopic examination have been used to detail the microstructural development within $\text{Ba}_2\text{YCu}_3\text{O}_{7-x}$ films for several processing conditions. Conditions that favor grain growth includes partial melting followed by recrystallization at lower temperatures. In these films, partial melting is induced by rapid thermal annealing at a temperature slightly above the peritectic melting temperature of $\text{Ba}_2\text{YCu}_3\text{O}_{7-x}$. Short firing duration prevents segregation of liquid and permits recrystallization of the correct phase at 920 °C.

Grains grow to the thickness of the film through repeated cycles of partial melting and recrystallization.

M7.208

TWO NON-CONTACT TECHNIQUES FOR CHARACTERIZATION OF THIN FILMS OF YBCO. C.A. Weiss, W.L. McLean and X.D. Wu, Physics Department, Rutgers University, Piscataway, NJ 08854; J. Barner and T. Venkatesan, Bellcore, Red Bank, NJ 07701.

Present research efforts in high T_c superconducting thin films have necessitated the need for non-contact techniques for film characterization. Two complementary techniques ideal for this purpose are the magnetically modulated microwave absorption (MAMMA) technique utilizing an ESR spectrometer and an AC magnetization technique.

We are using both these techniques to examine the properties of multilayer thin films of YBCO and Pr alloyed YBCO. The MAMMA technique is less subject to shielding effects and is better suited for the study of multilayers as opposed to AC susceptibility measurements. Measurements on thin films made by both techniques would be compared to illustrate their advantages and shortcomings.

M7.209

STRUCTURAL AND SUPERCONDUCTING PROPERTIES OF YBCO THIN FILMS ON $\text{Zr}(\text{Y})\text{O}_2$ SUBSTRATES. Q. Li*, G. Linker, J. Geerk, O. Meyer, and X. X. Xi*, Kernforschungszentrum Karlsruhe, Institute fuer Nukleare Festkoerperphysik, P. O. Box 3640, D-7500 Karlsruhe, FRG; *Physics Department, Rutgers University, Piscataway, NJ 08854

The growth feature of YBCO thin films on (100) and randomly cut single crystal $\text{Zr}(\text{Y})\text{O}_2$ substrate produced by hollow cathode magnetron sputtering was studied by He ion channeling and X-ray diffraction measurement. In both cases films with T_{c0} about 90 K and c-axis perpendicular to the surface were obtained. However, the films on randomly cut substrates showed no channeling effects whereas those on (100) substrates revealed good channeling behaviors with a X_{\min} value of 10% and a standard deviation of crystallite misorientation of 0.1°. Detailed studies of inclined channeling effects indicated that the crystal planes of YBCO films were azimuthally adjusted with a rotation of 45° about the substrate normal in order to reduce the lattice mismatch between YBCO and (100) $\text{Zr}(\text{Y})\text{O}_2$ substrate. The critical current density of films on the (100) substrates was $2 \times 10^6 \text{ A/cm}^2$ at 77 K which was one order of magnitude higher than that for films on randomly cut substrates.

M7.210

ANNEALING BEHAVIOR OF $\text{Ba}_2\text{YCu}_{3+x}\text{O}_{7+y}$ THIN FILMS T. Siegrist and E. Coleman, AT&T Bell Labs, Murray Hill, NJ 07974.

The annealing behavior of $\text{Ba}_2\text{YCu}_{3+x}\text{O}_{7+y}$ films grown by coevaporation of BaF_2 , Y and Cu on SrTiO_3 has been studied as a function of temperature. Upon annealing at temperatures below 800 °C, the phase forming first is $\text{Ba}_2\text{YCu}_4\text{O}_8$, independent of the starting stoichiometry. Higher temperatures, above approximately 825 °C are needed for $\text{Ba}_2\text{YCu}_3\text{O}_7$ to crystallize. Attempts to grow ordered intermediate phases between $\text{Ba}_2\text{YCu}_3\text{O}_7$ and $\text{Ba}_2\text{YCu}_4\text{O}_8$ are in progress.

M7.211

PROPERTIES OF THIN FILMS OF $\text{YBa}_2\text{Cu}_3\text{O}_7$ PREPARED BY COEVAPORATION OF Y, Cu AND BaF_2 . I. D. Raistrick, D. N. Sinha, F. H. Garzon, J. G. Beery and D. K. Wilde. Los Alamos National Laboratory, Los Alamos, NM.

We have prepared films of $\text{YBa}_2\text{Cu}_3\text{O}_7$ on single-crystal substrates of SrTiO_3 and LaGaO_3 by e-beam coevaporation of Y and Cu metals and thermal evaporation of BaF_2 . The properties of the films have been studied as a function of substrate material, thickness and post-deposition anneal conditions. The microstructure consists of a layer of strongly c-axis oriented material close to the interface and a less dense layer of a-axis oriented material on the free surface. Considerable variation in the grain size and the orientation of the film can be achieved by varying the film thickness and anneal temperature and time. The best films have critical currents in excess of 1 MA/cm² at 65 K in zero field and 0.1 MA/cm² in 7 T. We have also measured the surface resistance of the films at 22 GHz. Films on LaGaO_3 have measured R_s as low as 0.2 mOhm at 4 K; films on SrTiO_3 are an order of magnitude less good. The current-voltage relations and the dependence of J_c on threshold voltage and temperature have been analyzed in terms of a weak link array and flux creep models.

M7.212

EFFECT OF BUFFER LAYERS ON THE SUPERCONDUCTING PROPERTIES OF YBCuO FILMS ON METALLIC SUBSTRATES. S. Witanachchi, J. Chang, Y. Z. Zhu, S. Patel and D. T. Shaw, Institute on Superconductivity, State University of New York at Buffalo, Bonner Hall, Buffalo, NY 14260

Plasma assisted laser deposition technique has been used to grow as-deposited $\text{Y}_{1-x}\text{Ba}_x\text{Cu}_3\text{O}_{7-x}$ films on metallic substrates-stainless steel and hastelloy (Ni-Co-Cr-Mo). Low deposition temperature reduces the interfacial diffusion and thereby improves the superconducting properties. Films deposited directly on the metallic foils show critical temperatures around 79K and critical currents around 2×10^3 A/cm² at 40K. Critical currents have been moved to the 10^5 A/cm² range by incorporating laser evaporated Ag, MgO, BaTiO_3 and MgAl_2O_4 buffer layers. Superconducting properties and microstructures of these films will be discussed.

M7.213

INTERFACES IN THIN FILM HIGH- T_c SUPERCONDUCTORS. Lisa A. Tietz, M. Grant Norton and C. Barry Carter, Department of Materials Science and Engineering, Cornell University, Ithaca, NY 14853.

Both homo- and hetero- phase boundaries play important roles in determining the properties of superconducting thin films. Several studies have suggested that grain-boundary structure and composition define the weak-link behavior of individual grain boundaries. Previous work has shown that oriented Y-Ba-Cu-O thin films can contain large numbers of coincident site lattice (CSL) type tilt boundaries. The film-substrate interface, in turn, controls epitaxy and can be a region of significant compositional variation in the film.

Grain boundaries and film-substrate interfaces in thin film Y-Ba-Cu-O high- T_c superconductors have been studied using transmission electron microscopy (TEM) and energy dispersive x-ray spectroscopy (EDS). The films were grown on (001)-oriented Y_2O_3 -stabilized ZrO_2 (YSZ) single-crystal substrates either by electron beam coevaporation of the metals or by laser evaporation from stoichiometric bulk samples. The film microstructure was characterized in both plan-view and cross-section.

Particular attention has been paid to the effects of film annealing since degradation of properties of Y-Ba-Cu-O films is known to occur due to reaction between film and substrate. Observation of as-deposited films have shown a Ba-enriched intermediate layer, 5nm thick, at the film-substrate interface. The prepared films were subjected to low temperature heat treatments in air for various times and the effects of this treatment on the interfacial regions determined.

M7.214

OXYGEN RESONANCE STUDY IN YBaCuO HIGH- T_c FILMS. Hiroki Kuwano*, Jian Li, Peter Revesz, James W. Mayer, Materials Science and Engineering, Cornell University, Ithaca NY 14853-1501, Yasuhiro Nagai, NTT Applied Electronics Labs., Musashino, Tokyo 180 JAPAN.

The $^{16}\text{O}(\alpha,\alpha')^{16}\text{O}$ elastic resonance near 3.045 MeV has been applied to quantify oxygen concentrations in thin RF-sputtered YBaCuO high- T_c films. A series of resonance RBS spectra corresponding to oxygen concentrations at different depth can be obtained by varying the incident energy from 3.043 MeV to above 3.160 MeV. This non-destructive method has been proved to be powerful in determining oxygen concentrations in YBaCuO films. RUMP computer simulation program¹ was used to evaluate the measured spectra. Good agreement between the experiment and theoretical data was found.

The correlation between resistivity and composition change, especially near the interfaces of YBaCuO films and sputtered MgO films, was investigated after annealing at 900 °C, 850 °C, 800 °C, 750 °C, and 700 °C. Big composition change near the interface between YBaCuO films and sputtered MgO films deposited on Si substrate was found after annealing at 900 °C in oxygen ambient. The YBaCuO film, deposited on sputtered MgO buffer film on Si substrate and then annealed at 850 °C, showed superconductivity, while the films annealed at the other temperatures didn't show superconductivity.

1. B. Blanpain, P. Revesz, L.R. Doolittle, K.H. Purser and J.W. Mayer, Nucl. Instr. and Meth. in Phys. Res. B34 (1988) 459.

*Permanent Address: NTT Applied Electronics Labs., Nippon Telegraph and Telephone Corporation, Musashino, Tokyo 180 JAPAN

M7.215

LINE BROADENING ANALYSES OF VARIOUSLY PREPARED YBaCuO SUPERCONDUCTING FILMS. M. Ece and R.W. Vook, Physics Department, Syracuse University, Syracuse, N.Y. 13244-1130 and John P. Allen, CVC Products, Inc., Rochester, N.Y. 14603-1886.

Integral breadth X-ray diffraction line broadening from high T_c superconducting films having an (00L) texture has been investigated. The $\text{Y}_{1-x}\text{Ba}_x\text{Cu}_3\text{O}_{7-x}$ films were deposited by rf magnetron sputtering and flash evaporation methods. Films were deposited on sapphire (Al_2O_3), MgO and SrTiO_3 buffer layers. The line broadening arising in these films deposited under various conditions and given different annealing treatments was studied. Films grown on SrTiO_3 / Al_2O_3 had a preferred orientation whereas the films directly deposited on Al_2O_3 were randomly oriented. These results were correlated with electrical resistance measurements.

M7.216

CATION INTERDIFFUSION AT YBCO/MgO INTERFACES. M. Lanham, J. Mayer, S.J. Golden, A.G. Evans and M. Rühle*, Materials Department, University of California Santa Barbara, CA. 93106, *MPI für Metallforschung, Stuttgart, FRG.

Analytical TEM investigation of YBCO films heat treated at 950°C for 30 minutes on MgO revealed an interdiffusion of Cu and Mg. The concentrations of the cations within individual

grains at the interface were quantitatively measured. Charge and stoichiometric considerations, as well as, the similar size of the cations strongly suggests that as Cu diffuses into Mg lattice sites in the substrate, Mg must diffuse into in the film (probably Cu sites). However, our data show that their diffusion rates are much different ($MgOD_{Cu}/YBCOD_{Mg}=30$); which indicates that the diffusion mechanism is complicated by the layered structure of the perovskite-like films. No impurity segregation was detected at the interface. Diffraction study of several YBCO grains confirms that the film c-axis is oriented perpendicular to the substrate, but that the a/b plane has no fixed orientation, indicating that no epitaxial relationship exists.

M7.217

MICROSTRUCTURE OF $YBa_2Cu_3O_{7-x}$ THIN FILMS GROWN ON SINGLE CRYSTAL $SrTiO_3$ Siu-Wai Chan, D. M. Hwang, and S. M. Sempere, Bellcore, 331 Newman Springs Rd., Red Bank, NJ 07701

Thin films of $YBa_2Cu_3O_{7-x}$ on single crystal $SrTiO_3$ substrates have been shown to support the highest critical current (J_c) of any form of this material. e -evaporation of Y, BaF_2 and Cu, and annealing in wet oxygen at $850^\circ C$ has yielded reproducible films with critical current [$J_c(77K)$] greater than $5 \times 10^5 A/cm^2$ among different laboratories. It is, therefore, important to examine the microstructure of these films to gain insights into the role of microstructure on supercurrent-carrying-capacity. $YBa_2Cu_3O_{7-x}$ thin films on (001) and (014) $SrTiO_3$ were prepared and cross-sectional samples were studied with transmission electron microscopy. Three types of orthogonally misoriented $YBa_2Cu_3O_{7-x}$ grains are observed to grow on both (001) and (014) surfaces of single crystal $SrTiO_3$ substrates. Specially, these grains have their c-axes aligned with one of the three $\langle 100 \rangle$ directions of cubic $SrTiO_3$. This ambiguity creates a 3-fold degenerate epitaxy of $YBa_2Cu_3O_{7-x}$ on $SrTiO_3$, which results in 90° -grain boundaries in the final $YBa_2Cu_3O_{7-x}$ thin films. These boundaries are perovskite-structure preserving and free of any extraneous phases. The presence of extraneous phases elsewhere in the films did not destroy the connectiveness of superconducting materials and therefore, they are not damaging to superconducting transport.

M7.218

XPS Analysis of Y - Ba - Cu - O and Zr - O Thin Films and Interfaces with Silicon Substrates

D.B. Fenner, *⁺ A.M. Viano, *⁺ J.B. Boyce, *⁺ and G.A.N. Connell.*

*Xerox Palo Alto Research Center, Palo Alto, CA 94304.

⁺ Physics Dept., Santa Clara Univ., Santa Clara, CA 95053.

Thin films of $Y_1Ba_2Cu_3O_x$, ZrO_2 , and related oxides have been deposited on Si(100) by laser ablation deposition, and characterized by several techniques including x-ray photoemission spectroscopy (XPS). Si was prepared by several techniques including thermal and native oxidation, as well as etching and passivation by hydrogen termination. Certain of these films (~ 250 nm thick) have excellent superconducting properties. Films of 2 - 5 nm thickness, transferred under dry N_2 and into UHV, allow XPS evaluation of the thermal and chemical stability of interfaces and nearby regions. Even for 5 nm films of YBCO deposited at moderate temperatures on 15 nm films of SiO_2/Si the Cu 2p core - level XPS lines are quite similar to those

of bulk YBCO, i.e., Cu II. The Y and Ba 3d lines often narrow to single oxidation states for these very thin films, while the O 1s has 2 or 3 components.

This project was supported in part by the NSF (DMR-8822353), and the Air Force OSR (F49620-89-C-0017-DEF).

M7.219

THE INFLUENCE OF THE SUBSTRATE SURFACE ON THE NUCLEATION AND GROWTH OF SUPERCONDUCTING THIN FILMS. S. Basu, N. Bordes, M. Cohen and M. Nastasi; Los Alamos National Laboratory, Los Alamos, NM 87545.

The quality of epitaxially grown superconducting thin films are dependant on the nature of the substrate surface. In this study, the surface of (100) oriented $SrTiO_3$ single crystal substrates have been modified by chemical etching, thermal annealing and mechanical polishing. The quality of these substrate surfaces have been characterized by ion beam channeling and surface profilometry. Thin $YBa_2Cu_3O_7$ superconducting films were then deposited on these substrates. The epitaxy of the deposited films have been characterized by ion beam channeling, X-ray spectroscopy and 4-point probe measurements. The films have also been characterized in cross section by transmission electron microscopy. This paper will present results on the role of the substrate surface on the nucleation and epitaxial growth of thin superconducting films.

M7.220

MICROSTRUCTURES OF Y123 FILMS ON $SrTiO_3$ AND $LaGaO_3$. T. Roy, T. E. Mitchell and I. D. Raistrick, Los Alamos National Laboratory, Los Alamos, NM 87545

Cross sections of electron beam deposited thin films of Y123 on (100) $SrTiO_3$ and $LaGaO_3$ have been examined using Transmission Electron Microscopy. The grains of Y123 seem to align themselves with the c-axis either perpendicular to the interface or parallel to the interface with the grains having the c-axis perpendicular to the interface forming the layer closest to the interface. In particular, an 8000Å film deposited on $LaGaO_3$ which showed low surface resistance was observed to have about a 3000-4000Å layer of c-perpendicular grains and the rest of the film was made up of widely spaced grains in the c-parallel orientation.

The interfaces between the film and substrate showed remarkably good epitaxy although in some regions evidence of other oxide phases were also seen at the interface. Films subjected to varying post deposition annealing treatments will be compared. Microstructural data from similar films deposited on each of the two substrates will also be presented and correlations between observed superconducting properties and corresponding microstructures will be made.

M7.221

INVESTIGATION OF POTENTIAL DIFFUSION BARRIERS BETWEEN $YBa_2Cu_3O_{7-x}$ AND SILICON. A. Lubig, Ch. Buchal and B. Stritzker, Institut für Schicht- und Ionentechnik, KFA Jülich, D-5170 Jülich, W. Germany

Thin films of ZrO_2 and noble metals on TiN have been examined as potential diffusion barriers between Si substrates and high temperature superconductors. As best result so far, a buffer layer of 250 nm ZrO_2 enabled the growth of a 200 nm film of $YBa_2Cu_3O_{7-x}$, which has been deposited by laser ablation. Rutherford backscattering analysis reveals some interdiffusion between $YBaCuO$ components and the ZrO_2 layer. This effect may account for the relatively low T_c of about 60 K.

Our typical deposition temperature for $YBaCuO$ -films is $780^\circ C$. At this temperature the buffer layer combination Si/TiN/Noble Metal is stable under vacuum ambient and Si outdiffusion is

successfully suppressed, but exposing the films to oxygen at this temperature results in catastrophic surface roughening due to oxidation of the film.

M7.222

EPITAXIAL AND SUPERCONDUCTING PROPERTIES OF $Y_1Ba_2Cu_3O_{7-x}$ FILMS ON FIVE PEROVSKITE SUBSTRATES.* R. Feenstra, J. D. Budai, S. J. Pennycook, M. F. Chisholm, M. D. Galloway, D. K. Christen, D. P. Norton, J. W. McCamy, D. H. Lowndes, and L. A. Boatner, Oak Ridge National Laboratory, P. O. Box 2008, Oak Ridge, TN 37831.

A comparison is made between the epitaxial and superconducting properties of $Y_1Ba_2Cu_3O_{7-x}$ (YBCO) films on $LaGaO_3$, $NdGaO_3$, $LaAlO_3$, $KTaO_3$, and $SrTiO_3$ substrates. One series of films, with varying thickness between 50 and 500 nm, was produced by coevaporation of Cu, Y, and BaF_2 , followed by a furnace anneal at 800–900°C in wet oxygen. In a second series, YBCO films were grown in situ by pulsed-laser ablation with maximum processing temperatures between 650–750°C. By comparing trends in the properties of the films as a function of thickness, a distinction is made between effects characteristic for each fabrication process and effects specific to the substrates.

Initial results are reported for superconducting YBCO films on doped $KTaO_3$ substrates: the semiconducting solid solutions $K_{1-x}(Sr,Ba)_xTaO_3$ and the ferroelectrics $KTa_{1-x}Nb_xO_3$.

*Research sponsored by the Division of Materials Sciences, U.S. Department of Energy under contract DE-AC05-84OR21400 with Martin Marietta Energy Systems, Inc.

M7.223

THE INTERFACE BETWEEN SILVER CONTACTS AND HIGH T_c SUPERCONDUCTORS M.D. McConnell and W.G. Morris, General Electric Corp. R. and D., Schenectady, N.Y.

Silver diffuses into the lattice of $YBa_2Cu_3O_6$ during the annealing of silver contacts at 500 deg. C. Depth profiles using Auger electron spectroscopy with a focused electron beam show a diffusion zone about 50 nm deep, as well as segregation of Ba and O to the surface of the contact. There appears to be a slight loss of silver from the surface region, which could be explained by enhanced concentration at grain boundaries. High resolution SEM analysis of a fracture surface did not reveal the presence of silver on the grain boundaries. Further work correlating diffusion rates with grain orientation will be discussed.

M7.224

STUDY OF EPITAXY OF $YBa_2Cu_3O_{7-x}$ BY THERMAL REGROWTH OF ION IMPLANTED AMORPHOUS LAYERS.

J.A. Martinez*, A. Inam and X.D. Wu, Physics Department, Rutgers University, Piscataway, NJ; and B. Wilkens, N.G. Stoffel, D. Hart, D.M. Hwang, L. Nazar and T. Venkatesan, Bellcore, Red Bank, NJ.

A 1650 Å crystalline thin film of $YBa_2Cu_3O_{7-x}$ pulsed laser deposited on MgO substrate was irradiated with 25 keV oxygen ions at a dose of 10^{16} ions/cm², producing a disordered layer at the surface of ~800 Å thick. Using RBS channelling as well as x-ray diffraction techniques the evolution of the recovery of the lattice was studied as a function of different isochronal annealing treatments. No changes in the composition of the

sample for a one hour anneal was observed up to 950°C. The channelling measurements indicate unambiguous epitaxial regrowth. The Arrhenius plot of the regrowth fraction obtained from the channelling spectra yielded an activation energy of the order of 0.8 eV for the epitaxial regrowth of the disordered layers. Results on isothermal anneals, TEM cross-sectional analysis and electronic transport in these layers will also be reported.

*Department de Fisica, UNLP, Argentina. Member of Carrera del Investigador Científico, CICPBA, Argentina, on fellowship of Conicet, Argentina.

M7.225

VERY LOW RESISTANCE ELECTRICAL CONTACTS TO TI-BASED HIGH T_c FILMS. J.E. Kwak, R. P. Hellmer, T. R. Castillo, R. Padilla, and D.S. Ginley, Sandia National Laboratories, Albuquerque, NM 87185-5800.

Electrical contacts can be a limiting factor in the eventual practical application, or even just the measurement, of high-critical-current-density samples of the high T_c superconductors. Ti-based films present special problems because: (1) the highest critical current densities have been obtained with films, (2) the effective volume of contact is restricted by the thinness of the films, and (3) techniques which produce good contacts to "123" materials do not work as well with Ti-based materials.

Here we report the results of contact studies on $Tl_2Ca_2Ba_2Cu_3O_{10}$ and $Tl_2CaBa_2Cu_2O_8$ films. The best contacts thus far (resistivities near 10^{-8} Ω-cm²) have been obtained by first backsputtering the contact area before sputtering 3000 Å of Ag, then 3000 Å of Au. Other metallurgies tested to date (Ag, Au, Pt, and Ti/Ag) have not produced comparable results. However, the contacts are not yet optimized, showing marginally metallic temperature dependence and a slight degree of rectification.

Thermal anneals at 500–600 C for up to 15 min. have not been found to improve the contact resistances, perhaps reflecting deleterious effects of Ag incorporation into the Ti-based superconductor. The top Au layer provides a good bonding surface and may serve to suppress Ag oxidation. The films show some damage during backsputter for contacts: 50 W of RF power for 1 min. in 30 μm Ar increased the room temperature resistivity ρ by about 20%. Lighter backsputtering (ie., in 3–5 μm Ar), which does not increase ρ and has been shown to etch 10–20 Å from the film surface, will be used for further contact studies.

M7.226

MEASUREMENTS OF SURFACE RESISTANCE OF HTS THIN FILMS FROM 0.5 to 40 GHz.* J. Steinbeck, RADCE/EAC, Hanscom AFB, MA 01731, D. E. Oates, and A. C. Anderson Lincoln Laboratory, Massachusetts Institute of Technology, Lexington, Massachusetts 02173.

Although superconductors have no dc losses, they have electrical losses at microwave frequencies which are important for electronic applications. The magnitude of the loss is determined by the surface resistance, R_s , of the material. We have measured R_s in polycrystalline films of YBCO and BSCCO deposited in our laboratories as well as oriented films made by other laboratories by codeposition techniques. The R_s of YBCO and BSCCO thin films has been measured in the frequency range between 0.5 and 40 GHz using a stripline-resonator technique. R_s for the films is proportional to frequency squared over the entire measurement range. The magnitude of R_s is, however, strongly dependent on film microstructure. Our measurements at 1 GHz and 4 K show that randomly oriented films have $R_s \approx 10^{-3}$ Ω (close to Cu) while oriented large-grain films have markedly lower $R_s \approx 2 \times 10^{-6}$ Ω, approaching the R_s of superconducting Nb. The magnitude of R_s rises to ~2 Ω and 10^{-3} Ω at 40 GHz for the randomly and preferentially oriented films, respectively. An effective penetration depth, λ_{eff} , has been determined from R_s using local electrodynamics.

We find that λ_{eff} is dependent on film microstructure and is $\sim 5 \mu m$ for high- R_s films, decreasing to $\sim 5000 \text{ \AA}$ for low- R_s films. The smaller values of λ_{eff} calculated for oriented films with large grains are in reasonable agreement with values of the YBCO penetration depth ($\sim 2000 \text{ \AA}$) reported in the literature. The use of the stripline resonator technique for temperature and magnetic-field-dependent measurements of R_s will also be discussed.

*This work was supported by the Department of the Air Force.

M7.227

Electric-field modulation of a Bi-Sr-Ca-Cu-O film with a plasma polymerized film as an insulator. Shin'ichi Morohashi, Hideo Suzuki, Kohtaroh Gotoh, Norio Fujimaki and Shinya Hasuo, FUJITSU Limited, 10-1 Morinosato Wakamiya Atsugi, JAPAN

High- T_c superconducting devices are expected as future electron devices. One of the technology to realize these devices is to utilize the field effect on the superconducting film. We must prepare very thin and flat superconducting film to obtain the field effect. Thin insulator without leak current is also necessary. We have investigated those technologies. We developed the fabrication of a thin Bi-Sr-Ca-Cu-O(BSCCO) film and the thin insulator. The BSCCO film(30 nm thickness) was deposited on MgO(100) substrate using ion beam sputtering technique. Following it, the patterning of this film was done using ion beam etching technique. The plasma polymerization using trifluoroethane gas was used to make the insulator(30 nm thickness). Gold metal was evaporated and patterned as a gate electrode.

We investigated how the current-voltage characteristic of this multilayered structure with Au gate/plasma polymerized film/BSCCO film was modulated with electric-field. The supercurrent decreased from 5.0 A to 3.6 A at 4.2 K when the gate voltage(-20 V) was applied to the gate electrode. This behavior is thought to be attributed to the electric-field modulation of the BSCCO film beneath the plasma polymerized film, formed by the gate voltage.

ACKNOWLEDGEMENT

This work was performed under the management of the Scientific Computer Research Association as a part of the Large Scale Project of AIST/MITI "R&D of Scientific Computing System" sponsored by NEDO(New Energy and Industrial Technology Development Organization).

M7.228

RESISTANCE TRANSITIONS OF ION-BEAM THINNED $YBa_2Cu_3O_7$ FILMS — AN APPROACH TO THE LIMITING THICKNESS OF ONE LATTICE CONSTANT A. F. Hebard, R. H. Eick, T. Siegrist and E. Coleman, AT&T Bell Labs, Murray Hill, NJ 07974.

Ion beam milling of c-axis oriented $YBa_2Cu_3O_7$ films is shown to give smooth films which superconduct at thicknesses approaching a lattice constant (11.6 Å). The milling is done at 10° grazing angles with 1 keV Xe^+ ions incident on a rotating substrate. Van der Pauw resistance transitions and SEM micrographs are used to characterize the films at each successive milling stage. Surface "basketweave" texture, identified as a-axis oriented material, is removed during the first stages of milling. The "electrical" film thickness, proportional to the reciprocal of the room-temperature sheet resistance, shows a linear dependence with milling time, thus indicating a uniform rate of removal of material with constant resistivity. The resistance transitions reflect metallic behavior over the entire range of thicknesses for all films which attain zero resistance. The zero resistance transition temperatures decrease uniformly with decreasing thickness with most of the change occurring for thicknesses less than 100 Å. The crossover to insulating behavior occurs at "electrical" thicknesses near 10 Å with a temperature independent sheet resistance above the onset of the superconducting transition having a value of approximately

7000 Ω/\square . This value is close to that predicted by theory and has been previously seen in low- T_c superconductors. Continued milling beyond this limit results in semiconducting behavior without a superconducting transition.

M7.229

TRANSPORT MEASUREMENTS ON SUPERCONDUCTING $YBa_2Cu_3O_7$ LINES, STEP EDGE STRUCTURES, AND ION BEAM DAMAGED LINES. Brian Moeckly, Daniel K. Lathrop, Gregory F. Redinbo, Stephen E. Russek, R.A. Buhrman, Cornell University, Ithaca, NY.

Superconducting $YBa_2Cu_3O_7$ thin films have been fabricated by laser ablation and high pressure reactive sputtering. Both techniques produce highly oriented films with excellent superconducting properties and morphology as deposited. The films deposited on MgO and $SrTiO_3$ have T_c 's greater than 85K and have been patterned to form submicron features. Critical currents and magneto-transport measurements have been used to study film nucleation and weak link formation at step edges formed by ion milling. Electrical measurements are correlated with film microstructure as seen by TEM studies. Similar measurements have been made to study the effects of optical and e-beam lithographic processing, pattern definition by ion milling, and exposure to 100-1000eV ion bombardment. The results of these measurements and their implications for device fabrication will be discussed.

M7.230

CRITICAL CURRENT DENSITY OF NARROW SUPERCONDUCTING THIN FILMS FABRICATED BY LASER ABLATION TECHNIQUES. L.W. Song, Y.H. Kao, Q.Y. Ying, J.P. Zheng, H.S. Kwok, Y.Z. Zhu, and D.T. Shaw, State University of New York at Buffalo, NY.

Variations of critical current density of narrow superconducting thin films as a function of temperature and magnetic field are investigated. Films with different geometry are prepared by laser ablation techniques. The width of narrow constriction is generally smaller than 100 micrometer and thickness is less than 200 nanometer. Near T_c , the critical current density J_c follows a $(1-t)^{3/2}$ dependence, where $t=T/T_c$. For t below 0.7, J_c shows pronounced deviation from this behavior. In a magnetic field, $J_c(H)$ decreases monotonically, showing a higher slope in the low field region when the field is applied perpendicular to the film surface. Microwave response of these narrow thin films in a magnetic field and changes in the current-voltage characteristics are also measured at different temperatures. These data are interpreted in terms of anisotropy, flux pinning, and Josephson weak links.

This research is supported by AFOSR and DOE.

M7.231

MAGNETIC EFFECT ON LOW-RESISTIVITY METAL-HIGH T_c SUPERCONDUCTOR CONTACTS. Yonhua Tzeng, Mitch Belser, Department of Electrical Engineering, Auburn University, Alabama 36849.

Low-resistivity metal-high T_c superconductor contacts can be fabricated in a number of ways using metals such as silver and gold. It has also been discovered that by mixing silver with $YBa_2Cu_3O_{7-x}$ ceramic superconductor, a composite superconductor can be made to have a higher critical current density as well as a very effective flux pinning.

When silver is deposited onto YBa₂Cu₃O_{7-x} to form an electrical contact, the interface between the normal metal silver and the superconductor behaves like the silver-superconductor composite. The flux trapping at the interface might cause problems to the electrical properties of the contact, especially after the contact is exposed to a magnetic field. It means that it will take some time for the low resistivity of the contact to recover from its high resistivity value after the magnetic field is removed. Therefore, a metal that does not enhance the flux trapping but forms low-resistivity contacts to superconductors is desirable. We will discuss the magnetic effect on silver-YBa₂Cu₃O_{7-x} superconductor contact as well as compare the silver contacts made in various ways with contacts made by other metals such as gold.

M7.232

WET CHEMICAL ETCHING OF HIGH-TEMPERATURE SUPERCONDUCTING FILMS IN EDTA SOLUTION.

E. K. Shokoohi, L. M. Schiavone, C. T. Rogers, A. Inam*, X. D. Wu*, L. Nazar, and T. Venkatesan, Bellcore, 331 Newman Springs Rd., Red Bank, NJ 07701; *Physics Department, Rutgers University, Piscataway, NJ 08854.

Developing suitable microfabrication techniques for thin films of high-temperature superconducting ceramics is of great importance to realizing the device potential of these films. To date, use of the existing etching techniques have been limited by problems such as very fast etch rates (0.5 $\mu\text{m}/\text{min}$), non-selectivity of the etch, difficulty of detecting the end-point, and potential T_c degradation due to material deterioration by the etch.

In this talk, we present a wet chemical etchant which selectively removes Y-Ba-Cu-O with a low etch rate. The etchant consist of ethylenediaminetetraacetic acid (EDTA) solutions in glycerol and water and can be conveniently used in standard photolithography. We use laser deposited Y-Ba-Cu-O films, 0.1 - 1.0 μm thick, on SrTiO₃, BaTiO₃, MgO and sapphire substrates. For a saturated solution of EDTA in water the process is reaction limited. The reaction rate for the bulk of the film is 0.14 $\mu\text{m}/\text{min}$, at room temperature, and 0.30 $\mu\text{m}/\text{min}$ at 80°C. A fast initial etching (0.4 $\mu\text{m}/\text{min}$) cleans the surface of the film from porous layers exposing the solid dense bulk of the film. Process induced T_c degradation is less than 1°K and no larger than the accuracy of the experimental measurements. Details of the processing conditions, the reaction kinetics, and their effect on the morphology and the physical properties of the films will be discussed.

M7.233

CHARACTERIZATION OF HIGH-TEMPERATURE SUPERCONDUCTING MATERIALS IN Y-Ba-Cu-O SYSTEMS.

Hiroshi Kezuka, Department of Electronics, Tokyo Engineering University, 1404-1 Katakura, Hachioji, Tokyo 192, and Tomomi Masaki, Nippon Electronics, Engineering College, 1404-1 Katakura, Hachioji, Tokyo 192, Japan

The Y-Ba-Cu-O Systems have been reported with superconducting transition temperatures (T_c) over 90K. In order to investigate the material characterization in Y-Ba-Cu-O systems, optical study would give us useful information for the films(1) and bulk materials. The purpose of this work is to obtain the optical properties of Y-Ba-Cu-O systems as a surface impedance.

All samples are characterized by X-ray diffraction and SEM with energy dispersive X-ray analysis.

In this paper we report the measurements of optical constants ($n^*=n-jk$) of Y-Ba-Cu-O systems for 99.99% (4N)-purity.

As a result, optical constants of typical superconducting Y-Ba-Cu-O systems are $n^*=1.750-j0.326$ with $T_c=90.3\text{K}$ for 4N-purity.

(1) H. Kezuka et al, proc. International Conf. Electronic Materials, June 13-15, 1988, Tokyo, Japan.

M7.234

YBa₂Cu₃O_{7-x} Thin-Film d.c. SQUIDS with Focused Ion Beam Fabricated Weak-Links. B. Dutta, Physics Department, Middlebury College, Middlebury, VT 05753; C. T. Rogers, A. Scherer, and T. Venkatesan, Bellcore, 331 Newman Springs Rd., Red Bank, NJ; X. D. Wu Physics Department, Rutgers University, Piscataway, NJ 08854.

We are investigating thin-film d.c. SQUID magnetometers fabricated from very high quality laser deposited YBa₂Cu₃O_{7-x} (YBCO). Because these films are non-granular, they display low flux noise and microwave loss and are thus expected to produce low-noise SQUID loops. However, the lack of naturally occurring grain junctions requires that we intentionally fabricate weak-links. At present, we are attempting to fabricate the weak-links using a focused liquid-metal Ga ion beam (roughly 50 nm spot size) to thin and damage narrow strips of YBCO in the SQUID loop. Preliminary data on single wires indicates that this process can be controlled to produce good weak-links. We have designed a variety of d.c. SQUID loop inductances and geometries and have used our multi-layer laser deposition capability to produce planar thin-film YBCO coupling coils with inductances ranging from 1 to 500nH. Such coils, in conjunction with controlled weak-link fabrication, should lead to optimized high- T_c SQUID performance.

M7.235

FABRICATION AND PROPERTIES OF HETERO-EPITAXIAL MULTILAYER STRUCTURES OF METAL-OXIDE SUPERCONDUCTORS

H. Dorsett, A. Inam and X. D. Wu, Physics Department, Rutgers University, Piscataway, NJ 08854; C. T. Rogers and T. Venkatesan, Bellcore, 331 Newman Springs Rd., Red Bank, NJ 07701.

For device applications of the new high T_c superconductors, we have demonstrated a variety of multilayer structures using the family of 90 K superconducting compounds. Ion beam channeling, transmission electron microscopy and X-ray diffraction studies will be presented showing the nearly single crystalline growth of lattice-matched multilayered structures. Heterostructures displaying SNS device characteristics, where N is Pr₁Ba₂Cu₃O_{7-x}, have already been demonstrated and progress in the fabrication of SIS junctions will be reported. Results obtained from Auger electron spectroscopy on the sharpness of the interfaces and the relative diffusion of cations at different deposition temperatures indicate best interface sharpness of < 1 nm.

M7.236

IONIZING RADIATION EFFECTS ON THIN FILM HIGH TEMPERATURE SUPERCONDUCTORS. Steven D. Mittleman, Barry A. Kirby, Alvin J. Drehman, Bruce L. MacDonald, Robert J. Andrews, Michael N. Alexander, Rome Air Development Center, Solid State Sciences Directorate, Hanscom Air Force Base, MA.

There are many applications of solid state devices, ICs, and other electronic components such as communication satellites where a predictable response to ionizing radiation is essential. In the case of some low temperature superconductors, defects formed by electron radiation can increase critical current densities (J_c). In our study, thin films of sputtered Y-Ba-Cu-O with a T_c greater than 85K were irradiated with 1 MeV electrons and Co-60 gamma rays up to an equivalent dose of 40 Mrads (Si). Significant changes in J_c were observed while the critical temperature, T_c , remained unchanged. All irradiations and J_c measurements were performed with the sample held below the transition temperature to avoid annealing effects. T_c measurements on irradiated samples were kept in a temperature range not exceeding 110K for the same reason.

A more complete analysis of J_c as a function of radiation dose, temperature during radiation, and material compositional variations will be presented.

M7.237

FABRICATION OF HIGH T_c SUPERCONDUCTING COMPOSITE STRUCTURES.

D. T. Shaw, S. Patel, J. Chang, S. Witanachchi, Y. Z. Zhu, L. Song, and Y. H. Kao. Institute on Superconductivity, State University of New York at Buffalo, Bonner Hall, Buffalo, NY 14260

Reported improvements in the superconducting properties of silver doped YBCO has led us to fabricate composite structures on Yttrium stabilized zirconia (YSZ) and stainless steel (SS) substrates. These layered structures such as YBCO/Ag/YBCO on YSZ and SS have been grown in-situ by laser ablation using a 193 nm ArF excimer laser. The thickness of YBCO was 0.1 to 0.3 μm and the silver layers were 0.015 to 0.05 μm . Substrate temperature was varied from 550°C to 650°C. The layered structure was heat treated at 400°C for 5 min. up to 1 hour to allow a fraction of the silver interlayer to diffuse into the YBCO. Zero resistance temperature varied from 77K to 83 K for the SS and 83K to 90K for YSZ. Critical currents at 40K by transport measurement was in excess of 7.5×10^5 amps/cm² for films on YSZ and 10^4 amps/cm² on SS. (some of the measurements were limited by the contact resistance). Mechanical straining of the film on SS showed a tolerance of ~0.2% strain for a fifty percent decrease in critical current. Results on Auger profile, critical temperature and currents of the composite structure will be presented, and the mechanical strain effect of SS supported film will be discussed.

M7.238

INFLUENCE OF METALLIC SILVER INFILTRATION ON THE MICROSTRUCTURE AND TRANSPORT PROPERTIES OF YBaCuO. L. Ryelandt, M. Cassart, A. Vandenbosch, F. Delannay and J-P. Issi. Unité de Physico-Chimie et de Physique des Matériaux, 1 Place Croix du Sud, B 1348 Louvain-la-Neuve, Belgium,

Wires of YBa₂Cu₃O_{7-x} have been prepared by swaging using silver for the metal sheath. The influence of the heat-treatment conditions on the microstructure and transport properties (i.e. thermal conductivity, thermoelectric power and electrical resistivity) has been investigated. The same measurements have been performed on bulk samples pressed and sintered between two silver sheets.

Due to the infiltration of silver into the superconductor, composite materials were obtained. The electrical resistivity was found to decrease by more than one order of magnitude. It was observed that the presence of silver inside the bulk of the superconducting ceramic affects the grain growth and the porosity, that it does not reduce the T_c and J_c values, and that it leads to a very small contact resistance between the oxide and the metal.

M7.239

HIGH T_c SUPERCONDUCTOR FIBERS FROM METALLO-ORGANIC PRECURSORS. K. C. Chen and K. S. Mazdiyasni, General Atomics, San Diego, CA.

Homogeneous stoichiometric solution of yttrium i-propoxide, barium i-propoxide and copper ethylhexanoate has been prepared. This solution was converted to a resin-like material and is readily re-dissolved by organic solvents. The viscosity could be reversibly adjusted by adding or removing solvents. Modifications in the solution chemistry have been made to reduce barium carbonate formation during organic pyrolysis.

Single phase superconducting YBa₂Cu₃O_{7-x} fibers have been continuously spun from the viscous solution. Compositions other than stoichiometry have been prepared to examine the possibility of forming nano-scale inclusions in the "123" fiber. Seeding with fine DyBa₂Cu₃O_{7-x} crystallites with assistance of magnetic field was used to achieve crystallographic alignment. The phase and microstructural evolution and electrical properties of the fibers will be discussed.

M7.240

FORMATION OF SPUTTERED Y-BA-CU-O SUPERCONDUCTING THIN FILM ON METAL SUBSTRATE. H. Hayakawa, Y. Iijima, N. Sadakata and O. Kohno, Tokyo Laboratory, Fujikura Ltd., Tokyo, Japan

For the application of the high temperature superconducting materials, it is important to fabricate composites on long flexible substrate without diminishing excellent superconducting performance. Metal alloy substrates are useful because their flexibility and thermal properties as a conductor. Meanwhile, films of well-aligned grains with preferred orientation and high critical current density have been reported through thin film processing. Sputtering is one of the method to fabricate thin films with good superconductivity, however, the thin layer of the films on the substrate may be easily contaminated by the diffused elements from the substrate during the deposition. In order to eliminate the degradation of the films, putting intermediate buffer layer which reduce the interaction was found to be effective to realize good superconductivity. In this paper, we report the effect of the intermediate buffer layer of SrTiO₃ on nickel based alloy. The buffer layers and Y-Ba-Cu-O thin film were prepared by sputtering. The substrate was heated 550-700°C during the deposition. The microscopic morphology of the layers and transporting J_c characteristics are discussed.

M7.241

A MULTIFILAMENT SUPERCONDUCTING WIRE OF Y-Ba-Cu-O, L.R. Motowidlo, G.M. Ozeryansky, IGC, Advanced Superconductors Inc., Waterbury, CT, R.D. Blaughter, D.W. Hazelton, J.A. Rice, Intermagnetics General Corporation, Guilderland, NY.

Long lengths of Multifilament Superconducting wire with a Ag matrix of high Tc Y-Ba-Cu-O ceramic superconductor have been prepared using a powder precursor approach. Monofilaments were initially cold drawn or hydrostatically extruded, restacked into a billet and cold drawn to final size. A 0.4mm diameter multifilament wire was obtained with 29 filaments (15 μ m) of Y Ba₂ Cu₃ O₇ around a central core of 123. Following wire drawing, the conductor was annealed in oxygen to completely equilibrate the 123 to obtain optimum superconducting properties.

Heat treatment schedules were varied to evaluate the influence on critical current density. Pre-reaction of the 123 powder precursor prior to billet assembly appears to produce the best results. Transport measurement at 1 μ V/cm sensitivity showed current density in excess of 10³ A/cm² at 77K. The maximum length achieved was nearly 500 feet. This paper will present the results to date with a projection for future work.

M7.242

110K SUPERCONDUCTING FIBERS OF [Bi,Pb(Sb)]₂Sr₂Ca₂Cu₃O_{10+x} Zhang Jincang, Henan Normal University, Xinxiang, China; He Aisheng, North University of Technology, Beijing, China; Huo Yujing, Xiang Jiong and He Yusheng, Tsinghua University, Beijing, China

Superconducting fibers in [Bi,Pb(Sb)]₂Sr₂Ca₂Cu₃O_{10+x} high Tc superconducting materials have been prepared by means of the laser-heated pedestal growth method (LHPG). The onset transition temperature reached is 120K and zero resistance temperature reached is 110K. The critical current density (Jc) is greater than 10³ A/cm² at about 77K. The minimum diameter of fibers have reached 35 μ m, of which the flexibility is quite good.

The growth condition and the thermal treatment were also studied. It was found that the slower growth rate and the smaller diameter will lead to a better quality of the fiber. At the moment, thermal treatment was still necessary for the fabrication of 2223 phase superconducting fiber.

X-ray diffraction and SEM results indicate that the fibers have highly aligned morphology with the a-axis paralleled to the growth direction. Such strong textured structure will provide optimized path for superconducting current along the fiber. Unlike the case for the 2212 phase Bi-based superconducting fiber, EDAX analysis showed that the deviations of composition from source rod are quite noticeable for all elements, except for that of Sr. However, it is believed that the existence of Pb and Sb is vital for the stability of 110K high temperature phase of the Bi-based superconducting fibers.

M7.243

COILS OF YBCO TEXTURED BY PARTIAL MELTING. Ningxia Tan, Antony J. Bourdillon, State University of New York at Stony Brook, N.Y.; and N. Savvides, CSIRO Division of Applied Physics, Sydney 2070, Australia.

The majority of anticipated applications of high temperature superconductors require material with critical current densities higher than are currently attained in bulk ceramics. Improvements in current carrying capacity and in mechanical strength of fibres can be obtained by means of

crystal growth by partial melting of Y-Ba-Cu-O which melts incongruently. Segregation of fluid products, by gravity, tends to occur upsetting the stoichiometry of the material and producing insulating phases which often form at grain boundaries. However if recrystallization is arranged parallel to a vertical thermal gradient enhanced stoichiometry results and insulating phases can be removed by zone refinement. Coils require texturing with tangential growth. These can be mounted on non-reacting formers which are rotated in a furnace operated at 960 degrees centigrade ambient, with a local vertical gradient near to 1025 degrees at the coil.

The microstructure and electrical properties of textured coils have been examined from material wound in various ways. Processing techniques are selected to overcome the loss of mechanical strength which occurs during partial melting. Experiments have been extended to (Bi,Pb)-Sr-Ca-Cu-O, where partial melting destabilizes the high temperature (110 K) superconducting phase.

M7.244

THERMAL ANNEALING STUDY OF HIGH-Tc YBaCuO AND BiSrCaCuO SUPERCONDUCTING WIRES. Y. D. Yao(a), J. W. Chen(b), Y. Y. Chen(a), W. S. Pern(a), I. N. Lin(c), P. C. Yao(c), S. J. Yang(c) and S. E. Hsu(c). (a). Institute of Physics, Academia Sinica, Taipei, Taiwan, R.O.C. (b). Department of Physics, National Taiwan University, Taipei, Taiwan, R.O.C. (c). Materials R & D Center, Chung Shan Institute of Science and Technology, Lungtan, Taoyuan, Taiwan, R.O.C.

High-Tc YBaCuO and BiSrCaCuO superconducting wires have been fabricated by powder metallurgy technique. Copper and silver tubes were used as the external jackets [1]. High critical current density have been observed in these wire-type superconductors. Thermal annealing treatments for all the wire-type samples were performed between 773 K and 1230 K. Magnetization studies show that the superconducting properties can be improved after properly thermal annealing of these samples with silver jacket. The superconducting properties of all the samples after thermal annealing will be reported and discussed according to the magnetization studies.

1. Y. D. Yao, J. W. Chen, W. S. Pern, M. T. Yeh, I. N. Lin, P. C. Yao, S. J. Yang and S. E. Hsu, Proc. Ann. Conf. Chin. Soc. Mat. Sci. P. 1131 (1989).

M7.245

STUDIES ON MICROSTRUCTURE - PROPERTY RELATIONSHIP OF YBa₂Cu₃O_{7-x} + Ag COMPOSITE WIRE. S. Samajdar and S.K. Samanta, Plasticity Laboratory, Department of Mechanical Engineering and Applied Mechanics, 2250 G. G. Brown, The University of Michigan, Ann Arbor, Michigan 48109-2125, USA.

Silver is known to act as a compatible metal host for designing a microcomposite system with the high temperature superconducting ceramic YBCO^{1,2}. The unique role played by nascent silver generated from the silver monoxide precursor during sintering as well as warm compaction of the powder mix is illustrated with the help of light optical micrography.

It is seen that electrical as well as mechanical properties of the bulk composite is significantly governed by its microstructure. The microstructure, in turn, could be controlled by suitable heat treatment and proper selection of the fabrication process parameters at every step. Attempting a structure-property-processing correlation, a microstructure controlled scheme for fabricating superconducting composite product of useful shapes is discussed.

Successful fabrication of thin (0.75 mm dia.) and long (450 mm) flexible wire following this route is also reported here.

- 1) S. K. Samanta et al. "A Novel Processing Technique for Fabrication of Flexible High T_c Superconducting Wire", to be published in J. Appl. Phys., November (1989).
- 2) S. Samajdar et al. "A Phenomenological Model on The Deformation Mechanism of $YBa_2Cu_3O_{7-x} + Ag_2O$ Composite" to be published in J. Mat. Sci. Lett. (1989).

M7.246

MICROWAVE PROPERTIES OF HIGH QUALITY Y-Ba-Cu OXIDE THIN FILMS FROM 0-100 GHz.

A. Inam and X. D. Wu, Physics Department, Rutgers University, Piscataway, NJ 08854; L. Nazar and T. Venkatesan, Bellcore, 331 Newman Springs Rd., Red Bank, NJ 07701.

We have performed intra- and extra-cavity microwave frequency (1-100 GHz) measurements on high quality $Y_1Ba_2Cu_3O_{7-x}$ superconducting thin films, on (100) $LaAlO_3$ substrates, fabricated by the pulsed laser deposition technique. These films exhibit superconducting transition temperatures > 90 K and critical current densities of 5×10^6 A/cm² at 77 K. Ion beam channeling and X-ray diffraction studies indicate that films grown on the $LaAlO_3$ substrate possess remarkably high crystalline quality. Microwave surface resistance values at 77 K for these films are found to be more than one to two orders of magnitude lower than for copper at 77 K for almost the entire frequency range explored. We believe that the reason for such low surface resistances in these films is the virtual absence of grain and phase boundaries coupled with the high degree of crystallinity. Our studies show that the residual resistance measured below T_c is at present dominated by losses occurring in the substrate and the cavities rather than by losses intrinsic to the Y-Ba-Cu oxide superconductor.

M7.247

MICROSTRUCTURE AND FLUX PINNING CHARACTERISTICS OF HIGH- T_c SUPERCONDUCTING TAPE PREPARED BY THE DIRECTIONAL MELT-GROWTH TECHNIQUE. M. Okada, R. Nishiwaki, T. Matsumoto, T. Kamo, K. Aihara, and S. Matsuda. Hitachi Research Laboratory of Hitachi Ltd., Hitachi, Ibaraki 319-12, Japan.; M. Seido, Metal Research Laboratory of Hitachi Cable Ltd., Tsuchiura, Ibaraki 300, Japan.

Dense and aligned high- T_c superconductor tapes with metallic sheath were prepared by a directional melt-growth technique. Critical current density and flux pinning characteristics were studied in relation to the oriented microstructures.

In our previous paper(1), we reported that the drawing-rolling technique is effective to enhance the J_c 's of silver sheathed high- T_c superconducting tapes. The J_c 's of the tape, however, decrease sharply in the external magnetic field, since the superconducting core consists of sintered polycrystalline. In this study, a directional melt-growth technique is applied to improve the crystallite alignment and the grain boundary weak-link in the Y-123 and Tl-2223 tapes.

It was observed that the plate shaped Y-123 or Tl-2223 crystals (1 to 10 mm long and 0.05 mm thick) including fine second phases (ex. Y-211 crystals) were aligned parallel to the surface of the tape. Critical current density and

flux pinning characteristics in the tape will be discussed.

- (1) M. Okada et al : Jpn. J. Appl. Phys. 27(1988)L2345.

M7.248

REPRODUCIBLE, LARGE-SCALE PRODUCTION OF THALLIUM-BASED HIGH TEMPERATURE SUPERCONDUCTORS. R. L. Gay, D. Stelman, J. C. Newcomb, J. M. Pechenik, and L. F. Grantham. Rockwell International, Rocketdyne Division, 6633 Canoga Avenue, Canoga Park, CA 91303

The Rocketdyne Division of Rockwell International has developed a large scale spray-calcination technique, generic to the preparation of ceramic high temperature superconductor (HTSC) powders. The technique has the advantage of producing homogeneously mixed powders on a fine scale. Production of both yttrium- and thallium-based HTSCs has been demonstrated using this technique.

In the Rocketdyne superconductor spray calciner, solutions of the desired composition are atomized as a fine mist into a hot gas. Evaporation and calcination are almost instantaneous, yielding an extremely fine, very reactive, and homogeneous oxide powder. The calciner is 30 inches in diameter and can produce relatively large amounts (approximately 100 g/h) of yttrium- or thallium based HTSC without carbon contamination. Metallic impurities are less than 600 ppm.

Bulk samples of the thallium-based HTSC have been cold-pressed and sintered, and an optimized temperature schedule was found to produce the 2-2-2-3 compound. Sintered samples were examined by x-ray diffraction and characterized by measurements of T_c . Critical temperatures in excess of 110 K were found.

M7.249

FABRICATION OF $Bi_2Sr_2Ca_nCu_{n+1}O_x$ THIN FILMS BY LASER ABLATION. J. Chang, S. Witanachchi, S. Patel and D. T. Shaw. Institute on Superconductivity, State University of New York at Buffalo, Bonner Hall, Buffalo, NY 14260

Different phases of $Bi_2Sr_2Ca_nCu_{n+1}O_x$ ($n = 1-4$) thin films were grown by laser ablation. A 193 nm ArF excimer laser was used. Films obtained were oriented with the c-axis perpendicular to the substrate surface. The c-axis lattice parameters were about 31 Å, 37 Å, 43 Å, and 49 Å corresponding to $n = 1, 2, 3$, and 4, respectively. The substrate temperature was kept in the range of 500°C to 650°C during the deposition. These phases can be controlled by varying the deposition rate and the oxygen pressure. The zero resistivity temperature of the as-grown 2212 phase films can approach 80K. The resistance dropping around 110K for the as-grown $n = 2-4$ phase films was difficult to detect. These films are always characteristic of semiconductors. After a rapid post-annealing, these films became superconducting with zero resistivity temperatures of up to 100K with a sharp decrease in resistivity at 110K. Fabrication and properties of these c-axis oriented $Bi_2Sr_2Ca_nCu_{n+1}O_x$ films will be reported in detail at the conference.

M7.250

FORMATION OF 2223 PHASE IN Bi(Pb)-Sr-Ca-Cu-O SYSTEM DURING ANNEALING PROCESS. Chen Liquan, Huang Zuwei, Huang Yuzhen, Bi Jianqing, Ni Rongming and Zhao Zhongxian, Institute of Physics, Academia Sinica, P.O.Box 603, Beijing, China

The formation process of 110k phase during high temperature annealing has been studied by EDX combined with R-T measurement and X-ray diffraction. Starting material with nominal composition $Bi_{1-x}Pb_xSr_2Ca_2Cu_3O_{10}$ was sintered at 860°C for 24 hrs in air. Pellets pressed with sintered powder were annealed at 880°C for various time.

Nine types of grains with different composition can be distinguished from dark regions. They are 2212, 2223, 1114, 1112, 1111 and those rich in Ca-Cu, Sr-Ca-Cu, Bi-Cu and Sr-Bi-Cu respectively. After one day annealing, the samples contain small amount of 2223 grains. The major grains are rich in Sr-Ca-Cu and Ca-Cu. The percentage of 2223 grains and 1114 (rich in Cu) increased steeply in the samples annealed for 2 to 3 days. As the annealing process lasted up to 4 to 5 days, the number of these two type grains reduced and that of 1112, 1111 grains increased. These four type of grains could be considered as 110k phase. When annealing time increased from 1 day to 5 days, the 110k phase increased from 18% to about 100%. The evolution of the grains is following: grains rich in Sr-Ca-Cu and Ca-Cu \rightarrow 1114 (rich in Cu) \rightarrow 1112 \rightarrow 2223 \rightarrow 1111. More longer time annealing will lead to further loss of Ca and Cu.

M7.251

ROUTES TO HIGH- T_c SUPERCONDUCTING Tl-Ba-Ca-Cu-O FILMS USING ORGANOMETALLIC CHEMICAL VAPOR DEPOSITION. Darrin S. Richeson, Lauren M. Tonge, Jing Zhao, Jiming Zhang, Henry O. Marcy, Tobin J. Marks, Bruce W. Wessels, and Carl R. Kannevurf, Science and Technology Center for Superconductivity and the Materials Research Center, Northwestern University Evanston, IL 60208.

Films of the Tl-Ba-Ca-Cu-O high- T_c superconductor can be prepared by several organometallic chemical vapor deposition routes. Two of these involve Ba-Ca-Cu-O films that are first prepared on yttria-stabilized-zirconia using the volatile metalorganic precursors Ba(heptafluorodimethyl-octanedionate)₂, Ca(dipivaloylmethanate)₂, and Cu(acetylacetonate)₂. Deposition is carried out at 5 torr pressure with argon as the carrier gas and water vapor as the reactant gas. Thallium is next incorporated in these films either by vapor diffusion using bulk Tl-Ba-Ca-Cu-O as the source, or by organometallic chemical vapor deposition using Tl(cyclopentadienide) as the source. The latter deposition is carried out at atmospheric pressure with an argon carrier and water-saturated oxygen reactant, followed by rapid thermal annealing. Both types of films consist primarily of the TlBa₂Ca₂Cu₃O_x phase, have preferential orientation of the CuO planes parallel to the substrate surface, and exhibit onset of superconductivity at -125 K with zero resistance by 105 K. Preliminary results of four-component Tl-Ba-Ca-Cu-O chemical vapor deposition onto various substrates will also be reported.

M7.252

EFFECT OF PROCESSING PARAMETERS AND POSTPROCESSING THERMAL CYCLING ON THE SUPERCONDUCTING PROPERTIES OF Ag/YBa₂Cu₃O_{7-x} WIRES. Miguel A. Ocampo, Emilio Orgaz, Centro de Investigación y Desarrollo CONDUMEX Blvd. Cervantes Saavedra 255, 11520 Mexico, D.F., Mexico, and Tatsuo Akachi, Instituto de Investigaciones en Materiales, UNAM, Apdo. Postal 70-360, 04510 Mexico, D.F., Mexico.

Preforms of silver tubes with YBa₂Cu₃O_{7-x} powder were drawn to obtain wires with diameters in the 0.25mm to 1.00mm range. Samples were sintered at 900 °C in oxygen for different times and post-oxygenation was performed in a closed camera at various oxygen pressures.

An improvement in the superconducting parameters T_c and J_c was observed as the pressure of oxygen was increased and as the thickness of the silver wall was decreased.

A small decrease in T_c was observed with thermal cycling of the samples between liquid nitrogen and room temperature. A wider study of this effect is under way.

Electrical measurements as well as SEM observations are presented.

M7.253

THE ROLE OF STRUCTURAL DEFECTS IN FLUX PINNING AND HIGH J_c IN THIN FILM Y-Ba-Cu-O SUPERCONDUCTORS R. Ramesh, D.M. Hwang, A. Inam, P. England, T. Venkatesan Bellcore, Red Bank, New Jersey 07701.

Thin film YBCO superconductors, deposited by the pulsed laser deposition technique, have been shown to have critical currents of up to 5×10^6 A/cm² at 77K. Additionally, these films have better resistance to magnetic field induced dissipation than single crystals of these cuprates. In this paper, we report results of detailed microstructural characterization of these films, and attempt to rationalize the transport properties obtained based upon the defect microstructure. The thin films consist of an intimate distribution of defects such as structural dislocations, intergrowths of the 1-2-4 phase, etc. This microstructure, consisting of a uniform distribution of structural defects may be the cause for the high critical currents obtained in thin films prepared by this technique.

M7.254

ELECTRON MICROSCOPY OF (Bi,Pb)-Sr-Ca-Cu-O WIRES WITH VARYING SINTER TIMES. Y. Feng*, R. E. Smallman*, I. P. Jones*, F. Wellhofer*, N. McN. Alford*, T. W. Button*, *Superconductivity Research Group, and School of Metallurgy and Materials, University of Birmingham, P.O. Box 363, Birmingham B15 2TT. U. K. *ICI Advanced Materials, Runcorn, Cheshire WA7 4QE. U. K.

(Bi, Pb)-Sr-Ca-Cu-O '2223' wires with varying sinter times have been investigated by parallel physical measurements and analytical electron microscopy. The numbers of phases present, their relative amounts, compositions and microstructure modulations with varying sinter times are reported and correlated with the superconducting properties. In particular, the recently reported long period (010) modulation in Pb doped '2223' is associated with the high T_c (105K) phase.

M7.255

FIELD AND TEMPERATURE-DEPENDENT SUSPENSION STUDIES OF HIGH TEMPERATURE SUPERCONDUCTORS. S.A. Solin, Michigan State University, East Lansing MI 48824 and NEC Research Institute*, Princeton, NJ 08540 and Y. Huang, Michigan State University, East Lansing, MI 48824.

We have employed a novel variable temperature-variable field/field gradient cryogenic levitometer, previously used¹ in levitation experiments, to study the orientationally dependent² suspension properties of the yttrium, bismuth, and thallium-based high T_c materials. Various morphological forms of the samples including pressed but unsintered pellets, sintered pellets and (heavily faulted e.g. twinned, syntactic intergrown, etc.) single crystals have been examined. As in the case of the levitation data, the zero-field-cooled suspension data exhibit a temperature and field dependent critical temperature, T_g above which suspension ceases but the transition to the nonsuspended state sharpens dramatically with increasing field and is in all cases much sharper than the corresponding transition at T_L to a nonlevitated state. Also the suspension data do not exhibit the low temperature slope discontinuity which is a dominant feature of the levitation data and has been associated with inter and intragranular weak links in the pellet and single crystal morphologies, respectively. These results will be explained using a modified version of the a field-gradient model which has successfully accounted for the levitation data.

Research supported by the MSU CFMR

* Current/permanent address

1. S.A. Solin and Y. Huang, Proc. Industry-University Adv. Matls. Conf., Denver, 1989, in press, and to be published.
2. S.A. Solin, N. Garcia, S. Vieira, and M. Hortal, Phys Rev. Lett. **60**, 744 (1988).

M7.256

X-ray Diffraction Study of the Crystallization Process of High T_c superconducting Bi-Glass Ceramics. Winnie Wong-Ng, Chwan K. Chiang, Stephen W. Freiman and Lawrence P. Cook, National Institute of Standards and Technology, Gaithersburg, MD 20899.

Glass-ceramic processing has been demonstrated to be a successful technique for the preparation of high T_c superconductor ceramic oxides. Two different compositions of glasses were prepared in the Bi-Pb-Sr-Ca-Cu-O system by melting starting powders in air at high temperature (1200°C), followed by rapid quenching. The study of the formation of glasses and their subsequent crystallization into high T_c superconducting glass-ceramics through a sequence of heat-treatment was carried out in order to understand the possible mechanism of the formation of high T_c materials and to improve the control of processing. X-ray powder diffraction, differential scanning calorimetry and scanning electron microscopy were used to study the characteristics associated with the crystallization process. This paper describes the characterization of these materials at different annealing stages, with an emphasis on the use of the X-ray technique. A comparison of phases formed in the two glasses will be made.

M7.257

ON THE IMPROVEMENT OF $\text{DyBa}_2\text{Cu}_3\text{O}_{7-x}$ PROPERTIES THROUGH BETTER SINTERING

The sintering of $\text{DyBa}_2\text{Cu}_3\text{O}_{7-x}$ has been improved by controlling powder size, sintering temperature, and sintering atmosphere. Sintering below the eutectic temperature has been explored for different temperatures and oxygen partial pressures. Sintering kinetics have been enhanced, yielding high density (up to 95%) and small grain size (down to 1.5 microns) with shorter sintering times and lower temperatures. Two sets of samples, one set containing 10 wt.% percent Ag_2O in the precursor powder and one undoped set were studied. The sintering rate decreased with decreasing temperature, even in samples sintered in low partial pressures of oxygen, (which increases the oxygen vacancy concentration). The addition of Ag_2O yielded a dispersion of Ag particles about one half the $\text{DyBa}_2\text{Cu}_3\text{O}_{7-x}$ grain size at grain boundary triple points. Ag tended to enhance grain growth slightly and did not improve the superconducting properties. Resistivity was as low as 220 $\mu\Omega\text{-cm}$ at 100K. Transport critical current densities were 5 times higher than previous larger grain size samples which were sintered above the eutectic temperature. The best of the new samples achieved $\sim 100 \text{ A/cm}^2$ at 4.2K in fields of 1-7 T. This improvement occurred in spite of more than twice as much grain boundary surface area. We conclude that the grain boundaries in sintered 123 compounds are not always barriers to current flow, and that increasing the proportion of non-basal plane faced grain boundaries is important in raising J_c .

M7.258

SOME OBSERVATIONS ON THE EFFECTS OF HIGH PRESSURES AND TEMPERATURES ON THE STABILITY OF $\text{Y Ba}_2\text{Cu}_3\text{O}_{7-x}$. R.K. Williams.

K. B. Alexander, J. Brynastad, T. J. Henson, D. M. Kroeger, G. C. Marsh and J. O. Scarbrough, Oak Ridge National Laboratory, Oak Ridge, TN.

Hot isostatic pressing and heat treatments in high pressure oxygen environments were used to study the effect of pressure on the stability of $\text{Y Ba}_2\text{Cu}_3\text{O}_{7-x}$. In an initial experiment, it was found that orthorhombic $\text{Y Ba}_2\text{Cu}_3\text{O}_{7-x}$ decomposed into a four phase mixture under an argon pressure of 2000 atmospheres at 925°C. Microanalysis showed that the phases present were tetragonal Y-123, Y-124, the 211 phase and $\text{Ba}_3\text{Cu}_5\text{O}_y$. It was found that the decomposition could be reversed by subsequent heat treatments at atmospheric pressure, but temperatures of 875°C or greater

were required to produce adequate kinetics. Samples swelled during the heat treatments at atmospheric pressure, and the voids formed were found to preferentially occur at grain boundaries. The void formation appears to be associated with internal oxygen rejection.

Further experiments showed that Y-123 is unstable at pressures as low as 40 atm. The polyphase, hot isostatically pressed material did not revert to Y-123 during a 48 hour heat treatment at 875°C in 40 atm oxygen. A cold pressed pellet of orthorhombic Y-123 powder was also exposed to 40 atm oxygen at 875°C and found to partially decompose, but some Y-123 was also present. Microprobe analysis showed that $\text{Ba}_3\text{Cu}_5\text{O}_y$ was one of the decomposition products. Since both hydrostatic and chemical effects are produced in oxygen, a second powder pellet was heat treated at 875°C in a gold capsule. Decomposition was more extensive in the hydrostatic experiment, and microprobe analysis showed that Y-123, Y-124 and $\text{Ba}_3\text{Cu}_5\text{O}_y$ were present. The T_c of this sample was 80K, indicating that the Y-123 was probably not fully oxidized.

*Research sponsored by the Office of Energy Storage and Distribution, Conservation and Renewable Energy, U.S. Department of Energy, under contract DE-AC05-84OR21400 with Martin Marietta Energy Systems, Inc.

M8.1

CONSIDERATIONS LIMITING CRITICAL CURRENTS IN HIGH-TEMPERATURE SUPERCONDUCTORS. M.

Tinkham, Harvard University, Cambridge, MA 02138.

This talk reviews the basic principles of superconductivity which limit the critical current, with particular reference to the high temperature superconductors. The conventional practical definition of a critical current density in terms of a voltage criterion such as 1 $\mu\text{V/cm}$ has no fundamental significance, since the result can depend strongly on the criterion chosen. This problem is particularly serious with the high-temperature superconductors because of the greater prominence of significant resistance due to flux creep effects at the higher temperatures. The relation between the conventional pinning approach to determination of J_c within a continuum picture and the weak link Josephson junction coupling approach within a granular picture will be discussed, together with experiments on fluxon pinning in artificial arrays of Josephson junctions. The possible importance of intrinsic pinning related to fluctuations of stoichiometry and the discrete atomic structure of the ideal crystal will be considered.

The research was supported in part by the ONR and the NSF.

M8.2

FLUX MOTION AND DISSIPATION IN CUPRATE SUPERCONDUCTORS. B. Batlogg, T. T. M. Palstra and L. F. Schneemeyer, AT&T Bell Laboratories, Murray Hill, NJ 07974.

Magnetic flux motion in cuprate superconductors poses challenging conceptual questions and is closely related to properties of practical importance. We have studied the systematics of dissipation below T_c in all classes of high T_c compounds and find highest dissipation in superconductors with largest electronic anisotropy. Activation energies for flux motion of order kT are observed in large portions of the H-T phase space, which makes thermally activated dynamics a dominant phenomenon in cuprate superconductors. This is in marked contrast to traditional superconductors.

M8.3

HYSTERETIC DEPENDENCE OF CRITICAL CURRENT ON APPLIED MAGNETIC FIELD AND MAGNETIC IRREVERSIBILITY LINE CROSSINGS IN POLYCRYSTALLINE $\text{YBa}_2\text{Cu}_3\text{O}_7$. Thomas R. Askew and Richard B. Flippen, Central Research and Development Dept., E. I. du Pont de Nemours and Company, Inc., Wilmington, DE.

It has recently been observed (1,2) that the transport critical current density at temperatures near 77K exhibits a complex dependence on sub-Tesla applied magnetic fields and the previous history of such field strengths applied to samples of $\text{YBa}_2\text{Cu}_3\text{O}_7$. The relationship of this effect to magnetic irreversibility line (MIL) crossings will be discussed. The position of the MIL is measured by SQUID magnetometer detection of the irreversibility point and by applied field induced shift in the absorption component of the AC susceptibility. Data from these two methods will be compared, along with hysteresis data for several different morphologies of polycrystalline $\text{YBa}_2\text{Cu}_3\text{O}_7$. An explanation in the context of grain boundary structural properties will be attempted.

1. T. Hikata, et. al. Jpn. J. Appl. Phys. **28**, L82 (1989).
2. J. O. Willis, et. al. IEEE Trans. Magn. **25**, 2502 (1989).

M8.4

DISSIPATIVE EFFECTS OF VORTEX MOVEMENTS IN $\text{YBa}_2\text{Cu}_3\text{O}_7$ MEASURED BY MAGNETOTHERMAL EFFECTS. Izio Rosenman and Charles Simon, Groupe de Physique des Solides, U. Paris 7, Paris, France; and Gaston Collin, Laboratoire de Physique des Solides, U. Paris-Sud, Orsay, France.

We have measured the heat production related to vortex movement in YBC single crystals with mass extending from 20mg to 1g when a magnetic field is smoothly applied to the sample maintained in quasi adiabatic conditions. Temperatures range between 2K and 15K, and fields up to 70 KOe were applied.

We observe highly anisotropic magnetothermal oscillations (MTO) correlated to flux jumps in the sample, the flux penetration in the sample being monitored simultaneously: the temperature rises very fast (<2 sec) up to 20K and then falls slowly with a thermal time constant (appr. 50 sec). The period of the oscillations, ranges from 5KOe to 10KOe depending on the crystallographic orientation relative to the magnetic field. The heat pulses occur when the magnetic pressure is sufficiently strong to overcome the pinning force, then, the vortex move suddenly and rearrange themselves in an order corresponding to the value of the applied magnetic field. This motion gives rise to the heat produced. The maximum temperature attained in an MTO "pulse" is hence a direct measure of the pinning energy. Below a minimum field sweep velocity no MTO appear, this is related to the time dependence of the vortex motion and gives information on the rate of flux creep, this minimum corresponds to the value necessary to compensate the flux creep. In the low field region (< 10 KOe) the temperature rises smoothly up to a maximum below the field at which the first heating burst occurs, and this corresponds to the value of the applied field necessary to full penetration of the field in the sample (The H^* field in Bean model). MTO is hence an alternative method to the magnetic measurements for the determination of the principal parameters of flux penetration and flux pinning in superconductors.

M8.5 ABSTRACT NOT AVAILABLE

M8.6

ON THE RESISTIVE STATE OF HIGH TEMPERATURE SUPERCONDUCTORS IN MAGNETIC FIELD.

Yasuhiro Iye, *The Institute for Solid State Physics, The University of Tokyo, Roppongi, Minato-ku, Tokyo 106 Japan.*

Magnetotransport studies in the superconducting transition region were carried out using thin film samples of $\text{Bi}_2\text{Sr}_2\text{CaCu}_2\text{O}_{8+y}$ and $\text{ErBa}_2\text{Cu}_3\text{O}_{7-y}$. Superconducting fluctuation effect on the Hall conductivity as well as on the diagonal conductivity was investigated and discussed in comparison with a theory by Fukuyama *et al.* The fluctuation contribution to the Hall conductivity, $\Delta\sigma_{xy}$, is negative in sign and shows a stronger singularity than $\Delta\sigma_{xx}$, as T_c is approached from above.

The magnetic-field-induced resistive state below T_c is currently attributed to flux creep phenomenon. By a precise angular dependence study, we demonstrate a complete absence of dependence on the relative angle between current and field. This poses a serious question to the conventional picture of Lorentz-force-driven flux motion. The Hall effect in the resistive state exhibits a complicated temperature and field dependence, including threshold behavior and sign reversal.

M8.7

ELECTRICAL TRANSPORT DISSIPATION EFFECTS IN EPITAXIAL $\text{Y}_1\text{Ba}_x\text{Cu}_3\text{O}_{7-x}$ THIN FILMS.* D. K. Christen, C. E. Klabunde, J. R. Thompson,** H. R. Kerchner, S. T. Sekula, R. Feenstra, and J. D. Budai, Oak Ridge National Laboratory, Oak Ridge, TN, and **The University of Tennessee, Knoxville, TN.

$\text{Y}_1\text{Ba}_x\text{Cu}_3\text{O}_{7-x}$ thin films, 300–350 nm thick, were produced by co-evaporation of Y, Cu, and BaF_2 onto single crystal substrates of SrTiO_3 , followed by annealing in wet oxygen at 850 °C. Depending on processing conditions and substrate orientation, the films possessed different epitaxy and dramatically different transport properties. The best c-axis oriented films deposited on (100) substrate surfaces had critical current densities J_c that approached estimated material limits, with $J_c > 1 \text{ MA/cm}^2$ in zero magnetic field at 85K. At a resistivity criterion of about $10^{-11} \Omega\text{-cm}$, J_c remains greater than $2 \times 10^5 \text{ A/cm}^2$ for magnetic fields H to 6T, applied parallel to the crystalline a-b planes and perpendicular to the transport direction. This value is nearly two orders-of-magnitude higher than for the similar geometry with H parallel to the c-axis, for which J_c decreases rapidly for $H \geq 2 \text{ T}$.

Depositions on (110) substrate surfaces produced triaxial films comprised of finely divided domains having [110] and <103>-type orientations. These films had significantly lower T_c and J_c values, and exhibited temperature-dependent critical current densities indicative of thick, normal-barrier weak-link arrays. In large magnetic fields and at small current densities the dissipative response was ohmic and exhibited behavior predicted by flux creep/flux flow models, with the deduced pinning potential barriers varying as H^{-1} over a wide temperature range below T_c .

*Research sponsored by the Division of Materials Sciences, U.S. Department of Energy under Contract No. DE-AC05-84OR21400 with Martin-Marietta Energy Systems, Inc.

M8.8

LOW FIELD RESISTIVE BEHAVIOR OF $\text{Bi}_2\text{Sr}_2\text{CaCu}_2\text{O}_8$. R. B. van Dover, L. F. Schneemeyer, and J. V. Waszczak, AT&T Bell Laboratories, 600 Mountain Ave., Murray Hill, NJ 07974

Measurements of the resistivity of $\text{Bi}_2\text{Sr}_2\text{CaCu}_2\text{O}_8$ in low magnetic fields ($H \parallel \hat{c}$) reveals threshold behavior. Below a certain field, H_{th} , the resistivity is small ($\rho < 10^{-4} \rho_n$) while above this field the resistivity increases approximately linearly. This behavior is observed both in single crystals and oriented polycrystalline samples, at low current densities ($\rho < 0.1 \text{ A/cm}^2$), and is inconsistent with a description that is in

terms of flux creep, for which $\rho \sim \sinh(c/B)$ where c is a constant. The threshold field is substantially greater than H_{c1H} and may be related to the novel vortex interactions that have been postulated for this material.

M8.9

MAGNETIC RELAXATION IN $\text{Bi}_2\text{Sr}_2\text{CaCu}_2\text{O}_{8+x}$ SINGLE CRYSTALS. E. Agostinelli, P. Filaci, D. Fiorani, A.M. Testa, I.T.S.E., C.N.R. Area della Ricerca, Rome, Italy; G. Balestrino, Dip. di Fisica, Università di Salerno, Salerno, Italy; P. Paroli, Dip. d'Ingegneria Meccanica, II Università di Roma, Italy; J. Tejada, Dep. de Física Fonamental, Barcelona, Spain

We report the results of critical current and relaxation measurements in a $\text{Bi}_2\text{Sr}_2\text{CaCu}_2\text{O}_{8+x}$ single crystal.

Magnetization cycles were performed at different temperatures applying the magnetic field parallel to the c axis.

With increasing temperature the reversible regime of the magnetization cycles is rapidly restricted to low fields. J_c becomes strongly field dependent at temperatures so low as 20 K and vanishes at 30 K in presence of moderate fields.

The average pinning energy was determined by measuring the time decay of the zero field cooled magnetization at 4.2 K for different values of the external field (1 kOe; 3 kOe; 10 kOe) applied parallel to the c axis. The decay was found to be logarithmic, in agreement with the classical flux creep model.

The deduced average pinning energy decreases with the applied field: $U = 2.4 \cdot 10^{-3}$ eV for $H=1$ kOe; $1.0 \cdot 10^{-3}$ eV for $H=3$ kOe; $8 \cdot 10^{-4}$ eV for $H=10$ kOe.

M9.1

ATOMIC SCALE CHARACTERIZATION OF DEFECTS AND INTERFACES BY Z-CONTRAST STEM. S. L. Pennycook, M. F. Chisholm, D. E. Jesson, R. Feenstra, D. Mashburn, D. P. Norton, J. W. McCamy, and D. H. Lowndes, Oak Ridge National Laboratory, Oak Ridge, TN 37831.

A new technique for high-resolution electron microscopy is providing direct information on the atomic scale structure and chemistry of defects and interfaces. Using a scanning transmission electron microscope (STEM) unambiguous images are obtained, even at interfaces, which in many cases are interpretable intuitively. Planar defects in $\text{YBa}_2\text{Cu}_3\text{O}_{7-x}$ clearly exist in both interstitial and substitutional form. The first plane of the superconductor at a film/substrate interface can be seen directly and correlated with the subsequent growth and final film properties. Though structurally sharp, these interfaces can be chemically diffuse. The chemistry of low-angle tilt boundaries has been investigated and correlates with the critical current behavior. At low tilt angles an array of partial dislocations results in a fraction of the boundary area having the correct 123 structure, the remainder having a faulted structure. At higher tilt angles these dislocations collapse into triangular amorphous zones which are chemically identical to the adjacent 123 phase. This is therefore an intrinsic structural relaxation and is not due to impurity segregation.

We have found evidence for anisotropic solid-phase-epitaxial growth following ion implantation. Along the c direction, growth is slow and surface nucleation of polycrystalline 123 material occurs. Growth parallel to the c planes occurs fast and would allow materials modification through conventional ion implantation and thermal processing. Preliminary experiments on layer-by-layer deposition using a rapidly rotating multiple target and timed pulsed laser ablation will be described.

*Research sponsored by the Division of Materials Sciences, U.S. Department of Energy under contract DE-AC05-84OR21400 with Martin Marietta Energy Systems, Inc.

M9.2

Characterization of Superconducting $\text{YBaCu}(\text{F})\text{O}$ Thin Films with Three Different Orientations *
X.K. Wang, D. X. Li, D. Q. Li, Y. H. Shen, J. Q. Zheng, R. F. H. Chang, and J. B. Ketterson, Materials Research Center and Science & Technology Center for Superconductivity, Northwestern University, Evanston, IL 60208, U.S.A.

Epitaxial thin films of $\text{YBaCu}(\text{F})\text{O}$ have been prepared with: (1) the a -axis perpendicular to (100) SrTiO_3 ; (2) the c -axis perpendicular to (100) SrTiO_3 ; (3) the [110] axis perpendicular to (110) SrTiO_3 . Films were fabricated using a multilayer deposition technique involving three electron-guns containing Y, BaF_2 , and Cu under a pressure of 5×10^{-5} Torr of O_2 . As-deposited films, which contained polycrystalline and amorphous regions, were later annealed in a furnace under a flowing O_2 - H_2O atmosphere. XRD patterns, SEM and HRTEM images confirm that the films are highly oriented, essentially epitaxial. The a -axis oriented film exhibits zero resistance at 80K and a critical current density of $2.9 \times 10^6 \text{ A/cm}^2$ at 4.2K while the c -axis oriented film exhibits a T_c of 88K and a J_c of $0.9 \times 10^6 \text{ A/cm}^2$ at 4.2K; The J_c values were determined magnetically. The [110]-orientation film shows the sharpest transition with a transition width of 1K and zero resistance at 85K. The relation between chemical composition, substrate orientation, annealing history, microstructure, and the resulting superconducting behavior will be discussed.

* Work supported by the NSF/S&T Center (DMR 89-117), the NSF/MRC (DMR-85-20280), and the Office of Naval Research (N00014-88-K-0106).

M9.3

DIRECT OBSERVATION BY TRANSMISSION ELECTRON MICROSCOPY OF THE EARLY STAGES OF GROWTH OF SUPERCONDUCTING THIN FILMS. M. Grant Norton, Lisa A. Tietz, Scott R. Summerfelt and C. Barry Carter, Department of Materials Science and Engineering, Cornell University, Ithaca, NY 14853.

The fabrication of high quality thin films often depends on the early stages of the growth process during which epitaxy is established. The substrate surface structure generally plays a critical role at this stage. Many observations of the high- T_c superconductor film-substrate interface structure and chemistry have been made by transmission electron microscopy (TEM) of cross-section samples. Ion-milling induced damage, however, can be severe in these specimens. In the present study, the early stages of the growth of high- T_c superconducting thin films of Y-Ba-Cu-O have been studied by TEM using a technique which requires no post-deposition specimen preparation.

Ultra thin films (10nm) were deposited either by laser evaporation from stoichiometric bulk samples or by electron beam coevaporation of the metals directly onto self-supporting, ion-thinned, single-crystal ceramic substrates. The prepared thin foil substrates were chemically cleaned and annealed prior to deposition to remove damage resulting from ion-milling. The annealing temperature was chosen to induce surface faceting of the substrate leading to a stable well-defined morphology. The substrates investigated include (001)-oriented MgO , (001)-oriented SrTiO_3 and the technologically important (100)-oriented LaAlO_3 . The films were examined using TEM in order to determine the film orientation, composition and microstructure.

Standard films, 200 nm thick, were prepared under identical conditions to the ultra thin films. These films were superconducting as formed, having critical temperatures above 80K.

M9.4

CHARACTERIZATION OF CROSS-SECTIONS OF TlBaCaCuO THIN FILMS ON MgO SUBSTRATES BY ANALYTICAL AND HIGH RESOLUTION ELECTRON MICROSCOPY. J. Mayer, M. Lanham, T.W. James*, A.G. Evans, and M. Rühle**, Materials Department, University of California, Santa Barbara, CA 93106; * Superconductor Technologies Inc., 460 Ward Drive, Santa Barbara, CA 93111; ** now at: Max-Planck-Institut für Metallforschung, D-7000 Stuttgart 1, F.R.Germany.

Cross-sectioned TEM specimens of thin TlBaCaCuO superconducting films on ceramic substrates have been obtained using a newly developed preparation technique. The superconductor/substrate interface as well as grain boundaries and defects in the superconductor have been characterized by means of analytical and high-resolution electron microscopy.

The c-axis of all investigated TlBaCaCuO grains was found to be perpendicular to the interface and parallel to a cube axis of the MgO substrate. However, results of measurements of the angles between the axes of both materials in the planes parallel to the interface indicate that no epitaxial orientation relationship exists. EDX analysis and lattice images show no indication for impurity segregation or the formation of an amorphous layer at the interface and along grain boundaries.

The presence of intergrowth was confirmed by high-resolution electron microscopy. In addition, planar defects are formed due to a faulted sequence of the individual atomic layers perpendicular to the c-axis. The chemical nature of such defects could be determined by a quantitative evaluation of high-resolution micrographs.

M9.5 ABSTRACT NOT AVAILABLE

M9.6

THE PREPARATION OF Bi₂Sr₂CaCu₂O₈ FIBERS BY THE FLOAT ZONE PROCESS. Linda Moulton, Joseph Brenner, Material Science Dept., Stanford University, Stanford, CA; Perla Peszkin, Robert S. Feigelson, Center for Materials Research, Stanford University, Stanford, CA; and Dan Gazit, Nuclear Research Center Negev, P.O. Box 9001, Beer Sheva 84190, Israel.

A miniaturized float zone process using laser heating has been found to have potential for producing Bi₂Sr₂CaCu₂O₈ fibers which can carry high critical currents.⁽¹⁾ Growth stability and rate are two key issues which need to be addressed if suitable samples are to be produced for both property evaluation and prototype devices. Studies on the influence of growth rate on structure and properties will be discussed, along with the effects of growth atmosphere and post-growth annealing. For the growth of small diameter fibers (~ 30 μm), starting material density, homogeneity, and size are critical issues to the growth of long lengths of high quality fiber. Work on different strategies for starting material preparation will also be discussed.

1) R. S. Feigelson, D. Gazit, D. K. Fork, and T. H. Geballe, "Superconducting Bi-Ca-Sr-Cu-O Fibers Grown by the Laser-Heated Pedestal Growth Method," *Science*, Vol. 240, 1642 (June 17, 1988).

M9.7

110K Bi-Ca-Sr-Cu-O SUPERCONDUCTING FIBERS BY GLASS-TO-CERAMIC PROCESS. Haixing Zheng, Yi Hu, Yun-Seung Choi, Ren Xu, Patrick Lin and J.D. Mackenzie, Department of Materials Science and Engineering, University of California-Los Angeles, Los Angeles, CA 90024

A major part of applications of high-T_c superconductors requires the materials in the form of wires or fibers. The glass formation of Bi(Pb)-Ca-Sr-Cu-O system provide the opportunities to fabricate the materials into the fibers by the well developed glass-to-ceramic technology. In this work the melt-spinning technique to produce Bi(Pb)-Ca-Sr-Cu-O glass fibers will be described. The studies of the thermal analysis, x-ray diffraction and SEM techniques suggest that Bi₂Sr₂CuO₆ phase (T_c < 22 K) first

crystallizes from glasses, then transforms into Bi₂CaSr₂Cu₂O₈ phase (T_c ~ 80 K) and Bi₂Ca₂Sr₂Cu₃O₁₀ phase (T_c ~ 110 K) results from the dissolution of Bi₂CaSr₂Cu₂O₈ phase and the liquid phase. The Bi(Pb)-Ca-Sr-Cu-O ceramic fibers with zero resistance at above 100 K have been prepared by heat treated the glass fibers in the low oxygen atmosphere. The effect of microstructure on the critical current density J_c of the fibers have been studied. Finally the mechanical properties of glass fibers and glass ceramic fibers will be presented.

M9.8

DEVELOPMENT OF A COMPOSITE TAPE CONDUCTOR OF Y-Ba-Cu-O,* R.D. Blaugher, D.W. Hazelton, J.A. Rice, Intermagnetics General Corporation, Guilderland, NY.

Samples of a "prototype" composite tape conductor have been successfully prepared consisting of a layer of (123) Y Ba₂ Cu₃ O₇ on a Ni substrate with an MgO buffer layer. Layers of 123 were applied to the MgO/Ni substrate using either a powder precursor technique or vapor deposition. The composite samples were initially sintered at 910°C and equilibrated in oxygen at 450°C. These samples demonstrated promising mechanical properties with good adhesion to the substrate, tolerance to thermal cycling and ability to withstand nominal bending deformation without any cracking of the superconductor. The superconducting properties showed 123 orthorhombic formation with T_c onset between 60 and 92K. The depression in T_c onset for some of the samples was attributed to high Ni and Mg diffusion into the 123. Additional melt processing was performed to improve the current density, maintain superconductor continuity and preserve the mechanical properties. Preliminary transport measurements on selected samples have exceeded 1,000 A/cm² at 77K. This paper will review the results to date and discuss the potential for fabricating long lengths of conductor with technologically useful current density.

*Supported in part by SDIO Contract SDIO 84-88-C-0049 and an award from NYSIS in conjunction with NYS ERDA.

M9.9

PREPARATION OF HIGH T_c OXIDE SUPERCONDUCTING TAPE BY RF MAGNETRON SPUTTERING. M. Fukutomi, Y. Tanaka, T. Asano, H. Maeda, National Research Institute for Metals, Tsukuba Laboratories, Tsukuba-shi, Ibaraki, Japan and H. Takahara, Mitsui Mining & Smelting Co. LTD., Central Research Laboratory, Ageo-shi, Saitama, Japan

The feasibility of preparing YBaCuO and BiSrCaCuO films on metallic substrates was discussed in an attempt to fabricate a superconducting tape. Deposition method employed was an rf magnetron sputtering. MgO buffer layers were found to be a favorable choice to prevent the adverse reaction between the superconducting film and the underlying substrate. The MgO buffer layers used had a (200) preferred grain orientation. Particular attention was given to the preferential resputtering effect due to the bombardment of negative ions during sputtering. The substrate-cathode configuration used to achieve stoichiometric film composition was described. Highly oriented YBaCuO films have been obtained on a Hastelloy-X tape with a MgO buffer layer. The highest zero resistance temperature obtained so far of the YBaCuO thin films on a metallic tape was 81.0K in its as grown state, and a critical current density was 200 A/cm² at 77.4K and 10⁴ A/cm² at 60K. Preliminary results of YBaCuO films deposited on a bundle of Chromel fine wires were also reported.

In the Bi-Sr-Ca-Cu-O system, superconducting films with T_c of 70K were prepared on silver tapes. Studies have been focused on the development of buffer layers which can withstand high temperature post annealing processes without the degradation of the superconducting films.

M9.10

PROCESSING AND PERFORMANCE OF METAL-CERAMIC FIBER REINFORCED HIGH TEMPERATURE SUPERCONDUCTOR. S. Salib, C. Vipulanandan, and T. Stone, Texas Center for Superconductivity, University of Houston, Houston, Texas 77204-5506.

Growing large single crystals of the superconducting Yttrium-Barium-Copper oxide ($\text{YBa}_2\text{Cu}_3\text{O}_{7-\delta}$) phase is difficult and hence there is continuing interest in the fabrication of bulk components from sintered polycrystalline aggregates of the superconducting material. Aggregation of $\text{YBa}_2\text{Cu}_3\text{O}_{7-\delta}$ powder by compact molding and sintering results in a porous ceramic with poor mechanical properties and hence improving the ceramic properties is of interest.

It has been clearly demonstrated that Silicon Carbide (SiC) whiskers significantly improved the strength of ceramics without improving their ductility. On the other hand, steel fibers could improve the ductility. The objectives of this study were to investigate the improvement in the mechanical properties of the superconducting ceramic due to metal, ceramic, and metal-ceramic fiber reinforcements. Beam specimens 60 mm long with 13-mm square cross-sections were prepared at various porosities by varying the uniaxial compaction pressure. The fibers were mixed with the calcined powder and compacted, sintered, and then allowed to cool at a slow rate. The SiC content was varied up to 25% by volume and steel percentage was limited to 3% by weight. In order to limit the reaction between the continuous steel reinforcements and superconducting ceramic, silver (Ag) coating was used. The mechanical properties of the specimens were evaluated by 3-point beam tests. Performance of the fiber-reinforced ceramic composite was evaluated at 77 K and 300 K, followed by microstructural studies.

The effect of steel and SiC fibers on the mechanical and electrical properties has been verified in terms of the fiber content. Steel and SiC fibers had no measurable effect on the critical temperature and Meissner effect of the superconducting ceramic. While SiC ceramic increased the strength, the steel fibers improved the ductility.

M9.11

PREPARATION OF HIGH T_c Bi-Pb-Sr-Ca-Cu-O SUPERCONDUCTING FIBER BY LASER HEATED PEDESTAL GROWTH METHOD. K. Tomomatsu, A. Kume, H. Tominaga, Fujikura Ltd. Kiba, Koto-ku, Tokyo 135, Japan

Highly oriented Bi-Pb-Sr-Ca-Cu-O superconducting fibers including the high T_c phase have been prepared by laser heated pedestal growth (LHPG) method.

The fibers with 0.2-0.5 mm diameter have been grown from a small melting zone at the top of the sintered rod whose nominal composition was $\text{Bi}_{1.5}\text{Pb}_{0.5}\text{Sr}_2\text{Ca}_2\text{Cu}_3\text{O}_y$. The as-grown fiber had highly oriented structure, though it did not show any superconducting transition. The result of DC SQUID measurement of the fiber annealed at 850°C for 100 hours exhibited the superconducting transition at 110 K and 75 K corresponding to both the high and the low T_c phases. The annealed fiber maintained the orientation, and the convergence measured by XRD of the high T_c phase's a-b plane from the longitudinal direction was less than $\pm 5^\circ$.

Meanwhile, we have investigated the pseudobinary phase diagrams near the composition for the low T_c phase [1] and the high T_c phase. The obtained phase diagrams suggest that only the low T_c phase can be solidified from the liquid phase, therefore the annealing process is needed to yield the high T_c phase. The relationships between the composition of the initial rod, fiber growth condition, post-annealing condition and the characteristics of the fiber will be also discussed.

[1] K. Tomomatsu et al, Appl. Phys. Lett. to be published

M10.1

THIN FILM PROCESSING FOR HIGH- T_c SUPERCONDUCTORS OF Bi-SYSTEM. Kiyotaka WASA, Central Res. Labs. Matsushita Electric Co. Ltd., Moriguchi, Osaka 570, Japan

Basic thin film deposition processes for the high- T_c superconductors of Bi-systems are described in relation to their structure and superconducting properties. For the rare-earth high- T_c superconductors YBC the thin film deposition processes are classified into three processes:

- 1) deposition below crystallizing temperature followed by annealing [process (1)],
- 2) deposition above crystallizing temperature followed by annealing [process (2)],
- 3) deposition above crystallizing temperature without postannealing [process (3)].

For the Bi-system there appear several superconducting phases including the low- T_c phase $\text{Bi}_2\text{Sr}_2\text{Ca}_1\text{Cu}_2\text{O}_x$ and the high- T_c phase $\text{Bi}_2\text{Sr}_2\text{Ca}_2\text{Cu}_3\text{O}_x$. Thin films with these superconducting phases are synthesized by a selection of the substrate temperature T_s during the deposition in the process (1) and/or (2): the high- T_c phase with $T_c=100$ K is synthesized at $T_s > 800^\circ\text{C}$; the low- T_c phase with $T_c=80$ K, at $T_s < 600^\circ\text{C}$. However, these films often comprise intergrowth structure between the different superconducting phase.

The close control of the superconducting phase has been achieved by the layer-by-layer deposition in the atomic layer epitaxy process. XPS analyses suggest that their superconducting properties are governed by the valence of Cu which could be controlled by the deposition and/or postannealing process.

M10.2

PROCESSING AND PROPERTIES OF Bi-Sr-Ca-Cu-Oxide SUPERCONDUCTING THIN FILMS. D.A. Rudman, J.T. Kucera, M.M. Matthiesen, D.G. Steel, L.M. Rubin, D.W. Face, J.M. Graybeal, T.P. Orlando; M.I.T., Cambridge, MA 02139.

We have investigated the processing conditions necessary to produce superconducting thin films in the Bi-Sr-Ca-Cu-O system by sputter deposition. Films with compositions of $\text{Bi}_2\text{Sr}_2\text{CaCu}_2\text{O}_x$ (2212) and $\text{Bi}_2\text{Sr}_2\text{Ca}_2\text{Cu}_3\text{O}_x$ (2223) are deposited by co-deposition from metallic targets onto single crystal MgO and polycrystalline Ag substrates. The formation of the superconducting phase is very sensitive to the exact processing conditions (time, temperature and oxygen partial pressure) in the post deposition anneal, leaving a relatively narrow processing window for the formation of optimum material. For the 2212 phase, the films are nearly single phase and highly textured (c-axis normal, with $T_c(R=0)=84$ K and $J_c(77\text{ K}, H=0) \sim 10^4$ A/cm²). For the "2223" phase the films are formed without lead, and are a mixture of 2212 and 2223, with a $T_c(R=0)=106$ K. We have used these films to study transport properties in these systems. The critical current is highly anisotropic with applied field direction, and shows evidence of flux lattice melting at high temperatures, similar to single crystals. These films are also being used to fabricate simple grain boundary SQUID'S, and results from these devices will be reported.

M10.3

HIGH- T_c UNDOPED AND Pb-DOPED Bi-Sr-Ca-Cu-O THIN FILMS PREPARED BY ORGANOMETALLIC CHEMICAL VAPOR DEPOSITION. J.M. Zhang, H.O. Marcy, L.M. Tonge, B.W. Wessels, T.J. Marks, and C.R. Kannewurf, Center for High Temperature Superconductivity and Materials Research Center, Northwestern University, Evanston, IL 60208

Highly oriented films of the high- T_c undoped and Pb-doped Bi-Sr-Ca-Cu-O (BSCCO) superconductors have been prepared by organometallic chemical vapor deposition (OMCVD) using the volatile metal-organic precursors $\text{Cu}(\text{acetylacetonate})_2$, $\text{Sr}(\text{dipivaloylmethanate})_2$, $\text{Ca}(\text{dipivaloylmethanate})_2$, triphenyl bismuth, and tetraphenyl lead. Deposition is carried out at 2 torr with argon as the carrier gas and oxygen and water vapor as reactants. For Pb introduction into BSCCO films, two OMCVD approaches have been investigated. In the first approach, Pb is introduced by alternating OMCVD deposition of BSCCO and PbO_x films. In the second approach, Pb is incorporated into an OMCVD-derived BSCCO film by vapor diffusion using PbO as the source. After post annealing, energy dispersive x-ray analysis indicates most of the Pb originally doped into the films is lost. X-ray diffraction data and scanning electron micrographs reveal that Pb doping significantly improves the film morphology and crystalline orientation in such films. Both types of films on [100] single crystal MgO consist predominantly of the $\text{Bi}_2(\text{Sr,Ca})_3\text{Cu}_2\text{O}_x$ phase and have high preferential orientation of the crystallite c axes perpendicular to the substrate surface. Four-probe resistivity measurements indicate the onset of film superconductivity at ~ 110 K and zero resistance by 80 K. Possible mechanisms for the improvement of BSCCO films due to Pb-doping will be discussed. Effects of different reactant gases (e.g. N_2O , O_2 and H_2O) and different substrates on the superconductivity of OMCVD-derived BSCCO films will also be reported.

M10.4

PREPARATION OF Bi-Sr-Ca-Cu-O SUPERCONDUCTING THIN FILMS BY MOCVD. Shinji Gohda and Yasuhiro Maeda, Hoxan Research Laboratories, Hoxan corporation, 5-2 Kikusui, Shiroishi-ku, Sapporo 003 Japan.

Bi-Sr-Ca-Cu-O thin films have been prepared on MgO substrates using a MOCVD technique at low pressure. It was found in this experiment that composition ratio and crystal structure of thin films could be exactly controlled by the evaporation temperature of source materials, the flow rate of carrier gas argon, the temperature of substrates and oxygen partial pressure. By changing these conditions, it was possible to construct various crystal structure of thin films, high- T_c phase ($c=37\text{\AA}$), low- T_c phase ($c=30\text{\AA}$) or a mixed phase of these. High- T_c phase films had the composition ratio of approximately $\text{Bi}_2\text{Sr}_2\text{Ca}_2\text{Cu}_3\text{O}_x$, on the other hand, low- T_c phase films were obtained within wide range of composition ratio. Triphenylbismuth for Bi and β -diketone metal chelates for Sr, Ca and Cu were used as source materials. Thin films were deposited on (100) MgO substrates at the temperature between 800°C and 850°C . The film thickness was about 3000\AA . $T_c(\text{onset})$ of 115K and $T_c(\text{end})$ of 81K could be obtained for a film with the mixed phase of high- T_c phase and low- T_c phase in as-deposited state. X-ray diffraction showed that this film had a good crystallinity with the c -axis perpendicular to the substrate. The composition ratio of the film was approximately $\text{Bi}_1\text{Sr}_1\text{Ca}_1\text{Cu}_2\text{O}_x$. J_c of the film with $T_c(\text{end})$ of 81K was $1.0 \times 10^3 \text{ A/cm}^2$ at 77K.

M10.5

THE SYNTHESIS OF THE HIGH- T_c PHASE OF Bi-Pb-Ca-Sr-Cu-O THIN FILM BY SINGLE TARGET MAGNETRON SPUTTERING.* R.L. Meng, Li Gao, P. H. Hor, Y. Y. Sun, Y. Q. Wang, and C. W. Chu, Texas Center for Superconductivity, University of Houston, Houston TX 77204-5506.

The greater chemical stability of the Bi-Ca-Sr-Cu-O (BCSCO) to the ambient environment may make BCSCO a good material for HTS applications, provided techniques can be developed for the synthesis of single-phase material or of material with zero resistance at temperatures $> 77\text{K}$. A single target rf magnetron sputtering technique has thus been used in conjunction with fine-tuning the sputtering conditions and starting target composition. We have succeeded in preparing Pb-doped BCSCO films on the (100) MgO-substrate with an onset-temperature above 107K and a zero resistance temperature above 95K. These films exhibit a critical current density of $\sim 5 \times 10^4 \text{ A/cm}^2$ at 77K. Structural analyses by X-ray diffraction show a strong preferred orientation with the c -axis perpendicular to the film. The results demonstrate that the optimization of the target composition and of the annealing condition over a narrow temperature region is critical. The effects of sputtering condition, composition Pb-doping and thermal annealing will be presented and discussed.

* Work supported in part by DARPA and TCSUH.

M10.6

MOLECULAR BEAM EPITAXY OF LAYERED Bi-Sr-Ca-Cu-O COMPOUNDS. D.G. Schlom, J.T. Sizemore, A.F. Marshall, Z.J. Chen, J.S. Harris, Jr., J.C. Bravman, M.R. Beasley, T.H. Geballe, Stanford University, Stanford, CA 94305; and J.N. Eckstein, I. Bozovic, K.E. von Dessenbeck, Varian Research Center, Palo Alto, CA 94303.

We have grown smooth epitaxial films of Bi-Sr-Ca-Cu-O compounds in a modified molecular beam epitaxy (MBE) machine. Some of the films grown in this way were superconducting as grown. Four conventional resistively heated furnaces were used to provide stable fluxes of the constituents. Ozone was introduced close to the substrate during growth. It provided sufficient oxidation for the *in situ* growth of superconducting films. The molecular beams (with the exception of the ozone beam) were periodically shuttered in order to encourage c -axis growth of $\text{Bi}_2\text{Sr}_2\text{Ca}_n\text{Cu}_{n+1}\text{O}_x$ phases. *In situ* reflection high energy electron diffraction (RHEED) was used to study the crystal structure of the films during growth under a variety of growth conditions.

X-ray diffraction indicated that films grown in this way contained layered 2201, 2212, 2223, and 2245 - like phases. Cross-sectional TEM images of these films confirm the ability of this technique to grow metastable layered structures.

M10.7

Applications of Rapid Thermal Processing (RTP) to High Temperature Superconductors. D.S. Ginley, J. F. Kwak, E. L. Venturini, R. J. Baughman, and B. Morosin, Sandia National Laboratories, Albuquerque, NM 87185, and J. W. Halloran and M. J. Neal, CPS Superconductor, Inc., Milford, MA 01757

We report the application of rapid thermal processing (RTP) to the Y-Ba-Cu-O and Ti-Ba-Ca-Cu-O systems for spun wires, thick and thin films. In all cases, we have been able to produce superconducting material while operating in a non-equilibrium thermodynamic regime. Using conventional sintering, the Y-123 materials suffer from the problems of oxygen loss and undergo an orthorhombic to tetragonal phase transition during cool down. Similarly, the Ti HTS materials show pronounced Ti loss at the temperatures where sintering and film growth occur. RTP of spun Y-123 wires for 1 sec. at 1025 °C under oxygen has produced excellent grain growth and T_c of up to 92K with no further processing. The normal state resistivity is typically $> 1\text{m}\Omega\text{-cm}$ and the highest critical current to date has been 300 A/cm², leaving room for substantial improvement. RTP of Ti HTS thin films 0.3 μm thick has shown no Ti loss with 1-2 sec processing times at the melting point of the films (950°C) and zero resistance to 60K has been obtained. RTP is shown to be a new alternative for HTS processing with enhanced control of morphology and texture and the potential to produce high quality films on low cost, potentially reactive substrates.

This work was performed at Sandia National Laboratories, supported by the U. S. Department of Energy, Office of Basic Energy Sciences, under Contract No. DE-AC04-76DP00789.

M10.8

A NEW HYBRID PVD/OMCVD ROUTE TO HIGH- T_c SUPERCONDUCTING THIN FILMS OF Ti-Ba-Ca-Cu-O. D.S. Richeson, L.M. Tonge, X.K. Wang, H.O. Marcy, T.J. Marks, R.P.H. Chang, J.B. Ketterson, and C.R. Kannevurf, Science and Technology Center for Superconductivity and the Materials Research Center, Northwestern Univ., Evanston, IL 60208

Superconducting thin films of Ti-Ba-Ca-Cu-O have been prepared by a unique hybrid technique that combines electron beam evaporation with organometallic chemical vapor deposition (OMCVD). Multilayer thin films of Ba-Ca-Cu-O are prepared by sequential evaporation of BaF₂, CaF₂, and Cu sources onto single crystal MgO (100) or yttria-stabilized zirconia (YSZ) substrates followed by annealing in a water vapor saturated oxygen atmosphere. Thallium is then incorporated into these films in either of two ways: (1) rapid annealing of the Ba-Ca-Cu-O film in the presence of bulk thallium superconductor or (2) via OMCVD using (cyclopentadienyl)thallium as the source. The resultant films consist of predominantly single phase $\text{Ti}_1\text{Ba}_2\text{Ca}_2\text{Cu}_3\text{O}_x$ with the Cu-O planes preferentially oriented parallel to the substrate surface. Resistivity measurements indicate superconducting onset temperatures above 120 K with zero resistance by 104 K. By eliminating the water vapor anneal, residual fluoride, originating from the sources, may be left in the film. This leads to formation of predominantly g -axis oriented crystallites of the $\text{Ti}_1\text{Ba}_2\text{Ca}_2\text{Cu}_2\text{-O}_x$ phase. Effects of different substrates and annealing conditions on the properties of these hybrid Ti-Ba-Ca-Cu-O films will also be discussed.

M10.9

THE EFFECT OF ANNEALING CONDITIONS ON MAGNETRON SPUTTERED SUPERCONDUCTING TI-BASED THIN FILMS. S.H. Liou, Department of Physics, University of Nebraska-Lincoln, Lincoln, NE 68588-0111

There are many superconducting phases in the Ti-Ba-Ca-Cu-O system, in particular the $\text{Ti}_2\text{Ba}_2\text{Ca}_2\text{Cu}_3\text{O}_{10}$ phase has demonstrated superconductivity up to 125K. The annealing steps have been shown to be a crucial determinant of film quality. In this study, we discuss the formation of the superconducting phase of Ti-based films with systematically varied post-annealing temperature and annealing time. Thin films of $\text{Ti}_2\text{Ba}_2\text{CaCu}_2\text{O}_8$ and $\text{Ti}_2\text{Ba}_2\text{Ca}_2\text{Cu}_3\text{O}_{10}$ were routinely prepared on a wide variety of substrates (Y-ZrO₂, MgO, and SrTiO₃ etc.) The microstructure and crystal structure of the films depend

very much on the heat treatment and the chemical composition. For examples: We observed more rod or long needle-like microstructure in the Ba-enriched sample. If the film was deposited on a Y-ZrO₂ instead of on a MgO substrate, we observed that a longer annealing time and a higher annealing temperature are needed in order to form the $\text{Ti}_2\text{Ba}_2\text{Ca}_2\text{Cu}_3\text{O}_{10}$ phase.

A detailed x-ray, electron micro-probe, and scanning electron microscopy were carried out to evaluate the structure of superconducting phases formed for each annealing condition. The interrelation between the microstructure, crystal structure, and composition will be presented.

* The work was supported by NASA Lewis Research Center Grant NAG3-866, and by the University of Nebraska Foundation.

M10.10

ATOMIC RESOLUTION ELECTRON MICROSCOPY OF Bi-CUPRATES, R.Ramesh, B.G.Bagley, J.M.Tarascon, Bellcore, Red Bank, New Jersey 07701; C.J.D.Hetherington, B.Simion and G.Thomas, National Center for Electron Microscopy, Materials and Chemical Sciences Division, Lawrence Berkeley Laboratory, 1 Cyclotron Road, Berkeley CA 94720.

We report recent results of electron microscopic studies on the Bi based cuprates. Using HREM in conjunction with conventional electron microscopy and microanalysis, different types of defects have been characterized. The superconducting phase exhibits frequent variations in the stacking sequence. Dislocations, observed inside the grains, either introduce or accommodate the shear in the a - b plane and the local composition fluctuations. Grain boundaries along the short edge are generally disordered, whereas those near the long edge generally have a thin layer of the lower T_c polytypoid with the a - b plane as the grain boundary plane. Coherent intra-granular boundaries (most likely rotational) at the BiO layer are also observed. The defects we observe and have characterized in polycrystalline samples, will be contrasted and compared with those observed in thin films deposited by evaporation techniques and single crystals prepared by flux growth.

The work at Lawrence Berkeley Laboratory is supported by the Director, Office of Energy Research, Office of Basic Energy Sciences, Materials Sciences Division of the U.S.Department of Energy under contract No. DE-AC03-76SF00098.

M10.11

STUDY ON THE ELEMENTARY STEPS OF THE EPITAXIAL GROWTH OF Bi-Sr-Ca-Cu-O ON THE SURFACE OF Si AND MgO BY MEANS OF RHEED AND PHOTOELECTRON SPECTROSCOPES. Takashi HANADA, Maki KAWAI, Tsutomu GODA and Shousuke TERATANI RLEM, Tokyo Institute of Technology, Midori-ku, Yokohama, 227 ; The Institute of Physical and Chemical Research, Wako-shi, 351-01, Japan

Copper contained oxide superconductors are known to have layered structures. Successful attempts of forming various layered structures on substrates such as SrTiO₃ or on MgO in the case of Bi-Sr-Ca-Cu-O superconductor have been reported so far. In this paper, an attempt to elucidate the elementary steps of the epitaxial growth during the film formation by means of RHEED, XPS and UPS is reported. Clean surface of Si(001) and MgO(001) are obtained. Surface structure and the electronic states of Bi, Sr, Ca or Cu overlayers evaporated on are observed and the surface reaction between these surface and O₂ or N₂O are examined. The surface dangling bond of Si decreases by Bi evapo-

ration and disappears at the surface coverage of unity. Further increase in the coverage causes the formation of new state by Bi overlayer. Introducing oxygen on to this surface at 400 °C leads to the silicon oxide formation in the region of $\theta < 1$, and that of bismuth oxide in $\theta > 1$ region. At $\theta = 1$, where the dangling bond of silicon was completely compensated by the Bi, neither Si nor Bi was oxidized. Cu oxidation on MgO(001) by oxygen was also examined. Cu²⁺ was formed when $\theta < 1$, and with rather low temperature (150 °C). Raising temperature to 400 °C leads to the reduction of Cu²⁺ oxide to Cu⁺ oxide and to the Cu⁰.

M10.12

TEM STUDY OF CVD-GROWN Bi-Sr-Ca-Cu-O THIN FILMS ON (001) MgO SUBSTRATES. O. Ueda, T. Kimura, H. Yamawaki, M. Ihara, and M. Ozeki, Fujitsu Laboratories Ltd., 10-1 Morinosato-Wakamiya, Atsugi 243-01, Japan

CVD-grown Bi-Sr-Ca-Cu-O thin films on (001)MgO substrates with T_c at 110K have been structurally evaluated for the first time by transmission electron diffraction(TED) and high resolution transmission electron microscopy(HRTEM).

From plan-view observation, the thin films are found to consist of large domains oriented in the c-axis, with diameters of 15-100 μ m. It is also proved that there are two dominant orientation relationships between the domains and the substrate, i. e., a or b axis in the domain corresponds to the $\langle 100 \rangle$ or $\langle 110 \rangle$ direction of the MgO substrate within 10°. These domains exhibit incommensurate order along the b-axis. In addition, we have observed microdomains in which the a-axes are oriented normal to each other.

Cross-sectional observation indicates that the interface between the thin film and the substrate is very abrupt. Intergrowths of five different perovskite-related layers along the c-axis with different thickness are successfully observed. In the thin film, 80K phases with c=3.0 nm are dominant and 110K phases with c=3.6 nm are less likely, which is very consistent with the results from X-ray diffraction. Three other phases are very rarely observed. Furthermore, boundaries where the layered structure is different on both sides are often found.

M11.1

PROXIMITY-EFFECT AND TUNNELING IN YBa₂Cu₃O₇/METAL LAYERED STRUCTURES. L.H. Greene, W.L. Feldmann, J.B. Barner, L.A. Farrow, P.F. Miceli, R. Ramest, B.J. Wilkens, B.G. Bagley, Bellcore, 331 Newman Springs Rd., Red Bank, NJ 07701, M. Giroud, CRTBT-CNRS, Grenoble, FR. and J.M. Rowell, Conductus, Sunnyvale, CA.

Superconductive tunneling into high-T_c films is hampered by the short coherence lengths and non-superconducting surface layers. These properties together cause a dramatic depression of the order parameter at the free surface. A normal metal in close proximity to the high-T_c surface should allow the observation of a proximity gap. Therefore, we are fabricating Superconductor-Normal-Insulator-Superconductor (SNIS) layered structures for proximity tunneling spectroscopy.

Superconducting films of YBa₂Cu₃O₇ are grown in-situ by rf-magnetron sputtering from a single, composite target. The films, grown on (001)-MgO substrates, are shiny and highly oriented. X-ray analysis shows resolution limited rocking curves of $< .3^\circ$. Micro-Raman scattering of ultra-thin films ($< 200 \text{ \AA}$) shows the films are twinned with a-b axes lying in the plane, parallel to the (010) edges of the substrate. The microstructure, as determined by TEM cross-sectional analysis, shows a high degree of c-axis epitaxy and an intergrowth structure with c-axis values ranging from 11.7 to 13.5 \AA . Small area ($5 \times 10^{-6} \text{ cm}^2$) SNS junctions of YBCO/Au/Pb show supercurrents (with I_c's ranging from $< 40 \mu\text{A}$ to $\sim 1 \text{ mA}$ for 150 to 300 \AA thick Au) as well as Shapiro steps, indicative of a proximity Josephson junction. The SNIS structures for proximity tunneling spectroscopy are fabricated by in-situ growth of YBCO/(Au or Ag)/Ta trilayers.

Upon exposure to laboratory ambient for a few minutes, the Ta surface oxidizes to form a relatively low resistance ($\sim 1 \Omega$ for 1 mm^2) tunnel barrier. This barrier is reproducible, insulating and continuous since a sharp Pb gap and phonons from the Pb counter-electrode are routinely observed.

M11.2

MAGNETIC FLUX PINNING IN YBa₂Cu₃O_x FILMS.*

H. R. Kerchner, R. Feenstra, J. O. Thomson,** J. R. Thompson,** D. K. Christen, S. T. Sekula, and L. A. Boatner, Solid State Division, Oak Ridge National Laboratory, Oak Ridge, TN, and **The University of Tennessee, Knoxville, TN

The magnetic hysteresis was studied at audio frequencies for YBa₂Cu₃O_x films of different epitaxial orientations on single-crystal SrTiO₃ and KTaO₃ substrates. Deposition by coevaporation of Y, BaF₂, and Cu was followed by an anneal in flowing, wet oxygen at 800-850 °C. Low amplitude, reversible ac response gives evidence of strong flux pinning, while high amplitude, hysteretic response is used to obtain the limited critical current density J_c. Magnetic flux creep, manifest in the audio-frequency data, is clearly evident in dc magnetization data on the same samples.

Exclusion of small ac magnetic field is nearly identical for all samples and only weakly dependent upon the large dc field and upon temperature. In contrast the J_c deduced from the high amplitude ac response is sensitive to film orientation and grain morphology. It fits a scaling law widely used for describing Nb₃Sn and most other Al₅ materials.

*Research sponsored by the Division of Materials Sciences, U.S. Department of Energy under contract DE-AC05-84OR21400 with Martin Marietta Energy Systems, Inc.

M11.3

CRITICAL CURRENT DENSITY AND MICROSTRUCTURE OF YBa₂Cu₃O_{7-x} THIN FILMS AS A FUNCTION OF FILM THICKNESS. A. Mogro-Campero, L.G. Turner, E.L. Hall, and N. Lewis, GE Research and Development Center, Schenectady, NY.

The critical current density (J_c) of the best quality thin films of YBa₂Cu₃O_{7-x} (YBCO) on single crystal SrTiO₃ has been reported^x to exceed 10^6 A cm^{-2} at 77K. By coevaporation of Y, BaF₂, and Cu and postannealing at 850 °C, we have made thin films of YBCO on SrTiO₃ with zero resistance transition temperatures of 90K and J_c exceeding 10^6 A cm^{-2} at 77K for a film thickness of about 0.5 μm . Sample thickness was varied from about 0.2 μm to 2.5 μm . J_c is observed to decrease rapidly for the thicker samples, with little or no change in transition temperature. J_c decreases to $3 \times 10^5 \text{ A cm}^{-2}$ for the thickest sample. The room temperature resistivity of the films increases with increasing thickness.

Planar and cross sectional samples were prepared and investigated by transmission electron microscopy to determine the microstructure as a function of film thickness, and to correlate these findings with the electrical transport measurements. The 0.2 and 0.4 μm films were epitaxial single crystals with the YBCO c-axis normal to the film plane. Above 0.4 μm in thickness, the films consisted of an $\sim 0.4 \mu\text{m}$ layer adjacent to the substrate with the c-axis normal to the film plane, on top of which was epitaxial material with the c-axis in the plane of the film. The thickness dependence of the critical current density is in qualitative agreement with the microstructural observations.

M11.4

MICROSTRUCTURE AND PROPERTIES OF MIXED $\text{YBa}_2\text{Cu}_3\text{O}_{7-x}$ AND $\text{Y}_2\text{Ba}_4\text{Cu}_8\text{O}_{16}$ THIN FILMS. A.F. Marshall, A. Kapitulnik, Stanford University, Stanford, CA 94305; K. Char, R.W. Barton, Conductus, Inc., Sunnyvale, CA 94086; and S.S. Laderman, Hewlett-Packard Co., Palo Alto, CA 94304

Studies on the formation of the $\text{YBa}_2\text{Cu}_3\text{O}_{7-x}$ (123) and $\text{Y}_2\text{Ba}_4\text{Cu}_8\text{O}_{16}$ (248) phases in post annealed Y-Ba-Cu-O thin films have shown that a variety of mixed phase faulted and unfaulted structures can occur depending on the source materials, film stoichiometry and annealing temperatures. These structures are of interest both because they give information about the mechanisms of phase transformation to the 123 and/or 248 phases, which compete in a given synthesis regime, and because they sometimes exhibit new superconducting properties. Highly faulted mixed phase films, for example, can have T_c 's of 95-96 K as compared with 90 K for well ordered 123 and 82 K for well ordered 248.

We have been studying the nature of these faulted structures using transmission electron microscopy. High resolution microscopy of cross-section specimens shows the influence of faults on the c-axis layering whereas diffraction contrast analysis of planar specimens is more effective in showing the interaction of the faults with twins and second phase precipitates. Initial observations of 248 faults in predominantly 123 material indicate the formation of a dislocation-like strain pattern through the films which may hinder the formation of the well-ordered 248 phase. A variety of localized structural changes are observed, some of which may influence T_c if occurring in higher concentration.

M11.5

A STUDY OF GRAIN BOUNDARIES IN HIGH T_c SUPERCONDUCTING $\text{YBa}_2\text{Cu}_3\text{O}_{7-x}$ THIN FILMS USING HIGH RESOLUTION ANALYTICAL STEM. D. H. Shin, J. Silcox, S. Russek, D. Lathrop, and R. A. Buhrman, Cornell University, Ithaca, NY.

Grain boundaries in thin films of high T_c $\text{YBa}_2\text{Cu}_3\text{O}_{7-x}$ superconductor have been investigated with high resolution electron imaging and nanoprobe energy dispersive x-ray analysis. Films of $\text{YBa}_2\text{Cu}_3\text{O}_{7-x}$ were made by either reactive evaporation, sputtering, or laser ablation, on substrates of MgO or yttria-stabilized zirconia. The samples generally show good superconducting properties with transition temperatures around 80 K and high critical current densities of $\geq 1 \times 10^6$ Amp/cm² at 4 K. Samples with a tail near the transition temperatures were also used in order to study the correlation between the grain boundary structure and the superconducting properties.

A VG HB501A STEM operating at 100 kV was used for atomic structure imaging in both bright field and annular dark field imaging modes ($C_s = 1.2$ mm, $\alpha_{\text{obj}} = 13$ mrad, $\theta_{\text{cyl}} = 4$ mrad) and for EDX microanalysis with a 10 Å spatial resolution.

High resolution lattice images indicate that the grain boundaries of thin films of $\text{YBa}_2\text{Cu}_3\text{O}_{7-x}$ are mostly clean and coherent. No boundary layers of finite thicknesses, which are commonly found in bulk sintered samples, have been observed. However, strain during film growth may cause deformation of the lattice structure near the grain boundaries and this may result in the amorphization of a narrow region where the strain is most severe. The EDX profiles across the grain boundaries also indicate no composition deviations such as may be due to a second phase or to segregation, confirming the observation that the grain boundaries are mostly clean.

M11.6

EPITAXIAL GROWTH OF HIGH T_c THIN FILMS AND SUPERLATTICES: PROGRESS TOWARDS THE ARTIFICIAL CONSTRUCTION OF HIGH T_c SUPERCONDUCTORS. Jean-Marc Triscone, Michael G. Karkut,

Olivier Brunner, Louis Antognazza, and Øystein Fischer, Université de Genève, DPMC, 24 Quai E.-Ansermet, 1211 Genève, Switzerland.

We have prepared in situ YBaCuO and DyBaCuO thin films and YBaCuO/DyBaCuO superlattices by single target dc magnetron sputtering. For the single thin films, the orientation perpendicular to the surface is either c-axis, mixed a- and c-axis, and (103) depending on the choice of the substrate. T_{c0} 's are between 87 and 90K, residual resistivity ratios between 2.5 and 3. For the epitaxial (103) films prepared on (110) SrTiO_3 , x-ray diffraction pole figures show that these layers are single crystals with the [010] direction parallel to [001] SrTiO_3 and thus the CuO planes make an angle of 45° with the normal to the film surface. Absolute values of the resulting anisotropic resistivity have been extracted by the Van der Pauw and Montgomery method. The upper critical fields are markedly different from those of c-axis films. We have also for the first time epitaxially grown superlattices of YBaCuO/DyBaCuO by dc magnetron sputtering onto SrTiO_3 and MgO substrates. For c-axis multilayers the wavelengths range from 24Å (twice the c-axis) to 300Å and x-ray diffractograms show satellites peaks characteristic of multilayers for each wavelength. The crystalline coherence is of the order of the film thickness. The 24Å wavelength sample consists of, on the average, alternate planes of Y and Dy. The multilayers are superconducting with T_{c0} 's between 85 and 89K, transition widths of 2K and resistivity ratios of about 3. These results suggest that artificial structuring of high temperature oxide superconductors is within reach.

M11.7 ABSTRACT NOT AVAILABLE

M11.8

TUNNELLING MEASUREMENTS ON THIN FILMS OF $\text{YBa}_2\text{Cu}_3\text{O}_{7-\delta}$. A. M. Cucolo*, J. M. Valles, J. M. Phillips, M. Gurvitch, R. C. Dynes, and J. P. Garno, AT&T Bell Laboratories, Murray Hill, NJ 07974.

We have fabricated tunnel junctions of the type $\text{YBa}_2\text{Cu}_3\text{O}_{7-\delta}$ /barrier/Pb that show reproducible dV/dI characteristics. The $\text{YBa}_2\text{Cu}_3\text{O}_{7-\delta}$ films were chemically etched and then exposed to the ambient in order to form a natural tunnel barrier. Below the T_c of the $\text{YBa}_2\text{Cu}_3\text{O}_{7-\delta}$ films a structure associated with superconductivity appears in the conductance as a function of voltage. We discuss differences and similarities of these features and those obtained on tunnel junctions on chemically etched $\text{YBa}_2\text{Cu}_3\text{O}_{7-\delta}$ single crystals.

*On leave from Physics Dept., University of Salerno, 84081 Boronissi, Italy

M11.9

USE OF Si-YBaCuO INTERMIXED SYSTEM FOR PATTERNING OF SUPERCONDUCTING THIN FILMS Q. Y. Ma, E. S. Yang, G. V. Treyz, C. Shu, R. M. Osgood, Jr., Microelectronics Sciences Laboratories and Center for Telecommunication Research, 1312 Mudd, Columbia University, New York, NY 10027; and Chin-An Chang, IBM T. J. Watson Research Center, Yorktown Heights, NY 10598

A Si-YBaCuO intermixed system has been formed using rapid thermal annealing of $\text{Cu/BaO/Y}_2\text{O}_3/\text{Si}$ layered structures, which were deposited on MgO substrates by electron-beam evaporation. The electrical, structural, and interfacial properties of the Si-YBaCuO system have been analyzed by resistivity, X-ray diffraction, scanning electron

microscopy, X-ray photoelectron spectroscopy and Auger depth profiling measurements. It was found that Si mixed with YBaCuO during annealing, thus creating an insulating film. The non-conducting Si-YBaCuO system has been used to pattern YBaCuO films. The patterning process was carried out by first patterning a silicon layer using conventional photolithography and laser direct-writing. After the YBaCuO film has been deposited on the patterned film and annealed at 980°C, the patterned region became superconducting separated by Si-YBaCuO intermixed areas. Micron-sized line features with zero resistance temperatures above 77 K have been demonstrated.

M11.10

HIGH SPEED INFRARED DETECTORS USING Y-Ba-Cu-O THIN FILMS. J.P. Zheng, Q.Y. Ying and H.S. Kwok, Institute on Superconductivity, State University of New York at Buffalo, Bonner Hall, Buffalo, NY 14260

We report a high speed IR detector using high T_c Y-Ba-Cu-O thin films. The film was grown by laser deposition without post-annealing and patterned into a microstrip by direct laser writing. With this detector, distinguishable fast and slow components were observed in the electrical response to laser radiation in the visible and infrared. The temperature, bias current, laser intensity and film thickness dependence indicated clearly that the slow component is due to thermal heating of the film and the fast component is clearly nonthermal in origin. The mechanism of the nonthermal response will be discussed.

Y-Ba-Cu-O thin films and a standard high speed gold-doped germanium detector were compared for CO₂ laser detection. It was found that the superconducting films were at least 89 times more sensitive in both the high speed nonthermal regime and the slow thermal regime with the same bias conditions. In the high speed regime, the detectors speeds were comparable within the instrument resolution of 10 ns.

M11.11

Josephson Weak-links Fabricated From Heteroepitaxial YBa₂Cu₃O_{7-x}/PrBa₂Cu₃O_{7-x}/YBa₂Cu₃O_{7-x} Multilayers. C. T. Rogers and T. Venkatesan, Bellcore, 331 Newman Springs Rd., Red Bank, NJ 07701; A. Inam, Physics Department, Rutgers University Piscataway, NJ 08854.

We have fabricated Josephson weak-link devices from heteroepitaxial multi-layers of YBa₂Cu₃O_{7-x}/PrBa₂Cu₃O_{7-x}/YBa₂Cu₃O_{7-x} with a fourth layer of Au deposited for ohmic contacts. All the layers are grown by laser deposition in a single cycle of our multiple target deposition system. We have isolated devices of area, A, from 2x10⁻⁵cm² to 2x10⁻⁷cm² with a four step process using standard photolithography and Argon ion milling. Our finished devices show Current-Voltage characteristics similar to those observed in the traditional Superconductor/Normal-metal/Superconductor (SNS). They show good scaling of the critical currents, I_c, with A and scaling of the resistances, R, with 1/A. Typical values of the I_cR product of 3-7mV are consistent with conventional SNS behavior. We observe both microwave induced constant-voltage current steps and modulation of the critical current in transverse field thus demonstrating both the a.c. and d.c. Josephson effect in these junctions. We will discuss both the device fabrication and performance.

M11.12

HIGH T_c SUPERCONDUCTOR MULTILEVEL STRUCTURES FORMED WITH Ta₂O₅ SPACER LAYERS.* Rabi S. Bhattacharya, Universal Energy Systems, Inc., Dayton, OH; Peter B. Kosel, University of Cincinnati, Cincinnati, OH; T. Peterson, Wright Patterson Air Force Base, WRDC/MLPO, Dayton, OH.

Important electronic devices can be realized with current state-of-the-art high-T_c superconductor thin films by forming multilevel structures separated by thin dielectric layers. It has been found that tantalum oxide can be effectively used as a spacer layer because of its high melting point (1800°C) and good chemical stability at the typical temperatures used to anneal thin films of the YBaCuO superconductor. Best results have been achieved by sputtering thin films from a preformed sintered target of YBaCuO in oxygen and depositing very thin films of tantalum oxide by electron beam evaporation through a shadow mask to form simple device patterns. Strontium titanate substrates and oxygen furnace annealing at 850°C have been used to promote epitaxial growth of the superconductive crystalline phase. In this way two level multilayer structures have been formed and the layer transition temperatures determined by resistance measurements. Both levels of YBaCuO have shown superconductivity after annealing. However, the second layer shows reduced abruptness in the transition curves.

Thin superconducting films with the smooth surfaces were obtained by sputtering from a sintered target whose chemical composition has been adjusted to produce films which were nearly stoichiometrically correct. Such films required only short annealing times and produced the least stress on the tantalum oxide layers.

* This work was supported by the Department of Air Force under SBIR Phase I Contract No. F33615-88-C-1795.

**SYMPOSIUM N:
TAILORED INTERFACES IN
COMPOSITE MATERIALS**

N

November 27 - 29, 1989

Chairs

Carlo G. Pantano
123 Steidle Building
Pennsylvania State University
University Park, PA 16802
(814) 863-2071

Eric J. H. Chen
E.I. duPont de Nemours & Co., Inc.
Experimental Station
E302/309
Wilmington, DE 19898
(302) 695-3030

Symposium Support

Air Force Office of Scientific Research
E.I. duPont de Nemours & Co., Inc.

**Proceedings published as Volume 170
of the Materials Research Society
Symposium proceedings series.**

SESSION N1: Micromechanics of Interfaces

Chairs: A. G. Evans
Monday Morning, November 27
America Center (W)

8:30 *N1.1

STRESS FIELD CHARACTERISTICS AND DATA INTERPRETATION IN INTERFACE MEASUREMENTS OF CERAMIC COMPOSITES, John F. Mandell, Montana State University, Department of Chemical Engineering, Bozeman, MT; Shyh-Hua Jao, Massachusetts Institute of Technology, Department of Civil Engineering, Cambridge, MA.

9:00 N1.2

A NEW MODEL FOR THE DEBONDING OF DISCONTINUOUS FIBERS IN AN ELASTIC MATRIX, Christopher K.Y. Leung and Victor C. Li, Massachusetts Institute of Technology, Department of Civil Engineering, Cambridge, MA.

9:15 N1.3

STICK-SLIP DURING FIBRE PULL-OUT, Robert Cook, Michael Thouless and David Clarke, IBM T.J. Watson Research Center, Yorktown Heights, NY.

9:30 N1.4

EFFECTS OF A FRICTIONAL INTERFACE ON THE LOAD DIFFUSION FROM A BROKEN FIBER IN A FIBER-REINFORCED COMPOSITE, Bulent Aksel, Cornell University, Theoretical and Applied Mechanics, Ithaca, NY; Dimitris C. Lagoudas, Rensselaer Polytechnic Institute, Civil Engineering, Troy, NY; and Chung-Yuen Hui, Cornell University, Theoretical and Applied Mechanics, Ithaca, NY.

9:45 N1.5

A CRITICAL EVALUATION OF THE USE OF THE MICROBOND METHOD FOR DETERMINATION OF COMPOSITE INTERFACIAL PROPERTIES, R.A. Haaksma and M.J. Cehelnik, Alcoa Laboratories, Surface Technology, Alcoa Center, PA.

10:00 BREAK

*Invited Paper

Short Course C-08, "Ceramic and Metal Matrix Composites," may be of interest to symposium attendees. Details regarding course dates and instructors are provided in the short course section of this program.

10:30 N1.6

TAILORED INTERFACES IN COMPOSITE MATERIALS, John G. Williams, Michigan Technological University, Chemistry and Chemical Engineering Department, Houghton, MI; Mary E. Donnellan, Naval Air Development Center, Aerospace Materials Division, Warminster, PA; M.R. James and W.L. Morris, Rockwell International, Mechanics of Materials Department, Thousand Oaks, CA.

10:45 N1.7

THE INTERFACE IN TUNGSTEN FIBER REINFORCED NIOBIUM METAL MATRIX COMPOSITES, Toni Grobstein, NASA Lewis Research Center, Cleveland, OH; and Hee Mann Yun, Cleveland State University and Resident Research Associate at NASA Lewis Research Center, Cleveland, OH.

11:00 N1.8

INTERFACE MICROMECHANICS AND TOUGHENING PROPERTIES OF DUCTILE INTERFACE LAYERS IN CERAMIC MATRIX COMPOSITES, E.P. Butler and E.R. Fuller, Jr., National Institute of Standards and Technology, Ceramics Division, Gaithersburg, MD; H.M. Chan, Lehigh University, Department of Materials Science and Engineering, Bethlehem, PA.

11:15 N1.9

BRIDGING PROCESSES IN DUCTILE METAL-REINFORCED BRITTLE MATRIX COMPOSITES, M.C. Shaw, D.B. Marshall, Rockwell International Science Center, Structural Ceramics Department, Thousand Oaks, CA; and A.G. Evans, University of California, Materials Department, Santa Barbara, CA.

11:30 N1.10

EFFECT OF COATING OF DUCTILE FIBERS ON THE TOUGHENING OF BRITTLE INTERMETALLICS, Hervé Déve, A.G. Evans and R. Mehrabian, University of California, Materials Department, Santa Barbara, CA.

SESSION N2: REACTIONS AT INTERFACES

Chair: A. Joshi
Monday Afternoon, November 27
America Center (W)

1:30 N2.1

INTERFACIAL REACTIONS OF REFRACTORY METALS NIOBIUM AND TANTALUM WITH CERAMICS SILICON CARBIDE AND ALUMINA, A. Joshi, H.S. Hu, and J. Wadsworth, Lockheed Palo Alto Research Laboratory, Research and Development Division, Palo Alto, CA.

1:45 N2.2

SILICON-BASED OXIDATION-RESISTANT COATINGS ON NIOBIUM METAL, P.D. Stupik, A.R. Barron, Harvard University, Department of Chemistry, Cambridge, MA; M.A. Nastasi and T. Jervis, Los Alamos National Laboratory, Los Alamos, NM.

2:00 N2.3
EFFECT OF AMBIENT ATMOSPHERE ON THIN FILM REACTION OF Si_3N_4 WITH Ti, S.B. Desu, Virginia Polytechnic Institute and State University, Department of Materials Engineering, Blacksburg, VA; and J.A. Taylor, AT&T Bell Laboratories, Allentown, PA.

2:15 N2.4
SPINEL INTERPHASE FORMATION AT $\text{Ni}/\text{Al}_2\text{O}_3$ INTERFACES - PROSPECTS FOR TAILORING INTERFACE TENACITY, Kevin P. Trumble, University of California, Santa Barbara, Materials Department, Santa Barbara, CA; Manfred Rühle, MPI für Metallforschung, Stuttgart, West Germany; Anthony G. Evans, University of California, Santa Barbara, Materials Department, Santa Barbara, CA.

2:30 N2.5
THE FORMATION OF PERIODIC STRUCTURES DURING SOLID STATE INTERACTIONS BETWEEN Pt AND SiC , T.C. Chou and A. Mishra, Engelhard Corporation, Research and Development, Edison, NJ.

2:45 N2.6
FIBRE-MATRIX REACTION ZONES IN MODEL SILICON CARBIDE - TITANIUM ALUMINIDE METAL - MATRIX COMPOSITES, P.J. Doorbar, Rolls-Royce, plc., Manufacturing Technology, Derby, United Kingdom; D.R. Baker and M.H. Loretto, University of Birmingham, School of Metallurgy and Materials Science, Birmingham, United Kingdom.

3:00 BREAK

3:30 N2.7
TRANSMISSION ELECTRON MICROSCOPY STUDIES OF SILICON NITRIDE/SILICON CARBIDE INTERFACES, H.-J. Kleebe and M. Rühle, University of California, Santa Barbara, Materials Department, Santa Barbara, CA; N. Corbin and C. Willkins, Norton Company, Advanced Ceramics Department, Northboro, MA.

3:45 N2.8
THE EFFECT OF TEMPERATURE ON THE CHEMISTRY AND MORPHOLOGY OF THE INTERPHASE IN AN $\text{SCS6}/\text{Ti-6Al-4V}$ METAL MATRIX COMPOSITE, C. Jones, University of Illinois, National Centre for Composite Materials Research, Urbana, IL, and Liverpool University, United Kingdom; C.J. Kiely, University of Illinois, Materials Research Laboratory, Urbana, IL, and Liverpool University, United Kingdom; and S.S. Wang, University of Illinois, National Centre for Composite Materials Research, Urbana, IL.

4:00 N2.9
IMPROVED INTERFACIAL ADHESION IN METAL MATRIX/METALLIC GLASS COMPOSITES, Uwe Köster and Margret Blank-Bewersdorff, University of Dortmund, Department of Chemical Engineering, Dortmund, West Germany.

4:15 N2.10
HIGH-TEMPERATURE EVALUATION OF THE NICKEL/GRAPHITE INTERFACE, Nea S. Wheeler, David S. Lashmore, and Alexander J. Shapiro, National Institute of Standards and Technology, Electrodeposition Department, Gaithersburg, MD.

4:30 N2.11
THE INFLUENCE OF INTERFACIAL MODIFICATION ON TENSILE STRENGTH OF GR/AL COMPOSITES, Chen Ho, Guoding Zhang, and Renjie Wu, Shanghai Jiao Tong University, Institute of Composite Materials, Shanghai, China.

SESSION N3: INTERFACES IN POLYMER COMPOSITES I

Chair: M. Tirrell
Tuesday Morning, November 28
America Center (W)

8:30 *N3.1
THERMOMECHANICAL STABILITY OF ORGANOSILANE AND ORGANOTITANATE INTERPHASES IN GLASS REINFORCED COMPOSITES, A.T. DiBenedetto, S. Connelly, J. Gomez, and G. Haddad, University of Connecticut, Chemical Engineering Department, Storrs, CT.

9:00 N3.2
FILAMENT FRAGMENTATION PHENOMENA, Juan C. Figueroa, E. I. duPont de Nemours & Co., Inc., Engineering Research and Development Division, Wilmington, DE; Linda S. Schadler and Campbell Laird, University of Pennsylvania, Materials Science and Engineering Department, Philadelphia, PA.

9:15 *N3.3
APPLICATION OF COLD PLASMA IN TAILOR-DESIGNING COMPOSITE INTERFACES, Nakho Sung, Tufts University, Laboratory of Materials and Interfaces, Medford, MA.

9:45 N3.4
THE EFFECTS OF FIBER SURFACE TREATMENTS BY A COLD PLASMA IN CARBON FIBER/BISMALEIMIDE COMPOSITE, Tao C. Chang and Bor Z. Jang, Auburn University, Materials Engineering Program, Department of Mechanical Engineering, Auburn, AL.

10:00 BREAK

10:30 *N3.5
TAILORED INTERPHASES IN FIBRE REINFORCED POLYMERS, Michael R. Piggott, University of Toronto, Department of Chemical Engineering, Ontario, Canada.

11:00 N3.6
A TEM STUDY OF AN ADHESIVE/SHEET MOLDING COMPOUND INTERFACE, Eduardo A. Kamenetzky and Raymond S. Farinato, American Cyanamid, Stamford Research Laboratories, Stamford, CT.

11:15 N3.7
STUDY OF TRANSCRYSTALLIZATION IN POLYMER COMPOSITES, Benjamin S. Hsiao and Eric J.H. Chen, E. I. duPont de Nemours & Co., Inc., Fibers Department, Pioneering Research Laboratory, Wilmington, DE.

11:30 N3.8
THE EFFECT OF SALT WATER ABSORPTION ON INTERFACIAL DEGRADATION IN POLYMERIC COMPOSITE MATERIALS, Walter L. Bradley and Tim Grant, Texas A&M University, Mechanical Engineering, College Station, TX.

11:45 N3.9
THE INFLUENCE OF WATER ON THE EPOXY RESIN-GLASS INTERPHASES, Robert Kosfeld, Thomas Marzi, Ulrich Schröder and Michael Hess, University of Duisburg, Department of Physical Chemistry, Duisburg, West Germany.

SESSION N4: INTERFACES IN POLYMER COMPOSITES II

Chair: A. T. DiBenedetto
Tuesday Afternoon, November 28
America Center (W)

1:30 *N4.1
INTRINSIC MATERIAL LIMITATIONS IN USING INTERPHASE MODIFICATION TO ALTER FIBER-MATRIX ADHESION IN COMPOSITE MATERIALS, Lawrence T. Drzal, Michigan State University, Composite Materials and Structures Center, East Lansing, MI.

2:00 N4.2
ACID/BASE PROPERTIES OF CARBON AND GRAPHITE FIBER SURFACES, Sheldon P. Wesson, TRI/Princeton, Princeton, NJ; and Ronald E. Allred, PDA Engineering, Materials Development Department, Albuquerque, NM.

2:15 N4.3
CORRELATION BETWEEN FIBRE SURFACE ENERGETICS AND FIBRE-MATRIX ADHESION IN CARBON FIBRE REINFORCED PEEK COMPOSITE, D.J. Hodge, B. Middlemiss and J.A. Peacock, ICI, Wilton Materials Research Centre, Cleveland, United Kingdom.

2:30 N4.4
EFFECT OF SURFACE OXYGEN ON ADHESION OF CARBON FIBER REINFORCED EPOXY COMPOSITES, P.W. Yip and S.S. Lin, Army Materials Technology Laboratory, Watertown, MA.

2:45 N4.5
INTERFACIAL EFFECTS OF PLASMA TREATMENT ON FIBER PULL-OUT, Umesh Gaur, TRI Princeton, Princeton, NJ; and Theodore Davidson, University of Connecticut, Center for Surface and Interface Research, Storrs, CT.

3:00 BREAK

3:30 N4.6
INTERPHASE BEHAVIOR IN CYCLIC FATIGUE OF MONOFILAMENT COMPOSITES, Linda S. Schadler, University of Pennsylvania, Department of Materials Science and Engineering, Philadelphia, PA; Juan C. Figueroa, E. I. duPont de Nemours & Co., Inc., Wilmington, DE; and C. Laird, University of Pennsylvania, Philadelphia, PA.

3:45 N4.7
INTERLAMINAR FRACTURE IN CARBON FIBER/THERMOPLASTIC COMPOSITES, J.A. Hinkley, NASA Langley Research Center, Hampton, VA; W.D. Bascom, University of Utah, Department of Materials Science and Engineering, Salt Lake City, UT; and R.E. Allred, PDA Engineering, Albuquerque, NM.

4:00 N4.8
EFFECTS OF SURFACE TREATMENTS ON TENSILE AND INTERFACE SHEAR STRENGTHS IN GLASS FIBER/RESIN MATRIX COMPOSITES, Albert A. Kruger, Battelle-Pacific Northwest Laboratory, Chemical Sciences, Richland, WA.

4:15 N4.9
INTERFACIAL INTERACTIONS IN SILICA REINFORCED SILICONES, M.I. Aranguren, C.W. Macosko, M. Tirrell and B. Thakkar, University of Minnesota, Department of Chemical Engineering and Materials Science, Minneapolis, MN.

4:30 N4.10
AN INTERFACIAL THERMODYNAMIC STUDY ON NTC PHENOMENON OF CONDUCTIVE HDPE COMPOSITES, Zhang Mingqiu and Zeng Hanmin, Zhongshan University, Materials Science Institute, Guangzhou, China.

SESSION N5: POSTER SESSION

Tuesday Evening, November 28
7:00 p.m. - 10:00 p.m.
America Ballroom (W)

N5.1 FRACTO-EMISSION STUDIES OF INTERFACIAL FAILURE IN COMPOSITES, J.T. Dickinson, L.C. Jensen, and B.A. Mielke, Washington State University, Department of Physics, Pullman, WA.

N5.2 INTERFACES WITH DISCONTINUITIES AND INTERPHASES WITH CONTINUOUSLY VARYING PROPERTIES IN COMPOSITE MATERIALS, C.S. Chen, General Dynamics, Structure and Materials Department, Ft. Worth, TX.

N5.3 A SOLID-STATE NMR STUDY OF THE PMMA-Al₂O₃ INTERFACE, Kariofilis Konstadinidis, University of Minnesota, Department of Chemical Engineering and Materials Science, Minneapolis, MN; John Evans and Matthew Tirrell, University of Minnesota, Department of Chemistry, Minneapolis, MN.

N5.4 SPREADING OF LIQUID DROPLETS ON CYLINDRICAL SURFACES: ACCURATE DETERMINATION OF CONTACT ANGLE, H. Daniel Wagner, The Weizmann Institute of Science, Polymeric Composites Laboratory, Department of Materials Research, Rehovot, Israel.

N5.5 AN OPTICAL METHOD TO CHARACTERIZE IMPREGNATION AND WETTING OF GLASS-FIBERS WITH EPOXY RESIN, Robert Kosfeld, Thomas Marzi, Ulrich Schröder, and Michael Hess, University of Duisburg, Department of Physical Chemistry, Duisburg, West Germany.

N5.6 THE INFLUENCE OF ANNEALING ON THE BEHAVIOUR OF EPOXY-GLASS INTERPHASES, Robert Kosfeld, Thomas Marzi, Ulrich Schröder, Michael Hess, University of Duisburg, Department of Physical Chemistry, Duisburg, West Germany.

N5.7 THE ROLE OF RESIDUAL STRESSES IN THE CRACKING OF A MODEL METAL-CERAMIC SYSTEM, $Al_2O_3/Ta(Ti)$, A.H. Bartlett, M. Rühle, and A.G. Evans, University of California, Santa Barbara, Materials Department, Santa Barbara, CA.

N5.8 THE STRENGTH AND FRACTURE OF CERAMIC/METAL BONDED SYSTEMS, M.Y. He and A.G. Evans, University of California, Materials Department, Santa Barbara, CA.

N5.9 CVD Mo AND W OXYCARBIDE COATINGS ON SiC YARN, Michael Kmetz, Beng Jit Tan, University of Connecticut, Department of Chemistry, Storrs, CT; Francis S. Galasso, United Technologies Research Center, East Hartford, CT; and Steven L. Suib, University of Connecticut, Department of Chemistry, and Department of Chemical Engineering, Storrs, CT.

N5.10 SOLID STATE BONDING OF Si_3N_4 and Ni, Jian-Yih Wang and Shu-En Hsu, Chung Shan Institute of Science and Technology, Materials Research and Development Center, Taiwan, China; and Yoichi Ishida, University of Tokyo, Institute of Industrial Science, Tokyo, Japan.

N5.11 CHEMICAL INTERACTIONS IN THE ALUMINUM-CARBON AND ALUMINUM-SILICON CARBIDE SYSTEMS, Benji Maruyama, Naval Research Laboratory, Washington, DC; Fumio S. Ohuchi, E. I. duPont de Nemours & Co., Inc., Experimental Station, Wilmington, DE; Llewellyn K. Rabenberg, The University of Texas at Austin, Center for Materials Science, Austin, TX.

N5.12 STABILITY AND REACTIONS AT COMPOSITE INTERFACES OF TITANIUM ALUMINIDES WITH POTENTIAL FIBER MATERIALS, J.A. DeKock, M.-X. Zhang, and Y.A. Chang, University of Wisconsin, Department of Materials Science and Engineering, Madison, WI; and O.Y. Chen, Pratt and Whitney, United Technologies, East Hartford, CT.

N5.13 CHARACTERIZATION OF INTERFACES IN SiC PARTICULATE-REINFORCED Al ALLOYS USING AEM, D.-Q. Huang, Y.-P. Lin, and B.W. Robertson, McMaster University, Department of Materials Science and Engineering, Ontario, Canada.

N5.14 THE DISLOCATION STRUCTURE AND ENERGY OF NiO-Pt INTERFACES, F.-S. Shieu and S.L. Sass, Cornell University, Department of Materials Science and Engineering, Ithaca, NY.

N5.15 EFFECT OF ANNEALING ON THE ALUMINUM/SiC INTERFACE STRUCTURE AND COMPOSITION, Qiong Li, Janez Megusar and James A. Cornie, Massachusetts Institute of Technology, Department of Materials Science and Engineering, Cambridge, MA.

N5.16 INTERFACE ELECTRONIC STRUCTURE OF TITANIUM ALUMINIDE COMPOSITES, D.D. Vvedensky and S. Crampin, Imperial College, Department of Physics, The Blackett Laboratory, London, England; M.E. Eberhart, Los Alamos National Laboratory, Department MST-6, Los Alamos, NM; J.M. MacLaren, Los Alamos National Laboratory, Department T-11, Los Alamos, NM; L. Christodoulou, Martin Marietta Laboratories, Baltimore, MD.

N5.17 A COMPARISON OF SOLID STATE REACTIONS IN MECHANICALLY DEFORMED MULTILAYERED COMPOSITES IN THE NI-TI AND NI-ZR SYSTEMS, B.E. White, M.E. Patt and E.J. Cotts, State University of New York at Binghamton, Department of Physics, Applied Physics and Astronomy, Binghamton, NY.

N5.18 AC SPECTROSCOPY OF COMPOSITE MATERIALS, R. Gerhardt, Rutgers University, Department of Ceramics, Piscataway, NJ.

N5.19 NONDESTRUCTIVE EVALUATION OF INTERFACIAL DAMAGE IN SiC/Al CONTINUOUS FIBER COMPOSITES, T.M. Breunig, S.R. Stock, and S.D. Antolovich, Georgia Institute of Technology, Mechanical Properties Research Laboratory and School of Materials Engineering, Atlanta, GA; J.H. Kinney, R.A. Saroyan, and Q.C. Johnson, Lawrence Livermore National Laboratory, Chemical and Materials Science Department, Livermore, CA; M.C. Nichols, Sandia National Laboratories, Materials Department, Livermore, CA; and U. Bonse, Dortmund University, Department of Physics, Dortmund, West Germany.

N5.20 INTERACTIONS OF ACRYLIC POLYMERS WITH ALUMINUM SURFACES, J. Scott Shaffer, and Arup K. Chakraborty, University of California, Berkeley, Center for Advanced Materials, Lawrence Berkeley Laboratory, and Department of Chemical Engineering, Berkeley, CA; H.T. Davis and Matthew Tirrell, University of Minnesota, Department of Chemical Engineering and Material Science, Minneapolis, MN.

N5.21 THE PRODUCTION OF MODULUS GRADIENTS AT INTERFACES, Andrew Garton, Gautam Haldankar and Edward Shockey, University of Connecticut, Polymer Program, Storrs, CT.

N5.22 SURFACE TREATMENT OF CARBON FIBERS FOR USE IN COMPOSITES WITH THERMOPLASTIC RESINS, Aharon Moshonov, Rafael Institute, Haifa, Israel; Hong Li, Georgia Institute of Technology, Atlanta, GA; and John D. Muzzy, Georgia Institute of Technology, Atlanta, GA.

N5.23 EFFECT OF Ti^+ , Ar^+ AND N^+ ION IMPLANTATION ON ARAMID FIBER ADHESIVE PROPERTIES, J. Kalantar, Michigan State University, Department of Chemical Engineering, East Lansing, MI; D.S. Grummon, Michigan State University, Department of Metallurgy, Mechanics and Materials Science, East Lansing, MI; I.H. Loh, Advanced Surface Technology, Inc., Waltham, MA; and R.A. Moody, Spire Corporation, Patriots Park/Bedford, MA.

N5.24 DETERMINATION OF FLEXIBLE INTERLAYER THICKNESS FOR FIBER REINFORCED COMPOSITES, King H. Lo, Robert W. Schmitz and William G. Gottenberg, Shell Development Company, Houston, TX.

SESSION N6: ADHESION AND STRENGTH OF INTERFACES

Chair: T. A. Michalske
Wednesday Morning, November 29
America Center (W)

8:45 ***N6.1**
MEASUREMENT OF MOLECULAR FORCES AT SILICA SURFACES, Bimal Thakkar and M. Tirrell, University of Minnesota, Department of Chemical Engineering and Materials Science, Minneapolis, MN; and Donald J. David, Monsanto Corporation, Saflex Technology, Springfield, MA.

9:15 **N6.2**
SURFACE FORCES AND ADHESION BETWEEN DIS-SIMILAR MATERIALS MEASURED IN VARIOUS ENVIRONMENTS, Douglas T. Smith and Roger G. Horn, National Institute of Standards and Technology, Ceramics Division, Gaithersburg, MD.

9:30 **N6.3**
MEASUREMENT OF INTERFACIAL FRACTURE ENERGY, L. Rosenfeld, J.E. Ritter, M.R. Lin and T.J. Lardner, University of Massachusetts, Mechanical Engineering Department, Amherst, MA.

9:45 **N6.4**
THE EFFECTS OF PLASTICITY ON THE FRACTURE RESISTANCE OF GOLD/ALUMINA INTERFACES, Ivar E. Reimanis, Brian J. Dalgleish, M. Rühle and Anthony G. Evans, University of California, Santa Barbara, Materials Department, Santa Barbara, CA.

10:00 BREAK

10:30 ***N6.5**
THE EFFECT OF A WEAK INTERFACE ON TRANSVERSE PROPERTIES OF A CERAMIC MATRIX COMPOSITE, R.A. Shimansky, H.T. Hahn and N.J. Salamon, The Pennsylvania State University, University Park, PA.

11:00 **N6.6**
THE EFFECT OF INTERFACIAL STRENGTH ON THE MECHANICAL BEHAVIOR OF LAMINATED CERAMICS, M.D. Stuart, C.J. Russo, M.P. Harmer, H.M. Chan and G.A. Miller, Lehigh University, Department of Materials Science and Engineering, Bethlehem, PA.

11:15 ***N6.7**
THE EFFECT OF FIBER COATINGS ON INTERFACIAL SHEAR STRENGTH AND THE MECHANICAL BEHAVIOR OF CERAMIC COMPOSITES, Richard A. Lowden, Oak Ridge National Laboratory, Metals and Ceramics Division, Oak Ridge, TN.

11:45 **N6.8**
IMPROVED PERFORMANCE IN MONOFILAMENT FIBER REINFORCED GLASS MATRIX COMPOSITES THROUGH THE USE OF FIBER COATINGS, William K. Tredway and Karl M. Prewo, United Technologies Research Center, East Hartford, CT.

SESSION N7: INTERFACES IN CERAMICS AND CERAMIC COMPOSITES

Chair: W. K. Tredway
Wednesday Afternoon, November 29
America Center (W)

1:30 ***N7.1**
INTERFACIAL MICROSTRUCTURE AND FRACTURE OF ALUMINA FIBER REINFORCED GLASS MATRIX COMPOSITES, T.A. Michalske, Sandia National Laboratories, Albuquerque, NM.

2:00 **N7.2**
THE ROLE OF TIN DIOXIDE (SnO_2) INTERPHASE IN THE MECHANICAL BEHAVIOR OF ALUMINA/GLASS COMPOSITE, M.H. Siadati and K.K. Chawla, New Mexico Institute of Mining and Technology, Materials Engineering Department, Socorro, NM.

2:15 N7.3

THE STRUCTURE OF INTERFACES RESULTING FROM WHISKER SURFACE PRETREATMENTS IN SiC WHISKER-REINFORCED CERAMIC MATRIX COMPOSITES, T.A. Nolan and L.F. Allard, Oak Ridge National Laboratory, High Temperature Materials Laboratory, Oak Ridge, TN; M.H. Rawlins, American Matrix, Inc., Knoxville, TN.

2:30 N7.4

THE EFFECT OF INTERFACE STRUCTURE ON THE FRACTURE OF Al/Al₂O₃ COMPOSITES, B.D. Flinn, F.W. Zok, F.F. Lange, M. Rühle, and A.G. Evans, University of California, Santa Barbara, Materials Department, Santa Barbara, CA.

2:45 N7.5

CREEP PROPERTIES AND INTERFACIAL MICROSTRUCTURE OF SiC WHISKER REINFORCED Si₃N₄, Anders H. Swan and Lena K.L. Falk, Chalmers University of Technology, Physics Department, Gothenburg, Sweden.

3:00 N7.6

HIGH TEMPERATURE FRACTURE OF SiC WHISKER REINFORCED Al₂O₃ MATRIX COMPOSITES, C. Mangin, J. Homeny, University of Illinois, Materials Science/Ceramics Department, Urbana, IL; and S.S. Wang, University of Illinois, Theory/Applied Mechanics Department, Urbana, IL.

3:15 N7.7

THE ROLE OF CRYSTALLIZATION OF AN INTERGRANULAR GLASSY PHASE IN DETERMINING GRAIN BOUNDARY RESIDUAL STRESSES IN DEBASED ALUMINA, Nitin P. Padture and Helen M. Chan, Lehigh University, Department of Materials Science and Engineering, Bethlehem, PA; Brian R. Lawn, National Institute of Standards and Technology, Ceramics Division, Gaithersburg, MD; and Michael J. Readey, Coors Ceramic Company, Golden, CO.

3:30 N7.8

THE EFFECT OF RESIDUAL GRAIN BOUNDARY STRESSES ON MECHANICAL PROPERTIES OF ALUMINA-BASED CERAMICS, J.D. French, H.M. Chan, M.P. Harmer, and G.A. Miller, Lehigh University, Department of Materials Science and Engineering, Bethlehem, PA.

N1.1

STRESS FIELD CHARACTERISTICS AND DATA INTERPRETATION IN INTERFACE MEASUREMENTS OF CERAMIC COMPOSITES. John F. Mandell, Montana State University, Bozeman, MT; and Shyh-Hua Jao, Massachusetts Institute of Technology, Cambridge, MA.

The interpretation of debonding events in various test methods for interface characterization of composite materials is inherently difficult due to the complex stress fields which exist along interfaces. The particular case of indentation-type tests which compressively load the ends of individual fibers has been investigated using a cylinder-type model and finite element analysis, with special attention to residual thermal stresses and the singular point at the corner of the fiber and the polished surface. Cases investigated include carbon and ceramic fibers, glass and glass-ceramic matrices with varying coefficients of thermal expansion, and specific modelling of carbon interphase regions.

The results show that the strength of the singularity at the fiber corner is generally weak if the fiber and matrix moduli are of similar order of magnitude. The presence of a carbon interphase tends to localize the singular zones. Anisotropy of carbon fibers has a significant effect, and they have been found in some cases to debond at the free surface solely due to residual stresses. The results appear to correlate data for a variety of different Nicalon fiber/glass-ceramic matrix systems where carbon interphase thickness and residual stresses are considered.

N1.2

A NEW MODEL FOR THE DEBONDING OF DISCONTINUOUS FIBERS IN AN ELASTIC MATRIX. Christopher K.Y. Leung and Victor C. Li, Department of Civil Engineering, M.I.T., Cambridge, MA 02139.

The mechanical properties of fiber composites are strongly influenced by the debonding of fibers. When an embedded fiber is loaded from one end, debonding can occur at both the loaded end and the embedded end. In existing theories, only debonding from the loaded end is considered. During debonding, stress transfer between fiber and matrix leads to continued decrease in fiber strain and increase in matrix strain. As the debonded zone length approaches the embedded fiber end, a point will be reached where the longitudinal displacement in the matrix is higher than that in the fiber, which is physically impossible. However, if debonding from both ends of the fiber is considered, the size of the debonded zones will be limited and so is the amount of stress transfer between fiber and matrix. Matrix displacement will then always remain lower than fiber displacement.

A new theory for fiber debonding which considers debonding from both ends of the fiber is proposed. A new way to interpret the single fiber pull-out test as well as the correlation of fiber debonding in a pull-out specimen and that in the composite will be discussed. The new theory will be compared with existing theories for various lengths, volume fractions and moduli of fiber. It is suggested that the new theory can extend the validity of existing theories from short fiber composites with low V_f and E_f to all general cases.

N1.3

STICK-SLIP DURING FIBRE PULL-OUT. Robert Cook, Michael Thouless, and David Clarke, IBM, Thomas J. Watson Research Center, Yorktown Heights, NY.

The mechanics associated with interfacial sliding and debonding is of paramount importance in determining the toughness of fibre-reinforced brittle-matrix composites. As a crack advances through such a composite it is straddled by fibres and, if the fibres are fairly brittle, only the energy lost when the debonded fibres slide against the matrix significantly influences the toughness. The mechanics of delamination and pull-out can most easily be studied by investigating a model system consisting of a single fibre embedded in a matrix. Here we present some

initial findings of the phenomena that occur during single fibre pull-out. In particular, we focus on the stick-slip behavior after delamination: the fibre sticks and the load in the fibre increases to a critical value, at which point the fibre suddenly slips to a new position and sticks again. The implications of these results for fibre-composite toughening models will be discussed.

N1.4

EFFECTS OF A FRICTIONAL INTERFACE ON THE LOAD DIFFUSION FROM A BROKEN FIBER IN A FIBER-REINFORCED COMPOSITE. Bulent Aksel, Theoretical and Applied Mechanics, Cornell Univ., Ithaca, N.Y.; Dimitris C. Lagoudas, Civil Engineering, Rensselaer Polytechnic Inst., Troy, N.Y.; and Chung-Yuen Hui, Theoretical And Applied Mechanics, Cornell Univ., Ithaca, N.Y.

The effects of a frictional interface on the load diffusion from a broken fiber to the surrounding matrix material and the extent of slip near the fiber break in a single-fiber reinforced composite of infinite extent are studied by using a finite element method. The numerically computed axial load carried by the fiber for the perfect bond case (high coefficient of friction) is first compared with analytical results. Then, the normal and shear stresses on the interface, the extend of the slip zone as well as the amount of the relative slip and the axial load of the fiber are evaluated for different frictional coefficients and material parameters for both the fiber and the matrix. A shear-lag analysis is also carried out for a closed form prediction of the fiber load diffusion, the relative slip and the extend of the slip zone, resulting in good agreement with the finite element method results.

N1.5

A CRITICAL EVALUATION OF THE USE OF THE MICROBOND METHOD FOR DETERMINATION OF COMPOSITE INTERFACIAL PROPERTIES. R.A. Haaksma and M. J. Cehelnik, Alcoa Laboratories, Alcoa Center, PA, 15069.

Although the microbond or microdebond method has been applied with increasing frequency to characterize interfacial adhesion in fiber reinforced composites, a number of serious questions remain regarding the interpretation of experimental data. This paper addresses variables in the microbond test procedure including intrinsic material properties, specimen preparation methods, force measurement and force application techniques.

The applicability and the limitations of the microbond test for characterization of the interfacial properties in composites will be considered through the discussion and evaluation of extensive results obtained in our laboratory. When experimental data, generated for several different fiber/resin combinations, is presented in the typical manner (plots of applied debonding force *versus* fiber embedded length), a consistent and previously unexplained trend has been observed. The possible origins of this effect, which produces apparent negative forces values on linear extrapolation to zero embedded length, will be explored in terms of specimen failure mechanisms. Experiments, conducted using various techniques for measurement and application of force (point loading *versus* circular contact), will also be discussed.

N1.6

TAILORED INTERFACES IN COMPOSITE MATERIALS. John G. Williams, Michigan Technological University, Houghton, MI; Mary E. Donnellan, Naval Air Development Center, Warminster, PA; M. R. James, Rockwell International, Thousand Oaks, CA; and W. L. Morris, Rockwell International, Thousand Oaks, CA.

The mechanical properties of the material surrounding a single carbon fiber in an epoxy matrix have been studied. Properties were determined within 100 nm of the fiber. A pronounced soft interphase was revealed adjacent to the fiber.

A single fiber was embedded in a small supported disk

of epoxy matrix. The fiber was loaded in tension. Examination of the surface displacements in the resin revealed that the matrix material within 250 nm of the fiber was substantially softer than the matrix far from the fiber. This interphase material was active in creep. Measurement of indentation properties of the matrix around a single fiber showed that the material close to the fiber exhibited an apparently high modulus due to restriction by the fiber. The implications of these findings are discussed.

N1.7

THE INTERFACE IN TUNGSTEN FIBER REINFORCED NIOBIUM METAL MATRIX COMPOSITES. Toni Grobstein, NASA Lewis Research Center, Cleveland, Ohio and Hee Mann Yun, Cleveland State University, Resident Research Associate at the NASA Lewis Research Center, Cleveland, Ohio.

The fiber/matrix interface of W/Nb composites was characterized by microhardness measurements and electron probe microanalysis which implied that its properties were between those of the fiber and the matrix. This was expected given that the tungsten/niobium phase diagram forms a continuous solid solution. The tensile and creep-rupture properties of the W/Nb composites were measured from 1300 to 1600 K, and these results were evaluated using the rule of mixtures. The projected strength of the interface region was taken into account in these calculations. In addition, Kirkendall void formation was observed at the fiber/matrix interface after long times at temperature. However, the interdiffusion between tungsten and niobium did not significantly degrade the axial creep-rupture strength of the unidirectionally reinforced composites at times up to 5000 hr at 1500 K. Both the tensile strength and the creep resistance of the tungsten fiber reinforced composites significantly exceed that of monolithic niobium alloys even when compared on a strength to density basis.

N1.8

INTERFACE MICROMECHANICS AND TOUGHENING PROPERTIES OF DUCTILE INTERFACE LAYERS IN CERAMIC MATRIX COMPOSITES. E. P. Butler and E. R. Fuller, Jr., National Institute of Standards and Technology, Gaithersburg, MD 20899; and H. M. Chan, Lehigh University, Bethlehem, PA 18015.

The toughening attributes that fibers engender to brittle ceramics arise from several phenomena, including crack deflection, fiber/matrix debonding, crack bridging, and frictional fiber pullout. These phenomena are critically dependent on properties of the fiber/matrix interface: the strength of the interface determines the crack path, either undeflected through the fibers or deflected along the interface causing debonding; the nature of interface bonding determines the degree of subsequent crack bridging and frictional pullout in the wake of the crack.

In this study we examine the influence of metallic interface layers on these phenomena. We use a model composite system in which SiC monofilaments with metallic coatings are embedded in a borosilicate matrix. Metals of various ductilities were used for the metallic interface layers, for example, Cu, Ni, and W-Co. Layer thicknesses were nominally from 1 μm to 20 μm . Micromechanics of the interface, debond strength and frictional pullout properties, were characterized by single fiber pull-out experiments. Toughening properties were measured with a fracture mechanics configuration, the double-cleavage, drilled compression specimen, in which individual fibers were inserted in the prospective path of the crack. Interface properties are correlated directly with the toughening properties. Crack/fiber interactions are discussed in terms of the ductility and thickness of the metallic interface.

N1.9

BRIDGING PROCESSES IN DUCTILE METAL-REINFORCED BRITTLE MATRIX COMPOSITES.

M.C. Shaw, Rockwell Int'l Science Center, Thousand Oaks, CA, University of California, Santa Barbara, CA; D.B. Marshall, Rockwell Int'l Science Center, Thousand Oaks, CA; A.G. Evans, University of California, Santa Barbara, CA.

The bridging mechanism of toughening in ductile-metal reinforced brittle matrix composite laminates will be discussed. Methods of experimentally determining the crack bridging tractions within the bridging zone of model copper/glass systems will be described. Results will be presented and compared to predictions of theoretical models, demonstrating the role of the interface, and its control through processing, in dictating the balance between composite strength and toughness.

N1.10

EFFECT OF COATING OF DUCTILE FIBERS ON THE TOUGHENING OF BRITTLE INTERMETALLICS. Hervé Dève, A.G. Evans, R. Mehrabian, University of California, Materials Department, Santa Barbara, CA 93106.

The toughening of Titanium Aluminides by coated ductile reinforcements was investigated. Model laminate specimens of γ -TiAl reinforced with TiNb alloys that were coated with either Al_2O_3 or Y_2O_3 were studied. The specimens were fabricated by diffusion bonding. Toughening was evaluated using a newly devised tensile testing method. In situ observation of the fracture/debonding process during tensile testing, using optical microscopy and scanning electron microscopy, was used to document the role of the mechanical response of the interfaces on the toughening of the composite. Correlation was made between the toughness of the composite, the fracture energy of the interfaces, the extent of debonding, the mechanical properties, and failure mode of the reinforcements.

N2.1

INTERFACIAL REACTIONS OF REFRACTORY METALS NIOBIUM AND TANTALUM WITH CERAMICS SILICON CARBIDE AND ALUMINA. A. Joshi, H.S. Hu and J. Wadsworth, Lockheed Palo Alto Research Laboratory, 3251 Hanover street, Palo Alto, CA 94304

Recent interest in the development of advanced metal matrix composites has prompted research on interfacial reactions of Nb and Ta with candidate reinforcements such as silicon carbide and alumina. Formation of reaction layers as small as 0.1 μm can be detrimental to composite strength and ductility and in some instances to the corrosion behavior, which suggests the importance of understanding the early stages of interfacial reactions. Thin films of Nb and Ta were sputter deposited on single crystal and polycrystalline silicon carbide and on sapphire substrates, and the nature and extent of reaction evaluated using Auger depth profiling and electron microscopy. In the Nb/SiC system, NbC_x is the first reaction product to form, but the overall extent of the reaction is dominated by the formation of the more stable NbC_3Si ternary phase. Little or no interfacial reaction was observed in the Nb/ Al_2O_3 system for up to 4 hours at 1100°C, which also suggests that Al_2O_3 may be a potential diffusion barrier to minimize reactions in the Nb/SiC system. Similar interesting observations were made in the Ta/SiC and Ta/ Al_2O_3 systems.

N2.2

SILICON-BASED OXIDATION-RESISTANT COATINGS ON NIOBIUM METAL. P.D. Stupik, A.R. Barron*, Department of Chemistry, Harvard University, Cambridge, MA 02138; M.A. Nastasi and T. Jervis, Los Alamos National Laboratory, Los Alamos, NM 87545.

Silicon coatings of varying thicknesses on niobium substrates were subjected to thermal, laser, and ion beam mixing, and the effectiveness of the different methods for the synthesis of graded interfaces was compared. The resulting metal/silicon interfaces were characterized by XPS, Auger and RBS. The morphology of the coatings were studied using SEM. The samples were baked under an oxygen atmosphere in order to assess the relative stabilities of the interfaces to thermal stress and oxidation.

N2.3

EFFECT OF AMBIENT ATMOSPHERE ON THIN FILM REACTION OF Si_3N_4 WITH Ti. S.B.Desu, Department of Materials Engineering, Virginia Polytechnic Institute and State University, Blacksburg, VA; and J.A.Taylor, AT&T Bell Laboratories, Allentown, PA.

The thin film reactions of Si_3N_4 with Ti were carried out in both argon and nitrogen under rapid thermal conditions. The reaction products were characterized by X-ray diffraction, Auger electron spectroscopy (AES), X-ray photoelectron spectroscopy, and transmission electron microscopy (TEM). The reaction between Si_3N_4 and Ti is a complex process which is not only influenced by temperature, but also by ambient atmosphere.

The Si_3N_4 and Ti reaction in argon at lower temperatures led to the formation of mostly Ti_5Si_3 at the interface, with some contaminant oxygen and nitrogen released from the reaction, uniformly dissolved throughout the unreacted Ti. At higher temperatures, a three layer structure, $\text{TiN}/\text{TiSi}_x/\text{TiN}$ on unreacted Si_3N_4 , was developed. Depending on temperature, the observed silicide phase was either Ti_5Si_3 or TiSi_2 (C54).

Based on the experimental observations, a mechanism of reaction is proposed and used to explain the formation of three-layered structure.

N2.4

SPINEL INTERPHASE FORMATION AT $\text{Ni}/\text{Al}_2\text{O}_3$ INTERFACES - PROSPECTS FOR TAILORING INTERFACE TENACITY. Kevin P. Trumble, Manfred Rühle*, and Anthony G. Evans, Materials Department, University of California, Santa Barbara, CA 93106; *now at: MPI für Metallforschung, Stuttgart, FRG.

The applicability of many metal-ceramic combinations as high temperature composite materials is ultimately limited by interfacial chemical reactivity. Among the chemical processes occurring at metal/ceramic interfaces, interphase formation has often been associated with dramatic changes in interface mechanical integrity. If amenable to processing control, interphase formation represents a potential means of tailoring interface tenacity and, in turn, composite mechanical performance.

In the $\text{Ni}/\text{Al}_2\text{O}_3$ system, nickel aluminate spinel (NiAl_2O_4) reaction layers have been found to form in numerous diffusion bonding and composite compatibility studies. Only recently, however, have the thermodynamics, kinetics, and atomistics governing the underlying reaction process been quantitatively elucidated. Specifically, an oxygen activity dependence of spinel interphase formation has been clearly identified, which provides a means of controlling the formation of spinel reaction layers at $\text{Ni}/\text{Al}_2\text{O}_3$ interfaces.

The oxygen activity effect is briefly reviewed in terms of the reaction

thermodynamics, kinetics, and atomistics. The presentation then focuses on the effect of spinel interphase layers on interface mechanical behavior. Interface fracture resistance measurements are correlated with the resulting fracture morphologies. The microstructural origins of the observed mechanical behavior are identified, establishing a sound basis for evaluating the potential for tailoring interface tenacity by controlling spinel interphase formation.

N2.5

THE FORMATION OF PERIODIC STRUCTURES DURING SOLID STATE INTERACTIONS BETWEEN Pt AND SiC. T. C. Chou and A. Mishra, R & D, Engelhard Corp., Edison, NJ

Interfaces between Pt and SiC are produced by diffusion bonding at temperatures from 800 to 1100°C. Periodic structures consisting of alternating layers of C/Pt₃Si, C/Pt₂Si and C/platinum silicides mixture are generated in the diffusion zone at 900, 1000 and 1100°C, respectively. The spacing between periodic layers decreases as a function of distance from the reaction interface. The interactions between Pt and SiC are extensive; the reaction rate constants were calculated to vary between 10^{-7} to 10^{-4} cm²/sec from 900°C to 1100°C. A direct decomposition of SiC into free C and Si, which immediately reacts with Pt forming platinum silicides, are evident. The formation of platinum silicides cause an interfacial melting between Pt and SiC at respective temperatures. Scanning Auger microscopy, laser Raman spectroscopy, secondary electron microscopy and x-ray diffraction were used to investigate the interactions. Composition profiling across the diffusion zone and chemistry of the periodic structures are examined. Raman spectroscopy indicates that carbon is in either a glassy state or highly ordered graphitic state, depending upon its location from the reaction interface. The mechanism of the periodic structure formation is discussed based on solid solubility limited phase separation during solidification of the interfacial melts.

N2.6

FIBRE-MATRIX REACTION ZONES IN MODEL SILICON CARBIDE - TITANIUM ALUMINIDE METAL - MATRIX COMPOSITES. P.J.Doorbar, Rolls-Royce plc., Derby, U.K.; D.R.Baker and M.H.Loretto, School of Metallurgy and Materials Science, University of Birmingham, Birmingham, U.K.

Titanium aluminide-based metal-matrix composites are currently being investigated to determine their suitability for high temperature engineering applications.

Model composites with TiAl, Ti₃Al, and Ti₃Al + β matrices, and coated SiC continuous fibre reinforcement, have been produced. The fibre-matrix reaction zones have been characterised by a combination of optical microscopy, SEM, TEM, EPMA, EELS, EDX, SAD and CBED.

Investigations reveal extensive multi-phase reaction zones in all the composites. The phase formation can be rationalised partly by reference to published phase diagram information. Complex carbides of Ti₂AlC or Ti₃AlC type appear to be major constituents of the reaction zones, and extensive β -depleted regions are present around fibres in the Ti₃Al + β matrices. TiC-type phases are, in all cases, present nearest to the fibre, and titanium silicides with dissolved Nb and Al are also observed as narrow bands in the reaction zones. There is some evidence of Al rejection from reaction zones into all of the matrices.

N2.7

TRANSMISSION ELECTRON MICROSCOPY STUDIES OF SILICON NITRIDE / SILICON CARBIDE INTERFACES. H.-J. Kleebe, M. Rühle, UCSB, Materials Dept., Eng. III, Santa Barbara, CA; and N. Corbin, C. Willkens, Norton Co., Northboro, MA.

Microstructural investigations of four silicon nitride based whisker-reinforced ceramic materials were performed using a 400 kV transmission electron microscope. Chemical analysis of interfacial regions and triple point grain junctions in these materials were obtained via energy-dispersive x-ray spectroscopy (EDS) and a parallel electron energy loss spectrometer (PEELS), attached to the microscope.

All materials were prepared under identical experimental conditions, including a HIPing cycle as the densifying step. Using two different whisker sources (Tokai-, AMI-whiskers) as well as uncoated and C-coated reinforcements the densified silicon nitride materials revealed marked differences in the resulting mechanical properties.

This investigation focusses on the microstructure and the chemical analysis of the interface between Si_3N_4 -matrix and SiC-whisker. Combined HREM- and EDS / PEELS-investigations reveal that the observed deviations in RT- mechanical properties are mainly influenced by the microstructural and chemical development of the interface. Thereby, this phenomenon can be closely related to the surface chemistry and the C-coating of the reinforcements. Moreover, a comparison between these whisker-reinforced and a bulk Si_3N_4 -material with similar mechanical properties will be presented.

N2.8

THE EFFECT OF TEMPERATURE ON THE CHEMISTRY AND MORPHOLOGY OF THE INTERPHASE IN AN SCS6/Ti-6Al-4V METAL MATRIX COMPOSITE. C. Jones, *C.J. Kiely, and S.S. Wang National Centre for Composite Materials Research, University of Illinois, Urbana, Illinois 61801; *Materials Research Laboratory, University of Illinois, Urbana, Illinois 61801. (C. Jones and C.J. Kiely are now at Liverpool University, England)

Using TEM, Auger spectroscopy, EDX and convergent beam electron diffraction, a thorough characterisation of the interphase region between SCS6 fibres and Ti-6Al-4V matrix in a metal matrix composite has been performed. The interphase region is shown to be very complex, consisting of numerous layers of varying compositions and thicknesses most of which originate from the coating applied to the fibre by the manufacturer. This coating consists of several layers of carbon each containing small but varied concentrations of SiC. However, chemical interaction has occurred between fibre and matrix resulting in the formation of a layer of TiC and another of $\text{Ti}_x\text{Si}_y(\text{C})$, the latter being sandwiched between the TiC and the matrix itself.

The changes in chemistry and morphology within this interphase region upon exposure to varying heat treatments have also been studied. These changes such as the formation of small TiC particles at one interface, and the narrowing of a protective pyrocarbon layer at another, induce fracture to occur at different places within the interphase upon heating. The reasons for this are explained. Evidence for a change in phase of a $\text{Ti}_x\text{Si}_y(\text{C})$ layer to the more thermodynamically stable Ti_5Si_3 is also given.

N2.9

IMPROVED INTERFACIAL ADHESION IN METAL MATRIX/ METALLIC GLASS COMPOSITES. Uwe Köster & Margret Blank-Bewersdorff, Dept. Chem. Eng., University of Dortmund, D-4600 Dortmund 50, F.R. Germany

Metallic glasses exhibit a combination of attractive properties, e.g. high strength combined with good ductility and corrosion resistance; in addition their casting geometry as thin ribbons made them interesting for the use as strengthening fibers in metal matrix composites. However, previous

efforts of incorporating metallic glass ribbons failed due to a severe lack of adhesion.

In other metal matrix composites it is well known that heat treatments can lead to an improved adhesion by diffusional bonding, but annealing of a metallic glass usually results in severe embrittlement. In some primary crystallizing glasses, however, embrittlement is reduced during primary crystallization, i.e. strength and ductility is regained in the partially crystallized state.

The interfacial reaction in a $\text{Fe}_{42}\text{Ni}_{42}\text{B}_{16}/\text{Ni}$ composites has been studied systematically by cross sectional TEM. During primary crystallization of $\gamma\text{-(Fe,Ni)}$ in the bulk of the ribbon, very fine γ -crystals grow epitaxially from the interface with the Ni matrix into the original glass, thus producing a new amorphous/crystalline interface with excellent adhesion.

This work was supported by the DFG: SFB 316-G3.

N2.10

HIGH-TEMPERATURE EVALUATION OF THE NICKEL/GRAPHITE INTERFACE. Nea S. Wheeler, David S. Lashmore and Alexander J. Shapiro, NIST, Gaithersburg, MD.

Typically, failure in metal matrix composites (MMC's) can be traced to the interface between the fiber and the matrix. Since interfacial failure may be due to one or more of a number of processes, it is important to identify the failure mechanism in order to determine the most appropriate means of improving the interfacial characteristics.

A nickel/graphite MMC was produced by electroplating nickel onto a 7 μm polyacrylonitrile (PAN) graphite fiber tow (3000 fibers/tow) to a thickness of approximately 0.5 to 1 cm. The MMC was cut into 5-7 sections which were then individually encapsulated in quartz ampules under a vacuum, of 10^{-5} Pa (10^{-7} torr) and heat treated at 600, 800 and 1100 °C for time ranging from minutes to hours. Scanning electron microscopy (SEM) was used to observe the composites before and after annealing. Degradation of the fibers at $T < 800$ °C was found to result from diffusion of the graphite into the matrix. At $T > 800$ °C, however, the data suggests that nickel diffuses into graphite parallel to the basal planes. Thus, any improvement in the nickel/graphite interface should involve a diffusion barrier to separate the fibers from the matrix.

This paper will discuss diffusion barriers which were deposited directly onto the fibers before application of the nickel matrix to inhibit nickel/carbon interdiffusion.

N2.11

THE INFLUENCE OF INTERFACIAL MODIFICATION ON TENSILE STRENGTH OF GR/AL COMPOSITES. Chen Ho, Guoding Zhang and Renjie Wu, Institute of Composite Materials, Shanghai Jiao Tong University, Shanghai 200030, P.R. China

Varying the composition of the matrix alloy has been a useful technique for tailoring the interfacial structure of metal matrix composites. Here we provide results of the influence of different interfacial structures on the mechanical properties for graphite fiber (M40) reinforced aluminum alloys. The composites are produced by Ti-B CVD coating on the fiber and then infiltrate with molten aluminum alloys. The composition of the Al alloy matrix are selected as Al-Ti (Ti oversaturated), Al-Cu-Mg system alloy and compare with pure Al. We note that Al-Ti alloy with Ti oversaturated matrix has a excellent improvement on the tensile strength of the composites. That is almost 100% coincide with the ROM predicted value even at 600°C higher temperature, but only 50% of ROM for Al-Cu-Mg system matrix.

XPS study reveals that the original Ti-B coating layer is a complex but loose structure, it includes Ti_2O_3 , TiB_2 , and Al_2O_3 mainly. This layer may prevent the interfacial reaction between fiber and Al alloys matrix in a different extent. The TEM micrograph shows the composite with Ti oversaturated Al-Ti matrix has a rather broad and distinct interphase, and remains it after higher temperature treatment, comparatively, for the interphase of pure Al matrix is narrow. We consider the original coating layer probably remains in a larger extent for the former case, since the matrix is Ti oversaturated, it may block the reduced Ti element diffuse into Al matrix. In the case of Al-Cu-Mg system matrix, it also has a broad but two phase structure of interphase. By means of SAM analysis, it is obviously Al_4C_3 and intermetallic compound $CuAl_2$ constructions, but not the original Ti compounds.

N3.1

THERMOMECHANICAL STABILITY OF ORGANOSILANE AND ORGANOTITANATE INTERPHASES IN GLASS REINFORCED COMPOSITES. A.T. DiBenedetto, S. Connelly, J. Gomez, G. Haddad, University of Connecticut, Storrs, CT. 06269.

The thermomechanical stability of a number of organosilane surface treatments for glass fibers used in fiber reinforced epoxy and polyester composites has been evaluated. The force transmission across the fiber/matrix interface was measured as a function of temperature and exposure to water using a fiber fragmentation test. Both the organosilane molecular structure and the treatment conditions were varied. In addition, a titanate/polyether sulfone coupling agent was synthesized in-situ on the surface of E-glass fibers. The effect of the titanate on the engineering properties of fiber reinforced polysulfone composites was assessed.

It was found that the effectiveness of the coupling agents was strongly dependent on treatment time and the level of water both in the treatment solution and on the fiber surfaces. Non-aqueous treatments promoted higher fiber strength, but required exceptionally long treatment times. The presence of phenyl substitution on amino silanes improved the thermal stability in epoxy and polyester composites, but modified the hydrolytic stability in a less predictable fashion. It was also found that the in-situ prepared titanate/polysulfone oligomer improved the static and fatigue properties of the polysulfone composites.

N3.2

FILAMENT FRAGMENTATION PHENOMENA. Juan C. Figueroa, E. I. du Pont de Nemours & Co., Inc., Wilmington, DE; Linda S. Schadler & Campbell Laird, University of Pennsylvania, Philadelphia, PA.

The effect of fiber surface treatments on the inter-relationship between the tensile strength of a filament and the shear strength of its interphase region is one of the central issues facing composite materials technologists today.

We demonstrate here that analysis of fragmentation phenomena in monofilament composites can simultaneously yield information about these two parameters. An analysis of critical fragment populations which leads to the determination of interphase strengths is presented here. This analysis considers issues such as the strain energy exchange between fiber and matrix during filament fracture, as well as interphase relaxation due to visco-elastic behavior.

PAN-derived carbon/polycarbonate monofilament composites were deformed parallel to the fiber direction in-situ to

optical microscopy monitoring to yield information about the evolution and attainment of critical fragment populations. Results show that interphase strength in this system is limited by the presence of weakly bound layers on the fiber surface.

N3.3

APPLICATION OF COLD PLASMA IN TAILOR-DESIGNING COMPOSITE INTERFACES. Nakho Sung, Laboratory for Materials and Interfaces, Tufts University, Medford MA 02155.

Low temperature plasma generated by glow discharge is a convenient tool for the surface modification. Depending on the type of gas and the reactor configuration used, the treatment varies from a simple change of surface chemistry, such as oxidation or aminization, to a grafting of polymers having different structure and thickness. Through the fiber surface treatment, therefore, composite interphase can be tailor designed. For example, in graphite fiber reinforced composites, fiber surface may be modified either by plasma of simple gas or by plasma polymerization of monomers such as acrylonitrile, depending on the nature of matrix. In aramid fiber/elastomer case, fiber can be modified by implanting flexible chain polymers through plasma-induced polymerization of butadiene. In all cases, interfacial properties, such as adhesion or load transfer efficiency, are strongly dependent on the structure of modified surfaces. In particular, wetting characteristics chemical reactivity, degree of cross-linking (or open structure), and thickness of the treated layer are important structural parameters in promoting adhesion through primary bondings and/or molecular interdiffusion mechanisms.

N3.4

THE EFFECTS OF FIBER SURFACE TREATMENTS BY A COLD PLASMA IN CARBON FIBER/BISMALEIMIDE COMPOSITE. Tao C. Chang and Bor Z. Jang, Materials Engineering Program, Department of Mechanical Engineering, Auburn University, AL 36849

The surfaces of carbon fibers (Hercules AU-4) were treated by a cold oxygen or ammonia plasma. Efforts were made to define the optimal conditions of plasma treatments by adjusting the operational parameters, e.g. flow rate of gas and plasma power. The change in surface composition of various treated carbon fibers was characterized by X-ray photoelectron spectroscopy (XPS). Elemental surface concentrations were calculated from the corrected XPS peak area. The fiber surface free energies and the proportions of polar and dispersive components were determined by the contact angle measurement using a micro-Wilhelmy technique which incorporated five liquids having a wide range of polar to dispersive free energy ratios. A two-component bismaleimide system (Matrimid™ 5292 CIBA-GEIGY) was used as a matrix for composites containing either untreated or treated fibers. Transverse tensile test was chosen as a primary method in studying the change of interfacial strength caused by plasma treatments. Scanning electron microscopy (SEM) was used to show the effect on the fiber surface topology and the fracture morphology of composites. A correlation was established between fiber surface properties and mechanical performance of composites.

N3.5

TAILORED INTERPHASES IN FIBRE REINFORCED POLYMERS.

Michael R. Piggott, Dept. of Chemical Engineering, University of Toronto, Toronto, Ontario, Canada.

The use of fibre coatings to enhance adhesion between fibres and polymers normally means that, in the fibre composite, some residue of the coating is present at the fibre-matrix interface. This constitutes the interphase. The mechanical properties of this material may be measured using special equipment developed to do simple fibre pull out tests. These tests have the advantage of revealing the interphase failure mode (i.e., brittle or ductile) as well as providing such data as work of fracture, yield stress, interfacial pressure and the coefficient of friction for post-debonding slip. The equipment may thus be used to monitor coatings designed to develop particular properties. Results obtained so far indicate some ductility and yielding with thermoplastic interphases, while thermoset interphases appear to be universally brittle, with small works of fracture (10-200 Jm⁻²). The ideal interphase should probably have a moderate yield stress, to give the composites adequate compression and yield strength. After yielding, the interphase should fail in such a way as to give long fibre debonds, so that the composite has good impact resistance through promotion of fibre pull outs. The pressure across the interphase should be controlled so that fibre pull out lengths are maximized.

N3.6

A TEM STUDY OF AN ADHESIVE / SHEET MOLDING COMPOUND INTERFACE. Eduardo A. Kamenetzky and Raymond S. Farinato, American Cyanamid, Stamford Research Laboratories, Stamford, CT.

The interface between an epoxy adhesive on sheet molding compound (SMC) was studied by TEM. The interface width is less than 20 nm where it is sharp and on the order of 40 nm where it is more diffuse. The interfacial area in the TEM sample is located first by the difference between adhesive and SMC microstructures. Where there are no microstructural features we can investigate further the location of the interface by using the Mg K α peak from magnesia thickener in the polyester matrix of the SMC. Calcium carbonate crystals in the SMC extend to within less than 25 nm of the interface. Measurements of interface extent and roughness indicate that there is intimate contact and good mechanical bonding between the adhesive and SMC.

The strength of an adhesive-SMC joint depends on the microstructure of the interphase as well as on the nature of the bonding of the adhesive to the polyester matrix of the SMC. The formation of this interphase region will be driven thermodynamically and be limited by the chemorheology of the curing adhesive. The surface and interfacial energetics of this epoxy-SMC system were evaluated using sessile drop advancing contact angles. Good mechanical bonding observed by TEM is consistent with a small advancing contact angle of 20° for the epoxy adhesive on the SMC at 121 °C which shows a good thermodynamic driving force for the intimate contact during the bonding process.

N3.7

STUDY OF TRANSCRYSTALLIZATION IN POLYMER COMPOSITES.

Benjamin S. Hsiao and Eric J. H. Chen, E. I. du Pont de Nemours & Co., Inc., Fibers Department, Pioneering Research Laboratory, Experimental Station, P.O. Box 80302, Wilmington, Delaware 19880-0302

Fiber surface induced transcrystallization has been reported in many composite systems. It is believed that the transcrystalline region exhibits different properties than the bulk matrix due to a different morphological arrangement. In this work, it is our intention to examine the surface-induced transcrystallization in the present composites and to discuss some possible attributes of this phenomenon. Some characterization techniques, including thermal analysis, optical microscopy, dynamic torsional test and small

angle light scattering were utilized to study the kinetics of transcrystallization; microdebonding was also adapted to study the interfacial shear strength of the transcrystalline layer.

N3.8

THE EFFECT OF SALT WATER ABSORPTION ON INTERFACIAL DEGRADATION IN POLYMERIC COMPOSITE MATERIALS. Walter L. Bradley and Tim Grant, Mechanical Engineering, Texas A&M University, College Station, TX 77843.

The effect of salt water moisture absorption on the interfacial strength has been studied using graphite and glass fibers in matrices of eight polymeric materials including both thermosetting and thermoplastic systems. The effect of moisture degradation has been measured using transverse tensile strength, comparing specimens which have not been immersed in salt water (simulated ocean environment) to those which have.

The details of the degradation process(es) have been studied using direct observation of the transverse tensile tests in the scanning electron microscope. Specimens polished to clearly reveal fiber ends and the matrix are loaded in the SEM and the nature of the fracture process noted. A comparison of the details of the fracture process(es) for transverse tensile tests on both dry specimens and ones previously immersed in salt water gives good indication of the nature of the degradation that results from salt water immersion, particularly distinguishing moisture degradation of the interface from moisture degradation of the matrix.

N3.9

THE INFLUENCE OF WATER ON THE EPOXY RESIN-GLASS INTERPHASES. Robert Kosfeld, Thomas Marzi, Ulrich Schröder, Michael Heß, University of Duisburg, Department of Physical Chemistry, D-4100 Duisburg, FRG.

The incorporation of water largely effects material properties of glass-fiber-epoxy resins. Experimentally it can be discriminated between incorporation of water in the polymer matrix and in the polymer-glass-interphase. Glass-transition temperature in the beginning of the water resorption at 70 °C is decreased but later remains constant at a distinct value indicating a change in the mechanism governing water the sorption. Parallel to this observation an additional deep temperature relaxation process is observed in the dynamic-mechanical experiment. This does not occur in the pure resin without glass-fibers and it indicates property changes in the polymer-glass-interphase.

N4.1

INTRINSIC MATERIAL LIMITATIONS IN USING INTERPHASE MODIFICATION TO ALTER FIBER-MATRIX ADHESION IN COMPOSITE MATERIALS. Lawrence J. Dzkal, Composite Materials and Structures Center, Michigan State University, East Lansing, MI 48824-1326

A very large percentage of studies seeking to improve fiber-matrix adhesion to alter composite properties are directed at the formation of primary chemical bonds between the reinforcement surface and the matrix. The dynamic events that occur when the fiber-matrix interface is formed lead to the creation of an interphase which can

have properties quite different from the matrix in addition to any chemical bond formation.

This study has been directed at elucidating the role of these interphase properties themselves on fiber-matrix adhesion. A reinforcement (AS-4 carbon fiber) with a quantifiable surface chemistry and in epoxy matrix have been kept constant through a series of experiments in which the distance between crosslinks of the matrix has been changed. The wettability of the fiber and the degree of chemical bonding to the fiber have not changed but the interfacial shear strength measured for each of these systems has decreased with decreasing matrix modulus. It will be shown that the properties of the matrix and the residual stresses created during processing limit the maximum interfacial shear stress that can be supported by the fiber-matrix interphase.

N4.2

ACID/BASE PROPERTIES OF CARBON AND GRAPHITE FIBER SURFACES. Sheldon P. Wesson, TRI/Princeton, Princeton, NJ; and Ronald E. Allred, PDA Engineering, Materials Dev. Dept., Albuquerque, NM.

Carbon and graphite fiber surfaces were analyzed by inverse gas chromatography, using Lewis acids and bases as probe adsorbates to determine the effect of electrooxidation and radio frequency glow discharge plasma treatments on surface acid/base properties. Adsorption isotherms computed from chromatograms were analyzed with the CAEDMON algorithm (Computed Adsorption Energy Distribution in the MONolayer) to obtain histograms of surface area fraction versus adsorption energy. Changes in surface heterogeneity revealed by adsorptive energy distributions were correlated with wetting data and surface chemical composition deduced from high resolution x-ray photoelectron spectroscopy.

Histograms from adsorption isotherms using the Lewis base show fiber surface energetics are bimodal, with most of the surface presenting dispersion force or weak acid/base attraction to the probe. A small surface fraction of acid sites shows strong chemisorptive properties, and this area fraction increases systematically with the degree of electrooxidation. RF glow discharge plasmas are effective at enhancing surface acidity, especially on high modulus graphite fibers that resist conventional electrooxidative processes.

Chemisorptive properties of acid sites were investigated by programmed thermal desorption of the Lewis base from fiber surfaces. Preliminary results suggest that plasma treatments activate the surface, while causing less physical damage to the near surface region of the fiber.

N4.3

CORRELATION BETWEEN FIBRE SURFACE ENERGETICS AND FIBRE-MATRIX ADHESION IN CARBON FIBRE REINFORCED PEEK COMPOSITE. D J Hodge, B Middlemiss and J A Peacock, ICI Wilton Materials Research Centre, PO Box No 90, Wilton, Cleveland, TS6 8JE, UK

Surface energies of carbon fibres at different levels of surface treatment have been determined by a wetting force technique and related to fibre-matrix adhesion in carbon fibre reinforced PEEK composite. The effect of oxidative surface treatment on the surface free energy is detailed, along with the changes in surface oxygen and nitrogen content, as determined by X-ray photoelectron spectroscopy (XPS). The work of adhesion has been calculated for the carbon fibres and thermoplastic, which correlate well with experimental determination of interfacial strength. The technique can therefore be used to predict adhesion levels in fibre reinforced composites.

N4.4

EFFECT OF SURFACE OXYGEN ON ADHESION OF CARBON FIBER REINFORCED EPOXY COMPOSITES. P. W. Yip and S. S. Lin, Army Materials Technology Laboratory, Watertown, MA 02172

Over the past 20 years, carbon fiber has become a major reinforcing substance for lightweight structural materials. The strength and the degree of a reinforcement is dependent on fiber surface chemistry and morphology. Yet the interaction between the fiber surface and the matrix for better adhesion is not clearly understood. The mechanical properties and ultimate performance of composites tie intimately with surface morphologies of the fibers.

In this paper, the adhesion mechanism involved in the fiber epoxy resin composites is examined. Three carbon fibers of different origins are treated by chemical reagents to modify fiber surfaces. The surface morphology and chemistry are studied by scanning electron microscope, X-ray photoelectron spectroscopy and scanning Auger microprobe techniques, and adhesion strength by the transverse tensile strength (TTS) of the fiber epoxy composites. The amounts of oxygen existing on the fiber surfaces are compared with TTS of the reinforced composites.

The surface morphologies of these three fibers after the treatments change considerably. The extent of oxidation on the carbon fiber surface is dependent on the chemical reagents, the surface structures and the fiber precursors. The degree of adhesion is not promoted substantially either by the amount of oxygen or by carbon oxygen functional groups on the fiber surface. The chemical treatments not only increase the abundance of oxygen on the surface, but also enhance surface roughness. The increased roughness in surface micro-domains is a major factor governing the carbon fiber-epoxy resin adhesion.

N4.5

INTERFACIAL EFFECTS OF PLASMA TREATMENT ON FIBER PULL-OUT Umesh Gaur, TRI Princeton, P.O. Box 625, Princeton, NJ 08542; Theodore Davidson, Center for Surface & Interface Res, Univ. of Connecticut, Storrs, CT 06269-3136.

Because of the accepted importance of the fiber-matrix interface for load transfer, toughness, and durability, we have worked to modify this interface by plasma treatments of the fiber component. The treatments involved low temperature non-equilibrium plasmas using one or more gases to oxidize or reduce the fiber surface. Treatments of the fibers-as yarn-were conducted for 10 minutes at pressures of 500 mTorr with input power of 50 watts at 13.56 MHz. ILSS was evaluated by the microbond technique [Gaur and Miller, *Composites Sci. and Tech.*, 34, 35 (1989)] in which a droplet of cured epoxy resin is sheared from the fiber. Aramid-epoxy showed an increase in ILSS from untreated at 30 MPa to 57 MPa after an oxidizing plasma treatment. With high modulus polyethylene fibers the initial value of ILSS, 1 MPa, was increased to 8 MPa by treatment with a non-oxidizing plasma. Further work is directed toward establishing changes in surface morphology and chemistry by SEM and XPS.

N4.6

INTERPHASE BEHAVIOR IN CYCLIC FATIGUE OF MONOFILAMENT COMPOSITES. Linda S. Schadler, U. of Pennsylvania, Philadelphia, PA; Juan C. Figueroa, E.I. du Pont de Nemours & Co. (Inc), Wilmington, Delaware; C. Laird, U. of Pennsylvania, Philadelphia, PA.

Macroscopic properties of continuous-filament composites are known to be dependent on fiber-matrix interphase behavior. Monofilament graphite/Polycarbonate composites have been

used as a model system to study the cyclic fatigue properties of the interphase region. The stress transfer efficiency (the ability of the interphase to transfer load from the matrix to the fiber) of the interphase was monitored using a modified critical length technique. In order to determine the role of the interphase in cyclic deformation, the interphase was varied by etching the fiber surface. Correlations between fiber surface energetics, morphology and matrix properties have been made with cyclic damage. It has been found that damage (reduction in interphase stress transfer efficiency) due to cycling transverse to the fiber direction depends on both strain rate and amplitude indicating a strong influence of the viscoelastic properties of the matrix on damage. However, the maximum damage, corresponding to a complete debonding of the matrix and fiber, depends predominantly on fiber surface morphology. Damage due to cycling in the longitudinal direction was observed only after fiber failure and is therefore dependent on fiber strength.

N4.7

INTERLAMINAR FRACTURE IN CARBON FIBER/THERMO-PLASTIC COMPOSITES. J. A. Hinkley, NASA Langley Research Center, Hampton, VA; W. D. Bascom, University of Utah, Salt Lake City, UT; and R. E. Allred, PDA Engineering, Albuquerque, NM.

Although commercial surface treatments and sizings generally produce strong interface in carbon fiber/epoxy composites, much less is known about how to optimize carbon fiber/thermoplastic systems. Several lines of evidence suggest that standard oxidative fiber treatments are inadequate.

This presentation will review embedded fiber tests, composite toughness data, and fractography, all of which point to the prevalence of interfacial failures in thermoplastic composites. Data on unidirectional composites made from the model resin poly(2,6-dimethylphenylene) oxide will be used to illustrate how interface effects can lead to a greater than two-fold variation in Mode I interlaminar toughness. Progress towards improving adhesion using plasma treatment of fibers will be reported. Finally, an unexpected case of resin degradation, apparently promoted by the fiber, will be described.

N4.8

EFFECTS OF SURFACE TREATMENTS ON TENSILE AND INTERFACE SHEAR STRENGTHS IN GLASS FIBER/RESIN MATRIX COMPOSITES. Albert A. Kruger, Pacific Northwest Laboratory^(a), Chemical Sciences, Richland, Washington 99352-0999

Fracture mechanics derived for materials containing distributions of tiny cracks is found to be contradictory with analyses of fatigue data for treated glass fibers. Furthermore, the supposition that microcracks are formed on the glass surface at the time of fabrication is inconsistent with the production of fibers with an apparent lack of statistical variation of breaking strengths, either before or after accelerated aging.

Arrhenius calculations on the results of zero stress fatigue experiments indicate that the rate-determining step of glass aging is consistent with an interstitial hopping of highly mobile cations. Surface treatments used to modify the chemical corrosion mechanism alter the performance of glass reinforced plastics (grp) composites. The effects of this chemistry on initial fiber strengths, resistance to aging, and preliminary composite properties are reported.

^(a) Operated for the U.S. Department of Energy by Battelle Memorial Institute under Contract DE-AC06-76RLO 1830

N4.9

INTERFACIAL INTERACTIONS IN SILICA REINFORCED SILICONES. M.I. Aranguren, C.W. Macosko, M. Tirrell and B. Thakkar, University of Minnesota, Minneapolis, MN 55455

Polydimethylsiloxanes give elastomers that are very stable under different environmental conditions and stay rubbery over a large range of temperatures. However, they are mechanically very weak and so they are reinforced with fumed silicas. The dramatic improvement of properties is not only due to the open structure of the silica aggregates that occlude part of the polymer but also to the great affinity of the filler and matrix.

We have worked with vinyl terminated polydimethylsiloxanes of different molecular weight ($M_n = 9000$ to 146000) and fumed silicas of different surface treatment. All the silicas were modifications of Aerosil 130 (Degussa), so that the surface silanols were replaced by methyl groups or methyl and vinyl groups.

Diffusive reflectance IR spectroscopy was used to characterize the surface of the silicas and the adsorption of the polymer. The amount of bound rubber (fraction of polymer in the uncured state that is "irreversibly" adsorbed to the filler) is a function of the concentration of silanols in the silica and the molecular weight of the polydimethylsiloxane. The bound rubber was measured by extraction in chloroform which only leaves the strongly adsorbed polymer and probably extracts occluded and entangled chains. The amount of adsorbed polymer per weight of filler is independent of the filler concentration.

The rheology of the uncured rubber can be qualitatively explained by a model where the aggregates are connected to each other through the polymer. The connections can be due to entanglements of the bulk-chains or direction polymer bridging of the aggregates. Experiments using a surface force apparatus to measure the forces due to the two types of connections are underway.

N4.10

AN INTERFACIAL THERMODYNAMIC STUDY ON NTC PHENOMENON OF CONDUCTIVE HDPE COMPOSITES Zhang Mingqiu and Zeng Hanmin, Materials Science Institute, Zhongshan University, Guangzhou, P.R.C.

NTC (Negative Temperature Coefficient) phenomenon has limited the application of conductive composites with crystalline polymer matrix in PTC (Positive Temperature Coefficient) sensitives, self-controlled heaters, etc. In this paper, the interfacial characteristic and resistance-temperature property of the conductive composites comprised of high density polyethylene (HDPE), carbon black (CB) and graphite (GR) were studied with the help of contact angle measurement technique in order to make out a possible mechanism of NTC and a way to control it. The experimental result showed that the composites exhibited PTC below the melting point of HDPE, but NTC above it. On the other hand, it was found that with increasing temperature, the interaction and wettability between fillers and the resin weakened linearly. When temperature went beyond the melting point of HDPE, those CB and GR particles which had been separated by the movement of polymer chain units previously could displace a little more easily to accumulate once again forming a number of continuous electric paths in such resin of better fluidity. Hence, the conductivity of composites were improved and NTC occurred. This was a process that the system free energy dropped owing to the reduction of interfacial area between fillers and resin during this reconnection of fillers. A survey of the spreading coefficient also proved this tendency. We considered that surface treatment which lowers surface entropy of fillers and resin would reduce NTC effect.

N5.1

FRACTO-EMISSION STUDIES OF INTERFACIAL FAILURE IN COMPOSITES.* I. T. Dickinson L. C. Jensen, and B. A. Mielke, Department of Physics, Washington State University, Pullman, WA 99164.

We present measurements of the particle emission (electron and photon emission) during and following the failure of interfaces associated with composite materials. Photon emission measurements on semi-transparent materials such as epoxy and silica glass allow the detection of interfacial failure occurring at surfaces *within the matrix*. Simultaneous measurements of electron emission determine the exact time when cracks reach the surface of the sample, thereby providing a path of escape from a fracture surface to the surrounding vacuum and therefore to the detector. Systems to be discussed include glass fibers embedded in epoxy with variations in interfacial bonding, a single metal rod in epoxy tested in a pull-out experiment, and a similar test involving a metal rod in a silicate glass. The likely mechanism for light production involves microdischarges resulting from fracture-induced charge separation at two dissimilar surfaces. We also present fracto-emission results from controlled interfaces, including treated fibers in epoxy, and fiber matrix interfaces degraded by exposure to water vapor at elevated temperatures. These components of fracto-emission can provide a means of monitoring the details of the debonding process on time scales down to the sub-microsecond level.

*Work supported by the National Science Foundation under Grant DMR 8601281, the Office of Naval Research under Contract N00014-87-K-0514, the Goodyear Tire Company, and the Washington Technology Center.

N5.2

INTERFACES WITH DISCONTINUITIES AND INTERPHASES WITH CONTINUOUSLY VARYING PROPERTIES IN COMPOSITE MATERIALS. C. S. Chen, General Dynamics, Ft. Worth, Tx.

The transition region between any two different components in the macroscopic composite is well known for its effect upon both the local and global behavior of the composites. For simplicity and for lack of detailed information, in most treatment, however, an ideal interface is often considered where the composite only has some discontinuities in properties. But the transport process, and the transfer of response between the different components, and some failure characteristics in composites, have indicated that the ideal interface treatment is no longer sufficient. Particularly for material design, the tailorable interphases may provide greater varieties of macroscopic composites for applications.

In this presentation, we attempt to explore some essentials of the transition regions by examining the wave propagation in composite materials consisting of two different material elements in alternation. When the composite exhibits discontinuities in properties, then a wave front shows the familiar attenuation at the interfaces where discontinuities occur. We show how the strength of the wave front decays because of the "ideal interfaces". But when the smooth transition interphases allowed, no decay occurs due to structure right at the wave front. We show that the strength of the wave front oscillates between two definite values. We only require that the second derivatives of some material properties be continuous in the interphases. Such constraint still allows many tailorable interphases. We also show that behind the wave front, a non-uniform convergence will transfer the continuous interphases to the discontinuous interfaces when the thickness of the transition regions shrink to zero.

N5.3

A SOLID-STATE NMR STUDY OF THE PMMA- Al_2O_3 INTERFACE Kariofilis Konstantinidis, John Evans and Matthew Tirrell, University of Minnesota, Minneapolis, MN

Chemical bonding, reactivity and polymer conformation are among the

phenomena that contribute to the adhesive strength of a polymer/metal-metal oxide interface. Carbon-13 solid-state NMR has been used to study these phenomena in the reactive adsorption of poly(methyl methacrylate) on porous aluminum oxide. Reaction of the ester side chain of the polymer with the surface hydroxyls is observed in agreement with IR results. Both the large extent of reaction (>50%) and indications of conformational changes upon adsorption suggest that polymer molecules adopt a flat configuration on the surface. The dependence of the extent of reaction on molecular weight and tacticity of the polymer will be discussed, together with the importance of such results in predicting and promoting polymer/metal adhesion.

N5.4

SPREADING OF LIQUID DROPLETS ON CYLINDRICAL SURFACES: ACCURATE DETERMINATION OF CONTACT ANGLE. H. Daniel Wagner, Polymeric Composites Laboratory, Department of Materials Research, The Weizmann Institute of Science, Rehovot 76100 (Israel).

The wetting of cylindrical monofilaments by liquid polymers is a problem of much scientific and technological importance. In particular, the characterization of the physicochemical nature of interfaces is a key problem in the field of advanced fibrous composites. The macroscopic regime contact angle, which reflects the energetics of wetting at the solid-liquid interface, is very difficult to measure by usual methods in the case of very thin cylindrical fibers.

In the present article two numerical methods are proposed for the calculation of macroscopic regime contact angles from the shape of a liquid droplet spread onto a cylindrical monofilament. These methods, which build on earlier theoretical treatments by Carroll, and Yamaki and Katayama, very much improve the accuracy of the contact angle obtained. Experimental results with an epoxy-aramid system are presented to demonstrate the high degree of accuracy of the methods proposed.

N5.5

AN OPTICAL METHOD TO CHARACTERIZE IMPREGNATION AND WETTING OF GLASS-FIBERS WITH EPOXY RESIN. Robert Kosfeld, Thomas Marzi, Ulrich Schröder, Michael Heß, University of Duisburg, Department of Physical Chemistry, D-4100 Duisburg, FRG.

The character of the interphase between bulk polymer and reinforcing filler or fiber is of great importance for the mechanical behaviour of the composite. An optical technique has been developed by Ehrenstein¹ which is suitable to follow the course of sorption of resin by fiber material. This technique has been modified and applied to the sorption and curing process in Epoxy-glass-fiber composites. Thus, in certain cases it is possible to observe these processes without damaging the sample and obtain more detailed information about polymer-filler interaction during the first stages of production. In further steps these informations may be correlated to mechanical properties of the composites.

¹ H.O. Willax, G.W. Ehrenstein, Kunststoffe 62 (1972) 887

N5.6

THE INFLUENCE OF ANNEALING ON THE BEHAVIOUR OF EPOXY-GLASS INTERPHASES. Robert Kosfeld, Thomas Marzi, Ulrich Schröder, Michael Heß, - University of Duisburg, Department of Physical Chemistry, D-4100 Duisburg, FRG.

Observation of the glass-transition region is suitable for investigation of processes being correlated with the existence of a polymer-filler interphase. Room temperature curing epoxy resins were used with

and without glass-fibers incorporated. After the curing process at room temperature the samples were annealed. The differences in the glass transition of filled and pure resins together with the chemical structure of the resins and the glass-fiber surface are discussed with respect to the interphase properties. Shifts of the transition temperature after annealing compared with unfilled resins indicates the presence of a interphase with good mechanical properties.

N5.7

THE ROLE OF RESIDUAL STRESSES IN THE CRACKING OF A MODEL METAL-CERAMIC SYSTEM, $\text{Al}_2\text{O}_3/\text{Ta}(\text{Ti})$.
A.H. Bartlett, M. Rühle, A.G. Evans, University of California Santa Barbara, Santa Barbara, Ca.

A model bimaterial system, $\text{Al}_2\text{O}_3/\text{Ta}(\text{Ti})$, has been devised in which the residual stresses due to thermal mismatch between the metal and the ceramic can be controlled by varying the composition of the $\text{Ta}(\text{Ti})$ alloy. Fractographic characterization using SEM has been employed to compare the observed cracking behavior with that predicted by calculations. Depending on the sign of the thermal mismatch, cracks can occur either in the ceramic or in the reaction product interface. Crack angles correlate with the direction of maximum principal stresses. The trajectories of steady state cracks in the ceramic are also predicted and compared with experiment.

TEM has been used to identify reaction phase products, and characterize the structure of the interface. Cracks intersecting the interface are observed, and the role of defects on interfacial crack propagation assessed.

N5.8

THE STRENGTH AND FRACTURE OF CERAMIC/METAL BONDED SYSTEMS. M. Y. HE AND A. G. EVANS, Materials Department, University of California, Santa Barbara, CA.

The strength of Al_2O_3 materials bonded using a ductile metal layer is investigated. Systematic elastic-plastic stress analysis has elucidated the stresses that exist at metal/ceramic bond interfaces as well as near the tip of a small edge crack adjacent to the interface. The macroscopic stress-strain relations are calculated as functions of the bond layer thickness, metal yield strength, thermal expansion mismatch, elastic properties of the two materials and the location of the edge crack. The effects of these stresses on the strength and fracture of the bonded systems are also predicted and compared with the experimental results.

N5.9

CVD Mo and W Oxy-carbide Coatings on SiC Yarn
Michael Retsch¹, Beng Jit Tan¹, Francis S. Galasso²
and Steven L. Suib^{1,3} 1. Dept. of Chemistry, U-60,
University of Connecticut, Storrs, CT 06269-3060.
2. United Technologies Research Center, East Hartford, CT
06108. 3. Dept. of Chem. Eng., U-60, University of
Connecticut, Storrs, CT 06269-3060.

SiC fibers have been coated with molybdenum and tungsten oxy-carbides by heating $\text{Mo}(\text{CO})_6$ or $\text{W}(\text{CO})_6$ to 375°C in flowing hydrogen in a chemical vapor deposition (CVD)

process under reduced pressure. X-ray powder diffraction data were used to characterize these coatings and results suggest that MoOC or WOC were formed. These materials have a variable composition ranging from $\text{M}_2\text{C}_{0.7}\text{O}_{0.6}$ to $\text{M}_2\text{C}_{0.6}\text{O}_{0.5}$. Coated fibers were used for tensile strength measurements and these experiments indicate that the fibers were not significantly degraded during the coating process. The MoOC coating can be converted into a Mo metal coating by heating at 800°C. Similar studies with the tungsten system showed that WOC coatings could also be produced that also showed good tensile strengths. X-ray photoelectron spectroscopy experiments have been used to study the oxidation states of the elements of the coatings. Mapping studies by scanning Auger microscopy have been used to determine the uniformity of such coatings and to study their thicknesses.

N5.10

SOLID STATE BONDING OF Si_3N_4 AND Ni. Jian-Yih Wang, Shu-En Hsu, Chung Shan Institute of Science and Technology, Taiwan, R.O.C.; and Yoichi Ishida, University of Tokyo, Tokyo, Japan.

Since the solid state bonding of Si_3N_4 and Ni has great applicability in the future, it becomes the most attractive topic in the fields of ceramic and metal. From the phase diagram, nickel can solute a fair amount of silicon and nitrogen. Therefore, the $\text{Si}_3\text{N}_4/\text{Ni}$ bonding might form the ideal bonding interface with no formation of reaction phase as in the case of $\text{Al}_2\text{O}_3/\text{Nb}$ bonding^[1,2].

The ceramic used here are Toshiba-made pressureless-sintering Si_3N_4 , added a little Y_2O_3 and Al_2O_3 as the sintering binder, and the nickel is a commercial material with 99.9% purity. Solid state bonding was achieved by placing Ni foil (1mm thick) in between two pieces of silicon nitride, loading 12 MPa and heating at 1223K for one hour, and then furnace cooled. JEM-1250 HVEM, JEM-2000EX HREM, and JEM-4000FX AEM were used for the observation and composition analysis of bonding interface.

The 4-point bonding strength of $\text{Si}_3\text{N}_4/\text{Ni}$ is about 200MPa. In addition to the direct bonding, an amorphous-like phase was found existing in some regions of the $\text{Si}_3\text{N}_4/\text{Ni}$ interface, which is responsible for the degradation of bonding strength. In view of the experimental results, the formation of amorphous-like phase is due to the gathering of Al_2O_3 and Y_2O_3 , used as the sintering binders of Si_3N_4 , in bonding interface via intergranular diffusion during the bonding process.

- [1] M. Florjancic, W. Mader, M. Rühle, M. Turwitt; J. de Physique, C4 (1985).
- [2] Y. Ishida, J. Y. Wang, T. Suga; MRS Proceeding (1988).

N5.11

CHEMICAL INTERACTIONS IN THE ALUMINUM-CARBON AND ALUMINUM-SILICON CARBIDE SYSTEMS. Benji Maruyama, Naval Research Laboratory, Wash. D.C.; Fumio S. Ohuchi, E.I. du Pont de Nemours Exp Station, Wilmington, DE; and Llewellyn K. Rabenberg, The University of Texas at Austin, Austin, TX.

The atomic structure of the interface by and large determines the ultimate mechanical properties of graphite and silicon carbide reinforced metal matrix composites. The results of XPS investigations of the reaction kinetics of aluminum-carbon and aluminum-silicon carbide systems will be presented. Of particular interest is the influence of water vapor and hydrated alumina on the reaction kinetics. The

implications of the results on our previously developed Oxidation Model of Carbide Formation and on the behavior of interfaces in commercial composites will be discussed.

N5.12

STABILITY AND REACTIONS AT COMPOSITE INTERFACES OF TITANIUM ALUMINIDES WITH POTENTIAL FIBER MATERIALS. J. A. Dekock, M.-X. Zhang and Y. A. Chang, Department of Materials Science and Engineering, University of Wisconsin, Madison, WI 53706, and O. Y. Chen, United Technologies, Pratt and Whitney, E. Hartford, Conn. 06108.

In the development of titanium-aluminum intermetallic compounds for structural applications at high temperatures, there is a need to have a fundamental understanding of the stability and reactions between the intermetallic matrix and potential fibers. The objective of our study is to provide such a fundamental understanding of interfacial stability and reactions between titanium aluminide with several potential fibers such as TiB_2 , Al_2O_3 and SiC. Preliminary experimental results will be presented and interpreted in terms of thermodynamic stabilities at the interfaces and multi-component diffusion theory.

N5.13

CHARACTERISATION OF INTERFACES IN SiC PARTICULATE-REINFORCED Al ALLOYS USING AEM. D-Q. Huang, Y-P. Lin and B.W. Robertson, Department of Materials Science & Engineering, McMaster University, Hamilton, Ontario, Canada L8S 4L7.

The behaviour of metal-matrix composite systems can depend strongly on the nature of the interface between the reinforcing material and the metal matrix. Recently, the high temperature mechanical behaviour of SiC particulate-reinforced Al alloys has received attention. A preliminary study by Corbin and Wilkinson [1] of a 2014 Al alloy with 20% SiC particulates suggests that an increase in overaging of this material results in a change of fracture mode, during tensile testing at 400°C, from one involving SiC particle/matrix decohesion to one involving only matrix failure. Electron microscope studies of the SiC/matrix interface regions of these materials have been undertaken using SEM, TEM and STEM and will be reported along with work on A356 high strength casting alloy (Alcan). Reference will be made to the importance of thin foil preparation to the value and interpretability of transmission EM results.

[1] S F Corbin and D S Wilkinson, Effects of temperature on the mechanical behaviour of a SiC particulate reinforced Al alloy, CIM Conference, Halifax, August 20-24, 1989.

N5.14

THE DISLOCATION STRUCTURE AND ENERGY OF NiO-Pt INTERFACES. E.-S. Shieu and S.L. Sass, Department of Materials Science and Engineering, Cornell University, Ithaca, NY.

The dislocation structure of Pt-NiO (001) interfaces was studied using electron microscopy and electron diffraction techniques. Specimens were produced by hot pressing polycrystalline Pt films onto thin NiO single crystals, and bulk Pt single crystals onto bulk NiO single crystals. The polycrystalline Pt specimens were used to determine the favored orientation relationships between the NiO and Pt, while the bulk NiO-Pt specimens were used to study the detailed structure of the interface.

Three categories of orientation relationships were identified: exact epitaxy with $(001)_{Pt} \parallel (001)_{NiO}$; $[110]_{Pt} \parallel [110]_{NiO}$; small rotations away from exact epitaxy about the common [001] direction; high index planes of Pt parallel to (001) of NiO. Theoretical calculations of the expected dislocation structures of

interfaces with the first two orientation relationships were made using a Bollmann-type analysis. The experimental observations and theoretical predictions were shown to be in good agreement. The energies of the interfaces having the first two orientation relationships were shown to be similar which is believed to be the reason why they both occur.

N5.15

EFFECT OF ANNEALING ON THE ALUMINUM/SiC INTERFACE STRUCTURE AND COMPOSITION. Qiong Li, Janez Megusar and James A. Cornie, Massachusetts Institute of Technology, Cambridge, MA

This research is concerned with determination of structure and composition of interfaces in the SiC coated graphite fiber/ aluminum matrix composite as a function of different processing parameters. As such, it will contribute toward better understanding of the role of interfaces in optimizing properties of metal matrix composites.

The effect of annealing has been studied by constructing graphite fiber/amorphous SiC and amorphous SiC/aluminum couples separately. Graphite and aluminum ribbons have been coated with a thin layer of amorphous SiC using plasma enhanced chemical vapor deposition (thickness of the SiC coating did not exceed 0.3µm). These specimens were subsequently annealed over a wide temperature range. Interface structures, including reaction zones, resulting from each anneal were examined on transverse sections by using high resolution transmission electron microscopy and scanning transmission electron microscopy.

In the previously published research we showed that formation of a reaction zone can be almost completely suppressed under appropriate conditions of aluminum pressure infiltration of graphite preforms. At this conference, results on annealing of the aluminum/amorphous SiC couples will be presented, with the emphasis on kinetics of a reaction zone formation.

N5.16

INTERFACE ELECTRONIC STRUCTURE OF TITANIUM ALUMINIDE COMPOSITES

D.D. Vvedensky and S. Crampin, The Blackett Laboratory, Imperial College, London SW7 2BZ, U.K., M.E. Eberhart and J.M. MacLaren, Los Alamos National Laboratory, Los Alamos, New Mexico 87545, L. Christodoulou, Martin Marietta Laboratories, 1450 South Rolling Road, Baltimore, Maryland 21227-3898.

The electronic structure of $TiAl$, TiB_2 , and $TiAl/TiB_2$ interfaces are studied with the layer Korringa-Kohn-Rostoker method. These interfaces occur in titanium aluminide composites produced by a casting process known as XD™, which provides the facility for engineering microstructures for certain specified properties. By examining and comparing the bonding in $TiAl$ and TiB_2 , the calculations reveal that bonding between the titanium and the boron at the interface is inhibited by the presence of aluminum. These results are further supported by varying the aluminum concentration at the interface. We also investigate the interface electronic structure of TiN/TiB_2 and TiC/TiB_2 interfaces, which are discussed in light of the above results in terms of the chemical and morphological stability of the interfaces and their implications for the deformation behavior of these materials.

N5.17

A COMPARISON OF SOLID STATE REACTIONS IN MECHANICALLY DEFORMED MULTILAYERED COMPOSITES IN THE NI-TI AND NI-ZR SYSTEMS*; B. E. White, M. E. Patt and E. J. Corra, Department of Physics, Applied Physics and Astronomy, State University of New York at Binghamton - Differential scanning calorimetry and x-ray diffraction analysis were utilized to monitor solid state reactions in codeformed, multilayered composites in two

different metal systems: Ni-Zr and Ni-Ti. Solid state reactions at temperatures below ≈ 600 K in the Ni-Zr system produce an amorphous alloy interlayer of up to 1000 Å on time scales of order 1 h, while we have observed that upon similar heat treatment the interdiffusion of the constituents of the Ni-Ti diffusion couple is significantly slower. A previous comparison of the rate of diffusion of Ni in α -Ti versus the rate of diffusion of Ni in α -Zr also revealed such a difference¹. Our results further indicate that a kinetic constraint exists on the formation of crystalline intermetallic compounds in these Ni-Ti diffusion couples similar to that previously observed in Ni-Zr diffusion couples. Upon heating Ni-Ti diffusion couples at a constant scan rate of 10 K/min the intermetallic compound NiTi is first observed by means of x-ray diffraction to form at ≈ 670 K. The formation of this intermetallic compound is observed to be thermally activated with an activation energy of 2.5 eV.

¹G. M. Hood R. J. Schultz, Phil. Mag. 26, 329 (1972).
*Supported by Research Corporation Grant C-2587.

N5.18

AC SPECTROSCOPY OF COMPOSITE MATERIALS. R. Gerhardt, Dept. of Ceramics, Rutgers University, P.O. Box 909, Piscataway, NJ 08855

Electrical properties such as dielectric constant and resistivity are very sensitive to compositional variations, presence of impurity phases as well as the spatial distribution of the phases in question. Therefore, it is expected that any combination of two materials used to make a composite will result in noticeable changes in the electrical behavior, especially if the properties of the end members are very different. Even more changes are predicted if interdiffusion between the phases has occurred. The changes can be detected by d.c. measurements but there are several reasons why a.c. measurements are preferable. One of them is that a.c. spectroscopy can separate the contributions from the different phases if the right frequency and/or temperature range are utilized and the other is that a lot more information can be derived non-destructively and in-situ if certain conditions are met. Examples of how this technique can be used to study interfacial reactions in composites will be presented.

N5.19

NONDESTRUCTIVE EVALUATION OF INTERFACIAL DAMAGE IN SiC/Al CONTINUOUS FIBER COMPOSITES. T.M. Braunig, S.R. Stock, S.D. Antolovich, Mechanical Properties Res. Lab. and Sch. of Mat. Eng., Georgia Inst. of Technology, Atlanta, GA 30332-0245; J.H. Kinney, R.A. Saroyan and Q.C. Johnson, Chem. and Mat. Sci. Dept., Lawrence Livermore Nat. Lab., Livermore, CA 94550; M.C. Nichols, Mat. Dept., Sandia Nat. Lab., Livermore, CA 94550; and U. Bonse, Dept. of Phys., Dortmund Univ., Dortmund, FRG.

X-ray Tomographic Microscopy (XTM) uses synchrotron x-radiation to section samples nondestructively with resolution approaching $1\mu\text{m}$ and with sensitivity to changes in linear absorption coefficients approaching 1%. Hundreds of slices can be recorded simultaneously using the XTM, and this volume of material can be observed throughout the course of a test. We report XTM of damage in a SiC aligned-fiber, Al matrix composite. The location and extent of microcracking revealed by XTM is analyzed in three dimensions and is compared to results obtained from destructive sectioning. Particular emphasis is placed on the role of

interface cracking in determining mechanical properties.

This research was partially supported by DOE W-7495-ENG-48, United Technology Corp.-Pratt & Whitney Aircraft Div., and Lockheed Aeronautical Systems Co.-Marietta, GA; and the experiments were done at Stanford Synchrotron Radiation Lab. which is supported by DOE, Office of Basic Energy Sciences and NIH Biotechnology Resource Prog., Div. of Res. Resources.

N5.20

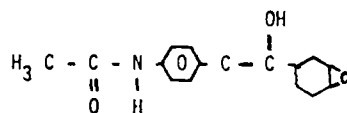
INTERACTIONS OF ACRYLIC POLYMERS WITH ALUMINUM SURFACES. J. Scott Shaffer, Arup K. Chakraborty, Center for Advanced Materials, Lawrence Berkeley Laboratory, and Department of Chemical Engineering, University of California, Berkeley, CA; H.T. Davis, Matthew Tirrell, Dept. of Chem. Eng. & Mat. Sci., University of Minnesota, MN.

The synthesis of interfaces between polymers and metallic substrates is of importance in the microelectronics, aerospace, automotive, and food packaging industries. In order to tailor these interfaces for specific applications it is imperative to elucidate the relationship between specific properties of the interface and the electronic structure of the substrate and the electronic and stereochemical structure of the polymer. In this work, we present an analysis investigating the fundamental molecular events that occur when acrylic polymers approach aluminum surfaces. We apply the density functional theory of the inhomogeneous electron gas within the framework of the local density approximation. The aluminum surface is modelled as a jellium, and interactions with oligomers of the polymer are treated using linear response theory and Green's functions. We report results for acrylic polymer adsorption that show the changes in the work function of the metal, the induced potential, and the charge density. The results are compared to our previous Hartree-Fock calculations for the interactions of PMMA with aluminum atoms, and the implications of our current studies for polymer adhesion are discussed.

N5.21

THE PRODUCTION OF MODULUS GRADIENTS AT INTERFACES. Andrew Garton, Gautam Haldankar and Edward Shockey, Polymer Program, University of Connecticut, 97 North Eagleville Road, Storrs, CT 06269-3136.

We have developed a range of additives for epoxy resins and polyimides which increase the modulus by $>50\%$, tensile strength by $>40\%$ and modify the fracture properties. The structure of a typical epoxy additive is shown below



These additives may be used to modify the bulk properties of the resin, or may be used as primers for metal or reinforcement surfaces. In the latter case, a modulus profile is set up at the interface, which results in improved stress transfer in adhesive bonds and composites.

N5.22

SURFACE TREATMENT OF CARBON FIBERS FOR USE IN COMPOSITES WITH THERMOPLASTIC RESINS. Aharon Moshonov, Rafael Institute, Haifa, Israel; Hong Li, Georgia Institute of Technology, Atlanta, Ga; and John D. Muzzy, Georgia Institute of Technology, Atlanta, Ga.

The paper describes a systematic study of surface treatment of carbon fibers by electrochemical oxidation using ammonium nitrite electrolyte. The fibers were oxidized in different reaction conditions, such as:

polarization potential, electrolyte concentration, solution temperature and duration of treatment. After oxidation the fibers were characterized by several methods. ESCA was adopted to analyze surface chemistry; SEM was used to study surface morphology and changes in fiber diameters; Thermal analyzer - to test the thermal stability of the treatment; Micro-mechanical tester was employed for single filament tensile tests and single filament critical length method for measurement of the fiber-polymer matrix interfacial strength.

It can be seen from the results that surface functionality involves carbon-oxygen bonds. Ten minutes treatment is sufficient to get uniformity in oxygen pick-up across the fibers bundle. No change in surface morphology was realized. The oxygen content on the surface of the fiber remains stable even after exposing them to high temperatures. The treatment improves the adhesion to the thermoplastic polymer and it does not reduce the mechanical properties of the fibers.

N5.23

EFFECT OF Ti^+ , Ar^+ AND N^+ ION IMPLANTATION ON ARAMID FIBER ADHESIVE PROPERTIES
J. Kalantar, Department of Chemical Engineering; D. S. Grummon, Department of Metallurgy, Mechanics and Materials Science; L. T. Drzal, Composite Materials & Structures Center, Mich. State Univ., E. Lansing, MI 48824; I. H. Loh, Advanced Surface Technology, Inc., Waltham MA 02154 and R. A. Moody, Spire Corp., Patriots Park/Bedford, MA 01730.

High performance synthetic fibers, such as the polyaramids, have high tensile strength, low density and high toughness, but suffer from poor fiber-matrix adhesion when used in polymer matrix composites. In the present study, ion implantation has been studied as a means to improve interfacial shear strength (ISS) in epoxy matrices. In addition to fiber-matrix adhesion properties, tensile and compressive strengths are reported for single fibers of duPont Kevlar-49 implanted with Ti^+ , Ar^+ and N^+ ions to doses between 1×10^{13} and 1×10^{15} ions/cm² at energies of 30 to 400 KeV.

Fiber compressive strengths were found to be unaffected by the irradiations, but tensile strength was diminished for implantations at higher energies and doses. Transmission electron micrographs show that fiber-matrix adhesion was significantly improved by ion implantation. However, critical length measurements in single fiber composite tension tests show that interfacial shear strength is improved only when the ion projected range exceeds 1 μ m. Together, these observations suggest that simply increasing fiber-matrix adhesion is insufficient to elevate ISS and that aramid fiber skin-core cohesion must also be improved.

N5.24

DETERMINATION OF FLEXIBLE INTERLAYER THICKNESS FOR FIBER REINFORCED COMPOSITES. King H. Lo, Robert W. Schmitz, and William G. Gottenberg, Shell Development Company, Houston, TX.

The influence of flexible interlayers/interphases on the performance of unidirectional fiber reinforced composites is studied. Micromechanical analysis based on the composite cylinders model is used to study the stiffness as well as the internal stress distributions within the composites. Based on the results of the micromechanics analysis, a criterion is proposed for the selection of optimal interlayer thickness for various composites. The proposed criterion gives results which seem to correlate well with some of the experimental data published in the literature.

N6.1

MEASUREMENT OF MOLECULAR FORCES AT SILICA SURFACES. Bimal Thakkar, M. Tirrell, University of Minnesota, Minneapolis, MN 55455; and Donald J. David, Monsanto Corporation, Springfield, MA 01151

Silica surfaces have recently been used in the Israelachvili surface forces apparatus. This has enabled us to measure the contact adhesion between two silica surfaces in air and dry nitrogen. The pull-off force (for dry N_2) divided by the mean radius of curvature of the cylindrical crossed-surfaces was measured as 500 ± 25 mN/m. This corresponds (using the JKR theory) to an adhesive energy between the surfaces of 52 ± 2.5 mJ/m². These numbers are comparable to those obtained between molecularly smooth mica and sapphire. We have gone on to use these as substrates for experiments in polymer adhesion to silica.

N6.2

SURFACE FORCES AND ADHESION BETWEEN DISSIMILAR MATERIALS MEASURED IN VARIOUS ENVIRONMENTS Douglas T. Smith and Roger G. Horn, National Institute of Standards and Technology, Gaithersburg, MD 20899.

The Israelachvili Surface Force Apparatus has been used extensively over the past decade to make detailed measurements of surface forces and adhesion between very smooth solids in various liquid and vapor environments. Most of those measurements have been made with mica surfaces, but we have recently developed a method of preparing smooth silica surfaces for use in place of the mica. The silica surfaces adhere in dry and humid atmospheres, but do not adhere when immersed in water.

The use of a second material not only broadens the scope of the Israelachvili technique, but also enables studies of forces and adhesion between dissimilar materials. In this talk we present results of such measurements for silica/mica and for silica sheets having different surface preparations, interacting in dry and humid atmospheres and in bulk aqueous solutions. We discuss the implications of these results for the fracture properties of interfaces.

N6.3

MEASUREMENT OF INTERFACIAL FRACTURE ENERGY. L. Rosenfeld, J. E. Ritter, M. R. Lin and T. J. Lardner, Mechanical Engineering Dept., Univ. of Massachusetts, Amherst, MA 01003.

The contact stresses resulting from indentation of a compliant coating on a rigid substrate causes a debond crack to initiate and propagate along the interface underneath the indenter. A fracture energy analysis of this indentation-induced debonding is presented. An expression for the strain energy release rate associated with the debond crack was obtained by modelling the debonded portion of the coating as an annular plate with plane stress conditions in the axial direction. Interfacial fracture toughness is derived in terms of indenter load, debond crack size, and the thickness and mechanical properties of the coating. Finite element analysis showed that the phase angle of loading, a measure of mixity of opening and shear along the surface of the debond crack, is about 45°. Good agreement was obtained between the model and experimental results on indentation-induced debonding of epoxy coatings on glass substrates. This analysis provides a basis for using indentation-induced debonding as a quantitative test technique for measuring interfacial fracture energy.

N6.4

THE EFFECTS OF PLASTICITY ON THE FRACTURE RESISTANCE OF GOLD/ALUMINA INTERFACES. Ivar E. Reimanis, Brian J. Dalgleish, M. Rühle, Anthony G. Evans, Materials Department, University of California, Santa Barbara, CA.

Gold/alumina interfaces are created by bonding highly

textured gold films (25 μ m) to single crystal alumina. Continuous examination of interface debonding is carried out by mechanical testing in situ in the optical microscope to examine the effect of plastic deformation on the energy of fracture of the interface. Fracture occurs at the interface and is accompanied by plastic deformation in the gold as evidenced by glide steps. Values of 20J/m² are measured for the fracture energy of the interface while values of 0.5J/m² are measured for the work of adhesion. The discrepancy between the fracture energy and work of adhesion has been quantitatively modeled on the basis of plasticity occurring in the gold during fracture. The contrast seen on fracture surfaces using differential interference in the optical microscope is used in conjunction with SEM, TEM, and x-ray diffraction to determine the extent and nature of plasticity. The interface chemistry is also discussed briefly with respect to stress corrosion.

N6.5

THE EFFECT OF WEAK INTERFACE ON TRANSVERSE PROPERTIES OF A CERAMIC MATRIX COMPOSITE R.A. Shimansky, H.T. Hahn, and N.J. Salamon, The Pennsylvania State University, University Park, PA

Although a weak interface leads to toughening of ceramic matrix composites under longitudinal tension, its effect on transverse properties is not well understood. The present paper provides the results of an analytical study into how transverse stiffness and strength are degraded by a weak interface.

A two-dimensional finite element model of a transverse representative volume element was used to study the effect of fiber/matrix debonding. In tension the fiber/matrix debonding was found to be almost equivalent to the absence of fibers. In compression, however, the degradation was rather minimal.

The ply failure in a cross-ply laminate was also analyzed using the fracture mechanics approach. The so-called inherent through-the thickness flaw model was used to show that the in situ ply failure stress could be much higher than the transverse tensile strength.

An experimental correlation was carried out to confirm the predicted effects of weak interface SiC/RBSN composite laminates.

N6.6

THE EFFECT OF INTERFACIAL STRENGTH ON THE MECHANICAL BEHAVIOR OF LAMINATED CERAMICS. M.D. Stuart, C.J. Russo, M.P. Harmer, H.M. Chan, G.A. Miller, Department of Materials Science & Engineering, Lehigh, University, Bethlehem, PA.

High purity alumina has been utilized as a model system to evaluate the effect of interface strength on the mechanical properties of laminated ceramics. Layers were prepared by tape casting followed by stacking to produce the bulk sample. The degree of interfacial bonding between layers was controlled by the pressure applied to the green sheet stacks during a uniaxial, warm pressing step prior to sintering. The interface spacing could also be regulated by varying the green sheet thickness.

Controlled flaws were introduced into the laminates perpendicular to the interfaces by indentation, and then propagated by loading samples in biaxial flexure. The resulting toughness and strength of the laminates have

been reported, and are discussed in terms of the mechanisms of energy dissipation by lateral cracking and of crack deflection at the interfaces.

N6.7

THE EFFECT OF FIBER COATINGS ON INTERFACIAL SHEAR STRENGTH AND THE MECHANICAL BEHAVIOR OF CERAMIC COMPOSITES. Richard A. Lowden, Oak Ridge National Laboratory, P.O. Box 2008, Oak Ridge, TN 37831-6063

Thin coatings deposited on ceramic fibers prior to densification employing chemical vapor infiltration techniques have been used to limit fiber-matrix bonding. Improvements in strength and toughness at room and elevated temperatures has been observed in SiC matrix composites fabricated from coated fibers. The properties of the fiber-matrix interface in fiber-reinforced ceramic composites have previously been examined utilizing an indentation method in which a standard microhardness indenter is used to push on fibers embedded in the ceramic matrix. Although semiquantitative results can be obtained, the measurements do not differentiate between debonding and frictional sliding. The depth-sensing Nanoindenter permits continuous measurement of force and displacement, therefore the instrument has been used to analyze debonding and frictional sliding in SiC matrix composites fabricated from fibers with various interfacial coatings. The results have been compared to those determined using the standard microhardness indenter. Correlations between interfacial phenomena and observed mechanical behavior have been made.

Research sponsored by the U.S. Department of Energy, AR&TD Fossil Energy Materials Program, under contract DE-AC05-84OR21400 with Martin Marietta Energy Systems, Inc.

N6.8

IMPROVED PERFORMANCE IN MONOFILAMENT FIBER REINFORCED GLASS MATRIX COMPOSITES THROUGH THE USE OF FIBER COATINGS. William K. Tredway and Karl M. Prewo, United Technologies Research Center, East Hartford, CT.

Fiber reinforced glass matrix composites are becoming an increasingly attractive material for many structural applications. The wide range of fibers available today makes it possible to tailor these composites for applications requiring vastly different properties. We have recently developed a technique which allows for the use of large diameter (100-144 μ m) monofilaments as the reinforcement for glass matrices, thus further extending the range of possibilities for creating tailored composites. The nature of the fiber-matrix interface is critical to the performance of these materials, with strong adhesion between the monofilaments and the glass resulting in poor composite strength and brittle fracture behavior. However, the use of coated monofilaments has resulted in a weaker fiber-matrix interface, with corresponding greater strengths and improved fracture toughness.

This presentation will discuss the mechanical performance of glass matrix composites reinforced with both uncoated and coated monofilaments. Analysis of the interfacial region using Auger, SEM, and TEM techniques will be discussed. The role of the interface in the control of composite behavior will be emphasized.

N7.1

INTERFACIAL MICROSTRUCTURE AND FRACTURE OF ALUMINA FIBER REINFORCED GLASS MATRIX COMPOSITES. T. A. Michalske, Sandia National Laboratories, Albuquerque, NM.

Silicon carbide fiber reinforced brittle matrix composites have been shown

to exhibit superior strength and fracture toughness over monolithic ceramics. Application of these structures at high temperature is limited by oxidation of the fibers while their use as electronic substrates is limited by the dielectric properties of the fiber. We have been investigating an all oxide composite system in order to develop oxidation resistant high dielectric constant composite structures. Polycrystalline alumina fiber reinforced glass matrix composites are used as the model system. We have studied three different fiber/matrix interface conditions: the direct alumina glass interface, an *in situ* grown zirconia interfacial layer, and a vapor deposited ZnO interfacial layer. Strong bonding at the glass alumina interface results in fiber failure ahead of the matrix crack. *In situ* zirconia layers promote fiber matrix debonding but severely reduce the fiber strength. Vapor deposited ZnO interfacial layers prevent interdiffusion at the fiber matrix interface and provide a low strength interfacial bond that is desirable for composite fracture toughness.

N7.2

THE ROLE OF TIN DIOXIDE (SnO_2) INTERPHASE IN THE MECHANICAL BEHAVIOR OF ALUMINA/GLASS COMPOSITE. M.H. Siadati and K.K. Chawla, New Mexico Institute of Mining and Technology, Socorro, NM 87801

Alumina (Al_2O_3) and glass form a strong chemical bond which is undesirable for toughness in a ceramic matrix composite. Tin dioxide interphase was incorporated to prevent this strong bond. Microprobe analysis studies indicated no evidence of diffusion between alumina and tin dioxide and very little between glass and tin dioxide. Indentation cracking method was applied to study the interaction of cracks with both rough and smooth alumina/tin dioxide interfaces. Indentations were placed on the alumina side at both 45 and 90 degrees with respect to the interface. In some cases, the cracks got stopped at or deflected along the interface. In many cases the cracks penetrated the interface, but they died out within the SnO_2 interphase.

Further investigation was carried out by means of four-point bend test. Fracture surfaces of these samples revealed secondary cracks perpendicular to the principal crack direction, indicating crack opening at weak alumina/tin dioxide interface. This secondary cracking involves additional energy expenditure in the fracture process, i.e., an improvement in toughness.

SnO_2 is, thus, a good diffusion barrier interphase with the necessary toughness enhancing characteristics (crack arresting/deflecting) for the alumina/glass composite.

N7.3

THE STRUCTURE OF INTERFACES RESULTING FROM WHISKER SURFACE PRETREATMENTS IN SiC WHISKER-REINFORCED CERAMIC MATRIX COMPOSITES* T. A. Nolan and L. F. Allard, High Temperature Materials Laboratory, Oak Ridge National Laboratory, Oak Ridge, TN 37831; M. H. Rawlins, American Matrix, Inc., Knoxville, TN 37922

Ceramic matrix composites reinforced with surface-modified SiC whiskers have shown differences in fracture toughness depending upon surface treatments such as acid washing, carbon deposition, and exposure to reducing or oxidizing atmospheres. Whisker surface crystallography prior to incorporation into the composites and the whisker-matrix interface structures after composite fabrication have been characterized by high resolution transmission electron microscopy. Interface structures differ depending upon modification treatment, and these differences have been related to

differences in mechanical properties of the composites.

*Research sponsored in part by the U.S. DOE, Assist. Sec. for Conservation and Renewable Energy, Office of Transportation Systems, as part of the High Temperature Materials Laboratory User Program, under contract DE-AC05-84OR21400 with Martin Marietta Energy Systems.

N7.4

THE EFFECT OF INTERFACE STRUCTURE ON THE FRACTURE OF $\text{Al}/\text{Al}_2\text{O}_3$ COMPOSITES. B. D. Flinn, F. W. Zok, F. F. Lange, M. Rühle, and A. G. Evans, University of California-Santa Barbara, Santa Barbara, CA 93106

The influence of interface structure and composition on the fracture toughness and fracture strength of a ductile dispersion toughened composite, (processed via the Lange et.al. method) has been investigated by alloying and heat treatment of the Al phase. Other researchers (Levi and Mehrabian, Met. Trans A, 1978) have shown that the addition of alloying elements such as Mg, Cu, and Si to the Al melt strongly effect the interface structure and properties of metal matrix composites ($\text{Al}_2\text{O}_3/\text{Al}$). Those results have been applied to ceramic matrix composites (Al_2O_3) reinforced with Al alloys.

The effect of precipitates and interphase formation on the debonding and fracture of the interface was studied. The interface structure and composition between the Al_2O_3 and the Al was characterized in TEM with microchemical analysis (EDS and PEELS). The debonding and interface failure was quantified in SEM by stereomicroscopy and high angle tilting. These results are correlated with the mechanical properties which show a strong R-curve behavior.

N7.5

CREEP PROPERTIES AND INTERFACIAL MICROSTRUCTURE OF SiC WHISKER REINFORCED Si_3N_4 . Anders H. Swan and Lena K.L. Falk, Chalmers University of Technology, Gothenburg, Sweden.

Whisker reinforced ceramic matrix composites have received a growing interest as potential structural ceramics due to the improved fracture toughness and creep properties of the material as compared with non-reinforced material. The most critical factor in determining the mechanical properties of whisker reinforced ceramics is the interfacial microstructure between the whiskers and the surrounding matrix. In this study, the creep properties of SiC whisker reinforced Si_3N_4 composites and a non-reinforced Si_3N_4 reference material have been studied using a 4-point bending test. The composites have been prepared by nitrided pressureless sintering using Y_2O_3 and Al_2O_3 as sintering aids. The microstructure of the composites has been studied using analytical transmission electron microscopy. In particular the interfaces between SiC whiskers and the surrounding matrix have been examined in order to explain the differences in creep behaviour.

High Temperature Fracture of SiC Whisker Reinforced Al₂O₃ Matrix Composites,

C. Mangin,* J. Homeny, S. S. Wang,
University of Illinois, Urbana, IL

As reported recently in the literature, the mechanical reliability of polycrystalline Al₂O₃ can be improved by the addition of SiC whiskers. In this study, the improvement of the fracture toughness of SiC whisker reinforced Al₂O₃ has been studied. The fracture toughness behavior of the composite as a function of temperature and whisker content and type is delineated. R-curves obtained under the various conditions are discussed. The nature of the interfaces between the SiC whiskers and the Al₂O₃ matrix and their consequence on the toughening mechanisms is discussed.

N7.7

THE ROLE OF CRYSTALLIZATION OF AN INTERGRANULAR GLASSY PHASE IN DETERMINING GRAIN BOUNDARY RESIDUAL STRESSES IN DEBASED ALUMINA. Nitin P. Padture, and Helen M. Chan, Lehigh University, Bethlehem, PA; Brian R. Lawn, N.I.S.T., Gaithersburg, MD; and Michael J. Readey, Coors Ceramic Company, Golden, CO.

The effect of grain size and crystallization of the intergranular glass on the R-curve behavior of Coors AD85 alumina has been studied. It was found that the grain size has a marked effect on the R-curve behavior, whereas crystallization of the intergranular glass has no effect. This latter result was somewhat surprising, in that crystallization would be expected to increase grain boundary residual stresses, and hence enhance R-curve behavior. TEM investigation revealed that anorthite, (the major crystalline intergranular phase) was highly twinned. It is postulated, therefore, that stress relaxation by high temperature deformation of anorthite is the predominant mechanism responsible for the lack of effect of crystallization on the R-curve behavior of Coors AD-85.

Comparison of microstructures of anorthite crystallized a) as an intergranular phase and b) from a bulk glass will be presented. High temperature hardness data (20-1500°C) obtained from anorthite will be compared with that of alumina. Based on the above results, a model for determining the magnitude and sign of intergranular residual stresses generated in Coors AD85 during crystallization of intergranular glass (and subsequent cooling to room temperature) will be presented.

N7.8

THE EFFECT OF RESIDUAL GRAIN BOUNDARY STRESSES ON MECHANICAL PROPERTIES OF ALUMINA-BASED CERAMICS. J. D. French, H. M. Chan, M. P. Harmer and G. A. Miller, Department of Materials Science and Engineering, Lehigh University, Bethlehem, PA.

One explanation which has been put forward to account for R-Curve behavior in non-transforming ceramics is the phenomenon of grain bridging across the crack walls. There is indirect evidence that residual grain boundary stresses play a significant role in enhancing grain bridging, and hence R-Curve characteristics in ceramics. In order to study this effect systematically, a series of two-phase alumina-based ceramics were processed containing 0 - 100% of a non-transforming second phase. The two second phase materials selected for this purpose were a) c-ZrO₂ (8 mol% YSZ) and b) Al₂TiO₅. Zirconia was chosen for its higher thermal expansion coefficient, $\alpha=10 \times 10^{-6}/^{\circ}\text{C}$ (cf. Al₂O₃, $\alpha=6.5 \times 10^{-6}/^{\circ}\text{C}$) and aluminum titanate was chosen for its severe thermal expansion anisotropy ($\Delta\alpha_{\text{max}}=23 \times 10^{-6}/^{\circ}\text{C}$). In both cases, the second phase addition acts as a means of pinning the matrix grains as well as a source of residual stress. The microstructures generated are duplex in nature (two distinct phases), and, in the zirconia case, extremely stable at high temperatures. Mechanical testing was performed using an indentation-strength-indenting (ISB) method. The effect of microstructure and volume fraction of second phase on the mechanical properties of the Al₂O₃-xZrO₂ and Al₂O₃-yAl₂TiO₅ ceramic composites will be discussed, together with results of high temperature hardness measurements.

SYMPOSIUM O: POLYMER BASED MOLECULAR COMPOSITES

0

November 27-30, 1989

Chairs

Dale W. Schaefer
Department 1810
Sandia National Laboratories
P. O. Box 5800
Albuquerque, NM 87185-5800
(505) 844-7937

James E. Mark
Mail Stop 172
Department of Chemistry
University of Cincinnati
Cincinnati, OH 45221
(513) 556-9292

Symposium Support

Allied-Signal, Inc.
Army Research Office
Dow Chemical Company
Dow Corning Corporation
E. I. duPont de Nemours & Co., Inc.
IBM Corporation
The Procter & Gamble Company
Rhône-Poulenc, Inc.
Union Carbide Corporation

**Proceedings published as Volume 171
of the Materials Research Society
Symposium proceedings series.**

SESSION 01: INORGANICS/EMULSIONS

Chairs: D. W. Schaefer and J. E. Mark
Monday Morning, November 27
Staffordshire (W)

8:30 *01.1

INORGANIC-ORGANIC COMPOSITES BY SOL-GEL TECHNIQUES, Helmut Schmidt and Rüdiger Nass, Fraunhofer-Institut für Silicatforschung, Ceramic Division, Würzburg, West Germany.

9:00 *01.2

NEW HYBRID INORGANIC-ORGANIC MATERIALS MADE BY THE SOL GEL METHOD: SYNTHESIS-STRUCTURE-PROPERTY BEHAVIOR, G.L. Wilkes, Bing Wang, Anthony Brennan, David Rodrigues and Hao-Hsin Huang, Virginia Polytechnic Institute and State University, Department of Chemical Engineering and Polymer Materials and Interfaces Laboratory, Blacksburg, VA.

9:30 01.3

CATALYTIC SYNTHESIS OF INORGANIC POLYMERS FOR HIGH TEMPERATURE APPLICATIONS AND AS CERAMIC PRECURSORS, Richard M. Laine, Jeffrey A. Rahn, Martin L. Hoppe, and Kay Youngdahl, University of Washington, Polymeric Materials Laboratory and Materials Science and Engineering Department, Seattle, WA.

9:45 01.4

CONDUCTING MULTILAYERED NANOCOMPOSITES: INTERCALATION OF CONJUGATED POLYMERS IN LAYERED MEDIA, Vivek Mehrotra, Taehyun Kwon, and Emmanuel P. Giannelis, Cornell University, Department of Materials Science and Engineering, Ithaca, NY.

10:00 BREAK

10:15 01.5

NYLON 6-CLAY HYBRID, Akane Okada, Masaya Kawasumi, Toshio Kurauchi, and Osami Kamigaito, Toyota Central Research and Development Laboratories, Inc., Aichi, Japan.

10:30 01.6

REINFORCEMENT OF ELASTOMERS BY THE IN-SITU PRECIPITATION OF FILLER PARTICLES, James E. Mark, University of Cincinnati, Department of Chemistry, Cincinnati, OH; Dale W. Schaefer, Sandia National Laboratories, Albuquerque, NM.

10:45 01.7

STRUCTURE-PROPERTY RELATIONSHIPS IN SILOXANE MOLECULAR COMPOSITES, D.W. Schaefer and J.E. Mark, Sandia National Laboratories, Albuquerque, NM; L. Jian, C.-C. Sun, D. McCarthy, C.-Y. Jiang, and Y.-P. Ning, University of Cincinnati, Department of Chemistry and the Polymer Research Center, Cincinnati, OH.

11:00 01.8

NMR IMAGING OF SILICA-SILICONE COMPOSITES, Leoncio Garrido and Jerome L. Ackerman, Massachusetts General Hospital, MGH NMR Center, Department of Radiology, Charlestown, MA; James E. Mark, University of Cincinnati, Department of Chemistry, Cincinnati, OH.

11:15 *01.9

SYNTHETIC POLYMERS IN WATER-IN-OIL MICRO-EMULSIONS, Françoise Candau, Institut C. Sadron, Department CRM-EAHP, CNRS-ULP, Strasbourg, France.

11:45 01.10

POLYMER BASED $\text{Si}_3\text{N}_4/\text{BN}$ COMPOSITES, Wayde R. Schmidt, Vijay Sukumar, William J. Hurley, Jr., Robert H. Doremus, and Leonard V. Interrante, Rensselaer Polytechnic Institute, Departments of Materials Engineering and Chemistry, Troy, NY.

SESSION 02: EMULSIONS/BLOCKS

Chairs: R. E. Cohen and J. P. Cohen-Addad
Monday Afternoon, November 27, 1989
Staffordshire (W)

1:30 *02.1

STABILIZED NANOPARTICLES OBTAINED FROM SYNTHETIC POLYMERIZABLE MICELLES AND VESICLES, Constantinos M. Paleos, NRC "Demokritos", Attiki, Greece.

2:00 02.2

THE PHYSICAL PROPERTIES OF MICROCELLULAR COMPOSITE FOAMS, Alice M. Nyitrai and Joel M. Williams, Los Alamos National Laboratory, Los Alamos, NM; and David Onn, University of Delaware, Newark, DE.

2:15 *02.3

BLOCK AND STATISTICAL COPOLYMERS OF DIPHENYLSILOXANE AND DIMETHYLSILOXANE, D.J. Meier, Michigan Molecular Institute, Midland, MI.

2:45 02.4

MULTIPHASE POLYMER SYSTEMS WITH CONTROLLED PHASE STRUCTURES, Claus D. Eisenbach, University of Bayreuth, Bayreuth, West Germany.

3:00 BREAK

*Invited Paper

3:15 Q2.5
SYNTHESIS AND EMULSIFICATION EFFECTS OF ISOTACTIC POLYSTYRENE/POLYBUTADIENE DIBLOCK COPOLYMERS, Luigi Cazzaniga and Robert E. Cohen, Massachusetts Institute of Technology, Department of Chemical Engineering, Cambridge, MA.

3:30 Q2.6
THE EFFECT OF PLANAR SURFACE CONSTRAINTS ON THE MICROPHASE SEPARATION OF STAR-DIBLOCK COPOLYMERS, Dwight W. Schwark and Edwin L. Thomas, Massachusetts Institute of Technology, Department of Materials Science and Engineering, Cambridge, MA; Chris S. Henkee, Dow Chemical Company, Midland, MI; and Lewis J. Fetters, Exxon Research and Engineering Company, Annandale, NJ.

3:45 Q2.7
PATH DEPENDENT MORPHOLOGIES OF A DIBLOCK COPOLYMER OF POLYSTYRENE/HYDROGENATED POLYBUTADIENE, Konstadinos Douzinas, Charles V. Berney, and Robert E. Cohen, Massachusetts Institute of Technology, Chemical Engineering Department, Cambridge, MA.

4:00 Q2.8
DYNAMIC IR STUDIES OF MICRODOMAIN INTERPHASES OF ISOTOPICALLY LABELED BLOCK COPOLYMERS, I. Noda, S.D. Smith, and C. Marcott, Procter and Gamble Company, Miami Valley Laboratories, Cincinnati, OH.

4:15 Q2.9
CO₂ DIFFUSION IN A POLYSTYRENE/POLYBUTADIENE BLOCK COPOLYMER WITH ORIENTED LAMELLAR DOMAINS, Dave Rein, Robert E. Cohen, and R.F. Baddour, Massachusetts Institute of Technology, Chemical Engineering Department, Cambridge, MA.

4:30 Q2.10
MORPHOLOGICAL CONTROL OF BLOCK COPOLYMERS FOR LOW GAS PERMEABILITY APPLICATIONS, Jeffrey Csernica, Robert E. Cohen and Raymond F. Baddour, Massachusetts Institute of Technology, Department of Chemical Engineering, Cambridge, MA.

SESSION Q3: RIGID-FLEXIBLE SYSTEMS

Chairs: R. W. Pekala and A. M. Nyitrai
Tuesday Morning, November 28
St. George B,C,D (W)

8:30 *Q3.1
LIGHT SCATTERING STUDIES OF THE STATE OF DISPERSION IN MOLECULAR COMPOSITES, Richard S. Stein and Sylvia Cohen Addad, University of Massachusetts, Lederle Graduate Research Center, Amherst, MA; Ben Hsaio, E. I. duPont de Nemours & Co., Inc., Pioneering Research Laboratory, Wilmington, DE; Russell Gaudiana, Polaroid Corporation, Cambridge, MA.

9:00 *Q3.2
RECENT ADVANCES IN THE MORPHOLOGY AND MECHANICAL PROPERTIES OF RIGID-ROD MOLECULAR COMPOSITES, Stephen J. Krause, Arizona State University, Department of Chemical, Bio, and Materials Engineering, Tempe, AZ; and Wenfang Hwang, Dow Chemical Company, Central Research - Advanced Polymeric Systems, Midland, MI.

9:30 Q3.3
RHEOLOGY OF BLENDS OF A RODLIKE POLYMER (PBO) AND ITS FLEXIBLE CHAIN ANALOG, V.S. Sullivan and G.C. Berry, Carnegie Mellon University, Department of Chemistry, Pittsburgh, PA.

9:45 Q3.4
PBZT MOLECULAR COMPOSITES WITH ADVANCED THERMOPLASTIC MATRICES, W. Michael Sanford and Gerard M. Prilutski, E. I. duPont de Nemours & Co., Inc., Fibers Department, Wilmington, DE.

10:00 BREAK

10:15 Q3.5
PBZT-BASED THERMOPLASTIC MOLECULAR COMPOSITES DEVELOPMENT; POLYAMIDE MATRIX SYSTEM, William C. Uy and E. Renee Perusich, E. I. duPont de Nemours & Co., Inc., Fibers Department, Wilmington, DE.

10:30 Q3.6
MORPHOLOGY AND FORMATION OF FIBRILLAR STRUCTURE IN PBO FIBER, C.C. Chau, J.H. Blackson, H.E. Klassen, and W.-F. Hwang, The Dow Chemical Company, Midland, MI.

10:45 Q3.7
MELT PROCESSABLE POLYMER COMPOSITES BASED ON THERMOTROPIC AND FLEXIBLE POLYMERS, G. Crevecoeur and G. Groeninckx, University of Leuven, Laboratory for Macromolecular and Structural Chemistry, Leuven, Belgium.

11:00 Q3.8
MOLECULAR COMPOSITES OF RODLIKE/FLEXIBLE POLYIMIDES, S.R. Rojstaczer, D.Y. Yoon, and W. Volksen, IBM Almaden Research Center, San Jose, CA; and M. Ree, IBM East Fishkill Facility, Hopewell Junction, NY.

11:15 Q3.9
STRUCTURE AND PROPERTIES OF BLENDS FROM POLY(CARBONATE) AND POLY(ETHYLENETERE-PHTHALATE-CO-P-HYDROXYBENZOATE): PHASE DIAGRAM AND MECHANICAL BEHAVIOUR, Robert Kosfeld, Frank Schubert, and Michael Hess, University of Duisburg, Department of Physical Chemistry, Duisburg, West Germany.

11:30 03.10

PHASES AND PHASE DIAGRAMS IN BLENDS OF POLYMER LIQUID CRYSTALS WITH ENGINEERING POLYMERS, Witold Brostow, University of North Texas, Center for Materials Characterization and Department of Chemistry, Denton, TX; Theodore S. Dziemianowicz, Himont U.S.A. Inc., Wilmington, DE; Michael Hess and Robert Kosfeld, Universität Duisburg, FB6 - Physikalische Chemie, Duisburg, West Germany.

11:45 03.11

STRUCTURE OF POLYQUINOLINE MOLECULAR COMPOSITE - A SMALL ANGLE SCATTERING STUDY, Wen-li Wu, National Institute of Standards and Technology, Polymers Division, Gaithersburg, MD; John K. Stille, Joseph W. Tsang, and Alex J. Parker, Colorado State University, Department of Chemistry, Fort Collins, CO.

SESSION 04: BLENDS/IPN's

Chairs: G. C. Berry and W. L. Wu
Tuesday Afternoon, November 28
St. George B,C,D (W)

1:30 *04.1

PHASE BEHAVIOR IN POLYMER BLENDS, William J. MacKnight and Frank E. Karasz, University of Massachusetts, Polymer Science and Engineering, Amherst, MA.

2:00 *04.2

SANS STUDIES OF BLENDS OF PROTONATED LINEAR POLYSTYRENE WITH CROSSLINKED DEUTERATED POLYSTYRENE, Robert M. Briber, National Institute of Standards and Technology, Polymers Division, Gaithersburg, MD.

2:30 04.3

DYNAMICS OF PHASE SEGREGATION IN POLY-P-PHENYLENE TEREPHTHALAMIDE AND AMORPHOUS NYLON BLENDS, J.C. Yang, T.I. Chen and T. Kyu, University of Akron, Center for Polymer Engineering, Akron, OH.

2:45 04.4

BLENDS OF CRYSTALLIZABLE POLYBUTADIENE ISOMERS, Maira Marx Nir and Robert E. Cohen, Massachusetts Institute of Technology, Department of Chemical Engineering, Cambridge, MA.

3:00 BREAK

3:15 04.5

FACTORS INFLUENCING PROPERTIES OF SAN/PMMA BLENDS, R. Subramanian, Y.S. Huang, J.F. Roach, and D.R. Wiff, GenCorp Research, Akron, OH.

3:30 04.6

DIELECTRIC STUDIES OF POLYESTER/POLYCARBONATE BLENDS, James M. O'Reilly and Joseph S. Sedita, Eastman Kodak Company, Corporate Research Laboratories, Rochester, NY.

3:45 *04.7

INTERPENETRATING POLYMER NETWORKS AND RELATED TOPOLOGICAL ISOMERS, Harry L. Frisch, State University of New York, Department of Chemistry, Albany, NY.

4:15 04.8

MOLECULAR MODELING OF INTERPENETRATING POLYMER NETWORKS (IPNs), W.B. Hammond and D.C. Prevorsek, Allied-Signal, Inc., Morristown, NJ.

4:30 04.9

FORMATION OF IPN TYPE THERMOPLASTIC MOLECULAR COMPOSITES, David A. Valia, General Dynamics Corporation, Convair Division, San Diego, CA.

SESSION 05: IONOMERS/STRUCTURE

Chairs: J. M. O'Reilly and I. Noda
Wednesday Morning, November 29
St. George B,C,D (W)

8:30 *05.1

MOLECULAR VARIABILITY IN IONOMERS, A. Eisenberg, McGill University, Department of Chemistry, Montreal, Canada.

9:00 05.2

BLOCK COPOLYMER IONOMERS: SULFONATED STYRENE-(ETHYLENE-CO-BUTYLENE)-STYRENE POLYMERS, R.A. Weiss and A. Sen, University of Connecticut, Department of Chemical Engineering/Polymer Science Program, Storrs, CT; L.A. Pottick and C.L. Willis, Shell Development Company, Westhollow Research Center, Houston, TX.

9:15 05.3

"GRAFT COPOLYMERS" FORMED BY SPECIFIC INTERACTIONS IN POLYSTYRENE AND POLYISOPRENE BASED IONOMERIC BLENDS, Sun Sasongko, M. Sabade, and R.A. Weiss, University of Connecticut, Polymer Science Department, Storrs, CT; and R. Jerome, University of Liege, Liege, Belgium.

9:30 05.4

MORPHOLOGY OF IONIC BLOCK COPOLYMERS BY SAXS, Jean-Pierre Guin, Alain Desjardins and Adi Eisenberg, McGill University, Chemistry Department, Montréal, Canada; Claudine E. Williams, LURE Université Paris-Sud, Department BAT 209 D, Orsay, France.

9:45 05.5

SMALL ANGLE X-RAY SCATTERING ON POLY(ETHYLENE-METHACRYLIC ACID) LEAD AND LEAD SULFIDE IONOMERS, Dan O. Wu and Benjamin Chu, State University of New York at Stony Brook, Department of Chemistry, Stony Brook, NY; and Walter Mahler, E. I. duPont de Nemours & Co., Inc., Central Research and Development Department, Wilmington, DE.

10:00 BREAK

10:15 05.6

POLYMER COMPOSITES WITH ELECTRONIC AND IONIC CONDUCTIVITIES, P. Audebert, N. Girault, M. Pineri, C.E.A., Groupe Physico-Chimie Moléculaire, Grenoble, France; and P. Audebert, Université Paris VII, Laboratoire d'Electrochimie Moléculaire, Paris, France.

10:30 *05.7

EXCIMER AND EXCITON FUSION OF BLENDS AND MOLECULARLY DOPED POLYMERS--A NEW MORPHOLOGICAL TOOL, Zhong-You Shi, Ching-Shan Li, Irene E. Newhouse and Raoul Kopelman, The University of Michigan, Department of Chemistry, Ann Arbor, MI.

11:00 05.8

THE ORDERED BICONTINUOUS DOUBLE DIAMOND STRUCTURE IN BLENDS OF DIBLOCK COPOLYMER AND HOMOPOLYMER, Karen I. Winey, University of Massachusetts, Polymer Science and Engineering Department, Amherst, MA; and Edwin L. Thomas, Massachusetts Institute of Technology, Materials Science Department, Cambridge, MA.

11:15 05.9

STUDIES ON THE MICROSTRUCTURE OF CORE-SHELL COPOLYMERS BY ELECTRON MICROSCOPY, R. Velázquez, UNAM, Instituto de Física, México, Mexico; A. Cruz, UNAM, Facultad de Química, México, Mexico; and V.M. Castaño, UNAM, Instituto de Física, México, Mexico.

11:30 05.10

STUDIES ON THE EXCESS FREE ENERGY AND THE COLLECTIVE DIFFUSION CONSTANT OF THE BLEND α -PS/PVME AND THE ISOTOPIC BLEND d -PS/PS WITH NEUTRON SMALL ANGLE SCATTERING, D. Schwahn, KFA Jülich GmbH, Institut für Festkörperforschung, Jülich, West Germany; K. Hahn, J. Streib, BASF Aktiengesellschaft, Polymer-, Festkörperphysik, Ludwigshafen, West Germany; and T. Springer, KFA Jülich GmbH, Institut für Festkörperforschung, Jülich, West Germany.

11:45 05.11

PROPERTIES AND STRUCTURE OF POLY(VINYL ALCOHOL) (PVA)/MELAMINE FORMALDEHYDE (MF) MOLECULAR COMPOSITES, Kecheng Gong and Xinghua Zhang, South China University of Technology, Polymer Structure and Modification Research Laboratory, Guangzhou, China.

SESSION OF: SYNTHESIS/ELECTRO-OPTICAL PROPERTIES

Chairs: C. D. Eisenbach and D. Q. Wu
Wednesday Afternoon, November 18
St. George B, C, D, W

1:30 *06.1

MORPHOLOGICAL CONSEQUENCES OF CATALYTIC HYDROGENATION OF POLYMERS IN THE BULK, Debra R. Gilliom, Sandia National Laboratories, Albuquerque, NM.

2:00 06.2

SYNTHETIC CONTROL OF MOLECULAR STRUCTURE IN ORGANIC AEROGELS, Richard W. Peralta, Lawrence Livermore National Laboratory, Chemistry and Materials Science Department, Livermore, CA.

2:15 06.3

SYNTHETIC PROCEDURES FOR PREPARING CROSS-LINKABLE ACRYLIC COMB-LIKE COPOLYMERS VIA MACROMONOMERS, G.-F. Cher and Frank A. Jones, North Dakota State University, Polymers and Coatings Department, Fargo, ND.

2:30 06.4

SYNTHESIS AND CHARACTERIZATION OF SEGMENTED COPOLYMERS OF A METHYLATED POLYAMIDE AND A THERMOTROPIC LIQUID CRYSTALLINE POLYESTER, Gregory T. Pawlikowski, R.A. Weiss, and S.J. Huang, University of Connecticut, Institute of Material Science, Storrs, CT.

2:45 06.5

MORPHOLOGY OF SOLVENT CAST DIBLOCK COPOLYMERS AND COPOLYMER-HOMOPOLYMER BLENDS CONTAINING "DURHAM" POLYACETYLENE, V. Sankaran, Massachusetts Institute of Technology, Department of Chemical Engineering, Cambridge, MA; R.R. Schrock, Massachusetts Institute of Technology, Chemistry Department, Cambridge, MA; and R.E. Cohen, Massachusetts Institute of Technology, Department of Chemical Engineering, Cambridge, MA.

3:00 BREAK

3:15 *06.6

AGGREGATION STRUCTURE AND ELECTRO-OPTICAL PROPERTIES OF (LIQUID CRYSTALLINE POLYMER)-(LOW MOLECULAR WEIGHT LIQUID CRYSTAL) COMPOSITE SYSTEM, Tisato Kajiyama, Kyushu University, Department of Applied Chemistry, Fukuoka, Japan.

3:45 06.7

(ABSTRACT WITHDRAWN)

4:00 Q6.8

ELECTRICALLY CONDUCTIVE COMPOSITE PREPARED BY TEMPLATE POLYMERIZATION OF PYRROLE INTO A COMPLEXED POLYMER, A. Mohammadi, D.W. Paul, O. Inganäs, J.O. Nilsson, and I. Lundström, Linköping Institute of Technology, Laboratory of Applied Physics, Department of Physics and Measurement Technology, Linköping, Sweden.

4:15 Q6.9

MIXED ALKALI-ALKALINE EARTH METAL PERCHLORATE POLYETHER COMPLEXED COMPOSITE POLYMER ELECTROLYTES: INVESTIGATION OF STRUCTURAL AND TRANSPORT PROPERTIES, A.N. Durga Rani, Indian Institute of Technology, Department of Physics, Madras, India; and P. Sathya Sainath Prasad, University of Minnesota, Corrosion Research Center, Department of Chemical Engineering and Materials Science, Minneapolis, MN.

SESSION 07: INTERFACES/MECHANICAL PROPERTIES

Chairs: W. M. Sanford and R. Subramanian
Thursday Morning, November 30
St. George B,C,D (W)

8:30 *07.1

DIBLOCK COPOLYMERS AT INTERFACES, Peter F. Green, Sandia National Laboratories, Albuquerque, NM.

9:00 07.2

SHORT TIME RELAXATION AT POLYMERIC INTERFACES, A. Karim, A. Mansour, and G.P. Felcher, Argonne National Laboratory, Materials Science Department, Argonne, IL; and T.P. Russell, IBM Almaden Research Center, Polymer Science Department, San Jose, CA.

9:15 07.3

NEUTRON REFLECTION STUDY OF SURFACE ENRICHMENT IN AN ISOTOPIC POLYMER BLEND, R.A.L. Jones, L. Norton, and E.J. Kramer, Cornell University, Materials Science Department, Ithaca, NY; R.J. Composto and R.S. Stein, University of Massachusetts at Amherst, Amherst, MA; T.P. Russell, IBM San Jose Research Division, San Jose, CA; G.P. Felcher, A. Mansour, and A. Karim, Argonne National Laboratory, Materials Science Department, Argonne, IL.

9:30 07.4

INTERDIFFUSION AND INTERFACIAL MOTION IN POLYMER BILAYERS, T.P. Russell, IBM Almaden Research Center, Polymer Science Department, San Jose, CA; A. Karim, A. Mansour, and G.P. Felcher, Argonne National Laboratory, Materials Science Department, Argonne, IL.

9:45 07.5

X-RAY REFLECTIVITY AND FLUORESCENCE MEASUREMENTS FROM POLYSTYRENE-CO-BROMOSTYRENE/POLYSTYRENE BLENDS, J. Sokolov, M.H. Rafailovich, and X. Zhao, Queens College, Department of Physics, Flushing, NY; W.B. Yun, Argonne National Laboratory, Argonne, IL; R.A.L. Jones and E.J. Kramer, Cornell University, Ithaca, NY; R.J. Composto, University of Massachusetts at Amherst, Amherst, MA; and B. Arun, Brooklyn College, Brooklyn, NY.

10:00 BREAK

10:15 07.6

SURFACE MODIFICATION AND SURFACE SEGREGATION PROPERTIES OF BLOCK COPOLYMERS, E. Parsonage and M. Tirrell, University of Minnesota, Department of Chemical Engineering and Materials Science, Minneapolis, MN; H. Watanabe, Osaka University, Department of Macromolecular Science, Osaka, Japan.

10:30 07.7

INTERFACIAL SEGREGATION EFFECTS IN MIXTURES OF HOMOPOLYMERS WITH COPOLYMERS, Vijay S. Wakharkar, Thomas P. Russell, and Vaughn R. Deline, IBM Almaden Research Center, San Jose, CA.

10:45 07.8

A NEW VARIABLE ANGLE FT-IR ELLIPSOMETER, J.L. Stehle, J.H. Lecat, J.P. Piel, O. Thomas and P. Evrard, SOPRA, Bois-Colombes, France; L.C. Hammond, ARIES/QEI, Concord, MA.

11:00 07.9

POLYMER MOLECULES AT INTERFACES: STUDIES BY SMALL-ANGLE NEUTRON SCATTERING, W.C. Forsman and B.E. Latshaw, University of Pennsylvania, Department of Chemical Engineering, Philadelphia, PA; and D.T. Wu, The Marshall Laboratory of the duPont Company, Philadelphia, PA.

11:15 07.10

MECHANICALLY INDUCED SILICA-SILOXANES MIXTURES, STRUCTURE OF THE ADSORBED LAYER AND PROPERTIES OF THE NETWORK STRUCTURE, J.P. Cohen-Addad, Laboratoire de Spectrometrie Physique, St. Martin d'heres, France.

11:30 07.11

THE EFFECT OF MASKED ISOCYANATES ON THE MECHANICAL PROPERTIES OF MY 720/DDS EPOXY RESIN, N. Rungsimuntakul, R.E. Fornes, and R.D. Gilbert, North Carolina State University, Fiber and Polymer Science Department, Raleigh, NC.

11:45 07.12

A STUDY OF SHORT METAL FIBER REINFORCED COMPOSITE MATERIALS, W.C. Chung, San Jose State University, Division of Technology, San Jose, CA.

SESSION 08: MISCELLANEOUS/
CONVENTIONAL COMPOSITES

Chairs: R. R. Haghighat and T. Kurauchi
Thursday Afternoon, November 30
St. George B,C,D (W)

1:30 *08.1

DEFORMATION BEHAVIORS OF POLYMER GELS IN ELECTRIC FIELD, T. Kurauchi, T. Shiga, Y. Hirose, and A. Okada, Toyota Central Research and Development Laboratories, Inc., Aichi, Japan.

2:00 08.2

BIAXIAL EXTRUSION OF POLYIMIDE LARC-TPI & LARC-TPI BLENDS, R. Ross Haghighat, Lucy Elandjian, Richard W. Lusignea, Foster Miller, Inc., Waltham, MA.

2:15 08.3

THE PROPERTIES OF RUBBER-CRUMB TOUGHENED POLYSTYRENE COMPOSITES OBTAINED THROUGH REINFORCING REACTION MOULDING, Kecheng Gong and Long-qui Zhong, South China University of Technology, Department of Polymer Science, Guangzhou, China.

2:30 08.4

FOURIER TRANSFORM RAMAN STUDIES OF SEMI-FLEXIBLE FLUOROCARBON CHAINS CONTAINING AN AROMATIC CORE, A. Schulte, V. Hallmark, R. Twieg, K. Song and J.F. Rabolt, IBM Almaden Research Center, San Jose, CA.

2:45 08.5

THE EFFECT OF LOW POWER AMMONIA AND NITROGEN PLASMAS ON CARBON FIBRE SURFACES, C. Jones, University of Illinois, National Centre for Composite Materials Research, Urbana, IL, and Liverpool University, IRC, Department of Physics, Liverpool, United Kingdom; and E. Sammann, University of Illinois, Materials Research Laboratory, Urbana, IL.

3:00 BREAK

3:15 08.6

(ABSTRACT WITHDRAWN)

3:30 08.7

DETERMINATION OF PARTICLE SIZE OF A DISPERSED PHASE WITH SMALL-ANGLE X-RAY SCATTERING, Frank C. Wilson, E. I. duPont de Nemours & Co., Inc., Polymer Products Department, Wilmington, DE.

3:45 08.8

THERMAL AND RHEOLOGICAL STUDY OF A THERMO-TROPIC LIQUID CRYSTALLINE POLYMER, H. Fruitwala, A.L. Cimecioglu, and R.A. Weiss, University of Connecticut, Institute of Material Science, Polymer Science Program and Department of Chemical Engineering, Storrs, CT.

4:00 08.9

BLENDS OF POLY(STYRENE-CO-MALEIC ANHYDRIDE) WITH MAIN-CHAIN NEMATIC POLYESTERS: PHASE BEHAVIOR AND MELT RHEOLOGY, J.J. Mara, R.B. Blumstein, A. Blumstein, University of Lowell, Polymer Science Department, Lowell, MA; and G. Kharas, Polysar, Inc., Leominster, MA.

01.1

INORGANIC-ORGANIC COMPOSITES BY SOL-GEL TECHNIQUES. Helmut Schmidt and Rüdiger Naß, Fraunhofer-Institut für Silicatforschung, Neunerplatz 2, D-6700 Würzburg, Fed. Rep. Germany

The incorporation of inorganic units into organic polymers on a finely divided or on a molecular scale can be a new challenge. Therefore, it is necessary to start from inorganic monomers or oligomers as precursors and to use chemical links to organic monomeric, oligomeric or even polymeric units. A suitable link can be a coordinative bond, e.g. complex formation between ligands bond to a polymeric chain and a metal atom of a ceramic precursor. Another suitable link is the Si-C bond with the Si fixed to a ceramic network via a Si-O bond. As ceramic precursors alkoxides undergoing a sol-gel reaction can be used, thus building up an inorganic backbone. For the formation of the organic polymeric chain, a variety of already known principles can be applied. Examples for the chemistry, structure to property relation and important applications for both basic principles with Si, Ti, Zr, and Al containing polymers are given.

01.2

NEW HYBRID INORGANIC-ORGANIC MATERIALS MADE BY THE SOL GEL METHOD: SYNTHESIS - STRUCTURE-PROPERTY BEHAVIOR. G. L. Wilkes, Bing Wang, Anthony Brennan, David Rodrigues and Hao-Hsin Huang, Virginia Polytechnic Institute & State University, Department of Chemical Engineering and Polymer Materials and Interfaces Laboratory, Blacksburg, VA.

Over the past few years, a number of network hybrid materials based on reactions between metal alkoxides and appropriately functionalized organic polymers/oligomers have been made. Under the appropriate conditions, a good dispersion of these components can be developed at the time of the sol gel reaction that promotes a high degree of mixing of these components in the final network structure. The presentation will focus on the range of synthesis that has been utilized to incorporate such metal alkoxides as those based on aluminum, silicon, titanium and zirconium. The organic oligomers will include such low T_g backbone materials as polydimethylsiloxane and polytetramethylene oxide as well as higher T_g backbone systems such as polyether ketone. In addition to the general synthesis, emphasis will also be distinctly placed on understanding the structure-property behavior of these materials utilizing mechanical and structural techniques such as dynamic mechanical spectroscopy, small angle x-ray scattering and transmission electron microscopy.

01.3

CATALYTIC SYNTHESIS OF INORGANIC POLYMERS FOR HIGH TEMPERATURE APPLICATIONS AND AS CERAMIC PRECURSORS: Richard M. Laine, Jeffrey A. Rahn, Martin L. Hoppe and Kay Youngdahl: Polymeric Materials Laboratory and Department of Materials Science and Engineering, University of Washington, Seattle, WA 98195

Titanium catalyzed redistribution of $-\text{[MeHSiO]}_x-$ and $-\text{[H}_2\text{SiNMe]}_x-$ in toluene leads to the formation of tractable inorganic polymers that can be spun or used to form films. The high temperature chemistry of these polymers will be discussed.

01.4

CONDUCTING MULTILAYERED NANOCOMPOSITES: INTERCALATION OF CONJUGATED POLYMERS IN LAYERED MEDIA. Vivek Mehrotra, Taehyun Kwon and Emmanuel P. Giannelis, Department of Materials Science and Engineering, Cornell University, Ithaca, NY 14853.

Intercalation compounds formed by the insertion of molecular layers in the galleries of a host structure offer new opportunities in designing multiphase systems with dispersion at the molecular level. Oxidative intercalation-polymerization of aniline, pyrrole, and thiophene in the intracrystalline region of layered silicates results in a new generation of conducting molecular composites. These materials consist of a multilayered structure with a periodicity of a few Angstroms in which molecular monolayers of the polymer are alternately stacked with the insulating host. Our discussion will concentrate on synthetic strategies and properties of the new layered nanocomposites.

01.5

NYLON 6-CLAY HYBRID. Akane Okada, Masaya Kawasumi, Toshio Kurauchi and Osami Kamigaito, Toyota Central Research and Development Laboratories, Inc., Nagakute, Aichi, Japan

Nylon 6 (polycaprolactam) has good properties and is a commonly used engineering polymer. It has been successfully reinforced by glass fiber or other inorganic materials. In these composites, polymer and additives are not homogeneously dispersed with each other under microscopic observation. If dispersion of polymer and additives could be achieved "in the dimension of molecules", the mechanical properties would be expected to be further improved and/or new unexpected features might appear from it. Clay is a potential candidate of the additive since it is composed of sheet silicates, 10 Å thick, and undergoes intercalation with organic molecules.

ϵ -Caprolactam was polymerized in the presence of montmorillonite, a clay, giving a nylon 6-clay hybrid (NCH). X-ray and TEM measurement revealed that each 10 Å layer dispersed in the nylon 6 matrix and that interlayer distance increased up to 214 Å from 12 Å of the clay mineral. Thus NCH has been proved a "polymer based molecular composite" or "nanometer composite". NCH could be injection-molded and showed excellent properties compared with nylon 6 such as tensile strength, modulus and heat resistance. Heat distortion temperature was heightened from 65 °C of nylon 6 to 145 °C of NCH which contains only 4 wt% (1.6 vol%) of clay.

Synthesis, structure and mechanism of improvement of properties of NCH will be discussed.

01.6

REINFORCEMENT OF ELASTOMERS BY THE IN-SITU PRECIPITATION OF FILLER PARTICLES. James E. Mark, University of Cincinnati, Department of Chemistry, Cincinnati, OH 45221-0172; and Dale W. Schaefer, Division 1810, P.O. Box 5800, Sandia National Laboratories, Albuquerque, NM 87185.

The goal of primary interest in these investigations was the development of novel methods for filling elastomeric networks. The techniques developed employ the in-situ precipitation of reinforcing fillers such as silica or a glassy polymer such as polystyrene either after, during, or before network formation.

The reaction involves decomposition of organometallic compounds, using a variety of catalysts and precipitation conditions, or free-radical polymerization of a suitable monomer. The effectiveness of the technique is gauged by stress-strain measurements carried out to yield values of the maximum extensibility, ultimate strength, and energy of rupture of the filled networks. Information on the filler particles thus introduced is obtained from density determinations, scattering measurements, and electron microscopy.

01.7

STRUCTURE-PROPERTY RELATIONSHIPS IN SILOXANE MOLECULAR COMPOSITES. D. W. Schaefer and J. E. Mark, Sandia National Laboratories, Albuquerque, NM 87185; and L. Jian, C.-C. Sun, D. McCarthy, C.-Y. Jiang, and Y.-P. Ning, Department of Chemistry and the Polymer Research Center, University of Cincinnati, Cincinnati, OH 45221

Small angle x-ray and neutron scattering techniques are used to study the structure of molecular composites composed of silica and polydimethylsiloxane. A variety of synthesis techniques are used for the precipitation of the hard silica phase. If the pre-existing siloxane network is swollen with tetraethylorthosilicate which is subsequently polymerized under basic conditions, the small angle scattering data is consistent with the existence of uniformly dense smooth surface particulate fillers consistent with previous electron microscopy data.

We tried several strategies in an attempt to produce ramified polymeric fillers. Polymerization at lower pH indeed gave dispersed fillers, but only at concentrations below that needed for effective reinforcement. At high filler concentrations we always found uniformly dense smooth surfaced fillers under solution polymerization conditions.

Two new classes of fillers prepared by polymerization under different conditions were discovered. The reaction of the swollen networks with ammonia vapor produced a bicontinuous network of silica and siloxane. In this case the continuous silica phase resulted in embrittled material.

The most promising reinforced elastomers reproduced by two-stage polymerization. In this case we find spinodal-like bicontinuous networks at large scales whereas at shorter length scales the fillers are dispersed, more like an interpenetrating network. In this case the mechanical properties are very desirable for reinforced elastomers, showing enhanced modulus with little loss of extensibility.

01.8

NMR IMAGING OF SILICA-SILICONE COMPOSITES. Leoncio Garrido and Jerome L. Ackerman, MGH NMR Center, Department of Radiology, Massachusetts General Hospital, 13th St., Bldg 149, Charlestown, MA 02129; James E. Mark, Department of Chemistry, University of Cincinnati, Cincinnati, OH 45221.

The design of materials having optimal properties for a given application requires knowledge on how the properties of interest depend upon their chemistry and structure at molecular level. NMR is very sensitive to both, the chemical composition and structure of a substance, and this is reflected in the chemical-shift spectrum as well as in the NMR relaxation parameters. Thus NMR imaging techniques offer the possibility of selectively map the distribution of a particular chemical species in a region of interest. Moreover, NMR imaging can also provide spatial information about changes in NMR properties that can be correlated with alterations in molecular structure.

This talk will introduce briefly the solid-state NMR imaging techniques and discuss their application to study silica-silicone composites. These materials are prepared using polydimethylsiloxane (PDMS) model networks reinforced by *in situ* precipitated silica (SiO₂). ¹H NMR images of the composites are obtained in which the contrast (differences in NMR signal intensity between different regions) is a function of proton density, spin-lattice (T₁) and spin-spin (T₂) relaxation times. These T₁ and T₂ maps represent a measure of molecular

mobility and they might be related to polymer-filler interactions and their distribution.

01.9

SYNTHETIC POLYMERS IN WATER-IN-OIL MICROEMULSIONS. Françoise Candau, (CRM-EAHP)CNRS-ULP, 6 rue Boussingault, 67083 Strasbourg Cédex, France.

High molecular weight water-soluble polymers are usually supplied in the form of water-in-oil emulsions which have advantages of low viscosity and easy storage and dissolution. Most uses in water treatment, flocculation, paper manufacture or mining fields require polymer latexes formed of finely dispersed particles. Polymerization in reverse micelles or microemulsions appears to be a promising technique, owing to the stability of the polymer latexes thus formed, as well as the high molecular weight and water solubility of the polymers themselves.

In this presentation, we discuss some aspects of the inverse microemulsion polymerization process, which can be directly correlated to the structural characteristics of the final latexes. An analysis is made on the role of monomer on the interfacial properties of the swollen micellar systems. These properties govern the stability of the latexes, a key parameter for industrial applications.

01.10

POLYMER BASED Si₃N₄/BN COMPOSITES. Wayne R. Schmidt, Vijay Sukumar, William J. Hurley, Jr., Robert H. Doremus, and Leonard V. Interrante, Departments of Materials Engineering and Chemistry, Rensselaer Polytechnic Institute, Troy, NY 12180-3590

Partially crystalline silicon nitride, with a specific surface area greater than 200 m²/g, is obtained by the pyrolysis of an organometallic, polymeric precursor under NH₃ to 1000°C. Additional heating to 1400°C under N₂ produces α-Si₃N₄. The addition of up to 15% boron nitride was found to affect the coarsening characteristics of amorphous silicon nitride by promoting surface area reduction and suppressing crystallinity. These results will be discussed as well as recent progress towards the preparation of BN molecular precursors and resulting Si₃N₄/BN composites obtained by combining the precursor systems.

02.1

STABILIZED NANOPARTICLES OBTAINED FROM SYNTHETIC POLYMERIZABLE MICELLES AND VESICLES. Constantinos M. Paleos, NRC "Demokritos", Aghia Paraskevi, 15310, Attiki, Greece.

Nanoparticles of 3-100nm in diameter can be formed by the polymerization of polymerizable micelles or vesicles.

Micellar polymerization was achieved either by solubilization of an appropriate monomer within a micelle, formed from conventional surfactants, or by polymerization of a polymerizable surfactant forming itself micelles. Depending on the position of the polymerizable group, at the head or at the tail, two types of polymerized micelles result i.e. with the backbone at the Stern region and those with the main chain at the lipophilic core.

Synthetic vesicles are more stable than micelles. In addition, the dependence of their structure and size on the mode of their formation allows greater flexibility than micelles. Topochemical addition and condensation polymerization was employed for their further stabilization. The binding of the surfactants may occur at various sites i.e. in one or both of the layers, and specifically at the surfactant head, in the middle or at the end of the lipophilic chains. Stabilized vesicles were also obtained from preformed polymers or ionenes and finally stabilization of conventional vesicles was also accomplished by appropriate coating of their surfaces.

Physical characterization including x-ray scattering, electron weight determination, fluorescence studies, electron microscopy, NMR were employed for their characterization.

02.2

THE PHYSICAL PROPERTIES OF MICROCELLULAR COMPOSITE FOAMS. Alice M. Nytray and Joel M. Williams, Los Alamos National Laboratory, Los Alamos, NM; and David Onn, University of Delaware, Newark, DE.

Recently we have reported on a new method of preparing microcellular composite foams. In this procedure an open-celled polystyrene foam is prepared by the polymerization of a high internal phase (water-in-oil) emulsion containing styrene, divinylbenzene, surfactant, free-radical initiator and water. After drying, the cells of the polystyrene foam are then filled with other materials such as aerogel or resoles. The physical properties of these materials e.g., surface area, density, thermal conductivity, and compressive strength will be presented.

02.3

BLOCK AND STATISTICAL COPOLYMERS OF DIPHENYLSILOXANE AND DIMETHYLSILOXANE. D.J. Meier, Michigan Molecular Institute, Midland, Michigan 48640.

Copolymers of diphenylsiloxane and dimethylsiloxane are of interest since they combine two siloxane components having very different properties. The polydiphenylsiloxane chain is inflexible, and the polymer (P) is a crystalline solid with a liquid crystalline or condic crystalline state below the very high melting (clearing) temperature. In contrast, the polydimethylsiloxane chain is highly flexible and the polymer (M) is a rubbery solid with a low melting temperature and a very low glass transition temperature. We have prepared a wide variety of block and statistical copolymers of these components, using anionic polymerization techniques to control molecular composition and molecular architecture.

The physical properties of the copolymers vary systematically with composition and architecture. Statistical or random copolymers with dimethylsiloxane as the major component are viscous liquids ($MW < 10^5$). In contrast, the diblock copolymer (P-M) with the same overall composition and molecular weight are grease-like, while the triblock copolymers (P-M-P) are tough elastomers. The block copolymers are molecular composites, in which the polydiphenylsiloxane component separates into crystalline microphases having a very uniform cylindrical or a lamellar morphology. The rods and lamellae have thicknesses comparable to the length of the polydiphenylsiloxane block, i.e., typically of the order of 100 Å.

Statistical copolymers of dimethylsiloxane and diphenylsiloxane with the latter as the major component are transparent solids at diphenylsiloxane concentrations below about 80%w. Such materials are of interest in use as radiation-resistant optical fibers⁽¹⁾, in which the diphenylsiloxane component is present in as high a concentration as possible to provide the radiation resistance, but with sufficient dimethylsiloxane in the copolymer to prevent crystallization of polydiphenylsiloxane and concomitant opacity.

(1) J. Walker and J. Harmon, personal communication.

02.4

MULTIPHASE POLYMER SYSTEMS WITH CONTROLLED PHASE STRUCTURES. Claus D. Eisenbach, University of Bayreuth, P.O.B. 101251, D-8580 Bayreuth, FRG.

In view of polymers as advanced materials it is a challenging task to mimic the elegant schemes of biological systems in self-organization phenomena, which ultimately lead to highly sophisticated tertiary structures with specific functions. The question is, if and to which extent these pattern can be transferred to the synthesis and design of new polymers with molecular control of the superstructure and with special and unique properties.

Our approach is the synthesis of segmented block copolymers with segments of uniform length and special molecular architecture. For polyetherurethane elastomers with regular primary structure it could be shown that a fractionated segregation of hard segments (4,4'-diphenylmethanebis(iminocarbonyl) or 1,4-bis(carbonyl)-

piperazine units and oxytetramethyleneoxy chain extender unit) occurs, which crystallize without chain folding. The lamellar thickness is directly proportional to the molecular length. However, by incorporating a more flexible unit in the relatively stiff hard segment, chain ences the superstructure and consequently the material properties, too. The structure-properties relationships of these model systems and the potential of tailoring the primary structure for creating new superstructures will be illustrated with particular examples and discussed.

02.5

SYNTHESIS AND EMULSIFICATION EFFECTS OF ISOTACTIC POLYSTYRENE/POLYBUTADIENE DIBLOCK COPOLYMERS. Luigi Carzaniga, Massachusetts Institute of Technology, Cambridge, MA, and Robert E. Cohen, Massachusetts Institute of Technology, Cambridge, MA.

A novel anionic synthesis technique for the stereospecific polymerization of styrene was used to prepared a set of well characterized isotactic polystyrene/polybutadiene (iPS/PB) diblock copolymers. The microphase separated morphologies of these diblocks were also studied with transmission electron microscopy of ultramicrotomed sections of molded and static cast films. Various thermal histories were imposed on the samples to study the effect of the crystallizable iPS on the microdomain structure. The blending of these copolymers with the respective homopolymers to form a crystallizable polystyrene/amorphous polybutadiene system is currently being investigated. Initial experiments show that these ternary blends exhibit a well ordered morphology which is attributed to the emulsifying effect of the iPS/PB diblock copolymers.

02.6

THE EFFECT OF PLANAR SURFACE CONSTRAINTS ON THE MICROPHASE SEPARATION OF STAR-DIBLOCK COPOLYMERS. Dwight W. Schwark and Edwin L. Thomas, Dept. of Mat. Sci. & Eng., MIT, Cambridge, MA; Chris S. Henkee, Dow Chemical Company, Midland, MI; Lewis J. Fetters, Exxon Research & Engineering Company, Annandale, N.J.

According to the strong segregation limit theories for linear diblock copolymers, the equilibrium bulk microdomain morphology is determined by the volume fraction of the components present. For star-diblock copolymers, in which the arms are composed of linear diblock chains, the equilibrium morphology is also dependent upon the composition. However, the microdomain morphology depends strongly on the number of arms. Increasing the arm number from 5 to 6, with the same overall sample composition, induces a morphological transition from hexagonally packed cylindrical microdomains to the ordered-bicontinuous double diamond (OBDD) structure.

In this series of experiments, the effect of planar surface constraints on the microphase separation was investigated. Transmission electron microscopy (TEM) was employed to examine the effect of both a single planar surface as well as two planar surfaces in close proximity, i.e. a thin film. In the thin film studies, the samples are asymmetric since the polymer/air surface and the polymer/substrate interface are different.

Similarities between linear and star-diblock copolymers in terms of the ordering of the microdomain morphologies at the surface and the presence of a surface layer of the lower surface tension component for both thick and thin specimens will be discussed. We also comment on the inhibition

of the OBDD structure as one approaches the surface of thick specimens or as the thickness of the thin film decreases. A comparison of the morphology of the thinnest regions in linear and star-diblocks will also be given. Important variables to consider are the location of the lower surface tension block (whether it is the inner or outer part of the arm), the overall sample composition, and the number of arms in the star.

02.7

PATH DEPENDENT MORPHOLOGIES OF A DIBLOCK COPOLYMER OF POLYSTYRENE/HYDROGENATED POLYBUTADIENE. Konstadinos Douzinas,; Charles V. Berney,; and Robert E. Cohen, Chem. Eng. Dept. M.I.T., Cambridge, MA.

A semi-crystalline diblock copolymer of Polystyrene/Hydrogenated Polybutadiene (SEB) was prepared by catalytic hydrogenation of a precursor, anionically polymerized, Polystyrene/Polybutadiene (SB) diblock copolymer.

Samples were cast from solution at temperatures below and above the melting point of the EB block. Changes in the microphase morphology were observed by TEM and SAXS. Annealing of the bulk copolymer also affected the observed morphology. The morphological changes are caused by competing mechanisms of crystallization versus phase separation. A qualitative phase diagram of the SEB/Solvent system is presented to put our observations in perspective.

02.8

DYNAMIC IR STUDIES OF MICRODOMAIN INTERPHASES OF ISOTOPICALLY LABELED BLOCK COPOLYMERS. I. Noda, S. D. Smith, and C. Marcott, The Procter & Gamble Company, Cincinnati, OH.

The transition region between microphase domains of block polymers, known as the interphase, is believed to play an important role in the development of unique properties of such copolymers. We used the combination of dynamic IR dichroism (DIRLD) spectroscopy and site-specific isotopic labeling of polymer chains to elucidate the degree of segmental interactions in the interphase region of styrene-isoprene diblock copolymers.

DIRLD spectroscopy measures the dynamic reorientations of submolecular constituents of a system which is perturbed by a small-amplitude strain. The technique is especially suited for probing the submolecular-level interactions of copolymer segments. Isotopic labeling using deuterium-substituted monomers enable us to differentiate the dynamic responses of well-defined parts of block segments, e.g., near the segment junction, chain end, or middle of the block.

The dynamic reorientations of isotopically labeled block copolymers were studied as functions of molecular weight, junction structure, and temperature. The reorientational motion of the polystyrene segment, especially near the block junction, was monitored around the glass transition temperature of the polyisoprene matrix. The degree of segmental mixing in the interphase region, which leads to the local plasticization of polystyrene by polyisoprene, was determined.

02.9

CO₂ DIFFUSION IN A POLYSTYRENE/POLYBUTADIENE BLOCK COPOLYMER WITH ORIENTED LAMELLAR DOMAINS. Dave Rein, Massachusetts Institute of Technology, Cambridge, MA; Robert E. Cohen, Massachusetts

Institute of Technology, Cambridge, MA; and R.F. Baddour, Massachusetts Institute of Technology, Cambridge, MA.

The solubility and diffusion coefficients of CO₂ in a polystyrene/polybutadiene (SB) block copolymer were measured in a pressure decay sorption apparatus. The morphology of the block copolymer films consisted of alternating S and B lamellae of approximately 100 Å thickness with excellent long range orientation perpendicular to the surface of the films. Diffusion behavior in the copolymer was simulated using homopolybutadiene and homopolystyrene data along with a finite difference model based on the well-ordered morphology. The comparison between measured and simulated diffusion coefficient values indicated that chain motions in the polybutadiene region of the block copolymer are restricted relative to those of homopolybutadiene owing to the connection with the polystyrene block.

02.10

MORPHOLOGICAL CONTROL OF BLOCK COPOLYMERS FOR LOW GAS PERMEABILITY APPLICATIONS. Jeffrey Csernica, Robert E. Cohen, Raymond F. Baddour, Massachusetts Institute of Technology, Cambridge, Massachusetts.

In many polymer applications where control of gas transport is required, it may be desirable to utilize heterogeneous polymer blends or block copolymers in which one component provides the necessary permeation characteristics, while the other improves material properties such as modulus or impact strength. If the application requires that a low permeability component provide transport qualities to the material (which will probably be the case in packaging and gas separations applications), the arrangement of the individual components will be critical, and must be one in which a diffusing species cannot circumvent the low permeability domains via high conductivity pathways.

Gas permeability coefficients were measured for several gases in two polystyrene-polybutadiene block copolymer systems. One exhibits a morphology of polybutadiene spheres (about 100 nm in diameter) in a polystyrene matrix; the second contains alternating lamellae (ca. 10 nm thick) which have been oriented perpendicular to the permeation direction by a thermomechanical processing technique. The measured permeabilities of these two materials are dominated by the transport behavior of the low permeability polystyrene component. Models are presented to describe transport in these microphase separated systems and to facilitate comparisons with the transport behavior of other two component polymer systems.

03.1

LIGHT SCATTERING STUDIES OF THE STATE OF DISPERSION IN MOLECULAR COMPOSITES. Richard S. Stein and Sylvia Cohen Addad, Polymer Research Institute, University of Massachusetts, Amherst, MA, Ben Hsiao, E. I. DuPont de Nemours Co, Inc., Wilmington DE 19898, and Russell Gaudiana, Polaroid Corporation, Cambridge, MA

Solutions of blends are prepared of stiff-chain polyesters and polyamides with flexible matrices by solvent casting. These are examined using the small-angle light scattering technique employing a photometric apparatus. Results

are analyzed using the Stein-Wilson extension of the Debye-Bueche theory in which the correlation functions for density and orientation fluctuations, $\gamma(r)$ and $f(r)$, and mean-squared fluctuations of the two average refractive index and its anisotropy, $\langle \eta^2 \rangle$ and $\langle \delta^2 \rangle$, respectively, are obtained. For a molecular dispersion, the correlation distances will be small and the anisotropy will be that of a single stiff molecule. Aggregation of rods is associated with an increase in the magnitude and size of the density fluctuations and a change in anisotropy fluctuations which depends upon the degree of correlation of orientation of the rods in the aggregate. Results thus far demonstrate that aggregates are present in all of the rod/coil composites prepared.

O3.2

RECENT ADVANCES IN THE MORPHOLOGY AND MECHANICAL PROPERTIES OF RIGID-ROD MOLECULAR COMPOSITES. Stephen J. Krause, Department of Chemical, Bio, and Materials Engineering, Arizona State University, Tempe AZ, 85287; and Wen-Fang Hwang, Central Research - Advanced Polymeric Systems, Dow Chemical Company, Midland MI, 48674

The concept of a self-reinforcing molecular composite of rigid-rod and flexible-coil polymer components was first proposed by Helminiak et al. (1) and fabricated by Hwang et al. (2) in the blend system of rigid-rod poly-p-phenylene benzobisthiazole (PBT) and semi-flexible coil poly-2,5(6) benzimidazole (ABPBI). After synthesis, the key to producing a rigid-rod molecular composite is to control morphology to disperse the reinforcing rod molecules as finely as possible in the matrix polymer such that they have a high ratio of length to width (aspect ratio) for efficient reinforcement. The rod component must not phase separate during processing. Morphological characterization techniques, which can measure the orientation and dispersion (or, conversely, the degree of phase separation), provide the tools for correlating theoretically predicted and measured mechanical properties. Application of new techniques for rigid-rod molecular composites will be discussed, including high resolution secondary and backscattered scanning electron microscopy and also Raman scattering for micromechanical characterization.

The modulus of the earliest rigid-rod molecular composite systems of the physical blend and the triblock copolymer of PBT/ABPBI were 1/2 to 3/4 of the theoretical value predicted by the "rule of mixtures" for the 30 PBT/70 ABPBI blend (120 GPa) and the triblock copolymer (100 GPa). Although these systems formed molecular composites, they did not have a glass transition temperature below the degradation temperature and could not be consolidated by thermal processing techniques. More recently, other systems which could potentially consolidate more easily, such as thermoplastic, thermoset, and in-situ rigid-rod molecular composite systems have been synthesized and explored, but the properties achieved have not yet approached those of the earlier aromatic heterocyclic systems. Limitations and possible improvements to such systems will be discussed.

1. T. E. Helminiak, F.E. Arnold, and C.L. Benner, and G.E. Husman, Am. Chem. Soc. Preprints, 16, 650 (1975).
2. W.-F. Hwang, D. Wiff, C.L. Benner, and T.E. Helminiak, J. Macromol. Sci. Phys., B22, 231 (1983).

O3.3

RHEOLOGY OF BLENDS OF A RODLIKE POLYMER (PBO) AND ITS FLEXIBLE CHAIN ANALOG, V. S. Sullivan and G. C. Berry, Carnegie Mellon University, Pittsburgh, PA 15213

Rheological properties of isotropic solutions of rodlike poly(1,4-phenylene-2,6-benzobisthiazole), PBO, coil-like poly(2,5-benzoxazole), ABPBO, and their miscible blends in solution will be described. Measurements include steady-state properties (the viscosity and recoverable compliance as functions of shear rate), transient properties (the recoverable compliance), and dynamic mechanical properties (the loss and storage compliances as functions of frequency). The distribution of retardation times deduced from the linear transient recoverable compliance is used together with a single-integral BKZ-type constitutive equation to estimate the nonlinear dependence on the shear rate, with reasonable success. The distribution of retardation times of the blends is broader than that for the rodlike chain, and tends to occur at longer times, reflecting a viscosity enhancement that occurs with the blends.

The linear (Newtonian) viscosity of solutions of the PBO polymer used are larger than those of the ABPBO polymer the same polymer concentrations. Nevertheless, the linear viscosity of blends of PBO and ABPBO tends to be nearly equal to a solution of PBO of the same total polymer concentration as the blend. This behavior will be discussed in terms of a model introduced in previous studies on miscible blends of rodlike and flexible chain polymers in solution. In this model, the rotational diffusion of the rodlike chain is severely constrained by the flexible chain polymer provided the reptational time constant for the latter is longer than the constraint release time for the rodlike component.

This work supported in part by a DARPA contract.

O3.4

PBZT MOLECULAR COMPOSITES WITH ADVANCED THERMOPLASTIC MATRICES. W. Michael Sanford and Gerard M. Prilutski, E. I. Du Pont de Nemours and Co., Experimental Station, P.O. Box 80302, Wilmington, DE 19880-0302

Thermoplastic molecular composites offer the potential for better economics and improvements in composite processing, and possibly performance, over conventional "string and glue" composites. The early development of molecular composite technology focused on polyamide matrix polymers; however, for many aerospace applications higher use temperatures and greater solvent resistance than that of polyamide matrices will be required. This paper describes work performed under contract to the U.S. Air Force to develop PBZT/thermoplastic molecular composites with high performance matrix resins into a viable technology.

A scalable process has been defined based on a novel mixed solvent/quaternary solution technology developed by Du Pont. Advantages of this process include better economics, superior processing performance, and improved MC fiber tensile properties versus prior art. Using this process we have obtained rule of mixtures properties in molecular composite fibers with matrix polymers offering use temperatures from 330 to 600°F. Consolidation of PBZT/PEKK fibrous preforms into uniaxial panels up to 10" x 15" has been demonstrated and material property evaluation and data base development are in progress. Uniaxial property levels achieved to date for all systems compare favorably with conventional "string and glue" PBZT/epoxy composites although compressive and shear performance may be limiting factors in MC applications.

O3.5

PBZT-BASED THERMOPLASTIC MOLECULAR COMPOSITES DEVELOPMENT; POLYAMIDE MATRIX SYSTEM. William C. Uy and E. Renee Perusich, E.I. Du Pont de Nemours & Co., Inc. Wilmington, DE.

Molecular composites (MC) are dispersions of rigid rod polymer molecules in a matrix of flexible coil polymers, formed by the coagulation of a solution containing these components. Thermoplastic molecular composites offer the potential for better economics and improvements in composite processing, and possibly performance, over conventional "string and glue" composites. This paper describes work performed under contract to the U.S. Air Force to develop PBZT/thermoplastic molecular composites into a viable technology.

A commercially viable MC spinning process has been defined based on a novel mixed solvent/quaternary solution technology developed by Du Pont. Advantages of this process include better economics, superior processing performance, and improved MC fiber tensile properties versus prior art. PBZT/polyamide MC fibers with tenacity/modulus of 332 ksi/29 Msi have been produced using this process. Adhesion equivalent to that obtained in conventional composites has been demonstrated. Uniaxial properties achieved to date compare favorably with conventional "string and glue" PBZT/epoxy composites although compressive and shear performance may be limiting factors in MC applications.

03.6

MORPHOLOGY AND FORMATION OF FIBRILLAR STRUCTURE IN PBO FIBER. S.C. Chau, J.H. Blackson, H.E. Clausen and W.F. Hawing, The Dow Chemical Company, Midland, MI.

Electron microscopy studies showed that the porous structure of organic fibers may contain fractal geometries; i.e., the pore spaces and geometric irregularities are self-similar upon variations of resolution. At the vicinity of a PBO fiber surface, the cross-sectional morphology showed dense fibrous aggregates with a degree of asymmetry in porosity along the radial direction. In the matrix, the pore size and porosity appeared to be slightly higher with the pores distributed randomly in the fibrous aggregates. The minimum observed aggregate size was about 100 Å or smaller. The fractal dimension of pores in PBO fiber as determined by using microscopy and image analyzing techniques was found to be 2.51 ± 0.06 . While the nonfibrillated fiber contained fibrous aggregates with random shapes, the fibrillated fiber showed a continuous fibril size distribution with no evidence of structural hierarchy. Based on these observations, a nucleation and growth model is suggested for the formation of fibrillar structure in PBO fiber with variations in the order of nucleation.

03.7

MELT PROCESSABLE POLYMER COMPOSITES BASED ON THERMOTROPIC AND FLEXIBLE POLYMERS.

G. Crevecoeur and G. Groeninckx; University of Leuven; Laboratory for Macromolecular and Structural Chemistry; Celestijnenlaan 200 F; 3030 Heverlee; Belgium

Thermotropic liquid crystalline polymers (TLCPs) can be blended with flexible polymers in the melt to lower the melt-viscosity of the latter and to form in situ reinforced polymer composites. Since the TLCP and the flexible polymer are generally immiscible, a two-phase system is obtained, in which the TLCP is dispersed as spheres or, more preferably, as fine fibrils, which reinforce the matrix in much the same fashion as conventional macroscopic composites, e.g. short fiber reinforced composites.

The systems studied contained as TLCP an aromatic polyester or polyester-amide, and the flexible polymer was either polystyrene (PS) or a miscible blend of PS and poly-(phenylene ether) (PPE). The blends were both injection moulded and spun into fibers. Experimental data will be presented in terms of morphology, mechanical and rheological properties, thermal and dynamic behaviour, and molecular orientation in the TLCP. Best reinforcement was found when sufficient elongational flow was applied during processing, and the viscosity of the flexible polymer was significantly higher than that of the TLCP. Morphological examination of these samples revealed a fibrous texture, with TLCP fibrils in the micron/sub-micron range, having very high aspect ratios (more than 100).

03.8

MOLECULAR COMPOSITES OF RODLIKE/FLEXIBLE POLYIMIDES. S. R. Rojstaczer, D. Y. Yoon, W. Volksen, IBM Research Division, Almaden Research Center, San Jose, CA 95120; and M. Rec, IBM East Fishkill Facility, Hopewell Jct., NY 12533.

Composites of rodlike and flexible polyimides have the potential to achieve the desired properties for application in microelectronic packaging by combining the required thermal and mechanical properties characteristic to the rigid component along with enhanced adhesion strength provided by the flexible polyimide.

We have employed the in-situ rod formation via imidization to obtain sub-micron scale phase separation of rodlike and flexible polyimides. Mixtures of the respective polyamic alkyl ester (PAE) and polyamic acid (PAA) in NMP solvent are therefore used for coating, followed by solvent evaporation and final thermal imidization. The ternary phase diagram of the NMP solvent/PAE/PAA system was determined for various PAA molecular weights. It is shown that the phase separated morphology of the fully imidized blends is primarily determined

during the initial thermal treatment involving the solvent evaporation, with only minor changes occurring during the in-situ rod formation via imidization process performed by thermal curing for 1 hour at 400°C. Transparent polyimide blends containing up to 25% weight fraction of the flexible component were obtained when the respective precursor solutions were rapidly dried either thermally at 150°C or at lower temperatures by microwave heating. Dynamical mechanical thermal analysis results indicate that phase separation takes place for all the compositions and molecular weights investigated. The size of the phase separated domains determined from scattering methods is used to establish the morphology-property relationship in rodlike/flexible polyimide molecular composites.

03.9

STRUCTURE AND PROPERTIES OF BLENDS FROM POLY(CARBONATE) AND POLY(ETHYLENETEREPHTHALATE-CO-P-HYDROXIBENZOATE): PHASE DIAGRAM AND MECHANICAL BEHAVIOUR. Robert Kosfeld, Frank Schubert, Michael Heß, University of Duisburg, Department of Physical Chemistry, D-4100 Duisburg, FRG.

Mixtures of liquid crystalline polymers with coil-shaped polymers exhibit a great potential in constructing advanced polymer materials. The properties of composites prepared from such polymers is strongly depending on the way of preparation and thermal history. The combination of polymers mentioned above is chosen to show the complexity of the phase diagrams obtained and the concentration dependence of some mechanical properties of these systems.

Depending on thermal history miscibility gaps and regions of partial miscibility are present and partial crystallization is observed due to nucleation of one component caused by the presence of the other.

Some results from simple processing experiments show interesting morphological features.

03.10

PHASES AND PHASE DIAGRAMS IN BLENDS OF POLYMER LIQUID CRYSTALS WITH ENGINEERING POLYMERS. Witold Brostow, Center for Materials Characterization and Department of Chemistry, University of North Texas, Denton, TX 76203-5371; Theodore S. Dziemianowicz, Himont U.S.A Inc., 800 Greenbank Road, Wilmington, DE 19808; Michael Hess and Robert Kosfeld, FB6 - Physikalische Chemie, Universität Duisburg, Postfach 10 16 29, D-4100 Duisburg 1, Federal Republic of Germany.

We continue studies¹⁻³ of blends of polymer liquid crystals (PLC) with ordinary engineering polymers (EP). We now focus on connections between mechanical and other properties and phase structures and phase diagrams. Pure PLC are already two-phase systems, addition of an EP complicates the situation further. In particular, we are concerned with phases which we call quasi-liquids, at temperatures between the glass transition and the melting point. These phases do not have the mobility usually associated with liquids - because of the presence of other constituents and also because of possible cold crystallization. Phase diagrams - involving nonequilibrium phases - will be connected to properties.

1. W. Brostow, T.S. Dziemianowicz, J. Romanski and W. Werber, Polymer Eng. & Sci. 1988, 28, 785.
2. R. Kosfeld, M. Hess and K. Friedrich, Mater. Chem. & Phys. 1987, 18, 93.
3. K. Friedrich, M. Hess and R. Kosfeld, Makromol. Chem. Symp. 1988, 16, 251.

O3.11

STRUCTURE OF POLYQUINOLINE MOLECULAR COMPOSITE-A SMALL ANGLE SCATTERING STUDY. Wen-li Wu, Polymers Division, NIST, Gaithersburg, MD; John K. Stille, Joseph W. Tsang and Alex J. Parker, Colorado State University, Fort Collins, CO.

The compatibility between a rigid rod and a flexible chain polyquinolines was characterized using a combination of small angle x-ray and neutron scattering (SAXS and SANS) techniques. In the past, the presence of microvoids had hampered the use of scattering techniques to quantify the solid state structure in polymer blends containing rigid rod molecules. In the present work both the SAXS and SANS measurements were performed and their intensities were reduced to their absolute scales.

Since the scattering contrast between the void and the polymer is grossly different for x-ray and neutron, the contribution from microvoids scattering can be filtered out, afterward the spatial arrangement of the rigid rod molecules can be determined.

The polyquinolines were synthesized through a solution polymerization of bis(0-aminoketone) with bis(ketomethylene) monomers. The flexible chain polymer has almost an identical composition as the rigid rod one, except there are two additional oxygen atoms per repeating unit for the flexible one.

The extent of molecular dispersion as well as its dependence on thermal treatments will be discussed.

O4.1

PHASE BEHAVIOR IN POLYMER BLENDS. William J. MacKnight and Frank E. Karasz, Polymer Science and Engineering, University of Massachusetts, Amherst, MA.

Mean Field Theories (Flory-Huggins, Lattice Gas, Equation of State) are capable of describing the essential features of the phase behavior of miscible polymer blends. The discussion will be restricted to flexible coil polymers and examples will be given in which specific interactions (i.e., hydrogen bonding), and the "copolymer repulsive effect" are responsible for miscibility or partial miscibility.

In the first category are blends of aromatic polybenzimidazoles and aromatic polyimides. Fourier Transform Infrared Spectroscopy has revealed that hydrogen bonding is responsible for the observed miscibility in these polymers.

The copolymer repulsive effect is well demonstrated by blends of sulfonylated poly(2,6-dimethyl-1,4 phenylene oxide) and poly(styrene-co acrylonitrile). In the case of these blends, six binary interaction parameters are required to describe the system. Despite the fact that 5 of the 6 are thermodynamically unfavorable for mixing, considerable regimes of copolymer compositions exist where miscibility occurs. This is due to the exceedingly large intramolecular repulsion between styrene and acrylonitrile segments.

O4.2

SANS STUDIES OF BLENDS OF PROTONATED LINEAR POLYSTYRENE WITH CROSSLINKED DEUTERATED POLYSTYRENE. Robert M. Briber, Polymers Division, National Institute of Standards and Technology, Gaithersburg, MD 20899.

SANS has been used to study mixtures of linear PSH with crosslinked PSD made by classical interpenetrating network (IPN) synthesis techniques where the linear chain (PSH) is dissolved in a mixture of the monomer of the second component (deuterated styrene) and crosslinking agent (DVB) which is then polymerized. The polymerization was performed at 130°C using AIBN as the initiator. Neutron scattering was performed at the NIST SANS facility. SANS indicates that phase separation occurs between the PSH and PSD during the polymerization at relatively low crosslink densities

($M_c = 16400$) with linear chains of $M_n = 43900$. This indicates that to produce true single phase samples very low crosslink densities must be used even with components which are compatible as linear chains. The SANS data as a function of linear chain length (at constant network density) and as a function of network density (at constant linear chain length) will be discussed in terms of the classical theory of swelling for a network in a solvent (generalized to a polymeric solvent) to show that contribution to the free energy from the stretching of the network chains is the reason for phase separation in such systems and not due to an isotope effect between the PSH and PSD. In addition, using the assumption of additivity of the mixing and elastic free energies the second derivative of the elastic free energy with respect to composition ($\partial^2 \Delta f_{1,2} / \partial \phi_2^2$) is obtained from the extrapolated zero angle scattering ($S(0)$).

O4.3

DYNAMICS OF PHASE SEGREGATION IN POLY-P-PHENYLENE TEREPHTHALAMIDE AND AMORPHOUS NYLON BLENDS, J. C. Yang, T. I. Chen and T. Kyu, Center for Polymer Engineering, University of Akron, Akron, Ohio.

Time-resolved light scattering has been employed to elucidate the dynamics of phase segregation of poly-p-phenylene terephthalamide (PPTA)/amorphous nylon (AN) molecular composites. Miscible PPTA/AN blends can be prepared from methane sulphonic acid solution by rapidly coagulating the solution in distilled water. The system, however, undergoes phase segregation upon thermal treatment and exhibits a lower critical solution temperature (LCST). Several temperature jump experiments were undertaken from ambient to a two-phase temperature region of 240, 250 and 260°C. Time-evolution of scattering profiles were analyzed in accordance with non-linear and dynamical scaling theories.

Acknowledgement: The support of this work by the U. S. Army Research Office is gratefully acknowledged.

O4.4

BLENDS OF CRYSTALLIZABLE POLYBUTADIENE ISOMERS. Maira Marx Nir and Prof. Robert E. Cohen, Massachusetts Institute of Technology, Dept. of Chemical Engineering, Cambridge, MA 02139

Blends of two crystallizable polybutadiene (PBD) isomers, syndiotactic 1,2 PBD and trans 1,4 PBD, have been extensively characterized in both crystallized and melt states. Although the chemical compositions of the two homopolymers are identical, their crystal structures and melting and glass transition temperatures are very dissimilar. As determined by WAXS, Rheovibron viscoelastometry, DSC, and microscopy, the crystallized blends exhibit phase-separated behavior over the full range of composition. The scale of heterogeneity in binary blends is less than 1μ and morphology is dependent on thermal history. Compatibility of the amorphous phases has been studied using mechanical spectrometry. Addition of amorphous 1,2/1,4 diblocks, as a means of emulsifying the blends, will also be discussed.

O4.5

FACTORS INFLUENCING PROPERTIES OF SAN/PMMA BLENDS. R. Subramanian, Y.S. Huang, J. F. Roach & D. R. Wiff, GenCorp Research, 2990 Gilchrist Road, Akron, Ohio 44305

The versatility of polymeric blends is reflected in the range of usable end properties that can be achieved through alterations in the composition and/or effective control of the morphologies of the mixtures. Solvent cast and melt mixed blends of SAN and PMMA have been studied to understand the influence of PMMA tacticity,

the acrylonitrile content of SAN copolymer and goodness of mixing on the properties of the final mixtures. The results show a shifting of the cloud point curves and the miscibility windows for the blends of SAN with different stereo-regular PMMAs. This is interpreted as being due to specific interactions between the acrylonitrile and methacrylate groups. The implications of this enhanced specific interaction on the processing conditions and subsequent improvement in mechanical properties will be discussed. The limits of mixing that can be achieved using currently available mixing procedures and the usefulness of the title blends as a model to predict phase behavior of a partially miscible system will also be discussed.

O4.6

DIELECTRIC STUDIES OF POLYESTER/POLYCARBONATE BLENDS. James M. O'Reilly and Joseph S. Sedita Corporate Research Laboratories, Eastman Kodak Company, Rochester, NY 14650

Some co-polyesters of ethylene glycol and cyclohexane dimethanol with terephthalic acid are miscible with polycarbonate when the polymers are prepared by extrusion at 285°C. These blends show a single T_g by DSC measurements and obey the Gordon-Taylor equation. The purpose of this study was to examine the relaxation behavior of these blends as a function of composition (25, 50, 75% wt) and to quantitatively assess the changes in the WLF coefficients with composition. The dielectric properties were measured with a DETA apparatus from Polymer Laboratories from -150 to 200°C at five frequencies (1, 3, 10, 28.5 and 100 kHz). The low temperature relaxation is not significantly affected by blend composition. Dipolar relaxation above T_g of the blends is typical of a single phase amorphous polymer. The distribution of relaxation times can be described by a Williams-Watts distribution function with $\beta=0.52$ to 0.57 over the range of composition. Free volume parameters, f and af , derived from the temperature dependence of the dielectric loss factor, depend on blend composition. f is lower for the blends than it is for the copolymers. The characteristic dielectric relaxation time at T_g is longer for the blends than it is for the copolymers. These results will be compared with enthalpy relaxation data on these blends and discussed in light of current models of glassy state relaxations.

O4.7

INTERPENETRATING POLYMER NETWORKS AND RELATED TOPOLOGICAL ISOMERS. Harry L. Frisch, Department of Chemistry, State University of New York, Albany, NY.

Interpenetrating polymer networks (IPN'S) and pseudo IPN'S have become increasingly important as novel, molecular, composite materials exhibiting chemically controlled degrees of phase separation. The scale of microphase separation can in some IPN'S be reduced so that single phase materials (exhibiting a single glass transition temperature) can be prepared from polymers whose linear chains are incompatible at almost all compositions. We discuss the synthesis, morphology and some thermal and mechanical properties of these macromolecular topological isomers including polymeric catenanes. We will present in particular recent results on the series of IPN'S of poly(2,6-dimethyl-1,4-phenylene oxide) with the compatible polystyrene, and the incompatible poly(methyl methacrylate), poly(butadiene), polyurethane acrylate, and poly(dimethylsiloxane). In the last system we can compare the behavior of the IPN'S, the pseudo IPN'S, polymeric catenane, graft and block copolymers as well as a highly mutually crosslinked copolymer.

O4.8

MOLECULAR MODELING OF INTERPENETRATING POLYMER NETWORKS (IPNs). W.B. Hammond and D.C. Prevorsek, Allied-Signal, Inc., P.O.Box 1021R, Morristown, N. J. 07962

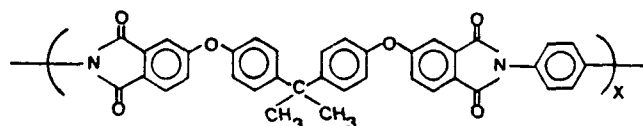
One way of generating nanometer structures is to start with a solution of a cross-linkable monomer and a high molecular weight polymer and carry out the cross-linking in a manner to produce minimal structural changes during the cross-linking process. This process produces

Interpenetrating Polymer Networks, IPNs, an important class of high performance polymers. We have used molecular modeling to study a class of IPNs prepared by cyclotrimerization of bisphenol-A dicyanate in the presence of a linear polymer such as polycarbonate. The cyclotrimerization of cyanates produces s-triazines linked by bisphenol-A bridges to form an open three dimensional network. Using oligomer structures to represent the polymer matrix, we have demonstrated that the network is flexible and can incorporate several strands of polycarbonate with net stabilization by van der Waals and electrostatic interactions. Molecular mechanics and dynamics calculations have been used to study the relationship between structure and physical properties of these materials. Procedures used to develop appropriate force field parameters for polymers will be discussed.

O4.9

FORMATION OF IPN TYPE THERMOPLASTIC MOLECULAR COMPOSITES. David A. Valia, General Dynamics Corporation, Convair Division, San Diego, Ca. 92138.

A novel approach for the production of thermoplastic molecular composites has been developed. Using the polyetherimide shown below as the matrix, an IPN type structure has been attained by synthesizing the rigid rod component in situ.



Data obtained from scanning electron microscopy, differential scanning calorimetry, thermogravimetric analysis, dynamic mechanical analysis and tensile type measurements will be presented. Results indicate that a homogeneous distribution of the rigid rod throughout the thermoplastic matrix has been obtained. The effect of using a novel method for attaining orientation of the rigid rod component will also be discussed.

O5.1

MOLECULAR VARIABILITY IN IONOMERS. A. Eisenberg, Department of Chemistry, McGill University, Montreal, Quebec, H3A 2K6 Canada.

Ionomers present the polymer chemist with an enormous range of opportunities for varying the molecular structure and properties of polymers. Even if one restricts oneself to a single polymer, e.g. styrene, and a single pendant ion, e.g. carboxylate, the range of structures is very large. For example, the ions can be attached to the backbone at random as in styrene-sodium methacrylate copolymers or they can be attached randomly to the *p* position of the phenyl ring, or can be even further from the backbone by the use of methylene spacers of various lengths. The structural variations affect the mechanical properties dramatically by affecting the morphology of the materials.

If one places the ions exclusively at one or both chain ends, the resulting block copolymers exhibit even more drastic morphological and bulk property changes. Furthermore, AB blocks yield micelles or inverted micelles, depending on the method of preparation, and can also be prepared as interfacial layers on water or between water and organic solvents, again exhibiting a range of unusual properties. If one allows the replacement of the carboxylate ion by, for example, a vinylpyridinium ion, further variation in properties becomes possible. Plasticizers are an additional parameter.

The ionomers, thus, present us with a most useful family of materials which allows for a dramatic variability in properties by allowing us to vary intermolecular interactions and therewith morphology of the systems.

05.2

BLOCK COPOLYMER IONOMERS: SULFONATED STYRENE-(ETHYLENE-CO-BUTYLENE)-STYRENE POLYMERS. R. A. Weiss and A. Sen, Univ. Connecticut, Storrs, CT; and L. A. Pottick and C. L. Willis, Shell Development Co., Houston, TX.

The polystyrene endblocks of a hydrogenated styrene-butadiene SBS block copolymer were lightly sulfonated in homogeneous solution. Sulfonate concentrations ranged from 2.5-18 mol%, and the free acid derivatives and the Na- and Zn-salts were prepared and characterized. The ionomeric nature of the modified block copolymers was demonstrated by their solubility behavior, solution properties, viscoelastic properties and their microstructure as determined by small angle x-ray scattering (SAXS).

Sulfonation increased the T_g of the styrene phase and also gave rise to a new rubbery plateau in the dynamic modulus above the styrene T_g . This plateau, which was a consequence of a physical network that formed from ionic interactions in the styrene blocks, persisted to nearly 300°C in the more highly substituted polymers. Thus, these materials consisted of three phases and two separate physical networks: one formed by 20-30 nm diameter spherical polystyrene microdomains dispersed in the rubbery matrix and the other formed by a 3-4 nm diameter ion-rich clusters within the styrene microphase. The introduction of the ionic network into the conventional block copolymer network resulted in significantly improved tensile properties for the block copolymer at elevated temperatures.

05.3

"GRAFT COPOLYMERS" FORMED BY SPECIFIC INTERACTIONS IN POLYSTYRENE AND POLYISOPRENE BASED IONOMERIC BLENDS. Sun Sasongko, M. Sabade and R. A. Weiss, University of Connecticut, Storrs, CT 06269-3136; and R. Jerome, University of Liege, Liege, Belgium.

This research considers the molecular architecture, morphology and properties of blends of a monofunctionalized polyisoprene and lightly sulfonated polystyrene (SPS). SPS was formed by sulfonation with acetyl sulfate of a narrow molecular weight distribution polystyrene ($M_n=39,000$; $M_w/M_n=1.08$). Ionomers containing 1.44, 3.58 mol% sulfonic acid or zinc sulfonate were blended with either stoichiometric or twice the stoichiometric amount (based on the acid functionality) of an ω -dimethylamino terminated polyisoprene ($M_n=3,800$; $M_w/M_n=1.23$). For the blends using the sulfuric acid derivatives, the two polymers interact by proton transfer; for the zinc sulfonate derivatives the interaction involves the formation of a transition metal complex. This interactions were studied by infrared spectroscopy.

The predominant molecular architecture is believed to be of a comb-like graft copolymer of the isoprene onto the polystyrene. The graft site, however, involves a physical, rather than a covalent bond that distinguishes these materials from more conventional graft or block copolymers or non-interacting physical blends. The consequences of the two different types of interactions, ionic and transition metal, on the bulk, solution, and rheological properties will be discussed and compared

with blends of comparable molecular weight unfunctionalized polymers and block copolymer with similar compositions and molecular weights.

05.4

MORPHOLOGY OF IONIC BLOCK COPOLYMERS BY SAXS. Jean-Pierre Gouin, Alain Desjardins and Adi Eisenberg, McGill University, Montréal, Canada, and Claudine E. Williams, LURE, Université Paris-Sud, Orsay, France.

SAXS experiments were done on well characterized AB and ABA block copolymers where the B blocks were poly(styrene) (200 to 1000 monomer units) and the A blocks were short (10 to 50 monomer units mainly) and were composed of either poly(vinyl-4-methylpyridinium iodide) or poly(cesium methacrylate). The materials were studied in the solid state. Various methods of preparing the samples were studied (casting, *in-situ* quaternization, freeze-drying).

The SAXS patterns all show a strong main peak and evidence of weaker peaks at higher angles. The main peak was attributed to a characteristic distance between the phase separated regions. The length of the short ionic blocks was shown to have a much greater effect on this characteristic distance than the length of the poly(styrene) blocks. An estimate of the morphological dimensions was obtained *via* space filling calculations based on the characteristic distance. The relative extent of the order between the phase separated regions was compared for the different architectures and methods of preparation by considering the peak widths.

05.5

SMALL ANGLE X-RAY SCATTERING ON POLY(ETHYLENE-METHACRYLIC ACID) LEAD AND LEAD SULFIDE IONOMERS. Dan O. Wu and Benjamin Chu (*), Chemistry Department, SUNY at Stony Brook, NY 11794-3400 and Walter Mahler, Central Research & Development Dept., Du Pont, Wilmington, DE 19898-0328

The morphology of ionomers: poly(ethylene-methacrylic acid) (EMA) lead salts (EMA/Pb) and lead sulfide compounds (EMA/PbS) has been studied by using the techniques of small angle x-ray scattering (SAXS), anomalous SAXS (ASAXS), and differential scanning calorimetry (DSC). EMA/Pb at ≤ 2 wt% exhibited two characteristic SAXS peaks which corresponded to the lamellar structure of the crystalline copolymer and the ionic structure of the Pb aggregates. With increasing Pb content, the lamellar peak retained its position but became less sharp and eventually vanished while the ionic peak grew and shifted to a lower value of q , with q being the scattering vector. DSC showed that the crystalline phase was present for all EMA/Pb samples and that the crystallinity decreased with increasing Pb content. PbS was made by a reaction of Pb ionomers with hydrogen sulfide. SAXS on EMA/BbS showed no ionic peak, but a peak located at the same q as the lamellar peak of Pb ionomers. ASAXS performed at the Pb L_3 absorption edge permitted the structural determination of pure Pb without interference of the lamellar peak. A schematic description of the ionomer structure will be presented.

05.6

POLYMER COMPOSITES WITH ELECTRONIC AND IONIC CONDUCTIVITIES. P. Audebert, N. Girault, M. Pineri, Groupe Physico-Chimie Moléculaire, DRF/SPh, Centre d'Etudes Nucléaires, 85X, 38041 Grenoble Cedex, France; and P. Audebert, Laboratoire d'Electrochimie Moléculaire, Université Paris VII, 75230 Paris Cedex 05, France.

Electronic and ionic conductive polymer composites are synthesized by an electropolymerization using pyrrole, bithiophene or aniline trifluoromethanesulfonate with a stiff, hydrophobic perfluorinated ionomer gel. An inert aqueous electrolyte is also used to insure the ionic conduction in the cell. The composites obtained have a high conductivity along with good mechanical properties (especially when they are annealed under pressure). Another method was developed consisting in the electropolymerization of the polyheterocycles into a swollen Nafion membrane inserted between the electrode and the electroactive gel prior to polymerization. This last method gave composite membranes which ally again a high electronic conductivity and mechanical properties similar to the initial unmodified membranes.

The composition and characteristics of the final polymers were investigated in relation with the composition of the initial gel, the polymerization currents and the applied potential.

The structures obtained for these materials correspond to that of the ionomer either in inverted micelle starting form or in the direct micellar form of the gels. The oxidized groups of the electron conductive polymer associate with the anionic sites of the ionomer. Ion exchange capacities have been measured.

05.7

EXCIMER AND EXCITON FUSION OF BLENDS AND MOLECULARLY DOPED POLYMERS--A NEW MORPHOLOGICAL TOOL. Zhong-You Shi, Ching-Shan Li, Irene E. Newhouse and Raoul Kopelman, Department of Chemistry, The University of Michigan, Ann Arbor, MI 48109-1055.

Exciton-exciton and exciton-excimer triplet fusion kinetics is monitored in medium molecular weight P1VN/PMMA solvent cast films with concentrations from 0.005 to 100% (weight), at temperatures of 77 to 300 K, via time resolved fluorescence and phosphorescence (10 ns to 10 sec). The heterogeneity exponent (h) is 0.5 for isolated P1VN chains, zero (classical) for pure P1VN and "fractal-like" throughout certain concentration regimes. However, h is not monotonic with blend concentration but rather oscillates between zero and 0.5. Correlation is made with morphology changes (phase separation, filamentation). The long-lived decays do fit stretched exponentials, with a parameter $\beta = 1 - h$. Furthermore, the blend topology is also studied with the aid of the time-modulation technique, in which the time-decays are obtained for different excitation durations, i.e., single pulse vs. cw or multiple-pulse laser excitation, but with equal global exciton densities at the start ($t = 0$) of the decays. As expected, the triplet exciton kinetics is dominated by short-range hops (about 5 Å) and thus monitors the primary topology of the chains. At concentrations below 0.01%, the excitons are constrained to a truly one-dimensional topology. At higher concentrations there is a fractal-like topology. Similar studies were conducted on naphthalene-doped PMMA (1-20% weight) and interpreted with the aid of computer simulations. The lower concentration samples are neither segregated nor random solution phases.

05.8

THE ORDERED BICONTINUOUS DOUBLE DIAMOND STRUCTURE IN BLENDS OF DIBLOCK COPOLYMER AND HOMOPOLYMER. Karen L. Winey, University of Massachusetts, Amherst, MA; and Edwin L. Thomas, Massachusetts Institute of Technology, Cambridge, MA.

We report the observation of the ordered bicontinuous double diamond (OBDD) structure in blends of poly(styrene-isoprene) diblock copolymers with homopolystyrene. Both components of the OBDD structure are continuous and periodic in three dimensions. The minority component of the OBDD resides in two

interpenetrating networks having diamond-cubic symmetry and constant mean curvature surfaces. The majority component resides in the continuous matrix between the two diamond channels. A lamellar diblock copolymer blended with homopolystyrene gives the OBDD with the homopolymer in the matrix. A small amount of homopolystyrene added to a cylindrical diblock copolymer, where polystyrene is the minority block, forms the OBDD with the homopolymer in the diamond channels.

The overall polystyrene volume fraction of the OBDD binary blends is approximately within the polystyrene volume fraction range established for pure diblock copolymers having the OBDD structure. However, obtaining the proper polystyrene volume fraction is not sufficient to produce the OBDD in a blend. A large amount of homopolystyrene added to a cylindrical diblock copolymer, where polystyrene is the minority block, macrophase separates rather than forming a polystyrene rich OBDD structure. Homopolymer solubility depends on the relative molecular weights of the homopolystyrene and the polystyrene block of the copolymer as well as the composition.

05.9

STUDIES ON THE MICROSTRUCTURE OF CORE-SHELL COPOLYMERS BY ELECTRON MICROSCOPY. R. Velázquez, A. Cruz* and V. M. Castaño, Instituto de Física, U.N.A.M., A. P. 20-364, México, D. F. 01000. *Facultad de Química, U.N.A.M., Cd. Universitaria, México, D. F.

Several structured copolymers (core-shell) have been studied by Transmission Electron Microscopy (TEM). The systems analyzed included styrene-butylacrylate with different compositions and preparation procedures. The microstructure found by TEM has been correlated to the chemical and physical properties of the copolymers. Special care has been dedicated to the interfacial characteristics of the materials.

05.10

STUDIES ON THE EXCESS FREE ENERGY AND THE COLLECTIVE DIFFUSION CONSTANT OF THE BLEND d-PS/PVME AND THE ISOTOPIC BLEND d-PS/PS WITH NEUTRON SMALL ANGLE SCATTERING. D. Schwahn, K. Hahn¹, J. Streib¹, and T. Springer IFF - KFA Jülich GmbH, 5170 Jülich, FRG ¹BASF Aktiengesellschaft, 6700 Ludwigshafen, FRG

Demixing and precipitation growth are of general interest in the application of polymer blends. We have carried out small angle neutron scattering (SANS) studies on the system PVME/d-PS having a lower critical solution temperature, and on the isotopic blend of polystyrene. Critical scattering and the domain growth rate have been studied for different temperatures and compositions of the components. Isotopic blends are ideal systems for testing theoretical models. In d-PS/PS ($M = 10^6$ dalton) the Flory-Huggins interaction parameter $\chi(\phi, T)$ as determined by SANS, yields binodal, the miscibility gap, and the corresponding spinodal line, with an upper critical temperature of 130 °C. From temperature relaxation experiments above T_c and from spinodal decomposition, the collective diffusion constant was determined. After 3 weeks of annealing at 125 °C, decomposition was observed which can be interpreted in terms of the Cahn-Hilliard-Cook theory for the early stages of decomposition.

05.11

PROPERTIES AND STRUCTURE OF POLY(VINYL ALCOHOL) (PVA)/MELAMINE FORMALDEHYDE (MF) MOLECULAR COMPOSITES. Kecheng Gong; and Xinghua Zhang, Polymer Structure and Modification Research Lab, South China University of Technology, Guangzhou, P.R. China.

The mechanical properties and structure of PVA/MP molecular composites have been studied in this paper. When PVA content was lower than a certain value (about 20% weight), the flexible strength and impact resistance were improved simultaneously. Although the impact resistance remained the previous trend when the PVA content went beyond the limit, the flexible strength tended to decrease.

The structure, morphology, heat-resistance and some other properties of the two-phase system were investigated by means of differential scanning calorimetry, thermogravimetry, infrared absorption spectrum and transmission and sweep electron microscopy. The results indicated that there was molecular composite structure in this two-component system and the chemical reaction including crosslinking between the components occurred. That gave the explanation of the effects of PVA on the mechanical properties and showed that the molecular composites are favourable for making full use of the macro-molecular potentiality.

O6.1

MORPHOLOGICAL CONSEQUENCES OF CATALYTIC HYDROGENATION OF POLYMERS IN THE BULK * Laure R. Collin, Sandia National Laboratories, Division 1811, Albuquerque NM 87185

When suitable catalysts are molecularly dispersed in polymers the polymers can be modified in the absence of added solvent. This paper describes the bulk catalytic hydrogenation of olefinic polymers with an emphasis on micro- and macro-scale morphology. Examples of the in-place conversion of an amorphous polybutadiene to crystalline polyethylene, a crystalline polybutadiene to amorphous polybutene, and crystalline polybutadiene to crystalline polyethylene will be provided. Modification of the centerblock of a polystyrene-polybutadiene triblock copolymer occurs with retention of the original morphology and domain size. A single component of a polymer blend can be selectively reacted in the bulk. For example, hydrogenation of a blend containing polybutadiene and polyisoprene resulted in preferential reaction of the disubstituted relative to the trisubstituted double bonds. Gross structural features attributable to initial fabrication will be described. Additionally, the possibility of obtaining a heterophase material by partial modification of a homophase polymer will be considered.

* This work was performed at Sandia National Laboratories supported by the U. S. Department of Energy under contract number DE-AC04-76DP00789.

O6.2

SYNTHETIC CONTROL OF MOLECULAR STRUCTURE IN ORGANIC AEROGELS Richard W. Pekala, Chemistry & Materials Science Department, Lawrence Livermore National Laboratory, Livermore, CA 94550

The sol-gel processing of metal alkoxides (e.g. tetramethoxy silane, tetraisopropoxy titanate) is a convenient method for tailoring the properties of inorganic materials at a molecular level. Sol-gel research has principally focused on the manipulation of silicate precursors to form polymeric or colloidal structures in solution. The hypercritical drying of crosslinked silica gels leads to the formation of a special class of open-celled foams referred to as aerogels. Aerogels have an ultrafine cell/pore size (< 1000 Å) and a morphology composed of interconnected particles with diameters less than 100 Å. This microstructure is responsible for the unusual optical, thermal, and acoustic properties of these materials.

Our research has focussed on organic syntheses which proceed through a sol-gel transition and can be controlled to produce aerogels with varying properties. Organic aerogels have been synthesized from the base catalyzed, aqueous reaction of resorcinol with formaldehyde. In this reaction, resorcinol (1,3-dihydroxy benzene) is a trifunctional monomer capable of adding formaldehyde in the 2,4 and/or 6 ring positions. These intermediate products condense into polymeric "clusters" with diameters ranging from 30-175 Å. The

resorcinol-formaldehyde (RF) "clusters" contain surface functional groups which lead to further crosslinking and eventual gel formation.

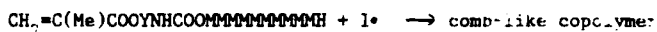
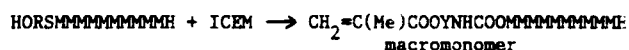
RF gels are hypercritically dried to form organic aerogels. The RF aerogels are dark red in color and transparent. Pyrolysis of the RF aerogels in an inert atmosphere leads to a vitreous carbon structure.

The catalyst concentration in the polymerization has been found to control the particle size, cell size, density, surface area, and modulus of the organic aerogels. In this paper, the chemical manipulation of the aerogel microstructure will be discussed. Characterization methods include SEM, TEM, BET nitrogen adsorption, and small angle scattering.

O6.3

SYNTHETIC PROCEDURES FOR PREPARING CROSS-LINKABLE ACRYLIC COMB-LIKE COPOLYMERS VIA MACROMONOMERS. G-F. Chen and Frank N. Jones, Polymers & Coatings Dept., North Dakota State University, Fargo, ND 58102

Synthesis of comb-like polymers and copolymers by polymerization of macromonomers is a subject of widespread scientific and technological interest. The macromonomers are commonly prepared by anionic, cationic or group transfer polymerization. We will report synthesis of copolymeric macromonomers by and comb-like copolymers by free-radical initiated polymerization using a functional chain transfer agent, a route which can be illustrated as follows:



[I· = initiator, M = mixed monomers, X and Y can be CH₂, CH₃.

This synthetic route works well in formation of non-functional and difunctional materials during the first step is minimized. Difunctional materials can result from termination by combination or from other reactions and are especially troublesome because they cause branching or gelation in the third step. It will be shown that by careful choice of monomers and reaction conditions in each step a wide variety of comb-like copolymers can be synthesized. Of particular interest are comb-like copolymers bearing mixtures of tines, some designed to impart cross-linkability and others designed to impart other desired properties to the materials.

O6.4

SYNTHESIS AND CHARACTERIZATION OF SEGMENTED COPOLYMERS OF A METHYLATED POLYAMIDE AND A THERMOTROPIC LIQUID CRYSTALLINE POLYESTER Gregory T. Pawlikowski, R. A. Weiss and S. J. Huang, University of Connecticut, Storrs, CT.

A block copolymer consisting of liquid crystalline polyester segments and methylated polyamide segments has been synthesized. Solution polycondensation of acid chloride end-capped poly-(terephthaloyl phenylhydroquinone) (LCP portion) with an amine terminated poly(N,N'-dimethylethylene sebacamide) was utilized to prepare the segmented copolymer.

Characterization by differential scanning calorimetry, infrared spectroscopy, thermogravimetric analysis, dynamic mechanical analysis, optical microscopy and scanning electron microscopy has been performed to verify the existence of the block copolymer and to evaluate its potential as a molecular composite material or self-reinforcing thermoplastic.

06.5

MORPHOLOGY OF SOLVENT CAST DIBLOCK COPOLYMERS AND COPOLYMER-HOMOPOLYMER BLENDS CONTAINING "DURHAM" POLYACETYLENE. Sankaran, V.; Schrock, R.R.; Cohen, R.E., Department of Chemical Engineering and Chemistry, Massachusetts Institute of Technology, Cambridge, MA.

Diblock copolymers of poly norbornene and 7,8-bis(trifluoromethyl)tricyclo[4.2.2.0^{2,5}]deca-3,7,9-triene were synthesized via ring opening metathesis polymerization using the catalyst $W(NAr)(CH^tBu)(O^tBu)_2$ [where $Ar = 2,6-C_6H_3^iPr_2$]. The second block is readily converted to "Durham polyacetylene" by heating to 120°C for 3.5 minutes. Solution cast films of these diblocks were studied using Transmission electron microscopy and Small angle X-ray scattering. Diblock copolymers with up to ten weight percent polyacetylene exhibit a morphology of polyacetylene spheres of ~250 Å diameter in a polynorbornene matrix. Also investigated was the effect on morphology of blending the diblocks with various amounts of polynorbornene.

06.6

AGGREGATION STRUCTURE AND ELECTRO-OPTICAL PROPERTIES OF (LIQUID CRYSTALLINE POLYMER)/(LOW MOLECULAR WEIGHT LIQUID CRYSTAL) COMPOSITE SYSTEM. Tisato Kajiyama, Dept. of Appl. Chem., Kyushu Univ., Hakozaki, Higashi-ku, Fukuoka, Japan

Reversible and bistable electro-optical effect based on light scattering was recognized for a binary composite composed of side chain type liquid crystalline polymer (LCP) and low molecular weight liquid crystal (LMWLC) of which chemical structure is similar to the mesogenic side chain of LCP. A light scattering state caused by the disorder of homeotropic alignment appeared below a threshold frequency. Furthermore, application of a 100 V a.c. field of 1 kHz made the transmission light intensity increased to 94 % within a few seconds. The optical heterogeneity in a smectic layer of the side chain group was caused by the difference of two forces based on both dielectric anisotropy of the side chain and the electrohydrodynamic motion of the main chain. Since application of a low frequency electric field induces an ionic current throughout the mixture film, it is reasonable to consider that an induced turbulent flow by an ionic current collapsed a fairly well organized large smectic layer into many small fragments, resulting in an increase in light scattering. The response speed of LCP to an applying electric field increased remarkably by mixing LMWLC. A smectic phase was observed in a fraction range above 55 wt% of LCP. In the case of a smectic mesophase, turbid and transparent states remained unchanged as it was, even though after removing an electric field.

Such a bistable and reversible light switching driven by two different frequencies could be newly realized by both characteristics of turbulent effect of LCP main chain and rapid response of LMWLC. We believe that the LCP/LMWLC mixture system is useful as a novel type of "light valve" exhibiting memory effect (bistable light switching).

06.7 ABSTRACT WITHDRAWN

06.8

ELECTRICALLY CONDUCTIVE COMPOSITE PREPARED BY TEMPLATE POLYMERIZATION OF PYRROLE INTO A COMPLEXED POLYMER. A. Mohammadi, D.W. Paul, O. Inganäs, J. O. Nilsson and I. Lundström, Laboratory of Applied Physics, Department of Physics and Measurement Technology, Linköping Institute of technology, S-581 83 Linköping, Sweden

Electrically conducting polymer composite films have been synthesized by the exposure of poly(4-vinylpyridine) complexed with cupric ions to pyrrole and water vapour. In order to immobilize optimum amount of the oxidant inside the polymer matrix, the ratio of poly(4-vinylpyridine)/cupric ion

= 1.8 was chosen. Polypyrrole was formed into this tailored structure by a template polymerization process.

Opaque polymer composite films with electrical conductivity up to 60 (Ωcm)⁻¹ have been obtained by this method. However, slightly coloured transparent composite thin films with a conductivity as high as 50 (Ωcm)⁻¹ were also produced.

The electrically conducting polymer composite films and the tailored complexed polymer have been characterized by XPS and IR spectroscopy, elemental analysis, EDX and scanning electron microscopy. The polymerization process was also followed by the use of a quartz crystal microbalance.

06.9

MIXED ALKALI-ALKALINE EARTH METAL PERCHLORATE POLYETHER COMPLEXED COMPOSITE POLYMER ELECTROLYTES : INVESTIGATION OF STRUCTURAL AND TRANSPORT PROPERTIES. A. N. DURGA RANI, Department of Physics, Indian Institute of Technology, Madras-600036, India and P. SATHYA SAINATH PRASAD, Corrosion Research Center, Department of Chemical Engineering & Material Science, University of Minnesota, Minneapolis, MN-55455, U.S.A.

Solid polymer electrolytes of the type $(1-x)\text{LiClO}_4 \cdot x\text{M}(\text{ClO}_4)_2$ (where M is an alkaline earth metal) in the composition range $0.05 < x < 0.5$ have been prepared by dissolving the alkali-alkaline earth perchlorate mixtures in acetonitrile and adding polyethylene oxide (PEO) to the solution in the O/Li ratio of 12:1 and 8:1. In these systems the complexation was accompanied by a considerable degree of ionic association and at low mixing levels, the complexes showed enhanced ionic conductivity when compared to pure $\text{LiClO}_4(\text{PEO})_8$ at room temperature. It is assumed that the heavier alkaline earth metal atoms act as dopants in creating defect structured composite polymers, where fast lithium ion conduction could be possible. At high mixing levels, the complexes exhibit low ionic conductivity values and it is assumed that coionic conduction.

a.c conductivity studies on these polymer electrolytes showed a dependence on both dopant concentration and temperature. Room temperature conductivities for some selective compositions were around $10^{-6} - 10^{-5}$ S/cm and the observed non-Arrhenius behaviour was analysed using the Vogel-Tammann-Fulcher equation and interpreted on the basis of the defect structure mechanisms in composite polymers.

Preliminary results on the structural aspects indicate the existence of octahedral and tetrahedral structures of alkaline earth metal cations with traces of water that is absorbed by the hygroscopic perchlorates in the process of sample preparation.

07.1

Diblock Copolymers at Interfaces* Peter F. Green, Sandia National Laboratories, Albuquerque N.M. 87185-5800

In multicomponent systems, such as diblock copolymers and polymer blends, the average composition in the vicinity of an interface differs from the bulk composition. In the special case of a free surface the lower surface energy component is preferentially located at the surface. Using different techniques we have investigated the interfacial properties of a series of symmetric diblock copolymers of polystyrene (PS) and polymethylmethacrylate (PMMA). Some of these copolymers were weakly segregated while others were highly segregated. Under equilibrium conditions secondary ion mass spectroscopy (SIMS) showed that the copolymer bulk microstructure was organized such that the PS and PMMA lamellae were parallel to the free surface; the polystyrene component was preferentially located at the free surface and the polymethylmethacrylate phase was preferentially located at the substrate (silicon) copolymer interface. X-ray photoelectron spectroscopy (XPS) measurements indicate that for the highly segregated copolymers the surface was composed only of PS and for the copolymers in the weak segregation limit the surface was composed of both PS and PMMA. The use of solvents was shown to dramatically alter the surface composition and the

organization of the bulk microstructure. We also investigated the interfacial activity of PS/PMMA copolymers in immiscible blends of PS and PMMA and at polymer metal interfaces using an ion beam analysis technique, elastic recoil detection (ERD). The interfacial activity was seen to be influenced considerably by the degree of compatibility of the copolymer and its composition. These findings will be discussed in light of mean field theory.

*This work, performed at Sandia National Laboratories, was supported by the U.S. Department of Energy under contract number DE-AC04-76DP00789

O7.2

Short time relaxation at polymeric interfaces, A. Karim, A. Mansour, G.P. Felcher, Argonne National Laboratory, T. P. Russell, Almaden Research Center.

Neutron reflection has been used to study the interdiffusion in polymer melts of high molecular weight polystyrene (PS) and deuterated polystyrene (d-PS). Bilayered samples of PS and d-PS were annealed at temperatures between the glass transition temperature, 100C, and 140C. For all annealing temperatures the interface showed a rapid initial broadening over distances up to 80Å, followed by a much slower diffusion process at longer times. The faster process could only be followed in detail at temperatures very close to T_g , where the time scale is of the order of few minutes. This process seems to be related to the relaxation of the Rouse segments of the polymer chains at the interface, with a characteristic time τ_B^1 associated with the relaxation of the polymer chain within the tube, but without a large scale spatial displacement of the entire polymer chain. Furthermore, the temperature dependence of τ_B is described by the empirical WLF scaling law.

1. C.W. Lantman, J.F. Tassin, P. Sergot, L. Monnerie, *Macromolecules*, 22, 483 (1989)

O7.3

NEUTRON REFLECTION STUDY OF SURFACE ENRICHMENT IN AN ISOTOPIC POLYMER BLEND. R.A.L. Jones, L. Norton, E.J. Kramer, Cornell Univ., R.J. Composto, R.S. Stein, Univ. of Massachusetts, T.P. Russell, IBM San Jose, G.P. Felcher, A. Mansour and A. Karim, Argonne National Laboratory.

We have measured neutron reflectivities from films of blends of deuterated polystyrene (d-PS) and protonated polystyrene (PS) before and after annealing, and used the results to determine the concentration versus depth profile of the films. After annealing, the surface appears to be enriched in d-PS, with a surface excess proportional to the bulk concentration of d-PS, in agreement with previous measurements using forward recoil spectrometry¹. The decay of the enhanced concentration into the bulk is over a length equal to approximately the bulk correlation length (~200 Å), in close agreement with that predicted by current mean-field theories². However the detailed decrease of the d-PS enrichment close to the surface does not follow the theory: while an almost exponential decay is predicted, the neutron reflection experiments show that the initial decay is a weaker function of depth over the first 50 Å.

1. Jones, Kramer, Rafailovich, Sokolov, Schwartz, *PRL* 62, 280 (1989)
2. I. Schmidt and K. Binder, *J. Physique* 46, 1631 (1985)

O7.4

Interdiffusion and interfacial motion in polymer bilayers, T.P. Russell, IBM-Almaden Research Center, A. Karim, A. Mansour, G.P. Felcher, Argonne National Lab.

Neutron reflection has been used to study the interdiffusion in bilayers of protonated and deuterated polystyrene of high molecular weight. Samples with molecular weight ratios ranging from 1:1 to 1:50 were annealed at different temperatures above the glass transition. The interdiffusion of species with different molecular weight causes a broadening of the interface which is consistent with an asymmetric distribution of density for a molecular weight ratio larger than 1:2. At the same time, the "interface" (which as seen by neutron reflection is defined as the position of maximum concentration gradient) moves during annealing, with a motion more pronounced the larger the difference in molecular weights. In a systematic series of measurements after different annealing times t , the interface motion was found to follow the predicted¹ macroscopic $t^{0.5}$ behaviour even for distances less than radius of gyration of the lighter species.

1. P.F. Green, C.J. Palmstrom, J.W. Mayer, and E.J. Kramer, *Macromolecules* 13, 880 (1980).

O7.5

X-RAY REFLECTIVITY AND FLOURESCENCE MEASUREMENTS FROM POLYSTYRENE-CO-BROMOSTYRENE/POLYSTYRENE BLENDS.

J. Sokolov, M.H. Rafailovich, X. Zhao, Queens College, W.B. Yun, Argonne National Laboratory, R.A.L. Jones, E.J. Kramer, Cornell University, R.J. Composto, Univ. of Mass. at Amherst and B. Arun, Brooklyn College.

We have measured the x-ray reflectivity and fluorescence from blends of hydrogenated polystyrene (PS) and polystyrene-co-bromostyrene (PBr₂S) of molecular weights ranging from 9.2K to 1.9M. The PBr₂S was prepared according to the procedure of Kambour and Bendler¹. The degree of bromination, x , was varied to control the miscibility of the blends. Highly immiscible blends ($x > 0.8$) were used to measure properties at sharp interfaces, while partially miscible blends ($x \leq 0.2$) were used to study segregation to surfaces in thin films. The lower surface energy component, PS, was enriched at the air-polymer interface. The PBr₂S component segregated to the Si surface forming a layer approximately 200Å wide. Detailed analysis of the results in terms of current mean field theories will be presented.

1. R.P. Kambour and J.T. Bender *Macromolecules* 19 (1986) 2679.

O7.6

SURFACE MODIFICATION AND SURFACE SEGREGATION PROPERTIES OF BLOCK COPOLYMERS E. Parsonage, M. Tirrell, University of Minnesota, Minneapolis, MN, H. Watanabe, Osaka University, Osaka, Japan

Block copolymers can be used as interfacial agents to compatibilize and modify heterogeneous material blends. As such, they can be used in such disparate areas as stabilizing colloidal dispersions and strengthening composite materials. We have been studying the properties of thin layers of

block copolymers which have been deposited by adsorption or spin-casting techniques. The purpose of this work has been to study the effect of the block copolymers on the interfacial properties of the system, and also how the interface affects the molecular configuration and morphology of the block copolymers near the interface. Block copolymers of styrene, isoprene and vinyl pyridine of various molecular weights have been synthesized by living anionic polymerization. The experimental techniques used to study these thin films include angle-resolved XPS, variable angle ellipsometry, radiotracer analysis and other techniques. The experimental results can in part be explained by a self-consistent field analysis of these model systems.

O7.7

INTERFACIAL SEGREGATION EFFECTS IN MIXTURES OF HOMOPOLYMERS WITH COPOLYMERS. Vijay S. Wakharkar, Thomas P. Russell and Vaughn R. Deline, IBM Research Division, Almaden Research Center, San Jose, CA 95120.

Secondary Ion Mass Spectroscopy (SIMS) has been used to study the surface and interfacial segregation of diblock copolymers in mixtures of the copolymer in the homopolymer. Symmetric, diblock copolymers of polystyrene (PS) and poly(methyl methacrylate) (PMMA), with either the PS or the PMMA homopolymers were investigated. In order to serve as a label in the SIMS measurements either block of the copolymer or the homopolymer is perdeuterated. Films cast from toluene solution onto silicon wafers were annealed above the glass transition temperature of either component. SIMS depth profiles were then obtained with an effective depth resolution of ca. 125Å. It was found that in mixtures of the copolymer with the PS homopolymer surface enrichment of the copolymer as well as segregation of the copolymer to the polymer/Si interface occurs. Prior to attaining equilibrium, the surface enrichment is accompanied by a prominent depletion of the copolymer beneath the surface. The surface excess increases as the bulk volume fraction of the copolymer in the mixture is increased from 1% to 10%. The time dependence of the surface enrichment was followed over a wide range of annealing times. At sufficiently long annealing times the concentration of the copolymer in the bulk of the film is quite low, the copolymer now being present either at the air/polymer interface or at the polymer/Si interface. The kinetics of the segregation process was found to be diffusion controlled. These segregation effects were found over a whole range of molecular weights of the homopolymer.

O7.8

A NEW VARIABLE ANGLE FT-IR ELLIPSOMETER.

J L Stehle, J H Lecat, J P Piel, O Thomas, P Evrard, SOPRA, 26/68 rue Pierre Joigneaux, 92270 Bois-Colombes, FRANCE. L C Hammond, ARIES/QEI, 5A1 Damonmill Square, Concord MA 01742, USA.

Use of a Fourier-transform interferometer integrated with a variable incidence angle ellipsometer extends the spectral range and capabilities of spectroscopic ellipsometry into the infrared. With a spectral range of 600 to 6000 cm^{-1} . Thick layers, such as epitaxial doped layers and polymers, can be analyzed.

A full description of this novel instrument will be given. Incidence angle can be varied automatically to enhance signal/noise and the ellipsometric data can be obtained together with vibrational absorption bands information to give a characteristic 'fingerprint' of the layers.

Examples of spectra of HCN polymer on nickel, DMHS on aluminum and PMMA on silicon will be presented for various incidence angles and layer thicknesses.

O7.9

POLYMER MOLECULES AT INTERFACES: STUDIES BY SMALL-ANGLE NEUTRON SCATTERING. W.C. Forsman and B.E. Latshaw, Department of Chemical Engineering, University of Pennsylvania, Philadelphia, PA., and D.T. Wu, The Marshall Laboratory of the duPont Company, Philadelphia, PA.

The nature of polymer molecules at the polymer-substrate interface plays an important role in determining the properties of composites. Small-angle neutron scattering holds the potential for comparing the conformation of macromolecules in the interface to their conformation in the bulk.¹⁻⁴ This paper describes experiments performed for that purpose.

The substrate was nearly-monodisperse 2000 Å silica particles, both bare and with grafted poly(butyl methacrylate). The particles were dispersed in isopropyl alcohol (IPA).

Scattering experiments were done at Brookhaven National Laboratory. We used mixtures of hydrogenous and deuterated IPA for contrast variation measurements. Particle concentrations were 1%, 5% and 10% by volume. The scattered intensities (after correcting for background scattering) were directly proportional to the particle concentration. We took this to mean that there is no contribution to the scattered intensity from interparticle interference over our range of experimental scattering angles. This is to be expected for particles as large as 2000 Å.

All the dispersions gave excellent signal-to-noise ratio. The difference between scattered intensities for bare particles and particles with grafted polymer could be interpreted in terms of the density profile of the grafted polymer segments in the interface.

O7.10

MECHANICALLY INDUCED SILICA-SILOXANE MIXTURES. STRUCTURE OF THE ADSORBED LAYER AND PROPERTIES OF THE NETWORK STRUCTURE.

J. P. Cohen-Addad, Laboratoire de Spectrometrie Physique, B.P. 87, 38402, St. Martin d'heres, France.

The mechanical mixing of silica particles with siloxane chains in a melt induces an adsorption process of chains upon the silica surface. This effect obeys a specific kinetics. The amount of polymer Q_s bound to silica through H-bonds is found to obey the law: $Q_s = aMn^8$ (square root of Mn) with Mn ranging from 2000 to 360000 g/mole. An interpretation of this law is given. It is illustrated from NMR investigations. A network structure is formed when the concentration of silica is high enough; mineral particles are connected to one another by polymer chains. An interpretation of swelling and stretching properties is given.

O7.11

THE EFFECT OF MASKED ISOCYANATES ON THE MECHANICAL PROPERTIES OF MY 720/DDS EPOXY RESIN.

N. Rungsimuntakul, R. E. Fornes, and R. D. Gilbert, North Carolina State University, Raleigh, NC 27695

The mechanical properties of epoxy resins and epoxy resin/graphite fiber composites are reduced by moisture absorption. Blocking of the residual functional groups in the cured MY 720/DDS epoxy resin significantly (~75%) lowers the equilibrium moisture absorption. Incorporation of masked isocyanates that deblock to release isocyanates in situ at the cure temperatures (150-177°C) also reduce the equilibrium moisture absorption by ~70%. Dynamic mechanical analyses and stress strain properties of the epoxy resins containing a number of masked isocyanates were studied to determine their effect on mechanical properties. The ultimate Tg of the epoxy is reduced by incorporation of masked isocyanate but not the actual Tg the dynamic moduli up to the Tg are relatively unaffected. Generally, the initial modulus, elongation at break and peak stress are equal or better than the unmodified resin.

A STUDY OF SHORT METAL FIBER REINFORCED COMPOSITE MATERIALS

Over the years, the conventional involvement of short fiber reinforced composites in electrical applications has been as electrical insulation. Contrary to this approach, with the increasing need of better electromagnetic interference (EMI) shielding and control of electrostatic charge Distribution (ESD) for computer, defense and some high tech structural components, it is expected that the development of conductive polymeric composite materials will grow strongly and significantly.

Although they can be used to replace some traditional materials, the deformation behavior of such short fiber reinforced composites have led to greater problems at the design and application stages. Stress concentration at short fiber ends is often of the major concern. Fracture in such composites where the damage will be initiated or accumulated is generally difficult to be predicted. An experimental investigation is therefore carefully designed and undertaken to systematically evaluate the mechanical properties as well as electrical properties. In this study, chopped Inconel 601 (nickel based) metal fiber with various lengths will be used to reinforce commercially available thermoset polyester resin. Mechanical testing such as tensile, impact, and flexure tests along with electrical measurements will be conducted to study the feasibility of using such composites. Fractographic examination by means of optical microscopy and scanning electron microscopy will be employed to help understand the fracture behavior and possible failure causes. The advantages and limitations of applying short metal fiber reinforced polymeric composites will further be addressed and discussed.

08.1

DEFORMATION BEHAVIORS OF POLYMER GELS IN ELECTRIC FIELD. I. Kurauchi, T. Shiga, Y. Hirose and A. Okada, TOYOTA Central Research and Development Laboratories, Inc., Nagakute, Aichi, Japan.

Polymer gels, "solid-liquid coexistent materials", can be called to be "biomimetic materials" because they consist of crosslinked polymer networks, ions and low molecules such as water. They must, therefore, have various possibilities as advanced functional polymers which can fulfill complicated and useful system functions. Polymer gels, "solid-liquid coexistent materials" may be the fifth material after metals, ceramics, polymers and composites.

Acrylic acid-acrylamide copolymer gels (PAA gels) swollen in water show three types of deformation under the influence of d.c. electric field in a solution; shrinking, swelling and bending. The type of deformation is determined on the fraction of sodium acrylate in a PAA gel, the shape of the PAA gel and how to set the gel between the anode and the cathode. When a rectangular gel is set parallel to the electrodes and d.c. field is applied to it, the bending can be observed. The bending speed of the PAA gel depends on the intensity of the applied electric field, the concentration of a salt in the solution and polyion in the gel.

The PVA-PAA gel (an IPN gel composed of polyvinyl alcohol) has high mechanical strength and the bending speed is equal to that of the PAA gel. It was applied to "robotic finger", which can pick up a fragile egg in safety. "Gel fish" was also made from the PVA-PAA gel. It can swim in water at the speed of about 2 cm/s by applying the alternative field.

08.2

BIAXIAL EXTRUSION OF POLYIMIDE LARC-TPI & LARC-TPI BLENDS

Biaxial extrusion of neat LARC-TPI polyimide and LARC-TPI Liquid Crystalline Polymer (LCP) blends were investigated as a part of an ongoing Phase II SBIR program funded by the National Aeronautics and Space Administration (NASA) at the Langley research center.

Films of neat LARC-TPI and LARC-TPI / LCP blends with nominal thicknesses of 0.001" and 0.002" with orientation of ~ 5 and

~ 30 degrees with respect to the machine direction were biaxially extruded using Foster Miller's proprietary extrusion technique. Thermal, mechanical, and physical characterization of the extrudates were carried out. Results revealed that LARC-TPI polyimide can be extruded into biaxially oriented films with relative ease. The neat LARC-TPI films were brittle. Incorporation of up to 20 percent by weight of an LCP however, made the polyimide more processible and reduced the coefficient of thermal expansion (CTE) by greater than 20 percent. The processing and properties of the extrudates will be discussed.

08.3

THE PROPERTIES OF RUBBER-CRUMB TOUGHENED POLYSTYRENE COMPOSITES OBTAINED THROUGH REINFORCING REACTION MOULDING. KeCheng Gong; And Long-gui Zhong; Department of Polymer Science, South China University of Technology, Guangzhou, P.R.China.

The rubber crumb toughened PS composites were prepared by reinforcing reaction moulding (RRM). It is found that the impact strength and break elongation of the RRM composite increase more remarkably with the increasing of crumb content, and they can be 10 times greater than those of pure PS when crumb content is 42%. Still, tensile strength and bend strength retain 50% of that of PS material. The RRM is better than mechanical blending in improving the mechanical properties of composite materials.

The crumb granularity and its distribution have great influences on the properties. Fig.3 shows that the impact strength is the greatest at the crumb granularity of 40 meshes, this is in compliance with Tuchman & Roson's result.

The analysis of dynamic mechanical performance figures reveals that there exists a complicated crosslinking network in the RRM composites and this structural characteristic is one of the necessities for high-impact tough polymer materials.

08.4

FOURIER TRANSFORM RAMAN STUDIES OF SEMIFLEXIBLE FLUOROCARBON CHAINS CONTAINING AN AROMATIC CORE. A. Schulte, V. Hallmark, R. Twigg, K. Song and J. F. Rabolt, IBM Research Division, Almaden Research Center, San Jose, CA 95120.

The molecular structures of a series of perfluoroalkane oligomers having two $F(CF_2)_n$ chains attached to a phenyl group in the para position have been characterized by FT and conventional Raman spectroscopy at ambient and low temperatures. From comparison with model compounds bands attributable to both the substituted phenyl ring and the perfluoroalkane chains could be assigned.

In particular, an intense low frequency vibration observed around 90 cm^{-1} has been found to undergo a 30 cm^{-1} shift to higher frequency when the temperature is lowered to -70°C . Evidence indicates that this band is attributable to a librational motion of the phenyl ring which is reduced in amplitude upon contraction of the lattice at low temperature.

In addition, Raman spectroscopy using a diamond anvil cell shows that the fluorocarbon chains containing an aromatic core exhibit different behavior than fluorinated alkanes with respect to the high pressure phase transition.

08.5

THE EFFECT OF LOW POWER AMMONIA AND NITROGEN PLASMAS ON CARBON FIBRE SURFACES. *C. Jones, National Centre for Composite Materials Research, University of Illinois, Urbana, Illinois 61801, and E. Sammann, Materials Research Laboratory, University of Illinois, Urbana, Illinois 61801 (*currently at IRC, Dept. of Physics, Liverpool University, Liverpool, England).

The effect of low power nitrogen and ammonia plasmas (<1W) on carbon fibre surfaces has been studied using XPS and SEM. A comparison is made between two PAN based fibres, a pitch based fibre, and single crystal graphite. Grazing angle techniques have been used to probe only the first 12-15 Å of the fibre surface. Plasma treatments were carried out in an *in situ* plasma treatment cell which was attached to a PHI 5400 X-ray photoelectron spectrometer. This enabled the immediate effects of the plasma to be studied before the treated surface was exposed to air. Both nitrogen and ammonia plasma treatments were successful in introducing amine functionality onto the fibre surface. Aliphatic and aromatic amine groups were detected. By comparing data collected at surface and bulk sensitive angles from the lower modulus PAN based fibres treated with an ammonia plasma, the aliphatic amines were present at a greater depth than those attached to an aromatic ring. This was not true for fibres treated with a nitrogen plasma where the ratio of aliphatic to aromatic amines remained constant. Ammonia plasmas also proved successful in removing all the oxygen containing species from the fibre surface. The higher modulus PAN based fibres were less prone to attack by these plasmas. By biasing the sample to a negative potential the number of amine groups increased dramatically and the chemistry of the surface became similar to that of the treated lower modulus fibres. Pitch based fibres were less reluctant to react. Increasing the biasing potential to several hundred volts did not significantly increase the number of amine groups incorporated onto the fibre surface. It was concluded that these groups adhered only to edge sites and/or defects on the fibre surface. Significant etching or pitting was not observed in SEM micrographs of these treated fibre surface even after sample biasing. Chemical change only occurred within the first few layers of the fibre and hence causing minimal damage to the fibre itself.

08.6 ABSTRACT WITHDRAWN

08.7

DETERMINATION OF PARTICLE SIZE OF A DISPERSED PHASE WITH SMALL-ANGLE X-RAY SCATTERING. Frank C. Wilson, DuPont Experimental Station, Wilmington, DE

Measures of median particle size and particle size distribution for one polymer dispersed in another have been determined from x-ray scans obtained on the ultra-high-resolution Bonse-Hart small-angle x-ray diffractometer. Correlation with electron microscopy results has been excellent. Depending upon the breadth of the distribution, particles up to about 1 micrometer in diameter have been characterized. The technique bases the analysis on the assumption of a log-normal particle-size distribution and characterizes the breadth of the distribution accordingly.

For typical samples containing particles with diameters ranging from 200 to 500 micrometers, intensity data are gathered between 0.002 and 0.16 degrees 2-theta and can be obtained in less than 30 minutes. Analysis of the data requires less than 10 minutes. The analysis assumes Rayleigh scattering from independent spheres and approximates this scattering with a Gaussian fit at low angles and an inverse 4th power fit at high angles. The matching of the modeled fit to the observed data is done with the invariant argument, $h^2 \times I(h)$. The data acquisition, reduction and presentation are all carried out on a lab-dedicated Hewlett-Packard minicomputer.

08.8

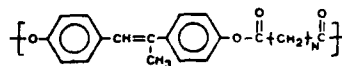
THERMAL AND RHEOLOGICAL STUDY OF A THERMOTROPIC LIQUID CRYSTALLINE POLYMER H. Fruitwala, A. L. Cimecioglu and R. A. Weiss Polymer Science Program and Dept. of Chemical Engineering, University of Connecticut, Storrs, CT 06269

A detailed study on a thermotropic copolyester based on 4,4'-dihydroxy, α - α' -dimethylbenzalazine was carried out. The soluble, nematic copolymer was enantiotropic and exhibited a relatively large mesophase range (~100 °C). Differential scanning calorimetry and thermogravimetric analysis were used to characterize the thermal transitions and thermal oxidative stability respectively. The liquid crystalline polymer has crystalline to nematic (K-N) and nematic to isotropic (N-I) transitions at ~155 °C and ~250 °C respectively. The transitions depended on the molecular weight and thermal history of the samples. Heating the polymer above the N-I transition significantly influenced the ability to form a mesophase. The complex viscosity (η^*) and the storage and loss moduli (G' and G'') were determined as a function of molecular weight using an oscillatory shear deformation. Thermal stability of the polymers was evaluated as a function of temperature and annealing time. The polymers exhibited good thermal stability up to the N-I transition (~250 °C). Prolonged annealing near or above the clearing point resulted in less than 1% weight loss, but about 10% reduction in the weight average molecular weight.

08.9

BLENDS OF POLY(STYRENE-CO-MALEIC ANHYDRIDE) WITH MAIN-CHAIN NEMATIC POLYESTERS PHASE BEHAVIOR AND MELT RHEOLOGY. J.J. Mara, R.B. Blumstein, A. Blumstein, Polymer Science Program, University of Lowell, Lowell, MA 01854, and G. Kharas, Polysar Inc., 31 Fuller St., Leominster, MA, 01453

Phase behavior and rheology under conditions of oscillatory shear were investigated for thermotropic main-chain nematic LCP's



and their blends with poly(styrene-co-maleic anhydride) (PSMA).

The following structural parameters were varied: LCP spacer length ($n=7$ and 10) and molecular mass; PSMA molecular mass and copolymer composition. Blends containing up to 30% LCP by weight were prepared from solution. Complex viscosity, loss and storage moduli were recorded in the isotropic and nematic temperature range of the LCP's. Strong negative deviations of melt viscosity relative to that of both parent polymers were observed, with a minimum occurring at low LCP concentrations (below 5% by weight). Results are interpreted in terms of LCP domain size and LCP/PSMA interactions.

SYMPOSIUM P: OPTICAL FIBER MATERIALS AND PROCESSING

P

November 27-29, 1989

Chairs

James W. Fleming
MTS/Room 6E-226
AT&T Bell Laboratories
600 Mountain Avenue
Murray Hill, NJ 07974
(201) 582-4499

George H. Sigel, Jr.
Fiber Optic Materials Research Program
Rutgers University
P.O. Box 909
Piscataway, NJ 08855-0909
(201) 932-4729

Shiro Takahashi
NTT Opto-Electronics Laboratory
NTT Corporation
Tokai-Mura, Naka-Gun
Ibaraki-Ken 319-11 Japan

Paul W. France
British Telecom Research Laboratory
Martlesham Heath Ipswich
IP5 7RE United Kingdom

Symposium Support

Air Products

Alcatel NV

AT&T Bell Laboratories

Corning Glass Works

DeSoto, Inc.

Heraeus Amersil

Johnson & Johnson

Nippon Mining Co. Ltd.

Nippon Telegraph & Telephone Corporation

Schott Fiber Optics, Inc.

Tosoh USA, Inc.

**Proceedings published as Volume 172
of the Materials Research Society
Symposium proceedings series.**

OPTICAL FIBER MATERIALS AND PROCESSING

November 27-29, 1989

SESSION P1: GENERAL FIBER PROCESSING I

Chairs: Peter C. Schultz
Monday Morning, November 27
Essex North East (W)

8:30 *P1.1
OVERVIEW OF FIBER OPTIC MATERIALS AND PROCESSING, S.R. Nagel, AT&T Technologies, Engineering Research Center, Princeton, NJ.

9:15 *P1.2
LIGHT SCATTERING STUDIES OF GAS-PHASE PARTICULATE SYNTHESIS, Alan J. Hurd, Sandia National Laboratories, Division 1152, Albuquerque, NM.

9:45 P1.3
ENTHALPY OF MIXING IN THE SYSTEM SILICA-GERMANIA: COMPARISON OF FLAME HYDROLYSIS MATERIAL TO HIGH TEMPERATURE FUSED GLASSES, P.D. Maniar and A. Navrotsky, Princeton University, Department of Geological and Geophysical Sciences, Princeton, NJ; and C.W. Draper, AT&T Technologies, Engineering Research Center, Princeton, NJ.

10:00 P1.4
MINIMUM NUMBER OF DEPOSITED LAYERS DURING PREFORM PREPARATION OF DISPERSION FLATTENED SINGLE MODE FIBERS, U. Ackerman, H. Bauch, R. Th. Kersten, U. Rutze, Schott Glaswerke, Mainz, West Germany.

10:15 BREAK

SESSION P2: GENERAL FIBER PROCESSING II

Chair: John B. MacChesney
Monday Morning, November 27
Essex North (W)

10:30 *P2.1
SOL-GEL PROCESSING FOR FIBER OPTIC APPLICATIONS, Ian M. Thomas, University of California, Lawrence Livermore National Laboratory, Livermore, CA.

11:00 P2.2
CONTINUOUS CASTING OF PARTICULATE SILICA GELS, E.M. Rabinovich, K.A. Jackson and Nonna A. Kopylov, AT&T Bell Laboratories, Murray Hill, NJ.

*Invited Paper

Short Course M-04, "Optoelectronic Materials, Processes, and Devices," may be of interest to symposium attendees. Details regarding course dates and instructors are provided in the short course section of this program.

11:15 P2.3
FLUID DYNAMICS INSTABILITIES IN DRAWN FIBERS, Charles Thompson and Arun Mulpur, University of Lowell, Department of Electrical Engineering, Laboratory for Advanced Computation, Lowell, MA.

11:30 P2.4
THERMAL MODELING OF THE OPTICAL FIBER DRAWING PROCESS, Haris Papamichael and Ioannis N. Miaoulis, Tufts University, Mechanical Engineering Department, Medford, MA.

11:45 P2.5
ACCELERATED COOLING OF OPTICAL FIBER, C.E. Polymeropoulos, V. Sernas, and S. Kyriacou, Rutgers University, Department of Mechanical and Aerospace Engineering, Piscataway, NJ.

SESSION P3: FIBER COATINGS

Chair: Rebecca Lu
Monday Afternoon, November 27
Essex North East (W)

1:30 *P3.1
DEPOSITION OF HERMETIC CARBON COATINGS ON SILICA FIBERS, R.G. Huff, F.V. DiMarcello, A.C. Hart, Jr. and K.L. Walker, AT&T Bell Laboratories, Murray Hill, NJ.

2:00 P3.2
SURFACE TREATMENTS AND COATING MATERIALS FOR SILICA FIBERS, Albert A. Kruger, Battelle-Pacific Northwest Laboratory, Chemical Sciences, Richland, WA.

2:15 P3.3
CHEMICAL REACTION AT GLASS/LIQUID INTERFACES, Kim F. Ferris and Larry R. Pederson, Pacific Northwest Laboratories, Materials and Chemical Sciences Department, Richland, WA.

2:30 P3.4
MODEL STRUCTURE OF THE VITREOUS SILICA SURFACE, B.P. Feuston and S.H. Garofalini, Rutgers University, Department of Ceramics and Institute for Engineered Materials, Piscataway, NJ.

2:45 P3.5
AN INVESTIGATION OF OPTICAL FIBER COATING PERFORMANCE IN EMBEDDED SENSING APPLICATIONS, R.A. Haaksma and M.J. Cehelnik, Alcoa Laboratories, Surface Technology Division, Alcoa Center, PA; and M.J. Kerkhoff, Alcoa Laboratories, Equipment Development Division, Alcoa Center, PA.

3:00 P3.6
FABRICATION OF OXIDE GLASS COATED FLUORIDE GLASS OPTICAL FIBERS FOR DURABILITY AND STRENGTH IMPROVEMENT, Yasutake Ohishi, Kazuo Fujiura and Shiro Takahashi, NTT Corporation, NTT Opto-Electronics Laboratories, Ibaraki, Japan.

3:15 BREAK

SESSION P4: ENVIRONMENTAL EFFECTS

Chair: Paul France

Monday Afternoon, November 27

Essex North East (W)

3:30 *P4.1

DIFFUSION OF HYDROGEN THROUGH HERMETIC CARBON FILMS ON SILICA FIBERS, P.J. Lemaire, K.S. Kranz, K.L. Walker, R.G. Huff and F.V. DiMarcello, AT&T Bell Laboratories, Murray Hill, NJ.

4:00 P4.2

ELECTRON PARAMAGNETIC RESONANCE STUDY OF THE HERMETIC, CARBON COATED, OPTICAL FIBER, Daryl Inniss, AT&T Bell Laboratories, Murray Hill, NJ.

4:15 P4.3

MATERIALS EFFECTS ON THE RADIATION SENSITIVITY OF SINGLE MODE OPTICAL FIBERS, E.J. Friebele, C.G. Askins, M.E. Gingerich, Naval Research Laboratory, Washington, DC; S.J. Hickey, Sachs Freeman Associates, Inc., Landover, MD; M.A. Putman, University of Maryland, College Park, MD; and C.M. Shaw, New York State College of Ceramics, Alfred University, Alfred, NY.

4:30 P4.4

EFFECT OF FIBER COMPOSITION AND STRESS ON THE RADIATION SENSITIVITY OF POLARIZATION-MAINTAINING FIBERS, M.E. Gingerich, Naval Research Laboratory, Washington, DC; S.J. Hickey, C.C. Harrington, Sachs Freeman Associates, Inc., Landover, MD; E.J. Friebele, Naval Research Laboratory, Washington, DC; and J.R. Onstott, 3M Center, St. Paul, MN.

4:45 P4.5

LUMINESCENCE MEASUREMENTS OF FUSED SILICA IN THE PRESENCE OF EXCIMER LASER RADIATION, N. Kuzuu, Nippon Silica Glass Yamaguchi Company, Shin-Nanyo Plant, Yamaguchi, Japan; Y. Komatsu and M. Murahara, Tokai University, Faculty of Engineering, Kanagawa, Japan.

5:00 P4.6

PHOTOLUMINESCENCE INDUCED BY 6.4 eV PHOTONS IN HIGH PURITY SILICA, T.E. Tsai and H.B. Lin, Geo Centers Inc., Fort Washington, MD; E.J. Friebele, Naval Research Laboratory, Washington, DC.

SESSION P5: HALIDE GLASSES AND FIBERS

Chair: Martin Drexhage

Tuesday Morning, November 28

Essex North East (W)

8:30 *P5.1

SYNTHESIS AND CHARACTERIZATION OF HEAVY METAL FLUORIDE GLASSES, P.W. France, S.F. Carter, M.W. Moore and J.R. Williams, British Telecom Research Laboratories, Martlesham-Heath, Ipswich, United Kingdom.

9:00 P5.2

PROCESS ANALYSIS IN THE SYNTHESIS OF FLUOROZIRCONATE GLASSES, M. Braglia, G. Cocito, M. Ferraris and G. Parisi, CSELT, Torino, Italy.

9:15 P5.3

EFFECT OF COMPOSITIONAL VARIATIONS AND PROCESSING ON THE OPTICAL SCATTERING OF ZBLAN GLASS, A.E. Neeves, W.A. Reed, M. Chui-Sabourin and A.J. Bruce, AT&T Bell Laboratories, Murray Hill, NJ.

9:30 P5.4

ORIGIN AND ELIMINATION OF SCATTERING CENTERS IN FLUORIDE GLASSES AND FIBERS, I. Aggarwal, Naval Research Laboratory, Washington, DC; J.S. Sanghera, University of Virginia, Charlottesville, VA; B. Harbison, L. Busse and P. Pureza, Naval Research Laboratory, Washington, DC.

9:45 P5.5

FABRICATION OF AlF_3 BASED GLASS FIBERS, M.R. Shahriari, T. Iqbal, P.R. Foy and G.H. Sigel, Jr., Rutgers University, Fiber Optic Materials Research Program, Piscataway, NJ.

10:00 P5.6

THE CHARACTERIZATION OF INFRARED TRANSMITTING OPTICAL FIBERS, R.D. Driver, G.M. Leskowitz, L.E. Curtiss, D.E. Moynihan and L.B. Vacha, IRIS Fiber Optics, Acton, MA.

10:15 P5.7

DESIGN PARAMETERS FOR FLUORIDE MULTIMODE FIBERS: EFFECTS OF COATING AND BENDING ON LOSS, L.E. Busse and I.D. Aggarwal, Naval Research Laboratory, Washington, DC.

10:30 BREAK

SESSION P6: CHALCOGENIDE AND

CHALCOHALIDE GLASSES

Chair: Shiro Takahashi

Tuesday Morning, November 28

Essex North East (W)

10:45 P6.1

PREPARATION AND PROPERTIES OF SELENIUM-TELLURIUM BASED CHALCOGENIDE AND CHALCOHALIDE GLASS, M.R. Tuzzolo, D.J. McEnroe and M.G. Drexhage, Galileo Electro-Optics Corporation, Sturbridge, MA.

11:00 P6.2
STRUCTURAL PRINCIPLES IN NON-OXIDE CHALCOGENIDE GLASSES, Hellmut Eckert, David Lathrop, Mark Drake, Kelly Moran and Mike Tullius, University of California at Santa Barbara, Department of Chemistry, Goleta, CA.

11:15 P6.3
PROPERTY-COMPOSITION RELATIONSHIP OF CHALCOGENIDE GLASSES CONTAINING GERMANIUM, Jay J.L. Yi and Peter R. Strutt, The University of Connecticut, Institute of Materials Science, Storrs, CT.

11:30 P6.4
TELLURIUM HALIDE GLASS FIBER FOR TRANSMISSION IN THE 8-12 μm REGION, X.H. Zhang, G. Fonteneau, H.L. Ma, J. Lucas, Université de Rennes, Laboratoire de Chimie Minérale D, Rennes, France.

11:45 P6.5
NEW STABLE IODIDE GLASSES IN THE Cd-As-I AND Cd-As-Ge-I SYSTEMS, Jong Heo and George H. Sigel, Jr., Rutgers University, Fiber Optic Materials Research Program, Piscataway, NJ.

12:00 P6.6
STRUCTURAL STABILITY OF TELLURIUM HALIDE GLASSES, Jay J.L. Yi and Peter R. Strutt, The University of Connecticut, Institute of Materials Science, Storrs, CT.

SESSION P6: CHALCOGENIDE AND CHALCOHALIDE GLASSES

Chair: Shiro Takahashi
Tuesday Afternoon, November 28
Essex North East (W)

1:30 P6.7
LASER IRRADIATION STUDIES OF IR-TRANSMITTING CHALCO-HALIDE GLASSES, Jean-Luc Adam, Carmen Ortiz and Jesse R. Salem, IBM Almaden Res. Center, San Jose, CA; and Xiang-Hua Zhang, Université de Rennes, Rennes, France.

1:45 P6.8
MECHANICAL STRENGTH OF LOW-DIMENSION GLASS FIBERS, K.A. Cergua, E.C. Behrman, and W.C. LaCourse, New York State College of Ceramics at Alfred University, Glass Division, Alfred, NY.

SESSION P7: POLYMERS AND PLANAR WAVEGUIDES

Chair: Bolesh Skutnik
Tuesday Afternoon, November 28
Essex North East (W)

2:00 *P7.1
ADVANCE OF PLASTIC OPTICAL FIBERS, Fumio Ide, Mitsubishi Rayon Company, LTD., Research and Development Department, Tokyo, Japan; Takashi Yamamoto, Mitsubishi Rayon Company, LTD., Central Research Laboratory, Hiroshima, Japan.

2:30 P7.2
LOW-LOSS GI PLASTIC OPTICAL FIBER AND NOVEL OPTICAL POLYMERS, Yasuhiro Koike and Yasuji Ohtsuka, Keio University, Yokohama, Japan.

2:45 *P7.3
SILICA-BASED SINGLE-MODE WAVEGUIDES AND THEIR APPLICATIONS TO INTEGRATED-OPTIC DEVICES, N. Takato and A. Sugita, NTT Corporation, NTT Opto-Electronics Laboratories, Ibaraki, Japan.

3:15 P7.4
POTENTIAL APPLICATION OF Bi(Pb)-Ca-Sr-Cu-O GLASSES FOR PREPARATION OF INTEGRATED OPTICAL FIBERS, Haixing Zheng and J.D. Mackenzie, University of California-Los Angeles, Department of Materials Science and Engineering, Los Angeles, CA.

3:30 BREAK

SESSION P8: CRYSTALLINE MATERIALS

Chair: Moni Saifi
Tuesday Afternoon, November 28
Essex North East (W)

3:45 P8.1
GROWTH OF OPTICAL QUALITY SAPPHIRE SINGLE CRYSTAL FIBERS, D.H. Jundt, M.M. Fejer and R.L. Byer, Stanford University, Applied Physics Department, Stanford, CA.

4:00 P8.2
THE GROWTH AND CHARACTERIZATION OF TUNGSTEN BRONZE STRONTIUM BARIUM NIOBATE SINGLE CRYSTAL FIBERS, Joyce Yamamoto and Amar Bhalla, Pennsylvania State University, Materials Research Laboratory, University Park, PA.

4:15 P8.3
PROTON EFFECTS IN KTiOPO_4 , P.A. Morris, M.K. Crawford, M.G. Roelofs and J.D. Bierlein, E. I. duPont de Nemours & Co., Inc., Experimental Station, Wilmington, DE; and G. Gashurov, Airtron, Litton Systems, Inc., Morris Plains, NJ.

4:30 P8.4

EXTENDED X-RAY ABSORPTION FINE STRUCTURE STUDY OF KNBO_3 , K.H. Kim, W.T. Elam and E.F. Skelton, Naval Research Laboratory, Washington, DC.

4:45 P8.5

ANALYSIS OF THERMAL VARIATION OF LENGTH AND REFRACTIVE INDEX OF LEAD FLUORIDE TO STUDY ITS OPTICAL PROPERTIES, Tarlok S. Aurora, Philadelphia College of Pharmacy and Science, Department of Math and Physics, Philadelphia, PA; Donald O. Pederson, University of Arkansas, Department of Physics, Fayetteville, AR; Stephen M. Day, Miami University, Oxford, OH.

SESSION 9: RARE EARTH DOPED GLASSES

Chair: E. Snitzer

Wednesday Morning, November 29

Essex North East (W)

8:30 *P9.1

MATERIALS AND PROCESSING REQUIREMENTS FOR EFFICIENT FIBER OPTIC NONLINEAR DEVICES, R.H. Stolen, AT&T Bell Laboratories, Holmdel, NJ.

9:00 P9.2

CONCENTRATION AND DISTRIBUTION OF Er AND Al IN SILICA-BASED FIBERS, D.W. Oblas, T. Wei, W.J. Miniscalco and B.T. Hall, GTE Laboratories, Incorporated, Waltham, MA.

9:15 P9.3

APPLICATION-SPECIFIC OPTICAL FIBRES MANUFACTURED FROM MULTICOMPONENT GLASSES, E.R. Taylor, M. Tachibana, J. Wang and D.N. Payne, University of Southampton, Optical Fibre Group, Department of Electronics and Computer Science, Southampton, United Kingdom.

9:30 P9.4

GLASSES FOR Er^{3+} -DOPED FIBER LASERS AND OPTICAL AMPLIFIERS, W.J. Miniscalco, L.J. Andrews, S. Zemon, B.T. Hall, T. Wei and R.C. Folweiler, GTE Laboratories Incorporated, Waltham, MA.

9:45 P9.5

EXCITED STATE CROSS SECTIONS FOR Er-DOPED GLASSES, S. Zemon, G. Lambert, W.J. Miniscalco, L.J. Andrews and B.T. Hall, GTE Laboratories Incorporated, Waltham, MA.

10:00 BREAK

10:15 *P9.6

RARE EARTH DOPED FIBERS, Elias Snitzer, Rutgers University, Fiber Optic Materials Research Program, Piscataway, NJ.

10:45 P9.7

INFRARED SPECTROSCOPY OF PROTONS IN KTiPO_4 , M.K. Crawford, P.A. Morris, M. Roelofs, E.I. duPont de Nemours & Co., Inc., Experimental Station, Wilmington, DE; and G. Gashurov, Airtron, Litton Systems, Inc., Morris Plains, NJ.

11:00 P9.8

OPTICAL ABSORPTION AND EMISSION IN RARE EARTH DOPED HEAVY METAL FLUORIDE GLASSES, R. Pafchek, E. Snitzer and G.H. Sigel Jr., Rutgers University, Fiber Optic Materials Research Program, Piscataway, NJ.

P1.1 ABSTRACT NOT AVAILABLE
P1.2

LIGHT SCATTERING STUDIES OF GAS-PHASE PARTICLE SYNTHESIS.
Alan J. Hurd, Division 1152, Sandia National Laboratories,
Albuquerque, NM 87185-5800

Although gas-phase reactions for the synthesis of glass and ceramic precursor particles offer many advantages, such as high purity and chemical nonspecificity, their products are difficult to assess in situ. Here experiments employing static and dynamic light scattering for two different systems, flame and plasma reactors, are discussed from the view of obtaining particle size and structure as a function of in situ position. With static light scattering, the conditions for probing particles' internal structure can often be met, as well as for a model-independent measure of size. Aerodynamic size and, in some cases, absolute mass can be obtained from dynamic light scattering; when combined with complementary (ex situ) data from small-angle x-ray or neutron scattering, a fairly complete picture of particle morphology can be constructed. Interpretation of selected results will be made by appealing to physical growth models.

This work was performed in collaboration with William L. Flower, Dale W. Schaefer, and Pauline Ho and was supported by Sandia National Laboratories under Department of Energy Contract No. DE-AC04-76-DP00789.

P1.3

ENTHALPY OF MIXING IN THE SYSTEM SILICA-GERMANIA:
COMPARISON OF FLAME HYDROLYSIS MATERIAL TO HIGH
TEMPERATURE FUSED GLASSES. P. D. Maniar, A. Navrotsky,
Department of Geological and Geophysical Sciences, Princeton
University, Princeton, NJ 08544; and C.W. Draper, AT&T,
Engineering Research Center, Princeton, N.J. 08540.

Germania doped silica glasses are of utmost importance as fiber optic material. We investigated the energetics of germania doped silica prepared by flame hydrolysis at 800 °C to understand the relation between structure and energetics and its dependence on preparation conditions. This was done by studying: 1) conventional high temperature fused glasses 2) untreated amorphous products of flame hydrolysis and 3) flame hydrolysis sample annealed to glass without melting.

Heats of solution, at 700 °C in molten lead borate, of fused silica-germania glasses, containing 0, 23, 26, 45, 74 and 100 mole percent germania, show ideal heats of mixing between the endmembers. This indicates that the fused glasses behave in a simple manner, with ideal substitution of Ge for Si in a tetrahedral framework. Flame hydrolysis samples (untreated and equivalent glasses) containing 0, 3, 23 and 26 mole percent germania have heats of solution that also plot on this ideal mixing line. This suggests that the flame hydrolysis material and annealed glasses are energetically very similar to their bulk-melted counterparts. This insensitivity of energetics to preparation conditions is consistent with our previous studies on silica prepared at various temperatures. It also suggests that short range order on the scale of nearest and next nearest neighbour dominates the energetics.

P1.4

MINIMUM NUMBER OF DEPOSITED LAYERS DURING PREFORM
PREPARATION OF DISPERSION FLATTENED SINGLE MODE
FIBERS. U. Ackerman, H. Bauch, R. Th. Kersten, U.
Rutze, Schott Glaswerke, W. Germany, 6500 Mainz,
Hattenbergstr. 10

The low pressure plasma-impulse-CVD process (1) is used for preparing dispersion flattened single mode (DFSM) fibers. In contrast to other fiber manufacturing processes, PICVD allows preparation of continuously designed refractive index profiles. Dispersion of less than 3.5ps/(nm km) between 1.25um and 1.6um was achieved. Zero dispersions of this profile are at 1.31um and 1.54um (2). In this paper the minimum number of layers necessary for preparation of such a continuously shaped refractive index is discussed.

(1) H. Bauch et al., Conf. Proc. SPIE 1985, Cannes, Vol. 584, 33 (1986)

(2) U. Fotheringham, Glotech. Ber. 62, 52 (1989)

P2.1

SOL-GEL PROCESSING FOR FIBER OPTIC APPLICATIONS*.
Ian M. Thomas, University of California, Lawrence
Livermore National Laboratory, P.O. Box 5508, L-490,
Livermore, CA.

The sol-gel process normally uses metal organic starting materials to prepare metal oxide products. Single or mixed oxides can be prepared and these can be in the form of bulk materials, coatings or fibers. The process has been the subject of investigations for many years, the amount of published material is increasing at an accelerating rate, and there has been some commercialization.

In the first part of the talk I will describe the sol-gel process in general with particular emphasis on its advantages and disadvantages over the more conventional procedures. In the second part I will concentrate on the preparation of optical fibers by this method and address the progress that has been made and the problems that have been encountered.

*Work performed under the auspices of the U.S. Department of Energy by Lawrence Livermore National Laboratory under Contract No. W-7405-ENG-48.

P2.2

CONTINUOUS CASTING OF PARTICULATE SILICA GELS.
E.M. Rabinovich, K.A. Jackson, and Nonna A.
Kopylov, AT&T Bell Laboratories, Murray Hill,
N.J.

Particulate silica gels have been used to prepare glass articles significantly larger than those made by the alkoxide process unless an autoclave is used. Usually the sols are cast in stoppered molds and pushed out from the mold after gelation. This is a slow process, and so we have carried out a study into the feasibility of transforming the batch process into a continuous process. In our process, the sol is pumped from a reservoir by a large metering pump, while the gelling agent is added by a smaller pump and admixed. The sol is delivered into a cylindrical mold where it gels while moving through the mold, either with or without heating. The activation energy for the gelation process was determined to be about 40 KJ/mol.

P2.3

Fluid Dynamics Instabilities in Drawn Fibers. Charles Thompson and Arum Mulpur Department of Electrical Engineering, Laboratory for Advanced Computation University of Lowell, Lowell, MA

The stability analysis of the equations governing drawn liquid fibers will be presented. Particular attention is given to the interaction between the winder and the fluid's motion. It will be shown that the terminal conditions presented by the winder assembly can influence both the spatial uniformity and growth rate of infinitesimal disturbances. The non-linear evolution of such disturbances will also be addressed and results presented. Preliminary results show that the nonlinear effect result in a supercritical bifurcation from the neutral stability point. Non-Newtonian models will also be considered.

[Work supported by Analog Devices Professorship]

P2.4

THERMAL MODELING OF THE OPTICAL FIBER DRAWING PROCESS.
Haris Papamichael and Ioannis N. Miaoulis*, Mechanical Engineering Department, Tufts University, Medford, MA 02155.

The fabrication process of glass optical fibers has been the subject of investigations through the years. These investigations were motivated by the need to improve the quality and increase the yield of optical fibers and optical multifiber systems. Although some studies have been performed in the area of thermal analysis of the fiber fabrication process, they usually focus on a specific, narrow range of parameters. The majority of the studies are performed for thin single (unsheathed) fibers (<0.2 mm). Very limited work has been done on modelling the thermal processing of thick fibers (>0.2 mm), and sheathed (core and clad) fibers, and most of the fabrication processes are performed on a costly trial and error basis. This paper presents a tool that we developed which the fiber fabrication community can use to predict the thermal behaviour of thin single, thick single, and core and clad fibers during processing. The thin fiber case was treated analytically and was treated as a fin. The variable convection transfer coefficient was calculated by the Karman-Pohlhausen technique. The study treated the air and glass properties as independent of temperature and separately as a function of temperature and results are compared with experimental findings. For the thick and core and clad fibers, where the one-dimensional treatment usually used for thin fibers does not apply, a finite difference technique was used for the numerical modeling of the processes. The results are presented in graphical form where the convective coefficients and temperature distributions are presented as a function of distance of the fiber from the furnace, for a wide range of diameters and drawing speeds. Comparison with experiments indicated close agreement.

P2.5

ACCELERATED COOLING OF OPTICAL FIBER. C. E. Polymenopoulos, V. Sernas, and S. Kyriacou, Dept. of Mechanical and Aerospace Engineering, Rutgers University, Piscataway, N. J. 08855.

An apparatus for accelerated cooling of optical fiber has been designed and tested using a 150 μ m diameter fiber drawn at speeds of up to 3 m/sec with Helium or Nitrogen as the cooling medium. Cooling was accomplished by passing the fiber through a 0.5 m long and 4 mm diameter water cooled tube, with the fiber moving in a direction opposite to the gas flow. To assure minimum cooling gas leakage from the cooling section the upstream gas plenum was kept at near atmospheric pressure, while the downstream plenum was at vacuum pressure. Gas flow rate was set using the measured pressure difference between the gas inlet and outlet. Using Helium and with the fiber moving at the maximum speed of 3 m/sec a mean cooling rate of approximately 5,000 $^{\circ}$ C/sec was measured within the cooling section which was positioned at a distance of 0.55 meters from the graphite furnace. The required gas flow rate was approximately 70 l/min resulting in a Reynolds number of approximately 2,400 based on the hydraulic diameter. Higher cooling rates can be achieved if the gas flow is increased, or if the tube wall temperature is reduced by refrigeration.

Analytical prediction of the fiber temperature using a finite difference solution of the conservation equations was in good

agreement with the experimental results. For the conditions tested the maximum local heat transfer coefficient was approximately 1,700 W/m^2 $^{\circ}$ C based on the local fiber and gas bulk temperatures. Additional computed results yielded the ratio of energy transfer to the gas and to the tube walls.

P3.1

DEPOSITION OF HERMETIC CARBON COATINGS ON SILICA FIBERS. R.G. Huff, F.V. DiMarcello, A.C. Hart, Jr., and K.L. Walker, AT&T Bell Laboratories, 600 Mountain Avenue, Murray Hill, NJ 07974

Carbon coated optical fibers have recently been shown to have excellent resistance to both static fatigue and hydrogen induced losses (1,2,3). The deposition technique used to form the carbon coating strongly affects the coating's ability to resist these degradation mechanisms. The system developed by AT&T utilizes an atmospheric CVD chamber in which a hydrocarbon gas is pyrolyzed on the fiber surface. The heat retained in the fiber from the fiber forming process is used to drive the reaction, and high draw speeds are typically used to attain the $\sim 900^{\circ}$ C temperature required to deposit the hermetic form of the carbon coating. Deposition rates of $\sim 1 \mu m$ m/sec are required to produce the ~ 500 \AA coating.

- 1) R.G. Huff, F.V. DiMarcello, A.C. Hart, Jr., "Amorphous Carbon Hermetically Coated Optical Fibers", Technical Digest, OFC 1989, paper TUG2.
- 2) K.E. Lu, M.T. Lee, D.R. Powers, S. Glaseman, "Hermetically Coated Optical Fibers", Technical Digest, Postdeadline Paper PD1, OFC 1989.
- 3) P.J. Lemaire, K.S. Kranz, K.L. Walker, R.G. Huff and F.V. DiMarcello, "Hydrogen Permeation in Optical Fibers with Hermetic Carbon Coatings", Electronic Letters, Vol. 24, No. 21, Pgs. 1323-1324, October 13, 1988.

P3.2

SURFACE TREATMENTS AND COATING MATERIALS FOR SILICA FIBERS. Albert A. Kruger, Pacific Northwest Laboratory^(a), Chemical Sciences, Richland, Washington 99352-0999

Following chemical treatment of the glass surface, application of a novel UV curable acrylic pre-polymer and subsequent polymerization yield strong fibers. This surface chemistry does not form a barrier or impermeable layer; rather, site-specific reactions giving rise to changes in the chemical reactivity of the surface. The initial tensile strength and resistance to aging of the silica fibers vary greatly with the treatment. Both static and dynamic fatigue experiments indicate significant modification of the aging process. Further, it is apparent that the Griffith flaw model is not applicable.

The polymer overcoat has good abrasion resistance, tear strength, low water vapor transmission rates, and adds no more than 5 dB/km of excess loss at -80° C.

P3.3

CHEMICAL REACTION AT GLASS/LIQUID INTERFACES.

Kim F. Ferris and Larry R. Pederson, Pacific Northwest Laboratories, Richland, WA 99352

Although the aqueous durability of ceramic materials and its relation with surface properties has been the subject of numerous studies, the basic processes at the reaction interface are still poorly understood. Dielectric effects from both the solid and solution phases can play a major role on reaction rates, while electric surface

charge phenomena can affect reaction rates through modifications in the local chemical environment. The electric surface charge on glasses can be varied through changes in solution ionic strength or by using organic/water mixtures as measured by pH-stat techniques. By using a silicic acid 'point charge' complex in the lattice sites surrounding silicic acid, a first order approximation can be made to the solid state dielectric effects. Combined with molecular spectroscopic data, such information can generate a molecular interpretation of initial surface structure and its evolution in reactive environments.

This work was supported by the U.S. Department of Energy, Office of Basic Energy Sciences under contract DE-AC06-76RLO 1830.

P3.4

MODEL STRUCTURE OF THE VITREOUS SILICA SURFACE*
B. P. Feuston and S. H. Garofalini, Dept. of Ceramics and Institute for Engineered Materials, Rutgers University, Piscataway, NJ 08855-0909

The surface structure of vitreous silica is investigated through molecular dynamics simulation. Comparison of the structure prior to fracture and after fracture and annealing allows identification of topological and bonding defect in the surface region. Identification of defects and their location are presented. Non-bridging oxygen (NBO) and edge-sharing tetrahedra are found to form on the oxygen terminated surface with 3-coordinated silica, 3-coordinated oxygen and 3-member rings just below the outermost atoms. An association between 3-membered rings and 3-coordinated oxygen is observed and its possible relationship to the Raman DZ defect peak will be discussed.

*Supported by Army Research Office, Grant No. DAAL03-86-K-0047

P3.5

AN INVESTIGATION OF OPTICAL FIBER COATING PERFORMANCE IN EMBEDDED SENSING APPLICATIONS.
R. A. Haaksma, M. J. Cehelnik and M. J. Kerkhoff, Alcoa Laboratories, Alcoa Center, PA, 15069.

The use of composite materials for aerospace applications has created an increasing need for developing nondestructive methods for assessment of composite performance. Embedded optical fiber sensor technology provides the potential for monitoring parameters of interest during processing and testing of composite materials as well as the opportunity for tracking properties over the lifetime of composite parts in service. The successful development of this technology depends on designing optical fiber sensor systems suitable for use in composite embedded sensing applications.

This paper focuses on the role played by optical fiber coatings in the design of embedded sensor systems. The performance of different optical fiber coatings under typical composite processing conditions will be discussed. Photomicrographs of test specimens containing embedded sensors will be presented which show delamination occurring at the coating/optical fiber interface in preference to the coating/epoxy resin interface. Based on this work, coating performance criteria will be outlined for use in the selection of appropriate fiber optic sensors for certain target applications in composites.

P3.6

FABRICATION OF OXIDE GLASS COATED FLUORIDE GLASS OPTICAL FIBERS FOR DURABILITY AND STRENGTH IMPROVEMENT, Yasutake Ohishi, Kazuo Fujiura and Shiro Takahashi, NTT Opto-Electronics Laboratories,

Tokai-Mura, Naka-Gun, Ibaraki-Ken, 319-11 Japan

Durability and mechanical strength of fluoride glass optical fibers are intrinsically inferior to those of silica and other oxide glass fibers. Many attempts to improve the properties of fluoride glass optical fibers have been made. However, effective techniques have not yet been developed.

It is expected that the improvement of durability and mechanical strength are attained by being coated with the oxide glasses. There are some oxide glasses whose thermal properties are matched to those of fluoride glasses.

Oxide glass coating is performed by jacketing fluoride preforms with oxide tubes. It is clarified by the thermal analyses that chemical reaction between fluoride and oxide glasses does not occur in the fiber drawing temperature range and begin to occur rapidly at the melting temperature of fluoride glasses. Using a lead oxide-based glass tube, smooth contact between fluoride and oxide glasses are confirmed.

P4.1

DIFFUSION OF HYDROGEN THROUGH HERMETIC CARBON FILMS ON SILICA FIBERS, P.J. Lemaire, K.S. Kranz, K.L. Walker, R.G. Huff, and F.V. DiMarcello, AT&T Bell Laboratories, 600 Mountain Avenue, Murray Hill, NJ, 07974.

Silica based optical fibers have been drawn with hermetic carbon coatings. These coatings are used to protect the silica portion of the fiber from undesirable loss increases and strength reductions caused by H_2 and H_2O , respectively. The hermetic properties of the carbon films have been evaluated using accelerated test conditions where the coated fibers were exposed to H_2 at elevated temperatures and hydrogen pressures. In-situ spectral loss monitoring has allowed us to measure changes in the characteristic optical loss features caused by either molecular H_2 or by species such as OH which form when hydrogen reacts with defects in the silica. By using long lengths of fiber it is thus possible to optically measure the extremely small amounts of hydrogen that penetrate the carbon films. At temperatures in the range of 100 to 145°C the diffusion of H_2 is readily modeled using classical diffusion theories for a composite cylinder, allowing calculation of the diffusion coefficient and of the solubility for H_2 in the carbon. At higher temperatures the diffusing H_2 is partially depleted by reaction with defects in the glass. For these conditions the inward diffusion of the H_2 and its reaction at defect sites tend to balance each other, giving rise to a constant, but extremely low, concentration of H_2 in the fiber.

P4.2

ELECTRON PARAMAGNETIC RESONANCE STUDY OF THE HERMETIC, CARBON COATED, OPTICAL FIBER. Daryl Inniss, AT&T Bell Laboratories, Murray Hill N.J.

Recently, a thin carbon film deposited on the surface of silica optical fibers has been shown to improve the fiber's resistance to static fatigue and hydrogen permeation. The carbon film is characterized by electron paramagnetic resonance spectroscopy. A single symmetrical resonance is observed, centered at the g value of 2.002. The lineshape is Lorentzian, suggesting spin delocalization. Intensity measurements ranging from 4K - 800K suggest that both conduction electrons and localized spin centers contribute to

the spin resonance. The localized spin centers may arise from point defects in the carbon film. The results are discussed in terms of specific structural models for the defects.

P4.3

MATERIALS EFFECTS ON THE RADIATION SENSITIVITY OF SINGLE MODE OPTICAL FIBERS, E.J. Friebele, C.G. Askins, M.E. Gingerich, S.J. Hickey*, M.A. Putnam**, C.M. Shaw***, Naval Research Laboratory, Washington, DC 20375 and W.H. Schmidt, Michigan State University, E. Lansing, MI 48824 (*Sachs Freeman Assoc., Inc., Landover, MD; **University of Maryland, College Park, MD; ***NYS College of Ceramics, Alfred University, Alfred, NY)

We have previously fabricated and irradiated a number of single mode fibers to a total dos of 2000 rads at -35C and fit the resultant recovery data to n^{th} -order kinetics (1). The "permanent" incremental loss determined from these data was used as a measure of the loss that would be induced by low dose rate fallout environments. Similar measurements have now been performed over a wide temperature range, and it has been found that the temperature dependence of the recovery parameters is determined by the composition of the core and cladding. Single mode fiber radiation response depends on fabrication parameters as well as dopant concentrations. The relationships between fabrication and kinetic parameters have been established through 3 techniques: orthogonal matrix analysis, multiple regression and multivariate analysis. A new experimental design to elucidate both one-way and two-way interactions between fabrication parameters and radiation response with good statistical significance and without confounding will be described.

(1) C.G. Askins, C.M. Shaw, T.e. Tsai, C.C. Harrington, M.E. Gingerich and E.J. Friebele, SPIE Vol. 992, pp. 74-83 (1988).

P4.4

EFFECT OF FIBER COMPOSITION AND STRESS ON THE RADIATION SENSITIVITY OF POLARIZATION-MAINTAINING FIBERS, M.E. Gingerich, S.J. Hickey*, C.C. Harrington* and E.J. Friebele, Naval Research Laboratory, Washington, DC 20375 and J.R. Onstott, 3M Center, St. Paul, MN 55144 (*Sachs Freeman Assoc., Inc., Landover, MD)

The radiation sensitivity of birefringent polarization-maintaining fibers has been shown to depend on the level of asymmetric stress applied to the Ge-doped silica core. (1) An implication of this result is that differential radiation-induced attenuation should be experienced along the two polarization axes. Measurements of the differential attenuation have been made during and after steady state ^{60}Co irradiations and following pulsed electron exposure to investigate this effect. The observed attenuation and the effect of the radiation exposures on the coupling between the two polarizations will be discussed. In addition, the radiation response of a new design of polarization-maintaining fibers, consisting of a very lightly Ge-doped silica core and depressed F-doped silica clad has been measured as a function of stress level. The effect of variations in the core composition and stress on the radiation sensitivity will be reported.

(1) E.J. Friebele, L.A. Brambani, M.E. Gingerich, S.J. Hickey and J.R. Onstott, submitted to Appl. Opt.

P4.5

LUMINESCENCE MEASUREMENTS OF FUSED SILICA IN THE PRESENCE OF EXCIMER LASER RADIATION
N.Kuzuu, Nippon Silica Glass Yamaguchi Co., Shin Nanyo, Yamaguchi 746, JAPAN.; Y.komatsu, Graduate student of Faculty Eng. Tokai Univ.; M.Murahara, Faculty of Eng. Tokai Univ. 1117 Kitakaname, Hiratsuka, Kanagawa 259-12, JAPAN.

Fused silica which were formed in the hydrogen-oxygen flame hydrolysis of SiCl_4 has absorption bands in the near-IR region but it can possess high optical transmission in the UV region. Thus this material could be used as a core for UV transmitting optical fiber. It has been observed that some samples of fused silica have structural defects that cause luminescence and thus absorption in this UV region.

We report on the luminescence behavior of the fused silica which has been irradiated by ArF excimer lasers. In this measurements, the emission spectrum of wide range were measured momentarily by diode array with image intensifier.

Irradiating with the ArF laser, it was seen that the intensity of luminescence at 650 nm varies inversely to the intensity of luminescence at 300 nm in different samples. A sample appearing no luminescence at 650 nm appears luminescence at 280 nm in place of at 300 nm. These two luminescence have different dependencies of intensity v.s. radiation time. From these results we conclude that luminescence at 650 and 300 nm are related with same origin, whereas the luminescence at 280 nm is caused by different origin from those two luminescence.

P4.6

PHOTOLUMINESCENCE INDUCED BY 6.4 eV PHOTONS IN HIGH PURITY SILICA, T.E. Tsai, H.B. Lin, GeoCenters, Inc., Fort Washington, MD 20744, E.J. Friebele, Naval Research Laboratory, Washington, DC 20375

Steady state photoluminescence in the visible range in high purity silica rods of suprasil at room temperature was studied using 6.4eV ($\lambda = 193\text{nm}$) photons as the excitation source. Electron spin resonance was used to monitor the induced paramagnetic centers. Broad luminescence bands at 2.8eV, 2.2eV and 1.9eV were observed. The relative intensities of these bands were altered by bringing the light to a focus inside the sample. Relative photoluminescence intensity was also studied as a function of laser pulse energy and irradiation time. For laser fluences up to 3000 J/cm², the intensity of 1.9eV band increases but that of 2.8eV band remains approximately the same. The growth of paramagnetic NBOHC centers was found to be correlated with that of 1.9eV band. These results will be discussed in relation to the radiolytic mechanism for defect generation in silica.

P5.1 ABSTRACT NOT AVAILABLE

P5.2

PROCESS ANALYSIS IN THE SYNTHESIS OF FLUOROZIRCONATE GLASSES, M. Braglia, G. Cocito, M. Ferraris and G. Parisi, CSELT, Torino, Italy

The synthesis process of high quality fluorozirconate glasses for infrared optical fibres is far away from optimization: the presence in glasses of OH groups, oxides and oxyfluorides causes high losses, strong crystallizations and unacceptable scattering values. (1,2)

During a glass synthesis process under nitrogen flow, IR spectroscopy and x-ray diffraction analyses on sever starting fluoride mixtures of ZBLAN composition

with 20-10-5-5% (weight) ammonium bifluoride, have been carried out. IR analysis reveal the presence of oxyfluoride and oxide species before melting, especially on samples without ammonium bifluoride, under inert atmosphere.

The glass quality has been improved by the addition of nitrogen trifluoride as reactive atmosphere during melting: IR spectra show a strong decrease of OH absorption in glasses prepared with 5-10-20% (weight) ammonium bifluoride. Electron spin resonance measurements (EPR) on gamma-irradiated glasses (5 Mrad) show the presence of the o_2^- signal, related with the presence of oxyfluorides or oxides. (3)

IR, XRD and EPR measurements on fluoride mixtures and the obtained glasses allow a strict control on the preparation process: this is important in the choice of times, temperatures and fluorinating agents for the improvement of the glass quality. Work is in progress in order to investigate other gaseous fluorinating agents. (4)

1. P.W. France, S.F. Carter, M.W. Moore, C.R. Day - Br. Telecom Technol. J. 5, 2 (1987) P.28
2. M. Braglia, M. Ferraris, G. Grego, G. Parisi, F. Taiariol Mat. Res. Bull 24, 6 (1989)
3. D.L. Griscom, P. Hart, J.M. Jewell, J.R. Shelby - J. of Non-Cryst. Sol. 103 (1988) p. 300
4. M.M. Broer, R.M. Atkins - J. Mater. Res. 3, 4 (1988) p. 755

P5.3

EFFECT OF COMPOSITIONAL VARIATIONS AND PROCESSING ON THE OPTICAL SCATTERING OF ZBLAN GLASS. A.E. Nerves, W. A. Reed, M. Chui-Sabourin and A. J. Bruce, AT&T Bell Laboratories, Murray Hill, NJ.

Molecular light scattering in the Mie and Rayleigh regime has been measured as a function of scattering angle at wavelengths between 0.6 and 2.6 μm on bulk samples of ZBLAN glasses. The effect of oxide and p-block additions as well as the effect of processing variations on the scattering have been measured. From an analysis of the angular scattering of both vertically and horizontally polarized beams the Rayleigh ratios, dysmetry and depolarization factors are determined as a function of wavelength. The average size of the scattering sites can be estimated in the range of 0.02 and 2.0 μm .

P5.4

Origin and Elimination of Scattering Centers in Fluoride Glasses and Fibers. I. Aggarwal, J. S. Sanghera*, B. Harbison, L. Busse and P. Pura, Naval Research Laboratory, Washington, D.C. 20375, *University of Virginia, Charlottesville, VA 22901

Fluorozirconate glasses are candidate materials for ultra-low loss optical fiber applications by virtue of their extremely low losses predicted in the mid-IR. In practice, the losses fall far short of the theoretically predicted value. This has been primarily attributed to both extrinsic absorption and scattering. While significant improvements have been made in reducing the absorption losses, the scattering losses still remain quite high. Although scattering losses on short lengths of fibers have given values as low as 0.025 dB/km at 2.35 μm , the losses on longer lengths exhibit Mie or wavelength independent behavior. The following paper/talk will describe both the nature and the origin of these scattering species. Based on this knowledge, the authors subsequently describe ways to eliminate the scattering centers.

P5.5

FABRICATION OF AlF_3 BASED GLASS FIBERS. M.R. Shahriari, T. Iqbal, P.R. Foy and G.H. Sigel, Jr., Rutgers University, Fiber Optic Material Research Program, Piscataway, NJ.

Several glass systems based on AlF_3 have been synthesized and fabricated into preforms by controlled melting and rotational casting or rod-in-tube techniques. High optical quality preforms have then been drawn into fibers using a specially modified drawing facility. The drawing tower is enclosed with a vertical glove box in which the levels of both moisture and oxygen are kept below 1 ppm during the drawing. The AlF_3 based glass fibers have shown dramatically superior chemical durability relative to the ZrF_4 based glass fibers. Selected optical, mechanical and thermal properties of these fibers will be presented. AlF_3 based glass fibers offer interesting opportunities for short range applications in the 2-4 micron region of the infrared such as sensing, remote spectroscopy and laser power delivery.

P5.6

THE CHARACTERIZATION OF INFRARED TRANSMITTING OPTICAL FIBERS. R.D. Driver, G.M. Leskowitz, L.E. Curtiss, D.E. Moynihan and L.B. Vacha, IRIS Fiber Optics, 40 Nagog Park, Acton, MA 01720

The authors will review the methods used to characterize infrared transmitting optical fibers. Emphasis will be placed on identifying potential sources of systematic error in fiber characterization measurements. Data will be presented on fiber strength for heavy metal fluoride and chalcogenide fibers. The methodology of fiber loss measurements will be discussed. The use of FTIR spectroscopic techniques for the measurement of fiber loss will be reviewed. Data will be presented for heavy metal fluoride, chalcogenide, sapphire and silver halide fibers. Fiber and preparation and fiber cleaving techniques will be reviewed. Data will be presented on the effects of fiber mode structure on fiber loss measurements. The competing processes of optical loss in fiber core, cladding and fiber buffer will be discussed.

P5.7

DESIGN PARAMETERS FOR FLUORIDE MULTIMODE FIBERS: EFFECTS OF COATING AND BENDING ON LOSS, L.E. Busse and I.D. Aggarwal, Naval Research Laboratory, Washington, DC

The potential for very long length repeaterless communications networks exists through the use of fluoride optical fibers, with minimum intrinsic loss predicted to be 0.01dB/km at 2.5 μm . Although in principle these fibers must be single mode, in practice fibers currently being made are multimode, due to their relative ease for fabrication. Loss effects due to coatings and bending in multimode fluoride fibers have not been addressed in the literature. In this paper it will be shown that due to the longer wavelength for fluoride vs. silica fibers, design parameters for step index fluoride fibers must be chosen carefully to avoid substantial induced loss due to typical UV polymer coatings and macrobending.

Numerical calculations for fluoride step index fiber structures have been made of these induced losses. Assuming a vacuum wavelength of 2.5 μm , ratios of clad/core diameters for > 90% of the modes suffering loss < 0.01dB/km were determined for various numerical apertures and core diameters. In addition, total induced losses were calculated assuming various made distributions in the fiber. It will be shown that large values of V, the normalized frequency, are needed to reduce such losses. Results of calculations of a minimum tolerable bend radius for a loss of < 10% of the total number of modes suggest that a large numerical aperture rather than core radius is generally preferable to achieve large values of V.

P6.1

PREPARATION AND PROPERTIES OF SELENIUM-TELLURIUM BASED CHALCOGENIDE AND CHALCOHALIDE GLASS, M.R. Tuzzolo, D.J. McEnroe and M.G. Drexhage, Galileo Electro-Optics Corporation, Galileo Park, PO Box 550, Sturbridge, MA 01566

Mid IR wavelengths are a spectral region which is significant for military, medical and industrial applications. Materials useful for IR transmission require low intrinsic and extrinsic attenuations, chemical durability and resistance to devitrification.

Chalcogenide glasses transmit infrared energy in the 2 to 14 micron wavelength region. Addition of tellurium to selenium based glasses produces lower attenuations at longer wavelengths due to a shift in the multiphonon edge. However, with increased tellurium content, lower transition temperatures and decreased stability often result. Addition of halogens to chalcogenides (chalcohalides) utilizes a steep exponential multiphonon edge to produce a low loss material at longer wavelengths. Iodine containing chalcohalides have been shown to be resistant to devitrification and show tailorable transition ranges.

Selenium-tellurium chalcogenide and iodine containing chalcohalide glasses were investigated for remote FTIR and low loss applications. Raw material pre-treatment techniques were employed that enable us to produce high purity glasses. Bulk glasses were characterized to determine which compositions provide the best properties, as required in today's commercial market. These measurements will be analyzed and the effects of pre-treatment, melting techniques and compositions will be discussed.

P6.2

STRUCTURAL PRINCIPLES IN NON-OXIDE CHALCOGENIDE GLASSES. Hellmut Eckert, David Lathrop, Mark Drake, Kelly Moran, and Mike Tullius, Department of Chemistry, University of California at Santa Barbara, Goleta, CA 93106.

Non-oxide chalcogenide glasses hold great promise for optical waveguide applications in the infrared region. Despite the significance of these systems, their structural organization is little understood to date. The various models used to describe the principles of glass-formation in non-oxide systems have often been conceptually divergent and sometimes contradictory for individual systems. In this contribution, we will present results from a first systematic effort to provide structural information for chalcogenide glasses by means of modern, state of the art, solid state NMR techniques. Results will be presented on the systems Si-Se, P-Se, Ge-P-Se, and P-S.

P6.3

PROPERTY-COMPOSITION RELATIONSHIP OF CHALCOGENIDE GLASSES CONTAINING GERMANIUM, Jay J.L. Yi and Peter R. Strutt, Institute of Materials Science, The University of Connecticut, Storrs, CT, USA

In-depth studies of property-composition relationship in chalcogenide glasses have revealed previously undiscovered structural features. For example, specific discoveries in the Ge-Se-Sb and similar systems were of (i) metastable phase separation for glasses with a high Se or S content (>70 at %), and (ii) abnormal behavior of some structural-sensitive properties (e.g. optical band-gap energy) for glasses with Se or S in the range of 60-70 at %. Structural and property characterization of the glasses involved using fourier transform infrared

spectroscopy, differential scanning calorimetry, thermomechanical analysis and other techniques; such features as spinodal decomposition and phase-separation were observed by scanning and transmission electron microscopy. In carefully studying the Ge-Se system, the liquidus curve (reported by H. Iser et al., 1982) was reexamined; this was found to have an s-shape at the phase-separation region. Another interesting finding was the dependence of the band-gap energy on composition in $(1-x)\text{GeSe}_2 \cdot x\text{Sb}_2\text{Se}_3$ glasses; this was not a linear relation but a curve with a maximum band-gap energy at 9 at % Sb.

P6.4

TELLURIUM HALIDE GLASS FIBER FOR TRANSMISSION IN THE 8-12 μm REGION, X.H. Zhang, G. Fonteneau, H.L. Ma, J. Lucas, Laboratoire de Chimie Minérale D, Université de Rennes, Campus de Beaulieu, 35042 Rennes, France

Glasses in the Te-Br-Se and Te-I-Se systems show potential low losses in the 8-12 μm region. They are very stable against crystallization and against moisture. The lowest losses of a single fiber at 10.6 μm measured using a CO_2 laser, is about 4dB/m. The essential diffusion centers in these fibers have been proved to be bubbles. Double crucible method was used to obtain fibers with core-cladding structure. The fiber with double indice shows much higher losses due to the incompatibility of the core-cladding glasses. A power delivery experiment was made using a single fiber having an attenuation of 5dB/m. The power density of about 42kw/cm² can be injected into the fiber without damaging this fiber.

P6.5

NEW STABLE IODIDE GLASSES IN THE Cd-As-I AND Cd-As-Ge-I SYSTEMS. Jong Heo and George H. Sigel, Jr., Fiber Optic Materials Research Program, Rutgers University, Piscataway, NJ

Non-fluoride halide glasses, especially iodides, are attractive candidates for optical fiber and lens materials operating in the mid-infrared region. However, their high hygroscopicity and poor thermal properties pose serious limitations to their practical applications. This study is focused on the glasses in the Cd-As-I and Cd-As-Ge-I systems for the purpose of developing water-resistant, thermally stable iodide glasses. Glasses in the former system are transparent out to 17 μm with a glass transition temperature of approximately 300°C. Preliminary water durability tests using FTIR showed no evidence of aqueous corrosion on the glass surface even after 24 hours at 70°C. Further, partial substitution of Ge for As improved the thermal properties of these glasses. Detailed experimental results on the optical, thermal and chemical properties will be discussed in comparison with the various types of infrared transmitting materials.

P6.6

STRUCTURAL STABILITY OF TELLURIUM HALIDE GLASSES, Jay J.L. Yi and Peter R. Strutt, Institute of Materials Science, The University of Connecticut, Storrs, CT, U.S.A.

In quantitative studies of the structural stability of Te-Cl and Te-Br glasses, specific attention has been devoted to determining the kinetics of their overall crystallization process in terms of time-temperature-transformation curves. This was established by using differential scanning calorimetry; the same technique was used to determine the glass composition range in which chemical decomposition occurs at elevated temperatures. The calorimetric studies reveal that the tendency of crystallization or thermal decomposition of these glasses is related to phase-diagram characteristics. Furthermore, results of x-ray radial distribution analysis of some of these glasses also indicated similar relationships. It seems that the

atomic arrangement of these glasses is not an idealized random arrangement as described by the classic Zachariasen-Warren model. Underlying causes for this deviation from a perfect random arrangement to one involving a degree of ordering (structural groups) is discussed.

P6.7

LASER IRRADIATION STUDIES OF IR-TRANSMITTING CHALCO-HALIDE GLASSES. Jean-Luc ADAM, Carmen ORTIZ, Jesse R. SALEM, IBM Research Division, San Jose, CA, U.S.A.; Xiang-Hua ZHANG, Université de Rennes I, Rennes, FRANCE.

The search for materials which transmit at the CO_2 wavelength has led to the discovery of new glasses based on tellurium and selenium and a halogen (Br, Cl or I). Because they transmit the $10.6\mu\text{m}$ line of the CO_2 laser, can be drawn into fibers and can be deposited as thin films, these materials have a tremendous potential for IR optical applications.

We have deposited amorphous thin films of the TeSeBr system by RF sputtering. We have studied for the first time laser irradiation of these thin films under experimental conditions which range from 20 to 300mW absorbed power and from 100ns to 1s laser pulse length. In some compounds, we have been able to induce structure changes for pulse lengths of 200ns or longer. For other compositions no crystallisation was observed by TEM except when annealed by the electron beam. We have measured the optical properties in the visible of these materials and their change induced by laser irradiation. We have measured their glass and melting temperatures as well as their calorimetric parameters. These were used in calculations of heatflow at the surface and into the sample which gave good agreement with our experimental results.

P6.8

MECHANICAL STRENGTH OF LOW-DIMENSION GLASS FIBERS. K. A. Cerqua, E. C. Behrman and W. C. LaCourse, New York State College of Ceramics at Alfred University, Alfred, NY.

Chalcogenide glasses present a unique opportunity for the study of the effect of dimensionality on the properties of amorphous systems. We present here results of our experiments on fibers of these materials. Strength in these fibers is related both to dimensionality, which is a continuously variable function of composition, and to drawing conditions, which produce ordering. A theoretical model incorporating both these effects is proposed and discussed.

P7.1

ADVANCE OF PLASTIC OPTICAL FIBERS. Fumio Ide, Mitsubishi Rayon Co., LTD., Chuo-ku, Tokyo Japan; and Takashi Yamamoto, Mitsubishi Rayon Co., LTD., Ohtake City Hiroshima-ken, Japan.

Plastic optical fibers, which are easier for handling and processing as well as cheaper in comparison with quartz type optical fibers, are calling strong attention for short distance optical communication system.

Progress of plastic optical fibers is reviewed. Furthermore their recent trend of development and their future prospect are discussed.

P7.2

LOW-LOSS GI PLASTIC OPTICAL FIBER AND NOVEL OPTICAL POLYMERS. Yasuhiro Koike and Yasuji Ohtsuka, Keio University, 3-14-1 Hiyoshi, Kohoku-ku, Yokohama 223, Japan.

Low-loss GI plastic optical fiber in which the attenuation of transmission was less than 200 dB/km near 650 nm wavelength was successfully obtained by heat-drawing GI preform rod. This rod was prepared by a new interfacial-gel

copolymerization technique where methyl methacrylate (MMA) and vinyl phenylacetate (VPAC) were placed in a PMMA tube and the copolymer phase was gradually formed from the gel phase on the inner wall of the tube, changing the radial composition of copolymer. The total scattering loss of the GI preform rod was less than 100 dB/km. The refractive index distribution of the GI plastic optical fiber was almost quadratic against the distance from the center axis, and the numerical aperture was 0.21.

Novel optical functional polymers were synthesized and characterized. Birefringence-free copolymer glasses which are quite transparent and homogeneous were prepared by the radical copolymerization of two monomers (M1 and M2) giving positive- and negative- birefringent homopolymers, respectively. Since the anisotropic polarization of the M1 monomer units is compensated by the M2 monomer units on the same polymer chain, the birefringence of the copolymer is zero on the length scale of several monomer units for any degree of orientation. Optically active amorphous polyacrylate glasses which act as new polarization modulators were synthesized. The application of these glasses for the rotation of the linear polarization phase and for the conversion of linear polarization to circular polarization which is different from the conventional principle of using inorganic crystals is discussed.

P7.3

SILICA-BASED SINGLE-MODE WAVEGUIDES AND THEIR APPLICATIONS TO INTEGRATED-OPTIC DEVICES. N. Takato and A. Sugita, NTT Opto-electronics Laboratories, Tokai, Ibaraki-ken, Japan

Low-loss SiO_2 -based single-mode waveguides are fabricated on Si substrates by flame hydrolysis deposition and reactive ion etching.

The waveguides loaded with a thin film heater operate as a phase shifter due to the refractive index dependence on temperature. The response time is relatively fast, 1 msec, because of the Si substrate heat sink. A novel phase shifter with an adiabatic structure preventing thermal diffusion to Si are also proposed for reduction of driving power.

Another important feature of the SiO_2 and Si combination is large stress-induced birefringence of the waveguide due to the difference in thermal expansion coefficients of these materials. Laser trimming adjustment of waveguide birefringence is proposed for constructing various polarization insensitive and sensitive devices.

Using these waveguide technologies, we have successfully developed not only passive devices such as couplers and demultiplexers but also active devices such as optical switches, tunable ring resonators, and optical frequency selection switches.

P7.4

POTENTIAL APPLICATION OF Bi(Pb)-Ca-Sr-Cu-O GLASSES FOR PREPARATION OF INTEGRATED OPTICAL FIBERS. Haixing Zheng and J.D. Mackenzie, Department of Materials Science and Engineering, University of California-Los Angeles, Los Angeles, CA 90024

Incorporation of an optical system (source, guides, modulates and detectors) into a fiber has great potential of applications. Bi_2O_3 -based glasses are one of important systems for preparation of this type of integrated fibers. Bi(Pb)-Ca-Sr-Cu-O glasses are infrared transmitting from 1.5 micron to 7.0 micron. Their refractive indices are in the vicinity of 2.9. Bi(Pb)-Ca-Sr-Cu-O glasses become superconducting after

crystallization. This superconducting glass ceramics can be used as the optical detectors based on the principle that photons will break the Cooper-pair electrons (superconducting electrons) and the materials change from superconducting to normally resistive. In this paper, the primary experimental results on (1) optical transmission; (2) fluorescence; and (3) electrical response of the Bi_2O_3 -based superconductors to the photons will be presented. The potential of Bi_2O_3 -based glasses for preparation of integrated optical fibers will be discussed.

P8.1

GROWTH OF OPTICAL QUALITY SAPPHIRE SINGLE CRYSTAL FIBERS, D.H. Jundt, M.M. Fejer and R.L. Byer, Applied Physics Department, Stanford University, Stanford, CA 94305

Void-free sapphire single crystal fibers with diameters of 110 μm and 60 μm and lengths of over 2m have been grown by the laser-heated pedestal growth method. The growth dynamics of the floating zone was studied and agrees well with theoretical predictions. The minimum loss of 0.5 dB/m was measured in the near infrared at 1064 nm. An absorption band centered at 400 nm results in losses of up to 20 dB/m in the visible. The fibers have potential applications in high temperature thermometry and in delivery systems for laser surgery. Absorption losses of 0.88 dB/m with a damage threshold higher than 1.2 kJ/cm² at 2936 nm made tissue ablation feasible with fibers several meters in length.

P8.2

THE GROWTH AND CHARACTERIZATION OF TUNGSTEN BRONZE STRONTIUM BARIUM NIOBATE SINGLE CRYSTAL FIBERS.

Joyce Yamamoto and Amar Bhatta, Materials Research Laboratory, The Pennsylvania State University, University Park, PA

Ferroelectric strontium barium niobate ($\text{Sr}_x\text{Ba}_{1-x}\text{Nb}_2\text{O}_6$) single crystal fibers have been grown using a laser heated pedestal technique (LHPG). $\text{Sr}_x\text{Ba}_{1-x}\text{Nb}_2\text{O}_6$ crystals have appealing photorefractive properties, and potential use in optical processing, data storage, and sensor applications. Previously, these crystals have only been grown in bulk form by the Czochralski technique where a major drawback in these crystals is the presence of compositional striations.

Single crystal fibers of compositions within the solid solution range ($x=0.25$ to $x=0.75$) were grown. Details of the growth technique will be presented. The effect of different growth parameters on the resulting crystal quality and their effect on property measurements will also be discussed.

Compositional striations were not detected in the $\text{Sr}_x\text{Ba}_{1-x}\text{Nb}_2\text{O}_6$ single crystal fibers.

P8.3

PROTON EFFECTS IN KTiOPO_4 , P.A. Morris, M.K. Crawford, M.G. Roelofs, J.D. Bierlein, E.I. du Pont de Nemours & Co, Inc., Experimental Station, Wilmington, DE 19880, G. Gashurov, Airtron, Litton Systems, Inc., 200 E. Hanover Ave., Morris Plains, NJ 07950.

KTiOPO_4 (KTP) is an optical crystal presently used for second harmonic generation and electro-optic applications. Defects have been studied in KTP crystals grown by the high and low temperature hydrothermal and flux techniques. The dominant defects present in KTP crystals grown by the hydrothermal techniques are protons. While the concentrations of protons in crystals grown by the various techniques is similar, the distribution and temperature

dependence of the OH^- sites are different. The effects of protons in KTP on the dielectric properties, ionic conductivity, and damage susceptibility have been studied. The relationship of the position and temperature dependence of the OH^- sites in the lattice to the observed properties is discussed.

P8.4

EXTENDED X-RAY ABSORPTION FINE STRUCTURE STUDY OF KNbO_3 , K.H. Kim (Naval Research Laboratory-National Research Council cooperative research associate), W.T. Elam, E.F. Skelton (Naval Research Laboratory)

Extended x-ray absorption fine structure of KNbO_3 was measured at the K edge of Nb, at various temperatures to include all phases of the material. KNbO_3 has the cubic perovskite structure and exhibits four distinct phases. Understanding the nature of its transitions will enhance the understanding of ferroelectrics in general. The experiments were done at NSLS X23A2 beamline in transmission mode and the data show excellent signal to noise ratio.

The first shell data were analyzed to determine the distances between Nb and O atoms. The single shell amplitude almost vanishes at $k \sim 7.4 \text{ \AA}^{-1}$ at all temperatures, indicating two distances with a separation of about 0.21 Å. Nonlinear fitting was used to determine the structure more carefully and data at all temperatures can be fit reasonably well with two Nb-O distances. This is in disagreement with the displacive model which implies only one Nb-O distance in the cubic phase and three distances in the tetragonal and orthorhombic phases. Cubic phase data cannot be fit with only one Nb-O distance. Tetragonal and orthorhombic phases data can be fit with three Nb-O distances, but the fit is not as good as two-distance fit.

The results suggest that the Nb atom is displaced along (111) direction relative to the O atoms in all phases. Thus, the transitions are not displacive, but have a strong order-disorder character. More quantitative analysis is being done to determine the distances accurately.

P8.5

ANALYSIS OF THERMAL VARIATION OF LENGTH AND REFRACTIVE INDEX OF LEAD FLUORIDE TO STUDY ITS OPTICAL PROPERTIES, Tarlok S. Aurora, Philadelphia College of Pharmacy and Science, Philadelphia, PA; Donald O. Pederson, University of Arkansas, Fayetteville, AR; Stephen M. Day, Miami University, Oxford, OH.

We have measured thermal expansion and refractive index variation in lead fluoride using a laser interferometer as a function of temperature. Data has been analyzed using Lorentz-Lorenz relation. Molecular polarizability, band gap and strain-polarizability parameter are studied as a function of temperature. They show a small variation with temperature. Near the superionic phase transition, the variation appears to be more pronounced. The results will be compared with those available for other fluorides.

P9.1

MATERIALS AND PROCESSING REQUIREMENTS FOR EFFICIENT FIBER OPTIC NONLINEAR DEVICES, R.H. Stolen, AT&T Bell Laboratories, Holmdel, NJ 07733

Nonlinear optics in an optical fiber can be used to make a variety of devices for the amplification or control of light. What keeps these devices out of the realm of practical application is the need for new materials and improvements in the guiding geometry itself. The problem is that even an enhancement such

as optical fiber interaction length does not bring the power requirements down to the 1-100mW range desired for compatibility with semiconductor laser sources. The most obvious approach is to try to replace the fused silica of the optical fiber core with a glass of large nonlinear response. This has proved to be difficult because improvements in nonlinear response seem to go along with linear loss, processing problems, and optical damage. The second approach which is now receiving more attention is to try to modify the properties of the guide itself both to increase the efficiency of the interaction and to optimize the fiber for the specific nonlinear device.

P9.2

CONCENTRATION AND DISTRIBUTION OF ER AND AL IN SILICA-BASED FIBERS. D.W. Oblas, T. Wei, W.J. Miniscalco and B.T. Hall, GTE Laboratories, Inc., Waltham, MA 02254

Rare earth doped optical fibers are now being widely investigated for their uses as lasers and amplifiers. Silica-based Er^{3+} -doped fibers offer the most potential for an optical amplifier in telecommunications applications. In order to refine the fabrication process and to optimize device performance, it is important to determine the concentrations and the distribution of Er along and across the fiber core as a function of process parameters. Furthermore, more accurate concentrations and Er profiles can improve the comparison of the cross sections among various Er-doped glasses.

Secondary ion mass spectrometry (SIMS) was used to measure the Er and Al distributions across and along Al/Er-codoped silica fibers and preforms prepared by a solution doping technique. Special (low melting) glass standards, containing known concentrations of Er, were prepared and used to calibrate the spectrometer to obtain the Er concentration quantitatively. It has been determined that the Er concentration varies along the core from 1260ppm to 530ppm by measuring three slices of the preform one-half inch apart. However, the Al concentration is more constant both across and along the core of these samples. Results will be presented for preforms prepared under a variety of conditions and with different codopants.

The concentrations were used to calculate Er emission and absorption cross sections which will be compared to the values obtained independently through decay measurements.

P9.3

APPLICATION-SPECIFIC OPTICAL FIBRES MANUFACTURED FROM MULTICOMPONENT GLASSES. E.R. Taylor, M. Tachibana, J. Wang and D.N. Payne, Optical Fibre Group, Department of Electronics and Computer Science, University of Southampton, Southampton SO9 5NH, UK

To date, silica has been widely used in special fibres for sensors, nonlinear optics and rare-earth-doped lasers and amplifiers. However, multicomponent glasses have a number of advantages in areas where low loss is not essential, since they can have enhanced magnetic, electric and acoustic responses. Furthermore, their third-order nonlinear coefficients can be an order of magnitude large. As rare-earth host materials, they allow tailoring of the local ionic environment which produces major changes in spectral properties, excited-state absorption, fluorescent lifetime and emission cross-sections.

We have fabricated optical fibres from both commercially-available and new multicomponent glass melts. With care and close attention to glass matching and processing conditions, fibres with losses close to the intrinsic loss of the bulk-glass precursors are obtainable using a modified rod-in-tube technique. The flexibility of the fabrication method provides a wide range of fibre designs for application in fibre devices, fibre sensors and fibre lasers.

F-series and SF-series glasses exhibit a useful combination of enhanced Verdet constant and high third-order nonlinearity. Fibres for nonlinear devices and fibre sensors have been fabricated from these glasses and the results of device testing will be presented.

P9.4

GLASSES FOR Er^{3+} -DOPED FIBER LASERS AND OPTICAL AMPLIFIERS. W.J. Miniscalco, L.J. Andrews, S. Zemon, B.T. Hall, T. Wei, R.C. Folweiler; GTE Labs., Inc., 40 Sylvan Rd., Waltham, MA 02254.

Widespread interest in Er^{3+} -doped optical fiber devices has been stimulated by reports of excellent performance for fiber lasers and amplifiers at 1.5 μm . The fibers have been made from silica codoped with combinations of germanium, phosphorus, and aluminum, or from fluorozirconate glass. Although there have been some measurements of the sensitivity of the gain and excited state absorption to codopants in silica fiber, the role of glass composition has not been extensively documented. Because the gain and signal/noise ratio of three-level devices are quite sensitive to the relevant cross sections, we have undertaken an investigation of the optical characteristics of Er^{3+} as a function of glass composition. The stimulated emission cross section at 1.5 μm and the absorption cross sections throughout the UV, visible, and infrared have been measured for silica, silicate, phosphate, fluorophosphate, and heavy metal fluoride glasses. Silica was found to have the smallest oscillator strength ($\approx 60 \text{ nm}$). Fluorophosphates are an intermediate case with bandwidths that increase with increasing fluorine to oxygen ratio. A notable exception to the general trend is Al-doped silica which has a bandwidth as large as a fluorophosphate. Low temperature photoluminescence and excitation spectra have been used to determine the magnitude of the Stark splittings and the inhomogeneous widths of the individual transitions. Because the overall Stark splittings are large ($\approx 400 \text{ cm}^{-1}$) compared to the inhomogeneous width ($\approx 10 \text{ cm}^{-1}$), the behavior of the system is expected to be largely homogeneous. The comparative advantages and disadvantages of the different glass compositions in active fiber applications will be discussed.

P9.5

EXCITED STATE CROSS SECTIONS FOR ER-DOPED GLASSES. S. Zemon, G. Lambert, W. J. Miniscalco, L. J. Andrews, and B. T. Hall, GTE Laboratories Inc., 40 Sylvan Road, Waltham, MA 02254

Erbium has been shown to be an important dopant for fiber lasers and amplifiers operating at 1550 nm. However, excited state absorption (ESA) occurs in several of the principal pump bands and is a major impediment to device implementation. In particular, for Er^{3+} -doped silica fibers pumped with AlGaAs diode lasers, strong ESA at $\approx 800 \text{ nm}$ seriously degrades performance. We present the results of ESA experiments on four glass compositions potentially useful for active fiber devices, i.e., phosphates, fluorophosphates, heavy-metal fluorides, and silicates. To our knowledge, Er^{3+} ESA has not been reported for glasses other than silica. A 647-nm pump and a dye-laser probe were employed to make the measurements in a

collinear configuration. Data were taken on bulk material because of the difficulty of synthesizing fibers for a large number of glasses. Saturation effects were used to estimate the population inversion and thus convert absorption data into cross sections. Data on ESA cross sections (σ_e) and ground state absorption cross sections (σ_g) will be presented for the region between 780 and 900 nm, which includes ESA bands at ≈ 800 and ≈ 850 nm. In the 800-nm band $\sigma_e \approx \sigma_g$ for the phosphates, fluorophosphates, and silicates. The heavy metal fluorides were found to have substantial populations in the upper excited states for our measurement conditions and ESA transitions originating from several of these states were identified. It is interesting to note that the oscillator strength of the 800-nm ESA band is at least a factor of four greater than that of the 850-nm band for all samples tested. These results will be compared to a calculation based upon the Judd-Ofelt approximation.

P9.6

RARE EARTH DOPED FIBERS, Elias Snitzer, Rutgers University, Fiber Optic Materials Research Program, PO Box 909, Piscataway, NJ 08855-0909

With diode and other laser sources, a number of rare earth transitions have been made to lase CW in end pumping of low loss silica or fluoride fibers. The latter is particularly interesting because its lower energy phonon spectrum permits efficient fluorescence from one than one level in some rare earths, such as Er and Tm, which gives added laser transitions and more efficient upconversion. The types of laser operation and fiber configurations will be reviewed.

P9.7

INFRARED SPECTROSCOPY OF PROTONS IN KTiOPO₄

M. K. Crawford, P. A. Morris, M. Roelofs, E. I. du Pont de Nemours & Co., Experimental Station, Wilmington, DE 19880
G. Gashurov, Airtron, Litton Systems, Inc., 200 E. Hanover Avenue, Morris Plains, NJ 07950

KTiOPO₄ (KTP) is a new nonlinear optical material which is finding considerable use in frequency generation and electro-optics. KTP can be grown hydrothermally or by flux methods, but the resulting materials are found to have different ionic conductivities and damage susceptibilities. We have undertaken a detailed infrared study of materials prepared in various ways, including temperature dependent observations, which illustrate distinct differences between samples. In particular, H⁺ defects, which exist in KTP as isolated OH⁻ ions, have complex polarized infrared spectra indicative of the number of distinct oxygen sites in the crystal. Both the H⁺ site distribution and the temperature dependences of the infrared linewidths for different OH⁻ sites are observed to vary in a reproducible and characteristic manner from sample to sample. Interpretation of the observations will be presented.

OPTICAL ABSORPTION AND EMISSION IN RARE EARTH DOPED HEAVY METAL FLUORIDE GLASSES.

R. Pafchek, E. Snitzer and G.H. Sigel Jr., Fiber Optic Materials Research Program, Rutgers Univ., N.J., 08854

Heavy metal fluoride glasses of ZBLAN composition have been selectively doped with varying concentrations of selected rare earth ions. The characteristics of both the emission and absorption spectra have been measured and contrasted with those of oxide glasses. Particular attention has been given to important laser parameters such as quantum efficiency, excited state lifetimes and concentration quenching versus rare earth concentration. In addition, the effects of co-doping the rare earths into the host glass have been studied. The potential implications of the work for laser device optimization will be discussed.

SYMPOSIUM Q:
ELECTRICAL, OPTICAL, AND
MAGNETIC PROPERTIES OF
ORGANIC SOLID STATE MATERIALS

Q

November 27 - December 1, 1989

Chairs

Long Y. Chiang
Exxon Research & Engineering Company
Clinton Township
Route 22, East
Annandale, NJ 08801
(201) 730-2565

Paul Chaikin
Department of Physics
Princeton University
Princeton, NJ 08544
(609) 452-4338

Dwaine Cowan
Department of Chemistry
The Johns Hopkins University
Baltimore, MD 21218
(301) 338-7425

Symposium Support

Air Force Office of Scientific Research

Allied-Signal, Inc.

Army Research Office

E. I. duPont de Nemours & Co., Inc.

Exxon Research and Engineering Company

GTE

IBM/Almaden Research Center

Matsushita Electric Industrial Company

Xerox Corporation

Proceedings published as Volume 173
of the Materials Research Society
Symposium proceedings series.

ELECTRICAL, OPTICAL, AND MAGNETIC
PROPERTIES OF ORGANIC SOLID STATE MATERIALS

November 27 - December 1, 1989

SESSION Q1: PLENARY SESSION

Chair: Donald R. Ulrich
Monday Morning, November 27
Essex South (W)

8:20 OPENING REMARKS

8:30 *Q1.1

CAN THE ORGANIC SOLID STATE PROVIDE THE NEXT GENERATION OF ELECTRICAL, OPTICAL AND MAGNETIC MATERIALS, Dwaine O. Cowan, The Johns Hopkins University, Department of Chemistry, Baltimore, MD.

9:00 *Q1.2

STABLE AND PROCESSIBLE CONDUCTING POLYMERS: OPPORTUNITIES FOR SCIENCE AND TECHNOLOGY, Alan J. Heeger, University of California, Santa Barbara, Institute for Polymers and Organic Solids, Santa Barbara, CA.

9:45 *Q1.3

NONLINEAR OPTICAL POLYMERS: CHALLENGES AND OPPORTUNITIES IN PHOTONICS, A.F. Garito, J.W. Wu, University of Pennsylvania, Department of Physics, Philadelphia, PA; G.F. Lipscomb and R. Lytel, Lockheed Palo Alto Research Laboratory, Palo Alto, CA.

10:30 BREAK

SESSION Q2: ORGANIC FERROMAGNETS (I)

Chair: Fred Wudl
Monday Morning, November 27
Essex South (W)

10:45 *Q2.1

ELECTRON-DONATING RADIALENES. POTENTIAL DONORS FOR MOLECULAR ORGANIC (SUPER)CONDUCTORS AND FERROMAGNETS, Zen-ichi Yoshida, Toyonari Sugimoto and Yoji Misaki, Kyoto University, Department of Synthetic Chemistry, Kyoto, Japan.

11:15 Q2.2

SYNTHESIS OF BULK HIGH SPIN DENSITY ORGANIC SOLIDS AS PRECURSORS TO ORGANIC FERROMAGNETS, Long Y. Chiang, Exxon Research and Engineering Company, Corporate Research Laboratory, Annandale, NJ; Ravindra B. Upasani, Princeton University, Department of Physics, Princeton, NJ; Dave P. Goshorn, Exxon Research and Engineering Company, Corporate Research Laboratory, Annandale, NJ.

*Invited Paper

11:45 Q2.3

FERROMAGNETIC INTERMOLECULAR INTERACTION AND CRYSTAL STRUCTURE OF α -NITRONYL NITROXIDE, Kunio Awaga, Tamotsu Inabe and Yusei Maruyama, Institute for Molecular Science, Okazaki, Japan.

SESSION Q3: CONDUCTING POLYMERS (I):
POLYANILINE

Chair: Alan G. MacDiarmid
Monday Afternoon, November 27
Essex South (W)

1:15 *Q3.1

THE POLYANILINES: A NOVEL CLASS OF CONDUCTING POLYMERS, A.G. MacDiarmid, University of Pennsylvania, Department of Chemistry, Philadelphia, PA; A.J. Epstein, The Ohio State University, Department of Physics and Department of Chemistry, Columbus, OH.

1:45 *Q3.2

POLYANILINE: AN OLD POLYMER WITH NEW PHYSICS, A.J. Epstein, The Ohio State University, Department of Physics and Department of Chemistry, Columbus, OH; and A.G. MacDiarmid, University of Pennsylvania, Department of Chemistry, Philadelphia, PA.

2:00 Q3.3

LOW ENERGY ELECTRONIC TRANSITIONS OF POLARON BANDS IN POLYANILINE, Sze Cheng Yang, Dan Zhang and Richard Cushman, University of Rhode Island, Department of Chemistry, Kingston, RI.

2:15 Q3.4

AQUEOUS COLLOIDAL DISPERSIONS OF POLYANILINE PARTICLES, S.P. Armes and M. Aldissi, Los Alamos National Laboratory, Materials Science and Technology Division, Los Alamos, NM.

2:30 Q3.5

INTERCALATIVE POLYMERIZATION OF CONDUCTIVE POLYMERS IN LAYERED INORGANIC HOSTS, Mercouri G. Kanatzidis, Chun-Guey Wu, Michigan State University, Department of Chemistry and Center for Fundamental Materials Research, East Lansing, MI; Henry O. Marcy, Donald C. DeGroot and Carl R. Kannewurf, Northwestern University, Department of Electrical Engineering and Computer Science, Evanston, IL.

2:45 Q3.6

EXTREME OXIDATION OF POLYTHIOPHENES, POLYPYRROLES, AND POLYANILINE: FINITE POTENTIAL WINDOWS OF HIGH CONDUCTIVITY, David Ofer, Richard M. Crooks, and Mark S. Wrighton, Massachusetts Institute of Technology, Department of Chemistry, Cambridge, MA.

3:00 BREAK

3:15 Q3.7
CHEMICAL AND PHYSICAL STUDIES OF SOLUBLE
PART OF EMERALDINE: ELECTRONIC AND MAGNETIC
PROPERTIES OF SHORT CHAIN SPECIES, R.
Laversanne, Centre de Recherche Paul
Pascal/CNRS, Pessac, France.

3:30 Q3.8
POLYANILINE AS A REVERSIBLY SWITCHABLE
MATERIAL, W.-R. Shieh, S.C. Yang, University
of Rhode Island, Department of Chemistry,
Kingston, RI; and C. Marzzacco, Rhode Island
College, Department of Physical Sciences,
Providence, RI.

3:45 Q3.9
MOISTURE EFFECTS IN THE CONDUCTING POLYMER,
POLYANILINE, J.P. Travers, C. Menardo and M.
Nechtschein, CENG, Grenoble, France; S.K.
Manohar and A.G. MacDiarmid, University of
Pennsylvania, Department of Chemistry,
Philadelphia, PA.

4:00 Q3.10
SPECTROSCOPIC AND MOLECULAR WEIGHT STUDIES
OF POLYTOLUIDINES, Y. Wei, K.F. Hsueh,
Drexel University, Department of Chemistry,
Philadelphia, PA; A. Ray, A.G. MacDiarmid,
J. Dykins, University of Pennsylvania,
Department of Chemistry, Philadelphia, PA;
and A.J. Epstein, The Ohio State University,
Department of Physics, Columbus, OH.

4:15 Q3.11
ELECTRICALLY CONDUCTIVE COMPOSITE OF POLY-
ANILINE AND POLY(p-PHENYLENE-TEREPH-
THALAMIDE), Xian-Tong Bi, Chun Wang and
Jing-sheng Bao, Academia Sinica, Institute
of Chemistry, Beijing, China.

4:30 Q3.12
INFRARED REFLECTION-ABSORPTION STUDY OF
ANILINE ELECTROPOLYMERIZATION ON STAINLESS
STEEL, F. Gaillard and G. Bouyssoux, Univer-
sité Claude Bernard-LYON I, Département de
Chimie Appliquée et Génie Chimique, Villeu-
rbanne, France; and S.N. Kumar, I.N.S.A.
LYON, Laboratoire de Physique de la Matière,
I.N.S.A. LYON, Villeurbanne, France.

4:45 Q3.13
ELECTRICAL PROPERTIES OF POLYANILINE-POLYMER
COMPOSITE FILMS, Kecheng Gong and Long-gui
Zhong, South China University of Technology,
Department of Polymer Science, Guangzhou,
China.

SESSION Q4: ORGANIC SUPERCONDUCTORS AND
ORGANIC METALS (I)
Chair: Gunzi Saito
Tuesday Morning, November 28
Essex South (W)

8:30 *Q4.1
PREPARATION AND PROPERTIES OF ORGANIC SUPER-
CONDUCTOR $K-(BEDT-TTF)_2Cu(NCS)_2$ AND ITS
RELATED MATERIALS, Gunzi Saito, The Univer-
sity of Tokyo, The Institute for Solid State
Physics, Tokyo, Japan.

9:00 *Q4.2
FERMI SURFACE OF ORGANIC METALS $\beta-(ET)_2IBr_2$
AND $\beta-(ET)_2I_3$ STUDIED BY MEANS OF GALVANO-
MAGNETIC MEASUREMENTS, V.N. Laukhin, M.V.
Kartsovnik, S.I. Pesotskii, USSR Ac. Sci.,
Institute of Chemical Physics,
Chernogolovka, USSR; P.A. Kononovich and
I.F. Schegolev, USSR Ac. Sci., Institute of
Solid State Physics, Chernogolovka, USSR.

9:30 *Q4.3
SUPERCONDUCTING AND NORMAL STATE PROPERTIES
OF BEDT-TTF BASED ORGANIC METALS, Madoka
Tokumoto, K. Murata, N. Kinoshita, H. Bando,
K. Yamaji and H. Anzai, Electrotechnical
Laboratory, Ibaraki, Japan.

10:00 Q4.4
HUBBARD PARAMETERS IN $(BEDT-TTF)_2X$ CRYSTALS,
Oliver H. LeBlanc, Jr., Margaret L. Blohm,
and Richard P. Messmer, General Electric
Corporate Research and Development, Schenec-
tady, NY.

10:15 BREAK

10:30 Q4.5
SPECIFIC HEAT MEASUREMENTS ON $K-(BEDT-TTF)_2-$
 $Cu(NCS)_2$, R.G. Goodrich and Jing-chun Xu,
Louisiana State University, Department of
Physics and Astronomy, Baton Rouge, LA;
Margaret Blohm and Oliver LeBlanc, General
Electric Research and Development Center,
Schenectady, NY.

10:45 Q4.6
PRESSURE DEPENDENCE OF THE STRUCTURAL AND
ELECTRONIC PROPERTIES OF ORGANIC SUPERCON-
DUCTORS, Daniel Chasseau, Jacques Gaultier,
Hamid Houbib, CNRS, Université de Bordeaux
I, Laboratoire de Cristallographie, Talence,
France; Laurent Ducasse, CNRS, Université de
Bordeaux I, Laboratoire de Physico-Chimie
Théorique, Talence, France; Mohammed Kurmoo
and Peter Day, Inorganic Chemistry Labora-
tory, Oxford, United Kingdom.

11:00 Q4.7
THIN FILM FORMATIONS OF CHARGE TRANSFER COMPLEXES WITH METALLIC PROPERTIES BY VACUUM EVAPORATION METHODS, M. Yudasaka and K. Nakanishi, Yokohama National University, Department of Materials Chemistry, Faculty of Engineering, Yokohama, Japan; H. Yamochi and G. Saito, University of Tokyo, Institute for Solid State Physics, Tokyo, Japan.

11:15 Q4.8
SYNTHESIS, CRYSTAL STRUCTURE AND SPECTROSCOPIC STUDIES OF NEW CT COMPOUNDS OBTAINED BY REACTION OF TTF AND THE POLYOXOANION $[Mo_6O_{19}]^{2-}$, D. Attanasio, C. Bellitto, M. Bonamico, V. Fares, P. Imperatori, and S. Patrizio, ITSE, CNR, Monterotondo (Roma), Italy.

11:30 Q4.9
A NEW SYNTHETIC METAL PRECURSOR: DIMETHYL-TETRATHIOTETRACENE AND RELATED COMPOUNDS, Toshio Maruo, Megh Singh and M. Thomas Jones, University of Missouri, St. Louis, Department of Chemistry, St. Louis, MO.

11:45 Q4.10
TETRANITROQUINODIMETHANE (TNQ) - ELECTRON-DEFICIENT PROTOTYPE FOR A NEW SERIES OF ORGANIC SOLID STATE MATERIALS, David J. Vanderah, Richard A. Hollins, Arnold T. Nielsen, and Chris Baun, Naval Weapons Center, Research Department, China Lake, CA.

SESSION Q5: ORGANIC METALS (II)

Chair: Michael Hanack
Tuesday Afternoon, November 28
Essex South (W)

1:00 *Q5.1
HIGHLY CONDUCTING COMPLEXES OF METALS WITH dmit AND dddt DITHIOLATE LIGANDS, E.B. Yagubskii, A.I. Kotov, L.I. Buravov, A.G. Khomenko, USSR Ac. Sci., Institute of Chemical Physics, Chernogolovka, USSR; V.E. Shklover, S.S. Nagapetyan, Yu.T. Struchkov, USSR Ac. Sci., A.N. Nesmeyanov Institute of Organoelement Compounds, Moscow, USSR; and L.Yu. Ukhin, Rostov State University, Institute of Physical and Organic Chemistry, Rostov, USSR.

1:30 *Q5.2
NEW ELECTRICALLY CONDUCTING SOLIDS BASED ON NICKEL(II) - BIS(1,3-DITHIOLE-2-THIONE-4,5-DISELENOLATE), A.M. Kini, H.H. Wang, M.A. Beno, U. Geiser, A.J. Schultz, K.D. Carlson, and J.M. Williams, Argonne National Laboratory, Chemistry and Materials Science Divisions, Argonne, IL.

1:45 Q5.3
BRIDGED MACROCYCLIC TRANSITION METAL COMPLEXES, A NEW TYPE OF SEMICONDUCTING MATERIALS, Michael Hanack, Andreas Hirsch, Armin Lange, Manfred Rein, Gunter Renz und Petra Vermehren, der Universität Tübingen, Lehrstuhl für Organische Chemie II, Institut für Organische Chemie, Tübingen, West Germany.

2:00 Q5.4
UNIAXIAL STRESS EFFECTS ON OPTICAL ABSORPTION SPECTRA OF HIGHLY ORIENTED IODINE DOPED PHTHALOCYANINE FILMS, Hiroaki Tsuyosi, Masako Yudasaka, Masatoshi Tanaka, Kazumi Nakanishi, and Susumu Kurita, Yokohama National University, Faculty of Engineering, Yokohama, Japan.

2:15 Q5.5
DISCOTIC LIQUID CRYSTALLINE PORPHYRINS: PHOTOPHYSICAL AND PHOTOELECTRICAL PROPERTIES OF LARGE-AREA CRYSTALLINE FILMS, Brian A. Gregg, University of Texas at Austin, Department of Chemical Engineering, Austin, TX; Marye Anne Fox and Allen J. Bard, University of Texas at Austin, Department of Chemistry, Austin, TX.

2:30 BREAK

SESSION Q6: CONDUCTING POLYMERS (II): POLYHETEROCYCLICS

Chair: Arthur J. Epstein
Tuesday Afternoon, November 28
Essex South (W)

2:45 Q6.1
LANGMUIR-BLODGETT FILMS OF CONDUCTING POLYMERS, T.A. Skotheim, X.Q. Yang, J. Chen, H.S. Lee, Brookhaven National Laboratory, Upton, NY; Y. Okamoto, Polytechnic University, Brooklyn, NY; M.L. denBoer, Hunter College of CUNY, New York, NY; M.F. Rubner, Massachusetts Institute of Technology, Cambridge, MA; S. Tripathy, University of Lowell, Lowell, MA.

3:00 Q6.2
LANGMUIR-BLODGETT MULTILAYER THIN FILMS OF ELECTRICALLY CONDUCTIVE POLYMERS, M.F. Rubner, I. Watanabe, K. Hong and R. Rosner, Massachusetts Institute of Technology, Department of Materials Science and Engineering, Cambridge, MA.

3:15 Q6.3
HETEROCYCLIC POLYMERS AND COPOLYMERS WITH CONTROLLED OPTOELECTRONIC PROPERTIES, Jose P. Ruiz, Kasinath Nayak, Dennis S. Marynick, and John R. Reynolds, The University of Texas at Arlington, Center for Advanced Polymer Research, Department of Chemistry, Arlington, TX.

3:30 **Q6.4**
SYNTHESIS, STRUCTURE, INFRARED SPECTRA, AND IODINE DOPING OF UNSUBSTITUTED POLYAZINES, William B. Euler and Benjamin C. Gill, University of Rhode Island, Department of Chemistry, Kingston, RI.

3:45 **Q6.5**
MODEL THIOPHENE OLIGOMERS: ELECTRONIC PROPERTIES AND THIN FILM DEVICES, Denis Fichou, Gilles Horowitz, and Francis Garnier, C.N.R.S., Laboratoire des Matériaux Moléculaires, Thiais, France.

4:00 **Q6.6**
PHOTOLUMINESCENCE, ESR, AND ODMR STUDIES OF PRISTINE AND PHOTODEGRADED POLY(3-HEXYLTHIOPHENE) FILMS AND SOLUTIONS, L.S. Swanson, L.R. Lichty, J. Shinar, Iowa State University, Ames Laboratory-USDOE and Physics Department, Ames, IA; and K. Yoshino, Osaka University, Department of Electrical Engineering, Osaka, Japan.

4:15 **Q6.7**
HELICAL CONFORMATIONS OF POLYTHIOPHENE, POLYPYRROLE AND THEIR DERIVATIVES, Miklos Kertesz and C.X. Cui, Georgetown University, Department of Chemistry, Washington, DC.

4:30 **Q6.8**
RESONANT RAMAN SCATTERING OF POLY-3-HEPTYLTHIOPHENE, C. Botta, A. Bolognesi, C. Catellani, and S. Luzzati, Istituto di Chimica delle Macromolecole, Milano, Italy.

4:45 ***Q6.9**
OPTICAL, ELECTROCHEMICAL AND STRUCTURAL PROPERTIES OF POLY(THIENYLENE VINYLENES) AND POLY(PHENYLENE VINYLENES), H. Eckhardt, K.Y. Jen, C.C. Han, L.W. Shacklette and R.L. Elsenbaumer, Allied-Signal, Inc., Morristown, NJ.

SESSION Q7: POSTER SESSION

Chair: Sze C. Yang
Tuesday Evening, November 28
7:00 p.m. - 10:00 p.m.
America Ballroom (W)

Q7.1 ENHANCEMENT OF THE MAGNETIC SUSCEPTIBILITY OF AN ORGANIC COMPLEX, G.J. Ashwell, A.T. Fraser, and P.J. Martin, Cranfield Institute of Technology, Centre for Molecular Electronics, Cranfield, United Kingdom.

Q7.2 NOVEL MATERIALS FOR OPTICAL DATA STORAGE, Geoffrey J. Ashwell and Marek Szablewski, Cranfield Institute of Technology, Centre for Molecular Electronics, Oal, United Kingdom.

Q7.3 EFFECTS OF IN-PLANE π' BONDING ON ELECTRONIC TRANSITION ENERGIES FOR INORGANIC POLYMERS, Kim F. Ferris, Battelle-Pacific Northwest Laboratory, Richland, WA.

Q7.4 SURFACE PLASMONS IN THIN FILM DIELECTRICS, S.M. Risser and K.F. Ferris, Battelle-Pacific Northwest Laboratory, Richland, WA.

Q7.5 PHYSICAL CHARACTERIZATION OF ORGANIC RADICALS BY LOW-FIELD ESR SPECTROMETRY, Mehdi Moussavi, Marc Beranger, Denis Duret, Nelly Kernevez, and Liliane Secourgeon, CEA-IRDI, Grenoble, France.

Q7.6 STUDIES ON THE FORMATION OF SWITCHING AND MEMORY STORAGE MATERIALS CONSTRUCTED FROM METALLO-ORGANIC CHARGE-TRANSFER SALTS, Hailing Duan, Dwaine O. Cowan, The Johns Hopkins University, Department of Chemistry, Baltimore, MD; and Jerome Kruger, The Johns Hopkins University, Department of Materials Science and Engineering, Baltimore, MD.

Q7.7 OPTICAL STUDIES OF POLYANILINES: EFFECTS OF ALKYL RING-SUBSTITUTION AND SOLVENT ENVIRONMENT, A. Ray, A.G. MacDiarmid, University of Pennsylvania, Department of Chemistry, Philadelphia, PA; J.M. Ginder and A.J. Epstein, Ohio State University, Department of Physics, Columbus, OH.

Q7.8 SPECTRO-ELECTROCHEMICAL STUDY OF RING-SUBSTITUTED POLYANILINE: POLY(2-METHOXYANILINE) AND POLY(2,5-DIMETHOXYANILINE), Robert Clark and Sze C. Yang, University of Rhode Island, Department of Chemistry, Kingston, RI.

Q7.9 ELECTRON PARAMAGNETIC RESONANCE STUDIES OF DONOR-ACCEPTOR SALTS IN POLYMER MEDIA, S.A. Jansen and Y.C. Fann, Temple University, Department of Chemistry and Materials Science, Philadelphia, PA.

Q7.10 HALL EFFECT AND MAGNETORESISTANCE IN UNDOPED POLY(3HEXYLTHIOPHENE), Azar Assadi, Christer Svensson and Magnus Willander, Linköping University, Department of Physics and Measurement Technology, Linköping, Sweden.

Q7.11 ELECTRON TUNNELING BETWEEN CHARGE DENSITY WAVE (CDW) AND NORMAL METAL AND BETWEEN TWO CDW's, Xiao Zhou Huang and Kazumi Maki, University of Southern California, Department of Physics, Los Angeles, CA.

Q7.12 BELOW-GAP PICOSECOND PHOTOCONDUCTIVE RESPONSE OF STRETCHED TRANS-POLYACETYLENE, A. Walser, R. Dorsinville, R.R. Alfano, City College of New York, Physics and Electrical Engineering Departments, New York, NY; G. Dellepiane, Università di Genova, Genova, Italy; and R. Tubino, Istituto di Fisica dell'Università, Sassari, and CNR, Istituto di Chimica delle Macromolecole, Milan, Italy.

Q7.13 THE PENN STATE 5-100 GHz FREE-SPACE MICROWAVE CHARACTERIZATION SETUP, Deepak K. Ghodgaonkar, Vijay K. Varadan, and Vasundara V. Varadan, Pennsylvania State University, Research Center for the Engineering of Electronic and Acoustic Materials, University Park, PA.

Q7.14 DONOR-ACCEPTOR MOLECULES FOR SECOND HARMONIC GENERATION, Malcolm R. McLean, Mamoun M. Badr, Larry R. Dalton, University of Southern California, Department of Chemistry, Los Angeles, CA; Robert L.S. Devine and William H. Steier, University of Southern California, Department of Electrical Engineering, Los Angeles, CA.

Q7.15 EFFECTS OF CONJUGATION LENGTH AND SUBSTITUENTS ON THE CONDUCTIVITY OF OXIDATIVELY DOPED α,ω -DIPHENYLPOLYENES, Linda S. Sapochak, Dave W. Polis, Art N. Bain, Larry R. Dalton, University of Southern California, Department of Chemistry, Los Angeles, CA; Charles W. Spangler, Northern Illinois University, DeKalb, IL.

Q7.16 CHARGE TRANSFER COMPLEX OF HEXAKIS (ALKYLTHIO) BENZENE WITH TETRAFLUOROTETRACYANOQUINODIMETHANE (t-EDTB)₂ TCNQF₄: A QUEST FOR TRIPLET STATE, Daniel Chasseau, Marc Alleaume, Georges Bravic, CNRS, Laboratoire de Cristallographie et Physique Cristalline, Rene Lapouyade, ENSCP Bordeaux Laboratoire de Photophysique et Photochimie Moleculaire, Talence, France; Jean-Pierre Morand, ENSCP Bordeaux, Talence France; Jacques Amiell and Pierre Delhaes, CNRS, Domaine Universitaire de Bordeaux I, Centre de Recherche Paul Pascal, Talence, France.

Q7.17 FERROMAGNETIC INTERACTIONS IN A SERIES OF SCHIFF-BASE METAL-ORGANIC POLYMERS, F. Palacio, J. Garin, J. Reyes, and F.J. Lazaro, C.S.I.C.-Universidad de Zaragoza, I.C.M.A., Zaragoza, Spain.

SESSION Q8: ORGANIC FERROMAGNETS (II)

Chair: J.B. Torrance

Wednesday Morning, November 29
Essex South (W)

8:15 *Q8.1

MAGNETISM IN DECAMETHYLFERROCENIUM TETRACYANOETHANIDE, [DMeFc]⁺[TCNE]⁻ AND RELATED SYSTEMS, Arthur J. Epstein, The Ohio State University, Department of Physics and Department of Chemistry, Columbus, OH; and Joel S. Miller, E. I. duPont de Nemours & Co., Inc., Central Research and Development Department, Wilmington, DE.

8:45 *Q8.2

FERROMAGNETIC INTERACTIONS IN ORGANIC SOLIDS: AN OVERVIEW OF THEORY AND EXPERIMENT, J.B. Torrance, IBM Almaden Research Center, San Jose, CA.

9:15 *Q8.3

RECENT PROGRESS IN THE PREPARATION OF ORGANIC METALS AND ORGANIC FERROMAGNETS, Fred Wudl, Fritz Closs, Pierre-Marc Allemand, Jordana Srdanov, Toshiyasu Suzuki, Heiki Isotalo, Hamid Kasmai, and Hideki Yamochi, University of California at Santa Barbara, Institute for Polymers and Organic Solids, Departments of Physics and Chemistry, Santa Barbara, CA.

9:45 *Q8.4

MAGNETIC PROPERTIES OF MICROCRYSTALLINE "POLY-(PHENYLDIACETYLENES)" CARRYING RADICAL OR CARBENE CENTERS ON THE SIDE CHAINS, Noboru Koga, Katsuya Inoue, Noriko Sasagawa, and Hiizu Iwamura, The University of Tokyo, Department of Chemistry, Tokyo, Japan.

10:15 BREAK

10:30 *Q8.5

ROLE OF TOPOLOGY IN SPIN ALIGNMENT OF ORGANIC MATERIALS, Koichi Itoh, Takeji Takui, Yoshio Teki and Takamasa Kinoshita, Osaka City University, Faculty of Science, Department of Chemistry, Osaka, Japan.

11:00 Q8.6

ROLE OF HIGH-SPIN MOLECULES AS MODELS FOR ORGANIC FERRO- AND FERRIMAGNETS, AND PI-TOPOREGULATED MAGNETIC POLYMERS, Takeji Takui, Masayuki Okamoto, Kazunobu Satoh, Toyohiro Shichiri, Yoshio Teki, Takamasa Kinoshita and Koichi Itoh, Osaka City University, Faculty of Science, Department of Chemistry, Osaka, Japan.

11:15 Q8.7

THERMAL STABILITY OF MAGNETIC PROPERTIES OF DEHYDROGENATED TRI-ARYLMETHANE RESINS, Michiya Ota, Gunma College of Technology, Maebashi, Gunma, Japan; and Sugio Otani, Gunma University, Faculty of Engineering, Kiryu-shi, Gunma, Japan.

11:30 **Q8.8**
POLYPHENOXY RADICALS : SYNTHESIS AND HOMO-POLYMERIZATION 3,5-DI-tert-BUTYL-4-HYDROXY-PHENYL DERIVATIZED OLEFINS AND METHACRYLATES, Ravindra B. Upasani, Exxon Research and Engineering Company, Annandale, NJ and Princeton University, Department of Physics, Princeton, NJ; Long Y. Chiang and Dave P. Goshorn, Exxon Research and Engineering Company, Corporate Research Laboratories, Annandale, NJ.

11:45 **Q8.9**
ORGANIC POLYRADICAL MODELS FOR ORGANIC MAGNETIC MATERIALS, David A. Modarelli, Frank C. Rossitto, Masaki Minato and Paul M. Lahti, University of Massachusetts, Department of Chemistry, Amherst, MA.

SESSION Q9: NON-LINEAR OPTICAL MOLECULES

Chair: J. Zyss

Wednesday Afternoon, November 29
Essex South (W)

1:00 ***Q9.1**
SYMMETRY, CHEMISTRY AND OPTICS: A COMBINED APPROACH TO MOLECULAR ENGINEERING IN NON-LINEAR OPTICS, J. Zyss, CNET (LA CNRS) Bagneux, France.

1:30 ***Q9.2**
NEW SECOND-ORDER NONLINEAR OPTICAL ORGANIC CRYSTALS, D.S. Donald, L.-T. Cheng, E. I. duPont de Nemours & Co., Inc., Central Research and Development Department, Experimental Station, Wilmington, DE; G. Desiraju, University of Hyderabad, School of Chemistry, Hyderabad, India; G.R. Meredith, and F.C. Zumsteg, E. I. duPont de Nemours & Co., Inc., Central Research and Development Department, Experimental Station, Wilmington, DE.

2:00 **Q9.3**
SYNTHESIS, THERMAL BEHAVIOR, AND SECOND-ORDER NONLINEAR OPTICAL PROPERTIES OF CONJUGATED, ACCEPTOR/DONOR COMPOUNDS, James F. Wolfe, Susan P. Ermer, Steven M. Lovejoy, Doris S. Leung, Ken Aron, Glenn A. Hansen, Lockheed Missiles and Space Company, Inc., Palo Alto, CA; and Steven P. Bitler, SRI International, Menlo Park, CA.

2:15 **Q9.4**
MATERIALS FOR A MULTIFREQUENCY PHOTOCHROMIC MEMORY, Geoffrey J. Ashwell and Marek Szablewski, Cranfield Institute of Technology, Centre for Molecular Electronics, Cranfield, United Kingdom.

2:30 **Q9.5**
ELECTRO-OPTIC AND NONLINEAR OPTICAL PROPERTIES OF 2,6-DIBROMO-N-METHYL-4-NITROANILINE (DBNMNA) CRYSTALS, Ajay Nahata, Keith A. Horn, and James T. Yardley, Allied-Signal, Inc., Morristown, NJ.

2:45 **Q9.6**
QUADRATIC NONLINEAR OPTICAL PROPERTIES OF DIVA CRYSTAL, Tatsuo Wada, C.H. Grossman, Shinji Yamada, Akira Yamada, A.F. Garito, and Hiroyuki Sasabe, Frontier Research Program (RIKEN), Saitama, Japan.

3:00 BREAK

3:15 **Q9.7**
EFFICIENT SECOND HARMONIC GENERATION OBSERVED IN HYDRAZONE DERIVATIVES OF AROMATIC ALDEHYDES, Richard S. Potember, Karen A. Stetyick, and Robert C. Hoffman, The Johns Hopkins University, Applied Physics Laboratory, Laurel, MD.

3:30 **Q9.8**
FERROELECTRICITY OF CHIRAL COMPOUNDS IN HIGHLY ORDERED SMECTIC PHASES, W. Haase, A.M. Biradar, and S. Wróbel, Institut für Physikalische Chemie, Technische Hochschule, Darmstadt, Federal Republic of Germany.

3:45 **Q9.9**
LANGMUIR-BLODGETT FILMS OF UNIDIMENSIONAL ORGANIC RECTIFIERS, Robert M. Metzger, University of Alabama, Department of Chemistry, Tuscaloosa, AL; and Charles A. Panetta, University of Mississippi, Department of Chemistry, University, MS.

4:00 **Q9.10**
L.B. FILM EXHIBITING COOPERATIVE SPIN TRANSITION, FOR 2D MOLECULAR MEMORY DEVICES, Philippe Coronel, Annie Ruaudel-Teixier and A. Barraud, CEA-IRDI-DESICP-DLPC/SCM, CEN.SACLAY, Gif-sur-Yvette, France.

4:15 **Q9.11**
EFFECTS OF MOLECULAR RIGIDITY ON ELECTRIC FIELD-INDUCED ALIGNMENT AND ORIENTATIONAL STABILITY OF DIPOLAR CHROMOPHORE COMPOSITES, H.E. Katz and M.L. Schilling, AT&T Bell Laboratories, Organic Chemistry Research and Development, Murray Hill, NJ; W.R. Holland, and K.D. Singer, AT&T Bell Laboratories, Engineering Research Department, Princeton, NJ.

4:30 **Q9.12**
ZINC TRIS(THIOUREA) SULFATE, A PROTOTYPE SEMIORGANIC NON-LINEAR OPTICAL MATERIAL, P.R. Newman, L.F. Warren, E.F. Wituchi, M.D. Ewbank, D.E. Cooper, Rockwell International Science Center, Thousand Oaks, CA; and G. Burdge, Laboratory for Physical Sciences, College Park, MD.

4:45 **Q9.13**
CARRIER INJECTION MECHANISM THROUGH ORGANIC/ORGANIC JUNCTIONS, Syun Egusa, Nobuhiro Gemma, Akira Miura, and Makoto Azuma, Toshiba Research and Development Center, Kawasaki City, Japan.

SESSION Q10: CONDUCTING POLYMERS (III):

POLYACETYLENE AND POLYSILANE

Chair: R. H. Friend

Thursday Morning, November 30
Essex South (W)

8:15 *Q10.1

INSULATOR-METAL TRANSITION AND CONDUCTION PROCESSES IN TRANS-POLYACETYLENE, E.W. Conwell, H.A. Mizes, and S. Jeyadev, Xerox Corporation, Webster Research Center, Webster, NY.

8:45 Q10.2

DETERMINATION OF CORRELATION PARAMETERS IN CONJUGATED POLYMERS, J. Tinka Gammel, D.K. Campbell, E.Y. Loh Jr., Los Alamos National Laboratory, Los Alamos, NM; S. Mazumdar, University of Arizona, Department of Physics, Tucson, AZ; and S.N. Dixit, Lawrence Livermore National Laboratory, Livermore, CA.

9:00 Q10.3

OPTICAL SPECTROSCOPY OF THE CHARGE ACCUMULATION LAYER IN POLYMERIC SEMICONDUCTOR MIS AND MISFET STRUCTURES, J.H. Burroughes, R.A. Lawrence, and R.H. Friend, Cavendish Laboratory, Cambridge, United Kingdom.

9:15 Q10.4

OPTICAL PROPERTIES OF POLYACETYLENE OLIGOMERS, H. Schaffer, R.R. Chance, Exxon Research and Engineering Company, Corporate Research, Annandale, NJ; K. Knoll, R.R. Schrock and R. Silbey, Massachusetts Institute of Technology, Chemistry Department, Cambridge, MA.

9:30 Q10.5

DECISIVE STEPS IN THE PRODUCTION OF HIGHLY CONDUCTING-CRYSTALLINE POLYMERS, Nicolas Theophilou, Institute for Polymers, Athens, Greece, and University of Pennsylvania, Department of Chemistry, Philadelphia, PA.

9:45 Q10.6

PHOTOCONDUCTIVE RESPONSE AND INTERCHAIN INTERACTIONS IN HIGHLY ORIENTED POLYACETYLENE, R. Tubino, Istituto di Fisica dell'Università', Sassari, and CNR, Istituto di Chimica delle Macromolecole, Milan, Italy; G. Dellepiane, Università' di Genova, Genova, Italy; and A. Walser, R. Dorsinville, R.R. Alfano, City College of New York, Physics and Electrical Engineering Departments, New York, NY.

10:00 Q10.7

¹³³Cs NMR STUDIES OF HIGHLY CESIUM DOPED POLYACETYLENE, F. Rachdi, P. Bernier, K. Zniber, USTL, Groupe de Dynamique des Phases Condensées, Montpellier, France.

10:15 Q10.8

REVERSIBLE PHOTOPRODUCTION OF STABLE CHARGED DEFECTS IN TRANS-POLYACETYLENE WITH MID-BAND-GAP PHOTOLYSIS, Carolyn F. Hoener, Lawrence Berkeley Laboratory, Laboratory of Chemical Biodynamics, Berkeley, CA, and University of Texas at Austin, Department of Chemistry, Austin, TX.

10:30 BREAK

10:45 Q10.9

CONDUCTING AND NONLINEAR OPTICAL POLYMERS FROM DIETHYNYLSILANES, T.J. Barton, S. Ijadi-Maghsoodi, Y. Pang, J. Shinar, Q.-X. Ni, Ames Laboratory/Iowa State University, Ames, IA; Z.V. Vardeny, University of Utah, Salt Lake City, UT; and S. Grigoros, Dow Corning Corporation, Midland, MI.

11:00 Q10.10

THERMALLY ACTIVATED CHARGE HOPPING TRANSPORT STUDIES IN A Σ -CONJUGATED POLYMER, L. Samuel and P.N. Sanda, IBM T.J. Watson Research Center, Yorktown Heights, NY; and R.D. Miller and D. Thompson, IBM Almaden Research Center, San Jose, CA.

11:15 Q10.11

FREE CARRIER BAND GAP IN POLY(PHENYL METHYL SILANE), R.G. Kepler and J.M. Zeigler, Sandia National Laboratories, Albuquerque, NM.

11:30 Q10.12

ESR STUDIES OF CHARGE TRANSPORT AND CARRIER DENSITY IN Σ -CONJUGATED POLYMER SYSTEMS, J.T. Riley, S.A. Jansen, Temple University, Philadelphia, PA; and Pia N. Sanda, IBM T.J. Watson Research Center, Yorktown Heights, NY.

11:45 Q10.13

THE DOPING OF POLY-p-PHENYLENE SULFIDE AND ITS OLIGOMERS: A SPECTROSCOPICAL STUDY, P. Piaggio, C. Cuniberti, G. Dellepiane, Università di Genova, Istituto di Chimica Industriale, Genova, Italy.

SESSION Q11: SPIN DENSITY WAVES

Chair: Paul Chaikin

Thursday Afternoon, November 30
Essex South (W)

1:30 *Q11.1

THE DYNAMICS OF SPIN DENSITY WAVES, George Grüner, University of California, Los Angeles, Dept. of Physics, Los Angeles, CA.

2:00 *Q11.2

BIDIRECTIONAL CRITICAL BEHAVIOUR AND COMPETITION BETWEEN ORDER PARAMETERS IN THE ORGANIC METAL (TMTSF)₂ClO₄, P. Garoche, F. Pesty, M. Heritier, Laboratoire de Physique des Solides, Université de Paris, Orsay, France.

2:30 ***Q11.3**

HIGH MAGNETIC FIELD PHASES OF THE (TMTSF)₂X (X = ClO₄, PF₆) CHARGE TRANSFER COMPLEXES, James S. Brooks, Boston University, Physics Department, Boston, MA.

3:00 **Q11.4**

HIGH FIELD MAGNETIZATION STEPS AT THE RE-ENTRANT METAL TO SPIN DENSITY WAVE LINE IN (TMTSF)₂ClO₄, M.J. Naughton, State University of New York at Buffalo, Buffalo, NY; R.V. Chamberlin, Arizona State University, Tempe, AZ; P.M. Chaikin, Princeton University, Princeton, NJ and Exxon Research and Engineering, Annandale, NJ; L.Y. Chiang, Exxon Research & Engineering, Annandale, NJ.

3:15 BREAK

3:30 **Q11.5**

A NEW THEORETICAL MODEL FOR THE SPIN DENSITY WAVE TRANSITIONS IN ORGANIC CHARGE TRANSFER SOLIDS, E.Y. Loh, Jr. and David K. Campbell, Los Alamos National Laboratory, Los Alamos, NM; and Sumit Mazumdar, University of Arizona, Physics Department, Tucson, AZ.

3:45 **Q11.6**

SOUND PROPAGATION IN CDW AND SDW, Attila Virosztek, University of Virginia, Charlottesville, VA; and Kazumi Maki, University of Southern California, Los Angeles, CA.

4:00 **Q11.7**

SOUND VELOCITY STUDIES OF THE BECHGAARD SALTS (TMTSF)₂ClO₄ AND (TMTSF)₂PF₆, X-D. Shi, University of Pennsylvania, Department of Physics, Philadelphia, PA and Princeton University, Department of Physics, Princeton, NJ; P.M. Chaikin, Princeton University, Department of Physics, Princeton, NJ and Exxon Research and Engineering Company, Annandale, NJ; L. Y. Chiang, Exxon Research and Engineering Company, Annandale, NJ; and R. Upasani, Princeton University, Department of Physics, Princeton, NJ and Exxon Research and Engineering Company, Annandale, NJ.

4:15 **Q11.8**

SOUND VELOCITY MEASUREMENTS IN (TMTTF)₂X (X = ReO₄, SbF₆) SALTS, S.E. Brown, H.H.S. Javadi, Los Alamos National Laboratory, Los Alamos, NM; and R. Laversanne, Centre de Recherche Paul Pascal, CNRS, Domaine Universitaire de Bordeaux, Talence, France.

4:30 **Q11.9**

QUANTUM HALL EFFECT AND RAPID OSCILLATIONS IN (TMTSF)₂PF₆ UNDER PRESSURE, S. Hannahs, J. Brooks, Boston University, Department of Physics, Boston, MA; W. Kang, Princeton University, Department of Physics, Princeton, NJ; P. Chaikin, Princeton University, Department of Physics, Princeton, NJ and Exxon Research and Engineering Company, Annandale, NJ; L. Chiang, Exxon Research and Engineering Company, Annandale, NJ; and R. Upasani, Princeton University, Department of Physics, Princeton, NJ and Exxon Research and Engineering Company, Annandale, NJ.

4:45 **Q11.10**

LOW TEMPERATURE ORIENTATIONAL DEPENDENCE OF THE MAGNETORESISTANCE IN (TMTSF)₂ClO₄: A SEARCH FOR MAGIC ANGLES, M.J. Naughton, O.H. Chung, State University of New York at Buffalo, Buffalo, NY; J.S. Brooks, Boston University, MA; P.M. Chaikin, Princeton University, Princeton, NJ and Exxon Research and Engineering Company, Annandale, NJ; and L.Y. Chiang, Exxon Research and Engineering Company.

SESSION Q12: NON-LINEAR OPTICAL POLYMERS (I)

Chair: Daniel J. Sandman
Friday Morning, December 1
Essex South (W)

8:00 ***Q12.1**

OBSERVATION OF NONLINEAR OPTICAL TRANSMISSION AND SWITCHING PHENOMENA IN POLYDIACETYLENE-BASED DIRECTIONAL COUPLER DEVICES, Paul D. Townsend, J.L. Jackel, Gregory L. Baker, J.A. Shelburne, and S. Etemad, Bellcore, Red Bank, NJ.

8:30 ***Q12.2**

POLYDIACETYLENE SIDE CHAINS AND ELECTRONIC STRUCTURE AND PROCESSES, Daniel J. Sandman, GTE Laboratories, Inc., Waltham, MA.

9:00 **Q12.3**

INVESTIGATIONS OF A NEW REVERSIBLE STRAIN INDUCED CHROMIC TRANSITION IN POLYDIACETYLENE ELASTOMERS, M.F. Rubner, R. Agrawal, and H. Beckham, Massachusetts Institute of Technology, Department of Materials Science and Engineering, Cambridge, MA.

9:15 **Q12.4**

SYNTHESIS AND PROPERTIES OF A FULLY CONJUGATED POLYDIACETYLENE: POLY(1,4-BIS(3-QUINOLYL)-1,3-BUTADIENE), Satya S. Talwar and M. Kamath, Indian Institute of Technology, Department of Chemistry, Bombay, India.

9:30 **Q12.5**

ORGANIC POLYMER SEMICONDUCTOR SUPERLATTICES, Samson A. Jenekhe and Wen-Chang Chen, University of Rochester, Department of Chemical Engineering, Rochester, NY.

9:45 **Q12.6**
LARGE THIRD-ORDER NONLINEAR OPTICAL PROPERTIES OF ORGANIC POLYMER SEMICONDUCTOR SUPERLATTICES, Samson A. Jenekhe and Wen-Chang Chen, University of Rochester, Department of Chemical Engineering, Rochester, NY; S.K. Lo, Honeywell Systems and Research Center, Minneapolis, MN; and Steven R. Flom, University of Minnesota, Department of Chemistry, Minneapolis, MN.

10:00 BREAK

10:15 **Q12.7**
A COUPLED INVESTIGATION OF QUADRATIC AND CUBIC NONLINEAR OPTICAL PROCESSES IN EXTENDED CHARGE TRANSFER POLYENES, M. Barzoukas, CNET (LA CNRS), Bagneux, France; M. Blanchard-Desce, College de France, Paris, France; F. Kajzar, CEA-CEN Saclay, Gif-sur-Yvette, France; J.M. Lehn, College de France, Paris, France; A. Messier, C. Sentein, CEA-CEN Saclay, Gif-sur-Yvette, France; J. Zyss, CNET (LA CNRS) Bagneux, France.

10:30 **Q12.8**
NONLINEAR OPTICAL STUDIES OF MIXED π -CONJUGATED POLYMER MULTILAYERS BY SECOND HARMONIC GENERATION, Hiroshi Koezuka, Tetsuyuki Kurata, Akira Tsumura, and Hiroyuki Fuchigami, Mitsubishi Electric Corporation, Materials and Electronic Devices Laboratory, Hyogo, Japan.

10:45 **Q12.9**
A NEW POLYOLEFIN MATERIAL "ZEONEX" FOR OPTICAL USES, Teiji Kohara, Masayoshi Ohshima, and Tadao Natsuume, Nippon Zeon Company, Ltd., Research and Development Center, Kawasaki, Japan, Masahiro Yamazaki, Nippon Zeon of America, Inc., White Plains, NY.

11:00 **Q12.10**
SYNTHESIS AND SECOND-ORDER NONLINEAR OPTICAL PROPERTIES OF NEW COUMAROMETHACRYLATE-METHYLMETHACRYLATE COPOLYMERS, R.A. Henry, C.M. Hoover, and G.A. Lindsay, Naval Weapons Center, Research Department, China Lake, CA; M.A. Mortazavi, A. Knoesen, and S.T. Kowel, University of California at Davis, Department of Electrical Engineering and Computer Science, Davis, CA.

11:15 **Q12.11**
NEW POLYMERS FOR ELECTROACTIVE APPLICATIONS, Mamoun M. Badr, David W. Polis, and Larry R. Dalton, University of Southern California Los Angeles, Department of Chemistry, Los Angeles, CA.

11:30 **Q12.12**
PHOTOEXCITATION SPECTROSCOPY OF PRECURSOR ROUTE POLY(THIOPHENE VINYLENE), D.D.C. Bradley, A.J. Brassett, N.F. Colaneri, R.H. Friend, R.A. Lawrence, Cavendish Laboratory, Cambridge, United Kingdom; and H. Murata, S. Tokito, T. Tsutsui, and S. Saito, Kyushu University, Department of Materials Science and Technology, Kasuga, Fukuoka, Japan.

11:45 **Q12.13**
SYNTHESIS AND CHARACTERIZATION OF NEW POLYMERS EXHIBITING LARGE OPTICAL NONLINEARITY: DERIVATIZED POLYANILINE AND COPOLYMER CONTAINING POLYANILINE SEGMENTS, Luping Yu, Mai Chen, Larry R. Dalton, University of Southern California, Department of Chemistry, Los Angeles, CA.

SESSION Q13: NON-LINEAR OPTICAL POLYMERS (II) AND COMPOSITES

Chair: Bryan E. Kohler
Friday Afternoon, December 1
Essex South (W)

1:30 **Q13.1**
THE 2^1A_g STATE IN LONG POLYENES: ELECTRONIC STRUCTURE, PHOTOINDUCED ABSORPTION AND THERMAL ISOMERIZATION, Bryan E. Kohler and Curtis Westerfield, University of California, Chemistry Department, Riverside, CA.

1:45 **Q13.2**
THEORETICAL CALCULATIONS ON NONLINEAR SUSCEPTIBILITIES OF ORGANIC MATERIALS, Yuzo Itoh, Tomoyuki Hamada, Atsushi Kakuta and Akio Mukoh, Hitachi Ltd., Hitachi Research Laboratory, Ibaraki, Japan.

2:00 **Q13.3**
NONLINEAR OPTICAL RESPONSE IN CONJUGATED POLYMERS - A THEORETICAL APPROACH, Mauro Pereira, Jr., University of Arizona, Optical Sciences Center, Tucson, AZ; S.W. Koch, University of Arizona, Physics Department and Optical Sciences Center, Tucson, AZ; Sumit Mazumdar, University of Arizona, Physics Department, Tucson, AZ; and S.N. Dixit, Lawrence Livermore National Laboratory, Livermore, CA.

2:15 **Q13.4**
ELECTRONIC STRUCTURES AND NONLINEAR OPTICAL PROPERTIES FOR CROSS-CONJUGATED POLYENE, Yuhei Mori and Yoshimichi Okano, ATR Optical and Radio Communications Research Laboratories, Kyoto, Japan.

2:30 **Q13.5**
ROTATIONAL DIFFUSION OF CHROMOPHORES INSIDE A GLASSY POLYMERIC FILM STUDIED BY ELECTRO-OPTICAL POLARIMETRY, Remi Meyrueix and Gerard Mignani, Rhone-Poulenc Recherches, Centre des Carrieres, Saint-Fons, France.

2:45 Q13.6

SECOND ORDER NONLINEAR OPTICS AND POLYMER PHYSICS OF CORONA POLED POLYMER FILMS, Hilary L. Hampsch, Northwestern University, Department of Materials Science and Engineering, Evanston, IL; Jian Yang and George K. Wong, Northwestern University, Department of Physics and Astronomy, Evanston, IL; and John M. Torkelson, Northwestern University, Depts. of Materials Science and Engineering and Chemical Engineering, Evanston, IL.

3:00 BREAK

3:15 Q13.7

THEORETICAL STUDIES OF THE NONLINEAR PROPERTIES OF 1-ARGININE PHOSPHATE AND DERIVATIVES, C.A. Langhoff, Dow Chemical, Midland, MI.

3:30 Q13.8

QUANTUM LATTICE FLUCTUATIONS AND NONLINEAR OPTICAL PROPERTIES OF CONDUCTING POLYMERS, J. Yu, B. Friedman and W.P. Su, University of Houston, Houston, TX.

3:45 Q13.9

THIRD ORDER NONLINEAR OPTICAL EFFECTS IN POLYCONDENSED THIOPHENE BASED POLYMERS, Lina Yang, R. Dorsinville, R.R. Alfano, City College of New York, Physics and Electrical Engineering Departments, New York, NY; C. Taliani, Consiglio Nazionale delle Ricerche, Istituto di Spettroscopia Molecolare, Bologna, Italy.

4:00 Q13.10

OPTICAL CHARACTERIZATION OF POLYDIACETYLENE LANGMUIR-BLODGETT FILM ON SILICON SUBSTRATES, P. Miller, A.M.K. Rahman, S.V. Broude, and S. Tripathy, University of Lowell, Departments of Physics and Chemistry, Lowell, MA.

4:15 Q13.11

MICRO-ENCAPSULATED CHIRAL POLYMER COMPOSITES, Vijay K. Varadan, Deepak K. Ghodgaonkar, Vasundara V. Varadan, and Akhlesh Lakhtakia, Pennsylvania State University, Research Center for the Engineering of Electronic and Acoustic Materials, University Park, PA.

4:30 Q13.12

ARTIFICIAL CHIRAL COMPOSITES, Vasundara V. Varadan, Deepak K. Ghodgaonkar, Vijay K. Varadan, and Akhlesh Lakhtakia, Pennsylvania State University, Research Center for the Engineering of Electronic and Acoustic Materials, University Park, PA.

4:45 Q13.13

POLYMER BLEND FOR RFI/EMI/EMC APPLICATIONS, Neil Williams, Vijay K. Varadan, and Vasundara V. Varadan, Pennsylvania State University, Research Center for the Engineering of Electronic and Acoustic Materials, University Park, PA.

Q1.1 ABSTRACT NOT AVAILABLE

Q1.2

STABLE AND PROCESSIBLE CONDUCTING POLYMERS: OPPORTUNITIES FOR SCIENCE AND TECHNOLOGY. Alan J. Heeger, Institute for Polymers and Organic Solids, University of California, Santa Barbara, Santa Barbara, CA 93106.

Recent advances in the synthesis and processing of conducting polymers have demonstrated that one can have materials with the electronic and optical properties of metals and semiconductors and the processing and mechanical advantages of polymers. This progress has opened the way to achieving a wide range of important configurations ranging from optical quality films (through spin casting) to highly oriented films and fibers through post-synthesis processing, using both pure conducting polymers and conducting polymers in blends and composites with other polymers.

The prospects for the achievement of high performance electronic and optical materials will be discussed with specific emphasis in two areas:

- (i) high electrical conductivity and
- (ii) optical and nonlinear optical properties.

In the area of electrical properties, we contrast two limits: "dirty" conductors where the transport is via carrier hopping such that $\sigma \sim 10$ S/cm or less, and true metals in which the carrier mean free path is many lattice constants. Analysis of similar limiting cases define the high performance optical and nonlinear optical properties of conducting polymers.

We conclude that conducting polymers represent a new class of electronic and optical materials with properties which range from those of commodities with routine properties to high performance materials which combine, for example, excellent electrical conductivity with high mechanical strength.

Q1.3

NONLINEAR OPTICAL POLYMERS: CHALLENGES AND OPPORTUNITIES IN PHOTONICS. A.E. Gatto and J.W. Wu, Dept. of Physics, University of Pennsylvania, Philadelphia, PA 19104; G.F. Lipscomb and R. Lytel, Lockheed Palo Alto Research Lab. O-9720, B-202, Palo Alto, CA 94304

Recent developments and advances in nonlinear and electro-optical materials will be discussed, with a special focus on nonlinear optical organic polymers.

Many materials classes have been studied to understand the physical properties and behavior of nonlinear optical responses at a fundamental level. Organic and polymeric systems are unique in that the macroscopic nonlinear responses, $\chi^{(2)}$ and $\chi^{(3)}$ can be traced back to the microscopic nonlinear optical susceptibilities of individual molecular units, allowing identification of nonlinear optical processes at a molecular level. According to a microscopic description of second and third order π -electron virtual excitation processes in low dimensional electronic conjugated structures, the strong correlations between π -electrons in reduced spatial dimensions, such as quasi-one or two dimensional molecules, are responsible for the large nonlinear optical responses of organic polymers. These processes lead to materials with exceptional nonlinear optical properties and are significant both for fundamental understanding and practical applications. Two classes of organic nonlinear optical materials will be discussed.

Optical bistability, a major subject in the nonlinear optics research, has been observed in an ultra-thin film polymer consisting of quasi-two dimensional (2D) conjugated discs of silicon naphthalocyanine (SINC) randomly distributed in a glassy matrix. The on-site electronic excitations of the quasi-2D discs exhibit Bloch type saturable absorption at fast timescales (10^{-9} - 10^{-12} sec). The nonlinear refractive index n_2 , obtained from the saturable absorption results is 1×10^{-4} cm²/kW, comparable to the value of GaAs.

Electro-optic polymers have been developed offering substantial advantages in electro-optic response, speed, fabricability and flexibility over conventional inorganic crystals. Current research toward fabricating electro-optic, organic integrated optical devices will be reviewed.

Q2.1

ELECTRON-DONATING RADIALENES. POTENTIAL DONORS FOR MOLECULAR ORGANIC (SUPER)CONDUCTORS AND FERROMAGNETS. Zen-ichi Yoshida, Toyonari Sugimoto and Yoji Misaki, Department of Synthetic Chemistry, Kyoto University, Yoshida, Kyoto 606 Japan.

Molecular organic systems having electrical and magnetic properties currently absorb much interest of theoretical and experimental scientists.

Although high-T_c ceramic superconductors have been discovered very recently, research on organic (super)conductors needs to be actively pursued with the aim of creating organic superconductors with high-T_c. Research on organic ferromagnetic materials is still in its infancy. Further development of the research on molecular organic (super)conductors and ferromagnets depends ultimately on the synthesis of reliable new organic donors.

From this point of view we have been investigating electron-donating [n] radialenes as new donors.

In this Symposium, preparation of the charge transfer complexes and radical cation salts of electron-donating [3], [4] and [5] radialenes (and related systems) and their electrical or magnetic property will be discussed along with their electrochemical and spectral properties.

Q2.2

SYNTHESIS OF BULK HIGH SPIN DENSITY ORGANIC SOLIDS AS PRECURSORS TO ORGANIC FERROMAGNETS. Long Y. Chiang, Ravindra B. Upasani¹ and Dave P. Goshorn, Corporate Research Laboratory, Exxon Research and Engineering Company, Annandale, NJ 08801; ¹Department of Physics, Princeton University, Princeton, NJ 08544.

We describe a synthetic approach to the preparation of bulk high spin density organic solids as a probe to organic ferromagnets utilizing an external doping process to achieve a molecular sequence of alternate donors and acceptors in different spin states for, in principle, the ground state ferrimagnets. We found that the introduction of arsenic pentafluoride into molecular crystals of charge transfer complexes disintegrates the long range order of crystal without rearranging the molecular stacking sequence of donor and acceptor. A high spin density solid can be made through AsF₅ doping of triplet donors at the solid state of materials. These spins were found to couple either ferromagnetically or weakly antiferromagnetically at various temperatures. In the case of doped HMT-HCHAT, a magnetic susceptibility with $\theta = 10.7$ K (125 - 300K) was observed, indicating a ferromagnetic coupling of spins. Below 125K the spin coupling becomes weakly antiferromagnetic with $\theta = -3.2$ K. Magnetic data of various charge transfer complexes of HMT and HOC will also be discussed.

Q2.3

FERROMAGNETIC INTERMOLECULAR INTERACTION AND CRYSTAL STRUCTURE OF α -NITRONYL NITROXIDE. Kunio Awaga, Tamotsu Inabe, and Yusei Maruyama, Institute for Molecular Science, Myodaiji, Okazaki 444, Japan.

There has recently been an increasing interest in organic/molecular ferromagnetism. α -nitronyl nitroxide, a stable organic radical of $S=1/2$, has an interesting molecular structure in this respect. Two NO groups are bonded by a carbon atom and the unpaired π electron is delocalized on the whole skeleton. This radical has, further, a strong spin polarization effect due to the short distance between the unpaired and non-bonding electrons. We have initiated a study of the electronic states and the magnetic behaviors of various α -nitronyl nitroxides.

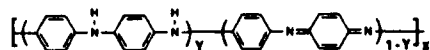
The temperature dependence of the magnetic susceptibilities and the field dependence of the magnetizations for three α -nitronyl nitroxides, 2-R-4,4,5,5-tetramethyl-4,5-dihydro-1H-imidazolyl-1-oxy 3-oxide (with R= phenyl(I), 3-nitrophenyl(II), 4-nitrophenyl(III)) have been measured. It is found that the intermolecular interaction is ferromagnetic (FM) in the crystal of III, while it is antiferromagnetic in I or II. The Weiss constant of III is +0.9 K. The magnetization curve of III at 2 K, the lower limit of the temperature measurements, almost corresponds to the theoretical one for $S=2$, and, therefore, it is certain that the FM interaction in III could cover more than 4 radicals.

Crystal structures of I and III have been determined by X-ray analysis. In III, a 2-D sheet structure is made by the weak intermolecular contacts between the O-atoms of NO groups and the N-atoms of NO₂ groups. The FM interaction would work in this sheet through these contacts. This contact is very similar to the coordination bonding between nitroxide and transition metal in some complexes.

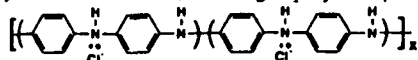
Q3.1

THE POLYANILINES: A NOVEL CLASS OF CONDUCTING POLYMERS* A. G. MacDiarmid, Dept. of Chemistry, Univ. of Penn., Phila., PA 19104, and A. J. Epstein, Dept. of Physics and Dept. of Chemistry, The Ohio State Univ., Columbus, OH 43210.

The polyanilines are a class of polymers the base form of which has the general formula



containing "y" reduced and (1-y) oxidized repeat groups. The value of "y" can in principle be varied continuously from y=1 to give the completely reduced material to y=0 to give the completely oxidized polymer. The "emeraldine" oxidation state (y=0.5) consists of alternating reduced and oxidized groups. It can be protonated i.e. "doped" by aqueous acids with a concomitant increase in conductivity of almost 10 orders of magnitude (to a maximum conductivity of 10^1 - 10^2 S/cm) forming a polysemiquinone radical cation such as



containing a delocalized half-filled broad polaron energy band. The polymer is readily solution processible into films and fibers which can be mechanically aligned, the doped forms of which have a conductivity parallel to the direction of alignment significantly greater than that of non-aligned material. X-ray studies show that the doped and undoped polymer exist in several different crystalline forms. A wide variety of derivatives can be synthesized by substitution on the ring or on the nitrogen.

*Supported in part by DARPA through a contract monitored by ONR.

Q3.2

POLYANILINE: AN OLD POLYMER WITH NEW PHYSICS*. A. J. Epstein, Dept. of Physics and Dept. of Chemistry, The Ohio State Univ., Columbus, Ohio 43210, and A. G. MacDiarmid, Dept. of Chemistry, Univ. of PA, Philadelphia, PA 19104.

Recent progress in the chemistry and processing of polyaniline has now enabled detailed chemical physical studies. X-ray diffraction studies show that emeraldine base can be prepared with a degree

of crystallinity up to fifty percent. Doping of this material occurs initially in the amorphous phase followed by doping into the crystalline regions. These materials are identified as Branch II of the emeraldine family. Emeraldine prepared directly as salt from solution is also up to ~50 percent crystalline (denoted Branch I) though its structure differs from Branch II materials. Dedoping of emeraldine salt I yields amorphous EB-I. Protonation of EB-I yields continuous growth of crystalline ES-I. Corresponding static and dynamic magnetic susceptibility experiments show that the protonated crystalline regions have a Pauli susceptibility corresponding to a metallic state while the protonated amorphous regions are nonmagnetic (spinless defects only). Photoinduced absorption studies of emeraldine base and leucoemeraldine base (LEB) show the presence of long-lived, photoexcited entities, including excitons (in EB) and massive polarons (in EB and LEB). Time-dynamic studies imply that the longevity of the photoexcited defects is associated with the roles of ring flipping and ring conformation in the polymer system. A new model for the effects of electron-lattice coupling via ring rotations is introduced. Extended charge transport studies of oriented and nonoriented films demonstrate the textured, granular metal nature of emeraldine salt. Though the highest dc conductivity measured approaches 100S/cm at room temperature, elimination of the barriers should lead to substantially higher conductivities. Potential new technologies based on the polyanilines, including nonlinear optics, optical information storage, and controlled microwave absorption are noted.

*Supported in part by DARPA through a contract monitored by U.S. O.N.R.

Q3.3

LOW ENERGY ELECTRONIC TRANSITIONS OF POLARON BANDS IN POLYANILINE. Sze Cheng Yang, Dan Zhang and Richard Cushman, University of Rhode Island, Chemistry Department, Kingston, RI 02881.

New absorption bands of polyaniline with transition energy less than 1 eV were studied by in-situ spectroelectrochemical methods. Depending on the preparation method and the substrate for thin film polymer, the transition occurs at either 0.9 eV as a single absorption band, or as a pair of bands at 1 eV and at 0.6 eV. The band intensity was studied as a function of the electrochemical potential and the pH of contacting electrolytes. Like the 1.5 eV and the 2.9 eV transitions, these near infrared transitions are related to the formation of polarons. However, details of our data indicate that the 0.9 eV band do not share with the 1.5 eV band the same lower electronic energy level of optical absorption transition. Implication to the assignment of electronic transitions are examined.

This work is supported in part by PPG Industries and by a contract administered by the Office of Naval Research from DARPA.

Q3.4

AQUEOUS COLLOIDAL DISPERSIONS OF POLYANILINE PARTICLES. S. P. Armes and M. Aldissi, Materials Science and Technology Division, Los Alamos National Laboratory, P. O. Box 1663, Los Alamos, NM 87545.

Colloidal polyaniline has been prepared in acidic aqueous media by a modified chemical polymerization of aniline in the presence of a tailor-made polymeric surfactant. The surfactant which acts as a steric stabilizer used in this study is poly(vinyl alcohol-co-vinyl acetate). This surfactant contains pendant aniline units which participate in the aniline polymerization, resulting in the formation of sterically-stabilized polyaniline particles which have a non-spherical "rice-grain" morphology.

It is shown that this novel form of polyaniline is more processable than the bulk powder that is normally obtained from a conventional chemical synthesis. The solid-state conductivity of solution-cast films or compressed pellets of these dispersions is surprisingly

high ($\approx 1 \text{ S/cm}$), despite the presence of the insulating outer layer of chemically-grafted stabilizer.

We have characterized these polyaniline colloids by a wide range of techniques including electron microscopy, cyclic voltammetry and Raman, visible absorption and X-ray photoelectron spectroscopy.

Q3.5

INTERCALATIVE POLYMERIZATION OF CONDUCTIVE POLYMERS IN LAYERED INORGANIC HOSTS. Mercouri G. Kanatzidis^(a), Chun-Guey Wu^(a), Henry O. Marcy^(b), Donald C. DeGroot^(b) and Carl R. Kannewurf^{(b)(a)} *Department of Chemistry and Center for Fundamental Materials Research, Michigan State University, East Lansing MI 48824 (b) Department of Electrical Engineering and Computer Science, Northwestern University, Evanston, IL 60208.*

Aniline, pyrrole and 2,2'-bithiophene can polymerize by *in-situ* oxidation/intercalation into layered $\text{V}_2\text{O}_5 \cdot n\text{H}_2\text{O}$ xerogels. The resulting products are novel laminated organic-inorganic molecular composites featuring alternating monolayers of conductive polymers and V_2O_5 slabs with interesting electrical properties. These materials differ from conventional (electro)chemically prepared conducting polymers because they are ordered (*vis a vis* amorphous) at least perpendicular to the V_2O_5 layers. They can also be obtained as free standing films. The V_2O_5 network is reduced in these reactions thus creating mobile carriers (small polarons) which reside on the vanadium oxide network. This creates two potentially competitive charge transport pathways, the organic polymer chains and the inorganic V_2O_5 slabs. Both pathways can be favored depending on the polymer/ V_2O_5 ratio. Chemical, spectroscopic, magnetic and electrical (conductivity and thermoelectric power) characterization of these materials will be presented. We show that both n-type and p-type as well as metallic and semiconducting properties can be achieved by controlling the polymer/ V_2O_5 ratio.

Q3.6

EXTREME OXIDATION OF POLYTHIOPHENES, POLYPYRROLES, AND POLYANILINE: FINITE POTENTIAL WINDOWS OF HIGH CONDUCTIVITY. David Ofer, Richard M. Crooks and Mark S. Wrighton, Department of Chemistry, Massachusetts Institute of Technology, Cambridge, MA 02139.

Many conjugated polymers show reversible electrochemical oxidation accompanied by large changes in their conductivity. We have extended the potential range where durable conducting polymers can be studied. We have investigated a number of polythiophenes, polypyrroles, and polyaniline by employing solvent/electrolyte media such as liquid $\text{SO}_2/[(n\text{-Bu})_4\text{N}]\text{AsF}_6$ where the electrochemical window is -0.2 to $+3.9 \text{ V}$ vs. SCE. Measurements of relative conductivity as a function of potential reveal that these polymers have finite potential windows of high conductivity, indicating that they only conduct in "mixed valence" states of fractional charge per repeat unit as is the case for organic charge-transfer salts. Potential dependent changes in electronic structure have been probed by *in situ vis-near IR* spectroscopy and related to cyclic voltammetry and changes in conductivity. In contrast to polyaniline, the highest occupied electronic band of poly(3-methylthiophene) appears to remain significantly populated at the most positive potentials where the polymer is durable, and the conductivity remains higher than that of the neutral polymer.

Q3.7

CHEMICAL AND PHYSICAL STUDIES OF SOLUBLE PART OF EMERALDINE: ELECTRONIC AND MAGNETIC PROPERTIES OF SHORT CHAIN SPECIES. R. Laversanne, CRPP / CNRS Château Brivazac F 33600 Pessac FRANCE

Polyaniline is well known as a conducting polymer for its original properties. One of the more striking is the possibility of switching between insulating and conducting phase by acid-base equilibrium. Yet the chemically prepared emeraldine is not perfectly characterized and a low molecular weight product is usually eliminated through light solvent extraction.

We present the results of investigations on this low molecular weight compounds. Chemical analysis indicate that not only the chain length is shorter than in the insoluble part of emeraldine, but oxidation level and chemical nature of the polymer are different.

On the other hand physical studies show that the electronic and magnetic behavior is fairly similar to this of the pristine emeraldine. In particular high conductivity, of the order of 1 Scm^{-1} is observed for highly protonated samples. Also the number of spin is protonation level dependent, but with a higher susceptibility of the unprotonated sample than in the corresponding emeraldine base.

The discussion will focus on the comparison between short chain species and what is usually called emeraldine and on the validity of transport theories used to describe this polymer.

Q3.8

POLYANILINE AS A REVERSIBLY SWITCHABLE MATERIAL. W.-R. Shieh, and S. C. Yang, University of Rhode Island, Chemistry Department, Kingston, RI 02881; and C. Marzocco, Rhode Island College, Department of Physical Sciences, Providence, RI 02908.

The electrical, optical and magnetic properties of conducting polymers are dramatically changed during an insulator-to-metal transition induced by doping. A reversal of this property-change can be achieved by undoping. If such externally controlled changes of properties are reversible over a large number of cycles the material is useful as a "smart" material that can adjust its electronic and optical properties on demand. In this study we examined the reversibility and cycling lifetime of electrochemical doping/undoping of polyaniline for its application as a smart material.

Polyaniline films coated on tin oxide or gold electrode were electrochemically switched to show clear-to-green color cycles while it undergoes insulator-to-metal transitions. Under suitable conditions polyaniline has cycling lifetime better than 100,000 cycles. The reason for the eventual loss of response was found to be the loss of ohmic contact at the interface between the polymer and the substrate instead of any irreversible chemical change of the polymer. The photochemical stability of polyaniline was also tested during the switching cycles. Results indicates polyaniline is a potentially useful "smart" material.

This work is supported in part by PPG Industries and by a contract administered by the Office of Naval Research from DARPA.

Q3.9

MOISTURE EFFECTS IN THE CONDUCTING POLYMER, POLYANILINE. J.P. Travas, C. Menardo, and M. Nechtschein, CENG, DRF/SPH/DSPE (UPR CNRS 216), 85X, 38041 Grenoble Cedex, France; S.K. Manohar and A.G. MacDiarmid, Department of Chemistry, University of Pennsylvania, Philadelphia, PA 19104-6323 (USA)

It has been known for a long time that polyaniline easily collects moisture and that hydration plays an important role in the transport properties. Conductivity (σ) and thermopower (S) have been measured as a function of the water vapour pressure. For any protonation level of polyaniline, hydration results in an increase of σ and a decrease of S . We have undertaken different studies in order to determine whether the

origin of the mechanisms which are responsible for these effects, is microscopic or macroscopic. We will present measurements of conductivity in poly-N-methyl-aniline, which show almost no dependence on the water vapour pressure. In this compound, most of the acidic protons are substituted by methyl groups. Several results concerning the moisture absorption process which have been obtained using proton NMR will be presented. In particular, we have shown that the absorption is a bulk process, water molecules being fixed on, or nearby, the acidic sites of polyaniline (protonated sites). These two results give arguments in favour of a microscopic origin of the observed effects.

Additional informations on the dynamics of the absorbed water molecules have been obtained. Two water phases exist 1) a solid phase composed of strongly fixed molecules and a "liquid" phase composed of mobile molecules. The role of the solid phase in a proton exchange mechanism between the polymer and the absorbed water will be pointed out.

Q3.10

SPECTROSCOPIC AND MOLECULAR WEIGHT STUDIES OF POLYTOLUIDINES. Y. Wei and K.F. Hsueh, Department of Chemistry, Drexel University, Philadelphia, PA 19104; A. Ray, A.G. MacDiarmid and J. Dykins, Department of Chemistry, University of Pennsylvania, PA 19104-6323 and A.J. Epstein, Department of Physics, The Ohio State University, Columbus, OH 43210-1106.

The base forms of poly(*o*-toluidine) and poly(*m*-toluidine) have been synthesized¹ and characterized by UV-visible, infrared and ¹H NMR spectroscopy. Assignments of the proton NMR signals have been facilitated by the use of model compounds. The distinction between benzenoid and quinoid methyl resonances in the NMR permits a semi-quantitative estimation of the oxidation states of the polytoluidines. Infrared studies are consistent with a polyaniline-type backbone having pendant methyl groups. Both polytoluidines appear to be essentially identical to each other and have conductivities of about 0.1 S/cm upon doping with 1M HCl. Field desorption mass spectrometry (FD-MS) gave a molecular weight of up to ~5,000. Gel-permeation chromatography of the same sample showed a bimodal elution pattern, suggesting that the FD-MS technique detects only the lower molecular weight fraction of the polymer. Despite this inherent limitation, FD-MS yields the interesting information that the polymer contains chains of both odd and even numbers of repeat units, necessitating the coexistence of different oxidation states in the base form of the polymer.

Q3.11

ELECTRICALLY CONDUCTIVE COMPOSITE OF POLYANILINE AND POLY(p-PHENYLENE-TEREPHTHALAMIDE), Xian-Tong Bi, Chun Wang, Jing-Sheng Bao, Institute of Chemistry, Academia Sinica, Beijing 100080, China.

The electrical properties and stability of polyaniline(PAn) prepared by chemical or electrochemical method are potentially attractive systems, but the poor processibility of PAn restrict their potential for applications.

It was known, the poly(p-phenylene-terephthalamide) (PPTA) can be used to make high modulus and high strength fibers by dry-jet-wet-spinning method.

In this paper, the improvement of the mechanical properties of PAn by processing the concentrated sulfuric acid solution of the mixture of chemically prepared conductive PAn powders and PPTA in different weight ratio are presented.

The concentrated sulfuric acid solution of PAn and PPTA were processed to films and threads, they are liquid crystalline conductive polymers with good mechanical properties.

The data of electrical conductivities and mechanical properties of the threads are given in the following table:

Weight ratio of PPTA/PAn	Tensile strength (N/mm ²)	Elongation at break, %	σ (s/cm)
4/1	12.5	4.0	1.5×10^{-4}
3/1	20.1	4.0	2.6×10^{-3}
2/1	41.2	4.0	2.3×10^{-1}

The X-ray diffraction and liquid crystal pictures of the composite are also reported.

Q3.12

INFRARED REFLECTION-ABSORPTION STUDY OF ANILINE ELECTRO-POLYMERIZATION ON STAINLESS STEEL. F. Gaillard, G. Bouyssoux, Département de Chimie Appliquée et Génie Chimique, CNRS UA-417, Université Claude Bernard-LYON I, 69622 Villeurbanne; and S.N. Kumar, Laboratoire de Physique de la Matière, CNRS UA-358, I.N.S.A. LYON, 20 Av. Albert Einstein, 69621 Villeurbanne, France.

Considerable work has been done recently on conducting polymers, and among them polyaniline. For such studies, FTIR in reflection-absorption mode has been shown to be a very powerful surface analysis technique.

Polyaniline films were grown on 304 L steel subjected to various surface treatments, such as degreasing, etching and anodization. The FTIR spectra of the films formed showed clear evidence for quinonic/aromatic alternating structure involving head to tail coupling. This was found to be independent of the thickness of the polymeric layer. The quinonic/aromatic ratio can be varied when the film is subjected to further dedoping treatments such as KOH immersion or electrochemical reduction.

The IR absorption due to the aromatic ring structure was observed after a certain induction period during the initial stages of electropolymerization. This was also confirmed by X-ray photoelectron spectroscopy. Low energy electron induced X-ray spectroscopy and X-ray fluorescence spectroscopy measurements. Results on FTIR measurements performed during the thermally induced structural changes of the polymer will also be presented.

Q3.13

ELECTRICAL PROPERTIES OF POLYANILINE--POLYMER COMPOSITE FILMS. KeCheng Gong; and Longgui Zhong; Department of Polymer Science, South China University of Technology Guangzhou, P.R. China.

Polyaniline--Polymer composite films through chemical oxidative polymerization using various oxidizing agents such as potassium chlorate, ammonium persulfate, hydrogen peroxide etc and employing a vinyl group polymer film as a base polymer were prepared in an acid medium. Their analysis by AES, IR spectroscopy and X-ray photoelectron spectroscopy shows that on these films polyaniline is an organic polymer of emeraldine basic structure and that it probably results from the coupling of chemically formed PhNH^+ radicals with the monomer. The WAXD spectroscopy shows that polyaniline--polymer composite films have some crystalline structural characteristics. These films are flexible, stable in air and homogeneous, and they display a conductivity of 10^{-4} -- $10^{-3} \text{ } \Omega^{-1} \text{ cm}^{-1}$ which is in the range of semiconductors.

Q4.1

PREPARATION AND PROPERTIES OF ORGANIC SUPERCONDUCTOR κ -(BEDT-TTF)₂Cu(NCS)₂ AND ITS RELATED MATERIALS. Gunzi Saito, The Institute for Solid State Physics, The University of Tokyo, Roppongi, Minato-ku, Tokyo 106, Japan.

Some important structural, physical and chemical aspects of an organic superconductor κ -(BEDT-TTF)₂Cu(NCS)₂, T_c of which is the highest among the organic superconductors so far known, will be discussed. Single crystals of the salt were prepared by electrocrystallization with three different electrolytes. The crystal structure indicates that dimerized BEDT-TTF molecules construct a two-dimensional (2D) conducting donor sheet in the bc plane which is sandwiched by the insulating anion sheets composed of polymerized Cu(NCS)₂ along the a-axis. Two kinds of sheets are linked by short atomic contacts between the terminal ethylene groups of BEDT-TTF and N and S atoms of the anion.

T_c of the BEDT-TTF-h₈ salt is 10.4K and its deuterated sample showed higher T_c by 0.5-0.6K (inverse isotope effect). Magnetic susceptibility measurements indicate that the salt is non-ideal class II superconductor and almost 100% of the perfect diamagnetism was observed below 7K. Upper critical field is anisotropic. H_{c2} values at 6K were about 13T and 0.5T in the 2D plane and normal to it, respectively. The ratio of GL coherence lengths were estimated as $\xi_{bc}(0): \xi_a(0) = 182\text{\AA}:9.6\text{\AA} = 19:1$. A Shubnikov-de Haas signal was observed which indicates the existence of the closed Fermi surface. Some other properties obtained by EPR, NMR, thermoelectric power, specific heat, tunneling spectroscopic measurements etc. and T_c of BEDT-TTF organic superconductors will be discussed for the molecular design of new organic superconductors. Some organic conductors related to κ -(BEDT-TTF)₂Cu(NCS)₂ will be also presented.

Q4.2

FERMI SURFACE OF ORGANIC METALS β -(ET)₂IBr₂ AND β -(ET)₂I₃ STUDIED BY MEANS OF GALVANOMAGNETIC MEASUREMENTS. V.N. Laukhin, M.V. Kartsovnik, and S.I. Pesotskii, Institute of Chemical Physics, USSR Ac.Sci., Chernogolovka, USSR; P.A. Kononovich, and I.F. Schegolev, Institute of Solid State Physics, USSR Ac.Sci. Chernogolovka, USSR.

Angular and field dependencies of the Shubnikov-de Haas oscillations and magnetoresistance have been studied in single crystals of the organic metals β -(ET)₂X (X = IBr₂ and I₃). For β -(ET)₂IBr₂ the electron orbits have been found to be open in the c-direction and closed in the ab-plane. Two types of the oscillations have been observed corresponding to the extreme ab-plane cross-sections values about 50 and 0.6% of the Brillouin zone area and to the cyclotron masses of 4.5 and 0.5m_e, respectively. The classical magnetoresistance part have been shown to oscillate with the field rotating in the ac- and b'c-crystal planes, that is likely associated with the Fermi surface peculiarities. A possible shape of the Fermi surface is discussed. For β -(ET)₂I₃ only slow oscillations at field directions close to H//c have been observed. The extreme cross-section value is about 1% of the corresponding Brillouin zone area.

Q4.3

SUPERCONDUCTING AND NORMAL STATE PROPERTIES OF BEDT-TTF BASED ORGANIC METALS. Madoka Tokumoto, K. Murata, N. Kinoshita, H. Bando, K. Yamaji and H. Anzai, Electrotechnical Laboratory, Tsukuba, Ibaraki 305, Japan

Recent progress on the superconducting and normal state properties characteristic to the BEDT-TTF based organic metals, including β -(BEDT-TTF)₂X and κ -(BEDT-TTF)₂Cu(NCS)₂, are presented. In addition to the low- and high- T_c states, with $T_c = 1$ K and 8 K, respectively, a new superconducting state with $T_c = 2$ K was found recently in β -(BEDT-TTF)₂I₃. Out of a systematic study on the β -(BEDT-TTF)₂X salts with the superconducting transition temperature (T_c) varying from 8 K to below 1 K, empirical rules for various factors governing T_c in this class of organic metals have been extracted.

In contrast to the quasi one-dimensional TMTSF based superconductors, two-dimensional nature of the electronic structure of BEDT-TTF salts has recently brought about a pronounced progress in the field of the Fermi surface study (Fermiology) on synthetic organic metals through observations of various quantum oscillations. In addition to the Shubnikov-de Haas and de Haas-van Alfen effects, a new oscillatory phenomenon characteristic to a quasi two-dimensional electronic system has been discovered in the angular dependence of magnetoresistance. The latter phenomenon is shown to be a new powerful tool in Fermiology.

Q4.4

HUBBARD PARAMETERS IN (BEDT-TTF)₂X CRYSTALS. Oliver H. LeBlanc, Jr., Margaret L. Blohm, and Richard P. Messmer, General Electric Corporate Research & Development, Schenectady, NY 12301.

Charge motion and spin exchange in (BEDT-TTF)₂X salts can be described by a two-dimensional Hubbard Hamiltonian. The relevant Hubbard parameters are computed for several of these salts, both superconducting and non-superconducting. An ab initio tight-binding method is used. Hartree-Fock LCAO molecular orbitals are determined for each unique BEDT-TTF molecule in the crystal structure. Orthogonalized linear combinations of these are used to compute intermolecular interactions between pairs of BEDT-TTF neutral molecules and +1 radical cations situated at nearest-neighbor lattice positions. One- and two-electron terms are included. Values are determined for: intermolecular transfer integrals (t_{ij}), on-site repulsions (U_{ii}), and nearest-neighbor repulsions (V_{ij}). The computed magnitudes of these parameters are consistent with the use of the tight-binding method. The calculations are repeated with small translational and rotational displacements of the molecules to determine the effects of lattice vibrations.

One-electron energy bands constructed from the t_{ij} , ignoring the U_{ii} and V_{ij} , are generally similar to those previously calculated by Mori and by Whangbo and their coworkers by semi-empirical, extended Huckel methods, but quite different from those found by Kubler et al. in β -(BEDT-TTF)₂I₃ using another ab initio technique, the augmented spherical wave method.

However, the U_{ii} and V_{ij} are so large (~2-3 eV) compared to the t_{ij} (~0.1eV) that the one-electron band model gives a poor description of the ground state and low-lying excited states of these systems. Evidently, a full treatment of the Hubbard Hamiltonian, with U_{ii} and V_{ij} taken into account, is needed.

Q4.5

SPECIFIC HEAT MEASUREMENTS ON κ -(BEDT-TTF)₂Cu(NCS)₂. R. G. Goodrich and Jing-chun Xu, Department of Physics and Astronomy, Louisiana State University, Baton Rouge, LA 70803-4001; and Margaret Blohm and Oliver LeBlanc, General Electric Research and Development Center, P. O. Box 8, Schenectady, NY 12301.

We have measured the specific heat of κ -(BEDT-TTF)₂Cu(NCS)₂ from 4 to 15 K. The superconducting

transition at 9.4 K is observed in a 5 mg powdered sample. Both the magnitude of the change in C_p at T_c and the temperature dependence of C_p below T_c indicate a strong coupling superconductor. If the lattice specific heat is assumed to contain contributions due to rigid body coupled translational and rotational modes between the two (BETF-TTF) molecules and independently the translational and rotational modes of the $\text{Cu}(\text{NCS})_2$, also treated as a rigid body, the phonon contribution to the specific heat in the measured temperature range can be represented by a Debye integral expression with a Debye temperature of 68 K. These results indicate that in the temperature range of the superconducting transition the dominate contribution to the phonon spectrum arises from these isolated molecular rigid body vibrations.

Q4.6

PRESSURE DEPENDENCE OF THE STRUCTURAL AND ELECTRONIC PROPERTIES OF ORGANIC SUPERCONDUCTORS. Daniel Chasseau, Jacques Gaultier, Hamid Houbib, Laboratoire de Cristallographie, URA 144 CNRS, Laurent Ducasse, Laboratoire de Physico-Chimie Théorique, URA 503 CNRS, Université de Bordeaux I, 33405 Talence Cedex (France), Mohammed Kurmoo and Peter Day, Inorganic Chemistry Laboratory, South Parks Road, Oxford OX1 3QR(U.K)

Physical properties of molecular superconductors are very sensitive to high pressure and a great number of experiments have been performed under these conditions. But, up to now, very few crystal structures have been determined by X-ray diffraction under pressure. We report here on the compressibility of the $(\text{TMTSF})_2\text{ClO}_4$ and $(\text{BEDTTTF})_2\text{-Cu}(\text{NCS})_2$ superconducting salts and on their structural and electronic properties derived from their high pressure crystal structure.

The pressure dependence of the cell parameters of $(\text{TMTSF})_2\text{ClO}_4$ has been studied up to 12 Kbar at room temperature. The compressibility has been calculated. The angle between the direction of the principal compressibility and the stacking axis is about 20 degrees at ambient pressure; it strongly increases with pressure. The magnitudes and the bulk modulus do not vary.

The crystal structures have been refined at 4, 6, 9.5 Kbar ($R=0.05$). The disorder of the perchlorate anion is reduced. The transfer integrals have been calculated; both normal and transverse overlaps strongly increase with pressure. At high pressure ($P > 12$ Kbar), the crystals become twinned and their three dimensional character disappears.

A similar study is currently in progress on the $(\text{BEDTTTF})_2\text{-Cu}(\text{NCS})_2$ superconducting salt which is up to now the molecular compound which exhibits the highest metal-superconductor transition temperature.

Q4.7

THIN FILM FORMATIONS OF CHARGE TRANSFER COMPLEXES WITH METALLIC PROPERTIES BY VACUUM EVAPORATION METHODS. M. Yudasaka and K. Nakanishi, Materials Chemistry, Faculty of Engineering, Yokohama National University, Tokiwadai 156, Hodogaya-ku, Yokohama 240, Japan
H. Yamochi and G. Saito, Institute for Solid State Physics University of Tokyo, 1-77-2 Roppongi, Minato-ku, Tokyo, Japan

A lot of charge transfer complexes are known to have metallic electrical properties. There have been known even those which behave like superconductors. So far, studies to obtain films of these charge transfer complexes have not been done enough.

Charge transfer complex films obtained in this study are TTF- I_2 and TMTSF- I_2 . They were obtained by double source evaporation of TTF and iodine or TMTSF and iodine under high vacuum. Iodine was evaporated by using a crucible whose temperature could be controlled down to about 100K. Temperature of quartz glass substrates were kept at room temperature.

The deposited films were confirmed to be really made of the charge transfer complexes by absorption spectra of infrared and visible regions. Electrical conductivities of the films were 1-10 S/cm. Properties of the films will be studied in detail.

Films of several other kinds of charge transfer complexes will be made by the same way and will be discussed their properties in detail, too.

Q4.8

SYNTHESIS, CRYSTAL STRUCTURE AND SPECTROSCOPIC STUDIES OF NEW CT COMPOUNDS OBTAINED BY REACTION OF TTF AND THE POLYOXOANION $[\text{Mo}_6\text{O}_{19}]^{2-}$. D. Attanasio, C. Bellitto, M. Bonamico, V. Fares, P. Imperatori, S. Patrizio, ITSE, CNR, Area della Ricerca di Roma, C.P.10, I-00016 Monterotondo (Roma), Italy.

Low-dimensional synthetic metals based on the one-electron organic donor TTF (tetrathiafulvalene) have been studied extensively in the last decade. Less attention has been paid to the TTF-derivatives where the counter ion is an inorganic molecular cluster, possibly in the mixed-valence state. The only few known examples show interesting electrical and magnetic properties. We have decided therefore to study the reaction of the donor molecules derived from TTF with the polyoxo-metalates having general formula $[\text{M}_6\text{O}_{19}]^{n-}$, where $M = \text{Mo}$ and W , $n = 2, 3$. Here we report the preparation and the structural data of two new compounds: $(\text{TTF})_3[\text{Mo}_6\text{O}_{19}]$ 1
 $(\text{TTF})_2[\text{Mo}_6\text{O}_{19}]$ 2

Both have been obtained by electrocrystallization technique from TTF and the $[\text{Mo}_6\text{O}_{19}]^{2-}$ anion in a mixture of acetonitrile and 1,1,2- $\text{C}_2\text{H}_3\text{Cl}_3$. The X-ray crystal and molecular structure of 1, refined to an $R = 0.025$, shows a one-dimensional stack of TTF, and each stack fits into channels formed by the anions. Within the stack a chain of trimers can be identified, the inter-trimeric distance being 3.51 Å. The infrared spectrum at r.t. is a typical spectrum of a TTF-mixed-valence derivative. The crystal structure and the physical properties of both compounds will be presented and discussed.

Q4.9

A NEW SYNTHETIC METAL PRECURSOR: DIMETHYLTETRA-THIOTETRACENE AND RELATED COMPOUNDS. Toshio Maruo, Megh Singh and M. Thomas Jones, Department of Chemistry, University of Missouri-St. Louis, St. Louis, MO 63121.

The electron donor tetrathiotetracene (TTT) forms charge transfer salts which at room temperature possess some of the highest electrical conductivities of any known synthetic metal. However, TTT is rather insoluble and hence difficult to purify. Thus, the synthesis and characterization of a new synthetic metal precursor, dimethyltetrathiotetracene (DMTTT), is described. Among the reasons for the synthesis of DMTTT are to obtain a compound with improved solubility and to investigate the question of whether a donor with symmetry of C_{2v} will resist undergoing the Peierls transition better than the parent compound which has symmetry of D_{2h} .

Cyclic voltammetry studies show that like its parent, DMTT, can be oxidized in two reversible one-electron steps. Each of the oxidation waves for DMTT is shifted to more negative potentials than those observed for TTT as expected for a dimethyl substituted TTT.

Both 1:1 and 2:1 DMTTX complexes have been prepared and characterized. Comparisons of physical properties and studies such as x-ray powder patterns, solid state ESR spectra, and electrical conductivities are reported. To date, these comparisons reveal considerable similarity between the properties of any given DMTT complex and its corresponding TTT complex.

Q4.10

TETRANITROQUINODIMETHANE (TNQ) - ELECTRON-DEFICIENT PROTOTYPE FOR A NEW SERIES OF ORGANIC SOLID STATE MATERIALS. David J. Vanderah, Richard A. Bellins, Arnold T. Nielsen, and Chris Baun, Research Department, Code 3853, Naval Weapons Center, China Lake, CA.

Recently we have synthesized a number of novel aromatic compounds substituted with two or more trimethyl groups. The title compound, TNQ, was prepared by vacuum pyrolysis of one of these, hexanitro-p-xylene (p-HNX), via 1,6-elimination of N_2O_4 . Clearly related to the more well known tetracyanoquinodimethane (TCNQ), TNQ is the first example of an quinodimethane system substituted with nitro groups. The TNQ system should be more electron-deficient than TCNQ owing to the stronger electron-withdrawing nature of the nitro group and thereby may give rise to complexes of enhanced electric and/or magnetic properties. Evidence of a charge-transfer complex of TNQ has been obtained.

In addition to TNQ, we are applying our synthetic methodology to prepare related systems. Our latest progress on the synthesis of other electron-deficient compounds containing nitro groups and new charge-transfer complexes derived from them will be presented.

Q5.1

HIGHLY CONDUCTING COMPLEXES OF METALS WITH dmit AND dddt DITHIOLATE LIGANDS. E.B. Yagubskii, A.I. Kotov, L.I. Buravov, and A.G. Khomenko, Institute of Chemical Physics, USSR Ac. Sci., Chernogolovka, USSR; V.E. Shklover, S.S. Nazapetyan, and Yu.T. Struchkov, A.N. Nesmeyanov Institute of Organoelement Compounds, USSR Ac. Sci., Moscow, USSR; and L.Yu. Ukhin, Institute of Physical and Organic Chemistry, Rostov State University, Rostov, USSR.

Highly conducting metal dithiolates have been synthesized based on anion $Au(dmit)_2^-$ ($dmit = 4,5$ -dimercapto - 1,3-dithiol - 2-thione) and cation $M(dddtt)_2^+$ ($M = Ni, Pt, Au$; $dddtt = 5,6$ -dihydro - 1,4-dithiin-2,3-dithiolate) complexes. Crystal structures and conducting properties have been studied. $[Au(dmit)_2]_2 \cdot Bu_4N$ and $[Au(dmit)_2]_2 \cdot Et_4N$ are characterized by the resistivity temperature dependence of the metallic type down to helium temperatures. The $[M(dddtt)_2]^+$ cation chelates represent a new class of dithiolene compounds and their salts are metal-complex analogs for the organic superconductors of BEDT-TTF cation-radical salts family. Till now only anion and neutral metal-complexes of dddt have been known which are

insulators. The behaviour of bond lengths changes in dddt by going from anion to cation complexes has been considered. The possibilities of the chemical modification for $[M(dddtt)]^+$ salts have been discussed. The nature of both metal and anion has been established to influence strongly the structure and conducting properties of these salts.

Q5.2

NEW ELECTRICALLY CONDUCTING SOLIDS BASED ON NICKEL(II) - BIS(1,3-DITHIOLE-2-THIONE-4,5-DISELENOL-ATE). A.M. Kini, H. H. Wang, M. A. Beno, U. Geiser, A. J. Schultz, K. D. Carlson and J. M. Williams, Chemistry and Materials Science Divisions, Argonne National Laboratory, Argonne, Illinois, 60439.

The metallo-organic compound nickel(II)-bis(1,3-dithiole-2-thione-4,5-dithiolate), commonly referred to as $[Ni(dmit)_2]^{2-}$, has recently yielded several electrically conducting and even superconducting materials. Encouraged by these findings and Nigrey's recent preparation of its selenium analog nickel(II)-bis(1,3-dithiole-2-thione-4,5-diselenolate), $[Ni(dsit)_2]^{2-}$, we have studied the electro-oxidation of $[Ni(dsit)_2]^{2-}$ with various cationic counterions. Our results thus far indicate that the stoichiometries [cation : $Ni(dsit)_2$ ratio] of the resultant solids depend on the cation size--larger cations favoring 1:1 and smaller cations favoring 1:2. Some of these solids structurally resemble κ -(BEDT-TTF) $_2Cu(NCS)_2$, an ambient pressure superconductor ($T_c = 10$ K). Details of the preparation, structural aspects, electrical properties and ESR results of these new materials will be presented.

Q5.3

BRIDGED MACROCYCLIC TRANSITION METAL COMPLEXES, A NEW TYPE OF SEMICONDUCTING MATERIALS. Michael Hanack, Andreas Hirsch, Armin Lange, Manfred Rein, Günter Renz und Petra Vermehren, Institut für Organische Chemie, Lehrstuhl für Organische Chemie II der Universität Tübingen, Auf der Morgenstelle 18, D-7400 Tübingen, West Germany

Bridged quasi onedimensional macrocyclic transition metal complexes $[MacML]_n$ using phthalocyanine (Pc), tetrabenzoporphyrine (TBP), 1,2- and 2,3-naphthalocyanines (1,2-; 1,3-Nc) as macrocycles (Mac) with $M = e.g. Fe, Ru, Co$ and $L = e.g. pyrazine (pyz), 1,4$ -diisocyanobenzene (dib), tetrazine (tz) exhibit interesting electrical properties. Regardless of the size of the bridging ligand after either chemical or electrochemical doping stable semiconducting compounds $[MacMLX]_n$ ($X = e.g. I, BF_4^-, ClO_4^- \dots$) are formed. For the first time the complete characterization of a soluble oligomer $[MacML]_n$ ($Mac = R_4Pc, M = Ru, L = dib$) by 1H -NMR spectroscopy is reported.

Some of these shish kebab complexes e.g. $[PcM(tz)]_n$, ($M = Fe, Ru$) or $[MacMCN]_n$; ($Mac = Pc, TBP; M = Co, Fe$) exhibit good semiconducting properties without additional external doping. Whether or not these compounds are intrinsic semiconductors will be discussed.

The synthesis of oligomeric bridged mixed valence compounds $[PcM^{3+}LPcM^{2+}L]_n$ ($M = \text{e.g. Fe}$) is another target of our work. We report here about first attempts to synthesize these oligomers.

Q5.4

Uniaxial Stress Effects on Optical Absorption Spectra of Highly Oriented Iodine Doped Phthalocyanine Films. Hiroaki Tsuyoshi, Masako Yudasaka, Masatoshi Tanaka, Kazumi Nakanishi, Susumu Kurita, Faculty of Engineering, Yokohama National University, 156 Tokiwadai, Hodogaya-ku, Yokohama 240, Japan

Highly oriented films of iodine doped Pd- and Ni-phthalocyanines are known to be obtained by iodine doping into Pd- and Ni-phthalocyanine epitaxial films which are available on mica by vacuum evaporation. The films have one dimensional like structures and show strong dichroism. Their absorption spectra are known to have large maxima around 620nm and 570nm when the incident light is polarized perpendicular and parallel to the one dimensional axis, respectively. We could see further a small maxima around 440nm in the parallel polarization case when the measurement temperature was lowered down to -180°C .

Uniaxial stress have been applied onto the films by mounting them on the piezoelectric transducer. The peak at 620nm and 505nm lost their intensity and shifted toward higher energy side by expansion along the one dimensional axis.

The results described above can be explained by ascribing the peak at 620nm to the $\pi-\pi^*$ transition of phthalocyanine molecules as usual, that of 505nm to I_2 , and that of 440nm to I_2^- .

Q5.5

DISCOTIC LIQUID CRYSTALLINE PORPHYRINS: PHOTO-PHYSICAL AND PHOTOELECTRICAL PROPERTIES OF LARGE-AREA CRYSTALLINE FILMS. Brian A. Gregg, Dept. of Chemical Engineering, Marye Anne Fox, Dept. of Chemistry, and Allen J. Bard, Dept. of Chemistry, University of Texas at Austin, Austin Tx.

The discotic liquid crystalline (DLC) phase can be used to form large-area, thin, crystalline arrays of one-dimensional conductors. A series of octaalkylporphyrins bearing different side chains have been synthesized including some with electron-withdrawing substituents at the meso positions. These materials are solids at room temperature and exhibit a single broad DLC phase before melting to isotropic liquids. The photophysical properties of thin films of these compounds are a strong function of the film order (crystallinity). There is evidence for ring-to-ring charge transfer state formation upon illumination of the most highly ordered films.

These materials have been capillary-filled into thin cells consisting of two sheets of indium-tin oxide glass separated by 1 - 5 μm spacers. Although completely symmetrical, such cells develop large, stable photovoltages and photocurrents when illuminated (e.g., $V_{oc} = 0.3\text{ V}$, $j_{sc} = 0.4\text{ mA/cm}^2$ under white light, 150 mW/cm^2). A model based on kinetically-controlled asymmetric exciton dissociation and photoinjection at the illuminated interface is presented to explain these results. This appears to be the first unambiguous example of a photovoltaic cell controlled entirely by interfacial kinetics. The predominance of the photoinjection process in these cells is attributed to the single-crystal-like character of the porphyrin films.

Q6.1

LANGMUIR-BLODGETT FILMS OF CONDUCTING POLYMERS I.A. Skotheim, X.Q. Yang, J. Chen, H.S. Lee, Brookhaven National Laboratory, Upton, NY 11973; Y. Okamoto, Polytechnic University, Brooklyn, NY 11201; M.L. denBoer, Hunter College of CUNY, New York, NY 10021; M.F. Rubner, MIT, Cambridge, MA 02139; S. Tripathy, University of Lowell, Lowell, MA 01854.

It has recently been demonstrated by several groups that Langmuir-Blodgett films can be constructed with polyheterocyclic conducting polymers based on alkylpyrroles and alkylthiophenes. In the case of alkylpyrroles, the heterocycle has a sufficient dipole moment to form a hydrophilic head group. 3-alkyl pyrroles with a sufficiently long hydrocarbon tail become surface active to produce single phase LB films which can be polymerized at the air-water interface. The films can be transferred to substrates to form highly anisotropic conducting multilayer structures. Although poly(3-alkyl thiophenes) are not surface active by themselves, high quality LB films can be formed with mixtures with stearic acid. We have made detail studies of the structure of these LB films with synchrotron radiation based spectroscopies. The molecular orientation of the films have been studied with x-ray absorption spectroscopy which separately reveal the orientation of the alkyl chains and the heterocycle headgroups. X-ray diffraction has been used to study the long range ordering of both monolayer and multilayer films. The intensity of x-rays emanating from a storage ring allows in-plane x-ray diffraction of monolayer films. The detailed results of these studies will be discussed.

Q6.2

LANGMUIR-BLODGETT MULTILAYER THIN FILMS OF ELECTRICALLY CONDUCTIVE POLYMERS. M. F. Rubner, I. Watanabe, K. Hong and R. Rosner, Department of Materials Science and Engin'g, MIT, Cambridge, MA 02139.

Well ordered multilayer thin films of a variety of conjugated polyheterocycles have been prepared using the Langmuir-Blodgett thin film technique. This technique allows, for the first time, control over the molecular architecture and superstructure of electroactive polymers. To date, two different methods have been established for the LB manipulation of these polymers. In one case, polypyrroles are synthesized directly at the air-water interface and subsequently fabricated into multilayer thin films. The second method involves the LB manipulation of mixed monolayers comprised of poly(3-alkyl thiophenes) and stearic acid. It has been found that stable monolayers created from mixtures containing as much as 80 mole % of poly(3-alkyl thiophenes) fitted with alkyl groups ranging from four to eighteen carbons can be manipulated into LB films using the traditional vertical lifting technique.

In both cases, it is possible to obtain multilayer structures which exhibit highly anisotropic electrical properties. The level of anisotropy can be further enhanced through the fabrication of novel organic superlattices comprised of molecular layers of conducting polymers alternating with insulating layers of surface active molecules. In some cases, conductivity anisotropies ($\sigma_{\parallel} / \sigma_{\perp}$) of over 10^{12} have been achieved. Thus, it is possible to fabricate novel molecular architectures which exhibit high in-plane conductivities (as large as 5 S/cm) and exceptionally low transverse conductivities (essentially insulating). The results of optical, infrared dichroism, capacitance (as a function of frequency and film thickness), and x-ray diffraction studies aimed at elucidating the structure and properties of these new thin films will be discussed.

Q6.3

HETEROCYCLIC POLYMERS AND COPOLYMERS WITH CONTROLLED OPTOELECTRONIC PROPERTIES. Jose P. Ruiz, Kasinath Nayak, Dennis S. Marynick and John R. Reynolds, Center for Advanced Polymer Research, Department of Chemistry, The University of Texas at Arlington, Arlington, TX, 76019-0065.

A series of aromatic polymers and copolymers have been investigated that contain a combination of 2,5-thienylene and 1,4-phenylene linkages. Bis-(1,4-thien-2-yl)phenylene monomers have been prepared with a variety of substituents on the 2,6-phenylene positions. Subsequent oxidative polymerization of this monomer, both chemically and electrochemically, yield a family of polymers containing a thiophene-phenylene-thiophene repeat unit. Theoretical modeling, using both PRDDO and ab initio methods, has been used to correlate thiophene-phenylene torsional angles with optical gaps. In addition, polymer band structure has been investigated using the Extended Hückel method.

Q6.4

SYNTHESIS, STRUCTURE, INFRARED SPECTRA, AND IODINE DOPING OF UNSUBSTITUTED POLYAZINES. William B. Euler, Benjamin C. Gill, Department of Chemistry, University of Rhode Island, Kingston, RI, 02881.

We have shown previously that the permethyl substituted polyazine ($(N-C(R)-C(R)-N)_x$, $R=CH_3$) is a linear, conjugated polymer that can be doped with iodine to give highly conducting powders. It was thought that the removal of the pendant methyl groups would lead to an improved polymeric conductor that would be analogous to polyacetylene.

Unsubstituted polyazine (PAZ) is synthesized from the condensation of glyoxal dihydrazone with glyoxal at room temperature in ethanol with acid catalysis. The IR spectra of product polymer shows a fairly intense and broad band at 3300 cm^{-1} due to OH groups. Some of this intensity may be due to occluded ethanol, but the primary source of OH is from nondehydrated imines, i.e., amino alcohols. This unusual structure arises from the hydrated nature of glyoxal, which is found as a trimeric dihydrate. Reaction in refluxing ethanol does not improve the dehydration significantly, while going to higher temperatures decomposes the glyoxal dihydrazone. The amino alcohol sites in the polymer chain act as conjugation breaks within the π system.

Despite the defects in the PAZ chains, the polymer can be doped with iodine into a conducting state. Room temperature conductivities as high as 0.1 $cm^{-1} ohm^{-1}$ can be attained. IR spectra of the doped and undoped polymers are similar, showing that no major structural changes have occurred. One new band does show up upon doping at about 1500 cm^{-1} which grows in intensity with doping level and is attributed to a bipolaronic type structure.

Q6.5

MODEL THIOPHENE OLIGOMERS: ELECTRONIC PROPERTIES AND THIN FILM DEVICES. Denis FLOCHU, Gilles HOROWITZ and Francis JABYER. C.N.R.S., Laboratoire des Matériaux Moléculaires 2, rue Henry Dunant- 94320, Thiais, France

In the field of conducting conjugated polymers, short oligomers of controlled chain length recently received much attention as model compounds towards a better understanding of the electronic properties of the corresponding polymers. The regioselective reconstruction of the chain sequence from the monomer unit by means of organic synthesis affords intermediate size molecules with a well-defined structure.

In this paper we illustrate this new approach to electronic polymers with alpha-conjugated thiophene oligomers ($\alpha-nT$) with $n = 3$ to 8. All oligothiophenes are individually synthesized. Thin solid films of controlled thickness are prepared on various substrates by vacuum sublimation.

In the first part, we discuss the optical spectra of the films in their neutral and doped states. Their third order optical nonlinearities have also been measured and MO calculations of the cubic nonlinear parameters have been performed as a function of the chain length and the inter-ring conformation. On the other hand, the highly stable radical cation $6T^{+}$ has been prepared and characterized: it may be considered as the basic polaron of polythiophene.

The second part focuses on the use of semiconducting $\alpha-6T$ thin films in building Schottky diodes and field-effect transistors. The main electric parameters of these devices are often superior to those of polythiophene: particularly, carrier mobilities as high as $10^{-2} cm^2 V^{-1} s^{-1}$ are obtained. Due to the good performances of the $\alpha-6T$ MISFET's, oligothiophenes appear to be very promising organic semiconductors.

Q6.6

PHOTOLUMINESCENCE, ESR, AND ODMR STUDIES OF PRISTINE AND PHOTODEGRADED POLY(3-HEXYLTHIOPHENE) FILMS AND SOLUTIONS. L. S. Swanson, L. R. Lichty, and J. Shinar, Ames Laboratory - USDOE* and Physics Department, Iowa State University, Ames, IA 50011-3020; K. Yoshino, Department of Electrical Engineering, Faculty of Engineering, Osaka University, Osaka 565, Japan.

The photoluminescence (PL), electron spin resonance (ESR), and optically detected magnetic resonance (ODMR) spectra of poly(3-hexylthiophene) films freshly cast from solution were measured as a function of 2.54eV irradiation in various gases and in vacuum. In the pristine films, the asymmetric ODMR spectra are decomposed into two gaussians 5G and 12G wide, split by $\Delta H = 2.4G$ at 9.4GHz and attributed to polarons, thus demonstrating charge conjugation symmetry breaking. At 20K, the narrow component is microwave saturated at lower power than the broad one. The 1.96eV exciton peak is very weak and the ODMR is absent in solution, hence both are suspected to result from interchain recombination events. Exposure of the films to either oxygen or above-gap photons alone does not noticeably affect the PL spectra, but an apparent photoinduced oxidation process quenches the PL and the ODMR. At -4mW excitation, the PL decay times are widely distributed from 35 - 6000 sec, possibly limited by O_2 diffusion at long times. The exciton peak and its sidebands decay more rapidly than the structureless component responsible for the ODMR.

*Operated for USDOE by Iowa State University under contract no. W-7405-Eng-82.

Q6.7

HELICAL CONFORMATIONS OF POLYTHIOPHENE, POLYPYRROLE AND THEIR DERIVATIVES. Miklos Kertesz and C.X. Cui, Department of Chemistry, Georgetown University, Washington, DC 20057.

Two stable conformations, a planar or nearly planar rod and a coil, have been located on the potential energy surfaces of several conducting polymers: polythiophene (PT), poly(3-methylthiophene) (PMeT), Polypyrrole (PPy) and poly(3-methylpyrrole) PMePy. The planar structure is slightly more stable for PT, PPy and PMePy, while the coil configuration is preferred for PMeT. This finding could explain the existence of the coil conformation for poly(3-butylthiophene) in solution and for doped PMeT and PPy in the solid phase. We have identified a quinoid coil form of PT by our calculations, which strongly supports the presence of a coil conformation of doped PT derivatives. The band gap and total energy as a function of conformation indicate that the thermochromic behavior of PT derivatives results from the change in conformation with temperature. Similar behavior is expected for PPy derivatives. Vibrational analysis for helical and planar conformation of PT has been carried out, which identifies experimental possibilities in distinguishing among the rod vs coil conformations. Similarities and differences with respect to polysilanes will be discussed.

Q6.8

RESONANT RAMAN SCATTERING OF POLY-3-HEPTYLTHIOPHENE C.Botta, A.Bolognesi, C.Catellani and S. Luzzati Istituto di Chimica delle Macromolecole, via Bassini 15, 20133 Milano, Italy. R. Tubino, dip. Fisica Università di Sassari.

We report resonant Raman scattering measurements on electrosynthesized poly-3-heptylthiophene, an interesting polymer which exhibit thermochromic and solvatochromic effects. The spectra of this

soluble conjugated polymer are obtained, at various temperatures, using different exciting wavelengths. Both as grown films and solutions has been studied. The results are discussed with reference to the specific electronic properties of the samples as monitored by their U.V.-Vis. absorption spectra.

Q6.9

OPTICAL, ELECTROCHEMICAL AND STRUCTURAL PROPERTIES OF POLY(THIENYLENE VINYLENES) AND POLY(PHENYLENE VINYLENES). H. Eckhardt, K.Y. Jen, C.C. Han, L.W. Shacklette, and R.L. Elsenbaumer, Allied-Signal, Inc., P.O. Box 1021R, Morristown, N.J. 07962

The electronic and electrochemical properties of poly(p-phenylene vinylene), poly(thienylene vinylene), and their derivatives with electron donating substituents such as methyl, methoxy, ethoxy, and butoxy groups were studied using electrochemical and optical techniques. It was found that electrochemically derived band gaps agree well with band gap values obtained from optical measurements. Substitution with electron donating groups substantially lowers both oxidation potentials and band gaps. A similar effect is attributed to the introduction of a vinylene linkage between aromatic rings along the polymer backbones of polyphenylenes and polythiophenes. Our results imply that through a proper choice of base polymer and substituents one can adjust the electrochemical potentials for the onset of oxidation and reduction as well as substantially red shift the absorption edge of these polymers. The ability to tailor these important properties provides these polymers with enormous application possibilities.

Q7.1

ENHANCEMENT OF THE MAGNETIC SUSCEPTIBILITY OF AN ORGANIC COMPLEX

The magnetic properties of $[1,2\text{-di}(4\text{-pyridinium})\text{-ethylene}]_x^{2+} [1,2\text{-di}(4\text{-pyridyl})\text{ethylene}]_{1-x}(\text{TCNQ})_3^{2-}$ are dependent upon the spin density which for this system can be readily varied. $X_{300\text{ K}}/X_{\text{Curie Law}} \approx 1$ for $x < \frac{1}{2}$, whereas for $x > \frac{1}{2}$ the ratio is less than unity and decreases with increasing values of x . In contrast, for $x \approx \frac{1}{2}$ the susceptibility is enhanced above the expected spin- $\frac{1}{2}$ Curie Law value. We have observed a spread of susceptibilities but all samples with $x \approx \frac{1}{2}$ have shown enhanced magnetic behaviour. Two samples gave $X_{300\text{ K}}/X_{\text{Curie Law}} = 8$.

Q7.2

NOVEL MATERIALS FOR OPTICAL DATA STORAGE

G.J. Ashwell, E.J.C. Dawney and M. Szablewski

Centre for Molecular Electronics, Cranfield Institute of Technology, Cranfield MK43 0AL, UK

The π -bridged donor-acceptor molecule, Z- β -(1-alkyl-4-pyridinium)- α -cyanostyryldicyanomethanide, shows a photochromic transition at 495 nm. The band is tunable and may be shifted by substitution, the wavelength being dependent, in part, upon the difference between the electron affinity and ionisation energy of opposite ends of the same

molecule. The synthesis and properties of several near infrared absorbing analogues, substituted at the acceptor end, will be reported and their photochromic and nonlinear optical properties will be assessed.

Q7.3

EFFECTS OF IN-PLANE π' BONDING ON ELECTRONIC TRANSITION ENERGIES FOR INORGANIC POLYMERS, Kim E. Ferris, Pacific Northwest Laboratory, Richland, WA 99352.

While the electronic structure of organic polymers is characterized by σ and out-of-plane π bonding networks, inorganic polymers also exhibit in-plane π' bonding interactions. The electronic transitions of these systems are often described in simple organic terms such as $n\text{-}\pi^*$ and $\pi\text{-}\pi^*$ excitations. The electronic structure of both these systems can be well described in terms of their molecular symmetry, even with the large bond polarity shown by such compounds as polyphosphazenes and siloxanes. However, with the presence of the in-plane π' bonding network, the optical transition energies for the inorganic systems are much higher. In this paper, we will present results comparing the electronic structure of pyridine and triazine as models for organic polymers, with those for the fluorophosphonitric trimer and tetramer as models for the polyphosphazenes.

This work was supported by the U.S. Department of Energy, Office of Basic Energy Sciences under contract DE-AC06-76RLO 1830.

Q7.4

SURFACE PLASMONS IN THIN FILM DIELECTRICS, S.M. Risser and K.F. Ferris, Pacific Northwest Laboratory, Richland, WA 99352

The optical response of thin film dielectrics films is influenced by phase homogeneity, interfacial strain, grain morphology, and the presence and distribution of voids. Different film deposition techniques have been found to generate distinct microstructures which perturb physical and optical properties from their bulk single crystal values. In small particle limit ($\lambda \gg d$), the mean field approach can be used for modelling the real part of the dielectric constant in terms of film microstructure. However, modelling of the microstructural effects is more complex when the size of the particles are approximately equal to the wavelength of light. We will report on work to theoretically model the optical properties of these particles using the retarded Maxwell's equations and the relation of these theoretically determined properties to the experimentally determined values.

Work supported by the U.S. Department of Energy, Office of Basic Energy Sciences under contract DE-AC06-76RLO 1830.

Q7.5

PHYSICAL CHARACTERIZATION OF ORGANIC RADICALS BY LOW-FIELD ESR SPECTROMETRY. Mehdi MOUSSAVI, Marc BERANGER, Denis DURET, Nelly KERNEVEZ and Liliane SECOURGEON, CEA-IRDI DLET/DSYS/SESA, BP 85 X 38041 GRENOBLE, FRANCE.

Electronic properties of organic materials are linked to their magnetic properties mainly studied by high field ESR spectroscopy. A low field (0.6 Gauss, 2 MHz) ESR spectrometer providing quantitative parameters is described. It gives informations such as frequency dependence of the linewidth, anisotropy of inhomogeneous line and also the values of T_1 , T_2 and the magnetic susceptibility using simple hypothesis.

The use of such a spectrometer is indispensable to establish a figure of merit for materials usable in ESR magnetometry. We present some results in many of known organic radicals: Lithium phthalocyanine, fluoranthene derivatives, N-doped polyacetylene etc.. The behaviour of these radicals is compared

to a radical anion salt, quinolinum bis tetracyanoquinodimethane considered as a reference.

The performances of this apparatus and a new 120 MHz ESR spectrometer which is under realization make their use envisageable for superconductor materials and also free radical solutions used in NMR magnetometers studies.

Q7.6

STUDIES ON THE FORMATION OF SWITCHING AND MEMORY STORAGE MATERIALS CONSTRUCTED FROM METALLO-ORGANIC CHARGE-TRANSFER SALTS Hailing Duan, Dwaine O. Cowan, Department of Chemistry; and Jerome Kruger, Department of Materials Science and Engineering, The Johns Hopkins University, Baltimore, MD21218.

Current controlled bistable switching and memory effects have been observed on metallo-organic charge-transfer salts, such as CuTCNQ and AgTCNQ, etc. These salts can be prepared by directly reacting metal donors with organo-acceptors in an acetonitrile solution. Metal donors both from transition groups and main groups have been tried. Different metal donors showed different reactivity with tetracyanoquinodimethane (TCNQ), as electron acceptor, in the formation of the charge-transfer salts. Electrochemical measurement has been employed to characterize the donor reactivity in the formation of the charge-transfer salts. SEM has also been used to examine the process of crystallization of the charge-transfer salts on a spherical single crystal of Cu. A possible mechanism of localized corrosion-crystallization process has been proposed for the formation of the charge-transfer salts.

Q7.7

OPTICAL STUDIES OF POLYANILINES: EFFECTS OF ALKYL RING-SUBSTITUTION AND SOLVENT ENVIRONMENT. A. Ray, A.G. MacDiarmid, Department of Chemistry, University of Pennsylvania, Philadelphia, PA 19014; J.M. Ginder and A.J. Epstein, Department of Physics, The Ohio State University, Columbus, OH 43210.

Methyl and ethyl ring-substituted derivatives of polyaniline have been synthesized and characterized by UV-visible-near IR spectroscopy. Optical spectra of the base forms in DMF solution suggest that the torsion angle between adjacent rings is increased by steric hindrance due to the alkyl groups in the substituted polyanilines, leading to blueshifts in the ~ 4 eV ("bandgap") and ~ 2 eV ("exciton") absorptions and an accompanying decrease in relative intensity of the "exciton" band. Steric considerations appear to override electronic effects of alkyl substituents.

The methyl ring-substituted derivative, poly(o-toluidine), is shown to exhibit solvatochromism. The "exciton" absorption shifts from 2.03 eV in pure N-methylpyrrolidinone to 2.19 eV in pure CH_2Cl_2 , accompanied by a loss in intensity relative to the "bandgap" absorption, with intermediate spectra observed in mixtures of these two solvents. The phenomenon is attributed to the presence of a more "rod-like" state in NMP as compared to a more "coil-like" state in CH_2Cl_2 .

The effects of alkyl substituents on acetic acid solution spectra of emeraldine salt will be discussed with respect to polaron band formation in these systems.^{1,2}

1. J.M. Ginder, A.J. Epstein, and A.G. MacDiarmid, to be published.
2. S. Stafstrom, J.L. Bredas, A.J. Epstein, H.S. Woo, D.B. Tanner, W.S. Huang, and A.G. MacDiarmid, *Phys. Rev. Lett.* 59, 1464 (1987).

*Supported in part by DARPA through a contract monitored by U.S. C.N.R.

Q7.8

SPECTRO-ELECTROCHEMICAL STUDY OF RING-SUBSTITUTED POLYANILINE: POLY(2-METHOXYANILINE) AND POLY(2,5-DIMETHOXYANILINE). Robert Clark and Sze C. Yang, University of Rhode Island, Department of Chemistry, Kingston, RI 02881.

Electronic absorption spectra of chemically modified polyaniline were studied as a function of the electrochemical potential and the degree of protonation. The chemical modification involves attaching one or two methoxy functional groups to the aromatic ring at carbon positions next to the C-N-C bridge.

The electronic absorption spectra of mono-methoxy substituted polyaniline are qualitatively similar to that of the un-substituted polyaniline. While the di-methoxy substituted polyaniline show dramatic change of number of bands and the position of bands.

The chemical modifications change the oxidation potentials and the pK_a of various oxidation and protonation forms of the polymer. The conditions for insulator/metal transitions are examined on a pH-potential phase diagram and are compared with that of the un-substituted and the methyl-substituted polyaniline. It is concluded that both steric and electronic influences of the methoxy substituents are important to the modification of its electronic property.

This work is supported in part by a contract administered by the Office of Naval Research from DARPA.

Q7.9

ELECTRON PARAMAGNETIC RESONANCE OF STUDIES OF DONOR-ACCEPTOR SALTS IN POLYMER MEDIA. S.A. Jansen and Y.C. Fann, Department of Chemistry and Materials Science, Temple University, Philadelphia, PA 19122.

Charge transfer complexes, their inherent electrical conductivity, magnetic properties and donor-acceptor redox relationships, have been a focus of much research in the last several years. One direction has been in the design of memory devices and applications in molecular electronics. Our work has focused on analysis of such processes in a polymeric film medium. Polycarbonate films of 7,7',8,8'-Tetracyanoquinodimethane (TCNQ) and o-tolidine complexes were studied by EPR spectroscopy from 100-300K. EPR spectra and magnetic susceptibility of the dispersed charge-transfer complexes will be presented and compared to the pristine materials. These studies were carried out as a function of donor/acceptor stoichiometry and concentration within the polymer matrix. Saturation studies show significant differences as the composition varies. In addition, the g-tensor and linewidth are strongly dependent on temperature and composition. A detailed molecular orbital study has aided in the analysis of the experimental data.

Q7.10

HALL EFFECT AND MAGNETORESISTANCE IN UNDOPED POLY(3-HEXYLTHIOPHENE). Azar Assadi, Christer Svensson and Magnus Willander, Dept. of Phys. and Measurement Technology, Linköping University, S-581 83 Linköping, Sweden.

Abstract.

We report studies of transport properties of thin films of undoped poly(3-hexylthiophene) (P3HT). The measurements were performed at room temperature on material fabricated by spinning a polymer solution onto oxidized silicon or glass, in some cases in the form of a field effect transistor [1]. The film thicknesses was in the order of 1000 Å. We studied magnetoresistance, field effect and Hall effect in these samples.

Transverse magnetoresistance was measured on films on glass. A positive magnetoresistance (DR/R) with an initial relative resistance increase rate of 0.073 T^{-1} was found. Transverse magnetoresistance was also studied by measuring the change of the field effect mobility with magnetic field. This measurement was performed using the field effect transistor structure. An initial mobility of $2.5 \cdot 10^{-5} \text{ cm}^2/\text{Vs}$ was reduced in a transverse magnetic field.

We also carried out Hall effect measurements on films on glass using a Van der Pauw electrode configuration. The measured Hall mobility was $1.1 \cdot 10^{-5} \text{ cm}^2/\text{Vs}$ and the charge carrier concentration was found to be $9.4 \cdot 10^{12} \text{ cm}^{-3}$.

This mobility is thus somewhat lower than the observed field effect value above.

The strong magnetoresistance observed may indicate that the charge carriers in P3HT have spins, i. e. are polarons.

[1] A. Assadi, C. Svensson, M. Willander and O. Inganäs, "Field effect mobility of poly(3-hexylthiophene)", *Appl. Phys. Lett.*, Vol. 53, pp. 195-197, 1988.

Q7.11

ELECTRON TUNNELING BETWEEN CHARGE DENSITY WAVE (CDW) AND NORMAL METAL AND BETWEEN TWO CDW's. XiaoZhou Huang and Kazumi Maki, Department of Physics, University of Southern California, Los Angeles, CA 90089-0484.

Making use of quasi-one dimensional Fröhlich model, we study the electron density of states and the tunneling current between CDW and normal metal and between two CDW's. Unlike the one dimensional model, the density of states of a CDW has a sharp peak at $\omega = \Delta(T) + \epsilon_0$, where $\Delta(T)$ is the order parameter and ϵ_0 is the unnesting parameter. The present result describes quite well a recent tunneling experiment by Ekino and Akimitsu on NbSe₃.

The tunneling current between two CDW's includes a term analogous to the Josephson current, which depends on the phase difference of two order parameters. However, unlike the Josephson effect there is no supercurrent between two CDW's. Further this term gives rise to an oscillating current when two CDW's slide with different velocities along the chain direction.

Q7.12

BELOW-GAP PICOSECOND PHOTOCONDUCTIVE RESPONSE OF STRETCHED TRANS-POLYACETYLENE A. Walser, R. Dorsinville, R. R. Alfano, Physics and Electrical Engineering, Depts. City College of New York 138th St. and Convent Ave. New York, New York 10031; G. Dellepiane, Università di Genova, Italy and R. Tubino Istituto di Fisica dell'Università, Via Vienna 2, Sassari and Istituto di Chimica delle Macromolecole, CNR, Milano Italy

The temperature dependence of the picosecond photoconductive response with above gap excitation for an highly oriented form of trans-polyacetylene was recently measured¹. Here, we wish to extend our past measurements of oriented samples and compare the temperature dependence of the photoconductive response with above gap excitation to that of below gap excitation. When the direction of the external dc field is parallel to the chain direction (1-d configuration) the fast response is independent of temperature while for current flow perpendicular to the chains (3-d configuration) the fast photoconductive response is temperature dependent. This response for the 1-d and 3-d configurations occur for both above and below gap excitation. The activation energy for above and below gap excitation is 0.048 eV and 0.063 eV respectively. The picosecond photo-conductive response for above and below gap excitation of trans-(CH)_x supports the theory that the mobile charged carriers (soliton and polarons) for both cases are one in the same.

The research at CCNY is supported in part by NASA and NSF.

1. A. Walser, A. Seas, R. Dorsinville, R. R. Alfano, R. Tubino, *Solid State Communications*, 62, 333 (1988)

Q7.13

THE PENN STATE 5-100 GHz FREE-SPACE MICROWAVE CHARACTERIZATION SETUP. Deepak K. Ghodgaonkar, Vijay K. Varadan and Vasundara V. Varadan, Research Center for the Engineering of Electronic and Acoustic Materials, 227 Hammond Building, Pennsylvania State University, University Park, PA 16802.

At our Center, we have set up a state-of-the-art free-space measurement apparatus for characterizing the electromagnetic reflection and/or transmission properties of planar samples in the 5-100 GHz frequency range. The heart of the apparatus consists of two spot-focussed antennas mounted on circular tracks on a horizontal table, while the brain is constituted by a HP8510B vector network analyzer. The system is fully automated and has been calibrated to yield reliable and accurate S-parameter measurements. Firmware-type algorithmic procedures have been designed to yield the complex electromagnetic properties of the samples as functions of frequency. Validation against known materials has been carried out. New data pertaining to materials such as ferrites, conducting polymers, and chiral materials will be presented.

Q7.14

DONOR-ACCEPTOR MOLECULES FOR SECOND HARMONIC GENERATION. Malcolm R. McLean, Mamoun M. Badr and Larry R. Dalton, Department of Chemistry, Robert L.S. Devine and William H. Steier, Department of Electrical Engineering, University of Southern California, Los Angeles, CA 90089-1062.

Present materials such as 2-methyl-4-nitroaniline (MNA) and LiNbO₃ have $\chi^{(2)}$ values in the usable regime for certain applications such as frequency doubling. However, although the magnitude of the $\chi^{(2)}$ effect in such materials is appreciable, there are many difficulties in using these materials in several important electro-optical applications. Clearly, the development of new materials with improved qualities is essential for device development. Theoretical calculations indicate that we can easily surpass the $\chi^{(2)}$ values of present materials. We are currently designing and synthesizing novel 3-ring aromatic materials with in built robustness as a foil against degradation. Precedent for their durability came from our experience with ladder polymers such as PQL, PTL, BBB and BBL. Initial experimentation involved corona poling in a poly-methylmethacrylate matrix followed by measurement of the β value at 1064 nm utilizing a Nd/Yag laser at its fundamental frequency. Results look promising, with a value higher than MNA and comparable to Disperse Red 1, but, more importantly, with minimal thermal or atmospheric degradation.

Q7.15

EFFECTS OF CONJUGATION LENGTH AND SUBSTITUENTS ON THE CONDUCTIVITY OF OXIDATIVELY DOPED α,ω -DIPHENYLPOLYENES. Linda S. Sapochak, Dave W. Polis, Art N. Bain, Larry R. Dalton, University of Southern California, Los Angeles, CA; and Charles W. Spangler, Northern Illinois University, DeKalb, IL.

It has been demonstrated that the oxidative doping of unsubstituted and substituted α,ω -diphenylpolyenes generate polaronic and bipolaronic intermediates that can be directly observed by absorption spectroscopy. Furthermore, the transitions have been shown to directly correlate with conjugation length and the electronic species are stabilized by donor substituents and destabilized by acceptor substituents. We now wish to report conductivity studies on these model compounds including the influence of conjugation length and effects of donor and acceptor substituents on the conductivity. The implications of these investigations on the metallic conducting state of these model systems provides important information for design of new electroactive materials.

Q7.16

CHARGE TRANSFER COMPLEX OF HEXAKIS (ALKYLTHIO) BENZENE WITH TETRAFLUOROTETRACYANOQUINODIMETHANE (t-EDTB)₂ TCNQF₄: A QUEST FOR TRIPLET STATE ! Daniel Chasseau, Marc Alléaume, Georges Bravic, Laboratoire de Cristallographie et Physique Cristalline, URA 144 CNRS; René Lapouyade, Laboratoire de Photophysique et Photochimie Moléculaire; Jean-Pierre Morand, ENSCP Bordeaux; Jacques Amiel and Pierre Delhaes, Centre de Recherche Paul Pascal CNRS, Domaine Universitaire de Bordeaux I, 33405 Talence Cedex (FRANCE)

In order to evaluate the potentiality of organic donor molecules for molecular/organic ferromagnets, with in principle C₃ molecular symmetry, as in the hexakis (alkylthio) benzene, we have prepared single crystals of the charge transfer complex of triethylene dithio benzene (t-EDTB) with TCNQF₄, which has been subsequently oxidized with bromine and arsenic pentafluoride gas.

The stoichiometry of this complex is 2:1 and it crystallizes in the triclinic system, space group P $\bar{1}$ with the following cell parameters: a=11.515, b=11.044, c=10.460 Å, α =111.50°, β =122.50°, γ =93.82°. The crystal structure consists of columns of alternating donor dyads and acceptors monads (DDADDA). The degree of charge transfer is estimated to be 0.2-0.3 from the methods based on bond lengths.

While (t-EDTB)₂·TCNQF₄ does not give a significant ESR spectrum, after treatment with the bromine gas a single line, centered around the free electron g value, appears without any evidence of either a ground or an excited triplet state. Oxidation process with AsF₅ is under investigation, using the strategy developed by Chiang and coworkers.

Q7.17

FERROMAGNETIC INTERACTIONS IN A SERIES OF SCHIFF-BASE METAL-ORGANIC POLYMERS. F. Palacio, J. Garin, J. Reyes and F.J. Lázaro, I.C.M.A., C.S.I.C. - Universidad de Zaragoza, 50009 Zaragoza (Spain)

The synthesis and magnetic properties of a series of metal-organic polymers of general formula $\{[M(C_{13}H_{17}N_3)_2]X \cdot 6H_2O\}_n$, where M = Fe(II) or Co(II) and X = SO₄²⁻, (NO₃)₂, (Cl⁻)₂, are reported. Magnetization and a.c. magnetic susceptibility measurements indicate the presence of strong ferromagnetic interactions in the materials.

The organic polymer is prepared from the polycondensation of a di-aldehyde with a diamine and it is diamagnetic. When the polymer is added to an aqueous solution of the corresponding metallic salt, the resulting material exhibits rather unusual magnetic properties.

The Fe-based polymers present rather high in-phase (χ') and out-of-phase (χ'') components of the ac magnetic susceptibility, with a maximum in χ' around 250 K. In the case of the Co-based ones the anomalies lie between 1 and 10 K. In the temperature range below the χ' maximum, the frequency dependence of the a.c. susceptibility and the magnetization are consistent with those of a blocked superparamagnet.

Q7.18 ABSTRACT WITHDRAWN

Q8.1

MAGNETISM IN DECAMETHYLFERROCENIUM TETRACYANO-ETHANIDE, [DMeFc]⁺[TCNE]⁻ AND RELATED SYSTEMS*. Arthur J. Epstein, Department of Physics and Department of Chemistry, The Ohio State University, Columbus, Ohio 43210; and Joel S. Miller, Central Research and Development Department, E.I. du Pont de Nemours & Company, Inc., Wilmington, DE 19880.

The three-dimensionally ordered ferromagnetic ground state of [DMeFc]⁺[TCNE]⁻ and its development from the paramagnetic state have been extensively studied utilizing a wide variety of techniques. The magnetic susceptibility for magnetic fields oriented parallel and perpendicular to the stacking axis is consistent with Heisenberg-like behavior, though the apparent exchange interaction differs for magnetic fields oriented parallel and perpendicular to the stacking axis. Neutron diffraction studies show the presence of increasing order below the Curie temperature, T_c = 4.8K. Specific heat experiments show a transition to the ordered state at 4.8K and reveal the dominance of one-dimensional interactions for T > T_c. AC susceptibility studies confirm the transition and reveal the presence of unusual loss mechanisms in the ferromagnetic state. Together these experiments lead to a perspective of a transition from predominately one-dimensional interactions for T > T_c to three dimensional ordering at T_c, to an anisotropic ferromagnetic state for T < T_c. Numerous critical constants have been estimated for these systems and show that the behavior is intermediate between Heisenberg and Ising-like as the material approaches the 3-D ferromagnetic transition. Selective i) replacement of the metal ion, ii) replacement of Me substituent groups with H, iii) use of C₆-ring ligands instead of C₅-ring ligands, and iv) replacement of TCNE with alternate acceptors has been carried out. These results are consistent with a model of configuration mixing of the lowest charge transfer excited state with the ground state developed earlier to understand the magnetic coupling in such systems.

* Supported in part by the U.S. Department of Energy Grant No. DE-FG02-86ER45271-A003.

Q8.2

FERROMAGNETIC INTERACTIONS IN ORGANIC SOLIDS: AN OVERVIEW OF THEORY AND EXPERIMENT. J. B. Torrance, IBM Almaden Research Center, San Jose, CA, U.S.A.

The simple model¹ for ferromagnetic interactions in a segregated stack of organic radicals is reviewed. In order to test this model, spin interactions between two benzene radical anions have been calculated² and shown to be indeed ferromagnetic. As an experimental test of this model, a series of cation radical salts of decacylene were prepared, but did not exhibit ferromagnetic interactions³. Organic ferromagnetism was found¹, however, in the polymeric system based on triaminobenzene. Recent polymerization studies⁴ of this system are also discussed.

¹J. B. Torrance, S. Oostra, and A. Nazzari, *Synth. Met.* 19, 709 (1987).

²P. S. Bagus and J. B. Torrance, *Phys. Rev.* B39, 7301 (1989).

³J. B. Torrance, P. S. Bagus, I. Johannsen, A. I. Nazzari, S. S. P. Parkin and P. Batail, *J. Appl. Phys.* 63, 2962 (1988).

⁴I. Johannsen, J. B. Torrance, and A. I. Nazzari, *Macromol.* 23, 566 (1989).

Q8.3

RECENT PROGRESS IN THE PREPARATION OF ORGANIC METALS AND ORGANIC FERROMAGNETS. Fred Wudl, Fritz Closs, Pierre-Marc Allemand, Gordana Srdanov, Toshiyasu Suzuki, Heiko Isotalo, Hamid Kasmai and Hideki Yamochi, Institute for Polymers and Organic Solids, Departments of Physics and Chemistry, University of California, Santa Barbara, California 93106

The preparation and properties of new organic metals based on bis(ethylenedioxy)tetrathiafulvalene (BEDO) will be presented. These include the AsF₆, PF₆, and N(CN)₂ salts as well as the three dimensional metal [(BEDO)₄I₃]. The results of electron spin resonance, magnetic susceptibility, and transport will be presented.

The preparation, epr, ENDOR, and magnetic susceptibility of a single crystal of a nitroxyl which has magnetic susceptibility behavior of a ferromagnet with a low transition temperature ($\theta = 0.9K$) will also be presented. Its properties will be correlated with its crystal structure and molecular orbital calculations. The former shows short inter hetero atom contacts and hetero atom-carbon contacts.

Q8.4

MAGNETIC PROPERTIES OF MICROCRYSTALLINE "POLY-(PHENYLDIACETYLENES)" CARRYING RADICAL OR CARBENE CENTERS ON THE SIDE CHAINS. Noboru Koga, Katsuya Inoue, Noriko Sasagawa, and Hiizu Iwamura*, Department of Chemistry, The University of Tokyo, 7-3-1 Hongo, Bunkyo-ku, Tokyo 113, Japan

According to the theories of topological symmetry of conjugated molecules and the EPR experiments on model dimers, the exchange coupling between radical centers attached to the phenyl rings is predicted to be ferromagnetic in poly(1-(m-or p-substituted phenyl)-1,3-butadiynes) obtained by topochemically controlled head-to-tail polymerization.

The 1-phenyl-1,3-butadiene derivatives (1 and 2, respectively) carrying stable t-butyl nitroxyls ($a_N = 1.35$ mT) and diazomethyl groups have been prepared. Mixed crystals of 1 and the corresponding hydroxylamine (<1:1) polymerized in the solid state at 100 °C to give black-violet microcrystals with metallic luster. A microcrystalline sample of 2 underwent spontaneous polymerization at room temperature when crystallized to give an insoluble polymer which was then photolyzed at cryogenic temperature to generate triplet carbene centers attached to the phenyl rings of the poly(phenyl-diacetylene).

Some of these microcrystalline polymeric samples were responsive to a magnet at room temperature. Magnetic susceptibility data of the two samples will

be discussed. Hydrogen bonding between the poly-diacetylene chains as estimated by X-ray crystal structure of 1 is considered to be responsible for increasing the dimension of the spin alignment.

Q8.5

ROLE OF TOPOLOGY IN SPIN ALIGNMENT OF ORGANIC MATERIALS. Koichi Itoh, Takeji Takui, Yoshio Teki, and Takamasa Kinoshita, Department of Chemistry, Faculty of Science, Osaka City University, Sugimoto, Sumiyoshi-ku, Osaka 558 Japan.

Since the detection of m-phenylenebis(phenylmethylene), the first organic high-spin molecule, in 1967, we have synthesized and characterized a series of organic high-spin molecules as models for organic ferromagnets and ferrimagnets. The molecular design for most of these compounds has been based on the utilization of pi spins in topologically-degenerate non-bonding MO's as well as of sigma spins in localized orbitals on the divalent carbon atoms of carbenes. In this paper, it is shown that the spin alignment in such organic compounds as determined by single crystal ESR is highly dependent on the topological nature of their molecular pi electron networks. This remarkable nature is further interpreted using the topological isomers of biphenyl-n,n'-bis(phenylmethylene) in terms of their spin density distributions which have been determined by a single crystal ENDOR technique and compared with theoretical values calculated on the basis of a generalized Hubbard model and the Heisenberg model; this is interesting because one of the isomers ($n=n'=3$) has the ground state whose spin multiplicity is predicted differently by molecular orbital and valence bond methods. Our approach has been extended to polymers in order to elucidate the origin of their magnetism. The results of their magnetic characterization will be discussed.

Q8.6

ROLE OF HIGH-SPIN MOLECULES AS MODELS FOR ORGANIC FERRO- AND FERRIMAGNETS, AND PI-TOPOREGULATED MAGNETIC POLYMERS. Takeji Takui, Masayuki Okamoto, Kazunobu Satoh, Toyohiro Shichiri, Yoshio Teki, Takamasa Kinoshita, and Koichi Itoh, Department of Chemistry, Faculty of Science, Osaka City University, Sugimoto, Sumiyoshi-ku, Osaka 558, JAPAN.

The quest for organic magnetism is the focus of current topics from both academic and industrial sides. Our continuing study of high-spin molecules as models for organic ferro- and ferrimagnets can be traced back to the detection of the first high-spin hydrocarbon, m-phenylenebis(phenylmethylene) in 1967 by one of the authors and to the proposal of pi-toporegulated ferromagnetic polymers. Our strategy for obtaining organic magnetism contains (1) molecular design for high-spin assemblies exploiting topologically-degenerate pi non-bonding MO's and (2) introduction of functional groups such as heteroatoms and methylene as bridges between high-spin assemblies in order to increase dimensionality of spin structure. In the latter study, exchange interaction via an ether bridge or via methylene between two high-spin assemblies has been examined by single-crystal ESR spectroscopy. Whether it is ferromagnetic or antiferromagnetic depends upon the substituted position of the bridge, demonstrating the importance of the topological nature in spin ordering. It turns out that superexchange interaction or hyperconjugation mechanism can dominate spin ordering between high-spin assemblies. Using the criteria obtained, model compounds for units of organic ferrimagnets have been synthesized and their spin structures have been determined. In order to elucidate spin ordering in organic compounds and ferromagnetic behavior originating from molecular/organic based moieties, it is indispensable to obtain information on the spin density distribution in their units such as high-spin molecules or radical sites. We have applied single-crystal ENDOR and TRIPLE techniques to typical types of high-spin molecules, one of which is the model unit of an organic ferrimagnet, and we have tested various spin-prediction theories in terms of the spin density distributions obtained.

Q8.7

THERMAL STABILITY OF MAGNETIC PROPERTIES OF DEHYDROGENATED TRI-ARYLMETHANE RESINS. Michiya Ota, Gunma College of Technology, Maebashi, Gunma 371, Japan; Sugio Otani Faculty of Engineering, Gunma University, Kiryu-shi Gunma 376, Japan

We have already reported^{1,2)} on the ferromagnetic behavior of tri-arylmethane resins. These resins were prepared by heating the mixture of aromatic compounds and aromatic aldehydes in the presence of acid catalyst.^{1,2)} Magnetic property appeared with dehydrogenation by photo-oxidation of methine proton. These dehydrogenated resins gave the magnetic hysteresis by vibrating sample magnetometer(VSM).

Recently, spin states of these resins are investigated from the standpoint of electron spin resonance(ESR) by Itoh's group. However, the stability of a magnetic property has not been discussed yet in details.

It was found that the magnetic properties disappeared by exposing the dehydrogenated resins to hydrogen halide(ex. HCl), activated O₂ and other fresh radical scavengers. This quenching behavior was observed by the VSM or the qualitative check named as "moving test on the water"¹⁾, that is, hysteresis loop disappeared to become diamagnetic and moving test was negative because the resin did not move on the surface of water after exposing.

This presentation will be further discussed on thermal stability of magnetic properties.

The authors wish to thank Prof. K. Itoh, Dr. T. Takui, and Dr. Y. Teki, Osaka City University for useful suggestions and discussions.

Reference

- 1) M. Ota, S.Otani et al., 57th JCS Annual Meeting, 3D410-

Q8.8

POLYPHENOXY RADICALS : SYNTHESIS AND HOMOPOLYMERIZATION OF 3,5-DI-*tert*-BUTYL-4-HYDROXYPHENYL DERIVATIZED OLEFINS AND METHACRYLATES¹. Ravindra B. Upasani², Long Y. Chiang, and Dave P. Goshorn, Corporate Research Laboratories, Exxon Research and Engineering Company, Annandale, NJ 08801.

Stable polyradicals can be used as precursors for organic ferromagnetic materials. We evaluated the thermal and chemical stability of various polyphenoxy radicals prepared through the modified synthetic methods. The monomeric 3,5-di-*t*-butyl-4-hydroxyphenyl derivatized olefins and methacrylates were prepared in multistep synthesis starting from 2,6-di-*t*-butylphenol. These monomers were polymerized in the presence of radical initiators at the refluxing temperature of aromatic solvents under an inert atmosphere. Stable phenoxy radicals can be obtained by the oxidation of polymers with lead oxide and other oxidant. These radicals were characterized by ESR and solid state magnetic susceptibility were measured at various temperatures.

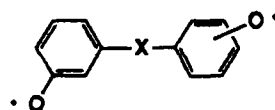
¹This work is supported by the National Science Foundation (DMR 8822532).

²Physics Department, Princeton University, Princeton, NJ 08544.

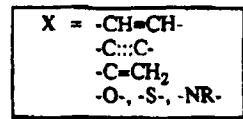
Q8.9

ORGANIC POLYRADICAL MODELS FOR ORGANIC MAGNETIC MATERIALS. David A. Modarelli, Frank C. Rossitto, Masaki Minato, and Paul M. Lahti, University of Massachusetts, Department of Chemistry, Lederle Graduate Research Tower, Amherst, MA 01003

Recent interest in synthesizing organic polyradicals with very high spin ground states has been spurred by the hope that macromolecular pi-conjugated polyradicals could have potential use as magnetic materials. We have been interested in synthesizing diradical and polyradical systems based on phenoxyl radical units linked by various conjugating units with different non-Kekule connectivity parities (see the generic diradical structural unit below). Experimental progress in synthesis and study of such model systems will be discussed.



generic diradical model



Q9.1

SYMMETRY, CHEMISTRY AND OPTICS : A COMBINED APPROACH TO MOLECULAR ENGINEERING IN NONLINEAR OPTICS.
J. Zyss - CNRS (LA CNRS 250) 196 Av. H. Ravera
 92220 BAGNEUX - FRANCE

The purpose of this work is twofold : first we point-out the relevance, towards nonlinear material definition and optimization, of Maxwellian propagative considerations beyond classical chemical and crystallographic criteria. Conversely, we show that these latter criteria, although often ignored in optical physics type of studies, may help considerably simplify propagative phenomena in complex low symmetry molecular crystals. We show that phase-velocity, group-velocity and group-velocity dispersion matching configurations are demanded, either independently or jointly, in order to enhance the yields of frequency conversion and parametric amplification processes. Such configurations are discussed within a simple geometrical framework which encompasses both phase-matched and unphase-matched, type I and type II, collinear and non-collinear processes. The trade-off between angular and spectral acceptance is quantitatively related to walk-off and group velocity matching and "optimized" phase-matched propagation geometries defined for various nonlinear crystals and laser pulse durations. Finally we propose to complement the usual oversimplified classification of nonlinear quadratic materials in terms of $d^2 n^3$ by a scale of more relevant parameters.

In the second part, we discuss frequently encountered low-symmetry biaxial molecular crystals. The complexity of optical studies in such media is due to the apparently arbitrary orientation of the optical dielectric framework which, by lack of crystalline symmetry, is not "overdetermined" along unit cell axis directions. We infer this orientation from the anisotropy of the molecular polarizability within a simple oriented gas model. We suggest a simple optical experiment to account for the departure of the Lorentz-Lorentz local field operator eigenframework from the optical dielectric axis.

Q9.2

NEW SECOND-ORDER NONLINEAR OPTICAL ORGANIC CRYSTALS. D. S. Donald, L.-T. Cheng, G. Desiraju*, G. R. Meredith and F. C. Zumsteg, E. I. du Pont de Nemours & Co., Central Research & Development Dept., Experimental Station, Wilmington, DE.

The design of molecular crystals with specific optical properties, which are thought to arise from constituent molecules' polarizability properties, is a desirable but currently unachievable goal. One can partially achieve this goal by choosing compounds with specific molecular attributes and empirically determine the manner in which these are translated into crystal properties. Besides the fact that there are no certain rules for prediction of crystal packing arrangements, there is also a problem in specifying molecular properties from what are today incomplete polarizability structure-property relationships. We have, realizing these limitations, identified new molecular crystals by a nonlinear optical (powder-SHG) scouting-screening program from lists of compounds chosen due to perceived desirable molecular properties. Examination of successful materials has revealed interesting, new alignment motifs. We will describe some of these materials and their preparation, relating molecular and crystal properties and structures.

*Current address: School of Chemistry, University of Hyderabad, Hyderabad, India

Q9.3

SYNTHESIS, THERMAL BEHAVIOR, AND SECOND-ORDER NONLINEAR OPTICAL PROPERTIES OF CONJUGATED, ACCEPTOR/DONOR COMPOUNDS. James F. Wolfe, Susan P. Ermer, Steven M. Lovejoy, Doris S. Leung, Ken Aron, Glenn A. Hansen, Lockheed Missiles and Space Co., Inc. Palo Alto, CA; and Steven P. Bitler, SRI International, Menlo Park, CA.

A series of new noncentrosymmetric compounds having both electron-accepting and electron-donating substituents on a conjugated, aromatic heterocyclic structure were synthesized and their spectroscopic, thermal, and solubility properties determined. Second harmonic generation (SHG) of the materials was studied by DC-induced SHG experiments. Although these materials are directly applicable to processing in guest/host systems, this study was designed to elucidate the relationship between structure and nonlinear optical activity, so that optimal structures could be chosen for attachment as polymer side-chains.

Because the compounds are comprised of the following four components: an electron-Acceptor, a Linking moiety, a Heterocyclic moiety, and an electron-Donating group, we call them ALHD compounds. The synthetic methodology relies first on the synthesis of a 2-phenylbenzazole that is substituted with both a primary and a secondary amine, the latter substituent providing the electron-donor and the primary amine providing a site for attachment of the electron-accepting moiety. A variety of electron-accepting groups were thus attached by a Schiff base formation with appropriate aldehydes and ketones.

The solubility of ALHD compounds could be modified by varying the alkyl substituents of the secondary amine. Those materials with long alkyl chains showed unique thermal behavior, including the formation of smectic phases at elevated temperature. DCSHG experiments to determine the molecular nonlinear susceptibilities will be discussed.

Q9.4

Materials For A Multifrequency Photochromic Memory

Geoffrey J. Ashwell and Marek Szablewski

Centre for Molecular Electronics, Cranfield Institute of Technology, Cranfield MK43 0AL, UK

TCNQ reacts with picolinium, lepidinium and quinaldinium salts to give zwitterionic materials of formula $D^+-CH=C(CN)-C_6H_4-C(CN)_2^-$, where D^+ is a heterocyclic group. The materials have large second order molecular hyperpolarisabilities and are also photochromic¹, the latter being attributed to intramolecular charge transfer and internal reorganisation with the formation of the neutral quinonoid form. Their LB films show sharp non-overlapping charge transfer bands and, by switching the components at different frequencies, multilayer films have the potential to store several bits per pixel. Three suitable materials with sharp, erasable, charge transfer bands at 495, 565 and 614 nm have been identified.

1. G.J. Ashwell, UK Patent Appl. 8907211.8 (1989).

Q9.5

ELECTRO-OPTIC AND NONLINEAR OPTICAL PROPERTIES OF 2,6-DIBROMO-N-METHYL-4-NITROANILINE (DBNMNA) CRYSTALS. Ajay Nahata,

Keith A. Horn and James T. Yardley, Allied-Signal, Inc., Engineered Materials Sector, Columbia Turnpike, Morristown, New Jersey

Single crystals of a new nonlinear optical material, 2,6-dibromo-N-methyl-4-nitroaniline (DBNMNA), have been prepared and found to belong to the orthorhombic system, polar space group Fdd2. Both the linear and quadratic electro-optic coefficients were measured at 633 and 810 nm. The refractive indices were obtained using a Brewsters angle technique for biaxial crystals. The nonlinear optical susceptibility for second harmonic

generation, d_{33} , was also measured at 1.06 and 1.62 microns by comparison with d_{11} of y-cut quartz. The second harmonic and electro-optic results are compared to a theoretical model in which the molecular nonlinear susceptibility, β_{xxx} , is assumed to be the only contributing tensor component.

Q9.6

QUADRATIC NONLINEAR OPTICAL PROPERTIES OF DIVA CRYSTAL. Tatsuo Wada, C. H. Grossman, Shinji Yamada, Akira Yamada, A. F. Garito and Hiroyuki Sasabe, Frontier Research Program (RIKEN), Wako, Saitama 351-01, Japan.

New organic nonlinear optical crystal: dicyano vinyl anisole (DIVA) has been grown from vapor by low pressure sublimation and from saturated solution by solvent evaporation. Evaporation rate was controlled by monitoring the vapor pressure of solvent. Crystallographic structure and quadratic nonlinear optical properties were investigated.

The methoxy groups are nearly aligned along the crystallographic b-axis, while the dicyano groups have approximately a 55° direction cosine to this axis. Molecular orientation in DIVA crystal with space group $P2_1$ is favorable for the highest possible value of phase-matchable coefficient.

Both TYPE I and TYPE II phase matched second harmonic generation (PMSHG) were observed from naturally grown faces of single crystals. Effective PMSHG was achieved at wavelengths from 0.8 to 1 μm . The effective TYPE I PMSHG coefficient (a combination of d_{21} , d_{23} and d_{25}) was determined as $d_{\text{eff}} = 4.9 \times 10^{-8} \text{ esu} = 40 \times d_{11}$ of quartz at a wavelength of 1.064 μm . Blue laser generation and optical parametric effects of DIVA crystal were also investigated.

Q9.7

EFFICIENT SECOND HARMONIC GENERATION OBSERVED IN HYDRAZONE DERIVATIVES OF AROMATIC ALDEHYDES. Richard S. Potember, Karen A. Stetyick, and Robert C. Hoffman, The Johns Hopkins University, Applied Physics Laboratory, Laurel, MD 20707-6099

Efficient second harmonic generation in 4-nitrobenzaldehyde hydrazone was first observed by Davydov et al. in 1977. Recently, we observed efficient second harmonic generation in analogous hydrazone derivatives of aromatic aldehydes formed by the condensation of the aldehyde with the appropriate hydrazine. The materials were tested using the widely-used Kurtz powder technique.

High SHG efficiencies were observed in 3-methoxy-4-nitrobenzaldehyde hydrazone (32 times ADP), 3-methoxy-4-nitrobenzaldehyde methylhydrazone (10 times ADP), 3-methyl-4-nitrobenzaldehyde hydrazone (25 times ADP), 1-naphthalenecarboxaldehyde hydrazone (5 times ADP) and 1-pyrenecarboxaldehyde phenylhydrazone (20 times ADP). The absorption edge of 4-nitrobenzaldehyde hydrazone (490 nm) was shifted to approximately 440 to 450 nm by adding methyl and methoxy donor groups adjacent to the acceptor group on the aromatic portion of the molecule. The absorption edge of 3-methoxy-4-nitrobenzaldehyde hydrazone, 3-methoxy-4-nitrobenzaldehyde methylhydrazone, 3-methyl-4-nitrobenzaldehyde hydrazone was 442 nm, 452 nm and 444 nm, respectively.

This work supported in part by the Dept. of the Navy contract N00039-89-C-5301.

Q9.8

FERROELECTRICITY OF CHIRAL COMPOUNDS IN HIGHLY ORDERED SMECTIC PHASES. W. Haase, A.M. Biradar, and S. Wróbel, Institut für Physikalische Chemie, Technische Hochschule, Petersenstr. 20, D-6100 Darmstadt, Federal Republic of Germany.

Ferroelectric liquid crystals showing a S_C^* -phase are truly a very spectacular material for the flat screen. The response time in the μ s-region is very short. Recently, several groups developed series of different materials showing some favourable properties as polarization, switching time, stability, etc. We are focussed on the related properties of the more crystal like chiral tilted phases.

A report is given on the bistability, polarization effect, switching time, and on the dielectric properties in the low and high frequency range of a mixture with a broad S_I^* -phase. Also the properties of single compounds with S_G^* - and S_F^* -phases are reported. Application aspects of higher ordered phases will be discussed.

Q9.9

LANGMUIR-BLODGETT FILMS OF UNIDIMENSIONAL ORGANIC RECTIFIERS*. Robert M. Metzger, Department of Chemistry, University of Alabama, Tuscaloosa, AL 35487-0336, USA, and Charles A. Panetta, Department of Chemistry, University of Mississippi, University, MS 38677, USA.

The Organic Rectifier Project seeks to assemble the unimolecular organic rectifier proposed in 1973 by Aviram and Ratner. This device would be a metal-organic-metal sandwich, in which the organic layer is a one-molecule thick Langmuir-Blodgett (LB) film of a suitable D- σ -A [donor-(covalent sigma bridge)-acceptor] molecule. We have prepared D- σ -A molecules where D = pyrene, bishexylaminophenyl (BHAP), or bisdodecylaminophenyl (BDDAP), σ = carbamate (C), & A = 2-bromo, 5-hydroxyethoxy-7,7,8,8-tetracyanoquinodimethan (BHTCNQ), 2-hydroxyethoxyTCNQ, and also hydroxymethoxyantraquinodimethan. The strongest LB films are obtained with D = BDDAP, but good films result even with D = BHAP. Some D- σ -A systems yield Z-type multilayers.

Crude attempts to measure through-film conductivity (and rectification) using sandwiches Al | BDDAP-C-BHTCNQ | Al (overlap area about 1-2 mm²) gave only open or short circuits. A scanning tunneling microscope experiment on a gold/silver/mica substrate yielded deceptive results.

*Research supported in part by NSF-DMR-88-01924, and by NSF-EPSCoR (Mississippi)

Q9.10

L.B. FILM EXHIBITING COOPERATIVE SPIN TRANSITION, FOR 2D MOLECULAR MEMORY DEVICES. Philippe Coronel, Annie-Ruaudel-Teixier and A. Barraud CEA-IRDI-DESICP-DLPC/SCM, CEN.SACLAY, 91191 GIF SUR YVETTE CEDEX (France)

Molecular electronics requires materials of molecular size exhibiting switching or memory properties. The Langmuir-Blodgett method (L.B.) and its variants provide controlled fabrication of molecular films one molecule thick and their

transfer onto solid supports. In these 2D monolayers, molecules are highly organized, so that complex organizations aimed at specific properties can be built. One of these, a semi-amphiphilic complex made of two SCN and two amphiphilic phenantrolines in a cis position, exhibits a spin transition around -20 °C. It switches from high spin ($S = 2$) at room temperature to low spin ($S = 0$) at low temperature. The transition does not follow the expected thermal Boltzmann statistics, but is rather steep, pointing out molecular cooperation. The L.B. film exhibits a hysteresis about 5 °C in width, while the parent 3D compound exhibits a hysteresis of less than 1 °C, but a much sharper transition. This apparently contradictory behaviour is ascribed to the high impurity content of the L.B. film in association with high intermolecular coupling.

Q9.11

EFFECTS OF MOLECULAR RIGIDITY ON ELECTRIC FIELD-INDUCED ALIGNMENT AND ORIENTATIONAL STABILITY OF DIPOLAR CHROMOPHORE COMPOSITES. H.E. Katz, M.L. Schilling, W.R. Holland, and K.D. Singer, AT&T Bell Laboratories, Murray Hill, NJ 07974, and Princeton, NJ 08540.

The fabrication of second order nonlinear optical materials requires the imposition of noncentrosymmetry on an ensemble of chromophores with large hyperpolarizabilities (β). The design of high- β chromophores is now very well understood, whereas the induction and maintenance of the noncentrosymmetry in noncrystalline materials remains a significant challenge. One of the leading methodologies for inducing chromophore alignment in amorphous electro-optic materials is to pole the chromophores in polymer films. Supramolecular organization and conformational rigidity may be engineered into chromophores and their surrounding matrices in order to increase the theoretical alignment achievable from a given electric field and the stability of the alignment at particular temperatures.

We have investigated the synthesis and electrical properties of rationally synthesized chromophore assemblies such as conformationally defined head-to-tail oligomers. Angles of dipole moment vectors of dimers in solution are in agreement with predictions based on x-ray structures of model compounds, with the dimers displaying enhanced electric field orientability compared with the isolated chromophores. We have also determined that conformationally unrestricted, monomeric azo dyes pole as relatively isolated molecules even when present in supersaturated solutions and in close proximity on polymer side chains in molten phases. However, covalent attachment of dyes to polymers enormously improves the temporal stability of aligned glassy materials, possibly due in part to inter-dye interactions. Materials simultaneously exploiting the concepts of directional assembly and direct polymer attachment of chromophores are being considered in order to maximize the long-term alignment obtainable in polymeric materials.

Q9.12

Zinc Tris(Thiourea) Sulfate, A Prototype Semiorganic Non-Linear Optical Material P.B. Newman, L. F. Warren, E. F. Witucki, M. D. Ewbank and D.E. Cooper, Rockwell International Science Center, 1049 Camino Dos Rios, Thousand Oaks, CA, 91320 and G. Burdge, Lab. For Physical Sciences, College Park, MD 20740

Zinc tris(thiourea) sulfate, $Zn[SC(NH_2)_2]_3SO_4$, is a prototype material in a newly discovered class of nonlinear optical compounds which we refer to as "semiorganic." These compounds are characterized by an organic constituent with a large second or third order molecular hyperpolarizability (β or γ), chemically bound within an inorganic salt forming a 3-D crystallographic lattice. The 3-D nature of the bonding in semiorganic materials represents a major advantage over

completely organic systems, which by virtue of their predominantly low-dimensional nature, generally grow only small needle-like crystals of very low optical quality. In addition to supplying the 3-D bonds which enables the growth of large optical quality crystals, the inorganic constituent apparently also contributes to the total NLO coefficients $\chi^{(2)}$ and $\chi^{(3)}$ via local field effects. The result is that in contrast to the expected effect of reducing the NLO behavior as a result of "diluting" the organic component, the inorganic component apparently increases the effect by being polarized by the field of the organic molecule. Experimental data showing both a significant $\chi^{(2)}$ and $\chi^{(3)}$ for this material, along with supporting data such as the region of transparency and the indices of refraction will be presented.

Q9.13

CARRIER INJECTION MECHANISM THROUGH ORGANIC/ORGANIC JUNCTIONS. Syun Egusa, Nobuhiro Gemma, Akira Miura and Makoto Azuma, Toshiba R&D Center, Kawasaki city, Japan.

Recently, great attention has been attracted on a novel organic EL device¹⁾ with multilayer structure achieving high brightness and low voltage drive. In this study, we have investigated the carrier injection mechanism through organic/organic junctions fabricated from electron transport(A) and hole transport(D) layers.

Several types of M/organic/M devices (M=Al, Au, ITO) were prepared by sequential evaporation of tetraphenylbenzidine(D molecule) and naphthaldiimide derivative(A molecule). The DC current, and the displacement current characteristics were measured by the low frequency ramp method.

For MAM and MDM devices, M/A and M/D junctions formed ohmic contact for electron and hole injections, respectively. For the MADM device, rectified characteristics were observed. For MADAM or MDADM devices, the DC currents were extremely suppressed. These results indicate that the D/A junction forms a blocking contact for a single carrier, while the existence of double carrier is needed for carrier flow through the D/A junction. The displacement current greater than the charging current was also observed in the low bias before the forward DC current flowed. It is suggested that the electron and hole injected from the respective electrodes accumulate in the D/A junction, and the resulting local high electric field induces the tunnel injection through the D/A junction.
1) Tung & VanSlyke, Appl. Phys. Lett., 51, 913 (1987)

Q10.1

INSULATOR-METAL TRANSITION AND CONDUCTION PROCESSES IN TRANS-POLYACETYLENE. E.M. Conwell, H.A. Mizes and S. Jeyadev, Xerox Corporation, Webster Research Center, Webster, NY

We have calculated the band structure for a chain of doped trans-polyacetylene using the electronic part of the SSH Hamiltonian plus the Coulomb potential arising from ions and charged solitons surrounding the chain. The calculations were done for the lattice structure of Na-doped polyacetylene and for another structure approximating that of iodine-doped polyacetylene. To agree with a number of experimental observations the donated electrons or holes were taken to be in soliton states at all dopant concentrations. Because screening depends on the calculated energy levels, specifically on the density of states at the Fermi energy, $\eta(E_F)$, in the metallic state, which in turn depend on the potential used to obtain them, self-consistency was required in the calculations. The energy level structure was found to depend strongly on the ion spacing, conveniently measured in terms of the average

spacing a of C-H's along the chain. For ion spacing 5a, characteristics of the Na ion-rich regions up to an average dopant concentration of ~6%, the chain remained semiconducting. For ion spacing 4a, which appears to characterize the next phase for Na doping, metallic behavior was found for a doped chain length of ~100 sites or more. Self-consistency was fulfilled with $\eta(E_F)$ equal to the measured value of the saturation Pauli susceptibility χ_p in the metallic state. In addition to accounting for the magnitude of χ_p in the metallic state, our model can account for a rapid rise in χ_p in the transition.

Conduction mechanisms in the "spinless conductivity" and metallic concentration ranges will be discussed.

Q10.2

DETERMINATION OF CORRELATION PARAMETERS IN π -CONJUGATED POLYMERS. J. Tinka Gammel, D.K. Campbell, E.Y. Loh, Jr.; Los Alamos National Laboratory, Los Alamos, NM 87544, S. Mazumdar, Department of Physics, University of Arizona, Tucson, AZ 85721; and S.N. Dixit, Lawrence Livermore National Laboratory, Livermore, CA 94550.

Using exact finite-size diagonalizations of extended Peierls-Hubbard Hamiltonians for systems of up to 15 sites, we study the excited state spectra of models for the finite oligomer analogs of *trans*- and *cis*-polyacetylene. We use a novel boundary condition averaging technique and a variety of other methods to extract maximal information from these small systems. For several electron-phonon couplings in the expected range, we discuss the extent to which we are able to find consistent values of the Hubbard on-site (U) and nearest-neighbor (V) correlation parameters such that the band gap, the 2^1A_g state, optical phonon frequency, and the optical absorptions for charged and neutral solitons and dimers occur in the experimentally expected ranges. Our results suggest that these correlation parameters are in the intermediate coupling regime ($U \simeq 2.5t_0$), beyond the range of perturbation theory.

* Supported by DOE

Q10.3

OPTICAL SPECTROSCOPY OF THE CHARGE ACCUMULATION LAYER IN POLYMERIC SEMICONDUCTOR MIS AND MISFET STRUCTURES. J. H. Burroughes, R. A. Lawrence and R. H. Friend, Cavendish Laboratory, Madingley Road, Cambridge CB3 0HE, UK.

We have been able to fabricate various semiconductor devices using Durham-route polyacetylene as the active semiconductor. The Metal-Insulator-Semiconductor (MIS) structure and the MISFET are of particular interest because, with the formation of charge accumulation and inversion layers, charge can be injected into the semiconductor without the need for chemical doping. Solitons are the lowest energy electronic excitations of polyacetylene, and we show here the various spectroscopic indications that the active charges in these structures have the character of charged solitons. These include the 'mid-gap' optical transition from soliton level to the band edge, the 'translation' IR active modes, and the Raman-active amplitude mode of the soliton. The Raman modes lie close to the amplitude modes of the dimerised chain, and are seen here for the first time by ratioing the Raman spectra off the active polyacetylene layer in the MISFET with and without the gate voltage present. These various spectroscopic measurements also allow measurement of the degree of order of the polymer at the interface with the insulator layer, and we find that various polymeric insulators give improved performance over that found in structures with silicon dioxide as the insulator layer.

Q10.4

OPTICAL PROPERTIES OF POLYACETYLENE OLIGOMERS.

H. Schaffer and R. R. Chance, Corporate Research, Exxon Research and Engineering Co., Annandale, NJ 08801; and K. Knoll, R. R. Schrock and R. Silbey, Chemistry Department, Massachusetts Institute of Technology, Cambridge, MA 02139.

Polyacetylene oligomers, with no chain substitution except for *t*-butyl caps at either end, have been prepared and isolated with the number of carbon-carbon double bonds, *n*, ranging from 1 to 13.¹ UV-vis absorption measurements of the all-trans molecules in several solvents, as well as in the solid state, show a dependence of the $1B_u \rightarrow 1A_g$ transition energy on environment polarizability that can be largely explained with a simple classical model. The Raman scattering spectra of the all-trans species as well as the alternating *cis*, *trans* molecules have been measured. While the carbon-carbon double bond frequency of the all-trans species decreases with increasing *n*, the single bond frequency increases with *n* to a maximum at *n*=5 before decreasing for *n*>5, perhaps due to coupling with the *t*-butyl end groups. At large *n*, Raman frequencies and absorption energies vary linearly with $1/n$. Extrapolation of these data, Raman and UV-visible, suggests that the familiar samples of *trans*-polyacetylene have conjugation lengths of roughly 20-30 double bonds.

1 K. Knoll and R. R. Schrock, J. Amer. Chem. Soc., in press.

Q10.5

DECISIVE STEPS IN THE PRODUCTION OF HIGHLY CONDUCTING-CRYSTALLINE POLYMERS.

Nicolas Theophilou*, Department of Chemistry, Univ. of Pennsylvania, Philadelphia, PA 19104-6323.

Different new catalyst based on transition metal compounds of groups IVb, Vb, VIb and VIIb combined with a reducing agent: $AlEt_3$ and $n-BuLi$, were used for the polymerization of acetylene. The obtained new polyacetylenes were characterized by SEM, STM, FTIR, ^{13}C NMR, WAXD and stretched mechanically, then doped with iodine, to the highly conducting regime (10^{-10} S/cm). The ESR studies of the catalyst, in connection with the polymerization kinetics, are in agreement with a uniform polymerization reaction related to the presence of one active species in the medium. By introducing some additional reducing agents, in the standard catalyst system ($Ti(OBu)_4 - AlEt_3$ -silicone oil), conductivities higher than 10^{-5} S/cm, after stretch-alignment and iodine doping of the polymer, were reached [1]. The structure and the electronic, electrical, magnetic and optical properties of the polymers will be discussed. We report also here a new technique, to increase the molecular order, crystallinity and conductivity of polyaniline [2]. Coherence lengths up to 400 Å were measured by WAXD and conductivities two orders of magnitude greater, than previously synthesized polyanilines were obtained.

[1] N. Theophilou and H. Naarmann, Makrom. Chem., Makrom. Symp. 24, 115 (1989); Synth. Met. 22, 1 (1987).

[2] N. Theophilou, S. Manohar, E. Scherr, US Pat. Ser #07/306,447, filed 02.02.1989.

*Institute for polymers, 6 Phidiou, Athens 10678, GREECE.

Q10.6

PHOTOCONDUCTIVE RESPONSE AND INTERCHAIN INTERACTIONS IN HIGHLY ORIENTED POLYACETYLENE R. Tubino Istituto di Fisica dell'Università, Via Vienna 2, Sassari and Istituto di Chimica delle Macromolecole, CNR, Milano Italy.

G. Dellepiane, Università di Genova, Italy and A. Walser, R. Dorsinville, R. R. Alfano, Physics and Electrical Engineering depts. City College of New York 138th St. and Convent Ave. New York, New York 10031;

The photoconductive response of highly oriented fibrous polyacetylene have been measured using a continuous wave laser for excitations above and below the energy gap as a function of temperature, laser polarization and direction of the current flow. The cw experimental data is interpreted using a modified Onsager theory for carrier photogeneration and their subsequent motion in low-dimensional lattices. The problem of interchain versus intrachain excitations of the carriers upon changing the laser polarization will be discussed on the basis of a tight binding model extended to include the effect of the electronic coupling between adjacent chains.

The research at CCNY is supported in part by NASA and NSF.

Q10.7

 ^{133}Cs NMR STUDIES OF HIGHLY CESIUM DOPED POLYACETYLENE

F. Rachdi, P. Bernier, K. Zniber
Groupe de Dynamique des Phases Condensées
U S T L 34060 Montpellier Cedex, France.

We report on ^{133}Cs NMR results of chemically highly doped polyacetylene. Two resonance lines were observed, corresponding roughly to metallic and ionic Cs states. The metallic one is strongly shifted from the standard reference (12000 ppm at room temperature) and has an unusual temperature dependence, considerably larger than in the pure metals. Such a behavior is observed for the first time in conducting polymers. It could be related to a significant density of conduction electrons residing on the dopant, which is organized in channels between the host lattice polyacetylene chains. Relaxation times versus temperature measurements on the Cs nuclei are in progress in order to check the Korringa like behavior.

Q10.8

REVERSIBLE PHOTOPRODUCTION OF STABLE CHARGED DEFECTS IN TRANS-POLYACETYLENE WITH MID-BAND-GAP PHOTOLYSIS. Carolyn E. Hoener, Laboratory of Chemical Biodynamics, Lawrence Berkeley Laboratory, Berkeley, CA Present address: Department of Chemistry, University of Texas at Austin, Austin, TX

Photoproduction and photodepletion of stable charged defects in *trans*-polyacetylene were observed, at low temperatures, by monitoring the IR signature of these defects: absorptions at 1368, 1289, 640 cm^{-1} (1053, 600 cm^{-1} for $(CD)_x$). These absorptions could be observed at long times (two to several hundred minutes) after photolysis, only when the sample was protected from photolysis by the probe beam, by blocking $\nu > 2,300$ cm^{-1} .

The location of these absorptions and the temperature dependence of their intensities were similar to those of previously observed photoinduced defects reported to have much shorter lifetimes ($\tau \sim ms$). The stable defects reported here can be produced at much lower photolysis energies ($\nu > 5,500$ cm^{-1}) than transient-photoinduced defects ($\nu > 9,000$ cm^{-1}). A mechanism for the photoproduction of stable defects, involving a two-photon process catalyzed by existing neutral defects, is proposed to explain this low onset.

The slow decay of these defects observed when the sample is kept in the dark is attributed to photoinduced depletion by blackbody irradiation. This process was slow enough to allow the wavelength dependence of photodepletion (observed at $2,800 < \nu < 8,000$ cm^{-1}) to be studied. The photodepletion was fastest near 4,500 cm^{-1} , suggesting that the defects possess an electronic absorption (with a peak near 4,500 cm^{-1}) similar to that observed directly for the transient-photoinduced defects.

Q10.9

CONDUCTING AND NONLINEAR OPTICAL POLYMERS FROM DIETHYNYLSILANES. T. J. Barton, S. Ijadi-Maghsoodi, Y. Pang, J. Shinar, Q.-X. Ni, Ames Laboratory/Iowa State University, Ames, IA; Z. V. Vardeny, University of Utah, Salt Lake City, UT; S. Grigoros, Dow Corning Corporation, Midland, MI.

Catalytic polymerization of diethynylsilanes [$R_2Si(C\equiv CH)_2$] produces polymers of molecular weights (M_w) up to 150,000 (PD ca. 2). These violet or blue polymers are soluble in a variety of organic solvents and are easily cast into coherent films. Although the films are electrical insulators, brief exposure to I_2 vapor affords conductivities up to 0.1 S/cm. The undoped films are photoconducting and light-induced ESR (LESER) has been measured as well as the ODMR.

Spectroscopic studies reveal that both I_2 -doping and steady-state photomodulation produce bipolarons. The effective e-e interaction energy (U_{eef}) is ca. 0.8 eV and E_g ca. 2 eV. Photobleaching recovery at 2 eV, measured with 75 fsec resolution, is almost one order of magnitude faster than ever reported for a conducting polymer.

Structural proposals for these novel polyacetylenes will be discussed in the context of 1H , ^{13}C -, and ^{29}Si -NMR, resonant Raman scattering, and ab initio and molecular dynamics calculations.

Q10.10

THERMALLY ACTIVATED CHARGE HOPPING TRANSPORT STUDIES IN A Σ -CONJUGATED POLYMER

L. Samuel and P.N. Sanda IBM T.J. Watson Research, Yorktown Heights, NY and R.D. Miller and D. Thompson IBM Almaden Research, San Jose, CA.

The σ -conjugated polysilanes have recently elicited much scientific interest, due to their novel properties and technological applications. They are composed of σ -bonded Si atoms along the backbone and two organic side groups attached to each Si atom. The charge transport properties of the polymers, as well as other physical properties, are strongly dependent on the nature of these groups. Charge transport in polysilanes is believed to involve fast transport along the Si chains and hopping transport between chains. Time of flight (TOF) spectroscopy and thermally stimulated current (TSC) measurements were performed in poly(methylphenylsilane), poly(p-methoxyphenylethylsilane) and poly(ethylphenylsilane) to study the influence of the substituent side groups on the hopping transport. The method of TSC, which is commonly used to study traps, was shown to be applicable for studying the bulk hopping transport, and its results were consistent with those obtained by TOF. The activation energies assigned to hopping transport ranged between 0.1-0.3eV and were dependent on the applied electric field. The nature of the field dependence of the activation energy varied with the substituents. A well defined peak was observed in the TSC spectra. The peak temperature, which was dependent both on the electric field and the heating rate, ranged between 100K-150K. When the samples were exposed to a high dose of UV radiation, a secondary peak at ~180K was observed, which was correlated with surface defect sites induced by the UV radiation.

Q10.11

FREE CARRIER BAND GAP IN POLY(PHENYL METHYL SILANE). R. G. Kepler and J. M. Zeigler, Sandia National Laboratories, Albuquerque, NM 87185.

Polysilanes are a new class of polymers which have recently been found to exhibit interesting and potentially very useful electronic properties. Some are excellent photoconductors and large nonlinear optical coefficients have been observed. These materials are of particular interest because their unusual properties are derived from σ electrons delocalized along the Si-Si backbone rather than from π electrons as in all the other intensely studied electronic polymers.

In earlier work on of photoconductivity in poly(phenyl methyl silane) we showed that hole transport is non-dispersive with a mobility of about $10^{-4}cm^2/Vs$ at 23°C and that electron transport cannot be observed. We also found that in the vicinity of the optical gap (about 3.5 eV) carrier generation by light involves the initial generation of excitons followed by the interaction of some of the excitons with the surface. We have now extended our carrier generation experiments to photon energies of 5.5 eV and see a large increase in the quantum efficiency for charge carrier generation beginning at about 4.6eV, indicative of a free carrier band-gap of that magnitude. We have been unable to observe carrier generation by two photon transitions, by exciton-exciton annihilation or by exciton photoionization but we have observed free holes generated uniformly throughout the sample by x-rays.

Q10.12

ESR STUDIES OF CHARGE TRANSPORT AND CARRIER DENSITY IN Σ -CONJUGATED POLYMER SYSTEMS J. T. Riley and S. A. Jansen, Temple University, Philadelphia, PA and Pia N. Sanda, IBM T. J. Watson Research Center, Yorktown Heights, NY

Irradiation of a homologous series of substituted polysilanes produces a magnetic state characterized by a single narrow ESR spectral envelope. This signal is associated with an activated magnetic state. The activation energy for each polymer in the series is reported and discussed in terms of the electronic structure. In addition, the spin density which is expected to be related to carrier density has been determined as a function of UV irradiation time. A kinetic study of the photodegradation of each polymer will also be presented.

Q10.13

THE DOPING OF POLY-p-PHENYLENE SULFIDE AND ITS OLIGOMERS: A SPECTROSCOPICAL STUDY. P. Piaggio, C. Cuniberti, G. Dellepiane Istituto di Chimica Industriale, Università di Genova, Corso Europa 30, I-16132 Genova, Italy,

Since the ultimate goal of research on conducting polymers is a combination of the mechanical properties of polymers with the electronic characteristics of metals, the class of sulfur-containing polymers, which is very attractive in this respect, is now receiving due attention. Poly-p-phenylene sulfide (PPS) is one of the polymers of this class which shows such interesting properties.

Contradictory interpretations of the spectroscopic features of PPS doped with different agents and at different doping levels may be found in the literature.

Purpose of this work is to attempt a rationalization of the existing interpretations by studying the electronic and vibrational spectra of doped PPS compared with those of its oligomers. The experimental data obtained with different sample morpho-

logies, different doping and dopant's nature will be presented and discussed. The time evolution of the spectral features after doping will also be analyzed.

For the understanding of the vibrational spectra after doping advantage will be taken from the vibrational assignment of pristine PPS and its oligomers recently proposed by the authors.

Q11.1

THE DYNAMICS OF SPIN DENSITY WAVES. George Grüner, University of California, Los Angeles, Dept. of Physics, 405 Hilgard Avenue, Los Angeles, CA. 90024.

While the dynamical response of superconducting and charge density wave ground states is well understood, relatively little is known about the dynamical behavior of spin density wave ground states. I will review the current status of the field by focussing on frequency dependent transport studies¹ in the model compounds $(\text{TMTSF})_2\text{X}$ with $\text{X} = \text{PF}_6$, NO_3 and ClO_4 . The observations are suggestive for a collective mode dynamics with effective mass and relaxation time close to the single particle mass and relaxation time observed in the metallic state, above the spin density wave transition. Pinning effects have been established through studies of alloys, and the experiments will also be related to observations² on nonlinear transport in these materials.

¹ G. Grüner, *Physica B + C* (to be published).
J. Carini, W.P. Beyermann, T.w. Kim, and G. Grüner, (to be published).

² S. Tomic, et al., *Phys. Rev. Lett.* **62**, 462 (1989).

Q11.2

BIDIMENSIONNAL CRITICAL BEHAVIOUR AND COMPETITION BETWEEN ORDER PARAMETERS IN THE ORGANIC METAL $(\text{TMTSF})_2\text{ClO}_4$. P. Garoche, F. Pesty, M. Heritier, Laboratoire de Physique des Solides, Université de Paris- Sud, 91405 Orsay, FRANCE.

In low dimensionnal conductors, the instability of the metallic state can lead to the formation at low temperature of a spin density wave state (S.D.W.) induced by the magnetic field. The critical behavior of the transition related to this metal insulator transition has been investigated by the measurement of both the specific heat and the thermal conductance in a fixed magnetic field. Above the second order phase transition, we observe a deviation from the mean field behavior whose temperature dependance is clearly associated with bidimensionnal gaussian fluctuations. At the partial reentrance point T_{cr} between S.D.W. subphases the specific heat displays a complex shape. Below T_{cr} it results simply from the vicinity of the two transition lines but just above T_{cr} the competition between order parameters leads to the formation of a non mean field specific heat anomaly. At the transition the thermal conduction along the less conducting axis c displays also a singularity, that is strongly reduced at the reentrance point. These two dimensionnal behaviors are analyzed in the framework of the quantized nesting model.

Q11.3

HIGH MAGNETIC FIELD PHASES OF THE $(\text{TMTSF})_2\text{X}$ ($\text{X} = \text{ClO}_4, \text{PF}_6$) CHARGE TRANSFER COMPLEXES. James S. Brooks,

Physics Dept., Boston University, Boston MA 02215.

The magnetic field induced spin density wave (FISDW) phases of the $(\text{TMTSF})_2\text{X}$ family of organic charge transfer salts continue to be the subject of active experimental and theoretical interest. The discovery of a re-entrant phase boundary from a spin density wave state to a metallic state has further stimulated this interest.¹ Although for $\text{X} = \text{ClO}_4$ the material is a superconductor below 1.3K, the material with $\text{X} = \text{PF}_6$ requires hydrostatic pressure in excess of 6 kbar to suppress a low temperature spin density wave state in favor of metallic / superconducting behavior. Indeed the role of the anion symmetry and ordering in the superconductivity and FISDW states is not yet fully understood, and complementary measurements in both materials are needed to resolve the problem.

This talk will focus on two relevant sets of measurements: 1) Recent specific heat measurements on $(\text{TMTSF})_2\text{ClO}_4$ at low temperatures and high magnetic fields (to 30 T) which yield a thermodynamic measurement of the re-entrant phase line, and show in addition the contribution of the so-called rapid oscillations to the specific heat in the region of the re-entrant phase line. 2) Magnetoresistance and Hall effect measurements on $(\text{TMTSF})_2\text{PF}_6$ which reveal striking integer Hall effect behavior in the FISDW state.

These new results will be discussed in light of recent theoretical work on the FISDW and re-entrant transitions.

* The author wishes to acknowledge N.A. Fortune, S.T. Hannahs, M.J. Graf, P.M. Chaikin, L.Y. Chiang, G. Montambaux, and J. Perenboom in connection with various aspects of this work.

1. See G. Montambaux et al., *Phys. Rev. B*, **39** 885 (1989) and references therein for a recent synopsis of this subject.

Q11.4

HIGH FIELD MAGNETIZATION STEPS AT THE REENTRANT METAL TO SPIN DENSITY WAVE LINE IN $(\text{TMTSF})_2\text{ClO}_4$. M.J. Naughton, State Univ. of N.Y. at Buffalo; R.V. Chamberlin, Arizona State Univ.; P.M. Chaikin, Princeton Univ. and Exxon Research; L.Y. Chiang, Exxon Research.

The magnetic field-induced spin density wave in the quasi-two dimensional conductor $(\text{TMTSF})_2\text{ClO}_4$ has been shown from magnetoresistance and Hall effect to be confined to fields between 4T and 27T at 0.5K, with a low field metallic state reappearing at higher fields.^[1] Previous magnetic measurements,^[2] while clearly detecting the FISDW phases, have not shown this reentrance. Here, we present measurements of the magnetization $M(H,T)$ in two samples of the title compound to 30T and 0.5K, where we show the first thermodynamic evidence of this unusual phase transition.

Two features are observed in $M(H)$ at $T=0.5K$, in addition to the usual cascade of FISDW phases: a slight diamagnetic increase at $B=24T$, followed by a sharp collapse toward $M=0$ at $B=26T$. At even higher fields, dHvA-type oscillations appear. The temperature dependence of these steps is identical to that determined as the reentrant line from resistance measurements. An analysis of the integrated energy $E - M\mu_H$ is consistent with a metallic ground state at the highest fields. The observation of two steps rather than one indicate a more complicated behavior than previously anticipated, and may assist in the understanding of this perplexing reentrant phenomenon.

1. M.J. Naughton, et al. *Phys. Rev. Lett.* **62**, 969 (1989)
2. R.V. Chamberlin, et al. *Phys. Rev. Lett.* **61**, 1189 (1988)

Q11.5

A NEW THEORETICAL MODEL FOR THE SPIN DENSITY WAVE TRANSITIONS IN ORGANIC CHARGE TRANSFER SOLIDS. E. Y. Loh, Jr. and David K. Campbell, Los Alamos National Laboratory, Los Alamos, NM 87545; and Sumit Mazumdar, Physics Department, University of Arizona, Tucson, AZ 85721.

It has previously been shown that the one-dimensional extended Hubbard model, in which the nearest-neighbor Coulomb repulsion between fermions is explicitly included, is the only theoretical model that can explain the high temperature behavior of the complete family of organic charge-transfer solids. It is now shown that an anisotropic two-dimensional version of the same model can explain the transitions to the spin density wave (SDW) phases in the TMTSF and TMTTF salts. We consider simultaneously (a) the pressure-induced spin-Peierls to SDW transition in TMTTF salts, (b) the magnetic-field-induced SDW transitions (FISDW) in the TMTSF salts, and (c) the absence of the SDW in the BEDT-TTF salts, and show that all of the above features can be explained within the same model. We use numerical techniques to examine the roles played by Coulomb interactions, bandfilling and anisotropy within the two-dimensional layer in detail, and show that the three distinct kinds of behavior in the three families of materials are expected within a quarter-filled extended Hubbard Hamiltonian with varying anisotropies. The highly specific role of the bandfilling is absent in previous mean-field theories. A new interpretation of the very high field transition (VHFT) in $(\text{TMTSF})_2\text{ClO}_4$ is given, and comparisons to experiments are made.

Q11.6

SOUND PROPAGATION IN CDW AND SDW. Attila Virosztek, University of Virginia, Charlottesville, VA; and Kazumi Maki, University of Southern California, Los Angeles, CA.

Making use of a quasi-one dimensional Fröhlich (or Hubbard) model, we study the sound propagation in a CDW (or SDW), within mean field theory. We include the quasi-particle damping in terms of randomly distributed impurities.

In general in a CDW (or SDW) ionic potential is screened by the quasi-particle and the phason. However, when the CDW (or SDW) is pinned the phason can not participate in the screening. Therefore in general the depinning of the CDW (or SDW) by an electric field decreases the sound velocity (as well as the elastic constants as observed). Further, due to the diffusion pole in the density-density correlation function, the quasi-particle contribution depends strongly on ω/Dq^2 . When $\omega/Dq^2 \ll 1$, the quasi-particle contribution is as important as in the collisionless limit¹ and the sound velocity increases in a CDW (or SDW) when the CDW is pinned, since the quasi-particles decrease rapidly in a CDW. On the other hand when $\omega/Dq^2 \gg 1$, the contribution of the quasi-particles is always negligible.

1. K. Maki and A. Virosztek, Phys. Rev. B **36**, 2910 (1987)

Q11.7

SOUND VELOCITY STUDIES OF THE BECHGAARD SALTS $(\text{TMTSF})_2\text{ClO}_4$ and $(\text{TMTSF})_2\text{PF}_6$ X.D. Shi^{1,2}, P. M. Chaikin^{2,3}, L. Y. Chiang³ and R. Upasani^{2,3}, ¹University of Pennsylvania, ²Princeton University, ³Exxon Research

We have used a vibrating reed technique to measure the sound velocity and attenuation in the Bechgaard salts through a number of transitions. In the ClO_4 salt the flexural and torsional modes have been used to observe changes in Young's and shear moduli through the anion ordering at 24 K, the superconducting transition at 1.4K and the Field Induced Spin Density Wave Transitions at temperatures down to 0.5K and fields to 10 Tesla. The FISDW transitions are seen as sharp increases in the moduli as carriers are progressively lost in higher field. In the PF_6 salt the ambient field spin density wave transition is studied.

Q11.8

SOUND VELOCITY MEASUREMENTS IN $(\text{TMTTF})_2\text{X}$ ($\text{X} = \text{ReO}_4$, SbF_6) SALTS. S.E. Brown, H.H.S. Javadi, Los Alamos National Laboratory, Los Alamos, New Mexico, 87545, and R. Laversanne, Centre de Recherche Paul Pascal, CNRS, Domaine Universitaire de Bordeaux I, 33405 TALENCE CEDEX FRANCE.

The TMTTF salts can undergo several types of transitions, including anion ordering at higher temperatures and a magnetic (Spin-Density Wave or Spin-Peierls) transition at lower temperatures. Also of interest is the so-called "structureless" transition for $\text{X} = \text{ReO}_4$, SbF_6 , and AsF_6 .

We have performed Young's Modulus measurements for $\text{X} = \text{ReO}_4$ and SbF_6 using the vibrating reed technique. Below the structureless transition, the rate of stiffening increases substantially. We interpret the results in terms of a decrease in the density of states and in that simple model extract estimates for the electron-phonon coupling constant λ . In the case of $\text{X} = \text{ReO}_4$, $\lambda \geq 0.04$, whereas for $\text{X} = \text{SbF}_6$, $\lambda \sim 0.02$.

Softening was observed at the transition in both cases, although it was much larger for $(\text{TMTTF})_2\text{ReO}_4$. The results are the first demonstration of phonon involvement in these transitions.

Q11.9

QUANTUM HALL EFFECT AND RAPID OSCILLATIONS IN $(\text{TMTSF})_2\text{PF}_6$ UNDER PRESSURE. S. Hannahs¹, J. Brooks¹, W. Kang², P. Chaikin^{2,3}, L. Chiang³, and R. Upasani^{2,3}, ¹Boston University, ²Princeton University and ³Exxon Research

We present magnetotransport data and the phase diagram derived from them for $(\text{TMTSF})_2\text{PF}_6$ under sufficient pressure that the zero field SDW is suppressed and the material is superconducting. Application of a large magnetic field perpendicular to the conducting plane then leads to the cascade of Field Induced Spin Density Wave transitions. The transitions are in good agreement with the Standard model for these transitions and in contrast to the more complicated behavior seen in the ClO_4 salt. In addition Hall and longitudinal resistivity indicates a behavior much closer to that observed in conventional Quantum Hall devices than in the ClO_4 salt or previous studies of PF_6 . We do observe the "rapid" SdH like oscillations in magnetoresistance at high field similar to those seen in ClO_4 , even though in the present case there is no evidence for anion ordering as some theories would require. The frequency of these oscillations is correlated with the characteristic fields for the FISDW's and with the superconducting T_c at different pressures.

Q11.10

LOW TEMPERATURE ORIENTATIONAL DEPENDENCE OF THE MAGNETORESISTANCE IN $(\text{TMTSF})_2\text{ClO}_4$: A SEARCH FOR MAGIC ANGLES. M.J. Naughton and O.H. Chung, State Univ. of N.Y. at Buffalo; J.S. Brooks, Boston Univ.; P.M. Chaikin, Princeton Univ. and Exxon Research; L.Y. Chiang, Exxon Research.

Lebed[1] has calculated that the anisotropic organic metals $(\text{TMTSF})_2\text{X}$, which undergo SDW ordering for magnetic fields greater than a few tesla oriented along the least conducting c^* -axis, should exhibit anomalous features for field directions away from this axis. In particular, he predicts a reduction in the FISDW threshold field when B is aligned at certain 'magic angles' to the c^* -axis, resulting from local commensurability between an electron's periodic motion in the b^* and c^* directions.

We have measured the low temperature magnetoresistance to 8T in the X-ClO_4 salt as a continuous function of the orientation of c^* with respect to B . At $T=70\text{mK}$, we observe from both angle and field sweeps the usual FISDW states, with the exception of one feature. The angular dependence shows a single resistance oscillation centered about halfway between c^* and b' . A similar anomaly has been seen previously by us and by Boebinger et al.[2] at higher temperatures and comparable orientation. We observe this oscillation to persist at fields below the known threshold field for the FISDW states (3-4T), which suggests either an origin independent of FISDW, or possibly the anomaly proposed by Lebed.

1. A.G. Lebed, J.E.T.P. Lett., **43**, 174 (1986).
2. G.S. Boebinger, et alia (preprint).

Q12.1

OBSERVATION OF NONLINEAR OPTICAL TRANSMISSION AND SWITCHING PHENOMENA IN POLYDIACETYLENE-BASED DIRECTIONAL COUPLER DEVICES. Paul D. Townsend, J. L. Jackel, Gregory L. Baker, J. A. Shelburne and S. Etemad, Bellcore, 331 Newman Springs Road, Red Bank, NJ 07701.

The large magnitude and ultrafast response of the electronic $\chi^{(3)}$ in polydiacetylenes makes them potentially attractive materials for applications in nonlinear optics. In particular, it may be possible to fabricate fast all-optical devices which require only relatively low threshold powers for switching. We developed techniques for fabricating directional coupler waveguide structures in thin films of soluble polydiacetylenes with the intention of evaluating the performance of the polymers in a prototype all-optical device format. A variety of nonlinear transmission and switching phenomena were observed in these devices, including slow thermal effects and ultrafast (picosecond) electronic effects. At $1.06\mu\text{m}$ the ultrafast electronic nonlinear phenomena were found to originate from intensity dependent changes in the imaginary part of the refractive index due to two-photon absorption effects. Recent measurements carried out at an operating wavelength of $1.3\mu\text{m}$ will also be reported.

Q12.2

POLYDIACETYLENE SIDE CHAINS AND ELECTRONIC STRUCTURE AND PROCESSES. Daniel J. Sandman, GTE Laboratories, Incorporated, 40 Sylvan Road, Waltham, MA 02254

The polydiacetylenes (PDA), a class of polymers whose main chain involves completely conjugated segments manifested by intense visible absorption, have a fully crystalline character assured by their synthesis involving topochemical and topotactic solid state polymerization resulting in macroscopic single crystal experimental samples. The observed thermal, electronic, optical, and magnetic properties of PDA are a sensitive function of the side chains present and specific side chain processes.

PDA have the largest value of the degenerate third order susceptibility ($\chi^{(3)}\omega$) of any material in the transparent spectral region where the temporal response is in the femtosecond regime. In the interest of enhancing ($\chi^{(3)}\omega$) in PDA, the crystal structure-linear spectrum relationship is discussed. With particular reference to the situation where the observed solid state spectrum of a PDA shifts to higher energy, evidence is presented which indicates that this spectral shift is associated with a change in the local crystallographic environment (side chain) without a change in main chain conformation.

Q12.3

INVESTIGATIONS OF A NEW REVERSIBLE STRAIN INDUCED CHROMIC TRANSITION IN POLYDIACETYLENE ELASTOMERS. M. F. Rubner, R. Agrawal and H. Beckham, Department of Materials Science and Engineering, MIT, Cambridge, MA 02139.

In-situ visible dichroism/tensile elongation studies of segmented polyurethanes containing conjugated polydiacetylene chains within their

hard segment domains have revealed a new reversible mechanochromic transition that manifests itself as a color change from blue to yellow during tensile elongation. This unusual strain induced transition, found in an elastomer whose hard segment structure is derived from hexamethylene diisocyanate and 5,7-dodecadiyne-1,12 diol, closely resembles the thermochromic transition also exhibited by this same material. The color change and the associated shift in the position of the polydiacetylene absorption band to higher energies is not simply an order-disorder transition but reflects a strain induced reorganization of the hard domain structure. It has been found that this blue to yellow transition is reversible as long as the material is not strained beyond about 350%.

Dichroism studies indicate that the hard segments of the copolymer orient perpendicular to the stretch direction during the initial stages of deformation. Such an orientation aligns the conjugated polydiacetylene chains along the stretch direction thereby producing a highly dichroic material. The level of residual orientation remaining after the material is relaxed back to its unstressed state depends strongly on the soft segment content of the copolymer. This represents the first reversible, mechanically induced chromic transition in a cross-polymerized diacetylene containing polymer.

Q12.4

SYNTHESIS AND PROPERTIES OF A FULLY CONJUGATED POLYDIACETYLENE: POLY(1,4-BIS(3-QUINOLYL)-1,3-BUTADIENE. Satya S. Talwar and M. Kamath, Department of Chemistry Indian Institute of Technology, Powai, Bombay India 400 076

Optical and electronic properties of polydiacetylenes (PDA) have attracted much attention. Some of the recent interest in PDA's is related to their large and fast non-linear optical response, making them good candidates for potential applications in ultrafast optical signal processing. Although the electronic and optical properties of PDA's are primarily dominated by the π -conjugated backbone, the substituent groups markedly influence the physical properties of polydiacetylenes. An aspect of the substituent effect that has remained under explored is the influence of formally π -conjugated substituents on the electronic properties of PDA's. Modification of the electronic and optical properties of PDA's with conjugating substituents may be expected through expansion of conjugation. Recent reports on conductivity of doped poly(bis(m -acetamidophenyl)butadiene) and spectral properties of 1-(N carbazoly)pent-1,3-dien-3-ol suggest such extension of conjugation. In this connection we report the synthesis of a fully conjugated polydiacetylene poly(1,4-bis(3-quinolyl)-1,3-butadiene)(Poly DQ). Results of our studies on the optical spectra and electrical conductivity of poly DQ will be presented. The long wavelength absorption in the PDA suggests extension of conjugation through backbone - side group interaction.

Q12.5

ORGANIC POLYMER SEMICONDUCTOR SUPERLATTICES. Samson A. Jenekhe and Wen-Chang Chen, Department of Chemical Engineering, University of Rochester, Rochester, New York 14627.

We report the synthesis and study of the first organic polymer semiconductor superlattices and observation of the predicted quantum size effects in the electronic and optical properties of such quasi one-dimensional semiconductor heterostructures. The organic semiconductor superlattices were designed as periodic multiblock conjugated copolymers $(A_xB_y)_m$, where A and B blocks have different band gaps. The optical properties were investigated as a function of the copolymer block length that allowed variation of

the superlattice period. Effects of a randomly variable periodicity was studied by synthesis of random multi-block conjugated copolymers. It will be shown that quantum well and superlattice heterostructures provide a rational and systematic approach to the molecular engineering of electronic, electro-optical, optical, and nonlinear optical properties in polymers.

Q12.6

LARGE THIRD-ORDER NONLINEAR OPTICAL PROPERTIES OF ORGANIC POLYMER SEMICONDUCTOR SUPERLATTICES. Samson A. Jenekhe and Wen-Chang Chen, Department of Chemical Engineering, University of Rochester, Rochester, New York 14627; S. K. Lo, Honeywell Systems and Research Center, Minneapolis, MN; and Steven R. Flom, Department of Chemistry, University of Minnesota, Minneapolis, MN.

We report an extensive study of the third-order nonlinear optical properties of a series of recently prepared organic polymer semiconductor superlattices using time and polarization dependent degenerate four wave mixing. At 532 nm, the picosecond $\chi_{xxxx}^{(3)}$ and $\chi_{xxxxy}^{(3)}$ were as large as 1.60×10^{-29} esu and 2.73×10^{-27} esu, respectively. At 568 nm, the nanosecond $\chi_{xxxx}^{(3)}$ and $\chi_{xxxxy}^{(3)}$ were as large as 1.80×10^{-28} esu and 2.42×10^{-26} esu, respectively. These are the largest third-order optical nonlinearities yet reported for any conjugated polymer. Important experimental trends in the structure-optical nonlinearity relationships will be described.

Q12.7

A COUPLED INVESTIGATION OF QUADRATIC AND CUBIC NONLINEAR OPTICAL PROCESSES IN EXTENDED CHARGE TRANSFER POLYENES
M. Barzoukas*, M. Blanchard-Desce**, F. Kajzar***, J.M. Lehn**, A. Messier***, C. Sentein**, L. Zyss*. "CNET (LA CNRS 250) 196 Av. H. Rava 92220 BAGNEUX - FRANCE; **Collège de France, 11 Place Marcelin Berthelot 75231 PARIS CEDEX 05; ***CEA-CEN Saclay 91191 GIF-SUR-YVETTE CEDEX - FRANCE

In the first part, nonlinear spectroscopic investigations combining electric-field induced second-harmonic generation (EFISH) with frequency dispersed third-harmonic generation (THG) in organic solutions /1,2/ are extended to newly synthesized long chain conjugated donor-acceptor polyenes /3/: in such molecules, as the γ and $\mu \beta /kT$ contributions are expected to be of the same order of magnitude, additional frequency dispersed measurements and adequate dispersion to relate $\gamma(-3\omega; \omega; \omega, \omega)$ from THG to $\gamma(-2\omega; \omega, \omega, \omega)$ from EFISH are performed. As opposed to a preliminary report /1/ where the cubic properties of paranitroaniline-like structures could indeed be neglected as compared to their quadratic properties, we show here that both contributions are non negligible. In the second part we report and discuss real and imaginary parts of the quadratic β and cubic γ hyperpolarizabilities of push-pull polyenes of increasing length /3/ as investigated by our coupled THG-EFISH methodology.

/1/ M. Barzoukas, P. Frémaux, D. Josse, F. Kajzar and J. Zyss MRS Symposium Series 109, 171 (1988)

/2/ F. Kajzar, I. Ledoux and J. Zyss Phys. Rev. A 36, 2210 (1987)

/3/ M. Barzoukas, M. Blanchard-Desce, D. Josse, J.M. Lehn and J. Zyss, Chem. Phys. 133, 323 (1989)

Q12.8

NONLINEAR OPTICAL STUDIES OF MIXED π -CONJUGATED POLYMER MULTILAYERS BY SECOND HARMONIC GENERATION Hiroshi Koezuka, Tetsuyuki Kurata, Akira Tsumura

and Hiroyuki Fuchigami, Mitsubishi Electric Corp., Materials & Electronic Devices Lab., Tsukaguchi-Honmachi 8-Chome, Amagasaki, Hyogo 661, Japan.

π -Conjugated polymers have been intensively investigated as candidates of nonlinear optical materials. Since nonlinear susceptibilities greatly depend on the degree of chromophore orientation, a Langmuir-Blodgett (LB) technique has been widely utilized to orient the chromophores. On the other hand, second harmonic generation (SHG) can be applicable to study the orientation of ultra-thin films. In this study, we have prepared mixed multilayers consisting of two kinds of π -conjugated system, that is, poly(3-hexyl-thiophene) (PHT) and amphiphilic pentacosanoic acid (DA). The orientation of the obtained multilayers having various mixing ratio of PHT to DA has been investigated primarily by a SHG Maker fringe method using a Q-switched Nd:YAG laser (1.06 μ m).

All the deposited LB films was Y-type. For SHG measurements the p-polarized harmonic radiation was observed only for s-(s+p) and p-(p+p) polarization of the fundamental. The SHG intensity increased with increasing ratio of PHT to DA. The SHG intensity clearly showed an odd-even effect relative to the deposited number of monolayers. From both the analyses of the observed Maker fringe patterns and the results of π -A isotherms the detailed orientation of mixed multilayers will be discussed.

Q12.9

A NEW POLYOLEFINE MATERIAL "ZEONEX" FOR OPTICAL USES
Teiji Kohara, Masayoshi Ohshima, and Tadao Natsuume, Nippon Zeon Co., Ltd., 1-2-1 Yako, Kawasaki-ku, Kawasaki, 210 Japan; Masahiro Yamazaki, Nippon Zeon of America, Inc., 50 Main Street, White Plains, New York 10606

Nippon Zeon Co., Ltd. has invented a new polyolefin polymer "ZEONEX", which has excellent properties for optical disc substrate. ZEONEX is an amorphous and transparent hydrocarbon polymer. It has high transmittance, small photoelastic coefficient, high heat resistance, low water absorption, low moisture permeability, and easy processing properties.

ZEONEX is made first by ring-opening polymerization of norbornene type monomers to intermediary polyolefin, which has unsaturated bonds in polymer main chain, then by hydrogenation to highly heat-resistant saturated hydrocarbon polymer. ZEONEX has rigid unsymmetric 5-membered ring structure in polymer main chain and has bulky substituents in the ring. Excellent features of ZEONEX are contributed by these structural characteristics.

We believe that ZEONEX is most suitable for single-sided optical discs, especially for uses in a large diameter discs. We have obtained 200 mm diameter discs, which have low retardation of birefringence less than 25 nm, by injection molding process. The molding conditions are similar to 130 mm diameter discs. The discs showed only quite small warpage even under the test conditions at 80°C and 90% RH. However, the discs made from PC showed a remarkably big warpage under the same conditions.

Q12.10

SYNTHESIS AND SECOND-ORDER NONLINEAR OPTICAL PROPERTIES OF NEW COUMAROMETHACRYLATE-METHYLMETHACRYLATE COPOLYMERS. R.A. Henry, J.M. Hoover, and G.A. Lindsay, Research Department, Code 3858, Naval Weapons Center, China Lake, CA 93555; and M.A.

Mortazavi, A. Knoesen, and S.T. Kowel, Department of Electrical Engineering and Computer Science, University of California, Davis, CA 95616.

The synthesis and second-order nonlinear optical properties of a new family of optically nonlinear polymers consisting of a coumarin dye attached to a poly(methylmethacrylate) (PMMA) backbone will be reported. Polymerizable coumaromethacrylate (CMA) monomers having alkyl spacers (C_2 to C_5) between the chromophore and the methacrylate group were prepared and copolymerized with methylmethacrylate (MMA) to yield CMA-MMA copolymers with high chromophore content (up to $9.8 \times 10^{20}/cm^3$) and glass transitions as high as $132^\circ C$. Spin cast films were prepared on BK7 substrates and oriented by corona-onset poling at elevated temperatures (COPET). The spectroscopic absorption and second harmonic generating properties of the poled CMA-MMA polymer films were measured as a function of chromophore density and alkyl spacer length, and were compared to results for poled guest-host systems such as PMMA-azo dye and PMMA-coumarin dye. Relative to PMMA - Disperse Red 1, CMA-MMA copolymer films exhibit larger and much more stable second-order nonlinear optical properties.

Q12.11

NEW POLYMERS FOR ELECTROACTIVE APPLICATIONS. Mamoun M. Badr, David W. Polis, and Larry R. Dalton, Department of Chemistry, University of Southern California Los Angeles, California 90089-0482

Polymers with enhanced third nonlinear susceptibilities can be achieved either by incorporating electroactive subunits in the polymer backbone or attaching them as pendant groups. Currently we are trying both approaches in order to maximize NLO properties of some polymeric systems. New random copolymers of styrene, p-aminostyrene and methylmethacrylate, with p-aminostyrene percentage covering the range 5-50%, have been synthesized and characterized by the conventional methods i.e., UV-VIS, IR, H^1 NMR, GPC, and thermal analysis. These polymers were then reacted with 4-chloro-7-nitrobenzofurazan to give bright orange polymers of which semi-transparent thin films were made. The degree of transparency depends on the amount of the electroactive units attached to the polymer.

We anticipate larger contributions from intermolecular processes at higher concentrations of electroactive subunits. We are also investigating the way the dye content affects the morphology of films since stacking of these units is expected at higher concentrations. Degenerate Four Wave Mixing measurements are currently underway. In addition, the synthesis of other functionalized random copolymers with different subunits of potentially high nonlinear optical properties is underway.

Q12.12

PHOTOEXCITATION SPECTROSCOPY OF PRECURSOR ROUTE POLY(THIOPHENE VINYLENE). D. D. C. Bradley, A. J. Brassett, N.F. Colaneri, R.H. Friend and R.A. Lawrence, Cavendish Lab, Madingley Rd, Cambridge CB3 0HE, UK; and H. Murata, S. Tokito, T. Tsutsui and S. Saito, Dept. of Materials Science and Technology, Kyushu University, Kasuga, Fukuoka 816, Japan.

Poly(thiophenevinylene) [PTV] is prepared via a sulphonium polyelectrolyte precursor, allowing the ready fabrication of fully dense thin films which are of interest for nonlinear optics and related applications. We report a study of the optical properties of PTV and its behaviour following photoexcitation. Photoexcitation above the bandgap (ca. 1.76 eV) gives rise to a transient spectrum in which absorption peaks ($-\Delta T/T = 3 \times 10^{-4}$) are seen at 0.43 and 1.0 eV. An additional oscillatory

structure appears in the vicinity of the band edge and at higher energies a broad bleaching band appears. The two main peaks are assigned to transitions involving bipolarons that are estimated to have a lifetime of order 3ms at 80K. The oscillatory structure is well correlated with the two intra-gap peaks in terms of its dependence upon intensity, temperature and chop-frequency and is assigned to a modulation of the band-edge caused by local electric fields in the vicinity of the charged bipolarons. No sub-bandgap luminescence is seen and the emission occurring in the absorptive region (a "hot" process) is very weak (comparable to the Raman scattering). On the basis of these results we discuss the nature of the confinement in PTV and the importance of non-radiative recombination pathways in quenching photoluminescence.

Q12.13

Synthesis and Characterization of New Polymers Exhibiting Large Optical Nonlinearity: Derivatized Polyaniline and Copolymer Containing Polyaniline Segments. Luping Yu, Mai Chen, Larry R. Dalton, Department of Chemistry, USC, LA, CA-90089-0482.

As part of a continuing exploration of organic polymers as nonlinear optical materials, a new derivatized polyaniline with carboxylic ester substituents and a copolymer containing derivatized polyaniline segments and aliphatic flexible chain have been synthesized via soluble precursors. The copolymer exhibits improved solubility and a defined absorption band-edge when compared to polymer. Degenerate four wave mixing (DFWM) measurements for copolymer indicate a third order susceptibility of 4.5×10^{-9} esu. The characterizations of derivatized polyaniline are in progress. Primary studies indicate that this polyaniline can be oxidized by electrochemical process to promote the electrical conductivity. A strong DFWM signal has been observed.

Q13.1

THE 2^1A_g STATE IN LONG POLYENES: ELECTRONIC STRUCTURE, PHOTOINDUCED ABSORPTION AND THERMAL ISOMERIZATION. Bryan E. Kohler and Curtis Westerfield, Chemistry Department, University of California, Riverside, CA 92521.

High resolution fluorescence and fluorescence excitation spectra have been obtained for the all-trans polyene 2,4,6,8,10,12,14,16-octadecaoctaene (16 conjugated carbon atoms). This is the longest discrete polyene for which such data are known. The 1^1A_g to 2^1A_g 0-0 band at $17,871\text{ cm}^{-1}$ is 4900 cm^{-1} below the 1^1B_u (band gap) transition at $22,770\text{ cm}^{-1}$. Both of these energies would have been predicted by fitting the J=0 excitation energies of shorter polyenes by a $1/N$ curve and extrapolating to $N=8$. The excitation energy and isomerization properties of the polyene 2^1A_g state can be extrapolated to polyenes of arbitrary conjugation length to give a consistent and quantitative accounting of the photoinduced absorption, thermal isomerization and nonlinear optical response observed for polyacetylene films.

Q13.2

THEORETICAL CALCULATIONS ON NONLINEAR SUSCEPTIBILITIES OF ORGANIC MATERIALS. Yuzo Itoh, Tomoyuki Hamada, Atsushi Kakuta, and Akio Mukoh, Hitachi Research Laboratory, Hitachi Ltd. 4026 Kuji-cho, Hitachi, Ibaraki, 319-12 Japan.

Under the oriented gas model approximation, we can calculate susceptibility of an organic crystal if the

molecular hyperpolarizability and the crystal structure are known. Semi-empirical (CNDO/S3-CI) and *ab initio* molecular orbital (MO) calculations are used to evaluate molecular hyperpolarizabilities. Crystal energy calculations, using empirical atom-atom pairwise potentials, are employed to evaluate the crystallization properties.

In the hyperpolarizability calculations, the semi-empirical MO calculations are applied to search for suitable materials for second harmonic generation (SHG) of a diode laser. The *ab initio* MO calculations are done for more rigorous analyses. Basis set dependence of the hyperpolarizability values calculated by a time independent perturbation and a coupled-perturbed Hartree-Fock (CPHF) methods is investigated.

Space group limiting calculations of crystal energy with the accelerating convergence method are performed to estimate the minimum energy crystal structures of organic nonlinear materials. The calculated structures agree well with the experimental ones.

The oriented gas model neglects the effect of intermolecular interactions by crystal packing on hyperpolarizability. The effect is estimated quantitatively by the *ab initio* MO calculations of super molecules of several typical organic nonlinear materials.

Q13.3

NONLINEAR OPTICAL RESPONSE IN CONJUGATED POLYMERS - A THEORETICAL APPROACH. Mauro Pereira, Jr., Optical Sciences Center, University of Arizona, Tucson, AZ 85721; S. W. Koch, Physics Department and Optical Sciences Center, University of Arizona, Tucson, AZ 85721; Sumit Mazumdar, Physics Department, University of Arizona, Tucson, AZ 85721; and S. N. Dixit, Lawrence Livermore National Laboratory, Livermore, CA 94550.

The nonlinear optical properties of organic conjugated polymers are theoretically investigated. We compute the differential transmission spectra (DTS) for conjugated polymers assuming a typical pump-probe geometry. The probe transmission is calculated both with and without the simultaneous excitation of the experimental system by a pump beam that is not collinear. Calculations are done for the simple Hincel (SSH), Hubbard and Pariser-Parr-Pople models, and both dipole-allowed one-photon states and dipole-forbidden two-photon states are included. The one-electron Hamiltonian is studied for the infinite chain length, while finite Hubbard and PPP chains are investigated within an exact numerical approach. The completely general expression for the DTS is evaluated without making use of any rotating wave approximation. The DTS is calculated for broad ranges of pump and probe frequencies to study absorption saturation, probe gain, photoinduced absorption, as well as the optical Stark effect.

Q13.4 ABSTRACT NOT AVAILABLE Q13.5

ROTATIONNAL DIFFUSION OF CHROMOPHORES INSIDE A GLASSY POLYMERIC FILM STUDIED BY ELECTROOPTICAL POLARIMETRY. Rémi MEYRUEIX and Gérard MIGNANI, Rhône-Poulenc Recherches, Centre des Carrières, 69192 SAINT-FONS CEDEX, France.

Amorphous polymers doped or functionalized with charge transfert chromophores appear to be a promising novel class of NLO material.

The dynamic of the chromophores when the film is subjected to an electrical poling field is studied both in the rubber and in the glassy state by electrooptical polarimetry. We present here the rigorous derivation of the second order susceptibility coefficients χ_{311} and χ_{111} from the phase shift between s and p waves crossing the film under incidence i. Our method is applied to some polymer matrix doped with the disperse red one azo dye.

Above the glassy temperature, T_g , the dopant dynamics is easily visualized by Kerr effect: the relaxation time is short ($\tau \approx 0,01$ s at $T_g + 5^\circ\text{C}$).

In the glassy state, disorientation as well as orientation can be achieved below T_g . The analysis of the SMOLUCHOVSKI equation shows that the rotation of the chromophore cannot be described by a single diffusion coefficient or a single relaxation time τ . We give results about the dependance of the relaxation time distribution with temperature, physical ageing, magnitude of the secondary transition, molecular weight and dopant/polymer dipolar interaction.

Q13.6

SECOND ORDER NONLINEAR OPTICS AND POLYMER PHYSICS OF CORONA POLED POLYMER FILMS. Hilary L. Hampsch^a, Jian Yang^b, George K. Wong^b, John M. Torkelson^{a,c}; ^aDepartment of Materials Science and Engineering, ^bDepartment of Physics and Astronomy, ^cDepartment of Chemical Engineering, Northwestern University, Evanston, IL.

Basic polymer physics phenomena, including relaxation and mobility, free volume, and free volume distributions were examined in glassy polymers doped with nonlinear optical (NLO) chromophores. Second order NLO effects such as second harmonic generation (SHG) and the linear electro-optic effect were examined as a function of time to investigate the temporal stability of dopant orientation in in-situ corona poled films of polystyrene, poly(methyl methacrylate), and bisphenol-A-polycarbonate doped with NLO dyes. In-situ corona poling was used to generate a strong electric field that oriented the dopants noncentrosymmetrically in the polymer matrix (required for SHG to occur). The SHG intensity decays when relaxations in the polymer glass allow the dopants freedom to rotate out of their poling-imposed noncentrosymmetric orientation. The SHG intensity was measured in-situ, directly in the beam path with time before and after physical and chemical modifications to the films, including physical aging and secondary bonding effects.

Physical aging, or sub- T_g annealing, was performed before and during poling in order to decrease and redistribute local free volume/decrease segmental mobility around the NLO dopants. Physical aging during poling led to an increase in temporal stability of the SHG intensity by densifying the matrix around the orienting dopants. Aging before poling decreased the fraction of dopants able to orient (decreased SHG intensity) but did not affect the shape of the SHG decay curve. Other variables examined included the effect of thermal history, poling temperature and time, and polymer polydispersity and molecular weight. Quenching from different temperatures above T_g led to different temporal stabilities of the SHG intensity. The effect of dopant/polymer interactions was studied by comparing NLO dopants of similar size but different ability to hydrogen bond to a given polymer matrix. Hydrogen bonding between the dopant and polymer significantly increased the temporal stability of the SHG intensity.

Q13.7

THEORETICAL STUDIES OF THE NONLINEAR PROPERTIES OF L-ARGININE PHOSPHATE AND DERIVATIVES. C. A. Langhoff, Dow Chemical, 1776 Bldg., Midland, MI 48674.

Recent work at the Lawrence Livermore National Laboratory has shown that L-arginine phosphate(LAP) is a good candidate for frequency conversion of Nd lasers. We have undertaken a quantum chemical study of LAP and several derivatives in an effort to understand the origin of its nonlinear properties. The semiempirical CNDO/S method was used to calculate the excited properties of the molecule and a conventional sum over states method was used to calculate the β tensor. Comparison of these results with measured values will be presented.

Q13.8

QUANTUM LATTICE FLUCTUATIONS AND NONLINEAR OPTICAL PROPERTIES OF CONDUCTING POLYMERS. J. Yu, B. Friedman, and W. P. Su, University of Houston, Houston, TX.

Quantum lattice fluctuations in the form of virtual soliton antisoliton ($S\bar{S}$) pairs have been shown to significantly affect the subgap absorption and the luminescence spectra of conjugated polymers. Within a tight binding model we have calculated the contribution of the virtual $S\bar{S}$ pairs to the cubic susceptibilities. The result can explain a pronounced two photon resonance peak in the third harmonic spectrum of trans-polyacetylene. Result for nondegenerate polymers will also be discussed.

Q13.9

THIRD ORDER NONLINEAR OPTICAL EFFECTS IN POLYCONDENSED THIOPHENE BASED POLYMERS. Lina Yang, R. Dorsinville, R. R. Alfano, Physics and Electrical Engineering Depts. City College of New York 138th St. and Convent Ave. New York, New York 10031; C. Taliani Istituto di Spettroscopia Molecolare Consiglio Nazionale delle Ricerche Via de'Castagnoli 1, 40126 Bologna, Italy

Third order nonlinear optical effects of polythiophene and a homologous series of polycondensed thiophene based polymers were investigated using the picosecond four wave mixing technique. For the first time, the dispersion of the cubic nonlinear susceptibility $\chi^{(3)}$ using four wave mixing above and below gap for several thin films samples of thiophene based polymers are reported. The $\chi^{(3)}$ for these polymers was found to be one of the largest and fastest.

The research at CCNY is supported by PSC and NSF.

Q13.10

OPTICAL CHARACTERISATION OF POLYDIACETYLENE LANGMUIR-BLODGETT FILM ON SILICON SUBSTRATES. P. Miller, A.M.K. Rahman, S.V. Brode, S. Tripathy, University of Lowell, Departments of Physics and Chemistry, Lowell, MA 01854

A bilayer of a surfactive polydiacetylene (15-8 PDA) has been deposited by langmuir-Blodgett (L.B.) technique on a smooth Silicon substrate. A commercial Lauda film balance was used to deposit the bilayer on a cleaned Silicon wafer.

The morphology of the deposited film has been studied by cross-polarized optical microscopy, and laser light scattering microscopy. Usual crystalline domains with size ranging from 5 to 50 μm can be seen between cross polarizers. Nonuniformities and voids in the film are observed by imaging the scattered light from a visible laser beam incident at grazing angle onto the film.

Raman scattering study on these bilayers have been carried out to investigate their vibronic structure. Information about vibronic levels from PDA has been used to define the extend of disorder and crystalline phase of the bilayer. Large enhancement of the scattering is obtained on local rough defects on the Si substrate.

Reference:

1. Y.J. Chen, S.K. Tripathy, G.M. Carter, B.S. Elman, E.S. Koteles and J. George, Jr, Solid State Comm. **58**, pp. 97-100 (1986).

Q13.11

MICRO-ENCAPSULATED CHIRAL POLYMER COMPOSITES. Vijay K. Varadan, Deepak K. Ghodgaonkar, Vasundara V. Varadan and Akhlesh Lakhtakia, Research Center for the Engineering of Electronic and Acoustic Materials, 227 Hammond Building, Pennsylvania State University, University Park, PA 16802.

In the past two years, we have extensively demonstrated the wide-ranging utility of chiral composites constructed at our Center. The composites are environmentally stable, and can be conveniently processed for RFI / EMI / EMC applications. The host material is a blend of silicone and non-silicone polymers, while microballoons made of a lossy chiral polymer constitute the inclusion phase. Extensive characterization tests conducted on our free-space microwave characterization facility over the 8-40 GHz range will be presented to demonstrate the remarkable properties of these composites.

Q13.12

ARTIFICIAL CHIRAL COMPOSITES. Vasundara V. Varadan, Deepak K. Ghodgaonkar, Vijay K. Varadan and Akhlesh Lakhtakia, Research Center for the Engineering of Electronic and Acoustic Materials, 227 Hammond Building, Pennsylvania State University, University Park, PA 16802.

Chiral media are commonly found in nature as the stereoisomers of organic chemistry, which exhibit the innate chirality of their molecules at optical frequencies. The geometric basis of chirality has been extended down to the GHz frequency range by suspending microminiature helices in a dielectric host material. Since the helices are chiral, the composite thus constructed is also (artificially) chiral. The host material can be simple polymers such as epoxy, or the more complicated conducting polymers. Properties of these artificial composites have been tested in the 8-40 GHz frequency range, and indicate their utility as EM shielding materials, microwave absorbers, as well as for other EMI / EMC / RFI purposes.

Q13.13

POLYMER BLEND FOR RFI / EMI / EMC APPLICATIONS. Neil Williams, Vijay K. Varadan and Vasundara V. Varadan, Research Center for the Engineering of Electronic and Acoustic Materials, 227 Hammond Building, Pennsylvania State University, University Park, PA 16802.

A conducting polymer blend made of silicone and non-silicone polymers has been developed at our Center. The silicone polymer is made of polysiloxane units with electron-withdrawing groups attached to silicone for a.c. conductivity. The non-silicone polymer is carbon-based and also has electron-withdrawing groups. D.C. conductivity may be imparted to the blend by adding tin tetrachloride powder. The polymer blend has been extensively tested in the 5-60 GHz frequency range using a free-space measurement setup described elsewhere in this Symposium. Our experimental results strongly indicate that this blend is suitable for RFI / EMI / EMC applications, and also for constructing microwave absorbing panels. It is environmentally stable, hydrophobic, and non-corrosive; and it can be applied to diverse surfaces in a variety of ways.

**SYMPOSIUM R:
MATERIALS SYNTHESIS UTILIZING
BIOLOGICAL PROCESSES**

R

November 28 - 30, 1989

Chairs

Peter C. Rieke
Materials & Chemical Sciences Center
Battelle-Pacific Northwest Laboratory
P.O. Box 999
Battelle Blvd.
Richland, WA 99352
(509) 375-2833

Mark Alper
Center for Advanced Materials
Lawrence Berkeley Laboratory and
Department of Molecular
& Cell Biology
University of California at Berkeley
Berkeley, CA 94720
(415) 486-6581

Paul D. Calvert
Arizona Materials Laboratories
University of Arizona
4715 E. Fort Lowell Road
Tucson, AZ 85712
(602) 322-2960

Symposium Support

Air Force Office of Scientific Research

Office of Basic Energy Sciences,
U.S. Department of Energy

**Proceedings published as Volume 174
of the Materials Research Society
Symposium proceedings series.**

MATERIALS SYNTHESIS UTILIZING
BIOLOGICAL PROCESSES

November 28 - 30, 1989

SESSION R1: BIOLOGICAL AND BIOMIMETIC
MINERALIZATION I

Chairs: Paul Calvert and Richard Blakemore
Tuesday Morning, November 28
Essex North Center (W)

8:30 *R1.1
BIOMINERALIZATION BY MAGNETIC BACTERIA,
Richard P. Blakemore, University of New
Hampshire, Microbiology Department, Durham,
NH.

9:00 *R1.2
DENTAL ENAMEL BIOMINERALIZATION: A PROSPEC-
TUS, Harold C. Slavkin, Malcolm L. Snead,
Margarita Zeichner-David, Eduardo C. Lau and
Alan G. Fincham, University of Southern
California, Los Angeles, School of Den-
tistry, Laboratory for Developmental Biol-
ogy, Department of Basic Sciences, Los
Angeles, CA.

9:30 *R1.3
BONE FORMATION: THE RULES FOR FABRICATING A
COMPOSITE CERAMIC, Arnold I. Caplan, Case
Western Reserve University, Skeletal
Research Center, Department of Biology,
Cleveland, OH.

10:00 BREAK

10:15 R1.4
CRYSTAL FORMATION WITHIN COLLAGEN FIBRILS: A
STUDY OF MINERALIZING TURKEY TENDON, S.
Weiner, Weizmann Institute of Science,
Structural Chemistry and Isotope Depart-
ments, Rehovot, Israel; W. Traub, J.
Moradian-Olkak, L. Addadi, Weizmann In-
stitute of Science, Structural Chemistry
Department, Rehovot, Israel; and W. J.
Landis, Children's Hospital, Harvard Medical
School, Boston, MA.

10:30 R1.5
MINERAL PHASE CHARACTERIZATION FROM IN VITRO
MINERALIZATION OF HUMAN OSTEOBLASTIC OS-
TEROSARCOMA CELLS, E.P. Paschalis, D.N.
Tatakis, R. Dziak and G.H. Nancollas, State
University of New York at Buffalo, Chemistry
Department, Buffalo, NY.

10:45 DISCUSSION

11:00 R1.6
CERAMIC OXIDE THIN FILM FORMATION UTILIZING
BIOLOGICAL PROCESSES, B.J. Tarasevich and
P.C. Rieke, Battelle-Pacific Northwest
Laboratory, Materials Sciences Department,
Richland, WA.

*Invited Paper

11:15 R1.7
A "BIO-MIMETIC" ROUTE TO BARIUM TITANATE
SHEETS, Paul Calvert, University of Arizona,
Department of Materials Science and En-
gineering, Tucson, AZ; R.A. Broad, Univer-
sity of Sussex, School of Chemistry, Sussex,
United Kingdom.

11:30 R1.8
SYNTHETIC SURFACES AS MODELS FOR BIOMINER-
ALIZATION SUBSTRATES, P.C. Rieke, B.J.
Tarasevich, S.B. Bentjen, Battelle-Pacific
Northwest Laboratory, Metals and Ceramics
Science Department, Richland, WA.

11:45 DISCUSSION

SESSION R2: BIOLOGICAL AND BIOMIMETIC
MINERALIZATION II

Chairs: Peter Rieke and Dave Eanes
Tuesday Afternoon, November 28
Essex North Center (W)

1:30 *R2.1
CALCIUM PHOSPHATE PRECIPITATION IN LIPOSOMAL
SUSPENSIONS, Edward D. Eanes, National
Institute of Standards and Technology,
Polymers Division, Gaithersburg, MD.

2:00 R2.2
KINETICS AND SOLUTION CHEMISTRY OF HYDROXYA-
PATITE FORMATION, Paul W. Brown and Mark T.
Fulmer, Pennsylvania State University,
Department of Materials Science and the
Materials Research Laboratory, University
Park, PA.

2:15 R2.3
THE NUCLEATION AND GROWTH OF CALCIUM PHOS-
PHATE ON SEPARATED SALIVARY PROTEIN FILMS,
A.A. Campbell and G.H. Nancollas, State
University of New York at Buffalo, Chemistry
Department, Buffalo, NY.

2:30 R2.4
THE INFLUENCE OF SALIVARY PROTEINS ON THE
GROWTH, AGGREGATION AND SURFACE PROPERTIES
OF HYDROXYAPATITE PARTICLES, M. Johnsson, C.
Richardson and G.H. Nancollas, State Univer-
sity of New York at Buffalo, Chemistry
Department, Buffalo, NY.

2:45 R2.5
THE EFFECTS OF PHOSPHOCITRATE AND CITRATE ON
THE CRYSTAL GROWTH AND PARTICLE SIZE DIS-
TRIBUTION OF HYDROXYAPATITE, C.F.
Richardson, M.S.A. Johnsson and G.H.
Nancollas, State University of New York at
Buffalo, Chemistry Department, Buffalo, NY.

3:00 DISCUSSION

3:15 BREAK

3:30 R2.6
THE MICROSTRUCTURES AND FORMATION OF BIOMINERALIZED BIVALVIA SHELLS, L.J. Huang and H-D. Li, Tsinghua University, Department of Materials Science and Engineering, Beijing, China.

3:45 R2.7
THE BERNAL SPIRAL AS A MODEL FOR THE STRUCTURE OF SOME BIOLOGICAL SYSTEMS, Gustavo Vázquez Polo and Miguel José Yacamán, UNAM, Instituto de Física, Mexico, Mexico.

4:00 R2.8
MECHANICAL PROPERTY-MICROSTRUCTURAL RELATIONSHIPS IN ABALONE SHELL, Mehmet Sarikaya, Katie Gunnison and İlhan A. Aksay, University of Washington, Department of Materials Science and Engineering, Seattle, WA.

4:15 R2.9
AN ELECTRON MICROSCOPY STUDY ON THE MICROSTRUCTURE OF THE STROMBUS GIGAS SHELL, V.J. Laraia Jr., M. Aindow and A.H. Heuer, Case Western Reserve University, Department of Materials Science and Engineering, Cleveland, OH.

4:30 R2.10
THE MICROINDENTATION BEHAVIOR OF SEVERAL MOLLUSK SHELLS, V.J. Laraia Jr., and A. H. Heuer, Case Western Reserve University, Department of Materials Science and Engineering, Cleveland, OH.

SESSION R3: ENZYMATIC SYNTHESIS OF MATERIALS IN CELL-FREE SYSTEMS

Chair: Mark Alper
Wednesday, November 29
Essex North Center (W)

8:30 MARK ALPER, OPENING REMARKS

8:45 R3.1
MATERIALS SYNTHESIS UTILIZING BIOLOGICAL PROCESSES, George M. Whitesides, Harvard University, Department of Chemistry, Cambridge, MA.

9:15 R3.2
THE USE OF PROTEINS IN THE SYNTHESIS OF POLYMERS AND THE MODIFICATION OF SILICON SURFACES, Lynn Oehler, Chris Hobbs, Mark Mastandrea and Mark Bednarski, University of California, Berkeley, Department of Chemistry and Center for Advanced Materials, Lawrence Berkeley Laboratory, Berkeley, CA.

9:45 R3.3
POLYMER SYNTHESIS BY FREE RADICAL ENZYME COUPLING REACTIONS IN SOLVENTS, J.A. Akkara, K. Senecal and D.L. Kaplan, US Army Natick, R&DE Center, Natick, MA.

10:00 R3.4
POLYMERIZATION OF PHENOLS CATALYZED BY PEROXIDASE - CONTROLS AND APPLICATIONS, A.R. Pokora and W.L. Cyrus Jr., Mead Central Research, Chillicothe, OH.

10:15 R3.5
BIOCATALYTIC SYNTHESIS OF POLYESTERS BY ENZYME-CATALYZED TRANSESTERIFICATION IN ORGANIC MEDIA, Cary J. Morrow, J. Shield Wallace, Gregory M. Bybee, Kristin B. Reda, and Mark E. Williams, University of New Mexico, Department of Chemistry, Albuquerque, NM.

10:30 DISCUSSION

10:45 BREAK

11:00 R3.6
ENZYMATIC SYNTHESIS OF ALKYDS, S. Geresh.

11:15 R3.7
ENZYMES AS AIDS IN POLYMER SYNTHESIS, G. Sudesh Kumar, Alchemie Research Centre, Thane, India.

11:30 R3.8
ENZYMATIC SYNTHESIS OF CHIRAL LACTONES AND POLYESTERS, Arie L. Gutman, Technion-Israel Institute of Technology, Department of Chemistry, Haifa, Israel.

11:45 DISCUSSION
SESSION R4: MATERIALS SYNTHESIS USING ALTERED OR SYNTHETIC GENES

Chair: David Tirrell
Wednesday Afternoon, November 29
Essex North Center (W)

1:30 R4.1
SITE-DIRECTED MUTAGENESIS FOR THE DESIGN OF ENZYMES FOR MATERIALS SYNTHESIS, Jack F. Kirsch and Mark Alper, University of California at Berkeley, Department of Molecular and Cell Biology, and Center for Advanced Materials, Lawrence Berkeley Laboratory, Berkeley, CA.

1:45 R4.2
SITE-SPECIFIC MUTAGENESIS WITH UNNATURAL AMINO ACIDS, Spencer J. Anthony-Cahill, Christopher J. Noren, Michael C. Griffith, Daniel J. Suich, Stephanie A. Robertson, Wenchuan Liang, and Peter G. Schultz, University of California at Berkeley, Chemistry Department, and Center for Advanced Materials, Lawrence Berkeley Laboratory, Berkeley, CA.

2:00 R4.3
MODIFICATION OF PROTEASES FOR PEPTIDE SYNTHESIS, Jeffrey A. Bibbs, Ziyang Zhong and Chi-Huey Wong, Research Institute of Scripps Clinic, LaJolla, CA and Center for Advanced Materials, Lawrence Berkeley Laboratory, Berkeley, CA.

2:15 DISCUSSION

2:30 R4.4
GENETICALLY CONTROLLED SYNTHESIS OF NEW POLYMERIC MATERIALS, Maurille J. Fournier and Thomas L. Mason, University of Massachusetts, Department of Biochemistry, Amherst, MA; Kevin P. McGrath and David A. Tirrell, University of Massachusetts, Department of Polymer Science and Engineering, Amherst, MA.

2:45 R4.5
SYNTHESIS OF A COLLAGEN ANALOG IN ESCHERICHIA COLI USING RECOMBINANT DNA TECHNOLOGY, Ina Goldberg and Anthony J. Salerno, Allied-Signal, Inc., Department of Biotechnology, Morristown, NJ.

3:00 R4.6
BIOLOGICAL PRODUCTION OF UNIFORM POLYPEPTIDES FOR OPTICAL APPLICATIONS, Carl W. Lawton, Herbert E. Klei, University of Connecticut, Department of Chemical Engineering, Storrs, CT; Linda D. Strausbaugh, University of Connecticut, Department of Molecular and Cell Biology, Storrs, CT; and Robert Crane, Wright Patterson Air Force Base, Materials Science Group, Dayton, Ohio.

3:15 DISCUSSION

3:30 BREAK

3:45 R4.7
GENETICALLY ENGINEERED ADHESIVE PROTEIN, Rebecca P. Link and Robert Strausberg, Genex Corporation, Gaithersburg, MD.

4:00 R4.8
ELASTOMERIC POLYPEPTIDE BIOMATERIALS, Dan W. Urry, University of Alabama at Birmingham, School of Medicine, Laboratory of Molecular Biophysics, Birmingham, AL.

4:15 R4.9
THE GENETIC PRODUCTION OF SYNTHETIC CRYSTALLINE PROTEIN POLYMERS, Joseph Cappello, Magda Marquet and Franco Ferrari, Protein Polymer Technologies, Inc., San Diego, CA.

4:30 R4.10
THE EXPRESSION OF SILK LIKE PROTEIN BY E. COLIVIA SYNTHETIC GENE EXRESSION, Nicholas V. Ashley, Cambridge Laboratory, PA Consulting Group - Technology, Herts, United Kingdom.

4:45 DISCUSSION

SESSION R5: MATERIALS PROPERTIES OF BIOPOLYMERS

Chairs: Paul Calvert and Steven Mann
Thursday Morning, November 30
Essex North Center (W)

8:30 R5.1
BIOPOLYMERIZATION AND BIOCRYSTALLIZATION EVENTS LEADING TO THE ASSEMBLY OF A CELLULOS MICROFIBRIL, R. Malcolm Brown Jr., The University of Texas at Austin, Department of Botany, Austin, TX.

9:00 R5.2
DESIGN AND ENGINEERING OF BIOPOLYMERS, ChoKyun Rha, Massachusetts Institute of Technology, Biomaterials Science Laboratory, Cambridge, MA.

9:15 R5.3
CHARACTERIZATION OF CHITOSAN BIOSYNTHETIC ENZYMES IN MUCOR ROUXII, Stephen J. Lombardi, Steven Arcidiacono and David I. Kaplan, US Army Natick Research, Development and Engineering Center, Natick, MA.

9:30 R5.4
RECENT STUDEIS ON THE BIOSYNTHESIS OF POLY-HYDROXYALKANOATES, Oliver P. Peoples and Anthony J. Sinskey, Massachusetts Institute of Technology, Department of Biology, Cambridge, MA.

9:45 DISCUSSION

10:00 BREAK

10:15 R5.5
INFLUENCE OF COPOLYMERIC STRUCTURE ON PROPERTIES OF POLY- β -HYDROXYALKANOATES (PHA), Robert H. Marchessault, Clevys Monasterios and Fred Morin, McGill University, Department of Chemistry, Quebec, Canada.

10:30 R5.6
EGGSHELL FORMATION IN THE HELMINTH FASCIOLA HEPATICA: FUTURE APPLICATION OF PRODUCTS TO SYNTHETIC MICROENCAPSULATION, Allison C. Rice-Ficht and Kathryn A. Dusek, Texas A&M University, Department of Medical Biochemistry and Genetics, College Station, TX; John Kochevar, Texas A&M University, Department of Medical Pathology, College Station, TX; J. Herbert Waite, University of Delaware, College of Marine Studies, Lewes, DE.

10:45 DISCUSSION

11:00 R5.7
CHARACTERIZATION AND STRUCTURE OF MUSSEL ADHESIVE PROTEINS, Richard A. Laursen, Jung-Jung Ou, Xiao-Tong Shen and Michael J. Connors, Boston University, Department of Chemistry, Boston, MA.

11:15 R5.8
CALCIUM MINERAL-PEPTIDE INTERACTIONS, A.P. Wheeler, Clemson University, Department of Biological Sciences, Clemson, SC; C. Steven Sikes, University of South Alabama, Mineralization Center, Mobile, AL.

11:30 R5.9
MOLECULAR RECOGNITION BETWEEN PROTEIN AND CRYSTAL: RELEVANCE TO BIOMINERALIZATION, L. Addadi, Weizmann Institute of Science, Structural Chemistry Department, Rehovot, Israel; A. Berman, Weizmann Institute of Science, Structural Chemistry and Isotope Departments, Rehovot, Israel; J. Moradian-Oldak Weizmann Institute of Science, Structural Chemistry Department, Rehovot, Israel; and S. Weiner, Weizmann Institute of Science, Structural Chemistry and Isotope Departments, Rehovot, Israel.

11:45 DISCUSSION

SESSION R6: STRUCTURE AND SELF-ASSEMBLY

Chairs: Paul Calvert and Malcolm Brown
Thursday Afternoon, November 30
Essex North Center (W)

1:30 R6.1
BIOMINERALIZATION: NEW ROUTES TO CRYSTAL ENGINEERING, Stephen Mann, University of Bath, School of Chemistry, Bath, United Kingdom.

2:00 *R6.2
ONTOGENETIC AND PHYLOGENETIC VARIATION OF FORM AND FUNCTION OF THE OCULAR LENS, J.G. Sivak, University of Waterloo, School of Optometry, Ontario, Canada.

2:30 R6.3
HIERARCHICAL STRUCTURE OF THE INTERVERTEBRAL DISC, J.J. Cassidy, A. Hiltner, and E. Baer, Center for Applied Polymer Research and Case Western Reserve University, Macromolecular Science Department, Cleveland, OH.

2:45 R6.4
BENDING, FOLDING, AND BUCKLING PROCESSES DURING BACTERIAL MACROFIBER MORPHOGENESIS, Neil H. Mendelson, University of Arizona, Department of Molecular and Cellular Biology, Tucson, AZ; John J. Thwaites, Cambridge University, Department of Engineering, Cambridge, United Kingdom.

3:00 DISCUSSION

3:15 BREAK

3:30 R6.5
MECHANICAL PROPERTIES OF BACTERIAL FIBERS, John J. Thwaites, Cambridge University, Department of Engineering, Cambridge, United Kingdom; and Neil H. Mendelson, University of Arizona, Department of Molecular and Cellular Biology, Tucson, AZ.

3:45 R6.6
GROWTH-PACKED PPT-A FIBER FOR THE REPLACEMENT OF NATIVE ASBESTOS, Han Sik Yoon, Korea Institute of Science and Technology, Department of Fiber Science, Seoul, Korea.

4:00 R6.7
COMPOSITE BIOMOLECULAR/SOLID STATE NANOSTRUCTURES, Kenneth Douglas and Noel A. Clark, University of Colorado, Physics Department, Boulder, CO; and Kenneth J. Rothschild, Boston, University, Physics Department, Boston, MA.

4:15 DISCUSSION

4:30 R6.8
DIAMETER QUANTIZATION IN CYLINDRICAL AGGREGATES OF CHLOROPHYLLS, D.L. Worcester, University of Missouri, Biology Department, Columbia, MO; T.J. Michalski, M.K. Bowman and J.J. Katz, Argonne National Laboratory, Chemistry Department, Argonne, IL.

4:45 R6.9
ENZYMATIC RESOLUTION OF BICYCLO[3.2.0]HEPT-2-EN-6-YL ESTERS, Norbert Klempier, Kurt Faber and Herfried Griengl, Graz University of Technology, Department of Organic Chemistry, Graz, Austria.

5:00 DISCUSSION AND CLOSING REMARKS

R1.1

BIOMINERALIZATION BY MAGNETIC BACTERIA. Richard P. Blakemore, Microbiology Department, University of New Hampshire, Durham, N. H. 03824.

At least a dozen morphologically distinct prokaryotic species take up iron and accumulate it some 20,000-fold over its extracellular concentration. They produce the iron oxide magnetite as an intracellular biomineralization product; as a consequence, each cell is magnetic. Magnetic bacteria exert control over the quantity, grain size, crystal morphology, distribution and orientation of magnetite within the cell in a species-specific manner. Other (non-magnetic) bacteria bioprecipitate magnetite extracellularly as an abundant but largely amorphous flocculent phase in the culture medium. Within cells of *Aquaspirillum magnetotacticum*, the most-studied magnetic bacterium, the mineral occurs as a core enclosed within a biological membrane; the entire structure comprising a "magnetosome".

The magnetosome membrane (which is obviously not required for bacterial magnetite formation) probably does control aspects of the biomineralization process in magnetic bacteria. Cell fractionation studies have revealed the chemical composition of the magnetosome vesicle membrane. Several proteins not found elsewhere in the cell are candidate proteins for sequence analysis and/or inclusion in artificial membrane vesicles to obtain *in vitro* control of magnetite formation.

Pertinent Japanese patents include applications of bacterial particles as magnetic toners (Canon, 21 Dec. 1987) and as substrates for immobilization of physiologically active substances (TDK 18 May, 1987) in addition to methods of separation and purification of the particles from cells (Hitachi 28 July, 1987).

R1.2

DENTAL ENAMEL BIOMINERALIZATION: A PROSPECTUS. Harold C. Slavkin, Malcolm L. Snead, Margarita Zeichner-David, Eduardo C. Lau and Alan G. Fincham, Laboratory For Developmental Biology, Department of Basic Sciences, School of Dentistry, University of Southern California, Los Angeles, CA. 90089-0191

It is becoming increasingly evident that recombinant DNA technology, physical-chemistry and selected biological processes can be coupled leading to the development of new "synthetic" biomaterials. One opportunity for such an interdisciplinary strategy is the development of dental restorative materials---human enamel. This summary and prospectus will highlight selected features related to dental enamel biomineralization. During vertebrate tooth dental enamel formation, fish through mammals, epithelium synthesize and secrete enamel proteins which serve to nucleate and regulate calcium hydroxyapatite crystal growth and orientation. Significant progress has been made in the isolation and characterization of these anionic as well as hydrophobic enamel proteins resulting in partial and complete amino acid sequences. In tandem, substantial progress has been made to identify, clone, sequence and express dental enamel cDNAs. More recent evidence has also provided specific time and position cellular localizations using *in situ* hybridization as well as chromosome mapping for the major amelogenin structural gene in both mouse and human. Synthetic oligopeptides have been used to study physical-chemical interactions related to biomineralization. How specific motifs within the primary structure and/or post-translational modifications of enamel proteins regulate enamel biomineralization remains, however, a critical issue towards developing a biotechnology to produce human enamel.

R1.3

BONE FORMATION: THE RULES FOR FABRICATING A COMPOSITE CERAMIC. Arnold I. Caplan, Skeletal Research Center, Dept. of Biology, Case Western Reserve University, Cleveland, OH 44106, USA

Bone is formed in a discrete series of fabrication steps by cells called osteoblasts. Osteoblasts arise in a sequence

of lineage steps from a stem cell through the stage of secretory activity; a few osteoblasts become encased in bone and are referred to as osteocytes. As a secretory cell, the osteoblast synthesizes and extrudes a unique *extracellular matrix* which concentrates calcium and phosphate to form the mineral phase of bone. Our studies of embryonic bone formation have uncovered several "rules" which govern the fabrication of bone, which is a "composite ceramic" of organic fibers (collagen) and mineral. These rules require that, for osteoblasts to form bone, they must congregate into cobblestone-like sheets with capillaries near their back. The capillaries are obligatory to oriented secretion of mineralizable matrix. Recent studies indicate that mineral itself can play a profound role in the orientation of the osteoblasts and the multiplication of the osteoprogenitor cells. Using porous Ca:P ceramics with marrow or marrow-derived cells, we can demonstrate that substantial numbers of osteoblasts bind to and are organized at the face of calcium phosphate. Although few in number, the osteoprogenitor cells divide and eventually these sheets make bone onto the surface of the porous ceramic. The new bone is in crystalline alignment with the ceramic surface and suggests that the ceramic surface may orient and actively stimulate the osteoblasts to make bone. In summary, the rules for bone formation are: (1) adequate number of osteoprogenitor cells, (2) capillaries, (3) sheets of osteoblasts, and (4) a Ca:P crystalline surface which supports *de novo* bone formation.

R1.4

CRYSTAL FORMATION WITHIN COLLAGEN FIBRILS: A STUDY OF MINERALIZING TURKEY TENDON. S. Weiner, W. Traub⁺, J. Moradian-Olkak⁺, L. Addadi⁺, Isotope and Structural Chemistry Depts.⁺, Weizmann Institute of Science, Rehovot, Israel and W.J. Landis, Children's Hospital, Harvard Medical School, Boston, MA.

Collagen is the framework protein that controls crystal formation in bone, dentin and tendon. Carbonate apatite crystals formed in association with the collagen fibril are all oriented with respect to their *c* axes. Studies of morphologies, sizes and electron diffraction patterns of individual mineral particles shows that the crystals are not unlike their synthetic counterparts. TEM images of individual mineralized turkey tendon fibrils embedded and examined in vitreous ice, show that the crystals are arranged in ordered parallel layers that form as stacked arrays across the fibril diameter. This motif is consistent with the crystals growing in grooves or channels formed by collagen gap regions being contiguous over large distances following the Katz-Li model. This 3-dimensional organizational pattern can extend between neighboring fibrils. Fibrils in the process of mineralizing have crystals with a wide range of sizes, many of which extended beyond one gap region in the fibril axis direction.

This study suggests that nucleation of carbonate apatite crystals is a controlled process causing *c* axis orientation, although it is not known whether this is inherent to collagen itself or is due to the presence of some additional component. Collagen, however, does not appear to constitute a rigid framework that confines crystal growth, but rather influences it in subtle ways, which have yet to be determined.

R1.5

MINERAL PHASE CHARACTERIZATION FROM *in vitro* MINERALIZATION OF HUMAN OSTEOBLASTIC OSTEOSARCOMA CELLS. E. P. Paschalis, D. N. Tatakis, R. Dziak and G. H. Nancollas, SUNY at Buffalo, Buffalo, NY

In an attempt to devise an easy and reliable method for the study and evaluation of the factors affecting biological mineralization, the characteristics of *in vitro* mineralization by two human osteoblastic osteosarcoma cell-lines were studied. Saos2 and G292 cells were seeded at 5E-4 cells/ml in McCoy's 5a medium with 10% fetal calf serum (FCS) (2ml/well of 6-well plate). After a

72 hr incubation period, the medium was changed to either McCoy's 5a with 10% FCS plus 50 µg/ml ascorbic acid and 10 mM β-Glycerophosphate (test) or same without β-Glycerophosphate (control). At 1, 2, 3 and 4 weeks the cell cultures were fixed with ethanol. After appropriate treatment, samples were examined by Scanning Electron Microscopy (SEM), Microprobe analysis (EDAX), X-Ray diffraction (XRD) and Fourier-transform infrared spectroscopy (FTIR). SEM pictures were taken of all the samples examined by EDAX. Only calcium was observed by EDAX analysis for all control and week 1 test samples. Test samples starting with the 2nd week, showed both calcium and phosphorus present. XRD and FTIR spectra indicated the presence of an amorphous phase in all test samples of weeks 2-4, whereas control samples were negative. These data suggest that human osteosarcoma cell-lines are capable of *in vitro* mineralization and that, under the conditions employed in this study, the mineralized phase is of an amorphous nature. We would like to thank NIH for the following grants in support of this work: DE03223, DE08240, DE07034, AR25271

R1.6

CERAMIC OXIDE THIN FILM FORMATION UTILIZING BIOLOGICAL PROCESSES. B. J. Tarasevich and P. C. Rieke, Pacific Northwest Laboratory, Richland, Washington 99352

Mineralization processes used by bioorganisms have been adapted for the nucleation and growth of ceramic oxide thin films onto surfaces from aqueous solutions. These strategies include the use of surfaces derivatized with specific functional groups that control the nucleation and growth and properties of materials deposited. Initial experiments have involved the precipitation of iron oxide materials onto functionalized polystyrene surfaces. Deposition resulted in the formation of thin films composed of densely packed, nanometer-sized crystallites. Various iron oxide phases were precipitated depending on the solution chemistry conditions; and relationships between the derivatized interfaces and the deposited minerals were investigated. Implications of this approach to thin film processing will be discussed.

R1.7

A "BIO-MIMETIC" ROUTE TO BARIUM TITANATE SHEETS Paul Calvert, Department of Materials Science and Engineering, University of Arizona, Tucson AZ 85712, and R.A. Broad, School of Chemistry, University of Sussex, BN1 9QJ, England.

Ceramic oxides can be formed by *in situ* precipitation in polymer films. A solution of polymer and alkoxide in a common solvent is cast and dried to form a polymer film. Treatment of this film with water or base converts the alkoxide to oxide within the polymer. The initial precipitate is an amorphous gel but this may convert to a crystalline precipitate.

Films of polymers containing dissolved barium and titanium alkoxides were cast. Treatment with water precipitated amorphous particles but extracted barium. Treatment of the film with boiling barium hydroxide caused crystalline barium titanate to form within the film.

Initial attempts to burn out the polymer and sinter the particulate sheet were unsuccessful because of the low packing density of the particles. Polybutylmethacrylate could be cast alkoxide levels corresponding to 65 wt% barium titanate. The polymer in this film was burnt out at 600°C and the residue sintered at 1330°C to a dense barium titanate layer.

An attraction of this approach to making ceramics is that it avoids problems due to the formation of hard agglomerates since particles do not come into contact from when they are first formed until when sintering starts.

R1.8

SYNTHETIC SURFACES AS MODELS FOR BIOMINERALIZATION SUBSTRATES. P. C. Rieke, B. J. Tarasevich, S. B. Bentjen, Pacific Northwest Laboratory, Richland, WA 99352

The structure-function relationship between biomineralization proteins and the growing mineral phase are difficult to study because of the uncertain composition, complex surface structure, and very low concentration of the proteins. Heterogeneous nucleation is promoted on surfaces which reduce the surface tension between the growing nuclei and the substrate. On organic protein surfaces factors such as ligand binding of cations, electrostatic attraction, van der Waals forces, functional group density, micro-regional mobility, and degree of order may play a role in the nuclei/substrate surface tension. Simpler artificial surfaces can substitute as model surfaces for the biological protein surfaces and provide a mechanism to systematically explore the physical and chemical substrate properties required for biomineralization.

We have drawn from recent work on surface modified polymers, Langmuir-Blodgett films and self-assembling monolayers to tailor make substrates as nucleation and/or crystal growth substrates. Sulfonic acid, carboxylic acid, and amine groups have been attached to various substrates. (Processes for attachment of other groups such as phosphates and multi-dentate ligands are being designed.) These three functional groups, a strong acid, weak acid and weak base respectively, provide a convenient series on which to compare the growth of various mineral phases. Methods of preparing these substrates and their relative effectiveness at promoting nucleation and/or crystal growth will be presented.

R2.1

CALCIUM PHOSPHATE PRECIPITATION IN LIPOSOMAL SUSPENSIONS. Edward D. Eanes, NIDR Research Associate Program, National Institute of Standards and Technology, Gaithersburg, MD.

Artificial lipid vesicles (liposomes) provide an *in vitro* approach for microencapsulating calcium phosphate precipitation reactions in a manner similar to that which occurs in matrix vesicles, the initial loci for extracellular mineralization in many skeletal tissues. Apatitic precipitates readily form within the aqueous interiors of liposomes prepared from phosphatidylcholine, dicetylphosphate, and cholesterol when the liposomal membranes enclosing pH 7.4 buffered 50 mM PO₄ solutions are made permeable to external 2.2 mM Ca²⁺ with ionophores. If the external Ca solution is rendered metastable with 1.5 mM PO₄, the apatitic precipitates rapidly expand to outside the liposomes as well.

Although originally developed as a model for matrix vesicle calcification, the latter observation that endogenously formed precipitates can readily seed metastable solutions outside the liposomes suggest that they may possibly be useful as vehicles to initiate spatially uniform precipitations in complex aqueous-polymeric or gel-like suspensions. The advantage that such a system has over direct seeding with exogenous apatite crystals is that the onset of the external precipitation can be controlled by the lipidic constituents. As an example, anionic lipidic membrane components such as phosphatidylserine (PS) can delay seeding for several hours. This protraction in initiating external precipitation results from PS-mediated attractions with inner membrane surfaces slowing movement of endogenous crystals to the outer liposome surface. Such delays could be useful in seeding systems where thorough dispersion of the reactants and setting of the gelling components may be desirable before precipitation commences.

R2.2

KINETICS AND SOLUTION CHEMISTRY OF HYDROXYAPATITE FORMATION. Paul W. Brown and Mark T. Fulmer, Department of Materials Science and the Materials Research Laboratory, The Pennsylvania State University, University Park, PA 16802.

It is possible to form hydroxyapatite at physiological temperature and ambient pressure by the reaction of particulate acidic and basic calcium phosphates. The reaction may be viewed as occurring at a metastable ternary invariant point in the system $\text{CaO-P}_2\text{O}_5\text{-H}_2\text{O}$, which involves the two solid reactants. The invariant solution is unstable with respect to hydroxyapatite, which precipitates from solution.

The kinetics of the above reaction and the morphologies of the hydroxyapatite reaction product will be discussed within the context of the selection of reactants and their respective particle sizes. The effects of homeopitaxy on kinetics and microstructure will also be considered.

Because hydroxyapatite formation occurs by a so-called "through solution mechanism," the species present in solution may exhibit a strong effect on both kinetics and morphology. Effects of common ions and biologically important inorganic ions, such as sodium, potassium and magnesium, will be discussed.

R2.3

THE NUCLEATION AND GROWTH OF CALCIUM PHOSPHATE ON SEPARATED SALIVARY PROTEIN FILMS. A.A. Campbell and G.H. Nancollas, University at Buffalo, Buffalo, New York.

The ability of proteins, when immobilized as films, to induce the formation of calcium phosphate mineral phases is of considerable interest. The Constant Composition (CC) method has been combined with a flow-through cell in order to investigate the nucleation and growth of calcium phosphate phases on immobilized films of bacteria, bacteria/saliva, and separated salivary proteins. These additives, although behaving as effective inhibitors when present in solution, nucleate calcium phosphate phases when deposited as layers on either glass or germanium surfaces. The morphologies of these deposits show differences depending on the nature of the films. The Constant Composition method enables detection of mineral deposition rates with a precision impossible to achieve using conventional crystal growth kinetics methods. Supported by NIDR #07585 and NIH #DE03223.

R2.4

THE INFLUENCE OF SALIVARY PROTEINS ON THE GROWTH, AGGREGATION AND SURFACE PROPERTIES OF HYDROXYAPATITE PARTICLES.

M. Johnsson, C. Richardson, G.H. Nancollas. Chemistry Dept. SUNY at Buffalo N.Y. 14214, USA.

The binding of salivary proteins to human enamel maybe an important factor in the protection against demineralization or excessive mineralization. The adsorption at hydroxyapatite (HAP) surfaces, of purified statherin, three cystatins and amylase has been investigated in saturated solutions of HAP. The influence of these proteins on the aggregation of HAP particles and the constant composition (CC) crystal growth rate of HAP in saturated solution has also been studied.

Statherin and one cystatin showed strong adsorption to HAP while amylase had a weaker affinity. The adsorption of the proteins influenced both the aggregation of the particles and the rate of mineralization of HAP

crystallites. An increase of almost 100% in average particle size was observed during the uptake of proteins at the HAP surfaces. Even at very low surface coverage ($0.5\text{-}1 \times 10^{-9}$ mol m^{-2}), strongly adsorbing proteins markedly decreased the HAP growth rates. Maximum inhibition was found at lower surface coverage for the cystatins compared to amylase. At surface coverages slightly greater than that required for maximum inhibition it appeared that the inhibiting influences actually decreased as the concentration of protein increased. Study supported by NIDR grant # DE07585.

R2.5

THE EFFECTS OF PHOSPHOCITRATE AND CITRATE ON THE CRYSTAL GROWTH AND PARTICLE SIZE DISTRIBUTION OF HYDROXYAPATITE. C.F. Richardson, M.S.A. Johnsson and G.H. Nancollas, SUNY at Buffalo, Buffalo, NY.

Several organic phosphates have been found to be good inhibitors of calcium phosphate precipitation. It is thus possible that phosphocitrate may be used as an *in vivo* inhibitor of calcification processes, such as tartar formation. This compound has been found to inhibit the crystal growth of hydroxyapatite (HAP), the primary constituent of enamel. A detailed understanding of the various effects of phosphocitrate and citrate, its hydrolysis product, on HAP may provide valuable information regarding mechanisms for the retardation of tartar formation.

In this study, the affinities of citrate and phosphocitrate, as well as a mixture of both compounds, toward HAP were investigated by equilibration adsorption experiments. The effects of both compounds on the crystal growth properties of HAP were investigated using the Constant Composition (CC) method, which enables precise kinetic data to be determined at constant solution parameters. In these experiments known amounts of each compound were adsorbed to the HAP seed surfaces prior to mineralization. Phosphocitrate, which exhibited a higher affinity toward HAP than did citrate, also showed greater inhibitory effects when present on the HAP surface. The effects of both compounds on the flocculation of HAP crystallites was studied by following the particle size distribution during the adsorption process. Supported by NIH grant #DE03223.

R2.6

THE MICROSTRUCTURES AND FORMATION OF BIOMINERALIZED BIVALVIA SHELLS. L.J. Huang and H-D. Li, Department of Materials Science and Engineering, Tsinghua University, Beijing, 100084, China.

The paper presents the detailed study of the structural features of the biomineralized bivalvia shells and a brief discussion of the growth mechanism of the different shell layers through a cell-controlled deposition process.

The *Cristaria plicata* (Leach), *Anodonta woodiana* (Lea) and *Lamprotula leai* (Grai) are selected as the prototypes in the present study. X-ray diffraction, Raman spectroscopy, optical microscope, ESCA, SEM and TEM are employed to study the structures of the shells. It is found that the periostracum, prismatic and pearl layer possesses quite different crystalline phases, respectively and each layer has more than one co-existed phases. The structure of the pearl layer is the most simple one and of a strong crystalline orientation. The prismatic layer can be further divided into two separate layers with a mismatch of two kinds

of prisms at the interface. Raman spectroscopy and ESCA analyses show that the biological molecules play a nontrivial role in forming the shells.

TEM study of the different parts of the mantle cells revealed that the microstructures of the cells and their functions in the orientation deposition of the crystalline phases. The fracture behaviors of the shells are also presented and characterized with the fractal approach.

R2.7

THE BERNAL SPIRAL AS A MODEL FOR THE STRUCTURE - OF SOME BIOLOGICAL SYSTEMS, Gustavo Vázquez Pólo and Miguel José Vacamán, Instituto de Física, Apdo. Postal 20364, UNAM.

It was pointed out by Boerdijk that a spiral --- structure can be generated by an array of tetrahedra. This structure was popularized by Bernal. It is shown that by the subsequent growth of different tetrahedra spiral structure formed by decahedra and icosahedra can be produced. These structures were termed decagonal and icosahedral spiral respectively. The diffraction pattern --- from those structures was calculated and it was shown the five fold symmetry and intrinsic incommensurability of the patterns. It is suggested that many structures in the Botanic world and --- some virus structures can be modelled by the decagonal and icosahedral spirals. The icosahedral spiral appears a likely model to explain the --- structure of some metallic glasses and of quasi-crystals approximations.

R2.8

MECHANICAL PROPERTY-MICROSTRUCTURAL RELATIONSHIPS IN ABALONE SHELL. Mehmet Sarikaya, Katie Gunnison, and Ilhan A. Aksay, Dept. of Materials Science and Engineering, University of Washington, Seattle, WA 98195.

Both the fracture toughness and strength properties of the species *Haliotis refuscens* (red abalone) shell in the nacre section display a unique combination of properties (K_{IC} , three-point-bend, of $\sim 10 \text{ MPa}\cdot\text{m}^{1/2}$, and fracture strength, four-point bend, of $\sim 200 \text{ MPa}$). These properties are related to the layered microstructure of the shell which is composed of CaCO_3 (95 v/o) and organic matter (5 v/o) in the "brick-and-mortar" configuration. Several toughening and strengthening mechanisms take part in the property increase which are related to the microarchitecture of this natural ceramic/polymer composite. The consequences of these results in the design and processing of synthetic components will be discussed.

Supported by AFOSR Grant No. AFOSR-88-0135.

R2.9

AN ELECTRON MICROSCOPY STUDY ON THE MICROSTRUCTURE OF THE *STROMBUS GIGAS* SHELL, V.J. Laraia, Jr., M. Aindow and A.H. Heuer, Department of Materials Science and Engineering, Case Western Reserve University, Cleveland, OH 44106.

Numerous organisms exhibit the ability to manufacture structural ceramic-polymer composites such as bone or shell. These biological hard tissues are of considerable materials interest as they are fabricated from physiologically abundant precursors at near ambient conditions. In this light, it is important to understand the mechanisms by which these tissues are formed in order that biological mineralization processes may be utilized or imitated in the manufacture of structural ceramic composites.

An electron microscopy study is presented of the shell from the saltwater mollusk *Strombus gigas*. This material is composed mostly of aragonite, the orthorhombic polymorph of CaCO_3 , with a

fine organic grain boundary phase. Scanning Electron Microscopy is used to show that the microstructure consists of hierarchical arrays of lamellae, typical of the crossed-lamellar microstructure. Examination of the finest units using Transmission Electron Microscopy reveals repeated twinning on the (110) plane. These twins have an average width of 5 nm with planar boundaries parallel to the twin plane. The atomic structure of these boundaries revealed using diffraction contrast and HREM suggests that they arise as a result of growth geometry rather than by any deformation twinning mechanism. These features and other defects in the lamellae are used to deduce possible growth mechanisms.

R2.10

THE MICROINDENTATION BEHAVIOR OF SEVERAL MOLLUSK SHELLS, V.J. Laraia, Jr. and A.H. Heuer, Department of Materials Science and Engineering, Case Western Reserve University, Cleveland, OH 44106.

Biological hard tissues are ceramic-polymer composites that employ a variety of microstructural designs, and possess extraordinary mechanical properties. For example, mollusk shell, which usually contains a very large fraction of the ceramic phase (CaCO_3), can have greater strength and toughness than many conventional ceramic materials. However, incompatibility between standard test specimen geometries and typical shell morphologies can cause difficulties in evaluating the mechanical behavior of these materials. These difficulties may be compounded by the fine scale and highly ordered (anisotropic) nature of the microstructures. Microindentation techniques provide information regarding bulk mechanical properties, such as hardness. Tests of this kind can also evaluate the mechanisms of deformation and fracture in a localized manner and permit a direct assessment of anisotropy in mechanical behavior. The results of Vickers and Knoop microindentation experiments are reported for shells exhibiting four distinct microstructural types: *nacreous*, *crossed-lamellar*, *prismatic* and *foliated*. The microstructural features are shown to play a crucial role in determining the morphology and extent of the damage zones about an indentation. Examples of delamination-induced lateral cracking, radial cracking along weak boundaries, and room temperature creep are discussed.

R3.1

MATERIALS SYNTHESIS UTILIZING BIOLOGICAL PROCESSES. George M. Whitesides, Department of Chemistry, Harvard University, Cambridge, MA 02139

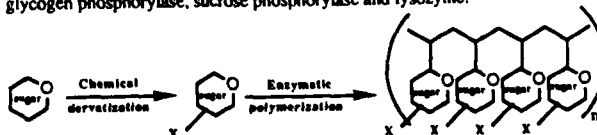
This talk will summarize some of the methods of biological synthesis of materials, including enzymology, fermentation and isolation from natural sources. The techniques of recombinant DNA technology offer, in principle, a range of new approaches to biological processing and to biologically-derived materials. The question of immediate current concern is: "What materials for what applications?" Some of the intrinsic properties of biologically derived materials will be discussed as background for answers to this question.

R3.2

THE USE OF PROTEINS IN THE SYNTHESIS OF POLYMERS AND THE MODIFICATION OF SILICON SURFACES Lynn Oehler, Chris Hobbs, Mark Mastandrea and Mark Rednarski Department of Chemistry and The Center for Advanced Materials, Lawrence Berkeley Laboratories University of California, Berkeley 94720

Proteins are a potentially valuable class of catalysts to synthesize polymers and new materials. We are engaged in a program to use enzymatic methods of polymerization and surface modification to prepare new polymeric materials from unnatural monomers. This methodology combines the power of chemical synthesis with the stereoselectivity of enzymatic polymerization reactions. This paper will focus on the progress we have made in the areas outlined below.

1) The chemical-enzymatic synthesis of fluorinated and sulfated polysaccharides using glycogen phosphorylase, sucrose phosphorylase and lysozyme:



2) The chemical and enzymatic modification of semiconductor materials and other polymers, and the use of these materials to study the interfacial properties associated with the binding of bacteria and viruses:



POLYMER SYNTHESIS BY FREE RADICAL ENZYME COUPLING REACTIONS IN SOLVENTS. J. A. Akkara, K. Senecal, and D. L. Kaplan, US Army Natick RD&E Center, Natick, MA 01760-5020.

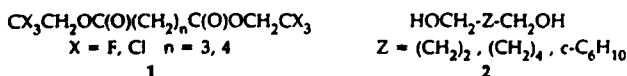
Polymers were synthesized from phenolic and aromatic amine compounds in the presence of hydrogen peroxide. These reactions were catalyzed by horse-radish peroxidase in organic solvents with small amounts of water at room temperature. Conditions for the synthesis of polymers with respect to reaction time and yield were studied with a number of monomers at different concentrations and solvents with different buffers over a pH range of 5.6 to 7.5. Polymers were prepared from para phenylphenol, 1-, and 2-naphthols, 1,3- and 1,5-naphthalene diols, aniline, benzidine, 8-hydroxyquinoline and isoquinoline either alone or in combinations. Physico-chemical properties of these enzymatically synthesized polymers were determined with respect to their melting point, solubility, electrical conductivity, elemental analysis, viscosity, molecular weight distributions, infrared absorption (including FTIR), thermal gravimetric analysis and differential scanning calorimetry. These enzyme catalyzed reactions produced polymers of molecular weight greater than 500,000 without copolymerizing agents such as formaldehyde. Moreover these coupling reactions were carried out under mild conditions of pH and temperature. In general the polymers synthesized have low solubility, high melting points and some degree of cross linking. These properties were further evaluated after chemical modifications of the polymers.

R3.4 ABSTRACT NOT AVAILABLE

R3.5

**BIOCATALYTIC SYNTHESIS OF POLYESTERS BY ENZYME-CATALYZED
TRANSESTERIFICATION IN ORGANIC MEDIA.** Cary J. Morrow, J. Shield
Wallace, Gregory M. Bybee, Kristin B. Reda, and Mark E. Williams, Department
of Chemistry, University of New Mexico, Albuquerque, NM 87131

Transesterification polymerization of bis(2,2,2-trichloroethyl) or bis(2,2,2-trifluoroethyl) alkaneidates, 1, with alkanediols, 2, can be effected at ambient temperature in organic solvents (e. g., ether, THF, hexane/methylene chloride) using porcine pancreatic lipase (PPL) as the catalyst. Molecular weights of the resulting $[AA + BB]_x$ polyesters approach 16,000 and polydispersities are usually narrow.



Using racemic bis(2,2,2-trichloromethyl) trans-3,4-epoxyhexanedioate, **3** as the diester monomer and 1,4-butanediol, **2**, $Z = (CH_2)_2$ as the diol monomer leads to an optically active polymer having an average degree of polymerization of 25 repeat units and a stereochemical purity estimated to be $\geq 96\%$.



The method has been extended to preparation of A-B oligomers and polymers using trichloroethyl and trifluoroethyl ω -hydroxyalkanoate monomers, 4.

Analysis of the progress of these polycondensations by high field NMR, VPC, and GPC, while they are under way, suggests the AA + BB cases may proceed preferentially through a "trimer" terminated at both ends by hydroxyl. An addition polymerization mechanism, in which the starting monomer is present throughout the polycondensation, is suggested for the A-B case.

The effect of monomer structure, various reaction conditions, and the apparent mechanisms, on the rate, degree of polymerization, regioselectivity, and stereoselectivity, of the polymerizations will be discussed.

R3.6 ABSTRACT NOT AVAILABLE

R3.7

ENZYMES AS AIDS IN POLYMER SYNTHESIS. G. Sudesh Kumar, Alchemie Research Centre, P. O. Box 155, Thane - 400 601, INDIA.

Polymer synthesis involving biocatalytic steps is an attractive route to chiral polymers, stereoregular polymers etc. Currently evolving non-aqueous enzyme chemistry is a valuable tool in macromolecular design.

Our work represents a novel enzyme-assisted synthesis of chiral polymers involving oxime acrylates as efficient irreversible acyl transfer agents and offers a novel biocatalytic intermediacy in macromolecular design.

We report porcine pancreatic lipase as an effective biocatalytic aid in the design and synthesis of alkyl resins from vegetable oils. The 1,3 specificity of lipases produces 2-monoacylglycerides resulting in uniform molecular order of the polymer.

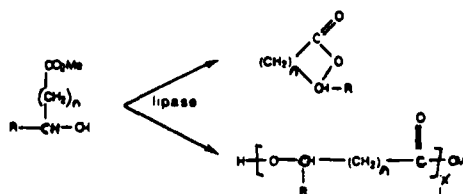
R3.8

Enzymatic synthesis of chiral lactones and polyesters

Arie L. Gutman
Department of Chemistry
Technion - Israel Institute of Technology
Haifa 32000, Israel

It is now well established that hydrolytic enzymes can function in anhydrous organic solvents, where they catalyse ester synthesis and ester exchange rather than hydrolysis.

We have found that lipases suspended in organic solvents are catalytically active towards esters of hydroxyacids and promote both the *intra* and the *intermolecular* transesterification reactions, leading to lactones and polymers respectively. The outcome depended on the chain-length and degree of substitution of the substrates. If a five-membered lactone could be formed, this was the exclusive product. A six-membered lactone was formed only if substituted in the 5 position. With shorter ($n \leq 2$) or longer ($n \geq 3$) chain-length hydroxyesters we observed formation of linear polymers. Using this approach we have prepared several polyesters, which in some cases contained more than 100 monomer units ($M.W. > 10,000$).



Our study shows that under these conditions the enzymes exhibit both enantioselectivity and prochiral selectivity and it provides a novel synthetic route to chiral lactones and polymers. These reactions are not possible in aqueous solutions where hydrolysis dominates.

R4.1

SITE-DIRECTED MUTAGENESIS FOR THE DESIGN OF ENZYMES FOR MATERIALS SYNTHESIS. Jack F. Kirsch and Mark Alper. Center for Advanced Materials, Lawrence Berkeley Laboratory and Department of Biochemistry, University of California at Berkeley, Berkeley, CA 94720

Enzymes produced by living organisms have been designed by evolution to perform under physiological conditions. The demands of this environment are very different from those that would allow for synthesis of useful materials. Enzymes that would be useful in materials synthesis must bind substrates that are likely to be quite different from cellular metabolites. Thus their active sites must be altered. Further, enzymes that would be useful in materials synthesis must have enhanced stability, including resistance to higher temperatures. This talk will summarize some recent results using site-directed mutagenesis to make predetermined changes in the amino acid sequence of enzymes to alter their substrate specificity and to enhance their thermal stability.

R4.2

SITE-SPECIFIC MUTAGENESIS WITH UNNATURAL AMINO ACIDS. Spencer J. Anthony-Cahill; Christopher J. Noren; Michael C. Griffith; Daniel J. Suich; Stephanie A. Robertson; Wenchuan Liang; and Peter G. Schultz, Center for Advanced Materials, Lawrence Berkeley Laboratory and Chemistry Dept., University of California, Berkeley, CA, 94720.

Recently a new method was described that extends the technique of oligonucleotide-directed mutagenesis by allowing for site-specific incorporation of unnatural amino acids into proteins. A chemically acylated suppressor tRNA inserts the desired unnatural amino acid into the growing peptide chain in response to an amber (UAG) stop message which can be generated at the codon in the gene corresponding to the amino acid residue of interest. Using this methodology we were able to substitute phenylalanine 66 in RTM B-lactamase with three phenylalanine analogs (Science, 1989, 244, 182). These results as well as recent attempts to optimize the methodology will be discussed.

R4.3

MODIFICATION OF PROTEASES FOR PEPTIDE SYNTHESIS. Jeffrey A. Bibbs, Ziyang Zhong; and Chi-Huey Wong, Center for Advanced Materials, Lawrence Berkeley Laboratory, Berkeley, CA 94720 and Department of Chemistry, Texas A&M University, College Station, Texas

Serine proteases are modified via active-site mutation to possess useful catalytic properties for polymerization of amino acid esters and for condensation of peptide segments. Several helical segments have been designed and synthesized for use as substrates for enzymatic polymerization.

R4.4

GENETICALLY CONTROLLED SYNTHESIS OF NEW POLYMERIC MATERIALS. Maurille J. Fournier and Thomas L. Mason, Department of Biochemistry, and Kevin P. McGrath and David A. Tirrell, Department of Polymer Science and Engineering, University of Massachusetts, Amherst, MA 01003.

Chemical methods of polymer synthesis are inherently limited by the

statistical nature of polymerization processes. As a result, the polymers currently in use are not pure materials, but instead are mixtures characterized by distributions of the important structural variables (molecular weight, composition, sequence and stereochemistry). The preparation of pure polymeric materials, and the use of polymers in applications that require precise structural control, can be realized only through the introduction of new synthetic methods. With this in mind, we have begun to develop molecular biological approaches to the preparation of new polymeric materials. The fidelity of protein biosynthesis, coupled with recent advances in the synthesis, cloning and expression of genes, offers the prospect of a new synthetic technique of unprecedented precision and remarkable scope. This lecture will describe the design, synthesis and expression of several new families of genes that encode amino acid copolymers of some potential interest in materials science.

R4.5

SYNTHESIS OF A COLLAGEN ANALOG IN *ESCHERICHIA COLI* USING RECOMBINANT DNA TECHNOLOGY. Ina Goldberg and Anthony J. Salerno, Allied-Signal Inc., Morristown, NJ.

Recombinant DNA techniques offer a rapid method for obtaining large quantities of structural proteins such as collagen. Poly(Gly-X-Y) can in principle be prepared by expressing an internally repetitive synthetic gene in a suitable microbial host. Such proteins, however, tend to be unstable due to the action of host proteases which recognize foreign polypeptides. In addition, highly repetitive nucleotide sequences can undergo deletions at high frequency in *E. coli*.

We constructed a family of synthetic genes coding for poly(Gly-Pro-Pro) which differ only in the number of repeating gene segments coding for the tripeptide unit. The *in vivo* levels of synthetic gene expression obtained show that the above polypeptide can be synthesized in *E. coli* but is labile compared to other cellular proteins. This degradation can be significantly reduced by the genetic inhibition of a bacterial protease system.

The synthetic collagen analog gene was observed to be highly unstable in *E. coli*, deleting at 9-base-pair intervals which correspond to one Gly-Pro-Pro unit. Experiments are currently in progress to analyze the various factors which may contribute to this genetic instability. Elucidating the processes which control the stability of synthetic genes and their corresponding proteins is essential for the future commercial production of novel biomaterials in microorganisms.

R4.6

BIOLOGICAL PRODUCTION OF UNIFORM POLYPEPTIDES FOR OPTICAL APPLICATIONS. Carl W. Lawton, and Herbert E. Klei, Department of Chemical Engineering; Linda D. Strausbaugh, Department of Molecular and Cell Biology, University of Connecticut, Storrs, CT; Robert Crane, Materials Science Group, Wright Patterson Air Force Base, Dayton, OH.

Recent advances in recombinant DNA technology have created the potential for engineering of protein molecules to specific uses beyond those normally considered for biomaterials. This research project has demonstrated the feasibility of producing polypeptides useful for laser filters and nonlinear optical applications.

Synthetic genes, ranging in size from 36 to 2000 base pairs, have been constructed from oligonucleotides using a restriction doubling technique. The synthetic genes have been inserted into a Protein A fusion expression system. Fused polypeptides from induced cells have been purified by affinity chromatography (IGG), cleaved with cyanogen bromide, and analyzed for sequence fidelity.

R4.7 ABSTRACT NOT AVAILABLE

R4.8

ELASTOMERIC POLYPEPTIDE BIOMATERIALS:

Dan W. Urry, Laboratory of Molecular Biophysics, School of Medicine, University of Alabama at Birmingham, Birmingham, Alabama.

Increasingly the term biomaterials has the added meaning of materials from biology. Two aspects of this sense of biomaterials are: 1) as this symposium features, materials made by biological (enzymatic) means, and 2) as presented in this report, biological polypeptide materials which may be made either by chemical or biological means. Poly (Val-Pro-Gly-Val-Gly) is a prominent member of this new class called elastomeric polypeptide biomaterials which have both medical and industrial applications. Interesting potential industrial applications are due to their capacity to function as chemomechanical transducers. This property is due to hydration mediated apolar-polar interaction free energies which provide for an efficient interconversion of chemical work and mechanical work and which provides fundamental driving forces for protein folding and assembly. The potential medical applications arise out of adjustable compliance, tissue compatibility, biodegradability with non-toxic products, ease of introduction of chemotactic and cell attachment peptides for directed tissue response. These properties allow consideration of temporary scaffoldings for reformation of natural artery, ligament, skin, etc. These biomaterials can be designed to elicit desired tissue responses.

R4.9

THE GENETIC PRODUCTION OF SYNTHETIC CRYSTALLINE

PROTEIN POLYMERS. Joseph Cappello, Magda Marquet and Franco Ferrari; Protein Polymer Technologies, Inc., 10655 Sorrento Vly. Rd., San Diego, CA, 92121.

Genetic and protein engineering are components of a new polymer chemistry which provide the tools for producing macromolecular polyamide copolymers of diversity and precision far beyond the current capabilities of synthetic polymer chemistry. The genetic machinery allows molecular control of chemical and physical chain properties. Nature has utilized this control to formulate protein polymers into fibers with extraordinary mechanical properties such as the strength and toughness of silk and the elasticity and resilience of mammalian elastin. The protein chains which make up these fibers consist of extensive repeating oligopeptide sequences. By producing synthetically designed protein chains containing many tandem repeats of only one repetitive sequence block (homoblock polymers), we are able to evaluate the inherent contribution of each repeat to the overall material properties. Using biotechnology, we have produced homoblock protein polymers consisting exclusively of silk-like crystalline blocks in quantities sufficient for material evaluation studies (10 to 100 grams). Silk-like homoblock polymers, as produced by microbial fermentation, exhibit measurable crystallinity both in solution and in solid state. The chain properties of the homoblock polymer can be changed by adding blocks of amino acids designed to contribute different structural properties. We have produced alternating copolymers of various amounts of silk-like and elastin-like blocks ranging from a ratio of 1:4 to 2:1, respectively. The crystallinity of each copolymer varies with the extent of crystalline block interruption. The ability to specifically engineer the mechanical properties of a fiber material is a potential outcome of this technology.

R4.10

THE EXPRESSION OF SILK-LIKE PROTEIN BY E.COLI VIA SYNTHETIC GENE EXPRESSION. Nicholas V. Ashley, PA Consulting Group - Technology, Cambridge Laboratory, Melbourne, Royston, Herts, SG8 6DP, UK

Silk is a protein fibre produced by spinning which is produced naturally by the larvae of the *Bombyx mori* moth and many other Arthropods. The *Bombyx mori* moth larva synthesizes the components of silk inside its body and extrudes them in the form of a fibre of silk which it spins into a cocoon. The *B. mori* silk fibre consists of twin filaments of the protein fibroin which are cemented or glued together by the protein sericin. These moth cocoons are the basis of commercial

natural silk production; the larvae produce fibres with a composition and structure that result in natural silk having a unique combination of properties of strength, softness and lustre, which cannot be matched by conventional manmade fibres.

Production of natural silk from these moth larva, however, is limited both in quantity and quality by geographical, political and other factors. As a result, the supply of natural silk is limited and prices are high. The objective of our work is to facilitate production of silk-like structural proteins, based on the protein fibroin of the silk fibre produced by the larvae of the *Bombyx mori* moth, and silk produced by various spiders. We ultimately intend to produce a family of silk-like proteins with superior physical properties to those found in nature.

Initially, a synthetic gene coding for the amino acid sequence (GAGAGSGGAAG(GAGAGS)_nY) was constructed to code for the block of 59 amino acids which comprise the crystalline domain of silk. This was interspersed with DNA to represent the amorphous region of the silk protein.

The synthetic gene was 3.3kb in size and cloned in E.coli. A silk like protein was expressed. The silk has been extracted, dissolved and fibres extruded.

R5.1

BIOPOLYMERIZATION AND BIOCRYSTALLIZATION EVENTS LEADING TO THE ASSEMBLY OF A CELLULOSE MICROFIBRIL.

R. Malcolm Brown, Jr., Department of Botany, The University of Texas at Austin, Austin, Texas 78712.

Until recently, very little was known of the steps leading to the biopolymerization of glucose units to form the B 1,4-linked glucan chain, the backbone of cellulose, nature's most abundant macromolecule and structural material. In addition, almost nothing was known about the subsequent crystallization events leading to the assembly of the cellulose microfibril. Now, polymerization has been accomplished *in vitro* using a cell free enzyme system. Interestingly, the *in vitro* synthesized glucan chains crystallize to form the cellulose II allomorph. *In vivo* synthesis usually yields the less thermodynamically metastable cellulose I allomorph; however, some living organisms such as the bacterium, *Sarcina* and the marine alga, *Halicystis*, synthesize cellulose II *in vivo*.

The site of cellulose microfibril assembly is known as the terminal complex (=TC) which was first elucidated using freeze etch/electron microscopy. TC's are associated with the cell membrane and often form elaborate geometrical assemblies of subunits which may control the crystalline allomorph, size and shape of the microfibril, degree of polymerization, etc.

This presentation will demonstrate the interesting relationship between the macrostructure of the enzyme complex and structure of its cellulosic product, the microfibril. From a structural point of view, this process is one of nature's most precise, genetically regulated bioprocesses, having existed since the early evolution of life on earth and diversified throughout the eons of time to be found among prokaryotic cells, plant cells, protists, animals, and possibly humans.

R5.2

Developments in modern biotechnology make stereo- and chiral-specific production of macromolecules with highly complex structures potentially possible. Thus, functional polymers can now be produced precisely according to design. Biological macromolecules and systems unique for the specific and intricately controlled functions, provide working models for the description and analysis of specific functions. The structure-property-function relationship becomes the critical, fundamental basis for the rational design of functional biopolymers. The structure-property-function relationship, the characterization, analysis and prediction of physical properties involved in molecular design are examined with the examples of flocculants (zooglan), dewatering agents (chitosan), spacefilling agents (glucan particles) and high-performance lubricants (hyaluronic acid).

Title: Design and Engineering of Biopolymer

R5.3

CHARACTERIZATION OF CHITOSAN BIOSYNTHETIC ENZYMES IN MUCOR ROUXII. Stephen J. Lombardi, Steven Arcidiacono, and David I. Kaplan. US Army Natick Research, Development and Engineering Center, Natick, MA 01760-5020

The enzymatic processes regulating the biosynthesis and deacetylation of chitin play a key role in the fundamental mechanism of growth, differentiation, nutrition in select fungal species. The chitin deacetylase of the dimorphic fungus, *Mucor rouxii* was purified 70.5-fold by ammonium sulfate precipitation, ion-exchange chromatography, and preparative polyacrylamide gel electrophoresis. The specific deacetylase activity was 94.7 nmol of acetyl groups (CH_3COO^-) released from the acetylated substrate glycol chitin per minute per milligram of protein. The deacetylase activity showed a pH optimum of 4.5 and varied markedly with the buffer employed. Column purified protein showed a K_m of $2.4 \times 10^{-4} \text{ M}$ to the soluble substrate glycol chitin. The column purified protein revealed a single polypeptide on polyacrylamide gel electrophoresis with an apparent molecular weight of 15,000 daltons. The chitin deacetylase activity of *Mucor rouxii* was independent of any bivalent metal ion (Mg^{++} , Mn^{++}) requirement for enzymatic activity. The enzyme activity was stable on storage at -20°C from 1-3 months and continued to demonstrate catalytic properties. Chitin synthetase, another key enzyme involved in the synthesis of chitosan is currently being characterized in similar fashion. In order to clarify the biosynthetic process for chitosan formation by chitin deacetylase/synthetase it is necessary to describe accurately conditions and factors influencing chitosan formation in vitro.

R5.4

Metabolic engineering via recombinant DNA provides an opportunity not only for the production of primary metabolites and antibiotics but has significant potential for manipulating the biosynthesis of complex carbohydrate and polyester biopolymers. Poly(β)-hydroxybutyrate (PHB), the polymeric ester of the C_4 monomer (D)- β -hydroxybutyrate, is an energy reserve material produced by a wide range of bacteria when grown under conditions of nutrient limitation. This polymer is particularly interesting in that it has the unique property of being a biodegradable thermoplastic material. Recent reports demonstrate that PHB is only one member of the family of polyhydroxyalkanoate (PHA) biopolymers which differ due to the incorporation of alternate subunits, e.g., C_3 , C_4 , C_5 , C_6 , etc. These features make this system particularly interesting for the emerging field of biopolymer engineering. In *Alcaligenes eutrophus* N16 the three enzymes of the PHB biosynthetic pathway, PHB polymerase, β -ketothiolase and acetoacetyl-CoA reductase are encoded by the *phbC-phbA-phbB* genes. The application of these genes for studying the enzymology of the pathway and manipulating PHA biosynthesis will be discussed.

Title: Recent Studies on the Biosynthesis of Polyhydroxyalkanoates

R5.5

INFLUENCE OF COPOLYMERIC STRUCTURE ON PROPERTIES OF POLY- β -HYDROXYALKANOATES (PHA). Robert H. Marchessault, Clevys Monasterios and Fred Morin, McGill University, Montreal, Quebec Canada

The influence of % valerate content on the solid state properties of poly- β -hydroxybutyrate (PHB) is critical for achieving suitable solid state characteristics of PHB/V plastics produced by ICI's BIOPOL subsidiary. For the butyrate/valerate family of bacterial co-polyesters, the change in T_g , T_m , optical rotation, polymorphism, crystallinity and crystallization rate are

well understood. The co-crystallization of the butyrate and valerate units is responsible for the observed isodimorphism in this series. It has the effect of allowing high crystallinity at all compositions for the PHB/V family. However, the crystals have conformational disorder which contributes favourably to the toughness characteristic of the copolymers.

The PHA family can be charted in terms of solid state characteristics by using the average sidechain length as the variable. In this situation: T_g , T_m , and crystalline fiber repeat show smooth variation in their values as a function of sidechain length. The crystallinity of the available materials is much less than for the PHB/V series and the basic thermoplastic character changes to thermal elastomeric for average sidechain length beyond C_3 or C_4 . The reason for this new physical characteristic of the material is not yet clear. All our samples are terpolymers which leads to crystallization difficulties.

NMR relaxation characteristics of the sidechain and backbone carbon atoms of solid samples has been studied over a range of temperatures well above the T_g of the samples. There is much greater motional freedom in the sidechain than in the helical backbone which can be thought of as a reinforcing molecular fiber in a matrix of mobile hydrocarbon.

R5.6

EGGSHELL FORMATION IN THE HELMINTH FASCIOLOA HEPATICA: FUTURE APPLICATION OF PRODUCTS TO SYNTHETIC MICROENCAPSULATION. Allison C. Rice-Fisher*, Kathryn A. Dusek*, John Koebeke* and J. Herbert Waite*, Department of Medical Biochemistry and Genetics*, Department of Medical Pathology*, Texas A & M University, College Station, TX 77840, and College of Marine Studies*, University of Delaware, Lewes, DE 19958.

Fasciola hepatica eggshell production has historically been attributed to a quinone-tanning process which involves cross-linking of proteins containing catecholic groups. We have demonstrated the presence of dihydroxyphenylalanine (DOPA) residues in the eggshells and in the peptide sequence of eggshell precursor proteins; several DOPA containing protein precursors of the shell have been purified and characterized. The major protein components are rich in glycine and DOPA residues and compose three major groups of 70 kDa, 31 kDa and 17 kDa in size. The 31 kDa protein, the major protein component by weight in the shell, has been purified and the amino acid composition and partial sequence determined. Genes encoding the 31 kDa protein have been isolated and sequenced revealing a family of related transcripts encoding proteins with similar amino acid composition and molecular weights. The composition of each cDNA closely reflects that determined through amino acid analysis of the purified protein; peptides derived from tryptic peptide sequences are present in each of the cDNAs investigated. Transcripts encoding the 31 kDa protein have been localized exclusively to the vitelline cells which are dedicated to shell production. Microheterogeneity observed in protein profiles of the purified 31 kDa protein appears due to the expression of up to six similar but nonidentical genes in the family rather than to posttranslational modifications. The 17kDa protein has also been purified and characterized revealing a repeating polymer containing not only DOPA and glycine but a very high histidine composition. The protein also exhibits microheterogeneity indicating a probable gene family.

A detailed study of the microencapsulation process developed by the worm for shell production is proceeding with the goal of mimicking the process *in vitro*; the long-term stability and non-antigenicity of these microcapsules would be advantageous for some applications. Recombinant 31 kDa and 17 kDa proteins are being produced *in vitro* for enzymatic oxidation and crosslinking *in vitro* using catechol oxidases produced by the worm as well as commercially available enzymes. These processes are being developed with the long term goal of producing improved microcapsules from eggshell protein precursors.

R5.7

CHARACTERIZATION AND STRUCTURE OF MUSSEL ADHESIVE PROTEINS. Richard A. Laursen, Jung-Jung Ou, Xiao-Tong Shen and Michael J. Connors, Department of Chemistry, Boston University, Boston MA 02215.

Many marine animals such as mussels and barnacles are able to anchor themselves to surfaces through the use of proteinaceous adhesives, which have the unique ability to form strong bonds in a wet environment. With eventual goal of developing wet-surface adhesives, we have carried out gene sequencing studies, using three species of mussel, in order to learn what structural characteristics give these proteins their special properties. Two classes of protein are revealed. Both are characterized by containing about 20% each of lysine and of tyrosine (or DOPA). However, the proteins from *Mytilus edulis* and *Mytilus californianus* consist primarily of tandem repeats of variations of the proline-rich decapeptide sequence, AKPSYPPTYK, while the protein from *Geukensia demissa* is rich in glycine and glutamine and is comprised of 11- and 13-residue variants, e.g., GKPTTYDAGYK, GQQKQTGYDTGYK and GGVQKTGYSGYK.

We propose that the repeat domains have definite folded structures, if not in solution, at least in the condensed (cross-linked) state that gives them their distinctive properties. In this respect, the mussel proteins may resemble collagen, which has both secondary structure and adhesive properties.

Supported by a grant from the Office of Naval Research.

R5.8

CALCIUM MINERAL-PEPTIDE INTERACTIONS. A.P. Wheeler, Dept. of Biological Sciences, Clemson University, SC; and C. Steven Sikes, Mineralization Center, University of South Alabama, Mobile.

Peptides have been synthesized by solid phase methods with structures which are in part based on experimentally-determined features of a major class of organic matrix phosphoproteins isolated from the calcium carbonate shell of the oyster. The matrix structures mimicked in the synthetic peptides included runs of aspartic acid (Asp), which were contrasted with peptides having other deployments of Asp with serine (Ser) and glycine (Gly). In addition, peptide-Ser was phosphorylated (PSer) and the hydrophobic carboxy-terminus of natural matrix was mimicked using polyalanine tails. The interaction of the various peptides with CaCO_3 as well as calcium phosphate was determined using a variety of crystallization assays and studies of adsorption of radio-labelled peptides to crystal surfaces.

In general, peptides that include runs of Asp regulate crystal nucleation and growth more effectively than those which contain $(\text{Asp-X})_n$ or $(\text{Asp-X-Y})_n$ sequences with X and Y being either Gly or Ser. Further, CaCO_3 crystals have a much higher binding capacity for polyAsp than for peptides with other deployments of Asp. Phosphorylation increases the regulatory activity and the crystal capacities of Asp/Ser - containing peptides. PolyAsp peptides having terminal PSer's are especially effective as regulators of CaCO_3 nucleation and the conversion of amorphous calcium phosphate to apatite. The activity of Asp₁₅ molecules in CaCO_3 nucleation assays is markedly increased by the addition of polyalanine tails.

R5.9

MOLECULAR RECOGNITION BETWEEN PROTEIN AND CRYSTAL: RELEVANCE TO BIOMINERALIZATION. L. Addadi, A. Berman⁺, J. Moradian-Oldak and S. Weiner⁺, Structural Chemistry and Isotope⁺ Depts., Weizmann Institute of Science, Rehovot, Israel.

In many mineralized tissues, common underlying processes are apparent in which the structured surfaces of acidic macromolecules or other organic molecules are involved in regulating mineralization via interactions at the interface with the forming crystals. Acidic glycoproteins extracted from mineralized tissues have been shown to selectively interact with specific crystal surfaces of calcium dicarboxylate crystals, of calcite and of some organic calcium phosphate derivatives. All these crystal surfaces present strikingly similar structural patterns. The protein-crystal interactions can thus be interpreted using common stereochemical rules, which appear to be transferable from one system to another. The varied operation of these rules can result in different control mechanisms. Thus acidic proteins extracted from mollusk shells, when adsorbed on a rigid matrix act as nucleators of oriented crystals of calcite. Similar proteins extracted from sea urchin skeletons act as controlled modulators of crystal growth and influence material properties, by being adsorbed at and occluded into calcite crystals during growth. Their mode of accommodation within the crystal is being studied using synchrotron X-ray radiation.

Thus the functions of these proteins in biomineralization seem to depend essentially on an accurate tuning of electrostatic interactions. Comparison between different systems provides information on the mechanism(s) of biological crystal growth, and hints at a general applicability of some basic molecular principles.

R6.1

BIOMINERALIZATION: NEW ROUTES TO CRYSTAL ENGINEERING. Stephen Mann, School of Chemistry, University of Bath, Bath BA2 7AY, UK.

This paper discusses the principal features of biomineralization in relation to the controlled crystallization of inorganic materials, and the modelling of these concepts in vitro. The biological strategies adopted in the regulation of nucleation and growth are; (a) the use of constrained reaction environments, (b) the synthesis of chemically and structurally specific organic macromolecules, and (c) the secretion of tailor-made additives of low and high molecular weight. Underlying these strategies is the concept of molecular recognition at interfaces comprising organic and inorganic surfaces. The structural, electrostatic and stereochemical aspects of these interfacial interactions will be described. Furthermore, the development of these ideas in synthetic systems involving the crystallization of CaCO_3 under Langmuir monomolecular films will be presented.

R6.2

ONTOGENETIC AND PHYLOGENETIC VARIATION OF FORM AND FUNCTION OF THE OCULAR LENS. J.G. Sivak, School of Optometry, University of Waterloo, Waterloo, Ontario, Canada, N2L 3G1

The lens of the vertebrate eye continues to grow and develop throughout life. New growth compresses older tissue toward the center, thereby producing a gradient refractive index distribution which has important implications in the control of longitudinal spherical aberration.

Lens size and shape varies widely among species; depending on whether the eye is used in air or underwater, or in nocturnal versus diurnal conditions. The lens of the typical aquatic eye, for example, is rigid and spherical in shape. Due to the neutralization of corneal refractive power in water, the lens is the only refractive element of the aquatic eye. Accommodative changes in ocular refractive power are produced by means of lens motion toward or away from the retina in aquatic forms and by change in lens shape in terrestrial species. Exaggerated change in lens shape accompanies diving behavior in certain aquatic birds in order to compensate for the loss of corneal refractive power in water.

Extensive alterations in lens size and shape and refractive index distribution are associated with the embryological development of the primate and avian eye. Recent results indicate that such changes do not significantly alter lens focal power. This suggests that ocular refractive development is controlled through growth of the globe (sclera and cornea) alone.

R6.3

HIERARCHICAL STRUCTURE OF THE INTERVERTEBRAL DISC. J.J. Cassidy, A. Hiltner, and E. Baer, Center for Applied Polymer Research and Case Western Reserve University, Cleveland, OH.

The hierarchical structure of the collagenous components of the intervertebral disc is characterized using optical microscope techniques. In the annulus fibrosus, the thickness of lamellae increases abruptly 2 mm inward from the edge of the disc, dividing the annulus into peripheral and transitional regions. Lamellae in the lateral and posterior annulus have a broad distribution of lamellar thicknesses. In alternate lamellae, fibers are inclined with respect to the vertical axis of the spine in a layup structure. From the edge of the disc inward to the nucleus, this interlamellar angle decreases from 62 to 45 degrees. Within lamellae, collagen fibers exhibit a planar crimped morphology. The plane of the waveform is inclined with respect to the spinal axis by the interlamellar angle. From the edge of the disc inward, the crimp angle increases from 20 to 45 degrees and the crimp period

decreases from 26 to 20 μm . A hierarchical model of the disc is presented that incorporates these morphological gradients.

Mechanical testing in load-deflection, stress relaxation, and creep modes reveals the response at each level of hierarchy to compression. The role water transport plays in determining the mechanical properties of the disc is also established. These mechanical data are analyzed with models that reflect the hierarchical composite structure.

R6.4

BENDING, FOLDING, AND BUCKLING PROCESSES DURING BACTERIAL MACROFIBER MORPHOGENESIS. Neil H. Mendelson, Dept. of Molecular and Cellular Biology, University of Arizona, Tucson, Arizona, and John J. Thwaites, Dept. of Engineering, Cambridge University

Bacterial macrofibers are multicellular structures produced by certain cultures of rod-shaped cells when cells do not separate from one another after septation. Chains of cells arise that twist as they grow. This twisting is thought to reflect either the geometry of assembly of the cell wall polymers or some aspect of their anisotropic behavior after insertion into the wall. The degree and direction of twisting is controlled by genetic and physiological factors such as growth temperature and the concentration of certain ions and other compounds in the growth medium. Twisting is ultimately responsible for a shape deformation of the cells into double-strand helical forms. The mechanical basis for shape determination and eventually macrofiber morphogenesis involves a folding process, the touching of elongating structures to themselves, blocked rotation, and shape deformation. In normal growth medium, time-lapse films reveal that writhing motions which lead to increased bending result in touching. In media of increased viscosity, bending is suppressed although elongation and rotation are unaffected. Folding occurs but now as a result of buckling. The forces responsible for both processes derive from growth and interaction of the cell surface with the growth medium. The helical shape once established is heritable. Whether the shape becomes "set" by cross-linking or other modification of the peptidoglycan remains to be determined.

R6.5

MECHANICAL PROPERTIES OF BACTERIAL FIBERS. John J. Thwaites, Dept. of Engineering Cambridge University, and Neil H. Mendelson, Department of Molecular and Cellular Biology, University of Arizona, Tucson, Arizona

Bacterial thread is the name given to a fibrillar fiber produced from cell-separation-suppressed mutants of *Bacillus subtilis*, which grow in long cellular filaments and produce in cultures aggregates that resemble randomly-laid textile webs. Threads are produced by steady withdrawal at the end of a sterile toothpick - for all the world like Carothers, 50 years ago! Individual filaments are drawn radially into the forming thread and adhere strongly to each other with axial alignment. Uniform threads up to 1 meter in length and 180 μm in diameter can be produced. Such threads contain about 50,000 filaments and upwards of 10^{10} cells.

Tests on thread show that peptidoglycan, which is the load-bearing polymer of the bacterial cell wall, behaves mechanically like other visco-elastic polymers. When dry its behavior is glassy, with high modulus; when wet, it is relatively weak and of low initial modulus. Relaxation data indicate a very wide spectrum of relaxation times. All the mechanical properties depend strongly on the RH of the test environment; they are also influenced by the ionic environment at the time threads are drawn.

Available evidence indicates that peptidoglycan is not crystalline. Nonetheless there is some degree of orientation in the bacterial cell wall. This is shown by the effect of enzyme attack on mechanical properties and by the twisted growth pattern of bacteria.

R6.6

Growth-packed PPT-A fiber for the replacement of native asbestors.

Poly-p-phenyleneterephthalamide (PPT-A) fibers made

by molecular growth and self ordering process had a similar structure to the native cellulose such as flax or lamie fibers. The unit fibrils that construct the fiber have an ultra fine thickness, high strength and modulus, as well as high heat resistance, which are the indispensable physical factors of synthetic fibers for the replacement of native asbestos. The growth-packing mechanism found in the formation of PPT-A fiber was something different from those currently debated for the interpretation of the native process. The oligomer chains which are scarcely soluble in polar solvent are preoriented by a biospinning or a similar action, and they are laterally supported by a large number of solvent bridges that connect between the polar groups of oligo-chains, by a linear association of solvent molecules. Thus, they form the 'gel crystal' which must be newly defined as a crystalline form which has a specific structure of three-dimensional molecular network, depending on the angles made by polar groups in oligo-chains. The chain growth, the formation of covalent bond between oligomers triggers the collapse of solvent bridges, resulting in the packing of the grown molecules by a lateral chain movement. The three-dimensional network structure of the fibrils inserting micro-cleavages between them is thus constructed by a subdivision of the gel crystal. The classical concept of fiber structure, the crystalline and amorphous regions and tie molecular theory must also be evaluated again with a different view that comes from the molecular growth-packing mechanism.

R6.7

COMPOSITE BIOMOLECULAR/SOLID STATE NANOSTRUCTURES Kenneth Douglas and Noel A. Clark, University of Colorado, Boulder, Colorado; and Kenneth J. Rothschild, Boston University, Boston, Massachusetts.

We demonstrate a process in which two dimensional protein crystals act as patterning elements for nanometer fabrication. In this process a two dimensional crystalline protein monolayer is deposited on a smooth substrate, metal coated by electron beam evaporation and then ion milled. Under ion milling this protein-metal heterostructure exhibits differential metal removal and rearrangement which varies on a protein molecular length scale. The result of this three-step parallel process is the fabrication of a 1 nm-thick metal film with 15 nm diameter holes periodically arranged on a triangular lattice of parameter 22 nm. These nanostructures are fabricated on both thin film and bulk substrates and are imaged by transmission electron microscopy (TEM) and scanning tunneling microscopy (STM) respectively.

R6.8

DIAMETER QUANTIZATION IN CYLINDRICAL AGGREGATES OF CHLOROPHYLLS. D.J. Worcester, University of Missouri, Columbia, MO; T.J. Michalski, M.K. Bowman & J.J. Katz, Argonne National Laboratory, Argonne, IL.

Neutron small-angle scattering measurements of several different chlorophylls hydrated in deuterated octane-toluene mixtures show that long, hollow cylinders of aggregated chlorophyll are formed. Clear secondary maxima are present in the scattering and the cylinder diameters are well determined, but depend on chlorophyll type. Our studies of numerous samples and several chlorophyll types provide strong evidence that there are only certain discrete values for the diameters, which are very nearly in the ratio of small integers. Thus, cylinders of Chla and Bchl_a are 11nm in diameter; Bchl_a and 2-Acetylchl_a, 21nm; and Bchl_a, 40-43nm. Substantial variability in size was found only for Chla/Chlb mixtures (35-50nm).

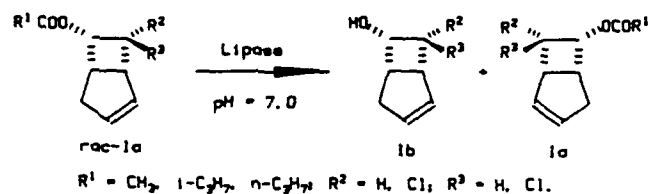
The quantization of diameters can be accounted for structurally if water molecules coordinate to the magnesium atom only on one side of the Chla macrocycle, but on either side of the Bchl_a and 2-

Acetylchla macrocycles. The additional acetyl groups in Bchla and 2-Acetylchla make water coordination possible on either side of the macrocycle without sacrifice of hydrogen bonding needed for aggregate formation and stability. The crucial structural consequence is that water coordination on either side of the macrocycles results in some of the macrocycles having opposing curvatures which cancel and therefore give the larger structures. An additional feature is that all chlorophyll macrocycles are equivalent in the Chla cylinders, but in the larger structures, pairs of macrocycles are the basic structural units. This suggests that there is particular stability to dimers of Bchla and of 2-Acetylchla.

R6.9

ENZYMATIC RESOLUTION OF BICYCLO[3.2.0]HEPT-2-EN-6-YL ESTERS. Norbert Klempier, Kurt Faber, Herfried Griengl; Institute of Organic Chemistry, Graz University of Technology, Stremayrgasse 16, A-8010 Graz, Austria

Both enantiomers of *endo*-bicyclo[3.2.0]hept-2-en-6-ol, a precursor of the Corey lactone, were obtained by means of a biocatalytic resolution using microbial lipases¹. Optimisation of the system with respect to substrate structure and the enzyme employed led to a procedure which gives rise to 1a and 1b in both $\geq 98\%$ e.e. when *rac*-1a ($R^1=CH_3$, $R^2=R^3=H$) was hydrolysed with lipase P from *Pseudomonas fluorescens* (Amano Pharm.Co.).



Other lipases (from *Candida cylindracea*, porcine pancreas and *Yarrowia* sp.) and derivatives bearing Chloro-atoms in the 7-position were less satisfactory with respect to both enantioselection and rate of reaction.

1 For a related investigation see: I.C.Cotterill, E.L.A.Macfarlane, S.M.Roberts, *J.Chem.Soc., Perkin Trans.1*, 1988, 3387.

SYMPOSIUM S: MULTI-FUNCTIONAL MATERIALS

S

November 29 - December 1, 1989

Chairs

Donald R. Ulrich
United States Air Force
Bldg. 410, Room B219
AFOSR/NC Bolling AFB
Washington, DC 20332-6448
(202) 767-4963

Alan J. Buckley
Research Director
Hoechst Celanese Research Company
86 Morris Avenue
Summit, NJ 07901
(201) 522-7788

Frank E. Karasz
Polymer Science & Engineering
Department of Materials Research
Laboratory
University of Massachusetts
Amherst, MA 01003
(413) 545-4783

George Gallagher-Daggitt
Ministry of Defence
Northumberland House
Northumberland Avenue
London WC 2N5 BT
United Kingdom
011-44-218-0550

Symposium Support

Air Force Office of Scientific Research

**Proceedings published as Volume 175
of the Materials Research Society
Symposium proceedings series.**

MULTI-FUNCTIONAL MATERIALS

November 29 - December 1, 1989

SESSION S1: MULTIFUNCTIONALITY IN CERAMICS/POLYMERS

Chairs: Donald R. Ulrich
Wednesday Afternoon, November 29
Essex North East (W)

1:30 *S1.1

NANODESIGNING OF MULTIFUNCTIONAL CERAMIC COMPOSITES, Ilhan A. Aksay, University of Washington, Department of Materials Science and Engineering, Seattle, WA.

2:00 *S1.2

NANOCOMPOSITES - THE MULTIFUNCTIONAL FAMILY OF MATERIALS, Rustum Roy, Pennsylvania State University, Materials Research Laboratory, University Park, PA.

2:30 *S1.3

SOL-GEL PROCESSING OF LARGE SILICA OPTICS, L.L. Hench, University of Florida, Gainesville, FL.

3:00 BREAK

3:15 S1.4

PHOTOACTIVE LIQUID CRYSTALLINE POLYMERS AS MULTIFUNCTIONAL MATERIALS, D. Creed, A.C. Griffin, C.E. Hoyle and K. Venkataram, University of Southern Mississippi, Departments of Chemistry and Polymer Science, Hattiesburg, MS.

3:30 *S1.5

MULTIFUNCTIONAL DEVICE APPLICATIONS OF NONLINEAR OPTICAL POLYMER MATERIALS, Rick Lytel and Ferris Lipscomb, Lockheed Missiles and Space Company, Inc., Research and Development Division, Palo Alto, CA.

4:00 *S1.6

EXPLORATORY STUDIES OF NEW NLO AND PIEZO-ELECTRIC POLYMERS, H.K. Hall, Jr., Anne B. Padias, Francesco Fuso, Zhende Ni and Michael A. Mitchell, University of Arizona, Chemistry Department, Tucson, AZ; Thomas Leslie, Hoechst-Celanese, Summit, NJ.

4:30 S1.7

POLYMER-SALT COMPLEXES, APPLICATION AND NATURE OF THE CHEMICAL BONDS, G.A. Nazri and D.M. MacArthur, General Motors Research Laboratories, Warren, MI; R. Aroca, University of Windsor, Windsor, Canada.

4:45 S1.8

STUDY ON DIOPSIDE WHISKERS PRECIPITATION TYPE HYDROXYAPATITE, T. Nonami, TDK Corporation, Research and Development Center, Chibaken, Japan.

*Invited Paper

SESSION S2: NON-LINEAR OPTICS IN MULTIFUNCTIONAL MATERIALS

Chair: Alan Buckley
Thursday Morning, November 30
Essex North East (W)

8:30 *S2.1

NOVEL ELECTROACTIVE AND NONLINEAR OPTICAL HETEROSTRUCTURES, Paras N. Prasad, State University of New York at Buffalo, Photonics Research Laboratory, Department of Chemistry, Buffalo, NY.

9:00 S2.2

ENHANCEMENT OF THIRD ORDER NONLINEARITY ON PHTHALOCYANINE COMPOUNDS, Masahiro Hosoda, Tatsuo Wada, Akira Yamada, Anthony P. Garito and Hiroyuki Sasabe, Frontier Research Program (RIKEN), Saitama, Japan.

9:15 *S2.3

TRANSPORT, OPTICAL PROPERTIES AND PHOTOEXCITATIONS IN LADDER TYPE POLYMERS, I. Belaish, D. Davidov and C. Rettori, Hebrew University of Jerusalem, Racah Institute of Physics, Jerusalem, Israel; M.R. McLean, L.R. Dalton and L.P. Yu, University of Southern California, Department of Chemistry, Los Angeles, CA.

9:45 BREAK

10:00 S2.4

DESIGN, CHARACTERIZATION, AND OPTICAL PROPERTIES OF PHOSPHAZENE-BASED POLYMERS, Gregory J. Exarhos and William D. Samuels, Battelle-Pacific Northwest Laboratory, Richland, WA; Kevin M. Crosby, Physics Department, Beloit, WI.

10:15 S2.5

ORGANIC, ORGANOMETALLIC AND POLYMERIC MATERIALS WITH UNUSUAL NONLINEAR OPTICAL AND ELECTRONIC PROPERTIES, Seth R. Marder and Joseph W. Perry, California Institute of Technology, Jet Propulsion Laboratory, Pasadena, CA; Eric J. Ginsburg, Christopher B. Gorman and Robert H. Grubbs, California Institute of Technology, Pasadena, CA.

10:30 S2.6

THIRD-ORDER OPTICAL NONLINEARITIES IN POLYMER COMPOSITES, Kenneth M. White, R. Ellen Harelstad, Cecil V. Francis and Diana J. Gerbi, 3M Company, Science Research Laboratory, St. Paul, MN; John Stevens and Peter C. Leung, 3M Company, Computational Science Center, St. Paul, MN.

10:45 *S2.7

SYNTHESIS AND PROPERTIES OF MULTIFUNCTIONAL POLYMERS, H.A. Goldberg, A.J. East, I.L. Kalnin, R.E. Johnson, H.T. Man, R.A. Keosian and D. Karim, Hoechst Celanese, Summit, NJ.

1:15 S2.8
MOLECULAR DESIGN OF SYNTHETIC POLYPEPTIDES OR NONLINEAR OPTICS, Takafumi Ishii, Tatsuo ada, Akira Yamada, Anthony F. Garito and Iroyuki Sasabe, Frontier Research Program RIKEN), Saitama, Japan.

1:30 *S2.9
MULTIFUNCTIONAL MACROMOLECULES - SOME DEVICE APPLICATIONS, Michael R. Worboys, Michael S. Riffith and Nicholas A. Davis, GEC-Marconi Research Centre, Essex, United Kingdom.

SESSION S3: MULTIFUNCTIONAL
INORGANIC MATERIALS

Chair: Ilhan A. Aksay
Thursday Afternoon, November 30
Essex North East (W)

1:30 *S3.1
MULTIFUNCTIONAL ENGINEERING MATERIALS-REVIEW AND PROJECTIONS, John D. Mackenzie, University of California at Los Angeles, Department of Materials Science and Engineering, Los Angeles, CA.

2:00 *S3.2
MULTIFUNCTIONAL FERROIC NANOCOMPOSITES, R.E. Ewning, H. Ikawa and S.E. McKinstry, Pennsylvania State University, Materials Research Laboratory, University Park, PA.

2:30 S3.3
APPLICATION OF SOL-GEL DERIVED NANOCOMPOSITES TO SOLID STATE EPITAXIAL GROWTH OF FILMS AND SELECTED SEMI-CONDUCTORS, Rustum Qay, S. Komarneni and A.M. Kazakos, Pennsylvania State University, Materials Research Laboratory, University Park, PA.

2:45 BREAK

3:00 S3.4
CONTROL OF $\text{YBa}_2\text{Cu}_3\text{O}_x$ AND BaTiO_6 SOL-GEL SOLUTION STRUCTURE BY CHEMICAL MODIFICATION WITH ORGANIC ACIDS, Haixing Zheng and J.D. Mackenzie, University of California-Los Angeles, Department of Materials Science and Engineering, Los Angeles, CA.

3:15 S3.5
POLY(ARYLENE ETHER) OR POLYIMIDE-SILICATE HYBRIDS VIA SOL-GEL ULTRASTRUCTURE PROCESSING, M. Spina, A. Brennan, G.L. Wilkes and J.E. McGrath, Virginia Polytechnic Institute and State University, Departments of Chemistry and Chemical Engineering, National Science Foundation Science and Technology Center: High Performance Polymeric Adhesives and Composites, Blacksburg, VA.

3:30 S3.6
PROTECTIVE COATINGS FOR HYPERSONIC VEHICLE APPLICATIONS, J. Covino and K. Klemm, Naval Weapons Center, Research Department, China Lake, CA.

3:45 *S3.7
HIGH COMPRESSIVE STRENGTH ORDERED POLYMER FIBERS AND FILMS VIA SOL-GEL MICROCOMPOSITE PROCESSING, Robert F. Kovar, R. Ross Haghighat and Richard W. Lusignea, Foster-Miller, Inc., Waltham, MA; Lawrence T. Drzal, Michigan State University, East Lansing, MI.

4:15 *S3.8
SOL-GEL ETALONS FOR ION LASERS, Nicholas J. Phillips, Loughborough University of Technology, Department of Physics, Loughborough, United Kingdom.

4:45 S3.9
DESIGNING PORE SIZE IN SILICA AND ALUMINO-SILICATE GELS, H. Kido, P.B. Malla and S. Komarneni, The Pennsylvania State University, University Park, PA.

SESSION S4: POLYMERS FOR ULTRASTRUCTURES

Chair: Frank E. Karasz
Friday Morning, December 1
Essex North East (W)

8:30 *S4.1
DIELECTRIC RELAXATION PROPERTIES AND ALIGNMENT BEHAVIOUR OF LIQUID-CRYSTALLINE SIDE-CHAIN POLYMERS, Graham Williams, University College of Swansea, Department of Chemistry, Swansea, United Kingdom; Frank E. Karasz, University of Massachusetts, Polymer Science and Engineering Department, Amherst, MA.

9:00 *S4.2
LIQUID CRYSTALLINE MATERIALS FOR POLYMER WITH ANISOTROPIC ULTRASTRUCTURES, George S. Attard, The University, Department of Chemistry, Southampton, United Kingdom.

9:30 S4.3
LIQUID CRYSTALS INCORPORATING METAL CENTRES, W. Haase, S. Gehring and B. Borchers, Institut für Physikalische Chemie, Technische Hochschule, Darmstadt, West Germany.

9:45 S4.4
DIELECTRIC PROPERTIES OF POLYMERIC LIQUID CRYSTALS WITH STRONG LATERAL DIPOLE GROUPS, W. Haase and M. Pfeiffer, Institut für Physikalische Chemie, Technische Hochschule, Darmstadt, West Germany.

10:00 BREAK

10:15 S4.5
SYNTHESIS AND PROPERTIES OF COMB-LIKE LIQUID CRYSTALLINE POLYMERS WITH ELECTROOPTICALLY ACTIVE MESOGENIC SIDE GROUPS, M. Maeda, R.S. Kumar, A. Blumstein and S.K. Tripathy, University of Lowell, Lowell, MA; P. Sixou and F. Faubert, Université de Nice, Laboratoire de Physique de la Matière Condensée, Nice, France.

10:30 S4.6
THERMOTROPIC CHIRAL NEMATIC POLYMERS AS OPTICAL MATERIALS, M.L. Tsai and S.H. Chen, University of Rochester, Department of Chemical Engineering and Laboratory for Laser Energetics, Rochester, NY.

10:45 *S4.7
MULTI-LAYERS THIN FILMS OF ACETALYZED POLY (VINYL ALCOHOL) DERIVATIVES OBTAINED BY THE LB METHOD AND THEIR OPTO-ELECTRONIC PROPERTIES, Kiyoshi Oguchi, Yasuhiko Yokoh, Kohei Sanui and Naoya Ogata, Sophia University, Department of Chemistry, Tokyo, Japan.

11:15 *S4.8
DIELECTRIC, TSC AND ELECTROMECHANICAL MEASUREMENTS ON SOME PROSPECTIVE N.L.O. POLYMERS, I.M. Ward, G.R. Davies and P.L. Carr, University of Leeds, Physics Department, Leeds, United Kingdom.

11:45 S4.9
SILICONE CONTAINING LIQUID CRYSTALLINE POLYURETHANES AND POLYESTER, Robert Kosfeld, Frank Braun, Lutz Willner and Michael Hess, University of Duisburg, Department of Physical Chemistry, Duisburg, West Germany.

SESSION S5: MULTIFUNCTIONAL DESIGN

Chair: George Gallagher-Daggitt

Friday Afternoon, December 1

Essex North East (W)

1:30 *S5.1
MICROSTRUCTURAL CONTROL IN SIDE CHAIN POLYMERS FOR OPTICAL APPLICATIONS, Tim Lemmon and Alan H. Windle, Cambridge University, Department of Materials Science and Metallurgy, Cambridge, United Kingdom.

2:00 S5.2
ZEOLITE LOADED POLYURETHANE FOAMS FOR ENVIRONMENTAL CONTROL, C.B. Frost, D.L. Lindner and J.E. Costa, Sandia National Laboratories, Livermore, CA.

2:15 *S5.3
PERIODIC AREA MINIMIZATION SURFACES IN MICROSTRUCTURAL SCIENCE, Edwin L. Thomas, Massachusetts Institute of Technology, Department of Materials Science and Engineering, Cambridge, MA.

2:45 S5.4
BEHAVIOR OF SUPERCONDUCTING CERAMIC-POLYMER COMPOSITE, C. Vipulanandan and S. Salib, University of Houston, Texas Center for Superconductivity, Houston, TX.

3:00 BREAK

3:15 S5.5
MICROSTRUCTURE OF PPTA/POLYPYRROLE COMPOSITE FIBERS, L.P. Rector, T.J. Marks and S.H. Carr, Northwestern University, Departments of Materials Science and Engineering and Chemistry and the Materials Research Center, Evanston, IL.

3:30 *S5.6
THEORY AND PRACTICE IN THE PREPARATION OF MULTIFUNCTIONAL MATERIALS CONTAINING DELOCALIZED π ELECTRONS, Larry R. Dalton, Rahel Vac, LuPing Yu and Linda Sapochak, University of Southern California, Department of Chemistry, Los Angeles, CA.

4:00 S5.7
MICROPHASE SEPARATION IN MULTIBLOCK COPOLYMER MELTS, Anne M. Mayes and Monica Olvera de la Cruz, Northwestern University, Department of Materials Science and Engineering, Evanston, IL.

4:15 S5.8
SEGMENTED ANISOTROPIC ISOTROPIC POLY ARYL ESTER POLY(ARYLENE ETHER) COPOLYMER MATERIALS, J.E. McGrath, K.L. Cooper, W. Waihamad, H. Huang, D. Chen and G.L. Wilkes, Virginia Polytechnic Institute and State University, Departments of Chemistry and Chemical Engineering, National Science Foundation Science and Technology Center: High Performance Polymeric Adhesives and Composites, Blacksburg, VA.

4:30 *S5.9
INORGANIC AND ORGANOMETALLIC PRINCIPLES IN THE DESIGN OF MULTIFUNCTIONAL MATERIALS, D. Michael P. Mingos, University of Oxford, Inorganic Chemistry Laboratory, Oxford, United Kingdom.

5:00 S5.10
MODELLING MICROSTRUCTURE IN MATERIALS THAT CONTAIN ANISOTROPIC PARTICLES, Christopher Viney, University of Washington, Department of Materials Science and Engineering, Seattle, WA; Larry A. Chick, Battelle Pacific Northwest Laboratory, Richland, WA.

S1.1

NANODESIGNING OF MULTIFUNCTIONAL CERAMIC COMPOSITES. Ilhan A. Aksay, Department of Materials Science and Engineering, University of Washington, Seattle, WA 98195

Processing of ceramic composites for multifunctional applications requires a precise control on compositional and density variations in the scale range of 10^{-9} m to 10^{-6} m. This presentation will review the methods of achieving this goal by utilizing combinations of colloidal particles and molecular precursors. Two basic needs will guide the presentation: (i) the need to consolidate powders as homogeneously as possible with respect to chemical and density fluctuations, and (ii) the need to shape complex geometries with a minimum degree of volume change (i.e., near-net-shape forming). Nanometer-sized particles provide the best solution for the first need but generally fail in the second category due to low density packing of particles. We will illustrate a variety of approaches to eliminate this low density problem while still retaining the control on nanodesigning. Examples will include an aluminum silicate ceramic with an optimum combination of optical and mechanical properties and HTSC ceramic fibers with a combination of mechanical and electrical properties.

S1.2

NANOCOMPOSITES—THE MULTIFUNCTIONAL FAMILY OF MATERIALS. Rustum Roy, Materials Research Laboratory, The Pennsylvania State University, University Park, PA 16802-4801.

Our synthesis in 1982 of nanocomposites made via the solution-sol-gel route has led to an unanticipatedly large family of materials, which can be tailored to perform large different functions. This review will encompass our own work on the chemical-structural properties (control of phase, of sintering temperature, of densification, of microstructure, of morphology, of reaction temperatures) but the work of others on optical and magnetic materials and even those with enhanced mechanical properties.

S1.3

SOL-GEL PROCESSING OF LARGE SILICA OPTICS. L. L. Hench, University of Florida, Gainesville, FL

Sol-gel processing offers the potential for near net shape casting of ceramics and glasses with ultrahigh purity and homogeneity. The current status of achieving these advantages in silica optical components of up to 75 mm diameter is discussed.

Two new types of optical silica have been developed using organometallic sol-gel processing. Fully dense (Type V) gel-silica has excellent optical transmission throughout the vacuum UV, UV, vis, NIR, and IR. Physical properties and structural characteristics of Type V gel-silica are generally equivalent or superior to the best grades of Types I-IV optical silicas; e.g., the coefficient of thermal expansion, OH content, and dispersion of Type V gel-silica is lower than Types I-IV. The UV cut-off of Type V gel-silica has been improved to < 180 nm, due to lower OH contents as shown by quantum cluster calculations.

Optically transparent porous gel-silicas are termed Type VIA, B, or C depending upon the total pore volume, density, surface area and microhardness. Type VIA gel-silica has a density that is 80-70% that of full density vitreous silica (Types I-V) with a total pore volume of 0.17 to 0.37 cc/g. The pores are interconnected with an average radius of only 1.2 nm and surface area of 290-800 m²/g. Type VIA silica can be impregnated with a broad range of optical polymers or compounds with excellent transmission out to 290-300 nm. Type VIB porous gel-silica has a smaller total pore volume and somewhat larger pore size. Type VIC has a density 95-100% of vitreous silicas with a UV cut-off to 185-165 nm.

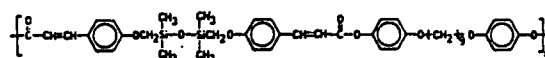
Both Types V and VI gel-silica offer the advantage of near net shape casting including the ability to form internal cavities using a lost wax process. Examples include a cast lightweight mirror with integral face plate and lightweight backing and porous substrates for scintillation counter, liquid crystal display, and planar waveguides.

Progressive improvements in process and defect control required to achieve scale-up to large sizes are illustrated.

S1.4

PHOTOACTIVE LIQUID CRYSTALLINE POLYMERS AS MULTIFUNCTIONAL MATERIALS. D. Creed, A.C. Griffin, C.E. Hoyle and K. Venkataram, Departments of Chemistry and Polymer Science, University of Southern Mississippi, Hattiesburg, MS, 39406.

The photochemistry and photophysics of polyarylcinnamate liquid crystals has been examined in thin films of these materials. Of particular interest is the [2+2] photocycloaddition reaction which leads to crosslinking (and insolubility) of these films. A typical structure is shown below. This polymer forms a clear,



amorphous film when cast from solution. The amorphous, cast polymer enters a LC (nematic) mesophase when heated above 70°C. The major photochemical reactions of this type of polymer are cyclobutane formation (leading to polymer crosslinking) and photo-Fries rearrangement. We will present evidence from absorption and fluorescence spectroscopy for formation of K-aggregates of the chromophores in the nematic LC phase. This effect leads to a wavelength dependence of the polymer photochemistry, both in the nematic mesophase and in the frozen nematic phase that is formed upon cooling the nematic polymer below its T_g. This can be exploited to produce exclusively the cyclobutane adduct.

S1.5

MULTIFUNCTIONAL DEVICE APPLICATIONS OF NONLINEAR OPTICAL POLYMER MATERIALS. Rick Lytel and Ferris Lipscomb, Research and Development Division, Lockheed Missiles and Space Co., Inc., D-9701, B-202, 3251 Hanover St., Palo Alto, CA 94304

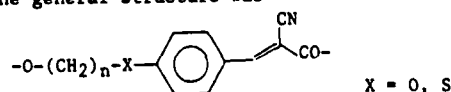
We describe a new, integrated approach for high-speed optical interconnection packages for integrated circuits. This approach is based upon the use of active polymer waveguides and switches to provide efficient light distribution and modulation in an integrated package.

We will first present a brief review of our recent work toward achieving practical electro-optic polymer waveguide devices. This will include recent experimental results on poling of channel waveguides, and device architectures, designs, and performance. We will then apply this work to a novel, integrated packaging approach using active polymer waveguides for interconnects and switches. This approach places specific requirements on the materials to ensure compatibility with package fabrication and assembly. We will present the technology, show its scope and applications, and its implications for polymer electro-optic materials.

S1.6

EXPLORATORY STUDIES OF NEW NLO AND PIEZOELECTRIC POLYMERS. H. K. Hall, Jr., Anne B. Padias, Francesco Fusco, Zhende Ni, Michael A. Mitchell, Thomas Leslie, Chemistry Department, University of Arizona, Tucson, AZ 85721

Earlier we synthesized the first AB polymers containing NLO-phores along the main chain. (J. Macromol. Sci.-Chem 1988) The general structure was



When the donor was oxygen, tractable NLO-active polymers with qualitatively good physical properties were obtained.

Now we have extended this work to sulfur as the donor atom. Again, good films capable of orientation were obtained. Methacrylate and acrylate polymers containing this NLO-phore in the side-chains were synthesized, permitting a comparison for the first time of main vs. side-chain placement.

We are synthesizing tetracyano-cyclopropane and -cyclobutane monomers as novel piezoelectric materials. Synthesis and polymerization of two styrene monomers containing the 2,2,3,3-tetracyano cyclobutane substituent will be described.

†Hoechst-Celanese, Summit, NJ 07901

SI.7

POLYMER-SALT COMPLEXES, APPLICATION AND NATURE OF THE CHEMICAL BONDS. G.A. Nazri, D.M. MacArthur, General Motors Research Laboratories, Warren, MI 48090, R. Aroca, University of Windsor, Windsor Ontario N9B 3P4, Canada

Polymer electrolytes are attracting interest because of potential application in solid state batteries and electrochromic windows. In this work, we report the performance of polymeric electrolytes in several galvanic cells. The nature of the chemical bonds and ion association in polymer-salt complexes were studied. The fundamental vibrational frequencies of the polymers and lithium salts were calculated and the band assignments agree quite well with the frequencies observed in Raman and IR spectra. The strong electrostatic interactions of the dissociated salt with the polymers induced changes in the intensity of the Raman bands and IR absorption bands of the polymer. The Raman and IR spectra of the polymer-salt complexes clearly show the existence of "free" ions, ion-pairs and salt cluster at various concentrations of the lithium salt. The maximum concentration of "free" ions deduced from the spectroscopy is in excellent agreement with the salt concentration required to obtain maximum ionic conductivity.

SI.8

STUDY ON DIOPSIDE WHISKERS PRECIPITATION TYPE HYDROXYAPATITE. T. Nonami TDK Corporation, R & D Center, 2-15-7 Higashi-Ohwada, Ichikawa-shi, Chiba-ken, 272, Japan

Hydroxyapatite (HAP) is a biocompatible material and has been used as an artificial bone or teeth material. However, the use range is often limited because of low mechanical strength.

Therefore, we investigated how to make the composite material in which whisker is distributed in matrix to give higher strength. The mixed powder of HAP and diopside was heated to make this composite material.

The sintering of HAP and the precipitation of whisker were examined, to find a method of making

them occur simultaneously.

Also, diopside was added to HAP and sintering at 1200°C for 2 hours was done. As a result of these investigations, diopside whisker of aspect ratio 10~15 was formed. Moreover, the glass phase of $\text{CaO-SiO}_2\text{-P}_2\text{O}_5\text{-MgO}$ system was generated at the interface of HAP and whisker. The bending strength of this sintered body was 300MPa and KIC was $3.2\text{MPa}\sqrt{\text{m}}$.

S2.1

NOVEL ELECTROACTIVE AND NONLINEAR OPTICAL HETEROSTRUCTURES. Paras N. Prasad, Photonics Research Laboratory, Department of Chemistry, State University of New York at Buffalo, Buffalo, NY.

This talk will focus on several novel Molecular and Polymeric Heterostructures prepared in our laboratory which have interesting electroactive and nonlinear optical properties. Time-resolved studies of excitation and carrier dynamics will be presented. The nonlinear optical response has been studied using second harmonic generation and femtosecond degenerate four wave mixing, the latter being used for the investigation of third-order nonlinear optical effects. Results will also be presented from optical waveguide studies.

S2.2

ENHANCEMENT OF THIRD ORDER NONLINEARITY ON PHTHALOCYANINE COMPOUNDS. Masahiro Hosoda, Tatsuo Wada, Akira Yamada, Anthony F. Garito and Hiroyuki Sasabe, Frontier Research Program (RIKEN), Wako, Saitama 351-01, Japan

Organic conjugated compounds which exhibit third order nonlinear optical effect and have excellent processability can be prospective candidates for some photoresponsive devices.

We report that macrocyclic compounds having two dimensional π -electron conjugated system, that is, soluble metallophthalocyanine derivatives show large third order nonlinear responses and can be easy to get a thin film of molecularly doped polymer by conventional spin coating technique. The alkyl-substituted metallophthalocyanines were synthesized and fully characterized. Third order nonlinear optical susceptibility ($\chi^{(3)}$) and molecular optical susceptibility (γ) of the thin film were determined by rotational Maker fringe measurement of optical third harmonic generation. Third order nonlinear optical susceptibility of alkyl-substituted metallophthalocyanine is 10^{-11} esu order. This value is a tenth magnitude of $\chi^{(3)}$ of non-substituted one showing almost the same magnitude as polydiacetylene. According to x-ray scattering and optical absorption spectroscopy of their two compounds, the above result was suggested to be dependent on the different stacking arrangements.

We will propose that a kind of intermolecular interaction on two-dimensional conjugated system plays an important role for the enhancement of third order optical nonlinearity.

S2.3

TRANSPORT, OPTICAL PROPERTIES AND PHOTOEXCITATIONS IN LADDER TYPE POLYMERS. I. Belash, D. Davidov and C. Rettori, Racah Institute of Physics, Hebrew University of Jerusalem, Israel; and M.R. McLean, L.R. Dalton and L.P. Yu, Department of Chemistry, University of Southern California, Los Angeles, California.

Ladder type polymers like BBB, BBL and PQL can be processed to achieve films with excellent planner alignment and mechanical properties. Heat treatment and pyrolysis can change the conductivity dramatically and can induce phase transformation to a new ladder-type polymer with high intrinsic conductivity (~ 200 s/cm). This phase transformation occurs at a pyrolysis temperature of $T_p \approx (600 \pm 50)^\circ\text{C}$. The conductivity is dominated by hopping between localized states according to the anisotropic variable range hopping model. The life-time of the photoexcitations at different wavelength of the exciting laser was studied by CW LESR and photoconductivity as well as by transient photoconductivity. The photogenerated spins decay slowly with two different characteristic times. The decay of the photogenerated charges is significantly faster. We demonstrate that the unique transport, optical and mechanical properties of ladder polymers may be used to fabricate fast switching devices. A device consisting of miniature conducting microstructure in a completely transparent insulating ladder polymer was developed in our laboratory.

S2.4

DESIGN, CHARACTERIZATION, AND OPTICAL PROPERTIES OF PHOSPHAZENE-BASED POLYMERS. Gregory J. Exarhos, and William D. Samuels, Pacific Northwest Laboratory, P.O. BOX 999, MS K2-44, Richland, WA 99352, and Kevin M. Crosby, Physics Department, Beloit College, Beloit, WI 53511.

Multifunctionality in linear inorganic polymer systems can be attained through replacement of functional side groups by organic or inorganic moieties or through the formation of homogeneous mixed polymer blends. Ongoing work in this laboratory has shown that the chemical nature of the substitutional side group in polyphosphazenes influences the dispersion-lubrication properties of colloidal suspensions thereby affecting particle packing during consolidation. A key parameter for these interactions was found to be the electron-withdrawing power of the substitutional group. Phosphazene polymers also exhibit desirable optical properties which can be exploited in device applications. For example, many of these phosphorus-nitrogen containing materials form clear transparent films with good transmission properties into the ultraviolet region of the spectrum. In addition, they exhibit good radiation and optical laser damage resistance.

Recent work in this laboratory involves the development of phosphazene polymers that exhibit non-linear optical activity. Modification of the intrinsic optical response of the phosphazene chain is achieved through substitution of functional side groups. The influence of side group electronegativity and extent of electron delocalization on optical properties will be presented.

S2.5

ORGANIC, ORGANOMETALLIC AND POLYMERIC MATERIALS WITH UNUSUAL NONLINEAR OPTICAL AND ELECTRONIC PROPERTIES. Seth R. Marder, Joseph W. Perry, Jet Propulsion Laboratory, California Institute of Technology, 4800 Oak Grove Drive, Pasadena, CA, 91109; Eric J. Ginsburg, Christopher B. Gorman and Robert H. Grubbs, Department of Chemistry, California Institute of Technology, Pasadena, CA, 91125.

A series of over 50 organic salts in which the cation has been designed to have a large molecular hyperpolarizability have been prepared. Variation of the counterion (anion) in many cases leads to molecules with very large macroscopic second-order optical nonlinearities as evidenced by the Kurtz powder technique. One salt has a second harmonic generation powder efficiency roughly 2000 times that of the

urea reference standard. X-ray studies demonstrate that for several of the compounds a highly polar orientation of the chromophore in the crystal lattice is achieved. The methodology has also successfully been applied to organometallic chromophores incorporating the ferrocenyl or ruthenocenyl moieties as the donors.

We have also been utilizing soluble well defined organometallic catalysts to prepare conjugated polymers by ring opening metathesis polymerization (ROMP). ROMP of substituted cyclooctatetraene monomers yields new polyacetylene derivatives which have a substituent on every eighth carbon (on the average). In many cases these polymers can be oxidatively doped to a conductive state. In the case of poly(octylcyclooctatetraene) a conductivity of $50 \Omega^{-1}\text{cm}^{-1}$ was observed. We are examining the third-order nonlinear optical properties of these materials. The substitution tends to make the polymers amorphous and as a result the materials exhibit much lower scattering losses than does the crystalline unsubstituted polyacetylene prepared by ROMP. Some of the polymers are soluble and thin films of these materials can be prepared by spin coating.

S2.6 ABSTRACT NOT AVAILABLE

S2.7

SYNTHESIS AND PROPERTIES OF MULTIFUNCTIONAL POLYMERS. H.A. Goldberg, A.J. East, I.L. Kalnin, R.E. Johnson, H.T. Man, R.A. Keosian, and D. Karim, Hoechst Celanese, 86 Morris Avenue, Summit, NJ.

Recent work aimed at developing new polymers which exhibit useful optical (and/or electro-optical) and piezoelectric properties will be presented. The materials under study include polymers with methacrylate backbones and nitrostilbene side chains as well as new polyvinylidene cyanide based copolymers. The synthesis of high purity monomers as well as the polymerizations will be described. In addition, pyro-electric, electro-optic, thermal, electrical and optical property data will be reported. The dependence of these properties (as well as important secondary properties such as thermal stability and mechanical properties) on composition, structure, and processing conditions will be discussed.

S2.8

MOLECULAR DESIGN OF SYNTHETIC POLYPEPTIDES FOR NONLINEAR OPTICS. Takafumi Ishii, Tatsuo Wada, Akira Yamada, Anthony F. Garito, and Hiroyuki Sasabe, Frontier Research Program (RIKEN), Hirosawa 2-1, Wako, Saitama, 351-01, Japan

Introducing electron donor and acceptor to highly conjugated π electron system is a common method to enhance molecular second order hyperpolarizability. However, this sometimes reduces transparency limiting its application severely.

Poly(γ -benzyl L-glutamate) (PBLG), a typical α -helical synthetic polypeptide, is known to have extraordinarily large molecular second order hyperpolarizability, β , (ex. $\beta = 5 \times 10^{-28}$ esu for PBLG, $M_w=550,000$) which arises from many carbonyl groups aligned parallel in a polymer chain, and this polymer shows excellent transparency. Large macroscopic nonlinear susceptibility may be achieved by controlling molecular orientation by regulating molecular weight, and there is a possibility to enlarge its molecular nonlinearity by chemical modification.

From this point of view, nitro group was introduced into side-chain of PBLG ($M_w=44,000$), in order to enhance microscopic hyperpolarizability, and we made co-polymers with poly(γ -dodecyl L-glutamate) to improve its solubility and fabricability. Second order molecular nonlinearity was determined by DCSHG measurement at a wavelength of 1064 nm.

S2.9

MULTIFUNCTIONAL MACROMOLECULES - SOME DEVICE OPTIONS.

Michael R. Worboys, Michael S. Griffith and Nicholas A. Davis, GEC-Marconi Research Centre, Great Baddow, Essex, U.K.

Multifunctional macromolecules are materials which exhibit more than one active function, e.g. nonlinearity and pyroelectricity, in the same material. This opens up new possibilities for device design and implementations. We have considered a number of possible devices and identified the material properties required for successful device implementation. In many cases it was found that at least two active properties were required. From the range of possible devices, the device options have been reduced to three classes of device, of which two proof-of-principle devices have been investigated and are now under construction.

This paper describes results of the initial fabrication and characterisation of the two proof-of-principle devices. The devices are a light modulated deformable mirror (using a photoconductor and a piezoelectric layer) and an optically modulated electro optic dual layer (using a photoconductor and an electro-optic layer).

S3.1

MULTIFUNCTIONAL ENGINEERING MATERIALS-REVIEW

AND PROJECTIONS. John D. Mackenzie, Department of Materials Science and Engineering, University of California, Los Angeles, CA 90024-1595

Multifunctional engineering systems made up of different material components each providing primarily a single function are well known. Frequently, even for a monofunctional application, the material component must already have an optimum set of properties to fulfill that function. It would be desirable to have multifunctional material components, but it is obvious that the development of such materials can be difficult. In this paper multifunctional engineering materials which have been successfully developed are reviewed. More recently, some new inorganic and inorganic-organic material systems have been developed on a laboratory scale. These include inorganic crystals, intercalated materials and nanocomposites. Their structure, microstructure, processing and properties will be discussed and projections made for their future applications.

S3.2

MULTIFUNCTIONAL FERROIC NANOCOMPOSITES. R.E. Newnham, H. Ikawa, S.E. McKinstry, Materials Research Laboratory, Pennsylvania State University, University Park, PA.

During the past decade, we have developed a large family of microcomposite materials for use as electromechanical transducers, PTC and NTC thermistors, piezoresistors, and chemical sensors. The constituent phases of such composites are typically on the scale of microns in at least one dimension. Recently, though, there is a sense of excitement as a number of different technologies come together in a synergistic manner to miniaturize and integrate composites into a wide variety of optoelectronic systems. In the field of ceramics, for example, the development of chemical preparation methods has led to an overall reduction in processing temperatures and the ability to prepare nanometer-sized particles. The simultaneous introduction of polyimides and other polymer systems stable at high temperatures allows, for the first time, the co-processing of ceramic and polymer nanocomposite systems for electronic applications.

Many of the whisker and precipitate strengthened materials used for structural components can be considered nanocomposites. This paper, however, concentrates on the recent developments in the field of electroceramic nanocomposites, laying particular emphasis on the role of the ferroic materials now utilized as soft ferrite transformers, barium titanate multilayer capacitors, toughened zirconia engine parts, lead zirconate-titanate transducers, and doped barium titanate PTC thermistors. The effect of nano-scale on both

the material property coefficients of these systems and on their phase transitions is also discussed.

S3.3

APPLICATION OF SOL-GEL DERIVED NANOCOMPOSITES TO SOLID STATE EPITAXIAL GROWTH OF OXIDES AND SELECTED SEMI-CONDUCTORS. Rustum Roy, S. Komarneni and A.M. Kazakos, Materials Research Laboratory, The Pennsylvania State University, University Park, PA 16802-4801.

We have extended our proof of solid state epitaxy in SSG derived nanocomposites such as ThSiO_4 [noncrystalline] + ThSiO_4 -[thorite] and ThSiO_4 -[noncrystalline] + ThSiO_4 -[huttonite] to cases where the crystalline phase is a single crystal.

Data will be presented on phases crystallizing from xerogels of the same composition deposited on clean single crystals (including different orientations) of Al_2O_3 ; spinel; TiO_2 ; Si; etc. These show varying degrees of oriented overgrowth from nearly single to slight morphological preference. For an example, boehmite coatings on Al_2O_3 single crystals led to the growth of needle-shaped grains with the same orientation as that of the single crystal while the same coatings on a polycrystalline α - Al_2O_3 substrate led to random overgrowth.

S3.4

CONTROL OF $\text{YBa}_2\text{Cu}_3\text{O}_x$ and BaTiO_6 SOL-GEL SOLUTION STRUCTURE BY CHEMICAL MODIFICATION OF ORGANIC ACIDS. Haixing Zheng and J.D. Mackenzie, Department of Materials Science and Engineering, University of California-Los Angeles, Los Angeles, CA 90024

Preparation of different forms (monoliths, films and fibers) of materials via sol-gel process require that the solutions have different structure. Modification of alkoxide solutions by organic acid slows down the hydrolysis rate and control the polymerization reaction, consequently yields the solutions with different structure. In this work, the effect of chemical modification of alkoxides ($\text{YBa}_2\text{Cu}_3(\text{OPr})_{13}$, and $\text{BaTi}(\text{OPr})_6$) by organic acids has been investigated. It is found that the connectivity of the oxide network increase with decreasing concentration of organic acids and thus change the solutions from spinal (fiber drawing solutions) to non-spinal. This change of the structure results in: (1) ease of the formation of desired phases; (2) denser microstructure with finer grains.

S3.5

POLY(ARYLENE ETHER) OR POLYIMIDE-SILICATE HYBRIDS VIA SOL-GEL ULTRASTRUCTURE PROCESSING. M. Spina, A. Brennan, G.L. Wilkes and J.E. McGrath, Departments of Chemistry and Chemical Engineering, National Science Foundation Science and Technology Center: High Performance Polymeric Adhesives and Composites, Virginia Polytechnic Institute and State University, Blacksburg, VA 24061.

Methodologies have been outlined and demonstrated which permit the well defined functionalization of high performance aromatic polymer precursors which allow utilization in ceramic type structure. The first example investigated has been to produce amino terminated poly(arylene ether)s or fully imidized polyimides which can be quantitatively derivatized to nadimide structures through the reaction of the amine functional oligomers with norbornene 2,3-dicarboxylic anhydride. The subsequent nadimides were quantitatively derivatized via hydrosilation reactions of dimethoxy or trimethoxy silane under chloroplatinic acid catalyzed conditions. The resulting tetra or hexa methoxy silanes were hydrolysed and co-condensed under conditions previously developed for siloxane modified materials to allow the desired structure to be produced by a sol-gel ultrastructure processing. The synthesis and characterization of these materials will be reported.

S3.6

PROTECTIVE COATINGS FOR HYPERSONIC VEHICLE APPLICATIONS. J. Covino AND K. Klemm, Research Department, Naval Weapons Center China Lake Ca. 93555-6001.

Protective coatings for both Ti-Al alloys and for C-C composites have been synthesized and characterized for hypersonic vehicle applications. Coatings of choice must show protection against oxygen and hydrogen both under mild environments of low flows and low temperatures as well as severe environments of high flows and high temperatures. Aluminum-silicate glass ceramics were chosen as coating candidates because they are materials which are stable to temperatures of 1500°C, are nonreactive to oxygen and have minimal reactivity with respect to hot hydrogen. This paper will discuss the chemistry of the coating synthesis and application as well as the characterization of such coatings.

The synthetic process used in this work is the sol-gel process. The desired chemical composition of the coatings was made by dissolving the corresponding metal alkoxides in and aqueous solution followed by a controlled dehydration and heat treatment to obtain stable coatings. Composition, viscosity, firing temperature and conditions were all important parameters which need to be controlled in order to obtain stable crack-free coatings.

The coatings were characterized using elemental analysis, X-ray diffraction, Scanning electron microscopy, heat treatments in both hydrogen and oxygen and some hydrogen permeation measurements. These measurements will be presented and discussed.

S3.7

HIGH COMPRESSIVE STRENGTH ORDERED POLYMER FIBERS AND FILMS VIA SOL-GEL MICROCOMPOSITE PROCESSING. Robert F. Kovar, R. Ross Haghghat and Richard W. Lusignea, Foster-Miller, Inc., 350 Second Avenue, Waltham, MA, and Lawrence T. Drzal, Michigan State University, East Lansing, MI.

Sol-gel glass microcomposite processing of poly(benzobisthiazole) (PBZT) films increased the compressive strength of PBZT/PEEK film laminates by more than four times. The presence of glass within microfibrillar regions of PBO/sol-gel glass microcomposite fibers inhibited micro-buckling during compression and greatly increased their resistance to compressive failure.

Studies of PBZT/sol-gel glass microcomposite film morphology conducted at UMass by E.L. Thomas and Penn State by C. Pantano indicated that sol-gel glass precursor solutions had condensed within PBZT films to produce a fine scale (100-300 Å) granular structure, homogeneously distributed throughout PBZT lamellae of microfibrils.

In a parallel effort, we have successfully extended sol-gel microcomposite processing technology to the improvement of compressive strength in ordered polymer fibers. Details concerning our results will be discussed.

S3.8

SOL-GEL ETALONS FOR ION LASERS. Nicholas J. Phillips, Department of Physics, Loughborough University of Technology.

This paper addresses developments in the understanding of intra cavity elements in ion lasers using sol-gel prepared glass. A novel form of interferometry was reported earlier this year at the Ilkley review meeting in which measurements of the thermal dispersion factor were discussed.

Following from these beginnings, we look again at the fabrication of working stalone for ion lasers with special emphasis on practical elements of high conversion efficiency. Of special interest are two cases of application: in the near ultra-violet part of the spectrum and applied to the generation of achromatic single mode behavior for polychromatic lasers used in multicolour holography.

S3.9

DESIGNING PORE SIZE IN SILICA AND ALUMINOSILICATE GELS. H. Kido, P. B. Malla and S. Komarneni, Materials Research Laboratory, The Pennsylvania State University, University Park, PA.

Porous solids are known to be ideal candidates for catalytic activities and for the study of the effect of confined space on the properties of fluids. An ability to design pores of varying size and uniform distributions in solids is very important to delineate the effect of varying degree of restrictive geometry on fluid properties. In addition, pore size and its structure are some of the most important parameters that govern the amount and the rate of vapor adsorption on the surfaces of solids, and consequently determine the shape of the adsorption isotherm. Large pores facilitate multilayer adsorption of vapors such as water and nitrogen and exhibit type II or type IV isotherm, whereas multilayer adsorption is physically not possible in small pores and therefore the adsorption follows type I isotherm. This paper aims at describing the synthesis of microporous silica gels of varying pore sizes and their water sorption properties.

A series of microporous silica gels of varying pore sizes (pore diameter <15 Å) were synthesized by hydrolyzing tetramethylorthosilicate (TMOS) with varying amounts of water. No catalyst or alcohol was added. Although the gelation time for all water/TMOS ratios (R) was approximately the same (about 3 hr), the pore size was found to be minimum at R = 4.96, and it increased with both increasing and decreasing R. The sample prepared at R = 4.96 exhibited moderate type I isotherm which changed to type IV with decreasing or increasing R. The effect of aluminum addition on the properties of gels was also investigated. A small decrease in pore size and an increase in sorption capacity was observed with the addition of a small amount of Al (Si:Al = 98:2). The addition of aluminum greater than or equal to 6% (Si:Al ≤ 94:6), however progressively increased both pore size and sorption capacity leading to type IV isotherm. The interpretation of the effect of R and amount of aluminum addition on pore size and shape of water isotherms will be discussed.

S4.1

DIELECTRIC RELAXATION PROPERTIES AND ALIGNMENT BEHAVIOUR OF LIQUID-CRYSTALLINE SIDE-CHAIN POLYMERS. Graham Williams, University College of Swansea, U.K., and Frank E Karasz, University of Massachusetts, Amherst, Mass., U.S.A.

A prerequisite for the use of liquid-crystalline (LC) side-chain polymers as media for digital, analogue and holographic optical data storage, for optical elements (e.g. erasable Fresnel zone plates) or for non-linear optics (e.g. second harmonic generation) is that films should be prepared in well-defined and reproducible states of macroscopic alignment. It is also important to have available direct methods for determining the nature and extent of the alignment of a particular film.

We describe the alignment behaviour of films of different LC side-chain polymers when they are subjected to electrical/thermal treatments. The alignment properties are monitored quantitatively using dielectric relaxation spectroscopy (10-10⁵ Hz). Certain polymers may be aligned homeotropically, planarly, or to any intermediate degree of alignment, using low or high frequency electric fields applied to films in the LC state or to films being cooled from the melt. The rates of field-induced alignment and field-free disalignment are strong functions of the sample temperature and its history.

The dielectric relaxation spectra vary systematically with the degree of macroscopic alignment of the sample and its temperature. The anisotropic dielectric relaxation behaviour may be explained in terms of molecular theory which predicts four relaxation modes for the anisotropic motions of the dipolar mesogenic groups. The permittivity data allow the director order parameter S_d to be determined for a sample having a uniaxial macroscopic alignment between homeotropic and planar. The time dependence of S_d may be determined from the dielectric data as a sample is aligned in an electric field (or disaligns by thermal processes) and such data may be interpreted using macroscopic continuum theory for the LC phase.

S4.2

LIQUID CRYSTALLINE MATERIALS FOR POLYMERS WITH ANISOTROPIC ULTRASTRUCTURES. George S. Attard, Department of Chemistry, The University, Southampton SO9 5NH, U.K.

Liquid crystalline phases are anisotropic fluid phases characterised by long-range orientational order and often varying degrees of spatial order. Liquid crystalline materials are classified as being either *thermotropic* or *lyotropic* depending on whether the driving force for the formation of the ordered phases is thermal or solvent-induced self-organisation. The rich polymorphism of both thermotropic and lyotropic liquid crystals can be exploited to produce novel polymers with controlled ultrastructure.

Materials with anisotropic ultrastructures can be obtained by constructing polymers with anisometric groups in the main-chain, as pendant side-chains, or a combination of both. The advantage of this approach is that a number of chemically distinct species may be incorporated into a single polymer chain without the problems of immiscibility normally encountered in multi-component systems. Using this approach it is therefore possible to design multifunctional materials whose properties are optimised with respect to particular applications. Examples of high T_g photoactive LC side-chain polymers with potential as n.l.o. materials will be described. In practice, the main disadvantage of this approach is that only a small subset of the varied LC polymorphism can be accessed. In order to achieve greater control on the ultrastructure a different approach is required. This involves the use of polymerisable LC monomers whose mesomorphic structure, whether lyotropic or thermotropic, can be locked by *in situ* polymerisation. The choice of polymerisable unit which is incorporated into a mesogenic monomer is dictated by the energetics of the polymerisation process and the range of thermal stability of the mesophase whose structure is to be retained in the polymer. Using this route it is possible to prepare polymers with a range of anisotropic ultrastructures. Examples of such polymeric materials derived from thermotropic and lyotropic LC phases will be described.

S4.3

LIQUID CRYSTALS INCORPORATING METALL CENTRES
W. Haase, S. Gehring, and B. Borchers, Institut für Physikalische Chemie, Technische Hochschule, Petersenstr. 20, D-6100 Darmstadt, Federal Republic of Germany.

Transitionmetal containing liquid crystals with e.g. Cu(II) show interesting physical properties such as optical absorption, paramagnetism, or magnetic co-operative phenomena, as well as the well known liquid crystalline properties.

We report on the syntheses, thermal data, and optical microscopy of some new monomeric Cu(II)-mesogens. These compounds show a broad liquid crystalline phase range. The strategies for the design of polynuclear mesogens and possible application aspects as 'Molecular Ferromagnets' are discussed. First results of magnetic investigations on dimeric Cu(II)-systems will be reported.

S4.4

DIELECTRIC PROPERTIES OF POLYMERIC LIQUID CRYSTALS WITH STRONG LATERAL DIPOLE GROUPS. W. Haase and M. Pfeiffer, Institut für Physikalische Chemie, Technische Hochschule, Petersenstr. 20, D-6100 Darmstadt, Federal Republic of Germany.

Recently, we and other groups have described the molecular dynamics of a series of side chain liquid crystalline polymers using dielectric spectroscopy and switching time experiments.

Now we report on the properties of compounds with strong lateral dipole groups as fluorine or cyano. Their influences on the different molecular modes are evaluated and characterized. The side chains used were phenylbenzoates or cyclohexylcyclohexanes, the main chains were polymethacrylates.

S4.5

SYNTHESIS AND PROPERTIES OF COMB-LIKE LIQUID CRYSTALLINE POLYMERS WITH ELECTROOPTICALLY ACTIVE MESOGENIC SIDE GROUPS
M. Maeda, R.S. Kumar, A. Blumstein, S.K. Tripathy, University of Lowell, Lowell, MA 01854; P. Sixou*, F. Faubert*, Laboratoire de Physique de la Matière Condensée, Université de Nice, Nice, France.

In an attempt to synthesize side chain liquid crystalline polymers containing NLO active moieties a number of p-substituted aromatic azomethine phenols with acceptor-donor substituents such as Me, N, Me, RO, NC and NO₂ were prepared and incorporated into a polymer chain as side groups. Liquid crystalline properties of low molecular compounds composed of such moieties were explored separately and as mixtures. Phase diagrams were established. These intermediate compounds of the type MO(CH₂)_n-OH (where M represents the substituted mesogen) show themselves interesting mesomorphic properties.

Methacrylic esters with such moieties were also synthesized. Polymers and co-polymer systems with acceptor-donor substituents were obtained. The properties of such systems were studied by various techniques including D.S.C., polarizing microscopy and thermally stimulated currents.

S4.6

THERMOTROPIC CHIRAL NEMATIC POLYMERS AS OPTICAL MATERIALS.
M.L. Tsai and S.H. Chen, Department of Chemical Engineering and Laboratory for Laser Energetics, University of Rochester, Rochester, New York 14627.

Liquid crystalline polymers have been demonstrated to have the potential of contributing to new technologies that are superior to existing ones based on holographic gratings, multilayer thin film interference coatings and low molar mass liquid crystals. Unfortunately, there is a shortage of polymeric materials that possess the desired thermotropic and optical properties. The focus of this talk is on issues related to the structure-property relationships:

- (1) Handedness of the helical structures presented by side-chain polymers in relation to the structural characteristics of the pendant chiral moiety.
- (2) Dependence of the helical twisting power on the chemical structures of both the chiral and the nematogenic monomers to facilitate the selective reflection wavelength tuning via comonomer ratio.

New polymer structures based on chiral building blocks other than the commonly used cholesteryl derivatives will be presented to address the afore-mentioned issues and to furnish new materials with improved properties for practical applications.

S4.7

MULTI-LAYERS THIN FILMS OF ACETALIZED POLY(VINYL ALCOHOL) DERIVATIVES OBTAINED BY THE LB METHOD AND THEIR OPTO-ELECTRONIC PROPERTIES. Kiyoshi Oguchi, Yasuhiko Yokoh, Kohei Sanui, and Naoya Ogata, Department of Chemistry, Sophia University, Tokyo 102, JAPAN.

Acetalized poly(vinyl alcohol) (PVA) derived from PVA and various aldehydes could form a perfect monolayer by means of Langmuir-Blodgett method, when an amphiphilic group was incorporated into the acetal group. It was found that the monolayer of the acetalized PVA could be deposited onto both hydrophobic and hydrophilic substrates with a deposition ratio of 1.0 so that Y-type multi-layers were obtained.

Multi-layers of the acetalized PVA were easily cross-linked by electron-beam exposure and the sensitivity was dependent on the length of alkyl

group on acetal group. The cross-linking reaction occurred due to the ring-scission of the acetal group and the resolution of patterns was higher than the films obtained by spin-coating, presumably owing to good molecular packings.

Various non-linear optical elements were incorporated into the acetal groups of PVA and their NLO properties were investigated. When p-nitro aniline was incorporated into the acetalized PVA, the multi-layer film exhibited a good second harmonic generation (SHG) and a new type of SHG active polymer was obtained. Conformations of the acetalized PVA and opto-electrical properties were discussed in forcus of NLO properties.

S4.8

DIELECTRIC, TSC AND ELECTROMECHANICAL MEASUREMENTS ON SOME PROSPECTIVE N.L.O. POLYMERS. Prof. I.M. Ward, Dr. G.R. Davies and Mr. P.L. Carr, Physics Department, University of Leeds, U.K.

Films of various non-linear optic or electroactive polymers have been made by solvent casting, dip coating or melt pressing techniques and poled using contact or corona poling. Most of the materials studied are methacrylate backbones with various NLO mesogens in side chains. These have kindly been provided by Hoescht-Celanese.

Such films must be poled in order to display second order NLO activity or piezoelectricity. Developing optimum poling conditions can then require lengthy sample preparation and measurement procedures. We have shown, in collaboration with Hoescht-Celanese, that the pyroelectric coefficient correlates well with the Pockels coefficient. Since the pyroelectric coefficient can be measured simply and rapidly it is a useful guide to the efficiency of poling. We have therefore used this measurement to optimise poling conditions, compare different materials and to study the stability of the polarisation produced. Dielectric loss spectra and TSC have also been used to study the relaxations occurring in these materials.

When compared with guest-host systems such as MNA in PMMA, these materials prove harder to pole, more brittle to handle but more stable in retention of their polarisation. These features seem correlated with the virtual absence of the sub- T_g relaxations found in PMMA.

S4.9

SILICONE CONTAINING LIQUID CRYSTALLINE POLYURETHANES AND POLYESTER. Robert Kosfeld, Frank Braun, Lutz Willner, Michael Heß, University of Duisburg, Department of Physical Chemistry, D-4100 Duisburg, FRG.

The results of a study are presented, where the possibility of creating liquid crystalline polyurethanes has been checked. Different types of aromatic urethane-structures were tested in combination with siloxane containing spacer groups. They are compared with corresponding ester-structures. The influence of the structure of the urethane-containing mesogenic hard segment as well as the composition of the soft segment has been investigated with respect to their potential of creating mesomorphic behaviour.

S5.1

MICROSTRUCTURAL CONTROL IN SIDE CHAIN POLYMERS FOR OPTICAL APPLICATIONS. Tim Lemmon and Alan Windle, Department of Materials Science and Metallurgy, Cambridge University, Pembroke Street, Cambridge, CB2 3QZ, UK.

The exploitation of the various functionalities which can be designed into organic systems is frustrated by the readiness with which all but the smallest molecules segregate into different phases. Multiphase structures are

particularly deleterious where one or more of the functionalities is optically based. Molecular miscibility is forced on the system by attaching the different active groups to a common polymer backbone.

The principles of microstructural control in the systems have been explored using a series of polymers with methacrylate backbones and 4-oxy-4'-nitrobiphenyl or 4-oxy-4'-nitrostilbene active groups attached through n-alkyl flexible spacer sequences.¹

Side-chain polymers with flexible spacers of three (CH_2) spacers have glass transitions of the order of 105°C. This range encompasses that of PMMA (the backbone polymer) so it is not surprising that halving the level of side group substitution has little effect on the T_g . There is no evidence of liquid crystallinity in the three-unit spacer materials, although they are optically birefringent cast and rapidly cooled between glass slides. In this condition the optic axis is normal to the plane of the specimen.

Six-unit spacers in biphenyl samples lead to a T_g of the order of 50°C, and expose a smectic liquid crystalline phase which has an upper transition at 77°C. Slow cooling through the mesophase leads to a highly scattering and optically useless glass. In the range from 77°C to 110°C the samples are clear but birefringent, again with their optic axes normal to the plane of the glass substrate although there is evidence of optical biaxiality below 95°C. This optical anisotropy is the result of the aligning influence of the glass surfaces and can be preserved in a clear glass by a suitably fast quench.

¹ Synthesised by Hoechst-Celanese Laboratories, Summit, NJ

S5.2

ZEOLITE LOADED POLYURETHANE FOAMS FOR ENVIRONMENTAL CONTROL. C. B. Frost, D. L. Lindner, J. E. Costa, Sandia National Laboratories, Livermore CA.

Over the past five years a series of zeolite loaded polyurethane foams have been developed by Sandia National Laboratories. These foams have shown the ability to perform in both structural and thermal roles while retaining the zeolite's capacity to sorb low molecular weight gases, particularly water vapor. These materials can be processed to yield a wide variety of densities, zeolite concentrations and geometrical shapes and volumes. By utilizing these materials in multi-functional roles we have been able to increase flexibility in packaging and protection in a wide range of applications. For example, large structures of rigid polyurethane foams have been used to provide structural stiffening while controlling moisture levels in enclosed volumes. We have also been able to demonstrate that loaded polyurethane foams can be use for protective potting of electronic devices.

This presentation will explain material preparation, processing, and applications. The material's chemical, mechanical and physical properties have been examined with a number of techniques and the results will be presented.

S5.3

PERIODIC AREA MINIMIZATION SURFACES IN MICROSTRUCTURAL SCIENCE, Edwin L. Thomas, Department of Materials Science and Engineering, MIT, Cambridge, MA

An A/B block copolymer consists of two macromolecules bonded together. In forming an equilibrium structure, such a material may separate into distinct phases, creating domains of component A and component B. A dominant factor in the determination of the domain morphology is area-minimization of the intermaterial surface, subject to fixed volume fraction. Surfaces that satisfy this mathematical condition are said to have constant mean curvature. The geometry of such surfaces strongly influences physical properties of the material and they have been proposed as structural models

in a variety of physical and biological systems. We have discovered domain structures in phase-separated diblock copolymers that closely approximate periodic constant mean curvature surfaces. Transmission electron microscopy and computer-simulation are used to deduce the three-dimensional microstructure by comparison of tilt series with two-dimensional image projection simulations of 3D mathematical models. Three structures are discussed: the first of which is the double diamond microdomain morphology associated to a newly discovered family of triply periodic constant mean curvature surfaces. Second, a doubly periodic boundary between lamellar microdomains, corresponding, to a classically known surface (called Scherk's First Surface) is described. Finally, we show a lamellar morphology in thin films and is apparently related to a new family of periodic surfaces.

S5.4

BEHAVIOR OF SUPERCONDUCTING CERAMIC-POLYMER COMPOSITE. C. Vipulanandan and S. Salib, Texas Center for Superconductivity, University of Houston, Houston, Texas 77204-5506.

Growing large single crystals of the superconducting Yttrium-Barium-Copper oxide ($\text{YBa}_2\text{Cu}_3\text{O}_{7.5}$) phase is difficult and hence there is continuing interest in the fabrication of bulk components from sintered polycrystalline aggregates of this superconducting material. Aggregation of $\text{YBa}_2\text{Cu}_3\text{O}_{7.5}$ powder by compact molding and sintering results in a porous ceramic with poor mechanical properties and hence improving the ceramic properties is of interest.

The objectives of this study are to investigate the effect of porosity on the ceramic behavior and to improve the mechanical properties of the superconducting ceramic using poly(methyl methacrylate) (PMMA) polymer. Both 12.5-diameter disk and 60-mm-long beam specimens were prepared at various porosities by varying the uniaxial compaction pressure from 30 to 350 MPa. The calcined powder was compacted, sintered, and then allowed to cool at a slow rate. The polymer was impregnated into the ceramic at room temperature. The mechanical properties of the specimens were evaluated by concentrically loading simply supported disk and beam specimens. Performance of the ceramic-polymer composite was also evaluated by thermocycling between 77 K and 300 K.

Density-pressure relationship has been developed for the compacted superconducting ceramic. The effect of PMMA impregnation on the mechanical and electrical properties has been verified in terms of the porosity. Polymer impregnation had no measurable effect on the critical temperature and Meissner effect of the superconducting ceramic. Linear and nonlinear property-porosity relationships have been developed for the ceramic and ceramic-polymer composite.

S5.5

MICROSTRUCTURE OF PPTA/POLYPYRROLE COMPOSITE FIBERS. L.P. Rector, T.J. Marks, and S.B. Carr, Departments of Materials Science and Engineering and Chemistry and the Materials Research Center, Northwestern University, 2145 Sheridan Road, Evanston, IL 60208.

Multifunctional fibers, exhibiting both excellent mechanical properties and electrical conductivity, have been prepared by combining poly(p-phenylene terephthalamide) (PPTA) and polypyrrole. A novel processing technique involving electropolymerization of pyrrole within a swollen PPTA fiber was employed. The electropolymerization occurs with a simultaneous collapse of the swollen fiber to produce a composite material with dispersed domains of the conductive phase. Continued electropolymerization produces an annular ring of polypyrrole on the fiber exterior, in analogy with previously reported work. Observations of the microstructure of these composite fibers by transmission

electron microscopy will be reported.

1 Gregory, R.V., Kimbrell, W.C., Kuhn, H.R., *Syn. Met.* 28, C823 (1989)

S5.6

THEORY AND PRACTICE IN THE PREPARATION OF MULTIFUNCTIONAL MATERIALS CONTAINING DELOCALIZED π -ELECTRONS. Larry R. Dalton, Rahel Vac, LuPing Yu, and Linda Sapochak, Department of Chemistry, University of Southern California, Los Angeles, CA 90089-0482.

Strong interchain polymer interactions are normally encountered for systems containing delocalized π -electrons. These interactions greatly reduce solubility with the result that polymers are difficult to prepare in high molecular weights and difficult to process into desired forms. Many types of functionality including nonlinear optical activity, electrical conductivity, high structural strength are incompatible with such limitations on polymer synthesis and processing. In this presentation we discuss general schemes for avoiding the problem of insolubility associated with traditional electroactive polymers. These methods are then used to prepare a variety of new electroactive polymers incorporating polyene and heteroaromatic structures. These polymers are then characterized and electroactivity properties are investigated for neutral, oxidized and reduced states of the polymers. The role of symmetry and the effects of substituents upon electroactivity is clarified. Finally, the discussion of homo and copolymer systems is extended to the consideration of composite systems.

S5.7

MICROPHASE SEPARATION IN MULTIBLOCK COPOLYMER MELTS. Anne M. Mayes and Monica Olvera de la Cruz, Department of Materials Science and Engineering, Northwestern University, Evanston, IL 60208.

Block copolymers undergo disorder-order transitions to periodic ordered structures, termed microphases, upon cooling. The microphase separation transition for triblock and star copolymer melts is investigated following a mean field approach proposed by Leibler for diblock copolymers. Continuous transitions are found in both systems at some composition f_{c} . In triblock melts three microphase morphologies are predicted - alternating lamellar structures, hexagonally packed cylinders, and bcc spheres. The windows of stability for the equilibrium morphologies are notably altered by varying the triblock architecture. In particular, some triblock systems have wide regions of stability for bcc structures with large spherical domains, suggesting improved mechanical properties. Corrections to the phase diagram when concentration fluctuations are included will be discussed.

S5.8

SEGMENTED ANISOTROPIC ISOTROPIC POLY ARYL ESTER POLY(ARYLENE ETHER) COPOLYMER MATERIALS. J.E. McGrath, K.L. Cooper, W. Waihamad, H. Huang, D. Chen and G.L. Wilkes, Departments of Chemistry and Chemical Engineering, National Science Foundation Science and Technology Center: High Performance Polymeric Adhesives and Composites, Virginia Polytechnic Institute and State University, Blacksburg, VA 24061.

Techniques have been refined for the synthesis of acetoxy or carboxy poly(arylene ether) systems which can be efficiently utilized as isotropic segment components in anisotropic-isotropic poly(arylate)-poly(ether) systems. The resulting materials allow for the introduction of either modest concentrations of liquid crystal structures which alter solvent resistance in the isotropic phase or for modest concentration of a segmented isotropic phase which permits improvements in the mechanical ductility under transverse conditions. The chemistry and morphological investigations

which have permitted these conclusions will be discussed along with preliminary mechanical properties.

S5.9

INORGANIC AND ORGANOMETALLIC PRINCIPLES IN THE DESIGN OF MULTIFUNCTIONAL MATERIALS. D. Michael P. Mingos, Inorganic Chemistry Laboratory, University of Oxford, South Parks Road, Oxford OX1 3QR, U.K..

The prospects of using the properties of inorganic solids with infinite structures in combination with the spectral, magnetic and chemical characteristics of co-ordination and organometallic compounds will be reviewed with particular reference to their potential applications in the electronics, sensors and optoelectronic fields.

Solid state inorganic chemistry provides a great variety of thermally stable and optically transparent host materials which have sufficiently large cavities for the incorporation of small molecules. These include zeolites with either spherical or cylindrical three dimensional cavities, layered compounds with infinite two-dimensional spaces and a variable third dimension, and pillared materials with intersecting one-dimensional channels. These structures may be chosen on the basis of a particular function and a second introduced via the incorporation of molecules in the cavities. Alternatively, they may be viewed as neutral structural materials and the multifunctionality can be introduced via the incorporation of molecules with different spectral or chemical properties.

As guest materials co-ordination and organometallic compounds have the following properties which are important in the context of multifunctionality : the ability to co-ordinate small molecules such as O_2 , SO_2 , H_2 reversibly, distinct reversible electrochemical properties, electronic transitions which show an enormous variation in extinction coefficients and oscillator strengths, polarised spectral transition and electrical conductivity properties.

S5.10

MODELLING MICROSTRUCTURE IN MATERIALS THAT CONTAIN ANISOTROPIC PARTICLES. Christopher Viney, Department of Materials Science and Engineering, University of Washington, Seattle, WA 98195; and Larry A. Chick, Battelle Pacific Northwest Laboratory, P.O. Box 999, Richland, WA 99352.

A thermodynamic analysis was developed by Flory to predict liquid crystalline phase separation in solutions of rod-like molecules. We have adapted this approach to model the formation of clusters in rigid-rod reinforced composites, initially for athermal behavior. In Flory's work, the necessary quantification of configurational entropy is obtained from a lattice model.

Our method uses a Monte Carlo simulation to calculate entropy, providing some significant advantages relative to the lattice model. Firstly, a number of approximations are eliminated from the calculations. Secondly, we are able to draw pictures of microstructures that are generated by random placement of rods, and so obtain a measure of the minimum domain (cluster) size as well as the minimum degree of order within domains. Given sufficient microstructural mobility (represented by simulated annealing), we expect coarsening of domain size and an increase in perfection of alignment to occur, towards the monodomain microstructure implicit to Flory's model. The average number of configurations that must be explored in order to achieve a given degree of coarsening can be related to coarsening times in real microstructures.

When extended to include "soft" interactions between rods, our studies will enable prediction of microstructure in a

variety of systems that contain rod-like structures. In liquid crystalline materials alone, this should facilitate control of non-linear optical properties, mechanical properties, and electrical conductivity.

SYMPOSIUM T: FRACTAL ASPECTS OF MATERIALS



November 28 - December 1, 1989

Chairs

J. H. Kaufman
IBM T.J. Watson Research Center
Room 13-105
P.O. Box 218
Yorktown Heights, NY 10598
(914) 945-1328

P. W. Schmidt
Physics Department
223 Physics Building
University of Missouri, Columbia
Columbia, MO 65211
(314) 882-8241

James E. Martin
Division 1152
Sandia National Laboratories
P.O. Box 5800
Albuquerque, NM 87185
(505) 844-9125

Symposium Support

Army Research Office

Cabot Corporation

E. I. duPont de Nemours & Company, Inc.

Exxon Research and Engineering Company

Ford Motor Company

IBM Corporation

Office of Naval Research

Schlumberger - Doll Research

**Extended Abstract Volume EA-20
published by the Materials Research Society.**

FRactal Aspects of Materials

November 28 - December 1, 1989

SESSION T1: PATTERN FORMATION AND GROWTH

Chair: B. Mandelbrot

Tuesday Morning, November 28
Staffordshire Room (W)

8:30 *T1.1

BREATH FIGURES: DROPLET CONDENSATION PATTERNS ON SURFACES, Charles M. Knobler, University of California, Los Angeles, Department of Chemistry and Biochemistry, Los Angeles, CA.

9:00 *T1.2

SELF-ORGANIZED CRITICALITY AND AVALANCHE DYNAMICS IN A DROPLET GROWTH MODEL WITH SLIDING, Fereydoon Family, Emory University, Department of Physics, Atlanta, GA.

9:30 *T1.3

FRACTALS AND NUCLEATION, W. Klein, Boston University, Physics Department, Boston, MA.

10:00 BREAK

10:30 T1.4

KINETICS OF SPINODAL DECOMPOSITION IN A POLYMER SOLUTION, R. Bansil and J. Lal, Boston University, Boston, MA.

10:45 T1.5

FRactal DIMENSIONS IN QUASICRYSTAL GROWTH MODEL, Z.M. Wang, York University, Physics Department, Ontario, Canada, and Chinese Academy of Sciences, Beijing, China; and K.Y. Szeto, York University, Physics Department, Ontario, Canada.

11:00 T1.6

PARTICLE-CLUSTER GROWTH OF AGGREGATES AT AN INTERFACE, C. Allain, M. Cloitre, Campus Universitaire, Lab FAST, Orsay, France.

11:15 T1.7

STATISTICAL PROPERTIES OF GENERALIZED AGGREGATION SYSTEM WITH INJECTION, H. Takayasu, Boston University, Department of Physics, Boston, MA; and Kobe University, Earth Science, Kobe, Japan.

*Invited Paper

Short Course C-09, "Fractals: Concepts and Applications in Materials Science and Engineering," may be of interest to symposium attendees. Details regarding course dates and instructors are provided in the short course section of this program.

11:30 T1.8

TWO-STAGE AGGREGATION OF A NON-AQUEOUS GOLD COLLOID, B.J. Oliver and C.M. Sorensen, Kansas State University, Department of Physics, Manhattan, KS; E.B. Zuckerman and K.J. Klabunde, Kansas State University, Department of Chemistry, Manhattan, KS.

SESSION T2: FRACTAL MEASURES AND PATTERN FORMATION II

Chair: Farid Abraham

Tuesday Afternoon, November 28
Staffordshire (W)

1:30 *T2.1

FRactal MEASURES OF POROUS MEDIA, Claude Tricot, École Polytechnique, Department of Applied Mathematics, Montreal, Canada.

2:00 T2.2

A LOCAL PERTURBATION NOTION APPLIED TO ROUGH SURFACE ANALYSIS, D. Wehbi, J.F. Quiniou, C. Roques-Carmes, ENSM-LMS, Besancon, France; and C. Tricot, École Polytechnique de Montréal, Montreal, Canada.

2:30 T2.3

ELECTROMAGNETIC AND OPTICAL WAVE SCATTERING FROM FRACTAL OBJECTS, Xiaoguang Sun and Dwight L. Jaggard, University of Pennsylvania, Moore School of Electrical Engineering, Philadelphia, PA.

3:00 BREAK

3:30 *T2.4

EVIDENCE OF CRITICAL BEHAVIOR IN A RANDOM FRACTAL AUTOMATION, G.M. Dimino, University of California at Santa Cruz, Physics Board of Studies, Santa Cruz, CA; and J.H. Kaufman, IBM Almaden Research Center, IBM Research Division, San Jose, CA.

4:00 T2.5

INFORMATION DIMENSION AS A MEASURE OF FRACTAL DISORDER, Panos Argyrakis, IBM Corporation, Scientific Engineering Computations, Kingston, NY.

4:30 T2.6

RANDOM WALK SIMULATION OF SOLVABILITY THEORY FOR THE SAFFMAN-TAYLOR PROBLEM, D.C. Hong, Lehigh University, Physics Department and Center for Polymer Science and Engineering, Bethlehem, PA; and H. Guo, McGill University, Physics Department, Quebec, Canada.

SESSION T3: FRACTURE

Chair: Paul Meakin
Wednesday Morning, November 29
Staffordshire (W)

8:30 T3.1

FLUCTUATIONS IN PHOTON EMISSION DURING EPOXY FRACTURE: EVIDENCE FOR CHAOS, Zhenyi Ma, J.T. Dickinson, and S.C. Langford, Washington State University, Department of Physics, Pullman, WA.

9:00 T3.2

FRACTURE AS A FRACTAL PROCESS: THEORY & EXPERIMENT, T.J. Mackin, J.J. Mecholsky Jr. and D.E. Passoja, The Pennsylvania State University, University Park, PA.

9:30 T3.3

STRUCTURE ANALYSIS OF FRACTURE SURFACES USING SCANNING TUNNELING MICROSCOPY, D.A. Bonnell and M.W. Mitchell, The University of Pennsylvania, Materials Science Department, Philadelphia, PA.

10:00 BREAK

10:15 T3.4

FRACTAL EFFECTS AND PERCOLATION OF MATERIAL FRACTURE, Dengshi Huang, Sichuan Economic Management College, Department of Basic Science, Chendu, China.

10:30 T3.5

FRACTAL NATURE OF FRACTURE SURFACE, Gongwen Peng and Decheng Tian, Wuhan University, Physics Department, Wuhan, China.

10:45 T3.6

PERCOLATION PROPERTIES OF RANDOM TWO-DIMENSIONAL POISSON FRACTURE NETWORKS, Kunal Ghosh, Jackson State University, Jackson, MS; Kevin Hestir, New Mexico State University, Las Cruces, NM; and Jane Long, Lawrence Berkeley Laboratory, Berkeley, CA.

11:00 T3.7

THE FRACTAL NATURE OF THE CRAZE PATTERN DEVELOPED IN MODE I FRACTURE OF POLYMERIC MATERIALS, Yuhong Ni and J.C.M. Li, University of Rochester, Materials Science Program, Mechanical Engineering Department, Rochester, NY.

11:15 T3.8

WEIBULL PLOTTING OF A FRACTAL DISTRIBUTION OF FLAWS, John F. Wight and James W. Laughner, Alfred University, New York State College of Ceramics, Ceramic Engineering Department, Alfred, NY.

11:30 T3.9

APPLICATION OF FRACTAL GEOMETRY TO DAMAGE MODELING IN ADVANCED MATERIALS, Ted L. Anderson, Texas A&M University, Department of Mechanical Engineering, College Station, TX.

JOINT SESSION T4/U10: SIZING AND SCALING EFFECTS

Chair: Bill Klein
Wednesday Afternoon, November 29
America North (W)

1:30 *T4.1/U10.1

FRACTAL STRUCTURE AND DYNAMICS OF TWO FLUID FLOW IN POROUS MEDIA, Jens Feder, University of Oslo, Department of Physics, Oslo, Norway.

2:00 T4.2/U10.2

NUMERICAL AND ANALYTICAL MODELS OF TRANSPORT IN POROUS CEMENTITIOUS MATERIALS, Edward J. Garboczi and Dale P. Bentz, National Institute of Standards and Technology, Building Materials Division, Gaithersburg, MD.

2:15 T4.3/U10.3

SIZING REQUIREMENTS FOR FLOW-THROUGH GEOCHEMICAL TESTS: THEORETICAL CONSIDERATIONS, MODEL RESULTS, AND IMPLICATIONS FOR THE INTERPRETATION OF TEST DATA, J.D. Hoover and E.C. Thornton, Westinghouse Hanford Company, Richland, WA.

2:45 T4.4/U10.4

A LAGRANGIAN REACTIVE TRANSPORT SIMULATOR WITH MULTIPLE PATHS AND STATIONARY-STATES: CONCEPTS, IMPLEMENTATION AND VERIFICATION, R.B. Knapp, University of California, Lawrence Livermore National Laboratory, Earth Sciences Department, Livermore, CA.

3:00 BREAK

3:30 *T4.5/U10.5

FRACTAL CHARACTERISTICS OF FRACTURE NETWORKS AND FLUID MOVEMENT IN ROCK, Christopher C. Barton, U.S. Geological Survey, Department MS 913, Denver, CO.

4:00 T4.6/U10.6

FLOW TO WELLS IN FRACTURED ROCK WITH FRACTAL STRUCTURE, Jim Poley, Kenzi Karasaki and Jane Long, Lawrence Berkeley Laboratory, Berkeley, CA; and John Barker, British Geological Survey, Oxfordshire, United Kingdom.

4:15 T4.7/U10.7

ANISOTROPIC SCALING OF INTERFACES IN POROUS MEDIA, Miguel A. Rubio, Haverford College, Department of Physics, Haverford, PA, and UNED, Madrid, Spain; Andrew Dougherty, Haverford College, Department of Physics, Haverford, PA; and Jerry P. Gollub, Haverford College, Department of Physics, Haverford, PA; and University of Pennsylvania, Philadelphia, PA.

4:30 T4.8/U10.8

SIZING AND SCALING REQUIREMENTS OF A LARGE-SCALE PHYSICAL MODEL FOR CODE VALIDATION, R. Khaleel, T. LeGore and J.D. Hoover, Westinghouse Hanford Company, Richland, WA.

4:45 T4.9/10.9

PERFORMANCE OF CONCRETE BARRIERS IN RADIOACTIVE WASTE DISPOSAL IN THE UNSATURATED ZONE, John C. Walton and Mark D. Otis, Idaho National Engineering Laboratory, Idaho Falls, Idaho.

SESSION T5: SURFACES I

Chair: A. Hurd

Thursday Morning, November 30
Staffordshire (W)

8:30 *T5.1

CAPILLARY CONDENSATION ON FRACTAL SURFACES, P. Pfeifer, J. Kenntner, University of Missouri, Physics Department, Columbia, MO; and M.W. Cole, Pennsylvania State University, Physics Department, University Park, PA.

9:00 T5.2

CHARACTERIZATION OF THE SURFACE FRACTAL DIMENSION AND ROUGHNESS OF EVAPORATED SILVER FILMS VIA ADSORPTION ISOTHERM MEASUREMENTS, J. Krim, V. Panella, and A. Sarkissian, Northeastern University, Physics Department, Boston, MA.

9:30 T5.3

HYDROGEN, NEON AND NITROGEN ADSORPTION ISOTHERMS ON POROUS VYCOR GLASS, T.E. Huber, Harvard University, Department of Physics, Cambridge, MA; and C.A. Huber, University of Puerto Rico, Rio Piedros, Puerto Rico.

10:00 BREAK

10:30 T5.4

(ABSTRACT WITHDRAWN)

11:00 T5.5

SMALL ANGLE X-RAY SCATTERING APPLIED TO INVESTIGATE THE FRACTAL PROPERTIES OF COAL AND OTHER POROUS CARBON-BASED MATERIALS, M. Reich, S. Russo, I.K. Snook, and H.K. Wagenfeld, Royal Melbourne Institute of Technology, Melbourne, Australia.

11:30 T5.6

SMALL ANGLE X-RAY AND NEUTRON SCATTERING FROM A FRACTAL DIFFUSION FRONT, Michel Rosso and Bernard Sapoval, Laboratoire de Physique de la Matière Condensée, Ecole Polytechnique, Palaiseau, France.

SESSION T6: SURFACES II

Chair: Jackie Krim

Thursday Afternoon, November 30
Staffordshire (W)

1:30 *T6.1

THE GROWTH OF SELF-AFFINE FRACTAL SURFACES, Paul Meakin, E. I. duPont de Nemours & Co., Inc., Central Research and Development, Wilmington, DE.

2:00 T6.2

PATTERN FORMATION AND CHARACTERIZATION FOR BIOLOGICAL MATERIALS, Charles Thompson and Kavita Chandra, University of Lowell, Laboratory for Advanced Computation, Department of Electrical Engineering, Lowell, MA.

2:30 T6.3

VISCOUS FINGERING EXPERIMENT WITH PERIODIC BOUNDARY CONDITIONS, J.V. Maher and Hong Zhao, Department of Physics and Astronomy, University of Pittsburgh, Pittsburgh, PA.

3:00 BREAK

3:30 T6.4

FRACTAL DIMENSION OF NATURAL POLYMERS, Louis Discitelle and Ronald Segars, U.S. Army Natick Research, Development and Engineering Center, Department STRNC-UE, Natick, MA.

4:00 T6.5

FRACTAL VS. SUB-FRACTAL: CLOUD RADIANCE AND OCEAN SURFACE DATA, Patricia H. Carter and Robert Cawley, U.S. Department of the Navy, Naval Surface Warfare Center, Silver Spring, MD.

4:30 T6.6

FRACTAL CHARACTERIZATION OF POROUS SILICA GELS BY GPC, Houqiang Li, Ying Li and Huaming Zhao, Sichuan University, Department of Chemistry, Chengdu, China.

SESSION T7: POSTER SESSION

Chair: V. Castano
Thursday Evening, November 30
7:00 p.m. - 10 p.m.
America Ballroom (W)

T7.1 A NEW TECHNIQUE TO DIFFERENTIATE BETWEEN GEMINATE AND NONGEMINATE RECOMBINATION OF EXCITONS IN DISORDERED MEDIA, Jagdish Prasad and Raoul Kopelman, The University of Michigan, Department of Chemistry, Ann Arbor, MI.

T7.2 STEADY-STATE REACTIONS ON FRACTALS: RATE LAWS AND SELF-ORGANIZATION, Eric Clement and Raoul Kopelman, The University of Michigan, Department of Chemistry, Ann Arbor, MI; and Leonard M. Sander, The University of Michigan, Department of Physics, Ann Arbor, MI.

T7.3 EXCITATION TIME MODULATION STUDIES OF MOLECULAR AGGREGATES IN DOPED POLYMERS, Zhong-You Shi, Irene E. Newhouse and Raoul Kopelman, The University of Michigan, Department of Chemistry, Ann Arbor, MI.

T7.4 PULSED VS. STEADY-STATE EXCITON RECOMBINATION KINETICS: EXPERIMENTS AND SIMULATIONS ON PORES, POWDERS AND RANDOM MEDIA, Stephen J. Parus, Zhong-You Shi and Raoul Kopelman, The University of Michigan, Department of Chemistry, Ann Arbor, MI.

T7.5 REACTANT TRAPPING AND STEADY-STATE SELF-ORDERING ON FRACTALS, Lola W. Anacker and Raoul Kopelman, The University of Michigan, Department of Chemistry, Ann Arbor, MI.

T7.6 HYDRODYNAMIC INSTABILITY IN CRYSTAL MELTS, Charles Thompson and Vineet Mehta, University of Lowell, Laboratory of Advanced Computation, Department of Electrical Engineering, Lowell, MA.

T7.7 GROWTH KINETICS IN A COAGULATION--FRAGMENTATION SYSTEM, Iman. M. Elminyami and C.M. Sorensen, Kansas State University, Department of Physics, Manhattan, KS.

T7.8 ROLE OF AGGREGATION IN THE FORMATION OF COLLOIDAL GOLD PARTICLES, Jun Liu, M. Sarikaya, W.Y. Shih, W.H. Shih, and I.A. Aksay, University of Washington, Washington Technology Center, Department of Materials Science and Engineering and Advanced Materials Program, Seattle, WA.

T7.9 THE EFFECT OF AGGREGATION ON COLLOID CATALYSTS, J.R. Melrose, Imperial College, The Blackett Laboratory, London, United Kingdom.

T7.10 MULTIPLE SCATTERING IN POWER-LAW CORRELATED MEDIA, J.R. Melrose, D. Sherrington, Imperial College, The Blackett Laboratory, London, United Kingdom; S. Sarker, RSRE, Worcester, United Kingdom.

T7.11 SMALL-ANGLE X-RAY SCATTERING STUDIES OF BONE POROSITY, Paul W. Schmidt, University of Missouri, Physics Department, Columbia, MO; David Avnir, The Hebrew University of Jerusalem, Department of Organic Chemistry, Jerusalem, Israel; A. Bivas, A. Weinreb, Hebrew University, Department of Physics, Jerusalem, Israel; Armin Röhl and David Nelson, University of Missouri, Physics Department, Columbia, MO.

T7.12 SMALL-ANGLE X-RAY SCATTERING FROM THE SURFACES OF REVERSED-PHASE SILICAS: POWER-LAW-SCATTERING EXPONENTS OF MAGNITUDES GREATER THAN FOUR, Paul W. Schmidt, University of Missouri, Physics Department, Columbia, MO; David Levy, The Hebrew University of Jerusalem, Department of Organic Chemistry, Jerusalem, Israel; Axel Höhr, University of Missouri, Physics Department, Columbia, MO; and David Avnir, The Hebrew University of Jerusalem, Department of Organic Chemistry, Jerusalem, Israel.

T7.13 FRACTAL DEGRADATION OF RADIATED MACROMOLECULES, Houqiang Li, Ying Li and Huaming Zhao, Sichuan University, Department of Chemistry, Chengdu, China.

T7.14 MULTIFRACTAL FEATURES OF THE FRACTAL AGGREGATES AT DIFFERENT STAGES, L.J. Huang, Tsinghua University, Department of Materials Science and Engineering, Beijing, China; B.X. Liu, Tsinghua University, Center of Condensed Matter and Radiation Physics, CCAST (World Lab), Department of Materials Science and Engineering, Beijing, China; J.R. Ding and H-D. Li, Tsinghua University, Department of Materials Science and Engineering, Beijing, China.

T7.15 COMPOSED RECURRANT SETS, Wen Zhi Ying, Li Jia Nong and Wang Han Fei, Wuhan University, Department of Mathematics, Wuhan, China.

T7.16 VISCOUS FINGERING ON 2D LATTICE MODELS NEAR THE PERCOLATION THRESHOLD, U. Oxaal, F. Boger, J. Feder and T. Jøssang, University of Oslo, Department of Physics, Oslo, Norway.

T7.17 THE FRACTAL DIMENSION OF PERCOLATION CLUSTERS, H.C. Akueze, and J. Stringer, Electric Power Research Institute, Palo Alto, CA.

T7.18 FRACTALS AND DIFFUSION PROCESSES, Hanna Nencka, Jarocin Pozn., Poland.

T7.19 LACUNARITY OF FRACTAL AGGREGATES, C. Allain and M. Cloitre, Campus Universitaire, Lab FAST, Orsay, France.

T7.20 LINEAR CORRELATION OF FRACTAL DIMENSION VERSUS MAGNETIC INTERACTION, B.X. Liu, Tsinghua University, Center of Condensed Matter and Radiation Physics, CCAST (World Lab), Department of Materials Science and Engineering, Beijing, China; and J.R. Ding, Tsinghua University, Department of Materials Science and Engineering, Beijing, China.

T7.21 FRACTAL MAGNETIZATION ON HIERARCHICAL LATTICES, W.A.M. Morgado, S. Coutinho and E.M.F. Curado, Centro Brasileiro de Pesquisas Físicas, Rio De Janeiro, Brazil.

T7.22 DYNAMIC PROPERTIES OF SOL-GELS, J.E. Martin and D. Adolf, Sandia National Laboratories, Albuquerque, NM.

T7.23 WAVELET TRANSFORMATION OF FRACTALS OBSERVED IN THIN SOLID FILMS, J.R. Ding and L.J. Huang, Tsinghua University, Department of Materials Science and Engineering, Beijing, China; and B.X. Liu, Tsinghua University, Center of Condensed Matter and Radiation Physics, CCAST (World Lab), Department of Materials Science and Engineering, Beijing, China.

T7.24 ANALYTICAL EXPRESSIONS FOR THE PERMEABILITY OF RANDOM TWO-DIMENSIONAL POISSON FRACTURE NETWORKS, Kevin Hestir, New Mexico State University, Las Cruces, NM; Jane Long, Lawrence Berkeley Laboratory, Earth Sciences Division, Berkeley, CA; and Kunal Ghosh, Jackson State University, Jackson, MS.

T7.25 FRACTAL ASPECTS OF HYDROGENATED AMORPHOUS AND MICROCRYSTALLINE SILICON, R.C. van Oort, J.C. van den Heuvel, M.J. Geerts, Delft University of Technology, Faculty of Electrical Engineering, Delft, The Netherlands.

T7.26 CHAIN COFORMATION OF IONOMERS IN A NON-POLAR SOLVENT, D.C. Hong, Lehigh University, Physics Department and Center for Polymer Science and Engineering, Bethlehem, PA.

T7.27 THE DIFFUSION COEFFICIENT OF A REPTATING POLYMER, J.M. Deutsch and T.L. Madden, University of California at Santa Cruz, Department of Physics, Santa Cruz, CA.

T7.28 DIFFUSION OF LINEAR POLYMERS IN GELS, S. Pajevic, R. Bensil, and C. Koňák, Boston University, Boston, MA.

T7.29 SYNERGETICS PARADIGM & DICHOTOMY AS A SPECIAL CASE OF MODERN THEORY OF CRITICAL PHENOMENA: FRACTAL-GEOMETRY = SCALE-INVARIANCE, Edward Siegel, Synergetics Paradigm and Dichotomy, San Francisco, CA.

T7.30 AUTOMATIC MATHEMATICAL CATASTROPHE ("AUTMATHCAT") AT EVEN INTEGER CRITICAL-DIMENSIONS $D=d_c^{st}=(1+1)=2$ & $D=d_c^{st}=(3+1)=4$ SUPERUNIVERSALITY IN MATHEMATICS DOMINATING PHYSICS, Edward Siegel, Synergetics Paradigm and Dichotomy, San Francisco, CA.

T7.31 SYNERGETICS PARADIGM & DICHOTOMY: SELF-ORGANIZED-CRITICALITY, AUTOMATIC MATHEMATICAL CATASTROPHES ("AUTMATHCATS"), MODERN THEORY OF CRITICAL PHENOMENA, INFINITE CONDUCTANCE FLUCTUATIONS, FRACTAL-CRYPTOGRAPHY, -LITHOGRAPHY, -FILIMENTATION-SUPERCONDUCTIVITY: SUPERUNIVERSALITY CLASS & CROSSOVER VIA DIMENSIONALITY UNCERTAINTY FLUCTUATION: FRACTAL-DIFFRACTAL CALCULUS, Edward Siegel, Synergetics Paradigm & Dichotomy, San Francisco, CA.

T7.32 SUPERUNIVERSALITY CLASS & CROSSOVER OF SYNERGETICS PARADIGM & DICHOTOMY MANIFESTATION OF CONSEQUENCES OF SCALE-INVARIANCE (=FRACTAL-GEOMETRY) THROUGHOUT PHYSICS DOMINATING PHYSICS, Edward Siegel, Synergetics Paradigm & Dichotomy, San Francisco, CA.

T7.33 DIMENSIONAL-CALCULUS OF DIMENSION-THEORY IMPLEMENTATION OF SYNERGETICS PARADIGM & DICHOTOMY "COMMON FUNCTIONING PRINCIPLE" PARSIMONY-OF-DICHOTOMY DOMINATION OVER SPECIFICITY-OF-COMPLEXITY, Edward Siegel, Synergetics Paradigm and Dichotomy, San Francisco, CA.

T7.34 FORMATION OF FRACTAL PATTERNS OF MoO_3-x CRYSTALS DURING PHASE TRANSFORMATION, Jizhong Zhang, Tsinghua University, Department of Materials Science and Engineering, Beijing, China.

T7.35 MULTIFRACTAL POROUS ROCK, J. Muller, J.L. McCauley, J.P. Hansen and A.T. Skjeltorp, Institute for Energy Technology, Kjeller, Norway.

T7.36 CHARACTERIZATION OF THE MECHANICAL FAILURE SURFACES OF ENERGETIC MATERIALS BY POWER SPECTRAL TECHNIQUES, M. Yvonne D. Lanzerotti, James J. Pinto, U.S. Army ARDEC, Picatinny Arsenal, NJ; and A. Wolfe, New York City Technical College, Brooklyn, NY.

SESSION T8: GELATION

Chair: D. Adolf
Friday Morning, December 1
Staffordshire (W)

8:30 *T8.1

BROWNIAN DYNAMICS OF BRANCHED POLYMERS, M.E. Cates, Cavendish Laboratory, Cambridge, United Kingdom.

9:00 T8.2

STATIC AND DYNAMIC PROPERTIES OF CONCENTRATED SOLUTIONS OF BRANCHED POLYMERS ELABORATED NEAR GELATION THRESHOLD, M. Delsanti, M. Adam, Service de Physique du Solide et de Résonance Magnétique, Gif-sur-Yvette, France; J.P. Munch, Université Louis-Pasteur, Laboratoire de Spectrométrie et d'Imagerie Ultrasonores, Strasbourg, France and Service de Physique du Solide et de Résonance Magnétique, Gif-sur-Yvette, France; and D. Durand, Université du Maine, Laboratoire de Chimie et Physico-Chimie Macromoléculaire, Le Mans, France.

9:30 *T8.3

DYNAMICS OF POLYMER GELATION, Michael Rubinstein, Eastman Kodak Company, Corporate Research Laboratories, Rochester, NY.

10:00 BREAK

10:30 T8.4

KINETIC GELATION IN SYSTEMS WITH AGGREGATION, BREAKUP, AND FLOW, R. Dennis Vigil and Robert M. Ziff, University of Michigan, Department of Chemical Engineering, Ann Arbor, MI.

11:00 T8.5

ELASTIC PROPERTIES OF COLLOIDAL GELS, W.H. Shih, J. Liu, W.Y. Shih, M. Sarikaya and I.A. Aksay, University of Washington, Washington Technology Center, Department of Materials Science and Engineering and Advanced Materials Technology Program, Seattle, WA.

11:15 T8.6

BRILLOUIN AND RAMAN SCATTERING FROM FRACTAL MATERIALS, J.L. Stehle, and P. Evrard, SOPRA, Bois-Colombes, France; V. Mazzacurati, Università degli Studi di Roma, Roma, Italy; G. Ruocco, Università degli Studi di L'Aquila, L'Aquila, Italy; and J.N. Willis and L.C. Hammond, ARIES/QEI, Concord, MA.

11:30 T8.7

MULTIFRACTAL STRUCTURE OF POLYMER-MODIFIED CEMENT PASTES, V.M. Castaño, UNAM, Instituto de Física, México, México; and P.W. Schmidt, University of Missouri, Physics Department, Columbia, MO.

SESSION T9: DLA, ELECTRODEPOSITION KINETICS

Chair: H.E. Stanley
Friday Afternoon, December 1
Staffordshire (W)

1:30 *T9.1

FIXED SCALE TRANSFORMATION APPROACH TO THE DIELECTRIC BREAKDOWN MODEL, L. Pietronero, Università di Roma, Roma, Italy; A. Erzan, University of Groningen, Groningen, The Netherlands; and Carl Everts, Yale University, New Haven, CT.

2:00 *T9.2

GEOMETRICAL MULTIFRACTALITY OF DIFFUSION LIMITED AGGREGATES, Tamas Vicsek, Emory University, Department of Physics, Atlanta, GA, and Institute for Techni Physics, Budapest, Hungary; Fereydoon Family, Emory University, Department of Physics, Atlanta, GA; and Paul Meakin, E.I. duPont de Nemours & Co., Inc., Wilmington, DE.

2:30 T9.3

ON THE MORPHOLOGY OF COPPER ELECTRODEPOSITS, J.R. Melrose, Imperial College, The Blackett Laboratory, London, United Kingdom; D.B. Hibbert, University of New South Wales, The Department of Analytical Chemistry, Sydney, Australia.

3:00 BREAK

3:15 T9.4

RANDOM WALKS AND THE DOUBLE LAYER IMPEDANCE, Thomas C. Halsey and Michael W. Leibig, The James Franck Institute and The University of Chicago, Department of Physics, Chicago, IL.

3:30 T9.5

BROWNIAN TRAIL RECTIFIED, Alan J. Hurd and Pauline Ho, Sandia National Laboratories, Albuquerque, NM.

3:45 T9.6

EQUILIBRIUM SIZE AND SHAPE OF RANDOM AGGREGATES, H.C. Akueze, and J. Stringer, Electric Power Research Institute, Palo Alto, CA.

4:00 T9.7

SELF-ORDERING AND KINETICS OF EXCITATIONS IN LOW DIMENSIONS AND DISORDERED MEDIA, Raoul Kopelman, Lola W. Anacker, Panos Argyrakis, Eric Clement, Laurel Harmond, Li Li, James S. Newhouse, Stephen J. Parus, Rodney Schoonover, The University of Michigan, Department of Chemistry, Ann Arbor, MI; and Leonard Sander, The University of Michigan, Department of Physics, Ann Arbor, MI.

4:30 T9.8
FRACTAL-LIKE EXCITON FUSION KINETICS IN
DILUTE POLYMER BLENDS, Raoul Kopelman,
Ching-Shan Li and Zhong-You Shi, The Univer-
sity of Michigan, Department of Chemistry,
Ann Arbor, MI.

4:45 T9.9
GROWTH PROBABILITY DISTRIBUTION OF DISCON-
TINUOUSLY BRANCHING TREE MORPHOLOGY DEVEL-
OPED AT AgCo/NaCl INTERFACE BY ION IRRADIA-
TION, B.X. Liu, Tsinghua University, Center
of Condensed Matter and Radiation Physics,
CCAST (World Lab), Department of Materials
Science and Engineering, Beijing, China; and
C.H. Shang, Tsinghua University, Department
of Materials Science and Engineering, Bei-
jing, China.

T1.1

BREATH FIGURES: DROPLET CONDENSATION PATTERNS ON SURFACES. Charles M. Knobler, Department of Chemistry and Biochemistry, UCLA, Los Angeles, CA.

Breath Figures are the patterns that form on surfaces when droplets of a partially wetting or non-wetting fluid nucleate and grow under conditions of constant supersaturation. Experimental studies by microscopy and light scattering of condensation of water on silanized glass surfaces have revealed two distinct stages of growth. In the early stages, droplets grow independently and the radius follows a power law $r \propto t^\alpha$. There is a crossover to coalescence-dominated growth in which the average radius $\langle r \rangle$ also follows a power law but with an exponent $\alpha' = 3\alpha$. In this regime, spatial correlations develop between droplets, the surface coverage and polydispersity remain constant, and the pattern is self-similar, depending only on a single characteristic length, $\langle r \rangle$. Insight into the process has been obtained by computer simulations, which reproduce the observations in detail, and by a scaling analysis, which shows that the relation between α and α' depends on the dimensionality of the droplets and that of the condensing surface. Connections will be made to other processes including the vapor deposition of metals.

T1.2

SELF-ORGANIZED CRITICALITY AND AVALANCHE DYNAMICS IN A DROPLET GROWTH MODEL WITH SLIDING. Fereydoon Family, Department of Physics, Emory University, Atlanta, GA 30322

What is the origin of the long-range spatial and temporal correlations that are commonly observed in many open dissipative systems? This question has attracted considerable attention in recent years. The existence of a stationary state in a simple model of sand pile has prompted Bak et al to propose that the type of scale-invariant avalanches that occur in the sand pile model might be related to the scaling and fractal behavior in other open systems. The existence of minimally stable states may explain the dynamics behind scaling and power law behavior generally observed in fractal systems.

We have investigated a model of droplet deposition, coalescence and avalanche. Our model may mimic processes such as the falling of dew on a cobweb or the flow of rain drops on a window pane. We begin by randomly adding droplets to a system and once a given droplet reaches a critical mass, it falls along a preferred direction in the system and in the process coalesces and removes all the droplets that it comes in contact with. We have used both lattice and off-lattice models and have investigated the basic dynamical features of the system, including the distribution of avalanche size and the time interval between avalanches. We find scaling behavior in some of the properties of the system, but no power law decay is observed in the auto-correlation function for mass transport. This suggests interesting differences between self-organized criticality in the sand pile model and the behavior of our model.

* This work was carried out in collaboration with Z. Cheng, P. Meakin, and S. Redner and was supported by ONR and Petroleum Research Fund.

T1.3

FRACTALS AND NUCLEATION. W. Klein, Boston University, Physics Department.

The classical theory of nucleation predicts that the decay from the metastable state is initiated by compact clusters or droplets with well defined interiors and surfaces that can be treated separately. Indeed, it is the free energy cost of creating the surface that is, according to the classical theory, responsible for the existence of the metastable state.

Computer simulations have indicated that the classical theory correctly describes the nucleation for systems with short range interactions (1,2) but not for systems with moderate and long range forces (3,4). In systems with long range interactions well defined spinodals (5,6) and the associated drop in surface tension produce critical droplets that are fractal in nature. (7,8)

We discuss the nature of nucleation in magnetic systems with long range forces as well as the implication of these results for the problem of crystallization.

1. D. Stauffer, A. Coniglio and D.W. Heermann, Phys. Rev. Lett. 49, 1299 (1982)
2. D.W. Heermann, A. Coniglio, W. Klein and D. Stauffer, J. Stat. Phys. 36, 447 (1984)
3. D.W. Heermann and W. Klein, Phys. Rev. Lett. 50, 1062 (1983)
4. L. Monette, W. Klein, M. Zuckermann, A. Khadir and R. Harris, Phys. Rev. B38 11607 (1988)
5. D.W. Heermann, W. Klein and D. Stauffer, Phys. Rev. Lett. 49, 1262 (1982)
6. M. Novotny, W. Klein and P. Rikvold, Phys. Rev. 333, 7729 (1986)
7. W. Klein and C. Unger, Phys. Rev. B28, 445 (1983)
8. C. Unger and W. Klein, Phys. Rev. B29, 2698 (1984)

T1.4

KINETICS OF SPINODAL DECOMPOSITION IN A POLYMER SOLUTION. R. Bansil and J. Lal, Boston University.

Spinodal decomposition in polymer systems is of interest because of their long range interactions. We studied the dynamics of spinodal decomposition in polystyrene-cyclohexane solution using small angle light scattering and quasi-elastic light scattering techniques. The light scattering set up consisted of a conical lens system which was used to measure the time evolution of the structure factor $S(K,t)$ at various times t after quenching the sample from a temperature in the one phase region to a temperature $T_q < T_c$ the spinodal temperature T_c . Qualitatively we observe the usual features of spinodal decomposition, i.e. a diffraction ring which collapses and grows in intensity with time. However a quantitative analysis of the data suggests that the scaling relations and growth laws differ from those found in polymer blends and solutions; for e.g. the wave vector $K \sim t^{-\alpha}$ where $\alpha = 1/2$ in contrast to the usual result $\alpha = 1/3$ for binary liquids. The scaling behavior of the structure factor $S(K,t)$ is also quite different and varies with quench depth. Results from two different molecular weights will be presented. Comparison on this system with polymer blends, polymer gels and binary mixtures will be discussed.

*Supported by NSF

T1.5

FRACTAL DIMENSIONS IN QUASICRYSTAL GROWTH MODEL Z.M. Wang* and K.Y. Szeo Physics Department, York University, Toronto, Ontario M3J 1P3, Canada

The fractal dimension of two-dimensional binary structures with five-fold symmetry is investigated using a quenched growth algorithm [1]. This algorithm has two sets of parameters: the interaction energies $E_{\alpha\beta}$ between the α and β species, and the linear box size ξ on the growing surface. We find various phases as a function of energy parameters. The box size is related to growth rate and diffusion process. The fractal dimensions using the radius of gyration [2] are calculated for systems up to 10,000 particles with different box sizes and in different phases. It is found that there are steps in the fractal dimension across a phase boundary.

[1]. K.Y. Sseto and Z.M. Wang. (1989), (submitted to Phys. Rev. B.) [2]. Stanley, H.E. (1977). J.Phys. A10, L211. P. 339.

* On leave from the Chinese Academy of Sciences (Beijing)

T1.6

PARTICLE-CLUSTER GROWTH OF AGGREGATES AT AN INTERFACE.

C. Allain, M. Cloitre, Lab. FAST, Bat. 502, Campus Universitaire, 91405 Orsay Cedex FRANCE.

Small particles trapped at an horizontal fluid interface by surface tension forces exert capillary forces one on the other. These forces make the particles stick together forming aggregates which exhibit self-similarity¹

In order to elucidate the growth mechanism, we have performed a detailed study of the capillary interaction. We have found that the vertical deformation of the interface plays the role of a potential which is the solution of the screened Laplace equation. The force to which is submitted a capillary monopole T placed in the capillary field C which derives from this potential is simply equal to $E=TC$. T and C are function of the geometry of the particle, of the different densities and of the contact angle. In addition, we can also calculate the capillary field around aggregates.

We have used these results to perform numerical simulations of particle-cluster aggregation induced by capillary forces. Single particles are launched far away from an origin by which they are attracted and where they stick irreversibly. The particles are not brownian and they move only because of the attractive interactions. This situation is completely different from the DLA model where the particles undergo a brownian motion. When the radius of the particles is of the order of the screening length, the aggregates are stringy with a fractal dimension of about 1.2. When the radius is lower than the screening length, the aggregates are compact at low length scales. These observations can be understood in terms of the properties of the capillary interaction.

¹C. Allain, M. Cloitre, in "Universalities in Condensed Matter", Springer-Verlag, Berlin, 1988, p.146.

T1.7

STATISTICAL PROPERTIES OF GENERALIZED AGGREGATION SYSTEM WITH INJECTION. H.Takayasu, Department of Physics, Boston Univ., Boston, MA02215 and Earth Science, Kobe Univ., Kobe 657, Japan

We theoretically analyze statistical properties of an irreversible system which is governed by random aggregation of real variables. In the presence of injection the system automatically chooses a critical stationary state having a power law distribution. The exponent of the power depends both on the spatial dimension and on the type of injection.

Applying this system to turbulence we give a theoretical explanation for the recent

experimental fact that the distribution of relative velocity in fully developed turbulence follows a Lorentzian.

We also report a strange multifractal property of this system, that is, the $f-\alpha$ spectrum is characterized by a single point (for example, $f=1, \alpha=3$) but the generalized dimension D , becomes a curve.

T1.8

TWO-STAGE AGGREGATION OF A NON-AQUEOUS GOLD COLLOID.* B.J. Olivier and C.M. Sorensen, Department of Physics, E.B. Zuckerman and K.J. Klabunde, Department of Chemistry, Kansas State University, Manhattan, KS 66506.

We have studied the dynamic behavior of a non-aqueous aggregating gold sol using quasi-elastic light-scattering (QELS). Pyridine has been used to displace the particle surface charge, inducing aggregation. By varying pyridine concentration different aggregation regimes were obtained.

The smaller pyridine concentrations resulted in a unique aggregation regime. In this regime a two-stage cluster growth process has been observed. The first stage of the growth process involves 4 to 5 nm spherical gold monomers aggregating and forming compact, larger gold spheres of approximately 30 nm radii. A second growth stage appears once the particles have obtained the approximate 30 nm radius. Here, the compact gold spheres aggregate to form ramified, seemingly fractal clusters. Each stage is characterized with a kernel homogeneity (λ). Preliminary analysis shows the first stage has $\lambda=1/3$ while the second stage displays nearly exponential cluster growth. *Supported by NSF Grant CBT8709622.

T2.1

FRactal MEASURES OF POROUS MEDIA. Claude Tricot, Department of Applied Mathematics, École Polytechnique, C.P. 6079, Succ. A, Montreal (Quebec) H3C 3A7, Canada.

A characteristic index for porous sets is the order of growth of the hole sizes. It may be, in specific cases, related to fractal parameters (dimension of the residual set, dimension of its boundary, fat-fractal exponent). Relationships between these parameters are investigated according to the topology of the set.

We show how to extend the same methodology to other problems such as:

- fractal dimension of aggregates
- two-sided dimension of a closed curve
- connected networks in the 3-dimensional space.

T2.2

A LOCAL PERTURBATION NOTION APPLIED TO ROUGH SURFACE ANALYSIS. D. Wehbi, J.F. Quiniou, C. Roques-Carnes, ENSMM-LMS, 25030 Besancon Cedex, France; and C. Tricot, École Polytechnique de Montréal, C.P. 6079, Succ. A., Montreal Quebec, Canada H3C 3A7.

Classical Fourier transforms give a global analysis of signals. In view of practical applications, we introduce a local approach based upon the concept of perturbation.

For a given curve T , the first step consists in the parameterization of T by a time-parameter t . Local arcs are the image of time-windows $[t - \epsilon, t + \epsilon]$, in which a perturbation $p(t, \epsilon)$ is measured.

The perturbation is minimal when the local arc is a straight segment. We may point out this general notion by using various

mathematical definitions. These definitions may use statistics (moment of order n , min and max-values), or geometrical parameters of T (convex hull, diameter,...).

The best suitable definition of $p(t,r)$ is selected according to the input - type of acquisition- or the output - efficiency of numerical calculations - data.

The order of growth of the average perturbation $\bar{p}(r)$ to 0 is related to the fractal dimensionality of T .

T2.3

ELECTROMAGNETIC AND OPTICAL WAVE SCATTERING FROM FRACTAL OBJECTS. Xiaoguang Sun and Dwight L. Jaggard, Moore School of Electrical Engineering, University of Pennsylvania, Philadelphia, PA 19104/6390.

In the coastline problem, the length of a rough coastline is determined by measurements using yardsticks of decreasing length. Since increasingly fine structure of the coastline can be measured or "seen" as the yardstick becomes shorter, its measured perimeter or length will increase. The rate at which this perimeter increases with decreasing yardstick size, is a quantitative measure of the coastline roughness and hence its fractal dimension. In the problem of wave interaction with fractal surfaces, the wavelength of the incident wave acts as a yardstick which probes the fractal nature of the rough surfaces at different scales as its size is varied. In this way, the increasingly fine structure of the rough objects can be "seen" as the wavelength becomes shorter. The fractal characteristics of these objects are embedded in their scattering properties as the wavelength is changed.

We consider the scattering of electromagnetic waves from a family of irregular rough objects characterized by bandlimited fractal functions such as the bandlimited Weierstrass function. This method provides a unified and realistic novel method for examining rough objects without the use of random functions and averaging techniques. We consider here canonical fractal objects such as fractally corrugated surfaces, fractally corrugated cylinders, and fractally fluted cylinders. The undisturbed incident field (Kirchhoff approximation or Born approximation) method is used in each case. We find analytical expressions and carry out numerical calculations for these fractal scattering problems. We relate the angular distribution of the scattering field to the fractal descriptors including the fractal dimension of these objects.

T2.4

EVIDENCE OF CRITICAL BEHAVIOR IN A RANDOM FRACTAL AUTOMATON. G. M. Dimino, Physics Board of Studies, U.C.S.C., Santa Cruz, CA; and J. H. Kaufman, I.B.M. Research Division, Almaden Research Center, San Jose, CA.

An automaton is described, in which growth is regulated by connectivity and a simple self screening constraint. As the strength of the screening is increased, the pattern evolves from compact to one dimensional, passing through an intermediate "critical" state. This state qualitatively resembles, and has a fractal dimension similar to that found in Witten-Sander aggregates, $D = 5/3$.

Finite size scaling of D vs. screening angle is observed, and the correlation length exponent ν is obtained. Since rotational symmetry is broken in this transition, we suggest that this is true critical behavior, with an effective temperature equal to $2\pi\theta$ where θ is the screening angle. A quantity, (mean deviation of the radial distribution function) is found to behave like an order parameter, and an exponent $\beta = 0.4 \pm 0.1$ extracted. The effective susceptibility has been calculated from correlations in this quantity, and it diverges with an exponent $\gamma = 1.4 \pm 0.2$. Other possible order parameters, and multifractal properties will be discussed.

T2.5

INFORMATION DIMENSION AS A MEASURE OF FRACTAL DISORDER. Panos Argyrakis, Department of Physics, 313-1, University of Thessaloniki, 54006 Thessaloniki, Greece.

A new picture is presented that studies dynamic phenomena on the usual fractal structure, such as the Sierpinski gasket, the percolation clusters, etc. by evaluating the well-known information function. This function has the form PlnP , i.e. an entropic form, where P is some type of probability measure. As an example we calculate the spectral dimension for a random walk on a fractal. We find that scaling is fully obeyed, and that the numerical values of the scaling exponents are in complete agreement with the previous "classical" way. We calculate all probability functions and show how the crossover to Euclidean behavior takes place.

T2.6

RANDOM WALK SIMULATION OF SOLVABILITY THEORY FOR THE SAFFMAN-TAYLOR PROBLEM. D.C. Hong, Physics Department and Center for Polymer Science and Engineering, Lehigh University, Bethlehem, PA 18015; H. Guo, Physics Department, McGill University, Montreal, Quebec, Canada H3A2T8.

We test the prediction of the solvability theory in the Saffman-Taylor problem by a random walk simulation. By a suitable modification of the surface tension in accord with the solvability theory, we observe a dynamically stable cusp to develop on the finger profile leading to a substantial reduction in the finger width. Identifying this cusp with that origination from the solvability theory, we find an excellent agreement between the solvability theory and the simulation results.

T3.1

FLUCTUATIONS IN PHOTON EMISSION DURING EPOXY FRACTURE: EVIDENCE FOR CHAOS.* Zhenyi Ma, J.T. Dickinson, and S. C. Langford, Department of Physics, Washington State University, Pullman, WA 99164.

The fracture of a number of materials is accompanied by the emission of visible light. This photon emission (phE, or triboluminescence) can be detected with a photomultiplier tube and digitized on sub-microsecond time scales. We have examined the time series defined by successive phE measurements for two materials, single crystal MgO and a brittle, unfilled epoxy, for evidence of chaos. Probability distributions, autocorrelation functions, Fourier transforms, and the correlation integral of Grassberger and Procaccia reveal nonstochastic fluctuations indicative of chaotic behavior associated with a low dimensional attractor. A significantly positive Lyapunov exponent estimate provides further evidence for chaos in the epoxy phE. We also report fractal dimension measurements of the epoxy fracture surface (D_s). We find that D_s is strongly correlated with a fractal measure (two-dimensional box dimension) of the phE data. This suggests that the progress of crack growth through the epoxy displays fractal features which are reflected in the accompanying phE. Possible correlations between D_s and other fracture parameters (e.g. fracture toughness) will also be discussed. phE from the unfilled epoxy will be compared with phE from a similar epoxy filled with alumina particles. The filled epoxy displays an important additional fracture mode (interfacial failure) and phE mechanism (involving charge separation at epoxy/alumina interface).

*Work supported by the National Science Foundation under Grant DMR 8601281, the Office of Naval Research under Contract N00014-87-K-0514, the McDonnell Douglas Independent Research and Development Fund, and the Washington Technology Center.

T3.2

FRACTURE AS A FRACTAL PROCESS: THEORY & EXPERIMENT. T.J. Mackin, J.J. Mecholsky, Jr., and D.E. Passoja, The Pennsylvania State University, University Park, PA 16802.

Fractal dimension was used to characterize the fracture surfaces of several polycrystalline, single crystal and glass ceramic fracture surfaces. The fractional part of the fractal dimensions were correlated with the critical stress intensity factor. From this correlation, an empirical equation was derived relating fracture energy and fractal dimension.

Recently, several theoreticians have proposed a relationship between fractal dimension and fracture energy. Furthermore, the quasi-static Griffith approach can be modified using fractals, again providing a theoretical basis for a fractal dimension-fracture energy relationship. This new approach, which will be called the fractal Griffith relation, will be presented along with several theoretical proposals from the literature. These models will be compared with the experimentally derived relationship.

T3.3

STRUCTURE ANALYSIS OF FRACTURE SURFACES USING SCANNING TUNNELING MICROSCOPY. D.A. Bonnell and M. W. Mitchell; The University of Pennsylvania, Philadelphia, PA 19104

The geometric structure of fracture surfaces could provide insight into fracture mechanisms, particularly in elastic materials where atomistic processes dominate. Fractal models have recently been invoked to describe fracture surface structure; however, surface roughness has proven difficult to quantify experimentally. The most common approaches to measuring surface roughness, sectioning to measure profiles and grinding to measure areas ('slit island'), require that a large number of measurements be made on each surface. The tediousness of these measurements precludes comprehensive analysis of a large number of surfaces. In contrast, topographic images acquired in a scanning tunneling microscope are easy to acquire and provide a high density digitization amenable to mathematical analysis. To explore this potential the spectral density and the variational horizontal element structuring method (HESM) of calculating fractal dimensional increments were tested on ideal "STM profiles" generated from a random number generator and the Weierstrass-Mandelbrot function with theoretical dimensional increments varying from 0.2 - 0.6. The characteristic noise in the tunneling signal was also quantified. This provided a measure of the uncertainty in our method and a comparison of fractal models to more conventional measures of surface roughness.

The structure of single crystal SiC and Si fracture surfaces were then imaged. Several conventional and fractal roughness parameters were calculated for each case. The variation of surface structure with fracture direction was determined, as were local variations with position. These observations will be discussed in terms of their implications to fracture mechanisms.

T3.4

FRACTAL EFFECTS AND PERCOLATION OF MATERIAL FRACTURE. Dengshi Huang, Department of Basic Science, Sichuan Economic Management College, Chendu, Sichuan, People's Republic of China.

The fracture of material is an important phenomenon whose study is of great practical importance. Mandelbrot and co-workers pointed out that fracture of material gives a statistical self-similar fractal and its fractal dimension is relevant to the properties of the materials. Recently, Ray et al and Sieradzki discussed two dimensional fracture by percolation theory.

The purpose of this paper is to research the relationship between the behavior of material fracture and the fractal dimension of the fractured surface as well as the scaling law of the relaxation modulus.

Obviously, the fractal dimension is closely related to the mechanical properties of material. It is shown that the mechanical behavior of material may be predicted by the measurement of the fractal dimension of the fracture surface.

T3.5

FRACTAL NATURE OF FRACTURE SURFACE. Gongwen Peng and Decheng Tian, Physics Department, Wuhan University, Wuhan, P.R.China

Abstract— A kinetic model is presented to simulate microscopically the crack propagation in solids composed of discrete atoms. The resulting fracture surface is found to be a fractal with dimension depending on the elastic constants of the material. For a 2-d lattice network consisting of 100 nodes in the x-direction and 50 nodes in the y-direction where the load is applied, we obtain the fractal dimensions of the fracture surfaces for two typical cases: $D=1.011 \pm 0.003$ for $K_x/K_y=1$; $D=1.248 \pm 0.017$ for $K_x/K_y=10$.

T3.6

PERCOLATION PROPERTIES OF RANDOM TWO-DIMENSIONAL POISSON FRACTURE NETWORKS. Kunal Ghosh,* Kevin Hestir,** and Jane Long, Lawrence Berkeley Laboratory, Berkeley, CA.

To study hydrological flow through cracks in solid material, a model has been proposed¹ which creates a two-dimensional network of fluid conducting lines, called fractures. In this paper, we discuss the expression for permeability using percolation theory. (The results from equivalent media theory are discussed in Ref. 1).

The permeability of such a system is the hydrological equivalent of the average DC electrical conductivity of a random resistor network. The important difference here is that the lattice is not regular. In particular, both the coordination number z and the normalized filling fraction p of this random lattice are calculated from the average number of intersections per fracture. Therefore, z is a function of p . Then the permeability K is expressed as $K \sim (p-p_c)^t$, where p_c is the percolation threshold.

We present the results of the permeability studies near p_c for a set of such random lattices with different fracture densities, as well as different distributions of length and/or orientation. The computed value of the critical exponent t gives $t \approx 1.1$. This is approximately the same universal value for regular 2-D lattices, independent of the lattice structure. Moreover, the p -dependent coordination number z has a value at p_c which obeys the universal law $z = d/(d-1)p_c$. The geometrical properties of the clusters near and above the percolation threshold are currently under investigation.

1. K. Hestir, J. Long, and K. Ghosh, this conference.

*Permanent address: Jackson State University, Jackson, MS

**Permanent address: New Mexico State University, Las Cruces, NM

T3.7

THE FRACTAL NATURE OF THE CRAZE PATTERN DEVELOPED IN MODE I FRACTURE OF POLYMERIC MATERIALS* Yuhong Ni, J. C. M. Li, Materials Science Program, Department of Mechanical Engineering, University of Rochester, Rochester, NY 14627

Dow Chemical ABS polymer with 17.5% rubber content is fractured in Mode I by using a compact tension specimen. The plastic zone developed before fracture has two distinct parts. A homogeneous cavity zone assumes a shape which seems to follow a critical hydrostatic tension criterion. Superposed in this zone and radiating from the crack tip are a set of finger-shaped crazes which seem to follow directions consistent

with the gradients of hydrostatic tension. These fingers possess the features of a Cantor set which has a fractal dimension of about 0.7. The density inside the fingers is about 20% lower than the original material. The stored energy of the finger region in the plastic zone is about 0.8 cal/g and can account for 80% of the toughness of the material. The size of the plastic zone is larger inside than at the surface of the specimen just opposite to the behavior of metals. The difference is explained by the different yield surfaces of the two materials. ABS containing varying rubber percentages are investigated also. The contribution of the fractal nature of the craze fingers to the fracture toughness of the polymers is discussed.

* Work supported by Dow Chemical Company.

T3.8

WEIBULL PLOTTING OF A FRACTAL DISTRIBUTION OF FLAWS. John F. Wight and James W. Laughner, NYS College of Ceramics, Alfred University, Alfred, NY 14802.

The Weibull modulus characterizes a material, giving an empirical relationship between load and risk of failure. The work presented here links the empirical Weibull modulus to a fractal flaw size distribution, giving the Weibull modulus a more theoretical basis.

A model of rods containing penny crack flaws is constructed. The flaw size distribution is characterized by a fractal dimension. The flaw size distribution in the rods is operated on by the Griffith theory yielding a strength distribution. Except at its extremes, the Weibull plot of the strength distribution is linear with a slope (Weibull modulus) equal to twice the fractal dimension of the flaw size distribution.

T3.9

APPLICATION OF FRACTAL GEOMETRY TO DAMAGE MODELING IN ADVANCED MATERIALS. Ted L. Anderson, Texas A&M University, Department of Mechanical Engineering, College Station, TX.

Many investigators have used the concepts of fractal geometry to characterize rough surfaces such as fracture surfaces. However, relatively few have recognized the potential of this subject to describe microstructural inhomogeneities such as second phase particles and microcracks. In the present work, the author assumes a material with a fractal distribution of microcracks, and then models the mechanical behavior of such a material.

If a material contains a self-similar distribution of microcracks, the microcrack density can be represented by a simple power law:

$$\rho(a_c) = \frac{N r(a > a_c)}{V} = \lambda a_c^{-D}$$

where a is a characteristic crack dimension, a_c is a reference crack size, λ is a constant, and D is the fractal dimension.

If the material is brittle, the largest microcrack that is sampled governs failure. In this case the above equation, combined with weakest link statistics and the Griffith failure criterion, leads to the well-known Weibull distribution for failure stress, with the Weibull shape parameter = $2D$. When a material exhibits stable microcrack growth, relatively simple expressions for global properties such as effective modulus and total fracture energy can be derived. The latter case represents an alternative to traditional continuum damage mechanics.

T4.1/U10.1

FRACTAL STRUCTURE AND DYNAMICS OF TWO FLUID FLOW IN POROUS MEDIA. Jens Feder, Department of Physics, University of Oslo, Box 1048 Blindern, 0316 Oslo 3, Norway.

The flow of fluids in porous media leads to displacement fronts that are fractal in many situations. We discuss results obtained in experiments on two-dimensional models. The dispersion of tracers, the invasion percolation at low displacement rates and the viscous fingering at high displacement rates are discussed. Symmetry breaking by gravity effects due to density differences leads to crossover phenomena that can be described by scaling functions. New results on the displacement in three-dimensional models are presented.

Fractal displacement processes exhibit dynamic scaling behavior characterized by new exponents, which we discuss in the context of invasion percolation.

T4.2/U10.2

NUMERICAL AND ANALYTICAL MODELS OF TRANSPORT IN POROUS CEMENTITIOUS MATERIALS. Edward J. Garboczi and Dale P. Bentz, National Institute of Standards and Technology, Building Materials Division, 226/B348, Gaithersburg, MD 20899.

Fluid flow under applied pressure gradients and ionic diffusion under applied concentration gradients in the pore space of a cementitious material are the key transport mechanisms that take place in these materials. Recent theoretical developments in the research labs of the oil exploration industry give new insight into how these processes can be successfully modeled at a fundamental level for cementitious materials. This talk will describe new computational methods for computing effective diffusion constants in models of porous materials, and analytical percolation-theory-based equations for predicting effective permeabilities. Digitized image modeling techniques developed at NIST will also be described.

T4.3/U10.3

SIZING REQUIREMENTS FOR FLOW-THROUGH GEOCHEMICAL TESTS, PART I. THEORETICAL CONSIDERATIONS. J.D. Hoover and E. C. Thornton, Westinghouse Hanford Company, P.O. Box 1970, Richland, WA 99352

A methodology for evaluating test apparatus size requirements has been applied to the sizing of flow-through tests used in the evaluation of coupled processes in open hydrothermal systems. The results of the sizing evaluation provide limits on the apparatus dimensions and test conditions required to yield results representative of the processes of interest. It is indicated from these evaluations that this information is critical in the design of flow-through tests and in the interpretation of test results. Size considerations, therefore, impact the use of flow-through test results in simulating the processes expected to occur in the near-field environment of a nuclear waste repository.

The main objective of this size evaluation is determination of the column dimensions and test conditions necessary to produce reactions pertinent to the processes of interest. The basis of the evaluation is treatment of the time required for reactions or processes of interest to occur, as the required column residence time for the fluid. Reaction paths and reaction times for model systems were determined using geochemical models involving reaction rate equations based on transition state theory. The range of appropriate column dimensions may then be obtained using expressions relating residence time to apparatus dimensions and flow conditions.

A finite range of appropriate column dimensions and test conditions exist for a given residence time requirement. However, determination of appropriate residence time depends on the purpose of the test and processes of interest. Factors such as test duration, sampling requirements, and engineering limitations must also impact the size and/or scale

requirements and these criteria can be used in the choice of the most practical combination of column dimensions and test conditions. It is indicated from the results of this study that size evaluations provide a technical basis for the design and construction of flow-through tests, and also for the interpretation of test results.

T4.4/U10.4

A LAGRANGIAN REACTIVE TRANSPORT SIMULATOR WITH MULTIPLE PATHS AND STATIONARY STATES: CONCEPTS, IMPLEMENTATION AND VERIFICATION. R. B. Knapp, L206, Earth Sciences Department, Lawrence Livermore National Laboratory, University of California, Livermore, California 94550

A geochemical software package which models static, single-path kinetic water-rock interactions, EQ3/6 [Wolery, T. J., Lawrence Livermore National Laboratory, UCRL-52658, 1979], has been modified to incorporate multiple-paths and stationary states under high Peclet number transport conditions in a Lagrangian reference frame [Lichtner, 1988]. These modifications permit calculation of reactive transport with reasonable computational requirements. Results from the new code, mpeq6, have been compared with analytical results for the simple HCl - SiO₂ system; excellent agreements were achieved. Results from mpeq6 have also been compared with published results [Lichtner, P., *Geochim. Cosmochim. Acta*, 52, 143-165, 1988] for a portion of the Al₂O₃ - HCl - K₂O - SiO₂ system. The results are in good qualitative and, in some cases, good quantitative agreement. However, the values of some variables differ substantially; these differences can be attributed to use of a different set of Al and Si aqueous species.

T4.5/U10.5

FRactal CHARACTERISTICS OF FRACTURE NETWORKS AND FLUID MOVEMENT IN ROCK. Christopher C. Barton, Box 25046, MS 913, Federal Center, Denver, CO 80225

Society's need to recover fluid resources (water, oil, and gas) from the Earth and to inject toxic waste materials in a reliable manner requires quantitative models to describe and predict the movement of fluids in rock. Existing models based on pore-space flow are inappropriate for study of the more rapid process of fluid flow through fracture networks. This type of flow is not a simple function of the fracture characteristics at any particular scale, but rather the integration of contributions at all scales.

The mathematical constructs of fractal geometry are uniquely suited to quantify and model relationships within complex systems that are statistically equivalent (that is, self-similar) at all scales. My results show that natural fracture networks in rock follow a fractal scaling law over six orders of magnitude. Detailed measurements of two-dimensional samples of three-dimensional fracture networks (at diverse scales in rocks of dissimilar age, lithology, and tectonic setting) show similar fractal dimensions in the range 1.6-1.8.

The small range in fractal dimension implies that a single physical process of rock fracturing operates over a wide range of scales, from microscopic cracks to large, regional fault systems. Independent field evidence has previously demonstrated that rock fracturing is an iterative process in which preexisting fractures influence the formation of subsequent fractures (such behavior is characteristic of fractal processes). The fractal behavior implies that fracture-network development is governed by a nonlinear equation. Fortunately, the ability of fractal mathematics to accurately quantify and model the system is not dependent on specific knowledge of this equation, as the equation has not yet been identified.

Knowledge that rock fracture networks are fractal allows use of data from a one-dimensional drill-hole sample to predict the two- and three-dimensional attributes of the fracture system. The spacing of fractures in drill holes is a fractal Cantor distribution, and the range of fractal dimension is 0.6-0.8, which is an integer dimension less than that of fracture-trace patterns exposed on two-dimensional, planar sections. The pattern of rock-matrix flow can exhibit fractal fingering, and matrix permeability is patchy in a manner analogous to fractal percolation clusters.

T4.6/U10.6

FLOW TO WELLS IN FRACTURED ROCK WITH FRACTAL STRUCTURE. Jim Polek, Kenzi Karasaki and Jane Long, Lawrence Berkeley Laboratory, Berkeley, CA; and John Barker, British Geological Survey, Wallingford, Oxfordshire, U.K.

Traditionally, models of fluid transport in rocks have been based on an integral (Euclidean) flow dimension. However, this assumption is not necessary and may not always be appropriate, especially for rocks with poorly connected fractures. Barker (1988) has formulated and solved the equation of flow to a well in a rock system characterized by an arbitrary flow dimension.

Using Sierpinski's carpet and a random percolating network, we generated two types of fractured rock systems with fractal properties. We then simulated hydraulic well tests in these systems. Both the fractal dimensions and the "radial" fractal dimensions of the systems were calculated using Orbach's (1986) method. The latter was calculated by accounting for only the radial component of the conductor. Of the two, we found that the radial fractal dimension better describes the physical processes occurring during a well test. The results from the well tests were in agreement with Barker's solution and a relationship between the slope of the pressure response curve and the radial fractal dimension was found. This relationship is significant because it could lead to a value for the fractal dimension of rock from field well test data. This field fractal dimension could then be used to estimate the rock's flow geometry and flow characteristics.

T4.7/U10.7

ANISOTROPIC SCALING OF INTERFACES IN POROUS MEDIA. Miguel A. Rubio, Haverford College, Haverford, PA, and UNED, Madrid, Spain; Andrew Dougherty, Haverford College, Haverford, PA; and Jerry P. Gollub, Haverford College, Haverford, PA, and University of Pennsylvania, Philadelphia, PA.

Two-fluid immiscible displacement may produce self-similar fractal interfaces, often described by invasion percolation or DLA models, for certain ranges of the relative viscosities and wetting properties of the fluids. These self-similar structures have the same scaling behavior in all directions.

Here we show that when the displacing fluid is more viscous and more efficient in wetting the medium, the interfaces are self-affine fractals, i.e., they show different scaling in different directions. We present experimental results on the interfaces obtained when water displaces air in a thin layer of glass beads. We have characterized the interfaces by computing their roughness (r.m.s. value of the interfacial width) as a function of length scale. The roughness shows power-law behavior with exponent $B = 0.73 \pm 0.03$, independent of the control parameter (capillary number, Ca). This exponent is related to the box dimension $2-B$, and the divider or compass dimension $1/B$. This behavior means that the interfaces are self-affine fractals with a box dimension of 1.27.

Supported by the NSF Low Temperature Physics Program DMR-8503543. M.A.R. was supported in part by a Fellowship of the NATO Scientific Committee.

T4.8/U10.8

SIZING AND SCALING REQUIREMENTS OF A LARGE-SCALE PHYSICAL MODEL FOR CODE VALIDATION. R. Khaleel, T. LeGore, and J. D. Hoover, Westinghouse Hanford Co., Richland, WA.

Post-closure performance assessment and the associated application of mathematical models play a critical role in assessing the long-term behavior of the engineered and natural barriers of a geologic repository. Although verification and benchmarking constitute an important part of determining model acceptability, it does not establish that the model is a reasonable approximation to physical reality. This is accomplished in the validation step in which model calculations are compared with data from controlled experiments.

Although in-situ field experiments provide useful data, information needed for model validation cannot be obtained from field observations alone because of the inherent uncertainties associated with the natural system. However, physical models, when properly scaled, constructed, and instrumented can provide the necessary information for validation of mathematical models and computer codes, and can overcome many of the uncertainties associated with large-scale in-situ testing. The

relationships between measurement, size, scaling, and discretization (block size) used in a numerical model must be incorporated in the conceptualization of a physical model. Sizing and scaling requirements of a large-scale physical model for hydrological testing are discussed. The justification for the minimum size of a physical model for hydrological testing can be based on the nature of heterogeneities introduced into the model. Results of numerical simulations used to determine the preliminary size requirements of a porous medium model are presented.

T4.9/U10.9

PERFORMANCE OF CONCRETE BARRIERS IN RADIOACTIVE WASTE DISPOSAL IN THE UNSATURATED ZONE. John C. Walton and Mark D. Otis, Idaho National Engineering Laboratory, P.O. Box 1625, Idaho Falls, Idaho 83415

Concrete barriers are an important component of many designs for disposal of radioactive waste in the unsaturated zone. In order to evaluate the effectiveness of the concrete barriers performance assessment models representing the material degradation and behavior must be developed. Models for evaluation of fluid flow and mass transport through concrete barriers located in the unsaturated zone are presented. Implications of the use of impermeable membranes in barrier design are discussed. The effectiveness of the concrete is shown to be dependent upon effective design. Concrete of highest quality may not always be desirable for use in waste disposal vaults.

T5.1

CAPILLARY CONDENSATION ON FRACTAL SURFACES. P. Pfeifer, J. Kennner, Physics Dept., University of Missouri, Columbia, MO 65203; and M.W. Cole, Physics Dept., Pennsylvania State University, University Park, PA 16802.

We extend our recent investigation of the Frenkel-Halsey-Hill theory of thick-film adsorption on fractal surfaces [Phys. Rev. Lett. **62**, 1997 (1989)] to include the effect of surface tension. The competition between long-range gas-solid interactions and surface tension leads to a regime where the coverage is lower than on a planar surface (FHH regime, intermediate film thicknesses) and a regime where the coverage may be higher than on a planar surface (capillary condensation, very thick films). The critical dimension below which the surface may adsorb more is $D = 8/3$. It leads to the surprising result that, at sufficiently high pressures, capillary condensation is most pronounced when the fractal dimension is low. The effect will be discussed in detail and will be applied to the experimental case of nitrogen adsorption on a self-affine silver surface.

T5.2

CHARACTERIZATION OF THE SURFACE FRACTAL DIMENSION AND ROUGHNESS OF EVAPORATED SILVER FILMS VIA ADSORPTION ISOTHERM MEASUREMENTS.* J. Krim, V. Panella and A. Sarkissian, Physics Department, Northeastern University, Boston, MA 02115

Adsorption studies have been carried out for a variety of evaporated silver films which have been deposited under controlled conditions onto the surface electrodes of a quartz crystal microbalance. These studies provide (a) an immediate determination of whether the film is smooth or rough and (b) if rough, an indication of pore morphology and fractal dimension. Surface structures ranging from amorphous to crystalline to self-affine fractals have been observed. In general, the surface area increases as the film thickness increases. Film thickness has little effect however on the

surface fractal dimension.

* Supported by NSF and PRF.

T5.3

HYDROGEN, NEON AND NITROGEN ADSORPTION ISOTHERMS ON POROUS VYCOR GLASS. * T. E. Huber and C. A. Huber, University of Puerto Rico, Rio Piedras, PR 00931.

The fractal properties of porous Vycor glass have been under some debate recently and the experimental determination of its surface area from the adsorption isotherms for simple adsorbates is of current interest. We have measured the adsorption isotherms of H_2 , D_2 and Ne in the temperature range from 15 to 77K in samples of porous Vycor glass. N_2 , at 77 K and 114 K, was also studied. The B.E.T model gives surface areas that are temperature dependent for all the gases studied. To understand this problem we have used the adsorption isotherm data to generate a thermodynamic characterization in the region of temperature and pressure covered. We obtain that a wide distribution of adsorption energies is necessary to explain the data. A model-independent adsorption isotherm is discussed which allows fitting of the data at all temperatures. Based on this model we discuss the scaling of the adsorption energy distribution function with molecular size and mass.

* Work supported by NSF-EPSCoR.

Present address: Department of Physics, Harvard University, Cambridge, MA 02138.

+ Present address: Francis Bitter National Magnet Laboratory, M.I.T., Cambridge, MA 02139.

T5.4 ABSTRACT WITHDRAWN

T5.5

SMALL ANGLE X-RAY SCATTERING APPLIED TO INVESTIGATE THE FRACTAL PROPERTIES OF COAL AND OTHER POROUS CARBON-BASED MATERIALS. M. Reich, S. Russo, I. K. Snook and H. K. Wagenfeld, Royal Melbourne Institute of Technology, Melbourne, VIC, AUSTRALIA

We use the Bale-Schmidt theory for the intensity of X-rays scattered through small angles (SAXS) by a porous solid with a fractal surface in conjunction with experimental SAXS data to estimate the surface fractal dimension, D of a wide range of porous, carbon based solids. The measured values of D vary over virtually the whole theoretically allowable range.

Further, we show that for a brown coal sample heated under nitrogen both the fractal dimension and extent of the surface are a function of the temperature. Below about 350°C the pore fractal dimension, D is 2.80 indicating a very convoluted surface whilst above 350°C the surface is becoming smooth, $D=2.0$.

T5.6

SMALL ANGLE X-RAY AND NEUTRON SCATTERING FROM A FRACTAL DIFFUSION FRONT Michel Rosso and Bernard Sapoval, Laboratoire de Physique de la Matière Condensée, Ecole Polytechnique, 91128 Palaiseau, France.

We have computed the small-angle scattering from simulated three dimensional (3D) diffusion fronts.

In 3D, the diffusion front (1) extends over a large concentration region over which it exhibits two different fractal behaviors. In a high concentration region, the front is a dense object with dimension 3. It behaves as an ordinary solid, but each of its points belongs to its surface. In the vicinity of a critical concentration p_c , which is a percolation threshold, the front is a more dilute object, with a fractal dimension 2.5.

Depending on whether the sample has its concentration restricted to the critical percolation region (with $D=2.5$), or extends over a broader concentration region we observe a mass fractal or a surface fractal behavior. This behavior is found for values of the wave vector q depending on the concentration gradient at p_c .

The interest of this exact calculation on a realistic model is to permit a quantitative analysis of experimental small angle scattering from various non homogeneous systems.

(1) M. ROSSO, J.F. GOUYET and B. SAPOVAL, Phys. Rev. Lett., **57**, 3195 (1986) and J.-F. GOUYET, M. ROSSO and B. SAPOVAL, Phys. Rev. **B37**, 1832 (1988)

T6.1

THE GROWTH OF SELF-AFFINE FRACTAL SURFACES.
Paul Meakin, E. I. du Pont de Nemours and Company,
Wilmington, DE

Simple models for growth and deposition lead to the formation of dense structures with rough surfaces that can be described in terms of self-affine fractal geometry. The growth of the surface roughness is characterized by two correlation lengths ($\xi_{||}$ and ξ_{\perp}). The correlation length ξ_{\perp} corresponds to the surface width and grow according to

$$\xi_{\perp} \sim t^{\beta}$$

where t is time. The correlation length $\xi_{||}$ describes the lateral distance over which fluctuations in the surface height persist and it grows according to

$$\xi_{||} \sim t^{\beta/\alpha} \sim t^{1/2}$$

where α is the Hurst exponent. The results of recent simulations and theoretical work for ballistic deposition at grazing incidence ($\theta \rightarrow \pi/2$ where θ is the angle of incidence) onto both a line and a plane will be described. In both cases the deposition process onto a d_s dimensional substrate can be mapped onto the coalescence of (d_s-1) dimensional objects and exact values for the exponents α and β in the limit $\theta \rightarrow \pi/2$ can be obtained.

Results from spatially correlated ballistic deposition simulations with and without restructuring (transfer of the deposited particle to the nearest local minimum) will be presented.

T6.2

Pattern Formation and Characterization for Biological Materials. Charles Thompson and Kavita Chandra. Department of Electrical Engineering, Laboratory for Advanced Computation University of Lowell, Lowell, MA

The problem of precipitate patterning in the formation of a porous biological materials is considered. In particular, we examine the temporal and spatial patterns generated by cellular calcification via an autocatalytic process. Preliminary results of a nonlinear model

describing the self-organization and pattern formation will be presented.

The relationship between cluster and pore size and on characterization of the fractal dimension will be addressed. The implication of the results to the application of textural analysis of porous biological materials using image-processing techniques will be discussed.

[Work supported by Analog Devices Professorship]

T6.3 ABSTRACT WITHDRAWN

T6.4

FRACTAL DIMENSION OF NATURAL POLYMERS. Louis Piscitelle and Ronald Segars, U.S. Army Natick Research, Development and Engineering Center, Natick, Massachusetts 01760-5020

The fractal dimension of powders obtained from the natural polymer Chitosan is shown to be dependent on both processing temperature and source (shrimp vs. crab). Measurement of the fractal dimension, thus, provides a means of characterizing Chitosan products. When coupled with other measurements, this parameter may prove useful in optimizing the functionality of Chitosan derivatives.

Obtaining uniform particle size distributions having different group means, or at least, accurately measuring the particle size distribution within a given group, is a difficult and critical step in determining the fractal dimension of a powder. Sieving, which was used in this study, may allow much larger particles to exist within a group if some of the particles are plate-like. If electrostatic forces occur, fines may attach to larger particles and fail to pass through the sieve whose mesh size is used to define the smallest particles within the group. Particle size distribution and even the mean value will be quite different from the values calculated from the mesh size of the sieves. These factors are shown to affect the determination of the fractal dimension.

T6.5

FRactal vs. SUB-FRACTAL: CLOUD RADIANCE AND OCEAN SURFACE DATA. Patricia H. Carter and Robert Cawley, NSWC, Silver Spring, MD.

The graph of a function or random process has a dimension that can be measured.^{1,2} In the case of a random process the dimension is typically fractal, but many nonfractal graphs also give a measured dimension larger than one. Hence, to implement a fractal characterization of experimental data it is desirable to be able to distinguish these possibilities. Previous experimental studies of infrared cloud radiance data have been consistent with a fractal hypothesis on the graphs of radiance against angle. The sub-fractal possibility, that the radiance function is differentiable but its derivative is not can be investigated by an analysis using measurement of a power law index of the amplitude spectrum. Results of analysis of infrared cloud data and ocean surface shape data will be presented indicating presence of fractal vs. sub-fractal characteristics.

1. Charles Adler, Patricia H. Carter and Robert Cawley, "A comparison of the fractal dimensions of cloud radiance graphs for two infrared color bands," in *Physics of phase space*, Y. S. Kim and W. W. Zachary, eds, Springer, L. N. Physics No. 278, 1987, p.45.

2. Patricia H. Carter and Robert Cawley, "Fractal characterization of infrared cloud radiance," in *Fractal aspects of Materials*, MRS fall meeting proceedings, 1987.

T6.6

FRactal CHARACTERIZATION OF POROUS SILICA GELS BY GPC. Houqiang Li, Ying Li, and Huaming Zhau, Department of Chemistry, Sichuan University, Chengdu 600064, The Peoples Republic of China.

Porous Media play an important role in many fields such as oil recovery, heterogeneous catalysts and Chromatography. The Characterization of porous silica gels (PSG) is of central importance in gel Chromatographic technique because of involving in separating polymers in laboratory. It has recently been shown that the PSG are statistically fractals. We have determined the fractal dimension of a series of porous silica gels by GPC.

T7.1

A NEW TECHNIQUE TO DIFFERENTIATE BETWEEN GEMINATE AND NONGEMINATE RECOMBINATION OF EXCITONS IN DISORDERED MEDIA. Jagdish Prasad and Raoul Kopelman, Department of Chemistry, The University of Michigan, Ann Arbor, MI 48109-1055.

Geminate formation and recombination of triplet excitons in 2,3-benzocarbazole/tetracene has been studied using a dynamic technique (pulse vs. steady state excitation). In tetracene, the mode of decay of the first excited singlet state is by fission (1) into two neighboring triplet excitons that can undergo geminate recombination. We monitored the geminate exciton recombination via delayed fluorescence using steady state and pulsed excitations. The decay rates for the 2,3-benzocarbazole/tetracene samples were than compared with the decay rates for nongeminate recombination in naphthalene samples. We find that the geminate recombination decay rates do not depend on the duration of the excitation (pulse length). For nongeminate recombination the decay rates do depend on the pulse length. Our work provides a new, dynamic technique to differentiate between geminate and nongeminate recombination of excitons. We expect similar effects for electron-hole and soliton recombinations.

1. S. Arnold, R. R. Alfano, M. Pope, W. Yu, P. Ho, R. Selsby, J. Tharrats and C. E. Swenberg, *J. Chem. Phys.* **64**, 5104 (1976).

T7.2

STEADY-STATE REACTIONS ON FRACTALS: RATE LAWS AND SELF-ORGANIZATION. Eric Clement and Raoul Kopelman, Department of Chemistry, The University of Michigan, Ann Arbor, MI 48109-1055; and Leonard M. Sander, Department of Physics, The University of Michigan, Ann Arbor, MI 48109-1120.

The $A + B \rightarrow 0$, $A + A \rightarrow 0$ and $A + T \rightarrow T$ (trapping) reactions are studied in fractal and Euclidean dimensions. Non-classical global rate-laws, particle distributions and critical dimensions are obtained. The reaction orders (exponents) depend on the type of reaction, the source term structure, the conservation laws and the dimensionality. Macroscopic, mesoscopic or microscopic self-ordering is observed, depending on the combination of the above specifications. The theoretical analyses are compared with Monte-Carlo simulations.

T7.3

EXCITATION TIME MODULATION STUDIES OF MOLECULAR AGGREGATES IN DOPED POLYMERS. Zhong-You Shi, Irene E. Newhouse and Raoul Kopelman, Department of Chemistry, The University of Michigan, Ann Arbor, MI 48109-1055.

Steady state vs. pulsed excitation decay kinetics were obtained for naphthalene doped PMMA (plexiglass). The triplet fusion kinetics for dilute samples depend drastically on the initial excitation kinetics. While the initial exciton densities are equal in both cases, the density distributions differ. The application of this technique to the study of heterogeneous samples is aided by model computer simulations on percolation clusters and fractal-like aggregates.

T7.4

PULSED VS. STEADY-STATE EXCITON RECOMBINATION KINETICS: EXPERIMENTS AND SIMULATIONS ON PORES, POWDERS AND RANDOM MEDIA. Stephen J. Parus, Zhong-You Shi and Raoul Kopelman, Department of Chemistry, The University of Michigan, Ann Arbor, MI 48109-1055.

The non-classical kinetics of exciton recombination in restricted geometries provides the foundation for a new experimental technique of probing the exciton dynamics and the sample topology. The phosphorescence and delayed fluorescence decays exhibit a dramatic dependence on the duration of the excitation. The comparison of pulsed and steady-state excitation provides information on the local topology of the sample and on the average hopping time of the exciton and the exciton diffusion length. This is possible because the distribution of the exciton population is non-Poissonian under steady-state excitation conditions. In addition, the pulse-created distribution also loses its Poissonian character with time. The experimental systems are: 1) Isotopic mixed naphthalene crystals above and below percolation; 2) Naphthalene crystalline powder; 3) Naphthalene embedded into porous glass. Except for the mixed crystals above the percolation concentration, all samples exhibit the non-classical effects typical of fractal-like topologies. The interpretation is aided by Monte-Carlo simulations.

T7.5

REACTANT TRAPPING AND STEADY-STATE SELF-ORDERING ON FRACTALS. Lola W. Anacker and Raoul Kopelman, Department of Chemistry, The University of Michigan, Ann Arbor, MI 48109-1055.

Supercomputer simulations (at the John von Neumann Center) of steady-state trapping reactions ($A + T \rightarrow T$) on a Sierpinski gasket (9843 sites) show both self-ordering [1] and anomalous (non-classical) reaction kinetics [2]. The reactants aggregate in the trap-free regions. This is similar to the behavior in one but not in three dimensions. The rate law exhibits an anomalous order: $Y = 2/d_s$ where d_s is the spectral (fractal, recurrence) dimension and Y is the trap-density exponent. However, the reactant-density exponent is classical ($X = 1$). We note that the overall order ($X + Y$) is the same as that of the $A + A$ reaction [2].

1. L. W. Anacker and R. Kopelman, *Phys. Rev. Lett.* **58**, 289 (1987).
2. L. W. Anacker, R. P. Parson and R. Kopelman, *J. Phys. Chem.* **89**, 4758 (1985).

T7.6

Hydrodynamic Instability in Crystal Melts. Charles Thompson and Vineet Mehta, Department of Electrical Engineering, Laboratory of Advanced Computation, University of Lowell, Lowell, MA

The hydrodynamic stability of semiconductor melts is considered. Special attention is paid to the Czochralski growth configuration. The parameter range in which the melt is unstable to three-dimensional disturbances is addressed. The temporal and spatial characteristics of the fluid velocity and temperature are obtained. It is shown that at high crystal rotation rates that linearly unstable disturbances propagate as three-dimensional waves confined to the boundary-layer at the liquid-solid interface. The relationship between the aforementioned flow characteristics and crystal morphology will be examined.

The effect of finite amplitude disturbances are also investigated. The results of a nonlinear stability analysis as well as the parametric dependence on bifurcation from the linearly unstable state will be presented.

[Work supported by Analog Devices Professorship]

T7.7

GROWTH KINETICS IN A COAGULATION--FRAGMENTATION SYSTEM * Iman, M. Elminyami and C.M. Sorensen, Department of Physics, Kansas State University, Manhattan, KS 66506.

We have numerically solved the Smoluchowski rate equation which included both coagulation and fragmentation kernels. A variety of kernels were used with different homogeneities. The mean aggregate size and number of clusters were found to evolve to equilibrium values in a characteristic time all dependent on the kernel homogeneities. During the evolutionary or non-equilibrium time regimes, the particle size distribution was found to exhibit scaling. These results confirm predictions made in reference 1.

*Supported by NSF Grant CBT8709622.

1. C.M. Sorensen, H.X. Zhang, and T.W. Taylor, *Phys. Rev. Lett.* **59**, 363 (1987).

T7.8

ROLE OF AGGREGATION IN THE FORMATION OF COLLOIDAL GOLD PARTICLES* Jun Liu, M. Sarikaya, W. Y. Shih, W. H. Shih, and I. A. Aksay, Department of Materials Science and Engineering and Advanced Materials Program, Washington Technology Center, University of Washington, Seattle, WA 98195

Formation of gold particles in colloidal solutions is studied. The gold particles are produced by reducing gold chloride with sodium citrate in water, and the process is studied at different stages by transmission electron microscopy. It is found that this process is very different from that of the classical nucleation and growth. As soon as the nuclei (about 2 nm) appear in the solution, they begin to aggregate. The aggregates grow to very large size (up to 0.2 μ m) and the fractal dimension increases with time. At later times, the aggregates break up into particles of smaller sizes. After a longer time, all the particles reach the same size (about 15nm in diameter). The

aggregation at early stages is due to van der Waals attraction between the particles. As the reaction progresses, the amount of charge on the particle surfaces, which is due to citrate adsorption increases and hence the total Coulomb energy of the system increases. When the Coulomb energy is large enough, the clusters break up. This is evidenced by the zeta potential measurements, which indicate that the charge on the particle surface gradually increases as the reaction proceeds. The size of the particles can be determined by minimizing the total interfacial energy of the system, which is the sum of the gold-water interfacial tension and the Coulomb energy. As a result, the particle size R is related to the citrate concentration C by the relation $R \sim C^{-0.66}$, which is in excellent agreement with experiments¹.

* This work is supported by AFOSR/DARPA under Contract No AFOSR-87-0114.

1. Goodman et al, *J. Microscopy*, Vol. 123, Pt 2, 201 (1981).

T7.9

THE EFFECT OF AGGREGATION ON COLLOID CATALYSTS. J.R. Melrose, The Blackett Laboratory, Imperial College, Prince Consort Road, London SW7 2BZ

Theoretical models for the large time effects of aggregation on the catalytic properties of metal colloids are developed within the framework of the electrochemical theory of the catalytic mechanism and recently proposed models for the extremes of cluster aggregation. In the case of fast aggregation of the colloid catalyst, the catalytic rate is generally predicted to decrease as a power law of time. In the case of slow aggregation catalytic rates are predicted to have an exponential decrease with time. One exceptional case gives a catalytic rate increasing with aggregation. Polydispersity could be important in the case of slow aggregations.

T7.10

MULTIPLE SCATTERING IN POWER-LAW CORRELATED MEDIA. J.R. Melrose, D. Sherrington, The Blackett Laboratory, Imperial College, Prince Consort Road, London SE7 2BZ, UK; S. Sarker, RSRE Gt Malvern, Worcs. U.K.

An analysis is made of multiple scattering in random media with power law correlations. In the leading approximation to Dyson's equation solutions for the frequency dependent attenuation and phase velocity are presented. These are discussed in the context of possible applications to seismology. Intensity effects will be discussed via the ladder approximation to the Bethe-Salpeter equation.

T7.11

SMALL-ANGLE X-RAY SCATTERING STUDIES OF BONE POROSITY* Paul W. Schmidt^(a), David Avnir^(b), Armin Röll^(a), and David Nelson^(a). (a) Physics Department, University of Missouri, Columbia, MO 65211. (b) Dept. of Organic Chemistry, the Hebrew University of Jerusalem, Jerusalem 91904, Israel.

The pores in normal and diseased bones have been studied by small-angle x-ray scattering. The scattering data give information about the structure on a scale from about 10 to 1,000 Å. Scattering data have been obtained both for the outer (cortical) and the less dense inner (trabecular) regions of the bones. Neutron scattering curves have been recorded in order to supplement the x-ray data. The scattering curves from the bone samples have been compared with the results from amorphous calcium phosphate samples prepared in the laboratory.

*Acknowledgement is made to the Donors of the Petroleum Research Fund, administered by the American Chemical Society, for support of this work.

T7.12

SMALL-ANGLE X-RAY SCATTERING FROM THE SURFACES OF REVERSED-PHASE SILICAS: POWER-LAW-SCATTERING EXPONENTS OF MAGNITUDES GREATER THAN FOUR*. Paul W. Schmidt^(a), David Levy^(b), Axel Höhr^(a), and David Avnir^(b). (a) Physics Department, University of Missouri, Columbia, MO 65211. (b) Dept. of Organic Chemistry, the Hebrew University of Jerusalem, Jerusalem 91904, Israel.

Small-angle x-ray scattering has been used to investigate the pore structure in fully and partially derivatized silicas on a scale from about 10 to 1,000 Å. In the derivatizing process, hydrocarbon chains were deposited on the pore surfaces of the silicas. There were hydrocarbon chains on all available sites in the commercial fully derivatized silicas. Silicas in which hydrocarbon chains were attached to different fractions of the available sites also were examined.

When $q\xi \gg 1$, where ξ is the average pore size, $q = 4\pi\lambda^{-1}\sin(\theta/2)$, λ is the wavelength, and θ is the scattering angle, the scattering intensity was proportional to $q^{-\alpha}$. The power-law-scattering exponent α was greater than 4.

The value of α depends on the form of the density change at the pore boundary. For a smooth pore boundary, in which the density undergoes a finite discontinuity from a value of zero in the pore to an essentially constant value in the body of the silica, $\alpha = 4$. When the pore boundary is fractal, $\alpha < 4$. The density transition in the derivatized silicas has been approximated by assuming that if x is the perpendicular distance into the silica from the pore surface, the density in the neighborhood of the pore boundary is proportional to x^β , with $0 < \beta \leq 1$. Calculations show that in this case $\alpha = 4 + 2\beta$.

*Acknowledgement is made to the Donors of the Petroleum Research Fund, administered by the American Chemical Society, for support of this work.

T7.13

FRAGMENTAL DEGRADATION OF RADIATED MACROMOLECULES. Houqiang Li, Ying Li and Huaming Zhao, Department of Chemistry, Sichuan University, Chengdu 610064, The People's Republic of China.

The degradation of the macromolecules radiated by the ray with high energy is an interesting phenomena whose study is of great theoretical and practical importance. Based on the facts of experiment, the relation between the degree of degradation and radiation dose is given by an empirical formula, however, up till now it has not been derived from theory. How to calculate it has been the focus of attention for some time. These questions are discussed by using the fractal theory in this paper.

T7.14

MULTIFRACTAL FEATURES OF THE FRACTAL AGGREGATES AT DIFFERENT STAGES. L.J.Huang, B.X.Liu*, J.R. Ding and H-D.Li, Department of Materials Science and Engineering, Tsinghua University, Beijing 100084 CHINA. *Also at Center of Condensed Matter and Radiation Physics, CCAST (World Lab.), Beijing.

Multifractal measure was employed to characterize the fractal aggregates of the iron oxide microspheres at different stages in thin amorphous films. It was found that these magnetic microspheres were initially open and stringy with a dimension of $D=1.35 \pm 0.05$. While the aggregates were subject to long term storage at ambient temperature, all the key parameters of the geometrical features of the aggregates, e.g. the leading singularities, the singularities of the scaling at the invaginated regions and the generalized dimensions, changed with time elapsed. The results also showed that the aggregates kept self-similarity, although the screening during evolution was suppressed by the solid state diffusion. We present the detailed dynamic evolution of these

parameters obtained from multifractal measure and the thermal stability of the fractal aggregates.

T7.15

COMPOSED RECURRENT SETS. Wen Z. Y., Li J. N. and Wang H. F., Department of Math., Wuhan Univ., Wuhan, P. R. China.

In this paper, we introduced the composed recurrent sets using a more general method than Dekking's, thus got a large amount of new fractals.

If one gives two substitutions θ_1, θ_2 over an alphabet A , let $\Sigma = \{\theta_1, \theta_2\}$, and suppose τ is a substitution over Σ , R the mirror image of Σ , then $R(\tau^n(\theta_1))$ is a composed substitution over A . Under certain conditions, for a given word w over A , we can associate each word $R(\tau^n(\theta_1))(w)$ with a compact subset K_n of \mathbb{R}^d by the similar method of Dekking. We proved that K_n converges to a compact subset K in Hausdorff metric and we obtain an estimation of the Hausdorff dimension of K which extends the results of Dekking and Bedford.

By this method we can obtain the fractal sets with several different scaling transformations. We can use this result to discuss the problems of quasicrystals and disorder systems.

T7.16

VISCOUS FINGERING ON 2D LATTICE MODELS NEAR THE PERCOLATION THRESHOLD. U. Oxaa, F. Boger, J. Feder and T. Jøssang, Department of Physics, University of Oslo, Norway.

Experiments with immiscible fluid-fluid displacement in two-dimensional porous models have been performed on geometrically well characterized models. By a photoetching technique we produce two-dimensional models of uniform pores on the nodes of a square lattice. The bonds connecting nearest neighbors are randomly given one of two permeabilities, k and $R \cdot k$, their ratio is kept fixed at $R = 10^{-4}$. The model is filled with a Newtonian high-viscosity fluid. This fluid is then displaced by centrally injecting air at constant pressure while allowing the viscous fluid to escape at the outer boundaries of the model. The resulting displacement patterns are photographed, digitized, analyzed and compared with the scaling predictions:

$$M(L) \sim L^{D_2} F(L/\xi, L/L_R), \quad \text{with } D_2 = 1.3$$

of Meakin et al. [1].

[1] P. Meakin, M. Murat, A. Aharony, J. Feder and T. Jøssang, *Diffusion-limited aggregation near the percolation threshold*, Physica A 155, 1-20 (1989)

T7.17

THE FRACTAL DIMENSION OF PERCOLATION CLUSTERS. H. C. AKUEZUE, and J. STRINGER, Electric power research Institute, Palo Alto, California 94303.

A Monte Carlo method is used to simulate a site percolation problem on a 2-dimensional square lattice. The variations of the radius of gyration's exponent, ρ , with the concentration, p , is studied in detail using two methods: a new simulation calculation method and the classical series procedure based primarily on the Martin's cluster enumeration algorithm. For the first time, the statistics of clusters up to the size 16 were studied in a series calculation.

The new computer simulation calculations indicate ρ is not a constant below or above p_c . Also the series calculations show that ρ is not constant at or below p_c and in the vicinity of p_c , ρ scales with p . Application of the new computer simulation calculation in estimating the fractal dimension of irregular coal agglomerated particles is also discussed.

T7.18

FRACTALS AND DIFFUSION PROCESS. Hanna Nencka, 63-200 Jarocin Pozn., woj. Kaliskie, Sportowa 2/12, Poland.

Proof of an existence of:

1. fractals with the same Hausdorff dimensions and different spectral dimensions ($d_H = d_H^1, d_s^1 \neq d_s^2$)
2. fractals with the different Hausdorff dimensions but the same spectral dimensions ($d_H \neq d_H^1, d_s^1 = d_s^2$)

is presented. The relationships between the space Δx and time Δt increments of a diffusion for this class of fractals are considered. The diffusion problems for the tree-like fractals are examined as well.

T7.19

LACUNARITY OF FRACTAL AGGREGATES. C. Allain, M. Cloitre, Lab FAST, Bat. 502, Campus Universitaire, 91405 Orsay Cedex FRANCE.

The lacunarity parameter has been introduced recently to characterize to what extent a fractal set is not translationally invariant. Unfortunately, the definitions available up to now in the literature lead to serious inconsistencies in the case of deterministic sets and they cannot be generalized to non deterministic objects such as fractal aggregates. In view of this, we propose a new definition of the lacunarity.

The idea consists in studying the distribution probability of the mass which is embedded in a box of arbitrary size shifted in all the possible manners onto the object under study. We define the lacunarity parameter as the mean square deviation of this mass probability distribution. This definition is quite general since it applies at any length scale to sets of arbitrary size which are not necessarily self-similar. In addition, it can be implemented easily in image processing systems to study experimental aggregates.

In the case of scale invariant objects, the lacunarity parameter follows a scaling law as a function of the box size. The exponent is related to the fractal dimension which can be determined by this way. The prefactor is taken as a measure of the lacunarity of the object. We test this new definition of the lacunarity on deterministic Cantor sets of various types and we check that all the inconsistencies encountered in the previous definitions disappear. Moreover, we establish its interest to characterize the geometry of experimental aggregates.

T7.20

LINEAR CORRELATION OF FRACTAL DIMENSION VERSUS MAGNETIC INTERACTION. B.X.Liu, Center of Condensed Matter and Radiation Physics, CCAST (World Lab.), Beijing and Dept. of Materials Science and Engineering, Tsinghua University, Beijing 100084, CHINA; and J.R.Ding, Dept. of Materials Science and Engineering, Tsinghua University, Beijing 100084, CHINA.

A systematic study on fractal aggregation of magnetic particles was performed. Four kinds of

magnetic particles, i.e. Fe_2O_3 , Co, Cr and Ni, aggregated on vapor-deposited Fe, Co, Cr and Ni thin films, respectively, resulting in the formation of fractal patterns. Transmission electron microscopy examination revealed that these patterns were the result of cluster-cluster aggregation.

A linear relationship between the fractal dimension of the aggregates and the effective atomic magneton number was found to be $D_f = Km + c$, where D_f refers to the fractal dimension, m refers to the effective atomic magneton number, K and c are constants found out to be 0.041 and 1.72 respectively. Accordingly, when the magnetic interaction among the aggregating particles reduces to zero, i.e. $m=0$, the corresponding fractal dimension is 1.72, which is just the value expected by the cluster-cluster aggregation model.

T7.21

FRACTAL MAGNETIZATION ON HIERARCHICAL LATTICES. W.A.M. Morgado, S. Coutinho and E.M.F. Curado, Centro Brasileiro de Pesquisas Fisicas, Rua Xavier Sigaud 150, CEP 22290, Rio De Janeiro, Brazil.

The local magnetization of the Ising and the Potts models on hierarchical lattices is studied by an iterative procedure. An exact recursion equation between the local magnetizations of the internal sites and the two ends of the primitive graph in a general hierarchical lattice is derived. The magnetization profile of a given path joining the two vertices of several lattices (e.g. diamond, Wheatstone bridge...) are exhibited showing near the critical temperature a fractal structure of high non-uniformities over the infinite range of resolution. The $f(\alpha)$ function characterizing how densely the singularities of the distribution of the local magnetization are distributed is also presented and discussed.

The exact critical exponent (β_L) of the local magnetization is calculated straightforwardly from the recursion equation. We found a nonconstant value for β_L increasing when we go deep inside the lattice. The exact critical exponent β for the magnetization of the whole lattice is also obtained. For the Ising model on the diamond and Wheatstone hierarchical lattices our figures for β recovers previous results obtained with (1) and without magnetic fields (2).

1. J.R. Melrose, J. Phys. A **16**, 3077 (1983).

2. A.O. Caride and C. Tsallis, J. Phys. A **20**, L667 (1987).

† Permanent address: Departamento de Fisica, Universidade Federal de Pernambuco, CEP 50739, Recife, Brazil.

T7.22

DYNAMIC PROPERTIES OF SOL-GELS. J. E. Martin and D. Adolf, Sandia National Laboratories, Albuquerque, NM 87185.

Gelling systems exhibit novel viscoelastic properties in the vicinity of the sol-gel transition. A scaling theory of these phenomena is presented, along with extensive measurements on silica and epoxy gels.

T7.23

WAVELET TRANSFORMATION OF FRACTALS OBSERVED IN THIN SOLID FILMS. J.R.Ding and L.J.Huang, Dept. of Materials Science and Engineering, Tsinghua University, Beijing 100084, CHINA; and B.X.Liu, Center of Condensed Matter and Radiation Physics, CCAST(World Lab.), Beijing and Department of

Materials science and Engineering, Tsinghua Uni., Beijing 100084, CHINA.

Fractal structures were observed in ion-irradiated Ni-Mo and Ni-Zr alloy films by transmission electron microscope examination. The fractal dimensions were determined to be 1.72 ± 0.02 and 1.4 ± 0.1 , respectively.

To study the local scaling properties of those observed fractals, wavelet transformation was performed. Since the fractals in our case were observed in the real physical process, the scale parameter "a" should be restricted within a relevant range. The different local scaling features of the fractals observed in the Ni-Mo and the Ni-Zr systems were compared. The $f-\alpha$ spectra yielded from wavelet transformation as well as from multifractal analysis proposed by Halsey et al. are also presented.

T7.24

ANALYTICAL EXPRESSIONS FOR THE PERMEABILITY OF RANDOM TWO-DIMENSIONAL POISSON FRACTURE NETWORKS. Kevin Hestir,* Jane Long, and Kunal Ghosh,** Lawrence Berkeley Laboratory, Berkeley, CA.

Hydrological studies of flow through cracks in solid material is modeled on a two-dimensional Poisson network of fluid conducting lines called fractures. The permeability of such random fracture networks can be studied using percolation theory and equivalent media theory, which are usually applied on regular lattices where the lattice elements are present with probability, p . In order to apply these theories to random systems, we must (1) define the equivalent to the case where $p = 1$, (2) define p in terms of the statistical parameters of the random network and (3) define the equivalent of the coordination number, z . An upper bound for permeability equivalent to the case of $p = 1$ is found by calculating the permeability of the fracture network with the same linear fracture frequency and infinitely long fractures. The permeability of networks with the same fracture frequency and finite fractures can be normalized by this maximum. An equivalent for p is found as a function of the connectivity, ζ , which is defined as the average number of intersections per fracture. The quantity ζ can be calculated from the distributions of fracture density, length and orientation. The equivalent p is defined by equating the average run length for a random network as a function of ζ to the average run length for a regular lattice as a function of p . Also, an average coordination number z can be calculated for the random systems as a function of ζ .

Thus defining p and z , we present in this paper, the expression for permeability based on equivalent media theory. (Percolation theory results are discussed in Ref. 1). Numerical studies provide strong support for this model. To apply the model to random length systems, the expression for ζ must be modified to remove short fractures which do not contribute to flow. This leads to a quantitative prediction of how permeability decreases as one removes shorter lines from a network.

1. K. Ghosh, K. Hestir, and J. Long, this conference.

*Permanent address: New Mexico State University, Las Cruces, NM

**Permanent address: Jackson State University, Jackson, MS

T7.25

FRACTAL ASPECTS OF HYDROGENATED AMORPHOUS AND MICROCRYSTALLINE SILICON.

R.C. van Oort, J.C. van den Heuvel, M.J. Geerts, Delft University of Technology, Faculty of Electrical Engineering, Mekelweg 4, Delft, the Netherlands.

The film surface of hydrogenated amorphous (a-Si:H) and microcrystalline (uc-Si:H) films etched in a hydrogen rf plasma were examined by using scanning electron microscopy. Microcrystalline silicon is a mixture of crystals imbedded in an a-Si:H matrix. Hydrogenated amorphous silicon generally is regarded as a material consisting of two phases. One phase of a high electrical quality and a high structural order, more or less imbedded in a second phase of poor

quality, containing a lot of hydrogen and many microvoids. This phase is of a low structural order. By etching the a- and uc-Si:H films in a hydrogen rf plasma one is able to reveal the various phases, the crystals of the uc-Si:H film and the phase of high quality in the a-Si:H type of film. The structures that become visible are fractal-like. In the case of the uc-Si:H type of film the fractals form a closed network. In the case of a-Si:H the fractals are segregated. The fractals can be regarded as crystalline in both the a- and uc-Si:H film. The existence of the fractals might be very important for a better understanding of the electrical and structural properties of the a- and uc-Si:H films.

T7.26

CHAIN CONFORMATION OF IONOMERS IN A NON-POLAR SOLVENT. D.C. Hong, Physics Department and Center for Polymer Science and Engineering, Lehigh University, Bethlehem, PA 18015.

We consider the conformation of ionomers that carry metallic group at each monomer site. This metallic group forms a point dipole in a non-polar solvent. In the presence of a strong electric field, the dipoles are expected to align themselves along the direction of the external field. In this limit, the exact renormalization group method yields the relation between the end-to-end distance R and the chain length N as: $R = N$ with $a = 2/d$ for $2 < d < 4$. The chain is thus fully stretched in 2 dimensions. A modified Flory theory also yields the same result. The relevance of our results to the experiment is also discussed.

T7.27

"FRACTAL ASPECTS OF MATERIALS"

THE DIFFUSION COEFFICIENT OF A REPTATING POLYMER. J.M. Deutsch and T.L. Madden, University of California at Santa Cruz, Santa Cruz, CA, 95064.

The dynamics of a polymer in a network of entanglements is studied. The viscosity and diffusion coefficient were studied in the repton model for up to 75 links. First we derive the correct procedure for calculating the three dimensional diffusion coefficient in this model. We find that the diffusion coefficient scales as $L^{2.3 \pm 0.1}$. This result is in marked contrast to the asymptotic L^2 prediction of reptation. We see that the asymptotic behavior of the diffusion coefficient must have corrections of the order of $L^{-1/2}$. This implies that fluctuations in the tube length cannot provide an adequate explanation for the experimental data. The viscosity is found to scale as $L^{3.49 \pm 0.13}$, in accord with experimental data and other numerical results.

T7.28

DIFFUSION OF LINEAR POLYMERS IN GELS. S. Pajevic, R. Bansil and, C. Koňák, Boston University.*

We have used photon correlation spectroscopy to study the diffusion of linear polystyrene (PS) with molecular weights ranging from 5,000 to 700,000 in methacrylate gels made by copolymerizing methyl methacrylate (MMA) and ethylene dimethacrylate (EDMA) in toluene. The linear polymer at a very dilute concentration was added to the mixture of monomers in toluene prior to gelation of MMA and EDMA. Since toluene is isorefractive with the MMA the measured correlation function determines the diffusion of the

linear polystyrene. Single exponential fits and 4th order cumulant analysis were used to determine the diffusion constant D as a function of M , the molecular weight of PS.

We found that D exhibits different scaling behavior depending on M . For low molecular weight PS $D \sim M^{-0.6}$ and D/D_0 is independent of M , (D_0 is the diffusion of PS in toluene) indicating a Stokes-Einstein type of diffusional mechanism. For PS with $M > M_c$, a critical molecular weight, we find $D \sim M^{-1.4 \pm 0.2}$ and $D/D_0 \sim M^{-1.2 \pm 0.2}$ characteristic of reptation. M_c depends on the extent of crosslinking in the gel. For very high molecular weight samples we observe diffusion constants much greater than would be predicted by reptation, and furthermore the molecular weight at which departure from reptation becomes evident decreases as the temperature or the amount of toluene is lowered. We believe that this is due to increasing incompatibility of the polymer and the gel. These results suggest that the diffusion of a polymer in a gel is more complex than predicted by the reptation model and that it is influenced strongly by the nature of the interaction with the gel matrix.

*Supported by NSF.

T7.29

SYNERGETICS PARADIGM & DICHOTOMY AS A SPECIAL CASE OF MODERN THEORY OF CRITICAL PHENOMENA: FRACTAL-GEOMETRY = SCALE-INVARIANCE. Edward Siegel, Synergetics Paradigm & Dichotomy, 183-14th Avenue, San Francisco, CA.94118.

Synergetics Paradigm & Dichotomy is manifestly shown step-by-step, to be a special case of the modern theory of critical phenomena, in fact having been prophesized by Ma and Toulouse & Pfeuty. As a fractal-Berry diffractal calculus, its dependence upon scaling-laws/relations of fractal-geometry is exactly equivalent to MTCP dependence upon scale-invariance, rediscovered in Bak et.al. "self-organized-criticality". Explicitly the 1:1 mapping equivalence is:

M.T.C.P. FUNCTION	1:1 MAP CRITICAL-EXPONENT	S.P.D. FUNCTION	"JOB"
$X(1/T-T_c) \approx 1/(1/T-T_c)^{\gamma}$	$\gamma \approx 1/n$	$X(w) \approx 1/w^n$	out
$\chi(1/T-T_c) \approx 1/(1/T-T_c)^{\nu}$	$\nu \approx 1/2$ $L \approx 2$	$\chi_L(w) \approx 1/w^L$	out
$A(1/T-T_c) \approx 1/(1/T-T_c)^{1-\nu}$	$\gamma \approx 2/3$ $? = ?$	$\sigma(w) \approx 1/w^?$	out
$G(r) \big _{T=T_c} \approx 1/r^{d-2+\gamma}$	$\gamma \approx 0$	$\begin{cases} SS: g(\underline{z}_r) = g(r)/\underline{z}^{d-D} \\ SA: g(\underline{z}_r) = g(r)/\underline{z}^{d-\Delta D} \end{cases}$	$\begin{matrix} in \\ vs \\ in \end{matrix}$
or			
$S(k) \big _{T=T_c} \approx 1/k^{2-\gamma}$	$\gamma \approx 0$	$\begin{cases} SS: S(\underline{k}/\underline{z}) = S(k)/\underline{z}^{d-D} \\ SA: S(\underline{k}/\underline{z}) = S(k)/\underline{z}^{d-\Delta D} \end{cases}$	$\begin{matrix} in \\ vs \\ in \end{matrix}$

connecting MTCP thermodynamic and transport functions: generalized susceptibility χ ; correlation/coherence length ξ ; pair correlation/distribution function χ_d ; equivalent to static structure factor/diffraction-pattern $S(k)$ to SPD analogs. Critical-exponent Fisher equality scaling-law $(2-\gamma) = \gamma/\nu$ explicitly expressed the SPD function connection equivalence: $[-\ln S(k)]_{T=T_c} / \ln k = [\ln(1/\chi) / \ln(1/\xi)]$ in MTCP equivalent to $[-\ln S(k, w=0) / \ln k] = [\ln(1/\chi) / \ln(1/\lambda)]$ in SPD exactly! I.S.-K.Ma, Modern Theory of Critical-Phenomena, Benj. (76)-p.496!

T7.30

AUTOMATIC MATHEMATICAL CATASTROPHE ("AUTMATHCAT") AT EVEN INTEGER CRITICAL-DIMENSIONS $D=d^{st}=(1+1)=2$ and $D=d^{st}=(3+1)=4$ SUPERUNIVERSALITY IN MATHEMATICS DOMINATING PHYSICS. Edward Siegel, Synergetics Paradigm & Dichotomy, 183-14th Ave. San Francisco, CA.94118.

Automatic mathematical catastrophe ("AUTMATHCAT") at even integer critical-dimensions (spacetime) $D=d^{st}=(1+1)=2$ and $D=d^{st}=(3+1)=4$ superuniversality in mathematics:
 • Fractal-Geometry "space"-filling "curves" at $D=d^{st}$ integer
 • Graph Theory of Polya and Rayleigh: recurrence($D=d^{st}=2$) versus transience($D=d^{st}=2$)

• Cauchy-(boundary-value)-problem solution versus non-solution for Hyperbolic Differential Equations (wave-equation, eikonal-equation, Huygens'-principle) of Courant & Hilbert for even versus odd integer spacetime dimensions
 • Knot Topology knot-to-un-knot unknotting above second even integer ($D=d^{st}=4$) dimension and nonexistence of topology below first even integer dimension ($D=d^{st}=2$)
 • Number Theory existence of first even integer as "the odd-est prime" being the only even prime number, thus the least common divisor of all even integers (dimensions) ... dominating the (Synergetics Paradigm & Dichotomy) superuniversality of physics;
 • Field Theory at $d^{st}=d^{st}_c=(1+1)=2$ and $d^{st}=d^{st}_c=(3+1)=4$ of Coleman and Brink-Nielsen very extensively throughout physics!
 • Modern Theory of Critical Phenomena phase-transition critical-dimensions at $D=d^{st}=(1+1)=2$ and $D=d^{st}=(3+1)=4$
 • Special [light-cone at $d^{st}=d^{st}_c=(3+1)=4$] and General (Takagi, Ooguri-...) Relativity
 • Mixed Bose-Einstein-Fermi-Dirac "anyon" Statistics of Wilczek bosons in even integer versus fermions in odd integer spacetime dimensions ...
 • Synergetics Paradigm & Dichotomy Superuniversality Class & Crossover Principle Fractal-Diffractal Calculus fractal-dimensionality uncertainty fluctuation upon Menger fractal-dimensionality (continuous) manifold with "AUTMATHCAT" at $D=d^{st}=2$

T7.31

SYNERGETICS PARADIGM & DICHOTOMY: SELF-ORGANIZED-CRITICALITY, AUTOMATIC MATHEMATICAL CATASTROPHES ("AUTMATHCATS"), MODERN THEORY OF CRITICAL PHENOMENA, INFINITE CONDUCTANCE FLUCTUATIONS, FRACTAL-CRYPTOGRAPHY, LITHOGRAPHY, FILAMENTATION-SUPERCONDUCTIVITY: SUPERUNIVERSALITY CLASS & CROSSOVER VIA DIMENSIONALITY UNCERTAINTY FLUCTUATION: FRACTAL-DIFFRACTAL CALCULUS. Edward Siegel, Synergetics Paradigm & Dichotomy, 183-14th Avenue, San Francisco, CA.94118 (with F.Young & A.Smith)

Synergetics Paradigm & Dichotomy superuniversality class & crossover is an ostensibly fractal-diffractal calculus upon a Menger continuous fractal dimensionality manifold, admitting derivative d/dD implemented via Aizawa-Fujisaka-Mandelbrot-Siegel fractal-dimensionality uncertainty fluctuations ΔD [self-affine & multifractal: $D = D_{mass}^{box} = D_{compass}^{mass}$...], with automatic-mathematical-catastrophes ("AUTMATHCATS") at even integer dimensions, throughout pure mathematics [topology (Jordan curve theorem, knot topology, graph theory, hyperbolic differential equation Cauchy-(boundary value)-problem solutions, number theory and "space"-filling of fractal-geometry) dominating/causing dimensionality-driven infinite conductance fluctuations throughout physics. Bak "self-organized-criticality" is identified as a special case; S.P.D. is manifestly demonstrated to be itself a special case of modern theory of critical phenomena by its characteristic universal critical-exponents, as has Bak's S.O.C. Other manifestations in: field theory, general relativity, elementary particle physics, special relativity, M.T.C.P., A.-I. cognition, biophysics, string theory, cosmology, quantum theory [Zitterbewegung I.C.F. with $1/f$ noise signature/"echo"=Heisenberg Uncertainty-Principle, manifestly proving exact equivalence of three Principles: Correspondence = Complementarity = Uncertainty!], Kaluza-Klein theories, Newton's law, nonlinear dynamics... abound and are exhaustively detailed. Superuniversal local-to-global phase-transition critical-phenomena with $1/f$ white-to- $1/f$ flicker [fluctuation-dissipation theorem-equivalent] noise and susceptibility power-spectra, infinite with d/dD , dominate physics as a (if not the) "common-functioning-principle"! , the consequence of scale-invariance, gauge-invariance and dimension!

T7.32

SUPERUNIVERSALITY CLASS & CROSSOVER OF SYNERGETICS PARADIGM & DICHOTOMY MANIFESTATION OF CONSEQUENCES OF SCALE-INVARIANCE (= FRACTAL-GEOMETRY) THROUGHOUT PHYSICS DOMINATING PHYSICS. Edward Siegel, Synergetics Paradigm & Dichotomy, 183-14th Avenue, San Francisco, CA.94118.

Synergetics Paradigm & Dichotomy special case of Modern Theory of Critical Phenomena (MTCP) exhibition of superuniversality class & crossover as direct consequence of self-similar versus self-affine fractal scaling-laws/relations upon Berry diffractal scaling-laws/relations, dominant scale-invariance symmetry consequence via Noether's theorem upon conservation-laws:

FRactal [r-space] →	DIFFRACTAL [k- &/or w-space]
SCALING-RELATION	ARP- DENSITY-OF-STATES POWER-SPECTRA
Self-Similar (D _d =2)	LOCAL- Constant NOISE-SUSCEPTIB.
$g(Z_r)=g(r)/Z_r^{D_d}$	IZATION N(w)=0 White White
Self-Affine (D _d =2)	DELOCAL- Linear (MLS) 1/w ⁰ 1/w ⁰
$g(Z_r)=g(r)/Z_r^{D_d}$	IZATION N(w)=n.w Flicker Flicker
	INFRA-RED DIV. 1/w ⁿ⁼¹ 1/w ⁿ⁼¹

where Anderson-Rayleigh-Polya (ARP) localization = locality is $e^{i(k \cdot r - w \cdot t)} e^{-\frac{1}{2} r \cdot r} e^{-\frac{1}{2} w \cdot w}$ with complex (non-conserved) wavevector/momentum $[k=k'+ik'']$ &/or frequency/energy $[w=w'+iw'']$ versus ARP-delocalization = globality plane-wave propagation $e^{i(k \cdot r - w \cdot t)}$ with real (conservation) $[k=k'; k''=0; w=w'; w''=0]$; SuperUniversal:

• QUANTUM THEORY^{1,2}: (Correspondence-Complementarity-Uncertainty) classical (d_s=2) = smooth path (particle) certainty $\delta x/\delta w$ CORRESPONDENCE = COMPLEMENTARITY = UNCERTAINTY $\delta x/\delta w$ quantum (d_s=2+ε) Zitterbewegung (wave) uncertainty $\delta x/\delta w$ • COSMOLOGY^{1,2}: pre-early non-physical universe vs. post-early physical universe with divergence at $D=d_c=(1+1)=2$ of: h&E, k_B & S; and "down" divergence of: N=I from 1 to finite & "c" from ∞. • BIOPHYSICS OF LIFE: (d=2) Davydov soliton -to- (D>2) Frohlich coherent electric polarization wave Bose-Einstein condensation of DelGuidice et.al., with Gol'danskii glassy biopolymer MLS. • ARTIFICIAL-INTELLIGENCE (COGNITION) • NONLINEAR DYNAMICS (Chaos) • QUANTUM FIELD THEORY • MODERN THEORY OF CRITICAL-PHENOMENA... 1&2. E. Siegel, Schrodinger Centenary (87); Fdns. of Mod. Phys. (87)

T7.33

DIMENSIONAL-CALCULUS OF DIMENSION-THEORY IMPLIMENTATION OF SYNERGETICS PARADIGM & DICHOTOMY "COMMON FUNCTIONING PRINCIPLE" PARSIMONY-OF-DICHOTOMY DOMINATION OVER SPECIFICITY-OF-COMPLEXITY. Edward Siegel, Synergetics Paradigm & Dichotomy 183-14th Avenue, San Francisco, CA. 94118.

Synergetics Paradigm & Dichotomy "common functioning principle" superuniversality class crossover ubiquitously all pervading throughout physics deriving from pure-mathematics, exhibiting automatic mathematical catastrophes ("AUTMATHCATS") at even-integer critical-dimensions:

LOCALITY ← PARSIMONY of → GLOBALITY
1/f⁰-WHITE ← DICHOTOMY → 1/f¹-FLICKER
[fluctuation-dissipation theorem-equivalent] noise and generalized-susceptibility power-spectrum, is derived via dimensional-calculus: Orthogonal to the fractional-calculus, with $\delta^D/\delta x^D$ operations, [integer dimensions for ordinary-calculus] dimensional-calculus dimensional-derivative $\delta/\delta D$ and dimensional-integral $\int \dots dD$ impliment Mandelbrot-Aizawa-Fujisaka² fractal-dimensional uncertainty fluctuations ΔD for self-affine and multi-fractals $D_{box} \neq D_{mass} \neq D_{compress}$ versus self-similar $D_{box} = D_{mass} = D_{compress}$. Upon a cylindrical Riemann-surface, implimentation of dimensional-derivative $\delta/\delta D$, orthogonal to ordinary- or fractional-derivatives, as a fibering exhibits "AUTMATHCATS" when operating upon equivalently: noise or generalized-susceptibility power-spectra $P(w; D) = (w; D)^{-1}/w^n(D)$ or critical-exponent $n(D)$ along this fiber-bundle. Inverse dimensional-integrals $\int \dots dD$ exhibit hysteresis flag of "AUTMATHCATS". Implimentation via Heaviside operational-calculus of Riemann-surface cylinder fibering results in: $(\delta/\delta D)[1/w^n(D)] = [(-\ln w/w^n(D))]/(\delta/\delta D)[n(D)] \delta(D-d_c)$ with $(\delta/\delta D)[n(D)] \delta(D-d_c) = [29(n(D))-1]/(\delta/\delta D)[n(D-d_c)] - n(d_c)/[n(d_c)]$ for d_c =even-integer critical-dimensions.
1. E. Siegel, Intl. Conf. on the Fractional Calculus, Koriyama (89)
SIAM Ann. Mtg., San Diego (89); Statphys-17, Rio de Janeiro (89)
2. B. Mandelbrot, Phys. Scripta 32, 257 (85); Y. Aizawa, Prog. Theo. Phys. 67, 982 (82); 68, 65 & 1864 (82); 69, 1416 (83); 70, 1249 (83); 70, 1204 (83); in Dimensions & Entropies in Chaotic Sys., Spring (86)

T7.34

formation of Fractal Patterns of MoO_{3-x} Crystals
During Phase Transformation.

The small pieces of molybdenum sheet were heated at 800°C in a particular oxidizing ambient. Some two-dimensional fractal patterns of MoO_{3-x} crystals grew during phase transformation. They are the results of Diffusion-Limited Cluster Aggregation (DLCA). Their fractal dimensions are different each other under the same

experimental condition, and are in a wide range. The electron diffraction experiments show that MoO_{3-x} crystals are single crystals. The possible growth mechanism of the fractal patterns is discussed.

T7.35

MULTIFRACTAL POROUS ROCK. J. L. McCauley, Physics Department, University of Houston, Houston, TX 77004, USA; J. Muller, A. T. Skjeltorp and J. P. Hansen, Institute for Energy Technology, N-2007 Kjeller, Norway.

The multifractal spectra of porespace of two different types of North Sea sandstone are measured using optical microscopy and a box-counting technique. The empirical results are described by a very simple planar Cantor set which is a multifractal Sierpinsky carpet. The good agreement between the data and the model shows that sandstone porevolume can be modelled by the simplest two-scale Cantor set on an octal tree.

T7.36

CHARACTERIZATION OF THE MECHANICAL FAILURE SURFACES OF ENERGETIC MATERIALS BY POWER SPECTRAL TECHNIQUES. M. Yvonne D. Lanzerotti, James J. Pinto, U.S. Army ARDEC, Picatinny Arsenal, NJ 07806 5000; and A. Wolfe, New York City Technical College, Brooklyn, NY 11201

Composition B is a composite energetic material containing 59% cyclotrimethylenetrinitramine (RDX), 40% TNT, and 1% wax. The nature of the fracturing of this material and the characterization of the fracture surfaces is of considerable practical and scientific interest. The fracture surfaces of the material under study are obtained by accelerating prepared samples in an ultracentrifuge. When the tensile or shear strength is exceeded a fracture surface is obtained. Using a diamond stylus profilometer, the topography of the fracture surface has been studied from a wavelength of 1.0 micron to nearly 1.0 centimeter. The spatial power spectra have been calculated from the data using a prolate spheroidal data window in the horizontal space domain prior to the employment of the fast Fourier transform algorithm. The power spectra are found to decrease with increasing spatial frequency. Peaks corresponding to the RDX particle size are observed in the Composition B power spectra. These peaks indicate that the fracture is occurring at the interface of the RDX and TNT grains in the composite, mixed material. The log of the root-mean-square roughness of the fractured surface interface is found to be directly proportional to the log of the profile length.

T8.1

BROWNIAN DYNAMICS OF BRANCHED POLYMERS. M. E. Cates, Cavendish Laboratory, Madingley Road, Cambridge CB3 0HE, UK.

The statics and dynamics of a quenched polymer sol are considered. An ideal quench is argued to have no effect on the fractal dimension of clusters. The hyper-scaling relation may be understood in terms of the excluded volume between flexible clusters of quenched network structure. The screening of hydrodynamics in a system with hyperscaling remains poorly understood, with Rouse and Zimm limits as bounds, but the real behavior probably lying in between. We consider how to modify existing results for quenched sols, so as to allow for slow reversible breaking of the cross-links. This is a first step toward the dynamical description of equilibrium sols.

T8.2

STATIC AND DYNAMIC PROPERTIES OF CONCENTRATED SOLUTIONS OF BRANCHED POLYMERS ELABORATED NEAR GELATION THRESHOLD. M. Delsanti (1), J.P. Munch (+,1), M. Adam (1) and D. Durand (2).

Synthesis of polydisperse randomly branched polymers near the gelation threshold are correctly described by percolation. Using the techniques of dynamic, static light scattering, and small-angle neutron scattering the space-time dependence of the structure factor of moderately concentrated solutions has been determined. In this concentration regime, the various polymers are no longer far away from each other as would occur in very dilute solution, and smaller polymers penetrate the largest ones. The main result is that increasing the polymer concentration, the profile of the dynamical structure factor goes from a stretched exponential function, with an exponent which decreases as concentration increases, to a power law function. The dynamical properties of these systems are similar to those observed in disordered media near the glass transition.

1. Service de Physique du Solide et de Résonance Magnétique, CEN-Saclay, 91191 Gif-sur-Yvette Cedex, France.
 2. Laboratoire de Chimie et Physico-Chimie Macromoléculaire, Unité associée au CNRS, Université du Maine, route de Laval, 72017 Le Mans, France.
- + Permanent address: Laboratoire de Spectrométrie et d'Imagerie Ultrasonores, Université Louis-Pasteur, 4, rue Blaise-Pascal, 67070 Strasbourg Cedex, France.

T8.3

DYNAMICS OF POLYMER GELATION. Michael Rubinstein. Corporate Research Laboratories, Eastman Kodak Company, Rochester, NY 14650

Gelation is a continuous phase transition well described by static scaling theories¹ (classical or critical percolation dependent on whether the linear sections between crosslinks are long or short).

A simple dynamic scaling theory² based on the Rouse model with the distribution of sizes of branched polymers determined by the critical percolation theory is in excellent agreement with recent experiments.

In the case of classical gelation with long linear entangled sections between crosslinks there is a time regime with dynamics dominated by entanglements crossing over at longer times to the Rouse regime.³

1. E. V. Patton, J. A. Wesson, M. Rubinstein, J. C. Wilson, and L. E. Oppenheimer, *Macromol.* **22**, 1946 (1989)
2. M. Rubinstein, R. H. Colby, and J. R. Gillmor in *Space-Time Organization in Macromolecular Fluids*, Eds. F. Tanaka, T. Ohta and M. Doi, Springer-Verlag, Berlin (1989)
3. M. Rubinstein, S. Zurek, T. C. B. McLeish, and R. C. Ball, submitted to *J. Physique* (Paris)

T8.4

KINETIC GELATION IN SYSTEMS WITH AGGREGATION, BREAKUP, AND FLOW. R. Dennis Vigil and Robert M. Ziff,

Department of Chemical Engineering, University of Michigan, Ann Arbor, MI.

We employ mean-field rate equations to study gelation in both open and closed systems undergoing aggregation and breakup. We consider the aggregation rate kernel $K_{ij} = ij$, which is known to lead to a gelation transition for irreversible aggregation in closed systems. We find that the existence of a gelation transition for aggregation-fragmentation depends upon the rate of breakup, the feed and removal rates, and in some cases also upon the initial conditions. Furthermore, our results show that the presence of breakup terms may lead to novel kinetic behavior. For example, consider a model of coagulation with single-particle breakoff, described by the aggregation kernel $K_{ij} = ij$ and fragmentation kernel $F_{ij} = \alpha((j+1)\delta_{i1} + (i+1)\delta_{j1})$. We find that the scaling exponent τ , which describes the large-size behavior of the steady-state size distribution for α above a critical value α_c , is $7/2$ rather than the usual value $5/2$, indicating that this process belongs to a new universality class of gelation. We conjecture a three-parameter scaling relation for the approach to gelation: $c_k = k^{-\tau} F(k/t^z, \epsilon k^\omega)$ with $\tau = 7/2$, $z = 2$, and $\omega = 1$, which describes the scaling of the size distribution c_k for $\epsilon \equiv (\alpha - \alpha_c) \rightarrow 0$, $k \rightarrow \infty$ and $t \rightarrow \infty$. We verify this form for limiting cases $t = \infty$, $\epsilon \rightarrow 0$ (approach to gelation of the steady-state solution) and $\epsilon = 0$, $t \rightarrow \infty$ (dynamics at the critical value of α).

T8.5

ELASTIC PROPERTIES OF COLLOIDAL GELS*. W. H. Shih,

J. Liu, W. Y. Shih, M. Sarikaya and I. A. Aksay, Department of Materials Science and Engineering, and Advanced Materials Technology Program, Washington Technology Center, University of Washington, Seattle, WA 98195

Elastic properties of colloidal gels are studied both experimentally and theoretically. In the scaling theory that we developed, a gel structure is modeled as close packing of fractal clusters formed by aggregation. Expressions for the elastic constant and the yield strain as a function of particle concentration are given. There are two regimes depending on the relative strength of the clusters and of the links between the clusters. In the strong-link regime, the elastic constant increases but the yield strain decreases with the particle concentration. In the weak-link regime, both the elastic constant and the yield strain increase with concentration. Crossover from the strong-link to the weak-link regime can occur as the concentration increases. Rheological study on silica gels clearly demonstrates the scaling behavior of each regime and the crossover. The rheologically deduced fractal dimension of the clusters is consistent with the light scattering measurements.

* This work is supported by AFOSR/DARPA under Contract No AFOSR-87-0114

T8.6

J. L. Stehle, P. Evrard, SOPRA, 26/68 rue Pierre Joigneaux, 92270 Bois-Colombes, FRANCE. V. Mazzacurati, Università degli Studi di Roma 'La Sapienza', 00185 Roma, ITALY. G. Ruocco, Università degli Studi di L'Aquila, 67100 L'Aquila, ITALY. J. N. Willis, L. C. Hammond, ARIES/QEI, 5A1 Damonmill Square, Concord MA 01742, USA.

Light scattering is a rapid, non-destructive technique for analysis of critical lengths in fractal materials. The shape of the low-frequency Raman and Brillouin spectra as important as their spectral positions. This data is difficult to observe, due to high stray light.

A new double spectrometer, used in double pass configuration (DMDP), has been developed, with a higher signal/noise ratio than a multi-pass Fabry Perot interferometer. This new instrument will be described.

Brillouin and Raman intensities can be measured in the same conditions, enabling calculation of absolute Raman intensities, by comparison with the Brillouin intensity, for a given laser power.

The first results obtained for transparent materials, including polymers, gels, glasses and AgI, will be presented.

T8.7

MULTIFRACTAL STRUCTURE OF POLYMER-MODIFIED CEMENT PASTES. V. M. Castaño, Instituto de Física, U.N.A.M., A.P. 20-364 México, D. F. 01000 and P. W. Schmidt, Physics Department 223 Physics Bldg., Univ. of Missouri, Columbia, MO 65211.

Several techniques, ranging from low angle X-ray and neutron scattering to digital processing of optical and electron microscopy micrographs have been utilized for studying various regimes of fractal structure in polymer-modified portland cement pastes. The results indicate clearly the role of polymer in capillary pores whereas gel porosity is not affected by the addition of polymeric materials. Also, a discussion of the relation between the mass and surface fractal dimensions obtained by the different experimental techniques is included.

T9.1

FIXED SCALE TRANSFORMATION APPROACH TO THE DIELECTRIC BREAKDOWN MODEL.

L. PIETRONERO, *Università di Roma, P.le A. Moro, 00185 Roma, Italy*, A. ERZAN, *University of Groningen, Melkweg 1, 9718 EP Groningen, The Netherlands*, and CARL EVERTSZ, *Yale University, Box 2155 Yale Station, New Haven, CT 06520, USA*

We discuss a new theoretical approach to the computation of the fractal dimension of clusters grown with the Dielectric Breakdown Model and the Diffusion-Limited Aggregation Model. This approach provides quantitative insight into the role of the screening and scale invariance of the Laplace equation in the formation of fractal patterns.

The approach exploits the scale invariance of the clusters which implies that knowledge of the distribution of the two diagrams needed in a dyadic coarse graining of clusters, can be obtained by considering their distribution at an arbitrary fixed scale. In the above approach, this distribution is obtained as the fixed point of the Fixed Scale Transformation. The box-counting dimension is then a simple function of this distribution.

We compare the theoretical results with those obtained from numerical simulations in the cylinder geometry and show a movie on the actual growth process.

T9.2

GEOMETRICAL MULTIFRACTALITY OF DIFFUSION LIMITED AGGREGATES, Tamas Vicsek, Department of Physics, Emory University, Atlanta, GA 30322, and Institute for Technical Physics, P.O. Box 76, H-1325 Budapest, Hungary, Fereydoon Family, Department of Physics, Emory University Atlanta, GA 30322, Paul Meakin, Du Pont de Nemours and Co., P.O. Box. 80356, Wilmington, DE, 19880.

Geometrical multifractals are complex patterns that can be described in terms of an infinite hierarchy of mass exponents corresponding to the local scaling of the mass. Since the distribution of growth probabilities in diffusion-limited aggregates (DLA) has been shown to be multifractal, it is natural to ask: Is DLA a geometrical multifractal or it can be described by a single fractal dimension?

We have used very large off-lattice DLA clusters and a generalized sand-box method Q which is particularly well suited for investigations of geometrical multifractality Q to study the scaling of the mass distribution in DLA. Our results show that the generalized dimensions $D(q)$ decrease monotonically with increasing q , demonstrating that DLA clusters are multifractal. We also show that the true fractal dimension of DLA clusters, $D(0)$, is larger than the usually accepted value, because the commonly used methods for the determination of the fractal dimension give $D(2)$.

T9.3

THE MORPHOLOGY OF COPPER ELECTRODEPOSITS.

J.R. Melrose, The Blackett Laboratory Imperial College, Prince Consort Road, London SW7 2BZ; D.B. Hibbert, The Department of Analytical Chemistry, University of New South Wales, P.O. Box 1, Kensington, Sydney 2033, Australia.

We report observations of the micron scale morphology of copper electrodeposits with emphasis on relating it to the morphology, fractal or dense radial, on the cm-scale.

We find that:

1. Concurrent changes of micron scale morphology and electrical resistance are observed.
2. Interfaces between dense radial and open cm-scale morphologies are composed of a three step transition between micron scale morphologies; many features of this transition are a challenge to understanding.
3. Under changing growth conditions it is possible to drive a metamorphosis from dense radial to open deposit; a concurrent metamorphosis is observed on the micron scale.

T9.4

RANDOM WALKS AND THE DOUBLE LAYER IMPEDANCE. Thomas C. Halsey, Michael W. Leibig, The James Franck Institute and the Department of Physics, The University of Chicago, Chicago, IL.

We present a numerical procedure, based on a random walk algorithm, for determining the analytic structure of the impedance of an ionic solution in contact with a perfectly polarizable metallic electrode, which may have a simple or fractal geometry. This technique is based on earlier work on a Green's function formulation of the impedance problem.¹

This technique applied to the problem of a deep groove yields the correct CPA type behavior. This procedure applied to a Diffusion Limited Aggregate, a DLA, indicates that DLA does not exhibit a CPA type impedance, but its analytic structure for small ω has a logarithmic dependence. We discuss the universality of this behavior.

¹T.C. Halsey, Phys. Rev. A **36**, 5877 (1987).

T9.5

BROWNIAN TRAIL RECTIFIED. Alan J. Hurd and Pauline Ho, Sandia National Laboratories, Department of Energy Contract No. DE-AC04-76-DP00789, Albuquerque, NM 87185-5800.

The experiments described here indicate when one of Nature's best fractals--the Brownian trail--becomes nonfractal.

In most ambient fluids, the trail of a Brownian particle is self-similar over many decades of length. The trail of a submicron particle suspended in an ordinary liquid, for example, recorded at equal time intervals, exhibits apparently discontinuous changes in velocity from the millimeter level (where convection or sedimentation can be important) down to molecular levels. Only when the time interval is shortened to 10^{-8} s does the velocity appear continuous.

In rarefied environments, this time resolution at which a Brownian trail is rectified from a curve without tangents to a smoothly varying trajectory is greatly lengthened, making it possible to study the kinetic regime by dynamic light scattering. Our recent experiments with particles in a plasma have demonstrated this capability. In this regime, the particle velocity persists over a finite "step length" allowing an analogy to an ideal gas with Maxwell-Boltzmann velocities; the particle mass could be obtained from equipartition. The cross over from ballistic flight to hydrodynamic diffusion was also seen.

This work was supported by Sandia National Laboratories under Department of Energy Contract No. DE-AC04-76-DP00789.

T9.6

EQUILIBRIUM SIZE AND SHAPE OF RANDOM AGGREGATES. H. C. AKUEZUE, and J. STRINGER, Electric power research Institute, Palo Alto, California 94303.

Random growth patterns can be observed in most physical systems that have evolved as a result of phase transformation reaction or diffusion. Thus a means whereby random growth phenomena can be fully understood and characterized is a topic of continued theoretical and practical interest. During random aggregation, the center of mass of the growing aggregate moves randomly much like a random-walker. The mean displacement of the center of mass is given by:

$$|r_i| \sim s^{(1/D)-1} \quad 1.$$

And:

$$\sum_i r_i \sim s^{1/D} \quad 2.$$

Large-scale computer simulation of DLA ($s \sim 10^6$) indicate D is different from the original calculated value of 1.66 by Sander and Witten based on cluster size of ~ 3600 . From equation 1 $|r| \rightarrow 0$ as $s \rightarrow \infty$ so that equation 2 can only be valid over certain s interval. As a consequence, representations 1 and 2 appear to be not valid in the cases of large-scale computer simulation results! The compromise can be recast in the form of the question: ARE THERE EQUILIBRIUM SIZES AND SHAPES (fractal Dimensions) IN RANDOM AGGREGATION? Kinetically and thermodynamically, the answer is yes. The kinetic equation that answers this intriguing question is discussed in terms of the fractal dimension and the parameters associated with the phenomena of the random-walking center of mass.

T9.7

SELF-ORDERING AND KINETICS OF EXCITATIONS IN LOW DIMENSIONS AND DISORDERED MEDIA. Raoul Kopelman, Lola W. Anacker, Panos Argyrakis, Eric Clement, Laurel Harmon, Li Li, James S. Newhouse, Stephen J. Parus, and Rodney Schoonover, Department of Chemistry, The University of Michigan, Ann Arbor, MI, 48109-1055; and Leonard Sander, Department of Physics, The University of Michigan, Ann Arbor, MI 48109-1120.

Diffusion-limited reaction kinetics becomes anomalous not only for fractals, with their anomalous diffusion, but also for low-dimensional (one and two) and disperse media, where the random walk is compact. We focus on annihilation, recombination and trapping reactions under non-equilibrium steady state (steady source) or batch (big bang) conditions. The typical reactions are: $A + A \rightarrow \text{Products}$, $A + B \rightarrow \text{Products}$ and $A + C \rightarrow C + \text{Products}$. We are interested in the global rate laws, and their relation to particle-particle distributions (e.g., pair-correlation and nearest-neighbor distribution functions) and in local rate laws (if definable). Anomalous reaction kinetics (more than classical kinetics) is particularly sensitive to initial conditions, source term structure, conservation laws (e.g., equal densities for A and B), excluded volume effects, and medium size, dimensionality and anisotropy. Analytical formalisms, scaling arguments, computer (and supercomputer) simulations and experiments (on chemical and physical reactions) all play an important role in the newly emerging picture.

1. L. W. Anacker and R. Kopelman, Phys. Rev. Lett. **58**, 289 (1987).

2. J. Prasad and R. Kopelman, Phys. Rev. Lett. **59**, 2103 (1987).

3. K. Lindenberg, B. J. West and R. Kopelman, Phys. Rev. Lett. **60**, 1777 (1988).

4. R. Kopelman, SCIENCE **241**, 1620 (1988).

T9.8

FRACTAL-LIKE EXCITON FUSION KINETICS IN DILUTE POLYMER BLENDS. Raoul Kopelman, Ching-Shan Li and Zhong-You Shi, Department of Chemistry, The University of Michigan, Ann Arbor, MI 48109-1055.

Exciton-exciton and exciton-excimer triplet fusion kinetics is monitored in medium molecular weight P1VN/PMMA films with concentrations from 0.005 to 100% (weight), at temperatures of 77 to 300 K, via time resolved fluorescence and phosphorescence (10 ns to 10 sec). The triplet-triplet annihilation is bimolecular at short times but pseudo-monomolecular at long times. Furthermore, the heterogeneity exponent (h) is 0.5 for isolated P1VN chains, zero (classical) for pure P1VN and "fractal-like" ($0 < h < 0.5$) throughout certain concentration regimes. However, h is not monotonic with blend concentration but rather oscillates between zero and 0.5. Correlation is made with morphology changes (phase separation, filamentation). The long-lived decays do fit stretched exponentials, with a parameter $\beta = 1 - h$. Distinction is also made between diffusion-limited and reaction-limited kinetic regimes. Furthermore, the blend topology is also studied with the aid of the time-modulation technique, in which the time-decays are obtained for different excitation durations, i.e., single pulse vs. cw or multiple-pulse laser excitation, but with equal global exciton densities at the start ($t = 0$) of the decays. As expected, the triplet exciton kinetics is dominated by short-range hops (about 5 Å) and thus monitors the primary topology of the chains. At concentrations below 0.01%, the excitons are constrained to a truly one-dimensional topology. At higher concentrations there is a fractal-like topology.

T9.9

GROWTH PROBABILITY DISTRIBUTION OF DISCONTINUOUSLY BRANCHING TREE MORPHOLOGY DEVELOPED AT AgCo/NaCl INTERFACE BY ION IRRADIATION. B.X.Liu, Center of Condensed Matter and Radiation Physics CCAST(World Lab.), Beijing and Dept. of Materials Science and Engineering, Tsinghua University, Beijing 100084, CHINA; and C.H. Shang, Dept. of Materials Science and Engineering, Tsinghua University, Beijing 100084, CHINA.

Discontinuously branching tree morphology (DBTM) is a new class of fractal structure having many common features with the lattice animals. Unlike all the previous observed fractal objects, DBTM patterns are composed of separated chain-like single-crystalline NaCl particles. Each DBTM can be viewed as a two-dimensional tree, which extends to a scale of 100 μm with self-similarity.

The scaling structures of the growth probability distribution were studied by putting a DBTM pattern in the Laplace field, and then measuring the growth probability as $P(\vec{r}, t) \sim |\nabla \phi(\vec{r}, t)|$.

The generalized dimensions $D(q)$ with $q \in (-10, 10)$, and the $f-\alpha$ formalism were also calculated to unravel the properties of the dynamic growth process.

**SYMPOSIUM U:
SCIENTIFIC BASIS FOR NUCLEAR
WASTE MANAGEMENT XIII**



November 27-30, 1989

Chairs

Virginia M. Oversby
Mail Stop L-310
Lawrence Livermore National Laboratory
P.O. Box 808
Livermore, CA 94550
(415) 423-2228

Paul W. Brown
168 Materials Research Laboratory
Pennsylvania State University
University Park, PA 16802
(814) 865-5352

Symposium Support

U.S. Department of Energy

**Proceedings published as Volume 176
of the Materials Research Society
Symposium proceedings series.**

SCIENTIFIC BASIS FOR NUCLEAR
WASTE MANAGEMENT XIII

November 27-30, 1989

SESSION U1: CEMENTITIOUS MATERIALS -
ASPECTS OF PERFORMANCE

Chairs: Paul Brown
Monday Morning, November 27
America North (W)

8:15 OPENING REMARKS

8:30 U1.1
NUCLEAR WASTE IMMOBILIZATION IN CEMENT-BASED MATERIALS: OVERVIEW OF FRENCH STUDIES, Pascal Bouniol, Eliane Revertegat, Jean Oliver, Philippe Gegout, Michel Jorda and Rosemarie Atabek, C.E.A, DRDD/SESD, CEN/FAR, Fontenay aux Roses, France.

9:00 U1.2
EFFECT OF CURING TEMPERATURE ON THE PROPERTIES OF CEMENTITIOUS WASTE FORMS, Ryan O. Lokken, John W. Shade and Paul F.C. Martin, Battelle-Pacific Northwest Laboratory, Richland, WA.

9:30 U1.3
BEHAVIOR OF CONCRETE AS A BARRIER MATERIAL FOR NUCLEAR WASTE DISPOSAL, R.J. James and Y.R. Rashid, ANATECH Research Corporation, La Jolla, CA.

9:45 U1.4
GROUTS AND CONCRETES FOR THE WASTE ISOLATION PILOT PROJECT (WIPP), Lillian D. Wakeley, U.S. Army Engineer Waterways Experiment Station, Vicksburg, MS.

10:00 BREAK

SESSION U2: CEMENTITIOUS MATERIALS -
ASPECTS OF DURABILITY

Chair: William Richmond
Monday Morning, November 27
America North (W)

10:30 *U2.1
ASSESSMENT OF THE PERFORMANCE OF CEMENT BASED COMPOSITE MATERIAL FOR RADIOACTIVE WASTE IMMOBILIZATION, M. Atkins, J. Cowie, F.P. Glasser, T. Jappy, A. Kindness and C. Pointer, University of Aberdeen, Department of Chemistry, Aberdeen, Scotland.

11:00 U2.2
DURABLE CONCRETE FOR A WASTE REPOSITORY-MEASUREMENT OF IONIC INGRESS, R.F. Feldman, J.J. Beaudoin, Institute for Research in Construction, National Research Council, Ottawa, Canada; and K.E. Philipose, Atomic Energy of Canada, Ltd., Waste Management Systems, Ontario, Canada.

*Invited Paper

11:30 U2.3
LOGNORMAL SIMULATION OF PORE EVOLUTION DURING CEMENT HARDENING, D. Shi, W. Ma and P.W. Brown, The Pennsylvania State University, Materials Research Laboratory, University Park, PA.

11:45 U2.4
MECHANISTIC MODEL FOR THE DURABILITY OF CONCRETE BARRIERS EXPOSED TO SULPHATE-BEARING GROUNDWATERS, Alan Atkinson and John A. Hearne, Harwell Laboratories, Materials Development Division, Oxon, United Kingdom.

SESSION U3: SORPTION AND
SPECIATION STUDIES

Chair: Greg Choppin
Monday Afternoon, November 27
America North (W)

1:30 U3.1
THE SOLUBILITY AND SORPTION OF URANIUM (VI) IN A CEMENTITIOUS REPOSITORY, M. Brownsword, A.B. Buchan, F.T. Ewart, R. McCrohon, G.J. Ormerod, J.L. Smith-Briggs and H.P. Thomason, Harwell Laboratory, Chemistry Division, Oxfordshire, United Kingdom.

1:45 U3.2
SPECIATION OF Pu(VI) IN NEAR-NEUTRAL TO BASIC SOLUTIONS VIA LASER PHOTOACOUSTIC SPECTROSCOPY, S. Okajima, J.V. Beitz, J.C. Sullivan and D.T. Reed, Argonne National Laboratory, Argonne, IL.

2:00 U3.3
MODELLING STUDIES OF SORPTION IN THE NEAR FIELD OF A CEMENTITIOUS REPOSITORY, A. Haworth, S.M. Sharland and C.J. Tweed, UKAEA, Harwell Laboratory, Theoretical Physics Division, Oxfordshire, United Kingdom.

2:30 U3.4
EVIDENCE OF LONG DISTANCE TRANSPORT OF NATURAL COLLOIDS IN A CRYSTALLINE ROCK GROUNDWATER, W.R. Alexander, R. Bruetsch, C. Degueldre, Paul Scherrer Institute, Villigen, Switzerland; and B. Hofmann, USGS, Denver, CO.

3:00 U3.5
ANALYTIC STUDIES OF COLLOID TRANSPORT, Y. Hwang, T.H. Pigford, P.L. Chambré, and W.W.-L. Lee, University of California, Berkeley, Department of Nuclear Engineering and Lawrence Berkeley Laboratory, Berkeley, CA.

3:15 BREAK

SESSION U4: CEMENTITIOUS MATERIALS -
ASPECTS OF LEACHING

Chair: William Bostick
Monday Afternoon, November 27
America North (W)

3:30 *U4.1

THE MICROSTRUCTURE OF ggbfs/OPC HARDENED CEMENT PASTES AND SOME EFFECTS OF ELEVATED TEMPERATURE LEACHING, I.G. Richardson, S.A. Rodger and G.W. Groves, University of Oxford, Department of Metallurgy and Science of Materials, Oxford, United Kingdom.

4:00 U4.2

THE EFFECTS OF TEMPERATURE ON THE LEACHING BEHAVIOR OF CEMENT WASTE FORMS, Mark Fuhrmann, Richard Pietrzak, John Heiser III, Eena-Mai Franz and Peter Colombo, Brookhaven National Laboratory, Radiological Sciences Division, Nuclear Waste Research Group, Upton, NY.

4:15 U4.3

THERMODYNAMIC MODELING OF CEMENTITIOUS WASTE FORM/GROUNDWATER INTERACTION AS A TOOL FOR LONG-TERM PERFORMANCE ASSESSMENT, Louise J. Criscenti and R. Jeff Serne, Battelle-Pacific Northwest Laboratory, Richland, WA.

4:30 U4.4

WASTE GROUT LEACH TESTS: PURSUIT OF MECHANISMS AND DATA FOR LONG-TERM PERFORMANCE ASSESSMENT, R. Jeff Serne, Battelle-Pacific Northwest Laboratory, Richland, WA.

SESSION U5: MODELING THE DISSOLUTION OF
NUCLEAR WASTE FORMS

Chairs: Werne Lutze and Carol Jantzen
Tuesday Morning, November 28
America North (W)

8:30 *U5.1

THERMODYNAMICS OF GLASSES FOR NUCLEAR WASTE DISPOSAL, Alexandra Navrotsky, Princeton University, Department of Geological and Geophysical Sciences, Princeton, NJ.

9:00 U5.2

A KINETIC MODEL FOR BOROSILICATE GLASS DISSOLUTION BASED ON THE DISSOLUTION AFFINITY OF A SURFACE ALTERATION LAYER, William L. Bourcier, Dennis W. Peifer, Kevin G. Knauss, Kevin D. McKeegan and David K. Smith, Lawrence Livermore National Laboratory, Livermore, CA.

9:30 U5.3

PREDICTION OF RADIOACTIVE WASTE GLASS DURABILITY BY THE HYDRATION THERMODYNAMIC MODEL: APPLICATION TO SATURATED REPOSITORY ENVIRONMENTS, Carol M. Jantzen, Westinghouse Savannah River Company, Aiken, SC.

10:00 BREAK

10:30 U5.4

CHEMISTRY OF GLASS CORROSION IN HIGH SALINE BRINES, B. Grambow, R. Müller, Hahn-Meitner-Institut Berlin, Berlin, Germany.

11:00 U5.5

THERMOKINETIC MODEL OF BOROSILICATE GLASS DISSOLUTION: CONTEXTUAL AFFINITY, T. Advocat, E. Vernaz, CEN-Valrhô, SDHA, Bagnols-sur-Cèze, France; J.L. Crovisier and B. Fritz, CNRS/CSGS, Strasbourg, France.

11:30 U5.6

COMPARISON OF THE LAYER STRUCTURE OF VAPOR PHASE AND LEACHED SRL GLASS BY USE OF AEM, B.M. Biwer, J.K. Bates, T.A. Abrajano Jr., Argonne National Laboratory, Argonne, IL; and J.P. Bradley, McCrone Environmental Services, Inc., Westmont, IL.

11:45 U5.7

DISSOLUTION MECHANISMS OF CaTiO_3 AND OTHER TITANATE PHASES IN THE SYNROC ASSEMBLAGE, S. Myhra, D.K. Pham, Griffith University, Division of Science and Technology, Nathan, Qld, Australia; R. St.C. Smart, South Australian Institute of Technology, School of Chemical Technology, Adelaide, Australia; and P.S. Turner, Griffith University, Division of Science and Technology, Nathan, Qld, Australia.

SESSION U6: WASTE GLASS
PERFORMANCE STUDIES

Chairs: Ned Bibler and Claude Sombret
Tuesday Afternoon, November 28
America North (W)

1:30 U6.1

A COMPARISON OF THE BEHAVIOR OF VITRIFIED HLW IN REPOSITORIES IN SALT, CLAY AND GRANITE. PART II: RESULTS, W. Lutze, Hahn-Meitner-Institut, Berlin, West Germany; M. Kawanishi, Abico Research Laboratory, Abico, Japan; J.A.C. Marples, Harwell Laboratory, Oxon, United Kingdom; and P. Van Iseghem, SCK/CEN, Mol, Belgium.

2:00 U6.2

COMPARISON OF SURFACE LAYERS FORMED ON SYNTHETIC BASALTIC GLASS, FRENCH R7T7 AND HMI BOROSILICATE NUCLEAR WASTE FORM GLASSES - MATERIALS INTERFACE INTERACTIONS TESTS, Michael J. Jercinovic, Stacy Kaser, Rodney C. Ewing, University of New Mexico, Department of Geology, Albuquerque, NM; and Werner Lutze, Hahn Meitner Institut, Berlin, West Germany.

2:30 U6.3

THE INTERACTION BETWEEN NUCLEAR WASTE GLASSES AND CLAY-II, P. Van Iseghem, K. Berghman and W. Timmermans, SCK/CEN, Mol, Belgium.

3:00 BREAK

3:30 U6.4
R7-T7 NUCLEAR WASTE GLASS BEHAVIOR IN MOIST CLAY: ROLE OF THE CLAY MASS/GLASS SURFACE AREA RATIO, N. Godon and E. Vernaz, CEN-Valrhô, SDHA/SEMC, Bagnols-sur-Cèze, France.

4:00 U6.5
PRODUCT CONSISTENCY LEACH TESTS OF SAVANNAH RIVER SITE RADIOACTIVE WASTE GLASSES, Ned E. Bibler, Westinghouse Savannah River Company, Aiken, SC; and John K. Bates, Argonne National Laboratory, Argonne, IL.

4:30 U6.6
THE REACTION OF SYNTHETIC NUCLEAR WASTE GLASS IN STEAM AND HYDROTHERMAL SOLUTION, W.L. Ebert and J.K. Bates, Argonne National Laboratory, Argonne, IL.

SESSION U7: POSTER SESSION
Tuesday Evening, November 28
7:00 - 10:00 p.m.
America Ballroom (W)

U7.1 ESTIMATION OF LONGEVITY OF PORTLAND CEMENT GROUT USING CHEMICAL MODELING TECHNIQUES, Stephen R. Alcorn, Mark A. Gardiner, IT Corporation, Albuquerque, NM; and William E. Coons, RE/SPEC, Inc., Albuquerque, NM.

U7.2 MODELLING OF THE EVOLUTION OF POREWATER CHEMISTRY IN A CEMENTITIOUS REPOSITORY, A. Haworth, S.M. Sharland and C.J. Tweed, UKAEA, Harwell Laboratory, Theoretical Physics Division, Oxfordshire, United Kingdom.

U7.3 A THEORETICAL STUDY OF THE EFFECT OF THE LEACH INTERVAL ON A SEMIDYNAMIC LEACH TEST, Roger D. Spence, Oak Ridge National Laboratory, Oak Ridge, TN.

U7.4 INTERACTION BETWEEN BLENDED CEMENTS AND A SULPHATE BEARING GROUND WATER, Susan L. Duerden, Peter L. Walton, and Amal J. Majumdar, Building Research Station, Watford, United Kingdom.

U7.5 (ABSTRACT WITHDRAWN)

U7.6 IMMOBILIZATION IN CEMENT OF ION EXCHANGE RESINS, Patrick Le Bescop, Pascal Bouniol and Michel Jorda, CEN, DRDD/SESD, CEN-FAR, Fontenay aux Roses, France.

U7.7 ENCAPSULATION OF RADIOIODINE IN CEMENTITIOUS WASTE FORMS, Mark Atkins and Frederik P. Glasser, University of Aberdeen, Department of Chemistry, Aberdeen, Scotland.

U7.8 EFFECT OF γ -RADIATION ON THE MICROSTRUCTURE AND MICROCHEMISTRY OF ggbfs/OPC CEMENT BLENDS, I.G. Richardson and G.W. Groves, University of Oxford, Department of Metallurgy and Science of Materials, Oxford, United Kingdom; and C.R. Wilding, UKAEA Harwell Laboratory, Materials Development Division, Oxfordshire, United Kingdom.

U7.9 HYDROGEN GENERATION IN MORTARS IMMOBILIZING WASTE CHLORIDE SALTS, Michele A. Lewis and David W. Warren, Argonne National Laboratory, Argonne, IL.

U7.10 POROSITY AND ION DIFFUSIVITY OF LATEX-MODIFIED CEMENT, T. Nishi, O. Kuriyama, M. Matsuda, K. Chino, Hitachi Ltd., Energy Research Laboratory, Hitachi, Japan; and M. Kikuchi, Hitachi Ltd., Hitachi Works, Hitachi, Japan.

U7.11 A COMPARISON OF THE BEHAVIOUR OF VITRIFIED HLW IN REPOSITORIES IN SALT, CLAY AND GRANITE. PART I: EXPERIMENTAL, L.A. Mertens, W. Lutze, Hahn-Meitner-Institut, Berlin, West Germany; J.A.C. Marples, Harwell Laboratory, Oxon, United Kingdom; and P. Van Iseghem, SCK/CEN, Mol, Belgium; E. Vernaz, CEA Valrhô, Bagnols-sur-Cèze, France.

U7.12 IN-SITU TESTING OF NUCLEAR WASTE FORMS IN A CLAY LABORATORY - RESULTS AFTER TWO YEARS CORROSION, P. Van Iseghem, W. Timmermans and B. Neerdael, SCK/CEN, Mol, Belgium.

U7.13 DISSOLUTION KINETICS OF A SIMPLE ANALOGUE NUCLEAR WASTE GLASS AS A FUNCTION OF pH, TIME AND TEMPERATURE, Kevin G. Knauss, William L. Bourcier, Kevin D. McKeegan, Celia I. Merzbacher, Son N. Nguyen, Frederick J. Ryerson, David K. Smith and Homer C. Weed, Lawrence Livermore National Laboratory, Livermore, CA.

U7.14 HYDROTHERMAL LEACHING OF R7-T7 BOROSILICATE GLASS, J. Caurel and E. Vernaz, CEN-Valrhô, SDHA/SEMC, Bagnols-sur-Cèze, France; D. Beaufort, Université de Poitiers, Laboratoire de Pétrologie des Alterations Hydrothermales, Poitiers, France.

U7.15 EFFECTS OF SURFACE-AREA-TO-SOLUTION VOLUME RATIO ON THE CHEMICAL DURABILITY OF NUCLEAR WASTE GLASSES, X. Feng, I.L. Pegg, Aa. Barkatt, P.B. Macedo, Catholic University of America, Vitreous State Laboratory, Washington, DC.

U7.16 ALTERATION OF MICROSTRUCTURE AND LEACHING PROPERTIES OF WEST VALLEY REFERENCE BY HEAT TREATMENT, A.C. Buechele, X. Feng, H. Gu, and I.L. Pegg, The Catholic University of America, Vitreous State Laboratory, Washington, DC.

U7.17 PARAMETRIC EFFECTS OF GLASS REACTION UNDER UNSATURATED CONDITIONS, J.K. Bates, T.J. Gerding and D.J. Wronkiewicz, Argonne National Laboratory, Argonne, IL.

U7.18 GROWTH RATES OF ALTERATION LAYERS AND ELEMENTAL MASS LOSSES DURING LEACHING OF BOROSILICATE NUCLEAR WASTE GLASS, Tsunetaka Banba and Takashi Murakami, Japan Atomic Energy Research Institute, Ibaraki, Japan.

U7.19 CHARACTERIZATION OF HIGHLY ACTIVE WASTES PRODUCED IN A HOT VITRIFICATION PLANT, J.P. Glatz, E. Toscano, M. Coquerelle and J. Fuger, Institute for Transuranium Elements, Commission of the European Communities, Karlsruhe, West Germany.

U7.20 THE LONG-TERM CORROSION AND MODELING OF TWO SIMULATED BELGIAN REFERENCE HIGH-LEVEL WASTE GLASSES - PART II, J. Patyn, P. Van Iseghem, W. Timmermans, SCK/CEN, Mol, Belgium.

U7.21 SIMULTANEOUS EVAPORATION OF Cs AND Tc DURING VITRIFICATION - A THERMOCHEMICAL APPROACH, H. Migge, Hahn-Meitner-Institut, Berlin, West Germany.

U7.22 THE EFFECT OF TEMPERATURE ON THE REDOX CONSTRAINTS FOR THE PROCESSING OF HIGH-LEVEL NUCLEAR WASTE INTO A GLASS WASTE FORM, Henry D. Schreiber, Charlotte W. Schreiber, Margaret W. Riethmiller and J. Sloan Downey, Virginia Military Institute, Center for Glass Chemistry, Lexington, VA.

U7.23 CALCULATION OF THE VISCOSITY OF NUCLEAR WASTE GLASS SYSTEMS, Ritesh P. Shah, E.C. Behrman and D. Oksoy, Alfred University, New York State College of Ceramics, Alfred, NY.

U7.24 CHARACTERIZATION OF MECHANICAL STRENGTHS FOR SIMULATED SOLIDIFIED HIGH LEVEL WASTE FORMS, Hiroshi Igarashi, Takeshi Takahashi, Power Reactor and Nuclear Fuel Development Corporation, Ibaraki, Japan.

U7.25 DIFFUSION OF CESIUM IN SODIUM-BOROSILICATE GLASSES USED FOR IMMOBILISATION OF NUCLEAR WASTE, E.G.F. Sengers and F.J.J.G. Janssen, N.V. Kema, R&D Division, Chemical Research Department, Et Arnhem, The Netherlands.

U7.26 ENTHALPIES OF MIXING AND INCIPIENT IMMISCIBILITY IN GLASSES IN THE SYSTEM $K_2O-SiO_2-La_2O_3$, A.J.G. Ellison and A. Navrotsky, Princeton University, Department of Geological and Geophysical Sciences, Princeton, NJ.

U7.27 GRAIN BOUNDARY INVENTORY AND UO_2 MATRIX DISSOLUTION STUDIES ON SPENT LWR FUEL, W.J. Gray, D.M. Strachan, and M.J. Apted, Battelle-Pacific Northwest Laboratory, Richland, WA.

U7.28 IDENTIFICATION OF SECONDARY PHASES FORMED DURING UNSATURATED REACTION OF UO_2 WITH EJ-13 WATER, J.K. Bates, B.S. Tani and E. Veleckis, Argonne National Laboratory, Argonne, IL.

U7.29 INVESTIGATIONS INTO THE ELECTRO-CHEMICAL LEACHING BEHAVIOUR OF UO_2 PELLETS IN VARIOUS SATURATED SALT SOLUTIONS, Ch. Keilling, P.-M. Heppner and G. Marx, Free University of Berlin, Institute for Inorganic and Analytical Chemistry, Radiochem. Division, Berlin, West Germany.

U7.30 A DEFORMATION AND THERMODYNAMIC MODEL FOR HYDRIDE PRECIPITATION KINETICS IN SPENT FUEL CLADDING, R.B. Stout, University of California, Lawrence Livermore National Laboratory, Livermore, CA.

U7.31 FLUORIDE INFLUENCE ON ZIRCALOY-4 CORROSION IN WATER AS A FUNCTION OF pH, TEMPERATURE AND FLUORIDE CONTENT, N.H. Uziemblo and H.D. Smith, Battelle-Pacific Northwest Laboratory, Richland, WA.

U7.32 CORROSION BEHAVIOR OF ZIRCALOY IN AQUEOUS MEDIA, Anna C. Fraker and Jonice S. Harris, National Institute of Standards and Technology, Gaithersburg, MD.

U7.33 POTENTIODYNAMIC POLARIZATION STUDIES OF CANDIDATE CONTAINER MATERIALS IN SIMULATED TUFF REPOSITORY ENVIRONMENTS, John A. Beavers and Neil G. Thompson, Cortest Columbus, Inc., Columbus, OH.

U7.34 MIGRATION BEHAVIOR OF URANIUM SERIES NUCLIDES IN ALTERED QUARTZ-CHLORITE SCHIST, T. Ohnuki, T. Murakami, K. Sekine, N. Yanase, H. Isobe and Y. Kobayashi, Japan Atomic Energy Research Institute, Department of Environmental Safety Research Institute, Ibaraki, Japan.

U7.35 MIGRATION OF ANIONIC SPECIES OF RADIOACTIVE COBALT THROUGH SOIL, Toshihiko Ohnuki, Japan Atomic Energy Research Institute, Department of Environmental Safety Research, Ibaraki, Japan; and David E. Robertson, Battelle-Pacific Northwest Laboratory, Chemical Science Department, Richland, WA.

U7.36 STUDY ON RELATION BETWEEN MIGRATION BEHAVIORS AND CHEMICAL FORMS OF COBALT, Shinzo Ueta, Naka Nuclear Development Center of Mitsubishi Metal Corporation, Ibaraki, Japan; and Naotake Katoh, Kogakuin University, Tokyo, Japan.

U7.37 GRIMSEL COLLOID EXERCISE, C. Degueldre, Paul Scherrer Institute, Villingen, Switzerland.

U7.38 AUTHIGENIC CLAY MINERALS IN THE RUSTLER FORMATION. WIPP SITE AREA, NEW MEXICO, Douglas G. Brookins, University of New Mexico, Department of Geology, Albuquerque, NM; Steven J. Lambert, Sandia National Laboratories, Albuquerque, NM; and David B. Ward, University of New Mexico, Albuquerque, NM.

U7.39 IN SITU OBSERVATION OF THE ALPHA/BETA-CRISTOBALITE TRANSITION USING HIGH VOLTAGE ELECTRON MICROSCOPY, Annemarie Meike, Lawrence Berkeley Laboratory, Materials and Chemical Sciences Division, Berkeley, CA; and William Glassley, Lawrence Livermore National Laboratory, Earth Sciences Division, Livermore, CA.

U7.40 ESTIMATION OF LONG-TERM DURABILITY OF BENTONITE FROM THE THERMAL HISTORY OF MURAKAMI DEPOSIT, JAPAN, G. Kamei, T. Arai, Y. Yusa, N. Sasaki, Power Reactor and Nuclear Fuel Development Company, Ibaraki, Japan; H. Takano, Dia Consultants Company, Tokyo, Japan.

U7.41 DIFFUSION OF SODIUM AND COPPER IN COMPACTED SODIUM BENTONITE AT ROOM TEMPERATURE, A. Muurinen, K. Uusheimo and M. Olin, Technical Research Centre of Finland, Reactor Laboratory, Espoo, Finland.

U7.42 THERMAL BEHAVIOUR OF BACKFILL MATERIAL FOR A NUCLEAR FUEL WASTE DISPOSAL VAULT, R.N. Yong and A.M.O. Mohamed, McGill University, Geotechnical Research Centre, Montreal, Canada; and S.C.H. Cheung, Atomic Energy of Canada Limited, Whiteshell Nuclear Research Establishment, Pinawa, Canada.

U7.43 A COUPLED CHEMICAL-MASS TRANSPORT SUBMODEL FOR PREDICTING RADIONUCLIDE RELEASE FROM AN ENGINEERED BARRIER SYSTEM CONTAINING HIGH-LEVEL WASTE GLASS, B.P. McGrail, D.W. Engel, M.J. Apted, A.M. Liebetrau, Battelle-Pacific Northwest Laboratory, Richland, WA; and N. Sasaki, Power Reactor and Nuclear Fuel Development Corporation, Ibaraki-ken, Japan.

U7.44 (ABSTRACT WITHDRAWN)

SESSION U8: SPENT FUEL PERFORMANCE

Chair: Lars Werme

Wednesday Morning, November 29
America North (W)

8:00 *U8.1
ACTINIDES CHEMISTRY AND SPENT FUEL PERFORMANCE STUDIES, G. Choppin

8:30 U8.2
OXIDATION OF UO_2 FUEL BY RADICALS FORMED DURING RADIOLYSIS OF WATER, S. Sunder, D.W. Shoesmith, Atomic Energy of Canada Limited, Whiteshell Nuclear Research Establishment, Geochemistry and Waste Immobilization Division, Pinawa, Canada; H. Christensen, Studsvik Energiteknik AB, Nyöping, Sweden; N.H. Miller and M.G. Bailey, Atomic Energy of Canada Limited, Whiteshell Nuclear Research Establishment, Geochemistry and Waste Immobilization Division, Pinawa, Canada.

9:00 U8.3
CONSTRAINTS BY EXPERIMENTAL DATA FOR MODELING OF RADIONUCLIDE RELEASE FROM SPENT FUEL, B. Grambow, Hahn-Meitner-Institut Berlin, Berlin, West Germany; L.O. Werme, SKB, Stockholm, Sweden; R. Forsyth, Studsvik Energiteknik AB, Nyköping, Sweden; and J. Bruno, Royal Institut of Technology, Department of Inorganic Chemistry, Stockholm, Sweden.

9:30 U8.4
STATISTICAL MODEL FOR GRAIN BOUNDARY AND GRAIN VOLUME OXIDATION KINETICS IN UO_2 SPENT FUEL, R.B. Stout, H.F. Shaw, University of California, Lawrence Livermore National Laboratory, Livermore, CA; and R.E. Einziger, Battelle-Pacific Northwest Laboratory, Richland, WA.

9:45 U8.5
MEASUREMENT OF SOLUBLE NUCLIDE DISSOLUTION RATES FROM SPENT FUEL, Charles N. Wilson, Battelle-Pacific Northwest Laboratory, Richland, WA.

10:00 BREAK

SESSION U9: CONTAINER AND FUEL CLADDING STUDIES

Chair: Sham Sunder

Wednesday Morning, November 29
America North (W)

10:30 U9.1
THEORETICAL MODELING OF CREVICE AND PITTING CORROSION PROCESSES IN RELATION TO CORROSION OF RADIOACTIVE WASTE CONTAINERS, John C. Walton, Idaho National Engineering Laboratory, Idaho Falls, ID.

11:00 U9.2
CORROSION PRODUCT IDENTIFICATION AND RELATIVE RATES OF CORROSION OF CANDIDATE METALS IN AN IRRADIATED AIR-STEAM ENVIRONMENT, Donald T. Reed, V. Swayambunathan, Argonne National Laboratory, Argonne, IL; and Richard A. Van Konynenburg, Lawrence Livermore National Laboratory, Yucca Mountain Project, Livermore, CA..

11:15 U9.3
A STUDY ON FABRICATION TECHNOLOGY OF CERAMIC OVERPACK - A CONCEPTUAL DESIGN AND FABRIAC-TION OF A FULL SCALE CERAMIC OVERPACK, T. Teshima, Y. Karita, NGK Insulators, Ltd., Nagoya, Japan; H. Ishikawa and N. Sasaki, Power Reactor and Fuel Development Corpora-tion, Ibaraki, Japan.

11:30 U9.4
AN INTERPRETATION OF THE HIGH-STRESS, LOW-TEMPERATURE CRACKING OF ZIRCALOY-4 SPENT FUEL CLADDING, H.D. Smith, Battelle-Pacific Northwest Laboratory, Richland, WA.

11:45 U9.5
A CORROSION LOCALIZATION ASSESSMENT OF THE MILD STEEL USED FOR NUCLEAR WASTE PACKAGE, Masatsune Akashi, Ishikawajima-Harima Heavy Industries Company, Ltd., Research In-stitute, Tokyo, Japan.

SESSION U10/T4: JOINT SESSION
SIZING AND SCALING EFFECTS

Chairs: Jim Kaufman and Virginia Oversby
Wednesday Afternoon, November 29
America North (W)

1:30 *U10.1/T4.1
FRACTAL STRUCTURE AND DYNAMICS OF TWO FLUID FLOW IN POROUS MEDIA, Jens Feder, University of Oslo, Department of Physics, Oslo, Nor-way.

2:00 U10.2/T4.2
NUMERICAL AND ANALYTICAL MODELS OF TRANSPORT IN POROUS CEMENTITIOUS MATERIALS, Edward J. Garboczi and Dale P. Bentz, National In-stitute of Standards and Technology, Build-ing Materials Division, Gaithersburg, MD.

2:15 U10.3/T4.3
SIZING REQUIREMENTS FOR FLOW-THROUGH GEOCHE-MICAL TESTS: THEORETICAL CONSIDERATIONS, MODEL RESULTS, AND IMPLICATIONS FOR THE INTERPRETATION OF TEST DATA, J.D. Hoover and E.C. Thornton, Westinghouse Hanford Company, Richland, WA.

2:30 U10.4/T4.4
A LAGRANGIAN REACTIVE TRANSPORT SIMULATOR WITH MULTIPLE PATHS AND STATIONARY-STATES: CONCEPTS, IMPLEMENTATION AND VERIFICATION, R.B. Knapp, University of California, Lawr-ence Livermore National Laboratory, Earth Sciences Department, Livermore, CA.

2:45 BREAK

3:15 U10.5/T4.5
FRACTAL CHARACTERISTICS OF FRACTURE NETWORKS AND FLUID MOVEMENT IN ROCK, Christopher C. Barton, U.S.Geological Survey, Department MS 913, Denver, CO.

3:45 U10.6/T4.6
FLOW TO WELLS IN FRACTURED ROCK WITH FRACTAL STRUCTURE, Jim Polek, Kenzi Karasaki and Jane Long, Lawrence Berkeley Laboratory, Berkeley, CA; and John Barker, British Geological Survey, Oxfordshire, United Kingdom.

4:00 U10.7/T4.7
ANISOTROPIC SCALING OF INTERFACES IN POROUS MEDIA, Miguel A. Rubio, Haverford College, Department of Physics, Haverford, PA; and UNED, Madrid, Spain; Andrew Dougherty, Haverford College, Department of Physics, Haverford, PA; and Jerry P. Gollub, Haver-ford College, Department of Physics, Haver-ford, PA; and University of Pennsylvania, Philadelphia, PA.

4:15 U10.8/T4.8
SIZING AND SCALING REQUIREMENTS OF A LARGE-SCALE PHYSICAL MODEL FOR CODE VALIDATION, R. Khaleel, T. LeGore and J.D. Hoover, West-inghouse Hanford Company, Richland, WA.

4:30 U10.9/T4.9
PERFORMANCE OF CONCRETE BARRIERS IN RADIOAC-TIVE WASTE DISPOSAL IN THE UNSATURATED ZONE, John C. Walton and Mark D. Otis, ID National Engineering Laboratory, Idaho Falls, ID.

SESSION U11: NEAR-FIELD STUDIED AND
PERFORMANCE ASSESSMENT

Chair: Henry Shaw
Thursday Morning, November 30
America North (W)

8:30 U11.1
LEACHING/MIGRATION OF UO₂-FUEL IN COMPACTED BENTONITE, Y. Albinsson, G. Skarnemark, M. Skälberg, Chalmers University of Technology, Department of Nuclear Chemistry, Göteborg, Sweden; R. Forsyth, Studsvik AB, Nyköping, Sweden; B. Torstenfelt, ABB-Atom, Västerås, Sweden; L. Werme, Swedish Nuclear Fuel and Waste Management, Stockholm, Sweden.

9:00 U11.2
MODELLING THE IN SITU PERFORMANCE OF BENTONITE-SAND BUFFER, H.S. Radhakrishna, K.-C. Lau, Ontario Hydro Research Division, Toronto, Canada; B.H. Kjartanson and S.C.H. Cheung, Atomic Energy of Canada Ltd., Whiteshell Nuclear Research Establishment, Pinawa, Canada.

9:15 U11.3
THE EFFECT OF CRACKS ON DIFFUSIVE MASS TRANSPORT THROUGH A CLAY BARRIER, Nava C. Garisto and Frank Garisto, Atomic Energy of Canada Ltd., Whiteshell Nuclear Research Establishment, Pinawa, Canada.

9:30 U11.4
FINAL DISPOSAL OF CEMENTITIOUS WASTE FORMS IN THE SWEDISH REPOSITORY FOR REACTOR WASTE (SFR), Jan S. Carlsson, Swedish Nuclear Fuel and Waste Management Company, (SKB), Stockholm, Sweden.

9:45 U11.5
MASS TRANSFER IN WATER-SATURATED CONCRETES, Alan Atkinson, Peter A. Claisse, Nicola M. Everitt, Andrew W. Harris and Alan K. Nickerson, Harwell Laboratories, Materials Development Division, Oxon, United Kingdom.

10:00 BREAK

10:30 U11.6
COUPLED FLOW OF HEAT AND MASS IN BARRIER MATERIALS AND ITS SIGNIFICANCE, S.C.H. Cheung, Atomic Energy of Canada Ltd., Whiteshell Nuclear Research Establishment, Pinawa, Canada.

10:45 U11.7
EFFECTIVE DIFFUSIVITY OF CARBON DIOXIDE AND IODINE THROUGH "G TUNNEL TUFF", Tevfik Bardakci, Franklin G. King and Maung Sein, North Carolina A&T State University, Greensboro, NC.

11:00 U11.8
¹⁴C TRANSPORT IN A PARTIALLY SATURATED, FRACTURED, POROUS MEDIUM, W. B. Light, P.L. Chambré, W.W.-L. Lee and T.H. Pigford, University of California, Berkeley, Department of Nuclear Engineering and Lawrence Berkeley Laboratory, Berkeley, CA.

11:15 U11.9
THE APPLICATION OF A COUPLED CHEMICAL TRANSPORT MODEL IN A TRIAL ASSESSMENT OF DEEP DISPOSAL OF LOW AND INTERMEDIATE LEVEL RADIOACTIVE WASTE, Steve Liew, Vea Economides, Adrian Dawes and David Read, WS Atkins Engineering Sciences, Epsom, United Kingdom.

11:30 U11.10
ANALYSIS OF MASS TRANSPORT IN AN ENGINEERED BARRIERS SYSTEM FOR THE DISPOSAL OF USED NUCLEAR FUEL, Nava C. Garisto and Dennis M. LeNeveu, Atomic Energy of Canada Ltd., Whiteshell Nuclear Research Establishment, Pinawa, Canada.

11:45 U11.11
ATTEMPTED VERIFICATION OF MATRIX DIFFUSION IN GRANITE BY MEANS OF NATURAL DECAY SERIES DISEQUILIBRIA, W.R. Alexander, Paul Scherrer Institute, Villingen, Switzerland; I.G. McKinley, NAGRA, Baden, Switzerland; A.B. MacKenzie, R.D. Scott, SURRC, Glasgow, Scotland; and J. Meyer, Min.-pet. Institute, University of Berne, Berne, Switzerland.

U1.1

NUCLEAR WASTE IMMOBILIZATION IN CEMENT-BASED MATERIALS: OVERVIEW OF FRENCH STUDIES, Pascal Bouniol, Eliane Revertegeat, Jean Oliver, Philippe Gegout, Michel Jorda, Rosemarie Atebek, C.E.A., DRDD/SESD, CEN/FAR, 92265 Fontenay aux Roses Cedex.

Cement-based materials are currently used in France for solidification of highly-salt-laden concentrates and ashes and for embedment of solid wastes. In the first case, the waste forms are considered to be "homogeneous" and are submitted to leach tests to evaluate radionuclide behavior. In the case of solid wastes, the whole package is regarded as a "heterogeneous waste form" and radionuclide confinement is ensured by an outer cover of pure mortar and measured using diffusion cells. In both cases the durability function is devolved to the concrete container and the waste package must abide by ANDRA specifications for Low Level Waste disposal.

An overview of the different problems to be solved is presented. Examples of cement-based matrices used to immobilize concentrates (containing F^- , Cl^- , SO_4^{2-} , NO_3^- , Na^+ and trace species) and phosphate ashes are given in relation to cement chemistry. It was demonstrated that, in the same cases, phosphate may improve waste form behavior. Experimental studies, undertaken to assess concrete durability obviously indicated that pH is the starting parameter of chemical degradation reactions. Ion nature (such as Cl^- , SO_4^{2-} , HCO_3^-/CO_3^{2-}) and concentration are secondary factors which only act on kinetics.

It was found that slag and fly ash cement has a better cesium retention ability and stronger resistance to chloride and sulfate attack than portland cement.

U1.2

EFFECT OF CURING TEMPERATURE ON THE PROPERTIES OF CEMENTITIOUS WASTE FORMS(a). Ryan O. Lokken, John W. Shade, and Paul F. C. Martin, Pacific Northwest Laboratory(b) Richland, WA 99352.

Current plans at Hanford for disposing various low-level liquid wastes include solidification using cementitious materials. This process, known as grouting, involves mixing liquid wastes with a blend of cementitious materials and pumping the resultant slurry to lined, underground concrete vaults. The total volume of the vaults is approximately 1.4 million gallons. As the grout slurry begins to solidify and harden, the temperature increases due to the exothermic hydration reactions. Adiabatic temperature increases of greater than 70°C have been measured in the laboratory. With a starting waste temperature of 45°C, the temperature of the grout in the vaults may approach 115°C.

A study is currently underway to assess the effects of long-term, high-temperature curing on the properties of grouts produced with simulated double-shell slurry feed (DSSF) waste. The waste was a salt solution containing high concentrations of sodium nitrate, sodium aluminate, and sodium hydroxide. The solids blend consisted of 47 wt% class F fly ash, 47 wt% ground blast furnace slag, and 6 wt% type I/II portland cement. The solids were mixed with the liquid waste at a ratio of 1080 g/L. Samples of laboratory-produced grout samples, cured at 75, 85, 95, 120, and 150°C, and samples cured in a 4000-gallon monolith, were characterized by scanning electron microscopy, x-ray diffraction, and thermal analysis to determine the effects of curing temperature on leachability, microstructure, phase compositions, and strength. Results of these activities are discussed.

- (a) Work supported by the U.S. Department of Energy under Contract DE-AC-76RL0 1830.
- (b) Operated for the U.S. Department of Energy by Battelle Memorial Institute.

U1.3

BEHAVIOR OF CONCRETE AS A BARRIER MATERIAL FOR NUCLEAR WASTE DISPOSAL R. J. James and Y. R. Rashid, ANATECH Research Corp., P.O. Box 9165, La Jolla, CA 92038.

A current method for disposal of nuclear waste is the immobilization of the waste in cement-based grout and burial in reinforced concrete vaults. The concrete vault provides the containment barrier to prevent leaching into the

environment. Because of heat generation in the waste, the concrete is subjected to elevated temperatures for the extent of the vault life. Under these conditions of elevated temperatures and long hold times, the effects of creep and cracking in concrete play a significant role in determining the structural and barrier integrity of the containment structure. Significant amounts of compressive strain due to creep in thermally loaded, confined structures may lead to split cracking due to the Poisson effect. If thermal gradients are present, cracking due to local bending may occur. In addition, and more importantly, for temperatures above 150 °F, the elastic modulus of concrete degrades with time even at constant temperature due to thermally activated damage. Since the stress due to thermal loads is proportional to the modulus, this requires continual redistribution of load that may lead to additional cracking.

This paper examines cracking in concrete as a means for evaluating long term functional requirements under barrier applications for nuclear waste disposal. A material model for concrete at elevated temperatures, including cracking, thermal creep, and stiffness degradation, has been developed based on available experimental data. Application of this model to underground, reinforced concrete structures under thermal loads will demonstrate the importance of creep and stiffness degradation in the structural design for barrier protection under extended life at elevated temperatures. The importance of capturing the correct temperature distributions and the thermal history of the structure in the analysis will also be demonstrated.

U1.4

GROUTS AND CONCRETES FOR THE WASTE ISOLATION PILOT PROJECT (WIPP). Lillian D. Wakeley, U.S. Army Engineer Waterways Experiment Station, P.O. Box 631, Vicksburg, MS 39181-0631, USA

The Structures Laboratory of the U.S. Army Engineer Waterways Experiment Station has conducted research on cement-based composites for the Waste Isolation Pilot Project (WIPP) since 1977, in cooperation with Sandia National Laboratories. Field testing requirements guided initial development of grouts. Concurrent and later laboratory studies explored the chemical stability and probable durability of these mixtures. Beginning in 1985, a series of small-scale seal performance tests at the WIPP prompted development of an expansive salt-saturated concrete. Important lessons learned from this ongoing work include: (1) carefully tailored mixtures can tolerate phase changes involving Ca, Al, and SO₄, without loss of structural integrity; (2) handling and placement properties are probably more crucial to the mixtures than is exact chemistry; and (3) for the environment of a geologic repository, demonstrated chemical durability will be the best indicator of long-term performance.

U2.1

ASSESSMENT OF THE PERFORMANCE OF CEMENT BASED COMPOSITE MATERIAL FOR RADIOACTIVE WASTE IMMOBILIZATION. M. Atkins, J. Cowie, F.P. Glasser, T. Jappy, A. Kindness and C. Pointer, Dept. of Chemistry, University of Aberdeen, Meston Walk, Old Aberdeen, AB9 2UE, Scotland.

The problem of predicting the future performance of cement-based systems is complicated by a poor understanding of the behaviour of cement systems at long ages, as well as of the complex interactions which can occur between cement and waste components - active as well as inactive - and with cement blending agents including fly ash, glassy slags and natural pozzolans. The progress achieved in developing a predictive capability is reviewed. Considerable success has been achieved in modelling the chemically-related features of cement based systems in terms of pH, E_h, and of element partition between solid and aqueous phases. The behaviour of model radwaste elements - iodine and uranium - has been studied in depth and indicate that both sorption and precipitation occur. U(VI), in particular, forms solubility-limiting compounds e.g. B uranophane. But in general, presently-available data are inadequate to predict many

cement-waste stream interactions, even for the inorganic constituents; future progress in modelling is likely to rely heavily on additions to the data base.

The repository environment will also condition chemical exchanges in cement-based systems. Progress is being made in predicting the impact of ground water components - Cl^- , SO_4^{2-} , CO_2 - on the performance of cement systems.

U2.2

DURABLE CONCRETE FOR A WASTE REPOSITORY - MEASUREMENT OF IONIC INGRESS. R.F. Feldman and J.J. Beaudoin, Institute for Research in Construction, National Research Council, Ottawa, Canada; and K.E. Philipose, Waste Management Systems, Atomic Energy of Canada Limited, Chalk River, Ontario, Canada, K0J 1J0.

A waste repository, labelled Intrusion Resistant Underground Structure (IRUS), for the belowground disposal of low level radioactive waste, is planned at Chalk River Nuclear Laboratories. It relies greatly on the durability of concrete for the required 500 years service life. A research program based on laboratory testing to design a durable concrete and to predict its useful engineered service life is in progress.

It has been established that the degradation of the concrete will depend on the rate of ingress of corrosive agents - chlorides and sulphate ions and CO_2 . Twenty mix formulations were developed to create various types and qualities of concrete, and to study their behaviour in different site environmental conditions. A total of 1000 concrete and 500 cement paste specimens with composition similar to the concrete binder are being exposed to 25 different combinations of the corrosive agents at 20°C and 45°C. Procedures to measure the ionic profiles and to determine the kinetics of diffusion of the ions in the various concretes have been developed. These incorporate modifications to SEM and EDXA techniques. Initial results from these measurements will be presented and discussed in terms of pore structure and permeability parameters of the concrete.

U2.3

LOGNORMAL SIMULATION OF PORE EVOLUTION DURING CEMENT HARDENING. D. SN, W. Ma, and P. W. Brown, Materials Research Laboratory, The Pennsylvania State University, University Park, PA 16802.

Many properties of cement-based systems are determined by the pore size distribution. Our capability to predict such properties depends on our capability to predict pore size distributions, given some basic characteristics of the cement matrix, in terms of materials chemistry, preparation and processing.

Preliminary work has been done to simulate the pore evolution during hardening of cement paste, based on a five-parameter lognormal model of size distribution of pores in hardened cement pastes. For cement pastes of different ages but otherwise identical, the pore size distributions may be reduced to a single, self-similar distribution curve, in terms of a dimensionless size which is the pore diameter divided by the median pore diameter. The location parameter, μ , is indicative of the curing time, while the shape parameter, σ , may be related to other factors, such as water-to-cement ratio and curing temperature.

This model may enable us to quantify the relationships among the pore size distribution of cement paste, the curing time, the curing temperature, and the water-to-cement ratio. Therefore, prediction of the pore size distribution of cement pastes based on a given set of curing conditions (time, temperature, water-to-cement ratio) becomes possible. Furthermore, this model may help predict properties dependent on pore structure, such as permeability and strength of hardened cement pastes, by relating such properties to parameters characteristic of the pore size distribution, μ and σ , rather than to the entire distribution of sizes.

U2.4

MECHANISTIC MODEL FOR THE DURABILITY OF CONCRETE BARRIERS EXPOSED TO SULPHATE-BEARING GROUNDWATERS Alan Atkinson and John A. Hearne, Materials Development Division, Building 429, Harwell Laboratory, Oxon, OX11 0RA, UK

Concretes are favoured materials for the construction of radioactive waste repositories in disposal strategies adopted by many countries. Their durability as structural materials and as physical barriers to radionuclide migration can be limited by their reaction with sulphate-bearing groundwater. In such a situation the concrete degrades by sulphate penetrating the concrete where it reacts with the hydrated cement to form expansive reaction products that cause stress and eventual disruption.

Data obtained from old concretes and accelerated tests have enabled an empirical relationship to be derived to describe the rate of this degradation, but this relationship is not founded on the mechanism of degradation itself. In the work described here the individual contributions to the mechanism have been examined in appropriate experiments in which diffusion, reaction and expansion have been quantified. These results have been integrated into a simple overall model in which the criterion for degradation is the accumulation of a critical quantity of stored elastic energy in the reaction zone. The results of this mechanistic model are in good quantitative agreement with those of the empirical model and enable extrapolations to be made to different concretes, cements and sulphate-bearing groundwaters.

U3.1

THE SOLUBILITY AND SORPTION OF URANIUM(VI) IN A CEMENTITIOUS REPOSITORY. Brownsword, M., Buchan, A. B., Ewart, F. T., McCrohon, R., Ormerod, G. J., Smith-Briggs, J. L. and Thomason, H. P. Chemistry Division, Harwell Laboratory, Oxfordshire, OX11 0RA, UK.

In the context of UK radioactive waste disposal, uranium and its daughters have been shown to make an important contribution to the overall risk assessment. The aqueous chemistry of uranium in the near-field is complicated by the multiple valency states that may exist, under these particular conditions of pH and redox potential, and by the possible formation of solid alkali and alkaline earth uranates. The research programme in support of the repository safety assessment carries out studies of the aqueous chemistry of uranium that include the aqueous speciation, characterisation of the solid phases that are in equilibrium with the repository water, measurement of the solubility of these solids and determination of the sorption onto the major near field substrates.

The paper describes some recent results of these experimental measurements and includes a study of the composition of the sodium and calcium uranates formed, under the conditions applicable to the near-field of a cementitious repository and the determination of their solubilities. Measurements of the sorption of uranium(VI) onto a slag cement and onto specimens of the same slag cement, aged artificially using hydrothermal and leaching treatments are also described.

U3.2

SPECIATION OF Pu(VI) IN NEAR-NEUTRAL TO BASIC SOLUTIONS VIA LASER PHOTOACOUSTIC SPECTROSCOPY.* S. Okajima, J. V. Beitz, J. C. Sullivan, and D. T. Reed, Argonne National Laboratory, 9700 South Cass Avenue, Argonne, IL 60439.

The high sensitivity technique of laser photoacoustic spectroscopy (LPAS) in combination with optical absorption spectroscopy was applied to the study of Pu(VI) speciation in systems important to their migration in the environment. Emphasis was on the hydroxo species formed although additional information on other groundwater-relevant ligands was obtained. Stability constants and speciation observed, based on the spectra obtained, are reported.

*This work was funded in part by developmental funds within Argonne National Laboratory and under the auspices of the Office of Basic Energy Sciences, Division of Chemical Sciences, U.S. Department of Energy, under contract number W-31-109-ENG-38.

U3.3

MODELLING STUDIES OF SORPTION IN THE NEAR FIELD OF A CEMENTITIOUS REPOSITORY A.Haworth, S.M.Sharland and C.J.Tweed, Theoretical Physics Division, Harwell Laboratory, UKAEA, Oxfordshire OX11 0RA, U.K.

Current plans for a low- and intermediate-level radioactive waste repository in the UK include a cement backfill. Sorption of radionuclides on to cement is an important process in limiting the aqueous concentrations in the near-field and is, therefore, likely to be of importance in constructing the safety case for a repository. Most experiments and modelling use a distribution coefficient approach. This quantifies sorption on to a material in terms of a simple linear isotherm, but does not take into account effects such as saturation of sites. The use of distribution coefficients for conditions other than those at which they were obtained may not be valid.

In this paper, we describe modelling studies of radionuclide transport through a cementitious backfill, based on a mechanistic interpretation of the processes. For this modelling we use the geochemical code PHREEQE and the coupled ionic transport/chemical equilibria code CHEQMATE. The predictions of the modelling will be compared with experimental data from various sorption experiments on cement.

U3.4

Evidence of long distance transport of natural colloids in a crystalline rock groundwater. W.R. Alexander, R. Bruetsch, C. Degueldre, Paul Scherrer Institute, 5232 Villigen, Switzerland and B. Hofmann, USGS, Denver CO 80225, USA.

The transport of radiocolloids (radionuclides in association with colloids) from the near field, through the geosphere, is recognised as a potential problem within current Swiss safety analysis models. Natural colloids could enhance doses to the biosphere by sorbing radionuclides released from a repository and then moving through fractured rock with minimal retardation, either by sorption on the rock or by filtration through the fracture infill.

NAGRA has therefore initiated a programme of research to study various aspects of colloid transport in both crystalline and sedimentary formations and, in this article, the results of a recent project are reported. An earlier study of the groundwater system of the Krunkelbach uranium prospect, Black Forest, West Germany, produced evidence of long distance transport of natural particles (> 450 nm nominal pore size filters) in the crystalline groundwaters. Newly produced samples which includes colloidal material (filters with nominal pore sizes in the range of 15-1000 nm were utilised) have been subjected to semi-quantitative analyses and the results have confirmed the earlier work on larger particles.

Stable isotope data implies that the groundwater recharge area lies within a gneiss formation some 5 km away from the uranium prospect. Colloid samples were collected within the prospect (at a depth of 240 m) and the Mg, Ti, Y and Zr contents of these colloids were found to be characteristic of the near by gneiss rather than the granite body which hosts the prospect.

The implications of such natural colloid generation and long distance transport are examined with respect to Swiss concepts for a crystalline rock radwaste repository.

U3.5

ANALYTIC STUDIES OF COLLOID TRANSPORT.

Y. Hwang, T. H. Pigford, P. L. Chambré, and W. W.-L. Lee, Department of Nuclear Engineering and Lawrence Berkeley Laboratory, University of California, Berkeley, CA 94720.

There is evidence that radionuclides move as colloids at the Nevada Test Site. Because of their ubiquitous nature, fast movement, and low retardation, it is important to study colloid transport in association with the planned repository at Yucca Mountain. We present some analytic studies of colloid transport in fractured porous rock, considering filtration as well as interaction between colloids and dissolved radionuclides.

Colloids of radioactive material can be expected in ground water in a geologic repository. Radioactive species released from a waste solid can appear as colloids by chemical reaction of the dissolved species with container material, by reduction in solubility and precipitation from cooling a near-saturated solution, from a change in the redox potential, or by sorption of a radioactive solute onto colloids that are already present in the ground water. Here we include "pseudocolloids" as colloids.

Colloids can transport radionuclides through geologic media at rates that can differ considerably from the solute transport rates. Current approaches for predicting colloid transport focus on the transport of the colloid itself and may not be adequate for predicting the long-term behavior of geologic repositories. Colloids of a given species can be expected to establish some kind of interaction with the solute of that species. Some colloids are likely to exhibit solubility, similar to that of a consolidated solid. Others, such as pseudocolloids, may exhibit sorption equilibrium between the solute concentration and the concentration of that species sorbed on the colloid. In either case, the interaction between the solute and colloid can be important in predicting long-term transport. Moreover, hydrogeologic transport through a fracture is likely to be accompanied by diffusion of solute into and out of the rock matrix surrounding the fracture.

We develop and solve differential equations for the interactive transport of colloids and solute. We discuss the analytic solutions and illustrate the importance of the various processes in colloidal transport, as steps towards developing more comprehensive models of colloid transport of radioactive species.

U4.1

THE MICROSTRUCTURE OF ggbfs/OPC HARDENED CEMENT PASTES AND SOME EFFECTS OF ELEVATED TEMPERATURE LEACHING. I.G.Richardson, S.A.Rodger and G.W.Groves, Department of Metallurgy and Science of Materials, University of Oxford, Parks Road, Oxford OX1 3PH, U.K.

Ground granulated blast-furnace slag (ggbfs)/Ordinary Portland cement (OPC) blends are possible materials for use in intermediate and low-level radioactive waste repositories. The microstructural development in neat OPC is reviewed. The effect of increasing the loading of ggbfs on the composition and microstructure of the hardened paste has been examined by a number of techniques, including transmission electron microscopy. The implications for performance are discussed. A ggbfs/OPC 9:1 blend which had been exposed, after normal hydration to aqueous leaching at 105°C was also examined. Marked changes in the microstructure and composition were observed.

U4.2

THE EFFECTS OF TEMPERATURE ON THE LEACHING BEHAVIOR OF CEMENT WASTE FORMS Mark Fuhrmann, Richard Pietrzak, John Heiser III, Eena-Mai Franz and Peter Colombo, Nuclear Waste Research Group, Brookhaven National Laboratory, Upton, NY, 11973.

The leaching mechanisms of simulated low-level radioactive waste forms are being determined as support for development of an accelerated leach test. Two approaches are being used: (1) comparisons of leaching data with results of a model that describes diffusion from a finite cylinder, and (2) observation of the leaching process at temperatures between 20°C and 65°C. To provide results that can be used for modeling, leaching at elevated temperatures must change neither the leaching mechanism nor the structural controls of leaching such as the porosity. Releases of cesium-137, strontium-85, calcium, sodium and potassium from plain portland cement, cement containing sodium sulfate and cement

containing incinerator ash have been determined under a variety of experimental conditions. To avoid experimental artifacts that could be misinterpreted as a release mechanism, minimal concentrations of ions in the leachate are necessary. Diffusion was observed to proceed without suppression when elemental concentrations in the leachate were less than 25 mg/L. Data from the leach tests were compared to model results for diffusion from the finite cylinder. While much of the data appears to be diffusion controlled, notable exceptions are cesium and sodium leached from cement/ash waste forms. For all samples activation energies ranging between 6 and 11 Kcal/mole have been calculated from the relationship of the effective diffusion coefficient to increasing temperature, close to the expected value of 5 Kcal/mole for diffusion. Solid phase analysis was performed to further examine the structural and mineralogical controls on leaching.

U4.3

THERMODYNAMIC MODELING OF CEMENTITIOUS WASTE FORM/GROUNDWATER INTERACTION AS A TOOL FOR LONG-TERM PERFORMANCE ASSESSMENT. Louise J. Criscenti and R. Jeff Serne, Pacific Northwest Laboratory, Richland, Washington 99352.

Experiments (i.e., static, modified ANS 16.1) have been conducted to study the leaching of elements from cementitious waste forms in groundwater. These experiments are completed in a short time period (150 days) and chemical equilibrium between the groundwater and waste form may not be achieved. Thermodynamic models can be used to determine if equilibrium between the waste form and groundwater has been established.

A conceptual model for the chemical interaction between a cementitious waste form and groundwater was developed and used with the MINTEQ computer code to predict the leachate compositions and solid phase assemblages that should be observed in several leaching experiments. The conceptual model includes (1) a modal analysis of the phases present in hydrated cement, (2) the chemical composition of the groundwater, and (3) a list of solid phases that may precipitate when the cement and groundwater react. To assist in developing the chemical model, MINTEQ calculations were performed on various leachate compositions from laboratory experiments to determine potential solubility controls. Once it can successfully predict the experimental results, the model can be used to investigate the long-term performance of a waste form.

The calculations indicate that the amount of carbonate present in the groundwater is a major factor influencing the stability of a waste form. Calculations using various partial pressures of CO₂ will be compared.

Pacific Northwest Laboratory is operated for the U.S. Department of Energy by Battelle Memorial Institute under Contract DE-AC06-76RLO 1830.

U4.4

WASTE GROUT LEACH TESTS: PURSUIT OF MECHANISMS AND DATA FOR LONG-TERM PERFORMANCE ASSESSMENT. R. Jeff Serne, Pacific Northwest Laboratory, P.O. Box 999 K6-81, Richland, WA 99352.

At Hanford low-level liquid nuclear waste is being mixed with cementitious forming materials (grout) to form solid monoliths. Prior to grouting each liquid waste, a performance assessment must be performed to evaluate the long-term environmental impact. These predictions rely upon a diffusion controlled conceptual release model and short-term laboratory leach data on small grout samples. This paper describes size scale-up and inventory scale-up experiments that evaluate whether diffusion does in fact control the release of radionuclides (e.g., ¹²⁹I, ⁹⁹Tc) and regulated chemicals (e.g., NO₃, NO₂, Se, Cr and F).

Size-scale up leach tests on cylindrical grout specimens (3.2cm dia.x3.2cm L to 30.4cm dia.x30.4cm L) were performed

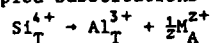
to evaluate whether leach rates follow the S/V dependency (geometric surface area to volume ratio) predicted by diffusion theory. After 200 days of leaching, species such as ⁹⁹Tc, NO₃, NO₂, Cr, Mo and Na show similar leach rates at all specimen sizes. However, the data suggest that simple diffusion theory (semi-infinite or finite source) is a less accurate predictor of observed leach rates than empirical relationships (see Cote and Constable 1987) that account for wash off, wash out and diffusion.

By changing the inventory of contaminants present in a waste form one can check whether diffusion or solubility processes appear to control leaching. Three sets of leach tests where ⁹⁹Tc, ¹²⁹I and Se were varied from (1X, 10X and 100X) were performed. Results to date suggest I leaching follows diffusion controlled release while Tc and Se are less well behaved (i.e., obey neither simple theory).

U5.1

THERMODYNAMICS OF GLASSES FOR NUCLEAR WASTE DISPOSAL. Alexandra Navrotsky, Department of Geological and Geophysical Sciences, Princeton University, Princeton, NJ 08544

Glasses containing nuclear waste typically have 5-10% or more of cations of high charge which perturb the aluminosilicate framework. Calorimetric studies of coupled substitutions



show the following trends. Greatest glass stabilization occurs when M is monovalent and large (e.g. Cs⁺), with thermodynamic stability decreasing with increasing z/r of M. For small alkaline earths (e.g. Mg²⁺) positive heats of mixing and a tendency toward clustering or unmixing develops. For cations of higher charge (e.g. La³⁺, Zr⁴⁺, Nb⁵⁺, Mo⁶⁺) this tendency is accentuated. Clustering on a microscopic scale implies that the local environment of these cations is independent of their concentration; the activity of the oxide component is virtually constant and relatively high and the system behaves more as a mechanical mixture than as a true solid solution. For consideration of the long-term stability, both kinetic and thermodynamic, of a waste-loaded glass, the relatively high thermodynamic activity of M-containing oxide implies a relative destabilization. However, because clustering may be pervasive, and only the volume fraction of the clusters changes with concentration of oxide, the reactivity of the waste form may be relatively insensitive to the degree of loading as long as a glass can be made.

U5.2

A KINETIC MODEL FOR BOROSILICATE GLASS DISSOLUTION BASED ON THE DISSOLUTION AFFINITY OF A SURFACE ALTERATION LAYER William L. Bourcier, Dennis W. Peifer, Kevin G. Knauss, Kevin D. McKeegan, and David K. Smith, Lawrence Livermore National Laboratory, Livermore, CA 94550

A kinetic model incorporated in the EQ3/6 geochemical modeling code is used to predict borosilicate waste glass dissolution rates. The dissolution rate is assumed to be controlled by the dissolution affinity of an alkali and boron-depleted altered surface layer on the glass. Model results predict the non-linear glass dissolution rate where the relatively rapid initial rate slows and approaches a linear release with time.

The model has been used to predict the results of static closed-system dissolution tests of a uranium-doped SRL-165 glass. The tests were performed in gold-bag and Teflon-lined stainless steel vessels from 100 to 250°C for up to 4 months in a dilute (0.003 molal) NaHCO₃ solution. The gold bag tests were used for solution sampling; the tests in Teflon run in parallel were used for solids characterization. Solids were analyzed using SEM, SIMS, x-ray diffraction, and nuclear reaction profiling methods.

Comparison of model and experimental results show that the release

rates of elements not strongly concentrated in surface layers or secondary phases (e.g. Li, B, Na) can be successfully predicted by the model. The release rates of elements that are concentrated in surface layers and secondary phases are more difficult to predict and accurate prediction is possible only if observed secondary phases are used to constrain species concentrations.

Work performed under the auspices of the U. S. Department of Energy by the Lawrence Livermore National Laboratory.

U5.3

PREDICTION OF RADIOACTIVE WASTE GLASS DURABILITY BY THE HYDRATION THERMODYNAMIC MODEL: APPLICATION TO SATURATED REPOSITORY ENVIRONMENTS. Carol M. Jantzen, Westinghouse Savannah River Company, Savannah River Site, Aiken, SC 29808.

The effects of groundwater chemistry on glass durability were examined using the hydration thermodynamic model. The relative durabilities of SiO_2 , tektites, basalts, waste glasses, medieval window glasses, and a frit glass were determined in tuffaceous J-13 groundwater, basaltic CR-4 groundwater, WIPP-B brine, and Permian-A brine using the MCC-1 test. For silicate groundwaters, the free energy of hydration, calculated from the glass composition and the final experimental pH, was linearly related to the logarithm of the measured silica concentration. The linear equation was identical to that observed previously for these glasses during MCC-1 testing in deionized water. The superposition of the line from the silicate groundwater and deionized water experiments occurs because the pH values for all the glasses tested in groundwater remained constant. Constant pH values decreased the calculated ΔG_{hyd} values while in turn, lower Si releases were measured. The slope defined by the groundwater and deionized water data is the theoretical slope, $\ln(1/2.303RT)$, for glass dissolution controlled by the dissolution of amorphous silica. For brines, the influence of the ion activity product (IAP) on the solubility of silica and other species was determined. Using the hydration thermodynamic model, nuclear waste glass durability in saturated repository environments can be predicted from the glass composition and the groundwater pH.

U5.4

CHEMISTRY OF GLASS CORROSION IN HIGH SALINE BRINES. B. Grambow, R. Müller, Hahn-Meitner-Institut Berlin, Glienicke Str. 100, D-1000 Berlin 39, FRG

This paper describes a geochemical model and a comparison to experimental data for glass corrosion in concentrated salt brines. Modeling was performed with the computer code EQ3/6. The brine chemistry was described with the Pitzer formalism [Pitzer 1973] for osmotic and activity coefficients.

The reaction path was calculated of a nuclear waste glass as a function of brine chemistry and of the formation of major alteration products. In agreement with the experimental data it was calculated that in MgCl_2 dominated brines a major alteration product are Mg rich clay minerals and due to the consumption of Mg by these products the pH decreases with the proceeding reaction. A constant pH and composition of alteration products is achieved, when the alkali release from the glass balances the Mg consumption. In the NaCl dominated brine MgCl_2 becomes exhausted by clay minerals. As long as there is still Mg left in solution the pH decreases. After exhaustion of Mg the pH rises with the alkali release from the glass and analcime is formed.

U5.5

THERMOKINETIC MODEL OF BOROSILICATE GLASS DISSOLUTION: CONTEXTUAL AFFINITY. T. Advocat & E. Vernaz, CEN-Valrhô, SDHA, BP 171, 30205 Bagnols-sur-Cèze Cedex, France; J.L. Crovisier & B. Fritz, CNRS/CSGS, 1 rue Blessig, 67000 Strasbourg, France.

Short and long term geochemical interactions of R7-T7 nuclear glass with water at 100°C were simulated with the DISSOL thermo-kinetic computer code. Both the dissolved glass quantity and the resulting water composition, saturation states and mineral quantities produced were calculated as a function of time.

The rate equation used in the simulation was first proposed by Aagard and Helgeson: $dc/dt = S/V \times k^+ \times (a_{\text{H}_2\text{O}})^n \times (1-Q/K)$. The predicted mineral phases were iron hydroxides, 2:1 clay mineral represented by an ideal solid solution model, manganese and zinc hydroxides, laumontite, strontianite, metastable amorphous silica, calcite and low albite. The calculated evolution of the glass/water system showed good agreement with short term experimental results (up to 1 year).

The best agreement with the one-year data was obtained with a reaction affinity calculated from silica activity (Grambow's hypothesis) rather than taking into account the activity of all the glass components as proposed by Jantzen and Plodinec.

Under near-equilibrium conditions, the reaction rate was proportional to the (Q/K) chemical affinity of the overall reaction. Under these conditions, chemical affinity was dependent on the stability or metastability of the reaction products. The dissolution rates observed experimentally at different SA/V ratios are therefore not intrinsically constant, but depend on the conditions under which reaction products form and on their physicochemical properties.

U5.6

COMPARISON OF THE LAYER STRUCTURE OF VAPOR PHASE AND LEACHED SRL GLASS BY USE OF AEM.* B. M. Biwer, J. K. Bates, T. A. Abrajano, Jr., Argonne National Laboratory, 9700 South Cass Avenue, Argonne, IL 60439; and J. P. Bradley, McCrone Environmental Services, Inc., 850 Pasquini Drive, Westmont, IL 60559.

The initial corrosion of nuclear waste glass in an underground repository may be expected to occur through interaction with water vapor prior to liquid water contact. The current U.S. underground repository site selected for characterization is located in the unsaturated zone where proper waste package design and emplacement will limit, if not exclude, groundwater contact with the waste glass even after breach of the waste form container. Analytical electron microscopy has been used to examine the detailed structure of 131 glass that has been reacted in water vapor under relative humidities ranging from 60 to 100%, temperatures between 75° and 200°C, and time periods up to two years. An intercomparison of the reaction progress and alteration products identified under the different reaction conditions provides insight as to the mechanisms controlling glass reaction. The results from the vapor phase reacted glasses are then compared to those from glass of similar composition that has been reacted under standard MCC-1 type conditions for time periods up to four years. 131 glass was chosen for study because it has been identified as a representative composition for the least durable DWPF glass to be produced for storage.

*Work supported by the U.S. Department of Energy, Office of Civilian Radioactive Waste Management, Yucca Mountain Project Office, under Contract Numbers W-31-109-Eng-38 and AX0848606.

U5.7

DISSOLUTION MECHANISMS OF CaTiO_3 AND OTHER TITANATE PHASES IN THE SYNROC ASSEMBLAGE

S. Myhra, D.K. Pham, R.St.C. Smart* and P.S. Turner, Division of Science and Technology, Griffith University, Nathan, Qld, Australia (* Now at: School of Chemical Technology, South Australian Institute of Technology, Adelaide, S.A. Australia).

Perovskite, hollandite and zirconolite are the major phases of the Synroc C titanate assemblage. The chemical durability in an aqueous environment of the separate minerals and the total assemblage is one of the most relevant performance criteria for the Synroc concept. Methodologies, incorporating complementary approaches with solution, surface and electron-optical analyses, have been developed for assessing performance in the epithermal and hydrothermal regimes. A detailed study of CaTiO_3 has been completed identifying the mechanisms which are operative as well as the kinetic and thermodynamic factors which affect the evolution of the system. It has been found that thermodynamic stability for CaTiO_3 can easily be engineered into the waste repository for $T < 90^\circ\text{C}$, while the same is probably more difficult to achieve at higher hydrothermal temperatures. A similar study, using a comparable methodology, is underway for hollandite. Preliminary results will be reported for the chemical durability of this phase.

U6.1

A COMPARISON OF THE BEHAVIOUR OF VITRIFIED HLW IN REPOSITORIES IN SALT, CLAY AND GRANITE. Part II: RESULTS. W. Lutze, Hahn-Meitner-Institut, Glienicke Strasse 100, 1000 Berlin 39, FRG., M. Kawanishi, Abiko Research Laboratory, Abiko, Chiba-pre, 270-11, Japan, J. A. C. Marples, Harwell Laboratory, Oxon OX11 0RA, UK., and P. van Iseghem, SCK/CEN, Boeretang 200, 2400 Mol, Belgium.

A 'Round Robin' test of the European Commission's "Repository Systems Simulation Leach Test" has been undertaken. This involved testing an inactive simulant of the French high-level waste glass SON68 (R7T7) containers which also held water, backfill, and either salt, clay or granite geological material. Ten laboratories undertook the granite option, six salt and three clay. The test procedure was closely specified and is given in detail in a companion paper.

Experiments with glass powder in contact with aqueous solutions were run for periods of time up to one year at 90°C and the solutions were analyzed for Si, B, Li and Mo (compulsory) and other corroded glass constituents (optional). The analytical results are discussed in terms of accuracy and precision and are used to evaluate and compare the performance of the glass (fig.1) under conditions representing those which might occur after disposal in future repository environments. The paper discusses the underlying corrosion mechanisms and the different degrees of corrosion in salt vs. clay and granite.

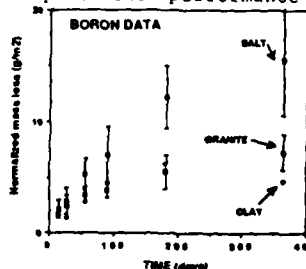


Fig. 1: Corrosion of HLW glass SON68 in salt, granite and clay, respectively.

U6.2

COMPARISON OF SURFACE LAYERS FORMED ON SYNTHETIC BASALTIC GLASS, FRENCH R7T7 AND HMI BOROSILICATE NUCLEAR WASTE FORM GLASSES - MATERIALS INTERFACE INTERACTIONS TESTS. Michael L. Jercinovic, Stacy Kaser, and Rodney C. Ewing, Dept. of Geology, Univ. of New Mexico, Albuquerque, NM 87131; Werner Lutze, Hahn Meitner Institut, Berlin GmbH, Glienicke Strasse, 1000 Berlin 39, F.R. Germany.

Surface precipitates have formed on basaltic and borosilicate nuclear waste form glasses during the 6 month, 1 year, and 2 year *in situ* Materials Interface Interactions Tests (MIIT) conducted at the WIPP site using WIPP Brine A as a leachant at 90°C . The surface layers were characterized by scanning electron microscopy, x-ray diffraction, electron microprobe analysis, and analytical electron microscopy.

The surface layers formed on synthetic basaltic glass are primarily Mg-chloride and halite with a minor silicate component. HMI borosilicate glass exposed to the same experiments have surface layers dominated by amorphous Mg-silicate with 6 month layers being overgrown by minor Mg-chloride, which is not seen after 1 year. Sub-micron sized anhydrite crystals have formed within the Mg-silicate layer. Minor dissolution pitting of the glass is seen in 1 and 2 year samples of the basaltic and HMI glasses, but is not as pervasive as is reported for basaltic glass altered naturally at low temperature in seawater. Natural alteration of basaltic glass results in the formation of clay-like Fe-Al silicate gel (palagonite) surface layers. Dissolution pitting of the French R7T7 glass during the MIIT experiments is more advanced than seen in either the synthetic basaltic glass or the HMI borosilicate glass. The R7T7 glass has surface layers of Mg-silicate, similar in composition to the surface layers formed on the HMI borosilicate glass.

The differences in surface layer compositions between synthetic basaltic glass compared to borosilicate waste form glasses in the *in situ* MIIT experiments may indicate a difference in corrosion behaviour between the two glass types when exposed to the repository environment. In addition, the differences between natural environments and those of waste repositories may limit the usefulness of natural analogues toward verification of models developed for use in the prediction of the long term corrosion of nuclear waste form glasses.

U6.3

THE INTERACTION BETWEEN NUCLEAR WASTE GLASSES AND CLAY-II. P. Van Iseghem, K. Berghman and W. Timmermans, SCK/CEN, Boeretang 200, B-2400 Mol, Belgium.

Results are summarized of an experimental programme which started as a continuation of an earlier programme (ref. 1), to evaluate the compatibility of the high level waste glasses of interest to Belgium (the Cogema R7T7 glass SON 68 and the Pamela glasses SM 513 and SM 527) with the clay repository host. The corrosion tests are performed in clay/claywater mixtures, in controlled Eh conditions, and consider inactive glasses, glasses tracers with Pu/Cs/Sr/Tc/..., and the presence of a γ irradiation field.

Some of the main indications after two year test duration are :

- Glass dissolution (B, Li, ...) occurs in a Si/Al/Fe equilibrated solution.
- Pu, Cs, Sr leach in similar way from the different glasses ; distribution coefficients, Kd, for Pu are glass dependent ; the Pu inventory leached in a mobile form (about 4×10^4 MW cut-off) is extremely small.
- The γ irradiation induces considerable hydrogen production, which decreases with higher clay concentration ; glass corrosion slightly decreases in a γ irradiation field.

The paper will discuss the results in terms of leaching mechanisms and source term determination.

U6.4

R7-T7 NUCLEAR WASTE GLASS BEHAVIOR IN MOIST CLAY: ROLE OF THE CLAY MASS/GLASS SURFACE AREA RATIO. N. Godon and E. Vernaz, CEN-Valrhé, SDHA, BP 171, 30205 Bagnols-sur-Cèze Cedex, France.

R7-T7 glass alteration in moist clay media was investigated with various clays. In contact with smectite 4a, selected in France as a potential engineered barrier material, the glass was significantly corroded: after 6 months the glass corrosion rate was practically the same as the initial alteration rate in double-distilled water. Substantially lower alteration was observed in contact with a "bentonite" (montmorillonite) activated by sodium carbonate.

Smectite 4a consumes silicon released by glass corrosion. This action retards the rise to high silicon concentrations in solution that diminish the glass corrosion rate. The duration of this phenomenon is proportional to the ratio between the clay mass (C) and the glass surface area (SA). Comparing the results of studies at variable C/SA ratios indicates that low glass corrosion rates are obtained more slowly at higher C/SA ratios.

Tests with ²³⁹Pu-doped R7-T7 glass have also shown that the radionuclide retention factor in the alteration film at the glass surface is only 6, compared with a factor of nearly 50 in double-distilled water under static conditions.

In order to determine the influence of clay activation by sodium (saturation of exchange sites by Na⁺) on glass alteration, tests were conducted with moist activated smectite 4a and unactivated bentonite.

This work highlights the importance of selecting the clay for possible use as an engineered barrier material. The interpretations advanced can provide guidelines for this selection.

U6.5

PRODUCT CONSISTENCY LEACH TESTS OF SAVANNAH RIVER SITE RADIOACTIVE WASTE GLASSES.

Ned E. Bibler, Westinghouse Savannah River Co., Aiken, SC, 29808; and John K. Bates, Argonne National Laboratory, Argonne, IL, 60439.

The Product Consistency Test (PCT) was developed at the Savannah River Site (SRS) to routinely verify the durability of nuclear waste glasses that will be produced in the Defense Waste Processing Facility. The PCT is a 7 day, crushed glass leach test in deionized water at 90°C. Final leachates are filtered and acidified prior to analysis. To demonstrate the reproducibility of the PCT when performed remotely, SRS and Argonne National Laboratory have performed the PCT on samples of two radioactive glasses. The tests were also performed in order to compare the releases of the radionuclides with the major nonradioactive glass components and to determine if an effect of radiation was present.

Results from the two laboratories for the releases of B, Li, Na, and Si, agreed within 10%. For the radionuclides Cs-137, Sb-125, Eu-154, and Sr-90, and alpha activity, the agreement was not as good (up to 2X difference) possibly due to different counting techniques at the two facilities. At both facilities, the normalized releases were in the same order, e.g. Li>B>Na>Si>Cs-137>Sb-125>Eu-154>Sr-90. The normalized releases for the nonradioactive elements and the final pH values in these tests agreed with those for nonradioactive glasses with similar composition indicating no significant effect of radiation.

U6.6

THE REACTION OF SYNTHETIC NUCLEAR WASTE GLASS IN STEAM AND HYDROTHERMAL SOLUTION. W. L. Ebert and J. K. Bates, Argonne National Laboratory, 9700 South Cass Avenue, Argonne, IL 60439.

Glass monoliths of the WVCN 50, WVCN 44, SRL 165, and SRL 202 compositions were reacted in steam and hydrothermally (static leaching) at temperatures between 90° and 200°C. The glass reaction resulted in the formation of leached surface layers in both environments. Secondary precipitates were formed on all glass types in the steam environment only. The assemblage of phases formed was unique to each glass type, but several precipitates were common to all glasses, including analcime and several calcium silicate phases. Reaction in steam is thought to occur in a thin layer of sorbed water which becomes

saturated with respect to the observed phases after only a few days of reaction. These phases establish lower equilibrium solution concentrations of several glass components which allow the glass reaction to proceed at a higher rate than in the hydrothermal environment. The reaction is accelerated in the sense that secondary phases form after a shorter reaction time in the steam environment than in the hydrothermal environment because of large differences in the glass surface area/leachant volume ratio. A knowledge of the secondary phases which form is crucial to the modeling effort of the repository program.

*Work supported by the U.S. Department of Energy, Office of Civilian Radioactive Waste Management, Yucca Mountain Project Office, under Contract Number W-31-109-Eng-38.

U7.1

ESTIMATION OF LONGEVITY OF PORTLAND CEMENT GROUT USING CHEMICAL MODELING TECHNIQUES. Stephen R. Alcorn and Mark A. Gardiner, IT Corporation, 5301 Central Avenue, NE, Albuquerque, NM 87108; and William E. Coons, RE/SPEC, Inc. 3815 Eubank Boulevard, NE, Albuquerque, NM 87111.

Portland cement-based grout is a favored candidate material for nuclear waste repository seals due to its low permeability, ability to be injected into narrow fractures, ability to self-heal, and apparent persistence. The long-term performance of this material is uncertain, since many phases which comprise cement are metastable. It may be assumed that cement-based grout will degrade with time and increase in permeability. Therefore, it is important to be able to estimate the duration of acceptable performance.

To address this issue, a two-part approach was taken: (1) characterize the chemical degradation that would occur from the interaction of grout with natural groundwater, and (2) assess the consequences with a permeability development model. To establish bounds, three scenarios were analyzed: (1) closed system (very slow flow/dissolution/precipitation), (2) dynamic (slow flow/dissolution/limited precipitation), and (3) open system (fast flow/dissolution). To assess the consequences of the chemical interactions, an empirical relationship between porosity and permeability was developed. Changes in grout performance with time were predicted by assuming a sequence of hydraulic heads that varied in response to changing repository conditions. Preliminary results indicate that cement grout may maintain acceptable performance for thousands to millions of years, providing its initial hydraulic conductivity is around 10⁻¹² m/sec, the grout mix is engineered to minimize the more soluble phases (e.g., ettringite), and it is emplaced at a site with elevated TDS groundwater where the local hydraulic gradient is low or repository repressurization times are short.

U7.2

MODELLING OF THE EVOLUTION OF POREWATER CHEMISTRY IN A CEMENTITIOUS REPOSITORY. A. Haworth, S.M. Sharland and C.J. Tweed, Theoretical Physics Division, Harwell Laboratory, UKAEA, Oxfordshire OX11 0RA, U.K.

The current UK concept for disposal of low- or intermediate-level nuclear waste comprises an underground repository with a largely cementitious backfill. The aqueous phase within the cement provides a high pH environment in which the solubilities of many nuclides are low and the rate of general corrosion of metal canisters is slow. Variation in porewater chemistry in the repository is likely to have implications for the release rates of nuclides. Several experimental studies on the effect of the interaction of seawater with cement are being carried out at Harwell as part of the Nirex Safety Assessment Research Programme. In particular, changes in the solution composition of the contact water are being investigated. Last year, a preliminary model of cement degradation was

developed using the coupled transport/chemical equilibrium code CHEQMATE. This model has been further developed for use in modelling the experimental studies to aid interpretation of results. In particular, mineral changes at the surface of the cement are investigated. Such changes may be important for both solution conditions in cracks within the backfill and adsorption of nuclides on to the surfaces.

U7.3

A THEORETICAL STUDY OF THE EFFECT OF THE LEACH INTERVAL ON A SEMIDYNAMIC LEACH TEST. Roger D. Spence, Oak Ridge National Laboratory, P. O. Box 2003, Oak Ridge, TN 37831-7273

A diffusion model is used to explore limitations of a standard leach procedure, specifically, the effect of the leach intervals for the ANSI/ANS-16.1 procedure. The suppression of the leach rate by allowing the concentration to build up, as in such semidynamic procedures, is well known and can be predicted by the diffusion model. The originators of this procedure were also aware of this effect, but leaching must proceed for a finite time in order to achieve detectable concentrations of a species. In fact, the model can be used to give the correlation between detection limit, starting sample concentration, measurable effective diffusion coefficient, and leach interval.

The ANSI/ANS-16.1 procedure specifies a leachant volume and a set of leach intervals spanning a total of 90 d. Using the initial and boundary conditions presented by this leach procedure, the second order partial differential equation representing Fick's second law is solved numerically using finite differences. This allows the prediction of the cumulative amount leached, taking into account the suppression of the driving force as the concentration increases during each interval. This prediction can be compared to the predicted amount leached without this suppression, that is the true dynamic case, for the same effective diffusion coefficient. The effective diffusion coefficients at which the difference between these two predicted values becomes significant was studied. The effect of varying the leach interval for a given effective diffusion coefficient is also explored. With these predictive tools, the limited resources of an experimental program can be concentrated on those situations that cannot be predicted by the model, such as nondiffusion mechanisms.

U7.4

INTERACTION BETWEEN BLENDED CEMENTS AND A SULPHATE BEARING GROUND WATER. Susan L. Duerden, Peter L. Walton, and Amal J. Majumdar. Building Research Station, Watford, UK.

Blended cement mixes containing pulverized fuel ash (pfa) and ground granulated blastfurnace slag (ggbs) with ordinary Portland cement (OPC) have been reacted with a sulphate bearing ground water for 9 months at 50° and 80°C and atmospheric pressure. The blends were 9:1 and 75:25 pfa or ggbs:OPC and are of interest to the radioactive waste disposal schemes currently under consideration in the UK.

Two types of specimens were used in the reaction, 150mm diameter and 50mm long cylinders, and 75µm powders prepared from the mixes after 7 days' hydration. The reaction products were examined by x-ray diffraction, differential scanning calorimetry and scanning electron microscopy.

After 28 days hydration in water some of the cylinders showed evidence of cracking when stored in air at 90% R.H. Heat evolution and volume change effects in these cylinders have been studied. During reaction of these cylinders with ground water the cracks act as loci for crystallization of ettringite and gypsum. For uncracked cylinders there is minimal interaction between cements and ground water after 9 months, but an outer layer of calcite and/or vaterite, approx. 3mm thick, was present in all reacted cylinders.

With powder specimens reactions proceed much faster. In the case of the 75:25 ggbs/OPC sample at 50°C the reaction products include the sulphate minerals ettringite, monosulphate and gypsum, and calcite. Hydrotalcite that forms during the first 7 days of initial curing persists in the presence of ground water, but calcium hydroxide disappears after 3 days. There is some indication that α-quartz begins to form after about 4 months.

U7.5 ABSTRACT WITHDRAWN

U7.6

IMMOBILIZATION IN CEMENT OF ION EXCHANGE RESINS. Patrick LE BESCOP; Pascal BOUNIOL; and Michel JORDA, C.E.A., DRDD/SESD, CEN-FAR, 92265 Fontenay aux Roses Cedex, FRANCE

Recent studies were carried out in FRANCE to improve ion exchange resin solidification in cement-based matrices. Work was conducted on different types of waste - cation, anion and mixed-bed resins - under regenerated and loaded states. Industrial applications could be found considering ion exchange resins from the water purification systems of COGEMA Reprocessing Plant (regenerated resins) and of PWR cooling circuits (loaded resins). The main objective is to reach a waste incorporation rate of at least 50% (in volume). Imposed acceptability criteria for subsurface disposal required that waste forms must be monolithic solids with a) no free standing water, b) no significant dimensional variations and no loss of mechanical integrity both after curing and during immersion testing, c) leach rates compatible with ANDRA specifications. Hydraulic cement formulations were developed taking into account waste chemistry, more precisely the presence of ions which inhibit setting. Two types of cement based material were investigated: Portland cement with additives and blended cement (named C.L.C) containing silica fume and smectite. Properties of cement-ion exchange resin waste forms (mechanical properties, shrinkage or swelling) as well as chemical interaction of the waste and the cement matrix were examined. The previous results mainly concerned "homogeneous waste forms" in which ion exchange resins were intimately mixed with the hydraulic binder. A new concept, allowing a higher incorporation rate, was promoted, considering the whole package as an "heterogeneous waste form". In this last case, radionuclide confinement was ensured by an outer cover of pure mortar.

U7.7

ENCAPSULATION OF RADIOIODINE IN CEMENTITIOUS WASTE FORMS. Mark Atkins and Frederik P. Glasser, Department of Chemistry, University of Aberdeen, Meston Walk, Aberdeen, AB9 2UE Scotland.

Risk assessment models applied to radioactive waste repository design disclose that iodine is one of the nuclides causing most concern. Computer calculations for these scenario studies assume that iodine, in the form of I⁻, is poorly sorbed on most geological materials. Thus it is important that iodine be retained at source, ie. within the vault, for as long as is practicable.

In the UK context, cements are likely to form a major part of the waste package for low and medium active wastes, and of engineered vault structures. These cements are likely to be blends of one form or another, including Portland cement blended with blast furnace slag, or fly ash. These materials are chemically reactive with OPC during the first 10¹-10⁶ years. It is important, therefore, to assess the effect of Portland cement and blending agent on iodine speciation and on iodine uptake by the constituent solid phases. Data are presented on uptake of I⁻ and IO₃⁻ on specific phases: Ca(OH)₂, calcium aluminosulphate hydrates, hydrotalcite and calcium silicate hydrogel (C-S-H). Precipitation of iodide as AgI, prior to cementation, is also considered.

Radiolytic effects on I are also described; the production of gaseous radioiodine (I_2) is potentially a serious problem.

U7.8

EFFECT OF γ -RADIATION ON THE MICROSTRUCTURE AND MICROCHEMISTRY OF ggbfs/OPC CEMENT BLENDS. I.G. Richardson and G.W.Groves, Department of Metallurgy and Science of Materials, University of Oxford, Parks Road, Oxford OX1 3PH, U.K.; and C.R.Wilding, Materials Development Division, UKAEA Harwell Laboratory, Oxfordshire OX11 0RA, U.K.

Ground granulated blast-furnace slag (ggbfs)/OPC blends are among the materials being considered as possible encapsulating matrices for low and intermediate level radioactive wastes. It is therefore desirable to identify any microstructural modifications which may result in these systems from exposure to ionizing radiations.

In order to investigate this, ggbfs/OPC blends were γ -irradiated to $>80\text{MGy}$ at 50°C over a period of 2 years. These were examined by electron optical, X-ray and thermal analysis techniques and the results compared with controls subjected to a similar hydration regime. The morphological and compositional similarities and differences revealed between the irradiated and control samples are presented and discussed.

U7.9

HYDROGEN GENERATION IN MORTARS IMMOBILIZING WASTE CHLORIDE SALTS.* Michele A. Lewis and David W. Warren, Argonne National Laboratory, 9700 So. Cass Avenue, Argonne, IL 60439.

A mortar formulation capable of immobilizing chloride salts containing fission product cesium and strontium has been developed. This formulation, which consists of cement, fly ash, slag, water, and 3 to 10 wt% LiCl-KCl salt, is strong and leach-resistant, and under irradiation only hydrogen gas is generated. The $G(\text{H}_2)$ value depended on temperature and chloride salt concentration and varied from 0.02 to 0.2. Higher salt concentrations led to higher hydrogen yields at 25°C but lower yields at 75 and 120°C . Steady state pressures were not attained. Mechanistic studies showed that reduced sulfur species in the slag primarily controlled the radiolysis mechanism in slag-containing mortars. Since hydrogen pressures were comparatively high (250 psig for a total dose of 500 Mrad) and since the feasibility of using venting to reduce hydrogen buildup was uncertain, several different methods to reduce hydrogen yields were investigated. These included the addition of small quantities of materials which function as electron scavengers, as oxidizers, or as precipitating agents for sulfides, the use of different containment materials, the partial dehydration of the waste form and the use of a hydrogen getter.

*Work supported by the U.S. Department of Energy, Nuclear Energy Research & Development Program, under Contract W-31-109-Eng-38.

U7.10

POROSITY AND ION DIFFUSIVITY OF LATEX-MODIFIED CEMENT.

T. Nishi, O. Kuriyama, M. Matsuda, K. Chino, Energy Research Lab., Hitachi Ltd.; and M. Kikuchi, Hitachi Works, Hitachi Ltd., Hitachi, JAPAN.

Latex-modified Portland cement was studied as a solidification agent for radioactive wastes. In order to predict the leaching rate of radionuclides from the cementitious waste forms using the mixing parameters such as water or latex content, the influence of these parameters was quantitatively estimated by porosity and ion diffusivity of hardened cement paste.

Total porosity of hardened cement paste decreased with water content and it was reduced by latex addition. Also the diffusion coefficient of ions decreased exponentially

with total porosity. Two experimental equations, by which total porosity was related to water and latex content and the diffusion coefficient of ions was related to total porosity, were derived from these results. The calculated results had good agreement with the measured ones.

U7.11

A COMPARISON OF THE BEHAVIOUR OF VITRIFIED HLW IN REPOSITORIES IN SALT, CLAY AND GRANITE. Part I: EXPERIMENTAL. L. A. Mertens, W. Lutze, Hahn-Meitner-Institut, Glienicke Strasse 100, 1000 Berlin 39, FRG., J. A. C. Marples, Harwell Laboratory, Oxon OX11 0RA, UK., and P. van Iseghem, SCK/CEN, Boeretang 200, 2400 Mol, Belgium, E. Vernaz, CEA Valrho, Marcoule BP 171, 30200 Bagnols sur Ceze, France.

Based on a universal "European Commission's Repository Systems Simulation Leach Test", a limited number of conditions were selected to be applied in a 'Round Robin' test in which 15 laboratories from 11 countries participated. Ten laboratories undertook the granite option, six salt and three clay. This contribution and a companion paper summarize the acquired information. The HLW borosilicate glass SON68 (R7T7), to be returned to and eventually disposed of in various geological repositories by Cogema's reprocessing customers, was tested in a standardized leach container developed and provided by CEA, Marcoule. The glass (2g of powder, 125-250 μm , and a coupon, 25x25x3mm, for each experiment) was prepared and delivered by CEA; together with crushed granite, sand, smectite and groundwater for the granite option. SCK-Mol provided the clay, smectite, sand and the recipe for claywater, HMI-Berlin the recipe for the rock salt composition. All materials were used in proportions and positions in the leach container as prescribed. The analytical method was the only variable to be chosen by the participants. After termination of the experiments (duration 14-364d, temperature 90°C), the concentrations of the glass constituents Si, B, Mo, Li, in solution had to be determined. Results for other elements (e.g., Zn, Sr, Na) and of surface analyses have been reported. The data base was used to evaluate the test procedure, the usage and versatility of the apparatus, and to identify analytical problems.

U7.12

IN-SITU TESTING OF NUCLEAR WASTE FORMS IN A CLAY LABORATORY - RESULTS AFTER TWO YEARS CORROSION. P. Van Iseghem, W. Timmermans and B. Neerdael, SCK/CEN, Boeretang 200, B-2400 Mol, Belgium.

Beginning of 1986, four tubes were introduced into the clay host formation from the underground Mol laboratory, at 220 m below surface level. About sixty-four waste form samples (40 x 15 x 5 mm) loaded on each tube, were brought directly in contact with the clay. One of the rigs is being held at ambient temperature for 5 years, two are heated at 90°C for respectively 2 and 5 years, and one is heated at 170°C for 5 years (ref. 1). These experiments are part of a large in-situ research programme, to demonstrate the suitability of the "Boom" clay layer at the Mol site as a waste repository host formation.

The paper discusses the results obtained from the first tube (two years at 90°C) which was retrieved by overcoring in August 1988. The main results are:

- The in-situ test was successful in terms of tube performance, operation (including retrieval), configuration (settling of the clay) and reliability of the results.
- The mass loss data and surface layer observations for the various glasses of interest (various CEC reference glasses) reveal a close similarity with parallel laboratory tests; the thickness of glass dissolved within two years varies between 40 and 325 μm .
- Glass composition effectively influences glass dissolution; the presence of canister and overpack corrosion products seems to enhance glass dissolution.

U7.13

DISSOLUTION KINETICS OF A SIMPLE ANALOGUE NUCLEAR WASTE GLASS AS A FUNCTION OF pH, TIME AND TEMPERATURE. Kevin G. Knauss, William L. Bourcier, Kevin D. McKeegan, Celia I. Merzbacher, Son N. Nguyen, Frederick J. Ryerson, David K. Smith and Homer C. Weed, Lawrence Livermore National Laboratory, Livermore, CA 94550

We have measured the dissolution rate of a simple five-component borosilicate glass (Na_2O , CaO , Al_2O_3 , B_2O_3 , SiO_2) using a flow-through system. The experiments were designed to measure the dissolution rate constant over the interval pH 1 through pH 13 at 3 temperatures (25, 50 and 70°C). Dilute buffers were used to fix pH as the glass dissolved. Solution and surface solid analyses provided information that are used to develop a kinetic model for glass dissolution.

Under all conditions we eventually observed linear dissolution kinetics. Above pH 8 or pH 9 dissolution was congruent and the gel layer was very thin. In strongly acidic solutions (pH 1 to pH 3) all components but Si were released in their stoichiometric proportions and a thick, Si-rich gel was formed. In mildly acidic to neutral solutions the gel was thinner and was both Si- and Al-rich, while the other components were released to solution in stoichiometric proportions. By varying the flow rate we demonstrated a lack of transport control of the dissolution rate.

The dissolution rates were found to be lowest at near-neutral pH and to increase at both low and high pH. A rate equation based on transition-state theory (TST) was used to calculate dissolution rate constants and reaction order with respect to pH over two pH intervals at each temperature. At 25°C between pH 1 and pH 7 the log rate constant for glass dissolution ($\text{g glass}/\text{m}^2\text{-d}$) was -0.77 and the order with respect to pH was -0.48. Between pH 7 and pH 13 the log rate constant for glass dissolution was -8.1 and the order with respect to pH was +0.51. The measured simple glass dissolution rate constants compare very well with constants estimated by fitting the same TST equation to experimental results obtained for SRL-165 glass and to dissolution rate estimates made for synthetic basaltic glasses.

U7.14

HYDROTHERMAL LEACHING OF R7-T7 BOROSILICATE GLASS.

J. Caurel and E. Vernaz, CEN-Valrhô, SDHA/SEMC, BP 171, 30205 Bagnols-sur-Cèze Cedex, FRANCE; D. Beaufort, Laboratoire de Pétrologie des Alterations Hydrothermales, Université de Poitiers, 40 avenue du Recteur Pineau, 86022 Poitiers Cedex.

The results of hydrothermal leach tests are intended to be used to predict long-term low-temperature glass dissolution. It is often assumed that experimental data can be extrapolated to other conditions using Arrhenius-type rate laws.

Hydrothermal leaching mechanisms and their temperature dependence in R7-T7 glass were investigated in static experiments lasting from 7 days to 1 year at 150°C and 250°C, and in 7-day experiments at temperatures from 100°C to 300°C. Leachates, surface layers, and crystalline products were analyzed by ICP, SEM, EMP, XRD, and cathodoluminescence. Activation energies of 24 to 33 $\text{kJ}\cdot\text{mol}^{-1}$ were obtained for the 7-day tests, and 70 $\text{kJ}\cdot\text{mol}^{-1}$ from established kinetics for boron at 150°C and 250°C for up to 6-months (the discrepancy is discussed below).

The formation of metastable alteration products and large cracks through the bulk glass result in a different chemical and physical system at 250°C than at lower temperatures. Arrhenius calculations between 250°C and 100°C obviously do not allow for this. The assumption of extrapolability will be discussed in light of these changes in the chemical and physical (SA/V) system rather than simple activation energy considerations alone.

U7.15

Effects of Surface-Area-to-Solution Volume Ratio on the Chemical Durability of Nuclear Waste Glasses. X. Feng, I. L. Pegg, Aa. Barkatt, P. B. Macedo. Catholic University of America, Vitreous State Laboratory, Washington DC 22064.

The ratio of glass surface area to solution volume is an important parameter that affects both dissolution and precipitation processes. The effect

of this ratio on chemical durability has been investigated in a number of studies. These studies reported that the leach rates decrease as the SA/V ratios increase for such nuclear waste glasses as PNL-7668, DWRG, and SRL-131. Most of these studies also found that glass leaching data for a range of times and SA/V can be represented by a single curve when plotted versus the product of SA/V and time. In this paper we report some of our findings concerning the SA/V effects on the durability of such nuclear waste glasses as WV205, WVCM47 and WVCM50 which suggest a rather more complicated behavior. We find that the leach rates of waste glasses do not always decrease as the SA/V increases. In fact, the effect is highly composition and SA/V dependent: in the same SA/V range, the leach rate of one glass may increase while that of another decreases with increasing SA/V. Similarly, for the same glass the leach rate may increase within one SA/V range but decrease within another. A consequence of these results is that the effect of (SA/V)t scaling is also composition and SA/V ratio dependent, and therefore the concentration data do not generally collapse into a single curve when plotted against (SA/V)t.

U7.16

ALTERATION OF MICROSTRUCTURE AND LEACHING PROPERTIES OF WEST VALLEY REFERENCE BY HEAT TREATMENT. A. C. Buechele, X. Feng, H. Gu, and I. L. Pegg, Vitreous State Laboratory, The Catholic University of America, Washington, D.C. 20064

Samples of West Valley reference glass WVCM-59 were subjected to isothermal heat treatment according to a systematic schedule of time-temperature combinations to simulate conditions which might be encountered during cooling after the glass is poured into canisters. Phases differentiating during heat treatment were observed, analyzed, and quantified using an SEM equipped with WDS, EDS and image processing and analyzing capabilities. A hitherto unobserved phosphorus-rich phase of indefinite morphology developed after 3 hours at 700°C and continued to grow in extent as time elapsed. Small amounts of rare metal (e.g. Rh, Ru, Pd) crystalline phases were always present in the as-melted glass and frequently served as nucleation sites during heat treatment. Iron-group spinels containing Fe, Ni, Cr, and Mn in variable proportions were the most common phases observed, appearing in quantities up to 3 vol% in heat treated glass. The formation of a thoria-ceria phase occurred at temperatures of 900°C and below but required a progressively longer time as the temperature was lowered. Acmites formed at temperatures of 700°C and below. MCC-3 tests were done to assess the durability of samples substantially altered in microstructure.

U7.17

PARAMETRIC EFFECTS OF GLASS REACTION UNDER UNSATURATED CONDITIONS.* J. K. Bates, T. J. Gerding, and D. J. Wronkiewicz, Argonne National Laboratory, 9700 South Cass Avenue, Argonne, IL 60439.

Eventual liquid water contact of high-level waste glass stored under the unsaturated conditions anticipated at the Yucca Mountain site will be by slow intrusion of water into a breached container/canister assembly. The water flow patterns under these unsaturated conditions will vary, and the Unsaturated Test method has been developed by the YMP to study glass reaction. The results from seven different sets of tests done to investigate the effect of systematically varying parameters such as glass composition, composition and degree of sensitization of 304L stainless steel, water

input volume, and the interval of water contact are discussed. Glass reaction has been monitored over a period of five years, and the parametric effects can result in up to a ten-fold variance in the degree of glass reaction.

*Work supported by the U.S. Department of Energy, Office of Civilian Radioactive Waste Management, Yucca Mountain Project Office, under Contract Number W-31-109-Eng-38.

U7.18

GROWTH RATES OF ALTERATION LAYERS AND ELEMENTAL MASS LOSSES DURING LEACHING OF BOROSILICATE NUCLEAR WASTE GLASS. Isunetaka Banba and Takashi Murakami, Japan Atomic Energy Research Institute, Tokai, Ibaraki 319-11, Japan.

MCC-1 static leaching experiments were carried out on a simulated waste glass in deionized water for up to 364 days at 90°C in order to examine the relationship between alteration layer thickness and elemental mass losses.

The thickness of the alteration layers increased linearly at a rate of 0.63 $\mu\text{m}/\text{day}$ for up to 91 days. After 91 days, however, the thickness was kept constant (about 60 μm) independent of time. The observed growth rate was in good agreement with the calculated one obtained by assuming that all boron in the leachates was due to the complete depletion of boron in the alteration layers. This means that shrinkage of the alteration layers is not significant, and suggests that the alteration layers retain their framework even after the depletion of part of the glass network formers and the recrystallization reported previously. The agreement of the leach rates also implies that the apparent release of elements from the glass almost ceases and the reaction between the alteration layers and the leachate plays a major role in the corrosion after 91-day leaching.

Two differently prepared layers, ethanol replacement of leachate and conventional air-drying before resin impregnation, revealed that the air-dried layers were thinner by about 5 percent because of shrinkage of the layers during air-drying.

U7.19

CHARACTERIZATION OF HIGHLY ACTIVE WASTE GLASSES PRODUCED IN A HOT VITRIFICATION PLANT, J.P. Glatz, E. Toscano and M. Coquerelle, and J. Fuger, Institute for Transuranium Elements, Commission of the European Communities, Karlsruhe, West Germany.

In the hot vitrification pilot plant operated by ENEA at JRC-Ispra were produced several high-level waste glass forms (up to 287 Ci/kg), containing 15 to 33 wt% fission products. These glasses were characterized in the hot cell laboratory at JRC-Karlsruhe.

The work comprised:

- mass and fission product distribution in the crucibles by gamma-scanning and radiography,
- microstructural and phase composition analysis by optical, SEM + EDAX and quantitative microscopy,
- leaching behaviour by the SOXHLET-method. The tests were performed on all glasses in water for 72 h. The analysis of the leachates was performed by ICP-MS and OES, and compared with the qualitative analysis by EDAX of the gel-layers found on the specimens after the dissolution tests.

Depending on glass and waste composition and loading, the products showed partial devitrification process or a two-glass system. In the partially devitrified glass, several precipitate morphologies were identified and analyzed. The precipitates, in the form of crystalline inclusions, were enriched in the main waste elements (metals, rare earths and actinides). In the two-glass system, the minor phase showed

a strong Al enrichment, with Cr and Ni as additional elements. Analysis of the leachates showed a good qualitative agreement with those performed on the gel-layers.

U7.20

THE LONG-TERM CORROSION AND MODELLING OF TWO SIMULATED BELGIAN REFERENCE HIGH-LEVEL WASTE GLASSES - PART II
J. Patyn, P. Van Iseghem, W. Timmermans, S.C.K./C.E.N., Boeretang 200 B-2400 MOL, Belgium
B. Grambow Hahn Meitner Institut Berlin, Glienicker Straße 100, 1000 Berlin 39, F.R. Germany

- ABSTRACT -

As part of a larger study to establish the performance of high level waste glass in repository conditions, long term phenomena related to the glass corrosion are being investigated, and modelling of the long term glass corrosion has been attempted. In a previous paper (ref 1) it was shown how for precursor glasses for two kinds of high level waste of importance for Belgium, modelling using the PHREEQE and GLASSOL codes could relatively well fit to the experimental data. The key role of Al_2O_3 on the long term behaviour was demonstrated. The experimental conditions were 90°C, $\text{SA.V}^{-1} = 10$ or 100m^{-1} , with distilled water as corrosion medium.

Recently, additional corrosion experiments in distilled water, but using powdered glass ($\text{SA.V}^{-1} = 7000\text{m}^{-1}$) at 90 or 120°C, provided a further confirmation about the final corrosion rate, but revealed also an additional corrosion accelerating (crystallisation ?) phenomenon in case of the high Al_2O_3 glass.

Modelling efforts at present managed to fit the calculated values with the experimental data, (but not the final acceleration) for the different SA.V^{-1} conditions.

The paper will discuss the experimental data, and the modelling approaches focusing the role of surface area to volume ratio (SA.V^{-1}), temperature and the Al_2O_3 content of the glass

U7.21

SIMULTANEOUS EVAPORATION OF Cs AND Tc DURING VITRIFICATION - A THERMOCHEMICAL APPROACH

H. Migge, Hahn-Meitner-Institut, Glienicker Strasse 100, 1000 Berlin 39, FRG

In vitrification of nuclear waste technetium tends to be lost substantially by evaporation. For the case that Cs is not present this behaviour was satisfactorily described by thermochemistry in the simple Tc-O system considering the predominance areas of the different oxides and the partial pressures of Tc_2O_7 above them. If Cs is present there are contradictory observations from the condensation products whether or not Tc evaporates simultaneously with Cs by forming gaseous CsTcO_4 . This compound - in contrast to solid CsTcO_4 - has not yet been identified experimentally. Its existence may be concluded, however, from the existence of the gaseous alkali-perrhenates. From comparison with these perrhenates the standard formation enthalpy and the entropies of condensed as well as of gaseous CsTcO_4 are estimated, and solid CsTcO_4 is assumed to melt above 1200K. Free energies of these compounds and tentative isothermal predominance area diagrams of the Cs-Tc-O system up to 1200K were calculated including isobars of the gases CsO , Cs_2O , TcO , Tc_2O_7 , and CsTcO_4 and their dependence on the condensed phase present. The pressure of gaseous CsTcO_4 above solid CsTcO_4 is very high even at lower temperatures ($\log p(\text{Pa}) = 3$ at 500K and $\log p(\text{Pa}) = 8.3$ at 1200K). From comparison with voltammetric and thermochemical results for borosilicate glass containing Tc it is concluded that condensed CsTcO_4 does exist in glass which contains Cs as well. Therefore, the appearance of condensates of CsTcO_4 during vitrification has to be expected. The pressure of CsTcO_4 decreases only slowly, if the oxygen or caesium potentials are reduced and condensed CsTcO_4 becomes unstable and condensed Tc, TcO_2 or Tc_2O_7 resp. are formed.

U7.22

THE EFFECT OF TEMPERATURE ON THE REDOX CONSTRAINTS FOR THE PROCESSING OF HIGH-LEVEL NUCLEAR WASTE INTO A GLASS WASTE FORM. Henry D. Schreiber, Charlotte W. Schreiber, Margaret W. Riethmiller, and J. Sloan Downey; Center for Glass Chemistry, Virginia Military Institute, Lexington, VA, 24450.

Efficient processing of high-level nuclear waste into a borosilicate glass matrix requires the consideration of the melt's redox properties. If the conditions that accompany the dissolution of the waste into the glass melt are too oxidizing, foaming problems may arise; conversely, if the conditions during processing are too reducing, sulfide and metal phases might precipitate from the melt and result in short circuiting between the electrodes.

Savannah River Laboratory glass frit #131 (SRL-131), the reference system for this study, is an alkali borosilicate glass whose redox chemistry has been extensively characterized at 1150°C. The oxidation-reduction equilibria of selected multivalent elements in this reference composition were investigated as a function of the imposed oxygen fugacity for several temperatures from 950°C to 1350°C.

The redox chemistry of the system defines an acceptable operating range in SRL-131 with respect to the imposed oxygen fugacity of about 10^{-5} to 10^{-12} atm at 950°C, of about 10^{-2} to 10^{-9} atm at 1150°C, and of about 10^0 to 10^{-7} atm at 1350°C in order to alleviate potential foaming problems at the upper limit and potential precipitation of metals and sulfides at the lower extreme. For the processing of the glass waste form, the previously prescribed range of 0.1 to 0.5 for $[Fe^{2+}]/[Fe^{3+}]$ in the resulting glass should be acceptable at all temperatures from 950°C to 1350°C.

U7.23

CALCULATION OF THE VISCOSITY OF NUCLEAR WASTE GLASS SYSTEMS. Ritesh P. Shah, E.C. Behrman, and D. Oksoy, New York State College of Ceramics, Alfred University, Alfred, NY 14802

Viscosity of one of the most important processing parameters and one of the most difficult to calculate theoretically, particularly for multicomponent systems like nuclear waste glasses. Here, we propose a semi-empirical approach based on the Fulcher equation, involving identification of key component variables, for which coefficients are then determined by regression analysis. Results are presented for a variety of glass systems, and compared both to experimental data and to statistical mechanical perturbation theory calculations.

U7.24

CHARACTERIZATION OF MECHANICAL STRENGTHS FOR SIMULATED SOLIDIFIED HIGH LEVEL WASTE FORMS. Hiroshi Igarashi, Takeshi Takahashi, Power Reactor & Nuclear Fuel Development Corp. (PNC), 4-33, Muramatsu, Tokai-mura, Ibaraki, 319-11, JAPAN

Various types of waste form have been developed and characterized in PNC to immobilize high level liquid waste generated from reprocessing nuclear spent fuel. Mechanical strength tests were made on simulated solidified high level waste forms which were borosilicate glass and diopside-glass-ceramic form. Commercial glasses were also tested for comparison with the waste forms.

Measured strengths were three-point bending strength, uniaxial compressive strength, impact strength by falling weight method, and vickers hardness. Fracture toughness and fracture surface energy were also measured by both of notch-beam and indentation technique. The strengths measured were evaluated with statistical errors.

The effect of change in composition was studied on the glass form. The change in waste content from 20 to 40 wt% did not influence the strength. No significant effect of the change of iron content in waste was observed. The difference in glass additives composition did not result in the change of strengths. The mechanical strengths measured of the glass forms were comparable with those of commercial glasses.

Clearer difference in the fracture toughness and fracture surface energy was observed between glass and glass-ceramic waste form. The fracture toughness of glass form by indentation test was about $0.7 \text{ MN/m}^{3/2}$ which was comparable with commercial glass. And fracture toughness of the glass-ceramic form was 30% higher than that of glass form.

U7.25

DIFFUSION OF CESIUM IN SODIUM-BOROSILICATE GLASSES USED FOR IMMOBILISATION OF NUCLEAR WASTE. E.G.F. Sengers and F.J.J.G. Janssen, N.V. KEMA, R&D Division, Chemical Research Department, P.O. Box 9035, 6800 ET Arnhem, The Netherlands.

Sodium-borosilicate glasses used for the immobilisation of nuclear waste were studied in experiments using concentration couples in order to determine the diffusion coefficient of Cs. The couples were made by pouring successively sodium-borosilicate glass and sodium-borosilicate glass containing 2 mol% cesiumoxide in alumina crucibles. Diffusion experiments were performed by heating the crucibles at various temperatures for five hundred hours. A scanning electron microscope, in combination with an energy dispersive spectrometer was used to determine concentration profiles.

In the temperature range 850 - 975 K diffusion coefficients between 10^{-18} and $10^{-15} \text{ m}^2/\text{s}$ were found. The activation energy for the cesium diffusion in that temperature range appears to be about 425 kJ/mol.

Diffusion coefficients for cesium diffusion have also been measured in glasses containing cesium and different amounts of other fission products, such as Sr and Zr, and impurities, such as Ca and Fe, and in simulated nuclear waste glasses. It can be concluded that the diffusion of cesium does not depend critically on the addition of other fission-product elements or other impurities.

U7.26

ENTHALPIES OF MIXING AND INCIPIENT IMMISCIBILITY IN GLASSES IN THE SYSTEM $\text{K}_2\text{O} \cdot \text{SiO}_2 \cdot \text{La}_2\text{O}_3$. A.J.G. Ellison and A. Navrotsky, Department of Geological and Geophysical Sciences, Princeton University, Princeton, NJ 08544

Enthalpies of mixing of quenched glasses along three joins have been determined using high-temperature solution calorimetry in molten $2\text{PbO} \cdot \text{B}_2\text{O}_3$ at 977 K. In $\text{K}_2\text{O} \cdot 5\text{SiO}_2 \cdot n\text{La}_2\text{O}_3$ and $\text{SiO}_2 \cdot n(\text{K}_2\text{O} \cdot \text{La}_2\text{O}_3)$ ($0 \leq n \leq 1$) glasses, the concentration of network-modifying cations and the ratio of non-bridging oxygen to silicon atoms (NBO/Si) increases with n . Along the join $(1-x)\text{K}_2\text{O} \cdot 5\text{SiO}_2 \cdot (x/3)\text{La}_2\text{O}_3$ ($0 \leq x \leq 0.75$), La is substituted for K in glasses with fixed NBO/Si. Despite differences in NBO/Si and the valences of K and La, enthalpies of mixing show no deviations from ideal mixing greater than -1 kJ/mol of the ternary system. $\text{K}_2\text{O} \cdot 5\text{SiO}_2 \cdot \text{La}_2\text{O}_3$ undergoes glass-glass phase separation at 1200 K, but the enthalpy of solutions of the clear glass and the phase-separated glass are identical within error.

These data indicate that phase-ordering (a precursor to liquid immiscibility) is present even at low La_2O_3 concentrations - increasing La_2O_3 adjusts the size and/or distribution of phase-ordered regions. Vibrational spectra of glasses in this system support this interpretation, and indicate that K and La do not share the same NBO; hence, phase-ordering is driven by the presence of La in the glass.

U7.27

GRAIN BOUNDARY INVENTORY AND UO_2 MATRIX DISSOLUTION STUDIES ON SPENT LWR FUEL. W. J. Gray, D. M. Strachan, L. E. Thomas, R. E. Einziger, and M. J. Apted. Pacific Northwest Laboratory, P. O. Box 999, Richland, WA 99352.

An experimental method is being developed for measuring the grain boundary inventory of radionuclides and for determining whether radionuclides within the UO_2 matrix of spent LWR fuel will dissolve congruently with the UO_2 . The method involves limited oxidation of spent fuel in air at low temperatures (150°C to 200°C). At these temperatures, spent LWR fuel oxidizes preferentially along the grain boundaries making the fuel fragments friable. This technique has been used successfully to prepare individual grains of irradiated UO_2 . Following oxidation, the spent fuel particles are mounted and thinned to permit examination by transmission electron microscopy (TEM). This analysis can show the presence of higher oxides, such as U_3O_8 , and provide assurance that the limited oxidation affected only the grain boundary material plus a few hundred nanometers of the UO_2 grain periphery.

Once the spent fuel has been dissociated into individual grains, the grain-boundary inventories of radionuclides can be measured. This is accomplished through a series of dissolution tests in which the solvent (e.g., dilute HCl) is changed and analyzed frequently. This technique gives an upper limit to the grain boundary inventory because it is not possible to prevent a small amount of the UO_2 grain periphery from oxidizing and subsequently dissolving. After the oxidized portions of the grains are completely removed, fluid-flow dissolution tests are used to determine whether the remaining UO_2 matrix material dissolves congruently. Water is pumped through a column containing spent fuel grains while the concentration of radionuclides in the column effluent is monitored. At high flow rates, the forward reaction rates of the various radionuclides can be measured and the degree of congruency determined.

U7.28

IDENTIFICATION OF SECONDARY PHASES FORMED DURING UNSATURATED REACTION OF UO_2 WITH EJ-13 WATER.* J. K. Bates, B. S. Jani, and E. Veleckis, Argonne National Laboratory, 9700 South Cass Avenue, Argonne, IL 60439.

The reaction of spent fuel under the unsaturated conditions anticipated to exist at the Yucca Mountain repository site will likely include contact between the fuel and small volumes of water under oxidizing conditions. To evaluate procedures that may be required to perform such testing, a set of parametric experiments has been conducted over a four-year period. One aspect of these experiments has been to identify the secondary phases that form during the reaction process. More than five distinct phases have been identified, including uranophane, boltwoodite, sklodowskite, and becquerelite. The methods used to identify the phases together with a temporal and spatial description as to how these phases formed with respect to the water flow pattern and cation depletion are discussed.

*Work supported by the U.S. Department of Energy Office of Civilian Radioactive Waste Management, Yucca Mountain Project Office, under Contract Number W-31-109-Eng-38.

U7.29

INVESTIGATIONS INTO THE ELECTROCHEMICAL LEACHING BEHAVIOUR OF UO_2 PELLETS IN VARIOUS SATURATED SALT SOLUTIONS

Ch. Keiling, P.-M. Heppner and G. Marx; Free University of Berlin; Institute for Inorganic and Analytical Chemistry; Radiochem. Div.; Fabbeckstr. 34-36; D-1000 Berlin - Dahlem (33); FRG

Within the frame of investigations into the safety aspects for direct waste disposal excluding spent fuel reprocessing experiments are made for characterizing the leaching behaviour of UO_2 pellets in various saturated salt solutions. The solutions taken into consideration are saturated NaCl solutions and also Q and R brines. The redox potentials for the various systems are realized electrochemically. Quite a number of electrode forms have been tested with respect to their applicability for performing measurements in solutions of significant high ionic strength. Using a newly developed UO_2 electrode the rest potentials of UO_2 electrodes have been determined in various systems. The corrosion rates could be potentiostatically obtained under a variety of different experimental conditions.

U7.30

A DEFORMATION AND THERMODYNAMIC MODEL FOR HYDRIDE PRECIPITATION KINETICS IN SPENT FUEL CLADDING

R. B. Stout, University of California-LLNL
P.O. Box 808, L-201, Livermore, CA 94550

ABSTRACT* Hydrogen is contained in the Zircaloy cladding of spent fuel rods from nuclear reactors. All the spent fuel rods placed in a nuclear waste repository will have a temperature history that decreases toward ambient; and as a result, most all of the hydrogen in the Zircaloy will eventually precipitate as zirconium hydride platelets. A model for the density of hydride platelets is a necessary sub-part for predicting Zircaloy cladding failure rate in a nuclear waste repository. A model is developed to describe statistically the hydride platelet density, and the density function includes the orientation as a physical attribute. The model applies concepts from statistical mechanics to derive probable deformation and thermodynamic functionals for cladding material response that depend explicitly on the hydride platelet density function. From this model, hydride precipitation kinetics depend on a thermodynamic potential for hydride density change and the inner product of a stress tensor and a tensor measure for the incremental volume change due to hydride platelets. The development of a material response model for Zircaloy cladding exposed to the expected conditions in a nuclear waste repository is supported by the U.S. DOE Yucca Mountain Project.

* Work performed under the auspices of the U.S. Department of Energy, Office of Civilian Radioactive Waste Management, Yucca Mountain Project Office, by the Lawrence Livermore National Laboratory under contract W-7405-ENG-48.

U7.31

"Fluoride Influence on Zircaloy-4 Corrosion in Water as a Function of pH, Temperature and Fluoride Content." (a)
N. Uziemblo and H. D. Smith, Pacific Northwest Laboratory, Richland Washington

The corrosion rate of Zircaloy-4 was determined in fluoride-doped water (100, 500, 1000ppm) using a pH stat system. The results were strong functions of pH, fluoride ion concentration and temperature. The calculated amount of corrosion using homogeneous corrosion rates correlated well with the observed weight loss exhibited by those same specimens. The weight loss indicates that the normal passivating film usually formed on Zircaloy in water is not present. This result is consistent with 1) observed increase in corrosion rate, 2) extensive pitting observed with scanning electron microscopy, 3) detected fluoride and

oxyfluoride compounds of zirconium on the surface observed via photo-electron spectroscopy, and 4) Zircaloy components in solution in the fluoride-doped water. Anodized Zircaloy specimens are observed to be attacked at a similar rate to the non-anodized material. Furthermore, specimens exhibit a temporary elevation of corrosion rate when they are cycled from high corrosion rate to low corrosion rate conditions. It can be concluded that fluoride in the water influences the corrosion rate of Zircaloy by modifying the passivation properties of the oxide film.

(a) The Yucca Mountain Project of the U.S. DOE is investigating the suitability of a site in the unsaturated zone at Yucca Mountain, Nevada, for a high-level waste repository.

(b) Pacific Northwest Laboratory is operated for the U.S. Department of Energy by Battelle Memorial Institute under Contract DE-AC06-76RLO 1830.

U7.32

CORROSION BEHAVIOR OF ZIRCALOY*IN AQUEOUS MEDIA

Anna C. Fraker and Jonice S. Harris, National Institute of Standards and Technology, Gaithersburg, MD 20899.

Zircaloy-2 (Zr-2) and Zircaloy-4 (Zr-4) are used as nuclear fuel cladding. Both alloys are more than ninety eight percent zirconium (Zr) and are highly corrosion resistant to various media. The thickness of nuclear fuel cladding is less than 1 mm, and it is important to establish whether the cladding will remain intact for the required time periods of nuclear waste storage. Electrochemical measurements using polarization techniques have been made on these alloys in aqueous media with a pH of 8.3 and varying ionic concentrations (1X and 10X) at temperatures of 22°C and 95°C.

Results of open circuit electrode potential measurements indicate that the Zircaloys passivate after immersion in the test media used. Anodic polarization measurements in concentrated media at 95°C show a passive region extending over a range of -400 millivolts to +850 millivolts where breakdown occurred. All potentials were measured versus a saturated calomel electrode (SCE). Cyclic polarization curves show the same passive region and breakdown potential and in addition, show hysteresis in the return portion of the curve. The hysteresis indicates possible susceptibility to localized corrosion, and selected experimental parameters were varied to investigate the reason for the hysteresis. Measured corrosion rates were low, but some white corrosion product was observed in one area after a thirty day exposure at 95°C.

Data will be presented and discussed in terms of corrosion rates, passivity, breakdown potential and susceptibility to localized corrosion under the conditions studied.

*Zircaloy is a registered trademark of the Westinghouse Electric Corp., Specialty Metals Division, Pittsburgh, PA

U7.33

POTENTIODYNAMIC POLARIZATION STUDIES OF CANDIDATE CONTAINER MATERIALS IN SIMULATED TUFF REPOSITORY ENVIRONMENTS. John A. Beavers and Neil G. Thompson, Cortest Columbus, Inc., Columbus, Ohio.

Cortest Columbus is investigating the long-term performance of container materials used for high-level waste packages as part of the information needed by the Nuclear Regulatory Commission to assess the Department of Energy's application to construct a geologic repository for high-level radioactive waste. In one task of the program, a cyclic potentiodynamic polarization (CPP) technique is being used to evaluate the corrosion behavior of the candidate container materials, which include copper-base alloys and Fe-Cr-Ni alloys. In order to evaluate the expected range of environmental variables (groundwater composition and temperature), a statistical

experimental design approach is being used. Complete matrices of CPP tests, which consist of 33 environments, have been completed on four candidate container materials; CDA 102 Copper, CDA 715 Copper-Nickel, Type 304L Stainless Steels and Incoloy Alloy 825. The test matrix was a Resolution IV experimental design for 15 environmental variables, including temperature and pH, species present in the groundwater, and those generated by radiolysis. In these environments, all four alloys tested exhibited a wide range of behavior including passive behavior, pitting, crevice corrosion and active corrosion. The CPP behavior of the Fe-Cr-Ni alloys was found to conform with a conventional interpretation of CPP curves while this was not the case for the copper-base alloys.

U7.34

MIGRATION BEHAVIOR OF URANIUM SERIES NUCLIDES IN ALTERED QUARTZ-CHLORITE SCHIST. T. Ohnuki, T. Murakami, K. Sekine, N. Yanase, H. Isobe and Y. Kobayashi, Department of Environmental Safety Research, Japan Atomic Energy Research Institute, Tokai, Ibaraki, 319-11, Japan

Migration behavior of uranium series nuclides in the altered quartz-chlorite schist has been studied utilizing data on the concentration distribution of uranium and thorium series nuclides at Koongarra in Australia. The distribution of $^{234}\text{U}/^{238}\text{U}$ and $^{230}\text{Th}/^{234}\text{U}$ activity ratios in the schist reveals that the migration behavior of uranium series nuclides differs between depths. The variation of $^{230}\text{Th}/^{234}\text{U}$ activity ratios against distance along the surface, intermediate and deep layers shows different trend in different layers. The X-ray diffraction patterns of the three rock samples collected at different layers show; quartz is found in all layers; chlorite is present only in the deep layer; kaolinite-smectite and goethite which are converted from chlorite, in the intermediate layer, and kaolinite-smectite, goethite and hematite which are converted from chlorite in the surface layer. Relationships between $^{234}\text{U}/^{238}\text{U}$ and $^{230}\text{Th}/^{238}\text{U}$ activity ratios along the surface, intermediate and deep layers reveal that the retardation factors of ^{234}U are greater by a factor of 1.1 and 1.9 than those of ^{238}U in the surface and intermediate layers, respectively. These suggest that different uranium adsorption between depths is probably due to different mineral assemblages.

U7.35

MIGRATION OF ANIONIC SPECIES OF RADIOACTIVE COBALT THROUGH SOIL. Toshihiko Ohnuki, Department of Environmental Safety Research, Japan Atomic Energy Research Institute, Shirakata, Tokai, Ibaraki, Japan and David E. Robertson, Chemical Science Department, Pacific Northwest Laboratories, Richland, WA.

The migration of an anionic species of ^{60}Co through soil has been examined utilizing data on the migration of radionuclides leached from an aqueous waste disposal site. Correlation coefficients between the concentrations of the anionic species of ^{60}Co and those of particulate, cationic and non-ionic species of ^{60}Co reveal that the anionic species of ^{60}Co was not interconverted with other species during migration. The cross-correlations between the concentrations of the anionic species of ^{60}Co gives a calculated retardation factor of the anionic species of ^{60}Co of approximately 19 being 1200 times lower than the laboratory measurements. The average concentration distribution of the anionic species

of ^{60}Co suggests that the migration of the anionic species of ^{60}Co consists of two migration fractions which was characterized by different migration mechanism.

U7.36

SHINZO UETA * AND NAOTAKE KATOH **

* Naka Nuclear Development Center of Mitsubishi Metal Corp., Mukohyama 1002-14, Naka-machi, Ibaraki 311-02, Japan.
**Kogakuin Univ., 1-24-2 Nishishinjuku, Tokyo 160, Japan.

Sorption is one of the most important mechanisms for the migration of radionuclide which released from the nuclear wastes. The sorption behaviors strongly depend on the chemical species of radionuclides. Therefore it is necessary to study on the migration from the point of view of chemical forms.

We carried out the column experiments, where Co was used as the tracer elements. The tracer solutions were prepared to treat three different chemical forms of Co^{2+} , $\text{Co}(\text{OH})_2$, and Co-EDTA . In the sand column which simulated the natural barrier, Co^{2+} and $\text{Co}(\text{OH})_2$ could be well retained and Co-EDTA showed no retardation.

On the contrary, Co-EDTA could be retained in the column filled with artificial absorbent, for example activated carbon and silica-alumina, then the distribution coefficients were about 60 ml/g in each case. In these experiments, the breakthrough curves of Co^{2+} , $\text{Co}(\text{OH})_2$, and Co-EDTA showed good agreements with the calculations which based on the ion exchange, filtration, and absorption model, respectively.

U7.37

GRIMSEL COLLOID EXERCISE. C. DEGUELDRE, Paul Scherrer Institute, CH-5232 Villigen, Switzerland

The Grimsel Colloid Exercise is an intercomparison exercise which consisted of an in situ sampling phase followed by a colloid characterization step. The goal of this benchmark, which involved 12 laboratories, is to evaluate both sampling and characterization techniques with emphasis on the colloid specific size distribution. The sampling took place at the Grimsel Test Site (NAGRA facility) and colloids were sampled from the water flowing in the granitic fracture. The production of colloid samples was carried out in duplicate by cross flow filtration (CEA, PSI) and by tangential flow filtration (AECL, UKAEA) while unfiltered water was also collected. CEA and PSI produced colloid samples on membranes changing both the pore size (3 - 450 nm) and the volume of water collected (20 - 150 ml). The colloid concentrates were yielded by tangential filtration with a cut-off of 1.5 (AECL) and 2.1 (UKAEA) nm respectively, the former concentrate being produced after a 1 μm prefiltration. While shipping and storage may affect the colloid samples, as well as the composition of both unfiltered/filtered water and concentrate samples, major element composition of the fluid samples was comparable for the chemical analysis groups. However, CO_2 contamination from the air decreases the pH from 9.6 to about 8 while increasing the total inorganic carbon. The exercise differentiates the colloid samples produced on site from those obtained after transfer of the fluid samples in the laboratory. The colloid concentration estimated by transmission electron microscopy and by gravimetry is around 10^{14} pt.l^{-1} for diameters larger than 10 nm. For colloids larger than 50 nm the concentration measured by scanning electron microscopy is about 10^{10} pt.l^{-1} . For colloids/particles larger than 450 nm, the concentration measured by gravimetry, scanning electron microscopy and single particle counting is about $2 \cdot 10^7$ pt.l^{-1} . On a weight basis, the total colloid and particle concentration measured by gravimetry, laser photoacoustic spectroscopy, chemical analysis of fluid samples, scanning electron microscopy, single particle counting and static light scattering is 200 ± 100 ppb. They consist of silica, illite/muscovite, biotite, calcium silicate, and organic material. These particles are negatively charged in the in situ conditions and the average cumulative specific size distribution is given by: $\log[\text{coll}] = 15.82(\pm 0.36) - 3.17(\pm 0.16)\log\phi$ with ϕ the colloid diameter ranging from 10 to 10,000 nm and $[\text{coll}]$ given in pt.l^{-1} . On the basis of an average site density of 3 nm^{-2} the calculated cation exchange capacity is of the order of nM and below the detection limit of the classical CEC tests. These results are discussed on the basis of the detection limit, lateral resolution and counting conditions of the techniques (precision) as well as the sample preparation (accuracy). The main recommendations are the need of in situ sampling, track of artefact production (e.g. ion retention, aggregation ...) and the minimization of potential contamination during sample preparation. Details on this study are published in a PSI/NAGRA/CEC report.

U7.38

AUTHIGENIC CLAY MINERALS IN THE RUSTLER FORMATION, WIPP SITE AREA, NEW MEXICO. Douglas G. Brookins, University New Mexico, Albuquerque, NM 87131; Steven J. Lambert, Sandia National Laboratories, Albuquerque, NM 87185; and David B. Ward, University of New Mexico, Albuquerque, NM 87131.

Transuranic waste is planned for disposal in the Late Permian evaporites of the Delaware Basin, southeastern New

Mexico, at the WIPP Site. The disposal horizon is located in the bedded halite of the Salado Formation, which is overlain by the impure halite-anhydrite (gypsum)-siltstone-mudstone of the Rustler Formation. The Rustler Formation also contains two dolomite members, the Magenta and Culebra, which transmit water. The Culebra Member is suspected to have actively interacted with waters at time(s) from the Late Permian to the present, and it is important to assess the reactivity of these waters in conjunction with WIPP Site stability.

We have investigated the Rb-Sr systematics of clay minerals from the Culebra Member and elsewhere in the Rustler Formation. By separating the less than 0.5 micron size material we are able to deal with presumed true authigenic clay minerals. The authigenic fraction is especially sensitive to chemical and isotopic exchange with waters, and exposure to large amount of water will reset the clay minerals to such a time. Our data yield a $250 \pm \text{Ma}$ Rb-Sr isochron, which is consistent with the Late Permian age of the Rustler Formation. This age is significant in that it demonstrates that these clay minerals have preserved their isotopic and chemical integrity since the Late Permian and have not been subjected to any pronounced interaction with waters since. This information lends further support to the suitability of the WIPP Site for transuranic waste disposal.

U7.39

IN SITU OBSERVATION OF THE ALPHA / BETA -CRISTOBALITE TRANSITION USING HIGH VOLTAGE ELECTRON MICROSCOPY. Annemarie Meike, Materials and Chemical Sciences Division, Lawrence Berkeley Laboratory, Berkeley, CA 94720; and William Glassley, Earth Sciences Division, Lawrence Livermore National Laboratory, Livermore, CA 94550.

To predict the behavior of the near-field environment of high-level radioactive waste containers, single phase dissolution and precipitation kinetics data are required. In the course of obtaining such data on cristobalite at LLNL, it was noted that synthetic cristobalite dissolved at rates slightly higher than natural cristobalite. Detailed characterization of the starting materials, using the 1.5 MeV High Voltage Electron Microscope (HVEM) at LBL, revealed that both samples contained beta-cristobalite and amorphous silica, in addition to alpha-cristobalite. To understand the mechanism responsible for the apparent metastable persistence of beta-cristobalite and amorphous silica, in-situ experiments were conducted on synthetic alpha-cristobalite using an environmental cell in which it was possible to introduce either dry CO_2 or a $\text{CO}_2 + \text{H}_2\text{O}$ vapor during heating and cooling sequences. Direct observation of electron diffraction patterns during the experiments suggests that the presence of water vapor affects the alpha-beta transition temperature, and may be responsible in part for the development of a stability field for amorphous silica at the transition. Preliminary results suggest that the temperature interval over which amorphous silica may persist could be several tens of degrees. The amorphous phase was not observed during the dry heating experiments. Because a high temperature, water-saturated vapor phase is expected to persist in the near-field environment for several hundred years, the chemical and mechanical properties of the proposed repository tuff may be modified by the development of amorphous silica from cristobalite. Further work is continuing in order to more precisely characterize the properties of this structural transition and its implications for near-field behavior.

Performed under contract W-7405-ENG-48 for Department of Energy Office of Civilian Radioactive Waste Management, Yucca Mountain Project.

U7.40

ESTIMATION OF LONG-TERM DURABILITY OF BENTONITE FROM THE THERMAL HISTORY OF MURAKAMI DEPOSIT, JAPAN. G. Kamei, T. Arai, Y. Yusa, N. Sasaki, Power Reactor & Nuclear Fuel Development Co., Tokai-mura, Ibaraki, Japan, H. Takano, Dia Consultants Company, Ikebukuro, Toshima-ku, Tokyo, Japan.

The illitization of smectite in natural environment affords information on the long-term durability of bentonite which is a candidate for buffer materials. Murakami bentonite deposit, central Japan, where the bentonite and rhyolitic intrusive are distributed, was surveyed and lateral varia-

tion of smectite to illite in the aureole of the rhyolite was studied.

Geochronology: The radiometric ages of some minerals from the intrusive rock and the clay deposit were measured. Comparison of the mineral ages (obtained by K-Ar, Rb-Sr, and fission track methods) with closure temperature estimates for the various isotopic systems has allowed the thermal history of the area. The age of the intrusion was 7.1 ± 0.5 Ma (at 350°C), and the cooling rate of the intrusive rock was estimated to be $30\text{--}60^\circ\text{C/Ma}$.

Durability of bentonite: The reported values of the fission track age of zircon in the bentonite around Murakami mine are mostly within the range from 16 to 18 Ma. The age of zircon in the bentonite obtained at Murakami mine is, however, 7.3 ± 0.4 Ma, which is very close to that of the intrusion. The latter value must be explained as the result of annealing for fission tracks in zircon. Hurford (1986) reported that minimum temperature of the annealing is taken to be 190°C for a $10\text{--}100^\circ\text{C/Ma}$ cooling rate. The annealing and the estimated cooling rate concludes that illitization was not scarcely occurred in $1.6\text{--}2.6$ Ma under the temperature range from 190°C to 100°C .

The waterchemistry related with the illitization was also discussed from the isotope-geochemical point of view.

U7.41

DIFFUSION OF SODIUM AND COPPER IN COMPACTED SODIUM BENTONITE AT ROOM TEMPERATURE A. Muurinen, K. Uusheimo and M. Olin, Technical Research Centre of Finland, Reactor Laboratory, Otakaari 3A, SF-02150 ESPOO, Finland

Compacted sodium bentonite has been considered as possible buffer material for final disposal of spent fuel in many countries. For safety analysis the migration mechanisms of substances in bentonite and the corresponding parameters must be known. In this research the diffusion mechanisms of sodium and copper in bentonite were studied experimentally at room temperature.

Diffusion of sodium seems to follow similar mechanisms as has been observed for cesium and strontium in several previous studies. The phenomena could be explained by some kind of diffusion of sorbed ions or surface diffusion. The measured apparent diffusivities of sodium varied from $5 \cdot 10^{-11}$ to $3 \cdot 10^{-10} \text{ m}^2/\text{s}$ and the effective diffusivities from $8 \cdot 10^{-11}$ to $1.6 \cdot 10^{-9} \text{ m}^2/\text{s}$ depending on the density of bentonite and the salt concentration of water solution.

Low solubility of copper caused precipitation thus interfering the diffusion experiments. However, the part of copper which did diffuse into bentonite seemed to follow the same type of mechanism as sodium. The measured apparent diffusivities of copper varied from $5 \cdot 10^{-12}$ to $5 \cdot 10^{-11} \text{ m}^2/\text{s}$.

U7.42

THERMAL BEHAVIOUR OF BACKFILL MATERIAL FOR A NUCLEAR FUEL WASTE DISPOSAL VAULT, R.N. Yong and A.M.O. Mohamed, Geotechnical Research Centre, McGill University, 8167 Sherbrooke Street W., Montreal, Quebec H3A 2K6, and S.C.H. Cheung, Atomic Energy of Canada Limited, Whiteshell Nuclear Research Establishment, Pinawa, Manitoba, Canada ROE 1L0.

One of the performance requirements of the backfill material in a nuclear fuel-waste disposal vault is to effectively conduct heat generated by the decay of the waste into the surrounding rock. This paper presents the experimental results of the thermal behaviour of the reference Canadian backfill material subjected to various temperature gradients. The results show that the time for the backfill material to establish thermal equilibrium under a tempera-

ture gradient is much shorter than that required for moisture equilibrium. The migration of moisture in the backfill has little effect on the heat transfer process.

U7.43

A COUPLED CHEMICAL-MASS TRANSPORT SUBMODEL FOR PREDICTING RADIONUCLIDE RELEASE FROM AN ENGINEERED BARRIER SYSTEM CONTAINING HIGH-LEVEL WASTE GLASS. B. P. McGrail, D. W. Engel, M. J. Apted, A. M. Liebetrau, Battelle, Pacific Northwest Laboratories, P. O. Box 999, Richland, WA 99352, and N. Sasaki, Power Reactor and Nuclear Fuel Development Corporation, Tokai-mura, Ibaraki-ken, Japan.

Battelle, Pacific Northwest Laboratories is assisting the Power Reactor and Nuclear Fuel Development Corporation of Japan (PNC) in developing models to predict the performance of an engineered barrier system (EBS) in a deep geologic repository for the permanent disposal of high-level nuclear waste. Mass transport models developed at the University of California-Berkeley and implemented in the Analytical Repository Source-Term (AREST) computer code for spent reactor fuel were modified to accommodate the borosilicate glass waste forms being considered by PNC. An analytical solution to the mass balance equations was derived that demonstrates the importance of understanding the kinetics of glass/water interactions to accurately predict diffusive mass transfer rates into the host rock. Preliminary results with the modified AREST code show that, unlike spent fuel, a distribution of containment failures over time does not significantly reduce the peak release of U-238 and Cs-135 from the glass relative to a limiting case in which all containers are assumed to fail simultaneously.

U7.44 ABSTRACT WITHDRAWN

U8.1 ABSTRACT NOT AVAILABLE

U8.2

OXIDATION OF UO_2 FUEL BY RADICALS FORMED DURING RADIOLYSIS OF WATER. S. Sunder, D.V. Shoesmith, H. Christensen*, N.H. Miller and M.G. Bailey, Geochemistry and Waste Immobilization Division, Atomic Energy of Canada Limited, Whiteshell Nuclear Research Establishment, Pinawa, Manitoba, Canada ROE 1L0; *Studsvik, S-611 82 Nykoping, Sweden.

Our studies have shown that the radical species, formed during radiolysis of water, are much more effective in causing UO_2 oxidation than the molecular oxidants formed during radiolysis of water or present in water from atmospheric sources. The effects of specific radicals on UO_2 oxidation were determined by controlling the solution chemistry, during radiolysis, to maximize the yield of a particular radical. The rate of oxidation of UO_2 during radiolysis was monitored by recording the corrosion potential of the UO_2 electrode as a function of time. Under steady-state conditions, the corrosion rate can be obtained from the corrosion potential by doing an electrochemical Tafel analysis. Our studies suggest that the oxidation of UO_2 in irradiated de-oxygenated solutions, consists of two stages. The first stage consists of the growth of a surface film of composition close to UO_2 , and similar in thickness to that obtained in unirradiated oxygenated solutions over longer exposure periods. For small doses, the rate of growth of this film appears to be proportional to the square root of the dose rate. The second stage consists of oxidative dissolution of this film (as UO_2^{2+}). This step mainly occurs at a higher dose. In irradiated oxygenated solutions, where O_2 radicals can reach concentrations of $10^{-6} \text{ mol}\cdot\text{L}^{-1}$, further surface oxidation to UO_2 , and other higher uranium oxides occurs. Our electrochemical results indicate the corrosion rates of UO_2 in irradiated solutions are substantially higher in the presence of dissolved oxygen than in its absence.

U8.3

CONSTRAINTS BY EXPERIMENTAL DATA FOR MODELING OF RADIONUCLIDE RELEASE FROM SPENT FUEL.

B. Grambow*, L.O. Werme**, R. Forsyth***, J. Bruno****, Hahn-Meitner-Institut Berlin, FRG; **SKB, Stockholm, Sweden; ***Studsvik, Nyköping, Sweden; ****Royal Institut of Technology, Stockholm, Sweden

In order to find constraints for the contributions to fission product release from spent UO₂ fuel we compared a large body of data of various fuel types from research projects in Canada, USA and Sweden. There is evidence that the release data of ⁹⁰Sr can be used to describe the degradation (oxidation/ dissolution) of the matrix. A compilation of ⁹⁰Sr release data under oxidic conditions from the Swedish, the Canadian and the US spent fuel corrosion program shows surprising quantitative similarities. After 1000 days typical fractional release rates of soluble radionuclides are 10⁻⁷/d. The rate of fuel alteration under oxidic conditions is either controlled by (1) the growth rate of secondary alteration products, (2) the solubility controlled dissolution rate of the matrix or (3) the rate of formation of oxidants by radiolysis. The various explanations and their quantitative contribution are discussed in the paper.

U8.4

STATISTICAL MODEL FOR GRAIN BOUNDARY AND GRAIN VOLUME OXIDATION KINETICS IN UO₂ SPENT FUEL¹

R.B. Stout and H.F. Shaw, Univ. of California - LLNL, P.O. Box 808, L-201, Livermore, CA 94550, and R.E. Einziger, Battelle - PNL, P.O. Box 999, Richland, WA 99352

The Yucca Mountain Project of the USDOE is investigating the suitability of a site in the unsaturated zone at Yucca Mtn., NV for a high-level nuclear waste repository. Most of the waste will consist of UO₂ spent fuel in Zircaloy-clad rods from nuclear reactors. If failure of both the waste containers and the cladding occurs within the lifetime of the repository, then the UO₂ will be exposed to oxygen in the air and higher oxides of uranium may form. The oxidation state of the spent fuel may affect its dissolution behavior if later contacted by water. A model for the kinetics of spent fuel oxidation under repository-relevant conditions is thus necessary to predict the behavior of the waste form for assessing the performance of the repository with respect to the containment of radionuclides. In spent fuel experiments, the UO₂ oxidation front initially propagates along grain boundaries followed by propagation into grain volumes. Thus, the oxidation kinetics is controlled by two processes and the oxidation of spent fuel fragments will depend on the density and physical attributes of grain boundaries. With this in mind, concepts from statistical mechanics are used to define a density function for grain boundaries per unit volume per unit species in a spent fuel fragment. Combining the integral forms of mass conservation and this grain boundary density function, a model for the global rate of oxidation for a spent fuel fragment is obtained. For rapid grain boundary oxidation compared to grain volume oxidation, equations of the model are solved and results compared to existing data.

¹Work performed under the auspices of the U.S. Department of Energy, Office of Civilian Radioactive Waste Management, Yucca Mountain Project Office, by the Lawrence Livermore National Laboratory under contract W-7405-ENG-48.

U8.5

MEASUREMENT OF SOLUBLE NUCLIDE DISSOLUTION RATES FROM SPENT FUEL. Charles M. Wilson, Pacific Northwest Laboratory, P. O. Box 999, Richland, WA 99352.

Laboratory tests are being initiated to gain a better understanding of potential soluble nuclide dissolution rates from spent fuel under proposed Yucca Mountain repository conditions. The release of actinide nuclides, which account for most of the long-term radioactivity in spent fuel, should be limited by solubility to levels sufficiently low to meet Nuclear Regulatory Commission controlled release limits. The release potential for soluble nuclides such as ⁹⁹Tc, ¹³⁵Cs, ¹²⁶Sn, ¹⁴C and ¹²⁹I, which account for about 1 - 2 % of the activity in spent fuel at 1000-years, is less certain. Factors potentially affecting soluble nuclide dissolution rates include degradation of the fuel structure by oxidation in the repository air atmosphere, temperature, and fuel characteristics such as fractional fission gas release.

Semi-static tests (total water changed each test cycle and periodic sample volumes replenished during test cycles) with low temperature oxidized fuel and "high gas release" fuel are being initiated. Semi-static tests are relatively simple and simulate potential dissolution scenarios in the repository, but do not measure the fuel matrix dissolution rate or indicate the degree to which soluble nuclides are preferentially dissolved from limited concentrations at grain boundaries. Flow-through tests are being developed to determine the degree to which soluble nuclides are preferentially released relative to fuel matrix dissolution rates. A challenging aspect of the flow-through test development is the measurement of soluble nuclides at concentrations that are much lower than in the semi-static tests. The rationale for conducting these types of tests, results from semi-static scoping tests with oxidized spent fuel, analytical requirements and results from preliminary flow-through tests are discussed.

U9.1

THEORETICAL MODELING OF CREVICE AND PITTING CORROSION PROCESSES IN RELATION TO CORROSION OF RADIOACTIVE WASTE CONTAINERS, John C. Walton, Idaho National Engineering Laboratory, P.O. Box 1625, Idaho Falls, Idaho 83415

A mathematical and numerical model for evaluation of crevice and pitting corrosion in radioactive waste containers is presented. The model considers mass transport, mass transfer at the metal/solution interface, and chemical speciation in the corrosion cavity. The model is compared against experimental data obtained in artificial crevices. Excellent agreement is found between modeled and experimental values. The importance of full consideration of complex ion formation in the aqueous solution is emphasized and illustrated.

U9.2

CORROSION PRODUCT IDENTIFICATION AND RELATIVE RATES OF CORROSION OF CANDIDATE METALS IN AN IRRADIATED AIR-STEAM ENVIRONMENT.* Donald T. Reed, V. Swayambunathan, Argonne National Laboratory, 9700 South Cass Avenue, Argonne, IL 60439; and Richard A. Van Konynenburg, Lawrence Livermore National Laboratory, Yucca Mountain Project, P. O. Box 5514, Livermore, CA 94551.

Yucca Mountain Project (YMP) is investigating the feasibility of constructing a high-level nuclear waste repository in the unsaturated zone of the Yucca Mountain located in Southwestern Nevada. The high-level nuclear waste container will initially be subjected to an air-steam environment with a gamma dose rate that may be in excess of 0.01 Mrad/h. To provide input to the YMP material selection process, a literature review was performed to identify the nature of the corrosion products formed on copper-based materials. In addition, short-term experiments were performed to identify the corrosion products formed as a function of irradiation conditions. These data are also reported.

*Work supported by the U.S. Department of Energy, Office of Civilian Radioactive Waste Management, Yucca Mountain Project Office, under Contract Number W-31-109-Eng-38.

U9.3

A STUDY ON FABRICATION TECHNOLOGY OF CERAMIC OVERPACK - A CONCEPTUAL DESIGN AND FABRICATION OF A FULL SCALE CERAMIC OVERPACK. T. Teshima, Y. Karita, NGK Insulators, Ltd., Suda-cho, Mizuho-ku, Nagoya, Japan; H. Ishikawa, and N. Sasaki, Power Reactor and Fuel Development Corp., Tokai-mura, Ibaraki, Japan.

Ceramic materials are being considered as candidate materials for overpacks because of their high durability. This paper describes the conceptual design and fabrication of a full-scale ceramic overpack.

The external pressure loading, equivalent to the initial rock pressures at the depth of 1000 m, was estimated to be in the range of 280-560 kg/cm². Materials investigated were porcelain for insulators, one of traditional ceramic, and Al₂O₃ with high purity of 99.7%, one of specialized ceramic. The selected design consisted of a cylindrical shell with hemispherical heads at each end. The design thickness of overpack is the sum of the structural thickness and corrosion allowance. The thickness required to resist the lithostatic pressure, estimated by the semi-empirical design equations for buckling of shells and finite element stress analyses is 119 mm for porcelain and 40 mm for Al₂O₃. The calculated corrosion thickness for 1000 years (based on preliminary corrosion test results) is 20 mm for porcelain and <1 mm for Al₂O₃, and leads to a design thickness of 150 mm for porcelain and 50 mm for Al₂O₃.

A full-scale overpack of porcelain, of dimensions 800 mm outer diameter x 2200 mm length x 150 mm wall thickness, was fabricated under the ordinary level of fabrication technology.

U9.4

*AN INTERPRETATION OF THE HIGH-STRESS, LOW-TEMPERATURE CRACKING OF ZIRCALOY-4 SPENT FUEL CLADDING. (a) H. D. Smith, Pacific Northwest Laboratory (b), Richland, Washington 99352.

Zircaloy spent fuel cladding is expected to inhibit the access of the repository environment to spent fuel and the subsequent release of radionuclides to the environment after failure of the waste package container. Experiments were conducted on Zircaloy-4 spent fuel cladding C-rings to ascertain their susceptibility to cracking under tuff repository conditions. (These spent fuel rods will be stored in a pressurized state.) This was accomplished by stressing the C-rings with a dead-weight load while they were exposed to 90°C well J-13 water. The stress levels ranged from 80 to 96% of the observed yield stress as determined from proportional limit testing of sibling Zircaloy-4 C-rings. The C-rings broke in 26 to 245 days, depending on the stress level. Fracture characteristics observed by optical microscopy and scanning electron microscopy show the development of transgranular fractures at the beginning of cracking of the C-rings. Rapid deformation produces only ductile failure. This indicates that stress corrosion cracking or delayed hydrogen cracking are the probable mechanisms initiating failure. Two experiments run in laboratory air took longer to fail but still failed. In all cases, the fracture surface and apparent initial crack growth rates were consistent with delayed hydrogen cracking as the cause of the C-ring failure.

(a)The Yucca Mountain Project of the U.S. DOE is investigating the suitability of a site in the unsaturated zone at Yucca Mountain, Nevada, for a high-level waste repository.
(b)Pacific Northwest Laboratory is operated for the U.S. Department of Energy by Battelle Memorial Institute under Contract DE-AC06-76RLO 1830.

U9.5

A CORROSION LOCALIZATION ASSESSMENT OF THE MILD STEEL USED FOR NUCLEAR WASTE PACKAGE. Masatsune Akashi, Research Institute, Ishikawajima-Harima Heavy Industries Co., Ltd., Tokyo, JAPAN

This paper describes a study of the corrosion behavior of high-level nuclear waste packages made of mild steels in the geological disposal. It has aimed at establishing the model estimates the corrosion allowance required to achieve a 1000-year life.

Series of galvanostatic tests, which can be modeled on the corrosion behavior governed by the diffusion of dissolved oxygen in the neutral environment. The maximum penetration depth and the depth distribution were measured for each specimen by a sophisticated ultrasonic inspection technique.

The Gumbel distribution model was applied to the analysis of each data set of maximum penetration depths. For the purpose of the prediction of corrosion allowance required, the distribution parameters were estimated due to the linear unbiased estimator method which allowed for extrapolation in space. The relations among the average penetration depth, the maximum penetration depth and the corrosion allowance required were discussed.

U10.1/T4.1

FRactal STRUCTURE AND DYNAMICS OF TWO FLUID FLOW IN POROUS MEDIA. Jens Feder, Department of Physics, University of Oslo, Box 1048 Blindern, 0316 Oslo 3, Norway.

The flow of fluids in porous media leads to displacement fronts that are fractal in many situations. We discuss results obtained in experiments on two-dimensional models. The dispersion of tracers, the invasion percolation at low displacement rates and the viscous fingering at high displacement rates are discussed. Symmetry breaking by gravity effects due to density differences leads to crossover phenomena that can be described by scaling functions. New results on the displacement in three-dimensional models are presented.

Fractal displacement processes exhibit dynamic scaling behavior characterized by new exponents, which we discuss in the context of invasion percolation.

U10.2/T4.2

NUMERICAL AND ANALYTICAL MODELS OF TRANSPORT IN POROUS CEMENTITIOUS MATERIALS. Edward J. Garboczi and Dale P. Bentz, National Institute of Standards and Technology, Building Materials Division, 226/B348, Gaithersburg, MD 20899.

Fluid flow under applied pressure gradients and ionic diffusion under applied concentration gradients in the pore space of a cementitious material are the key transport mechanisms that take place in these materials. Recent theoretical developments in the research labs of the oil exploration industry give new insight into how these processes can be successfully modeled at a fundamental level for cementitious materials. This talk will describe new computational methods for computing effective diffusion constants in models of porous materials, and analytical percolation-theory-based equations for predicting effective permeabilities. Digitized image modeling techniques developed at NIST will also be described.

U10.3/T4.3

SIZING REQUIREMENTS FOR FLOW-THROUGH GEOCHEMICAL TESTS THEORETICAL CONSIDERATIONS. **J. D. Hoover** and E. C. Thornton, Westinghouse Hanford Company, P.O. Box 1970, Richland, WA 99352

A methodology for evaluating test apparatus size requirements has been applied to the sizing of flow-through tests used in the evaluation of coupled processes in open hydrothermal systems. The results of the sizing evaluation provide limits on the apparatus dimensions and test conditions required to yield results representative of the processes of interest. It is indicated from these evaluations that this information is critical in the design of flow-through tests and in the interpretation of test results. Size considerations, therefore, impact the use of flow-through test results in simulating the processes expected to occur in the near-field environment of a nuclear waste repository.

The main objective of this size evaluation is determination of the column dimensions and test conditions necessary to produce reactions pertinent to the processes of interest. The basis of the evaluation is treatment of the time required for reactions or processes of interest to occur, as the required column residence time for the fluid. Reaction paths and reaction times for model systems were determined using geochemical models involving reaction rate equations based on transition state theory. The range of appropriate column dimensions may then be obtained using expressions relating residence time to apparatus dimensions and flow conditions.

A finite range of appropriate column dimensions and test conditions exist for a given residence time requirement. However, determination of appropriate residence time depends on the purpose of the test and processes of interest. Factors such as test duration, sampling requirements, and engineering limitations must also impact the size and/or scale requirements and these criteria can be used in the choice of the most practical combination of column dimensions and test conditions. It is indicated from the results of this study that size evaluations provide a technical basis for the design and construction of flow-through tests, and also for the interpretation of test results.

U10.4/T4.4

A LAGRANGIAN REACTIVE TRANSPORT SIMULATOR WITH MULTIPLE PATHS AND STATIONARY STATES: CONCEPTS, IMPLEMENTATION AND VERIFICATION. **R. B. Knapp**, L206, Earth Sciences Department, Lawrence Livermore National Laboratory, University of California, Livermore, California 94550

A geochemical software package which models static, single-path kinetic water-rock interactions, EQ3/6 [Wolery, T. J., Lawrence Livermore National Laboratory, UCRL-52658, 1979], has been modified to incorporate multiple-paths and stationary states under high Peclet number transport conditions in a Lagrangian reference frame [Lichtner, 1988]. These modifications permit calculation of reactive transport with reasonable computational requirements. Results from the new code, mpeq6, have been compared with analytical results for the simple HCl - SiO₂ system; excellent agreements were achieved. Results from mpeq6 have also been compared with published results [Lichtner, P., *Geochim. Cosmochim. Acta*, 52, 143-165, 1988] for a portion of the Al₂O₃ - HCl - K₂O - SiO₂ system. The results are in good qualitative and, in some cases, good quantitative agreement. However, the values of some variables differ substantially; these differences can be attributed to use of a different set of Al and Si aqueous species.

U10.5/T4.5

FRACTAL CHARACTERISTICS OF FRACTURE NETWORKS AND FLUID MOVEMENT IN ROCK. Christopher C. Barton, Box 25046, MS 913, Federal Center, Denver, CO 80225

Society's need to recover fluid resources (water, oil, and gas) from the Earth and to inject toxic waste materials in a reliable manner requires quantitative models to describe and predict the movement of fluids in rock. Existing models based on pore-space flow are inappropriate for study of the more rapid process of fluid flow through fracture networks. This type of flow is not a simple function of the fracture characteristics at any particular scale, but rather the integration of contributions at all scales.

The mathematical constructs of fractal geometry are uniquely suited to quantify and model relationships within complex systems that are statistically equivalent (that is, self-similar) at all scales. My results show that natural fracture networks in rock follow a fractal scaling law over six orders of magnitude. Detailed

measurements of two-dimensional samples of three-dimensional fracture networks (at diverse scales in rocks of dissimilar age, lithology, and tectonic setting) show similar fractal dimensions in the range 1.6-1.8.

The small range in fractal dimension implies that a single physical process of rock fracturing operates over a wide range of scales, from microscopic cracks to large, regional fault systems. Independent field evidence has previously demonstrated that rock fracturing is an iterative process in which preexisting fractures influence the formation of subsequent fractures (such behavior is characteristic of fractal processes). The fractal behavior implies that fracture-network development is governed by a nonlinear equation. Fortunately, the ability of fractal mathematics to accurately quantify and model the system is not dependent on specific knowledge of this equation, as the equation has not yet been identified.

Knowledge that rock fracture networks are fractal allows use of data from a one-dimensional drill-hole sample to predict the two- and three-dimensional attributes of the fracture system. The spacing of fractures in drill holes is a fractal Cantor distribution, and the range of fractal dimension is 0.6-0.8, which is an integer dimension less than that of fracture-trace patterns exposed on two-dimensional, planar sections. The pattern of rock-matrix flow can exhibit fractal fingering, and matrix permeability is patchy in a manner analogous to fractal percolation clusters.

U10.6/T4.6

FLOW TO WELLS IN FRACTURED ROCK WITH FRACTAL STRUCTURE. **Jim Polek**, Kenzi Karasaki and Jane Long, Lawrence Berkeley Laboratory, Berkeley, CA; and John Barker, British Geological Survey, Wallingford, Oxfordshire, U.K.

Traditionally, models of fluid transport in rocks have been based on an integral (Euclidean) flow dimension. However, this assumption is not necessary and may not always be appropriate, especially for rocks with poorly connected fractures. Barker (1988) has formulated and solved the equation of flow to a well in a rock system characterized by an arbitrary flow dimension.

Using Sierpinski's carpet and a random percolating network, we generated two types of fractured rock systems with fractal properties. We then simulated hydraulic well tests in these systems. Both the fractal dimensions and the "radial" fractal dimensions of the systems were calculated using Orbach's (1986) method. The latter was calculated by accounting for only the radial component of the conductor. Of the two, we found that the radial fractal dimension better describes the physical processes occurring during a well test. The results from the well tests were in agreement with Barker's solution and a relationship between the slope of the pressure response curve and the radial fractal dimension was found. This relationship is significant because it could lead to a value for the fractal dimension of rock from field well test data. This field fractal dimension could then be used to estimate the rock's flow geometry and flow characteristics.

U10.7/T4.7

ANISOTROPIC SCALING OF INTERFACES IN POROUS MEDIA. Miguel A. Rubio, Haverford College, Haverford, PA, and UNED, Madrid, Spain; **Andrew Dougherty**, Haverford College, Haverford, PA; and **Jerry P. Gollub**, Haverford College, Haverford, PA, and University of Pennsylvania, Philadelphia, PA.

Two-fluid immiscible displacement may produce self-similar fractal interfaces, often described by invasion percolation or DLA models, for certain ranges of the relative viscosities and wetting properties of the fluids. These self-similar structures have the same scaling behavior in all directions.

Here we show that when the displacing fluid is more viscous and more efficient in wetting the medium, the interfaces are self-affine fractals, i.e., they show different scaling in different directions. We present experimental results on the interfaces obtained when water displaces air in a thin layer of glass beads. We have characterized the interfaces by computing their roughness (r.m.s. value of the interfacial width) as a function of length scale. The roughness shows power-law behavior with exponent $\beta = 0.73 \pm 0.03$, independent of the control parameter (capillary number, Ca). This exponent is related to the box dimension

2-B, and the divider or compass dimension 1/B. This behavior means that the interfaces are self-affine fractals with a box dimension of 1.27.

Supported by the NSF Low Temperature Physics Program DMR-8503543. M.A.R. was supported in part by a Fellowship of the NATO Scientific Committee.

U10.8/T4.8

SIZING AND SCALING REQUIREMENTS OF A LARGE-SCALE PHYSICAL MODEL FOR CODE VALIDATION. R. Khaleel, T. LeGore, and J. D. Hoover, Westinghouse Hanford Co., Richland, WA.

Post-closure performance assessment and the associated application of mathematical models play a critical role in assessing the long-term behavior of the engineered and natural barriers of a geologic repository. Although verification and benchmarking constitute an important part of determining model acceptability, it does not establish that the model is a reasonable approximation to physical reality. This is accomplished in the validation step in which model calculations are compared with data from controlled experiments.

Although in-situ field experiments provide useful data, information needed for model validation cannot be obtained from field observations alone because of the inherent uncertainties associated with the natural system. However, physical models, when properly scaled, constructed, and instrumented can provide the necessary information for validation of mathematical models and computer codes, and can overcome many of the uncertainties associated with large-scale in-situ testing. The relationships between measurement, size, scaling, and discretization (block size) used in a numerical model must be incorporated in the conceptualization of a physical model. Sizing and scaling requirements of a large-scale physical model for hydrological testing are discussed. The justification for the minimum size of a physical model for hydrological testing can be based on the nature of heterogeneities introduced into the model. Results of numerical simulations used to determine the preliminary size requirements of a porous medium model are presented.

U10.9/T4.9

PERFORMANCE OF CONCRETE BARRIERS IN RADIOACTIVE WASTE DISPOSAL IN THE UNSATURATED ZONE. John C. Walton and Mark D. Otis, Idaho National Engineering Laboratory, P.O. Box 1625, Idaho Falls, Idaho 83415

Concrete barriers are an important component of many designs for disposal of radioactive waste in the unsaturated zone. In order to evaluate the effectiveness of the concrete barriers performance assessment models representing the material degradation and behavior must be developed. Models for evaluation of fluid flow and mass transport through concrete barriers located in the unsaturated zone are presented. Implications of the use of impermeable membranes in barrier design are discussed. The effectiveness of the concrete is shown to be dependent upon effective design. Concrete of highest quality may not always be desirable for use in waste disposal vaults.

U11.1

LEACHING/MIGRATION OF UO₂-FUEL IN COMPACTED BENTONITE. Y. Albinsson, G. Skarnemark, M. Skälberg, Department of Nuclear Chemistry, Chalmers University of Technology, S-412 96 Göteborg, Sweden; R. Forsyth, Studsvik AB, S-611 82 Nyköping, Sweden; B. Torstenfelt, ABB-Atom, S-721 63 Västerås, Sweden; L. Werme, Swedish Nuclear Fuel and Waste Management, Box 5864, S-102 48 Stockholm, Sweden.

In the Swedish concept for final disposal of high-level radioactive waste, bentonite clay (BC) has

been proposed as a suitable backfill material. It is therefore important to investigate the influence of BC on the corrosion of spent UO₂-fuel and on the release behaviour of fission products (FP's) and actinides (An's). In this investigation the leaching/migration of FP and An's from spent fuel pellets into highly compacted BC is measured.

The release and migration of the FP's Cs, Eu and Tc and the An's U, Pu, Am and Cm is measured after different contact times (0.3, 0.5 and 1.1 a). Experiments aiming at longer contact times are in progress. In some cases small amounts (0.5-1%) of Cu, Fe or vivianite have been added to the BC.

The results indicate a high mobility of Cs. The An's have a very low mobility. After 1.1 year, Pu has diffused less than 0.5 mm away from the fuel. Am and Cm appear to be somewhat more mobile. The behaviour of Eu is similar to that of An(III). Tc has a high mobility in BC, except in the case of iron addition.

U11.2

MODELLING THE IN SITU PERFORMANCE OF BENTONITE-SAND BUFFER. H.S. Radhakrishna, K.-C. Lau, Ontario Hydro Research Division, Location KR252, 800 Kipling Avenue, Toronto, Ontario, Canada M8Z 5S4, B.H. Kjartanson and S.C.H. Cheung, Atomic Energy of Canada Limited, Whiteshell Nuclear Research Establishment, Pinawa, Manitoba, Canada ROE 1L0.

In the Canadian nuclear fuel waste management concept, a number of engineered barriers, such as the waste containers and the bentonite-sand buffer, are used to inhibit the transport of radionuclides. The buffer material is also required to effectively conduct the heat from the waste containers to the surrounding rock. This paper examines the principal processes occurring in the buffer before water saturation takes place, and the impacts of such processes on buffer performance. Particular emphasis is placed on the modelling of heat and moisture transfer. Numerical simulations show that the temperature distribution can be reasonably predicted by the Philip-DeVries model, while the moisture distribution is found to be sensitive to the transport coefficients, and also depends on the hydraulic boundary conditions.

U11.3

THE EFFECT OF CRACKS ON DIFFUSIVE MASS TRANSPORT THROUGH A CLAY BARRIER. Nava C. Garisto and Frank Garisto, Atomic Energy of Canada Limited, Whiteshell Nuclear Research Establishment, Pinawa, Manitoba, Canada ROE 1L0

Clay-based barriers are often proposed as engineered sealing systems for underground disposal vaults of used nuclear fuel. Thus, in the Canadian conceptual vault design, each used-fuel container is emplaced in a vertical borehole in rock and surrounded by a compacted buffer material, made up of a mixture of sodium bentonite and sand. There is some evidence, however, that the buffer may be susceptible to fracturing due to, for example, cementation or moisture depletion.

In this paper we estimate numerically the consequences of fracturing on radionuclide diffusion through a finite buffer layer. The cases studied represent hypothetical crack widths and density of cracks in a reference system based on the Canadian conceptual vault design.

The results indicate that for swept away boundary conditions at the buffer/rock interface, the total flux through the cracked buffer system is, as expected, greater than through the corresponding uncracked buffer. However, the effect of the cracks, which depends on the crack's width and the inter-crack spacing, is relatively small.

Moreover, for the case in which the rock at the buffer/rock interface is intact and thus, the mass transport of material

from the buffer into the rock is small, the effects of cracks on the total release flux is negligible.

U11.4

FINAL DISPOSAL OF CEMENTITIOUS WASTE FORMS IN THE SWEDISH REPOSITORY FOR REACTOR WASTE (SFR). Jan S Carlsson, Swedish Nuclear Fuel and Waste Management Co (SKB), P O Box 5864, S-102 48 Stockholm, SWEDEN.

Disposal of LLW/ILW from the operation of Nuclear Power Plants in Sweden takes place in an underground repository (SFR) close to the Nuclear Power Plant in Forsmark. The waste is mainly spent ion exchange resins solidified in cement or bitumen. Approximately 90% of the radionuclide inventory will be allocated to a concrete silo surrounded by bentonite, at the time of sealing. This paper focus on requirements on ion exchange resins immobilized in cement for final disposal in the SFR silo.

Apart from general requirements on the design (dimensions, weight etc) and management (marking, documentation etc) the requirements could be divided into groups with respect to:

- radiological, chemical and mechanical properties

To ensure a diffusion scenario for transport of radionuclides from the silo the surrounding clay (bentonite) barrier has to be intact.

Gas production inside the silo, or swelling of waste packages, could crack the silo walls.

All requirements on a waste package and how they are fulfilled are described in a Waste Type Description.

U11.5

MASS TRANSFER IN WATER-SATURATED CONCRETES

Alan Atkinson, Peter A Claisse, Nicola M Everitt, Andrew W Harris, and Alan K Nickerson, Materials Development Division, Building 429, Harwell Laboratory, Oxon, OX11 0RA, UK

Cements and concretes are often considered as barriers helping to contain radionuclides in waste repositories. The performance of cementitious material as a mainly physical barrier to the escape of dissolved radionuclides depends on the mass transfer characteristics of the chosen material(s). In particular the diffusion and sorption behaviour of individual radionuclides and the water permeability are important. These parameters also influence the way in which the chemistry of the concrete is imposed on the rest of the repository and, in addition, the transport of gas through concretes controls the way in which gases escape from the repository. These parameters have been measured for a variety of cementitious materials covering different types of structural concrete and cementitious backfills; all possible repository construction materials. Diffusion measurements have been made using aqueous iodide, strontium and caesium ions and tritiated water as diffusing species. The results show that diffusion of tritiated water is much more rapid from that of other species whilst the transport of strontium and caesium is hindered by sorption; particularly in materials containing blast furnace slag. The transport of gas through these materials has been found to be very sensitive to the degree of water saturation and is extremely low in fully saturated structural concretes. Cementitious backfills have, nevertheless, been identified that have appreciable gas transport even when almost saturated.

The consequences of the results for the performance of cementitious barriers are discussed.

U11.6

COUPLED FLOW OF HEAT AND MASS IN BARRIER MATERIALS AND ITS SIGNIFICANCE, S.C.H. Cheung, Atomic Energy of Canada Limited, Whiteshell Nuclear Research Establishment, Pinawa, Manitoba, Canada ROE 1L0.

In a nuclear fuel waste disposal vault, simultaneous non-congruent flow of heat, fluid and solutes due to differences of temperature, hydraulic potential and solute concentration will occur in the water-saturated clay-sealing material. The coupled processes have been assessed by a method that uses irreversible thermodynamic processes. The theoretical results show that the coupling effects depend on the relative magnitude of the gradient of the temperature, solute concentration and hydraulic potential as well as the permeabilities of the sealing materials and of the rock. For the Canadian disposal concept, the results indicate that mass transport in the saturated buffer and backfill should be controlled mainly by molecular diffusion.

U11.7

EFFECTIVE DIFFUSIVITY OF CARBON DIOXIDE AND IODINE THROUGH "G TUNNEL TUFF". Tefik Bardakci, Franklin G. King, and Maung Sein, North Carolina A&T State University, Greensboro, NC, 27411.

The Topopah Spring Member of the Paintbrush Tuff in Yucca Mountain, Nevada is a prime candidate for the site of the first national high level radioactive waste repository. One of the questions to be answered in characterizing the site is the extent of diffusion of radioactive gases, such as carbon dioxide and iodine, to the accessible environment. The objectives of this study were to measure the effect of temperature and water content on the effective diffusivity of carbon dioxide and the effect of temperature on the effective diffusivity of iodine through Topopah Spring Tuff and to characterize the pore structure of Topopah Spring Tuff. Since Topopah Spring Tuff samples were not made available, experiments were conducted with tuff samples from a nearby location called Rainier Mesa Ash flow from "G" tunnel.

Information obtained on the diffusion of gases through tuff provides data to determine whether the Nuclear Regulatory Commission and Environmental Protection Agency regulations can be met. There is presently no available data for the diffusion of carbon dioxide and iodine, which are released from the nuclear waste, through tuff.

The effective diffusivity of carbon dioxide and iodine through "G" tunnel tuff were determined using a steady-state method (counter diffusion) and an unsteady-state method respectively. Results show that the effective diffusivity of carbon dioxide and iodine through dry tuff increased with temperature. The effective diffusivity of carbon dioxide decreased as the moisture content of the "G" tunnel tuff increased. An empirical correlation was obtained to estimate the effective diffusivity of carbon dioxide as a function temperature and the percent saturation. Specific surface area and pore volume of the samples were determined using a mercury porosimeter. A scanning electron microscope was utilized to further characterize the porous structure of the tuff samples.

U11.8

¹⁴C TRANSPORT IN A PARTIALLY SATURATED, FRACTURED, POROUS MEDIUM. W. B. Light, P. L. Chambré, W. W.-L. Lee, and T. H. Pigford, Department of Nuclear Engineering and Lawrence Berkeley Laboratory, University of California, Berkeley, CA 94720.

Radioactive gases released from waste placed in the partially saturated rock would have a direct pathway to the biosphere. This presents a new problem in assessing the potential health impacts of such releases, and in complying with regulations.

We analyse the transport of ¹⁴C in an unsaturated, fractured, porous medium with gas-phase advection and dispersion. Gases released into a partially saturated, fractured rock move in the fractures, while pore water is held inside the rock matrix. First we assess the interaction of ¹⁴C in CO₂ with bicarbonate ion in ground water as a possible retardation mechanism. Then we treat the combined fracture and pore matrix as an equivalent porous medium with local carbon-distribution equilibrium between the gas and liquid phases.

Our results indicate that liquid in the rock matrix between fractures will reach essentially the same equilibrium concentration as the liquid at the fracture walls when the modified Peclet number $Lq_g/\epsilon K_D D_l$ is much less than unity, where L is half the distance between fractures, q_g is the gas Darcy velocity, ϵ is the porosity, K_D is the equilibrium distribution coefficient defined as the molar concentration of liquid-phase carbon divided by the molar concentration of gas-phase carbon, and D_l is the liquid-phase diffusion coefficient.

We then solve the equation for the transport of ¹⁴C in an equivalent porous medium. With the retardation just described the advection velocity v and dispersion coefficient D obtained for ¹⁴C are

$$v = \frac{q_g}{\epsilon[(1-S) + SK_D]} \quad D = \frac{(1-S)D_g + SK_D D_l}{(1-S) + SK_D}$$

where S is the liquid saturation and D_g is the dispersion coefficient for the gas phase. The solution is based on space-time-invariant values for ϵ , S , K_D , q_g , D_g , and D_l . Using parameter values from the Yucca Mountain SCP we predict peak ^{14}C concentrations at the ground surface comparable to the USNRC limit for unrestricted areas of $10^{-7} \mu\text{Ci}/\text{cm}^3\text{-Air}$. In the paper we present predicted ^{14}C concentrations from point or plane sources, with either an impulse or band-release source term.

U11.9

THE APPLICATION OF A COUPLED CHEMICAL TRANSPORT MODEL IN A TRIAL ASSESSMENT OF DEEP DISPOSAL OF LOW AND INTERMEDIATE LEVEL RADIOACTIVE WASTE

Steve Liew, Vea Economides, Adrian Dawes and David Read, WS Atkins Engineering Sciences, Woodcote Grove, Ashley Road, Epsom, Surrey, United Kingdom KT18 5BW.

The UK Department of the Environment is developing an independent capability to evaluate proposals made for the deep underground disposal of low and intermediate level radioactive wastes. Coupling of chemical processes with hydrodynamic transport has been identified as an important element of the assessment strategy and a suite of models has now been developed which fully couple thermodynamic mass action expressions to advection-diffusion terms.

This paper illustrates the use of the CHEMTARD (Chemical Transport Adsorption Redox and Decay) code by reference to studies on waste disposal and natural analogue sites within the UK. The role of such methods within the overall DOE methodology is highlighted through a trial assessment of deep disposal beneath Harwell, Oxfordshire.

The feasibility of employing a mechanistic approach to quantifying sorption processes is explored and comparisons drawn with more simple analytical models based on linear adsorption isotherms. The implications for risk assessment practices reliant on the assumption of "conservative" parameter distributions or worst case estimates is discussed.

U11.10

ANALYSIS OF MASS TRANSPORT IN AN ENGINEERED BARRIERS SYSTEM FOR THE DISPOSAL OF USED NUCLEAR FUEL. Nava C. Garisto and Dennis M. LeNeveu, Atomic Energy of Canada Limited, Whiteshell Nuclear Research Establishment, Pinawa, Manitoba, Canada R0E 1L0.

The Vault Model has been developed to assess the performance of engineered barriers in a conceptual geological disposal vault for used nuclear fuel. It represents container failure, release of radionuclides from used fuel and mass transport of released radionuclides through the clay-based sealing materials surrounding the waste containers. This paper focuses on mass-transport processes represented by the Vault Model, including diffusion, convection and retardation.

In particular, we present results of several scoping calculations carried out with the Vault Model. We consider cases where the clay-based barriers are represented by either a one- or a two-layer system adjacent to an intact rock and a case where the two clay-based barriers are adjacent to a highly fractured rock.

These calculations provide insight into the model and produce test cases for comparison with both relatively simple analytical estimates and similar computer codes, as they become available. The analytical estimates generally support the Vault Model results and thus enhance our confidence in the accuracy of the Vault Model calculations.

U11.11

ATTEMPTED VERIFICATION OF MATRIX DIFFUSION IN GRANITE BY MEANS OF NATURAL DECAY SERIES DISEQUILIBRIA. W.R. Alexander, Paul Scherrer Institute, 5232 Villigen, Switzerland; I.G. McKinley, NAGRA, 5401 Baden, Switzerland; A.B. MacKenzie, R.D. Scott, SURRC, Glasgow G75 0QU, Scotland and

J. Meyer, Min.-pet. Institute, University of Berne, 3012 Berne, Switzerland.

According to the Swiss concept for the disposal of radioactive waste, the material will be placed in deep rock formations to ensure that only small amounts, if any, of radionuclides released from the waste packages ever reach the surface and so enter the biosphere. It is, however, likely that the rock formation will be fractured and that advection along the fractures will be the dominant mechanism of radionuclide transport from the repository.

It has been suggested that, in systems where such advective flow is dominant, radionuclides might gain access to the rock surrounding the fractures by diffusion in a connected system of pores or microfractures - the so called "matrix diffusion".

Matrix diffusion is difficult to study in the laboratory due to the very slow transport rates involved but one approach which can circumvent this and other problems involves the study of the natural decay series in profiles perpendicular to water bearing fractures. The preferential mobility of U and Th daughters relative to their parents can enhance their removal from the bulk rock, by diffusion, to the fractures. This transport of natural decay series radionuclides is thus analogous to the diffusion of solute from a fracture into the rock as considered in safety analysis models.

In this paper we present a detailed study of a rock core in which there are clear signs of water-rock interactions in and around a fracture with an especially striking indication of Radium remobilisation across the fracture. The geochemical data are interpreted with the aid of a detailed mineralogical examination of the core in conjunction with data from laboratory sorption experiments. A more realistic definition of matrix diffusion is presented and the implications of the results with respect to mathematical representations of such mechanisms in safety assessment models are discussed.

SYMPOSIUM V: MACROMOLECULAR LIQUIDS



November 27 - December 1, 1989

Chairs

Cyrus R. Safinya
Room LC-334
Exxon Research & Engineering Company
Route 22 East
Annandale, NJ 08801
(201) 730-2887

Phil A. Pincus
Materials Department
College of Engineering
University of California at
Santa Barbara
Santa Barbara, CA 93106
(805) 961-4685

Samuel Safran
Room LC-346
Exxon Research & Engineering Company
Route 22 East
Annandale, NJ 08801
(201) 730-2886

Symposium Support

Exxon Research and Engineering Company

**Proceedings published as Volume 177
of the Materials Research Society
Symposium proceedings series.**

MACROMOLECULAR LIQUIDS

November 27 - December 1, 1989

SESSION V1: PHASE BEHAVIOR AND STRUCTURE: POLYMERS

Chair: C. R. Safinya

Monday Morning, November 27
Essex Center W

8:15 ***V1.1**

LINEAR AND STAR POLYMERS IN THE LIQUID STATE, William W. Graessley, Lewis J. Fetters, Mireille Adam, and Andrea D. Kiss, Exxon Research and Engineering Company, Corporate Research Laboratories, Annandale, NJ.

8:45 **V1.2**

COOPERATIVE EFFECTS IN STRAINED POLYMERIC NETWORKS, Bertrand Deloche and Paul Sotta, Université de Paris Sud, Laboratoire de Physique du Solide (CNRS-LA2), Orsay, France; and Jean Herz, Institut Charles Sadron, Strasbourg, France.

9:00 ***V1.3**

PHASE BEHAVIOR AND STRUCTURE OF WEAKLY CHARGED COPOLYMERS, Jean-François Joanny, Institut Charles Sadron, Strasbourg, France; and Ludwik Leibler, E.S.P.C.I., Paris, France.

9:30 **V1.4**

CURVATURE ELASTICITY AND STRUCTURES OF SURFACTANTS AND BLOCK CO-POLYMERS, Zhen-Gang Wang and S.A. Safran, Exxon Research and Engineering, Annandale, NJ.

9:45 **V1.5**

BLOCK COPOLYMER AGGREGATES IN A SYSTEM OF TWO IMMISCIBLE SOLVENTS, N. Brandon and M. Tirrell, University of Minnesota, Department of Chemical Engineering and Materials Science, Minneapolis, MN; A. Halperin, Hebrew University, The Fritz Haber Research Center for Molecular Dynamics, Jerusalem, Israel.

10:00 BREAK

10:30 **V1.6**

STRUCTURE OF ZWITTERIONIC ASSOCIATING POLYMERS, Y. Shen, C.R. Safinya, M. Adam, K.S. Liang, L. Fetters, J. Stokes, and R. Chance, Exxon Research and Engineering Company, Corporate Research, Annandale, NJ.

*Invited Paper

Short Course C-09, "Fractals: Concepts and Applications in Materials Science and Engineering," may be of interest to symposium attendees. Details regarding course dates and instructors are provided in the short course section of this program.

10:45 **V1.7**

BLOCK COPOLYMER MICELLES IN A SELECTIVE SOLVENT, Mahn Won Kim, Su-Nin Liu, and T.C. Chung, Exxon Research and Engineering Company, Annandale, NJ.

11:00 ***V1.8**

STRUCTURAL AND DYNAMIC PROPERTIES OF POLYMERIC GELS, S.J. Candau, Université Louis Pasteur, Laboratoire de Spectrométrie et d'Imagerie Ultrasonores, Strasbourg, France.

11:30 **V1.9**

SLOW FLUCTUATIONS IN SWOLLEN POLYMER GELS, J.V. Maher and M.W. Di Francesco, University of Pittsburgh, Department of Physics and Astronomy.

11:45 **V1.10**

CHARACTERIZATION OF CURING PROCESSES IN POLYMERIC SYSTEMS, AT VARIOUS STOICHIOMETRIC RATIOS, USING ULTRASONIC WAVES, A. Shefer, Ben-Gurion University, Chemical Engineering Department, Beer-Sheva, Israel; G. Gorodetsky, Ben-Gurion University, Physics Department, Beer-Sheva, Israel; and M. Gottlieb, Ben-Gurion University, Chemical Engineering Department, Beer-Sheva, Israel.

SESSION V2: PHASE BEHAVIOR AND STRUCTURE: SURFACTANT SYSTEMS

Chair: S. A. Safran

Monday Afternoon, November 27
Essex Center (W)

1:30 ***V2.1**

EXPERIMENTAL DATA AND THEORETICAL INTERPRETATION OF PHASE SEPARATION IN PROTEIN WATER SOLUTIONS WITH APPLICATION TO CATARACT DISEASE, G.B. Benedek, D. Blankschtein, M. Kondo, P. Schurtenberger, J.A. Thomson, G.M. Thurston, and M.C. Wiener, Massachusetts Institute of Technology, Department of Physics and Center for Materials Science and Engineering, Cambridge, MA.

2:00 ***V2.2**

NOVEL LIQUID CRYSTALLINE PHASES OF TOBACCO MOSAIC VIRUS, R.B. Meyer, Brandeis University, Department of Physics, Waltham, MA.

2:30 **V2.3**

DIFFUSE X-RAY SCATTERING STUDIES OF LYOTROPIC TUBULAR PHASES, E.B. Sirota, E.Y. Sheu, C.R. Safinya, and K.S. Liang, Exxon Research and Engineering Company, Corporate Research, Annandale, NJ.

2:45 ***V2.4**

SURFACTANTS IN SOLUTION: EXPERIMENTAL EXAMPLES OF FLUCTUATING MEMBRANES, Didier Roux, Centre de Recherche Paul Pascal, Domaine Universitaire, Talence, France.

3:15 BREAK

3:45 *V2.5

ELECTRON MICROSCOPY OF COMPLEX FLUIDS, Yeshayahu Talmon, Technion-Israel of Technology, Department of Chemical Engineering, Haifa, Israel.

4:15 V2.6

SYNCHROTRON X-RAY SCATTERING STUDIES OF THE LYOTROPIC L_3 PHASE, N. Lei, C.R. Safinya, K.S. Liang, E.B. Sirota, and R. Plano, Exxon Research and Engineering Company, Corporate Research, Annandale, NJ.

4:30 V2.7

BICONTINUOUS STRUCTURE OF THE "ANOMALOUS ISOTROPIC PHASES L_3 " AND MICELLAR- L_3 PHASE TRANSITIONS, A.M. Bellocq, D. Gazeau, and D. Roux, C.N.R.S., Centre de Recherche Paul Pascal, Pessac, France; and E. Freysz, Université de Bordeaux I, Centre de Physique Moléculaire optique et Hertzienne, Talence, France.

4:45 V2.8

FLEXIBILITY AND INTERACTION MEASUREMENTS IN DILUTE LAMELLAR PHASES BY DYNAMIC LIGHT SCATTERING, F. Nallet and D. Roux, Domaine Universitaire, Centre de Recherche Paul Pascal, Talence, France; and J. Prost, Ecole Supérieure de Physique et de Chimie Industrielles, Paris, France.

SESSION V3: NON-NEWTONIAN FLOW

Chair: W. Graessley

Tuesday Morning, November 28

Essex Center (W)

8:15 *V3.1

NONLINEAR FLOW BEHAVIOR OF HIGH MOLECULAR WEIGHT POLYMERS, Dale S. Pearson, University of California, Santa Barbara, Department of Chemical and Nuclear Engineering and Materials Department, Santa Barbara, CA.

8:45 V3.2

RHEOLOGICAL AND KINETIC PROPERTIES OF SEMI-DILUTE SOLUTIONS OF ELONGATED MICELLES, S.J. Candau, G. Waton, and F. Merikhi, Université Louis Pasteur, Laboratoire de Spectrométrie and d'Imagerie Ultrasonores, Strasbourg, France; and R. Zana, Institut Charles Sadron, Strasbourg, France.

9:00 V3.3

LIGHT SCATTERING EVIDENCE FOR "WORM-LIKE" MIXED DETERGENT-DIACYLPHOSPHATIDYLCHOLINE (PC) MICELLES, R. Chamberlin, G. Thurston, and G. Benedek, Massachusetts Institute of Technology, Cambridge, MA; D. Cohen and M. Carey, Harvard Medical School, Boston, MA.

9:15 *V3.4

SHEAR FLOW AND ISOTROPIC-LAMELLAR TRANSITIONS, S.T. Milner, AT&T Bell Laboratories, Murray Hill, NJ.

9:45 *V3.5

LANDAU THEORY OF THE NEMATIC TO SMECTIC-A TRANSITION UNDER SHEAR FLOW, R. Bruinsma, University of California, Los Angeles, Physics Department, Los Angeles, CA.

10:15 BREAK

10:45 V3.6

NONEQUILIBRIUM X-RAY DIFFRACTION STUDY OF THE NEMATIC-SMECTIC-A TRANSITION UNDER SHEAR FLOW, C.R. Safinya, E.B. Sirota, R. Plano, and N. Lei, Exxon Research and Engineering Company, Corporate Research, Annandale, NJ.

11:00 V3.7

KINETICS OF THE LATE STAGE GROWTH IN THE PHASE SEPARATION OF A CRITICAL BINARY MIXTURE, Serge Lacelle and Franco Cau, Université de Sherbrooke, Quebec, Canada.

11:15 *V3.8

SELF-DIFFUSION AND RHEOLOGY OF WEAKLY IN-HOMOGENEOUS BLOCK COPOLYMERS, Scott T. Milner and Glenn H. Fredrickson, AT&T Bell Laboratories, Murray Hill, NJ; Frank S. Bates and Jeffrey H. Rosedale, University of Minnesota, Department of Chemical Engineering and Materials Science, Minneapolis, MN.

11:45 V3.9

SCALING ANALYSIS OF SHEAR THINNING IN POLYMER SOLUTIONS, Y. Rabin, Weizmann Institute of Science, Chemical Physics Department, Rehovot, Israel; and H.C. Ottinger, ETH-Zentrum, Institut für Polymere, Zurich, Switzerland.

SESSION V4: COLLOIDS

Chair: N. A. Clark

Tuesday Afternoon, November 28

Essex Center (W)

1:30 *V4.1

EFFECT OF THE STABILIZING COATING AND THE PRESENCE OF FREE POLYMER ON THE CRYSTALLIZATION PHENOMENA OF COLLOIDAL SUSPENSIONS, C. Smits, J.K.G. Dhont, and H.N.W. Lekkerkerker, University of Utrecht, Van't Hoff Laboratory, Padualaan, The Netherlands.

2:00 V4.2

CHARGE AND SIZE POLYDISPERSITY EFFECTS ON THE SCATTERING PROPERTIES AND THE HIGH FREQUENCY ELASTICITY OF COLLOIDS, B. D'Aguanno, Rudolf Klein, and N. Wagner, Universität Konstanz, Fakultät für Physik, Konstanz, West Germany.

2:15 *V4.3

DYNAMICS OF CONCENTRATED COLLOIDS, D.A. Weitz, Exxon Research and Engineering Company, Annandale, NJ.

2:45 V4.4

NON-DIFFUSIVE BROWNIAN MOTION STUDIED BY DIFFUSING WAVE SPECTROSCOPY, D.J. Pine, Haverford College, Department of Physics, Haverford, PA; D.A. Weitz, Exxon Research and Engineering Company, Annandale, NJ; P.N. Pusey and R.J.A. Tough, Royal Signals and Radar Establishment, Worchestershire, United Kingdom.

3:00 V4.5

DIELECTRIC RELAXATION IN CONCENTRATED SOLUTIONS OF INVERTED MICELLES, J. Sowa, S. Bhattacharya, M.J. Higgins, and J.S. Huang, Exxon Research and Engineering Company, Annandale, NJ.

3:15 BREAK

3:45 *V4.6

FORMULATION AND PROCESSING OF COLLOIDAL DISPERSIONS, William B. Russel, Princeton University, Department of Chemical Engineering, Princeton, NJ.

4:15 V4.7

SEDIMENTATION STUDIES IN NEARLY HARD-SPHERE SUSPENSIONS, Steven E. Paulin and Bruce J. Ackerson, Oklahoma State University, Department of Physics, Stillwater, OK.

4:30 V4.8

NUCLEATION OF COLLOIDAL CRYSTALS, D.J.W. Aastuen, C. Swindal, J. Pieper, and N.A. Clark, University of Colorado, Department of Physics, Boulder, CO.

4:45 *V4.9

FLOW PROPERTIES OF CONCENTRATED COLLOIDAL SUSPENSIONS, J.W. Goodwin and R.W. Hughes, University of Bristol, Department of Physical Chemistry, Bristol, United Kingdom.

5:15 V4.10

CRYSTALS UNDER SHEAR AND THE MELTING TRANSITION, Mark J. Stevens, The Johns Hopkins University, Department of Physics and Astronomy, Baltimore, MD; James F. Belak, The Johns Hopkins University, Department of Physics and Astronomy, Baltimore, MD, and Lawrence Livermore National Laboratories, Livermore, CA; and Mark O. Robbins, The Johns Hopkins University, Department of Physics and Astronomy, Baltimore, MD.

SESSION V5: APPLICATIONS OF COMPLEX FLUIDS

Chair: R. B. Meyer

Wednesday Morning, November 29

Essex Center (W)

8:15 *V5.1

RHEOLOGY OF PHASE SEPARATED BLOCK COPOLYMER MELTS, H. Henning Winter, University of Massachusetts, Department of Chemical Engineering, Amherst, MA.

8:45 *V5.2

MICROEMULSION PERFORMANCE FLUIDS, Jan Bock, Exxon Research and Engineering Company, Corporate Research, Annandale, NJ.

9:15 *V5.3

APPLICATIONS OF FERROELECTRIC LIQUID CRYSTAL (FLC) ELECTRO-OPTIC DEVICES, Noel A. Clark, University of Colorado, Department of Physics and Center for Optoelectronic Computing Systems, Boulder, CO.

9:45 *V5.4

MICROSCOPIC PROCESSES IN MICROEMULSION POLYMERIZATIONS, Francoise Candau, CNRS-ULP, ICS, Strasbourg, France.

10:15 BREAK

10:45 *V5.5

THE BEHAVIOR OF ELECTRIC FIELD DEPENDENT FLUIDS UNDER DYNAMIC STRESSES, Frank E. Filisko, The University of Michigan, Materials Science and Engineering, Ann Arbor, MI.

11:15 V5.6

DEPENDENCE OF THE LOCATION OF DIACETYLENIC GROUP ON THE SIZE OF THE VESICLES FROM 1,2 DIACYL PHOSPHOCHOLINES, Alok Singh, Naval Research Laboratory, Bio/Molecular Engineering Branch, Washington, DC; S. Marchywka, Geo-Centers Inc., Ft. Washington, MD; and R. Shashidhar, Naval Research Laboratory, Bio/Molecular Engineering Branch, Washington DC; and Geo-Centers Inc., Ft. Washington, MD.

11:30 V5.7

FORMATION OF METAL COLLOIDS IN INVERSE MICELLES AND MICROEMULSIONS, J.P. Wilcoxon and R. Williamson, Sandia National Laboratories, Albuquerque, NM.

11:45 V5.8

STRUCTURE AND PROPERTIES OF RESORCINOL-FORMALDEHYDE GELS, Stephan A. Letts, S. Buckley and F.M. Kong, University of California, Lawrence Livermore National Laboratory, Livermore, CA.

SESSION V6: INTERFACIAL BEHAVIOR:

SOLID/LIQUID, LIQUID/LIQUID

Chair: P. S. Pershan

Wednesday Afternoon, November 29

Essex Center (W)

1:30 *V6.1

STUDY OF POLYMER ADSORPTION PHENOMENA ON A SOLID SUBSTRATE, Mahn Won Kim, Exxon Research and Engineering Company, Annandale, NJ.

2:00 *V6.2

MODULATED PHASES AND CHIRAL DISCRIMINATION IN AMPHIPHILIC MONOLAYERS AT THE WATER/AIR INTERFACE, David Andelman, School of Physics and Astronomy, Tel-Aviv University, School of Physics and Astronomy, Tel-Aviv, Israel.

2:30 *V6.3

WETTING ON HETEROGENEOUS SOLID SURFACES, S. Garoff, Carnegie Mellon University, Department of Physics, Pittsburgh, PA.

3:00 BREAK

3:30 V6.4

STATISTICAL THERMODYNAMICS OF PHASE TRANSITIONS IN SURFACTANT MONOLAYER FILMS, R.S. Cantor, Dartmouth College, Department of Chemistry, Hanover, NH.

3:45 V6.5

X-RAY REFLECTIVITY OF A POLYMER MONOLAYER AT THE WATER/VAPOR INTERFACE, M.L. Schlossman, D.K. Schwartz, E. Kawamoto, G. Kellogg, P.S. Pershan, Harvard University, Department of Physics and Division of Applied Sciences, Cambridge, MA; M.W. Kim and T.C. Chung, Exxon Corporation Research Laboratory, Annandale, NJ.

4:00 V6.6

SURFACE ADSORPTION STUDIES BY OPTICAL SHG, Viola Vogel, C. Mullin, and Y.R. Shen, University of California, Berkeley, Department of Physics, Berkeley, CA; and Mahn Won Kim, Exxon Research and Engineering Company, Annandale, NJ.

4:15 V6.7

X-RAY REFLECTIVITY STUDIES OF SOLID/LIQUID CRYSTAL INTERFACES, B.M. Ocko, Brookhaven National Laboratory, Physics Department, Upton, NY.

4:30 V6.8

X-RAY REFLECTIVITY STUDIES OF POLYELECTROLYTE ADSORPTION AT THE SOLUTION-VAPOR INTERFACE, M.L. Schlossman, E.H. Kawamoto, D.K. Schwartz, and P.S. Pershan, Harvard University, Department of Physics and Division of Applied Sciences, Cambridge, MA; M.W. Kim and D. Peiffer, Exxon Corporate Research Laboratory, Annandale, NJ.

4:45 V6.9

NRA STUDIES ON THE INTERFACE FORMATION IN POLYMER MIXTURES BELOW THE CRITICAL POINT, Ullrich Steiner, Jacob Klein and Omer Zak, Weizmann Institute of Science, Department of Polymer Research, Rehovot, Israel; Kumar Chaturvedi, FBLJA World Laboratory Project, Geneva, Switzerland; Georg Krausch and Gunther Schatz, University of Konstanz, Department of Physics, Konstanz, West Germany.

SESSION V7: EXOTIC SYSTEMS: 1

Chair: D. R. Nelson

Thursday Morning, November 30
Essex Center (W)

8:00 *V7.1

TWO-COMPONENT GRAFTED POLYMER LAYERS, T.A. Witten, University of Chicago, Chicago, IL; and S.T. Milner, Exxon Corporate Research, Annandale, NJ.

8:30 *V7.2

LONG-RANGE INTERACTIONS AND RIGIDITY OF POLYMERS AND SURFACES, Mehran Kardar, Massachusetts Institute of Technology, Physics Department, Cambridge, MA.

9:00 *V7.3

STATISTICAL BEHAVIOR OF ELASTIC MEMBRANES, S. Leibler, C.E.N.-Saclay, Service De Phys. Theorique, Gif-Sur-Yvette, France.

9:30 BREAK

9:45 V7.4

DEHYDRATION OF PROTEIN POLYMERS IN CONCENTRATED NEMATIC SOLUTIONS, Judith Herzfeld and Reinhard Hentschke, Brandeis University, Department of Chemistry, Waltham, MA.

10:00 V7.5

APPLICATIONS OF SCALING THEORIES FOR POLYMER ADSORPTION TO PROTEIN PARTITIONING IN TWO-PHASE AQUEOUS POLYMER SYSTEMS, Nicholas L. Abbott, Daniel Blankschtein, and T. Alan Hatton, Massachusetts Institute of Technology, Department of Chemical Engineering, Cambridge, MA.

10:15 V7.6

PHASE BEHAVIOR OF NONIONIC AMPHIPHILE AND NONIONIC POLYMER IN AQUEOUS SOLUTION, Klaus R. Wormuth, Exxon Research and Engineering Company, Annandale, NJ.

10:30 V7.7

LAYERED LIQUID CRYSTALS AND SUPERCONDUCTORS: THE COMPLETE STORY, G. Srajer, R. Pindak, J.W. Goodby and M.A. Waugh, AT&T Bell Laboratories, Murray Hill, NJ; J.S. Patel, Bell Communications Research, Redbank, NJ.

10:45 V7.8

THERMAL PROPERTY EVOLUTION TOWARD EFFECTIVELY TWO-DIMENSIONAL SUBSTRATE-FREE SYSTEMS, R. Geer and C.C. Huang, University of Minnesota, Department of Physics, Minneapolis, MN; R. Pindak and J.W. Goodby, AT&T Bell Laboratory, Murray Hill, NJ.

11:00 V7.9

DYNAMIC RIGIDITY PERCOLATION IN INVERTED MICELLES, L. Ye, D.A. Weitz, Ping Sheng, S. Bhattacharya, J.S. Huang, and M.J. Higgins, Exxon Research and Engineering Company, Annandale, NJ.

11:15 V7.10
PHASE SEPARATION IN A LIPID/WATER/UREA MICELLAR SYSTEM, Bruce L. Carvalho, Massachusetts Institute of Technology, Department of Materials Science and Engineering, Cambridge, MA; Sow-Hsin Chen, Massachusetts Institute of Technology, Department of Nuclear Engineering, Cambridge, MA; and John S. Huang, Exxon Research and Engineering Company, Annandale, NJ.

11:30 V7.11
THE STRUCTURE OF THE BORDER LAYER BETWEEN GEL AND WATER, Zenon Bochynski, Adam Mickiewicz University, Institute of Physics, Non-Crystalline Materials Division, Grunwaldzka, Poland.

SESSION V8: COMPLEX FLUIDS

Chair: Phil Pincus
Thursday Afternoon, November 30
Essex Center (W)

1:30 V8.1
INTERACTION BETWEEN GRAFTED POLYMERIC BRUSHES, Gary S. Grest and Michael Murat, Exxon Research and Engineering Company, Annandale, NJ.

1:45 V8.2
EFFECT OF MOLECULAR WEIGHT ON THE HIGH FREQUENCY BULK MODULUS, OF WELL CHARACTERIZED POLY(DIMETHYLSILOXANE) POLYMERS, A. Shefer, Ben-Gurion University, Chemical Engineering Department, Beer-Sheva, Israel; J.R. Emery and D. Durand, Université du Maine, Le Mans, France; M. Gottlieb, Ben-Gurion University, Chemical Engineering Department, Beer-Sheva, Israel; and G. Gorodetsky, Ben-Gurion University, Physics Department, Beer-Sheva, Israel.

2:00 V8.3
SURFACE MODES ON CONCENTRATED POLYMER SOLUTIONS AND GELS, James L. Harden, Philip A. Pincus, University of California, Santa Barbara, College of Engineering, Materials Department, Santa Barbara, CA; and Harald Pleiner, Universität Essen, FB Physik, Essen, West Germany.

2:15 V8.4
MECHANICAL PROPERTIES OF CROSSLINKED SEMIDILUTE POLYMER SOLUTIONS NEAR AND FAR FROM THE GELATION THRESHOLD, C. Allain, Campus Universitaire, Lab. FAST, Orsay, France; L. Limat, ESPCI, Lab. Physico-chimie Théorique, Paris, France; and L. Salomé, CRPP, Pessac, France.

2:30 V8.5
"AGGREGATION IN BLOCK COPOLYMER SOLUTIONS," M. Olvera de la Cruz, Northwestern University, Department of Materials Science and Engineering, Evanston, IL.

2:45 V8.6
MICELLIZATION OF TRIBLOCK COPOLYMERS WITH POORLY SOLVATED END BLOCKS, N.P. Balsara and M. Tirrell, University of Minnesota, Department of Chemical Engineering and Materials Science, Minneapolis, MN; T.P. Lodge, University of Minnesota, Department of Chemistry, Minneapolis, MN.

3:00 V8.7
X-RAY REFLECTION AND SCATTERING STUDIES OF THE WATER-VAPOR INTERFACE, D.K. Schwartz, M.L. Schlossman, E. Kawamoto, G. Kellogg and P.S. Pershan, Harvard University, Department of Physics and Division of Applied Sciences, Cambridge, MA; and B.M. Ocko, Brookhaven National Laboratory, Department of Physics, Upton, NY.

3:15 BREAK

3:45 V8.8
X-RAY STUDIES OF CYTOCHROME C MONOLAYERS BOUND TO LANGMUIR-BLODGETT FILMS AND SELF-ASSEMBLED MONOLAYERS, J.M. Pachence, S. Amador, and J.K. Blasie, University of Pennsylvania, Chemistry Department, Philadelphia, PA.

4:00 V8.9
DOMAIN SHAPE INSTABILITIES IN A TWO-DIMENSIONAL BINARY FLUID MIXTURE: EPIFLUORESCENCE MICROSCOPY AND DIGITAL IMAGE ANALYSIS, M. Seul and M.J. Sammon, AT&T Bell Laboratories, Murray Hill, NJ.

4:15 V8.10
X-RAY REFLECTIVITY OF A LONG CHAIN FATTY ACID MONOLAYER AT THE WATER/VAPOR INTERFACE, M.L. Schlossman, D.K. Schwartz, E. Kawamoto, G. Kellogg and P.S. Pershan, Harvard University, Department of Physics and Division of Applied Sciences, Cambridge, MA.

4:30 V8.11
STUDY OF FATTY ACID MONOLAYERS DEPENDENCE ON CATIONIC INTERACTIONS BY ELLIPSOMETRY, Mahn Won Kim, Exxon Research and Engineering Company, Annandale, NJ; Bryan B. Sauer, Hyuk Yu, Mehran Yazdanian, and George Zografi, University of Wisconsin, Department of Chemistry and School of Pharmacy, Madison, WI.

4:45 V8.12
ELECTROHYDRODYNAMIC FLOW DYNAMICS IN THICK LIQUID CRYSTAL CELLS, David H. Van Winkle and Jit Gurung, Florida State University, Tallahassee, FL; and Rand Biggers, Naval Coastal Systems Center, Panama City, FL.

5:00 V8.13
RADIAL CREEPING FLOW BETWEEN PARALLEL DISKS OF ROD-LIKE NEMATIC LIQUID CRYSTALS: TEXTURES AND INSTABILITIES, Alejandro D. Rey, McGill University, Department of Chemical Engineering, Quebec, Canada.

SESSION V9: POSTER SESSION

Chair: E. B. Sirota
Thursday Evening, November 30
7:00 p.m. - 10:00 p.m.
America Ballroom (W)

V9.1 DYNAMICS OF MIXTURES OF INTERACTING COLLOIDS USING DIFFUSING WAVE SPECTROSCOPY, Xia Qiu, University of Pennsylvania, Philadelphia, PA; and Exxon Research and Engineering Company, Annandale, NJ; H.D. Ouyang, Lehigh University, Bethlehem, PA; D.A. Weitz, Exxon Research and Engineering Company, Annandale, NJ; D.J. Pine, Haverford College, Haverford, PA; and P.M. Chaikin, Exxon Research and Engineering Company, Annandale, NJ and Princeton University, Princeton, NJ.

V9.2 GRAVITY EFFECT ON WEAKLY CONCENTRATED GEL PHASES, C. Allain, Campus Universitaire, Lab. FAST, Orsay, France; and C. Amiel, Lab. Physico-chimie des Biopolymères, Thiais, France.

V9.3 A COMPUTER MODEL FOR THE AVERAGE "CLUSTER" SIZE IN POLYMER AGGREGATES, A.C. Balazs, J.Y. Hu, S. Lewandowski and A.P. Lentvorski, University of Pittsburgh, Materials Science and Engineering Department, Pittsburgh, PA; C. Lantman, Mobay Corporation, Pittsburgh, PA.

V9.4 PGSE-NMR & SANS FROM TPB BASED MICROEMULSIONS, Paul M. Lindemuth, University of Missouri-Rolla, Department of Chemistry, Rolla, MO; Boualem Hammouda, University of Missouri-Columbia, Research Reactor Facility, Columbia, MO; Joseph R. Duke, Frank D. Blum, and Raymond L. Venable, University of Missouri-Rolla, Department of Chemistry, Rolla, MO.

V9.5 SOL-GEL SILICATE FORMATION - pH AND TEMPERATURE DEPENDENCE, Anselmo M. Elias, Maria E. Elias and Maria M. Nunes, Lisbon University, Chemistry Department, Lisboa, Portugal.

V9.6 SIMPLE THEORY FOR PERSISTENT-FLEXIBLE LIQUID CRYSTAL POLYMERS BEYOND THE SECOND VIRIAL APPROXIMATION, Reinhard Hentschke, Brandeis University, Department of Chemistry, Waltham, MA.

V9.7 THE EFFECT OF PRESSURE ON THE CRITICAL TEMPERATURE OF FOUR-COMPONENT MICROEMULSIONS, J. Goyette and T.K. Bose, Université du Québec à Trois-Rivières, Trois-Rivières, Canada; J. Thoen, Katholieke Universiteit, Leuven, Belgium; J.R. Lalanne, Centre de Recherche Paul Pascal, Talence, France.

V9.8 THE MECHANICAL PROPERTIES OF THIXOTROPIC GELS AND THEIR EFFECT ON ATTENUATION IN OPTICAL FIBER COMMUNICATION CABLES, C.R. Taylor and B.J. Overton, AT&T Bell Laboratories, Norcross, GA.

V9.9 ELECTROSTATIC AND SCREENING EFFECTS ON THE DYNAMIC ASPECTS OF POLYELECTROLYTE SOLUTIONS: "POLY(P-PHENYLENE VINYLENE) PRECURSOR IN METHANOL," H. Mattoussi, K.H. Langley, and F.E. Karasz, University of Massachusetts, Polymer Science Department, Amherst, MA.

V9.10 ATOMIC STRUCTURE OF ALLOY-PARTICLES OBTAINED AS COLLOIDAL SUSPENSIONS, Gabriela Díaz Guerrero, Roberto Hernández, Laura Cabrera and Miguel José Yacamán, UNAM, Instituto de Física, México, México.

V9.11 MICROSCOPIC STRUCTURE AND DYNAMICS OF CONFINED POLYMER MELTS, Ioannis Bitsanis, University of Florida, Gainesville, FL; and George Hadziioannou, IBM Almaden Research Center, San Jose, CA.

V9.12 MOLECULAR DYNAMICS STUDY OF PHASE STRUCTURE IN BINARY MIXED COLLOIDS, Raymond D. Mountain, National Institute of Standards and Technology, Gaithersburg, MD; and D. Thirumalai, University of Maryland, IPST, College Park, MD.

V9.13 WEIGHTED-DENSITY THEORY OF PHASE TRANSITIONS IN FLUIDS COMPOSED OF ANISOTROPIC PARTICLES, John F. Marko, The University of Chicago, The James Franck Institute, Chicago, IL; and W.A. Curtin, BP Research and Development, Cleveland, OH.

SESSION V10: EXOTIC SYSTEMS: II

Chair: J. D. Litster
Friday Morning, December 1
Essex Center (W)

8:00 *V10.1
WHAT CAN WE LEARN FROM COMPUTER SIMULATIONS OF MACROMOLECULAR LIQUIDS? Gary S. Grest, Exxon Research and Engineering Company, Annandale, NJ.

8:30 *V10.2
LYOTROPIC LIQUID CRYSTALS, P.S. Pershan, Harvard University, Department of Physics and Applied Sciences, Cambridge, MA.

9:00 *V10.3
SIMULATIONS OF CONTACT LINE MOTION: SLIP AND
THE DYNAMIC CONTACT ANGLE, Mark Robbins and
Peter Thompson, The Johns Hopkins Univer-
sity, Department of Physics and Astronomy,
Baltimore, MD.

9:30 BREAK

10:00 V10.4
QUASIPARTICLE MEDIATED MELTING IN TWO DIMEN-
SIONS, M.A. Glaser and N.A. Clark, Univer-
sity of Colorado, Department of Physics,
Boulder, CO.

10:15 V10.5
INTERACTIONS BETWEEN CHARGED MACROIONS IN
SOLUTION, M.J. Stevens and M.O. Robbins, The
Johns Hopkins University, Department of
Physics and Astronomy, Baltimore, MD.

10:30 V10.6
THE EFFECT OF HYDROSTATIC PRESSURE ON LI-
QUID-LIQUID PHASE SEPARATION IN MICELLAR
SOLUTIONS OF C8-LECITHIN AND WATER, K.
Helmerson, P. Schurtenberger, G.M. Thurston,
T. Kushida, S. Angehrn, and G.B. Benedek,
Massachusetts Institute of Technology,
Department of Physics and Center for Materi-
als Science and Engineering, Cambridge, MA.

10:45 V10.7
MOLECULAR-THERMODYNAMIC FRAMEWORK TO PREDICT
MICELLIZATION, PHASE BEHAVIOR AND PHASE
EQUILIBRIA OF MICELLAR SOLUTIONS, D.
Blankschtein and S. Puvvada, Massachusetts
Institute of Technology, Department of
Chemical Engineering, Cambridge, MA.

11:00 V10.8
A MODEL FOR ORIENTATIONAL AND TRANSLATIONAL
ORDERING IN MICELLAR AND OTHER REVERSIBLY
ASSEMBLING SYSTEMS, Mark P. Taylor and
Judith Herzfeld, Brandeis University, De-
partments of Chemistry and Physics, Waltham,
MA.

11:15 V10.9
REEXAMINATION OF OSMOTIC PRESSURE MEASURE-
MENTS IN SELF-ASSEMBLING SYSTEMS, S. Puvvada
and D. Blankschtein, Massachusetts Institute
of Technology, Department of Chemical En-
gineering, Cambridge, MA.

11:30 V10.10
DIELECTRIC SPECTROSCOPY OF COMPLEX LIQUIDS
AND SOLUTIONS FROM KHZ TO 20 GHZ, Yan-Zhen
Wei and S. Sridhar, Northeastern University,
Department of Physics, Boston, MA.

V1.1

LINEAR AND STAR POLYMERS IN THE LIQUID STATE. William W. Graessley, Lewis J. Fetters, Mireille Adam and Andrea D. Kiss, Corporate Research Laboratories, Exxon Research & Engineering Company, Annandale, NJ 08801.

The properties of polymeric liquids vary widely with molecular size (typically 10-100 nm for long flexible chains), molecular architecture (linear or star, for the case here) and the polymer concentration (dilute solutions to the melt state). Architecture affects dilute solution behavior primarily through the internal segment density, which is small (ca. 1%) for linear chains but increases progressively with f , the number of arms in polymeric stars ($f \geq 3$). Thus, static and dynamic measures of size move toward a "fuzzy sphere" relationship with one another as f increases, internal dynamics are suppressed, and there is some evidence for liquid-like ordering near the overlap concentration. Some properties, e.g., the osmotic pressure, become independent of architecture at higher concentrations, but chain entanglement increasingly dominates the global dynamics and affects the relaxation of linear chains and stars in quite different ways. The much slower dynamics of stars are governed by arm length; the number of arms is now relatively unimportant. Theoretical aspects and some analogies with microgels and end-associated polymers will be discussed briefly.

V1.2

COOPERATIVE EFFECTS IN STRAINED POLYMERIC NETWORKS. Bertrand Deloche, Paul Sotta, Laboratoire de Physique du Solide (CNRS-LAZ), Université de Paris Sud, Orsay 91405, France; and Jean Herz, Institut Charles Sadron, Strasbourg 67083, France.

The orientational segmental order in uniaxially strained rubbers is studied with the deuterium-NMR. The method exploits the observation of residual quadrupolar interactions related to the mean degree of segmental order in the deformed network. The experimental facts are the following:

- (1) An uniaxial dynamics of the chain segments along the direction of the applied force.
- (2) An orientation of diluent probes (solvent molecules or polymer chains).
- (3) A concentration effect depending on the nature of the swelling agent (solvent molecules or polymer chains).

These observations show that the stress-induced orientation involve cooperative orientational correlations between chain segments (and diluents). This result leads to add an anisotropic contribution to the Flory interaction parameter. Inclusion of such a correction in a mean field description of polymer networks enables us to account for our observations and to discuss some aspects of rubber elasticity (stress-strain relationship, solvent-dependent maximum in the dilation modulus).

V1.3

PHASE BEHAVIOR AND STRUCTURE OF WEAKLY CHARGED COPOLYMERS. Jean-François Joanny, Institut Charles Sadron, 67083 Strasbourg Cedex, France; and Ludwik Leibler, E.S.P.C.I., 10, Rue Vauquelin, 75231 Paris Cedex 05, France.

We discuss static properties of weakly charged polyelectrolyte solutions which can be viewed as a special class of copolymers. We show that systems with a hydrophobic backbone may undergo a microphase separation transition (MST) into oppositely charged domains. At low copolymer concentration micelle formation is expected. At higher concentrations various mesophases should be present. As salt is added to the solution a usual macroscopic phase separation (precipitation of polymer chains).

We also discuss phase separation in solutions containing both weakly charged and neutral polymers. We show that the presence of electric charges dramatically affects phase diagrams. The results may be of some importance for understanding certain biological systems containing weakly charged proteins.

V1.4

CURVATURE ELASTICITY AND STRUCTURES OF SURFACTANTS AND BLOCK CO-POLYMERS. Zhen-Gang Wang and S. A. Safran, Exxon Research and Engg., Rt. 22 E., Clinton Twp., Annandale, NJ 08801

The curvature elastic free energy is a useful starting point for the understanding of the structure and phase transitions of membranes, microemulsions, and vesicles. Microscopic models of the elastic constants and the spontaneous curvature can lead to interrelationships between these quantities. Spring-like models are discussed for the case of short-chain surfactants, while a description of grafted polymers is used to study the case of block-copolymer membranes. Particular attention is focused on the origin of the saddle-splay elastic constant, which can stabilize ordered, bicontinuous structures of constant mean curvature. The phase diagram showing the competition of these structures with lamellar, cylindrical, and spherical phases is presented and discussed in light of recent experiments.

V1.5

BLOCK COPOLYMER AGGREGATES IN A SYSTEM OF TWO IMMISCIBLE SOLVENTS. N. Brandon, M. Tirrell, and A. Halpern.

Block copolymers in a mixture of two immiscible solvents can form 'swollen micelles'. The polymer acts as a surfactant solubilizing one solvent in the other. A model is proposed for the dependence of the aggregation number and the aggregate size (or curvature) on system parameters such as the molecular weight of the blocks or the solvent/polymer interaction parameter. The model utilizes scaling concepts proposed for grafted polymers and micelles in a single solvent, also including the contribution of a second solvent and interfacial tension between the two phases. It is found that the system parameters depend strongly on the inner block molecular weight and the interfacial tension.

Systems of polystyrene-quaternized polyvinyl pyridine block copolymers with varying molecular weights in mixtures of immiscible solvents will be investigated using dynamic light scattering.

V1.6

STRUCTURE OF ZWITTERIONIC ASSOCIATING POLYMERS. Y. Shen, C. R. Safinya, M. Adam, K. S. Liang, L. Fetters, J. Stokes, and R. Chance, Exxon Research and Engineering Co., Corporate Research, Route 22 East, Annandale, NJ 08801.

We have carried out x-ray scattering studies in melts of a series of linear polyisoprenes with highly polar sulfo-zwitterion groups at one end. The zwitterion end groups cause aggregation in good solvents for polyisoprene. The aggregation number depends strongly on the molecular weight of the polyisoprene tails and on the polarity of the solvent. Molecular mechanics simulations of the interactions between the zwitterion head groups suggest tubelike or disklike structures for the aggregates. Spherical structures are not energetically favorable. High resolution synchrotron x-ray scattering studies were carried out for six different (chain) molecular weights between 2000 and 22,000. For low molecular weights (between 2000 and 4000) a tubular structure is found with the tubes organized on a well-defined, two-dimensional triangular lattice with very large domain sizes >2000 Å. A structural phase transition to a cubic (bcc) phase with long range order is observed to occur for molecular weights >10,000. The lattice spacing increase over the molecular range was between 95 Å (for MW=2000) and 206 Å (for MW=22,000). For the high

molecular weight melts, annealing transforms the structure from (bcc) (with long range order) to an (fcc) glass-like phase.

V1.7

BLOCK COPOLYMER MICELLES IN A SELECTIVE SOLVENT
Mahn Won Kim, Su-Nin Liu, and T. C. Chung Exxon Research and Engineering Company Rt.22 East Annandale, NJ 08801

Block copolymer (A-B) shows the fascinating structures, such as the lamellar, cylindrical and spherical shape, in a bulk due to its unique chemical structure which possess the ability to form a stable interface between two incomparable mixture of polymers. Not only in a bulk, it is also well known that the block copolymers form micelles in a selective solvent which is very good solvent for one(A) of the diblock but poor solvent for the other segment(B). In this case, B segments form a dense core and A segments make a shell to be solubilize in the solvent.

In this talk, we present the aggregation number and the hydrodynamic radius of a micelle as a function of the number of B monomer by static and dynamic light scattering and compare the results with the surfactant micelles.

V1.8

STRUCTURAL AND DYNAMIC PROPERTIES OF POLYMERIC GELS.
S.J. Candau, Laboratoire de Spectrométrie et d'Imagerie Ultrasonores, Université Louis Pasteur, 4, rue Blaise Pascal, 67070 Strasbourg Cedex, France.

Networks composed of crosslinked polymer chains are of great interest, not only for their unique physical and chemical behaviour, but also for their possible technological applications. Network structures can be obtained by covalent crosslinking (irreversible gels) or physical processes (reversible gels). In this presentation, the macroscopic equilibrium and dynamic properties of gels are discussed in relation with the microscopic structure. Special emphasis is given to the ionized aqueous gels which are more and more frequently encountered in industrial practice.

V1.9

SLOW FLUCTUATIONS IN SWOLLEN POLYMER GELS.* J. V. Maher and M. W. Di Francesco, Department of Physics and Astronomy, University of Pittsburgh, PA 15260.

We have used light scattering to measure slow fluctuations in swollen polyacrylamide gels (7% polymer by weight). Fluctuations are at the lower limit of detectability by light scattering when pure water is used as a solvent, but the light scattering signal can be enhanced several orders of magnitude by either using a binary-liquid solvent or introducing a low concentration of 0.05 micron polystyrene spheres into an otherwise pure-water solvent. While the same fluctuations are observed in either case, we have emphasized measurements with the binary-liquid solvent, since in this case we can tune the scattering strength by changing the temperature in the neighborhood of the solvent's critical point. The system shows only weak fluctuations in the frequency range $0.1 \text{ Hz} < f < 100 \text{ Hz}$ and exhibits previously-reported solvent-relaxation behavior at higher frequencies¹. Strong fluctuations are observed in the very low frequency regime $5 \times 10^{-4} \text{ Hz} < f < 0.1 \text{ Hz}$. While these strong fluctuations generally grow in amplitude as frequency is reduced, they do not show typical $1/f$ or even power law behavior over most of their range.

* Supported by the DOE on grant # DE-FG02-84ER45131.
1. K. X. Xia and J. V. Maher, Phys. Rev. A37, 3626 (1988).

V1.10

CHARACTERIZATION OF CURING PROCESSES IN POLYMERIC SYSTEMS, AT VARIOUS STOICHIOMETRIC RATIOS, USING ULTRASONIC WAVES.
A. Shefer, G. Gorodetsky and, M. Gottlieb, Ben-Gurion University, Beer-Sheva, 84105, Israel

Ultrasonic wave measurements have been employed in recent years, as a non-destructive, non-interfering technique for the characterization of polymers (1). Continuing our previous work (2) on ultrasonic wave propagation studies in curing covalent networks, we studied the effect of reaction stoichiometry on the evolving molecular structure and gel point. During the process of network formation the reacting system undergoes a phase transition, from a viscoelastic liquid into a viscoelastic solid (gel).

Vinyl terminated linear poly(dimethylsiloxane) molecules were crosslinked by means of the hydrosilation reaction with a four functional hydride silane crosslinker. The various stoichiometric ratios, r , of the reacting systems were created by introducing different amounts of the crosslinker ($r=0.45$ to $r=2.34$) (where the stoichiometric ratio was $r=[\text{-Si-H}]/[\text{-Si-CH=CH}_2]$). In order to characterize the structural changes in the reacting polymeric systems as a function of their theoretically calculated distance from the gel point, we measured the relative longitudinal wave velocity using the acoustic interferometer, at a frequency of 10MHz with a resolution of 0.001%. Dilatometric measurements provided information on often neglected, changes in the density of the systems. The extent of the crosslinking reaction was monitored simultaneously by IR spectroscopy.

It was found that longitudinal wave velocity increases during the course of these reactions. The magnitude of this increase is proportional to the crosslink density of the network being formed. Above the balanced stoichiometric ratio ($r=1.0$) no additional increase was observed, both in the relative wave velocity and density changes. Wave velocity results exhibit a step like increase around the sol-gel transition point for all the stoichiometric ratios studied whereas density increases linearly as the crosslinking reaction proceeds towards gelation. Since both wave velocity and density are observed to increase as a function of reaction conversion, it is clear that the measured increase in wave velocity is due to the true change in the value of the longitudinal bulk modulus.

1.Hartmann B., in "Methods in Experimental Physics"

R. A. Fava editor, Vol 16, Academic Press, NY, (1980).

2.Shefer A., Gorodetsky G., and Gottlieb M., Proc. MRS Fall Meeting, p.534 (1988).

V2.1

EXPERIMENTAL DATA AND THEORETICAL INTERPRETATION OF PHASE SEPARATION IN PROTEIN WATER SOLUTIONS WITH APPLICATION TO CATARACT DISEASE G.B. Benedek, D. Blankschtein, M. Kondo, P. Schurtenberger, J.A. Thomson, G.M. Thurston and M.C. Wiener, Department of Physics and Center for Materials Science and Engineering, MIT, Cambridge, MA

We present measurements of both the liquid-liquid coexistence curve¹ and the solid-liquid phase boundary for aqueous solutions of the bovine lens protein γ -crystallin. We observe that the liquid-liquid phase separation is in fact metastable relative to the solid-liquid phase boundary. We shall also present a Gibbs free energy model for these protein-water solutions in an effort to obtain theoretically all the equilibrium properties including the location and shape of the phase boundaries. Application of this data to the problem of cataract diseases in the eye lens will be discussed.

¹J.A. Thomson, P. Schurtenberger, G.M. Thurston and G.B. Benedek PNAS(USA) 84:7079 (1987)

V2.2 ABSTRACT NOT AVAILABLE

V2.3

DIFFUSE X-RAY SCATTERING STUDIES OF LYOTROPIC TUBULAR PHASES. E. B. Sirota, E. Y. Sheu, C. R. Safinya, and K. S. Liang, Exxon Research and Engineering Co., Corporate Research, Route 22 East, Annandale, NJ 08801.

We have carried out diffuse x-ray scattering studies in the lyotropic tubular phases of the ternary (SDS/water/dodecane) and quaternary (with added cosurfactant) systems. In the ternary system, at three water to surfactant ratios (W/S, by weight), we investigated the structural transitions along the

appropriate dodecane dilution lines. The x-ray data exhibit the following distinctive features. First, at $W/S=1, 1.5,$ and 2 with no oil, the systems exhibit pure tubular structure packed on a hexagonal lattice. Second, for $W/S=1$, the hexagonal lattice evolves and exhibits a structural transition to an oblique lattice at $V_0=0.18$ (V_0 =oil volume fraction). Third, at $W/S=1.5$, the structure changes at $V_0=0.12$ from hexagonal through an intermediate phase, in which broad peaks are established, to a distorted center rectangular phase. In these phases as a function of increasing intertubular distance, we analyze the thermal diffuse scattering which allows us to measure the bulk elastic moduli.

V2.4

SURFACTANTS IN SOLUTION: EXPERIMENTAL EXAMPLES OF FLUCTUATING MEMBRANES. Didier Roux, Centre de Recherche Paul Pascal, Domaine Universitaire, F-33405 Talence Cedex, France.

Surfactants in solution give rise to many fascinating structures which can be considered as phases of surfaces. The structure and stability of these phases can be often understood in terms of the elastic energy of the surfactant film (membrane). In most of the cases, the bending constant κ related to deformations of the membrane is quite large and thermal fluctuations of the film are negligible. In some interesting cases, it is possible to make the membrane so flexible that thermal fluctuations (undulations) are important.

Flexible membranes lead to ordered structures such as dilute lamellar phases where the interactions between membranes are dominated by undulation forces coming from the steric hindrance of the undulations. The measurements of elastic constants of lamellar phases allow to obtain quantitative information upon flexibility and interactions between membranes.

Besides lamellar phases, flexible membranes can fill space randomly leading to isotropic phases of connected films. Two different cases may exist depending on the monolayer or bilayer character of the film. Monolayer corresponds to bicontinuous microemulsion where oil and water domains are separated. Bilayer leads to bicontinuous structure of the same solvent (oil or water). This latter case (sponge phase) has very interesting properties related to the special symmetry (in and out) of this phase. The effect of thermal fluctuations on membranes allows an understanding of the phase behavior and the thermodynamical properties of these phases.

V2.5

ELECTRON MICROSCOPY OF COMPLEX FLUIDS. Yeshayahu Talmon, Department of Chemical Engineering, Technion-Israel of Technology, Haifa 32000, Israel.

Transmission electron microscopy can provide high resolution direct images of liquid systems, if they can be made compatible with the high vacuum in the instrument, and with the low penetration power of the electron beam. Thus, the challenge is specimen preparation while preserving the original microstructure of these normally labile systems. In recent years we have developed techniques and equipment to prepare thermally-fixed (ultra-rapidly cooled, i.e., vitrified) specimens of microstructured fluids. Preparation is carried out under controlled conditions to prevent structural rearrangement during specimen handling from the original vial to the microscope. We have applied the technique to directly visualize a wide range of complex fluids systems: micelles, vesicles, liposomes, lyotropic liquid crystals, and gels, in synthetic and biological systems. The technique will be briefly described along with recent applications, including new developments such as "on the grid processing" for growing new phases in the specimen, and "time-resolved cryo-transmission electron microscopy",

a technique to investigate dynamical processes in liquid systems, e.g., phase transformations, by direct imaging of thermally-fixed specimens.

V2.6

SYNCHROTRON X-RAY SCATTERING STUDIES OF THE LYOTROPIC L_3 PHASE. N. Lei, C. R. Safinya, K. S. Liang, E. B. Sirota, and R. Plano, Exxon Research and Engineering Co., Corporate Research, Route 22 East, Annandale, NJ 08801.

We have carried out a high resolution small angle synchrotron x ray scattering study of the lyotropic L_3 phase in the quaternary system of SDS, pentanol, dodecane and water. This phase is found in the vicinity of the dilute lamellar phase, which consists of stacks of extremely flexible membrane sheets. We studied the L_3 phase as a function of dodecane dilution with volume fraction between 0.45 to 0.86. We have analyzed our data within the context of two different models. First, we consider an elastic description of the L_3 phase consisting of a phase of randomly oriented self-avoiding sheets with a persistence length of the order of 1000Å. Second, we fit the x-ray structure factor to a form derived from a recent lattice model of G. Gompper and M. Schick (preprint, July 1989).

1C. R. Safinya, D. Roux, G. S. Smith, S. K. Sinha, P. Dimons, N. A. Clark and A. M. Bellocq, Phys. Rev. Lett. **57**, 2718 (1986).

V2.7

BICONTINUOUS STRUCTURE OF THE "ANOMALOUS ISOTROPIC PHASES L_3 " AND MICELLAR- L_3 PHASE TRANSITIONS. A.M. Bellocq, D. Gazeau, D. Roux, Centre de Recherche Paul Pascal, C.N.R.S. Château Brivazac, Pessac, and E. Freysz, Centre de Physique Moléculaire optique et Hertzienne, Université de Bordeaux I, 33405 Talence Cedex, France.

Anomalous flow birefringent phases, sometimes designated as L_3 , have been identified in both the water-rich and the oil-rich parts of the phase diagram of the water (NaCl)-dodecane-pentanol-SDS system. Conductivity and neutron scattering results provide evidence that the structure of these phases consists of a highly connected, sponge-like, random bilayer-continuous surface. The surfactant surface separates, depending upon the system, either two water-continuous domains or two oil-continuous domains. The data are consistent with a recent theoretical model (M. Cates et al, Europhys. Lett. **5**, 733, 1988). In some conditions of salinity and temperature, the L_3 phase and the micellar phase (L_1 or L_2) form a single continuous region. The transition from micellar to bicontinuous structures will be examined.

V2.8

FLEXIBILITY AND INTERACTION MEASUREMENTS IN DILUTE LAMELLAR PHASES BY DYNAMIC LIGHT SCATTERING. F. Nallet, D. Roux, Centre de recherche Paul-Pascal, Domaine universitaire, 33405 Talence cedex, France; and J. Prost, Ecole supérieure de physique et de chimie industrielles, 10 rue Vauquelin, 75231 Paris cedex 05, France.

Dynamic light scattering measurements on oriented samples of dilute lyotropic smectics have been performed. The hydrodynamics of two-component smectics A is applied to describe the fluctuation spectrum in our multicomponent samples. The experimentally relevant hydrodynamic mode is the *undulation/baroclinic* mode, which arises from the coupling between concentration and layer displacement fluctuations.

Two elastic constants, the layer compressibility modulus (at constant chemical potential) \bar{B} and the bending modulus K , are extracted from its

anisotropic dispersion relation. Membrane flexibility (K) and intermembrane interactions (B) have been studied along a dilution line, with smectic repeating distances in the range 4-35 nm. The results support the view of flexible membranes (flexibility of the order of $k_B T$) interacting by means of the Helfrich's steric interaction.

Measurements of the flexibility as a function of the chemical composition of the membranes (cosurfactant length) have been performed.

V3.1

NONLINEAR FLOW BEHAVIOR OF HIGH MOLECULAR WEIGHT POLYMERS. Dale S. Pearson, Department of Chemical and Nuclear Engineering and Materials Department, University of California, Santa Barbara, CA 93106.

High molecular weight polymer liquids are frequently subjected to high speed flow conditions that produce very nonlinear effects. Typical observations are (1) a steady state viscosity that changes rapidly with the applied deformation rate, (2) a stress relaxation modulus which is a strong and even unstable function of the applied strain, and, after the inception of flow, (3) transient stresses that greatly exceed their steady state values. Responses of this type are observed at all concentrations, but are most dramatic in concentrated solutions and melts. Because polymers are typically processed at high flow rates, it is important to develop an explanation for this type of behavior. The past ten years have been a period of remarkable progress in this direction. The strong nonlinearities have been shown to be a result of entanglement effects which arise naturally in concentrated liquids. Such interactions modify the behavior of both rigid rod polymers and flexible coil polymers. This talk will review the physical principles and the constitutive equations which are required to describe the flow of these systems. Successes that have been achieved and problems that remain unsolved will be covered.

V3.2

RHEOLOGICAL AND KINETIC PROPERTIES OF SEMI-DILUTE SOLUTIONS OF ELONGATED MICELLES. S.J. Candau, G. Waton, F. Merikhi, Laboratoire de Spectrométrie & d'Imagerie Ultrasonores, Université Louis Pasteur, 4, rue Blaise Pascal, 67070 Strasbourg Cedex, France; and R. Zana, Institut Charles Sadron, 6, rue Boussingault, 67083 Strasbourg Cedex, France.

Aqueous micelles of ionic surfactants adopt an anisodiametric shape at high ionic strength. An increase of surfactant concentration induces a micellar growth leading to very elongated flexible micelles which behave in many respects like polymers. Rheological data suggest that the flow properties of these systems can be described by a model of reptation truncated by the kinetics of fragmentation-coagulation of the micelles. In this paper we present results of T-Jump experiments with light scattering detection, performed in cetyltrimethylammonium bromide aqueous solutions. The characteristic micellar kinetics relaxation time has been studied as a function of salt concentration, surfactant concentration and temperature. The rheological behaviour of the semi-dilute solutions of elongated micelles is discussed in the light of the T-Jump results. The activation energy for the scission of the micelles is determined from the combined results of T-Jump and rheological experiments.

V3.3

LIGHT SCATTERING EVIDENCE FOR "WORM-LIKE" MIXED DETERGENT-DIACYLPHOSPHATIDYLCHOLINE (PC) MICELLES R. Chamberlin, G. Thurston, G. Benedek, MIT, Camb., MA; D. Cohen, & M. Carey, Harvard Med. Sch., Bos., MA

Using static and dynamic light scattering, we examined the micellar systems tabulated. Each mixed detergent - egg yolk PC (EYPC) solution examined can be diluted from a one phase (micellar) into a two phase (lamellar plus aqueous) system. Upon dilution toward the two phase boundary, the apparent radius of gyration R_g , the apparent hydrodynamic radius R_h , and the apparent molecular weight M_{app} , all appeared to diverge. In spite of this divergence, the ratios $R_h/M_{app}^{1/2}$ ($= A$), and R_g/R_h ($= B$), had weak variation and similar values for all EYPC systems: $A = 1.8 \times 10^{-2}$ nm/(gm/mole)^{1/2}, and $B = (1.6 \pm 1)$. Remarkably, this is the same behavior observed for A and B in di-C₈ and di-C₇ PC solutions which form "worm-like" locally cylindrical micelles. The value of A is inconsistent with a previous EYPC disk micelle model¹ since it yields a disk thickness of only 1nm instead of the assumed 5nm for an EYPC bilayer. The behavior of A and B is consistent with a hydrodynamic theory² for flexible "worm-like" structures in solution. In the limit that the "worm" contour length is much greater than the "worm" persistence length, ξ_p , the theory predicts $A = 1.5$, and $A = 8.84 \times 10^{-3} \times [\xi_p]^{1/2} / r$ nm/(gm/mole)^{1/2} where r is the radius of the "worm" cross section. If $r = 2.5$ nm, the length of an EYPC molecule, then A gives $\xi_p = 26$ nm.

PC	Detergent (D)	[D]/[PC] (mol. rat.)	[NaCl] (M)	Temp (°C)	Conc. (mg/ml)	A X 10 ² (nm/(gm/mole) ^{1/2})
EYPC	NaCholate	1.0	.15	20.0	13 - 50	1.66 ± .06
EYPC	NaCholate	1.0	.4	20.0	10 - 50	1.82 ± .06
EYPC	NaCholate	0.8	.15	20.0	18 - 100	1.79 ± .13
EYPC	NaTaurocheno- deoxycholate	1.7	.15	20.0	1 - 100	1.73 ± .33
EYPC	Octylglucoside	8	.15	20.0	11 - 100	1.81 ± .13
Di-C ₈	none	0	0	55.0	1 - 5	1.88 ± .09
Di-C ₇	none	0	0	20.0	2 - 30	1.94 ± .07

¹N. A. Mazer, G. B. Benedek, M. C. Carey, *Biochemistry*, 19, 601 (1980)

²H. Yamakawa, M. Fujii, *Macromolecules*, 6, 407 (1973)

V3.4

SHEAR FLOW AND ISOTROPIC-LAMELLAR TRANSITIONS. S. T. Milner, AT&T Bell Laboratories, 600 Mountain Ave., Murray Hill, NJ 07974.

In systems such as lyotropic liquid crystals, certain microemulsions, and block copolymers, a nearly second-order transition from an isotropic state to a lamellar phase is observed. In these transitions, nonlinear fluctuation terms lower the mean-field transition temperature T_c and drive the transition first order. We consider the effect of simple shear on these systems, showing that shear suppresses the fluctuations and raises T_c . In a range of temperatures, the lamellar phase can be induced by applying shear. We obtain an effective potential under shear in the disordered phase, and conclude that the transition under shear remains first order, though very weakly so at high shear rate. The mechanism for suppression of fluctuations suggests that lamellar ordering first occurs with wavevector normal to the shear plane.

*Work performed in collaboration with M. E. Cates, Cavendish Laboratory, Cambridge University.

V3.5

LANDAU THEORY OF THE NEMATIC TO SMECTIC-A TRANSITION UNDER SHEAR FLOW.* R. Bruinsma, Physics Department, UCLA, Los Angeles, CA 90024.

Shear flow distorts the microstructure of fluids if the Deborah number De becomes comparable to one. In complex fluids, exotic hydrodynamic effects are often seen in this regime. We compute within Landau theory the structure factor $S(q)$ of a sheared nematic close to the nematic to smectic-A phase transition. As a function of increasing Deborah number, the pretransitional smectic-A (cybotactic) clusters become increasingly more geometrically restricted, evolving from their usual three dimensional ellipsoidal shape for $De \ll 1$ to an extremely anisotropic one-dimensional shape for $De \gg 1$. We discuss the predictions of Landau theory for x-ray diffraction

experiments for various orientations of the nematic director. The suppression of pre-transitional critical fluctuations by shear flow is found to raise the transition temperature T_{NA} , and peculiarly, T_{NA} is found to depend on the orientation of the director. These distortions of the microscopic cybotactic clusters for $De \gg 1$ by shear flow are also reflected on the macroscopic level. The classical theory of the dynamics of nematics, due to Erickson, Leslie and Parodi (ELP), is found to be incomplete. We compute the new "normal forces" which must be added to ELP hydrodynamics for large De and we discuss their consequence, in particular the analog of shear-thinning for liquid crystals.

* in collaboration with C. R. Safinya

V3.6

NONEQUILIBRIUM X-RAY DIFFRACTION STUDY OF THE NEMATIC-SMECTIC-A TRANSITION UNDER SHEAR FLOW. C. R. Safinya, E. B. Sirota, R. Plano, and N. Lei, Exxon Research and Engineering Co., Corporate Research, Route 22 East, Annandale, NJ 08801.

We report on x-ray scattering studies of the microscopic structure of the nematic (N) and the smectic-A (SmA) phases in (8CB) under dynamic "steady-state" shear flow conditions carried out in an x-ray Couette-cell. In the nematic phase, we find a director-flip-transition as the SmA fluctuations increase on approaching the SmA phase. We associate this transition with the microscopic renormalization of the Miesowicz viscosity η_b predicted by W. L. McMillan (Phys. Rev. A, 9, 1720 (1974)) to be proportional to the square root of the SmA susceptibility measured by x-rays. As a function of decreasing temperature in the vicinity of the SmA phase, we find an abrupt transition (rather than the expected continuous transition) to a regime where the pretransitional (SmA) fluctuations (e.g. the cybotactic domains) are distorted and suppressed along the shear. The distorted structure allows us to directly measure the (SmA) order parameter relaxation time as a function of shear rate. We find that as a function of increasing shear rate the N-SmA transition temperature T_{NA} increases initially but eventually, above a critical shear rate decreases, so that in the (shear rate-T) plane we find a reentrant nematic phase. We associate the initial rising of T_{NA} with the suppression of critical fluctuations due to shear flow.

V3.7

KINETICS OF THE LATE STAGE GROWTH IN THE PHASE SEPARATION OF A CRITICAL BINARY MIXTURE. Serge Lacelle and Franco Cau, Dept. de Chimie, Université de Sherbrooke, Sherbrooke, Québec, Canada J1K 2R1.

The effects of shear flow on the phase separation processes in the critical binary mixture aniline/cyclohexane have been studied with natural abundance ^{13}C nuclear magnetic resonance spectroscopy. The ^{13}C lineshapes were monitored as a function of temperature quenches in the unstable region of the coexistence curve. From the resonance linewidths are inferred average lifetimes of molecules in a phase. Assuming a diffusive mechanism for interphase transport yields time-dependant domain sizes $R(t)$. Power laws $R \sim t^x$ are observed. Crossovers in the growth exponents x are also observed. These results will be discussed in light of existing theories on critical fluctuations under shear, hydrodynamic percolation, and late stage growth.

V3.8

SELF-DIFFUSION AND RHEOLOGY OF WEAKLY INHOMOGENEOUS BLOCK COPOLYMERS. Scott T. Milner and Glenn H. Fredrickson, AT&T Bell Laboratories, 600 Mountain Ave., Murray Hill, NJ 07974; Frank S. Bates and Jeffrey H. Rosedale, University of Minnesota, Dept. of Chemical Engineering and Materials Science, 421 Washington Ave., S.E., Minneapolis, MN 55455.

We discuss the self-diffusion and rheological properties of block copolymer melts that are weakly microphase separated, or in the pretransitional disordered phase. Oscillatory shear measurements on a model saturated hydrocarbon diblock copolymer indicate a breakdown of time-temperature superposition and detect unusually large shear and normal stresses. We have investigated single-molecule and collective mechanisms for this anomalous behavior, both related to the presence of large amplitude composition fluctuations in such systems. A particularly striking prediction is that the energetic barrier to self-diffusion is a small fraction of $k_B T$ in the weakly ordered phase, in apparent violation of the Lindeman criterion for melting.

V3.9

SCALING ANALYSIS OF SHEAR THINNING IN POLYMER SOLUTIONS. Y. Rabin, Chemical Physics Department, Weizmann Institute of Science, Rehovot, Israel 76100; and H.C. Ottinger, Institut für Polymere, ETH-Zentrum, CH-8092 Zurich, Switzerland.

Introducing the notion of a "shear blob" defined as a segment of a polymer on the scale of which the tension along the chain balances the viscous shearing force, we reproduce Onuki's prediction for the shear thinning of intrinsic viscosity

$$[\eta] \sim \dot{\gamma}^{-\alpha}$$

where $\dot{\gamma}$ is the shear rate, $\alpha = 1 - (1/3\nu)$ and ν is the Flory exponent. A new prediction for the shear thinning of the normal stress coefficients (Ψ_1, Ψ_2) is

$$[\Psi_i] \sim \dot{\gamma}^{-2\alpha}$$

Furthermore, if the Rabin-Kawaski conjecture about the suppression of the excluded-volume effect in strong shear is correct, we predict that $\alpha = 1/3$, independent of solvent quality.

V4.1

EFFECT OF THE STABILIZING COATING AND THE PRESENCE OF FREE POLYMER ON THE CRYSTALLIZATION PHENOMENA OF COLLOIDAL SUSPENSIONS. C. Smits, J.K.G. Dhont and H.N.W. Lekkerkerker, Van't Hoff Laboratory, University of Utrecht, Padualaan 8, 3584 CH Utrecht, The Netherlands.

Visual observations and preliminary light scattering experiments on the crystallization process in various colloidal systems are reported. In the first place we studied the influence of the stabilizing coating of the colloidal particles on the rate of crystallization. The various coatings give rise to different ranges of the repulsive interaction. This is found to have a pronounced effect on the rate of crystallization. Furthermore we investigated the effect of free polymer added to the dispersion. It appears that addition of free polymer has a dramatic effect on the crystallization phenomena.

V4.2

CHARGE AND SIZE POLYDISPERSITY EFFECTS ON THE SCATTERING PROPERTIES AND THE HIGH FREQUENCY ELASTICITY OF COLLOIDS. B. D'Aguzzo, Rudolf Klein and N. Wagner, Fakultät für Physik, Universität Konstanz, D-7750 Konstanz, FRG.

Polydispersity in charge and size of colloidal particles strongly influences the static light scattering $I(k)$ and the first cumulants $\Gamma(k)$ of the dynamic correlation function. These effects are calculated by solving the Ornstein-Zernike integral equation for the microstructure with the thermodynamically consistent Roger-Young (RY) closure for a multicomponent mixture of up to 10 components.

Comparison of monodisperse calculation with Monte Carlo simulations demonstrates the superiority of the RY closure for interparticle potentials of screened Coulomb type over the Percus-Yevick and hypernetted chain closures. The results for $I(k)$ and $\Gamma(k)$ for polydisperse systems show significant difference from results obtained by treating the system as an effectively monodisperse one. For $I(k)$ a large increase is found at small k as well as a shift in the main peak. These results have immediate consequences for the experimental determination of the charge on the colloidal particles from the main peak in $I(k)$. Finally, high-frequency elastic moduli, which can be expressed in terms of static structure factors and the above results, are predicted as functions of concentration and polydispersity.

V4.3

DYNAMICS OF CONCENTRATED COLLOIDS.* D.A. Weitz, Exxon Research and Engineering Co., Rt. 22 E, Annandale, NJ 08801.

The interactions between colloidal particles, and between the particles and the surrounding fluid, play a major role in determining the dynamics of concentrated suspensions. Here we discuss different applications of light scattering to study the dynamics in concentrated colloidal suspensions. When the particles are comparable to the wavelength of light, a concentrated suspension will typically scatter light very strongly. This can be exploited through the use of Diffusing Wave Spectroscopy (DWS), which is an extension of traditional dynamic light scattering to the multiple scattering regime. New physics can be explored with DWS as it allows the motion of the particles to be measured on very short length scales. We exploit this feature to study the hydrodynamic interactions that influence the nature of Brownian motion at very short time scales. The dynamics at even faster time scales, or higher frequencies, are dominated by the acoustic behavior of the suspensions. If the multiple scattering can be eliminated, the acoustic properties can be studied through the use of Brillouin scattering. Again, these properties are strongly influenced by the interactions between the particles. Here, we investigate the relationship between the particle correlations, as characterized by the structure factor, and the propagation of acoustic modes through the suspension. The combination of these techniques enables us to explore new regimes of $S(q, \omega)$ for concentrated suspensions, and thus study the dynamics of the colloidal particles.

* in collaboration with L. Ye, Ping Sheng, D.J. Pine, and P.N. Pusey.

V4.4

NON-DIFFUSIVE BROWNIAN MOTION STUDIED BY DIFFUSING WAVE SPECTROSCOPY. D.J. Pine, Department of Physics, Haverford College, Haverford, PA 19041, D.A. Weitz, Exxon Research and Engineering Co., Rt. 22 E, Annandale, NJ 08801, P.N. Pusey and R.J.A. Tough, Royal Signals and Radar Establishment, Malvern, Worcestershire WR14 9PS, UK.

The trajectory of a Brownian particle on time scales comparable to the viscous damping time reflects the interplay between the short range, random molecular forces and the long range, hydrodynamic forces on the particle. For short times, the particle motion is "ballistic", while at long times, the motion is diffusive. The nature of the transition from ballistic to diffusive motion is determined by the interaction of the particle with the surrounding fluid. The flow field, or vorticity, established in the fluid when the particle moves, reacts back on the Brownian particle, resulting in a persistence of the motion. This is manifested as a "long-time tail" in the decay of the velocity autocorrelation function. Thus, the nature of the short-time, non-diffusive, Brownian motion and the transition to diffusive trajectories are sensitive functions of the hydrodynamic interactions between a colloidal particle and the surrounding fluid. We use diffusing wave spectroscopy (DWS), the analysis of temporal fluctuations of multiply-scattered laser light. This technique extends traditional dynamic light scattering to the strongly multiple-scattering regime, and can be used to probe the motion of Brownian particles at length scales of only a few angstroms, much less than the wavelength of light. We clearly observe the non-diffusive motion of Brownian particles at early times and the slow approach to the asymptotic diffusive motion.

V4.5

DIELECTRIC RELAXATION IN CONCENTRATED SOLUTIONS OF INVERTED MICELLES. J. Sowa, S. Bhattacharya, M. J. Higgins and J. S. Huang, Exxon Research and Engineering Company, Route 22 East, Annandale, NJ 08801.

Low-frequency dielectric relaxation studies show anomalous behavior in concentrated solutions of inverted micelles in oil. A new and slow relaxation process appears at high concentrations accompanied by a conductivity anomaly. This is suggestive of the formation of some yet-unknown large-scale structure. Similarities and dissimilarities with glassy relaxation in liquids are noted in the variations of the relaxation times with temperature, volume fraction of surfactants and oil chain-length.

V4.6

FORMULATION AND PROCESSING OF COLLOIDAL DISPERSIONS. William B. Russel, Department of Chemical Engineering, Princeton University, Princeton, NJ 08544-5263

Colloidal dispersions appear during the processing of chemicals and materials in a number of contexts that require control of macroscopic properties, particular phase behavior and rheology, through manipulation of the chemistry. This talk will survey several applications, including the colloidal processing of ceramics, the formulation of coatings, solid-liquid separations, and waste water treatment, and attempt to identify the relevant fundamental science involved.

V4.7

SEDIMENTATION STUDIES IN NEARLY HARD - SPHERE SUSPENSIONS. Steven E. Paulin and Bruce J. Ackerson, Department of Physics, Oklahoma State University, Stillwater, OK 74078 - 0444.

Results are presented for sedimentation studies of suspensions in a liquid of micron diameter "nearly hard" colloidal spheres consisting of polymethylmethacrylate (PMMA) cores stabilized sterically by a thin layer of poly-(12-hydroxystearic acid). The particles are dispersed in a mixture of decalin and tetralin in proportion chosen to nearly match the particle refractive index, thus providing nearly transparent samples. A series of samples having different volume fractions of particles are prepared and allowed to settle at one g. In each sample a dense crystalline solid develops and grows upward from the bottom, and a clear supernatant boundary appears and descends from the top. Depending on the initial particle volume fraction the central region evidences a liquid, crystal, or coexisting crystal and liquid ordering of particles having a sharp boundary. Measurements are made of these boundary regions as a function of time. In addition light scattering diffraction studies are conducted to monitor crystalline solid lattice constants as a function of time and height in the sample. From these data sedimentation velocities for dense suspensions are determined as a function of volume fraction and suspension phase behavior. Particle interactions are examined in the dilute limit. Model hard sphere sedimentation rates and equations of state are tested by comparison of these data with a numerical solution of a diffusion-sedimentation equation.

V4.8

NUCLEATION OF COLLOIDAL CRYSTALS. D.J.W. Aastuen, C. Swindal, J. Pieper, and N.A. Clark, Department of Physics, University of Colorado, Boulder, CO 80309.

The number of bcc colloidal crystal nucleation events per unit volume-per unit time (n_c) in a supercooled (shear melted) colloidal liquid is found to increase strongly with the degree of supercooling. The evolution with in-

creasing n_g from recrystallization by nucleation and growth to glass formation will be discussed.

Supported by NSF DMR 8512071.

V4.9

FLOW PROPERTIES OF CONCENTRATED COLLOIDAL SUSPENSIONS. J.W. Goodwin; and R.W. Hughes, Department of Physical Chemistry, University of Bristol, Cantock's Close, Bristol BS8 1TS, England.

As the volume fraction of a suspension of spheres is increased non-Newtonian flow is observed. Shear thinning behaviour is often seen whilst at higher concentrations dilatancy may occur. The volume concentration at which non-Newtonian behaviour is initially found is a function of both the particle size and the range of the inter-particle forces.

Suspensions of hard spheres are Newtonian up to volume fractions, ϕ , approaching 0.5. For particles where there is a weak attractive colloid potential start to show shear thinning behaviour at $\phi > 0.3$. Both a low stress limiting viscosity and viscoelasticity can be measured for such suspensions. When there are long range electrostatic forces acting between the particles, viscoelastic behaviour can be found at $\phi < 0.2$.

All these systems can be analysed in terms of an equilibrium structure and the colloid potentials. For strongly attractive or coagulated systems this is not the case and non-equilibrium structures are produced.

Examples of each of these systems will be given and some of the models used for predicting the behaviour will be discussed.

V4.10

CRYSTALS UNDER SHEAR AND THE MELTING TRANSITION.* Mark J. Stevens, James F. Belak,** and Mark O. Robbins, Department of Physics and Astronomy, The Johns Hopkins University, Baltimore, MD 21218

We have studied the effect of shear on crystals with a screened-Coulomb (Yukawa) interparticle interaction. This potential gives a good description of the equilibrium properties of a well studied experimental system: charge-stabilized colloidal crystals. We use an extension of the Parrinello-Rahman molecular-dynamics method to impose a constant shear-rate ' γ '. In simulations at low shear-rates, we find a solid-like state with planes of particles sliding over each other. The density of stacking faults increases with ' γ '. At high shear rates, we find an enhanced diffusion perpendicular to the shear direction and the calculated structure factor indicates ordering of particles into strings. At even higher shear rates, the solid melts and we observe the spherical structure factor characteristic of the fluid state. Microscopic mechanisms, by which these crystals propagate shear, will also be discussed. *Work supported by National Science Foundation Grant No. DMR-8553271

**Permanent address: Lawrence Livermore Laboratories, Livermore, CA 94550

V5.1

RHEOLOGY OF PHASE SEPARATED BLOCK COPOLYMER MELTS. H. Henning Winter, University of Massachusetts, Department of Chemical Engineering, Amherst, MA 01003, USA

Block copolymers with micro phase-separated structure in the molten state (above the melting and glass transition temperatures of both blocks) exhibit striking rheological behavior which determines their processing and their application. The 3-dimensional interface of the microphase separated structure strongly reduces the molecular mobility. Some systems have been reported to exhibit yield stress or gel behavior. However, most molten block copolymer melts seem to be liquids with long relaxation times. The long relaxation modes are determined by the interface while the short ones remain mostly unaffected by phase separation.

Large strains alter the phase separated structure with the effect that the molecular mobility increases by about one order of magnitude. Even then, the molecular mobility is so low that it prevents the recovery of the equilibrium structure. Therefore, processing flows effectively produce a microphase separated structures which strongly depend on strain and temperature history. The molecules are not altered by this process.

Rheological phenomena will be reviewed for systems with amorphous and with liquid crystalline short blocks.

V5.2

MICROEMULSION PERFORMANCE FLUIDS. Jan Bock, Corporate Research, Exxon Research & Engineering Co. Rt. 22 East, Annandale, NJ 08801

Microemulsions are thermodynamically stable mixtures of two immiscible fluids, such as oil and water, and one or more surfactants or cosurfactants. These systems have a rich micro-structure and phase behavior which can take the form of a variety of multi-phase and single phase oil- or water-continuous or bicontinuous fluids with unique and useful properties. The thermodynamic stability and ultra-low interfacial tension are reasons that microemulsions are used as displacement fluids for chemically enhanced oil recovery. In addition, the clarity, high solubilization capacity and high interfacial area suggest other uses for these "performance fluids".

The relationship between surfactant structure and the phase behavior and properties of microemulsions is the key to their design. Through the proper selection of surfactants, microemulsion phase continuity can be tailored for a variety of applications. Water-continuous microemulsions can be designed for water based lubricants or metal working fluids. Oil-continuous microemulsions are being studied in water containing fuels for reduced emissions. Bicontinuous microemulsions are proving useful for separating oil and water from refinery sludge. Proper surfactant selection also leads to high water and oil solubilization in microemulsions which in turn results in improved effectiveness in these applications.

V5.3

APPLICATIONS OF FERROELECTRIC LIQUID CRYSTAL (FLC) ELECTRO-OPTIC DEVICES. Noel A. Clark, University of Colorado, Department of Physics and Center for Optoelectronic Computing Systems, Boulder, CO 80309.

I will review the device applications of microsecond speed, surface bistable FLC electro-optic effects, emphasizing high information content displays, spatial light modulators for optical computing, and optical switches.

Work supported by NSF CDR 8622236 and ARO DAAL-03-86-K-0053.

V5.4

MICROSCOPIC PROCESSES IN MICROEMULSION POLYMERIZATIONS. Françoise Candau, ICS (CRM-EAHP) CNRS-ULP, 6 rue Boussingault, 67083 Strasbourg Cedex, France.

Microemulsions are attractive media for polymerization reactions, because they can lead under appropriate conditions to high molecular weight polymers entrapped within small-sized stable particles. We describe here some characteristics of the polymerization of hydrophilic monomers in microemulsions stabilized by anionic or nonionic surfactants. Incorporation of monomer in the starting systems induces a change of the curvature of the surfactant monolayer resulting in a percolative behavior. Eventually, the radius of curvature becomes so large that the globular configuration transforms toward a bicontinuous structure. A correlation is established between the mechanism of the particle growth during the polymerization and the percolative behavior of the micellar systems. The different steps of the building up of the polymer latex particles has been investigated.

V5.5

THE BEHAVIOR OF ELECTRIC FIELD DEPENDENT FLUIDS UNDER DYNAMIC STRESSES. Frank E. Filisko, The University of Michigan, Materials Science and Engineering, Ann Arbor, MI 48109.

Fluids whose rheological properties are a strong function of applied electric field were first observed in the 1940's by W. Winslow. In their simplest form these fluids are suspensions of a nonconductive particulate phase in a nonconductive liquid phase. For years these fluids were of intellectual curiosity only due to severe constraints imposed on them by the requirement for large amounts of absorbed water on the particulate phase. With the recent discovery of particulate systems which produce field active suspensions without adsorbed water, interest in these fluids has reawakened both commercially and intellectually. The strong possibility that the phenomenon is related to fundamental chemistry/physics implies that when adequately understood, materials can be synthesized or formulated to optimize desirable properties. Furthermore, characterizing and modeling the behavior of these fluids represents a considerable challenge in itself. In this presentation we will discuss recent developments in understanding molecular mechanisms responsible for the phenomenon as well as the rheological behavior of ER fluids in response to a dynamic stress.

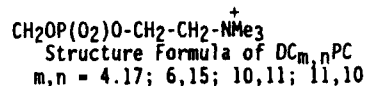
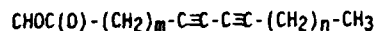
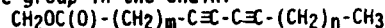
V5.6

DEPENDENCE OF THE LOCATION OF DIACETYLENIC GROUP ON THE SIZE OF THE VESICLES FROM 1,2 DIACYL PHOSPHOCHOLINES. Alok Singh¹, S. Marchywka² and R. Shashidhar^{1,2}

¹Bio/Molecular Engineering Branch, Naval Research Laboratory, Washington, D.C. 20375-5000; ²Geo-Centers Inc., Ft. Washington, MD 20744

It has been observed in our laboratory that molecules of 1,2bis(tricoso-10,12 diynoyl)-sn-Glycero-3-phosphocholine (DCg,gPC), a diacetylenic lipid, self-assemble into different structural forms when dispersed in water depending upon the methods of preparation and thermal cycling. Aqueous dispersion of this lipid upon sonication above the chain melting temperature produces small unilamellar vesicles (SUV's). The diameter of these SUV's can be determined by light scattering techniques (auto-correlation method). In order to understand the

specific role of the diacetylenic group on the macroscopic structures exhibited by the lipid dispersion, we have determined the hydrodynamic diameters of vesicles formed by aqueous dispersions of a series of lipids, viz, DC_{m,n}PC (see figure). These lipids have been so chosen that although the total chain length is the same for them, the position of the diacetylenic group within a chain is different. It is observed that the hydrodynamic diameter of the vesicles is dependent on the position of the diacetylenic group in the chain.



V5.7

FORMATION OF METAL COLLOIDS IN INVERSE MICELLES AND MICROEMULSIONS. J. P. Wilcoxon (Organization 1152), and R. Williamson (Organization 1843), Sandia National Laboratories, Albuquerque, NM 87185.

We describe the formation of a variety of metal colloids (e.g. Au, Pt, Ir, Pd, Rh, Re, Ni, Fe, and Hg) in nonionic and ionic surfactant systems. We show how the underlying microheterogeneous structure of micellar solutions can be manipulated to control the properties of colloids formed by either photochemical or chemical reduction of metal salts. Conversely, using the Au system as an example, we illustrate how the formation of structures in various regions of the phase diagram (e.g. a lamellar region, near a three phase body (bicontinuous region), or near a critical point can be used to gain information concerning the underlying structure. Such techniques as electron microscopy or small angle x-ray scattering which are basically sensitive only to the metal (high Z) structures can then be used to draw inferences concerning the precursor microemulsion structure. We demonstrate control of size, particle density, and structure by manipulation of the system temperature and composition and discuss the underlying reaction mechanism for photochemical (laser) reduction of metal salts in surfactant systems.

*This work performed at Sandia National Laboratories, Albuquerque, NM and supported by the U.S. Department of Energy under Contract No. DE-AC-04-76DP00789.

V5.8

STRUCTURE AND PROPERTIES OF RESORCINOL-FORMALDEHYDE GELS*, Stephan A. Letts, S. Buckley, and F.M. Kong, University of California, Lawrence Livermore National Laboratory, Livermore, California

Foams made from condensation polymerized resorcinol-formaldehyde (RF) gels are being considered for use in direct-drive laser fusion targets. Our goals are to produce a mechanically strong foam and determine the relationship between gel and foam properties. We are studying the gels by both scanning and transmission electron microscopy and viscometry to determine the structure of the materials and the effects of processing conditions.

RF gel shear properties were measured using an oscillatory viscometer. We studied the effects of both cure temperature and catalyst concentration (Na₂CO₃) on the solution viscosity. We have found that the viscosity of the solution of mixed reactants increased from a water-like viscosity of 0.01 poise to 100 poise in a time period of approximately 30 minutes. We believe that particles are formed during polymerization. As polymerization occurs the polymer phase separates into a colloidal suspension. Gelation results much later

(500 to 2,000 minutes) from aggregation of the particles into the "strings of pearls" morphology of the gels and dried foam.

We have also used freeze-fracture TEM to observe the morphology of particles in the solution and gel. We find a structure of aggregated spherical particles approximately 200 Å in diameter. This structure compares well with structures seen by SEM and TEM in supercritically dried foams.

*Work performed under the auspices of the U. S. Department of Energy by the Lawrence Livermore National Laboratory under contract number W-7405-ENG-48.

V6.1

STUDY OF POLYMER ADSORPTION PHENOMENA ON A SOLID SUBSTRATE* Mahn Won Kim, Exxon Research and Engineering Company Rt.22 East Annandale, NJ 08801

The phase retardation angle, $\Delta\phi$, as a function of the incident angle was measured to study adsorption and depletion of polymers near a solid substrate from a solution using an evanescent-wave ellipsometry technique. A lightly sulfonated ionomer dissolved in polar solvent displayed an appreciable interfacial adsorption layer, while the nonionic precursor in ethyl acetate exhibits a depleted concentration profile. The results are in good agreement with adsorption or depletion layer profiles obtained previously by other techniques, i.e. X-ray fluorescence for polymer adsorption and optical fluorescence evanescent wave technique for depletion.

Furthermore, the results show that ionomer adsorption from a relatively dilute polymer solution is strongly dependent on the sulfonate level of the ionomer and the nature of substrate. Depletion layer formation occurs at all sulfonate levels when the polymers are in contact with a hydrophilic surface. Except a lowest anionic charge, the ionomers are observed to preferentially adsorb onto a hydrophobic substrate.

*This work was done in collaboration with Drs. D. G. Peiffer, H. Hsiung, Th. Rasing Y. R. Shen, and Mr. W. Chen.

V6.2

MODULATED PHASES AND CHIRAL DISCRIMINATION IN AMPHIPHILIC MONOLAYERS AT THE WATER/AIR INTERFACE. David Andelman, School of Physics and Astronomy, Tel-Aviv University, Tel-Aviv 69978, Israel.

Recently, modulated phases of insoluble monolayers of fatty acids and phospholipids spread on the water/air interface have been observed by fluorescence microscopy experiments. We propose a theoretical explanation of this observation by including electrostatic (dipolar) interactions in the total free energy calculation for the monolayer. Dipoles can originate from two sources: neutral amphiphiles have a permanent dipole and charged amphiphiles have an induced one. Modulated phases are found to be stable in two different limits: close to the liquid-gas transition and at low temperatures. Several phases with stripe and hexagonal symmetry are predicted and the phase transition between them are calculated.

Phospholipids and other biological molecules have one or more chiral centers that are responsible for chiral discrimination and chiral specificity in biological processes. Langmuir monolayers of chiral amphiphiles offer one of the simplest realization of chiral mixtures because of their two-dimensional character. We calculate the chiral discrimination for a particular type of model molecule--an amphiphile with a tripodal head moiety. The

chiral discrimination depends on the intergroup interaction and tends to favor homochirality for electrostatic interactions and heterochirality for van der Waals interactions. Phase diagrams for racemic mixtures that form conglomerates and racemates are calculated.

V6.3

Wetting on Heterogeneous Solid Surfaces. S. Garoff, Dept. of Physics, Carnegie Mellon University, Pittsburgh, PA 15213.

Wetting and spreading of a fluid on a solid are highly complex phenomena. Real surfaces are both rough and chemically heterogeneous on many length scales and this non-ideal character has dramatic effects on the wetting properties of these surfaces. Using a variety of experimental and theoretical techniques, we have examined wetting and spreading on heterogeneous surfaces.

Submonolayer coverages of surfactant molecules on solid surfaces are often composed of islands of these molecules and thus produce surfaces with heterogeneous wetting properties. For these patchy surfaces (and most ambient surfaces), contact angle hysteresis and unsteady motion of the contact line are characteristic of the wetting behavior. A simple model of the energy of such a system has been used to explain these phenomena. This model bears resemblance to that describing the motion of domain walls past impurities in a ferromagnet, the origin of Barkhausen noise. To examine wetting in a more controlled fashion, wetting and spreading on surfaces with microfabricated heterogeneities have been experimentally probed. These experiments mimic many of the essential features on naturally heterogeneous surfaces. Finally, x-ray reflection measurements have been used to examine the effects of surface heterogeneity on the structure of the ultrathin wetting layers which extend beyond bulk menisci of fluids at rest or moving on a solid. We found that the roughness and heterogeneity of the solid surface manifest themselves in the roughness of the fluid/vapor interface of the film, in the irregularity of the terminating boundary of the film, and in the hysteretic pinning of that terminating boundary.

V6.4

STATISTICAL THERMODYNAMICS OF PHASE TRANSITIONS IN SURFACTANT MONOLAYER FILMS. R. S. Cantor, Department of Chemistry, Dartmouth College, Hanover, N.H. 03755.

In recent work [J. Chem. Phys. 90, 4431; 4440 (1989)], a lattice statistical mechanical method has been developed to predict structural and thermodynamic properties of fluid phases of surfactant monolayer films at the interface between water and a hydrophobic solvent. This approach incorporates translational and conformational degrees of freedom of the surfactants and accounts for chain/solvent/water mixing energy in nearest-neighbor approximation. In addition to the liquid-gas transition, a fluid-fluid phase transition is predicted to occur at high surface densities (σ). We examined the predicted σ -dependence of two structural order parameters: the solvent concentration profile and a measure of the degree of surfactant translational freedom. With increasing σ , the chains are predicted to react predominantly through loss of translational freedom, until virtually all translational freedom is lost at $\sigma=0.6$, although a considerable amount of solvent remains "trapped" within the flexible chains. Further compression results in a shift in the chain conformational distribution favoring extended conformations that pack more efficiently, thus ejecting previously trapped solvent and resulting in an internal condensation of chain segments - the high-density transition. The low-density transition can be viewed as a two-dimensional demixing of chains (retaining trapped solvent) and "free" solvent between the chains.

In monolayers of mixed chain length, the high density transition is predicted to exhibit azeotropy. If the chains differ sufficiently in length, heterogeneous azeotropy is predicted, the phase diagrams resembling those of bulk *n*-alkane/water mixtures in the critical region.

V6.5

X-RAY REFLECTIVITY OF A POLYMER MONOLAYER AT THE WATER/VAPOR INTERFACE. M.L. Schlossman, D.K. Schwartz, E. Kawamoto, G. Kellogg, P.S. Pershan (Department of Physics and Division of Applied Sciences, Harvard University, Cambridge, MA 02138), M.W. Kim and T.C. Chung (Exxon Corporation Research Laboratory, Annandale, NJ)

X-ray reflectivity of a co-poly 1,2-butadiene/butyl alcohol (50% random substitution) monolayer at the water/vapor interface was measured from the critical angle to $Q_z = 0.6 \text{ \AA}^{-1}$ (where Q_z is the transferred momentum normal to the interface). On a Langmuir trough, the monolayer was prepared at three different surface pressures, all in the high pressure saturated region of the isotherm. Preliminary analysis allows us to determine the width of the vapor/monolayer interface, the maximum electron density of the monolayer, and the position of that maximum from the vapor/monolayer interface. The width of the vapor/monolayer interface for the two lower pressures can be predicted from the theoretical form for thermal capillary waves using *in situ* measurements of the surface tension; for the highest pressure monolayer, the width of the interface is larger than predicted by capillary wave theory. The position of the maximum in the electron density moves further from the interface, away from the vapor, as the pressure increases. The maximum observed value of the monolayer electron density is approximately 10% larger than that of the bulk polymer.

Work supported by the National Science Foundation under grants NSF-DMR-88-12855 and NSF-DMR-86-14003.

V6.6

SURFACE ADSORPTION STUDIES BY OPTICAL SHG, Viola Vogel, C. Mullin, Y. R. Shen, Dept. of Physics, University of California, Berkeley, California 94720, Mahn Won Kim, Exxon Research and Engineering Company Rt. 22 East Annandale, New Jersey 08801

The high surface specificity of optical second harmonic generation (SHG) makes the technique to be an ideal tool for time resolved surface adsorption studies. SHG allows to measure directly the surface excess as well as the average orientation of the adsorbed molecules. In this talk, we will focus an adsorption process of surfactants of the air/liquid interface with the aim to prove theoretical models relating surface pressure and surface excess as well as to study orientational phase transitions.

V6.7

X-RAY REFLECTIVITY STUDIES OF SOLID/LIQUID CRYSTAL INTERFACES. B.M. Ocko, Physics Department, Brookhaven National Laboratory, * Upton, NY 11973.

Liquid crystals exhibit diverse wetting phenomena since both orientational as well as positional order can be induced by an interface at temperatures where the bulk phase is disordered. For the present study the x-ray reflectivity technique, which is directly related to the ordering along the surface normal direction, has been extended to the liquid/solid interface. X-ray reflectivity measurements have been carried out at the National Synchrotron Light Source. Studies have been conducted in the isotropic phase of the cyanobiphenyl compounds (10CB, 11CB, 12CB) at alkylsiloxane coated silicon surfaces (C10, C12, C18). These results indicate that the (Smectic A) layering transitions do not depend on the length of the alkylsiloxane hydrocarbon chain. For 12CB three distinct layering transitions are observed, whereas five transitions are observed at the air interface. In addition, the layering transition temperatures are shifted

with respect to the transitions at an air interface. The measured reflectivities have been fit to simple density profiles and the smectic order parameters for the first two layers are consistent with mean field theory.

References

1. B.M. Ocko, A. Braslau, P.S. Pershan, J. Als-Nielsen, and M. Deutsch, Phys. Rev. Lett. vol. 57, p. 94 (1986).

* This work was supported by the Division of Material Research, U.S. Department of Energy, under contract No. DE-AC02-76CH00016.

V6.8

X-RAY REFLECTIVITY STUDIES OF POLYELECTROLYTE ADSORPTION AT THE SOLUTION-VAPOR INTERFACE. M.L. Schlossman, E.H. Kawamoto, D.K. Schwartz and P.S. Pershan (Department of Physics and Division of Applied Sciences, Harvard University); M.W. Kim and D. Peiffer (Exxon Corporate Research Laboratory)

Synchrotron X-ray reflectivity studies of the vapor-liquid interface of polyelectrolyte solutions were carried out at Brookhaven National Laboratory. Several concentrations of dilute solutions (0.1-5 wt. %) of co-poly (styrene/rubidium-sulfonated styrene [8.4% random substitution]) in dimethyl sulfoxide (Rb-SPS; molecular weight 100 K) and co-poly (vinyl pyridine/brominated vinyl pyridine [65.8% r. s.]) in water (Br-PVP; MW 143 K) were prepared. X-rays were scattered from the surfaces of these solutions, and the specularly reflected intensity measured over 9 orders of magnitude from the critical angle to $Q_z = 0.5 \text{ \AA}^{-1}$. Compared with the Fresnel reflectivity (from an idealized sharp interface between vapor and a homogeneous phase of the same density as the bulk solution), the Br-PVP system exhibits an enhancement of reflected intensity, whereas the Rb-SPS system exhibits a diminished reflectivity. Data from the Br-PVP solutions indicate a 20% enhancement of surface electron density over that of the bulk in a region $\sim 10 \text{ \AA}$ from the surface, whereas the Rb-SPS data indicate a depletion of interfacial electron density.

Work supported by the National Science Foundation under grants NSF-DMR-88-12855 and NSF-DMR-86-14003.

V6.9

NRA STUDIES ON THE INTERFACE FORMATION IN POLYMER MIXTURES BELOW THE CRITICAL POINT. Ulrich Steiner, Kumar Chaturvedi¹, Omer Zak, Georg Krausch², Günther Schatz² and Jacob Klein. Department of Polymer Research, Weizmann Institute, Rehovot 76100, Israel.

Mixtures of polystyrene (hPS) and deuterated polystyrene (dPS) are weakly incompatible and thus characterized by a small interaction parameter χ . Upon heating a bilayer of hPS and dPS to a temperature below, but close to the critical temperature of the mixture, the polymers will not interdiffuse freely, but a finite interfacial region will be formed. Based on a known $\chi \sim 10^{-4}$ the equilibrium width is expected to be of a few tens of nm.

Nuclear Reaction Analysis (NRA), a profiling technique which employs the $^2\text{H}(^3\text{He}, ^4\text{He})^1\text{H}$ reaction has been used to study the interfacial structure of a bilayer of hPS and dPS. This technique has a resolution which is significantly higher than that of comparable ion-beam techniques which use elastic scattering; this allows us to measure the structure with ca. 10nm resolution.

Using this technique, we measured directly the composition profile at the interface of the hPS/dPS bilayer. We have shown, that it grows with time to some limiting interfacial width at

sufficiently long times. The variation of the interfacial width with temperature is in fair agreement with the prediction of mean field theories.

We are currently investigating the development of the interface width with time and are also using our approach to characterize the coexistence features of this system. Results will be given and compared to theoretical predictions.

1. FBLJA World Lab. Project, CERN, CH-1211 Geneva Switzerland.
2. Dept. of Physics, University of Konstanz, D-7750 Konstanz, FRG.

V7.1

TWO-COMPONENT GRAFTED POLYMER LAYERS T. A. Witten University of Chicago, Chicago IL 60637 and S. T. Milner, Exxon Corporate Research, Annandale NJ 08801.

Polymers in a liquid often have strong effects on liquid-liquid and liquid-solid interfaces. In this talk we consider the distinctive effects of polymers attached densely to such an interface *by one end*, so that each chain is obliged to elongate substantially. Such dense grafting may be attained by adsorbing end-functionalized polymers [H. T. Taunton, C. Toprakcioglu, L. J. Fetters, and J. Klein *Nature* 332 712 (1988)] or copolymers [S. Granick, S. Patel, and M. Tirrell, *J. Chem. Phys.* 85 5370 (1986)] to a solid surface, or at a polymer-polymer interface [D. J. Kinning, K. I. Winey and E. L. Thomas, *Macromolecules* 21 3502 (1988)]. The stretched polymers endow the grafted layer with considerable stored free energy, making it resist bending, compression and the entry of unattached chains.

In this talk we consider the effects on this high-energy grafted layer when two immiscible grafted polymers are present. We discuss how the segregation of the two species is influenced by the grafting constraint and by their relative molecular weights.

V7.2

LONG-RANGE INTERACTIONS AND RIGIDITY OF POLYMERS AND SURFACES. Mehran Kardar, Physics Department, Massachusetts Institute of Technology, Cambridge, MA 02139.

We examine the effects of long-range interactions, e.g. Coulomb repulsions, in polymers and surfaces. An important consequence of such interactions is a strong resistance to bending, which in many cases leads to macroscopically flat morphologies. Thermal fluctuations around the flat shape leads to a characteristic roughness exponent. Even screened Coulomb interactions can result in large bending energies. For membranes we calculate the dependence of the effective bending energy, and the resulting persistence length, on the screening distance. This amounts to extending the concept of the "Odijk length" from polymers to surfaces.

Y. Kantor and M. Kardar, *Europhys. Lett.* 9, 53 (1989).

V7.3

STATISTICAL BEHAVIOR OF ELASTIC MEMBRANES. S. Leibler, Service De Phys. Theorique, C.E.N.-Saclay, F-91190 Gif-Sur-Yvette, Cedex France.

Polymerized membranes are two-dimensional objects built with molecules tightly bound together. Simple examples are given by phospholipid bilayers with crosslinked molecules, thin polymeric films or networks of proteins forming permanent or temporary structures in a cell. Recently, these systems have attracted attention of theoretical physicists because of their rich thermodynamic behavior. When the elastic constants of a polymerized membrane (e.g. the bending modulus) are of order $k_B T$, the thermal fluctuations can induce various statistical phenomena such as crumpling transitions, buckling

transitions, surprising shape transformations, etc. We shall present here a short review of these phenomena, and describe some recent analytical and numerical results concerning the polymerized membranes. We shall also suggest some possible directions for further experimental studies as well as mention several possible applications for these systems.

V7.4

DEHYDRATION OF PROTEIN POLYMERS IN CONCENTRATED NEMATIC SOLUTIONS.¹ Reinhard Hentschke and Judith Herzfeld, Department of Chemistry, Brandeis University, Waltham, Massachusetts 02254-9110.

Protein fibers (e.g., actinfilaments, microtubules, and sickle cell hemoglobin fibers), formed by the reversible association of quasispherical protein monomers, contain substantial solvent. At high concentrations, solutions of these fibers become non-ideal due to interactions between the elongated particles. One manifestation of this non-ideality is the spontaneous alignment of the fibers. Model calculations, involving simple intra- and inter-aggregate interactions leading to polymerization and alignment, agree well with osmotic pressure measurements of sickle cell hemoglobin solutions in the region of the phase transition. However, at higher concentrations the theory cannot fit the experimental data unless solvent can be squeezed out of the fiber under stress. We find that a linear potential for fiber dehydration gives osmotic pressures results consistent with the experimental data. Under these conditions, substantial fiber dehydration occurs with increasing protein concentration beyond the alignment transition. This shows that particle interactions sufficient to cause alignment are also sufficient to squeeze significant amounts of solvent out of sickle cell hemoglobin fibers.

1. Supported by NIH grant HL-36546 and a fellowship to RH from the Deutsche Forschungsgemeinschaft.

V7.5

APPLICATIONS OF SCALING THEORIES FOR POLYMER ADSORPTION TO PROTEIN PARTITIONING IN TWO-PHASE AQUEOUS POLYMER SYSTEMS. Nicholas L. Abbott, Daniel Blankschtein, T. Alan Hatton, Department of Chemical Engineering, Massachusetts Institute of Technology, Cambridge, MA 02139 USA.

The ability of proteins to distribute unevenly between the phases of biphasic aqueous polymer systems is well established experimentally. In particular, the importance of protein size, phase-forming polymer size and polymer concentration has been previously measured.

Despite this large body of experimental data, a relatively poor understanding of molecular mechanisms causing the observed partitioning exists. An alternative to recent statistical-mechanical and virial expansion type models to describe characteristic features of protein partitioning in two-phase aqueous polymer systems is proposed. The new approach applies scaling concepts developed in polymer physics to the interaction of polymers with colloidal particles (i.e., proteins) to provide a computationally-simple yet molecular thermodynamic description of the protein partitioning problem. The dimensional arguments capture the universal features of polymer solution behavior in simple analytic expressions, and appear capable of describing characteristic features of the experimentally measured protein partition coefficients.

V7.6

PHASE BEHAVIOR OF NONIONIC AMPHIPHILE AND NONIONIC POLYMER IN AQUEOUS SOLUTION. Klaus R. Wormuth, Exxon Research and Engineering Co., Route 22 East, Clinton Township, Annandale, NJ 08801.

A relatively unexplored area of research, the

phase behavior of polymer and surfactant mixtures, is systematically examined. Nonionic amphiphile ($C_{12}E_6 = CH_3(CH_2)_{11}[O(CH_2CH_2)_6OH]$) mixed with nonionic polymer (polyethylene oxide) present richly varying phase behavior as a function of temperature and composition when the molecular weight of the amphiphile and polymer are changed. As the amphiphile is stretched from the weakly-associating alcohol $C_{12}E_6$ to the strongly-associating surfactant $C_{18}E_6$, miscibility with polymer is greatly reduced. A qualitative description of the phase behavior is achieved by treating the surfactant micelle as a polymer, and treating polymer-polymer interactions with a model based on Flory-Huggins solution thermodynamics.

V7.7

LAYERED LIQUID CRYSTALS AND SUPERCONDUCTORS: THE COMPLETE STORY. G. Srajer, R. Pindak, J. W. Goodby, M. A. Waugh, AT&T Bell Laboratories, Murray Hill, NJ; and J. S. Patel, Bell Communications Research, Redbank, NJ.

The application of a twist distortion to a layered, smectic-A liquid crystal phase is analogous to the application of a magnetic field to a superconductor¹. In the latter case, the magnetic field is either expelled (type-I) or incorporated in a lattice of flux lines (type-II). Until now, this analogy has been only partially fulfilled, because all known smectic-A materials displayed type-I behavior.

In this talk we report high-resolution x-ray and optical data on well aligned samples which unambiguously confirm the existence of a smectic-A phase exhibiting type-II behavior, that is, rather than expel twist, the locally layered phase incorporates it in a macroscopic helical structure involving an array of defects which are, presumably, screw dislocations. The resultant new phase is referred to as a smectic-A*². Our optical studies confirm the helical structure since aligned samples selectively reflect circularly polarized light. The pitch of the helix is $\sim 0.4 \mu m$, obtained by measuring the wavelength of the reflected light. Furthermore, x-ray measurements demonstrate that, firstly, the layer correlations extend, at least, 4000 Å and, secondly, the layers are oriented parallel to the helical axis. Finally, detailed reciprocal space scans reveal that the scattering from the A* phase is consistent with that expected from the "Twist Grain Boundary" (TGB) phase recently proposed by Renn and Lubensky³. The TGB phase is the liquid crystal analog of the superconductor Abrikosov flux lattice.

1. P.G. de Gennes, *Solid State Commun.* **10**, 753 (1972).
2. J.W. Goodby, et al. *Nature* **337**, 449 (1989).
3. S.R. Renn and T.C. Lubensky, *Phys. Rev. A* **38**, 2132 (1988).

V7.8

THERMAL PROPERTY EVOLUTION TOWARD EFFECTIVELY TWO-DIMENSIONAL SUBSTRATE-FREE SYSTEMS.* R. Geer and C.C. Huang, Dept. of Physics, University of Minnesota, Minneapolis, MN 55455; R. Pindak and J.W. Goodby, AT&T Bell Laboratory, Murray Hill, NJ 07974.

A high-resolution free-standing liquid-crystal film calorimeter has been developed to investigate the temperature dependence of the heat capacity of substrate-free liquid-crystal films. We have observed a clear evolution of the heat-capacity anomaly from the films of the liquid-crystal compound 650BC as the film are reduced in thickness from 20 to 4 molecular layers near their bulk smectic-A-hexatic-B transition. Here 650BC refers to n-hexyl-4'-n-pentylxybiphenyl-4-carboxylate. For the films with thickness between 5 and 20 molecular layers, a second transition can be resolved about 0.5 K above the main transition temperature. We propose that the higher-temperature transition signals an ordering of the surface layers of the films while the lower-temperature transition involves an ordering of the interior layers. In contrast, the 4-layer films show a single and sharp heat-capacity peak (FWHM = 200 mK) without thermal hysteresis. This heat-capacity anomaly can be described by a cusp-like power-law expression. Experimentally, for the first time we demonstrate the capability to measure heat-capacity anomaly in an effectively

two-dimensional substrate-free system. The theory on 2D XY transitions predict no sharp anomaly at the transition temperature. Our experimental results on 4-layer film disagree with this theoretical prediction.

*Supported in part by a NSF grant

V7.9

DYNAMIC RIGIDITY PERCOLATION IN INVERTED MICELLES. L. Ye, D.A. Weitz, Ping Sheng, S. Bhattacharya, J.S. Huang and M.J. Higgins, *Exxon Research and Engineering Co., Rt. 22E, Annandale, NJ 08801*.

We report the unusual viscoelastic properties of inverted micelles of AOT in decane. The volume fraction of the micelles, ϕ , can be varied, while their radius remains fixed. There is a weak, short-range attractive interaction between the micelles, and the characteristic times scale of this interaction, τ_c , determines their behavior. On time scales long compared to τ_c , their diffusive motion ensures that the micelles are dynamically dispersed in the surrounding oil. By contrast, on time scales short compared to τ_c , the micelles form instantaneous, random clusters, which at sufficiently high ϕ , form a connected network. These time-dependent correlations result in a surprising viscoelastic behavior in this relatively simple fluid. We account for the ϕ -dependence of the viscoelastic properties by means of a static effective medium approximation for an elastic composite. We account for the frequency dependence of the viscoelastic properties through the parameters describing the micelle phase. The variation of these parameters also reflects the frequency dependence of the correlations between the micelles. At high frequencies, the micelle phase exhibits a solid-like behavior which supports shear at $\phi > 0.2$. This high-frequency rigidity of the surfactant micelle phase exhibits power-law scaling with ϕ . We interpret this as dynamic rigidity percolation.

V7.10

PHASE SEPARATION IN A LIPID/WATER/UREA MICELLAR SYSTEM. Bruce L. Carvalho, Department of Materials Science and Engineering, M.I.T., Cambridge, MA 02139; Sow-Hsin Chen, Department of Nuclear Engineering, M.I.T., Cambridge, MA 02139; and John S. Huang, Exxon Research and Engineering Company, Annandale, NJ 08801

It is well known [1] that the dioctanoylphosphatidylcholine (diC8PC)/water system exhibits liquid-liquid phase separation with an upper consolute temperature at around $T_c = 46^\circ C$. We have found [2] that the consolute temperature can be dramatically lowered by the addition of a small amount of urea. The lowering of T_c is found to be a linear function of the mole fraction of added urea. We compare the measured cloud point curves at various urea concentrations with a recent thermodynamic theory [3]. The three basic parameters of this theory are: $\Delta\mu$, the free energy advantage of micellar growth; C , an effective free energy of monomer-monomer interaction; and γ , the ratio of the effective monomer volume to the volume of a water molecule. This theory can be made to fit the cloud point curves with a set of urea dependent parameters, $\Delta\mu$, C and γ . We also use small angle neutron scattering to obtain $\Delta\mu$ and static light scattering techniques to extract $\Delta\mu$, C and γ for the system diC8PC/heavy water/[urea]=1 Molar. These two independent measurements serve as a test of this recent theory.

- [1] Tausk, R. J. M.; Overbeek, J. Th. G., *Biophys. Chem.*, **2**, 53(1974).
- [2] Carvalho, B. L.; Briganti, G.; Chen, S. H., *J. Phys. Chem.*, **93**, 4282(1989).
- [3] Blankenshtein, D.; Thurston, G. M.; Benedek, G. B., *Phys. Rev. Lett.*, **54**, 955(1985).

THE STRUCTURE OF THE BORDER LAYER BETWEEN GEL AND WATER.
Zenon Bochyński, Non-Crystalline Materials Division,
Institute of Physics, Adam Mickiewicz University, 60-780
Poznań 2, Grunwaldzka 6, Poland.

A system of silica gel-water of different degree of filling the gel structure with water molecules was studied. A newly elaborated method of X-ray diffraction analysis was applied. This method is based on stage approximation of the following structures, by differentiation of the radial distribution functions:

- the structure of pure silica gels type $\text{SiO}_2\text{-R}_2\text{O}_3$,
- the structure of hydrated silica gels type $\text{SiO}_2\cdot x\text{H}_2\text{O-R}_2\text{O}_3$,
- the structure of the border layer between water and silica gel type $\text{SiO}_2\text{-H}_2\text{O-R}_2\text{O}_3$, and
- the structure of pure water $\text{H}_2\text{O-R}_2\text{O}_3$.

The changes in structural parameters of gels dependent on the refinement of the gels grains and the degree of thermal ageing were determined. In the next step, the structure and character of the border sorption layer formed in the process of surface filling with water was investigated. The structure of the border layer in the process of formation of subsequent water absorption layers was analyzed by the way of stage saturation. Structural parameters of the layers of water absorbed in the gels as well as of the locally ordered/unbound/complexes of pure water, were determined. The obtained structural parameters enabled us to construct structural models of silica gels and the border layer between gel and water.

V8.1

INTERACTION BETWEEN GRAFTED POLYMERIC BRUSHES.
Gary S. Grest and Michael Murat, Exxon Research and Engineering Company, Annandale, NJ 08801.

Equilibrium properties of end-grafted polymers constrained between parallel plates as well as the force between such plates are studied using molecular dynamics simulations. Polymers consisting of 10 to 150 monomers are grafted randomly at an average surface coverage of ρ_a onto one of the two parallel plates immersed in a good solvent. ρ_a is taken to be large enough to induce overlap and consequent stretching of the chains. For infinite separation of the plates and intermediate values of ρ_a , we find a monomer density profile in reasonable agreement with the parabolic form predicted by the self consistent field theory of Milner *et al*¹. We also find that the density of the free ends is non-zero everywhere within the brush, in agreement with that theory. For separations smaller than the contact separation, we monitor these properties as well as the interpenetration of the brushes and the force between the plates. We find that the amount of interpenetration can be described by a simple scaling function for different values of N and ρ_a . The force vs. separation curves agree well with the experimental results of Taunton *et al*² and with the predictions of both the scaling³ and self consistent field¹ theories.

1. S. T. Milner, T. A. Witten and M. E. Cates, *Macromolecules* **21**, 2610 (1988).
2. H. J. Taunton, C. Toprakcioglu and J. Klein, *Macromolecules* **21**, 3336 (1988).
3. P.-G. de Gennes, *C. R. Acad. Sci. Paris* **300**, 839, (1985).

V8.2

EFFECT OF MOLECULAR WEIGHT ON THE HIGH FREQUENCY BULK MODULUS, OF WELL CHARACTERIZED POLY(DIMETHYLSILOXANE) POLYMERS. A. Shaffer*, J. R. Emery*, D. Durand*, M. Gottlieb**, and G. Gorodetsky**.

*Université du Maine, Le Mans, France, and
**Ben-Gurion University, Beer-Sheva, 84105, Israel

Comparison of the high frequency bulk modulus of five well characterized linear poly(dimethylsiloxane) (PDMS) polymers indicates that the bulk modulus is strongly affected by intermolecular spacing which is a consequence of polymer-polymer interaction. The objective of

this study was to shed some light on the bulk modulus-structure relation in polymers of which very little is known.

The bulk modulus was evaluated from ultrasonic wave velocity measurements (at 8MHz using the conventional pulse method(1)), density measurements, and published data on the PDMS shear modulus values at this frequency (2).

The bulk modulus was observed to go through a maximum at the critical molecular weight for chain entanglements, and then decrease as the molecular weight is further increased. Density was also observed to exhibit the same behaviour as a function of molecular weight. It is suggested that because of the high tangled nature of the polymer structure, beyond the critical molecular weight for entanglements, close packing is impossible. At higher molecular weights because of imperfect chain packing, molecular forces, which fall off rapidly with increasing molecular separation are account for the observed phenomenon. The magnitude of polymer packing structure with respect to its molecular weight can be estimated from the known values of specific volume or density (3).

1. Mason W. P., *Physical Acoustics- Principles and methods*, Vol 1-Part A, (Academic Press, N.Y. 1964)
2. Barlow A. J., Harrison G., and Lamb J., *Poc. Roy. Soc. Ser., A*, **282** (1964)
3. Broadhurst M. G., and Mopsik F. L., *J. Chem. Phys.*, **52**, 3634 (1970)

V8.3

SURFACE MODES ON CONCENTRATED POLYMER SOLUTIONS AND GELS.
James L. Harden and Phillip A. Pincus, Materials Department, College of Engineering, University of California, Santa Barbara, CA; and Harald Pleiner, FB Physik, Universität Essen, D4300, Essen 1, F.R.G.

We present a coupled two-fluid model for surface modes on concentrated polymer solutions and swollen gels. This model is used to derive a surface mode dispersion relation and surface amplitude autocorrelation function in the limit of strong coupling. We discuss the effect of chain diffusion and surface tension on the nature of these modes.

V8.4

MECHANICAL PROPERTIES OF CROSSLINKED SEMIDILUTE POLYMER SOLUTIONS NEAR AND FAR FROM THE GELATION THRESHOLD.
C. Allain, Lab. FAST Bat. 502, Campus Universitaire 91405 Orsay Cedex FRANCE; L. Limat, Lab. Physico-chimie Théorique, ESPCI 10 rue Vauquelin 75231 Paris Cedex FRANCE; and L. Salomé, CRPP, Château Brivazac 33600 Pessac FRANCE

When a polymer solution is mixed with a crosslinker solution, various phases are formed depending on the respective concentrations of the polymer and of the crosslinker: sols, gels, precipitates or inhomogeneous gels. We have investigated the rheological properties of the sols and gels formed at a constant concentration in polymer (Hydrolysed Polyacrylamide) for various concentration in crosslinker (Chromium III). Using a magnetic levitation sphere rheometer, we have measured the variations of the steady state zero shear viscosity and of the steady state linear elastic modulus. A detailed spectroscopic study¹ has allowed us to determine the number of crosslinks formed in the same range of polymer and crosslinker concentrations.

In the vicinity of the gelation threshold, the divergence of the viscosity and the increase from zero of the elastic modulus have been interpreted in terms of critical behaviour. The values of the exponents have been found in good agreement with the predictions of the scalar percolation model². The prefactors and the width of the critical region have been interpreted in relation with the gelation of semidilute polymer solutions.

Finally, the variation of the viscosity in the limit of the very low crosslink concentrations has been related to the concentration in crosslinks at the critical point.

¹ C. Allain and L. Salomé, in "Biological and Synthetic Polymer Networks", Elsevier Applied Science; Amsterdam (1988)

² C. Allain and L. Salomé, *Macromol.*, **20**, 2957 (1987)

V8.5

"AGGREGATION IN BLOCK COPOLYMER SOLUTIONS. M. Olvera de la Cruz, Department of Materials Science and Engineering, Northwestern University, Evanston, IL. 60208.

The ability to produce block copolymers has led to new materials with unique properties. The chemical connectivity of incompatible blocks forces segregation to occur at distances of the order of the block sizes. In block copolymer melts, the segregated domains form periodic ordered structures termed microphases. Most block copolymers are strongly incompatible. In such cases, in order to ensure equilibrium microphase separated samples, the microphases are prepared from solution. Microphase separation in semidilute solutions of block copolymers in nonselective good solvents is analyzed. The solvent effects on the thermodynamics in the weak segregation limit are discussed. The transitions between microphase morphologies as a function of block copolymer concentration are studied. The analysis is extended to describe local aggregation in randomly cross linked A and B chains in non-selective good solvent.

V8.6

MICELLIZATION OF TRIBLOCK COPOLYMERS WITH POORLY SOLVATED END BLOCKS N.P. Balsara, M. Tirrell, T.P. Lodge, University of Minnesota, Minneapolis, MN

The present work is aimed at exploring the possibility of micellization of ABA triblock copolymers in solvents that preferentially dissolve the middle block. Spherical micelles in these systems would consist of a core containing A blocks, surrounded by loops of B blocks. The existence of this microstructure has not yet been proved. In fact, the absence of micelles in these systems has been reported by a number of workers. Dynamic light scattering measurements on solutions of polyvinylpyridine-polystyrene-polyvinylpyridine in toluene indicate that these systems can form micelles. It is found that the length of the middle block (polystyrene) has a large influence of the micellization characteristics.

V8.7

X-RAY REFLECTION AND SCATTERING STUDIES OF THE WATER-VAPOR INTERFACE. D.K. Schwartz, M.L. Schlossman, E. Kawamoto, G. Kellogg, P.S. Pershan (Department of Physics and Division of Applied Sciences, Harvard University, Cambridge, MA 02138), and B. M. Ocko, (Department of Physics, Brookhaven National Laboratory, Upton, NY 11973)

To test predictions relating the RMS width of the water-vapor interface to thermally-excited capillary waves,¹ we have measured both the x-ray reflectivity from the water surface and diffuse scattering away from the specular reflection. Surface tension γ and water cleanliness were measured *in situ* on a Langmuir trough in a vapor-controlled environment. The prediction for the RMS surface roughness is $\sigma^2 = (k_B T / 2\pi\gamma) \ln(q_{\max}/\Delta q)$, where q_{\max} is an upper cutoff of the order of $\pi/(\text{molecular radius})$ and Δq is determined by the spectrometer resolution. We measured this roughness by means of specular reflectivity at three values of Δq and obtained excellent agreement with theory with the single free parameter $\pi/q_{\max} = 1.45 \text{ \AA}$. By comparison, the radius of the water molecule is 1.93 \AA . We measured the scattering at wave-vectors corresponding to these capillary waves and obtained line shapes in excellent agreement with theory with no free parameters.

¹A. Braslau, P. S. Pershan, G. Swislow, B. M. Ocko, J. Als-Nielsen, *Phys. Rev. A*, Vol. 38, p. 38, 1988.

Work supported by the National Science Foundation under grants NSF-DMR-88-12855 and NSF-DMR-86-14003.

V8.8

X-RAY STUDIES OF CYTOCHROME C MONOLAYERS BOUND TO LANGMUIR-BLODGETT FILMS AND SELF-ASSEMBLED MONOLAYERS. J.M. Pachence, S. Amador, and J.K. Blasie, Chemistry Department, 231 South 34th Street, University of Pennsylvania, Philadelphia, PA 19104.

We have recently developed methods for deriving the profile structure of Langmuir-Blodgett (LB) lipid films having one to five bilayers from x-ray diffraction data. For example, we have employed these techniques to determine the location of a monolayer of cytochrome c, an important electron transfer protein, either electrostatically or covalently bound to the surface of various LB lipid films via nonresonance x-ray diffraction. Furthermore, the location of the heme-Fe atoms within the electron density profile of the cytochrome c/LB lipid film was indicated to $\pm 3 \text{ \AA}$ accuracy using resonance x-ray diffraction. To further characterize this system, optical linear dichroism was used to determine the orientation of the cytochrome c heme group relative to the plane of the surface.

Cytochrome c molecules have also been bound covalently to self-assembled monolayers of trichlorosilylundecyl thiol. We have underway x-ray scattering and electron transfer kinetics experiments on these cytochrome c monolayers and on the complexes they form with associated electron transfer proteins. X-ray interferometry techniques using monolayers of these protein complexes bound to the surfaces of synthetic inorganic multilayer substrates are under investigation as a means of directly determining the structure of the protein complexes.

V8.9

DOMAIN SHAPE INSTABILITIES IN A TWO-DIMENSIONAL BINARY FLUID MIXTURE: EPIFLUORESCENCE MICROSCOPY AND DIGITAL IMAGE ANALYSIS. M. Seul and M. J. Sammon, AT&T Bell Laboratories, 600 Mountain Ave., Murray Hill, NJ 07094.

A series of domain shape instabilities in a binary fluid mixture of surfactants confined to an air-water interface has been investigated by means of epifluorescence microscopy. The formation of domains of finite extent in this surfactant monolayer is the result of a competition of short-range attractive (vdW) and long-range repulsive (dipole-dipole) interactions which leads to the appearance of modulated phases in a variety of condensed matter systems. Digital image processing techniques have been employed to perform a spectral analysis of domain wall configurations, revealing characteristic signatures of the shape instabilities and permitting the study of shape fluctuations. The nature of the instabilities is discussed in light of current theoretical models.

V8.10

X-RAY REFLECTIVITY OF A LONG CHAIN FATTY ACID MONOLAYER AT THE WATER/VAPOR INTERFACE. M.L. Schlossman, D.K. Schwartz, E. Kawamoto, G. Kellogg, P.S. Pershan (Department of Physics and Division of Applied Sciences, Harvard University, Cambridge, MA 02138).

X-ray reflectivity of Lignoceric acid ($\text{CH}_3(\text{CH}_2)_{22}\text{CO}_2\text{H}$) at the vapor/water ($\text{pH} = 2$ using HCl) interface was measured at room temperature from the critical angle to $Q_z = 0.6 \text{ \AA}^{-1}$ (where Q_z is the transferred momentum normal to the interface). A measurement of surface pressure vs. area/molecule (from 17 to $30 \text{ \AA}^2/\text{molecule}$) exhibits one flat region in the isotherm. The reflectivity, which is related to the derivative of the electron density normal to the interface, was measured throughout the isotherm. Preliminary analysis allows a determination of the electron density in the tail-region, the overall thickness of the monolayer, and the electron density in the head group. Changes in the electron density in the head group as a function of pressure were observed. The overall thickness of the monolayer increases with increasing pressure. Perhaps the most striking observation is that, for the highest pressures, the head group region gets thicker, indicating that the head groups rearrange normal to the interface.

Work supported by the National Science Foundation under grants NSF-DMR-88-12855 and NSF-DMR-86-14003.

V8.11

STUDY OF FATTY ACID MONOLAYERS DEPENDENCE ON CATIONIC INTERACTIONS BY ELLIPSOMETRY Mahn Won Kim, Exxon Research and Engineering Company Rt. 22 East Annandale, NJ 08801, and Bryan B. Sauer, Hyuk Yu, Mehran Yazdani and George Zografis, Dept. of Chemistry and School of Pharmacy, Univ. of Wisconsin, Madison, WI 53706

Fatty acids monolayers with chain lengths of 15, 16, 18, and 22 carbons were studied on aqueous substrates containing hydrochloric acid, cadmium chloride, and lead chloride using a phase modulated ellipsometry instrument. The change in ellipsometric phase angle $\delta\Delta$ was found to be linearly dependent on chain length with the same coefficient for all three cations whereas the magnitude of $\delta\Delta$ was shown to be different. The proportionality constant with respect to chain length was modeled in terms of the refractive index contributions of the hydrocarbon tails, giving thicknesses in agreement with those obtained by other techniques. The magnitudes of $\delta\Delta$ were analyzed in terms of film refractive index anisotropy, whereby our results were shown to be consistent with anisotropic refractive indices obtained by other methods. They were also examined relative to pH values and cation concentration, and the results are discussed in terms of a refractive index increase due to the interaction of carboxylates with divalent cations.

V8.12

ELECTROHYDRODYNAMIC FLOW DYNAMICS IN THICK LIQUID CRYSTAL CELLS. David H Van Winkle* and Jit Gurung[†], Department of Physics, Florida State University, Tallahassee FL 32312, and Rand Biggers, Naval Coastal Systems Center, Panama City FL 32407

High voltage, low frequency AC electric fields are used to induce hydrodynamic flow in 1.3 cm diam. X .63 cm thick cylindrical cells, of methoxy-benzilidene-n-butylaniline (MBBA). MBBA has a negative dielectric anisotropy and a positive conductivity anisotropy. In thin liquid crystal cells, the effects of an AC electric field on the sample are reasonably well understood. Below a critical frequency, flow cells which are Williams domains, form above a critical voltage. Above that frequency, molecular reorientation without flow develops above a critical electric field. When flow cells are established the thermal transfer rate of the samples is enhanced. This enhancement has been studied for driving frequencies ranging from 20 to 720 Hz, with maximum enhancement observed at 130 Hz. Both the threshold voltage for onset of flow and the flow patterns as a function of voltage and frequency have been studied using image processing techniques. Results correlating the optical observations with the previously measured effective thermal conductivity enhancement will be presented.

* Supported by an ASEE-ONR Summer Faculty Research Fellowship and the Center for Materials Research and Technology at Florida State University.

† Supported by an NSF Undergraduate Summer Research Fellowship, permanent address Davidson College, Davidson, NC 28036.

V8.13

Radial Creeping Flow Between Parallel Disks of Rod-Like Nematic Liquid Crystals: Textures and Instabilities. Alejandro D. Rey, Department of Chemical Engineering, McGill University, Montreal, Quebec, Canada H3A 2A7.

Three similarity solutions of the Leslie-Ericksen equations for low molar mass rod-like nematics are obtained for pressure-driven radial out-flow between concentric parallel disks. There are two competing hydrodynamic effects: extensional flow (strongest at the centerline) and shear (strongest near the bounding surfaces). At low pressure drops the in-plane orientation is stable and the centerline orientation is in the direction of flow. The relaxation of this mode after cessation of flow is of the order of seconds. As the pressure drop is increased an orientation instability sets in. The elongational torques twist the material out of the flow plane; right and left rotations are possible. The mechanism is analogous to the magnetic Fredericksz transition with the character of a second order phase transition. Since the elongational torques weaken as distances from the axis of the disks increase there is a critical radius at which in-plane and out-of-plane orientational modes meet. The relaxation after cessation of flow is of the order of minutes for the out-of-plane modes. There is a second critical pressure drop at which the orientation returns back to the flow plane. This transition is analogous to the cholesteric-nematic transition in the presence of a magnetic field. The new mode is oriented in the direction of flow at the centerline. The relaxation after cessation of flow is effected by the nucleation of disclination line defects. The time scale is of the order of half-hour. The relaxation is analogous to nucleation and growth in a first order phase transition.

V9.1

DYNAMICS OF MIXTURES OF INTERACTING COLLOIDS USING DIFFUSING WAVE SPECTROSCOPY Xia Qiu^{1,2}, H. D. Ou-Yang³, D. A. Weitz², D. J. Pine⁴ and P. M. Chaikin^{2,5}, ¹University of Pennsylvania, ²Exxon Research and Engineering Co., ³Lehigh University, ⁴Haverford College, ⁵Princeton University

In the strong multiple scattering regime, the photon intensity autocorrelation function depends on an average of the dephasing caused by the motion of the component species. We report on how data for mixtures of colloidal particles can be deconvoluted to obtain the dephasing from one of the species (and therefore the mean square displacement as a function of time for this species) when the motion of the other species and the mean free paths are known. The system under consideration consists of a few large spheres suspended in a sea of much smaller spheres which are either Brownian or strongly interacting and crystalline or glass like.

V9.2

GRAVITY EFFECT ON WEAKLY CONCENTRATED GEL PHASES. C. Allain, Lab. FAST, Bat. 502, Campus Universitaire 91405 Orsay Cedex FRANCE; and C. Amiel, Lab. Physico-chimie des Biopolymères, CNRS 2-8 rue H. Dunant 94320 Thiais FRANCE.

The nature of the phases formed by copolymerisation of bi- and quadri-functional monomers depends on the different concentrations in monomers. If one or the other of these is low, the macromolecules at the end of the chemical reaction have a finite size and a sol with a viscous behaviour is formed. On the other hand, if the two concentrations are large enough, an infinite network extends through the medium and a gel exhibiting an elastic behaviour is formed. In disagreement with this simple scheme, we have observed that between the two domains where sols and gels are formed, there exist a range of concentration in which the samples exhibit a phase segregation with a viscous zone laying above an elastic one. In order to elucidate the origin of this phenomenon, we have performed a rheological study as a function of the total monomer concentration, keeping constant the ratio of the concentrations in quadri- and bi-functional monomers.

In the intermediate range, we have observed that the rheological properties do not reach an equilibrium value even when the time elapsed from the sample preparation largely exceeds the achievement of the chemical reaction. In the range without segregation, the variations of the viscosity and of the elastic modulus measured at the end of the chemical reaction versus the total monomer concentration, c , have been interpreted in terms of scaling behaviour and fitted with $(c-c_c)$ power laws. The determination of the critical concentration c_c performed

independantly on the viscous points and on the elastic points has lead to a single value of c_c equal to the lower bond of the intermediate range of concentrations, showing that the phases with segregation are gel phases.

Moreover, an estimate of the sedimentation kinetics and a calculation of the deformation of the polymer network under its own weight, which is governed by the osmotic longitudinal modulus, allows us to conclude that the gravity is at the origin of the segregation observed in weakly concentrated gel phases near the gelation critical point.

V9.3

A COMPUTER MODEL FOR THE AVERAGE "CLUSTER" SIZE IN POLYMER AGGREGATES. A. C. Balazs, J. Y. Hu, S. Lewandowski, A. P. Lentvovski and C. Lantman*, Materials Science and Engineering Department, University of Pittsburgh, Pittsburgh, PA 15261, *Mobay Corp., Pittsburgh, PA 15205-9741

We have developed a computer simulation, in three-dimensions, for the reversible diffusion-limited aggregation of triblock amphiphilic polymers. In this model, both ends of the chain represent the terminal hydrophobic groups, while the backbone of the chain is hydrophilic. In aqueous solutions, such chains self-assemble to form extensive aggregates. Within these aggregates, the hydrophobic segments are grouped together in "clusters". Through these simulations, we examine how the average cluster size varies as the number of chains in the aggregate increases and as the lifetime of the association between these hydrophobes is varied. Since values for the average cluster size have, at present, not been attainable through laboratory experiments, these computer experiments play an important role as a predictive tool.

V9.4

PGSE-NMR & SANS FROM TPB BASED MICROEMULSIONS. Paul M. Lindemuth, Department of Chemistry, University of Missouri-Rolla, Rolla, MO; Boualem Hammouda, Research Reactor Facility, University of Missouri, Columbia, MO; Joseph R. Duke, Department of Chemistry, UMR; Frank D. Blum, Department of Chemistry, UMR; Raymond L. Venable, Department of Chemistry, UMR.

Small angle neutron scattering (SANS) and pulsed-gradient spin-echo (PGSE) NMR are used to investigate the inverse microemulsion region of the phase diagram of the tetradecylpyridinium bromide (TPB) - 85% heptane/15% pentanol - water system. Observations of the self-diffusion coefficients for water via PGSE-NMR show several distinct transitions within the water-in-oil (w/o) region, one of which involves the ordering of compact closed structures into a percolating network prior to the onset of bicontinuous morphology. Conductivity measurements were used to corroborate judgements based on the NMR data. A smaller isotropic region proximate to the lamellar liquid crystalline region exhibits a complete inversion of phase relative to the w/o region.

SANS measurements have been performed on TPB based microemulsions containing D_2O . A simple model assuming spherical aggregates interacting with a hard sphere potential has been used to extract aggregate (heavy water - Stern layer) sizes and packing fractions. A clear transition from the isolated aggregate scattering regime to the interaggregate dominated scattering regime has been observed as the heavy water concentrations were increased from approximately 5 to 25% by weight.

V9.5

SOL-GEL SILICATE FORMATION - pH AND TEMPERATURE DEPENDENCE. Anselmo M. Elias, Maria E. Elias and Maria M. Nunes, Chemistry Department, Lisbon University, Campo Grande, C1 - 59, 1700 Lisboa, Portugal.

The optical and physical properties of produced gels and finished preforms are strongly dependent on sol-gel processing conditions.

In previous work we have reported the effect of OH-group on the attenuation of silica optical fiber preforms. In this paper we report the effect of pH and temperature on the rate of hydrolysis and condensation reactions. Silicate prepared from hydrolysis of tetramethoxysilane in methanol-water mixture, using α -picoline as a DCCA. Typical values of pH started slightly above 7 and drop to the range of 4 as the hydrolytic polymerisation proceeds. Several instrumental limitations are posed to the use of typical methods of pH measurements. As expected the pore size distribution for silica gels is highly dependent on the gelation temperature and aging.

V9.6

SIMPLE THEORY FOR PERSISTENT-FLEXIBLE LIQUID CRYSTAL POLYMERS BEYOND THE SECOND VIRIAL APPROXIMATION.¹ Reinhard Hentschke, Department of Chemistry, Brandeis University, Waltham, Massachusetts 02254-9110.

Khokholov and Semenov² have proposed a theory for long persistent chains that quite accurately describes the liquid crystalline behavior of dilute solutions of long homogeneous bend-elastic macromolecules. In this work, the KS approach is extended by replacing their second virial description of excluded volume effects by Lee's generalization of the Carnahan-Starling equation.³ This yields results for the order parameter and the equation of state for persistent-flexible polymers which are valid over a wide range of polymer concentrations. Comparisons with experimental data yield excellent agreement for large polymer axial ratios, where rigid particle theories deviate strongly from the experimental results.

1. Supported by NIH grant HL-36546 and a fellowship to RH from the Deutsche Forschungsgemeinschaft.

2. A. R. Khokholov and A. N. Semenov, *Physica* **108A**, 546 (1981); **112A**, 605 (1982).

3. S. Lee, *J. Chem. Phys.* **87**, 4972 (1987).

V9.7

THE EFFECT OF PRESSURE ON THE CRITICAL TEMPERATURE OF FOUR-COMPONENT MICROEMULSIONS. J. Goyette and T.K. Bose, Université du Québec à Trois-Rivières, Trois-Rivières, Canada, G9A 5H7; J. Thoen, Katholieke Universiteit Leuven, 3030 Leuven, Belgium; J.R. Lalanne, Centre de Recherche Paul Pascal, 33405 Talence, France.

Four-component microemulsions composed of n-decane, water, n-pentanol and sodium dodecylsulfate (SDS) with critical points on a line, show large deviations from Ising behavior near a critical end point (CEP) on the critical line (1). Refractive index anomalies recently reported (2) for these microemulsions are also not Ising-like and could not be characterized in a satisfactory way in terms of power-law expressions.

In this paper we present data for the pressure dependence of the critical temperature (dT_c/dP) for several of these microemulsions. For all the microemulsions investigated so far, negative dT_c/dP values, substantially decreasing near the CEP, are obtained.

From the negative sign of dT_c/dP it can be concluded that if there is any critical contribution of a density anomaly to the refractive index n , it must be opposite to the anomaly for n recently reported by Rebhouch and Lalanne (2). On the basis of two-scale-factor universality, combining dT_c/dP with correlation-length critical amplitudes, we also find that a density anomaly is very likely unobservable experimentally.

(1) A.M. Bellocq, P. Honorat, D. Roux, *J. Phys. (Paris)* **46**, 743 (1985).

(2) N. Rebhouch, J.R. Lalanne, *J. Chem. Phys.*, **90**, 1175 (1989).

THE MECHANICAL PROPERTIES OF THIXOTROPIC GELS AND THEIR EFFECT ON ATTENUATION IN OPTICAL FIBER COMMUNICATION CABLES. C. R. Taylor, Bob J. Overton, AT&T Bell Laboratories, Norcross, GA.

A colloidal gel typically is a semi-liquid substance comprising a thickening agent in a liquid carrier. All types of gelling agents form network structures in which the carrier is held by capillary forces. When a low stress is applied to a gel the material acts substantially solid-like, but if the stress is above a critical value the material flows and the viscosity decreases rapidly, a behavior frequently described as thixotropic.

Colloidal gels have been used as communication cable filling compounds. In optical fiber cables it is essential that, in addition to waterblocking, the filling gel maintain the optical fibers in a low stress state so that signal attenuation is minimized. While the shear modulus has been considered the prime variable for optimizing performance of optical fiber cable filling compounds, we find that a further parameter must be controlled. This parameter is the critical stress at which the gel yields.

We develop a simple, experimental approach to evaluate the appropriate particle content for a fumed silica/mineral oil fiber optic cable filling gel, a content that provides a low critical yield stress while maintaining other desirable properties such as low temperature mechanical characteristics and very low oil syneresis. Further, we establish the relationship between the critical yield stress (and strain) of a filling gel and the transmission performance of the encapsulated optical fibers.

ELECTROSTATIC AND SCREENING EFFECTS ON THE DYNAMIC ASPECTS OF POLYELECTROLYTE SOLUTIONS: "POLY(P-PHENYLENE VINYLENE) PRECURSOR IN METHANOL" H. Matlousi, K. H. Langley, F. E. Karasz, Polymer Science Department, University of Massachusetts, Amherst, MA

We present a QELS study of a synthetic polyelectrolyte compound: Poly(p-phenylene vinylene) derivative dissolved in methanol. The dynamical aspects of these solutions are found to be strongly dependent on whether, or not, we have added small ions. For salt-free solutions, we measured two different diffusion coefficients, D_c and D_s , attributed respectively to cooperative and center of mass motions. The small value of the hydrodynamical correlation length ξ_H , deduced from D_c , reflects the large interpenetration of polyions in salt-free solutions. The chains are, consequently, highly expanded even though not rod-like in shape. The addition of even a small amount of sodium chloride progressively modifies the solution's behavior. First we measured only one diffusion coefficient when c_s exceeds a certain threshold. The effective diffusion coefficient measured for these solutions depends both on the ionic strength and the polymer concentration. The type of variation of D_{eff} versus c_p and versus c_s , is compared to previous work achieved on either polyelectrolytes and ionomers materials or on micelles.⁽¹⁾ The set of data are also quantitatively compared to theoretical considerations as the electrostatic model.^(2,3)

1. M. Won Kim, D. G. Peiffer, *J. Chem. Phys.*, **83**, 4159 (1985).
2. P. Doherty, G. B. Benedek, *J. Chem. Phys.*, **61**, 5426 (1974); and ref. included.
3. S. G. Lin, W. L. Lee, J. M. Schurr, *Biopolymers*, **17**, 1041 (1978).

ATOMIC STRUCTURE OF ALLOY-PARTICLES OBTAINED AS COLLOIDAL SUSPENSIONS. Gabriela Díaz, Roberto Hernández, Laura Cabrera and Miguel José Vacamán, Instituto de Física, U.N.A.M. Apartado Postal 20364, 01000, México, D.F.

Small bimetallic particles (Au-Pd, Pt-Rh, Pt-In and Pt-Ru), were prepared as colloidal sols. The particles were analyzed using High resolution Electron Microscopy, X-ray microanalysis, energy loss and microdiffraction. The shape and size of the particles was controlled by the preparation conditions. We report a systematic study of the different particle shapes, that can be produced. It is found that a higher proportion of the particles have triangular, icosahedral or decagonal shape. High resolution microscopy -- shows that the surface of the particles is rougher than that of similar particles obtained by vacuum evaporation. The roughness of the precipitated particles might have interesting consequences for its catalytic properties. It is shown that --- alloys are observed in most cases.

MICROSCOPIC STRUCTURE AND DYNAMICS OF CONFINED POLYMER MELTS. Ioannis Bitsanis, Department of Chemical Engineering, University of Florida, Gainesville, FL and George Hadziioannou, IBM Almaden Research Center, San Jose, CA.

We performed a series of equilibrium and flow molecular dynamics simulations of dense polymer melts confined between structureless, planar walls.

The melt density varied in an oscillatory manner next to the solid walls. The effect of the solid surface on the melt density was screened after 2-3 molecular diameters and the layering of the polymer segments was found to be much weaker than that observed in simple fluids as a result of the limitations imposed by the segment connectivity. The effect of the wall on the shape of individual chains was similarly restricted to the portions of the chain in the immediate wall vicinity. Chains in the wall vicinity were strongly shrunk in the direction normal to the wall and slightly swollen in the two directions parallel to the wall.

The mobility of the chains in the direction normal to the wall was reduced significantly and the effect was more pronounced in the presence of strong wall-segment attraction. The mobility parallel to the walls was only slightly affected even for chains in the immediate wall vicinity. Finally, the maximum relaxation time of the chains was quite insensitive to the presence of the solid surfaces and the effective viscosity of strongly confined oligomers was found to retain essentially its bulk value up to pore widths only three segment diameters wide.

MOLECULAR DYNAMICS STUDY OF PHASE STRUCTURE IN BINARY MIXED COLLOIDS. Raymond D. Mountain, NIST, Gaithersburg, MD 20899; and D. Thirumalai, University of Maryland, College Park, MD 20742.

The results of a series of molecular dynamics simulations of binary mixtures of colloidal particles interacting via pairwise additive potentials of DVLO type are reported. The parameters for the potentials were chosen to be consistent with realistic systems. We have varied the composition and volume fraction and have determined the resulting phase structure of the mixtures.

We find that liquid, crystalline, and glassy states are possible, depending primarily on the volume fraction. The importance of the factor in the interaction resulting from the finite size of the colloids is illustrated by comparing

results obtained with and without this term. It is found to be very important for interesting conditions. This confirms other results obtained by analytic and simulation methods.

This approach is useful for static properties but is unable to describe time correlated properties since the hydrodynamic interactions between the colloids is missing. The status of this currently active research topic will be reviewed.

V9.13

WEIGHTED-DENSITY THEORY OF PHASE TRANSITIONS IN FLUIDS COMPOSED OF ANISOTROPIC PARTICLES. John F. Marko, The James Franck Institute, The University of Chicago, Chicago, IL 60637; and W. A. Curtin, BP Research & Development, 4440 Warrensville Center Road, Cleveland, OH 44128.

A nonperturbative approach to the density-functional description of phase transitions in fluids composed of anisotropic particles is presented. Based on the weighted density approach developed for systems with spherically symmetric interparticle interactions[1], this theory is exact to second order in density deviations from the isotropic phase, and at higher orders exactly satisfies all sum rules that can be expressed in terms of the two-body direct correlations.

This theory has been applied to the description of phase transitions in hard-particle fluids. The description of the structure of ordered phases near crystallization transitions is greatly improved in comparison to the commonly used second-order theory. For transitions to the nematic phase, it is found that the higher-order contributions do not modify the predictions of the second-order theory. Accurate two-body liquid structure appears to be the key factor leading to an improved description of the nematic phase.

[1] W. A. Curtin and N. W. Ashcroft, Phys. Rev. A 32, 2909 (1985); A. R. Denton and N. W. Ashcroft, Phys. Rev. A 39, 4701 (1989).

V10.1

WHAT CAN WE LEARN FROM COMPUTER SIMULATIONS OF MACROMOLECULAR LIQUIDS? Gary S. Grest, Exxon Research & Engineering Company, NJ 08801.

I will describe how computer simulations techniques, particularly molecular dynamics, can be useful for investigating the static and dynamic properties of macromolecular liquids. For polymeric systems, I will show how simulations can be applied to study a wide variety of systems, such as linear, ring and star polymers from the dilute, single chain limit to a dense melt consisting of many long, entangled chains. For a dense polymer melt, I will present our recent results¹ which cover the entire regime from the non-entangled regime (Rouse) to highly entangled regime (reptation). The results indicate that the reptation model provides a very good description of the dynamics of the chains in the entangled regime, while Rouse model provides an excellent description of the dynamics of short chains. Extensions of the technique to study polymer networks and surface phenomena will also be discussed.

1 K. Kremer, G. S. Grest and I. Carmesin, Phys. Rev. Lett. 61, 566 (1988); K. Kremer and G. S. Grest (to be published).

V10.2 ABSTRACT NOT AVAILABLE

V10.3

SIMULATIONS OF CONTACT LINE MOTION: SLIP AND THE DYNAMIC CONTACT ANGLE.* Mark Robbins and Peter Thompson, Dept. of Physics and Astronomy, The Johns Hopkins University, Baltimore, MD 21218.

The usual no-slip boundary condition of hydrodynamics leads to divergences in the stress and energy dissipation when the contact line between a fluid interface and a solid moves. Since the measured dissipation is finite, either the no-slip condition or hydrodynamics must break down. However, experiments have been unable to determine the source of this breakdown since all theories predict the same behavior at large distances from the contact line.

We present results of detailed Molecular Dynamics simulations for a single fluid and two immiscible fluids confined between solid walls and sheared in a Couette geometry. A wide range of shear rates and wall and fluid properties were studied. Little or no slip occurred at the solid walls in single fluid simulations. However, at strong wall-fluid couplings or equal wall and fluid densities epitaxial ordering was induced in the first few fluid layers. This locking leads to jerky stick-slip dynamics in these layers.

Steady-state velocity fields and interfaces were obtained in two fluid simulations. Changes with capillary number in the interface shape and dynamic contact angle were consistent with experiment and macroscopic theory. Computed velocity fields showed that the usual no-slip boundary condition broke down within about two atomic spacings from the contact line. This slip appeared to be associated with the breakdown of local hydrodynamics at atomic scales: Microscopic results for the pressure-stress tensor differed from the Navier-Stokes expression in the slip region. We attribute this to non-local contributions to the stress from all atoms within the range of interactions. These non-local effects only become apparent when velocity gradients vary on atomic scales.

*Supported by the National Science Foundation Grant No. DMR-8553271.

V10.4

QUASIPARTICLE MEDIATED MELTING IN TWO DIMENSIONS. M.A. Glaser and N.A. Clark. Department of Physics, University of Colorado, Boulder, CO 80309.

We show, using computer simulation and two-dimensional (2d) colloids, that the 2d simple liquid local structure is a tiling-like mosaic of square and triangle lattice. This structure is obtained in a model where in the 2d melting transition is a quasiparticle (QP) condensation in which the QP's are square lattice cells condensed by attractive short range interactions into tiling structures.

Supported by NSF DMR 8512071.

V10.5

INTERACTIONS BETWEEN CHARGED MACROIONS IN SOLUTION.* M.J. Stevens and M.O. Robbins, Department of Physics and Astronomy, The Johns Hopkins University, Baltimore MD 21218.

For small counterion densities, interactions between charged macroions in solution have been effectively characterized by the Poisson-Boltzmann Equation (PBE). However, at sufficiently large densities, interactions between counterions are no longer negligible and the PBE breaks down. Monte Carlo (MC) simulations and hypernetted chain (HNC) calculations for parallel charged plates show that the interaction may change from repulsive to attractive in this limit. We have developed a simple local density functional theory that incorporates the strong correlations at high counterion densities, and is equivalent to the PBE at low densities. Like more complicated MC and HNC calculations, our theory gives attractive interactions at high densities. We find the origin is collapse of counterions on to the plates when a critical density is exceeded. We have also performed complementary MC simulations of counterions and spherical macroions in solution. As expected from the analytic

theory, counterions collapse onto the macroions at high densities.
*Supported by the National Science Foundation Grant No. DMR-8553271.

V10.6

THE EFFECT OF HYDROSTATIC PRESSURE ON LIQUID-LIQUID PHASE SEPARATION IN MICELLAR SOLUTIONS OF C₈-LECITHIN AND WATER K. Helmersson, P. Schurtenberger, G.M. Thurston, T. Kushida, S. Angehrn and G.B. Benedek, Department of Physics and Center for Materials Science and Engineering, MIT, Cambridge, MA

We report measurements of the location of the coexistence curve for binary liquid phase separation and of the hydrodynamic radii of micelles in solutions of C₈-lecithin and water, at hydrostatic pressures between 1 atm and 800 atm. We find that increased hydrostatic pressure dramatically reduces the critical temperature T_c for liquid-liquid phase separation, by approximately 23°K over the 800 atm range. The hydrodynamic radii of the C₈-lecithin micelles, at dilute amphiphile concentration, remains constant as a function of the applied pressure. We interpret our experimental findings in terms of the pressure dependence of two phenomenological parameters, C and $\Delta\mu$, which govern the strength of intermicellar interactions and the extent of micellar growth, respectively, within a Gibbs free energy model¹ of micellar solutions.

¹D Blankschtein, G.M. Thurston and G.B. Benedek, *J. Chem. Phys.* 85:7268 (1986)

V10.7

MOLECULAR-THERMODYNAMIC FRAMEWORK TO PREDICT MICELLIZATION, PHASE BEHAVIOR AND PHASE EQUILIBRIA OF MICELLAR SOLUTIONS. D. Blankschtein and S. Puvvada, Department of Chemical Engineering, Massachusetts Institute of Technology, Cambridge, MA 02139 USA.

We will present a molecular-thermodynamic framework which is capable of predicting (i) micelle formation and growth, (ii) micellar solution phase behavior, and (iii) phase equilibria of surfactant-water micellar solutions.

The theory incorporates the effects of surfactant molecular architecture, that is, chemical structure and conformation of hydrophobic and hydrophilic surfactant moieties, on: (i) interfacial tension reduction at the micellar core-water interface due to surfactant adsorption and surface curvature, (ii) steric and packing effects associated with the spatial conformations adopted by the hydrophobic and hydrophilic moieties, and (iii) electrostatic interactions between the hydrophilic moieties at the micellar core-water interface. A detailed comparison with experimental findings in aqueous solutions of nonionic, ionic, and zwitterionic surfactants will be presented.

V10.8

A MODEL FOR ORIENTATIONAL AND TRANSLATIONAL ORDERING IN MICELLAR AND OTHER REVERSIBLY ASSEMBLING SYSTEMS.¹ Mark P. Taylor and Judith Herzfeld, Departments of Chemistry and Physics, Brandeis University, Waltham, Massachusetts 02254-9110.

Liquid crystalline order is a feature common to many reversibly assembling systems, such as micelle forming surfactants, polymerizing proteins and linearly aggregating polyaromatic molecules. The order observed in these inherently polydisperse systems may be translational as well as orientational, i.e., nematic, smectic (lamellar) and columnar (hexagonal) phases are possible. The temperature and concentration dependent phase behavior exhibited by such systems is often remarkably complex, due to the coupling between the aggregate size, orientation and position distributions. We have developed a model of such reversibly

assembling systems which fully accounts for the coupling between these distributions. A phenomenological description of aggregate assembly is utilized in conjunction with a scaled particle calculation of the configurational entropy of the polydisperse system. The interparticle potential is modeled as a hard-core surrounded by a short-range repulsive step. Translational order is incorporated by imposing cell boundaries in the relevant dimensions, an approach that gives good agreement with Monte Carlo results for monodisperse systems.² We compare the calculated phase behavior with experimental data and report model results for the temperature and concentration dependence of the aggregate size distribution, the orientational order parameter, and the periodicity of translational ordering.

1. Supported by NIH grant HL-36546.
2. M. P. Taylor, R. Hentschke and J. Herzfeld, *Phys. Rev. Lett.* 62, 800 (1989).

V10.9

REEXAMINATION OF OSMOTIC PRESSURE MEASUREMENTS IN SELF-ASSEMBLING SYSTEMS. S. Puvvada and D. Blankschtein, Department of Chemical Engineering, Massachusetts Institute of Technology, Cambridge, MA 02139 USA.

The peculiarities of membrane osmotic pressure measurements in self-assembling systems such as micellar solutions will be discussed. It will be shown that in certain cases these measurements can yield the weight-average micellar molecular weight, M_w , instead of the conventional number-average micellar molecular weight, M_n . The implications of this rather striking result for the evaluation of the degree of polydispersity, $\alpha = M_w/M_n$, and the associated extent of micellar growth in micellar solutions will be examined. In this respect, a reexamination of membrane osmotic pressure measurements in aqueous micellar solutions of the nonionic surfactant n-dodecyl hexaoxyethylene glycol monoether (C₁₂E₆) will be presented.

V10.10

DIELECTRIC SPECTROSCOPY OF COMPLEX LIQUIDS AND SOLUTIONS FROM KHZ TO 20 GHZ. Yan-Zhen Wei and S. Sridhar, Department of Physics, Northeastern University, Boston, MA 02115.

Dielectric spectroscopy is a powerful probe of order and disorder, particularly when carried out over a broad frequency range. We have recently developed a technique which enables quasi-continuous measurements upto 20 GHz in liquids. The technique has been applied to a variety of systems: ionic aqueous solutions, aqueous solutions of biopolymers and proteins, and polymeric liquids and solutions.

In solutions of bio-polymers such as poly-lactic acids and poly-vinyl alcohol in methylene chloride, we observe an excluded volume effect which is frequency- and molecular weight dependent. In aqueous solutions of proteins such as myoglobin, similar effects are observed due to the hydration shell, from which we deduce its size and the relaxation time of the hydration water. In LiCl/H₂O solutions, as a function of concentration, effects due to dissociated ions and undissociated ion pairs are observed. At very high concentrations and/or low temperatures, cooperative effects occur - the low temperature data can be explained in terms of mode coupling theories. Presently we are studying polymeric liquids such as poly-isoprene, to examine the normal mode and segmental mode relaxation, and possible entanglement effects.

* Supported by PRF-ACS.

**SYMPOSIUM W:
FLY ASH AND COAL CONVERSION
BY-PRODUCTS CHARACTERIZATION,
UTILIZATION AND DISPOSAL VI**

W

November 29 - December 1, 1989

Chairs

R. L. Day
Department of Civil Engineering
University of Calgary
Calgary, Alberta
Canada T2N 1N4
(403) 220-7489

F. P. Glasser
Department of Chemistry
University of Aberdeen
Meston Walk
Old Aberdeen
AB9 2UE
SCOTLAND
0224 27 2906

Symposium Support

Electric Power Research Institute

Gas Research Institute

Iowa Fly Ash Affiliates

Mining & Mineral Resources Research Institute

Ortech International

Western Fly Ash Research, Development & Data Center

**Proceedings published as Volume 178
of the Materials Research Society
Symposium proceedings series.**

FLY ASH AND COAL CONVERSION
BY-PRODUCTS CHARACTERIZATION,
UTILIZATION AND DISPOSAL VI

November 29 - December 1, 1989

SESSION W1:

Chair: R. L. Day
Wednesday Afternoon, November 29
Adams Room (W)

1:15 OPENING BY SYMPOSIUM CHAIRS

1:20 INTRODUCTION BY SESSION CHAIR

1:30 *W1.1

DATABASE OF CHEMICAL, MINERALOGICAL AND PHYSICAL PROPERTIES OF NORTH AMERICAN FLY ASH, G.J. McCarthy and Jody K. Solem, North Dakota State University, Fargo, ND; O.E. Manz and D.J. Hassett, University of North Dakota, Grand Forks, ND.

2:15 W1.2

THE ROLE OF GLASSY PHASES IN THE CEMENTITIOUS REACTIVITY OF FLY ASHES AND SLAGS, R.T. Hemmings and E.E. Berry, Matex Consultants Inc., Mississauga, Canada.

2:45 BREAK

3:15 W1.3

THE SPECIFIC HEAT OF COAL ASHES, L.L. Isaacs and R. Ledesma, The City College, Department of Chemical Engineering, New York, NY.

3:45 W1.4

ANALYSIS OF COAL FLY ASH BY BULK AND SURFACE CHARACTERIZATION TECHNIQUES, M. Bellotto and C. Boni, CISE Tecnologie Innovative, Materials and Technology Division, Milan, Italy; A. Caridi, CISE Tecnologie Innovative, Materials and Technology Division, Milan, Italy, and CNEA, Buenos Aires, Argentina; E. Cereda and C. Chemelli, CISE Tecnologie Innovative, Materials and Technology Division, Milan, Italy; G.M. Braga Marazzan, CISE Tecnologie Innovative, Materials and Technology Division, Milan, Italy, and Istituto di Fisica Generale Applicata dell'Università, Milan, Italy; and M. Scagliotti, CISE Tecnologie Innovative, Materials and Technology Division, Milan, Italy.

4:15 W1.5

MICROSTRUCTURE, MASS TRANSPORT AND DENSIFICATION OF SLAG-CEMENT PASTES, Q.L. Feng and F.P. Glasser, University of Aberdeen, Department of Chemistry, Old Aberdeen, Scotland.

*Invited Paper

4:45 W1.6

A STATISTICAL INVESTIGATION ON PARTICLE TO PARTICLE VARIATION OF FLY ASH USING, SEM-AIA-EDAX TECHNIQUE, L.E. Barta, G. Vámos, Institute of Energy, Budapest, Hungary; M.A. Toğan, J.D. Teare, J.M. Beér, A.F. Sarofim, Massachusetts Institute of Technology, The Energy Laboratory and Department of Chemical Engineering, Cambridge, MA.

SESSION W2:

Chair: F. P. Glasser
Thursday Morning, November 30
Adams Room (W)

8:20 SESSION CHAIR REMARKS

8:30 W2.1

OXYANION SUBSTITUTED ETTRINGITES: SYNTHESIS, CHARACTERIZATION AND AQUEOUS STABILITY, P. Kumarathasan and G.J. McCarthy, North Dakota State University, Fargo, ND; D.J. Hassett and D.F. Pflughoeft-Hassett, University of North Dakota, Grand Forks, ND.

9:00 W2.2

COMPARISON BETWEEN NATURAL WEATHERING PROCESSES AND FORCED LEACHING OF CLASS-F FLY ASH, A. Andrade, Y.M.A. Coenegracht, G.G. Hollman, H.S. Pietersen, and R.D. Schuiling, Institute of Earth Science, Geochemistry Department, Utrecht, The Netherlands.

9:30 W2.3

EFFECT OF CALCIUM ADDITIVES ON SULFUR CAPTURE AND PUZZOLANIC ACTIVITY OF FLYASH IN COAL WATER FUEL FLAMES, M.A. Togan, T. Paloposki, J.D. Teare and J.M. Beér, Massachusetts Institute of Technology, Department of Chemical Engineering, Cambridge, MA; M. Rini and R.C. LaFlesh, Combustion Engineering, Inc., Windsor, CT; L.E. Barta and G. Vámos, Institute of Energy, Budapest, Hungary.

10:00 BREAK

10:30 W2.4

MICROPROBE STUDY OF CHEMICAL INTER-GRAIN VARIATION IN CLASS-F FLY ASH: APPLICATION OF FUZZY C-MEANS CLUSTER ANALYSIS AND NON-LINEAR MAPPING, Hans S. Pietersen and Jan M. Bijen, Delft Technical University, Faculty of Civil Engineering, Materials Science Section, Delft, The Netherlands; Simon P. Vriend and Rene E.P. Poorter, Institute of Earth Science, Geochemistry Department, Utrecht, The Netherlands.

11:00 W2.5

EVOLUTION OF LIME AND MICROSTRUCTURAL DEVELOPMENT IN FLYASH-PORTLAND CEMENT SYSTEMS, Joseph A. Larbi and Jan M. Bijen, Delft Technical University, Faculty of Civil Engineering, Materials Science Section, Delft, The Netherlands.

11:30 W2.6
ACTIVITY OF SULPHUR-FIXED ASH FROM DESULPHURING COMBUSTION OF HIGH-SULFUR COAL IN FLUIDIZED BED FOR BUILDING MATERIALS, Lien Huizhen and Jiang Jiabiao, Tsinghua University, Department of Civil Engineering, Beijing, China.

SESSION W3:

Chair: P. L. Pratt
Thursday Afternoon, November 30
Adams Room (W)

1:20 CHAIR'S REMARKS & ANNOUNCEMENTS

1:30 *W3.1
STUDIES ON MECHANISM OF DEVELOPMENT OF PHYSICAL AND MECHANICAL PROPERTIES OF HIGH VOLUME FLY-ASH CEMENT PASTES, Rolf F. Feldman, National Research Council Canada, Institute for Research in Construction, Ottawa, Canada.

2:15 W3.2
REACTIVITY OF FLY ASH AT HIGH pH, H.S. Pietersen, A.L.A. Fraay, and J.M. Bijen, Delft Technical University, Faculty of Civil Engineering, Materials Science Section, Delft, The Netherlands.

2:45 BREAK

3:15 W3.3
AGGLOMERATION OF HIGH CALCIUM FLY ASH FOR UTILIZATION: I. PHYSICAL PROPERTIES, Kenneth L. Bergeson, Carol L. Kilgour, and Scott Schlorholtz, Iowa State University, Department of Civil and Construction Engineering, Ames, IA.

3:45 W3.4
AGGLOMERATION OF HIGH CALCIUM FLY ASH FOR UTILIZATION: II. BINDING MECHANISMS AND LEACHING BEHAVIOR, Carol L. Kilgour, Kenneth L. Bergeson, and Scott Schlorholtz, Iowa State University, Department of Civil and Construction Engineering, Ames, IA.

4:15 W3.5
STUDY ON THE PROPERTIES OF SEPARATED CLASS F FINE FLY ASH, T.C. Sheu, S.T. Kuo, and L.W. Quo, Taiwan Power Company, Power Research Institute, Taiwan, China.

4:45 W3.6
REACTIVITY OF FLY ASH-PORTLAND CEMENT- $\text{Ca}(\text{OH})_2$ - $\text{CaSO}_4 \cdot 2\text{H}_2\text{O}$ MIXTURES, R.L. Berger, and Shamba Wang, University of Illinois, Department of Civil Engineering, Urbana, IL.

SESSION W4:

Chair: R. F. Feldman
Friday Morning, December 1
Adams Room (W)

8:20 CHAIR'S REMARKS & ANNOUNCEMENTS

8:30 *W4.1
THE PRACTITIONERS VIEW OF FLY ASH UTILIZATION, Ronald H. Mills, University of Toronto, Toronto, Canada.

9:15 *W4.2
USE OF FLY ASH IN CONCRETE - A EUROPEAN VIEW, Peter L. Pratt, Imperial College, Department of Materials, London, United Kingdom.

10:00 BREAK

10:30 W4.3
RESISTANCE OF FLY ASH MORTARS TO SULPHATE ATTACK IN A CONTROLLED ENVIRONMENT, Robert L. Day and J. Konecny, University of Calgary, Department of Civil Engineering, Alberta, Canada.

11:00 W4.4
PERFORMANCE OF A FLY ASH STABILIZED PAVEMENT, Joakim G. Laguros, University of Oklahoma, Civil Engineering Department, Norman, OK; and Curt Hayes, Oklahoma Department of Transportation, Research Department, Oklahoma City, OK.

11:30 W4.5
THE EFFECT ON CEMENT MORTAR AND CONCRETE BY ADMIXTURE OF SPRAY DRYING ABSORPTION PRODUCTS, Kirsten G. Jeppesen, The Technical University of Denmark, The Institute of Mineral Industry, Lyngby, Denmark.

SESSION W5:

Chair: G. J. McCarthy
Friday Afternoon, December 1
Adams Room (W)

1:20 SESSION CHAIR REMARKS

1:30 W5.1
EVALUATING THE USE OF PONDED FLY ASH IN A ROADWAY BASE COURSE, David W. Hunsucker, and R. Clark Graves, University of Kentucky, Kentucky Transportation Center, Lexington, KY.

2:00 W5.2
STATE-OF-THE-ART IN MWC ASH DISPOSAL TECHNIQUES AND DESIGN REQUIREMENTS, Keith E. Forrester, Wheelabrator Environmental Systems, Inc., Environmental Engineering, Danvers, MA.

2:30 W5.3
ENVIRONMENTAL ASSESSMENT OF BOTTOM ASH USED
IN ROAD STABILIZATION, Asmarre Atalay and
Joakim G. Laguros, University of Oklahoma,
Civil Engineering and Environmental Science,
Norman, OK.

3:00 CLOSING REMARKS, SESSION CHAIRS

W1.1

DATABASE OF CHEMICAL, MINERALOGICAL AND PHYSICAL PROPERTIES OF NORTH FLY ASH. G.J. McCarthy and Jody K. Solem, North Dakota State University, Fargo; O.E. Manz and D.J. Hassett, University of North Dakota, Grand Forks, ND.

Fly ash from electrical generating stations is an inherently variable material due to differences in the chemistry of the source coal, in the coal preparation, in the combustion conditions and in ash collection and handling methods. Because no two utilities have all of these factors in common, each plant's fly ash is unique, and may vary itself with time. If one wishes to obtain generic information relevant to the utilization or disposal of this material, it must be done by applying statistical procedures to a large database. With support from electrical utilities and fly ash marketers, preparation of such a database incorporating results from more than 500 North American fly ashes is nearing completion. The principal components of the database are information on the power plant and its coal, major oxides chemical analyses, the mineralogy (crystalline compounds) and ASTM C 618 physical properties. Although the emphasis is on fly ash derived from combustion of lignite and subbituminous coal, data for bituminous coal fly ash are also included. Chemical composition and XRD mineralogy "fingerprints" of various classes of fly ash have been established. Statistical analyses of variability in fly ash chemistry and mineralogy have also been performed.

W1.2

THE ROLE OF GLASSY PHASES IN THE CEMENTITIOUS REACTIVITY OF FLY ASHES AND SLAGS. R.T. Hemmings and E.E. Berry, MATEX Consultants Inc., Mississauga, Ontario, Canada.

Coal fly ashes and rapidly cooled metallurgical slags are largely composed of non-crystalline or glassy aluminosilicates. It is generally accepted that much of the cementitious reactivity of these materials arises from chemical reactions between alkaline pore solutions and glass constituents. Reactivity in glasses results from the combined effects of chemical composition, thermal history and surface conditions. The products of reaction are largely determined by the leachability of glass components and the ionic status of the pore water. The paper presents a critical review of the experimental and theoretical basis for current understanding of glass reactivity as it relates to the use of fly ashes and slags in cemented systems. Directions for future research and the basis for a general theory of reactivity among supplementary cementing materials are also considered.

W1.3

THE SPECIFIC HEAT OF COAL ASHES. L.L. Isaacs and R. Ledesma, Department of Chemical Engineering, The City College, New York, NY.

Coal ashes were prepared at 1000K from the Argonne Premium Coal (APS) samples suite. Specific heats were measured between 120K and 700K. The specific heats were correlated with ash composition.

W1.4

ANALYSIS OF COAL FLY ASH BY BULK AND SURFACE CHARACTERIZATION TECHNIQUES. M. Bellotto¹, C. Boni¹, A. Caridi^{1,2}, E. Cereda¹, C. Chemelli¹, G.M. Braga Marazzan^{1,2}, M. Scagliotti¹.
1 CISE Tecnologie Innovative, P.O. BOX 12081, 20134 Milan, Italy - 2 Istituto di Fisica Generale Applicata dell'Università, Milan, Italy

This paper presents an overview of techniques for bulk and surface characterization of fly ash. Examples are reported for analysis of NBS

Standard Reference Materials, as well as of integral and size fractionated coal fly ashes. A better knowledge of coal fly ash elemental composition, structural characteristics and of inter- and intra-particle heterogeneity is needed for the understanding and quantification of the physical and chemical processes related to fly ash formation and reactivity. Its reactivity is relevant to the utilization, disposal and collection of particulate emissions by electrostatic precipitators.

The techniques applied for bulk elemental analysis are PIXE and PIGE. Electron microscopy has been used to investigate fly ash morphology, while its mineralogy has been studied by means of XRD. The glass in coal fly ash has been investigated using microfocus Raman spectroscopy. Surface characterization tools, Auger and X-ray photoelectron spectroscopies, have been used to analyze the samples and to obtain radial composition profiles of individual particles.

* Work performed under ENEL-DSR/CISE contract
** On leave from CNEA, Buenos Aires, Argentina

W1.5

MICROSTRUCTURE, MASS TRANSPORT AND DENSIFICATION OF SLAG-CEMENT PASTES. Q.L. Feng and F.P. Glasser, Department of Chemistry, University of Aberdeen, Old Aberdeen, AB9 2UE, Scotland.

An important property of well-cured slag-cement blends is their low permeability. The densification process in slag-cement blends has been followed by electron microscopy and electron microanalysis to determine changes to the matrix microstructure and mineralogy. Briefly, Mg in the slag remains on the site of former glassy slag grains, but combines with enough Al to give a hydrotalcite phase: some Ca and Si also remain, probably as C-S-H, but much Ca and Si migrate into the paste matrix. This transfer of chemical substance provides the driving force for matrix densification. Mass balance calculations are used to support these observations and to generalize on them, so the extent of densification potential can be calculated for various blend proportions as well as for slags having different chemical compositions. Specimen calculations are presented. Quality assurance of slag is to be optimized. The ability to calculate the potential for densification, at least in principle, is seen as an important step forward in design for durability.

W1.6

A Statistical Investigation on Particle to Particle Variation of Flyash using SEM-AIA-EDAX Technique

I.E. Barna, G. Vámos
Institute of Energy
Budapest, Hungary

M.A. Toqan, J.D. Teare, J.M. Beer, A.F. Sarofim

The Energy Laboratory and
Department of Chemical Engineering
Massachusetts Institute of Technology
Cambridge, Massachusetts 02139

ABSTRACT

Prediction of the binding characteristics of fly ash in concrete is of great interest for fly ash utilization. Correlations between fly ash pozzolanic activity and chemical composition/morphology based on bulk analyses are inadequate due to the strong particle to particle variation of fly ash properties. In an answer to this problem scanning electron microscopy combined with automated image analysis and energy dispersive X-ray analysis (SEM-AIA-EDAX) used previously for the study of mineral inclusion distributions in coal has been extended to the analyses of large numbers of individual fly ash particles.

Results of an analytical statistical treatment of the experimental data show that this technique can provide information on the variation of the size and chemical composition of individual fly ash particles and can therefore be used for the evaluation of different types of fly ash in respect of their usability in concrete.

W2.1

OXYANION SUBSTITUTED ETTRINGITES: SYNTHESIS, CHARACTERIZATION AND AQUEOUS STABILITY. P. Kumarathasan and G.J. McCarthy North Dakota State University, Fargo; D.J. Hassett and D.F. Pflughoeft-Hassett, University of North Dakota, Grand Forks, ND.

Long-term batch leaching studies of composites of lignite combustion and gasification ashes with a calcium-based scrubber waste have shown the prominent formation of ettringite [$\text{Ca}_6\text{Al}_2(\text{SO}_4)_3(\text{OH})_{12} \cdot 26\text{H}_2\text{O}$] in the solids, in parallel with reductions in solution concentrations of potentially hazardous elements such as boron and selenium. In nature, boron is known to substitute for sulfur in several minerals in the ettringite group (charlesite, sturmanite) and a selenate analog of ettringite was reported many years ago. The possibility that oxyanions such as $\text{B}(\text{OH})_4$, SeO_4 , AsO_4 , CrO_4 , MoO_4 and VO_4 might be precipitated from hazardous waste solutions as low solubility substituted ettringites is the basis for an ongoing study. Substituted ettringites of each of these oxyanions have been prepared and characterized chemically and by x-ray powder diffraction. The stability of the prototype sulfate ettringite, and of borate and selenate substituted ettringites, has been measured in aqueous solutions with varying pH and solution constituent concentrations.

W2.2

COMPARISON BETWEEN NATURAL WEATHERING PROCESSES AND FORCED LEACHING OF CLASS-F FLY ASH. A. Andrade, Y.M.A. Coenegracht, G.G. Hollman, H.S. Pietersen & R.D. Schuiling. Inst. of Earth Sci., Dept. Geochem., 3508 TA Utrecht, The Netherlands.

In lysimeters the natural weathering process of three class-F fly ashes was studied. The ashes were classified according to their alkaline content into acid, neutral or alkaline. In the upper section of the beds organic C is slightly increased after 4 yrs of weathering. The density of the neutral fly ash is slightly decreased. The density of acid and alkaline fly ash increased and concretions have been formed. In the alkaline fly ash this is due to local cementation by calcite. In acid fly ash the concretions are enriched in a number of major and minor elements. Only sulfur shows significant mobility. Hardly any signs of soil development are detected. Under natural conditions trace elements will be leached over a very long time period.

Column leaching experiments with mild acids and complexing agents were conducted in order to check if the natural leaching process can be accelerated. Strong acids (pH=1) appeared most effective, although large quantities of major elements were also leached. Weak acids combined with complexing compounds are more selective with respect to a number of hazardous elements, but less effective. A few heavy metals remain present in high concentrations, although in a less mobile form. Forced leaching of fly ashes before dumping may eliminate most of the environmental problem of mobilisation of heavy metals.

W2.3

Effect of Calcium Additives on Sulfur Capture and Pozzolanic Activity of Flyash in Coal Water Fuel Flames

Using coal water fuels (CWF), a flame investigation was carried out to determine the effects of the pretreatment of CWFs by calcium additives upon the efficiency of in-flame sulfur capture and flyash pozzolanic activity.

To this effect, seven coal-water fuels were used, the first of which served as base fuel without additive sorbent while the other seven contained one of two types of sorbents. Three of the latter fuels were prepared by admixing to the base fuel varying amounts of calcium acetate solutions, while calcium hydroxide particles, in varying amounts were admixed to the remaining three coal water fuels.

In the combustion tests, flyash samples were collected from the exit of a furnace and analyzed by Scanning Electron Microscopy in conjunction with Automated Image Analysis and Energy Dispersive X-Ray Spectroscopy (SEM-ALA-EDAX) for elemental distribution of calcium and sulfur in the fly ash particles. Particle size distributions of the sampled solids were determined using a laser diffraction particle size analyzer (Malvern) and X-ray diffraction and SEM-EDAX measurements were made on hardened flyash-water mixture to determine the pozzolanic activity of the flyash.

Of the two additives used the calcium acetate was more effective in capturing sulfur; 71% sulfur reduction was obtained with a mole ratio of Ca/S = 1.8. Both the calcium acetate and calcium hydroxide additives produced improved flyash pozzolanic activity.

W2.4

MICROPROBE STUDY OF CHEMICAL INTER-GRAIN VARIATION IN CLASS-F FLY ASH: APPLICATION OF FUZZY C-MEANS CLUSTER ANALYSIS AND NON-LINEAR MAPPING. Hans S. Pietersen and Jan M. Bijen, Fac. of Civ. Eng., Materials Sci. Sec., Delft Tech. Univ., 2628 CN Delft, The Netherlands; Simon P. Vriend and Rene E.P. Poorter, Inst. of Earth Sci., Geochemistry Dept., 3508 TA Utrecht, The Netherlands.

The chemistry of individual grains of several Class F fly ashes has been investigated by electron microprobe analysis. Both bulk fly ash as well as size and density separated fractions were analyzed. The analysis of low concentrations of the light alkaline elements was given special attention. In order to obtain structure in the large dataset obtained, a combination of two multivariate statistical procedures was applied. The method involved the use of both fuzzy c-means cluster analysis (FCM) and non-linear mapping (NLM) techniques and allowed for a quick visual interpretation of the fly ash analysis. It provided information which is not obtained through the use of the commonly used classical two- or three dimensional data representation plots alone. The cluster analysis of all ash data indicated that a model of 5-6 clusters could best explain the chemical differences between several class-F fly ashes. Most clusters showed an inverse relation between SiO_2 and Al_2O_3 , combined with different levels of Fe, Ca, Mg and/or K and Na. Inter-grain variation of individual fly ashes showed, on a smaller scale, similar variations. The results of the cluster analysis were related with fly ash -reactivity and -glass content data.

W2.5

EVOLUTION OF LIME AND MICROSTRUCTURAL DEVELOPMENT IN FLYASH-PORTLAND CEMENT SYSTEMS. Joseph A. Larbi and Jan M. Bijen, Delft Technical University, Faculty of Civil Engineering, Materials Science Section, Stevinweg 1, 2628 CN Delft, The Netherlands.

The evolution of calcium hydroxide, $\text{Ca}(\text{OH})_2$ and the development of microstructure during the early hydration of flyash-portland cement systems have been investigated. During the first one month of hydration, the lime content of flyash-portland cement mortars was found to be significantly higher than those of the reference mortars. After one month of hydration, however, the lime content in the flyash-portland cement mortars began to decrease.

The study also showed that the chemistry of the pore solution in contact with the hydrating cement system and the glass content of the flyashes exerted major influences on the rate of evolution of lime in the flyash-portland cement mortars.

Pore size distribution analysis by means of mercury intrusion porosimetry revealed higher capillary porosity in the flyash-portland cement mortars than the plain mortars for the same water/(cement+flyash) ratios during the first one month of hydration.

The results of the lime content in the mortars and the pore size distribution studies were supported by scanning electron microscope analysis on fractured surfaces of similar mortar specimens which revealed large, better-crystallized calcium hydroxide plates at the paste-aggregate as well as the paste-flyash interfaces during the first one month of hydration.

W2.6

ACTIVITY OF SULPHUR-FIXED ASH FROM DESULPHURING COMBUSTION OF HIGH-SULFUR COAL IN FLUIDIZED BED FOR BUILDING MATERIALS. Lian Huizhen and Jiang Jiabiao, Dept. of Civil Engineering, Tsinghua University, Beijing, P.R. of China.

Adding a kind of novel desulphurizer into fluidized bed, amount of the sulphur-fixed ash from combustion of high-sulphur coal (named sulphur- fixed boiling slag) can be over 30%.

It is known that activity of boiling slag is better than that of fly ash, and the boiling slag can be used as active blending materials in portland cement. But another fact has been proved by experiments as follow: The sulphur-fixed boiling slag has cementitious property itself. The slag was mixed with water ($w/c=0.44$) and formed without any other materials, the compressive strength of that specimen came up to over 10 Mpa after steam curing, even more than 20 Mpa depending on its composition, and that of another specimen with the same composition by adding with lime of 8% came up to over 20 Mpa (compared with above mention 10 Mpa). Therefore, activity of the sulphur-fixed boiling slag is better than that of sulphur-free boiling slag as a cementitious material.

In accordance with present studies, it is found that factors of influence on the activity are substantially involved with $f\text{-CaO}$ content, sulphur content and $(\text{CaO}+\text{SO}) / (\text{SiO} + \text{AlO})$ ratio, etc. So that the quality and practice of sulphur-fixed boiling slag used as cementitious materials can be appreciated and controlled.

W3.1

STUDIES ON MECHANISM OF DEVELOPMENT OF PHYSICAL AND MECHANICAL PROPERTIES OF HIGH VOLUME FLY ASH-CEMENT PASTES. Rolf F. Feldman, National Research Council Canada, Institute for Research in Construction, Ottawa, Ontario, Canada, K1A 0R6

Workers at CANMET, Ottawa, Canada, have shown that high volumes of fly ash can be used in structural concrete. This work was performed to elucidate the possible mechanisms of strength and pore structure development in cement pastes containing 45 to 56 percent of a type F Ligan, Nova Scotia fly ash.

Cement paste mixtures containing 45 and 56 percent fly ash each at W/S of 0.35 and 0.30 were prepared using a lignosol based superplasticizer and cured for 6 months. During curing, thermal analysis, pore size distribution, SEM, permeability, porosity, compressive strength and modulus of elasticity data were obtained.

Results showed that relatively high values of mechanical properties may be obtained at relatively early times. The following factors may explain this observation.

- (a) At early times the blended pastes have effectively a high water-cement ratio (≈ 0.70).
- (b) The initial cement reaction is accelerated.
- (c) The fly ash - Ca(OH)_2 reaction commences at a period earlier than 3 days probably because of the large volume of fly ash used, provides a relatively large amount of the more reactive material.
- (d) Cement matrix and residual unreacted fly ash form a good mechanical bond.
- (e) A relatively homogeneous hydrate product with low Ca(OH)_2 content and low C/S ratio CSH produces a stronger body.

W3.2

REACTIVITY OF FLY ASH AT HIGH pH. H.S. Pietersen, A.L.A. Fraay and J.M.J.M. Bijen, Delft Tech. Univ., Fac. of Civ. Eng., Materials Science Section, 2628 CN Delft, The Netherlands.

The reaction of fly ash in concrete is only initiated after one or more weeks. In this incubation period the fly ash behaves as a more or less inert material and serves as a precipitation nucleus for Ca(OH)_2 and C-S-H gel originating from cement hydration. The occurrence of this incubation period can be explained by the strong dependency of the glass breakdown on the alkalinity of the pore water. The process of glass breakdown increases if the pH becomes higher than approx. 13.2, a situation which only occurs in cement pore waters after some days. The fly ash reactivity is also related to glass content, particle size and temperature.

In order to compare the reactivity of several Dutch class F fly ashes, size and density separated fractions of different fly ashes were reacted with a number of alkaline activators with a pH ranging from 13 to 13.7. The composition of both the reacted and unreacted fly ash fractions was analyzed using microprobe analysis, QXRD, SEM and TEM. Samples of the solution were analyzed after several time intervals and thus apparent activation energies could be calculated. Particle size and glass content appeared to be the major variables concerning fly ash reactivity. The effect of small differences in glass composition on ash reactivity is not entirely clear as most glasses contained varying amounts of crystalline inclusions.

W3.3

AGGLOMERATION OF HIGH CALCIUM FLY ASH FOR UTILIZATION: 1. PHYSICAL PROPERTIES. Kenneth L. Bergeson, Carol L. Kilgour & Scott Schlorholtz, Department of Civil & Construction Engineering, Iowa State University, Ames, IA.

Inability of the Iowa fly ash industry to meet their demands for fly ash during the peak construction months led the Iowa Fly Ash Affiliates Group to investigate storage alternatives available for high-calcium fly ashes. Conventional, closed storage facilities are extremely expensive and currently not cost effective. In addition the industry is faced with the rising costs of landfill disposal. This paper presents the results of utilizing the rapid self-cementitious properties of high-calcium ashes to agglomerate them into discrete aggregate size particles for stockpiling. The two fly ashes used in this study contained 25 to 30 percent calcium. Water was used as an agglomerating medium. Agglomeration was accomplished using three types of commercial equipment as follows: continuous rotary pan agglomerator, continuous auger agglomerator and a batch turbine agglomerator. All units produced relatively well graded aggregate material differing primarily in particle shape and texture. Production agglomeration capacity of all units range up to 50 tph. Previous work on laboratory bench studies of pan-agglomerated materials, stored under water for

over one year, indicated high particle stability and no tendency for mass cementing. Research work discussed includes; gradation and abrasion testing; strength and durability as an artificial aggregate in concrete; strength and durability as a treated and untreated base material; and use of the fine fraction for soil stabilization. Agglomerated pellets were also reground using a newly developed, energy efficient, micronizing technique. Research results using the reground ash in concrete and soil stabilization are also discussed.

W3.4

AGGLOMERATION OF HIGH CALCIUM FLY ASH FOR UTILIZATION: II. BINDING MECHANISMS AND LEACHING BEHAVIOR. Carol L. Kilgour, Kenneth L. Bergeson and Scott Schlorholtz, Department of Civil & Construction Engineering, Iowa State University, Ames, IA

Agglomeration provides an economical means of storing Iowa fly ash resources for future use in construction as a base material, as a soil stabilization agent, and in concrete. Agglomerates were produced from two fly ashes using three commercial size agglomeration procedures. Evaluation of the chemical, mineralogical and morphological nature of the agglomerates shows that each of the three procedures used one or more of the following binding mechanisms: Solid bridges caused by chemical reaction, adsorption layers, molecular and electrostatic forces, and interlocking.

It is envisaged that the many potential uses of the agglomerated material could eventually result in the complete utilization of Iowa fly ash. At present, however, disposal of the agglomerates must be considered. Compared to dry fly ash disposal, agglomeration offers the advantages of reduced ash volume, easier handling and prevention of primary pollution. However, the possibility of groundwater contamination by leachate from the agglomerated material needs careful consideration.

This paper discusses the binding mechanisms used in the three agglomeration techniques and presents the results of the authors' work on leaching properties deemed important for agglomerate disposal.

W3.5

Study On The Properties Of Separated

Class F Fine Fly Ash

Consistent quality of fly ash is the main key to utilize it. In this study, we tried to use separation technique to improve the properties of fineness and ignition loss of fly ash.

In the experiment, fly ash was passed through dry sievers of No.200, No.300, and No.400 mesh. Chemical characteristics and physical properties of each classified fine fly ash were studied. Cement in mortar and paste were replaced with 10%, 20%, 30%, 40% and 50% of sieved and unsieved fly ash. Flowability, setting time, curing condition, compressive strength, shrinkage, and sulfate resistance of each formulated mixture were tested. The results showed as follows:

- (1) Ignition loss of separated fine fly ash is greatly reduced. It is good for cement and concrete mixing.
- (2) Fly ash passed No.300 sieve has good properties, high yield and economic processing cost.
- (3) Cement Products and ready mixed concrete which contain the fine fly ash, passing No.300 mesh,

replacing cement not more than 30%, can get advantages of both quality improvement and cost lowering.

W3.6

REACTIVITY OF FLY ASH-PORTLAND CEMENT- $\text{Ca}(\text{OH})_2$ - $\text{CaSO}_4 \cdot 2\text{H}_2\text{O}$ MIXTURES. R. L. Berger and Shamba Wang, Department of Civil Engineering, University of Illinois, 208 N. Mathews, Urbana, IL.

The influence of additions of $\text{Ca}(\text{OH})_2$ up to 15% and $\text{CaSO}_4 \cdot 2\text{H}_2\text{O}$ up to 8% on the reactivity and strength development of portland cement-fly ash pastes was investigated. Samples were batched on water/solid volume basis to ensure a equal initial porosity. Fly ash reactivity determined by $\text{Ca}(\text{OH})_2$ consumption ranged from 7% to 12%. Additions of $\text{Ca}(\text{OH})_2$ increased fly ash reactivity but not strength. $\text{CaSO}_4 \cdot 2\text{H}_2\text{O}$ additions resulted in equal or greater 90 day strengths than control samples.

W4.1

THE PRACTITIONERS VIEW OF FLY ASH UTILISATION. Ronald H. Mills, University of Toronto, Toronto, Ontario M5S 1A4.

Partial substitution of Portland cement (PC) with fly ash (FA) offers the practitioner increased scope for optimal utilisation of materials but requires careful evaluation of the resulting blended cement beyond the basic age-strength relationship. Nevertheless, characteristic strength is invariably specified, and for the practitioner, the cost of meeting this requirement depends on workability, the rate of strength gain and the influence of variability. The blend may be characterised by a mass efficiency factor which is the mass ratio of PC to FA which will yield the same target strength at fixed maturity and workability. Alternatively, the maturity efficiency factor may be determined as the ratio of log maturity values for the cements to reach a given target strength. Both efficiency factors incorporate important economic parameters of interest to the practitioner.

The glassy character of FA means that its inclusion attracts calcium hydroxide and sodium and potassium ions released into solution by the PC component. The risk of alkali-aggregate reaction is thus reduced. This characteristic may prove to be of such over-riding importance that a new approach to mix design is necessary. The essence of such an approach would be the provision of sufficient FA to absorb reactive species released by the PC. This might involve increased PC + FA and water, with concomitant reduction in aggregate and in fineness modulus.

Dimensional changes such as shrinkage and creep affect the distribution of load between steel and concrete in columns, the deflection of beams and slabs and cracking where displacements are restrained. In the case of PC concrete, both creep and shrinkage depend on the volume ratio of hydration products and the movement of pore water caused by drying and by mechanical load. The nature of the hydration products varies with PC/FA ratio and thus quantities such as the internal surface area, the hydraulic mean radius of pores and the effective modulus - the ratio of stress to total strain - must be evaluated.

W4.2

USE OF FLYASH IN CONCRETE - A EUROPEAN VIEW. Peter L. Pratt, Department of Materials, Imperial College, Prince Consort Road, London SW7 2BP, England.

The use of flyash in concrete is presented from the European point of view. The usage varies by country from as high as 96% in the case of Holland, to 10% in the UK. Beneficiation of the flyash is being used to improve the properties of the final concrete while mixed blends of flyash with silica fume and superplasticiser are being developed to make high grade, high strength concretes. Studies of the consumption of flyash by the pozzolanic reaction with calcium hydroxide are becoming more and more sophisticated and details of the pozzolanic calcium aluminate and calcium silicate hydrates are becoming increasingly clear. Their role in aiding strength development and in improving the durability of concrete is well

established and a number of different ways in which they can reduce chloride attack, carbonation and alkali-silica reaction has been identified. The importance of proper curing of the low-lime Class F flyashes commonly available in Europe is well understood but the conditions necessary for this to occur are not always employed on construction sites. Recent work in the UK has determined the effect of relative humidity upon the pozzolanic reaction and the hydration reaction and from this it should be possible to determine adequate curing regimes for a wide range of sizes of concrete structure and of drying conditions.

W4.3

RESISTANCE OF FLY ASH MORTARS TO SULPHATE ATTACK IN A CONTROLLED ENVIRONMENT. Robert L. Day and J. Konecny, Dept. of Civil Engineering, University of Calgary, Alberta, Canada

Sulphate-expansion tests were performed on mortar bars manufactured with two types of subbituminous fly ash and two types of cement. One fly ash was from Alberta, Canada while the second, a high-calcium ash, was from the United States. Ordinary and sulphate-resistant cements were used in the examination.

Bars were exposed to attack when they reached a given strength level. Some bars were soaked in a mixed solution of sodium and magnesium sulphate under controlled conditions; the pH of each solution was maintained at either 7 or 9.5 by regular additions of sulphuric acid. For other bars the pH of the solution was uncontrolled and was allowed to reach its natural equilibrium state. Behaviour of bars in water baths where pH was maintained constant was also examined. Bars were soaked in individual three-bar groups so that possible correlation between (a) amount of acid added and (b) linear bar expansion with time could be observed. Post-expansion examinations included strength degradation, qualitative X-ray analysis and thermal analysis.

Results show some interesting correlations, or lack thereof, between acid addition and sulphate attack. Mortars made with the Alberta ash performed better than the corresponding control mortars; however, in a mixed magnesium/sodium solution expansions were much greater than in previous tests where only sodium sulphate was used. Bars made with the U.S. ash performed very poorly under all conditions.

W4.4

PERFORMANCE OF A FLY ASH STABILIZED PAVEMENT. Joakim G. Laguros, the University of Oklahoma, Norman, OK; Curt Hayes, ODOT, Oklahoma City, OK.

An expansive shale roadbase, stabilized with a Class C (high-calcium) fly ash received a 6-inch asphaltic surface and the highway was opened to traffic six years ago. Periodic sampling and visual observations indicate that the performance of the pavement test sections are above average.

Analyses of field samples showed that fly ash, either alone or mixed with lime and cement, was effective in ameliorating the texture and plasticity of the shale and imparting strength to it on a long term basis. Pavement deflections and the extent of cracking have not increased beyond acceptable levels during the six year period.

XRD studies show a reduction of the areas under the peaks and the SEM observations reveal a dense degree of packing and reduction of the void areas. These modifications occur during the first two years of service and any changes beyond that period appear to be minor.

W4.5

THE EFFECT ON CEMENT MORTAR AND CONCRETE BY ADMIXTURE OF SPRAY DRYING ABSORPTION PRODUCTS. Kirsten G. Jeppesen, The Institute of Mineral Industry, The Technical University of Denmark, DK-2800 Lyngby.

Studies of the SDA-containing mortars mentioned at the MRS Fall Symposium 1987 have been continued and the state of the sulphur has been tested.

A full scale project concerning 3 front elements from concrete containing 20 and 30 wt.% spray drying absorption products (SDA) is kept under observation for development of strength, mineralogical composition and corrosion for the 2. year.

The use of SDA as filler for mortar and concrete has been studied and methods for decomposing the SDA-agglomerates has been developed. In addition the influence of chemical composition and grain size distribution in SDA has been studied.

An untraditional frost-thaw experiment has been made which includes SDA- and PC-mortars shows the effect of superplasticizers.

The setting time and water requirement for mortars containing different kinds and quantities of SDA have been studied.

The possibility of using SDA containing 4% Cl from NaCl in seawater (processwater) is under examination.

W5.1

EVALUATING THE USE OF PONDED FLY ASH IN A ROADWAY BASE COURSE. David Q. Hunsucker, Kentucky Transportation Center, Lexington, KY; and R. Clark Graves, Kentucky Transportation Center, Lexington, KY.

This report summarizes findings of laboratory and field trial evaluations of ponded fly ash as a component of a stabilized aggregate base course. Ponded fly ash is the fine portion of pond ash which is a by-product of coal burning processes and is disposed of by sluicing to a disposal pond.

Three stabilized aggregate base mixtures containing various proportions of dense graded aggregate, ponded fly ash, and hydrated lime were evaluated in the laboratory relative to maximum dry density, optimum moisture content, unconfined compressive strength, and static chord modulus of elasticity. The mixture that was selected for field trial evaluation had the highest unconfined compressive strength and consisted of 84% dense graded aggregate, 11% ponded fly ash, and 5% hydrated lime.

A 750-foot section of a 22-foot wide roadway was constructed in May 1988. Approximately 83 tons of ponded fly ash were utilized in constructing the experimental base. Prior to construction, in-place California Bearing Ratio tests, moisture content determinations and Road Rater deflection tests were performed to characterize the prepared subgrade. The stabilized aggregate base was placed in one 8-inch lift. During construction, relative compaction and moisture content of the base material were monitored by means of nuclear devices. Post construction evaluations included Road Rater deflection tests on the base and asphaltic concrete layers, and coring to obtain samples for laboratory evaluation.

To date, the section containing the stabilized aggregate base is performing very well in comparison to the conventionally designed section.

W5.2

STATE-OF-THE-ART IN MWC ASH DISPOSAL TECHNIQUES AND DESIGN REQUIREMENTS.

Keith E. Forrester, PE, Wheelabrator
Environmental Systems, Inc., 55 Ferncroft
Road, Danvers, MA 01923.

This paper presents the current practices employed by WES at its state-of-the-art ash landfills. The use of ash as an engineered material versus the disposal as a loose waste is the major direction of land application now being employed. By utilizing simple civil engineering methods, historically used in soil cement and standard soil foundation applications, this MWC ash is treated more like an aggregate cement matrix than a solid waste.

The application of the methods results in phenomenal physical and geotechnical/geochemical changes within the mixed MWC ash. Subsequent design considerations for ash runoff control, treatment and storage are discussed as well as suggested design changes for leachate collection and control, daily cover/interim cover/final cover use and post closure site utilization.

Empirical and laboratory demonstrated parameter changes in K_d , transport kinetics, runoff coefficients, density, UCS, visual observations, triaxial strengths and solubility/leaching results are presented in defense of the papers conclusions and recommendations for future MWC ash disposal practices.

W5.3

ENVIRONMENTAL ASSESSMENT OF BOTTOM ASH USED IN
ROAD STABILIZATION. Asmarre Atalay and Joakim G.
Laguros, Univeresity of Oklahoma, Civil Engineer-
ing and Environmental Science, Norman, Oklahoma.

Large amounts of fly ash and bottom ash are being produced by electric power plants and other facilities. While both fly ash and bottom ash are currently being disposed in land fills, fly ash is found to be a useful admixture to cement to make concrete. The usefulness of bottom ash as a soil stabilizer for unpaved roads is also being recognized. However, because of the levels of trace metals and organics present in the ash, there is increasing interest on the environmental problems that may result from the surface application of these wastes.

Soil, water and vegetation samples were collected from sites where bottom ash had been used to stabilize unpaved roads in Oklahoma. Similar samples were also collected from a fly ash stabilized road in the subsurface, and from a fly ash disposal site. In addition, fly ash, bottom ash, and coal samples were analyzed for metals and organics contents. Metals were analyzed by an Inductively Coupled Plasma (ICP) and the organics by a Gas-liquid Chromatograph.

Results indicated that fly ash used in the roadbed had no significant effect on the vegetation and water quality in the immediate vicinity. Surface applied bottom ash showed significant leaching of trace metals into the nearby streams and lakes, however, it had no detrimental effect on the surrounding vegetation.

SYMPOSIUM X:
FRONTIERS OF MATERIALS RESEARCH
A Series of Authoritative Reviews
for the Nonspecialist



November 27 - 30, 1989

Chair

Rustum Roy
Materials Research Laboratory
The Pennsylvania State University
University Park, PA 16802
(814) 865-3421

FRONTIERS OF MATERIALS RESEARCH
A Symposium Crossing All Symposia
Nonspecialist

November 27 - December 1, 1989

Chair: Rustum Roy

TV SESSION: THE NEW FRONTIERS

Monday, November 27

12:00 - 1:30 p.m.

Staffordshire Room (W)

The Society will initiate this year an experiment in new ways of reporting research results.

Five papers reporting the "hottest," up-to-the-minute advances in the field and representative of the scope of materials research will be broadcast live by satellite to industrial research laboratories, universities and others.

For satellite hook-ups in your institution, call NTU for industry (303-484-0565) or PBS for universities (1-800-257-2578).

12:05 *XNF1.1

NEW STEELS BY DESIGN, G.B. Olson, Department of Materials Science and Engineering and Materials Research Center, Northwestern University, Evanston, IL.

12:20 *XNF1.2

DIAMOND SCHOTTKY DIODES BASED ON GROWTH OF THICK ($>100\mu$) B-DOPED HOMOEPITAXIAL FILMS, G. Gildenblat, S.A. Grot, C.W. Hatfield, C.R. Wronski, A.R. Badzian, T. Badzian and R. Messier, The Pennsylvania State University, University Park, PA.

12:35 *XNF1.3

MATERIALS SYNTHESIS UTILIZING BIOLOGICAL PROCESSES, Lynn Oehler, Chris Hobbs, Mark Mastandrea and Mark Bednarski, Lawrence Berkeley Laboratories, The Center for Advanced Materials, Berkeley, CA.

12:50 *XNF1.4

LIQUID CRYSTALLINE MATERIALS FOR POLYMER WITH ANISOTROPIC ULTRASTRUCTURES, G.S. Attard, The University, Southampton, United Kingdom.

1:05 *XNF1.5

PULSED UV-LASER PROCESSING FOR ULTRA-HIGH-SPEED DEVICE TECHNOLOGY, Thomas W. Sigmon, Stanford University, Stanford, CA; Kurt H. Weiner, Lawrence Livermore National Laboratory, Livermore, CA; and Paul G. Carey, Siemens, Munich, West Germany.

*Invited Paper

SESSION X2

Tuesday, November 28

12:05 - 1:25 p.m.

Staffordshire Room (W)

12:05 *X2.1

LOW-TEMPERATURE PROCESSING OF NOVEL HIGH T_c SUPERCONDUCTING THIN FILMS AND APPLICATIONS, J. Narayan, North Carolina State University, Raleigh, NC.

12:45 *X2.2

REVIEW AND STATUS OF LANXIDE'S TECHNOLOGIES FOR REINFORCED CERAMICS AND METALS, A.W. Urquhart, Lanxide Corporation, Newark, DE.

SESSION X3

Wednesday, November 29

12:05 - 1:25 p.m.

Staffordshire Room (W)

12:05 *X3.1

NANOCOMPOSITE APPROACHES TO NOVEL PROPERTIES IN POLYMERS, D. Ulrich, Air Force Office of Scientific Research, Washington, DC.

12:45 *X3.2

SUPERCONDUCTOR STATUS II: PHYSICS OF HIGH T_c SUPERCONDUCTIVITY, R.C. Dynes, AT&T Bell Laboratories, Murray Hill, NJ.

SESSION X4

Thursday, November 30

12:05 - 1:25 p.m.

Staffordshire Room (W)

12:05 *X4.1

ADVANCES IN ZEOLITES AND OTHER MICROPOROUS MATERIALS, David Vaughan, Exxon Research and Development, Annandale, NJ.

12:45 *X4.2

SYNTHETIC METALS: A NOVEL ROLE FOR ORGANIC POLYMERS, Alan MacDiarmid, University of Pennsylvania, Philadelphia, PA.

XNF1.1

NEW STEELS BY DESIGN, G.B. Olson, Department of Materials Science and Engineering and Materials Research Center, Northwestern University, Evanston, IL.

Nucleation of a fine dispersion of optimal-stability equilibrium austenite has produced record fracture toughness in AF1410 steel, using state-of-the-art 'design' by combining detailed characterization, thermodynamics (via THERMOCALC) and kinetics of precipitation and coarsening. This has led to the conceptual design of new steel compositions for specific high performance applications. New compositions have been designed for enhanced transformation dilatancy for greater transformation toughening.

XNF1.2

DIAMOND SCHOTTKY DIODES BASED ON GROWTH OF THICK (>100 μ) B-DOPED HOMOEPITAXIAL FILMS, G. Gildenblat, S.A. Grot, C.W. Hatfield, C.R. Wronski, A.R. Badzian, T. Badzian and R. Messier, The Pennsylvania State University, University Park, PA.

Using microwave plasma CVD we have been able to deposit B-doped single crystal (and polycrystalline) homoepitaxial diamond layers >150 μ thick on natural single crystals. Schottky diodes with excellent rectifying characteristics were obtained using a single crystal homoepitaxial base. As in the case of Schottky diodes with a polycrystalline diamond base, diode characteristics are controlled by deep acceptors.

Additional treatment of the homoepitaxial film surface can induce the transition from rectifying to ohmic behavior of the metal/CVD diamond contacts.

XNF1.3

MATERIALS SYNTHESIS UTILIZING BIOLOGICAL PROCESSES, Lynn Oehler, Chris Hobbs, Mark Mastandrea and Mark Bednarski, Lawrence Berkeley Laboratories, The Center for Advanced Materials, Berkeley, CA.

We report on a program to use enzymatic methods of polymerization and surface modification to prepare new polymeric materials from unnatural monomers in the areas outlined below. (1) The chemical-enzymatic synthesis of fluorinated and sulfated polysaccharides using glycogen phosphorylase, sucrose phosphorylase and lysozyme; (2) the chemical and enzymatic modification of semiconductor materials and other polymers, and the use of these materials to study the interfacial properties associated with the binding of bacteria and viruses.

XNF1.4

LIQUID CRYSTALLINE MATERIALS FOR POLYMERS WITH ANISOTROPIC ULTRASTRUCTURES, G.S. Attard, The University, Southampton, United Kingdom.

Materials with anisotropic ultrastructures can be obtained by constructing polymers with anisometric groups in the main-chain, as pendant side-chains, or a combination of both. Using this approach it is therefore possible to design multifunctional materials whose properties are optimised with respect to particular applications. Examples of high T_g photoactive LC side-chain polymers with

potential as n.l.o. materials will be described. In order to achieve greater control on the ultrastructure another approach is required. This involves the use of polymerisable LC monomers whose mesomorphic structure, whether lyotropic or thermotropic, can be locked by in situ polymerisation. Using this route it is possible to prepare polymers with a range of anisotropic ultrastructures. Examples of such polymeric materials derived from thermotropic and lyotropic LC phases will be described.

XNF1.5

PULSED UV-LASER PROCESSING FOR ULTRA-HIGH-SPEED DEVICE TECHNOLOGY, Thomas W. Sigmon, Stanford University, Stanford, CA; Kurt H. Weiner, Lawrence Livermore National Laboratory, Livermore, CA; and Paul G. Carey, Siemens, Munich, West Germany.

We have used pulsed uv-laser doping and selective epitaxy for vertical scaling of junctions for silicon MOS and bipolar structures and fabrication of selective heterostructure layers. Successful applications in the fabrication of submicron MOSFETs and narrow base bipolar transistors in silicon will be presented. Results, both structural and electrical, on the fabrication of heterostructures layers in the Ge_xSi_{1-x} and In_xGa_{1-x}As material systems will be presented.

X2.1

LOW-TEMPERATURE PROCESSING OF NOVEL HIGH T_c SUPERCONDUCTING THIN FILMS AND APPLICATIONS, J. Narayan, North Carolina State University, Raleigh, NC.

This talk reviews the progress made in the formation of superconducting thin films. Epitaxial films which can sustain current densities up to 6.0x10⁶ A cm⁻² at 77K have been fabricated using "in-situ" pulsed laser deposition techniques. Details of epitaxial growth and correlations between microstructure and superconducting properties of high-T_c thin films will be highlighted.

X2.2

REVIEW AND STATUS OF LANXIDE'S TECHNOLOGIES FOR REINFORCED CERAMICS AND METALS, A.W. Urquhart, Lanxide Corporation, Newark, DE.

This paper is intended to update the MRS audience on the current status of Lanxide's novel technologies for ceramic and metal matrix composites. Included will be a short review of the processing methods, a description of properties and performance characteristics achieved, and a brief summary of applications being addressed and the current commercialization status.

X3.1 ABSTRACT NOT AVAILABLE

X3.2

SUPERCONDUCTOR STATUS II: PHYSICS OF HIGH T_c SUPERCONDUCTIVITY, R.C. Dynes, AT&T Bell Laboratories, Murray Hill, NJ.

The number of known high T_c phases and our understanding of the physics underlying high T_c superconductivity have both grown dramatically in the three years since La_{2-x}Ba_xCuO₄ was identified as a 30K superconductor. Recent advances include measurements of reproducible tunneling data on YBa₂Cu₃O₇. This talk summarizes the current state of research on high temperature superconducting oxides.

X4.1 ABSTRACT NOT AVAILABLE

X4.2 ABSTRACT NOT AVAILABLE

**SYMPOSIUM Y:
SPECIALTY CEMENTS WITH
ADVANCED PROPERTIES**

Y

November 27-29, 1989

Chairs

Barry E. Scheetz
Materials Research Laboratory
Pennsylvania State University
University Park, PA 16802
(814) 865-3539

Ivan Odler
Tech Universitat
Clausthal Zehntnerstrasse
2A Clausthal-Zellerfeld
West Germany
011-49-5323-722251

Hamlin Jennings
Northwestern University
Technological Institute
2145 Sheridan Road
Evanston, IL 60208
(312) 491-4655

Albert Landers
Armstrong World Industries
2500 Columbia Avenue
Lancaster, PA 17603
(717) 396-5352

Symposium Support

CEMCOM Corporation

Geochemical Corporation

W. R. Grace & Company

Pennsylvania State University Chemically
Bonded Ceramics Consortium

Pyrament Division of Lone Star Industries

**Proceedings published as Volume 179
of the Materials Research Society
Symposium proceedings series.**

SPECIALTY CEMENTS WITH ADVANCED PROPERTIES

November 27-29, 1989

SESSION Y1: PHOSPHATE CEMENTS

Chair: A. Landers

Monday Morning, November 27
Adams Room (W)

8:30 INTRODUCTION BY SYMPOSIUM CHAIRS

8:40 INTRODUCTION BY SESSION CHAIR, A. Landers

8:45 *Y1.1

SELF-SETTING CALCIUM PHOSPHATE CEMENT, Laurence C. Chow, American Dental Association Health Foundation, Paffenbarger Research Center, National Institute of Standards and Technology, Rockville, MD.

9:30 Y1.2

THE SOLUTION CHEMISTRY OF CALCIUM PHOSPHATE CEMENT, Paul W. Brown, David Sample and Nancy Hocker, Pennsylvania State University, Department Materials Science, University Park, PA.

10:00 Y1.3

CALCIUM PHOSPHATE DENTAL CEMENT, Like Xie, and E.A. Monroe, Alfred University, New York State College of Ceramics, Alfred, NY.

10:30 BREAK

10:45 Y1.4

LOW-TEMPERATURE (<300°C) PHOSPHATE CERAMICS FROM REACTIVE ALUMINAS, M.R. Silsbee, R. Steinke, D.M. Roy, D. Agrawal and R. Roy, Pennsylvania State University, The Materials Research Laboratory, University Park, PA.

11:15 Y1.5

INVESTIGATIONS ON PHOSPHATE CEMENTS HARDENING AT ROOM TEMPERATURE, Alfred Zürz and Ivan Odler, Technical University of Clausthal, Institute of Nonmetallic Materials, Clausthal-Zellerfeld, West Germany.

SESSION Y2: SPECIAL PROCESSING (I) - DSP

Chair: L. Struble

Monday Afternoon, November 27
Adams Room (W)

12:55 INTRODUCTION BY L. STRUBLE

1:00 *Y2.1

ELEVATED TEMPERATURE BEHAVIOR OF DSP-TYPE CEMENTS, Sean Wise, CEMCOM Corporation, Lanham, MD.

*Invited Paper

1:45 Y2.2

PORE STRUCTURE OF DSP PASTES DETERMINED BY LOW ANGLE SCATTERING, T.A. Bier, University of Illinois, Center for Cement Composite Materials, Urbana, IL; J. Olek, D. Winslow, Purdue University, Department of Civil Engineering, West Lafayette, IN; and J.F. Young, University of Illinois, Center for Cement Composite Materials, Urbana, IL.

2:15 BREAK

SESSION Y2: RELATED TOPICS WITH GENERAL INTEREST (I)

Monday Afternoon, November 27
Adams Room (W)

2:30 Y2.3

A STUDY OF LOW POROSITY POLYMERIZED β -C₂S PASTE, Lu Ping, Zhao Jin and Shen Wei, Tongji University, Department of Materials Science and Engineering, Shanghai, China.

3:00 Y2.4

MORPHOLOGY AND LONG TERM BEHAVIOR OF POLYMER CEMENT CONCRETE (PCC), K.P. Grosskurth, Technical University Braunschweig, Institut für Baustoffe, Massivbau und Brandschutz, Braunschweig, West Germany.

3:30 Y2.5

PREPARATION AND PROPERTIES OF ZNO-PAA CEMENTS, A. Padilla, A. Vázquez, UNAM, Instituto de Investigaciones en Materiales, México, México; V.M. Castaño, UNAM, Instituto de Física, México, México.

4:00 Y2.6

MICROSTRUCTURE, MASS TRANSPORT AND DENSIFICATION OF SLAG-CEMENT PASTES, Q.L. Feng and F.P. Glasser, University of Aberdeen, Department of Chemistry, Old Aberdeen, Scotland.

4:30 Y2.7

HIGH WATER CEMENT RATIO CLAY CEMENT GROUTS, Stephan A. Jefferis, Queen Mary College, University of London, Department of Civil Engineering, London, United Kingdom.

SESSION Y3: NEW CEMENT SYSTEMS

Chair: Paul W. Brown

Tuesday Morning, November 28
Adams Room (W)

8:25 INTRODUCTION BY SESSION CHAIR, Brown

8:30 *Y3.1

STRATLINGITE-HYDROXYGARNET CEMENTS FROM CaO-Al₂O₃-SiO₂ GLASSES, John F. Macdowell, Corning Inc., Corning, NY.

9:15 Y3.2
CHARACTERIZATION AND CEMENTITIOUS BEHAVIOR OF A NEW REACTIVE ALUMINA, D.K. Agrawal, M.R. Silsbee, and R. Roy, Pennsylvania State University, The Materials Research Laboratory, University Park, PA.

9:45 Y3.3
THE HYDRATION AND CALCINATION MECHANISM OF CALCIUM ALUMINATE BASED ULTRA-HIGH STRENGTH CEMENT WITH CALCIUM SULPHOALUMINATE COMPOUND, Iwao Mino, Etsuo Sakai, Asaaki Nishioka, Denki Kagaku Kogyo K.K. Research Center, Tokyo, Japan; and Masaki Daimon, Tokyo Institute of Technology, Department of Inorganic Materials, Tokyo, Japan.

10:15 BREAK

10:30 *Y3.4
PYRAMENT -- A CEMENT FOR THE 21ST CENTURY-- AVAILABLE NOW, William D. Kirkpatrick, Lone Star Industries, Research and Development II, Pyrament Division, Houston, TX.

11:15 Y3.5
NEW RAPID SETTING ALKALI ACTIVATED CEMENT COMPOSITIONS, D.M. Roy and M.R. Silsbee, Pennsylvania State University, The Materials Research Laboratory, University Park, PA.

11:45 Y3.6
CORROSION BEHAVIOR OF CONCRETE MADE WITH PYRAMENT CEMENT, Harovel G. Wheat, University of Texas at Austin, Mechanical Engineering Department, Austin, TX.

12:15 Y3.7
ALKALI ACTIVATED SLAG AND PORTLAND/SLAG ULTRAFINE CEMENTS, William J. Clarke, Geochemical Corporation, Ridgewood, NJ; and Maan Helal, Northwestern University, Evanston, IL.

SESSION Y4: SPECIAL PROCESSING (II) - MDF
Chair: I. Odler
Tuesday Afternoon, November 28
Adams Room (W)

1:25 INTRODUCTION BY SESSION CHAIR,
I. Odler

1:30 *Y4.1
MDF - AN OVERVIEW, J. Francis Young, University of Illinois, Urbana, Center for Cement Composite Materials, Urbana, IL.

2:15 Y4.2
FRACTURE TOUGHNESS OF MACRO-DEFECT-FREE (MDF) CEMENTS BY INDENTATION TECHNIQUE, Yeong-Shyung Chou, J.J. Mecholsky Jr., M.R. Silsbee, D.M. Roy, J. Adair, and P. Heiland, Pennsylvania State University, The Materials Research Laboratory, University Park, PA.

2:45 Y4.3
THE CHEMISTRY OF MDF CEMENTS PRODUCED FROM POLYACRYLAMIDE-CEMENT WATER PASTES, M.R. Silsbee, D.M. Roy, Pennsylvania State University, Materials Research Laboratory, University Park, PA.

3:15 BREAK

3:30 Y4.4
IMPROVING THE WATER RESISTANCE OF MACRO-DEFECT-FREE CEMENT, M. Berg, P.P. Russell and J.F. Young, University of Illinois, Center for Cement Composite Materials, Urbana, IL.

4:00 Y4.5
A VIEW OF MDF PASTES, M.R. Silsbee, M. Perez-Pena and D.M. Roy, Pennsylvania State University, The Materials Research Laboratory, University Park, PA.

4:30 Y4.6
PORTLAND CEMENT - BASED MDF CEMENTS, J. Falkner, and J. Francis Young, University of Illinois, Urbana, Center for Cement Composite Materials, Urbana, IL.

SESSION Y5: RELATED TOPICS WITH GENERAL INTEREST (II)

Chair: P. Pratt
Wednesday Morning, November 29
Adams Room (W)

8:25 INTRODUCTION BY P. PRATT

8:30 Y5.1
CHEMICALLY BONDED CERAMICS, Paul W. Brown, Pennsylvania State University, Department of Materials Science, University Park, PA.

9:00 Y5.2
THE PROPERTIES OF GYPSUM - FREE PORTLAND CEMENTS, Tomáš Vřetěčka, Building Research Institute, Prague, Czechoslovakia; František Škvára and Jaroslav Hrazdír, Czechoslovakia Academy of Science, Institute of Glass and Ceramics Chemistry, Prague, Czechoslovakia; and Pius Ďurovec, Cementwork Prachovice, Prachovice, Czechoslovakia.

9:30 Y5.3
LEACHABILITY OF CEMENT SOLIDIFIED INCINERATOR WASTE, Tahar El-Korchi, Worcester Polytechnic Institute, Worcester, MA; David L. Gress and Robin Collins, University of New Hampshire, Department of Civil Engineering, Durham, NH.

10:00 BREAK

10:15 Y5.4

THE CHEMISTRY OF AL-TOBERMORITE AND ITS COEXISTING PHASES AT 175°C, Mary W. Barnes and Barry E. Scheetz, Pennsylvania State University, Materials Research Laboratory, University Park, PA.

10:45 Y5.5

NUMERICAL SIMULATION OF THE FREEZING PROCESS AND HYDRAULIC PRESSURE FIELDS IN A CEMENTITIOUS MATRIX, Tahar El-Korchi, John M. Sullivan Jr. and Andreas N. Alexandrou, Worcester Polytechnic Institute, Worcester, MA.

11:15 Y5.6

STRUCTURE AND PROPERTIES OF ALKALI SILICATE BASED BINDERS, Ivan Odler and Ulrich Hennicke, Technical University of Clausthal, Institute of Nonmetallic Materials, Clausthal-Zellerfeld, West Germany.

11:45 CLOSING REMARKS BY SYMPOSIUM CHAIR

Y1.1 ABSTRACT NOT AVAILABLE

Y1.2 ABSTRACT NOT AVAILABLE

Y1.3

CALCIUM PHOSPHATE DENTAL CEMENT. Like Xie and E. A. Monroe, New York State College of Ceramics, Alfred University, Alfred, NY, 14802.

Cement systems composed of mixtures of various calcium phosphate powders and aqueous solutions of H_3PO_4 , $Ca(OH)_2$ or Na_2SiO_4 which can yield a reaction product of hydroxyapatite, $Ca_5(PO_4)_3(OH)$, were investigated. The investigated powder mixtures contained tetracalcium phosphate ($Ca_4P_2O_9$) plus one of the following: brushite ($CaHPO_4 \cdot 2H_2O$), monetite ($CaHPO_4$), tricalcium phosphate ($Ca_3(PO_4)_2$), and octacalcium phosphate ($Ca_8H_2(PO_4)_6 \cdot 5H_2O$). In order to determine the optimal conditions for cement setting reactions, first reactions of powder mixture in dilute solutions were performed. Using these dilute solution reactions as a foundation, cement systems were then formulated. The reaction products of cement system were characterized by both powder X-ray diffraction analysis and infrared spectroscopy.

The cement system of tetracalcium phosphate and brushite hardened into a solid composed of hydroxyapatite within a reasonable short time. The setting time and strength depended on both composition and content of liquid. Additives of CaF_2 and hydroxyapatite promoted the formation of hydroxyapatite and reduced the setting time.

The biocompatibility was also investigated by implanting cement into the jaw bone of rats for up to 12 weeks, and evaluating them both clinically and histologically by microscopy and SEM. The results indicated that the cement containing tetracalcium phosphate and brushite was the optimum composition for both biocompatibility and short setting time.

Y1.4

LOW-TEMPERATURE (< 300 °C) PHOSPHATE CERAMICS FROM REACTIVE ALUMINAS. M.R. Sijbeek, R. Steinke, D.M. Roy, D. Agrawal, R. Roy, The Materials Research Laboratory, Pennsylvania State University, University Park, Pa.

Reactive aluminas including rapidly calcined gibbsites offer exciting potential for forming ceramic materials at low temperatures. New x-ray amorphous aluminas will react with water at room temperatures to form compacts with 10 - 50 MPa tensile strengths, via viscous slurries. The cementitious behavior of these materials has been examined. The results of TGA, X-ray, SEM, isothermal calorimetry, mechanical properties and other characterization techniques as applied to these systems will be discussed.

Y1.5

INVESTIGATIONS ON PHOSPHATE CEMENTS HARDENING AT ROOM TEMPERATURE: Alfred Zürz and Ivan Odler, Technical University of Clausthal, Clausthal-Zellerfeld, Fed. Rep. Germany

Cements with high early strength can be prepared from magnesium oxide MgO and various soluble phosphates. The strength depends strongly on the quality of the MgO employed and the kind of phosphate and retarder used. In this paper various phosphate binder systems have been studied and their strength properties and structure are reported. Intensive investigations were done especially on the system $MgO/(NH_4)_2HPO_4$.

Y2.1 ABSTRACT NOT AVAILABLE

Y2.2

PORE STRUCTURE OF DSP PASTES DETERMINED BY LOW ANGLE SCATTERING. T. A. Bier¹, J. Olek², D. Winslow² and J. F. Young¹ (1) Center for Cement Composite Materials, University of Illinois, Urbana, IL; (2) School of Civil Engineering, Purdue University, W. Lafayette, IN.

DSP (Densified with Small Particles) cement pastes were prepared using a high alite Portland cement and varying amounts of high quality by-product silica fume. Previous work has shown that DSP pastes have a particularly fine pore structure which is very sensitive to removal of water. Even solvent replacement drying is likely to cause permanent changes. Thus saturated pastes were examined by low angle scattering with varying hydration times and fume contents. The results will be compared to those obtained by nitrogen adsorption studies on pastes dried by methanol replacement.

Y2.3

A STUDY OF LOW POROSITY POLYMERIZED B-C₂S PASTE. Lu Ping, Zhao Jin and Shen Wei, Department of Materials Science and Engineering, Tongji University, Shanghai 200092, China.

A high active B-C₂S is used in this paper to prepare polymerized hardened paste with low porosity by compacting under pressure of 250 MPa in water/solid ratio of 0.12. XRD, MIP, SEM-EDPA and GPC techniques are employed to detect micro-structure of the paste before and after adding inorganic complex ion Fe^{2+} and Ni^{2+} or organic silane VTES.

The test results indicate that the inorganic ions and organic silane can take part in polymerizing reaction during hydration of the B-C₂S paste, it makes the content of polymer in it distinctly increase, and average C/S ratio decrease to lower than 0.8. The intrinsic properties of C-S-H gel in the paste thus can be greatly improved, resulting in further development of mechanical strength of this low porosity paste. The highest compressive strength has achieved 316 MPa. Meanwhile, the fracture energy of the materials increases and the brittleness decreases.

Y2.4

MORPHOLOGY AND LONG TERM BEHAVIOUR OF POLYMER CEMENT CONCRETE (PCC). K. P. Großkurth, Institut für Baustoffe, Massivbau und Brandschutz, TU Braunschweig, West-Germany.

PCC represents a heterogeneous material whose properties, compared with conventional concrete, are additionally influenced by the strongly temperature dependent polymeric behaviour. In the hydraulic binder film-formed polymers obviously form a second coherent co-matrix system which couples to the surface of the aggregates and intersperses the hydrated cement in the form of links and porous polymeric membranes. Therefore the polymeric co-matrix system is able to absorb and transfer power due to its structural conditions. Because of their visco-elastic state under normal temperature conditions film-formed polymer additives are only able to increase deformability and to decrease the elastic modulus and strength of concrete. To get an stabilization effect the temperature of application has to range below the glass transition temperature of the polymer.

For the use of modified concrete it is important to have good knowledge of its long-term behaviour of strength and deformability. The test results of compressive strength show that the delayed rise of strength increases with rising polymer content: PCC with polymer to cement ratio of $p/c = 0.15$ will achieve strength of ordinary cement concrete only after two years. The structure of polymeric

matrix may be the reason for the delayed hydration. The polymeric intermediate layers obstruct diffusion processes as these processes take place in cement hydration. Investigations of PCC-creep under constant stress indicate rising deformability with increasing polymer content, because of their visco-elastic state the polymeric intermediate layers form slip planes in the binder.

Y2.5

PREPARATION AND PROPERTIES OF Zn O- PAA CEMENTS. A Padilla, A. Vázquez, Instituto de Investigaciones en Materiales, U.N.A.M., A. P. 70-360, México, D. F. 04510 and V. M. Castaño, Instituto de Física, U.N.A.M., A. P. 20-364, México, D. F. 01000.

Special low-temperature-processed cements based in ZnO and polyacrylic acid (PAA) were prepared. A detail study of the influence of various physico-chemical parameters (i.e. viscosity, solids content, polymer content, PH, etc.) upon the performance of the resulting material is presented. Also, the mechanical properties (elastic modulus, fracture toughness, etc.) of the cements were analyzed as well as the corresponding microstructure by using electron microscopy.

Y2.6

MICROSTRUCTURE, MASS TRANSPORT AND DENSIFICATION OF SLAG-CEMENT PASTES. Q.L. Feng and F. P. Glasser, Department of Chemistry, University of Aberdeen, Old Aberdeen, AB9 2UE, Scotland.

An important property of well-cured slag-cement blends is their low permeability. The densification process in slag-cement blends has been followed by electron microscopy and electron microanalysis to determine changes to the matrix microstructure and mineralogy. Briefly, Mg in the slag remains on the site of former glassy slag grains, but combines with enough Al to give a hydrotalcite phase: some Ca and Si also remain, probably as C-S-H, but much Ca and Si migrate into the paste matrix. This transfer of chemical substance provides the driving force for matrix densification. Mass balance calculations are used to support these observations and to generalize on them, so the extent of densification potential can be calculated for various blend proportions as well as for slags having different chemical compositions. Specimen calculations are presented. Quality assurance of slag is to be optimized. The ability to calculate the potential for densification, at least in principle, is seen as an important step forward in design for durability.

Y2.7

HIGH WATER CEMENT RATIO CLAY CEMENT GROUTS Stephan A. Jefferis, Queen Mary College, University of London, U.K.

High water/cement ratio clay cement grouts now find wide application in the formation of underground cut-off walls for groundwater control and toxic waste containment. To form a cut-off wall a trench is excavated and kept continuously filled with the fluid grout which must stabilise the excavation much as a drilling fluid stabilises an oilwell during drilling. On completion of the excavation the grout must set to form a material with strength and permeability comparable to that of a clay. The grouts therefore have to meet rather unusual specifications.

In addition to their use in the field it has been found that they can offer great advantages in the laboratory as modelling materials for cement systems. The high water cement ratio makes them very sensitive to shear level during mixing, cement admixtures, deleterious chemicals, etc. Their properties are also highly sensitive to the use of fly ash and ground granulated blast furnace slag as cement replacements. In particular it is found that the percentage replacement rather than the absolute quantity is significant and it is possible to design a material that gets weaker as the total quantity of cementitious material is increased -

an effect yet to be observed in concrete. The grouts are of relatively high permeability compared with concrete and so the effects of deleterious chemicals can be investigated quite rapidly. For example it is possible to demonstrate a chromatographic separation of adsorbed species - a phenomena that will occur in concrete but only over a very extended timescale. In summary these grouts are useful not only in the field for their special application but also in the laboratory as modelling materials that may shed new light on the behaviour of cementitious systems and in a much shorter timescale than concrete or low water cement ratio grouts.

Y3.1 ABSTRACT NOT AVAILABLE

Y3.2

CHARACTERIZATION AND CEMENTITIOUS BEHAVIOR OF A NEW REACTIVE ALUMINA. D.K. Agrawal, M.R. Silsbee and R. Roy, Materials Research Laboratory, The Pennsylvania State University, University Park, PA 16802-4801.

Highly reactive alumina (from Rhone-Poulenc) which is x-ray amorphous, offers a great potential as an Al-source precursor for forming low temperature chemically bonded ceramics. This alumina was characterized for its thermal behavior, structure, hydration reaction kinetics using XRD, TGA, DTA, IR, isothermal calorimetry, and the data are compared with those of other conventional aluminas and precursors such as α -Al₂O₃, gibbsite and boehmite. The results of hydration studies will also be presented.

Y3.3

THE HYDRATION AND CALCINATION MECHANISM OF CALCIUM ALUMINATE BASED ULTRA-HIGH STRENGTH CEMENT WITH CALCIUM SULPHOALUMINATE COMPOUND Iwao Mino*, Etsuo Sakai*, Asaaki Nishioka*, Masaki Daimon**, *DENKI KAGAKU KOGYO K.K. Research Center, 3-5-1 Asahi-cho Machida-shi, Tokyo, 194, JAPAN, **Dept. of Inorganic Materials, Tokyo Institute of Technology, 2-12-1 O-okayama-cho Meguro-ku, Tokyo, 152, JAPAN

The authors have reported about the calcium aluminate based ultra-high strength cement, or the densified system containing homogeneously arranged ultra-fine particles (DSP), with highly improved bending strength and relatively large hardening shrinkage. This report deals with the hydration and calcination mechanism of calcium aluminate based DSP with calcium sulphoaluminate. The hardening shrinkage becomes nearly zero, and very high bending strength can be obtained by calcining at 300-600 °C. The starting materials are a calcium aluminate compound, silica fume, calcium sulphoaluminate and superplasticizer, and the water to solid ratio is 0.15-0.25. The hydration and calcination mechanism and morphology are studied by means of XRD, thermal analysis (DSC), Hg-porosimetry and SEM/EDS. The main hydration products are C₃AH₆, AH₃ and ettringite, forming a densely packed structure together with a large amount of unreacted cement particles. The hardening shrinkage is remarkably reduced, because of the ettringite formation in the early stage. The bending strength is about 55MPa, when calcined at 600 °C. C₃A₇ and CS are identified by XRD, needle-shaped skeleton of ettringite crystals are observed by SEM. It is suggested that chemically bonding substances are C₃A₇, amorphous Al₂O₃, and CS in calcined calcium aluminate based DSP with ettringite.

Y3.4 ABSTRACT NOT AVAILABLE

Y3.5

NEW RAPID SETTING ALKALI ACTIVATED CEMENT COMPOSITIONS, D.M. Roy and M.R. Silsbee, The Materials Research Laboratory, Pennsylvania State University, University Park, Pa.

Recently a new rapid setting cement composition has been marketed under the trade name "Pyrament". This cement is an alkali-activated

blended cement composition that relies on the action of soluble alkalis on fine-grained non-crystalline aluminosilicates to produce high early strengths. This report examines possible reaction mechanisms of "synthetic" compositions developed in our own laboratory. The possibility of utilizing these rapid setting compositions to produce MDF cements is also addressed. Comparisons are made with the properties of manufactured "Pyrament" cement.

Y3.6

CORROSION BEHAVIOR OF CONCRETE MADE WITH PYRAMENT CEMENT. Harovel G. Wheat, Mechanical Engineering, University of Texas at Austin

The corrosion resistance of concrete specimens made using cement having the trade name Pyrament has been determined by means of polarization resistance and Electrochemical Impedance Spectroscopy. Three water-cement ratios were tested, namely 0.25, 0.27, and 0.29. Based on tests conducted on samples continuously immersed in a 3.5 % NaCl solution as well as those subjected to alternating wetting and drying conditions for over a year, the specimens have exhibited remarkable corrosion resistance. The results of electrochemical testing as well as surface analysis data will be given.

Y3.7

ALKALI ACTIVATED SLAG AND PORTLAND/SLAG ULTRAFINE CEMENTS. William J. Clarke, Geochemical Corporation, Ridgewood, NJ; and Maan Helal, Northwestern University, Evanston, IL.

Ultrafine Alkali Activated Slag (AAS) and Portland/Slag (P/S) cements have been commercially available in the United States for 2 and 5 years respectively. Ultrafine cements have been researched at Northwestern University for 6 years.

Particle size of the ultrafine slag is 2 percent at 7 micron and 50 percent at 3 micron... ultrafine portland/slag is 2 percent at 10 micron and 50 percent at 4 micron.

Chemical composition of the slag is 35 percent SiO_2 , 16 percent Al_2O_3 and 43 percent CaO . Composition of the 50 percent portland/50 percent slag cement is between portland and slag.

Both ultrafine cements permeate fine sands at higher water cement ratio. Viscosity plays an important part in the permeation mechanism... both grouts are below 10 cps at 2:1 water cement ratio. This low viscosity is obtained through superplasticizing with naphthalene sulfonate and acrylic acid polymers.

Application of the ultrafine cements includes dam grout curtain rehabilitation, consolidation grouting and nuclear and hazardous waste containment. One hundred and twenty metric ton of portland/slag cement has been used for hazardous waste containment at Niagara Falls, New York.

Y4.1 ABSTRACT NOT AVAILABLE

Y4.2

FRACTURE TOUGHNESS OF MACRO-DEFECT-FREE (MDF) CEMENTS BY INDENTATION TECHNIQUE. Yeong-Shyung Chou, J. J. Mecholsky, Jr., M. Silsbee, D. M. Roy, J. Adair, P. Heiland, Materials Research Laboratory, The Pennsylvania State University, University Park, PA 16802.

The fracture toughness of MDF cement with different polymer contents has been investigated by the indentation-strength method and fracture surface analysis. Samples were cut into beams, indented at loads from 1Kg to 15Kg and broken in 3-point flexure. It was found that the fracture toughness obtained by these two different techniques showed good agreement for the low (3 v%) polymer cement. R-curve behavior, i.e., increasing crack-growth-resistance was also observed.

The ultimate (apparent) toughnesses are $1.3 \text{ MPa}\cdot\text{m}^{1/2}$ for low (3 v%) polymer content and $2.2 \text{ MPa}\cdot\text{m}^{1/2}$ for high (8 v%) polymer content cement. Electron micrographs showed a sponge-like microstructure for the high polymer cement and microcracking for the low polymer cement. The effects of microstructure on fracture toughness are discussed.

Y4.3

THE CHEMISTRY OF MDF CEMENTS PRODUCED FROM POLYACRYLAMIDE-CEMENT WATER PASTES. M.R. Silsbee and D.M. Roy, The Materials Research Laboratory, Pennsylvania State University, University Park, Pa.

It is generally accepted that the role of the polymers in these systems is more complex than simply acting as a processing aid. The polymer interacts in some way with the cations released from the cement to form a metal cross-linked polymer gel. Studies on complex formation in polymer gels have shown that there is often an unusual specificity in the ions resulting in the highest degree of complexation. In addition gelation often occurs only within a narrow pH regime. Hence, the results shown here will attempt to examine the effects of altering the cement chemistry on strength development in calcium silicate cement based systems.

Y4.4

IMPROVING THE WATER RESISTANCE OF MACRO-DEFECT-FREE CEMENT. M. Berg, P. P. Russell and J. E. Young, Center for Cement Composite Materials, Univ. of Illinois, Urbana, IL 61801

Macro-defect-free cement composites made with calcium aluminate cement and polyvinylalcohol exhibit hygroscopic behavior with concomitant strength loss.

The rate of moisture up-take will be discussed and the success of various strategies to control it will be considered. Changes in the proportion of polymer used and the addition of cross-linking agents, such as boric acid, and a chromium (III) complex, have been studied. The use of silane coupling agents is another promising approach.

Y4.5

A VIEW OF MDF PASTES. M.R. Silsbee, M. Perez-Pena, and D.M. Roy, The Materials Research Laboratory, Pennsylvania State University, University Park, Pa.

The addition of water soluble polymers to cements pastes (MDF cements) has been examined. The microstructures observed are distinctly different from those found in more traditional materials. The hydration products formed tend to be produced in lesser amounts and with different morphologies as compared to traditional materials. The results of SEM, EDX and automated image analysis techniques will be presented.

Y4.6 ABSTRACT NOT AVAILABLE

Y5.1 ABSTRACT NOT AVAILABLE

Y5.2

THE PROPERTIES OF GYPSUM - FREE PORTLAND CEMENTS Tomáš Všetěčka, Building Research Institute (VÚPS) Prague, František Škvára, Jaroslav Hrazdára, Institute of Glass and Ceramics Chemistry, Czechoslovak Academy of science, Pius Ůrovec, CEMENT-WORK Prachovice.

Gypsum-free Portland cements (GF cements) comprise the system ground clinker with a specific area of 350-500 m^2kg^{-1} - grinding aid-a surface-active substance with hydroxyl groups (sulphonated polyphenolate)-alkali carbonate. The physics-chemical character and the amount of the grinding aid play an important part in the process of liquefaction and hydration of GF cements. The primary advantage of GF cements is based on the workability of pastes, mortars and concrete at low water-to-cement ratios, due to the synergic effect of the re-

gulating admixtures (grinding aid-surface active sub.-alkali carbonate). Using various proportions of the regulating admixtures, it is possible to control, with a high degree of reliability, the hydration process and thus also the required properties of the composites. The GF cements characteristically very high early strengths within 1-24 hours (mortars 2-6 MPa after 2 h, 30-50 MPa after 24 h and 60-100 MPa after 28 days, compressive strength of concrete, 25-60 MPa within 24 h and 60-110 MPa after 28 days; in the case of special concrete, 20-30 MPa, 80-100 MPa and more than 140 MPa after 8 hours, 24 hours and 28 days respectively). Additional specific properties of the GF cements include setting and hardening at sub-zero temperatures, resistance to aggressive media. Industrial production of the GF cements was started in 1989.

Y5.3

LEACHABILITY OF CEMENT SOLIDIFIED INCINERATOR WASTE. Tahar El-Korchi, Worcester Polytechnic Institute, Worcester, MA 01609, David L. Gress, and Robin Collins, University of New Hampshire, Durham, N.H. 03824.

The leachability of cement solidified incinerator waste was conducted using a weak acid. The release of heavy metals (i.e. As, Cd, Pb, Cr) from the cement based matrix was observed as a function of pH and alkalinity of the leachate.

Microstructural characterization of the matrix was conducted prior and during the leaching process using scanning electron microscopy and X-ray mapping. The heavy metals affected the morphological features of the early hydration products as well as the crystalline formation of the heavy metal complex.

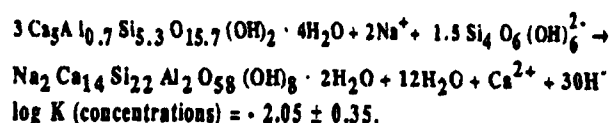
Solubility of the metal and effective release was highly dependent on the pH of the leachate and neutralization of the alkalinity. The metal release is also dependent on the physico-chemical integrity of the hydration products.

A leaching model is proposed based on metal release and microstructural dependence. A local leaching front is recognized as an integral part of the rate of metal release combined with diffusion and/or dissolution from the silica rich residual skeleton.

Y5.4

THE CHEMISTRY OF AL-TOBERMORITE AND ITS COEXISTING PHASES AT 175°C. Mary W. Barnes and Barry E. Scheetz, The Pennsylvania State University, University Park, Pennsylvania.

Synthesis of Al-tobermorite were made at 175°C at Ca/Si = 0.7 - 1.16 and Al/(Al + Si) = 0.12. Two regions were observed. At Ca/Si < 1 in the presence of Na, reyerite coexists with tobermorite. Ca is low, approximately 0.0003 molal, while Si is high about 0.01 molal. At Ca/Si = 1 only tobermorite was observed. At Ca/Si > 1 hydrogarnet coexists with tobermorite, Ca is relatively high about 0.003 molal, and Si is relatively low, equal to or less than 0.002. Because the interlayer spacing of tobermorite is constant for this series at 11.41 ± 0.02 Å, the Al content of the solid is assumed to be constant and equal to the analyzed value for the solid products of the runs at Ca/Si = 1.0, in which only tobermorite was observed: Al = 0.7 mol/5 mol Ca. The Na content observed in these same solids depended on the degree of rinsing; for a double-rinsed sample Na = 0.1 mol/5 mol Ca. It is therefore concluded that under these conditions, Na + Al does not substitute for Si. The tobermorite-reyerite reaction may be written:



Y5.5

NUMERICAL SIMULATION OF THE FREEZING PROCESS AND HYDRAULIC PRESSURE FIELDS IN A CEMENTITIOUS MATRIX. Tahar El-Korchi, John M. Sullivan, Jr. and Andreas N. Alexandrou, Worcester Polytechnic Institute, Worcester, MA 01609

In severe cold climates, damage to concrete structures can be caused by frost action or cycles of freezing and thawing. The degree and mechanism of freeze-thaw deterioration is a complex phenomenon and depends on the microstructure of the particular material as well as environmental conditions. Current practice for evaluation of cementitious materials to freeze-thaw cycles involves lengthy and costly experimental procedures. Hence, it is very desirable to predict the freeze-thaw durability of construction materials based on physico-chemical characteristics of the matrix. For this purpose a numerical model has been developed that predicts the solidification process and hydraulic pore pressures in saturated porous materials.

The nonlinear, coupled governing equations are used in both the frozen and unfrozen phases. The hydraulic pressure generated by the volume expansion of water during freezing is solved assuming a perfectly elastic continuum. Realistic pore size distributions in cementitious materials are simulated. The temperature dependency of the thermal properties (specific heat capacity, thermal conductivity and latent heat of fusion) is incorporated in the numerical model. Due to the large range of pore sizes in cementitious materials the freezing point depression plays a major role in the transient simulation and is handled as a function of local curvature of the interface. The interfacial boundary conditions preserve the balance between the sensible heat transported away from the interface into the frozen and unfrozen zones and the latent heat of fusion released during solidification at the interface. Additionally, the microscopic behavior of the interface due to local pore size distribution effects are incorporated.

Results are compared to various analytic solutions where available and to existing experimental data. The simulations predict the transient solidification front and hydraulic pore pressure fields within the porous matrix with fidelity.

Y5.6

STRUCTURE AND PROPERTIES OF ALKALI SILICATE BASED BINDERS. Ivan Odler and Ulrich Hennicke, Technical University of Clausthal, Clausthal-Zellerfeld, Fed.Rep.Germany

Water solutions of sodium silicate $\text{Na}_2\text{O} \cdot x \text{SiO}_2$ react with sodium fluosilicate Na_2SiF_6 to yield SiO_2 and NaF. This reaction is associated with a setting and hardening of the system. The hardened material consist of anamorphous SiO_2 matrix with embedded NaF. Within the present paper the kinetics of the reaction, the structure of the hardened material and its properties are reported.

AUTHOR/SPEAKER INDEX

This index indicates the paper number for authors, sessions for session chairs, and symposia for symposium organizers. The following typical examples show the code system whereby individuals are referenced:

- | | |
|-----------|---|
| A2.1 | Author of Paper Number A2.1
(Symposium A, Second Session, First Paper) |
| G3 | Session Chair for Session G3
(Third Session of Symposium G) |
| J | Symposium Organizer for Symposium J |
| A1.1/H1.1 | Joint Session (Symposium A and Symposium H) |

AASTUEN, D.J.W., V4.8
ABBOTT, KATHLEEN S., K2.6
ABBOTT, NICHOLAS, L., V7.5
ABDUL-RAZZAQ, W., D10.19
ABE, HITOSHI, M5.10
ABE, TAKAO, G18.7
ABELE, J.C., E6.2
ABELES, B., D9.1, H3.9, J7.14
ABELL, J.S., M7.165
ABERNATHY, C.R., G8.2, G19.2
ABRAHAM, FARID, T2
ABRAJANO, T.A., JR., U5.6
ABUL-FADL, ALI, D8.8
ACHUTHURAMAN, V.S., M4.13
ACKERMAN, JEROME L., O1.8
ACKERMAN, U., F1.4
ACKERSON, BRUCE, J., V4.7
ACKLAND, G.J., G18.24
ACOSTA, DWIGHT R., C9.24
ACOSTA, RAUL E., K3.9
ADACHI, H., M7.15
ADAIR, J., Y4.2
ADAM, JEAN-LUC, P6.7
ADAM, M., T8.2
ADAM, MIREILLE, V1.1, V1.6
ADAMS, P.M., A9.7, D10.15, G20.3
ADAMS, S., E4.4A
ADAMSKI, JOSEPH A., G9.26
ADDAD, SYLVIA COHEN, O3.1
ADDADI, L., R1.4, R5.9
ADOLF, D., T7.22, T8
ADONCECCHI, V., L4.6
ADVOCAT, T., U5.5
AERS, G.C., G18.12
AESCHLIMANN, M., A10.4
AGARWAL, ANURADHA M., G10.5
AGGARWAL, I.D., P5.4, P5.7
AGGARWAL, S.L., J6.2
AGNELLO, P.D., D7.6
AGOSTINELLI, E., M8.9
AGRAWAL, D.K., Y1.4, Y3.2
AGRAWAL, R., Q12.3
AGUIERO, A., L5.13
AHERN, BRIAN S., G9.26, M7.30
AHLGREN, W.L., E2.4, E2.6, E8.5
AHLSTROM, M., G3.5
AHMED, F., F9.8
AHMED, H., A8.7
AHN, C.C., D10.15
AHN, H., A9.16
AHRENKIEL, RICHARD K., G9.4
AI, C.C., F3.5
AI, REBECCA, A9.1
AIHARA, K., M7.247
AIKAWA, I., H7.3
AINDOW, M., F8.4, R2.9
AISHENG, HE, M6.11, M7.242
AITA, CAROLYN RUBIN, H4.5, H6.13
AJTOKA, T., H7.3
AJURIA, S.A., A10.5
AKAGI, TATSUO, M4.11, M7.252
AKAGI, YOSHIRO, D12.1, K5.12
AKAHORI, T., I3.6
AKASAKA, Y., H7.8
AKASHI, MASATSUNE, U9.5
AKIMOTO, KOICHI, C5.1
AKITA, K., B2.8
AKKARA, J.A., R3.3
AKSAY, ILHAN A., M7.105, R2.8, S1.1, S3, T7.8, T8.5
AKSEL, BULENT, N1.4
AKUEZUE, H.C., T7.17, T9.6
ALAYA, S., G4.5
ALBER, I., C13.4
ALBIN, DAVID S., H6.6
ALBIN, SACHARIA, F4.7
ALBINSON, Y., U11.1
ALBRIGHT, D.E., H5.4
ALCORN, STEPHEN R., U7.1
ALDEBERT, P., O5.6
ALDISSI, M., Q3.4
ALDRICH, DAVID, C10.5
ALEXANDER, DALE E., A6.1
ALEXANDER, K.B., M7.258
ALEXANDER, MICHAEL N., M7.174, M7.236
ALEXANDER, W.R., U3.4, U11.11
ALEXANDROU, N., Y5.5
ALFANO, R.R., Q7.12, Q10.6, Q13.9
ALFORD, N. MCN., M7.254
ALFORD, T.L., A2.8, A7.8
ALJISHI, S., H1.7
ALKIS, M.H., A3.5
ALLAIN, C., T1.6, T7.19, V8.4, V9.2
ALLARD, L.F., C9.31, M7.3
ALLARDO, PEDRO GRIMA, E8.8
ALLEAUME, MARC, Q7.16
ALLEMAND, PIERRE-MARC, Q8.3
ALLEN, CHARLES W., A2.1
ALLEN, E.L., G9.16
ALLEN, JOHN P., M7.215
ALLEN, ROLAND E., M7.9
ALLEN, SUSAN D., B2.4, B2.5, B3
ALLEN, JR., S.J., D1.3
ALLRED, DAVID D., D9.4, E1.5, E3.4
ALLRED, RONALD E., N4.2, N4.7
ALLRED, WORTH P., E1.5
ALONSO, R.G., E10.10
ALP, E.E., M7.2
ALPER, MARK, R., R3, R4.1
ALTELARREA, H., G9.31
ALTMAN, M., C3.1
ALTSHULER, ANATOLY M., F2.11, F3.3, F3.5, F4.10, F5.2, L5.5
AMADOR, S., V8.8
AMARATUNGA, G.A.J., F5.12
AMATO, A., M7.106
AMATO, CARMELA C., L2.9
AMEN, M.S., A6.4
AMIEL, C., V9.2
AMIELL, JACQUES, Q7.16
AMIRTHARAJ, P.M., E1.4
AN, D.K., G18.11
ANACKER, LOLA W., T7.5, T9.7
ANASTASIADIS, S.H., J2.9, J2.10
ANDELMAN, DAVID, V6.2
ANDERSEN, H.H., A4.6
ANDERSEN, L.-U. AEN, A3.1
ANDERSON, A.C., M7.226
ANDERSON, E.E., M7.63, M7.68
ANDERSON, G.B., A9.4, H3.4
ANDERSON, G.W., B4.4
ANDERSON, GREGORY C., A7.7
ANDERSON, K.K., K2.2
ANDERSON, L.W., F3.14
ANDERSON, MICHAEL P., J5.10
ANDERSON, PHILIP W., M1.1
ANDERSON, ROBERT A., G7.4, G18.38
ANDERSON, TED L., T3.9
ANDERSON, W.A., D2.11, G9.17
ANDERSON, W.T., B4.7
ANDERSSON, T.G., C11.3
ANDO, KEN, M7.22
ANDO, Y., D6.2
ANDRADE, A., W2.2
ANDREADIS, T.D., A6.2, A6.3
ANDRESHAK, JOSEPH C., B5.14
ANDREWS, J.W., I2.6
ANDREWS, L.J., P9.4, P9.5
ANDREWS, ROBERT J., M7.140, M7.174, M7.236
ANDRIKIDIS, C., M7.177
ANGEHRN, S., V10.6
ANGELINI, P., A7.2
ANGELUCCI, R., A9.2
ANJARD, RONALD P., K5.10
ANKNER, J.F., J2.4
ANGHENO, LIU, M4.9
ANTHONY, B., I3.3, I3.4
ANTHONY, L., D10.36, D10.39
ANTHONY, THOMAS R., F1.2
ANTHONY-CAMILL, SPENCER J., R4.2
ANTOGNAZZA, LOUIS, M1.6
ANTOLOVICH, S.D., N5.19
ANTONELLI, A., F4.9, G10.2
ANZAI, H., Q4.3
AOKI, S., M7.181
APTED, M.J., U7.27, U7.43
ARAI, T., U7.40
ARAI, TOSHIHIRO, H2.5
ARANGUREN, M.I., N4.9
ARBET, V., D10.15, Q20.3
ARCANGELI, C., C9.16
ARCIDIACONO, STEVEN, R5.3
ARCISZEWSKA, M., E10.12
ARENDT, P.N., M7.196
ARENDT, R.H., M6.9, M7.129
ARGYRAKIS, PANOS, T2.5, T9.7
ARIAS, J.M., E6.4, E8
ARJAVALINGAM, G., K4.2
ARKO, A.J., M7.3
ARMES, S.P., Q3.4
ARMIENTO, C.A., D7.9, D10.45
ARMIGLIATO, A., A9.2
ARNOLD, G.W., A9.3
ARNOLD, D.J., E9.4
ARONA, R., S1.7
ARON, KEN, Q9.3
ARORA, B.M., G9.11, G9.12, G9.37
ARRIGA, O., G9.40
ARST, M.C., B5.19
ARUN, B., O7.5
ASAI, T., B2.9
ASANO, JUNKO, D2.6
ASANO, T., M9.9
ASHBURN, J.R., M7.63, M7.68
ASHLEY, C.S., J6.8
ASHLEY, NICHOLAS V., R4.10
ASHOK, S., F4.8, H6.11
ASHWELL, GEOFFREY J., Q7.1, Q7.2, Q9.4
ASKER, THOMAS R., M8.3
ASKINS, C.G., P4.3
ASOM, M.T., D10.27, D10.48
ASSADI, AZAR, Q7.10, Q7.18
ASSALI, L.V.C., G5.3, G18.39
ASTHANA, A., M7.173
ATASEK, ROSEMARIE, U1.1
ATALAY, ASMARRE, W5.3
ATKINS, MARK, U2.1, U7.7
ATKINSON, ALAN, U2.4, U11.5
ATTANASIO, D., Q4.8
ATTARD, GEORGE S., S4.2, XNF1.4
ATWAL, K.P., M7.95
ATWATER, HARRY A., A1.3, A10.3, D9.2
AUCIELLO, O., A6.4
AUCOUTURIER, M., G6.5
AUDEBERT, P., O5.6
AUGUSTUS, P.D., A8.7
AUNER, G.W., A3.5
AURORA, TARLOK S., P8.5
AUVERT, G., B6.10
AU YANG, S.Y., E9.1
AVADHANI, S.V., H6.4
AVALOS, MIGUEL, C13.2
AVERBACK, R.S., A6.42
AVNIR, DAVID, T7.11, T7.12
AWADELAKARIM, O.O., G1.2, G18.22
AWAGA, KUNIO, Q2.3
AXE, JOHN, E., J1.1
AYERS, J.E., D2.7
AZIZ, M.J., A8, A10.3
AZUMA, MAKOTO, Q9.13
BABA, T., G15.2
BACHMANN, FRIEDRICH G., B6.1, B6.11
BACHMANN, KLAUS J., D6.11, F2.1, F9.9
BACHMANN, PETER K., I4.1
BACHOWSKI, STEVEN, G9.26, M7.30
BACHRACH, R.Z., A9.4, H3.4
BADDOUR, RAYMOND F., O2.9, O2.10
BADR, MAMOUN M., Q7.14, Q12.11
BADZIAN, A.R., F4.2, F4.8, XNF1.2
BADZIAN, T., F4.2, F4.8, XNF1.2
BAER, E., R6.3
BAERI, P., A10.11
BAERT, K., H7.6
BAETZOLD, ROGER C., M7.85
BAGLEY, B.G., I2.7, M10.10, M11.1
BAGLIN, J.E.E., A1.9
BAI, BENJAMIN J., F1.4
BAI, G., D10.50
BAI, J.N., L5.12
BAI, P., A6.5, H6.15
BAI, XINDE, A6.9
BAILEY, M.G., U8.2
BAIN, ART N., Q7.15
BAIN, C., B5.7
BAIOCCHI, F.A., B5.11
BAJAJ, KRISHAN K., G14, G14.1
BAKER, D.R., N2.6
BAKER, GREGORY L., Q12.1
BAKKER, ALOYSIUS F., C8.1
BAKRY, ASSEM, G9.4
BALACHANDRAN, U., M7.8, M7.44, M7.45, M7.51, M7.125
BALASUBRAMANIAN, LALITA A., D10.29
BALAZS, A.C., V9.3
BALDO, F.M., A3.9, M1.8
BALESTRINO, G., M8.9
BALK, P., D11.10
BALLADORE, JEAN-LOUIS, I4.7
BALLINGALL, J.M., D7.2
BALLINI, Y., D10.2
BALLUTAUD, D., G6.5
BALOOCH, M., M7.186
BALSARA, N.P., V8.6
BAMFORD, THOMAS A., D6.3
BANBA, TSUNETAKA, U7.18
BANDO, H., Q4.3
BANDYOPADHYAY, A.K., H1.10
BANERJEE, RATNABALI, H1.10
BANERJEE, S., G9.11, I3.3, I3.4
BANEY, RONALD H., M7.46
BANSAL, NAROTTAM P., M7.148
BANSIL, R., T1.4
BANTSEKOV, S.V., F4.5, F9.3
BAO, JING-SHENG, Q3.11
BAO, X.J., G9.49
BAOREN, ZHANG, M4.9
BARAFF, G.A., G17.1
BARANOWSKI, J.M., G17.2, G17.5
BARATTA, G., A10.11
BARBER, Z.H., M7.166
BARBER, D., G11.3
BARBOUR, J.C., A2, A2.8, M7.117
BARCZYNSKA, J., G9.7
BARD, ALLEN J., Q5.5
BARDACKI, TEVFIK, U11.7
BARDEN, PAUL E., M4.8
BARDIN, T.T., A1.9, G9.10
BAREFIELD, E.K., M7.171
BARFKNECHT, ANDREW, K, K5
BARIBEAU, J.-M., D10.18, D10.20
BARIMANI, ARMAN, A6.20
BARKATT, AA., U7.15
BARKER, JOHN, T4.6/U10.6, U10.6/T4.6
BARMAN, D., F2.11
BARNARD, J.A., D10.24
BARNER, J.B., M7.208, M11.1
BARNES, MARY W., Y5.4
BARNES, P.A., G9.10
BARNETT, S.J., B4.2
BARNIER, SUZANNE, H6.5
BARR, DONALD E., K1
BARRAUD, A., Q9.10
BARRERA, E.V., C9.27, C9.28
BARRON, A.R., L6.7, N2.2
BARRY, J., G18.32
BARSKI, A., D10.47
BARTA, L.E., W1.6, W2.3
BARTLETT, A.H., N5.7
BARTLETT, R.J., M7.3
BARTOLI, JR., FIL J., E, E6, E9.2, E9.3, E9.4
BARTOLOME, J., M7.21
BARTON, CHRISTOPHER C., T4.5/U10.5, U10.5/T4.5
BARTON, R.W., M11.4
BARTON, T.J., Q10.9
BARTRAM, M.E., L2.1
BARUA, A.K., H1.10
BARUS, A.M., K5.6
BARZOUKAS, M., Q12.7
BASA, D.K., F8.2
BASCOM, W.D., N4.7
BASEMAN, ROBERT J., B5.5, B5.14
BASSANI, J.L., C13.4
BASSEL, R.H., A6.3
BASU, S., A9.5, M7.219
BATABYAL, A.K., H1.10
BATCHELOR, D., B6.9
BATES, FRANK, S., V3.8
BATES, JOHN K., U5.6, U6.5, U6.6, U7.17, U7.28
BATEY, J., I2.9
BATLOGG, B., M2.2, M7.33, M8.2
BATSON, P.E., F3.1
BAUCH, H., P1.4

BAUER, C.L., D1.10, K7.8
BAUER, E., C3.1
BAUERLE, D.W., B7.1
BAUGH, DELROY A., C9.10, D10.4, D10.28
BAUGHMAN, R.J., M7.141, M7.157, M10.7
BAULES, P., M2.7
BAUMAN, J., H1.4
BAUMGARTNER, J.W., F6.7
BAUN, CHRIS, Q4.10
BEALL, GEORGE H., K1.5
BEAN, J.C., A2.2, D5.3, D5.6
BEASLEY, M.R., M10.6
BEAUDOIN, J.J., U2.2
BEAUFORT, D., U7.14
BEAULAIGUE, L., M7.2, M7.3
BEAVERS, JOHN A., U7.33
BECKER, M.F., A8.8, A9.23
BECKHAM, H., Q12.3
BECLA, P., E10.1, E10.7
BEDAIR, S.M., B4.5, D4.8, D8.4, D12.7, G12.2
BEDNARSKI, MARK, R3.2, XNF1.3
BEECH, F., J3.8, K3.10
BEER, J.M., W1.6, W2.3
BERRY, J.G., M7.173, M7.211
BEHRMAN, M., A9.58
BEHRMAN, E.C., P6.8, U7.23
BEIN, THOMAS, H2.8
BEITZ, J.V., U3.2
BELAISH, I., S2.3
BELAK, JAMES, P., V4.10
BELAN, R.M., M7.201
BELL, L.D., C6.1
BELLITTO, C., Q4.8
BELLOCO, A.M., V2.7
BELLOTTO, M., W1.4
BELSER, MITCH, M7.231
BELT, ROGER F., M7.169
BELTRAN, A., M7.21
BELTRAN, D., M7.21
BEMELMANS, H., A9.27, G16.4
BENCHIGUER, T., G9.34
BENDER, G.A., M7.149
BENDEK, G.B., V2.1, V3.3, V10.6
BENDEK, R., A6.42
BENNETT, B.L., M7.72
BENNETT, BRIAN R., D12.4
BENNETT, J.C., M7.147
BENNETT, LAWRENCE H., D10.19, M7.13, M7.154
BENNETT, P.A., C10.4
BENO, M.A., Q5.2
BENSIL, R., T7.28
BENSON, B.W., G18.26
BENTJEN, S.B., R1.8
BENTZ, DALE P., T4.2/U10.2
U10.2/T4.2
BENYATTOU, TAHA, Q2.5
BERANGER, MARC, Q7.5
BERDING, MARTHA A., E7.4A
BERG, M., Y4.4
BERGER, R.L., W3.6
BERGER, S.D., B4.10
BERGESON, KENNETH, L., W3.3, W3.4
BERGHMAN, K., U6.3
BERGMAN, P., D10.42, G14.2, G14.4
BERGSTROM, D.S., A4.7
BERGSTROM, DEBORA F., M7.46
BERK, N.F., J7.5, J7.6
BERKOWITZ, M., C8.2
BERMAN, A., R5.9
BERNARD, C., L1.1
BERNEY, CHARLES V., O2.7
BERNHARDT, ANTHONY F., B, B1
BERNHOLC, J., F4.9, F6.6, G, G10, G10.2, G11, G18
BERNIER, P., Q10.7
BERRY, E.E., W1.2
BERRY, G.C., O3.3, O4
BERRY, W.B., F6.11
BERTOLET, DAN, D10.41, D11.3
BESCOF, PATRICK LE, U7.6
BESMAN, THEODORE M., L, L2.5, L3.2, L5, L5.3
BEUERHANN, THOMAS, B7.5
BEVAN, M.J., E8.3
BEVK, J., C9.40
BEYE, A.C., G3.3, G3.4, G9.40
BHADRA, R., A11.3
BHALLA, AMAR S., M7.195, P8.2
BHARGAVA, R., M7.102
BHAT, I.B., E7.2
BHATTAGAR, M.C., A9.22
BHATTACHARYA, P.K., D7.8
BHATTACHARYA, RABI S., A9.6, A9.41, M11.12
BHATTACHARYA, S., V4.5, V7.9
BHIDE, V.G., H6.14
BI, JIANQING, M7.250
BI, XIAN-TONG, Q3.11
BIALY, S., B3.3
BIBBS, JEFFREY A., R4.3
BIBLER, NED E., U6, U6.5
BIEGELSEN, DAVID K., C1.1, C2.3
BIER, T.A., Y2.2
BIERLEIN, J.D., P8.3
BIGGERS, RAND, V8.12
BIJEN, JAN M., W2.4, W2.5, W3.2
BINGZONG, LI, D10.7
BIRADAR, A.M., Q9.8
BIRNBOIM, MEYER H., H4.6, H6.12
BIRTSCHER, ROBERT C., A4.7, A8.10, J7.10
BISHOP, S.G., F2.9, F6.8, G4
BISI, O., C9.16
BISWAS, PRATIM, M7.42, M7.70
BISWAS, R., J6.9
BISWAS, SAMBHU N., E8.9
BITTER, STEVEN P., Q9.3
BITSANIS, IOANNIS, V9.11
BITTENSOR, S.N., B2.2
BIUNNO, N., L5.6
BIVAS, A., T7.11
BIWER, B.M., U5.6
BIZNEK, M.E., M7.45, M7.51
BLACK, D.R., J7.7
BLACK, JERRY G., B, B2, B2.3
BLACKSON, J.H., O3.6
BLAKEMORE, RICHARD P., R1, R1.1
BLANCHARD-DESCHE, M., Q12.7
BLANK-BEWERSDORFF, MARGRET, N2.9
BLANKSCHEIN, DANIEL, V2.1, V7.5, V10.7, V10.9
BLASIE, J.K., V8.8
BLAUGHER, R.D., M7.241, M9.8
BLENDELL, J.E., M7.13
BLISS, D.E., G17.4
BLOCKER, MARK, K5.5
BLOHM, MARGARET L., Q4.4, Q4.5
BLOOM, IRA, M7.156
BLOOMER, T.E., M7.122
BLUM, FRANK, D., V9.4
BLUMSTEIN, A., O8.9, S4.5
BLUMSTEIN, R.B., O8.9
BOATNER, L.A., M7.185, M7.192, M7.222, M11.2
BOBONNEAU, FLORENCE, H5.2
BOCHYNSFI, ZENON, V7.11
BOCK, JAN, V5.2
BOCKRIS, J. O'M., I3.7
BOCQUET, A.E., M7.7
BODE, M., A3.4, G12.1
BOEUP, J.-P., I1.2
BOGER, F., T7.16
BOGY, D.B., H5.3
BOHN, C.T., M7.125
BOHR, J., A4.6
BOKHIMI, M7.66
BOLAND, JOHN J., C6.4, C9.6, M7.76
BOLEY, M.S., M7.131
BOLOGNESI, A., Q6.8
BOLT, JOHN, K4.4
BOMAN JR., R.C., G20.3
BONAMICO, M., Q4.8
BONAR, J.M., D7.4
BONI, C., W1.4
BONNELL, D.A., T3.3
BONSE, U., N5.19
BOOKER, G.R., G13.3
BOULCHAND, FUNIT, M7.42, M7.70
BORCHERS, B., S4.3
BORCHERS, J., J2.8
BORDES, M., A7.3, M7.219
BORNSTEIN, J.T., G18.51
BORRESSEN, PETER, A, A3, A3.8, A6, A7.8, A9, A11.5
BORGHESI, A., G18.5
BORGHES, G., A9.27, Q16.4
BORISENKO, V.E., C9.36
BORLAND, J.O., B5.19
BORNEHANN, H.J., M7.83
BORRIGO, J.M., G9.3
BOSCH, J., G9.31
BOSE, D.K., L4.10
BOSE, T.K., V9.7
BOSTICK, WILLIAM, U4
BOSWELL, F.W., M7.147
BOSZO, FORONC, B2.6
BOTEV, A.A., F4.5
BOTTA, C., Q6.8
BOTTIGER, J., A3.1
BOTTKA, N., G9.36
BOUCHARD, A.M., J6.9
BOUILOV, L.L., F4.5
BOUX, J., L5.9
BOULDIN, D., H1.5
BOUNIOU, PASCAL, U1.1
BOURCIER, ROY J., A11.7
BOURCIER, WILLIAM L., U5.2, U7.13
BOURDILLON, A.J., M7.177, M7.243
BOURGET, LAWRENCE P., F3.13
BOURGAIN, JACQUES C., G4.5, G15.3, G16.5
BOUSSOUX, G., Q3.12
BOWER, A., D4.2
BOWLER, A., C7.5
BOWMAN, M.K., R6.8
BOWMAN JR., ROBERT C., A9.7, D10.15, E6.6, G20.3, J5.2
BOYA, D., L2.11
BOYCE, J.B., A9.4, H3.4, H4.3, M3.8, M7.183, M7.218
BOYD, DAVID, F8.12
BOYD, I.W., M3.10
BOYS, D.R., A8.7
BOZOVIC, I., M10.6
BOZO, F., B2.6
BRADDOCK, W.D., A9.52
BRADLEY, D.D.C., Q12.12
BRADLEY, J.P., U5.6
BRADLEY, KENNETH, J7.4
BRADLEY, WALTER L., N3.8
BRADSHAW, J., J2.7
BRAGLIA, M., P5.2
BRANDON, N., V1.5
BRANDEN, BODIL, B3.12
BRASEN, D., A2.9
BRASSETT, A.J., Q12.12
BRAUERS, A., D11.10
BRAUN, FRANK, S4.9
BRAUN, RUDIGER, B5.18
BRAUNSTEIN, G., G9.18
BRASIC, GEORGES, Q7.16
BRAVMAN, J.C., D2.5, M10.6
BREAU, L., I3.3, I3.4
BREDELL, L.J., A3.10
BREITSCHWERTD, A., G6.4, H3.5
BRELVI, M., D10.50
BREMER, T., A7.5
BRENNAN, ANTHONY, O1.2, S3.5
BRENNAN, T.M., G9.41, G16.2
BRENNER, JOSEPH, M9.6
BREUNIG, T.M., N5.19
BREWER, J.A., M7.201
BREWER, P.D., B1.7
BREY, L., C2.2
BRIBER, ROBERT M., O4.1
BRICE, D.K., A1.2
BRICENO, MAURO, C9.2
BRIDGES, F., M3.8, M7.183
BRILLSON, L.J., E2.2
BRINGANS, R., C, C4, C9
BRINGLEY, JOSEPH F., M6.2, M6.3, M7.56
BRINKER, C.J., J6.8, J6.12
BRINKMAN, A.W., E8.6
BROAD, R.A., R1.7
BRODSKY, B., D10.10
BRODY, H.D., M7.139
BRODY, PHILIP S., A9.12
BROKMEYER, H.G., J3.4
BRONNER, G., B4.1
BROOKINS, DOUGLAS G., U7.38
BROOKS, JAMES S., Q11.3, Q11.9, Q11.10
BROOKS, KENNETH, M5.12
BROSTOW, WITOLD, O3.10
BROUDE, S.V., F2.11, F3.3, Q13.10
BROVKA, P., A6.35, A6.36
BROW, R.K., A9.3
BROWER, KEITH L., G4.2
BROWN, A.R., G11.1
BROWN, APRIL S., D7.1
BROWN, D.R., M7.196
BROWN, D.W., A2.6
BROWN, GAIL J., G4.4, G17.3
BROWN, M., M3.10
BROWN, P.D., E8.6
BROWN, PAUL W., R2.2, U, U1, U2.3, Y1.2, Y3, Y5.1
BROWN, ROBERT A., G18.10
BROWN, S.E., Q11.8
BROWN JR., R. MALCOLM, R5.1, R6
BROWNSWORD, M., U3.1
BRUCE, A.J., P5.3
BRUELY, J., F3.1
BRUESCH, R., U3.4
BRUINSMA, R., V3.5
BRULEY, J., F3.1
BRUNNER, OLIVIER, M11.6
BRUNO, J., U8.3
BRUS, LOUIS, H2.1
BRUYNSERAEDE, YVAN, A2.12, C11.1, D6.5, D10.30, M7.75
BRYDEN, W.A., F8.9, F8.10, F9.5
BRYNESTAD, J., M7.118, M7.258
BUCHAL, CH., A7.5, M7.221
BUCHAN, A.B., U3.1
BUCHTA, R., L3.4
BUCK, M., F1.7
BUCKETT, MARY I., A9.8
BUCKLEY, ALAN J., S, S2
BUCKLEY, S., V5.8
BUDA, F., G6.3
BUDAI, J.D., M3.3, M7.118, M7.192, M7.222, M8.7
BUDIL, M., G10.4
BUDNICK, JOSEPH I., M4.12, M7.10, M7.97
BUECHELEGU, A.C., U7.16
BUEHLER, E.C., F3.4, H1.3
BUHRER, WILLI, J4.3
BUHRMAN, R.A., M7.188, M7.229, M11.5
BUITING, M.J., L3.9
BULARZIK, JOSEPH, M6.3
BULLOUGH, TIM J., A6.6
BUNOD, P., G9.34
BURAYOV, L.I., Q5.1
BURDEG, G., Q9.12
BURGESE JR., D., L1.4, L2.12
BURILA, C.T., M4.12
BURNEMSTER, C.P., M7.108
BURNS, C.J., L6.8
BURNS, G., M7.112
BURNS, GERALD, M7.29
BURNS, R.P., D6.4, D6.11
BURROUGHS, J.H., Q10.3
BUSHAN, B., H5.3
BUSSE, L.E., P5.4, P5.7
BUSSMANN, U., A2.11
BUSTARRET, E., H3.8, H6.10
BUTLER, E.P., N1.8
BUTLER, J.E., F2.9, F3.11
BUTLER, J.R., C10.4
BUTLER, S.R., M7.50
BUTTON, T.W., M7.254
BUYERS, WILLIAM J.L., J6.12
BYBEE, GREGORY M., R3.5
BYER, R.L., P8.1
CABANEL, R., D10.47
CABANISS, G., G19.2
CABRERA, LAURA, V9.10
CACOURIS, T., B5.20
CADWELL, L.A., D8.11
CAI, Y.M., Q1.3
CAIHAO, WANG, E8.10
CALDERON, HECTOR, J4.10
CALDES, M.T., M7.151
CALVERT, PAUL D., R, R1, R1.7, R5, R6
CAMARATA, R.C., D4.3, D6, D6.6
CAMON, HENRI, I4.7
CAMPBELL, A.A., R2.3
CAMPBELL, DAVID K., Q10.2, Q11.5

CAMPBELL, I.H., H1.2, H5.4
 CAMPISANO, S.U., A2.5
 CAMPUZANO, J.C., M7.2, M7.3
 CARDAN, FRANCOISE, O1.9, V5.4
 CARDAN, S.J., V1.8, V3.2
 CARNOON, ROWLAND M., K4.8
 CANTOR, B., A10.9
 CANTOR, R.S., V6.4
 CANUT, B., A8.5, G18.13
 CAO, D.X., A7.10, A9.18
 CAPASSO, FEDERICO, D8.1
 CAPLAN, ARNOLD I., R1.3
 CAPPELLI, E., L4.6
 CAPPELLO, JOSEPH, R4.9
 CAPRILE, C., C3.5
 CAR, R., G6.3
 CARDONE, F., G12.3
 CAREY, M., V3.3
 CAREY, PAUL G., B1.3, XNF1.5
 CARIDI, A., W1.4
 CARIM, ALTAF H., C9.30, M7.47, M7.77
 CARLTON, KAREN L., L2.2
 CARLSON, K.D., Q5.2
 CARLSSON, JAN S., U11.4
 CAROSELLA, C.A., A6.7
 CARPENTER, LESLIE E., M7.46
 CARR, P.L., S4.8
 CARR, S.H., S5.5
 CARRINGTON, W.A., F2.9, F3.11
 CARROLL, D.W., L6.8
 CARTER, C. BARRY, C4.4, C9.22, C12.6, C13, D1.3, D10.5, G20.2, K6.5, L2.8, M7.188, M7.213, M9.3
 CARTER, PATRICIA H., T6.5
 CARTER, S.F., P5.1
 CARTER, W.B., M7.171
 CARUSO, R., G8.4
 CARVALHO, BRUCE, L., V7.10
 CASANOVE, M.J., M2.7
 CASEY, KELLY G., B3.12
 CASPARY, R., M7.106
 CASSANHO, A., M7.28
 CASSART, M., M7.12, M7.238
 CASSIDY, J.J., R6.3
 CASTANO, V.M., O5.9, T7, T8.7, Y2.5
 CASTILLO, T.R., M7.225
 CATALAN, A.B., A11.9
 CATANA, A., C10.2
 CATELLANI, C., Q6.8
 CATES, M.E., T8.1
 CAD, FRANCO, V3.7
 CAUDRON, R., J4.8
 CAULET, J., D1.4, D10.2
 CAUREL, J., U7.14
 CAVA, R.J., J3.8, M2.2
 CAVADIAS, S., I1.7
 CAVENETT, B., E4.4A
 CAWLEY, ROBERT, T6.5
 CAZZANIGA, LUIGI, O2.5
 CECONE, G., C3.5
 CEDER, G., M7.69
 CEHELNIK, M.J., N1.5, P3.5
 CELII, F.G., F2.3
 CELLIER, F., L5.10
 CENTANNI, MICHAEL A., M7.11
 CEREDA, E., W1.4
 CEREZO, ALFRED, D8.10
 CERQUA, K.A., P6.8
 CERRI, ALBERTO, J4.12
 CERULLO, M., A5.1, D5.7
 CEYER, S.T., B5.16
 CHABAL, Y.J., C7.6
 CHADI, D.J., G16.1, G17
 CHAFFIN, JOHN H., M7.169
 CHAIKIN, PAUL M., Q, Q11, Q11.4, Q11.7, Q11.9, Q11.10, V9.1
 CHAILLOUT, C., M6.1
 CHAKI, T.K., A6.8
 CHAKOUMAKOS, BRYAN C., M2.4, M7.64, M7.124
 CHAKRABARTI, U.K., B5.11, G8.4
 CHAKRABORTY, ARUP K., N5.20
 CHAKRABORTY, R.N., A6.26
 CHAMBERLIN, R., V3.3
 CHAMBERLIN, R.V., Q11.4
 CHAMBEROD, A., D10.21
 CHAMBERS, F., C11.1
 CHAMBERS, G.P., A6.17
 CHAMBRE, P.L., U3.5, U11.8
 CHAMPAGNE, B., M7.55
 CHAN, HELEN M., M4.2, M7.43, M7.86, M1.8, M6.6, M7.7, M7.8
 CHAN, K.K., F5.12
 CHAN, SIU-WAI, M7.217
 CHAN, W.K., D1.1
 CHANCE, R.R., Q10.4, V1.6
 CHAND, N., C4.3
 CHANDRA, DIPANKAR, E7.7, E7.9
 CHANDRA, KAVITA, T6.2
 CHANDRASEKHAR, G.V., M7.29
 CHANDRASEKHAR, H.R., D11.6, E9.10
 CHANDRASEKHAR, MEERA, D11.6, D12, E9.10
 CHANDVANKAR, S.S., G9.37
 CHANG, C.C., M3.2
 CHANG, CHIN-AN, M11.9
 CHANG, H.L.M., L6.3, L6.4
 CHANG, I.T.H., A10.9
 CHANG, J., M7.212, M7.237, M7.249
 CHANG, K.-T., H1.5
 CHANG, K.H., D7.8
 CHANG, L., M7.133
 CHANG, L.L., D11.6, E9.7
 CHANG, R.P.H., M9.2, M10.8
 CHANG, S.J., D10.15, G20.3
 CHANG, S.L., C7.5
 CHANG, TAO C., N3.4
 CHANG, Y.A., K5.8, K7.4, K7.5, N5.12
 CHAO, P.C., D7.2
 CHAPPLE-SOKOL, J.D., I2.9
 CHAR, K., M7.183, M11.4
 CHARASSE, MARIE-NOELLE, G2.5
 CHARBONNIER, M., A8.5, G18.13
 CHASON, E., A1.2, A8
 CHASSEAU, DANIEL, Q4.6, Q7.16
 CHATER, R., A2.11
 CHATFIELD, C., L3.5
 CHATURVEDI, KUMAR, V6.9
 CHATURVEDI, U.K., A6.26
 CHAU, C.C., O3.6, S5.6
 CHAUDHRY, M. IQBAL, F6.11
 CHAUDHURI, J., D6.7, E2.8
 CHAUSSEMY, G., A8.5, G18.13
 CHAWLA, K.K., N7.2
 CHAYAHARA, A., A6.33
 CHEEKS, T.L., D1, D1.1, D1.2, D1.3
 CHEMELLI, C., W1.4
 CHEN, A.-B., E7.4A
 CHEN, B., L5.6
 CHEN, C.H., M6.5, M7.33
 CHEN, C. JULIAN, K
 CHEN, C.K., A9.21
 CHEN, C.S., N5.2
 CHEN, D., S5.8
 CHEN, DE HUAI, M7.164
 CHEN, ERIC J.H., N, N3.7, M7.92
 CHEN, G.-F., O6.3
 CHEN, HEMING, A6.9
 CHEN, HSIO-CHENG, A9.9
 CHEN, IN-GANN, M7.82
 CHEN, J., Q6.1
 CHEN, J.C., D10.36, D10.39
 CHEN, J.F., D10.36
 CHEN, J.G., M7.131
 CHEN, J.T., B5.19
 CHEN, J.W., M7.244
 CHEN, JUN, B5.3
 CHEN, K., M7.78
 CHEN, K.C., M7.178, M7.239
 CHEN, L., H3.10
 CHEN, L.F., M7.168
 CHEN, LIQUAN, M7.250
 CHEN, M.-C., E1.6
 CHEN, MAI, Q12.13
 CHEN, O.Y., N5.12
 CHEN, Q., M4.13
 CHEN, QING-MING, A9.10, B5.15
 CHEN, SAMUEL, G9.13, G9.18
 CHEN, SHUGUANG, F8.8, H6.8
 CHEN, SOW-HSIN, J2.3, J7.4, S4.6, V7.10
 CHEN, T.I., O4.3
 CHEN, W.K., D10.36, D10.39
 CHEN, W.M., D10.43, G6.2, G9.20, G18.14, G18.43
 CHEN, WEN-CHANG, Q12.5, Q12.6
 CHEN, Y.L., A11.9
 CHEN, Y.Y., M7.244
 CHEN, Z.J., M10.6
 CHENG, A.Y., G9.49
 CHENG, F.S., M7.63, M7.68
 CHENG, H., E3.3
 CHENG, H.Y., M7.63, M7.68
 CHENG, HERMAN C.T., L1.9
 CHENG, K.-Y., G9.30
 CHENG, L.-T., Q9.2
 CHENG, T.T., F8.4
 CHENG, Y.-T., A3.5, A3.6, A11.9
 CHENG, YUANDA, D10.25
 CHENGLU, LIN, A6.31, A9.48, H6.7
 CHEONG, S.W., M7.3
 CHERN, C., M5.13
 CHEUNG, S.C.H., U7.42, U11.2, U11.6
 CHEVALIER, J.-P., M7.110
 CHEVALIER, J., G9.51
 CHIARELLI, R., H6.9
 CHIANG, C.K., M7.13
 CHIANG, CHWAN, K., M7.154, M7.256
 CHIANG, CHWAN-KANG, A9.12
 CHIANG, JUSTIN, I2.3
 CHIANG, LONG Y., Q, Q2.2, Q8.8, Q11.4, Q11.7, Q11.9, Q11.10
 CHIAROTTI, GUIDO L., G6.3
 CHICK, LARRY A., S5.10
 CHEN, C.J., D2.5
 CHILTON, B.T., D5.4
 CHIN, T.S., M7.99, M7.153, M7.160, M7.178
 CHING, W.Y., M7.6
 CHINO, K., G9.34, U7.10
 CHINOV, P.B., D7.6
 CHISHOLM, M.F., C9.32, C11.6, D10.12, M7.222, M9.1
 CHIU, RAYMOND C., M7.159
 CHIU, SHIH-LIANG, K3.9
 CHO, N.-H., H5.3
 CHO, S.J., A6.10
 CHOE, G., A6.23
 CHOE, H.S., A6.10
 CHOI, C.S., J5.6
 CHOI, D.S., A6.10
 CHOI, J.-O., B5.10
 CHOI, JAE-SUNG, M7.40
 CHOI, Y.W., D7.7, D10.34
 CHOI, YUN-SEUNG, M9.7
 CHONG, P.J., B2.9
 CHOPPIN, GREG, U3, U8.1
 CHOPRA, K.L., A9.22
 CHOU, HENRY, J4.6
 CHOU, P., D10.13, M5.9
 CHOU, T.C., N2.5
 CHOU, TSU-WEI, L1.10
 CHOU, Y.T., K6.8
 CHOU, YEONG-SHYUNG, Y4.2
 CHOW, GAN-MOOG, A9.11
 CHOW, H.M., M7.139
 CHOW, LAURENCE C., Y1.1
 CHRISSEY, D.B., M3.12
 CHRISTEN, DAVID K., M, M5, M7.118, M7.222, M8.7, M11.2
 CHRISTENSEN, H., U8.2
 CHRISTODOULOU, L., N5.16
 CHRISTOFFEL, E., G9.34
 CHRISTOU, A., B4.4, B4.7, D10.33
 CHU, BENJAMIN, O5.5
 CHU, C.-J., F6.13, H5.2
 CHU, C. JUDITH, F1.4
 CHU, C.W., M7.120, M10.5
 CHU, H.N., F3.14
 CHU, MARGARET S.Y., U7.44
 CHU, PAUL, M, M1
 CHU, WEI-KAN, A7.9, F4.4, F4.11
 CHU, X., E2.3
 CHU, YOUYI, C9.19
 CHUANG, T.J., F1.7
 CHUANG, TIEN-MIN, H7.10
 CHUI-SABOURIN, M., P5.3
 CHUNG, KWAN SOO, H3.2
 CHUNG, O.H., Q11.10
 CHUNG, T.C., V1.7, V6.5
 CHUNG, W.C., O7.12
 CHYI, J.-I., C2.5
 CIMA, MICHAEL J., M7.139, M7.158, M7.159, M7.207
 CIMECIOGLU, A.L., O8.8
 CIPOLLI, R., M4.12
 CLAISSE, PETER A., U11.5
 CLANCY, FAULETTE, A4.2, C8.3
 CLARK, NOEL A., R6.7, V4, V4.8, V5.3, V10.4
 CLARK, ROBERT, Q7.8
 CLARKE, D.R., G7.3
 CLARKE, DAVID, N1.3
 CLARKE, S., C8.4, D8.7, D10.23
 CLARKE, WILLIAM J., Y3.7
 CLAUS, H., M7.3
 CLAXTON, P.A., D2.7
 CLAY, K.J., F5.12
 CLEM, T.R., M7.80
 CLEMENS, B.M., C13.6
 CLEMENT, ERIC, T7.2, T9.7
 CLEVENGER, L.A., G18.34
 CLIFTON, P.A., E8.6
 CLINE, J.P., J7.7
 CLOITRE, M., T1.6, T7.19
 CLOSS, FRITZ, Q8.3
 COCITO, G., P5.2
 COCKAYNE, B., E5.5
 COENEGRACHT, Y.M.A., W2.2
 COGAN, S.F., M4.5
 COGORDAN, J.A., M7.1
 COHEN, D., V3.3
 COHEN, JEROME B., J1.6, J3
 COHEN, M.R., A7.3, A10.7
 COHEN, MARVIN L., M1.2, M7.219
 COHEN, P.I., D8.2
 COHEN, R.M., F5.11
 COHEN, ROBERT E., O2, O2.5, O2.7, O2.9, O2.10, O4.4, O6.5
 COHEN-ADDAD, J.P., O2, O7.10
 COLANERI, N.F., Q12.12
 COLE, H.S., B3.1
 COLE, M.W., G9.15, G9.17, T5.1
 COLEMAN, E., M7.210, M7.228
 COLIJN, P.F., A9.56
 COLLIN, GASTON, M8.4, M7.114
 COLLINS, A.T., F1.1, F2.7
 COLLINS, ALIKI K., L3.8
 COLLINS, G.J., I4.4
 COLLINS, JOSHUA, L1.6
 COLLINS, R.T., D7.5
 COLLINS, ROBIN, Y5.3
 COLLIS, W.J., D8.8
 COLOMBO, PETER, U4.2
 COMITA, PAUL B., B1.4, B1.6
 COMPAN, ALVIN, A9.7, E6.6, G15.5
 COMPOSTO, RUSSELL J., J7.12, O7.3, O7.5
 CONNELL, G.A.N., M3.8, M7.183, M7.218
 CONNELL, S.H., G18.36
 CONNELLY, S., N3.1
 CONNORS, MICHAEL J., R5.7
 CONRAD, H., J6.7
 CONRAD, JOHN R., A9.31
 CONTINENZA, ALESSANDRA, F8.13
 CONWELL, E.W., Q10.1
 COOK, J.G., A6.11
 COOK, JR, J.W., E4.6, E6.5, E6.8, E8.7, E9.2, E9.4
 COOK, LAWRENCE P., A9.12, M7.111, M7.154, M7.256
 COOK, ROBERT, N1.3
 COOK, STEPHEN J., A4.2
 COOKE, D.W., M7.72, M7.196
 COONEY, E.C., A9.13
 COONS, WILLIAM E., U7.1
 COOPER, B.R., C9.13
 COOPER, D.E., Q9.12
 COOPER, E.A., M7.44
 COOPER, K.L., S5.8
 COOPER, L., D10.48
 COPEL, M., D5.8
 COQUERELLE, M., U7.19
 CORBETT, J.M., M7.147
 CORBETT, JAMES W., G18.27, G18.51
 CORBIN, N., N2.7
 CORDTS, B.F., A6.39

CORNIE, JAMES A., N5.15
CORONEL, PHILIPPE, Q9.10
CORTESI, E., A6.25
COSANDRY, P., C13.1
COSTA, J.E., S5.2
COTTEL, C.M., G19.3
COTTE, J.M., D10.17
COTTS, E.J., N5.17
COUTINHO, S., T7.21
COVINO, J., S3.6
COWAN, DWAIN O., Q, Q1.1, Q7.6
COWERN, N.E.B., G18.3
COWIE, J., U2.1
CRAMPIN, S., N5.16
CRANE, ROBERT, R4.6
CRANFORD, M.K., M7.29, P8.3, P9.7
CREED, D., S1.4
CREUSET, J., D10.47
CREVECOEUR, G., O3.7
CRISCENTI, LOUISE J., U4.3
CRISMAN, E.E., D10.38
CRONIN, J.P., M7.140
CROOKS, RICHARD M., Q3.6
CROS, BERNARD, I4.7
CROSBY, KEVIN M., S2.4
CROVISIER, J.L., U5.5
CROW, JOHN D., K2.1
CROW, M.L., J3.9
CRUZ, A., O5.9
CSERNICA, JEFFREY, O2.10
CUANG, HAO-HSIN, O1.2
CUCCOLO, A.M., M1.9, M11.8
CUI, C.X., Q6.7
CULBERTSON, R.J., A9.24
CULLIS, A.O., A10.9, C9.22, E5.5
CUMBERBATCH, TOBY J., H2.9, M4.8
CUN, C.-C., O1.7
CUNIBERTI, C., Q10.13
CUNNINGHAM, J., G12.1
CUNNINGHAM, JACK E., D, D3
CUOMO, J.J., A1.1, A1.8, F5.4, F5.10, M7.194
CURADO, E.M.F., T7.21
CURACHI, TOSHIO, O1.5
CURTIN, W.A., V9.13
CURTINS, H., H1.4
CURTISS, L.E., P5.6
CUSHMAN, RICHARD, Q3.3
CUSTER, J.S., A2.3, A9.14
CUSHAW, CALVIN, F3.7
CYRUS JR., W.L., R3.4
CZARNECKI, JERRY, F3.12, L2.13
CZYZEK, G., M7.83

D'AGUANNO, B., V4.2
D'EMIC, CHRISTOPHER, M7.56
D'EVELYN, MARK, F1.4
DA SILVA, E.C.F., G18.39
DABROWSKI, B., M2.10, M6.6, M7.38
DACOL, P.H., M7.112
DADSON, B.W., D4.6
DAHL, M., E10.7
DAHL-PETERSEN, SVEND, M7.146
DAHREN, U., C9.33
DAI, MINGJIANG, A6.9
DAIMON, MASAKI, Y3.3
DALGLEISH, BRIAN J., N6.4
DALTON, LARRY R., Q7.14, Q7.15, Q12.11, Q12.13, S2.3, S5.6
DALY, J.T., D10.38
DAMAM, G., D10.49, D12.10
DAMILIN, B., B5.23
DAMMEFAER, S., O4.1
DANYLUK, STEVEN, K7.7
DAS, A., K4.1
DAS, R., F5.5, F6.7, G9.32
DAS, S.R., A6.11
DASGUPTA, A., M9
DASS, M. LAWRENCE A., L3.7
DATYE, A.K., C9.31
DAUTREMOY-SMITH, W.C., A9.26, G18.41
DAVID, DONALD J., N6.1
DAVID, M.I.F., J3.5, J3.11
DAVIDOV, D., S2.3
DAVIDSON, B.N., I3.8
DAVIDSON, J.L., S5.22
DAVIDSON, THEODORE, N4.5

DAVIES, G.R., S4.8
DAVIES, GORDON, F2.12, G18.18
DAVIS, C., M7.48
DAVIS, H.T., N5.20
DAVIS, JOHN, D12.3
DAVIS, M.E., M7.74
DAVIS, NICHOLAS A., S2.9
DAVIS, R.L., J3.6
DAVIS, ROBERT F., F6.2, F6.6, F6.7, F7.7, L3.1
DAWES, ADRIAN, U11.9
DAY, PETER, Q4.6
DAY, ROBERT, L., W, W1, W4.3
DAY, STEPHEN M., P8.5
DAYAN, D., F8.9, F9.5
DE, BHOLA N., G18.45
DE BATIST, R., M7.170
DE CARLO, J., E8.11
DE FONTAINE, D., M7.69
DE HOSSON, J.T.H.M., A9.15
DE KILJSE, TH.H., A9.56
DE JONGE, W.J.M., E10.8
DE LA FUENTE, G.F., M7.21
DE MIERRY, P., G6.5
DE REUS, R., A3.3
DE UNAMUNO, S., B5.9
DEAK, PETER, C9.15, F5.3, G18.27
DEAL, MICHAEL D., G9.16, G9.25, G12.4
DEANE, STEPHEN, M4.8
DEAVILLEZ, R.R., G18.34
DEEDS, H.A., M7.118
DEGROOT, DONALD C., Q3.5
DEGUEDRE, C., U3.4, U7.37
DEGUIRE, MARK R., M7.148
DEICHER, M., G5.5
DEKOCK, J.A., N5.12
DEL AGNEL, P., M7.98
DEL ALAMO, JESUS A., D12.4
DELANNAY, F., M7.12, M7.238
DELAYEN, J.R., M7.125
DELEO, G.G., G6.1
DELHAES, PIERRE, Q7.16
DELIN, VAUGHN R., O7.7
DELLEPIANE, G., Q7.12, Q10.6, Q10.13
DELOCHE, BERTRAND, V1.2
DELSANTI, M., T8.2
DEMCHENKO, A.I., A6.36
DENBOER, M.L., Q6.1
DENNIS, B.S., A9.43, A9.44
DEFOTIER, S., D10.2
DESFOYDT, J.M., E3.3
DESCHIEPPE, P., H7.6
DESIRAJU, G., Q9.2
DESJARDINS, ALAIN, O5.4
DESU, S.B., L1.5, L4.5, L6.5, N2.3
DEUTSCH, J.M., T7.27
DEVANE, G., C11.1
DEVE, HERVE, N1.10
DEVENISH, ROBERT W., A6.6
DEVINE, R.A.B., I2.10, I4.6
DEVINE, ROBERT L.S., Q7.14
DEVITO, RICHARD, M7.169
DEWAMES, R.E., E6.4
DEWAN, H.S., M7.60
DHAR, N.K., E1.4
DHARMA-WARDANA, M.W.C., D10.18
DHONT, J.K.G., V4.1
DI FRANCESCO, M.W., V1.9
DI MARZIO, D., E8.11
DIAMOND, S., E9.8
DIAS, A.G., H1.8
DIBENEDDETTO, A.T., N3.1, N4
DICILLIO, J., M7.11
DICKINSON, J.T., N5.1, T3.1
DICKINSON, L.T., B3.9
DIDOMENICO, L., M7.202
DIECKMANN, R., J4.2
DIERKER, S.B., A9.43, A9.44, J7.8, J7.9
DIETRICH, H., C11.2
DIORIO, MARK S., M5.4
DIMARCELLO, F.V., P3.1, P4.1
DIMINO, G.M., T2.4
DINARDO, R., J2.7
DING, J.R., A9.28, L5.12, T7.14, T7.20, T7.23
DINGLEY, D.J., D6.2
DINGRONG, QIAN, E10.11

DINWIDDIE, RALPH B., K6.2
DIP, A., D8.4
DISCHLER, B., G19.5
DIXIT, S.N., Q10.2, Q13.3
DIXON, JOHN M., M7.4
DLUBEK, G., A9.31
DMOCHOWSKI, J.E., G16.2
DMOSKI, W., J1.7
DO CARMO, M.C., G18.18
DOBACZEWSKI, L., G16.2
DOBSON, J.F., M7.7
DODABALAPUR, A., D11.7
DODD, R. ARTHUR, A9.31
DODSON, BRIAN W., D, D4.7, D10
DOGGETT, W.O., E5.8
DOHYA, A., K1.4
DOLL, G.L., M7.28
DOMINGUEZ, J.M., M7.98
DONALD, D.S., Q9.2
DONG, QIN, H6.7
DONNELLAN, MARY E., N1.6
DONOVAN, E.P., A6.7
DOORBAR, P.J., N2.6
DORRUS, ROBERT H., O1.10
DORMAN, D., M7.102
DORNEN, A., G1.3, G5.4
DORSETT, H., M7.235
DORSINVILLE, R., Q7.12, Q10.6, Q13.9
DOUGHERTY, ANDREW, T4.7/U10.7
DOUGLAS, KENNETH, R6.7
DOUZINAS, KONSTADINOS, O2.7
DOVE, DEREK B., M7.76
DOVEK, M.M., C3.3
DOW, J.D., G14.6
DOWEN, P.A., B3.3, C7.4
DOWNER, M.C., A9.16
DOWNEY, J. SLOAN, U7.22
DOWNING, R. GREGORY, J5.1, J5.2
DOYAMA, MASAO, M7.84
DOYLE, B.L., A6.19
DOYLE, J.P., M7.194
DOYLE, N.J., E8.3
DRAKE, J.M., J7.14
DRAKE, MARK, P6.2
DRAPER, C.W., P1.3
DRAVID, VINAYAK, P., C4.5
DREHM, ALVIN J., M7.174, M7.236
DREIFUS, D.L., E4.6, E7.10
DRESSSELHAUS, M.S., M7.28
DREXHAGE, MARTIN G., P5, P6.1
DRISCOLL, T., H2.6
DRIVER, R., M7.177
DRIVER, R.D., P5.6
DROOPAD, R., D10.35, G13.3
DRZAL, LAWRENCE T., N4.1, S3.7
DU, HONGHUA, L6.2
DU, J., H6.15
DU, R., D6.1, J2.8
DUAN, HAILING, Q7.6
DUBE, C., G18.46
DUBOWSKI, J.J., E9.9
DUCASSE, LAURENT, Q4.6
DUDLEY, MICHAEL, D9.3, D10.29, G18.49, J1.4
DURDEN, SUSAN L., U7.4
DUESBERY, M.S., G18.28
DUH, K.G.H., D7.2
DUKE, CHARLES B., C9.14
DUKE, JOSEPH, R., V9.4
DULINETS, U.C.H., A6.36
DUMAIS, M.W., M7.174
DUMAS, PH., M7.49
DUNCAN, W.M., D8.4, E1.6
DUNHAM, SCOTT T., G10.5
DUNLOP, G.L., C11.3
DUPAS, G., D10.2
DUPUIS, N., D11.9
DUPUIS, R.D., G19.4
DURA, J.A., J2.4
DURAND, D., T8.2, V8.2
DUREL, V., D10.2
DURET, DENIS, Q7.1
DURLE, V., D10.2
DUROSE, K., E8.6
DUROVEC, PIUS, Y5.2
DUSANE, R.O., H6.14
DUSEK, J.T., M7.8
DUSEK, KATHRYN A., R5.6

DUTCHER, JOHN R., D6.8
DUTTA, B., M7.234
DUTTA, M., G9.15
DWIGHT, K., E10.7
DWIR, B., M5.8
DYER, PAUL N., L4, L4.3, L4.7
DYKINS, J., Q3.10
DYMENT, F., A9.58
DYNES, R.C., M1.9, M5, M11.8, X3.2
DYRBYE, K., A3.1
DZIAK, R., R1.5
DZIEMIANOWICZ, THEODORE S., O3.10
DZIOBA, STEVEN, I2.5

EAGLESHAM, DAVID J., A5.1, C5.3, C10.1, D1.5, D5, D5.3, D5.7
EAMES, DAVE, R2
EAMES, EDWARD D., R2.1
EAST, A.J., S2.7
EASTMAN, DEAN E., K1.1
EASTMAN, J.A., J1.9
EATON, H.E., M4.12
EBE, HIROJI, E2.8
EBERHART, N.E., N5.16
EBERT, W.L., U6.6
ECE, M., M7.215
ECKERT, HELLMUT, H2.8, P6.2
ECKHARDT, H., Q6.9
ECKSTEIN, J.N., M10.6
ECONOMIDES, VEA, U11.9
ECONOMOU, N.P., B2.2
EDGE, RON, J3.3
EDWARDS, ARTHUR H., F5.3
EDWARDS, JR, D., B2.2
EPPELSON, K.R., M7.171
EGAMI, T., J1.7
EGLAID, K., M7.70
EGUSA, SYUN, Q9.13
EHRICH, D.J., B2.2
EICHHAMMER, W., G18.4
EICK, R.H., M7.228
EICKHOFF, THOMAS, D11.11
EINLOTH, M.C., M7.125
EINSET, ERIK O., L1.3
EINZIGER, R.E., U8.4
EISENBACH, CLAUD D., O2.4, O6
EISENBERG, ADI, O5.1, O5.4
EK, B.A., D1.9
EKLUND, ELLIOTT A., A5.4
EL-BAYOUMI, O.H., M7.140
EL-GHOR, M.K., A8.3, A9.17
EL-KORCHI, TAHAR, Y5.3, Y5.5
EL-MASRY, N.A., D2.12, D4.8, D8.4, G12.2
ELAM, W.T., P8.4
ELANDJIAN, LUCY, O8.2
ELENA, M., A6.12
ELIAS, ANSELMO, M., V9.5
ELIAS, MARIA, E., V9.5
ELLIMAN, R.G., A2.2, A2.7, A8.1, A8.9
ELLIOTT, N.E., M7.196
ELLISON, A.J.G., U7.26
ELLISON, C.L., F5.11
ELMAN, B., D7.9, D10.32, D10.45, D11.3
ELMINYAMI, IMAN M., T7.7
ELSENBAUMER, R.L., Q6.9
ELSTON, T.C., L1.7
ELWELL, DENNIS F., M7.46
EMANUELSSON, P., G18.44
EMERY, J.R., V8.2
ENCK, R.C., K5.1, K6.3
ENDOH, YASUYUKI, E5.7
ENGEL, D.W., U7.43
ENGELHARDT, T., H2.2
ENGLAND, CRAIG D., D6.8
ENGLAND, J.M.C., A8.7
ENGLAND, P., M7.253
ENGLE, GEORGE, L5.4
ENGLISH, G.R., L2.8
ENJALBERT, R., M2.7
ENNEN, H., G19.5
ENOMOTO, N., M7.143
EOM, C.B., M5.6, M7.130
EPPELSON, J.E., J1.9, J5.3
EPSTEIN, ARTHUR J., Q3.1, Q3.2, Q3.10, Q6, Q7.7, Q8.1
ERA, KOH, F9.2

ERCK, R.A., A6.13
 ERDEMIR, A., A6.13
 ERES, DJULA, D10.12
 ERICKSON, ANDREW N., M5.4
 ERMER, SUSAN P., Q9.3
 EROKHIN, YURI N., B5.23
 ERWIN, R.W., J2.8
 ERWIN, STEVEN C., F5.1
 ERZAN, A., T9.1
 ESAKI, L., D11.6
 ESCHBACH, P.A., B3.9
 ESCHRICH, TIMOTHY C., D4.10
 ESCUDERO, R., M2.11
 ESROM, HILMAR, B3.4, B7.11
 ESPER, E., K7.2
 ESTLE, T.L., G7.1
 ETEMAD, S., Q12.1
 ETOH, H., D10.14
 ETOH, K., A6.41
 ETZ, EDGAR S., M7.100
 EVANS, WILLIAM B., Q6.4
 EVANS, A.G., M7.216, M9.4, N1.9, N1.10, N2.4, N5.7, N5.8, N6.4, N7.4
 EVANS, JOHN, F8.12, N5.3
 EVANS, K.R., D7.7
 EVERITT, NICOLA M., U11.5
 EVERTSZ, CARL, T9.1
 EVETTS, J.E., M7.166
 EVRAD, P., D10.44, O7.8, T8.6
 EWART, F.T., U3.1
 EWBANK, M.D., Q9.12
 EWEN, B., J6.1
 EWING, RODNEY, C., U6.2
 EXARHOS, GREGORY J., F8.11, S2.4

 FABBRI, R., A9.2
 FABER JR., JOHN, J1.6, J3.10, J7.10
 FABER, KURT, R6.9
 FACE, D.W., M10.2
 FAHEY, P.M., D10.17, G10.3
 FAINCHTEIN, R., F8.9, F9.5
 FAIZ, M., M7.2, M7.3
 FALCO, CHARLES M., D6.8, M7.176
 FALK, LENA K.L., N7.5
 FALKNER, J., Y4.6
 FAMILY, FEREYDOON, T1.2, T9.2
 FAN, HANJIE, A9.1
 FAN, Y.B., J7.3
 FAN, YU-DIAN, A9.10, B5.15
 FANG, T.D., G9.45
 FANG, ZHAOQIANG, G9.21
 FANGGAO, CHANG, M6.11
 FANN, Y.C., Q7.9
 FARABAUGH, EDWARD N., A9.12, F3.6
 FARAGO, B., J6.1, J6.8
 FARES, V., Q4.8
 FARINATO, RAYMOND S., N3.6
 FARLOW, G.C., A9.37
 FARNETH, W.E., M7.29
 FARNOUX, B., J2.1
 FARROW, L.A., M11.1
 FARROW, R.F.C., D2, D2.5
 FASTNACHT, R.A., M7.74
 FASTOW, R., E7.1
 FATEMI, M., C11.2, G18.42
 FATHAUER, R.W., D1, D1.11, D10.3
 FAUBERT, F., S4.5
 FAUCHET, PHILIPPE M., H, H1.2, H2, H4.2, H5.4, H6
 FAURIE, J.P., E2.2, E2.3
 FAVRE, R., L5.9
 FEDER, JENS, T4.1/U10.1, T7.16, U10.1/T4.1
 FEENSTRA, R., C, C2, C6, C12, M3.3, M7.192, M7.222, M8.7, M9.1, M11.2
 FEI, WANG HAN, T7.15
 FEIGELSON, ROBERT S., M9.6
 FEIL, W.A., L6.9
 FEILD, C.A., M7.112
 FEILE, R., M3.6
 FEJER, M.M., P8.1
 FELCHER, GIAN P., J2, J2.3, J7.12, O7.2, O7.3, O7.4
 FELDMAN, ALBERT, F3.6
 FELDMAN, L.C., A3.4, D10.9
 FELDMAN, R.D., G9.44
 FELDMAN, ROLF P., U2.2, W3.1, W4
 FELDMANN, W.L., M11.1
 FENDORF, M., M7.113
 FENG, AIGUO, M5.12
 FENG, HONG, D10.7
 FENG, O.L., W1.5, Y2.6
 FENG, QINGRONG, M7.145
 FENG, SONG L., G15.3
 FENG, Y., M7.254
 FENG, X., U7.15, U7.16
 FENG, Z.C., D11.8
 FENNER, D.B., C2.3, M3.8, M7.218
 FENSKE, G.R., A3.9, A6.13
 FERNIE, P.A., B5.22
 FERRARI, FRANCO, R4.9
 FERRARIS, M., P5.2
 FERRIS, KIM P., Q7.3, Q7.4, P3.3
 FETTERS, LEWIS J., J6.1, O2.6, V1.1, V1.6
 FEUSTON, B.P., P3.4
 FICHO, DENIS, Q6.5
 FIELDS, J.L., K5.1
 FIGUEROA, J., H1.8
 FIGUEROA, JUAN C., N3.2, N4.6
 FILACI, P., M8.9
 FILIPKOWSKI, MARK, M7.10
 FILISKO, FRANK, E., V5.5
 FINCHAM, ALAN G., R1.2
 FINNERS, J., D11.10
 FINEL, A., J4.8
 FINGER, F., H1.4
 FINK, TOBIN, A9.52
 FINKMAN, E., E7.3
 FINNEMORE, D.K., M7
 FINSTAD, T.G., D13
 FIORANI, D., M8.9
 FISCHER, D.W., G9.2
 FISCHER, ØYSTEIN, M11.6
 FISCHER, T.E., C9.5
 FISCHMAN, G.S., M7.61, FISHER, G.B., A9.13
 FISHER, R.A., M7.106
 FITZGERALD, E.A., D5.5, D10.27, D10.48
 FITZPATRICK, B.J., E4.2
 FIX, RENAUD M., L6.6
 FLAMM, D.L., I2.8
 FLEISCHER, E.L., A7.8
 FLEISHNER, PAUL F., M7.46
 FLEMING, JAMES W., P
 FLEMING, ROBERT M., M2.5, M5.2, M7.33
 FLEMINGS, M.C., M7.139
 FLINN, B.D., N7.4
 FLIPPEN, RICHARD B., M8.3
 FLOM, STEVEN R., Q12.6
 FLOREZ, T.T., D1.1, G20.2
 FLOTTMANN, T., K7.2
 FLUSS, M.J., J4.5
 FLYNN, C.P., D4, D6.1, J2.4, J2.8
 FOGARASSY, E., B5.9, B7.3, B7.7
 FOILES, S.M., C13.7
 FOLKERTS, T.J., M6.7
 FOLLSTAEDT, DAVID M., A10.6, A11, A11.7
 FOLWEILER, R.C., P9.4
 FONER, S., E10.1
 FONS, P., A4.3
 FONSTEAD, C., D8
 FONSTAD, C.G., D10.37
 FORTCUBERTA, J., M7.25
 FONTENEAU, G., P6.4
 FORD, W.K., C7.5, C9.9
 FORK, D.K., M3.8, M7.183
 FORNES, R.E., O7.11
 FORRESTER, KEITH, E., W5.2
 FORSMAN, W.C., O7.9
 FORSYTH, R., U8.3, U11.1
 FORTIN, E., D11.9
 FORTMANN, C.M., H5.4
 FORTUNATI, K., M7.120
 POSTER, K., C8.2
 FOTIADIS, DIMITRIOS I., L1.3
 FOULON E., B7.7
 FOUNTAIN, G.O., I3.5, I4.5
 FOURNIER, MAURILLE J., R4.4
 FOWLER, W.B., G6.1
 FOX, ALAN G., K4.8
 FOX, MARYE ANNE, Q5.5
 FOY, P.R., P5.5
 FRAAY, A.L.A., W3.2
 FRADIN, F., M1
 FRAKER, ANNA C., U7.32
 FRANCE, PAUL W., P, P4, P5.1
 FRANCIOSI, A., C3.5, E7.6, E10.3, G12.6
 FRANCIS, CECIL V., S2.6
 FRANCISCO, EDGARDO, L2.13
 FRANSEN, T., L2.10
 FRANZ, EENA-MAI, U4.2
 FRASER, A.T., Q7.1
 FRAUNDORF, P., C9.29
 FREDRICKSON, GLENN H., V3.8
 FREEDMAN, ANDREW, B3.7, B4.6
 FREELAND, P.E., D5.5, D10.27, D10.48
 FREEMAN, ARTHUR J., P8.13
 FREEMAN, G.B., L1.7
 FREER, B.S., C9.40
 FREIMAN, W., M7.256
 FREITAS, JR., J.A., F2.9, F6.8
 FRELTOFT, TORSTEN, M7.146
 FRENCH, J.D., N7.8
 FREUND, L.B., D4, D4.2
 FREYSZ, E., V2.7
 FRICKE, J., J6.7
 FRIEBELE, E.J., P4.3, P4.4, P4.6
 FRIEDLAND, E., A3.10
 FRIEDMAN, B., Q13.8
 FRIEND, R.H., Q10, Q10.3, Q12.12
 FRIPP, ARCHIBALD, E7.4A
 FRISCH, HARRY L., O4.7
 FRITZ, B., U5.5
 FRITZ, I.J., G9.41
 FRÖHLINGS DORF, J., M3.6
 FRONCZEK, FRANK R., M6.4
 FROSCNER, KENNETH E., C9.38
 FROST, C.B., S5.2
 FRUITWALA, H., O8.8
 FU, Q., E3.6
 FUCHIGAMI, HIROYUKI, Q12.8
 FUCHS, C., B5.9, B7.3
 FUERTES, A., M7.151
 FUGER, J., U7.19
 FUHRMANN, MARK, U4.2
 FUJIKAWA, Y., F6.14
 FUJIMAKI, NORIO, M7.227
 FUJIMORI, NAOKI, F, P5.8
 FUJIMOTO, I., D8.3
 FUJIMOTO, J.G., K2.2
 FUJIMOTO, M., E4.5
 FUJIMOTO, MASATOMO, D2.10
 FUJIOKA, H., H7.2
 FUJISAKI, YOSHIHISA, G9.39
 FUJISAWA, T., G15.2
 FUJIURA, KAZUO, P3.6
 FUKUDA, T., G18.47
 FUKUI, K., H7.11
 FUKUSHIMA, HIROTO, G9.24
 FUKUTOMI, M., M9.9
 FULLER, E.R., JR., M7.111, N1.8
 FULMER, MARK T., R2.2
 FUOSS, P., A9.43
 FURDYNA, J.K., E9.6, E10.10, J2.5
 FURUKAWA, SEIJIRO, D2.6
 FURUKAWA, SHOJI, H4.1
 FUSE, MOTOMASA, A9.50
 FUSO, FRANCESCO, S1.6
 FUTUTOMI, M., M9.9
 GABBE, D.R., M7.28
 GABILLI, E., A9.2
 GADNEY, HARRY D., L6.10, L6.11
 GAIDUK, P., G18.2
 GAIER, J.R., M7.31
 GAILLARD, D., L5
 GAILLARD, F., Q3.12
 GALASSO, FRANCIS S., L4, L4.8, N5.9
 GALEZ, PHILIPPE, M7.114
 GALLAGHER, P.K., M7.104
 GALLAGHER-DAGGIT, GEORGE, S, S5
 GALLARDO, PEDRO GRIMA, E8.8
 GALLIGAN, J.M., E1.8
 GALLOIS, BERNARD, I2.7, L, L1, L2.4, L5.2, L6.2, M5.13
 GALLOWAY, M.D., M7.222
 GALTIER, PIERRE, G2.5
 GALT, J., M2.7
 GAMMEL, J. TINKA, Q10.2
 GAMMON, DANIEL, C9.8
 GAMO, KENJI, B4.8
 GAN, ZIZHAO, M7.145
 GANAPATHI, L., M7.59
 GAO, L., M10.5
 GARBAUSKAS, M.F., M6.9, M7.129
 GARBOCZI, EDWARD J., T4.2/U10.2 U10.2/T4.2
 GARCIA-VAZQUEZ, VALENTIN, M7.176
 GARDINER, MARK A., U7.1
 GARDNER, J.D., K4.6
 GARFUNKEL, E., B4.9
 GARG, D., L4.3
 GARHART, JONATHAN, M5.12
 GARIN, J., Q7.17
 GARISTO, FRANK, U11.3
 GARISTO, NAVA C., U11.3, U11.10
 GARITO, ANTHONY P., C9.11, Q1.3, Q9.6, S2.2, S2.8
 GARNIER, FRANCIS, Q6.5
 GARNO, J.P., M1.9, M11.8
 GAROCHE, P., M7.121, Q11.2
 GAROFALINI, S.H., B4.9, P3.4
 GAROFF, S., V6.3
 GARONE, P.M., A10.8, G11.7, G18.40
 GAROSSHEN, T.J., E1.8
 GARRIDO, LEONCIO, O1.8
 GARRISON, BARBARA J., A4.1
 GARSADDEN, ALAN, I1.1
 GARTON, ANDREW, N5.21
 GARZON, P.H., M7.173, M7.211
 GASHUROV, G., P8.3, P9.7
 GASKILL, D. KURT, D12.3, G9.36
 GATES, STEPHEN M., M7.56
 GATESMAN, ANDREW, F3.13
 GAUDIANA, RUSSELL, O3.1
 GAUFRES, R., L2.11
 GAULTIER, JACQUES, Q4.6
 GAUR, UMESH, N4.5
 GAUZZI, A., M5.8
 GAY, R.L., M7.248
 GAYLE, FRANK W., M6.4
 GAZEAU, D., V2.7
 GAZIT, DAN, M9.6
 GEBALLE, T.H., M5.6, M5.7, M7.183, M10.6
 GEDDO, M., G18.5
 GEER, R., V7.8
 GEERK, J., A7.1, H3.3, M5.5, M7.209
 GEERTS, M.J., H3.3, T7.25
 GEGOUT, PHILIPPE, U1.1
 GEHLHOFF, W., G18.44
 GEHRING, S., S4.3
 GEIS, M.W., F4.1
 GEISER, U., Q5.2
 GELINAS, C., M7.55
 GELLINGS, P.J., L2.10
 GEMMA, NOBUHIRO, Q9.13
 GENQING, YANG, A9.20, A9.48
 GEOHEGAN, D.B., M7.193
 GEORGE, PATRICIA M., A9.60
 GERBERICH, W.W., D4.5
 GERBI, DIANA J., S2.6
 GERDING, T.J., U7.17
 GERESH, S., R3.6
 GERHARDT, R.A., J7.7, N5.18
 GERLING, MARIA, D11.5
 GERRARD, N.D., G19.4
 GERRITS, C.E.P., E10.8
 GERRITSEN, H.J., D10.38
 GEURTS, JEAN, C7.3, D11.10
 GHASAS, S.V., H6.14
 GHANDHI, S.K., D2.7, D7.6, E7.2, E8.1, G3.1, G9.3
 GHATAK, KAMAKHYA P., E8.9
 GHODGAONKAR, DEEPAK K., Q7.13, Q13.11, Q13.12
 GHOSH, KUNAL, T3.6, T7.24
 GIALANELLA, S., A6.12
 GIANNELIS, EMMANUEL P., K4.3, O1.4
 GIAPIS, KONSTANTINOS P., E4.4
 GIBALA, R., D7.8
 GIBB, K., D11.9
 GIBBERMAN, M., M7.11
 GIBSON, J.M., C, C1, C4.3, C5, C12.1, C12.2, G19.3
 GIBSON, W.M., D1.7, D2.7, D10.3

GIEBULTOWICZ, T.M., J2.5
 GIESS, EDWARD A., K4
 GIESSEN, B.C., M4.6, M7.92, M7.115
 GILBERT, R.D., O7.11
 GILCHRIST, H.L., D1.1, D1.2
 GILDENBLAT, G.S.H., F4.2, XNF1.2
 GILES, N.C., E6.1
 GILES, ROBERT, F3.13
 GILL, BENJAMIN C., Q6.4
 GILLIOM, LAURA R., O6.1
 GILMER, GEORGE H., C8.1
 GINDER, J.M., Q7.7
 GINGERICH, M.E., P4.3, P4.4
 GINLEY, D.S., M4, M7.117, M7.141, M7.157, M7.225, M10.7
 GINSBURG, ERIC J., S2.5
 GINSBAULT, N., O5.6
 GIROLAMI, G.S., L6.1
 GIROUD, M., M11.1
 GISLASON, H.P., G3.5
 GIUNTA, G., L4.6
 GLADFELTER, WAYNE L., F8.12
 GLADSTONE, D.J., B5.16
 GLASER, E., G15.4
 GLASER, M.A., V10.4
 GLASS, JEFFREY T., F, F2.1, F3.4, F5.5
 GLASSER, F.P., U2.1, U7.7, W, W1.5, W2, Y2.6
 GLASSLEY, WILLIAM, U7.39
 GLATZ, J.P., U7.19
 GLEASON, KAREN K., C12.4, F2.4
 GLENBOCKI, D.J., D11
 GLENBOCKI, OREST J., D12.5
 GLINKA, C.J., J7.5, J7.6
 GODA, TSUTOMU, M10.11
 GODBEY, DAVID J., C1.4, D10.11, D10.16
 GODDARD III, WILLIAM A., M1.5
 GODDARD, N., U6.4
 GOFF, J.P., J6.11
 GOHDA, SHINJI, M10.4
 GOLDBERG, H.A., S2.7
 GOLDBERG, INA, R4.5
 GOLDEN, S.J., M7.122, M7.216
 GOLDMAN, L.M., D9.2, D9.7
 GOLDOYS, E., G9.7
 GOLLUB, JERRY P., T4.7/U10.7
 U10.7/T4.7
 GOLTZENÉ, A., G9.34
 GOMEZ, J., N3.1
 GOMPEF, F., J6.9
 GONDHALEKAR, V., D6.7
 GONG, J.-R., D4.8
 GONG, KECHANG, O5.11, O8.3, Q3.13
 GONINI, A., C13.7
 GONSALVES, J., E3.6
 GONSALVES, KENNETH, L6, L6.2
 GONZÁLEZ-GALBET, J., M7.151
 GONZÁLEZ-HERNANDEZ, J., E1.5
 GOODBY, J.W., V7.7, V7.8
 GOODMAN, D.W., L2.3
 GOODMAN, G.L., M2.3
 GOODMAN, P., M7.7
 GOODRICH, R.G., Q4.5
 GOODWIN, J.W., V4.9
 GOODWIN, MICHAEL W., E7.9
 GOORSKY, M., B2.7, G12.3
 GOPALAM, B.S.V., H6.4
 GORDON, ROY G., L6.6
 GORETTA, KENNETH C., M4.7, M7.51, M7.65, M7.150, M7.156
 GORMAN, CHRISTOPHER B., S2.5
 GORODETSKY, G., V1.10, V8.2
 GÖSELE, ULRICH M., G9.5, G20.4
 GOSHORN, DAVE P., Q2.2, Q8.8
 GOSSARD, A.C., D8, D10.42, D10.43, G9.20, G14.2, G14.3, G14.4
 GOSSETT, C.R., M3.12
 GOTO, SHIGEO, G9.39
 GOTO, T., L3.3
 GOTO, TOSHIO, H1.1
 GOTOH, KOHTAROH, M7.227
 GOTOH, S., M7.58
 GOTTENBERG, WILLIAM G., N5.24
 GOTTLIEB, M., V1.10, V8.2
 GOTTSLEBEN, OLIVER, B3.5
 GOUGH, J.S., E7.4
 GOUIN, JEAN-PIERRE, O5.4
 GOVEA, L., M2.11
 GOW, T.R., D8.11
 GOYETTE, J., V9.7
 GRABAEK, L., A4.6
 GRABOW, MARCIA H., C8.1
 GRABOWSKI, K.S., M3.12
 GRADER, G.S., M6.8
 GRAESSLEY, WILLIAM W., V1.1, V3
 GRAHAM, R.J., K6.7
 GRAHAM, W.R., D2.1, D2.3
 GRABOW, B., U5.4, U8.3
 GRANDE, P.L., A9.58
 GRANIER, VINCENT, B5.1
 GRANT, TIM, N3.8
 GRANTHAM, L.F., M7.248
 GRAVES, R. CLARK, W5.1
 GRAVESTIEN, D.J., D11.2
 GRAY III, GEORGE T., J4.11
 GRAY, W.J., U7.27
 GRAYBEAL, J.M., M10.2, M7.204
 GRAZMAN, BRENT L., U5.1
 GREEN, A.J., M7.171
 GREEN, DAVID J., L4.7
 GREEN, M.L., A2.9
 GREEN, PETER F., O7.1
 GREENBLATT, M., M7.36, M7.155
 GREENE, J.E., A4.3, F7.2, I3.1
 GREENE, L.H., M11.1
 GREENLIEF, C. MICHAEL, M7.56
 GREER, JAMES A., M7.189
 GREGG, BRIAN A., Q5.5
 GRESS, DAVID L., Y5.3
 GREST, GARY, S., V8.1, V10.1
 GREUTER, FELIX, M7.52
 GREVE, D.W., M7.201
 GRIDER, D.T., B6.9
 GRIENGL, HERFRIED, R6.9
 GRIESS, M., G18.30
 GRIFFIN, A.C., S1.4
 GRIFFIN, JAMES, G9.29
 GRIFFITH, MICHAEL C., R4.2
 GRIFFITH, MICHAEL S., S2.9
 GRIGORAS, S., Q10.9
 GRIMALDI, M.G., A10.11
 GRIMMEISS, H.G., G1.1, G2.2, G18.44
 GRIMSDITCH, M.H., A11.3, C11.1
 GROBSTEN, TONI, N1.7
 GROENINCKX, G., O3.7
 GRONSKY, R., M7.95, M7.108, M7.113, M7.120
 GROSSKURTH, K.P., Y2.4
 GROSSMAN, C.H., Q9.6
 GROSSMANN, G., G2.2
 GROT, S.A., F4.2, XNF1.2
 GROTHAUS, JEFF, M7.42
 GROVENOR, CHRIS R.M., D8.10, E6.3
 GROVES, G.W., U4.1, U7.8
 GRUBBS, ROBERT H., S2.5
 GRUMMON, D.S., N5.23
 GRUNEBaum, D., G1.3
 GRUNER, GEORGE, Q11.1
 GRUNTHANER, F.J., C6.1
 GU, C., M7.3
 GU, H., U7.16
 GUARISCO, D., A10.4
 GUARNIERI, C. RICHARD, A1.8, F5.4
 GUBSER, D., M10
 GUENAI, B., D1.4
 GUÉRIN, R., D10.2
 GUERRERO, E., G18.8
 GUERRERO, GABRIELA DIAZ, V9.10
 GUIDO, L.J., G20.1
 GUILINGER, T.R., A6.19
 GUILLOT, GÉRARD, G2.5
 GUITTARD, MICHELIN, H6.5
 GUIVARC'H, A., D1.4, D10.2
 GUNGOR, M.N., K4.6
 GUNNISON, KATIE, R2.8
 GUNSHOR, R.L., E2.1, E3.5, E3.6, E3.7, E4, E10.5
 GUO, H., T2.6
 GUO, J., M7.2
 GUO, T., C7.5, C9.9
 GUO, X.S., B5.21
 GUO, YANGMING, F8.8
 GUO, YUEJIN, M1.5
 GUPTA, ARUNAVA, B5.5, M3.13, M7.112
 GUPTA, C.K., L4.10
 GUPTA, J., M7.194
 GURER, E., G18.26
 GURUNG, JIT, V8.12
 GURVITCH, M., M1.9, M6.5, M11.8
 GUSMAN, M.I., M7.130
 GUSTAFSSON, ANDERS, D11.5
 GUTMAN, ARIE L., R3.8
 GUTMANN, RONALD J., H7.10
 GUZMAN, L.A., A6.12
 GUZMAN, O., M7.98
 GYORFFY, B.L., J2.6, J4.7
 HA, D.H., M7.144
 HA, N.T., G18.41, G19.4
 HAAKSMA, R.A., N1.5, P3.5
 HAARER, D., B3.10
 HAASE, D.G., M7.48
 HAASE, M.A., E3.3
 HAASE, W., Q9.8, S4.3, S4.4
 HABA, BELGACEM, B5.5
 HABERMEIER, H.-U., M3.5
 HABU, K., M7.136
 HACHICHA, M.A., H3.8, H6.10
 HACKER, NIGEL P., F2.2
 HACKEY, J.P., M4.5
 HADDAD, G., N3.1
 HADZITIOANNOU, GEORGE, V9.11
 HAEGEL, N.M., A8.11, D2.12, G2.4
 HAGBERG, J., M7.138, M7.200
 HAGEROTT, M., E3.6
 HAGGERTY, J.S., M7.139
 HAGHIGHAT, R. ROSS, O8, O8.2, S3.7
 HAHN, H.T., N6.5
 HAHN, K., O5.10
 HAILE, SOSSINA, M., J1.8
 HAILS, J.E., B4.2, E8.2
 HAINES, M., E4.4A
 HALBOUT, J.-M., K4.2
 HALDANKAR, GAUTAM, N5.21
 HALDER, N.C., G9.14
 HALL, B.T., P9.2, P9.4, P9.5
 HALL, E.L., M11.3
 HALL JR., H.K., S1.6
 HALLER, E.E., G, G1.2, G7, G8, G9, G17.4
 HALLER, W., J7.5, J7.6
 HALLIN, C., D10.42, G14.4
 HALLMARK, V., O8.4
 HALLORAN, J.W., M10.7
 HALPERIN, A., V1.5
 HALSEY, THOMAS C., T9.4
 HAMADA, TOMOYUKI, Q13.2
 HAMAKAWA, Y., H5.1
 HAMANAKA, KOICHI, M7.197
 HAMBOURGER, P.D., M7.11
 HAMERS, R.J., C7.1
 HAMILTON, JR., W.J., E2.4, E2.6, E8.5
 HAMM, R.A., G19.3
 HAMMOND, L.C., C9.4, D10.44, L2, L2.7, O7.8, T8.6
 HAMMOND, W.B., O4.8
 HAMMOUDA, BOUALEM, V9.4
 HAMPSCH, HILARY L., Q13.6
 HAN, C.C., J6.2, J6.4
 HAN, C.C., Q6.9
 HAN, J., E3.6
 HAN, JEONG W., E4.6, E6.1, E6.5, E6.7, E6.8, E9.2
 HAN, M.K., H5.1
 HAN, P.D., M7.132, M7.133
 HAN, S.C., M7.23
 HANABUSA, MITSUGU, B6.7
 HANACK, MICHAEL, Q5, Q5.3
 HANADA, TAKASHI, M10.11
 HANAK, THOMAS, G9.4
 HANIOGOFKY, J.A., M7.171
 HANN, J., B5.19
 HANNA, JUN-ICHI, H1.9, H3.6
 HANNAHS, S., Q11.9
 HANSEN, A., L6.11
 HANSEN, GLENN A., Q9.3
 HANSEN, J.P., T7.35
 HANTZIS, C., F3.3
 HARA, A., G18.47
 HARA, KUNHIKO, D8.12
 HARA, M., B1.5
 HARA, MASAHICO, C9.11
 HARA, S., P6.12
 HARADA, N., M7.162
 HARAI, I., G18.47
 HARBISON, B., P5.4
 HARBISON, J.P., D1.1, D1.2, G20.2
 HARDEN, JAMES L., V8.3
 HARE, T., M7.48
 HARELSTAD, R. ELLEN, S2.6
 HARGIS, I.G., J6.2
 HARIMA, H., M5.11
 HARIU, TAKASHI, E4.3
 HARLAN, CHARLENE P., U7.44
 HARMER, MARTIN P., M4.2, M7.43, N6.6, M7.8
 HARMOND, LAUREL, T9.7
 HARPER, R.L., E6.1
 HARRINGTON, C.C., P4.4
 HARRIOTT, LLOYD R., B3.6
 HARRIS, ANDREW W., U11.5
 HARRIS, J.H., K5.2, K6.7
 HARRIS, JONICE S., U7.32
 HARRIS, R.D., K5.1, K6.3
 HARRIS, STEPHEN J., F1.8
 HARRIS JR., J.S., M10.6
 HARRISON, H.B., A9.18, B2.3
 HARRISON, JOSEPH G., G18.37
 HARRISON, STEVEN A., U8.1
 HARRISON, WILLIAM T.A., H2.8
 HARRUS, ALAIN S., I2, I2.1
 HART, D., M7.224
 HART JR., A.C., P3.1
 HARTFORD, E.H., M5.2
 HARTITT, B., G18.4
 HASEGAWA, H., J6.2
 HASH, MC., M7.156
 HASHIMOTO, FUMIO, G18.25
 HASHIMOTO, SHIN, D1.7, D1.9, D1.11, D2.7, D10.3, D10.8
 HASHIMOTO, T., J6.2
 HASHIMOTO, TSUNEYUKI, A9.50
 HASPER, ALBERT, L2.6
 HASSETT, D.J., W1.1, W2.1
 HASTIE, JOHN W., A9.12
 HASUE, SHINYA, M7.227
 HATALIS, MILTIADIS K., E5.3, H2.3
 HATFIELD, C.W., F4.2, XNF1.2
 HATTA, S., M7.15
 HATTANGADY, S.V., F7.3, I3.5, I4.5
 HATTON, T. ALAN, V7.5
 HAU, TSING, M7.160
 HAUGAN, T., M7.167
 HAUGE, ROBERT H., F1.4, F3.15
 HAUGSTAD, G., C3.5, E7.6, E10.3, G12.6
 HAUS, H.A., K2.2
 HAUS, J.W., H6.12
 HAUSTAD, G., E7.6, E10.3
 HAVEN, V.E., D2.12
 HAWARADA, HIROSHI, F5.7
 HAWORTH, A., U3.3, U7.2
 HAYAKAWA, H., M7.240
 HAYASHI, EIJI, M7.84
 HAYASHI, K., M7.135
 HAYASHI, NOBUYUKI, A2.4
 HAYASHI, S., M7.15
 HAYASHI, SHIGENORI, F5.9
 HAYES, CURT, W4.4
 HAYES, W., J6.11
 HAYNES, T.E., A8.12, D10.12, F8.6
 HAYRI, ERIC A., M7.34
 HAYTER, JOHN, B., J1.3
 HAZELTON, D.W., M9.8, M7.241
 HE, J.-W., L2.3
 HE, M.Y., N5.8
 HE, MICHAEL, N5.5, N5.6
 HEADRICK, R.L., C10.1, D10.9
 HEALD, S.M., C9.27, C9.28, C13.6, M7.88
 HEALY, P.C., M7.7
 HEARNE, JOHN A., U2.4
 HEB, MICHAEL, N3.9
 HEBARD, A.F., M6.8, M7.228
 HEBLE, BRIAN, L1.9
 HECHT, M.H., C6.1
 HEEGER, ALAN J., Q1.2

HEGDE, M.S., M3.2
 HEILAND, P., Y4.2
 HELMAN, D., E10.1, E10.4, E10.7, H6.3
 HENNEY, P.A., D2.1
 HENRICH, M., G10.4
 HEISER, JOHN, III, U4.2
 HELAL, MAAN, Y3.7
 HELLMAN, E.S., M5.2
 HELLMER, R.P., M7.225
 HELLSTROM, E.E., M7.79
 HELMERSON, K., V10.6
 HEMBREE JR., D.M., L5.3
 HEMGENT, P.L.F., A2.11, A6.14, A6.31
 HEMMINGS, R.T., W1.2
 HENCH, L.L., S1.3
 HENKKE, CHRIS S., O2.6
 HENNICKS, ULRICH, Y5.6
 HENRY, A., G18.22, G18.43
 HENRY, M.O., G9.53, G18.18
 HENRY, R.A., Q12.10
 HENSLEY, D.W., M7.177
 HENSON, T.J., M7.258
 HENTSCHKE, REINHARD, V9.6
 HENZLER, M., C3.2
 HEO, JONG, P6.5
 HEPP, A.F., M7.31
 HEPPNER, P.-M., U7.29
 HEREMANS, J.P., M7.28
 HERITIER, M., Q11.2
 HERMAN, IRVING P. B6.5, E10.5
 HERMAN, M.H., D10.46, D11.7, G9.35, G9.36
 HERNANDEZ, ROBERTO, C13.2, V9.10
 HERRERO, C.P., G6.4, H3.5
 HERRON, NORMAN, H2.8
 HERTL, W., A7.8
 HERZ, JEAN, V1.2
 HERZFELD, JUDITH, V7.4, V10.8
 HERZINGER, CRAIG M., D12.6
 HESS, DENNIS W., I, I1, I2.3
 HESS, MICHAEL, N3.9, M5.5, M5.6, O3.9, O3.10, S4.9
 HESS, NANCY J., F8.11
 HESS, PETER, B1.8, B5.18
 HESTIR, KEVIN, T3.6, T7.24
 HESTINGTON, C.J.D., M10.10
 HEUER, A.H., R2.9, R2.10
 HEUSER, BRENT J., J5.3
 HEUSINKVELD, M.M.D., L2.10
 HEWAK, D.W., B3.2
 HEYMAN, J., G1.2
 HIBBERT, D.B., T9.3
 HICKEY, S.J., P4.3, P4.4
 HICKMAN, J.J., B5.7
 HIDAKA, H., B2.8
 HIGASHI, G.S., B7.10, C7.6
 HIGGINS, M.J., V4.5, V7.9
 HIGGS, V., G2.3
 HILL, C., A8.7
 HILL, D.N., M7.171
 HILL, H., B4.2
 HILL, I., H6.15
 HILL, M., M7.13, M7.111
 HILL III, W.T., M3.11
 HILLAIRET, J., D10.21
 HILLEKE, R.O., J2.3
 HILLS, GRAHAM W., I2.1
 HILTNER, A., R6.3
 HILTON, ROBERT M., G9.26
 HIMPEL, F., C12
 HINKLEY, J.A., M4.7
 HINKS, D.G., M2.10, M6.6, M6.7, M7.38
 HINTERMANN, H., L4.2, L4.3
 HIPPSLEY, C.A., J5.11
 HIRABAYASHI, I., M7.14, M7.128
 HIRABAYASHI, M., F9.6
 HIRAI, M., C9.1
 HIRAI, T., L3.3
 HIRAKI, AKIO, F2.8, F4.6, F5.7, H3.7
 HIRAMOTO, HIROO, K3.1
 HIRAO, MASAHICO, C8.5
 HIRASHITA, N., H7.3
 HIRATA, G., H5.1
 HIROSAWA, ICHIRO, C5.1
 HIROSE, MASATAKA, I4.2
 HIROSE, Y., O8.1
 HIRSCH, ANDREAS, Q5.3
 HIRTZ, J.P., D10.47
 HIRVONEN, J.-P., A3.7, A6.34, A9.19, A10.7
 HIRVONEN, J.K., A1.6, A6.34
 HITOTSUYANAGI, H., M7.135
 HITTERMAN, R.L., J3.10, M6.9
 HJALMARSON, HAROLD P., G9.41, G15, G16.3
 HO, CHEN, N2.11
 HO, H.L., D1.10
 HO, KWOK-LUN, F8.12
 HO, PAUL S., K3, K3.9
 HO, PAULINE, T9.5
 HO, PIN, D7.2
 HO, SHI LUN, C8.5
 HOBBS, ANTHONY, R8.4
 HOBBS, CHRIS, R3.2, XNF1.3
 HOBSON, W.S., A8.11, B5.11, B5.12, G2.4, G8.4, G19.2
 HOCKER, NANCY, Y1.2
 HOCKETT, R.S., F3.2
 HODES, G., H2.2
 HODGE, D.J., M4.3
 HOENER, CAROLYN F., Q10.8
 HOFF, H.A., F3.11, M7.96, M7.101
 HOFFLINGER, B., B4.3
 HOFFMAN, ALON, M3.9
 HOFFMAN, C.A., E9.2, E9.3, E9.4
 HOFFMAN, DAVID M., L6.6
 HOFFMAN, ROBERT C., Q9.7
 HOFFMANN, B., U3.4
 HOGGINS, J.T., F5.11
 HOHR, AXEL, T7.12
 HOLDEN, T.M., J5.8
 HOLLAND, D., M7.165
 HOLLAND, O.W., A2.10, A8.3, B4.12
 HOLLAND, W.R., Q9.11
 HOLLEMAN, JISK, L2.6
 ROLLINS, RICHARD A., Q4.10
 HOLLMAN, G.G., W2.2
 HOLLOWAY, KAREN, C10.3
 HOLMA, MARIANNE, F6.3, M5.12
 HOLONYAK JR., N., G20.1
 HOLTZ, P.O., D10.42, D10.43, G9.20, G14.2, G14.3, G14.4
 HOLTZBERG, F., M7.112
 HOMENY, J., N7.6
 HOMER, VICKI, J3.3
 HOMEWOOD, K.P., A6.14
 HONEYCUTT, J.W., D2.2
 HONG, D.C., T2.6, T7.26
 HONG, D.J.L., M7.20, M7.27, M7.67, M7.86
 HONG, K., Q6.2
 HONG, M., A3.4
 HONG, Q.Z., D5.3, D10.22, G9.42, G18.35
 HONGLEIE, SHEN, A9.20
 HONMA, N., G18.31
 HOOD, E.S., C7.5
 HOOVER, J.D., T4.3/U10.3, T4.8/U10.8, U10.3/T4.3, U10.8/T4.8
 HOOVER, J.M., Q12.10
 HOPKINS, L.C., G19.3
 HOPPE, MARTIN L., O1.3
 HOR, P.H., M4.1, M10.5
 HORIE, C., H4.4
 HORN, K.M., A1.2
 HORN, KEITH A., Q9.5
 HORN, ROGER G., M6.2
 HOROWITZ, GILLES, Q6.5
 HORRIGNA, J.A., M7.174
 HOSHI, N., A6.41
 HOSHINO, M., G13.2
 HOSHINO, TAIZO, E7.5
 HOSHINOCHI, S., M5.11
 HOSODA, MASAHIRO, S2.2
 HOUBIB, HAMID, Q4.6
 HOUGHTON, D.C., D5.9, D10.18, D10.20
 HOWARD, W., F2.5
 HOWE, ARTHUR T., B6.6
 HOWELL, R.H., J4.5
 HOYLE, C.E., S1.4
 HRAZDÍRA, JAROSLAV, Y5.2
 HRUSKA, JANE, G18.45
 HSAO, BEN, O3.1
 HSEIH, K.C., C9.34
 HSIAO, BENJAMIN S., N3.7
 HSIEH, HORNGMING, A6.42
 HSIEH, JULIAN J., I2.8
 HSIUNG, L., D1.9
 HSU, C.H., M7.160
 HSU, JUNG-KUEI, D10.41
 HSU, N.J., M5.9
 HSU, SHU-EN, L4.2, M7.153, M7.244, N5.10
 HSU, T., I3.3, I3.4
 HSU, W.C., D7.10
 HSUEH, K.F., Q3.10
 HU, EVELYN L., B5.6
 HU, H.S., N2.1
 HU, J.Y., V9.3
 HU, MU-SAN, K3.8
 HU, REN YUAN, A3.9
 HU, Y.-Z., I2.6
 HU, YI, H9.7
 HUA, B.Y., D11.9
 HUANG, C.C., V7.8
 HUANG, D., F2.5
 HUANG, D.-Q., N5.13
 HUANG, DENGSHI, T3.4
 HUANG, HAO-HSIN, O1.2, S5.8
 HUANG, J.S., A11.6
 HUANG, JOHN S., J6.1, J7.14, V4.5, V7.9, V7.10
 HUANG, L.J., A6.15, A9.28, R2.6, T7.14, T7.23
 HUANG, S.J., O6.4
 HUANG, T.W., M7.153, M7.160
 HUANG, XIAO ZHOU, Q7.11
 HUANG, Y., M7.255
 HUANG, Y.S., O4.5
 HUANG, YEMING, M7.73
 HUANG, YUZHEN, M7.250
 HUANG, ZUWEI, M7.250
 HUBBARD, K.M., M7.196
 HUBER, C.A., E10.4, H2.7, H6.3, T5.3
 HUBER, D., G18.8
 HUBER, T.E., H2.7, T5.3
 HUBLER, G.K., A6.7
 HUDSON, JOHN B., L2.9
 HUFF, RICHARD G., P3.1, P4.1
 HUFF, W., M7.70
 HUGGINS, H.A., B4.10
 HUGHES, R.W., V4.9
 HUGILL, K.J., D8.7
 HUGUET, P., L2.11
 HUI, CHUNG-YUEN, N1.4
 HUI, TAN, H6.7
 HUIZHEN, LIAN, W2.6
 HULL, R., C11, D5.6, D7.4
 HULTS, W.L., M7.72
 HUMPHREYS, COLIN J., A6.6, D5.10
 HUMPHREYS, T.P., F7.3
 HUNERMANN, MICHAEL, C7.3
 HUNG, M.P., M7.99, M7.153, M7.160
 HUNG, Z.H., M7.160
 HUNSUCKER, DAVID W., W5.1
 HUNT, R.W., G18.12
 HUNTER, B.A., J3.6
 HUNTER, J., E4.4A
 HURD, ALAN J., P1.2, T5, T9.5
 HURLEY, WILLIAM J., O1.10
 HURT, JOHN C., K6
 HUSSEY, BRIAN W., B5.5
 RUSSIEN, S.A., D4.8
 HUTCHINGS, C.W., C7.4
 HUTCHINGS, M.T., J5.11, J6.11
 HUTH, G.C., M7.23
 HWAN, LEWIS, L4.8
 HWANG, D.M., M7.217, M7.224, M7.253
 HWANG, IN DUK, G9.19
 HWANG, JUNG TAE, H3.2
 HWANG, S., E6.5, E6.8, E7, E8.7
 HWANG, WEN-FANG, O3.2, O3.6
 HWANG, Y., U3.5
 HYBERTSEN, MARK S., C4.2, M1.3
 HYLDTOFT, JENS, M7.146
 HYNES, ANTHONY J., I1.6
 IANNO, N.J., G18.4
 IBÁÑEZ, R., M7.21
 IBBOTSON, DALE E., I, I2.8, I3
 ICHIMURA, M., G10.6
 IDE, FUMIO, P7.1
 IDZERDA, Y.U., D6.10
 IESIKOV, YU M., A9.39
 IGARASHI, H., M7.89
 IGARASHI, HIROSHI, U7.24
 IHARA, M., M10.12
 IHARA, SIGEO, C8.5
 IJIMA, Y., M7.240
 IJADI-MAGHSOODI, S., Q10.9
 IKAWA, H., S3.2
 IKEDA, MASAHII, B6.7
 IKEGAWA, S., M2.9
 IMAJIS, A., D10.33
 IMAJIS, S., A9.21, A9.36
 IMAI, K., M7.143
 IMPERATORI, P., Q4.8
 INABE, TAMOTSU, Q2.3
 INAM, A., M3.2, M7.224, M7.232, M7.235, M7.246, M7.253, M11.11
 INANAS, C., O6.8
 INGELS, MARTIN, H3.5, H6.1
 INGUVA, R., H6.12
 INNIS, DARYL, P4.2
 INOKUMA, TAKAO, H2.5
 INOUE, KATSUYA, Q8.4
 INOUE, KEN-ICHI, A6.16
 INOUE, N., C2.4
 INOUE, Y., H7.8
 INSPEKTOR, A., F1.10
 INTERRANTE, CHARLES G., U8.1
 INTERRANTE, LEONARD V., L2.9, O1.10
 INUSHIMA, TAKASHI, F5.9
 IPOSHI, T., H7.8
 IQBAL, T., P5.5
 IRENE, E.A., I2.6
 IRMSCHER, R., A7.5
 IRVINE, S.J.C., B4.2, E7.4, E8.2
 ISAACS, L.L., W1.3
 ISAKOV, I.F., A6.29
 ISHIBASHI, K., C10.6, D10.1
 ISHIBASHI, KIYOTAKA, A6.16
 ISHIBASHI, TADAO, G9.38
 ISHIDA, KOICHI, C5.2
 ISHIDA, YOICHI, N5.10
 ISHIGE, K., M7.128
 ISHIHARA, SHIM-ICHIRO, I1.9
 ISHII, TAKAFUMI, S2.8
 ISHIKAWA, H., U9.3
 ISHIKAWA, JUNZO, A1.7
 ISHIKAWA, KAZUHIRO, M7.84
 ISHIKAWA, MITSURU, H2.5
 ISHIMURA, T., H7.11
 ISHINO, MARIKO, D12.1, K5.12
 ISLAM, Q., C10.5
 ISOBE, H., U7.34
 ISOGAI, A., C9.26
 ISOTALO, HEIKI, Q8.3
 ISSI, J.-P., M7.12, M7.238
 ITO, HIROSHI, D8.12, G9.38
 ITO, K., A6.41
 ITO, TOSHIMICHI, H3.7
 ITOH, HIROSHI, M7.94
 ITOH, KENJI, S5.9
 ITOH, KOICHI, Q8.5, Q8.6
 ITOH, M., H7.2, H7.3
 ITOH, YOSHIKO, G9.24
 ITOH, YUZO, Q13.2
 IWAMI, M., C9.1
 IWAMURA, HIIZU, Q8.4
 IYE, YASUHIRO, M8.6
 IYER, SHANTHI N., D8.8
 IYER, SUBRAMANIAN S., D1.9, D5.1, G14.5
 IZQUIERDO, R., B6.8
 IZUMIYA, H., E4.5
 IZZARD, M., H7.9
 JACKEL, J.L., Q12.1
 JACKMAN, J.A., E9.9
 JACKMAN, R., M3.10
 JACKMAN, T.E., G18.12
 JACKSON, K.A., D10.48, P2.2
 JACKSON, KOBLAR A., F1.6, G18.37
 JACKSON, S.L., G9.30
 JACOBSON, A.J., M6.6
 JACOBSON, D.C., A2.3, A5.1, A9.14, A9.43, A9.44, G18.33
 JACOBSON, M.I., K3.7
 JAGANNADHAM, K., D4.9, M9.5
 JAGANNATH, C., D7.9, D10.32
 JAGANNATHAN, R., K7.1

JAGER, W., G12.5
JAGGARD, DWIGHT L., T2.3
JAHAN, M.S., M7.72
JAIN, AMITABH, A9.22
JAKE, R.A., M7.171
JAMES, A.C.W.P., M7.33
JAMES, J.B., E8.5
JAMES, J.H., M5.8
JAMES, K., E1.7
JAMES, M.R., N1.6
JAMES, R.B., G9.49
JAMES, R.D., L3.2
JAMES, R.J., U1.3
JAMES, T.W., M9.4
JANG, BOR Z., N3.4
JANG, H.K., A6.10
JANG, JIN, H3.2
JANKOWSKI, A.F., D6, D6.7, D9.6
JANOT, CHR., J1.7
JANSEN, F., F3.4
JANSSEN, S.A., Q7.9, Q10.12
JANSSEN, F.J.J.G., U7.25
JANSSEN, G.C.A.M., L3.6
JANSSEN, K.T.F., A9.47, G18.3
JANTING, J., A3.1
JANTZEN, CAROL M., U5, U5.3
JANZ, S., C11.4
JANZEN, E., G4.6, G9.47
JAO, SHYH-HUA, N1.1
JAPPY, T., U2.1
JARDINE, A. PETER, D10.29, F1.5
JASINSKI, JOSEPH M., I1.5
JAVADI, H.H.S., Q11.8
JAWOROWSKI, A.E., G18.48
JAYANETTI, J., C9.27
JEFFERIS, STEPHAN A., Y2.7
JEMIAN, P.R., J7.7, L6.11
JEN, K.Y., Q6.9
JENDRICH, U., G11.5
JENEKHE, SAMSON A., Q12.5, Q12.6
JENG, NANSENG, G10.5
JENG, S., K3.3
JENG, S.J., H7.4
JENG, Y.H., K3.9
JENG, Y.L., M7.45
JENNETT, NIGEL M., D6.2
JENNINGS, C., M7.2, M7.3
JENNINGS, HAMLIN, Y
JENNISON, D.R., M1.3
JENSEN, J.E., B1.7
JENSEN, KLAUS F., E4.4, F8.12, I4.9, L1.3, L1.11
JENSEN, L.C., N5.1
JENSEN, H.P., M7.28
JEON, HYEONGTAG, C10.5, D2.2
JEON, YOUNG JIN, A8.8, A9.23, B5.13
JEONG, J., G4.3
JEPPESSEN, KIRSTEN, G., W4.5
JERCINOVIC, MICHAEL J., U6.2
JEROME, R., O5.3
JEROMINEK, H., B3.2
JERVIS, T.R., A9.19, A10.7, N2.2
JESSON, DAVID E., C9.32, C11.6, M9.1
JEYADEV, S., Q10.1
JEZEWSKI, M., G17.2
JIABTAO, JIANG, W2.6
JIAMIN, ZHANG, E10.11
JIAN, L., O1.7
JIANG, X.P., M7.139
JIANG, XIANG-LIU, F3.10
JIANGOU, ZHANG, M4.9
JIANKUN, ZHOU, A6.30
JIAO, K.L., D2.11, G9.17
JIMENEZ, JORGE R., D1.9
JIN, H.-S., M7.206
JIN, M.H., E1.7
JIN, S., M7.74
JIN, SHU, H1.7
JIN, XINGYUN, M7.73
JINCANG, ZHANG, M6.11, M7.242
JIONG, XIANG, M6.11, M7.242
JOANNY, JEAN-FRANCOIS, V1.3
JOHANSEN, A., A4.6
JOHN, D., E1.2
JOHN, P., B5.22, B7.9
JOHNSON, C., J2.7
JOHNSON, D.D., J2.6, J4.4, J4.7
JOHNSON, D.L., M7.45
JOHNSON, E., A4.6, A11.1
JOHNSON, E.A., A9.24
JOHNSON, HERBERT H., A3.8
JOHNSON, Q.C., N5.19
JOHNSON, R.E., S2.7
JOHNSON, R.I., A9.4, H3.4
JOHNSON, S.M., E1.1, E2.4, E2.6, E8.5, M7.130
JOHNSON, STEVEN T., A8.9, G9.6
JOHNSON, W.L., A3.2
JOHNSON, M.S.A., R2.4, R2.5
JONES, C., E1.7
JONES, C., N2.8, O8.5
JONES, E.D., D10.46
JONES, FRANK N., O6.3
JONES, I.P., M7.254
JONES, K.A., I4.6
JONES, K.S., A8.11, A9.25, B5.12
JONES, K.W., M7.71
JONES, M. THOMAS, Q4.9
JONES, R.A.L., O7.3, O7.5
JONKER, B.T., D6.9, D6.10, E10.6
JOOS, B., G18.28
JORDA, MICHEL, U1.1, U7.6
JORGENSEN, J.D., J, J1.7, M2, M6.6, M6.9, M7.38
JOS, H.F.F., G18.3
JOSHI, A., N2, N2.1
JOSSANG, T., T7.16
JOYCE, B.A., D8.7
JUBBER, M., B5.22
JUDY, J.H., F3.8
JULIEN, CHRISTIAN, H6.5
JUNDT, D.H., P8.1
JUNG, CHANG YOUNG, H3.2
JUNGBLUT, FRANK, A6.20
JUNK, P.C., B2.3
JUNLIAN, YAN, M4.9
JUNSHENG, WANG, M4.9
JUPINA, MARK A., C12.3
KAATZ, F.H., D2.3
KABYSHEV, A.V., A9.29
KACZOR, P., G16.2
KADOIWA, K., D2.8
KADONO, MASAYA, F5.9
KADOTA, YOSHINORI, G9.24
KAHEN, K.B., G9.8, G9.9
KAIM, R.E., A9.47
KAISER, DEBRA L., M6.4
KAISER, WILLIAM J., C6.1, C7
KAJDA, JACEK M., K5.3
KAJIHARA, S., F4.9
KAJIYAMA, TISATO, O6.6
KAJZAR, F., Q12.7
KAKALIOS, J., D9, D9.8
KAKUTA, ATSUSHI, Q13.2
KALANTAR, J., N5.23
KALEJS, J.P., G18.46
KALIDINDI, S.R., L1.5
KALISHER, M.H., E8.5
KALNIN, I.L., S2.7
KALOYEROS, ALAIN E., F6.3, M5.12
KALYANIWALLA, N., H6.12
KAMATH, M., Q12.4
KAMEDA, M., H7.1
KAMEHARA, N., K5.11
KAMEI, G., U7.40
KAMENETZKY, EDUARDO A., N3.6
KAMIGAITO, OSAMI, C9.26, O1.5
KAMIJOH, K., G9.40
KAMINSKI, PAWEZ, G2.6
KAMITAKAHARA, W.A., J6.9
KAMIURA, YOICHI, G18.25
KAMLOTT, G.W., M7.74
KAMO, AKIRA, H1.9
KAMO, M., F2.7
KAMO, T., M7.142, M7.247
KAMP, M., D11.10
KANAI, MASAKI, M3.4
KANATZIDIS, MERCOURI G., Q3.5
KANBAYASHI, SHIGERU, H7.5
KANEHORI, KEIICHI, M7.172
KANG, W., Q11.9
KANICKI, J., H7.4
KANNEWURF, CARL R., M7.180, M7.251, M10.3, M10.8, Q3.5
KANT, R.A., A6.17
KAO, C.T., A8.12
KAO, Y.C., D2.9, D7.3, D9.3, G18.49
KAO, Y.H., M7.71, M7.191, M7.230, M7.237
KAO, Y.J., G2.4
KAPITULNIK, A., M11.4
KAPLAN, DAVID L., R3.3, R5.3
KAPUR, M., I3.7
KARAKASHIAN, A.S., F2.11, F3.3, F5.2
KARAM, N.H., D2.12
KARASAKI, KENZU, T4.6/U10.6, U10.6/T4.6
KARASZ, FRANK E., O4.1, S, S4.1, S5, V9.9
KARDAR, MEHRAN, V7.2
KARFUNKEL, U., G18.36
KARIM, A., J7.12, O7.2, O7.3, O7.4
KARIM, D., S2.7
KARIMI, M., C9.17
KARITA, Y., U9.3
KARUT, MICHAEL G., M11.6
KARLICKER, JR., R.F., A9.26
KARMARKAR, M.M., C5.4
KARTHEUSER, E., E10.9
KARTSOVNIK, M.V., Q4.2
KASE, J., M4.3
KASER, STACY, U6.2
KASMAI, HAMID, Q8.3
KATAOKA, I., A6.41
KATAYAMA-YOSHIDA, HIROSHI, G9.46
KATO, T., G13.2
KATO, TERUO, M7.90
KATO, Y., D8.5
KATOH, NAOTAKE, U7.36
KATZ, A., A9.26
KATZ, H.E., Q9.11
KATZ, J.J., R6.8
KAUFEL, G., B5.4
KAUFMAN, JIM H., T, T2.4
KAWAI, MAKI, M10.11
KAWAI, SHICHI, B2.9, M3.4
KAWAI, TOMOJI, M3.4, M7.62
KAWAMOTO, E.H., V6.5, V6.8, V8.7, V8.10
KAWAMOTO, J., C9.2
KAWANISHI, M., U6.1
KAWANO, A., C9.2
KAWARADA, HIROSHI, F2.8, F4.6, F5.7
KAWARADA, MONTONOBU, F1.9
KAWASAKI, M., C9.23
KAWASAKI, RYODOU, M5.10
KAWASUMI, MASAYA, O1.5
KAWATA, YUTAKA, A6.16
KAY, ERIC, I4.8
KAZUMATA, YUKIO, M7.90
KAZAKOS, A.M., S3.3
KEAR, B.H., M5.13, M7.137
KEARLEY, G.J., J2.2
KEELEY, JOSEPH T., L3.8
KEILING, CH., U7.29
KEILMANN, F., G3.6
KELLER, R., D4.5, G5.5
KELLETT, B.J., M5.8
KELLOCK, A.J., A1.9
KELLOGG, G., V6.5, V8.7, V8.10
KELLY, M.J., A6.19
KELNER, G., F6.5
KEMA, N.V., U7.25
KENNEDY, T.A., G1.5, G15.4
KENNEDY, W., M1.10
KENNEDY, J., T5.1
KENZER, D., M7.45
KEOSIAN, R.A., S2.7
KEPLER, R.G., Q10.11
KERAMIDAS, V.G., D1.1
KERCHNER, H.R., M7.118, M8.7, M11.2
KERKHOFF, M.J., P3.5
KERNEVEZ, NELLY, Q7.5
KERR, D., G4.1
KERSTEN, R.TH., P1.4
KERTESZ, MIKLOS, Q6.7
KES, P.H., M8.5
KESSELMAN, M., E8.11
KESTERNICH, W., J7.11
KETTERSON, J.B., D10.10, M9.2, M10.8
KEUCH, T.F., G12.3
KEZUKA, HIROSHI, M7.233
KHALEEL, R., T4.8/U10.8, U10.8/T4.8
KHAN, H.R., M7.107
KHANDROS, IGOR Y., K7.3
KHANTHA, M., C9.21
KHARAS, G., O8.9
KHASANOV, O.L., A9.31
KHOMENKO, A.G., Q5.1
KIDO, H., S3.9
KIDO, Y., C9.2
KIEFL, R.F., G7.1
KIELE, J.A., E1.1
KIELY, C.J., C2.5, C9.34, N2.8
KINBLE, R., G1.3, G5.4
KIKUCHI, H., M7.143
KIKUCHI, M., U7.10
KIKUCHI, RYOICHI, M7.40, M7.105
KIKUCHI, TORU, K5.9
KILGOUR, CAROL, L., W3.3, W3.4
KILNER, J.A., A2.11
KIM, C.S., E1.8
KIM, CHEOL J., M7.148
KIM, H., J7.3
KIM, H.K., A6.18
KIM, H.M., D10.36, D10.37
KIM, H.S., B7.2, M3.7
KIM, HONGDOO, J6.4
KIM, J., K4.7
KIM, JEHA, D6.8
KIM, K.H., P8.4
KIM, M.H., D10.24
KIM, MAHN WON, V1.7, V6.1, V6.5, V6.6, V6.8, V8.11
KIM, S.-J., D10.50
KIM, S.S., A6.10, A6.18, I4.3
KIM, SUNG CHUL, H3.2
KIM, T.S., D2.9, D7.3
KIM, Y., C11.5, G9.44, G12.1
KIM, Y.C., M7.118
KIM, Y.H., K4.7
KIM, Y.W., F7.2
KIM, YOON-GI, B3.3
KIM, YOUNG K., C9.10, D10.4, D10.28
KIMBALL, C.W., M2.10, M7.38
KIMBARA, K., K1.4
KIMERLING, L.C., A9.26, D10.48, G4.3, G12
KIMURA, R., E5.1
KIMURA, T., M10.12
KINDNESS, A., U2.1
KING, A.H., C9.20
KING, FRANKLIN G., U11.7
KING, J.S., J5.3
KINGON, A.I., A6.4, M7.48
KINGSLEY, B., M7.163
KINI, A.M., Q5.2
KINNEY, J.H., N5.19
KINOMURA, A., A6.33
KINOSHITA, MAKOTO, M7.62
KINOSHITA, N., Q4.3
KINOSHITA, TAKAMASA, Q8.5, Q8.6
KIRBY, BARRY A., M7.236
KIRIAKIDIS, G., B4.7
KIRKPATRICK, WILLIAM D., Y3.4
KIRSCH, JACK F., R4.1
KIRCH, S.J., B4.11
KISHIDA, SHUNJI, B2.1
KISS, ANDREA, D., V1.1
KISTENMACHER, T.J., F8.9, F8.10, F9.5
KITABATAKE, M., A4.3
KJARTANSON, B.H., U11.2
KLABUNDE, C.E., M8.7
KLABUNDE, K.J., T1.8
KLASSEN, H.E., O3.6
KLATT, M., J3.4
KLEEBE, H.-J., E2.4, N2.7
KLEI, HERBERT E., R4.6
KLEIN, BILL, T4/U10
KLEIN, JACOB, V6.9
KLEIN, MAX, L2.4
KLEIN, RUDOLF, V4.2
KLEIN, W., T1.3
KLEM, J.F., G9.41
KLEMM, K., S3.6
KLEMPER, NORBERT, R6.9
KLEVERMAN, M., G1.1, G2.2, G4.6, G9.47
KLOSOWSKI, P., J2.5

KLUG-WEISS, PETRA, M7.52
 KLUMPP, A., B7.6
 KMETZ, MICHAEL, N5.9
 KMIRC, R., M7.83
 KNAPP, JAMES A., A, A4, A5, A6, A6.19, A9, A10
 KNAPP, R.B., T4.4/U10.4, U10.4/T4.4
 KNAUSS, KEVIN G., U5.2, U7.13
 KNIGHT, A.E.W., B2.3
 KNIGHT, D., F1.10
 KNOBLER, CHARLES M., T1.1
 KNOBSEN, A., Q12.10
 KNOLL, K., Q10.4
 KNOTES, OTTO, A6.20
 KNOWLES, JAMES, F3.2
 KNOX, ROBERT, A9.9
 KNUDSEN, JOHN P., A9.7, J5.2
 KO, KEI-YU, G9.13, G9.18
 KOB, RICHARD, F5.13
 KOBASHI, K., F3.4
 KOBAYASHI, A., B2.9
 KOBAYASHI, HISAO, A2.4
 KOBAYASHI, M., E2.1, E3.5, E3.6, E3.7
 KOBAYASHI, M., M5.11
 KOBAYASHI, NAOTO, A2.4, F9.7
 KOBAYASHI, Y., U7.34
 KOCH, C.C., M7.48, M10
 KOCH, R., M1.4, M8
 KOCH, S., D10.47
 KOCH, S.W., Q13.3
 KOCH, THOMAS L., K2.4
 KOCHVAR, JOHN, R5.6
 KODAS, TOIVO T., B1.4, M7.47
 KOEPKE, B., M4.13
 KOESTNER, R.J., E1.6
 KOEZUKA, HIROSHI, Q12.8
 KOGA, K., F6.14
 KOGA, NOBORU, Q8.4
 KOGELSCHATZ, ULRICH, B7.11
 KOH, SUNG OK, H3.2
 KOHARA, S., M7.147
 KOHARA, TEIJI, Q12.9
 KOHLER, BRYAN E., Q13, Q13.1
 KOHNO, O., M7.181, M7.240
 KOIDL, P., G19.5
 KOIKE, J., A11.3
 KOIKE, YASUHIRO, P7.2
 KOJIMA, KAZUYOSHI, M7.197
 KOLAWA, E., H6.13
 KOLBAS, R.M., E7.10
 KOLLENBRANDER, K.D., I1.8
 KOLIN, N.G., A9.54
 KOLODZIEJSKI, L.A., E2.1, E3.7, E10.5
 KOMARNENI, S., M7.60, M7.195, S3.3, S3.9
 KOMATSU, Y., P4.5
 KOMEN, Y., A9.18
 KOMIYA, TOHRU, H1.9
 KONAGAI, M., E5.1
 KONAK, C., T7.28
 KONDO, M., V2.1
 KONDO, NAOTO, D2.10
 KONDOH, S., M4.3
 KONECNY, J., W4.3
 KONG, P.M., V5.8
 KONG, H.S., F6.7
 KONKEL, W.H., E1.1
 KONOMI, I., C9.2
 KONONOVICH, P.A., Q4.2
 KONSTANTINIDIS, KARIOFILIS, N5.3
 KOPCSAY, G.V., K4.2
 KOPELMAN, RAUL, O5.7, T7.1, T7.2, T7.3, T7.4, T7.5, T9.7, T9.8
 KOPILOV, N., P2.2
 KOPT, R.F., D10.46, G9.51
 KOPYLOV, NONNA A., P2.2
 KORDAS, G., M7.45
 KOREN, G., M3.13, M7.112
 KORSHUNOV, P.P., A9.54
 KORTAN, A.R., D10.48
 KOSOL, PETER B., M11.12
 KOSFELD, ROBERT, N3.9, N5.5, N5.6, O3.9, O3.10, S4.9
 KOSHINO, NAGAOKI, F1.9
 KOSHIZUKA, N., M7.58
 KOSTER, UWE, K7.6, N2.9
 KOSTORZ, GERNOT, J4, J4.3, J4.10, J4.12
 KOSUGE, S., K4.5
 KOTECKI, D.E., H7.4
 KOTELES, EMIL S., D7.9, D10.32, D10.41, D10.45, D11, D11.3
 KOTOV, A.I., Q5.1
 KOVAC, CAROLINE A., K7
 KOVALCHICK, J., D10.9
 KOVALEV, D.I., E5.9
 KOVAR, ROBERT F., S3.7
 KOWALCZYK, S.P., K4.7
 KOWEL, S.T., Q12.10
 KOZAK, MATTHEW W., U7.44
 KOZUBOWSKI, J., D4.5
 KOZUCH, D.M., G6.1, G8.2
 KRAJEWSKI, J.J., M2.2
 KRAMER, E.J., O7.3, O7.5
 KRANZ, K.S., P4.1
 KRASKO, GENRICH L., C9.25
 KRAUSCH, GEORG, V6.9
 KRAUSE, B., M7.37
 KRAUSE, STEPHEN J., A6.39, G18.32, O3.2
 KRAUSS, A.R., A6.4
 KRAMITZ, D., J5.5
 KREBS, J.J., D6.9, D6.10, E10.6
 KREMER, R.E., E6.2
 KRIM, JACKIE, T5.2, T6
 KRINGHOF, P., G11.6
 KRISHNAMURTHY, SRINIVASAN, E7.4A
 KRISHNAN, K.M., H5.3
 KRISHNAN, MAHADEVAIYER, K7.1
 KRISHNASWAMY, J., B4.12, F3.17
 KROEGER, D.M., M11, M7.258
 KROL, A., M7.191
 KRUEGER, S., J1.5, J7.7
 KRUGER, ALBERT A., N4.8, P3.2
 KRUGER, JEROME, Q7.6
 KRÜGER, U., M3.6
 KRUSIUS, J.P., K1.3
 KRUSOR, B.S., C2.3
 KU, H.C., M7.153
 KUBO, Y., M7.89
 KUCERA, J.T., M7.204, M10.2
 KUDRIAVTSEVA, E.A., A9.54
 KUECH, THOMAS F., B2.7, B4, D7.5, G12.3
 KUENTZLER, R., M7.107
 KUJIRAI, HIROSHI, H1.9
 KUKIMOTO, H., E3.2, G15.2
 KULKARNI, P., H6.14
 KULLBERG, M.L., M7.44, M7.45
 KULLEN, P., A6.34
 KUMAGAI, K., H7.11
 KUMAR, ASHOK, D10.13, M5.9, M7.59
 KUMAR, BINOD, H6.2
 KUMAR, G. SUDESH, R3.7
 KUMAR, R.S., S4.5
 KUMAR, S.N., A8.5, G18.13, Q3.12
 KUMARATHASAN, P., W2.1
 KUMASHIRO, YUKINOBU, A2.4, F9.6, F9.7
 KUME, A., M9.11
 KUN, LIU, E10.11
 KUO, CHENG-TZU, L4.2
 KUO, P.K., F4.3
 KUO, S.T., W3.5
 KUO, Y.H., M7.168
 KUPPERMAN, D.S., J3.10
 KURATA, TETSUYUKI, Q12.8
 KURAUCHI, T., O1.5, O8, O8.1
 KURIACOSE, J.C., A9.42
 KURIHARA, KAZUAKI, F1.9
 KURITA, SUSUMU, Q5.4
 KURIYAMA, O., U7.10
 KURK, MORGAN, D4.10
 KURMOO, MOHAMMED, Q4.6
 KURODA, KEN'ICHI, M7.197
 KURTZ, S.R., G16.3
 KUSAKA, MASAHICO, C9.1, G9.22
 KUSAKABE, Y., M5.11
 KUSHIDA, T., V10.6
 KUSHNARENKO, V.P., A9.39
 KUST, ROBERT P., A7.9
 KUSZKO, W., G17.2
 KUWANO, HIROKI, M7.214
 KUWANO, Y., H7.1
 KUZUU, N., P4.5
 KVAM, E.P., D5.10
 KWAK, J.F., M7.117, M7.141, M7.157, M7.225, M10.7
 KWO, J., M5.1
 KWOK, CHEE-KIN, H6.13
 KWOK, H.S., B7.2, K3.3, M1.7, M3.7, M7.230, M11.10
 KWON, TAEHYUN, O1.4
 KYRIACOU, S., P2.5
 KYU, T., O4.3
 LABUN, P.A., K6.7
 LACELLE, C., D10.31, D11.9
 LACELLE, SERGE, V3.7
 LACKEY, W.J., L3
 LACKEY, W.J., M7.171
 LACOURSE, W.C., P6.8
 LADDERMAN, S.S., M5.6, M11.4
 LAFFORET, J., L2.11
 LAFLESH, R.C., W2.3
 LAGALLY, M.G., F3.14
 LAGASSE, M.J., K2.2
 LAGOS, B., M4.5
 LAGODAS, DIMITRIS C., N1.4
 LAGUROS, JOAKIM, G., W4.4, W5.3
 LAHTI, PAUL M., Q8.9
 LAI, WILLIAM, C9.38
 LAIA, J.R., L6.8
 LAIBINIS, P., B5.7
 LAIBOWITZ, R.B., M7.112
 LAINE, RICHARD M., O1.3
 LAIRD, CAMPBELL, N3.2, N4.6
 LAKHTAKIA, AKHLESH, Q13.11, Q13.12
 LAKIS, R.L., M7.50
 LAKSHMI, R.P. VIJAYA, E1.9
 LAL, J., T1.4
 LALANNE, J.R., V9.7
 LALEVIC, B., M7.137
 LAM, C.H., H1.5
 LAM, D.J., L6.3, L6.4
 LAM, NGHI Q., A4.4
 LAMAZE, GEORGE P., J5.1
 LAMBERT, G., G3.2, P9.5
 LAMBERT, STEVEN J., U7.38
 LAMBLE, G.M., C13.6
 LAMBRECHT, W.R.L., C13.3, F6.9
 LAMOREAUX, R.H., M7.130
 LAN, JIAN, M7.145
 LANAGAN, M.T., M7.8, M7.125
 LAND, DAVID J., K4.10
 LANDERS, ALBERT, Y. Y1
 LANDIN, S.M., K5.6
 LANDIS, W.J., R1.4
 LANFORD, W.A., B5.21
 LANG, C.A., C3.3
 LANGE, ARMIN, Q5.3
 LANGE, F.F., M7.122, M7.4
 LANGER, J.M., G2, G16.2
 LANGFORD, S.C., B3.9, T3.1
 LANGHOFF, C.A., Q13.7
 LANGLAND, JOHN K., J5.1
 LANGLEY, K.H., V9.9
 LANGOUCHE, G., A2.12, A9.27, D10.30, G16.4
 LANHAM, M., M9.4, M7.216
 LANSARI, Y., E4.6, E6.7, E6.8, E8.7, E9, E9.4
 LANTMAN, C., V9.3
 LANZEROTTI, M. YVONNE D., T7.36
 LAPOUYADE, RENE, Q7.16
 LARBALESTIER, D.C., M7.257
 LARAIA JR., V.J., R2.9, R2.10
 LARBI, JOSEPH, A., W2.5
 LARDNER, T.J., N6.3
 LARSEN, A. NYLANDSTED, G11.6, G18.2
 LARSEN, KIM KYLLESBECH, G18.2
 LARSON, ALLEN C., J5.4
 LASHMORE, DAVID S., J2.7, N2.10
 LATHROP, DANIEL K., M7.229, M11.5
 LATHROP, DAVID, P6.2
 LATSHAW, B.E., O7.9
 LATUSHKO, YA. I., G18.21
 LAU, EDUARDO C., R1.2
 LAU, K.-C., U11.2
 LAU, KEI MAY, D10.41, D11.3
 LAUGHLIN, K.B., B5.16
 LAUGHNER, JAMES W., T3.8
 LAUGIER, A., A8.5, G18.13
 LAUGIER, J., D10.21
 LAUKHIN, V.N., Q4.2
 LAURSEN, RICHARD A., R5.7
 LAVERSANNE, R., Q3.7, Q11.8
 LAVOIE, C., B6.8
 LAWLER, J.E., F3.14
 LAWN, BRIAN R., M7.7
 LAWRENCE, D.J., G9.8
 LAWRENCE, M., M7.48
 LAWRENCE, R.A., Q10.3, Q12.12
 LAWSON, A.C., J4.11
 LAWTON, CARL W., R4.6
 LAY, K.W., M7.24
 LAZARE, SYLVAIN, B5.1
 LAZAREVA, O.I., F4.5, F9.3
 LAZARO, F.J., Q7.17
 LE CORRE, A., D1.4
 LE, JING-QI, F3.10
 LEBLANC, JR. OLIVER H., Q4.4, Q4.5
 LECAT, J.H., C9.4, L2.7, O7.8
 LECHTER, W.L., M7.96, M7.101
 LEDESMA, R., W1.3
 LEE, C.B., M7.185, M7.187, M7.205
 LEE, C.J., K3.3
 LEE, D.R., A8.12
 LEE, F., D8.11
 LEE, H.K., M7.144
 LEE, H.S., Q6.1
 LEE, H.W., B2.4
 LEE, J.G., M7.36
 LEE, J.W., D10.50, G18.41
 LEE, JEONG Y., B5.13
 LEE, K-S., D12.8
 LEE, K.M., G4.3
 LEE, K.W., M7.144
 LEE, M.B., E8.11
 LEE, N.L., A9.13
 LEE, S.-TONG, G9.13, G9.18
 LEE, SEUNG KYU, H3.2
 LEE, SUKMOCK, D6.8
 LEE, W.H., C3.4
 LEE, W.W.-L., U3.5, U11.8
 LEE, YONG-HEE, D6.4, D6.11, F2.1
 LEFKOW, A.R., F3.14
 LEGORE, T., T4.8/U10.8, U10.8/T4.8
 LEGUES, F.K., D2.7, D5.8, D10.17, G7.5
 LEGRICE, Y.M., F2.6, F3.4, H4.3
 LEGROS, R., G9.51
 LEHMAN, J.L., G9.15
 LEHN, J.M., Q12.7
 LEI, N., V2.6, V3.6
 LEIBER, J., D11.10
 LEIBERICH, A., C9.18
 LEIBLER, MICHAEL W., T9.4
 LEIBLER, LUDWIK, V1.3
 LEIBLER, S., V7.3
 LEIDERER, P., M3.6
 LEITE, J.R., G5.3, G18.39
 LEKKERKERKER, H.N.W., V4.1
 LEMAIRE, P.J., P4.1
 LEMMON, TIM, S5.1
 LENAHA, PATRICK M., C12.3
 LENEVEU, DENNIS M., U11.10
 LENG, LIM POH, A6.27
 LENTVORSKI, A.P., V9.3
 LEPPÄVUORI, S., M7.200, M7.138
 LESKOWITZ, G.M., P5.6
 LESLIE, THOMAS, S1.6
 LETTS, STEPHAN, A., V5.8
 LEU, JINPERNG, I4.9
 LEUNG, CHRISTOPHER K.Y., N1.2
 LEUNG, DORIS S., Q9.3
 LEUNG, PETER C., S2.6
 LEUSINK, G.J., L3.6
 LEVER, R.F., G11.2
 LEVI, A.P.J., D10.9
 LEVKOFF, J., C9.18
 LEVOSKA, J., M7.138, M7.200
 LEVY, DAVID, T7.12
 LEVY, DAVID H., C12.4
 LEWALT, M.T., G3
 LEWANDOWSKI, S., V9.3
 LEWIS, JONATHAN H., D8.8
 LEWIS, M., H2.6
 LEWIS, MICHELE A., U7.9
 LEWIS, N., M11.3
 LEY, L., H1.7
 LI, CHE-YU, K

LI, CHENGGEN, M7.73
 LI, CHING-SHAN, O5.7, T9.8
 LI, D., E3.5, E3.7
 LI, DEJEI Q., M7.37, M9.2
 LI, D.X., M9.2
 LI, GUZHONG, M7.145
 LI, HENG-DE, A6.15, A9.10, B5.15, R2.6, T7.14
 LI, HONG, N5.22
 LI, HOU, F3.18, F3.19
 LI, HOUQIANG, T6.6, T7.13
 LI, J.C.M., T3.7
 LI, JIAN, F9.7, G18.35, K5.7
 LI, L., M7.168
 LI, LI, T9.7
 LI, LIAN, F4.10, L5.5
 LI, Q., J7.11
 LI, Q., M5.5, M7.209
 LI, QIONG, N5.15
 LI, S., M7.155
 LI, VICTOR, C., N1.2
 LI, WANGPEI, A6.9
 LI, Y.H., A8.1
 LI, YING, T6.6, T7.13
 LIANG, K.S., V1.6, V2.3, V2.6
 LIANG, WENCHUAN, R4.2
 LIAO, Y.X., J1.9
 LIANG, QI, F3.18, F3.19
 LICHTY, L.R., Q6.6
 LICK, W.J., E2.6
 LIDDLE, J. ALEX, D8.10, E6.3
 LIEBETRAU, A.M., U7.43
 LIEFTING, J.R., A8.4, A8.6, A9.30
 LIEW, STEVE, U11.9
 LIGHT, W.B., U11.8
 LIGHTOWLERS, E.C., G2.3, G9.53, G18.18
 LIMMATA, E., F6.13
 LILIENTELD, DAVID A., A3, A11.5
 LIMAT, L., V8.4
 LIN, C.A., M7.99
 LIN, C.H., M7.160, M7.178
 LIN, CHIN, M7.145
 LIN, FUYU, E5.3, H2.3
 LIN, GUANG H., I3.7
 LIN, H.B., P4.6
 LIN, I.N., M7.244
 LIN, JIAN-YANG, B2.5
 LIN, M.R., N6.3
 LIN, M.Y., J7.14
 LIN, PATRICK, M9.7
 LIN, R., D8.11
 LIN, R.J., M5.3, M7.161
 LIN, S.S., N4.4
 LIN, SHUHAN, F8.8, H6.8
 LIN, T.L., D10.8
 LIN, Y.-P., N5.13
 LINDEFELT, U., G18.23
 LINDEMUTH, PAUL, M., V9.4
 LINDNER, D.L., S5.2
 LINDQUIST, JOHN M., A9.60
 LINDSAY, G.A., Q12.10
 LINDSTROM, J.L., G6.2, G18.22
 LINDSTROM, J.N., L3.5
 LING, XINSHENG, M7.10
 LINK, REBECCA P., R4.7
 LINKER, G., A7.1, M5.5, M7.209
 LINNARSSON, M., G4.6, G9.47
 LIQU, S.H., M10.9
 LIQU, Y., F1.10
 LIUPMAN, JOSEPH D., A9.21, A9.36
 LIPSOMB, G. FERRIS, Q1.3, S1.5
 LISHAN, DAVID G., B5.6
 LIST, R.S., M7.3
 LITSTER, J.D., V10
 LITTLE, D., L5.13
 LIU, B., F4.4
 LIU, B.X., A6.15, A9.28, A11.8, L5.12, T7.14, T7.20, T7.23, T9.9
 LIU, D.Z., M7.23
 LIU, H., B4.5
 LIU, H.-Y., D7.3, D9.3, E1.3, E1.6, G18.49
 LIU, J., M7.82
 LIU, J.Z., M1.8, M7.3
 LIU, J.Z., M7.2
 LIU, JOYCE C., G7.5, K7.9
 LIU, JUN, T7.8, T8.5
 LIU, L., M7.130
 LIU, P.L., D10.36, D10.39, K3.3
 LIU, R., M7.3
 LIU, SU-NIM, V1.7
 LIU, TAO, K6.8
 LIU, W.C., D7.10
 LIU, X., E10.6
 LIU, Y.S., B3.1
 LIU, ZUNXIAO, M7.145
 LIZHI, CHEN, A9.49
 LO, KING H., N5.24
 LO, S.K., Q12.6
 LOCKWOOD, D.J., D10.18
 LOCQUET, J.-P., C11.1
 LODGE, T.P., V8.6
 LOEHMAN, R.E., M7.77
 LOH, I.H., N5.23
 LOH JR, E.Y., Q10.2, Q11.5
 LOHMANN, W., K7.2
 LOKKEN, RYAN O., U1.2
 LOMBARDI, STEPHEN J., R5.3
 LOMBARD, S., A2.5
 LONG, G.G., J1.5, J6, J7.7, L6.11
 LONG, JANE, T3.6, T4.6/U10.6, T7.24, U10.6/T4.6
 LONGO, M., F3.17
 LOONG, C.-K., M2.3
 LOPATA, J., G6.1, G8.2, G8.4, G18.41
 LOPATIN, V.V., A9.29, F9.4
 LOPES, V.C., E7.8
 LOPEZ-CRUZ, ELIAS, E1.5
 LORA, F., M7.21
 LORENZEN, LISELOTTE, M7.146
 LORETTO, D., B4.10, C4.3
 LORETTO, M.H., N2.6
 LOUR, W.S., D7.10
 LOURENCO, M.A., A6.14
 LOVEJOY, STEVEN M., Q9.3
 LOW, S., J5.9
 LOWDEN, P., L5.13
 LOWDEN, RICHARD A., L3.2, N6.7
 LOWE, W., D10.27, D10.48
 LOWNDES, DOUGLAS H., D10.12, M3.3, M7.192, M7.222, M9.1
 LOZYKOWSKI, H.J., E4.8
 LU, ENLIAN, H2.4, H6.9
 LU, F., M7.78
 LU, JIONG PING, L5.11
 LU, REBECCA, P3
 LU, T.-M., A6.5, F5.17
 LU, W.X., A8.4, A8.6, A9.30
 LU, Y., M7.137
 LU, Y.F., A6.33, B3.8
 LU, Z., E4.2
 LU, ZHANGDE, B5.3
 LUBIG, A., M7.221
 LUCAS, J., P6.4
 LUCOVSKY, GERALD, H1.3, I, I2.4, I3.8, I4, I4.3
 LUDTKA, G.M., J5.8
 LUPTMAN, H.S., D10.9, G18.41, G19.4
 LUJAN JR., MANUEL, J5.4
 LUND, J.C., F9.8
 LUNDSTOM, I., O6.8
 LUO, H., E10.10, J2.5
 LUO, J.S., M7.110
 LUO, L., D1.7
 LUPO, JAMES A., C13.5
 LUSIGNEA, RICHARD W., O8.2, S3.7
 LUTH, H., D11.10
 LUTZ, M., A10.4
 LUTZE, WERNE, U5, U6.1, U6.2, U7.11
 LUX, R.A., I4.6
 LUYBERG, M., G12.5
 LUZEAU, P., D10.47
 LUZZATI, S., Q6.8
 LUZZI, D.E., A9.51
 LYMAN, CHARLES, E., C4.5
 LYND, L., M4.12, M7.97, M7.182
 LYNN, K.G., C9.27
 LYTEL, RICK, Q1.3, S1.5
 MA, E., G18.34
 MA, H.L., P6.4
 MA, J.S., P4.6
 MA, Q.Y., M11.9
 MA, W., U2.3
 MA, WEI PING, H4.6, H6.12
 MA, ZHENYI, T3.1
 MAAREF, H., G4.5
 MACARTHUR, D.M., S1.7
 MACAULAY, JOHN B., A5.3
 MACCHESNEY, JOHN B., P2
 MACDIARMID, ALAN G., Q3, Q3.1, Q3.2, Q3.9, Q3.10, Q7.7, X4.2
 MACDONALD, A.J., M7.174
 MACDONALD, BRUCE L., M7.236
 MACDONALD, W.A., J7.13
 MACDOUGALL, JAMES E., H2.8
 MACDOWELL, JOHN F., K1.5, Y3.1
 MACEDO, P.B., U7.15
 MACEWEN, S.R., J5.8
 MACFARLANE, J.C., M7.177
 MACHARRIE, JR, R., D10.27, D10.48
 MACHONKIN, M.A., F3.4
 MACKENZIE, A.B., U11.11
 MACKENZIE, JOHN D., F6.13, H5.2, M9.7, P7.4, S3.1, S3.4, S4
 MACKENZIE, ROSS A.D., D8.10, E6.3
 MACKIN, T.J., T3.2
 MACKNIGHT, WILLIAM J., O4.1
 MACLAREN, J.M., N5.16
 MACOSKO, C.W., N4.9
 MACRANDER, ALBERT T., D8.8
 MADAKSON, P., A6.21, K7.9
 MADAR, R., L1.1
 MADDEN, T.L., T7.27
 MADHUKAR, A., D8.9
 MAEDA, H., M9.9
 MAEDA, M., S4.5
 MAEDA, YASUHIRO, M10.4
 MAES, HERMAN E., A9.35
 MAETA, HIROSHI, M7.90
 MAEX, K., A2.9, A2.12, D10.30
 MAEX, M.A., M7.72
 MAGNO, R., G9.50
 MAGNOTTA, VINCENT L., L4.7
 MAGRUDER, R.H., A7.4
 MAHAJAN, S., D1.10, K7.8
 MAHER, D.M., A9.26, D5.10
 MAHER, J.V., T6.3, V1.9
 MAHLER, WALTER, O5.5
 MAIER, M., G19.5
 MAILHOT, C., D7.5
 MAJZRZAK, C.F., J2.4, J2.7, J2.9, J2.10
 MAJUMDAR, AMAL J., U7.4
 MAKHMUDOV, N.A., A9.31
 MAKI, KAZUMI, Q7.11, Q11.6
 MAKIHARA, H., K5.11
 MAKINO, DAISKE, K5.9
 MAKITA, Y., G3.3, G3.4, G9.40
 MAKSIMOV, A.K., A9.39
 MALAFSKY, GEOFFREY P., A6.22, C1.4, D10.11
 MALHERBE, J.B., A3.10
 MALIK, R.J., D7.4
 MALLA, P.B., S3.9
 MAN, H.T., S2.7
 MANAKO, T., M7.89
 MANASREH, M.O., G9.1, G9.2, G17.3
 MANDELBRIT, B., T1
 MANDELL, JOHN F., N1.1
 MANDICH, M.L., I1.8
 MANGIN, C., N7.6
 MANIAR, P.D., P1.3
 MANKIEWICH, P., M11.7
 MANN, M.E., M7.69
 MANN, STEVEN, R5, R6.1
 MANNAERTS, J.P., A3.4
 MANOHAR, S.K., Q3.9
 MANORY, RAFAEL, M3.9
 MANSFIELD, J.F., D7.8
 MANSFIELD, S., K5.6
 MANSOUR, A., J7.12, O7.2, O7.3, O7.4
 MANTESE, J.V., A11.9
 MANTINI, M.J., D6.4, D6.11, I4.5
 MANTL, S., A11.2
 MANZ, O.E., W1.1
 MAPLE, M. BRIAN, M5.4
 MARA, J.J., O8.9
 MARCAZZAN, G.M. BRAGA, W1.4
 MARCHESSAULT, ROBERT H., R5.5
 MARCHYKWA, S., V5.6
 MARCOTT, C., O2.8
 MARCOTTE, V.C., K5.8, K7.4
 MARCY, HENRY O., M7.180, M7.251, M10.3, M10.8, Q3.5
 MARDER, SETH R., S2.5
 MARFEST, G., A9.34
 MARFAING, J., A9.32
 MARFAING, YVES, E2.5
 MARGRAVE, JOHN L., F1.4, F3.15
 MARINE, W., A9.32
 MARINELLI, WILLIAM J., L2.2
 MARINO, J., M7.11
 MARITN, P.J., Q7.1
 MARK, JAMES E., O, O1, O1.6, O1.7, O1.8
 MARKELZ, A., M7.95
 MARKERT, K.M., C7.1
 MARKIEWICZ, R.S., M4.6, M7.19, M7.78, M7.92
 MARKO, JOHN, F., V9.13
 MARKS, LAURENCE D., A9.1, A9.8, A9.33, A9.59, M7.37
 MARKS, T.J., L6.9, M7.180, M7.251, M10.3, M10.8, S5.5
 MARKUNAS, R.J., D6.4, D6.11, F7.3, I3.5, I4.5
 MAROUDAS, DIMITRIS, G18.10
 MARPLES, J.A.C., U6.1, U7.11
 MARQUET, MAGDA, R4.9
 MARRAKCHI, G., G4.5
 MARSELLA, J., E10.7
 MARSH, G.C., M7.258
 MARSHALL, A.F., M10.6, M11.4
 MARSHALL, D.B., N1.9
 MARTIN, A., P5.17
 MARTIN, H., K3.4
 MARTIN, JAMES E., T, T7.22
 MARTIN, P.A., D7.2
 MARTIN, P.J., Q7.1
 MARTIN, PAUL F.C., U1.2
 MARTINEZ, A., E9.2
 MARTINEZ, J.A., M7.224
 MARTINEZ-MIRANDA, L.J., D2.1
 MARUCCO, J.-F., M7.114
 MARUO, TOSHIO, Q4.9
 MARUYAMA, BENJI, N5.11
 MARUYAMA, KENJI, E2.8, E8.4
 MARUYAMA, YUSEI, Q2.3
 MARWICK, A.D., G7.5
 MARK, D.T., M6.6
 MARK, G., U7.29
 MARYNICK, DENNIS S., Q6.3
 MARZI, THOMAS, N3.9, N5.5, N5.6
 MARZIK, JAMES, M7.175
 MARZZACCO, C., Q3.8
 MASAKI, TOMOMI, M7.233
 MASCHER, P., G4.1
 MASEL, R.I., C3.4, D8.11
 MASHBURN, D.N., M3.3, M7.193, M9.1
 MASHIMOTO, YOHKO, D12.2
 MASI, JAMES V., P6.10
 MASON, T.O., M7.44, M7.51
 MASON, THOMAS L., R4.4
 MASTANDREA, MARK, R3.2, XNF1.3
 MASUDA, HIROMU, M7.14
 MATARAS, D., I1.7
 MATERA, G., F3.17
 MATES, T., K3.4
 MATHEV, A., J2.4
 MATHEVET, J.P., A6.37
 MATHINE, D.L., E3.6
 MATHIOT, D., G6.5
 MATHUR, K., K4.10
 MATHUR, R., L5.2
 MATLOCK, J.H., G18.1
 MATSUBARA, ICHIRO, M7.62
 MATSUBARA, T., M4.3
 MATSUDA, AKIHISA, H1.1
 MATSUDA, KOICHIRO, G9.22
 MATSUDA, M., U7.10
 MATSUDA, S., M7.142, M7.247
 MATSUI, JUNJI, C5.1
 MATSUI, MASAOKI, M7.84
 MATSUMOTO, T., G13.2
 MATSUMOTO, T., M7.247
 MATSUMOTO, Y., H5.1
 MATSUNAGA, JUN'ICHI, H7.5
 MATSUNAMI, HIROYUKI, F6.1, F6.4
 MATSUOKA, HIROSHI, M7.84

MATSUSHITA, Y., P6.14
 MATSUYAMA, T., H7.1
 MATTHIJSSEN, M.M., M7.198, M10.2
 MATTINGLY, PAUL A., U7.44
 MATTOUSST, H., V9.9
 MATTSOON, J., D10.10
 MATUS, L.G., P6.7
 MATZ, R., B3.10
 MAYER, J., M9.4
 MAYER, JAMES W., A7.8, D5.3,
 D10.22, P9.7, G9.42, G18.35,
 K5.7, M7.214
 MAYER, K.M., G3.3, G3.4, G9.40
 MAYER, THOMAS M., I2.6, I3.2
 MAYES, ANNE M., S5.7
 MAZDIYASNI, K.S., M7.239
 MAZIASZ, P.J., A11.4
 MAZUMIT, SUMIT, Q10.2, Q11.5,
 Q13.3
 MAZUR, J.H., E9.9
 MAZZACURATI, V., T8.6
 MAZZONE, A.M., A4.5, A6.24
 MCARDLE, J., M4.13
 MCCALLUM, J.C., A7.2, A9.34
 MCCAMY, J.W., M3.3, M7.192,
 M7.222, M9.1
 MCCANDLISH, L.E., M7.137
 MCCARRON, E.M., M7.29
 MCCARRON, III, EUGENE M., M7.35
 MCCARTHY, D., O1.7
 MCCARTHY, G.J., W1.1, W2.1, W5
 MCCARTY, K.F., M6.7
 MCCAULEY, J.L., T7.35
 MCCOLLUM, M.J., G9.30
 MCCONNELL, M.D., M7.223
 MCCROHON, R., U3.1
 MCCULLOCH, DOUGLAS, A9.40
 MCDANIEL, D., M7.70
 MCDANIEL, DARL, M7.42
 MCDEWITT, B.T., D8.4, D12.7,
 G12.2
 MCDEVITT, S., E1.2
 MCDEVITT, T., A6.34
 MCELFRISH, MICHAEL W., M6.2
 MCENROE, D.J., P6.1
 MCGILL, T.C., E4.1, E5
 MCGONTAGL, M., B5.16
 MCGRAIL, B.P., U7.43
 MCGRATH, J.E., S3.5, S5.8
 MCGRATH, KEVIN P., R4.4
 MCGUIGAN, K.G., G9.53, G18.18
 MCGUIRE, T.R., J3.9, M3.13
 MCHARGUE, C.J., A7, A7.2, A9.34,
 A9.37
 MCINTYRE, C.R., E10.2
 MCINTYRE, PAUL C., M7.159
 MCKAY, R.I., B2.3
 MCKEAGAN, KEVIN D., U5.2, U7.13
 MCKENNA, D.C., D10.26
 MCKERNAN, STUART, C4.4, C9.22,
 K6.5
 MCKINLEY, I.G., U11.11
 MCKINSTRY, S.E., S3.2
 MCLEAN, G., J7.13
 MCLEAN, MALCOLM R., Q7.14, S2.3
 MCLEAN, W.L., M7.208
 MCLENAGHAN, A.D.W., J7.13
 MCMAHON, R.A., A8.7
 MCMILLAN, J.M., M7.184
 MCMILLS, L., M7.155
 MCNAMARA, KAREN M., F2.4
 MEAKIN, PAUL, T3, T6.1, T9.2
 MEACARTNEY, M.L., M4.13
 MECHOLSKY JR, J.J., T3.2, Y4.2
 MEGUSAR, JANEZ, N5.15
 MEHRABIAN, R., N1.10
 MEHRER, H., G12.5
 MEHROTRA, VIVEK, K4.3, O1.4
 MEHTA, A., M7.20, M7.27, M7.86
 MEHTA, VINEET, T7.6
 MEI, GUANO, H4.6
 MEI, P., G20.2
 MEIER, D.J., Q2.3
 MEIER, F., A10.4
 MEIKE, ANNEMARIE, U7.39
 MEILER, J., B3.10
 MELAMUD, MORDECHAI, J7.1
 MELIM, V.J., M2.10
 MELKOTE, RAJESH R., L1.11
 MELMAN, P., D7.9, D10.32,
 D10.45, D11.3
 MELROSE, J.R., T7.9, T7.10, T9.3
 MENARDO, C., Q3.9
 MENDELSON, NEIL H., R6.4, R6.5
 MENDOZA, EDGAR, L6.10, L6.11
 MENG, R.L., M7.120, M10.5
 MENKE, D.R., E3.5, E3.6
 MEREDITH, G.R., Q9.2
 MERIKHI, F., V3.2
 MERK, E., G1.2
 MERLI, M., A9.2
 MERTENS, G., M3.5
 MERTENS, L.A., U7.11
 MERTENS, PAUL W., A9.35
 MERTENS, R., H7.6
 MERZ, J.L., D10.42, D10.43,
 E1.7, E4.8, G9.20, G14.2,
 G14.3, G14.4
 MERZBACHER, CECILIA I., U7.13
 MESHII, M., A11.3
 MESKOOB, M., M7.137
 MESSIER, A., Q12.7
 MESSIER, RUSSELL, F, F1.10,
 F4.2, F4.8, XNP1.2
 MESSINA, CARLA G., U8.1
 MESSNER, RICHARD P., Q4.4
 METZGER, ROBERT M., Q9.9, Q13
 MEUFFELS, P., J3.7, M7.39
 MEUNIER, M., B6.8
 MEYER, J., U11.11
 MEYER, J.R., E9.2, E9.3, E9.4
 MEYER, O., A7.1, M5.5, M7.209
 MEYER, R.B., V2.2, V5
 MEYERSON, B.S., D10.17
 MEYRUEIX, REMI, Q13.5
 MEYUAPPAN, M., B5.2
 MIAOULIS, IOANNIS N., A9.21,
 A9.36, P2.4
 MICELI, P.P., D1.3, M11.1
 MICHALSKE, T.A., L2.1, N6, M7.1
 MICHALSKI, T.J., R6.8
 MICHEL, D., M7.110
 MICHEL, D.J., G18.28
 MICHEL, J., G4.3
 MICHELAKIS, C., B4.7
 MIDDLEHOEK, JAN, L2.6
 MIDDLEMAN, STANLEY, L1.9
 MIDDLEMISS, B., M4.3
 MIELKE, B.A., N5.1
 MIGGE, H., U7.21
 MIGLIORATO, P., H7.9
 MIGNANI, GERARD, Q13.5
 MILLER, B., M6.5
 MILLER, G.A., M6.6, M7.8
 MILLER, G.R., K6.1
 MILLER, JOEL S., Q8.1
 MILLER, N.H., U8.2
 MILLER, P., Q13.10
 MILLER, R., B3.3
 MILLER, R.D., Q10.10
 MILLET, P., M2.7
 MILLS, GORDON, J5.9
 MILLS, M.J., C13.1
 MILLS, R.H., W4.1
 MILNE, W.I., F5.12, H7.9
 MILNER, S.T., V7.1
 MILNER, SCOTT T., V3.4, V3.8
 MILNES, A.G., D1.10, G9.21,
 G9.23, K7.8
 MILSTEIN, JOSEPH B., F4.10, L5.5
 MINATO, MASAKI, Q8.9
 MINEMURA, TETSUROH, D2.6
 MINFORD, E., L4.7
 MINGOS, TAO, H6.7
 MINGOS, D. MICHAEL P., S5.9
 MINI, S.M., M7.2
 MINIER, M., D1.4, D10.2
 MINISALCO, W.J., P9.2, P9.4,
 P9.5
 MINO, IWAQ, Y3.3
 MINOMURA, SHIGERU, G9.22
 MIOTKOWSKI, I., E9.10
 MIRAVITLES, C., M7.25, M7.151
 MISAKI, YOJI, Q2.1
 MISAWA, S., P6.12
 MISHIMA, A., Q7.10
 MISHIMA, OSAMU, P9.1, P9.2
 MISHRA, A., N2.5
 MISHRA, UMESH K., D7.1
 MITCHEL, W.C., G4.4
 MITCHELL, A.W., M6.6, M6.7,
 M7.38
 MITCHELL, I.V., G18.12
 MITCHELL, M.W., T3.3
 MITCHELL, MICHAEL A., S1.6
 MITCHELL, RICHARD L., E5.4
 MITCHELL, T.E., A9.5, M7.220
 MITSUI, K., D2.8
 MITTEMEIJER, E.J., A9.56
 MIURA, AKIRA, Q9.13
 MIYAJIMA, M., M7.128
 MIYAKE, KIYOSHI, A1.5
 MIYAO, M., D1.8, D10.14
 MIYASATO, TATSURO, H4.1
 MIYATAKE, T., M7.58
 MIYAUCHI, KATSUKI, M7.172
 MIYAZAKI, SEIICHI, I4.2
 MIZES, H.A., Q10.1
 MIZUKI, JUN'ICHIRO, C5.1
 MIZUNO, FUMIO, M7.14
 MIZUTA, M., G15.2
 MO, DANG, H6.8
 MOAZED, K.L. F5.6
 MODARELLI, DAVID A., Q8.9
 MOECKLY, BRIAN, M7.229
 MOGRO-CAMPERO, A., M11.3
 MOHAMED, A.M.O., U7.42
 MOHAMMAD, F., H6.14
 MOHAMMADI, A., O6.8
 MOHRLE, MARTIN, G8.5
 MOINI, AHMAD, J7.2
 MOLLER, H.J., G11.5, G18.30
 MOLLER, KARIN, H2.8
 MOLNAR, B., P6.5, F8.7, G15.4
 MOLVA, E., G9.34
 MONASTERIOS, CLEVYS, R5.5
 MONEMAR, B., D10.42, D10.43,
 G2.1, G3.5, G4.6, G6.2,
 G9.20, G9.47, G14.2, G14.4,
 G18.14, G18.15, G18.16,
 G18.19, G18.22, G18.43
 MONROE, E.A., Y1.3
 MONTIE, E.A., D11.2
 MONTOYA, A., M7.98
 MOODENBAUGH, A.R., M7.18,
 M7.57, M7.88
 MOODY, R.A., N5.23
 MOON, B.M., M7.137
 MOONEY, J.B., M7.163
 MOONEY, PATRICIA M., G15.1
 MOONEY, P.M., G16
 MOORE, C., M7.134
 MOORE, F.G., E6.2
 MOORE, G., M7.45
 MOORE, J.A., B5.10
 MOORE, M.W., P5.1
 MORADIAN-OLDAK, J., R1.4, R5.9
 MORAN, KELLY, P6.2
 MORAND, JEAN-PIERRE, Q7.16
 MORANTE, J.R., G9.31
 MORDKOVICH, VIKTOR N., B5.23
 MORE, K.L., F8.6, L3.2, L5.3,
 MOREHEAD, P.P., G11.2
 MORELLI, D.T., M7.28
 MORGADO, W.A.M., T7.21
 MORGAN, J.S., F8.10, F9.5
 MORI, M., G3.4
 MORI, YUHEI, Q13.4
 MORI, YUSUKE, F2.8, F4.6, F5.7
 MORIMOTO, T., M4.3
 MORIN, FRED, R5.5
 MORISHIGE, YUKIO, B2.1
 MORKOC, H., C2.5
 MORON, L., A6.12
 MOROHASHI, SHIN'ICHI, M7.227
 MOROSIN, B., M7.141, M7.157,
 M10.7
 MORRIS, D., D10.31
 MORRIS, N., A8.11
 MORRIS, P.A., P8.3, P9.7
 MORRIS, W.G., M7.223
 MORRIS, W.L., N1.6
 MORRIS, G.W., M7.166
 MORRISH, A.A., F3.11
 MORROW, CARY J., R3.5
 MORSSINKHOF, R.W.J., L2.10
 MORTAZAVI, M.A., Q12.10
 MOSHONOV, AHARON, N5.22
 MOSE, III, T.S., M7.171
 MOSS, S.C., J, J4.6
 MOSSET, ALAIN, I4.7
 MOSSMAN, DARYL L., A9.60
 MOSTOLLER, M.E., J4.6
 MOTOHIRO, TOMOYOSHI, C9.26
 MOTOOKA, T., C12.5
 MOTOWIDLO, L.R., M7.241
 MOULTON, LINDA, M9.6
 MOUNIER, SUZANNE, D1.3, D10.5
 MOUNTAIN, RAYMOND, D., V9.12
 MOUNTZIARIS, T.J., L1.3
 MOUROU, GERARD, A9.9
 MOUSSAVI, MEHDI, Q7.5
 MOUSSAVI-MADANI, M., G18.36
 MOUSTEFAONI, R., G9.51
 MOY, LARRY P., M7.175
 MOYLAN, CHRISTOPHER, B5
 MOYNIHAN, D.E., P5.6
 MUCHA, J.A., I2.8
 MUELLER, M.H., J7.10
 MUKAIDA, M., L3.3
 MUKOH, AKIO, Q13.2
 MULLER, HEINRICH G., B6.12
 MULLER, J., T7.35
 MULLER, J.C., G18.4
 MULLER, R., U5.4
 MULLIN, C., V6.6
 MULLIN, J.B., B4.2, E7.4, E8.2,
 MULLINS, J.T., E8.6
 MULLINS, W.M., C9.5
 MURPUR, ARUN, P2.3
 MURAKATA, C., G18.31
 MUNCH, J.P., T8.2
 MUNDER, H., D11.10
 MUNDSCHAU, M., C3.1
 MUNEKATA, H., E9.7
 MUNGER, R., M7.103
 MUNIR, Z.A., A2.6
 MURAHARA, MASATAKA, B1.9, B2.10,
 B4.11, P4.5
 MURAKAMI, E., D10.14
 MURAKAMI, S., E8.4
 MURAKAMI, TAKASHI, U7.18, U7.34
 MURAT, MICHAEL, V8.1
 MURATA, H., Q12.12
 MURATA, K., Q4.3
 MURAY, JULIUS J., A5.3
 MURUTANI, T., D2.8
 MURPHY, D.W., M7.33
 MURRAY, B.W., A1.6
 MURRAY, JEFF J., G9.25
 MURRAY, R., G11.1
 MUSE, J., A8.12
 MUSKET, R.G., A2.6
 MUSOLF, J., D11.10
 MURINEN, A., U7.41
 MUZZY, JOHN D., N5.22
 MYBURG, G., A3.10
 MYCIELSKI, A., E10.7, E10.11,
 E10.12
 MYERS, DWIGHT L., M7.54
 MYERS, SAMUEL M., A11.7
 MYHRA, S., M7.7, U5.7
 NA, RUDIGER, O1.1
 NAEVEN, R., M7.39
 NAGAI, YASUHIRO, M7.214
 NAGAPETIAN, S.S., Q5.1
 NAGATA, M., M7.135
 NAGATA, SEIICHI, I1.9
 NAGAYA, S., M7.128
 NAGEL, S.R., P1.1
 NAGELS, P., M7.170
 NAHATA, AJAY, Q9.5
 NAHM, S., D6.9
 NAHORY, R.E., D1.1, D1.2
 NAKABEPPU, P., H7.11
 NAKADA, K., K4.5
 NAKAGAWA, K., D1.8, D10.14
 NAKAGAWA, M., M7.128
 NAKAHIGASHI, KIYOTAKA, M7.53
 NAKAJIMA, YOSHIHARU, D12.1,
 K5.12
 NAKAMURA, H., C9.1
 NAKAMURA, N., D1.8
 NAKANISHI, KAZUMI, Q4.7, Q5.4
 NAKANO, M., M7.199
 NAKANO, S., H7.1
 NAKATA, T., P6.14
 NAKATANI, ALAN I., J6.4
 NAKAYAMA, SATOSHI, I3.6
 NAKAYAMA, Y., G3.4
 NALLET, F., V2.8
 NAMAVAR, F., A6.25, A9.24

NAMBA, SUSUMU, A6.16, A6.33, A9.46, B3.8, B4.8
 NANCOLLAS, G.H., R1.5, R2.3, R2.4, R2.5
 NANIISHI, YASUSHI, D2.10
 NAOE, MASAHICO, K6.4
 NARASIMHAN, K.L., G18.17
 NARAYAN, JAGDISH, B4.12, C9.35, D4.9, D10.13, F3.17, L5.6, M, M3, M3.1, M5.9, M7.59, M7.185, M7.187, M7.190, M7.205, M9.5, X2.1
 NARAYANASAMY, A., J1.9
 NARDUCCI, D., F5.4, F5.10
 NASH, ALEXIS S., M4.7, M7.150
 NASH, PHILIP, M4.7, M7.150
 NASS, RUDIGER, O1.1
 NASTASI, M.A., A3.7, A7.3, A9.5, A10.7, M7.196, M7.219, N2.2
 NASU, K., Q7.10
 NATSUUME, TADAO, Q12.9
 NAUGHTON, M.J., Q11.4, Q11.10
 NAVARRO, J.M., M7.151, M7.21
 NAVROTSKY, ALEXANDRA, M6.3, F1.3, U5.1, U7.26
 NAYAK, KASINATH, Q6.3
 NAZAR, L., M7.224, M7.246, M7.232
 NAZARE, M.H., F2.12, G9.53
 NAZRI, G.A., S1.7
 NEAL, M.J., M10.7
 NECHTSCHIN, M., Q3.9
 NEERDAEL, B., U7.12
 NEERINCK, DOMINIQUE, C11.1, D6.5
 NEEVES, A.E., P5.3
 NEIFELD, R.A., M3.11
 NELSON, A.J., D10.13
 NELSON, C.D., M7.123, M7.126
 NELSON, D.R., V7
 NELSON, DAVID, T7.11
 NELSON, H.H., F2.3
 NEMANTCH, R.J., C10.5, D2.2, F2.6, F3.4, F3.17, F7.3, H1.3, H4.3
 NEMIROVSKY, Y., E7.1
 NENCKA, HANNA, T7.18
 NETTER, P., L4.9
 NEUDECK, G.W., B4.3
 NEUGEBAUER, C.A., K1
 NEUMANN, D.A., J2.4, J2.7, J7.3
 NEUMARK, G.F., E4.2
 NEVES, A.J., F2.12
 NEWBURY, P.R., E4.2
 NEWCOMB, J.C., M7.248
 NEWHOUSE, IRENE E., O5.7, T7.3
 NEWHOUSE, JAMES S., T9.7
 NEWMAN, K.E., G13
 NEWMAN, P.R., Q9.12
 NEWMAN, R.C., G11.1, G19
 NEWNHAM, ROBERT E., K4.1, S3.2
 NEWSAM, J.M., M6.6
 NG, M.F., M7.207
 NGUYEN, MY N., K5.5
 NGUYEN, SON N., U7.13
 NI, Q.-X., Q10.9
 NI, RONGMING, M7.250
 NI, YUHONG, T3.7
 NI, ZHENDE, S1.6
 NICCUM, JEFF T., B6.6
 NICHOLS, C.S., G7.3
 NICHOLS, M.C., N5.19
 NICHOLSON, D.M., J4.4, J4.5, J4.7
 NICKEL, J., M7.95
 NICKERSON, ALAN K., U11.5
 NICOL, JACQUELINE M., J6.10, J7.3
 NICOLET, M.-A., D10.50
 NIEH, C.W., D1.11, D10.3, D10.8
 NIELSEN, ARNOLD T., Q4.10
 NIELSEN, BENT, C9.27
 NIGAM, A.K., A6.26
 NIGAVEKAR, A.S., H6.14
 NIINA, T., F6.14
 NIJS, J., H7.6
 NILSSON, J.O., O6.8
 NING, Y.-P., O1.7
 NINOMIYA, K., B5.17
 NIR, MOIRA MARX, O4.4
 NISHI, T., U7.10
 NISHIJIMA, YOSHITO, E2.8
 NISHIKUNI, M., H7.1
 NISHIMATSU, S., B5.17
 NISHIMURA, K., F5.5
 NISHIMURA, T., D2.8, H7.8
 NISHINA, Y., H4.4
 NISHINE, S., D8.3
 NISHINO, HIRONORI, F6.1
 NISHIOKA, ASAAKI, Y3.3
 NISHIWAKI, R., M7.247
 NIWA, K., K5.11
 NOAD, J.P., D10.40
 NODA, I., O2.8, O5
 NODA, S., C9.26
 NOGAMI, J., C3.3
 NOH, D.W., M5.13
 NOLAN, T.A., N7.3
 NOLTE, D.D., G17.4
 NOMURA, SHUNJI, M7.22
 NONAMI, T., S1.8
 NONG, LI JIA, T7.15
 NONOYAMA, H., M7.135
 NORNEN, CHRISTOPHER J., R4.2
 NORMAN, A.G., G13.3
 NORRIS, P., M5.13
 NORTHROP, G.A., G1.4, G14.5
 NORTHROP, J.E., C2.1, C8
 NORTON, D.P., M3.3, M7.192, M7.222, M9.1
 NORTON, L., O7.3
 NORTON, M. GRANT, K5.3, K6.9, M7.188, M7.213, M9.3
 NOTIS, MICHAEL R., C4.5, K5.4, K6.6, K6.8, M4.10
 NOUFI, ROMMEL, H6.6
 NOVAK, D., B4.9
 NOWAK, RAINER, B1.8
 NUMAN, MUHAMMAD Z., A6.27
 NUNES, A.C., J3.9
 NUNES, MARIA, M., V9.5
 NURMIKKO, A.V., E2.1, E3.6
 NUTT, GERALD L., C9.38
 NYGREN, E., A8.1, G18.50
 NYITRAY, ALICE M., O2.2, O3
 O'BRIEN, D.F., M7.171
 O'BRYAN, H.M., M4, M7.74, M7.104
 O'HERN, M.E., A9.37
 O'KEEFE, M.A., C9.33
 O'REILLY, JAMES M., J6.5, O4.6, O5
 OATES, D.E., M7.226
 OBER, C.K., K3.4
 OBLAS, D.W., P9.2
 OBRADORS, X., M7.151
 OCAMPO, MIGUEL A., M4.11, M7.252
 OEHLER, LYNN, XN1.3
 OCKO, B.M., V6.7, V8.7
 ODA, T., G9.40
 ODEH, I.M., B7.9
 OEDLER, IVAN, Y, Y1.5, Y4, Y5.6
 OEHLER, LYNN, R3.2
 OEHLERS, M., D11.10
 OEHLER, G.S., G6.2
 OELHAFEN, P., C5.5
 OFER, DAVID, B5.7, Q3.6
 OGALIE, S.B., D8.9
 OGASAWARA, M., G18.31
 OGATA, NAOKA, S4.7
 OGAWA, TOMOYA, G9.27
 OGUCHI, KIYOSHI, S4.7
 OGUCHI, TAMIO, G9.46
 OGURA, TORU, M7.62
 OH, E., E10.10
 OH, MIN-SEOK, M4.10
 OH, SEYONG, K7.3
 OH, T.S., K4.7
 OHDOMARI, I., P6.12
 OHISHI, YASUTAKE, P3.6
 OHMI, SHINYA, D8.12
 OHNISHI, H., M5.11
 OHNISHI, M., H7.1
 OHNISHI, N., G3.3, G3.4, H7.1
 OHNO, H., E9.7
 OHNUKI, TOSHIHIKO, U7.34, U7 35
 OHSAWA, A., G18.47
 OHSHIMA, MASAYOSHI, Q12.9
 OHSHIMA, T., D1.8
 OHSHITA, Y., F8.1
 OHSUKA, YASUJI, P7.2
 OHUCHI, FUMIO S., N5.11
 OKADA, AKANE, O1.5, O8.1
 OKADA, M., M7.247
 OKADA, Y., E4.5, H1.2
 OKAJIMA, S., U3.2
 OKAMOTO, H., H5.1
 OKAMOTO, MASAYUKI, Q8.6
 OKAMOTO, P.R., A11.3
 OKAMOTO, S., H7.1
 OKAMOTO, Y., Q6.1
 OKANO, YOSHIMICHI, D8.3, Q13.4
 OKAOTO, YASUNARI, K5.12
 OKOSHI, MASAYUKI, B1.9
 OKSOY, D., U7.23
 OKUHIRA, H., B5.17
 OKUNUKI, MASAHICO, A9.57
 OLAJOS, J., G1.1, G2.1
 OLANDER, D.R., M7.186
 OLANDER, E., B5.4
 OLEGO, D., E2.3
 OLEK, J., Y2.2
 OLIN, M., U7.41
 OLIVER, B.J., T1.8
 OLIVER, JEAN, U1.1
 OLSCHNER, F., P9.8
 OLSEN, B.L., M7.184
 OLSON, B.L., M7.5
 OLSON, C.G., M7.3
 OLSON, C.W., M7.122
 OLSON, G.B., C9.25, XN1.1
 OLSON, G.L., A5.2, B1.7
 OLVERA DE LA CRUZ, MONICA, S5.7, V8.5
 OMLING, P., G18.44
 ONGA, SHINJI, H7.5
 ONIYAMA, H., E5.2
 ONN, DAVID G., K4.4, K6.2, O2.2
 ONO, M., K4.5
 ONSTOTT, J.R., P4.4
 OOKA, KOHJI, K5.12
 OPILA, ELIZABETH J., M7.32
 OPPENHEIM, I.C., A1.4
 OPRYSKO, MODEST M., K2.3
 ORGAZ, EMILIO, M4.11, M7.252
 ORLANDO, T.P., M7.204, M10.2
 ORMEROD, G.J., U3.1
 ORTAL, C., G9.49
 ORTIZ, CARMEN, P6.7
 OSAKA, J., C2.4
 OSAKI, SHIGEMORI, I3.6
 OSBURN, C.M., A9.53, D10.6
 OSGOOD JR, R.M., B5.20, M1.9
 OSOFSKY, M.S., M2.8, M3.12, M7.96, M7.101
 OSSICINI, STEFANO, C9.16
 OSTLING, M., L3.4
 OTA, MICHIO, Q8.7
 OTANI, SUGIO, Q8.7
 OTIS, MARK D., T4.9/U10.9, U10.9/T4.9
 OTSUKA, AKIRA, I1.9
 OTSUKA, N., E3.5, E3.6, E3.7
 OTT, KEVIN, M7.47, M7.72
 OTT, MARY L., G9.18
 OTTENHEIM, J.J.M., A9.47
 OTTINGER, H.C., V3.9
 OTTOLINI, L., G18.5
 OU, JUNG-JUNG, R5.7
 OU-YANG, H.D., V9.1
 OURMAZD, A., A3.4, C9.40, C11.5, G9.44, G12.1
 OVERSBY, VIRGINIA M., T4/U10, U
 OVERTON, B.J., V9.8
 OVIEDO-RAO, R., M2.11
 OWENS, B., D11.3
 OXALD, U., T7.16
 OYAMA, T., M7.128
 OYOSHI, KEIJI, A6.32
 OZAKI, S., I3.6
 OZERI, M., G13.2, M10.12
 OZERYANSKY, G.M., M7.241
 OZTURK, M.C., B6.9
 PAASCHALIS, E.P., R1.5
 PACHENCE, J.M., V8.8
 PADDOCK, CAROLYN A., K2
 PADIAS, ANNE B., S1.6
 PADILLA, A., Y2.5
 PADMANABHAN, K.R., A1.4, A3.5, C5.4
 PADMANABHAN, R., K3.10
 PADTURE, NITIN P., M7.7
 PAFCHER, R., P9.8
 PAGE, JOHN H., J6.12
 PAGE, R.A., J1.5
 PAGNON, D., D10.47
 PAIK, SUN M., C9.12
 PAINE, DAVID C., D4.10
 PAINE, R.T., C9.31
 PAJEVIC, S., T7.28
 PAJOT, BERNARD, G8.1
 PAKULA, K., E10.12
 PALACIO, F., Q7.17
 PALEOS, CONSTANTINOS M., O2.1
 PALMSTRØM, CHRIS J., C4.4, D1.1, D1.3, D10.5, G20.2
 PALOPOSKI, T., W2.3
 PALSTRA, T.T.M., M8.2
 PAN, M.H., M7.155
 PANDELISEV, KIRIL, I1.3
 PANELLA, V., T5.2
 PANETTA, CHARLES A., Q9.9
 PANG, S.J., M7.168
 PANG, Y., Q10.9
 PANISH, M.B., G19.3
 PANKOVE, J., A2.10
 PANKOVE, JACQUES I., F7.1
 PANTANO, CARLO G., N
 PANTELIDES, S.T., G10.1
 PANTOJAS, V., D9.1
 PAPAMICHAEL, HARRIS, F2.4
 PAPANICOLAOU, N.A., B4.4
 PARAT, K.K., E7.2
 PARBROOK, P.J., E5.5
 PARETZKIN, BORIS, M7.111
 PARK, N.R., A8.12, D6.4
 PARISE, JOHN B., M7.35
 PARISI, G., P5.2
 PARK, B., G18.33, G18.50
 PARK, HAI WOONG, K7.7
 PARK, I.S., G9.48
 PARK, J.C., M7.144
 PARK, K.-H., D10.26
 PARK, SIN CHONG, G9.19
 PARK, WON-WOO, A8.8
 PARKER, ALEX J., O3.11
 PARKER, G.R., A1.6, A6.34
 PARKER, J.C., L6.3, L6.4
 PARKER, S.D., D10.35, G13.3
 PARKINSON, B.A., C9.7
 PARKINSON, W.J., L5.1
 PARKS, C.C., H7.4
 PARKS, D., M7.82
 PAROLI, P., M8.9
 PARRETTA, A., L4.6
 PARRINELLO, M., G6.3
 PARSONAGE, E., O7.6
 PARSONS, G.N., H1.3, I2.4, I3.8
 PARTRIDGE, JULIAN P., K
 PARUS, STEPHEN J., T7.4, T9.7
 PASCHALIS, E.P., R1.5
 PASCHER, H., E10.10
 PASHLEY, D.W., D10.35
 PASHMAKOFF, BOYILL I., B3.11
 PASK, J.A., M7.77
 PASKO, J.G., E6.4
 PASSELL, L., J2.7
 PASSOJA, D.E., T3.2
 PASTEL, PAUL, F5.16
 PASTOL, Y., K4.2
 PATEL, J.S., V7.7
 PATEL, S., M7.167, M7.191, M7.212, M7.237, M7.249
 PATHAK, RAMJI, A6.26
 PATRIZIO, D., A9.6, A9.41
 PATRIZIO, S., Q4.8
 PATT, M.E., N5.17
 PATTERSON, DONALD E., F3.15
 PATTILLO, S.G., L6.8
 PATYN, J., U7.20
 PAUL, D., M7.25
 PAUL, D.W., O6.8
 PAULEAU, Y., B6.10
 PAULIKAS, A.P., M7.3
 PAULIN, STEVEN, E., V4.7
 PAULSSON, GERT, D11.5
 PAVUNA, D., M5.8
 PAWLKOWSKI, GREGORY T., O6.4
 PAWLOWSKI, W.P., K3.7
 PAYNE, D.A., M7.132, M7.133
 PAYNE, D.N., P9.3
 PAZOL, BRIAN G., M7.169

PEACOCK, J.A., M4.3
 PEARAR, P.J., G9.1, G9.35
 PEARSALE, THOMAS P., D11.1
 PEARSON, DALE, S., V3.1
 PEARTON, S.J., A8.11, B5.11,
 B5.12, D10.46, G6.1, G8.2,
 G8.4, G18.41, G19.2
 PECHENIK, J.M., M7.248
 PECK JR, W.F., M2.2
 PEDERSEN, K., C11.4
 PEDERSON, DONALD O., P8.5
 PEDERSON, LARRY R., B3.9, P3.3
 PEDERSON, MARK R., F1.6, G18.37
 PEDRAZA, D.F., A9.38, A11.4
 PEERCY, P.S., A10, A10.3, A10.6,
 D4.1, M7.117
 PEGG, I.L., U7.15, U7.16
 PERRSSON, P.E. F2.3
 PEI, SHIYU, M6.6, M7.38
 PEICHUN, YANG, F3.18, F3.19
 PEIPER, DENNIS W., U5.2
 PEIPER, D., V6.8
 PEISL, J., J4.1
 PEKALA, RICHARD W., O3, O6.2
 PELLEGRINO, JOSEPH G., D2.4,
 G9.29
 PENFOLD, J., J2.11
 PENG, GONGWEN, T3.5
 PENG, J.L., M7.26, M7.106
 PENG, P., M7.86
 PENG, WEIMIN, M2.10
 PENNEY, T., M7.5
 PENNYCOOK, S.J., A2.10, A8.3,
 A9.17, C9.32, C11.6, M7.222,
 M9.1
 PENSL, G., G1.3
 PEOPLES, OLIVER P., R5.4
 PEOPPEL, ROGER B., M4.7
 PEREIRA, ESTELA, G9.52
 PEREIRA, JR, MADRO, Q13.3
 PEREPEZKO, J.H., A10.6
 PEREZ, A., A9.34, G9.31
 PEREZ, J.A., H2.7
 PEREZ-PENA, M., Y4.5
 PERIC, ALEKSANDAR D., U7.5
 PERKINS, J., E10.7
 PERKINS, RAYMOND, E3.4
 PERKOWITZ, S., D11.8
 PERN, W.S., M7.244
 PERNG, C.P., M7.178
 PERNO, L.H., M7.160, M7.177
 PEROVIC, D.D., D5.9
 PERRST, M., G12.5
 PERRIERE, J., B5.9
 PERRY, C.H., D12.8, D12.9, M7.78
 PERRY, JOSEPH W., S2.5
 PERKANS, PETER D., D9, D9.1,
 F5.17, H2.4, H2.6, H3.9, H4,
 H6.9
 PERSHAN, P.S., C9.40, V6, V6.5,
 V6.8, V8.7, V8.10, V10.2
 PERUSICH, E. RENEE, O3.5
 PESOTSKII, S.I., Q4.2
 PESTY, P., Q11.2
 PESZKIN, PERLA, M9.6
 PETERKIN, JANE E., G18.45
 PETERMAN, D.J., E7.6
 PETERSEN, DONALD R., M7.46
 PETERSEN, J.W., G11.6
 PETERSON, D.L., G9.8
 PETERSON, E.J., M7.196
 PETERSON, G.G., M7.182
 PETERSON, S.C., M7.207
 PETERSON, T., M11.12
 PETHICA, JOHN B., C6.3
 PETIT, J.B., F6.7
 PETKIE, R., A6.28
 PETROU, A., E10.6
 PETROV, V.V., G18.21
 PETRUZZELLO, J., E2.3
 PETRY, W., J3.1
 PETTAVIN, SERGE, I4.7
 PFIFFER, R.L., I2.10, I4.6
 PFIFER, P., T5.1
 PFIFER, L.N., A5.1, D10.49,
 D12.10
 PFIFER, M., S4.4
 PFIFER, W., G5.5
 PFLUGHOFF-HASSETT, D.F., W2.1
 PHAM, D.K., U5.7
 PHAN, V., H7.4
 PHELPS, A.W., F2.5
 PHILIPPOSE, K.E., U2.2
 PHILLIPS, GREG, F3.13
 PHILLIPS, J.M., M11.8
 PHILLIPS, N.E., M7.106
 PHILLIPS, NICHOLAS J., S3.8
 PHILLIPS, RICHARD, F3.7
 PHILLIPS, RICHARD J., D10.49
 PHIPPS, M., A6.11
 PIAGGI, A., G18.5
 PIAGGIO, P., Q10.13
 PICCIOLLO, J.J., M7.8
 PICKART, S.J., J3.9
 PICKERING, MICHAEL A., L3.8
 PICKETT, WARREN E., F1.6, P5.1
 PICRAUX, S.T., A1.2
 PIEL, J.P., C9.4, L2.7, O7.8
 PIERSON, J., V4.8
 PIETTERSEN, H.S., W2.2
 PIETTERSEN, HANS S., W2.4, W3.2
 PIETRONERO, L., T9.1
 PIETRZAK, RICHARD, U4.2
 PIGFORD, T.H., U3.5, U11.8
 PIGGOTT, MICHAEL R., N3.5
 PIHLSTROM, B., I4.4
 PIKE, W.T., D4.4
 PINCUS, PHIL, V, V8, V8.3
 PINCZUK, A., D10.49, D12.10
 PINDAK, R., V7.7, V7.8
 PINE, D.J., V4.4, V9.1
 PINERI, M., O5.6
 PING, LU, Y2.3
 PING, LIU, D10.7
 PINNAVAIA, THOMAS J., J7.2, J7.3
 PINOL, S., M7.25
 PINSKI, F.J., J2.6, J4.4, J4.5,
 J4.7
 PINTO, HAIM, J7.1
 PINTO, JAMES J., T7.36
 PINZONE, C.J., G19.4
 PIROUZ, P., F8.3, F8.4
 PISCITELLE, LOUIS, T6.4
 PISTOL, MATS-ERIK, D11.5
 PIVAC, B., G18.5
 PLANO, M.A., G9.30
 PLANO, R., V2.6, V3.6
 PLECAS, ILIJA B., U7.5
 PLEINER, HARALD, V8.3
 PLUMMER, J.D., G9.16
 POATE, J.M., A2.3, A5.1, A9.14,
 A9.43, A9.44, D5.3, G18.33
 POEHLER, T.O., F8.9, F8.10, F9.5
 POEPEL, ROGER B., M4.7, M7.8,
 M7.51, M7.45, M7.150
 POETZINGER, JANET L., K7.3
 POGANY, A.P., A8.1, A9.18,
 POGGI, A., A9.2
 POGREBNJAK, A.D., A9.31, A9.39
 POINTER, C., U2.1
 POKER, D.B., A1, A7.6
 POKORA, A.R., R3.4
 POLEK, JIM, T4.6/U10.6,
 U10.6/T4.6
 POLIS, DAVID W., Q7.15, Q12.11
 POLLAK, FRED H., D, D8.4, D10,
 D11.6, D12, D12.7
 POLMAN, A., A10.2
 POLO, GUSTAVO VAZQUEZ, R2.7
 POLONIS, DOUGLAS H., A11.7
 POLYMERPOULOS, C.E., P2.5
 PONCE, F., A9.4
 POND, R.C., C4.1, C10
 PONGRATZ, P., G18.8
 POORTER, RENE E.P., W2.4
 PORSCHKE, E., J3.7
 POST, RICHARD S., F3.13
 POSTHILL, J.B., D6.4, D6.11,
 F7.3, F9.9, I3.5, I4.5
 POTEMBER, RICHARD S., Q9.7
 POTEMSKI, R., B2.7, G12.3
 POTREPKA, D.M., M4.12, M7.182
 POTT, D., F9.3
 POTTER, D.I., A9.13
 POTTICK, L.A., O5.2
 POTTS, J.E., E3.3
 PÖTZL, H.W., G10.4, G18.8
 POUDOULEC, A., D10.2
 POWELL, J.A., F8.3
 POWELL, R.C., F7.2
 PRABHAKAR, E.N., H6.3
 PRABASH, M., E9.10
 PRASAD, JAGDISH, T7.1
 PRASAD, K., H1.4
 PRASAD, P. SATHYA SAINATH, O6.9
 PRASAD, PARAS N., S2.1
 PRASAD, R.K., M7.190
 PRASAD, RAM, M7.127
 PRASK, H.J., J5.6
 PRATT, JR, W.P., M7.123, M7.126
 PRATT, P., Y5
 PRATT, PETER, L., W3, W4.2
 PRATER, STEVEN, A7.7, A9.40
 PREMCHANDRAN, V., G18.17
 PREVORSEK, D.C., O4.8
 PREMO, KARL M., N6.8
 PRICE, D.L., C9.13
 PRICE, DAVID L., J6.6
 PRICE, JACK L., K4.10
 PRICE JR, PETER E., B1.4
 PRIEMMEYER, H.G., J5.7
 PRILUTSKI, GERARD M., O3.4
 PRINCE, E., J1.8
 PRINZ, G.A., D6.9, D6.10, E10.6
 PRIOR, K., E4.4A
 PROKES, S.M., C11.2, D5, D5.2,
 G18.42
 PROKHORENKO, T.A., A9.54
 PROKO, J.G., A1.9, G9.10
 PROST, J., V2.8
 PROUGH, STEVEN D., K1.2
 PRUCNAL, PAUL R., K2.5
 PRYOR, R.W., F4.3
 PUREZA, P., P5.4
 PURPURA, J.W., M7.80
 PUSA, P., M7.200
 PUSEY, P.N., V4.4
 PUTMAN, M.A., P4.3
 PUTNIS, ANDREW, F5.12, H2.9
 PUVVADA, S., V10.7, V10.9
 PYNN, ROGER, J1.2
 QADRI, SYED B., D10.11
 QAYYUM, A., B7.9
 QIAN, Q.-D., E3.5
 QIU, J., E3.5
 QIU, X., V9.1
 QU, J., C13.4
 QUATE, C.F., C3.3
 QUINIOU, J.F., T2.2
 QUINN, W.E., I2.7
 QUN, ZHOU, E10.11
 QUO, L.W., W3.5
 RABEAU, THOMAS, C9.40
 RABENBERG, LLEWELLYN K., N5.11
 RABIN, Y., V3.9
 RABINOVICH, E.M., P2.2
 RABOLT, J.F., J2.3, O8.4
 RACHDI, F., Q10.7
 RADELAAR, S., L3.6
 RADHAKRISHNA, H.S., U11.2
 RADLER, MICHAEL, J., J1.6
 RADLOU, H.B., M6.7, M7.26,
 M7.106
 RADPOUR, F., D10.13, M5.9
 RADZIMSKI, ZBIGNIEW J., G18.29
 RAFAILOVICH, M.H., L6.11, O7.5
 RAGER, B., B6.11
 RAGHAVACHARI, KRISHNAN, B7.10,
 C7.6
 RAGHAVAN, K., C8.2
 RAHMAN, A.M.K., F2.11, Q13.10
 RAHN, JEFFREY A., O1.3
 RAI, A.K., A9.6, A9.41, D5.2
 RAI, D.K., H6.2
 RAINEY, V., J5.11
 RAISANEN, A., C3.5, E7.6,
 E10.3, G12.6
 RAISTRICK, I.D., M7.173,
 M7.211, M7.220
 RAIZMAN, A., E1.2
 RAJ, RISHI, L5.11
 RAJALAKSHMI, R., G9.12
 RAJAN, KRISHNA, A6.28, D1.9,
 M7.93
 RAJARSHI, S.V., H6.4
 RAJENDRAN, S., G18.46
 RAJESWARAN, G., G9.8, G9.17
 RALSTON, J.D., G19.5
 RAMACHANDRAN, V., M7.203
 RAMANATHAN, K.V., A1.8, A6.28,
 D1.9
 RAMANUJACHARY, K.V., M7.36,
 M7.155
 RAMDANI, J., B4.5, G12.2
 RAMDAS, A.K., E9.10, E10.10
 RAMADASS, G.A., M7.203
 RAMESH, R., M7.253, M10.10,
 M11.1
 RAMIREZ, J.C., D4.2
 RAMSTEINER, M., G19.5
 RAND, S.C., F2.10
 RANI, A.N. DURGA, O6.9
 RANI, V.K. MADHUSMITHA, E1.9
 RAO, C.N.R., M2.6
 RAO, T.S., D11.8
 RAO, V.R.S., A9.42
 RAPAKOULIAS, D.E., I1.7
 RASHID, Y.R., U1.3
 RASTON, C.L., B2.3
 RATH, B.B., F3.11
 RAUSCH, W., H7.4
 RAVINDRA, N.M., C9.3
 RAVINDRANATHAN, P., M7.195
 RAWLINS, M.H., M7.3
 RAY, II, R.D., M7.79
 RAY, A., Q3.10, Q7.7
 RAYNE, R.J., M7.149
 RAZAVI, F.S., M7.147
 READ, DAVID, U11.9
 READE, R.P., M7.184
 READER, A.H., L3.9
 READEY, MICHAEL J., M7.7
 READEY, S.E., A9.4, H3.4
 RECTOR, L.P., S5.5
 REDA, KRISTIN B., R3.5
 REDDY, B.K., E1.9
 REDDY, K.V., B6.6
 REDDY, D. RAJA, E1.9
 REDINBO, GREGORY F., M7.229
 REDKAR, S., B5.19
 REDMAN, D.A., F2.10
 REDWING, R., F3.14
 REDWING, R., H2.6
 REE, M., O3.8
 REEBER, ROBERT R., A7.9
 REED, DONALD T., U3.2, U9.2
 REED, W.A., P5.3
 REENTS, W.D., JR, I1.8
 REESON, K.J., A2.11
 REEVES, G.A., M7.196
 REHN, LYNN E., A2.1, A3.9, A6.1,
 A8.10, A11.3, M1.8
 REICH, M., T5.5
 REICHENAUER, G., J6.7
 REICHMAN, JOSEPH, E4.7
 REID, R.G., D8.4, D12.7
 REIMANIS, IVAR E., N6.4
 REIN, DAVE, O2.9
 REIN, MANFRED, Q5.3
 REINERT, P.D., E2.6
 REINHARD, LESZEK, J4.3
 REITZE, D.H., A9.16
 REMNEV, G.E., A6.29
 RENGAN, A., F3.17
 RENTSCHLER, J.A., A3.4, G9.44
 RENZ, GUNTER, Q5.3
 RESNICK, PAUL R., K3.5
 REST, J., A4.7
 RETTORI, C., S2.3
 REVCOLEVSKI, A., C4.5
 REVERTEGAT, ELAINE, U1.1
 REVESZ, PETER, A1.6, A7.8, F9.7,
 M7.214
 REY, ALEJANDRO, D., V8.13
 REYES, J., Q7.17
 REYES-GASGA, J., M7.119
 REYNOLDS, C.L., G9.36
 REYNOLDS, DONALD C., G14.1
 REYNOLDS, JOHN R., Q6.3
 RHA, CHOKYUN, R5.2
 RHINE, WENDELL E., M7.158,
 M7.159
 RHYNE, J.J., J2.5, J2.8
 RIBEAU COURT, J-P., M7.121
 RIBBS, MICHEL, I4.7
 RICE, J.A., M9.8, M7.241
 RICE-FICHT, ALLISON C., R5.6
 RICHARDS, D.R., M6.6, M7.38
 RICHARDS, R. RONALD, M7.54
 RICHARDS, R.W., J7.13
 RICHARDSON, C., R2.4, R2.5
 RICHARDSON, CLIFF F., C8.3

RICHARDSON, I.G., U4.1, U7.8
RICHARDSON JR., J.W., J7.10
RICHERT, BRENT A., M7.9
RICHESON, D.S., M7.251, M10.8
RICHMAN, R.M., M7.31
RICHMOND, ELIEZER DOVID, C9.37, D2.4
RICHMOND, WILLIAM, U2
RICHTER, D., J6.1, J6.8
RICHTER, WOLFGANG, C7.3, D11.11
RICOULT, DANIEL, C9.22
RIDGWAY, M.C., A2.2, A2.7
RIDGWAY, MARK C., G9.6
RIEKE, PETER C., R, R1.6, R1.8, R2
RIETHMILLER, MARGARET W., U7.22
RIGGS, M.L., M7.163
RILEY, J.T., Q10.12
RILLO, C., M7.21
RING, TERRY, T5.4
RINI, M., W2.3
RIOS-JARA, DAVID, M4.11
RISSE, S.M., Q7.4
RITSKO, JOHN J., K2
RITTER, C., J3.4
RITTER, J.E., N6.3
RITZ, K.N., B5.19
ROACH, J.F., O4.5
ROBBINS, MARK O., V4.10, V10.3, V10.5
ROBERTS, C., D10.38
ROBERTS, E., M7.140
ROBERTS, J.C., B4.5
ROBERTSON, B.W., N5.13
ROBERTSON, DAVID E., U7.35
ROBERTSON, STEPHANIE A., R4.2
ROBINSON, A.K., A2.11
ROBINSON, B.J., D5.4
ROBINSON, HEYWARD G., G12.4
ROBINSON, I.K., C10.1, D10.9
ROBISON, J.H., G18.48
ROCKETT, A., C2.5, C9.34
ROCKWELL, BENJAMIN, D11.6
RODBELL, K.P., B5.21
RODGER, S.A., U4.1
RODITI, E., D10.33
RODMACQ, B., D10.21
RODRIGUES, CARLOS O., C9.15
RODRIGUES, DAVID, O1.2
RODRIGUEZ, M.A., M7.81
RODRIGUEZ-CARVAJAL, J., M7.151
RODRIGUEZ, S., E10.9
ROELOFS, M.G., P8.3, P9.7
ROGERS, C.T., M7.232, M7.234, M7.235, M11.11
ROGERS JR., J.W., L2.1
ROITBURD, ALEXANDER, M7.13, M7.91
ROUSTACZER, S.R., O3.8
ROLFE, S., E9.9
ROLIN, T.D., M7.63, M7.68
ROLL, ARMIN, T7.11
ROLLET, A.D., A7.3
ROMAND, M., A8.5
RONAY, MARIA, G11.4
ROORDA, S., A9.14, A9.43, A9.44
ROOT, JOHN H., J5.8, J6.12
ROPARS, G., D1.4
ROQUES-CARMES, C., T2.2
ROSE, KENNETH, H1.5, H7.10
ROSEDALE, JEFFREY, H., V3.8
ROSEN, MERVINE, A6.2, A6.3
ROSENBERG, ROBERT, B, B7
ROSENBERGER, P., L1
ROSENFELD, L., N6.3
ROSENFELDER, S., M7.140
ROSENGREEN, A., M7.163
ROSENMAN, IZIO, M8.4
ROSNER, DANIEL E., L1.6
ROSNER, R., Q6.2
ROSS, C.A., D9.7
ROSS, P.M., C12.1
ROSSABI, J., G9.15
ROSSBITO, FRANK C., Q8.9
ROSSO, MICHEL, T5.6
ROTH, A.P., D10.31, D11.9
ROTH, J.A., A5.2
ROTH, ROBERT S., M7.111
ROTHSCHILD, KENNETH J., R6.7
ROTHSCHILD, MORDECHAI, B2.2, B6
ROUCAU, C., M2.7
ROUSINA, R., D10.40
ROUTBORT, J.L., M7.65, M7.156
ROUX, DIDIER, V2.4, V2.7, V2.8
ROWELL, J.M., M11.1
ROWELL, N.L., D10.18
ROY, D.M., Y1.4, Y3.5, Y4.2, Y4.3, Y4.5
ROY, R.A., A6.28, M7.194
ROY, RUSTUM, M7.195, S1.2, S3.3, X, Y1.4, Y3.2
ROY, T., A9.5, M7.220
ROYLE, A., E7.4
ROZGOONYI, G.A., D2.2
ROZGOONYI, GEORGE A., G18.29
RUADDEL-TEIKIER, ANNIE, Q9.10
RUBART, W.S., A9.25
RUBIN, L.M., M10.2
RUBIN, M.D., H5.3
RUBINSTEIN, MICHAEL, T8.3
RUBIO, MIGUEL A., T4.7/U10.7, U10.7/T4.7
RUBNER, M.P., Q6.1, Q6.2, Q12.3
RUCKENSTEIN, E., M7.152
RUCKMAN, M.W., C9.28
RUDD, G., B4.9
RUDDER, R.A., F7.3, I4.3, I4.5
RUDMAN, D.A., M7.198, M7.204, M10.2
RÜHLE, MANFRED, E2.4, M7.216, M9.4, N2.4, N2.7, N5.7, N6.4, N7.4
RUIZ, JOSE P., Q6.3
RUNGSIMUNTAKUL, N., O7.11
RUOCO, G., T8.6
RUPICH, M.W., M4.5
RUPP, B., J3.7
RUPP JR, L.W., M2.2
RUPPERT, A.P., D9.1, H6.9
RUSH, J.J., J2.7, J7.3
RUSSEK, STEPHEN E., M7.188, M7.229, M11.5
RUSSEL, S.D., B6.4
RUSSEL, WILLIAM, B., V4.6
RUSSELL, P., B6.9
RUSSELL, P.P., Y4.4
RUSSELL, S., K5.7
RUSSELL, THOMAS P., J2.9, J2.10, J7, O7.2, O7.3, O7.4, O7.7
RUSSELL, WILLIAM, F5.13
RUSSO, C.J., N6.6
RUSSO, R.E., M7.184, M7.186
RUSSO, S., T5.5
RUTZE, U., P1.4
RYAN, R.W., D7.4
RYELANDT, L., M7.12, M7.238
RYERSON, FREDERICK J., U7.13
SABA, F., M3.10
SABADE, M., O5.3
SABATINI, R.L., M7.57, M7.164
SABO, K.A., M7.163
SABOCHICK, MICHAEL J., A4.4, C13.5
SACKS, ROBERT N., D4.10
SADAKATA, N., M7.181, M7.240
SADANA, D.K., A9.25
SADNICK, LARRY P., D8.6, D10.4, G9.43
SAENGER, K.L., M7.194
SAFARI, A., M7.137
SAFINYA, C.R., V, V1, V1.6, V2.3, V2.6, V3.6
SAFRAN, S.A., V, V1.4, V2
SAGGESE, S.J., P5.5
SAHA, N.C., K4.9
SAIFI, MONI, P8
SAITO, GUNZI, Q4, Q4.1, Q4.7
SAITO, S., Q12.12
SAITO, TAKAYUKI, K5.9
SAKAI, AKIRA, C5.2
SAKAI, ETSUO, Y3.3
SAKAI, KAZUPUMI, G9.27
SAKASHITA, MASAO, E7.5
SAKORAFOS, K.G., K3.7
SAKUMA, E., F6.12
SAKURAI, S., J6.2
SAKURAI, T., M2.9
SALAMA, K., M4.4
SALAMANCA-YOUNG, L., D6.9
SALAMON, M.B., J2.8
SALAMON, N.J., N6.5
SALEM, JESSE R., P6.7
SALERNO, ANTHONY J., R4.5
SALES, BRIAN C., M2.4, M7.64
SALIB, S., M9.10, S5.4
SALINAS-RODRIGUEZ, A., J5.8
SALONE, L., V8.4
SALZBERG, A.P., H2.7
SAMADAR, S., M7.245
SAMANTA, S.K., M7.245
SAMARITA, N., E9.6, E10.10, J2.5
SAMESHIMA, T., B1.5
SAMITIER, J., G9.31
SAMMANN, E., O8.5
SAMMON, M.J., V8.9
SAMPERE, S.M., M7.217
SAMPLE, DAVID, Y1.2
SAMUEL, L., Q10.10
SAMUELS, WILLIAM D., S2.4
SAMUELSON, LARS, D11.5
SANCHEZ, FRANCISCO H., A9.45
SANCHIS, M.J., M7.21
SANDA, H., A9.46
SANDA, PIA N., Q10.10, Q10.12
SANDER, L.C., J7.5, J7.6
SANDER, LEONARD M., T7.2, T9.7
SANDHU, G.S., F4.4, F4.11
SANDMAN, DANIEL J., Q12, Q12.2
SANDS, T., D1.1, D1.2, D1.3
SANFORD, W. MICHAEL, O3.4, O7
SANGANERIA, M., D4.9
SANGHERA, J.S., P5.4
SANHONG, ZHANG, C9.19
SANKARAN, V., O6.5
SANTIAGO-AVILES, J.J., D2.1
SANTORO, A., J3.8, M6.10
SANUI, KOHEI, S4.7
SAPIÑA, F., M7.21
SAPOCHAR, LINDA S., Q7.15, S5.6
SAPOVAY, BERNARD, T5.6
SARFAK, M., J4.8
SARHOLT-KRISTENSEN, L., A4.6
SARIKAYA, MEHMET, M7.105, R2.8, T7.8, T8.5
SARIN, V.K., L4.1
SARIS, P.W., A3.3, A8.4, A8.6, A9.30, A9.47, A9.56
SARKAR, D., G18.17
SARKER, S., T7.10
SARKISSIAN, A., T5.2
SAROFIM, A.F., M1.6
SAROVAN, R.A., N5.19
SARRADIN, JOEL, I4.7
SARTWELL, B.D., A6.17
SASABE, HIROYUKI, C9.11, Q9.6, S2.2, S2.8
SASAGAWA, NORIKO, Q8.4
SASAKI, KENICHI, F1.9
SASAKI, N., M7.199, U7.40, U7.43, U9.3
SASAKI, TAIZO, G9.46
SASAKI, Y., H4.4
SASONGKO, SUN, O5.3
SASS, S.L., N5.14
SASTRY, SHANKAR M.L., C9.29
SATIYA, S.K., J2.7, J2.9, J2.10
SATO, Y., F2.7
SATOH, K., G9.34
SATOH, KAZUNOBU, Q8.6
SATOH, T., M7.199
SATOU, HIDETAKA, K5.9
SATOU, K., M7.162
SATOU, M., A6.33
SATTLEBERGER, A.P., L6.8
SAUER, BRYAN, B., V8.11
SAVINO, E., A9.58
SAVOVA, EVDOKIA B., B3.11
SAVVIDES, N., M7.177, M7.243
SAWANO, K., M7.13
SAWYER, WILLIAM D., G18.6
SAYERS, D.E., C10.5
SCAGLIOTTI, M., M1.4
SCARBROUGH, J.O., M7.258
SCARDI, P., A6.12
SCARMOZZINO, R., B5.20
SCHAAFSMA, D., D10.38
SCHAAKE, HERB F., E, E1.3, E3, E3.2, M7.119
SCHABES-RECHKIMAN, PABLO, C13.2, M7.119
SCHACHAM, S.E., E7.3
SCHACHINGER, EWALD, M7.9
SCHADLER, LINDA S., N3.2, M4.6
SCHAEFER, DALE W., J6.8, J6.12, O, O1, O1.6, O1.7
SCHAFER, H., Q10.4
SCHATZ, GUNTHER, V6.9
SCHATZLER, R., J6.7
SCHAUER, W., M5.5
SCHBETZ, BARRY E., Y, Y5.4
SCHEGOLEV, I.F., Q4.2
SCHENCK, PETER K., A9.12
SCHERER, A., M7.234
SCHETZINA, JAN F., E, E1, E4.6, E5.8, E6.1, E6.5, E6.7, E6.8, E7.10, E8.7, E9.2, E9.4, E9.5
SCHIAVONE, L.M., M7.232
SCHILLING, L.L., M7.129
SCHILLING, M.L., Q9.11
SCHILLING, W., J4.2
SCHIRBER, J.E., M7.141
SCHIRBER, J.E., M7.157
SCHLESINGER, T.E., G9.21, G9.23, G9.49, M7.201
SCHLETTE, A., G5.4
SCHLOM, D.G., M10.6
SCHLORHOLTZ, SCOTT, W3.3, W3.4
SCHLOSSMAN, M.L., V6.5, V6.8, V8.7, V8.10
SCHLUTER, MICHAEL, M1.3
SCHMID, P.E., C10.2
SCHMID, UWE, G18.9
SCHMIDT, HELMUT, O1.1
SCHMIDT, PAUL W., T, T7.11, T7.12, T8.7
SCHMIDT, WAYDE R., O10
SCHMITZ, K.M., G9.17
SCHMITZ, ROBERT W., N5.24
SCHNEEMAYER, LYNN F., M, M1.9, M2, M2.5, M6.5, M6.8, M7.33, M8.2, M8.8
SCHNEIDER, J.W., G7.1
SCHÖPFELD, BERND, J4.3, J4.12
SCHOOINOVER, RODNEY, T9.7
SCHOWALTER, L.J., D, D1.9, D2.7, D3
SCHREIBER, CHARLOTTE W., U7.22
SCHREIBER, HENRY D., U7.2
SCHREMS, M., G18.8
SCHREUTELKAMP, R.J., A8.4, A8.6, A9.30, A9.47
SCHREY, F., C5.3, D1.6
SCHROCK, R.R., O6.5, Q10.4
SCHRODER, J., J5.7
SCHROEDER, ULRICH, N3.9, N5.5, N5.6
SCHROEDER, H., J7.11
SCHROEDER, JOHN, H2.4
SCHROEDER, THOMAS D., M7.100
SCHUBERT, FRANK, O3.9
SCHUHL, A., D10.47
SCHUHMACHER, BERND, K7.6
SCHUILLING, R.D., M2.2
SCHULBERG, M.T., B5.16
SCHULER, CLAUDS, M7.52
SCHULER, SIEGFRIED, B6.12
SCHULLER, IVAN K., C9.12, C11.1, D6.5, M7.75
SCHULTE, A., O8.4
SCHULTZ, A.J., Q5.2
SCHULTZ, K., C7.2
SCHULTZ, P.J., G18.12
SCHULTZ, PETER C., P1
SCHULTZ, PETER G., R4.2
SCHURTENBERGER, P., V2.1, V10.6
SCHUSTER, D., J4.2
SCHWAB, C., G7.1, G9.34
SCHWAHN, D., J7.11, O5.10
SCHWARK, DWIGHT W., O2.6
SCHWARTZ, D.K., V6.5, V6.8, V8.7, V8.10
SCHWARTZ, DANIEL S., C9.29
SCHWARTZ, P.V., A10.8, G11.7, G18.40
SCHWARZ, S.A., G11.7, G18.40, G20.2
SCHWEIKA, WERNER E., J4.2, J4.5, J4.9
SCHWEISS, P., M7.114
SCHILLA, C.J., D10.17, G12.3
SCOTT, BRUCE A., M6.2, M6.3, M7.56
SCOTT, M., M7.134

SCOTT, R.D., U11.11
SCOVILLE, N.A., L3
SCOZZAFAVA, MARY ROSE, M7.158
SEAGER, CARLETON H., G7.4,
G18.38
SEALY, B.J., A8.11
SECOURGEON, LILIANE, Q7.5
SEDIRA, JOSEPH S., Q4.6
SEDLACEK, J.H.C., B2.2
SEEBAUER, E.G., C7.2
SEEGER, D.E., B4.11
SEEHRA, M.S., M7.31
SEGALL, B., C13.3, F6.9,
SEGARS, RONALD, T6.4
SEGHER, EJELOUL, G2.5
SEGUMILLER, A., M3.13
SEIBERLING, L., A9.25
SEIBT, M., G18.30
SEIDO, M., M7.247
SEIN, MAUNG, U11.7
SEKI, H., F1.7
SEKINE, K., U7.34
SEKULA, S.T., M7.118, M8.7,
M11.2
SELINDER, T.I., F8.5
SELLSCHOP, J.P.F., G18.36
SELM, PATHI, M7.60
SELVAMANICKAM, V., M4.4
SEN, A., O5.2
SEN, S., E1.1
SENECAL, K., R3.3
SENGERS, E.G.F., U7.25
SENGUPTA, DIPANKAR, G9.6
SENTEIN, C., Q12.7
SEONG, T.Y., G13.3
SEPIC, J., E1.2
SERNAS, V., P2.5
SERNE, R. JEFF, U4.3, U4.4
SESHAN, K., H7.4
SETO, H., D8.3
SEUL, M., V8.9
SEUNTJENS, J.M., M7.257
SEXTON, D.A., B6.4
SHABANOV, N.N., A9.39
SHACKLETTE, L.W., Q6.9
SHADE, JOHN W., U1.2
SHADLER, LINDA S., N3.2, N4.6
SHAFFER, M.W., M7.5
SHAFFER, J. SCOTT, N5.20
SHAH, A., H1.4
SHAH, A., M7.167
SHAH, K.S., F9.8
SHAH, RITESH P., U7.23
SHAH, S., D6.7, E2.7
SHAHIARI, M.R., P5.5
SHAKED, HAGAI, J7.1
SHALEK, P.D., L5.1
SHANABROOK, B.V., C9.8, C11.2
SHANE, J., D10.49
SHANG, C.H., A11.8, T9.9
SHAOQI, PENG, F5.15
SHAPIRA, Y., E10.2
SHAPIRO, ALEXANDER, N2.10
SHAPIRO, ANDREW A., M7.46
SHAPIRO, M.J., M7.171
SHAPIRO, S.M., J. J1, J3.2, J4.6
SHARAN, S., B4.12, D4.9
SHARLAND, S.M., U3.3, U7.2
SHARMA, D.K., G9.37, G18.17
SHARMA, R., G9.17
SHARMA, R.K., K4.9
SHARMA, R.P., M1.8
SHARMA, S.N., H1.10
SHASHIDHAR, R., V5.6
SHAULOV, A., M7.102
SHAVER, D.C., B2.2
SHAW, C.M., P4.3
SHAW, D.T., B7.2, M3.7, M7.167,
M7.191, M7.212, M7.230,
M7.237, M7.249
SHAW, HENRY F., U8.4, U11
SHAW, J.L., E2.2
SHAW, M.C., N1.9
SHAW, T.M., M7.29
SHEFER, A., V1.10, V8.2
SHELBURNE, J.A., Q12.1
SHELBY, R., G9.50
SHELDON, B.W., L2.5
SHELDON, R.N., M6.7, M7.26,
M7.106
SHEN, H., D11.6
SHEN, HUI-MIN, M7.109, M7.116
SHEN, LEI, G9.21
SHEN, WEI, Y2.3
SHEN, X.-L., M7.121
SHEN, XIAO-TONG, R5.7
SHEN, Y., V1.6
SHEN, Y.H., M9.2
SHEN, Y.R., V6.6
SHENG, PING, V7.9
SHENG, T., I4.4
SHER, A., E1.2, E7.4A, M7.163
SHER, C.J., M7.191
SHERRINGTON, D., T7.10
SHERWOOD, R.C., M7.74
SHEU, E.Y., V2.3
SHEU, S., C7.2
SHEU, T.C., W3.5
SHI, D., U2.3
SHI, DONGLU, M4.7, M7.51,
M7.131, M7.150, M7.156
SHI, L.T., M7.87
SHI, T., L6.5
SHI, X.-D., Q11.7
SHI, ZHONG-YOU, O5.7, T7.3,
T7.4, T9.8
SHIBATA, H., G3.3, G3.4, G9.40
SHIBATA, SUSUMU, M5.10
SHIBATA, TOMOHIRO, D2.10
SHICHANG, ZOU, A6.30, A6.31,
A9.20, A9.48, A9.49, H6.7
SHICHIRI, TOYOHIRO, Q8.6
SHIEH, W.-R., Q3.8
SHIELDS, T.C., M7.165
SHIEU, F.-S., N5.14
SHIGA, T., O8.1
SHIGENAKA, NAOTO, A9.50
SHIGETA, M., D8.3
SHIH, W.H., T7.8, T8.5
SHIH, W.Y., T7.8, T8.5
SHIM, T.E., C10.6, D10.1
SHIMAKAWA, Y., M7.89
SHIMANOE, KENGO, E7.5
SHIMANSKY, R.A., N6.5
SHIMAWAKI, H., D8.5
SHIMIZU, A., G9.40
SHIMIZU, H., G18.31
SHIMIZU, ISAMU, H1.9, H3.6, H5
SHIMOHATA, KENJI, M7.16
SHIMOMYAMA, J., M4.3
SHIN, D.H., M11.5
SHIN, K.C., G9.48
SHIN, KISOO, C9.20
SHIN, S.H., E6.4
SHINAR, J., Q6.6, Q10.9
SHINDE, S., J3.9
SHINOHARA, KOJI, E2.8, E8.4
SHINOZAKI, D.M., K3.6
SHOHARA, Y., M7.128
SHI T. H., H3.6
SHIK SHI, KENSUKE, M7.94
SHIRAKAWA, KOUICHI, B2.10, B4.11
SHIREY, L.M., F8.7
SHIVASHANKAR, S.A., A1.8, J3.9
SHKLOVER, V.E., Q5.1
SHOCKEY, EDWARD, N5.21
SHOESMITH, D.W., U8.2
SHOKOOHI, F.K., M7.232
SHONE, M., E4.2
SHORT, K.T., A2.9, B4.10
SHRIVASTAVA, SADHNA, A9.22
SHRODER, R.E., H4.3
SHU, C., M11.9
SHU, Y.Z., M7.230
SHURTLEFF, J. KEVIN, E3.4
SIADATI, M.H., M7.2
SICIGNANO, A., E4.2
SIEGAL, M.P., D2.1
SIEGEL, EDWARD, T7.29, T7.30,
T7.31, T7.32, T7.33
SIEGEL, R.W., J1.9
SIEGRIST, THEO, M2.5, M7.210,
M7.228
SIERADZKI, K., D4.3, D6.6
SIFFERT, P., B7.7, G18.4
SIGALOVSKY, J., M7.115
SIGEL JR., GEORGE H., P, P5.5,
P6.5, P9.8
SIGMON, T.W., B1.3, XNP1.5
SIGMUND, H., B7.6
SIKES, C. STEVEN, R5.8
SILBEY, R., Q10.4
SILCOX, J., M11.5
SILLETTI, A., D10.32
SILLMON, R.S., G9.36
SILSBEE, M.R., Y1.4, Y3.2,
Y3.5, Y4.2, Y4.3, Y4.5
SILVERANS, R.E., A10.10
SIMON, B., M10.10
SIMKO, J.P., I2.6
SIMMONS, J.J., M7.61
SIMON, CHARLES, M8.4
SIMONS, DONALD G., K4.10
SIMPSON, P.J., G18.12
SINGER, K.D., Q9.11
SINGH, A.K., M7.185, M7.187,
M7.190, M7.205
SINGH, ALOK, V5.6
SINGH, J.P., J3.10, M7.65
SINGH, K., L4.10
SINGH, MEGH, Q4.9
SINGH, R., D10.13
SINGH, RAJIV K., L5.6, M3.1,
M5.9, M7.205
SINGH, SHRI, R., A9.33
SINGLE, RICHARD, F6.3
SINHA, D.N., M7.211
SINHA, S., M5.9
SINHA, S.K., M6.6, J7.14
SINKE, W.C., A9.14, A9.43,
A9.44, A10.2, L5.7
SINKLER, W., A9.51
SINSKEY, ANTHONY J., R5.4
SIROTA, E.B., V2.3, V2.6, V3.6,
V9
SIVAK, J.G., R6.2
SIVANANTHAN, S., E2.2
SIVARAM, SIVA, L3.7
SIVERTSEN, J.M., F3.8
SIXOU, P., S4.5
SIZEMORE, J.T., M10.6
SJOSTRAND, M.E., L3.5
SKALBERG, M., U11.1
SKARNEMARK, G., U11.1
SKELTON, E.F., P8.4
SKJELTORP, A.T., T7.35
SKLAD, P.S., A7.2, A9.34
SKOPEL, W., M8
SKOTHEIM, T.A., Q6.1
SKUDLIK, H., G5.5
SKUTNIK, BOLESLE, P7
SKVARA, FRANTISEK, Y5.2
SLAOUI, A., B7.7
SLAVKIN, HAROLD C., R1.2
SLEIGHT, ARTHUR W., M2.1, M6
SLIKERMAN, W., F6.12
SLUITER, M., J4.4
SLUZEMSKI, D.A., K5.8
SMALLMAN, R.E., M7.254
SMART, R. St.C., U5.7
SMITH, A.W., L1.8
SMITH, D.A., A1.8
SMITH, D.C., L6.8
SMITH, D.L., D7.5
SMITH, DAVID J., D10.25
SMITH, DAVID K., U5.2, U7.13
SMITH, DONALD L., I2.2
SMITH, DORAN D., A9.52, G9.15
SMITH, DOUGLAS T., N6.2
SMITH, F.W., F3.9, F8.2
SMITH, G., M7.191
SMITH, G.A., D1.7, D10.26
SMITH, H.D., U7.31, U9.4
SMITH, H.J.T., M7.103
SMITH, J.L., M7.72
SMITH, K., E10.7
SMITH, LEIGH M., G3.1
SMITH, P.L., A9.53, D10.6
SMITH, P.M., D7.2
SMITH, P.W., E5.5
SMITH, PATRICK M., A10.3
SMITH, R.J., A6.18
SMITH, S.D., Q2.8
SMITH-BRIGGS, J.L., U3.1
SMITS, C., V4.1
SMYTH, D.M., M7.20, M7.27,
M7.86
SNEAD, MALCOLM L., R1.2
SNEED, B.P., E7.10
SNITZER, ELIAS, P9, P9.6,
P9.8, Q8
SNOECK, E., M2.7
SNOOK, I.K., T5.5
SNOW, D.B., M4.12
SNYDER, ERIC J., A5.4
SNYDER, LAWRENCE C., C9.15,
F5.3, G18.27
SNYDER, PAUL G., D12.6
SNYDER, R., M7.134
SNYDER, R.L., M7.61, M7.81
SOBERS, R.G., D10.50
SOBOLEV, N.A., A9.54
SODERHOLM, L., M2.3
SOE, SUNG MOO, H3.2
SOETA, A., M7.142
SOKOLINA, G.A., F4.5, F9.3
SOROLOV, J., L6.11, O7.5
SOLAL, P., J4.8
SOLEH, JODY K., W1.1
SOLER, M., A9.26
SOLIN, S.A., J7.3, M7.255
SOLLER, MARC, M7.175
SOLMI, S., A9.2
SOLTYKA, A.J., D2.11
SOMBRET, CLAUDE, U6
SOMERK, R.E., M7.166
SOMMER, M., F3.9
SONDER, EDWARD, M2.4, M7.64,
M7.124
SONG, J.H., A6.18
SONG, K., O8.4
SONG, L., M7.237
SONG, L.W., M7.71, M7.191,
M7.230
SONI, N.C., M7.127
SOOD, D.K., A7.10
SORENSEN, C.M., T1.8, T7.7
SOTIRCHOS, STRATIS V., L1.12
SOTTA, PAUL, V1.2
SOUCAIL, B., D11.9
SOULEN, JR. R.J., M7.149
SOULEN, JR. ROBERT J., M7.17
SOWA, ERIC C., C13.7
SOWA, J., V4.5
SPAEPEN, F., A9.14, A9.43,
A9.44, D9.2, D9.7, G18.33,
G18.50
SPANGLER, CHARLES W., Q7.15
SPEAR, K.E., F2.5, L1.2
SPENCE, J.C.H., C6.2
SPENCE, ROGER D., U7.3
SPENCER, J.T., B3.3
SPENCER, MICHAEL, G9.29
SPENCER, MICHAEL D., H2.9
SPINELLA, C., A2.5
SPINU, M., S3.5
SPRAGUE, J.A., A6.3, M3.12
SPRINGER, T., O5.10
SPRINGHOLZ, G., B7.6
SQUILLANTE, MICHAEL R., M7.175
SRAJER, G., V7.7
SRIDANOV, GORDANA, Q8.3
SRIDHAR, S., M1.10, V10.10
SRINANTH, K., F4.8, H6.11
SRINIVAS, B., A9.42
SRINIVASAN, R., B3.12, M7.203
SRINIVASAN, T.T., K4.1
SRIVASTAVA, A.K., G9.11, G9.37,
G18.17
SRIVATSA, A.R., D10.13, F3.17
SROLOVITZ, D., D7.8
STADELMANN, P., C10.2
STAHLBUSH, ROBERT, D12.3
STAMPANONI, M., A10.4
STANLEY, H.E., T9
STANNARD, J.E., E1.1
STARR, T.L., L1.7, L1.8
STATON-BEVAN, A.E., D10.35
STAUNTON, J.B., J2.6, J4.7
STAVOLA, M., G5, G6, G6.1, G8.2
STEARNS, LAURA C., M7.43
STEARNS, MARY BETH, D10.25
STECHER, E.B., M1.3
STEEDS, J.W., E9.8
STEEL, D.G., M10.2, M7.204
STEELE, BRIAN C.H., K5.3, K6.9
STEGEMAN, GEORGE I., D6.8
STEHLER, J.L., C9.4, D10.44,
L2.7, O7.8, T8.6
STEIDELL, C.A., K4
STEIER, WILLIAM H., Q7.14
STEIGERWALD, M.L., B7.10
STEIN, RICHARD S., J7.12, O3.1,
O7.3

STEINBECK, J., M7.226
 STEINBRUCH, CH., A6.5
 STEINER, D., G5.5
 STEINER, ULLRICH, V6.9
 STEINFELD, J.I., B7.8
 STEINKE, R., Y1.4
 STELLA, A., G18.5
 STELMAN, D., M7.248
 STEMMET, M.C., G18.36
 STERN, STANLEY H., K4.10
 STETTYCK, KAREN A., Q9.7
 STEVENS, JOHN, S2.6
 STEVENS, MARK, J., V4.10, V10.5
 STEVENS, ROBERT E., L4.7
 STEVENSON, DAVID A., G9.25 G12.4
 STEWART, A.M., M7.7
 STILLER, JOHN K., O3.11
 STILLMAN, G.E., G8.3, G9.30
 STINESPRING, CHARTER D., B3.7, B4.6
 STINSON, M.G., A9.53
 STINTON, D.P., L5.3, L6
 STOBBS, W.M., C12.1
 STOCK, S.R., N5.19
 STOCKS, G.M., J2.6, J4.4, J4.5, J4.7
 STOFFEL, N.G., M7.224
 STOGNIJ, A.I., B5.8
 STOKES, J., V1.6
 STOLEN, ROGER H., P9.1
 STOLK, P.A., A10.2
 STOLWIJK, N.D., G1.3, G12.5
 STOLZ, P., G1.3
 STONE, D.S., K7.5
 STONE, T., M9.10
 STORCH, D.R., M7.191
 STOUT, R.B., U7.30, U8.4
 STOVAIA, M., G6
 STRACHAN, D.M., U7.27
 STRADLING, R.A., G13.3
 STRAUSBAUGH, LINDA D., R4.6
 STRAUSBERG, ROBERT, R4.7
 STREETMAN, B.C., D11.7
 STREHLAU, B., A7.1
 STREIB, J., O5.10
 STREIT, DWIGHT C., D8.6, G9.43
 STREITZ, F., D6.6
 STRINGER, J., T7.17, T9.6
 STRINGFELLOW, G.B., G13.1
 STRITZKER, B., M3.6, M7.221
 STROEVE, P., J2.3
 STROM, U., F2.9
 STRONGIN, DANIEL R., B1.6
 STRUBBE, L., Y2
 STRUCHKOV, YU.T., Q5.1
 STRUTT, PETER R., A9.11, L5.8, P6.3, P6.6
 STUART, M.D., N6.6
 STUCKY, GALEN D., H2.8
 STUKE, MICHAEL, B3.4, B3.5, B7.5
 STUPIK, P.D., L6.7, N2.2
 STUPP, SAMUEL I., K3.2
 STURM, J.C., A10.8, G11.7, G18.40
 STUTZ, C.E., D7.7
 STUTZMANN, M., G6.4, H1.7, H3.5, H6.1
 SU, M.Y., M7.37
 SU, W.P., Q13.8
 SUAHARA, K., H7.8
 SUBRAMANIAN, R., O4.5, O7
 SUCK, J.B., J6.9
 SUENAGA, M., C9.23, M7.18, M7.57, M7.88, M11
 SUEZAWA, M., G5.2
 SUGA, T., M7.128
 SUGAHARA, K., H7.8
 SUGII, NOBUYUKI, M7.172
 SUGIMOTO, TOYONARI, Q2.1
 SUGIMOTO, Y., B2.8
 SUGITA, A., P7.3
 SUGIYAMA, H., G9.40
 SUH, E.-K., E10.10
 SUI, ZHIFENG, E10.5
 SUIB, STEVEN L., L4.8, N5.9, SUICH, DANIEL J., R4.2
 SUKOW, C.A., P7.3
 SUKUMAR, VIJAY, O.10
 SULEK, J., M7.65
 SULLIVAN, J.C., U3.2
 SULLIVAN, JOHN M., JR., Y5.5

SULLIVAN, V.S., O3.3
 SUMINO, K., G5.2
 SUMMERFELT, SCOTT R., C12.6, L2.8, M9.3
 SUMMERFIELD, G.C., J5.3
 SUN, C.C., O1.7
 SUN, J., M5.6
 SUN, JIA-SHU, A9.55
 SUN, LIN-HAI, M7.109
 SUN, QING, D10.31
 SUN, XIAOQUANG, T2.3
 SUN, Y.Y., M10.5
 SUN, YUNXI, M7.145
 SUNDARAM, M., D10.42, D10.43, G9.20, G14.2, G14.3, G14.4
 SUNDER, SHAM, U8.2, U9
 SUNDRGREN, J.-E., F8.5
 SUNG, NAKHO, N3.3
 SUNIL, D., L6.11
 SUNSHINE, STEVEN A., M2.5
 SURI, A.K., L4.10
 SUZUKI, HIEDO, M7.227
 SUZUKI, NORIO, A6.16
 SUZUKI, S., C10.6, D10.1
 SUZUKI, T., D8.3, M7.142
 SUZUKI, TAKAMASA, D8.12
 SUZUKI, TOSHIYASU, Q8.3
 SUZUKI, TETSUYA, E7.5
 SVEINBJORNSSON, E.O., G3.5
 SVENSSON, B.G., G18.15
 SVENSSON, CHRISTER, Q7.10, Q7.18
 SVENSSON, J.H., G18.15, G18.16
 SWAGTEN, H.J.M., E10.8
 SWAMINATHAN, V., G8.4
 SWAN, ANDERS H., M7.5
 SWANSON, L.S., Q6.6
 SWANSON, M.L., A8.12, F4.4, F4.11
 SWARTZENDRUBER, LYDON J., D10.19, M6.4, M7.13
 SWAYAMBUNATHAN, V., U9.2
 SWIECH, W., C3.1
 SWINDAL, C., V4.8
 SWITZER, JAY A., D10.49
 SYLLAIOS, A.J., E7.8
 SZABLEWSKI, MAREK, Q7.2, Q9.4
 SZAFRANEK, I., G8.3, G9.30
 SZETO, K.Y., T1.5
 SZILAGYI, A., E2.6
 SZUSZKIEWICZ, W., E10.11
 TABATA, HITOSHI, M3.4
 TABATABAIE, N., D1.1, D1.2, D1.3
 TACHIBANA, K., M5.11
 TACHIBANA, M., P9.3
 TAGAMI, TAKASHI, A6.32
 TAGUCHI, TSUNEMASA, E5.6, E5.7
 TAI, NYAN-HWA, L1.10
 TAKAGI, S., F9.6
 TAKAHARA, H., M9.9
 TAKAHASHI, JUNICHI, B6.3
 TAKAHASHI, K., E5.1
 TAKAHASHI, SHIRO, P, P3.6, P6
 TAKAHASHI, T., K6.4
 TAKAHASHI, TAKESHI, U7.24
 TAKAI, MIKIO, A6.16, A6.33, A9.46, B3.8, G9.24
 TAKAMI, H., M7.143
 TAKAMORI, TAKESHI, M7.76
 TAKANO, H., U7.40
 TAKAOKA, GIKAN H., A1.7
 TAKARABE, KEN-ICHI, G9.22
 TAKASAKI, K., H7.2
 TAKATA, T., M7.58
 TAKATO, N., P7.3
 TAKAYASU, H., T1.7
 TAKECHI, M., G13.2
 TAKEDA, A., G10.6
 TAKEDA, FUMIO, K6.4
 TAKEDA, M., G10.6
 TAKEMURA, Y., E5.1
 TAKEUCHI, S., M7.142
 TAKEYAMA, T., G18.20
 TAKUI, TAKEJI, Q8.5, Q8.6
 TALIANI, C., Q13.9
 TALLEY, P.L., F4.3
 TALMON, YESHAYAHU, V2.5
 TALWAR, DEVKI N., G9.45
 TALWAR, SATYA S., Q12.4
 TAMARGO, MARIA C., E2, E3.1
 TAMOR, M.A., F5.14

TAN, BENG JIT, L4.8, N5.9.
 TAN, N.X., M7.177
 TAN, NINGXIA, M7.243
 TAN, TEH Y., G9.5, G9.13, G9.18, G20.4
 TAN, ZHENGQUAN, M4.12, M7.97
 TANAKA, AKINORI, H2.5
 TANAKA, KAZUNOBU, H, H3, H6
 TANAKA, M., H7.1, M7.136
 TANAKA, MASATOSHI, Q5.4
 TANAKA, S., M7.58, M7.128
 TANAKA, SHOJI, M7.14
 TANAKA, SHUHEI, A6.32
 TANAKA, Y., M9.9
 TANAYA, M., B2.8
 TANG, HUA, B6.5
 TANG, P.F., K7.8
 TANI, B.S., U7.28
 TANI, TAKAYUKI, I3.6
 TANIGAWA, HIDEO, M7.62
 TANIGUCHI, HIROSHI, K5.12
 TANINO, H., E4.5
 TANIOKU, MASAMI, M7.197
 TANOU, H., G9.40
 TANOU, HISAO, A2.4
 TANSKI, WILLIAM J., D4.10
 TAO, Z., M7.71
 TARASCON, J.M., M10.10
 TARASEVICH, B.J., R1.6, R1.8
 TAREY, RAM D., A9.22
 TARN, J.C.L., D4.8
 TASCH, A., I3.3, I3.4
 TASKAR, N.R., E7.2
 TATAKIS, D.N., R1.5
 TATSUMI, TORU, C5.2
 TAUBER, A., M3.11
 TAUC, J., H3.10
 TAYLOR, E.R., P9.3
 TAYLOR, GARY, B1.1
 TAYLOR, J.A., N2.3
 TAYLOR, J.A.T., K5.6, M7.49
 TAYLOR, K.N.R., M7.165, J3.6
 TAYLOR, M.J., P5.6
 TAYLOR, MARK, P., V10.8
 TAYLOR, RAYMOND L., L3.8
 TEARE, J.D., W1.6, W2.3
 TEATE, A.A., G9.14
 TEDROW, P.M., M7.174
 TEEGARDEN, DAVID, J6.5
 TEEPE, M., M7.45
 TEIXEIRA, M.E., K3.7
 TEJADA, J., M8.9
 TEKI, YOSHIO, Q8.5, Q8.6
 TEMKIN, HENRY, B3.6
 TEMST, KRISTIAAN, D6.5
 TEN, YE-YUNG, F4.10, L5.5
 TERAGUCHI, N., E5.1
 TERATAHI, SHOUSUKE, M10.11
 TEREMETSKAYA, I.G., F4.5
 TERRY, J.C., M7.163
 TESHIMA, T., U9.3
 TESSMER, G.J., D7.2
 TESTA, A.M., M8.9
 TETREULT, T.G., A1.6, A6.34
 THAKKAR, BIMAL, N4.9, N6.1
 THAKUR, R.P.S., D10.13, M5.9
 THEIL, J.A., I4.3
 THEILER, T., G3.6
 THEIS, N., G15.1
 THELANDER, MICHAEL W., E5.8
 THEODORE, N.D., G20.2
 THEOPHILOU, NICOLAS, Q10.5
 THEWALT, M.L.W., G3, G5.1, G18.43
 THIEL, F.A., D10.48
 THILDERKVIK, A-L., G2.2
 THIRUMALAI, D., V9.12
 THIYAGARAJAN, P., J7.2, J7.4
 THOEN, J., V9.7
 THOMAS, EDWIN L., O2.6, O5.8, S5.3
 THOMAS, G., M10.10
 THOMAS, G.A., D10.48
 THOMAS, G.J., C13.1
 THOMAS, IAN M., P2.1
 THOMAS, L.E., U7.27
 THOMAS, O., O7.8
 THOMAS, P.A., C3.4
 THOMAS, P.M., A9.26, D10.50
 THOMAS, R.L., F4.3
 THOMASON, H.P., U3.1

THOMPSON, C.V., A9.21, A10.5, G18.34
 THOMPSON, CHARLES, P2.3, T6.2, T7.6
 THOMPSON, D., Q10.10
 THOMPSON, D.A., D5.4
 THOMPSON, J.G., M7.7
 THOMPSON, J.R., M7.118, M8.7, M11.2
 THOMPSON, MICHAEL O., A2.3, A4, A5, A9.14, A10.1, A10.3
 THOMPSON, MICHAEL R., C9.14
 THOMPSON, NEIL G., U7.33
 THOMPSON, PETER, V10.3
 THOMPSON, PHILLIP E., D12.3
 THOMPSON, R.D., D1.9
 THOMSON, J.A., V2.1
 THOMSON, J.O., M11.2
 THONKE, K., G1.3, G5.4
 THORNE, JAMES, E3.4
 THORNTON, E.C., T4.3/U10.3, U10.3/T4.3
 THORNTON, J.A., P7.2
 THORNTON, R.P., A8.1
 THOULESS, MICHAEL, N1.3
 THUMIM, DAVID, F3.12, L2.13
 THURSTON, G.M., V2.1, V3.3, V10.6
 THWAITES, JOHN J., R6.4, R6.5
 TIAN, DECHENG, T3.5
 TIANG, X.D., E4.8
 TIDSWELL, I.M., C9.40
 TIEFEL, T.H., M7.74
 TIEN, J., H7.4
 TIERNEY, E., I2.9
 TIETZ, LISA A., C12.6, L2.8, M7.188, M7.213, M9.3
 TIGGES, C.P., M7.141, M7.157
 TIMANS, P.J., A8.7
 TIMBRELL, P., D10.20
 TIMMERMAN, W., U6.3, U7.12, U7.20
 TIMMONS, MICHAEL L., G9.4
 TINSIT, R., C11.4
 TIN, C.C., G9.10
 TINKHAM, M., M8.1
 TIRRELL, DAVID A., R4, R4.4
 TIRRELL, MATTHEW, N3, N4.9, N5.3, N5.20, N6.1, O7.6, V1.5, V8.6
 TISCHLER, J.Z., D10.12
 TISSINK, H.C., A3.3
 TITZE, HEINZ, D11.5
 TIWARI, P., M7.187
 TKACZYK, I.E., M7.24
 TOBY, B.H., J1.7
 TODD, JOHN D., C6.3
 TOKAREV, V.V., A6.35, A6.36, B5.8
 TOKITO, S., Q12.12
 TOKUMOTO, MADOKA, Q4.3
 TOMADAKIS, MANOLIS, L1.12
 TOMASCH, G.A., P7.2
 TOMASI, A., A6.12
 TOMINAGA, H., M9.11
 TOMKINSON, J., J2.2
 TOMOMATSU, K., M9.11
 TOMPA, G.S., E2.6, M5.13
 TOMSIA, A.P., M7.77
 TONG, B.Y., H6.15
 TONG, X., C10.4
 TONGE, L.M., L6.9, M7.180, M7.251, M10.3, M10.8
 TONNEAU, D., B6.10
 TOQAN, M.A., W1.6, W2.3
 TORKELSON, JOHN M., Q13.6
 TORNG, C.J., P3.8
 TORRANCE, J.B., Q8, Q8.2
 TORSTENFELT, B., U11.1
 TOSCANO, E., U7.19
 TOSCANO, PAUL J., F6.3
 TOTH, L.E., M7.149
 TOUGH, R.J.A., V4.4
 TOULOUSE, J., M7.67
 TOUZEAU, M., D10.47
 TOWN, S.L., J3.6
 TOWNSEND, PAUL D., Q12.1
 TOYODA, KOICHI, B1.9
 TRACY, BRYAN, L3.7
 TRAIL, STEVEN S., M6.2, M6.3, M7.56

TRAUB, W. R1.4
 TRAUTMAN, P., G17.5
 TRAVERSE, J.P., Q3.9
 TRAVERSE, AGNES, A6.37, A6.38
 TREDWAY, WILLIAM K., N6.8, N7
 TREGILGAS, J.H., E1.6
 TREVINO, S.F., J7.3
 TREY, G.V., M11.9
 TRICOT, CLAUDE, T2.1, T2.2
 TRIFTSCHAUER, W., C9.27
 TRIPATHY, S., Q6.1, Q13.10, S4.5
 TRISCONE, JEAN-MARC, M11.6
 TROMBETTA, J.M., G1.5
 TROMP, RUUD M., C1.2, C3, D5.8
 TROULLIER, N., E10.3
 TRUCKS, G.W., C7.6
 TRUMBLE, KEVIN P., N2.4
 TSAI, CHUANG CHUANG, H, H1, H6
 TSAI, M.L., S4.6
 TSAI, MING-JIN, M7.32
 TSAI, PATRICIA, M5.4
 TSAI, T.E., P4.6
 TSANG, JOSEPH W., O3.11
 TSAO, J.Y., A1.2, A10.3, D4.6
 TSENG, FEN-CHU, F1.5
 TSENG, W., C9.8, C11.2
 TSU, D.V., I4.3
 TSUDA, S., H7.1
 TSUEI, C.C., M3.13
 TSUJI, HIROSHI, A1.7
 TSUKAMOTO, TAKEO, A9.57
 TSUMURA, AKIRA, Q12.8
 TSURUOKA, TAJIJI, M5.10
 TSUTSUI, KAZUO, D2.6
 TSUTSUI, T., Q12.12
 TSUYOSI, HIROAKI, Q5.4
 TU, AN, F5.17, H2.6
 TU, C., D7
 TU, C.W., G9.51
 TU, K.N., G18.34, M7.87, M9
 TUBINO, R., Q7.12, Q10.6
 TUCHMAN, JUDAH A., E10.5
 TUCKER, J.H., G11.1
 TULCHINSKI, D., G18.51
 TULCHINSKY, VICTOR, F6.3
 TULKE, A., K7.2
 TULLER, HARRY L., M7.32
 TULLIUS, MIKE, P6.2
 TUNG, R.T., C5.3, C10.1, D1.5, D1.6, D2
 TURCHI, P.E.A., J4.4, J4.5
 TURCHINSKAYA, M., M7.13
 TURNER, B., M3.11
 TURNER, L.G., M11.3
 TURNER, P.S., U5.7
 TUSZYNSKI, JACK A., M7.4
 TUTKEN, T., G11.5
 TUTTLE, JOHN R., H6.6
 TUZZOLO, M.R., P6.1
 TWARDOWSKI, A., E10.8, E10.12
 TWEED, C.J., U3.3, U7.2
 TWESTEN, RAY, C5.4
 TWIEG, R., O8.4
 TWIGG, MARK E., D2.4, D10.11, D10.16
 TYNDALL, GEORGE W., B6.2, F2.2
 TZENG, YONHUA, F3.7, M7.231
 UCHIKAWA, FUSAOKI, M7.53
 UDA, TSUYOSHI, C8.5
 UDAGAWA, E., K5.11
 UEDA, O., E8.4, G13.2, M10.12
 UEDA, TETSUZO, F6.1
 UEDA, Y., F6.14
 UETA, SHINZO, U7.36
 UETANI, T., F6.14
 UHEYAMA, M., M7.135
 UGOLINI, D., C5.5
 UHLMANN, D.R., M7.140
 UKHIN, L.YU, Q5.1
 ULLAL, HARIN S., D10.13, E5.4
 ULLMAIER, H., J7.11
 ULRICH, DONALD R., Q1, S, S1, X3.1
 UNION, D.M., Q9.28
 UNO, N., M7.143
 UPASANI, RAVINDRA B., Q2.2, Q8.8, Q11.7, Q11.9
 URBAN, K., Q12.5
 URISU, TSUNEO, B6.3
 UROUHART, A.W., X2.2
 URRY, DAN W., R4.8
 USHIJIMA, TOSHIE, M7.16
 USUI, A., D8.5
 USUI, S., B1.5
 UTSUMI, YUICHI, B6.3
 UUSHEIMO, K., U7.41
 UUSIMAKI, A., M7.138, M7.200
 UY, WILLIAM C., O3.5
 UZIEMBLA, N.H., U7.31
 V. D. PERS, N.M., A9.56
 VAC, RAHEL, S5.6
 VACHA, I.B., P5.6
 VAIDYA, K.J., M7.122
 VAISHNAVA, P.P., M7.123, M7.126
 VAKMIN, DAVID, J5.10
 VAKNIN, D., M6.6
 VALEK, L.P., M7.11
 VALIA, DAVID A., O4.9
 VALLADARES, J., D10.49, D12.10
 VALLES JR., J.M., M1.9, M11.8
 VALLET, M., M7.151
 VALLEY, GEORGE C., G9.33
 VAMOS, G., W1.6, W2.3
 VAN DE WALLE, CHRIS G., C1.3, G7.2
 VAN DE WALLE, G.F.A., D11.2
 VAN DEN HEUVEL, J.C., H3.3, T7.25
 VAN DER JEUGD, C.A., L3.6
 VAN DER SPIEGEL, J., D2.3
 VAN DER VEEN, J.F., F6.12
 VAN DOVER, ROBERT B., M7.74, M8.8
 VAN DRIEL, H., C11.4
 VAN GORKUM, A.A., D11.2
 VAN HOOK, JERROLD, M7.189
 VAN HOVE, M., A10.10
 VAN ISEGHEM, P., U6.1, U6.3, U7.11, U7.12, U7.20
 VAN KONYENBURG, RICHARD A., U9.2
 VAN MAAREN, A.J.P., L5.7
 VAN OORT, R.C., H3.3, T7.25
 VAN RAAP, MARCELA B. FERNANDEZ, A9.45
 VAN ROSSUM, M., A10.10
 VAN VECHTEN, JAMES A., G18.9, G20
 VAN WINKLE, DAVID, H., V8.12
 VANACKEN, J., A2.12, D10.30, M7.75
 VANDENBOSCH, A., M7.12, M7.238
 VANDERAH, DAVID J., Q4.10
 VANDERAH, T.A., M2.8, M6
 VANDERBILT, DAVID, C2.2
 VANDERSTRAETEN, HANS, C11.1, D6.5
 VANDERVOORT, K., M7.131, M7.3
 VANDEVYVER, M., G9.45
 VANHELLEMONT, J., A2.12, D10.30
 VANTOMME, A., A2.12, D10.30
 VARADAN, VASUNDARA V., M7.60, Q7.13, Q13.11, Q13.12, Q13.13
 VARADAN, VIJAY K., M7.60, Q7.13, Q13.11, Q13.12, Q13.13
 VARDENY, Z.V., H3.10, Q10.9
 VARHUE, WALTER, F5.16, I1.3
 VASE, PER, M7.146
 VATERLAUS, A., A10.4
 VAUDIN, MARK D., A9.12
 VAUGHAN, DAVID, X4.1
 VAZIRI, M., E3.6
 VAZQUEZ, ARMANDO, C13.2, Y2.5
 VEAL, B.W., M7.3
 VEIRS, D.K., H5.3
 VELAZQUEZ, R., O5.9
 VELECKIS, E., U7.28
 VENABLE, RAYMOND, L., V9.4
 VENKATARAM, K., S1.4
 VENKATASUBRAMANIAN, R., G3.1, G9.3
 VENKATESAN, T., M3, M3.2, M7.202, M7.208, M7.224, M7.232, M7.234, M7.235, M7.246, M7.253, M11.11
 VENTURINI, E.L., M7.117, M7.141, M7.157, M10.7
 VEPREK, STAN, H1.6
 VERGAMINI, PHILLIP J., J5.4
 VERMEHREN, PETRA, Q5.3
 VERNAZ, E., U5.5, U6.4, U7.11, U7.14
 VERNON, S.M., D2.11, D2.12, D10.34
 VIANO, A.M., M7.218
 VICENTE, L., M7.98
 VICSEK, TAMAS, T9.2
 VIDALI, G., C7.4, C9.17
 VIGIL, R. DENNIS, T8.4
 VILLARRUBIA, J.S., C6.4, C9.6
 VILLERET, MURIELLE, E10.9
 VINCENT, C., L5.9
 VINCENT, H., L5.9
 VINEY, CHRISTOPHER, S5.10
 VIPULANANDAN, C., M9.10, S5.4
 VIROSZTEK, ATTILA, Q11.6
 VISHWANATHAN, R., D8.9
 VISITSERNGTRAKUL, S., A6.39, G18.32
 VITEK, V., C9.21, C13.4, G18.24
 VITTORI, V., L4.6
 Vlieg, E., D10.9
 VLOEBERGH, H., A2.12, D10.30
 VOGEL, VIOLA, V6.6
 VOGT, R.N., M7.125
 VOISIN, P., D11.9
 VOLKERT, C.A., A8.2
 VOLKSEN, W., O3.8
 VON BARDELEBEN, HANS J., G4.5, G9.33, G15.3, G16.5
 VON DESSONNECK, K.E., M10.6
 VON HEGEN, M. HORN, C3.2
 VON MOLNAR, S., E9.7, E10
 VON NEIDA, A.E., A8.11
 VOOR, R.W., M7.215
 VOORRIPS, A.C., A3.3
 VREDENBERG, A.M., A3.3, A9.56
 VREELAND, THOMAS T., JR., D10.50
 VRIEND, SIMON, P., W2.4
 VSETECKA, TOMAS, Y5.2
 VVEDENSKY, D.D., C8.4, D8.7, D10.23, N5.16
 WACHS, A.L., J4.5
 WADA, N., J7.3
 WADA, T., G10.6
 WADA, TATSUO, S2.2, S2.8, Q9.6
 WADSWORTH, J., N2.1
 WAGENFELD, H.K., T5.5
 WAGNER, H. DANIEL, N5.4
 WAGNER, N., V4.2
 WAGNER, S., H1.2, H3.1, H7
 WAHAB, Q.U., F8.5
 WAHL, GEORG, B3.4
 WAHLBECK, PHILLIP G., M7.54
 WAIHAMAD, W., S5.8
 WAITE, J. HERBERT, R5.6
 WAKELEY, LILLIAN D., U1.4
 WAKHARKAR, VIJAY S., O7.7
 WALKER, G.F., K4.7
 WALKER, J.F., D7.4
 WALKER, K.L., P3.1, P4.1
 WALL, A., G12.6
 WALLACE, J., E4.4A
 WALLACE, J. SHIELD, R3.5
 WALSER, A., Q7.12, Q10.6
 WALSER, R.M., A6.23, A8.8, A9.23
 WALSH, D., A6.19
 WALTON, JOHN C., T4.9/U10.9, U9.1, U10.9/T4.9
 WALTON, PETER L., U7.4
 WALUKIEWICZ, W., G17.4, G19.1
 WANG, BING, C1.2
 WANG, C., F6.6, H1.3, I3.8
 WANG, CHUN, Q3.11
 WANG, F.F.Y., F1.5
 WANG, G.-C., D10.26
 WANG, G.-J., C13.4
 WANG, H.H., Q5.2
 WANG, J., P9.3
 WANG, JENQDAW, L5.11
 WANG, JIAN-YIH, N5.10
 WANG, K.L., D10.15, G18.42, G20.3
 WANG, LU-MIN, A8.10
 WANG, N., Q1.3
 WANG, P.D., G13.3
 WANG, P.T., D10.17
 WANG, PING, M7.41
 WANG, QI, D9.4
 WANG, R.L., D7.10
 WANG, S., B4.9
 WANG, S.S., N2.8, M7.6
 WANG, SHAMBA, W3.6
 WANG, SHU-LIN, H3.9
 WANG, SHUQJIN, B5.3
 WANG, TE-NING, M7.109
 WANG, W., D7
 WANG, W.I., D11.6
 WANG, X., A9.16
 WANG, X.K., M9.2, M10.8
 WANG, X.Q., M7.67
 WANG, X.W., M7.134
 WANG, XIAOMEI, E10.1, E10.7
 WANG, Y.L., M7.57, M7.88
 WANG, Y.Q., M10.5
 WANG, Y.T., D11.4
 WANG, YE-NING, M7.116
 WANG, YING, H2.8
 WANG, YUH-LIN, B3.6
 WANG, Z.L., A8.6
 WANG, Z.M., T1.5
 WANG, ZHEN-GANG, V1.4
 WARD, DAVID B., U7.38
 WARD, I.D., D10.46, D11.7, G9.35, G9.36
 WARD, I.M., S4.8
 WARNOCK, J., E10.6
 WARREN, DAVID W., U7.9
 WARREN, G.W., D10.24
 WARREN, JAMES W., L5.4
 WARREN, L.F., Q9.12
 WAS, GARY S., A6.1, A11.2
 WASA, KIYOTAKA, M7.15, M10.1
 WASZCZAK, J.V., M1.9, M6.5, M8.8
 WATABE, HIROKUNI, C9.1, H3.7
 WATANABE, H., O7.6
 WATANABE, I., Q6.2
 WATANABE, NOBUO, A9.57
 WATARI, T., K1.4
 WATERMAN, JAMES, D12.3
 WATKINS, LINWOOD, F4.7
 WATKINS, MAURICE, J5.10
 WATKINS, STEVEN F., M6.4
 WATKINS, THOMAS, L4.7
 WATON, G., V3.2
 WAUGH, M.A., V7.7
 WEATHERLY, G.C., D5.9
 WEBB, J.B., D10.40, D11.8
 WEBER, JORG, G7.6, G18.6
 WEBSTER, GEORGE A., J5.9
 WEBSTER, PETER J., J5.9
 WEED, HOMER C., U7.13
 WEEKS, R.A., A7.4
 WEHBI, D., T2.2
 WEI, CHONGDE, M7.145
 WEI, J., F4.6
 WEI, L., F4.3
 WEI, T., P9.2, P9.4
 WEI, TIAN, A6.40
 WEI, Y., Q3.10
 WEI, YAN-ZHEN, V10.10
 WEIMER, K.P., A3.10
 WEIMER, R., F1.10
 WEINBERGER, B.R., M4.12, M7.97, M7.182
 WEINER, JOSEPH S., D10.49, D12.10
 WEINER, KURT H., B1.3, XNF1.5
 WEINER, S., R1.4, R5.9
 WEINREB, A., T7.11
 WEINSTEIN, R., M7.82
 WEIPING, CAI, A6.40
 WEIR, B.E., A9.26, D10.48
 WEISS, C.A., M7.208
 WEISS, R.A., O5.2, O5.3, O6.4, O8.8
 WETTZ, D.A., V4.3, V4.4, V7.9, V9.1
 WELCH, D.O., M7.88
 WELLAND, M.E., F5.12
 WELLHOFER, F., M7.165, M7.254
 WELP, U., M2.3, M7.131
 WEMAN, HELGE, G18.19
 WENHAI, WU, E8.10
 WENK, RUDY, J5.4
 WENTZCOVICH, RENATA M., F8.13
 WERDER, D.J., M6.5, M7.33
 WERME, LARS O., U8, U8.3, U11.1

WESSELS, B.W., L6.9, M7.180,
 M7.251, M10.3
 WESSON, SHELTON P., M4.2
 WEST, J.A., A10.3
 WEST, K.W., A5.1, D10.49, D12.10
 WEST, S., M7.140
 WESTCOTT, MICHAEL R., E5.3, H2.3
 WESTENDORP, J.F.M., A9.47
 WESTERFIELD, CURTIS, Q13.1
 WESTWOOD, ALISTAIR D., K5.4,
 K6.6
 WESTWOOD, DAVID I., D11.11
 WEYERS, M., D11.10
 WEYEN, H., M7.170
 WHALEY, G.J., D8.2
 WHANG, C.N., A6.10, A6.18
 WHEALON, W.J., K7.5
 WHEAT, HAROVEL G., Y3.6
 WHEELER, A.P., R5.8
 WHEELER, NEA S., N2.10
 WHITE, ALICE E., A2.9, B4.10
 WHITE, B.E., N5.17
 WHITE, C.W., A7.2, A8.3, A9.34,
 A9.37
 WHITE, J.W., J1.9
 WHITE, KENNETH M., S2.6
 WHITE, T.J., M7.7
 WHITE, W.B., F2.5
 WHITEHAIR, S.J., F5.4
 WHITESIDES, GEORGE M., B5.7,
 R3.1
 WHITTAKER, E.A., L2
 WICHERT, TH., G5.5
 WIE, C.R., D7.7, D10.34, D10.36,
 D10.37
 WIENER, M.C., V2.1
 WIESMANN, H., M7.164
 WIFF, D.R., O4.5
 WIGHT, JOHN F., T3.8
 WIJARANAKULA, W., G18.1
 WILBY, M.R., C8.4
 WILCOXON, J.P., V5.7
 WILDE, D.K., M7.173, M7.211
 WILDING, C.R., U7.8
 WILKENS, B.J., D1.2, I2.7,
 M7.224, M11.1
 WILKES, G.L., O1.2, S3.5, S5.8
 WILKINS, B., C11.2
 WILLANDER, MAGNUS, F8.5, Q7.10,
 Q7.18
 WILLE, L.T., M7.108
 WILLIAMS, C., N2.7
 WILLIAMS, CLAUDINE E., O5.4
 WILLIAMS, G.M., E5.5
 WILLIAMS, GRAHAM, S4.1
 WILLIAMS, J.M., Q5.2
 WILLIAMS, J.R., P5.1
 WILLIAMS, J.S., A2.2, A2.7,
 A8.1, A8.9
 WILLIAMS, JOEL M., O2.2
 WILLIAMS, JOHN G., N1.6
 WILLIAMS, K.E., M7.198
 WILLIAMS, MARK E., R3.5
 WILLIAMS, NEIL, Q13.13
 WILLIAMS, R.L., D10.35, G13.3
 WILLIAMS, R.K., M7.258
 WILLIAMS, R. STANLEY, A5.4,
 C9.10, D10.4, D10.28
 WILLIAMS, ROBIN H. D11.11
 WILLIAMSON, R., V5.7
 WILLIS, C.L., O5.2
 WILLIS, J.N., D10.44, T8.6
 WILLNER, LUTZ, S4.9
 WILNER, M., F3.5, G9.28
 WILSON, A., B1.2
 WILSON, CHARLES N., U8.5
 WILSON, FRANK C., O8.7
 WILSON, J.I.B., B5.22, B7.9
 WILT, D.P., D10.50
 WILTZIUS, P., J7.8, J7.9
 WINDLE, ALAN H., S5.1
 WINKER, K., A9.4, H3.4
 WINEY, KAREN I., O5.8
 WINOGRAD, NICHOLAS, A6.22
 WINSLOW, D., Y2.2
 WINTER, H.H., V5.1
 WISE, SEAN, Y2.1
 WISTROM, RICHARD E., A3.8
 WITANACHCHI, S., M7.167, M7.191,
 M7.212, M7.237, M7.249
 WITHROW, S.P., A2.10, A7, F8.6
 WITTEN, T.A., V7.1
 WITTMER, M., C5.5, G10.3
 WITUCHI, E.F., Q9.12
 WOLD, A., E10.7
 WOLF, S.A., M7.17
 WOLFE, A., T7.36
 WOLFE, JAMES F., Q9.3
 WOLFF, P.A., E9.1, E10.2
 WOLFF, S., H3.1
 WOLFORD, D.J., G, G1, G1.4,
 G3.1, G9, G14.5
 WOLKOW, EUGENE, L6.10, L6.11
 WONG, CHI-HUEY, R4.3
 WONG, D., G9.23
 WONG, GEORGE K., Q13.6
 WONG, K.W., M7.6
 WONG, PETER, L6.10
 WONG, S.K., H6.15
 WONG, S.P., F5.15
 WONG-NG, WINNIE, M6.4, M7.100,
 M7.111, M7.154, M7.256
 WOO, J.J., A6.18
 WOOLF, DAVID A., D11.11
 WOOLAM, JOHN A., D12.6, G18.45
 WORBOYS, MICHAEL R., S2.9
 WORCESTER, D.L., R6.8
 WORLOCK, J.M., D12.8, D12.9
 WORMHOUDT, JODA C., I1.4
 WORMUTH, KLAUS, R., V7.6
 WORONIECKA, JULITA E., B4.10
 WORTHINGTON, T.K., M7.112
 WORTMAN, J.J., B6.9
 WORZALA, FRANK, A9.31
 WRIGHT, ALBERT F., J4.12
 WRIGHT, P.J., E5.5
 WRIGHT, W.H., E7.8
 WRIGHTON, MARK S., B5.7, Q3.6
 WRÓBEL, J., G16.2
 WRÓBEL, J.M., E9.9
 WRÓBEL, S., Q9.8
 WRONKIEWICZ, D.J., U7.17
 WRONSKI, C.R. F4.2, XNF1.2
 WU, C.H., F5.14
 WU, C.M., M7.178
 WU, CHUN-GUEY, Q3.5
 WU, D.T., O7.9
 WU, DAN Q., O5.5, O6
 WU, DONG HO, M1.10
 WU, J., D9.3, G18.49
 WU, J.M., Q1.3
 WU, JIN, M7.116
 WU, KE, M7.145
 WU, M.F., A2.12, D10.30
 WU, NAI-LIH, M7.152
 WU, P.T., M5.3, M7.161
 WU, RENJIE, N2.11
 WU, RONGZHI, G18.27
 WU, T.B., M7.178
 WU, WEN-LI, J6.3, O3.11, O4
 WU, X.-M., P5.17
 WU, X.D., M3.2, M7.202, M7.208,
 M7.224, M7.232, M7.234,
 M7.235, M7.246
 WU, X.S., B5.3
 WU, YEUN-JUNG, D9.1, H3.9
 WU, Z.L., M7.23
 WU, Z.Q., D11.4
 WUDL, FRED, Q2, Q8.3
 WUENSCH, B., J5
 WUENSCH, B.J., J1.8
 WUENSCH, DARRELL L., B6.6
 WUYTS, B., M7.75
 WUYTS, K., A10.10
 WYNN, J.D., A9.26
 XI, WANG, A6.30
 XI, X.X., A7.1
 XI, X.X., M3.2, M5.5, M7.209
 XIA, W., A7.6
 XIANGHUAL, LIU, A6.30
 XIAO, Q.P., D1.11, D10.3, D10.8
 XIAO, TONGSAN D., L5.8
 XIAO, ZHIGANG, G18.29
 XIAOLIAN, SHEN, D10.7
 XIE, LIKE, Y1.3
 XIE, K.M., M7.23
 XIE, Y.-H., D5.5
 XIN, PU, F3.18, F3.19
 XIN, XU, B7.8
 XING, G.C., F9.9
 XIU, L.S., D11.4
 XU, HONGGI, G18.23
 XU, J.J., L6.3, L6.4
 XU, JING-CHUN, Q4.5
 XU, M., K3.3
 XU, MING, M7.131
 XU, REN, M9.7
 XU, X.L., A9.49
 XU, YOUWEN, C9.23, M7.18,
 M7.57, M7.88
 XU, Z., M7.133
 XU, ZHENG, B4.8
 XU, ZI-RAN, M7.109
 XUE, LIXIN, M7.145
 YACAMÁN, MIGUEL JOSE, C13.2,
 M7.119, R2.7, V9.10
 YAGUBSKII, E.B., Q5.1
 YALAN, XU, M4.9
 YALISOVE, S.M., C4.3, C10.1,
 D1.5
 YAMADA, A., G3.3, G3.4, G9.40
 YAMADA, AKIRA, C9.11, S2.2,
 S2.8, Q9.6
 YAMADA, I., A6.41
 YAMADA, SHINJI, Q9.6
 YAMADA, TADATOSHI, M7.16
 YAMADA, YOICHI, E5.6
 YAMADA, YUTAKA, M7.22
 YAMAGA, S., E5.2
 YAMAGATA, K., H7.7
 YAMAGUCHI, K., M7.58
 YAMAGUCHI, T., F6.14, M7.181
 YAMAHITA, T., M2.9
 YAMAJI, K., Q4.3
 YAMAMOTO, JOYCE, P8.2
 YAMAMOTO, K., M5.6
 YAMAMOTO, K., M7.162
 YAMAMOTO, TAKASHI, P7.1
 YAMAMOTO, Y., C10.6, D10.1,
 F8.5
 YAMASHITA, HIROSHI, M7.62
 YAMASHITA, TOMOHISA, M7.22
 YAMASUCHI, H., M2.9
 YAMAUCHI, SATOSHI, E4.3
 YAMAWAKI, H., M10.12
 YAMAZAKI, MASAHITO, Q12.9
 YAMAZAKI, SHUMPEI, F5.9
 YAMACHI, H., Q4.7
 YAMACHI, HIDEKI, Q8.3
 YAN, B.D., D10.24
 YAN, T., M7.206
 YANAGISAWA, E., M4.3
 YANASE, N., U7.34
 YANG, A.B., M7.3
 YANG, BING, F3.10
 YANG, C.S., M7.179
 YANG, C.Y., M7.88
 YANG, CHIH H., A1.3
 YANG, E.H., M11.9
 YANG, G.-R., F5.17, H6.15
 YANG, HSINJIN, J6.5
 YANG, J., F8.3
 YANG, J.C., O4.3
 YANG, JIAN, Q13.6
 YANG, KAI-YUEH, M5.4
 YANG, LINA, Q13.9
 YANG, S.J., M7.244
 YANG, SZE CHENG, Q3.3, Q3.8,
 Q7, Q7.8
 YANG, X.Q., Q6.1
 YANG, Y.C., F3.5
 YANG, YING-HU, F3.10
 YANG, Z., E6.7, E8.7, E9.5
 YAO, GONG-DA, D9.3, D10.29,
 G18.49
 YAO, HUADE D., A9.7, G15.5
 YAO, J.Y., C11.3
 YAO, P.C., M7.153, M7.244
 YAO, T., E4.5
 YAO, Y.D., M7.152, M7.71,
 M7.244
 YARBROUGH, WALTER A., F1.3
 YARDLEY, JAMES T., Q9.5
 YAROSHETSKII, I.D., E5.9
 YASUMATSU, TATSURO, H3.7
 YAZDANIAN, MEHRAN, V8.11
 YE, L., V7.9
 YEH, MILDRED, B3.12
 YEH, N.C., M1.6
 YEH, T., F3.8
 YEN, TYAN-YWAN, L4.2
 YI, G.-J., E4.2
 YI, JAY J.L., P6.3, P6.6
 YIN, X., D8.4, D12.7
 YING, HAN, H6.7
 YING, Q.Y., B7.2, M1.7, M3.7,
 M7.230, M11.10
 YING, WEN ZHI, T7.15
 YIP, P.W., N4.4
 YIRU, ZHOU, M4.9
 YOKOH, YASUHIKO, S4.7
 YOKOTA, YOSHIHIRO, F2.8, F4.6,
 F5.7
 YOKOYAMA, SHOICHI, M7.16
 YONEDA, ERIKO, M7.22
 YONEHARA, T., F4.6, H7.7
 YONEKAWA, MASARU, B2.10, B4.11
 YONEMITSU, T., A6.41
 YONETA, MINORU, G18.25
 YONG, R.N., U7.42
 YOO, WOO SIK, F6.4
 YOON, D.Y., O3.8
 YOON, HAN SIK, R6.6
 YOSHIDA, KIICHI, M7.53
 YOSHIDA, S., F6.12
 YOSHIDA, ZEN-ICHI, Q2.1
 YOSHIKAWA, A., E5.2
 YOSHIKAWA, K., M7.199
 YOSHINO, HISASHI, M7.22
 YOSHINO, J., G15.2
 YOSHINO, K., Q6.6
 YOSHIZAKI, KIYOSHI, M7.53
 YOUNG, J. FRANCIS, Y2.2, Y4.1,
 Y4.4, Y4.6
 YOUNGDAHL, C.A., M7.8
 YOUNGDAHL, KAY, O1.3
 YOUNGDALE, E.R., E9.2
 YOUNGMAN, R.A., K5.2, K6.7
 YOUSHAN, CHEN, A6.30
 YOUYI, CHU, C9.19
 YU, A.J., D5.3
 YU, C.F., E4.2
 YU, HYUK, V8.11
 YU, JAOHUA, E10.3
 YU, J., Q13.8
 YU, LUPING, Q12.13, S2.3, S5.6
 YU, NING, A7.9
 YU, SHAOFENG, G9.5
 YU, T.H., D7.2
 YU, XIAOHUA, C3.5, E7.6, E10.3
 YU, Z., I4.4
 YUDASAKA, MASAKO, Q4.7, Q5.4
 YUE, A.S., M7.179
 YUEHUI, YU, A6.31
 YUGAI, V.M., A9.39
 YUJING, HUO, M7.242
 YUN, HEE MANN, N1.7
 YUN, SUN JIN, B5.13
 YUN, W.B., O7.5
 YUSA, Y., U7.40
 YUSHENG, HE, M6.11, M7.242
 YUZUN, GAO, G18.20
 ZABEL, H., J2.4
 ZACHARIAH, M.R., L1.4
 ZAHN, DIETRICH R.T., D11.11
 ZAHURAK, S., M7.33
 ZAIDI, M.A., G4.5
 ZAJAC, GERRY W., B6.6
 ZAK, OMER, V6.9
 ZAKUTAEV, A.N., A6.29
 ZANA, R., V3.2
 ZANDER, W., M3.6
 ZANDIAN, M., E6.4
 ZAROVSKI, D.I., C9.36
 ZAWADZKI, P., M5.13
 ZAWISLAK, F.C., A9.58
 ZAZOUI, MIMOUN, G15.3
 ZEICHNER-DAVID, MARGARITA, R1.2
 ZEIDLER, J.R., P5.6
 ZIEGLER, J.M., Q10.11
 ZELLER, M.V., F6.11
 ZEMANSKI, JOHN M., G9.6
 ZENON, S., G3.2, P9.4, P9.5
 ZENG, HANMIN, N4.10
 ZHANG, B.X., A8.6
 ZHANG, DAN, Q3.3
 ZHANG, FANG-QING, F3.10
 ZHANG, GUODING, M2.11
 ZHANG, HONGMEI, K4.4
 ZHANG, J.M., M7.251, M10.3
 ZHANG, J.P., A9.59
 ZHANG, JINOWEN, M7.41

ZHANG, JIZHONG, T7.34
 ZHANG, KAIMING, P8.8
 ZHANG, LIJIE, M4.2
 ZHANG, M.-X., K7.4, N5.12
 ZHANG, MINGQIU, N4.10
 ZHANG, S.-L., L3.4
 ZHANG, X., D10.35
 ZHANG, X-G., C13.7
 ZHANG, XIANG-HUA, P6.4, P6.7
 ZHANG, XINGHUA, O5.11
 ZHANG, Y.-J., M4.13
 ZHANG, Y.-Z., M7.168
 ZHANG, YANPING, B7.5
 ZHAO, B.-R., M71.68
 ZHAO, HONG, T6.3
 ZHAO, HUAMING, T6.6, T7.13
 ZHAO, J., M7.31, M7.180, M7.251
 ZHAO, JIARONG, A9.12
 ZHAO, JIN, C9.3, Y2.3
 ZHAO, MEIYU, M7.73
 ZHAO, O.-X., D10.42, G14.4
 ZHAO, X., O7.5
 ZHAO, XUE-SHU, H2.4
 ZHAO, YONG, G18.45
 ZHAO, ZHONG-XIAN, M7.250
 ZHAO, ZHONGXIAN, M7.41
 ZHENG, HAIKING, M9.7, P7.4, S3.4
 ZHENG, J.-P., B7.2, M7.230,
 M11.10
 ZHENG, J.-Q., M9.2
 ZHENG, LONGRU, G9.13, G9.17
 ZHENG, X.-L., E10.4, E10.7
 ZHENG, XIAOCI, A9.31
 ZHENG, Y., M2.10, M6.7, M7.38
 ZHENWU, XUAN, F3.18, F3.19
 ZHONG, LONG-GUI, O8.3, Q3.13
 ZHONG, Y., B6.9
 ZHONG, ZIYANG, R4.3
 ZHOU, D., M7.70
 ZHOU, DERONG, M7.42
 ZHOU, L., M7.168
 ZHOU, TIAN-QUN, G18.29
 ZHOU, W., A7.10
 ZHOU, W., D12.9
 ZHOU, X., L5.12
 ZHOU, Y., M7.2
 ZHU, J., G11.3
 ZHU, JANE G., C4.4, D1.3, D10.5,
 D10.22, G9.42
 ZHU, JIN-SONG, M7.116
 ZHU, Y., C9.23
 ZHU, Y.-Z., M7.212, M7.237,
 M7.191
 ZHUANG, W.-H., D11.4
 ZIEGLER, C.-K., E2.6
 ZIELINSKI, W., D4.5
 ZIFF, ROBERT M., T8.4
 ZINCK, J.-J., B1.7
 ZINGG, RENE P., B4.3
 ZINOV'EV, N.-N., E5.9
 ZIWEI, FANG, A9.48
 ZNIBER, K., Q10.7
 ZOCCO, T.-G., A9.19
 ZOGRAPF, GEORGE, V8.11
 ZOK, F.-W., N7.4
 ZOLLNER, STEFAN, H6.1
 ZOU, C., B5.7
 ZUCKERMAN, E.-B., T1.8
 ZUHR, RAY A., A, A1, A6, A7.4,
 A9, A9.17, F8.6
 ZUMSTEG, F.-C., Q9.2
 ZUNDEL, T., G7.6
 ZURZ, ALFRED, Y1.5
 ZUYAO, ZHOU, A9.20, A9.48, A9.49
 ZWEIBEL, KENNETH, E5.4
 ZYSS, J., Q9, Q9.1, Q12.7

■ MRS PUBLICATIONS ■

MRS Symposium Proceedings

Volume

- 1—Laser and Electron-Beam Solid Interactions and Materials Processing
- 2—Defects in Semiconductors
- 3—Nuclear and Electron Resonance Spectroscopies Applied to Materials Science
- 4—Laser and Electron-Beam Interactions with Solids
- 5—Grain Boundaries in Semiconductors
- 6—Scientific Basis for Nuclear Waste Management IV
- 7—Metastable Materials Formation by Ion Implantations
- 8—Rapidly Solidified Amorphous and Crystalline Alloys
- 9—Materials Processing in the Reduced Gravity Environment of Space
- 10—Thin Films and Interfaces
- 11—Scientific Basis for Nuclear Waste Management V
- 12—In Situ Composites IV
- 13—Laser-Solid Interactions and Transient Thermal Processing of Materials
- 14—Defects in Semiconductors II
- 15—Scientific Basis for Nuclear Waste Management VI
- 16—Nuclear Radiation Detector Materials
- 17—Laser Diagnostics and Photochemical Processing for Semiconductor Devices
- 18—Interfaces and Contacts
- 19—Alloy Phase Diagrams
- 20—Intercalated Graphite
- 21—Phase Transformations in Solids
- 22—High Pressure in Science and Technology
- 23—Energy Beam-Solid Interactions and Transient Thermal Processing
- 24—Defect Properties and Processing of High-Technology Nonmetallic Materials
- 25—Thin Films and Interfaces II
- 26—Scientific Basis for Nuclear Waste Management VII
- 27—Ion Implantation and Ion Beam Processing of Materials
- 28—Rapidly Solidified Metastable Materials
- 29—Laser-Controlled Chemical Processing of Surfaces
- 30—Plasma Processing and Synthesis of Materials
- 31—Electron Microscopy of Materials
- 32—Better Ceramics Through Chemistry
- 33—Comparison of Thin Film Transistor and SOI Technologies

Volume

- 34—The Physical Metallurgy of Cast Iron
- 35—Energy Beam-Solid Interactions and Transient Thermal Processing/1984
- 36—Impurity Diffusion and Gettering in Silicon
- 37—Layered Structures, Epitaxy, and Interfaces
- 38—Plasma Synthesis and Etching of Electronic Materials
- 39—High-Temperature Ordered Intermetallic Alloys
- 40—Electronic Packaging Materials Science
- 41—Advanced Photon and Particle Techniques for the Characterization of Defects in Solids
- 42—Very High Strength Cement-Based Materials
- 43—Fly Ash and Coal Conversion By-Products: Characterization, Utilization, and Disposal
- 44—Scientific Basis for Nuclear Waste Management VIII
- 45—Ion Beam Processes in Advanced Electronic Materials and Device Technology
- 46—Microscopic Identification of Electronic Defects in Semiconductors
- 47—Thin Films: The Relationship of Structure to Properties
- 48—Applied Materials Characterization
- 49—Materials Issues in Applications of Amorphous Silicon Technology
- 50—Scientific Basis for Nuclear Waste Management IX
- 51—Beam-Solid Interactions and Phase Transformations
- 52—Rapid Thermal Processing
- 53—Semiconductor-on-Insulator and Thin Film Transistor Technology
- 54—Thin Films—Interfaces and Phenomena
- 55—Biomedical Materials
- 56—Layered Structures and Epitaxy
- 57—Phase Transitions in Condensed Systems—Experiments and Theory
- 58—Rapidly Solidified Alloys and Their Mechanical and Magnetic Properties
- 59—Oxygen, Carbon, Hydrogen, and Nitrogen in Crystalline Silicon
- 60—Defect Properties and Processing of High-Technology Nonmetallic Materials
- 61—Defects in Glasses
- 62—Materials Problem Solving with the Transmission Electron Microscope
- 63—Computer-Based Microscopic Description of the Structure and Properties of Materials

For more information stop by the MRS Publications Desk or contact the MRS Publications Dept., 9800 McKnight Road, Pittsburgh, PA 15237; phone 412-367-3012; fax 412-367-4373.

■ MRS PUBLICATIONS ■

Volume

- 64—Cement-Based Composites: Strain Rate Effects on Fracture
- 65—Fly Ash and Coal Conversion By-Products: Characterization, Utilization and Disposal II
- 66—Frontiers in Materials Education
- 67—Heteroepitaxy on Silicon Technology
- 68—Plasma Processing
- 69—Materials Characterization
- 70—Materials Issues in Amorphous-Semiconductor Technology
- 71—Materials Issues in Silicon Integrated Circuit Processing
- 72—Electronic Packaging Materials Science II
- 73—Better Ceramics Through Chemistry II
- 74—Beam-Solid Interactions and Transient Processes
- 75—Photon, Beam and Plasma Stimulated Chemical Processes at Surfaces
- 76—Science and Technology of Microfabrication
- 77—Interfaces, Superlattices, and Thin Films
- 78—Advances in Structural Ceramics
- 79—Scattering, Deformation and Fracture in Polymers
- 80—Science and Technology of Rapidly Quenched Alloys
- 81—High-Temperature Ordered Intermetallic Alloys, II
- 82—Characterization of Defects in Materials
- 83—Physical and Chemical Properties of Thin Metal Overlayers and Alloy Surfaces
- 84—Scientific Basis for Nuclear Waste Management X
- 85—Microstructural Development During the Hydration of Cement
- 86—Fly Ash and Coal Conversion By-Products: Characterization, Utilization and Disposal III
- 87—Materials Processing in the Reduced Gravity Environment of Space
- 88—Optical Fiber Materials and Properties
- 89—Diluted Magnetic (Semimagnetic) Semiconductors
- 90—Materials for Infrared Detectors and Sources
- 91—Heteroepitaxy on Silicon Technology II
- 92—Rapid Thermal Processing of Electronic Materials
- 93—Materials Modification and Growth Using Ion Beams
- 94—Initial Stages of Epitaxial Growth
- 95—Amorphous Silicon Semiconductors—Pure and Hydrogenated
- 96—Permanent Magnet Materials
- 97—Novel Refractory Semiconductors
- 98—Plasma Processing and Synthesis of Materials

Volume

- 99—High-Temperature Superconductors
- 100—Fundamentals of Beam-Solid Interactions and Transient Thermal Processing
- 101—Laser and Particle-Beam Chemical Processing for Microelectronics
- 102—Epitaxy of Semiconductor Layered Structures
- 103—Multilayers: Synthesis, Properties, and Nonelectronic Applications
- 104—Defects in Electronic Materials
- 105—SiO₂ and Its Interfaces
- 106—Polysilicon Films and Interfaces
- 107—Silicon-on-Insulator and Buried Metals in Semiconductors
- 108—Electronic Packaging Materials Science III
- 109—Nonlinear Optical Properties of Polymers
- 110—Biomedical Materials and Devices
- 111—Microstructure and Properties of Catalysts
- 112—Scientific Basis for Nuclear Waste Management XI
- 113—Fly Ash and Coal Conversion By-Products: Characterization, Utilization, and Disposal IV
- 114—Bonding in Cementitious Composites
- 115—Specimen Preparation for Transmission Electron Microscopy of Materials
- 116—Heteroepitaxy on Silicon: Fundamentals, Structures, and Devices
- 117—Process Diagnostics
- 118—Amorphous Silicon Technology
- 119—Adhesion in Solids
- 120—High-Temperature/High-Performance Composites
- 121—Better Ceramics Through Chemistry III
- 122—Interfacial Structure, Properties, and Design
- 123—Materials Issues in Art and Archaeology
- 124—Microwave Processing of Materials
- 125—Materials Stability and Environmental Degradation
- 126—Advanced Surface Processes for Optoelectronics
- 127—Scientific Basis for Nuclear Waste Management XII
- 128—Processing and Characterization of Materials Using Ion Beams
- 129—Laser and Particle-Beam Modification of Chemical Processes on Surfaces
- 130—Thin Films: Stresses and Mechanical Properties
- 131—Chemical Perspectives of Microelectronic Materials
- 132—Multicomponent Ultrafine Microstructures
- 133—High Temperature Ordered Intermetallic Alloys III

For more information stop by the MRS Publications Desk or contact the MRS Publications Dept., 9800 McKnight Road, Pittsburgh, PA 15237; phone 412-367-3012; fax 412-367-4373.

■ MRS PUBLICATIONS ■

Volume

- 134—**The Materials Science and Engineering of Rigid-Rod Polymers**
- 135—**Solid State Ionics**
- 136—**Fly Ash and Coal Conversion By-Products: Characterization, Utilization and Disposal V**
- 137—**Pore Structure and Permeability of Cementitious Materials**
- 138—**Characterization of the Structure and Chemistry of Defects in Materials**
- 139—**High Resolution Microscopy of Materials**
- 140—**New Materials Approaches to Tribology: Theory and Applications**
- 141—**Atomic Scale Calculations in Materials Science**
- 142—**Non-Destructive Monitoring of Materials Properties**
- 143—**Synchrotron Radiation in Materials Research**
- 144—**Advances in Materials, Processing and Devices in III-V Compound Semiconductors**
- 145—**III-V Heterostructures for Electronic/Photonic Devices**
- 146—**Rapid Thermal Annealing/Chemical Vapor Deposition and Integrated Processing**
- 147—**Ion Beam Processing of Advanced Electronic Materials**
- 148—**Chemistry and Defects in Semiconductor Heterostructures**
- 149—**Amorphous Silicon Technology 1989**
- 150—**Materials for Magneto-Optic Data Storage**
- 151—**Growth, Characterization, and Properties of Ultrathin Magnetic Films and Multilayers**
- 152—**Optical Materials: Processing and Science**
- 153—**Interfaces between Polymers, Metals, and Ceramics**
- 154—**Electronic Packaging Materials Science IV**
- 155—**Processing Science of Advanced Ceramics**
- 156—**High Temperature Superconductors: Relationships between Properties, Structure, and Solid-State Chemistry**

Proceedings from the 1989 MRS Fall Meeting

Titles from the 1989 Fall Meeting are available for a limited time at special pre-publication prices. Place your advance order during the meeting at the MRS Publications Desk, or contact MRS.

Volume/Symposium

- 157/A—**Beam Solid Interactions: Physical Phenomena**, J.A. Knapp, P. Borgesen, R.A. Zehr, 1990
- 158/B—**In-Situ Patterning: Selective Area Deposition and Etching**, R. Rosenberg, A.F. Bernhardt, J.G. Black, 1990
- 159/C—**Atomic Scale Structure of Interfaces**, R.D. Bringans, R.M. Feenstra, J.M. Gibson, 1990

- 160/D—**Layered Structures: Heteroepitaxy, Superlattices, Strain, and Metastability**, B.W. Dodson, L.J. Schowalter, J.E. Cunningham, F.H. Pollak, 1990
- 161/E—**Properties of II-VI Semiconductors: Bulk Crystals, Thin Films, Quantum Well Structures and Dilute Magnetic Systems**, J.F. Schetzina, F.J. Bartoli, Jr., H.F. Schaake, 1990
- 162/F—**Diamond, Boron Nitride, Silicon Carbide and Related Wide Bandgap Semiconductors**, J.T. Glass, R.F. Messier, N. Fujimori, 1990
- 163/G—**Impurities, Defects and Diffusion in Semiconductors: Bulk and Layered Structures**, J. Bernholc, E.E. Haller, D.J. Wolford, 1990
- 164/H—**Materials Issues in Microcrystalline Semiconductors**, P.M. Fauchet, C.C. Tsai, K. Tanaka, 1990
- 165/I—**Characterization of Plasma-Enhanced CVD Processes**, D.E. Ibbotson, D.W. Hess, G. Lucovsky, 1990
- 166/J—**Neutron Scattering for Materials Science**, S.M. Shapiro, S.C. Moss, J.D. Jorgensen, 1990
- 167/K—**Advanced Electronic Packaging Materials**, J. Partridge, C-Y. Li, C.J. Chen, A. Barfknecht, 1990
- 168/L—**Chemical Vapor Deposition of Refractory Metals and Ceramics**, T.M. Besmann, B.M. Gallois, 1990
- 169/M—**High Temperature Superconductors: Fundamental Properties and Novel Materials Processing**, J. Narayan, C.W. Chu, L.F. Schneemeyer, D.K. Christen, 1990
- 170/N—**Tailored Interfaces in Composite Materials**, C.G. Pantano, E.J.H. Chen, 1990
- 171/O—**Polymer Based Molecular Composites**, D.W. Schaefer, J.E. Mark, 1990
- 172/P—**Optical Fiber Materials and Processing**, J.W. Fleming, G.H. Sigel, S. Takahashi, P.W. France, 1990
- 173/Q—**Electrical, Optical and Magnetic Properties of Organic Solid-State Materials**, L.Y. Chiang, D.O. Cowan, P. Chaikin, 1990
- 174/R—**Materials Synthesis Utilizing Biological Processes**, P.D. Calvert, M. Alper, P.C. Rieke, 1990
- 175/S—**Multi-Functional Materials**, D.R. Ulrich, F.E. Karasz, A.J. Buckley, G. Gallagher-Daggitt, 1990
- 176/U—**Scientific Basis for Nuclear Waste Management XIII**, V.M. Oversby, P.W. Brown, 1990
- 177/V—**Macromolecular Liquids**, C.R. Safinya, S.A. Safran, P.A. Pincus, 1990
- 178/W—**Fly Ash and Coal Conversion By-Products: Characterization, Utilization and Disposal VI**, R.L. Day, F.P. Glasser, 1990
- 179/Y—**Specialty Cements with Advanced Properties**, H. Jennings, A.G. Landers, B.E. Scheetz, I. Odler, 1990

For more information stop by the MRS Publications Desk or contact the MRS Publications Dept., 9800 McKnight Road, Pittsburgh, PA 15237; phone 412-367-3012; fax 412-367-4373.

■ MRS PUBLICATIONS ■

Volume

- EA-1—Laser Chemical Processing of Semiconductor Devices
- EA-2—Graphite Intercalation Compounds
- EA-3—Alloy Phase Diagrams
- EA-4—Fractal Aspects of Materials: Metal and Catalyst Surfaces, Powders and Aggregates
- EA-5—Beam Induced Chemical Processes
- EA-6—Fractal Aspects of Materials
- EA-7—Nonlinear Optical Materials
- EA-8—Graphite Intercalation Compounds
- EA-9—Superconducting Materials
- EA-10—Fractal Aspects of Materials II
- EA-11—High Temperature Superconductors

Extended Abstracts

Volume

- EA-12—Structure-Property Relationships in Optical Materials
- EA-13—Fractal Aspects of Materials: Disordered Systems
- EA-14—High-Temperature Superconductors
- EA-15—Diamond and Diamond-Like Materials Synthesis
- EA-16—Graphite Intercalation Compounds: Science and Applications
- EA-17—Fractal Aspects of Materials: Disordered Systems
- EA-18—Selected Topics in Electronic Materials
- EA-19—Technology Update on Diamond Films
- EA-20—Fractal Aspects of Materials (from 1989 Fall Meeting)

MRS Communications

Communications on the Materials Science and Engineering Study, compiled by MRS, 1986

MRS Conference Proceedings

Code

- VLSI—Tungsten and Other Refractory Metals for VLSI Applications
- VLSI II—Tungsten and Other Refractory Metals for VLSI Applications II
- TMC—Ternary and Multinary Compounds
- V-III—Tungsten and Other Refractory Metals for VLSI Applications III

Code

- AMEC—Atomic and Molecular Processing of Electronic and Ceramic Materials: Preparation, Characterization and Properties
- MFSO—Materials Futures: Strategies and Opportunities
- V-IV—Tungsten and Other Refractory Metals for VLSI Applications IV

Proceedings of the MRS International Meeting on Advanced Materials

(May 30-June 3, 1988 in Tokyo, Japan)

- IMAM-1—Symposium N: Biomaterials; Symposium P: Ionic Polymers; Symposium Q: Ordered Polymers for High Performance Materials
- IMAM-2—Symposium I: Hydrogen-Absorbing Materials; Symposium O: Catalytic Materials
- IMAM-3—Symposium B: Rapid Quenching; Symposium C: Powder Preparation
- IMAM-4—Symposium A: Composites; Symposium G: Corrosion/Coating of Advanced Materials
- IMAM-5—Symposium J: Structural Ceramics; Symposium M: Fracture Mechanics
- IMAM-6—Symposium D: Superconductivity

- IMAM-7—Symposium E: Superplasticity
- IMAM-8—Symposium F: Joints of Metals and Ceramics
- IMAM-9—Symposium H: Shape Memory Materials
- IMAM-10—Symposium K: Multilayers
- IMAM-11—Symposium L: Microstructure-Property Relationship in Magnetic Materials
- IMAM-12—Symposium R: Photoresponsive Materials
- IMAM-13—Symposium S: Advanced Cements and Chemically Bonded Ceramics
- IMAM-14—Symposium T: Biosensors

Also available: ICEM-International Conference on Electronic Materials

(June 13-15, 1988, Tokyo, Japan)

For more information stop by the MRS Publications Desk or contact the MRS Publications Dept., 9800 McKnight Road, Pittsburgh, PA 15237; phone 412-367-3012; fax 412-367-4373.

FRONTIERS of MATERIALS SCIENCE

Tutorials on the "frontier topics" of materials research
available from MRS on VHS and U-Matic.

TITLE AND SPEAKER

Defect Engineering in Semiconductors
(H.C. Gatos, MIT)

Recent Advances in Polymers
(H. Mark, Polytechnic Institute of New York)

Superconductor Design and Application
(E.W. Collings, Battelle Columbus Laboratories)

Tribology Update
(K.C. Ludema, University of Michigan)

Mechanics of Electronic Packaging Materials
(H. Hieber, Philips GmbH)

A Case History of Materials Development:
Optical Fibers
(J.B. MacChesney, AT&T Bell Laboratories)

State of the Art Non-Destructive Evaluation
(R. Green, Jr., Johns Hopkins University)

New Materials Technology for Highways
(R. Decker, University Science Partners)

Fractals and Disorderly Growth (P. Meakin, E.I. duPont de
Nemours & Company)

Ultrathin Film Growth from Langmuir Blodgett to Self-Assembly
(A. Ulman, Eastman Kodak Company)

Failure Analysis in Materials Research
(M. Louthan Jr., Savannah River Laboratory)

Properties of Hydrogenated Amorphous Silicon
(R. A. Street, Xerox Palo Alto Research Center)

Also available on VHS and U-Matic: "High Temperature Superconductors," tapes of two recent MRS Symposia;
and Linus Pauling's Plenary Address at the 1989 MRS Spring Meeting.

*The new, comprehensive
monograph by two
respected authorities
in the field...*

ATOM PROBE MICROANALYSIS:

Principles and Applications to Materials Problems

by
M.K. Miller, Oak Ridge National Laboratory
G.D.W. Smith, University of Oxford

Comprehensive coverage.

The first monograph to address this increasingly important subject, *Atom Probe Microanalysis* offers a practical guide to the process and technique of studying materials at the atomic level. It provides an up-to-date introduction for nonspecialists as well as helpful reference for those already working in the field.

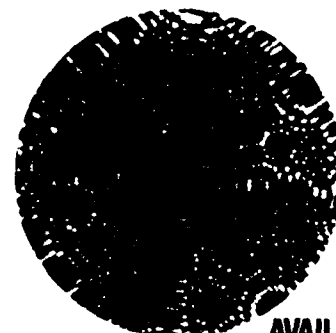
Excellent for classroom use.

Material presented in *Atom Probe Microanalysis* has been successfully tested in the classroom. Drs. Miller and Smith introduced their popular short course on the atom probe at the 1987 MRS Fall Meeting in Boston, and since that time the book has served as a core reference for that class.

Course Review Copies:

Instructors may examine *Atom Probe Microanalysis* at no charge for 15 days. Contact the MRS Publications Department at (412) 367-3012 for details.

**Visit the MRS
Publications Desk
for more information**



**AVAILABLE
ONLY FROM THE
MATERIALS
RESEARCH SOCIETY**

Order Information:

Atom Probe Microanalysis
ISBN: 0-931837-99-5
Order Code: APM
\$40.00 MRS Members
\$47.00 U.S. List
\$56.00 Elsewhere

MRS accepts check or money order (payable in U.S. Dollars), purchase order, and Visa, MasterCard and Diner's Club cards. Order from the Materials Research Society, Publications Department, 9800 McKnight Road, Pittsburgh, PA 15237 U.S.A., telephone (412) 367-3012; fax (412) 367-4373.

*In Europe, Africa, and the Middle East order from: Clarke Associates Europe Ltd, 13a Small Street, Bristol BS1 1DE, England, telephone 0272 268964, Fax 0272 226437

■ 1990 SPRING MEETING ■

April 16-21, San Francisco, California

Meeting Chairs

John C. Bravman
Stanford University
Department of Materials
Science & Engineering
Building 550
Stanford, CA 94305
Telephone (415) 723-3698
FAX (415) 725-4034

C. Jeffrey Brinker
Sandia National Laboratories
Division 1846
P.O. Box 5800
Albuquerque, NM 87185
Telephone (505) 846-3552
FAX (505) 846-5064

William H. Butler
Oak Ridge National Laboratory
Building 4500S
P.O. Box 2008, MS 114
Oak Ridge, TN 37831-6114
Telephone (615) 574-4845
FAX (615) 574-7721

SYMPOSIUM A

BETTER CERAMICS THROUGH CHEMISTRY IV

C.J. Brinker, Sandia National Laboratories,
(505) 846-3552, FAX (505) 846-5064
D.E. Clark, University of Florida, (904) 392-7660,
FAX (904) 392-6359
Donald R. Ulrich, Air Force Office of Scientific
Research, (202) 767-4963
Brian J.J. Zelinski, Arizona Materials Laboratories,
(602) 322-2977, FAX (602) 322-2993

SYMPOSIUM B

ADVANCED METALLIZATIONS IN MICROELECTRONICS

Avishay Katz, AT&T Bell Laboratories, (201) 582-2261,
FAX (201) 582-5917
Shyam P. Murarka, Rensselaer Polytechnic Institute,
(518) 276-2978, FAX (518) 276-8761
Ami Appelbaum, Rockwell International Corporation,
(214) 996-6522, FAX (214) 996-5545

SYMPOSIUM C

POLYSILICON THIN FILMS AND INTERFACES

Bruha Raicu, Integrated Technology Associates,
(408) 773-8614; FAX (408) 235-7028
T. Kamins, Hewlett-Packard, (415) 857-5470,
FAX (415) 857-5308
Carl V. Thompson, Massachusetts Institute of
Technology, (617) 253-7652, FAX (617) 258-8539

SYMPOSIUM D

CRITICAL CURRENTS IN HIGH-TEMPERATURE SUPERCONDUCTORS

John R. Clem, Iowa State University, (515) 294-4223,
FAX (515) 294-0689
Jack W. Ekin, National Institute of Standards &
Technology, (303) 497-5448, FAX (303) 497-5316
Sungho Jin, AT&T Bell Laboratories, (201) 582-4076,
FAX (201) 582-2913
Donald M. Kroeger, Oak Ridge National Laboratory,
(615) 574-5155, FAX (615) 574-6073

SYMPOSIUM E

HIGH RESOLUTION ELECTRON MICROSCOPY OF DEFECTS IN MATERIALS

Robert Sinclair, Stanford University, (415) 723-1102,
FAX (415) 725-4034
Ulrich Dahmen, University of California, Berkeley,
(415) 486-4627, FAX (415) 486-4888
David J. Smith, Arizona State University,
(602) 965-4540

SYMPOSIUM F

DEGRADATION MECHANISMS IN III-V COMPOUND SEMICONDUCTOR DEVICES & STRUCTURES

V. Swaminathan, AT&T Bell Laboratories,
(201) 582-4981, FAX (201) 582-5917
Stephen J. Pearton, AT&T Bell Laboratories,
(201) 582-4757, FAX (201) 582-5917
Omar Manasreh, Wright Research & Development
Center, (513) 255-4474, FAX (513) 255-5375

SYMPOSIUM G

MATERIALS ISSUES IN ART AND ARCHAEOLOGY II

James R. Druzik, Getty Conservation Institute,
(213) 822-2299; FAX (213) 821-9409
Pamela B. Vandiver, Smithsonian Institution,
(301) 238-3734, FAX (301) 238-3667
George Wheeler, Metropolitan Museum of Art,
(212) 570-3858, FAX (212) 570-3879

SYMPOSIUM H

MATERIALS FOR SENSORS AND SEPARATIONS

Marc Anderson, University of Wisconsin-Madison,
(608) 262-2470, FAX (608) 262-0454
John Armor, Air Products and Chemicals, Inc.,
(215) 481-5792, FAX (215) 481-4600
D. Jed Harrison, University of Alberta, (403) 492-2790,
FAX (403) 492-8231
Antonio J. Ricco, Sandia National Laboratories,
(505) 846-4947, FAX (505) 846-2009

SYMPOSIUM I

ALLOY PHASE STABILITY AND DESIGN

G. Malcolm Stocks, Oak Ridge National Laboratory,
(615) 574-5163, FAX (615) 574-7721
David P. Pope, University of Pennsylvania,
(215) 898-9837, FAX (215) 898-1130
Anthony F. Giamei, United Technologies Research
Center, (203) 727-7172, FAX (203) 727-7669

SYMPOSIUM J

THIN FILM STRUCTURES AND PHASE STABILITY

Bruce M. Clemens, Stanford University, (415) 725-7455,
FAX (415) 725-4034
William L. Johnson, California Institute of Technology,
(818) 356-4433, FAX (818) 795-1547

SYMPOSIUM K

THIN FILMS: STRESSES AND MECHANICAL PROPERTIES II

Warren Oliver, Oak Ridge National Laboratory,
(615) 576-7245, FAX (615) 574-7721
Mary Doerner, International Business Machines,
(408) 284-8369, FAX (408) 256-8481
George Pharr, Rice University, (713) 527-8101, Ext.
3573, FAX (713) 285-5136, Bitnet: PHARR@RICE
Franz R. Brotzen, Rice University, (713) 527-8101,
FAX (713) 285-5136

SYMPOSIUM L**MICROWAVE PROCESSING OF MATERIALS**

William B. Snyder, Oak Ridge National Laboratory, (615) 576-2178, FAX (615) 574-8216
Willard H. Sutton, United Technologies Research Center, (203) 727-7639, FAX (203) 727-7669
D. Lynn Johnson, Northwestern University, (312) 491-3584, FAX (312) 491-4133
Magdy F. Iskander, University of Utah, (801) 581-6944, FAX (801) 581-8692

SYMPOSIUM M**PLASMA PROCESSING AND SYNTHESIS OF MATERIALS**

Diran Apelian, Drexel University, (215) 895-1541, FAX (215) 895-4929
Julian Szekeley, Massachusetts Institute of Technology, (617) 253-3236, FAX (617) 253-8124

SYMPOSIUM N**LASER ABLATION FOR MATERIALS SYNTHESIS**

David C. Paine, Brown University, (401) 863-1457, FAX (401) 863-1157
John C. Bravman, Stanford University, (415) 723-3698, FAX (415) 725-4034

SYMPOSIUM O**AMORPHOUS SILICON TECHNOLOGY - 1990**

P.C. Taylor, University of Utah, (801) 581-4484, FAX (801) 581-4801
Malcolm J. Thompson, Xerox PARC, (415) 494-4561, FAX (415) 494-4919
P.G. LeComber, University of Dundee, United Kingdom, 44-382-23181, FAX 44-382-201604
Y. Hamakawa, Osaka University, Japan, 81-6-844-1151, FAX 81-6-853-1362
Arun Madan, Colorado, (303) 526-9016, FAX (303) 526-1718

SYMPOSIUM P**SURFACE AND NEAR SURFACE STRUCTURE OF POLYMER INTERFACES**

Jeffrey A. Kelber, Sandia National Laboratories, (505) 844-5436, FAX (505) 844-9624
Ralph G. Nuzzo, AT&T Bell Laboratories, (201) 582-5486
Matthew V. Tirrell, University of Minnesota, (612) 625-0192, FAX (612) 626-7246
Ernesto Occhiello, Istituto Guido Donegani, Italy, FAX (39) 321-44-7378

SYMPOSIUM Q**ATOMIC SCALE CALCULATIONS OF STRUCTURE IN MATERIALS**

Michael A. Schluter, AT&T Bell Laboratories, (201) 582-3106
Murray S. Daw, Sandia National Laboratories, (415) 294-2198, FAX (415) 294-3231

SYMPOSIUM R**INTERMETALLIC MATRIX COMPOSITES**

Donald L. Anton, United Technologies Research Center, (203) 727-7174, FAX (203) 727-7879
Robert McMeeking, University of California, Santa Barbara, (805) 961-4583, FAX (805) 961-8124
Daniel Miracle, United States Air Force, Wright-Patterson AFB, (513) 255-9833, FAX (513) 255-9792
Patrick Martin, Los Alamos National Laboratory, (505) 667-8168, FAX (505) 667-1754

SYMPOSIUM S**PHYSICAL PHENOMENA IN GRANULAR MATERIALS**

Theodore H. Geballe, Stanford University, (415) 723-0215, FAX (415) 723-0010
Ping Sheng, Exxon Research & Engineering, (201) 730-2870, FAX (201) 730-3042
G.D. Cody, Exxon Research & Engineering, (201) 730-3022; FAX (201) 730-3042

SYMPOSIUM T**SUPERPLASTICITY IN METALS, CERAMICS, AND INTERMETALLICS**

Merrieta J. Mayo, Sandia National Laboratories, (505) 846-3551, FAX (505) 846-5064
Jeffrey Wadsworth, Lockheed Missile & Space Co., Inc., (415) 424-2234, FAX (415) 354-5415
Masaru Kobayashi, Technological University of Nagaoka, Japan, 0258-46-6000, Ext. 7120, FAX 0258-46-6972
Amiya K. Mukherjee, University of California at Davis, (916) 752-1776; FAX (916) 752-8058

SYMPOSIUM U**MATERIALS INTERACTIONS RELEVANT TO THE PULP, PAPER AND WOOD INDUSTRIES**

June D. Passaretti, Pfizer Minerals Research Center, (215) 861-3431, FAX (215) 861-3412
Daniel Caulfield, USDA Forest Service, (608) 231-9436, FAX (608) 231-9592
Rustum Roy, Pennsylvania State University, (814) 865-3421, FAX (814) 865-2326
Vance Setterholm, USDA Forest Service, (608) 264-5878; FAX (608) 264-5692

SYMPOSIUM V**EPITAXIAL HETEROSTRUCTURES**

Don W. Shaw, Texas Instruments, Inc., (214) 995-4788, FAX (214) 995-5539
John C. Bean, AT&T Bell Laboratories, (201) 582-3324, FAX (201) 582-3901
Vassilis G. Keramidas, Bellcore, (201) 758-3353, FAX (201) 758-9626
Paul S. Peercy, Sandia National Laboratories, (505) 844-4309, FAX (505) 846-2009

SYMPOSIUM W**WORKSHOP ON SPECIMEN PREPARATION FOR TRANSMISSION ELECTRON MICROSCOPY OF MATERIALS II**

Ron Anderson, IBM, (914) 892-2225, FAX (914) 892-2555

SYMPOSIUM X**FRONTIERS OF MATERIALS RESEARCH**

Robert A. Huggins, Stanford University, (415) 723-4110, FAX (415) 725-4034

SYMPOSIUM Y**FERROELECTRIC THIN FILMS**

Angus I. Kingon, North Carolina State University, (919) 737-2347, FAX (919) 737-3419
Edward R. Myers, National Semiconductor, (408) 721-2258, FAX (408) 736-8503

■ FUTURE MRS MEETINGS ■

1990 Spring Meeting: April 16-21

San Francisco Marriott Hotel
San Francisco, CA

Meeting Chairs:

John C. Bravman (415) 723-3698; FAX (415) 725-4034
C. Jeffrey Brinker (505) 846-3552; FAX (505) 846-5064
William H. Butler (615) 574-4845; FAX (615) 574-7721
Abstract Deadline: November 15, 1989

1990 Fall Meeting: November 26 - December 1

Boston Marriott Hotel and Westin Hotel/Copley Place
Boston, Massachusetts

Meeting Chairs:

Robert Hull (201) 582-6455; FAX (201) 582-3901
Gregory J. McCarthy (701) 237-7193; FAX (701) 237-7050
Frans Spaepen (617) 495-3760; FAX (617) 495-9837
Abstract Deadline: July 1, 1990

1991 Spring Meeting: April 29 - May 3

Anaheim Marriott Hotel
Anaheim, California

Meeting Chairs:

A.K. Hays (505) 844-7632; FAX (505) 844-1543
Ernesto E. Marinero (408) 927-2016; FAX (408) 927-2100
Carl V. Thompson (617) 253-7652; FAX (617) 258-8539
Abstract Deadline: November 15, 1990

1991 Fall Meeting: December 2-7

Boston Marriott Hotel and Westin Hotel/Copley Place
Boston, Massachusetts

Meeting Chairs:

Julia M. Phillips (201) 582-4428; FAX (201) 582-2521
Michael M.J. Treacy (201) 730-2755; FAX (201) 730-3042
Man H. Yoo (615) 574-5165; FAX (615) 574-7721
Abstract Deadline: July 1, 1991

International Conference on Electronic Materials-1990:

September 17-19

Newark, New Jersey

Co-sponsored by:

Materials Research Society, European Materials Research Society,
and the Japan Society of Applied Physics

Abstract Deadline: May 1, 1990

R.P.H. Chang (312) 491-3598; FAX (312) 491-4181
Takeo Sugano (813) 812-2111 #6675; FAX (813) 818-5706
Van Tran Nguyen (33) 76 76 40 69; FAX (33) 76 90 34 43

International Conference on New Diamond Sciences and Technology (ICNDST-90):

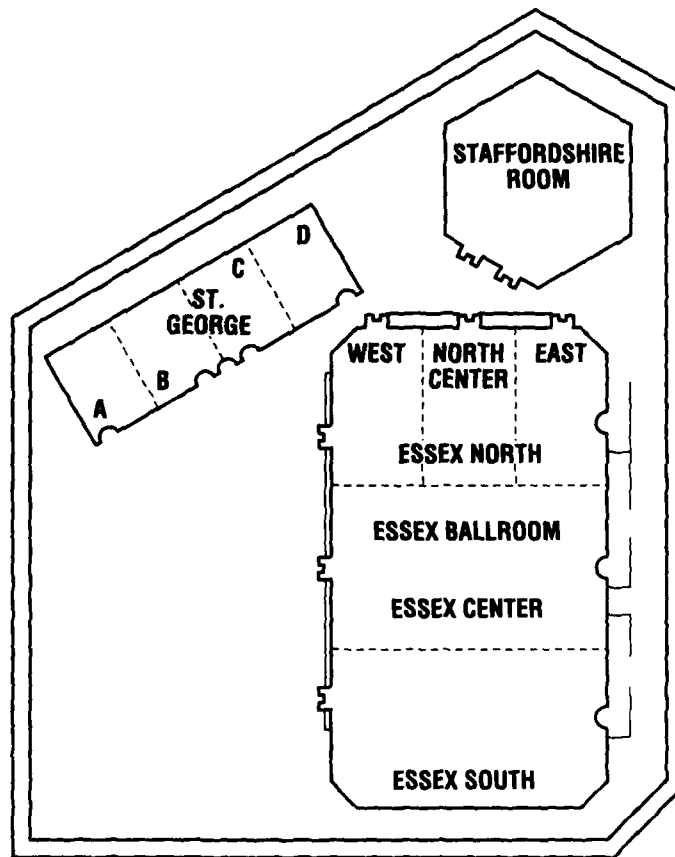
September 23-27

Crystal City, Virginia

Co-sponsored by:

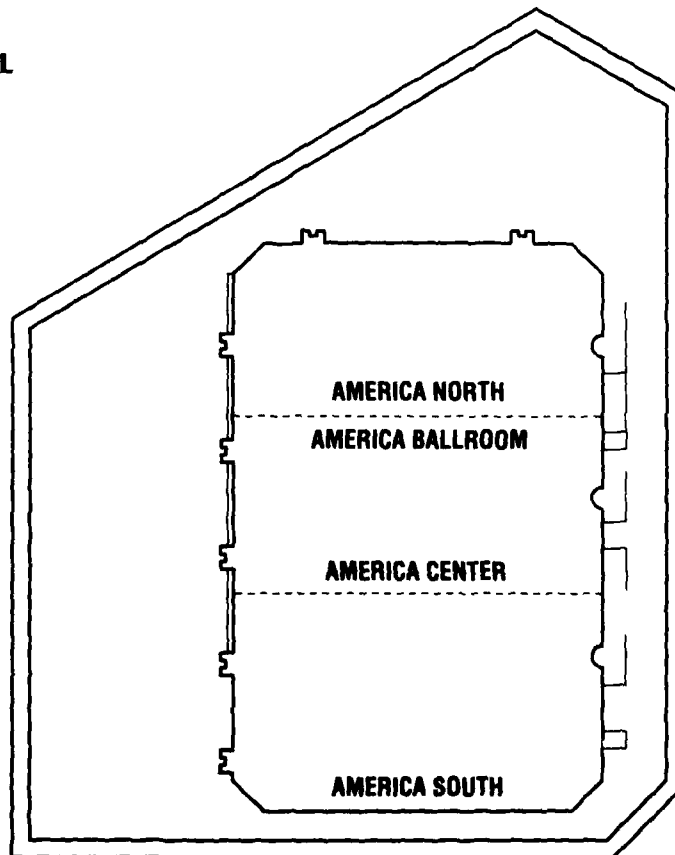
Materials Research Society and the Electrochemical Society

Russell Messier (814) 865-3423; FAX (814) 865-2326



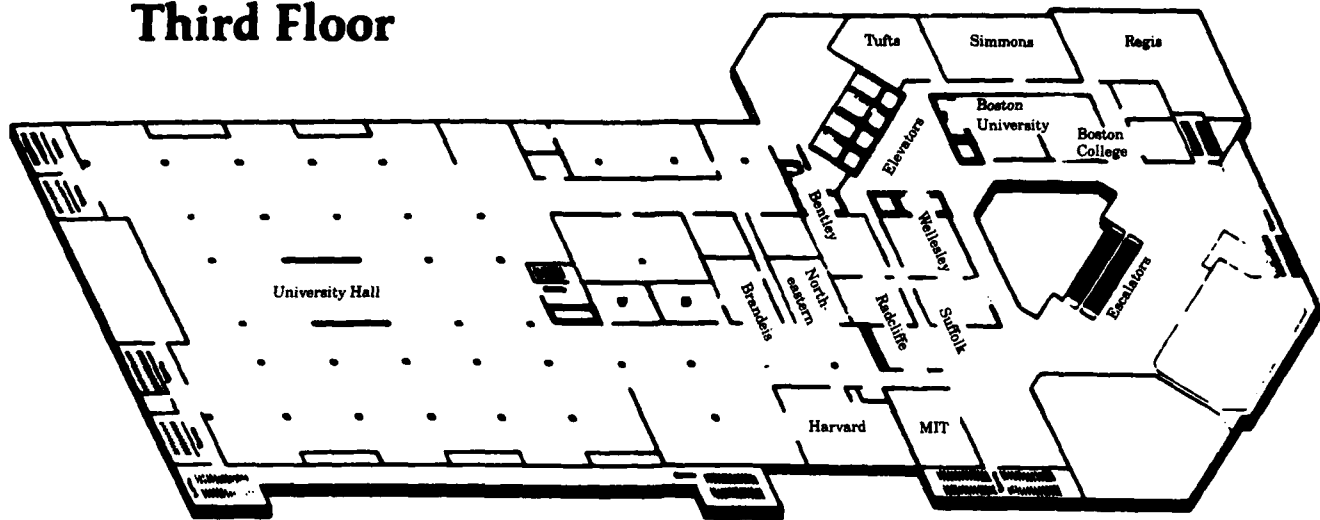
THIRD FLOOR

THE WESTIN HOTEL

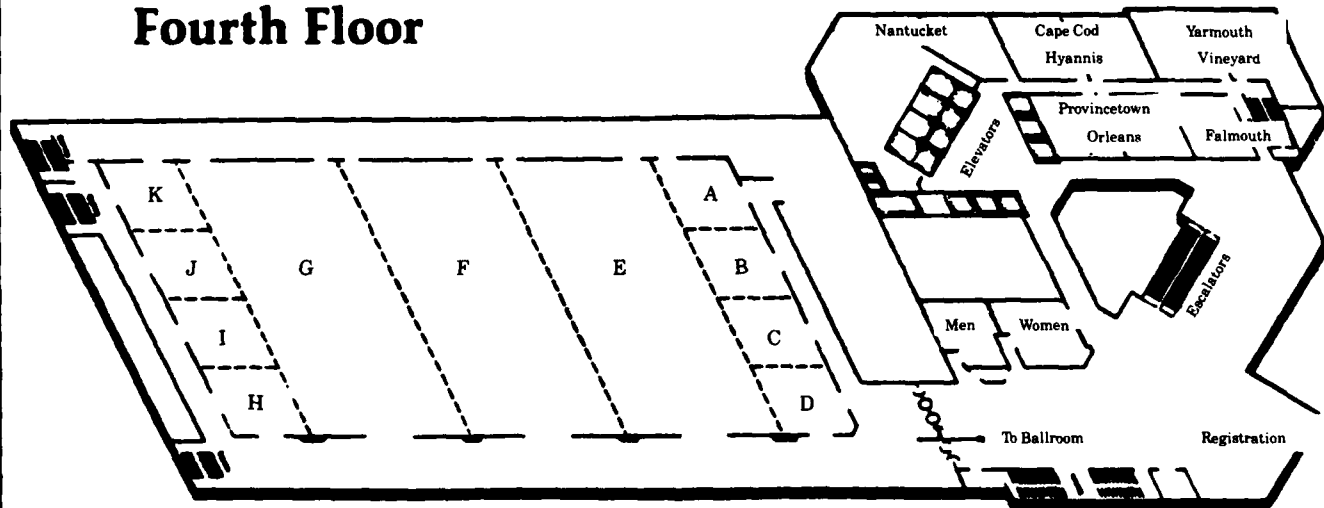


FOURTH FLOOR

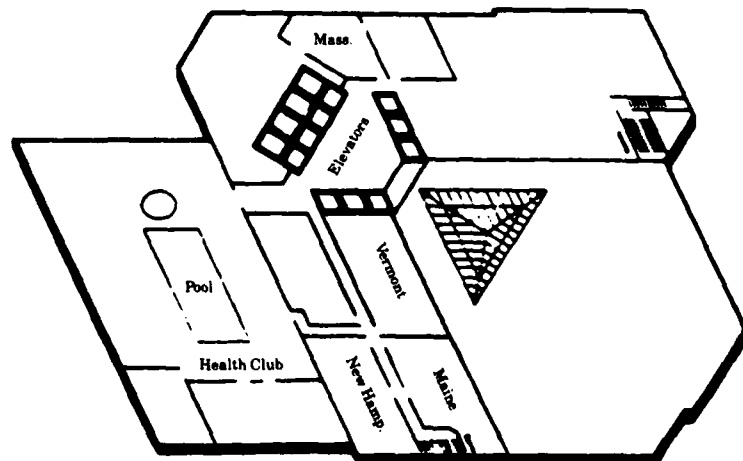
Third Floor



Fourth Floor



Fifth Floor



Marriott
HOTELS • RESORTS

BOSTON MARRIOTT HOTEL COPLEY PLACE

1989 FALL MEETING ACTIVITIES LOCATOR

	SUNDAY NOV. 26	MONDAY, NOV. 27		
		a.m.	p.m.	eve
A: Beam-Solid Interactions		Salon E (M)		
B: In Situ Patterning				
C: Atomic Scale Structure		Salon A/B (M)		
D: Layered Structures		Salon C/D (M)		Salon C/D (M)
E: Properties of II-VI Semiconductors		Salon H/I (M)		
F: Wide Bandgap Semiconductors				
G: Defects in Semiconductors		Salon F (M)		
H: Microcrystalline Semiconductors				
I: Plasma-Enhanced CVD		Yarmouth/Vineyard (M)		
J: Neutron Scattering		Salon J/K (M)		
K: Electronic Packaging		Provincetown/Orleans (M)		
L: CVD Refractory Metals/Ceramics				
M: High-Temperature Superconductors		Salon G (M)		
N: Interfaces in Composites		Essex NW (W)		
O: Polymer Based Molecular Composites		America Center (W)		
P: Optical Fiber Materials		Staffordshire (W)		
Q: Organic Solid-State Materials		Essex NE (W)		
R: Materials Synthesis/Biological Processes		Essex South (W)		
S: Multi-functional Materials				
T: Fractals				
U: Nuclear Waste Management		America North (W)		
V: Macromolecular Liquids		Essex Center (W)		
W: Fly Ash and Coal Conversion By-Products				
X: Frontiers of Materials Research		Staffordshire (W) 12:05-1:25 p.m.		
Y: Specialty Cements		Adams (W)		
Meeting Registration	Fourth Floor (M) 4:00-9:00 p.m.	Fourth Floor (M) 7:00 a.m.-7:00 p.m.		
Manuscript Room				
Equipment Exhibit				
MRS Short Courses	M-05, C-09	M-05, M-06, C-01, C-06, C-09, C-14, C-16, P-05, F-08		

6:00 p.m. Plenary Session
Salon E, Marriott Hotel
Robert N. Noyce

TUESDAY, NOV. 28			WEDNESDAY, NOV. 29			THURSDAY, NOV. 30			FRIDAY, DEC. 1		SAT. DEC. 2
a.m.	p.m.	eve	a.m.	p.m.	eve	a.m.	p.m.	eve	a.m.	p.m.	
Salon E (M)		America Ballroom (W)				Salon E (M)		America Ballroom (W)	Salon E (M)		
			Salon E (M)			Salon A/B (M)		America Ballroom (W)	Salon A/B (M)		
Salon A/B (M)		America Ballroom (W)	Salon A/B (M)								
Salon C/D (M)			Salon C/D (M)			Salon C/D (M)		America Ballroom (W)	Salon C/D (M)		
Salon H/I (M)			Salon H/I (M)			Salon H/I (M)			Salon H/I (M)		
America South (W)		America Ballroom (W)	America South (W)			America South (W)		America Ballroom (W)	America S (W)		
Suffolk (M)			Suffol (M)			Suffolk (M)			Suffolk (M)		
Salon F (M)		America Ballroom (W)	Salon F (M)			Salon F (M)		America Ballroom (W)	Salon F (M)		
			Salon J/K (M)			Salon J/K (M)		America Ballroom (W)	Salon J/K (M)		
Yarmouth Vineyard (M)						Yarmouth Vineyard (M)					
Salon I/K (M)			Yarmouth Vineyard (M)								
Provincetown Orleans (M)		America Ballroom (W)	Provincetown Orleans (M)								
			Essex NW (W)			Essex NW (W)			Essex NW (W)		
Salon G (M)			Salon G (M)		America Ballroom (W)	Salon G (M)			Salon G (M)		
Essex NW (W)			America Lobby (W)			America Lobby (W)			America Lobby (W)		
America Center (W)		America Ballroom (W)	America Center (W)								
St. George (W)			St. George (W)			St. George (W)					
Essex NE (W)			Essex NE (W)								
Essex South (W)		America Ballroom (W)	Essex South (W)			Essex South (W)			Essex South (W)		
Essex NC (W)			Essex NC (W)			Essex NC (W)					
				Essex NE (W)		Essex NE (W)			Essex NE (W)		
Staffordshire (W)			Staffordshire	America North (W)		Staffordshire (W)		America Ballroom (W)	Staffordshire (W)		
America North (W)		America Ballroom (W)	America North (W)			America North (W)					
Essex Center (W)			Essex Center (W)			Essex Center (W)		America Ballroom (W)	Essex Center (W)		
				Adams (W)		Adams (W)					
Staffordshire (W) 12:05-1:25 p.m.			Staffordshire (W) 12:05-1:25 p.m.			Staffordshire (W) 12:05-1:25 p.m.					
Adams (W)			Adams (W)			Adams (W)					
Fourth Floor (M) 7:30 a.m.-5:00 p.m.			Fourth Floor (M) 7:30 a.m.-5:00 p.m.			Fourth Floor (M) 7:30 a.m.-5:00 p.m.			Fourth Floor (M) 7:30 a.m.-noon		

Marrriott Hotel: Cape Cod Hyannis - 4th Floor
Westin Hotel: St. George A - 3rd Floor
Open Daily 7:30 a.m. - 5:30 p.m.

University Hall (M) Noon - 7:00 p.m. Deli Lunch Noon - 1:30 p.m. Reception 5:00 - 7:00 p.m.	University Hall (M) 9:30 a.m. - 5:00 p.m. Deli Lunch Noon - 1:30 p.m.	University Hall (M) 9:30 a.m. - 2:00 p.m. Deli Lunch Noon - 1:30 p.m.		M-04, C-03, C-06, C-20, P-06, P-12, P-14, P-15, F-04	M-04, C-03, C-06, P-06 P-14, F-04
C-01, C-19, P-16, F-01, F-08	C-01, C-19, P-16, F-01, F-08	C-19, P-16 F-02, F-04			